F1103

R

REVUE ROUMAINE DE CHIMIE

[illegible]LVA

Tome 18
N° 1
Janvier 1973
RRCHAX, 18, *1*, 1—186 (1973)

ÉDITIONS DE L'ACADÉMIE DE LA RÉPUBLIQUE SOCIALISTE DE ROUMANIE

Rev. Roumaine Chim. 18, *1*, p. 1—186 (1973), Bucarest

COMITÉ DE RÉDACTION

Rédacteur en chef :

I. G. MURGULESCU, membre de l'Académie de la République Socialiste de Roumanie

Rédacteurs en chef adjoints :

A. T. BALABAN et V. EM. SAHINI, membres correspondants de l'Académie de la République Socialiste de Roumanie

Collège de rédaction :

C. DRĂGULESCU, RALUCA RIPAN, CR. SIMIONESCU, membres de l'Académie de la République Socialiste de Roumanie ; EM. BRATU, ECATERINA CIORĂNESCU-NENITZESCU, P. SPACU, membres correspondants de l'Académie de la République Socialiste de Roumanie ; MARGARETA AVRAM, I. D. MARCHIDAN, G. NIAC et D. SĂNDULESCU

La Revue Roumaine de Chimie paraît 12 fois par an. Toute commande de l'étranger (fascicules ou abonnements) sera adressée à Intreprinderea Rompresfilatelia, Boîte postale 2001, telex 011631, Bucarest, Roumanie

Les manuscrits, les livres et les revues proposés en échange, ainsi que toute correspondance seront envoyés à la rédaction :

REVUE ROUMAINE DE CHIMIE
23, Str. Dumbrava Roşie, Bucarest, Roumanie

ÉDITIONS DE L'ACADÉMIE DE LA RÉPUBLIQUE SOCIALISTE DE ROUMANIE
3 bis, Str. Gutenberg, Bucarest

REVUE ROUMAINE
DE
CHIMIE

SZÁGOS MŰSZAKI KÖNYVTÁR
CIÓS

Tome 18, N° 1 Janvier 1973

Page

S. SOLACOLU and D. POPESCU-HAŞ, The mineralizing action of F^- ions in vitroceramic structures of the $Na_2O-MgO-Al_2O_3-SiO_2$-system on volume effects 3–10

S. STERNBERG and LUCIA BEJAN, Thermodynamic properties of the reciprocal mixtures of fused salts : $AgCl+(K, Rb, Cs)$.I . . . . 11–22 B4.

R. DINESCU et M. CERCHEZ, Les équilibres de phase du système $NaO^2-CaO-Al_2O_3-SiO_2$. Equilibres de phase dans le sous-système $NaO^2.\,Al_2O_3.\,6SiO_2-CaO.\,Al_2O_3.\,2SiO_2-3Al_2O_3.\,2SiO_2-Al_2O_3$ intéressant la céramique superalumineuse 23–34

AL. CECAL et I. A. SCHNEIDER, Réactions d'échange isotopique entre Tl(III) complexé et $^{204}Tl(I)$ 35–42

C. DRĂGULESCU, T. SIMONESCU and MARIA TOTAN CURTUI, Study of the thorium-purpurin complex by butanol extraction 43–48

C. DRĂGULESCU and NICOLETA VÎLCEANU, Uranyl-pyrophosphate complexes. III. The monopyrophosphato-pentauranyl cation complex. 49–52

C. DRĂGULESCU, NICOLETA VÎLCEANU and I. JULEAN. Uranyl-pyrophosphate complexes. IV. Precipitation reactions of the pyrophosphato-uranylate complex anions with the Ag^+ ion 53–58

C. DRĂGULESCU and NICOLETA VÎLCEANU, Uranyl-pyrophosphate complexes. V. The precipitation reaction of the sodium bis-pyrophosphato-uranylate complex with the Cd^{2+} ion 59–62

N. S. BIRADAR and V. H. KULKARNI, Schiff base complexes with IV and V group metals 63–71

MARIA MAVRODIN-TĂRĂBÎC, L'étude des espèces ioniques formées par l'hydrolyse de l'ion d'uranium hexavalent . . . . 73–88 K

L. KLASINC, N. TRINAJSTIĆ and E. POP, Theoretical study of isomeric thienylfurans 89–98

M. VLASSA, MARIA IONESCU and J. FABIAN, Electronic structure and transitions of 1, 2, 3-trimethoxyacridine 99–109

FELICIA CORNEA, CORNELIA FULEA et A. O. FULEA, Relations concernant la structure électronique et la réactivité de quelques thioamides . . . 111–121

A. BALOG, D. BREAZU, VIORICA VOINESCU, MARGARETA HERMAN, E. VARGHA and E. RAMONȚIAN, Peptides. XII. Behaviour of the mixed anhydrides of some amino acids N-protected with β-ketoesters. 123–129

Rev. Roumaine Chim. **18**, *1*, p. 1–186 (1973), Bucarest

M. VOICU, F. BADEA and ANCA VOICU, Kinetics of solvolytic reactions. IV. Transition state in the π-route of the acetolysis of 5H-dibenzo [a, d]-cyclohepten-5-yl-(β-ethyl) tosylate 131–144

I. C. POPESCU, C. LITEANU and V. CIOVÎRNACHE, Characterization of the ceramic ion-selective membrane-electrodes. IV. Influence of the obtaining conditions of Ag_2S membrane upon the working of Ag^+-selective membrane-electrode 145–153

C. LITEANU and A. CONSTANTINESCU, Paper thermochromatography. XVII. The separation of leucine and isoleucine in temperature gradient 155–159

TIBERIU NĂȘCUȚIU, Le comportement des ions inorganiques en chromatographie sur papier avec solvants à base d'alcools—acides 161–174

GH. FURNICĂ, MARIA TOADER, ELISABETA TURCITU et ȘTEFANIA BULAN, L'étude du mécanisme physico-chimique de la sorption des isotopes radio-actifs par certaines macromolécules inorganiques polyélectrolytiques. I. La sorption physique et chimique par la diatomite, la montmorillonite, la kieselguhr, le silicagel, le kaolin et la calcite, des radionucléides des éléments I, P, Na, Cs, Sr, Ba, Zn, Cu, Co, Mn et Fe 175–185

Revue Roumaine de Chimie, 18, 1, 3–10 (1973)

THE MINERALIZING ACTION OF F^- IONS IN VITROCERAMIC STRUCTURES OF THE $Na_2O-MgO-Al_2O_3-SiO_2$-SYSTEM ON VOLUME EFFECTS

S. SOLACOLU and D. POPESCU-HAŞ
Polytechnical Institute, Chair of Physical Chemistry of Silicates and Oxide Compounds
Str. Polizu, 1, Bucharest, Romania

Received July 24, 1972

Volume effects which occur upon heating a vitreous structure of the $Na_2O-MgO-Al_2O_3-SiO_2$-system using fluorine as a nucleator were investigated. Two plastic deformation areas preceding the appearance of crystalline phases were revealed by the dilatometric curves. The correspondence between temperatures at which plastic deformation areas and those of exothermal peaks on the ATD curves confirms the two stages involved in the formation and crystallization of microphases in vitroceramic masses with fluorine. The difference in the expansion coefficients of masses in various primary structuration compartments shows that structuration is based on the relations of phase heat equilibrium. The predominance of a certain type of structures, in various vitroceramic masses investigated, indicates the selectivity impressed by F^- ions as nucleators on these masses.

1. INTRODUCTION

Both vitreous microphases and crystalline phases occurring in vitroceramic structures obtained by low-temperature crystallization are usually not equilibrium phases and are different from the others found in ceramic masses with the same oxide composition [1,2,3]. They are generally metastable phases and their composition, respectively, the characteristics impressed on vitroceramic masses depend on the heat treatment during crystallization.

Mg^{2+} and Al^{3+} ions in tetrahedral coordination may participate, together with Si^{4+} ions in the formation of vitreous structures [4,5,6] and having larger ionic radius, vitreous structures will be looser or more com-

---

[1] I. I. Kitsigorodski and R. I. Hodowskaia, "Slekloobraznoie" – vol. I, Izd. Akad. S.S.S.R., Moskva-Leningrad, 1963, p. 31.

[2] R. I. Hodowskaia and N. M. Pavluşkin, *Neorganiceskie materiali*, **3**, 1908 (1967).

[3] D. Popescu-Haş, Doctorial thesis, Polytechnical Institute of Bucharest, 1971, p. 127.

[4] E. I. Galiant, *Doklady Akad. Nauk S.S.S.R.*, **137**, 1425 (1961).

[5] L. I. Aiswert, *J. Soc. Glas. Technol.*, **38**, 479 (1954).

[6] K. O. Botvinik and A. G. Jaroker, *Neorganiceskie materiali*, **3**, 1638 (1967).

pact, depending on the larger or smaller number of (MgO_4) (AlO_4) tetrahedra involved in their formation and causing variations in density and in volume.

Our investigations regarding the microstructure of vitroceramic masses of the $Na_2O-MgO-Al_2O_3-SiO_2$ - system showed that the proportion of tetrahedral coordination and penetration of Mg^{2+} and Al^{3+} ions into the composition of solid solutions — the structure of α-quartz appearing as metastable phases in these masses — varies in relation to the MgO and Al_2O_3 content and to the heat treatment during crystallization. [2,3,7]

Taking into account these considerations, the present paper investigates the volume effects obtained on heating certain vitreous structures of the $Na_2O-MgO-Al_2O_3-SiO_2$-system, using fluorine as a nucleator.

2. EXPERIMENTAL APPROACH

The glasses studied were melted in an electric furnace with a platinum-rhodium crucible of own construction. Fluorine-free glasses were melted at a temperature of 1500° for 120 minutes and glasses containing fluorine were melted at 1450° for 60 minutes. Fluorine mixtures were dried prior to melting at 110°, to reduce fluorine losses during the melting process.

The $5 \times 5 \times 50$ mm and $5 \times 5 \times 25$ mm samples were shaped by pressing the melt into metallic moulds and rapidly cooling it thereafter until a temperature of 500° was reached; the cooling rate was then controlled in an electric annealing kiln.

Volume effects were determined by a Leitz—Wetzlar dilatometer.

3. EXPERIMENTAL RESULTS

3.1. VITREOUS STRUCTURES OF THE $Na_2O-MgO-Al_2O_3-SiO_2$ PHASE EQUILIBRIUM SYSTEM

Usually, the melting temperature is of 1500° in glass industry furnaces, hence the compositions of the investigated vitreous structures were placed in the area delimited by the conical projection of the isotherme of 1500° of the $MgO-Al_2O_3-SiO_2$ ternary system in the section corresponding to 10% Na_2O content in the $Na_2O-MgO-Al_2O_3-SiO_2$-system.

Since the $Na_2O-MgO-Al_2O_3-SiO_2$ quaternary system was not investigated, the primary crystallization volumes of components have not yet been delimited; because the 10% Na_2O section is very close to $MgO-Al_2O_3-SiO_2$ ternary system, it was assumed that the position of the compositions investigated in the primary crystallization volumes of the quaternary system corresponds to the primary crystallization compartments of components in the basic ternary system, within the limit of admissible errors.

---

[7] S. Solacolu and D. Popescu-Haş, *Rev. Roumaine Chim.*, **17**, 319 (1972).

Compositions investigated in various primary crystallization compartments presented a same content of SiO_2 while Al_2O_3 and MgO contents varied; the 10% Na_2O content remained constant in all compositions.

The research regarding the volume effects involved in the formation of vitroceramic structures took into account the following objectives:

— occurrence of new phases, structural changes and variation of rheological characteristics during crystallization by heat treatment;

— variation in volume effects in relation to temperature and whether the value of expansion coefficients is similar to the specific value of compounds corresponding to the primary crystallization compartments involving the investigated compositions.

3.2. SYNTHESIS OF VITREOUS STRUCTURES

The raw materials used in the synthesis of the studied glasses were: vein-quartz with a 99.75% 0.1 mm finely-ground SiO_2 content, pure calcinated alumina, magnesium oxide for analysis, sodium carbonate for analysis and pure cryolite.

Mixtures were subjected to gravimetric determination and homogenized in ball-mills. Each mixture was melted three times for homogeneity purposes; specimens were shaped from glasses melted for the third time.

The absence of crystalline phases in the resulting vitreous structures was controlled by X-ray diffraction and by polarized light microscopy.

4. DISCUSSION OF RESULTS

4.1. GLASSES WITHOUT F⁻ ION AS A NUCLEATOR

Figure 1 presents the relative expansion curves of some representative fluorine-free masses denoted by $S_1 - S_7$ symbols whose composition is situated in the primary crystallization compartments of the Na_2O-$-MgO-Al_2O_3-SiO_2$-system.

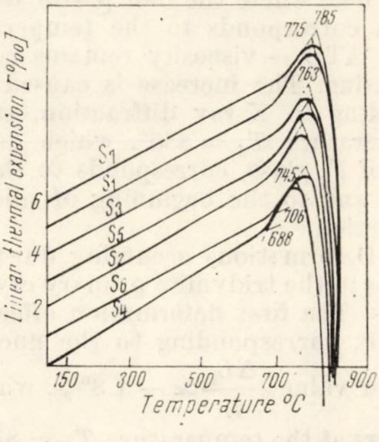

Fig. 1. — Relative expansion curves of fluorine-free glasses of the $Na_2-MgO-Al_2O_3-SiO_2$-system.

The dilatometric curves of investigated fluorine-free glasses are typical for the dilatometric curves of glasses and present three characteristic areas.

The first area corresponds to the practically linear expansion and the average expansion coefficient is $\alpha_{10}^{640} = 7.1 \ldots 8.1 \times 10^{-6}\,°C^{-1}$. The second area corresponds to the so-called dilatometric anomalies due to structural changes occurring in vitreous phase at temperatures ranging between 600°... 720° and 745°... 785°. The third area corresponds to the viscous flow.

4.2. GLASSES WITH F⁻ IONS AS NUCLEATORS

The dilatometric curves of glasses in the $Na_2O-MgO-Al_2O_3-SiO_2$-system with F^--ions as nucleators denoted by $F_1 - F_6$ symbols present inflections that indicate, on the one hand, the variation of rheological characteristics in relation to temperature and, on the other hand, the occurrence of new phases and structural changes producing volume variations.

In general, as temperature increases following plastic deformation effects, viscosity of glasses is lowered to a certain point; it then remains constant for a short period of time called "nucleation" period of crystallization, due to the occurrence of new phases, and starts increasing thereafter. The mass becomes rigid and begins again to expand.

4.2.1. *Volume effects in tridymite masses.* The dilatometric curves of glasses in this primary crystallization compartment compared to ATD curves (fig. 2a) show that, in addition to the temperature corresponding to structural changes in vitreous state, these glasses present four other temperatures which delimit two plastic deformation areas. At temperature $T_2 - 640°$ where the first plastic deformation area ends for F_1 glass — and which corresponds to the temperature of the first exothermic peak on curve ATD — viscosity remains constant for a moment and then starts increasing. The increase is caused by the occurrence of fluorides which, according to X-ray diffraction, start crystallizing at this temperature. Temperature $T_4 = 835°$, which delimits the second plastic deformation area of F_1 glass, corresponds to the second exothermic peak on the ATD curve and to the beginning of silicate crystallization according to X-ray diffraction.

Deformations occurring due to plastic deformation in vitroceramic masses in the tridymite primary crystallization compartment have medium values. The first deformation effect which appears at temperature $T_2 = 640°$, corresponding to the nucleation of fluoride crystals, presents a smaller value $\frac{\Delta L_1}{L} \simeq -1.8‰$, while the second effect which no longer appears at the temperature $T_4 = 835°$, corresponding to silicate nucleation, presents an almost double value $\frac{\Delta L_2}{L} \simeq -3.2‰$.

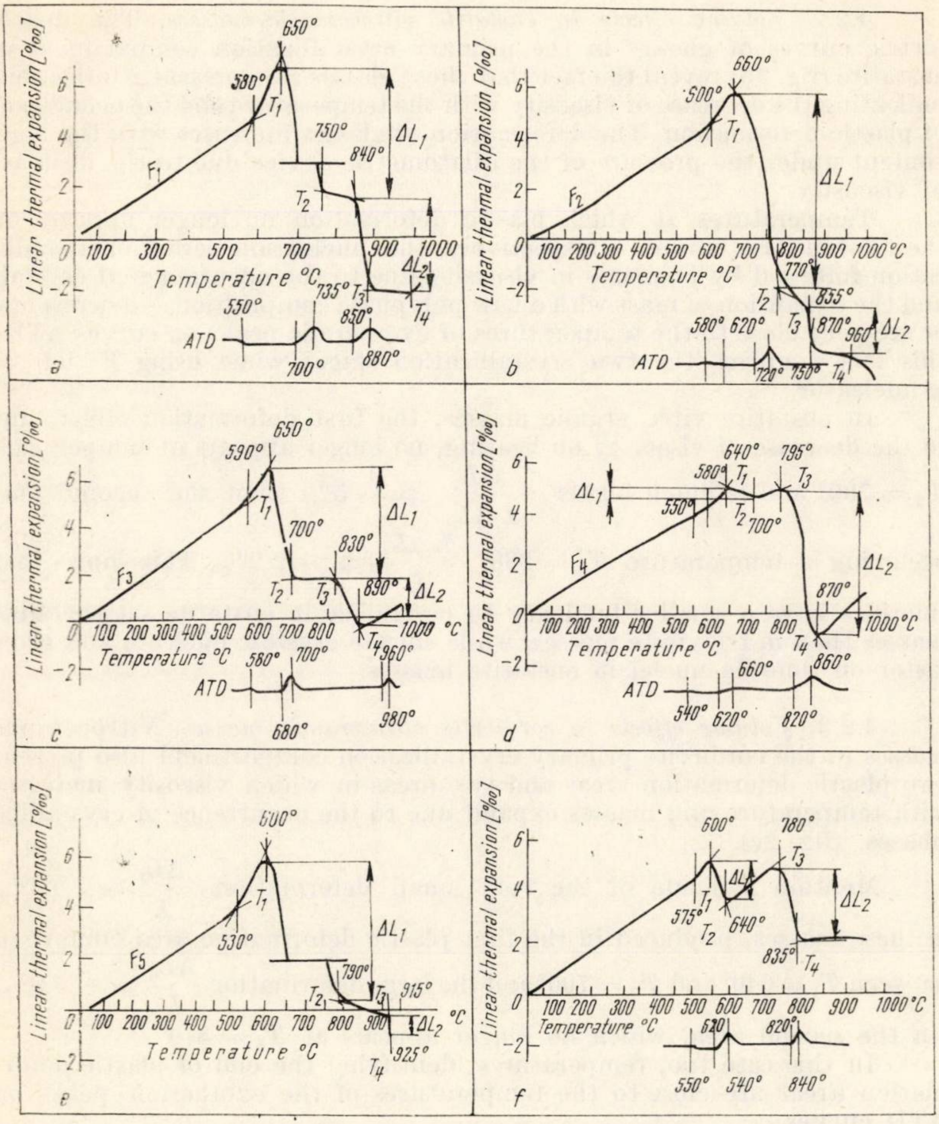

Fig. 2. — Volume effects involved in heat expansion and ATD characteristic to F$^-$ nucleated vitroceramic masses of the $Na_2O-MgO-Al_2O_3-SiO_2$-system.

a – tridymite, *b* – enstatite, *c* – cordierite, *d* – forsterite, *e* – spinel, *f* – sapphirine vitroceramics.

This shows that fluorides nucleate at higher viscosities than do silicates in tridymite vitroceramic masses.

4.2.2. *Volume effects in enstatite vitroceramic masses.* The dilatometric curves of glasses in the primary crystallization compartment of enstatite (fig. 2b) reveal the fact that these glasses also present 2 inflections indicating the decrease of viscosity with the temperature and the occurrence of plastic deformation. The deformation of glasses increases with the MgO content under the pressure of the dilatometric device due to the decrease of viscosity.

Temperatures at which plastic deformation no longer appears on the dilatometric curves — respectively the nucleation period of crystallization followed by increases in viscosity due to the occurrence of crystals and the expansion of mass with a new polyphase composition — correspond or are very close to the temperatures of exothermic peaks on curves ATD ; this fact confirms the two crystallization stages when using F^- ion as a nucleator.

In enstatite vitroceramic masses, the first deformation effect, due to the decrease of viscosity on heating, no longer appears at temperature $T_2 = 700°$ and is much higher $\frac{\Delta L_1}{L\Delta L_2} \simeq -5\%$ than the second one, occurring at temperature $T_4 = 890°$ $\frac{L\Delta L_2}{L} \simeq -2.2^0/_{00}$. This shows that fluorides have a smaller tendency to crystallize in enstatite vitroceramic masses than in tridymite masses, while silicate crystals nucleate and grow faster on fluoride nuclei in enstatite masses.

4.2.3. *Volume effects in cordierite vitroceramic masses.* Vitroceramic masses in the cordierite primary crystallization compartment also present two plastic deformation areas and two areas in which viscosity increases with temperature and masses expand due to the occurrence of crystalline phases. (fig. 2c).

Mention is made of the very small deformation $\frac{\Delta L_1}{L} \simeq -0.4^0/_{00}$ in these masses, produced in the first plastic deformation area comprised between $T_1 = 640°$ and $T_2 = 700°$ and the large deformation $\frac{\Delta L_2}{L} \simeq -5.8^0/_{00}$ in the second area, which no longer appears at $T_4 = 870°$.

In this case too, temperatures identifying the end of plastic deformation areas are close to the temperatures of the exothermic peaks on ATD curves.

A characteristic phenomenon for these masses is the fact that fluoride nucleation occurs during the heating process involving the lowest reduction of viscosity.

4.2.4. *Volume effects in forsterite, spinel and sapphirine vitroceramic masses.* The volume effects revealed by the dilatometric curve of those glasses (fig. 2d, f, g) are generally similar to those glasses investigated in the other primary crystallization compartments. Each of them presents two plastic deformation areas which end at temperatures close to the exothermic peaks on ATD curves.

A particularity of glasses with composition situated in these primary crystallization compartments and characterized by a lower-than 50% SiO_2 content, is the very large deformation in the first dilatometric plastic deformation area (forsterite $\frac{\Delta L_1}{L} \simeq -2\%$ and sapphirine $\frac{\Delta L_1}{L} \simeq -5\%$) which indicates the lowest viscosity at which nucleation of fluoride crystals occurs.

Viscosity increases at temperatures beyond those involved in the nucleation of crystallization due to the occurrence of crystalline phases and masses with a new phase composition present an almost constant expansion or a slight contraction due to crystallization.

4.3. ACTION OF F^- IONS ON THE STRUCTURE AND VOLUME EFFECTS IN VITROCERAMIC MASSES

Table 1 presents the average expansion coefficients α_{20}^{300} of vitro ceramic masses treated at 850° and 950° for 60 minutes and at 1000° under the heating conditions which correspond to the determination of the dilatometric curve. The values of the expansion coefficients of vitroceramic masses subjected to heat treatment at various temperatures are not specific for the compounds corresponding to the primary crystallization compartments in which they are situated.

Table 1

Volume effects and heat expansion of fluorine-nucleated ceramic masses of the $Na_2O-MgO-Al_2O_3-SiO_2$-system

Vitroceramic masses	Plastic deformation		$\alpha_{20}^{300} \times 10^{-6}$			
	$\frac{\Delta L_1}{L} \cdot 10^3$	$\frac{\Delta L_2}{L} \cdot 10^3$	Glass	Vitroceramics subjected to heat treatment at temperatures of :		
				850°	950°	1000°
Tridymite	− 1.8	−3.2	8.5	11.5	12.00	12.5
Enstatite	− 5.0	−2.2	8.6	12.1	13.5	13.5
Cordierite	− 0.4	−5.0	7.5	10.4	11.5	11.6
Forsterite	−20	−2.0	8.1	13.5	14.6	14.7
Spinel	− 7.5	−2.0	7.7	15.2	15.3	15.3
Sapphirine	−50	−0.8	8.0	—	—	12.3

Within this system, cordierite glasses as well as cordierite vitroceramic masses present the least volume effects due to heat expansion. This shows that the incipient cordierite vitreous microphases have a remarcable heat stability, similar to the cordierite crystalline phases. The volume behaviour to temperature is different in the various vitroceramic masses of this system which, from point of view of dilatometry, follow the criterion of the primary crystallization compartments of crystalline phases. This shows that the structuration of vitreous microphases is oriented and is according with the relations of crystalline phase heat equilibrium of the system and varies in relation to the primary phase crystallization compartment including the mass composition; it divides vitroceramic masses into : tridymite, cordierite forsterite, spinel and sapphirine.

The small differences among the expansion coefficients of the vitroceramic masses in various primary crystallization compartments are due to the small proportion of the crystalline phases specific to each compartment compared to the preponderating crystalline phase which is represented by one single type of fluorosilicate belonging to the mica family (phlogopite).

5. CONCLUSIONS

1. The similarity between temperatures causing crystallization nucleation and viscosity increases with the increase of temperature and the temperatures of the exothermic peaks on the ATD curve confirm the two crystallization stages of fluorine-nucleated vitroceramic masses of the $Na_2O-MgO-Al_2O_3-SiO_2$-system. The first stage, according to X-ray diffraction, corresponds to fluoride crystallization and the second, to fluorosilicates.

2. Viscosity at which fluorine nucleation occurs in masses of the $Na_2O-MgO-Al_2O_3-SiO_2$-system decreases with the increase in the MgO content.

3. Cordierite vitrocearmic masses present the highest viscosity at which nucleation of fluoride crystals occurs.

4. The volume behaviour involved in heat expansion of vitroceramic masses having compositions situated in various primary crystallization compartments shows that the structuration of vitreous microphases is based on the relations of phase heat equilibrium of the system and divides vitroceramic masses into : tridymite, enstatite, cordierite, forsterite, spinel and sapphirine.

5. Crystallization as a preponderant phase of a single type of fluorosilicate belonging to the mica family (phlogopite), in all fluorine-nucleated vitroceramic masses of the primary crystallization compartment of the $Na_2O-MgO-Al_2O_3-SiO_2$-system, subjected to heat treatment between 850–1000°, indicates the selectivity impressed by F^- ions as nucleators on the crystallization of these masses.

Revue Roumaine de Chimie, **18**, *1*, 11–22 (1973)

THERMODYNAMIC PROPERTIES OF THE RECIPROCAL MIXTURES OF FUSED SALTS : AgCl+(K, Rb, Cs)I

S. STERNBERG and LUCIA BEJAN

Institute of Physical Chemistry, Str. Galați 31, Bucharest, Romania

Received May 16, 1972

The partial molar thermodynamic properties of AgI in reciprocal mixtures of fused salts AgCl + KI, AgCl + RbI and AgCl + CsI have been calculated from e.m.f. measurements of the formation galvanic cells. The thermodynamic functions ; $\Delta\mu_{AgI}$, ΔS_{AgI} and ΔH^{M}_{AgI} from the experimental data are compared with those calculated from the enthalpies of the exchange reactions AgI + MeCl = = AgCl + MeI where Me = K, Rb, Cs, taking into account the polarization energy of the anion by the two cations.

1. – INTRODUCTION

In previous papers [1–3] a thermodynamic study of reciprocal systems of fused salts AgI + KCl, AgI + KBr, AgI + RbCl and AgI + CsCl was presented.

In this paper we present the thermodynamic study of reciprocal mixtures of AgCl + KI, AgCl + RbI and AgCl + CsI based on e.m.f. measurements of the formation cells :

$$Ag(s)\ \|AgCl(l,\ x_1) + KI(l,\ x_2)\|\ I_2(g,\ 1\ atm)\ \text{graphite}$$

$$Ag(s)\ \|AgCl(l,\ x_1) + RbI(l,\ x_2)\|\ I_2(g,\ 1\ atm)\ \text{graphite}$$

and

$$Ag(s)\ \|AgCl(l,\ x_1) + CsI(l,\ x_2)\|\ I_2(g,\ 1\ atm)\ \text{graphite}$$

For the study of these systems we used formation cells with iodine electrode, because the equilibrium :

$$MeX + 1/2\ I_2 \rightleftarrows MeI + 1/2\ X_2$$

is practically completely shifted to the left.

---

[1] S. STERNBERG and L. BEJAN, *Rev. Roumaine Chim.*, **14**, 303 (1969).

[2] S. STERNBERG and L. BEJAN, *J. Chem. Thermodynamics*, **2**, 341 (1970).

[3] S. STERNBERG and L. BEJAN, *Rev. Roumaine Chim.*, **16**, 175 (1971).

Details of the cell and the characteristics of the reversible iodine electrode have been given in previous works.[1,4,5] The e.m.f.'s were measured using a "Solartron" type L.M. 1440.2 digital voltmeter. E.m.f.'s measurements were effected for different molar fractions at different temperatures. The reproducibility of the experimental values was of 1-2 mV.

Pure chemical salts were used. AgCl, KI, RbI and CsI were first melted and purified by bubbling with gaseous halogenated acids.

2. – RESULTS AND DISCUSSION

In reciprocal mixtures one must consider a chemical reaction, e.g. in the present case :

$$\mathrm{AgI}(l) + \mathrm{MeCl}(l) \rightleftarrows \mathrm{AgCl}(l) + \mathrm{MeI}(l)$$

where Me = K, Rb, Cs. The phase diagrams[6] of these systems indicate that the mixtures AgI + MeCl are stable pairs while the mixtures AgCl + MeI are unstable pairs, being transformed into the corresponding stable pairs.

In previous works the mixtures situated on the left side of the equilibrium were studied, while in this paper the right side systems, namely the unstable pairs will be dealt with.

The e.m.f.'s *vs.* temperature for different molar fractions of the mixtures AgCl + (K, Rb, Cs)I are listed in tables 1–3. The functions $E = f(T)$ were obtained from about 20–30 points by the least squares method calculated with a computer. Since the unstable pairs of salts in the melt are transformed into stable pairs giving rise to AgI, the thermodynamic functions of AgI in the corresponding mixtures have been computed.

The partial molar chemical potential of silver iodide in the mixture, $\Delta\mu_{\mathrm{AgI}}$ – namely the difference between the chemical potential μ_1 of AgI in the mixture with the molar fraction $x_1 = x_{\mathrm{AgCl}}$ and the chemical potential μ^0 of pure AgI – was computed from e.m.f.'s measurements :

$$\Delta\mu_{\mathrm{AgI}} = \mu_1 - \mu^0 = -\mathcal{F}[E(x_1) - E^0] \qquad (1)$$

where E^0 refers to cells with pure AgI while $E(x_1)$ refers to cells with mixture.

The partial molar entropy was calculated from thermal coefficients :

$$\Delta S_{\mathrm{AgI}} = S_1 - S^0 = -\mathrm{d}(\mu_1 - \mu^0)/\mathrm{d}T = \mathcal{F}\left[\frac{\mathrm{d}E(x_1)}{\mathrm{d}T} - \frac{\mathrm{d}E^0}{\mathrm{d}T}\right] \qquad (2)$$

---

[4] S. Sternberg, I. Adorian and I. Galasiu, *J. Chim. phys.*, **62**, 63 (1965).

[5] S. Sternberg, I. Adorian and I. Galasiu, *Rev. Roumaine Chim.*, **11**, 581 (1966).

[6] N. K. Voskresenskaia, N. N. Evseeva, S. I. Berul and I. P. Verescetina in "Spravocihnik po plavkosti sistem iz bezvodnyn neorganicheskikh solei " tome 2, Editor Izdatelstvo Akademii Nauk U.R.S.S., Moscow, Leningrad, 1961, p. 159, 176, 146.

Table 1

Experimental e.m.f. values E expressed as smoothed functions of temperature T, and derived thermodynamic functions at 973 K of AgI in AgCl+ KI mixtures containing mole fraction x_1 of AgCl

x_{AgCl}	$a_{AgI} = x_{Ag^+} \cdot x_{I^-}$	$\frac{E}{V}$	$\frac{\mu_1 - \mu^0}{cal \cdot mol^{-1}}$		$\frac{S_1 - S^0}{cal \cdot K^{-1}\ mol^{-1}}$		$\frac{H_1 - H^0}{cal \cdot mol^{-1}}$	
			Exp.	Calc. rel. (11)	Exp.	Calc. rel. Temkin	Exp.	Calc. rel (8)
$x_{Ag} = 1$	1	$0.5238 - 0.272 \times 10^{-3}\,(T - 973)$	—	—	—	—	—	—
0.7	0.21	$0.5843 - 0.130 \times 10^{-3}\,(T - 973)$	−1395	−1402	3.275	3.102	+1792	+1436
0.6	0.24	$0.5703 - 0.159 \times 10^{-3}\,(T - 973)$	−1072	−1048	2.606	2.943	+1464	+1556
0.55	0.2475	$0.5695 - 0.142 \times 10^{-3}\,(T - 973)$	−1054	−1020	2.998	2.775	+1863	+1532
0.5	0.25	$0.5694 - 0.148 \times 10^{-3}\,(T - 973)$	−1052	−1090	2.860	2.755	+1731	+1446
0.4	0.24	$0.5847 - 0.140 \times 10^{-3}\,(T - 973)$	−1404	−1517	3.044	2.836	+1558	+1087
0.3	0.21	$0.6186 - 0.147 \times 10^{-3}\,(T - 973)$	−2186	−2344	2.883	3.102	+ 619	+ 494
0.25	0.1875	$0.6386 - 0.102 \times 10^{-3}\,(T - 973)$	−2648	−2924	3.921	3.327	+1167	+ 123
0.2	0.16	$0.6642 - 0.087 \times 10^{-3}\,(T - 973)$	−3238	−3635	4.266	3.642	+ 913	− 284

Table 2

Experimental e.m.f. values E expressed as smoothed functions of temperature T, and derived thermodynamic functions at 973 K of AgI in AgCl +RbI mixtures containing mole fraction x_1 of AgCl

x_{AgCl}	$\frac{E}{V}$	$\frac{\mu_1 - \mu^0}{cal \cdot mol^{-1}}$		$\frac{S_1 - S^0}{cal \cdot K^{-1}\ mol^{-1}}$		$\frac{H_1 - H^0}{cal \cdot mol^{-1}}$	
		Exp.	Calc. rel. (11)	Exp.	Calc. rel. Temkin	Exp.	Calc. rel (8)
$x_{AgI}=1$	$0.5238-0.272\times10^{-3}(T-973)$	—	—	—	—	—	—
0.8	$0.5896-0.137\times10^{-3}(T-973)$	−1517	−2294	3.113	3.642	+1511	+1143
0.7	$0.5799-0.124\times10^{-3}(T-973)$	−1294	−1587	3.413	3.102	+2027	+1331
0.6	$0.5816-0.156\times10^{-3}(T-973)$	−1333	−1367	2.675	2.836	+1270	+1306
0.5	$0.5867-0.162\times10^{-3}(T-973)$	−1451	−1570	2.537	2.755	+1018	+1030
0.4	$0.6043-0.144\times10^{-3}(T-973)$	−1856	−2193	2.952	2.836	+1016	+ 480
0.3	$0.6339-0.130\times10^{-3}(T-973)$	−2539	−3260	3.275	3.102	+ 647	− 345
0.2	$0.6566-0.117\times10^{-3}(T-973)$	−3063	−4866	3.575	3.642	+ 416	−1429

Table 3

Experimental e.m.f. values E expressed as smoothed functions of temperature T, and derived thermodynamic functions at 973 K of AgI in AgCl + CsI mixtures containing mole fraction x_1 of AgCl

x_{AgCl}	$\frac{E}{V}$	$\frac{\mu_1 - \mu^0}{\text{cal} \cdot \text{mol}^{-1}}$		$\frac{S_1 - S^0}{\text{cal} \cdot \text{K}^{-1}\ \text{mol}^{-1}}$		$\frac{H_1 - H^0}{\text{cal} \cdot \text{mol}^{-1}}$	
		Exp.	Calc. rel. (11)	Exp.	Calc. rel. Temkin	Exp.	Calc. rel. (8)
$x_{AgI} = 1$	$0.5238 - 0.272 \times 10^{-3} (T - 973)$	—	—	—	—	—	—
0.8	$0.5952 - 0.140 \times 10^{-3} (T - 973)$	−1647	−2301	3.044	3.642	+1315	+1197
0.7	$0.5835 - 0.177 \times 10^{-3} (T - 973)$	−1377	−1684	2.191	3.102	+ 755	+1291
0.6	$0.5888 - 0.173 \times 10^{-3} (T - 973)$	− 1499	−1590	2.283	2.836	+ 722	+1132
0.5	$0.6045 - 0.158 \times 10^{-3} (T - 973)$	−1861	−1948	2.629	2.755	+ 674	+ 699
0.4	$0.6253 - 0.150 \times 10^{-3} (T - 973)$	−2341	−2746	2.814	2.836	+ 397	− 24
0,3	$0.6553 - 0.136 \times 10^{-3} (T - 973)$	−3033	−4016	3.136	3.102	+ 19	−1041

while the partial molar heat of mixing of AgI was computed using the relation :

$$\Delta H_{\mathrm{AgI}} = H_1 - H^0 = \mu_1 - \mu^0 + T(S_1 - S^0) \tag{3}$$

Tables 1—3 contain also the values of the partial molar thermodynamic functions of AgI, both those resulting from experimental data and those computed Flood, Førland and Grjotheim theory,[7] taking into account the deviations from the random distribution.

According to Temkin[8] the partial molar entropy of silver iodide in AgCl + MeI mixtures, where Me = K, Rb, Cs is given by the relation :

$$S_1 - S^0 = - R\{\ln x(\mathrm{Ag}^+)x(\mathrm{I}^-)\} = - R \ln x_1x_2 \tag{4}$$

Førland[9] suggests a corrected relation for the configurational entropy in the expression of which one takes into account the deviations from the random distribution (the quasichemical theory) :

$$S_1 - S^0 = - R \ln x_1x_2 - 1/2x_1x_2\,[x_1 + x_2 - 3x_1x_2]\,\frac{(\Delta H')^2}{zRT^2} \tag{5}$$

According to Flood, Førland and Grjotheim[7] the first term of the partial molar heat of mixing due to the interaction between the nearest neighbours (cation-anion), is :

$$\Delta H_{\mathrm{AgI}} = H_1 - H^0 = x_1x_2\,\Delta H \tag{6}$$

where ΔH refers to the above ionic exchange reaction.

Førland[9] considers also the existence of certain variations of the energies of ionic interactions between the following nearest neighbours (cation-cation and anion-anion interactions), similar to those occurring in binary mixtures of fused salts :

$$\Delta H^{\mathrm{M}}_{\mathrm{AgI}} = H_1 - H^0 = x_1x_2\,\Delta H + x_2^2(x_1b_{\mathrm{Cl}} + x_2b_{\mathrm{I}}) + x_1^2(x_2b_{\mathrm{Me}} + x_1b_{\mathrm{Ag}}) +$$
$$+ x_2x_1\,[x_2(b_{\mathrm{Ag}} - b_{\mathrm{Me}}) + x_1(b_{\mathrm{I}} - b_{\mathrm{Cl}})] \tag{7}$$

where the b parameters are the interaction parameters in equations of the type $H_1^{\mathrm{E}} = bx_2^2$, of the four binary mixtures which can form a reciprocal system. The index letters refer to the common ion of the binary mixture.

---

[7] H. Flood, T. Førland and K. Grjotheim, *Z. anorg. Chem.*, **276**, 289, (1954).

[8] M. Temkin, *Acta Physicochim. U.R.S.S.*, **20**, 411, (1945).

[9] T. Førland in "Fused Salts" Editor B. R. Sundheim, McGraw-Hill Book Company, New York, 1964, p. 63—164.

If one considers also the deviations from the random distribution one obtains the relation :

$$\Delta H^{M}_{AgI} = H_1 - H^0 = \Delta H_{AgI}(\text{eqn. } 7) - x_1x_2(x_1 + x_2 - 3x_1x_2)\frac{(\Delta H')^2}{zRT} \quad (8)$$

The partial molar chemical potential of AgI is computed from the equations :

$$\Delta\mu_{AgI} = \Delta H_{AgI}(\text{eqn. } 6) - T\,\Delta S_{AgI}(\text{eqn. } 4) \quad (9)$$

$$\Delta\mu_{AgI} = \Delta H_{AgI}(\text{eqn. } 7) - T\,\Delta S_{AgI}(\text{eqn. } 4) \quad (10)$$

$$\Delta\mu_{AgI} = \Delta H_{AgI}(\text{eqn. } 8) - T\,\Delta S_{AgI}(\text{eqn. } 6) \quad (11)$$

The relations (6—11) have been applied to the computation of the partial molar thermodynamic functions of AgI in the systems AgCl + + (K, Rb, Cs)I, where x_1 refers to the weighed molar fraction of AgCl and x_2 to that of alkali iodide (K, Rb, Cs)I.

Førland and co-workers[10] have applied this theory to the AgBr + + NaCl system, taking for $\Delta H'$ a value selected so that a good agreement with the experimental values of entropy has been observed.

We applied the theory of Flood, Førland and Grjotheim to the systems previously studied,[1-3] but some changes in the method of computation of $\Delta H'$ have been effected; namely we consider the following value resulting from relation[2]:

$$\Delta H' = \Delta H + \frac{\Sigma b_i}{2} \quad (12)$$

where ΔH was selected so as to supply a value in good agreement with the experimental values of the corresponding partial molar functions. In the case of AgCl + (K, Rb, Cs)I systems the values which were selected for $\Delta H'$, were those used for the stable salt pairs.

Table 4 contains the heats of reaction (ΔH) for stable pairs previously studied as well as $\frac{\Sigma b_i}{2}$ terms taken from the literature[5,11-14] and the values of $\Delta H'$ resulting from equation (12).

---

[10] T. Førland and T. Ostwald in "Selected Topics in High-Temperature Chemistry", Universitetsforlaget, Oslo, 1966, p. 15.

[11] S. Sternberg and C. Herdlicka, *Rev. Roumaine Chim.*, **13**, 13 (1968).

[12] O. J. Kleppa and L. Hersh, *J. Chem. Phys.*, **42**, 1309, 3752 (1965).

[13] S. Sternberg, I. Adorian and I. Galasiu, *Electrochim. Acta*, **11**, 385 (1966).

[14] S. Sternberg, I. Adorian, *Electrochim. Acta*, **13**, 1647 (1968).

Table 4

Enthalpies of reaction

Salt pair	$\Delta H/\mathrm{cal\cdot mol^{-1}}$		$\Sigma b_i/2$	$\Delta H'$
	from thermochemical data	from our experimental results [1-3]	$\mathrm{cal\cdot mol^{-1}}$	$\mathrm{cal\cdot mol^{-1}}$
AgI+KCl	+9179	+8600	−1911	+6689
AgI+RbCl	+7936	+8600	−3603	+4997
AgI+CsCl	+7670	+8500	−5250	+3250

Tables 1–3 give also the thermodynamic activities of AgI in the corresponding mixtures computed by the Temkin relation,

$$a_{\mathrm{AgI}} = x_{\mathrm{Ag^+}} \cdot x_{\mathrm{I^-}} = x_1 x_2 \tag{13}$$

as well as the values of thermodynamic functions of AgI resulting both from experimental data and computed from the relations (6), (8), (11). Experimental and computed results are in satisfactory agreement.

The partial molar chemical potentials of AgI in the three mixtures AgCl + KI, AgCl + RbI and AgCl + CsI are plotted in figures 1–3. The theoretical curves are computed using relations (9)–(11) and the points represent the experimental data. It may be seen that all the curves present a maximum. The theoretical curves computed from equation (9) present the maximum at $x_1 = 0.5$, while both theoretical curves computed from relations (10) and (11) in which the interaction parameters are considered, have the maxima shifted to molar fractions x_1 higher than 0.5. For the AgCl + KI system the maximum is shifted to $x_1 = 0.55$, for the AgCl + + RbI at $x_1 = 0.6$, while for the AgCl + CsI system the maximum is located at $x_1 = 0.63-0.65$.

Figures 1–3 show that the experimental maxima are also shifted with respect to $x_1 = 0.5$, the order of sequence being the same as for the theoretical maxima. The correction for the ordering process has a small value in all cases. The AgCl + RbI and AgCl + CsI systems show a higher deviation of the experimental points corresponding to extreme values of molar fractions when the concentration of AgI in the mixture is small. Deviations have been observed also for the stable systems [1-3] with low concentration of AgI. In the case of dilute reciprocal solutions the theory of Flood and Førland might probably require some corrections.

The shape of the $\Delta\mu_{\mathrm{AgI}} - x_1$ curves can be explained as follows: since the ordering effect has a small value and, hence may be neglected, the chemical potential $\Delta\mu_{\mathrm{AgI}}$ can be calculated using the relation:

$$\Delta\mu_{\mathrm{AgI}} = \Delta H x_1 x_2 + f(b_i) + RT \ln x_1 x_2 \tag{14}$$

The term $\Delta H x_1 x_2$ is positive and represents the component of the heat of mixing which results from the heat of the exchange reaction. The term $f(b_i)$ represents the component of the heat of mixing resulting

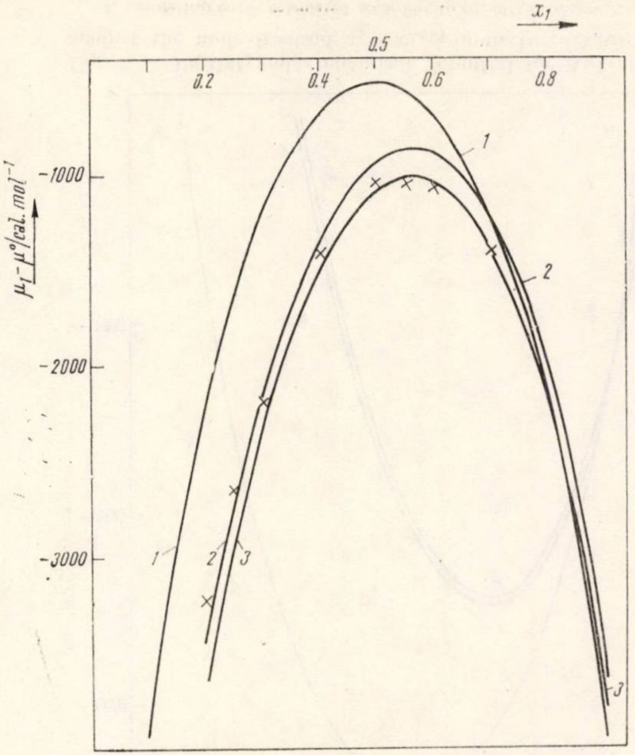

Fig. 1. – Partial molar chemical potential for AgI plotted against the mole fraction $x_1 = x_{AgCl}$ in mixtures AgCl+KI.

1, Theoretical curve calculated according to eq. (9); *2*, theoretical curve calculated according to eq. (10); *3*, theoretical curve calculated according to eq. (11); × × × – ~ Experimental points.

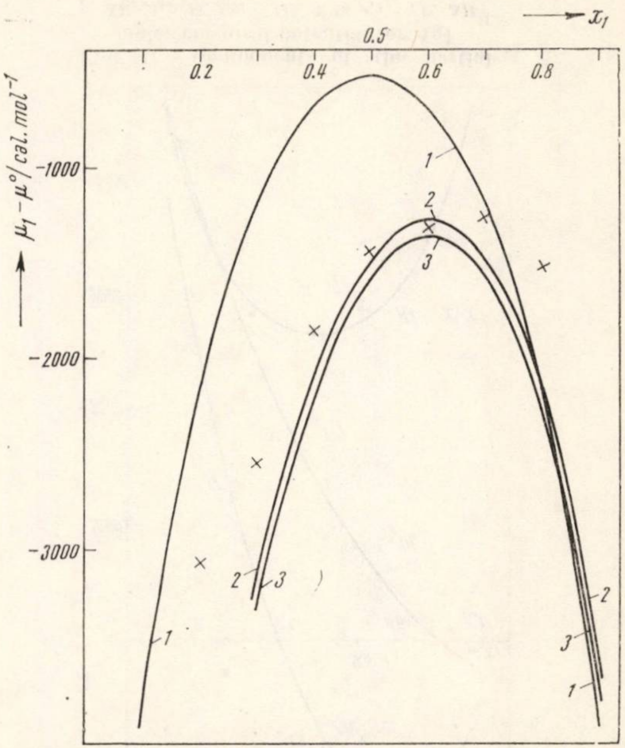

Fig. 2. – Partial molar chemical potential for AgI plotted against the mole fraction $x_1 = x_{AgCl}$ in mixtures AgCl+RbI.

1, Theoretical curve calculated according to eq. (9); *2*, theoretical curve calculated according to eq. (10); *3*, theoretical curve calculated according to eq. (11); × × × – ~ Experimental points.

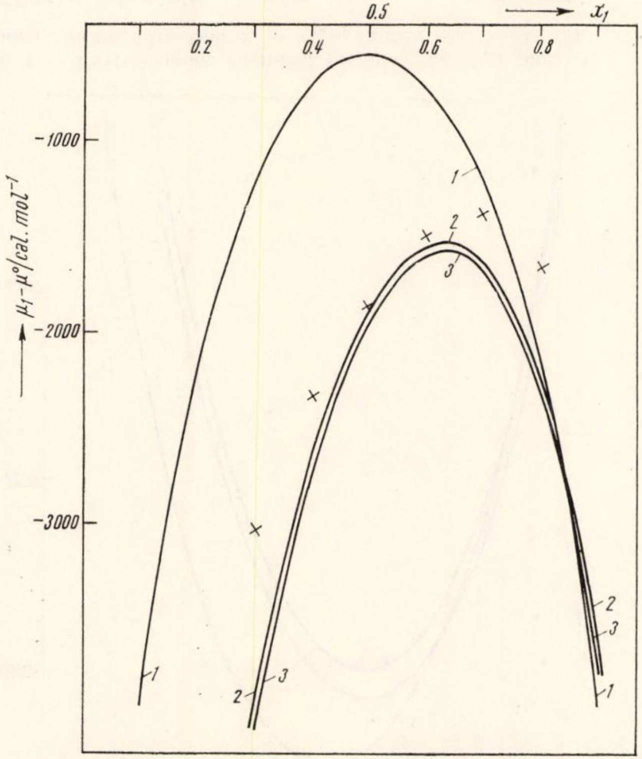

Fig. 3. — Partial molar chemical potential for AgI plotted against the mole fraction $x_1 = x_{AgCl}$ in mixtures AgCl+CsI.

1, theoretical curve calculated according to eq. (9); *2*, theoretical curve calculated according to eq. (10); *3*, theoretical curve calculated according to eq. (11); × × × — ≃ Experimental points.

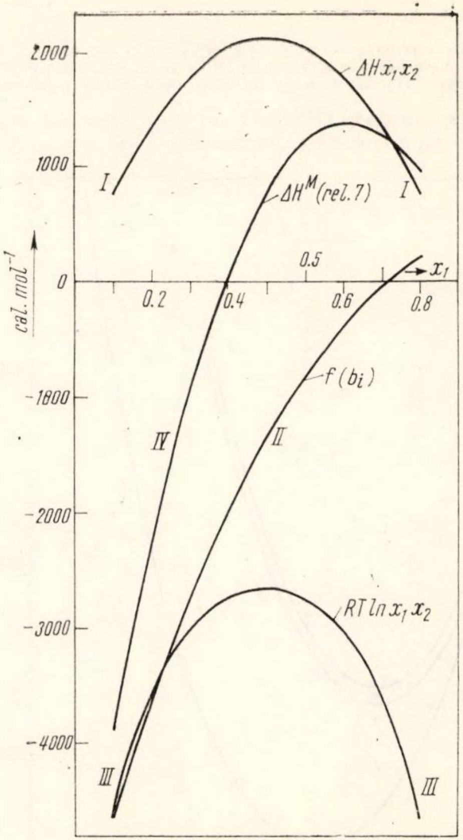

Fig. 4. — Components of the partial molar chemical potential for AgI

I, $\Delta H x_1 x_2$; II, $f(b_i)$; III, $R \ln x_1 x_2$; IV, ΔH^M (eq. 7).

from the contributions of polarization and London energies. The value of $f(b_i)$ results from equation (7). The term $RT \ln x_1x_2 = - T\Delta S$ results from the mixing entropy of a system with four different ions and is always negative.

In figure 4 all the three terms are plotted. The first and the third terms have a maximum for the fraction $x_1 = 0.5$ (curves I and III). This maximum results from the product $x_1x_2 = a_{\mathrm{AgI}}$ which represents the thermodynamic activity of silver iodide computed after Temkin :

$$a_{\mathrm{AgI}} = x_{\mathrm{Ag}^+} . x_{\mathrm{I}^-}$$

This behaviour results actually from the reciprocal system,character of the melt studied. From the combination of these two terms (curves I and III fig. 4) one obtains $\Delta\mu_{\mathrm{AgI}}$ given by relation (9), and having a maximum for $x_{\mathrm{AgCl}} = 0.5$ (e.g. curve 1 from fig. 3).

The second term, $f(b_i)$, is always negative in the case of the systems studied by us, because their polarization energies are higher than London's [13,14,1-3] ones. It should be mentioned that these energies are not characteristic of the reciprocal mixtures. As in the case of binary mixtures the values of these energies depend firstly on the ratio $\mathrm{Ag}^+/\mathrm{Me}^+$. A curve without a maximum is obtained, since in this case the product x_1x_2 does not occur in the corresponding equation. Curve IV which results from the combination of curves I and II has the maximum shifted to $x_1 = 0.7$, while from curves III and IV the chemical potential $\Delta\mu_{\mathrm{AgI}}$ results which is represented by a curve having the maximum shifted to $x_1 \simeq 0.7$ (e.g. curve 2 of fig. 3).

Thus it has been proved that the shift of the maximum is due in fact to the exothermal polarization energy. The shift increases from K to Cs in the same order as the polarization energy for the binary mixtures with a common anion.

Figure 5 gives the experimental partial molar chemical potentials of AgI in the three mixtures. In all cases $\Delta\mu_{\mathrm{AgI}}$ are negative. The partial molar chemical potential of AgI increases in absolute value in the order :

$$\mathrm{AgCl} + \mathrm{CsI} < \mathrm{AgCl} + \mathrm{RbI} < \mathrm{AgCl} + \mathrm{KI}$$

just as in the case of the stable pairs AgI + MeX.[1-3] Table 4 shows that the less positive is the heat term $\Delta H'$, the more negative is $\Delta\mu_{\mathrm{AgI}}$.

For all the three systems studied, the heats of the exchange have very closely approaching values (experimental values of ΔH, table 4). The difference found for the expression of $\Delta\mu_{\mathrm{AgI}}$ arises from the term $\Sigma b_i/2$ and ultimately from the polarization energies which increase in absolute value in the following order :

$$|b_{\mathrm{Ag-K}}| < |b_{\mathrm{Ag-Rb}}| < |b_{\mathrm{Ag-Cs}}|$$

Thus it has been proved that in the case of the unstable as well as stable systems[1-3] it is absolutely necessary to take into account the correction term $f(b_i)$ in order to make an exact estimation of the mixing thermodynamic properties.

Figure 6 gives the plots of the partial molar entropies of mixing of AgI in the mixture AgCl + RbI. The third curve represents the graphically averaged values of ΔS^M_{AgI} determined experimentally.

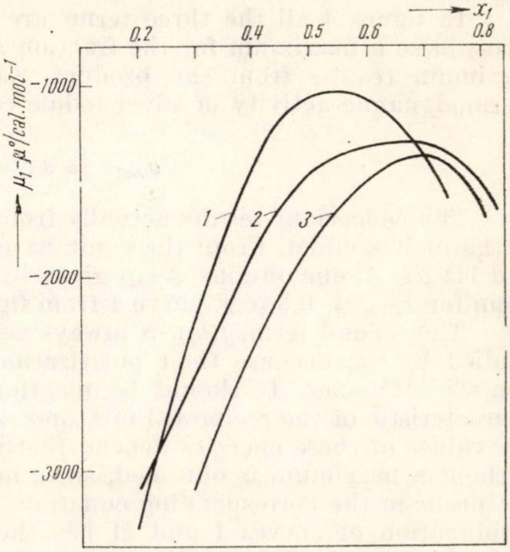

Fig. 5. — Experimental partial molar chemical potentials $\Delta\mu_{AgI}$ for AgI plotted against the mole fraction $x_1 = x_{AgCc}$ in mixtures :

1, (AgCl + KI) ; 2, (AgCl + RbI) ; 3, (AgCl + + CsI).

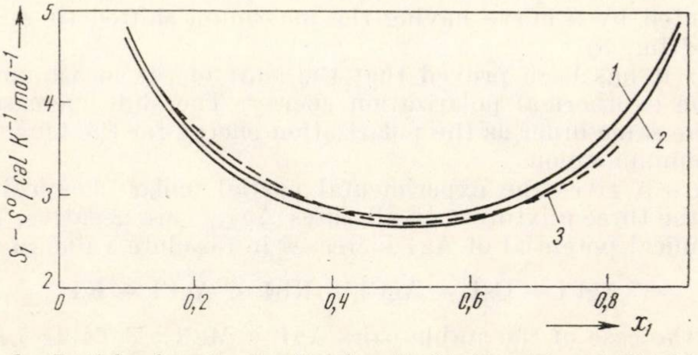

Fig. 6. — Partial molar entropies of mixing of AgI in the mixture AgCl + RbI.

1, Theoretical curve calculated according to equation (4) ; 2, theoretical curve calculated according to equation (5) ; Curve 3 represents the graphically averaged values of ΔS^M_{AgI} determined experimentally.

As may be seen from the figure 6 the ordering correction of the mixing entropy is very small and the experimental values occur between the two theoretical curves. A similar behaviour with respect to the mixing entropy is observed also in the other two systems.

Acknowledgement. The calculations have been carried out on the IBM System 360/30 computer by M. Ciopec [15] from the Institute of Physical Chemistry, Bucharest, to whom we wish to express our thanks.

[15] M. Ciopec and D. I. Marchidan, *Rev. Roumaine Chim.* (in print).

Revue. Roumaine de Chimie, **18**, *1* 23–34 (1973)

LES ÉQUILIBRES DE PHASE DU SYSTÈME $Na_2O-CaO-Al_2O_3-SiO_2$.

ÉQUILIBRES DE PHASE DANS LE SOUS-SYSTÈME $Na_2O.Al_2O_3.6SiO_2-CaO.Al_2O_3.2SiO_2-3Al_2O_3.2SiO_2-Al_2O_3$ * INRÉRESSANT LA CÉRAMIQUE SUPERALUMINEUSE

R. DINESCU et M. CERCHEZ

Centre de Chimie Physique, 23 str. Dumbrava Roşie, Bucarest

Reçu le 10 juillet 1972

On a déterminé les relations de paragenèse quaternaire d'équilibre dans la zone alumineuse du système $Na_2O-CaO-Al_2O_3-SiO_2$, en délimitant le sous-système V $Na_2O.\ Al_2O_3.\ 6SiO_2-CaO.\ Al_2O_3.\ 2SiO_2-3Al_2O_3.\ 2SiO_2-Al_2O_3$; on a établi la surface quaternaire divariante $3Al_2O_3.\ 2SiO_2-Al_2O_3$. Dans le sous-système V sont déterminées des relations quantitatives qui permettent d'obtenir les phases coexistantes au traitement termique jusqu'à 1600° et on a élaboré un système modulaire de corrélation des conditions de paragenèse avec les propriétés des masses alumineuses du système.

1. INTRODUCTION

Dans des travaux antérieurs [1,2] on a déterminé les équilibres de phase dans la zone acide et alumineuse du sous-système $NAS_6-CAS_2-A_3S_2$-S.**)

La classification modulaire proposée [1] délimite les domaines de composition qui correspondent aux masses réfractaires de silice,semi-acides, silico-argileuses et alumino-argileuses, ainsi qu'aux masses de céramique fine alumino-siliceuses usuelles.

Le présent travail développe l'étude des équilibres de phase dans le sous-système adjacent : $NAS_6-CAS_2-A_3S_2-A$, noté avec le numéro V (fig. 1), sous-système qui intéresse les réfractaires et les porcelaines superalumineuses. Ce sous-système doit être examiné conjointement avec le sous-système I, $NAS_6-CAS_2-A_3S_2-S$, étant donné que l'incongruence dans le système quaternaire de la mullite déplace la courbe limite quaternaire G_7G_8 afférente au sous-système V, dans ce même système [2].

*) Dans ce travail on désigne par Al_2O_3 la phase de haute température: αAl_2O_3 (corindon).
**) N–Na_2O, C–CaO, A–Al_2O_3, S–SiO_2.

---

[1] R. Dinescu et M. Cerchez, *Chimie et Industrie*, **104**, 255 (1971).
[2] R. Dinescu et M. Cerchez, *Silicates Industriels*, **36**, 151 (1971).

La méthode de travail utilisée a été antérieurement décrite.[1,2] Les points invariants et les conditions d'emplacement dans le sous-système $NAS_6-CAS_2-A_3S_2-A$ sont présentés dans le tableau 1.

Tableau 1

Points invariants et conditions d'encadrement dans le sous-système $NAS_6-CAS_2-A_3S_2-A$

Symbole	Sous-système Equation d'encadrement	Points et courbes caractéristiques	Composition oxydique Na_2O % CaO % Al_2O_3 % SiO_2 %	Température °C	Bibliographie
CV	$NAS_6-CAS_2-A_3S_2-A$	G_7-G_8	Courbe univariante quaternaire	1104–1512	
TI F_1	$NAS_6-CAS_2-A_3S_2$ $-S-0{,}43A+1{,}55N+58{,}7<0$	—	Pseudo-système ternaire	—	
BI f_1	$NAS_6-A_3S_2$ $S+0{,}77-83{,}6<0$	—	Pseudo-système binaire	—	3,4 5,6
BII f_2	NAS_6-CAS_2 $S+1{,}49A-97{,}8>0$	—	Solution solide	—	7
BIII f_3	$CAS_2-A_3S_2$ $S+0{,}43A-59{,}0>0$	—	Pseudo-système binaire	—	3,5 6,8, 9
TII F_2	$NAS_6-A_3S_2-A$ $-S-A-N+100>0$	G_7	11,2 – 20,0 68,8	1104	3,4, 5,6
BIV f_4	A_3S_2-A $S+A-100<0$	e_{12}	– – 21,4 78,6	~1850	4,5 6,10 11,12
BV f_5	NAS_6-A $S+0{,}85A-85{,}3>0$	e_{13}	11,8 – 21,0 67,2	1108	3,4 5,6
TIII F_3	$CAS_2-A_3S_2-A$ $-S-A-C+100>0$	G_8	–15,6 36,6 47,8	1512	3,5 6,8, 9
BVI f_6	CAS_2-A $-S-0{,}68A+68{,}2<0$	e_{14}	– 19,2 31,8 41,0	1547	3,5 6,8, 9
TIV F_4	NAS_6-CAS_2-A $-S-0{,}68A+1{,}17N+68{,}2<0$	$e_{13}-e_{14}$	Courbe univariante ternaire	1108–1547	

[3] * * * « Diagrammes d'équilibres thermiques calibrées pour applications quantitatives » Ed. The American Ceramic Society Columbus-Ohio, 1969.

[4] J. F. Schairer et N. L. Bowen, *Amer. J. Sci.*, **245**, 196 (1947); 253, 681 (1955); **254**, 129 (1956); **256**, 581 (1958).

[5] E. F. Osborne et A. Muan, « Phase Equilibrium Diagrams of Oxide Systems », Ed. The American Ceramic Society, 1960-dans 6.

[6] E. M. Levin, C. R. Robbins et H. F. Mc Murdie, « Phase Diagrams for Ceramists », Ed. The American Ceramic Society inc., Columbus-Ohio, 1964, p. 123, 181, 219.

[7] N. L. Bowen, *Amer. J. Sci.*, **36**, 164 (1915) — dans 6.

[8] G. A. Rankin et F. E. Wright, *Amer. J. Sci.*, **36**, 1 (1915) — dans 6.

[9] I. Olshansky, *Doklady Akad. Nauk S.S.S.R.*, **76**, 93 (1951).

[10] N. A. Toropov et F. Ya. Galahov, *Izvest. Akad. Nauk S.S.S.R., Otdel. Khim. Nauk*, **9**, 1 (1958); *Voprosy Petrograf. Mineral Akad. Nauk S.S.S.R.*, **2**, 245 (1953).

[11] P. P. Budnicov et S. G. Treswjatschi, *Silikat Techn.*, **12**, 396 (1961).

[12] Sh. Aramaky et R. Roy, *J. Amer. Ceram. Soc.*, **42**, 644 (1959); **45**, 229 (1962).

Des déterminations expérimentales préalables ont démontré que la courbe G_7G_8 peut être assimilée à une droite (tableau 2).

Dans le présent travail on a déterminé la surface quaternaire divariante qui sépare le volume de cristallisation primaire de la mullite de celui du corindon (αAl_2O_3).

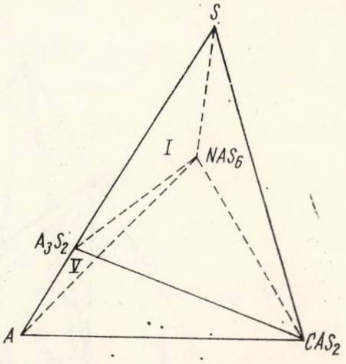

Fig. 1. — Sous-systèmes avec $3Al_2O_3.2SiO_2$ dans le système quaternaire $Na_2O-CaO-Al_2O_3-SiO_2$.

Tableau 2

Températures théoriques et expérimentales de fusion des masses afférentes à la courbe G_7-G_8

Composition oxydique				$t_{\text{théorique}}$ (°C)	t_{exp} (°C)
Na_2O %	CaO %	Al_2O_3 %	SiO_2 %		
5,96	7,26	27,68	59,10	1300	1330
3,24	11,02	31,25	54,49	1400	1410
0,50	14,82	34,83	49,85	1500	1490

2. ÉQUILIBRES THERMIQUES DE PHASE DES MASSES QUATERNAIRES QUI CRISTALLISENT PRIMAIREMENT LA MULLITE ET LE CORINDON

Dans la figure 2 on présente la surface quaternaire divariante $e_{12}-G_7-G_8$, qui sépare les compartiments de cristallisation primaire de la mullite et du corindon.

Sur la surface quaternaire divariante $e_{12}-l-G_7-G_8-m$ (figure 2) s'établit l'équilibre thermique suivant :

$$A + A_3S_2 \rightleftarrows \text{liq } e_{12}lG_7G_8m \qquad (1)$$

On observe que l'intersection — suivant la courbe lm — du pseudo-système ternaire $NAS_6-CAS_2-A_3S_2$ avec la surface divariante $e_{12}-G_7-G_8$

montre l'extension des volumes de cristallisation primaire de la mullite et du corindon dans le sous-système NAS$_6$—CAS$_2$—A$_3$S$_2$—S, ainsi que dans le sous-système NAS$_6$—CAS$_2$—A_3S_2—S.

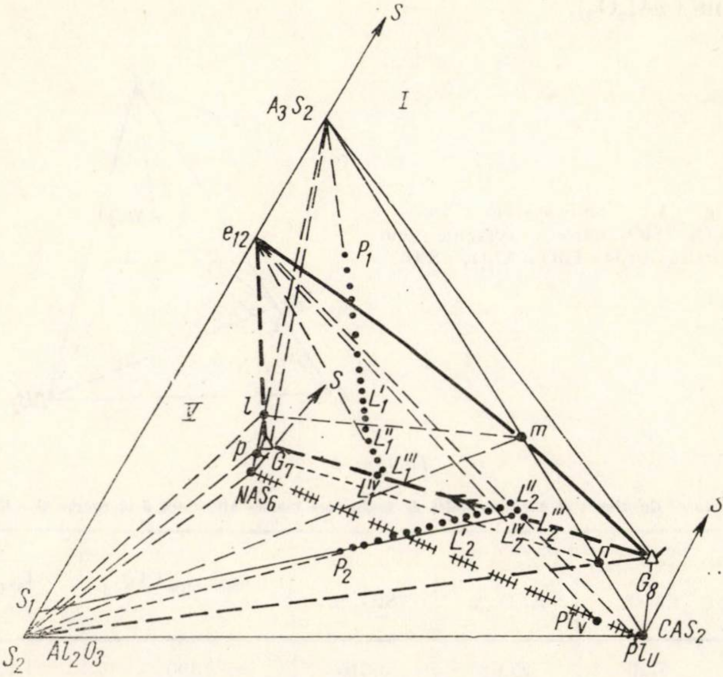

Fig. 2. — Équilibres de phase dans le sous-système NAS$_6$—CAS$_2$—A_3S_2—A et partiellement dans le sous-système NAS$_6$—CAS$_2$—A_3—S_2—S.

2.1. MASSES SITUÉES DANS LE SOUS-SYSTÈME V NAS$_6$—CAS$_2$—A_3S_2—A

On observe que, dans le volume contenant les masses à alumine en excès par rapport à celle des points de la surface A_3S_2—G_7—G_8 (figure 2), on trouve deux volumes de cristallisation primaire afférentes au sous-système V : celui de la mullite A_3S_2—m—l—e_{12}, celui du corindon A—e$_{12}$—l—p—n—m.

a) Les masses situées dans le volume A_3S_2—m—l—e_{12} cristallisent primairement la mullite et la phase liquide finale se situe sur la courbe univariante quaternaire G_7—G_8 (figure 2, masse P$_1$).

b) Les masses situées dans le volume A—e_{12}—l—p—n—m cristallisent primairement le corindon et présentent une phase liquide finale située également sur la courbe limite G_7—G_8 (figure 2, masses P_2).

Dans le tableau 3 on indique les équations des volumes de cristallisation primaire de la mullite et du corindon dans le sous-système NAS$_6$—CAS$_2$—A_3S_2—A.

Tableau 3

Équations des volumes de cristallisation de la mullite ($A_3S_2-m-l-e_{12}$) et du corindon ($A-e_{12}-l-p-n-m$) dans le sous-système $NAS_6-CAS_2-A_3S_2-A$ et des volumes de cristallization de la mullite ($A_3S_2-m-G_8-G_7-l$) et du corindon ($l-m-n-p-G_7-G_8$) dans le sous-système $NAS_6-CAS_2-A_3S_2-S$

Volume	Plan limite	Équation de plan limite	Équation du volume
	a) Sous système	$NAS_6-CAS_2-A_3S_2-A$	
$A_3S_2-m-l-e_{12}$ (phase primaire mullite)	$A_3S_2-l-e_{12}$ $A_3S_2-m-e_{12}$ A_3S_2-m-1	$P_1=S+A+N-100=0$ $P_2=N=S+A+C-100=0$ $P_3=S+0{,}42A-1{,}59N-58{,}34=0$	$P_1<0$; $P_2<0$; $P_3>0$
$A-e_{12}-l-p-n-m$ (phase primaire corindon)	$A-p-n$ $A-e_{12}-G_8$ $A-e_{12}-G_7$ $l-p-n-m$ $(NAS_6-CAS_2-A_3S_2)$	$P_4=S+0{,}755A-0{,}75N-75{,}51=0$ $P_5=N=S+A+C-100=0$ $P_6=S+A+N-100=0$ $P_7=-S-0{,}43A+1{,}54N+58{,}95=0$	$P_4>0$; $P_5<0$; $P_6<0$; $P_7>0$
	b) Sous-système	$NAS_6-CAS_2-A_3S_2-S$	
$A_3S_2-m-G_8-G_7-l$ (phase primaire mullite)	A_3S_2-m-l $l-m-G_8-G_7$ $(e_{12}-G_7-G_8)$ $A_3S_2-G_7-G_8$	$P_3=S+0{,}42A-1{,}59N-58{,}34=0$ $P_8=S+0{,}61A-0{,}93N-70{,}63=0$ $P_9=S+0{,}57A-0{,}97N-69{,}35=0$	$P_3<0$; $P_8>0$; $P_9>0$
$-m-n-p-G_7-G_8$ (phase primaire corindon)	$n-p-G_7-G_8$ $(A-n-p)$ $l-m-n-p$ $l-m-G_8-G_7$ $(e_{12}-G_7-G_8)$	$P_4=0$ $P_7=0$ $P_8=0$	$P_4>0$; $P_7<0$; $P_8<0$

2.2. MASSES SITUÉES DANS LE SOUS-SYSTÈME $NAS_6-CAS_2-A_3S_2-S$

a) Eu égard à l'incongruence de la mullite dans les systèmes ternaires et quaternaires, les masses situées dans le volume $l-m-n-p-G_7-G_8$, qui font partie du sous-système $NAS_6-CAS_2-A_3S_2-S$, cristallisent primairement le corindon ; la mullite apparaît comme phase secondaire par la dissolution de l'alumine, quand la composition de la phase liquide se situe sur la courbe G_7-G_8. Le liquide final possède la composition située sur la courbe univariante E_2-E_4 (le trajet de fusion parcourt également la surface $E_2E_4G_7G_3$ dans le sous-système $NAS_6-CAS_2-A_3S_2-S$ *).

Dans les figures 2 et 3 sont représentées conjointement avec le sous-système $NAS_6-CAS_2-A_3S_2-A$, les fractions des volumes qui font partie du sous-système $NAS_6-CAS_2-A_3S_2-S$.

Le trajet de fusion d'une masse P_3 située dans le volume $l-m-p-n-G_7-G_8$ est indiqué dans la figure 3.

---

* Voir les travaux antérieurs. [1, 2]

b) Dans le même sous-système se trouvent également placées les masses du volume $A_3S_2—l—G_7—G_3—m$ (figure 3) qui cristallisent primairement la mullite et qui terminent la solidification toujours avec un liquide sur la courbe $E_2—E_4$. Dans le tableau 3 sont aussi indiquées les équations

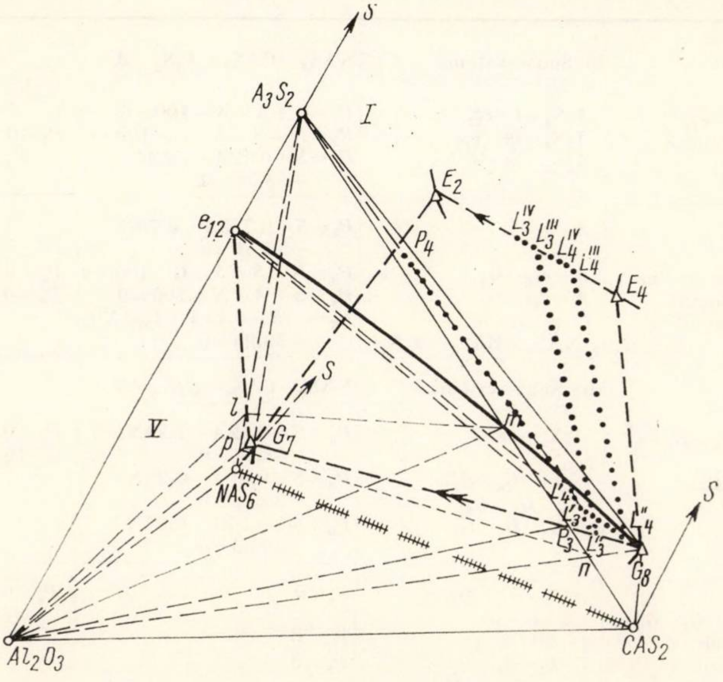

Fig. 3. — Le compartiment de cristallisation primaire de la mullite et les phases de cristallisation de la masse fondue P dans le sous-système $NAS_6—CAS_2— A_3S_2—S$ (les volumes $l—m—p—n—G_7—G_8$ et $A_3S_2—m—G_7—G_8—l$).

$$t_{P_3} \cdots t_{L_3^{I}} \quad A \rightleftarrows \text{liq } P_3 \ldots L_3^{I}$$

$$t_{L_3^{I}} \cdots\cdot t_{L_3^{II}} \quad A + A_3S_2 \rightleftarrows \text{liq } L_3^{I} \ldots L_3^{II}$$

$$t_{L_3^{II}} \cdots t_{L_3^{III}} \quad A_3S_2 + \text{ss}Pl_3^{II} \ldots \text{ss}Pl_3^{III} \rightleftarrows \text{liq } L_3^{II} \ldots L_3^{III}$$

$$t_{L_3^{III}} \cdots t_{L_3^{IV}} \quad S + A_3S_2 + \text{ss}Pl_3^{III} \ldots \text{ss}Pl_4^{IV} \rightleftarrows \text{liq } L_3^{III} \ldots L_3^{IV}$$

$$t_{L_3^{IV}} \quad S + A_3S_2 + \text{ss}Pl_3^{IV} \rightleftarrows \text{liq } L_3^{IV}$$

de définition des surfaces qui delimitent ce volume. On observe que le volume $A_3S_2—l—G_7—G_8—m$ est très étroit, se trouvant pratiquement dans la limite des erreurs de lecture sur le diagramme.

Sur la figure 3 on présente le trajet de cristallisation d'une masse P_4 de ce volume.

En même temps que la délimitation de la surface quaternaire divariante $A_3S_2—A$ et en considérant les déterminations présentées dans les travaux antérieurs [1,2], on a complètement défini le compartiment de cristallisation primaire de la mullite.

3. RELATIONS QUANTITATIVES POUR LA DÉTERMINATION DES PHASES D'ÉQUILIBRE PENDANT LE TRAITEMENT THERMIQUE DES MASSES SUPERALUMINEUSES DANS LE SOUS-SYSTÈME $NAS_6-CAS_2-A_3S_2-A$

Le calcul de la proportion d'équilibre du corindon et de la masse fondue d'une part et du corindon de la mullite de la masse fondue d'autre part est illustré dans le volume $A-e_{12}-l-p-n$ et respectivement sur la surface quaternaire divariante, à des températures allant jusqu'à 1600° ; le calcul est réalisé par l'application des relations du centre de gravité suivant le mode de travail indiqué dans des travaux antérieurs [1,2], en assimilant les surfaces isothermes à des plans, la composition des phases étant déterminée analytiquement.

Les isoplèthes et les isothermes de la surface $e_{12}-l-m-G_7-G_8$ sont indiquées dans la figure 4 ; on observe sur cette figure la position rapprochée des isothermes, dans la zone de 20 à 35% Al_2O_3, ce qui montre la grande influence sur les propriétés réfractaires exercée par la teneur en Al_2O_3 sur ces masses. Dans le tableau 4 on indique les formules qui permettent de déterminer les composants de phase d'équilibre en fonction de la composition oxydique et de la température de cuisson, dans le volume de cristallisation primaire de l'alumine, dans le sous-système $NAS_6-CAS_2-A_3S_2-A$.

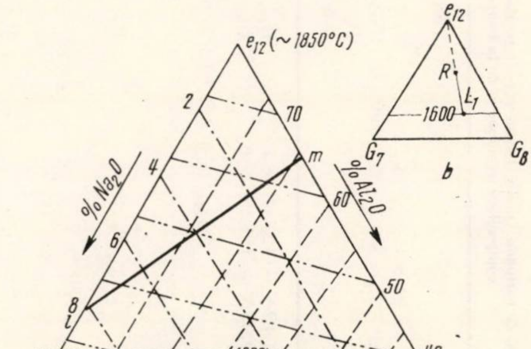

Fig. 4. — La surface quaternaire divariante $e_{12}-G_7-G_8$:

a) Isothermes et isoplètnes; b) Trajet de fusion et solidification

Le trajet typique de fusion est représenté sur la figure 2 (masse P_2).

Tableau 4

Équations des volumes des masses fondues et des masses de corindon + masse fondue et les formules de détermination des composants d'équilibre, qui dépendent de la composition oxydique et de la température

			Volume $A-l-m-n-p$(du volume $A-e_{12}-l-m-G_7-G_8$)	
Équation des plans limites	1) $\alpha A - e_{12}-G_8$ $P_5 = S+A+C-100=0$	2) $\alpha A-e_{12}-G_7$ $P_6=S+A+N-100=0$	3) $l-m-n-p$ $(NAS_6-CAS_2-A_3S_2)$ $P_7 = S-0{,}43A+0{,}69N+$ $+58{,}95=0$	4) $l-m-G_7-G_8$ $P_8 = S+0{,}61A-0{,}93N-$ $-70{,}63=0$
Équations des plans isothermes	$I_{1200} = S + 2{,}14A + 1{,}12N - 125{,}00 = 0$ $I_{1300} = S + 1{,}71A + 0{,}33N - 108{,}36 = 0$		$I_{1400} = S + 3{,}46A + 1{,}70N - 168{,}10 = 0$ $I_{1500} = S + 1{,}59A + 0.054N - 105{,}26 = 0$	
		$I_{1600} = S + 1{,}64A - 0{,}39N - 112{,}60 = 0$		
Équation du volume des masses fondues	$P_5<0$	$P_6<0$	$P_7>0$	$I_{1200-1600}>0$
Équation du volume des masses d'alumine et de phase liquide	$P_5 < 0$	$P_6 < 0$	$P_7 > 0$	$I_{1200-1600}< 0$

Température (°C)	Corindon %	Phase liquide %
1200	1,124S + 2,405A + 1,259N − 140,50	−1,124S − 2,405A − 1,259N + 248,50
1300	1,596S + 2,279A + 0,527N − 172,97	−1,596S − 2,729A − 0,527N + 272,97
1400	0,562S + 1,945A + 0,955N − 94,47	−0,502S − 1,945A − 0,955N + 194,47
1500	1,861S + 2,959A + 0,100N − 195,89	−1,861S − 2,959A − 0,100N + 295,89
1600	1,946S + 3,191A + 0,759N − 219,12	−1,946S − 3,191A − 0,759N + 319,12

Des exemples de calcul des compositions de phase des trois masses superalumineuses à la température de 1600° sont indiqués dans les tableaux 5 et 6.

Tableau 5

Calcul de la composition de phase de deux masses superalumineuses cuites à 1600°C dans le volume $A - e_{12} - l - p - n - m$

Dénomination		Méthode de calcul	Résultats	
			Masse alumineuse I	Masse alumineuse II
Composition oxydique de la masse (%)		—	$SiO_2 = 22$ $Al_2O_3 = 73$ $Na_2O = 2$ $CaO = 3$	$SiO_2 = 9$ $Al_2O_3 = 90$ $Na_2O = 0,5$ $CaO = 0,5$
Caractérisation modulaire		Formules (2) (3) (4)	$S_A = 8,8$ $S = 22,7$ $C = 6,0$	$S_A = 65,31$ $S = 11,1$ $C = 5,0$
Équation du volume corindon + masse fondue		Tableau 3	$P_4 = 0,10$ $P_5 = -2,0$ $P_6 = -3,0$ $P_7 = 8,7$	$P_4 = 1,06$ $P_5 = -0,5$ $P_6 = -0,5$ $P_7 = 19,75$
Corindon	Limite	$\% Al_2O_3$	73	90
	Réel	Tableau 4	58,15	85,96
Phase liquide (%)		Tableau 4	41,85	14,04
Composition oxydique de la phase liquide		Par différence de la composition oxydique de la masse et du corindon réel	$SiO_2 = 52,6$ $Al_2O_3 = 35,5$ $CaO = 7,14$ $Na_2O = 4,76$	$SiO_2 = 64,12$ $Al_2O_3 = 28,76$ $CaO = 3,56$ $Na_2O = 3,56$

Du tableau 5 résulte le puissant effet fondant des oxydes alcalins et alcalino-terreux ; les deux oxydes ensemble en proportion de 1% dans le mélange initial produisent environ 4% de phase liquide.

Il résulte du tableau 6 la grande quantité de phase liquide (27,8%) qui se forme à la température de 1600° en présence de 4% somme d'oxyde de sodium et d'oxyde de calcium.

Tableau 6

Calcul de la composition de phase d'une masse réfractaire mullite-corindon cuite à 1600°C sur la surface quaternaire divariante $e_{12}-G_7-G_8$

Dénomination	Méthode de calcul	Résultats
Composition oxydique (%)	—	$SiO_2=21,6$ $Na_2O=1,0$ $Al_2O_3=74,2$ $CaO=3,0$
Caractérisation modulaire	Formules (2) (3) (4)	$S_A=11,7$ $S=5,7$ $C=7,6$
Valeur de l'équation du volume de corindon + masse fondue	Tableau 3	$P_4=+1,4$ $P_6=-3,0$ $P_5=-1,0$ $P_7=+7,1$
Composition oxydique du point R (%)	Figure 4	$SiO_2=42,1$ $Na_2O=2,0$ $Al_2O_3=49,7$ $CaO=6,2$
Composition oxydique de la phase liquide (%)	Figure 4	$SiO_2=51,2$ $Na_2O=2,8$ $Al_2O_3=49,7$ $CaO=9,1$
Equation de la droite L_1PS_1	Par les points P et L_1	$\frac{S-21,6}{51,2-21,6}=\frac{A-74,2}{36,9-74,2}=\frac{N-1,0}{2,8-1,0}$
Composition oxydique du point S_1 (%)	Intersection de la droite $L_1\,PS$ avec la droite $A+S-100=0$	$SiO_2=5,2$ $Al_2O_3=94,8$
Phase liquide (%)	Relation du centre de gravité [1]	27,8
Phases solides totales (%)	Relation du centre de gravité [1]	72,2
Corindon (%)	Du total des phases solides	64,5
Mullite (%)	Du total des phases solides	7,7
Al_2O_3 théorique	% Al_2O_3	74.2

4. SYSTÈME MODULAIRE POUR LES MASSES CÉRAMIQUES SUPERALUMINEUSES

Le système modulaire proposé réalise la corrélation des propriétés des masses superalumineuses avec les conditions de paragenèse du sous-système $NAS_6 - CAS_2 - A_3S_2 - A$, suivant la méthode indiquée antérieurement.[1]

a) *Degré de saturation par rapport à l'alumine* (S_A). La saturation en alumine représente les quantités théoriques de Al_2O_3 en excès, en comparaison de la quantité d'Al_2O_3 liée chimiquement. En exprimant en équivalents molaires il résulte :

$$S_A = \%\,Al_2O_3 - (1{,}82\%\,CaO + 1{,}65\,Na_2O - 2{,}55\%\,SiO_2) \qquad (2)$$

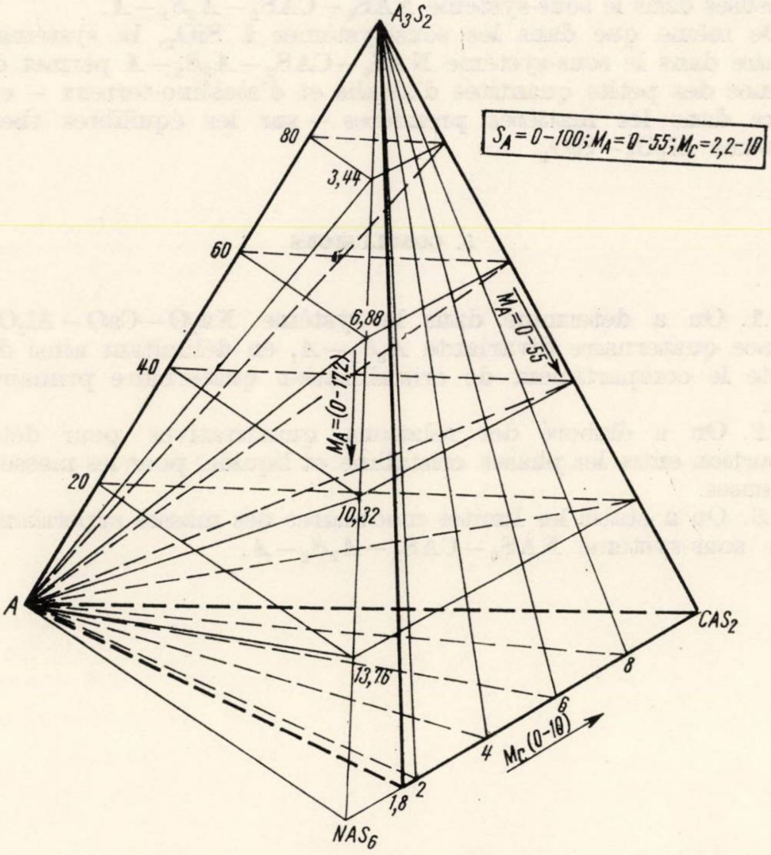
A_3S_2
$S_A=0-100; M_A=0-55; M_C=2,2-10$
80
60
40
20
3,44
6,88
10,32
13,76
1,8
$M_A=(0-17,2)$
$M_A=0-55$
A
CAS_2
NAS_6
2
4
6
8
$M_C(0-10)$

Fig. 5. — Position des masses superalumineuses dans le sous-système $NAS_6 - CAS_2 - A_3S_2 - A$.

Revue Roumaine de Chimie, 18, 1, 23–34 (1973)

Le lieu géométrique des masses ayant un degré égal de saturation représente des plans parallèles au plan $NAS_6-CAS_2-A_3S_2$.

b) *Le module S* est le rapport :

$$S = \frac{\%CaO + \%Na_2O}{\%SiO_2} 100 \qquad (3)$$

Le lieu géométrique des masses ayant le même S est représenté par des plans qui convergent des côtés $NAS_6-A_3S_2$ et $CAS_2-A_3S_2$, dans le sommêt Al_2O_3 du tétraèdre.

c) *Le module C* est formulé de la même façon que dans le cas des masses du sous-système à SiO_2 *, étant donné que le lieu géométrique des masses à C égal représente des plans qui convergent du côté NAS_6-CAS_2 sur l'arrête $Al_2O_3-SiO_2$ du tétraèdre.

On indique dans la figure 5 les limites modulaires des masses superalumineuses dans le sous-système $NAS_6-CAS_2-A_3S_2-A$.

De même que dans les sous-systèmes à SiO_2, la systématisation modulaire dans le sous-système $NAS_6-CAS_2-A_3S_2-A$ permet d'établir l'influence des petits quantités d'alcalis et d'alcalino-terreux — existants toujours dans les matières premières — sur les équilibres thermiques du système $Al_2O_3-SiO_2$.

5. CONCLUSIONS

5.1. On a déterminé dans le système $Na_2O-CaO-Al_2O_3-SiO_2$ la surface quaternaire divariante A_3S_2-A, en délimitant ainsi de façon complète le compartiment de cristallisation quaternaire primaire de la mullite.

5.2. On a élaboré des relations quantitatives pour déterminer la proportion entre les phases cristalline et liquide, pour les masses superalumineuses.

5.3. On a établi les limites modulaires des masses superalumineuses dans le sous-système $NAS_6-CAS_2-A_3S_2-A$.

---

*) $C = \frac{\%CaO}{\%Na_2O + \%CaO} 10. \qquad (4)$

Revue Roumaine de Chimie, **18**, *1*, 35–42 (1973)

RÉACTIONS D'ÉCHANGE ISOTOPIQUE ENTRE Tl(III)–COMPLEXÉ ET ^{204}Tl(I)

AL. CECAL et I. A. SCHNEIDER

Université « Al. I. Cuza », Faculté de Chimie, 11, str. 23 August, Jassy, Roumanie

Reçu le 7 juillet 1972

Le but de ce travail est de déterminer l'influence de quelques combinaisons complexes du Tl(III) et de la nature de la liaison métal-ligand sur les paramètres cinétiques et thermodynamiques caractéristiques de la réaction d'échange isotopique pour le système ^{204}Tl(I)–Tl(III). On y estime les valeurs du temps de semi-échange, des constantes de vitesse, des énergies et entropies d'activation et aussi du facteur préexponentiel.

INTRODUCTION

Il est bien connu que l'échange isotopique donne des indications précises sur la structure des combinaisons complexes et sur la nature de la liaison métal-ligand. Les auteurs du présent travail tâchent d'établri l'influence exercée par la structure et le type de liaison d'une combinaison complexe sur les paramètres qui caractérisent les réactions d'échange isotopique.

Dans ce but, on a préparé 14 composés complexes du Tl(III) avec un certain nombre de ligands organiques choisis de telle sorte qu'il existe entre eux et le métal central différentes sortes de liaison chimique. On a poursuivi ensuite chez les différentes combinaisons complexes, l'échange entre le ^{204}Tl(I) et le Tl(III) – complexé, la variation des paramètres cinétiques et thermodynamiques spécifiques de la réaction mentionnée

PARTIE EXPÉRIMENTALE

L'échange isotopique dans le système ^{204}Tl(I)–Tl(III)—complexé a été étudié par la synthèse des combinaisons complexes : Tl(III)-8-hydroxyquinoléine, Tl(III)-5, 7-dibromo-8-hydroxyquinoléine [1–2], Tl(III)-acide-8-hydroxyquinoléine-7-sulfonique, Tl(III)-acide-7-iodo-8-hydroxyquinoléine-5-sulfonique [3], $HTlBr_4$. pyridine, $HTlBr_4$. α-picoline, $HTlBr_4$. quinoléine, [4]

---

[1] F. Feigl, *Nature*, **163**, 436 (1948).

[2] F. Feigl et L. Baumfeld, *Analyt. Chim. Acta*, **3**, 83 (1949).

[3] Al. Cecal et I. A. Schneider, *Inorg. Chim. Acta*, **5**, 623 (1971).

[4] G. Sandri, *Mikrochim. Acta*, **2**, 253 (1958).

$HTlBr_4$. 2,6-lutidine, $HTlBr_4$. 2,4,6-collidine,[5] $HTlBr_4$. diantipyrylméthane,[6] Tl(III)-2, 2′-dipyridyl, Tl(III)-1, 10-phénanthroline,[7-9] Tl(III)-diéthyldithiocarbamate[10] et Tl(III)-thénoyltrifluoroacétone.[11] Les complexes obtenus à l'état solide ont été dissous dans de l'alcool éthylique, auquel on a ajouté de l'eau jusqu'à la proportion 75 alcool : 25 eau.

Le Tl(I) radioactif nous a été procuré par l'Institut de Physique Atomique sous forme de $^{204}TlNO_3$ solide. Celui-ci a été dissous dans de l'acide azotique (33%) et à la solution on a ajouté du $TlNO_3$ comme porteur. On a déterminé la concentration totale du Tl monovalent par voie gravimétrique.[12]

On a introduit des quantités différentes de réactants dans des flacons de 250 ml, en ajoutant une solution tampon $CH_3COOH-CH_3COONa$ (0,2 M) et une solution de KNO_3 pour régler le pH et la force ionique (à 0,5). Pour poursuivre la cinétique de la réaction d'échange, on a fait à des intervalles de temps, de chaque échantillon, une extraction de 2 ml solution. La séparation des deux états d'oxydation du thallium a été réalisée par la méthode de Harbottle et Dodson[13], en précipitant le Tl(I) sous forme de Tl_2CrO_4. On a lavé et filtré le précipité respectif en posant le volume de la solution à 40 ml. De cette solution on a pris une quote-part de 14 ml, dont on a mesuré l'activité avec un compteur d'immersion dans le liquide (VA–Z–410) lié à un compteur électronique de type VSP–1960. On a poursuivit les réactions d'échange jusqu'à l'équilibre, c'est-à-dire, jusqu'à ce que les dernières 2–4 lectures de l'activité eussent donné des valeurs approximativement constantes.

RÉSULTATS ET DISCUSSIONS

L'estimation des paramètres cinétiques : le temps de semi-échange (en heures) et la constante de vitesse (en l/mole.h) a été faite en partant de la relation de McKay[14-16]. Dans ce but, on a tracé des droites en coordonnées : $-\log(1 - F)$ en fonction du temps, de sorte, que pour la valeur $F = 1/2$ du facteur d'échange sur l'ordonnée, corresponde sur l'abscisse la valeur du temps de semi-échange ($t_{1/2}$). En déterminant ce paramètre, on a calculé la constante de vitesse :

$$k = \ln 2 / [t_{1/2}(a + b)]$$

Les résultats obtenus sont indiqués sur les tableaux 1–3.

---

[5] AL. CECAL et I. A. SCHNEIDER, *Zhur. analit. Khim*, **26**, 1432 (1971).

[6] A. I. BUSEV et V. G. TIPTOVA, *Zhur. analit. Khim*, **15**, 291 (1960).

[7] G. I. SUTTON, *Austral. J. Chem.* **11**, 120 (1958).

[8] F. I. KULBA et V. E. MIRONOV, *Zhur. neorg. Khim*, **4**, 1393 (1959).

[9] F. I. KULBA et V. E. MIRONOV, *Zhur. neorg. Khim*, **4**, 1398 (1959).

[10] H. BODE, *Z. analyt. Chem*, **144**, 165 (1955).

[11] V. Z. AMARIEI, «Dissertatsia na soiskanie uchenoi stepeni kandidata khimicheskikh nauk, M.G.U., Moscou, 1969.

[12] A. I. BUSEV et V. G. TIPTOVA, *Zhur. analit. Khim*, **14**, 28 (1959).

[13] G. HARBOTTLE et R. W. DODSON, *J. Amer. Chem. Soc.*, **73**, 2442 (1951).

[14] H. A. MC KAY, *Nature*, **142**, 997 (1938).

[15] AL. CECAL, *Studii și cercetări Chim.* Acad. București, **20**, 31 (1972).

[16] AL. CECAL, *Studii și cercetări Chim.* Acad. București, **20**, 197 (1972).

Tableau 1

Paramètres cinétiques : $t_{1/2}$ (en heures) et k (en mole/l.h), caractéristiques des réactions d'échange isotopique étudiées pour différentes concentrations des réactants (pour t = 21,4°C et pH = 3,6)

Réaction d'échange	Concentrations des réactants (ions g/l) × 10^4						
	[Tl$^+$] [Tl^{3+}] 6,0 6,0	[Tl$^+$] [Tl^{3+}] 9,0 6,0	[Tl$^+$] [Tl^{3+}] 12,5 6,0	[Tl$^+$] [Tl^{3+}] 17,5 6,0	[Tl$^+$] [Tl^{3+}] 6,0 4,0	[Tl$^+$] [Tl^{3+}] 6,0 2,5	[Tl$^+$] [Tl^{3+}] 6,0 1,5
^{201}Tl$^+$ – $(C_9H_6NO)_3Tl$	283,2 2,03	255,2 1,89	187,2 1,99	168,0 1,86	336,3 2,07	376,8 2,18	426,2 2,16
^{204}Tl$^+$ – $(C_9H_4NOBr_2)_3Tl$	258,2 2,22	213,6 2,16	165,6 1,99	141,6 2,09	312,0 2,22	325,6 2,20	417,6 2,21
^{201}Tl$^+$ – $(C_9H_6NO_4S)_3Tl$	261,6 2,20	237,6 1,98	175,2 2,13	162,8 1,91	280,8 2,46	338,8 2,40	420,0 2,20
^{204}Tl$^+$ – $(C_9H_5NO_4SI)_3Tl$	280,8 2,05	252,0 1,93	200,8 1,89	162,2 1,89	324,0 2,13	372,0 2,19	424,7 2,17
^{204}Tl$^+$ – $HTlBr_4 \cdot C_5H_5N$	244,8 2,75	201,2 2,59	172,8 2,66	139,2 2,62	242,2 2,85	292,8 2,78	336,0 2,75
^{204}Tl$^+$ – $HTlBr_4 \cdot C_6H_7N$	213,6 2,80	189,4 2,63	163,2 2,69	124,8 2,71	252,0 2,75	288,0 2,82	333,6 2,76
^{204}Tl$^+$ – $HTlBr_4 \cdot C_7H_9N$	194,4 2,69	177,6 2,69	148,8 2,71	112,8 2,82	235,2 2,94	273,6 2,97	327,6 2,82
^{204}Tl$^+$ – $HTlBr_4 \cdot C_8H_{11}N$	177,6 3,04	156,0 2,96	132,0 2,83	108,2 2,84	230,6 3,00	256,8 [illegible]	321,8 3,03
^{204}Tl$^+$ – $HTlBr_4 \cdot C_9H_6N$	163,2 3,53	141,6 3,36	117,6 3,38	110,8 3,38	196,8 3,33	256,8 3,37	316,6 3,31
^{204}Tl$^+$ – $HTlBr_4 \cdot C_{23}H_{24}N_4O_2$	146,4 3,64	117,6 3,62	100,8 3,71	79,2 3,73	216,0 3,29	252,0 3,22	314,4 3,48
^{204}Tl$^+$ – $[Tl\ dip_2](NO_3)_3$	369,6 1,66	338,4 1,43	288,0 1,49	247,2 1,49	412,8 1,67	465,6 1,75	506,4 1,82
^{204}Tl$^+$ – $[Tl\ ph_2](NO_3)_3$	386,4 1,49	357,6 1,39	304,8 1,22	271,2 1,29	441,6 1,56	506,4 1,60	576,0 1,60
^{204}Tl$^+$ – $(C_5H_{10}NS_2)_3Tl$	276,0 2,09	232,8 1,98	182,4 2,05	156,0 1,89	297,6 2,23	369,4 2,20	444,0 2,08
^{204}Tl$^+$ – $(C_8H_3O_2SF_3)_3Tl$	208,8 2,76	180,0 2,56	165,0 2,59	124,8 2,57	264,0 2,63	290,4 2,80	336,0 2,75

Tableau 2

L'interdépendance entre la température du milieu réactant et les paramètres correspondant à l'échange isotopique entre ^{204}Tl(I) et Tl(III) complexé (la concentration des réactants est choisie égale à 0,00060 ions g/l et pH = 3,6)

Réaction d'échange	Paramètres cinétiques	Température °C			
		8,2	21,4	30,1	38,7
$^{204}Tl^{+} - (C_9H_6NO)_3Tl$	$t_{1/2}$ k	338,0 1,71	283,2 2,03	244,8 2,35	232,8 2,47
$^{204}Tl^{+} - (C_9H_4NOBr_2)_3Tl$	$t_{1/2}$ k	304,8 1,89	258,2 2,22	201,6 2,86	160,8 3,38
$^{204}Tl^{+} - (C_9H_6NO_4S)_3Tl$	$t_{1/2}$ k	307,2 1,87	261,6 2,20	204,6 2,82	163,2 3,35
$^{204}Tl^{+} - (C_9H_5NO_4SI)_3Tl$	$t_{1/2}$ k	374,4 1,54	280,8 2,05	213,2 2,70	168,0 3,43
$^{204}Tl^{+} - HTlBr_4 \cdot C_5H_5N$	$t_{1/2}$ k	316,8 1,82	244,8 2,75	184,8 3,72	112,8 5,11
$^{204}Tl^{+} - HTlBr_4 \cdot C_6H_7N$	$t_{1/2}$ k	307,2 1,87	213,6 2,80	141,4 4,08	105,4 5,46
$^{204}Tl^{+} - HTlBr_4 \cdot C_7H_9N$	$t_{1/2}$ k	290,4 1,98	194,4 2,96	139,2 4,15	93,6 6,16
$^{204}Tl^{+} - HTlBr_4 \cdot C_8H_{11}N$	$t_{1/2}$ k	252,0 2,28	177,6 3,04	136,8 4,21	76,8 7,51
$^{204}Tl^{+} - HTlBr_4 \cdot C_9H_6N$	$t_{1/2}$ k	220,8 2,61	163,2 3,53	117,9 4,90	72,0 8,01
$^{204}Tl^{+} - HTlBr_4 \cdot C_{23}H_{24}N_4O_2$	$t_{1/2}$ k	208,8 2,76	146,4 3,65	96,0 6,01	57,6 10,01
$^{204}Tl^{+} - [Tl\ dip_2](NO_3)_3$	$t_{1/2}$ k	420,0 1,37	369,6 1,66	271,2 2,12	232,8 2,47
$^{204}Tl^{+} - [Tl\ ph_2](NO_3)_3$	$t_{1/2}$ k	465,6 1,33	386,4 1,49	278,4 2,07	235,2 2,45
$^{204}Tl^{+} - (C_5H_{10}NS_2)_3Tl$	$t_{1/2}$ k	345,6 1,66	276,0 2,09	192,0 3,00	156,0 3,69
$^{204}Tl^{+} - (C_8H_3O_2SF_3)_3Tl$	$t_{1/2}$ k	290,6 1,98	208,8 2,76	156,0 3,69	94,4 6,11

Par des représentations de type Arrhenius ($\log k$ fonction de $1/T$) on déduit les valeurs des énergies d'activation et celles du facteur préexponentiel. Après la détermination des valeurs du facteur préexponentiel,

Tableau 3

L'influence du pH sur les réactions d'échange isotopique étudiées (la concentration des réactants est choisie égale à 0,00060 ions g/l et la température égale à 21,4°C)

Réaction d'échange	Paramètres cinétiques	pH			
		3,6	4,2	4,8	5,6
$^{204}Tl^{+} - (C_9H_6NO)_3Tl$	$t_{1/2}$ k	283,2 2,03	280,6 2,04	270,4 2,16	261,4 2,26
$^{264}Tl^{+} - (C_9H_4NOBr_2)_3Tl$	$t_{1/2}$ k	258,2 2,22	230,4 2,50	216,0 2,67	206,1 2,86
$^{204}Tl^{+} - (C_9H_6NO_4S)_3Tl$	$t_{1/2}$ k	261,0 2,20	235,2 2,45	218,4 2,64	204,0 2,82
$^{204}Tl^{+} - (C_9H_5NO_4SI)_3Tl$	$t_{1/2}$ k	280,8 2,05	252,0 2,28	237,6 2,42	220,8 2,61
$^{204}Tl^{+} - HTlBr_4 \cdot C_5H_5N$	$t_{1/2}$ k	244,8 2,75	202,0 2,85	177,2 3,29	156,0 4,33
$^{204}Tl^{+} - HTlBr_4 \cdot C_6H_7N$	$t_{1/2}$ k	213,6 2,80	174,8 3,30	156,0 3,69	122,4 4,71
$^{204}Tl^{+} - HTlBr_4 \cdot C_7H_9N$	$t_{1/2}$ k	194,4 2,96	172,4 3,34	146,2 3,94	120,0 4,80
$^{204}Tl^{+} - HTlBr_4 \cdot C_8H_{11}N$	$t_{1/2}$ k	177,6 3,04	160,8 3,59	144,0 4,00	117,6 4,90
$^{204}Tl^{+} - HTlBr_4 \cdot C_9H_6N$	$t_{1/2}$ k	163,2 3,53	141,6 4,07	136,4 4,68	112,8 5,11
$^{204}Tl^{+} - HTlBr_4 \cdot C_{23}H_{24}N_4O_2$	$t_{1/2}$ k	146,4 3,64	136,8 4,21	110,6 5,21	98,4 5,86
$^{204}Tl^{+} - [Tl\ dip_2](NO_3)_3$	$t_{1/2}$ k	369,4 1,66	304,8 1,89	276,0 2,09	244,0 2,35
$^{204}Tl^{+} - [Tl\ ph_2](NO_3)_3$	$t_{1/2}$ k	386,4 1,49	342,2 1,68	297,6 1,92	266,4 2,16
$^{204}Tl^{+} - (C_5H_{10}NS_2)_3Tl$	$t_{1/2}$ k	276,0 2,09	254,4 2,26	237,6 2,42	220,8 2,61
$^{204}Tl^{+} - (C_8H_3O_2SF_3)_3Tl$	$t_{1/2}$ k	208,8 2,76	188,9 3,04	163,2 3,53	138,2 4,14

on peut établir les valeurs des entropies d'activation.[17] Toutes ces valeurs sont réportées au tableau 4.

---

[17] S. W. Benson, « The Foundations of Chemical Kinetics », Mc. Graw Hill, New York, 1960.

Tableau 4

Valeurs des énergies et entropies d'activation et des logarithmes du facteur préexponentiel qui caractérisent les réactions étudiées

Réaction d'échange	E kcal/mole	log A	$-\Delta S$ cal/mole·degré
$^{204}Tl^{+} - (C_9H_6NO)_3Tl$	7,912	6,110	30,768
$^{204}Tl^{+} - (C_9H_4NOBr_2)_3Tl$	8,698	6,752	27,811
$^{204}Tl^{+} - (C_9H_4NO_4S)_3Tl$	8,375	6,518	28,924
$^{204}Tl^{+} - (C_9H_5NO_4SI)_3Tl$	8,231	6,384	29,505
$^{204}Tl^{+} - HTlBr_4 \cdot C_5H_5N$	14,534	11,090	7,856
$^{204}Tl^{+} - HTlBr_4 \cdot C_6H_7N$	15,026	11,473	6,089
$^{204}Tl^{+} - HTlBr_4 \cdot C_7H_9N$	15,457	11,806	5,487
$^{204}Tl^{+} - HTlBr_4 \cdot C_8H_{11}N$	16,008	12,197	2,355
$^{204}Tl^{+} - HTlBr_4 \cdot C_9H_7N$	16,974	12,980	+0,836
$^{204}Tl^{+} - HTlBr_4 \cdot C_{23}H_{24}N_4O_2$	18,400	13,912	+5,210
$^{204}Tl^{+} - [Tl\ dip_2](NO_3)_3$	7,589	5,820	32,098
$^{204}Tl^{+} - [Tl\ ph_2](NO_3)_3$	7,360	5,636	33,045
$^{204}Tl^{+} - (C_5H_{10}NS_2)_3Tl$	11,408	8,736	18,547
$^{204}Tl^{+} - (C_8H_3O_2F_3S)_3Tl$	12,212	9,442	15,237

L'influence du pH sur les paramètres cinétiques mène à la conclusion qu'il existe deux chemins différents et concurrents pour la réaction d'échange,[18] l'un indépendant de la concentration des ions d'hydrogène et l'autre dépendant de cette concentration.

Les données présentées plus haut laissent voir qu'il y a une différence prononcée entre les paramètres cinétiques et thermodynamiques caractéristiques des réactions d'échange isotopique soumises à notre examen, en fonction du type de combinaison complexe et de la nature de la liaison métal-ligand dans cette combinaison. On observe que les paramètres respectifs varient, dans le même groupe de combinaisons complexes, en fonction du substituent greffé au noyau de base, chose très importante pour la clarification de l'effet produit par les substituents sur la réactivité de la molécule organique respective.

Pour les combinaisons complexes du Tl(III), par exemple avec la 8-hydroxyquinoléine et ses dérivés, les substituents $R = Br$, SO_3H et I introduits dans la position 7 du noyau de la 8-hydroxyquinoléine influencent différemment la liaison $0-Tl$.[19-21]

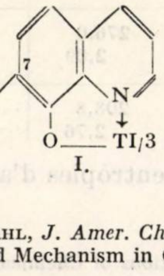

I.

---

[18] R. J. Prestwood et A. C. Wahl, *J. Amer. Chem. Soc.*, **71**, 3137 (1949).

[19] C. K. Ingold, « Structure and Mechanism in Organic Chemistry », Cornell University Press, Ithaca, New York, 1953.

[20] C. K. Ingold, « Introduction to Structure of Organic Chemistry », G. Bell and Sons Ltd. Londres, 1960.

[21] E. H. Rodd, « Chemistry of Carbon Compounds », Elsevier, Amsterdam, 1957.

Le brome ayant l'effet inductif le plus accentué produit une attraction plus prononcée sur les électrons extérieurs de l'atome d'oxygène, affaiblissant la liaison O—Tl et facilitant le transfert d'électrons du ^{204}Tl(I) au Tl(III) du complexe. Au point de vue de la possibilité de perturbation des orbitaux électroniques de l'oxygène, le groupement SO_3H aura sans doute un effet plus puissant que celui du I, d'où l'on peut déduire que pour le complexe Tl(III) - acide 8-hydroxyquinoléine-7-sulfonique, l'échange isotopique avec le ^{204}Tl(I) sera plus rapide que pour le complexe Tl(III)-acide 7-iodo-8-hydroxyquinoléine-5-sulfonique.

Pour les complexes d'addition entre l'acide tétrabromothallique et les bases pyridiniques ou avec le diantipyrylméthane, on constate que l'échange est plus rapide lorsque dans la molécule organique respective on introduit des substituents CH_3 (α-picoline, 2,6-lutidine, 2, 4, 6-collidine) ou bien un cycle benzénique (quinoléine). L'étude des spectres IR, par exemple, montre que la structure de ces combinaisons complexes est (II)

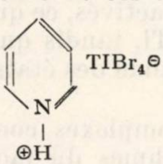

II.

L'addition de l'ion hydrogène à l'azote du cycle pyridinique (ou bien à l'un des atomes d'oxygène dans le diantipyrylméthane) influencera la distribution de la charge positive en l'orientant seulement sur le noyau respectif et non sur les substituents. L'introduction de nouveaux substituents agrandira la distance entre le noyau positif et l'ion négatif $[TlBr_4]^-$, en affaiblissant l'interaction entre les ions. En même temps, l'ion $[TlBr_4]^-$ approchera l'ion $^{204}Tl^+$ en facilitant la réalisation d'un complexe intermédiaire par des ponts de brome, par lesquels le transfert électronique entre les deux états d'oxydation du Tl aura lieu.

Chez les derniers complexes étudiés, on a constaté que l'échange isotopique entre le ^{204}Tl(I) et le Tl(III) complexé avec la thénoyltrifluoroacétone est plus rapide que pour les autres complexes. Ce fait peut s'expliquer par l'attraction plus grande exercée par le noyau du thiophène et surtout par les trois atomes de fluor sur les électrons des orbitaux des atomes d'oxygène, diminuant la densité de charge autour de ces atomes et affaiblissant la liaison entre l'ion métallique central et le ligand (III)

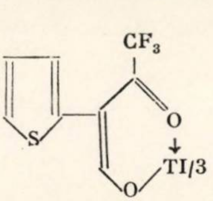

III

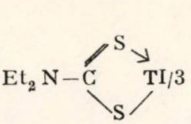

IV

Pour le complexe du Tl(III) et le diéthyldithiocarbamate on constate un échange isotopique lent dû aux liaisons C=S et C—S qui, ayant un caractère électronégatif appréciable, attireront les électrons du reste de la molécule organique et agrandiront la stabilité des liaisons S–Tl et S → Tl (IV).

L'échange isotopique pour les complexes avec le dipyridyl et la phénanthroline est très lent puisque, entre les complexes cationiques qu'ils forment avec le Tl(III) et l'ion $^{204}Tl^+$ approchant, il y aura une forte répulsion électrostatique.[22]

On suppose que pour la réalisation du transfert d'électrons il se forme des complexes activés dans lesquels, entre le $^{204}Tl(I)$ et le Tl(III) s'interpose soit une molécule d'eau, soit des ions Br^- ou OH^-.

La probabilité d'existence de ces intermédiaires est différente pour les divers complexes et on peut l'estimer soit par les valeurs de l'entropie d'activation soit par celles du facteur préexponentiel.

Les valeurs élevées de l'entropie d'activation dénotent une très faible stabilité de ces complexes activés, ce qui explique l'échange lent entre les deux états d'oxydation du Tl, tandis que les valeurs plus petites sont associées à une stabilité plus grande des états de transition et à un échange isotopique plus rapide.

Pour les combinaisons complexes coordinatives (neutres ou cationiques), les valeurs des logarithmes du facteur préexponentiel montrent qu'il existe des effets stériques appréciables et que pour réaliser l'état de transition qui facilite l'échange isotopique, il est nécessaire que le réactant non complexé s'approche d'une certaine direction ; si ces conditions ne sont pas satisfaites, la réaction d'échange n'aura pas lieu. Chez les complexes d'addition de l'acide tétrabromothallique avec des bases organiques, il n'y a pas d'effet stérique appréciable et le $^{204}Tl(I)$ peut s'approcher de n'importe quelle direction.

---

[22] Al. Cecal et I. A. Schneider, *Radiochem. Radioanalyt. Letters* **12**, 39 (1972).

Revue Roumaine de Chimie, **18**, *1*, 43–48 (1973)

STUDY OF THE THORIUM-PURPURIN COMPLEX BY BUTANOL EXTRACTION

C. DRĂGULESCU, T. SIMONESCU and MARIA TOTAN CURTUI

Ministry of Education, Timişoara Chemical Centre, Bd. Mihai Viteazul 24
"Babeş-Bolyai" University, Faculty of Chemistry, Cluj, str. Arany Janos 11
Timişoara University, str. Pestalozzi 16

Received June 7, 1972

The optimum conditions of thorium extraction with a butanol solution of purpurin in the presence of trichloroacetic acid have been established. The composition and the stability of the complex were determined in butanol medium, the instability constant being $K = 1.02 \cdot 10^{-7}$. The extractive-spectrophotometric method elaborated was used for the determination of thorium from certain alloys and monasitic earths.

Literature references data present purpurin (P) as coloured reagent for aluminium [1] and for germanium colorimetric determination. [2] The complexes of this trihydroxyantraquinonic derivate with rare earths as : La, Ce, Pr, Nd, Sm, were studied spectrophotometrically in 95% ethanol. [3] The composition and stability of certain complexes of thorium with ligands from polyhydroxyantraquinonic derivate series (alizarin, quinalizarin and carminic acid) [4,5] were determined by extractive spectrophotometric methods within the works carried out in our laboratory.

The aim of this paper is to establish the extraction conditions of thorium in the presence of trichloroacetic acid with butanol solution of purpurin, as well as the study of the complex formed in 1-butanol for the elaboration of an extractive spectrophotometric method for the determination of thorium.

---

[1] E. F. Labanova, E. I. Kleshchelîskaya and L. I. Korchenenkova, *Sbornik. Tr. Vses. Zaoch. Politekh. Inst. Nr.* 39, **1967**, 46 *Chem. Abstr.* **69**, 15632f (1968).

[2] M. Finkelsteinate and J. C. Garjonyte, *Zhur. Khim. Obshchest.*, **13**, 593 (1968).

[3] J. Ahmad, N. Ahmad and S. M. F. Rahman, *J. Indian Chem. Soc.*, **44**, 485 (1967).

[4] C. Drăgulescu, T. Simonescu, G. Nemeş and M. Totan, *Rev. Roumaine Chim.*, **15**, 563 (1970).

[5] C. Drăgulescu, T. Simonescu, G. Nemeş and M. Totan, "Lucrările celei de a III-a Conferinţe naţionale de Chimie Analitică" Braşov, vol. IV, 1971, p. 103.

EXPERIMENTAL

Apparatus. The absorption spectra were recorded with a SP 800 "Unicam" spectrophotometer, Cambridge, England, and the other spectrophotometric determinations were made with Carl Zeiss Jena DDR "Spekol" spectrophotometer. The pH measurements were made with MV–11 Calmann & Grahnert Dresden DDR pH-meter.

Reagents : 10^{-2}M thorium nitrate solution was prepared dissolving about 5.52 g$Th(NO_3)_4 \cdot . xH_2O$ Merck (with a content of min 46 % ThO_2) in 1.000 ml bidistilled water. The titre of solution was determined gravimetrically as ThO_2.

– $1 \cdot 10^{-3}$ and $2 \cdot 10^{-2}$M thorium nitrate solutions were obtained by dilution.

– $1 \cdot 10^{-3}$ M purpurin solution in 1-butanol was prepared dissolving, by slight heating, 0.0256 g Merck purpurin in 100 ml 1-butanol.

– approx. 2M trichloroacetic acid (TCA) solution was obtained by dissolving a corresponding quantity of Merck trichloroacetic acid in bidistilled water.

– 1-butanol, the fraction between 117 and 118.5° obtained at the distillation of fermentation butanol, was used.

Method

20 ml of butanol solution of purpurin is added to 20 ml aqueous solution containing 0.2 ml about 2 M TCA (pH = 2.5), and a known quantity of thorium nitrate. It is stirred for two minutes and the phases are separated. The butanol phase is collected in a calibrated flask and is completed to 25 ml with 1-butanol. After extraction, thorium content in water solution is determined spectrophotometrically with thoron.[6]

RESULTS AND DISCUSSION

A red-coloured complex is found at extraction of thorium from aqueous solution with a butanol solution of purpurin. Absorption curves of this complex at various pH extractions, in comparison with absorption curves of purpurin in the same conditions are represented in Figure 1. As Figure 1 illustrates, purpurin presents the maximum absorption at 478 nm in the whole pH range in which the determinations were made. The absorption maximum of the thorium-purpurin complex, /Th–P/, is placed at a wavelength much different from that of the pure ligand. Regarding the absorption curve 6 from figure 1 (drawn for optimum extraction condition) the 533 nm wavelength was chosen for determination.

The influence of pH and trichloroacetic acid concentration was studied to establish optimum extraction conditions. The curves in Figure 1 indicate the optimum pH of extraction and formation of the /Th–P/ complex as being 2.5.

There is no /Th–P/ complex formation in pH range 0.6–1.0 and at pH values higher than 3, thorium precipitates, and this makes the determination difficult. Total extraction is practically achieved in the pH range of 2.5–3, after one extraction.

---

[6] M. Pinta "Recherche et dosage des éléments traces" Dunod, Paris, 1962, p. 611.

The percentage distribution curve of thorium depending on trichloroacetic acid concentration represented in Figure 2 shows that the trichloroacetic acid influences much the extraction of thorium with butanol solution of purpurin. In the absence of trichloroacetic acid, a percentage extraction of only 8.6% is obtained.

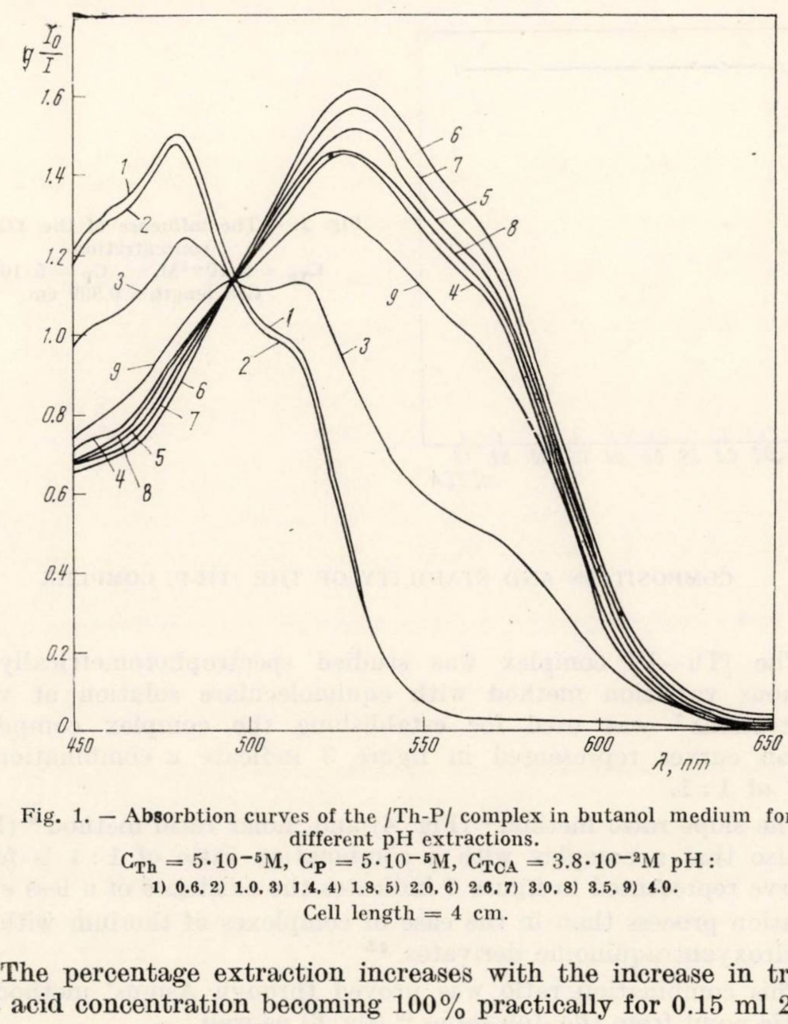

Fig. 1. — Absorbtion curves of the /Th-P/ complex in butanol medium for different pH extractions.
$C_{Th} = 5 \cdot 10^{-5}$M, $C_P = 5 \cdot 10^{-5}$M, $C_{TCA} = 3.8 \cdot 10^{-2}$M pH:
1) 0.6, 2) 1.0, 3) 1.4, 4) 1.8, 5) 2.0, 6) 2.6, 7) 3.0, 8) 3.5, 9) 4.0.
Cell length = 4 cm.

The percentage extraction increases with the increase in trichloroacetic acid concentration becoming 100% practically for 0.15 ml 2M TCA acid in aqueous solution. Since in these conditions the phases are separated very slowly, 0.2 2M TCA acid was used when the phases were well separated.

Following the kinetics of formation reaction of the /Th–P/ complex in 1-butanol, in established extraction conditions, it is noticed that the formation of the complex does not need long time and this allows measurements to be made immediately after the separation of the phases. The complex formed is stable for at least fourteen days.

Lambert Beer's law is observed over the concentration range where the work was carried out. It is observed up to 10 μg at least.

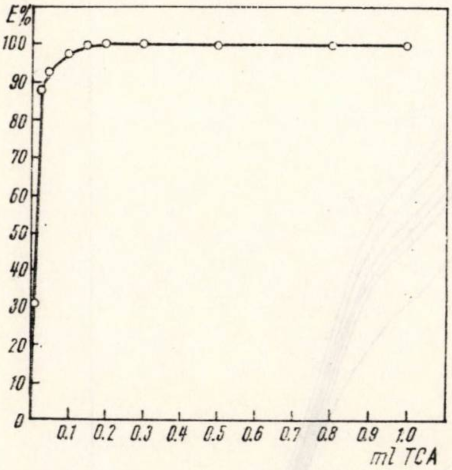

Fig. 2. — The influence of the TCA—acid concentration
$C_{Th} = 5 \cdot 10^{-5}$M, $C_P = 5 \cdot 10^{-5}$ M
Cell length = 0.999 cm.

COMPOSITION AND STABILITY OF THE /TH-P/ COMPLEX

The /Th—P/ complex was studied spectrophotometrically. The continuous variation method with equimoleculare solution at various concentrations[7] was used for establishing the complex composition. The Job curves represented in figure 3 indicate a combination ratio /Th : P of 1 : 1.

The slope ratio method[8] (Fig. 4) and molar ratio method[9] (Fig. 5) show also that a complex with a combination ratio of 1 : 1 is formed. The curve represented in figure 5 indicates the existence of a less evident dissociation process than in the case of complexes of thorium with other polyhydroxyantraquinonic derivates.[4,5]

This combination ratio was proved through Asmus' method with isosbestic point from the Job series[10] (fig. 6) as well.

The instability constant was counted by the method of Harvey and Manning,[8] $K = 1.02 . 10^{-7}$.

[7] P. Job, *Ann. Chim. (France)*, **9**, 113 (1928).
[8] A. E. Harvey and D. L. Manning, *J. Amer. Chem. Soc.*, **72**, 4488 (1950).
[9] J. H. Yoe and A. L. Jones, *Ind. Eng. Chem. Analyt. Ed.*, **16**, 111, (1944).
[10] E. Asmus, *Z. analyt. Chem.*, **193**, 81 (1963).

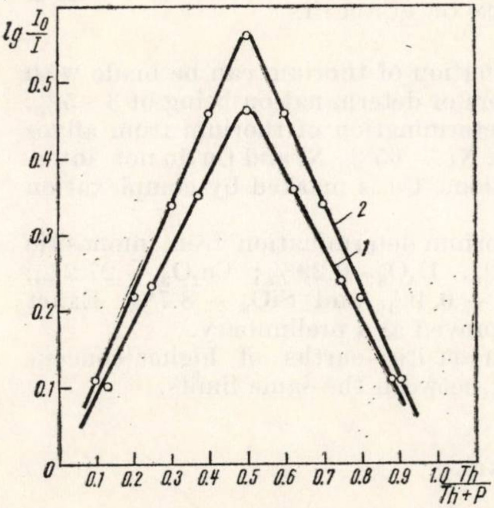

Fig. 3. – Continuous variation method for the /Th-P/ complex
1) $C_{total} = 4\cdot10^{-5}$ M, 2) $C_{total} = 5\cdot10^{-5}$ M
Cell length = 4 cm.

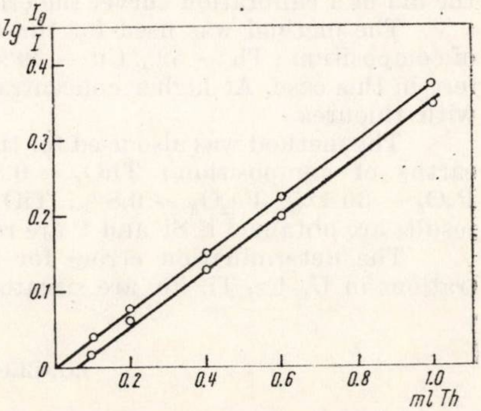

Fig. 4. – Slope ratio method for the /Th-P/ complex $C_{constant\ component} = 2.4\cdot10^{-4}$ M
Cell length = 0.999 cm.

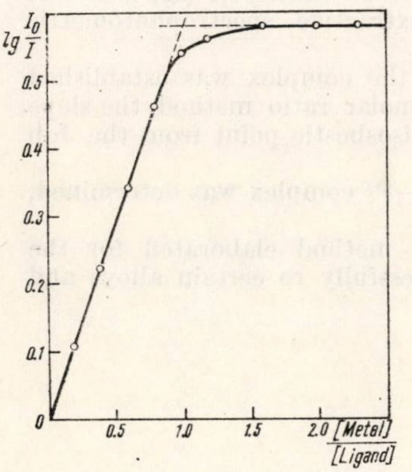

Fig. 5. – Molar ratio method for the /Ph-P/ complex
$C_{Th} = 2\cdot10^{-4}$M Cell length = 0.999 cm.

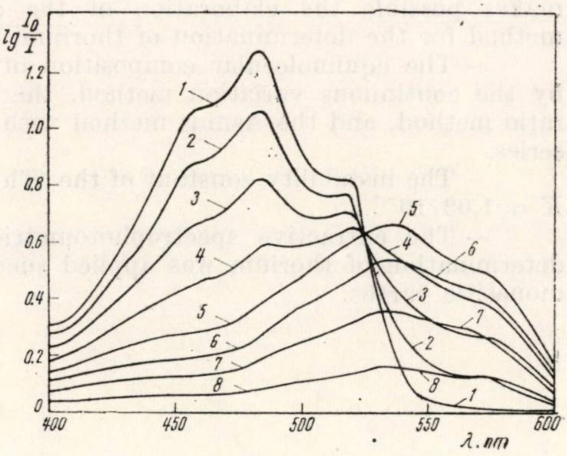

Fig. 6. – Absorbtion curves of continuous variation series $C_{total} = 4\cdot10^{-5}$M C_{Th}:
1) $0.4\cdot10^{-5}$M, 2) $0.8\cdot10^{-5}$M, 3) $1.2\cdot10^{-5}$M,
4) $1.6\cdot10^{-5}$M, 5) $2.0\cdot10^{-5}$M, 6) $2.4\cdot10^{-5}$M,
7) $2.8\cdot10^{-5}$M, 8) $3.2\cdot10^{-5}$M.
Cell length = 4 cm.

EXTRACTIVE SPECTROPHOTOMETRIC DETERMINATION OF THORIUM WITH BUTANOL SOLUTION OF PURPURIN

The spectrophotometric determination of thorium can be made with the aid of a calibration curve, the errors of determination being of 3–5%.

The method was used for the determination of thorium from allyos of composition : Th – 5%, Cu – 30%, Ni – 65%. Ni and Cu do not interfere in this case. At higher concentrations, Cu is masked by complexation with thiourea.

The method was also used for thorium determination from monasitic earths of composition : ThO_2 – 9.8%, U_3O_8–0.29% ; Ce_2O_3 – 27.2%, P_2O_5 – 30.1%, Fe_2O_3 – 0.8%, TiO_2 – 0.4%, and SiO_8 – 8.7%. Exact results are obtained if Si and P are removed as a preliminary.

The determination errors for monasitic earths of higher concentrations in U, Ce, Ti, Fe, are situated between the same limits.

CONCLUSIONS

– The optimum extraction and formation conditions of the /Th–P/ complex were established.

– The trichloroacetic acid makes possible the extraction of thorium with a butanol solution of purpurin in the pH range 2.5–3.

– Percentage extractions of 100% are obtained after one extraction only.

– Lambert-Beer's law is applied up to at least 10.2 μg, and this makes possible the elaboration of the extractive spectrophotometric method for the determination of thorium.

– The equimolecular composition of the complex was established by the continuous variation method, the molar ratio method, the slope ratio method, and the Asmus method with isosbestic point from the Job series.

– The instability constant of the /Th–P/ complex was determined, $K = 1{,}02 \cdot 10^{-7}$.

– The extractive spectrophotometric method elaborated for the determination of thorium was applied successfully to certain alloys and monasitic earths.

Revue Roumaine de Chimie, 18, 1, 49–52 (1973)

URANYL-PYROPHOSPHATE COMPLEXES. III[1] THE MONOPYROPHOSPHATO-PENTAURANYL CATION COMPLEX

C. DRĂGULESCU and NICOLETA VÎLCEANU

Centre of Chemistry
Bd. Mihai Viteazul 24, Timişoara, Romania

Received May 8, 1972

The formation of one single monopyrophosphato-pentauranyl cation complex, $[(UO_2)_5H_2P_2O_7]^{8+}$, was found spectrophotometrically, in the 0.83–3.00 pH range. Its formation constant after the Newman and Hume method is $K_q = 0.0344$.

Literature data concerning the complex combinations of the uranyl cation with oxyacid ligands show that, together with numerous anion-complexes, there are cation complexes as well. Thus, the following combinations have been identified without being separated from the solution: $[(UO_2)_2CO_3]^{2+}$, [2] $[UO_2(SCN)]^+$, [3] $[(UO_2)_2SO_4(H_2O)_{10}]^{2+}$. [4] In the class of pyrophosphate complexes some metal-pyrophosphate cation complexes have been found. These were presented in the monographical work. [5]

Uranyl-pyrophosphate cation complexes have not been mentioned in the previous literature in this field. For the first time this type of combination was mentioned in our work,[6] where we have shown the formation of a series of successive complex combinations in the system $UO_2^{2+} - P_2O_7^{4-}$. The dissolution of the combinations $(UO_2)_2P_2O_7$ and $Na_2(UO_2)_3(P_2O_7)_2$ in an excess of uranyl salt, is an indication for the formation of complexes with a higher proportion of uranyl cation in the molecule.

In the previous note,[6] on the basis of radiometric titration and radioelectrophoretic determinations the possibility of formation of some uranyl-pyrophosphate cation complexes, which can be expressed by the formula $[(UO_2)_mP_2O_7]^{(2m-4)+}$, where $m = 2-5$, was shown.

---

[1] Part. II. C. DRĂGULESCU, N. VÎLCEANU and I. JULEAN, *Z. anorg. Chem.*, **376**, 196 (1970).

[2] I. I. CHERNYAEV, "Complex Compounds of Uranium", Jerusalem 1966, Israel Program for Scientific Translation, "Kompleksnye Soedinenya Urana", Izdatelsstvo Nauka, Moskva, 1964.

[3] S. AHRLAND, *Acta Chem. Scand.*, **3**, 1067 (1949).

[4] V. A. SHUBIN, G. B. POLUEKTOV, N. P. GALKIN and A. A. MAIOROV, *Zhur. neorg. Khim.*, **6**, 2319 (1961).

[5] C. DRĂGULESCU and N. VÎLCEANU, *Studii şi Cercetări Chim. Acad. R.S.R.*, **17**, 357 (1969).

[6] C. DRĂGULESCU, I. JULEAN and N. VÎLCEANU, *Rev. Roumanie Chim.*, **10**, 809 (1965).

In order to obtain additional data concerning the formation of the cationic complex combinations, the experimental procedure adopted was the spectrophotometric titration technique. This method permitted the determination of the combination ratio metal-ligand as well as the evaluation of the formation constant of the resulted complex.

EXPERIMENTAL

Reagents :

— $UO_2(NO_3)_2 . 6H_2O$ *p.a.* Merck

— $Na_4P_2O_7 . 10H_2O$ *p.a.* Merck

— $H_4P_2O_7$ *p.a.*, obtained through the passing of a $Na_4P_2O_7$ solution over a Dowex 50 × 12 column.

— The solutions of the different pyrophosphoric species $H_3P_2O_7^-$, $H_2P_2O_7^{2-}$, $HP_2O_7^{3-}$ were prepared from $H_4P_2O_7$ 0.1M and $Na_4P_2O_7$ 0.1M accomplishing mixtures in the proper stoichiometric ratio. The purity of the pyrophosphoric anions was verified through the paper chromatography technique, applying the monodimensional ascendent chromatographic method with acid solvent.[7] The concentration of the pyrophosphoric species has been determined by conductometric or pH-metric titrations with NaOH 0.1M.

— $NaClO_4 . H_2O$ *p.a.* Merck, has been used for the maintaining of the constant strength, $\mu = 0.1$.

Apparatus

— Unicam SP 800 spectrophotometer, with quartz cells;

— pH-meter 25 Radiometer (Copenhagen) with G 202C glass electrode and K 401 calomel electrode.

RESULTS

The spectrophotometric titration of 4×10^{-2} moles $UO_2(NO_3)_2$ with $H_4P_2O_7$ 1×10^{-3}M pH = 1.92 — 0.85, $NaH_3P_2O_7$ 1×10^{-3} M pH = 1.92 — 1.20, $Na_2H_2P_2O_7$ 1×10^{-3} M pH = 1.92 — 1.60 (figures 1 and 2), and $Na_3HP_2O_7$ 1×10^{-3} M pH = 1.92 — 2.40, at the wave length of 420 and 408 mμ, respectively show that irrespective of the reagent, at the molar ratio UO_2^{2+}/pyrophosphoric species = 5/1, the titration curve exhibits a point of inflexion.

The titration of 4×10^{-2} moles $UO_2(NO_3)_2$ with $Na_4P_2O_7$ 1×10^{-3} M pH = 1.92—3.00, leads to a straight line up to the ratio 5/1 between the reaction partners, where the presence of a precipitate stops the titration.

On the other hand, at the molar ratio UO_2^{2+}/pyrophosphoric species = = 5/1 for all the titrations, i.e. on the pH interval between 0.85—3.00, the value of the absorbance is the same for the two wave lengths considered to be ($A = 0.66$ for $\lambda = 420$ mμ and $A = 0.43$ for $\lambda = 408$ mμ). We estimate that those represent proofs for the formation of one single complex at the molar ratio 5/1 between the reagents, to which (taking into consideration the pH of the solutions) the probable composition $[(UO_2)_5H_2P_2O_7]^{8+}$ corresponds.

---

[7] H. Grunze and E. Thilo, "Die Papierchromatographie der kondensierten Phosphate", Akademie Verlag, Berlin, 1955, p. 3—12.

We have spectrophotometrically determined the value of the formation constant of this complex after the Newman and Hume method.[8]

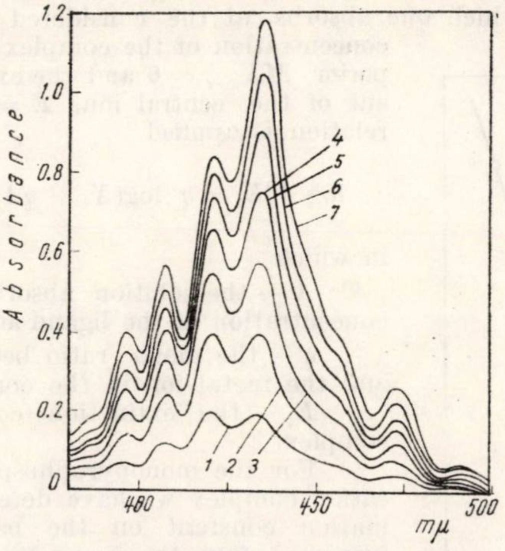

Fig. 1. — Absorbtion spectra of the following solutions :

1, 4.0×10^{-2} moles $UO_2(NO_3)_2 + 2.0 \times 10^{-3}$ moles $Na_2H_2P_2O_7$;
2, 4.0×10^{-2} moles $UO_2(NO_3)_2 + 4.0 \times 10^{-3}$ moles $Na_2H_2P_2O_7$;
3, 4.0×10^{-2} moles $UO_2(NO_3)_2 + 6.0 \times 10^{-3}$ moles $Na_2H_2P_2O_7$;
4, 4.0×10^{-2} moles $UO_2(NO_3)_2 + 8.0 \times 10^{-3}$ moles $Na_2H_2P_2O_7$;
5, 4.0×10^{-2} moles $UO_2(NO_3)_2 + 1.0 \times 10^{-2}$ moles $Na_2H_2P_2O_7$;
6, 4.0×10^{-2} moles $UO_2(NO_3)_2 + 1.2 \times 10^{-2}$ moles $Na_2H_2P_2O_7$;
7, 4.0×10^{-2} moles $UO_2(NO_3)_2 + 1.4 \times 10^{-2}$ moles $Na_2H_2P_2O_7$,
reference : $UO_2(NO_3)_2$ 4.0×10^{-2}M ; $\mu = 0.1(NaClO_4)$; pH = 1.92 – 1.60.

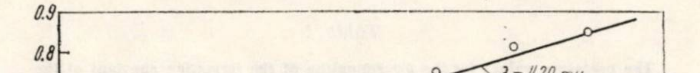

Fig. 2. — Spectrophotometric titration of 4.0×10^{-2} moles $UO_2(NO_3)_2$ with $Na_2H_2P_2O_7$ 0.1 M.

---

[8] L. Newman and D. N. Hume, *J. Amer. Chem. Soc.*, **79**, 4571 (1957).

If the ratio K_{q+r}/K_q is sufficiently large it might be necessary to determine K_q when the central atom concentration (M_t) is in great excess to the concentration of the ligand added (X_t). In the case two species are present, out of which one absorbs, at the considered wavelength, the concentration of the complex immediately superior $MX_{q+r} = 0$ and the extinction coefficient of the central ion, $E = 0$, the following relation is applied

$$\log A/E_q = q\{\log(X_t - qA/E_q)\} + \log K_q$$

in which

A — the solution absorbance at the X_t concentration of the ligand added;

q — the molar ratio between the ligand and the metal ion in the complex;

E_q — the extinction coefficient of the complex.

For the monopyrophosphato-pentauranyl cation complex we have determined the formation constant on the basis of the data furnished from the figure 1; $q = 0.2$, $E_q = 21$. Table 1 presents the necessary values for the determination of the formation constant of the monopyrophosphato-pentauranyl cation complex.

Figure 3 contains the determination of the formation constant of the complex $[(UO_2)_5H_2P_2O_7]^{8+}$. The value of the formation constant is $K_q = 0.0344$.

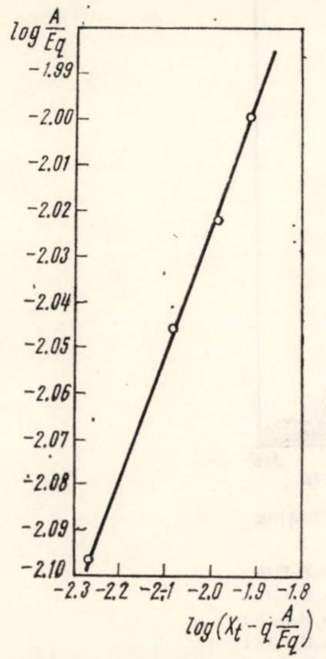

Fig. 3. — Determination of the constant of the complex formation $[(UO_2)_5H_2P_2O_7]^{8+}$.

Table 1

The necessary values for the determination of the formation constant of the monopyrophosphato-pentauranyl cation complex

spectrum	$A_{422m\mu}$	$\log A/E_q$	$\log(X_t - qA/E_q)$
3	0.135	−2.187	−2.328
4	0.165	−2.097	−2.267
5	0.185	−2.046	−2.086
6	0.200	−2.002	−1.985
7	0.210	−2.000	−1.921

Revue Roumaine de Chimie, 18, 1, 53–58 (1973)

URANYL-PYROPHOSPHATE COMPLEXES. IV[1]

PRECIPITATION REACTIONS OF THE PYROPHOSPHATO-URANYLATE COMPLEX ANIONS WITH THE Ag^+ ION

C. DRĂGULESCU, NICOLETA VÎLCEANU and I. JULEAN

Centre of Chemistry
Bd. Mihai Viteazul 24, Timişoara, Romania

Received June 11, 1972

The formation of the following complex salts: $Ag_6[UO_2(P_2O_7)_2]$, $Ag_4Na_2[UO_2(P_2O_7)_2]$, $AgNa[UO_2(P_2O_7)]$ and $Ag_2[UO_2(P_2O_7)]$, compounds derived from the bis- and monopyrophosphato-uranylate complex anions, have been evidenced conductometrically and radiometrically.

The titration series of the pyrophosphoric anions with the UO_2^{2+} cation[2] has permitted us, by following the combination ratio of the reaction partners as a pH function, to establish the formation and the composition of the uranyl-pyrophosphate complexes.

For highly soluble complexes that are to be found in the solution, in the form of soluble sodium salts difficult to isolate, we tried an indirect way of checking their composition, by precipitation with salts of heavy metals. In this way, the sodium ions may be either partially or totally replaced by other metallic ions, having a greater ionic radius.

The bis- and monopyrophosphato-uranylate complexes precipitate with a series of metallic ions like: Ag^+, Cd^{2+}, Zn^{2+}, Co^{2+}, Ni^{2+} etc. They may be thus separated from the solution under the form of some still uninvestigated complex salts.

EXPERIMENTAL

Reagents:

- $UO_2(NO_3)_2 \cdot 6H_2O$ *p.a.* Merck
- $Na_4P_2O_7 \cdot 10H_2O$ *p.a.* Merck
- $Na_4{}^{32}P_2O_7$ *p.a.* prepared in the thermic decomposition of $Na_2H^{32}PO_4$ *p.a.* at 550°.

---

[1] C. Drăgulescu and N. Vîlceanu, *Rev. Roumaine Chim.*, Part III, **18**, *1*, 49–52, (1973).
[2] C. Drăgulescu, N. Vîlceanu and I. Julean, *Z. anorg. Chem.*, **376**, 196 (1970).

— The bis- and monopyrophosphato-uranylate complexes were prepared from $UO_2(NO_3)_2$ 0.1M and $Na_4P_2O_7$ 0.1M in stoichiometric ratio.

— $AgNO_3$ *p.a.* and $^{110}AgNO_3$ *p.a.* Merck

— $NaClO_4.H_2O$ *p.a.* Merck

Apparatus

The conductometric titration was effected with a Metrohm-Herisau conductoscop. In the radiometric titration we have used a Vakutronik VAM 16D counter, with Geiger-Müller MTS—17 and VAZ—410 counters.

DISCUSSION OF THE RESULTS

We give below the precipitation titrations of the bis- and mono-pyrophosphato-uranylate complex anions (the paper electrophoretic method has permitted us to put into evidence, by the migration direction of the complexes, only the sign of their charge).

a. The precipitation reaction of the bis-pyrophosphato-uranylate complex anion with the Ag^+ cation.

Figures 1, 2 and 3 show the titration of the bis-pyrophosphato-uranylate complex anion with $AgNO_3$ and vice versa. The conductometric titration curve (curve 1, figure 1) shows a substantial increase in the conductivity of the solution. This is owing to the reagent added. After the addition of about 2 ml $AgNO_3$ 0.1 M there appears a yellow-white voluminous precipitate in the solution. The conductivity of the solution remains constant all along its formation. After reaching the molar ratio of one mole bis-pyrophosphato-uranylate complex to 4 Ag^+ atoms, the conductivity of the solution slowly increases until the mentioned ratio reaches the value 1/6; then the conductivity of the solution registres an important increase depending on the excess of the reagent added.

The curve of the reversed conductometric titration (curve 2, figure 1), shows a very slight increase in the conductibility as far as the molar ratio, complex/Ag^+ = 1/6. From the beginning of the titration one can observe the appearance of the above mentioned voluminous precipitate. The conductivity of the solution continues to increase, function of the excess of the bis-pyrophosphato-uranylate complex added.

The diagram of the radiometric titration of the bis-pyrophosphato-uranylate complex (marked with ^{32}P) with $AgNO_3$ (curve 1, figure 2) shows, in accordance with the analogous conductometric titration, that the formation of the precipitate does not take place immediately, but only after exceeding the solubility of the precipitate. Accordingly, the radioactivity of the solution is constant up to 2 ml reagent addition. The appearance of the precipitate (which engages the marked P atom) is accompanied by a strong decrease of the radioactivity up to the only inflexion point on the titration diagram, corresponding to the molar ratio, complex/Ag^+ = 1/6.

Working with ^{110}Ag and with the unmarked complex (figure 2, curve 2) the radioactivity of the solution increases at the beginning, owing to the marked reagent, but falls with the formation of the precipitate and remains constant during the formation of the precipitate. After the

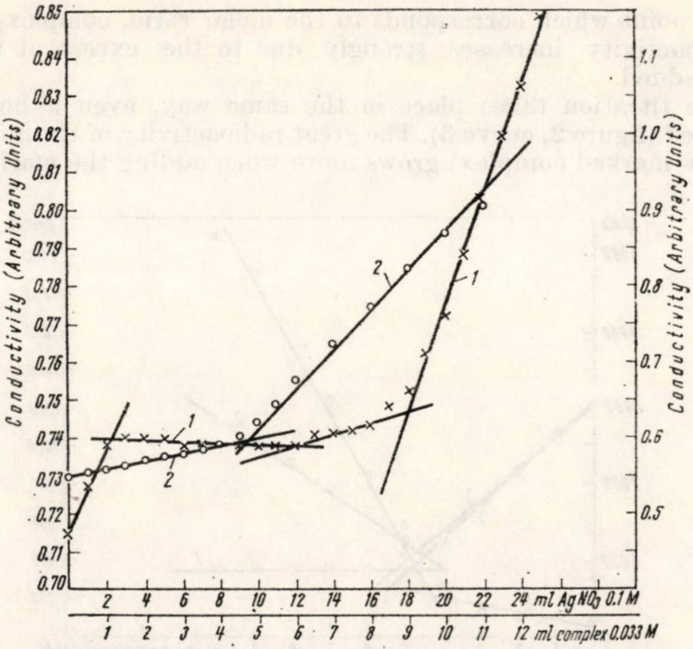

Fig. 1. – Conductometric titration of the sodium bis-pyrophosphato-uranylate complex (3 ml $UO_2(NO_3)_2$ 0.1M + 6 ml $Na_4P_2O_7$ 0.1M) with $AgNO_3$ 0.1M (curve 1). Conductometric titration of 10 ml $AgNO_3$ 0.1M with the sodium bis-pyrophosphato-uranylate complex (prepared from $UO_2(NO_3)_2$ 0.1M and $Na_4P_2O_7$ 0.1M in stoichiometric ratio) (curve 2).

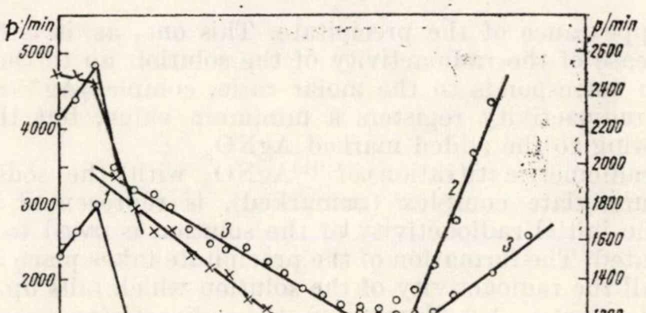

Fig. 2. – Radiometric titration of the sodium bis-pyrophosphato-uranylate complex (3 ml $UO_2(NO_3)_2$ 0.1M + 6 ml $Na_4P_2O_7$ 0.1M) with $AgNO_3$ 0.1M:

1, complex marked with ^{32}P; *2*, $AgNO_3$ marked with ^{110}Ag; *3*, both reaction partners are marked.

inflexion point which corresponds to the molar ratio, complex/$Ag^+ = 1/6$, the radioactivity increases strongly due to the excess of the marked reagent added.

The titration takes place in the same way, even if both reagents are marked (figure 2, curve 3). The great radioactivity of the initial solution (owed the marked complex) grows more when adding the marked reagent, until the appearance of the precipitate. This one, as it is formed, leads to the decrease of the radioactivity of the solution up to the equivalence point which corresponds to the molar ratio, complex/$Ag^+ = 1/6$; in this point, the radioactivity registers a minimum value, but then increases strongly, owing to the added marked $AgNO_3$.

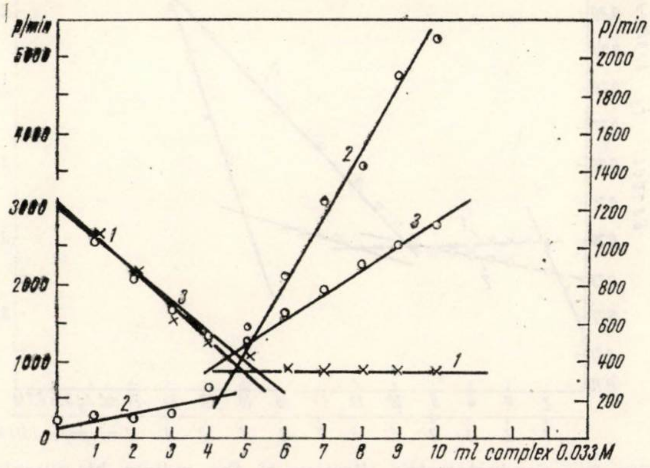

Fig. 3. — Radiometric titration of 10 ml $AgNO_3$ 0.1M with the sodium bis-pyrophosphato-uranylate complex (prepared from $UO_2(NO_3)_2$ 0.1M and $Na_4P_2O_7$ 0.1M in stoichiometric ratio:
1, $AgNO_3$ marked with ^{110}Ag; 2, complex marked with ^{32}P; 3, both reaction partners are marked.

The radiometric titration of $^{110}AgNO_3$ with the sodium-bis-pyrophosphato-uranylate complex (unmarked), is represented by curve 1, figure 3. The initial radioactivity of the solution is owed to ^{110}Ag, which is to be titrated. The formation of the precipitate takes place immediately; it engages all the radioactivity of the solution which falls up to the molar ratio, complex/$Ag^+ = 1/6$. Further on, the radioactivity remains constant.

Working in the variant with unmarked and complex marked $AgNO_3$ (curve 2, figure 3), the curve of the radiometric titration shows a reverse form than the preceding one: the radioactivity is nearly constant, all along the duration of the precipitate formation, until it reaches the same molar ratio, complex/Ag = 1/6, after which it increases strongly (the added complex is marked).

Curve 3 of figure 3 shows the development of the radiometric titration of silver nitrate with sodium bis- pyrophosphato-uranylate complex, both reaction partners being marked. The initial radioactivity of the solution owed to ^{110}Ag decreases when the complex is added, all along the formation period of the precipitate. After the equivalence, marked by the inflexion point which corresponds to the molar ratio, complex/$Ag^+ = 1/6$, the radioactivity registers an important increase in accordance with the marked reagent added.

Comparing the results of the conductometric and radiometric titrations, both direct and reverse ones, in all the investigated variants, we could observe the certain formation of the insoluble combination at the molar ratio, complex/$Ag^+ = 1/6$, corresponding to the $Ag_6[UO_2(P_2O_7)_2]$, after the following scheme :

$$\{[UO_2(P_2O_7)_2]^{6-} + {}_6Na^+\} + {}_6(Ag^+ + NO_3^-) \rightleftarrows$$

$$\rightleftarrows Ag_6[UO_2(P_2O_7)_2] + {}_6(Na^+ + NO_3^-)$$

Unlike all the other titrations, the conductometric titration of the sodium bis-pyrophosphato-uranylate complex with Ag^+ (curve 1, figure 1) also shows the formation of an intermediate compound at the molar ratio, complex/$Ag^+ = 1/4$. In this case the reaction could develop as follows :

$$\{[UO_2(P_2O_7)_2]^{6-} + {}_6Na^+\} + {}_4(Ag^+ + NO_3^-) \rightleftarrows$$

$$\rightleftarrows Ag_4Na_2[UO_2(P_2O_7)_2] + {}_4(Na^+ + NO_3^-)$$

Adding the reagent, the formed precipitate transforms itself in the final product of the reaction $Ag_6[UO_2(P_2O_7)_2]$.

b. The precipitation reaction of the monopyrophosphato-uranylate anion complex with the Ag^+ cation.

Figures 4 and 5 show the precipitation reactions of the sodium monopyrophosphato-uranylate complex with the Ag^+ cation (the reverse titration have not been conclusive and, therefore, we do not present them).

The conductometric titration curve (figure 4) shows an increase in the conductivity of the solution, owing to the reagent added. The compound which is being formed is soluble, at the beginning, until approximately 2 ml $AgNO_3$ is added when the precipitation begins. The first inflexion point of the conductometric curve corresponds to the molar ratio, complex/$Ag^+ = 1/1$. As the reagent is added, the conductivity of the solution increases a little up to the molar ratio 1/2, after which it increases much as the reagent is excessively added.

The radiometric titration curves of the complex marked with Ag^+ (curve 1, figure 5) show, at the beginning, that the radioactivity of the solution is constant and the compound formed is soluble; then it falls owing to the engagement of the complex in the precipitate up to the only equivalence point corresponding to the molar ratio, complex/$Ag^+ = 1/1$.

The same experimental result is obtained by working with marked Ag^+ (curve 3, figure 5). The radioactivity of the solution grows owing to the addition of the marked reagent and formation of the soluble compound.

With the appearance of the precipitate and during its formation, the radioactivity falls strongly up to the molar ratio, complex/$Ag^+ = 1/1$, and then remains constant.

Curve 2, figure 5 shows the evolution of the titration in the case that both reaction partners are marked. In this instant too, the radioactivity of the solution increases owing to the solubility of the formed compound and then suddenly falls. The inflexion point of the diagram at the ratio 1/1 of the components shows the end of the reaction when the radioactivity increases again.

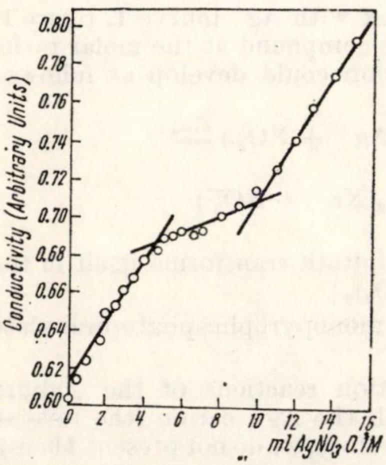

Fig. 4. — Conductometric titration of the sodium monopyrophosphato-uranylate complex (5 ml $UO_2(NO_3)_2$ 0.1M + 5 ml $Na_4P_2O_7$ 0.1M) with $AgNO_3$.

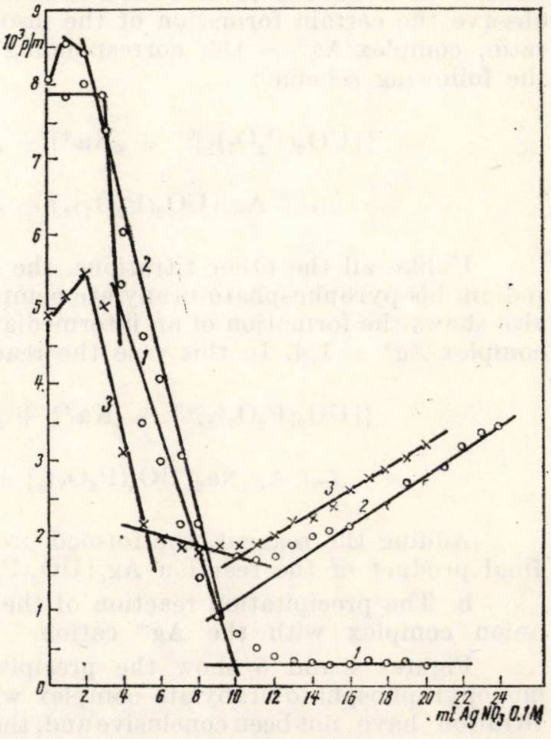

Fig. 5. — Radiometric titration of the sodium monopyrophosphato-uranylate complex (10 ml $UO_2(NO_3)_2$ 0.1M + 10 ml $Na_4P_2O_7$ 0.1M) with $AgNO_3$: *1*, complex marked with ^{32}P; *2*, both reaction partners are marked; *3*, $AgNO_3$ marked with ^{110}Ag.

Both the data of the conductometric titration and the radiometric ones point to the formation of a compound at the molar ratio, monopyrophosphato-uranylate complex/$Ag^+ = 1/1$, $AgNa[UO_2(P_2O_7)]$. Unlike the radiometric titration, the conductometric titration shows that the reaction continues, by replacing the second sodium atom and formation of a compound at the molar ratio, complex/$Ag^+ = 1/2$, $Ag_2[UO_2(P_2O_7)]$.

Revue Roumaine de Chimie, 18, *1*, 59 – 62 (1973)

URANYL-PYROPHOSPHATE COMPLEXES. V[1]

THE PRECIPITATION REACTION OF THE SODIUM BIS-PYROPHOSPHATO-URANYLATE COMPLEX WITH THE Cd^{2+} ION

C. DRĂGULESCU and NICOLETA VÎLCEANU

Centre of Chemistry, Bd. Mihai Viteazul 24, Timişoara, Romania

Received June 11, 1972

The conductometric and potentiometric study of the reaction of sodium bis-pyrophosphato-uranylate complex with $Cd(NO_3)_2$, shows the successive formation of the following combinations:

$Na_2Cd[UO_2(NaP_2O_7)_2]$, $Na_2Cd[CdUO_2(P_2O_7)_2]$ and $Cd_2[CdUO_2(P_2O_7)_2]$.

From the group of divalent metals which precipitated with the sodium bis-pyrophosphato-uranylate complex,[2,3] we have chosen the Cd^{2+} ion for study.

EXPERIMENTAL

Reagents:

- $UO_2(NO_3)_2 \cdot 6H_2O$ *p.a.* Merck
- $Na_4P_2O_7 \cdot 10H_2O$ *p.a.* Merck
- $Cd(NO_3)_2 \cdot 4H_2O$ *p.a.* Merck

Apparatus:

The conductometric titration was effected with a Metrohm Herisau conductoscop.

The potentiometric titration was accomplished with a Radiometer (Copenhagen) pH-meter 25, with a cadmium metallic indicator electrode and a saturated calomel electrode as reference. The titration was made very slowly, with a 40 minutes interval between the readings.

DISCUSSION OF THE RESULTS

Figures 1 and 2 present the conductometric, respectively potentiometric titration of the sodium bis-pyrophosphato-uranylate complex with $Cd(NO_3)_2$.

---

[1] C. Drăgulescu, N. Vîlceanu and I. Julean, Part IV, *Rev. Roumaine Chim.*, **18**, 53–59 (1973).

[2] C. Drăgulescu, I. Julean and N. Vîlceanu, *Rev. Roumaine Chim.*, **10**, 809 (1965).

[3] C. Drăgulescu, N. Vîlceanu and I. Julean, *Z. anorg. Chem.*, **376**, 196 (1970).

The conductometric titration diagram (figure 1), through the three inflexion points, indicated the formation of three combinations at the molar ratio, complex/Cd^{2+} = 1/1, 1/2 and 1/3. All along the titration, the conductibility increases, the segments of the straight line have different slopes.

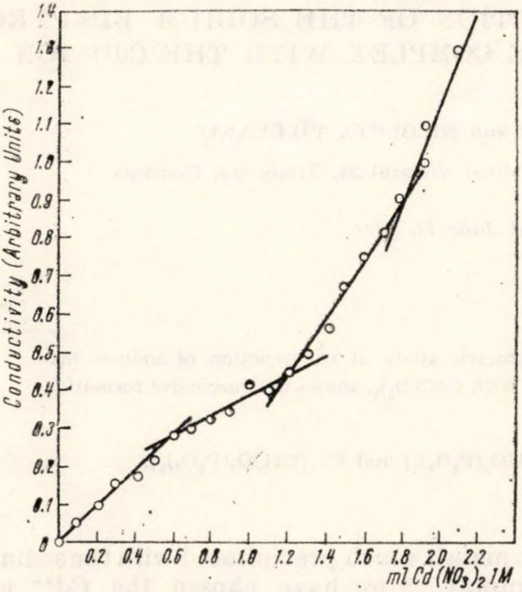

Fig. 1. — Conductometric titration of the sodium bis-pyrophosphato-uranylate complex (6 ml $UO_2(NO_3)_2$ 0.1M + 12 ml $Na_4P_2O_7$ 0.1M) with $Cd(NO_3)_2$ 1M.

The formation of a white-green precipitate takes place immediately but it dissolves again in the solution of the complex. After the addition of 0.3 ml reagent, it appears and maintains all along the titration.

Unlike the conductometric titration of the sodium bis-pyrophosphato-uranylate complex with the Ag^+ ion, [1] which shows the substitution of the six Na^+ ions from the complex $\{[UO_2(P_2O_7)_2]^{6-} + {}_6Na^+\}$ in two stages (at first four and then the last two), the titration with Cd^{2+} shows that the process takes place in three stages, with the gradual substitution of each ${}_2Na^+$ ions with one Cd^{2+} ion.

Through the three equivalent points at the molar ratio, sodium bis-pyrophosphato-uranylate complex/Cd^{2+} = 1/1, 1/2 and 1/3, the potentiometric titration curve shows, in agreement with the conductometric data, the formation of three combinations. Up to equivalence (1), which corresponds to the first potential jump, owing to the fact that the potential of the cadmium electrode is becoming more and more positive, one conclude that there appear Cd^{2+} ions in the system in this part of the titration. After the first equivalence, as the potential of the cadmium electrode becomes more and more negative, it seems that the Cd^{2+} ions disappear gradually from the system (equivalence (2)). The third point of equivalence may be interpreted in the same way as the first one.

The potentiometric titration curve permits the following interpretation for the processes that take place :

In the first stage of the reaction there is an ionic change in the external sphere of coordination of the complex between two Na^+ ions and one Cd^{2+} ion.

In the second part of the reaction (up to equivalence (2)), the titration diagram shows that a slow process of captivating the Cd^{2+} begins, by engaging them in the internal sphere of the complex, where a Cd^{2+} ion replaces two Na^+ ions. Such a behaviour is in accordance with the results obtained by Lambert and Watters[4] which show that at $pH > 8.87$ one must take into consideration the formation of the $[Na(P_2O_7)]^{3-}$ complex.

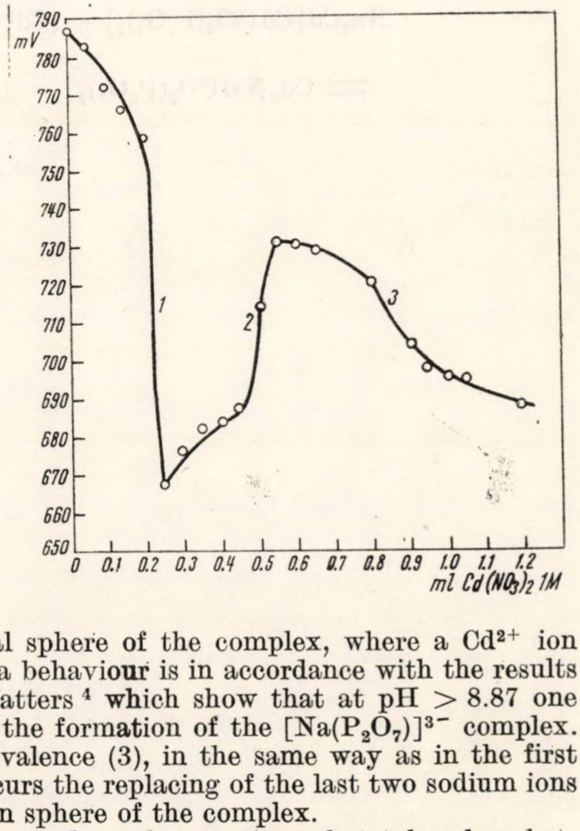

Fig. 2.—Potentiometric titration of the sodium bis-pyrophosphato-uranylate complex (3 ml $UO_2(NO_3)_2$ 0.1M + 6 ml $Na_4P_2O_7$ 0.1 M) with $Cd(NO_3)_2$ 1M.

In the end, up to equivalence (3), in the same way as in the first part of the titration, there occurs the replacing of the last two sodium ions from the external coordination sphere of the complex.

We may schematically reproduce the reactions that take place between the sodium bis-pyrophosphato-uranylate complex and Cd^{2+} ions as follows :

— up to equivalence (1) :

$$\{_4Na + [UO_2(NaP_2O_7)_2]^{4-}\} + (Cd^{2+} + {}_2NO_3^-) \rightleftarrows$$

$$\rightleftarrows Na_2Cd\,[UO_2(NaP_2O_7)_2] + {}_2(Na^+ + NO_3^-)$$

---

[4] S. M. Lambert and J. I. Watters, *J. Amer. Chem. Soc.*, **79**, 4262 (1957).

— up to equivalence (2) :

$$Na_2Cd[UO_2(NaP_2O_7)_2] + (Cd^{2+} + {}_2NO_3^-) \rightleftarrows$$

$$\rightleftarrows Na_2Cd[CdUO_2(P_2O_7)_2] + {}_2(Na^+ + NO_3^-)$$

— up to equivalence (3) :

$$Na_2Cd[CdUO_2(P_2O_7)_2] + (Cd^{2+} + {}_2NO_3^-) \rightleftarrows$$

$$\rightleftarrows Cd_2[CdUO_2(P_2O_7)_2] + {}_2(Na^+ + NO_3^-)$$

Revue Roumaine de Chimie, 18, 1, 63–71 (1973)

SCHIFF BASE COMPLEXES WITH IV AND V GROUP METALS

N. S. BIRADAR * and V. H. KULKARNI
Department of Chemistry, Karnatak University, Dharwar, India

Received April 28, 1972

A few IV and V group metal complexes have been prepared with bis (salicylidene-4-aminoacetophenone)-benzidine and bis(salicylidene-4-aminoacetophenone)-*p*, *p*'-diaminodiphenyl sulphide, and characterized by elemental analysis. They are yellow to orange-yellow coloured amorphous substances, insoluble in common organic solvents. The infrared spectra of these complexes have been studied, and possible structures have been proposed.

INTRODUCTION

The bidentate Schiff bases containing a variety of donor sites are numerous, and the complexes with those bases rank among the most studied and best characterized ones.[1-4] Recently, in an exhaustive review on the multidentate chelating agents, Goodwin [5] gives a critical account of various designs of the multidentate Schiff bases, and the steric-factors influencing the geometry of the ligands. However, in these recent years, Broomhead, Robinson [6] and Wilson, Rose [7] synthesized, and characterized a new heptadentate Schiff base and its nickel (II) complex.

All these observations establish that there is no much information available on the multidentate Schiff base complexes of IV and V group metals. It is of interest to study the stereochemistry of these metals when complexed with various multidentate Schiff bases.

In this paper we wish to report the synthesis and characterization of the IV and V group metal complexes with the following new Schiff bases.

---

* To whom all the correspondence should be addressed.

[1] R. H. Holm, G. W. Everette Jr. and A. Chakravorty, *Prog. Inorg. Chem.*, **7**, 83 (1966).

[2] L. Sacconi, *Coord. Chem. Rev.*, **1**, 192 (1966).

[3] S. Yamada, E. Ohno, Y. Kuge, A. Takeuchi, and K. Yamanouchi, *Coord. Chem. Rev.*, **3**, 247 (1968).

[4] B. O. West, *New Pathways Inorg. Chem.*, (1968) 303 ; *Chem. Abstr.*, **70**, 120604s (1969).

[5] H. A. Goodwin, "Chelating Agents and Metal Chelates" Edt. by F. P. Dwyer and D. P. Mellor, Academic Press, New York, 1964.

[6] J. Broomhead and D. Robinson, *Austral. J. Chem.*, **21**, 1356 (1968).

[7] L. T. Wilson and N. J. Rose, *J. Amer. Chem. Soc.*, **90**, 604 (1968).

I. Bis-(salicylidene-4-aminoacetophenone) benzidine
II. Bis-(salicylidene-4-aminoacetophenone)-*p*, *p*′-diaminodiphenyl sulphide.

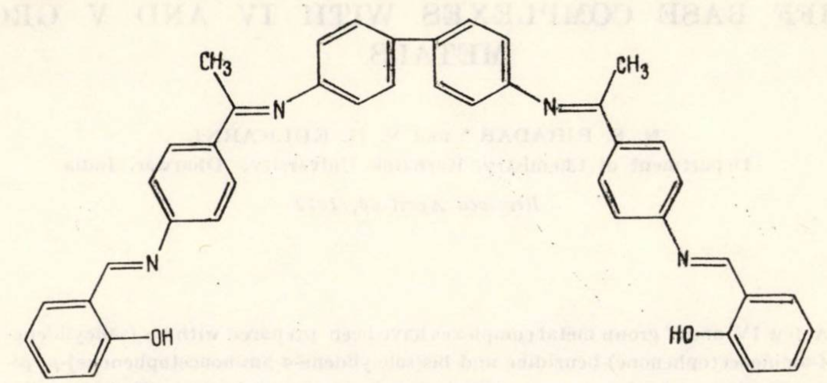

I

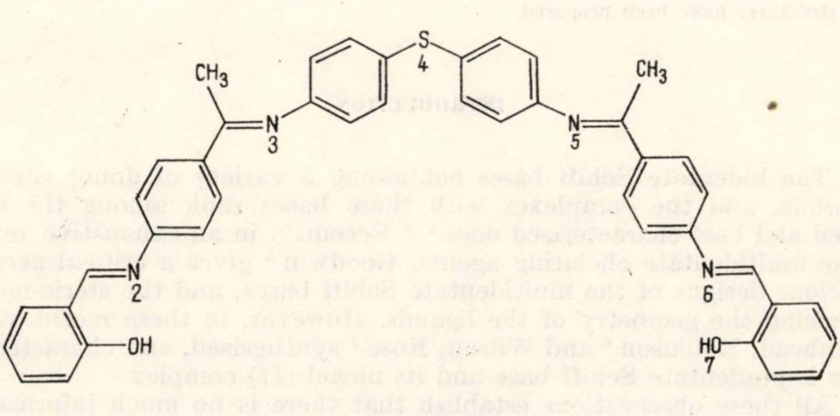

II

EXPERIMENTAL

Tin (IV) and titanium (IV) chlorides and zirconyl chloride were of Riedel grade. Niobium (V) chloride was of Fluka grade. Oxovanadium (V) chloride was prepared by the known method.[8] *p*, *p*′-diaminodiphenyl sulphide was prepared by the method reported elsewhere.[9]

PREPARATION OF THE SCHIFF BASES

Salicylaldehyde and 4-aminoacetophenone in 1 : 1 molar ratio were refluxed for an hour on a water bath. The reaction mixture was cooled and salicylidene-4-aminoacetophenone was separated.

---

[8] G. Brauer, "Handbook of Preparative Inorganic Chemistry" Vol. 2; Academic Press, New York, 1965, p. 1264.

[9] S. R. Safir, S. Kushner L. M. Braucone and Y. Subbaraw, *J. Org. Chem.*, 13 924 (1948).

Further, salicylidene-4-aminoacetophenone and a diamine (benzidine or *p, p'*-diaminodiphenylamine) were mixed in 1 : 2 molar ratio in a large excess of alcohol and refluxed for two hours. The solid separated was filtered, washed with alcohol and dried in vacuum over fused calcium chloride.

PREPARATION OF THE COMPLEXES

1. *Tin (IV) Complex* : Tin (IV) chloride in absolute alcohol was mixed with a little excess of Schiff base in an alcohol medium and refluxed for 3–4 hours at 70–80°. The solvent was vapourized away and consequently the temperature was raised to 180° and maintained around 180° till the HCl gas ceased to evolve. The solid formed was extracted with alcohol and filtered. The dry mass was powdered and extracted in a Soxhlet apparatus using absolute alcohol.

	% Sn	% N	% Cl	
1. $(C_{42}H_{32}N_4O_2)SnCl_2$	14.45	6.92	8.52	Found
	14.59	6.88	8.72	Calcd.
2. $(C_{42}H_{32}SN_4O_2)SnCl_2$	13.94	6.70	8.25	Found
	14.03	6.62	8.40	Calcd.

2. *Titanium (IV) complex* : The same procedure as above was followed to prepare this complex :

	% Ti	% N	% Cl	
3. $(C_{42}H_{32}N_4O_2)TiCl_2$	6.35	7.60	9.45	Found
	6.45	7.54	9.56	Calcd.
4. $(C_{42}H_{32}SN_4O_2)TiCl_2$	6.00	7.32	9.00	Found
	6.18	7.23	9.16	Calcd.

3. *Complex with* $ZrOCl_2$: The method for preparing these complexes is reported elsewhere.[10]

	%Zr	%N	%Cl	
5. $(C_{42}H_{32}N_4O_2)ZrCl_2$	11.53	7.20	8.97	Found
	11.60	7.14	9.03	Calcd.
6. $(C_{42}H_{32}SN_4O_2)ZrCl_2$	11.36	6.95	8.76	Found
	11.15	6.84	8.68	Calcd.

4. *Oxovanadium (V) complex* : $VOCl_3$ in carbon tetrachloride was treated with a slight excess of Schiff base with vigorous shaking and left for several hours till the evaluation of HCl gas ceased. The precipitated complex was filtered and washed with carbon tetrachloride and finally with ether. The dry mass was powdered and extracted in a Soxhlet apparatus till it was free from the reagent, then washed with ether and dried at 50–60°.

	% V	% N	% Cl	
7. $(C_{42}H_{32}N_4O_2)VOCl$	6.89	7.81	4.75	Found.
	7.01	7.71	4.89	Calcd.
8. $(C_{42}H_{32}SN_4O_2)VOCl$	6.99	7.43	4.65	Found
	6.72	7.38	4.68	Calcd.

5. *Niobium (V) complex* : The same procedure as above was followed :

---

[10] N. S. BIRDAR and V. H. KULKARNI, *J. Karn. Univ. (Science)*, **15**, 10 (1970).

	% Nb	% N	% Cl	
9. $(C_{42}H_{32}N_4O_2)NbCl_3$	11.01	7.00	12.75	Found
	11.28	6.80	12.92	Calcd.
10. $(C_{42}H_{32}SN_4O_2)NbCl_3$	10.52	7.00	12.30	Found
	10.86	6.55	12.46	Calcd.

ANALYSIS

Metal ions, chloride and nitrogen in these complexes were determined by the standard methods.[11]

PHYSICAL MEASUREMENTS

Details of the physical measurements are the same as those given in our previous paper.[12]

RESULTS AND DISCUSSION

All the complexes are yellow in colour, amorphous and insoluble in almost all common organic solvents. They are soluble to a limited extent in DMF and DMSO.

The molar conductance values in DMF at the concentration 10^{-3} M show that these are non-electrolytes in DMF.

The base I contains four C=N, and two OH groups. The infrared spectrum of salicylidene-4-aminoacetophenone shows a strong band at 1690 cm^{-1} and it is attributed to the C=O stretch. It is known that C=O group shows a strong band around 1705 cm^{-1} and it is sensitive to the conjugation.[12] In the Schiff base I this band disappears and the band due to the C=N stretch appears around 1590 cm^{-1}. This suggests clearly that the C=O group of the salicylidene-4-aminoacetophenone has been utilized in the reaction with the NH_2 groups of the benzidine. This base can be compared with the typical hexadentate ligand III reported by Sarma and Bailar,[13] bis (salicylidene) trithylenetetramine.

On the grounds of steric factors they have shown that the Schiff base III prefers the configuration IV.

The Schiff base under present investigation is of aromatic origin and possesses all the coordinating sites on the *para* positions and only two peripheral hydroxy groups are on the *ortho* positions. This makes the molecule bulky, and the coordination groups on the *para* positions promote the steric hindrance. It can generate O—N—N and N—N—O sequences which are necessary for the sexadentate behaviour. But the mode of situation of the donor groups shows that the molecule is very much strained to act as a sexadentate ligand.

These chlorides of group IV and V metals form complexes with 1 : 1 stoichiometry with this base and these are all non-electrolytes.

---

[11] A. I. Vogel, "Text Book of Quantitative Inorganic Analysis", Longmans, London, 1961.

[12] N. S. Biradar and V. H. Kulkarni, *J. Inorg. Nuclear Chem.*, **33**, 2451 (1971).

[13] B. Das Sarma and J. C. Bailar Jr., *J. Amer. Chem. Soc.*, **77**, 5476 (1955).

The infrared spectrum of the ligand I shows an intense band at 1590 cm^{-1} and is assigned to the mixture of C=N and C=C stretching vibrations. This band splits into two bands on complex formation and one band appears around 1613 cm^{-1} and the other appears around 1587 cm^{-1}. The band at higher frequency is attributed to the C=N stretch in the complexes. The broad, weak band assignable to the intramolecular hydrogen bonded-OH disappears in the complexes, showing that the oxygen metal bonds have been formed between metals and the ligand.

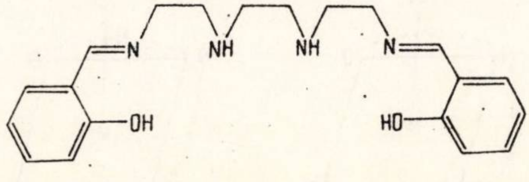

III

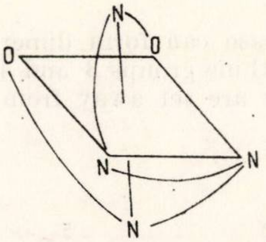

IV

It has been established that the metal ligand vibrations occur in the 600—400 cm^{-1} region.[14] The *trans* complexes are shown to have only one ν(M — N) vibration while the *cis* complexes show two ν(M — N) vibrations. [15] The titanium (IV) complex shows two bands in the region 550—530 cm^{-1} and are assigned to the ν(Ti—N) vibrations. This suggests that the complex favours the *cis* configuration.

From the above discussion, it can be concluded that the hydroxy groups 1 and 6 are involved in the complex formation and azomethine groups are coordinated to the central metal ion. This information helps to predict structures VA, B for these complexes.
The construction of the model shows that the molecule is flexible enough to allow the azomethine groups 2 and 5 and hydroxy groups 1 and 6 to take part in the complexation, to result the complex of the type (A). If the azomethine groups 3 and 4 form coordinate bonds with the central metal ion (as shown in B), it requires the stabilization of the twelve membered rings instead of two six-membered rings (as shown in A). In addition to this the *para* — azomethine groups 3 and 4 in the molecule present

---

[14] D. M. Adams, "Metal Ligand and Related Vibrations" Edward Ernold, London, 1967.
[15] S. C. Jain and R. Rievest, *J. Inorg. Nuclear Chem.*, **32**, 1117 (1970).

the added steric hindrance, thus preventing the formation of alternate structure (B).

It may be thought that like bis (salicylidene) benzidine, which fails to form monomeric complexes on the grounds of steric-factors, and forms

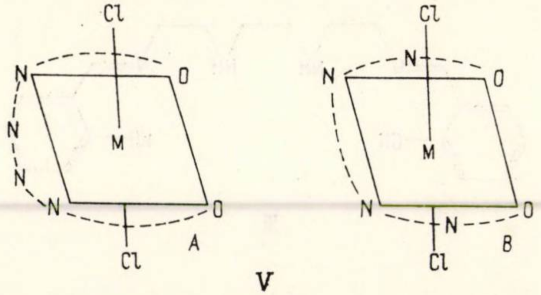

V

dimeric complexes, this base can form dimeric complexes of type C. In this case also the azomethine groups 3 and 4 may not take part in the complex formation as they are set away from the position suitable for coordination.

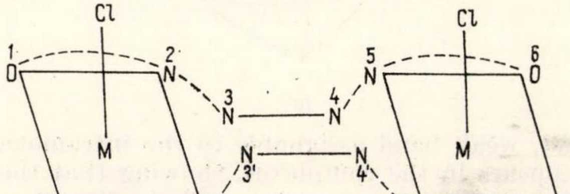

C

It seems possible in view of the known dimeric complexes of bis (salicylidene) benzidine [16,17] and other similar type of Schiff bases [18,19].

The complex of oxovanadium (V) with this base shows two distinct IR bands in the V=O stretching region, indicating that the complex exists in the dimeric form. Ginsberg *et al.* [20] also notice such type of doubling in the case of oxovanadium (IV) complexes with substituted salicylidene-*o*-aminophenols. It has already been shown that the base favours to form *cis* complexes, analogous to bis (salicylidene) benzidine and bis (salicylidene)-*p*-phenylenediamine.

This discussion helps us to realize that the IV group metal complexes with this ligand prefer to exist in the *cis* dimeric structure having coor-

---

[16] C. G. Macarovici, E. Perte and E. Motiu, *Rev. Roumaine Chim.*, **11**, 53 (1966).

[17] P. Pfeiffer and H. Pfitzner, *J. prakt. Chem.*, **145**, 243 (1936).

[18] P. Pfeiffer, E. Breith, E. Lubbe and T. Tsumaki, *Liebigs Ann. Chem.*, **503**, 84 (1933).

[19] P. Pfeiffer, Th. Hesse, H. Pfitzner, W. Scholl and H. Thielert, *J. prakt. Chem.*, **1049**, 217 (1937).

[20] A. P. Ginsberg, E. Koubeck and H. J. Williams, *Inorg. Chem.*, **5**, 1656 (1966).

dination number six. Two chlorides occupy the *trans* positions in the octahedron. In the case of oxovanadium (V) the coordination number is six, and the *trans* positions are occupied by the oxygen and chloride (type D).

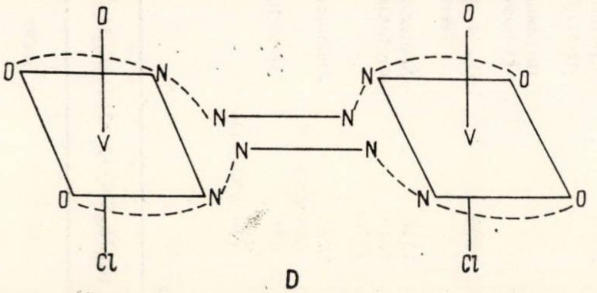

D

Niobium (V) forms 1 : 1 complex and it has lost two of its five chlorides in the reaction. It is shown to be non-electrolyte in DMF, hence the complex has coordination seven. There is no simple arrangement known for this coordination number. But in view of the majority of the known complexes having 1 : 4 : 2 stereochemistry [21] these complexes may be regarded to have this stereochemistry.

The condensation of salicylidene-4-aminoacetophenone with *p*, *p'*-diaminodiphenyl sulphide yields the Schiff base II.

This base contains seven hetero-atoms positioned in appropriate places required for the coordination. Two hydroxy groups (1 and 7), four azomethine groups (2, 3, 5 and 6) and one sulphur group (4) present in the molecule make us include this base in the heptadentate ligand group. It can be said that the pyramidal disposition of the sulphur bonds removes the steric hindrance to some extent. The base II is comparatively more flexible than the base I. Like base I, this base also contains all the coordinating centres on the *para* positions.

The IR spectrum of the base shows a strong band at 1626 cm^{-1} and is assigned to the C=N stretch. This band shows considerable shift on complexation (Table 1) suggesting that the coordination has formed between the metal ion and the azomethine nitrogen. The band due to intramolecular hydrogen bonded —OH is not observed in the complexes.

From the above observations it is possible to propose the two structures *E* and *F* for these complexes :
In both cases the central —S— is removed far away from the position suitable for coordination. The steric hindrance does not permit the azomethine groups 3 and 5 to take part in the coordinate bond formation.

The IR spectrum of oxovanadium (V) shows double bands in the V=O stretching region (Table 1), and titanium (IV) complex shows two bands in the ν(M—N) region (Table 1) showing that the complex favours the *cis* form. These observations help us to conclude that all the complexes with this base II can exist in the dimeric form (G).

---

[21] Barraclough, J. Lewis and R. S. Nyholm, *J. Chem. Soc.*, **1959**, 3552.

Table 1

Infrared frequencies (in cm^{-1}) of Schiff bases and their complexes and assignments

S. No.	Ligand I	$(C_{42}H_{32}N_4O_2)SnCl_2$	$(C_{42}H_{32}N_4O_2)TiCl_2$	$(C_{42}H_{32}N_4O_2)ZrCl_2$	$(C_{42}H_{32}N_4O_2)VOCl$	$(C_{42}H_{32}N_4O_2)NbCl_3$	Assignments
1	2865	2957	2950	3030	2899	3030	=CH and aromatic CH stretching vibration
2	2564	—	—	—	—	—	Intramolecular H-bonded-OH
3	1590	1613	1650	1630	1613	1620	C=N stretching vibration
	—	1575	1610	1580	1587	1580	Aromatic C=C stretching vibrations
	1550	1538	1550	1540	1550	1610	
	1460	1515	1470	1480	—	1470	
4	1260	1350	1290	1295	1320	1295	Phenolic C–O
			545 wν(Ti–N)	—	990	550 ν(Nb–N)	
			515 s		ν(V=O)	520	stretching vibration
					970		
			485 mν(Ti–O)	—		440 ν(Nb–O)	

Table 2

Bis(salicylidene-4-aminoacetophenone)-p,p'-diaminodiphenylsulphide

S.No.	Ligand II	$(C_{42}H_{32}SN_4O_2)SnCl_2$	$(C_{42}H_{32}SN_4O_2)TiCl_2$	$(C_{12}H_{32}SN_4O_2)ZrCl_2$	$(C_{42}H_{32}SN_4O_2)VOCl$	$(C_{42}H_{32}SN_4O_2)NbCl_3$
1	2899	2941	2899	3000	2857	3030
2	2632	—	—	—	—	—
3	1626	1613	1600	1620	1587	1600
4	1587	1585	1582	1580	1562	—
	1567	—	1538	1540	1538	1530
	1493	1515	1497	1480	—	1500
5	1285	1350	1360	1320	1300	1320
					100 ν(V=O)	— ν(Nb–N
					961	520
						480 ν(Nb–O)

These are non-electrolytes and have 1 : 1 stoichiometry, hence they have the coordination number six (including the complex with oxovanadium (V)).

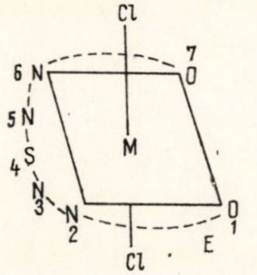
Cl
7
6 N
O
5 N
M
4 S
N 3
N 2
O 1
Cl

E

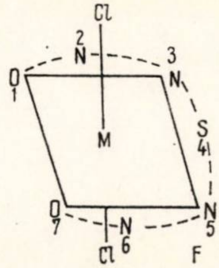
Cl
2 N
3 N
O 1
M
S 4
O 7
N 6
N 5
Cl

F

Niobium (V) complex is also non-electrolyte and has 1 : 1 stoichiometry hence it is hepta coordinated. In view of the majority of the hepta coordinated niobium (V) complexes having 1 : 4 : 2 stereochemistry,[21] these complexes may be considered to have the same stereochemistry.

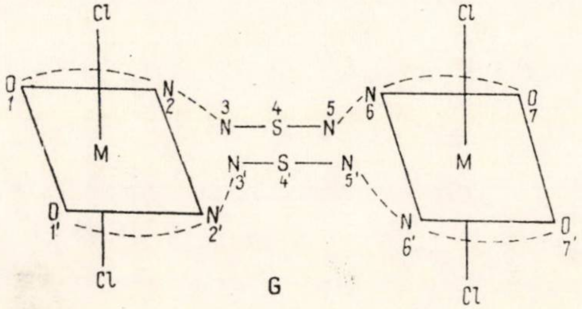
Cl
O 1
N 2
3 N
4 S
5 N
N 6
O 7
Cl
M
M
N 3'
S 4'
N 5'
O 1'
N 2'
N 6'
O 7'
Cl
Cl

G

Acknowledgement. One of the authors (V.H.K.) is grateful to the Karnatak University for the financial assistance.

Revue Roumaine de Chimie, **18**, *1*, 73–88 (1973)

L'ÉTUDE DES ESPÈCES IONIQUES FORMÉES PAR L'HYDROLYSE DE L'ION D'URANIUM HEXAVALENT

MARIA MAVRODIN-TĂRĂBÎC

Centre de Chimie Physique, 31, str. Galaţi, Bucarest

Reçu le 2 février 1972

On a déterminé, par des méthodes spectrophotométriques et pH-métriques, la nature et la stabilité des espèces ioniques formées par l'hydrolyse de l'ion d'uranium hexavalent, en milieu inerte d'acide perchlorique. On a démontré que, dans un domaine de pH supérieur à 2,5, l'hydrolyse de l'ion UO_2^{2+} a lieu par une suite de réactions qui dépendent du pH et qui conduisent à la formation des complexes polynucléaires du type $U_2O_5^{2+}$ et $U_3O_8^{2+}$, caractérisés par les valeurs moyennes des constantes d'équilibre $K_1 = 1 . 10^{-6}$ et $K_2 = 1 . 10^{-7}$.

Les études effectuées sur les solutions des sels d'uranium hexavalent ont démontré que l'ion U^{6+} n'existe pas dans les solutions aqueuses. Même dans les solutions les plus acides c'est exclusivement l'ion UO_2^{2+} qui se forme, celui-ci pouvant être considéré comme un premier terme d'une série de produits d'hydrolyse.[1–3]

La détermination et la caractérisation des espèces ioniques qui résultent de l'hydrolyse des sels d'uranium hexavalent est très importante, tant au point de vue pratique — vu le rôle que cet élément joue dans les différents domaines de la science appliquée et la technique moderne — qu'au point de vue théorique, étant donné la complexité des réactions qui ont lieu dans les systèmes : « sels d'uranium hexavalent — eau». L'importance de l'étude est illustrée par le grand nombre de travaux publiés, ces derniers temps, dans ce domaine.[4–16]

[1] J. Sutton, *J. Chem. Soc.*, *1–2/S*, 5 **1949**, 275.

[2] S. Ahrland, *Acta Chem. Scand.*, **3**, 374 (1949).

[3] J. Fancherre, *Compt. rend.*, **227**, 1367 (1948).

[4] S. Hietanen, *Acta Chem. Scand.*, **8**, 1607 (1954).

[5] L. G. Sillen, *Acta Chem. Scand.*, **8**, 299 (1954).

[6] S. Hietnen, L. G. Sillen, *Acta Chem. Scand.*, **13**, 1828 (1959).

[7] J. Komar, *Zhur. analit. Khim.*, **10**, 236 (1955).

[8] J. A. Hearne, *J. Chem. Soc.*, **1957**, 168.

[9] A. I. Zhukov, *Zhur. priklad. Khim.*, **35**, 696 (1962).

[10] D. Cole, *J. Phys. Chem.*, **71**, 2771 (1967).

[11] H. S. Dunsmore, S. Hietanen, L. G. Sillen, *Acta Chem. Scand.*, **17**, 2644 (1965).

[12] U. Schedin, M. Frydman, *Acta Chem. Scand.*, **22**, 115 (1968).

[13] A. Robert, *Acta Chem. Scand.*, **22**, 250 (1968).

[14] P. A. Hurnitz, *J. Phys. Chem.*, **71**, 4142 (1967).

[15] K. Whittaker, *J. Phys. Chem.* **69**, 2319 (1965).

[16] C. Drăgulescu, J. Julean, *Rev. Roumaine Chim.*, **7**, 815 (1962).

Les recherches entreprises en vue d'éclaircir le mécanisme de l'hydrolyse n'ont pas réussi à déterminer complètement la composition du système à cause de la complexité des réactions et du grand nombre des espèces ioniques théoriquement possibles, dont la formation est conditionnée par une série de paramètres du milieu tels que : pH, concentration, température, nature des ions qui coexistent dans la solution, force ionique, etc.

Vu que les conclusions auxquelles ont abouti les différents chercheurs sont souvent contradictoires, l'étude des réactions qui ont lieu dans les systèmes « sel d'uranium hexavalent — eau » reste encore très actuelle.

★

Compte tenu des considérations ci-dessus, dans ce travail on s'est proposé de :

— déterminer la nature des espèces ioniques résultant de l'hydrolyse de l'uranium ;

— caractériser l'évolution des réactions mises en évidence en fonction d'une série de paramètres du milieu tels que : pH, force ionique, concentration, nature des ions coexistant dans la solution, etc.

L'analyse qualitative de la nature des réactions qui ont lieu dans les systèmes : « sel d'uranium hexavalent — eau » a été faite par voie spectrophotométrique, l'étude quantitative des réactions mises en évidence s'effectuant à l'aide des titrages pH-métriques.

Pour éviter les erreurs, les études ont été réalisées en utilisant du perchlorate d'uranyle, étant donné que l'ion UO_2^{2+} ne forme pas de complexes avec l'ion ClO_4^-.

PARTIE EXPÉRIMENTALE

RÉACTIFS

Perchlorate d'uranyle, $UO_2(ClO_4)_2\ 6H_2O$ (*p.a.* Th. Schuchardt). On a préparé une solution « stock » approximativement 0,1 N, dont on a obtenu, en diluant avec de l'eau bidistillée, les solutions de perchlorate d'uranyle de différentes concentrations : 0,02 N, 0,05 N, 0,01 N, 0,001 N.

Les concentrations de ces solutions ont été vérifiées par voie gravimétrique (évaporation et calcination à l'état d'oxyde U_3O_8).

— *Perchlorate de sodium*, $NaClO_4$ (*purum*, Merck). Il a été utilisé après trois recristallisations et séchage à 110°.

— *Hydroxyde de sodium* (*p.a.* Merck). Les solutions utilisées ont été préparées en diluant une solution « stock » approximativement 0,1 N. La concentration des solutions de NaOH a été établie avec du phtalate acide de kalium.

— *Acide perchlorique*, $HClO_4$ (*p.a.* Merck) de concentration d'environ 75 %. On a utilisé des solutions approximativement 0,1 N, analysées par titrage alcalimétrique.

APPAREILS

Les déterminations spectrophotométriques ont été effectuées à l'aide d'un spectrophotomètre Karl Zeiss Jéna VSU 1.

Pour les titrages pH-métriques on a utilisé un pH-mètre Radiometer – Copenhagen (électrodes de verre et calomel). Les déterminations ont été faites dans une installation fermée spécialement construite.

MODE DE TRAVAIL

L'étude spectrophotométrique a été effectuée en déterminant les courbes d'absorption des solutions de perchlorate d'uranyle à :

a) *concentration constante* (0,02 N) et pH variable (1,6 ; 2 ; 2,5 ; 3 et 4) – pour tirer des conclusions en ce qui concerne l'évolution de l'hydrolyse en fonction du pH – et à

b) pH constant (1,6) et concentration variable (0,02 ; 0,04 et 0,01 M) – pour tirer des conclusions sur la nature des composés–résultant de l'hydrolyse, en fonction de la concentration.

Les différentes valeurs du pH ont été obtenues en ajoutant de l'acide perchlorique, respectivement de l'hydroxyde de sodium. Les solutions ont été maintenues à une force ionique constante $I = 1$, en utilisant comme milieu ionique le perchlorate de sodium. Les déterminations ont été faites à une température d'environ 22°.

Les *déterminations pH-métriques* ont été effectuées en titrant les solutions d'uranyle avec du NaOH. Pour tirer des conclusions sur l'influence de la concentration sur la nature des espèces ioniques qui se forment par l'hydrolyse, on a travaillé avec des solutions de perchlorate d'uranyle de différentes concentrations, comprises entre 0,1 – 0,001 M.

L'influence de la force ionique a été évaluée en effectuant des déterminations, pour chaque concentration, à quatre forces ioniques : I = 0,5 ; 1 ; 1,5 et 2, réalisées avec du $NaClO_4$.

Les déterminations ont été faites par le titrage direct de la solution de perchlorate d'uranyle avec du NaOH. On a travaillé dans un large domaine de pH, les titrages pH-métriques étant considérés terminés à l'apparition d'un précipité stable, de couleur orange, de polyuranate. Les titrages ont été répétés trois fois, les valeurs du pH représentées graphiquement et utilisées dans les calculs étant des valeurs moyennes. Les valeurs d'équilibre ont été obtenues après 60 secondes d'agitation.

RÉSULTATS ET DISCUSSIONS SUR LA NATURE ET LA STABILITÉ DES ESPÈCES IONIQUES FORMÉES PAR L'HYDROLYSE DE L'ION U^{6+}

1. L'ÉTUDE SPECTROPHOTOMÉTRIQUE

La formation des produits d'hydrolyse, en fonction du pH, a été mise en évidence qualitativement en déterminant les courbes d'absorption caractéristiques de la solution de perchlorate d'uranyle à différentes valeurs du pH.

Tel qu'on le voit dans la figure 1, les courbes d'absorption obtenues au pH =1,6 ; 2 et 2,5 sont identiques, ce qui confirme que, dans ce domaine de pH, il ne se forme qu'un seul ion, l'ion UO_2^{2+} ; au pH = 3, on obtient une courbe d'absorption évidemment déviée, ce qui indique un déplacement de l'équilibre dans le sens de l'hydrolyse de l'ion UO_2^{2+}, qui commence au pH 2,5 et continue, en s'accentuant, à mesure que le pH de la solution augmente. Des courbes d'absorption représentées dans la figure 1, on constate que les espèces ioniques formées par l'hydrolyse de l'ion UO_2^{2+} (pH $> 2,5$) se caractérisent par des coefficients molaires d'extinction supérieurs à celui de l'ion UO_2^{2+}.

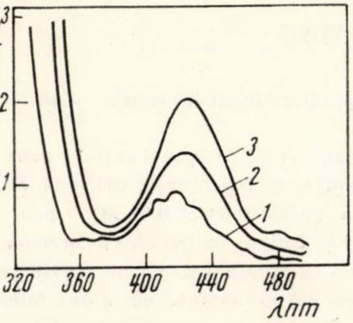

Fig. 1. — Variation du spectre d'absorption de la solution de perchlorate d'uranyle 0,01 M, en fonction du pH. courbe *1* : pH = 1,6 ; 2 et 2,5 ; courbe *2* : pH = 3, courbe *3* : pH = 4)

Le fait que, à un certain pH, l'allure des courbes d'absorption est identique pour toutes les concentrations considérées, écarte l'hypothèse de la formation des produits polymères du type $(UO_2)_2$, $(UO_2)_3 \ldots (UO_2)_n$.

2. L'ÉTUDE pH-MÉTRIQUE

2.1. LA DÉTERMINATION DE LA NATURE DES ESPÈCES IONIQUES FORMÉES PAR L'HYDROLYSE

L'étude quantitative des équilibres hydrolytiques du système : « perchlorate d'uranyle — eau » a été effectuée par le titrage pH-métrique des solutions de perchlorate d'uranyle, caractérisées par des concentrations variant entre 0,001—0,05M et par les forces ioniques $I = 0,5$; 1 ; 1,5 et 2.

Les données expérimentales obtenues en travaillant dans le domaine de pH $= 2,5-10$ sont représentées dans les figures 2—5.

En analysant les courbes de titrages des solutions de perchlorate d'uranyle on observe que :

— L'allure générale des courbes est semblable, à toutes les concentrations et forces ioniques, ce qui indique que, dans le domaine de concentration considéré (0,05—0,001 M), la nature des réactions qui ont lieu dans le système est la même.

— Les courbes de titrage présentent deux points d'inflexion situés au pH $= 4,5-5$ et, respectivement, au pH > 6. Ces deux points d'inflexion correspondent à des valeurs du pH qui varient avec la concentration des solutions considérées, mais leur propriété caractéristique est que le rapport : mol. UO_2^{2+} : équivalents de NaOH correspondant à la première inflexion : équivalents de NaOH correspondant à la seconde inflexion est le même pour toutes les concentrations et les forces ioniques : 1 : 1,68 ; 2,36 ou 3 : 5 : 7.

Les équivalents de NaOH ont été calculés aux points d'inflexion, déterminés — pour toutes les concentrations et forces ioniques — à l'aide

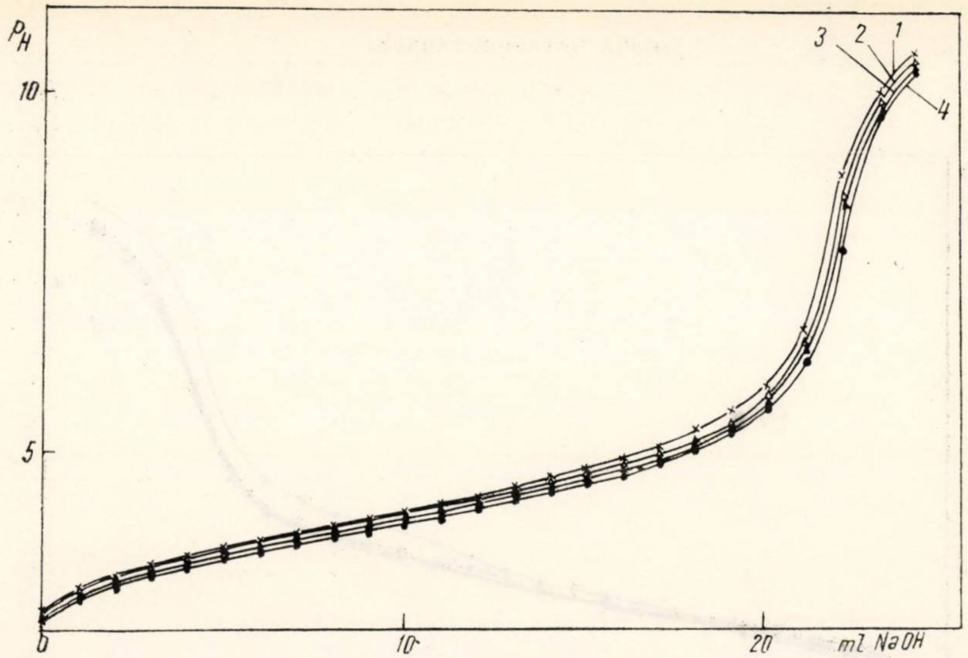

Fig. 2. — Courbes de titrage pH-métrique des solutions de perchlorate d'uranyle 0,05 M (I = 0,5 (*1*);
I = 1 (*2*); *I* = 1,5 (*3*); *I* = 2(*4*)).

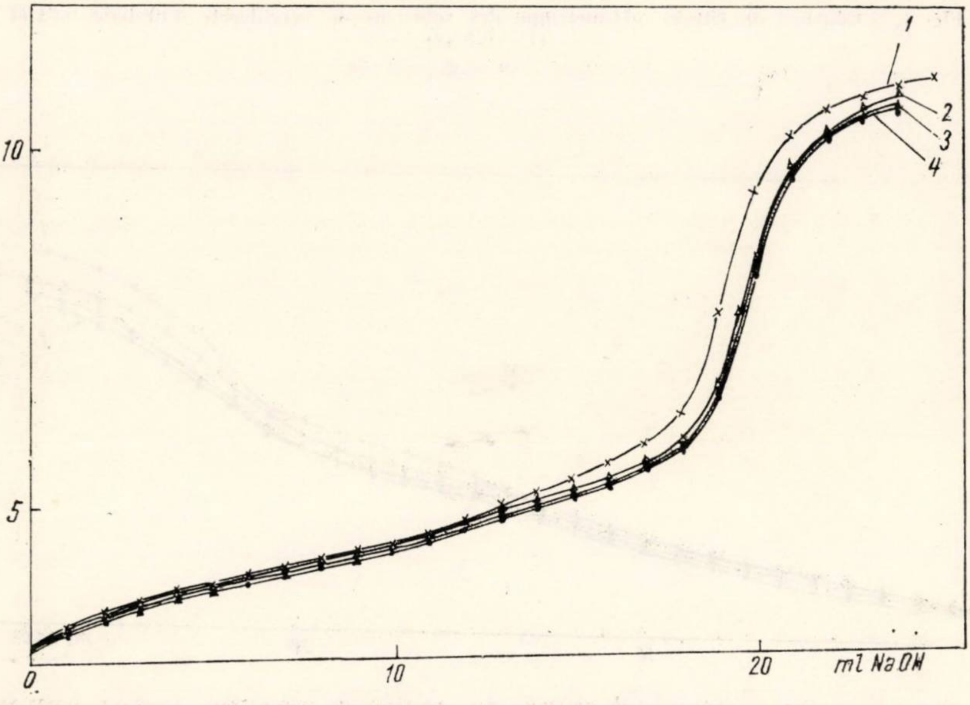

Fig. 3. — Courbes de titrage pH-métrique des solutions de perchlorate d'uranyle 0,02 M (I = 0,5 (*1*);
I = 1 (*2*); *I* = 1,5 (*3*) et *I* = 2 (*4*)).

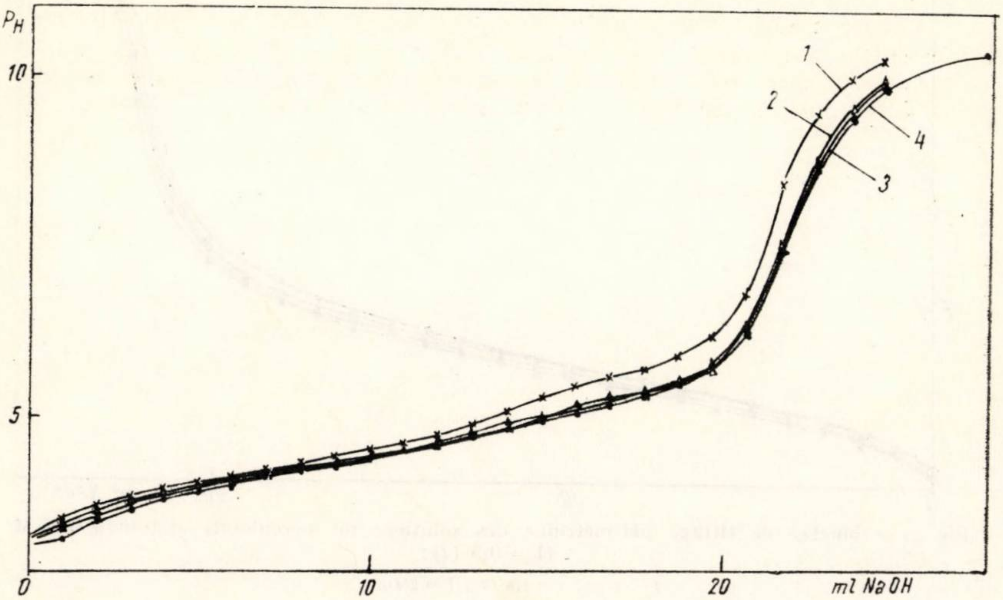

Fig. 4. — Courbes de titrage pH-métrique des solutions de perchlorate d'uranyle 0,01 M ($I = 0,5$ (*1*);
$I = 1$ (*2*); $I = 1,5$ (*3*) et $I = 2$ (*4*)).

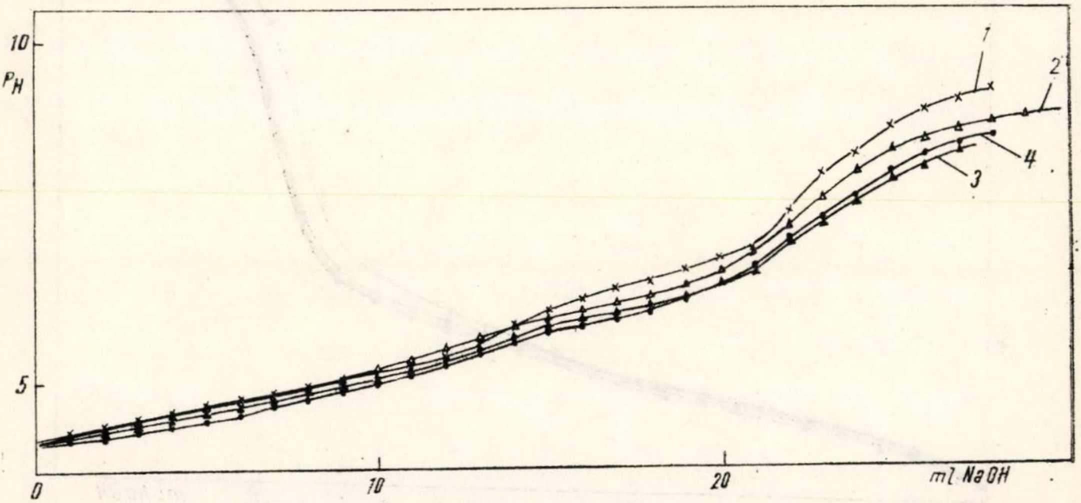

Fig. 5. — Courbes de titrage pH-métrique des solutions de perchlorate d'uranyle 0,001 M ($I = 0,5$ (*1*);
$I = 1$ (*2*); $I = 1,5$ (*3*) et $I = 2$ (*4*)).

des courbes différentielles. (Dans la figure 6 on a représenté quelques-unes de ces courbes.)

Les rapports $UO_2^{2+} : OH^- = 3 : 5 : 7$ indiquent que les réactions d'hydrolyse impliquent trois ions UO_2^{2+} et cinq ions OH^- (pour la première inflexion) et trois ions UO_2^{2+} et 7 ions OH^- (pour la deuxième inflexion) et plaident pour un mécanisme d'hydrolyse qui – en accord avec Sutton /1/ –

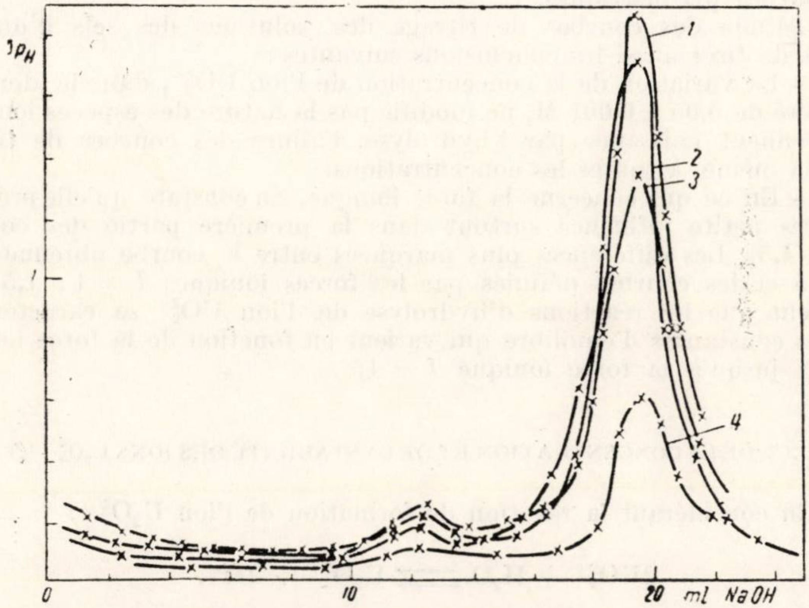

Fig. 6. — Courbes différentielles de titrage pH-métrique des solutions de perchlorate d'uranyle de concentration variée : $C = 0{,}05$ M (*1*) ; $C = 0{,}02$ M (*2*) ; $C = 0{,}01$ M (*3*) ; $C = 0{,}001$ M (*4*).

— peut être représenté par la chaîne réactionnelle :

$$2UO_2^{2+} + H_2O \rightleftarrows U_2O_5^{2+} + 2H^+ \qquad \text{(a)}$$

$$U_2O_5^{2+} + UO_2^{2+} + H_2O \rightleftarrows U_3O_8^{2+} + 2H^+ \qquad \text{(b)}$$

$$U_3O_8^{2+} + H_2O \rightleftarrows U_3O_8(OH)^+ + H^+ \qquad \text{(c)}$$

$$U_3O_8(OH)^+ + H_2O \rightleftarrows U_3O_8(OH)_2 + H^+ \qquad \text{(d)}$$

$$U_3O_8(OH)_2 + H_2O \rightleftarrows U_3O_8(OH)_3^- + H^+ \qquad \text{(e)}$$

$$U_3O_8(OH)_3^- + H_2O \rightleftarrows U_3O_8(OH)_4^{2-} + H^+ \text{ etc.} \qquad \text{(f)}$$

Les réactions (a) et (b) qui conduisent à la formation des ions polymères caractérisés par des ponts d'oxygène ($U_2O_5^{2+}$ et $U_3O_8^{2+}$) sont représentées par la première partie ascendante de la courbe de titrage.

La réaction (c), d'addition d'un ion OH^- à l'ion $U_3O_8^{2+}$, est marquée par un premier saut du pH. La formation de l'anion $U_3O_8(OH)_3^-$ (la réaction e) est indiquée par la seconde inflexion de la courbe de titrage située à des valeurs du pH > 6. On peut considérer que l'addition des ions OH^- continue et que dans le système il se forme des anions du type $U_3O_8(OH)_4^{2-}$... ..., etc., processus qui ne peut être défini et limité par l'analyse directe des courbes pH-métriques.

L'étude des courbes de titrage des solutions des sels d'uranyle permet de tirer aussi les conclusions suivantes :

— La variation de la concentration de l'ion UO_2^{2+}, dans le domaine considéré de 0,05 à 0,001 M, ne modifie pas la nature des espèces ioniques qui prennent naissance par l'hydrolyse, l'allure des courbes de titrage étant la même, à toutes les concentrations.

— En ce qui concerne la force ionique, on constate qu'elle présente une très petite influence surtout dans la première partie des courbes (pH $> 4{,}5$). Les différences plus marquées entre la courbe obtenue pour $I = 0{,}5$ et les courbes définies par les forces ioniques $I = 1$; 1,5 et 2 indiquent que les réactions d'hydrolyse de l'ion UO_2^{2+} se caractérisent par des constantes d'équilibre qui varient en fonction de la force ionique surtout jusqu'à la force ionique $I = 1$.

2.2. CALCUL DE LA CONCENTRATION ET DE LA STABILITÉ DES IONS $U_2O_5^{2+}$ ET $U_3O_8^{2+}$

En considérant la réaction de formation de l'ion $U_2O_5^{2+}$:

$$2UO_2^{2+} + H_2O \rightleftarrows U_2O_5^{2+} + 2H^+,$$

si q = ml solution de NaOH de concentration c mole/l, ajoutés, par titrage, à p = ml solution de perchlorate d'uranyle de concentration m (mole/l) et $u = UO_2^{2+}$; $v = U_2O_5^{2+}$; $h = H^+$; $K_w/h = OH^-$ — les concentrations des différentes espèces ioniques qui participent à la réaction, on peut écrire les relations (1) (qui exprime le bilan de l'uranium) et (2) qui exprime l'électroneutralité de la solution) :

$$u + 2v = pm/p + q \tag{1}$$

$$2u + 2v + h + qc/p + q = \frac{2pm}{p+q} + \frac{K_w}{h} \tag{2}$$

dans lesquelles :

$\dfrac{qc}{p+q}$ représente la concentration de l'ion Na^+

et

$\dfrac{2\,pm}{p+q}$ — la concentration de l'ion ClO_4^-.

En résolvant les équations (1) et (2) (*p*, *m*, *q* et *c* sont connus des données initiales et *h* est déterminé par calcul à l'aide des données pH-métriques), on obtient $u = UO_2^{2+}$ et $v = U_2O_5^{2+}$, en équilibre au pH considéré.

En connaissant *u* et *v*, la constante de stabilité de l'ion $U_2O_5^{2+}$ se détermine à l'aide de la relation :

$$K_1 = \frac{vh^2}{u^2} \tag{3}$$

Dans ce travail on a étudié la formation de l'ion $U_2O_5^{2+}$ dans des solutions de perchlorate d'uranyle de différentes concentrations et forces ioniques.

On a effectué des calculs pour un domaine de pH, dont la limite supérieure ($\simeq 4 - 4{,}5$) a été déterminée par le commencement de la précipitation.

Les résultats obtenus en utilisant la relation (3) qui considère que, dans un certain domaine de pH, coexistent dans la solution seulement les ions UO_2^{2+} et $U_2O_5^{2+}$, sont présentés dans les tableaux 1–16. (Les études ont été effectuées sur des solutions de différentes concentrations et forces ioniques ; les conditions exactes de travail sont mentionnées dans chaque tableau).

Tableau 1

Concentrations, à l'équilibre, des espèces ioniques UO_2^{2+} et $U_2O_5^{2+}$ formées par l'hydrolyse du perchlorate d'uranyle 0,0455 M, à $I = 0{,}5$

pH	UO_2^{2+} mole/l	$U_2O_5^{2+}$ mole/l	K_1
2,79	0,04390	0,00080	$1{,}06 \cdot 10^{-6}$
3,30	0,02910	0,00395	$1{,}16 \cdot 10^{-6}$
3,45	0,02303	0,00598	$1{,}38 \cdot 10^{-6}$
3,70	0,01301	0,00849	$1{,}90 \cdot 10^{-6}$
3,81	0,00890	0,00955	$2{,}80 \cdot 10^{-6}$
3,92	0,00590	0,01040	$4{,}30 \cdot 10^{-6}$
4,02	0,00253	0,01123	$15{,}00 \cdot 10^{-6}$

Tableau 2

Concentrations, à l'équilibre, des espèces ioniques UO_2^{2+} et $U_2O_5^{2+}$ formées par l'hydrolyse du perchlorate d'uranyle 0,0455 M, à $I = 1$

pH	UO_2^{2+} mole/l	$U_2O_5^{2+}$ mole/l	K_1
2,71	0,04360	0,00095	$1{,}80 \cdot 10^{-6}$
3,41	0,02300	0,00600	$1{,}63 \cdot 10^{-6}$
3,67	0,01300	0,00850	$2{,}20 \cdot 10^{-6}$
3,79	0,00900	0,00950	$3{,}00 \cdot 10^{-6}$
4,00	0,00260	0,01120	$16{,}50 \cdot 10^{-6}$

Tableau 3

Concentrations, à l'équilibre, des espèces ioniques UO_2^{2+} et $U_2O_5^{2+}$ formées par l'hydrolyse du perchlorate d'uranyle 0,0455 M, à $I = 1,5$

pH	UO_2^{2+} mole/l	$U_2O_5^{2+}$ mole/l	K_1
2,71	0,04360	0,00095	$1,80 \cdot 10^{-6}$
3,21	0,02900	0,00400	$1,70 \cdot 10^{-6}$
3,37	0,02296	0,00602	$2,02 \cdot 10^{-6}$
3,50	0,01830	0,00685	$1,98 \cdot 10^{-6}$
3,64	0,01300	0,00850	$2,63 \cdot 10^{-6}$
3,74	0,00900	0,00950	$3,80 \cdot 10^{-6}$
3,86	0,00590	0,01630	$7,90 \cdot 10^{-6}$
3,99	0,00252	0,01124	$18,4 \cdot 10^{-6}$

Tableau 4

Concentrations, à l'équilibre, des espèces ioniques UO_2^{2+} et $U_2O_5^{2+}$ formées par l'hydrolyse du perchlorate d'uranyle 0,0455 M à $I = 2$.

pH	UO_2^{2+} mole/l	$U_2O_5^{2+}$ mole/l	K_1
2,70	0,04360	0,00095	$1,80 \cdot 10^{-6}$
3,14	0,02889	0,00405	$2,53 \cdot 10^{-6}$
3,30	0,02290	0,00605	$2,80 \cdot 10^{-6}$
3,55	0,01300	0,00850	$3,90 \cdot 10^{-6}$
3,65	0,00890	0,00955	$5,80 \cdot 10^{-6}$
3,74	0,00580	0,01040	$10,01 \cdot 10^{-6}$
3,87	0,00250	0,01120	$30,20 \cdot 10^{-6}$

Tableau 5

Concentrations, à l'équilibre, des espèces ioniques UO_2^{2+} et $U_2O_5^{2+}$ formées par l'hydrolyse du perchlorate d'uranyle 0,0182 M ,à $I = 0,5$.

pH	UO_2^{2+} mole/l	$U_2O_5^{2+}$ mole/l	K_1
3,10	0,01741	0,00039	$0,97 \cdot 10^{-6}$
3,37	0,01408	0,00121	$1,08 \cdot 10^{-6}$
3,74	0,00882	0,00259	$1,08 \cdot 10^{-6}$
3,90	0,00667	0,00316	$1,10 \cdot 10^{-6}$
3,99	0,00460	0,00370	$1,81 \cdot 10^{-6}$
4,11	0,00272	0,00413	$3,31 \cdot 10^{-6}$
4,22	0,00154	0,00453	$6,8 \cdot 10^{-6}$

Tableau 6

Concentrations, à l'équilibre, des espèces ioniques UO_2^{2+} et $U_2O_5^{2+}$ formées par l'hydrolyse du perchlorate d'uranyle 0,0182 M, à $I=1$

pH	UO_2^{2+} mole/l	$U_2O_5^{2+}$ mole/l	K_1
3,38	0,01409	0,00120	$1{,}02\cdot10^{-6}$
3,59	0,01119	0,00195	$0{,}90\cdot10^{-6}$
3,74	0,00882	0,00259	$1{,}07\cdot10^{-6}$
3,89	0,00667	0,00316	$1{,}30\cdot10^{-6}$
3,99	0,00460	0,00370	$1{,}81\cdot10^{-6}$
4,11	0,00272	0,00413	$3{,}31\cdot10^{-6}$
4,22	0,00154	0,00453	$6{,}80\cdot10^{-6}$

Tableau 7

Concentrations, à l'équilibre, des espèces ioniques UO_2^{2+} et $U_2O_5^{2+}$, formées par l'hydrolyse du perchlorate d'uranyle 0,0182 M, à $I=1{,}5$

pH	UO_2^{2+} mole/l	$U_2O_5^{2+}$ mole/l	K_1
3,05	0,01732	0,00044	$1{,}13\cdot10^{-6}$
3,56	0,01117	0,00196	$1{,}10\cdot10^{-6}$
3,70	0,00880	0,00259	$1{,}30\cdot10^{-6}$
3,85	0,00666	0,00317	$1{,}40\cdot10^{-6}$
3,98	0,00459	0,00370	$1{,}90\cdot10^{-6}$
4,20	0,00153	0,00453	$7{,}60\cdot10^{-6}$

Tableau 8

Concentrations, à l'équilibre, des espèces ioniques formées par l'hydrolyse du perchlorate d'uranyle 0,0182 M, à $I = 2$

pH	UO_2^{2+} mole/l	$U_2O_5^{2+}$ mole/l	K_1
3,10	0,01741	0,00039	$0{,}97\cdot10^{-6}$
3,29	0,01399	0,00125	$1{,}60\cdot10^{-6}$
3,47	0,01111	0,00199	$1{,}70\cdot10^{-6}$
3,65	0,00878	0,00261	$1{,}63\cdot10^{-6}$
3,75	0,00663	0,00318	$2{,}09\cdot10^{-6}$
3,87	0,00456	0,00371	$3{,}20\cdot10^{-6}$
4,14	0,00152	0,00453	$10{,}00\cdot10^{-6}$

Tableau 9

Concentrations, à l'équilibre, des espèces ioniques UO_2^{2+} et $U_2O_5^{2+}$, formées par l'hydrolyse du perchlorate d'uranyle 0,0091 M, à $I = 0{,}5$

pH	UO_2^{2+} mole/l	$U_2O_5^{2+}$ mole/l	K_1
3,27	0,00857	0,00026	$1{,}01\cdot10^{-6}$
3,52	0,00703	0,00058	$1{,}07\cdot10^{-6}$
3,70	0,00570	0,00090	$1{,}10\cdot10^{-6}$
3,85	0,00463	0,00118	$1{,}09\cdot10^{-6}$
3,98	0,00364	0,00143	$1{,}09\cdot10^{-6}$
4,09	0,00279	0,00165	$1{,}48\cdot10^{-6}$
4,18	0,00191	0,00184	$2{,}20\cdot10^{-6}$
4,27	0,00126	0,00201	$3{,}40\cdot10^{-6}$

Tableau 10

Concentrations, à l'équilibre, des espèces ioniques, UO_2^{2+} et $U_2O_5^{2+}$, formées par l'hydrolyse du perchlorate d'uranyle 0,0091 M, à $I = 1$

pH	UO_2^{2+} mole/l	$U_2O_5^{2+}$ mole/l	K_1
3,27	0,00700	0,00060	$1{,}33\cdot10^{-6}$
3,64	0,00567	0,00091	$1{,}37\cdot10^{-6}$
3,80	0,00462	0,00119	$1{,}25\cdot10^{-6}$
3,92	0,00362	0,00144	$1{,}58\cdot10^{-6}$
4,02	0,00268	0,00165	$2{,}07\cdot10_{-6}$
4,14	0,00190	0,00184	$2{,}62\cdot10^{-6}$
4,21	0,00126	0,00202	$4{,}73\cdot10^{-6}$

Tableau 11

Concentrations, à l'équilibre, des espèces ioniques formées par l'hydrolyse du perchlorate d'uranyle 0,0091 M, à $I = 1{,}5$

pH	UO_2^{2+} mole/l	$U_2O_5^{2+}$ mole/l	K_1
3,17	0,00843	0,00033	$2{,}1\ \cdot10^{-6}$
3,36	0,00690	0,00065	$2{,}52\cdot10^{-6}$
3,54	0,00561	0,00094	$2{,}35\cdot10^{-6}$
4,15	0,00125	0,00202	$6{,}3\ \cdot10^{-6}$
4,25	0,00065	0,00217	$15{,}9\cdot10^{-6}$

Tableau 12

Concentrations, à l'équilibre, des espèces ioniques formées par l'hydrolyse du perchlorate d'uranyle 0,0091 M, à $I = 2$

pH	UO_2^{2+} mole/l	$U_2O_5^{2+}$ mole/l	K_1
3,15	0,00840	0,00035	$2{,}4\cdot10^{-6}$
3,69	0,00457	0,00121	$2{,}3\cdot10^{-6}$
3,84	0,00360	0,00145	$2{,}2\cdot10^{-6}$
3,96	0,00267	0,00166	$2{,}7\cdot10^{-6}$
4,07	0,00190	0,00185	$3{,}6\cdot10^{-6}$
4,17	0,00126	0,00202	$5{,}7\cdot10^{-6}$
4,29	0,00066	0,00066	$12{,}9\cdot10^{-6}$

Tableau 13

Concentrations, à l'équilibre, des espèces ioniques formées par l'hydrolyse du perchlorate d'uranyle 0,00091 M, à $I = 0,5$

pH	UO_2^{2+} mole/l	$U_2O_5^{2+}$ mole/l	K_1
4,12	0,000835	0,000037	$0,30 \cdot 10^{-6}$
4,27	0,000680	0,000070	$0,42 \cdot 10^{-6}$
4,38	0,000548	0,000101	$0,55 \cdot 10^{-6}$
4,49	0,000445	0,000127	$0,65 \cdot 10^{-6}$

Tableau 14

Concentrations, à l'équilibre, des espèces ioniques formées par l'hydrolyse du perchlorate d'uranyle 0,00091 M, à $I = 1$

pH	UO_2^{2+} mole/l	$U_2O_5^{2+}$ mole/l	K_1
4,12	0,000835	0,000037	$0,30 \cdot 10^{-6}$
4,48	0,000444	0,000128	$0,70 \cdot 10^{-6}$
4,60	0,000350	0,000150	$0,76 \cdot 10^{-6}$

Tableau 15

Concentrations, à l'équilibre, des espèces ioniques formées par l'hydrolyse du perchlorate d'uranyle 0,00091 M, à $I = 1,5$

pH	UO_2^{2+} mole/l	$U_2O_5^{2+}$ mole/l	K_1
4,13	0,000836	0,000037	$0,29 \cdot 10^{-6}$
4,20	0,000670	0,000075	$0,66 \cdot 10^{-6}$
4,25	0,000642	0,000108	$0,82 \cdot 10^{-6}$
4,37	0,000477	0,0001328	$1,05 \cdot 10^{-6}$
4,47	0,000341	0,000154	$1,40 \cdot 10^{-6}$
4,60	0,000253	0,000173	$1,68 \cdot 10^{-6}$

Tableau 16

Concentrations, à l'équilibre, des espèces ioniques formées par l'hydrolyse du perchlorate d'uranyle 0,00091 M, à $I = 2$

pH	UO_2^{2+} mole/l	$U_2O_5^{2+}$ mole/l	K_1
4,07	0,000825	0,000042	$0,45 \cdot 10^{-6}$
4,19	0,000669	0,000075	$0,68 \cdot 10^{-6}$
4,26	0,000535	0,000107	$1,09 \cdot 10^{-6}$
4,37	0,000435	0,000132	$1,20 \cdot 10^{-6}$
4,42	0,000336	0,000157	$2,00 \cdot 10^{-6}$
4,54	0,000250	0,000175	$2,27 \cdot 10^{-6}$
4,68	0,000158	0,000191	$2,41 \cdot 10^{-6}$

Tel qu'on le voit dans les tableaux 1–16 et les figures 7 et 8, la constante K_1 présente, dans le domaine de pH dans lequel on peut considérer que dans la solution coexistent seulement les ions UO_2^{2+} et $U_2O_5^{2+}$, une valeur moyenne d'environ 1.10^{-6}, en accord avec les données de la littérature. [1-3]

À un certain pH, situé dans le domaine de 3,6 à 4 (la valeur exacte dépend des paramètres qui caractérisent le milieu de réaction) on constate une augmentation brusque de la valeur déterminée pour la constante K_1, ce qui prouve que, à partir de cette valeur de pH, les espèces ioniques qui coexistent dans la solution près de l'ion UO_2^{2+} et $U_2O_5^{2+}$ se forment dans des quantités qui ne peuvent plus être négligées. (Pour ce domaine de pH, l'équation (3) ne conduit plus à des valeurs correctes.)

Le pH qui correspond à cette augmentation brusque de la valeur de la constante K_1 limite le domaine dans lequel on peut considérer que, dans la solution, il se forme, comme produits d'hydrolyse de l'ion U^{6+}, seulement les ions UO_2^{2+} et $U_2O_5^{2+}$.

En ce qui concerne la formation et la stabilité des ions $U_3O_8^{2+}$, en considérant la réaction :

$$U_2O_5^{2+} + UO_2^{2+} + H_2O \rightleftharpoons U_3O_8^{2+} + 2H^+,$$

si on applique le principe de l'électroneutralité, on peut écrire la relation :

$$2u + 2v + 2w + h = \frac{2\,pm - qc}{(p+q)} \tag{4}$$

dans laquelle w, u, v et h représentent les concentrations (mole/l) des ions $U_3O_8^{2+}$ (w), UO_2^{2+}(u), $U_2O_5^{2+}$ (v) et H^+ (h). (Les autres symboles p, m, q et c ont les mêmes significations que pour la relation (3).)

En résolvant l'équation (4) on obtient $w = U_3O_8^{2+}$ en équilibre, dans les conditions de pH, concentration et force ionique considérées.

En connaissant $u = UO_2^{2+}$, $v = U_2O_5^{2+}$ et $w = U_3O_8^{2+}$, la constante de stabilité de l'ion $U_3O_8^{2+}$ peut être calculée à l'aide de la relation :

$$K_2 = \frac{wh^2}{uv} \tag{5}$$

Dans ce travail on a étudié la formation de l'ion $U_3O_8^{2+}$ dans des solutions de perchlorate d'uranyle de différentes concentrations et forces ioniques. (Les résultats sont représentés dans les figures 9–10.)

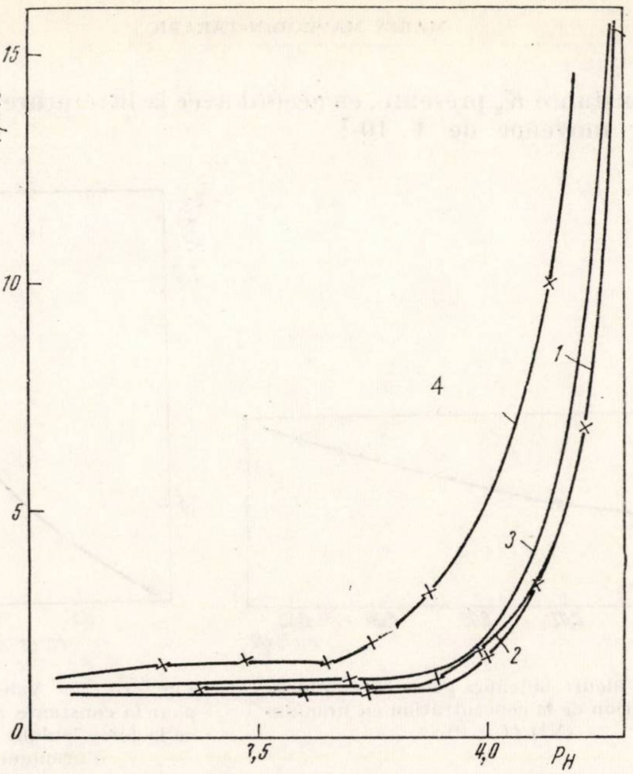

Fig. 7. — Valeurs obtenues pour la constante K_1, en travaillant sur des solutions de perchlorate d'uranyle caractérisées par concentration constante (0,02 M) et forces ioniques variées :
$I = 0,5$ (*1*) ; $I = 1$(*2*) ; $I = 1,5$ (*3*) et $I = 2$ (*4*).

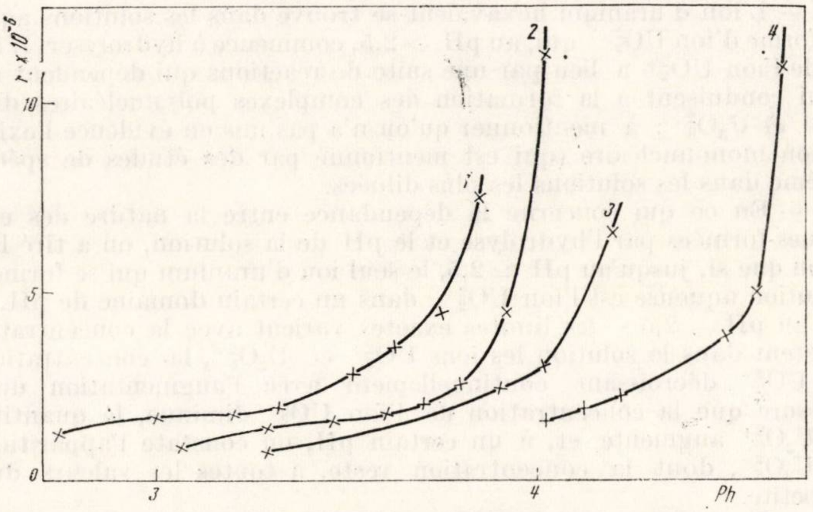

Fig. 8. — Valeurs obtenues pour la constante K_1, en travaillant sur des solutions de perchlorate d'uranyle caractérisées par force ionique constante ($I = 1$) et concentrations variées :
$C = 0,05$M(*1*) ; $C = 0,02$ M (*2*) ; $C = 0,01$ M(*3*) et $C = 0,001$ M (*4*).

La constante K_2 présente, en accord avec la littérature de spécialité, [1] une valeur moyenne de $1 . 10^{-7}$.

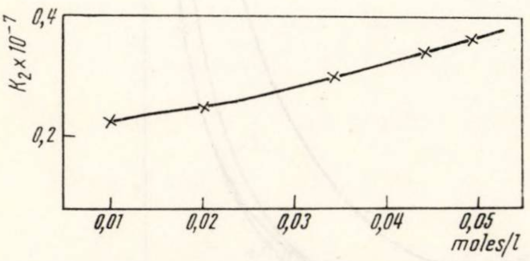

Fig. 9. — Valeurs obtenues pour la constante K_2, en fonction de la concentration en uranium (VI) ($I = 0$).

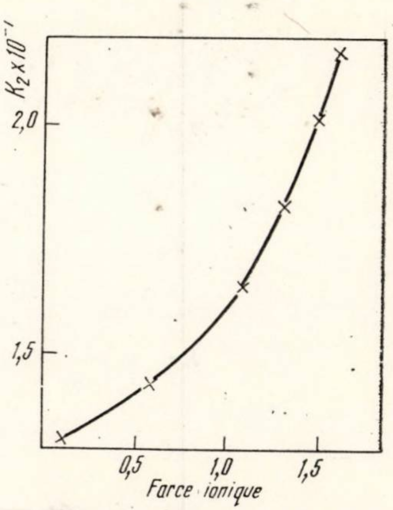

Fig. 10. — Valeurs obtenues pour la constante K_2, en fonction de la force ionique de la solution d'uranium (VI).

CONCLUSIONS

— L'ion d'uranium hexavalent se trouve dans les solutions aqueuses sous forme d'ion UO_2^{2+} qui, au pH $> 2{,}5$, commence à hydrolyser. L'hydrolyse de l'ion UO_2^{2+} a lieu par une suite de réactions qui dépendent du pH et qui conduisent à la formation des complexes polynucléaires, du type $U_2O_5^{2+}$ et $U_3O_8^{2+}$; à mentionner qu'on n'a pas mis en évidence l'existence de l'ion mononucléaire (qui est mentionné par des études de spécialité) ni même dans les solutions les plus diluées.

— En ce qui concerne la dépendance entre la nature des espèces ioniques formées par l'hydrolyse et le pH de la solution, on a tiré la conclusion que si, jusqu'au pH $\simeq 2{,}5$, le seul ion d'uranium qui se forme dans la solution aqueuse est l'ion UO_2^{2+}, dans un certain domaine de pH, supérieur au pH $= 2{,}5$ — les limites exactes varient avec la concentration — coexistent dans la solution les ions UO_2^{2+} et $U_2O_5^{2+}$, la concentration des ions UO_2^{2+} décroissant continuellement avec l'augmentation du pH. À mesure que la concentration de l'ion UO_2^{2+} diminue, la quantité des ions $U_2O_5^{2+}$ augmente et, à un certain pH, on constate l'apparition des ions $U_3O_8^{2+}$, dont la concentration reste, à toutes les valeurs du pH, très petite.

— La stabilité des ions $U_2O_5^{2+}$ et $U_3O_8^{2+}$ se caractérise par les valeurs moyennes des constantes d'équilibre, $K_1 = 1.10^{-6}$ et $K_2 = 1.10^{-7}$ et augmente avec la force ionique de la solution.

Revue Roumaine de Chimie, **18**, *1*, 89–98 (1973)

THEORETICAL STUDY OF ISOMERIC THIENYLFURANS

L. KLASINC, N. TRINAJSTIĆ

Institute "Rugjer Bošković", P.O.B. 1016, 41001 Zagreb, Croatia, Yugoslavia

and E. POP

Chemical-Pharmaceutical Research Institute, Str. Fabricii 126, Cluj, Romania

Received June 2, 1972

Molecular orbital calculations in the framework of Pariser-Parr (P—P) theory have been applied to some ground state properties and to UV spectra of the four isomeric thienylfurans. The good agreement is obtained with the experiment for the first $\pi - \pi^*$ electronic transition. No conclusion could be reached about preferred conformational arrangements on the grounds of only the P—P calculations for *syn* and *anti* forms, because the results of calculations for both forms agree rather closely with the experimental values. Extended Hückel MO results indicate that the 2, 3′- and 2, 3′-thienylfurans have planar *syn* conformation, while 3, 3′-thienylfuran planar *anti* conformation. For 3, 2′-isomer there is no distinction between the two planar forms. Bond length calculations predicted a very long bond between the heterocycles, which have preserved to a great extent the geometries of individual furan and thiophene ring systems.

The four isomeric thienylfurans : 2-(2′-thienyl)furan (*1*), 3-(2′-thienyl) furan (*2*), 2-(3′-thienyl) furan (*3*), and 3-(3′-thienyl) furan (*4*), have recently been synthesized.[1] These molecules belong to the class of the isomeric compounds consisting of two heterocyclic five-membered rings separated by an essential single bond (~ 1.46 Å) and are of current interest.[1–15]

---

[1] H. Wynberg, H. J. M. Sinnige and H. M. J. C. Creemers, *J. Org. Chem.*, **36**, 1011 (1971).

[2] H. Wynberg and A. Logothetis, *J. Amer. Chem. Soc.*, **78**, 1960 (1956).

[3] H. Wynberg, A. Logothetis and D. Ver Ploeg, *J. Amer. Chem. Soc.*, **79**, 1972 (1957).

[4] H. Wynberg and A. Bantjes, *J. Org. Chem.*, **24**, 1421 (1959).

[5] S. Gronowitz and H. O. Karlsson, *Arkiv Kemi*, **17**, 89 (1961).

[6] H. Wynberg, *Angew. Chem.*, **75**, 453 (1963).

[7] H. Wynberg and A. Kraak, *J. Org. Chem.*, **29**, 2455 (1964).

[8] R. Grigg, J. A. Knight and M. V. Sargent, *J. Chem. Soc.*, **C, 1966,** 976.

[9] H. Wynberg and J. W. Van Reijèndem, *Rec. Trav. chim.*, **86**, 382 (1967).

[10] N. Trinajstić and A. Hinchliffe, *Croat. Chem. Acta*, **40**, 163 (1968).

[11] T. Živković and N. Trinajstić, *Canad. J. Chem.*, **47**, 697 (1969).

[12] M. J. S. Dewar and N. Trinajstić, *J. Amer. Chem. Soc.*, **92**, 1453 (1970).

[13] A. Skanche, *Acta Chem. Scand.*, **24**, 1389 (1970).

[14] A. Almenningen, O. Bastiansen and P. Svendsäs, *Acta Chem. Scand.*, **12**, 1671 (1958).

[15] G. J. Visser, G. J. Heeres, J. Wolters and A. Vos, *Acta Cryst.*, **B 24**, 467 (1968)

Some molecules of this class of compounds: bithienyls (2,2′-(*5*), 2,3′-(*6*), and 3,3′-(*7*)) and bifuryls (2,2′-(*8*), 2,3′(-*9*), and 3,3′-(*10*)) have been previously reported and their chemical and spectral properties investigated.[2-9] The skeletal structures of isomeric thienylfurans (*1—4*), bithienyls (*5—7*), and bifuryls (*8—10*) in *anti* forms are shown in Fig. 1.

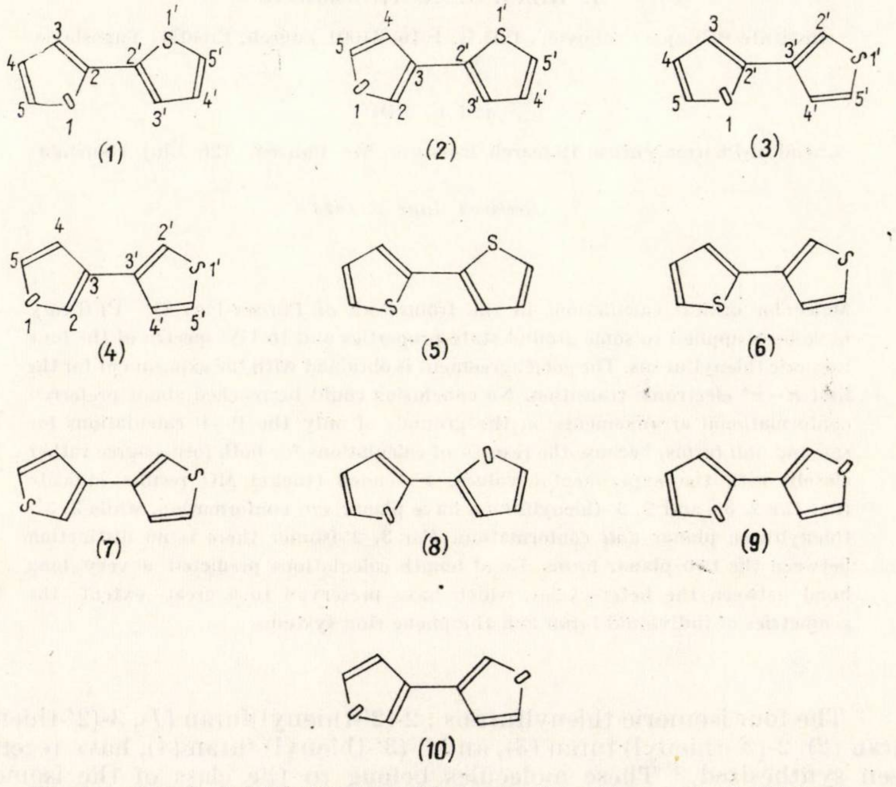

Fig. 1. — Atomic skeletal structure of isomeric thienylfurans (*1—4*), bithienyls (*5—7*), and bifuryls (*8—10*) in *anti* form.

We have studied thienylfurans (*1—4*) using the semi-empirical method of Pariser and Parr[16] (P—P) in order to interpret their electronic spectra. The P—P method has been shown to be a very reliable method for studying the electronic spectra of various kinds of hydrocarbons and heteroconjugated systems.[17,18] Since the formalism of the P—P method has been presented rather extensively in recent monographs,[17-19] need not to be repeated here. The standard set of parameters for C, O, and S is used. The values of the one-center electron repulsion integrals and one-electron core resonance integrals are given in Table 1. The two-center electron repulsion integrals have been determined in the Mataga-Nishimoto manner.[20]

---

[16] R. Pariser and R. G. Parr, *J. Chem. Phys.*, **21**, 466, 767 (1953).

[17] J. N. Murell, "Theory of the Electronic Spectra of Organic Molecules", Methuen, London, 1963.

[18] T. E. Peacock, "Electronic Properties of Aromatic and Heterocyclic Molecules", Academic Press, London, 1965.

[19] R. G. Parr, "The Quantum Theory of Molecular Electronic Structure", Benjamin, New York, 1963.

Table 1

Values of the parameters used in the calculations [a)]

Atom (X)	Valence state	W_X(eV)	γ_{XX}(eV)	β_{C-X}(eV)	r_{C-X}(Å)
C	trtrtr	11.16	11.13	−2.390	1.400
O	$tr^2trtr\ \pi^2(\rangle O)$	33.00	21.53	−2.000	1.370
S	$tr^2trtr\ \pi^2(\rangle S)$	22.88	13.05	−1.800	1.720

a) R. Pariser and R. G. Parr, *J. Chem. Phys.*, **21**, 466, 767 (1953); N. Solany, F. W. Birss and J. B. Greennshields, *Canad. J. Chem.*, **43**, 1569 (1965); F. P. Billingsley, II and J. E. Bloor, *Theoret. Chim. Acta*, **11**, 325 (1968); M. J. S. Dewar and N. Trinajstić, *J. Amer. Chem. Soc.*, **92**, 1453 (1970).

In the present calculations sulphur is considered without *d*-orbital participation. Reasons for this are several: the experience of various authors in their studies,[21−24] our recent work on the ground and excited states of σ-bivalent sulphur compounds.[12,25−27] Finally, some recent *ab initio* SCF MO calculations on very small molecules (H_2S)[28] or ions (α-sulphinyl carbanion)[29] have shown that the 3d-AO′ s of σ-bivalent sulphur are too high in energy[30,31] to have much importance in bonding.

All calculations have been carried out with a FORTRAN program coded for a CEA 90−40 computer.

RESULTS AND DISCUSSIONS

Thienylfurans consist of the two heterocyclic ring systems (furan and thiophene) separated by one essential carbon (sp^2)-carbon (sp^2) single bond. These compounds are expected to appear in planar *syn* or planar *anti* (or twisted) forms. There are no experimental evidences concerning conformations of thienylfurans available as yet. However, there are some experimental studies reported for related systems, e.g.: 2,2'-bithienyl (*5*) and 3,3'-bithienyl (*7*). The electron diffraction studies of 2,2'-bithienyl vapour [14] show that the thiophene ring systems in this molecule are twisted in an *anti* form and have practically the same dimensions as thiophene itself. [32] It has also been found that the length of the bond joining the two thiophene rings ($C_2-C'_2$) is 1.48 Å. This bond is only a little (0.032 Å) shorter than the single bond (1.512 Å) between the two sp^2-hybridized carbon atoms. This implies the very small π-interaction between the two rings. On the other hand, the x-ray studies [15] on 2,2'-bithienyl, 2,3'-bithienyl, and 3,3'-bithienyl have shown these molecules planar in *anti* forms. The interring distance is again found to be rather long, e.g.: 1.49 Å (*5*), 1.46 Å (*6*), and 1.48 Å (*7*), respectively. Some theoretical studies[10-14] on bond lengths in bithienyls agreed with these findings. Similarly, the theoretical studies by Skancke [15] predicted the *anti* form of 3,3'-bithienyl to be more stable than *syn* form, and the angle of twist 30° and 150° for the two forms relative to *syn* form. However, there was no such a clear distinction between the planar and twisted forms of 2,2'-bithienyl; the planar form being somewhat less favourable than non-planar one.

---

[20] N. Mataga and K. Nishimoto, *Z. phys. Chem.* (*Frankfurt*), **13**, 140 (1957).

[21] H. Lumbroso and R. Passerini, *Bull. Soc. chim. France*, **1957**, 311.

[22] K. Boček, A. Mangini and T. Zahradnik, *J. Chem. Soc.*, **1963**, 255.

[23] R. Gerdil and E. A. C. Lucken, *J. Amer. Chem. Soc.*, **87**, 213 (1965).

[24] G. di Leonardo and C. Zauli, *J. Chem. Soc.*, **A 1969**, 1305.

[25] A. Hinchliffe and N. Trinajstić, *Theor. Chim. Acta*, **10**, 458 (1968).

[26] N. Trinajstič, *Tetrahedron Letters*, **1968**, 1529.

[27] L. Klasinc and N. Trinajstić, *Tetrahedron*, **27**, 4045 (1971).

[28] S. Polezzo, M. P. Stabilini and M. Simonetta, *Mol. Phys.*, **10**, 609 (1969).

[29] S. Wolfe, A. Rauk and I. G. Csizmadia, *J. Amer. Chem. Soc.*, **89**, 5710 (1967).

[30] S. Wolfe, A. Rauk and I. G. Csizmadia, *Canad. J. Chem.*, **47**, 113 (1969); *J. Amer. Chem. Soc.*, **91**, 1567 (1969).

[31] S. Wolfe, A. Rauk, L. M. Tel and I. G. Csizmadia, *Chem. Comm.*, **1971**, 96.

In the light of these structural possibilities in bithienyls we have carried out P—P calculations for the planar *syn* and planar *anti* forms of the four isomeric thienylfurans. Some trial calculations have been performed at earlier stages of this work with the assumed starting interring distance of 1.40 Å, but it converged to the final value of 1.46 Å. Calculated bond orders were converted to bond lengths using the expression of Coulson and Golebiewski. [33] As a result of these trial calculations the value of 1.46 Å as the interring distance was adopted in all present calculations. In our earlier work [13] on the electronic structure of bithienyls and bifuryls we have found the same thing: interring bond orders always converged to such values of bond orders which gave, through the Coulson-Golebiewski bond order-bond length relationship, the bond lengths of 1.46—1.48 Å.

The calculated singlet-singlet transition energies (ΔE, eV) and oscillator strengths of the isomeric thienylfurans for both models considered (*syn*: 1.46 Å and *anti*: 1.46 Å) are reported in Table 2. The electronic transition energies and oscillator strengths have been calculated by a limited configuration interaction (LCI) procedure. The experimental data (ΔE, eV and log ε) are also given in Table 2.

We attributed the calculated values: (*1*) = 4.02 (4.01), (*2*) = = 4.22 (4.20), (*3*) = 4.48 (4.49) and (*4*) = 4.64 (4.64) to the first $\pi - \pi^*$ transition (all results in eV values; the results for planar *syn* conformations are reported in brackets). The corresponding experimental values are: (*1*) = 4.19, (*2*) = 4.54, and (*3*) = 4.44 (all results in eV values). There is no low lying $\pi - \pi^*$ band reported in 3-(3'-thienyl)furan. The difference between the calculated and experimental values is of the order of 0.2 Å; the calculated values being always lower. The second $\pi - \pi^*$ transition is always less intense. The calculated values: (*1*) = 5.27 (5.27), (*2*) = 5.37

---

[32] B. Bak, D. Christensen, L. Hansen-Nygaard and J. Rastrup-Andersen, *J. Mol. Spectroscopy*, **7**, 58 (1961)

[33] C. A. Coulson and A. Golebiewski, *Proc. Phys. Soc.*, **78**, 1310 (1961).

Table 2

Calculated and experimental* singlet-singlet transition energies (ΔE) of isomeric thienyl furans

Molecule	Conformation	Δ E (eV) and oscillator strengths (in brackets)						
2−(2′−thienyl) furan (*1*)	*syn*	4.01(1.05);	5.27(0.01);	5.52(0.02);	6.00(0.30);	6.03(0.02);	6.80(0.01)	
	anti	4.02(1.06);	5.27(0.08);	5.50(0.05);	5.97(0.01);	6.06(0.03);	6.98(0.87)	
	Experiment	4.19(4.04);	5.39(2.11);					
3−(2′−thienyl) furan (*2*)	*syn*	4.20(0.74);	5.37(0.03);	5.54(0.01);	5.84(0.11);	6.07(0.13);	6.76(0.35)	
	anti	4.22(0.75);	5.37(0.03);	5.57(0.07);	5.84(0.27);	6.04(0.05);	6.81(0.49)	
	Experiment	4.54(3.89);						
2−(3′−thienyl) furan (*3*)	*syn*	4.49(0.79);	5.00(0.00);	5.52(0.46);	5.69(0.08);	6.54(0.17);	6.59(0.00);	6.86(0.46)
	anti	4.48(0.81);	5.03(0.01);	5.56(0.37);	5.68(0.00);	6.55(0.19);	6.61(0.03);	6.84(0.54)
	Experiment	4.44(4.13);	5.44(4.09);					
		4.59(4.12);						
3−(3′−thienyl) furan (*4*)	*syn*	4.64(0.61);	5.13(0.02);	5.56(0.22);	5.70(0.05);	6.51(0.34);	6.66(0.00);	6.87(0.03)
	anti	4.64(0.62);	5.13(0.02);	5.56(0.22);	5.70(0.05);	6.51(0.34);	6.65(0.01);	6.86(0.03)
	Experiment		5.12(3.88);					

* Experimental data from Ref. 1, Solvent : (96%) ethanol.

(5.37), (*3*) = 5.03 (5.00) and (*4*) = 5.13 (5.13) are attributed to the second $\pi - \pi^*$ transition (all values in eV). The corresponding experimental values are: (*1*) = 5.39, (*3*) = 5.44, and (*4*) = 5.12 (all values in eV). There is no second $\pi - \pi^*$ transition reported in 3-(2′-thienyl) furan. Agreement between the experiment and calculation is again reasonably good, if we accept the assignement made; the average difference between the calculated and experimental values being 0.1 — 0.4eV. Examination of the calculated results shows no difference between the two possible conformational forms. Calculated values for both models: planar *syn* and planar *anti*, are in similar agreement with the experiment. To elaborate this further we have also carried out P—P calculations for planar *syn* and planar *anti* forms of bithienyls and bifuryls with the interring distance of 1.46 Å. The plots of the calculated lower $\pi - \pi^*$ transition energies (ΔE) of thienylfurans, bithienyls and bifuryls (see for these results Table 3) for both possible planar conformations vs. experimental values [1] are shown in Figs. 2 and 3. The agreement with experiment in both cases is almost identical. The points lie reasonably close to a straight line, the correlation coefficients being 0.972 (0.970) and the standard deviation 0.0508 eV (0.0513 eV). Results for planar *syn* forms are given in brackets. The slopes of the least-squares lines (0.915 and 0.898) are close to the theoretical unit value. Apparently the spectral data are not sufficient enough to predict the most preferred conformation in these systems. The excitation energies in these molecules, which consist of two conjugated subsystems joined by one single bond, do not depend on the molecule as a whole, but on the individual subsystems. [34] These were analysed for bithienyls by Wachters and Davies [34] using the local energy method of Longuet-Higgins and Murrell.[35] Wachters and Davies found hardly any difference in transition energies of the two forms, but the corresponding oscillator strengths did differ in the case of 3,3′-bithienyl.

It is obvious that in order to elucidate this question some other theoretical approach must be used. The Extended Hückel Theory (EHT) may be more fruitful in this respect, because there are some clear indications that EHT is a suitable semi-empirical MO method [36-38] for predicting the preferred conformations. EHT theory was applied to the problem of the preferred conformations of isomeric thienylfurans.[39] The preliminary

---

[34] A. J. H. Wachters and D. W. Davies, *Tetrahedron*, **20**, 2841 (1964).

[35] H. C. Longuet-Higgins and J. N. Murrell, *Proc. Pyhs. Soc.*, **A 68**, 601 (1955).

[36] J. R. Hoyland, "Molecular Orbital Studies in Chemical Pharmacology", L. B. Kier, Springer-Verlag, New York, p. 31.

[37] L. B. Kier, "Molecular Orbital Theory in Drug Research", Academic Press, New York, 1971.

[38] V. Galasso, G. De Alti and A. Bigotto, *Tetrahedron*, **27**, 991 (1970); V. Galasso and G. De Alti, *Tetrahedron*, **27**, 4947 (1971); V. Galasso and N. Trinajstić, *Tetrahedron*, **28**, 000 (1972).

[39] V. Galasso and N. Trinajstić, to be published.

EHT results show that in 2-(2′-thienyl) furan and 2-(3′-thienyl) furan the planar *syn* form is more stable, while in 3-(3′-thienyl) furan the planar *anti* is more stable. In the case of 3-(2′-thienyl) furan there is no clear distinction obtained between either of these forms. Besides, no tendency to deviate from planarity is shown by any of these systems.

Bond orders are reported in Table 4. The interring bond orders were converted to the corresponding bond lengths using two different

Table 3

Calculated and experimental * lower singlet-singlet transition energies (ΔE) of Isomeric bithienyls and bifuryls

MOLECULE	CONFORMATION		EXPERIMENT
	syn	*anti*	
2,2′–bithienyl	4.07(1.19)	4.08(1.18)	4.12 (4.11)
(*5*)	5.30(0.01)	5.31(0.00)	5.04 (3.79)
	5.53(0.01)	5.52(0.08)	
	6.01(0.23)	5.97(0.00)	
2,3′–bithienyl	4.57(0.88)	4.56(0.88)	4.40 (4.12)
(*6*)	5.02(0.05)	5.03(0.06)	5.28 (3.97)
	5.55(0.50)	5.61(0.36)	
	5.68(0.13)	5.68(0.14)	
3,3′–bithienyl	4.72(0.72)	4.66(0.42)	4.77 (4.05)
(*7*)	5.11(0.00)	5.12(0.03)	
	5.59(0.23)	5.66(0.08)	
	5.68(0.10)	5.68(0.76)	5.85 (4.35)
2,2′–bifuryl	4.00(1.13)	3.98(0.97)	4.21(4.09)–4.41
(*8*)	5.26(0.00)	5.27(0.00)	(4.27)
	5.56(0.00)	5.51(0.02)	5.56 (3.32)
	5.99(0.19)	5.89(0.00)	5.71 (3.31)
2,3′–bifuryl	4.52(0.69)	4.51(0.71)	4.59 (4.06)
(*9*)	4.98(0.02)	4.99(0.03)	4.79(sh)–4.88(sh)
	5.37(0.49)	5.41(0.37)	
	5.66(0.03)	5.66(0.01)	5.79 (sh)
3,3′–bifuryl	4.67(0.57)	4.60(0.28)	
(*10*)	5.11(0.00)	5.09(0.02)	5.12 (3.88)
	5.41(0.24)	5.47(0.62)	
	5.67(0.03)	5.65(0.02)	

* Experimental data from Ref. 1.

bond order-bond length relations[11,33] :

$$L_{CC} = 1.532 - \frac{0.242\ p_{CC}}{1 + 0.420\ p_{CC}}\ (\text{Å}) \qquad (\text{I})^{11}$$

and

$$L_{CC} = 1.517 - 0.180 \qquad (\text{Å}) \qquad (\text{II})^{33}$$

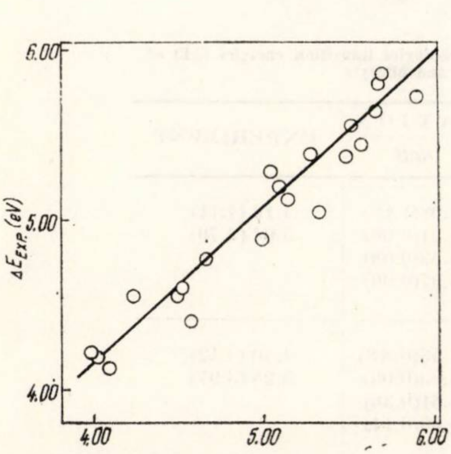

Fig. 2. — The plot of experimental vs. calculated lower $\pi-\pi^*$ transition energies for *anti* forms.

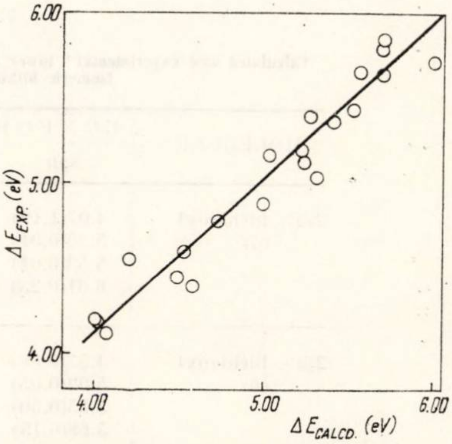

Fig. 3. — The plot of experimental vs. calculated lower $\pi-\pi^*$ transition energies for *syn* forms.

The following calculated values are obtained for the interring distance :

Molecule	Bond	Predicted interring distance (in Å)	
		(I)	(II)
(1)	2—2′	1.45	1.45
(2)	3—2′	1.46	1.46
(3)	2—3′	1.46	1.45
(4)	3—3′	1.46	1.46

These results suggest that the experimental interring distances in thienylfurans should be foundat about 1.46 Å.

The inspection of the other bond orders shows that the geometries of ring systems are very alike to those of the individual molecules making up the isomeric thienylfurans, e.g. : thiophene and furan.

We report in Table 5 calculated molecular geometry for 2-(2′-thienyl) furan as an example and experimental geometries of thiophene[32] and

Table 4

Bond orders

MOLECULE	CONFORMATION	BOND i–j										
		1–2	1–5	2–3	3–4	4–5	Interring Bond order	1′–2′	1′–5′	2′–3′	3′–4′	4′–5′
2–(2′–thienyl) furan (1)	*syn*	0.373	0.369	0.763	0.532	0.816	0.373	0.403	0.398	0.756	0.536	0.809
	anti	0.377	0.376	0.760	0.535	0.814	0.370	0.409	0.404	0.754	0.539	0.806
3–(2′–thienyl) furan (2)	*syn*	0.377	0.373	0.773	0.531	0.816	0.339	0.404	0.398	0.768	0.538	0.826
	anti	0.380	0.374	0.772	0.530	0.817	0.341	0.407	0.399	0.768	0.538	0.816
2–(3′–thienyl) furan (3)	*syn*	0.375	0.372	0.772	0.528	0.819	0.345	0.407	0.400	0.765	0.535	0.810
	anti	0.377	0.373	0.772	0.527	0.818	0.344	0.410	0.402	0.764	0.535	0.809
3–(3′–thienyl) furan (4)	*syn*	0.373	0.372	0.781	0.526	0.820	0.317	0.403	0.396	0.775	0.532	0.825
	anti	0.375	0.372	0.781	0.526	0.820	0.318	0.403	0.397	0.775	0.532	0.825

furan. [40] The following linear relationships for converting the bond orders to CS [11] and CO [41] bond lengths have been used :

$$L_{CS} = 1.829 - 0.262\ p_{CS}$$

$$L_{CO} = 1.437 - 0.165\ p_{CO}$$

It is clearly seen that both ring systems have geometries very similar to those of furan and thiophene; the overall difference between two sets of values being only 0.007 Å.

Table 5

Calculated bond lengths in 2-(2′-thienyl) furan (1)

BOND	BOND	LENGTH (Å)
1–2	1.730	(1.718)^{a}
1–5	1.730	(1.718)^{a}
2–3	1.380	(1.370)^{a}
2–2′	1.450	(1.423)
3–4	1.421	(1.423)^{a}
4–5	1.370	(1.370)^{a}
1′–2′	1.369	(1.371)^{b}
1′–5′	1.370	(1.371)^{b}
2′–3′	1.381	(1.361)
3′–4′	1.420	(1.431)
4′–5′	1.372	(1.361)

a) Bond distances of thiophene from Ref. 32
b) Bond distances of furan from Ref. 40.

---

[40] B. Bak, D. Christensen, W. B. Dixon, L. Hansen-Nygaard, J. M. Anderson and M. Schottländer, *J. Mol. Spectroscopy*, **9**, 124 (1962).

[41] Adapted from G. Häfelinger, *Chem. Ber.*, **103**, 2922 (1970).

Charge densities are reported in Table 6. Oxygen and sulphur each contribute two electrons to the π system, and the charge densities on oxygen and sulphur acquire positive charges in every case. The acquired positive charge is smaller on oxygen than sulphur, due to a larger value of the ionization potential for oxygen. In other words, the π electrons of oxygen are more firmly bound than those on sulphur. The charge densities on carbon atoms are pretty evenly distributed and carbon atoms acquire negative charge in every case.

Table 6

π-Electron Densities

MOLECULE	CONFORMATION	II – ELECTRON DENSITIES									
		1	2	3	4	5	5′	4′	3′	2′	1′
2–(2′–thienyl) furan (*1*)	*syn*	1.801	1.052	1.050	1.044	1.063	1.053	1.058	1.054	1.056	1.770
	anti	1.793	1.047	1.058	1.048	1.063	1.049	1.067	1.061	1.052	1.762
3–(2′–thienyl) furan (*2*)	*syn*	1.795	1.042	1.058	1.047	1.067	1.053	1.066	1.056	1.059	1.751
	anti	1.794	1.040	1.062	1.049	1.066	1.053	1.070	1.061	1.050	1.756
2–(3′–thienyl) furan (*3*)	*syn*	1.798	1.043	1.051	1.059	1.063	1.056	1.061	1.060	1.045	1.766
	anti	1.796	1.048	1.056	1.054	1.059	1.055	1.063	1.062	1.044	1.763
3–(3′–thienyl) furan (*5*)	*syn*	1.797	1.059	1.047	1.045	1.065	1.058	1.060	1.050	1.059	1.759
	anti	1.797	1.054	1.047	1.045	10.65	1.058	1.060	1.050	1.059	1.759

Revue Roumaine de Chimie, **18**, *1*, 99–109 (1973)

ELECTRONIC STRUCTURE AND TRANSITIONS OF 1, 2, 3-TRIMETHOXYACRIDINE

M. VLASSA, MARIA IONESCU

Institute of Chemistry, Str. Donath 59–65, Cluj, Romania

and

J. FABIAN

Department of Chemistry, Technical University Dresden, The German Democratic Republic

Received May 12, 1972

The reactivity indices (π-electron density, π-bond order, free valence index, superdelocalizability index), the bond lengths and the electronic transition (singlet-singlet, singlet-triplet and triplet-triplet) of 1,2,3-trimethoxyacridine (I) and of parent compound acridine, were computed by a SCF–LCI* method. The calculated electronic energies are in good agreement with experimental data.

INTRODUCTION

In connection with current investigation on 1, 2, 3-trimethoxyacridine derivatives [1,2] we calculated the π-electronic transitions and the reactivity of 1, 2, 3-trimethoxyacridine (I). For comparison, the π-electronic structure and electronic transitions of the unsubstituted compound, acridine, **were also computed.

A better knowledge of the physical properties might be important in order to understand the chemical and photochemical behaviour of compound I.

The reactivity is discussed by means of π-reactivity indices. The limits of such a consideration are well known. Among the excited states only the states resulting from $\pi - \pi^*$ transitions were calculated.

METHOD OF CALCULATION

The calculations were performed by the SCF–LCI(PPP) method. For computing the transition energies, the interactions between the monoexcited configurations were set up from HMO and SCF functions. Those configurations which use electronic transitions between the four highest occupied and the four lowest virtual molecular orbitals were selected.

---

* LCI = Limited configuration interaction.

** The following abbreviations were used in the text : A for acridine, and TMA for 1, 2, 3-trimethoxyacridine.

[1] M. Ionescu and M. Vlassa, *Rev. Roumaine Chim.*, **16**, 743 (1971).

[2] M. Ionescu, M. Vlassa and I. Goia, *J. prakt. Chem.*, **314**, 441 (1972).

The PPP calculations were performed by following the Mataga-Nishimoto procedure [3] for two center repulsion integrals. This approximation is successfully used in the calculation of the electronic distribution, ionization potential and spectral data of heterocyclic compounds.

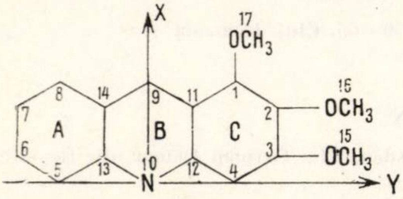

I

Fig. 1. — Coordinate system used for 1,2, 3,-trimethoxyacridine (I).

The π-electronic system of the 1, 2, 3-trimethoxyacridine molecule consists of a number of 20 π-electrons delocalized over 17 centers. The molecule is assumed to be planar (C_s symmetry group) with an idealized bond distance of $r_{CC} = r_{CN} = r_{CO} = 1.40$ Å. The coordinate system used is given in figure 1.

For resonance integrals we chose the following value: $\beta_{CC} = \beta_{CN} = \beta_{CO} = -2.38$ eV (PPP/1). For comparison, with the data which will be published in a forthcoming paper on the N-oxides, an enlarged value for β_{CN}($\beta_{CN} = -2.636$ eV) was used in a second computation (PPP/2). This value was derived from π-bond order p_{CN} of acridine-N-oxide given by Mantsch and co-workers using the following linear β/p relations[4]:

$$\beta_{CC} = -0.51\,p - 2.04 \text{ eV} \quad (1)$$

$$\beta_{CN} = -0.53\,p - 2.34 \text{ eV} \quad (2)$$

The one center repulsion integrals $\gamma_{\mu\mu}$ and the core integrals U_μ were taken from the literature [5,6]: $\gamma_{CC} = 8.25$ eV, $\gamma_{NN} = 9.50$ eV, $\gamma_{OO} = 12.60$ eV; $U_C = 8.72$ eV, $U_N = 11.72$ eV and $U_O = 20.72$ eV.

An initial set of orthogonalized eigenvectors obtained by a Hückel approximation ($h_{\dot{N}} = 0.5$, $h_{\ddot{O}} = 2$; $k_{CC} = k_{CO} = 1$ and $k_{CN} = 1.1075$) were taken to construct the self-consistent molecular orbitals.

The molecular orbitals obtained from simple Hückel and PPP's procedures, respectively, were used then as a basis for a configuration interaction treatment (HMO—LCI with the same parameters as for PPP/2).

---

[3] K. Nishimoto and N. Mataga, *Z. phys. Chem.* (Frankfurt), **12**, 335 (1957).

[4] K. Nishimoto and L. Forster, *Theor. Chim. Acta*, **5**, 155 (1966); *Chem. Phys.*, **71**, 409 (1967).

[5] H. H. Mantsch, W. Seiffert and V. Zanker, *Rev. Roumaine Chim.*, **14**, 125 (1969).

[6] F. Dörr, C. Hohlneicher and S. Schneider, *Ber. Bunsengesellscaft Phys. Chem.* **70**, 803 (1966).

The π-electronic system of the acridine molecule consists of a number of 14 π-electrons, delocalized over 14 centers. The molecule is also planar (C_{2V} symmetry group), the bond distances r_{CC} and r_{CN} were both taken as 1.40 Å. The same coordinate system was considered as for 1, 2, 3-trimethoxyacridine (I). The electronic structure of acridine was calculated only with parameters used in the PPP/1 computation.

The input data used in these calculations are shown in Table 1.

Table 1

The input data for acridine (1 – 14) and for 1, 2, 3-trimethoxyacridine (1 – 17)

Center	Coordinate		Ionization potential eV	Electron affinity eV	Number of contributing electrons
	X	Y			
1	2.420	2.800	8.72	0.47	1
2	3.630	2.100	8.72	0.47	1
3	3.630	0.700	8.72	0.47	1
4	2.420	0.000	8.72	0.47	1
5	2.420	0.000	8.72	0.47	1
6	3.630	0.700	8.72	0.47	1
7	3.630	0.700	8.72	0.47	1
8	2.420	2.800	8.72	0.47	1
9	0.000	2.800	8.72	0.47	1
10	0.000	0.000	11.72	2.22	1
11	1.210	2.100	8.72	0.47	1
12	1.210	0.700	8.72	0.47	1
13	1.210	0.700	8.72	0.47	1
14	1.210	2.100	8.72	0.47	1
15	4.840	0.000	20.72	12.00	2
16	4.840	2.800	20.72	12.00	2
17	2.420	4.200	20.72	12.00	2

The CC, CO and CN bond lengths were estimated by two methods :

a) using the relations given by Nishimoto and Forster, [4] which assume that the differences between the double bond distances are all 1.80 Å :

$$r_{CC} = 1.517 - 0.180\ p \text{ Å} \quad (3)$$

$$r_{CN} = 1.451 - 0.180\ p \text{ Å} \quad (4)$$

$$r_{CO} = 1.410 - 0.180\ p \text{ Å} \quad (5)$$

b) using Jenkins' relation [7] :

$$d = \frac{1}{A + B(1 + p)} \text{ Å} \qquad (6)$$

where the constants A/B are 0.2868/0.1334 for CC bonds and 0.316/0.144 for CN bonds. A good agreement was observed for the values of the CC and CN bond lengths calculated by these two procedures.

---

[7] H. O. Jenkins, *J. Amer. Chem. Soc.*, **77**, 3168 (1955).

The calculations were carried out on an Elliot 503 b computer with an autocode program.

RESULTS AND DISCUSSION

The bond order (p_μ), the π-electronic density (q_μ), the bond length ($r_{\mu\mu}$), the free valence index (F_μ), as well as the superdelocalizability index (S_μ) were obtained for 1, 2, 3-trimethoxyacridine (I) and for acridine starting from these coefficients and orbital energies.[8] The results of our calculations are shown in Tables 2–6.

Table 2

Calculated electron density for acridine (q_μ^{A}) and for 1, 2, 3-trimethoxyacridine (q_μ^{TMA}) · (PPP/1)

Center	q_μ^{A}			q_μ^{TMA}			$q_\mu = q_\mu^{TMA} - q_\mu^{A}$		
	S_0	S_1 S_2	T_1 T_2	S_0	S_1 S_2	T_1 T_2	S_0	S_1 S_2	T_1 T_2
1	0.992	0.971	0.975	0.999	0.892	0.966	0.007	−0.079	−0.009
		1.040	0.989		1.045	1.015		0.005	0.050
2	1.008	0.979	0.971	1.056	0.968	1.006	0.048	−0.011	0.035
		0.937	1.015		0.972	0.991		0.035	−0.024
3	0.978	0.996	1.006	0.959	1.000	1.008	−0.02	0.004	0.002
		0.972	0.976		0.914	1.006		−0.058	0.030
4	1.005	0.946	0.960	1.094	0.919	0.991	0.089	−0.027	0.031
		1.034	0.952		1.105	1.106		−0.029	0.154
5	1.005	0.946	0.960	1.007	1.027	0.973	0.002	0.081	0.013
		1.034	0.952		1.040	0.976		0.006	0.024
6	0.978	0.994	1.006	0.984	1.022	1.009	0.006	0.028	0.003
		0.972	0.976		1.008	1.022		0.036	0.046
7	1.008	0.979	0.971	1.015	1.018	0.990	0.007	0.039	0.019
		0.937	1.015		0.952	0.970		0.015	−0.045
8	0.992	0.971	0.750	0.995	1.044	1.000	0.003	0.073	0.250
		1.040	0.989		1.055	1.010		0.015	0.021
9	0.906	1.040	1.018	0.920	1.014	1.069	0.014	−0.026	0.051
		1.077	1.027		1.118	1.040		0.041	0.013
10	1.299	1.275	1.270	1.311	1.333	1.293	0.012	0.058	0.023
		1.383	1.311		1.399	1.333		0.016	0.019
11	1.015	1.015	1.015	1.038	1.056	1.055	0.023	0.041	0.040
		0.950	1.012		0.994	1.054		0.044	0.042
12	0.901	0.936	0.930	0.900	0.939	0.928	−0.001	0.003	−0.002
		0.837	0.887		0.852	0.848		0.015	−0.039
13	0.900	0.936	0.930	0.904	0.934	0.935	0.004	−0.002	0.005
		0.837	0.887		0.860	0.866		0.023	−0.021
14	1.015	1.015	1.015	1.023	1.016	1.020	0.008	0.001	0.005
		0.950	1.012		0.963	1.029		0.013	0.017
15	—	—	—	1.927	1.927	1.929	—	—	—
					1.892	1.931			
16	—	—	—	1.940	1.912	1.921	—	—	—
					1.899	1.903			
17	—	—	—	1.929	1.889	1.907	—	—	—
					1.931	1.900			

---

[8] L. Salem, "The Molecular Orbital Theory of Conjugated System", W. A. Benjamin Inc., New York, 1966.

Table 3

Calculated reactivity indices of 1, 2, 3-trimethoxyacridine (I)

Center	π-electron density		Free valence number							Superdelocalizability index *		
	HMO	PPP/2	HMO	PPP/2	PPP/1					S_E	S_N	S_R
					S_0	S_1	S_2	T_1	T_2			
1	0.979	1.000	0.238	0.263	0.263	0.345	0.306	0.306	0.435	—	—	—
2	0.046	1.056	0.231	0.245	0.245	0.290	0.349	0.288	0.348	—	—	—
3	0.934	0.961	0.185	0.202	0.205	0.247	0.321	0.246	0.239	—	—	—
4	1.163	1.095	0.535	0.485	0.478	0.601	0.507	0.618	0.603	0.728	0.268	0.498
5	1.026	1.008	0.463	0.464	0.457	0.491	0.494	0.531	0.644	0.505	0.420	0.463
6	0.983	0.986	0.408	0.408	0.408	0.438	0.502	0.443	0.411	0.330	0.410	0.371
7	1.016	1.015	0.409	0.409	0.408	0.433	0.525	0.446	0.511	0.412	0.370	0.394
8	0.985	0.996	0.458	0.460	0.460	0.494	0.496	0.528	0.640	0.406	0.489	0.447
9	0.920	0.928	0.510	0.530	0.509	0.661	0.620	0.658	0.583	0.399	0.646	0.523
10	1.253	1.288	—	—	—	—	—	—	—	0.544	0.424	0.489
11	1.040	1.037	0.130	0.120	0.128	0.138	0.218	0.135	0.144	—	—	—
12	0.956	0.905	0.121	0.186	0.130	0.156	0.245	0.137	0.219	—	—	—
13	0.952	0.909	0.119	0.129	0.126	0.141	0.244	0.137	0.188	—	—	—
14	1.019	1.022	0.110	0.113	0.111	0.127	0.215	0.121	0.121	—	—	—
15	1.902	1.927	—	—	—	—	—	—	—	—	—	—
16	1.920	1.939	—	—	—	—	—	—	—	—	—	—
17	1.906	1.929	—	—	—	—	—	—	—	—	—	—

* Superdelocalizability index was calculated using only HMO coefficients and energy.

From the data in the Table 2 it can be seen how the presence of the methoxy groups (with + *M* effect) changes the electron density distribution relatively to the parent compound, acridine. The electron density of the nitrogen atom increases, the 1, 2, 3-trimethoxyacridine molecule being more basic than the parent compound (see tables 2 and 3).

For 1, 2, 3-trimethoxyacridine (I) we could verify the rule observed by Tiutulkov and co-workers,[9] namely that the basicity of the excited singlet state (S_1) is greater and that of the excited triplet state (T_1) is lower than the one of the ground state (see Table 2). For acridine our calculations pointed out that the excited singlet state (S_1) has a lower basicity than the ground state ($q_{\mathrm{N}}^{\mathrm{O}} = 1.299$ and $q_{\mathrm{N}}^{S_1} = 1.275$; Tiutulkov[9] found $q_{\mathrm{N}}^{\mathrm{O}} = 1.118$ and $q_{\mathrm{N}}^{S_1} = 1.135$), however the excited triplet state (T_1) has a lower basicity than the ground state.

The electron density of the 1, 2, 3-trimethoxyacridine molecule is greater than of the parent compound acridine (see Table 2), especially in the *C* and *B* rings (see Fig. 1), with the exception of the C_3 ring atom. The influence of the three methoxy groups in the vicinal positions 1, 2 and 3 lowers the electron density at C_3 and increases it mostly at $C_4(q_4 = +0.089)$. Since the electron density is increased in 1, 2, 3-trimethoxyacridine (I), the electrophilic substitution takes place easier than in the case of acridine (especially at C_4, $F_A = 0.458$ and $F_{\mathrm{TMA}} = 0.601$).

---

[9] N. Tiutulkov, F. Fratev and P. Petrov, *Theor. Chim. Acta*, **8**, 236 (1967).

Table 4

Calculated free valence number of acridine

Center	Free valence number					
	HMO	PPP/1				
		S_0	S_1	S_2	T_1	T_2
1	0.460	0.462	0.537	0.498	0.550	0.689
2	0.409	0.408	0.452	0.452	0.461	0.478
3	0.409	0.410	0.456	0.466	0.445	0.471
4	0.460	0.458	0.546	0.492	0.546	0.679
5	0.460	0.458	0.546	0.492	0.546	0.679
6	0.409	0.410	0.456	0.466	0.445	0.471
7	0.409	0.408	0.452	0.452	0.461	0.478
8	0.460	0.462	0.537	0.498	0.550	0.681
9	0.520	0.516	0.674	0.610	0.684	0.576
10	—	—	—	—	—	—
11	0.106	0.109	0.121	0.235	0.121	0.148
12	0.106	0.128	0.142	0.282	0.138	0.172
13	0.106	0.128	0.142	0.282	0.138	0.172
14	0.106	0.109	0.121	0.235	0.121	0.148

The nucleophilic substitution which is characteristic for the C_9 position, has the same probability for both molecules ($F_A = 0.516$ and $F_{TMA} = 0.509$).

By inspecting the reactivity indices for the carbon atoms of compound I (see Table 3), the tendency to electrophilic substitution decreases in the order : $4 > 5 > 7$ (for acridine this order is $2 = 7 > 4 = 5$ [10,11] identical with our results, see table 4).

As with acridine, the position 9 remains the most probable center for nucleophilic and radicalic substitution ; the reactivity of the carbon atoms towards nucleophilic substitution is $9 > 8 > 6$.

The electron density of I has the same characteristics for the PPP/2 computation as for the simple Hückel method (Tables 3 and 5).

As shown by the free valence values the reactivity is increased in the excited singlet and triplet states, while the bond lengths are not changed.

The bond lengths calculated for acridine in this work, are in good agreement with the bond lengths of the acridine molecule as determined by x-ray diffraction [12] (see Table 5).

The bond lengths and the bond orders for the ground state and for the excited states (S_1, S_2, T_1 and T_2) of 1, 2, 3-trimethoxyacridine (I) are listed in Table 6.

The computed energies for the singlet-singlet, singlet-triplet and triplet-triplet transitions of acridine and of 1, 2, 3-trimethoxyacridine (I) are summarized in Tables 7—10, along with their transition moments, the direction of the transition moments, the oscillator strengths, the configurational weights as well as the experimental values.

---

[10] C. A. Coulson, P. Daudel and R. Daudel, *Bull. Soc. chim. France*, **1948**, 1181.

[11] H. C. Longuet-Higgins and C. A. Coulson, *J. Chem. Soc.*, **1949**, 971.

[12] P. C. Philips, *Acta Cryst.*, **9**, 237 (1956).

Table 5

Calculated bond order and bond lengths of acridine

Bond	Bond order						Bond lengths						
	HMO	PPP/1					HMO	PPP/1					Experimental data [12]
	S_0	S_0	S_1	S_2	T_1	T_2	S_0	S_0	S_1	S_2	T_1	T_2	
1–2	0.606	0.583	0.513	0.523	0.519	0.559	1.342	1.346	1.359	1.356	1.358	1.350	1.34
2–3	0.485	0.500	0.512	0.381	0.517	0.542	1.430	1.427	1.425	1.448	1.424	1.419	1.43
3–4	0.606	0.608	0.529	0.561	0.524	0.578	1.408	1.408	1.422	1.416	1.424	1.413	1.39
4–5	0.606	0.529	0.608	0.661	0.524	0.574	1.408	1.408	1.422	1.416	1.424	1.413	1.39
5–6	0.485	0.500	0.512	0.381	0.517	0.542	1.430	1.427	1.425	1.448	1.424	1.419	1.43
6–11	0.535	0.521	0.565	0.541	0.557	0.459	1.421	1.423	1.415	1.420	1.417	1.434	1.43
7–8	0.737	0.753	0.621	0.699	0.628	0.594	1.384	1.381	1.405	1.391	1.404	1.428	1.37
8–9	0.586	0.569	0.655	0.504	0.659	0.677	1.411	1.415	1.399	1.426	1.398	1.397	1.42
11–12	0.737	0.753	0.620	0.699	0.628	0.594	1.384	1.381	1.405	1.391	1.404	1.428	1.37
9–10	0.737	0.755	0.625	0.679	0.612	0.587	1.384	1.381	1.404	1.395	1.407	1.411	1.37
12–13	0.586	0.569	0.655	0.504	0.659	0.667	1.411	1.421	1.399	1.426	1.398	1.397	1.42
13–14	0.737	0.755	0.625	0.679	0.612	0.587	1.384	1.381	1.404	1.395	1.407	1.411	1.37
1–6	0.606	0.583	0.513	0.528	0.519	0.559	1.342	1.346	1.359	1.356	1.358	1.350	1.34
2–7	0.535	0.521	0.565	0.541	0.558	0.459	1.421	1.423	1.415	1.420	1.417	1.434	1.43
3–10	0.535	0.515	0.570	0.555	0.570	0.464	1.421	1.424	1.414	1.417	1.414	1.433	1.43
5–14	0.535	0.515	0.570	0.555	0.570	0.464	1.421	1.424	1.414	1.417	1.414	1.433	1.43

The data in the Tables 7–10 and in Fig. 2 show a good agreement between the calculated transition energies and the experimental values. The values of the angle of the transition moments are also in agreement with the Platt classification of these bands (^1L_a, ^1L_b and ^1B_b).

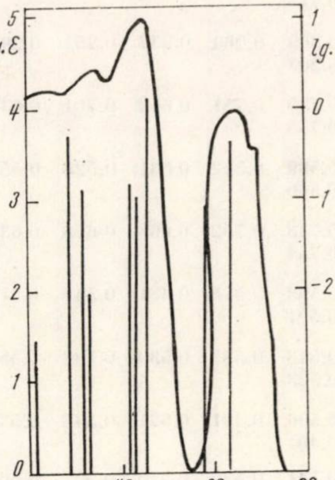

Fig. 2. — Comparison of experimental and calculated spectral characteristics of 1, 2, 3-trimethoxyacridine (log ε = log f + 4 ; lit. [13])

The calculated and experimental data point out that the long wave length absorptions present a red shift in comparison with the parent

---

[13] I. Fabian, A. Melhorn and R. Zahradnik, *J. Phys. Chem.*, **73**, 3975 (1968).

Table 6

Calculated bond order and bond lengths of 1, 2, 3-trimethoxyacridine

Bond	Bond order						Bond lengths					
	HMO/ PPP/2	S_0 (PPP/1)	S_1 (PPP/1)	S_2 (PPP/)	T_1 (PPP/1)	T_2 (PPP/1)	HMO/ PPP/2	S_0 (PPP/1)	S_1 (PPP/1)	S_2 (PPP/1)	T_1 (PPP/1)	T_3 (PPP/1)
1−2	0.593 0.593	0.580	0.530	0.496	0.532	0.521	1.358 1.344	1.347	1.315	1.362	1.345	1.357
2−3	0.470 0.483	0.487	0.516	0.403	0.512	0.525	1.439 1.430	1.429	1.424	1.444	1.425	1.422
3−4	0.627 0.628	0.626	0.558	0.566	0.553	0.576	1.408 1.404	1.404	1.417	1.410	1.417	1.413
4−5	0.596 0.601	0.597	0.513	0.556	0.521	0.573	1.422 1.409	1.409	1.425	1.413	1.423	1.414
5−6	0.486 0.499	0.504	0.522	0.404	0.521	0.512	1.436 1.427	1.426	1.423	1.444	1.423	1.425
6−11	0.534 0.513	0.523	0.578	0.535	0.563	0.452	1.427 1.425	1.423	1.413	1.420	1.416	1.436
7−8	0.685 0.724	0.719	0.601	0.637	0.602	0.659	1.398 1.387	1.388	1.409	1.402	1.409	1.398
8−9	0.544 0.533	0.535	0.619	0.454	0.623	0.574	1.424 1.421	1.421	1.406	1.435	1.405	1.414
9−10	0.683 0.715	0.654	0.535	0.629	0.552	0.518	1.398 1.388	1.388	1.421	1.404	1.418	1.424
10−17	0.305 0.263	0.264	0.332	0.251	0.297	0.292	1.355 1.363	1.362	1.350	1.365	1.356	1.357
11−12	0.735 0.755	0.751	0.663	0.701	0.638	0.636	1.338 1.381	1.382	1.398	1.391	1.402	1.402
12−13	0.589 0.569	0.572	0.631	0.528	0.551	0.655	1.423 1.415	1.414	1.403	1.422	1.400	1.399
13−14	0.733 0.754	0.752	0.668	0.678	0.635	0.566	1.390 1.381	1.382	1.397	1.395	1.403	1.415
1−6	0.593 0.591	0.578	0.481	0.548	0.511	0.580	1.358 1.345	1.347	1.322	1.352	1.359	1.346
2−7	0.548 0.523	0.535	0.530	0.588	0.550	0.469	1.431 1.423	1.421	1.422	1.411	1.418	1.433
3−10	0.506 0.491	0.491	0.521	0.545	0.532	0.487	1.432 1.429	1.429	1.423	1.419	1.423	1.429
5−14	0.541 0.519	0.520	0.570	0.557	0.569	0.526	1.426 1.424	1.423	1.414	1.417	1.415	1.422
8−15	0.318 0.273	0.274	0.265	0.320	0.261	0.259	1.354 1.367	1.361	1.360	1.352	1.363	1.357
9−16	0.273 0.239	0.238	0.288	0.300	0.269	0.292	1.361 1.361	1.367	1.358	1.356	1.362	1.363

Table 7

Calculated and experimental singlet-singlet transition energies of 1, 2, 3-trimethoxyacridine *

N°	Transition energies (eV)			Transition moment M (Å)	Oscillator strength *f*	Angle of the transition	Configurational weight %	Experimental values of the transition energies (eV)
	HMO	PPP/1	PPP/2	PPP/1	PPP/1	PPP/1	PPP/1	
1	2.94	2.87	2.93	1.006	0.254	268°33′34″	10−11 : 96.61	3.17
2	3.67	3.50	3.56	1.061	0.345	5°10′13″	9−11 : 80.87	3.43
3	4.00	3.89	3.97	0.538	0.098	138°45′07″	8−11 : 96.29	
4	4.78	4.63	4.66	2.036	1.681	0°21′43″	10−12 : 75.77	4.76
5	4.89	4.76	4.79	0.059	0.131	138° 4′29″	10−13 : 93.21	
6	5.11	4.91	4.98	0.695	0.208	182°52′26″	7−11 : 60.18	5.33
7	5.55	5.43	4.43	0.138	0.009	240° 7′35″	10−14 : 60.77	
8	5.67	5.50	5.54	0.594	0.170	195°52′33″	9−13 : 99.22	
9	5.89	5.73	5.75	1.052	0.556	295° 6′25″	9−12 : 70.26 10−14 : 25.13	6.01
10	6.27	6.14	6.14	0.090	0.004	74°10′55″	8−12 : 56.34 9−13 : 26.78	
11	6.43	6.30	6.32	0.980	0.535	262°50′49″	8−13 : 74.64	
12	6.56	6.34	6.42	0.521	0.151	147°40′50″	9−14 : 58.36	

* The symmetry for all the excited states is *A′*, the transition being allowed for both *x* and *y* polarization.

Table 8

Calculated and experimental singlet-singlet transition energies of acridine. (PPP/1)

N°	Transition energies (eV)	Transition moment M (Å)	Oscillator strength *f*	Angle of the transition	Configurational weight %	Experimental values of the transition energies [14] (eV)
1	3.10	1.081	0.318	270° 0′5″	7−8 : 97.61	3.28
2	3.66	0.882	0.249	180° 0′0″	6−8 : 78.08	3.48
3	4.04	0.350	0.043	0° 0′14″	5−8 : 98.06	
4	4.84	2.233	2.111	180° 0′0″	7−9 : 78.42	4.98
5	4.88	0.597	0.152	180° 0′0″	7−10 : 96.97	5.14
6	5.14	0.057	0.002	90° 1′53″	4−8 : 46.03	
7	5.65	0.142	0.001	89°59′25″	4−8 : 47.96 7−11 : 29.93	
8	5.74	0.101	0.005	90° 0′25″	6−10 : 31.91 7−11 : 27.39	
9	5.99	0.900	0.423	270° 0′4″	6−9 : 72.30	
10	6.43	0.131	0.001	269°59′11″	5−9 : 56.53 6−10 : 42.28	
11	6.53	0.326	0.061	239°59′59″	6−11 : 63.12	
12	6.57	1.274	0.935	269°59′59″	5−10 : 81.87	

---

[14] V. Zanker and W. Flügel, *Z. Naturforsch.*, **19**b, 376 (1964).

Table 9

Calculated singlet-triplet and triplet-triplet transition energies of 1,2,3 – trimethoxyacridine

N°	Singlet-triplet transition energies (eV)			Triplet-triplet transition energies (PPP/1) (eV)				
	HMO	PPP/1	PPP/2	Energies (eV)	Transition moment M (Å)	Oscillator stregth f	Angle of the transition	Configurational weight %
1	1.78	1.74	1.82	1.12	0.746	0.055	195°22′47″	8–11 : 46.15
2	2.91	2.86	2.88	1.26	0.215	0.005	283°11′18″	9–11 : 68.65
3	3.06	3.00	3.06	2.20	0.656	0.083	178°11′9″	10–12 : 64.73
4	3.98	3.94	4.01	2.31	0.456	0.042	293°43′32″	7–11 : 40.02
5	4.19	4.04	4.17	2.50	1.396	0.426	202°59′46″	7–11 : 19.02
6	4.24	4.23	4.21	2.64	1.453	0.488	166°59′38″	10–13 : 25.16
7	4.39	4.40	4.43	3.02	0.184	0.009	105°51′44″	9–12 : 70.15
8	4.81	4.76	4.77	3.57	0.310	0.030	69°22′22″	8–12 : 77.14
9	5.32	5.31	5.30	3.64	0.340	0.037	96°2′50″	9–13 : 50.72
10	5.48	5.38	5.41	3.81	0.102	0.009	182°39′0″	9–14 : 58.10 7–13 : 26.09
11	5.80	5.55	5.69	4.22	0.258	0.025	258°26′42″	8–13 : 53.55 10–14 : 32.66
12	5.96	6.03	6.00					

Table 10

Calculated singlet-triplet and triplet-triplet transition energies of acridine (PPP/1)

N°	Singlet-triplet transition energies (eV)	Triplet-triplet transition energies (eV)	Transition moment M (Å)	Oscillator strength f	Angle of the transition	Configurational weight %
1	1.78	1.20	0.603	0.038	0°0′1″	5–8 : 64.71 7–10 : 30.12
2	2.98	1.41	0.199	0.005	0°0′18″	6–8 : 94.90
3	3.19	2.24	0.426	0.036	359°59′59″	7–9 : 77.63
4	4.02	2.50	0.681	0.131	269°59′59″	4–8 : 39.61 7–11 : 25.73
5	4.29	2.57	0.177	0.007	269°59′38″	7–11 : 35.52 4–8 : 32.38
6	4.36	2.73	1.945	0.904	0°0′0″	7–10 : 46.96 5–8 : 29.36
7	4.52	3.09	0.159	0.007	269°59′56″	6–9 : 80.36
8	4.88	3.75	0.037	0.000	90°1′18″	5–9 : 59.70
9	5.53	3.83	0.328	0.036	269°59′49″	6–10 : 38.79 4–8 : 25.59
10	5.61	3.97	0.043	0.001	0°0′37″	6–11 : 66.59
11	5.76	4.53	0.339	0.044	89°59′44″	5–10 : 53.82 7–11 : 37.71
12	6.14					

compound, acridine. At shorter wave lengths a very intense transition follows, which in comparison with the corresponding transition of the parent compound experience a hypsochromic shift.

Table 11 shows the dipole moments of acridine and for 1, 2, 3-trimethoxyacridine (I). The calculated value for the S_0 state of acridine is in good agreement with the experimental value.[15] The direction of the calculated dipole moment is 270°0′8″ for acridine (towards the nitrogen atom) and 228°58′40″ for compound I (towards the $N-C_{13}$ bond).

Table 11

Calculated dipole moment for acridine and 1, 2,3-trimethoxyacridine

Compound	State	Dipole moment (D)	Experimental data
1, 2, 3-trimethoxyacridine	S_0	3.884	
	S_1	9.441	
	S_2	6.580	
	T_1	4.850	
	T_2	4.407	
acridine	S_0	1.856	1.940 [15]
	S_1	0.829	
	S_2	1.457	
	T_1	1.159	
	T_2	0.299	

The ability of a molecule to function as donor in a donor-acceptor complex is measured by the ionization potential. The molecular ionization potential and the electron affinity is related to the energy of the highest occupied (HOMO) and lowest virtual orbital energy (LVMO), respectively.[16] When one-center integral is used, the ionization potential equals the amount of HOMO energy :

$$IP = |e_{\mathrm{HOMO}}|$$

and the electron affinity equals the amount of LVMO energy :

$$EA = |e_{\mathrm{LVMO}}|$$

For 1, 2, 3-trimethoxyacridine (I) $IP = 7.22$ eV and $EA = 1.93$ eV (PPP/1). Our calculations give for the ionization potential of acridine the value 7.71 eV (experimental value 7.70 eV[17]). This suggests that 1, 2, 3-trimethoxyacridine (I) has a lower electron affinity relatively to acridine ($2.24_{\mathrm{A}} - 1.93_{\mathrm{TMA}} = 0.31$ eV).

EXPERIMENTAL

The uv spectrum of 1, 2, 3-trimethoxyacridine (I) was recorded in hexane solution ($c = 0.00283$ mg/ml) on a Carl Zeiss Jena SPECORD spectrometer. 1, 2, 3-Trimethoxyacridine was prepared by a method reported in a previous paper.[2]

---

[15] Z. V. Puskareva and Z. J. Kokoşko, *Doklady Akad. Nauk S.S.S.R.*, **93**, 97 (1953).

[16] T. L. Kunii and H. Kuroda, *Theor. Chim. Acta*, **11**, 97 (1968).

[17] A. Terenin and T. Vilessova "Advances in Photochemistry", vol. 2, Interscience Publishers, New York, 1964, p. 385.

is in good agreement with the experimental value.[illegible] The direction of the [illegible] dipole moment is [illegible] for [illegible] (toward the nitrogen atom) and [illegible] for compound 1 [illegible].

[illegible]

[illegible]	[illegible]	[illegible]	[illegible]
[illegible]	[illegible]	[illegible]	[illegible]

The ability of a molecule to function as donor in a donor-acceptor complex is measured by the ionization potential. The molecular ionization potential and the electron affinity is related to the energy of the highest occupied (HOMO) and lowest virtual orbital energy (LVMO), respectively. If [illegible] is used, the ionization potential equals the minus of HOMO energy:

$$IP = -\varepsilon_{HOMO}$$

and the electron affinity equals the minus of LVMO energy:

$$EA = -\varepsilon_{LVMO}$$

For 1,3,5-trimethoxybenzene (1) IP = [illegible] eV and EA = [illegible] eV [illegible]. Our calculations give for the ionization potential of acridine the value [illegible] eV (experimental value 7.70 eV). This suggests that 1,3,5-trimethoxybenzene (1) has a lower electron affinity relatively to acridine ([illegible] = 0.41 eV).

EXPERIMENTAL

The UV spectrum of 1,3,5-trimethoxybenzene (1) was recorded in hexane solution [illegible]. 1,3,5-Trimethoxybenzene was [illegible] reported in a previous paper.[illegible]

[illegible]

[illegible] Theor. Chim. Acta, 11, 97 (1968).

[illegible] "Advances in Photochemistry", vol. 2, Interscience Publishers, New York, [illegible].

[illegible]

Revue Roumaine de Chimie, 18, *1*, 111–121 (1973)

RELATIONS CONCERNANT LA STRUCTURE ÉLECTRONIQUE ET LA RÉACTIVITÉ DE QUELQUES THIOAMIDES

FELICIA CORNEA *, CORNELIA FULEA * et A. O. FULEA **

* Laboratoire de Chimie organique, Faculté de Chimie, Université de Bucarest
** Laboratoire de Physique-Chimie des macromolécules, Faculté de Chimie, Université de Bucarest

Reçu le 12 fevrier 1972

Pour expliquer la manière dont la structure électronique détermine la réactivité de quelques thioamides, on a appliqué la méthode des orbitales moléculaires en utilisant l'approximation Hückel et la technique ω, pour neuf thioamides. Pour le groupement fonctionnel thioamidique et thioamidique protoné on a pris en considération les structures suivantes : $-C(:S)NH_2$; $-C(:NH)SH$; $-C(:\overset{+}{S}H)NH_2$ et $-C(:\overset{+}{N}H_2)SH$. Dans ce travail on utilise pour la première fois un système complet de paramètre pour ces formes :

$$\alpha_{\dot{S}} = \alpha + 0,5\beta \; ; \; \alpha_{\ddot{S}} = \alpha + \beta \; ; \; \alpha_{\overset{+}{S}} = \alpha + 1,5\,\beta$$

$$\beta_{C=S} = \beta_{C-S} = \beta_{C=\overset{+}{S}} = 0,6\beta \; ; \quad \alpha_{\dot{N}} = \alpha + 0,5\beta$$

$$\alpha_{\ddot{N}} = \alpha + 1,5\beta \; ; \; \alpha_{\overset{+}{N}} = \alpha + 2\beta \; ; \; \beta_{C=N} = \beta$$

$$\beta_{C-N} = 0,8\beta \; ; \; \beta_{C=\overset{+}{N}} = \beta \; ; \; \alpha_{CH_2,CH_3} = \alpha + 2\beta$$

$$\beta_{C-CH_2,\, C-CH_3} = 0,7\beta$$

On a calculé les niveaux d'énergie des électrons π, l'énergie de résonance et les diagrammes de charge, pour les quatre formes des thioamides étudiés. Compte tenu des données obtenues par calculs on estime la tautomérie des thioamides, l'orientation de la substitution électrophile par le groupement thioamidique et la capacité d'accepteur d'hydrogène.

1. INTRODUCTION

Les recherches effectuées dans le domaine des thioamides ont abordé, en particulier, le problème de la synthèse et de la réactivité de ces substances. Des études théoriques ont été aussi effectuées en utilisant la méthode des orbitales moléculaires.

Les méthodes de calcul présentent intérêt au cas où les résultats sont en bonne concordance avec les données obtenues par déterminations expérimentales.

Le modèle de Janssen[1] pour les dérivés thiocarbonyliques a conduit à de bons résultats , tant par la méthode HMO simple, que par la technique ω. On a obtenu une bonne concordance pour les énergies de transition $n \to \pi^*$ et $\pi \to \pi^*$ calculées et déterminées expérimentalement pour quelques dérivés thiocarbonyliques.[1-3] Aussi, autres propriétés, comme la force basique de quelques thioamides et dérivés de la thiourée,[4] les constantes de dissociation de quelques thiocétoacides,[5] déterminées expérimentalement sont-elles en concordance avec les résultats obtenus par calcul.

Sandström[6] a appliqué le modèle de Janssen aux thioacétamide, thiobenzamide et thioacrylamide. Pour les thioacétamide et thiobenzamide on a calculé les niveaux d'énergie, la distribution de la charge, l'ordre de liaison et l'énergie de transition $n \to \pi^*$ et $\pi \to \pi^*$ tant pour l'état fondamental, que pour l'état excité mais pour le thioacrylamide seulement pour l'état fondamental.

La force basique des thioamides a été discutée uniquement pour le thioacétamide, sans prendre en considération l'hyperconjugaison.

Dans la présente note on a effectué une étude théorique pour quelques thioamides qui peuvent être considérés comme premier terme d'une série, en utilisant la méthode HMO simple et la technique ω.

2. LE CHOIX DES PARAMÈTRES

Bien que d'autres paramètres aient été proposés pour les dérivés thiocarbonyliques,[7] le modèle de calcul proposé par Janssen est fréquemment utilisé grâce aux bons résultats obtenus.

Dans ce travail les paramètres de Janssen sont utilisés seulement pour les liaisons $C{=}S$ et $C{-}S$, vu que son travail[1] ne mentionne pas tous les paramètres nécessaires pour décrire les quatre structures possibles du groupement thioamidique. Pour les liaisons $C{=}\overset{+}{S}$, ont été employés les paramètres indiqués par Sandström,[6] tandis que pour les liaisons $C{-}N$, $C{=}N$ et $C{=}\overset{+}{N}$ les paramètres donnés dans plusieurs travaux de Streitwieser[8] et Pullman.[9] Dans la présente note nous avons employé pour la première fois, un système complet de paramètres pour les quatre formes du groupement thioamidique, dont les valeurs sont indiquées dans le tableau 1.

---

[1] M. J. Janssen, *Rec. Trav. chim.*, **79**, 1066 (1960).

[2] M. J. Janssen, et J. Sandström, *Tetrahedron*, **20**, 2339 (1964).

[3] M. J. Janssen, *Rec. Trav. chim.*, **79**, 464 (1960).

[4] M. J. Janssen, *Rec. Trav. chim.*, **81**, 650 (1962).

[5] M. J. Janssen, *Rec. Trav. chim.*, **82**, 931 (1963).

[6] J. Sandström, *Acta Chem. Scand.*, **16**, 1616 (1962).

[7] A. Mehlborn et J. Fabian, *Z. Chem.*, **5**, 420 (1965).

[8] A. Streitwieser, « Molecular Orbital Theory of Organic Chemists », Ch. 4 et 5, Wiley, New York, 1961.

[9] B. Pullman et A. Pullman, « Quantum Biochemistry », Chap. 3, Interscience Publishers, New York, Londres, 1963.

Les groupements $-CH_3$ et $-CH_2-$ ont été assimilés à un hétéroatome qui contribue avec une paire d'électrons au système conjugué. Ce modèle « hétéroatomique » de la hyperconjugaison a donné de bons résultats notamment pour les calculs effectués par la technique ω. [8]

Selon, la technique ω, l'intégrale coulombienne pour un atome r se modifie en fonction de la densité des électrons π à cet atome, q_r et un paramètre sans dimension ω, avec une valeur qui varie entre les limites de 0,33 à 1,8. Dans ce travail $\omega = 1{,}4$ — valeur fréquemment utilisée. Ainsi, l'intégrale coulombienne est définie par la relation :

Tableau 1

Paramètres utilisés pour les calculs dans la présente note

Liaison		h_x	k_x
N	$\mathrm{C-\underset{\vert}{\ddot{N}}-}$	1,5	0,8
	$\mathrm{-C=N-}$	0,5	1
	$\mathrm{C=\underset{\vert}{\overset{+}{N}}-}$	2	1
S	$\mathrm{C-S-}$	1	0,6
	$\mathrm{C=S}$	0,5	0,6
	$\mathrm{C=\overset{+}{S}-}$	1,5	0,6
CH_2, $CH_3=X$		2	0,7

$$\alpha_{r'} = \alpha_r + \omega(n_r - q_r)\beta_{CC}$$

où n_r représente le nombre d'électrons avec lequel l'atome participe à la conjugaison, et qui peut être 1 ou 2.

L'intégrale de résonance se modifie en fonction de la longueur de la liaison rs notée R_{rs} et est obtenue par la relation

$$\beta_{rs'} = \beta_{rs} \exp\left[-(R_{rs} - 1{,}397)/0{,}3106\right]$$

Les calculs ont été effectués à l'aide d'une machine de calcul IBM—360, conformément à un programme élaboré par P. Gund de l'Université de Massachusetts.

3. DISCUSSION DES RÉSULTATS

On a effectué des calculs pour les thioamides suivants : thioformamide I, thioacétamide II, phénylthioacétamide III, thiobenzamide IV, thioacrylamide V, cinnamthioamide VI, thio-urée VII, dithiobiuret VIII et dithiomalonamide IX, en considérant pour le groupement thioamidique et thioamide protoné les structures suivantes :

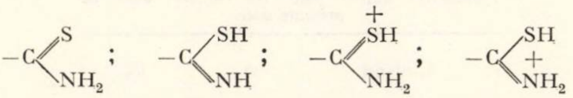

Ces thioamides ont été choisis tels que, sur la base des résultats obtenus, l'on puisse tirer des conclusions sur l'influence des différents radicaux ou groupes d'atomes par l'effet électromère sur la structure électronique du groupement thioamidique.

Compte tenu de toutes les données obtenues par calcul, on apprécie la tautomérie thioamide-isothioamide, l'orientation de la substitution électrophile par le groupement thioamidique lié d'un noyau benzénique et la capacité d'accepteur d'hydrogène des thioamides étudiés.

Pour les thioformamide, phénylthioacétamide, cinnamthioamide, dithiobiuret et dithiomalonthioamide on n'a pas fait jusqu'à présent de calculs par la méthode des orbitales moléculaires.

LA TAUTOMÉRIE THIOAMIDE – ISOTHIOAMIDE

La possibilité d'un équilibre tautomère dans le cas des thioamides est basée, au point de vue théorique, compte tenu de la structure du groupement thioamidique. L'élément structurel essentiel existant dans la molécule d'un thioamide est constitué par le système tricentrique, non saturé, et dans certaines conditions bien déterminées, ont lieu dans ce système des réarrangements par des migrations 1—3.

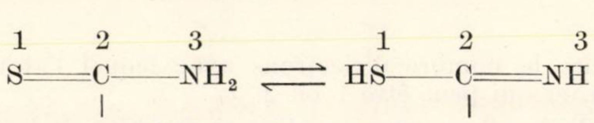

$$\overset{1}{S}=\underset{|}{\overset{2}{C}}-\overset{3}{NH_2} \rightleftharpoons \overset{1}{HS}-\underset{|}{\overset{2}{C}}=\overset{3}{NH}$$

Cette condition structurale qui conditionne l'apparition de la tautomérie dans la classe des thioamides a conduit à plusieurs études dans le but de mettre en évidence l'existence de cet équilibre, par la détermination de la présence de la forme thioamide ou isothioamide (soit par méthodes chimiques [10] soit par méthodes physiques).

Dans ce sens on donne quelques exemples. Par la comparaison des spectres UV de quelques dérivés convenablement substitués par les spectres des dérivés de référence, Hantzsch[11] montre que, généralement, les thioamides se trouvent sous forme thiocarbonylique. L'étude de 2-mercaptobenzothiazole[12] et de 2-thiopyridone[13] mettent en évidence que la forme thiocarbonylique est prédominante.

---

[10] A. E. A. Werner, *Sci. Proc. Roy. Dublin Soc.*, **22**, 387 (1941), *Chem. Abstr.*, **35**, 54159 (1941).

Les spectres en IR indiquent la forme thionique pour quelques dérivés de la thio-urée,[14] généralement, la forme mésomère $\overset{-}{S}\text{— —}C=\overset{+}{N}H_2$ pour les thioamides,[15] dans une quantité appréciable, et pour les thioamides cycliques[16] et le dithiobiuret,[17] on observe aussi une faible bande qui correspond au groupement —SH, fait qui, dans ce cas, est un argument plaidant pour la présence des deux formes tautomères dans les conditions données.

L'apparition de deux signaux dans le spectre RMN de la thioacétanilide est considérée par certains auteurs comme un argument pour l'existence des formes tautomères.[18] D'autres auteurs[19] considèrent cependant cette constatation comme un argument pour l'existence de deux isomères de type s-*cis* et s-*trans*.

Bien que les deux formes des thioamides (la forme thiocarbonylique et iminothiolique) n'eussent pas été séparées comme on a réussi pour d'autres substances qui présentent le phénomène de la tautomérie, souvent la forme isothioamidique est citée pour expliquer notamment le mécanisme de quelques réactions chimiques des thioamides.

Généralement on considère que l'équilibre est déplacé vers la forme thiocarbonylique.

La constante d'équilibre tautomère K_t[9] est déterminée par la relation :

$$RT \ln K_t = -\Delta G$$

où :

$$\Delta G = \Delta H - T\Delta S$$

Vu que dans le cas de la tautomérie n'a pas lieu un changement du degré d'ordre du système dans les deux formes tautomères, la constante d'équilibre sera déterminée par la variation d'enthalpie du système, fait qui peut être écrit :

$$\Delta H = \Delta H_{\text{conj}} + \Delta H_{H-\text{liaison}}$$

---

[11] A. Hantzsch, *Ber.*, **64**, 661 (1931).

[12] H. P. Koch, *J. Chem. Soc.*, **1949**, 401.

[13] M. H. Palmer, « The Structures and Reactions of Heterocyclic Compounds », Chap. II, Edward Arnold Ltd., Londres, 1967.

[14] A. K. Chibisov et Yu. A. Pentin, *Zhur. obshchei Khim.*, **1961**, 11.

[15] K. A. Jensen, *Acta Chem. Scand.*, **17**, 551 (1963).

[16] E. S. Levin et G. N. Rodionova, *Doklady Akad. Nauk S.S.S.R.*, **164**, 684 (1965); **172**, 607 (1967).

[17] K. A. Jensen, H. R. Baccaro et O. Buchardt, *Acta Chem. Scand.*, **17**, 163 (1963).

[18] A. J. Speziale et L. R. Smith, *J. Org. Chem.*, **28**, 3492 (1963).

[19] J. D. Rae, *Canad. J. Chem.*, **45**, 1 (1967).

Donc, pour voir quelle est la forme tautomère la plus stable, il faut calculer l'énergie de conjugaison pour les deux formes et la variation de l'énergie quand on passe de la liaison N—H à la liaison —S—H.

$\Delta H_{\text{conjugaison}}$ représente la différence entre les énergies de conjugaison ΔE, caractéristiques des deux formes tautomères :

$$\Delta H_{\text{conj}} = \Delta E_1 - \Delta E_2$$

où déloc = délocalisation

$$\Delta E = E_{\text{déloc}} - E_{\text{loc}}$$

Dans le tableau 2 sont données les valeurs ΔE en unités β pour les quatre formes des thioamides (non protoné et protoné), calculées tant par la méthode HMO simple que par la technique ω.

L'étude des données indiquées dans le tableau 2 révèle que pour la forme thiocarbonylique, ΔE présente, dans tous les cas, des valeurs plus grandes que pour la forme iminothiolique (isothioamidique). Il faut ajouter aussi le fait, que l'énergie de la liaison SH est plus petite avec — 0,7455 β respectivement 12,3 *k*cal/mole que la liaison N—H. [20]

Les valeurs obtenues par la technique ω pour les différences $\Delta E_{\text{thione}} - \Delta E_{\text{thiole}}$ sont plus grandes que celles obtenues par la méthode HMO simple.

L'analyse des données indiquées dans le tableau 2 permet d'observer l'influence de l'introduction d'un noyau benzénique, dans la molécule d'un thioamide sur la valeur ΔE. De cette manière si on compare les valeurs obtenues pour les thioamides II et III et aussi pour les thioamides V et VI, on observe une croissance de la valeur ΔE obtenue tant par la méthode HMO simple que par la technique ω pour la forme thioamidique et isothioamidique.

D'autre part, la comparaison du thioamide III avec IV révèle de petites différences entre les valeurs ΔE, fait qui indique une forte hyperconjugaison du groupement $-CH_2$ avec le reste de la molécule.

Le thioformamide I qui, généralement, peut être considéré comme un groupement thioamidique « pur » présente les plus petites valeurs ΔE, pour les deux formes (par les deux méthodes utilisées), comparativement aux autres thioamides.

Le thioacétamide II et la thio-urée VII peuvent être considérés comme dérivés de I par la substitution de l'atome d'hydrogène par le groupement $-CH_3$ et respectivement NH_2 ; les données du tableau 2 indiquent des valeurs plus grandes de ΔE pour VII que pour II.

Le dithiobiuret VIII et le dithiomalonamide IX peuvent être considérés comme dérivés de la thio-urée VII et du thioacétamide par la substitution d'un atome d'hydrogène par le groupement $CSNH_2$ ce qui conduit à une augmentation de la valeur ΔE si on compare VII et II.

---

[20] L. Pauling, « The Nature of the Chemical Bonds », Chap. 3 IIIe ed., Cornell University Press, Ithaca, New York, 1960.

Tableau 2

Valeurs ΔE en unités β

N°	Formule du thioamide	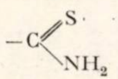		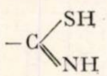		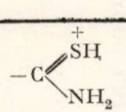		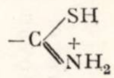	
		H	ω	*H*	ω	*H*	ω	*H*	ω
I	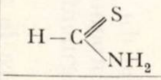	0,4447	1,4495	0,2433	0,7843	0,5892	1,0221	0,3866	0,4553
II	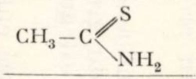	0,6009	0,5725	0,4512	0,9958	0,8893	1,3141	0,6679	0,7582
III	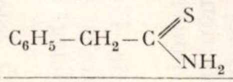	2,8522	3,8841	2,6023	3,2082	3,0302	3,5142	2,8181	2,9548
IV	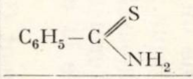	2,9141	3,5858	2,6552	2,9193	3,0773	3,1428	2,8559	2,5653
V	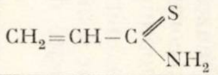	0,9729	1,9919	0,7015	1,3259	1,1433	1,5473	0,9161	0,9700
VI	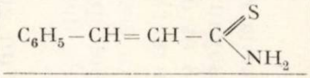	3,4499	4,1432	2,1618	2,4768	3,6329	3,6884	3,3970	3,1052
VII	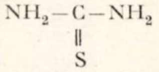 $NH_2-\underset{\underset{S}{\|}}{C}-NH_2$	0,8462	1,7282	0,5659	1,0477	1,0360	1,4513	0,8239	0,8494
VIII	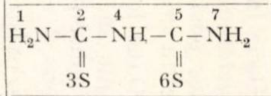 $\overset{1}{H_2N}-\underset{\underset{3S}{\|}}{\overset{2}{C}}-\overset{4}{NH}-\underset{\underset{6S}{\|}}{\overset{5}{C}}-\overset{7}{NH_2}$	1,6557	3,4183	1,3874 1,6596	2,7400($N^1=$) 2,7035($N^4=$)	1,8452	3,0684	1,6255($\overset{+}{N}_1$) 1,7254($\overset{+}{N}_4$)	2,5139 2,5159
IX	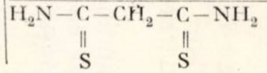 $H_2N-\underset{\underset{S}{\|}}{C}-CH_2-\underset{\underset{S}{\|}}{C}-NH_2$	1,3908	3,3263	1,1452 1,5831	2,6509($N^1=$) 2,6475($C^4=$)	1,5641	2,9571	1,3541	2,3986

ORIENTATION DE LA SUBSTITUTION ÉLECTROPHILE PAR LE GROUPEMENT CSNH$_2$

Le groupement fonctionnel $-CSNH_2$ par sa structure et l'effet électronique exercé oriente la substitution électrophile sur le noyau benzénique dans la position *méta* (position 3 et 5).

Le calcul de la distribution de la densité de la charge dans la molécule permet d'obtenir des informations sur les positions où peut se produire l'attaque d'un réactant électrophile où nucléophile.

Dans le tableau 3 sont indiquées les densités de la charge pour les thioamides III, IV et VI.

Tableau 3

Valeurs de densité de la charge dans le noyau benzénique

Le thioamide	Position	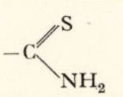 $-C(=S)-NH_2$		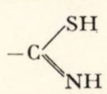 $-C(-SH)=NH$		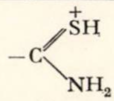 $-C(=\overset{+}{S}H)-NH_2$		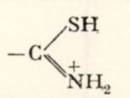 $-C(-SH)=\overset{+}{N}H_2$	
		H	ω	H	ω	H	ω	H	ω
III	2,6	1,0261	1,0201	1,0280	1,0203	1,0246	1,0177	1,0254	1,0169
	3,5	0,9986	1,0059	0,9986	1,0059	0,9987	1,0051	0,9987	1,0049
	4	1,0188	1,0155	1,0203	1,0157	1,0174	1,0134	1,0182	1,0127
IV	2,6	0,9435	0,9931	0,9663	0,9940	0,9155	0,9761	0,9247	0,9715
	3,5	1,0015	0,9978	1,0011	0,9981	1,0020	0,9922	1,0021	0,9906
	4	0,9505	0,9941	0,9714	0,9949	0,9247	0,9784	0,9342	0,9739
VI	2,6	0,9631	0,9973	0,9782	0,9978	0,9456	0,9898	0,9520	0,9875
	3,5	1,0005	0,9991	1,0004	0,9992	1,0007	0,9964	1,0007	1,9956
	4	0,9653	0,9975	0,9799	0,9979	0,9484	0,9900	0,9549	0,9877

Dans la molécule du thiobenzamide, où le groupement CSNH$_2$ est lié directement au noyau benzénique, la densité de la charge est maximale dans les positions 3 et 5, comme on pouvait prévoir, compte tenu de la nature du groupement thioamidique.

Dans le cas du cinnaméthioamide, l'influence du groupement thioamidique se transmet par l'intermédiaire du groupement $-CH=CH-$ et en conséquence la densité de la charge est augmentée aussi dans les positions 3 et 5.

L'existence d'un groupement CH$_2$ placé entre le noyau benzénique et le groupement thioamidique dans la molécule du phénylthioacétamide modifie la distribution de la charge. Le groupement CH$_2$ étant un substituent de premier ordre oriente la substitution électrophile dans les positions *ortho* et *para* (ou 2, 4 et 6).

Le diagramme de la distribution de la charge indique dans ce cas que les positions 2, 4 et 6 ont une valeur de la densité électronique plus élevée que les autres positions.

En ce qui concerne les formes tautomères iminothioliques (isothioamidiques), la substitution électrophile est orientée dans les mêmes positions que dans les formes thioniques (thioamidiques).

Vu que la substitution électrophile a lieu d'habitude en milieu acide, nous avons aussi pris en considération les deux formes protonées correspondantes pour les deux formes tautomères.

Dans ce cas, la densité de la charge est aussi augmentée dans les positions 3 et 5 pour les thioamides IV et VI et dans les positions 2, 4 et 6 pour le thioamide III.

LA CAPACITÉ D'ACCEPTEUR D'HYDROGÈNE DES THIOAMIDES

L'existence dans le groupement thioamidique des deux atomes qui possèdent des doublets électroniques libres (l'azote et le soufre) a conduit à des discussions contradictoires concernant l'atome qui peut fixer le proton.

Sur la base des résultats de quelques recherches effectuées dans le domaine des amides et thioamides, en utilisant la méthode spectrale (spectroscopie UV, IR, RMN) on a tiré la conclusion que la protonation a lieu au niveau de l'atome d'oxygène dans le cas des amides et au niveau de l'atome de soufre dans le cas des thioamides. [21]

Ainsi, comme on observe dans le tableau 2, les données indiquées montrent que les énergies de conjugaisons des deux formes protonées à l'atome de soufre, ou à l'atome d'azote sont différentes.

Dans tous les cas les valeurs ΔE sont plus grandes pour les formes protonées à l'atome de soufre, fait qui est en concordance avec les constatations expérimentales.

Les valeurs des indices de charges calculées pour l'atome de soufre et d'azote dans la forme thioamide et isothioamide mettent en évidence la différence entre ces deux formes à l'état fondamental et l'importance des effets électromères dynamiques dans la fixation d'un proton.

Les données indiquées dans le tableau 4 permettent de tirer quelques conclusions sur l'influence de la nature des radicaux et sur l'influence de la structure des thioamides VII, VIII et IX (tableau 5) grâce à laquelle ces thioamides sont fréquemment utilisés comme réactifs, pouvant former des complexes.

Les auteurs remercient encore une fois M. Mircea Gheorghiu, qui a eu l'amabilité de mettre à leur disposition le programme de calcul.

---

[21] A. M. White et D. H. O'Brien, *Chem. Rev.*, **70**, 561 (1970).

Tableau 4

Indices de charge pour l'atome de soufre et d'azote (les thioamides I–VI)

Le thioamide	S				N			
	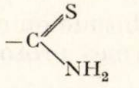 $-C\begin{smallmatrix}\nearrow S\\ \searrow NH_2\end{smallmatrix}$		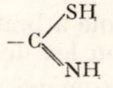 $-C\begin{smallmatrix}\nearrow SH\\ \searrow NH\end{smallmatrix}$		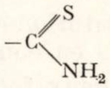 $-C\begin{smallmatrix}\nearrow S\\ \searrow NH_2\end{smallmatrix}$		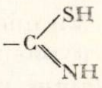 $-C\begin{smallmatrix}\nearrow SH\\ \searrow NH\end{smallmatrix}$	
	H	ω	*H*	ω	*H*	ω	*H*	ω
I	1,5997	1,8880	1,8763	1,8603	1,8010	1,9035	1,3675	1,2214
II	1,6760	1,2480	1,8871	1,8718	1,8222	1,9111	1,4437	1,2757
III	1,6745	1,2445	1,8871	1,8715	1,8225	1,9110	1,4417	1,2723
IV	1,6236	1,1963	1,8881	1,8683	1,8299	1,9099	1,3936	1,2256
V	1,6311	1,1953	1,8907	1,8684	1,8361	1,9099	1,4007	1,2248
VI	1,6458	1,1976	1,8942	1,8702	1,8446	1,9113	1,4125	1,2259

Revue Roumaine de Chimie, 18, 1, 111–121 (1973)

Tableau 5

Indices de charge pour l'atome de soufre et d'azote (les thioamides VII – IX)

Le thioamide	S						N					
	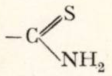 $-C(=S)NH_2$		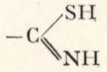 $-C(SH)=NH$				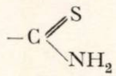 $-C(=S)NH_2$		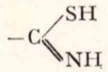 $-C(SH)=NH$			
	H	ω	=S		−S−		*H*	ω	=N−		−N<	
			H	ω	H	ω			*H*	ω	*H*	ω
VII	1,7149	1,2655	—	—	1,8937	1,8753	1,8356	1,9135	1,4858	1,2916	1,8776	1,9169
VIII	1,6914	1,2557	1,7006($N^1=$) 1,7298($N^4=$)	1,2563 1,2562	1,8910 1,8546	1,8740 1,8430	1,8309($N^{1,7}$) 1,7216(N^4)	1,9127 1,8470	1,4606($N^1=$) 1,3613($N^4=$)	1,2823 1,2728	1,7490(N^4) 1,8327(N^7) 1,8528(N^1) 1,8438(N^7)	1,8497 1,9127 1,9169 1,8985
IX	1,6657	1,2427	1,6699($N^1=$) 1,7403($C^4=$)	1,2430 1,2605	1,8862 1,8653	1,8712 1,8692	1,8207	1,9107	1,4334($N^1=$)	1,2706	1,8213(N^7) 1,8555(N^1) 1,8603(N^7)	1,9108 1,9145 1,9180

Revue Roumaine de Chimie, **18**, *1*, 123–129 (1973)

PEPTIDES. XII[*]

BEHAVIOUR OF THE MIXED ANHYDRIDES OF SOME AMINO ACIDS[**] N-PROTECTED WITH β-KETOESTERS

A. BALOG, D. BREAZU, VIORICA VOINESCU, MARGARETA HERMAN, E. VARGHA[**]
and E. RAMONŢIAN

Institute for Chemical and Pharmaceutical Research, Str. Fabricii 126, Cluj, Romania

Received March 6, 1972

The pivaloyl, isobutyroyl and benzoyl mixed anhydrides of AE– and CP–C-phenylglycines undergo at the pH 2 a simultaneous acyl migration and splitting of the AE or CP protecting groups, followed by the formation of the corresponding N-acyl C-phenyl-glycine (2). A similar reaction was observed in the case of the pivaloyl mixed anhydrides of some other AE-amino acids and by the benzoyl mixed anhydride of AE–L–PheOH. The mixed anhydrides formed from AE–Gly–OK and Phth–Gly–Cl leads by acyl migration to the dipeptide Phth–Gly–Gly–OH. The conditions in which the above reaction takes place without racemization, as well as the probable mechanism of the acyl migration are discussed.

In our earlier papers[1,2] we have shown the advantages presented in the peptide synthesis by the alkaline or dicyclohexylammonium salts of the amino acids N-protected with β-ketoesters or β-diketones, using the mixed anhydrides method. For the preparation of the mixed anhydrides, in the peptide synthesis we have used pivaloyl chloride, benzoyl chloride, ethyl chloroformate etc. The temperature was below – 5° and the reaction time 15–20 min. The formation of the mixed anhydride was performed by adding a drop of N-methylmorpholine.[3] Using for the aminolysis amino acid esters or peptide esters, the N-protected peptide esters could be obtained in high yields (over 70–80%).

---

[*] Peptides XI. A. BALOG, D. BREAZU, C. DAICOVICIU, E. VARGHA, L. BEU and F. GÖNCZY, *Rev. Roumaine Chim.*, **16**, 1601 (1971).

[**] The abbreviations of amino acids correspond to the rule submitted by the IUPAC-IUB-Comission on Biochem. Nomenclature, *Z. physiol. Chem.*, **348**, 256 (1967).

Other abbreviations used : AE = 1-ethoxycarbonyl-propen-2-yl ; CP = 2-ethoxycarbonyl-cyclopenten-1-yl ; TMA = trimethylacetyl (pivaloyl) ; TEA = triethylamine ; Phth = phthaloyl ; THF = tetrahydrofuran ; Bz = benzoyl ; DMA = dimethylacetyl (izobutyroyl).

[***] The Department of Organic Chemistry, Babeş-Bolyai University, Str. Arany J. 11, Cluj, Romania.

[1] A. BALOG, D. BREAZU, E. VARGHA, F. GÖNCZY and L. BEU. *Rev. Roumanie Chim.*, **15**, 1375 (1970).

[2] A. BALOG, E. VARGHA, D. BREAZU, L. BEU and F. GÖNCZY, *ibid.*, **15**, 1391 (1970).

[3] G. R. FOSKER, J. H. C. NAYLER and F. A. WILCOX, *Brit. Pat.*, 991, 586, Beecham Research Laboratories Ltd. Brentford, 1962 ; *Chem. Zentr.*, **1967**, 33–1856.

Under these conditions, a disproportionation of the mixed anhydrides to symmetric ones — a very frequent side reaction in the case of the N-acylamino acid mixed anhydrides — was not observed.

The mixed anhydrides of the amino acids N-protected with β-ketoesters or β-diketones react normally with sodium methoxide in benzene or with methanol in the presence of TEA. [4] Thus, the methanolysis of the AE—C-phenylglycyl-pivaloyl mixed anhydride leads to AE—C-phenylglycine methyl ester in 93% and respectively 74% yield.

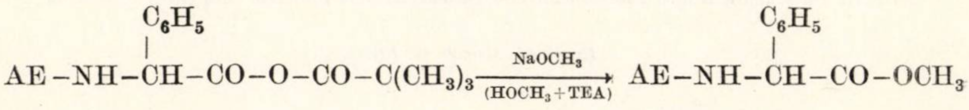

$$\mathrm{AE{-}NH{-}\overset{\displaystyle C_6H_5}{\overset{|}{C}}H{-}CO{-}O{-}CO{-}C(CH_3)_3 \xrightarrow[(HOCH_3+TEA)]{NaOCH_3} AE{-}NH{-}\overset{\displaystyle C_6H_5}{\overset{|}{C}}H{-}CO{-}OCH_3} \qquad (1)$$

A partial racemization (12–13%) occurs during the esterification. When 20% excess of sodium methoxide was used a complete racemization was observed.

The mixed anhydrides of the amino acids N-protected with β-ketoesters show an interesting behaviour in acidic media. By treating their solution with hydrochloric acid to pH 2 a transposition takes place in which the acylic rest from the carboxyl migrates to the amino group, with the subsequent splitting of the N-protecting rest (AE or CP). In this way, the mixed anhydrides of the C-phenylglycine N-protected with acetoacetic or cyclopentanone-2-carboxylic ester yield N-acyl-C-phenylglycines (table 2).

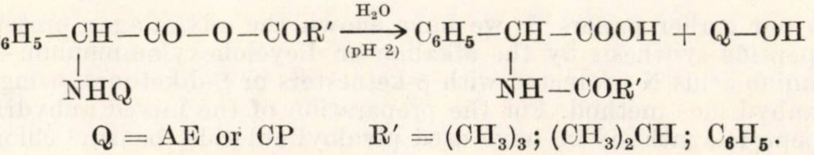

$$\mathrm{C_6H_5{-}\underset{\displaystyle NHQ}{\underset{|}{C}}H{-}CO{-}O{-}COR' \xrightarrow[(pH\ 2)]{H_2O} C_6H_5{-}\underset{\displaystyle NH{-}COR'}{\underset{|}{C}}H{-}COOH + Q{-}OH} \qquad (2)$$

$\mathrm{Q = AE}$ or $\mathrm{CP} \qquad \mathrm{R' = (CH_3)_3;\ (CH_3)_2CH;\ C_6H_5}$.

The above reaction can be easily controlled by titration with alkali, when only one mole of hydroxide is consumed per mole of mixed anhydride. The acyl migration does not seem to be influenced by time, as the same quantity of the hydroxide was consumed at different intervals ranging from 5 to 240 minutes (table 1A). Nor seems the temperature to influence it sensibly, as the same results are obtained at temperatures between — 5° and + 25° (table 1B). It may be affirmed that under the above mentioned conditions no hydrolisis and disproportionation occur.

In order to check the final N-acylated products after the migration, we synthesized them by direct acylation methods. Physical constants of both products were identical.

When for the formation of the mixed anhydrides from dicyclohexylammonium salts of the C-phenylglycine N-protected with β-ketoesters a catalytic amount of N-methylmorpholyne was used, a complete racemization took place. This behaviour is due to the phenylglycine structure which has a special sensitivity towards racemization in the presence of bases.[5] In the absence of this catalyst it was necessary to extend the reaction time for the formation of the mixed anhydride from 5–10 minutes to 30 minutes. In this manner the N–TMA–D-phenylglycine was obtained by acylic migration with a high optical purity.

---

[4] D. A. Johnson, *J. Amer. Chem. Soc.*, **75**, 3636 (1953).

Table 1

The consumption of sodium hydroxide pro mole of mixed anhydride

A		B	
The reaction time min	NaOH consumption equivalent	Temperature °C	NaOH consumption equivalent
10	0.98	−5	0.96
60	0.96	0	1.27
120	0.97	+10	1.14
240	1.00	+25	1.08

A. The reaction was performed following the general method, at a temperature below 0°. The reaction time refers to the period between the acidulation and the alkaline titration of the reaction mixture.

B. After the acidulation to pH 2 the reaction time was in all cases 2 hrs.

If for the acidulation to pH 1,5 methanolic hydrochloric acid was added (anhydrous media) the acyl migration occurs as above. Using an excess of methanolic hydrochloric acid, the 0 → N acyl shift was followed by esterification with the formation of the N–TMA–C-phenylglycine methyl ester, identical with that prepared from N–TMA–C-phenylglycine and diazomethane.

We have also studied the acyl migration and the simultaneous splitting of the N-protecting group in the case of the pivaloyl mixed anhydride of the following amino acid derivatives: AE–GlyOH, AE–L–ValOH, AE–L–LeuOH and AE–L–IleOH. The reaction took place according to our expectations and the corresponding N-pivalic derivatives were obtained in overall yield 60% (table 2). The products were identified by direct acylation of the respective amino acids with pivaloyl chloride according to the Schotten-Baumann method.

In the case of the L-alanine and L-phenylalanine, the N-pivaloyl derivatives resulted by acyl migration could not be crystallized, but the mixed anhydride obtained from AE–PheOH and benzoyl chloride yielded N-benzoyl-L-phenylalanine (yield over 80%) identical with that mentioned in the litterature.[6]

---

[5] D. G. Neilson and D. F. Ewing, *J. Chem. Soc.*, **1966**, 393.

[6] M. Goodman and L. Levine, *J. Amer. Chem. Soc.*, **86**, 2918 (1964).

In the case of the mixed anhydride obtained from the AE—Gly—OK and phthaloylglycyl chloride the acyl migration followed by the splitting of the N-protecting group (AE) led to N-phthaloylglycyl-glycine

$$\mathrm{AE-NH-CH_2-COOK} \xrightarrow{\mathrm{Cl-CO-CH_2-NPhth}} \mathrm{AE-NH-CH_2-CO-O-CO-}$$

$$\mathrm{-CH_2-NPhth} \xrightarrow[(\mathrm{pH}=2)]{\mathrm{H_2O+}} \mathrm{PhthN-CH_2-CO-NH-CH_2CO_2H} \qquad (3)$$

The melting point of our product was lower with 14—15° than that described[7] owing to the presence of the N-phthaloylglycine, that could not be removed not even by repeated recrystallizations. The product (m.p. 216—218°) was converted by means of the cyanomethyl tosylate[2] into N-phthaloylglycyl-glycine cyanomethyl ester, identical with the same derivative obtained[2] from glycine cyanomethyl ester hydrochloride and phthaloylglycyl chloride.

Regarding the mechanism of the acyl migration described here, it seems reasonable to admit a certain analogy with the intramolecular transposition observed by Weygand and co-workers[8,9] in the case of symmetric anhydride of glycine or alanine N-protected with trifluoroacetyl group. The transposition takes place in the presence of ethanolic dicyclohexylamine and leads to the corresponding N-trifluoroacetyl dipeptide and ethyl trifluoroacetate.

In our case, the migration occurs under the catalytic action of acids and follows also an intramolecular mechanism: yields are high and no disproportionation or dipeptide formation was observed. It can be presumed that in the first step a protonated form (I) of the anhydride group appears[10] which allows the nucleophilic attack of the nitrogen on the acid partner's carbonyl

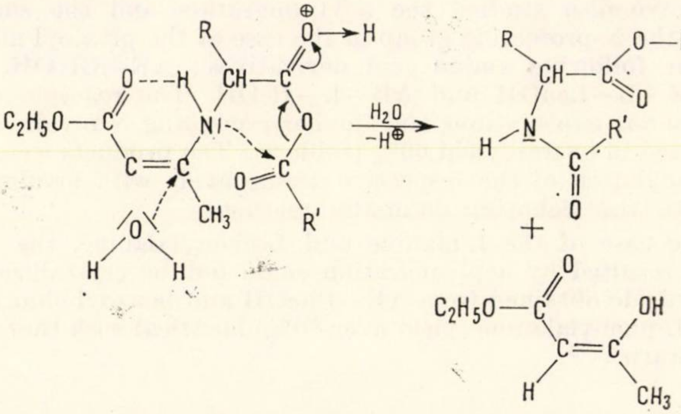

---

[7] M. Bodanszky, *Acta Chim. Acad. Sci. Hung.*, **10**, 335 (1957).

[8] F. Weygand and M. Reiher, *Chem. Ber.*, **88**, 26 (1955).

[9] F. Weygand and U. Glöchler, *ibid.*, **89**, 653 (1956).

[10] V. Gold and J. Hilton. *J. Chem. Soc.*, **1955**, 843.

On the other hand, the nucleophilic character of the nitrogen atom is strengthened by the enaminic form, which supposes an intramolecular hydrogen bond. In the next step, the acylation of the amino group takes place with subsequent reforming of the carboxyl group and the hydrolytic removal of the protecting group.

The acyl migration observed by the mixed anhydrides of the amino acids N-protected with β-ketoesters has not a general character. Thus, it does not occur in the case of the mixed anhydrides of the C-phenylglycine N-protected with benzoylacetone or 2,6-dimetoxybenzoylacetone, because of the marked stability of the protecting groups. [1]

EXPERIMENTAL

All melting points were performed in glass capillaries and are uncorrected. The analytical samples were dried over P_2O_5 for 3—4 hrs at 64° and 16—20 Torr. The specific rotations were determined in tubes of 2 dm at 20—24° (Metra 400/a-Prague polarimeter).

1. *Acyl-migration. General method.* 10 mmoles of potassium or dicyclohexylammonium salt of the amino acid N-protected with acetylacetic, respectively, cyclopentanon-2-carboxylic ester was dissolved in 40 ml of THF and cooled in ice-salt bath for 4—5 min. 10 mmoles of acid chloride (1.2 ml pivaloyl or benzoyl chloride) was added and the mixture was cooled further for 15 min. The formed precipitate (consisting in potassium or dicyclohexylammonium chloride) was filtered and washed three times with THF.

The cooled solution of the mixed anhydride was treated with hydrochloric acid 25% to pH 1.5—2. After standing for 1 hr with cooling and 1 hr at room temperature, the mixture was concentrated in vacuum to 1/5 of the volume. A light excess of 5% sodium bicarbonate was added. The aqueous solution was extracted twice with ether and acidulated to pH 1—2. The N-acylamino acid precipitated by storage and cooling was filtered and dried. The raw product was crystallized from an adequate solvent (see Table 2).

2. *N-Pivaloyl-C-phenylglycine.* a) The mixed anhydride was prepared from 1.6 g (5 mmoles) of *potassium N-(1-ethoxy-carbonyl-propen-2-yl)-D-phenylglycinate* and 0.6 ml pivaloyl chloride in 30 ml THF, following the above described method. After treatment with hydrochloric acid, the usual work-up afforded 0.75 g (74%) of *N-pivaloyl-D-phenylglycine*, melting at 133—134°.

b) In the same way, but using a drop of N-methylmorpholine as catalyst for the formation of the mixed anhydride, after the transposition, 0.8 g (83%) N-pivaloyl-DL-phenylglycine was obtained $[\alpha]_D = 0°$ ($c = 1$, EtOH); m.p. 152—153° (from aqueous ethanol); mixed melting point with a sample prepared following the Schotteng-Baumann method did not depress.

		C	H	N	
$C_{13}H_{17}NO_3$ (235.3)	Calcd.	66.31	7.28	5.95	
	Found	66.52	7.83	6.02	(Kjeldahl)

c) The mixed anhydride was prepared according to the 2.*a* (from 2.35 g (5 mmoles) of *dicyclohexylammonium N-(2-ethoxycarbonyl-cyclopenten-l-yl)-phenylglycinate*. After the filtration of the dicyclohexylammonium hydrochloride, the solution of the mixed anhydride was treated with 25% methanolic hydrochloric acid to pH 1.5. The work-up following the general method gave 0.8 g (68%) of *N-pivaloyl-D-phenylglycine*. $[\alpha]_D$: —167° ($c = 1$, ethanol); m.p. 133—136°, without depression by mixing with the sample obtained according to *Schotten-Baumann*'s method.

Table 2

N-Acylamino acids obtained by acyl migration

N°	N-Acylamino-acid**	Yield %	M.p.° (solvent)[a]	$[\alpha]_D^{20-24°}$	Formula (M. weight)	Analyses Calc./Found C	H	N
1	TMA−Gly−OH	63[b]	133−134 (LP.−Ac)	−	$C_7H_{13}NO_3$ (159.2)	52.82 52.79	8.23 8.27	8.80 8.50
2	TMA−L−Ile−OH	68	105−106[c] (EtOH/H_2 01 : 1)	−6,1(c=1, DMF) +32.5 (c=1, AcOEt)	$C_{11}H_{21}NO_3$ (215.3)	61.37 61.70	9.83 10.04	6.51 6.80
3	TMA−L−Leu−OH	56	151−152[d] (EtOH/H_2O 1 :1)	−28.7 (c=1, MeOH) −12.2 (c=1, AcOEt)	$C_{11}H_{21}NO_3$ (215.3)	61.37 61.86	9.83 10.20	6.51 6.61
4	Bz−L−Phe−OH	82	140−141[e] (H_2O)	36.6 (c=1, dioxan)	$C_{16}H_{15}NO_3$ (269.3)	−	−	−
5	Bz−D−Phg−OH[f]	63	191−193[g] (EtOH/H_2O)	−119.5 (c=1,EtOH)	$C_{15}H_{13}NO_3$ (255.3)	70.58 69.84	5.13 5.76	5.49 5.42
6	Bz−L−Phg−OH[f]	67	192−193 (EtOH/H_2O)	+119.8 (c=1,EtOH)	−	−	−	−
7	DMA-D-Phg-OH	65	121−122 (EtOH/H_2O)	−184 (c=1.2,EtOH)	$C_{12}H_{15}NO_3$ (221.3)	65.13 64.76	6.83 6.98	6.33 6.71
8	TMA-D-Phg-OH	74	137−139 (MeOH/H_2O)	−168.5 (c=1,EtOH)	$C_{13}H_{17}NO_3$ (235.3)	66.36 66.52	7.28 7.47	5.95 6.03
9	TMA-L-Val-OH	85	138−140 (B21)	+11.4 (c=1, DMF) 0° c=1, MeOH) −20.1 (c=1, AcOEt)	$C_{10}H_{19}NO_3$ (201.3)	59.67 60.20	9.52 9.90	6.96 7.03

a, Abbreviations for the solvents : MeOH = methanol ; EtOH = ethanol ; LP = benzine b.p. 70 − 80° ; Ac = acetone ; DMF = dimethyl formamide AcOEt = ethyl acetate ; Bzl = benzene.

b, After recrystallization.

c, By direct acylation : yield 76% ; m.p. 105 − 106° without depression with N° 2.

d, By direct acylation : yield 96% ; m.p. 150 − 152° without depression with N° 3.

e, Lit. [6] M.p. 142 − 143° (corr.) ; $[\alpha]_D^{20}$ + 38.74 (c = 1.6, dioxan).

f, The mixture of the D izomer (N°. 5) and L izomer (N° 6) has m.p. 176 − 177°. The lit. [10] indicates for the N-benzoyl-DL-phenylglycine m.p. 177.5°

g, The product obtained by direct acylation m.p. 192 − 195° ; $[\alpha]_D^{20}$ − 120.3° c = 1, EtOH) ; Lit. [11] m.p. 186 − 187° ; $[\alpha]_D^{25}$ − 84.3° (c = 1.4, 1N NaOH) ; and [12] m.p. 187 − 188° ; $[\alpha]_D$ − 84.1, respectively.

---

[11] S. G. COHEN, R. M. SCHULTZ and S. Y. WEINSTEIN, *J. Amer. Chem. Soc.*, **88**, 5315 (1966).

[12] S. MINOVICI, *Bul. Soc. Chim. Romania*, **2**, 8 (1920) ; *Chem. Abstr.*, **14**, 3228 (1920).

3. *N-Pivaloyl-C-phenylglycine methyl ester.* a) The mixed anhydride was prepared following the 2. *b*) and after filtration, the solution was treated with an excess of 25 % methanolic hydrochloric acid (5 ml). After 30 minutes cooling and 1 hour storage at room temperature, the reaction mixture was washed successively with water, 5 % sodium bicarbonate solution, water. The organic layer was dried over Na_2SO_4. After the removal of the solvent and the recrystallization of the residue 0.9 g (72 %) of *N-pivaloyl-DL-phenylglycine methyl ester* was obtained; $[\alpha]_D$: 0° ($c = 1$, methanol); m.p. 148–149° (ethanol).

$C_{14}H_{19}NO_3$ (249.2)	Calcd.	C 67.45	H 7.68	N 5.64
	Found	67.25	8.00	5.60

b) The methylic ester obtained from *N-Pivaloyl-DL-C-phenylglycine* and ethereal diazomethane presented m.p. 148.5–149° and showed no depression when mixed with the above product.

4. *Phthaloyl-glycylglycine.* 2.3 g (10 mmoles) of *potassium N-(1-ethoxycarbonyl-propen-2-yl)-glycinate* suspended in 25 ml of acetonitrile was treated dropwise under stirring and cooling at – 5°, with 2.2 g (10 mmoles) of phthaloylglycyl chloride dissolved in 15 ml of acetonitrile. After a standing of 1 hour 2 N hydrochloric acid was added slowly to pH 2. The stirring was continued for 30 minutes at – 5° and for 30 minutes at room temperature. Addition of 30 ml water yielded a white precipitate that was filtered and washed successively with water and methanol.

After recrystallization from water resulted 2.1 g (81 %) product with m.p. 216–218° (after two recryst, from water Lit. [7] indicates for the same product m.p. 230–233°.

N-Phthaloyl-glycylglycine cyanomethyl ester. 0.8 g (3 mmoles) of phthaloyl-glycylglycine obtained as above was suspended in 5 ml of anhydrous acetone and was treated with 0.45 ml of TEA and 0.6 g (3 mmoles) of cyanomethyl tosylate.

The mixture was stirred for 2 hours. The precipitate formed by adding 75 ml water was filtered and dried. Yield 0.72 g (80 %); m.p. 203–204° (from ethanol) without depression by mixing with the ester obtained from glycine cyanomethyl ester hydrochloride and phthaloylglycine chloride. [2]

5. *The methanolysis of the mixed anhydrides.*

N-(1-Ethoxycarbonyl-propen-2-yl)-C-phenylglycine methyl ester. The mixed anhydride, obtained following the general method from 10 mmoles of AE-D-phenylglycine potassium salt and 1.2 ml of pivaloyl chloride, was treated at – 10° with 110 ml 0.1 N benzenic solution of sodium methoxide. The mixture was stirred for 1 hour and was allowed to stand for several hours at room temperature. The solvent was removed under *vacuum*. By treating the gelatinous residue with water, 2.6 g (93 %) of raw ester was precipitated, m.p. 67–91°. After recrystallization from light benzine (b.p. 60–80°) m.p. 75–76°; $[\alpha]_D^{20} + 191°$ ($c = 1$, methanol). The same product obtained using methyl tosylate according to literature [2] has m.p. 80–81° and $[\alpha]_D^{20} + 259°$ ($c = 1$, methanol).

b) The mixed anhydride obtained as described before at *a*) was treated, under cooling in ice-salt bath, with 1.5 ml methanol and 1.6 ml TEA. After 6 hours storage at room temperature the reaction mixture was poured into water (200 ml). The separated oil solidified gradually yielding 2.05 g (74 %) product with m.p. 75–76° (benzine).

Note. The use of 10–20 % excess of sodium methoxide afforded the DL-product, m.p. 101–102° (benzine); $[\alpha]_D^{21}$: 0° (m.p. according to lit. [2] : 104–105°)

Revue Roumaine de Chimie, 18, 1, 131–144 (1973)

KINETICS OF SOLVOLYTIC REACTIONS. IV.[1]

TRANSITION STATE IN THE π-ROUTE OF THE ACETOLYSIS OF 5H-DIBENZO [a, d]-CYCLOHEPTEN-5-YL-(β-ETHYL) TOSYLATE

M. VOICU*, F. BADEA * and ANCA VOICU **

Organic Chemistry Laboratory,
* Polytechnic Institute, str. Polizu 1, Bucharest
** Institute of Organic Chemistry, Splaiul Independenţei 204 bis, Bucharest

Received July 31, 1972

5H-Dibenzo [a, d] cyclohepten-5-yl-(β-ethyl) tosylates, **1**, substituted in the *para* position in benzene ring with respect to the double bond, were prepared. Rate constants for the acetolysis, activation parameters, salt effects, and variation of the ratio of uncyclized (*B*), to cyclized products (*C*), with the sodium acetate concentration, were studied. The ratio *B*/*C* varies linearly with the sodium acetate concentration, as has been previously observed for the unsubstituted tosylate, **1**–H. The assisted rate constants and *R* terms (equation 2) are well correlated in a $\rho-\sigma^n$ treatment; these are discussed as evidence for a bridged transition state in the π-route reaction.

In the acetolysis of the tosylate **1**–H, two types of reaction products are formed[2]: the unrearranged acetate **2**(*B*), on the one hand, and the bridged products **3**(*C*), on the other hand. The formation of the latter products involves the double bond (π-route).

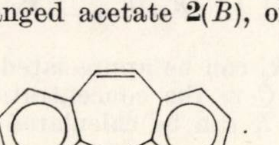

1

(X=H, Cl, CH_3, OCH_3)

---

[1] Part. III, M. Voicu, F. Badea and A. Bucur, *Rev. Roumaine Chim.*, **17**, 1539 (1972).

[2] E. Ciorănescu, M. Banciu, R. Jelescu, M. Rentzea, M. Elian and C. D. Nenitzescu, *Rev. Roumaine Chim.*, **14**, 911 (1969).

The kinetic treatment of the NaOAc-buffered acetolysis has revealed that sodium acetate is involved in the formation of all reaction products,[3] the mechanism depicted in Chart I being in good agreement with the published results.

Chart I

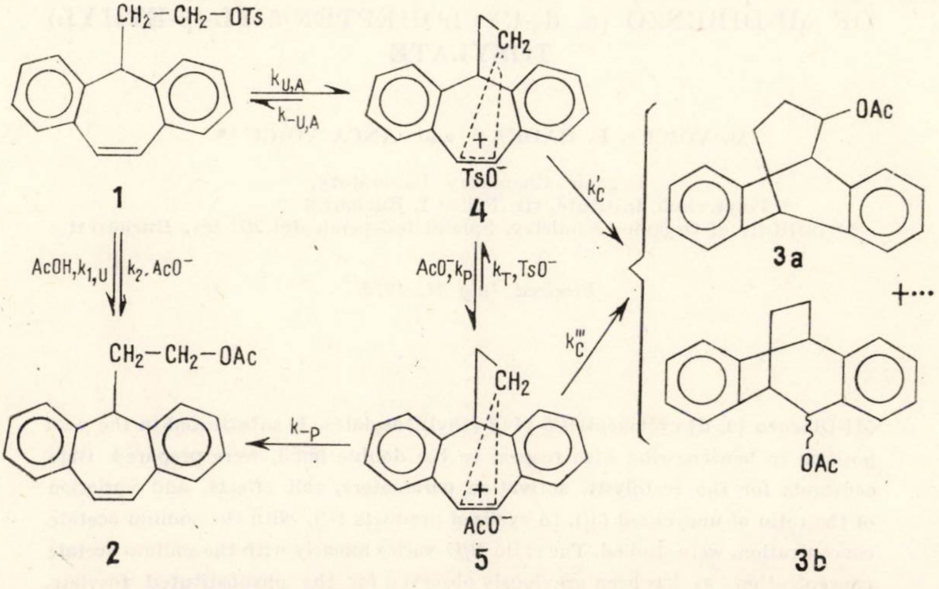

According to that reaction mechanism, the ratio between the unrearranged and rearranged products (B/C) is given by relationship[3] (1)

$$\frac{B}{C}=\frac{k_{1,\mathrm{U}}}{k_{\mathrm{U,A}}}+\left[\frac{k_{\mathrm{P}}/k'_{\mathrm{C}}}{1+k'''_{\mathrm{C}}/k_{-\mathrm{P}}}+\frac{k_2}{k_{\mathrm{U,A}}}\right]\cdot[\mathrm{NaOAc}] \qquad (1)$$

in which $k_{1,\mathrm{U}}$, $k_{\mathrm{U,A}}$ and k_2 can be appreciated from the kinetic data and the plot of the ratio B/C *vs* the concentration of sodium acetate. From the same plot the term R can be calculated:

$$R=\frac{k_{\mathrm{P}}/k'_{\mathrm{C}}}{1+k'''_{\mathrm{C}}/k_{-\mathrm{P}}} \qquad (2)$$

It was considered that this term measures the relative stability of the intermediate[3] of the π-route.

In an effort to find other examples which would satisfy the relationships (1) and (2), ring substituted derivatives of **1**—H (**1**—X, X = Cl, CH_3 and CH_3O) have been studied in this work. It was hoped that if relationship (1) holds up in these cases too, a better understanding of the R

---

[3] M. Voicu and F. Badea, *Rev. Roumaine Chim.*, **14**, 929 (1969).

factor could be acquired. It was anticipated that the free energy relationships could give a better hint regarding the structure of the first formed intermediate. Indeed, in Chart I, the cation in the ion pairs **4** and **5** was considered to be the bridged ion **6**. However, the nature of the rearranged formed products are also in agreement with a benzylic ion **7**, or with a phenonium ion **8**.

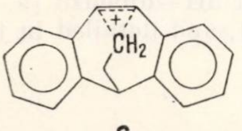

6

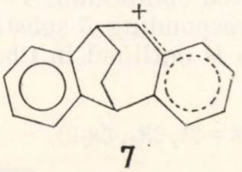

7

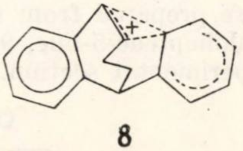

8

Bartlett and Sargent[4] pointed out some time ago: "in view of the difficulty of examining the structures of short lived ions, and the greater difficulty of examining transition states, the effect of substitution at different sites may be the best available criterion of the nature of the transition state in an ionization". In this respect, the substitution of the aromatic rings in **1**$-$X seemed to us promising.

It is well known that the solvolysis of benzylic derivatives is best correlated with Brown's σ^+ constants,[5] high negative reaction constants ρ being observed[6] (*t*-cumyl chloride, $\rho = -4.9$; 1-phenylcyclopentyl chloride, $\rho = -4.5$; 2-phenyl-2-*exo*-norbornyl chloride, $\rho = -4.3$). A similar correlation with $k_{U,A}$ values should be checked up if the benzylic ion **7** would be formed in the rate determining step.

For phenonium ion reactions, similar free energy relationships have been observed, the reaction constants ρ being comparatively lower than the values observed in benzylic ion reactions (6- and 7-substituted benzonorbornen-2-*exo*-yl brosylates,[7] $\rho = -3.3$ or[8] -2.8; neophyl brosylates,[9] $\rho = -3.0$; 6, 7-disubstituted- *anti*-9-benzonorbornenyl brosylates,[10] $\rho = -2.6$; 6-substituted-*anti*-9-benzonorbornenyl brosylates,[11] $\rho = -2.4$). The rate constants, at least for the *p*-methoxy derivatives, are greater than for the $\rho - \sigma$ treatment (*trans*-2-arylcyclopentyl tosylate[12]; 1-aryl-2-propyl tosylate[13]; 2-arylethyl tosylate[14]). If the phenonium ion **8** is formed in the rate determining step of the solvolysis of **1**$-$X derivatives, a value of the reaction constant of about -2 or -3 should be expected.

---

[4] P. D. Bartlett and G. D. Sargent, *J. Amer. Chem. Soc.*, **87**, 1297 (1965).

[5] H. C. Brown and Y. Okamoto, *J. Amer. Chem. Soc.*, **80**, 4979 (1958).

[6] H. C. Brown and K. Takeuchi, *J. Amer. Chem. Soc.*, **88**, 5336 (1966).

[7] H. Tanida, J. Ishitobi, T. Irie and T. Tsushima, *J. Amer. Chem. Soc.*, **91**, 4512 (1969).

[8] D. V. Braddon, G. A. Wiley, J. Dirlam and S. Winstein, *J. Amer. Chem. Soc.*, **90**, 1901 (1968).

[9] R. Heck and S. Winstein, *J. Amer. Chem. Soc.*, **79**, 3432 (1957).

[10] H. Tanida and H. Ishitobi, *J. Amer. Chem. Soc.*, **88**, 3663 (1966).

[11] H. Tanida, *J. Amer. Chem. Soc.*, **85**, 1703 (1963).

[12] C. J. Kim and H. C. Brown, *J. Amer. Chem. Soc.*, **91**, 4287 (1969).

[13] C. J. Lancelot and P. von R. Schleyer, *J. Amer. Chem. Soc.*, **91**, 4291 (1969).

[14] M. G. Jones and J. L. Coke, *J. Amer. Chem. Soc.*, **91**, 4284 (1969).

Smaller absolute values of the ρ constants ($|\rho| \ll 2$) should be observed if the bridged ion **6** is initially formed, the delocalization of the positive charge in ion **6** being less important as in the ions **7** and **8**.

RESULTS

Syntheses. The substituted compounds **1**$-$Cl, **1**$-CH_3$ and **1**$-OCH_3$ were prepared from the corresponding 3-substituted 5H$-$dibenzo [a, d] cycloheptene-5-one, 9$-$X, as is outlined in Chart II, and detailed in the experimental section.

Chart II ($X = Cl, CH_3, CH_3O$)

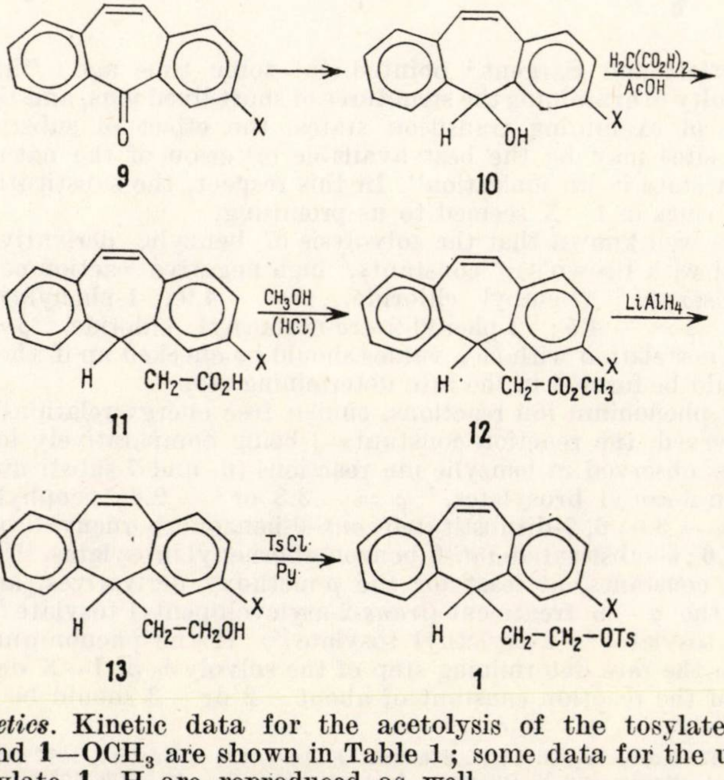

Kinetics. Kinetic data for the acetolysis of the tosylates **1**$-$Cl, **1**$-CH_3$ and **1**$-OCH_3$ are shown in Table 1; some data for the unsubstituted tosylate **1**$-$H are reproduced as well.

Reaction products. No attempt has been undertaken to prove the exact structure of the reaction products formed in the acetolysis of **1**$-$Cl, **1**$-CH_3$ and **1**$-OCH_3$. The ratio between the unrearranged and rearranged products, B/C, was determined spectrophotometrically on the absorbtion of stilbene system in B, [3] as a function of the concentration of the added sodium acetate. The results are plotted in Figure 1.

From the observed kinetics in the absence of sodium acetate (Table 1), and the intercept of the straight lines in figure 1, the assisted rate constants, $k_{U,A}$, and the pseudounimolecular rate constants, $k_{1,U}$ could be calculated (Table 2).

Table 1

Kinetic data for the acetolyses of 5H-dibenzo [a, d] cyclohepten-5-yl-(β-ethyl) tosylates, 1

Compound	Temperature °C	[NaOAc] mmoles/l	a) $10^4 \cdot k$ $\sec^{-1}$	$\Delta H^{\neq 298}$ kcal/mole	$\Delta S^{\neq 298}$ e.u.	c) b^{110}_{NaOAc}
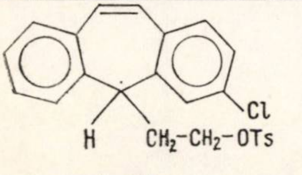 **1-Cl**	75.0	—	0.0302			
	95.0	—	0.258			
	110.0	—	1.09	26.6	−7.7	3.12
	110.0	20.75	1.17			
	110.0	41.00	1.25			
	110.0	61.70	1.29			
	110.0	204.0	1.78			
1−H b)	110.0	—	2.04	25.4	−9.8	0.868
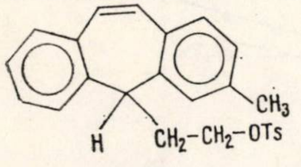 **1-CH₃**	75.0	—	0.0880			
	80.0	—	0.156			
	95.0	—	0.711			
	110.0	—	2.98	26.0	−7.2	0.697
	110.0	61.20	3.11			
	110.0	123.4	3.25			
	110.0	204.0	3.39			
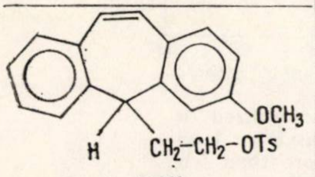 **1-OCH₃**	75.0	—	0.126			
	100.0	—	1.70			
	110.0	—	4.24	26.2	−6.0	0.527
	110.0	63.0	4.56			
	110.0	124.0	4.68			
	110.0	206.0	4.90			

a) Spectrophotometric measurements ; b) Ref. 3 ; c) Normal salt effect.[15]

The terms R could be calculated from the slopes of the straight lines in Figure 1, if the values of the bimolecular rate constants, k_2, are known. It has been shown previously,[3] that both $k_{1,\mathrm{U}}$ and k_2 can be determined from the corresponding rate constants $k_{1,\mathrm{S}}$, $k_{2,\mathrm{S}}$ of the saturated analogue **14**.

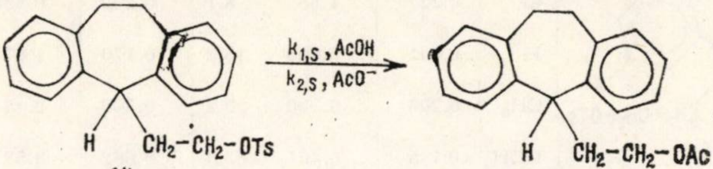

14 **15** (3)

$$\text{rate} = k_{1,\mathrm{S}} \cdot [14] + k_{2,\mathrm{S}} \quad [14] . [\mathrm{NaOAc}] \tag{4}$$

---

[15] A. H. Fainberg and S. Winstein, *J. Amer. Chem. Soc.*, **78**, 2763 (1956).

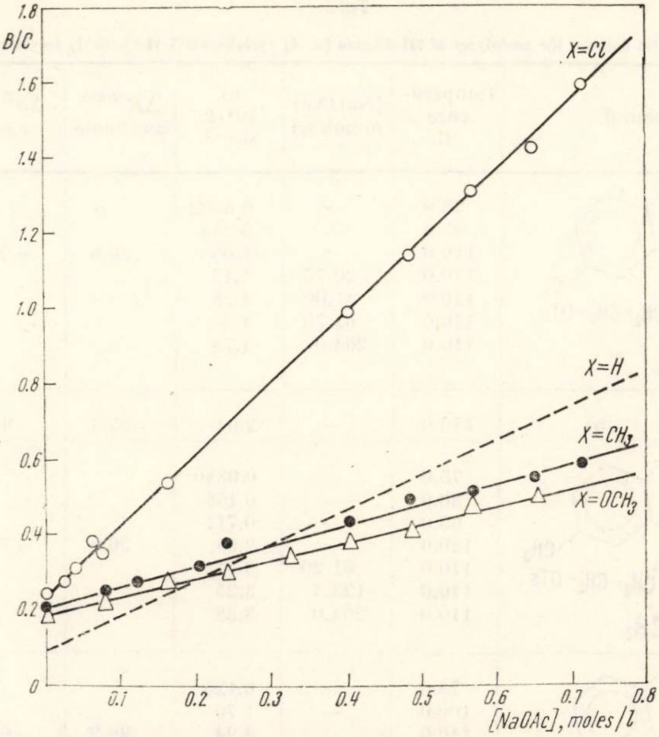

Fig. 1. – Dependence of the ratio B/C of uncyclized to cyclized products of the acetolyses of the tosylates **1** on sodium acetate concentration, at 110°, for more than ten half-lives; $[\mathbf{1}] = (7\ldots 10)\cdot 10^{-5}$ moles/l.

Table 2

Detailed kinetic data for the acetolyses of the tosylates 1. at 110°

Compound	X	$\left(\frac{B}{C}\right)_0$	slope of Figure 1 $l\cdot mole^{-1}$	a) $\frac{k_U}{k_S}$	$10^4\cdot k_{1,U}$ sec^{-1}	$10^4\cdot k_{U,A}$ sec^{-1}	R
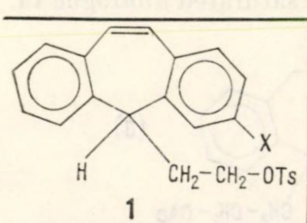 **1**	Cl	0.227	1.88	8.1	0.202	0.888	1.49
	H	0.091	0.909	15.2	0.170	1.87	0.72
	CH_3	0.206	0.530	22.2	0.509	2.47	0.39
	OCH_3	0.185	0.461	33.0	0.662	3.58	0.36

a) k_S is the rate constant of the saturated unsubstituted compound, **14**, assuming that it is regardless of the substituent (see the following discussion in the text) ; $k_S = 1.34\cdot 10^{-5}$ sec^{-1}, at 110°, Ref. [3].

Pritzkow and Schöppler[16] have shown that the bimolecular rate constants of the reaction of the primary tosilates, $R-CH_2-OTs$ with acetate ion in acetic acid are only slightly affected by the nature of the α radical, R : in our reaction, a slight structural change occurs in the γ substituent of a γ—Ar′ γ-Ar-propyl linkage. It is therefore reasonable to assume that the rate constant k_2, would be not seriously affected by the nature of the substituent in one of the γ-aryl rings. The R values from Table 2 were thus calculated from the known value k_2, for the unsubstituted saturated derivative, **14**.

---

[16] W. PRITZKOW and K. H. SCHÖPPLER, *Chem. Ber.*, **95**, 834 (1962)

DISCUSSIONS

THE ASSISTED IONIZATION OF 1–X DERIVATIVES

The validity of relationship (1) was also confirmed by the herein reported results. The ratio between the unrearranged and rearranged products (B/C) varies linearly with the sodium acetate concentration in the substituted series (**1**–X, X=Cl, CH_3, OCH_3), as it does in the case of the unsubstituted tosylate, [3] **1**–H. The observed rate constants increase as the electron-repelling effect of the substituent in the aromatic ring is increasing, indicating a charge delocalization in the aromatic ring in the rate determining step. However, the assisted rate constants, $k_{U,A}$ (Table 2) are not correlated with σ^+ values, excluding thus the formation of a benzylic ion **7** in the rate determining step. The data recorded in Table 2 are best fitted with σ^n values, [17] indicating either a phenonium ion **8**, or a bridged ion **6** (Figure 2).

The small negative value ($\rho_{U,A} = -1.17$) of the slope of the correlation line in Figure 2, rules out the phenonium ion **8**, and suggests, as the most probable intermediate of the initial step, the bridged ion **6**. As Bartlett and Sargent have shown, [4] the rate of the formation of bridged ions in π-route reactions depends upon the nucleophilicity of the double bond; the reactivity of the double bond in **1**–X derivatives is expected to be modified by the inductive effect of the substituent in the aromatic ring, in perfect agreement with the observed $\rho_{U,A}$ value.

The analysis of the term R (2) is another proof for the mechanism given in Chart I. This term can be splitted into two factors, a stability factor, S, and a delocalization factor, D :

$$R = \frac{k_P}{k'_C} \cdot \frac{k_{-P}}{k_{-P} + k'''_C} = S \cdot D \qquad (5)$$

The first factor, $S = k_P/k'_C$, measures the ability of the ion pair **4** to discern between different nucleophiles (NaOAc and AcOH, respectively); its value will be greater, the greater the stability of the ion pair.

The delocalization factor, $D = k_{-P}/(k_{-P} + k'''_C)$, represents the molar fraction of the ion pair **5** which reacts to give the unrearranged acetate, B. Its value depends upon the charge distribution in the bridged ion **6**–X; the smaller its value, the greater the charge in the ω position.

---

[17] M. van Bekkum, P. E. Verkade and B. M. Wepster, *Rec. Trav. chim.*, **78**, 815 (1959).

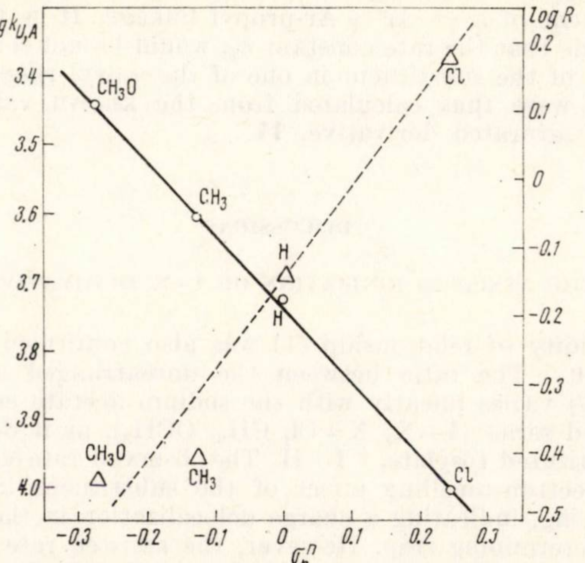

Fig. 2. — The $\rho - \sigma^n$ treatment of the anchimerically assisted rate constants. $k_{U,A}$, at 110° (solid line; $_{U,A}\rho = -1.17$, $r = 0.99$), and of the relative stability factor, R (dashed line; $\rho_R = +1.22$, $r = 0.86$), in the acetolyses of the tosylates **1**.

The delocalization factor, D, measures also the weight of the retro-π-route in this system *).

The R values given in Table 2 seem to be governed by the D-factors. Indeed, it is expected that the charge in the ω position will be more developed in **6**—OCH$_3$ (smallest R-value), and less developed in **6**—Cl (highest R-value), in agreement with the calculated R-values.

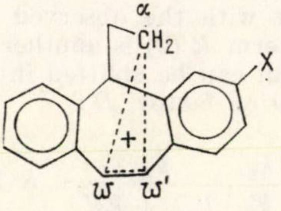

6—X

Similar stability factors, $S = k_P/k'_C$, are expected for bridged ions, **6**—X, but very different values should be anticipated for benzylic ion **7**.

---

*) Felkin and Lion[18] claimed to have discovered the first example of a retro-π-route reaction. Our previous work[3] have already discussed the retro-π-route observed[2] in the acetolysis of the 5H-dibenzo[a, d] cyclohepten-5-yl(β-ethyl) tosylate, **1**—H.

[18] H. Felkin and C. Lion, *Tetrahedron*, **27**, 1375 (1971).

If the stability factors are not very different from each other, a linear free energy relationship of the *R* terms is expected, and this will be essentially a *D*-factor correlation.

D-factors measure also the disappearance of the developed charge in the ionization step. The *R* terms should therefore correlate in their turn with σ^n values, and the sign of the ρ_R parameter should be positive. This was really found to be the case : $\rho_R = +1.22$ (Fig. 2).

Neither from relation (5), nor from figure 3a, it could not have been expected the nearly perfect identity between the absolute values of ρ_R and $\rho_{U,A}$. Indeed, the transition state for the formation of the unrearranged acetate **2** from the ion pair **5** should not be very different from the transition state of the return from the ion pair **4** (Hammond's postulate [19]). A smaller positive value than the absolute value of $\rho_{U,A}$ should have been expected for ρ_R.

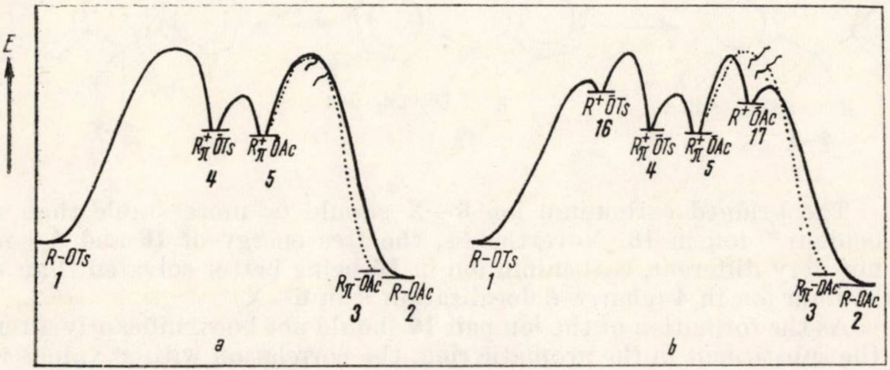

Fig. 3. — Potential energy plot for the acetolysis of **1**$-$X derivatives. a. According Chart I (assisted ionization); b. According Chart III (unassisted ionization).

The found equality

$$|\rho_{U,A}| \approx |\rho_R| \tag{6}$$

is easily interpreted (Figure 3 b), if the mechanism depicted in Chart I is only slightly modified.

$$k_{U,A} = \frac{k_H}{k_{-H}} \cdot k_1 = K_H \cdot k_1 \tag{7}$$

According to Chart III, the initial ionization is not assisted by the double bond, a tight ion pair, **16**, being thus formed. ***The observed anchimeric assistance of the double bond is thus the result of the rearrangement of the ion pair* 16 *in the bridged ion pair* 4*, which lowers the weight of the reversible reaction,*** k_{-H}.

---

[19] G. S. Hammond, *J. Amer. Chem. Soc.*, **77**, 334 (1955).

Chart III

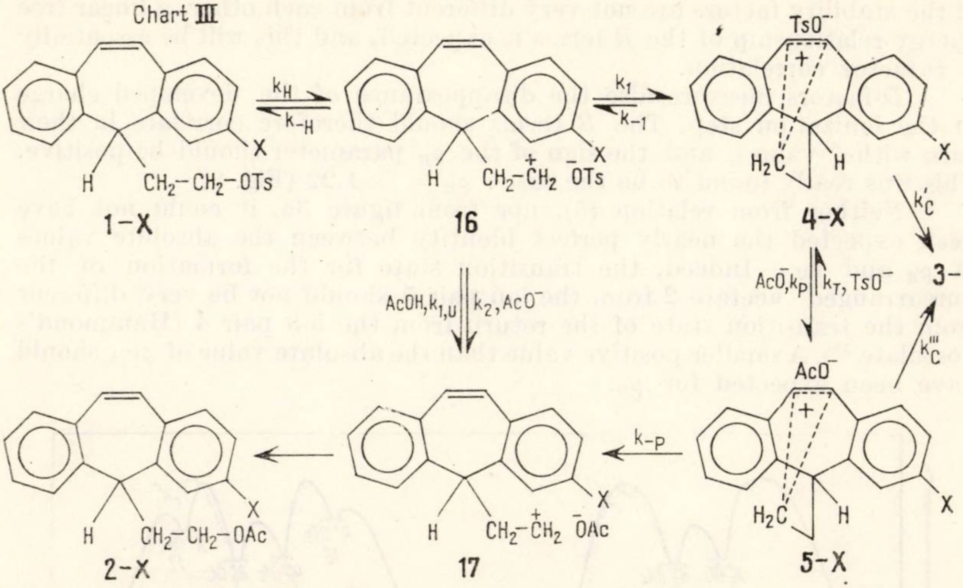

The bridged carbonium ion **6**−X should be more stable than the carbenium[20] ion in **16**. Nevertheless, the free energy of **16** and **4** could be not very different, carbenium ion in **16** being better solvated than the carbonium ion in **4** (charge delocalization[21] in **6**−X).

As the formation of the ion pair **16** should not be significantly altered by the substituent in the aromatic ring, the correlation with σ^n values will depend upon the second step (the formation of the bridged ion pair **4**), and this step would be similar to the reverse reaction, **5**−X → **17** (see Chart III and Figure 3b).

Our interpretation of the anchimeric assistance is in agreement with other known data which will be discussed in another paper.

THE BIMOLECULAR ROUTES IN THE FORMATION OF UNCYCLIZED PRODUCT

The bimolecular routes in the formation of the uncyclized product, **2**−X, labelled in Chart I with $k_{1,U}$ for AcOH and k_2 for AcO- are not essentially different from the retro-π-route in formation of **2**. According to Chart III, either tight ion pair **16**, or ion pair **4** can react with NaOAc. The direct formation of **2**−X from **16**, or the rearrangement of **16** into **4** are similar ; in both reactions, a carbenium ion center in **16** is either captured by a double bond, or by another nucleophile, NaOAc.

The pseudounimolecular reaction ($k_{1,U}$ in Table 2), deserves some further comments. Both electron-repelling and attracting substituents increase the rate constant, $k_{1,U}$ for the unsubstituted derivative, **1**−H.

---

[20] G. A. Olah, *J. Amer. Chem. Soc.*, **94**, 808 (1972).

[21] H. C. Brown, *Chem. Soc. (London), Special Publ.*, **16**, 140 (1962).

The last three rate constants $k_{1,U}$ in Table 2 (X=H, CH_3 and OCH_3) correlate with Brown's σ^+ parameters; the slope, $\rho = -0.52$ agrees fairly well with the ρ parameters for the *ortho*-alkylation of toluene[22] ($\rho = -0.45 .. -0.62$). The capture of the carbenium ion center in **16** by the neighbouring aromatic rings could be an explanation; an Ar_2-5 assisted solvolysis seems attractive. However, the small ratio of this reaction in the overall process of the 1–X acetolysis has not enabled us to bring some other support of that mechanism.

Unimolecular ionization in acidic solvents such as carboxylic acids must be a general route in the solvolysis, even if the radical carrying the leaving group is a primary one. The validity of this assumption is confirmed by the similar ρ values of the NaOAc-buffered acetolysis of primary tosylates (a value $\rho = +1$ can be calculated from the data published by Pritzkow and Schöppler[16]) and the value $\rho_{U,A} = -1.17$ ($\rho_{U,A}$ measures the change in the nucleophile, the double bond, and should therefore have an inverted sign).

EXPERIMENTAL

Melting points are uncorrected. IR spectra were recorded with a double-beam Jena U.R.–20 spectrophotometer. NMR spectra were obtained on a Varian A–60A spectrometer, using TMS as internal standard.

3-Substituted-5H-dibenzo [*a, d*] *cyclohepten-5-ones*, **9**, are known compounds : **9**–Cl[23]; **9**–CH_3[23]; **9**–OCH_3.[24]

3-Substituted-5H-dibenzo [*a, d*] *cyclohepten-5-ols*, **10** :

– **10**–CH_3[25] and **10**–OCH_3[24] are known compounds;

– **10**–Cl was prepared by reducing **9**–Cl with sodium borohydride in methanol, as **10**–CH_3[25]. After two recrystallizations from ligroin, **10**–Cl melted at 140–2°. Anal. : Found : C, 73.31 ; H, 4.70 ; Cl, 15.30. Calcd. for $C_{15}H_{11}ClO$: C, 74,23 ; H, 4.57 ; Cl, 14,61 %. IR spectrum (CCl_4, cm^{-1}) : 1045 s, 3638 s.

3-Substituted-5H-dibenzo [*a, d*] *cyclohepten-5-yl-acetic acids*, **11**. The used procedure is based on that reported earlier [26,2] for the unsubstituted acid, **11**—H.

A solution of **10**–X and malonic acid in anhydrous acetic acid (molar ratio, 1 : 2 : 50) was heated under reflux for 20 hrs. Evaporation under reduced pressure gave an oily residue which was dissolved in ether. The resulting solution was extracted with a 10 % sodium hydroxide solution. When acidified with hydrochloric acid under cooling, a crystalline precipitate appeared.

– **11**–Cl : 97 % yield, m.p. 158–9° (ethanol-water, 2 : 1). Anal. : Found : C, 71.45 ; H, 4.87 ; Cl, 12.64. Calcd. for $C_{17}H_{13}ClO_2$: C, 71.71 ; H, 4.61 ; Cl, 12.45 %. IR spectrum (CS_2, cm^{-1}) : 735 m, 760 m, 786 s, 830 s, 1710 vs, 2600–3200 m, broad.

---

[22] F. Badea, "Mecanisme de Reacţie în Chimia Organică", Ed. Ştiinţifică, Bucureşti, 1971, p. 324.

[23] N. V. Koninklijke, *Pat. Brit.* 943, 604 (1963) ; *Chem. Abstr.*, **61**, 4293 (1964).

[24] G. Berti, A. Daseltino, G. Gregori and F. Marcini, *Ann. Chim.* (*Ital.*), **52**, 514 (1962).

[25] C. van der Stelt, A. F. Harms and W. Th. Nauta, *J. Med. Pharm. Chem.*, **4**, 335 (1961) ; *Chem. Abstr.*, **56**, 7241 (1962).

[26] C. van der Stelt, A. Haasjes, H. M. Tersteege and W. A. Nauta, *Rec. Trav. chim.*, **84**, 1466 (1965).

— **11**—CH_3 : 77% yield, m.p. 177—8° (ethanol). Anal. : Found : C, 81.68 ; H, 6.35. Calcd. for $C_{18}H_{16}O_2$: C, 81.79 ; H, 6.10%. IR spectrum (CS_2, cm^{-1}) : 745 m, 757m, 766m, 790m, 830s, 930m, broad, 1310s, 1710vs, 2400—3300m, broad.

—**11**—OCH_3 : 80% yield, m.p. 158—9° (ethanol, 90%). Anal. : Found . C, 76.39 ; H, 5.90. Calcd. for $C_{18}H_{16}O_3$: C, 76.11 ; H, 6.07%.

Methyl esters of 3-substituted-5H-dibenzo [a, d] cyclohepten-5-yl-acetic acids, **12**.

The corresponding acid **11** was dissolved in methanol (molar ratio, 1 : 200) previously saturated with gaseous hydrochloric acid. This solution was refluxed for 20 hrs. Most of the alcohol was removed by distillation (reduced pressure, steam bath), and the resulting solution was diluted with ether. This extract was washed with water, then with a 10% sodium carbonate solution, again with water, and dried over anhydrous sodium sulfate. The solvent was removed under reduced pressure, yielding a colourless oil.

— **12**—Cl : virtually quantitative yield, m.p. 52—3° (methanol). Anal. : Found : C, 72.25 ; H, 5.28 ; Cl, 12.21. Calcd. for $C_{18}H_{15}ClO_2$: C, 72.36 ; H, 5.06 ; Cl, 11.87%. IR spectrum (CCl_4, cm^{-1}) : 1165vs, 1247vs, 1300s, 1743vs.

— **12**—CH_3 : 92% yield. Anal. : Found : C, 81.22 ; H, 6.91. Calcd. for $C_{19}H_{18}O_2$: C, 81.99 ; H, 6.52%.

— **12**—OCH_3 : 90% yield. IR spectrum (CCl_4, cm^{-1}) : 1159s, 1263s, 1743vs.

3-Substituted-5H-dibenzo [a, d] cyclohepten-5-yl-(β-ethanol), **13**.

A solution of **12** in anhydrous ether was added for a period of 3/4 hr to a stirred mixture of an equal amount of lithium aluminium hydride and ether. The mixture was heated at reflux for 2 hrs, and left overnight, then cooled with ice, and a 10% solution of sulfuric acid was then added. The aqueous layer was extracted four times with ether. The combined organic layers were washed with water and dried over anhydrous sodium sulfate. The solvent was removed under reduced pressure to give a colourless liquid in virtually quantitative yield. The NMR data listed in Table 3 were in agreement with the assigned position of the substituent.

— **13**—Cl : The vapour phase chromatogram showed a major peak (98.8% of total area). Anal. : Found : C, 74.36 ; H, 5.94 ; Cl, 11.92. Calcd. for $C_{17}H_{15}ClO$: C, 75.41 ; H, 5.59 ; Cl, 13.09%. IR spectrum (CCl_4, cm^{-1}) : 1040vs, 3648 m.

—**13**—CH_3 : m.p. 68—9° (ethanol). The vapour phase chromatogram of this material showed a major peak (95.3% of total area). Anal. : Found : C, 85.88 ; H, 7.29. Calcd. for $C_{18}H_{18}O$: C, 86.36 ; H, 7.25%. IR spectrum (CCl_4, cm^{-1}) : 1040vs, 3648m.

— **13**—OCH_3 : The vapour phase chromatogram showed a major peak (94.9% of total area). Anal. : Found : C, 80.65 ; H, 7.21. Calcd. for $C_{18}H_{18}O_2$: C, 81.16 ; H, 6.76%. IR spectrum (CCl_4, cm^{-1}) : 1041vs, 3639m.

Tosylates of 3-substituted-5H-dibenzo [a, d] cyclohepten-5-yl-(β-ethanol), **1**. The tosylates **1**—Cl and **1**—CH_3 were prepared essentially following the mentioned procedure [2] for the unsubstituted tosylate, **1**—H.

The alcohol **13** was dissolved in dry pyridine, and solid *p*-toluenesulfonyl chloride (molar ratio, 1 : 40 : 1.1) was added. The mixture was swirled until all the chloride had dissolved. The solution was kept at 0° for 4 days, during which time large crystals of pyridine hydrocloride formed. A solution of ice-water and hydrochloric acid was added and the mixture extracted three times with methylene chloride. The combined extracts were washed successively with dilute hydrochloric acid, water, diluted sodium carbonate solution, and water ; the solution was then dried over anhydrous magnesium sulfate, and methylene chloride was removed at 30° under reduced pressure. A clear oil separated ; after several days this oil solidified to produce white needles of tosylate.

Table 3

NMR spectra of the alcohols 13a)

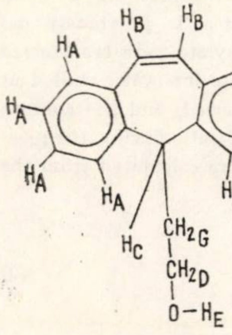

13

X	H_y		δ ppm	J Hz
Cl	7 H_A	multiplet	6.85 – 7.30	
H	8 H_A	multiplet	7.10 – 7.40	
CH_3	7 H_A	multiplet	6.80 – 7.15	
OCH_3	7 H_A	multiplet	7.00 – 7.50	
Cl	2 H_B	singlet	6.70	—
H	2 H_B	singlet	6.82	—
CH_3	2 H_B	singlet	6.70	—
OCH_3	2 H_B	singlet	6.82	—
Cl	1 H_C	triplet	4.08	7.5
H	1 H_C	triplet	4.15	8.0
CH_3	1 H_C	triplet	4.08	7.5
OCH_3	1 H_C	triplet	4.18	7.0
Cl	2 H_D	triplet	3.12	6.0
H	2 H_D	triplet	3.20	6.0
CH_3	2 H_D	triplet	3.10	6.0
CH_3O	2 H_D	triplet	3.33	6.0
Cl	1 H_E	singlet	2.83	—
H	1 H_E		....	—
CH_3	1 H_E	singlet	2.75	—
CH_3O	1 H_E		....	—
Cl				—
H	1 H_F		....	—
CH_3	3 H_F	singlet	2.25	—
OCH_3	3 H_F	singlet	3.83	—
Cl	2 H_G	quartet	1.80	
H	2 H_G	quartet	1.85	
CH_3	2 H_G	quartet	1.82	
OCH_3	2 H_G	quartet	1.98	

a) In carbon tetrachloride; tetramethylsilane as reference.

— **1**–Cl: m.p. 106–7° (ethanol). Anal: Found: C, 67.68; H, 5.07; Cl, 8.48. Calcd. for $C_{24}H_{21}ClO_3S$: C, 67.83; H, 4.98; Cl, 8.34%. IR spectrum (CS_2, cm^{-1}): 1175vs, 1186vs, 1368vs.

— **1**–CH_3: 77% yield, m.p. 155–6° (ethanol). Anal.: Found: C, 73.93; H, 6.32; S, 7.67. Calcd. for $C_{25}H_{24}O_3S$: C, 74.22; H, 5.98; S, 7.93%. IR spectrum (CCl_4, cm^{-1}): 1176vs, 1188vs, 1368vs.

— **1**–OCH_3: A 0.3 g sample (1.12 mmoles) of **13**–OCH_3 was dissolved in 0.5 ml of anhydrous ether and 0.14 ml of dry pyridine; 0.25 g (1.31 mmoles) of *p*-toluenesulfonyl chloride was added and the solution was kept at 0° for 2 days. This procedure [27] gave 0.4 g (85% yield) of **1**–OCH_3, m.p. 77–9° (methanol). Anal.: Found: C, 71.68; H, 5.99; S, 6.93. Calcd. for $C_{25}H_{24}O_4S$: C, 71.20; H, 5.72; S, 7.71%. IR spectrum (CCl_4, cm^{-1}): 1176vs, 1187s, 1370s.

---

[27] R. Huisgen and G. Seidl, *Chem. Ber.*, **96**, 2740 (1963).

The ratio of the uncyclized to cyclized products, B/C, was measured spectrophotometrically, [3] taking advantage of the 293 mμ absorption band corresponding to the stilbene system of the compounds **1** and **2**. The applicability of the Lambert-Beer's law was verified. The extinction coefficients are : $\varepsilon_{1-\mathrm{Cl}} = 15{,}030$; $\varepsilon_{1-\mathrm{CH_3}} = 13{,}460$; $\varepsilon_{1-\mathrm{OCH_3}} = 13{,}150$.

When the reaction is completed (more than ten half-lives), the ratio of the uncyclized to cyclized products (the double bond is involved in the formation of the cyclized products and they do not contain the stilbene system) was calculated from the equation [3] :

$$\left(\frac{B}{C}\right)_{\infty} = \frac{E_{\infty}}{E_0 - E_{\infty}} \tag{8}$$

Kinetic measurements were performed in anhydrous acetic acid containing a small amount of acetic anhydride. [3] Sodium acetate solutions were obtained as is previously described.[3] Solutions of desired concentration (about 10^{-5} moles/l) of tosylate were transferred in sealed tubes and thermostated. They were withdrawn at appropriate intervals, chilled at room temperature (in these conditions the reaction is practically quenched) and the content was introduced in spectrophotometric cuve. As the constance of the *B/C* ratio during the reaction time had been demonstrated in these cases, the rate constants were calculated from the equation (9), which gave the real constant :

$$k = \frac{2.303}{t} \log \frac{E_0 - E_{\infty}}{E - E_{\infty}} \tag{9}$$

Acknowledgements. The authors wish to express their special gratitude to Professor Ecaterina Ciorănescu-Nenitzescu for helpful guidance throughout the progress of this research. They thank Miss E. Sliam and Mrs. V. Daniel for elementary analyses, M. Elian for IR spectra and F. Chiraleu for NMR spectra.

Revue Roumaine de Chimie, **18**, *1*, 145–153 (1973)

CHARACTERIZATION OF THE CERAMIC ION-SELECTIVE MEMBRANE-ELECTRODES. IV *

INFLUENCE OF THE OBTAINING CONDITIONS OF Ag_2S MEMBRANE UPON THE WORKING OF Ag^+-SELECTIVE MEMBRANE-ELECTRODE

I. C. POPESCU, C. LITEANU and V. CIOVÎRNACHE

"Babeş-Bolyai" University, Department of Analytical Chemistry,
Str. Arany János 11, Cluj, Romania

Received March 11, 1972

Results of a detailed study concerning the influence of the obtaining conditions of the Ag_2S ceramic membrane (granulation, pressing pressure and membrane thickness) upon the electrode function and electric resistance of Ag_2S membrane-electrode are presented. Statistical interpretation of the experimental results leads to the conclusion that in the region explored the parameters studied do not affect the electrode function of the Ag^+-selective membrane-electrode.

In a previous paper some characteristics and applying of a new type of Ag^+-selective membrane-electrode has been shown. [1]

The functional element which gives the selectivity of the membrane electrode, is made of Ag_2S powder. By quasi-stationary double faced pressing this gives a rigid ceramic compact with variable thickness and diameter.

Fixing the so-obtained membrane at the extremity of an electrochemically inactive tube, one obtains a membrane-electrode with good selectivity for Ag^+ ion. [2]

Based on these preliminary results, it has further on been tested if, and to what extent, a number of factors as : powder granulosity, pressing-pressure and membrane thickness, have an influence upon the electrode function *E*-*p*Ag. At the same time, the electrical resistance of the membranes obtained in various conditions has been evaluated. In the following part, the results of the measurements accomplished in this sense are shown together with their statistical interpretation.

---

* Part III. C. Liteanu and I. C. Popescu, *Stud. Univ. Babeş-Bolyai, Chem.*, **17**, 45 (1972).

[1] C. Liteanu, I. C. Popescu and S. B. Domşa, Romanian Patent, 67066 (1971).

[2] C. Liteanu, I. C. Popescu and V. Ciovîrnache, *Talanta*, **19**, 985 (1972).

EXPERIMENTAL PART

The Ag_2S powder has been obtained by precipitation with H_2S from an aqueous $AgNO_3$ solution. The precipitate, after washing (free of H_2S) and drying (24 h at 105°) has been finely powdered and washed with CCl_4 (in order to remove the sulphur traces). After eliminating CCl_4 it was powdered again under C_6H_6 in an agate mortar. The dried precipitate (24 h at 105° under stirring) has been sorted by mechanical sieving in five fractions; 1) < 0.05 mm, 2) 0.05–0.125 mm, 3) 0.125–0.16 mm, 4) 0.16–0.25 mm; 5) 0.25–0.5 mm.

The pressing has been carried out in a rigid matrix. The surface of the membranes obtained was of 1 cm.^{2}

The membrane-electrode was made according to the previously reported procedure[1], with the only difference that the potential of the inner face of the membrane has been taken over by a platinum electrode through a mercury layer.

Thus, recording of the electrode function $E-p$Ag corresponds to the measurement of e.m.f. of the following cell:

$$(-)\text{SCE} \left\| \begin{array}{l}\text{bridge of 0.1M KNO}_3\\ \text{agar-agar}\end{array} \right\| \begin{array}{l}\text{test}\\ \text{solution}\end{array} \left| \begin{array}{l}\text{Ag}_2\text{S}\\ \text{membrane}\end{array} \right| \text{Hg, Pt } (+) \tag{1}$$

The test solutions of different pAg have been obtained by diluting an exactly 0.1M $AgNO_3$ solution prepared by weighing.

E.m.f. has been measured with an electronic potentiometer (Radelkis OH 102). The test solution was magnetically stirred. The working temperature was of 25 ± 0.1°.

RESULTS

A. THE ELECTRODE FUNCTION

The influence of granulation of the Ag_2S powder. From the Ag_2S powder fractions obtained membranes have been pressed. The electrode function $E-pAg$ of the corresponding membrane-electrodes has been traced, both at variable ionic strength and at $\mu = 0.1$ M (obtained by adjusting the concentration of the test solutions with KNO_3). The pressing pressure has been of 24 t/cm². Results of the e.m.f. measurements of the cell (1) at $\mu =$ variable and $\mu = 0.1$ M are presented in table 1.

In table 1 are also given the coefficients E_0 and $2.303 \times RT/F$ from the equation of the electrode function (calculated by means of the least square method)

$$E = E_0 - \frac{2.303\ RT}{F} p\text{Ag} \tag{2}$$

corresponding to the studied electrodes, as well as the dispersion of the experimental values referred to the values calculated from the equation of the straight line (2)

$$s^2 = \sum_{1}^{n} \frac{[E_{i\,(\text{exp})} - E_{i\,(\text{calc})}]^2}{n-2} \tag{3}$$

Table 1

Influence of the granulation on the electrode function

Fraction	< 0.05		$0.05-0.125$		$0.125-0.16$		$0.16-0.25$		$0.25-0.50$	
Thickness (mm)	3.55		5.27		4.84		4.85		4.83	
	E(mV)		E(mV)		E(mV)		E(mV)		E(mV)	
pAg	μ=var.	$\mu=0.1$	μ=var.	$\mu=0.1$	μ=var.	$\mu=0.1$	μ=var.	$\mu=0.1$	μ=var.	$\mu=0.1$
	1	2	3	4	5	6	7	8	9	10
6.0	372.0	360.0	368.0	365.0	362.0	345.0	316.0	322.0	312.0	326.0
5.0	420.0	397.0	435.0	402.0	420.0	396.0	378.0	368.0	366.0	368.0
4.0	480.0	455.0	486.0	459.0	486.0	455.0	435.0	422.0	420.0	424.0
3.0	546.0	515.0	552.0	520.0	552.0	518.0	498.0	486.0	480.0	487.0
2.0	604.0	578.0	608.0	582.0	608.0	580.0	556.0	545.0	540.0	546.0
1.0	660.0	640.0	664.0	644.0	660.0	641.0	608.0	610.0	608.0	611.0
0.0	704.0	—	708.0	—	706.0	—	656.0	—	640.0	—
E_0	712.3	691.1	717.3	694.9	715.8	698.7	644.0	662.3	651.0	662.5
$\frac{2.302\ RT}{F}$	57.1	57.2	57.1	57.0	57.6	59.8	57.2	58.1	56.7	57.8
s^2	42.6	71.7	45.0	80.5	57.6	16.5	33.4	45.7	67.0	59.0

The influence of the pressing pressure. From Ag_2S powder corresponding to the fraction 0.05—0.125 membranes have been pressed at different pressures. Results of the $E-p$Ag measurements at $\mu =$ variable and $\mu = 0.1$ M are given in table 2 together with the coefficients corresponding to the equation (2) and dispersion value (3).

The influence of the membrane thickness. From the fraction 1 (< 0.05) membranes of different thickness have been pressed. The pressing pressure was the same in all of the cases (24 t/cm^2). Results of the e.m.f. measurements of the cell (1), at $\mu =$ variable and $\mu = 0.1$ M, together with the coefficient values from the equation (2) and with the value of the expression (3) are given in table 3.

Experimental results presented in tables 1—3 have been submitted to a statistical analysis in order to establish if the factors examined affect the behaviour of the electrode or not. The analysis included the statistical testing of the identity of two straight lines, [3] chosen from the same group of experiments such that to seem to be, at the first sight, the most different. If an insignificant difference is observed, this conclusion will be simplicitly extended upon the whole group of experiments. Further on, a calculation example is given corresponding to the data tabulated in table 1 (columns 1, 3, 5, 7 and 9).

In the first place, it was tested with the aid of the bilateral F criterion, if the most different regressional dispersions (s_5^2 and s_4^2, defined

---

[3] B. B. Nalimov, „Primenenie matematiceskoi statistiki pri analize vescestva", Moskva 1960, p. 103—106.

Table 2

The influence of the pressing pressure on the electrode function

Pressure (10^3 At/cm^2)	16		20		26		34		40	
Thickness (mm)	2.41		3.00		2.20		2.63		2.29	
	E(mV)		E(mV)		E(mV)		E(mV)		E(mV)	
pAg	μ=var.	$\mu = 0.1$	μ=var.	$\mu = 0.1$	μ=var.	μ=0.1	μ=var.	μ=0.1	μ=var.	μ=0.1
	1	2	3	4	5	6	7	8	9	10
7.0	140.0	—	124.0	—	114.0	—	116.0	—	150.0	—
6.0	180.0	160.0	168.0	186.0	164.0	192.0	162.0	199.0	194.0	222.0
5.0	240.0	214.0	228.0	228.0	229.0	225.0	221.0	256.0	228.0	249.0
4.0	312.0	304.0	300.0	294.0	300.0	288.0	300.0	290.0	330.0	320.0
3.0	376.0	378.0	366.0	362.0	366.0	256.0	364.0	358.0	394.0	387.0
2.0	433.0	438.0	422.4	426.0	422.4	418.0	420.0	420.0	452.2	450.0
1.0	487.0	504.0	477.0	483.0	476.0	480.0	473.0	480.0	506.0	510.0
0.0	534.0	—	525.0	—	523.2	—	525.0	—	552.0	—
E_0	543.4	551.1	535.4	544.5	535.4	536.0	524.2	538.0	563.7	567.3
$2.302\frac{RT}{F}$	58.8	59.1	58.7	61.3	60.4	60.1	60.2	60.0	59.8	60.3
s^2	83.6	742.3	73.0	55.7	83.0	156.0	78.0	115.0	90.6	152.0

by the equation (3), are significantly different or not. Since

$$F_{\text{calc}} = \frac{s_5^2}{s_4^2} = 2.68 < F_{\text{tab}\ [\alpha = 0.02\ (5.5)]} = 11.00 \tag{4}$$

it follows that the two most different regressional dispersions do not differ significantly. That is why, with the aid of the equation

$$\overline{s}^2 = \frac{(n_3 - 2)\, s_3^2 + (n_5 - 2)\, s_5^2}{n_3 + n_5 - 4} \tag{5}$$

(where $n_3 = n_5 = 7$ stand for the number of experimental points corresponding to the two straight lines), the weighted mean dispersion has been calculated for the straight lines which have the most different slopes (table 1, columns 5, 9).

Using this weighted mean dispersion ($\overline{s}^2 = 62.3$) the dispersion of the difference of the two slopes from equation (2) has been evaluated

$$s^2_{b_3 - b_5} = \overline{s}^2 \left[\frac{1}{\sum\limits_1^n x_{3i}^2 - n_3 \overline{x}_3^2} + \frac{1}{\sum\limits_1^n x_{5i}^2 - n_5 \overline{x}_5^2} \right] \tag{6}$$

Table 3

Influence of the membrane thickness on the electrode function

Thickness (mm)	0.68		1.07		1.57		1.98		2.96		3.64		6.30	
	E(mV)		E(mV)		E(mV)		E(mV)		E(mV)		E(mV)		E(mV)	
pAg	μ = var.	μ=0.1	μ = var.	μ=0.1	μ = var.	μ=0.1	μ = var.	μ=0.1	μ = var.	μ=0.1	μ = var.	μ=0.1	μ = var.	μ=0.1
	1	2	3	4	5	6	7	8	9	10	11	12	13	14
7	348.0	—	—	—	340.0	—	348.0	—	328.0	—	340.0	—	336.0	—
6	380.0	393.0	372.0	384.0	372.0	384.0	376.0	384.0	378.0	375.0	368.0	384.0	364.0	378.0
5	444.0	444.0	432.0	432.0	432.0	429.0	432.0	432.0	426.0	423.0	426.0	426.0	426.0	423.0
4	504.0	504.0	492.0	492.0	492.0	489.0	492.0	492.0	483.0	483.0	486.0	486.0	480.0	480.0
3	585.0	570.0	570.0	559.0	570.0	555.0	573.0	558.0	558.0	549.0	564.0	552.0	558.0	546.0
2	637.0	648.0	628.0	620.0	624.0	616.0	627.0	620.0	620.0	600.0	620.0	613.0	616.0	608.0
1	690.4	692.0	680.0	682.0	678.0	679.0	680.0	680.0	672.0	672.0	674.0	672.0	668.0	670.0
0	738.0	—	728.0	—	725.0	—	726.0	—	720.0	—	720.0	—	715.0	—
E_0	746.9	759.1	735.4	740.3	732.4	735.5	733.1	738.6	726.1	725.2	726.8	728.9	721.2	725.6
$2.302\ \frac{RT}{F}$	58.8	62.1	58.6	60.6	58.1	60.0	57.5	60.3	58.0	59.5	57.7	59.0	57.4	59.4
s^2	148.5	81.5	143.7	56.5	130.7	39.0	172.6	28.0	79.3	42.5	158.2	50.0	154.6	47.5

where: $x_{3_i}^2$ and $x_{5_i}^2$ stand for the squares of pAg values in table 1, columns 5 and 9, respectively; $-\overline{x}_3^2$ and $\overline{x}_5^2$ stand for the squares of the mean pAg values in table 1 columns 5 and 9, respectively.

With the aid of these values ($s^2_{\mathrm{b_3-b_5}} = 4.45$) the value

$$t_{\mathrm{calc}\ (b_3-b_5)} = \frac{b_3 - b_5}{s_{b_3-b_3}} = 0.43 < t_{\mathrm{tab}\ [\alpha = 0{,}02;\ K = 10]} = 3.17 \tag{7}$$

Since the variable "t"$_{\mathrm{calc}}$ < "t"$_{\mathrm{tab}}$ it results that the deviation from the parallelism of the two straight lines is statistically insignificant.

In order to prove the identity of the two straight lines it was observed that

$$\overline{x}_3 = \overline{x}_5 = 3.00 \tag{8}$$

where: $\overline{x}_3$, $\overline{x}_5$ stand for the mean values of pAg in table 1, columns 5 and 9, respectively. That is why, in order to establish the identity of the two straight lines, it would be necessary and sufficient that also

$$\overline{E}_3 \equiv \text{statistically } \overline{E}_5 \tag{9}$$

where $\overline{E}_3$ and $\overline{E}_5$ stand for the mean value of E in table 1, columns 5 and 9, respectively.

By using the bilateral "t" criterion, the following relation has been obtained, indeed.

$$t_{\mathrm{calc}\ (\overline{E}_3\ -\ \overline{E}_5)} = 1.04 < t_{\mathrm{tab}\ [\alpha\ =\ 0{,}02;\ \mathrm{K}\ =\ 12]} = 3.06 \tag{10}$$

consequently, the two straight lines are statistically identical.

B. ELECTRIC CONDUCTIVITY

The electric conductivity of the membranes obtained has been measured by means of the connection given in fig. 1, using a Radelkis OK 102 type conductometer (*c*).

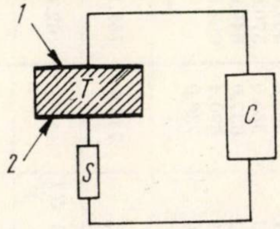

Fig. 1. — Schematic diagram of the working device for conductivity measurements at room temperature.

1,2 — Pt contacts (plates); *T* — tablet; *S* — spring; *C* — conductivity meter;

In order to realize reproducible measurements, it was necessary to assure firstly a constant pressing force of the contacts on the surface of the pellet. Therefore, the spring (*R*) which is the support of the mobile contact (2) was always compressed to a constant length. Meanwhile, in order to eliminate the influence of the membrane thickness upon the conductivity values measured, the specific conductivity has been calculated by referring the measured values to the membrane thickness (these membranes have a surface of 1 cm^2). In table 4 the mean results of three conductivity measurements ($t=25°$) are presented for each membrane obtained in different conditions.

Table 4

Influence of the granulation and pressing pressure on the membrane conductivity

Fraction	Number of used membranes	Pressure of pressing (10^{-3} At/cm^2)	σ ($10^3 \Omega^{-1}$cm^{-1})
<0.05	5	16	84.6± 6.75
<0.05	1	20	*256.5±24.5
<0.05	1	26	*117.2±25.3
<0.05	1	34	73.4±24.3
0.05 −0.125	4	16	17.9± 5.5
0.05 −0.125	2	20	19.5± 3.9
0.05 −0.125	2	26	14.0± 5.8
0.05 −0.125	2	34	21.2± 7.6
0.05 −0.125	3	40	16.8± 3.6
0.125−0.16	5	16	33.1± 9.6
0.125−0.16	3	20	70.5±16.6
0.125−0.16	3	26	58.2±15.6
0.125−0.16	2	34	68.5± 9.2
0.16 −0.25	5	16	11.4± 3.3
0.16 −0.25	2	20	20.8± 3.1
0.16− 0.25	3	26	24.6± 4.6
0.16 −0.25	3	34	28.8± 3.4
0.25 −0.50	5	16	6.1± 0.8
0.25 −0.50	3	20	14.9± 1.3
0.25 −0.50	3	26	20.9± 3.7
0.25 −0.50	3	34	21.8± 5.5

* dubious experimental values.

Further on, conductivity measurements have been performed at different temperatures. Previously, the thermogram of the Ag_2S powder used has been recorded (fig. 2).

From the thermogram, the possibility of performing measurements in the 50−530° interval has been established. Practically, measurements have been carried out in the 50−190° interval using the connection given in fig. 3. Data obtained are shown in fig. 4. By means of the least square method the equation of the $\sigma(\Omega^{-1}\ \mathrm{cm}^{-1})$ vs T(K) dependence has been calculated.

$$\sigma = 580 \times e^{-4.58 \times 10^3/T}$$

and $E^{\neq} = 0.43$ eV.

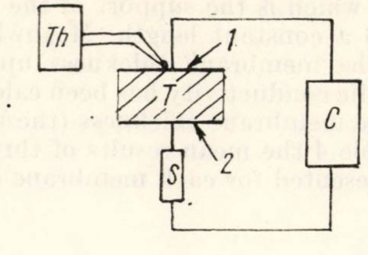

Fig. 2. — Schematic diagram of the device used for conductivity measurements at various temperatures.
1, 2-Pt contacts (plates) ; $T-Ag_2S$ tablet ; S-spring ; C-conductivity meter ; Th-thermocouple.

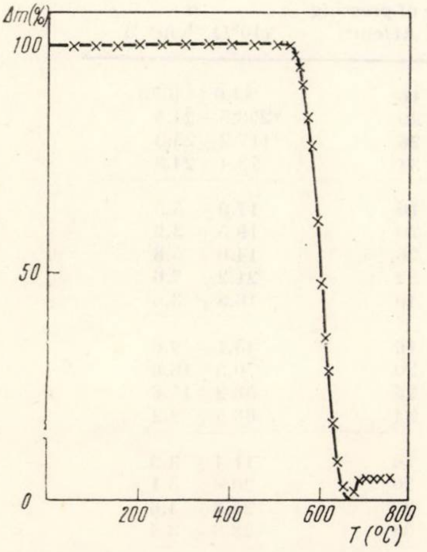

Fig. 3. — Thermogram for used Ag_2S.

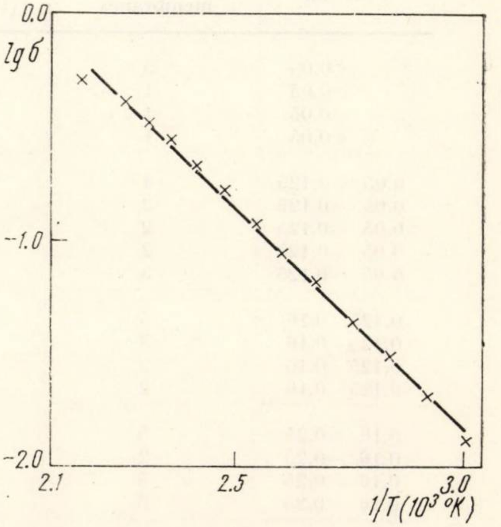

Fig. 4. — Dependence of the Ag_2S electric conductivity on temperature.

DISCUSSION AND CONCLUSIONS

The electrode function. The experimental data collected and their statistical interpretation have proved that neither the granulosity and the thickness of the membrane, nor the pressing pressure have any influence upon the electrode function, certainly, in the region investigated by us. Evidently in elaboration of a membrane with optimal properties, one must take into account and other points of view too, such as economicity, mechanical resistance and so on.

Electric resistance. The values in table 4 indicate also the significant independence of the conductivity values from the obtaining conditions of the membrane (granulosity and pressure). However, it must be noticed that the conductivity values characteristic for the Ag_2S powder compacts

($20 - 50 \times 10^{-3}\ \Omega^{-1}\ cm^{-1}$ on an average) are very small as compared to the Ag_2S crystals $500-800\ \Omega^{-1}\ cm^{-1}$.

The temperature dependence of the conductivity obeys an increasing exponential law, proving, in this way, the mixed character of the conductivity of the Ag_2S powder compacts.

In conclusion, the Ag_2S powder compacts, obtained at pressures between 16–40 t/cm^2, allow Ag^+ -selective membrane-electrodes, with good electrochemical properties, to be obtained.

Revue Roumaine de Chimie, **18**, *1*, 155–159 (1973)

PAPER THERMOCHROMATOGRAPHY. XVII *
THE SEPARATION OF LEUCINE AND ISOLEUCINE IN TEMPERATURE GRADIENT

C. LITEANU and A. CONSTANTINESCU

"Babeş-Bolyai" University, str. Arany Janos, 11, Cluj, Military Academy, Şos. Panduri nr. 68–70, Bucharest, Romania

Received March 21, 1972

The separation of leucine from isoleucine in temperature gradient on continuous strip chromatograms and on chromatograms with baffles was studied. The growing effect of the chromatographic column length was determined in temperature gradient conditions for both forms of the chromatograms used. In the case of the chromatogram with baffles a greater increase of the separation effect of the temperature gradient was observed ; this favours the separation of the two amino acids which in the conditions of the isothermal chromatography have very close R_f values.

The separation of leucine and isoleucine from complex mixtures cannot be achieved by ascending and descending chromatography with different solvent systems, [1-5] including Mathias isothermic chromatography. [6] The papers published by one of the authors have demonstrated the possibility of chromatographic separation of some anorganic and organic compounds having very close R_f values, by using the temperature gradient. [7-17] Therefore using the solvent system n-butanol + acetic acid + water (4 : 1 : 5 v/v) we aimed to separate leucine and isoleucine by applying the temperature gradient process to a variant of Mathias chromatogram, worked out by us.

---

* This paper was read at the Third National Conference of Analytical Chemistry held at Braşov, September, 1971. Part. XVI : S. Gocan, C. Ciupala-Costea, T. Hodisan and C. Liteanu, **17**, 1069 (1971).

[1] L. B. Rockland and J. C. Underwood, *Analyt. Chem.*, **26**, 1557 (1954).
[2] T. Wieland, *Angew. Chem.*, **60**, 313 (1951).
[3] S. M. Partridge, *Biochem. J.*, **42**, 238 (1948).
[4] G. Biserte and M. Dautrevaux, *Prod. probl. pharm.*, **8**, 374 (1963).
[5] K. N. Saxena and J. R. Grandi, *J. Chromatog.*, **8**, 546 (1962).
[6] W. Mathias, *Naturwiss.*, **41**, 17 (1954).
[7] C. Liteanu and S. Gocan, *Stud. Univ. Babeş-Bolyai, Chem.*, **6**, 99 (1961).
[8] *Idem, ibid.*, **7**, 99 (1962).
[9] *Idem, ibid.*, **11**, 74 (1966).
[10] *Idem, Rev. Chim. Acad. R.P.R.*, **7**, 1041 (1962).
[11] *Idem, Rev. Roumaine Chim.*, **9**, 651 (1964).
[12] *Idem, ibid.*, **10**, 1054 (1965).
[13] *Idem, Bull. Soc. chim. France*, **1969**, 1416.
[14] *Idem, ibid.*, **1967**, 3836.
[15] S. Gocan and C. Liteanu, *Rev. Roumaine Chim.*, **9**, 715 (1964).
[16] C. Liteanu, F. Margineanu and D. Macarovici, *Rev. Roumaine Chim.*, **12**, 503 (1967).
[17] C. Liteanu and N. Dulamita, *Rev. Roumaine Chim.*, **13**, 437 (1968).

With this end in view, the chromatographic paper has two baffles coupled in series, continued by an ascending chromatographic migration band (fig. 1).

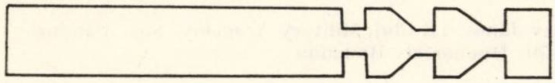

Fig. 1. – Paper chromatogram with baffles.

The chromatographic chamber used is described in a previous paper [13] and the working techniques are the same as in the above mentioned papers. We have first used isothermal chromatography on a paper provided with the two baffles, after which increasing temperature differences between the lower and upper parts of the paper (temperature gradient) were applied, until a satisfactory separation was obtained, the spots of the two amino-acids becoming tangent.

The behaviour of leucine and isoleucine on continuous paper chromatographic strips without baffles was studied concomitantly both isothermically and in temperature gradient, with the same Δt values and the same working time. The data obtained are summarized in tables 1 and 2.

For $\Delta t = 40°$ (t. grad $= 5.88°/\text{cm}$) the separation of leucine and isoleucine can be taken into consideration for both chromatogramic forms.

The optimum estimation criterion for the efficiency of chromatographic separation obtained is the comparison of the "growing of the chromatographic column length" effect in temperature gradient conditions, which can be calculated by means of the Liteanu & Gocan [14] relation

$$(R_f)_{t.\text{grad}} = (R_f)_{\text{isoth}} \times \frac{V + \Delta V}{V} \tag{1}$$

where V is the volume of the mobile phase and ΔV the additional volume of eluent which leaves the chromatographic column owing to the unsaturated atmosphere and its condensation on the eluent surface in the beaker.

By substituting the data in table 1 for t. grad $= 5.88°/\text{cm}$ in relation (1), one obtains :

a) for a paper chromatogram with baffles :

$$0.04 = 0.01 \times \frac{V + \Delta V}{V}$$

or $0.01\ \Delta V = 0.03$ V ; i.e. $\Delta V = 3$ V and because $V = lA_M$ (A_M is the mobile phase section and l is the startfront eluent distance), it results that : $\Delta l = 3l$ i.e. $\Delta l = 3 \times 6.8 = 20.4$ cm.

b) for the paper chromatogram without baffles:

$$0.03 = 0.01 \times \frac{V + \Delta V}{V}$$

was obtained, and, finally $\Delta V = 2V$, i.e. $\Delta l = 2l = 2 \times 6.9 = 13.8$ cm.

The paper chromatogram with baffles increases even more the separation effect of the temperature gradient favouring the separation of these two amino-acids, which in isothermal conditions have very close R_f values.

VERIFICATION OF THE GOCAN-LITEANU RELATION

Gocan and Liteanu [15] have established the following relation between the R_f and the temperature gradient in partition chromatography, on verified paper and on cellulose thin layer [16-17]

$$R_f = \frac{1}{1 + \alpha_0 k_0 - \frac{\alpha_0 k_0}{\text{grad}.l.t.}\,\text{grad}.t.} = \frac{1}{1 + \alpha_0 k_0\left(1 - \frac{\text{grad}.t}{\text{grad}.l.t.}\right)} \qquad (2)$$

where grad. t. l. is the temperature gradient for $R_f = 1$, and $\alpha_0 k_0$ has the same significance as the product αk of the fundamental equation [18] for partition chromatography, i.e. for grad. $t = 0$

$$R_f = \frac{1}{1 + \alpha k} \qquad (3)$$

We intended to verify the validity of relation (2) and, by applying the temperature gradient to the new variant of the chromatogram form used by us.

The data in table 2 were obtained by using, as already shown, the system: n-butanol + acetic acid + water (4 : 1 : 5 v/v) as eluent, in isothermal conditions and afterwards in temperature gradient on paper.

In fig. 2 is represented the variation of R_f values with the temperature gradient and in fig. 3 the values of the αk product depending on the temperature gradient.

One can notice (fig. 2) that the R_f values increase with the temperature gradient and the liniarity of αk values increasing with the gradient (fig. 3) proves the validity of relation (2) even if the open chromatographic column, having the form represented in fig. 1, has been used.

---

[18] R. Consden, A. H. Gordon and A. J. P. Martin, *Biochem. J.*, **38**, 224 (1944).

The value of the limiting temperature gradient could not be experimentally determined as it requires high temperatures at the upper part of the chromatographic chamber.

For leucine *t. l.* grad = 21.5 and for isoleucine *t. l.* grad = 42 are obtained graphically.

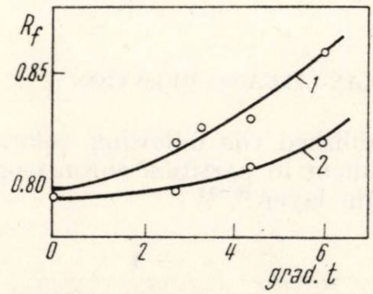

Fig. 2. — Variation of R_f values with the temperature gradient : *1*, leucine ; *2*, isoleucine.

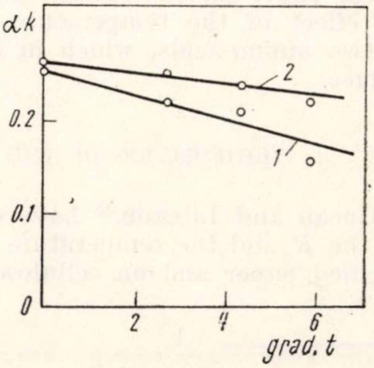

Fig. 3. — The values of the αk product depending on the temperature gradient : *1*, leucine ; *2*, isoleucine.

CONCLUSIONS

By combining the temperature gradient with an open (paper) chromatographic column provided with two baffles at the lower part, leucine could be separated from isoleucine. It was meanwhile proved that the baffles increase the positive effect of the temperature gradient in the separation of these amino-acids.

Table 1

The values R_f of leucine and isoleucine depending on the temperature
— Paper : Schleicher — Schüll 2040 a
— Solvent : n-butanol + acetic acid + water (4 : 1 : 5 : v/v)

Time (h)	t_1	t_2	Temp. grad. (°C/cm)	Leucine		Isoleucine	
				R_f		R_f	
				Chromatograms with baffles	Continuous strip chromatograms	Chromatograms with baffles	Continuous strip chromatograms
1.5	20	20	0	0.80	0.65	0.79	0.64
1.5	20	60	5.88	0.86	0.70	0.82	0.67

The data in the tables are the average values obtained by 5 determinations

Table 2

The values R_f and αR of leucine and isoleucine depending on the temperature gradient

Leucine					Isoleucine				
Temp. (°C)		αk	Temp. grad (°C/cm)	$R_{f_{\text{exp}}}$	Temp. (°C)		αk	Temp.grad. (°C/cm)	$R_{f_{\text{exp}}}$
t_1	t_2				t_1	t_2			
20	20	0.25	0	0.80	20	20	0.26	0	0.79
20	40	0.22	2.70	0.82	20	40	0.25	2.70	0.80
20	50	0.21	4.28	0.83	20	50	0.24	4.28	0.81
20	60	0.16	5.88	0.86	20	60	0.22	5.88	0.82

The data in the tables are the average values obtained by 5 determinations

Revue Roumaine de Chimie, **18**, *1*, 155–159 (1973)

Revue Roumaine de Chimie, 18, 1, 161–174 (1973)

LE COMPORTEMENT DES IONS INORGANIQUES EN CHROMATOGRAPHIE SUR PAPIER AVEC SOLVANTS À BASE D'ALCOOLS – ACIDES

TIBERIU NĂȘCUȚIU
Institut de physique atomique, B.P. 35, Bucarest, Roumanie

Reçu le 30 juin 1972

On a étudié le comportement d'environ 60 ions inorganiques en solvants d'alcools et d'acide chlorhydrique 1–10N (1 : 1), d'alcools – acide nitrique ou d'alcools – HF 40 % – HCl 6N (en différentes proportions), pour établir les possibilités de séparation. Dans les discussions l'ordre des ions pris en considération est celui de leur disposition dans le système périodique des éléments.

Une série de travaux, publiés par nous ces dernières années, portent sur l'étude de l'efficience de la séparation d'un nombre accru d'ions inorganiques (environ 60), en utilisant les mélanges de solvants : alcools et acide chlorhydrique, alcools et acide nitrique ou alcools, acide hydrofluorique et acide chlorhydrique, en diverses proportions et concentrations. Ces études indiquent tant les solvants donnant la répartition la plus uniforme des ions inorganiques sur l'entier chromatogramme, que le comportement des ions respectifs, en mélange de solvants : alcools et acides. Sur ce dernier sujet, nous allons faire, en ce qui suit, une discussion de caractère général, en traitant les ions considérés dans l'ordre de leur disposition dans le système périodique des éléments.

Les séparations ont été effectuées en utilisant les solvants suivants :

Alcool méthylique – HCl 1, 2, 4, 6, 8, 10N (1 : 1)

Alcool éthylique – HCl 2, 4, 6, 8, 10N (2 : 1)

Alcool *n*-propylique – HCl 1, 2, 4, 6, 8, 10N (1 : 1)

Alcool *iso*-butylique – HCl 1, 2, 4, 6, 8, 10N (1 : 1)

Alcool tertiaire-butylique – HCl 1, 2, 4, 6, 8, 10N (1 : 1)

Alcool *n*-amylique – HCl 1, 2, 4, 6, 8, 10N (1 : 1)

Alcool *iso*-amylique – HCl 4, 6, 8, 10N (1 : 1)

Alcool tertiaire amylique – HCl 2, 4, 6N (1 : 1)

Alcool benzylique – HCl 10, 12N (4 : 1)

Alcool benzylique — alcool éthylique — HCl 6, 8N (2 : 2 : 1)

Alcool méthylique — HNO_3 — 1, 2, 4, 6, 8, 10N (2 : 1)

Alcool éthylique — HNO_3 — 2, 4, 6N (2 : 1)

Alcool éthylique — HF 40% — HCl 6N (75 : 5 : 20)

Alcool éthylique — HF 40% — HCl 6N (95 : 2 : 5)

Alcool *iso*-propylique — HF 40% — HCl 6N (75 : 5 : 20)

Alcool *n*-butylique — HF 40% — HCl 6N (75 : 5 : 20)

Alcool *iso*-amylique — HF 40% — HCl 10N (80 : 5 : 15)

MODE OPÉRATOIRE

Nous avons utilisé des solvants organiques et des acides de différentes provenances, à pureté « pour chromatographie » ou bien « pour analyse ».

Les éléments utilisés ont été dissous en HCl 1N, excepté les substances à tendance d'hydrolyse, qui ont été dissoutes en HCl 6N. Au cas des éléments ayant des isotopes radioactifs à propriétés adéquates, les solutions ont été préparées par dilution des métaux ou des oxydes respectifs, irradiés, au préalable, dans le réacteur nucléaire (v. tableau 1).

Les séparations ont été effectuées par chromatographie ascendante, sur papier Whatman N° 1 (garanti pour chromatographie), dimensions 30 × 30 cm. Le point d'application a été tracé à une distance de 3 cm au-dessus de l'extrémité inférieure de la feuille de papier. Les solutions des ions à séparer ont été déposées sur la feuille de papier à l'aide d'une pipette, à des intervalles de 2—3 cm, les taches initiales ayant les diamètres de 0,5 à 0,8 cm. Dans chaque tache ont été déposés 0,05—35 μg d'élément. Ensuite les chromatogrammes ont été séchés à l'air (environ une heure) ou sous courant d'air chaud et introduits dans les chambres chromatographiques pendant 8—15 heures, afin d'équilibrer l'humidité. Le développement a duré 4—25 heures, fonction de la vitesse de migration du solvant. Lorsque le solvant s'est déplacé à environ 20 cm de la ligne d'application, les chromatogrammes ont été séchés à l'air et soumis aux opérations de révélation avec réactifs de couleur ou par mesures de radiotactivité.

Notre étude comprend presque tous les éléments du système périodique, à l'exception des éléments du groupe des gaz nobles, de certains éléments radioactifs (Fr, Ra, Ac, Pa, Tc, transuraniens) et de quelques éléments produisant des anions (C, N, O, S, B, Si et Ge).

Pour chaque groupe d'éléments ont été effectués 2—3 chromatogrammes, les valeurs R_F, indiquées dans les tableaux étant les moyennes des valeurs obtenues par voie expérimentale. Les erreurs individuelles n'ont pas dépassé de plus de $\pm$ 0,02 les valeurs R_F inscrites dans les tableaux.

Tableau 1

Substances utilisées pour la détermination des valeurs R_F et les possibilités de révélation

Substance inactive	Isotope radioactif	Produit irradié	Réactif de couleur
LiCl	—	—	Quinalizarine solution saturée + NH_3
NaCl	^{22}Na(import), ^{24}Na	Na_2CO_3	$AgNO_3$ 0,1N et réactif Beestecher
KCl	^{42}K	K_2CO_3	,,
RbCl	^{86}Rb	$RbNO_3$	,,
CsCl	^{134}Cs	$CsNO_3$	,,
$CuCl_2$	^{64}Cu	Cu	$K_4Fe(CN)_6$ solution 5%
$AgNO_3$	^{110m}Ag	Ag	Na_2S solution 5%
$[AuCl_4]H$	^{198}Au	Au	$SnCl_2$ 3% en HCl 4N
$BeCl_2$	^{7}Be	Li	Quinalizarine solution saturée + NH_3
$MgCl_2$	—	—	,,
$CaCl_2$	^{45}Ca	$Ca(NO_3)_2$	,,
$SrCl_2$	^{89}Sr	$SrCO_3$	Acide rubéanique 0,5% en C_2H_5OH 95% + NH_3
$BaCl_2$	—	$BaCO_3$	,,
$ZnCl_2$	^{65}Zn	Zn	Dithizone 0,001% en $CHCl_3$
$CdCl_2$	$^{115,115m}Cd$	Cd	Na_2S solution 5%
$HgCl_2$	^{203}Hg	$Hg_2(NO_3)_2$	Dithizone 0,001% en $CHCl_3$
$ScCl_3$	^{46}Sc	Sc_2O_3	Quinalizarine solution saturée + NH_3
YCl_3	^{90}Y	Y_2O_3	,,
$LaCl_3$	^{140}La	La_2O_3	,,
$Ce(NO_3)_4 2NH_4NO_3 . 6H_2O$	$^{1\ 1}Ce$	$Ce(NO_3)_4 . 2NH_4NO_3 . 6H_2O$	,,
$PrCl_3$	^{142}Pr	Pr_6O_{11}	,,
$NdCl_3$	^{147}Nd	Nd_2O_3	,,
$SmCl_3$	^{152}Sm	Sm_2O_3	,,
$EuCl_3$	^{152}Eu	Eu_2O_3	,,
$GdCl_3$	^{159}Gd	Gd_2O_3	,,
$TbCl_3$	^{160}Tb	Tb_4O_7	,,
$DyCl_3$	^{165}Dy	Dy_2O_3	,,
$ErCl_3$	$^{169,171}Er$	Er_2O_3	,,
$YbCl_3$	^{175}Yb	Yb_2O_3	,,
$LuCl_3$	^{177}Lu	Lu_2O_3	,,
$AlCl_3$	—	—	,,
$GaCl_3$	^{72}Ga	Ga	,,
$InCl_3$	^{116}In	In	,,
$TlCl_3$	^{204}Tl	Tl	Dithizone 0,001% en $CHCl_3$
$ZrOCl_2$	$^{95}Zr+^{95}Nb$	$OZr(NO_3)_2$	Quinalizarine solution saturée en $C_2H_5OH+NH_3$
$HfOCl_2$	—	—	,,
$Th(NO_3)_4$	—	—	,,
$SnCl_2$	^{119}Sn	Sn	Dithizone 0,001% en $CHCl_3$
$[SnCl_6](NH_4)_2$	—	—	,,
VO_3NH_4	—	—	Pyrogallol 5% en $C_2H_5OH+ + NH_3$
PO_4HNa_2	^{32}P	P_2O_5	—
AsO_4H_3	^{76}As	As_2O_5	KI 3% en HCl 1N
$SbCl_3$	$^{122,124}Sb$	Sb	Dithizone 0,001% en $CHCl_3$
$SbCl_5$	$^{122,124}Sb$	—	,,

Tableau 1 (suite)

Substances utilisées pour la détermination des valeurs R_F et les possibilités de révélation

Substance inactive	Isotope radioactif	Produit irradié	Réactif de couleur
$BiCl_3$	^{210}Bi	$Bi(OH)(NO_3)_2$	Na_2S 5%
$CrCl_3$	^{51}Cr	$K_2Cr_2O_7$	—
$[Mo_7O_{24}](NH_4)_6$	^{99}Mo	MoO_3, Na_2MoO_4	$SnCl_2$ 3% en HCl 4N + + NH_4SCN
WO_4Na_2	^{187}W	WO_3, W	,,
$UO_2(NO_3)_2$	—	—	$K_4[Fe(CN)_6]$ 5%
SeO_3Na_2	—	—	KI 3% en HCl 1N
SeO_4H_2	—	—	,,
TeO_3Na_2	^{131}Te+autres isotopes	TeO_2	,,
TeO_6H_6	^{131}Te+autres isotopes	TeO_6H_6	,,
OsO_4+NaOH+ + HCl	$^{191}Os+^{193}Os$	OsO_4	—
$[PoCl_6]H_2$	^{210}Po	$Bi(OH)(NO_3)_2$	—
$MnCl_2$	^{56}Mn	$Mn(NO_3)_2$	Quinalizarine solution saturée en $C_2H_5OH+NH_3$
ReO_4H	^{188}Re	Re	$SnCl_2$ 3% en HCl 4N+ +NH_4SCN
$FeCl_3$	^{59}Fe	Fe	$K_4[Fe(CN)_6]$ 5%
$CoCl_2$	^{60}Co	Co	Na_2S 5%
$NiCl_2$	^{65}Ni	$Ni(NO_3)_2$	Diméthylglioxine 1% en $C_2H_5OH+NH_3$
$[RhCl](NH_4)_2$	—	—	$SnCl_2$ 3% en HCl 4N
$[IrCl_6]Na_2$	^{192}Ir	Ir	—
$PdCl_2$	—	$PdCl_2$	$SnCl_2$ 3% en HCl 4N
$[PtCl_4]H_2$	^{197}Pt	Pt	,,
$[PtCl_6]H_2$	^{197}Pt	Pt	,,

RÉSULTATS ET DISCUSSIONS

Li, *Na*, *K*, *Rb*, *Cs*. Dans les solvants d'alcools — HCl ou HNO_3, les métaux alcalins se déplacent sous forme de taches compactes. Les vitesses de migration diminuent au fur et à mesure que la chaîne de l'alcool croît, donc à mesure que décroît le caractère polaire du solvant. C'est pourquoi les meilleures séparations s'obtiennent par les solvants à base d'alcool méthylique.

Li, Na et K ont des vitesses de migration différentes, tandis que chez les métaux alcalins lourds ces vitesses sont presque similaires, les valeurs R_F du rubidium étant plus proches de celles du potassium que de celles du césium. Chez ce groupe la vitesse de migration n'est pas fonction du poids atomique, les valeurs R_F du césium et parfois celles du rubidium dépassant les valeurs R_F du potassium.

Aucun des solvants utilisés ne sépare en totalité les ions de ce groupe d'une manière satisfaisante. Les solvants :

a) alcool méthylique — HCl 4—8N (1 : 1) ;

b) alcool éthylique — HCl 2—4N (2 : 1) ;

c) alcool tertiaire-butylique — HCl 2—4N (1 : 1) séparent les métaux alcalins légers (v. tableau 2), tandis que le solvant à base d'alcool isobutylique – HCl 12N (1 : 1) sépare bien les quantités réduites (< 5 µg) de Cs ($R_F = 0{,}52$) et de Rb^+ ($R_F = 0{,}29$).

Tableau 2

Séparation des métaux alcalins

Solvants	Valeurs R_F					Bibliographie
	Li^+	Na^+	K^+	Rb^+	Ca^+	
Alcool méthylique HCl 4N (1 : 1)	0,86	0,56	0,44	0,47	0,52	[1]
Alcool méthylique HCl 6N (1 : 1)	0,84	0,53	0,40	0,45	0,50	[1]
Alcool éthylique HCl 8N (1 : 1)	0,78	0,47	0,33	0,42	0,47	[1]
Alcool éthylique HCl 2N (2 : 1)	0,67	0,43	0,25	0,26	0,28	[2]
Alcool éthylique HCl 4N (2 : 1)	0,65	0,36	0,20	0,19	0,24	[2]
Alcool tertiaire-butilique HCl 2N (1 : 1)	0,90	0,72	0,59	0,58	0,60	[3]
Alcool tertiaire-butylique HCl 4N (1 : 1)	0,88	0,64	0,52	0,51	0,55	[3]

En solvants fluorhydriques, le lithium développe la plus grande vitesse de migration, mais la tache respective présente une traînée. Les ions des autres métaux alcalins restent sur la ligne de départ. C'est pourquoi les solvants fluorhydriques sont adéquats pour la séparation d'un grand nombre d'éléments d'ions de métaux alcalins. Dans ce but nous recommandons le solvant composé d'alcool iso-propylique – HF 40% – HCl 10N (80 : 5 : 15). [4]

Be, *Mg*, *Ca*, *Sr*, *Ba*. Dans tous les solvants chlorhydriques les métaux de ce groupe se déplacent d'après leur poids atomique, le béryllium ayant les valeurs R_F les plus élevées. Le baryum produit des désagréments à cause du fait que la tache est pourvue d'une traînée s'allongeant à mesure que s'acroît la normalité du HCl.

L'acide nitrique n'imprime pas de différences essentielles dans l'ordre de migration de ces éléments. L'acide fluorhydrique précipite le magnésium, le calcium, le strontium et le baryum sous forme de fluorures et les taches respectives restent sur la ligne d'application ou s'éloignent très peu de celle-ci. La solubilité en HCl des fluorures de magnésium et de calcium imprime à ces ions une tendance de migration, mais les taches respectives présentent une petite proéminence frontale. Le béryllium, qui a une tendance de complexation sous forme de fluorure, se détache nettement des autres éléments de ce groupe.

---

[1] T. NĂŞCUŢIU, *Rev. Roumaine Chim.*, **9**, 273 (1964) et *Studii şi Cercetări Chim. Acad., Bucureşti*, **12**, 273 (1964).

[2] T. NĂŞCUŢIU, *Rev. Roumaine Chim.*, **10**, 989 (1965) et *Studii şi Cercetări Chim. Acad., Bucureşti*, **13**, 1025 (1965).

[3] T. NĂŞCUŢIU, *Rev. Roumaine Chim.*, **12**, 845 (1967).

[4] T. NĂCUŞŢIU, *Rev. Roumaine Chim.*, **12**, 839 (1967).

Nous soulignons le fait, que tant en solvants d'alcool amylique — HCl 4N — qu'en solvants à base d'alcool benzylique, les ions de ce groupe restent sur la ligne d'application, seul le béryllium se déplace, mais avec des valeurs R_F très basses.

Les solvants les plus indiqués dans la séparation de ces éléments sont consignés dans le tableau 3.

Tableau 3

Séparation des éléments Be, Mg, Ca, Sr, Ba

Solvants	Valeurs R_F					Bibliographie
	Be^{2+}	Mg^{2+}	Ca^{2+}	Sr^{2+}	Ba^{2+}	
Alcool méthylique HCl 8N (1 : 1)	0,84	0,72	0,57	0,36	0,17	1
Alcool méthylique $HNO_3$6N (2 : 1)	0,89	0,78	0,66	0,48	0,29	1
Alcool méthylique HN_3 8N (2 : 1)	0,87	0,73	0,62	0,40	0,28	1
Alcool méthylique HNO_3 10N (2 : 1)	0,85	0,71	0,59	0,41	0,26	1
Alcool éthylique HNO_3 4N (2 : 1)	0,79	0,56	0,37	0,26	0,12	2
Alcool éthylique HNO_3 6N (2 : 1)	0,77	0,50	0,30	0,21	0,10	2
Alcool *n*-propylique HCl 6N (1 : 1)	0,74	0,53	0,40	0,27	0,15	5
Alcool tertiaire-butylique HCl 4N (1 : 1)	0,83	0,71	0,57	0,45	0,33	3

Sc, Y, La, lanthanides. Guedes de Carvalho [6] a étudié le comportement des éléments de ce groupe dans des solvants à base d'alcool butylique — HCl et a vérifié l'observation de Lederer concernant la succession des lanthanides sous forme d'une courbe sinusoïdale, plus ou moins accentuée, selon la concentration de l'acide contenu par le solvant. Une étude plus détaillée sur le comportement des éléments de ce groupe a été faite par Maia et Carvalho, [7] qui ont conclut que les solvants étudiés ne permettent pas une séparation satisfaisante de ces éléments.

Nos essais ont suivi surtout la possibilité de séparation des terres rares des autres éléments et non pas leur séparation individuelle.

Le scandium possède la plus grande vitesse de migration en tous les solvants étudiés, étant suivi par l'yttrium et par le lanthane, les valeurs R_F de l'yttrium étant plus proches des valeurs R_F du lanthane que de celles du scandium. Une séparation entre le lanthane et les lanthanides n'a pas été possible avec aucun des solvants essayés.

---

[5] G. Popa et T. Năşcuţiu, *Rev. Roumaine Chim.*, **13**, 315 (1968).

[6] R. A. Guedes de Carvalho, *Analyt. Chim. Acta*, **16**, 555 (1957).

[7] M. O. Maia et R. A. Guedes de Carvalho, *J. Chromatog.*, **8**, 245 (1962).

Pour la séparation du scandium de l'yttrium nous recommandons le solvant d'alcool éthylique – HCl 8N (2 : 1). Les valeurs R_F pour Sc^{3+} et Y^{3+} sont 0,43 respectivement 0,19.

La séparation du Sc, Y et La peut être réalisée avec de l'alcool éthylique – HCl 4N (2 : 1). Les valeurs R_F sont : $Sc^{3+} = 0{,}58$; $Y^{3+} = 0{,}36$; $La^{3+} = 0{,}26$; lanthanides = 0,25–0,33.

En solvants fluor-chlorhydriques, les éléments de ce groupe précipitent sous forme de fluorures et restent sur la ligne d'application.

Ti, Zr, Hf, Th. En mélanges d'alcools supérieurs et d'acide chlorhydrique à normalité élevée, le titane se déplace sous forme d'une tache compacte.

Une bonne séparation du titane des autres éléments s'obtient avec le solvant d'alcool benzylique – HCl 12N (4 : 1). Dans le voisinage de la tache du Ti (R_F = 0,28) sont situés Co (R_F = 0,35), In (R_F = 0,57), Ru (R_F = 0,20), Be (R_F = 0,20) et Li (R_F = 0,17)[8].

En solvants fluorhydriques, le fluorure complexe de titane se déplace avec une vitesse appréciable, se situant dans la partie supérieure ou centrale des chromatogrammes. Dû à ce fait, avec ces solvants le titane peut être séparé de quelques éléments qui l'accompagnent souvent et dont la séparation à l'aide de solvants chlorhydriques n'est pas possible.

Dû à la tendance accentuée d'hydrolyse, le zirconium et le hafnium causent des inconvénients dans la chromatographie sur papier. Dans les solvants étudiés, même à normalités d'acide élevées, les taches des deux éléments ont des traînées plus ou moins accentuées, selon la concentration de l'acide et la nature de l'alcool.

En solvants chlorhydriques, la charge élevée de ces ions diminue la vitesse de migration, les taches respectives étant situées dans le voisinage de la ligne d'application.

La migration des deux éléments sous forme de fluorures complexes est plus acceptable, mais une détermination quantitative ne peut être réalisée, vu qu'une petite quantité de ces éléments reste à la ligne d'application, étant fortement absorbée par le papier filtre pendant le séchage des chromatogrammes avant la révélation. L'utilisation d'un chromatogramme non séché améliore la situation, mais les valeurs R_F sont insuffisamment reproductibles.

Avec aucun des solvants étudiés n'a été obtenue une séparation efficace entre le zirconium et le hafnium.

Le thorium se déplace sous forme d'une tache d'aspect régulier. En solvants chlorhydriques cet élément développe une relative basse vitesse de migration, se situant dans la partie inférieure des chromatogrammes ayant les valeurs R_F proches de celles du hafnium et des lanthanides. La séparation de ces trois groupes d'éléments n'est possible avec aucun des solvants étudiés.

En solvants fluorhydriques, excepté ceux à base d'alcool éthylique, le thorium précipite à la ligne d'application.

---

[8] G. Popa, T. Năşcuţiu et V. Iliescu, *Rev. Roumaine Chim.*, **13**, 447 (1968).

V, *Nb*, *Ta*. Dans tous les solvants étudiés, le vanadium se déplace sous forme de tache compacte. Par contre, dans les solvants chlorhydriques et nitriques, le niobium et le tantale précipitent sur la ligne d'application, les taches respectives ayant une proéminence frontale. C'est pourquoi les valeurs R_F des deux éléments n'ont pas été déterminées.

La tendance de complexation sous forme de fluorures rend meilleur le comportement chromatographique de ces éléments, vu qu'en solvants fluorhydriques le niobium et le tantale se déplacent lorsque les valeurs R_F sont élevées, tandis que le vanadium lorsque ces valeurs sont basses ou moyennes.

La séparation des trois éléments peut être réalisée avec les solvants indiqués dans le tableau 4.

Tableau 4

Séparation de V^V, Ta^V et Nb^V

Solvants	Valeurs R_F			Bibliographie
	V^V	Ta^V	Nb^V	
Alcool *n*-butylique HF 40%–HCl 6N (75 : 5 : 20)	0,15	0,89	0,60	[4]
Alcool iso-amylique HF 40%–HCl 10N (80 : 5 : 15)	0,06	0,32	0,83	[4]

Des séparations exceptionnelles, tant entre le niobium et le tantale, qu'entre ces éléments et le hafnium (zirconium) ont été obtenues avec le solvant d'alcool iso-butylique – HF 40% – acide oxalique ou tartrique 0,5N (35 : 2 : 3).[9]

Cr, *Mo*, *W*, *U*. Dû à la réduction des ions CrO_4^{2-} ou $Cr_2O_7^{2-}$ à Cr^{3+} en solvants chlorhydriques, les taches respectives sont munies d'une traînée ou d'une proéminence frontale. C'est pourquoi nous avons étudié seulement le comportement des ions Cr^{3+}.

En milieu d'acide chlorhydrique ou nitrique, le tungstène précipite sous forme d'acide tungsténique et reste à la ligne d'application. Les études à ^{187}W ont montré que les taches respectives ont des proéminences frontales qui s'allongent simultanément à l'augmentation de la normalité de l'acide du solvant. Cela explique pourquoi le tungstène empêche la séparation des éléments ayant des valeurs R_F basses ou moyennes.

En solvants fluor-chlorhydriques le tungstène manifeste une tendance de migration. Les valeurs R_F résultent aussi bien du rapport entre la concentration de l'acide fluorhydrique et celle de l'acide chlorhydrique, que de la nature de l'alcool.

La séparation des trois éléments peut être réalisée avec un grand nombre de solvants chlorhydriques, à condition que l'acide chlorhydrique ait une concentration de 1–2N.

Mn, *Tc*, *Re*. Les ions MnO_4^- sont réduits en milieu chlorhydrique à des valeurs inférieures ; de la sorte, le comportement de cet élément a dû être étudié sous forme de Mn^{2+}.

La migration du technétium n'a pas été étudiée ; le rhénium se trouvait dans la solution sous forme d'ion ReO_4^-.

---

[9] T. Năşcuţiu et A. Grigorovici, *Rev. Roumaine Chim.*, **10**, 449 (1965).

Vu que les ions Mn^{2+} manifestent une faible tendance de complexation, les valeurs R_F sont remarquablement plus réduites que celles des ions ReO_4^-, ce fait étant plus accentué lors de la diminution du caractère polaire de l'alcool et de l'augmentation de la concentration de l'acide du solvant.

Fe, Co, Ni. Les éléments de ce groupe se déplacent dans l'ordre : $Fe^{3+} > Co^{2+} > Ni^{2+}$, leurs taches étant assez uniformes.

En HCl à normalités réduites, les valeurs R_F du cobalt et du nickel sont proches, tandis qu'à des normalités élevées, la stabilité du chlorure complexe de nickel est réduite et, par conséquent, l'on obtient des séparations assez bonnes. Le tableau 5 indique quatre solvants adéquats pour séparer le cobalt du nickel.

Tableau 5

Séparation de Co^{2+} et Ni^{2+}

Solvants	Valeurs R_F		Bibliographie
	Co^{2+}	Ni^{2+}	
Alcool *n*-propylique–HCl 10N (1 : 1)	0,45	0,26	5
Alcool *n*-amylique–HCl 10N (1 : 1)	0,36	0,21	10
Alcool iso-amylique–HCl 8N (1 : 1)	0,40	0,17	10
Alcool iso-amylique–HCl 10N (1 : 1)	0,57	0,27	10

Le nombre des solvants en état de séparer les trois éléments de ce groupe est plus réduit (v. le tableau 6).

Tableau 6

Séparation de Fe^{3+}, Co^{2+}, et Ni^{2+}

Solvants	Valeurs R_F			Bibliographie
	Fe^{3+}	Co^{2+}	Ni^{2+}	
Alcool iso-butylique HCl 12N (1 : 1)	1	0,60	0,25	11
Alcool *n*-amylique HCl 10N (1 : 1)	0,76	0,37	0,21	10
Alcool benzylique–HCl 12N (4 : 1)	1	0,36	0,05	8

Les métaux platiniques. Pour préparer les solutions nécessaires à la séparation, nous avons utilisé les substances suivantes : $K_2[RuCl_6]$, $(NH_4)_3[RhCl_6]\cdot 3H_2O$, $PdCl_2$, OsO_4, Ir, $K_2[PtCl_4]$ et $H_2[PtCl_6]\cdot xH_2O$.

Après l'irradiation dans le réacteur nucléaire, OsO_4 a été dissous en NaOH, évaporé presque à sec et redissous en HCl 6N. Les réactions qui ont eu lieu peuvent être formulées comme suit :

---

[10] T. NĂŞCUŢIU et V. ILIESCU, *Rev. Roumaine Chim.*, **12**, 853 (1967).

[11] T. NĂŞCUŢIU, *Studii şi Cercetări Chim. Acad. Bucureşti*, **9**, 719 (1961).

$$OsO_4 + 2NaOH = Na_2[OsO_4(OH)_2]$$

$$Na_2[OsO_4(OH)_2] + 6HCl = Na_2[OsO_2Cl_4] + H_2O$$

Pendant la migration Os (VI) est réduit à Os (IV)

$$[OsO_2Cl_4]^{2-} + 4H^+ + 4Cl^- = [OsCl_6]^{2-} + Cl_2 + 2H_2O$$

L'irridium métallique a été solubilisé par fusion avec un mélange de NaOH et $NaNO_2$. En reprenant la fusion, on obtient un mélange de chlorures complexes de Ir (III) et Ir (IV).

Les solvants à base d'alcools inférieurs déplacent les ions de ce groupe dans la partie supérieure des chromatogrammes et aucune séparation convenable ne peut avoir lieu. De plus, les taches sont allongées ou bien munies de traînées. La diminution de la polarité de l'alcool mène à la formation de taches plus uniformes et à des séparations de paires ou de groupes de trois de ces éléments. Quelques ions de ce groupe, par exemple Rh^{IV}, Os^{VI}, Pt^{IV}, etc., forment des taches doubles, soit à cause de la formation d'espèces complexes stables différentes, soit dû à l'action réductrice de la cellulose. Les meilleures séparations ont été obtenues avec les solvants consignés dans le tableau 7.

Tableau 7

Séparation des métaux platiniques

Solvants	Valeurs R_F							Bibliographie
	Ru^{III}	Rh^{IV}	Pd^{2+}	Os^{IV}	Ir^{IV}	Pt^{II}	Pt^{IV}	
Alcool iso-butylique HCl 8N (1 : 1)	0,31	0,43	0,68	0,69	0,39	1,65	0,75	11
Alcool iso-butylique HCl 12N (1 : 1)	0,25	0,34	0,48	0,56	0,27	0,45	0,53	11
Alcool *n*-amylique HCl 10N (1 : 1)	0,25	0,25	0,47	0,65	—	0,60	0,59	10
Alcool iso-amylique HCl 6N (1 : 1)	0,12	0,11	0,56	0,74	—	0,70	0,70	10

Les solvants nitriques et fluorhydriques ne sont pas adéquats à la séparation des métaux platiniques.

Cu, Ag, Au. Les ions d'argent précipitent sous forme de chlorures et restent à la ligne d'application. A mesure que la normalité de l'acide augmente dû à la formation de chlorures complexes, les taches respectives reçoivent une proéminence frontale. C'est pourquoi nous recommandons la précipitation initiale des ions Ag et l'élimination du précipité par centrifugation.

En solvants nitriques les ions d'argent sont réduits pendant l'équilibrage de l'humidité du chromatogramme avec l'humidité de la chambre chromatographique et deux taches se produisent : l'une reste à la ligne d'application (comme argent métallique) et l'autre se déplace. La réduction des ions d'argent peut être évitée si le temps de saturation ne dépasse pas 8 heures.

L'or est aussi réduit à forme métallique, même en solvants chlorhydriques et peut former des taches doubles. En solvants à acide nitrique cet élément se déplace sous forme de taches allongées ; sa séparation d'autres éléments n'est pas satisfaisante. En solvants à HF—HCl les ions de l'or ont des vitesses de migration élevées et se localisent au front du solvant.

La séparation du cuivre de l'or se réalise le mieux en solvants peu polaires et à HCl concentré. L'or se déplace au front du solvant ou dans sa proximité ; le cuivre se déplace à valeurs R_F moyennes.

Pour la séparation Cu—Ag—Au, nous recommandons le solvant d'alcool iso-amylique — HF 40% — HCl 6N (75 : 5 : 20) ; les valeurs R_F sont les suivantes :

$$Cu^{2+} = 0{,}25,\ Ag^{+} = 0{,}00 :\ [AuCl_4]^{-} = 1{,}00$$

Zn, *Cd*, *Hg*. Les ions Hg^{2+} se déplacent à la vitesse la plus grande. A des normalités basses de l'HCl, ces ions sont suivis par Zn^{2+} et Cd^{2+} et à normalités plus élevées de 6N HCl l'ordre de migration change dans le sens $Hg^{2+} > Cd^{2+} > Zn^{2+}$. Le fait que les ions Hg^{2+} ont des valeurs R_F élevées est dû à la faible dissociation du chlorure mercurique et l'inversion observée aux Cd—Zn est due au caractère complexant plus fortement manifesté par le cadmium.

Les valeurs R_F de ces ions sont suffisamment rapprochées, de telle façon qu'une séparation peut être réalisée seulement avec des solvants ayant la normalité de l'acide chlorhydrique inférieure à 2,5. La décroissance de la normalité diminue considérablement les valeurs R_F du zinc et du cadmium par rapport à celles du mercure.

Le solvant pour la séparation la plus efficace des éléments de ce groupe est composé par :
alcool *n*-amylique — HCl 1N (1 : 1) [10].

Les R_F ont les valeurs suivantes :

$$Hg^{2+} = 0{,}60,\ Zn^{2+} = 0{,}18,\ Cd^{2+} = 0{,}08$$

Al, *Ga*, *In*, *Tl*. La faible tendance de complexation manifestée par Al^{3+} détermine cet ion à se déplacer surtout en solvants à teneur de HCl à normalité élevée et à valeurs R_F basses.

L'indium se déplace à des valeurs R_F moyennes et Ga^{3+} et Tl^{3+} sont localisés à des valeurs R_F supérieures. Les ions Tl^{3+}, ayant un caractère plus prononcé de complexation que le gallium, la migration des deux derniers éléments est différenciée dans un milieu faiblement chlorhydrique.

En solvants à HNO_3 l'ordre de migration change dans le sens que les ions Tl^{3+} ont la vitesse de migration la plus élevée. La succession aluminium, gallium et indium diffère selon le cas et une séparation efficace entre les trois éléments n'a pu être réalisée. En solvants à HF—HCl, la compétition entre la complexion du gallium sous forme de fluorure ou de chlorure nous permet de distancer cet élément à la valeur R_F désirée. En certains de ces solvants l'aluminium reste à la ligne de départ, la tache respective ayant une proéminence frontale.

Les solvants adéquats à la séparation des éléments de ce groupe sont ceux du tableau 8.

Tableau 8

Séparation de Tl^{3+}, Ga^{3+}, In^{3+}, et Al^{3+}

Solvants	Valeurs R_F				Bibliographie
	Tl^{3+}	Ga^{3+}	In^{3+}	Al^{3+}	
Alcool iso-butylique—HCl 4N(1 : 1)	0,96	0,63	0,44	0,14	11
Alcool *n*-amylique—HCl 4N(1 : 1)	0,98	0,53	0,18	0,01	10
Alcool iso-amylique—HCl 4N(1 : 1)	1,00	0,83	0,20	0,01	10
Alcool benzylique—alcool éthylique HCl 8N(2 : 2 : 1)	0,98	0,82	0,42	0,10	8
Alcool éthylique—HF 40 % HCl 6N(95 : 2 : 3)	1,00	0,30	0,65	0,00	4
Alcool iso-propylique—HF 40 % HCl 6N (74 : 5 : 20)	1,00	0,55	0,35	0,00 PF	4

Ge, Sn, Pb. Le comportement du germanium n'a pas été étudié. Les ions Sn^{2+} et Sn^{IV} ne peuvent être séparés par aucun des solvants essayés.

Les ions Pb^{2+} précipitent sous forme de chlorure et restent à la ligne d'application ou se déplacent à des concentrations de HCl plus élevées, sous forme d'une tache allongée, en dérangeant l'identification des ions à R_F basses ou moyennes.

En solvants à teneur en alcool méthylique et HNO_3, les ions de plomb et de stanium se déplacent sous forme de taches assez uniformes, mais ne peuvent être séparés.

Des écarts entre ces ions s'obtiennent en solvants fluorhydriques.

P, As, Sb, Bi. Les trois premiers éléments, en état de valence maximale, se déplacent à des valeurs R_F élevées ; comme suite, leur séparation est difficile. Par contre, le Bi^{3+} se déplace à des valeurs R_F moyennes, ce qui permet la séparation de ses homologues inférieurs.

L'antimoine, dû à sa tendance d'hydrolyse, cause parfois des désagréments, les taches respectives étant pourvues de traînées visibles, surtout lorsqu'on travaille avec de grandes quantités de substance (< 15 µg) et avec des concentrations basses en acide chlorhydrique. En solvants nitriques, l'antimoine se déplace sous forme d'une bande occupant une grande partie du chromatogramme et empêchant de la sorte l'analyse des autres ions.

En solvants chlorhydriques, une séparation efficace des quatre éléments n'a pas été réalisée, mais un écart entre les ions $PO_4{}^{3-}$ et AsO_4^{3-} a été obtenu avec le solvant d'alcool méthylique — HCl 2N (R_F : $PO_4^{3-} = 0,77$; $AsO_4^{3-} = 0,87$). De bonnes séparations entre les ions As^{V}, Sb^{V} et Si^{3+} peuvent être obtenues avec des solvants à base d'alcool benzylique (v. le tableau 9) et entre As^{V} et Sb^{V}, avec des solvants fluorhydriques (v. tableau 10).

Tableau 9

Séparation de As^{V}, Sb^{V} et Bi^{III}

Solvants	Valeurs R_F			Bibliographie
	As^{V}	Sb^{V}	Bi^{III}	
Alcool benzylique – HCl 12N (4 : 1)	0,64	0,83	0,42	8
Alcool benzylique – HCl 10N (4 : 1)	0,57	0,83	0,33	8

Tableau 10

Séparation de As^{V} et Sb^{V}

Solvants	Valeurs R_F		Bibliographie
	As^{V}	Sb^{V}	
Alcool éthylique – HF 40%–HCl 6N (75 : 5 : 20)	0,90	0,70	4
Alcool éthylique – HF 40%–HCl 6N (95 : 2 : 5)	0,85	0,60	4
Alcool iso-propylique – HF 40%–HCl 6N (75 : 5 : 20)	0,81	0,32	4
Alcool *n*-butylique – HF 40%–HCl 6N (75 : 5 : 20)	0,75	0,55	4

Se, Te, Po. La séparation des ions SeO_3^{2-} et TeO_3^{2-} peut être obtenue en plusieurs solvants à teneur en HCl ou HNO_3 diluée (v. le tableau 11). L'augmentation de la concentration de l'acide diminue les différenciations entre les valeurs R_F, tandis qu'une augmentation de la proportion d'alcool dans le solvant imprime un écart plus adéquat entre les deux taches.

La séparation du sélénium et du tellure ayant des valences supérieures peut être obtenue avec un nombre réduit de solvants. Le fait est dû à la tendance du Te (VI) de former des iso-polyacides qui se déplacent sous forme de taches allongées.

Pour la séparation du Se^{IV}, Te^{IV}, Se^{VI} et Te^{VI} peuvent être utilisés les solvants groupés dans le tableau 12.

Tableau 11

Séparation de SeO_3^{2-} et TeO_3^{2-}.

Solvants	Valeurs R_F		Bibliographie
	SeO_3^{2-}	TeO_3^{2-}	
Alcool éthylique – HCl 2N (2 : 1)	0,71	0,38	2
Alcool *n*-propylique – HCl 1N (1 : 1)	0,71	0,46	5
Alcool iso-butylique – HCl 1N (1 : 1)	0,56	0,66	11
Alcool iso-butylique – HCl 2N (1 : 1)	0,07	0,23	11
Alcool *n*-amylique – HCl 2N (1 : 1)	0,35	0,08	10
Alcool éthylique – HF 40%–HCl 6N(95 : 2 : 5)	0,67	0,35	4
Alcool méthylique – HNO_3 2N (2 : 1)	0,80	0,52	1
Alcool éthylique – HNO_3 4N (2 : 1)	0,74	0,42	2

Tableau 12

Séparation de Se^{IV}, Te^{IV}, Se^{VI} et Te^{VI}

Solvants	Valeurs R_F				Bibliographie
	Se^{IV}	Te^{IV}	Se^{VI}	Te^{VI}	
Alcool propylique – HCl 10N (4 : 1)	0,59	0,85	0,33	0,08	8
Alcool benzylique – HCl 12N (4 : 1)	0,65	0,93	0,56	0,14	8

CONCLUSIONS

Les données presentées ci-dessus nous conduisent à l'affirmation que les solvants d'alcool et d'acide chlorhydrique, en différentes normalités et proportions, permettent la séparation d'un grand nombre d'ions inorganiques. Les solvants étudiés ont été utilisés pour la séparation des produits résultés dans différentes réactions nucléaires, tant en vue de l'identification et de la détermination quantitative, qu'en vue d'obtenir des épreuves ayant une pureté radiochimique adéquate aux mesures de constantes radioactives.

Revue Roumaine de Chimie, **18**, *1*, 175–185 (1973)

L'ÉTUDE DU MÉCANISME PHYSICO-CHIMIQUE DE LA SORPTION DES ISOTOPES RADIO-ACTIFS PAR CERTAINES MACROMOLÉCULES INORGANIQUES POLYÉLECTROLYTIQUES. I

LA SORPTION PHYSIQUE ET CHIMIQUE PAR LA DIATOMITE, LA MONTMORILLONITE, LA KIESELGUHR, LE SILICAGEL, LE KAOLIN ET LA CALCITE, DES RADIONUCLÉIDES DES ÉLÉMENTS I, P, Na, Cs, Sr, Ba, Zn, Cu, Co, Mn et Fe

GH. FURNICĂ, MARIA TOADER, ELISABETA TURCITU et ŞTEFANIA BULAN
Institut d'Hygiène et de la Santé Publique, 1–3, str. Dr Leonte, Bucarest, 15

Reçu le 8 février 1972

Les suspensions et les sédiments des bassins de surface ont la capacité de retenir de nombreux isotopes radio-actifs d'une solution aqueuse. On étudie la capacité de sorption des divers composants chimiques des suspensions et des sédiments des bassins de surface, comme la diatomite, la montmorillonite, la kieselguhr, le silicagel (gel de silice), le kaolin et la calcite. Sont utilisés les isotopes radio-actifs des éléments chimiques suivants : I, P, Na, Cs, Sr, Ba, Zn, Cu, Co, Mn et Fe. On étudie aussi l'action éluante de l'eau sur la capacité de rétention des isotopes par ces macromolécules, pour déterminer l'aspect physique ou chimique de sorption des isotopes par les substances chimiques utilisées.

La pollution radio-active du milieu ambiant par les effluents radioactifs est un processus associé à l'élargissement des domaines d'utilisation de l'énergie nucléaire et des isotopes radio-actifs.

Les isotopes radio-actifs dissous peuvent être accumulés par la sorption dans les sédiments et dans les suspensions des eaux naturelles[1-9]. L'équilibre physico-chimique entre les phases solides et les phases

---

[1] C. L. COMAR, « Radiological Concentration Processes », Pergamon-Press, Londres, 1967, p. 1.

[2] R. BITTEL, *Rapport EUR*–**3877**/1968–CEA, Fontenay-aux-Roses.

[3] V. VOICU, *Igiena*, **18**, 331 (1969).

[4] A.I.E.A., « Evacuation des déchets radio-actifs dans le sol », Vienne, 1966, Collection « Sécurité », n° 10.

[5] A.I.E.A., « Evacuation des déchets radio-actifs en eau douce », Vienne, 1963, Collection Sécurité, n° 15.

[6] GH. FURNICĂ et V. VOICU, *Rev. Roumaine Chim.*, **15**, 1087 (1970).

[7] GH. FURNICĂ, *Igiena*, **17**, 135 (1968).

[8] J. L. VEROT et J. M. BLUM, *Contract Euratom*, **1967**, 3452 ; **1968**, 4192.

[9] Public Health Service « Radiological Surveillance Studies at a Boiling Water Nuclear Power Reactor », U.S. Dept. of Health, Maryland, 1970.

liquides des bassins de surface déterminent le processus d'accumulation des isotopes radio-actifs dissous. Les plus importants composants chimiques des suspensions des eaux naturelles sont, selon diverses publications scientifiques,[2] la calcite (50%), les argiles (28%), la dolomite (10%), le quartz (10%) et les produits organiques (2%). On a considéré que la composition moyenne des sédiments des eaux naturelles diffère de celle des suspensions. Ainsi Wanderer et d'autres considèrent que les sédiments ont la composition suivante[10] : produits organiques (34%), quartz (28%), calcite (18%) et argiles (20%).

En considérant que la bentonite montmorillonitique, la diatomite, la kieselguhr, le silicagel et le kaolin sont les composants chimiques les plus fréquents dans les sédiments et dans les suspensions, nous avons étudié la capacité de sorption des isotopes radio-actifs par ces substances, tenant compte des propriétés d'échangeurs d'ions des substances mentionnées.[11-12] La présente note comprend l'étude de la sorption des isotopes radio-actifs des éléments chimiques I, P, Na, Cs, St, Ba, Zn, Cu, Co, Mn et Fe, ainsi que les conclusions sur la forme physique ou chimique de la rétention des isotopes par les macromolécules inorganiques étudiées.

MÉTHODE DE TRAVAIL

On a utilisé la bentonite montmorillonique ayant la composition : 69,6% SiO_2 ; 17,8% Al_2O_3 ; 2,03% Fe_2O_3 ; 1,4% CaO ; 0,6% Na_2O — K_2O et la diatomite ayant la composition : 73% SiO_2 ; 9,5% Al_2O_3 ; 3,8% Fe_2O_3 ; 1,5% TiO_2 ; 2,5% CaO ; 3,5% MgO ; 1,0% Na_2O ; 1,2% K_2O et 0,2% P_2O_5. Selon les études aux rayons X toutes les bentonites utilisées appartiennent au type montmorillonite calcique.[13] Le silicagel (gel de silice) utilisé, produit Merk, en perles de 2—5 mm, a été séché à 105°C, ayant un contenu maximal de 3% H_2O. La kieselghur (terre silicée) et le kaolin sont aussi des produits commerciaux, purifiés et calcinés. Le marbre a été utilisé sous forme de poudre blanche avec une granulation maximale de 0,3 mm.

La phase solide, après l'imbibition avec de l'eau distillée, a été maintenue en contact permanent pendant 24—48 heures avec la solution radio-active dans des fioles de centrifuge, dans le rapport : 2 g de terres actives et 50 ml de solution radio-active. Après 48 heures, on a séparé la phase liquide par centrifugation pendant 10 mn à 2500 tours/mn et ensuite on a mesuré radiométriquement, par décantation à l'aide de pipettes, l'activité de la phase solide. On a calculé les résultats en pour cent de l'activité retenue par la phase solide. Pour une détermination précise on a aussi mesuré l'activité retenue par le verre des fioles. La radio-activité a été déterminée directement dans les fioles, au moyen d'un compteur (détecteur à scintillations) *gamma* à puits, type NaI (Tl), connecté à l'échelle de comptage F.H. — 49. L'activité *bêta* a été mesurée à l'aide d'un compteur proportionnel, à circulation de CH_4, en géométrie 50%, de type F.H. — 409 A.

Les solutions radio-actives utilisées, ayant l'activité spécifique de l'ordre de 100 pCi/ml à 1 nCi/ml, proviennent des solutions obtenues au réacteur atomique I.F.A. Bucarest et de l'Amersham, initialement concentrées, et diluées dans notre laboratoire. Les isotopes ont été les suivants : ^{131}I, ^{32}P, ^{22}Na, ^{134}Cs, ^{85}Sr, ^{131}Ba, ^{64}Cu, ^{57}Co, ^{54}Mn et ^{59}Fe.

---

[10] G. Wanderer, «Actes du Symposion International de Radioécologie», Cadarache, France, C.E.A., 1969, p. 165.

[11] C. B. Amphlett, «Inorganic Ion Exchanges». Elsevier Publish, Comp. Amsterdam, 1964, p. 28—170.

[12] E. V. Egorov et I. D. Novikov, «Deistvie ionizuruischik izluchenii na ionoobmenye materialy», Atomizdat, Moscou, 1965.

Après détermination radiométrique, la phase solide a été lavée avec de l'eau déminéralisée, en réalisant une proportion de 80 ml d'eau par 1 g de terre. Après lavage, la phase solide a été séparée par centrifugation, l'activité retenue étant mesurée encore une fois radiométriquement.

RÉSULTATS

Les résultats concernant la sorption des radionuclides par la bentonite, la diatomite, la kieselguhr, le kaolin et le marbre (la calcite) sont représentés, en pour cent, sur les figures 1–6, et ceux concernant l'influence éluante de l'eau sur la rétention des isotopes radio-actifs par les macromolécules mentionnées dans les figures 7–12. Ces résultats obtenus de l'étude simultanée de 4 échantillons, révèlent des erreurs expérimentales allant de 0,5 à 3,3%, ce qui permet de tirer les conclusions suivantes :

En conditions statiques les isotopes ^{134}Cs, ^{85}Sr, ^{65}Zn, ^{64}Cu, ^{57}Co, ^{54}Mn et ^{69}Fe dissous dans la solution aqueuse sont retenus dans une proportion de 91 à 99% par la bentonite montmorillonitique, tandis que les isotopes ^{22}Na et ^{131}Ba seulement de 40 à 70%. L'isotope ^{32}P est retenu en proportion de 20% et l'isotope ^{131}I de 2 à 5% (fig. 1).

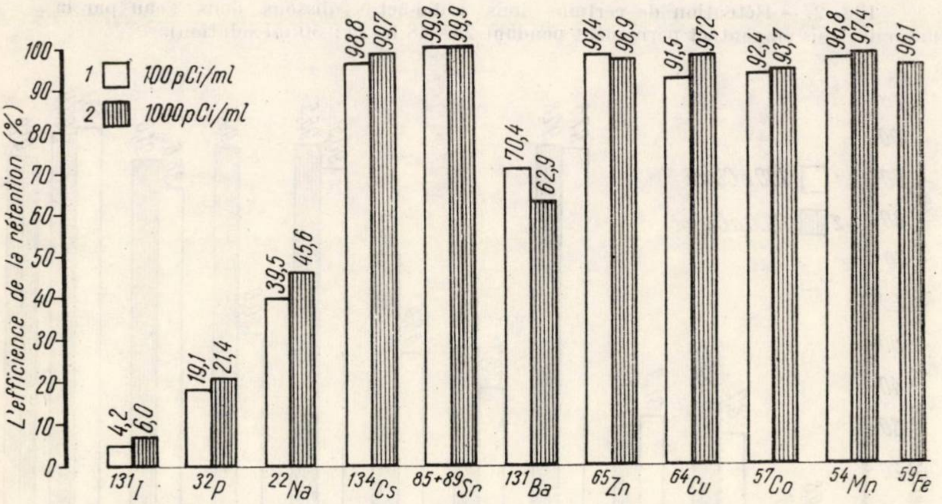

Fig. 1. — Rétention de certains ions radio-actifs dissous dans l'eau, par la montmorillonite mis en contact permanent pendant 24–48 h (2g : 50 ml solution).

Le kieselguhr et le silicagel réagissent de manière différente, vu que le premier retient de 90 à 99% d'isotopes ^{134}Cs, ^{65}Zn, ^{64}Cu, ^{57}Co, ^{54}Mn et ^{59}Fe, le second retenant dans cette proportion seulement le nucléide ^{57}Co. La rétention par la kieselguhr des isotopes ^{131}Ba et ^{64}Cu diffère en fonction de l'influence de la concentration de la solution radio-active. On a aussi remarqué que les isotopes ^{32}P, ^{22}Na, ^{85}Sr et ^{131}Ba sont retenus dans une proportion inférieure à 50% (fig. 3—4).

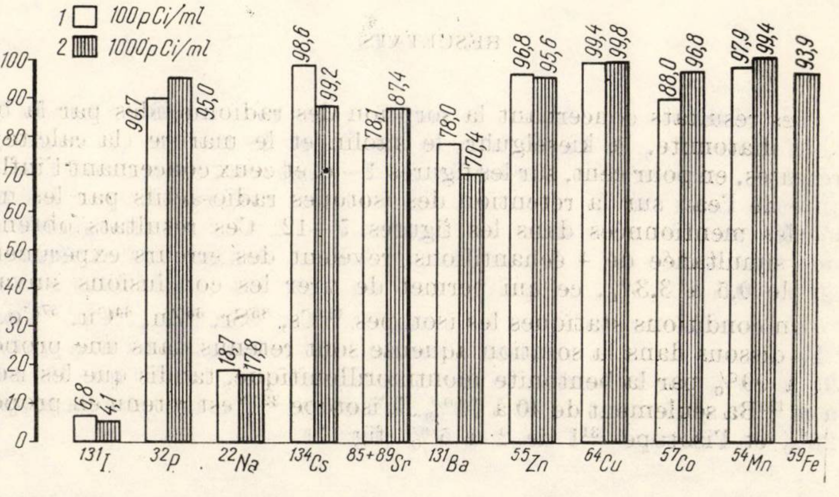

Fig. 2. — Rétention de certains ions radio-actifs dissous dans l'eau par la diatomite mis en contact permanent pendant 24—48 h (2g : 50 ml solution).

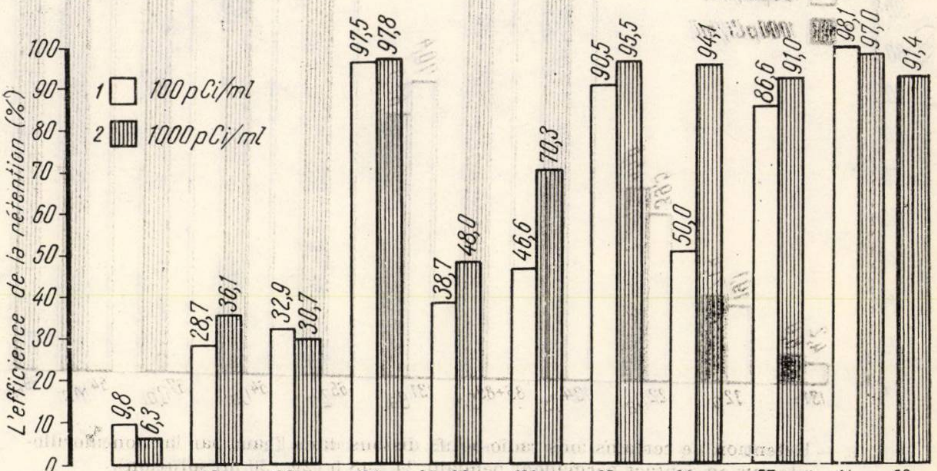

Fig. 3. — Rétention de certains ions radio-actifs dissous dans l'eau par la kieselguhr mis en contact permanent pendant 24—48 h (2 g : 50 ml solution).

Le kaolin présente certaines particularités, retenant les isotopes ^{32}P, ^{134}Cs, ^{65}Zn, ^{64}Cu, ^{57}Co, ^{54}Mn et ^{59}Fe, dans une proportion dépassant 50%, tandis que le nucléide ^{22}Na est retenu à 73% et les nucléides ^{85}Sr et ^{131}Ba

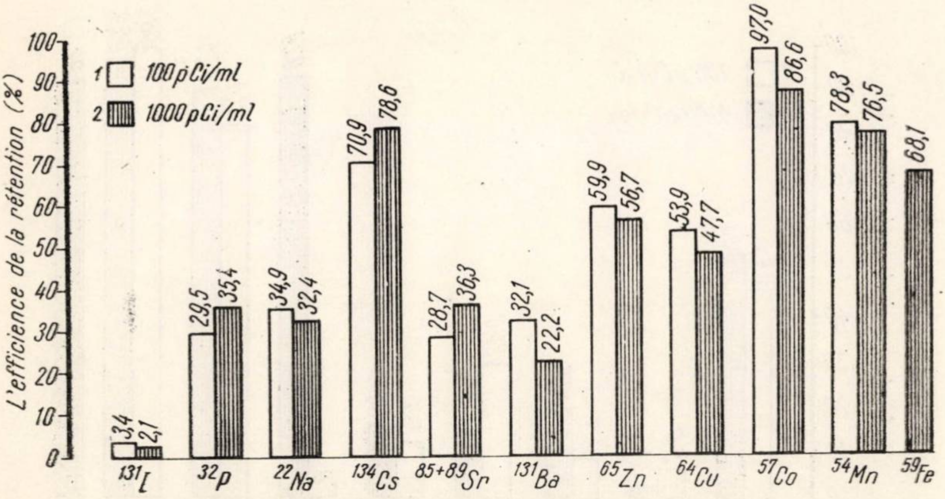

Fig. 4. — Rétention de certains ions radio-actifs dissous dans l'eau par le silicagel mis en contact permanent pendant 24—48 h (2 g : 50 ml solution).

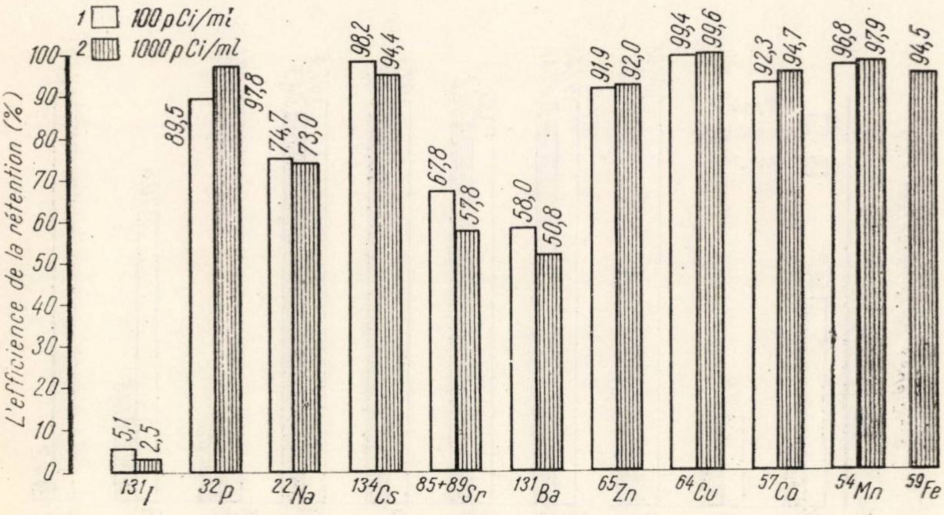

Fig. 5. — Rétention de certains ions radio-actifs dissous dans l'eau, par le kaolin, mis en contact pendant 24—48 h (2 g : 50 ml solution).

sont retenus de 50 à 60% (fig. 5). La calcite du marbre retient jusqu'à 90% les isotopes ^{64}Cu, ^{57}Co, ^{54}Mn et ^{59}Fe et seulement de 45 à 50% le nucléide ^{32}P. Les isotopes ^{22}Na, ^{134}Cs, ^{85}Sr et ^{131}Ba sont retenus dans une proportion inférieure à 30% (fig. 6).

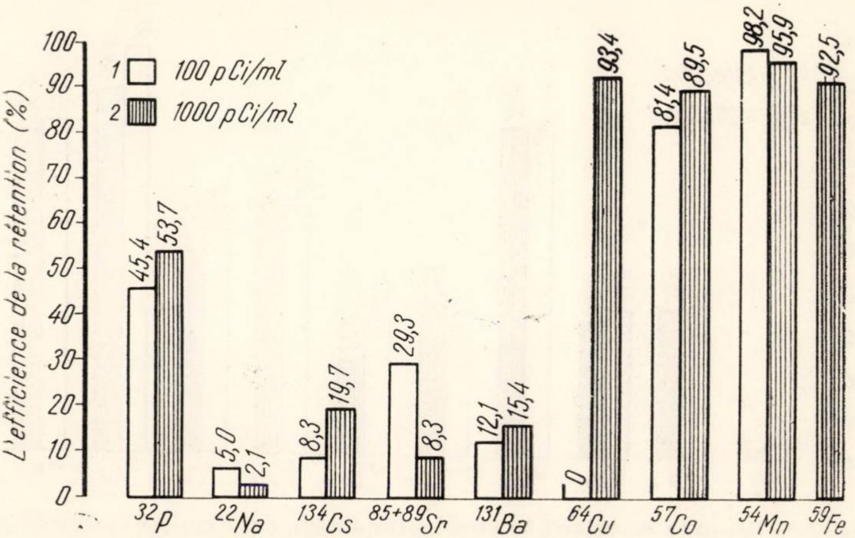

Fig. 6. — Rétention de certains ions radio-actifs, dissous dans l'eau, par le marbre, mis en contact permanent pendant 24—48 h (2 g : 50 ml solution).

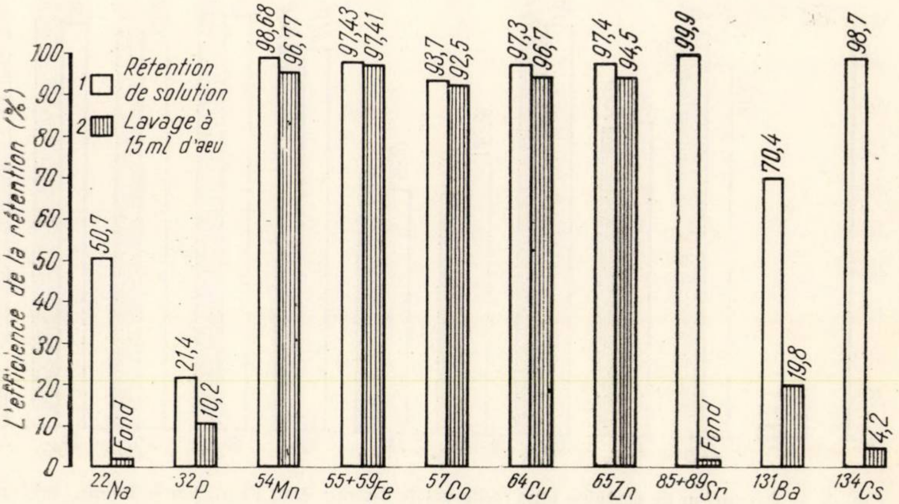

Fig. 7. — Influence sur l'efficience de la rétention des ions radio-actifs par la montmorillonite, après un contact pendant 24—48 h sous l'action éluante de l'eau.

Les résultats représentés sur les figures 7—12 font ressortir dans les conditions statiques l'effet éluant de l'eau sur la rétention des isotopes par les macromolécules inorganiques étudiées.

---

[13] VL. LAMBRINO et GH. FURNICĂ, *Compt. rend. de l'Acad. Bulgare de Sciences*, **22**, 1111 (1969).

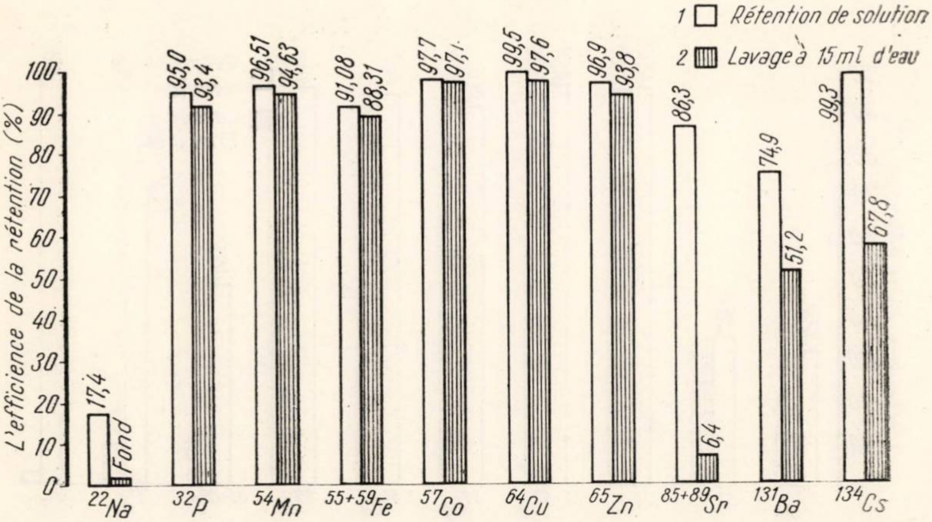

Fig. 8. — Influence sur l'efficience de la rétention des ions radio-actifs par la diatomite, après un contact pendant 24—48 h, sous l'action éluante de l'eau.

On a remarqué au cas de la monmorillonite que les nucléides ^{22}Na, ^{85}Sr et ^{134}Cs sont élués dans une proportion de 90%, le nucléide ^{32}P à 50% et le radionucléide ^{131}Ba dans une proportion dépassant 75% (fig. 7). La diatomite perd par élution 90% de nucléide ^{22}Na, 85% de nucléide ^{85}Sr, plus que 25% de nucléide ^{131}Ba et plus que 40% de nucléide ^{134}Cs (fig. 8). Les radionucléides ^{54}Mn, ^{59}Fe, ^{57}Co, ^{64}Cu et ^{65}Zn retenus par la diatomite et la montmorillonite sont élués seulement dans une proportion de 3 à 7% par l'eau, tandis que ^{32}P, retenu par la diatomite, est élué seulement dans une proportion de 3 à 4%.

La kieselguhr (fig. 9) retient les isotopes ^{54}Mn, ^{59}Fe, ^{57}Co, ^{64}Cu dans une proportion élevée, mais l'élution par l'eau provoque une élimination moyenne de 2 à 14%. On a aussi remarqué que ^{32}P retenu par la kieselguhr dans une proportion de 36% est élué jusqu'à 15%, par lavage avec de l'eau, donc ^{22}Na est élué jusqu'à 20%. Les nucléides ^{65}Zn, ^{85}Sr, ^{131}Ba et ^{134}Cs sont élués dans une grande proportion jusqu'à 40—95%. Le silicagel (fig. 10) perd en petite quantité les nucléides ^{54}Mn, ^{59}Fe, ^{57}Co, ^{64}Cu et ^{65}Zn (1 — 6%), mais l'effet éluant est plus intense pour les isotopes ^{22}Na, ^{32}P, ^{85}Sr, ^{131}Ba et ^{134}Cs.

Les nucléides ^{32}P, ^{54}Mn, ^{59}Fe, ^{57}Co, ^{64}Cu et ^{65}Zn retenus par le kaolin (fig. 11) dans une proportion élevée sont ensuite éliminés en petite quantité par l'effet éluant de l'eau (de 1 à 9%). Les nucléides ^{134}Cs et ^{131}Ba sont élués dans une proportion de 30 à 33%, tandis que les isotopes ^{22}Na et ^{85}Sr sont éliminés par l'eau à 99%. Il est intéressant de mentionner que la calcite du marbre (fig. 12) a retenu des quantités plus élevées de ^{54}Mn,

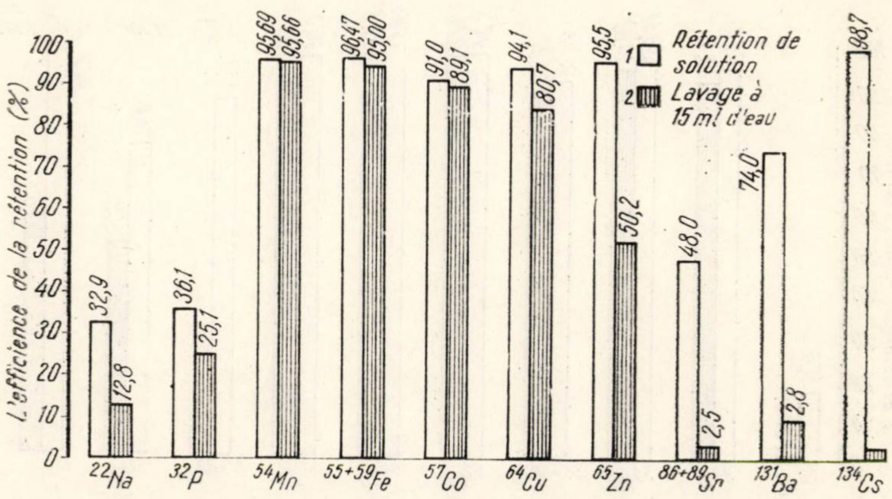

Fig. 9. — Influence sur l'efficience de la rétention des ions radio-actifs par le kieselguhr, après un contact de 24 à 48 h, sous l'action éluante de l'eau.

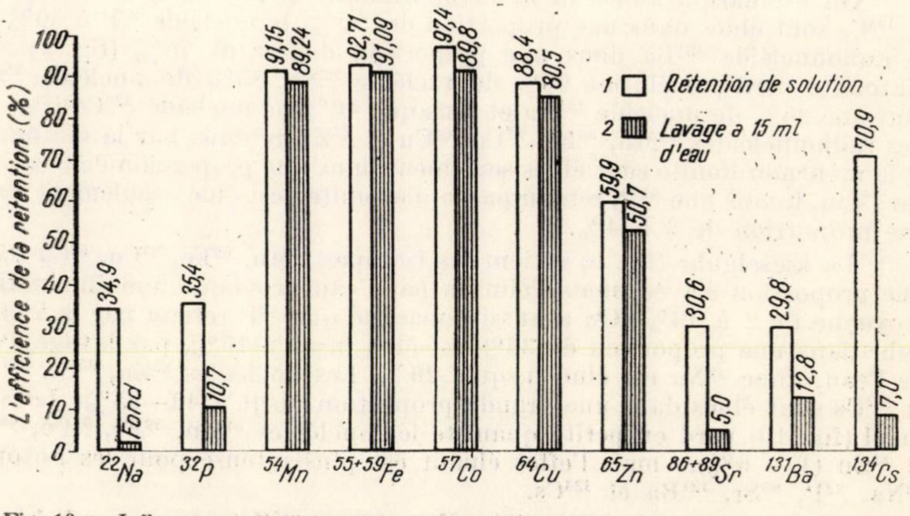

Fig. 10. — Influence sur l'efficience de la rétention des ions radio-actifs par le silicagel, après un contact de 24 à 48 h, sous l'action éluante de l'eau.

^{59}Fe, ^{57}Co et ^{64}Cu, de nucléides qui sont après élués en petites proportions (de 1 à 6%). Le nucléide ^{134}Cs retenu dans une petite proportion est éliminé aussi en petites quantités. Dans le cas des nucléides ^{32}P et ^{131}Ba les quantités retenues par le kaolin sont éluées jusqu'à 50%.

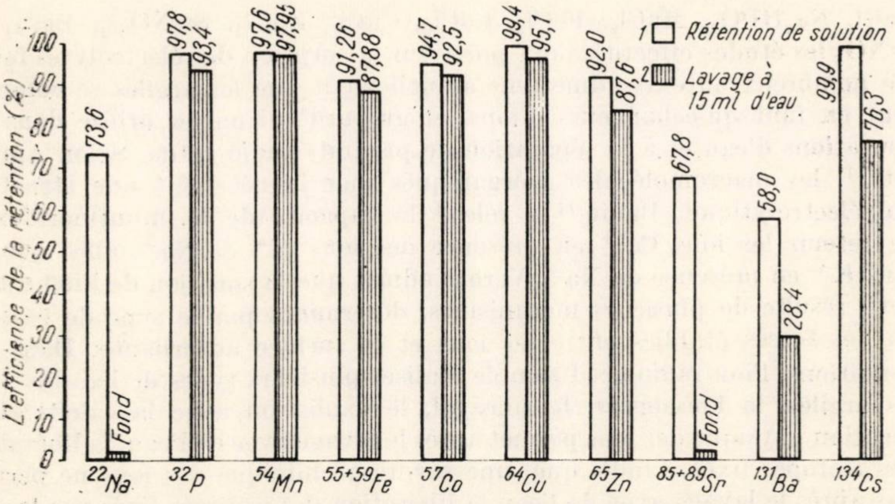

Fig. 11. — Influence sur l'efficience de la rétention des ions radio-actifs par le kaolin, après un contact de 24 à 48 h, sous l'action éluante de l'eau.

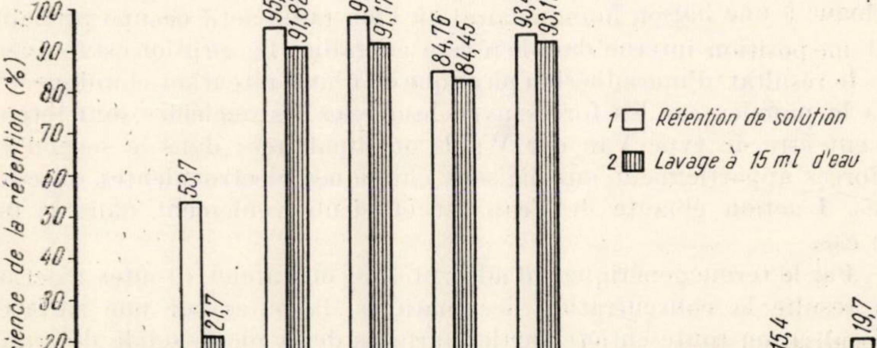

Fig. 12. — Influence sur l'efficience de la rétention des ions radio-actifs par le marbre, après un contact de 24 à 48 h, sous l'action éluante de l'eau.

DISCUSSIONS

Les résultats obtenus révèlent la différence de la capacité de sorption des divers ions radio-actifs par les macromolécules inorganiques étudiées. Compte tenu que toutes les combinaisons chimiques utilisées ont été :

NaCl, Na_2HPO_4, $MnCl_2$, $FeCl_3$, $CoCl_2$, $CuCl_2$, $ZnCl_2$, $Sr(NO_3)_2$, $BaCl_2$ et $CsNO_3$ les études effectuées ont porté sur la sorption des électrolytes forts. De nombreux auteurs admettent actuellement que les argiles se comportent en tant qu'échangeurs d'ions, et aujourd'hui on les utilise dans les épurations d'eau et à la séparation de produits radio-actifs. Selon Amphlett, [11] les macromolécules inorganiques mentionnées ont une structure polyélectrolytique. Banin [14] a relevé la capacité de la montmorillonite de retenir les ions Ca^{2+} en présence des ions K^+ et Na^+, ainsi que les ions K^+ en présence de Na^+. Verot [8] admet que la sorption de l'ion radioactif résulte de plusieurs mécanismes, déterminés par le type de liaisons ou des forces établies entre les ions et la surface adsorbante. Dans ces conditions, l'ion radio-actif semble réaliser plusieurs types de liaisons avec les argiles, la kieselguhr, le silicagel, le kaolin ou avec la calcite. Une sorption physique des ions permet après le lavage avec de l'eau, la libération des isotopes fixés, tandis que, une sorption chimique des ions ne permet pas après le lavage avec de l'eau la libération des isotopes fixés par la surface absorbante. Dans ces conditions, Bittel admet que l'ion radio-actif semble réaliser avec le substratum deux principaux types de liaison [2] : une liaison relativement labile analogue à une liaison hétéropolaire où l'ion radio-actif peut être remplacé par d'autres ions et une autre liaison (analogue à une liaison homopolaire) où l'ion radio-actif occupe probablement une position interne dans le réseau cristallin. La sorption est fréquemment le résultat d'une adhésion physique ou d'une rétention chimique. [15,16] Dans le premier cas les forces avec lesquelles les nucléides sont retenus peuvent être de type Van der Waals ou dipolaires ; dans le second cas ces forces appartiennent aux liaisons chimiques électrovalentes ou covalentes. L'action éluante de l'eau est efficiente seulement dans le premier cas.

Par le terme générique « d'adsorption », on entend « toutes réactions d'où résulte la concentration des matières dissoutes sur une surface ». La localisation toute entière sur les surfaces de la phase solide détermine la sorption « secondaire ». Dans d'autres conditions la sorption devient de type « primaire » pour les mécanismes de réactions impliquant la rétention dans des graines (ou des réseaux cristallins). Par conséquent, on peut admettre que les trois paramètres les plus importants déterminant le comportement d'un système hétérogène envers la sorption d'un constituant ionique d'une solution aqueuse sont les suivants : le pouvoir d'échange (de sorption) ; la constante d'équilibre chimique ou d'échange isotopique et la diffusion.[17-30] Nos résultats montrent que la sorption des ions radio-actifs des éléments Na, Cs, Ba et Sr en contact avec la montmorillonite se déroule dans une proportion de 80 à 90% à l'aide des forces non chimiques. Cette proportion baisse de 30 à 50% en contact avec la diatomite. La kieselguhr retient physiquement ces ions radio-actifs dans une proportion de 10 à 55%, tandis que le kaolin retient chimiquement les radio-ions Cs* et Ba^{2+} dans une proportion de 45 à 75%. La calcite maintient chimiquement l'isotope Cs dans une proportion de 85%, tandis que les isotopes de Ba sont fixés dans une proportion de 50% et l'ion $H_2PO_4^-$ dans une proportion de 45%. Les ions radio-actifs des nucléides du Mn, Fe, Co, Cu et Zn sont retenus chimiquement par la montmorillonite et la diatomite dans une proportion de 85 à 100%.

---

[14] A. Banin, *Israel J. Chem.*, 6, 27 (1968).

[15] S. Ţilenski, « Chimie Coloidală », Ed. tehnică, Bucarest, 1964, p. 193, 422.

[16] C. Niac, « Chimie fizică », Ed. didactică și pedagogică, Bucarest, 1966, p. 472.

Les résultats mentionnés permettent de conclure que la sorption des ions radio-actifs d'une solution aqueuse par les macromolécules inorganiques peut être attribuée à la formation des liaisons physiques ou chimiques entre ces deux groupes des substances. La proportion des liaisons physiques ou chimiques formées dépend de la nature chimique des ions et de la structure des groupements chimiques des macromolécules inorganiques. Nos résultats démontrent en même temps la nécessité d'effectuer des études suivies concernant la nature de la liaison chimique entre les divers ions radio-actifs retenus et les macromolécules inorganiques mentionnées.

---

[17] I. S. Kulikov, « Folosirea izotopilor radioactivi în metalurgie », Ed. tehnică, Bucarest, 1957, p. 182.

[18] W. F. Kisselew, *Z. Chem.*, **7**, 369 (1967).

[19] A. N. Frumkin et O. Zarubina, *Zhur. fiz. Khim.*, **2**, 545 (1931).

[20] N. A. Șilov, *Z. phys. Chem.*, **13**, 188 (1928); **14**, 211 (1930).

[21] A. Banin, « Clays and Clay Minerals », Pergamon Press, New York, 1966, p. 133.

[22] Hwa-Sheng Cheng, *Health Physics*, **14**, 353 (1968).

[23] H. Sherry et H. Walton, *J. Phys. Chem.*, **71**, 1457 (1967).

[24] M. Rinando et M. Milas, *Compt. rend.*, (C), **269**, 1190, 1280 (1969).

[25] S. Solacolu, « Chimie fizică a silicaților », Ed. tehnică, Bucarest, 1968, p. 69.

[26] A. P. Ruțcov, « Chimie coloidală », Ed. tehnică, Bucarest, 1960, p. 107.

[27] T. Ionescu, « Schimbători de ioni », Ed. tehnică, Bucarest, 1964, p. 97.

[28] Th. G. Sahama et K. Rankama, « Geochimia », Ed. tehnică, Bucarest, 1970, p. 222.

[29] A. V. Dumanski, « Coloizii », Ed. de Stat, Bucarest, 1949, p. 394.

[30] R. Bittel et C. Boursat, *Bull. du groupe français des Argiles*, **11**, 9 (1959); **12**, 89 (1960).

Revue Roumaine de Chimie, 18, 1, 175–185 (1973)

OS MŰSZAKI KÖ
CIÓS

[illegible]

[illegible]

[illegible]

NOTE POUR LES AUTEURS

La *Revue Roumaine de Chimie* publie des articles en anglais, français, russe, allemand ou espagnol. Les auteurs sont priés d'envoyer des articles, notes, communications et comptes rendus inédits.

Les manuscrits seront dactylographiés à deux intervalles. Les tableaux seront dactylographiés sur feuilles séparées, de même que la légende des figures. Les diagrammes seront tracés à l'encre de Chine sur papier calque. Les tableaux et les figures seront numérotés par des chiffres arabes, en nombre strictement nécessaire. Prière de ne pas inscrire les mêmes données dans les tableaux et les figures. Les formules chimiques seront incluses dans le texte ; en outre, elles seront transcrites sur des feuilles séparées. Les auteurs sont priés d'indiquer les caractères italiques (en soulignant les lettres au crayon), ainsi que tout autre caractère spécial. L'ordre des références bibliographiques sera celui de leur mention dans le texte ; le nom de l'auteur sera précédé de l'initiale du prénom ; les publications périodiques seront présentées suivant les prescriptions internationales. Les références seront ajoutées à la fin de l'article ; elles paraîtront comme des notes, au bas de la page. Le texte sera précédé d'un résumé, comprenant 15 lignes au maximum.

L'entière responsabilité du contenu des articles appartient aux auteurs. On publie des articles dus aux collaborateurs roumains ou étrangers. Les auteurs recevront 50 tirés à part.

PRINTED IN ROMANIA

1973 MAI 1 9

TRAVAUX PARUS AUX ÉDITIONS DE L'ACADÉMIE DE LA RÉPUBLIQUE SOCIALISTE DE ROUMANIE

P. BALTĂ et E. BALTĂ, **Introducere în chimia fizică a stării vitroase** (Introduction à la chimie physique de l'état vitreux), 1971, 240 p., 15,50 lei.

LYDIA-MARIA VAICUM, **Biodegrabilitatea detergenţilor** (Biodégrabilité des détergents), 1971, 254 p., 16 lei.

TIBERIU NĂSCUŢIU, **Metode radiometrice de analiză** (Méthodes radiométriques d'analyse), 1971, 346 p., 19,50 lei.

I. ZUGRĂVESCU et I. STOICESCU-CRIVETZ, **Polimeri heterociclici** (Polymères hétérocycliques), 1971, 190 p., 9,50 lei.

CRISTOFOR SIMIONESCU, C. V. UGLEA, **Fracţionarea compuşilor macromoleculari** (Fractionnement des composés macromoléculaires), 1969, 292 p., 18,50 lei.

I. MAXIM, **Materiale nucleare** (Matériaux nucléaires), 1969, 444 p., 30 lei.

CRISTOFOR SIMIONESCU et CLEOPATRA VASILIU-OPREA, **Mecanochimia compuşilor macromoleculari** (La mécanochimie des composés macromoléculaires), 1967, 344 p., 23,50 lei.

CORNEL BODEA et collab., **Tratat de biochimie vegetală**, partea I, **Fitochimie** (Traité de biochimie végétale, Ire partie, Phytochimie), Ier vol., 1964, 747 p. + 4 annexes + 2 pl., 41 lei; IIe vol., 1965, 1262 p., 1 pl., 56 lei; IIIe vol., 1967, 773 p., 35 lei.

V. GHEŢIE et V. MICUŞAN, **Analiza imunochimică. Teorie şi practică** (Analyse immunochimique. Théorie et pratique), 1966, 369 p., 28 lei.

R. PORTOCALĂ et L. POPA, **Acizii ribonucleici celulari şi virali** (Les acides ribonucléiques cellulaires et viraux), 1966, 375 p., 8 pl., 26 lei.

I.P.I. —c. 2052

43 426

Lei 25.—

F 1103

R

PETEFALVA

REVUE ROUMAINE DE CHIMIE

Tome 18

N° 2

Février 1973

RRCHAX, 18, *2*, 187–352 (1973)

ÉDITIONS DE L'ACADÉMIE DE LA RÉPUBLIQUE SOCIALISTE DE ROUMANIE

Rev. Roumaine Chim.

18, *2*, p. 187–352 (1973), Bucarest

COMITÉ DE RÉDACTION

Rédacteur en chef:

I. G. MURGULESCU, membre de l'Académie de la République Socialiste de Roumanie

Rédacteurs en chef adjoints:

A. T. BALABAN et V. EM. SAHINI, membres correspondants de l'Académie de la République Socialiste de Roumanie

Collège de rédaction:

C. DRĂGULESCU, RALUCA RIPAN, CR. SIMIONESCU, membres de l'Académie de la République Socialiste de Roumanie; EM. BRATU, ECATERINA CIORĂNESCU-NENITZESCU, P. SPACU, membres correspondants de l'Académie de la République Socialiste de Roumanie; MARGARETA AVRAM, I. D. MARCHIDAN, G. NIAC et D. SĂNDULESCU

La Revue Roumaine de Chimie paraît 12 fois par an. Toute commande de l'étranger (fascicules ou abonnements) sera adressée à Intreprinderea Rompresfilatelia, Boîte postale 2001, telex 011631, Bucarest, Roumanie

Les manuscrits, les livres et les revues proposés en échange, ainsi que toute correspondance seront envoyés à la rédaction:

REVUE ROUMAINE DE CHIMIE
23, Str. Dumbrava Roşie, Bucarest, Roumanie

ÉDITIONS DE L'ACADÉMIE DE LA RÉPUBLIQUE SOCIALISTE DE ROUMANIE
3 bis, Str. Gutenberg, Bucarest

ORSZÁGOS MŰSZAKI KÖNYVTÁR DOKUMENTÁCIÓS KÖZPONT

REVUE ROUMAINE DE CHIMIE

Tome 18, Nr. 2 Février 1973

Page

I. G. MURGULESCU, E. POPA and EUGENIA IVANA, Electronic absorption spectra of silver halides in passing from solid to molten state 189–193

ILEANA IOSIF, I. A. SCHNEIDER and C. VOLANSCHI, Some aspects of the cool flame and low-temperature ignition of methane . . . . . . 195–201 R

S. SOLACOLU, M. CERCHEZ and E. SEGAL, Kinetics of the formation reactions of oxydic compounds in solid phase through differential thermal analysis . . . . 203–210 Bef

IUDITA ADORIAN, Temperature and concentration dependence of molar polarization in binary mixtures of polar liquids with nonpolar solvent . . 211–219

S. STERNBERG and T. VIŞAN, The determination of the diffusive and capacitive current in the chronopotentiometry of the molten salt systems $(Na,Ag)NO_3$ and $(K, Ag)NO_3$ 221–231

OV. MATEIOVICI, Study of electrochemical forming of surface oxides on the active carbon electrode 233–238

O. IORDACHE, MARCELA MUNTEAN and I. TEOREANU, Stochastic modelling of chemical processes 239–246

FLORICA POPEA, CRISTINETA MĂRCULESCU and CONSTANŢA PÎRLOG, New uranyl compounds with pyrimidine derivatives 247–255

EUGENIA GÂRD, F. CHIRALEU, ILEANA I. STĂNOIU and A. T. BALABAN, Isotopic exchange of active methyl hydrogens. VII. Kinetic study of 2,4,6-trimethylpyrylium salts in deuterium oxide 257–261

M. IOVU and ANCA ANGELESCU, Phenyl benzyl sulphides 263–268

IOSIF DRIMUŞ und IOAN T. IONESCU, Der Einfluss der Kettenlänge einiger *n*-Alkane auf ihre Peroxydierungsgeschwindigkeit mit molekularem Sauerstoff, in flüssiger Phase . . . . 269–274 R

R. BACALOGLU und B. D. BADER, Neue organische Pigmente – Isatinderivate. III. Studium der IR-Spektren einiger 2-Arylaminoindoxyle und 3-Aryliminooxindole 275–282

F. KEREK und I. MOŢOC, Matrizielle Charakterisierung der Struktur und Topologie der organischen Verbindungen. I. Konstitution 283–288

I. MOŢOC und F. KEREK, Matrizielle Charakterisierung der Struktur und Topologie organischer Verbindungen. II. Konfiguration, Chiralität . . . 289–296

ALI ALI KHALAF, Modern Friedel-Crafts chemistry. I. Cyclialkylations of some secondary and tertiary phenylalkyl chlorides in the presence of the mild $AlCl_3/CH_3NO_2$ and $FeCl_3$ catalysts 297–304

N. COBIANU, C. BOGHINĂ, B. MĂRCULESCU and I. AMĂLINEI, On the reactivity of N-vinylcaprolactam in radicalic polymerization 305–317

Rev. Roumaine Chim. **18**, *2*, 187–352 (1973), Bucarest

Page

CANDIN LITEANU and IONEL CĂTĂLIN POPESCU, Studies on the electroanalytical behaviour of membrane-electrodes under current. I. Current-membrane potential curves for the parchment membrane-electrode impregnated with $BaSO_4$ 319–326

CR. I. SIMIONESCU, I. BENEDEK, SILVIA IOAN, N. ASANDEI and MONIQUE GALIN, Copolymerization reactions using organic titanium derivatives-aluminum alkyl complexes. VII. Structural aspects of acrylonitrile-methylmethacrylate copolymers prepared by the use of the soluble Ziegler-Natta catalyst system: bis(cyclopentadienyl)-titanium-dichloride-triethylaluminum 327–346

I. INŢA and P. MĂRGINEANU, The ferromagnetic resonance of nickel-chromia catalyst 347–352

Revue Roumaine de Chimie, **18**, *2*, 189–193 (1973)

ELECTRONIC ABSORPTION SPECTRA OF SILVER HALIDES IN PASSING FROM SOLID TO MOLTEN STATE

I. G. MURGULESCU, E. POPA and EUGENIA IVANA

Center of Physical Chemistry
Str. Galaţi 31, Bucharest — 13, Romania

Received September 22, 1972

Electronic absorption spectra of silver halides in passing from solid to molten state were obtained. A bathochromic shift of the absorption band edge with temperature was observed. The observed energy jumps at melting points and bathochromic effect are explained as due to the same structural modification.

1. INTRODUCTION

The resemblance of the ultraviolet absorption spectra of AgCl, AgBr and AgI [1–5] with those of alkali halides is well-known.

The AgCl absorption spectrum in solid state at 20 K is composed of a broad maximum at about 50,000 cm^{-1} and another at 42,000 cm^{-1} (doublet).

The same general characteristics may be noticed for the Ag Br spectrum at 20 K, that is a continuous absorption in the range of 50,000 cm^{-1}, a maximum at 34,500 cm^{-1} and another at 39,000 cm^{-1}.

Similarly, AgI has a continuous absorption in ultraviolet and a maximum at about 23,600 cm^{-1}.

However, in contrast to the alkali halides, silver halides have absorption tails which extend towards longer wavelength. The origin of these long wavelength absorption tails has been a matter of speculation for many studies. [3,5–9]

---

[1] Y. Okamoto, *Nach. Akad. Wiss. Göttingen*, 2A, **14**, 275 (1956).
[2] S. Tutihasi, *Phys. Rev.*, **105**, 882 (1957).
[3] F. C. Brown, T. Masumi, and H. H. Tippins, *J. Phys. Chem. Solid.*, **22**, 101 (1961).
[4] F. Moser and F. Urbach, *Phys. Rev.*, **102**, 1519 (1956).
[5] F. Seitz, *Rev. Mod. Phys.*, **23**, 328 (1951).
[6] F. Seitz and F. C. Brown, Intern. Conf. Sci. Photo Liège, 1959.
[7] W. Martienssen, Proc. Intern. Conf. Semicond. Phys. Prague, 1961.
[8] B. L. Ioesten and F. C. Brown, *Phys. Rev.*, **148**, 919 (1966).
[9] S. K. Suri and H. K. Henisch, *Phys. Stat. Sol.* (b), **44**, 627 (1971).

In the literature, AgCl and AgBr were investigated in the molten state,[10,11] and the influence of the temperature upon the absorption band edge was studied.

This work reports the absorption spectra of AgCl, AgBr, and AgI in passing from solid to molten state.

2. EXPERIMENTAL PART

The absorption measurements were carried out with a "Specord UV-VIS" Carl Zeiss Jena recording spectrophotometer.

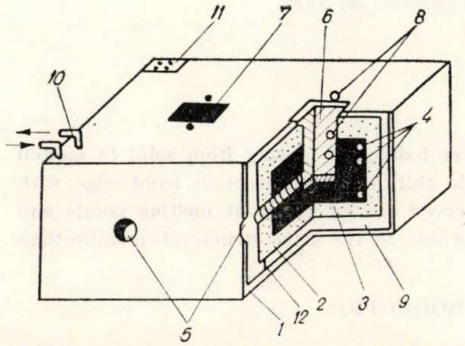

Fig. 1. — Furnace for high temperatures.

1, Cooling mantle; *2*, Asbestos layer; *3*, Ceramic block for warming; *4*, Warming resistance; *5*, Windows for the double monochromatic beam; *6*, Cell room; *7*, Cover of the cell room; *8*, Holes for the thermocouples; *9*, Air layer; *10*, Pipe for cooling water; *11*, Panel of the electric supply; *12*, Metallic housing.

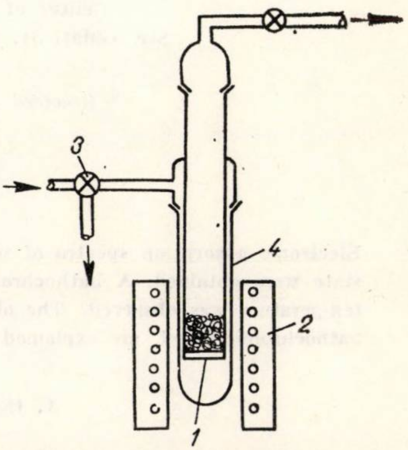

Fig. 2. — Drying and filtering apparatus.

1, Glass frit; *2*, Furnace; *3*, Two way top; *4*, AgX.

The usual cells holder was replaced by a furnace (fig. 1) permitting temperatures up to 700°.

The temperature uniformity inside the furnace has been controlled by two Pt—Pt, Rh thermocouples placed in two different sites.

On account of the very strong absorption of the melt, cells with a thickness of about 10 μ have been used. These were filled and sealed under vacuum.

The silver halides were prepared from diluted solutions of $AgNO_3$, respectively with KCl, KBr and KI previously recrystallized. The silver salts obtained in this way were dried and purified with the installation presented in fig. 2.

An argon stream, previously purified and dried, is passed through a G-3 glass frit, on which the salt is to be found.

The system of purification is composed of a tube of glass filled with metallic copper and two tubes of glass filled respectively with P_2O_5 and silicagel.

The temperature is gradually raised by means of the furnace (fig. 2) in which the lower part of the installation is introduced.

---

[10] C. D. Thurmond, *J. Amer. Chem. Soc.*, **75**, 3928 (1953).

[11] B. R. Sundheim and J. Greenberg, *J. Chem. Phys.*, **28**, 439 (1958).

Near to the melting point and after the melting of the salt, a dried current of HX gas is passed through.

For removing of HX, the installation is washed with argon, 2–3 h after melting. Then the melt is filtered. All the preparing and purifying operations have been performed in darkness, due to the sensitivity of the silver halides to light.

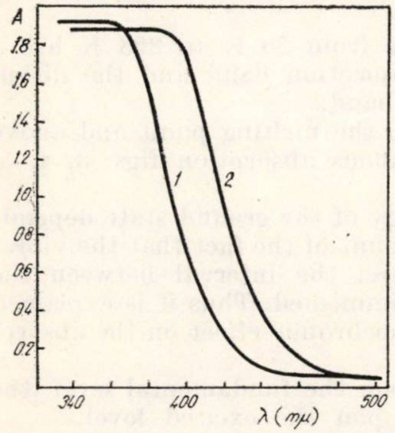

Fig. 3. — Absorption spectrum of AgCl.

1, $t = 400°$ (solid) ; $t = 470°$ (melt).

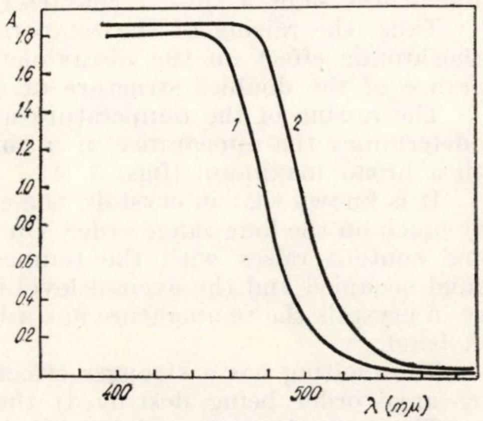

Fig. 4. — Absorption spectrum of AgBr.

1, $t = 425°$ (solid) ; *2*, $t = 470°$ (melt).

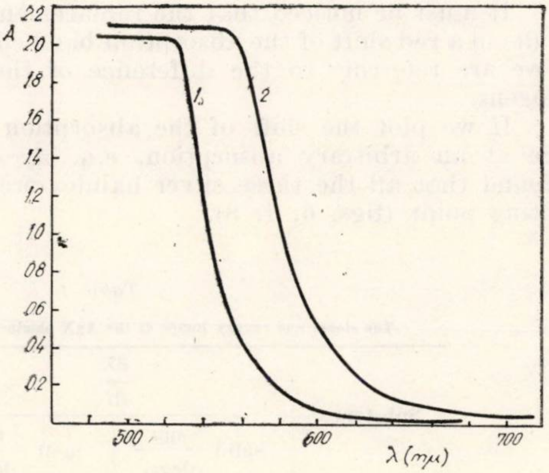

Fig. 5. — Absorption spectrum of AgI.

1, $t = 530°$ (solid) ; *2*, $t = 580°$ (melt).

3. RESULTS AND DISCUSSIONS

The absorption spectra of AgCl, AgBr and AgI are presented in figs. 3, 4 and 5.

After examining the spectra, we found that these present a continuous absorption with a broad maximum at about 380 mμ ($t = 470°$) for AgCl and at about 460 mμ ($t = 470°$) for AgBr.

For AgI we found a very strong absorption between 400—550 mμ without any maximum. The absorption suddenly diminishes at about 555 mμ ($t = 580°$). We can also notice a shift of the edge of the absorption band with the temperature, to low energies, both in the molten and solid state.

The studies on AgX absorption spectra in the solid state at low temperatures show a similar characteristic.

Thus, the raising of the temperature from 20 K to 293 K has a bathochromic effect on the ultraviolet absorption band and the disappearance of the doublet structure of the band.

The raising of the temperature up to the melting point and above it, determines the appearance of a continuous absorption (figs. 3, 4, 5) with a broad maximum (figs. 3, 4).

It is known that in crystals, the energy of the ground state depends very much on the long-range order. On account of the fact that the vibrational content raises with the temperature, the interval between the ground occupied and the excited level is diminished. Thus it is explained why in crystals the temperature has a bathochromic effect on the absorption band.

The melting has a stronger effect upon the fundamental level (the long-range order being destroyed) than upon the excited level.

Thus, the fundamental band being strongly delocalized, the energetic interval between the levels diminishes and the spectrum will occur at longer wavelength.

It must be noticed that the replacement of the Cl^- with Br^- and I^- results in a red shift of the absorption band edge, which is easily explained, if we are referring to the difference of the electronic affinity of the halogens.

If we plot the shift of the absorption band edge (the wavelength edge at an arbitrary absorption, e.q. $A = 1$) against temperature, it is found that all the three silver halides present finite jumps (Δ) at the melting point (figs. 6, 7, 8).

Table 1

The slopes and energy jumps of the AgX obtained from plots no 6, 7, 8

Substance	$\frac{d\lambda}{dt}$ solid $\frac{m\mu}{degr.}$	$\frac{d\lambda}{dt}$ melt $\frac{m\mu}{degr.}$	Δ (cm^{-1})
AgCl	0.363	0.20	982
AgBr	0.28	0.15	825
AgI	0.15	0.11	850

In table 1 the values of these jumps (Δ) and also the slopes $d\lambda/dt$ of the absorption band edge are inserted, both in the solid and molten state (the columns 2, 3).

The slopes of the absorption band edge in the solid state are greater than those in the molten one.

This fact proves that the temperature determines more structural modifications in the solid than in the molten state. The values of these slopes decrease from AgCl to AgI both in solid and molten state and there are small differences between those of the molten state.

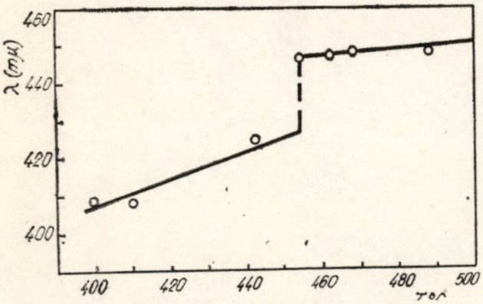

Fig. 6. — Temperature variation of the absorption band edge of AgCl.

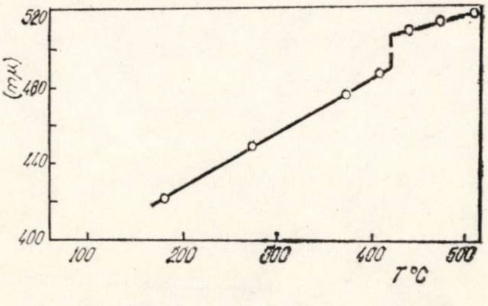

Fig. 7. — Temperature variation of the absorption band edge of AgBr.

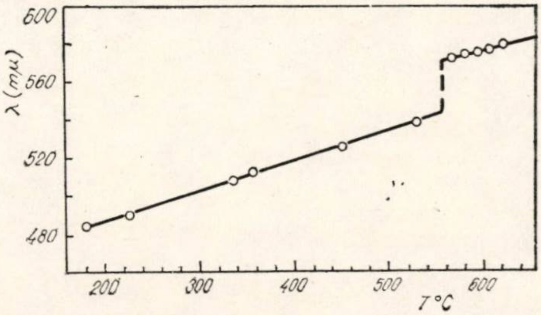

Fig. 8. — Temperature variation of the absorption band edge of AgI.

These results are also in concordance with other physicochemical properties [12-14] of the silver halides in their passing from solid to molten state (the change of the melting volume, the heat of melting etc.).

---

[12] A. R. Ubbelohde, "Melting and Crystal Structure", Oxford Univ. Press, 1965, p. 144.

[13] G. I. Janz, "Molten salts handbook", Acad. Press, New York, 1967, p. 187.

[14] A. R. Ubbelohde, *Proc. Chem. Soc.*, **1960**, 332.

Revue Roumaine de Chimie, **18**, *2*, 195–201 (1973)

SOME ASPECTS OF THE COOL FLAME AND LOW-TEMPERATURE IGNITION OF METHANE

ILEANA IOSIF, I. A. SCHNEIDER and C. VOLANSCHI

Centre of Physical Chemistry
Str. Galaţi, 31, Bucharest 13, Romania

Received July 20, 1972

The methane oxidation initiated by nitric acid was investigated in a dynamical system at 557°. The emission spectrum of the cool flame was recorded in order to understand the complex physical and chemical processes which lead to the appearance of the flame phenomenon. By modifying the conditions of the reaction in a series of experiments, the ignition phenomenon was studied.

The slow oxidation of hydrocarbons has been the object of extended experimental and theoretical [1–5] works, which have indicated the existence of two temperature-dependent mechanisms, i.e. high-temperature and low-temperature regions. [6]

The transition between these two temperature regions is frequently associated with the appearance of some interesting effects, such as the negative temperature coefficient, the cool flame and the ignition phenomenon.

The appearance of the "cool flame" was observed as far back as 1924 in a work related to the oxidation of octane. [7] Extending this work to some paraffins, olefines, naphthenes, aldehydes and ethers, [8,9] Prettre noticed the absence of the cool flame in methane and ethane.

However, in 1953 Gray, [10] studying the oxidation of ethane in the 500°–600° temperature range, and somewhat later Vanpée, [11] studying

---

[1] D. M. Newitt and L. S. Thorness, *J. Chem. Soc.*, 1656 (1937).

[2] R.A. Day and R. N. Pease, *J. Amer. Chem. Soc.*, **63**, 2234 (1940).

[3] J. H. Knox and R. G. W. Norrish, *Trans. Faraday Soc.*, **50**, 928 (1954).

[4] J. H. Knox and R. G. W. Norrish, *Proc. Roy. Soc.*, **A 221**, 151 (1953).

[5] C. N. Hinshelwood, *Proc. Roy. Soc.*, **A 205**, 375 (1951).

[6] C. H. Yang and B. F. Gray, *J. Phys. Chem.*, **73**, 3395 (1969).

[7] J. C. Pope, E. J. Dykstra and G. Edgar, *J. Amer. Chem. Soc.*, **51**, 1875, 2203 (1924).

[8] M. Prettre, P. Dumanois and P. Laffitte, *Compt. rend.*, **191**, 329, 414 (1932).

[9] M. Pettre, *Bull. Soc. chim., France*, **51**, 1132 (1932).

[10] J. A. Gray, *J. Chem. Soc.*, **1953**, 741.

[11] M. Vanpée, *Compt. rend.*, **234**, 804 (1956).

the oxidation of methane in statical conditions, succeeded to evidence the flame phenomenon in these two first members of the parafinic series too. More detailed studies concerning the phenomenon of cool flame in methane were carried out later[12-14] and these revealed the various factors which influence the phenomenon.

In this work, the emission spectrum of the cool flame was recorded, in order to understand more accurately the complex chemical and physical processes which lead to the flame phenomenon.

EXPERIMENTAL

Tne working technique was similar with that described in an earlier paper.[14] To record the emission spectrum, a Carl-Zeiss Jena spectrograph with glass optics was used.

The dynamical conditions of the reaction permitted to maintain the flame steady as position and intensity, during the 5–7 hr which were necessary to obtain an emission spectrum.

RESULTS AND DISCUSSIONS

The spectrum of the cool flame obtained in the air oxidation reaction of methane, initiated by nitric acid is shown in Fig. 1.

For comparison, in Fig. 2 is shown the spectrum of the cool flame obtained for heptane-air mixture[15] with a quartz Hilger spectrograph.

It can be seen that a correspondence exists between the wavelengths of the bands in these two spectra, on the one hand, and the band wavelengths reported by Emeleus[16] for the cool flame of ether, on the other. The spectrum of the cool flame was first described by Emeleus and later identified by Kondratiev[17] as being the fluorescence spectrum of formaldehyde, the main bands lying in the 3600–4500 Å range.

According to the results of Walsh,[18] the reaction in which the excited formaldehyde is formed must be exothermic to the extent of at least 77 kcal/mol.

Taking this into account, the following radicalic reactions may be proposed, even if their probabilities of taking place are relatively low[6]: $H + H\dot{C}O \rightarrow HCHO^{*}$ (e) electronically excited knowing that the dissociation energy of the C–H band is 87 Kcal.

Since several vibrational states correspond to a given electronic state, it is plausible to admit that the most probable transition is that between the electronically excited state and the first vibrational level

---

[12] J. Egret, L. R. Sochet and M. Lucquin, *Bull. Soc. chim., France*, **1965**, 2205.

[13] A. B. Nalbandian, I. Iosif and I. A. Schneider, *Rev. Roumaine Chim.*, **13**, 672 (1968).

[14] I. Iosif and I. A. Schneider, *Rev. Roumaine Chim.*, **15**, 1827 (1970).

[15] W. J. Levedahl and H. P. Broida, *Analyt. Chem.*, **24**, 1776 (1952).

[16] H. J. Emeleus, *J. Chem. Soc.*, **1926**, 2948.

[17] V. N. Kondratiev, *Z. Phys.*, **63**, 322 (1930).

[18] A. D. Walsh, *Trans. Faraday Soc.*, **43**, 305 (1947).

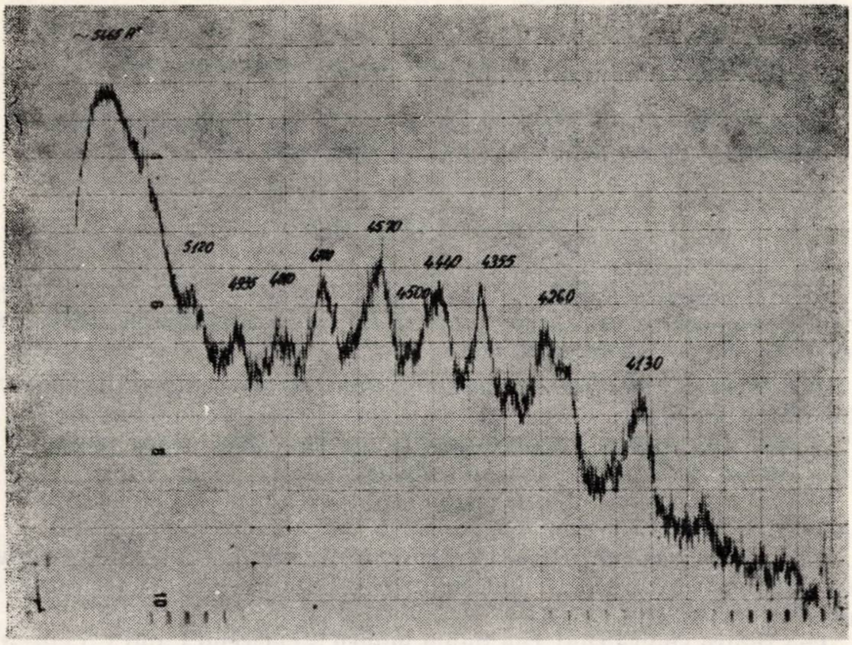

Fig. 1. — Spectrum of the cool flame of methane.

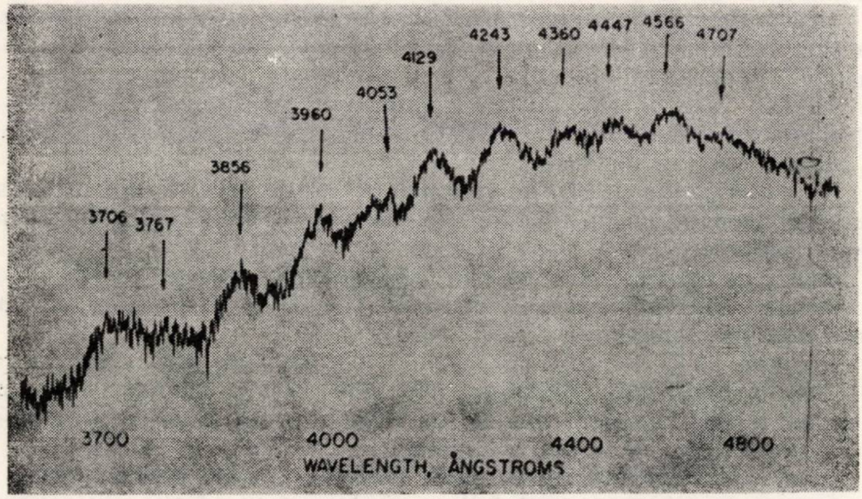

Fig. 2. — Spectrum of the cool flame of n–heptane. 15

of the lower electronic state; this transition is accompanied by light emission:

$$\mathrm{HCHO^*\,(e)} \xrightarrow{h\nu} \mathrm{HCHO^*\,(v)}\ \text{vibrationally excited.}$$

Several transitions follow between various vibrational levels of the lower electronic state, with thermal energy release:

$$\mathrm{HCHO^*} \xrightarrow{q} \mathrm{HCHO}$$

In consequence, light emission should appear first in the form of a bluish flame, and it should be followed by thermal emission; this picture agrees with the experimental facts.

The intensity of the thermal emission increases towards the front of the flame since:

— the vibrational deactivation is unlikely and takes place at low rate as compared to the electronic deactivation,

— the vibrational deactivation appears after the electronic deactivation.

This effect was confirmed experimentally and is illustrated in Fig. 3, where the temperature distribution in the flame is shown for three different flow rates.[14]

The figure shows that the flame length is between 1 and 1.5 cm, while the temperature difference between the top and the base of the flame is of about 200—250°.

It was shown experimentally [15] that in the range of low temperatures, after the preliminary formation of the cool flame, the self-ignition appears, which is a characteristic of all branching-chain reactions.

In the case of the initiated oxidation reaction of methane, the ignition phenomenon was observed to appear when the methane amount was reduced in the mixture.

This fact is shown in Fig. 4, which gives the variation of ΔT versus initiator concentration (HNO_3) for various compositions of the air-methane gaseous mixture.

One can see that the ignition phenomenon appears in the case of low methane content mixtures, in which the flame turns from bluish to yellow and the temperature raises above 1200°.

For the 1000 cm^3/min air + 200 cm^3/min CH_4 and 1200 cm^3/min air + 200 cm^3/min CH_4 mixtures, the self-ignition would be possible for higher initial temperatures of the reactor or by a preheating of the gaseous mixture.

After an interval of temperature increase, an interval in which the temperature remains constant follows, independent of the initiator concentration in the mixture or the composition of the air—CH_4mixture.

We should also note the existence of the two ignition limits as a function of the concentration of nitric acid.

From Fig. 4 a continuity may be seen to exist between the cool flame effect and the ignition effect; the cool flame represents a large part of the reaction.

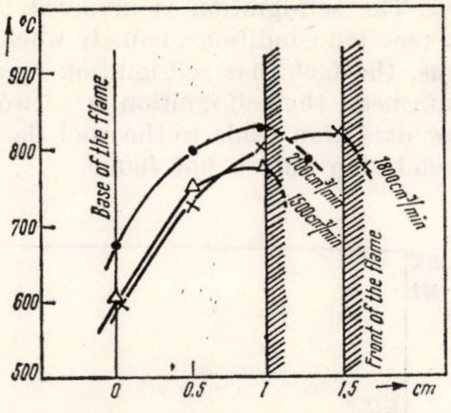

Fig. 3. – Temperature distribution in the flame.

Fig. 4. – The limits of the self-ignition as a function of HNO_3 concentration, for various compositions of the air-methane mixture and $T_i = 557°$.

1, 1000 cm^3/min air + 200 cm^3/min CH_4; *2*, 1200 cm^3/min air + 200 cm^3/min CH_4; *3*, 1400 cm^3/min air + 200 cm^3/min CH_4; *4*, 1600 cm^3/min air + 200 cm^3/min CH_4.

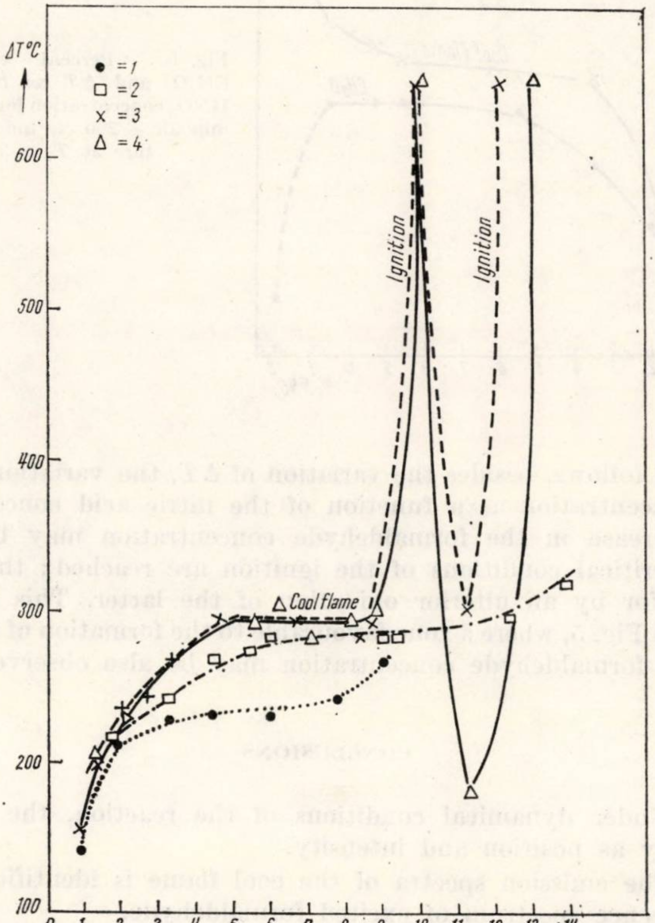

The self-ignition is involved here as a result of modifications in the reaction conditions, namely when some critical conditions are reached. Thus, the fact that self-ignition appears after cool flame formation [15] is confirmed; the self-ignition is a two-step process: in the first step, the slow oxidation leads to the cool flame formation, which becomes in the second step only a hot flame.

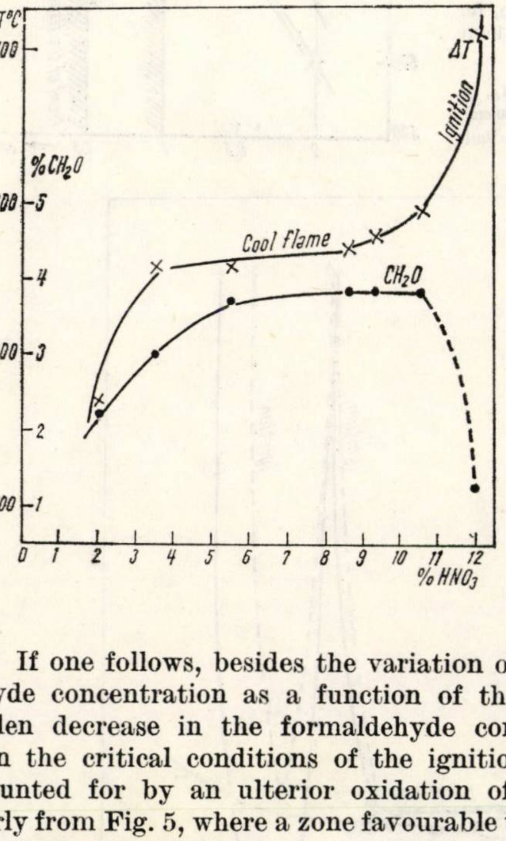

Fig. 5. — Percent variation of CH_2O and ΔT as functions of HNO_3 concentration for a 1400 cm³/min air + 200 cm³/min CH_4 mixture at $T_i = 557°$.

If one follows, besides the variation of ΔT, the variation of formaldehyde concentration as a function of the nitric acid concentration, a sudden decrease in the formaldehyde concentration may be observed when the critical conditions of the ignition are reached; this could be accounted for by an ulterior oxidation of the latter. This fact results clearly from Fig. 5, where a zone favourable to the formation of a maximum and steady formaldehyde concentration may be also observed.

CONCLUSIONS

1 — Under dynamical conditions of the reaction, the cool flame is stationary as position and intensity.

2 — The emission spectra of the cool flame is identified as being the fluorescence spectrum of excited formaldehyde.

3 — Both the cool flame and the ignition are favoured in low methane content mixtures.

4 — There is a continuity between the cool flame phenomenon and the ignition phenomenon; the cool flame constitutes an important part of the reaction.

5 — It is confirmed that the hydrocarbon self-ignition at low temperatures is a two-stage process; in the first stage, the slow oxidation leads to the cool flame formation and the reaction development in the second stage leads to the hot flame formation.

Revue Roumaine de Chimie, **18**, *2*, **208**–210 (1973)

KINETICS OF THE FORMATION REACTIONS OF OXYDIC COMPOUNDS IN SOLID PHASE THROUGH DIFFERENTIAL THERMAL ANALYSIS *)

S. SOLACOLU, M. CERCHEZ and E. SEGAL

Institute of Physical Chemistry, Str. Galați 31,
Bucharest-9, Romania

Received July 10, 1972

For reactions which take place without variation of weight

$$nA\,(s) + mB\,(s) \rightarrow A_nB_m(s) - \Delta H\;^{**)}$$

a kinetic study is undertaken making use of the data given by the differential thermal analysis. An original method, based on the use of kinetic equations established in the hypothesis that the analysed processes are controlled by diffusion, was devised.

1. INTRODUCTION

The use of differential thermal analysis to the study of the kinetics of chemical reactions is recommended by different authors. [1–3] The method is based on the direct proportionality existing between the reaction enthalpy, that can be measured, and the quantity of reacted substance. [3] The thermogravimetric methods and the methods using differential thermal analysis, were especially applied to investigate the kinetics of heterogeneous decomposition reaction taking place with gas release. [1,2,4–8] The methods of determining the reaction kinetics, from DTA data, for the formation reactions of oxydic compounds, of the following form:

$$nA(s) + mB(s) \rightarrow A_nB_m(s) - \Delta H \qquad \text{(I)}$$

---

*) Communicated at the 3rd National Conference of Pure and Applied Physical Chemistry, Bucharest, 4–7 Sept, 1972.

**) exothermal process

[1] D. Fătu, *J. Thermal Anal.*, **1**, 285 (1969).

[2] G. Berggren, *J. Thermal Anal.*, **1**, 265 (1969).

[3] S. Speil, *Chem. Abstr.*, **38**, 6234 (1944).

[4] H. I. Borchardt and F. D. Daniel, *J. Amer. Chem. Soc.*, **79**, 41 (1957).

[5] E. S. Freeman and B. Carroll, *J. Phys. Chem.*, **62**, 394 (1958).

[6] L. Reich, *J. Inorg. Nucl. Chem.*, **28**, 1329 (1966).

[7] V. Satava and F. Skvara, *J. Amer. Ceram. Soc.*, **52**, 591 (1969).

[8] A. W. Coats and P. Redfern, *Nature*, **201**, 68 (1964).

are unknown. The kinetics of these reactions, which take place without a weight variation in the system, can not be determined by thermogravimetry.

We present below a kinetic study of a type (I) chemical process using the data of differential thermal analysis.

An original method was therefore worked out, based on the use of some kinetic equations established in the hypothesis that the processes submitted to analysis are controlled by diffusion.

To illustrate the proposed method, we present below the determination of the kinetic formation parameters of bismuth titanate $4Bi_2O_3 \cdot TiO_2$ which is a member of the bismuth titanate class with important uses in the field of dielectric ceramics and especially for masses having ferroelectrical properties.[9,10] For this compound the reaction kinetics is unknown.[11]

2. CALCULATION TECHNIQUE

2.1. DEDUCTION OF RELATIONSHIPS USED TO CALCULATE THE KINETIC PARAMETERS. CALCULATION PROCEDURE BY PROCESSING THE KINETIC EQUATION IN INTEGRAL FORM IN NON-ISOTHERMAL WORKING CONDITIONS

We shall consider as an example the kinetic equation suggested by Jander for the chemical processes, with a reaction rate controlled by tridimensional diffusion.[7,12]

Jander's equation may be written in the following form

$$1 - 2(1-\alpha)^{1/3} + (1-\alpha)^{2/3} = kt^{*)} \qquad (1)$$

After differentiation and rearrangement one obtains

$$[(1-\alpha)^{-2/3} - (1-\alpha)^{-1/3}]\,\mathrm{d}\alpha = \frac{3}{2}k\,\mathrm{d}t \qquad (2)$$

But

$$\frac{\mathrm{d}T}{\mathrm{d}t} = a \qquad (3)$$

where a – is the heating rate and

$$k = Z\exp(-E/RT) \qquad (4)$$

where

Z – is the pre-exponential factor
E – the activation energy (cal/mol)
R – the gas constant (cal/mol^{-1} K^{-1})
T – the absolute temperature (K).

---

*) It was noted : α – the transformation degree, t – the time, k – the kinetic constant.

[9] L. E. Cross and R. C. Pohanka, *Mater. Res. Bull.*, **6**, 939 (1971).

[10] R. E. Newnham, R. W. Wolfe and J. F. Dorian, *Mater. Res. Bull.*, **6**, 1029 (1971).

[11] Gh. Morar, *Rev. Roumaine Chim.*, (in printing).

[12] C. Kröger and J. Blömer, *Z. anorg. Chem.*, **280**, 51 (1955).

After replacing relations (3) and (4) in equation (2), inclusion of the numeric fraction in the constant $\left(\frac{3k}{2} = k_0\right)$ and integration, there results the following equation for the entire display field of the reaction

$$\int_0^{\alpha} [(1-\alpha)^{-2/3} - (1-\alpha)^{-1/3}]\, d\alpha = \frac{k_0}{a} \int_{T_0}^{T_\alpha} \exp\left(-\frac{E}{RT}\right) \tag{5}$$

To solve the integral in the right member of the equation (5) (temperature), we have used an approximate method, generally employed.[8] We thus obtained

$$\frac{1}{2}[1 + (1-\alpha)^{2/3}] - (1-\alpha)^{1/3} = \frac{k_0\, RT^2}{3aE}\left(1 - \frac{2RT}{E}\right) \exp\left(-\frac{E}{RT}\right) \tag{6}$$

which after logarithmation becomes

$$\log \frac{1}{T^2}\left\{\frac{1}{2}[1 + (1-\alpha)^{2/3}] - (1-\alpha)^{1/3}\right\} = \log \frac{k_0 R}{3aE}\left(1 - \frac{2RT}{E}\right) - \frac{E}{4.575\ T} \tag{7}$$

If one admits that the total area A between the DTA curve (fig. 1) and the base line is proportional to the entire quantity of transformed substance, and the area a, limited by the DTA curve, the base line and the ordinate corresponding to moment t_i, is proportional to the quantity of substance transformed till that moment, the transformation degree of equation (7) may be expressed by

$$\alpha = \frac{a}{A} \tag{8}$$

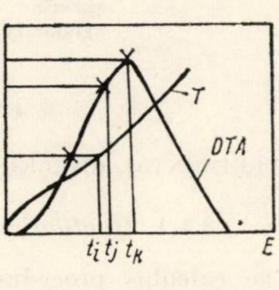

Fig. 1. — Diagram of the variation of the sample temperature and of the temperature difference between the sample and the actionless substance versus time.

By introducing it into equation (7), there results

$$\log \frac{1}{T^2}\left\{\frac{1}{2}\left[1 + \left(1 - \frac{a}{A}\right)^{2/3}\right] - \left(1 - \frac{a}{A}\right)^{1/3}\right\} = \log \frac{k_0 R}{3aE}\left(1 - \frac{2RT}{E}\right) - \frac{E}{4.575\ T} \tag{9}$$

To determine the activation energy we notice that the plotting of values

$$\log \frac{1}{T^2} \left\{ \frac{1}{2} \left[1 + \left(1 - \frac{a}{A} \right)^{2/3} \right] - \left(1 - \frac{a}{A} \right)^{1/3} \right\} \quad \text{versus} \quad \frac{1}{T}$$

leads to a line with a slope bound to the activation energy by the relation

$$E \text{ (cal/mol)} = 4.575 \ \mathrm{tg}\, \beta. \tag{10}$$

Table 1 gives the analogous calculation formulae for other known kinetic equations, usually applied to reactions with a rate controlled by diffusion phenomena.

Table 1

Calculus relations of reaction kinetics for formation mechanisms of solid phase compounds with the reaction rate controlled by diffusion

N⁰	Equation	Diffusion type	Name of equation	Calculation formula of activation energy. Procedure of processing the integral equation
1.	$\alpha^2 = 2kt$	Unidimensional diffusion	Jander [13]	$\log \frac{1}{T^2} \frac{\left(\frac{a}{A}\right)^2}{2} = \log \frac{kAR}{aE} \left(1 - \frac{2RT}{E}\right) - \frac{E}{4.575\ T}$
2.	$[1-(1-\alpha)^{1/3}]^2 = kt$	Tridimensional diffusion spheric symmetry	Jander [13]	$\log \frac{1}{T^2} \left\{ \frac{1}{2} \left[1 + \left(1 - \frac{a}{A}\right)^{2/3} \right] - \left(1 - \frac{a}{A}\right)^{1/3} \right\} = \log \frac{k_0}{3a} \frac{R}{E} \left(1 - \frac{2RT}{E}\right) - \frac{E}{4.575\ T}$
3.	$1 - \frac{2}{3}\alpha - (1-\alpha)^{2/3} = kt$	Tridimensional diffusion spheric symmetry	Ginstling-Brounshtein [14]	$\log \frac{1}{T^2} \left\{ \frac{3}{2} \left[1 - \left(1 - \frac{a}{A}\right)^{2/3} - \alpha \right] - \frac{a}{A} \right\} = \log \frac{k_0}{a} \frac{RT^2}{E} \left(1 - \frac{2RT}{E}\right) - \frac{E}{4.575\ T}$

3. EXPERIMENTAL RESULTS

3.1. EXPERIMENTAL CHECKING OF THE PROPOSED CALCULUS RELATIONS

3.1.1. *Qualitative study of $4Bi_2O_3 \cdot TiO_2$ formation*

The calculus procedure was applied for checking the formation reaction of compound $4Bi_2O_3 \cdot TiO_2$, recently identified as such, and not as a term in a solid solution.[15]

---

[13] W. Jander, *Z. anorg. Chemie*, **163**, 1, 29 (1927); **166**, 31 (1927); **168**, 113 (1928); *Angew. Chem.*, **41**, 79 (1928).

[14] P. P. Budnicov and A. M. Ginstling, "Reacţii v smesiah tverdykh veshchestv", Gosud. Izd. po stroitelstvu, arhitecture i stroitelnîm materialam, Moscova, 1961, p. 261.

[15] E. I. Speranskaia, I. S. Rez, L. V. Kozlova, V. M. Skorikov and V. I. Slavov, *Izvest. Akad. Nauk S.S.S.R., Neorg. Mater.*, **1**, 232 (1965).

Figure 2 gives the DTA curve of the stoichiometric mixture of Bi_2O_3 and TiO_2. Three thermal effects are pointed out on the curve: an exothermal one between 610 and 700° having a maximum at 670°, and two endothermal ones with the maxima at 730° and respectively at 865°.

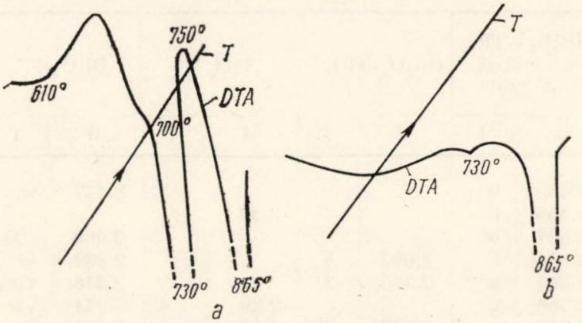

Fig. 2. — Differential thermal analysis of the stoichiometric mixture $4Bi_2O_3 + TiO_2$.
a) initial oxydic mixture; b) mixture calcinated at 725°.

In agreement with Speranskaia *et al.*,[15] the endothermal effects are ascribed to the polymorphous transformation $\beta Bi_2O_3 \rightarrow \alpha Bi_2O_3$ and, respectively, to the fusion $4Bi_2O_3 \cdot TiO_2 (s) \rightarrow 4Bi_2O_3 \cdot TiO_2 (l)$. The exothermal effect with a maximum at 670° was ascribed by us to the formation, in solid phase, of the compound $4Bi_2O_3 \cdot TiO_2$. The checking of this hypothesis was confirmed by thermal analysis of the sample calcinated at 725° (figure 2b). We notice that only the melting effect of the formed compound appears markedly on the curve, fact showing the actual formation of $4Bi_2O_3 \cdot TiO_2$; the attenuation up to nearly the base line of the polymorphous transformation effect of Bi_2O_3 shows that the largest part of the Bi_2O_3 quantity has reacted.

The checking of the compound formation was also carried out by roentgenography through analysis of the mixture calcinated at 725° and 575°. At 725° the characteristic lines $4Bi_2O_3 \cdot TiO_2$ were identified besides the TiO_2 and BiO_3 lines (table 2). We mention the fact that owing to the numerous coincidences between $4Bi_2O_3 \cdot TiO_2$ and Bi_2O_3, and to the fact that the solid phase reaction is in an incipient phase, only the intensive individual lines, characteristic for the initial oxides and for titanate, were considered decisive for identification.

The fact that among the Bi_2O_3 lines, the intense lines with $d = 1.63 - 1.65$ Å (20–100) and $d = 1.65 - 1.75$ Å (70–100) are missing, also proves the important desintegration of the initial oxide network at the reaction with TiO_2.

3.1.2. *Kinetic study of $4Bi_2O_3 \cdot TiO_2$ formation. Discussion of results*

For quantitative measurements in reaction kinetics the recording of DTA curves was carried out with the thermoderivatograph M.O.M.-Budapest, in air, with the sensitivity of the DTA galvanometer at 1/2.

Heating rate : 10°/minute. The fineness of the oxides used corresponds to a granulation < 60 μm.

Table 2

X-ray diffraction intensities of the stoichiometric mixture $4Bi_2O_3 + TiO_2$ calcinated at 725°* (CuK_α)

$4Bi_2O_3 + TiO_2$ calcinated at 725°		$4Bi_2O_3 \cdot TiO_2$ [15]		TiO_2 **		Bi_2O_3 ***		Identified phases
d	I	d	I	d	I	d	I	
3.483	w					3.477	w	Bi_2O_3
3.455	i			3.48	i			TiO_2
2.897	w					2.900	35	Bi_2O_3
2.675	i	2.697	8			2.634	vi	$Bi_2O_3 + 4Bi_2O_3 \cdot TiO_2$
2.367	w	2.395	2			2.348	vw	$Bi_2O_3 + 4Bi_2O_3 \cdot TiO_2$
2.266	w			2.29	4	2.241	vw	$Bi_2O_3 + TiO_2$
2.048	w	2.077	2	2.15	v.w	2.140	w	
						2.034	vw	$Bi_2O_3 + 4Bi_2O_3 \cdot TiO_2 + TiO_2$
1.967	m	1.991	4	2.05	12	1.955	m	$Bi_2O_3 + 4Bi_2O_3 \cdot TiO_2$
1.829	m	1.848	3			1.826	m	$Bi_2O_3 + 4Bi_2O_3 \cdot TiO_2$
1.497	i	1.493	6	1.49	20	1.460	i	$Bi_2O_3 + 4Bi_2O_3 \cdot TiO_2 + TiO_2$
1.425	i	1.441	4	1.45	20	1.422	w	$Bi_2O_3 + 4Bi_2O_3 \cdot TiO_2 + TiO_2$
		1.413	1					
1.378	w	1.381	3			1.372	w	$Bi_2O_3 + 4Bi_2O_3 \cdot TiO_2$
1.309	w	1.357	1	1.34	i			$4Bi_2O_3 \cdot TiO_2 + TiO_2$
1.244	w	1.250	3	1.25	4	1.277	i	$Bi_2O_3 + 4Bi_2O_3 \cdot TiO_2 + TiO_2$
1.215	i	1.211	7			1.220	90	$Bi_2O_3 + 4Bi_2O_3 \cdot TiO_2$
1.196	i	1.196	7			1.200	90	$Bi_2O_3 + 4BiO_3 \cdot TiO_2$
1.176	i	1.181	7	1.17	w	1.190	90	$4Bi_2O_3 \cdot TiO_2 + TiO_2$

* vw, very weak ; w, weak ; m, medium ; i, intensive ; vi, very intensive.

** Anatas (99.6 %) calcinated at 1400°. The intensity of the diffraction lines expressed in numbers, characterized d according to Mirkin[16] ; they were mentioned, as in the comparison proofs made by us we did not find them.

*** Bi_2O_3 (99.96 %) calcinated at 900°. The intensity of the diffraction lines expressed in numbers, characterized d according to A.S.T.M.[17] ; they were mentioned, as in the comparison proofs undertaken by us we did not find them.

The values of the surfaces of the exotherm effect on the DTA curve corresponding to the different moments of the reaction were initially determined, both by planimetric calculation and by weighing the copying paper cut to correspond to the surface after plotting the effect.

As the gravimetric methods give marked nonconformities for very small values of the transformation gradient (table 3), owing to the variation of the paper density and to the weighing errors, only the data obtained by planimetric calculus were capitalized for kinetic calculations.

Figure 3 gives graphically the reaction kinetics calculated according to Jander's equation (9).

As it results from relation (10), the value of the activation energy is of 229 kcal/mol (fig. 3).

---

[16] L. I. Mirkin, "Spravocinic po rentghenomustructurnomu analizu policristalov", Izd. Gosud. fizico matematicheskoi literatury, Moscow, 1961, p. 545.

[17] A.S.T.M. 2–0547.

To check the order of magnitude of the activation energy of the reaction, we have used the approximate calculation method of considering the dynamic process as an infinity of isothermal processes. [7,18] The logarithm of the rate constant for different time periods was thus calculated, and plotted versus $\frac{1}{T}$ (fig. 4).

Table 3

Comparison between the values of the surfaces determined on the DTA curve by planimetric calculation and by gravimetry

t (°C)	Planimetry		Gravimetry	
	Surface (cm²)	Ratio of growth	Surface (mg)	Ratio of growth
630	0.2		2.85	
		5.5		2.93
640	1.1		8.35	
		2.27		2.41
650	2.5		20.10	
		2.44		2.18
660	6.1		43.80	
		1.64		1.61
670	10.0		70.75	
		1.41		1.41
680	14.1		99.90	
		1.21		1.21
697	17.1		120.10	

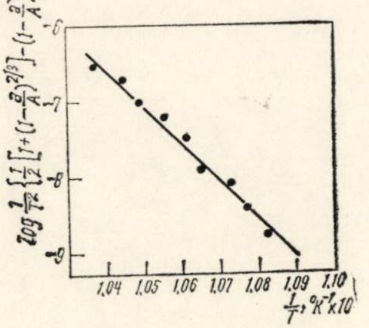

Fig. 3. — Checking of the relation (9) corresponding to the formation of $4Bi_2O_3 \cdot TiO_2$ between 610–700° from the stoichiometric oxydic mixture.

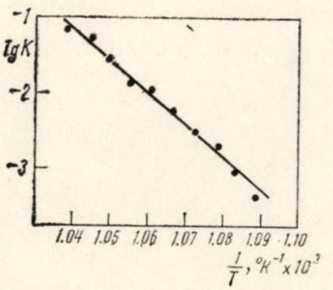

Fig. 4. — Plotting of the logarithm of the reaction rate constant versus $\frac{1}{T}$.

---

[18] D. Cismaru, *St. cerc. fiz.*, **6**, 435 (1955); *St. cerc. chim.*, **5**, 119 (1957); **5**, 673 (1957); **6**, 539 (1958).

This method gives the value of the activation energy at 200 kcal/mol showing a satisfactory agreement with the order of magnitude of the value determined by the preceeding method.

The initially obtained value of 229 kcal/mol is considered as a significant value, as this method, generally used to determine the reaction kinetics, is recommended as more precise.[8,19]

The high value of the activation energy shows a maximum energetic contribution to the formation of this titanate of the same order of magnitude as, for instance, in the case of Pb_2SiO_6 formation.[20]

4. CONCLUSIONS

1. — Calculus expressions of the activation energy were established for chemical reactions of the type

$$nA\,(s) + mB\,(s) \rightarrow A_nB_m(s) - \Delta H$$

based on the data obtained from the DTA curve, in the hypothesis that the reaction rate is controlled by diffusion phenomena.

2. — For exemplification, the kinetics of the formation reaction of $4Bi_2O_3 \cdot TiO_2$ between 610 and 700°, of the initial stoichiometric mixture of Bi_2O_3 and TiO_2 oxides, according to Jander equation, was presented.

---

[19] I. G. Murgulescu and E. Segal, *Studii și Cercetări Chim. Acad. R.P.R.*, **15**, 261 (1967).

[20] R. Jagitsch *et al.*, *Arkiv. Kemi, Mineral Geol.*, **15 A**, 6 (1942); **22 A**, 2 (1946).

Revue Roumaine de Chimie, **18**, *2*, 211 – 219 (1973)

TEMPERATURE AND CONCENTRATION DEPENDENCE OF MOLAR POLARIZATION IN BINARY MIXTURES OF POLAR LIQUIDS WITH NONPOLAR SOLVENT

IUDITA ADORIAN

Department of Physical Chemistry, Polytechnical Institute
Str. Polizu 1, Bucureşti, Romania

Received July 27, 1972

Dielectric constants, refractive indices and densities of cyclohexane-nitrobenzene, cyclohexane-chlorobenzene and cyclohexane-ethyl benzoate mixtures have been measured at various concentrations and temperatures. Positive deviations from additivity of the molar polarization and the molar volumes are reported. The temperature dependence on the orientation polarization of the polar components, at various concentrations is discussed.

The study of molar polarization of polar liquids in nonpolar solvents was the object of various papers in the period 1920–1940, especially in view of the determination of permanent electric moments at law concentration. Subsequently, the area of these studies extended to include the investigation of the dielectric behaviour of liquid mixtures in the full range of concentrations, with the purpose of obtaining some information about the molecular interactions, from the exhibited deviations from additivity.

Along this line of investigation are to be mentioned the experimental works of Williams, [1] Smyth, [2] e.a., as well as those of Wolfke, [3] Malsch, [4] van Arkel and Snoek [5] that attempted to account for dipolar interactions by introducing some formal corrections in the expression of the polarization. The theoretical treatment of the mutual influence of the permanent dipoles in liquid state was first made by Debye, [6] Onsager, [7] Kirkwood [8] and developed subsequently by others. [9-11] In recent years the dielectric behaviour of liquid mixtures became a subject of interest for many investigators. [12-21] This regain of interest can be explained both by the fact that the theoretical progress makes possible a better interpretation of the results and by the development of new experimental techniques (study of dielectric relaxation, i.r. spectrography, NMR), which yield informations mutually complementary to the study of electrostatic polarization.

---

[1] J. W. Williams, *J. Amer. Chem. Soc.*, **48**, 1888 (1926); **49**, 1676, 2408, 2916 (1927); **50**, 94, 362 (1928); **51**, 2332. 2350 (1929); **52**, 1356, 1831 (1930); **53**, 2096 (1931).

[2] C. P. Smyth, *J. Amer. Chem. Soc.*, **50**, 1536, 1547, 1883 (1928); **51**, 1736, 3312, 2330 (1929); **52**, 1824, 2227, 3546 (1930); **53**, 527, 545, 1296, 2115, (1931).

[3] M. Wolfke, *Phys. Z.*, **29**, 713 (1928); **31**, 498 (1930).

[4] J. Malsch, *Phys. Z.*, **33**, 383 (1932).

[5] A. E. von Arkel and J. Snoek, *Phys. Z.*, **33**, 662 (1932); **35**, 187 (1934).

[6] P. Debye, *Phys. Z.*, **36**, 100, 193 (1935).

In the present paper, results concerning concentration and temperature dependence or orientation polarization in low frequency field, of polar liquids dissolved in nonpolar solvent, are presented. The behaviour of some benzene derivatives: nitrobenzene, chlorobenzene and ethyl benzoate in mixture with cyclohexane has been studied. The investigated concentration range was $x_2 = 0.1-0.9$ (x_2 — mole fraction of the polar component). The temperature range investigated (15°—70°) covers the greatest part of the temperature range in which the above mentioned systems are in the liquid state.

EXPERIMENTAL PART

Substances used: nitrobenzene p.a. dried on P_2O_5 and distilled $n_D^{20} = 1.5525$; chlorobenzene p.a. distilled $n_D^{20} = 1.5244$; ethyl benzoate p.a. distilled $n_D^{20} = 1.5048$ and cyclohexane dried on P_2O_5 and distilled $n_D^{20} = 1.4260$.

Measurements of dielectric constants were carried out with a heterodyne beat apparatus at a frequency of 0.5 MHz (stabilized with a piesoelectric quartz crystal). There is a linear relationship between the value read on the scale of the apparatus and the measured capacity. The cells used consisted of two concentric cylinders with 9.37 pF and 12.8 pF effective capacity, respectively.

Density measurements have been carried out with a pycnometer with a volume of $14.5181 + 0.0003\ (t - 20°)$ cm^3.

Measurements of the refractive index were performed by means of a Pulfrich refractometer. As monochromatic light source a sodium vapour lamp was used.

---

[7] L. Onsager, *J. Amer. Chem. Soc.*, **58**, 1486 (1936).

[8] J. G. Kirkwood, *J. Chem. Phys.*, **4**, 592 (1936); **7**, 911 (1939).

[9] Iu. K. Syrkin, *Doklady Akad. Nauk. S.S.S.R.*, **35**, 43 (1942).

[10] A. D. Buckingham and R. E. Raab, *Trans. Faraday Soc.*, **55**, 377 (1959).

[11] R. H. Cole, *J. Chem. Phys.*, **39**, 2602 (1963).

[12] A. V. Celiano, P. S. Gentile and M. Cefola, *J. Chem. Eng. Data*, **7**, 391, (1962).

[13] S. K. K. Jatkar and V. K. Phansolkar, *J. Univ. Poona Sci. Technol.*, **22**, 49 (1962).

[14] Ko Kimura and Ryoichi Fujishiro, *Bull. Chem. Soc. Japan*, **35**, 85 (1962).

[15] O. A. Osipov, M. A. Pamina, O. E. Kashirenina, G. V. Nemirov and I. K. Shelamov, *Zhur. obshchei Khim.*, **31**, 3153 (1961).

[16] V. V. Coremkyna, I. A. Vakelov and M. I. Shahparonov, *Vestnik. Mosk. Univ. Ser. II. Khim.*, **19**, I, 33 (1964).

[17] C. Brot, *J. Chim. phys.*, **61**, 139 (1964).

[18] J. Hurwic and J. Markuze, *Roczniki Chem.*, **39**, 1885 (1966).

[19] Iu. Ia. Fiolkov, V. A. Tsenderovskaia and O. K. Kudra, *Ukrain. khim. Zhur.* **32**, 239 (1966).

[20] H. Loiseleur, J. C. Merlin and R. A. Paris, *J. Chim. phys.*, **64**, 634 (1967).

[21] A. N. Campbell and E. M. Kartzmark, *Canad. J. Chem.*, **47**, 619 (1969).

The temperature of the pycnometer, dielectric-cell and refractometer was kept constant within ±0.1° using a Höppler ultrathermostate with external circulation. The temperature was measured in three points of the circuit.

The solutions used were prepared freshly in glass flasks with ground cap and the concentrations were established by weighing on an analytical balance.

RESULTS

The dielectric constants of the cyclohexane-nitrobenzene, cyclohexane-chlorobenzene and cyclohexane-ethyl benzoate mixtures at various values of the mole fraction x_2, of the polar component and at various temperatures are presented in table 1.

Table 1

Dielectric constant of mixtures, $\varepsilon_{1,2}$

Cyclohexane — nitrobenzene

t°C / x_2	1	0.8944	0.7992	0.6559	0.6030	0.4965	0.4072	0.3064	0.2061	0.0953	0
15	35.56	30.89	26.71	21.09	19.23	15.31	12.28	9.22	6.45	3.93	2.03
20	34.33	30.05	26.09	20.60	18.76	14.98	12.05	9.10	6.38	3.90	2.02
25	33.47	29.47	26.50	20.17	18.34	14.69	11.82	8.95	6.29	3.84	2.02
30	32.69	28.86	25.11	19.76	17.97	14.45	11.60	8.79	6.22	3.79	2.01
40	31.07	27.61	24.08	19.02	17.28	13.92	11.17	8.46	6.05	3.71	2.00
50	29.95	26.62	23.12	18.32	16.58	13.32	10.76	8.22	5.89	3.67	1.99
60	28.76	25.66	22.26	17.65	16.03	12.93	10.49	7.99	5.68	3.62	1.975
70	27.73	24.72	**21.5**4	16.93	—	12.64	10.14	7.79	5.55	—	1.96

Cyclohexane — chlorobenzene

t°C / x_2	1	0.8947	0.7985	0.7048	0.6023	0.4998	0.3984	0.2900	0.2056	0.0857	0
15	5.73	5.34	4.94	4.56	4.16	—	3.39	3.00	2.71	2.302	2.03
20	5.64	5.27	4.87	4.50	4.11	3.73	3.35	2.97	2.69	2.290	2.02
25	5.56	5.19	4.80	4.44	4.06	3.68	3.31	2.94	2.67	2.279	2.02
30	5.47	5.12	4.74	4.39	4.00	3.64	3.28	2.92	2.65	2.267	2.01
40	5.33	4.99	4.63	4.28	3.92	3.57	3.22	2.87	2.61	2.241	2.00
50	5.18	4.86	4.52	4.18	3.83	3.49	3.16	2.82	2.58	2.218	1.99
60	5.05	4.75	4.41	4.09	3.75	3.42	3.10	2.78	2.54	2.195	1.975
70	4.93	4.64	4.31	4.00	3.67	3.36	—	2.74	2.50	2.177	1.96

Cyclohexane — ethyl benzoate

t°C / x_2	1	0.8984	0.8016	0.7012	0.6046	0.4947	0.3981	0.3017	0.1916	0.1005	0
15	6.29	5.92	5.58	5.18	4.771	4.280	3.858	3.409	2.983	2.502	2.03
20	6.20	5.83	5.48	5.10	4.697	4.220	3.812	3.373	2.956	2.482	2.02
25	6.11	5.74	5.40	5.03	4.635	4.174	3.768	3.333	2.925	2.468	2.02
30	6.01	5.67	5.33	4.97	4.585	4.122	3.727	3.301	2.899	2.454	2.01
40	5.83	5.52	5.19	4.84	4.475	4.030	3.644	3.233	2.855	2.428	2.00
50	5.67	5.37	5.06	4.74	4.363	3.952	3.585	3.183	2.806	2.398	1.99
60	5.53	5.24	4.94	4.61	4.282	3.892	3.508	3.137	2.771	2.369	1.975
70	5.40	5.12	4.85	4.54	4.196	3.832	3.472	3.093	2.736	2.340	1.96

Revue Roumaine de Chimie, **18**, *2*, 211–219 (1973)

Table 2

Refractive indices of mixtures, $n_{1,2}$

Cyclohexane — nitrobenzene

t°C \ x_2	1	0.8944	0.7992	0.6559	0.6030	0.4965	0.4072	0.3064	0.2061	0.0953	0
15	1.55471	1.54175	1.52831	1.50831	1.50190	1.48820	1.47643	1.46390	1.45193	1.43908	1.42847
20	1.55246	1.53835	1.52570	1.50691	1.49936	1.48588	1.47437	1.46171	1.44933	1.43638	1.42597
25	1.54995	1.53635	1.52367	1.50433	1.49775	1.48366	1.47222	1.45952	1.44713	1.43377	1.42327
30	1.54766	1.53406	1.52146	1.50190	1.49519	1.48103	1.46966	1.45683	1.44472	1.43127	1.42047
40	1.54298	1.52962	1.51734	1.49794	1.49079	1.47721	1.46569	1.45303	1.44000	1.42657	1.41519
50	1.53836	1.52534	1.51327	1.49462	1.48675	1.47310	1.46121	1.44873	1.43487	1.42137	1.40994
60	1.53347	1.52093	1.50931	1.49004	—	1.46917	1.45663	1.44472	1.42847	1.41638	1.40453
70	1.52927	1.51806	1.50562	1.48696	—	—	1.45373	1.43989	—	1.41142	1.39972

Cyclohexane — chlorobenzene

t°C \ x_2	1	0.8974	0.7985	0.7048	0.6023	0.4998	0.3984	0.2900	0.2056	0.0857	0
15	1.52692	1.51536	1.50507	1.49528	1.48473	—	1.46490	1.45433	1.44652	1.43588	1.42847
20	1.52438	1.51281	1.50255	1.49280	1.48230	1.47183	1.46201	1.45173	1.44401	1.43317	1.42597
25	1.52164	1.51034	1.50001	1.49032	1.47986	1.46946	1.45942	1.44923	1.44151	1.43087	1.42327
30	1.51905	1.50785	1.49747	1.48762	1.47721	1.46699	1.45713	1.44652	1.43898	1.42797	1.42047
40	1.51372	1.50274	1.49242	1.48259	1.47221	1.46191	1.45233	1.44171	1.43397	1.42287	1.41519
50	1.50831	1.49775	1.48753	1.47800	1.46728	1.45693	1.44753	1.43648	1.42897	1.41788	1.40994
60	1.50311	1.49290	1.48298	1.47339	1.46260	1.45213	1.44201	1.43147	1.42417	1.41271	1.40453
70	1.49775	1.48801	1.47878	1.46808	1.45783	1.44702	—	1.42647	1.41877	1.40777	1.39972

Cyclohexane — ethyl benzoate

t°C \ x_2	1	0.8984	0.8016	0.7012	0.6046	0.4947	0.3981	0.3017	0.1916	0.1005	0
15	1.50703	1.50030	1.49395	1.48656	1.47918	1.47094	1.46220	1.45413	1.44502	1.43668	1.42847
20	1.50479	1.49812	1.49137	1.48434	1.47751	1.46808	1.45982	1.45173	1.44251	1.43417	1.42597
25	1.50255	1.49575	1.48927	1.48181	1.47428	1.46579	1.45743	1.44973	1.44030	1.43167	1.42327
30	1.50030	1.49357	1.48705	1.47996	1.47242	1.46370	1.45523	1.44733	1.43798	1.42937	1.42047
40	1.49595	1.48927	1.48269	1.47565	1.46827	1.45903	1.45133	1.44281	1.43306	1.42437	1.41519
50	1.49166	1.48531	1.47839	1.47134	1.46340	1.45513	1.44612	1.43818	1.42837	1.41937	1.40994
60	1.48743	1.48123	1.47526	1.46649	1.45903	1.45083	1.44201	1.43377	1.42347	1.41490	1.40453
70	1.48259	1.47663	1.47035	1.46220	1.45473	1.44632	1.43768	—	1.41867	1.40994	1.39972

Table 3

Densities of mixtures, $d_{1,2}$

Cyclohexane — nitrobenzene

t°C / x_2	1	0.8944	0.7992	0.6559	0.6030	0.4965	0.4072	0.3064	0.2061	0.0953	0
15	1.2082	1.1606	1.1178	1.0539	1.0308	0.9853	0.9471	0.9055	0.8643	0.8197	0.7827
20	1.2029	1.1568	1.1126	1.0493	1.0260	0.9803	0.9426	0.9008	0.8594	0.8149	0.7777
25	1.1985	1.1520	1.1079	1.0445	1.0214	0.9754	0.9376	0.8957	0.8546	0.8102	0.7730
30	1.1932	1.1472	1.1029	1.0394	1.0163	0.9705	0.9327	0.8907	0.8498	0.8053	0.7634
40	1.1834	1.1373	1.0929	1.0293	1.0063	0.9605	0.9228	0.8809	0.8398	0.7956	0.7588
50	1.1728	1.1275	1.0832	1.0196	0.9965	0.9507	0.9130	0.8710	0.8302	0.7859	0.7492
60	1.1635	1.1177	1.0736	1.0100	—	0.9412	0.9035	0.8613	0.8205	0.7762	0.7394
70	1.1537	—	1.0634	—	—	0.9314	0.8935	0.8515	0.8107	—	0.7291

Cyclohexane — chlorobenzene

t°C / x_2	1	0.8947	0.7985	0.7048	0.6023	0.4998	0.3984	0.2900	0.2056	0.0857	0
15	1.1119	1.0745	1.0407	1.0084	0.9735	—	0.9062	0.8715	0.8448	0.8087	0.7827
20	1.1065	1.0691	1.0353	1.0031	0.9683	0.9344	0.9013	0.8665	0.8401	0.8047	0.7777
25	1.1012	1.0636	1.0300	0.9978	0.9638	0.9292	0.8961	0.8615	0.8352	0.7989	0.7730
30	1.0956	1.0584	1.0247	0.9926	0.9578	0.9240	0.8911	0.8565	0.8302	0.7940	0.7684
40	1.0847	1.0475	1.0140	0.9821	0.9474	0.9137	0.8808	0.8465	0.8203	0.7845	0.7588
50	1.0737	1.0367	1.0032	0.9714	0.9371	0.9032	0.8706	0.8362	0.8102	0.7744	0.7492
60	1.0630	1.0260	0.9926	0.9609	0.9266	0.8928	0.8604	0.8263	0.8004	0.7648	0.7394
70	1.0521	1.0152	0.9820	0.9503	0.9161	0.8825	—	0.8161	0.7903	0.7548	0.7291

Cyclohexane — ethyl benzoate

t°C / x_2	1	0.8984	0.8016	0.7012	0.6046	0.4947	0.3981	0.3017	0.1916	0.1005	
15	1.0516	1.0226	1.0077	0.9773	0.9597	0.9242	0.9030	0.8702	0.8408	0.8148	0.7827
20	1.0469	1.0178	1.0030	0.9725	0.9549	0.9195	0.8985	0.8655	0.8362	0.8101	0.7777
25	1.0421	1.0130	0.9983	0.9678	0.9503	0.9147	0.8936	0.8606	0.8314	0.8054	0.7730
30	1.0375	1.0083	0.9936	0.9630	0.9455	0.9100	0.8890	0.8559	0.8267	0.8006	0.7684
40	1.0280	0.9988	0.9843	0.9535	0.9361	0.9004	0.8791	0.8463	0.8172	0.7911	0.7588
50	1.0186	0.9893	0.9748	0.9440	0.9267	0.8910	0.8697	0.8368	0.8076	0.7814	0.7492
60	1.0094	0.9800	0.9655	0.9348	0.9174	0.8814	0.8603	0.8273	0.7981	0.7718	0.7394
70	1.000	0.9706	0.9562	0.9252	0.9079	0.8718	0.8507	0.8176	0.7884	0.7623	0.7291

In table 2 the refractive indices and in table 3 the densities of the above mentioned mixtures are reported.

The dielectric constants exhibit negative deviations from the additivity in the cyclohexane-nitrobenzene and cyclohexane-chlorobenzene system and positive ones in the cyclohexane-ethyl benzoate system. By increasing the temperature the dielectric constants decrease and the departures from additivity too. The densities of the mixtures decrease linearly with the temperature and present small negative deviations from additivity. The refractive indices are quasi-additive.

The molar polarizations $P_{1,2}$ of the mixtures have been calculated by Debye's equation

$$P_{1,2} = \frac{\varepsilon_{1,2} - 1}{\varepsilon_{1,2} + 2} \cdot \frac{M_{1,2}}{d_{1,2}} = P_1x_1 + P_2x_2 \tag{1}$$

where $\varepsilon_{1,2}$ and $d_{1,2}$ are the dielectric constants and the density of the mixtures respectively, and $M_{1,2} = x_1M_1 + x_2M_2$ (x_1 and x_2 being the mole fractions of the nonpolar and the polar component respectively).

In fig. 1 the 20° isotherms of the molar polarization of the three mixtures are presented, as calculated by equation (1). Positive deviations from additivity are observed in all cases, the largest one in the case of the cyclohexane-nitrobenzene system. Large positive molar polarization deviations are usually observed simultaneously with large negative deviations of the dielectric constant. [18] The deviations from ideal behaviour decrease with increasing temperature.

Molar polarizations of the mixtures calculated by the Kirkwood-Onsager equation

$$P = \frac{(\varepsilon - 1)(2\varepsilon + 1)}{9\varepsilon} \cdot \frac{M_{1,2}}{d_{1,2}} \tag{2}$$

vary linearly with the concentration in the cyclohexane-chlorobenzene and cyclohexane-ethyl benzoate systems and present a small deviation from additivity in the cyclohexane-nitrobenzene system.

The molar refraction calculated by the Lorenz equation

$$R_{1,2} = \frac{n_{1,2}^2 - 1}{n_{1,2}^2 + 2} \cdot \frac{M_{1,2}}{d_{1,2}} \tag{3}$$

varies linearly with the concentration in each case.

In fig. 3 the $R_{1,2} = f(x_2)$ isothermes at 20° are presented.

In fig. 4 the molar volumes at 20° of the three mixtures are presented. Small positive deviations from the ideal state are observed, which decrease with increasing temperature. The excess volumes at two temperatures for the cyclohexane-chlorobenzene and cyclohexane-nitrobenzene mixtures are presented in figures 5 and 6.

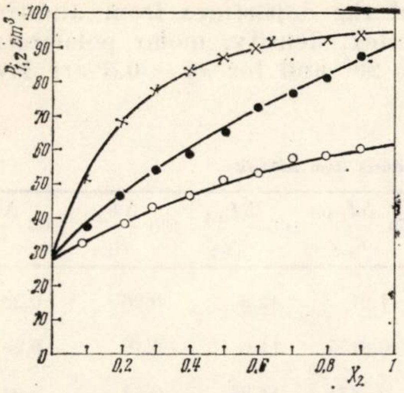

Fig. 1. — Molar polarization calculated with equation (1) of the cyclohexane-nitrobenzene x, cyclohexane-chlorobenzene o and cyclohexane-ethyl benzoate• mixtures.

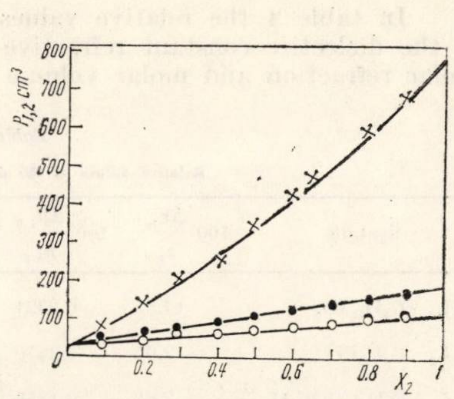

Fig. 2. — Molar polarization calculated with equation (2) of the cyclohexane-nitrobenzene x, cyclohexane-chlorobenzene o and cyclohexane-ethyl benzoate• mixtures.

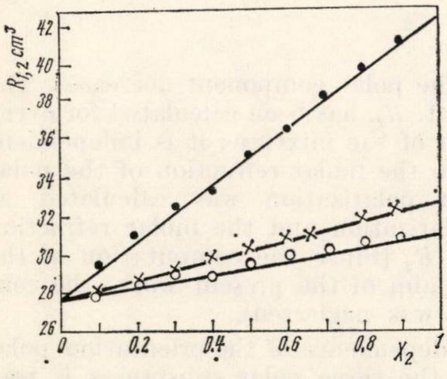

Fig. 3. — Molar refraction of the cyclohexane-nitrobenzene x, cyclohexane-chlorobenzene o and cyclohexane-ethyl benzoate• mixtures.

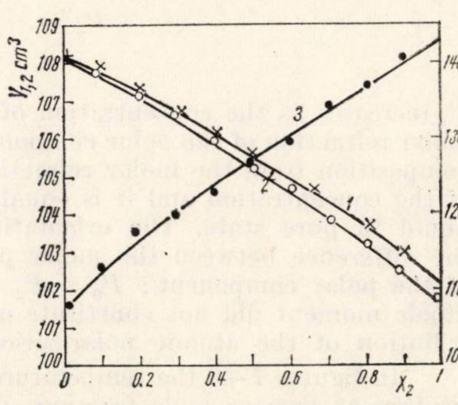

Fig. 4. — Molar volume of the cyclohexane-nitrobenzene. 1, x, cyclohexane-chlorobenzene 2, and cyclohexane-ethyl benzoate 3, mixtures. (the right-hand scale concerns the cyclohexane-ethyl benzoate mixture).

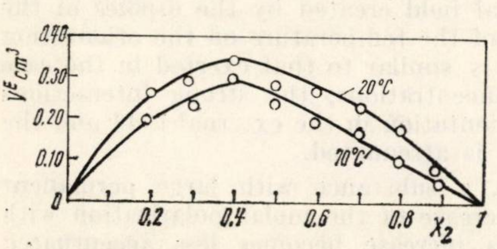

Fig. 5. — Integral excess molar volume of the cyclohexane-chlorobenzene mixture.

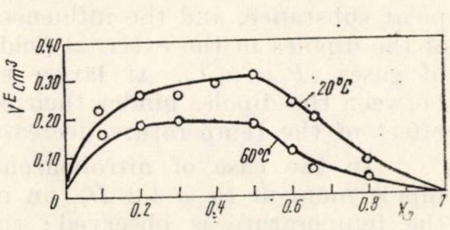

Fig. 6. — Integral excess molar volume of the cyclohexane-nitrobenzene mixture.

In table 4 the relative values of the departures from additivity of the dielectric constant refractive index, density, molar polarization, molar refraction and molar volume at 20° and for $x_2 = 0.5$ are given.

Table 4

Relative values of the departures from additivity

System	$100\,\frac{\Delta\varepsilon_{1,2}}{\varepsilon_{1,2}}$	$100\,\frac{\Delta n_{1,2}}{n_{1,2}}$	$100\,\frac{\Delta d_{1,2}}{d_{1,2}}$	$100\,\frac{\Delta P_{1,2}}{P_{1,2}}$	$100\,\frac{\Delta R_{1,2}}{R_{1,2}}$	$100\,\frac{\Delta V_{1,2}}{V_{1,2}}$
$C_6H_{12}-C_6H_5NO_2$	−17.55	−0.2221	−1.01	42.8	0.26	0.29
$C_6H_{12}-C_6H_5Cl$	− 2.65	−0.2270	−0.8175	11.6	0.10	0.28
$C_6H_{12}-C_6H_5COOC_2H_5$	2.68	0.1855	0.7875	11.25	0.54	0.94

Based on equation (1) the molar polarization of the polar component can be calculated

$$P_2 = \frac{P_{1,2} - P_1 x_1}{x_2} \tag{4}$$

P_2 increases as the concentration of the polar component decreases. The molar refraction of the polar component, R_2, has been calculated for every composition from the molar refraction of the mixture; it is independent of the concentration and it is equal to the molar refraction of the polar liquid in pure state. The orientation polarization was calculated as the difference between the molar polarization and the molar refraction of the polar component: $P_0 = P_2 - R_2$ (Since the computation of the dipole moment did not constitute an aim of the present work, the contribution of the atomic polarization was neglected).

In figures 7—9 the temperature dependence of the orientation polarization at various mole fractions of the three polar substances is presented. It is to be noted that the orientation polarization decreases with increasing temperature for chlorobenzene and ethyl benzoate, the increase being more marked as the concentration of the polar component gets smaller. The dispersion of the polar molecules in the nonpolar liquid diminishes the effect of the internal field created by the dipoles of the polar substance, and the influence of the temperature on the orientation of the dipoles in the external field is similar to that exerted in the case of gases ($P = a/T$). At larger concentrations, the strong interactions between the dipoles hinder their orientation in the external field and the effect of the temperature decrease is attenuated.

In the case of nitrobenzene, a substance with large permanent dipole moment ($\mu = 4.2\ D$), an increase of the molar polarization with the temperature is observed; this increase becomes less accentuated as the concentration decreases, and at small concentrations a decrease of the molar polarization can be observed as in the previous two cases. This reversal of the slope was observed also at other strongly polar substances. [2] The behaviour of the nitrobenzene in pure state and at high concentration can be explained by the existence of associations of the dipoles, that dissimulate to some extent the dipole moment. With increasing temperature dissociation takes place and the molar polarization increases. With small concentrations there is no association and the effect of the temperature consists in a randomization of the orientation of the free dipoles relative to the external field.

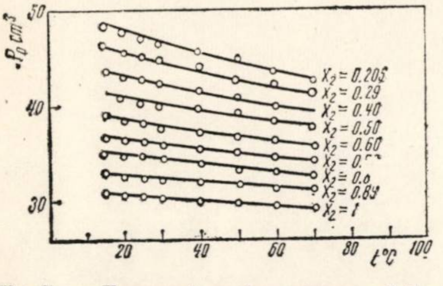

Fig. 7. — Temperature dependence of the orientation polarization of chlorobenzene.

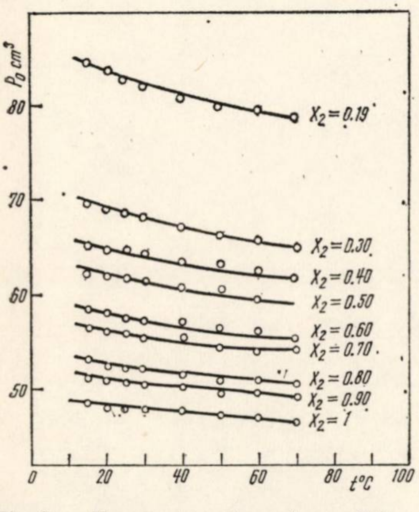

Fig. 8. — Temperature dependence of the orientation polarization of ethyl benzoate.

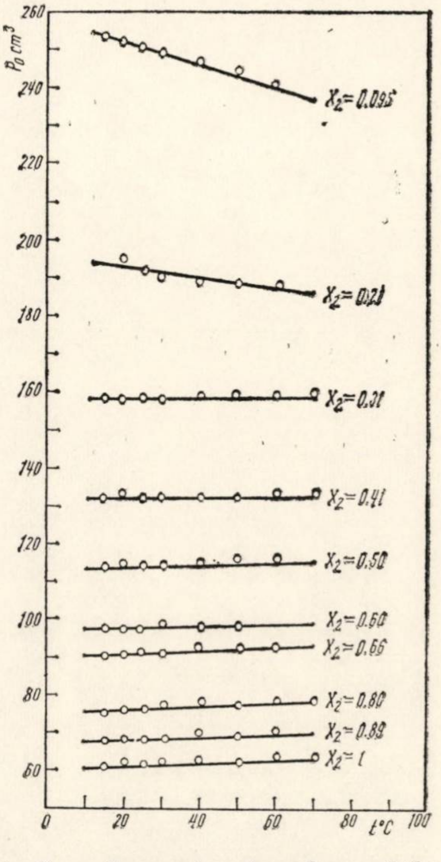

Fig. 9. — Temperature dependence of the orientation polarization of nitrobenzene.

Acknowledgement. The author wishes to thank Prof. I. G. Murgulescu for his advice, suggestions and support offered to carry out this work.

Revue Roumaine de Chimie, 18, 2, 221–231 (1973)

THE DETERMINATION OF THE DIFFUSIVE AND CAPACITIVE CURRENT IN THE CHRONOPOTENTIOMETRY OF THE MOLTEN SALT SYSTEMS (Na, Ag)NO_3 AND (K, Ag)NO_3

S. STERNBERG and T. VIŞAN

Department of Physical Chemistry and Electrochemistry, Polytechnic Institute of Bucharest, Romania

Received July 7, 1972

The chronopotentiometric method has been applied in the molten alkali nitrates systems, $NaNO_3-AgNO_3$ and KNO_3-AgNO_3, for $AgNO_3$ concentrations of $0.5 - 2 \times 10^{-2}$ mole $\cdot l^{-1}$ and current densities of $5 - 30 \times 10^{-3}$ A $\cdot$ cm^{-2}. It was shown that the capacitive current may be neglected in optimal conditions. At low concentrations and high current densities the chronopotentiograms are strongly distorted by the electric double layer charging. A method to correct the transient of the distorted chronopotentiogram and to estimate the capacitive current is proposed.

In recent years, the chronopotentiometric method has been applied to many binary systems of molten salts, by recording the potential-time curves through galvanostatic polarization.

Assuming that the transport of the ion to the electrode is effected exclusively by the semi-infinite linear diffusion process, the interdiffusion coefficient (D) can be calculated using Sand's equation

$$\tau^{1/2} = \frac{\pi^{1/2} nFD^{1/2} c}{2i} \qquad (1)$$

where

τ — chronopotentiometric transient

i — current density

c — ion concentration

n — number of electrons which participate at the electrode reaction

F — Faraday's constant.

The transient is measured on the chronopotentiogram by one of the graphical methods proposed.[1-4]

Fig. 1 represents a typical chronopotentiogram which illustrates the procedure for the determination of the transient. This procedure will be referred to as "the graphical method of Reinmuth".[3] It should be mentioned that in this method, the precise measurement of the potential variation is not necessary; only the exact evaluation of the transient τ is required.

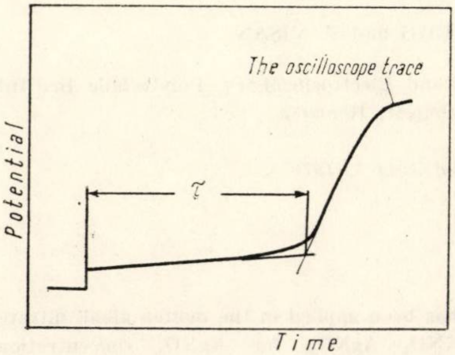

Fig. 1. — A typical chronopotentiogram. τ — the transient.

In deducing equation (1) it has been assumed that the electrical current was entirely used in the faradic process. In reality, because the potential varies continuously in time, a fraction of the total current is used for charging the electrical double layer, i.e. there exists a diffusive (faradic) and a capacitive current, i_F and i_c, which satisfy the relation

$$i = i_F + i_c \tag{2}$$

In the following, an analysis of the role of the capacitive current during the cathodic chronopotentiometric polarization in fused salt solutions is presented. At the same time, it is interesting to note that the problem is of practical importance. Thus, in very diluted solutions, or for high current densities, the capacitive current becomes sufficiently great and, consequently, for a correct interpretation of the experimental chronopotentiograms, it is necessary to estimate it.

Under these conditions, the chronopotentiograms are strongly distorted, so that the direct measurement of the transient by drawing tangents at the potential-time curve, becomes inapplicable.

The present paper suggested, in a first approximation, a method for determining the transient, starting from Nernst's relation, which for

---

[1] L. Gierst and A. L. Juliard, *J. Phys. Chem.*, **57**, 701 (1953).

[2] P. Delahay and T. Berzins, *J. Amer. Chem. Soc.*, **75**, 2486 (1953).

[3] W. H. Reinmuth, *Analyt. Chem.*, **33**, 485 (1961).

[4] C. D. Russell and J. M. Peterson, *J. Electroanalyt. Chem.*, **5**, 467 (1963).

the linear semi-infinite diffusion takes the following form

$$E = E^{\circ} + \frac{RT}{nF} \ln\left(c - \frac{2it^{1/2}}{\pi^{1/2} nFD^{1/2}}\right) \tag{3}$$

If E and E_1 represent the cathodic potentials corresponding to the variable time t and to the fixed time t_1 (t_1 may be also zero), then we find the equation

$$\Delta E = E - E_1 = \frac{RT}{nF} \ln \frac{\pi^{1/2}\, nFD^{1/2}c - 2it^{1/2}}{\pi^{1/2}\, nFD^{1/2}c - 2it_1^{1/2}} \tag{4}$$

We could write the equation (4) in the following form

$$1 - \exp\left(\frac{nF\Delta E}{RT}\right) = \frac{2i}{\pi^{1/2}\, nFD^{1/2}\, c}\left[t^{1/2} - t_1^{1/2} \exp\left(\frac{nF\Delta E}{RT}\right)\right] \tag{5}$$

The quantity ΔE is measured at different times t (maintaining t_1 at a fixed value). In a system having the co-ordinates : $1 - \exp\left(\frac{nF\Delta E}{RT}\right)$ and $t^{1/2} - t_1^{1/2} \exp\left(\frac{nF\Delta E}{RT}\right)$ a curve is obtained, the initial linear portion of which, extrapolated for the ordinate equal to 1 ($\Delta E \to -\infty$), gives the measured transient $\tau_m^{1/2}$.

We shall call this procedure of transient evaluation "the $E - t$ linear equation method" or shortly "the $E - t$ method".

By this method we obtain a first correction of the chronopotentiograms, through an improved determination of the transient. The transient obtained by the $E - t$ method is corrected, by introducing in the Sand's equation a faradic current $i_F = i - i_c$.

The capacitive current is computed from the relation

$$i_c = -C_{dl}\frac{\mathrm{d}E}{\mathrm{d}t} = C_{dl}\frac{RT}{nF}\frac{1}{2\,t^{1/2}\,(\tau^{1/2} - t^{1/2})} \tag{6}$$

In relation (6), C_{dl} represents the differential capacity of the double layer per surface unit, the capacity being considered constant for a certain potential range.

The second factor of the same relation results from the differentiation of the relation (3), at the same time, taking into account Sand's equation. [5]

It is clear that equation (6) has an approximate character because the current density i of equation (3) has been considered constant.

---

[5] Iu. K. Delimarskii, A. V. Gorodyskii and V. V. Kuzmovich, *Coll. Czech. Chem. Comm.*, **25**, 3056 (1960).

In reality, one must consider the faradic current i_F, which varies in time.

Such a treatment was applied by De Vries on the basis of a programme, using a computer. [6]

We shall further use equation (6) for an approximate computation of the capacitive current.

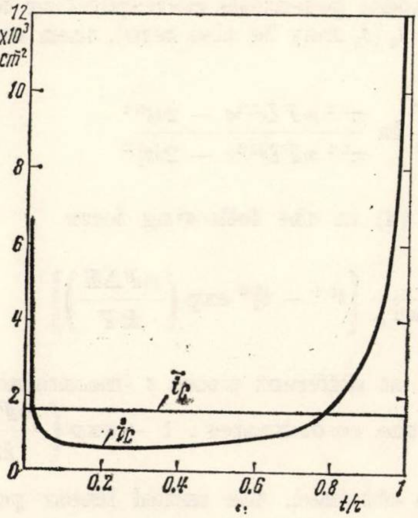

Fig. 2. — The capacitive current in $NaNO_3-AgNO_3$ system. $c_{AgNO_3} = 0.5 \times 10^{-2}$ mole$\cdot l^{-1}$, $i = 15 \times 10^{-3}$ A$\cdot$cm^{-2}, $t = 350°$.

Fig. 2 represents the capacitive current i_c computed by relation (6) for a distorted chronopotentiogram. It may be seen that for a sufficiently great time interval (*ca* 0.8 τ), i_c does not vary too much; thus one can take an average capacitive current with the aid of which one may proceed to a second correction of the chronopotentiograms.

EXPERIMENTAL

The determinations were performed in the molten alkali nitrates systems $NaNO_3-AgNO_3$ and KNO_3-AgNO_3, with $AgNO_3$ concentrations of $0.5-2.0 \times 10^{-2}$ mole$\cdot$l^{-1} and current densities of $5-30 \times 10^{-3}$ A$\cdot$cm^{-2}, on a cathode platinum plate. The temperature was maintained constant at 350 ± 0.5°, and the recording of the potential-time curves was effected directly on the photographic paper from cathode-ray oscillograph.

The electrical assembling, the cell, the electrodes and the working procedure are described elsewhere. [7]

RESULTS AND DISCUSSION

Fig. 3 shows a distorted chronopotentiogram, for which the drawing of the tangents for the measurement of the transient becomes very difficult. Fig. 4 shows the $E - t$ method proposed by us for the determination of the transient, through extrapolation of the linear portion of the curve plotted in the coordinates expressed in (5). In this last figure, the chronopotentiogram is a little distorted owing to the low capacitive current, which is practically negligible.

---

[6] W. T. De Vries, *J. Electroanalyt. Chem.*, **17**, 31 (1968); **18**, 467 (1968).

[7] S. Sternberg and C. Herdlicka, *Rev. Roumaine Chim.*, **14**, 991 (1969); **15**, 343 (1970).

In this situation, the transient obtained by the $E - t$ method is practically equal to that obtained by the Reinmuth's graphical method.

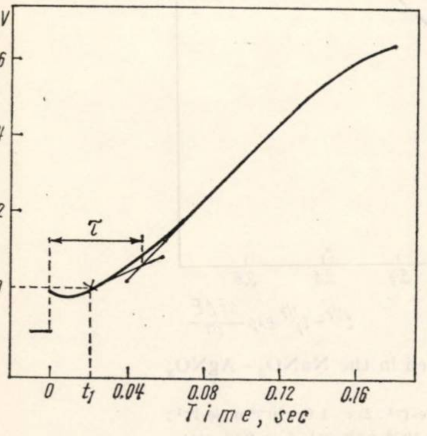

Fig. 3. — A distorted chronopotentiogram in the KNO_3-AgNO_3 system. $c_{AgNO_3} = 0.5 \times 10^{-2}$ mole·l^{-1}, $i = 10 \times 10^{-3}$ A·cm^{-2}, $t = 350°$.

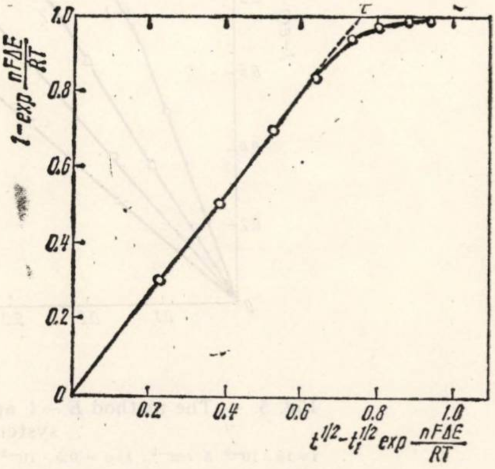

Fig. 4. — The determination of the transient by the method proposed by us (the $E - t$ method). $c_{AgNO_3} = 2.0 \times 10^{-2}$ mole·l^{-1}, in the $NaNO_3 - AgNO_3$ system; $i = 10 \times 10^{-3}$A·cm^{-2}, $t_1 = 0.05$ sec.

In the case of more diluted solutions of Ag^+ ions, the deviation from linearity of the initial portion is more and more pronounced (figs. 5 and 6) and corresponds to a greater distortion of the potential-time curves.

In order to verify the different procedures for the correction of the capacitive current, the interdiffusion coefficient of the Ag^+ ion has been computed from the transients measured by the $E - t$ linear equation method.

In the concentration range used by us, the interdiffusion coefficient D_{Ag^+} is a constant which depends only on the nature of the solvent. Tables 1 and 2 contain the results obtained in this way for D_{Ag^+} in the molten salt systems, $NaNO_3-AgNO_3$ and KNO_3-AgNO_3, at different concentrations and current densities (column 7). Under our working conditions the transients had values ranging between 0.015 and 0.75 seconds.

Tables 1 and 2 contain also the values of the interdiffusion coefficient calculated from direct readings of transients by the Reinmuth's graphical method (column 6). At high concentrations and low current densities the results obtained by the two methods are in very good agreement. In tables 1 and 2 the interdiffusion coefficients obtained from undistorted chronopotentiograms are marked with the sign *.

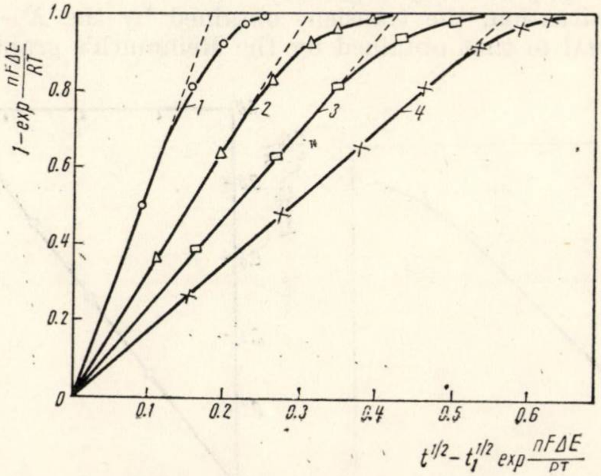

Fig. 5. — The method $E - t$ applied in the $NaNO_3-AgNO_3$ systems.
$i = 15 \times 10^{-3}$ A·cm^{-2}; 1) $c = 0.5 \times 10^{-2}$ mole·l^{-1}; 2) $c = 1.0 \times 10^{-2}$ mole·l^{-1}; 3) $c = 1.5 \times 10^{-2}$ mole·l^{-1}; 4) $c = 2.0 \times 10^{-2}$ mole·l^{-1} $t_1 = 0.01$ sec.

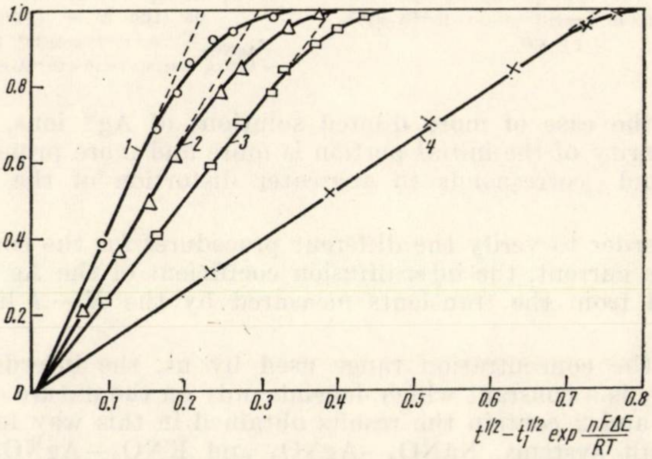

Fig. 6. — The method $E - t$ applied in the KNO_3-AgNO_3 systems.
$i = 10 \times 10^{-3}$ A·cm^{-2}; 1) $c = 0.5 \times 10^{-2}$ mole·l^{-1}; 2) $c = 0.75 \times 10^{-2}$ mole·l^{-1}; 3) $c = 1.0 \times 10^{-2}$ mole·l^{-1}; 4) $c = 2.0 \times 10^{-2}$ mole·l^{-1} $t_1 = 0.01$ sec.

On the basis of these results the following average values have been adopted:

$D_{Ag^+} = 2.54 \times 10^{-5}$ cm^2·s^{-1} in the $NaNO_3-AgNO_3$ system, and $D_{Ag^+} = 1.93 \times 10^{-5}$ cm^2·s^{-1} in the KNO_3-AgNO_3 system, at the temperature of 350°. These data are in agreement with other previously obtained results. [7] In the case of distorted chronopotentiograms, improved values of the interdiffusion coefficients are obtained.

Table 1

Interdiffusion coefficient values of silver ion in $NaNO_3 - AgNO_3$, at 350°

$C_{AgNO_3} \times 10^2$ $\frac{\text{mole}}{1}$	$i \times 10^3$ $\frac{\text{A}}{\text{cm}^2}$	Transient τ_s sec	Percent capacitive current $i_c/i \times 100$, %		Interdiffusion coefficient $D_{Ag^+} \times 10^5$, cm²/s			Percent deviation %	
			eq. (7)	graphical integration (fig. 2)	Reinmuth's method (D')	$E - t$ method	$E - t$ method and correction (D'')	$\frac{D' - D_{Ag^+}}{D_{Ag^+}} \times 100$	$\frac{D'' - D_{Ag^+}}{D_{Ag^+}} \times 100$
0.50	5.0	0.186	7.0	2.0	2.60	2.91	2.79	2.4	9.8
	7.5	0.0825	9.4	2.8	3.06	3.15	2.95	20.5	16.1
	10.0	0.0465	11.0	4.5	3.83	3.22	2.95	50.8	16.1
	12.5	0.0297	16.0	7.2	4.25	3.80	3.29	67.3	29.6
	15.0	0.0206	20.0	11.4	6.10	4.00	3.12	140.3	22.8
0.75	5.0	0.417	2.6	1.6	2.94	2.68	2.58**	15.8	1.6
	7.5	0.186	9.4	1.75	3.30	3.10	3.05	30.0	20.1
	10.0	0.098	7.5	2.0	4.00	3.00	2.88	57.5	13.4
1.00	5.0	0.742	1.0	0.8	2.80	2.60	2.55**	10.2	0.4
	7.5	0.575	1.35	1.6	2.55	2.61	2.53**	0.4	−0.4
	10.0	0.186	2.0	1.9	2.88	2.65	2.55**	13.4	0.4
	12.5	0.119	1.6	1.85	2.76	2.64	2.54**	8.7	0
	15.0	0.0825	5.3	3.0	3.38	2.84	2.68	33.1	5.5
	17.5	0.0609	5.7	4.0	3.35	2.86	2.63	31.9	3.5
	25.0	0.0297	13.7	4.0	4.00	3.42	3.15	57.5	24.0
1.50	10.0	0.417	−2.0	0.7	2.49*	2.53*	2.50*	−2.0	−1.6
	15.0	0.186	−2.0	1.2	2.63*	2.53*	2.48*	3.5	−2.4
	20.0	0.104	1.25	1.3	2.68*	2.61*	2.54*	5.5	0
2.00	10.0	0.742	0	0.8	2.50*	2.54*	2.51*	−1.6	−1.2
	15.0	0.330	0.07	0.67	2.39	2.54*	2.51*	−5.9	−1.2
	20.0	0.186	0.75	1.0	2.67*	2.59*	2.54*	5.1	0
	25.0	0.119	1.60	1.1	2.77	2.62*	2.56*	9.1	0.8
	30.0	0.0825	2.35	1.25	2.62*	2.60*	2.54*	3.1	0

The $8^{-\text{th}}$ column of the above tables contains the interdiffusion coefficient computed by considering only the diffusive current i_F, and leaving out the capacitive current i_c from the total current.

For a correct evaluation of the capacitive current it is necessary to know the value of the average capacity of the electrical double layer C_{dl}, which is obtained by recording the potential-time curves in the supporting electrolyte, under galvanostatic conditions.[8] Our determinations gave the following values: 120 $\mu F \cdot cm^{-2}$ in $NaNO_3$ and 100 $\mu F \cdot cm^{-2}$ in KNO_3.

An average capacitive current has been estimated by the graphical integration of equation (6) (see fig. 2).

In this way, a considerable improvement of the interdiffusion coefficients with respect to the true values is obtained (column 8), in some cases (the values marked with **) correct values of interdiffusion coefficients being obtained even from distorted chronopotentiograms.

Table 2

Interdiffusion coefficient values of silver ion in $KNO_3 - AgNO_3$, at 350°

$C_{AgNO_3} \times 10^2$ mole/1	$i \times 10^3$ A/cm²	Transient τ_s sec	Percent capacitive current $i_c/i \times 100$, %		Interdiffusion coefficient $D_{Ag^+} \times 10^5$, cm²/s			Percent deviation %	
			eq. (7)	graphical integration (fig. 2)	Reinmuth's method (D')	$E-t$ method	$E-t$ method and correction (D'')	$\frac{D'-D_{Ag^+}}{D_{Ag^+}} \times 100$	$\frac{D''-D_{Ag^+}}{D_{Ag^+}} \times 100$
0.5	5.0	0.141	6.0	3.6	2.36	2.16	2.00**	22.3	3.6
	7.5	0.0625	6.7	5.35	2.45	2.20	1.99**	27.0	3.1
	10.0	0.0352	14.5	7.0	2.74	2.48	2.14	42.0	10.9
	12.5	0.0225	16.8	8.0	3.84	2.86	2.42	99.0	25.4
	15.0	0.0157	21.4	8.7	4.33	3.15	2.64	124.0	36.8
0.75	5.0	0.317	4.0	1.2	2.14	2.10	2.05**	10.9	6.7
	7.5	0.141	6.0	2.0	2.35	2.18	2.07**	21.8	7.3
	10.0	0.0792	6.0	2.0	3.30	2.20	3.07	71.0	59.0
1.0	5.0	0.562	1.4	0.8	2.02	1.97	1.94**	4.7	0.5
	7.5	0.250	3.6	1.2	2.30	2.12	2.07**	19.2	7.3
	10.0	0.141	2.0	1.5	2.25	2.14	2.06**	16.6	6.7
2.0	7.5	1.000	0	0	1.93*	1.93*	1.93*	0	0
	10.0	0.562	0.6	0.6	1.93*	1.95*	1.93*	0	0
	20.0	0.141	−0.4	0.9	1.98*	1.92*	1.91*	2.6	−1.0
	30.0	0.0625	0.67	1.67	1.91*	1.94*	1.90*	−1.0	−1.5

In the last two columns of the tables 1 and 2 there are listed the relative deviations of the interdiffusion coefficient calculated after the Reinmuth's graphical method (D') and after the method suggested by us (D'').

As can be seen, by the application of two successive corrections, a considerable improvement of the interdiffusion coefficients is obtained even from the most distorted chronopotentiograms.

---

[8] R. S. Rodgers and L. Meites, *J. Electroanalyt. Chem.*, **16**, 1 (1968).

Thus, it may be concluded that the two determining processes which take place at the cathode are the diffusion and the charging of the electrical double layer.

The deviations which however exist between D'' and D_{Ag^+} can be explained by the approximate character of the expression of the capacitive current (eq. 6).

From the true values of the interdiffusion coefficients D_{Ag^+} a theoretical τ_s can be calculated for every chronopotentiogram, namely a value corresponding to the total current i.

Comparing the transient τ_s with that measured by the $E - t$ linear equation, one can estimate an experimental average capacitive current, namely

$$\frac{i - i_c}{i} = \frac{\tau_s^{1/2}}{\tau_m^{1/2}} \tag{7}$$

In the 4-th and 5-th columns of tables 1 and 2, the values of the ratio $\frac{i_c}{i} \times 100$, calculated by equations (6) and (7), are compared.

As can be seen, the experimental ratio i_c/i is twice the ratio calculated from relation (6).

Some authors have tried to correlate the value of the percent capacitive current $\frac{i_c}{i} \times 100$, with a parameter in the expression of which a term representing the electrical double layer capacity occurs. Rodgers and Meites [8] give tabulated values for the correction of the direct reading transient, depending on the different values of the quantity $\frac{C_{dl}}{i\,\tau_s}$.

Our experimental results are not within the limits set in the correction tables found in the literature, but a linear dependence between the experimental i_c/i ratio and $\frac{C_{dl}}{i\,\tau_s}$ has been noticed, as also results from fig. 7.

De Vries [6] has resolved the differential equation of diffusion depending on a so-called "distorting parameter" K, which can be defined by the expression

$$K = \frac{C_{dl} \cdot RT}{n^2 F^2 (\pi D \tau)^{1/2}\, c} = \frac{2iC_{dl}\, RT}{n^3 F^3 \pi D c^2} \tag{8}$$

Thus, the distortion of the potential-time curves owing to the double layer charging depends only upon the distorting parameter K. [6,9]

---

[9] D. Deroo, J. Guitton and J. Besson, *J. Chim. phys.*, **67**, 1097 (1970).

Other authors [10,11] have suggested that this parameter has twice the previous value, while an obvious distortion occurs for values of the parameter more than 0.001.

Taking into account the relation (1), the relation (8) can be put in the form

$$K = \frac{RT}{2nF} \cdot \frac{C_{dl}}{i\tau_s} \tag{9}$$

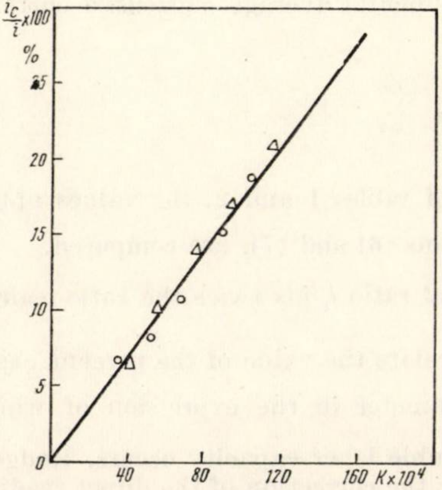

Fig. 7. — The relation between the percent capacitive current and the distorting parameter.

○ – for the $NaNO_3-AgNO_3$ systems.
Δ – for the KNO_3-AgNO_3 systems.

From the slope of the straight line represented in fig. 7, the following proportionality relation is obtained

$$\frac{i_c}{i} = 1 - \frac{\tau_s^{1/2}}{\tau_m^{1/2}} = 17.2\,K \tag{01}$$

A linear proportionality relation between $\frac{i_c}{i}$ and K can be also deduced from relation (6).

Putting in this last relation $t = \alpha \cdot \tau$, we obtain

$$\frac{i_c}{i} = \frac{RT}{2nF} \frac{C_{dl}}{\beta i \tau_s} \tag{11}$$

where $\beta = \alpha^{1/2} - \alpha$.

---

[10] M. L. Olmstead and R. S. Nicholson, *Analyt. Chem.*, **42**, 796 (1970).
[11] O. Dracka, *Coll. Czech. Chem. Comm.*, **34**, 2627 (1969).

Fig. 8 shows the variation of β as a function of the ratio $\alpha = \frac{t}{\tau}$. By graphical integration and averaging, we obtain for the mean value $\bar{\beta} = 0.14$.

Substituting this in relation (9) we obtain

$$\frac{i_c}{i} = 7.1\,K \tag{12}$$

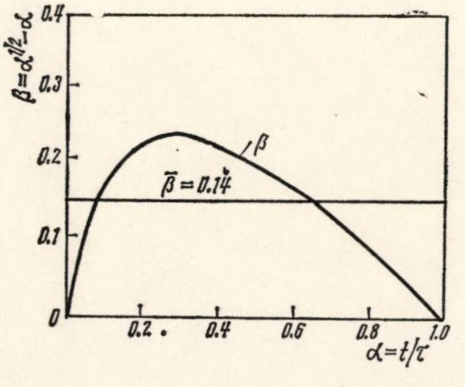

Fig. 8. — The dependence of β on the ratio $\alpha = t/\tau$.

As can be seen, the computed proportionality factor is approximately one half of that obtained from relation (9), which has been determined from experimental data. The disagreement results from the approximate character of the equation (6) in which the current i and, consequently, the transient τ_s have been considered constant.

The correction of the capacitive current, using the method suggested by De Vries, requires a very complicated computation to complete the correction tables.

The semi-empirical relation (10) proposed by us can be used for a direct correction of the capacitive current.

From the experimental data obtained by us, it also follows that under certain conditions of concentration and current densities (when the ratio $\frac{C_{dl}}{i\tau_s}$ is low), one obtains "quasi-ideal" chronopotentiograms, to which the Reinmuth's graphical method can be successfully applied, for a correct calculation of the transients and of the interdiffusion coefficients in molten salts.

Revue Roumaine de Chimie, **18**, *2*, 233–238 (1973)

STUDY OF ELECTROCHEMICAL FORMING OF SURFACE OXIDES ON THE ACTIVE CARBON ELECTRODE

OV. MATEIOVICI

Military Academy,
Şos. Panduri 60, Bucureşti, Romania

Received June 15, 1972

The formation of oxides compounds on active carbon electrode was investigated by means of the charging curves method. After a previous cathodic polarization up to zero value of the potential, the electrode was anodically polarized with a current of 90 μ amp (that is 7.5×10^{-9} amp/cm^2) up to the potential of + 1,200 mvolts (*vs.* normal hydrogen electrode). From the form of the charging curve, the presence of two oxide types was ascertained, but their structure was not determined. No influence of the chemisorbed gases, such as AsH_3, on the surface of the electrode was observed. The form of the charging curves is strongly dependent on temperature. Thus, the amount of oxygen which can be desorbed increases with temperature. On the basis of this phenomenon, the active electrochemical oxygen concept was introduced for the case of an active carbon electrode. From this point of view, the same potential of the active carbon electrode is expressed as different amounts of oxygen for constant pH and temperature values.

The electrochemical phenomena of the active carbon are based on the potential difference existing between surface oxides (the combinations *in situ* of carbon with oxygen) and the electrolyte solution. These surface oxides are not so well defined. They depend on many factors, that is : the raw material of the active carbon, its treatment both during activation and post-activation and so on.

Generally speaking, one can distinguish between three forms of oxygen sorption : physically adsorbed oxygen, chemically adsorbed oxygen and chemisorbed oxygen. The ratio between these three forms of oxygen lies in the same factors mentioned before.

Austen and Ingram[1] established, by the paramagnetic resonance method, that free radicals form on the surface of the active carbons. Garten and Weiss [2] state that on the surface of different carbons there are quinone and hydroquinone groups. Active carbons which have an intermediary structure between quinone and hydroquinone must be assumed. [2]

---

[1] I. Austen and A. Ingram, *Chem. and Ind.*, **37**, 981 (1956).

[2] S. Garten and W. Weiss, *Austral. J. Chem.*, **8**, 68 (1955).

By infrared spectroscopic method, hydroxyl and carbonyl groups were detected as a result of the reactions between O_2, O_3 and H_2O and active carbons. [3-5] Between the activation temperature and the properties of the active carbons, a strong relationship was observed. [6] But not all carbon-oxygen compounds are active in oxidation reactions.

Rideal and Wright [7,8] pointed out that oxidation action is not due to the oxygen found in the stable oxides form.

Davtian and co-workers [9] showed that in SO_2 oxidation, on the surface of the active carbons, take part some surface oxides which are easily desorbed at the room temperature and in vacuum.

Frumkin [10] and later Davtian [11] investigated the surface compounds on the active carbon electrode by means of the charging curves.

In the present work, new aspects regarding surface oxides forming are emphasized.

EXPERIMENTAL TECHNIQUE

In this work an active carbon electrode made by wood char was used. The mass of the electrode was small and varied between 1.5—1.7 mg. The electrode was completely immersed into solution. The cell made of glass, was closed and thermostated. As a comparison electrode, the calomel electrode was used and the potentials were referred to normal hydrogen electrode.

The electrochemical forming of surface oxides was studied by means of the charging curves method.

The electrolyte was 0.02 M. H_2SO_4 solution. For the preparation of the solution, twice-distilled water was used.

EXPERIMENTAL RESULTS

1 — The chemisorbed oxygen amount can be determined from the length of the charging curve. The charging curve was taken by cathodic polarization with a current of 3 μ amp starting from the steady potential (+650 m volts) up to zero value. The temperature was 25°. Inasmuch, as the specific area of the electrode was 1.2 m^2, a current density of 2.5×10^{-10} amp/cm^2 results.

The form of the charging curve is represented in figure 1.

---

[3] R. Smith and D. A. Young, *Trans. Faraday Soc.*, **62**, 2880 (1966).

[4] V. I. Lygin, N. V. Kovaleva, N. N. Kavtaradze and A. V. Kiselev, *Kolloid. Zhur.*, **22**, 334 (1960).

[5] J. B. Donnet, F. Hueber, N. Pearl and J. Jaeger, *J. Chim. phys.*, **60**, 426 (1963).

[6] W. M. Wright, *Proc. Cambridge Phil. Soc.*, **23**, 187 (1926).

[7] E. K. Rideal and W. M. Wright, *J. Chem. Soc.*, **1925**, 1347.

[8] Idem, *J. Chem. Soc.*, **1926**, 3182.

[9] O. K. Davtian and Yu. A. Tcai, *Zhur. fiz. Khim.*, **35**, 992 (1961).

[10] A. N. Frumkin, *Uspekhi Khim.*, **18**, 9 (1949).

[11] O. K. Davtian and Yu. A. Tcaci, *Zhur. fiz. Khim.*, **35**, 2727 (1961).

Taking into account the adsorption pseudocapacitance it results an amount of chemisorbed oxygen of 500 μ equivalents/g. From the fact that on the charging curve, two distinct regions characterized by two flats can be seen: one of them at the potential of +570—580 m volts, which lies on 8—10 m coulombs, and the other, at the potential of about 300 m volts, which lies on about 40 m coulombs, would suppose that two individual oxides exist here.

2 — The electrode was purified of oxygen for six days, by cathodic polarization up to zero potential. The polarization was made with a current of 3 μ amp. Onto the electrode, N_2 free oxygen was bubbled for a few hours. The charging curve was taken at the current of 90 μ amp and 25° temperature.

Both during cathodic polarization, that is for oxygen desorption, and during the drawing of the charging curve, high purity AsH_3 was bubbled onto the electrode for a few minutes. When the potential was + 1,200 m volts, the current was switched off and inverted for oxygen desorption up to zero potential value and then a new charging curve was drawn. Three similar curves were obtained and their aspect is shown in figure 2. Two distinct domains on the charging curves are distinguished: first a linear portion up to about + 1,000 m volts, and the second, a flatter portion over + 1,000 m volts.

No effect by bubbling AsH_3 onto electrode was observed in what concerns the length and the form of charging curves.

3 — To investigate the variation of the charging curves form with temperature, in figure 3 two curves at + 5° are plotted. As can be seen, for the small temperature, the reproductivity between two determinations is better. Also, for the small temperature the charging curve begins to incline for a greater potential.

4 — It is of interest to know in what way the oxygen could be desorbed from the electrode surface at once after its chemisorption. The same current of polarization as above was used both for anodic and for cathodic polarization 90 μ amp (Fig. 4).

The working temperature was 25°. In this case, half a quantity of electricity necessary for obtaining the potential of + 1,200 m volts is used to get up to zero potential.

Another question in connection with the quantity of oxygen maintained as electrochemical active oxygen was focused by the next experience. Thus, for the temperature of + 7°, 35 μ coulombs/cm^2 are necessary up to zero potential, while for the temperature of + 25°, 52 μ coulombs/cm^2 are necessary. Two curves (potential vs. quantity of electricity) are plotted in Figure 5.

5 — To detect some disturbance regarding the charging curve with time, the electrode was polarized with a cathodic current of 3 μ amp for 15 days. For this current a very stable zero dynamic potential was obtained. After the electrode was purified in this way, two charging curves were taken for two temperatures: +7° and +25°. In this case, in spite of the fact that the purification time of the electrode by polarization varied in large limits, no discrepancy between the length and the

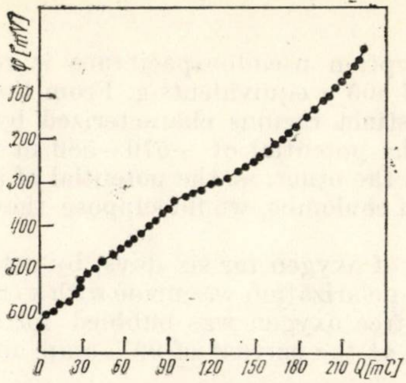

Fig. 1. — Cathodic charging curve of the active carbon electrode.

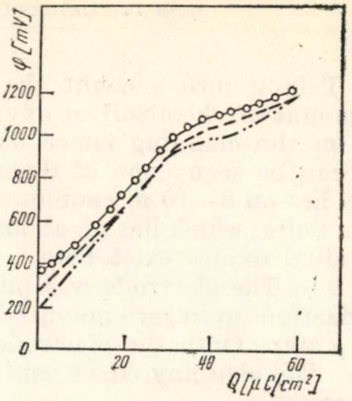

Fig. 2. — Charging curves of the active carbon electrode ($T = 25°$).

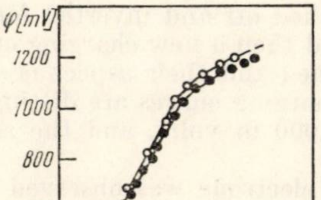

Fig. 3. — Charging curves of the active carbon electrode ($T = 5°$).

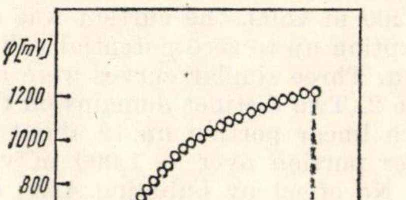

Fig. 4. — Anodic (above) and cathodic charging curves of the active carbon electrode.

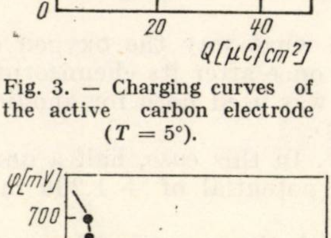

Fig. 5. — Variation of the potential, at the oxygen desorption, with the quantity of electricity at the temperatures of 25° (curve *1*) and of 7° (curve *2*).

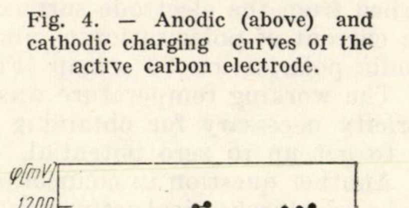

Fig. 6. — Form of the charging curves after a cathodic polarization of the electrode for 15 days, up to zero value of potential at the temperature of 25°, (curve *1*) and at the temperature of 7° (curve *2*).

form of the charging curves were observed as visible in figure 6, by comparison with the curves given in figures 2 and 3. From this fact, an independence of the form of the charging curves on the time results.

DISCUSSION AND CONCLUSIONS

It is beyond any doubt that the electrochemical phenomena investigated on the active carbon electrode are based on the active surface compounds. It is very difficult, if not impossible, to define all compounds existing between some intervals on the charging curve and, therefore, no effort in this respect was made in the present work.

However, some assurances were established.

Thus, the amount of oxygen, which may be electrochemisorbed on the electrode here investigated, is always the same for the same current value. It can be imagined that on the other active carbon electrode (i.e. coconut shells) the amount of electrochemisorbed oxygen could be different. The form of two charging curves showed a better reproductivity for the curves taken at the lower temperature.

This is probably due to a better definition of the surface oxides. It is interesting to note that no effect was observed if on the surface of the electrode other gases (i.e. AsH_3) are chemisorbed.

In other words, it seems that the surface of the active carbon electrode is characterized by two areas : an active electrochemical area and a chemical area. No interference between these two areas was observed for this electrode.

A remarkable fact lies also in the independence of the length and the form of the charging curve on the cathodic polarization time up to zero dynamic potential value. This phenomenon proved that a limit time exists in the purification of the electrode, beyond which, the time (hence, the quantity of electricity) is ineffective.

By polarization of the electrode with a small current which varies from 1×10^{-9} amp to 3×10^{-6} amp, the electrode potential deviates from the value of the steady potential, function of the current polarity. If the current is maintained between these limits and is kept rigorously constant, the potential is established at one value which persists as long as the electrode is polarized.

This potential was named the "dynamic potential".

The dynamic potential is very constant provided that both pH and temperature are constant.

However, if one proceeds to the interruption of the cathodic polarization current, the dynamic potential fades away and the steady potential is established again. The steady potential of the active carbon electrode, in 0.02 M. H_2SO_4 solution, is $+650-750$ m volts. (*vs*. the normal hydrogen electrode).

From the fact that the electrode may get up to the same potential but with different amounts of oxygen, depending on the temperature, proves that only a part of the oxygen is electrochemically active. The rest has no importance from the electrochemical point of view. Unfortunately, it is difficult to find a rigorously mathematical relation between the potential and the electrochemically active oxygen concentration (for given pH and temperature values).

The charging curves method pointed out the complexity of the phenomenon, giving some information with respect to the state of the surface.

Revue Roumaine de Chimie, 18, 2 239—246 (1973)

STOCHASTIC MODELLING OF CHEMICAL PROCESSES

O. IORDACHE, MARCELA MUNTEAN and I. TEOREANU

Polytechnic Institute, Str. Polizu 1, Bucharest, Romania

Received July 17, 1972

In the present paper a general mathematical model for the irreversible evolution in discrete stages of some chemical processes is presented. The model is adapted for the hardening process of silicate binders. A good concordance with the experimental results is obtained.

1. INTRODUCTION

The evolution of chemical processes is often essentially influenced by a great number of factors having as result a probabilistic comportment. Consequently, to describe such processes, stochastic models are recommended instead of deterministic ones.

The advantages of stochastic models result mainly from their congruence with the intimate mechanism of the process development. Sometimes, the results obtained with stochastic models can also be found by deterministic models, but the considerations regarding the development of the process as a whole and in large intervals of time, as are usually done for deterministic models, often hinder even the essence of the studied phenomena. The stochastic models give also, along with the average values of the parameters, the differences from these values. The stochastic models use statistical parameters obtained directly from experiment or intuitively chosen when the difficulties do not permit to explain the cause of a certain comportment of the phenomenon but the necessities impose the knowledge of the concrete mode of the process development.

The stochastic models are important for the study of some problems, for example : the kinetics of chemical reactions (i.e. autocatalytic, chain reactions and especially polymerization ones), the structure formation of certain materials (coagulation, restructuring, felting of polymers, hardening of binders, fatigue of materials), transport phenomena (mass, heat, momentum), growth phenomena (crystallization, coalescence, etc.).

In the present paper a general mathematical model for the irreversible evolution, in discrete states, is presented. A discussion of the way in which, depending on the process, the necessary statistical parameters are chosen, as well as the way of interpreting the process according with the particular values of the parameters. The models are then applied for the hardening of the constituents of portland cement clinker and especially for the hardening of tricalcium silicate.

2. MATHEMATICAL MODEL

Let us denote by $X(t)$ the stochastic variable with discrete values $1, 2 \ldots n$, representing the evolution step of the process (e.g. the polycondensation degree), by $P_{ij}(\tau, t)$, the transition probability defined as

$$P_{ij}(\tau, t) = \text{Prob}\,\{X(t) = j \mid X(\tau) = i\}\ (t \geqslant \tau \geqslant 0)$$

(the probability that the polycondensation degree at time t to be j, if, at the previous time τ, it was i), by $q_i(t)$ the intensity function defined as

$$q_i(t) = \lim_{\Delta t \to 0} \frac{1 - P_{ij}(t, t + \Delta t)}{\Delta t}$$

(the probability that the polycondensation degree $X(t)$ to change in the interval $(t, t + \Delta t)$ is $q_i(t)\,\Delta t$, if at time t, it was i), by $Q_{ij}(t)$, the probability of relative transition defined as

$$q_i(t)\,Q_{ij}(t) = \lim_{\Delta t \to 0} \frac{P_{ij}(t, t + \Delta t)}{\Delta t}$$

(conditional probability that the polycondensation degree to become j at time $(t + \Delta t)$, if it has been i, at time t and in the interval $(t, t + \Delta t)$ it has changed).

The aim of this paper is to determine the transition probabilities $P_{ij}(\tau, t)$ which actually offer concrete values for the fraction of the substance arrived in the state j, at time t, if at the previous time τ, it has been in the state i.

Making the hypothesis that the successive changes are independent (Markov process, without memory), the probabilities follow the Kolmogorov-Feller's equations [1]

$$\begin{aligned} \frac{\partial P_{ij}(\tau, t)}{\partial t} &= -\,q_i(t)\,P_{ij}(\tau, t) + \sum_{k=0}^{\infty} q_k(t)\,Q_{ij}(t)\,P_{ik}(\tau, t) \\ \frac{\partial P_{ij}(\tau, t)}{\partial \tau} &= q_i(\tau)\left[P_{ij}(\tau, t) - \sum_{k=0}^{\infty} Q_{ij}(\tau)\,P_{kj}(\tau, t)\right] \end{aligned} \qquad (1)$$

---

[1] W. FELLER, "An introduction to probability theory and its applications", vol. I., second ed., Academic Press, New York, 1960.

In the particular case of the polycondensation process by successive adding of monomer units, the equations (1) become

$$\frac{\partial P_n(t)}{\partial t} = -\lambda(n, t)\, P_n(t) + \lambda(n-1, t)\, P_{n-1}(t). \tag{2}$$

In Eq. (2) $\tau = 0$, $i = 1$ was considered as initial state (that is, the polycondensation process starts from the monomer) and the following notations were made

$$q_n(t) = \lambda(n, t)$$

$$P_{1n}(0, t) = P_n(t).$$

$P_n(t)$ represents the probability that the polycondensation degree be n at time t, if initially it was 1 ; actually, as in the polydisperse silicate systems, the number of particles is practically great, $P_n(t)$ represents also the fraction of the n-silicate in the mixture.

Equation (2) shows that the variation in time of the quantity of n-silicate at time t, $\frac{\partial P_n(t)}{\partial t}$ is due to the decrease of the n-silicate, $-\lambda(n, t)\, P_n(t)$, as a result of the reaction with intensity $\lambda(n, t)$ by which this n-silicate becomes $(n+1)$-silicate, as well as by the increase of the quantity of n-silicate, $\lambda(n-1, t)\, P_n - 1\,(t)$, due to the reaction of $(n-1)$-silicate which, with the intensity $\lambda(n-1, t)$, becomes n-silicate at time t.

The model described by (2) is connected with a given phenomenon by the parameter $\lambda(n, t)$, that is by the particular way by which the change intensity depends on the polycondensation degree at time t. The justification of the dependence is found in the mechanism itself, and it is, at the same time, an explanation of the mechanisms proposed to explain some experiments. The parameter $\lambda(n, t)$ is analogous to the rate constants of the processes used in deterministic treatment (for example in the chemical kinetics). This parameter appears as a synthetic indication of this process evolution. It constitutes a powerful tool, permitting the expression, of some different and complicated phenomena, in a working manner, using simple and intuitive equations like equation (2). It must be mentioned that, due to its character of statistical estimator, it avoids sometimes the explanation of the physicochemical process.

In what follows, some particular cases of dependence of parameter λ on the polycondensation degree n and the time t will be analysed.

Case 1. (C_1) The intensity function of the transition is constant $\lambda(n, t) = \lambda$.

This is the hypothesis of equal reactivity. The rate constant of the polycondensation process remains constant throughout the process evolution. This hypothesis was used by Flory [2] in the case of polycondensation by addition without termination.

From the physical point of view this hypothesis is connected with the invariance of the electronic structure of the functional groups with the increase of n, with the absence of steric hindrance, and with the fact that in the system the only process taking place is the polycondensation. In the case of the hardening of silicate binders these assumptions do not hold; here the steric and spatial hindrances, which appear as the silicate chains grow and the hardening process develops, led to a decrease of λ with n, while the process of formation of hardened structure determines a slowing in time of the polycondensation process.

For the assumption of equal reactivity the distribution of n-mer is of Poisson type. From (2) one obtains

$$P_n(t) = \frac{(\lambda t)^{n-1}}{n!} e^{-\lambda t}. \tag{3}$$

This distribution is suited to a good description of a simple phenomenon like vinyl polymerization. The polycondensation process of calcium silicates, due to the above reasons is not governed by (3), except for small times. The distribution (3) shows a decrease of the monomer quantity in time and an increase followed by a decrease and then by an asymptotic stabilization of the quantity of dimer, trimer etc.

Case 2 (C_2). The intensity function depends on state and does not depend on time: $\lambda(n, t) = \lambda(n) = \lambda n$.

In this case the reactivities of the mers are different for different states but are independent on time. It means that some motives appear in the system for the variation of the transition intensity with the state of the system (modifications due to the conjugation of the electronic structure, steric hindrance etc.) but there are not other phenomena superimposed on those studied.

The distribution of the n-mer in time is

$$\begin{cases} P_n(t) = \beta_n \sum\limits_{k=1}^{\infty} \dfrac{1}{\alpha_{nk}} e^{-\lambda n t} \\ \\ P_1(t) = e^{-\lambda_1 t} \end{cases} \tag{4}$$

where

$$\alpha_{nk} = \prod_{\substack{i=1 \\ i \neq k}}^{n} \gamma_{ik} \qquad \text{for } K \leqslant n,$$

and

$$\gamma_{ik} = \lambda_i - \lambda_k$$

---

[2] J. P. Flory, "Principles of polymer chemistry", Cornell University Press, Ithaca, New York, 1953.

These equations maintain the general characteristics of the Poisson distribution (to which the distribution given by (4) tends, when $\lambda_i = \lambda =$ constant) but (4) is more comprehensive because it permits to describe some phenomena for which the evolution from a state to another determines essential changes.

The result is useful for the study of the kinetics of some consecutive reactions. It may characterize, for example, a phenomenon like the condensation of the silicic acid. The polycondensation of the hydrated calcium silicates can not be described by (4), but only at small times of hardening, when the parallel structuring phenomena have not a great development.

Case 3 (C_3). The intensity function depends only on time not on state $\lambda(n, t) = \lambda(t)$.

Such a dependence may appear when in a system, like in C_1, different phenomena take place; for example if the polycondensation or polyaddition reaction of some simple substances is controlled by diffusion, then the effect of the diffusion is manifested by a particular dependence on the time of the parameter λ. Sometimes a strong dependence on time may hide a weak dependence on n.

In the case of cooling the silicate glass, for which the polymerization process was often treated in the C_1 hypothesis, the dependence on time may appear when the polycondensation of silicates is accompanied by solidification.

The distribution of the n-mer is

$$P_n(t) = [1 - \beta(t)]\,[\beta(t)]^{n-1} \tag{5}$$

where

$$\beta(t) = 1 - e^{\gamma(t)}$$

and

$$\gamma(t) = -\int_0^t \lambda(\tau)\, d\tau$$

This distribution maintains the general characteristics of the distributions obtained in C_1 and C_2, that is, the decrease in time of the quantity of the monomer and the increase, followed by the decrease and the stabilization of the polymer quantity.

In the case of the hardening of the silicate binders where the formation of the hardened structure leads to a very strong dependence on time of the polycondensation rate, the above distribution may represent a rather good approximation, especially when the number of the functional groups, — OH, is constant.

Case 4 (C_4). The intensity function depends both on time and state.

This situation corresponds to the case of inequal reactivity and superposition of phenomena in the system. This is the most complicated situation, from the mathematical point of view but is the situation most often found in practice.

In this case, the main problem is to define, using a qualitative description of the phenomena and the experimental facts, the dependence of the parameter λ on time and degree of polycondensation.

The hardening of the silicate binders, particularly of the tricalcium silicate, results from a partial superposition of three processes : the hydration — hydrolysis of the binder with the formation of gelic calcium hydrosilicates and the coagulation of these hydrosilicates, the polycondensation and crystallization of the formed calcium hydrosilicates and the formation of the hardening structure.

These three phenomena superpose one another in such a way that the polycondensation (which is preceded, at molecular scale, by hydration — hydrolysis process and followed by structuring) can be characterized only by an intensity function, dependent on time and degree of polycondensation.

The dependence on the polycondensation degree is explained by steric hindrance, by a possible modification of the number of functional groups, by the inclusion in the hardened structure of molecules with high polycondensation degree, by the appearance of cyclic polymers, etc.

The dependence on time may be explained by the strong decrease of the reaction rates due to the development of the hardened structure which strongly hinders the phenomenon.

The polycondensation is characterized by two statistical parameters : β, the fractional decrease of the intensity of the process for an increase with a unity of the polycondensation degree, at constant time, and γ, the fractional decrease of the intensity of the process in a unit time, at a constant degree of condensation

$$\beta = -\frac{1}{\lambda}\left(\frac{\partial \lambda}{\partial n}\right)_t$$

$$\gamma = -\frac{1}{\lambda}\left(\frac{\partial \lambda}{\partial t}\right)_n \qquad (6)$$

The above relations show that the variation in time and with the polycondensation degree of λ is so much the bigger, the bigger is λ. Therefore, the more rapid processes decay rapidly and the slow ones decay slowly.

The use of these parameters is based on the assumption, confirmed by experience, that a particular pair of values of β and γ characterize a certain binder (for example $3\ CaO.SiO_2$). It results, therefore, that β and γ depend on the nature of the substances present and depend very little on time and on polycondensation degree. This very property imposes and permits their use.

With β and γ defined by (6) it results

$$\lambda(n, t) = e^{-\beta n} e^{-\gamma t} \tag{7}$$

The solution of the equation (2) is therefore

$$P_n(t) = e^{-\int_0^t \lambda(n,t)\mathrm{d}t} \int_0^t \lambda(n-1, t) P_{n-1} e^{\int_0^t \lambda(n,t)\mathrm{d}t} \mathrm{d}t \tag{8}$$

3. COMPARISON WITH THE EXPERIMENT

The above result is compared to the results obtained by Lentz.[3] A good correlation is obtained using for β and γ the values of 2/3, respectively 1/3, that is for an increase by a unity of the polycondensation degree λ decreases by 66 % of its value and for a unit time elapse λ decreases by 33% of its value. Therefore, the dependence of λ on n and t is very strong and this is due especially to the structuring phenomena which hinder the polycondensation. The intensities of the transition vary so much with n and t, that for a certain n, the advance of the polycondensation is unlikely to vary (and this is one of the reasons that the presence of high n-hydrosilicates is not found in the experiment); experimentally, values of the order of tenths are obtained for n, and for a certain time, the reaction is practically stopped. This situation corresponds to that found in reality, where after 1–3 months the polycondensation reactions practically do not advance any more.

With the above values for β and γ and using the graphical integration the results shown in table 1 for 3 $CaO.SiO_2$ are obtained :

Table 1

The distribution of hydrosilicates

Time	1 day	7 days	28 days	3 months	4 years	14.7 years
Hydromonosilicate-$P_1(t)$	65	27	23	22	21.5	21
Hydrodisilicate-$P_2(t)$	17	30	34	34	33.2	33
Hydrotrisilicate-$P_3(t)$	2	7	7.5	7.2	7	7

The comparison with the experiment shows a good concordance up to 3 months of hydration time (fig. 1). For larger periods of time the concordance is weaker; the fact may be due to the structuring phenomena which take away variable quantities of n-hydrosilicate from the reaction medium.

---

[3] G. Lentz, "Symposium on structure of portland cement paste and concrete", Academic Press, Washington, 1966.

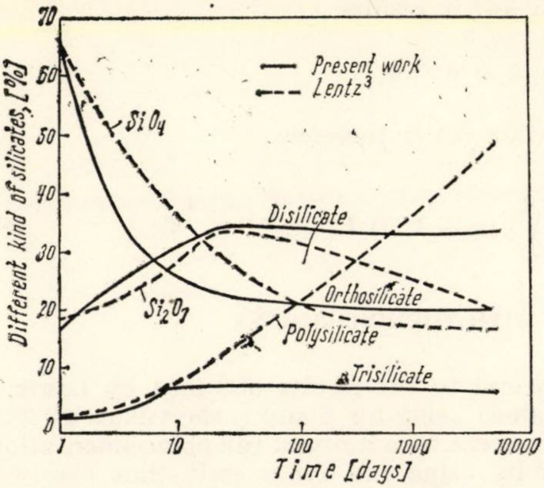

Fig. 1. — The concentration of polysilicates in tricalcium silicate pastes.

The present stochastic model, which can be applied to the hardening of silicate binders, makes evident two statistical parameters β and γ. Their systematic study for different binder classes may be useful. These parameters characterize, from the polycondensation process point of view, the nature of the binder and the nature of the substances present in the binder mass (ions, etc.).

Revue Roumaine de Chimie, **18**, *2*, 247–255 (1973)

NEW URANYL COMPOUNDS WITH PYRIMIDINE DERIVATIVES

FLORICA POPEA, CRISTINETA MĂRCULESCU and CONSTANŢA PÎRLOG

Centre of Physical Chemistry, Str. Dumbrava Roşie 23, Bucharest, Romania

Received July 4, 1972

In this paper, 3 new uranyl compounds of the general formula $ML_2 \cdot nH_2O$ are presented ($M = UO_2$; $L =$ barbituric acid, thiobarbituric or 5-ethyl-barbituric acid). They are characterized by thermal behaviour, X-ray diffraction studies, u.v. and visible reflectance spectra, as well as i.r. vibration spectra.

In a previous paper, a spectrophotometric study on the behaviour of the uranyl ion, in the presence of barbituric (AB) and thiobarbituric (ATB) acid, in aqueous, ethanol, methanol and acetone solution was reported.[1]

In this work, some new, solid compounds obtained in the reaction of the uranyl ion with the same reagents, are presented. Having in view the reactivity of the position 5 and the tautomery involved for the hydrogen atoms in the positions 1,3 of the pyrimidine ring,[2,3] researches concerning the reaction of the uranyl ion with some 5-substituted derivatives of the barbituric acid, were also performed. Both 5-bis-substituted derivatives (5,5-phenyl-ethyl-barbituric and 5,5-diethyl-barbituric acid) did not allow to obtain a compound. With alloxan, although it includes a high reactive CO in the position 5, presumably undergoing an oxido-reduction reaction in aqueous solution, no unitary compound was obtained.[4]

Considering that the presence of a free hydrogen atom at the C_5 prompts the reactivity of the ligand towards the metallic ion, we managed syntheses with monosubstituted derivatives of the barbituric acid, namely with 5-aminobarbituric, 5-nitrosobarbituric (violuric), 5-nitrobarbituric (dilituric) and 5-ethylbarbituric acid. In the reactions of the 5-amino-, 5-nitroso- or 5-nitro-barbituric acids with uranyl ion, no unitary solid product was obtained, although, both with violuric [5,6] and dilituric acids[7-10] unitary, solid compounds with numerous metallic ions have been quoted in the literature, some of these reactions providing gravimetric methods used in the determination of these ions. Microscopic studies are also reported on the crystals obtained in the reaction between the uranyl ion and the violuric acid. [11] Only 5-ethyl-barbituric acid (5-EB) leads to the formation of an uranyl compound of the same type as those of the barbituric and thiobarbituric acids ones, suggesting the presence of the ethyl radical in C_5 to promote the labilization of the neighbouring hydrogen atoms.

---

[1] Fl. Popea and C. Pîrlog, *Rev. Roumaine Chim.*, **13**, 473 (1968).

[2] Sundaresa Soundararajan, *Trans. Faraday Soc.*, **54**, 1147 (1958).

[3] D. J. Brown, "The Pyrimidines", Interscience publishers, New York, 1962, p. 1—30.

[4] C. D. Neniţescu, "Chimie Organică", vol. 2, Editura Didactică şi pedagogică, Bucureşti, 1963, p. 729.

These would be consistent with the failure to obtain solid, unitary compounds in the reaction of the uranyl ion with the barbituric acids nonsubstituted in C_5, but substituted in the 1 (1-phenylbarbituric acid) and 1,3 positions (1,3-biphenylbarbituric acid).

The compounds obtained are of the $ML_2.nH_2O$ type ($M = UO_2$, L = AB, ATB, or 5-EB) and were synthesized using the direct reaction, in aqueous solution, of stoichiometric amounts of the uranyl nitrate hexahydrate towards the respective acid, respecting severely the conditions indicated.

EXPERIMENTAL

STARTING MATERIALS

The following reagents were graded and used without additional purification:

$UO_2(NO_3)_2 \cdot 6H_2O$ ANALAR; barbituric acid. $2H_2O$ Carlo Erba; Alloxan—Chinoin; 5-nitrobarbituric (dilituric) acid, 5,5-diethyl-barbituric acid and 5,5-phenyl-ethyl-barbituric acid — E. Merck; 5-aminobarbituric and 5-nitrosobarbituric acid — Fluka. The following ones were synthesized and purified in the laboratory by methods reported in the literature: thiobarbituric acid, [12] 5-ethyl-barbituric acid, [13] 1-phenyl-barbituric acid and 1,3-biphenyl-barbituric acid. [14]

SYNTHESIS OF THE COMPOUNDS

$UO_2[AB]_2 \cdot 4 \cdot H_2O$ (I) An aqueous suspension of 0.002 M AB·$2H_2O$ was treated with dilute NaOH to give the pH=5.4 (the final volume not exceeding 30 ml) and heated to 75—80°. 0.001 M solid uranyl nitrate was added, stirring vigorously and keeping the same tem-

---

[5] S. Vallados–Dubois and J. Lemerle, *Compt. rend.*, **260**, 145 (1965). Chem. Abstr., **62**, 11208^a (1965).

[6] M. Ziegler and D. Glemser, *Mikrochim. Acta*, **1956**, 1515.

[7] F. Mihai and B. Roch, *Bul. St. şi tehnic al Inst. Politeh. Timişoara*, **3**, 245 (1958).

[8] F. Mihai and B. Roch, *Studii şi Cercetări Chim. Acad. R.P.R.*, **7**, 303 (1960).

[9] F. Mihai and B. Roch, *Bul. Şt. şi tehnic al Inst. Politeh. Timişoara*, **5**, 369 (1960).

[10] F. Mihai, *Rev. Roumaine Chim.*, **11**, 657 (1966); *Chem. Abstr.*, **65**, 11738^d (1966),

[11] J. W. van Ligten and H. van Velthuyzen, *Mikrochim. Ichnoanalyt. Acta*, 759 (1964); *Chem. Abstr.*, **61**, 12607^g (1964).

[12] D. Michael, *J. Prakt. Chem.*, **49**, 38 (1894).

[13] E. Fischer, A. Dilthy, *Liebigs Ann. Chem.*, **335**, 357 (1904).

[14] A. Killen Macbeth, Th. Nunan and D. Traill, *J. Chem. Soc.*, **1926**, 1232.

perature for about 5′; the solution turned turbid. On cooling at room temperature, a bright yellow precipitate separated, which was filtered after about 30′, washed with 10 ml 50% ethanol (aqueous solution) and air dried.

$UO_2[ATB]_2 \cdot 5H_2O$ (II) 35 ml warm water (70–75°) was poured over 0.002 M ATB and a fairly clear solution was obtained; then, 0.001 M solid uranyl nitrate was added warming with agitation at the same temperature for other 5′. The solution turned brown, became gradually yellow and on cooling at room temperature the separated orange yellow precipitate was filtered after about 30′, washed and dried like the compound (I).

$UO_2[5\text{-}EB]_2 \cdot H_2O$ (III). A mixture of 0.002 M 5-EB and 10 ml water ($pH = 2.8-3$) was treated with diluted NaOH to reach $pH = 3.4$ and warmed at 60–65°. Then 0.001 M uranyl nitrate was added, stirred vigorously and continually heated at the same temperature for other 5′. The solution, red-coloured on the addition of the uranyl nitrate, changed gradually to yellow, then following the separation of the orange, crystalline precipitate. After cooling at the room temperature and settling (for about 30′) the product was filtered, washed with cold water (+4°) and air dried.

The composition of the 3 new compounds was established on the basis of the chemical analysis, (the analytical data and their colour are summarized in table 1) namely: the metal was determined as oxide (U_3O_8) by ignition, while nitrogen, carbon and hydrogen by microcombustion.

Table 1

Analytical data

Compound	Colour	U%		C%		H%		N%	
		calcd.	*found*	*calcd.*	*found*	*calcd.*	*found*	*calcd.*	*found*
(I)	canary-yellow	39.92	40.23	16.48	16.61	2.54	2.48	9.39	9.47
(II)	yellow-orange	36.94	36.96	14.91	14.92	2.50	2.48	8.66	8.50
(III)	orange	39.18	39.32	24.42	24.20	2.70	3.08	9.29	9.51

The shining microcrystals of (I), (II) and (III) are stable at room temperature, but decompose on heating. They are practically insoluble in common solvents (water, ethanol, methanol, acetone, ether, CCl_4, TBF, THF, DMSO, DMF, ethyl acetate, benzene) and only sparingly soluble in warm water. The compounds were characterized by thermal studies, by X-ray diffraction studies, electronic and i.r. spectra.

APPARATUS

The thermal studies were performed by means of a MOM E. Paulik, J. Paulik-L. Erdey Derivatograph and by using the Boetius heat table. The X-ray diffraction patterns were recorded on the URS. 50. IM equipment; the intensity data were collected on a diffractometer with Geiger–Müller counter. The reflectance spectra were drawn on a VSU-1 C. Zeiss-Jena spectrophotometer and the i.r. spectra were recorded on a UR-20 C. Zeiss-Jena spectrophotometer.

RESULTS AND DISCUSSION

Thermal behaviour. In order to determine the number and the bonding of the water molecules in the new compounds, the thermal curves were recorded in the 30°—300° temperature range with a 5°/min. rate, in air atmosphere, using Al_2O_3 as standard. An amount of 0.4—0.5 g was taken for each sample.

The TG and DTG curves (fig. 1) indicate for the compound (I) a 11.31 % loss of weight between 150° and 230° corresponding to $4.H_2O$ for a molecule of anhydrous compound, followed by a weak slope. The DTA curve reveals at 155° the starting of a transformation with endothermic effect, its maximum value, at 210°, corresponding to the removal of the crystallization water.

The TG and DTG curves in fig. 2 evidence a smooth decrease of the weight, beginning with 60°. Between 90° and 130°, the water is expelled with an increased rate, the 11.22 % loss of weight corresponding to 4 water molecules. The following 2.75 % loss of weight, between 130° and 210° is developed with a smoother slope and corresponds to the removal of another water molecule. Starting with this temperature, the horizontal level appears, which characterizes an anhydrous compound. The DTA curve reveals an endothermic, striking effect, between 100° and 130°, with a maximum at 100°, and another one much weaker between 190° and 230° with a maximum at 208°. As can be seen, the thermal curves allow to conclude that one of the 5 water molecules is differently bound in the compound.

For (III) like for (II), the thermogravimetric analysis indicates a slight loss of weight (4 %) between 100 and 280°. The endothermic effect corresponding to the removal of the water is very weak with a maximum only at 185°.

As can be seen in table 2, the values obtained for the crystallization water, by means of the thermogravimetric analysis, agree with those calculated on the basis of the chemical data.

Table 2

% crystallization water content

Compound	% water content	
	Calculated on analytical data	Found by thermogravimetric analysis
(I)	12.08	11.31
(II)	13.97	13.97
(III)	3.01	4.00

In addition, the thermal behaviour of the compounds was also followed with a Boetius heating plate.

Starting with 140°, compound (I) presents some modifications, which reach a maximum effect at 200°—220°. At 265°—300° the product undergoes decomposition.

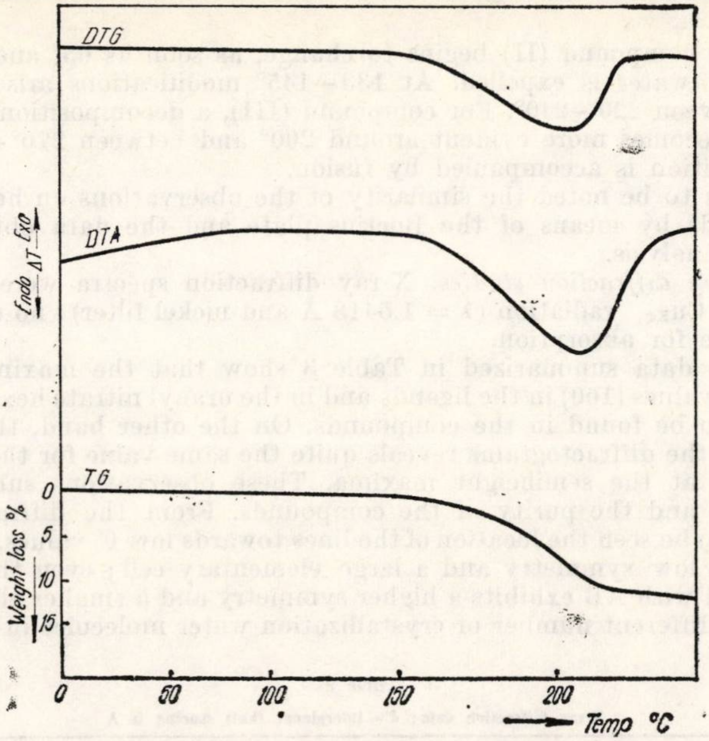

Fig. 1. — Thermal curves for $UO_2\,[AB]_2 \cdot 4H_2O$ (I).

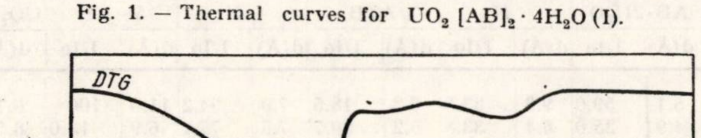

Fig. 2. — Thermal curves for $UO_2\,[ATB]_2 \cdot H_2O$ (II).

The compound (II) begins to change, as soon as 65° and between 104—115° water is expelled. At 133—145° modifications arise, emphasized between 220—240°. For compound (III), a decomposition observed at 140° becomes more evident around 200° and between 270°—300° the decomposition is accompanied by fusion.

It is to be noted the similarity of the observations on heating the compounds by means of the Boetius plate and the data obtained by thermal analysis.

X-ray diffraction studies. X-ray diffraction spectra were recorded using the $Cu_{K\alpha_1}$ radiation ($\lambda = 1.5418$ Å and nickel filter); no correction was made for absorption.

The data summarized in Table 3 show that the maxima of the intensity values (100) in the ligands and in the uranyl nitrate hexahydrate, are not to be found in the compounds. On the other hand, the examination of the diffractograms reveals quite the same value for the breadth measured at the semiheight maxima. These observations substantiate the unity and the purity of the compounds. From the diffractograms it is also to be seen the location of the lines towards low θ° values, accounting for a low symmetry and a large elementary cell; even though the compound with AB exhibits a higher symmetry and a smaller elementary cell. The different number of crystallization water molecules in the com-

Table 3

X-ray diffraction data; d = interplanar (hkl) spacing in Å

I		$AB \cdot 2H_2O$		II		ATB		III		5—EB		$UO_2(NO_3)_2 6H_2O$	
d (Å)	I/Io	d(Å)	I/Io	d(Å)	I/Io	d(Å)	I/Io	d(Å)	I/Io	d(Å)	I/Io	d(Å)	I/Io
7.2	38.3	5.1	59.0	9.3	33.8	6.3	18.5	7.9	94.2	11.0	100	6.7	60.0
6.2	75.3	4.9	25.0	6.4	33.8	5.2	90.7	7.5	77.1	6.9	13.0	6.5	95.0
5.9	26.0	4.4	21.0	6.2	61.2	4.8	11.1	6.5	20.0	5.5	90.0	5.8	85.0
5.1	100	4.3	28.4	5.3	100	4.6	20.3	5,5	100	5.0	75.0	5.7	87.5
4.4	53.4	4.1	11.4	4.6	27.4	4.1	29.6	5.3	85.7	4.8	13.0	4.3	80.0
4.2	53.4	3.9	31.8	4.5	35.4	3.9	53.7	5.2	20.(1)	4.4	24.0	4.3	100
3.9	47.9	3.6	11.3	3.7	70.9	3.6	64.8	4.9	25.7	4.3	13.0	3.8	32.5
3.8	23.2	3.3	36.3	3.7	70.9	3.3	100	4.5	34.2	3.9	14.0	3.7	42.5
3.7	64.3	3.3	23.8	3.4	17.7	3.2	77.7	4.2	45.7	3.7	81.0	3.6	35.0
3.6	46.5	3.1	100	3.4	17.7	3.2	77.7	4.1	42.8	3.5	13.0	3.3	62.5
3.4	42.4	3.0	50.0	3.2	56.4	3.1	55.5	4.0	82.8	3.4	23.0	3.3	85.0
3.1	32.1	2.9	23.8	3.1	32.2	3.0	20.3	3.9	40.0	3.2	13.0	3.2	15.0
3.0	20.5	2.8	28.4	3.0	32.2	2.8	29.6	3.8	22.8	3.1	20.0	2.9	17.5
2.9	36.9	2.7	42.0	2.9	48.3	2.7	20.4	3.6	31.4	3.0	88.0	2.8	22.5
2.8	21.2			2.8	37.0	2.6	16.7	3.5	25.7	2.8	22.0	2.7	25.0
2.8	21.9			2.6	24.1	2.5	18.5	3.1	14.3	2.6	32.0	2.7	12.5
2.7	23.2			2.4	38.7	2.4	16.7	3.1	14.3	2.5	14.0	2.6	35.0
2.6	13.7			2.4	22.5	2.3	18.5	3.0	28.5	2.4	14.0	2.5	37.5
2.5	26.0			2.4	17.7	2.3	16.7	2.9	22.8	2.2	14.0	2.5	50.0
2.4	34.2			2.3	14.5	2.2	20.3	2.8	22.8	2.1	13.0	2.4	35.0
2.4	23.2			2.2	12.9	1.9	20.3	2.8	28.5	2.0	12.0	2.4	22.5
2.3	24.6			2.2	35.4	1.8	22.2	2.7	28.5			2.3	37.5
2.2	17.8			2.2	29.0	1.8	20.3	2.6	20.0			2.2	12.5
2.2	26.0			2.0	29.0	1.7	11.1	2.6	11.4			2.2	25.0
2.2	12.3			1.9	11.3			2.3	14.3			2.2	25.0
2.2	12.3			1.9	11.3			2.2	17.1			2.1	30.0
2.1	13.7			1.9	12.9			2.1	22.8			2.1	20.0
2.1	16.4			1.8	11.3			1.9	14.3			2.0	12.5

pounds evidence the fact that they do not belong to the same structure type, as a consequence of the lack of isomorphic relations.

Electronic spectra. The reflectance spectra were drawn at room temperature within 260 nm (38,461 cm^{-1}) — 1200 nm (8,333 cm^{-1}) range, using MgO as standard.

Figures 3, 4, and 5 show that the absorption bands proper to the uranyl ion appearing at 410 nm (24,390 cm^{-1}) and 315 nm (31,740 cm^{-1}) are assigned to the transition $^1\Sigma_g^+ \rightarrow {}^3\pi_u^-$, respectively $^1\Sigma_g^+ \rightarrow {}^1\Sigma_u^-$ or $^1\Delta_{2u}$.[15]

As far as the absorption maxima of the ligands are concerned, they appear in the u.v. range at about 300 nm (30,303 cm^{-1}) and can be ascribed

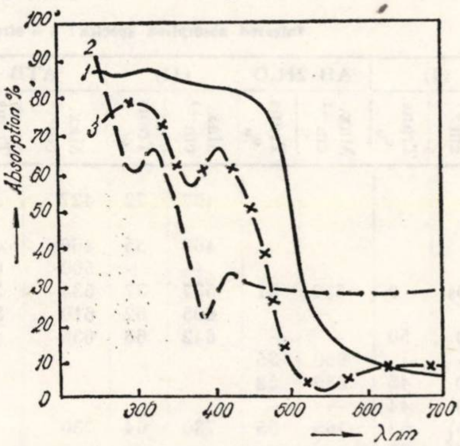

Fig. 3. — Reflectance spectra for:
1 – $UO_2[AB]_24H_2O$; 2 – $AB.2H_2O$;
3 – $UO_2(NO_3)_26H_2O$

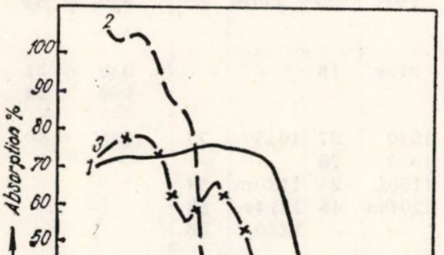

Fig. 4. — Reflectance spectra for:
1 – $UO_2[ATB]_25H_2O$; 2 – ATB;
3 – $UO_2(NO_3)_2.6H_2O$

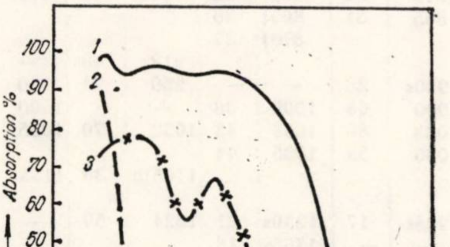

Fig. 5. — Reflectance spectra for:
1 – $UO_2[5-EB]_2.H_2$; 2 – 5 – EB;
3 – $UO_2(NO_3)_2.6H_2O$

---

[15] S. P. Mc. Glynn and J. K. Smith, *J. Mol. Spectroscopy*, **6**, 188 (1961).

to a transition n → π* from the nonbonding orbital of the nitrogen to the π antibonding orbitals of the pyrimidine ring. [16] The other absorption maxima in the region 430 nm (23,255 cm^{-1}) — 450 nm (22,200 cm^{-1}) could be ascribed to the presence of the substituents in the pyrimidine ring.

As can be seen, the shape of the absorption curves of the compounds present the maxima proper to the ligands, as weak inflexions. *Infrared spectra.* The i.r. spectra were recorded within the 400—1800 cm^{-1} range, using solid substances pelleted with KBr and they are given in table 4.

Table 4

Infrared absorption spectra; s = strong, m = medium sh = shoulder

(I)		AB·$2H_2O$		(II)		ATB		(III)		5—EB		$UO_2(NO_3)_2 6H_2O$	
Max. cm^{-1}	Trans. %	Max. cm^{-1}	Trans. %	Max. cm^{-1}	Trans %	Max. cm^{-1}	Trans. %	Max. cm^{-1}	Trans. %	Max. cm^{-1}	Trans. %	Max. cm^{-1}	Trans. %
				427	72	427	53	430	60	420	60		
										440	62		
				466	55	466	41						
				—	—	500	69	525	41	515	62		
550s	9	550s	21	537	37	534	39	570s	10	—	—	560	56
				605	52	610	35						
640	50	—	—	642	66	635	40	637	55	640	78		
—	—	660	35					660	55				
690	45	680	52					—	—	680	80		
710	44	—	—					700	54			700	57
745	53	765	55	730	64	730	42	—	—	745	66	750	49
775	30												
810	34	800	42	810	48	810	30	788s	30	790 m	62	810	63
865	51	860	36										
		870	37										
				912	40	—	—	912s	18	—	—	930	34
950s	28	—	—	950	74	940	50					960	29
1000	68	1000	36	—	—	1000	42						
1033	66	1058	48	1032	70	1035	39	1040	67	1045	77	1035	50
1085	59	1085	44					1080	70	—	—		
				1165m	36	1155s	6	1150s	24	1180m	64		
								1200m	48	1214s	53		
1225s	17	1230s	21	1224	50	—	—	—	—	1240	56		
—	—	1265s	18										
1290s	3	—	—	—	—	1280	25					1290	18
				1300	24	1300	25						
—	—	1330s	14					1330s	4	1340s	54		
1368s	3	—	—	1365m	37	1350s	14	1350	4	—	—		
—	—	1400s	18	1390	42	1400sh	24	1380s	4	1370s	36	1390	10
				1450m	45	1440s	26	—	—	1420	56		
								—	—	1450s	46		
1480s	16	1490	31					1485s	13	—	—	1540	13
—	—	1560s	16	1540—									
				60s	35	1540s	13	1580	0.5	—	—		
1600s	0.5	—	—	1600—									
				40s	20	1600sh	24	1640s	0.5	—	—	1620	53
1650sh	9	1670s	32	—	—	1640m	29	1680s	6	—	—		
1712s	4	1720s	8	—	—	1690	36	1720s	4	1720s	24		

---

[16] J. P. Phillips, "Spectra-Structure Correlation" Academic Press, New York, London, 1964, p. 114—120; 152—155.

The uranyl ion, with an almost linear arrangement of the chemical bonds $O{=}U{=}O$, presents an absorption maximum in the 930–960 cm^{-1} range,[17] which is found again in the uranyl nitrate.

The literature does not report sufficiently accurate data concerning the assignment of the absorption bands exhibited by the ligands, AB, ATB and 5-EB, the present study being limited only to the bands proper to the pyrimidine ring.[18,19]

The absorption bands assigned to the pyrimidine ring, 1402 cm^{-1}, 1467 cm^{-1} and 1570 cm^{-1} due to the in-plane vibrations and the absorption bands within the 724–680 cm^{-1} range ascribed to the out-of-plane vibrations, are found again in the compounds with the uranyl ion, with more or less obvious changes in their frequencies and intensity.

As can be seen, in the compound (I), the absorption maxima at 690 cm^{-1}, 1480 cm^{-1} and 1600 cm^{-1}, in (II) the absorption maxima at 730 cm^{-1}, 1390 cm^{-1}, 1450 cm^{-1} and 1600–1640 cm^{-1} and in (III) the absorption maxima, at 730 cm^{-1}, 1380 cm^{-1}, 1485 cm^{-1}, 1640 cm^{-1} and 1680 cm^{-1}, characterized the pyrimidine ring.

The absorption maxima of the uranyl ion (at 930 and 960 cm^{-1}) reappear in the mentioned compounds, namely in (I) at 950 cm^{-1}, in (II) at 912 and 950 cm^{-1} and in (III) at 912 cm^{-1}.

It must be mentioned that in (II), the appearing band, at 1540 cm^{-1} is ascribed[20] to the $-\mathrm{S}-\mathrm{C}\langle$ group also present in the ATB.

CONCLUSIONS

As results from the chemical and physical investigations performed in the present note, the three compounds herein studied contain ligands reacting more probable in the enolic form, the pyrimidine structure being consistent with the spectral behaviour of the compounds in i.r., as well as in u.v., and visible range.

Acknowledgement. The authors express their gratitude to Dr. D. Todor for the thermal measurements, to R. Giuşcă, for the registration of the diffractograms and to M. Elian for the registration of the i.r. spectra. The authors are indebted to Dr. C. Lepădatu, D. Cismaru and to D. Ciomîrtan for their assistance in the interpretation of the data.

---

[17] K. Nakamoto, "Infrared Spectra of Inorganic and Coordination Compounds", J. Wiley & Sons, Inc., New York, 1962, p. 77, 92.

[18] T. S. Hermann and I. M. Black, *J. Appl. Spectroscopy*, **20**, 413 (1966).

[19] R. C. Lord, A. L. Marston and F. A. Milles, *Spectrochim. Acta*, **9**, 113 (1957).

[20] Y. Sat, *Bull Chem. Research Inst. of non-aqueous solutions Tohoku Univ.*, **6**, 9 (1956).

Revue Roumaine de Chimie, 18, 2, 257–261 (1973)

ISOTOPIC EXCHANGE OF ACTIVE METHYL HYDROGENS. VII.[1]

KINETIC STUDY OF 2,4,6-TRIMETHYLPYRYLIUM SALTS IN DEUTERIUM OXIDE

EUGENIA GÂRD*, F. CHIRALEU**, ILEANA I. STĂNOIU* and A. T. BALABAN*

* Institute of Atomic Physics, P.O.B. 35, Bucharest, Romania
** Centre of Organic Chemistry, Bucharest, Romania

Received September 30, 1972

The NMR spectra at various temperatures and pH values, of buffered deuterium oxide solutions of 2,4,6-trimethylpyrylium chloride or trifluoromethanesulphonate show a rapid decrease of the 4-methyl proton peak and a slower decrease of the peak due to the 2- and 6-methyl protons. Rate constants, activation energies and the pH dependence indicate a mechanism of the exchange *via* methylenepyrans (anhydrobases). Non-buffered solutions yield kinetic data indicating a pH lower than 1.

INTRODUCTION

2,4,6-Trimethylpyrylium salts (I) exchange fairly rapidly their nine methyl hydrogens in deuterium oxide, and very slowly their two β-standing hydrogens. Infrared spectra[2] or isotopic analyses[3] do not distinguish α- from γ-methyl groups; however, nuclear magnetic resonance spectra[4] give rise to distinct peaks for the α-methyl groups (τ 7.10 in SO_2) and the γ-methyl group (τ 7.26 in SO_2); previous observations indicated that the γ-methyl hydrogens exchange more rapidly than α-methyl hydrogens, both in 2,4,6-trimethylpyrylium perchlorate which contains the two kinds of methyl groups in the same molecule,[5] and in 2,4-diphenyl-6-methylpyrylium as compared with 2,6-diphenyl-4-methylpyrylium salts.[6]

---

[1] Part VI, E. GÂRD, I. I. STĂNOIU, A. T. BALABAN and F. CHIRALEU, *Rev. Roumaine Chim.*, **14**, 247 (1969).

[2] A. T. BALABAN, G. D. MATEESCU and M. ELIAN, *Tetrahedron*, **18**, 1083 (1962).

[3] A. T. BALABAN, E. GÂRD and C. N. RENȚIA, *Abh. Dtsch Akad. Wiss. Berlin, Kl. Chem., Geol., Biol.*, 659 (1964).

[4] A. T. BALABAN, G. R. BEDFORD and A. R. KATRITZKY, *J. Chem. Soc.*, **1964**, 1646.

[5] E. GÂRD, A. VASILESCU, G. D. MATEESCU and A. T. BALABAN, *J. Labelled Comp.*, **3**, 196 (1967).

[6] E. GÂRD, I. BALLY, A. VASILESCU, A. ARSENE and A. T. BALABAN, *ibid.*, **1**, 182 (1965).

A kinetic study of the deuteration of I in non-buffered and buffered medium is now described.

EXPERIMENTAL PART

2,4,6-Trimethylpyrylium chloride.[7] 2,4,6,-Trimethylpyrylium perchlorate[8] was introduced into a cold stirred mixture of 5% aqueous sodium hydrogen carbonate and benzene. The benzene layer was rapidly dried over sodium sulphate, then dry hydrogen chloride was bubbled into this benzene solution of 2,4,6-trimethylpyrylium pseudobase (4-methyl-3-hepten-2,6-dione) in the cold. A dark oily lower layer of 2,4,6-trimethylpyrylium chloride separated. The benzene layer was discarded and the very hygroscopic chloride was freed from benzene by keeping in an evacuated desiccator over phosphorus pentoxide and potassium hydroxide until a thick crystalline suspension resulted (a white pure product may be obtained by spreading this suspension on a porous plate in a dry box). If the evacuation is continued until all benzene leaves, the product is yellowish. The product can be stored for a few days in an evacuated desiccator. On longer storing it darkens. Alternatively, the pseudobase can be extracted by benzene from a mixture of aqueous trimethylpyrylium chloroferrate and sodium acetate.

2,4,6-Trimethylpyrylium trifluoromethanesulphonate (*triflate*) was prepared from acetic anhydride, *t*-butanol and trifluoromethanesulphonic acid.[9]

The properties of 2,4,6-trimethylpyrylium salts presented in Table 1 make it clear that the perchlorate cannot be employed in kinetic studies owing to its low solubility and that the triflate is the most advantageous.

Table 1

Properties of 2,4,6-trimethylpyrylium salts

Property	Perchlorate	Chloride	Triflate
Non-explosive	No	Yes	Yes
Water-soluble	Slightly	Yes	Yes
Non-hygroscopic	Yes	No	Yes
Conservable	Yes	No	Yes

NMR Spectra. The isotopic exchange was performed in NMR vials which were filled with a freshly prepared solution of 2,4,6-trimethylpyrylium salt in deuterium oxide or in a buffered ($NaOD + D_3PO_4$) deuterium oxide solution of different pH values (35—100 mg salt in 0.5 ml D_2O, i.e. 30—100 moles D_2O per mole I). The spectra were determined with a Varian A 60-A spectrometer at various intervals and at different temperatures, recording the aromatic and methyl proton peaks as well as the respective integral curves. The aromatic proton peak serves as an internal standard since its area is practically constant (the relative exchange rate for the aromatic protons being much smaller than the rates for methyl protons).[5] Heights *h* of integral curves for the methyl peaks were measured; where necessary, slight corrections were made by comparison with the aromatic proton peak which was assumed to be constant; ratios $h_\gamma/h_{0\gamma}$ and $h_\alpha/h_{0\alpha}$ were plotted semi-logarithmically against the time. By the method of least squares, straight lines were determined which fit the experimental points, yielding k_γ and k_α values (table 2). Since the initial $h_{0\alpha}/h_{0\gamma}$ ratio must be 2, and starts to increase because h_γ decreases more rapidly than h_α, this gives an internal check for the real zero time of the experiment, which must agree within fractions of a minute with the measured zero time.

---

[7] A. T. Balaban, *Compt. rend.*, **256**, 4041 (1963).

[8] A. T. Balaban and C. D. Nenitzescu, *Org. Synth.*, **44**, 98 (1964); *Org. Synth. Coll. Vol.* 5, in press.

[9] A. T. Balaban and A. J. Boulton, *Org. Synth. Coll. Vol.* 5, in press.

Table 2

Kinetic data for isotopic exchange with D_2O of methyl protons in 2,4,6-trimethylpyrylium salts

Anion	pH	Temp. °C	α-Methyl			γ-Methyl			$\frac{k_\gamma}{k_\alpha}$
			k_α sec^{-1}	$T_{1/2,\alpha}$ h	$k_{\alpha,\,calc}$ sec^{-1}	k_γ sec^{-1}	$T_{1/2,\gamma}$ h	$k_{\gamma,\,calc}$ sec^{-1}	
Cl	1.07	38	—	—	—	$8.30 \cdot 10^{-5}$	2.26	$8.47 \cdot 10^{-5}$	—
		50	—	—	—	$4.30 \cdot 10^{-4}$	0.43	$4.48 \cdot 10^{-4}$	—
		62	—	—	—	$9.80 \cdot 10^{-4}$	0.19	$1.01 \cdot 10^{-3}$	—
Cl	2.07	38	—	—	—	$9.69 \cdot 10^{-5}$	1.759	$1.10 \cdot 10^{-4}$	—
		50	$3.69 \cdot 10^{-5}$	4.75	$4.05 \cdot 10^{-5}$	$6.48 \cdot 10^{-4}$	0.240	$8.05 \cdot 10^{-4}$	17.6
		62	$4.86 \cdot 10^{-5}$	3.80	$5.08 \cdot 10^{-5}$	$1.25 \cdot 10^{-3}$	0.162	$1.19 \cdot 10^{-3}$	25.6
		70	$1.16 \cdot 10^{-4}$	1.61	$1.20 \cdot 10^{-4}$	$1.60 \cdot 10^{-3}$	0.125	$1.54 \cdot 10^{-3}$	13.8
F_3CSO_3	2.50	38	$2.27 \cdot 10^{-5}$	8.25	$2.33 \cdot 10^{-5}$	$3.55 \cdot 10^{-4}$	0.54	$3.58 \cdot 10^{-4}$	15.6
		50	$1.13 \cdot 10^{-4}$	1.58	$1.27 \cdot 10^{-4}$	$1.36 \cdot 10^{-3}$	0.127	$1.51 \cdot 10^{-3}$	12.1
		62	$2.90 \cdot 10^{-4}$	0.65	$2.96 \cdot 10^{-4}$	$2.25 \cdot 10^{-3}$	0.058	$3.33 \cdot 10^{-3}$	7.7
Cl	3.70	38	$3.44 \cdot 10^{-5}$	5.50	$3.33 \cdot 10^{-5}$	$6.58 \cdot 10^{-4}$	0.295	$6.55 \cdot 10^{-4}$	19.1
		50	$1.30 \cdot 10^{-4}$	1.50	$1.28 \cdot 10^{-4}$	$1.27 \cdot 10^{-3}$	0.105	$1.84 \cdot 10^{-3}$	13.1
		62	$2.71 \cdot 10^{-4}$	0.55	$3.50 \cdot 10^{-4}$	$2.93 \cdot 10^{-3}$	0.078	$2.47 \cdot 10^{-3}$	10.8
		70	$5.13 \cdot 10^{-4}$	0.32	$6.00 \cdot 10^{-4}$	—	—	—	—
Cl	[a]	38	$2.16 \cdot 10^{-6}$	86	$2.25 \cdot 10^{-6}$	$5.16 \cdot 10^{-5}$	3.1	$6.22 \cdot 10^{-5}$	23.8
		55	$5.22 \cdot 10^{-6}$	29	$6.66 \cdot 10^{-6}$	$3.19 \cdot 10^{-4}$	0.56	$3.45 \cdot 10^{-4}$	61.1
		62	$1.59 \cdot 10^{-5}$	10.8	$1.79 \cdot 10^{-5}$	$4.15 \cdot 10^{-4}$	0.44	$4.40 \cdot 10^{-4}$	26.1
		70	$6.38 \cdot 10^{-5}$	3.7	$5.22 \cdot 10^{-5}$	$7.92 \cdot 10^{-4}$	0.20	$9.66 \cdot 10^{-4}$	12.3
		87	$1.40 \cdot 10^{-4}$	1.0	$1.97 \cdot 10^{-4}$	—	—	—	—
F_3CSO_3	[a]	62	$1.87 \cdot 10^{-5}$	9.8	$1.97 \cdot 10^{-5}$	$3.67 \cdot 10^{-4}$	0.52	$3.39 \cdot 10^{-4}$	19.6

[a] No buffer added.

The experimental points h/h_0 also yield in the semilogarithmic plot *versus* time half-lives $T_{1/2,\gamma}$ and $T_{1/2,\alpha}$ for the times when $\log(h/h_0) = 1.7$. These half-lives determined by visual interpolation may be used to compute $k_{\alpha,\mathrm{calc}}$ and $k_{\gamma,\mathrm{calc}}$ which are less accurate than those determined by the method of least squares but are comparable with them (table 2).

Though the pH of the solution does not change during the exchange and the isotopic composition of the solvent remains practically constant owing to the large excess of D_2O, some plots show slight departure from linearity, especially in the initial and final regions;

the former is probably due to the processes of dissolution and reaching the prescribed temperature which are not instantaneous; when the exchange has resulted in extensive deuteration, the integration of small NMR peaks becomes affected by larger errors because of the unfavourable signal-to-noise ratio.

DISCUSSION OF THE RESULTS

Experimental results are presented in table 2 which gives k_α and k_γ in function of temperature and pH value of the buffer solution for 2,4,6-trimethylpyrylium chloride and trifluoromethanesulphonate. The more reliable value, determined through the method of least squares, is listed first; k_{calc} is determined from $T_{1/2}$ by a less precise method.

From the data it is apparent that in the range of temperatures 40—100°, the ratio of deuterium exchange rates for the γ- and α-methyl group in I varies between ca. 8 and 20, in agreement with the average ratio of about 10 reported earlier, [5] and shows the tendency to decrease with increasing temperature. Therefore, to achieve a selective deuteration of the γ-methyl group (which can be useful in synthetic work for obtaining various labelled compounds from pyrylium salts [10,11]) it is advisable to have lower exchange temperatures, and therefore slower reactions.

A plot of log*k* *versus* pH reveals that at a given temperature the rate of exchange increases with the pH of the solution.

Experiments in non-buffered medium (table 2) show that the rate of exchange of the non-buffered solutions of trifluoromethane-sulphonate or chloride is very low, and corresponds in fact to an extrapolated pH of about 0.5.

The variation of the rate with temperature is reflected in the activation enthalpies (table 3) determined from the data in table 2 by a least-squares linearization. Very slow (α-methyl exchange at pH 2.07) or very fast reactions (γ-methyl exchange at pH 3.70) are affected by larger errors and have therefore been omitted from table 3. The trend evident from table 3 is that the higher are the pH values the lower is the activation barrier and that α-methyl groups have an activation energy higher than γ-methyl with 2.5—4 k cal/mole.

The above kinetic data are compatible with a mechanism involving the transfer of a proton from a methyl group of I to a base, followed by a rapid reaction of the resulting methylenepyran with a deuteron originating from the solvent. A molecular orbital calculation of the α- *versus* γ-methylenepyran [12,13] reveals the higher delocalization in the latter, more symmetrical pyran, which is formed more rapidly than the former, despite the lower π-electron density of α- than of γ-positions, evidenced

---

[10] A. T. Balaban, E. Gârd, A. Vasilescu and A. Barabas, *J. Labelled Comp.*, **1**, 266 (1965).

[11] A. Barabas, E. Gârd, A. Vasilescu and A. T. Balaban, *ibid.*, **2**, 359 (1966).

[12] A. T. Balaban and C. C. Renția, *Rev. Roumaine Chim.*, **11**, 1193 (1966), note added in proof.

[13] G. V. Boyd, *ibid.*, **12**, 1133 (1967).

both by NMR experiments[4] and by theoretical calculations.[14] However, with less electronegative heteroatoms the situation is reversed, as pointed out by Tupitsyn and Zatsepina for pyridinium salts, where α-methyl groups exchange faster than γ-methyl groups.[15,16]

Table 3

Arrhenius parameters for the isotopic exchange of 2,4,6-trimethylpyrylium in deuterium oxide

Anion	pH	α-Methyl			γ-Methyl		
		E_a kcal/mole	log A	$\Delta H\neq$ kcal/mole	E_a kcal/mole	log A	$\Delta H\neq$ kcal/mole
Cl	*a*	20.5	12.064	19.9	18.1	11.928	17.5
Cl	1.07	—	—	—	21.6	14.530	21.0
Cl	2.07	—	—	—	19.6	13.225	19.0
F_3CSO_3	2.5	22.2	14.424	21.6	16.2	11.437	15.6
Cl	3.7	17.6	11.392	17.0	—	—	—

a No buffer added.

---

[14] G. V. Boyd and A. T. Balaban, *ibid.*, **14**, 1575 (1969).

[15] N. N. Zatsepina, L. Yu. Kaminsky and I. F. Tupitsyn, *Organic Reactivity* (*Reakts. Sposobnost. Org. Soedin.*), **6**, 442 (1969).

[16] N. N. Zatsepina, A. V. Kirova and I. V. Tupitsyn, *ibid.*, **5**, 70 (1968).

Revue Roumaine de Chimie, 18, 2, 263–268(1973)

PHENYL BENZYL SULPHIDES

M. IOVU and ANCA ANGELESCU

University of Bucharest, Physics Departments

Chair of Chemistry, Şos. Panduri 90, Bucharest, Romania

Received May 18, 1972

The method previously described by us, in the synthesis of polyethers and aromatic bis-ethers was applied also to the synthesis of phenyl benzyl sulphides. For the synthesis of phenylbenzyl sulphides, the thiophenol or the *p*-methylthiophenol were converted into alkali thiophenolates by treating with sodium hydroxide. After the removal of the water (resulted from the reaction) by azeotropic distillation with ethanol and benzene mixture, the thiophenolates were treated with the chloromethylated derivative. The corresponding sulphides resulted.

Discovering an easy method for the synthesis of aromatic polyethers [1] and bis-ethers, [2,3] we passed to the synthesis of aromatic sulphides and we used the same method.

For the first time, in the synthesis of phenyl benzyl sulphide the reaction between sodium thiophenolate and benzyl chloride has been used.[4] But, to obtain the anhydrous sodium thiophenolate, prior to our investigations, the authors[4] have synthesized the sodium methoxide, of sodium and methanol, followed by the reaction between methoxide and thiophenol.

According to Brintzinger, Schmahl and Witte [5] the phenyl benzyl sulphide was obtained together with another reaction product, from chloromethylsulphochloride ($ClCH_2SCl$) and benzene, in carbon disulphide in the presence of aluminium chloride as catalyst.

More recently [6] the reaction between phenol and benzyl mercaptans in the presence of the hydrochloric acid in a closed tube has been used for the synthesis of phenyl benzyl sulphide. The authors of this method obtained a liquid product. The authors [4,5] of the above method obtained solid products with m.p. 40–41° and respectively m.p. 44°.

[1] M. Iovu and M. Manolescu, Patent R.S.R. 61.805 (1969).
[2] M. Iovu, *Rev. Roumaine Chim.*, **16**, 1223 (1971).
[3] M. Iovu, *Rev. Roumaine Chim.*, **17**, (1972).
[4] R. L. Schriner, H. C. Struck and W. J. Jorison, *J. Amer. Chem. Soc.*, **52**, 2060 (1930).
[5] H. Brintzinger, H. Schmahl and H. Witte, *Chem. Ber.*, **85**, 338 (1952).
[6] S. Oae and R. Kiritani, *Bull. Chem. Soc. Japan*, **38**, 1381 (1965).

Among the substituted phenyl benzyl sulphides, only *p*-tolyl benzyl sulphide was synthesized from *p*-methyl thiophenol and benzyl chloride. *p*-Tolyl benzyl sulphide has m.p. 44°. [7]

In some other papers we have shown the possibility to obtain polyethers [1] and aromatic bis-ethers [2,3] by using the condensation of aromatic chloromethylated derivatives with alkali phenoxides in non-aqueous medium, without the aid of a catalyst.

According to our method, the alkali phenoxides have been obtained from phenols and alkali hydroxides (and not from alkali alkoxide or alkali metal and phenol) in a mixture of solvents (ethanol and benzene) in which the phenol is soluble. The resulting water is removed by azeotropic distillation (as a mixture of ethanol-benzene-water). The anhydrous alkali phenolate is treated, in the same mixture of solvents (ethanol-benzene), with the halogenated derivative.

The condensation takes place at 70–75° with formation of alkali chloride and the corresponding ethers, which precipitated. These are easily separated from the solvents, by filtering and the sodium chloride is removed by water washing.

The method used for polyethers and aromatic bis-ethers synthesis is applied with good results for phenyl benzyl sulphides synthesis too, without essential changes.

Thus, to obtain sodium thiophenolate we have used thiophenol, sodium hydroxide and a mixture of benzene and ethanol, too, as a reaction medium, which permits the removal of the water, resulting from the reaction, as an azeotropic ethanol-water-benzene mixture :

$$ArSH + NaOH \rightarrow ArSNa + H_2O$$

When introducing the chloromethyl derivative, the nucleophilic attack of the thiophenolate ion on the halogenated derivative takes place, for instance :

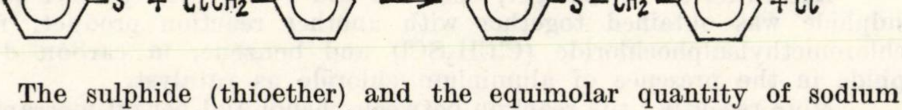

The sulphide (thioether) and the equimolar quantity of sodium chloride result, and they precipitate.

The sulphides with a higher melting point precipitate together with the sodium chloride and can be separated by filtering from the solvents and from the unreacted dissolved raw materials.

The sodium chloride is removed by water washing on the filter. The sulphide is recrystallized from ethanol.

The sulphides with a lower melting point do not crystallize in the reaction mixture at the same time with sodium chloride ; to separate them, they are washed with water in a separatory funnel when the sodium chloride and a part of the unreacted raw materials are removed. Then, some of the sulphides crystallize in the solution separated in the separatory funnel, after cooling and then, their recrystallization from ethanol follows. Other sulphides are not crystallized and they are purified by distillation in vacuum.

---

[7] E. FROMM, *Liebigs Ann. Chem.*, **396**, 75 (1931).

In this paper we present 8 sulphides, 6 of them being unknown. All the 8 sulphides are synthesized from thiophenol or *p*-methylthiophenol and benzyl chloride, 1-chloromethyl-4-methyl-benzene, 1-chloromethyl-2,4-dimethylbenzene or 1-chloromethyl-2,5-dimethylbenzene, using the new method.

RESULTS AND DISCUSSIONS

Table 1 gives the structural formulas of the synthesized sulphides, their melting points (or their boiling points) the microanalytical results of sulphur determination, λ_{max} and ε_{max} from UV spectrography and their yields.

By studying the data we notice that the melting points increase at the substitution of a methyl radical on the aromatic nuclei not directly connected with the sulphur atom and they are to a little extent influenced by the substitution of the methyl radical on the aromatic nuclei directly connected with the sulphur atom. The melting points decrease at the sulphides in which the aromatic nuclei not directly connected with the sulphur atom are substituted for two methyl radicals. If none of the methyl radicals is in the *para* position, the sulphides are liquid.

The synthesized sulphides, characterized by a direct connection with the sulphur function (thioether) of a benzenic nucleus and of a second one through an intermediary methylene group, $Ar-S-CH_2-Ar$, can be considered as mixt ones.

This fact is also shown by the wavelength value of the maximum of UV absorption. For these sulphides, the wavelength value is to be found between 255 and 259 nm (table 1), while for the aliphatic sulphides [8] the wavelength is to be found at about 210 nm and for the diphenyl sulphides [8] at about 280 nm.

The sulphides synthesized by us hardly absorb in the 200—210 nm area, characteristic of the aliphatic sulphides.

The wavelength values corresponding to the UV absorption maxima of an intensive band (table 1) demonstrate the presence of a less intensive bathochrom effect in the substitution of the benzenic nuclei, which are connected with a methyl radical in the *para* position.

In the IR spectra of the sulphides synthesized by us, the absorption band for the C—S bond could not be singled out; this is weak and is to be found in the 600—700 cm^{-1} area, where the absorption takes place also due to the out-of-plane vibrations of the aromatic nucleus.

---

[8] R. Passerini, "Organic sulfur compounds", vol. I, Pergamon Press, New York — N. Kharash editor, 1961, p. 57.

Table 1

Phenyl benzyl sulphides

Sulphides	Formula	S % *calculated* / *found*	Melting (boiling) point °C	λ_{max} nm	ε_{max}	Yield %
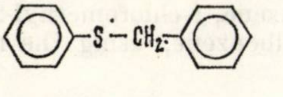	$C_{13}H_{12}S$	16.00 15.89	39.5	255.4	0.330	80
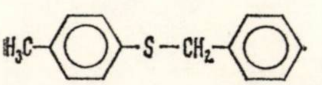	$C_{14}H_{14}S$	15.85 15.47	43	257	0.242	63
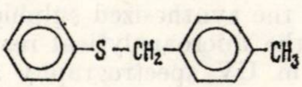	$C_{14}H_{14}S$	15.85 15.65	69	256	0.393	70
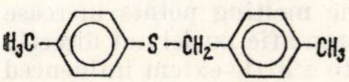	$C_{15}H_{16}S$	14.05 14.03	67.5–68	259	0.324	70
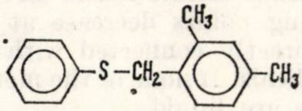	$C_{15}H_{16}S$	14.05 13.97	44.5–45.5	256	0.445	51
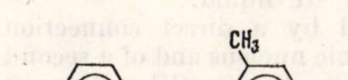	$C_{16}H_{18}S$	13.50 13.24	47–48	259	0.272	17
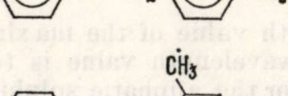	$C_{15}H_{16}S$	14.05 14.09	173–174 (/3 mm)	256	0.268	51
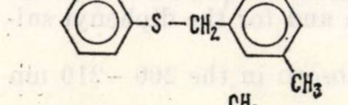	$C_{16}H_{18}S$	13.50 13.32	166–167 (/2 mm)	258	0.364	50

We have obtained phenyl benzyl sulphide with the highest yield. The yields diminished with the increase of the number of methyl radicals substituted on the aromatic nuclei.

In this case, the yields are very small because the sulphides do not crystallize in the reaction mixture. On washing the reaction mixture in the separatory funnel and then during distillation many losses are recorded.

EXPERIMENTAL

Thiophenol and 4-methyl thiophenol were obtained by reducing benzenesulphochloride and toluenesulphochloride with zinc and sulphuric acid (33%).[9]

Benzyl chloride was a "Riedel" commercial product.

1-Chloromethyl-*p*-toluene was synthesized by photochemical chlorination of *p*-xylene with sulphuryl chloride, using benzoyl peroxide as activator.

1-Chloromethyl-2,4-dimethylbenzene and 1-chloromethyl-2,5-dimethylbenzene were synthesized by chloromethylation of *m*-xylene and *p*-xylene, using paraformaldehyde, hydrochloric acid and phosphoric acid.

The determination of the sulphur was made by the oxidation of sulphides with oxygen in the presence of platinum catalyst, and with hidrogen peroxide, followed by volumetric determination of sulphuric acid.[10]

The UV spectra were obtained with the Specord, Zeiss-Yena, spectrophotometer, and the IR spectra with the UR-20, Zeiss-Yena, apparatus.

SYNTHESIS OF PHENYL BENZYL SULPHIDE

In a double-necked, 50 ml flask, ground joint, equipped with an ascending refrigerator and a thermometer, we have inserted 2.754 g thiophenol (1/40 mol), 1.010 g NaOH (1/40 mol plus an excess of 1/4000 mol) and 30 ml of ethanol-benzene mixture (in the ratio 1 : 1 in volume). The mixture is heated to the boiling point for 3 hours, till the sodium thiophenolate forms. The reflux refrigerator is then changed to a distillation refrigerator and 15 ml azeotropic mixtures are distilled to remove the water resulting from the reaction. After cooling of the flask, 3.139 g benzyl chloride (1/40 mol) are added, the distillation refrigerator is again changed for the refluxing one, to which a tube with calcium chloride is connected and is heated for 3 hours at 65—67°. Sodium chloride first forms, which precipitates and then sulphide which becomes abundent after cooling of the reaction flask to 5°.

The reaction mixture is filtered, when the solid sodium chloride and the solid sulphide separate from the solvent and the liquid unreacted raw materials. The solid mixture is now water washed to remove sodium chloride. The precipitate is dried in vacuum; 4.012 g phenyl benzyl sulphide results and after two recrystallizations its melting point will be 39.5°.

The 4-methyl-phenyl benzyl sulphide, phenyl 4-methyl benzyl sulphide and 4-methylphenyl 4-methyl-benzyl sulphide were obtained in a similar way.

Phenyl 2,4-dimethyl-benzyl sulphide and 4-methyl-phenyl 2,4-dimethyl-benzyl sulphide did not crystallize from the reaction mixture, and that is why it was washed with water in the separatory funnel to remove the sodium chloride and a part of the unreacted thiophenol.

The product of the synthesis of phenyl 2,4-dimethyl-benzyl sulphide was distilled in vacuum, after drying on calcium chloride.

From the fraction distilled at 148—150°/2 mm, after cooling, phenyl 2,4-dimethylbenzyl sulphide crystallized; after the recrystallization from anhydrous ethanol, the melting point is 45.5—46.5°.

---

[9] Weygand–Hilgetag, "Organisch-Chemische Experimentierkunst" 3. Auflage, Johann Ambrosius Barth–Verlag, Leipzig, 1964, S. 711.

[10] T. N. Kasterina, L. S. Kalinina, "Analiza chimică a rășinilor sintetice și a materialelor plastice" — traducere din limba rusă, Ed. Tehnică, București, 1965, p. 42.

4-Methyl-phenyl 2,4-dimethyl-benzyl sulphide crystallized from the dry washed product, without any distillation, at a reduced pressure.

Phenyl 2,5-dimethyl-benzyl sulphide and 4-methyl-phenyl 2,5-dimethyl-benzyl sulphide have been identically processed, but they still remained liquid after distillation in vacuum.

Phenyl 2,5-dimethyl-benzyl sulphide has b.p. 173—174°/3 mm, with $\rho_{20} = 1.0742$ and $n_D^{20} = 1.6120$; $MR_{calc} = 72.186$, $MR_{found} = 73.715$.

4-Methylphenyl 2,5-dimethylbenzyl sulphide has b.p. 166—167°/2 mm with $\rho_{20} = 1.0501$ and $n_D^{20} = 1.6011$; $MR_{calc} = 77.228$, $MR_{found} = 77.801$.

CONCLUSIONS

The method described in our first paper, for the aromatic bis-ethers synthesis, may be used with good results for aromatic sulphides synthesis too.

Anhydrous, alkali thiophenolates can be obtained by treating phenyl-mercaptans with sodium hydroxide and the removal of water derived from the reaction, by azeotropic distillation.

Anhydrous alkali thiophenolates react easily with dichloromethylated derivatives in ethanol-benzene mixture.

Phenyl benzyl sulphide and tolyl benzyl sulphide have their melting points identical with the products synthesized in other ways. Other sulphides synthesized by us are not yet described.

Revue Roumaine de Chimie, 18, 2, 269–274 (1973)

DER EINFLUSS DER KETTENLÄNGE EINIGER *n*-ALKANE AUF IHRE PEROXYDIERUNGSGESCHWINDIGKEIT MIT MOLEKULAREM SAUERSTOFF, IN FLÜSSIGER PHASE

I. DRIMUŞ und I. T. IONESCU

Aus dem Laboratorium für Organisch-Chemische Technologie
Technische Hochschule, Bukarest, Calea Victoriei 149

Eingegangen am 24. Juni 1972

In flüssiger Phase wurden *n*-Dekan, *n*-Dodekan, *n*-Tetradekan, *n*-Oktadekan, *n*-Eikosan, *n*-Tetrakosan und *n*-Pentatriakontan mit molekularem Sauerstoff oxydiert. Mit Peroxyde als Initiatorem, wächst die Ansammlung von peroxydischem Sauerstoff in der Reaktionsmasse, bei kleinen Umsätzen, mit der Temperatur, Reaktionsdauer und Kettenlänge. Es wurde eine Gleichung zwischen der Zahl der Kohlenstoffatome der *n*-Alkanmolekülen und der Reaktionsgeschwindigkeit festgestellt.

Das Verhältnis zwischen der Oxydierungsgeschwindigkeit der *n*-Alkane und deren Kettenlänge wurde bisher nur wenig studiert.

Einige Verfasser haben in Gasphase, andere, in flüssiger Phase gearbeitet. Es wurden verschiedene Katalysatoren angewendet und die Oxydierung bis zu Alkoholen und Ketonen, von einigen Verfassern, von anderen wieder, bis zu Carbonsäuren geleitet.

Cullis [1] schreibt den Einfluß der Methylgruppen aus den Molekülen der *n*-Alkane zu, daß deren Oxydierungsgeschwindigkeit folgende Werte hat; CH_3-CH_3 ... 0,0011 ; $CH_3-CH_2-CH_3$ ... 0,1 ; $CH_3-(CH_2)_2-CH_3$ ... 0,5 ; $CH_3-(CH_2)_3-CH_3$ ... 7,5 ; $CH_3-(CH_2)-CH_3$ ... 200 und $CH_3-(CH_2)_8-CH_3$ ... 1380.

Zilberg und Smirnova oxydierten mit molekularem Sauerstoff n-$C_{12}H_{26}$, n-$C_{13}H_{28}$, n-$C_{14}H_{30}$ und n-$C_{15}H_{32}$, in flüssiger Phase, mit Cobaltstearat als Katalysator; sie bemerkten, daß die Reaktionsgeschwindigkeit gleichmäßig mit der Zahl der Methylengruppen in den Molekülen ansteigt.[2]

Tiscovski land, daß bei der Oxydierung der Alkane, in flüssiger Phase, mit molekularem Sauerstoff, in Gegenwart von Mangannaphthenat, die Reaktionsgeschwindigkeit der Säurenbildung mit der Länge der Kohlenwasserstoffkette wächst.[3]

---

[1] C. F. Cullis und M. F. R. Muclaacy, *Rev. Inst. franç. Pétrole*, **4**, 283 (1949).

[2] G. A. Zilberg und S. N. Smirnova, *Doklady Akad. Nauk S.S.S.R.*, **166**, 643 (1966).

[3] V. K. Tiscovski, *Zhur. priklad. Khim.*, **30**, 493 (1957).

In der vorliegenden Arbeit wurde die Oxydierung von *n*-Alkanen mit $C_{10}...C_{35}$ durch Einblasen von Sauerstoff, in flüssiger Phase, ohne Katalysatoren, ausgeführt. Die Induktionsperiode wurde ausgelassen, da man Spuren von Peroxyd verwendet hat. Der Oxydierungsverlauf wurde durch Bestimmung des peroxydischen Sauerstoffs in der Reaktionsmasse verfolgt.

Es sei bemerkt, daß die Reaktion sehr empfindlich ist, und daß die angesammelte Peroxydmenge nicht nur von der Natur des *n*-Alkans, von Temperatur und Oxydierungsdauer, sondern sehr stark, auch von Menge und Verteilugungsgrad des Sauerstoffes, wie auch von Form, Größe und Baumaterial des Reaktors abhängt.

DAS AUSLASSEN DER INDUKTIONSPERIODE

Führt man fein verteilten Sauerstoff durch einen flüssigen *n*-Alkan, bei geeigneter Temperatur, so beginnt die Reaktion nach einer mehr oder weniger kurzen Induktionsperiode, durch Ansammlung von Peroxyden in der flüssigen Masse. Durch viele gleichzeitige, aufeinanderfolgende und angeleitete Reaktionen treten mit der Zeit in der Reaktionsmasse verschiedene mono-, di-, und polisubstituierte Verbindungen, so wie auch Abbauprodukte in immer größerer Zahl und Menge auf.

Wir haben uns mit der Ansammlungsperiode der Peroxyde in Abhängigkeit von Zeit befaßt. Um vergleichbare Ergebnisse zu erzielen, mußte man die Induktionsperiode auslassen.

Um die Reaktion einzuleiten, bzw. die Induktionsperiode auszulassen, schlugen Geisler, Asinger und Wien vor, dem in den Reaktor eingeführten Sauerstoff, Ozon beizumischen; zu demselben Zweck gebrauchte Emanuel Stickstoffdioxyd. [4,5]

Wir konnten keine löslichen Salze von Schwermetallen (Co, Mn, Cr, usw.) verwenden, da diese Katalysatoren, obwohl sie die Induktionsperiode beseitigen, die Peroxyde mit großer Geschwindigkeit zerlegen und so die *n*-Alkane zu Verbindungen mit höherem Oxydierungsgrad (hauptsächlich Carbonsäuren) oxydieren.

In unserem Fall konnte die Induktionsperiode ausgelassen werden, entweder durch eine Vorbehandlung der Reaktionsmasse mit 0,1 $mg.g^{-1}$ eines geeigneten Peroxyds, [6] oder durch die Ausführung der Oxydierung in einem Feld ionisierender Strahlungen sowie auch durch Vorbestrahlen der zu oxydierenden *n*-Alkane mit uv-Strahlungen, γ- [7,8] Strahlungen oder Ultraschall. [9]

---

[4] G. Geisler, F. Asinger und H. Wien, *Chem. Ber.*, **92**, 958 (1959).

[5] N. M. Emanuel, *Zhur. fiz. Khim.*, **30**, 847 (1956).

[6] G. Ioanid, I. Drimuş, A. Drăguţ und M. Klang, Rum. Patent, no. 41933, 24 feb. 1961,

[7] I. Drimuş, G. Ioanid, A. Drăguţ, V. Dumitrescu und P. Vasilescu, Rum. Patent. no. 2541–41642, 24 feb. 1961.

[8] I. Drimuş und C. Florescu, *Bul. Inst. Politeh. Bucureşti*, (1972) (unter Druck).

[9] I. Drimuş, V. Pribnov, R. Avram und I. Frorea, *Bul. Inst. Politeh. Bucureşti*, **23**, 119 (1961).

Nach dem Start, hat man die Ansammlung der Peroxyde, bei der Oxydierung eines n-Alkans, bei vergleichbaren Bedingungen, in Abhängigkeit von Zeit und Temperatur, studieren können.

Abb. 1 stellt die bei der Oxydierung des n-Dodekans mit molekularem Sauerstoff erhaltenen Ergebnisse dar. Man bemerkt, daß in den ersten 6 Stunden, bei niedrigeren Temperaturen, die Sauerstoffansammlung, linear verläuft; nur bei höheren Temperaturen erscheint ein Maximum.

Gleichartige Kurvenfamilien geben auch die in der gegenwärtigen Arbeit studierten höheren und niedrigeren Homologe des n-Dodekans.

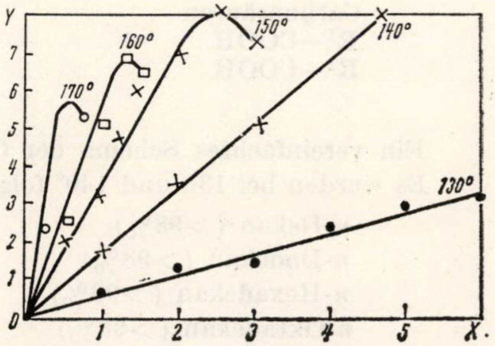

Abb. 1. — Die Oxydierung des n-Dodekans. Die Ansammlung von peroxydischem Sauerstoff in Abhängigkeit von Zeit und Temperatur (Reaktor von 150 cm^3).

X = Oxydierungsdauer (Stunden); Y = Peroxydzahl (mg O/g).

Um vergleichbare Ergebnisse zu erhalten, wurden verschiedene n-Alkane je 3 Stunden, bei 130 und 140° oxydiert, in Bedingungen, in welchen die von uns studierten n-Alkane lineare Ansammlungen von peroxydischem Sauerstoff in der Reaktionsmasse weisen.

Der Mechanismus der Alkanoxydierung ist nicht vollständig geklärt. Wahrscheinlich bilden Alkylhydroperoxyde die erste Stufe der Oxydierung. Nachher, bei größeren Umsätzen, treten in der Reaktionsmasse, unter anderen Ketone, Carbonsäuren usw. auf. Diese Produkte peroxydieren sich wiederum.

Bei kleinen Umsätzen (am Anfang der Oxydierung und bei mäßigen Temperaturen) kann man annehmen, daß die (jodometrisch bestimmte) Peroxydzahl der Reaktionsmasse den Alkylhydroperoxyden entspricht aber mit wachsendem Umsatz, haben die Peroxyde (Hydroperoxyde) der Zwischenprodukte ein größeres Gewicht.

In der Reaktionsmasse gelöste oder dispergierte Salze von Schwermetallen (Fe, Co, Ni Mn, Cr, usw.) wiedersetzen sich, wie gezeigt, der Peroxydansammlung.[8] So, zum Beispiel, in Gegenwart von 0,1% Cobaltnaphthenat, treten Peroxyde nur als Spuren auf, obwohl der Oxydierungsprozeß zur Bildung von Alkoholen, Ketonen, Carbonsäuren usw. mit größerer Geschwindigkeit stattfindet.

In unseren Arbeiten haben wir nur sehr reine Kohlenwasserstoffe verwendet und die Verunreinigungen mit Salzen von Schwermetallen, die die Peroxydansammlung unvorteilhaft beeinflussen könnten, gemieden.

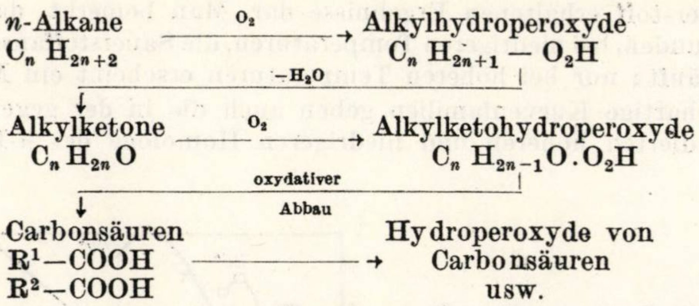
n-Alkane
$C_n H_{2n+2}$
O_2
Alkylhydroperoxyde
$C_n H_{2n+1} - O_2H$
$-H_2O$
Alkylketone
$C_n H_{2n} O$
O_2
Alkylketohydroperoxyde
$C_n H_{2n-1} O . O_2H$
oxydativer
Abbau
Carbonsäuren
$R^1 - COOH$
$R^2 - COOH$
Hydroperoxyde von
Carbonsäuren
usw.

Ein vereinfachtes Schema der Oxydierung von *n*-Alkane.

Es wurden bei 130 und 140° folgende Kohlenwasserstoffe oxydiert:

n-Dekan ($>98\%$)
n-Dodekan ($>98\%$)
n-Hexadekan ($>98\%$)
n-Oktadekan ($>98\%$)
n-Eikosan ($>95\%$)
n-Tetrakosan ($>95\%$)
n-Pentatriakontan.

Diese Stoffe waren alkenefrei; ihre Verunreinigungen waren nahe gelegene, höhere und niedrigere Homologe. Sie wurden aus natürlichen Fettsäuren synthesisiert.

Die Oxydierung wurde durch Einleitung von fein verteiltem Sauerstoff in das, vorher mit 100 ppm Alkylperoxyde behandeltem Kohlenwasserstoff, ausgeführt. Man arbeitete ohne metallische Katalysatoren.

Die Peroxadzahl wurde jodometrisch bestimmt.

Wie aus Abb. 2 hervorgeht, verläuft in den ersten 180 Minuten die Ansammlung des peroxydischen Sauerstoffes linear, im Einklang mit der Gleichung:

$$C = A . t . n .$$

wo: C = mg aktiver Sauerstoff pro Gramm oxydierte Substanz; t = Oxydierungszeit, in Minuten; n = Zahl der Kohlenstoffatome aus dem zu oxydierenden *n*-Alkanmolekül; A = eine spezifische Konstante für den verwendeten Apparat und die Arbeitstemperatur, ausgedrückt in mg aktivem Sauerstoff pro Gramm oxydierte Substanz und Minute.

Mit dem von uns verwendeten Apparat, war der mittlere Wert für A_{130° $7{,}65 . 10^{-4}$ mg 0/g.min, und für A_{140° $2{,}39 . 10^{-3}$ mg O/g.min.

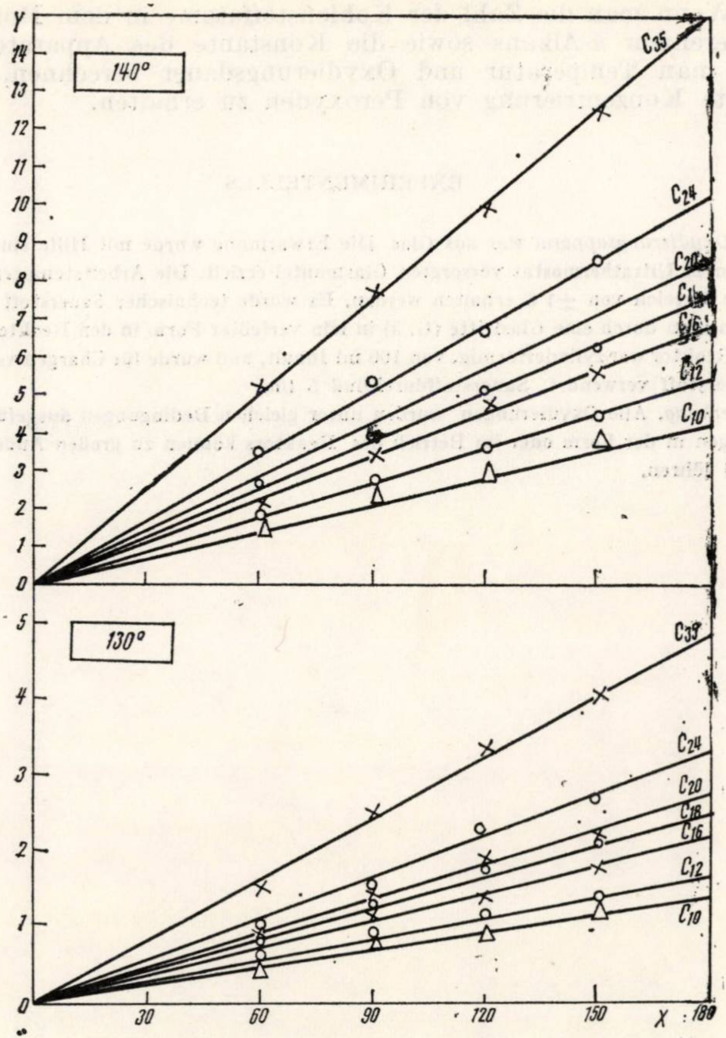

Abb. 2. — Ansammlung von aktivem Sauerstoff in der Reakionsmasse bei der Oxydierung einiger *n*-Alkane bei 130° und 140°.
X = Oxydierungsdauer (Minuten) ; Y = Peroxydzahl (mg O/g).

SCHLUSSFOLGERUNG

1. Die Peroxydierungsgeschwindigkeit der *n*-Alkane (C_{10}—C_{35}), bei Temperaturen von 130 und 140°, wächst gleichmäßig mit der Zahl der Kohlenstoffatome in dem Molekül.

2. Um vergleichbare Ergebnisse zu erzielen muß man die Anwesenheit metallilscher Katalysatoren vermeiden und die Reaktionsmasse vorher mit organischen Peroxyden behandeln („Besamung").

3. Wenn man die Zahl der Kohlenstoffatome in dem Molekül des zu oxydierenden *n*-Alkans sowie die Konstante des Apparates kennt, so kann man Temperatur und Oxydierungsdauer berechnen, um die erwünschte Konzentrierung von Peroxyden zu erhalten.

EXPERIMENTELLES

Der Oxydierungsapparat war aus Glas. Die Erwärmung wurde mit Hilfe eines mit Glyzerin aus einem Ultrathermostat versorgten Glasmantel erzielt. Die Arbeitstemperatur konnte konstant im Bereich von ±1°C erhalten werden. Es wurde technischer Sauerstoff (99 %) verwendet, den man durch eine Glasfritte (G. 3) in fein verteilter Form in den Reaktor einführte.

Der Reaktor war zylinderförmig, von 100 ml Inhalt, und wurde für Chargen von je 100 ml Kohlenwasserstoff verwendet. Sauerstoffdurchfluß 5 l/h.

Anmerkung. Alle Oxydierungen wurden unter gleichen Bedingungen ausgeführt. Kleine Veränderungen in der Form oder im Betrieb des Reaktors können zu großen Änderungen der Peroxydzahl führen.

Revue Roumaine de Chimie, **18**, *2*, 275–282 (1973)

NEUE ORGANISCHE PIGMENTE–ISATINDERIVATE. III

STUDIUM DER IR-SPEKTREN EINIGER 2-ARYLAMINOINDOXYLE UND 3-ARYLIMINOOXINDOLE

R. BACALOGLU und B. D. BADER

Vom Lehrstuhl für organische Chemie der Fakultät für industrielle Chemie,
Timişoara, Str. Bocşa 6 und vom Forschungslaboratorium der industriellen Gruppe
für Petrochemie, Piteşti, Şos. Giurgiului 127

Eingegangen am 19. Mai 1972

Es wurden die Spektren der im Titel genannten Verbindungen im Bereich 400 bis 4000 cm^{-1} untersucht. Durch Auslegen der dem heterozyklischen System charakteristischen Bande wurden die Strukturen der untersuchten Verbindungen festgelegt und Überlegungen über die Art ihrer Assozierung in der Kristallstruktur unternommen.

Im Rahmen der bisherigen Forschungen wurde eine Reihe von Pigmenten, Derivate des Aminoindoxyls, [2] sowie eine andere Reihe Derivate des Iminooxindols [1,2] synthetisiert, welche reelle Anwendungsmöglichkeiten zum Einfärben von Polyolefinen und Polyvinylchlorid bieten. Zur besseren Kenntnis der Eigenschaften dieser Verbindungen sowie zur Bestimmung ihrer Struktur haben wir ein Studium durch IR-Spektroskopie vorgenommen.

ERGEBNISSE UND DISKUSSION

a) 2-ARYLAMINO-INDOXYLE

Die untersuchten 2-Arylamino-indoxyle wurden durch die Reaktion des 2-Chlorindolenin-3-ons (Isatin-2-chlorid) mit verschiedenen Diaminen in *o*-Dichlorbenzol bei Erwärmen unter Rückfluß erhalten.

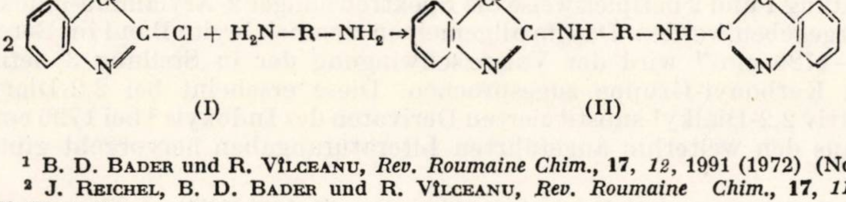

(I) (II)

---

[1] B. D. Bader und R. Vîlceanu, *Rev. Roumaine Chim.*, **17**, *12*, 1991 (1972) (Note II).

[2] J. Reichel, B. D. Bader und R. Vîlceanu, *Rev. Roumaine Chim.*, **17**, *11*, 1889 (1972) (Note I).

Das Isatin-2-chlorid wurde seinerseits nach älteren Literaturangaben durch Chlorierung des Isatins mit PCl_5 in Chlorbenzol hergestellt.

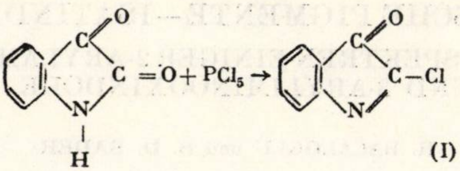

(I)

Die Struktur der letzten Verbindung wurde bis heute noch nicht vollkommen durch physiko-chemische Messungen bestätigt.

Tabelle 1

Die wichtigsten Banden des 2-Aminoindoxyl-Systems in Verbindungen der Struktur II

Symbol	Diamin entsprechend R aus Struktur II	Valenzschwingungen entsprechend (cm^{-1})				
		C=O	C=N	N−H	C−N	
					N-Indoxyl	N-Aryl
IV	1,4-Phenylendiamin	1715	1610	3400 2850	1310	1210
V	1,3-Phenylendiamin	1710	1605	3400 sehr breit	1320	1200
VI	2,4-Touilendiamin	1715	1610	3400 sehr breit	1320	1200
VII	Benzidin	1710	1610	3400 2850	1250	1190
VIII	*o*-Tolidin	1710	1605	3350 2850	1270	1190
IX	*o*-Dianisidin	1715	1610	3370 2850	1250	1200
X	1,5-Diaminoanthrachinon	1720	1600	3400 sehr breit	1260	1200
XI	1,4-Diaminoanthrachinon	1715	1610	3400 sehr breit	1270	1200

In Tabelle 1 werden die wichtigsten, den Schwingungen des 2-Aminoindoxyl-System entsprechenden Bänder zusammengefaßt, während in Abbildung 1 und 2 beispielsweise die Spektren einiger 2-Arylamino-indoxyle wiedergegeben werden. Das im allgemeinen ziemlich breite Band im Bereich 1710—1720 cm^{-1} wird der Valenzschwingung der in Stellung 3 befindlichen Karbonyl-Gruppe zugesprochen. Diese erscheint bei 2,2-Diaryl-, respektiv 2,2-Dialkyl-substituierten Derivaten des Indoxyls [3] bei 1720 cm^{-1}. Wie aus den weiterhin angeführten Literaturangaben hervorgeht gibt es anscheinend keine klaren Unterschiede zwischen der Lage der Bande, welche den Valenzschwingungen der Karbonylgruppen aus Stellung 2 und 3 entsprechen, weshalb für die Klärung dieses Strukturteiles die untersuchten Schwingungen keine besondere Anzeigen liefern.

---

[3] B. Wittkop und A. Ep, *J. Amer. Chem. Soc.*, **73**, 5664 (1951).

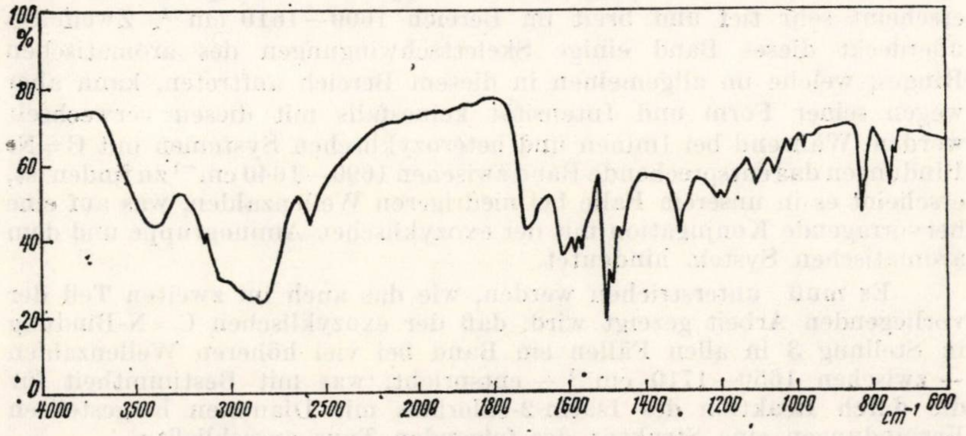

Abb. 1. — Das Infrarotspektrum des Bis-(Indolenin-3-on-2-yl)-phenylendiamins-1,4 in KBr-Preßling (600—4000 cm^{-1}).

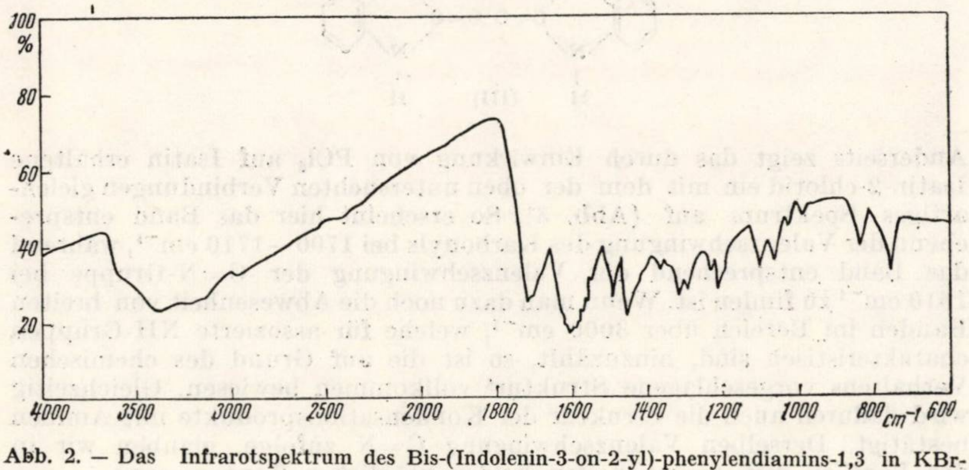

Abb. 2. — Das Infrarotspektrum des Bis-(Indolenin-3-on-2-yl)-phenylendiamins-1,3 in KBr-Preßling (600—4000 cm^{-1}).

Da die untersuchten Verbindungen zweifellos Assozierungen durch Protonbindungen aufweisen, welche im allgemeinen die Lage des Bandes welches der Karbonylgruppe entspricht beeinflussen, wobei eine Verschiebung gegen kleinere Wellenzahlen mit ca. 10—20 cm^{-1} zu verzeichnen ist, und da Ketone mit Karbonylgruppen an 5-Atomringen allgemein dieses Band bei 1745 cm^{-1} aufweisen, wird es klar, daß dieses Band keinesfalls deutlich durch Konjugation der Ketongruppe mit den ungesättigten Gruppen des Systems wie – aromatischer Ring und Doppelbindungen $C=N$ – beeinflußt wird.

Das der Valenzschwingung der Gruppe $C=N$ entsprechende Band erscheint sehr tief und breit im Bereich 1600–1610 cm^{-1}. Zweifellos überdeckt dieses Band einige Skelettschwingungen des aromatischen Ringes, welche im allgemeinen in diesem Bereich auftreten, kann aber wegen seiner Form und Intensität keinesfalls mit diesen verwechselt werden. Während bei Iminen und heterozyklischen Systemen mit $C=N$ Bindungen das entsprechende Band zwischen 1690–1640 cm^{-1} zu finden ist, erscheint es in unserem Falle bei niedrigeren Wellenzahlen, was auf eine hervorragende Konjugation mit der exozyklischen Aminogruppe und dem aromatischen System hindeutet.

Es muß unterstrichen werden, wie das auch im zweiten Teil der vorliegenden Arbeit gezeigt wird, daß der exozyklischen $C=N$-Bindung in Stellung 3 in allen Fällen ein Band bei viel höheren Wellenzahlen – zwischen 1650–1710 cm^{-1} – entspricht, was mit Bestimmtheit für die durch Reaktion des Isatin-2-chlorides mit Diaminen hergestellten Verbindungen eine Struktur des folgenden Typs ausschließt:

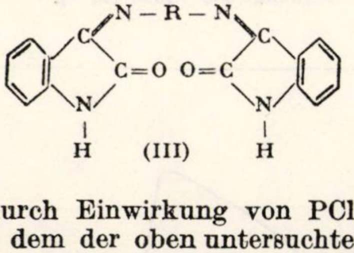
(III)

Anderseits zeigt das durch Einwirkung von PCl_5 auf Isatin erhaltene Isatin-2-chlorid ein mit dem der oben untersuchten Verbindungen gleichartiges Spektrum auf (Abb. 3). So erscheint hier das Band entsprechend der Valenzschwingung des Karbonyls bei 1700–1710 cm^{-1}, während das Band entsprechend der Valenzschwingung der $C=N$-Gruppe bei 1610 cm^{-1} zu finden ist. Wenn man dazu noch die Abwesenheit von breiten Banden im Bereich über 3000 cm^{-1}, welche für assozierte NH-Gruppen charakteristisch sind, hinzuzählt, so ist die auf Grund des chemischen Verhaltens vorgeschlagene Struktur[4] vollkommen bewiesen. Gleichzeitig wird dadurch auch die Struktur der Kondensationsprodukte mit Aminen bestätigt. Derselben Valenzschwingung $C=N$ zufolge, glauben wir in der Lage zu sein zwischen den beiden möglichen Tautomeren:

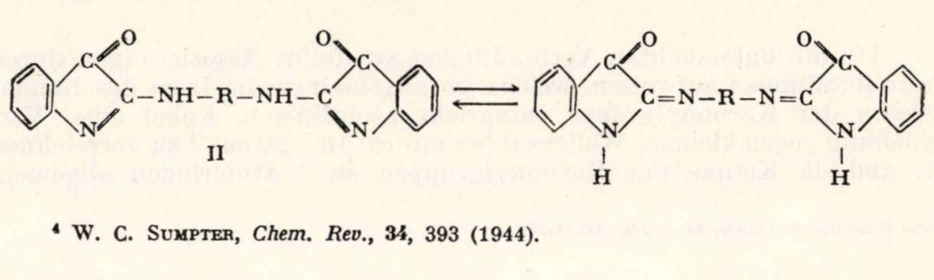
II

---

[4] W. C. Sumpter, *Chem. Rev.*, **34**, 393 (1944).

denjenigen mit endozyklischer C=N-Gruppe auf Grund der wie weiter oben schon genannten niedrigwelligen Stellung des Bandes, sowie der Analogie mit dem Spektrum des Isatin-2-chlorids als reell zu betrachten.

Es wurde auch in anderen ähnlichen Fällen schon bewiesen, daß für exozyklische C=N-Bindungen Banden bei höheren Frequenzen charakteristischer sind als für endozyklische, wie das auch aus dem folgenden Beispiel hervorgeht[5]:

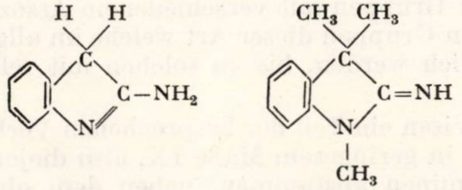

$\nu_{C=N}$ 1642 cm^{-1} 1653 cm^{-1}

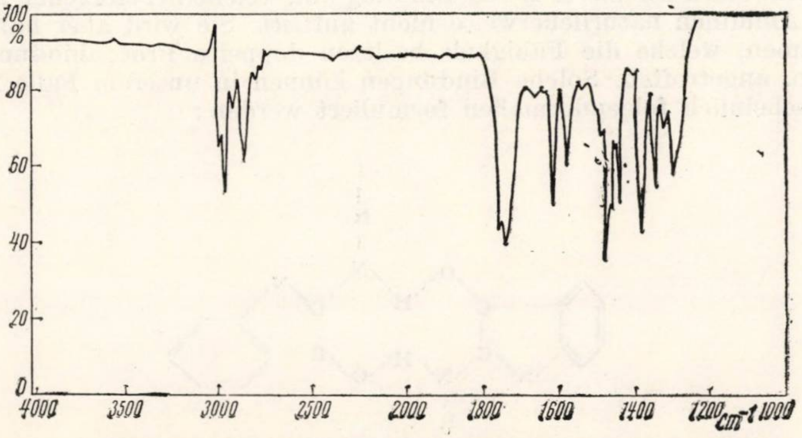

Abb. 3. — Das Infrarotspektrum des Isatin-2-chlorids in Chloroform-Lösung (1000—4000 cm^{-1}).

2-Arylamino-indoxyle weisen im Bereich 1200—1320 cm^{-1} zwei im allgemeinen intensive Banden auf, welche den Valenzschwingungen C—N zugesprochen werden können. Solche Schwingungen für aromatische Amine beispielsweise sind allgemein für ein Band im Bereich 1250—1360 cm^{-1} verantwortlich, welches um so mehr nach höheren Wellenlängen verschoben wird, je stärker die Bindung einen Doppelbindungscharakter aufweist. In unserem Falle ist es sehr wahrscheinlich, daß infolge der sehr bedeutenden Konjugation zwischen dem Indoxyl-System und den unbeteiligten Elektronen des Stickstoffatoms das Band zwischen 1230—1320 cm^{-1} der Bindung Stickstoff-Indoxyl entspricht. Das Band zwischen 1190—1200 cm^{-1} ist wahrscheinlich der Bindung Stickstoff-aromatisches System zuzuschreiben.

---

[5] J. Kebrle und K. Hoffmann, *Helv. chim. Acta*, **39**, 116 (1956).

Im Bereich 3270–3400 cm^{-1} weisen alle untersuchten Spektren ein oder zwei sehr breite Banden auf, welche auf durch Protonbindungen assozierte N–H Gruppen hinweisen. Wie aus Tabelle 1 und Vergleich der Abbildungen 1 und 2 hervorgeht, können alle untersuchten Verbindungen von diesem Standpunkt in zwei Kategorien eingeteilt werden. Einerseits weisen alle Verbindungen ein äußerst breites Band auf, welches bei cca. 2500 cm^{-1} anfängt und bei 3400 cm^{-1} ein Maximum besitzt. Dieses Band ist auf N–H-Gruppen mit verschiedenem Assozierungsgrad zurückzuführen, von freien Gruppen dieser Art welche im allgemeinen bei 3450 – 3490 cm^{-1} ersichtlich werden, bis zu solchen mit relativ kräftiger Assozierung.

Anderseits weisen ein Teil der besprochenen Verbindungen und zwar IV, VII, VIII und in geringerem Maße IX, also diejenigen, die von paradisubstituierten Aminen abstammen, neben dem obengenannten Band, ein zweites gleichfalls breites Band um 2850 cm^{-1} auf. Dieses weist auf eine sehr stark assozierte N–H Bindung hin, welche bei einfachen Aminen oder Amidinen natürlicherweise nicht auftritt. Sie wird aber häufig bei Systemen, welche die Fähigkeit besitzen doppelte Protonbindungen zu bilden, angetroffen. Solche Bindungen können in unserem Falle höchstwahrscheinlich folgendermaßen formuliert werden:

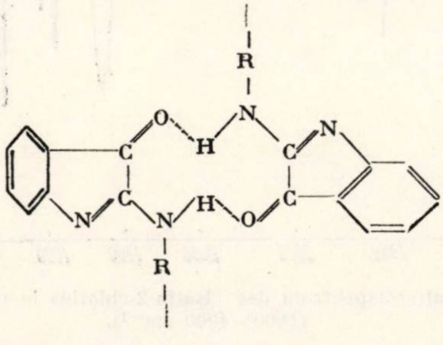

Die von metasulbstituierten Aminen oder Diaminoanthrachinone abstammenden Verbindungen können aus anscheinend sterischen Gründen solche Protonbindungen nicht bilden.

b) 3-ARYLIMINO-OXINDOLE

Die untersuchten 3-Arylimino-oxindole wurden durch die Reaktion des 3,3-Dichlorisatins mit aromatischen Diaminen, [2] wie auch durch direkte Kondensation des Isatins mit aromatischen Diaminen in Gegenwart von Polyphosphorsäure, [1] hergestellt. Die auf den zwei Synthesewegen erhaltenen Produkte sind identisch wie es aus dem Vergleich der IR-Spektren der beiden Derivate des *p*-Phenylendiamins ersichtlich wird (Abb. 4).

In Tabelle 2 werden die dem Oxindol-System charakteristischen wichtigsten Banden aufgeführt, welche über die Struktur der untersuchten

Verbindungen Aufschluß geben sollen.

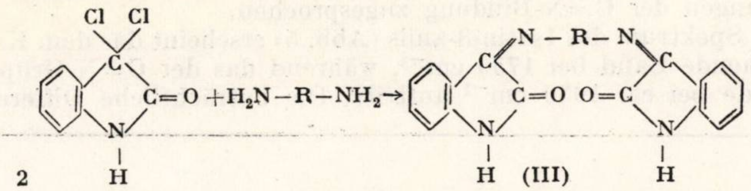

Tabelle 2

Die wichtigsten Banden des 3-Aryliminooxindol-Systems in Verbindungen der Struktur III

Symbol	Diamin entsprechend R aus Struktur III	Valenzschwingungen entsprechend (cm⁻¹)			
		C=O	C=N	N−H	C−N
XII	1,4-Phenylendiamin	1730	1710	3400 3200	1300, 1240 1200
XIII	Benzidin	1710	1710	3400 3200	1300, 1240 1200
XIV	*o*-Tolidin	1720	1710	3370 3200	1300, 1250

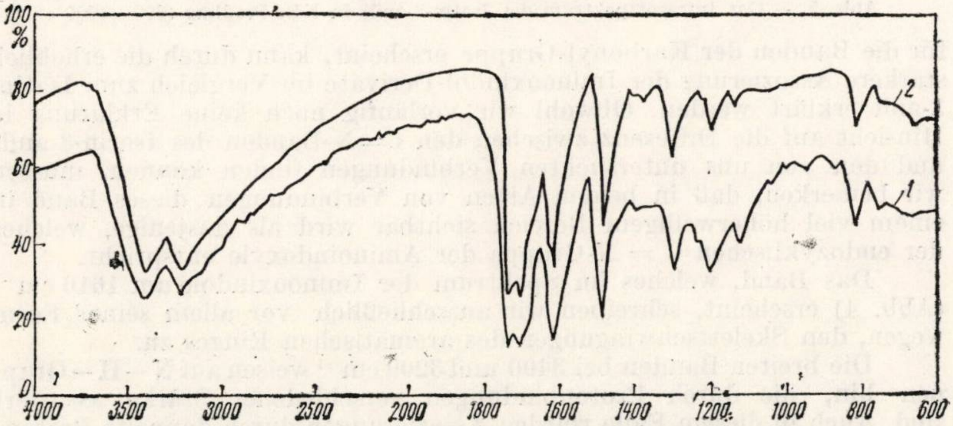

Abb. 4. — Die Infrarotspektren des Bis-(Indolin-2-on-3-yliden)-phenylendiamins-1,4 in KBr-Preßlingen (600−4000 cm⁻¹) erhalten durch:

1, Reaktion des 3,3-Dichlorisatins mit *p*-Phenylendiamin; *2*, direkte Kondencation des Isatins mit *p*-Phenylendiamin.

Das Oxindol und seine verschieden substituierten Derivate weisen ein Band im Bereich 1710−1740 cm⁻¹ auf, welches der Ketongruppe zugesprochen wird,[6−9] wodurch seine Keton-Struktur bestätigt wird.

In unserem Falle, erscheint dieses Band im gleichen Bereich jedoch viel breiter, woraus man das Vorhandensein eines Dubletts klar ersehen kann (Abb. 4). Wir haben das Maximum um 1710−1730 cm⁻¹ den Schwin-

---

[6] E. Wenkert, A. K. Bose und T. L. Reid, *J. Amer. Chem. Soc.*, **75**, 5514 (1953).
[7] A. Kellie, D. G. O'Sullivan und P. W. Sadler, *J. Chem. Soc.*, **1956**, 3809.
[8] H. E. Baumgarten und P. L. Creger, *J. Amer. Chem. Soc.*, **82**, 4634 (1960).
[9] H. E. Baumgarten, P. L. Creger und R. L. Zey, *J. Amer. Chem. Soc.*, **82**, 3977 (1960).

gungen des Karbonyls, während dasjenige bei 1710 cm^{-1} den Valenzschwingungen der C=N-Bindung zugesprochen.

Im Spektrum des Isatin-3-anils (Abb. 5) erscheint das dem Karbonyl entsprechende Band bei 1750 cm^{-1}, während das der C=N-Gruppe entsprechende bei ca. 1650 cm^{-1} auftritt. Die beträchtliche Differenz, die für die Banden der Karbonyl-Gruppe erscheint, kann durch die erheblich stärkere Assozierung der Iminooxindol-Derivate im Vergleich zum Isatin-3-anil erklärt werden. Obwohl wir vorläufig noch keine Erklärung in Hinsicht auf die Differenz zwischen den C=N-Banden des Isatin-3-anils und den von uns untersuchten Verbindungen finden können, müssen wir bemerken, daß in beiden Arten von Verbindungen dieses Band in einem viel höherwelligem Bereich sichtbar wird als dasjenige, welches der endozyklischen C = N-Gruppe der Aminoindoxyle entspricht.

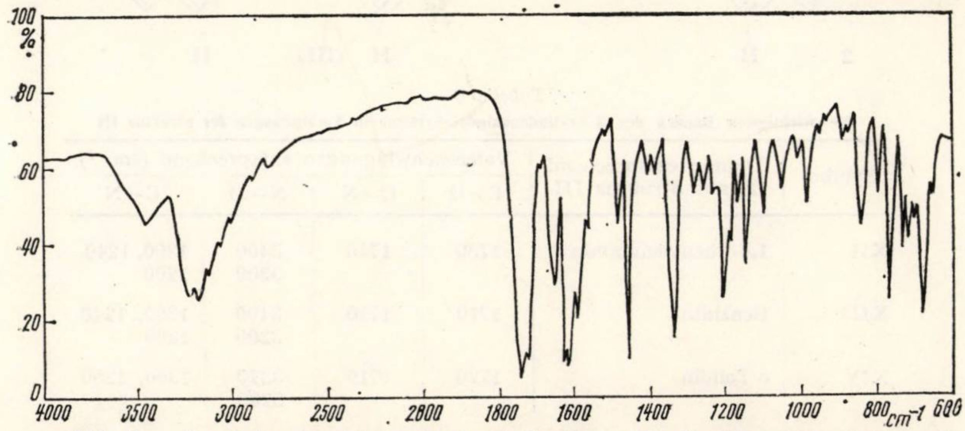

Abb. 5. — Das Infrarotspektrum des Isatin-3-anils in KBr-Preßling (600—4000 cm^{-1}).

Das Band, welches im Spektrum der Iminooxindole um 1610 cm^{-1} (Abb. 4) erscheint, schreiben wir ausschließlich vor allem seiner Form wegen, den Skelettschwingungen des aromatischen Ringes zu.

Die breiten Banden bei 3400 und 3200 cm^{-1} weisen auf N—H—Gruppen hin, die durch Protonbindungen verschiedener Stärke assoziert sind. Auch in diesem Falle wurden Assozierungen durch doppelte Protonbindungen für die Schwingungen um 3200 cm^{-1} verantwortlich gemacht:

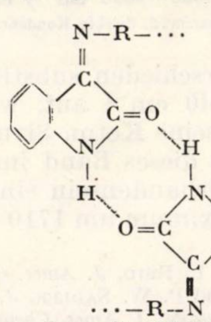

Den Valenzschwingungen der C—N-Bindung wurde eine Gruppe von Banden zwischen 1300 und 1200 cm^{-1} zugesprochen.

Revue Roumaine de Chimie, **18**, *2*, 283–288 (1973)

MATRIZIELLE CHARAKTERISIERUNG DER STRUKTUR UND TOPOLOGIE DER ORGANISCHEN VERBINDUNGEN. I

KONSTITUTION

F. KEREK und I. MOŢOC

Aus dem Organisch-chemischen Laboratorium des
Polytechnischen Instituts „Traian Vuia"
Timişoara Postfach 103

Eingegangen am 22. Juni 1972

Es wird für die Beschreibung der Konstitution der einfachen organischen Verbindungen ein Matrix-Formalismus verwendet. Analog mit den gewöhnlichen Matrizen war es möglich, eine Konstitutionsmatrix als Summe der Elementenmatrizen zu schreiben. Die verwendete Matrix erlaubt einen einfachen mathematischen Ausdruck der Bedingungen der Konstitutionsisomerie und verschiedener diesbezüglicher Probleme.

1. EINLEITUNG

Man kennt zahlreiche Versuche, die Struktur und einige Eigenschaften der organischen Verbindungen mathematisch zu beschreiben. In diesem Sinne verdienen jene erwähnt zu werden, die eine systematische Klassifizierung zum Gegenstand haben, [1] oder jene die die Einführung von Daten in die Computern verfolgen, [2] oder andere dieser Art. [3]

Eine besondere Kategorie stellen die verschiedenen Versuche dar, in der Chemie bekannte mathematische Formalismen anzuwenden, wie zum Beispiel die Graphentheorie, [4,5] die Topolgie [6–8] und andere, [9,10] mit welchen man eine genauere Ausdrucksweise der zahlreichen chemischen Phänomene anstrebt.

---

[1] L. C. Thomas, „A New Chemical Structure Code for Data Storage and Retrieval in Molecular Spectroscopy", Verlag Heyden and Son, London, 1968.

[2] L. Spialter, *J. Amer. Chem. Soc.*, **85**, 2012 (1963); *J. Chem. Documentation*, **4**, 261 (1964). G. Read und D. J. Stone, *J. Chem. Soc.* (*C*), **1966**, 906.

[3] J. J. Mulckhuyse, *Synthese*, **12**, 257 (1960).

[4] C. Berge, „Théorie des graphes et ses applications" 2-te Ausgabe, Verlag Dunod, Paris, 1963.

[5] A. T. Balaban, *Rev. Roumaine Chim.*, **12**, 875 (1967); *Tetrahedron*, **25**, 2949 (1969).

[6] G. Schill, *Liebigs Ann. Chem.*, **693**, 182 (1966).

[7] H. P. Schulz, *J. Org. Chem.*, **30**, 1361 (1965).

[8] V. Prelog, *Nachr. Chem. Techn.*, **14**, 229 (1966); *Chem. Brit.*, **4**, 382 (1968).

[9] E. Ruch und A. Schönhofer, *Theor. Chim. Acta*, **19**, 295 (1970).

[10] E. Ruch und A. Schönhofer, *Theor. Chim. Acta*, **10**, 91 (1968); E. Ruch, *Theor. Chim. Acta*, **11**, 183 (1968).

Eine dritte Kategorie von Autoren versucht grundlegend neue Lösungen zu diesem Problem zu finden. Hierzu gehören in erster Reihe Ugi und seine Mitarbeiter, [11,12] welchen, unter Anwendung einiger Elemente der modernen Mathematik (Mengen, Topologie, usw.), die Ausarbeitung eines allgemein anwendbaren Klassifikations- und Nomenklatursystems gelang.

Unsere Arbeit stellt einen Versuch dar, die Konstitution sowie die Topologie der Moleküle organischer Verbindungen in einer matriziellen Sprachweise auszudrücken, einschließlich die wichtigsten stereoisomerischen Beziehungen.

2. KONSTITUTIONSMATRIZEN

Durch die Adoptierung einer einheitlichen Symbolisierung der verschiedenen Strukturelemente können wir jeder chemischen Verbindung eine Matrix $\mathfrak{M}$ zuordnen, welche deren Konstitution eindeutig darstellt.

Zur Veranschaulichung werden wir zuerst die matrizielle Darstellung im konkreten Fall eines azyklischen Kohlenwasserstoffes: 2,3,3-Trimethyl-5-äthyl-4-t-butyl-heptan (I) zeigen, und anschließend die Verallgemeinerungsmöglichkeiten dieser Methode.

Bezeichnen wir mit 1 ein Kohlenstoffatom (mit 0 ÷ 3 Wasserstoffatomen), mit O ein Wasserstoffatom, mit 2,3, usw. die Radikale Äthyl-, Propyl- usw., während $\bar{3}$, $\bar{4}$ die entsprechenden iso-Formen darstellen, so kann die Konstitution obiger Verbindung (I), in Bezugnahme auf die Hauptkette * (nach der Nomenklatur IUPAC [13]) mit Hilfe folgender Matrix $\mathfrak{M}$, vom Typ n×3 wiedergegeben werden:

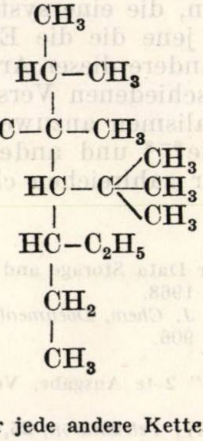

$$\mathfrak{M}(\mathrm{I}) = \begin{bmatrix} 0 & 1 & 0 \\ 0 & 1 & 1 \\ 1 & 1 & 1 \\ 0 & 1 & 4 \\ 0 & 1 & 2 \\ 0 & 1 & 0 \\ 0 & 1 & 0 \end{bmatrix} \qquad M_{42} = \bar{4} = \begin{bmatrix} 0 & 1 & 0 \\ 1 & 1 & 1 \end{bmatrix} \qquad M_{52} = \begin{bmatrix} 0 & 1 & 0 \\ 0 & 1 & 0 \end{bmatrix} \qquad (\mathrm{I})$$

---

* oder jede andere Kette.

[11] I. Ugi, D. Marquarding, H. Klusacek, G. Gokel und P. Gillespie, *Angew. Chem.*, **82**, 741 (1970).

[12] P. Gillespie, P. Hoffman, H. Klusacek, D. Marquarding, S. Pfohl, F. Ramirez, E. A. Tsolis und I. Ugi, *Angew. Chem.*, **83**, 691 (1971).

[13] „IUPAC Nomenclature of Organic Chemistry". 1957, Butterworths, London, 1958.

Für die Substituenten dieser Kette, mit drei oder mehreren Kohlenstoffatomen, ergibt sich, ebenfalls in der ausführlichen matriziellen Schreibungsform, eine sekundäre Matrix, wie es zum Beispiel $\overline{4}$ im obigen Beispiel ist *.

Verallgemeinernd können wir also sagen, daß man einer bestimmten organischen Verbindung eine Matrix $\mathfrak{M}$ zuordnen kann, welche eindeutig ihre Konstitution beschreibt. Für besondere Fälle kann man von der Matrix $n \times 3$ zur Matrix $n \times 1$ oder $n \times 2$ durch Partition übergehen.

Je nach der Art der Kette (Haupt- oder Nebenkette) welcher man die Matrix zuordnet, d.h. also in Bezugnahme auf die Restriktionsbedingungen welche bei ihrer Konstruktion gestellt wurden, unterscheidet man zwei Typen von Matrizen von der Form $n \times 3$:

i) Die Matrix $\mathfrak{M}$-Hauptmatrix, welche die Konstitution des Moleküls in Bezugnahme auf die Hauptkette charakterisiert. In der entwickelten Form (siehe Beziehung (3)) beschreibt sie aber eindeutig die Konstitution des gesamten Molekülaufbaues.

ii) Die Matrizen M, sekundäre genannt, welche Nebenmatrizen[14-17] der Matrix $\mathfrak{M}$ sind. Weil auch die Elemente einer Matrix M Nebenmatrizen vom Typ M sein können, kommen wir überein, einen zusätzlichen Begriff zu definieren, und zwar: Die Spezies k einer Konstitutionsmatrix. Die Spezies der Matrix $\mathfrak{M}$ ist, laut Definition, gleich mit 1 ($k = 1$). Die Elemente der Matrix $\mathfrak{M}$ zerlegt man in Matrizen vom Spezies 2 ($k = 2$), die man mit ${}^2M$ bezeichnet. Die Elemente der Matrix ${}^2M$ zerlegt man in ${}^3M$, usw. Im allgemeinen: M ist vom Spezies k (${}^kM$), wenn sie in der Matrix vom Spezies $k - 1$ (${}^{k-1}M$) Element ist.

Die Matrix $\mathfrak{M}$ besteht also aus:

$$\mathfrak{M} = \begin{bmatrix} {}^2M_{11} & 1 & {}^2M_{12} \\ \cdots & \cdots & \cdots \\ {}^2M_{l1} & 1 & {}^2M_{l2} \\ \cdots & \cdots & \cdots \\ {}^2M_{n^11} & 1 & {}^2M_{n^12} \end{bmatrix}$$

Man kann erkennen, daß $\mathfrak{M}$ die Matrix darstellt, die der Hauptkette (bestehend aus n^1 Kohlenstoffatomen) des Kohlenwasserstoffes oder dessen Derivate zugeordnet ist. Die Matrix $\mathfrak{M}$ kann man als folgende Summe schreiben:

$$\mathfrak{M} = \sum_{\text{alle } (l,p)} {}^2M_{lp} \, {}^{n^1}m_{lp} + {}^{n^1}m_{00} \tag{1}$$

---

* **Übereinkunftsgemäß vernachlässigt man die Zeilen 0 0 0, welche vor der ersten Zeile der Matrizen $\mathfrak{M}$ und M stehen müßten, bzw. nach der letzten Zeile der Matrix $\mathfrak{M}$ folgen müßten.**

[14] G. Cohen, „Eléments de Calcul Matriciel, à l'usage des E.N.S.A.M. et Ecoles d'Ingénieurs", Dunod, Paris, 1962.

[15] D. Michal, „Matrice and Tensor Calculus", Wiley, New York, 1966.

[16] H. Schwerdtfeger, „Introduction to Linear Algebra and Theory of Matrices", Verlag Noordhoff, Groningen, 1950.

[17] D. Pham, „Techniques du calcul matriciel", Verlag Dunod, Paris, 1962.

Es wird die folgende Zerlegungsweise gewählt [13-16]:

$$\mathfrak{M} = {}^2M_{11}\begin{bmatrix} 1 & 0 & 0 \\ \cdots & \cdots & \cdots \\ 0 & 0 & 0 \\ \cdots & \cdots & \cdots \\ 0 & 0 & 0 \end{bmatrix} + {}^2M_{12}\begin{bmatrix} 0 & 0 & 1 \\ \cdots & \cdots & \cdots \\ 0 & 0 & 0 \\ \cdots & \cdots & \cdots \\ 0 & 0 & 0 \end{bmatrix} + {}^2M_{n1}\begin{bmatrix} 0 & 0 & 0 \\ \cdots & \cdots & \cdots \\ 0 & 0 & 0 \\ \cdots & \cdots & \cdots \\ 1 & 0 & 0 \end{bmatrix} +$$

$$+ {}^2M_{n2}\begin{bmatrix} 0 & 0 & 0 \\ \cdots & \cdots & \cdots \\ 0 & 0 & 0 \\ \cdots & \cdots & \cdots \\ 0 & 0 & 1 \end{bmatrix} + \begin{bmatrix} 0 & 1 & 0 \\ 0 & 1 & 0 \\ \cdots & \cdots & \cdots \\ 0 & 1 & 0 \\ \cdots & \cdots & \cdots \\ 0 & 1 & 0 \end{bmatrix} \qquad (2)$$

Es folgt aus der Gleichheit von (1) mit (2), daß:

$$^{n1}m_{00} = \begin{bmatrix} 0 & 1 & 0 \\ 0 & 1 & 0 \\ \cdots & \cdots & \cdots \\ 0 & 1 & 0 \\ \cdots & \cdots & \cdots \\ 0 & 1 & 0 \end{bmatrix}$$

Andererseits sind ${}^{n1}m_{lp}$ Matrizen, die alle Elemente gleich Null haben, außer dem Element (l, p), das gleich 1 ist. Man kann diese Zerlegung der Matrix $\mathfrak{M}$ in einer allgemein gültigen Form schreiben:

$$\mathfrak{M} = {}^{n1}m_{00} + \sum_{\text{alle }(l,\,p)} \sum_{\text{alle }k} \sum_{\text{alle }(l',\,p')} ({}^{k+1}M_{l'p'} \cdot {}^{k+1}m_{l'p'}) \cdot {}^{n1}m_{lp} \qquad (3)$$

wo: $l = 1, 2, \ldots, n;$ $\quad p = 1, 2$

$l' = 1, 2, \ldots, n;$ $\quad p' = 1, 2$

$k = 1, 2, \ldots;$

die gegebene Werte annehmen können.

Für das Hervorheben eines bestimmten Liganden (l_0, p_0) der Hauptkette C_{n^1} benützt man die folgende Zerlegungsweise :

$$\mathfrak{M} = {}^{1n}m_{00} + \sum_{(lp)\neq(l_0p_0)} {}^2M_{lp}\cdot{}^{n^1}m_{lp} + {}^2M_{l_0p_0}\cdot{}^{n^1}m_{l_0p_0} \tag{4}$$

Eine konkrete Anwendung der Gleichung (3) auf die Verbindung (II) führt uns zu dem Ausdruck (5) :

$$CH_3-C(CH_3)_2-CH_2-CH[C(CH_3)_3]-(CH_2)_2-CH_3 \tag{II}$$

$$\begin{aligned}\mathfrak{M} = {}&{}^7m_{00} + {}^7m_{21} + {}^7m_{22} + {}^7m_{42}\cdot({}^2m_{00} + {}^2m_{21} + {}^2m_{22} + 0\cdot{}^2m_{11} + 0\cdot{}^2m_{12}) + \\ &+ 0\cdot({}^7m_{11} + {}^7m_{12} + {}^7m_{31} + {}^7m_{32} + {}^7m_{51} + {}^7m_{52} + {}^7m_{61} + {}^7m_{62} + \\ &+ {}^7m_{71} + {}^7m_{72}).\end{aligned} \tag{5}$$

Im Falle der Verbindung (III) erhält man den Ausdruck (6) :

$$CH_3-C(CH_3)_2-C[C(CH_3)_3]_2-C(CH_3)_2-CH_3 \tag{III}$$

$$\begin{aligned}\mathfrak{M} = {}&\begin{bmatrix} 0 & 1 & 0 \\ 1 & 1 & 1 \\ 4 & 1 & 4 \\ 1 & 1 & 1 \\ 0 & 1 & 0 \end{bmatrix} = {}^5m_{00} + {}^5m_{21} + {}^5m_{22} + {}^5m_{41} + {}^5m_{42} + ({}^5m_{31} + {}^5m_{32})\cdot \\ &\cdot({}^2m_{00} + 0\cdot{}^2m_{11} + 0\cdot{}^2m_{21} + 0\cdot{}^2m_{12} + {}^2m_{21} + {}^2m_{22}) + \\ &+ 0\cdot({}^5m_{11} + {}^5m_{21} + {}^5m_{41} + {}^5m_{42}).\end{aligned} \tag{6}$$

3. KONSTITUTIONSISOMERIE

Die matrizielle Behandlung der Konstitutionsisomerie besteht in der Bestimmung der Bedingungen, unter welchen man die Matrix $\mathfrak{M}$ und die Matrizen M aufbaut.

In der folgenden Ausführung stellen (lp), $(l'p')$ die Elemente aus den Positionen (lp), beziehungsweise $(l'p')$ dar. Wir werden nun die Kettenisomerie im Alkan $C_x H_{2x+2}$ $(x = 1, 2, \ldots)$ behandeln :

Die erste Isomeriebedingung ist :

$$\sum_{l=1}^{n^1}\sum_{p=1}^{2}(l,p) = x - n^1 \tag{7}$$

$$\sum_{l'=1}^{k+2_n}\sum_{p'=1}^{2}(l',p') = {}^k(l'\,p') - {}^{k+1}q \tag{8}$$

In diesen Beziehungen stellen n^1 und q die Dimensionen der Haupt- beziehungweise der sekundären Matrizen dar. Mit ${}^k(l'p')$ wurde das Element $(l'p')$ aus der Matrix M der Spezies k bezeichnet. Die nächste Bedingung ist tatsächlich ein mathematischer Ausdruck der IUPAC-Nomenklaturkonvention [17] bezüglich der Länge der Haupt- und Nebenketten. Es wird gezeigt, daß die Länge der Nebenkette, die vom Zentrum j abzweigt, folgende zwei Bedingungen erfüllen muß:

a.) Für die Matrix $\mathfrak{M}$:

$$ {}^1j - 1 \geqslant {}^2q \leqslant {}^1n - ({}^1j + 1). \tag{9}$$

In der obigen Ungleichung ziehen wir das Gleichheitszeichen in Betracht, wenn:

$a - 1$: die Anzahl der Elemente $(lp) \neq 0$ der Nebenmatrix $(>j) \times 3$ ist.

$a - 2$: die Anzahl der Elemente $(lp) \neq 0$ der Nebenmatrix $(<j) \times 3$ größer oder gleich mit der Anzahl der Elemente $(l'p') \neq 0$ der Matrix $q \times 3$ ist.

b.) Für die Matrizen M:

$$ {}^kj - 1 \geqslant {}^{k+1}q. \tag{10}$$

Die Bedingung, in welcher in obiger Beziehung auch das Gleichheitszeichen gültig wird, ist jene, die oben mit $a - 1$ bezeichnet wurde.

Dank der Existenz der gleichwertigen Stellungen auf einer Hauptkette beschreiben zwei Matrizen die gleiche chemische Konstitution wenn:

$$\begin{bmatrix} {}^2M_{11} & 1 & {}^2M_{12} \\ \cdot\;\cdot\;\cdot & \cdot\;\cdot\;\cdot & \cdot\;\cdot\;\cdot \\ {}^2M_{n^11} & 1 & {}^2M_{n^12} \end{bmatrix} = \begin{bmatrix} {}^2M_{n^11} & 1 & {}^2M_{n^12} \\ \cdot\;\cdot\;\cdot & \cdot\;\cdot\;\cdot & \cdot\;\cdot\;\cdot \\ {}^2M_{11} & 1 & {}^2M_{12} \end{bmatrix} \tag{11}$$

Andere Möglichkeiten, die zur Gleichwertigkeit der Matrizen führen würden, schließt man durch folgende Bedingungen (12) aus:

$$\begin{aligned} (l\ 1) &< (l\ 2); \quad & l &= 1, 2, \ldots, n^1 \\ (l'\ 1) &< (l'\ 2); \quad & l' &= 1, 2, \ldots, q. \end{aligned} \tag{12}$$

Die Bestimmung der Anzahl der Kettenisomere einer chemischen Verbindung besteht also darin, die Anzahl der nichtgleichwertigen Matrizen $\mathfrak{M}$, die ihr zugeordnet wurden, zu finden.

4. SCHLUSSFOLGERUNGEN

Der hier vorgeschlagene Matrix-Formalismus der Konstitution einfacher organischer Verbindungen erlaubt eine anschauliche Ausdrucksweise der dazugehörigen Probleme. Unter anderen, scheint diese Schreibweise versprechend für die Computereinführung von Konstitutionsdaten, sowie auch für eine mathematische Formulierung der wichtigsten topologischen Beziehungen, die sich gegenwärtig noch in ihrer Ausarbeitung befindet.

Revue Roumaine de Chimie, **18**, *2*, 289–296 (1973)

MATRIZIELLE CHARAKTERISIERUNG DER STRUKTUR UND TOPOLOGIE ORGANISCHER VERBINDUNGEN. II

KONFIGURATION, CHIRALITÄT

I. MOŢOC und F. KEREK
Aus dem Organisch-chemischen Laboratorium des
Polytechnischen Instituts „Traian Vuia"
Timişoara Postfach 103

Eingegangen am 22. Juni 1972

Für eine anschauliche mathematische Charakterisierung der molekularen Topologie wird eine kanonische Matrix vorgeschlagen. Diese, zusammen mit einigen Operatoren ($\mathcal{C}$, $\mathcal{L}$, *F*, *T*) erlauben eine einfache mathematische Ansdrucksweise des Verfahrens zur Bestimmung der molekularen Chiralität sowie der verschiedenen stereoisomeren Beziehungen. Beachtlich sind die Vergleiche zwischen dem mathematischen und chemischen Sinne dieser Gleichungen, wie zum Beispiel: die den enantiomeren Konfigurationen zugeordneten Matrizen stehen im Verhältnis Matrix-transponierte Matrix.

1. EINLEITUNG

In unserer vorhergehenden Arbeit [1] wurden die Prinzipien der matriziellen Beschreibung der Konstitution organischer Verbindungen dargelegt. Im folgenden wird versucht, dieselbe mathematische Methode in der Beschreibung der topologischen Eigenschaften der Moleküle anzuwenden.

Die chemische Topologie beschäftigt sich, laut Prelogs Definition, [2,3] mit den Eigenschaften der geometrischen Figuren, die mit der momentanen oder „time average" Topographie der chemischen Teilchen (also damit, was man gewöhnlich als räumliche Anordnung der Atome im Molekül bezeichnet) isomorph oder homöomorph sind.

In einer topologischen Behandlung eines Molekülaufbaus kommt den metrischen Parametern eine beschränkte Bedeutung zu, d.h. man operiert nicht in einem metrischen Raum. Jedoch auf diese Art und

---

[1] F. Kerek und I. Moţoc, *Rev. Roumaine Chim.*, Rev. Roumaine Chim., dieses, Heft, S. 285

[2] V. Prelog, Abstr. Roger Adams Award Lecture 1969, ACS Meeting, Salt Lake City, Utah.

[3] V. Prelog, *Chem. Brit.*, **4**, 382 (1968).

Weise erzielt man eine Verallgemeinerung der Probleme, denn der metrische Raum ist ein Sonderfall des afinen Raumes. [4]

Die Idee der topologischen Behandlung der Stereoisomerie und der damit zusammenhängenden Erscheinungen fand interessante Anwendungen. [5] Ebenso erzielte man spektakuläre experimentelle Beweise für einige „rein"-topologische Isomeriefälle. [6-9]

Besondere Beachtung in der Reihe der theoretischen Ausführungen verdienen die Arbeiten von Ruch und seinen Mitarbeitern. [10-12] Sie haben, unter anderen, eine umfassende Theorie der Chiralitätsfunktionen und der damit verbundenen Phänomene aufgestellt.

Arbeiten von grundlegender Bedeutung sind die kürzlich erschienenen Artikel von Ugi und Mitarbeiter, [13,14] welche die Thematik der Molekularstruktur behandeln, in einem sowohl den statischen als auch den dynamischen Problemen allgemein anwendbaren mathematischen Formalismus. Die Verfasser haben zu diesem Zweck Elemente der modernen Mathematik (Mengen, Gruppen, Permutationen usw.) erfolgreich verwendet.

Von Anfang an weisen wir darauf hin, daß diese Arbeit keine ähnliche, die Gesamtheit der strukturellen Probleme umfassende Behandlung beabsichtigt! Es wird versucht, nur eine einfache und anschauliche mathematische Struktur für die Charakterisierung der häufigsten Aspekte struktureller Beziehungen zu finden. Der Zweck einer solchen Umschreibung der chemischen Realität in mathematischen Modellen ist, mit diesen Modellen mathematische Operationen ausführen zu können, um nachher die entsprechenden Schlußfolgerungen mit Hilfe von chemischen Ausdrücken zu erläutern.

Es sei noch hinzugefügt, daß die Behandlung der mit der Stereoisomerie zusammenhängenden Beziehungen, nur auf die topologischen Aspekte der Probleme beschränkt wird. Ebenso wird es einfachheitshalber in jedem Fall versucht, die in Betracht gezogenen strukturellen Elemente, nach Möglichkeit, auf ein Minimum zu beschränken. Mit anderen Worten, es werden nur jene strukturellen Elemente behandelt, die eine bestimmte Rolle in der analysierten Struktureinheit haben.

Es ist möglich, daß die Anwendung des matriziellen Formalismus in einigen besonderen Fällen, infolge der Vereinfachungstendenz weniger erfolgreich sein wird.

---

[4] J. Garsoux, „Espaces vectoriels topologiques et distributions", Dunod, Paris **1963**.

[5] E. L. Muetterties, *J. Amer. Chem. Soc.*, **91**, 1636; 3098; 4115 (1969).

[6] E. Wasserman, *Sci. American*, **207**, 94 (1962).

[7] A. Lüttringhaus, F. Cramer, H. Prinzbach und F.M. Henglein, *Liebigs Ann. Chim.*, **613**, 185 (1958).

[8] V. Prelog und H. Gerlach, *Helv. Chim. Acta.*, **47**, 2288 (1964).

[9] H. Gerlach, J. A. Owtschinnikov und V. Prelog, *Helv. Chim. Acta*, **47**, 2294 (1964).

[10] E. Ruch und A. Schönhofer, *Theor. Chim. Acta.*, **10**, 91 (1968).

[11] E. Ruch, *Theor. Chim. Acta.*, **11**, 183 (1968).

[12] E. Ruch und A. Schönhofer, *Theor. Chim. Acta.*, **19**, 225 (1970).

[13] I. Ugi, D. Marquarding, H. Klusacek, G. Gokel und P. Gillespie *Angew. Chem.*, **82**, 741 (1970); P. Gillespie, P. Hoffmann, H. Klusacek, D. Marquarding, S. Pfohl, F. Ramirez, E. Tsolis und I. Ugi, *Angew. Chem.*, **83**, 691 (1971).

[14] I. Ugi und P. Gillespie, *Angew. Chem.*, **83**, , 980; 982 (1971).

2. KONFIGURATION

2.1. DEFINITION. ALLGEMEINE BETRACHTUNGEN

Zahlreiche Verfasser haben in letzter Zeit auf das Fehlen einer vollkommenen, zufriedenstellenden Definition des Begriffes der Konfiguration, beziehungsweise der Konformation hingewiesen. [15–17]

Es ist in diesem Rahmen nicht angebracht, die verschiedenen Seiten dieser Problematik zu behandeln. [18] Trotzdem ist es notwendig, den Sinn, in dem die betreffenden Begriffe im folgenden verwendet werden, klarzulegen.

Im Rahmen einer auf topologische Aspekte beschränkten Behandlung muß die *Konfiguration* als ein topologisches Modell der relativen räumlichen Anordnung der Liganden in bezug auf ein Strukturelement betrachtet werden, ohne die verschiedenen, durch relative Torsionsbewegungen um internukleare Achsen des Moleküls erzeugbaren Varianten, in Betracht zu ziehen.

Für die folgenden Ausführung werden die, durch solche Drehungen erhaltenen und geläufig als *Konformationen* bezeichneten Varianten, ebenfalls vom topologischen Standpunkt aus betrachtet.

Das Problem der Molekularchiralität spielt natürlich im Rahmen der Gesamtheit der stereoisomeren Beziehungen eine grundlegende Rolle. Wir übernehmen die Definition des Begriffes in dem von Kelvin gegebenen Sinn (1904), [19] mit der Bemerkung, daß wir uns in erster Reihe auf die geläufigen, d.h. auf die von Ruch und Mitarbeiter mit *a* bezeichneten Typen von Molekularchiralität beziehen.

Zu Beginn werden wir die Konvention zur Spezifikation der zentralen Chiralität nach Cahn, Ingold und Prelog [20] vom mathematischen Standpunkt aus behandeln, da sie eine grundlegende Bedeutung in der Diskussion der mit der Chiralität zusammenhängenden chemischen Aspekte hat.

2.2. DAS CAHN, INGOLD, PRELOG-VERFAHREN ZUR BESTIMMUNG DER MOLEKULAREN CHIRALITÄT

Dieses Verfahren umfaßt eigentlich folgende Teile :

— Ein Set von Instruktionen, welche die prioritäre Ordnung der Liganden festlegen und zusammenfassend als Standard-Sequenzregel bekannt sind, die wir künftighin mit I bezeichnen werden.

— Die Instruktionen, welche die konventionelle Betrachtungsweise des Chiralitätselements betreffen, die wir mit *K* bezeichnen werden.

---

[15] R. S. Cahn und V. Prelog, „Report on Symposium, on Stereochemical Concepts and Nomenclature", London 1968.

[16] IUPAC Tentative Rules for the Nomenclature of Organic Chemistry Section E. Fundamental Stereochemistry, *J. Org. Chem.*, **35**, 2849 (1970).

[17] * * * *Nachr. Chem. Techn.*, **17**, 443 (1969).

[18] G. Ostrogovich und F. Kerek, „Kompendium der Elemente der Stereochemie", Polytechnisches Institut Timişoara, 1971.

[19] „Chiral heißt jede geometrische Figur, die mit ihrem Spiegelbild nicht kongruent ist", Lord Kelvin, Baltimore Lectures (1884); L. Whyte, *Nature*, **180**, 513 (1957); **182**, 198 (1958).

[20] R. S. Cahn, C. K. Ingold und V. Prelog, *Angew. Chem.*, **78**, 413 (1966).

In Funktion von diesen Bedingungen kann der Sinn der Chiralität in jedem Fall eindeutig als *R* (rectus) oder *S* (sinister), beziehungsweise als *P* (plus) oder *M* (minus) bestimmt werden.

2.3. STANDARD-SEQUENZREGEL

Die Spezifikation des Sinnes der Chiralität drängt in jedem Fall die Differenzierung der Liganden eines Chiralitätszentrums auf, deren Anzahl $\mathcal{N}$ gewöhnlich zwischen 2 und 6 liegt : $2 \leqslant \mathcal{N} \leqslant 6$.

Ganz allgemein gesehen, kann man von der Menge der möglichen Liganden $\overline{\psi}$ sprechen :

$$\overline{\psi} = \{\psi_N\} \qquad (N = 1, 2, \ldots, \infty)$$

Die Menge aller möglichen Liganden $\overline{\psi}$ ist unendlich und zählbar. Laut der Standard-Sequenzregel können wir den nichtidentischen Elementen ψ dieser Menge $[\psi \in \overline{\psi}]$ Indices N zuordnen. Die Zuordnung des Index N erzielt man durch eine isomorphe Abbildung, d.h. einem gegebenen Liganden entspricht ein einziger Index. Da die Menge N der natürlichen Zahlen aufgrund der Beziehung „ist größer" (d.h. $>$) vollkommen geordnet ist, wird auch die Menge $\overline{\psi}$ durch die isomorphe Natur der Abbildung total geordnet sein.

$$N > N' \text{ bedeutet, daß auch } \psi_N > \psi_{N'} \tag{I}$$

3. CHARAKTERISIERUNG DER KONFIGURATION DURCH EINE KANONISCHE MATRIX

Von topologischem Standpunkt aus ist die Konfiguration eines Strukturelements durch die relative räumliche Anordnung der diesem Element zugeordneten Liganden definiert.

Für gewöhnliche organische Verbindungen bleibt die Zahl der Liganden, die eine definierende Rolle für den Sinn der Konfiguration haben, begrenzt, und zwar : $2 \leqslant \mathcal{N} \leqslant 4$.

Alle diese Liganden gehören der vollkommen geordneten Menge $\overline{\psi}$ an. Im Falle von vier, einem Chiralitätselement zugeordneten Liganden ist die Anordnung derselben in einer Matrix vom Typ 2×2 anschaulich und vorteilhaft dargestellt :

$$M^* = \begin{bmatrix} \psi_{11} & \psi_{12} \\ \psi_{21} & \psi_{22} \end{bmatrix} \qquad \psi_{ij} \in \overline{\psi} \ (i, j = 1, 2) \tag{1}$$

Um eine eindeutige Beziehung zwischen der chiralen Struktur und der zugeordneten Matrix herzustellen sind die folgenden Bemerkungen besonders notwendig :

— Der Ligand letzten Ranges nach der Standard-Sequenzregel (I) nimmt die Position ψ_{22} in der Matrix M^* ein.

— Die Hauptdiagonale der Matrix stellt die entfernteste Kante des Tetraeders dar (Bedingung *K* von Cahn, Ingold und Prelogs Verfahren). Abbildung (1) veranschaulicht diese zwei Konventionen:

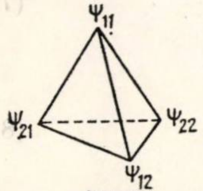

Abb.(1)

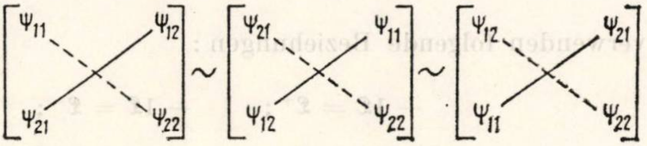

$$\begin{bmatrix}\psi_{11} & \psi_{12}\\ \psi_{21} & \psi_{22}\end{bmatrix} \sim \begin{bmatrix}\psi_{21} & \psi_{11}\\ \psi_{12} & \psi_{22}\end{bmatrix} \sim \begin{bmatrix}\psi_{12} & \psi_{21}\\ \psi_{11} & \psi_{22}\end{bmatrix} \qquad (2)$$

Zieht man das Element ψ_{22} letzten Ranges $\equiv 0$ in Betracht, dann erhalten obige Matrizen folgende kanonische Form *M*:

$$M = \begin{bmatrix}\psi_{11} & \psi_{12}\\ \psi_{21} & 0\end{bmatrix} \quad M' = \begin{bmatrix}\psi_{21} & \psi_{11}\\ \psi_{12} & 0\end{bmatrix} \quad M'' = \begin{bmatrix}\psi_{12} & \psi_{21}\\ \psi_{11} & 0\end{bmatrix} \qquad (3)$$

Alle drei Matrizen beschreiben ein und dieselbe Konfiguration, wie das im folgenden gezeigt wird.

3.1. SPEZIFIKATION DER ZENTRALEN CHIRALITÄT

Wir definieren einen Operatoren $\mathcal{C}^\varphi$ mit folgenden Eigenschaften:

$$\mathcal{C}^1 M = M' \quad \mathcal{C}^2 M = \mathcal{C}^1 M' = M'' \quad \mathcal{C}^1 M'' = M \qquad (4)$$

$$M = \mathcal{C}^0 M = \mathcal{C}^2 M' = \mathcal{C}^1 M''$$

d.h. verallgemeinert:

$$\mathcal{C}^\varphi a = a \qquad (a = \text{Skalar})$$

$$\mathcal{C}^\varphi = \mathcal{C}^1 \mathcal{C}^{\varphi-1} \longleftrightarrow \mathcal{C}^\varphi = \mathcal{C}^{\varphi-3k} \qquad (5)$$

wo: $k = 0, 1, \ldots$ und $\varphi \geqslant 3$.

Daraus folgt, daß der Operator $\mathcal{C}^\varphi$ eine zirkulare Permutation mit Elementen, die mit ψ_{22} nichtidentisch sind, und zwar im Uhrzeigersinn aufstellt.

Gegeben ist auch der Operator $\mathcal{L}$, der eine zirkuläre Permutation der Liganden ψ_{11}, ψ_{12}, ψ_{21} in der von der Standard-Sequenzregel dieser Liganden festgelegten Reihenfolge aufstellt. Man kann also schreiben:

$$\mathcal{C}^\varphi M = \lambda \mathcal{L} M. \qquad (6)$$

Aus der Beziehung (6) folgt, daß der Skalar λ die Werte $\lambda = \pm 1$ annimmt, d.h. jedwelche Matrix von chiraler Konfiguration erfüllt eine der folgenden Gleichungen :

$$\mathcal{C}^{\varphi} = \mathcal{L}\,; \qquad \mathcal{C}^{\varphi} = -\,\mathcal{L}\,; \tag{7}$$

Wir verwenden folgende Beziehungen :

$$+\,1\mathcal{L} = \mathcal{L}^{+}\,; \qquad -\,1\mathcal{L} = \mathcal{L}^{-}\,; \tag{8}$$

Also werden die Gleichungen (7) :

$$\mathcal{C}^{\varphi} = \mathcal{L}^{+}\,; \qquad \mathcal{C}^{\varphi} = \mathcal{L}^{-}\,; \tag{9}$$

Wir bemerken, daß die Anwendung dieser Operatoren der Drehung der Verbindung um die Achse $C - \psi_{22}$ auf folgende zwei Arten gleichkommt :

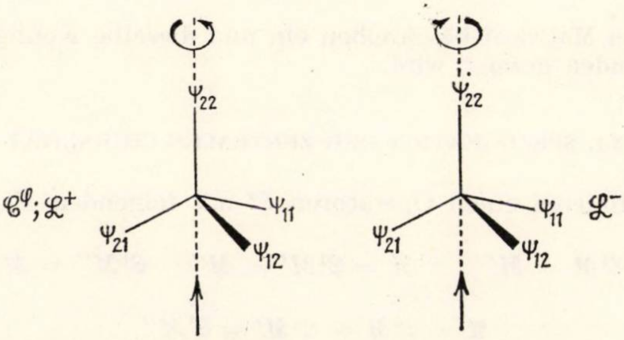

Durch unmittelbares Berechnen kann man zeigen, daß :

$$\mathcal{C}^{\varphi}\mathcal{L}^{+} = \mathcal{L}^{+}\mathcal{C}^{\varphi} \qquad \mathcal{C}^{\varphi}\mathcal{L}^{-} = -\,\mathcal{L}^{-}\mathcal{C}^{\varphi}$$

$$\mathcal{L}^{+} = -\,\mathcal{L}^{-} \longleftrightarrow \mathcal{L}^{-} = -\,\mathcal{L}^{+}$$

Faßt man obige Eigenschaften zusammen, so :

$$\mathcal{C}^{\varphi}\mathcal{L}^{-} = -\,\mathcal{L}^{-}\mathcal{C}^{\varphi} = \mathcal{L}^{+}\mathcal{C}^{\varphi} = \mathcal{C}^{\varphi}\mathcal{L}^{+}$$

Man kann also behaupten, daß die Matrix M eine Konfiguration $R(M_R)$, beziehungsweise $S(M_S)$ definiert, je nachdem, ob sie die Gleichung :

$$\mathcal{C}^{\varphi}M_R = \mathcal{L}^{+}M_R$$

oder :

$$\mathcal{C}^{\varphi}M_S = \mathcal{L}^{-}M_S$$

erfüllt. Mit anderen Worten, verwirklicht die Teilung der Menge $\lambda = \{M\}$ in zwei Klassen (Untermengen), λ_R und λ_S, so daß:

$$\lambda_R U \lambda_S = \lambda; \qquad \lambda_R \cap \lambda_S = \Phi$$

Das heißt, daß λ_R und λ_S disjunkt sind, da es keine Matrix M gibt, die sowohl λ_R als auch λ_S angehört.

Gegeben sei nun eine Matrix M_R, d.h. $\mathfrak{C}^{\varphi} M_R = \mathfrak{L}^{+} M_R$. Gegeben ist auch M_R^T, die transponierte Matrix von M_R. Durch unmittelbares Berechnen findet man:

$$-\mathfrak{C}^{\varphi} M_R^T = \mathfrak{L}^{+} M_R^T$$

oder:

$$-[-\mathfrak{C}^{\varphi} M_R^T] = -\mathfrak{L}^{+} M_R^T \tag{10}$$

Das heißt:

$$\mathfrak{C}^{\varphi} M_R^T = \mathfrak{L}^{-} M_R^T \tag{11}$$

Also $M_R^T \in \lambda_S$, was soviel bedeutet wie: $M_R^T \equiv M_S$
Die Transponierung ($|^T$) führt zur Inversion der Konfiguration. Also die beiden Klassen von Konfigurationsmatrizen verwandeln sich eine in die andere durch die Transponierung ihrer Elemente.

Folglich stehen die den zwei enantiomeren Konfigurationen entsprechenden Matrizen im Verhältnis Matrix und ihre transponierte Matrix zueinander.

Für jede Konfigurationsmatrix M des Chiralitätszentrums eines Moleküls (mit einem einzigen Chiralitätszentrum) kann man folgende Chiralitätsgleichungen schreiben:

$$\mathfrak{C}^{\varphi} M = \mathfrak{L}^{+} M \qquad \mathfrak{C}^{\varphi} M^T F = \mathfrak{L}^{-} M^T F \tag{12}$$

oder:

$$\mathfrak{C}^{\varphi} M = \mathfrak{L}^{-} M \qquad \mathfrak{C}^{\varphi} M^T F = \mathfrak{L}^{+} M^T F \tag{13}$$

Mit F wurde folgende Matrix bezeichnet:

$$F = \begin{bmatrix} \delta & 0 \\ 0 & \delta \end{bmatrix}$$

wo δ der Operator ist, welcher folgende Operation ausführt:

$$[a_{ji}]\delta = [a_{ji}]^T = [a_{ij}]$$

F besitzt die Eigenschaft:

$$F.F = E$$

wo :

$$E = \begin{bmatrix} 1 & 0 \\ 0 & 1 \end{bmatrix}$$

Aus den Gleichungen (12) und (13) folgt, daß die aufeinanderfolgende Anwendung der Operation F und beziehungsweise $|^T$ die Widerspiegelung des Moleküls in seiner Gesamtheit darstellt. Durch F wird die konfigurative Inversion der Liganden, durch die Transposition T aber wird dieselbe Operation beim betreffenden Zentrum erzielt.

SCHLUSSFOLGERUNGEN

Die Anwendung der matriziellen Struktur bei der Charakterisierung der Konfiguration ermöglichte die Festlegung einiger analytischer Ausdrücke (Gleichungen). Diese ermöglichen eine kurzgefaßte Beschreibung des Chiralitätssinnes, der Enantiomeriebeziehung im Falle der zentralen Chiralität.

Es ist wichtig zu bemerken, daß sich die matrizielle Beschreibung schon lange Zeit als beste Methode zur Beschreibung der Vektor- und Tensorprobleme bewährt hat. Diese Parallele erlaubt unter anderen, die verschiedenen Chiralitätserscheinungen als vektorielle Probleme zu betrachten.

Vorläufig werden wir in unserer folgenden Arbeit [21] die axiale, konformationelle Chiralität und andere spezielle Chiralitätsfälle betrachten.

---

[21] F. Kerek und I. Moţoc (noch unveröffentlicht).

Revue Roumaine de Chimie, 18, 2, 297–304 (1973)

MODERN FRIEDEL-CRAFTS CHEMISTRY. I

CYCLIALKYLATIONS OF SOME SECONDARY AND TERTIARY PHENYLALKYL CHLORIDES IN THE PRESENCE OF THE MILD $AlCl_3/CH_3NO_2$ AND $FeCl_3$ CATALYSTS

ALI ALI KHALAF

Department of Chemistry, Assiut University, Assiut,
Arab Republic of Egypt

Received July 26, 1972

Chlorides (1) through (8) were prepared and their reactions in the presence of $AlCl_3/CH_3NO_2$ and $FeCl_3$ catalysts were investigated. In the presence of these mild catalysts, the chlorides underwent clean cyclidehydrohalogenations to give the corresponding indans and tetralins in yields much better than those reported previously from the cyclidehydrations of the corresponding alcohols with either sulphuric or phosphoric acid. The results, in general, demonstrated that Fiedel-Crafts cyclialkylations provide a very useful simple method for preparing indan and tetralin derivatives.

In 1966, Khalaf and Roberts[1] investigated, among other things, the cyclialkylations of certain phenylalkyl chlorides in the presence of aluminum chloride as catalyst. Utilising modern instrumental methods of separation and identification, these authors recognized two important facts about these reactions: First, certain generalizations regarding the extent or lack of accompanying rearrangements that have been made by other workers[2] are too broad, and some of the experimental data upon which these generalizations were reached are virtually incorrect. Secondly, with the strong catalyst aluminum chloride, the cyclialkylation reactions were frequently accompanied by other side reactions, especially intermolecular polyalkylation and hydride exchange. For example, the latter reaction was held responsible for the formation of isopentylbenzene in the $AlCl_3$-catalyzed cyclization of both 2-chloro-2-methyl-4-phenylbutane and 1-chloro-2-methyl-4-phenylbutane and of isohexylbenzene in the cyclization of 2-chloro-2-methyl-5-phenylpentane[1]. These side reactions which result in the production of compounds with boiling points very close to those of the expected cyclic products place very serious limitations on the synthetic potentialities of these aluminum chloride-catalyzed cyclialkylations. For this reason, it was found of interest to study the utilization of mild catalysts such as $FeCl_3$ and $AlCl_3/CH_3NO_2$ complex in an attempt to eliminate or, at least, to minimize the observed undesirable side reactions. Frequently, the use of the mild $AlCl_3/CH_3NO_2$ catalyst has been shown to be advantageous, both in industrial processes and in laboratory syntheses, not only because it inhibits all the side reactions that are initiated by the abstraction of hydride ions,[3-8] but also because it has a uniform activity and a constant physical state.[9]

---

[1] A. A. Khalaf and R. M. Roberts, *J. Org. Chem.*, 31, 89 (1966).

[2] G. Baddeley and R. Williamson, *J. Chem. Soc.*, 1956, 4647.

In the present work, the Friedel-Crafts cyclialkylations of the tertiary chlorides **1** to **6** and of the secondary chlorides **7** and **8** were investigated in the presence of both $AlCl_3/CH_3NO_2$ and $FeCl_3$ catalysts.

RESULTS AND DISCUSSION

The results of the cyclialkylation reactions of chlorides (**1**) through (**8**) are summarized in Table 1 and schematically in equations (A) to (H).

Table 1

Cyclialkylation Reactions of Secondary and Tertiary Phenylalkyl Chlorides in the Presence of $AlCl_3/CH_3NO_2$ and $FeCl_3$ Catalysts [a]

Exp. N°	Starting chloride (N°)	Catalyst	Solvent	Products	Yield[b] %
1	2-Chloro-2-methyl-4-phenylbutane (**1**)	$AlCl_3/CH_3NO_2$	P.E.[c]	1,1-Dimethylindan	79
2	2-Chloro-2-methyl-4-phenylbutane (**1**)	$AlCl_3/CH_3NO_2$	CS_2	1,1-Dimethylindan	60
3	2-Chloro-2-methyl-4-phenyl butane (**1**)	$AlCl_3/CH_3NO_2$	P.E.	1,1-Dimethylindan	65
4	2-Chloro-2-methyl-4-(*o*-tolyl)butane (**2**)	$AlCl_3/CH_3NO_2$	P.E.	1,1,4-Trimethylindan	75
5	2-Chloro-2-methyl-4-(*o*-tolyl)butane (**2**)	$FeCl_3$	P.E.	1,1,4-Trimethylindan	73
6	2-Chloro-2-methyl-4-(*m*-tolyl)butane (**3**)	$AlCl_3/CH_3NO_2$	P.E.	1,1,5-(56 %) and 1,1,7-trimethylindan (44 %).	70
7	2-Chloro-2-methyl-4-(*m*-tolyl)butane (**3**)	$FeCl_3$	P.E.	1,1,5-(60 %) and 1,1,7-trimethylindan (40 %)	65
8	2-Chloro-2-methyl-4-(*p*-tolyl)butane (**4**)	$AlCl_3/CH_3NO_2$	P.E.	1,1,6-trimethylindan	72

---

[3] C. D. Nenitzescu, I. Necşoiu, A. Glatz and M. Zalman, *Chem. Ber.*, **92**, 10 (1959).

[4] M. Inatome, K. W. Greenlee, J. M. Derfer and C. E. Boord, *J. Amer. Chem. Soc.*, **74**, 292 (1952).

[5] R. M. Roberts and S. E. McGuire, *J. Org. Chem.*, **35**, 102 (1970).

[6] A. A. Khalaf and R. M. Roberts, *J. Org. Chem.*, **35**, 3717 (1970).

[7] R. M. Roberts, A. A. Khalaf and R. N. Greene, *J. Amer. Chem. Soc.*, **86**, 2846 (1964).

[8] L. Schmerling and J. P. West, *J. Amer. Chem. Soc.*, **76**, 1917 (1954).

[9] L. Schmerling, *Ind. Eng. Chem.*, **40**, 2072 (1948); Understandably chloride, 3 gave a mixture of the two isomeric trimethylindans 14 and 15 because it has two positions available for ring closure, one *ortho* and another *meta* to the aromatic methyl group.

(continued)

Exp. N°	Starting chloride (N°)	Catalyst	Solvent	Products	Yield[b] %
9	2-Chloro-2-methyl-4-(*p*-tolyl)butane (**4**)	$FeCl_3$	P.E.	1,1,6-trimethylindan	68
10	2-Chloro-2-methyl-5-phenylpentane (**5**)	$AlCl_3/CH_3NO_2$	P.E.	1,1-Dimethyltetralin	74
11	2-Chloro-2-methyl-5-phenylpentane (**5**)	$FeCl_3$	P.E.	1,1-Dimethyltetralin	76
12	2-Chloro-2-methyl-6-phenylhexane (**6**)	$AlCl_3/CH_3NO_2$	P.E.	1-Isopropyltetralin	68
13	2-Chloro-2-methyl-6-phenylhexane (**6**)	$FeCl_3$	P.E.	1-Isopropyltetralin	65
14	3-Chloro-5-phenylpentane (**7**)	$AlCl_3/CH_3NO_2$	P.E.	1-Methyltetralin	75
15	3-Chloro-5-phenylpentane (**7**)	$FeCl_3$	P.E.	1-Methyltetralin	70
16	2-Chloro-5-phenylpentane (**8**)	$AlCl_3/CH_3NO_2$	P.E.	1-Methyltetralin	83
17	2-Chloro-5-phenylpentane (**8**)	$FeCl_3$	P.E.	1-Methyltetralin	76

[a] All reactions were carried out at room temperature for a total reaction time of one hour using the ratios specified in the experimental part.

[b] Determined by distillation in some cases and by vpc analysis using internal standards in some other cases.

[c] Petroleum ether (b.p. 60 – 80°).

As indicated in the experimental section, the results were obtained by treating the chlorides with mild $AlCl_3/CH_3NO_2$ and $FeCl_3$ catalysts in carbon disulphide and/or petroleum ether solvent at a room temperature of 25°.

From the results of Table 1, it can be seen that the $AlCl_3/CH_3NO_2$ and $FeCl_3$ treatments produced 1,1-dimethylindan (**10**) from 2-chloro-2-methyl-4-phenylbutane (**1**), 1,1,4-trimethylindan (**12**) from 2-chloro-2-methyl-4-(*o*-tolyl)butane (**2**), a mixture of 1,1,5- (**14**) and 1,1,7-trimethylindane (**15**) from 2-chloro-2-methyl-4-(*m*-tolyl)butane (**3**), 1,1,6-trimethylindan (**17**) from 2-chloro-2-methyl-4-(*p*-tolyl)butane (**4**) 1,1-dimethyltetralin (**19**) from 2-chloro-2-methyl-5-phenylpentane (**5**), 1-isopropyltetralin (**22**) from 2-chloro-2-methyl-6-phenylhexane (**6**) and 1-methyltetralin (**25**) from both 3-chloro-5-phenylpentane (**7**) and 2-chloro-5-phenylpentane (**8**). Previously, we have shown that the $AlCl_3$ catalyzed cyclization produced a mixture of 1,1-dimethylindan and isopentylbenzene from chloride (**1**) and a mixture of 1,1-dimethyltetralin and isohexylbenzene from chloride (**5**). Parallelly, it has been found in this work that the $AlCl_3$-induced cyclization of the tertiary chloride (**4**) gave a mixture

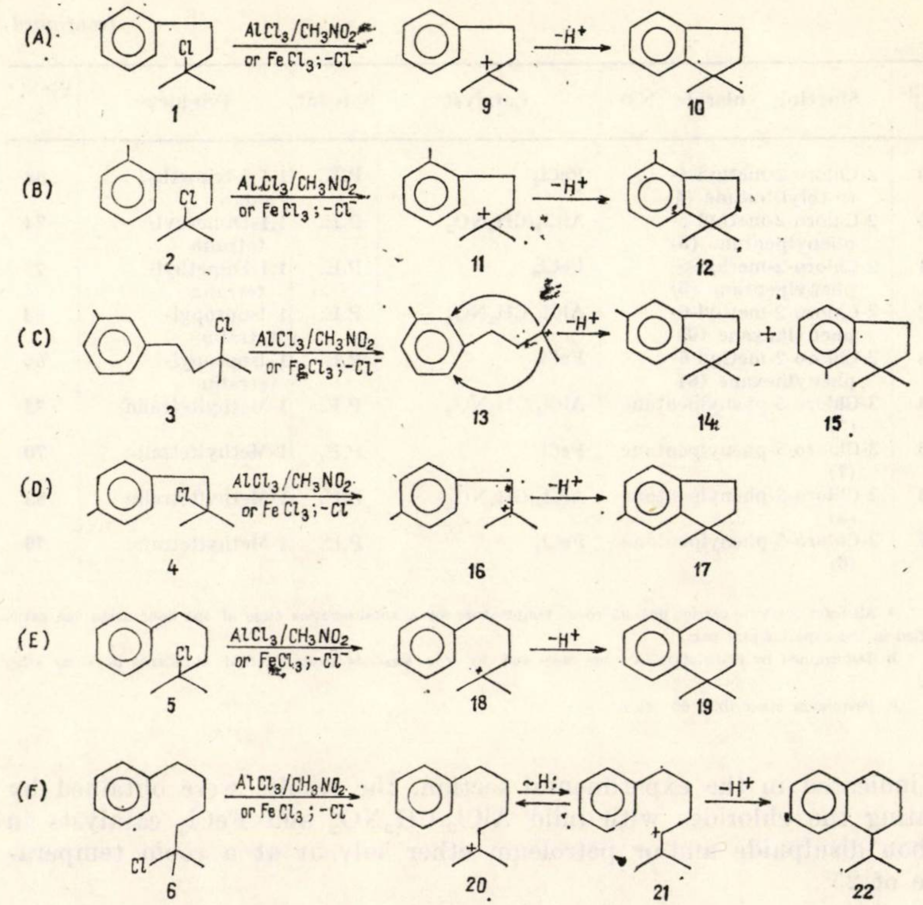
(A)
Cl
AlCl₃/CH₃NO₂
or FeCl₃; -Cl⁻
-H⁺
1
9
10
(B)
Cl
AlCl₃/CH₃NO₂
or FeCl₃; -Cl⁻
-H⁺
2
11
12
(C)
Cl
AlCl₃/CH₃NO₂
or FeCl₃; -Cl⁻
-H⁺
+
3
13
14
15
(D)
Cl
AlCl₃/CH₃NO₂
or FeCl₃; -Cl⁻
-H⁺
4
16
17
(E)
Cl
AlCl₃/CH₃NO₂
or FeCl₃; -Cl⁻
-H⁺
5
18
19
(F)
Cl
AlCl₃/CH₃NO₂
or FeCl₃; -Cl⁻
~H:
-H⁺
6
20
21
22
(G)
Cl
AlCl₃/CH₃NO₂
or FeCl₃; -Cl⁻
~H:
-H⁺
7
23
24
25
(H)
Cl
AlCl₃/CH₃NO₂
or FeCl₃; -Cl⁻
-H⁺
8
24
25

of the cyclialkylation product (17) and the hydride-exchange product, 2-methyl-4-(*p*-tolyl)butane (26), see equation (I).

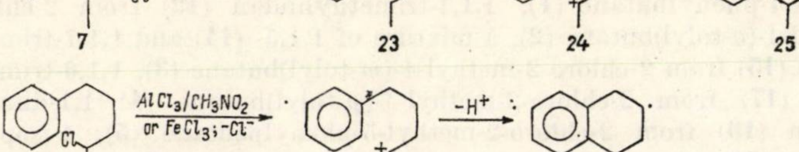
(I)
Cl
AlCl₃
+
4
17
26

The production of the latter compound in the presence of the strong catalyst $AlCl_3$, can reasonably be rationalized in terms of a secondary dealkylation reaction which can be visualized as shown in equation (J).

(J)

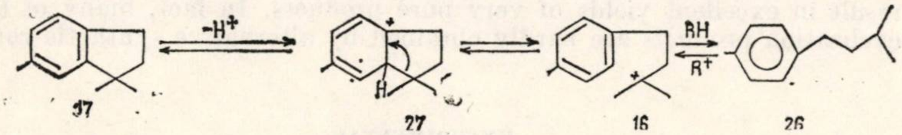

An experimental support for the equation (J) was found in the fact that the treatment of the trimethylindan (**17**) with $AlCl_3$ under conditions similar to those used in the cyclialkylation reaction resulted in the production of the ring-opening product (**26**).

Comparing the results obtained from the cyclizations of chlorides (**1**) to (**8**) in the presence of $AlCl_3/CH_3NO_2$ or $FeCl_3$ catalyst with those obtained from the cyclization of the same chlorides in the presence of $AlCl_3$ catalyst or of the corresponding alcohols [10,11,12] in the presence of H_2SO_4 or H_3PO_4 catalyst, one can make the following observations :

1 — In cyclizing the chlorides, the use of the mild catalysts, $AlCl_3/CH_3NO_2$ and $FeCl_3$ instead of the strong catalyst $AlCl_3$ successfully inhibits undesirable secondary carbonium ion processes such as those outlined in equation (J) and whose occurrence leads to the production of isopentylbenzene from chloride (**1**), of *p*-isopentyltoluene from chloride (**4**) and of isohexylbenzene from chloride (**5**).

2 — Carbonium ion rearrangements occurring prior to the cyclization step cannot be avoided under any of the applied conditions. Thus, starting with either the chlorides or the corresponding alcohols and using either a strong or a mild catalyst, rearrangements such as the secondary-to-tertiary carbonium ion rearrangement (20)→(21) of equation (F) and the secondary-to-secondary carbonium ion rearrangement (23)→(24) of equation (G) do always occur. The deriving force for most of these rearrangements lies in the known [1,10,12] fact that a six-membered ring formation is favoured over either a five- or a seven-membered ring formation.

3 — Usually, better yields of the cyclization products are obtained from the $AlCl_3/CH_3NO_2$- or $FeCl_3$-catalyzed cyclidehydrohalogenations of the chlorides than from the H_2SO_4 or H_3PO_4 catalyzed cyclidehydrations of the corresponding alcohols, especially in systems involving tertiary ring closure to indans. For example, the yields of the cyclization products from the $AlCl_3/CH_3NO_2$-catalyzed reactions of chlorides (**1**), (**2**), (**3**), and (**4**) were respectively 79, 75, 70 and 72% while the yields from the H_2SO_4-catalyzed reactions of the corresponding alcohols [10,11] were 57, 40, 15 and 50% respectively.

---

[10] A. A. Khalaf and R. M. Roberts, *J. Org. Chem.*, **34**, 3571 (1969).

[11] A. A. Khalaf and R. M. Roberts, *J. Org. Chem.*, **36**, 1040 (1971).

[12] R. O. Roblin, Jr., D. Davidson and M. T. Bogert, *J. Amer. Chem. Soc.*, **57**, 151 (1935), and references therein.

In conclusion, the results of this work demonstrated the usefullness of the mild catalysts, $AlCl_3/CH_3NO_2$ and $FeCl_3$ in effecting the cyclialkylation reactions of secondary and tertiary phenylalkyl chlorides. As these catalysts inhibit secondary carbonium ion reactions, they always result in excellent yields of very pure products. In fact, many of these cyclization products are hardly obtained by alternative synthetic routes.

EXPERIMENTAL

ANALYTICAL PROCEDURES

Vapour-phase chromatographic (v.p.c.) analyses were made using a Pye Series 104 chromatograph with a Polyethylene Glycol Adipate (PEGA) and a Methyl Silicone Gum (SE-30) columns. Infrared (i.r.) analyses were done using a Unicam SP 200 G Grating I.R. Spectrophotometer and a Beckman IR5A Spectrophotometer. Nuclear Magnetic Resonance (n.m.r.) analyses were carried out using a Varian Associates A-60 spectrometer with carbon tetrachloride as solvent and TMS as internal standard. Microanalyses were performed by the Microanalytical unit of the Chemistry Department of Assiut University, Assiut, Egypt.

SYNTHESIS OF REQUIRED MATERIALS

I. *Synthesis of Starting Chlorides*

A. *Tertiary Chlorides.* The intermediate carbinols, 2-hydroxy-2-methyl-4-phenylbutane, 2-hydroxy-2-methyl-4-(*o*-tolyl)butane, 2-hydroxy-2-methyl-4-(*m*-tolyl)butane, 2-hydroxy-2-methyl-4-(*p*-tolyl)butane, 2-hydroxy-2-methyl-5-phenylbutane and 2-hydroxy-2-methyl-6-phenylbutane were prepared according to the methods previously described by Khalaf and Roberts [1,11] for the first five carbinols and by Roblin, Davidson and Bogert [12] for the last carbinol. These carbinols were converted to the corresponding chlorides by the action of concentrated hydrochloric acid in the presence of anhydrous calcium chloride as described below.

In a typical experiment, 0.1 mole of carbinol and 30 ml of concentrated hydrochloric acid were placed in a separatory funnel and the resulting mixture was saturated with anhydrous calcium chloride and shaken thoroughly for about 15 minutes. After shaking, the layers were allowed to separate and the upper organic layer was taken and washed first with 5% sodium bicarbonate solution and secondly with water, then dried over anhydrous calcium chloride. The dry product was distilled under reduced pressure to give the pure chloride.

Applied to 2-hydroxy-2-methyl-4-phenylbutane, the above procedure gave 2-chloro-2-methyl-4-phenylbutane (1) in 80% yield: b.p. 83–86 (2.4–2.5 mm.), lit.[1] b.p. 84–85° (2.5 mm.).

Similarly, 2-hydroxy-2-methyl-4-(*o*-tolyl)butane gave 2-chloro-2-methyl-4-(*o*-tolyl)-butane (2) in 75% yield: b.p. 83–85° (2.4 mm.).

Anal. Calcd. for $C_{12}H_{17}Cl$: Cl, 18.06. *Found*: Cl, 17.63.

2-Hydroxy-2-methyl-4-(*m*-tolyl)butane gave 2-chloro-2-methyl-4-(*m*-tolyl)butane (3) in 76% yield: b.p. 86–88° (2.6 mm.).

Anal. Calcd. for $C_{12}H_{17}Cl$: Cl, 18.06. *Found*: Cl, 18.50.

2-Hydroxy-2-methyl-4-(*p*-tolyl)butane gave 2-chloro-2-methyl-4-(*p*-tolyl)butane (**4**) in 82% yield: b.p. 82–84° (2.2–2.3 mm.). The n.m.r. spectrum of this chloride had a singlet at 6.97 ppm (four aromatic hydrogens) a low-field part of an AA′BB′ system located between 2.90 and 2.59 ppm (methylene group adjacent to the aromatic ring), a singlet at 2.27 ppm (aromatic methyl), high-field part of the AA′BB′ system located between 2.12 and 1.77 ppm (second methylene group) and a singlet at 1.55 ppm (two aliphatic methyls).

Anal. Calcd. for $C_{12}H_{17}Cl$: Cl, 18.06. *Found*: Cl, 18.06.

2-Hydroxy-2-methyl-5-phenylpentane gave 2-chloro-2-methyl-5-phenylpentane (**5**) in 79% yield: b.p. 113–115° (8.2 mm.); lit.[1] b.p. 112–113° (8 mm.).

2-Hydroxy-2-methyl-6-phenylhexane gave 2-chloro-2-methyl-6-phenylhexane (**6**) in 78% yield: b.p. 110–112° (1 mm.).

Anal. Calcd. for $C_{13}H_{19}Cl$: Cl, 16.86. *Found*: Cl, 16.60.

It is to be noted that the infrared spectra of all of the above chlorides showed no hydroxyl absorption

B. *Secondary Chlorides.* The intermediate carbinols, 3-hydro-5-phenylpentane and 2-hydroxy-5-phenylpentane were prepared essentially as described by Khalaf and Roberts[1] for the former carbinol and by Roblin, Davidson and Bogert[12] for the latter carbinol. The two carbinols were converted into the corresponding chlorides by treatment with thionyl chloride in pyridine according to the following typical procedure.

A solution of 0.05 mole of the carbinol in 0.06 of pyridine was placed in a 100-ml three-necked flask equipped with a reflux condenser, a pressure-equalizing dropping funnel, a thermometer and a stirring magnet. The flask was then surrounded by an ice bath and the stirrer was started while 0.06 mole of freshly distilled thionyl chloride was added from the dropping funnel at such a rate that the temperature of the reaction mixture did not rise above 10°. After addition was complete, the reaction mixture was stirred at room temperature for two hours and at 50° for one hour then decomposed by pouring over ice. The organic product was extracted with ether, washed repeatedly with ice-cold water then with 10% sodium bicarbonate solution and again with cold water. The washed solution was dried over anhydrous calcium chloride and distilled under reduced pressure.

Applied to 3-hydroxy-5-phenylpentane, the above procedure gave 3-chloro-5-phenylpentane: b.p. 92–94° (3.1 mm.); lit. b.p. 91° at 3.0 mm[1] and 100° at 12 mm[2].

Similarly, 2-hydroxy-5-phenylpentane gave 2-chloro-5-phenylpentane: b.p. 90–91° (3.0 mm.); lit[2]. b.p. 100° (12 mm.).

II. *Synthesis of Final Products*

The required 1,1-dimethylindan (**10**), 1,1,4-trimethylindan (**12**), 1,1,5-trimethylindan (**14**), 1,1,7-trimethylindan (**15**), 1,1,6-trimethylindan (**17**), 1,1-dimethyltetralin (**19**), 1-methyltetralin (**25**) and *p*-isopentyltoluene (**26**) were prepared as previously reported by Khalaf and Roberts.[1,11] Details concerning the preparation of compounds (**10**), (**19**) and (**25**) are given in reference [1] and those concerning the preparation of compounds (**12**), (**14**), (**15**), (**17**), and (**26**) are given in reference.[11]

The required 1-isopropyltetralin was prepared by the reaction of isopropylmagnesium bromide with 1-tetralone followed by reduction of the resulting 1-hydroxy-1-isopropyltetralin by hydrogen and palladium on carbon in glacial acetic acid containing little perchloric acid.[13] The product obtained had a b.p. of 99–100° at 0.53 mm.; lit.[12] b.p.: 247° at atmospheric pressure.

---

[13] R. M. Roberts, G. A. Ropp and O. K. Neville, *J. Amer. Chem. Soc.*, **77**, 1764 (1955).

CYCLIALKYLATION PROCEDURES

a) *Using $AlCl_3/CH_3NO_2$ as catalyst*

To a 50-ml, two-necked, round-bottomed flask equipped with a magnetic stirrer, a pressure-equalizing dropping funnel and a reflux condenser fitted with a calcium chloride tube was placed 0.002 mole of anhydrous $AlCl_3$, 0.02 mole of nitromethane and subsequently 30 ml of solvent (CS_2 or petroleum ether, b.p. 60–80°). To this was added dropwise (over a period of 15 minutes) a solution of 0.02 of the phenylalkyl chloride in 20 ml of the same solvent. After the addition was complete, the reaction mixture was allowed to stir at room temperature for another 45 minutes, then decomposed with a 5% hydrochloric acid solution. Using a separatory funnel, the organic layer was separated, washed first with water and secondly with a 5% sodium bicarbonate solution and again with water, followed by drying over anhydrous sodium carbonate. The solvent was distilled under atmospheric pressure and the hydrocarbon residue was distilled under vacuum.

b) *Using $FeCl_3$ as catalyst*

The above procedure was again followed except that the $AlCl_3/CH_3NO_2$ catalyst was replaced by anhydrous $FeCl_3$.

c) *Using $AlCl_3$ as catalyst*

The procedure was also the same except that the catalyst was the strong $AlCl_3$ with no added nitromethane. Only chloride 4 was cyclized under such conditions.

Data concerning catalyst, solvent, yields and compositions of final products are summarized in Table 1.

TREATMENT OF 1,1,6-TRIMETHYLINDAN (17) WITH $AlCl_3$

In a 50-ml, one-necked, round-bottomed flask, equipped with a magnetic stirrer and a reflux condenser fitted with calcium chloride tube was placed 0.16 g (0.001 mole) of 1,1,6-trimethylindan, 20 ml of petroleum ether (b.p. 60–80°) and 0.014 g (0.0001 mole) of $AlCl_3$ and the mixture was stirred at room temperature for one hour. The mixture was decomposed and the organic layer was separated, washed and dried in the usual manner, then analyzed by vapour-phase chromatography to show that the product was a mixture of 1,1,6-trimethylindan (28%) and *p*-isopentyltoluene (72%).

IDENTIFICATION OF THE REACTION PRODUCTS

The products obtained from the above reactions were identified by comparison of their physical properties, their spectroscopic data and their vapour-phase chromatography retention times with those of the hydrocarbons prepared by unequivocal procedures.

Revue Roumaine de Chimie, 18, 2, 305–317 (1973)

ON THE REACTIVITY OF N-VINYLCAPROLACTAM IN RADICALIC POLYMERIZATION

N. COBIANU*, C. BOGHINĂ*, B. MĂRCULESCU* and I. AMĂLINEI**

* Laboratory of Macromolecular Chemistry,
Polytechnic Institute, Bucharest, Romania
** Research Department of UFS Săvineşti,
Romania

Received August 2, 1972

The copolymerization of acrylonitrile (I) with N-vinylcaprolactam (II) in solution in the temperature range of 55–70° was studied. The reactivity ratios, r_{ij}, of this pair of monomers were determined the following values being obtained :

$$r_1^{55°} = 0.29 \qquad r_1^{65°} = 0.30 \qquad r_1^{70°} = 0.27$$

$$r_2^{55°} = 0.18 \qquad r_2^{65°} = 0.15 \qquad r_2^{70°} = 0.09$$

For the determination of the Q_2 and e_2 constants for N-vinylcaprolactam (NVC) the copolymerization processes in the styrene (ST) – NVC and methyl methacrylate (MMA) – NVC systems at 70° were also studied. The values of the reactivity ratios are :

$$\text{ST} - \text{NVC}: \qquad r_1 = 19.1 \qquad r_2 = 0.027$$

$$\text{MMA} - \text{NVC}: \qquad r_1 = 5.3 \qquad r_2 = 0.05$$

The average values of the Q and e parameters are the following :

$$Q_2 = 0.116 \qquad e_2 = -1.1$$

1. INTRODUCTION

The study of the synthesis and polymerization of N-vinylcaprolactam (NVC) has been promoted by the physico-chemical properties of polyvinylpyrrolidone, a product which has been obtained in 1940–1950.

Although, from its obtaining,[1-3] many years have passed, data regarding the polymerization of NVC[3-6] and its radicalic copolymerization[7-11] are still scarce. Up to now, only the reactivity ratios for the binary copolymerization of NVC with phenyl vinyl ether,[9] buthyl methacrylate[10] and vinyl acetate (AV)[11] have been determined. The patent literature is richer and reveals many areas of utilization of such polymers.

In order to obtain more accurate information regarding the reactivity of NVC, the study of the binary copolymerization with acrylonitrile (AN), styrene (ST) and methyl methacrylate (MMA) was carried out.

2. EXPERIMENTAL

a. MATERIALS

NVC was obtained according to the method of literature. The product, purified and encapsulated under argon, was redistilled under vacuum before being used. The fraction used in the experiments had a refractive index, $n_D^{20} = 1.5135$.

AN, ST and MMA were purified according to the usual methods. The commercial α, α'-azobisisobutyronitrile (AIBN) as radical initiator was twice recrystallized from ethanol ($F_p = 102.5^\circ$).

The N,N-dimethyl formamide (DMF) was for three hours refluxed under vacuum on calcium hydride followed by double distillation ($n_D^{25} = 1.4268$).

The dioxan as pure solvent ($n_D^{20} = 1.4224$) was obtained by refluxing it on metallic sodium and then it was rectified using a column with twenty theoretical plates.

b. POLYMERIZATION PROCEDURE

Copolymerization reactions were carried out in glass ampoules with two arms[12]; before filling with monomer and initiator solutions, they were dried under vacuum and then filled with argon.

---

[1] W. Reppe, H. Krzikalla, O. Dornheim and R. Sauerbier, (to I. G. Farbenind) U. S. Pat. 2.317.763, (1943); *Chem. Abstr.*, **37**, 6057^1 (1943).

[2] W. E. Hanford and D. L. Fuller, *Ind. Eng. Chem.*, **40**, 1179 (1948).

[3] F. M. Shostakovskii, *Izvest. Akad. Nauk S.S.S.R., Otdel khim. Nauk*, **1953**, 108; F. M. Shostakovskii, F. P. Sidelkovskaya and M. G. Zelenskaya, *Doklady Akad. Nauk S.S.S.R., Otdel. khim. Nauk*, **1952**, 643; F. M. Shostakovskii, N. A. Medzikovskaya and M. G. Zelenskaya, *Izvest. Akad. Nauk S.S.S.R., Otdel. khim. Nauk*, **1952**, 682.

[4] F. M. Shostakovskii and M. G. Zelenskaya, *Izvest. Akad. Nauk S.S.S.R., Otdel. khim. Nauk*, **1952**, 690.

[5] O. F. Solomon, M. Corciovei and C. Boghină, *J. Appl. Polymer Sci.*, **12**, 1843 (1968).

[6] O. F. Solomon, D. S. Vasilescu and V. Tărărăscu, *J. Appl. Polymer. Sci.*, **13**, 1 (1969).

[7] F. M. Shostakovskii, F. P. Sidelkovskaya and A. M. Homutov, *Izvest. Akad. Nauk S.S.S.R., Otdel. khim. Nauk*, **1955**, 919.

[8] G. E. Ham, *Textile Res. J.*, **24**, 597 (1954).

[9] F. P. Sidelkovskaya, M. I. Askarov and F. Ibragimov, *Vysokomol. Soedineniya*, **A 3**, 976 (1961).

[10] F. Ibragimov, D. Mukhamadaliev and T. G. Gafurov, *Vysokomol. Soedineniya*, **A 12**, 1475 (1970).

[11] El Sabban, M. Zaki, S. I. Dimitrieva and A. I. Meos, *Vysokomol. Soedineniya*, **B 12**, 243 (1970).

[12] T. Otsu an H. Inoue, *Makromol. Chem.*, **128**, 31 (1969).

After filling, one of the arms was closed, and the ampoules were conditioned by three cycles of freezing at $-100°$, air-removal at 10^{-2} mm, filling with purified argon, and warming at 30°. Finally, the ampoules brought at normal pressure with argon were closed, and the solutions at the reaction temperature were rapidly mixed. After a sufficient reaction time as to obtain a small conversion, the copolymerization reaction is stopped by abrupt freezing near the congelation temperature. The copolymers with ST and MMA were isolated from the solution by precipitating them with petroleum ether. The precipitation of the copolymers with AN was carried out with methyl alcohol for the feed containing at least 50% mole AN and for the other situations with ethyl ether.

c. VISCOSITY MEASUREMENT

Intrinsic viscosities of copolymers were calculated using the data obtained with diluted solutions (copolymer concentration less than 0.2 g/dl) with Ubbelohde viscosimeter. The viscosity was measured in DMF for the copolymers with AN and in toluene for the other ones. The intrinsic viscosity was calculated using the following relationship[13]

$$|\eta| = \eta_{sp}/c\,(1+0.333\,\eta_{sp})$$

d. ANALYSES OF THE COPOLYMERS

The composition of the copolymers was determined according to Dumas classical micromethod. Due to the infusibility of the copolymers with high content in AN, on the one hand, and to the wetability of the copolymers with high content in NVC, on the other hand, the samples were broken up (the particle size less than 0.4 mm), dried up under high vacuum and stored under anhydrous conditions before analysis.

3. RESULTS AND DISCUSSION

3.1. KINETIC ASPECTS OF THESE BINARY COPOLYMERIZATIONS

The copolymerization of NVC with AN in homogeneous solution was carried out at different initial compositions of the feed and at three temperatures 55, 65 and 70°. Some kinetic data regarding the dependence of the initial copolymerization rate on feed composition are given in table 1. Figure 1 sums up the influence of the factors discussed above.

It is found out that the total rate of copolymerization reaches a maximum a little far from that corresponding to the equimolecular feed. Table 2 gives the results obtained for the copolymerization of ST with NVC at 70° and at a concentration of the initiator of $1.73 \cdot 10^{-3}$ mole/l.

---

[13] O. F. Solomon and B. Gottesman, *Makromol. Chem.*, **104**, 177 (1967).

Although the copolymerization reaction takes place in bulk (more than 90% of the reaction volume is taken by the monomers, the remaining being DMF), the rate of the process is much smaller than in the previous case. Figure 2 presents the dependence of the reduced copolymerization rate on the initial feed composition. It can be seen that the

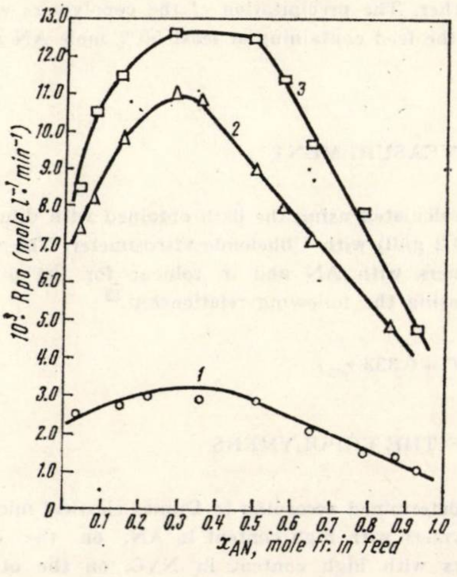

Fig. 1. — Dependence of copolymerization rate upon the composition feed for the AN—NVC system.

$(M_1)_0 + (M_2)_0 = 2.8$ mole/l. $(AIBN)_0 = 7.5 . 10^{-4}$ mole/l. Solvent: DMF

1, 55°; *2*, 65°; *3*, 70°

Table 1

Copolymerization of acrylonitrile (M_1) with N-vinyl caprolactam (M_2) initiated by AIBN at 55°C in the presence of DMF: $(M_1)_0 + (M_2)_0 = 2.8$ mole/l. $(AIBN)_0 = 7.5 \cdot 10^{-4}$mole/l

(M_1) in monomers (mole — %)	Reaction time (min)	Conversion %	N % Dumas	(M_1) in copolymer (mole fraction)	Rate of copolymerization 10^3 R_{po} (mole/l. min)	$[\eta]$* (ml/g)
3.6	50	3.42	13.26	0.390	2.47	94.1
14.3	55	4.31	14.10	0.463	2.80	116.3
21.4	60	5.28	14.34	0.482	3.04	126.9
35.7	70	6.60	14.50	0.494	2.96	127.7
50.0	70	7.13	15.26	0.550	2.99	124.9
64.3	75	6.12	15.86	0.591	2.17	109.2
78.6	90	6.49	17.98	0.712	1.64	113.3
86.2	100	6.39	17.93	0.709	1.48	—
92.9	110	5.24	19.59	0.786	1.11	102.9

* Solvent DMF; 25°C, Polymer concn. ⩽ 0.2 g/dl.

Table 2

Copolymerization of styrene (M_1) with N-vinyl caprolactam (M_2) initiated by AIBN at 70°C in the presence of DMF : $(AIBN)_0 = 1.73 \cdot 10^{-3}$ mole/l

$(M_1)_0 + (M_2)_0$ (mole/l)	(M_1) in monomers (mole − %)	Reaction time (min)	Conversion %	N % Dumas	(M_1) in copolymer (mole fraction)	Rate of copolymerization $10^4 \cdot R_{po}$ (mole/l · min)	$[\eta]^*$ (ml/g)
6.726	6.5	140	0.44	4.39	0.634	2.56	—
6.780	12.8	199	0.95	2.65	0.789	4.00	32.6
6.915	25.2	170	1.40	1.60	0.876	6.88	—
7.040	37.1	140	1.67	1.04	0.921	10.30	56.8
7.172	48.5	102	1.52	0.69	0.948	13.12	66.5
7.320	59.5	65	1.12	0.52	0.961	15.25	74.4
7.425	70.2	75	2.00	—	0.970**	21.45	72.5
7.559	80.5	65	2.00	—	0.980**	23.60	81.5
7.718	90.4	55	1.80	—	0.990**	25.80	90.9

* Solvent toluene, 25°C, Polymer conc. 0.05 ... 0.2 g/dl
** From Fig. 5

copolymerization rate increases proportionally to the ST molar fraction in feed. In this case, NVC acts as a retarder of the polymerization process.

As regards the binary system α-methylstyrene — NVC, the experiments carried out under favourable conditions (bulk polymerization, reaction time : 35 h for 70° and 100 h for 55°) for the obtaining of the products with a relatively high molecular weight, have showed that no proper copolymerization process takes place but probably one of oligomerization type. The reaction products are not precipitable in the nonsolvents of both homopolymers.

For the binary system MMA—NVC the total copolymerization rate increases monotonously with the comonomer molar fraction, tending quasi-exponentially to the total rate of the homopolymerization reaction of MMA under the same conditions. The results are presented in figure 3 and table 3.

3.2. CALCULATION OF THE REACTIVITY RATIOS

3.2.1. The AN—NVC system. The literature [8,14] does not mention the data which can be used to calculate the reactivity ratios for this

---

[14] G. I. Kudriavtsev, Z. A. Rassolova, T. A. Romanova, M. A. Jarkova and E. A. Vasilieva-Sokolova, *Khim. Volokna*, **1966**, 3.

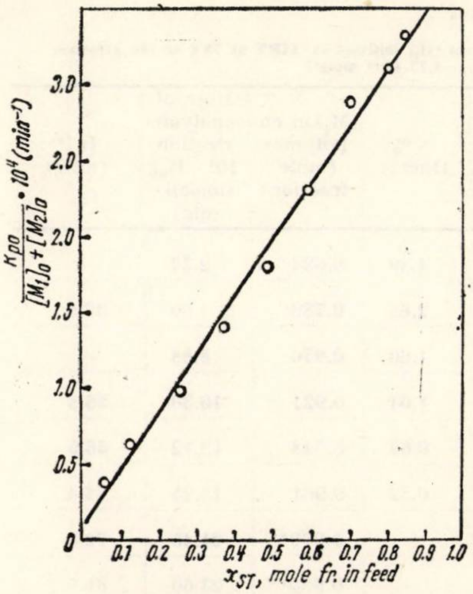

Fig. 2. — Copolymerization rate against composition feed for the ST—NVC system at 70°.

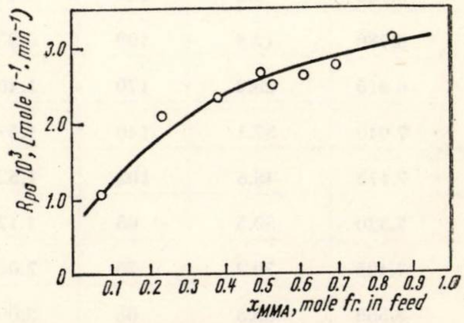

Fig. 3. — Copolymerization rate against composition feed for the MMA—NVC system.

$(M_1)_0 + (M_2)_0 = 2$ mole/l. $(AIBN)_0 = 1\cdot10^{-3}$ mole/l*
Solvent: dioxan; 70°.

Table 3

Copolymerization of methyl methacrylate (M_1) with N-vinyl caprolactam (M_2) initiated by AIBN at 70°C in the presence of 1,4-dioxan: $(M_1)_0 + (M_2)_0 = 2$ mole/l, $/AIBN/_0 = 1\cdot10^{-3}$ mole/l

(M_1) in monomers (mole— %)	Reaction time (min)	Conversion (%)	N % Dumas	(M_1) in copolymer (mole fraction)	[η]* (ml/g)
100.0	40	7.25	—	1.000	73.1
84.6	49	7.41	0.775	0.944	—
69.2	50	6.38	1.020	0.925	66.5
61.5	60	7.13	1.435	0.894	58.5
53.8	60	6.70	1.635	0.877	58.1
50.0	60	6.90	1.870	0.859	57.8
38.5	60	6.00	2.420	0.814	—
23.1	60	5.43	3.460	0.726	52.3
7.7	50	2.32	5.400	0.545	—

* Solvent toluene, 25°C, Polymer concn. 0.2 ... 0.23 g/dl.

pair of monomers. Data regarding the composition of the obtained copolymers, for different initial feed, are given in tables 1 and 4.

The monomer/copolymer composition curve for the AN–NVC system is presented in figure 4.

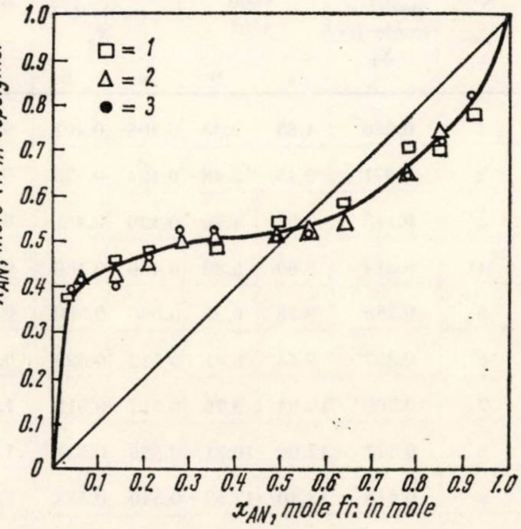

Fig. 4. — Monomer/copolymer composition curve for radical copolymerization of the AN–NVC system.

1, 55°; *2*, 65°; *3*, 70°

One observes that these three copolymerization processes at temperatures between 55° and 70°, led approximatively to the same monomer/copolymer composition curve, which shows an important tendency for the alternation of the mers. On the base of $Q_2 = 0.081$ and $e_2 = -1.55$ constants given by Sidelkowskaia *et al.*,[9] a more pronounced alternation had to be anticipated. A least square method was used for calculation of the reactivity ratios for this system.[15]

For these three temperatures, the reactivity ratios have the following values :

— temperature 55° $n = 8$ (n — the number of feeds for which the copolymerizations were done)

$$r_1 = 0.29 ; \quad r_2 = 0.18$$

— temperature 65° $n = 11$

$$r_1 = 0.30 ; \quad r_2 = 0.15$$

— temperature 70° $n = 11$

$$r_1 = 0.27 \quad r_2 = 0.09.$$

---

[15] P. W. Tidwell and G. A. Mortimer, *J. Polymer Sci.*, A, 3, 369 (1965).

Table

Experimental and calculated data for determining of the

N°	Experimental data					Calculated			
	Feed composition (mole fr) X_1	Copolymer yield (%)		Copolymer composition (mole fr.) X_1		$R = \frac{x_1}{x_2}$	$\rho = \frac{X_1}{X_2}$		$\frac{R}{\rho}$
		a	b	a	b		a	b	a
1	0.036	4.83	2.33	0.408	0.401	0.0373	0.6892	0.6694	−0.01682
2	0.071	5.45	3.48	0.424	0.420	0.0764	0.7361	0.7241	−0.02739
3	0.143	7.26	4.70	0.426	0.411	0.1669	0.7422	0.6978	−0.05798
4	0.214	6.80	5.30	0.456	0.466	0.2723	0.8382	0.8727	−0.05256
5	0.286	9.18	6.25	0.500	0.530	0.4006	1.0000	1.1277	0.00000
6	0.357	9.45	6.61	0.512	0.528	0.5552	1.0492	1.1186	0.02604
7	0.500	10.04	9.70	0.517	0.515	1.0000	1.0704	1.0619	0.06577
8	0.571	12.00	10.71	0.526	0.521	1.3310	1.1097	1.0877	0.13157
9	0.643	13.40	12.59	0.540	0.553	1.8011	1.1739	1.2371	0.26680
10	0.786	4.75	12.21	0.656	0.651	3.6729	1.9070	1.8653	1.7469
11	0.857	11.29	9.43	0.738	0.727	5.9930	2.8168	2.6630	3.8654
a: 65°C, b: 70°C.								Σ	5.9477

It can be seen that the reactivity ratio r_1 remains practically unchanged, while the reactivity ratio r_2 having smaller values, decreases approximately twice for an increase of temperature from 55° to 70°.

3.2.2. The ST−NVC system. As in the previous case, the copolymerization with ST is less described in literature. [7] The experimental study of the reactivity of NVC, in this binary system, offers new data for a deeper analysis. The experimental results regarding the analysis of the copolymers obtained from processes with various initial compositions of the feed are shown in table 2. Figure 5 presents the monomer/copolymer composition curve for the copolymerization of the ST with NVC.

One may observe that during copolymerization the feed becomes continuously richer in NVC.

The reactivity ratios for this system were calculated using a least square method and Fineman-Ross's method. [16] Using the least square method, for $n = 4$ (the other feeds with $x_{ST} > 0.485$ led to compositions susceptible to great errors) the following values are obtained :

$$r_1 = 18.5 \quad \text{and} \quad r_2 = 0.014.$$

---

[16] M. Fineman and S. D. Ross, J. Polymer Sci., 5, 259 (1950).

4

acrylonitrile (M_1) N-vinyl caprolactam system constants

data						
$(\rho-1)$	$10^3\frac{R^2}{\rho}$		$\frac{R^3}{\rho^2}(\rho-1)$		$\frac{R^4}{\rho^2}$	
b	a	b	a	b	a	b
-0.01842	2.0187	2.0784	$-3.395\cdot10^{-5}$	$-3.828\cdot10^{-5}$	$4.075\cdot10^{-6}$	$4.320\cdot10^{-6}$
-0.02911	7.9296	8.0610	$-2.172\cdot10^{-4}$	$-2.346\cdot10^{-4}$	$6.288\cdot10^{-5}$	$6.498\cdot10^{-5}$
-0.07228	36.530	39.919	$-2.176\cdot10^{-3}$	$-2.885\cdot10^{-3}$	$1.408\cdot10^{-3}$	$1.593\cdot10^{-3}$
-0.03972	88.460	84.963	$-4.649\cdot10^{-3}$	$-3.375\cdot10^{-3}$	$7.825\cdot10^{-3}$	$7.218\cdot10^{-3}$
0.04536	160.48	142.31	0.000	$6.455\cdot10^{-3}$	$2.534\cdot10^{-2}$	$2.025\cdot10^{-2}$
0.05886	293.79	275.56	$7.65\cdot10^{-3}$	$1.622\cdot10^{-2}$	$8.631\cdot10^{-2}$	$7.593\cdot10^{-2}$
0.05829	934.23	941.75	$6.144\cdot10^{-2}$	$5.489\cdot10^{-2}$	$8.728\cdot10^{-2}$	$8.868\cdot10^{-1}$
0.10732	1,596.4	1,628.71	$2.1\cdot10^{-1}$	$1.748\cdot10^{-1}$	2.548	2.653
0.34519	2,763.4	2,622.20	$7.373\cdot10^{-1}$	$9.052\cdot10^{-1}$	7.636	6.876
1.7038	7,074.4	7,232.20	12.36	12.32	50.04	52.30
3.7425	12,750.6	13,487.0	49.28	50.47	162.6	181.9
4.902	25,709	26,465	62.65	63.94	223.82	244.80

The data regarding the linearization of the differential equation of copolymers composition, using Fineman and Ross's method, are presented in figure 6.

As it results from figure 6, the reactivity ratios values are :

$$r_1 = 19.1 \text{ and } r_2 = 0.027.$$

The better values for these reactivity ratios seem to be those determined by Fineman and Ross's method, taking into account the reduced number of experiments considered in the least square calculation.

Making a parallel with the binary system ST$-$Vinyl acetate (AV) for which $r_1 = 55$ and $r_2 = 0.01$, [17] one may observe that the radicalic reactivity of NVC is greater than that of AV.

3.2.3. The MMA$-$NVC system. Taking into account the fact that the constants Q_1 and e_1 of the two reference monomers from the binary system were presented above, the tentative to a better approximation of the constants Q_2 and e_2 for NVC imposed an analysis of a system with a comonomer with a polarity between that of ST and that of AN. MMA was chosen. As for the ST—NVC system, the reactivity ratios were determined by means of those two methods of linearization presented above.

---

[17] F. R. Mayo, C. Walling, F. M. Lewis and W. F. Hulse, *J. Amer. Chem. Soc.*, **70**, 1523 (1942).

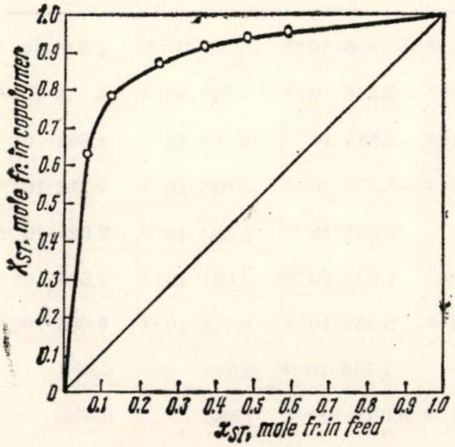

Fig. 5. — Monomer/copolymer composition curve for radical copolymerization at 70° of the ST—NVC system.

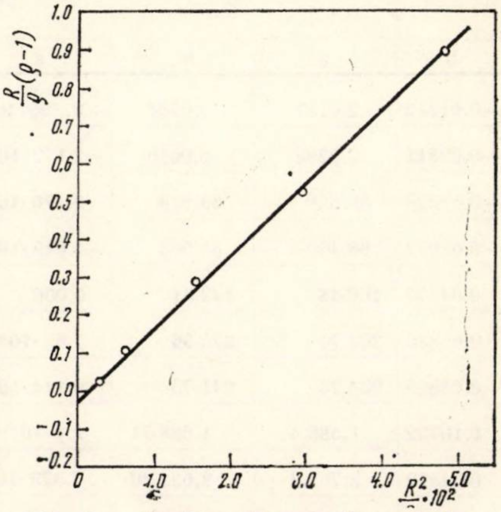

Fig. 6. — Graphic determination of the ST—NVC system constants after Fineman-Ross.

Using the least square method, for $n = 6$, the following values resulted :

$$r_1 = 5.3 \text{ and } r_2 = 0.05$$

and by means of Fineman-Ross's method (figure 7) the following values were obtained :

$$r_1 = 5.0 \text{ and } r_2 = 0.03.$$

There is a good concordance between the values obtained by these two methods.

The monomer/copolymer composition curve of the MMA—NVC system which is given in figure 8, is intermediate as related to those regarding the binary copolymerization of NVC with AN and ST but closer to that of ST.

Table 5 presents the reactivity ratios r_{ij} at 70° for the systems which were studied.

One may observe that the product $r_i\, r_j$ has the smallest value for the AN—NVC system and the highest one for the ST—NVC system, when the reactivity ratios for the second system are determined using the Fineman-Ross's method. This fact seems to be a supplemental argument for a more accurate determination of the reactivity ratios r_{ST} and r_{NVC} by means of this method.

The binary copolymerization systems of the NVC contain partners with a very different polarity (strong and weak electron accepting monomers), which in the propagation reaction give macroradicals stabilized in a higher or smaller extent by $p - \pi$ conjugation. All radicals of the partners are more stable (therefore, less reactive) than the NVC radical.

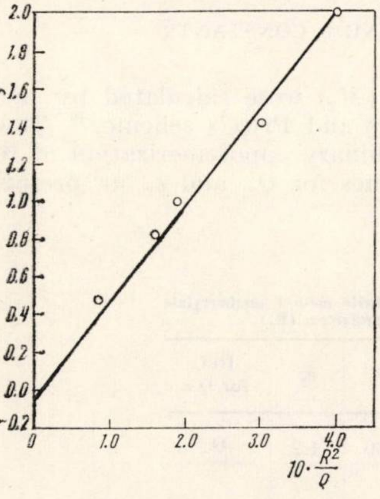

Fig. 7. — Graphic determination of the MMA — NVC system constants after Fineman-Ross.

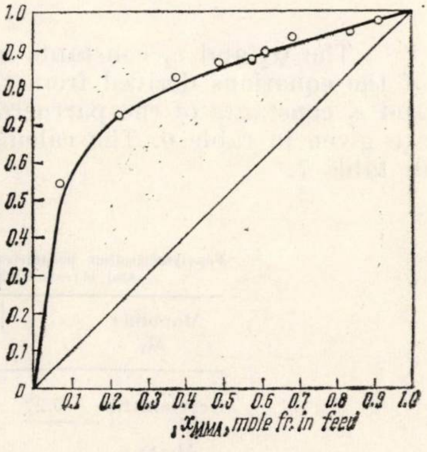

Fig. 8. — Monomer/copolymer composition curve for radical copolymerization at 70° of the MMA—NVC system.

In all these systems the tendency of this radical for cross propagation, is evidenced. Since also $r_{AN} < 1$, one believes that the propagation reactions in this system are dominated by polarity. The reverse polarity

Table 5

Values of the copolymerization constants for the monomer pairs styrene-vinyl caprolactam; methyl methacrylate-vinyl caprolactam; acrylonitrile-vinyl caprolactam

M_1	r_1		r_2		$r_1 . r_2$	
	Least-squares method	Fineman-Ross method	Least-squares method	Fineman-Ross method	Least-squares method	Fineman-Ross method
Styrene	18.5	19.1	0.014	0.027	0.259	0.515
Methyl metacrylate	5.3	5.00	0.05	0.03	0.265	0.15
Acrylonitrile	0.27	—	0.09	—	0.0246	—

of the two monomers lowers much the energy of the activated complexes of the cross addition. The probability of homopropagation of AN being much diminished, it becomes important only for feeds with a high content of this monomer.

3.3. CALCULATION OF Q AND e CONSTANTS

The Q_2 and e_2 constants for NVC (M_2) were calculated by means of the equations derived from the Alfrey and Price's scheme.[18] The Q_1 and e_1 constants of the partners of the binary copolymerization of NVC are given in table 6. The calculated values for Q_2 and e_2 ar presented in table 7.

Table 6

Copolymerization parameters foracrylonitrile methyl methacrylate and styrene: with N-vinyl caprolactam (M_2)

Monomer M_1	r_1	r_2	Q_1	e_1	Ref. for Q,e
Acrylonitrile	0.27	0.09	0.60	1.2	19
Methyl methacrylate	5.0	0.03	0.74	0.4	19
Styrene	19.1	0.027	1.00	−0.8	18

Table 7

Q, e Parameters for N-vinyl caprolactam (M_2)

N-vinyl caprolactam M_2	M_1			Average parameters
	Acrylonitrile	Methyl methacrylate	Styrene	
e_2	−0.73	−0.96	−1.61	−1.1
Q_2	0.210	0.082	0.056	0.116

The average constant $e_2 = -1.1$ demonstrates a donor effect of the substituent of this vinylic monomer lower than that supposed from the copolymerization with phenyl ether,[9] with AV[11] or that resulted from the copolymerization with ST, in the last case the decisive factor of the process being that of the conjugation.

The value $e_2 = -1.1$ anticipates a relative weak tendency of NVC for a cationic polymerization. This fact is in good agreement with the experimental data obtained for the cationic polymerization of N-vinylpyrrolidone with boron trifluoride[20] and with the value obtained by

---

[18] T. Alfrey and C. C. Price, *J. Polymer Sci.*, **2**, 101 (1947).

[19] L. J. Young, *J. Polymer Sci.*, **54**, 411 (1961).

[20] C. E. Schildknecht, A. O. Zoss and F. Grosser, *Ind. Eng. Chem.*, **41**, 2891 (1949).

Alfrey [21] for N-vinylpyrrolidone. Comparing the average values of Q and e of NVC, with those of AV ($Q_{AV} = 0.02$ and $e_{AV} = 0.5$ [22]) one may evidence the following:

— The radicalic reactivity of NVC is higher than that of AV, while the reactivity of the radicals is in a reverse ratio. From this point of view it is evident that the stabilization of the radical:

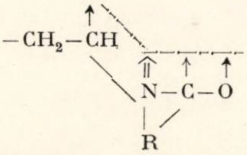

is firmer than that of the radical:

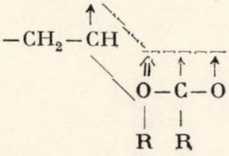

which one explains by the lower potential energy of the conjugated lactamic system than that of the acetoxy system.

— The energy difference between the two systems consists in fact in the stronger electronegative character of the esteric oxygen, as compared to that of the amidic nitrogen.

— As regards the values e of the two monomers, in the case of NVC the donor effect in front of the acceptor partners is more pronounced, which can be explained by the difference in the electronegativity showed above.

As it has been experimentally observed in the copolymerization with strong electron accepting monomers (AN) there is a total copolymerization rate higher than in the copolymerization processes with weaker electron accepting monomers (MMA) and all the more so with amphoter partners (ST).

In the copolymerization with monomers which have strong electrophilic substituents one may expect the copolymerization rate to reach a maximum for the equimolecular feed.

---

[21] J. F. Bork and L. E. Coleman, *J. Polymer Sci.*, 43, 413 (1960).

[22] L. J. Young and C. C. Kennedy, In "Copolymerization", Edited by G. E. Ham, Interscience Publishers, New York, 1964, p. 862.

Revue Roumaine de Chimie, **18**, *2*, 319–326 (1973)

STUDIES ON THE ELECTROANALYTICAL BEHAVIOUR OF MEMBRANE-ELECTRODES UNDER CURRENT. I

CURRENT-MEMBRANE POTENTIAL CURVES FOR THE PARCHMENT MEMBRANE-ELECTRODE IMPREGNATED WITH $BaSO_4$

CANDIN LITEANU and IONEL CĂTĂLIN POPESCU

Chair of Analytical Chemistry, "Babeş-Bolyai", University,
Cluj, Romania

Received September 11, 1972

Some new current-membrane potential measurements for $BaSO_4$-parchment membrane-electrode are exposed. The measurements ranged in the rectification domain. A Tafel diagram is suggested for the interpretation of the results. A kinetic hypothesis is also proposed for understanding the behaviour of $BaSO_4$-parchment membrane-electrode in dynamic state conditions.

The great majority of studies and uses referring to the membrane-adjacent solution electrochemical system, is meant to capitalize on the behaviour of this system when the net current passing through it is extremely feeble ($10^{-12}-10^{-14}$ A). This is especially the case for working the ion selective membrane-electrodes.

There exist nevertheless some research fields dealing with phenomena connected to the behaviour of permselective membranes through which a relative higher electric current passes, as for instance : electrodialysis,[1] rectifying of alternating electric current,[2-5] conductometric titration with indicating resistance[6-8] and a variant of coulometric generation.[9] The method of passing a current through the membranes has also lead to interesting results in the study of working mechanism of membranes,[10] and of the transitory response of glass electrodes,[11-14] as well as in potentiometric titration.[15-16]

---

[1] N. Lakshminarayanaiah, *Chem. Rev.*, **65**, 491 (1965).

[2] C. Liteanu and Gh. Rădulescu, *Rev. Roumaine Chim.*, **14**, 1257 (1969).

[3] Gh. Rădulescu, C. Liteanu and E. Marinescu, *Stud. Univ. Babeş-Bolyai, Chem.*, **14**, 33 (1969).

[4] Gh. Rădulescu, C. Liteanu and G. Steinbrecher, *J. Chim. phys.*, **68**, 1412 (1971).

[5] Gh. Rădulescu, G. Steinbrecher and C. Liteanu, *J. Chim. phys.*, **68**, 1403 (1971).

[6] C. Liteanu and E. Hopîrtean, *Rev. Roumaine Chim.*, **12**, 517 (1967).

[7] C. Liteanu and L. Gerghariu-Mîrza, *Rev. Roumaine Chim.*, **15**, 1871 (1970).

[8] C. Liteanu and L. Ghergheariu-Mîrza, *Talanta*, **19**, 980 (1972).

[9] R. B. Hanselman and L. B. Rogers, *Analyt. Chem.*, **32**, 1240 (1960).

The present note gives some new results on the electrochemical behaviour of the membrane-electrode of parchment impregnated with $BaSO_4$, obtained by interpreting the current-membrane potential curves plotted in a dynamic state. The investigated domain corresponds to the rectifying region ($0.65\ \text{V} < E_m < 0.90\ \text{V}$) signalled in similar studies on this type of electrode.[17,18]

EXPERIMENTAL

The membrane-electrode of pergament impregnated with $BaSO_4$ was used in the form described by Liteanu and Mioşcu.[19] Some constructive changes were nevertheless necessary: a platinated Pt electrode (plate 1 cm × 1 cm) was introduced into the membrane-vase. Another platinated Pt electrode of identical form and dimensions was set outside. This couple of electrodes, symmetrically set on each side of the membrane, has served to apply the external polarization tension.

During the whole experiments $Ba(OH)_2\ 5 \times 10^{-2}$ N was used as internal solution and $H_2SO_4\ 5 \times 10^{-2}$ N as external solution. The external solution was stirred magnetically.

The polarization tension was picked up from the cylinder of a polarograph (Radelkis OH 102) turning with a suitable and known speed. The intensity of the electric current passing through the membrane is directly registered by the polarograph.

The potential of the membrane-electrode was estimated by measuring at 10 seconds interval with an electronic potentiometer (Radiometer TTT1) the emf of the electrochemical chain:

$$(+)\ \text{ESC}\,\big|\,\text{Ba(OH)}_2\ 5\times10^{-2}\ \text{N}\,\big|\,\text{membrane}\,\big|\,\text{H}_2\text{SO}_4\ 5\times10^{-2}\,\big|\,\text{ESC}\ (-) \qquad (1)$$

The block-draft of the working device is given in figure 1.

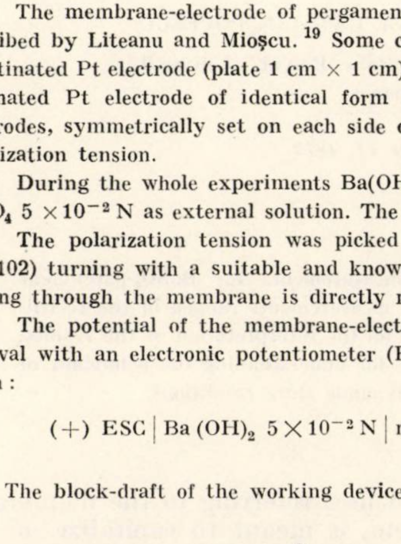

Fig. 1. — The schematic diagram of the working assembly: *1*, polarograph; *2*, working cell; *3*, $BaSO_4$-parchment membrane; *4*, Pt-platined electrodes; *5*, SCE; *6*, potentiometer.

---

[10] G. Eisenman, J. P. Sandblom and J. L. Walker, Jr., *Science*, **155**, 965 (1967).
[11] R. P. Buck, *J. Electroanalyt. Chem.*, **18**, 363 (1968).
[12] R. P. Buck, *J. Electroanalyt. Chem.*, **18**, 381 (1968).
[13] R. P. Buck and I. Krull, *J. Electroanalyt. Chem.*, **18**, 387 (1968).
[14] A. Wikby and G. Johansson, *J. Electroanalyt. Chem.*, **23**, 23 (1969).
[15] P. Bersier, J. Bersier and F. Hügli, *Helv. Chim. Acta*, **42**, 2514 (1959).
[16] R. Geyer and P. Niklas, *Z. analyt. Chem.*, **177**, 166 (1960).
[17] P. Hirsch–Ayalon, *Electrochim. Acta*, **10**, 773 (1965).
[18] E. P. Honig and J. H. Th. Hengst, *Electrochim. Acta*, **15**, 491 (1970).
[19] C. Liteanu and M. Mioșcu, *Rev. Roumaine Chim.*, **10**, 903 (1965).

EXPERIMENTAL RESULTS

Considering the parchment-membrane electrode impregnated with $BaSO_4$, separating the $Ba(OH)_2$ from the H_2SO_4, analogous to a $n - p$ junction,[20,21] one has called inverse polarization the application of a tension between the Pt electrodes thus directed that the electrode sunk in the hydroxide solution positivates versus the one sunk in the acid solution. The inverse situation was called direct polarization.

Inverse polarization. Proceeding to the dynamic raising of the current-membrane potential curve, one has applied an external polarization tension varying linearly with the time between the electrodes, according to the relationship

$$E = k \cdot t \tag{2}$$

where $k = 8.33 . 10^{-3}$ V/sec.

The results of the $I - t$ or $E_m^{'} - t$ recordings are reproducible. Two typical curves are presented in figure 2.

To clear up the reasons for the apparition of the null ordinate domain on the $I - t$ curve (fig. 2, curve 2), one has proceeded to the shifting of the zero point of the recorder, thus putting into evidence the passing of a current having an inverse direction to the polarization one. Figure 3 gives two $I - t$ curves obtained in the two above mentioned ways.

By correlating $I - t$ data with $E_m - t$ data, the curve $I - E_m$ corresponding to the inverse polarization represented on figure 4 was obtained.

The curve $I - E_m$ can surprisingly be partially linearized by the Tafel type diagrams. Thus, making use of the data in figure 4 and considering as overvoltage of the membrane electrode (η) the positive difference between the value of the potential of the inverse polarized electrode and the value of the potential of the resting electrode, one has noticed that :

— for values of $\eta < 0.1$ V, that curve $I - E_m$ admits equation

$$\eta = K \cdot I^* \tag{3}$$

where $I^* = I - I_0$, and I_0 is the intensity of the current passing through the membrane when $\eta = 0$. The experimental data according to the equation (3) are rendered in figure 5.

— for values of $\eta > 0.1$ V, the curve $I - E_m^{'}$ takes a linear form according to the equation (4)

---

[20] H. Reiss, *J. Chem. Phys.*, **21**, 1209 (1953).

[21] C. S. Fuller, *Rec. Chem. Progr.*, **17**, 75 (1956).

$$\eta = A + B.\lg I^* \qquad (4)$$

where A and B are two constants, and I^*, is as above defined. A corresponding representation appears in figure 6.

From $I - t$ data (fig. 2, curve 2), correlated to the values of the external polarization tension, according to the equation (2), one has graphically computed (method of tangents) the evolution of the cell resistance in time ($R - t$). Then, correlating the $E_m - t$ data (fig. 2, curve 1) with the $R - t$ data obtained above, one has plotted curve $R - E_m$ (fig. 7). One obtains a curve with a marked maximum corresponding to the value of the equilibrium potential of the membrane-electrode.

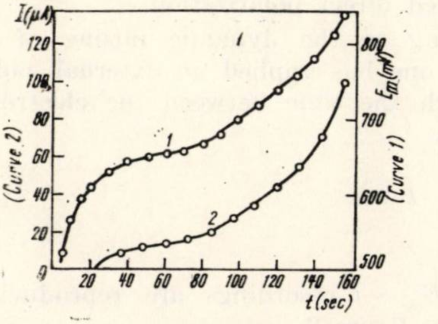

Fig. 2. – The $E_m - t$ (*1*) and $I - t$ (*2*) curves for reverse polarization.

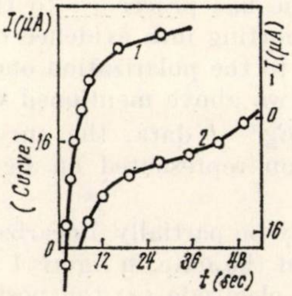

Fig. 3. – The $I - t$ curves with (*1*) and without (*2*) polarograph nul point removal.

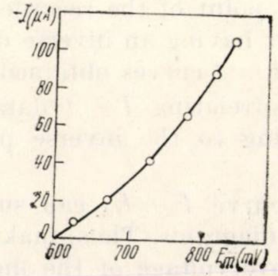

Fig. 4. – The $I - E_m$ curve for reverse polarization.

Direct polarization. Following the same method as in the case of inverse polarization, one has plotted the curve $I - t$ and $E_m - t$. By correlating these data one has obtained the curve $I - E_m$ for direct polarization. This was represented together with the curve $I - E_m$ of inverse polarization, giving the global $I - E_m$ curve, rendered by figure 8.

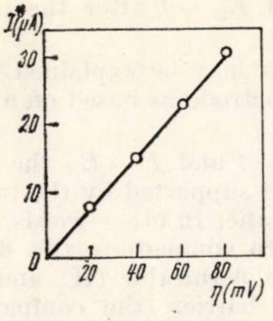

Fig. 5. — The linearization of $I^* - E_m$ curve, for $\eta < 0.1$ V.

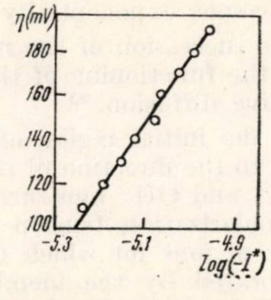

Fig. 6. — The linearization of $I^* - E_m$ curve, for $\eta > 0.1$ V.

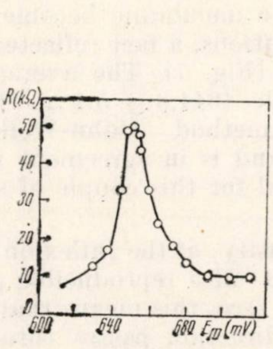

Fig. 7. — The $R - E_m$ curve for reverse polarization.

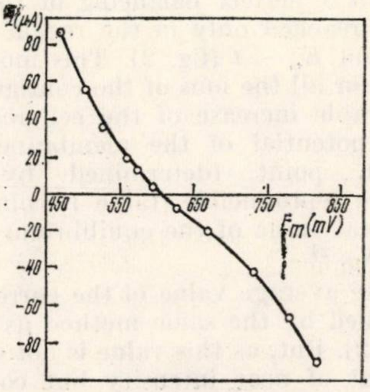

Fig. 8. — The whole $I - E_m$ curve for $BaSO_4$-parchment membrane-electrode.

$I > 0$ direct polarization; $I < 0$ reverse polarization.

DISCUSSIONS

By analysing the curves $I - t$, $E_m - t$ and $R - E_m$ corresponding to inverse polarization, one may note:

1. In the field of relatively small external polarization, a current contrary to the direction of the polarization passes through the membrane. The potential of the membrane-electrode decreases abruptly, reaching the resting value with the annulment of the current.

2. In the region in which the polarization tension nears the resting value of the membrane-electrode potential, an inflexion point appears on the curves $I - t$ and $E_m - t$, and curve $R - E_m$ simultaneously presents a maximum.

3. The shape of the curves $I - t$ and $E_m - t$ after the inflexion point becomes exponentially increasing.

The succession of the noted phenomena may be explained by considering the functioning of the membrane-electrode as based on a process of selective diffusion. [22]

In the initial region of the curves $I - t$ and $I - E_m$ the current contrary to the direction of the polarization is supported by the transport of the H^+ and OH^- ions through the membrane. In other words, as long as the polarization tension is insufficient to compensate the diffusion tendency of ions for which the membrane is permeable (H^+ and OH^-), unequilibrated by the membrane potential barrier (the compartments are shorted outside by connection to the tension source), the ions will penetrate undisturbed the membrane. The very moment the outer polarization tension equilibrates this tendency, the potential of the membrane returns to the resting value.

But a perfect balancing of the diffusion tendency of the H^+ and OH^- is reached only in the region of the inflexion point on the curves $I - t$ and $E_m - t$ (fig. 2). This moment the membrane becomes impermeable for all the ions of the contiguous solutions, a fact reflected by the considerable increase of the cell resistance (Fig. 7). The average value of the potential of the membrane-electrode (644.8 ± 5.1 mV) at the inflexion point (determined by the method Hahn-Weiler [23]) is therefore reproducible (table 1, column 3) and is in agreement with the theoretical value of the equilibrium potential for this couple of solutions (645 mV). [24]

The average value of the current intensity, at the inflexion point — determined by the same method as above is also reproducible (table 1, column 2). But, as this value is not equal to zero, this means that at rest, a current of near intensity but contrary direction passes through the membrane. This is a discharge current, made of H^+ and OH^- ions. It is probably caused by the unsuited porosity of the support. The immediate result is the establishment for the resting potential of a value inferior to that of the equilibrium potential, and a more remote result is the desactivation of the membrane-electrode.

The continuous increase of the membrane-electrode potential appears after the installation of the concentration polarization. The passing of the current is based either on the penetration of the membrane by the Ba^{2+} and SO_4^{2-} ions, or, less likely, on the electrolysis of water in the membrane.[17,18]

Regarding the Tafel-type interpretation of curve $I - E_m$, we must recall that the theory of these diagrams can also be adopted by the phenomena studied by us. For the time being, based on the analogy between the $BaSO_4$-parchment membrane system and a $n - p$ junction, [18] one can explain the use of Tafel type diagrams to interpret the curve $I - E_m$, obtained in the case of inverse polarization.

---

[22] C. LITEANU and I. C. POPESCU, *Talanta*, **19**, 974 (1972).

[23] F. L. HAHN and G. WEILER, *Z. analyt. Chem.*, **69**, 417 (1926).

[24] P. HIRSCH-AYALON, *Rec. Trav. chim.*, **75**, 1065 (1956).

Table 1

The current intensity (I^*) and the membrane-electrode potential (E_i) values corresponding to the inflexion points and the various I^*-E_m curves

Current number	I^* (uA)	E_i (mV)
1	8.8	644
2	7.2	642
3	10.2	646
4	9.6	641
5	12.2	646
6	11.2	644
7	9.6	643
8	14.2	655
9	12.6	654
10	7.8	633
	$\bar{I}^* = 10.2 \pm 1.0$	$\bar{E}_i = 644.8 \pm 5.1$

$k = 9$; $t = 2{,}26$; $\alpha = 0.95$.

The following equation is well known

$$i = i_s(e^{VF/RT} - 1) \tag{6}$$

where : i is the net current through the junction ; i_s is the exchange current, characteristic to the type of junction ; V is the potential difference applied to the junction ; all the other notations have the usual meaning). If we write

$$V = \eta \tag{7}$$

and

$$i = I^* \tag{8}$$

and consider that only the electric potential difference $(E - E_m)$ is the force supporting the passage of current (I^*) through the membrane we easily rediscover the empiric equations (3) and (4).

Thus, when $\eta < (RT/F)$, taking into account the relations (7) and (8) we can transform the relation (6), by series development of the exponential function, obtaining

$$I^* = i_s\eta/(RT/F) \tag{9}$$

a relationship showing a linear dependency $\eta - I^*$, appearing in figure 5.

Also, when $\eta > (RT/F)$, one can neglect the second term of the equation (6), and based on equations (7) and (8), one obtains

$$I^* = i_s\, e^{F\eta/RT} \tag{10}$$

a relationship putting into evidence a linear dependency $\eta - \lg I^*$, as in figure 6. The slope of the experimental line (237 mV) differs from its theoretical value ($2.303\ RT/F = 59$ mV, at $T = 298°$ K). In fact this discrepancy between the experimental results and the theoretical previsions is general when one makes use of the $n-p$ junction model to interpret the current-tension characteristics of the systems : bipolar membrane adjacent solutions.[2–5]

Revue Roumanie de Chimie, **18**, **2**, 327–346 (1973)

COPOLYMERIZATION REACTIONS USING ORGANIC TITANIUM DERIVATIVES-ALUMINUM ALKYL COMPLEXES. VII*

STRUCTURAL ASPECTS OF ACRYLONITRILE-METHYLMETHACRYLATE COPOLYMERS PREPARED BY THE USE OF THE SOLUBLE ZIEGLER-NATTA CATALYST SYSTEM: BIS (CYCLOPENTADIENYL)-TITANIUM-DICHLORIDE-TRIETHYL-ALUMINUM**

CR. I. SIMIONESCU*, I. BENEDEK*, SILVIA IOAN*, N. ASANDEI* and MONIQUE GALIN**

*"P. Poni" Institute of Macromolecular Chemistry, Jassy, Romania
** Centre de Recherches sur les Macromolecules, Strasbourg, France

Received June 17, 1972

This paper deals with the structural investigation of the acrylonitrile — methylmethacrylate copolymers synthesized by the use of the homogeneous Ziegler-Natta type catalyst system: bis (cyclopentadienyl)-titanium dichloride-triethylaluminum.

In some previous works, [1–6] the kinetics and the mechanism of the acrylonitrile copolymerization with acrylic-, vinyl aromated- comonomers and with epichlorohydrine, using the Ziegler-Natta type soluble catalyst, constituted by bis(cyclopentadienyl)-titanium-dichloride-triethylaluminum has been investigated.

Continuing our work in this field, the following presentation will concern mainly with the results obtained as regards the structure of the acrylic copolymers prepared with the above mentioned homogeneous catalyst.

---

* Part VI: CR. I. SIMIONESCU, SILVIA IOAN, I. BENEDEK and N. ASANDEI, of this series is published in Revue Roumaine Chim., **17**, 2003–2011, 1972.

** This paper includes a part of the dissertation submitted by Benedek.

[1] CR. I. SIMIONESCU, N. ASANDEI, I. BENEDEK and C. UNGURENAȘU, *European Polymer J.*, **5**, 449 (1969).

[2] CR. I. SIMIONESCU, N. ASANDEI, I. BENEDEK and C. UNGURENAȘU, *European Polymer J.*, **6**, 925 (1970).

[3] I. BENEDEK, N. ASANDEI and CR. I. SIMIONESCU, *European Polymer J.*, **7**, 995 (1971).

[4] CR. I. SIMIONESCU, I. BENEDEK and N. ASANDEI, *European Polymer J.*, **7**, 1549 (1971).

[5] CR. I. SIMIONESCU, N. ASANDEI and I. BENEDEK, *European Polymer J.*, **7**, 1561 (1971).

[6] CR. I. SIMIONESCU, I. BENEDEK, SILVIA IOAN and N. ASANDEI, unpublished results.

EXPERIMENTAL PART

The homopolymers and the copolymers of acrylonitrile (AN) and methylmetacrylate (MMA) were prepared using the same polymerization procedure as that previously used.[1-6]

Data on the thermal stability were obtained with the aid of a M.O.M. Derivatograph (in air).

The flash pyrolysis has been performed using 10 μg polymer samples. The pyrolysis was undertaken by the use of an induction pyrolyzer (Curie point), the degradation products being analysed by vapour-phase chromatography.

The N.M.R. spectra were recorded, by the use of a J.E.O.L. 60 MHz apparatus, at 160° (solvent $CDCl_3$, internal reference TMS).

X-ray investigations, T.U.R. M-60 apparatus, were performed using the $K\alpha$ ray of the copper.

Gravimetric average molecular weights M_w have been determined by a P.C.L. Peaker type, light scattering apparatus.

RESULTS AND DISCUSSION

The physico-mechanical properties of typical AN-MMA copolymers were checked and some examples taken from our studies will serve to illustrate their characteristics. The obtained results are summarized in Table 1.

Table 1

Physico-mechanical characteristics of the MMA-AN copolymers prepared by the $Cp_2TiCl_2-AlEt_3$ catalyst

N %	Tensile strength Kgf/cm²	tgδ %	Specific resistance Ω·cm	Resistance to sparking KV/mm
4.72	422	2	$4.50 \cdot 10^{15}$	12.0
5.10	422	1	$1.40 \cdot 10^{15}$	23.6
4.50	420	2	$1.42 \cdot 10^{14}$	26.5

It is seen from this table, that our copolymers (similarly to the technical MMA) possess very good mechanical and electrical properties. In order to bring the results in agreement with our concept of polymerization kinetics and mechanism let us focus our attention on the structural investigation of these materials. The purpose of this work is mainly to discuss some structure kinds of these polymers, i.e. solubility, crystallinity, thermal stability, structural homogeneity, sequence distribution and tacticity.

SOLUBILITY

On returning to the I.R. spectra of the AN-MMA copolymers the products appear to have a rather different character from that of free radical- or ionic polymers. The differences may arise partially from the existence of cyclized structures in polymers. In accordance with this finding, an insoluble fraction (in usual solvents, e.g., chloroform, or N,N-dimethylformamide) of these polymers has been found.

For further evaluations an average value of 10–30 per cent must be considered, for this insoluble fraction, depending on the synthesis conditions (e.g. temperature and aluminium/titanium ratio).

THERMAL STABILITY

Thermogravimetric data provide a further experimental evidence, supporting the idea that the AN-MMA copolymers prepared by the $Cp_2TiCl_2-AlEt_3$ catalyst contain some cyclized structures. The results show clearly the presence of destruction regions situated at temperatures above 400°, and furthermore, an important unpyrolysed residue content. Results are given in table 2.

Table 2

Derivatographic analysis data

Polymer	Catalyst	Residue % g	Destruction interval,°	Maximum decomposition temperature,° $T_{M_1}, T_{M_2}, T_{M_3}$	Activation energy Kcal/mole	Reaction order n
PAN	Cp_2TiCl_2 $-AlEt_3$	50	120–180	150 ; 345 ; 610	—	—
PMAN	Cp_2TiCl_2 $-AlEt_3$	3.68	210–255 255–413	270 ; 342 ;	50.60	2.0
	AIBN	4.12	50–250 250–413	155 ; 355 ;	32.70	0.7
PMMA unpurified polymer		16.60	200–425	330	—	—
PMMA purified by 1 reprecipitation		smaller than 5	—	335	40.58	2.5
PMMA purified by 2 reprecipitations	Cp_2TiCl_2 $-AlEt_3$	smaller than 5	—	360	34.50	0.5
PAMMA purified by 3 reprecipitations		smaller than 5		370	35.27	0.3
P(AN–MMA)′		4.52	220–430	375	37.90	2.0
P(AN–MMA)″	Cp_2TiCl_2 $-AlEt_3$	4.10	200–280 280–407 407–495	265 ; 338	51.40	1.4
P(AN–MMA)*		17.30	255–430 430–600	375	—	—

Observations : ′results obtained by crucibles ; ″by plates ; unfractionated polymer (*)

As it results from table 2, a difference concerning the composition of the calcination residue regarding fractionated or unfractionated polymer can be accounted for. Assuming that, for the first case in residuum constitution only the rests of catalyst chemically bonded participate, for the latter case it could be expected that both the chemically bonded promoters residue and the cyclised structures contribute to the formation of the unpyrolysed residuum.

The thermogravimetrical analyses of polyacrylonitrile indicates the existence of three destruction domains, as can be seen in the figure 1 (the maximum temperatures are reported in table 2).

The interpretation of the first destruction domain seems to be somewhat difficult, as it is situated more below the decomposition domain of the free radical PAN. The second interval, situated at 300°, can be assigned to the linear PAN, and the last, situated above 800°, to the cyclized PAN. We remark that polymethacrylonitrile (PMAN) characterized by the existence of two destruction domains, possesses this first domain at a higher temperature in comparison to PAN (see Fig. 2).

Fig. 2 represents the derivatograms of the PMAN synthesized by free radicalic and Ziegler type catalyst.

Making use of these data, by the aid of the Freeman-Caroll [7] method, one can calculate the activation energies for the main destruction domain (200–400°), as can be seen in Fig. 3.

The literature data, [8] show that the use of this method permits to obtain overall activation energy values, which can be used (together with the initial decomposition temperatures) for thermal stability characterization. As can be seen in table 2, the reported values differ, depending on the polymer nature. One can constate an increased thermal stability for PMAN prepared by homogeneous catalyst with respect to free radicalic polymer.

It can be observed from figure 1, that PMMA synthesized by homogeneous catalyst is characterized by an increased thermal stability and a singular decomposition domain, with respect to the other two homopolymers (which present some decomposition processes).

The thermogravimetric study of the AN-MMA copolymers synthesized by the homogeneous catalyst, gives the results compiled in figures 4 and 5.

As can be seen from the data presented in the above figures, the copolymers investigated by us, present a relatively high thermal stability with respect to PMMA. It is generally assumed that one can characterize quantitatively the thermal stability of the polymers on the basis of the activation energies and of the destruction order. These data are reported in table 2.

Furthermore, in order to evaluate quantitatively the influence of the impurities on the thermal behaviour of the polymers, some measures with purified (by successive reprecipitation) and unpurified PMMA were realized (the chloroform-ethanol system as a solvent precipitant one for

---

[7] E. S. Freeman and B. Caroll, *J. Phys. Chem.* **,62**, 398 (1958).

[8] L. H. Flynn and L. A. Wall, *J. Res. Nat. Bur. Stand., Sect. A*, **70 A**, 513 (1966)

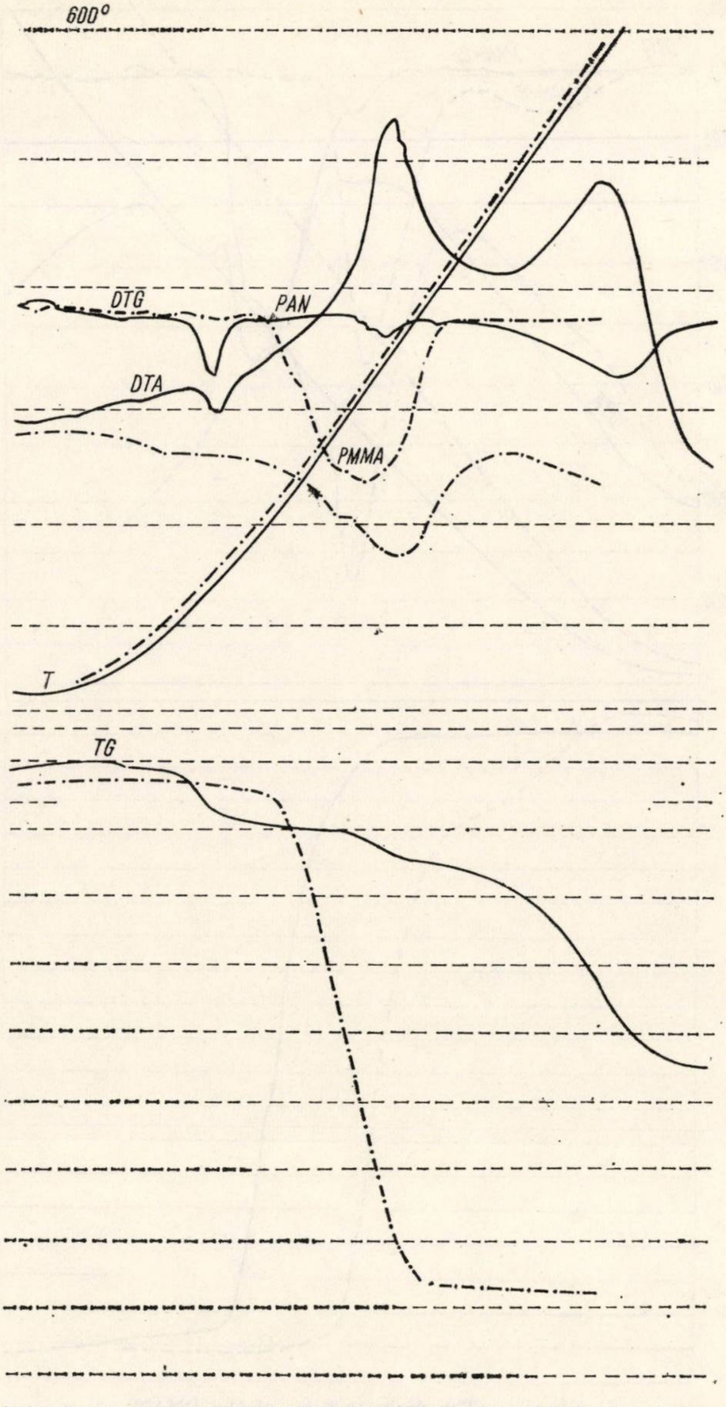

Fig. 1. — The derivatograms of the PAN and PMMA prepared by the $Cp_2TiCl_2-AlEt_3$ catalyst system.

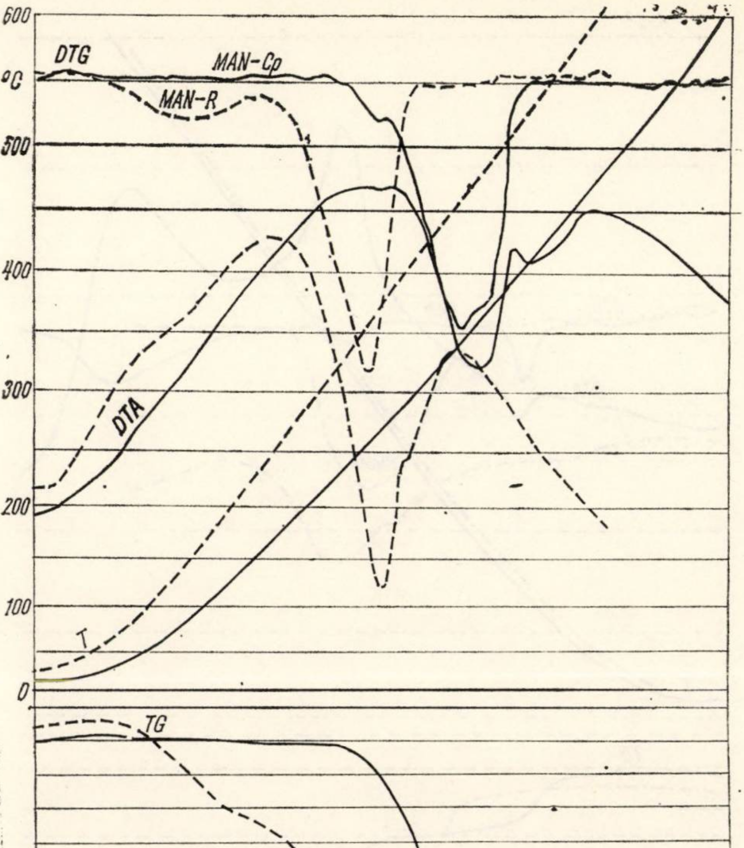

Fig. 2. – The derivatograms of the PMAN.

MAN – R = free radicalic **PMAN** ;
MAN – Cp = **PMAN** obtained by the $Cp_2TiCl_2 - AlEt_3$ catalyst.

polymer purification has been used). The results are summarized in table 2. As can be seen from the data of table 2, the activation energy values differ with ±5 Kcal/mole, depending on the polymer purification degree;

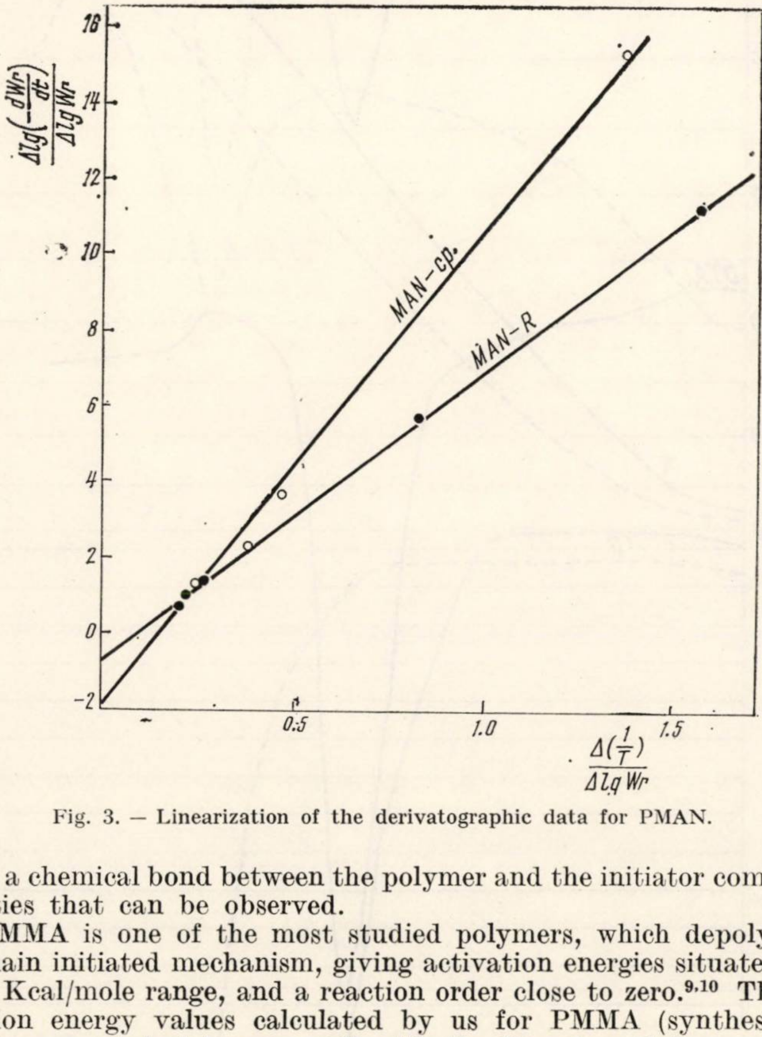

Fig. 3. — Linearization of the derivatographic data for PMAN.

there is a chemical bond between the polymer and the initiator components impurities that can be observed.

PMMA is one of the most studied polymers, which depolymerizes by a chain initiated mechanism, giving activation energies situated in the 32—42 Kcal/mole range, and a reaction order close to zero.[9,10] Thus, the activation energy values calculated by us for PMMA (synthesized by homogeneous catalysis) agree well with the literature data.

It can be observed, that the calculation errors which may derive on the one hand from the different degrees of purification of the polymers and, on the other hand, from the method itself, make the obtained "n" and "E" values to be only orientatively used.

---

[9] N. Grassie, "Khimia Protsesov Distructsii Polimerov", Izd. Inostrannoi Literatury, Moskva, p. 32.

[10] L. A. Wall and J. H. Flynn, *Chem. and Techn.*, **35**, 1157 (1962).

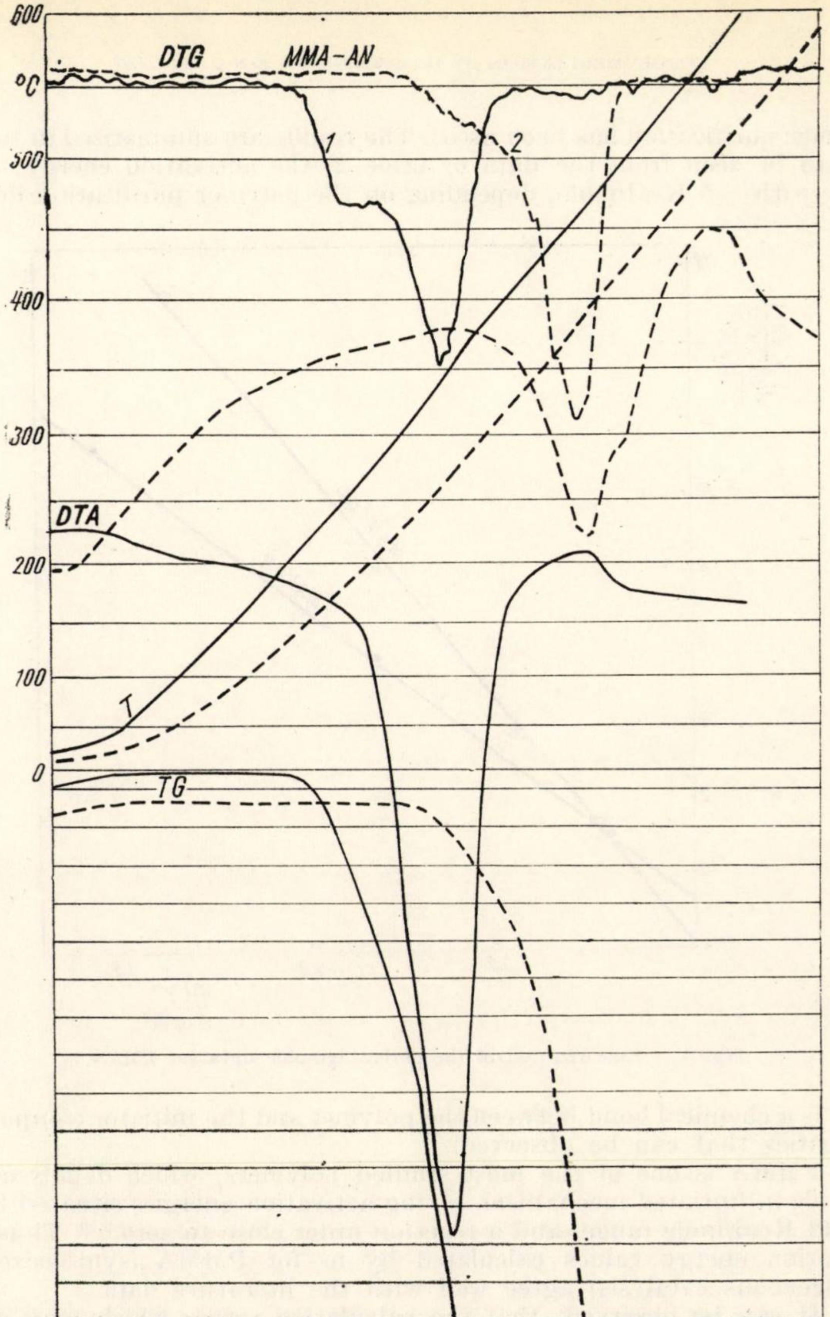

Fig. 4. – The derivatograms of the MMA-AN copolymer prepared by the $Cp_2TiCl_2-AlEt_3$ catalyst :

1, Results obtained by warming plates ; *2*, Results obtained by crucibles.

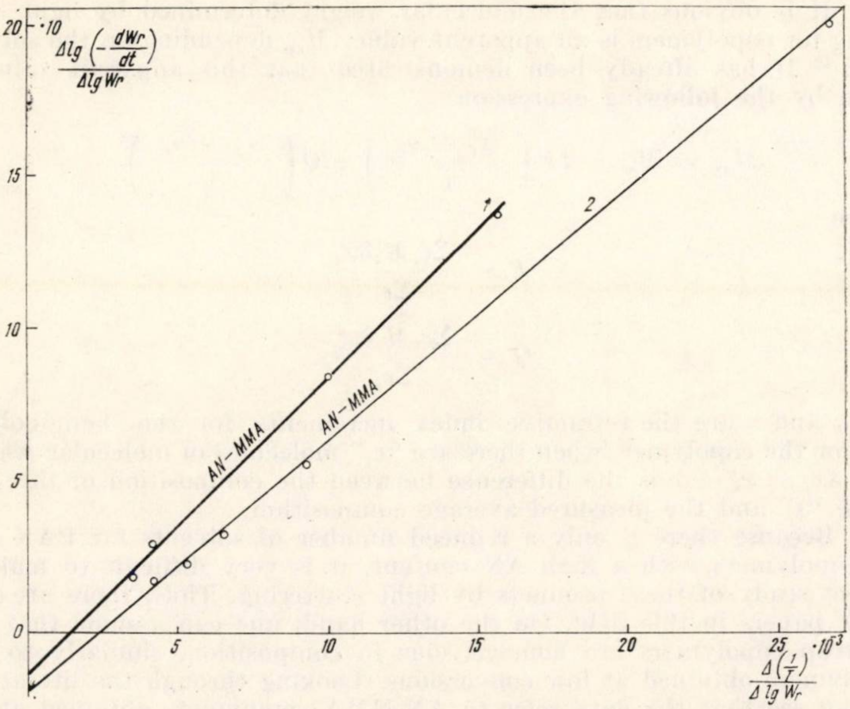

Fig. 5. — Linearization of the MMA-AN copolymer derivatographic data :
1, Results obtained by warming plates; *2*, Results obtained by crucibles.

STRUCTURAL HOMOGENEITY

Preliminary experiments taught us that the polymers have a structure composed by a soluble fraction and an insoluble one. Thus the techniques involving the assay of solution might be applied only to the soluble fraction examination.

It could be expected for the PMAN (which is soluble in usual solvents) study to give some structural data also applicable to PAN. However, it is safe to say, that the extrapolation of PMAN solubility and thermal resistance data for PAN is doubtful. One can constate, that PMAN contains reduced quantities of unpyrolised residue with respect to PAN (see table 2) and a reduced hot acetone insoluble fraction content (smaller than 10%). Therefore, the insoluble (cyclised) structure content is little and the increased „solubility index" value denotes the lack of crystallinity and stereoregularity.[11]

In addition, structural homogeneity (molecular weight and composition polydispersity) data for the soluble polymer fractions were reported.

---

[11] Yasushi Yoh, Toshio Yoshihara, Yahide Kotake, Yoshikatsu Imai and Seiki Kurihara, *J. Polymer. Sci.*, **A 1**, 605 (1967).

It is obvious that the molecular weight determined by light scattering for copolymers is an apparent value, M_{ap} depending on the solvent used.[12] It has already been demonstrated that this apparent value is given by the following expression

$$M_{ap} = M_w + 2P\left(\frac{\nu_A - \nu_B}{\nu}\right) + Q\left(\frac{\nu_A - \nu_B}{\nu}\right)^2 \tag{1}$$

where

$$P = \frac{\Sigma c_i M_i \delta x_i}{\Sigma c_i} \tag{2}$$

$$Q = \frac{\Sigma c_i M_i \delta x_i^2}{\Sigma c_i} \tag{3}$$

ν_A, ν_B and ν are the refractive index increments for the homopolyers and for the copolymer, when there are "c_i" molecules of molecular weight M_i ; $\delta x_i = x_i - x$ is the difference between the composition of the molecule "i" and the measured average composition.

Because there is only a reduced number of solvents for PAN and for copolymers with a high AN content, it is very difficult to make a correct study of these products by light scattering. Thus, there are only a few papers in this field. On the other hand, one can assume that the azeotrop copolymers are homogeneous in composition, similarly to the copolymers obtained at low conversions. Looking through the literature, we can see that the data refer to AN-MMA copolymers obtained at reduced conversions, having an assumed compositional homogeneity.[13] In order to simplify the measurements, the homopolymer treatment (in a singular solvent) is used for these copolymers.

In our case, there are new polymers with unknown compositional distribution and thus the simplified study is not applicable. Consequently, a great number of solvents have been used in order to determine M_{ap} values.

Refractive index increments for M_{ap} determination are calculated by additivity, in some cases they being practically verified. The dependence of refractive index increments of the polymer solutions as a function of the solvents refractive index, is described in figure 6.

Using the data of figure 6 for the light scattering measurements of the AN-MMA copolymers the following structural characteristics (cop. 1) were obtained :

As can be seen in Table 3, the determined parameters, i.e. the radius of giration $(\overline{R}_0^2)_{1/2}$ and the second virial coefficient (A_2) agree well with the literature data.[13]

A typical Zimm diagram for the AN-MMA copolymer is presented in figure 7.

It is known that the existence of a linear distribution of the apparent molecular weights, as a function of $\nu_A - \nu_B/\nu$, denotes the compositional homogeneity of the investigated copolymer. The graphical representation of the data of Table 3 gives a parabola, providing the compositional heterogeneity of the copolymer (see Fig. 8).

---

[12] H. Benoit, *Ber. Bunsengesellschaft Phys. Chem.*, **70**, 286 (1966).

[13] Y. Shimura, *Bull. Chem. Soc. Japan*, **40**, 273 (1967).

The parameters P and Q of this parabola characterize quantitatively the polymer heterogeneity, by the following values : $M_w=1.1717\cdot10^6$;

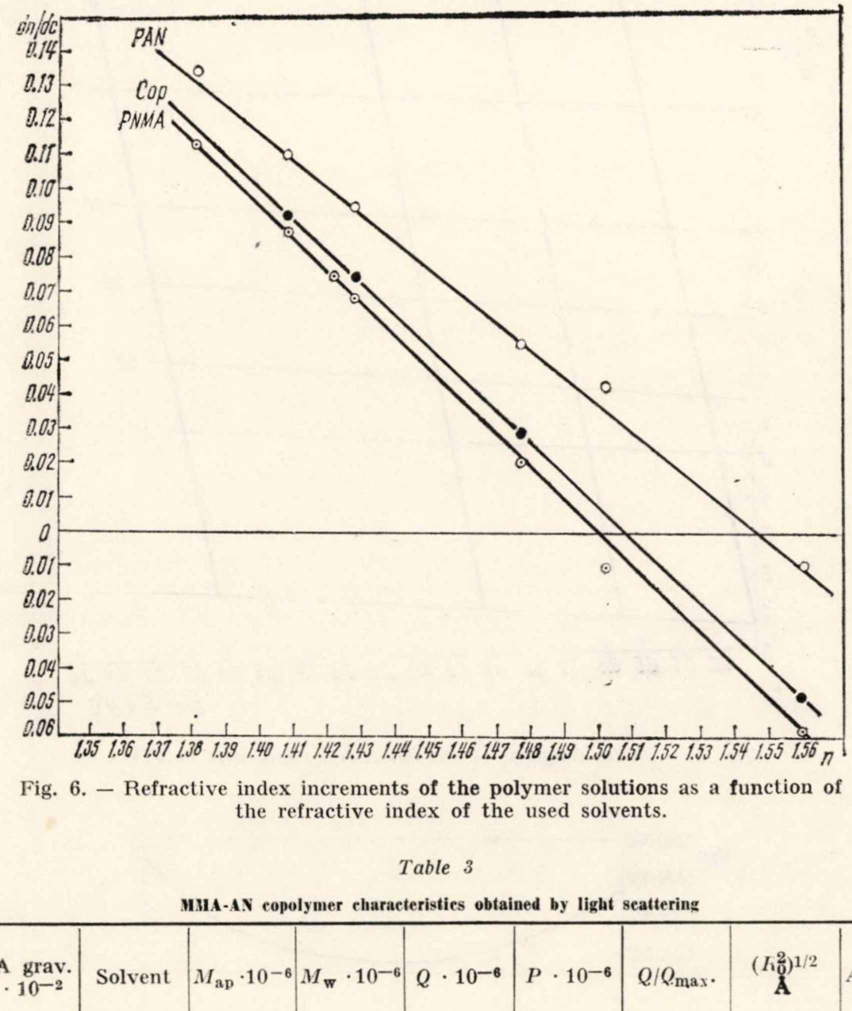

Fig. 6. — Refractive index increments of the polymer solutions as a function of the refractive index of the used solvents.

Table 3

MMA-AN copolymer characteristics obtained by light scattering

MMA grav. % $\cdot 10^{-2}$	Solvent	$M_{ap}\cdot10^{-6}$	$M_w\cdot10^{-6}$	$Q\cdot10^{-6}$	$P\cdot10^{-6}$	$Q/Q_{max}\cdot$	$(\bar{h}_0^2)^{1/2}$ Å	$A_2\cdot10^3$
0.810	DMF	1.001	1.172	0.575	−0.337	0.330	831	0.428
	THF	1.039					822	0.306
	DMSO	1.200					581	0.148

$P=0.3375\cdot(-10^6)$; $Q=0.5750\cdot10^6$. The obtained experimental data show that the AN-MMA copolymer prepared by Ziegler-Natta catalysis

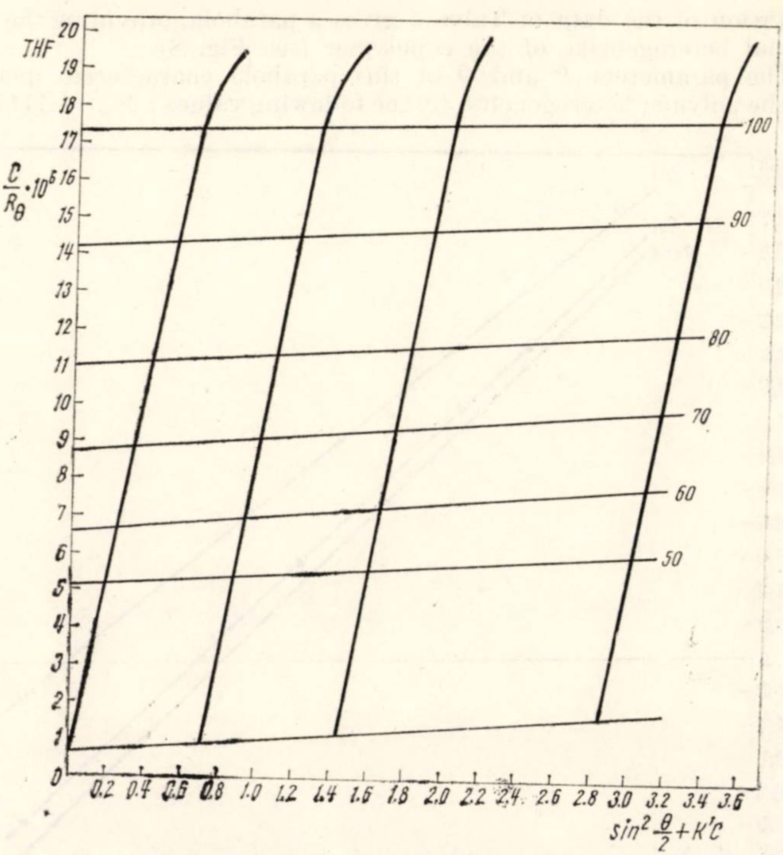

Fig. 7. — **Zimm diagram of the MMA-AN copolymer in THF.**

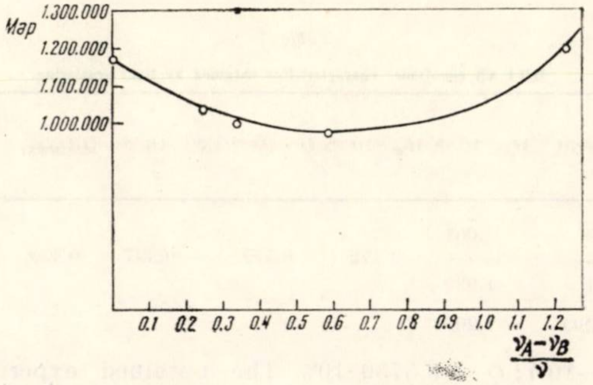

Fig. 8. — $M_{ap} = f\left(\frac{\nu_A - \nu_B}{\nu}\right)$.

is heterogeneous in composition. The comparative examination of the above summarized data, with respect to those calculated for acrylonitrile-styrene copolymers, [6] illustrates the existence of a difference, concerning the copolymer heterogeneity, between AN-MMA and AN-St copolymers. The AN-MMA copolymer has a more reduced compositional heterogeneity. This is due probably to the differences existing in the mechanism of the two discussed polymerization processes. [1-5] Thus, on the basis of our preliminary experiments, an ionic-coordination mechanism for AN-MMA copolymers and a concurrent mixed mechanism for AN-St copolymers has been assumed.

CRISTALLINITY

By X ray investigation of the PAN and PMAN soluble fractions no crystallinity has been found. On the other hand, both PMMA and the MMA-AN copolymer possess some crystallinity. The X ray diagram of a MMA-AN copolymer (cop. 1) is presented in figure 9.

As can be seen from figure 9, the MMA-AN copolymer has a per cent crystallinity index of 40. Supplemental data concerning the structural ordering of copolymers can be obtained by I.R. spectroscopic investigations using parallely and perpendicularly polarized light. The I.R. spectrum of MMA-AN copolymer recorded in polarized light is presented in Fig. 10. The total absence of dichroism is surprising (partially due probable to an insufficient orientation of the film formed by the technique of evaporation on a mercury surface and constant load straining).

SEQUENCE DISTRIBUTION

The flash pyrolysis data, concerning the MMA-AN copolymers prepared by homogeneous Ziegler-Natta catalysis demonstrate the existence of structures which are different from that of the copolymers obtained by free radicalic mechanism. One can constate that the main degradation products are AN and MMA. The dependence of the monomer yield of the destruction processus, as a function of the copolymer composition, is presented in figure 11.

The curves *a* and *b* represent the yield in AN and MMA for free radicalic copolymers pyrolysed in the same conditions, [14] and the points noted by *A* and *B* correspond to the copolymers prepared by homogeneous Ziegler-Natta catalysis. One can constate that these products have a different behaviour. The AN yield is much more and the MMA yield is also reduced with respect to the radical copolymer of the same composition.

---

[14] M. Galin, J. Guillot and A. Guyot, *J. Macromol. Sci. Chem.*, **A 4**, 19 (1970).

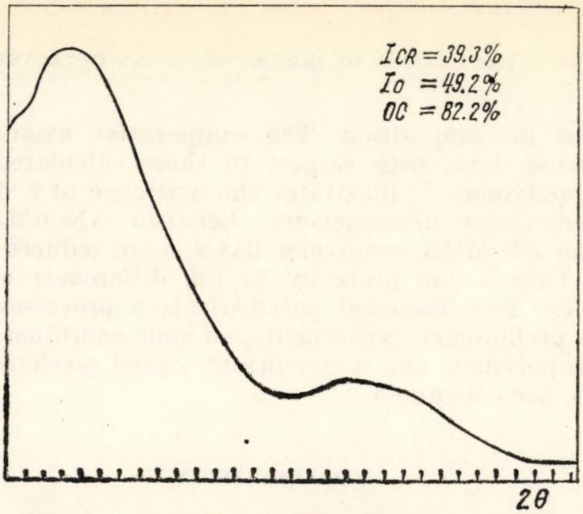

Fig. 9. — *X* ray diagram of the MMA-AN copolymer.

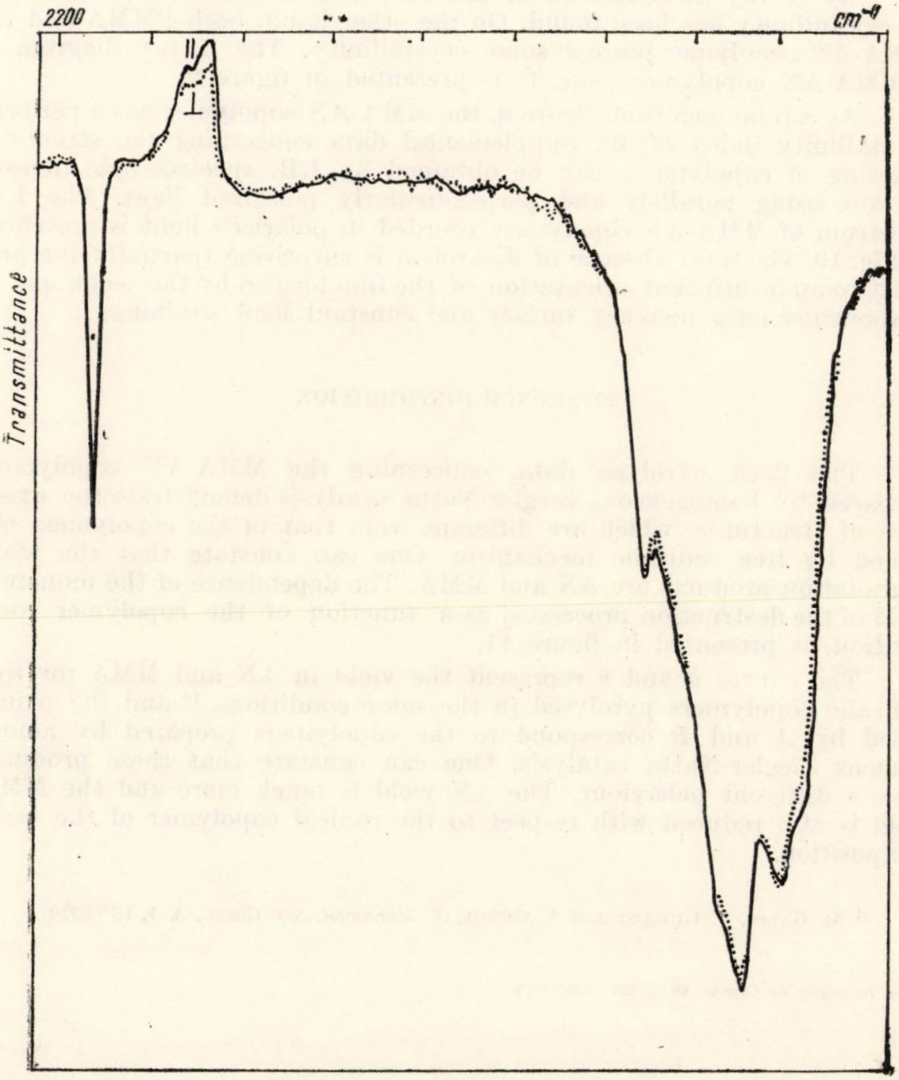

Fig. 10. — I.R. spectra of the MMA-AN copolymer in polarized light.

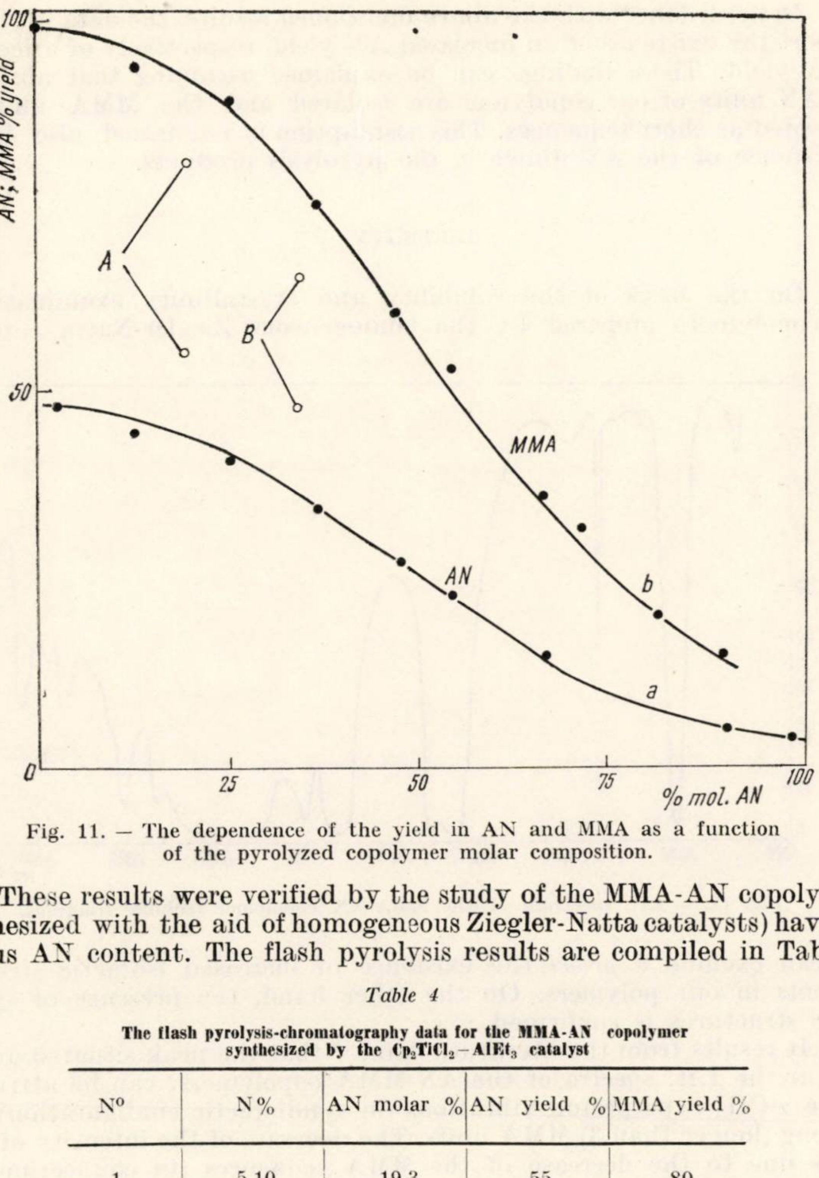

Fig. 11. — The dependence of the yield in AN and MMA as a function of the pyrolyzed copolymer molar composition.

These results were verified by the study of the MMA-AN copolymers (synthesized with the aid of homogeneous Ziegler-Natta catalysts) having a various AN content. The flash pyrolysis results are compiled in Table 4.

Table 4

The flash pyrolysis-chromatography data for the MMA-AN copolymer synthesized by the $Cp_2TiCl_2-AlEt_3$ catalyst

N°	N %	AN molar %	AN yield %	MMA yield %
1	5.10	19.3	55	80
2	6.00	22.7	67	76
3	8.15	30.8	60	55
4	8.44	31.9	57	67
5	8.61	32.5	55	68
6		25.5	42	87
7		37.0	36	74

Observation : N° 1 − 5 refer to the MMA − AN copolymer obtained by the $Cp_2TiCl_2-AlEt_3$ catalyst ; N° 6,7 refer to the free-radicalic MMA-AN copolymers with a 70 − 30%, respectively 50 − 50%, comonomer constant.

In accordance with the above mentioned results, the data of Table 4 support the existence of an increased AN yield, respectively of a decreased MMA yield. These findings can be explained assuming that almost all the AN units of our copolymer are isolated and the MMA units are imbedded as short sequences. This assumption is confirmed also by the inexistence of the AN dimer in the pyrolysis products.

TACTICITY

On the basis of the solubility and crystallinity examination of the copolymers prepared by the homogeneous Ziegler-Natta catalysis, one can exclude *a priori* the existence of increased isotactic structure contents in our polymers. On the other hand, the presence of syndiotactic structures is confirmed.

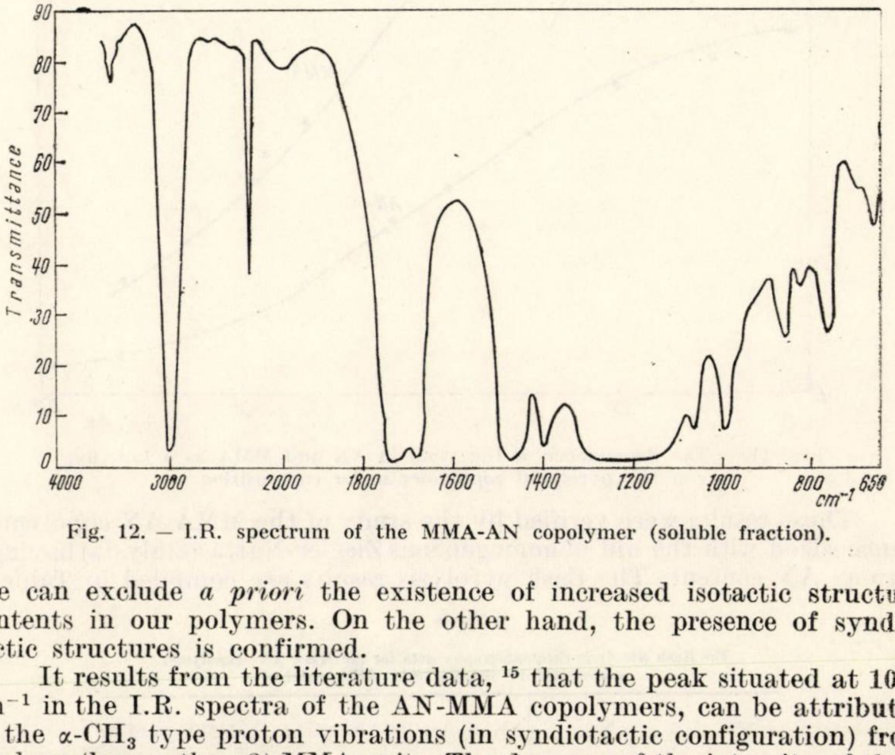

Fig. 12. — I.R. spectrum of the MMA-AN copolymer (soluble fraction).

It results from the literature data,[15] that the peak situated at 1060 cm^{-1} in the I.R. spectra of the AN-MMA copolymers, can be attributed to the α-CH_3 type proton vibrations (in syndiotactic configuration) from the long (longer than 3) MMA units. The decrease of the intensity of these bands due to the decrease of the MMA sequences (in connection with the band situated at 840 cm^{-1}, which characterizes also the MMA units, but is independent of the configuration) with the increase of the AN content in copolymer can be observed.

The I.R. spectrum of the AN-MMA copolymer is reported in Fig. 12.

As can be seen from Fig. 12, there are characteristic vibrations at 1060 cm^{-1} for the syndiotactic units in the copolymer spectrum.

---

[15] R. Schmolke, H. Herma and V. Groebe, *Faserforschung*, **16**, 598 (1965).

The literature [16] mentions the presence of a singlet at 6.42 τ (which can be attributed to the methoxy protons) and of three singlets situated at 8.65 ; 8.77 ; and 8.88 τ (assigned to the methyl protons from the isotactic, heterotactic and syndiotactic triads) in the N.M.R. spectra of the PMMA.

The N.M.R. spectra of the AN-MMA copolymer are presented in figure 13.

It is demonstrated that the presence of AN units in the AN-MMA copolymer determines some changes in the bands. [17] In the methoxy region two new bands appear. The first is situated at 6.35 τ and increases while the AN content of the copolymer increases. At a higher content than 30 AN per cent, a new peak situated at 6.32 appears. Our spectra contain all these three bands situated at 6.32 ; 6.35 and 6.42 τ (noted by A, A_1 and B).

It is known that the methoxy proton resonance in PMMA presents a tacticity independent singlet. Thus, the new bands can be attributed to the two MMA units which are situated in the neighbourhood of the AN units, and the nitrile group's paramagnetic influence gives a shift of the resonance to the reduced values of the magnetic field.

Concerning the α-methyl protons, one can observe also the presence of two new bands at 8.62 and 8.71 τ in agreement with the literature data. [17] The intensity of the band situated at 8.62 τ increases while the copolymer AN content increases as well; the intensity of the bands situated at 8.77 and 8.88 τ decreases with the increase of the AN content in the copolymer. Therefore, in spectra of our copolymer appear four bands (noted by D, E, F, G) situated at 8.66 ; 8.76 and 8.86 τ (the observed shifts in the position of the bands can be attributed to the solvent). The D and E bands are attributed to the AN units of the copolymer, and the F and G bands exist also for homopolymer).

Under the assumption that isotactic diads exist in our copolymer, two new symmetrical doublets centered about 7.6 and 8.3 τ (the methylene region in the 8.0 τ neighbourhood is not sufficiently resolved) must appear. Practically, in our spectra there are not these bands. In consequence, the D and E bands can not be attributed to the α-CH_3 protons, from the isotactic triads. On the basis of the literature data [17] the D band can be due to the isolated MMA units, situated between two AN units.

The bad resolution of the spectra does not permit the interpretation of β-CH_2 domain of the MMA and AN units and that of the CH protons from AN. Practically, the overlapping of the α-CH and of the methoxy absorption (probably, because of the weak polymer solubility) is observed.

With the following relationship, [16] the molar per cent content of MMA in copolymer, by the methoxy groups intensity (X), integral α-CH_3,

---

[16] J. Guillot, A. Guyot and Pham Quang Tho, *J. Macromol. Sci. Chem.*, **A 2**, 1303 (1968).

[17] Pham Quang Tho, J. Guillot and A. Guyot, *Compt. rend.*, **264**, 2019 (1967).

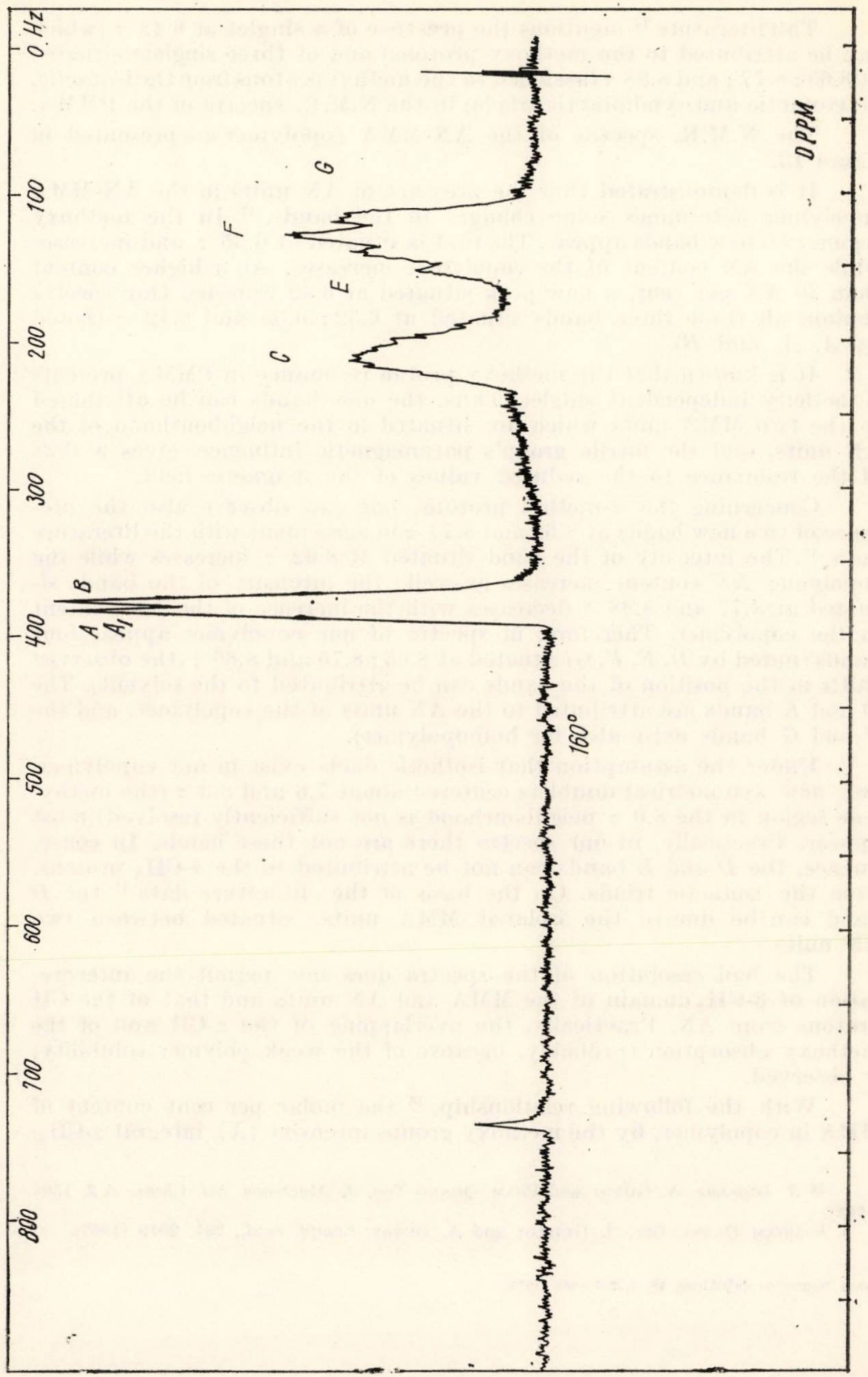

Fig. 13. — R.M.N. spectrum of the MMA-AN copolymer.

CH_2, α-CH intensity (Y) and the α-CH_3 groups intensity (Z) determination, can be calculated

$$\text{MMA }\% = \frac{X}{X + Y - 2X/3} = \frac{Y}{Z + Y - 2Z/3} \qquad (4)$$

The results of our calculus agree well with the nitrogen analysis data.

The average numerical length of the MMA sequences ($L_{MMA}n$) can be obtained from the examination of OCH_3 bands. The B band can be attributed to the internal ($n - 2$) units of the MMA sequences having n length ; the A and A_1 bands correspond to the terminal units of the sequences. The following formula holds for the ratio of intensities

$$I\,(B)/I\,(A + A_1) = (n - 2)/2 \qquad (5)$$

Then we have

$$L_{MMA}n = 2\,(1 + I\,(B)/I\,(A + A_1)) = 4.90 \qquad (6)$$

It seems therefore that the copolymer contains short sequences formed by five MMA units. These results verify the conclusions derived from our previous pyrolysis experiments.

Supplemental data, concerning the short sequences, by α-CH_3 analysis can be obtained. In PMMA these bands are triad tacticity sensible. For the copolymers, the possibility of a cotacticity [18] must be determined. As can be seen, the D band (due to the isolated units) is not sufficiently resolved. For the latter reasons, for tacticity evaluation, we discuss only the internal units of the long MMA sequences.

The data suggest, that the D band can be attributed to the MMA_1 units and the E band to the MMA_2 sequences. A very small part of this band is due to the isotactic triads from the long MMA sequences. The F band is constituted, on the one hand, from the heterotactic triads of the long MMA sequences and from the terminal units of the long MMA_x ($x > 3$) sequences, on the other hand. The G band can be attributed to the syndiotactic triads of the long MMA sequences.

In consequence, concerning the proportion of different structural units in the copolymer, the following values can be approximated : 12.5 % isolated MMA_1 units ; 12.5 % MMA_2 units ; 25 % long heterotactic sequences ; 50 % long syndiotactic units. The syndiotactic units participate with about 70 % proportion in the constitution of the long MMA sequences (which represent 75 % of the long MMA units).

A similar conclusion, concerning the presence of syndiotactic MMA units by acid hydrolysis of the polymer, was drawn. It is known that isotactic PMMA differs from that syndiotactic by the acid hydrolysis rate. [19,20] The isotactic polymer is completely hydrolysed in concentrated sulphuric acid in about one hour (at 55°). The hydrolysis rate of the syndiotactic polymer is more reduced. For a 85 per cent hydrolysis degree of the syndiotactic polymer at least 24 hours are needed. In our case, for the PMMA prepared with the homogeneous catalyst, a 13.4 per cent degree of hydrolysis (in standard conditions) after one hour was found. Consequently, the good chemical resistance supports the hypothesis of a syndiotactic configuration.

---

[18] F. A. Bovey, *J. Polymer Sci.*, **62**, 197 (1962).

[19] G. Smets and W. E. De Loeker, *J. Polymer Sci.*, **45**, 461 (1960).

[20] G. Smets and W. E. De Loeker, *J. Polymer Sci.*, **40**, 203 (1959).

CONCLUSIONS

In order to characterize the structure (structural and compositional homogeneity, thermal stability, structural ordering, sequence distribution, tacticity, solution properties of the macromolecular chains) of MMA-AN copolymers synthesized with the homogeneous Ziegler-Natta type catalyst $Cp_2TiCl_2-AlEt_3$, several experimental techniques (i.e. derivatographic analysis, I.R., N.M.R. and X-ray spectroscopy, acid hydrolysis, pyrolysis-chromatography and light scattering) were used. The physico-mechanical properties of the polymers has also been investigated.

The solubility study, the thermal and I.R. spectroscopy showed the presence of cyclised structures and of a residual initiator content in the polymers.

The products contain a soluble fraction and an insoluble one. The soluble fractions characterized by an advanced compositional heterogeneity and a mean degree of ordering (crystallinity index of 40%), have very good physico-mechanical properties and a notable thermal stability (their heterogeneity being smaller than that of the corresponding AN-St copolymer).

For the same overall tacticity (70% of the long MMA sequences are syndiotactic) that of corresponding free-radicalic obtained copolymer, the MMA-AN copolymer prepared by the homogeneous Ziegler-Natta type catalysts, present a completely different sequence distribution, characterized by the existence of isolated AN units, separated from short MMA sequences (with an average length of 5 units).

Revue Roumaine de Chimie, **18**, 2, 347 – 352 (1972)

THE FERROMAGNETIC RESONANCE OF NICKEL-CHROMIA CATALYST

IOAN INŢA and PETRE MĂRGINEANU

University of Braşov, Department of Physics, str. Karl Marx 50, Braşov, Romania
and
Institute of Atomic Physics, str. Donáth, 59 – 105, Cluj, Romania

Received February 21, 1972

By ferromagnetic resonance experiments at room temperature and in X-band (9350 MHz), two quantities have been determined : the g-spectroscopic splitting factor for $Ni-Cr_2O_3$ catalyst samples and several nickel catalyst samples on other oxide supports (MgO, Al_2O_3, SiO_2, ZnO, CeO_2) and an effective magnetization M_{ef} for $Ni-Cr_2O_3$ catalysts. The former quantity is independent of the nickel concentration in the catalyst or the type of the oxide support. At the M_{ef} variation on the nickel concentration a sudden decrease appears at the concentration of 10 – 15 % Cr. We put this variation on the account of the exchange interaction through the oxide support.

1. INTRODUCTION

In the last time, the Ferromagnetic Resonance Method (FMR) has begun to be used in the study of nickel catalysts.[1-3] Due to the obtained results the FMR investigations may offer new information on the physical properties of catalysts. For instance, by FMR studies we may obtain interesting information on the adsorption phenomenon of gases on catalyst,[2] and also some indications referring to the influence the physical properties of catalyst have upon the catalytic ones.[1]

However, one must not neglect the fact that the catalysts which contain ferromagnetic metals are generally very complex physical systems and due to this, the interpretation of FMR spectra becomes extremely difficult. For example, the nickel catalysts on oxide support, important in heterogeneous catalysis[4] are presented as polycristalline powders in which the ferromagnetic metal is dispersed as grains of different sizes within the mass of the oxide support. For such samples very large FMR adsorption lines are obtained, which emphasize the existence of many complex inner interactions (inside the ferromagnetic grain, among these grains, respectively between the grains and the oxide support).

---

[1] J. Yasamura and S. Abe, *Nature*, **207**, 1192 (1965).

[2] A. Andreev and P. W. Selwood, *J. Catalysis*, **8**, 375 (1967).

[3] A. A. Slinkin and A. Fedorova, *Kinetika i Kataliz*, **3**, 655 (1968).

[4] I. E. Germain, in "Catalyse heterogene", Dunod, Paris, 1959, chap. 5.

There are a few tests [3] for the establishing of the factors which influence the shape and width of the FMR lines, their dependence upon temperature, the shape and size of ferromagnetic metal grains, their concentration in catalyst and the type of the oxide support. The experimental technique used in obtaining the FMR lines in several works appeared until now, have some drawbacks, the most important being the fact that it does not offer the possibility to investigate the internal magnetic fields of the catalyst samples as powders.

In our work we try to obtain a better estimation of FMR parameters by using an experimental technique specific of the ferromagnetic metal samples having a disc shape. Researches were made about $Ni-Cr_2O_3$ catalysts, important especially for the isotopic exchange reaction of deuterium between water vapour and hydrogen.[5] We have recorded the spectroscopic splitting factor variation, g, the effective magnetization M_{ef} and the variation of the FMR line width, as function of the nickel concentration in the catalyst. In several tests, the support is made of Zn, Al, Mg, Si and Ce oxide.

2. EXPERIMENTAL

The nickel catalysts on oxide supports have been prepared by the method described in.[6] For FMR measurements samples have been prepared as thin catalyst powder layer (diameter $= 0.01-0.03$ mm), fixed on a microscope glass slide of 4×4 mm^2, by means of a polyvinilic glue. These samples have been glued with silver paste in the centre of the plane wall of a cylindrical cavity (with the mode TE_{111}), where the high frequency magnetic field has the maximum value and the electric one is null. Thus, an electric contact has been achieved between the catalyst layer and the wall of the cavity without modifying sensibly the geometry of the cavity.

The FMR measurements have been carried out with the JES$-$3B installation, using the X-band (9350 MHz), at room temperature. The derivatives of the absorption curves of FMR have registered for two orientations of the magnetic field outside the plane of the catalyst layer, namely: parallel ($H_{||}$) and perpendicular ($H_{\perp}$) to this plane.

In figure 1 are shown the FMR lines obtained for the $Ni-Cr_2O_3$ (80% Ni) and $Ni-ZnO$ (60% Ni) samples. Differences between the intensity and the position on the axis of the static field H of the FMR lines are noticed for the two orientations used. For all the investigated samples, the FMR lines corresponding to the perpendicular orientation appear at a field $H_{\perp}$ greater than $H_{||}$. This dependence of the position of the FMR maximum absorption upon the orientation of the external magnetic field against the catalyst layer plane, can be ascribed to an effective demagnetization field that appears at the perpendicular orientation ($H_{\perp}$) of the external field due to the interactions among the metallic nickel grains.

If these grains are spherical, their demagnetization field is null*) and assimilating the catalyst layer to a thin magnetic film whose effective magnetization M_{ef} is created by the interactions from among the metallic grains, the resonance conditions for the two orientations will be[7]:

---

[5] G. M. Murphy, in "Production of Heavy Water", McGraw-Hill, New York, 1951.

[6] P. Mărgineanu and A. Olariu, *J. Catalysis*, **8**, 359 (1967).

*) It becomes practically zero for nonspherical grains too, due to their random orientation.

$$\omega_{\parallel} = \gamma \, [(H_{\parallel} + 4\pi M_{ef}) \cdot H]^{\frac{1}{2}} \quad (1)$$

$$\omega_{\perp} = \gamma \, (H_{\perp} - 4\pi M_{ef}) \quad (2)$$

We notice that measuring $H_{\parallel}$, $H_{\perp}$, $\omega_{\parallel}$ and $\omega_{\perp}$, g and M_{ef} can be concomitantly determined.

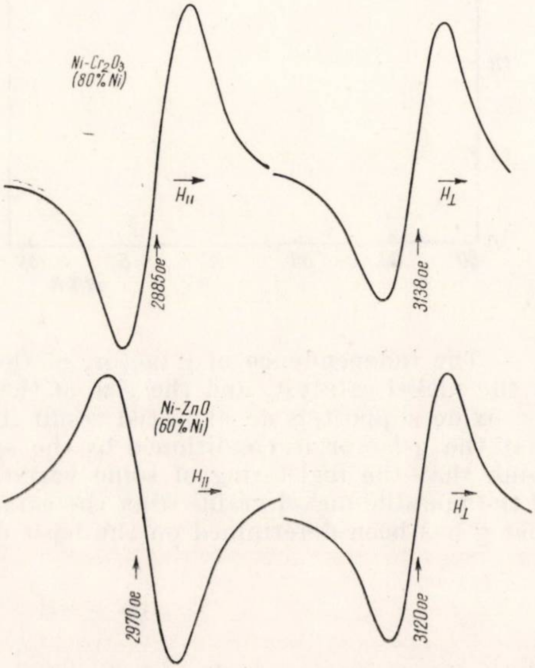

Fig. 1. — Absorption curves of FMR for $N_1-Cr_2O_3$ and $Ni-ZnO$ catalyst samples.

The static magnetic field ($H_{\parallel}$ and $H_{\perp}$) has been measured with a NMR sonde with the precision of ±8 oe and the microwave frequency with a reference cavity, the error being below 0.1 %. The width of the FMR lines has been measured by the distance between the two maxima of the derivative of the FMR absorption curve on the axis of the static field H.

3. RESULTS AND DISCUSSION

Figure 2 presents the values of the g-spectroscopic splitting factor for $Ni-Cr_2O_3$ samples, having atomic nickel concentration between 60% and 100% and for some nickel catalyst samples, on ZnO, MgO, Al_2O_3, SiO_2 and CeO_2 supports.

From figure 2 one may notice that the g-factor does not depend upon the catalyst composition or the type of its oxide support. The g-mean value being g = 2.22±0.08, it is perfectly corresponding to the value obtained for colloidal nickel ($g = 2.22 \pm 0.02$) by Bagguley.[8,9] For pure metallic nickel in bulk state $g = 2.20$ has been obtained.[10]

---

[7] I. Inţa and R. Baican, *Rev. Roumaine Phys.*, **14**, 673 (1969).

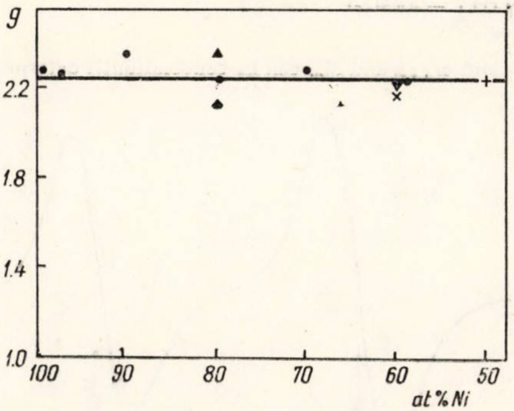

Fig. 2. — g-Factor for nickel catalyst samples on oxide supports (● : Ni — Cr_2O_3 sintered; ▲ : Ni — ZnO; ■ : Ni — MgO; ♦ : Ni — Al_2O_3; X : Ni SiO_2; + : Ni — C_eO_2)

The independence of g-factor, of the metallic nickel concentration in the nickel catalyst, and the size of the nickel grains and the type of the oxide support, is an expected result if we take into account the fact that the g-factor is conditioned by the spin-orbit interaction only. We think that the registering of some variation for g, function of the size of the metallic nickel grains from the catalyst is due not only to the fact that g has been determined on the basis of the resonance condition,

$$\omega = \gamma H \tag{3}$$

where the magnetocrystalline fields of the metallic nickel grains and of the demagnetization ones are neglected, but also to the perturbation which is determined by the catalyst probe in the resonance cavity. This perturbation (given by the eddy currents and the change in the cavity geometry) increases with the electrical conductivity of the catalyst. By using a catalyst layer in electric contact with the cavity wall, this drawback of the methods used until now [2] can be avoided.

The fact that the value of the resonance field at the perpendicular orientation ($H_{\perp}$) is greater than that corresponding to the parallel one ($H_{\parallel}$) for all the measured samples, urges us to allow the appearance of a demagnetization effective field $4 \# \pi M_{ef}$ directed perpendicularly to the plane of the catalyst layer. As it has been shown above, this field cannot be ascribed to the metallic nickel grains. Watching the M_{ef} variation upon the atomic chrome concentration of the catalyst (figure 3), we notice that a sudden decrease of it appears within the range 10—15% Cr.

---

[8] D. M. S. Bagguley and N. S. Harvick, *Proc. Phys. Soc.*, A **67**, 648 (1954).

[9] D. M. S. Bagguley, *Proc. Roy. Soc.*, A **228**, 549 (1955).

[10] N. Bloembergen, *Phys. Rev.*, **78**, 572 (1950).

We should remark that such a decrease in the same concentration range can be obtained for the electric conductivity of the $Ni-Cr_2O_3$ catalyst [6], emphasizing its passing from a metallic behaviour to a semiconductor one.

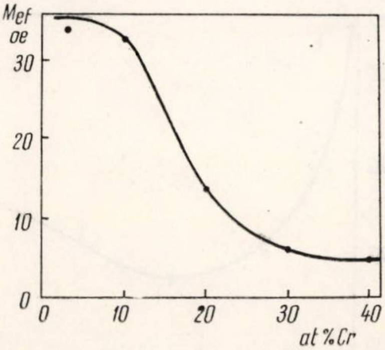

Fig. 3. — Dependence of effective magnetization of Cr — concentration in $Ni-Cr_2O_3$ catalysts.

Since the effective magnetization value M_{ef} is small in comparison with the value of the saturation catalyst,[11] we may consider that M_{ef} is created by the interactions from among the metallic nickel grains. Among these grains dipole-dipole interactions and exchange interactions by means of the oxide support can appear, given by the conductivity electrons. This type of interaction was suggested by Evdokimov. [12,13] The dipole-dipole interactions, being interactions with long range action, bring about an effective magnetic field whose intensity decreases gradually according to the "dilution" of the ferromagnetic metal in catalyst and therefore they cannot underlie the interpretation of the M_{ef} variation upon the nickel concentration in the catalyst.

The indirect exchange interactions have a small range action. They occur between the spins of some neighbouring grains, separated by an oxide layer, by means of the conductivity electrons. At a certain thickness of the oxide layer, for which the electric conductivity decreases at once [6] the number of the conductivity electrons will diminish determining a reduction of the exchange interactions through the support and therefore of the effective magnetization M_{ef}.

In figure 4 the dependence of the FMR width line ($\Delta H_{\parallel}$ and $\Delta H_{\perp}$) upon nickel concentration is graphically represented.

The presence of a minimum of this variation situated in the same concentration range (80–85% Ni) can be related to the disappearance of exchange interactions through the support. At great nickel concentrations the width of the resonance line increases markedly due to the intensifying of interactions from among the nickel crystals. The gradual

---

[11] M. Moraru, *Rev. Roumaine Phys.*, **14**, 823 (1969).

[12] V. B. Evdokimov and M. N. Kuznesov, *Zhur. fiz. Khim.*, **40**, 2406 (1966).

[13] V. D. Kozalov and V. B. Evdokimov, *Zhur. fiz. Khim.*, **40**, 1854 (1966).

ORSZÁGOS MŰSZAKI KÖNYVTÁR DOKUMENTÁCIÓS KÖZPONT 1883

width increase of the line at concentrations less than 80% Ni, emphasizes the influence of the interactions from among the ferromagnetic metal and oxide grains (probably of ferro-antiferromagnetic type). In complex physical systems as the catalyst powders on oxide supports, the excitement of a uniform precession mode in FMR is out of question. In such substance lots of resonance modes, whose resonance frequency depends on the size and direction of the saturation magnetization vector of each grain, might probably appear. By dipole and exchange interactions their precession movements can be coupled, so that the width of the line diminishes.[14] As soon as the exchange interactions through the support disappear, the action of this effect diminishes and thus the line width will increase.

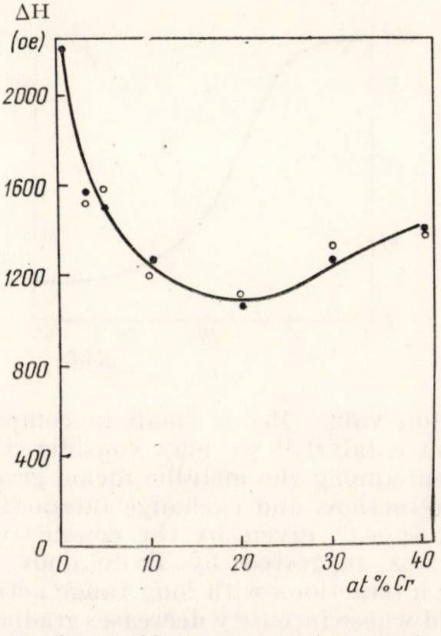

Fig. 4. — Dependence of the FMR line width on Cr-concentration in $Ni-Cr_2O_3$ catalysts (○ : $\Delta H_{\parallel}$; ● : $\Delta H_{\perp}$)

It is to be remarked that the catalytic activity of the $Ni-Cr_2O_3$ catalyst is maximum within the nickel concentration range for which the sudden variation of its electric conductivity and of the effective magnetization M_{ef} are obtained. This enables us to imagine the following mechanism which can contribute to the catalytic activity increase : for nickel concentrations, where M_{ef} decreases at once, the exchange interaction through the support, among metallic nickel grains, has maximum fluctuations and these amplify the Van der Waals forces, increasing, in this way the activity of the catalyst.

---

[14] S. Geschwind and A. M. Clogston, *Phys. Rev.*, **108**, 49 (1957).

NOTE POUR LES AUTEURS

La *Revue Roumaine de Chimie* publie des articles en anglais, français, russe, allemand ou espagnol. Les auteurs sont priés d'envoyer des articles, notes, communications et comptes rendus inédits.

Les manuscrits seront dactylographiés à deux intervalles. Les tableaux seront dactylographiés sur feuilles séparées, de même que la légende des figures. Les diagrammes seront tracés à l'encre de Chine sur papier calque. Les tableaux et les figures seront numérotés par des chiffres arabes, en nombre strictement nécessaire. Prière de ne pas inscrire les mêmes données dans les tableaux et les figures. Les formules chimiques seront incluses dans le texte; en outre, elles seront transcrites sur des feuilles séparées. Les auteurs sont priés d'indiquer les caractères italiques (en soulignant les lettres au crayon), ainsi que tout autre caractère spécial. L'ordre des références bibliographiques sera celui de leur mention dans le texte; le nom de l'auteur sera précédé de l'initiale du prénom; les publications périodiques seront présentées suivant les prescriptions internationales. Les références seront ajoutées à la fin de l'article; elles paraîtront comme des notes, au bas de la page. Le texte sera précédé d'un résumé comprenant 15 lignes au maximum.

L'entière responsabilité du contenu des articles appartient aux auteurs. On publie des articles dus aux collaborateurs roumains ou étrangers. Les auteurs recevront 50 tirés à part.

PRINTED IN ROMANIA

TRAVAUX PARUS AUX ÉDITIONS DE L'ACADÉMIE DE LA RÉPUBLIQUE SOCIALISTE DE ROUMANIE

P. BALTĂ et E. BALTĂ, **Introducere în chimia fizică a stării vitroase** (Introduction à la chimie physique de l'état vitreux), 1971, 240 p., 15,50 lei.

LYDIA-MARIA VAICUM, **Biodegrabilitatea detergenţilor** (La Biodégrabilité des détergents), 1971, 254 p., 16 lei.

TIBERIU NĂSCUŢIU, **Metode radiometrice de analiză** (Méthodes radiométriques d'analyse), 1971, 346 p., 19,50 lei.

I. ZUGRĂVESCU et I. STOICESCU-CRIVETZ, **Polimeri heterociclici** (Polymères hétérocycliques), 1971, 190 p., 9,50 lei.

I. MAXIM, **Materiale nucleare** (Matériaux nucléaires), 1969, 444 p., 30 lei.

CRISTOFOR SIMIONESCU, C. V. UGLEA, **Fracţionarea compuşilor macromoleculari** (Fractionnement des composés macromoléculaires), 1969, 292 p., 18,50 lei.

CRISTOFOR SIMIONESCU et CLEOPATRA VASILIU-OPREA, **Mecanochimia compuşilor macromoleculari** (La mécanochimie des composés macromoléculaires), 1967, 344 p., 23,50 lei.

CORNEL BODEA et collab., **Tratat de biochimie vegetală, partea I, Fitochimie** (Traité de biochimie végétale, Ire partie, Phytochimie), Ier vol., 1964, 747 p. + 4 annexes + 2 pl., 41 lei ; IIe vol., 1965, 1262 p., 1 pl., 56 lei ; IIIe vol., 1967, 773 p., 35 lei.

V. GHEŢIE et V. MICUŞAN, **Analiza imunochimică. Teorie şi practică** (Analyse immunochimique. Théorie et pratique), 1966, 369 p., 28 lei.

R. PORTOCALĂ et L. POPA, **Acizii ribonucleici celulari şi virali** (Les acides ribonucléiques cellulaires et viraux), 1966, 375 p., 8 pl., 26 lei.

D. PURDELEA et R. VÎLCEANU, **Chimia compuşilor organici ai fosforului şi ai acizilor lui** (La chimie des composés organiques du phosphore et de ses acides), 1965, 540 p., 37 lei.

I.P.I. — c. 2167

43 426

Lei 25.—

F 1103

R REFERÁLVA

REVUE ROUMAINE DE CHIMIE

TOME 18
Nº 3
Mars 1973
RRCHAX, 18, 3, 353–520 (1973)

ÉDITIONS DE L'ACADÉMIE DE LA RÉPUBLIQUE SOCIALISTE DE ROUMANIE

Rev. Roumaine Chim. 18, 3, p. 353–520 (1973), Bucarest

COMITÉ DE RÉDACTION

Rédacteur en chef:

I. G. MURGULESCU, membre de l'Académie de la République Socialiste de Roumanie

Rédacteurs en chef adjoints:

A. T. BALABAN et V. EM. SAHINI, membres correspondants de l'Académie de la République Socialiste de Roumanie

Collège de rédaction:

C. DRĂGULESCU, RALUCA RIPAN, CR. SIMIONESCU, membres de l'Académie de la République Socialiste de Roumanie; EM. BRATU, ECATERINA CIORĂNESCU-NENITZESCU, P. SPACU, membres correspondants de l'Académie de la République Socialiste de Roumanie; MARGARETA AVRAM, D. I. MARCHIDAN, G. NIAC et D. SĂNDULESCU

La Revue Roumaine de Chimie paraît 12 fois par an. Toute commande de l'étranger (fascicules ou abonnements) sera adressée à Întreprinderea de comerţ exterior — Rompresfilatelia, Boîte postale 2001, telex 011631, Bucarest, Roumanie

Les manuscrits, les livres et les revues proposés en échange, ainsi que toute correspondance seront envoyés à la rédaction :

REVUE ROUMAINE DE CHIMIE

23, Str. Dumbrava Roşie, Bucarest, Roumanie

ÉDITIONS DE L'ACADÉMIE DE LA RÉPUBLIQUE SOCIALISTE DE ROUMANIE
3 bis, str. Gutenberg, Bucarest

REVUE ROUMAINE
DE
CHIMIE

Tome 18, N° 3 Mars 1973

Page

I. G. MURGULESCU and IOANA DEMETRESCU, The kinetics of reactions between benzhydryl bromide and normal alcohols · · · · · · · · · · 355–360

V. E. SAHINI and MARINA OLTENEANU, Solvent effect on the anharmonicity of the C=O vibration of acetophenone and benzophenone · · · · · · · 361–365

G. DE MARIA, L. MALASPINA, G. BARDI and R. GIGLI, Simultaneous determination by Knudsen effusion-microcalorimetric technique of the vapour pressure and sublimation enthalpy of antimony trifluoride. Vapour pressure of bismuth trifluoride · · · · · · · · · · · · · · · 367–375

RODICA VÎLCU and ZOICA CENUȘE, Isothermal equilibrium and calculation of excess functions in the benzene-isobutyl alcohol system · · · · · · 377–385

RODICA VÎLCU and C. MISDOLEA, Significant structures theory of ionic binary liquid mixtures : heat capacities, compressibility coefficients and thermal-expansion coefficients · 387–398

P. BALTĂ and L. DOLLINGHER, Influence of alkaline cations on the sensitivity of the phototropic glasses with AgCl · · · · · · · · · · · · · · · · · · · 399–404 Bq

P. SPACU and EUGENIA IVAN, New compounds of yttrium and lanthanides with derivatives of anthranilic acid. I. The N,N bis(carboxy methyl) anthranilic acid (ANDA) · 405–416

Z. FINTA, CS. VÁRHELYI and J. ZSAKÓ, Kinetics and mechanism of substitution reactions of complexes. XLIII. Basic hydrolysis of $[Co(DH)_2(H_2O)(NCS)]$ · 417–424

FLORICA POPEA and CRISTINETA MĂRCULESCU, New thorium complexes with pyrimidine derivatives · · · · · · · · · · · · · · · · · · · 425–430 R

SCHELY AVRAMOVICI, I. DRUȚĂ and I. ZUGRĂVESCU, On some derivatives of the hydrazinocarboxylic acid. II. Syntheses and spectral data 431–439

MARGARETA AVRAM, I. G. DINULESCU, C. D. NENITZESCU, R. A. Y. JONES, A. R. KATRITZKY and R. J. WYATT, Configurations of substituted dibenzobicyclo[3.2.1]octadienes · · · · · · · · · · · · · · · 441–447

FLAVIAN CUIBAN, Peptide syntheses with N-(acyl-*o*-nitrophenyl)-substituted amino acids · 449–461 R

FLAVIAN CUIBAN, An improved synthesis of optically pure N^{α}-methyl-lysine 463–468

V. FĂRCĂȘAN and I. CRISTEA, Dibenzofurans I. The formylation of 3-di-

Rev. Roumaine Chim. **18**, *3*, p. 353–520 (1973), Bucarest

api

methylamino-dibenzofuran by the Vilsmeier-Haack method · · · · · · 469–472

M. IOVU et S. RADU, Condensation du 4,4′-azodiphénoxyde de sodium avec les dérivés chlorométhylés du benzène · · · · · · · · · · · · · · · · · · 473–478

ALI ALI KHALAF, Modern Friedel-Crafts Chemistry. II. Rearrangements accompanying benzene alkylations with 1- and 2-hydroxy-2-methyl-1-phenylpropane, 1- and 2-chloro-2-methyl-1-phenylpropane and 2-methyl-1-phenyl-1-propene in the presence of Friedel-Crafts catalysts · · · 479–487

V. V. BADIGER and M. Y. M. JAMKHANDI, Analogues of chloramphenicol. II. Synthesis of 2-chloroacetamido-1-(4′-chloro-3′-nitro-phenyl)propane-1,3-diol · 489–492

I. PETRARIU, CORNELIA LUCA, IG. POINESCU and M. DIMA, Quaternary basic ammonium polyelectrolytes. I. Quaternization reaction of some tertiary amines containing hydroxylic groups with chloromethylated polystyrene · 493–500

GR. TEODORESCU, Methods for the determination of tolazoline. Visible and infrared spectra of the combination with ammonium reineckate · · · · 501–506

SILVIU-DUMITRU POPESCU, Polarographic determination of anthraquinone, 2-chloroanthraquinone and 2-aminoanthraquinone · · · · · · · · · · 507–510

MARIA FITI, Mechanism of radiolytic reduction of Cr^{VI} in aqueous solutions 511–517

COMPTE RENDU · 519–520

Revue Roumaine de Chimie, **18**, *3*, 355–367 (1973)

THE KINETICS OF REACTIONS BETWEEN BENZHYDRYL BROMIDE AND NORMAL ALCOHOLS

I. G. MURGULESCU and IOANA DEMETRESCU

Physical Chemistry Department, Bucharest University, Bd. Republicii 13, Romania

Received October 27, 1972

The kinetics of the reactions between benzhydryl bromide and the first four alcohols of the normal series was studied, in the temperature range 0–55°. The results were compared with those regarding the alcoholysis of the benzhydryl chloride.

INTRODUCTION

The solvolysis of benzhydryl bromide[1–4] was less studied than the solvolysis of the benzhydryl chloride. [5–12] We carried out this work in order to compare the kinetics of the alcoholysis reactions of the two halides of the same class.

EXPERIMENTAL

The benzhydryl bromide we used has been prepared in our laboratory according to known methods. [13–15] The methyl and ethyl alcohols have been anhydrized using 4 Å molecular sieves. The propyl and butyl alcohols were Merck anhydricum. The water in the alcohols has been determined by means of Karl Fisher's reagent and the following quantities were found: 0.025% in CH_3OH, 0.03% in C_2H_5OH, 0.19% in C_3H_7OH and 0.05% in C_4H_9OH.

---

[1] J. Horman and M. J. Strauss, *J. Chem. Educ.*, **2**, 118 (1969).

[2] A. D. Mease, M. J. Strauss, J. Horman, K. J. Andrews and R. M. Keefer, *J. Amer. Chem. Soc.*, **90**, 1797 (1968).

[3] M. J. Strauss, L. J. Andrews and R. M. Keefer, *J. Amer. Chem. Soc.*, **90**, 3473 (1968).

[4] T. Benfey, O. Hughes, E. D. and C. K. Ingold, *J. Chem. Soc.*, **1952** (2488).

[5] F. Kiy and A. Ward, *J. Amer. Chem. Soc.*, **58**, 2398 (1935).

[6] A. Ward, *J. Chem. Soc.*, **1927**, 2285.

[7] I. G. Murgulescu and Fl. Bărbulescu, *Rev. Roumiane Chim.*, **8**, 153 (1963).

[8] I. G. Murgulescu and I. Demetrescu, *Rev. Roumaine Chim.*, **16**, 781 (1971).

[9] S. Altscher, R. Baltzly and I. Blackman, *J. Amer. Chem. Soc.*, **74**, 3649 (1952).

[10] T. Farinacci and L. Hammett, *J. Amer. Chem. Soc.*, **59**, 2542 (1937).

[11] A. Fainberg, S. Winstein and E. Grunwald, *J. Amer. Chem. Soc.*, **79**, 4146 (1957).

[12] I. G. Murgulescu and I. Demetrescu, *Rev. Roumaine Chim.*, **17**, 595 (1972).

[13] J. Norris, R. Thomas and B. Brown, *Ber. dtsch. chem. Ges.*, **43**, 2959 (1910).

[14] A. Curtot, *Liebigs Ann. Chim.*, **5**, 80 (1916).

[15] C. G. Swain and C. B. Scott, *J. Amer. Chem. Soc.*, **75**, 141 (1953).

The concentrations have been determined by a direct conductometric method, using both calibration curves given in a previous work [16] and calibrations made directly in the reaction medium. The measurements have been made by means of a CK Radiometer conductometer, with a relative errror of about 1 %. The concentrations have been checked titrimetrically with 0.032 m sodium methoxide in the presence of phenolphthalein.

RESULTS

The rate of the reaction

$$(C_6H_5)_2CHBr + ROH \rightarrow (C_6H_5)_2CHOR + HBr$$

is given by the well-known equation

$$dx/dt = k\,(a - x)\,(b - x), \tag{1}$$

were x is the diminution of concentration, while a and b are the initial concentrations of the reactants.

The alcohol being in excess, x is negligible with respect to b and equation (1) takes a simpler form, which, being integrated, gives

$$k = \frac{2.303}{bt} \log \frac{a}{a - x} \tag{2}$$

The equation (2) could be written as

$$\log\,(a - x) = -\,\frac{bk}{2.303}\,t - \log a, \tag{3}$$

which makes evident the possibility of determining the rate constant from the slope of the straight line : $\log\,(a - x) = f\,(t)$. The method is illustrated in figure 1 for the case of butyl alcohol at 40° ; k was found to be 0.11 $cm^3\ mol^{-1}\ sec^{-1}$.

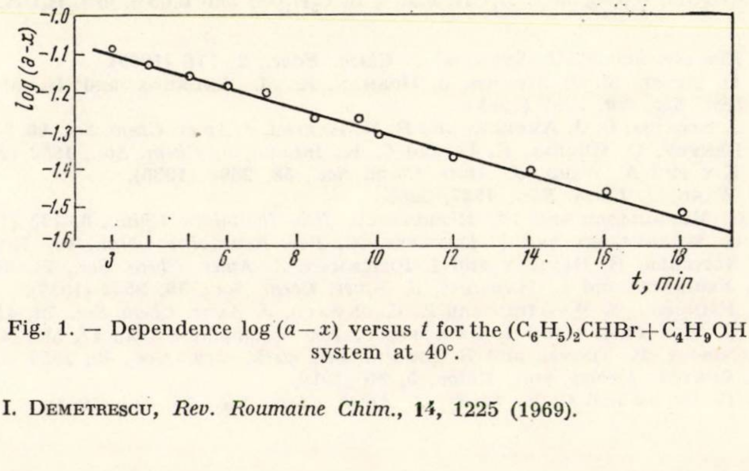

Fig. 1. — Dependence $\log\,(a-x)$ versus t for the $(C_6H_5)_2CHBr + C_4H_9OH$ system at 40°.

---

[16] I. Demetrescu, *Rev. Roumaine Chim.*, **14**, 1225 (1969).

We worked with two initial halide concentrations (0.1 n and 0.2 n) and no change in the value of the rate constants was noticed.

In table 1 we give the rate constants of the alcoholysis reactions between benzhydryl bromide and the first four alcohols of the normal series. It may be seen that the rate constants show a decrease as the chain of alcohol grows longer. The values are much larger than the rate constants of the reactions between benzhydryl chloride and alcohols, convincingly illustrating the reactivity scale of halides in protic solvents ($k_{I^-} > k_{Br^-} > k_{Cl^-}$).

Table 1

Rate constants for the $(C_6H_5)_2CHBr$ + ROH systems
k cm^3 mol^{-1} s^{-1}

ROH	0°	15.5°	20°	25°	30°	35°	40°	45°	50°	55°
CH_3OH	0.0155	0.18	0.36	0.87	—	—	—	—	—	—
C_2H_5OH	—	—	0.07	0.16	0,32	0,52	—	—	—	—
C_3H_7OH	—	—	—	—	0.052	0.093	0.184	0.671	—	—
C_4H_9OH	—	—	—	—	—	—	0.11	0.24	0.54	0,74

Plotting log k *versus* $1/T$ (fig. 2) gave straight lines which enabled us to calculate the energy of activation and the preexponential factor, using the least squares method.

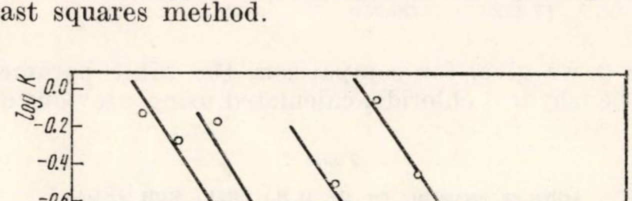

Fig. 2. — Dependence log k versus $1/T$ for the $(C_6H_5)_2CHBr$ + ROH system

1, R=CH_3; *2*, R=C_2H_5; *3*, R=C_3H_7; *4*, R=C_4H_9.

According to the well-known equations of the activated complex theory

$$\Delta^*H = E - RT \tag{4}$$

$$\Delta^*S = 2.303\left(R\log\frac{A}{T} - \log\frac{k}{h}\right) \tag{5}$$

$$\Delta^*G = \Delta H - T\Delta S^* \tag{6}$$

the other activation parameters were calculated. ΔH^* is the variation of the activation enthalpy. ΔS^* the variation of the activation entropy. ΔG^* the variation of the free activation energy, E the activation energy. A the preexponential factor, T the temperature. k, h and R are the Boltzmann's, Planck's and gas constants, respectively.

The activation parameters are listed in table 2.

Table 2

Activation parameters for $(C_6H_5)_2CHBr$ + ROH the systems

ROH	log A	$E_{[cal]}$	$\Delta S^*_{[ue]}$	$\Delta H^*_{[cal]}$	$\Delta G^*_{[cal]}$
CH_3OH	18.6503	25,580	+24.87	24,990	17,120
C_2H_5OH	18.5975	26,490	+24.50	25,890	18,460
C_3H_7OH	20.3706	29,600	+31.73	28,940	19,440
C_4H_9OH	17.8988	26,950	+21.23	26,300	19,440

In table 3 we give, for comparison, the same parameters for the alcoholysis of benzhydryl chloride, calculated using previous data. [7,8]

Table 3

Activation parameters for the $(C_6H_5)_2$ CHCl + ROH systems

ROH	log A	$E_{[cal]}$	$\Delta S^*_{[ue]}$	$\Delta H^*_{[cal]}$	$\Delta G^*_{[cal]}$
CH_3OH	12.415	15960	− 3.38	18900	19990
C_2H_5OH	12.008	19500	− 5.29	18850	20550
C_3H_7OH	11.725	19400	− 7.04	18740	21020
C_4H_9OH	11.602	19370	− 7.60	18730	21190
$C_5H_{11}OH$	11.373	19350	− 8.66	18710	21510
$C_6H_{13}OH$	11.210	19040	− 9.40	18390	21430
iC_3H_7OH	13.956	20210	+ 3.18	19570	18540
iC_4H_9OH	13.35	19410	+ 0.33	18770	18660
i$C_8H_{17}OH$	11.771	17870	− 6.84	17230	19440
sec C_3H_7OH	10.1702	17400	−14.17	16760	21340
sec C_4H_9OH	9.7916	17600	−15.91	16960	22100

As may be seen from the tables 2 and 3, the alcoholysis reactions of the benzhydryl bromide are characterized by much larger activation energies than the corresponding reactions of benzhydryl chloride, denoting that the reactions of bromide are much more influenced by temperature. We also notice differences in the activation entropy, this one being large and positive in the case of the reactions with benzhydryl bromide, and negative as a rule in the case of the reactions with benzhydryl chloride (except for the systems formed with secondary alcohols).

Like in the case of many other related reactions, which do not involve substantial changes in the structure or in the medium characteristics, it can be seen that the enthalpies and entropies of activation given in the tables 2 and 3 verify a linear relation of the form. [17,18]

$$\Delta H^* = \Delta H_0^* + \beta \Delta S^* \qquad (7)$$

where ΔH_0^* is the intercept of the straight line for $\Delta S^* = 0$ and β the slope, having dimensions of a temperature.

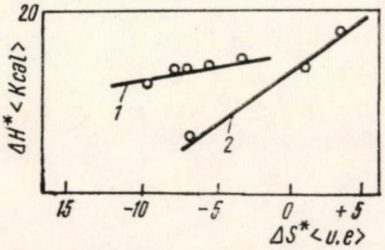

Fig. 3. — Dependence ΔS^* *versus* ΔH^* for the alcoholysis of benzhydryl chloride.

1, $(C_6H_5)_2CHCl + nROH$; *2*, $(C_6H_5)_2CHCl + i-ROH$.

The equation (7) is often called the isokinetic equation as $\Delta G^* = \Delta H^* =$ constant, when $T = \beta$ and the reactions satisfying it have the same speed.

In figure 3 the dependence of ΔS^* on ΔH^* is given for the alcoholysis reactions of benzhydryl chloride; the straight line (1) corresponds to the reactions with normal alcohols and the line (2) to the reactions with isoalcohols.

The results for the alcoholysis of benzhydryl bromide are not conclusive from this point of view.

The two straight lines in figure 3 are not parallel as we might expect for systems of reactions having the same mechanism. Assuming a mixed mechanism [10,19] for the alcoholysis reactions of benzhydryl halides, that difference in slope may be accounted for by the different weights of the unimolecular and bimolecular mechanisms. This mechanism might also explain the variation of the activation entropy, from marked negative values, characteristic for the slow bimolecular reactions between dipoles, to large positive values, contradicting the image of a dipolar activated complex.

The fact that the systems with benzhydryl bromide do not verify the Laidler-Eyring equation, [20] the plot of log k as a function of the

---

[17] J. E. LEFFLER, *J. Org. Chem.*, **20**, 1202 (1955).

[18] J. E. LEFFLER, *J. Org. Chem.*, **31**, 533 (1966).

[19] M. VOICU, *Studii şi Cercetări Chim. Acad. R.S.R.*, **17**, 717 (1969).

[20] S. GLASSTONE, K. J. LAIDLER and M. EYRING, „The theory of rate processes", New York, London, 1941, p. 419.

Kirkwood ratio $(D - 1)/(2D + 1)$ being not a straight line as it was in the case of systems with benzhydryl chloride, [8,21] may be accounted for, in the same way, accepting the mixed mechanism.

In conclusion, we can assert, taking also into account the data concerning, the solvolysis of benzhydryl halides, [1-11] the salt effects, and the mass law effect, that these solvolyses imply, besides the bimolecular mechanism, more or less pronounced characteristics of the monomolecular mechanism.

---

[21] I. Demetrescu, *Rev. Roumaine Chim.*, 15, 1721 (1970).

Revue Roumaine de Chimie, **18**, *3*, 361–365 (1973)

SOLVENT EFFECT ON THE ANHARMONICITY OF THE C=O VIBRATION OF ACETOPHENONE AND BENZOPHENONE

V. E. SAHINI and MARINA OLTENEANU

Centre of Physical Chemistry, Ministry of Education
Galaţi 31, Bucharest, Romania

Received October 10, 1972

We studied the effect of weak hydrogen bond formation on the mechanical and electrical anharmonicity of the C = O vibration. On passing from interaction such as collision complexes to interactions by means of weak hydrogen bonds the C = O vibration becomes more harmonic.

Many theoretical works consider that the modifications of the mechanical and electrical anharmonicity are responsible to some extent for the important perturbations of the stretching vibrations of polar vibrators. [1,2,3]

Earlier experimental results obtained by Lüttke, Mecke and Greinacher [4] for water in various organic bases show that the effect of hydrogen bond formation is to decrease the mechanical anharmonicity as compared to that of the gaseous monomer.

Bell and Barrow [5] assigned the splits of the bands corresponding to the overtones of the ν_{OH} of methanol and phenol to the existence of two minima of the potential surfaces, using an explanation given by Detoni and Hadži [6] and Blinc and Hadži. [7]

Sokolov [8] pointed out that the existence of two potential minima is hardly probable.

In a more recent work, Barrow [9] explained these splits by Fermi resonance between the overtones of ν_{OH} stretching vibrations and a combination which involves the OH deformation mode.

---

[1] G. Bratož and D. Hadži, *J. Chem. Phys.*, **27**, 991 (1957).

[2] H. L. Frisch and G. L. Vidale, *J. Chem. Phys.*, **25**, 982 (1956).

[3] D. Hadži and H. W. Thomson, "Hydrogen Bonding", Pergamon Press, New York, 1957.

[4] E. Greinacher, W. Lüttke and R. Mecke, *Z. Electrochem.*, **59**, 23 (1955).

[5] C. L. Bell and G. M. Barrow, *J. Chem. Phys.*, **31**, 300 (1959).

[6] S. Detoni and D. Hadži, *J. Chem. Soc.*, **3163** (1955).

[7] R. Blinc and D. Hadzi, *Spectrochim. Acta*, **16**, 852 (1960).

[8] N. D. Sokolov, „Vodorodnaia Sviazi", vol. 7, Izdatelstvo Nauka, Moskow, 1964.

[9] G. M. Barrow, *Spectrochim. Acta*, **16**, 799 (1960).

Experimentally there is no doubt on the existence of these splits for strong hydrogen bonds. Possibly the low values obtained by different authors for the anharmonicity are due to the fact that they used for calculations the stronger high frequency band.

Barthomieu and Sandorfy,[10] Durocher and Sandorfy[11] and Foldes and Sandorfy[12] undertook a more sistematical study of the overtones of the ν_{OH} and ν_{NH} stretching vibrations.

By comparing the frequencies of the ν_{NH} fundamentals and of overtones of some secondary amines in pure liquids and in carbon tetrachloride solutions they found that the self-association leads to a decrease of the mechanical anharmonicity of the first overtone.

For stronger hydrogen bonds (alcohols, phenol) Durocher, Foldes and Sandorfy found for multimer that the mechanical anharmonicity is approximately twice that for the monomer vibration ν_{OH}.

Couzi and van Huong,[13] in a study concerning the change of the anharmonicity of ν_{OH} vibration of phenol, found that in nonpolar solvents the anharmonicity values are roughly the same as for the gas phase. For weak hydrogen bonds there is a decrease, while in strong accepter proton solvents the mechanical anharmonicity increases markedly.

Lüttke, Mecke, Barthomieu and Sandorfy[14] found an important decrease of the electrical anharmonicity for the ν_{OH} and ν_{NH} vibrations.

On the contrary, Couzi and van Huong[13] showed that the apparent absorption intensity of the band corresponding to the first overtone of the ν_{OH} vibration is markedly weaker as that of the fundamental and is in no way influenced by the molecular interactions.

We have considered interesting to follow the influence of some interactions through weak hydrogen bonds upon the overtones of the $C = O$ vibrator for benzophenone and acetophenone.

EXPERIMENTAL

The benzophenone p.a. was recrystallized several times from ethanol. The acetophenone p.a. was purified by successive recrystallizations and carefully dried.

The solvents, spectrochemical grade, were dried on molecular sieves (4 Å, Carlo Erba) and distilled under molecular sieves just before use.

The used concentrations were 0.05 M/L for the fundamentals and 0.5 M/L for the overtone region.

The spectra were recorded with a U.R. 10 C Zeiss-Jena spectrophotometer. The wavelength calibration was made with water vapours and the linearization was made electronically.

The apparent integrated intensities were calculated without wing corrections.

[10] C. Barthomieu and C. Sandorfy, *J. Mol. Spectroscopy*, **15**, 15 (1965).
[11] G. Durocher and C. Sandorfy, *J. Mol. Spectroscopy*, **15**, 22 (1965).
[12] A. Foldes and C. Sandorfy, *J. Mol. Spectroscopy*, **20**, 262 (1966).
[13] M. Couzi and P. van Huong, *Spectrochim. Acta*, **26** A, 94 (1970).
[14] W. Lüttke and R. Mecke, *Z. Electrochem.*, **53**, 241 (1949).

RESULTS AND DISCUSSION

The bands corresponding to $\nu_{C=O}$ stretching vibrations of benzophenone and acetophenone in carbon tetrachloride are symmetrical and become more asymmetrical by solving the compounds in dichloromethane, dibromomethane and chloroform.

The bands corresponding to the first overtone, $2\nu_{c=o}$, for both ketones are symmetrical, except if we use chloroform as a solvent.

Using mixed solvents for studying the shape of the bands corresponding to the first overtone we did not observe the appearance of submaxima, contrary to the facts observed by Josien and co-workers [15] and by us [16] for the fundamentals.

The absorption maxima of the fundamentals and overtones do not shift with solvent change in pure solvents.

Table 1 show the frequencies of the fundamentals and overtones and the mechanical anharmonicities calculated from these frequencies for both ketones in the considered solvents.

Table 1

Frequencies of the fundamentals and of the first overtones and the mechanical anharmonicity of the C = O vibration for benzophenone and acetophenone

	Acetophenone			Benzophenone		
solvent	$\nu_{01(cm^{-1})}$	$\nu_{02(cm^{-1})}$	$\omega_e x_e$	$\nu_{01(cm^{-1})}$	$\nu_{02(cm^{-1})}$	$\omega_e x_e$
CCl_4	1692	3359	14	1667	3308	13
CH_2Cl_2	1683	3349	9	1657	3298	8
CH_2Br_2	1681	3343	10	1656	3295	9
$CHCl_3$	1681	3347	8	1656	3297	8

It can be observed that by solving benzophenone and acetophenone in dichloromethane, dibromomethane and chloroform there is a decrease of the mechanical anharmonicity for the C = O vibrator relative to that calculated for both ketones in carbon tetrachloride.

To account for the behaviour of the electrical anharmonicity we study the shape of the absorption bands corresponding to the fundamentals $\nu_{C=O}$ and the overtones $2\nu_{C=O}$.

From tables 2 and 3 one can observe that the apparent integrated intensity of the fundamental vibrations rises by an order of magnitude at hydrogen bond formation in agreement with the results for other compounds containing C = O group. For the overtones there is no change on passing from the nonpolar solvent to the polar ones, in agreement

---

[15] J. Lascombe and M. L. Josien, "Advances in Molecular Spectroscopy", vol. 2, Pergamon Press, New York, 1962, p. 843.

[16] V. E. Sahini and M. Feldman, *Rev. Roumaine Chim.*, **13**, 527 (1968).

Table 2

Molar extinction coefficients, apparent absorption intensities and half bandwidths of the fundamentals and the first overtones of the C=O vibration for benzophenone

	ν_{01}			ν_{02}			A'_{02}/A'_{01}
solvent	$\varepsilon_1(1\cdot mol^{-1}cm^{-1})$	$A'_{01}\,(1\cdot mol^{-1}\ cm^{-2})$	$^1\Delta\nu_{1/2}(cm^{-1})$	$\varepsilon_2\,(1\cdot mol^{-1}\ cm^{-1})$	$A'_{02}(1\cdot mol^{-1}\ cm^{-2})$	$^2\Delta\nu_{1/2}(cm^{-1})$	
CCl_4	1385	1362	12.2	13.93	300	23	0.22
CH_2Cl_2	1072	12,275	15	11.08	298	30	0.02
CH_2Br_2	1072	11,972	14.6	11.42	319	26.6	0.02
$CHCl_3$	996	18.077	20.6	10.00	337	40.6	0.01

Table 3

Molar extinction coefficients, apparent absorption intensities and half bandwidths of the fundamentals and the first overtones of the C=O vibration for acetophenone

	ν_{01}			ν_{02}			A''_{02}/A''_{01}
solvent	$\varepsilon_1(1\cdot mol^{-1}cm^{-1})$	$A''_{01}(1\cdot mol^{-1}\ cm^{-2})$	$^1\Delta\nu_{1/2}(cm^{-1})$	$\varepsilon_2\,(1\cdot mol^{-1}\ cm^{-1})$	$A''_{02}\,(1\cdot mol^{-1}\,cm^{-1})$	$^2\Delta\nu_{1/2}\ (cm^{-1})$	
CCl_4	1321	1184	11.7	11.6	278	25	0.23
CH_2Cl_2	1162	12.612	14	9.7	265	27	0.02
CH_2Br_2	1142	13.119	14.6	9.6	295	34	0.02
$CHCl_3$	1009	17.886	18.6	8.3	280	42	0.01

with the results of van Huong and Couzi [13] for the first overtone of the ν_{OH} stretching vibration of phenol.

Thus for benzophenone the values of the apparent integrated intensities are approximately 280 L mol^{-1} cm^{-2} and for acetophenone, 300 L mol^{-1} cm^{-2}.

It is well konwn that the existence of an electrical anharmonicity in a diatomic molecule leads to a nonlinear dependence of the dipole moment variation on the internuclear distance and M can be expressed as :

$$M = M_0 + M_1 r + M_2 r^2 + M_3 r^3 + \dots$$

Neglecting the higher terms, Russel and Thomson [17] have showed that in the diatomic oscillator approximation we can write

$$(A_{02}/A_{01}) = X_e\, 1 - (2B/ar_e)^2$$

where $B = M_2/M_1$ and a is the Morse constant in the potential function. From the values of the ratios A_{02}/A_{01} we can see that there is an important decrease of the electrical anharmonicity of the $C = O$ group for both ketones in CH_2Cl_2, CH_2Br_2 and $CHCl_3$.

From tables 2 and 3 one can also observe a decrease of the molar extinction coefficients of the fundamentals, in agreement with earlier results.

For the corresponding overtones, there is an important decrease as compared with those of the fundamentals (by two orders of magnitude) but the values are of the same order of magnitude for carbon tetrachloride and for the polar solvents.

The small decrease observed on passing from carbon tetrachloride to chloroform follows the increase in the hydrogen bond strength. One can also see from tables 3 and 4 that the values of the half bandwidths of the overtones are twice those for the fundamentals, both for the nonpolar solvent and the polar one. Attempts to correlate these latter values to those of the apparent integrated intensities and molar extinction coefficients has not led to any significant results.

CONCLUSIONS

1. On passing from interactions such as collision complexes to interactions by means of weak hydrogen bonds, there is a decrease of the mechanical anharmonicity of the $C = O$ vibration for the ketones under consideration.

2. The molar extinction coefficients of the overtones and the ratios of the apparent integrated intensities of the overtones and fundamentals decrease with the increase of the hydrogen bonding strength.

Therefore, in the cases discussed above for the interactions, by means of weak hydrogen bonds, the $C = O$ vibration becomes more harmonic.

---

[17] R. A. Russel and H. W. Thomson, *Proc. Roy. Soc.*, **234**, 318 (1956).

with the results of van Thong and [illegible] for the first overtone of the [illegible] stretching vibration of phenol.

For the fundamentals the values of the apparent integrated intensities are approximately 260 L mol^{-1} cm^{-2} and for the overtones [illegible] L mol^{-1} cm^{-2}.

It is well known that the intensity of an vibrational transition of a diatomic molecule leads to a nonlinear dependence of the dipole moment variation on the internuclear distance and M can be expressed as

$$M = M_0 + M_1 [illegible] + M_2 [illegible] \ldots$$

Neglecting the higher terms, Russell and Thompson[illegible] have shown that in the harmonic oscillator approximation one can write:

$$[illegible]$$

where $\beta = M_2/M_1$ and a is the Morse constant in the potential function. From the values of the ratios A_2/A_1 we can see that there is an important decrease of the electrical anharmonicity of the [illegible] group for both ketones in CH_2Cl_2, CH_2Br_2 and $CHCl_3$.

From tables 2 and 3 one can also observe a decrease of the molar extinction coefficients of the fundamentals, in agreement with earlier results.

For the corresponding overtones, there is an important decrease as compared with those of the fundamentals (by two orders of magnitude) but the values are of the same order of magnitude in carbon tetrachloride and for the polar solvents.

The small decrease observed on passing from carbon tetrachloride to chloroform follows the increase in the hydrogen bond strength. One can also see from tables 3 and 4 that the values of the half band-widths of the overtones are twice those for the fundamentals, both for the non-polar solvent and the polar one. Attempts to correlate these latter values to those of the apparent integrated intensities and molar extinction coefficients has not led to any significant results.

CONCLUSIONS

1. On passing from intermolecular [illegible] as collision complexes to [illegible] by means of weak hydrogen bonds, there is a decrease of the mechanical anharmonicity of the C=O vibration for the ketones under consideration.

2. The molar extinction coefficients of the overtones and the ratios of the apparent integrated intensities of the overtones and fundamentals decrease with the increase of the hydrogen bonding strength.

Therefore, in the cases discussed above for the interactions by means of weak hydrogen bonds, the C=O vibration becomes more harmonic.

[illegible] and H. W. Thompson, Proc. Roy. Soc., [illegible]

[illegible]

Revue Roumaine de Chimie, 18, 3, 367–375 (1973)

SIMULTANEOUS DETERMINATION BY KNUDSEN EFFUSION-MICROCALORIMETRIC TECHNIQUE OF THE VAPOUR PRESSURE AND SUBLIMATION ENTHALPY OF ANTIMONY TRIFLUORIDE. VAPOUR PRESSURE OF BISMUTH TRIFLUORIDE

G. DE MARIA, L. MALASPINA, G. BARDI and R. GIGLI

Laboratorio di Chimica-Fisica ed Elettrochimica, Istituto Chimico, Università di Roma, Roma, Italy

Received September 22, 1972

The Knudsen vapour pressure and sublimation enthalpy of SbF_3 were simultaneously determined on the temperature range 375–455 K utilizing a Calvet microcalorimeter, with a method based on the differential calorimetry combined with the Knudsen effusion technique. The relative equations on the investigated temperature range are as follows:

$$\Delta H^0_{sub}(T) = (25987 \pm 36) - (5.28 \pm 0.09)\,T \text{ cal mole}^{-1}$$

$$\log_{10} p_{torr} = (11.48 \pm 0.06) - (5176 \pm 23)/T.$$

The sublimation enthalpy values at 298 K obtained from the microcalorimetric data and by second and third-law treatment of the vapour pressure data are: ΔH^0_{298} (calorimetric) = 24407 ± 71 cal mole^{-1}, ΔH^0_{298} (second-law) = 24385 ± 105 cal mole^{-1} and ΔH^0_{298}(third-law) = 24409 ± 54 cal mole^{-1}. The thermodynamic functions of $SbF_{3(g)}$ molecule were also evaluated on the temperature range 298–1000 K. The vapour pressure values of BiF_3 were determined on the temperature range 669–838 K utilizing a vacuum thermobalance. The data relative to the sublimation process are as follows:

$$\log_{10} p_{torr} = (11.79 \pm 0.09) - (9797 \pm 70)/T;$$

$$\Delta H^0_{298} \text{ (second-law)} = 47726 \pm 320 \text{ cal mole}^{-1};$$

$$\Delta H^0_{298} \text{ (third-law)} = 48077 \pm 233 \text{ cal mole}^{-1}.$$

INTRODUCTION

There is little information in the literature about the vapour pressure and the sublimation enthalpy of the antimony and bismuth trifluorides. These compounds have been investigated only by Cubicciotti [1,2] by means of a transpiration method. In the present work, the antimony trifluoride has been studied utilizing a method based on the combination

---

[1] D. Cubicciotti, *High Temp. Sci.*, **1**, 268 (1969).

[2] D. Cubicciotti, *J. Electrochem. Soc.*, **115**, 1138 (1968).

of the microcalorimetry with the classical Knudsen effusion technique. This method allows to obtain simultaneously, the values of vapour pressures and sublimation enthalpy of the compound investigated at well-known temperatures.

Using this procedure, already successfully applied to cadmium, [3] zinc and tellurium [4] and to benzoic acid and anthracene, [5] the sublimation enthalpy value, directly determined by microcalorimetry, can be compared with the values obtained by the second and third-law treatment of the vapour pressure data.

Due to a temperature range too high for the employment of the apparatus utilized for the antimony trifluoride, the vapour pressure of bismuth trifluoride was determined by measuring the rate of mass loss in Knudsen conditions, using a thermobalance.

EXPERIMENTAL

A. SbF_3

The microcalorimetric measurements were carried out utilizing a SETARAM Calvet differential microcalorimeter [6] described elsewhere. [7] The two twin microcalorimeter elements are placed symmetrically in a kanthal block, and the differential thermal flow is measured by means of two thermopiles in opposition, each one consisting of 396 Pt; Pt – 10% Rh thermocouples and connected with a galvanometer. The thermogram is recorded by means of a spot following recorder actuated by the same galvanometer. The assembly utilized for the evaporation experiment, consisting of two identical devices placed in the working and reference cells of the microcalorimeter, is described in detail in previous works. [3-5] The proportionality between thermal power and galvanometric deflection i.e. the instrument constant (P/Δ), was determined by Joule effect [3-5] at each experimental temperature.

The temperatures were measured by a previously calibrated Pt; Pt – 10% Rh thermocouple placed in the center of the calorimetric block.

B. BiF_3

The rate of mass loss in the Knudsen conditions of the samples was measured by means of a null Ugine-Eyraud mod. B. 60 SETARAM microbalance. The reaction chamber, a silica-glass tube, 60 cm high and 17 mm in diameter, was heated along its whole length by means of a cylindrical coaxial graphite resistance. The Knudsen cells were suspended to the balance beam and placed in the center of the isothermal zone of the reaction chamber (about 15 cm long) determined in a former experiment. The mass loss of the samples was recorded at temperatures maintained constant within $\pm 1°$ by means of an efficient thermoregulation device.

The temperatures of the samples were measured with a previously calibrated Pt; Pt – 10% Rh thermocuple inserted in an identical cell placed immediately beneath the effusion cell and recorded simultaneously with the sample loss. A differential pumping system for the reaction chamber, balance housing and for the furnace allowed to obtain a vacuum of not less than 1×10^{-5} torr. Both compounds 99.99% purity, Alfa Inorganics Co., were evaporated in platinum Knudsen cells, with effusion holes of different diameter (see Tables 3 and 4) drilled into platinum sheets 0.1 mm thick.

---

[3] L. Malaspina, R. Gigli and G. Bardi, *J. Chem. Thermodynamics*, **3**, 827 (1971).

[4] L. Malaspina, R. Gigli and G. Bardi, *Rev. Int. Hautes Tempér. et Réfract.*, **9**, 131 (1972).

[5] L. Malaspina, R. Gigli and G. Bardi, in press on *J. Chem. Phys.*

[6] E. Calvet and H. Pratt, "Microcalorimétrie, Applications Physico-Chimiques et Biologiques", Masson, Paris, 1956.

[7] L. Malaspina, R. Gigli and V. Piacente, *Rev. Int. Hautes Tempér. et Réfract.*, **8**, 211 (1971).

RESULTS

A. VAPOUR PRESSURE AND SUBLIMATION ENTHALPY OF $SbF_3(s)$

The simultaneous measurements of the sublimation enthalpy and of the vapour pressure were carried out by measuring the area of the thermogram relative to the quantitative evaporation in the Knudsen conditions of the sample with the same experimental procedure used in the previous works.[3-5] The investigated temperature range was 375 to 455 K. Use was made of the well-known expressions

$$\Delta H^0_{\text{sub}}(T) = 1/4.186 \, \frac{M}{m} \, (P/\Delta)\,(A/v) \tag{1}$$

$$p_{(\text{torr})} = \frac{2.256 \times 10^{-2} \times 760}{S} \, (\mathrm{d}m/\mathrm{d}t)\,(T/M)^{1/2}(1/K) \tag{2}$$

where

$\Delta H^0_{\text{sub}}(T)$ = the value of sublimation enthalpy at absolute temperature T (cal mole^{-1})
p = vapour pressure (torr)
m = mass of the sample evaporated (g)
P/Δ = microcalorimeter constant (watt mm^{-1})
A = area of the thermogram (mm^2)
v = recording speed of the thermogram (1/12 mm s^{-1})
S = effusion hole area (cm^2)
$(\mathrm{d}m/\mathrm{d}t)$ = rate of mass loss (g s^{-1})
K = Clausing correction factor[8]

According to the mass spectrometric investigation by Cubicciotti[1] we considered that within the investigated temperature range the vapour phase in equilibrium with the condensed SbF_3 consists only of SbF_3 molecules.

In order to check the reproducibility of the data, three vaporizations were carried out at each temperature. The values of the sublimation enthalpy so determined and the mean values are given in Table 1. The least square treatment of the experimental mean values of $\Delta H^0_{\text{sub}}(T)$ as function of T (plotted in Figure 1) gives the equation

$$\Delta H^0_{\text{sub}}(T) = (25987 \pm 36) - (5.28 \pm 0.09)\,T. \tag{3}$$

---

[8] S. Dushman, "Scientific foundation of vacuum technique", John Wiley and Sons, N.Y., 1958, pp. 90–111.

Table 1

Enthalpy of sublimation $\Delta H^{\circ}_{\text{sub}}$ (T) of SbF_3

T (K)	10^5 P/Δ (watt mm^{-1})	m (mg)	A (mm^2)	$\Delta H^{\circ}_{\text{sub}}$ (T) cal $mole^{-1}$	
374.5	7.17	11.59	3020	23935	
	7.15	13.85	3620	23942	23934
	7.19	14.63	3800	23925	
384.5	7.31	35.87	9120	23811	
	7.36	37.35	9480	23932	23876
	7.34	34.96	8880	23885	
388.4	7.39	32.46	8174	23841	
	7.40	37.57	9455	23859	23833
	7.37	35.09	8845	23800	
392.8	7.52	49.89	12352	23853	
	7.49	51.31	12717	23782	23812
	7.50	48.07	11907	23800	
397.1	7.53	79.50	19602	23786	
	7.55	84.68	20872	23841	23785
	7.51	80.46	19844	23729	
402.3	7.58	117.47	28675	23705	
	7.60	106.69	26040	23764	23753
	7.61	121.33	29605	23789	
408.3	11.00	154.00	25944	23741	
	10.99	178.53	30080	23722	23749
	11.02	164.61	25944	23783	
412.8	11.11	204.74	34122	23721	
	11.10	220.69	36784	23702	23728
	11.13	233.80	38962	23762	
418.8	11.05	98.85	16544	23693	
	11.04	107.76	18040	23677	23701
	11.07	113.59	19008	23732	
424.2	11.14	217.28	36000	23646	
	11.15	222.38	36840	23664	23664
	11.16	216.60	35880	23683	
429.2	11.20	253.22	41750	23657	
	11.17	260.27	42919	23598	23631
	11.19	234.97	38744	23638	
437.6	11.26	317.99	51894	23541	
	11.28	287.24	46872	23581	23581
	11.30	335.98	54823	23622	
443.5	11.40	551.75	89012	23561	
	11.38	581.87	93874	23521	23555
	11.41	567.98	91630	23582	
450.2	11.44	551.11	88320	23488	
	11.47	554.59	88872	23548	23521
	11.46	533.91	85560	23528	
455.2	11.52	605.85	96448	23495	
	11.54	645.67	102784	23535	23488
	11.49	667.74	106304	23434	

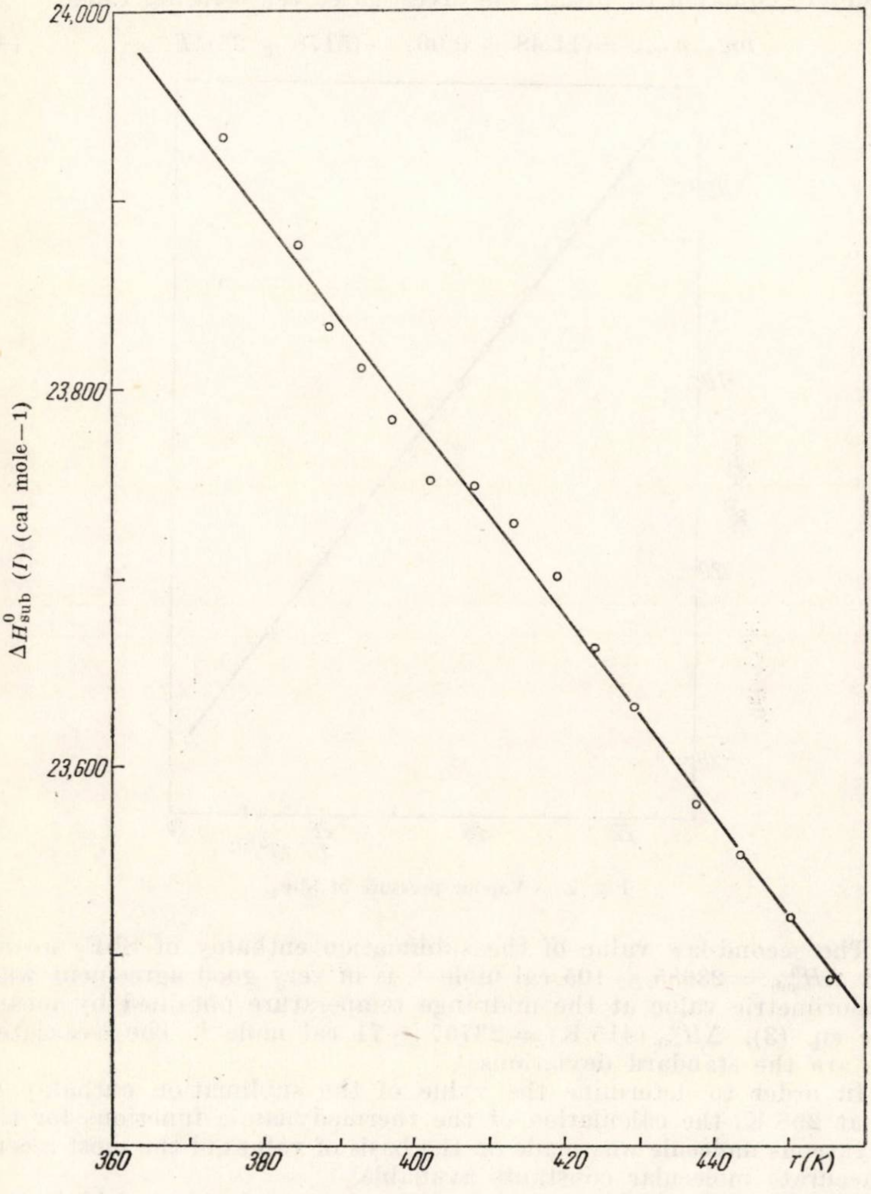

Fig. 1. — Sublimation enthalpy of SbF_3 determined by microcalorimetry.

The experimental average vapour pressure values of SbF_3 are listed in Table 3 and plotted as function of $1/T$ in Figure 2. The relative least square equation is, within the investigated temperature range

$$\log_{10} p_{(\mathrm{torr})} = (11.48 \pm 0.06) - (5176 \pm 23)/T. \qquad (4)$$

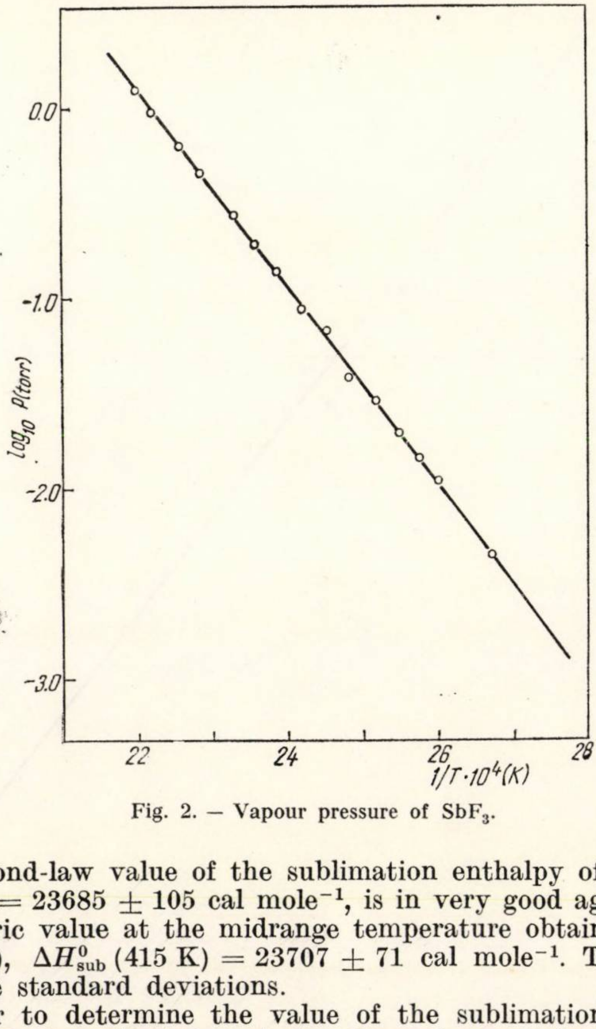

Fig. 2. — Vapour pressure of SbF_3.

The second-law value of the sublimation enthalpy of SbF_3 so obtained $\Delta H^0_{\mathrm{sub}} = 23685 \pm 105$ cal mole^{-1}, is in very good agreement with the calorimetric value at the midrange temperature obtained by means of the eq. (3), $\Delta H^0_{\mathrm{sub}}$ (415 K) $= 23707 \pm 71$ cal mole^{-1}. The associated errors are the standard deviations.

In order to determine the value of the sublimation enthalpy of SbF_3 at 298 K, the calculation of the thermodynamic functions for the SbF_3 gaseous molecule was made on the basis of values of the most recent and accurate molecular constants available.

A pyramidal structure and a symmetry number $\sigma = 3$ [1,9-11] was assumed for the SbF_3 molecule. The Sb-F values for internuclear $d_{\mathrm{Sb-F}} =$

---

[9] S. Konaka and M. Kimura, *Bull. Chem. Soc. Japan*, **43**, 1693 (1970).

[10] C. Matsumura and H. Takeo, "Symposium on molecular structure", Fukuota, Oct., 15, 1969.

[11] T. R. Manley and D. A. Williams, *Spectrochimica Acta*, **21**, 1467 (1965).

$= 1.879 \pm 4 \times 10^{-3}$ Å, and the bond angle $\alpha = 95 \pm 0.8°$, recently determined [9], were utilized.

The values for the vibration frequencies 666 and 298 cm^{-1}, non-degenerate, and 622 and 210 cm^{-1}, doubly degenerate, reported by Timoshinin [12] were used. The electronic contribution was assumed to be negligible. [1,13] The thermodynamic functions so evaluated are reported in Table 2.

Table 2

Thermodynamic functions calculated for SbF_3 (g) molecule

T (K)	$-(G^0_T - H^0_{298})/T$ (cal K^{-1} $mole^{-1}$)	$(H^0_T - H^0_0)$ (cal $mole^{-1}$)	S^0_T (cal K^{-1} $mole^{-1}$)	C_p (cal K^{-1} $mole^{-1}$)
298.15	71.85	3585	71.85	16.144
300	71.86	3615	71.95	16.176
350	72.06	4443	74.51	16.912
400	72.51	5303	76.81	17.467
450	73.11	6188	78.89	17.889
500	73.78	7091	80.79	18.215
550	74.50	8008	82.54	18.470
600	75.24	8937	84.16	18.672
650	75.98	9875	85.66	18.835
700	76.72	10820	87.06	18.967
750	77.46	11771	88.37	19.077
800	78.18	12727	89.60	19.168
850	78.88	13687	90.77	19.244
900	79.58	14651	91.87	19.309
950	80.25	15618	92.92	19.364
1000	80.93	16586	93.93	19.409

The aforementioned second-law and calorimetric sublimation enthalpy of SbF_3 at the midrange temperature were thus reduced to 298 K utilizing the heat content values determined in this work for SbF_3 (g) and those reported by Cubicciotti [1] for the condensed phase. These values are ΔH^0_{sub} (298 K) (second-law) $= 24385 \pm 105$ cal $mole^{-1}$ and ΔH^0_{sub} (298 K) (calorimetric) $= 24407 \pm 71$ cal $mole^{-1}$.

The third-law treatment of the experimental vapour pressure data determined in this work is shown in Table 3. The $(G^0_T - H^0_{298})/T$ values calculated in this work for SbF_3 (*g*) and those reported in literature for solid SbF_3 were utilized. One obtains an average value of ΔH^0_{sub} (298 K) $=$ $= 24409 \pm 54$ cal $mole^{-1}$.

---

[12] V. S. Timoshinin and S. V. Khandozhko, *Zh. Prikl. Spektrosk.*, **7**, 959 (1967).

[13] P. A. G. O'Hare, A.N.L. 7456, Nov., 1968.

Table 3

Vapour pressure and sublimation enthalpy of SbF_3 calculated by the third-law method

T (K)	d (mm)	$(\mathrm{d}m/\mathrm{d}t)\times 10^{6}$[a] ($\mathrm{g\ s^{-1}}$)	p[b] (torr)	$-R\ln p$ (atm) ($\mathrm{cal\ K^{-1}\ mole^{-1}}$)	$-\Delta(G^0_T - H^0_{298})/T$ ($\mathrm{cal\ K^{-1}\ mole^{-1}}$)	ΔH^0_{298} (sub) ($\mathrm{cal\ mole^{-1}}$)
374.5	1.0	1.279	4.446×10^{-3}	23.946	41.27	24423
384.5	1.0	3.149	1.109×10^{-2}	22.130	41.25	24368
388.4	1.0	4.037	1.429×10^{-2}	21.617	41.22	24407
392.8	1.0	5.450	1.941×10^{-2}	21.018	41.21	24443
397.1	1.0	8.179	2.931×10^{-2}	20.198	41.19	24379
402.3	1.0	10.584	3.820×10^{-2}	19.672	41.17	24476
408.3	1.0	18.599	6.745×10^{-2}	18.542	41.16	24374
412.8	1.0	24.200	8.831×10^{-2}	18.007	41.13	24410
418.8	0.5	8.763	1.406×10^{-1}	17.128	41.10	24384
424.2	0.5	12.072	1.949×10^{-1}	16.432	41.08	24396
429.2	0.5	16.880	2.742×10^{-1}	15.755	41.07	24389
437.6	0.5	28.496	4.667×10^{-1}	14.698	41.03	24387
443.5	0.5	38.637	6.383×10^{-1}	14.076	41.01	24429
450.2	0.5	57.409	9.550×10^{-1}	13.275	40.98	24426
455.2	0.5	73.704	1.244	12.749	40.97	24451
					average value	24409 ± 54[c]

[a] For each temperature, the value of the rate of weight loss, $(\mathrm{d}m/\mathrm{d}t)$, was calculated as an average of three experimental values (see Table 1) which practically coincide.

[h] Values corrected by Clausing factor equal to 0.9091 and 0.8330 for diameter (d) of the effusion hole equal to 1.0 and 0.5mm respectively.

[c] Twice the standard deviation of the mean.

Table 4

Vapour pressure and sublimation enthalpy of BiF_3 calculated by the third-law method

T (K)	d (mm)	$(\mathrm{d}m/\mathrm{d}t)\times 10^{6}$[a] ($\mathrm{g\ s^{-1}}$)	p[b] (torr)	$-R\ln p$ (atm) ($\mathrm{cal\ K^{-1}\ mole^{-1}}$)	$-\Delta(G^0_T - H^0_{298})/T$ ($\mathrm{cal\ K^{-1}\ mole^{-1}}$)	ΔH^0_{298} (sub) ($\mathrm{cal\ mole^{-1}}$)
669	1.1	0.685	1.514×10^{-3}	26.088	45.55	47926
695	1.1	1.675	5.331×10^{-3}	23.585	45.35	47910
695	1.1	1.605	5.108×10^{-3}	23.672	45.35	47970
709	1.1	2.913	9.360×10^{-3}	22.464	45.33	48065
714	1.1	3.990	1.287×10^{-2}	21.832	45.30	47932
716	1.1	3.906	1.262×10^{-2}	21.873	45.30	48096
725	1.1	5.044	1.639×10^{-2}	21.352	45.26	48294
726	1.1	5.585	1.817×10^{-2}	21.146	45.25	48203
732	1.1	7.059	2.306×10^{-2}	20.674	45.25	48256
741	1.1	9.560	3.141×10^{-2}	20.061	45.17	48336
744	1.1	10.378	3.418×10^{-2}	19.892	45.13	48376
752	0.4	2.227	6.390×10^{-2}	18.647	45.13	47960
757	1.1	18.982	6.307×10^{-2}	18.675	45.07	48225
761	0.4	3.047	8.794×10^{-2}	18.020	45.07	48011
772	0.4	4.700	1.366×10^{-1}	17.137	45.00	47970
779	0.4	6.272	1.832×10^{-1}	16.556	44.95	47913
789	0.4	8.781	2.580×10^{-1}	15.874	44.91	47959
793	0.4	9.985	2.942×10^{-1}	15.613	44.88	47970
801	0.4	11.060	3.270×10^{-1}	15.403	44.85	48263
802	0.4	12.410	3.677×10^{-1}	15.169	44.84	48127
810	0.4	17.810	5.303×10^{-1}	14.442	44.80	47986
818	0.4	20.269	6.070×10^{-1}	14.176	44.75	48200
830	0.4	35.190	1.061	13.069	44.70	47948
832	0.4	35.505	1.058	13.064	44.70	48060
838	0.4	44.355	1.354	12.598	44.62	47949
					average value	48077 ± 233[b]

[a] Values corrected by Clausing factor equal to 0.9167 and 0.800 for diameter (d) of the effusion hole equal to 1.1 and 0.4 mm respectively.

[b] Twice the standard deviation of the mean.

B. VAPOUR PRESSURE OF $BiF_3(s)$

The thermogravimetric measurement of the vapour pressure of BiF_3 (*s*) was carried out on the temperature range 669 to 838 K. The vapour phase in equilibrium with the solid trifluoride was also assumed to be composed only of BiF_3 molecules on the investigated temperature range.[2]

The vapour pressure values obtained by utilizing the eq. (2) are listed in the Table 4.

The $\log p$ vs $1/T$ plot is shown on Figure 3. The least-square treatment of the experimental data gives, within the investigated temperature range, the equation

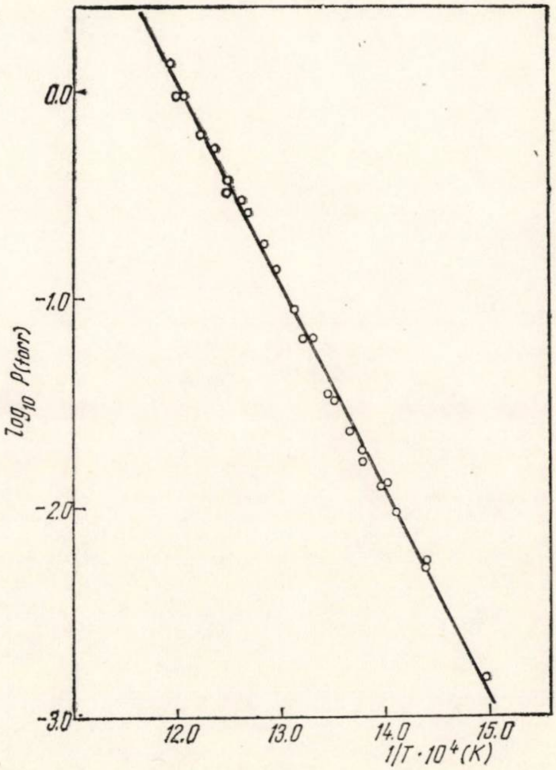

Fig. 3. — Vapour pressure of BiF_3.

$$\log_{10} p_{(\mathrm{torr})} = (11.79 \pm 0.09) - (9797 \pm 70)/T. \qquad (5)$$

The relative second-law value of the sublimation enthalpy of BiF_3 is $\Delta H^0_{\mathrm{sub}}(745\ \mathrm{K}) = (44832 \pm 320)$ cal mole^{-1}.

The corresponding value at 298 K, obtained utilizing the heat content data reported by Cubicciotti[2] for the condensed and vapour phases, is $\Delta H^0_{\mathrm{sub}}(298\ \mathrm{K}) = (47726 \pm 320)$ cal mole^{-1}. The third-law treatment of the experimental vapour pressure data, utilizing the free energy function values reported in the literature[2] is also given in Table 4. An average value of $\Delta H^0_{\mathrm{sub}}(298\ \mathrm{K}) = (48077 \pm 233)$ cal mole^{-1} for the bismuth trifluoride was obtained.

Revue Roumaine de Chimie, 18, 3, 377–385 (1973)

ISOTHERMAL EQUILIBRIUM AND CALCULATION OF EXCESS FUNCTIONS IN THE BENZENE-ISOBUTYL ALCOHOL SYSTEM

RODICA VÎLCU and ZOICA CENUȘE

Chair of Chemical Thermodynamics and Electrochemistry, Bucharest University,
Bd. Republicii 13, Romania

Received October 12, 1972

Isothermal vapour-liquid equilibria were measured in the benzene-isobutyl alcohol system at 45 and 55°. The measured data were employed to calculate the values of excess quantities.

Recently, a considerable effort has been made to formulate more general rules governing the behaviour of components of binary mixtures in the vapour – liquid phase equilibrium which could substitute the somewhat lengthy experimental procedures. This effort is based primarily on a detailed descriptive study of binary systems of suitably chosen homologous series. Attention is paid mainly to systems displaying considerable deviations from ideal behaviour, e.g. mixtures of polar substances with nonpolar ones.

The study of the benzene-butyl alcohols binary systems was started with the aim to contribute to this kind of description. The present work presents the results of the measurement of the isothermal vapour-liquid equilibria of the benzene-isobutyl alcohol system at 45 and 55°.

EXPERIMENTAL

PREPARATION OF PURE SUBSTANCES

Benzene of the reagent grade purity for cryoscopy (Belgium) was used; the water content with Karl-Fischer reagent was 0.00336%.

Isobutyl alcohol was a pure reagent (Austria) which was redistilled; only after this distillation the physical constants were in good agreement with the literature data; the water content with Karl-Fischer reagent was 0.00455%.

The physical properties of the reagents were indicated in table 1.

Table 1

Physical properties of the reagents

Substance	Refractive index (n_D^{25})		Boiling point (°C)		d (g/ml)		P_c (atm)	T_c (°C)
	experimental	liter.	experimental	liter.	experimental	liter.		
benzene	1.4975	1.49715[1]	80.1	80.07 [2]	0.8738	0.8740 [2]	50.1 [4]	290.5 [4]
isobutyl alcohol	1.3940	1.3938 [2]	107.8	108.01 [2]	0.7985	0.7979 [3]	42.39 [5]	276.7 [5]

ANALYSIS OF MIXTURES

Composition of the equilibrium mixture was determined by measuring the refractive index at 25° with an Abbé refractometer having a precision of about $\pm 2.10^{-4}$. In this case a calibration graph was necessary.

Results of the measurements are presented in table 2 and in figure 1.

Table 2

Dependence of refractive index on composition in the benzene-isobutyl alcohol system

$x^L_{C_6H_6}$	0.0564	0.0726	0.0883	0.1394	0.1410	0.1412	0.2078	0.2088	0.2726	0.2735	0.3412
n_D^{25}	1.3991	1.4005	1.4000	1.4066	1.4065	1.4070	1.4130	1.4133	1.4197	1.4192	1.4248
$x^L_{C_6H_6}$	0.3426	0.3429	0.4080	0.4127	0.4764	0.4791	0.5399	0.6087	0.6098	0.6699	0.7377
n_D^{25}	1.4263	1.4266	1.4330	1.4333	1.4380	1.4400	1.4470	1.4523	1.4225	1.4585	1.4650
$x^L_{C_6H_6}$	0.7993	0.8675	0.9317	0.9324							
n_D^{25}	1.47181	1.4797	1.4885	1.4894							

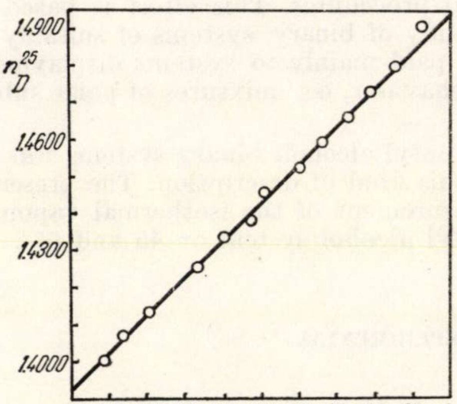

Fig. 1. — The calibration graph.

---

[1] A. K. Kenneth and F. I. Mathews, *J. Chem. Eng. Data*, **15**, 182 (1970).

[2] J. Timmermans, "Physico-Chemical Constants of Pure Organic Compounds", vol. 2, Elsevier Publishing Co. Inc., New York, 1950.

[3] "International Critical Tables of Numerical Data Physics, Chemistry and Technology", vol. 3. McGraw-Hill Book Company Inc. New York, 1928, p. 27.

[4] J. Landolt-Börnstein, "Physikalisch-Chemische Tabellen", Verlag Van Julius Springer Berlin, 1929, p. 442.

[5] D. Ambrose and R. Townsend, *J. Chem. Soc.*, **1963**, 3614.

APPARATUS

The apparatus which was set up for measurements was one of Swietoslawsky equilibrium type previously described in detail.[6]

The temperature was adjusted with a thermoregulator to ± 0.05°.

Two cylinders, one of 2 l and another of 60 l served as vacuum reservoires. Regulation of pressure was attained handly with a capilar stopcock by means of a manometer, allowing to read pressure with a precision of about 1 mm Hg, which was satisfactory with respect to the fact that heating system permitted to control the temperature with an accuracy of ± 0.05°.

EXPERIMENTAL RESULTS

The measurements in the benzene-isobutyl alcohol system rises no difficulty and the experimental data were indicated in the table 3 and in figures 2 and 3.

Table 3

Measured data in the benzene-isobutyl alcohol at 45 and 55°

	45°			55°	
$x^L_{C_6H_6}$	$x^V_{C_6H_6}$	P(mmHg)	$x^L_{C_6H_6}$	$x^V_{C_6H_6}$	P(mmHg)
0	0	40.45	0	0	71.30
0.0235	0.062	79.1	0.056	0.148	91.5
0.114	0.224	106.5	0.134	0.292	158.6
0.171	0.302	129.9	0.192	0.412	183.7
0.221	0.395	140.4	0.265	0.505	210.2
0.300	0.462	162.4	0.330	0.545	223.5
0.388	0.526	173.7	0.402	0.518	264.6
0.471	0.598	187.6	0.506	0.628	277.9
0.529	0.615	194.5	0.534	0.662	283.1
0.601	0.665	207.5	0.615	0.685	301.8
0.645	0.692	212.5	0.734	0.769	332.8
0.668	0.723	220.3	0.792	0.801	339.6
0.716	0.735	224.5	0.892	0.825	338.0
0.790	0.793	230.1	0.933	0.845	337.7
0.903	0.845	227.9	1	1	326.95
0.976	0.929	225.1			
1	1	223.50			

The system is azeotropic at 45 and 55° and the azeotropic point did not vary with the temperature.

The used constants of the Antoine equation (log $P = A - B/t + C$) were indicated in table 4.

In the figure 4 were indicated the equilibrium diagrams at 45 and 55°.

---

[6] R. Vîlcu and Z. Cenușe, *Rev. Roumaine Chim.*, **16**, 1635 (1971).

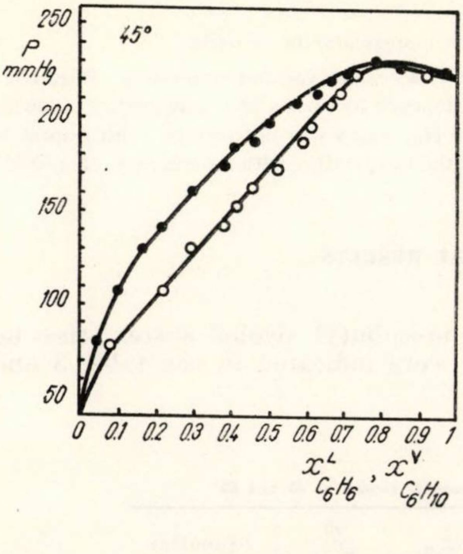

Fig. 2. — Dependence of the total pressure (P) vs. benzene equilibrium composition ($x^L_{C_6H_6}$) of the liquid phase at 45°.

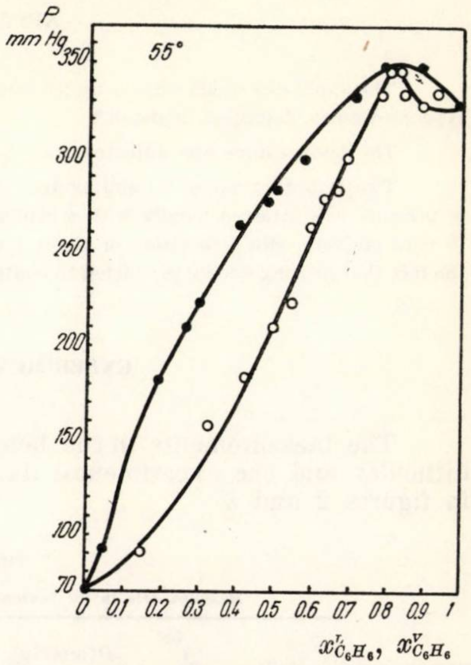

Fig. 3. — Dependence of the total pressure (P) vs. benzene equilibrium composition ($x^L_{C_6H_6}$) of the liquid phase at 55°.

Table 4

The constants of Antoine equation

Substance	A	B	C
benzene [7]	6.98745	1206.35	220.237
isobutyl alcohol [8]	8.19613	1697.44	212.610

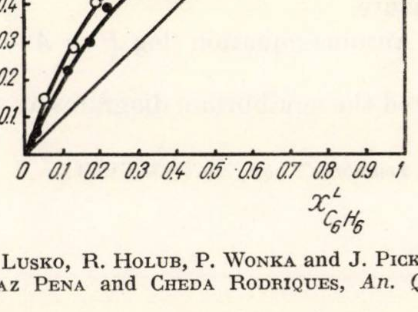

Fig. 4. — Equilibrium diagrams ($x^L_{C_6H_6} - x^V_{C_6H_6}$) at 45 and 55°.

---

[7] J. LUSKO, R. HOLUB, P. WONKA and J. PICK, *Coll. Czech. Chem. Comm.*, **35**, 385 (1970).

[8] DIAZ PENA and CHEDA RODRIQUES, *An. Quim.*, **66**, 721 (1970).

In the effort to introduce into the calculations a correction for the real behaviour of the vapour phase we calculated the activity coefficients with the relation:

$$\ln \gamma_i = \ln x_i^V P / x_i^L P_i^0 + (B_{ii} - V_i)(P - P_i^0)/RT + P\delta_{ij}(1 - x_i^V)^2/RT \quad (1)$$

where

$$\delta_{ij} = 2B_{ij} - B_{ii} - B_{jj}$$

For pure nonpolar gases an excellent correlation for the second virial coefficient B_{ii} has been given by Pitzer and Curl[9] based on the theorem of corresponding states. It has the form

$$P_{c_i} B_{ii} / RT_{c_i} = f_B^{(0)}(T_r) + \omega_i f_B^{(1)}(T_r) \quad (2)$$

where P_{c_i} is the critical pressure of i, T_{c_i} is the critical temperature of i, ω_i is the acentric factor of i and T_r is the reduced temperature, T/T_{c_i}. The acentric factor is defined by

$$\omega_i = -\log(P_i^s / P_{c_i}) - 1.000 \quad (3)$$

where P_i^s is the saturation vapour pressure of i at $T/T_{c_i} = 0.7$. The empirically determined functions $f_B^{(0)}(T_r)$ and $f_B^{(1)}(T_r)$ are

$$f_B^{(0)}(T_r) = 0.1445 - 0.330/T_r - 0.1385/T_r^2 - 0.0121/T_r^3 \quad (4)$$

$$f_B^{(1)}(T_r) = 0.073 + 0.46/T_r - 0.50/T_r^2 - 0.097/T_r^3 - 0.0073/T_r^8 \quad (5)$$

For pure polar gases O'Connell and Prausnitz[10] have developed a new empirical correlation on an extended corresponding states theorem of the form

$$P_{c_i} B_{ii} / RT_{c_i} = f_B^{(0)}(T_r) + \omega_{H_i} f_B^{(1)}(T_r) + f_\mu(\mu_R, T_r) + \eta_i f_a(T_r) \quad (6)$$

The symbol ω_{H_i} stands for the acentric factor of the polar component homomorph (a homomorph of a polar molecule is a nonpolar molecule having approximately the same size and shape as those of the polar molecule).

The empirical function $f_\mu(\mu_R, T_r)$ depends on the reduced temperature T_r and on the reduced dipole moment defined by

$$\mu_R = 10^2 \mu_i^2 P_{c_i} / T_{c_i}^2 \quad (7)$$

---

[9] K. S. Pitzer and R. F. Curl, *J. Amer. Chem. Soc.*, **79**, 2369 (1957).

[10] J. P. O'Connell and J. M. Prausnitz, *Ind. Eng. Chem. Proc. Design. and Development*, **6**, 245 (1967).

where μ_i is the dipole moment of component i in Debye units.

For $\mu_R > 4$ f_μ is given by

$$\begin{aligned} f_\mu(\mu_R, T_r) = &- 5.237220 + 5.665807 (\ln \mu_R) - 2.133816 (\ln \mu_R)^2 + \\ &+ 0.2525373 (\ln \mu_R)^3 + 1/T_r x [5.769770 - 6.181427 (\ln \mu_R) + \\ &+ 2.283270 (\ln \mu_R)^2 - 0.2649074 (\ln \mu_R)^3] \end{aligned} \tag{8}$$

Equation (8) is not applied for molecules of very low polarity ($\mu_R < 4$) because of the logaritmic terms and for such molecules one should use $f_\mu(\mu_R, T_r) = 0$, as in our case.

$$(\mu_{\text{isobutyl alcohol}} = 1.64).$$

The association constant η_i is an empirically determined quantity which reflects the tendency of a component, e.g. alcohols, to associate with itself. The association function is given by

$$f_a(T_r) = \exp [6.6 (0.7 - T_r)] \tag{9}$$

The values of η_i are determined by Prausnitz, from the difference between experimental data and results obtained from the equations (4), (5) and (6).

The form of equation (9) is governed by the behaviour of the most associating substances. Generally, the association function contributes with a significant quantity to the total second virial coefficient at a temperature near and below the normal boiling point.

In order to estimate cross coefficient, B_{ij}, the previously presented correlating equations for pure components, we used with suitable combinatory rules for the various parameters. When i is a polar substance and j is a nonpolar one, equations (4), (5) and (8) are used for B_{ij}, where for $T_{c_{ij}}$ is used equation

$$T_{c_{ij}} = (T_{c_i} \cdot T_{c_j})^{1/2} \tag{10}$$

For ω_{ij} Prausnitz used

$$\omega_{ij} = (\omega_{H_i} + \omega_j)/2 \tag{11}$$

Equation (12) is used for $P_{c_{ij}}$

$$P_{c_{ij}} = 4T_{c_{ij}}[P_{c_i} \cdot V_{c_i}/T_{c_i} + P_{c_j} \cdot V_{c_j}/T_{c_j}]/(V_{c_i}^{1/3} + V_{c_j}^{1/3})^3 \tag{12}$$

where V_c is the critical volume.

If reliable critical volume data are not available, they should be estimated with the relation

$$V_c = RT_c(0.293 - 0.08\ \omega)/P_c \tag{13}$$

The calculated values of the second virial coefficient of benzene, B_{11} and of isobutyl alcohol, B_{22}, are tabulated in tables 5 and 6.

Table 5

The values of the second virial coefficient B_{11} at 45 and 55°

Substance	Temperature (°C)	B_{11} (ml/mol)	ω	d (g/ml)	M(g)	V(ml/mol)
benzene	45	−1245.08	0.211	0.8575 [11]	78.114	93.13
	55	−1145.12	0.211	0.83870 [11]	78.114	98.82

Table 6

The values of the second virial coefficient B_{22} at 45 and 55°

Substance	Temp (°C)	B_{22} (ml/mol)	ω	d(g/ml)	M(g)	V(ml/mol)	$\mu_R^{(D)10}$	η_i^{10}
isobutyl	45	−194.19	0.215	0.78327 [3]	73.116	93.34	1.64	0.49
isobityl alcohol	55	−219.43	0.215	0.77608 [3]	73.116	94.21	1.64	0.49

The values of the cross coefficient B_{12} and of δ were indicated in table 7.

Table 7

The values of B_{12} and δ

Temperature (°C)	B_{12} (ml/mol)	(nl/mol)
45	−1291.36	−1143.45
55	−1189.36	−1014.17

With these values of B_{11}, B_{22} and δ ln γ_1 and ln γ_2 were calculated and tabulated in table 8.

The thermodynamical consistency of the data was checked graphically using the Gibbs-Duhem equation

$$\int_0^1 \ln \frac{\gamma_2}{\gamma_1}\, \mathrm{d}x_2^L = 0. \tag{14}$$

---

[11] "Manualul inginerului chimist", vol. II, Ed. Tehnică, București, 1955, p. 1059.

Table 8

The values of the ln γ_1 and ln γ_2 at 45° and 55° in the benzene-isobutyl alcohol system

45°			55°		
$x^L_{C_6H_6}$	ln γ_1	ln γ_2	$x^L_{C_6H_6}$	ln γ_1	ln γ_2
0.0235	−0.063	0.631	0.056	−0.291	0.145
0.114	−0.061	0.834	0.134	0.056	0.596
0.171	0.028	0.993	0.192	0.248	0.624
0.221	0.118	0,989	0.265	0.207	0.680
0.300	0.108	1.123	0.330	0.125	0.749
0.388	0.053	1.197	0.402	0.153	0.955
0.471	0.064	1.253	0.506	0.055	1.068
0.529	0.012	1.134	0.534	0.072	1.048
0.601	0.027	1.452	0.615	0.028	1.232
0.645	0.019	1.508	0.734	0.063	1.386
0.668	0.058	1.503	0.792	0.049	1.504
0.716	0.029	1.634	0.892	−0.046	2.023
0.790	0.032	1.714	0.933	−0.670	2.343
0.903	−0.047	2.185			
0.976	−0.042	2.787			

The measured isothermal data were correlated using a third Van Laar equation

$$\log \gamma_1 = A_{12}(1 + A_{12}x_1^L/A_{21} \cdot x_2^L)^{-2} \tag{15}$$

and a third order Margules equation

$$\log \gamma_1 = x_1^{L2}\,(2A_{21} - A_{12}) + 2x_1^{L3}(A_{12} - A_{21}) \tag{16}$$

The constants of these equations are listed in table 9.

Table 9

The constants of the Van Laar and Margules equations

Temperature (°C)	Equation type	A_{12}	A_{21}
45	Van Laar 3	3.653	43.628
	Margules 3	2.640	−16.331
55	Van Laar 3	2.151	34.300
	Margules 3	8.761	−18.589

From the mentioned equilibrium data the excess quantities G^E (cal/mol) were estimated and the values are given in table 10 as well as in figure 5.

These data presented a maximal value for 45° at $x^L_{C_6H_6} = 0.24$ and $G^E = 517.44$ cal/mol and for 55° at $x^L_{C_6H_6} = 0.26$ and $G^E = 346.68$ cal/mol.

Table 10

The values of G^E cal/mol) for the benzene-isobutyl alcohol system at 5 and 55°

45°		55°	
$x^L_{C_6H_6}$	G^E(cal/mol)	$x^L_{C_6H_6}$	G^E(cal/mol)
0.0235	388.59	0.056	75.37
0.114	402.67	0.134	327.31
0.171	523.55	0.192	345.03
0.221	503.54	0.265	346.68
0.300	517.44	0.330	339.45
0.388	476.15	0.402	395.40
0.471	438.09	0.506	347.13
0.529	341.67	0.534	329.28
0.601	376.51	0.615	307.24
0.645	346.18	0.734	259.34
0.688	321.68	0.792	219.79
0.716	306.49	0.892	110.91
0.790	243.53	0.933	58.46
0.903	186.58		
0.976	163.37		

The decrease of the free excess enthalpy, G^E is dus to the decrease of the number of associates with increase of the temperature.

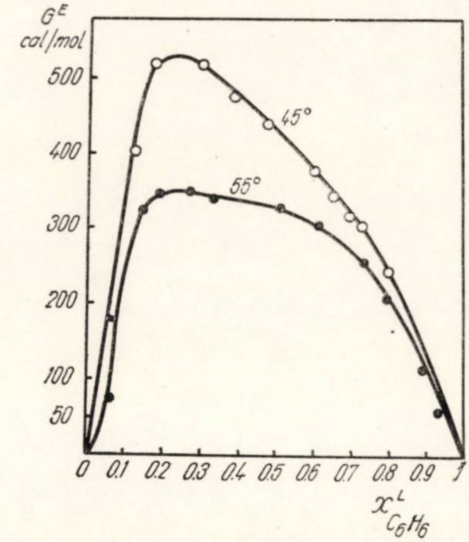

Fig. 5. — Diagrams of G^E(cal/mol) at 45 and 55° of the benzene-isobutyl alcohol system.

For this system no calorimetric data could be found in the literature for the temperatures used in our experiments.

Revue Roumaine de Chimie, **18**, *3*, 387–398 (1973)

SIGNIFICANT STRUCTURES THEORY OF IONIC BINARY LIQUID MIXTURES: HEAT CAPACITIES, COMPRESSIBILITY COEFFICIENTS AND THERMAL-EXPANSION COEFFICIENTS

RODICA VÎLCU and C. MISDOLEA

Physico-Chemical Institute, str. Galaţi 31, Bucharest, Romania

Received October 2, 1972

The heat capacity at constant volume, as well as the compressibility and the thermal-expansion coefficient of the binary systems of molten salts K(Cl—Br), Na(Cl—Br) and Cl(Na—K) were calculated at 1073 K, 1173 K and 1273 K, by taking the theory of significant structures as a model of the liquid state. The computed data allow, by comparing them with the experimental data, to discuss some aspects of the theory.

INTRODUCTION

The heat capacity, the thermal-expansion coefficient and the compressibility coefficient can offer, for any model of the liquid state, conclusive verifications. By computing these quantities, the partition function, at which the considered model arrives, can be more thoroughly analysed because the expressions contain derivatives of the first and second order in respect to the temperature as well as to the volume. This permits to verify the hypothesis of the theory and the manner of expressing mathematically these hypotheses. In a previous paper, [1] we computed these quantities for the ionic liquids KCl, KBr, NaCl, and NaBr, the model under study being the theory of the significant structures. [2] When the theory is extended to binary systems [3,4] the computation of the heat capacity, of the thermal — expansion coefficient and of the compressibility constitutes a still more necessary verification.

---

[1] R. Vîlcu and C. Misdolea, *J. Chem. Phys.*, **46**, 906 (1967).

[2] C. Carlson, H. Eyring and T. Ree, *Proc. Natl. Acad. Sci. U.S.A.*, **46**, 333 (1960)

[3] K. Liang, H. Eyring and R. P. Marchi, *Proc. Natl. Acad. Sci. U.S.*, **52**, 1107 (1964)

[4] S. M. Ma and H. Eyring, *J. Chem. Phys.*, **42**, 1920 (1965).

The partition function of an ionic liquid, according to the theory of significant structures, is [2]

$$Z_i = \left\{ \frac{\exp\left[(E_{s_i}/2RT)(V_i/V_{s_i})^{1/3}\right]}{[1-\exp(-\theta_i/T)]^3} \left[1 + n_{h_i} \exp\left(-\frac{a_i E_{s_i} (V_i/V_{s_i})^{1/3}}{2n_{h_i} RT}\right)\right]\right\}^{2N\frac{V_{s_i}}{V_i}} \times \tag{1}$$

$$\times \left[\frac{(2\pi m_i kT)^{3/2}}{h^3} \frac{8\pi^2 I_i kT}{h^2} \frac{1}{1-\exp(-h\nu_i/kT)} \frac{\mathrm{e}V_i}{N}\right]^{N\frac{V_i - V_{s_i}}{V_i}}$$

In this formula, as well as in the following ones, index *i* takes the values 1 or 2, according to whether it concerns the liquid 1 or 2 as constituent of the binary system. The quantities appearing in the expression of the partition function are :

E_{s_i},	the sublimation energy at the melting point
θ_i,	the Einstein characteristic temperature of the solid at the melting point
V_i,	the molar volume of the liquid
V_{s_i},	the molar volume of the solid at the melting point
n_{h_i},	the supplementary number of accesible positions of a molecule, besides the equilibrium position

$$n_{h_i} = n_i \frac{V_i - V_{s_i}}{V_{s_i}}, \quad n_i = C_i \frac{V_{s_i}}{V_i}$$

where C_i is the coordination number

a_i,	a parameter related to the energy necessary to a molecule for occupying one of its accessible positions
m_i,	the mass of the molecule
I_i,	the moment of inertia of the diatomic gaseous salt molecule
ν_i,	the vibration frequency of the gaseous molecule in its fundamental state.

The Helmholtz free energy of a mole of liquid, $F_i = -RT \ln Z_i$ is expressed by

$$F_i = -RT\left[\frac{2}{x_i}(\sigma_1^{(i)} + \sigma_2^{(i)} - \eta_i) + \left(1 - \frac{1}{x_i}\right)\left(\gamma_i + \ln \frac{eV_{s_i}}{N} x_i\right)\right] \tag{2}$$

where $x_i = V_i/V_{s_i}$, with the notations

$$\sigma_1^{(i)} = \frac{E_{s_i}}{2RT} x_i^{1/3} \tag{3}$$

$$\sigma_2^{(i)} = \ln\left[1 + n_i(x_i - 1)\exp\left(-\frac{a_i E_{s_i}}{2n_i RT}\,\frac{x_i^{1/3}}{x_i - 1}\right)\right] \tag{4}$$

$$\eta_i = 3\ln\left[1 - \exp\left(-\theta_i/T\right)\right] \tag{5}$$

$$\gamma_i = \ln\left[\frac{(2\pi m_i kT)^{3/2}}{h^3}\,\frac{8\pi^2 I_i kT}{h^2}\,\frac{1}{1 - \exp(-h\nu_i/kT)}\right] \tag{6}$$

Since the heat capacity at constant volume is equal to the internal energy variation, with regard to the temperature, whose expression is

$$U_i = RT^2\,(\partial \ln Z_i/\partial T)v \tag{7}$$

we shall obtain

$$C_{v_i} = \frac{RT}{x_i}\left[4\left(\frac{\partial\sigma_1^{(i)}}{\partial T} + \frac{\partial\sigma_2^{(i)}}{\partial T} - \frac{\partial\eta_i}{\partial T}\right) + 2T\left(\frac{\partial^2\sigma_1^{(i)}}{\partial T^2} + \frac{\partial^2\sigma_2^{(i)}}{\partial T^2} - \frac{\partial^2\eta_i}{\partial T^2}\right) + (x_i - 1)\left(2\frac{\partial\gamma_i}{\partial T} + T\frac{\partial^2\gamma_i}{\partial T^2}\right)\right] \tag{8}$$

The coefficients of thermal expansion and of isothermal compressibility for the components 1 and 2 are deduced from the equations of definition

$$\alpha_i = \frac{(\partial V_i/\partial T)_P}{V_i} \tag{9}$$

$$\beta_{T_i} = -\frac{(\partial V_i/\partial P)_T}{V_i} \tag{10}$$

The derivatives occurring in the above relations are deduced from the pressure formula, i.e. from the state equation according to the significant structures theory. Starting from the formula $P = -(\partial F_i/\partial V_i)_T$ and taking into account that $x_i = V_i/V_{s_i}$, we obtain

$$P = \frac{RT}{V_{s_i} x_i^2}\left[-2(\sigma_1^{(i)} + \sigma_2^{(i)} - \eta_i) + 2x_i\left(\frac{\partial\sigma_1^{(i)}}{\partial x_i} + \frac{\partial\sigma_2^{(i)}}{\partial x_i}\right) + \gamma_i + \ln\frac{V_{s_i}}{N}\,x_i + x_i\right]. \tag{11}$$

According to whether i is equal to 1 or to 2, two expressions will be obtained, identical as to their form, one of which corresponding to component 1, used in the computations of this component, and another to component 2, necessary in the calculations of component 2. The derivative $(\partial V_i/\partial T)_P$ is calculated indirectly by the relation

$$\left(\frac{\partial V_i}{\partial T}\right)_P = -\left(\frac{\partial P}{\partial T}\right)_{V_i} \Big/ \left(\frac{\partial P}{\partial V_i}\right)_T \tag{12}$$

The previously presented relations, as well as the manner of deducing them, were given in the preceding paper, [1] where we computed the heat capacity, the thermal-expansion coefficient and the isothermal compressibility coefficient of the pure ionic liquids NaCl, NaBr, KCl, KBr. They were resumed here, on the one hand, so as to make unitary the present paper that deals with binary mixtures and, on the other hand, because some changes have intervened in the notations. The necessary parameters for these computations were equally given in the above mentioned paper. [1]

Following the general method for establishing the partition function of a binary system [3,4] we deduce the following expression [5] for the ionic liquids

$$\begin{aligned} Z_{12} = \Bigg\{ & \frac{(X_1+X_2)!}{X_1!\,X_2!} \left(\frac{\exp[(E_s/2RT)\,(V/V_s)^{1/3}}{[1-\exp(-\theta_1/T)]^3} \Bigg\{ 1 + n_h \exp \times \right. \\ & \left. \times \left[- \frac{aE_s\,(V/V_s)^{1/3}}{2n_h\,RT} \right] \Bigg\} \right)^{2X_1 \frac{V_s}{V}} \times \left[\frac{(2\pi\, m_1\, kT)^{3/2}}{h^3}\, \frac{8\pi^2 I_1 kT}{h^2} \times \right. \\ & \left. \times \frac{1}{1-\exp(-h\nu_1/kT)}\, \frac{eV}{N} \right]^{X_1 \frac{V-V_s}{V}} \times \\ & \times \left(\frac{\exp[(E_s/2\,RT)\,(V/V_s)^{1/3}}{[1-\exp(-\theta_2/T)]^3} \Bigg\{ 1 + n_h \exp\left[- \frac{a\,E_s\,(V/V_s)^{1/3}}{2n_h\,RT} \right] \Bigg\} \right)^{2X_2 \frac{V_s}{V}} \times \\ & \times \left[\frac{(2\pi\, m_2\, kT)^{3/2}}{h^3}\, \frac{8\,\pi^2 I_2\, kT}{h^2}\, \frac{1}{1-\exp(-h\nu_2/kT)}\, \frac{eV}{N} \right]^{X_2 \frac{V-V_s}{V}} \end{aligned} \tag{13}$$

where $n_h = n\,\dfrac{V-V_s}{V}$, while X_1 and X_2 are the molar-fractions of the two components.

The expression of the binary partition function contains the parameters of the two component liquids, as well as the characteristic parameters of the mixture. They are E_s, V_s, V, a and n. The volume V is calculated with density data of the mixture, while the other parameters are calculated with the aid of the following formula

---

[5] R. Vîlcu and C. Misdolea, *J. Chem. Phys.*, **45**, 3414 (1966).

$$E_s = (X_1 \sqrt{E_{s_1}} + X_2 \sqrt{E_{s_2}})^2$$

$$V_s = (X_1 \sqrt[3]{V_{s_1}} + X_2 \sqrt[3]{V_{s_2}})^3$$

$$a = X_1 a_1 + X_2 a_2$$

$$n = X_1 n_1 + X_2 n_2$$

From the partition function (13) we deduce the Helmholtz free energy of the binary system

$$F_{12} = - RT \ln Z_{12} = - RT \left[\ln \frac{(X_1 + X_2)!}{X_1 !\, X_2 !} + \frac{2}{x} (\sigma_1 + \sigma_2) - \right.$$

$$\left. - \frac{2}{x} (X_1 \eta_1 + X_2 \eta_2) + \left(1 - \frac{1}{x}\right) \left(X_1 \gamma_1 + X_2 \gamma_2 + \ln \frac{V_s}{N} x + 1\right)\right] \tag{14}$$

where $x = V/V_s$.

The following notations were adopted

$$\sigma_1 = \frac{E_s}{2RT} x^{1/3} \tag{15}$$

$$\sigma_2 = \ln \left[1 + n(x-1) \exp\left(- \frac{aE_s}{2n\,RT} \frac{x^{1/3}}{x-1}\right)\right] \tag{16}$$

Quantities σ_1 and σ_2 are characteristic of the mixtures while the other quantities γ_1, γ_2, η_1 and η_2 are characteristic of the components.

The heat capacity at constant volume is obtained by the same method as in the case of the components, from internal energy

$$U = RT^2 \left(\frac{\partial \ln Z_{12}}{\partial T}\right)_V$$

which has to be derived with regard to the temperature. We obtain

$$C_V = \frac{RT}{x}\left\{4\left[\frac{\partial\sigma_1}{\partial T}+\frac{\partial\sigma_2}{\partial T}-\left(X_1\frac{\partial\eta_1}{\partial T}+X_2\frac{\partial\eta_2}{\partial T}\right)\right]+\right.$$

$$+\,2T\left[\frac{\partial^2\sigma_1}{\partial T^2}+\frac{\partial^2\sigma_2}{\partial T^2}-\left(X_1\frac{\partial^2\eta_1}{\partial T^2}+X_2\frac{\partial^2\eta_2}{\partial T^2}\right)\right]+ \tag{17}$$

$$\left.+\,(x-1)\left[2\left(X_1\frac{\partial\gamma_1}{\partial T}+X_2\frac{\partial\gamma_2}{\partial T}\right)+T\left(X_1\frac{\partial^2\gamma_1}{\partial T^2}+X_2\frac{\partial^2\gamma_2}{\partial T^2}\right)\right]\right\}$$

The thermal-expansion coefficient and the isothermal compressibility are deduced from the following relations

$$\alpha = \frac{(\partial V/\partial T)\;P}{V} \tag{18}$$

$$\beta_T = -\,\frac{(\partial V/\partial P)_T}{V} \tag{19}$$

As in the case of the components, the derivatives from relations (18) and (19) shall be obtained by means of the pressure formula

$$P = -\,(\partial F_{12}/\partial V)_T = \frac{RT}{V_s\,x^2}\left[-\,2\,(\sigma_1+\sigma_2)+2x\left(\frac{\partial\sigma_1}{\partial x}+\frac{\partial\sigma_2}{\partial x}\right)+\right. \tag{20}$$

$$\left.+\,2\,(X_1\,\eta_1+X_2\,\eta_2)+(X_1\gamma_1+X_2\gamma_2)+\ln\frac{V_s}{N}\,x+x\right]$$

The derivative $(\partial V/\partial T)_P$ is obtained in the same way as (12)

$$\left(\frac{\partial V}{\partial T}\right)_P = -\left(\frac{\partial P}{\partial T}\right)_V \Bigg/ \left(\frac{\partial P}{\partial V}\right)_T \tag{21}$$

RESULTS

Computations were made for systems with a common cation K(Cl—Br) and Na(Cl—Br) as well as for the system with a common anion Cl(Na—K). In order to follow the variation with the temperature of the computed quantities, three temperatures were considered, namely 1073 K, 1173 K and 1273 K. The molar fractions, with which the computations were made, were determined with the aid of the data available for the densities.[6-8]

Formula (17) gave the heat capacities at a constant volume. For the Na(Cl—Br) system they are to be found in table 1. In this table, as in those for other systems, there are equal data concerning the components so as to make the comparations possible. No experimental data concerning C_v are available for the mixtures of ionic liquids. The heat capacities at constant volume are given in table 2 for the K(Cl—Br) system and in table 3 for the Cl(Na—K) system.

Table 1

Heat capacity at constant volume (cal/mole K) for Na(Cl–Br) system

X_{NaCl}	$T = 1073$ K		$T = 1173$ K		$T = 1273$ K	
	Calc	*Exptl* [9]	*Calc*	*Exptl* [9]	*Calc*	*Exptl* [9]
0.0	11.059 [1]	11.900	10.861 [1]	11.800	10.689 [1]	11.700
0.2	11.076	—	10.865	—	10.686	—
0.4	11.100	—	10.877	—	10.694	—
0.5	11.114	—	10.893	—	10.710	—
0.6	11.134	—	10.896	—	10.703	—
0.8	11.171	—	10.911	—	10.706	—
1.0	11.226 [1]	11.700	10.951 [1]	11.400	10.737 [1]	11.300

Table 2

Heat capacity at constant volume (cal/mole K) for the K(Cl–Br) system

X_{KCl}	$T = 1073$ K		$T = 1173$ K		$T = 1273$ K	
	Calc	*Exptl* [9]	*Calc*	*Exptl* [9]	*Calc*	*Exptl* [9]
0.0	11.170 [1]	11.600	10.971 [1]	11.500	10.791 [1]	11.300
0.2	11.180	—	10.975	—	10.792	—
0.4	11.182	—	10.978	—	10.792	—
0.5	11.182	—	10.982	—	10.800	—
0.6	11.188	—	10.986	—	10.804	—
0.8	11.200	—	11.100	—	10.817	—
1.0	11.210 [1]	11.100	11.013	10.900	10.836 [1]	10.800

Table 3

Heat capacity at constant volume (cal/mole K) for the Cl(Na–K) system

X_{NaCl}	$T = 1073$ K		$T = 1173$ K		$T = 1273$ K	
	Calc	*Exptl* [9]	*Calc*	*Exptl* [9]	*Calc*	*Exptl* [9]
0.0	11.213 [1]	11.100	11.013 [1]	10.900	10.836 [1]	10.800
0.2075	11.188	—	10.961	—	10.767	—
0.5123	11.184	—	10.937	—	10.736	—
0.7294	11.206	—	10.944	—	10.736	—
1.0	11.226 [1]	11.700	10.951 [1]	11.400	10.737	11.300

---

[6] I. G. Murgulescu and St. Zuca, *Rev. Roumaine Chim.*, **10**, 129 (1965).

[7] St. Zuca and L. Ionescu-Vasu, *Rev. Roumaine Chim.*, **12**, 1285 (1967).

[8] E. R. van Artsdalen and V. S. Yaffe, *J. Phys. Chem.*, **59**, 118 (1955).

[9] J. O'M Bockris and N. E. Richards, *Proc. Roy. Soc.* (*London*), **A 241**, 44 (1957).

The thermal-expansion coefficient was computed with the aid of formulae (18) and (21). From the density variation with temperature, that is known for all three systems, [6–8] the experimental values of this coefficient can be deduced

$$\alpha = -\frac{1}{\rho}\left(\frac{\partial \rho}{\partial T}\right)_P$$

The excess thermal-expansion coefficient was computed with formula

$$\alpha^E = \alpha - (\ \Phi_1\alpha_1 + \ \Phi_2\alpha_2)$$

where Φ_1 and Φ_2 indicate the volumetric fractions of the two components The results are to be found in tables 4, 5, and 6.

Table 4

Thermal-expansion coefficient for the Na(Cl – Br) system

X_{NaCl}	T = 1073 K				T = 1173 K				T = 1273 K			
	$\alpha \times 10^4$ ($°K^{-1}$)		$\alpha^E \times 10^4$ ($°K^{-1}$)		$\alpha \times 10^4$ ($°K^{-1}$)		$\alpha^E \times 10^4$ ($°K^{-1}$)		$\alpha \times 10^4$ ($°K^{-1}$)		$\alpha^E \times 10^4$ ($°K^{-1}$)	
	Calc	*Exptl*[7]	*Calc*	*Exptl*	*Calc*	*Exptl*[7]	*Calc.*	*Exptl*	*Calc.*	*Exptl*[7]	*Calc.*	*Exptl*
0.0	4.77[1]	3.58	—	—	4.43[1]	3,71	—	—	4.31[1]	3.85	—	—
0.2	4,67	3,59	−0.03	0.02	4.32	3.72	−0.02	0.02	4.20	3.86	−0.01	0.03
0.4	4.62	3.50	−0.04	−0.05	4.21	3.63	−0.03	−0.05	4.08	3.77	−0.03	−0.06
0.5	4.58	3.38	−0.05	−0.16	4.14	3.50	−0.06	−0.18	3.98	3,63	−0.08	−0.19
0.6	4.55	3.52	−0.05	−0.02	4.10	3.65	−0.04	−0.02	3.96	3.78	−0.03	−0.02
0.8	4.50	3.60	−0.03	0.07	4.02	3.73	−0.01	0.08	3.88	3.87	0.01	0.08
1.0	4.47[1]	3.50	—	—	3.91[1]	3.63	—	—	3.74[1]	3.76	—	—

Table 5

Thermal-expansion coefficient for the K(Cl – Br) system

X_{KCl}	T = 1073 K				T = 1173 K				T = 1273 K			
	$\alpha \times 10^4$ ($°K^{-1}$)		$\alpha^E \times 10^4$ ($°K^{-1}$)		$\alpha \times 10^4$ ($°K^{-1}$)		$\alpha^E \times 10^4$ ($°K^{-1}$)		$\alpha \times 10^4$ ($°K^{-1}$)		$\alpha^E \times 10^4$ ($°K^{-1}$)	
	Calc	*Exptl*[6]	*Calc*	*Exptl*	*Calc*	*Exptl*[6]	*Calc*	*Exptl*	*Calc*	*Exptl*[6]	*Calc*	*Exptl*
0.0	5.19[1]	4.01	—	—	4.92[1]	4.18	—	—	4.83[1]	4.36	—	—
0.2	5.15	4.05	−0.01	0.09	4.87	4.22	0.001	0.10	4.79	4.40	0.02	0.10
0.4	5.13	4.07	−0.02	0.17	4.83	4.24	0.01	0,18	4,76	4,43	0.05	0.20
0.5	5.13	3.95	−0.01	0.08	4.81	4.12	0.01	0.09	4.71	4.29	0.03	0.10
0.6	5.11	3.95	−0.01	0.11	4.78	4.11	0.01	0.12	4.69	4.28	0.04	0.12
0.8	5.08	3.88	−0.02	0.11	4.71	4.04	0.002	0.12	4.61	4.21	0.02	0.13
1.0	5.06[1]	3.70	—	—	3.84	3.84	—	—	4.51[1]	4.00	—	—

Table 6

Thermal-expansion coefficient for the Cl(Na – K) system

X_{NaCl}	T = 1073 K				T = 1173 K				T = 1273 K			
	$\alpha \times 10^4$ ($°K^{-1}$)		$\alpha^E \times 10^4$ ($°K^{-1}$)		$\alpha \times 10^4$ ($°K^{-1}$)		$\alpha^E \times 10^4$ ($°K^{-1}$)		$\alpha \times 10^4$ ($°K^{-1}$)		$\alpha^E \times 10$ ($°K^{-1}$)	
	Calc	*Exptl.*[8]	*Calc*	*Exptl.*	*Calc*	*Exptl*[8]	*Calc*	*Exptl*	*Calc*	*Exptl*[8]	*Calc*	*Exptl*
0.0	5.06[1]	3.86	—	—	4.65[1]	4.03	—	—	4.51[1]	4.20	—	—
0.2075	4.99	3.88	0.02	0.08	4.54	4.04	0.01	0.08	4.43	4.21	0.04	0.09
0.5123	4.80	3.73	0.003	0.04	4.30	3.88	−0.02	0.03	4.16	4.03	−0.01	0.03
0.7294	4.65	3.64	−0.02	0.03	4.11	3.78	−0.04	0.03	3.95	3.92	−0.04	0.03
1.0	4.47[1]	3.49	—	—	3.91[1]	3.61	—	—	3.74[1]	3.75	—	—

No experimental data are available for the isothermal compressibility. The speed of the ultrasounds in the component liquids as well as in their binary mixtures allows to compute the adiabatic compressibility.[10,11] The theoretical data concerning this coefficient are computed with the formula

$$\beta_s = \frac{\beta_T}{\gamma} \tag{22}$$

where $\gamma = C_p/C_v$, while for C_p we have the relation

$$C_p = C_v + \frac{\alpha^2 VT}{\beta_T} \tag{23}$$

The excess adiabatic compressibility is

$$\beta_s^E = \beta_s - (\Phi_1 \beta_{s_1} + \Phi_2 \beta_{s_2})$$

The results concerning K(Cl—Br) and Cl(Na—K) systems are registered in tables 7 and 8.

No experimental data concerning the Na(Cl—Br) system are available for β_T nor for β_s. The theoretical results are registered in table 9.

DISCUSSIONS

The examination of the computation results for the heat capacities at constant volume shows that the significant structures theory leads to results in good concordance with the experimental data. The variation

---

[10] S. Sternberg and V. Vasilescu, *Rev. Roumaine Chim.*, **12**, 1187 (1967).

[11] S. Sternberg and V. Vasilescu, *Rev. Roumaine Chim.*, **15**, 1665 (1970).

Table

Isothermal and adiabatic compressibility

X_{KCl}	T = 1073 K						T =	
	$\beta_T \times 10^{12}$ (cm²/dyn)		$\beta_s \times 10^{12}$ (cm²/dyn)		$\beta_s^E \times 10^{12}$ (cm²/dyn)		$\beta_T \times 10^{12}$ (cm²/dyn)	
	Calc	*Exptl* [9]	*Calc*	*Exptl* [10]	*Calc.*	*Exptl*	*Calc*	*Exptl* [9]
0.0	29.37[1]	43.80	13.32	31.48	—	—	32.50[1]	52.10
0.2	27.91	—	12.60	30.29	−0.16	−0.31	30.87	—
0.4	26.61	—	11.96	29.43	−0.21	−0.23	29.39	—
0.5	26.10	—	11.70	29.17	−0.16	−0.01	28.57	—
0.6	25.44	—	11.38	—	−0.16	—	27.78	—
0.8	24.06	—	10.71	27.54	−0.17	−0.08	26.08	—
1.0	22.97[1]	38.40	10.16	26.50	—	—	24.51[1]	45.70

Table

Isothermal and adiabatic compressibility

X_{NaCl}	T = 1073 K						T =	
	$\beta_T \times 10^{12}$ (cm²/dyn)		$\beta_s \times 10^{12}$ (cm²/dyn)		$\beta_s^E \times 10^{12}$ (cm²/dyn)		$\beta_T \times 10^{12}$ (cm²/dyn)	
	Calc	*Exptl* [9]	*Calc*	*Exptl* [11]	*Calc*	*Exptl*	*Calc*	*Exptl* [9]
0.0	22.97[1]	38.40	10.51	26.48	—	—	24.51[1]	45.70
0.2075	22.00	—	9.89	26.71	−0.13	1.17	23.53	—
0.5123	19.80	—	9.15	25.21	−0.07	1.25	20.89	—
0.7294	17.93	—	8.43	23.41	−0.13	0.73	18.73	—
1.0	15.86[1]	28.70	7.61	20.82	—	—	16.42[1]	33.80

with temperature is also correctly represented : the computations show, moreover, a diminution with the temperature as is also observed experimentally. In all three systems, however, at all temperatures, the computed C_v increases for the component for which the experimental data indicate a diminution. No experimental data of the heat capacities are yet available for the binary systems of ionic liquids. The thermal expansion coefficient does not offer such a good concordance as that of the heat capacities, particularly at 1073 K temperature. It is though satisfactory, especially at higher temperature; so, at 1273 K, the concordance is good and sometimes even quite good. But this good concordance is due to the fact that the initial computed values, higher than the experimental ones, diminish with temperature, while the experimental values increase with temperature, so that at 1273 K they are near enough to one another. For α^E, the concordance is no more good even at 1273 K. But in this case, the magnitude order being 10^{-6} against 10^{-4} for α, the experimental values can be strongly influenced by the errors appearing at the determination of the density. Isothermal as well as adiabatic compressibility show a distinct non-concordance with the experimental data. For the isothermal compressibility, the computed data are hardly higher

for the K(Cl−Br) system

= 1173 K				*T* = 1273 K					
$\beta_s \times 10^{12}$ (cm^2/dyn)		$\beta_s^E \times 10^{12}$ (cm^2/dyn)		$\beta_T \times 10^{12}$ (cm^2/dyn)		$\beta_s \times 10^{12}$ (cm^2/dyn)		$\beta_s^E \times 10^{12}$ (cm^2/dyn)	
Calc	*Exptl*[10]	*Calc*	*Exptl*	*Calc*	*Exptl*[9]	*Calc*	*Exptl*[10]	*Calc*	*Exptl*
15.22	36,78	—	—	37.06[1]	62.10	17.61	43.28	—	—
14.43	35.34	−0.11	−0.39	35.33	—	16.74	41.59	−0.05	−0.43
13.71	34.58	−0.12	−0.03	33.75	—	15.96	40.98	0.03	0.32
13.32	34.30	−0.14	−0.27	32.51	—	15.39	40.72	−0.09	0.76
12.94	—	−0.13	—	31.61	—	14.95	—	−0.06	—
12.14	32.01	−0.12	−0.15	29.57	—	13.99	37.50	−0.04	−0.21
11.39	30.82	—	—	27.41[1]	54.70	12.99	36.08	—	—

8

for the Cl(Na−K) system

= 1173 K				*T* = 1273 K					
$\beta_s \times 10^{12}$ (cm^2/dyn)		$\beta_s^E \times 10^{12}$ (cm^2/dyn)		$\beta_T \times 10^{12}$ (cm^2/dyn)		$\beta_s \times 10^{12}$ (cm^2/dyn)		$\beta_s^E \times 10^{12}$ (cm^2/dyn)	
Calc	*Exptl*[11]	*Calc*	*Exptl*	*Calc*	*Exptl*[9]	*Calc*	*Exptl*[11]	*Calc*	*Exptl*
11.39	30.87	—	—	27.41[1]	54.70	12.97	36.23	—	—
11.22	31.15	0.30	1.47	26.72	—	12.98	36.19	0.53	1.45
10.32	29.21	0.20	1.51	23.55	—	11.91	34.19	0.35	1.96
9.47	26.84	0.01	0.77	21.01	—	10.90	31.01	0.07	0.84
8.52	23.72	—	—	18.34[1]	40.00	9.79	27.18	—	—

Table 9

Isothermal compressibility $\beta_T \times 10^{12}$ (cm^2/dyn) for the Na(Cl−Br) system

X_{NaCl}	*T* = 1073 K		*T* = 1173 K		*T* = 1273 K	
	Calc	*Exptl*[9]	*Calc*	*Exptl*[9]	*Calc*	*Exptl*[9]
0.0	22.46[1]	33.60	24.27[1]	38.60	27.23[1]	44.90
0.2	21.05	—	22.65	—	25.46	—
0.4	19.75	—	21.02	—	23.50	—
0.5	19.02	—	20.01	—	22.16	—
0.6	18.32	—	19.40	—	21.71	—
0.8	17.11	—	18.06	—	20.34	—
1.0	15.86[1]	28.70	16.42[1]	33.80	18.33[1]	40.00

than the half of the experimental data, while for the adiabatic compressibility, the non-concordance is still greater. The variation with temperature is however correctly represented. The computed data indicate an increase with the temperature and the experimental ones confirm it. In the computation of the heat capacity at constant volume, only the derivatives of the various parts of the partition function with regard to the temperature appear. The good concordance between the theoretical data and the experimental ones indicate that the intervention of the temperature in the expression of the partition function is correct. The disagreement between the theoretical values of the isothermal and adiabatic compressibility – in the expressions of which appears the derivative of the partition function with regard to the volume – and the experimental values, shows that the partition function has no formulation able to reflect correctly enough the structure of the liquid.

Revue Roumaine de Chimie, **18**, *3*, 399–404 (1973)

INFLUENCE OF ALKALINE CATIONS ON THE SENSITIVITY OF THE PHOTOTROPIC GLASSES WITH AgCl

P. BALTĂ * and L. DOLLINGHER **

* Polytechnic Institute, Str. Polizu 1, Bucharest
** Centre of Physical Chemistry, Str. Galaţi 31, Bucharest, Romania

Received September 2, 1972

Continuing the previous investigations, phototropic glasses on B_2O_3 basis have been studied, to which small quantities of alkaline oxides were added. It was established that the sensitivity of the simple phototropic glasses changes inversely proportional with the coordination number of the alkaline cation met in the composition. The phenomenon has been correlated with the influence of the alkaline cations on the separation process of the vitrous microphases. The study of the X-ray fluorescence of silver confirms the hypothesis presented in one of our previous papers, according to which silver chloride and complexes including boron and alkaline cation are met in these glasses under the form of metallic silver.

1. INTRODUCTION

In one of our previous works [1] we have revealed the possibility of outlining the specific influence of the cation in a phototropic glass with maximum simplified composition, when introduced together with the network formator and silver chloride, having in view the possibility of obtaining new data in connection with the mechanism of the process that takes place in the phototropic glasses with AgCl.

We report hereby a new series of results obtained on the same simple B_2O_3 glass following the investigations carried on in this field.

2. EXPERIMENTAL

We have synthetized phototropic glasses having compositions presented in table 1. The mixture of raw material was melted and maintained at 850° for one hour. After that, plates with a thickness of 2 mm have been obtained. The glasses were thermically treated at 250°, 275° and 300° for 15, 30 and 60 minutes to lend them phototropic properties.

---

[1] P. Baltă, L. Dollingher and M. Cîrstea, *Rev. Roumaine Chim.*, **17**, 25 (1972).

Transmission measurements were performed on these samples, in the same way as reported in our previous papers, [2,3] depending on the duration of ultraviolet irradiation, also recording the X-ray fluorescence spectra of silver.

Table 1

Synthesized glasses of (% molar) composition: M_2O = 2.28%; AgCl = 0.675%; B_2O_3 = 97.045%

Composition of raw material mixture (g)	Glass				
	19	20	15	16	17
$B(OH)_3$	200	—	—	—	—
B_2O_3	—	98	95.59	93.28	90.14
$AgNO_3$	1.7	1.66	1.62	1.59	1.53
HCl (conc)	10 cc	—	—	—	—
NaCl	—	3.82	—	—	—
KCl	—	—	4.81	—	—
RbCl	—	—	—	7.66	—
CsCl	—	—	—	—	9.64

3. RESULTS AND DISCUSSIONS

As the sensitivity of these glasses to ultraviolet radiations, as well as the thermal fading rate, are influenced by previous thermal treatments, as can be seen in figure 1 for the case of glass containing Na_2O, all samples were submitted to the same thermal treatment: 30 minutes at 275°.

The measurement results of the transmission changes, depending on the duration of the ultraviolet irradiation of constant intensity, are presented in figure 2.

An order of the obtained curves according to the alkaline cation contained is noticed. The most sensitive is the glass not containing alkaline cations (glass 19, table 1) but which, owing to the mixture of raw materials and to the melting conditions, contains hydrogen. After 420 seconds of irradiation, the transmission of this glass decreases to about 42%, as compared with the initial one considered 100%. The cesium glass has the lowest sensitivity, its transmission decreasing to about 70%, after the same period of irradiation.

A very interesting fact, namely that the variation of the equilibrium transmission (after 420 seconds of irradiation) is directly proportional to the coordination number of the contained cations is presented in figure 3.

The sensitivity of the respective glass decreases depending on the increase of the coordination number. This correlation suggests the idea that the sensitivity decrease could be determined by a separation tendency

---

[2] P. BALTĂ, E. BALTĂ and L. DOLLINGHER, *Rev. Roumaine Chim.*, **16**, 1315 (1971).

[3] P. BALTĂ and E. BALTĂ, "Introducere în chimia fizică a stării vitroase", Ed. Acad., București, 1971.

of the vitrous microphases. Concurrently with the rise of the coordination number, it is possible that the Cl⁻ ion contained in the alkaline chloride should be kept to a greater extent in the coordination sphere of the respective cation, and, consequently, the silver halide should hardly separate as big enough grains.

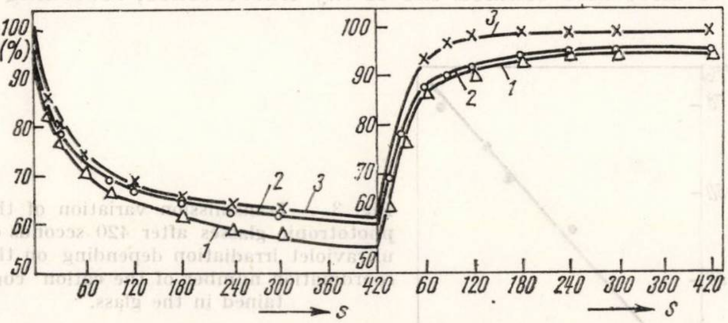

Fig. 1. — Colouring curves at irradiation with UV rays (a) and fading when heating at 200° (b) of phototropic glass No. 20 (Table 1) containing Na⁺ ions, thermically treated before irradiation, in the following conditions :
1) 15 min at 275°; 2) 30 min at 275°; 3) 60 min at 275°.

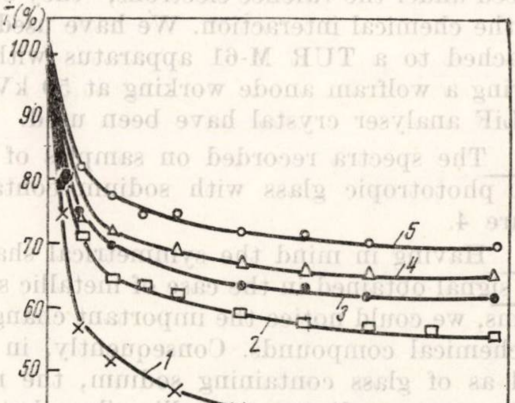

Fig. 2. — Transmission variation of the phototropic glass samples with different cations, when irradiated with ultraviolet rays :
1) glass 19; 2) glass 20; 3) glass 15; 4) glass 16; 5) glass 17, from Table 1.

Taking into account the fact that the number of alkaline cations is the same for all glasses, it is natural that this tendency should grow concurrently with the coordination number.

As a matter of fact it is known that the separation tendency of the vitrous microphases decreases from the glasses containing Na_2O to those containing K_2O, Rb_2O and Cs_2O. If the electromicroscopical pictures confirm this theory, it will allow to prove scientifically the mechanism by which the network modifier cations affect the properties of the phototropic glasses containing AgCl.

For obtaining information regarding the existence of silver in these glasses, we have also studied the X-ray fluorescence, recording the $K_3\beta_2$ peak of silver from $\lambda = 1458$ Å representing the behaviour of the electrons placed under the valence electrons,[4] they being strongly enough influenced by the chemical interaction. We have used a HZG 1 RFA 1 spectrometer attached to a TUR M-61 apparatus with a FS 35 Ö fluorescence tube having a wolfram anode working at 50 kV tension and 20 mA intensity. A LiF analyser crystal have been used.

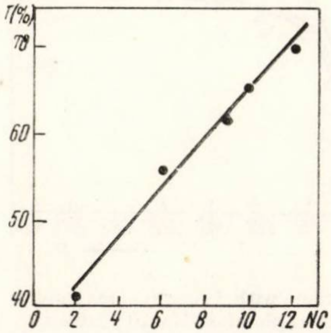

Fig. 3. — Transmission variation of the phototropic glasses after 420 seconds of ultraviolet irradiation depending on the coordination number of the cation contained in the glass.

The spectra recorded on samples of metallic silver, silver chloride and phototropic glass with sodium containing silver are presented in figure 4.

Having in mind the symmetrical shape and the high amplitude of the signal obtained in the case of metallic silver, not influenced by foreign atoms, we could notice the important changes appeared in silver occurring in chemical compounds. Consequently, in the case of silver chloride as well as of glass containing sodium, the maximum of 21°15′ is noticed again corresponding to metallic silver but it is also noticed a widening of the band to the angles with higher values.

Ligand field greatly influences the properties of the transitional ions.

The fluorescence emission is therefore expected to differ from that of the pure metal in case of Ag^+ ion surrounded by Cl^- ions. Consequently, the second emission maximum of AgCl occurred at 21°30′ can be supposed to correspond to silver bound as AgCl. The occurrence of metallic silver in AgCl is not suprising, taking into account the fact that it decomposes easily in the presence of light, and it has been exposed to X-rays during the experimental.

---

[4] K. SAGEL, "Tabellen zur Röntgen Emision und Absorbtion Analyse", Springer Verlag, Berlin, 1959.

In the spectrum recorded on the phototropic glass we could notice a prominent peak corresponding to metallic silver, a lower peak in the position of AgCl and a third one at 21°45′ that could be assigned to Ag partially or totally surrounded by oxygen ions, namely occurred under the form of silver borate or as sodium and silver borate or chloroborate, as reported in one of our previous papers.[1]

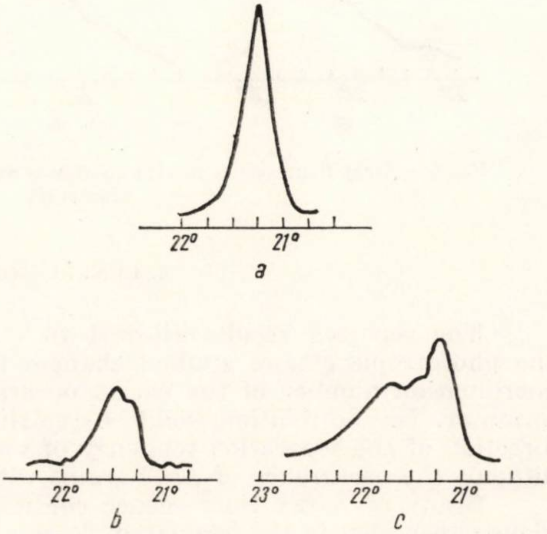

Fig. 4. — Line $K_3\beta_2$ met in the X-ray fluorescence spectrum of metallic silver (a), of silver contained in silver chloride (b), and in the phototropic glass with-sodium(c).

The widening of this band exceeding 22° seems to confirm the presence of a series of complexes in which the ligand properties influenced by boron and sodium change to a sufficient extent for justifying the widening of the emitted band.

It can be noticed the fact that the direction of the ligand field influence is the same as in the case of charge transfer.[3]

The intensity rise of the ligand field from chlorine to oxygen brings about a shifting of the emission maximum to lower energies.

The presence in the second coordination sphere of alkaline ions (in the case of complexes) brings about a new rise of the ligand field because of a rise of their polarizability and, consequently, the widening of the emitted band to longer wavelengths.

In figure 5 it is ascertained that the general aspect of the recorded spectra remains the same in the case of all glasses containing alkaline ions. It is nevertheless noticed a general decrease of intensity from the glass containing sodium to that with cesium.

It is possible that this effect should be correlated with the decrease of the concentration of fluorescence centres because of silver dispersion, that, as we have previously reported, increases in the same direction.

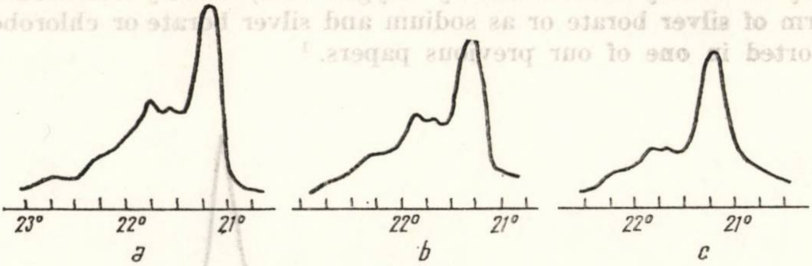

Fig. 5. — X-ray fluorescence spectra on glasses with sodium (a), potassium (b), and cesium (c).

4. CONCLUSIONS

The reported results allowed to establish that the sensitivity of the phototropic glasses studied changes inversely proportional with the coordination number of the cation occurring together with the network formator. This correlation could be explained by the decrease in the same direction of the separation tendency of vitrous microphases, making more difficult the occurrence of AgCl grains with big enough dimensions.

Study of X-ray fluorescence confirms the idea, reported in a previous paper, that in the irradiated glasses, silver occurs, from the chemical point of view, in three states : as metallic silver, silver chloride and under the form of complexes as silver borates or chloroborates, or double borates of silver and sodium.

The above data represent a contribution to a more profound and accurate understanding of the phototropic glasses structure and of the mechanism of the occurring processes.

Revue Roumaine de Chimie, **18**, 3, 405-416 (1973)

NEW COMPOUNDS OF YTTRIUM AND LANTHANIDES WITH DERIVATIVES OF ANTHRANILIC ACID. I

THE N,N BIS (CARBOXY METHYL) ANTHRANILIC ACID (ANDA)

P. SPACU and EUGENIA IVAN

Research Center of Physical Chemistry
Str. Dumbrava Roşie, 23, Bucharest, Romania

Received October 2, 1972

New compounds of yttrium and lanthanides were synthetized with N,N bis (carboxy methyl) anthranilic acid (ANDA) having the general formula : [Ln ANDA] · $3H_2O$; Ln = La, Ce, Pr, Nd, Sm, Eu, Gd, Tb, Dy, Ho, Er, Yb and Y. They are also chemically characterized by electronic spectra in ultraviolet and visible ranges, IR spectra and Debyegrams, to characterize the chemical bonding of these compounds and to suggest a structural formula.

There are rather few published papers on the synthesis of the compounds with carboxy methyl derivatives of anthranilic acid.

Young *et al*[1] giving a series of values for the stability of the complexes of bivalent metals with anthranilic acid and its derivatives, shows the attaching effect of acetic groups to amino nitrogen on the stability, as reflected in the sequence : anthranilic acid < anthranilic monochloroacetic acid < anthranilic diacetic acid. This may be due to the fact that the number of chelate rings increases as the carboxy methyl groups are introduced step by step to anthranilic acid.

The N,N bis (carboxy methyl) anthranilic acid (ANDA) belongs to the class of complexons derivated from monoamine, having a betainic structure in solution :

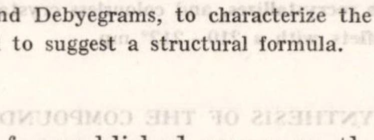

(1)

---

[1] A. Young and T. R. Sweet, *J. Am. Chem. Soc.*, **80**, 800 (1958).

According to the kind of metallic ions, ANDA may behave as a tridentate ligand, as well as a quadridentate one. [2-8]

In the present paper we have studied the compounds formed by ANDA with trivalent ions of yttrium and lanthanides.

A compound of lanthanum with ANDA corresponding to the formula : La ANDA.4 H_2O was isolated from 95% Et OH, [4] but appears as a very hygroscopic compound.

EXPERIMENTAL

MATERIALS

The chlorides and nitrates of yttrium and the lanthanides were obtained from the respective oxides Johnson-Mathey of 99.9% purity, excepting Eu_2O_3 — of 98% purity, by processing with diluted 1 : 1 chlorhydric acids, respectively nitric acid, Merck.

The N,N bis (carboxy methyl) anthranilic acid or anthranil diacetic acid (ANDA), $C_{11}H_{11}NO_6$, was synthetized making use of the directives found in literature [1,8] in the following way : the mixture of anthranilic and monochloracetic acids, in a 1 : 3 ratio is passed into a neutral solution of NaOH—2n and anhydrous Na_2CO_3 is refluxed for 3 hours, continuously correcting the pH at 7. By acidulation and boiling with HCl (at pH = 2) it precipitates the anthranil diacetic acid, which recrystallizes, and colourless crystalls are obtained in the form of unfluorescent brilliant leaflets with a 210—212° mp.

SYNTHESIS OF THE COMPOUNDS

The lanthanide compounds with ANDA were obtained in two ways :

1) To a solution (0.04 M) lanthanide or yttrium chloride 50 ml with a pH = 4.5—5.5 (according to the lanthanide) is added 50 ml of the reactive obtained in the following way : 5 g of ANDA are dissolved in NH_4OH—2n, and heated to remove the excess of ammonia. The solution is filtered, 20 ml of ethanol are added and one completes with water in a calibrated flask of 500 ml (pH = 4.5). The pH of the solutions mixture falls to 3, and the precipitation takes place in time. The alcohol favours the apparition and agglomeration of the precipitate, but the precipitates obtained are gelatinous and the yield in the compound is low.

2) 0.5 g of ANDA are solved (heated) in 25 ml of water (pH = 2) and the lanthanide chloride solution is added (0.3 g $LnCl_3$ aq in 25 ml water). The ratio ANDA : Ln = 1 : 1. After 15 minutes of heating on a water bath, by stirring there appears a crystalline precipitate which during one hour is enriched and deposited.

---

[2] T. Tomita, E. Kyuno and R. Tsuchiya, *Bull. Chem. Soc. Japan*, **42**, 947 (1969).

[3] C. Drăgulescu, T. Simonescu and R. Anton, *Studii și cercetări St. Chim. Timișoara*, VI (1—2), 21 (1959).

[4] C. Drăgulescu, T. Simonescu, I. Menessy and R. Anton, *Studii și Cercetări St. Chim. Timișoara* *VIII* (1—2), 9 (1961).

[5] C. Drăgulescu, R. Pomoje and I. Menessy, "Omagiu Raluca Ripan", 225 (1966).

[6] C. Drăgulescu, S. Policec and T. Simonescu, *Talanta*, **13**, 1451, 1543 (1966); **17**, 557 (1970).

[7] C. Drăgulescu, I. Menessy, M. Pîrlea and A. Ferencz, *Bull. Soc. Chim. Fr.* **(1967)**,4740.

[8] C. Drăgulescu, R. Pomoje, I. Menessy and M. Pîrlea, *Rev. Roumaine Chim.*, **15**, 1029, 1543 (1970).

If the ANDA solution is neutralized at pH = 6 – 7 with NH_4OH-2n, the precipitation takes place immediately and quantitatively. The deposited precipitate is filtered, washed with warm water and then with anhydrous ethanol to remove the unreacted ANDA excess.

The substances are dried in free air, at room temperature.

The whole series of compounds with yttrium and the following lanthanides : La, Ce, Pr, Sm, Eu, Gd, Tb, Dy, Ho, Er, Yb were obtained by the second method ; correcting the pH with NH_4OH-2n.

CHEMICAL ANALYSIS

The lanthanide was determined by direct combustion at the respective oxide. N, C, H were determined by microanalysis.

The absorption spectra in ultraviolet for ANDA were carried out for the 10^{-4} M methanol and dioxan solutions (pH = 4) and for aqueous 2.10^{-3} M solutions with pH : 4.5 , 8.2 and 9.3 (in the presence of NH_4OH).

The reflexion spectrum ($\lambda = 250-400$ mm) was measured for the solid ligand in 1 : 4 and 1 : 5 dilutions with MgO.

For all the synthetized compounds we have only measured the reflexion spectra in ultraviolet, in 1 : 5 dilution, and in visible range ($\lambda = 360-1100$ mm) on the substance itself, using MgO for reference.

The reflexion spectra of Pr, Nd, Dy, Ho and Er nitrates were also determined, considered as reference aquo ions.

The measurements on solutions were carried out at a spectrophotometer Carl Zeiss VSU-2 and those on tablets on a spectrophotometer Carl Zeiss VSU-1, having the reflexion device attached.

IR spectra were achieved at a UR-10 spectrophotometer on KBr, tablets in the 400–4000 cm^{-1} field for ANDA and the compound of neodymium with water [Nd ANDA].3 H_2O and without water (heated to 230° – the minimal point on the curve DTA).

The X rays diffraction spectra were achieved at a TUR M-60 apparatus for ANDA and all the compounds by the method of Debye-Scherrer powders. The following radiations were used according to the absorption of lanthanides.

Table 1

Selection of X diffraction conditions for lanthanides

Lanthanide	Radiation	[A°]	Filter
La, Ce, Pr, Nd	Cr K_{α_1}	2.28962	V
Sm	Fe K_{α_1}	1.93597	Mn
Eu, Gd	Co K_{α_1}	1.78892	Fe
Tb, Dy	Ni K_{α_1}	1.65784	Co
Y, Ho, Er, Yb	Cu K_{α_1}*	1.54051	Ni

* Radiation CuK_{α_1} was used for ANDA.

The recording of the films was carried out at a Carl Zeiss microphotometer with a recorder.

For ANDA and the compounds Y, Er and Yb the diffraction spectra were also recorded at a diffractometer HZG-1 (RDG) using the radiation $CuK_{\alpha 1}$.

The conversion of the θ angles into d [A°] was made by means of the tables of A. J. Rose.

RESULTS AND DISCUSSIONS

The results of the chemical analysis are given in table 2.

Table 2

Analytical data

Found	La = 31.85 %	C = 29.69 %	H = 3.60 %	N = 3.17 %
Calculated $LaC_{11}H_8NO_6.3H_2O$	La = 31.35 %	C = 29.81 %	H = 3.18 %	N = 3.16 %
Found	Ce = 31.80 %	C = 29.51 %	H = 3.70 %	N = 3.18 %
Calculated $CeC_{11}H_8NO_6.3H_2O$	Ce = 31.53 %	C = 29.73 %	H = 3.18 %	N = 3.15 %
Found	Pr = 31.80 %	C = 29.93 %	H = 3.52 %	N = 3.00 %
Calculated $PrC_{11}H_8NO_6.3H_2O$	Pr = 31.66 %	C = 29.68 %	H = 3.17 %	N = 3.14 %
Found	Nd = 32.34 %	C = 29.10 %	H = 3.48 %	N = 2.88 %
Calculated $NdC_{11}H_8NO_6.3H_2O$	Nd = 32.16 %	C = 29.46 %	H = 3.15 %	N = 3.13 %
Found	Sm = 32.95 %	C = 28.64 %	H = 3.36 %	N = 2.83 %
Calculated $SmC_{11}H_8NO_6.3H_2O$	Sm = 33.07 %	C = 28.96 %	H = 3.10 %	N = 3.08 %
Found	Eu = 33.18 %	C = 28.66 %	H = 3.38 %	N = 2.70 %
Calculated $EuC_{11}H_8NO_6.3H_2O$	Eu = 33.31 %	C = 29.06 %	H = 3.09 %	N = 3.07 %
Found	Gd = 33.89 %	C = 28.54 %	H = 3.32 %	N = 2.73 %
Calculated $GdC_{11}H_8NO_6.3H_2O$	Gd = 34.07 %	C = 28.62 %	H = 3.06 %	N = 3.03 %
Found	Tb = 34.51 %	C = 28.80 %	H = 3.20 %	N = 2.85 %
Calculated $TbC_{11}H_8NO_6.3H_2O$	Tb = 34.31 %	C = 28.46 %	H = 3.04 %	N = 3.02 %
Found	Dy = 34.74 %	C = 28.23 %	H = 3.85 %	N = 2.73 %
Calculated $DyC_{11}H_8NO_6.3H_2O$	Dy = 34.82 %	C = 28.30 %	H = 3.03 %	N = 3.00 %
Found	Ho = 34.89 %	C = 27.57 %	H = 3.14 %	N = 2.68 %
Calculated $HoC_{11}H_8NO_6.3H_2O$	Ho = 35.15 %	C = 28.16 %	H = 3.01 %	N = 2.98 %
Found	Er = 35.60 %	C = 27.54 %	H = 3.05 %	N = 2.70 %
Calculated $ErC_{11}H_8NO_6.3H_2O$	Er = 35.47 %	C = 28.02 %	H = 2.99 %	N = 2.97 %
Found	Yb = 36.21 %	C = 27.64 %	H = 3.55 %	N = 2.67 %
Calculated $Yb\,C_{11}H_8NO_6.3H_2O$	Yb = 36.25 %	C = 27.68 %	H = 2.96 %	N = 2.93 %
Found	Y = 22.38 %	C = 33.23 %	H = 3.74 %	N = 3.45 %
Calculated $YC_{11}H_8NO_6.3H_2O$	Y = 22.61 %	C = 33.61 %	H = 3.59 %	N = 3.56 %

Based on the chemical data it was established that the chemical formula for the synthetized compounds corresponds to the ratio 1:1 Ln/ANDA with $3H_2O$($C_{11}H_8O_6N$ Ln.$3H_2O$). Only in the case of the lanthan compound, synthetized by the first method there is the chemical formula La ANDA.$4H_2O$.

Found: La = 30.60; C = 28.60; H = 3.90%, N = 3.09%

Calculated for $LaC_{11}H_8O_6N$ La = 30.12; C = 28.65; H = 3.49% N = 3.04%.

The compounds obtained are not hygroscopic, are stable in time, and do not melt up to 250—280°.

Regarding the colour, this is in the shade of lanthanides, respectively: white for Y, La, Eu, Gd, Tb, Dy and Yb; cream for Ce, Sm, Ho; light green for Pr; light lavender for Nd and pink for Er.

The solubility of the compounds obtained is very low, less than 10^{-3} M, in the majority of organic solvents. This fact has limited the spectrophotometric study only to measurements on solid substance.

The reflexion spectra of the ligand and their synthetized compounds present 2 maxima each in ultraviolet at:

$\lambda_1 = 355 - 365$ nm
$\lambda_2 = 265 - 268$ nm for ANDA

and

$\lambda_1 = 302 - 306$ nm
$\lambda_2 = 255 - 258$ nm for [Ln ANDA].$3H_2O$

In figure 1 are represented the reflexion spectra in ultraviolet, in 1 : 5 dilution with MgO for ANDA and compounds with Y, La and Ce. The other compounds with lanthanides present similar spectra and the plotting of all the curves on the same figure was impossible.

In the absorption spectra of the ligand in methanol or dioxan, absorption bands are not precisely outlined, and among the absorption spectra in aqueous solutions at different pH 4.5, 8.2, 9.3, figure 1 represents (the dotted line) the spectrum presenting the band at 302 nm.

Between the reflexion spectrum of the ligand and the compounds one notices a difference of 50 nm at the λ_1 band. The band at 302—306 nm appears only in the absorption spectrum of the ligand in solutions with pH > 7. This was interpreted [4] as the possibility of a betanic structure, in which the nitrogen becomes tetracoordinated.

The presence of this band also in the spectra of the studied compounds, is an indication that in the compounds, the nitrogen is tetracoordinated by coordination to the lanthanid ion, and ANDA can then behave as a quadridentate ligand. This fact is fully confirmed by the IR spectra.

In the reflexion spectra in visible range ($\lambda = 360-1100$ nm) shifts were located for certain bands of the compounds with Pr, Nd, Dy, Ho and Er, given the respective aquo ions, towards higher wave lengths.

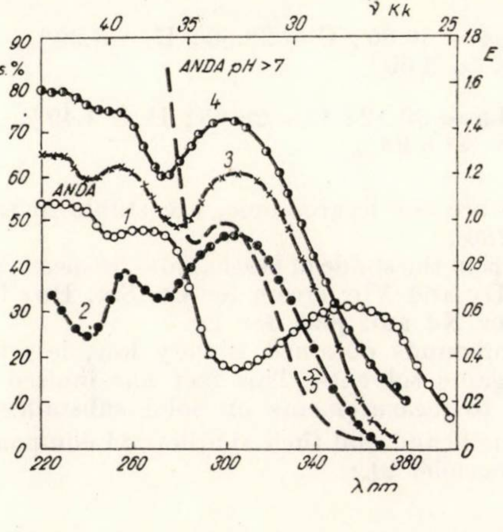

Fig. 1. — Reflexion spectra in ultraviolet in 1/5 dilution with MgO for : *1.* ANDA ; *2.* [Y ANDA]$.3H_2O$; *3.* [La ANDA]$.3H_2O$; *4.* [Ce ANDA]$.3H_2O$ and absorption spectra for *5.* ANDA in aqueous solution, with a pH = 9.3.

From these shifts, the average covalence degrees of the chemical bond were calculated, according to the formula [9] :

$$\delta' = \frac{1-\beta'}{\beta'} . 100 \text{ where}$$

β' = nephelauxetic ratio, and is given by the ratios :

$\beta' = \frac{\beta_{\text{complex}}}{\beta_{\text{aquoion}}} = \frac{\tilde{\nu}_{\text{complex}}}{\tilde{\nu}_{\text{aquoion}}}$ where $\tilde{\nu}_c$ and $\tilde{\nu}_{aq}$ are the wave numbers of the same transitions in the complex and respectively in the aquo ion.

Table 3

Spectral data in visible range for [Pr ANDA] . $3H_2O$

Band assignment	$\tilde{\nu}_{aq}$ cm^{-1}	$\tilde{\nu}_c$ cm^{-1}	β'	δ'
$^3P_2$	22675	22471	0.99100	0.91
$^3P_1$	21459	21321	0.99356	0.65
$^3P_0$	20833	20703	0.99375	0.63
$^1D_2$	17006	16997	0.99829	0.17

S. P. SINHA, *Spectrochim. Acta*, **32**, 57 (1966).

Table 4

Spectral data in visible range for [Nd ANDA] . $3H_2O$

Band assignment	$\tilde{\nu}_{aq}$ cm^{-1}	$\tilde{\nu}_c$ cm^{-1}	β′	δ′
$^2G_{9/2}$	19723	19607	0.99411	0.59
$^4G_{7/2}$	19230	19138	0.99521	0.48
$^4G_{5/2}$	17391	17391	1	0
$^4F_{9/2}$	14925	14814	0.99256	0.75
$^4F_{7/2}$ $^4S_{3/2}$	13698	13605	0.99321	0.68
$^2H_{9/2}$ $^4F_{5/2}$	12738	12658	0.99371	0.63
$^4F_{3/2}$	11695	11627	0.99418	0.58

Table 5

Spectral data in visible range for [Dy ANDA] . $3H_2O$

Band assignment	$\tilde{\nu}_{aq}$ cm^{-1}	$\tilde{\nu}_c$ cm^{-1}	β′	δ′
^4G	27472	27472	1	0
^4G	25835	25773	0.99760	0.24
	22222	22222	1	0
	13333	13333	1	0

Table 6

Spectral data in visible range for [Ho ANDA]. $3H_2O$

Band assignment	$\tilde{\nu}_{aq}$ cm^{-1}	$\tilde{\nu}_c$ cm^{-1}	β′	δ′
$^5G_5$	24096	24038	0.99759	0.24
$^5F_1$	22271	22222	0.99779	0.22
$^5F_3$	20790	20661	0.99379	0.62
$^5F_4$	18691	18621	0.99625	0.37
$^5F_4$	15586	15625	0.99611	0.39

As may be noticed from tables 3—7, the parameter δ′ takes still higher positive values in the case of compounds with Pr and Nd and positive values, but smaller, and even equal to zero for compounds with Dy, Ho and Er. This shows a more marked covalence of the chemical bond in the compounds having for central ion the lanthanide with f^2 (Pr) and f^3 (Nd) then the respective aquo ions, and this covalence decreases, becoming smaller, or even equal for those compounds in which the lanthanide ion has the lager f more completely occupied with electrons.

Table 7

Spectral data in visible range for [Er ANDA] . $3H_2O$

Band* assignment	$\tilde{\nu}_{aq}$ cm^{-1}	$\tilde{\nu}_c$ cm^{-1}	β′	δ′
$^2G_{9/2}$	27548	27472	0.99662	0.34
$^4G_{11/2}$	26455	26455	1	0
$^2H_{9/2}$	24630	24630	1	0
$^4F_{3/2}$	22675	22624	0.99775	0.22
$^4F_{7/2}$	20661	20576	0.99588	0.41
$^2H_{11/2}$	19305	19230	0.99611	0.39
$^4S_{3/2}$	18621	18518	0.99446	0.56
$^4F_{9/2}$	15444	15384	0.99611	0.39

* The assignment of spectral terms was made according to literature.[9,10]

IR spectra for ANDA and the compound [Nd ANDA].$3H_2O$ and the compound dehydrated at 230° [Nd ANDA] are given in figure 2.

The peaks corresponding to the characteristic vibrations in the IR spectra of [Nd ANDA].$3H_2O$ and [Nd ANDA] are summarized in table 8.

Table 8

IR Spectral data

Compound	$\nu_{C=C}$ cm^{-1}	$\nu_{C=O}$ cm^{-1}				ν_{N-H} cm^{-1}	ν_{O-H} cm^{-1}
		Un-ionic	Aryl chelates	COO$^-$ asym.	COO$^-$ sym.		
ANDA	1600—1608	1730	1695	1550—1570 1600—1608	1420 1460	3350	2517—2560
NdANDA.$3H_2O$	1585—1610	—	1610	1550—1565 1590—1610	1418—1422 1458	3500—3200	
Nd ANDA	1590—1610	—	1645 1610	1555—1565 1590—1610	1420—1422 1460	3500—3200	

The assignment was made according to literature.[11,12]

---

[10] N. K. DUTT, A. GUPTA, *J. Inorg. Nucl. Chem.*, 33, 4188 (1971).

[11] L. J. BELLAMY, "The infrared spectra of complex molecules", London Methuen et Co. Ltd., New York, John Wiley et sons. INC, 1959.

[12] NAKAMOTO KAUZO, "Infrared spectra of inorganic and coordination compounds", John Wiley et sons. INC, New York, London, Izdatelsvo "Mir", Moscova, 1966.

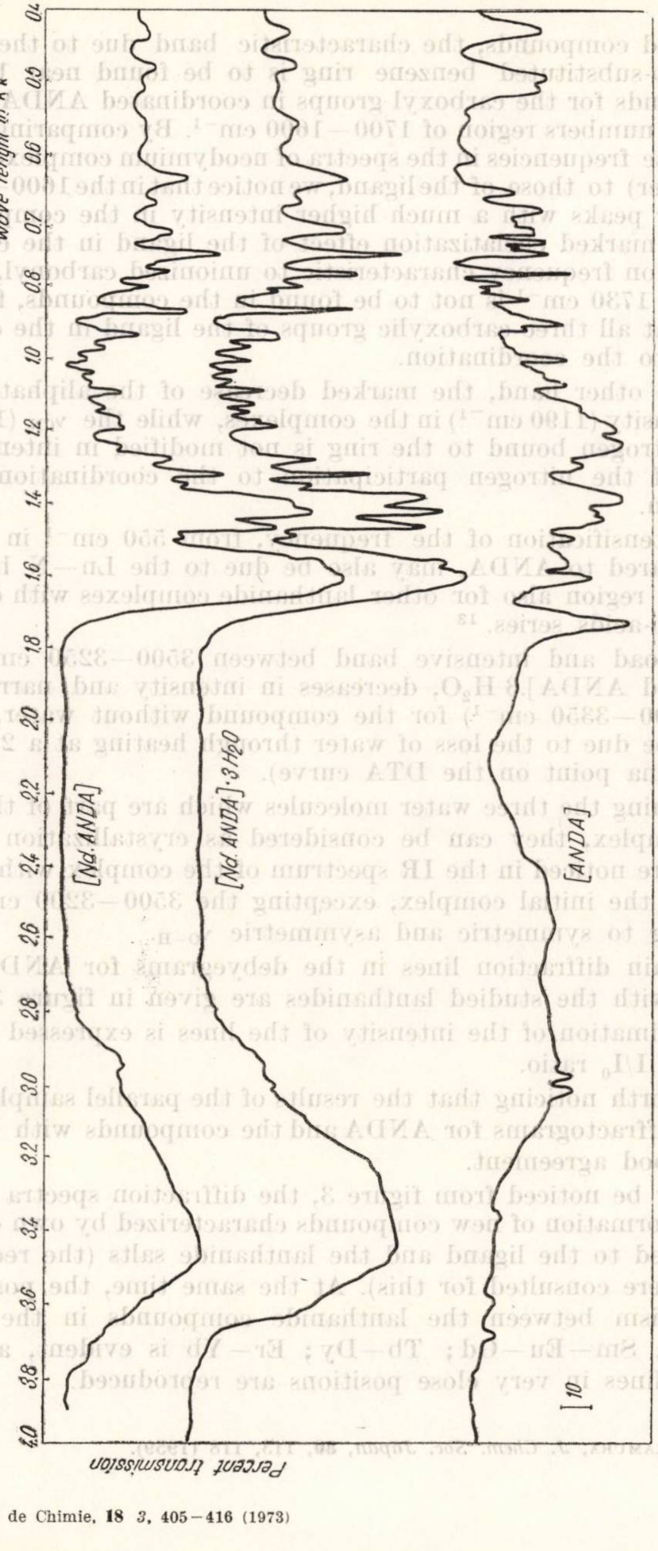

Fig. 2.— IR spectra for ANDA and compounds [Nd ANDA].$3H_2O$ and [Nd ANDA].

In all studied compounds, the characteristic band due to the stretching $\nu_{C=C}$ in *ortho*-substituted benzene ring is to be found near 1600 cm^{-1}, while the bands for the carboxyl groups in coordinated ANDA are shown within wave numbers region of 1700—1600 cm^{-1}. By comparing the intensities of these frequencies in the spectra of neodymium complexes (with, or without water) to those of the ligand, we notice that in the 1600–1700 cm^{-1} there appear peaks with a much higher intensity in the complexes, thus proving the marked chelatization effect of the ligand in the compounds. The absorption frequency characteristic to unionized carbonyl, appearing in ANDA at 1730 cm^{-1} is not to be found in the compounds, from where it results that all three carboxylic groups of the ligand in the compounds participate to the coordination.

On the other hand, the marked decrease of the aliphatic ν_{CN} frequency intensity (1190 cm^{-1}) in the complexes, while the ν_{CN} (1380—1375 cm^{-1}) for nitrogen bound to the ring is not modified in intensity, is an indication of the nitrogen participation to the coordination with the lanthanid ion.

The intensification of the frequency, from 550 cm^{-1} in the complexes compared to ANDA, may also be due to the Ln—N bond, identified in this region also for other lanthanide complexes with derivatives of the amino-acids series. [13]

The broad and intensive band between 3500—3250 cm^{-1} of the spectrum [Nd ANDA].3 H_2O, decreases in intensity and narrows down its field (3500—3350 cm^{-1}) for the compound without water, an effect which may be due to the loss of water through heating at a 230° temperature (minima point on the DTA curve).

Concerning the three water molecules which are part of the initially prepared complex, they can be considered as crystallization water, as no changes are noticed in the IR spectrum of the complex without water, compared to the initial complex, excepting the 3500—3200 cm^{-1} region corresponding to symmetric and asymmetric ν_{O-H}.

The main diffraction lines in the debyegrams for ANDA and its compounds with the studied lanthanides are given in figure 3.

The estimation of the intensity of the lines is expressed in percentages by the I/I_0 ratio.

It is worth noticing that the results of the parallel samples, debyegrams and diffractograms for ANDA and the compounds with Y, Er and Yb are in good agreement.

As may be noticed from figure 3, the diffraction spectra of X rays confirm the formation of new compounds characterized by own diffraction lines compared to the ligand and the lanthanide salts (the record cards of JCPDS were consulted for this). At the same time, the possibility of an isomorphism between the lanthanide compounds in the sequence Ce—Pr—Nd; Sm—Eu—Gd; Tb—Dy; Er—Yb is evident, as a series of intensive lines in very close positions are reproduced.

---

[13] K. Nakamura, *J. Chem. Soc. Japan*, **80**, 113, 118 (1959).

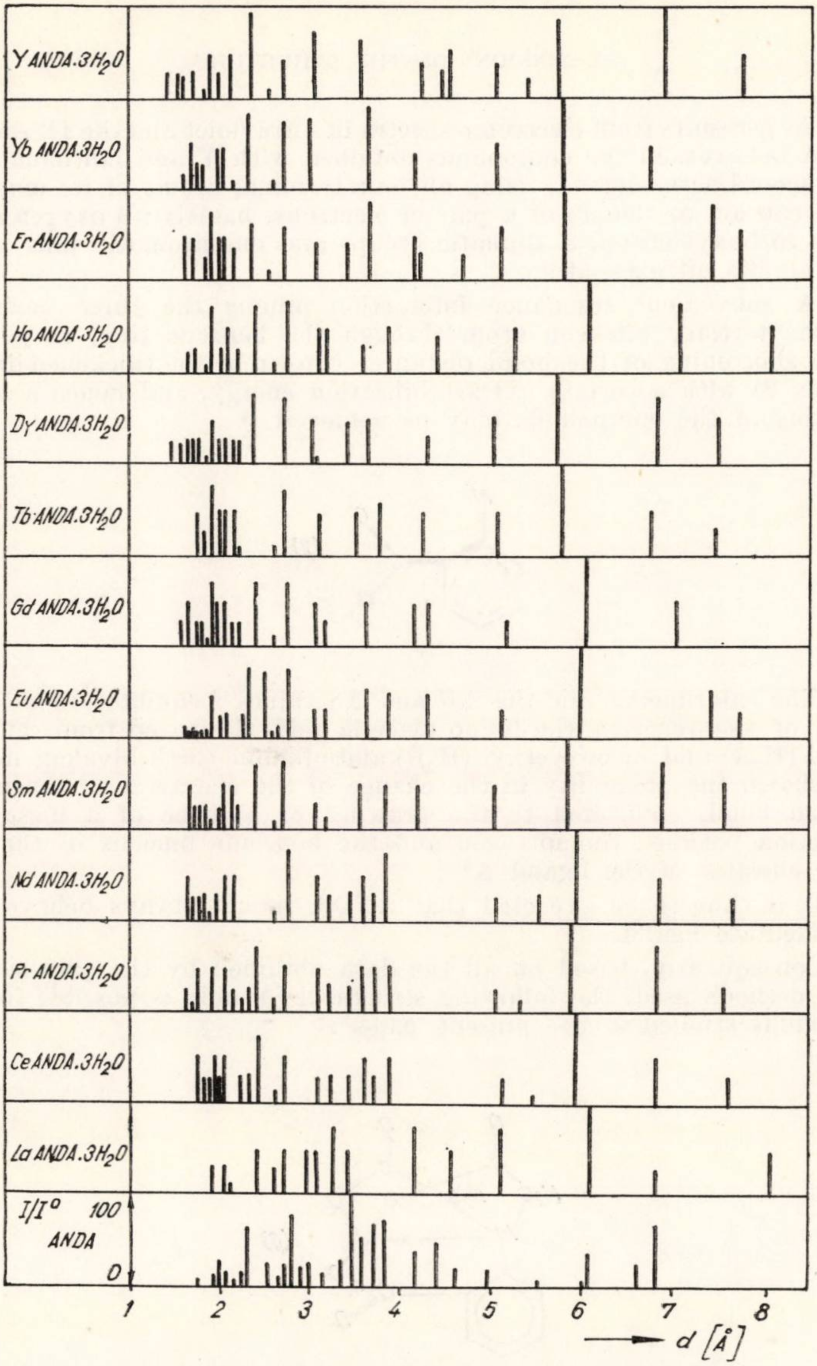

Fig. 3. — Diffraction spectra of X rays for ANDA and compounds [Ln ANDA].$3H_2O$, where Ln = La, Ce, Pr, Nd, Sm, Eu, Gd, Tb, Dy, Ho, Er, Yb and Y.

DISCUSSIONS ON THE STRUCTURE

As it results from electronic spectra in ultraviolet and the IR spectra, ANDA behaves, in the compounds obtained with Y and lanthanides, as a tetracoordinated ligand, using all four terminal atoms of its molecule, which can act as donors of a pair of electrons, namely: 3 oxygen atoms of the carboxyl group, 2 aliphatic groups and one aromatic plus a tertiary aminic nitrogen atom.

A convenient resonance interaction among the three carboxyls and the tertiary nitrogen atom through the benzene ring, may result in the shortening of the bond distances (shown by the thickened lines — formula 2) with a certain extrastabilization energy, and hence a higher chelating of the compounds may be achieved.[14]

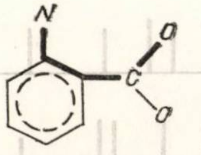

(2)

The calorimetric and the ΔH and ΔS values[15] equilibrium measurements of the reaction the imino diacetic acids derivated from carboxyphenyl (H_3A) and carboxyethyl (H_3B) and alkaline-earth bivalent metals, have shown the possibility in the change of the character of the metal-nitrogen bond, connected to the presence or absence of a mesomeric interaction between the nitrogen and the benzenic nucleus in the case of the chelates of the ligand A^{3-}.

It is thus to be expected that ANDA should always behave as a quadridentate ligand.

Consequently, based on all the data obtained by the physico-chemical methods used, the following structural formula is possible for the compounds studied in the present paper:

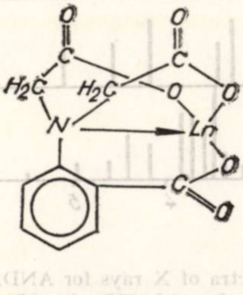

(3)

---

[14] A. E. Martell and M. Calvin, "Chemistry of the metal chelate compounds", New York Prentice Hall INC., New York, 1956, p. 156.

[15] E. Uhling and A. Martin, *J. Inorg. Nuclear. Chem.*, **31**, 2781 (1969).

Revue Roumaine de Chimie, **18**, *3*, 417–424 (1973)

KINETICS AND MECHANISM OF SUBSTITUTION REACTIONS OF COMPLEXES. XLIII*

BASIC HYDROLYSIS OF $[Co(DH)_2(H_2O)(NCS)]$

Z. FINTA, CS. VÁRHELYI and J. ZSAKÓ

Faculty of Chemistry, Chair of Physical Chemistry, Babeş-Bolyai University,
str. Arany János 11, Cluj, Romania

Received August 2, 1972

Synthesis and IR spectrum of $[Co(DH)_2(H_2O)(NCS)] \cdot 2\ H_2O$ are described. In basic solutions a protolytic equilibrium takes place. The acid form undergoes an aquation with $\Delta H_1^{\neq} = 32.4$ *k*cal/mole, presumably by an S_N1 pathway. The basic form participates to an olation reaction with $\Delta H_2^{\neq} = 22.5$ *k*cal/mole presumably on an $S_N^{\neq}2$ pathway. Results are compared with those obtained with the analogous dinitro- and nitro-aquo derivatives.

The aquo-acido-bis-dioximato-cobalt (III) non electrolytic complexes are formed as intermediates during the aquation of $(Co\ (Diox.H)_2X_2]^-$ type complex anions in acid solutions (where Diox. H_2 stands for a molecule of an α-dione-dioxime). Thus, aquation of $(Co\ (DH)_2\ Cl_2]^-$, $[Co(DH)_2Br_2]^-$, $Co(DH)_2I_2]^-$ (DH_2 = dimethylglyoxime) in dilute solutions leads in the first stage to the formation of $(Co(DH)_2(H_2O)Cl]$, $[Co(DH)_2(H_2O)Br]$ and $[Co(DH)_2(H_2O)I]$, respectively. [1–4] These compounds are known also in crystalline state, obtained by heating of aqueous suspensions of the $H[Co(DH)_2X_2]$ type complex acids. [5–6]

Some of the sparingly soluble halogeno-aquo-non-electrolytes are formed as the main product of the oxydation of a mixture of CoX_2, NaX and Diox. H_2, e.g. the following complexes : [Co(Niox. $H)_2(H_2O)Cl]$,[Co(Niox. $H)_2(H_2O)Br]$, [Co(Niox. $H)_2(H_2O)I]$. [7] (Niox. H_2 = cyclohexane diondioxime).

---

* Part XLII : Cs. Várhelyi, J. Zsakó and Z. Finta, *Z. anorg. Chem.*, (1972), in press.

[1] J. Zsakó, Cs. Várhelyi and Z. Finta, *Stud. Univ. Babeş-Bolyai Chem.*, **14**, 17, 51 (1969).

[2] Cs. Várhelyi, Z. Finta and J. Zsakó, *Rev. Roumaine Chim.*, **14**, 1133 (1969).

[3] Z. Finta, J. Zsakó and Cs. Várhelyi, *Z. phys. Chem. (Leipzig)*, **242**, 200 (1969).

[4] A. V. Ablov, *Izvest. Sektora Platiny*, **30**, 67 (1955).

[5] A. V. Ablov and N. M. Samus, *Zhur. neorg. Khim.*, **5**, 852 (1960).

[6] A. V. Ablov and G. P. Syrzova, *Zhur. neorg. Khim.*, **1**, 687 (1956).

[7] L. Szotyori and Cs. Várhelyi, *Veszprémi vegyipari Egy. Közl.*, 1973 (in press).

The analogous α-benzyldioximato derivatives [Co (Diph. H)$_2$–(H$_2$O)Cl], [Co(Diph. H)$_2$(H$_2$O)Br] which are also very sparingly soluble, have been obtained from [Co(Diph. H)$_2$Cl$_2$]$^-$ and [Co(Diph. H)$_2$Br$_2$]$^-$, by treating them with water.[8]

In the case of the [Co(DH)$_2$(H$_2$O)(NCS)] and [Co(DH)$_2$(H$_2$O)(NCSe)] type derivatives of the pseudohalogens, treatment with ammonia of the corresponding bis-dioximato-diacido complexes is necessary.

Thus the above mentioned thiocyanato-non-electrolyte has been obtained by Ablov and co-workers by means of aquation of [Co(DH)$_2$(NO$_2$)(NCS)]$^-$ in dilute ammoniacal solution.[9]

In the present paper [Co(DH)$_2$(H$_2$O)(NCS)]·2 H$_2$O has been synthesized as described in the experimental part. IR spectrum of the complex obtained is given in fig. 1.

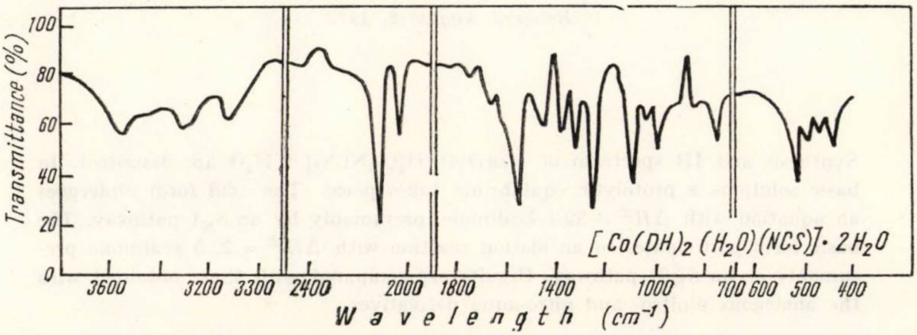

Fig. 1. – IR spectrum of [Co(DH)$_2$(H$_2$O)(NCS)]·2 H$_2$O.

The weak bands characteristic for the short O–H...O hydrogen bridges, observed in the case of [Co(DH)$_2$(amine)$_2$]X[10] and H[Co(DH)$_2$X$_2$][11] type complexes, too, appear at 2360 cm^{-1} (weak) and at 1720–1740 cm^{-1} (weak). These bands plead also in this case for a *trans* geometric configuration. The stretching vibration frequencies $\nu_{C=N}$ and ν_{C-S} characteristic for the coordinated NCS group appear at 2114 (very strong) and 820–830 cm^{-1} (medium), respectively. Their position and intensity is almost the same as in the case of [Co(DH)$_2$(NCS)$_2$]$^-$, i.e. the complex studied is also an isothiocyanato derivative, NCS is linked to Co through the N atom,[11–13] contrary to the thiocyanato complexes of Pt, Pd and Hg.

In acid solutions of [Co(DH)$_2$(H$_2$O)(NCS)] no aquation reaction occurs. In the case of the [Co(DH)$_2$(NCS)$_2$]$^-$ ion only the first NCS$^-$ can be exchanged for water molecules. Even this reaction affords a considerably high activation enthalpy of 32.2 Kcal/mole and leads to an equilibrium shifted towards the dithiocyanatocomplex. The equilibrium constant of reaction

---

[8] A. V. Ablov and G. P. Syrzova, *Zhur. neorg. Khim.*, **7**, 2066 (1962).

[9] A. V. Ablov, N. M. Samus and V. Popov, *Doklady Akad. Nauk. S.S.S.R.*, **106**, 665 (1956).

[10] R. Ripan, Cs. Várhelyi and E. Hamburg, *Stud. Univ. Babeș-Bolyai Chem.*, **9** (2), 33 (1964).

[11] A. Nakahara, *Bull. Chem. Soc. Japan.*, **28**, 473 (1955).

[12] M. Chamberlain and J. C. Bailar, *J. Amer. Chem. Soc.*, **81**, 6412 (1959).

[13] J. Fujita, K. Nakamoto and M. Kobayashi, *J. Amer. Chem. Soc.*, **78**, 3295 (1956).

$$[Co(DH)_2(NCS)_2]^- + H_2O \rightleftarrows [Co(DH)_2(H_2O)(NCS)] + NCS^- \quad (1)$$

is of the order of magnitude of 10^{-5}. [14]

In basic solutions the situation may be fundamentally changed. The aquo-non-electrolytic type complexes $[Co(DH)_2(H_2O)X]$ show the behaviour of weak acids with an acidity constant of about 10^{-7}—10^{-8}. [15-17]

In basic solutions, due to the equilibrium

$$[Co(DH)_2(H_2O)(NCS)] \rightleftarrows [Co(DH)_2(OH)(NCS)]^- + H^+ \quad (2)$$

a complex anion, similar to $[Co(DH)_2(NCS)_2]^-$, appears, which may suffer an aquation. On the other hand, in strongly basic media another protolytic equilibrium takes place, implying the break up of a O—H..O hydrogen bridge, [18] the corresponding acidity constant being of the order of magnitude of 10^{-12}. [16 19]

Presumably, the equilibrium :

$$[Co(DH)_2(OH)(NCS)]^- \rightleftarrows [Co(DH)(D)(OH)(NCS)]^{-2} + H^+ \quad (3)$$

makes easier the liberation of NCS^- ions.

On the basis of the above considerations one can expect the aquation of the complex studied to take place with a measurable rate. Our experiments were consistent with this presumption. By measuring the concentration of the liberated NCS^- ions as function of time, OH^- concentration and temperature, reaction has been observed to be apparently of first order. Logarithmic plot of c_0/c versus time showed a good linearity, as seen from several examples given in fig. 2.

From the slope of the straight lines obtained, apparent first order rate constants k_{exp} have been derived. Results are presented in table 1.

Influence of OH^- concentration on k_{exp} values is completely different from that observed in the case of $[Co(DH)_2(H_2O)(NO_2)]$, where a protolytic equilibrium of the type (3) and the aquation of both forms have been observed. [17] Rate constants k_{exp} presented in table 1 show a nearly linear increase at higher OH^- concentration, and at lower ones they approach a limiting value. This suggests the idea, that reaction (3) plays the part of a pre-equilibrium and the exchange of NCS^- for OH^- takes place with both species I and II, but the pathway of the reaction is different. Species I undergoes an aquation

---

[14] Z. Finta, Cs. Várhelyi and J. Zsakó, *J. Inorg. Nuclear Chem.*, **32**, 3013 (1970).

[15] D. M. Palade, T. N. Voloh, N. A. Breslavskaia and T. N. Golyshina, *Zhur. neorg. Khim.*, **15**, 2698 (1970).

[16] Cs. Várhelyi, J. Zsakó and M. Zsigmond, *Stud. Univ. Babeş-Bolyai, Chem.*, **16** (2), 53 (1971).

[17] J. Zsakó, Z. Finta and Cs. Várhelyi, *J. Inorg. Nuclear Chem.*, **34**, 2887 (1972).

[18] A. V. Ablov and M. P. Filippov, *Zhur. neorg. Khim.*, **5**, 2717 (1960).

[19] J. P. Birk, P. Boon-Chock and J. Halpern, *J. Amer. Chem. Soc.*, **90**, 6959 (1968)

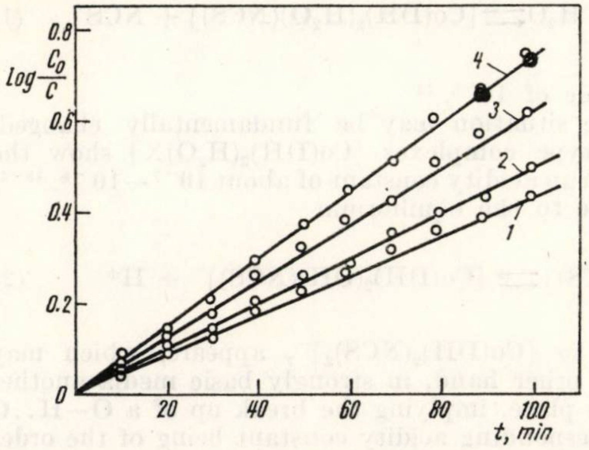

Fig. 2. — Determination of apparent first order rate constants at 40°:

1) $[OH^-] = 0.127$ M; 2) $[OH^-] = 0.215$ M; 3) $[OH^-] = 0.303$ M; 4) $[OH^-] = 0,391$ M.

$$[Co(DH)_2(OH)(NCS)]^- + H_2O = [Co(DH)_2(OH)(H_2O)] + NCS^- \quad (4)$$

Table 1

Apparent first order rate constants of the aquation of $[Co(DH)_2(OH)(NCS)]^-$ ($k_{exp} \times 10^5$)

t° $[OH^-]$ mole/l	18	21	24	25	27	30	35	38	40
0.083	—	—	—	—	—	3.52	7.50	11.8	16.8
0.127	—	—	—	—	—	3.75	7.53	11.8	16.6
0.171	—	—	—	—	—	4.12	8.25	12.7	17.4
0.215	—	—	—	—	—	4.81	9.40	14.2	19.1
0.259	—	—	—	—	—	5.40	10.6	15.7	21.0
0.303	—	—	—	—	—	6.23	12.1	17.8	23.5
0.347	—	—	—	—	—	7.10	13.4	19.7	26.0
0.391	—	—	—	—	—	7.92	15.2	22.0	28.4
0.505	—	—	—	5.67	—	—	—	—	—
0.523	2.36	3.43	5.06	—	7.48	—	—	—	—
0.611	—	—	5.98	—	8.82	—	—	—	—
0.675	—	—	—	7.43	—	—	—	—	—
0.699	2.90	4.35	6.71	—	9.92	—	—	—	—
0.787	—	—	7.48	—	—	—	—	—	—
0.845	—	—	—	9.20	—	—	—	—	—
0.875	3.82	5.62	8.51	—	—	—	—	—	—

followed by a rapid deprotonation

$$[Co(DH)_2(OH)(H_2O)] = [Co(DH)_2(OH)_2]^- + H^+ \quad (5)$$

due to the alcalinity of solution. In the case of species II a second order olation reaction may be presumed, according to the equation

$$[Co(DH)(D)(OH)(NCS)]^{2-} + OH^- = [Co(DH)(D)(OH)_2]^{2-} + NCS^- \quad (6)$$

On the basis of this scheme the following relation can be derived

$$k_{\text{exp}} = -\frac{K}{K_w}(k_{\text{exp}} - k_2\,[OH^-])\,[OH^-] + k_1 \quad (7)$$

where K stands for the equilibrium constant of reaction (3), k_1 and k_2 for the rate constants of reactions (4) and (6), respectively, and K_w for the ionic product of water.

Since at high OH^- concentration equilibrium (3) must be shifted towards the formation of species II and the activation energy required for reaction (4) is presumably rather high, one may assume reaction (6) to be practically the only reaction taking place at low temperatures and high OH^- concentrations.

At temperatures between 18 and 27° a large excess of OH^- has been used and second order rate constants of reaction (6) may be derived simply by deviding k_{exp} by $[OH^-]$. Values are presented in table 2.

Table 2

Second order rate constants for reaction (6) ($k_2 \times 10^5$, $M^{-1}\ s^{-1}$)

$[OH^-]$ mole/l	18°	21°	24°	25°	27°
0.505	—	—	—	11.2	—
0.523	4.51	6.56	9.67	—	14.3
0.611	—	—	9.79	—	14.4
0.675	—	—	—	11.0	—
0.699	4.15	6.22	9.60	—	14.2
0.787	—	—	9.50	—	—
0.845	—	—	—	10.9	—
0.875	4.37	6.42	9.72	—	—

The rather good constancy of the k_2 values obtained for different OH^- concentrations are consistent with the scheme presumed. The graphical plot of log k_2/T versus $1/T$ (fig. 3) enabled us to derive the following activation enthalpy and entropy values:

$$\Delta H_2^{\neq} = 22.5 \pm 0.4 \text{ kcal/mole}; \quad \Delta S_2^{\neq} = -1.2 \pm 1.1 \text{ Cl.}$$

By using these parameters, the following k_2 values can be calculated:

t°	18	21	24	25	27	30	35	38	40
$k_2 \times 10^5$, $M^{-1}s^{-1}$	4.28	6.45	9.61	10.9	14.2	20.7	38.8	55.8	70.9

which enabled us to derive K and k_1 values according to eq. (7). The graphical plot of $k_{\exp}$ versus $(k_{\exp} - k_2[OH^-])[OH^-]$ gave the straight lines represented in fig. 4.

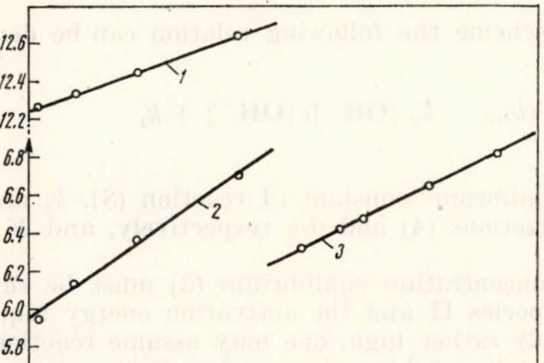

Fig. 3. — Determination of thermodynamic and kinetic parameters of the reactions (3)—1, (4)—2and (6)—3.

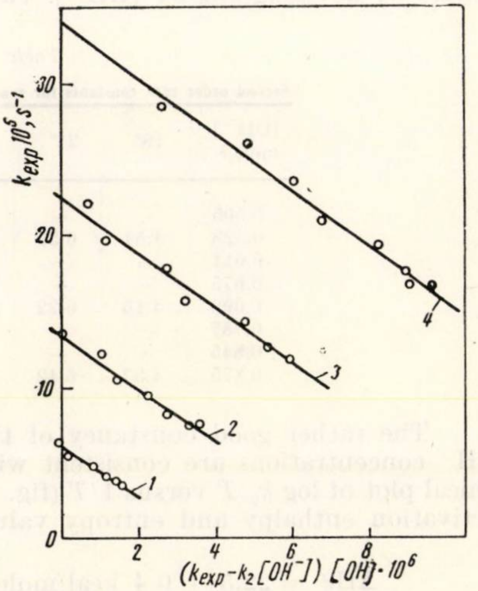

Fig. 4. — Graphical determination of k_1 and K on the basis of equation (7), 1—30°, 2—35°, 3—38°, 4—40°.

From the zero concentration ordinate and from the slope of the straight lines obtained, k_1 and K values given in table 3 have been derived. For K_w literature data [20] have been used.

---

[20] K. P. MISCHENKO and A. A. RAVDEL, "Kratkii spravochnik fizikokhimicheskikh velicin", Izd. Khimia, Moscow, 1965, p. 106.

Activation enthalpy and entropy values for reaction (4) have been derived by using the linear relationship between $\log k_1/T$ and $1/T$ and reaction enthalpy and entropy for reaction (3) in a similar way, by performing the graphical plot of $\log K$ versus $1/T$ (see fig. 3).

Table 3

Rate constants of reaction (4) and equilibrium constants of reaction (3)

$t°$	$k_1 \times 10^5, s^{-1}$	$K \times 10^{13}$
30	5.86	2.30
35	13.3	3.54
38	22.5	4.67
40	34.0	5.32

Results obtained are the followin :

$$\Delta H_1^{\neq} = 32.2 \pm 0.5 \text{ kcal/mole}; \quad \Delta S_1^{\neq} = 28.4 \pm 1.3 \text{ Cl}$$

$$\Delta H = 16.1 \pm 0.3 \text{ kcal/mole}; \Delta S = -4.8 \pm 1.0 \text{ Cl}$$

DISCUSSION

Data derived from kinetic measurements plead for the correctness of our scheme presumed, i.e. there is a protolytic pre-equilibrium, which involves the break up of one of the O–H..O hydrogen bridges. Due to this equilibrium the complex studied showed the behaviour of a weak acid, viz. it is a weaker acid than the analogous dinitro- and nitro-hydroxo complexes. [17] It is apparent the coordinated nitro and thiocyanato group to have a considerable *cis*-effect. Meanwhile, the smaller the acidity constant, the larger the reaction enthalpy of the acid dissociation.

The species $[Co(DH)_2(OH)(NCS)]^-$ undergoes an aquation according to equation (4).

The activation enthalpy has nearly the same value as for the aquation of the species $[Co(DH_2)(DH)(NCS)_2]$.

This is not surprising, since the electrostatic effect compensates the difference between the *trans* effect of the OH and NCS groups. The negative charge of species I makes easier the break up of the Co–NCS bond as compared to neutral molecules, but in the case of the species $[Co(DH_2)(DH)(NCS)_2]$ the presence of another NCS group in *trans* position has nearly the same effect.

The species $[Co(DH)(D)(OH)(NCS)]^{2-}$ undergoes an olation reaction described by equation (6).

The activation enthalpy required is with 10 kcal less, than for species I. The higher negative charge alone cannot explain such a large difference and one may presume also a difference in mechanism. The very low activation enthalpy value and the partial reaction order with regard to OH^- ions suggests the idea the mechanism of reaction (6) to be S_N2, and that of reaction (4) S_N1.

In the case of the analogous dinitro- and nitro-hydroxocomplexes instead of the olation a very aquation reaction has been observed. One can presume the different behaviour to be the result of steric hindrance, which makes impossible the S_N2 olation pathway in the case of coordinated nitro-groups.

EXPERIMENTAL

Synthesis of $[Co(DH)_2(H_2O)(NCS)] \cdot 2\,H_2O$. 0.1 moles of cobalt acetate (25 g) and 0.3 moles of KCNS (30 g) are solved in 500 ml water, the hot solution of 0.2 moles of dimethylglyoxime (23 g) in about 0.8 l ethanol is added and the mixture is oxidized by bubbling air for 5–6 hours. The precipitate of $Co^{II}[Co(DH)_2(NCS)_2]_2$, formed as by-product, is filtered and the brown solution is treated, under continuous stirring with 50–60 ml 10 p.c. ammonia, added drop by drop.

Light brown crystalline product is formed. It is filtered, washed several times with water and dried on air. Yield : 70 %.

Anal. Found : Co = 15.15 ; S = 8.10 ; H_2O (cryst. water) = 8.60. *Calc.* for $Co(C_4H_7\,N_2O_2)_2$ H_2O (NCS)$\cdot 2\,H_2O$; Co = 15.03 ; S = 7.99 ; H_2O (cryst. water) = 8.98.

IR spectrum has been recorded in KBr pellets, by means of a UR 10 Carl Zeiss Jena spectrophotometer, from 400–4000 cm^{-1}.

Kinetic measurements. Samples weighed have been solved in distilled water preheated to the working temperature. Standard NaOH solution has been added in order to ensure the needed OH^- concentration (taking into account the base necessary for the aquo-hydroxo transformation) and standard $NaNO_3$ solution, necessary for the ionic strength of 1 M. Samples of the complex of about 5×10^{-3} M were kept in ultrathermostat at working temperature, with an accuracy of $\pm$ 0.1°. 9 different working temperatures were used between 18 and 40°. Samples of 5 ml were taken out at different intervals, acidified with HNO_3, and the concentration of the NCS^- ions liberated was determined by means of potentiometric titrations. In the titrations 10^{-2} M $AgNO_3$ solution has been used. Indicatory electrode : silver wire.

Revue Roumaine de Chimie, **18**, *3*, 425–430 (1973)

NEW THORIUM COMPLEXES WITH PYRIMIDINE DERIVATIVES

FLORICA POPEA and CRISTINETA MĂRCULESCU

Centre of Physical Chemistry,
Str. Dumbrava Roşie, 23 Bucharest

Received August 17, 1972

In the present note, the new thorium compounds of the $ML_4 \cdot nH_2O$ type (M= Th ; L =barbituric or thiobarbituric acid), their chemical analyses, thermal behaviour, X-ray diffraction data, reflectance and i.r. spectra, are reported.

Following the researches concerning the reactivity of pyrimidine derivatives with 5f elements, in a previous work, the thorium nitrate-water-violuric (isonitrosobarbituric) acid system was studied spectrophotometrically [1].

Recently, [2] based on the reactivity of the 5-position and on the tautomery of the hydrogen atoms in the 1,3—positions of the pyrimidine ring, there has been interest to obtain solid compounds in the reaction of the uranyl ion with pyrimidine derivatives.

The present article describes the results on the investigations aimed to obtain new solid thorium compounds in the reaction with barbituric, thiobarbituric, monosubstituted at the C_5 barbituric acids (5-aminobarbituric and 5-ethylbarbituric acids), and with nonsubstituted at the C_5 (1-phenyl and 1,3-biphenyl)-barbituric acids.

The only unitary products obtained, are of the general formula $ML_4 \cdot nH_2O$ (M = Th ; L = AB or ATB). They resulted from the direct reaction, in aqueous solution, in stoichiometric amounts of thorium nitrate pentahydrate and barbituric (AB) or thiobarbituric acid (ATB) maintaining strictly the conditions indicated.

EXPERIMENTAL

Reagents. Thiobarbituric acid, 5-ethylbarbituric acid, 1-phenyl and 1,3-biphenylbarbituric acid were synthesized and purified, using the classical methods.

The following reagents (reagent grade), were used without additional purification : $Th(NO_3)_4 \cdot 5H_2O$ E. Merck, $AB \cdot 2H_2O$ — Carlo Erba and 5-aminobarbituric acid — Fluka.

---

[1] F. Popea and A. C. Banciu, *Rev. Roumaine Chim.*, **15**, 1319 (1970).

[2] F. Popea, C. Mărculescu and C. Pîrlog, *Rev. Roumaine Chim.*, under press.

Syntheses of Th[AB]$_4$·2H$_2$O *and* Th[ATB]$_4$·9H$_2$O

The two compounds were prepared by the same procedure. A 20 ml. aqueous suspension of 0.002 M AB·2H$_2$O or ATB was heated on boiling. The clear solution obtained (yellow with ATB) was treated with 0.0005 M thorium nitrate pentahydrate, stirring vigorously and keeping the same temperature for 5′ more. The solution became turbid and on cooling at room temperature, the compound I separated after 2 hours and II after only 60′. They were filterd, washed with 10 ml water, ethanol, ethilic ether and air dried.

The composition of the 2 compounds was determined based on the chemical analysis and namely : the metal by ignition as oxide (ThO$_2$), nitrogen, carbon and hydrogen by microcombustion.

Anal.		Th%	C%	H%	N%	H$_2$O%
I —	*calcd.*	29.88	24.74	2.08	14,43	4.28
	found	29.83	24,71	2.38	14.39	—
II —	*calcd.*	24.00	19.87	3.13	11.59	16,77
	found.	24.07	20.04	3.31	11.95	16.47

The white shining compound I microcrystals are stable at room temperature for a long time, but the II white-yellowish ones decompose on heating ; they are practically insoluble in the common solvents (ethanol, methanol, acetone, ethylic ether, T.H.F., D.M.F. and DMSO) and insoluble even in warm water.

The thermal behaviour, X-ray diffraction data, u.v. and visible reflectance spectra as well as the vibration i.r. spectra of the compounds were also studied.

RESULTS AND DISCUSSIONS

THERMAL BEHAVIOUR

The thermal curves were recorded on a MOM E. Paulik, J. Paulik—L. Erdey Derivatograph in the 30°—300° thermal range, in air atmosphere, with a 5°/min rate, using Al$_2$O$_3$ as standard and an amount of 0.4—0.5 g. for each sample.

For the compound II, the TG and DTG curves (fig. 1) reveal a continuous loss of weight between 50° and 200° ; the 16.47% value in agreement with the 16.77% one, calculated based on the analytical data corresponds to 9 water molecules for a molecule of anhydrous compound. Starting with this temperature, till 280° a horizontal level follows, characteristic for the anhydrous substance, and then a more abrupt loss of weight due to its decomposition. The DTA curve indicates an endothermic effect, with a maximum at 170°, and at 285° begins the decomposition with exothermic effect.

The thermal analysis was not conclusive for the II compound. The TG curve evidences a continuous loss of weight between 205° and 300°, but does not allow to recognize the end of the water removal, due probably to the simultaneous decomposition of the compound.

The thermal behaviour of the compounds was followed also with a Boetius heating plate.

On heating, at about 100°, Th[AB]$_4$·2H$_2$O begins to expel water and appear modifications, emphasized with the rise of the temperature. At 250° changes of the colour are observed, as a consequence of the

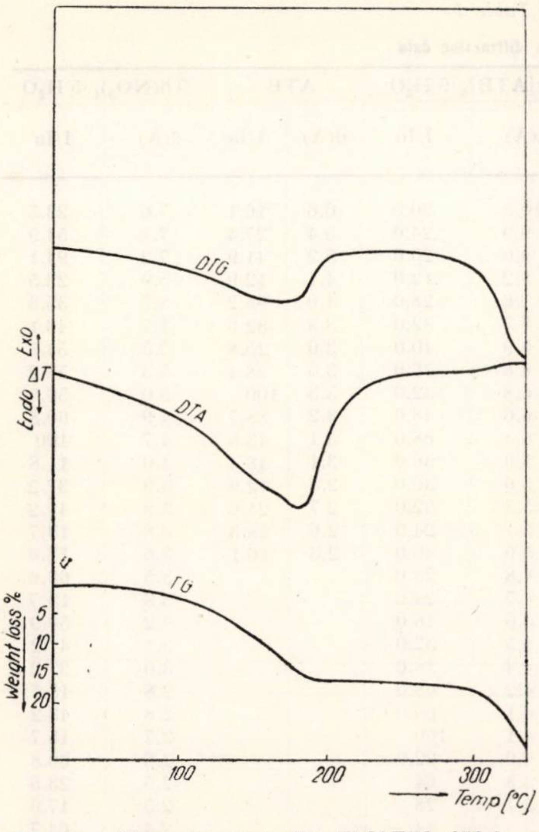

Fig. 1. — Thermal curves for Th[ATB]$_4$·9H$_2$O.

decomposition undergone by the whole mass, till 320°, but no net melting point can be observed.

As soon as 75°, Th[ATB]$_4$·9H$_2$O exhibits variations of the volume and a movement in the whole mass, till 235°, the beginning of the decomposition. The effect reaches a maximum at 285° and a sulfur odour is perceived, although till 320°, a sharp melting point can not be observed. As to be seen, the observations on heating the compounds by means of a Boetius heating table agree with those obtained by the thermal curves.

X-RAY DIFFRACTION STUDIES

The X-ray diffraction spectra were recorded on a URS. 50. IM equipment and the intensity data were collected on a diffractometer with Geiger-Müller counter. The Cu$_{K\alpha1}$ radiation ($\lambda = 1.5418$ Å and nickel filter) was used; no correction was made for the absorption.

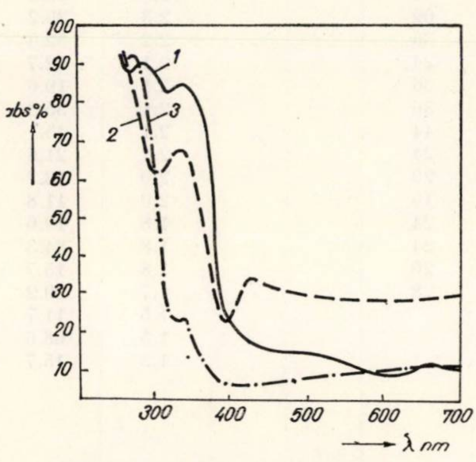

Fig. 2. — Reflectance spectra for:
1, Th[AB]$_4$.2H$_2$O. *2*, AB.2H$_2$O. *3*, Th(NO$_3$)$_4$.5H$_2$O.

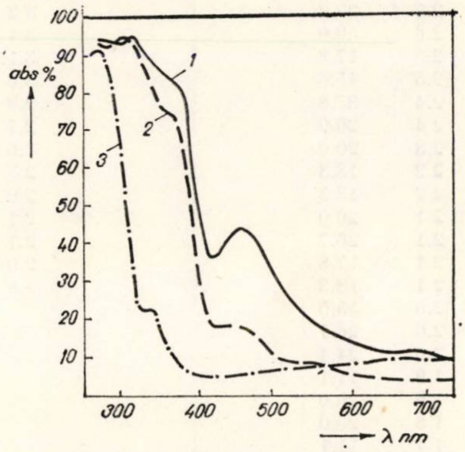

Fig. 3. — Reflectance spectra for:
1, Th[ATB]$_4$.9H$_2$O. *2*, ATB. *3*, Th(NO$_3$)$_4$.5H$_2$O.

Table 1

X-ray diffraction data

$Th[AB]_4 \cdot 2\,H_2O$		$AB \cdot 2\,H_2O$		$Th[ATB]_4 \cdot 9\,H_2O$		ATB		$Th(NO_3)_4 \cdot 5\,H_2O$	
d(Å)	I/Io	d(Å)	I/Io	d(Å)	I/Io	d(Å)	I/Io	d(Å)	I/Io
9.7	28.9	7.1	14.0	10.5	20.0	6.6	16.1	7.6	23.5
8.3	17.8	5.9	15.0	9.9	24.0	5.4	27.4	7.4	54.9
7.0	15.5	4.9	100	9.0	20.0	5.2	41.9	7.2	94.1
6.6	66.7	4.3	38.0	8.2	12.0	4.1	12.9	5.9	23.5
6.3	35.6	4.1	10.0	7.6	28.0	4.0	95.2	5.7	35.3
6.1	44.4	3.9	100	7.3	32.0	3.8	32.3	5.7	43.1
5.7	26.7	3.3	100	6.9	40.0	3.6	25.8	5.5	54.9
5.4	24.4	3.2	27.0	6.8	36.0	3.5	98.4	5.3	56.9
5.3	33.3	3.0	43.0	6.8	32.0	3.3	100	5.0	56.9
5.1	32.2	2.9	46.0	6.6	48.0	3.2	88.7	4.9	60.8
4.9	40.0	2.8	100	6.4	68.0	3.1	43.5	4.7	100
4.8	100	2.6	17.0	5.9	36.0	3.1	48.4	4.0	11.8
4.5	35.6	2.5	27.0	5.6	36.0	2.8	12.9	3.9	37.2
4.4	8.9	2.5	12.0	5.3	32.0	2.7	21.0	3.9	41.2
4.2	17.8	2.4	16.0	5.1	24.0	2.6	19.3	3.8	13.7
4.1	24.4	2.3	13.0	5.0	40.0	2.3	16.1	3.6	17.6
3.9	35.6	1.9	13.0	4.8	28.0			3.5	68.6
3.8	35.6	1.8	11.0	4.7	24.0			3.3	13.7
3.7	17.8			4.6	16.0			3.2	56.9
3.6	15.6			4.5	32.0			3.1	41.2
3.5	26.7			4.4	16.0			3.0	37.2
3.5	17.8			4.2	68.0			2.8	15.7
3.4	33.3			4.1	60.0			2.8	43.2
3.3	11.1			4.1	100			2.7	15.7
3.2	53.3			4.0	92.0			2.6	60.8
3.1	33.3			3.8	64			2.5	23.5
3.0	26.6			3.7	28			2.5	17.6
2.9	46.7			3.5	44			2.4	64.7
2.8	40.0			3.4	28			2.4	37.2
2.7	13.3			3.3	40			2.3	76.5
2.7	22.2			3.2	60			2.3	39.2
2.6	40.0			3.1	36			2.2	52.9
2.5	17.8			3.1	24			2.1	62.7
2.5	15.6			3.0	36			2.1	19.6
2.4	37.8			2.9	36			2.1	35.3
2.4	20.0			2.7	44			2.1	45.1
2.3	20.0			2.6	24			2.1	21.6
2.2	13.3			2.3	20			2.0	13.7
2.2	13.3			2.0	16			2.0	11.8
2.1	20.0			2.1	24			1.8	19.6
2.1	26.7			2.1	24			1.8	84.3
2.1	17.8			2.0	20			1.8	15.7
2.1	13.3			1.8	28			1.7	39.2
2.0	15.5							1.5	11.7
2.0	26.7							1.5	68.6
2.0	24.4							1.5	15.7
1.9	11.1								
1.9	20.0								
1.8	20.0								
1.7	11.1								
1.7	17.8								
1.6	15.6								
1.5	13.3								

d = interplanar (hkl) spacing in Å

Table 2

Infrared absorption spectra

$Th[AB]_4 \cdot 2\ H_2O$		$AB \cdot 2\ H_2O$		$Th[ATB]_4 \cdot 9\ H_2O$		ATB		$Th(NO_3)_4 \cdot 5\ H_2O$	
Max. cm^{-1}	Trans. %	Max. cm^{-1}	Trans. %	Max. cm^{-1}	Trans. %	Max. cm^{-1}	Trans. %	Max. cm^{-1}	Trans. %
				—	—	427	53		
				470	36	466	41		
				—	—	500	69		
555s	11	550s	21	545s	20	534m	39	550	54
				606	50	610	35		
650	60	660	35	642	41	635	40		
705	47	680	52						
762	47	765	55	707	50	730	42	755s	30
795	33	800	42	800	38	810	30	812s	45
840	42	—	—						
865	52	860—70	36—37	868	50	—	—		
1000	70	1000	36	1020	60	1000	42		
						1035	39	1045s	31
				1180	23	1155s	6		
1223s	19	1230s	21	1230	30	—	—		
—	—	1265s	18	—	—	1280	25		
1295s	5	—	—	1296s	14	1300	25	1315s	13
1360s	13	1330s	14			1350s	14	1345s	9
1380s	8	—	—	1388s	15			1390	43
1405s	18	1400s	18			1400sh	24		
				1450	44	1440s	26		
1480s	23	1490m	31						
—	—	1560s	16	1540—50s	28	1540s	13	1520s	10
1620s	18	—	—	1610s	4	1600sh	24		
1640sh	3	1670s	22	1640s	4	1640m	29	1620	33
1735s	8	1720s	8						

s=strong; m=medium; sh=shoulder.

As to be seen (table 1) the compounds are unitary and pure, free of thorium nitrate and of ligand. On the other hand, the diffractograms exhibit well defined lines in the region of small Bragg θ° angles. This observation substantiates a low symmetry and a large elementary cell. The different number of crystallization water molecules in these compounds, indicates their lack of symmetry.

ELECTRONIC SPECTRA

The reflectance spectra were recorded with a VSU-1 Jena spectrophotometer, at room temperature from 260 nm (38,461 cm^{-1} to 1200 nm (8.333 cm^{-1}) using MgO as a standard.

Thorium [3] does not exhibit a proper absorption in the visible range and the absorption curves of I and II have only the general shape of those of the ligands, with some shifts and changes in the intensity.

As may be seen, in figs. 2 and 3, the absorption maxima present in the ligands at about 300 nm (30.303 cm^{-1}) reappear in I at 285 nm (3.588 cm^{-1}) and at 330 nm (3.333 cm^{-1}) and in II at 315 nm (3.174 cm^{-1}) and the absorption maxima in the 420 nm (2.325 cm^{-1}) — 450 nm (2.222 cm^{-1})

---

[3] CL. DUVAL, "Traité de micro-analyse minérale", vol. 2, Presses scientifiques internationales, Paris, 1955, p. 70, p. 95.

range reappear in I at 395—405 nm (2.531—2.469 cm^{-1}) and in II at 455 nm (2.197 cm^{-1}).

Generally, as for the corresponding uranyl compounds, the characteristic absorption maxima of the ligands appear much weakened or as simple inflexions in the two compounds.

INFRARED SPECTRA

The vibration spectra, in the infrared were recorded on a UR-20 C. Zeiss spectrophotometer within the 400—1800 cm^{-1} range, using the technique of the pelleted powders (with KBr).

As may be seen in table 2, the absorption bands assigned to the pyrimidine ring, are present in the AB and the ATB ligands and also appear in the two new corresponding compounds, with more or less important changes in their position and their intensity. The absorption maxima at 1402, 1460 and 1570 cm^{-1}, due to the in-plane vibrations of the pyrimidine ring are to be found at 1400, 1490 and 1560 cm^{-1} in $AB.2H_2O$ and in the compound I at 1405, 1480 and 1620—40 cm^{-1}; in ATB at 1400, 1440 and 1600—40 cm^{-1}, and in the compound II at 1388, 1450, and 1610—40 cm^{-1}. The bands ascribed to the out-of-plane vibrations at 680—724 cm^{-1} appear at 680 cm^{-1} in $AB.2H_2O$, at 730 cm^{-1} in ATB and reappear at 705 cm^{-1} in I. In the compound II, this band is to be found at 707 cm^{-1} but much weaker probably due to the environment of the 9 water molecules of the compound.

In addition, the absorption band at 1540 cm^{-1}, characteristic for the $-S-\acute{C}=$ vibration is to be seen in ATB and appears also in the compound II.

CONCLUSIONS

The two new compounds obtained and characterized by chemical analysis and physical data, may suggest the enolic form as being more probable for the ligands in the reaction with thorium ion. The assumption is also supported by the spectral studies.

Revue Roumaine de Chimie, 18, 3, 431–439 (1973)

ON SOME DERIVATIVES OF THE HYDRAZINOCARBOXYLIC ACID. II

SYNTHESES AND SPECTRAL DATA

SCHELY AVRAMOVICI, I. DRUȚĂ and I. ZUGRĂVESCU

Department of Organic Chemistry "Al. I. Cuza" University, Iassy, Romania

Received August 10, 1972

The synthesis of some hydrazonocarboxylic esters, previously obtained by the condensation of the corresponding semicarbazones with monochloroacetic acid, was carried out now directly. It was also proved that some products considered to have a 3-ketimino-2,4-oxazolidindione structure or a 4-oxazolone-2-hydrazonic one, are also hydrazonocarboxylic esters. The structure of the products is investigated by chemical analysis and IR and NMR spectral data.

In a previous paper, [1] the results obtained in the study of the condensation reaction between monochloroacetic acid and some semicarbazones of unsaturated aromatic ketones were published. In these cases the formation of different kinds of products with close analytical values was possible, whose structures were difficult to be elucidated. On the basis of elementary analysis and IR spectra, we have attributed a 3-ketimino 2,4-oxazolidindione structure (I) to the products isolated by the condensation of the studied semicarbazones with monochloroacetic acid in isopentyl alcohol in the presence of the triethylamine, and a 4-oxazolone 2-hydrazone structure (II) to the products isolated when the condensation takes place in ethyl alcohol in the presence of natrium acetate:

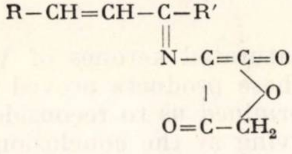
I

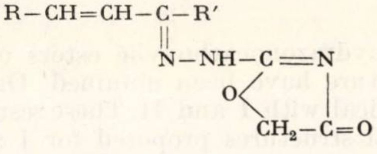
II

Then, the study was extended to the semicarbazones of saturated aromatic aldehydes and ketones. [2] We have proved that the reaction, in various alcohols used as solvents, leads to the separation of hydrazonocarboxylic esthers (III) as main products :

---

[1] S. Avramovici, I. Gabe and I. Zugrăvescu, *Anal. Sti. Univ. "Al. I. Cuza", Iaşi, Sect. I*, **10** (2), 165 (1964).

[2] Part I. S. Avramovici, I. Druţă, I. Gabe and I. Zugrăvescu, *Rev. Roumaine Chim.*, **16**, 1237 (1971).

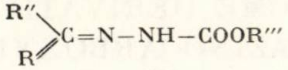

$$\begin{matrix}R'' \\ R\end{matrix}\!\!>\!C=N-NH-COOR'''$$

III

The structure which has been attributed to the final products was deduced from the interpretation of the analytical and spectral data, because the intermediaries which appeared in the different stages of the reaction could not be isolated.

In the present paper the possibility of III-type products obtained in another way of synthesis was studied. This made it possible for us to confirm the structures previously supposed. For this purpose, the isopentyl and *n*-hexyl esters of the hydrazinocarboxylic acid (IV), the new products were prepared and afterwards condensated with the same aromatic aldehydes and ketones :

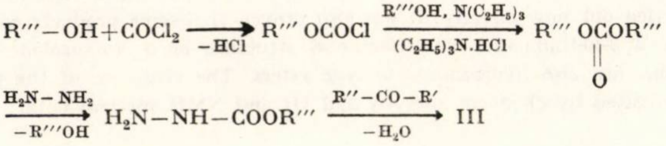

$$R'''-OH+COCl_2 \xrightarrow[-HCl]{} R'''\,OCOCl \xrightarrow[(C_2H_5)_3N.HCl]{R'''OH,\ N(C_2H_5)_3} R'''\,O\underset{\underset{O}{\|}}{C}OR'''$$

$$\xrightarrow[-R'''OH]{H_2N-NH_2} H_2N-NH-COOR''' \xrightarrow[-H_2O]{R''-CO-R'} III$$

IV

After obtaining these results the problem was put whether the I and II structures corresponded to reality. In order to see if these products are not also hydrazonocarboxylic esters we have achieved the condensation of the ethylic and isopentylic esters of the IV-type hydrazinocarboxylic acid with the unsaturated aromatic ketones initially used for the synthesis of the semicarbazones, which led to the products of previously attributed I and II structures. According to the reaction :

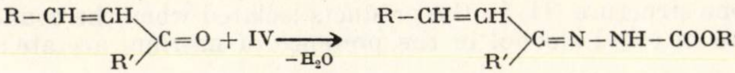

$$\begin{matrix}R-CH=CH \\ R'\end{matrix}\!\!>\!C=O + IV \xrightarrow[-H_2O]{} \begin{matrix}R-CH=CH \\ R'\end{matrix}\!\!>\!C=N-NH-COOR'''$$

V

the hydrazonocarboxylic esters of some unsaturated ketones of V-type structure have been obtained. On analysis these products proved to be identical with I and II. These results has determined us to reconsider the initial structures proposed for I and II, arriving at the conclusion that these products are not 3-ketimino 2,4-oxazolidindiones (I) or 4-oxazolon 2-hydrazones (II) but, hydrazonocarboxylic esters of V-type.

For the interpretation of the IR and NMR spectra the products III-H, V-G and V-H, mentioned in table 1, which served as comparison term, were also synthesized.

In all, nine hydrazones of the isopentyl ester, two hydrazones of the *n*-hexyl ester and five hydrazones of the ethyl ester of the hydrazinocarboxylic acid, corresponding to the III and V structures, have been separated and identified.

The IR spectra were registered with a SP 200 UNICAM spectrophotometer, using the KBr pellet technique; the most important and characteristic bands are given in table 2.

The NMR spectra were registered with a 60 MC JEOL apparatus at 20°, using as solvent $DCCl_3$ or CCl_4. The data are shown in table 3.

The IR and NMR spectra of the seven products described in the previous paper[2] are identical and they are not reproduced in the present work. The tables 2 and 3 contain only the characteristic spectral data of some of the newly synthesized products. From the beginning we must mention that these data are similar to those presented in the previous note. What is different is the presence of the olefinic double band which can be very well identified in the NMR spectra.

The two olefinic protons in the case of the V—A and V—E compounds provided two doublets in the NMR spectra, situated in the interval $\delta = 6-7.18$ ppm with a coupling constant particularly great, namely $j = 16$ c/s. In the cases of V—C and V—F compounds these protons are placed in the interval $\delta = 6.5-7.33$ ppm, the coupling constant being comprised between 8.3—8.6 c/s.

As in the case of the products discussed in the previous work, the IR spectra of those compounds are characterized by the presence of the corresponding $\rangle C{=}O$ ester group, located between 1690—1740 cm^{-1} and that corresponding to the antisymmetrical vibration $\rangle C{-}O{-}C\langle$ between 1230—1290 cm^{-1}. The ester group can be noticed also in the NMR spectra, in which the protons from the α-ester position appear between $\delta = 4.16-4.27$ ppm; the protons attached to the β-esteric carbon appear at about $\delta = 1.33$ ppm in the $-CH_3$ case group and at about $\delta = 1.66$ ppm in the $-CH_2-$ case group. Otherwise, the presence of this grouping in the NMR spectra represents the most important proof of a III or V-type linear structure formed in all the cases. The forming of I or II-type structures would have led to the absence of the signals and coupling corresponding to the esters alkyl groups and to the appearance of a singlet representing the methylenic group from the cycle in the NMR spectra. In the case of the I-type compounds, this singlet would have been situated round the value $\delta = 5.1$ ppm and in the case of type II compounds at $\delta = 5.2$ ppm, which was not noticed.

Concerning the —NH— group, the characteristic band in IR spectra is present in the 3200—3300 cm^{-1} region, while in the NMR spectra the proton of this group furnished a singlet situated at δ varying between 7.55—8.48 ppm, according to the structure. The presence of this proton in all spectra also represented a proof that instead of the supposed cyclic structures I we must take into account the V formulated structures.

Table 1

Hydrazonocarboxylic esters

Prod. nº	Formulae with the proton specifications (see table 3 with NMR spectra)	Identical with	From ref.
III-A	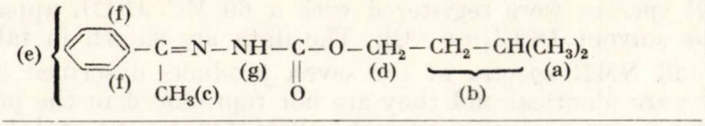	X_1	1
III-B	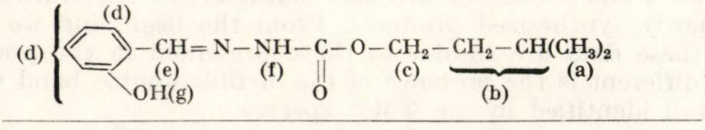	X_2	1
III-C	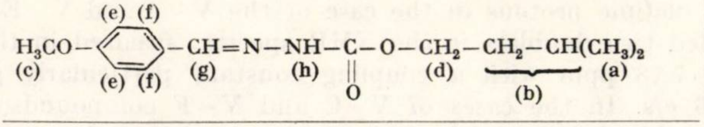	X_3	1
III-D	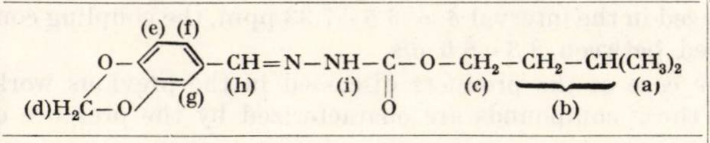	X_4	1
III-E	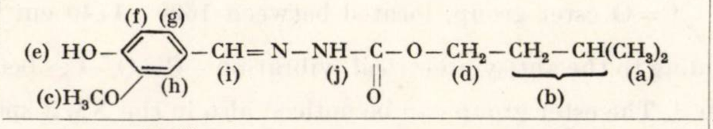	X_5	1
III-F	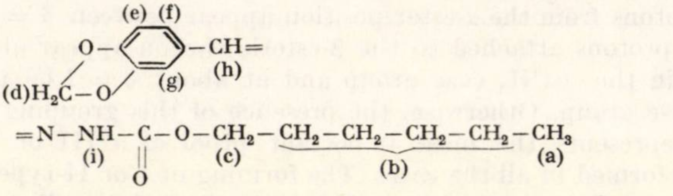	X_6	1
III-G	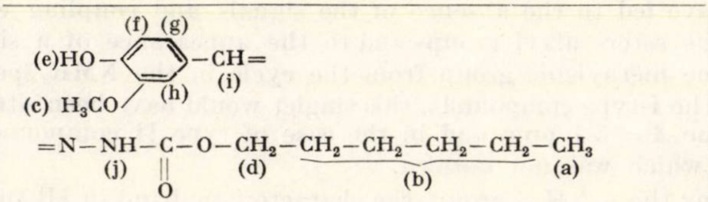	X_7	1
III-H	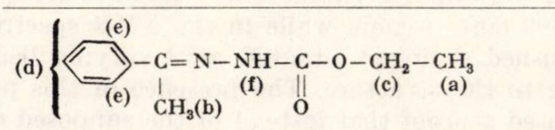		3

---

[3] K. v. Auwers and W. Daniel, *J. Prakt. Chem.*, 2 **110**, 256 (1925).

Table 1 (continued)

Prod. n°	Formulae with the proton specifications (see table 3 with NMR spectra)	Identical with	From ref.
V-A	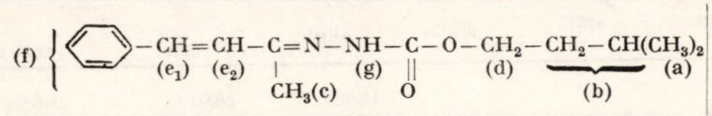	B_1	2
V-B	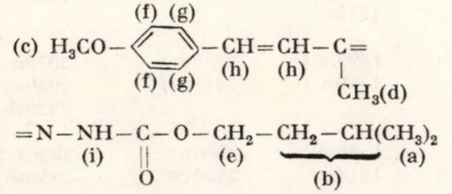	B_2	2
V-C	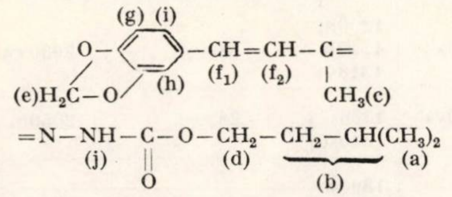	B_3	2
V-D	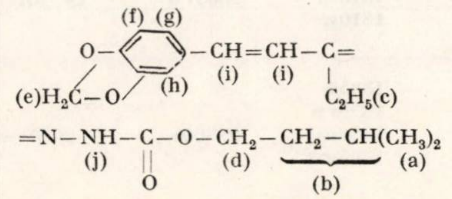	B_4	2
V-E	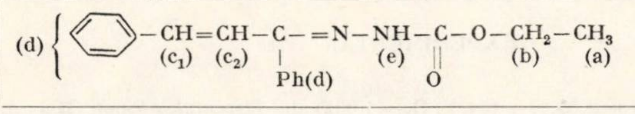	A_1	2
V-F	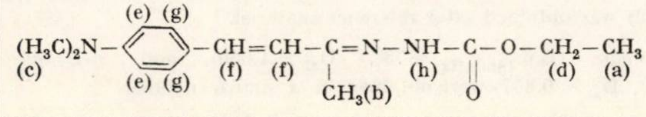	A_2	2
V-G	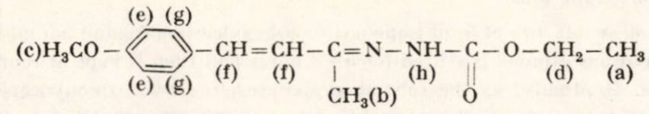		
V-H	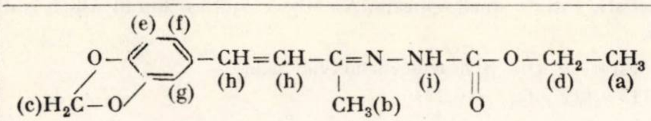		

Table

IR spectra of the

Prod. n°	$\diagup\dot{C}=\dot{C}\diagdown$ arom.	$\diagup\!\!\!\diagup CH-$ arom.	$>C=C<$ aliph.	$\diagdown\!-CH\diagup$ aliph.	$-CH_2-$ sym.	$-CH_2-$ antisym.
V-A	1590m 1545s } 1500w } s	3040w	964s	1386w 1342w 1315w	2880w 2850vw	2968m } 2930w } m
V-B	1540m } 1520w } vs	3040w } 20152 } w	975s	1390m } 1370w } m	2880w } 2845w } m	2970m } 2940sh } m 2920sh }
V-C	1580s 1520s } 1515sh } vs	3050w	970s	1386m 1318m	2900w 2800vw	2990s } 2950sh } s
V–E	1575m 1505vs	3090w 3020w	970s	1390m 1350w 1318vs	2850sh	2930vw
V–F	1560sh } 1535s } vs	3050sh } 3000w } m	960vs	1366s } 1340sh } s	2830w	2950m
V-G	1580m } 1540s } sl	3020m	969s	1390w 1345sh 1310w	2860vw	2950sh
III–H	1550s 1500m	3000m	980m	1385w 1370vw 1320sh } 1305w } m	2830vw	2950vw

EXPERIMENTAL

1. *Isopentylchloroformate* (B.p. $=154.3°$, $D_{15}=1.032$) and *Isopentylcarbonate* ($B.p._{17mmHg} = 105-110°$, $D_{15} = 0.912$) was obtained after reference material.[4]

2. *n-Hexylchloroformate* ($B.p._{18mmHg} = 78°$, $D_{22} = 1.066$) and *n-Hexylcarbonate* ($B.p._{10mmHg} = 132-138°$, $D_{24} = 0.857$) were obtained in a similar manner.

3. *The hydrazinocarboxylic esters.*

The general method. A mixture of 5 ml isopentyl or *n*-hexylcarbonate and 2.5 ml hydrazinehydrate in 10 ml anhydrous ethanol is stirred for 6–8 hours and then is kept at room temperature for a long time. Gradually, as the solvent evaporates, the hydrazinohydrate smell disappears and a characteristic esteric smell appears. An oily, colourless liquid which is distilled at low pressure remains.

– The isopentyl ester of the hydrazinocarboxylic acid.
$B.p._{12mmHg} = 115-122°$, $D_{20} = 0.977$

---

[4] B. Bose, *Liebigs Ann. Chem.*, **205**, 227 (1880).

2

hydrazonocarboxylic esters

aliph.	–C–O–C–		>C=O	>C=N–	–NH–	Subst. arom. ring
deform	ether	ester	ester			
1470w 1450w } m		1276w 1245sh } sl 1230sh	1735w 1715w } vs	1635w	3228ml	775w 750m } s
1470m 1440m } m	1065s 1032s	1280w 1255m } sl 1230w	1728w 1715w } vs	1610s	3225s	778m 740m
1485m 1450s	1065m 1040s } sl	1283w 1260m } sl 1230s	1708vs	1620m 1600m	3230m	772 m 730w
1475w 1450m } sl 1430w		1270w 1218vs	1725m 1702m } sl	1625vs	3200w	780sh 770s } s 753sh
1480sh 1450m } m		1270m 1240s } sl	1725m 1700m } vs	1610vs	3250m	815s 780m
1485vw 1470w } m 1450w	1050vs	1290w 1255sh } sl 1238sh 1180m	1730m 1707m } vs	1625sh 1612s } s	3280m	835m 818w } m 780m
1470w 1450m } m		1240vsl	1730w 1705w } sl	1610m	3240m	880m 830w 770vs

– The *n*-hexyl ester of the hydrazinocarboxylic acid.

B.p.$_{14mmHg}$ = 140–144°, D_{20} = 0.983.

– The ethyl ester of hydrazinocarboxylic acid was obtained after reference material.[3]

4. *The hydrazonocarboxylic esters*

The general method. To a mixture of 1.5 mole ester of the hydrazinocarboxylic acid and 1 mole carbonilic compound solved in a small quantity of alcohol, 2–3 drops of acetic acid are added. In some cases the condensation products separate immediately, in others it is necessary to stir or to heat for a short time. As sometimes, a partial transesterification takes place at the same time with condensation, it is indicated to use, both at synthesis and at recrystallization, the alcohol which had esterificated the hydrazinocarboxylic acid. The recrystallization is done by alcohol, alcohol-water or ethylacetate.

Thus, all the products presented in table 1 were separated with 50–80% efficiency. Their analytical data are synthesized in table 4. In some cases their melting points differ. They are in general a little higher than in the previous papers,[1,2] because of their higher purity.

Table 3

NMR spectra of the hydrazonocarboxylic esters

Prod. n°	δ ppm	N° prot.	Multiplicity	J c/s	Attribute	Solvent	Observations
V−A	0.95	6	doublet	6	$H_{(a)}$	CCl$_4$	superpos. sign. (δ = 1.4−1.8)
	1.63	3	multiplet	6 and 7.1	$H_{(b)}$		
	2	3	singlet	—	$H_{(c)}$		
	4.16	2	triplet	7.1	$H_{(d)}$		
	6.69	1	doublet	16	$H_{(e_1)}$ or $H_{(e_2)}$		
	6.74	1	doublet	16	$H_{(e_2)}$ or $H_{(e_2)}$		
	7.15	5	multiplet	—	$H_{(f)}$		sign. between δ = 6.97−7.45
	8.48	1	singlet	—	$H_{(g)}$		
V−C	0.95	6	doublet	6	$H_{(a)}$	CDCl$_3$	
	1.58	3	multiplet	6 and 7.2	$H_{(b)}$		
	2.01	3	singlet	—	$H_{(c)}$		superpos. sign. (δ = 1.2−1.7)
	4.23	2	triplet	7.2	$H_{(d)}$		
	5.88	2	singlet	—	$H_{(e)}$		
	6.72	2	singlet	—	$H_{(f_1)}$ or $H_{(f_2)}$		
	6.73	1	doublet	8.3	$H_{(g)}$		
	6.88	1	singlet	—	$H_{(h)}$		
	7.1	1	doublet	8.3	$H_{(i)}$		long range coupling
	7.95	1	singlet	—	$H_{(j)}$		
V−E	1.2	3	triplet	7.2	$H_{(a)}$	CDCl$_3$	
	4.2	2	quadriplet	7.2	$H_{(b)}$		
	6.15	1	doublet	16	$H_{(c_1)}$ or $H_{(c_2)}$		
	7.18	1	doublet	16	$H_{(c_1)}$ or $H_{(c_2)}$		
	7.2	10	multiplet	—	$H_{(d)}$		sign. between δ = 6.9−7.5
	7.55	1	singlet	—	$H_{(e)}$		
V−F	1.34	3	triplet	7.2	$H_{(a)}$	CDCl$_3$	
	1.98	3	singlet	—	$H_{(b)}$		
	2.93	6	singlet	—	$H_{(c)}$		
	4.27	2	quadriplet	7.2	$H_{(d)}$		
	6.57	2	doublet	8.6	$H_{(e)}$		
	6.77	2	singlet	—	$H_{(f)}$		
	7.27	2	doublet	8.6	$H_{(g)}$		long range coupling
	7.69	1	singlet	—	$H_{(h)}$		
V−G	1.32	3	triplet	7	$H_{(a)}$	CDCl$_3$	
	2	3	singlet	—	$H_{(b)}$		
	3.75	3	singlet	—	$H_{(c)}$		
	4.27	2	quadriplet	7	$H_{(d)}$		
	6.77	2	doublet	8	$H_{(e)}$		
	6.78	2	singlet	—	$H_{(f)}$		
	7.31	2	doublet	8	$H_{(g)}$		long range coupling
	8.05	1	singlet	—	$H_{(h)}$		
III−H	1.35	3	triplet	7	$H_{(a)}$	CCl$_4$	
	2.16	3	singlet	—	$H_{(b)}$		
	4.16	2	quadriplet	7	$H_{(c)}$		
	7.07	3	multiplet	—	$H_{(d)}$		
	7.52	2	multiplet	—	$H_{(e)}$		sign. between δ = 8.4−8.15
	8.28	1	—	—	$H_{(f)}$		

Table 4

Analytical data of the hydrazonocarboxylic esters

Prod. n°	NAME	Molecular formula (°C)	Mp {found lit.*	** MW {calc. found	C% {calc. found	H% {calc. found	N% {calc. found
III–A	Isopentyl acetophenone-hydrazinecarboxylate	$C_{14}H_{14}O_2N_2$	82 75	248 226.3	67.70 67.90	8.06 8.05	11.29 11.03
III–B	Isopentyl 3-(2-hydroxybenzylidene) hydrazinecarboxylate	$C_{13}H_{18}O_3N_2$	146 146	250 246.9	62.40 62.52	7.20 7.09	11.20 11.32
III–C	Isopentyl 3-(4-methoxybenzylidene) hydrazinecarboxylate	$C_{14}H_{20}O_3N_2$	93 89	264 255.9	63.63 63.18	7.57 7.56	10.60 10.63
III–D	Isopentyl 3-(3.4-methylenedioxybenzylidene)-hydrazinecarboxylate	$C_{14}H_{18}O_4N_2$	89 94	278 276.9	60.43 60.56	6.49 6.71	10.08 9.98
III–E	Isopentyl 3-(3-hydroxy 4-methoxybenzylidene)-hydrazinecarboxylate	$C_{14}H_{20}O_4N_2$	136 136	280 276.1	60.00 60.08	7.14 7.33	10.00 9.87
III–F	n-Hexyl 3-(3,4-methylenedioxybenzylidene) hydrazinecarboxylate	$C_{15}H_{20}O_4N_2$	133 123	292 299.1	61.64 61.58	6.85	9.59 9.56
III–G	n-Hexyl 3-(3-hydroxy 4-methoxybenzylidene) hydrazinecarboxylate	$C_{15}H_{22}O_4N_2$	90 85	294 291.1	61.22 61.73	7.48 8.08	9.52 10.01
III–H	Ethyl acetophenone-hydrazinecarboxylate	$C_{11}H_{14}O_2N_2$	120 120	206 197.5	64.07 63.98	6.79 6.65	13.5 13.97
V–A	Isopentyl benzylidene-acetonehydrazynecarboxylate	$C_{16}H_{22}O_2N_2$	145 145	272 271.1	70.07 69.51	8.02 7.79	10.21 9.70
V–B	Isopentyl 3-(4-methoxybenzylideneacetone) hydrazinecarboxylate	$C_{17}H_{24}O_3N_2$	145 145	304 277.2	67.10 66.85	7.89 7.53	9.21 9.58
V–C	Isopentyl 3-(3,4-methylenedioxybenzylideneacetone) hydrazinecarboxylate	$C_{17}H_{22}O_4N_2$	154 160	318 309.5	64.15 64.29	6.91 6.78	8.80 8.88
V–D	Isopentyl 3-(3,4-methylenedixybenzylidenemethyl ethylcetone) hydrazinecarboxylate	$C_{18}H_{24}O_4N_2$	152 152	332 312.1	65.06 64.75	7.22 7.11	8.43 8.90
V–E	Ethyl benzylideneacetophenone hydrazinecarboxylate	$C_{18}H_{18}O_2N_2$	142 142	294 303	73.47 73.80	6.12 6.25	9.52 9.97
V–F	Ethyl 3-(4-N-dimethyl benzylideneacetone) hydrazinecarboxylate	$C_{15}H_{21}O_2N_3$	215 213	275 282.2	65.45 65.14	7.63 7.83	15.27 16.13
V–G	Ethyl 3-(4-methoxybenzylideneacetone) hydrazinecarboxylate	$C_{14}H_{181}O_3N_2$	187	262 242.3	64.12 63.63	6.87 6.45	10.69 10.64
V–H	Ethyl 3-(3,4-methylene dioxybenzylideneacetone) hydrazinecarboxylate	$C_{14}H_{16}O_4N_2$	196	276 260.1	60.87 59.97	5.80 5.56	10.14 9.69

* The reference is indicated in table 1.

** Molecular weight was determined by the Rast-method.

Revue Roumaine de Chimie, **18**, *3*, 431–439 (1973)

Revue Roumaine de Chimie, **18**, *3*, 441 – 447 (1973)

CONFIGURATIONS OF SUBSTITUTED DIBENZOBICYCLO [3.2.1]OCTADIENES*[1]

MARGARETA AVRAM, I. G. DINULESCU and C. D. NENITZESCU
Organic Chemical Institute, Bucharest, Romania

RICHARD A. Y. JONES, A. R. KATRITZKY and R. J. WYATT
School of Chemical Sciences, University of East Anglia, Norwich, NOR 88 C

Received October 6, 1972

The configurations of dibenzobicyclo[3,2,1]octadienes prepared by solvolysis and the course of further transformations of dibromodibenzo-bicyclo[4,2,0] octadiene are confirmed and the mechanisms elucidated.

There is a long-standing, hitherto unresolved, discrepancy regarding the configuration of dibenzobicyclo[3, 2, 1]octadienes (**1**). In 1964 we published chemical evidence [2] and NMR data [3] for the configuration of a series of these compounds, which were in good agreement *except* for one compound which appeared to possess the *exo*-4-acetoxy-*syn*-8-bromo structure on NMR but the *endo*-4-acetoxy-*syn*-8-bromo structure on chemical evidence (*cf* **1**). We have now confirmed the *exo* configuration for this compound, shown that the corresponding hydroxy compound [2] (the NMR of which was not previously [3] investigated) also possess the *exo* configuration, and elucidated the mechanisms of the reaction sequences which appeared earlier to suggest the opposite configurations at the 4-position.

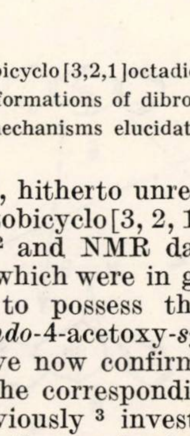

1

Solvolyses of dibromodibenzobicyclo[4, 2, 0]octadiene (**2**) give [2] C_4-substituted *syn*-8-bromodibenzobicyclo [3,2,1]octadienes : acetolysis yields the 4-acetoxy derivative (**3**), hydrolysis yields the 4-hydroxy deri-

---

[*] This paper is dedicated by the surviving authors to the memory of Professor C. D. Nenitzescu.

[1] This paper is considered as Part XXXVI in the Series "Application of Proton Magnetic Resonance Spectroscopy to Structure Problems". Part XXXV, see E. Boldignon, A. Sigor, I. J. Fletcher, A. R. Katritzky and J. R. Lea, *J. Chem. Soc.* (*B*), **1970**, 1567.

[2] I. G. Dinulescu, M. Avram, Gh. D. Mateescu and C. D. Nenitzescu, *Chem. and Ind.*, **1964**, 2023; *Rev. Roumaine Chim.*, **9**, 351 (1964).

[3] A. R. Katritzky and B. Wallis, *Chem. and Ind.*, **1964**, 2025.

vative (**4**), and in the presence of AgBr **2** is isomerized to the 4-bromo-compound (**5**). The same products were obtained [2] from dibenzobicyclo [2,2,2] octadiene (**6**) by reaction with bromine in acetic acid, by reaction with bromine in a mixture of tetrahydrofuran and water, and by simple addition of bromine, respectively. Chemical evidence was correctly adduced for the *endo*-orientation of the bromine at C-4 in **5**; the *endo*-configuration for the acetoxy and hydroxy groups in **3** and **4** appeared at that time to follow from simple transformations from **5**. However, Cristol and coworkers [4] independently reported the formation of **3** and **4** from **6**, assigning them the *exo*-configurations given in the structures (*cf*-also Ref. [5]).

Scheme 1

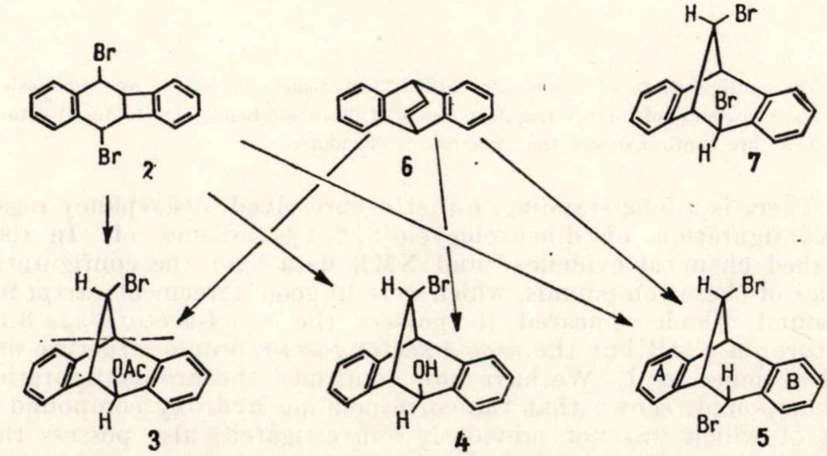

The isomerization of **2** with an ionizing catalyst also yields the *endo*-dibromide **5** which is the thermodynamically stable isomer; Cristol and coworkers [6] concluded that in general *endo*-4-substituted compounds are more stable than their *exo*-analogues (*cf* **1**). The course of addition of bromine to **6** is probably subject to steric effects. In the addition of the less bulky chlorine at C-8, Cristol and coworkers [7] found that a mixture of 12% *syn*-8-*endo*-4-dichloro-derivative and 88% *exo*-derivative was formed.

PHYSICAL EVIDENCE AND ASSIGNMENT OF CONFIGURATIONS

(a) *Dipole moments*. We have determined the dipole moments of compounds **3**, **4** and **5** (Table 2) from the data recorded in Table 1. By the method of Table 3 we are able to show that the bromo-compound does indeed possess the *endo*-configuration (**5**). Unfortunately, several uncertainties, particularly the unknown rotational isomerism around the C—O bond, precludes any clear conclusion from dipole moments regarding the configuration of the hydroxy and the acetoxy compounds.

---

[4] S. J. Cristol, F. P. Parungo and D. E. Plorde, *J. Amer. Chem. Soc.*, **87**, 2870 (1965).

[5] B. B. Jarvis, J. B. Yount and T.-H. Yang, *J. Org. Chem.*, **37**, 797 (1972).

[6] S. J. Cristol, F. P. Parungo, D. E. Plorde and K. Schwarzenbach, *J. Amer. Chem. Soc.*, **87**, 2879 (1965).

[7] S. J. Cristol, R. P. Arganbright and D. D. Tanner, *J. Org. Chem.*, **28**, 1374 (1963).

Table 1

Dipole moment measurements* of dibenzobicyclo[3,2,1]octadienes at 25° benzene

$10^6 w$	$10^6 (v_1 - v_{12})$	$10^6 (\varepsilon_{12} - \varepsilon_1)$
exo-4-Acetoxy-*syn*-8-*bromo* (**3**)		
1598	781	1664
2160	1109	2299
4219	2101	4436
syn-8-Bromo-*exo*-4-hydroxy (**4**)		
3201	1494	7806
8426	4004	20.940
syn-8-*endo*-4-Dibromo (**5**)		
2400	1553	3176
3437	2184	4537
4757	2986	6201
8315	—	10.840

* w= Weight fraction of solute. ε = dielectric constant. v = specific volume. The suffixes 1 and 12 refer to solvent and solution respectively.

Table 2

Dipole moments of dibenzobicyclo[3,2,1]octadienes at 25° in benzene

Compound	$\frac{d\varepsilon^a}{dw}$	$\frac{-dv^a}{dw}$	$T^P - 2\infty$	E^P	μ (D)^a
exo-4-Acetoxy-*syn*-8-bromo (**3**)	1.053±0.007	0.499±0.008	134.0	80.5	1.62±0.02
syn-8-Bromo-*exo*-4-hydroxy (**4**)	2.49 ±0.02	0.476±0.004	201.0	71.1	2.52±02
syn-8-*endo*-4-Dibromo-(**5**)	1.301±0.005	0.628±0.008	145.1	77.0	1.82±0.02

[a] Errors are quoted as ± one standard deviation based on least square plots; they are thus errors of experimental precision, but do not include errors arising from assumptions, in particular from the neglect of A^P.

Table 3

Calculated component and total moments for endo (5) and exo dibromo compounds (7)

Dipole component	Model used			Angle		Total moment (D)
	Compound	Moment D	Ref.	θ^a	Φ^b	
Ring A and *ortho*-alkyl groups	hydrindene	0.53	[c]	50	90	—
Ring B and *ortho*-alkyl groups	*o*-xylene	−0.58	[d]	60	−60	—
Bridge-Br	bromocyclopentane	2.16	[e]	55	90	—
exo-Br	[f]	1.97	—	50	60	4.49[g]
endo-Br	[f]	1.97	—	150	−10	2.00[g]

[a] Φ is angle to Z-axis; [b] θ is angle to x-axis of projection of the moment in the xy plane where the Z-axis is defined as bisecting the C—C—C bridge angle and the zy plane is defined as containing the bridge C—Br bond. [c] N. V. Sidgwich and H. D. Springall, *J. Chem. Soc.*, 1532 (1936). [d] C. P.Smyth and S. O. Morgan, *J. Am. Chem. Soc.*, **49**, 1030 (1927); L. Tigsnik, *Z. physik Chem.* **B13**, 425 (1931). [e] J. D. Roberts and V. C. Chambers. *J. Am. Chem. Soc.* **73**, 5030 (1951) [f] The C—Br component of $PhCH_2Br$]μ=1.87 D, see C. P. Smyth and W. S. Wallis. *J. Am. Chem. Soc.*, **53**, 527 (1931)] calculated by assuming C—C—Br = 110° and $C_{alk} - C_{ar}$ moment = 0.43 D. [g] cf measured moment of 1.82 D.

Table 4

Infrared unassociated ν OH band frequencies (cm⁻¹) for dibenzobicyclo [3,2,1] octadienes [a]

Substituents		Frequency for 4-OH group	
8 Position	4 Position	*exo*	*endo*
syn-Bromo	OH, H	3585	—
syn-Bromo	OH, Me	3570	—
H	OH, H	3620	3588
H	OH, Me	3625	3588

[a] Measured in CCl_4.

(b) *Infrared spectra.* The position of the unassociated νOH stretching band (Table 4) for 4-*endo*- and 4-*exo*-alcohols show that the *endo*-compounds have the lower frequency, but that the frequency of the *exo*-compounds is lowered by an 8-*syn* bromine substituent, which is in a favourable position for intramolecular hydrogen bonding with the hydroxy group (*cf* **8**). The infrared evidence is particularly helpful for relating the methyl series compounds with the desmethyl derivative (see later).

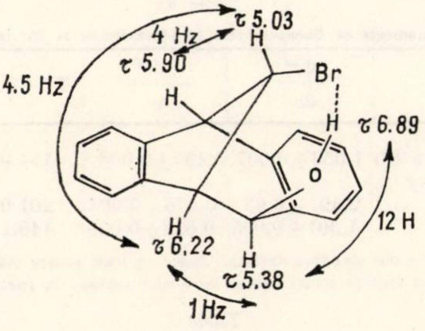

· 8

(c) *NMR spectra.* The spectra of the bromo-hydroxy derivative **8** shows clearly that it is the *exo*-hydroxy compound : in particular the small J_{45} is characteristic ; [5] other J and τ values are in good agreement with previous work on these compounds. [3] The large coupling between the *endo*-H and the hydroxy-H is further evidence for intramolecular hydrogen bond formation which holds these two hydrogens at a dihedral angle near 180°.

CHEMICAL EVIDENCE AND ELUCIDATION OF REACTION MECHANISM

The product of the reduction of the acetoxy derivative (**3**) with $LiAlH_4$ is affected by the purity of the reagent. Different specimens of $LiAlH_4$ gave either the *exo*- (**9**) or the *endo*-4-hydroxy compound (**10**) or a mixture of both. The structure of the alcohols **9** and **10** and of the corresponding acetoxy derivatives are supported by their spectra. Both alcohols (**9** and **10**) give on oxidation the same ketone (**11**).[4]

We first thought that the *exo*-alcohol (**9**) was initially formed in the reduction, and that it was converted into **10** in the presence of strong alkali in some reagent specimens. However, the *exo*-alcohol (**9**) (obtained by solvolysis of dibenzobicyclo [2,2,2] octadienol tosylate)[8] is recovered unchanged after heating with bases, e.g. KOH/EtOH. The *exo*-alcohol (**9**) on heating with sodium hydride in THF is converted in high yield to the ketone **11**;[9,10] similarly the alcohol **4** is converted to the ketone **12**. Reduction of the ketone **11** with $LiAlH_4$ gives as chief product the *endo*-alcohol (**10**) (92.5%) with a little isomer **9** (7.5%) as shown by Cristol and co-workers[4] and confirmed by us. However, reduction of the bromoketone **12** with $LiAlH_4$ gives the *exo*-alcohol **4**. The difference in the behaviour of the ketones (**11** and **12**) on reduction with $LiAlH_4$ must be ascribed to steric hindrance in **12** by the bromine atom at C-8 which directs attack of hydride ion from the less hindered *endo*-direction.

Scheme 2

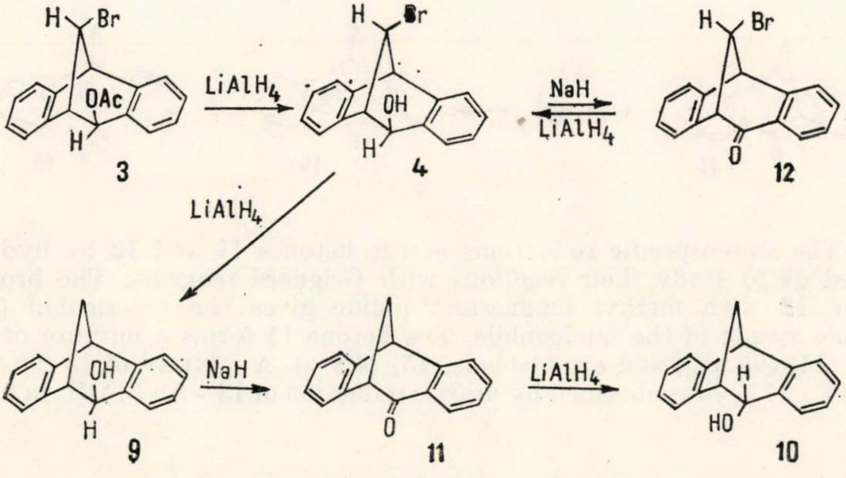

These results support the mechanism of Scheme 2 for the formation of *exo*- (**9**) and *endo*-alcohols (**10**) from the bromoacetoxy derivative (**3**).

[8] E. Ciorănescu, A. Mihai, G. Mihai, M. Elian and C. D. Nenitzescu, *Rev. Roumain Chim.*, **10**, 175 (1965).

[9] E. Ciorănescu, A. Mihai and C. D. Nenitzescu, unpublished.

[10] For the oxidation of secondary alcohols to ketones in the presence of strong bases see W. von E. Doering and R. M. Haines, *J. Amer. Chem. Soc.*, **76**, 482 (1954); R. Cornubert and W. Kondrachoff, *Compte rend.*, **245**, 1362 (1957); B. Alexandre, R. Cornubert, Y. Fagnoni and W. Kondrachoff, *Bull. Soc. chim. France*, **1960**, 661; A. le Berre, *Bull. Soc. chim. France*, **1961**, 1193.

The initialy formed bromohydrin (**4**) is further reduced by $LiAlH_4$ to the *exo*-alcohol (**9**) which reacts with NaH (if this is present to give the ketone **11**, which in turn is reduced with $LiAlH_4$ stereospecifically to yield *endo*-alcohol (**10**). If any bromo-ketone (**12**) is formed from **4**, it is reduced by excess $LiAlH_4$ back to **4** again.

Scheme 3

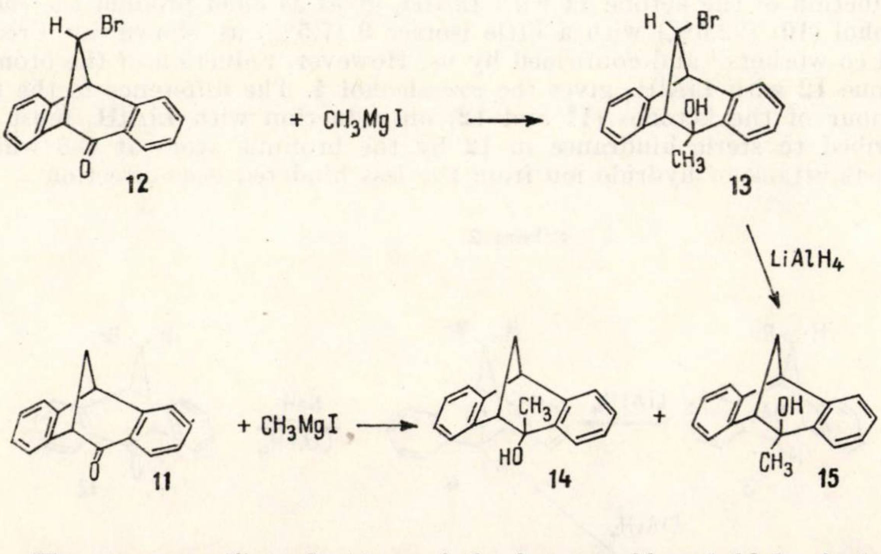

The stereospecific reductions of the ketones **11** and **12** by hydride ion led us to study their reactions with Grignard reagents. The bromo-ketone **12** with methyl magnesium iodide gives the *exo*-alcohol (**13**), by *endo* attack of the nucleophile. The ketone **11** forms a mixture of the *endo*- (**14**) (95.2%) and *exo*-alcohols (**15**) (4.8%). A mixture of **15** (96.3%) and **14** (3.7%)was obtained by drastic reduction of **13** with $LiAlH_4$ inTHF.

EXPERIMENTAL

IR spectra were recorded with double beam Jena UR-20 and Perkin-Elmer Model 21 spectrophotometers. The NMR spectra were determined with Perkin-Elmer R 10 and Varian A 60-A instruments (TMS as internal standard). Gas-liquid chromatographic analyses were carried out on a Carlo Erba Model GD gas chromatograph, using 20% Carbowax 20 M, 1 m, 2 mm columns, H_2 (120 ml/min) as carrier gas, and a column temperature at 225°.

Reduction of exo-4-*acetoxy*-syn-8-*bromo*-2,3,6,7-*dibenzobicyclo*$_0$3,2,1]*octa*-2,6-*diene*(**3**) *with lithium aluminium hydride.* [Note : the $LiAlH_4$ reagent used varied in quality and came from different sources.] A. 3.5 g (10 mmol) **3** in anhydrous THF (60 ml) was heated under reflux for 48 hr with $LiAlH_4$ (2.0 g), then water was added, the ethereal solution was washed with water and evaporated. The oily residue was recrystallized from cycloheaxne yielding the *endo*-hydroxy compound **10** (1.7 g; 77%), m.p. 145°. (*Found*: C, 86.15; H, 6.43. *Calcd.* for $C_{16}H_{14}O$: C, 88.45, H, 6.35%). The alcohol **10** yielded an acetate m.p. 132° after recrystallization from MeOH. (*Found*: C, 81.95; H, 6.12. *Calcd.* for $C_{18}H_{16}O_2$: C, 81.80; H, 6.10%).

B. 0.5 g **3** in THF (10 ml) was heated under reflux for 48 hr with $LiAlH_4$ (0.5 g) and NaH (0.1 g). Treatment as in A above yielded the *exo*-hydroxy compound **9** with 2% **10**.

C. 1 g **3** in THF (20 ml) was heated under reflux for 48 hr in argon with $LiAlH_4$ (1 g) and LiH (0.3 g). Treatment as in A yield only the *exo*-alcohol **9**.

D. 3.5 g **3**, THF (60 ml) and $LiAlH_4$ (2 g) were heated under reflux for 48 hr. Treatment as in A yielded only the *exo*-alcohol **9**.

Reaction of the ketone **11** *with lithium aluminium hydride.* 1 g **11** in ether (25 ml) were heated under reflux 1 hr with $LiAlH_4$ (1 g). Treatment as before gave a mixture of **10** and **9** in the ratio 92.5 : 7.2, determined by gas-liquid chromatography.

Reaction of the ketone **12** *with lithium aluminium hydride.* 0.5 g bromo-ketone **12** in ether (20 ml) was left with $LiAlH_4$ (0.5 g) for 3 hr at room temperature. Treatment as before yielded bromo-alcohol **4** (0.4 g; 80%), with IR and NMR spectra identical to those of an authentic sample.

Reaction of the bromo-alcohol **4** *with sodium hydride.* 0.5 g **4** in THF (10 ml) was heated under reflux for 8 hr with NaH (0.3 g). Treatment as before gave bromo-ketone **12** (0.3 g), with IR spectrum identical to that of an authentic sample.

Attempts to isomerize exo-*alcohol* **9** *to* endo-*alcohol* **10**. A. The *exo*-alcohol **9** (0.5 g) in THF (10 ml) was heated under reflux with NaH (0.3 g) for 4 hr. $LiAlH_4$ (0.3 g) was added and the mixture heated under reflux for 4 hr. Treatment as before yielded the *endo*-alcohol **10** (identified by m.p. and IR spectrum).

B. 0.5 g **9** in THF (10 ml) when heated under reflux with NaH (0.3 g) and $LiAlH_4$ (0.3 g) for 2 hr yielded **9** and **10** in the ratio 66 : 33, determined by gas-liquid chromatography.

C. 1 g **9** in THF (20 ml) when heated under reflux with $LiAlH_4$ (0.5 g) for 48 hr gave only the starting material.

D. **9** was recovered unchanged after heating under reflux for 24 hr with 20% alcoholic KOH.

Attempts to isomerize exo-*alcohol* **4**. **4** gave rise only to starting material when heated under reflux for 24 hr with 20% alcoholic KOH.

Reaction of the ketone **11** *with methyl mangesium iodide.* 1.0 g **11** in ether (20 ml) was added dropwise to a solution of methyl magnesium iodide [prepared from Mg (0.4 g) and MeI (2.5 g) in ether (20 ml)] and the mixture kept at room temperature overnight. Work-up as before followed by chromatography on alumina with ether gave an oil (0.6 g) which contained **14** and **15** in the ratio 95.2 : 4.8, determined by gas-liquid chromatography (*Found*: C, 85.51; H, 7.05. *Calcd.* for $C_{17}H_{16}O$: C, 86.41; H, 6.82%).

Reaction of the bromo-ketone **12** *with methyl magnesium iodide.* 1.0 g **12** was treated as above to yield the *exo*-alcohol **13** (0.7 g), m.p. 105° after recrystallization from MeOH (*Found*: C, 64.95; H, 5.02; Br, 25.65. *Calcd.* for $C_{17}H_{15}BrO$: C, 64.78; H, 4.80; Br, 25.36%).

Removal of bromine from **13** *with lithium aluminium hydride.* Bromo-alcohol **13** (0.5 g) in THF (15 ml) was heated under reflux for 48 hr with $LiAlH_4$ (0.5 g). Treatment as before and chromatography on alumina with ether gave rise to **15** and **14** in the ratio 96.3 : 3.7 as determined by gas-liquid chromatography.

Acknowledgement. We thank Professor S. J. Cristol for helpful correspondence and access to unpublished data.

Revue Roumaine de Chimie, **18**, *3*, 449–461 (1973)

PEPTIDE SYNTHESES WITH N-(ACYL-*o*-NITROPHENYL)-SUBSTITUTED AMINO ACIDS

FLAVIAN CUIBAN

Department of Industrial Chemistry, Polytechnical Institute "Traian Vuia",
Timişoara, POB 103, Romania

Received October 27, 1972

Several N-acylated amino acids with *o*-nitrophenyl-acetyl or 2-methyl-2-*o*-nitrophenoxy-propionyl groups were synthetized and their behaviour during peptide syntheses was investigated. Better results were obtained with 2-methyl-2-*o*-nitrophenoxy-propionyl protected amino acids, which can be prepared with good yields without racemization. After peptide bond synthesis, the acyl residue is readily removed as cyclic lactam, by catalytic reduction under mild conditions and the aminopeptide is easily separated. Optical activity was preserved if in peptide bond syntheses mixed anhydrides or carbodiimides were used but only racemic products were obtained with acid chlorides of protected amino acids.

The use of *o*-nitrophenoxy-acetic and chloroacetic as aminoprotecting groups during peptide synthesis [1,2] could not be extended, because heating is necessary for removal of the protecting groups; this heating can favour some unwished secondary reactions. The study of the reduction of α- and β-*o*-nitrophenyl substituted amides, showed [3] that mainly *o*-nitrophenylacetic (**1**) and 2-methyl-2-(*o*-nitrophenoxy)-acid amides (**2**) present a pronounced tendency to lactamize after hydrogenation. Lactams result even at room temperature and the primary amine involved in carboxyl function amidation is eliminated. This behaviour suggested the possibility of using acids (**1**) and (**2**) as aminoprotecting groups in peptide synthesis. [4] In this paper, experiments are described for this purpose.

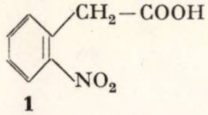

1

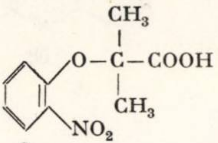

2

The acylation of amino acids with acid chlorides (**1** and **2**), in aqueous media buffered at $pH = 8-10$, did not yield satisfactory results because the acid chloride hydrolyzes partially. Good results were obtained when

---

[1] R. W. Holley and A. D. Holley, *J. Amer. Chem. Soc.*, **74**, 3069 (1952).

[2] S. Akabori, S. Sakakibara and Y. Shimonishi, *Bull. Chem. Soc. Japan*, **31**, 784 (1958); **34**, 739 (1961).

[3] F. Cuiban, *Rev. Roumaine Chim.*, **17**, 897 (1972).

[4] F. Cuiban, *Tetrahedron Letters*, **27**, 2471 (1971).

the corresponding *p*-nitrophenyl esters were used instead of acid chlorides (whose preparation was described in a previous study [3]). N-Acylated amino acids (**3**—**13**) from table 1 were obtained without difficulties (see experimental part) as esters or free acids, depending on the raw material. Only compound (**4**) was obtained in two ways: by glycine acylation and by ester (**3**) hydrolysis. It was established on this occasion that for lysine diacylated products (**6** and **7**) are easily obtained; also the procedure enables to acylate selectively the terminal amine, but separation of pure product is more difficult. Details will be discussed in another work.

In order to test the elimination possibilities of acyl protecting groups from amino acids, catalytical reduction in standard conditions was used, adapting it to the case of *o*-nitrophenyl-substituted amides. [3] Diacylated lysine derivatives (**6** and **7**) and protected phenylalanine (**10**) were used as model substances. Phenylalanine can be considered as a representative of the other protected amino acids, since it does not raise special problems at the elimination process of the protecting groups. Using a diamino acid such as lysine, the order in which the two acyl groups are eliminated could be observed. The protecting group elimination was checked by TLC, on samples taken at various intervals and by separating the reaction products.

Considering the results obtained in the catalytic reduction of α- and β-*o*-nitrophenyl acid amides from the previous work, [3] the simplified reactions, which could occur in the reduction of N^{α}, N^{ε}-di(*o*-nitrophenyl acetyl)-lysine are given in scheme 1.

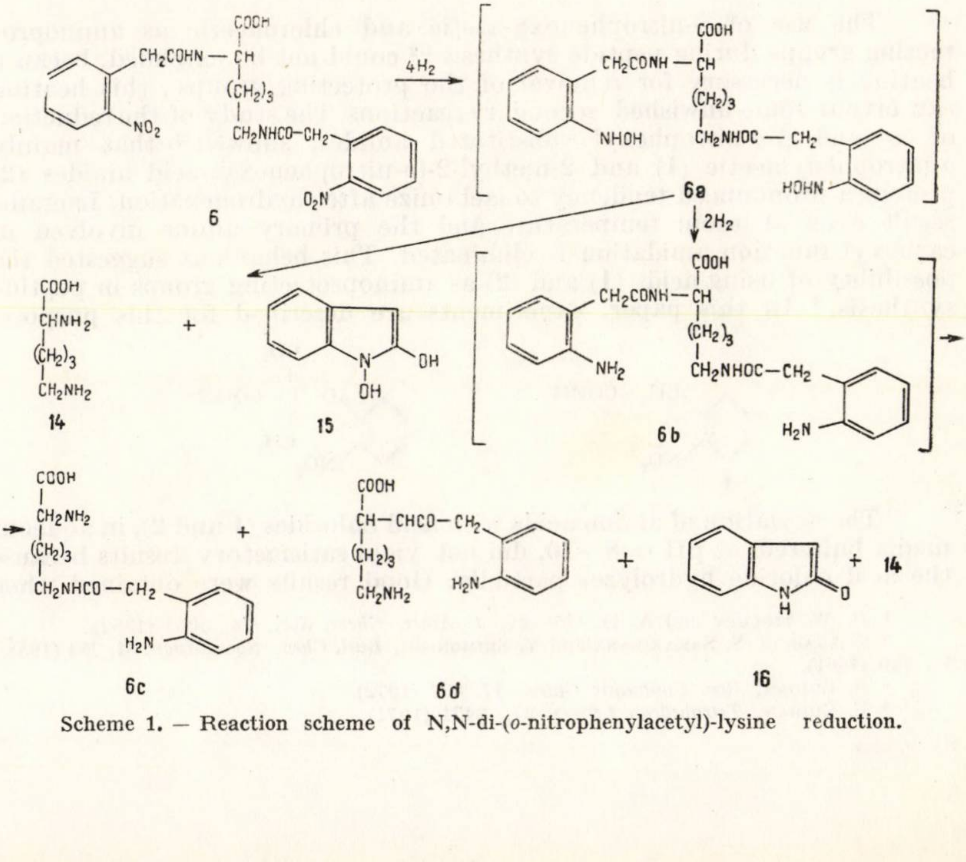
COOH
CH₂COHN — CH
(CH₂)₃
NO₂
CH₂NHCO–CH₂
O₂N
6
4H₂
COOH
CH₂CONH — CH
(CH₂)₃
NHOH
CH₂NHOC — CH₂
HOHN
6a
2H₂
COOH
CHNH₂
(CH₂)₃
CH₂NH₂
14
N
OH
OH
15
COOH
CH₂CONH—CH
(CH₂)₃
NH₂
CH₂NHOC—CH₂
H₂N
6b
COOH
CH₂NH₂
(CH₂)₃
CH₂NHCO — CH₂
H₂N
6c
COOH
CH—CHCO—CH₂
(CH₂)₃
CH₂NH₂
H₂N
6d
N
H
O
16
14

Scheme 1. — Reaction scheme of N,N-di-(*o*-nitrophenylacetyl)-lysine reduction.

Table 1

N-Protected amino acids

No.	Name	Formula	Analysis Calcd./Found			m.p. °C	α_D^{25}	Yield %	Recrystallizing solvent
			C	H	N				
3	N-*o*-Nitrophenylacetyl ethyl glycinate	$C_{12}H_{14}N_2O_5$	54.13 54.30	5.30 5.20	10.52 10.50	122–124	—	98	EtOAc or H_2O
4	N-*o*-Nitrophenylacetyl-glycine	$C_{10}H_{10}N_2O_5$	50.42 50.40	4.31 4.30	11.76 11.70	141	—	75	EtOH
5	N-*o*-Nitrophenylacetyl diethyl-L-glutamate	$C_{17}H_{22}N_2O_7$	55.70 55.38	6.05 5.78	7.64 7.70	78–80	−30 (C = 2, MeOH)	74	EtOAc + petr. ether
6	N$^{\alpha}$, N$^{\varepsilon}$-Di-(*o*-nitrophenylacetyl)-L-lysine	$C_{22}H_{24}N_4O_8$	55.80 55.60	5.11 5.30	11.85 11.64	165–167	+12.9 (C = 1.4, sol. $NaHCO_3$ 5 %),	96	Me_2CO
7	N$^{\alpha}$, N$^{\varepsilon}$-Di-(2-methyl-2-*o*-nitrophenoxypropionyl)-L-lysine	$C_{26}H_{32}N_4O_{10}$	55.70 55.73	5.75 5.80	9.99 10.20	62	−2.4 (C = 2, AcOH)	71	Et_2O
8	N$^{\varepsilon}$-(Benzyloxycarbonyl)-N$^{\alpha}$-(2-methyl-2-*o*-nitrophenoxypropionyl)-L-lysine	$C_{24}H_{29}N_3O_8$	59.10 59.50	5.99 6.20	8.68 8.50	oil	−14.2 (C = 1.7, sol. $NaHCO_3$5%)	83.5	—
9	N-(2-Methyl-2-*o*-nitrophenoxypropionyl)-D,L-phenylalanine	$C_{19}H_{20}N_2O_6$	61.25 61.20	5.41 5.42	7.52 7.45	151	—	87	MeOH
10	N-(2-Methyl-2-*o*-nitrophenoxypropionyl)-L-phenylalanine	$C_{19}H_{20}N_2O_6$	61.25 61.30	5.41 5.45	7.52 7.60	138	−15 (C = 1.4 MeOH)	84.5	MeOH
11	N-(2-Methyl-2-*o*-nitrophenoxypropionyl)-L-valine	$C_{15}H_{20}N_2O_6$	55.54 55.62	6.21 6.11	8.63 8.60	11	−7.5 (C = 4, MeOH)	70.5	—
12	N-(2-Methyl-2-*o*-nitrophenoxypropionyl)-D,L-leucine	$C_{16}H_{22}N_2O_6$	56.79 56.80	6.55 6.60	8.27 8.30	123	—	73	EtOH–H_2O
13	N-(2-Methyl-2-*o*-nitrophenoxypropionyl)-L-leucine	$C_{16}H_{22}N_2O_6$	56.79 57.00	6.55 6.80	8.27 8.40	95	−32 (C = 2, MeOH)	60	EtOH–H_2O

In our experimental conditions, neither hydroxylaminic derivatives (**6a**) resulted by partial reduction, nor 1,2-dihydroxyindole (**15**) could be evidenced in the reaction medium. At the end of the hydrogenation, most of the product appears as lysine (**14**) together with the corresponding equivalent of 2-hydroxyindole (**16**) alone with small quantities of monoacylated reduction products either in position ε (**6c**) or in α (**6d**). In TLC, they appear with very different Rf values, and are distinguished by ninhydrine colouring. For the N^{ε}-acylated derivative (**6c**) the colouring appears immediatly at cool, while the N^{α}-acylated (**6d**) derivative is coloured by ninhydrine only on warming or during a longer time at room temperature. Judging from the size of the spots and their colour intensity, the N^{ε}-acylated product (**6c**) appears in greater amount, and unlike (**6d**), traces of (**6c**) can be observed on the chromatogram even after preserving the reaction mixture for 24 hours at room temperature. By solvent elimination at 40—50°,the entire lysine appears free, indicating the full elimination of the protecting groups.

On hydrogenation of the diacylated derivative of lysine (**7**) with 2-methyl-2-(*o*-nitrophenoxy)-propionic acid, when hydrogen absorption stops, the entire amount of lysine occurs as free product. The reduced monoacylated derivatives, similar to products (**6c** and **6d**), were never obtained, but only the lactam and lysine (**14**) according to the reaction scheme 2.

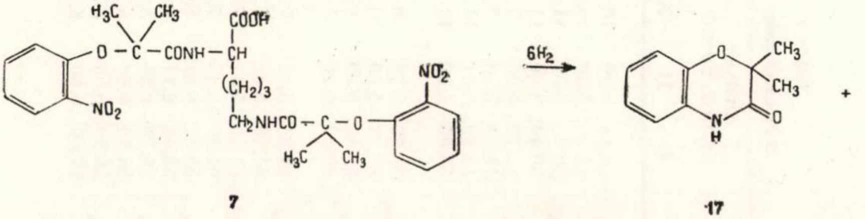

Scheme 2. — The reduction of N,N-di-(2-methyl-2-*o*-nitrophenoxy-propionyl)-lysine.

The acyl residue elimination on reduction of the protected phenylalanine (**10**), occurred according to a similar scheme, yielding free phenylalanine and lactam (**17**). In all cases, the deprotected amino acid is obtained unracemized, in practically quantitative yield. Owing to the water insolubility of the secondary cyclic derivatives (**16**), and (**17**) respectively, the separation of free amino acids was achieved very easily. It was observed from these data, that unlike the model amides studied in the previous work, [3] in the case of acylated amino acids, perceptible differences in the elimination of *o*-nitrophenylacetyl protecting groups appeared in opposition to 2-methyl-(*o*-nitrophenoxy)-propionyl, the latter being eliminated more easily.

Although some other acyl groups for protecting the amine function in peptide synthesis are easily eliminated, they cannot be widely employed because in the activation stage of the carboxyl group, racemization occurs on account of azlactone formation. [5] The decomposition of the acylamino acids was noticed, when converted in acid chlorides [6] with $SOCl_2$ or PCl_5;

---

[5] A. Hillmann and G. Hillmann, *Z. Naturforsch.*, **6b**, 340 (1951).

[6] J. C. Sheehan and D. H. Jang, *J. Amer. Chem. Soc.*, **80**, 1154 (1958).

the peptide yields were poor, when the azide[7] method was used. The danger of racemization is greater in peptide syntheses with acylamino acids and it varies in function of the activation method (acid chloride, mixed anhydride, active ester, etc.) and experimental conditions (temperature, solvent nature, pH, etc.).

In order to investigate the racemization tendency and to test the behaviour of 2-methyl-2-(*o*-nitrophenoxy)-propionic amino acids for peptide bond formation, model substances with optically active amino acids were prepared, and different activation methods frequently applied for peptide preparation, were used. Finally, optical activity of different synthetized products was compared to authentic samples. Protected phenylalanine (**10**) was condensed with ethyl glycinate by means of acid chloride, mixed anhydride (with carbonic ester) or N,N′-dicyclohexylcarbodiimide (DCC). After total deprotection of the product (**20**) optical purity of phenylalanylglycine (**23**) was compared to optically pure product.[8]

(i) — As it appears in scheme 3, L-phenylalanine (**10**) was condensed with ethyl glycinate by means of acid chloride and yielded a completely racemized product. Racemization occurs even in the obtaining of acid chloride (**18**), since the solution resulted at chlorination lacks optical activity, while in alkaline hydrolysis the racemic protected amino acid results (**9**). By ethereal extraction of the acid chloride (**18**) an optically inactive product was separated, by which IR spectroscopy offers the characteristic absorption of azlactones in the 1835—1840 cm^{-1} range. This absorption band completely disappears on treating with triethylamine and *p*-nitrophenol in accordance with the results published by Young,[9] referring to base-catalyzed racemization of acylpeptides.

(ii)—In opposition to acid chloride activation *via* mixed anhydrides, dipeptide (**20**) was obtained, and after saponification of (**22**) and elimination of the protecting group, phenylalanyl glycine (**23**) presented optical activity as indicated in the literature. The condensation yield *via* mixed anhydrides is not quantitative (61.5%). By adequate processing of the reaction product, the unreacted carboxyl component (**10**) having initial optical activity, was isolated.

The obtention of an optically active product is in contradiction to the general remarks of several authors,[10–12] who noticed an advanced racemization, when mixed anhydrides for amino acid activation were used.

(iii)—Condensation of acyl-phenylalanine (**10**) with ethylglycinate in the presence of N,N′-dicyclohexylcarbodiimide affords very good yields (98%), and the resulted product (**20**—**23**) is optically pure dipeptide. The unreacted carboxyl component isolated from the reaction mixture, preserves full initial optical activity just as in the case of mixed anhydrides.

---

[7] F. R. King, J. W. Clark-Lewis, D. D. A. Kidd and R. Smith, *J. Chem. Soc.*, **1954**, 1039.

[8] J. C. Sheehan, D. W. Chapman and R. W. Roth, *J. Amer. Chem. Soc.*, **74**, 3822 (1952).

[9] I. Antonovici and G. T. Young, *J. Chem. Soc.*, **1967**, 595.

[10] V. du Vigneaud and C. E. Meyer, *J. Biol. Chem.*, **99**, 143 (1932—1933).

[11] R. A. Boissonnas, *Adv. Org. Chem.*, **3**, 159 (1963).

[12] N. A. Smart, G. T. Young and M. W. Williams, *J. Chem. Soc.*, **1960**, 3903.

The experimental data obtained by mixed anhydride and DCC activation of the carboxyl group, demonstrate that racemization does not occur. The formation of an azlactone from mixed anhydride **(19)** or from the activated compound **(21)** is probably hindered by a steric effect, owing to the presence of the two bulky methyl groups in the proximity of the reaction center. Consequently, the intramolecular attack of the carbonyl oxygen on the activated carboxyl group from **(19)** and **(21)**, in order to form azlactone, hardly occurs or is even prevented. In the case of acid chloride the steric effect of the two methyl groups is not detectable, on account of the smaller volume of chlorine in relation to the substituents of the activated compounds **(19)** and **(21)**.

The following experimental data also plead to support this explanation. The conversion of acyl-phenylalanine **(10)** into anilide **(24)** by means of the acid chloride, results in the total loss of optical activity, while with mixed anhydride **(19)** optically active **(24)** was obtained.

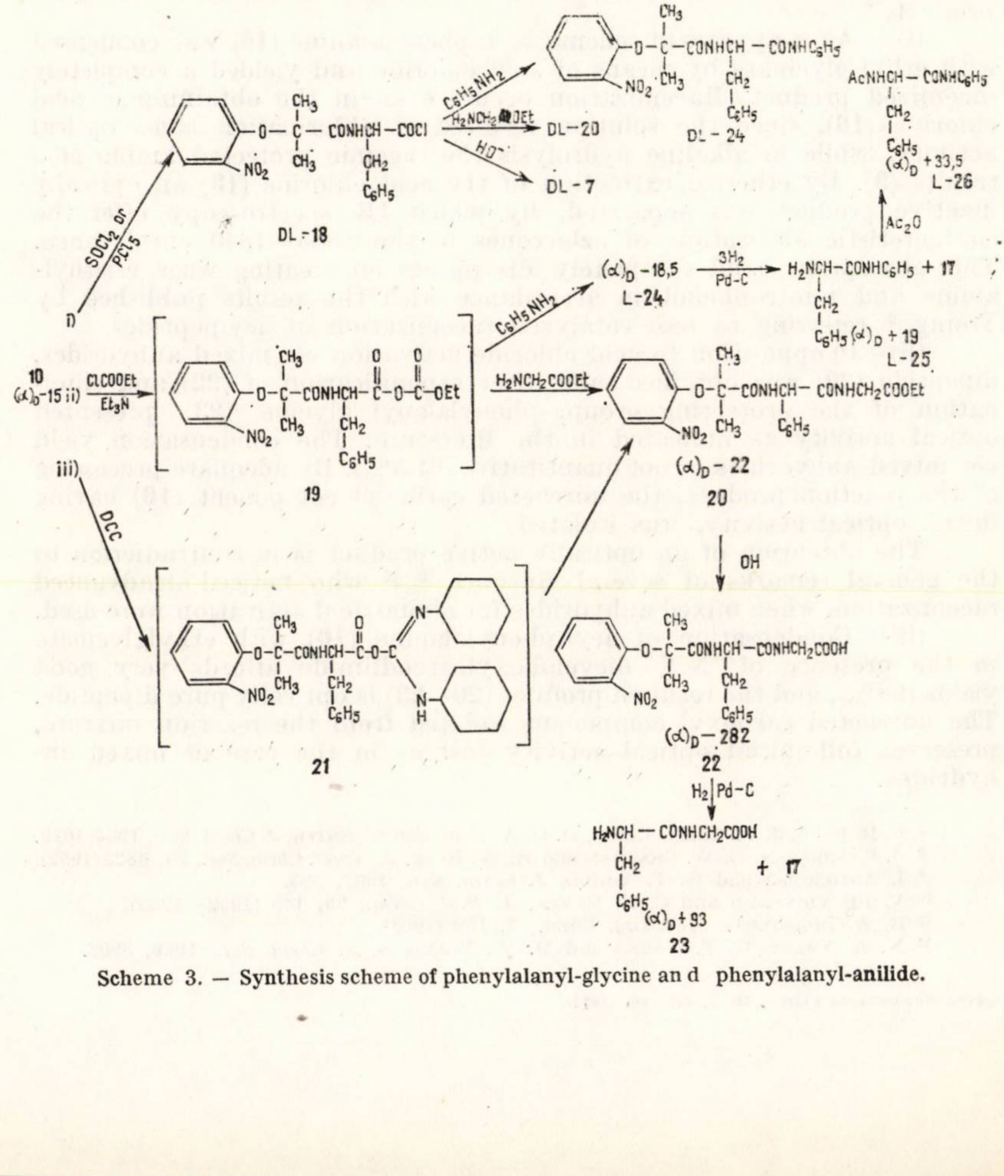
10
(α)D -15 i)
i)
ii)
iii)
ClCOOEt
Et3N
SOCl2 or PCl5
DL - 18
DL - 20
DL - 7
DL - 24
C6H5NH2
H2NCH2COOEt
HO⁻
AcNHCH — CONHC6H5
(α)D +33,5
L-26
Ac2O
(α)D -18,5
L-24
3H2
Pd-C
H2NCH-CONHC6H5 + 17
(α)D + 19
L-25
19
20
(α)D - 22
DCC
21
OH
22
(α)D - 282
H2 Pd-C
H2NCH — CONHCH2COOH
+ 17
(α)D + 93
23

Scheme 3. — Synthesis scheme of phenylalanyl-glycine an d phenylalanyl-anilide.

Phenylalanyl-anilide **(25)** separated after catalytic hydrogenation, has the same optical activity as the optically pure product described in the literature, [8] and the acetylated derivative **(26)** has a greater positive rotation than **(25)**.

Also 2-methyl-2-(*o*-nitrophenoxy)-propionyl-alanyl-L-leucine **(13)** behaves in a similar manner with the protected phenylalanine (see scheme 4). The anilide **(28)** resulted from acid chloride **(27)** is racemic, while the anilide formed *via* mixed anhydride, after deprotecting **(30)** by catalytic reduction and benzoylation, yields benzoyl-L-leucyl-anilide **(31)** having the same optical activity as that described in literature. [13]

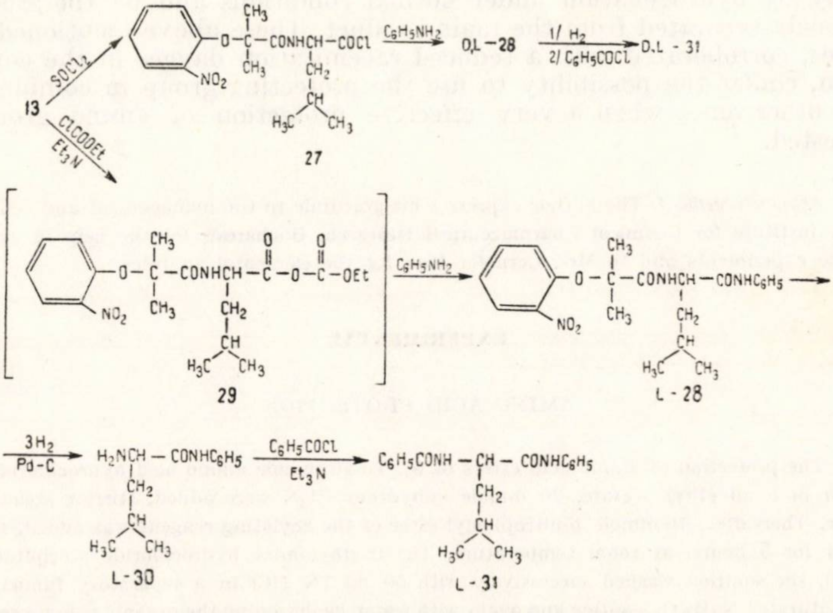

Scheme 4. — Leucyl-anilide synthesis scheme.

As may be seen from scheme 3, 2-methyl-2-(*o*-nitrophenoxy)-propionyl-peptide ester **(20)** can be used further in peptide synthesis. The two protecting groups can be selectively eliminated. By base-catalysed hydrolysis, free acid **(22)** results. By catalytical reduction, the protecting group of the amine was eliminated. Reduction time is very short, and as it was demonstrated by the chromatograms at the end of hydrogen adsorption, the protecting group is eliminated fully under the form of 3,3-dimethylbenzomorpholone **(17)**. The separation of the amine component, free from products resulted after protecting group elimination, involves no complication.

From the given data and those described in the experimental part, it can be concluded that the protection of amino groups by the 2-methyl-

---

[13] M. Bergman and H. Fraenkel-Conrat, *J. Biol. Chem.*, **119**, 707 (1937).

2-(*o*-nitrophenoxy)-propionyl residue can find applications in peptide synthesis, having at the same time some peculiarities which could offer advantages in relation to the used reagents and the experimental techniques. The acylation agent is prepared easily, is pure and stable, enables the achievements of high protecting yields, without racemization danger, such as occurs in the case of phthalyl, formyl or trifluoroacetyl groups. The protecting groups confer a better crystallinity to the protected amino acids (especially in comparison to urethanes), stability in acid media and undefined stability. The presence of the nitro group in the peptide molecule enables the determination of very small amounts of products by U.V. absorption at 255 nm. Elimination of the protecting group occurs simply by hydrogenation under normal conditions and by the products are easily separated from the main product. These above mentioned properties, corroborated with a reduced racemization danger in the condensation, confer the possibility to use the protecting group in combination with other ones, when a very effective protection of amino group is requested.

Acknowledgement. The author expresses his gratitude to the management and colleagues of the Institute for Chemical Pharmaceutical Research, Bucharest, for the help in carrying out the experiments and to Mrs. Cornelia Ioan for the elemental analyses.

EXPERIMENTAL

AMINO ACID PROTECTION

The protection of amino acid esters (**3, 5**). To 10 mmole amino acid hydrochloride, suspended in 5 ml ethyl acetate, 20 mmole anhydrous Et_3N were added, stirring steadily for 1 hour. Thereafter, 10 mmole *p*-nitrophenyl ester of the acylating reagent was added, stirring further for 5 hours, at room temperature. The triethylamine hydrochloride precipitate was filtered, the solution washed successively with 50 ml 1N HCl in a separatory funnel, then with saturated $NaHCO_3$ solution and again with water, maintaining the organic volume constant by fresh solvent addition. After drying the solution on anh. Na_2SO_4, the solvent was removed in vacuum and the residue recrystallized from an adequate solvent.

Saponification of the protected amino acid ester (**3**). To the solution of 10 mmole N-protected amino acid ester in 30–50 ml *t*-butanol, 15 mmole aqueous solution of 2N NaOH was added, stirring for 2–3 hours, at room temperature. After complete hydrolysis, that can be controlled by TLC on silica plates, 40 ml water was added and the solvent removed in vacuum, with a rotatory evaporator. The residue solved in 40 ml water, acidulated to pH = 6 and the unreacted product was extracted with ethyl ether. The ice-cooled aqueous solution was acidulated to pH = 2, when the N-protected amino acid separated, filtered, dried and recrystallized from an adequate solvent.

Amino acid acylation (**4, 8, 9–13**). To the solution of 25 mmole $KHCO_3$ in 15 ml water and 10 mmole amino acid, a solution of 10 mmole *p*-nitrophenyl ester of the acylating agent in 10 mmole acetone was added under stirring. Several times, some part of the acylating agent precipitated, but by prolonging its stirring at room temperature for 2 hours, a homogeneous solution was obtained. The mixture was heated to reflux for 2–4 hours controlling the disappearance of free amino acid on silica plates. Eluent- benzol : acetone : acetic acid (60 : 35 : 5 in volume); free amino acid was evidenced by means of ninhydrine solution.

Acetone was removed in vacuum, the residue dissolved in 70 ml distilled water, acidulated to pH = 6, and *p*-nitrophenol and the unreacted ester were extracted 3 times with 15 ml ethyl acetate. Solvent traces were eliminated in vacuum from the aqueous solution, and N-acylated amino acid was precipitated, from the ice-cooled solution with HCl 10%, until pH = 2. When the amino acid did not crystallize satisfactorily, the sedimented oil was extracted with ethyl acetate and, after drying and solvent removal, it was recrystallized from a suitable solvent.

Lysine diacylation (**6**,**7**). To the solution of 10 mmole lysine base in 15 ml 1 molar $NaHCO_3$, 20 mmole *p*-nitrophenyl ester of the acylating acid, dissolved in 40 ml acetone, was added. The mixture heated for 3 hours to reflux on a water bath, provided a homogeneous solution. With TLC (on silica with sec$-$BuOH : HCOOH : H_2O = 75 : 15 : 10) a prelevated sample indicated the full reaction of lysine into the diacylated derivative and a small amount of N^{ε}-acylated derivative.

The solvent was removed in vacuum, the residue dissolved in 30 ml water, treated with HCl 10% to pH = 6 and the resulted *p*-nitrophenol has been extracted with ethyl acetate. To the 0° cooled aqueous solution HCl was added till pH = 1, when the diacylated product precipitated. For the removal of lysine and monoacylated derivative traces, the precipitate was extracted with 2 portions of 25 ml dichloromethane, the unified extracts were washed successively with 20 ml 2N HCl and water. The solution was dried over Na_2SO_4 and after solvent removal in vacuum, the residue was recrystallized from the solvent mentioned in table 1.

THE ELIMINATION OF PROTECTING GROUPS FROM AMINO ACIDS

To the Pd$-$C 5% (0.5 g) catalyst in 10 ml glacial acetic acid, previously hydrogenated, [3] 1 mmole protected amino acid, solved in 10 ml glacial acetic acid, was added. The theoretical amount of hydrogen was absorbed in 10$-$30 minutes, thereafter absorption stopped. Reduction and cleavage processes of the protecting groups were controlled with TLC (on silica G plates, by means of the solvent system sec-BuOH : H_2O : HCOOH = 75 : 10 : 15, and iodine vapour colouring or ninhydrine solution).

The catalyst filtered on a cellite layer was washed with acetic acid. The solution was concentrated in vacuum, eliminating acetic acid in an advanced manner by adding water to the residue and evaporating. The residue was treated with 5 ml water, 1 mmole HCl, and the resulting lactam separated by filtering. For full elimination of the cyclized product, the aqueous solution was extracted by ethyl ether, and processed in order to separate the free amino acid.

For the separation of monoamino-monocarboxyl acids, the solution was neutralized to pH = 6, when the amino acid crystallized. Concerning lysine, the monohydrochloride solution was concentrated to a small volume, and precipitated with alcohol or acetone. The deprotection yield is quantitative. The separated amino acids have equal specific rotation values to the initial ones. The lactams separated by cyclization do not colour with a solution of FCl_3 5% (N-hydroxy-lactams are absent) and do not depress the melting point, in a mixture with authentic products. [3]

SYNTHESIS OF THE PEPTIDE BOND AND ANILIDES; CONTROL OF RACEMIZATION

2-*Methyl*-2-(*o-nitrophenoxy*)-*propionyl-D,L-phenylalanyl-ethyl glycinate* (*D,L*-**24**)

i. To 3.72 g (10 mmole) protected L-phenylalanine (**10**) dissolved in 50 ml anhydrous benzol, 1.45 ml (20 mmole) $SOCl_2$ was added, and refluxed 2 hours on a water bath. The excesses of $SOCl_2$ and solvent were removed in vacuum, while the residue was solved in 50 ml anhydrous benzol.

To a suspension of 5.6 g (40 mmole) glycine ethyl ester hydrochloride acid in 50 ml chloroform, a KOH solution (3.5 g in 3.5 ml water) was added under very strong stirring. To the separated chloroformic layer, dried over anh. K_2CO_3, filtered and cooled to $-10°$, the solution of acid chloride in benzene was added under stirring. The mixture was kept for 2 hours at room temperature, washed successively with 30 ml solution of HCl 5%, water, saturated $NaHCO_3$ solution and again water. By acidifying the aqueous bicarbonate solution previously resulted, 0.18 g acyl-phenylalanine (m.p. 147–149°) was separated. After recrystallization from water-alcohol (m.p. 150–151°), it was similar to the racemic product of acylated phenylalanine (**9**). *Calcd.* : $C_{19}H_{20}N_2O_6$, C : 61.25 ; H : 5.51 ; N : 7.52 ; *Found* : C : 61.20 ; H : 5.42 ; N : 7.45%. $(\alpha)_D^{25} = 0$.

The organic solution was dried over anh. Na_2SO_4, the solvent removed in vacuum and the residue mixed with 10 ml anh. Et_2O and let to crystallize at cool. By filtering, 4.03 g D,L-**24**) m.p. 130–133°) were separated, in 88% yield. After recrystallization from abs. methanol, (m.p. 134–135.5° ; $(\alpha)_D^{25} = 0$ (c = 2, MeOH abs.) *Calcd.* : $C_{23}H_{27}N_3O_7$, C : 60.38 ; H : 5.94 ; N : 9.18 ; *Found* : C : 60.6 ; H : 5.98 ; N : 9.20%.

The product synthetized from (**9**) and ethyl glycinate has the same properties.

2-*Methyl*-2-(*o-nitrophenoxy*)-*propionyl-L-phenylalanyl-ethyl glycinate* (L-**24**).

ii. (*via* N,N′-Dicyclohexyl carbodiimide ; DCC)

To the solution of 3.72 g (10 mmole) (**10**) in 20 ml anhydrous dioxane and 20 ml dichloromethane, 1.03 g (10 mmole) freshly distilled ethyl glycinate was added, cooled to $-10-15°$. Under energetic stirring, 2.06 g (10 mmole) DCC, solved in 10 ml dichloromethane, was added dropwise, stirring further for 2 hours permitting temperature to increase until room temperature. After standing over night, one drop of glacial acetic acid was added, stirred for an hour, the resulted dicyclohexylurea filtered, and washed with dioxan. The solution was evaporated and the crystalline residue was dissolved in 150 ml dichloromethane. It was successively washed with 50 ml HCl 5%, water, saturated $NaHCO_3$ solution, again with water and then dried on anh. Na_2SO_4. Acidulating the aqueous $NaHCO_3$ solution, 0.13 g (**10**) were recovered, m.p. 132–134°.

The drying agent was eliminated by filtering, the solvent removed and the residue recrystallized in 12 ml absolute methanol. 3.97 g (**24**) crystalline, white product was achieved, with m.p. 138° (87% yield) ; $(\alpha)_D^{25} = -22$ (c = 2.29, absolute methanol). *Calcd.* : $C_{23}H_{27}N_3O_7$, C : 60.38 ; H : 5.94 ; N : 9.18 ; *Found* : C : 60.6 ; H : 6.10 ; N : 9.12%.

The experiment repeated with greater amounts of reagents yielded 98% of the theory.

iii. (*via* Mixed anhydride method)

To the solution of 3.72 g (10 mmole) (**10**) in 10 ml purified dichloromethane, 1.4 ml (10 mmole) anh., freshly distilled Et_3N were added. Cooled to $-15°$, 0.95 ml (10 mmole) freshly distilled ClCOOEt, dissolved in 3 ml dichloromethane were added dropwise, under stirring. After 15 min, 1.03 g (10 mmole) freshly distilled ethyl glycinate, solved in 30 ml dichloromethane were added, stirred at low temperature for 30 min and post-reacted for 2 hours at room temperature. The reaction mixture was washed successively with 30 ml HCl 5% solution, water, saturated $NaHCO_3$ solution and again with water. By acidulating the $NaHCO_3$ solution, 0.6 g 2-methyl-2-(*o*-nitrophenoxy)-propionyl-L-phenylalanine (**10**) with m.p. 130–134°, were recovered.

After drying the solution over Na_2SO_4, the solvent was removed in vacuum, the residue mixed with 10 ml absolute Et_2O, and put to crystallize at cool. After filtering, 2.35 g (L **20**) m.p. 135–137° were obtained, that increased to 138° when recrystallized from absolute methanol; 65% yield. *Calcd.* : $C_{23}H_{27}N_3O_7$, C : 60.38 ; H : 5.94 ; N : 9.18 ; *Found* : C : 60.4 ; H : 6.00 ; N : 9.14%. $(\alpha)_D^{25} = 21.8$ (c = 2, absolute methanol).

2-*Methyl*-2-(*o-nitrophenoxy*)-*propionyl-L-phenylalanyl-glycine* (**22**)

To a suspension of 4.72 g (**20**) (10.32 mmole) in 110 ml *t*-butyl alcohol, 10 ml 2N NaOH were added. A yellow homogeneous solution was obtained after stirring for 1 hour. It was stirred in addition for 2 hours, added 150 ml water, and the solvent removed in vacuum, by a rotatory evaporator. The residue was solved in 100 ml water, acidulated to pH = 6, and the traces of unreacted products were extracted 3 times with 20 ml Et_2O.

The solvent traces were eliminated from the aqueous solution, and after cooling to 0°, acidifying to pH = 2, a yellow product, crystallizing in time, was achieved. After filtering in vacuum, drying over P_2O_5, 4 g (**22**) m.p. 110–112° and $(\alpha)_D^{25} = -212$ (c = 2, abs. methanol) were achieved. Yield-90%. Through recrystallization with abs. methanol-ether 1:1, the melting point increases to 124–126° and $(\alpha)_D^{25} = -282$. *Calcd.* : $C_{21}H_{23}N_3O_7$, C : 58.73 ; H : 5.39 ; N : 9.78 ; *Found* : C : 58.70 ; H : 5.80 ; N : 9.68%.

L-Phenylalanyl-glycine (**23**)

To a suspension of 1.5 g g Pd–C 5% catalyst in 20 ml acetic acid hydrogenated at room temperature, 1.24 g (2.84 mmole) 2-methyl-2-(*o*-nitrophenoxy)-propionyl-L-phenylalanyl-glycine (**22**) solved in 20 ml acetic acid was added and the reduction was continued. Hydrogen absorption stopped after 30 min, while TLC (on silica G plates, with $C_6H_6 : CH_3COCH_3 : CH_3COOH = 60 : 35 : 5$) indicates the full cleavage of the protecting group. The free peptide remains at start, while the initial product has Rf = 0.5 (colouring with iodine and ninhydrine solution). Samples do not give positive reaction with $FeCl_3$ 5% solution and neither on diazotization and coupling with β-naphthol.

The catalyst was filtered on a cellite layer, and the solvent removed in vacuum. To the oil-like residue, 3 ml 1N HCl solution and 5 ml water were added; 0.5 g 3,3-dimethylbenzmorpholone was separated by filtering. The aqueous solution was 3 times extracted with 20 ml Et_2O in order to eliminate the cyclized product traces and concentrated in vacuum. The residue was solved with 5 ml water, neutralized with a solution of Et_3N 5% to pH = 6 and concentrated in vacuum. The residue was triturated with 15 ml acetone, and the free peptide filtered. In order to remove triethyl amine hydrochloride, the precipitate was refluxed with 10 ml chloroform, yielding 0.62 g L-phenylalanyl-glycine, m.p. 250–252° (decomposition). Crystalline product was obtained after recrystallization from water-acetone and dried over P_2O_5, m.p. 258–260° (decomposition). $(\alpha)_D^{25} = 93$ (c = 2, water). *Calcd.* : $C_{11}H_{14}N_2O_3$ 1/2 H_2O, C : 57.12 ; H : 6.54 ; N : 12.1 ; *Found* : C :. 57.20 ; H : 6.70 ; N : 12.17%.

2-*Methyl*-2-(*o-nitrophenoxy*)-*propionyl-D,L-phenylalanyl-anilide* (D, L-**24**)

To the solution of 1.20 g (3.22 mmole) 2-methyl-2-(*o*-nitro-phenoxy)-propionyl-L-phenylalanine (**10**) in 16 ml anh. benzene, heated to reflux on a water bath, 0.8 g (6.72 mmole) $SOCl_2$ were added. The solvent and $SOCl_2$ excess were removed in vacuum after 2 hours, and the residue solved with 20 ml anh. benzene. To the ice-cooled solution of 0.30 ml (3.22 mmole) aniline and 0.46 ml (3.22 mmole) triethylamine in 20 ml benzene, a solution of benzene-acid chloride was added. It was kept over night and washed successively with 20 ml water, 2N HCl saturated $NaHCO_3$ solution and again with water. After drying over natrium sulphate, the benzene solution was concentrated to sicc., while the oil-like residue, recrystallized from acetic acid, yielded 0.91 g white crystalline D,L anilide (**24**), m.p. 158—159°, soluble in Et_2O, insoluble in petroleum ether; $(\alpha)_D^{25} = 0$ (c = 2, abs. methanol); *Calcd.*: $C_{25}H_{25}N_3O_5$, C: 67.09; H:5.63; N: 9.39; *Found*: C: 67.10; H: 5.70; N: 9.50%.

2-Methyl-2-(o-nitrophenoxy)-propionyl-L-phenylalanyl-anilide (L-**24**)

To the solution of 3.72 g (**10**) (10 mmole) in 40 ml dichloromethane, 1.4 ml (10 mmole) Et_3N was added, cooling at —15° with ice and salt. 0.95 ml (10 mmole) ClCOOEt, solved in 10 ml dichloromethane were dropped, stirred for 30 min at low temperature, and 1 ml (11 mmole) aniline dissolved in 10 ml dichloromethane was added. It was stirred for 1 hour at low temperature and kept over night, at room temperature.

The reaction mixture was thoroughly washed successively with 20 ml HCl 10% water, saturated $NaHCO_3$ solution, and again with water. Acidulating the aqueous bicarbonate solution, 2.12 g unreacted (**10**) crystallized. After drying the organic solution over anh. Na_2SO_4 and solvent removal in vacuum, 2 g white, crystalline anilide (L **24**), m.p. 138—140° was obtained. The yield is quantitative, considering the recovered product (**10**) too. After recrystallization from EtOH and drying over P_2O_5, m.p. 142°; $(\alpha)_D^{25} = -18.5$ (c = 1.85, abs. methanol). *Calcd.*: $C_{25}H_{25}N_3O_5$, C: 67.05; H: 5.65; N: 9.39; *Found*: C:67.00; H:5.80; N: 9.25%.

L-Phenylalanyl-anilide (**25**)

After catalytical reductive removal of the protecting group of (**24**) under standard conditions, L-phenylalanyl-anilide had close properties to those described in literature,[8] m.p. 70—73°; $(\alpha)_D^{25} = 18.5$ (c = 1.85, absolute methanol).

N-acetyl-L-phenylalanyl-anilide (L **26**)

To the solution of 0.24 g (1 mmole) L-phenylalanyl-anilide (**25**) in 10 ml 1N HCl, 1 ml saturated $NaHCO_3$ solution and 1 ml Ac_2O were added. After 30 min, 1 ml Ac_2O was still added, heated to boiling, and acetic acid added until a clear solution was obtained. After cooling, 0.25 g (**26**) crystallized, m.p. 193—195°, in 88.5% yield. Recrystallized from abs. methanol, m.p. increased to 195—196°. $(\alpha)_D^{25} = 33.5$ (c = 2.7, glacial acetic acid). *Calcd.*: $C_{17}H_{18}N_2O_2$, C:71.30; H: 6.33; N: 9.78; *Found*: C:71.20; H: 6.40; N: 9.50%.

2-*Methyl*-2-(*o-nitrophenoxy*)-*propionyl-D,L-leucyl-anilide* (D,L-**28**)

Starting from the acylated L-leucine (**13**) derivative, by acid chloride conversion (**27**), as described at the suitable product of L-phenylalanine (**24**), the racemized anilide was obtained, m.p. 140—144°, in 77% yield. The melting point remains unchanged, after recrystallization from ethyl alcohol. $(\alpha)_D^{25} = 0$ (c = 2, abs. methanol) *Calcd.*: $C_{22}H_{27}N_3O_7$, C: 63.9; H: 6.58; N: 10.16; *Found*: C: 64.20; H: 6.80; N: 10.30%.

N-Benzoyl-D,L-leucyl-anilide (D,L-**31**)

To a suspension of 1 g Pd—C 5% in 20 ml acetic acid, previously hydrogenated, the solution of 1.25 g (3 mmole) (D,L **28**) in 20 ml glacial acetic acid was added. After the absorption of the theoretical hydrogen amount (205 ml), the catalyst was filtered on a cellite layer and washed with acetic acid. TLC (on silica G with chloroform : ethyl acetate = 4:1, iodine vapour and ninhydrine colouring) evidenced the total disappearance of the initial product (Rf = 0.7), the deprotected product appeared at start while 3,3-dimethyl-benzmorpholone at Rf = 0.77.

To the filtered solution, 3.2 ml HCl 1N and 5 ml water were added, and acetic acid was removed in vacuum. The residue resolved with 5 ml water, separated 0.5 g 3,3-dimethyl-benzmorpholone after filtering m.p. 165—167°, while the solution did not yield positive $FeCl_3$ reaction, thus not containing N-hydroxy-lactam.

The aqueous solution was concentrated to sicc in vacuum, dried over P_2O_5, yielding 0.72 g leucyl-anilide hydrochloride, very deliquescent, in 100% yield. The product was solved with 15 ml water, neutralized with 2N NaOH, pH = 9—10, and the base extracted 3 times with 15 ml Et_2O. After drying the ethereal solutions over anh. Na_2SO_4, it was treated with 1 ml Et_3N, ice-cooled, and to this added 0.5 ml anh. benzoyl chloride. Finally, 0.57 g, white, crystalline N-benzoyl-D,L-leucyl-anilide, m.p. 179—180°, was obtained; melting point 196°, after recrystallization from ethyl alcohol. *Calcd.* : $C_{19}H_{22}N_2O_5$, C : 73.52 ; H : 7.14 ; N : 9.02 ; *Found* : C : 73.70 ; H : 7.30 ; N : 9.05 %.

2-Methyl-2-(o-nitrophenoxy)-propionyl-L-leucyl-anilide (L-**28**)

The synthesis procedure was similar to that adopted for L-phenylalanyl-anilide (L-**24**), *via* mixed anhydride, in a 70.5 % yield ; a white product resulted when crystallized from ethyl alcohol. M.p. 127—128°. $(\alpha)_D^{25} = -13$. (c = 1.5, abs. methanol). *Calcd.* : $C_{22}H_{27}N_3O_5$, C : 63.90 ; H : 6.58 ; N : 10.16 ; *Found* : C : 64.00 ; H : 6.70 ; N : 10.25 %.

N-Benzoyl-L-leucyl-anilide (L-**31**)

Deprotection and benzoylation of product (L-**28**) were executed similarly to the racemized product. Melting point 214—215°. $(\alpha)_D^{25} = 10.75$ (c = 1.5, glacial acetic acid), after recrystallization from ethanol. *Calcd.* : $C_{19}H_{22}N_2O_2$, C : 73.52 ; H : 7.14 ; N : 9.02 ; *Found* : C : 73.60 ; H : 7.20 ; N : 9.05 %.

Revue Roumaine de Chimie, 18, 3, 463 – 468 (1973)

AN IMPROVED SYNTHESIS OF OPTICALLY PURE N^{α}-METHYL-LYSINE

FLAVIAN CUIBAN

Department of Industrial Chemistry, Polytechnical Institute "Traian Vuia"
Timişoara, POB 103, Romania

Received October 27, 1972

A procedure for the selective protection of the terminal amino group of lysine by acylation with 2-methyl-2-(*o*-nitrophenoxy)-propionic acid was established, which permitted the synthesis of N^{α}-methyl-L-lysine.

The discovery of numerous N-methylated amino acids in peptide antibiotics isolated from microorganisms, stimulated the study of synthetical obtention of N-methyl-amino acids. Amino acid methylation, preserving the optical purity, was reported recently [1]. In the case of amino acids such as lysine which also possess another amino function, susceptible to be methylated, it was proposed [1] to protect it by means of the benzyloxycarbonyl group, frequently used in peptide syntheses. The above authors found however the partial cleavage of the protecting group during the synthesis and the appearance of secondary products difficult to eliminate.

Considering the high stability and easy removal of a new protecting group tested in peptide synthesis, [2] it appeared interesting to use it in the synthesis of N^{α}-methyl-lysine (**1**). As it is known, the nitro group is not reduced by some complex hydrides. [3] Therefore, we protected the lysine terminal amine by acylation with 2-methyl-2-(*o*-nitrophenoxy)-propionic acid. The succession of reactions in N^{α}-methyl-lysine synthesis is indicated in scheme 1.

In the reductive methylation of compound (**4**) there is no danger of splitting the protecting group, while by its elimination from compound (**5**) the N^{α}-benzyl residue is also eliminated.

Some difficulties were encountered in the synthesis of compound (**2**), the N^{ε}-acylated derivative of lysine. Although it was affirmed [4] that lysine can be acylated selectively at the terminal amine by means of

---

[1] P. Quitt, J. Hellerbach and K. Vogler, *Helv. Chim. Acta*, **46**, 327 (1963).

[2] F. Cuiban, *Tetrahedron Letters*, **27**, 2471 (1971). *Rev. Roumaine Chim.* (under press).

[3] R. T. Coutts and D. G. Wibberley, *J. Chem. Soc.*, **1963**, 4610.

[4] H. Zahn and H. R. Falkenburg, *Liebigs Ann. Chem.*, **636**, 117 (1960).

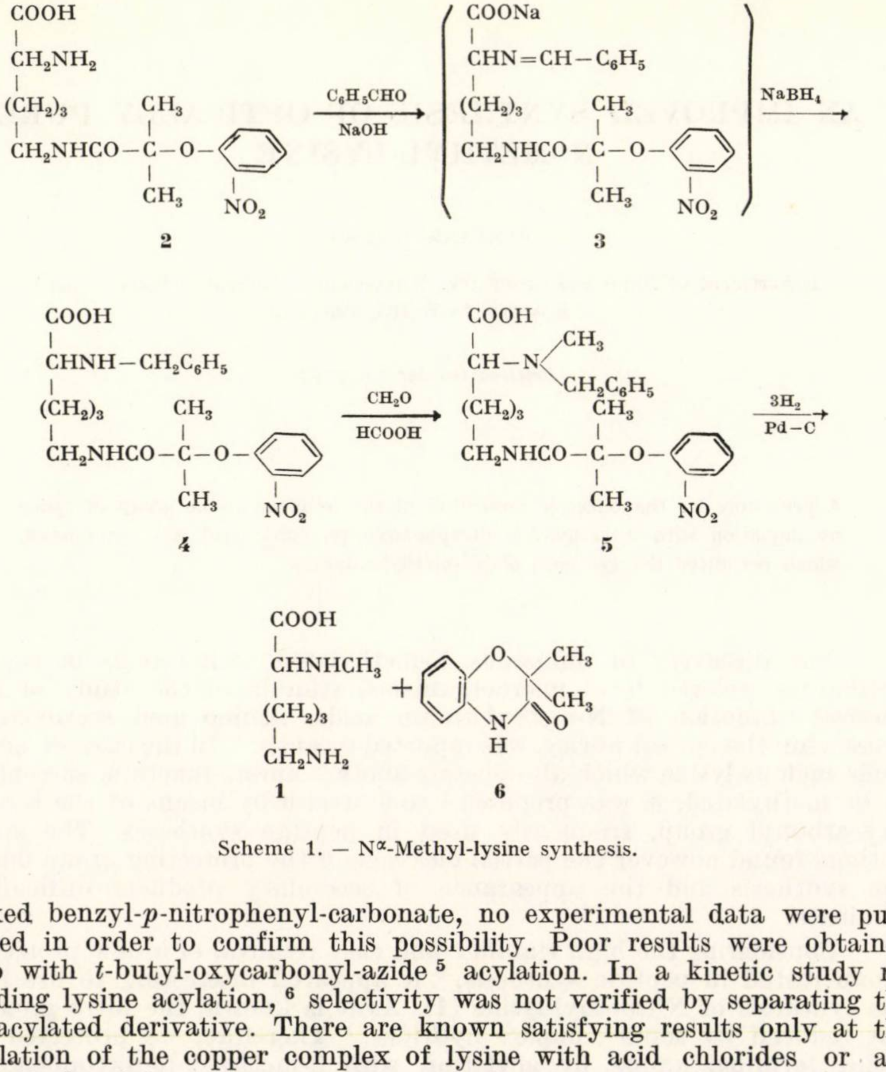

Scheme 1. — N^{α}-Methyl-lysine synthesis.

mixed benzyl-*p*-nitrophenyl-carbonate, no experimental data were published in order to confirm this possibility. Poor results were obtained also with *t*-butyl-oxycarbonyl-azide [5] acylation. In a kinetic study regarding lysine acylation, [6] selectivity was not verified by separating the N^{ε}-acylated derivative. There are known satisfying results only at the acylation of the copper complex of lysine with acid chlorides or anhydrides[7] and thus our experiments were directed especially towards these methods.

Similarly to the preparation of acylamino acids, from the previous work, [2] 2-methyl-2-(*o*-nitrophenoxy)-propionic acid chloride could not be used, on account of the competitive hydrolysis with the acylation reaction. The acylation experiments of lysine copper complex with mixed anhydride **(7)** (see scheme 2), prepared after standard techniques *in situ*, conducted to important amounts of N^{ε}-ethyl-oxycarbonyl-lysine (**8**), along with the N^{ε}-acylated derivative (**2**).

---

[5] R. Schwazer and W. Rittel, *Helv. Chim. Acta*, **44**, 159 (1961).

[6] J. Leclerc and L. Benoiton, *Canad. J. Chem.*, **46**, 1047 (1968).

[7] A. Neuberger and F. Sanger, *Biochem. J.*, **37**, 515 (1943).

The N$^{\varepsilon}$-ethyl-carbamate (**8**) was separated by repeated recrystallizations and was identical to the product synthetized by the acylation of lysine copper-complex.

The amount of urethane (**8**) varies from 15 to 50% depending on the experimental conditions. Although both products (**2** and **8**) were evidenced chromatographically in the cupric complex stage (**2a** and **8a**), their separation for preparative goals did not succeed.

The occurrence of urethane (**8**) in the reaction mixture is due to the nonselective attack of the terminal lysine amine on the mixed anhydride (**7**), owing probably to the steric hindrance and to the structure of the copper complex of lysine.

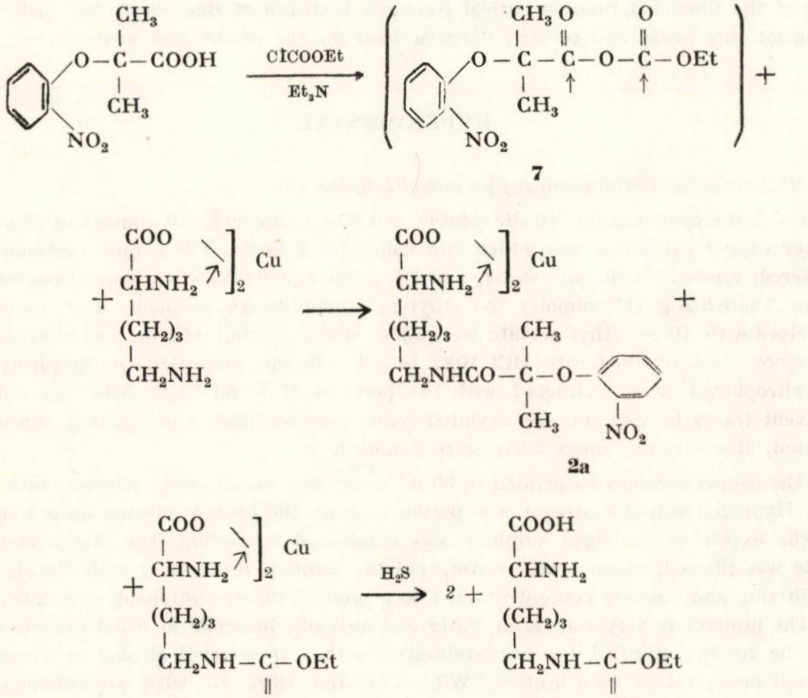

Scheme 2. — N$^{\varepsilon}$-2-Methyl-2-(*o*-nitrophenoxy)-propionyl-lysine synthesis *via* mixed anhydride

The complex of lysine can be acylated with satisfactory results by means of the 2-methyl-2-(*o*-nitrophenoxy)-propionic acid *p*-nitrophenyl ester. The complex reaction product incorporated the copper lysine complex and the cupric salt of the 2-methyl-2-(*o* nitrophenoxy)-propionic acid as impurities from the ester hydrolysis.

However, it is possible, by using *p*-nitrophenyl ester, to acylate predominantly the terminal amine even from the uncomplexed lysine.

It is necessary then to use lysine in excess and, for pure product separation, to resort to ion exchange chromatography. The yield is only 40% in the latter case (for details, see experimental part).

The course of the synthesis after reaction scheme 1 does not encounter difficulties. Very good yields were met at every stage, and N^{α}-methyl-lysine had a slightly higher melting point and specific rotation than those described in the literature.[1] The established procedure can be applied for both enantiomers and may be extended to other diamino acids.

Acknowledgement. The author expresses his gratitude to the management and colleagues of the Chemical Pharmaceutical Research Institute of Bucharest, for their help in carrying out this work, and to Mrs. Cornelia Ioan for the combustion analyses.

EXPERIMENTAL

N^{ε}-2-methyl-2-(o-nitrophenoxy)-propionyl-L-lysine (**2**)

i — Via copper complex. To the solution of 1.62 g lysine 90% (10 mmole) in 25 ml water, 2 g basic copper carbonate was added and boiled for 2 hours. The copper carbonate excess was filtered, washed with hot water, and 2.5 g (30 mmole) $NaNCO_3$ were dissolved in the solution. There 5.2 g (15 mmole) 2-methyl-2-(*o*-nitrophenoxy)-propionic acid *p*-nitrophenyl ester, solved with 10 ml ethyl acetate were added under stirring. Stirring was continued for 12 hours more, then acidified with HCl 10% to pH = 6, the unreacted *p*-nitrophenyl ester and *p*-nitrophenol were extracted with two portions of 50 ml Et_2O. After the removal of the solvent traces in vacuum, the acylated lysine complex (**2a**) was filtered, washed with water and, after drying, about 2.5 g were obtained.

The copper-complex suspended in 30 ml water was solved under stirring, with 0.35 ml H_2SO_4. Hydrogen sulphide stream was passed through the heated solution on a water bath, while the excess of hydrogen sulphide was eliminated by boiling. The precipitated copper sulphide was filtered, washed with water, and the solution neutralized with $BaCO_3$ powder. After filtering and vacuum concentration, 1.76 g product (**2**) was obtained, m.p. 205°, in 50% yield. The product is very soluble in water and alcohols, insoluble in usual organic solvents. It can be further purified by recrystallization either from ethyl alcohol or by solving in water and precipitation from acetone. With TLC (on silica G, with sec-butanol : formic acid : water = 75 : 15 : 10), it was unitary chromatographical, Rf = 0.58; $\varepsilon = (255\ \mathrm{nm})\ 2.68 \cdot 10^3$ in glacial acetic acid, which permitted quantitative determination. $(\alpha)_D^{25} = 9$ (c = 1.25 in 2N HCl). *Calcd*: $C_{16}H_{23}N_3O_6$, C : 54.38; H : 6.56; N : 11.89.

Found: C : 54.20; H : 6.70; N : 11.90%.

ii — Direct acylation. To a solution of 20 mmole lysine in 12 ml water, 10 mmole 2-methyl-2-(*o*-nitrophenoxy)-propionic acid *p*-nitrophenyl ester, dissolved with 40 ml acetone, were added under stirring. Stirring was continued at room temperature for 8 hours. After heating and refluxing for 3 hours more on water bath, the solvent was removed by means of a rotatory evaporator. The residue dissolved in 50 ml water, acidulated with HCl, pH = 6, then *p*-nitrophenol and the unreacted ester were extracted successively with 20 ml ethyl acetate. To the aqueous solution 20 mmole HCl solution was added, while the precipitated N-diacylated lysine derivative was separated either by filtering, or extraction by means of ethyl acetate or ethyl ether.

The aqueous solution removed from solvent traces was passed over a strong acid cationite column (Dowex 50 or Zerolit 225) 1.5 × 15 cm. Initially, the column was washed with water up to the elimination of chlorine ions from the eluate, then with 1 % ammonia solution, collecting the pH = 5—11 fraction, which gave positive reaction with ninhydrine soaked paper. The collected fraction was concentrated in vacuum for ammonia removal and passed over a weak cationite acid column of carboxyl type (Amberlite IRC 50), with close sizes to the fist cationite column. The column was eluted by aqueous ammonia solutions of increasing concentrations, 0.25, 0.5.1 %, then the pH = 4.5—7.5 fraction collected, which gave positive ninhydrine reaction and contained the N^{ε}-acylated derivative of lysine. The almost pure product was achieved by vacuum concentration to sicc. The fraction collected further at pH = 7—11, contained unreacted lysine and small quantities of N^{ε}-acylated derivative. It can be introduced into a new reaction.

iii — Mixed anhydride acylation (**7**). Usual techniques were performed for anhydride preparation, with tetrahydrofurane as solvent. The precipitated complex contained both products (**2a** and **8a**), while the urethane *ratio* was greater with increasing tetrahydrofuran concentration. The composition of the mixture was established by UV spectroscopy of N^{ε}-[2-methyl-2-(*o*-nitrophenoxy)-propionyl]-lysine. The urethane separation could be achieved only after hydrogenation of the mitxure in order to eliminate the protective group from (**2**), which was subsequently separated of the resulting lysine, by ion exchange chromatography, as described at *ii*.

N^{ε}-*Ethyloxycarbonyl-L-lysine* (**8**). To the solution of 5.90 g lysine 90 % base (36.4 mmole) in 100 ml water, 15 ml 2N HCl and 9 g basic copper carbonate were added, and boiled under stirring for 2 hours. After filtering the copper carbonate excess and adjusting to pH = 9 with 2N natrium hydroxide solution, cooled to 5°, and 5.92 g (54.5 mmole) ClCOOEt was added dropwise under stirring, adding in the meantime hydroxide for constant pH. The precipitate was filtered, washed with water and ethyl alcohol, yielding after drying 9.3 g cupric complex (**8a**), m.p. 252° (decomposition). The precipitate suspended in 200 ml water, was treated by hydrogen sulphide stream, at boiling on water bath, hot filtered and let to crystallize after cooling. After concentrating the mother solution, altogether 6.7 g, in 80 % yield, a white, crystalline product was obtained; m.p. 264° (decomposition), chromatographical unitary (on silica G plates, with sec-butanol : formic acid : water = 75 : 15 : 10, Rf = 0,48), $(\alpha)_D^{25} = 16.5$ (c= 1.58 in 2N HCl). *Calcd* : $C_9H_{18}N_2O_4$, C : 49.52 ; H : 8.3 ; N : 12.83 ; *Found* : C : 49.80 ; H : 8.50 ; N : 12.80 %.

N^{α}-*Benzyl*-N^{α}-*[2-methyl-2-(*o*-nitrophenoxy)-propionyl]-L-lysine* (**4**)

To the solution of 2.74 g (7.75 mmole) (**2**) solved with 20 ml water, 4 ml solution of 2N NaOH was added, then dropping under vigorous stirring 0.8 ml (8 mmole) freshly distilled benzaldehyde. To the cleared solution, 1 g $NaBH_4$ solved with 4 ml ice cooled water was added in portions. Stirring was continued for some hours, then benzaldehyde and $NaBH_4$ treatment repeated, with the same amounts. After stirring for 5 hours, hydrochloric acid was added dropwise, very slowly, as to reach pH = 8. The separated precipitate from (**4**) was water washed, the mother solution and water extracted 3 times by 10 ml Et_2O to eliminate benzaldehyde and benzyl alcohol. From the aqueous solution acidified to pH = 6, another amount of (**4**) precipitated, altogether 2.3 g, in 67 % yield. Recrystallized from ethyl alcohol, in diluted acids and alkalis soluble yellow crystals were obtained, m.p. 210—212°. $(\alpha)_D^{25} = 13.2$ (*c* = 1.6, in acetic acid : 1N HCl, 1 : 1). With TLC (on silica G, with sec-butanol : formic acid : water = 75 : 15 : 10), it appeared unitary with Rf = 0.7, while with iso-BuOH : NH_3 10 % = 85 : 15, Rf = 0.43. It was very poorly coloured with ninbydrine. By successive spraying with a 10 % solution of *p*-nitrobenzoic acid chloride in petroleum ether and pyridine, the plates were coloured blue. *Calcd.* : $C_{23}H_{29}N_3O_6$, C : 62.28 ; H : 6.58 ; N : 9.48 ; *Found* : C : 64.20 ; H : 6.70 ; N : 9.40 %.

N^{α}-(Methyl, benzyl), N^{ε}-[2-methyl-2-(o-nitrophenoxy)-propionyl]-L-lysine (**5**)

To the solution of 1.1 g (2.5 mmole) (**4**) in 4 ml 98 % formic acid, 0.25 ml (3 mmole) 40 % formol solution was added, then heated on water bath until CO_2 emission stopped. Formic acid was removed in vacuum, then treated by ethyl alcohol for full formic acid removal. The residue dissolved with ethyl alcohol, precipitated by means of ethyl ether, and filtered rendered 1.05 g yellow crystals of (**5**) m.p. 151°, in 92 % yield. The melting point increased to 155°, after recrystallization from hydroalcoholic mixture (3 : 1) and was unitary chromatographical (on silica G, with sec-BuOH : HCOOH : H_2O = 75 : 15 : 10, iodine vapour colouring), Rf = 0.62. It did not colour with ninhydrine. The product is soluble in dilute solutions of acids and alkalis, insoluble in water. $(\alpha)_D^{25} = 18.8$ (c = 1.6 in 1N HCl : acetic acid 1 : 1). *Calcd.* : $C_{24}H_{31}N_3O_2$, C : 63.00 ; H : 6.83 ; N : 9.18 ; *Found* : C : 63.20 ; H : 7.00 ; N : 9.30 %.

N^{α}-Methyl-L-lysine (**1**)

A suspension of 0.5 g 5 % Pd—C in 10 ml acetic acid was hydrogenated until the hydrogen absorption stopped. To this catalyst, 0.457 (1 mmole) (**5**) solved in 10 ml glacial acetic acid was added and hydrogenation proceeded ; the theoretical amount of hydrogen, 90 ml, was absorbed in 1 hour. After filtering the catalyst, solvent removal in vacuum, 0.5 ml 2N HCl and 5 ml water were added, while the insoluble 3,3-dimethyl-benzmorpholone (**6**) was extracted by Et_2O, in 3 portions.

The aqueous solution concentrated to a small volume, precipitated with 30 ml absolute ethanol, 0.14 g N^{α}-methyl-L-lysine, as monochlorohydride, crystalline product, m.p. 254—257° (decomposition), in quantitative yield. Literature [1] m.p. 250—253°. $(\alpha)_D^{25} = 31$ (c = 1, in 6N HCl). If necessary, it can be recrystallized from an alcohol-acetone mixture. *Calcd.* : $C_7H_{16}N_2O_2 \cdot HCl$, C : 42.74 ; H : 8.71 ; N : 14.24 ; Cl^- : 18.04 ; *Found* : C : 42.80 ; H : 8.75 ; N : 14.30 ; Cl^- : 19.00 %.

Revue Roumaine de Chimie, **18**, *3*, 469–472 (1973)

DIBENZOFURANS I. THE FORMYLATION OF 3-DIMETHYLAMINO-DIBENZOFURAN BY THE VILSMEIER-HAACK METHOD

VALER FĂRCĂŞAN and IOAN CRISTEA
Department of Chemistry, University Babeş-Bolyai, Cluj,
str. Arany Janos 11

Received July 31, 1972

By the formylation of 3-dimethylamino-dibenzofuran (I) under the conditions of the Vilsmeier-Haack reaction the aldehydes III and IV were obtained and their structure proved.

There are only few data [1,2,3] concerning the formylation of dibenzofuran derivatives by the Vilsmeier-Haack method [4] and the synthesis of dimethylamino-formyl-dibenzofurans has not been described yet in the literature. These reasons determined us to investigate the behaviour of 3-dimethylamino-dibenzofuran (I) under the conditions of the Vilsmeier-Haack reaction.

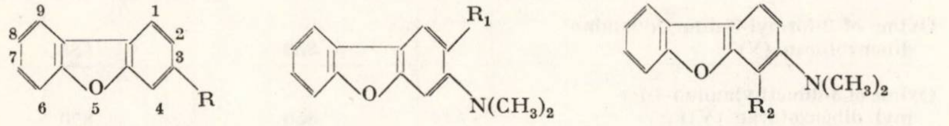

I : $R = N(CH_3)_2$ III : $R_1 = CHO$ IV : $R_2 = CHO$

II : $R = H$ V : $R_1 = CHNOH$ VI : $R_2 = CHNOH$

IX : $R = NH_2$ VII : $R_1 = CHN{-}NHC_6H_3(NO_2)_2$ VIII : $R_2 = CHN{-}NHC_6H_3(NO_2)_2$

Compound I was allowed to react with dimethylformamide in the presence of phosphorus oxychloride. From the crude product two compounds, A and B, were isolated by column chromatography (alumina Brockmann III – eluent toluene).

---

[1] J. A. Hogg, *Iowa State Coll., J. Sci.*, **20**, 15 (1945).

[2] H. Gilman, S. Avakian, J. A. Hogg and R. G. Johnson, *J. Amer. Chem. Soc.*, **75**, 6310 (1953).

[3] Cl. Rontier, Ng. Ph. Buu-Hoï and R. Royer, *J. Chem. Soc.*, **1956**, 4276.

[4] A. Vilsmeier and A. Haack, *Ber. dtsch. chem Ges.*, **60**, 121 (1927).

The bands at 1685 cm^{-1} in the i.r. spectrum as well as the peaks at $\delta = 10.26$ and 10.50 (p.p.m.) in the n.m.r. spectrum indicate the presence of the formyl group. The elemental analyses of these substances, their oximes and 2,4-dinitrophenylhydrazones, show that A and B are isomeric monoformyl derivatives. For the two isomers the structures III and IV are the most probable, taking into account the electrophilic nature of the Vilsmeier-Haack reagents, [5] the electronic effects exerted by the dimethylamino group and the lack of reactivity of dibenzofuran (II) under the conditions used by us for the formylation of 3-dimethylamino-dibenzofuran (I).

The lower melting point and the higher R_f of *A* as compared to *B* suggests a less polar character, which is in better agreement with formula III.

If the i.r. spectra of substances *A* and *B* are compared with those of their oximes (V and VI), 3-dimethylamino-dibenzofuran (I) and dibenzofuran (II), in the range 800 — 900 cm^{-1} (see table 1), a sharp band at 830 cm^{-1} can be observed in the spectra of both *B* and VI, which is absent in the spectra of the other compounds. This band may be assigned to C—H out-of-plane bending of the two adjacent hydrogens in the substituted benzene ring. [6] This can be taken as an argument for the validity of the structure IV assigned to B.

Table 1

IR spectra of I, II, III, IV, V and VI in the range 800 – 900 cm^{-1}

Compound	$1/\lambda\ cm^{-1}$							
Dibenzofuran (II)			846		853			
Diemethylamino-dibenzofuran(I)	818			850				895
2-Formyl-3-dimethylamino-dibenzofuran (III)			840			865	875	
3-Dimethylamino-4-formyl-dibenzofuran (IV)	815	*830*	840			868	888	
Oxime of 2-formyl-3-dimethylamino dibenzofuran (V)				853			885	
Oxime of 3-dimethylamino-4-formyl dibenzofuran (VI)		*828*		850			870	

The n.m.r. spectra are consistent with the formulae III respectively IV for compounds *A* and *B*. Indeed, the aromatic region, in the n.m.r. spectrum of *A*, comprise, apart from the other expected signals, two singlets corresponding to the more shielded 4-proton ($\delta = 7.14$) and the one less shielded in position 1 ($\delta = 8.32$). The same region, in the spectrum of *B*, shows two doublets ($\delta = 7.91$ and 6.96, respectively) determined by the coupling of protons 1 and 2, the last being the more shielded. The coupling constant $J_{12} = 9$ cps, is within the usual range of coupling constants for *ortho* protons in bezene derivatives.[7]

---

[5] G. A. OLAH, "Friedel-Crafts and related reactions", vol. 3, part 2, Interscience Publishers a Division of John Wiley and Sons. Inc., New York—London—Sydney, 1964, p. 1211.

[6] M. AVRAM and GH. D. MATEESCU, "Spectroscopia în infraroşu. Aplicaţii în chimia organică", Editura tehnică, Bucureşti, 1966, p. 272.

The above raported data show that by the formylation of 3-dimethylamino-dibenzofuran (I) two isomeric aldehydes are formed. By comparing the yields (III higher than IV) the preference of the electrophilic reagent in the Vilsmeier-Haack reaction for the position 2 of I is clarely pointed out.

With a view to obtain a deeper insight in the structure of oximes V and VI, we recorded their i.r. spectra. Both compounds show an intense band around 3300 cm^{-1}, due to the associated hydroxyl group. Taking into account the papers of Palmer and Werbin[8] or Hadzi and Premru[9] this fact suggests that the two oximes are in the *sin* (α) form and are associated as dimers.

The hydrogen bonds are stronger in the case of VI (ν_{OH} 3300 cm^{-1}) than in that of V (ν_{OH} 3360 cm^{-1}).

EXPERIMENTAL*

3-Dimethylamino-dibenzofuran (I)

A mixture of 1 g 3-amino-dibenzofuran (IX),[10] 1.75 g sodium bicarbonate, 5 ml water and 1.6 ml dimethyl sulfate were stirred at 10°, until the evolution of carbon dioxide ceased. Then the excess of dimethyl sulfate was decomposed with concentrated ammonia and water. The precipitate was filtered and recrystallized from ethanol. m.p. 96–97°, identical with that one already reported.[11]

Formylation of 3-dimethylamino-dibenzofuran (I)

To a mixture of 1.5 ml ice-cooled DMFA and 0.5 ml phosphorus oxychloride 1 g I was stepwise added. The mixture was warmed on a steam-bath for 2 hours and then poured on 25 g ice.

The pH was adjusted at 6 with a solution of sodium acetate (5 g in 13 ml water) and allowed to stand at room temperature for some hours. The oil which separated was extracted with chloroform. (The mother-liquor was neutralized with sodium bicarbonate and extracted in its turn with chloroform). The chloroform extracts were dried on anhydrous sodium sulfate, and the solvent removed to afford an oil. This was dissolved in toluene and chromatographied on an alumina (Brockmann III) column, using toluen as eluent. Two yellow zones were formed and the two corresponding fractions were evaporated to dryness, yielding the aldehyde *A* (III) (the first which leaves the column) and *B* (IV).

---

* Melting points (uncorrected) were esstimated on Boetius microstage. For recording the i.r. spectra (in KBr pellets), a double-beam Carl-Zeiss Jena UR-20 spectrophotometer was used.
The proton n.m.r. spectra were measured in deuterochloroform (TMS as reference) on a Tesla BS 487 B (80 MHz) apparatus.

[7] R. M. Silverstein and G. C. Bassler, "Spectrometric identification of organic compounds", Sec. ed., John Wiley and Sons. Inc., New York–London–Sydney, 1967, p. 145.

[8] A. Palm and H. Werbin, *Canad. J. Chem.*, **31**, 1004 (1953).

[9] D. Hadzi and L. Premru, *Spectrochim. Acta*, **23** A, 35 (1967).

[10] V. Fărcăşan, S. Florea and L. Beju, *Stud. Univ. Babeş-Bolyai. Chim.*, **15** (1), 63 (1970).

[11] W. H. Kirkpatrick and P. T. Parker, *J. Amer. Chem. Soc.*, **57**, 1123 (1935).

The aldehyde III (0.6 g 53%) was dissolved in 30 ml warm methanol, filtered, and water was added dropwise under stirring to the ice cooled solution, until yellow needles appeared. M.p. 49°. i.r. 754, 1120, 1195, 1235, 1430, 1470, 1610, 1640, 1688, 2810, 2960 cm^{-1}.

Anal. Calcd. for $C_{15}H_{13}NO_2$: C, 75.28 ; H, 5.47 ; N, 5.85.

Found : C, 75.5 ; H, 5.8 ; N, 5.5.

The aldehyde IV (0.3 g 25.5%) was recrystallized from *n*-heptane. M.p. 84°, yellow needles. i.r. 752, 1030, 1122, 1135, 1190, 1400, 1430, 1470, 1610, 1686, 2968 cm^{-1}.

Anal. Calcd. for $C_{15}H_{13}NO_2$: C, 75.28 ; H, 5.47 ; N, 5.85.

Found : C, 75.7 ; H, 5.9 ; N, 6.1.

2,4-Dinitrophenyl-hydrazones

To 0.3 g aldehyde (III or IV) dissolved in 10 ml ethanol, a solution of 0.2 g 2,4-dinitrophenyl-hydrazine and 0.5 ml concentrated hydrochloric acid in 10 ml ethanol was added and the mixture heated on a steam-bath for 30 minutes. The hot mixture was filtered and the precipitate washed with boiling ethanol. The crude products were recrystallized from dimethylformamide.

Compound VII : m.p. 278°, red needles.
Anal. Calcd. for $C_{21}H_{17}N_5O_5$: N, 16.69.
Found : N, 16.6.
Compound VIII : m.p. 248°, red needles.
Anal. Calcd. for $C_{21}H_{17}N_5O_5$: N, 16.69.
Found : N, 16.4.

Oximes

A solution of 2.1 g hydroxylamine hydrochloride in 6 ml water was treated with a solution of 3.5 g potassium hydroxide in 3.5 ml water and then added to a solution of 2.8 g aldehyde (III or IV) in 250 ml ethanol. The mixture was heated on a steam-bath for 2 hours, then poured into 500 ml water and neutralized with diluted sulfuric acid. The precipitate was filtered and washed with water. The crude product was recrystallized from carbon tetrachloride.

Compound V : m.p. 151°, needles. i.r. 760, 930, 972, 1000, 1120, 1210, 1285, 1460, 1480, 2945 cm^{-1}.

Anal. Calcd. for $C_{15}H_{14}N_2O_2$: N, 11.01.

Found : N, 10.9.

Compound VI : m.p. 181°, white yellow plates. i.r. 760, 950, 970, 1032, 1150, 1190, 1200, 1328, 1420, 1470 cm^{-1}.

Anal. Calcd. for $C_{15}H_{14}N_2O_2$: N, 11.01.

Found : 11.1.

Acknowledgements. The authors are grateful to Dr. I. Silberg for valuable discussions regarding n.m.r. spectra.

Revue Roumaine de Chimie, **18**, *3*, 473–478 (1973)

CONDENSATION DU 4,4′-AZODIPHÉNOXYDE DE SODIUM AVEC LES DÉRIVÉS CHLOROMÉTHYLÉS DU BENZÈNE

M. IOVU et S. RADU

Faculté de Chimie, Université de Bucarest,
Splaiul Independenţei, 89, Bucarest

Reçu le 22 septembre 1972

La préparation des biséthers par la condensation des phénoxydes de sodium avec les dérivés chlorométhylés en utilisant une nouvelle méthode facile, consistant dans la formation des phénoxydes alcalins anhydres, par l'éloignement de l'eau résultée de la réaction des phénols avec du NaOH, par distillation azéotrope avec un mélange d'éthanol-benzène et puis la réalisation de la réaction de condensation avec le phénoxyde anhydre, toujours en milieu d'éthanol-benzène, nous a conduit à cette étude. La condensation des 4,4-azodiphénoxydes alcalins avec les dérivés chlorométhylés n'est pas décrite dans la littérature. En utilisant la méthode décrite antérieurement on a obtenu le 4,4′-azodiphénoxyde de sodium anhydre qui a été condensé en milieu d'éthanol-benzène avec divers dérivés monochlorométhylés du benzène substitué.

Dans une série d'articles, [1–4] nous avons présenté la synthèse des biséthers avec la formule générale $Ar-O-CH_2-Ar-CH_2-O-Ar$, où le radical aryle représente un noyau benzénique substitué par un ou plusieurs radicaux méthyle, cyclohexyle ou par le groupe nitro.

Ces biséthers ont été synthétisés à l'aide de phénoxydes de sodium anhydres, obtenus par une méthode originale, qui consiste dans l'éloignement de l'eau résultée de la réaction des phénols avec du NaOH, par distillation d'un mélange azéotrope éthanol -benzène -eau, en utilisant un mélange (1 : 1 en volume) d'éthanol-benzène. L'eau a été éloignée par un mélange d'éthanol-benzène qui est aussi indiqué comme milieu de réaction pour la condensation ultérieure du phénoxyde de sodium avec le dérivé chlorométhylé.

---

[1] M. Iovu, *Rev. Roumaine Chim.*, **16**, 1223 (1971).

[2] M. Iovu et N. Nicolau, *Rev. Roumaine Chim.*, **16**, 1919 (1971).

[3] M. Iovu, *Rev. Roumaine Chim.*, **17**, 1261 (1972).

[4] M. Iovu, N. Miclovici et S. Creţu, *Rev. Roumaine Chim.*, **17**, 1417 (1972).

Dans cet article, nous présentons les résultats de la condensation du 4,4'-azodiphénoxyde de sodium avec les dérivés monochlorométhylés suivants : chlorométhyl-benzène, chlorométhyl-2,4-diméthyl-benzène, chlorométhyl-2,5-diméthyl-benzène, chlorométhyl-3,5-diméthyl-benzène, chlorométhyl-2,4,6-triméthyl-benzène et chlorométhyl-4-phényl-benzène.

Le 4,4'-azodiphénoxyde de sodium, anhydre, a été obtenu par traitement du 4,4'-azodiphénol avec l'hydroxyde de sodium (solide) en milieu d'éthanol-benzène et l'éloignement de l'eau sous forme d'un mélange azéotrope eau-éthanol-benzène. Le phénoxyde anhydre est additionné de dérivé chlorométhylé. L'azobisésther résulte par l'action nucléophile de l'anion phénoxydique sur le dérivé chlorométhylé. Les réactions qui ont lieu sont :

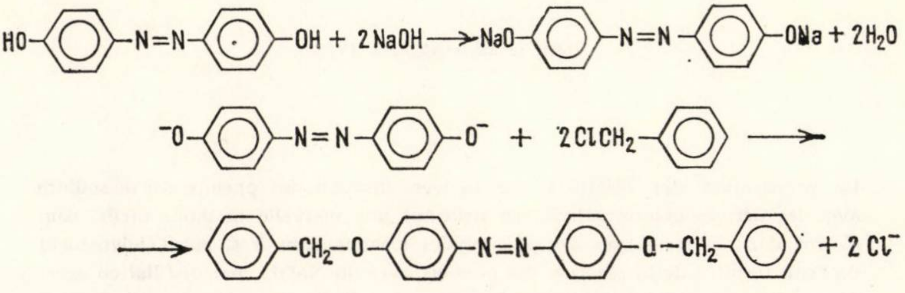

L'azobisésther formé précipite avec le chlorure de sodium ; ces composés se séparent des solvants par filtration, puis le chlorure de sodium est éloigné par lavage avec de l'eau, sur le filtre.

L'azobisésther séché est recristallisé à l'aide d'un mélange d'éthanol-benzène (en différents rapports en fonction de la solubilité).

Les conditions de travail sont les mêmes pour tous les composés synthétisés, indifféremment des matières premières.

RÉSULTATS ET DISCUSSION

Les azobisésthers, les résultats de l'analyse élémentaire de C, H, N, leurs températures de fusion et les rendements sont indiqués dans le tableau 1.

Tous ces azobisésthers sont solides, ayant une couleur jaune et fondent à températures élevées (comparativement aux bisésthers synthétisés antérieurement, [1-4] qui ne contiennent pas la fonction azo).

On peut observer dans le tableau 1 que les valeurs des températures de fusion pour les trois isomères : 4,4'-bis (2,4- diméthyl-benzyloxy) azobenzène, 4,4'-bis (2,5-diméthyl-benzyloxy) azobenzène et 4,4'-bis (3,5-diméthyl-benzyloxy) azobenzène sont très proches, les positions des radicaux méthyle sur les noyaux benzéniques influençant très peu les températures de fusion.

Bien que la réaction de condensation du 4,4'-azodiphénoxyde de sodium avec les dérivés chlorométhylés soit totale, les rendements ne sont

Tableau 1

Azobiséthers

Éthers	Formule	C % Calculé Trouvé	H % Calculé Trouvé	N % Calculé Trouvé	Point du fusion °C	Rend., %
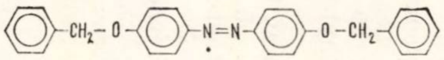	$C_{26}H_{22}O_2N_2$	79,16 78,99	5,61 5,62	7,10 7,16	199	73,2
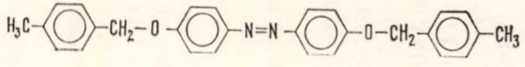	$C_{28}H_{26}O_2N_2$	79,59 79,12	6,20 6,08	6,63 6,34	230–230,5	78,5
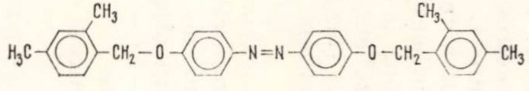	$C_{30}H_{30}O_2N_2$	79,97 79,66	6,71 6,24	6,22 6,51	192–193	78,2
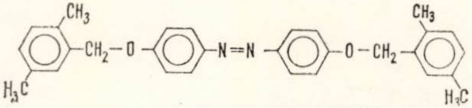	$C_{30}H_{30}O_2N_2$	79,97 79,60	6,71 6,47	6,21 6,59	190–191	84,3
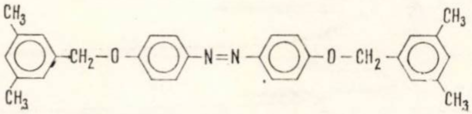	$C_{30}H_{30}O_2N_2$	79,97 79,81	6,71 6,82	6,21 6,45	190,5–191	63,4
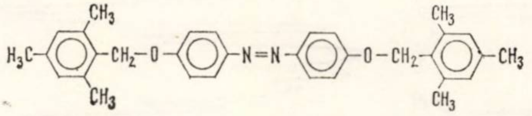	$C_{32}H_{34}O_2N_2$	80,30 79,89	7,15 7,32	5,86 5,71	234,5–245	50,1
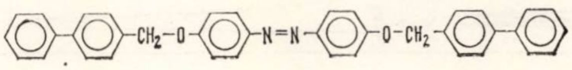	$C_{38}H_{30}O_2N_2$	83,50 83,05	5,53 5,36	5,12 5,00	190,5–191,5	68,5

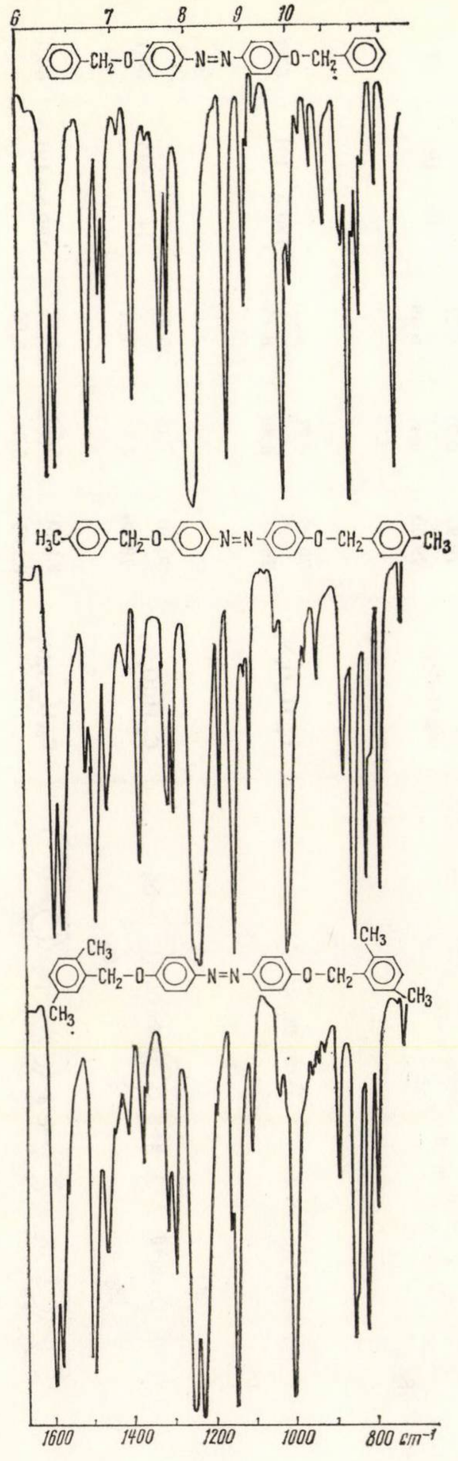

pas élevés, parce qu'on a travaillé dans des quantités grandes de solvant, avec des quantités petites de matières premières, en suivant la préparation des produits d'une grande pureté.

L'étude spectrale en IR met en évidence des bandes d'absorption dues aux vibrations caractéristiques des éthers et azodérivés.

Tous les composés présentent une bande d'absorption intense à 1010 + 10 cm^{-1} attribuée à la fréquence symétrique de la liaison C–O–C. Par exemple, pour les composés dont les spectres sont représentés dans la figure 1 on trouve les valeurs suivantes : $\nu C-O-C_{sym} = 1019\ cm^{-1}$ pour le 4,4'-bis(benzyloxy)azobenzène, 1016 cm^{-1} pour le 4,4'-bis(4-méthylbenzyloxy)azobenzène et 1016 cm^{-1} pour le 4,4'-bis(2,5-diméthyl-benzyloxy)azobenzène.

Cette bande se superpose à celle due à $\nu C-H$.

Aussi, tous les azobiséthers absorbent-ils fortement dans la région très étroite autour de la valeur 1150 cm^{-1}, ce qu'on doit aux vibrations asymétriques de la fonction éther. Pour les composés dont les spectres sont réportés dans la figure 1, $\nu C-O-C_{asym}$ a les valeurs suivantes : 1152 cm^{-1} pour le 4,4'-bis(benzyloxy)azobenzène, 1148 cm^{-1} pour le 4,4'-bis(4-méthyl-benzyloxy) azobenzène et 1149 cm^{-1} pour le 4,4'-bis(2,5-diméthyl-benzyloxy)azobenzène.

En comparant les valeurs des longueurs d'onde où absorbent les azobiséthers synthétisés par nous, qui ont un caractère mixte d'éther aliphatique et d'éther aromatique ($-Ar-O-CH_2-Ar$), on constate que celles-ci se trouvent entre les valeurs caractéristiques des éthers

Fig. 1. — Spectres IR des 4,4'-bis(benzyloxy)azobenzène, 4,4'-bis-(4-méthylbenzyloxy)azobenzène et du 4,4'-bis(2,5-diméthylbenzyloxy)azobenzène.

aliphatiques ($\nu_{sym} = 940$ cm^{-1} et $\nu_{asym} = 1070$ à 1050 cm^{-1}) et les valeurs des éthers aromatiques ($\nu_{sym} = 1040$ à 1020 cm^{-1} et $\nu_{asym} = 1250$ cm^{-1}).

Dans les spectres IR est présente une bande de 1410 à 1408 cm^{-1}, de faible intensité, pouvant être attribuée aux liaisons N=N, en accord avec des données de Fatiadi.[5] La seconde bande qui selon l'auteur mentionné se trouve de 1579 à 1558 cm^{-1}, dans le cas des composés synthétisés par nous, comme on peut voir dans la figure 1, est superposée aux bandes d'absorption caractéristiques des noyaux benzéniques de 1600 ± ± 25 cm^{-1} et 1580 ± 20 cm^{-1}, qui, à la différence des autres éthers aromatiques,[1,3,4] apparaissent très intenses aux azobiséthers.

PARTIE EXPÉRIMENTALE

Le 4,4'-azodiphénol a été obtenu par réduction en milieu alcalin (KOH) du *p*-nitrophénol.[6]

Le chlorométhylbenzène a été un produit commercial-Riedel. Le 4-méthyl-chlorométhylbenzène a été obtenu par chloration photochimique du *p*-xylène avec du SO_2Cl_2.

Le chlorométhyl-2,4-diméthyl-benzène et le chlorométhyl-2,5-diméthyl-benzène ont été obtenus par chlorométhylation du *m*-xylène, respectivement du *p*-xylène.

Le chlorométhyl-3,5-diméthyl-benzène a été obtenu par chloration photochimique du mésytylène avec du SO_2Cl_2, en utilisant comme initiateur le peroxyde de benzoyle. Cette réaction, ainsi que le produit obtenu ne sont pas décrits dans la littérature.

Le chlorométhyl-2,4,6-triméthyl-benzène a été obtenu par chlorométhylation du mésitylène, en utilisant du formaldéhyde 30%, de l'acide chlorhydrique conc., en tétrachlorure de charbon.

Le 4-chlorométhyl-biphényle a été obtenu par chlorométhylation du biphényle avec du paraformaldéhyde, de l'acide chlorhydrique conc. et du $ZnCl_2$ en acide acétique et éther de pétrole.

Les spectres IR ont été obtenus en pastilles KBr à l'aide d'un appareil Perkin-Elmer 157.

Synthèse du 4,4'-bis(benzyloxy)azobenzène

Dans un ballon à double col de 100 ml (avec rodage de 14,5), muni d'un réfrigérant ascendant et d'un thermomètre, on a introduit 5,35 g (1/40 mole) de 4,4'-azodiphénol, 2 g de NaOH (1/20 mole), 20 ml d'éthanol anhydre et 20 ml de benzène. Le mélange est chauffé à l'ébullition jusqu'à ce que NaOH réagit avec le 4,4'-azodiphénol, en formant un phénoxyde de sodium, partiellement soluble dans le mélange de solvants.

Après environ une heure de chauffage au point d'ébullition, le réfrigérant ascendant est substitué par un réfrigérant pour distillation de 15 ml de mélange azéotrope eau-éthanol-benzène, donc pour l'éloignement de l'eau résultée de la réaction. On ajoute ensuite 6,32 g

---

[5] A. J. Fatiadi, *J. Res. Nat. Bur. Stand.*, A **71**, 277 (1967).
[6] R. Willstätter et M. Benz, *Ber. dtsch. chem. Ges.*, **39**, 3492 (1906).

(1/20 mole) de chlorométhyl-benzène (avec un petit excès), mais le réfrigérant de distillation est changé de nouveau par l'un de reflux, le chauffage étant fait à l'aide d'une lampe à incandescence de 2,5 W à 65—67°. La réaction du chlorométhylbenzène avec le 4,4'-azodiphénoxyde de sodium a lieu, en formant dans le milieu de réaction le chlorure de sodium, qui précipite.

L'azobiséther précipite plus tard, quand la quantité formée est un plus grande, donc la solubilité plus petite, à la température du travail.

Après 5 heures de chauffage, le chauffage est arrêté, mais le ballon où a eu lieu la réaction est laissé refroidir à la température ambiante, pour précipiter une quantité maximale d'azobiséther.

La séparation de l'azobiséther et du chlorure de sodium de la solution qui contient des matières non soumises à la réaction est effectuée par filtration. Une quantité petite d'alcool (2—3 ml) est ajoutée sur le filtre, puis le précipité est lavé à de l'eau et séché dans l'étuve à 105°.

On obtient 7,21 g de 4,4'-bis(benzyloxy)azobenzène. Rendement 73,2 %.

Le rendement dépend de la quantité de solvant dans laquelle a lieu la réaction et du rapport éthanol-benzène.

A une dilution élevée le rendament est petit, parce que une partie d'azobiséther reste en solution, mais la pureté du produit séparé est plus grande.

La température de fusion a été déterminée après des recristallisations répétées dans un mélange d'éthanol-benzène (1 : 1 en volume).

Les autres éthers, mentionnés dans le tableau 1, ont été synthétisés de façon identique.

CONCLUSIONS

Le présent article montre que la réaction du 4,4'-azodiphénoxyde de sodium avec les dérivés monochlorométhylés du benzène ou du benzène substitué avec divers substituents a lieu en bonnes conditions, dans un mélange d'éthanol-benzène, à la température d'ébullition du mélange.

On peut obtenir des azobiséthers avec la formule générale :

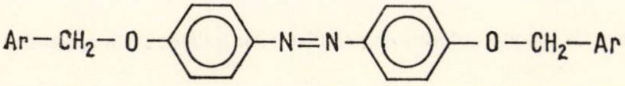

où Ar représente un aryle, substitué ou non substitué.

Revue Roumaine de Chimie, **18**, *3*, 479–487 (1973)

MODERN FRIEDEL-CRAFTS CHEMISTRY. II[1]

REARRANGEMENTS ACCOMPANYING BENZENE ALKYLATIONS WITH 1- AND 2-HYDROXY-2-METHYL-1-PHENYLPROPANE, 1- AND 2-CHLORO-2-METHYL-1-PHENYLPROPANE AND 2-METHYL-1-PHENYL-1-PROPENE IN THE PRESENCE OF FRIEDEL-CRAFTS CATALYSTS

ALI ALI KHALAF
Chemistry Department, University of Assiut,
Assiut, Arab Republic of Egypt

Received July 26, 1972

The alkylations of benzene with 1- and 2-hydroxy-2-methyl-1-phenylpropane, with 1- and 2-chloro-2-methyl-1-phenylpropane and with 2-methyl-1-phenyl-1-propene (β,β-dimethylstyrene) in the presence of various Friedel-Crafts catalysts have been investigated. The results of these alkylations were found to be very much similar to those obtained from the alkylations of benzene with neophyl halides and isobutylene dihalides under the same conditions. With the strong catalyst $AlCl_3$, these alkylations gave mixtures consisting of 1,2-diphenyl-2-methylpropane, 1,1-diphenyl-2-methylpropane and DL- and *meso*-2,3-diphenylbutane. With weak catalysts such as $AlCl_3/CH_3NO_2$, $FeCl_3$ or H_2SO_4, the first two isomers were formed only and both of the latter forms were missing from the product mixtures. In all cases, however, the first two isomers were produced in an equilibrium ratio of 2 of the first isomer to 1 of the second. Mechanisms were suggested to account for the results obtained.

In 1952 Somerville and Spoerri [2] reported that the aluminum chloride-catalyzed alkylation of benzene with both 1-hydroxy-2-methyl-2-phenylpropane (neophyl alcohol) and the corresponding 1-chloro-2-methyl-2-phenylpropane (neophyl chloride) gave 1,2-diphenyl-2-methylpropane mixed with varying amounts of the rearrangement product 2,3-diphenylbutane. Similar results were also reported by these [2] and other workers from the $AlCl_3$-catalyzed alkylations of benzene with isobutylene dihalides [3,4,5,6] (1,2-dihalo-2-methylpropanes) which were shown [6] to proceed through the intermediate formation of neophyl halides.

---

[1] Part I: A. A. Khalaf, preceding paper in this Journal.

[2] W. T. Somerville and P. E. Spoerri, *J. Amer. Chem. Soc.*, **74**, 3803 (1952).

[3] K. Sisido and V. Jasikawa, *J. Amer. Chem. Soc.*, **70**, 1608 (1948).

[4] L. Schmerling, I. West and R. Welch, *J. Amer. Chem. Soc.*, **78**, 5406 (1956); **80**, 576 (1958).

[5] L. V. Bugrova and I. P. Tsukervanik, *Zhur. obshchei Khim.*, **32**, 3575 (1962); *Chem. Abstr.*, **58**, 11242 g (1963).

[6] L. V. Bugrova and I. P. Tsukervanik, *Zhur. org. Khim.*, **1** (4), 714 (1965); *Chem. Abstr.*, **63**, 5542 f (1965).

In 1966, the alkylation of benzene with both neophyl chloride and isobutylene dibromide was reinvestigated by Khalaf and Roberts[7] who, with the help of modern instrumental methods of analysis, have discovered that the products from these reactions are more complex than previously described. According to these workers, the products obtained from both halides were mixtures consisting of 1,2-diphenyl-2-methylpropane, 1,1-diphenyl-2-methylpropane and DL- and *meso*-2,3-diphenylbutane in alkylations catalyzed by $AlCl_3$ and of the first two isomers only in aklylations catalyzed by $AlCl_3/CH_3NO_2$ or $FeCl_3$. In all cases, however, the first two isomers were consistantly produced in an equilibrium ratio of about 2 : 1, respectively. To account for the products obtained in the alkylations of benzene with isobutylene dibromide ((**1**), X=Cl) and neophyl chloride (**3**), X=Br) in the presence of Friedel-Crafts catalysts, Khalaf and Roberts[7] suggested the carbonium ion mechanism outlined in equations I–VI of Scheme I:

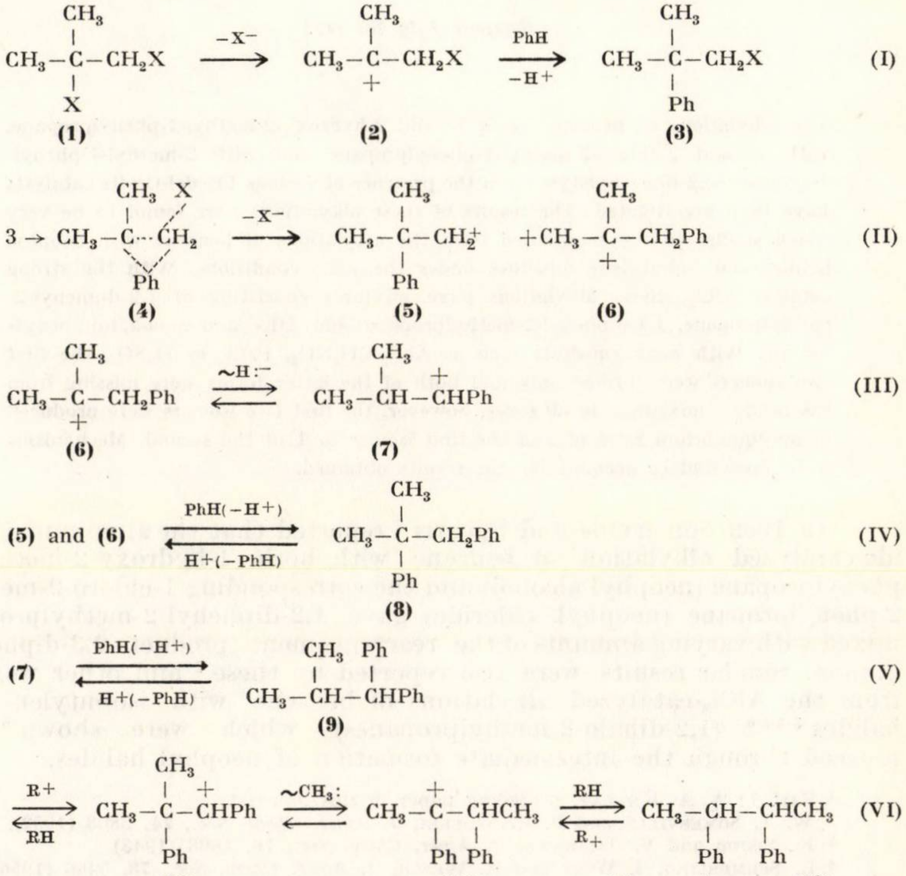

Scheme I

---

[7] A. A. Khalaf and R. M. Roberts, *J. Org. Chem.*, **31**, 926 (1966).

The production of an equilibrium mixture of (**8**) and (**9**) from the reaction of benzene with either neophyl chloride or isobutylene dibromide, even when the weak catalysts were used, was attributed by the authors to a rapid equilibration of the tertiary carbonium ion 6 (which is produced as an intermediate in both cases) with the secondary benzylic ion (**7**) by a 1,2-hydride shift (equation III) prior to the second alkylation that leads to the formation of (**8**) and (**9**) (equations IV and V).

In the light of the above mechanism, it is assumed that Friedel-Crafts alkylations of benzene with any other systems that may lead to the generation of the tertiary ion 6 or of the secondary benzylic ion 7 should give alkylation mixtures similar to those reported previously from isobutylene dihalide (**1**) and neophyl halide (**3**). To test this reasonable assumption, the present paper was devoted to investigate the Friedel-Crafts alkylation of benzene with 1- and 2-hydroxy-2-methyl-1-phenyl-propane, with 1- and 2-chloro-2-methyl-1-phenylpropane and with 2-methyl-1-phenyl-1-propene.

RESULTS AND DISCUSSIONS

The conditions and results of the alkylation experiments are summarized in the accompanying Table 1. It can be seen from the obtained results that the alkylation of benzene with both the chlorides and the alcohols gave similar alkylation mixtures whose compositions were dependent upon the type of catalyst and conditions employed. Thus, using the mild catalysts $AlCl_3/CH_3NO_2$ and $FeCl_3$, resulted in the formation of the usual equilibrium mixture which consists of 1,2-diphenyl-2-methylpropane and 1,1-diphenyl-2-methylpropane in a ratio of 2 : 1. The same equilibrium mitxure was also obtained when benzene was alkylated with 2-methyl-1-phenyl-1-propene in the presence of sulphuric acid as the catalyst. Using the strong catalyst $AlCl_3$, however, resulted in the formation of more complex alkylation mixtures consisting of the aforementioned 1,1- and 1,2-diphenyl-2-methylpropane isomers in addition to DL — and *meso*—2,3—diphenylbutane. It is to be noted that both of the latter forms of 2,3-diphenylbutane were missing in alkylations catalyzed by mild catalysts and that the first two isomers were again present in the established equilibrium composition of 2 :1.

The formation of DL- and *meso*-2,3-diphenylbutane in the presence of the strong catalyst $AlCl_3$ and not in the presence of the weak $AlCl_3/CH_3NO_2$ and $FeCl_3$ catalysts can reasonably be explained in terms of the known ability of $AlCl_3$ to abstract hydride ions. [7] Thus, in the presence of this hydride abstracting catalyst, one can visualize the formation of both forms of 2,3-diphenylbutane occurring through the route (**8**) → (**10**) → → (**11**) → (**12**) (eq. VI of Scheme I and Scheme II). The latter route was formerly supported by the fact that treatment of a pure sample of 1,2-diphenyl-2-methylpropane with $AlCl_3$ gave a mixture in which DL- and *meso*-2,3-diphenylbutane were present. None of the latter forms were obtained, however, when $AlCl_3/CH_3NO_2$ and $FeCl_3$ catalysts were used.[7]

Mechanistically, the results of Table 1 can plausibly be rationalized in terms of the carbonium ion processes outlined in Scheme II.

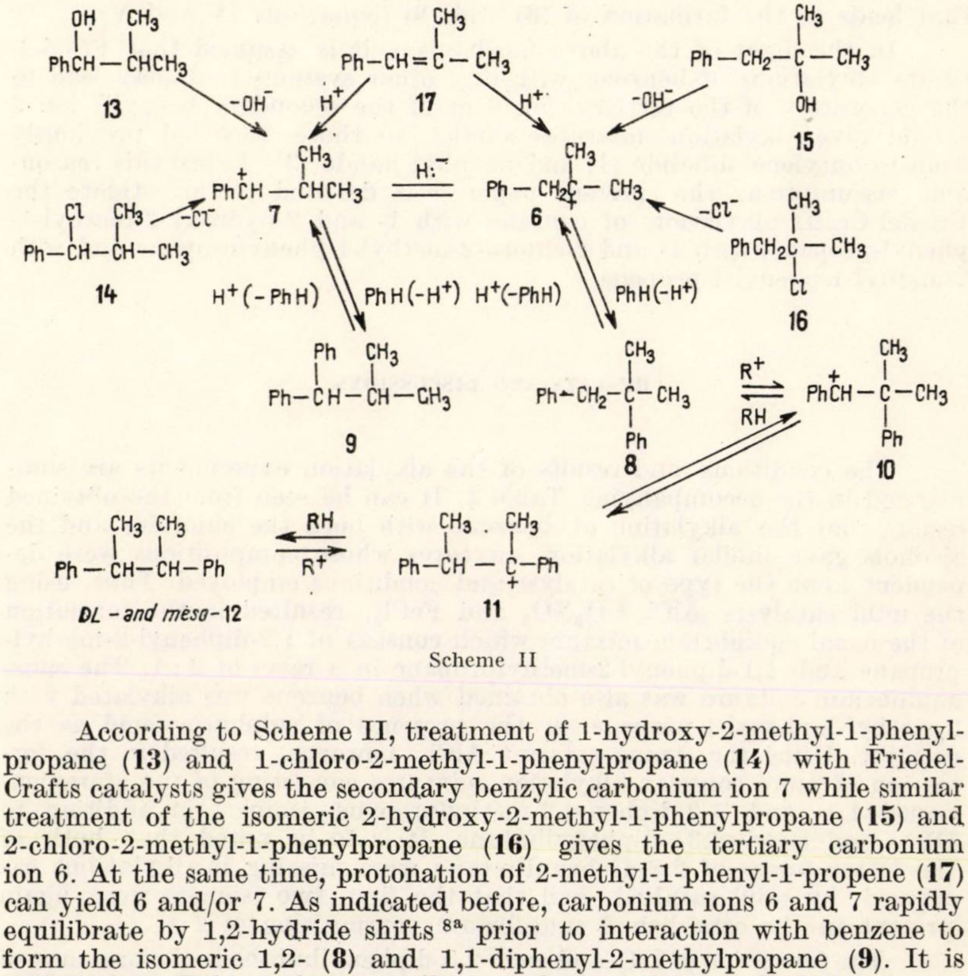

Scheme II

According to Scheme II, treatment of 1-hydroxy-2-methyl-1-phenylpropane (**13**) and 1-chloro-2-methyl-1-phenylpropane (**14**) with Friedel-Crafts catalysts gives the secondary benzylic carbonium ion 7 while similar treatment of the isomeric 2-hydroxy-2-methyl-1-phenylpropane (**15**) and 2-chloro-2-methyl-1-phenylpropane (**16**) gives the tertiary carbonium ion 6. At the same time, protonation of 2-methyl-1-phenyl-1-propene (**17**) can yield 6 and/or 7. As indicated before, carbonium ions 6 and 7 rapidly equilibrate by 1,2-hydride shifts[8a] prior to interaction with benzene to form the isomeric 1,2- (**8**) and 1,1-diphenyl-2-methylpropane (**9**). It is evident from Table 1 that regardless of which of the five alkylating agents (**13**), (**14**), (**15**), (**16**) or (**17**) is used as starting material, and of whether $AlCl_3$, $AlCl_3/CH_3NO_2$, $FeCl_3$ or H_2SO_4 is used as catalyst, compounds (**8**) and (**9**) are produced in a ratio corresponding to their equilibrium composition. However, it is only in the presence of $AlCl_3$ which has the power to generate carbonium ion (**10**) that the two forms of 2,3-diphenylbutane are actually formed.

[8a] In contrast, in SbF_5-FSO_3H solvent systems Olah and his collaborators have observed only the secondary benzylic cation, phenylisopropylcarbonium ion 8, as the static stable species, which is generated from 1-hydroxy-2-methyl-1-phenyl-propane (13). This demonstrates that in the strong SbF_5-FSO_3H acid system, the secondary benzylic phenylisopropylcarbonium ion (7) appears to be more stable than the tertiary dimethyl-benzylcarbonium ion (6).

In concluding the present discussion, it is worthwhile to mention that the results of Table 1, which show that at equilibrium, compounds (**8**) and (**9**) are present in a ratio of 2 : 1, augment our previous suggestion [8b] that isomer (**8**) is more thermodynamically stable than isomer (**9**). It is also interesting to know that in alkylating arenes with systems leading to the intermediate formation of ions such as (**5**), (**6**) or (**7**), one should expect carbonium ion rearrangements of the type observed in this work and which result in alkylation mixtures composed of various isomers. In fact, further studies to illustrate this are currently under way.

EXPERIMENTAL

ANALYTICAL PROCEDURES

The infrared spectra (i.r.) were done using either a Pye Unicam Sp 200 G Grating IR Spectrophotometer or a Beckman IR-5A Spectrophotometer. A Varian A-60 spectrometer was used for nuclear magnetic resonance (n.m.r.) analysis . Vapour-phase chromatographic analyses (v.p.c.) were carried out using either a Pye Series 104 chromatograph or a Beckman GC-2A instrument. The columns used were : a) 12-ft, 30% silicone gum rubber SE-30 ; b) 12 ft, 15% Bentone-34, c) 12-ft 20% DEGA, d) 5-ft, 3% PEGA, e) 5-ft, 3% DNP.

A. SYNTHESIS OF STARTING MATERIALS AND FINAL PRODUCTS

Synthesis of Starting Materials

Synthesis of 1-Hydroxy-2-methyl-1-'phenylpropane (**13**). This was prepared by the condensation of phenylmagnesium bromide with isobutyraldehyde. In a typical preparation, phenylmagnesium bromide was prepared as usual from 9.6 g. (0.4 g atom) of magnesium turnings, a small crystal of iodine, 62.8 g. (0.4 mole) of bromobenzene and a total of 250 ml of dry ether. To the resulting Grignard reagent, a solution of 36.0 g isobutyraldehyde in 50 ml dry ether was added under cooling and strring. After additon was completed, the reaction mixture was stirred at room temperature for 3 hr and under reflux for another hour. The reaction mixture was then cooled and decomposed by treating with a saturated solution of ammonium chloride. The organic layer was separated, washed with water and dried over anhydrous sodium sulphate. Distillation of the ether under atmospheric pressure left a residue which upon careful distillation under vacuum gave 36 g (60% yield) of the desired alcohol : b.p. 75—79° (1.1—1.2 mm). Reported [9] b.p. : 75—77° at 1.2 mm.

[8b] R. M. Roberts, A. A. Khalaf and R. N. Greene, *J. Amer. Chem., Soc.*, **86**, 2846 (1964).

[9] M. V. Grignard, *Ann. Phys.*, **24**, 467 (1901).

Synthesis of 2-Hydroxy-2-methyl-1-phenylpropane (**15**). This compound was made by the condensation of acetone with benzylmagnesium chloride. In a typical run, benzylmagnesium chloride was prepared as directed[10] from 14.4 g. (0.60 g-atom) of magnesium, a small crystal of iodine, 75.9 g. (0.60 mole) of benzyl chloride, and a total of 300 ml of dry ether. To the resulting Grignard reagent, a solution of 40.6 g (0.7 mole of pure dry acetone in 100 ml dry ether was added under cooling, at such a rate that gentle refluxing occurred. After addition, the reaction mixture was stirred for three hours at room temperature and for another half an hour at reflux temperature. The reaction mixture was then cooled and decomposed with a saturated ammonium chloride solution. The ether layer was separated, washed three times with water and dried over anhydrous sodium sulphate. The ether was removed and the residue was carefully distilled under vacuum to give 68 g (76% yield) of pure 2-hydroxy-2-methyl-1-phenylpropane : b.p. 77–78° (1.2 mm.). Reported b.p. 112–114 at 12 mm[11,12] and 127–128° at 14 mm.[13]

Synthesis of 1- (**14**) *and 2-Chloro-2-methyl-1-phenylpropane* (**16**). These two isomers were prepared by treatment of the respective alcohols with thionyl chloride in pyridine.[14] In a typical treatment, 0.12 mole of thionyl chloride was added with cooling and stirring to a solution of 0.1 mole of the alcohol in 0.12 of pyridine. After addition, the mixture was stirred at room temperature for 2 hr and at 40–50° for 1 hr, then decomposed with cold water. The organic layer was extracted with ether, washed first with cold water, secondly with 5% sodium carbonate and finally with cold water, then dried over anhydrous sodium sulphate. The ether was distilled at atmospheric pressure and the residue was carefully distilled under vacuum.

Applied to 1-hydroxy-2-methyl-1-phenylpropane (**13**) the above procedure gave 1-chloro-2-methyl-1-phenylpropane in 60% yield : b.p. 86–89° (14–15 mm). Reported[15] b.p. : 53° (0.6 mm).

Similarly, 2-hydroxy-2-methyl-1-phenylpropane (**15**) gave 2-chloro-2-methyl-1-phenylpropane (**16**) in 65%. Yield : b.p. 53–55° (0.7 mm). Reported[16] b.p. : 86–87° (9–10 mm). The n.m.r. spectrum of the compound showed the aromatic protons (main peak) at 2.86 T (relative area 5), benzylic protons at 7.03 T (relative area 2) and methyl protons at 8.56 T (relative area 6).

Synthesis of 2-Methyl-1-phenyl-1-propene (*β,β-Dimethylstyrene* (**17**). This was prepared by the dehydration of 1-hydroxy-2-methyl-1-phenylpropane by treatment with 15% sulphuric acid following standard procedures.[17,18] The produced 2-methyl-1-phenyl-1-propene (**17**) was distilled under vacuum : b.p. 70–73° (12.0–12.5 mm). Reported[19] b.p. : 70.5–71.5° (12 mm).

---

[10] H. Gilman and W. E. Catlin, *Org. Syn.*, Coll. Vol. I, 471 (1941).

[11] N. D. Zelinsky and M. W. Gawedowskaja, *Ber. dtsch. chem. Ges.*, **61**, 1052 (1928).

[12] G. A. Olah, C. U. Pittman, Jr., E. Nemanworth and M. B. Comisarow, *J. Amer. Chem. Soc.*, **88**, 5571 (1966).

[13] A. Glages, *Ber. dtsch. chem. Ges.*, **37**, 1723 (1904).

[14] F. C. Whitmore and F. A. Karnatz, *J. Amer. Chem. Soc.*, **60**, 2536 (938).

[15] P. A. Levene and L. A. Makeska, *J. Biol. Chem.*, **70**, 355 (1926). P. A. Levene and R. E. Marker, *ibid.*, **97**, 381 (1932).

[16] G. T. Davis and H. Tanida, *J. Amer. Chem. Soc.*, **84**, 1606 (1962).

[17] C. F. H. Allen and S. Converse, *Org. Syn.*, Coll. Vol. I, 226 (1941).

[18] D. J. Cram, *J. Amer. Chem. Soc.*, **71**, 3887 (1949).

[19] C. Ruechardt, *Chem. Ber.*, **94**, 2599 (1961).

B. *Synthesis of Final Products*

Synthesis of 1,2-Diphenyl-2-methylpropane (**8**). The compound was obtained by the coupling of benzylmagnesium chloride with 2-chloro-2-phenylpropane following essentially the procedure of Khalaf and Roberts[7] : b.p. 145–147° (12.8 mm), lit.[7] b.p. 148–150° (11 mm).

Synthesis of 1,1-Diphenyl-2-methylpropane (**9**). The title compound was prepared starting with phenylmagnesium bromide and methyl isobutyrate following the procedure described by Khalaf and Roberts.[7] The intermediate 1,1-diphenyl-2-methyl-1-propanol was directly reduced to the hydrocarbon using hydrogen and palladium on carbon in glacial acetic acid containing little perchloric acid. The product obtained had a boiling point of 123–124° at 6.4 mm; lit[7] b.p. 168–169° at 29 mm.

Synthesis of DL- and meso-2,3-Diphenylbutane (**12**). These two isomers were obtained by Grignard coupling of 1-bromo-1-phenylethane following literature procedures.[2, 20] The DL-isomer, b.p. 159–160° at 32 mm and lit[7] b.p. 111–112° at 1.8 mm was obtained in 14% yield and the *meso*-isomer, m.p. 124–126° and lit.[7] m.p. 126–127°, was obtained in 21% yield.

ALKYLATION PROCEDURES

In all alkylations, the reactions were carried in a two-necked, round-bottomed flask, equipped with a mechanical stirrer, a pressure equalizing dropping funnel and a reflux condenser fitted with a calcium chloride tube. The catalyst and 90% of the required amount of benzene were introduced into the flask and the alkylating agent dissolved in the rest of benzene was added dropwise (over a period of 30 minutes) through the funnel, while the reactants in the flask were stirred and cooled to about 10–15°. After the addition was complete, the reaction mixture was stirred at room temperature for the rest of the time, then decomposed with water and extracted with ether. The ether layer was washed with water, dried over anhydrous sodium carbonate and the ether was distilled at atmospheric pressure.

In reactions catalyzed by mild catalysts, the identities and relative yields of the products were both determined by v.p.c. analysis and comparison of retention times of the constituents with those of authentic samples under identical conditions. In these reactions, the absolute yields of the products were also determined by v.p.c. using 2,2-diphenylbutane[7] as an internal standard.

In reactions catalyzed by $AlCl_3$, the reaction products were first distilled to obtain a forerun of a mixture of *sec*- and isobutylbenzene and secondly the diphenylated fractions were freed from solid *meso*-2,3-diphenylbutane by successive chilling to 0° and filtration. The identities and relative yields of the liquid diphenylated isomers were then determined by v.p.c. analysis and compared with authentic samples as before.

Data concerning reaction conditions, mole ratios of reactants, compositions and yields of products are summarized in Table 1.

---

[20] A. I. Lepin, *J. Russ. Phys. Chem. Soc.*, **44**, 1190 (1912).

Table 1

Alkylations of benzene with 1- and 2-Hydroxy-2-methy-1-phenylpropane with 1- and 2-Chloro-2-methyl-1-phenylpropane and 2-Methyl-1-phenyl-1-propene [a]

Exp. N°	Reactans	Mole ratios of reactants	Time[b]	Composition of diphenylated products[c], %	Yield[d]
	SECTION A: *With 1-Hydroxy-2-methyl-1-phenylpropane* (**13**)				
1	Alcohol $-C_6H_6-H_2SO_4$	1 : 10 : 1	3	1,2-Diphenyl-2-methylpropane (66 %) and 1,1-diphenyl-2-methylpropane (34 %)	30
2	Alcohol $-6_6H_6-AlCl_3-CH_3NO_2$	1 : 10 : 1.2 : 6	3	1,2-Diphenyl-2-methylpropane (68 %) and 1,1-diphenyl-2-methylpropane (32 %)	59
3	Alcohol $-C_6H_6-AlCl_3-CH_3NO_2$	1 : 10 : 1.2 : 6	24	1,2-Diphenyl-2-methylpropane (67 %) and 1,1-diphenyl-2-methylpropane (33 %)	50
4	Alcohol $-C_6H_6-AlCl_3$	1 : 10 : 1.2	2	1,2-Diphenyl-2-methylpropane (29 %), 1,1-diphenyl-2-methylpropane (61 %), *meso*-2,3-diphenylbutane (6 %), and DL-2,3-diphenylbutane (4 %)	49[e]
5	Alcohol $-C_6H_6-AlCl_3$	1 : 10 : 1.2	10	1,2-Diphenyl-2-methylpropane (42 %), 1,1-diphenyl-2-methylpropane (20 %), *meso*-2,3-diphenylbutane (16 %) and DL-2,3-diphenylbutane (12 %)	46[e]
	SECTION B: *With 2-Hydroxy-2-methyl-1-phenylpropane* (**15**)				
6	Alcohol-$C_6H_6-H_2SO_4$	1 : 10 : 1	3	1,2-Diphenyl-2-methylpropane (68 %) and 1,1-diphenyl-2-methylpropane (32 %)	62
7	Alcohol $-C_6H_6-AlCl_3-CH_3NO_2$	1 : 10 : 1.2 : 6	3	1,2-Diphenyl-2-methylpropane (66 %) and 1,1-diphenyl-2-methylpropane (34 %)	75
8	Alcohol $-C_6H_6-AlCl_3$	1 : 10 : 1.2	2	1,2-Diphenyl-2-methylpropane (58 %), 1,1-(diphenyl-2-methylpropane (28 %), *meso*-2,3-diphenylbutane (8%) and DL-2,3-diphenylbutane (6 %)	57[e]
	SECTION C: *With 2-Methyl-1-phenyl-1-propene* (**17**)				
9	Alkene $-C_6H_6-H_2SO_4$	1 : 10 : 0.5	3	1,2-Diphenyl-2-methylpropane (67 %) and 1,1-diphenyl-2-methylpropane (35 %)	35

Exp. N°	Reactants	Mole ratios of reactants	Time[b]	Composition of diphenylated products[c], %	Yield[d]
	SECTION D : *With 1-Chloro-2-methyl-1-phenylpropane* (**14**)				
10	Chloride – 6_6H_6 – $FeCl_3$	1 : 10 : 0.1	3	1,2-Dipheny-2-methylpropane (65%) and 1,1-diphenyl-2-methylpropane (35%)	48
11	Chloride – C_6H_6 – $AlCl_3$ – CH_3NO_2	1 : 10 : 0.1 : 0.6	3	1,2-Diphenyl-2-methylpropane (66%) and 1,1-diphenyl-2-methylpropane (34%)	50
12	Chloride – C_6H_6 – $AlCl_3$	1 : 10 : 0.1	2	1,2-Diphenyl-2-methylpropane (62%), 1,1-diphenyl-2-methylpropane(29%), *meso*-2,3-diphenylbutane (5%) and DL-2,3-diphenylbutane (4%)	43[e]
13	Chloride – C_6H_6 – $AlCl_3$	1 : 10 : 0.1	10	1,2-Diphenyl-2-methylpropane (55%), 1,1-diphenyl-2-methylpropane (27%), *meso*-2,3-diphenylbutane (10%) and DL-2,3-diphenylbutane (8%)	38[e]
	SECTION E : *With 2-Chloro-2-methyl-1-phenylpropane* (**16**)				
14	Chloride C_6H_6 – $FeCl_3$	1 : 10 : 0.1	3	1,2-Diphenyl-2-methylpropane (68%) and 1,1-diphenyl-2-methylpropane(32%)	76
15	Chloride – C_6H_6 – $AlCl_3$ – CH_3NO_2	1 : 10 : 0.1 : 0.6	3	1-2-Diphenyl-2-methylpropane (66%) and 1,1-diphenyl-2-methylpropane (34%)	79
16	Chloride – C_6H_6 – $AlCl_3$	1 : 10 : 0.1	3	1,2-Diphenyl-2-methylpropane (60%), 1,1-Diphenyl-2-methylpropane (28%), *meso*-2,3-diphenylbutane (8%) and DL-2,3-diphenybutane (8%)	73[e]
17	Chloride – C_6H_6 – $AlCl_3$	1 : 10 : .0	10	1,2-Diphenyl-2-methylpropane (54%), 1,1-diphenyl-2-methylpropane (26%), *meso*-2,3-diphenylbutane (12%) and DL-2,3-diphenylbutane (8%)	55[e]

a) Reactions were carried out as described in the experimental section. b) Tota time before work-up; time for addition of alkylating agent to benzene and catalyst was about 30 minutes. c) Distribution of isomers calculated from v.p.c. analysis and isolation of solid *meso*-2,3-diphenylbutane. d) Combined yield of diphenylbutane based on alkylating agent. e) Yields in these cases were determined by distillation. In these $AlCl_3$ catalyzed alkylations a forerun of a mixture of *sec*- and isobutylbenzene amounting to about 7 to 15 weigth per cent yield of the total distillable product was also obtained.

Revue Roumaine de Chimie, **18**, *3*, 489–492 (1973)

ANALOGUES OF CHLORAMPHENICOL. II

SYNTHESIS OF 2-DICHLOROACETAMIDO-1-(4′-CHLORO-3′-NITROPHENYL)PROPANE-1,3-DIOL

V. V. BADIGER and M. Y. M. JAMKHANDI

Department of Chemistry, Karnatak University, Dharwar-3

Received July 7, 1972

3-Nitro-4-chlorophenacyl bromide (I) on treatment with potassium phtalimide yields the corresponding phtalimido derivative (II). Hydroxymethylation of II followed by Meerwein-Ponndorf-Verley reduction yields racemic *threo*-2-phthalimido-1-(3′-nitro-4′-chlorophenyl)-propane-1,3-diol (IV). The basic hydrolysis of IV gives racemic threo-2-amino-1-(3′-nitro-4′-chlorophenyl) propane-1,3-diol (V) which is resolved by crystallization of the d- and l-salts on treatment with ammonia and subsequent condensation with methyl dichloroacetate to give d- and l-*threo*-2-dichloroacetamido-1-(3′-nitro-4′-chlorophenyl)propane-1,3-diol (VI).

The chemical stability and the ready synthesis of chloramphenicol as well as the relative simplicity of its structure make this antibiotic a popular model for studying the effect of variations in structure on biological activity. Although a large number of analogues of chloramphenicol have been prepared and studied in biological system, the specific structural requirements for maximum antibacterial activity have not been fully determined. Comparison of the relative activities of various analogues suggest that the D-*threo*-2-dichloroacetamido-1,3-propanediol is essential to the activity and the optimum biological activity is dependent on the electron-rich substituents in the aromatic ring. [1] While working on the structure-activity relationships of various analogues of chloramphenicol, Bambas *et al.*, suggested that a halogen atom rather than a nitro group in the *para* position might enhance the activity of the molecule.[2]

On the basis of this premise, and as a part our general programme in the continued search for new antibacterial agents, [3] we have prepared another analogue of chloramphenicol containing both nitro group and chlorine atom in the benzene ring.

[1a] M. C. Rebstock, "Medicinal Chemistry", edited by A. Burger Interscience Publishers Inc. N. Y., 1960, p. 917.

[b] J. R. E. Hoover and B. Blank, *J. Medicin. pharm. Chem.*, **6**, 628 (1963).

[2] L. L. Bambas, H. D. Troutman and L. M. Long, *J. Amer. Chem. Soc.*, **72**, 4445 (1950).

[3] V. V. Badiger and M. Y. M. Jamkhandi, *Indian J. Chem.*, **9**, 198 (1971).

The synthetic route chosen for the preparation of *d*- and l-*threo*-2-dichloroacetamido-1-(3′-nitro-4′-chlorophenyl)propane-1,3-diol (IV) is based on the method of Caldwell and Scheweiker.[4]

3-Nitro-4-chloroacetophenone served as a starting material for the reaction sequence. Bromination of 3-nitro-4-chloroacetophenone in the α-position afforded 3-nitro-4-chlorophenacyl bromide (I) which on treatment with potassium phthalimide yielded the corresponding phthalimido derivative II. Hydroxymethylation of II was achieved in ethanolic solution using 37—38% aqueous formaldehyde and sodium bicarbonate. The resulting 2-phthalimido-3-hydroxy-1-(3′-nitro-4′-chlorophenyl)-1-propanone (III) was converted to dl-*threo*-2-phthalimido-1-(3′-nitro-4′-chlorophenyl) propane-1,3-diol (IV) using Meerwein-Ponndorf-Verley reduction. The dl-*threo* configuration was assigned on analogy with the work of earlier workers.[5] Compound IV was hydrolysed by warm alcoholic potassium hydroxide to dl-*threo*-2-amino-1-(3′-nitro-4′-chlorophenyl)-propane-1,3-diol (V). The racemic base V was resolved by crystallization of the d- and l-salts of d-camphorsulfonic acid from isopropyl alcohol. The less soluble salt, m.p. 199—200°, $[\alpha]_D^{30} - 3.2°$ (methanol) upon treatment with ammonium hydroxide gave a (—) base, m.p. 88—89°, $[\alpha]_D^{30} - 17.5°$ (ethyl acetate).

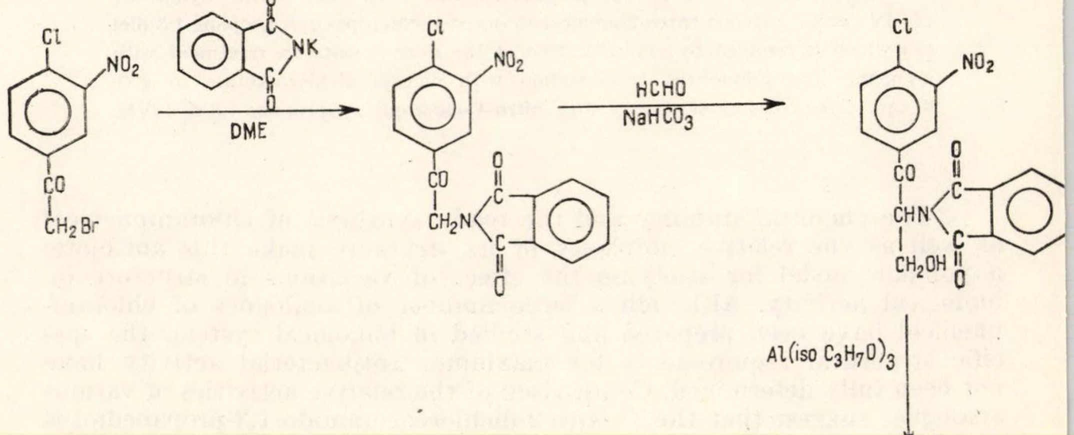
Cl
NO2
CO
CH2Br
NK
DME
Cl
NO2
CO
CH2N
HCHO
NaHCO3
Cl
NO2
CO
CHN
CH2OH
Al(iso C3H7O)3
Cl
NO2
HO—C—H
H—C—N
CH2OH
KOH
C2H5OH
Cl
NO2
HO—C—H
H—C—NH2
CH2OH
Cl2CH·COOCH3
Cl
NO2
HO—C—H
H—C—NHCOCHCl2
CH2OH

W. T. CALDWELL and G. C. SCHEWEIKER, *J. Amer. Chem. Soc.*, **75**, 5884 (1953).

[5] N. P. BUU-HOI, N. D. KUONG and N. H. KHOI, *J. Chem. Soc.*, **1951**, 255.

The more soluble salt, m.p. 188–189°, $[\alpha]_D^{30} + 24.0°$ (isopropyl alcohol), yielded, on treatment with ammonia, a (+) base, m.p. 165–66°, $[\alpha]_D^{30} + + 25.5°$ (methanol). The resolved (+) and (−) bases were separately condensed with methyl dichloroacetate to give N-dichloroacetyl derivatives, m.p. 196–98°, $[\alpha]_D^{30} + 18.5°$ (ethyl acetate) and m.p. 182–83°, $[\alpha]_D^{30} - 18.18°$ (ethyl acetate) respectively.

EXPERIMENTAL PROCEDURE

3-NITRO-4-CHLOROPHENACYLBROMIDE (I)

3-Nitro-4-chloroacetophenone (0.5 mole) dissolved in glacial acetic acid (300 g) was warmed and treated with bromine (0.5 mole) dropwise. After the addition, the reaction mixture was stirred for half an hour and poured on crushed ice. The solid material was filtered and washed with ice water. It was crystallized from ethanol in colourless needles, m.p. 84°, yield 81%, (lit. [6] m.p. 84°).

PHTHALIMIDO-3-NITRO-4-CHLOROACETOPHENONE (II)

Potassium phthalimide (0.27 mole) was added to a solution of (0.0253 mole) of 3-nitro-4-chlorophenacyl bromide (I) in 20 ml of dimethylformide. The reaction was slightly exothermic. The temperature was rising to 55° in 5 minutes and the temperature dropped slowly to 25°. After the addition of 30 ml of chloroform the mixture was poured into 100 ml of water. The aqueous phase was separated and extracted with 2 × 100 ml portions of chloroform. The combined chloroform extract was washed with 20 ml of 0.2 N sodium hydroxide solution to remove the unreacted phthalimide and then with 20 ml of water. After drying over anhydrous sodium sulfate, the chloroform was removed, the crystalline residue was triturated with 40 ml of ether to give phthalimido-3-nitro-4-chloroacetophenone as yellow powdery needles, m.p. 170–72°, yield, 60%.

Analyses for $C_{16}H_2ClN_2O_5$: *Calc.* C, 49.35 ; H, 2.5 ;
Found : C, 48.86 ; H, 2.7.

3-NITRO-4-CHLORO-β-(HYDROXYMETHYL)-α-PHTALIMIDOACETOPHENONE (III)

A suspension of 2.0 g (0.0057 mole) of the 3-nitro-4-chlorophthalimidoacetophenone in 5 ml of 37–38% aqueous formaldehyde and 20 ml of 95% ethanol containing a small amount if sodium bicarbonate was stirred at room temperature for two hours. The mixture was poured in ice water and the solid was filtered and dried to give 2.2 g of 3-nitro-4-chloro-β-(hydroxymethyl)-α-phthalimidoacetophenone. It was crystallized from ethyl acetate in shining yellow crystals, m.p. 189–90° yield, 3.1 g.

Analyses for $C_{17}H_{11}ClN_2O_5$: *Calc.* : C, 54.47 ; H, 2.9 ;
Found : C, 54.77 ; N, 2.9.

dl-*threo*-2-Phthalimido-1-(3-nitro-4-chlorophenyl)propane-1,3-diol (IV)

3-Nitro-4-chloro-β-(hydroxymethyl)-α-phthalimidoacetophenone (6.4 g) was added to a hot solution of 8.0 g of aluminum isopropoxide in 70 ml of isopropyl alcohol in a 100 ml flask equipped with a Hans condenser. After a few minutes an opaque red-brown solution was formed and removal of acetone was continued for four hours when the acetone test was negative. During the last 15 minutes the distillation was rapid.

[6] H. G Garg, *J. Indian Chem. Soc.*, **38**, 59 (1961).

The thick red brown residue was allowed to cool just below the reflux temperature before 10 ml of water were added. The mixture was refluxed for 15 minutes and filtered. During the refluxing the colour changed to light yellow. The residue was treated twice by refluxing with 25 ml portions of 80% aqueous isopropyl alcohol. The combined extracts were concentrated *in vaccuo*. The residue was refluxed with 25 ml of ethyl acetate until the oily material had dissolved. The ethyl acetate was removed under reduced pressure. The solid obtained was recrystallized from ethylene dichloride in light yellow needles, m.p. 190—91°, yield, 3.0 g.

Analyses for $C_{17}H_{13}ClN_2O_5$: *Calc.* : C, 54.18 ; H, 3.4 ;
Found : C, 54.00 ; H, 3.6.

dl-*threo*-2-Amino-1-(3′-nitro-4′-chlorophenyl)propane-1,3-diol (V).

3.0 g dl-*threo*-2-phthalimido-1-(3′-nitro-4′-chlorophenyl) propane-1,3-diol was added by stirring to 7.0 ml of hot alcoholic solution of 87% (0.85 mole) potassium hydroxide and stirring was continued for 30 minutes after addition was complete. The orange solution was diluted with 40 ml of cold water and made slightly acidic with hydrochloric acid. The light yellow crystalline product was filtered off, washed well with cold water and dried. It was recrystallized from glacial acetic acid, m.p. 157—58°, yield 2.5 g.

Analyses for $C_9H_{11}ClN_2O_4$: *Calc.* : C, 43.81 ; H, 4.49 ;
Found : C, 44.00 ; H, 4.60.

Resolution of dl-*threo*-3-Nitro-4-chlorophenyl-2-amino-1,3-propanediol. (*Threo* series)

2.0 g of dl-*threo*-3-nitro-4-chlorophenyl-2-amino-1,3-propanediol and 2.0 g of d-camphorsulfonic acid (BDH) were dissolved in 40 ml of isopropyl alcohol by heating on steam bath for 10 minutes. After standing overnight at room temperature 870 mg of salt were obtained. Recrystallization from isopropyl alcohol gave pure ld-salt, m.p. 199—200°. $[\alpha]_D^{30} - 3.2°$ (methanol).

The mother liquor from the first crop of 870 mg of crude ld-salt (m.p. 199—200°) was diluted with two volumes of ether. A crop of 1.7 g was recrystallized from isopropyl alcohol to yield 1.4 g, m.p. 188—89°.

$[\alpha]_D^{30} + 24.0°$ (isopropyl alcohol).

l- and d-3-Nitro-4-chlorophenyl-2-amino-1,3-propanediol.

A sample of 615 mg of d-camphorsulfonate of the l-base was dissolved in 10 ml of distilled water and pH adjusted to 10 with ammonium hydroxide. The precipitated base was filtered after 20 minutes and recrystallized from ethyl acetate, m.p. 88—89°, yield 410 mg.

$[\alpha]_D^{30} - 17.5°$ (ethyl acetate).

The d-base, m.p. 165—166°, was prepared from the corresponding d-camphorsulfonate.

$[\alpha]_D^{30} + 25.5°$ (methanol).

1-N-Dichloroacetamido-1-(3′-nitro-4′-chlorophenyl)-2-amino-1, 3-propanediol. VI

A mixture of the foregoing amine (300 mg) and methyl dichloroacetate (0.5 ml) was kept at 80° for 3 hours. The precipitate obtained on treatment with light petroleum-ether was crystallized from ethyl acetate in light yellow crystalline solid, m.p. 196—97°, yield 150 mg.

$[\alpha]_D^{30} + 18.75°$ (ethyl acetate).

d-N-Dichloroacetamido-1-(3′-nitro-4′-chlorophenyl)-2-amino-1,3-propanediol.

A mixture of foregoing amine (279 mg) and methyl dichloroacetate (0.5 ml) was kept at 80° for 3 hours. The precipitate obtained on treatment with light petroleum-ether was crystallized from ethyl acetate in light yellow needles, m.p. 182—83°, yield 115 mg.

$[\alpha]_D^{30} - 18.18$ (ethyl acetate).

Acknowledgement. We thank Prof. S. Siddappa, Head of the Department of Chemistry, for his interest in the work. We also thank Sri V. A. Desai for the analytical data recorded. One of us (M.Y.M.J.) is grateful to the Ministry of Education, Government of India, for providing a research training scholarship.

Revue Roumaine de Chimie, 18, 3,493 – 500 (1973)

QUATERNARY BASIC AMMONIUM POLYELECTROLYTES. I

QUATERNIZATION REACTION OF SOME TERTIARY AMINES CONTAINING HYDROXYLIC GROUPS WITH CHLOROMETHYLATED POLYSTYRENE

I. PETRARIU, CORNELIA LUCA, IG. POINESCU and M. DIMA

Institute of Macromolecular Chemistry "P. Poni"
Jassy, Aleea Gr. Ghica Vodă Nr. 41 A

Received June 27, 1971

The amination reaction of the chloromethylated polystyrene with dimethyl-2-hydroxyethylamine, dimethyl-2-hydroxypropylamine and diethyl-2-hydroxyethylamine has been studied and the poly[(*p*-vinylbenzyl)dimethyl-2-hydroxyethyl-ammonium chloride], poly[(*p*-vinylbenzyl)dimethyl-2-hydroxypropylammonium chloride] and poly[(*p*-vinylbenzyl) diethyl-2-hydroxyethylammonium chloride] were obtained. The reaction took place initially in the homogeneous medium and then continued in heterogeneous medium. The polyelectrolytes obtained are completely soluble in water.

Polyelectrolytes of the quaternary ammonium salts type began to be more and more studied and their use in different fields extended very much in the last time.

These polyelectrolytes can be used as catalysts in different chemical reactions, bactericides, algicides, emulsifiers, adsorbants in chromatography and as coagulation agents to remove the acid substances of aqueous solutions. Also they can be used successfully in different chemical processings, cosmetics, plastics, textiles and water treatments.

In the present paper the optimum synthesis conditions of the [(*p*-vinylbenzyl)dimethyl-2-hydroxyethyl ammonium chloride], [(*p*-vinylbenzyl)dimethyl-2-hydroxypropyl ammonium chloride] and [(*p*-vinylbenzyl)diethyl-2-hydroxyethyl ammonium chloride] type polyelectrolytes as well as their thermal stability and behaviour in solution were studied.

The syntheses have been achieved through the chloromethylation of the polystyrene and amination of the chloromethylated polystyrene with some tertiary amines containing hydroxylic groups.

The general reactions are :

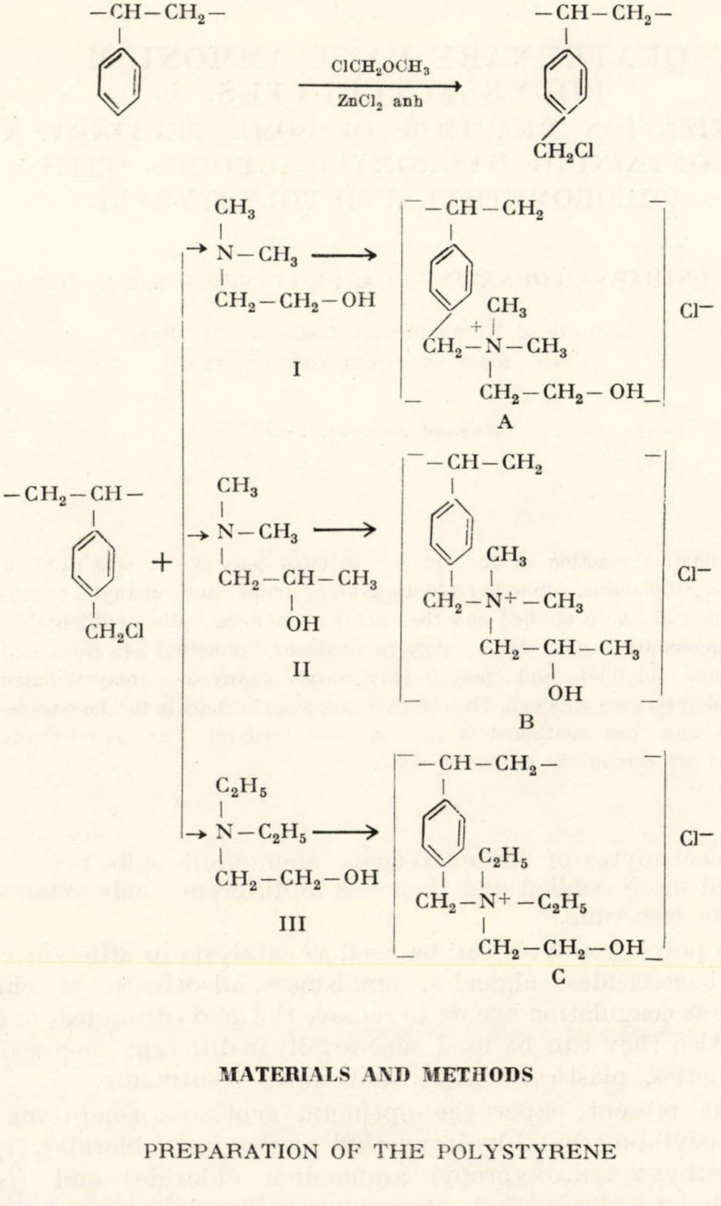
ClCH₂OCH₃
ZnCl₂ anh
–CH–CH₂–
CH₂Cl
CH₃
N–CH₃
CH₂–CH₂–OH
I
CH₂–N⁺–CH₃
CH₂–CH₂–OH
Cl⁻
A
CH₂–CH–CH₃
OH
II
B
C₂H₅
N–C₂H₅
III
CH₂–N⁺–C₂H₅
C

MATERIALS AND METHODS

PREPARATION OF THE POLYSTYRENE

Polystyrene has been prepared by suspension polymerization and purified by twice precipitating a dioxan solution in methanol[1]. The molecular weight of the purified polystyrene as determined by the viscosimetrie method (Ubbelohde with suspension level) was 17,160.

---

[1] I. Petrariu and J. Stamberg, *Coll. Czech. Chem. Comm.*, **32**, 798 (1967).

The monochlormethylether was prepared according to the method described by Pepper and Paisley.[2] The fraction with b.p. 58–60°, $n^{25} = 1.3949$, obtained by redistillation of the resulting product, has been used.

Obtaining of chloromethylated polystyrene [ClPS]. Polystyrene synthetized as above was chloromethylated according to literature procedure data,[3] to a content of 23.23% Cl, which corresponded to a molar conversion of 100%, monosubstitution of the aromatic nuclei being assumed.

Amination of the chloromethylated polystyrene. The amination reaction of the chloromethylated polystyrene with dimethyl-2-hydroxyethylamine (DMEA), dimethyl-2-hydroxypropylamine (DMPA) and diethyl-2-hydroxyethylamine (DEEA) was carried out in a three-neck flask, fitted with a mercury seal stirrer, a reflux condenser closed with an anhydrous calcium chloride tube, and a thermometer, at 40°, in anhydrous benzene.

The chloromethylated polystyrene and amines were taken in a molar ratio varying between 1 : 1 and 1 : 15 and reaction times of 1–48 hours.

After amination, the polyelectrolyte was filtered, washed with anhydrous benzene to eliminate the excess amine and dried in vacuum. Then, the resulting polyelectrolyte was purified by solving in anhydrous methanol and precipitated with vigorous stirring in anhydrous ethyl ether. The precipitated product was washed with anhydrous ethyl ether and dried to a constant weight in a vacuum oven at 40°. The conversion degree of the quaternary ammonium compounds was determined from the nitrogen content of the resulted compound.

Dimethyl 2 hydroxyethyl amine has been prepared according to Handard's and Inglod's indication.[4]

Diethyl 2 hydroxyethyl amine and dimethyl 2 hydroxypropyl amine (Lab. BDH reagent) were redistilled before use.

The solvent utilized was the anhydrous benzene on metallic sodium.

Ultraviolet spectra were measured on a Unicam SP 800 spectrophotometer using 1 cm quartz cuvettes.

The derivatograms were obtained on a F. Paulik, J. Paulik and L. Erdey derivatograph, in air with a heating regime of 12°/min.

Viscosimetric measurements were made at 25° in an Ubbelohde suspended level type viscosimeter.

RESULTS AND DISCUSSIONS

In order to find the optimum amination conditions of chloromethylated polystyrene with the above mentioned amines, we decided to observe the influence of different factors (the molar ratio, the amination reaction time etc.) on the transformation degree α.

The optimum conversion temperature was found to be 40° in order to avoid the chemical degradation of quaternary ammonium polyelectrolytes.

---

[2] K. W. Pepper and H. M. Paisley, *J. Chem. Soc.*, 1953, 4097.

[3] G. D. Jones, *Ind. Eng. Chem.*, **44**, 2688 (1952).

[4] W. Handard and C. K. Ingold, *J. Chem. Soc.*, 1927, 1013.

Amination with an excess of tertiary amine can result in a total or partial replacement of chlorine atoms in the chloromethylated polystyrene. Figure 1 shows that at a 1 : 2 molar ratio ClPS : amines of type I, II, III and reaction temperature of 40° in anhydrous benzene dimethyl-2-hydroxyethylamine proves to be the most reactive, respective the polyelectrolyte *A* reaching in 8 hours a transformation degree of 91.2% while the polyelectrolyte *B* attains 75.73% and the polyelectrolyte *C* only 9.09% conversion.

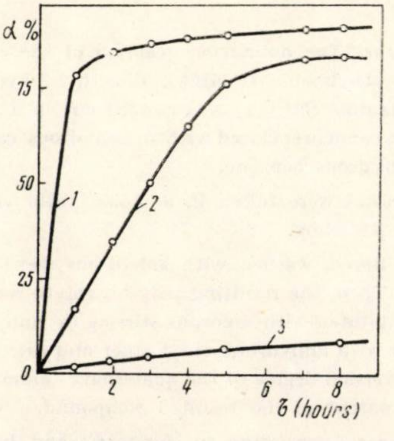

Fig. 1. — Influence of the amination duration (in hours) on the conversion degree α. Reaction conditions: ClPS/amines molar ratio 1/2, 40°, reaction medium=anhydrous benzene ; α=molar conversion degree.

1, polyelectrolyte *A* ; 2, polyelectrolyte *B* ; 3, polyelectrolyte *C*.

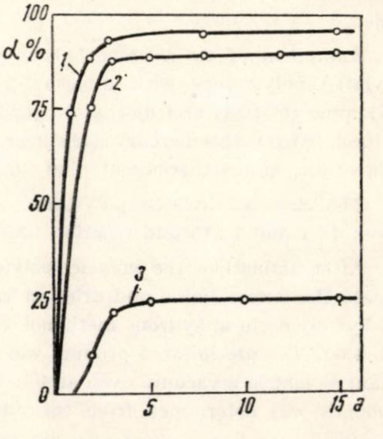

Fig. 2. — Influence of conversion degree α versus ClPS/amines molar ratio in anhydrous benzene ; α = molar conversion degree. *a* = amine moles for 1 mole of chloromethylated polystyrene. Reaction conditions : 40° ; 5 hours.

1, polyelectrolyte *A* ; 2, polyelectrolyte *B* ; 3, polyelectrolyte *C*.

Attempts to enhance the degree of transformation more than 9.09% for polyelectrolyte *C* by increasing the time of the amination reaction have not yielded the desired results. After 48 hours, the degree of transformation was only 14.7%.

In order to increase much more the amination degree of polyelectrolyte *C* as the other polyelectrolytes, the amination process was carried out at higher molar ratios, namely ClPS : amines varying between 1 : 1 and 1 : 15, reaction time 5 hours and temperature 40°. As one can observe from figure 2, the amination degree is 94.0% for the polyelectrolyte *A*, 89% for the polyelectrolyte *B* and 24% for the polyelectrolyte *C*.

A clear image of the maximum amination conditions of these three polyelectrolyte types, is shown in table 1.

The impossibility of a completely amination of the ClPS in the case of amine III, in the above described reaction conditions, may be due to steric factors hindering the interaction of the amination agent with

Table 1

Variation of the maximum conversion degree of chloromethylated polystyrene with the kind of amine; molar ratio ClPS/amine = 1/3, temperature 40°C, reaction medium: anhydrous benzene

Amine	Reaction time hours	Maximum conversion %
Dimethyl-2-hydroxyethylamine	5	94
Dimethyl-2-hydroxypropylamine	5	89
Dicthyl-2-hydroxyethylamine	48	52

each elementary link of the chloromethylated polystyrene as the molecular volume of the amine III is much larger than of the other two amines used in the amination reaction.

A series of viscosimetric measurements of aqueous solutions of the polyelectrolytes *A*, *B*, *C* were carried out (fig. 3).

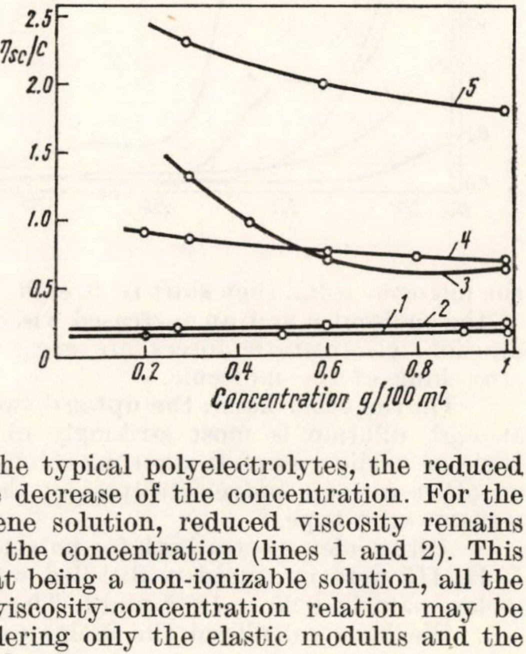

Fig. 3. — Reduced viscosity of unquaternized polymer in anhydrous benzene solution and quaternary ammonium polyelectrolytes of *A*, *B* and *C*-types in aqueous solution.

1, chloromethylated polystyrene; *2*, linear polystyrene; *3*, polyelectrolyte of type *A*; *4*, polyelectrolyte of type *C*; *5*, polyelectrolyte of type *B*.

It is well known that for the typical polyelectrolytes, the reduced viscosity η_{sc}/C increases with the decrease of the concentration. For the unquaternized polymers in benzene solution, reduced viscosity remains unchanged with the variation of the concentration (lines 1 and 2). This may be explained by the fact that being a non-ionizable solution, all the macromolecules are coiled and viscosity-concentration relation may be theoretically calculated by considering only the elastic modulus and the relaxation time of the coiled molecules.

The increase of η_{sc}/C with decreasing concentration is much more visible in the case of *A* and *B* polyelectrolytes, because these have a higher conversion degree (94% and 89%, respectively) than *C* polyelectrolyte whose conversion degree is 52% only. An explanation of this viscosity behaviour can be given. In the flowing liquid the molecules lie athwart to the shear lines and these influence the viscosity by their length number and resistance to elongation. To a large extent, at high concentration, the polyelectrolyte molecules are close together and the reduced viscosity η_{sc}/C represents normal values.

On dilution, the molecules of quaternized polymers which have ionizable groups, begin to space out and, due to the positive charge of the nitrogen atom, they start to stretch. This causes an increased extension of the molecules and an increased viscosity. For a still higher degree of dilution, electrostatic forces are great enough to produce a maximum stretching of the molecule.

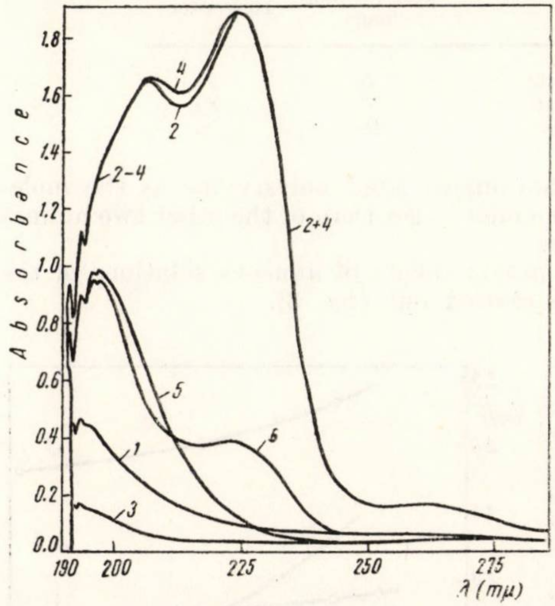

Fig. 4. – U.V. spectra of I, II and III amines and of *A*, *B*, *C* polyelectrolytes.

1, amine I; 2, polyelectrolyte *A*; 3, amine II; 4, polyelectrolyte *B*; 5, amine III; 6, polyelectrolyte *C*.

On the other hand, the upward sweep of the reduced viscosity curve at high dilution is most strikingly observed with polymers containing basic ar acidic groups in aqueous solutions. This finding was also proved on other cationic polyelectrolytes of the polyvinyl – chloroacetate quanternary salts type.[5]

Ultraviolet spectra both for polyelectrolytes *A*, *B*, *C* and the amines I, II, III were measured in distilled water, at a concentration of 1/4000 molar, namely 0.25×10^{-3} mol/l. The results are shown in fig. 4.

We have calculated the molar extinctions ε for the characteristic peaks of the polyelectrolytes *A*, *B* and *C* ($\varepsilon = D/lc$, $D = \log I_0/I$ is the optical density, c = concentration in moles per liter and l = width of the solution layer).

Curves 1, 3 and 5 represent ultraviolet absorption spectra for I, II and III amines. The amines show characteristic peaks at 192, 194 and 196 mμ. These peaks are partially due to the water absorption, because in the curve of water absorption, peaks with less intensity appear in this region.

---

[5] J. P. Newport and R. J. Reyholds, *S. C. I. Monograph*, **26**, 131 (1967).

Curves 2, 4 and 6 show absorption spectra of the *A*, *B* and *C* polyelectrolytes. In the 190–200 mμ region one observes the same peaks as in the case of the above mentioned amines with the difference that here new peaks appear at 207 mμ and 225 mμ. There is also a broader peak at 262 mμ but with less intensity. In the case of *C* polyelectrolyte peaks appear at 225 mμ and 262 mμ only. The peak at 225 mμ is characteristic for the quaternary nitrogen. [6] The ultraviolet absorption spectra may be a control of nitrogen quaternization, because the strong absorption due to N^+ appears at wave lengths of 225 mμ where tertiary nitrogen has no absorption.

In the case of *A* and *B* polyelectrolytes the molar extinction coefficients for the peaks at 207, 225 and 262 mμ have the same values, namely : $\varepsilon_{207\mathrm{m}\mu} = 6640$; $\varepsilon_{262\mathrm{m}\mu} = 640$ and $\varepsilon_{\max} = 7480$ at 225 mμ.

As for the *C* polyelectrolyte, the peaks at 225 mμ and 262 mμ have smaller molar extinction coefficients, namely : $\varepsilon_{\max} = 1540$ at 225 mμ and $\varepsilon_{262\mathrm{m}\mu} = 240$. It is to be noted that the values of molar extinction coefficients for $\chi = 225$ mμ which are characteristic for N^+ agree with the molar transformation degree α.

With respect to the thermal behaviour, differences have been found between polystyrene and the other chemical modified compounds as chloromethylated polystyrene and the three polyelectrolytes *A*, *B* and *C*. These differences consist both in a changed degradation mechanism, illustrated by the decomposition of the unique process of polystyrene and a modification of thermal stability, both conclusions being supported by the data presented in figure 5 and table 2.

The size of this modification can be quantitatively appreciated from the weight loss curves (fig. 5).

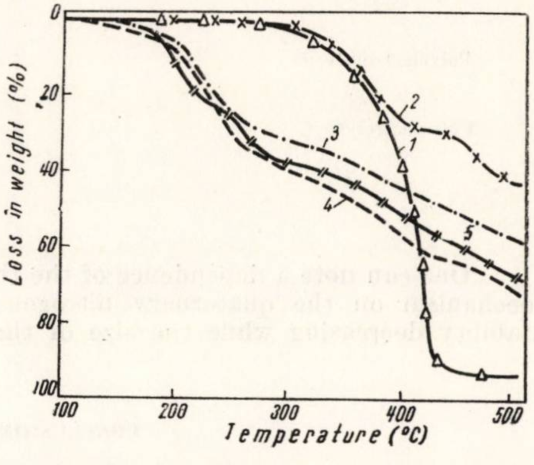

Fig. 5. — Thermogravimetric curves of polystyrene, of chloromethylated polystyrene and those of *A*, *B* and *C* polyelectrolytes.

1, polystyrene ; *2*, chloromethylated polystyrene ; *3*, polyelectrolyte *A* ; *4*, polyelectrolyte *B* ; *5*, polyelectrolyte *C*.

From fig. 5 one can note that polystyrene (curve 1) has a great thermal stability up to 350°, then a sharp weight loss takes place between 350–450°. By chloromethylation (curve 2), thermal stability does not change too much in the 100—400° interval, but the weight losses over this temperature are smaller then in the case of polystyrene. By the quaternization of chloromethylated polystyrene one obtains the three polyelectrolytes *A*, *B* and *C*. The polyelectrolytes show at lower temperature 100—350° a less thermal stability than the polystyrene and chloromethylated polystyrene, but at a higher temperature, at about 500°, the weight losses of the polyelectrolytes are smaller than those of the initial polymer (polystyrene). The conclusions concerning the thermal stability are referring to the initial product of decomposition. At higher temperatures, the stability of the products resulted in the first stage of decomposition is different.

---

[6] B. D. Coleman and R. M. Fuoss, *J. Amer. Chem. Soc.*, **77**, 5472 (1955).

This can be due to their dissimilar structure, because subsequent degradation processes (not to be met with at polystyrene) take place at different intervals of temperature and with variable losses of weight, as we can observe from table 2.

Table 2

DTG analyses data of linear polystyrene and its chemical transformation products (rate of heating 12°/min, max temp 900°C)

Product	Number of degradation processes	Field of temp °C	Loss of weight %
Polystyrene	1	260—450	91
Chloromethylated polystyrene	3	245—420	28.75
		420—510	14.75
		510—900	—
Polyelectrolyte *A*	3	145—310	31.30
		310—440	17.00
		440—600	31.40
Polyelectrolyte *B*	3	150—310	38.50
		330—450	22.60
		450—900	—
Polyelectrolyte *C*	4	150—220	16.66
		220—320	20.77
		320—430	17.20
		450—605	35.00

One can note a dependence of the thermal stability and degradation mechanism on the quaternary nitrogen substituents size, the thermal stability decreasing while the size of the substituents increases.

CONCLUSIONS

The amination reaction of the chloromethylated polystyrene with dimethyl-2-hydroxyethylamine, dimethyl-2-hydroxypropylamine and diethyl-2-hydroxyethylamine has been studied. The polyelectrolyte thus obtained were characterized from the point of view of their thermal stability and their behaviour in aqueous solution.

Revue Roumaine de Chimie, **18**, *3*, 501 – 506 (1973)

METHODS FOR THE DETERMINATION OF TOLAZOLINE VISIBLE AND INFRARED SPECTRA OF THE COMBINATION WITH AMMONIUM REINECKATE

GRIGORE TEODORESCU

Polytechnic Institute of Bucharest
Department of Inorganic and Analytical Chemistry
Str. Polizu, 1, Bucharest, Romania

Received August 12, 1972

The present paper presents methods of determining the tolazoline based upon its combination with ammonium reineckate, the dissolving of the obtained compound in acetone followed by the precipitation of the reineckate anion as silver reineckate and the titration of the silver nitrate excess with ammonium thiocyanate. Since the obtained compound is soluble in acetone, forming a coloured solution, the tolazoline has been determined colorimatrically as well. The structure of the obtained compound has been assigned by the determination of the molecular mass, by means of visible spectra for ammonium reineckate and tolazoline reineckate. In order to determine the structure of tolazoline reineckate, infrared spectrum of tolazoline and of its compound, obtained by combination with ammonium reineckate has also been recorded.

The tolazoline (benzazoline, periphen), 2-benzyl-4,5-dihydroimidazole hydrochloride abr. CBI, is a blood-vessel dilator able to generate a rise of the blood flow, being used for troubles of peripheric vessels.

The known analytical determination of tolazoline is based upon the titration of the chloride anion. The method can be precise only with a chemically pure product (free of HCl or NaCl). In order to determine a less pure substance (as it may appear in the process of its manufacture), we considered necessary to improve the method of determination of the pure substance, a method based upon the reaction of tolazoline with ammonium reineckate, $NH_4[Cr(NCS)_4(NH_3)_2]$, abr. $(Rc^-NH_4^+)$, a reagent that we also used for the determination of other substances.[1-10]

---

[1] P. Spacu and Gr. Teodorescu, *Rev. Chim.*, *(București)*, **8**, (1), 41 (1957).
[2] Gr. Teodorescu, *Bul. Inst. Politeh. București*, **29** (5), 83 (1967).
[3] Gr. Teodorescu and Il. Niculescu, *Bul. Inst. Politeh. București*, **30**, (1), 17 (1968).
[4] Gr. Teodorescu, *Bul. Inst. Politeh. București*, **31** (3), 51 (1969).
[5] Gr. Teodorescu, *Bul. Inst. Politeh. București*, **31** (4), 45 (1969).
[6] Gr. Teodorescu, *Bul. Inst. Politeh. București*, **31** (5), 61 (1969).
[7] Gr. Teodorescu, *Bul. Inst. Politeh. București*, **32** (1), 43 (1970).
[8] Gr. Teodorescu, *Bul. Inst. Politeh. București*, **32** (4), 79 (1970).
[9] Gr. Teodorescu, *Bul. Inst. Politeh. București*, **33** (1), 67 (1971).
[10] Gr. Teodorescu, *Rev. chim. anal. București*, **1** (2), 75 (1972).

METHOD

The reaction takes place even in a neutral aqueous solution, as tolazoline hydrochloride contains a quaternary nitrogen atom.

Tolazoline is precipitated with a mole $Rc^-NH_4^+$ according to the equation :

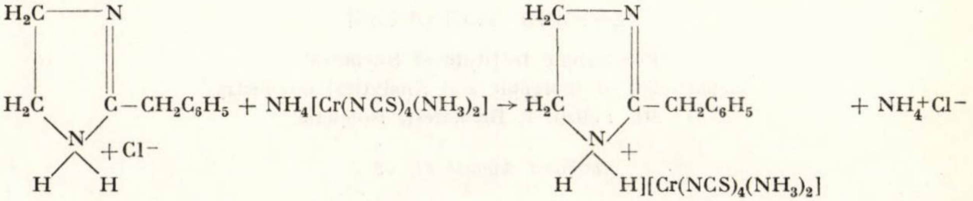

The obtained combination is insoluble in water and soluble in acetone.

The reaction with $Rc^-NH_4^+$ was also used in the determination of tolazoline by volumetric, colorimetric and spectral methods.

1. VOLUMETRIC METHOD

The aqueous solution of tolazoline is precipitated with 2% $Rc^-NH_4^+$ according to the above mentioned equation.

The resulting violet-pink precipitate is filtered, washed with water and dissolved in acetone.

The acetone solution is treated with silver nitrate solution in excess. Silver reineckate precipitates according to the equation :

$$[Cr(NCS)_4(NH_3)_2]^- + Ag^+ \rightarrow Ag[Cr(NCS)_4(NH_3)_2]$$

After filtering and washing of the product, the excess of silver nitrate is titrated with thiocyanate in the presence of iron (III) ammonium alum as an indicator.

1.1. *Experimental part*

25 ml Solution containing 0.01 g substance (CB I) per 1 vol (0.25 g in all) are quantitatively brought in a standard flask of 250 ml with distilled water.

Samples of 10−24 ml are taken out of this solution and precipitated with an approximately equal volume of freshly prepared 2 % $Rc^-NH_4^+$ solution, by gradually adding and continuously stirring, until the solution above the precipitate becomes dark violet-red. The obtained product is filtered on a G_3 filtrable crucible, carried along by means of 0.1 % $Rc^-NH_4^+$ solution and with cold (4° C) distilled water until the solution becomes colourless, and in the end washed two times with 5−10 ml ether.

The compound is directly dissolved in 10−20 ml acetone on a filtrable crucible which is then washed with 20−30 ml distilled water, the whole solution being collected in a 250 ml flask. 100 ml distilled water, 15 ml silver nitrate 0.1 N and 2 drops of nitric acid

2 N are added. The silver reineckate is precipitated. The precipitate is filtered, then washed with distilled water by decanting and the filtrate is collected together with the washing water in a 750 ml titrating decanter. In the same decanter, 2 ml saturated solution of iron (III), ammonium alum (about 40 %) and 3–4 drops of nitric acid 2 N are added, and the excess of silver nitrate is titrated by means of ammonium thiocyanate 0.1 of factor = 1.0638.

To 1 ml silver nitrate 0.1 N corresponds 0.01965 g tolazoline. The results are given in Table 1.

Table 1

Determination of CBI by volumetric method

CBI sample	CBI in samples determined with $Rc^- NH_4^+$	CBI in samples determined with $R_c^- NH_4^+$	Statistical data
g	g	%	
0.0100	0.0100	100	$N = 10$
0.0120	0.0119	99.77	$\overline{X} = 99.62$
0.0140	0.0138	98.57	$S = 0.565$
0.0160	0.0160	100	$S_{\overline{X}} = 0.17$
0.0170	0.0170	100	t = Student variable
0.0200	0.0200	100	$t_{(P=95\%\,;\ \nu=9)} = 2.26$
0.0210	0.0208	99.04	out of tables
0.0220	0.0220	100	Result = 99.62 ± 0.38
0.0240	0.0240	100	

2. COLORIMETRIC METHOD

2.1. *Method*

CBI is precipitated with $Rc^-NH_4^+$, in the same way as by the volumetric method, in molar ratio 1 : 1. Since the product is soluble in acetone forming a red-coloured solution, CBI can be easily determined colorimetrically as well.

2.2. *Procedure*

The analysis is carried out by the method of standard curves. A $Rc^-NH_4^+$ solution of $T = 0.0140$ g/ml was used, from which corresponding volumes were taken into 100 ml standard flasks, diluted in 50 ml acetone and filled up to the mark with distilled water, so that solutions of concentrations $T = 0.000147$; 0.000294 ; 0.000441 ; 0.000588 were obtained.

A Lange photocolorimeter was used, with green filters ($\lambda = 533$ nm) and the standard curve was determined.

Samples containing 0.0140–0.0240 g/ml were taken out of the CBI solution of $T = 0.0010$ g/ml and precipitated with $Rc^-NH_4^+$ as in the volumetrical method. After filtering and washing, the samples were quantitatively dissolved in acetone, the solutions being col-

Table 2

Results of the colorimetration of CBI reineckate

CBI sample	Determined CBI	Determined CBI	Statistical data
g	g	%	
0.000140	0.000138	98.57	$N = 5$
0.000180	0.000177	98.34	$\overline{X} = 98.55$
0.000200	0.000197	98.50	$S = 0.2924$
0.000220	0.000218	99.01	$S_{\overline{X}} = 0.14$
0.000240	0.000236	98.34	t = Student variable
			$t_{(P=95\%;\ \nu=4)} = 2.78$ (out of tables)
			Result : 98.55 ± 0.39

lected in 100 ml standard flasks which were then filled up to the mark with distilled water. After homogenization they were measured colorimetrically (Table 2).

3. SPECTRAL STUDY

3.1. *Characterization of visible spectrum of tolazoline reineckate*

The structure of the substance obtained from CBI and $Rc^{-}NH_4^{+}$ through the above mentioned method can be assigned by determining its molecular mass by means of the absorbance (A) and of the absorptivity (K) of visible spectra.

A common feature of the visible spectra for $Rc^{-}NH_4^{+}$ and for CBI reineckate is that the absorption maxima (λ_{max}) are nearly the same, namely $\lambda_{max} = 520-525$ nm (diagram 1) for $Rc^{-}NH_4^{+}$ (in ethanol 95%) and $\lambda_{max} = 525$ nm (diagram 2) for CBI reineckate (in ethanol 95% as well).

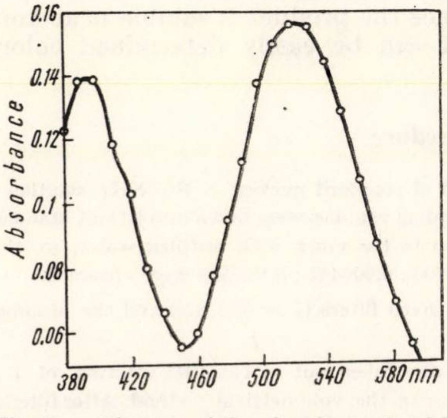

Fig. 1. — Diagram of the absorbancy in visible for ammonium reineckate $g_1 = 0.1\%$; $1 = 0.5$ cm; solvent = 95% ethanol.

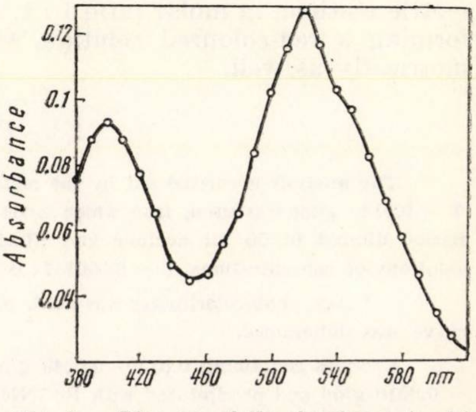

Fig. 2. — Diagram of the absorbancy in visible for tolazoline reineckate $g_1 = 0.1$; $1 = 0.5$ cm; solvent = 95% ethanol.

The absorptivity was determined (K) according to the following relation, with $R_c^-NH_4^+$ in ethanol 95% at a concentration $c = 0.00297$ mole $R^-NH_4^+$, in a 0.5 cm long absorption cell and for an absorbance (A) read on diagram 1 and corresponding to the value $\lambda_{max} = 520-525$ nm. Since the determination was made with $l = 0.5$ cm, value A will be doubled for $l = 1$ cm.

$$K_{(ethanol)} = 2 \times 0.154/0.00297 = 103.7$$

Value K, determined for $Rc^-NH_4^+$, can be considered, within limits of admissible errors, as being also available for CBI reineckate, as λ_{max} for CBI reineckate is equal (or nearly so) to λ_{max} for $Rc^-NH_4^+$ (diagrams 1 and 2).

In order to determine the molecular mass (M_d) the following relation will be used:

$$M_d = g_1/100 \times K/A\,.1.1000 \tag{1}$$

In case $g_1 = 0.1$ g CBI reineckate per 100 ml solution and $l = 1$ cm, relation (1) becomes:

$$M_d = K/A. \tag{2}$$

Practically, the determination of visible absorption of CBI reineckate in 95% ethanol is carried out. The absorbance for $\lambda_{max} = 520-530$ nm at a concentration of 0.1% and in a cell of $l = 0.5$ cm, under given conditions, is 0.108. For $l = 1$ cm, value A is doubled. Replacing K in relation (2) by the determined value for $Rc^-NH_4^+$, the molecular mass is obtained:

$$M_d = \frac{103.7}{2 \times 0.108} = 480. \tag{3}$$

If this value is compared with that of the calculated molecular mass ($M_c = 479.4$), they are seen to be very close, which proves the monoreineckate structure.

A spectrophotometer Zeiss VSU-1 with tubs, whose length was of 0.5 cm and 1 cm, was used.

3.2. *Characterization of tolazoline reineckate in infrared*

The infrared spectrum of CBI reineckate has also been recorded for the structural characterization of the compound.

The IR spectrum of CBI reineckate has been interpreted by comparing it with the $Rc^{-}NH_4^{+}$ spectrum (Table 3).

The IR spectrum of the complex presents bands found in the IR spectrum of ammonium reineckate, which can be attributed to the NH_3 and NCS groups in the reineckate anion of the compound (Table 4); they appear at 490 (δ_{NCS}), 1270 $\overset{\text{Sym}}{\underset{\text{N-H}}{\delta\,\mathrm{NH_3}}}$, 2100 ($\nu_{C-N}$), 3170−3310 $\overset{\text{Sym}}{\underset{\text{N-H}}{\nu\,\mathrm{NH_3}}}$

It also shows bands corresponding to the organic base (Table 4). These bands, at 465 cm^{-1}, 525 cm^{-1}, 749 cm^{-1}, 1300 cm^{-1}, 1620 cm^{-1}, 2680 cm^{-1}, 2970 cm^{-1}, appear also in the spectrum of the compound, where they are slightly altered in position and intensity.

Table 3

IR spectrum of ammonium reineckate

ν (cm^{-1})		T %
472 (w)	δNCS	62
509 (w)		57
718 (i)	NH_3	39
833 (w)	νC−S	76
965		76
1265 (i)	$\delta^{Sym}_{NH_3}$	34
1405 (i)	δNH_4^{+}	32
1605	(H_2O)	50
2059	νC-N	14
2125 (i)		1
3015 (vw)		38
3160 (w)		30
3195 (vw)	νNH_3	32
3238 (w)		28
3315 (w)		27

Table 4

IR spectral bands of tolazoline and of the product obtained with ammonium reineckate

Tolazoline spectrum		Tolazoline reineckate spectrum		
$\bar{\nu}$ (cm^{-1})	T %	$\bar{\nu}$ (cm^{-1})	T %	Attributions
425 (w)	76	425 (w)	85	alkali band
465 (i)	52	460 490 (i)	50	δNCS
525 (i)	48	525 (i)	58	alkali band
625 (w)	70	625 (w)	69	
645 (w)	58	—	—	
700 (i)	35	700 729 (i)	40	alkali band
749				
—	—	780 (w)	73	
820 (w)	66	820 (w)	83	
855 (w)	74			
—	—	915 (w)	82	
950 (w)	78	—	—	
1040 (w)	62	1050 (w)	74	
1210 (i)	38	1205 (w)	70	
—	—	1270 (i)	36	Sym δNH_3 N−H
1300 (i)	20	1300 (w)	55	
1430 (i)	36	1500 (i)	60	
1620 (i)	9	1600 1620 (i)	31	alkali band
		2100 (i)	1	νC−N
2680 (i)	30	2645 (w)	74	alkali band
2970 (i)	8	2980 (w)	52	alkali band
3070	9			
		3170 (m)		
		3230 (m)	23	Sym νNH_3 N−H
		3310 (w)		

Revue Roumaine de Chimie, 18, 3, 507–510 (1973)

POLAROGRAPHIC DETERMINATION OF ANTHRAQUINONE, 2-CHLOROANTHRAQUINONE AND 2-AMINOANTHRAQUINONE

SILVIU-DUMITRU POPESCU

Institute of Chemical Researches
Splaiul Independenței, 202, Bucharest, Romania

Received March 24, 1972

By using dimethylformamide as the most suitable solvent, a solution of ammonium acetate as support of basic electrolyte, and by adding a gelatine solution to suppress the maxima, a new polarographic method for determining anthraquinone, 2-chloroanthraquinone and 2-aminoanthraquinone has been achieved. After removing the oxygen, the organic compound is polarographed, the reduction taking place in a domain of which the potential of deposits corresponds to an appreciable value and is reported to the mercury dropping electrode.

Anthraquinone is an organic compound with wide uses in the dye technology. For this reason, the search for rapid and accurate dosage methods for this substance represents an analytical problem of high practical interest.

Among the analytical methods, polarography gives the most conclusive results. The polarographic method described in the present note offers high advantages compared to the similar methods already reported in the literature. Thus, a polarographic method based on the anthraquinone determination in LiCl or LiOH media [1] implied a lesser precision and is less easy to handle as a working technique, especially due to the presence of LiCl, which is a hygroscopic salt. Other authors [2] have suggested the polarographic determination of anthraquinone by using acetic acid and ammonium acetate as the base electrolyte, which may cause the inconvenience that benzoylbenzoic acid, as an impurity, forms further polarographic steps which could falsify the analytical results.

Finally, when sulphuric acid was used[3] the sensitivity of the polarographic method was noticeably lowered and the sample processing became too intricate.

---

[1] R. P. Lastovski and Iu. I. Weinstein, „Analiza tehnică în industria produselor intermediare și a coloranților", vol. 2, Ed. tehno-științifică de Stat pt. literatură chimică, Moscova, 1958.

[2] T. Isshiki and K. Tada, *Pharm. Bull.*, **2**, 266 (1954).

[3] J. C. James, *Trans. Faraday Soc.*, **47**, 1240 (1951).

The advantage of the polarographic method, as described below, consists in the possibility of removing all these difficulties which affect the course of the analysis, and in its exactness, rapidity and simplicity, as the experimental tests carried out in laboratory have shown to be fulfilled.

Anthraquinone polarography is based on the anthraquinone reduction up to anthrahydroquinone, according to the following reaction scheme:

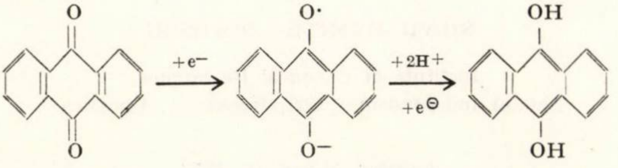

Anthraquinone Semiquinone Anthrahydroquinone

The reduction potentials are reproducible and characteristic for the aforementioned derivative, and the existing impurities do not influence the analysis.

EXPERIMENTAL

REAGENTS

1. Pure N,N′-dimethylformamide
2. Ammonium acetate, 5 M solution
3. Solution of gelatine 1 %
4. Standard solutions of anthraquinone and 2-aminoanthraquinone.

A. *Standard solution of anthraquinone*

0.1 g of anthraquinone p.a. are weighed and dissolved in N,N′-dimethylformamide, the solution being transferred into a graduated flask of 100 ml and brought up to the mark with the same organic solvent (1 ml standard solution = 1 mg anthraquinone).

B. *Standard solution of 2-aminoanthraquinone*

0.1 g 2-aminoanthraquinone p.a. is weighed and then introduced into a graduated flask of 100 ml dissolved and brought up to the mark using N,N′-dimethylformamide in the same way as for anthraquinone (1 ml standard solution = 1 mg 2-aminoanthraquinone).

The standard solutions are left to stay in a dark place.

APPARATUS

The measurements were carried out on a LP_{60} polarograph with a Sefram-Graphispot recorder having a maximum sensitivity of 0.25 μA.

An electrolytic condenser of 180 μF was connected to the terminals of the Sefram recorder, this capacity being necessary to remove the current oscillations during the formation and detachment of the mercury drops.

A capillary of 0.07 mm was used as a dropping electrode, the flow rate of mercury being of one drop for each 3 seconds.

PROCEDURE

A sample of 0.1 g is weighed and introduced into a graduated flask of 100 ml, and then dissolved and brought to the graduation mark with dimethylformamide.

After a good homogenization, a 5 ml solution is introduced with a volume pipette into a graduated flask of 25 ml, to which 4 ml of 5 M of ammonium acetate solution as well as 1 ml of gelatine solution 1% is then added.

The content is once more homogenized and slightly cooled and reached to the graduation with dimethylformamide.

The samples are left to stay in a dark place for 5 min, and bubbled with methane or nitrogen (30 min), polarographed at potentials comprised within −0.42 V and −0.56 V, the capillary tube having a flow rate of one drop per three seconds.

The samples were recorded in comparison to a standard obtained under the same experimental conditions.

For 2-aminoanthraquinone the standard used was prepared from the same substance of *p.a.* purity.

The concentration of anthraquinone is given by the formula :

$$\% C = (H_p \cdot C_{et} / H_{et} \cdot G) \cdot 100$$

where :

C = is the concentration of the sample,

H_p = the step height of the sample (in mm),

H_{et} = the step height of the standard (in mm),

C_{et} = the standard concentration in mg/ml,

G = the sample weight expressed in grams.

CONCLUSIONS

1. The method is reproducible and the errors do not exceed ± 1% which is confirmed by the calibration curve of anthraquinone as shown in figure 1.

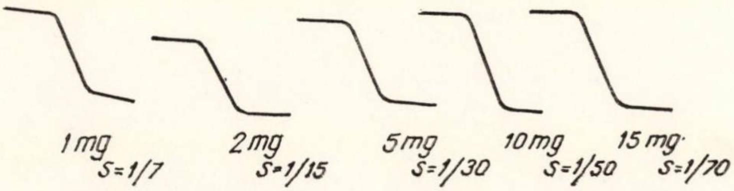

Fig. 1. — Calibration curves of the anthraquinone standard at various concentrations.

2. The curves recorded at different periods of time are quite similar, no changes being observed with their heights.

3. Impurities, such as benzoylbenzoic acid (fig. 2-b), phtalic anhydride (fig. 2-c), phenanthrene (fig. 2-d), anthracene (fig. 2-e), carbazole (fig. 2-f), and maleic anhydride (fig. 2-g) did not influence the polarographic analysis, even at the 1 : 10 anthraquinone/impurity ratio.

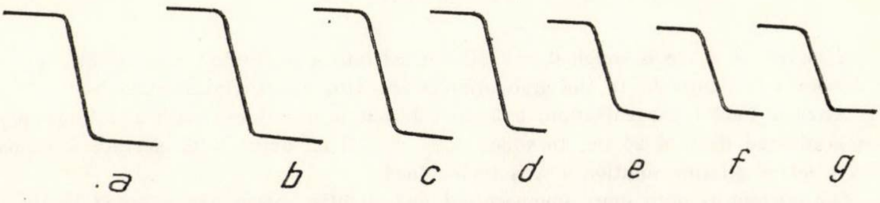

Fig. 2. — Comparative polarograms of anthraquinone for various impurities introduced :

a. – anthraquinone (standard), 5 mg S = 1/20 ; b. – benzoylbenzoic acid, 50 mg S = 1/20 ; c. – phtalic anhydride, 50 mg S = 1/20 ; d. – phenanthrene, 50 mg S = 1/20 ; e. – anthracene, 50 mg S = 1/30 ; f. – carbazole, 50 mg S = 1/30 ; g. – maleic anhydride, 50 mg S = 1/30.

The samples of anthraquinone should be kept in a dark place in order to remove the occurrence of photochemical or oxidation reactions.

Revue Roumaine de Chimie, **18**, *3*, 511–517 (1973)

MECHANISM OF RADIOLYTIC REDUCTION OF Cr^{VI} IN AQUEOUS SOLUTIONS

MARIA FITI

Institute of Atomic Physics, P. O. Box 35, Bucharest, Romania

Received October 8, 1972

The mechanism of Cr^{VI} reduction to Cr^{III} hydrated electrons and hydrogen atoms is discussed. In the presence of specific OH radical scavengers, such as alcohols, the Cr^{VI} reduction occurs with $G(-Cr^{VI}) = G(Cr^{III})$ depending on Cr^{VI} concentration, acidity, additives and dose-rate. In neutral, deaerated solutions and in the presence of *t*-butanol the reduction occurs directly by e^-_{aq} and H ($G_{red} = G_H + G_{e_{aq}} = 3.2$) because $G - Cr^{VI} \simeq 1/3\, G_{red} = 1.05 \pm 0.05$. In the presence of methanol and in acid solutions $G\,(-Cr^{VI})$ exceeds largely the value required by the above equation; the reduction is controlled by chain reaction mechanism, propagated by the H, HO_2 and $.CH_2OH$ radicals.

INTRODUCTION

The Cr^{VI} as chromate and/or dichromate ions are quite resistant to radiolysis in its pure, neutral, and aerated aqueous solution because the ions reduced by e^-_{aq} and H atoms are oxidized back by OH radicals issuing from water radiolysis.

It is well known that the chromate and dichromate anions are very powerful oxidizing agents. In their aqueous solutions, subjected to ionizing radiation, it is expected that they would react with reducing species, e^-_{aq} and H, present in these conditions.

The overall equation of water radiolysis is

$$H_2O \rightarrow e^-_{aq},\ H,\ OH,\ H_2O_2,\ H_2 \qquad (A)$$

with the G values as follows:

$$G_{e^-_{aq}} = 2.70, \quad G_{OH} = 2.70, \quad G_H = 0.45$$

$$G_{H_2} = 0.55, \quad G_{H_2O_2} = 0.70.$$

The rate constants of chromate and dichromate reactions with e_{aq}^- have been measured by pulse radiolysis method [1,2]:
$k(CrO_4^{2-}) = 1.8 \times 10^{10}$ mol^{-1} s^{-1}, $k(Cr_2O_7^{2-}) = 4.4 \times 10^{10}$ mol^{-1} s^{-1}
A Cr^{V} transient is presumably formed, by the reaction of either e_{aq}^- or H atom and it is reoxidized back by OH radical reaction with an estimated rate constant of 5×10^{10} mol^{-1} s^{-1}. It is also noted [2] that the transient species goes back to the original compound by a second order process.

The apparent stability of Cr^{VI} is due to opposite processes and for this reason there are quite few data on the detailed mechanism of radiolytic reduction of chromate and dichromate anions in aqueous solution.

For practical and theoretical reasons, it is of interest to have more information on the reactions which occur and we are reporting here new relevant data on the reduction mechanism.

EXPERIMENTAL

Materials. Analytical grade Merck potasium chromate and potasium dichromate is used to make up the solutions in triply distilled water. All other materials were of analytical grade purity, without further purification except *t*-butanol which was purified by three recrystallizations.

Irradiations were carried out in 10 ml samples, contained in cylindrical Pyrex vessels, at the 2 MeV electron beam, delivered by a linear accelerator and to the γ-rays produced by stopping the above electron beam through the tungsten windows. The dose-rates available with these facilities were of 1.6×10^{18} eV ml^{-1} s^{-1}, for the electron beam and 4.8×10^{15} eV ml^{-1} s^{-1}, for γ-rays.

Analysis. The Cr^{VI} concentration was followed spectrophotometrically at $\lambda = 374$ nm, the chromate anion absorption peak. The dichromate solutions were analysed as chromate, adding NaOH 4% aqueous solution to irradiated dichromate solution. [3]

Trivalent chromium was identified from its green Cr_2O_3 oxide and by conversion to a violet trioxalate complex, [4], that may be read at $\lambda = 420$ or 560 nm.

The yield of molecular hydrogen was determined by gas chromatography, on a molecular sieve 5 A column, with argon as carrier gas.

The hydrogen was extracted from solutions using a modified Van Slyke extractor.

In solutions containing methanol, we identified carbonyl group of formaldehyde by its specific reaction with 2–4 dinitrophenylhidrazine.

RESULTS AND DISCUSSIONS

A. NEUTRAL SOLUTIONS

As we expected the pure, deaerated solution of CrO_4^{2-} ions of low concentrations, irradiated to electron and γ-rays beam gives a very low yield of $G(-Cr^{VI}) \simeq 0.10$.

---

[1] J. K. Thomas, S. Gordon and E. J. Hart, *J. Phys. Chem.*, **68**, 1524 (1964).

[2] J. H. Baxendale, E. M. Fielden and J. P. Keene, *Proc. Roy. Soc.*, **A286**, 320 (1965).

[3] J. M. Kolthoff and P. I. Elving, "Treatise on Analytical Chemistry", Part III, vol. 8, Wiley Interscience, New York, 1968, p. 273.

[4] H. M. Hershensen, "Ultraviolet and Visible Absorption Spectra". Academic Press, New York, 1959, p. 1945.

The reactions which occur are essentially the following:

$$Cr^{VI} + e_{aq}^{-}(H) \rightarrow Cr \tag{1}$$

$$Cr^{V} + OH \rightarrow Cr^{VI}. \tag{2}$$

In order to avoid the reaction (2) we added to the Cr^{VI} solutions powerful and specific OH scavengers, namely alcohols as: methanol, ethanol, *t*-butanol etc., which react with OH and H, but are quite unreactive towards e_{aq}^{-}:

$$CH_3OH + OH \rightarrow .CH_2OH + H_2O \tag{3}$$

$$CH_3OH + H \rightarrow .CH_2OH + H_2 \tag{4}$$

The organic radical produced from these reactions, is usually a strong reducing species leading to the corresponding aldehyde:

$$M^{n+} + .CH_2OH \rightarrow M^{(n-1)+} + H_2C{=}O + H. \tag{5}$$

In the particular case of *t*-butanol, the radical formed by reactions like (3) and (4) is quite unreactive [5] and consequently the only reducing radicals are e_{aq}^{-} and H, issuing from water radiolysis.

In order to study the reduction by these species, we used *t*-butanol as OH scavenger. Its reactivity towards H atom is also very small as it appears from the rate constants [6]:

$$k_H = 1.0 \times 10^5 \text{ mol}^{-1} \text{ s}^{-1}, \quad k_{OH} = 2.8 \times 10^8 \text{ mol}^{-1} \text{ s}^{-1}.$$

The results concerning the Cr^{VI} reduction, in neutral solutions containing *t*-butanol, are given in the table 1.

Table 1

$G(-Cr^{VI})$ in neutral aqueous solution of CrO_4^{2-} in the presence of *t*-butanol

CrO_4^{2-}, N / *t*-butanol, M	2×10^{-4}	5×10^{-4}	10^{-3}	2×10^{-3}	5×10^{-3}	Dose-rate $eV\cdot ml^{-1}\,s^{-1}$
0.1	0.30	0.30	0.30	0.35	0.35	1.6×10^{18}
1.0	0.25	0.25	0.25	0.30	0.35	electron beam
0.1	0.80	0.85	0.95	1.05	1.10	4.8×10^{15}
1.0	0.70	0.75	0.80	0.95	1.10	γ-rays

---

[5] J. H. BAXENDALE, M. A. I. RODGERS and M. D. WARD, *J. Chem. Soc.*, *A*, **1970**, 1246.
[6] M. ANBAR and P. NETA, Israel Atomic Energy Commission, Report—IA 1079, 1966.

In these conditions the Cr^{VI} reduction is due mainly to e^-_{aq} because $G_{e^-_{aq}} = 2.70$ is much higher than $G_H = 0.55$ and, which is more, H atoms could be also scavenged by *t*-butanol.

We verified the scavenging of primary H atoms by *t*-butanol by measuring the $G(H_2)$ as well. This value is essentially equal to $G_{H_2} = 0.45$, provided by water radiolysis, but for large concentrations of *t*-butanol and small concentrations of chromate ions we observed a small increase of measured yield up to $G(H_2) = 0.70$.

For 2×10^{-4} N, CrO_4^{2-} and 2M *t*-butanol we obtained this maximum value which shows the high reactivity of CrO_4^{2-} ions towards H atoms, compared with that of *t*-butanol.

From the above results it is clear that $G(-Cr^{VI})$ can be explained by the e^-_{aq} and H atom reactions such that:

$$Cr^{VI} + e^-_{aq}(H) \rightarrow Cr^{V} \tag{1}$$

$$Cr^{V} + e^-_{aq}(H) \rightarrow Cr^{IV} \tag{6}$$

$$Cr^{IV} + e^-_{aq}(H) \rightarrow Cr^{III} \tag{7}$$

These reactions lead to the $G(-Cr^{VI})$ value required by stoichiometric relation:

$$G(-Cr^{VI}) = G(Cr^{III}) = 1/3\ G_{red} \tag{B}$$

As we see from table 1, the $G(-Cr^{VI})$, obtained by γ-rays irradiation at quite small dose-rate, satisfies that relation while, in the case of large dose-rate of pulsed electron beam irradiations, $G(-Cr^{VI})$ is roughly three times smaller.

This large dose effect is due to the bimolecular decay of the Cr^{V} transient, fact which also has been shown by pulse radiolysis experiments:[2]

$$2Cr^{V} \rightarrow Cr^{VI} + Cr^{IV} \tag{8}$$

or:

$$Cr^{V} + Cr^{IV} \rightarrow Cr^{VI} + Cr^{III} \tag{9}$$

These reactions obviously supress the reduction, because the Cr^{VI} is partially back reformed.

It must be noticed that $G(-Cr^{VI})$ practically does not depend on Cr^{VI} concentration; the small concentration effect from table 1 is correlated to the corresponding small scavenging effect of H atoms by *t*-butanol.

B. ACID SOLUTIONS

The results concerning the radiolytic reduction of Cr^{VI} ions in acid solutions are quite different from the previous ones, in neutral solutions.

$G(-Cr^{VI})$ is higher in absence of any alcohol and depends strongly on Cr^{VI} concentration, acidity and dose-rate.

The obtained results are plotted in figure 1.

The dose-rate effect is smaller than before; in irradiation the $G(-Cr^{VI})$ is twice higher than in electron beam irradiation. The Cr^{VI} concentration effect is high and also we must notice the effect of acidity which is quite significant (curves 2 and 3).

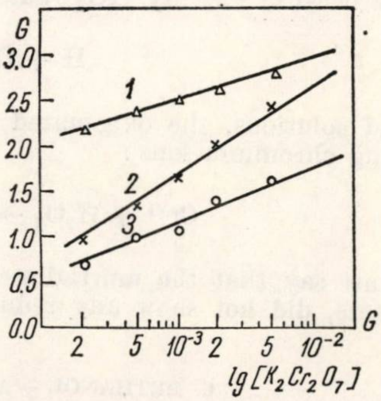

Fig. 1. — $G(-Cr^{VI})$ in $K_2Cr_2O_7$ acid solutions.

1) 0.8 N H_2SO_4, $4.8 \cdot 10^{15}$ eV ml^{-1} s^{-1}, γ-rays;
2) 0.8 N H_2SO_4, $1.6 \cdot 10^{18}$ eV $ml^{-1} s^{-1}$, electron-beam;
3) 0.2 N H_2SO_4, $1.6 \cdot 10^{18}$ eV ml^{-1} s^{-1}, electron-beam.

The results show that $G(-Cr^{VI})$ largely exceeds the required stoichiometric value of 1/3 G_{red}, from relation (B).

It is known that in these conditions because of reaction

$$e^-_{aq} + H^+ \rightarrow H \tag{10}$$

we have all reducing species as H atoms.

We repeated the experiment in aerated solutions and the results showed that the presence of O_2 does not only inhibit the reduction of Cr^{VI} but even induce a small increase of $G(-Cr^{VI})$. It is very difficult to explain all these results by H atoms reduction, which only initiate this process:

$$Cr_2O_7^{2-} + H \rightarrow CrO_3^- + CrO_4^{2-} + H^+ \tag{11}$$

We suppose that the Cr^V transient, as CrO_3^-, in these conditions reacts further with water to give rise to a reducing species to develop a chain reduction, as follows:

$$CrO_3^- + H_2O \xrightarrow{H^+} CrO_2 + HO_2 + H_2 \tag{12}$$

$$H_2 + OH \rightarrow H + H_2O \tag{13}$$

The HO_2 and H radicals reduce further the Cr^{VI}, or its transient valence states, until Cr^{III}:

$$Cr^{VI} + HO_2 \rightarrow Cr^V + O_2 + H^+ \tag{14}$$

In this hypothesis the back oxidation by OH radicals can not overcome this chain reduction process even in the absence of any OH scavenger. The dose-rate effect is probably due to the competition between reactions (12) and (8). The last one is faster in electron beam irradiation.

In the presence of oxygen it is possible that the reactions are quite similar because initially HO_2 radical is also formed, as follows :

$$H + O_2 \rightarrow HO_2. \tag{15}$$

In acid solutions, the oxigenated water issuing from radiolysis is also reducing chromium ions :

$$Cr^{VI} + H_2O_2 \rightarrow Cr^{IV} + 2H^+ + O_2 \tag{16}$$

We must say that the unirradiated acid solutions, used in these experiments, did not show any reduction effect of Cr^{VI} ions.

C. METHANOL – AQUEOUS SOLUTIONS

As we expected, using instead of *t*-butanol, another alcohol such as methanol or ethanol, the radiolitic reduction of Cr^{VI} could be higher because of reducing ability of the organic radical formed in reactions (3) and (4).

We investigated in detail the Cr^{VI} reduction, in the presence of methanol, and the obtained results show that $G(-Cr^{VI})$ is higher in both acid and neutral solutions.

In the case of 10^{-3} N K_2CrO_4 neutral solutions, the dependence of G values, of $G(Cr^{VI})$ and $G(H_2)$, on methanol concentration is shown in figure 2.

As we see, both these yields increase with methanol concentration increasing.

Obviously, these results lead us to involve $.CH_2OH$ radical in the reducing mechanism, because only the G_H value and the known reactivity of methanol ($K_{OH} = 6 \cdot 10^8$ mol^{-1} s^{-1} and $K_H = 1.6 \cdot 10^6$ mol^{-1} s^{-1}) cannot explain the above results. If $.CH_2OH$ is unreactive, in neutral solution, for the biggest methanol concentration, the yield of measured hydrogen should obey the following relation :

$$G(H_2) = G_H + G_{H_2} = 1.0 \tag{C}$$

The $G(H_2)$ exceeds the above value, which means that H atom secondary formed *via* reaction (5) is partially scavenged in reaction (4). In this way the radicals H and $.CH_2OH$ develop the chain reduction of chromium ions and H_2 formation.

In acid solutions, as we see in figure 3, the reduction yield is more increasing because of the reaction (12). In these conditions, the chain mechanism is complex because of many reactions involved.

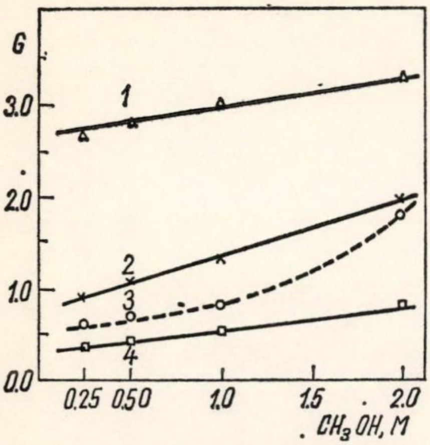

Fig. 2. – $G(-Cr^{VI})$ and $G(H_2)$ in K_2CrO_4 neutral solutions, in presence of methanol.
——— $G(-Cr^{VI})$, - - - - $G(H_2)$

1) 10^{-3} N K_2CrO_4, $4.8 \cdot 10^{15}$ eV $ml^{-1}s^{-1}$, γ-rays;
2) and 3) 10^{-3} N K_2CrO_4, $1.6 \cdot 10^{18}$ eV $ml^{-1}s^{-1}$, electron-beam;
4) $2 \cdot 10^{-4}$ N K_2CrO_4, $1.6 \cdot 10^{18}$ eV $ml^{-1}s^{-1}$, electron-beam.

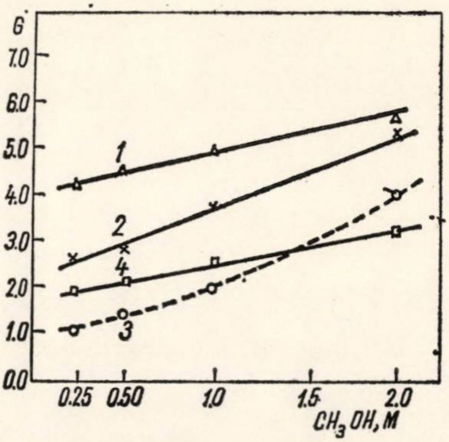

Fig. 3. – $G(-Cr^{(VI)})$ and $G(H_2)$ in 10^{-3} N $K_2Cr_2O_7$ acid solutions.
——— $G(-Cr^{VI})$, - - - - $G(H_2)$

1) 0.8 N H_2SO_4, $4.8 \cdot 10^{15}$ eV $ml^{-1}s^{-1}$, γ-rays;
2) and 3) 0.8 N H_2SO_4, $1.6 \cdot 10^{18}$ eV $ml^{-1}s^{-1}$, electron-beam;
4) 0.2 N H_2SO_4, $1.6 \cdot 10^{18}$ eV $ml^{-1}s^{-1}$, electron-beam.

The dose rate and Cr^{VI} concentration effects are even bigger and the $G(H_2)$ increases considerably too.

It can be concluded that the radiolytic reduction of Cr^{VI} by H and e^-_{aq} occurs by a simple, direct mechanism. The reduction yield can be considerably increased using either specific OH scavengers and/or organic additive such as alcohols which generate active reducing radicals and develop chain reactions.

In acid solution the reduction yield is big even in the absence of OH scavengers, owing to water reaction with Cr^{V} transient, which also develops chain reduction of dichromate.

Revue Roumaine de Chimie, 18, 3, 511–517 (1973)

COMPTE RENDU

N. RIEHL. "Einführung in die Lumineszenz" (Introduction to luminiscence), Verlag Karl Thiemig, München, 1971, XV + 351 p.

Luminiscence phenomena are an object of growing interest from the theoretical as well as from the practical point of view. Research work on the emission of light of free atoms and molecules has brought a decisive contribution to the study of their quantic properties and their structure, while the luminiscence of condensed matter has offered important informations on the structure of solid bodies and energy transfer. The mechanism of luminiscence differs according to different types of solid bodies. It is these differences in the mechanism of different luminiscence types which present a major scientific interest and which are at the origin of many practical uses, such as : oscillograph screens, X-Ray lamps, luminiscent dyes, luminiscent plates and diodes, luminiscence microscopy, scintillation detectors, etc.

All these problems would require several volumes to be duely analysed and described, but such a work would soon be obsolete because of the rapid progress achieved in this domain.

The author, with the cooperation of F. Fischer, H. E. Gumlich, E. Krantz, H. Lange, H. Scharmann, A. Schmillen and H. Vogel has got together this compendium, aiming to offer a general information on the main lines of research and use of luminiscence.

The first chapter clarifies the terms of "fluorescence" (when the emission of light ceases immediately after the excitation is stopped) and "phosphorescence" (when it still continues). However, the classification according to the category of luminiscent substance seems better suited and has been adopted by the authors. General information about the composition and obtention of these substances is also to be found in this first chapter. There are two types of substances with luminiscent properties : those with atoms and molecules having own luminiscent properties, and those which acquire these by doping with alien atoms or by lattice flaws. There exists a "cathodic luminiscence", a "photoluminiscence", a "radioluminiscence", an "electroluminiscence" and a "chemiluminiscence", according to the energetic excitation sources bringing about the luminiscence phenomenon. The luminiscence due to flame ("candoluminiscence") and the one due to crystall clivage ("triboluminiscence") are special cases.

The second chapter deals with luminiscent substances of the zinc sulphide group, its activators, and their different properties. The dependence of luminiscence yield upon temperature, energy transfer, behaviour of luminiscent substances with several sorts of activators, absorption and emission spectra, photon interaction, etc. are also studied in this chapter. Finally, the main practical uses of these luminophores are examined and commented upon. The third chapter dwells on luminiscent substances containing oxygen and those of the rare earths group and the way of obtaining them by synthesis reactions in solid phase.

Chapter four is intended to halogenate luminiscent substances and their different uses. As a matter of fact, these were the first fluorescent substances discovered and the name itself comes from fluorit, the mineral first in use in this domain.

"Thermoluminiscence" is treated in chapter five and "Electroluminiscence" in chapter six, while the last chapter deals with the "physical bases of the possibility to apply luminiscence to organic substances". It, therefore, deals with the luminiscent features of fluoresceine, anthracene, phenantren, naphtalene, eosive salicilic acid and their derivates. Their luminiscence qualities are very useful in scintillation techniques and in luminiscent microscopy.

Each chapter ends with a minute speciality bibliography and the whole work is accompanied by an alphabetical index, making it very handy and useful not only to specialists but also to students and technicians.

Al. Fruma

NOTE POUR LES AUTEURS

La *Revue Roumaine de Chimie* publie des articles en anglais, français, russe, allemand ou espagnol. Les auteurs sont priés d'envoyer des articles, notes, communications et comptes rendus inédits.

Les manuscrits seront dactylographiés à deux intervalles. Les tableaux seront dactylographiés sur feuilles séparées, de même que la légende des figures. Les diagrammes seront tracés à l'encre de Chine sur papier calque. Les tableaux et les figures seront numérotés par des chiffres arabes, en nombre strictement nécessaire. Prière de ne pas inscrire les mêmes données dans les tableaux et les figures. Les formules chimiques seront incluses dans le texte ; en outre, elles seront transcrites sur des feuilles séparées. Les auteurs sont priés d'indiquer les caractères italiques (en soulignant les lettres au crayon), ainsi que tout autre caractère spécial. L'ordre des références bibliographiques sera celui de leur mention dans le texte ; le nom de l'auteur sera précédé de l'initiale du prénom ; les publications périodiques seront présentées suivant les prescriptions internationales. Les références seront ajoutées à la fin de l'article ; elles paraîtront comme des notes, au bas de la page. Le texte sera précédé d'un résumé comprenant 15 lignes au maximum.

L'entière responsabilité du contenu des articles appartient aux auteurs. On publie des articles dus aux collaborateurs roumains ou étrangers. Les auteurs recevront 50 tirés à part.

PRINTED IN ROMANIA

1973 JUN 21

TRAVAUX PARUS AUX ÉDITIONS DE L'ACADÉMIE DE LA RÉPUBLIQUE SOCIALISTE DE ROUMANIE

P. BALTĂ et E. BALTĂ, **Introducere în chimia fizică a stării vitroase** (Introduction à la chimie physique de l'état vitreux), 1971, 240 p., 15,50 lei.

LYDIA-MARIA VAICUM, **Biodegrabilitatea detergenţilor** (La biodégrabilité des détergents), 1971, 346 p., 19,50 lei.

I. ZUGRĂVESCU et. L. STOICESCU-CRIVETZ, **Polimeri heterociclici** (Polymères hétérocycliques), 1971, 190 p., 9,50 lei.

I. V. MAXIM, **Materiale nucleare** (Matériaux nucléaires), 1969, 444 p., 30 lei.

CORNEL BODEA et collab., **Tratat de biochimie vegetală**, partea I, **Fitochimie** (Traité de biochimie végétale, Ire partie, Phytochimie), Ier vol., 1964, 747 p. + 4 annexes + 2 pl., 41 lei ; IIe vol., 1965, 1962 p., 1 pl., 56 lei ; IIIe vol., 1967, 773 p., 35 lei.

CRISTOFOR SIMIONESCU et CLEOPATRA VASILIU-OPREA, **Mecanochimia compuşilor macromoleculari** (La méchanochimie des composés macromoléculaires), 1967, 344 p., 23,50 lei.

V. GHEŢIE et V. MICUŞAN, **Analiza imunochimică. Teorie şi practică** (Analyse immunochimique. Théorie et pratique), 1966, 369 p., 28 lei.

R. PORTOCALĂ et L. POPA, **Acizii ribonucleici celulari şi virali** (Les acides ribonucléiques cellulaires et viraux), 1966, 375 p., 8 pl., 26 lei.

I.P.I. – c. 2524

43 426

Lei 25.–

F1103

[illegible]

REVUE ROUMAINE DE CHIMIE

TOME 18
N° 4
Avril 1973

RRCHAX, **18**, *4*, 521–734 (1973)

ÉDITIONS DE L'ACADÉMIE DE LA RÉPUBLIQUE SOCIALISTE DE ROUMANIE

Rev. Roumaine Chim. **18**, *4*, p. 521–734 (1973), Bucarest

COMITÉ DE RÉDACTION

Rédacteur en chef :

I. G. MURGULESCU, membre de l'Académie de la République Socialiste de Roumanie

Rédacteurs en chef adjoints :

A. T. BALABAN et V. EM. SAHINI, membres correspondants de l'Académie de la République Socialiste de Roumanie

Collège de rédaction :

C. DRĂGULESCU, RALUCA RIPAN, CR. SIMIONESCU, membres de l'Académie de la République Socialiste de Roumanie ; EM. BRATU, ECATERINA CIORĂNESCU-NENITZESCU, P. SPACU, membres correspondants de l'Académie de la République Socialiste de Roumanie ; MARGARETA AVRAM, D. I. MARCHIDAN, G. NIAC et D. SĂNDULESCU

La Revue Roumaine de Chimie paraît 12 fois par an. Toute commande de l'étranger (fascicules ou abonnements) sera adressée à Întreprinderea Rompresfilatelia, Boîte Postale 2001, telex 011631, Bucarest, Roumanie

Les manuscrits, les livres et les revues proposés en échange, ainsi que toute correspondance seront envoyés à la rédaction :

REVUE ROUMAINE DE CHIMIE
23, Str. Dumbrava Roşie, Bucarest, Roumanie

ÉDITIONS DE L'ACADÉMIE DE LA RÉPUBLIQUE SOCIALISTE DE ROUMANIE
3 bis, str. Gutenberg, Bucarest, Roumanie

REVUE ROUMAINE
DE
CHIMIE

SZÁGOS MŰSZAKI KÖNYVTÁR ÉS DOKUMENTÁCIÓS KÖZPONT 1983

Tome 18, N° 4 Avril 1973

Page

I. G. MURGULESCU and IOANA DEMETRESCU, On the mechanism of the reactions between benzyl bromide and alcohols 523–529

A. GIOABĂ, V. EM. SAHINI and ELENA VOLANSCHI, NMR spectra of some phenoxatellurine derivatives 531–536

D.P. LAZĂR and J. TURKEVICH, Methyl radicals on porous Vycor glass as studied by ESR spectroscopy 537–547

M. CONTINEANU, TATIANA ONCESCU and R. N. SCHINDLER, Kinetics and mechanism of the thermal decomposition of azibenzyl. I. Decomposition in benzene solution 549–556

Z. MOSER, K. FITZNER and L. ZABDYR, On the equilibrium constant of the side reaction in the concentration cell in dilute Cd–Pb liquid solutions . . 557–567

П. ПУТАНОВ, Ж. ЙОВАНОВИЧ и Р. ХЕРАК, Влияние добавок и восстановительной среды на формирование фазового состава в катализаторе для низкотемпературной конверсии окиси углерода . . . 569–573

BOJANA D. ALEKSIĆ and ANA TERLECKI-BARIČEVIĆ, Investigation of some properties of the ammonia synthesis catalysts obtained by melting natural magnetite 575–581

C. DRĂGULESCU, ANA NIMARĂ, I. JULEAN and D. MARANDIUC, Polarographic behaviour of bismuth (III) in acid perchlorate solutions 583–588

P. SPACU and EUGENIA IVAN, New compounds of yttrium and lanthanides with N, N′-ethylenedianthranilic acid (EDAN) 589–598

ILEANA ALBESCU, Contributions to the study of lanthanides with biguanide derivatives. V. Lanthanide compounds with hydrochloric paludrine 599–608

MARIA MAVRODIN-TĂRĂBÎC, Contribution à l'étude de l'hydrolyse de l'ion UO_2^{2+} en milieu perchlorique 609–621

I. TEOREANU and MARIA GEORGESCU, The role of clinker and of calcium chloride in the hardening process of some silicate slags 623–634

A. T. BALABAN, Chemical graphs. XVIII. Graphs of degrees four or less, isomers of annulenes, and nomenclature of bridged polycyclic structures 635–653

F. KEREK und I. MOŢOC, Matrizielle Charakterisierung der Struktur und Topologie der organischen Verbindungen III. Konformation, Chirale Konformeren 655–665

ELENA IŞFAN and A. BARABÁS, Heterocyclic organoboron compounds. XV. Boronium chelate salts and beryllium chelates of 1,3-ketoenols with disturbed resonance in the chelate ring 667–676

Revue Roumaine Chim. **18**, *4*, 521–734 (1973), Bucarest

D. SUCIU, Electronic spectra and acidity constants of some 2-amino-5-substituted thiazoles 677–683

I. SIMITI, MIOARA COMAN, I. SCHWARTZ, Contributions to the study of heterocycles. XXIV. A study of intermediates in the Hantzsch reaction. A new method to obtain 5-acetylthiazole derivatives 685–694

D. A. ISĂCESCU, I. V. IONESCU, FLORIADA GULUȚĂ, C. RONCEA and D. MIHĂIȚĂ, Studies in the polyethylene field. VI. Pressure-volume-temperature-crystallinity relationship in high-pressure additive-containing polyethylene 695–715

L. KÉKEDY and F. MAKKAY, Zero current bipotentiometric indication with pretreated electrodes. I. Oxidimetric titration of Fe(II) using platinum electrodes 717–722

LUCIA BEU and JANA RUSSU, The synthesis and spectrophotometric studies on benzoyl cyanide phenylhydrazones 723–732

COMPTE RENDU 733

Revue Roumaine de Chimie, 18, 4, 523–529 (1973)

ORSZÁGOS MŰSZAKI KÖNYVTÁR ÉS DOKUMENTÁCIÓS KÖZPONT 1883

ON THE MECHANISM OF THE REACTIONS BETWEEN BENZYL BROMIDE AND ALCOHOLS

I.G. MURGULESCU and IOANA DEMETRESCU

The Faculty of Chemistry, Chair of Physical Chemistry, Bd. Republicii 13, Bucharest, Romania

Received October 26, 1972

The results of studying the systems formed by benzyl bromide alcoholysis with normal alcohols[1], primary isoalcohols[2] and secondary alcohols[3] are analysed. The activation parameters of these systems are calculated and the observed compensation effects are discussed accepting a linear correlation of the entropy and enthalpy factors. The results lead to a sequence of reaction mechanisms.

The benzyl halides solvolysis[4–11] has been the subject of numerous kinetic studies but, unfortunately, the obtained results led to contradictory interpretations. To contribute to the elucidation of some ambiguities we have comparatively analysed the results obtained previously in the benzyl bromide alcoholysis with normal, secondary and isoalcohols.

In table 1 we give the values of the activation energy, preexponential factors, free activation entropy, enthalpy and energy, for all studied systems.

One can see that the activation entropies and enthalpies are correlated. Figure 1 shows the compensation effect in the assumption of the isokinetic equation.[12,13]

The isokinetic equation is:

$$\Delta H^{\neq} = \Delta H_0^{\neq} + \beta \Delta S^{\neq} \qquad (1)$$

---

[1] I. G. MURGULESCU and I. DEMETRESCU, *Rev. Roumaine Chim.*, **15**, 141 (1970).

[2] I. G. MURGULESCU and I. DEMETRESCU, *Rev. Roumaine Chim.*, **16**, 1483 (1970).

[3] I. G. MURGULESCU and I. DEMETRESCU, *Rev. Roumaine Chim.*, **17**, 599 (1972).

[4] H. von HALBAN and W. GAST, *Z. Phys. Chem.*, **91**, 591 (1916).

[5] C. BEVAN, E. HUGHES and C. K. INGOLD, *Nature*, **171**, 301 (1953).

[6] J. W. BAKER, *J. Chem. Soc.* **1934**, 1987.

[7] J. W. BAKER, *J. Chem. Soc.* **1936**, 1448.

[8] B. BENSLEY and C. KOHNSTAM, *J. Chem. Soc.* **1957**, 4747.

[9] C. GEORGOULIS, J. LANDAIS and C. VILLE, *J. Chim. phys.*, **67**, 450 (1970).

[10] S. WINSTEIN, E. GRUNWALD and H. JONES, *J. Amer. Chem. Soc.* **73**, 2700 (1951).

[11] J. HYNE, R. WILLE and R. WARKA, *J. Amer. Chem. Soc.* **84**, 2914 (1962).

[12] J. E. LEFFLER, *J. Org. Chem.*, **20**, 1202 (1955).

[13] J. E. LEFFLER, *J. Org. Chem.*, **31**, 533 (1966).

Table 1

Activation parameters for the $C_6H_5\,CH_2\,Br$ + ROH system

ROH	log *A*	*E*	$\Delta H^{\neq}$	$\Delta S^{\neq}$	$\Delta G^{\neq}$
CH_3OH	12.138	22420	21730	− 5.27	23540
C_2H_5OH	11.480	21500	20820	− 8.29	23660
C_3H_7OH	11.184	21130	20450	− 9.65	23760
C_4H_9OH	10.408	20140	19457	−13.20	24670
iso-C_4H_9OH	10.72	20100	19420	−11.77	23460
iso-C_5H_7OH	9.63	19200	18520	−16.77	24271
iso-$C_8H_{17}OH$	8.55	18500	17810	−21.75	25380
sec-C_3H_7OH	7.77	16500	15820	−25.26	23800
sec-C_4H_9OH	7.068	16200	15510	−28.54	25440

where H_0 is the intercept for $\Delta S^{\neq} = 0$, and β, having the dimensions of a temperature, the slope of the straight line. The equation (1) is called "isokinetic", because putting it in the equation defining the free activation energy,

$$\Delta G^{\neq} = \Delta H^{\neq} - T\Delta S^{\neq} \tag{2}$$

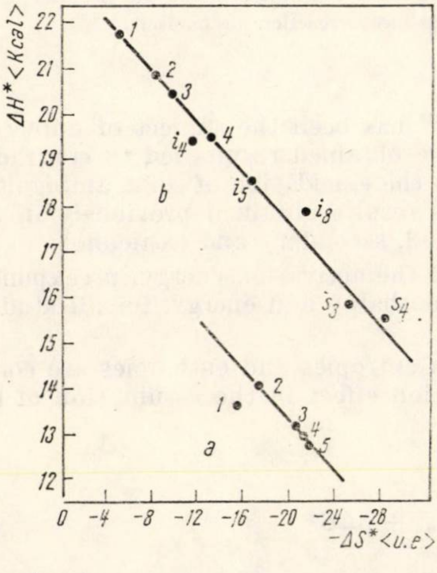

Fig. 1. — Compensation effects for the systems:

a) C_6H_5COCl + ROH;

b) $C_6H_5CH_2Br$ + ROH: 1. CH_3OH; 2. C_2H_5OH; 3. C_3H_7OH; 4. C_4H_9OH; 5. $C_6H_{13}OH$; i_4 = *i*-C_4H_9OH; i_5 = *i*-$C_5H_{11}OH$; i_8 = *i*-$C_8H_{17}OH$; s_3 = sec-C_3H_7OH; s_4 = sec-C_4H_9OH.

we get

$$\Delta G^{\neq} = \Delta H_0^{\neq} + (\beta - T)\,\Delta S^{\neq} \tag{3}$$

and we can see that at $T = \beta$, $\Delta G^{\neq} = \Delta H_0^{\neq}$ = constant; this means that the reactions obeying equation (1) have the same rate at the temperature $T = \beta$.

Related systems verifying an isokinetic equation could be supposed to have a common mechanism. However, such interpretations must be carefully made taking into account the experimental errors affecting the values of both entropy and enthalpy.

As we can see from figure 1, the entropies and enthalpies follow a straight line. The isokinetic temperature is as much as 2°. We also can see that the reactions formed by the alcoholysis of benzoyl chloride[14] have the same isokinetic temperature; this indicates a common mechanism for the alcoholysis of the two compounds. Since for the latter it has been admitted, due to a series of reasons,[15-17] a bimolecular mechanism, we could argue in favour of a bimolecular mechanism in the case of the alcoholysis of benzyl bromide either.

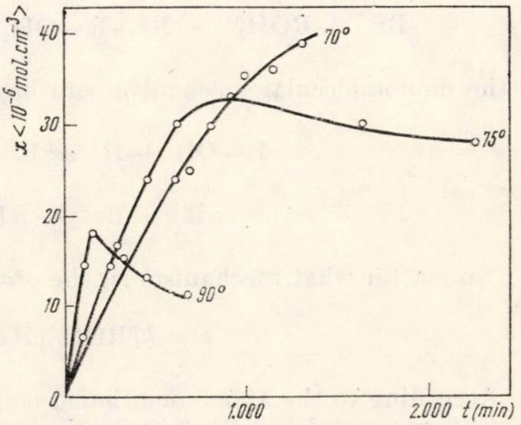

Fig. 2. — Variation of HBr concentration in time for the $C_6H_5CH_2Br + i\text{-}C_8H_{17}OH$ system.

It is interesting to notice that the points having a greater distance from the straight line correspond to alcohols with more carbon atoms in molecule, both in case of isoalcohols and in case of secondary alcohols; in such cases some changes in the kinetic mechanism could have taken place.

These observations were completed by some other experimental facts found in the case of systems with a long reaction time, e.g. in the case of the isooctyl alcohol. In that case we found that the variation in time of the acid concentration shows a maximum (fig. 2). As we have shown in a previous work,[2] at the same time the quantity of water in the system was increasing. The decrease of the acidity was interpreted as being due to the consumption of the acid in a reaction with the alcohol. The reaction between the acid and the alcohol was followed up leading to the conclusion that at a temperature less than 50° it has a negligible weight in the case of alcoholysis reactions finishing in 20 hours at most. Under other conditions, however, it is highly probable that the reaction between acid and alcohol become competitive with the halide alcohol reaction.

---

[14] I. G. Murgulescu and I. Demetrescu, *Rev. Roumaine Chim.* **14**, 149 (1969).
[15] A. Kivinen, *Suomen Kemistilehti B*, **36**, 163 (1963).
[16] A. Kivinen, *Suomen Kemistilehti B*, **38**, 210 (1965).
[17] A. Kivinen and A. Viitala, *Suomen Kemistilehti B*, **40**, 19 (1967).

As the displacement of the halogen is preceded by a rapid equilibrium, bimolecular and unimolecular mechanisms were successively suggested, like in most similar two-step reactions.[18-21]

The bimolecular scheme is represented by the equations :

$$R-OH + H^+ \rightleftarrows ROH_2^+$$

$$Br^- + ROH_2^+ \rightarrow [Br-R-OH_2] \rightarrow Br-R + H_2O$$

and the monomolecular mechanism can be represented by

$$R-OH + H^+ \rightleftarrows R^+ + H_2O$$

$$R^+ + Br^- \rightarrow RBr$$

No matter what mechanism is, the observed kinetics is of the second order

$$v = k[ROH][HBr]$$

According to the above mentioned considerations and to some other arguments presented in a previous work,[2] taking into account the existing results regarding the alcoholysis of benzyl chloride,[9] we consider that the alcoholysis of benzyl bromide is represented by the following sequence of successive reactions

$$C_6H_5-CH_2Br + ROH \rightarrow C_6H_5CH_2OR + H^+Br^-, \qquad (a)$$

a pseudo-monomolecular reaction followed by the acid-alcohol reaction; taking into account the mechanism discussed above, this reaction could be as follows

$$ROH + HBr \overset{fast}{\rightleftarrows} ROH_2^+ + Br \qquad (b)$$

$$ROH_2^+ + Br^- \xrightarrow{slow} RBr + H_2 \qquad (c)$$

2nd order,

or

$$ROH_2^+ \xrightarrow[slow]{} R^+ + H_2O \xrightarrow[fast]{} RBr \qquad (d)$$

1st order

$$RBr + ROH \xrightarrow[very\ slow]{} ROR + HBr \qquad (e)$$

By reactivity reasons the reaction (e) could be neglected as against (c) and (d).

---

[18] S. Kilpi, *Z. phys. Chem.*, **141**, A 424 (1929).

[19] S. Kilpi, *Z. phys. Chem.*, **166**, A 285 (1933).

[20] E. Grunwald and S. Winstein, *J. Amer. Chem. Soc.*, **69**, 2051 (1947).

[21] M. Bennett and F. Reynolds, *J. Chem. Soc.*, **1935**, 131.

The equilibrium

$$ROH_2^+ + H_2O \underset{2}{\overset{1}{\rightleftarrows}} H_3O^+ + ROH$$

could also exist, reflecting the competition of nucleophylic effects of water and alcohol.

The above image would correspond theoretically to any system formed by benzyl bromide and alcohols, for any alcohol. Examining the rate constants at various conversions [1,2,3] for the same system in the same temperature conditions, a diminution of the rate constant can be observed beginning at advanced conversion. This limit from which the diminution of the rate constant exceeds the experimental errors, changes from one alcohol to another, decreasing as the chain of the alcohol grows longer; our experimental data indicate that for the systems formed with alcohols having more than 4–5 carbon atoms, the reaction between acid and alcohol has an important contribution.

As regards the formal kinetic solution of this problem, according to some approximations already used for similar cases [22] only the reaction (a) of the sequence was taken into account, except for the system with isooctyl alcohol.

In the case of this alcohol we chose a method starting with the integration of the rate equation. [9]

If a is the initial concentration of benzyl bromide, y the concentration of octyl bromide and x the concentration of the acid, the rate equation will be

$$\frac{dx}{dt} = k_1(a - x - y) - k_2x^2 \tag{3}$$

This equation describes correctly the variation of the concentration in the sequence of reactions which is schematically:

$$\begin{array}{l} C_6H_5CH_2Br + ROH \xrightarrow{k_1} C_6H_5CH_2OR + H^+Br^- \\ (a - x - y) \end{array}$$

$$Br^- + ROH_2^+ \xrightarrow{k_2} RBr + H_2O$$

The solution of the equation is not a simple one.
The equation can be put in the form

$$\frac{dx/dt}{a - x - y} = k_1 - \frac{k_2x^2}{a - x - y} \tag{4}$$

which allows a very convenient graphically solving, using the straight line

$$\frac{dx/dt}{a - x} = f\left(\frac{x^2}{a - x}\right) \tag{5}$$

---

[22] D. Roberts, H. Young and S. Winstein, *J. Amer. Chem. Soc.*, **64** 2157 (1942).

In this way we use only that part of the curve of the variation of the acid concentration in time for which y is negligible (the part before the maximum in fig. 2); the straight line obtained has the slope $-k_2$ and the intercept for $\left(\frac{x^2}{a-x}\right) = 0, k_1$. The obtained values are given in table 2.

Table 2

The rate constants k_1 and $k'_2 = k_2/b$ for the $C_6H_5CH_2Br + i\text{-}C_8H_{17}OH$ system

k ($s^{-1}\,mol^{-1}cm^3$)	70°	75°	90°
k_1	$7.06 \cdot 10^{-4}$	$9.90 \cdot 10^{-4}$	$26.3 \cdot 10^{-4}$
k'_2	$1.94 \cdot 10^{-1}$	$2.89 \cdot 10^{-1}$	3.74

Plotting log k versus $1/T$ allows the calculation of the following values for the activation parameters

$$E = 16\,110 \text{ cal} \qquad E = 37\,730 \text{ cal}$$

$$\Delta S^{\neq} = -24.30 \text{ cal/degree}$$

$$\Delta H^{\neq} = 15\,530 \text{ cal}$$

$$\Delta G^{\neq} = 23\,990 \text{ cal}$$

The activation energy E_2 of the reaction between the solvent and hydrobromic acid indicates that this reaction is strongly affected by temperature, which is to be expected if the evolution of the curves in fig. 2 is taken into account. This value fully agrees with the activation energies given in the literature for the reactions between acid and alcohol.[9,23] Correspondingly the values of k_2 given for the alcoholysis of benzyl chloride by methyl alcohol[9] ($k'_2 = 4.75\ s^{-1}mol^{-1}\,cm^3$ at 80°, $k'_2 = 1.50\ s^{-1}mol^{-1}\,cm^3$ at 70° and $4.2 \times 10^{-1} s^{-1}mol^{-1}\,cm^3$ at 60°) are of the same order of magnitude and lead to comparable activation energies.

The interpretation of the benzyl halides alcoholysis as a sequence of reactions explains the diminution tendency of rate constant in these systems observed in other kinetic studies. Therefore, this diminution cannot be interpreted as a mass law effect and cannot be an argument for a unimolecular mechanism; moreover, the older hypothesis, according to which benzyl compounds have the tendency to react according to SN_1 substitutions, was lately infirmed.

---

[23] C. Hinshelwood, *J. Chem. Soc.*, **1935**, 599.

Studying the variation of the activation entropy and of the ratio between the activation heat capacity and the activation entropy, $\Delta C^{\neq}/\Delta S^{\neq}$, for SN_1 and SN mechanisms, Kohnstam suggested this ratio as criterion for the mechanism: from known activation entropies for SN_1 and SN_2 reactions and from the $\Delta S^{\neq}$ value observed at substitution in benzyl halide undergoing solvolysis, he calculated the solvolytic percent of SN_1 and SN_2.

In the majority of cases fractional part of SN_2 was much greater than that of SN_1.

Isotopic exchange of benzyl chloride with chlorine follows also an SN_2 mechanism.

In spite of literature contradictions, we consider that the solvolysis benzyl halides in alcoholic medium are complex bimolecular reactions.

Revue Roumaine de Chimie, 18, 4, 523–529 (1973)

Revue Roumaine de Chimie, **18**, *4*, 531–536 (1973)

NMR SPECTRA OF SOME PHENOXATELLURINE DERIVATIVES

A. GIOABĂ, V. EM. SAHINI and ELENA VOLANSCHI

Department of Physical Chemistry
Bd. Republicii 13, Bucharest

Received November 4, 1972

The NMR spectra of 10,10 – and 2,8-substituted derivatives of phenoxatellurine are given and discussed. The deshielding of the protons at the 1,9 sites evidences charge modifications in the benzene rings which are accounted for by semi-empirical MO-calculations.

The previous papers [1,2] were concerned with the electronic spectra and CT-complexes of phenoxatellurine and its derivatives. It is well known that the electronic spectra furnish information especially on the energy levels of the molecule. The charge distribution in the ground state and its change under the influence of solvents or substituents are better reflected, according to several authors [3,4] by the proton chemical shifts in the NMR spectra. Therefore, the object of this paper is to present the NMR spectra of phenoxatellurine and some disubstituted derivatives and to correlate them with changes of the charge distribution in the heterocycle.

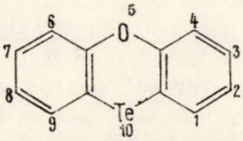

Fig. 1. — The numbering used in this paper.

EXPERIMENTAL PART

The compounds contained in Table 1 (numbering as in fig. 1) were synthetized by literature methods.[5-8] Their NMR spectra were recorded at a HNM–C 60–HL Spectrometer at 60 Mc and a TESLA–487 B Spectrometer at 80 Mc, in $CDCl_3$ and DMSO–d_6 with TMS as internal standard.

---

[1] A. Gioabă, V. Em. Sahini and E. Volanschi, *Rev. Roumaine Chim.*, **15**, 501 (1970).
[2] A. Gioabă, V. Em. Sahini and E. Volanschi, *Rev. Roumaine Chim.*, **15**, 309 (1970).
[3] P. J. Black, R. D. Brown and M. L. Heffernan, *Austral. J. Chem.*, **20**, 1305 (1967).
[4] J. B. Cobb and J. D. Memory, *J. Chem. Phys.*, **50**, 4262 (1969).
[5] H. D. K. Drew, *J. Chem. Soc.*, **223**, 3054 (1926).
[6] G. Vasiliu and A. Gioabă, *Rev. Chim.* (*București*), **20**, 357 (1969).
[7] A. Gioabă and G. Vasiliu, *Anal. Univ. București Ser. Șt. Naturii Chimie*, **15**, 89 (1966).
[8] G. Vasiliu and A. Gioabă, *Rev. Chim.* (*București*), **19**, 253 (1968).

A general remark made throughout this work was that excepting the fluoro-compounds, the 2,8-disubstituted derivatives give uncompletely resolved spectra. It was firstly thought this could be due to their poor solubility in the solvents used; therefore, $SOCl_2$ was also employed for 2,8-dimethyl, 10,10-dichlorophenoxatellurine, but in spite of the better solubility in this solvent, the resolution was not improved. In the case of the 2,8-dimethyl derivatives the broadening of the signals of the 1,9 and 3,7 protons could be due, according to Pople, [9] to the unresolved quartet determined by the interaction with the methyl protons.

Table 1

The compounds studied and the references for their synthesis

Phenoxatellurine [5]	2,8-Difluoro-phenoxatellurine [6]	2,8-Dimethyl-phenoxatellurine [7]*	2,8-Dichloro-phenoxatellurine [8]
10,10-Dichlorophenoxatellurine [5]	10,10-Dichloro-2,8-difluoro-phenoxatellurine [6]	10,10-Dichloro-phenoxatellurine [7]	10,10-Dichloro-phenoxatellurine [8]
—	—	10,10-Dibromophenoxatellurine [7]	—
10,10-Diiodophenoxatellurine [5]	10,10-Diiodo-2,8-difluorophenoxatellurine [6]	—	—

* In our previous work [1] the melting point of this compound appeared erroneous. The real value is m.p. = 75–76°.

RESULTS AND DISCUSSION

From all the compounds studied only the spectrum of phenoxatellurine was recently mentioned in literature by Calder *et al.* [10]. These authors remark the greater solvent dependence of two protons and, by analogy with similar compounds, assign their chemical shifts to the 1, 9 positions (fig. 1). Our results for the unsubstituted phenoxatellurine are in good agreement with this statement, pointing out a shift of the signal of these protons from 7.49 ppm in $CDCl_3$ to 7.62 ppm in DMSO-d_6.

As the NMR spectra of the phenoxatellurine derivatives are dependent on the substituent position, they will be discussed separately in function of the site of substitution.

A. TELLURIUM – SUBSTITUTED DERIVATIVES

As it was pointed out by Balkau, Fuller and Heffernan [11] the usefulness of the electronegative substituted derivatives (at the heteroatom) in helping to assign the spectrum of the parent compound lay in the possibility that only H_1 and H_9 might be severely displaced, the remaining protons being fairly remote from the site of substitution.

In order to check this, the spectrum of 10,10-diiodophenoxatellurine was analysed in the ABCX approximation and the results compared to those of Calder *et al.* for the parent compound.

---

[9] J. A. Pople, W. G. Schneider and H. J. Bernstein, "High-resolution nuclear magnetic resonance", McGraw-Hill Book Comp., New York, 1959, p. 353.

[10] J. C. Calder, R. B. Johns and J. M. Desmarchelier, *Austral. J. Chem.*, **24**, 325 (1971).

[11] F. Balkau, M. W. Fuller and M. L. Heffernan, *Austral. J. Chem.*, **24**, 2293 (1971).

Table 2

Spectral parameters of 10,10-disubstituted phenoxatellurines

Compound	δ_1	δ_2	δ_3	δ_4	J_{12}	J_{13}	J_{14}	J_{23}	J_{24}	J_{34}	Solvent
Phenoxatellurine[10]	7.64	7.07	7.30	7.26	7.62	1.57	0.41	7.54	1.17	8.20	acetone
10,10-Diiodo-phenoxatellurine	8.003	7.19	7.43	7.36	7.60	1.50	0.40	7.50	1.50	8.20	DMSO-d_6
10,10-Dichlorophenoxatellurine	8.14	—	—	—	—	—	—	—	—	—	,,

As may be seen from fig. 2b the poor resolution of the spectrum of the 10,10-dichloroderivative prevented the analysis of the whole spectrum, so that only $\delta_{1,9}$ could be determined. It is visible from Table 2 that two protons in the molecule are strongly deshielded by the electronegative substitution at the tellurium atom. We consider this to be a valid argument for the assignment of the low fields signal to the 1,9 positions. The fact that their chemical shifts are in the order of electronegativity of the halogens supports the idea that the modification of the NMR spectrum on the 10,10-substitution is primarily due to inductive effects.

B. RING - SUBSTITUTED DERIVATIVES

The relevant chemical shifts of the 2,8 and simultaneously 2,8-10,10-substituted derivatives are contained in Table 3. As may be observed, the

Table 3

Approximate parameters^a) of the proton resonance spectra of the 2,8- and 10,10-substituted phenoxatellurines

Compound	δ_1	δ_3	δ_4	J_{12}	J_{13}	J_{14}	J_{23}	J_{24}	J_{34}	Compound	$\delta_{1,9}$
2,8-Difluoro-phenoxatellurine	7.48	5.05	7.18	7.6	2.5	0.6	7.5	2.4	8.5	2,8-Dimethyl-phenoxatellurine ($CDCl_3$)	7.20
2,8-Difluoro-10,10-diiodo-phenoxatellurine^b)	7.75	—	—	—	—	—	—	—	—	2,8-Dimethyl-10,10-dibrom-phenoxatellurine ($CDCl_3$)	7.64
2,8-Difluoro-10,10-dichloro-phenoxatellurine	7.89	7.38	7.50	7.5	2.3	0.6	7.5	2.4	8.5	2,8-Dimethyl-10,10-dichlorophenoxatellurine	7.98

a) The spectra of the simultaneously 2,8- and 10,10-substituted derivatives were analysed in the ABMX approximation which accounts satisfactorily for the observed spectrum.

b) The spectrum of 2,8-difluoro-10,10-diiodophenoxatellurine in DMSO is an example of "deceivingly simple' spectrum of ABMX type (4 lines) and only the chemical shift of the 1,9 protons could be determined.

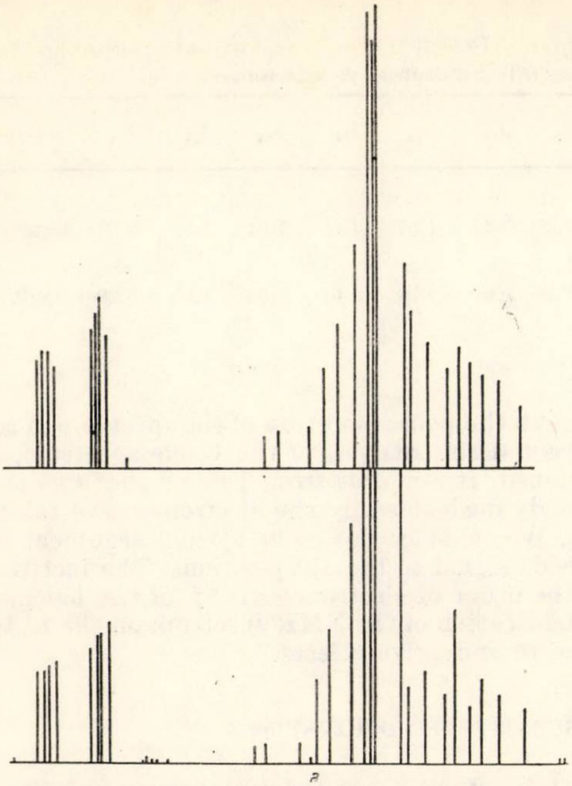

Fig. 2a. – Spectrum of 10,10-diiodophenoxatellurine in DMSO : experimental (upper spectrum) and calculated with the parameters contained in Table 2 (down).

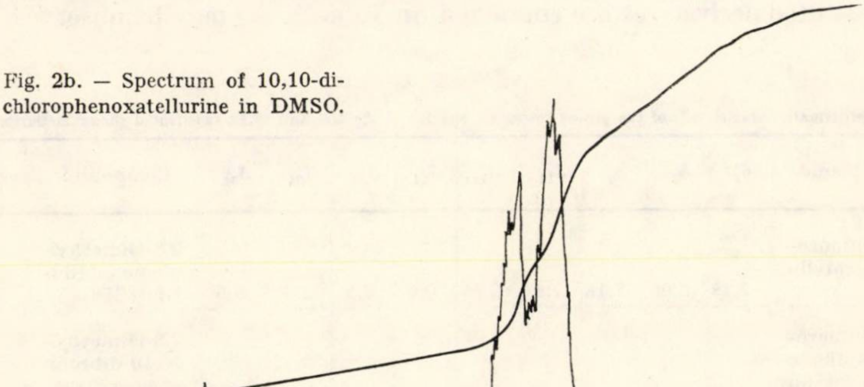

Fig. 2b. – Spectrum of 10,10-dichlorophenoxatellurine in DMSO.

2,8-substitution with fluorine and methyl shifts the 1,9 protons to higher fields *vs*. those of the parent compound. The effect of the electronegative 10,10-substitution discussed before is also evident for simultaneously 2,8-and 10,10-substituted compounds.

Several authors [3,4] think that a quantitative correlation may be established between the excess charge on the carbon atoms, Δq, and the shift of the proton bound to it, δ. Although the precise form of such a relationship is still discussed, many authors think it holds also for heterocyclic molecules. The system studied is of course too large and there are few data about the tellurium atom in organic compounds to permit the development of any quantitative dependence.

Fig. 3. — Experimental (a) and calculated (b) spectrum (parameters from Table 3) of 2,8-difluorophenoxatellurine.

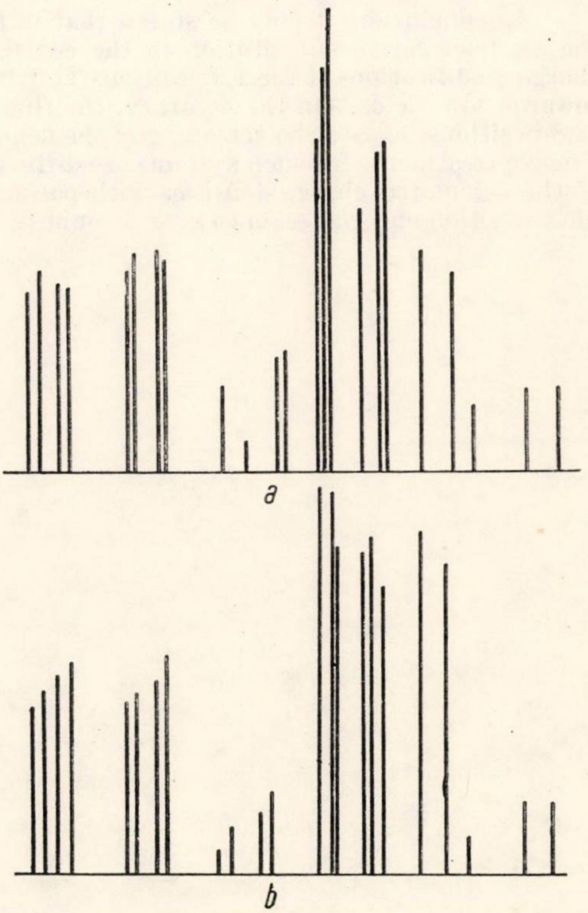

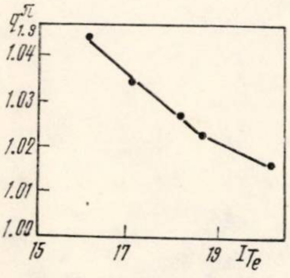

Fig. 4. — The dependence of the π-charge density of the 1,9 positions (calculated SCF — PPP) on the ionization potential of the tellurium atom.

However, semi-empirical SCF-MO calculations in the frame of the Pariser-Parr-Pople method were performed; basic assumptions and choice of parameters are discussed elsewhere [12], in connection to the electronic spectra. It was supposed that the electronegative substitution at the tellurium atom will enhance its ionization potential and it was found that the most sensitive were the 1,9 positions.

Fig. 4 shows a regular decrease of the 1,9-charge density with the increasing I. P. of the tellurium atom. This decrease is parallel to the observed shift towards low fields of the 1,9 protons on the electronegative substitution at the tellurium atom.

In conclusion, it may be stated that in the case of phenoxatellurine the electronegative substitution in the central ring brings about greater charge modifications at the 1,9 positions, shifting the signal of these protons towards low fields. On the contrary, the fluoro-substitution in the rings (2,8-positions) causes the screening of the neighbouring 1,9 protons. Quantitative treatments for such systems are difficult to perform but the trends of the calculated charge densities with parameters calibrated for electronic transition energies seem to give account for the observed shifts.

---

[12] V. Em. Sahini and E. Volanschi, *Rev. Roumaine Chim.*, to be published.

Revue Roumaine de Chimie, **18**, *4*, 537–547 (1973)

METHYL RADICALS ON POROUS VYCOR GLASS AS STUDIED BY ESR SPECTROSCOPY

D. P. LAZĂR* and JOHN TURKEVICH**

* Physical Chemistry Department "Al. I. Cuza" University, Jassy, Calea 23 August nr. 11, Romania

** Frick Chemical Laboratory, Princeton University, Princeton, New Jersey, U.S.A.

Received January 28, 1972

The practical procedures for preparing methyl radicals from methyl iodide adsorbed on porous Vycor glass are presented; then the ESR spectra of the methyl radical are in detail described following both temperature and microwaves-power influence on the methyl radicals decay. Chemical treatment of the glass support and its influence on the methyl radical lifetime are also reported.

EXPERIMENTAL PROCEDURE

Methyl radicals were prepared by u.v. light irradiation at liquid nitrogen temperature of methyl iodide adsorbed on porous Vycor glass rods (Vycor glass rods were of 1.5 mm diameter and 20 mm long, 40 Å pores size, Corning nr. 7930). The irradiation was carried out with a low pressure mercury lamp (110 volts input 5,000 volts output, 500 watts power) at a distance of 2 to 3 cm from the quartz tube containing Vycor rod sample which was, as a preliminary, immersed into a Dewar vessel (suitable for ESR measurements) filled with liquid nitrogen. The ESR Dewar vessel used for u.v. light irradiation was similar to the one used for the proper measurements, i.e. having a long transparent quartz tube at the bottom. Irradiation was carried out in a ESR Dewar vessel different from the one used for measurements to avoid the signals generated by the u.v. irradiation in the quartz of the ESR Dewar vessel.

The quartz used for the sample tubes containing Vycor samples, as well the Vycor glass, did not develop a signal on irradiation. After irradiation, the sample tube, having in a Vycor glass rod, was rapidly transferred (to avoid iceing) from one Dewar vessel filled with liquid nitrogen to the other Dewar vessel also containing liquid nitrogen.

To record ESR spectra, a VARIAN Spectrometer Md. V. 4500 operating at 9.5 kcycles/s, with a multi-purpose cavity mode TE_{102} was employed; the magnetic field was modulated at 100 KHz and was controlled by a Field Dial regulator V–FR 2200. All ESR measurements were made at liquid nitrogen temperature, except for cases when the temperature rise influence, was studied.

The Vycor glass rods, as received, were first treated with concentrated nitric acid, then with distilled water and heated in vacuum for 10–12 hours at 600°. Some of the Vycor samples were treated for 12 hours at room temperature with aqueous sodium tetraborate solutions (2.00 %–0.2 % – 0.1 % and 0.05 %) and others were treated with aqueous solutions of hydrogen fluoride (0.5 %–0.35 % – 0.25 % and 0.1 %).

Treatment with HF solutions having concentrations greater than 0.5% caused decrease in the size of the Vycor rods used.

The Vycor samples were placed in quartz tubes suitable for ESR measurements and these tubes were sealed through quartz-pyrex graded seals to stopcocks having standard tape joints which permitted attachment to a conventional vacuum system.

The sample was pumped off for at least 12 hours at 600° using a mercury diffusion pump; it was then cooled down in vacuum to room temperature; after this the sample was contacted for 2 minutes with vapours of freshly distilled methyl iodide at room temperature. After methyl iodide adsorption, the sample was pumped off for 15 minutes at room temperature, then transferred to the quartz Dewar vessel filled with liquid nitrogen and irradiated with u.v. light. Unless otherwise stated, the u.v. irradiation time was 15 minutes.

RESULTS

The ESR spectrum of the methyl radical consisted of four strong sharp lines centered at $g = 2$, each line having satellites. Frequently, 2 additional lines due to hydrogen atoms were observed.

The four sharp methyl radical lines have a separation of 22.1 G, which was constant to 1% in a given hyperfine complex structure and varied from measurement to measurement by at most 2%.

The intensities of lines under normal measurement conditions (microwaves power attenuation = 10 dB; modulation amplitude of 1.5 gauss; scan: 500 G/10 min) were in the ratio of 1.00/3.76/4.07/1.28 for magnetic field values of 3185.5/3214.7/3235.4/3251.1 G.

This result is in good agreement with the ratio 1.0/3.7/4.1/1.3 previously reported by Turkevich and Fujita. [1]

These former values markedly differ from the theoretical values of 1.0/3.0/3.0/1.0 experimentally confirmed for the methyl radical in aqueous solution by Turkevich and Mickevich. [2]

The line-width was 2.8 G, a value previously reported by Turkevich and Fujita [1] for the methyl radical on silica and, therefore, much wider than the value of 1.2 G found by Turkevich and Mickevich [2] for the methyl radical in solution.

Measurements were carried out to determine the effect of microwaves power and modulation amplitude on the intensity and width of the hyperfine structure. It was found that at 15 dB power attenuation the modulation amplitude has a large effect on the line intensities.

As is shown in Table 1, lines 1 and 2 (numbered from the lower field side) exhibit a maximum intensity at modulation 400 (= 1.5 G) while lines 3 and 4 at modulation 300 (= 1.2 G).

Distorsion of the lines was observed if the modulation amplitude was increased above 600 (= 2.25 G).

---

[1] J. Turkevich and Y. Fujita, *Science*, **152**, 1659 (1966).

[2] D. Mickevich and J. Turkevich, *J. Phys. Chem.*, **72**, 2703 (1968).

Table 1

Influence of the field modulation

Modulation (dial settings)	Line intensities (a.u.)				Line ratios (line 1 as unit)			
	1	2	3	4	1	2	3	4
1	5.8	21.95	25.5	12.5	1	3.78	4.45	2.16
2	9.8	53.80	84.4	18.8	1	5.49	8.61	1.92
5	23.0	128.0	151.0	51.0	1	5.57	6.57	2.22
10	48.0	236.0	269.0	92.0	1	4.92	5.60	1.93
25	131.0	426.0	670.0	182.0	1	3.25	5.11	1.39
50	225.0	1154.0	1547.0	484.0	1	5.13	6.88	2.15
100	452.0	2352.0	3108.0	800.0	1	5.20	6.88	1.77
160	730.0	3555.0	4340.0	1195.0	1	4.87	5.95	1.64
200	925.0	4190.0	4725.0	1435.0	1	4.53	5.11	1.55
250	1040.0	4420.0	5050.0	1530.0	1	4.25	4.86	1.47
320	1225.0	4805.0	5410.0	1650.0	1	3.92	4.42	1.35
400	1600.0	4860.0	5300.0	1616.0	1	3.04	3.31	1.01
500	1340.0	4875.0	5150.0	1590.0	1	3.64	3.84	1.19
600	1345.0	4790.0	4950.0	1485.0	1	3.56	3.68	1.10
800	1295.0	4465.0	4600.0	4370.0	1	3.48	3.45	1.06
1000	1205.0	4108.0	4192.0	1296.0	1	3.41	3.48	1.08
2000	904.0	2900.0	2932.0	904	1	3.21	3.24	1.0

Conditions : F = 3205 G ; Sc = 500 G/10 min ; Att = 15 dB ; L = 100 ;
R = 2 ; U.V. time = 6 hrs
T = −196°C ; untreated Vycor rod

Note : for all tables included the following abbreviations are used ;
F = magnetic field intensity ; Sc = Scan ; Att = power attenuation ;
L = amplification level ; R = time response ;
Md = modulation amplitude ; U.V. time = U.V. time irradiation ;
T = temperature ; a.u. = arbitrary units.

Table 2

Influence of microwaves power (for Md = 400)

Microwaves power (dB)	Line-intensities (a.u.)				Line ratios (Line 4 as unit)			
	1	2	3	4	1	2	3	4
0	285.50	933.75	886.25	253.75	1.11	3.68	3.49	1
3	396.25	1308.75	1231.25	343.75	1.15	3.81	3.58	1
6	872.5	2750.00	2625.00	735.00	1.19	3.74	3.57	1
10	1295.00	4320.00	4030.00	1320.00	0.98	3.27	3.05	1
15	1616.00	5300.00	4860.00	1600.00	1.01	3.31	3.04	1
20	1425.00	4670.00	4255.00	1115.00	1.28	4.19	3.82	1
25	830.00	2950.00	2575.00	695.00	1.19	4.24	3.71	1

Conditions : F = 3205 G ; Sc = 500 G/10 min; L = 100 ; R = 2 ; T = 196°C; U.V. time = 5 hrs untreated Vycor rod.

The influence of microwaves power was determined both at modulation 400 and modulation 10 (= 0.375 G). At modulation 400, the hyperfine line of the spectrum seems to saturate at powers greater than 15 dB setting.

Table 3

Influence of the microwaves power (Modulation = 10).

Field (gauss)	Power (dB)	Line (n^0)	Length (l) (m.m)	Width (w) (m.m)	W^2 (mm^2)	Signal intensity $(w^2.1)\times10^3$
1	2	3	4	5	6	7
3185.5 gauss	0	1	91.30	31.00	961.00	87.739
	3		151.56	24.20	585.64	88.759
	6		236.40	18.80	353.44	83.553
	10		429.00	16.50	272.25	116.795
	15		752.00	12.50	156.25	117.500
	20		860.00	11.90	141.61	121.784
	25		859.00	11 00	121.00	103.939
3214.7 gauss	0	2	81.80	31.60	998.50	81.682
	3		125.00	27.20	739.84	92.480
	6		195.00	21.80	475.24	92.671
	10		341.88	17.90	320.41	109.541
	15		442.80	15.10	220.00	100.958
	20		442.80	14.30	204.49	90.548
	25		300.00	12.0	144.00	43.200
3235.4 gauss	0	3	94.00	32.00	1024.00	96.256
	3		146.64	22.10	488.41	65.754
	6		241.75	17.00	289.00	69.685
	10		447.00	14.80	219.00	97.893
	15		779.20	13.00	169.00	131.684
	20		1013.75	12.30	151.29	153.370
	25		814.40	10.20	104.00	84.697
3259.1 gauss	0	4	32.35	25.40	645.56	20.871
	3		49.25	24.80	615.04	30.291
	6		73.84	20.20	408.04	30.130
	10		127.37	15.00	225.00	28.658
	15		208.80	11.80	139.24	34.073
	20		240.50	10.80	116.64	28.052
	25		201.00	10.80	116.64	23.445

Conditions: Sc = 10 G/10 min.; $R = 1$; $L = 100$
$T = -196$°C; u.v. time = 6 hrs
untreated Vycor rod.

At modulation 10 the saturation effect starts at powers greater than 20 dB.

The width of the lines decrease in all cases with power, being 402 mili-gauss at the lowest power and modulation used.

The intensities of the four lines of the hyperfine spectrum are seriously different depending on the modulation amplitude, the best line-ratios being those which were observed at higher modulations. Measurements at 35 KHz/s, attenuation of 15 dB and modulation of 20 (= 0.75 G) gave the same spacing between the hyperfine lines as was obtained at 9.5 KHz/s when a ratio of line intensities of 1.0/2.75/2.37/0.73 was obtained. The line width was of 2.0 G.

In addition to the four main peaks of methyl radical spectrum (Fig. 1), nine satellite-peaks were observed. Eight of these satellites can be divided into two groups symmetrically placed around the main peaks.

The separation between the two outermost peaks is of 76.26 G while the separation between the penultimate lines of the main peaks of the methyl radical spectrum is of 71.46 G, resulting a difference of 4.80 G between the above given values. We assign these eight satellite peaks to a splitting produced in the main peaks by the natural abundance of C^{13} isotope. Turkevich and Fujita [1] found a difference of 38.5 G but using 55% enriched C^{13}, and characterized the methyl group as being a planar free-moving radical. On the basis of our present results, we must conclude that the methyl group is a planar radical rotating around the axis perpendicular to the plane. [3]

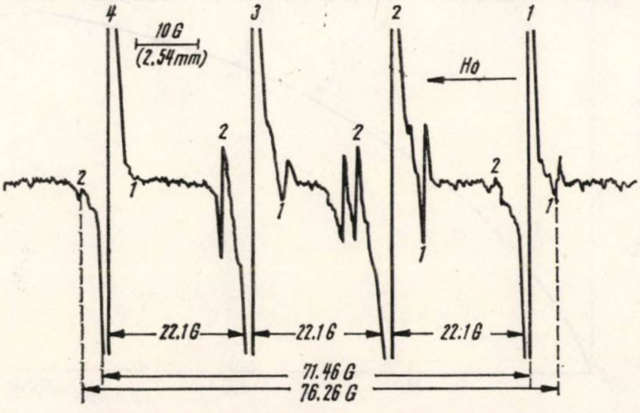

Fig. 1. — Electron spin resonance spectrum of methyl radicals from the U.V. light photolysis of methyl iodide on porous Vycor glass ($T = -196°C$).

Conditions: $F = 3205$ G; Sc = 1 KG/100 min; Att = 10 dB; Md = 10; $R = 2$; $L = 1\,000$; U. V. time = 6 hrs; untreated Vycor; Chart speed = 2.54 cm/min; Chart calibration: 1 cm = 3.937 G).

No peaks were found at a difference of 38.5 G characteristic for a planar free moving methyl radical nor at 300 G characteristic for a tetrahedral configuration of CH_3 radical.

The difference between our present results and that reported by Turkevich and Fujita [1] must be ascribed to the higher concentration of methyl radicals used in the present work and hence to the scarcity of methyl radicals (2% from the possible maximum concentration of methyl radicals) in the Turkevich-Fujita experiments.

The separation between the four peaks of the first group of satellite-lines is of 22.8/19.8/24.2 G, and 22.1/22.0/22.1 G respectively, for the second group, while the main peaks separations are of 22.1 G.

The intensity of the satellite-lines was about 1% of the second line of the main spectrum when for the C^{13} abundance it should be of 0.5%, since in the ESR methyl spectrum there are two C^{13} lines for each C^{12}

---

[3] Ţ. Cole, H. O. Pritchard, N. R. Davidson and H. M. Mc. Conell, *Mol. Phys.*, **1**, 406 (1958).

line. The ninth satellite-peak [*] was observed at a distance of 7.33 G from the peak number 2 on the low field side. Peak 2 (main spectrum) also shows a shoulder on each side separated by 4.2 G [**].

Very often a hydrogen atom spectrum consisting of two lines separated by 491 G was recorded and having an intensity of 0.4% of the smallest methyl peaks. Its lines were very sharp being 0.4 G at 25 dB power attenuation and for a field modulation of 0.1 G.

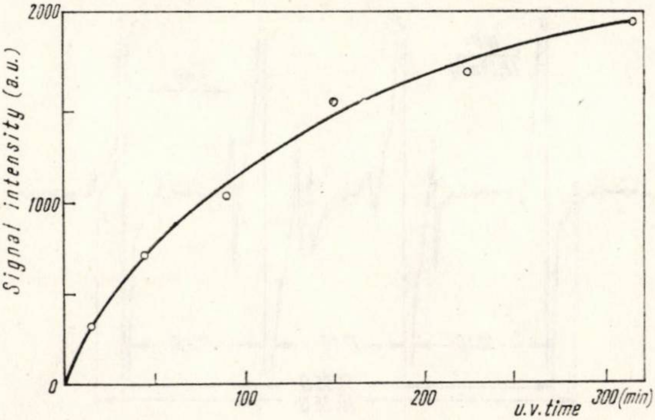

Fig. 2. – Influence of U.V. irradiation time (untreated Vycor rod).

The hydrogen spectrum saturated very easily and the above given value of the line-width may be an upper limit.

A small asymmetric signal was observed at $g = 4$.

U.V. time irradiation effect. The intensity of the ESR signal rose steadily with that of irradiation and, as Fig. 2 shows, approaches a limiting value when the opposite reaction

$$CH_3I \rightleftharpoons CH_3 + I \qquad (1)$$

reaches the equilibrium state. It should be noted that the signal after fifteen minutes u.v. irradiation was easily measured at a level of amplification of 40 and after 315 minutes u.v. irradiation at a level of 5. A level of 2 000 could be used before the noise of the instrument interfers with the methyl signals.

DECAY OF THE METHYL RADICALS AS A FUNCTION OF TEMPERATURE

The ESR signal of the methyl radicals decays as the temperature is raised from the liquid nitrogen temperature to room temperature, where the equilibrium of the opposite reaction (1) is shiften to the left, restoring the initial product. The procedure consisted in keeping the sample at liquid nitrogen temperature in a Dewar flask (filled with liquid nitrogen), then bringing it into a hole of a cylindrical aluminium block (placed into another Dewar flask) cooled to the desired temperature with liquid nitrogen. The temperature of the aluminium block was controlled with a calibrated chromell-alumel thermocouple.

---

[*] The ninth satellite is due to the Dewar vessel.

[**] These shoulders cannot be seen in Fig. 1.

The sample was kept at a certain fixed temperature for at least ten minutes (thermostation time interval) just sufficient to allow thermal equilibrium between sample and aluminium block and then again brought into the ESR Dewar to the temperature of liquid nitrogen for measurements. Experiments showed that at a given temperature the decrease of the ESR signal takes place very rapidly, perhaps in less then the ten minutes used as the measurement time interval, then the ESR signal decreases slowly with time as Fig. 3 shows.

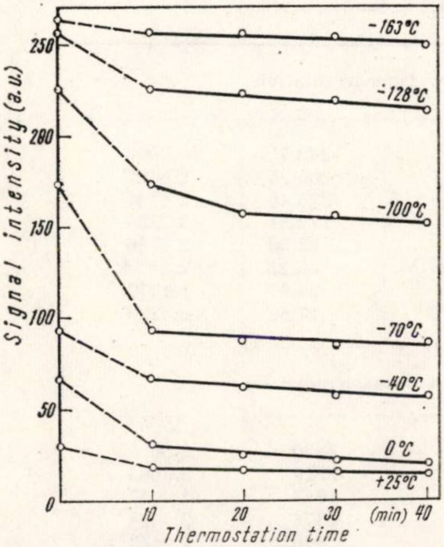

Fig. 3. – Curves of temperature and time decay of methyl radicals after fifteen minutes U.V. irradiation.

(Conditions: $F=3205$ G; $Sc=500$ G/10 min; $L=100$; $R=2$; Att$=15$ dB; untreated Vycor rod (see also the footnote under Table 4).

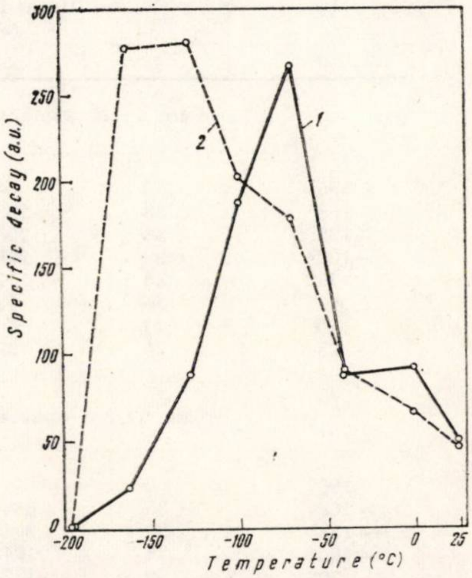

Fig. 4. – Specific decay of methyl radicals concentration for two distinct cases: 15 and 315 minutes U.V. time irradiation, respectively.

(Note: specific decay for 15 min U.V. time irradiation is ten times smaller than the specific decay for 315 min U.V. time irradiation).

Conditions: the same as for Fig. 3

Legend: *1*, full line = 15 min U.V. time; *2*, dotted line = 315 min U.V. time.

The main diminution of the signal takes place within the shortest time interval for measurements (namely in the first ten minutes). If we plot this decrease as a function of temperature we find that the greatest drop of the methyl radical concentration occurs at about − 70°. There is a discontinuity in the evolution of the decay process in the temperature range between − 70° and + 25°, this diminution having, as it seems to us, a periodical character (Fig. 4).

Table 4

Temperature and time decay of methyl radicals for two distinct cases : a/15 minutes u.v. irradiation b/315 u.v. time irradiation

Temp. °C	T °C	Reference signal intensity (a.u.)	Signal intensity (a.u.)	Specific decay $\frac{100-\Delta.10^2}{T}$
0	1	2	3	4
Case a : 15 minutes u.v. time irradiation				
−196°	0	—	263.75	0.0000
−163°	33	263.75	256.25	2.9327
−128°	33	256.25	225.40	2.5131
−100°	28	225.40	172.51	2.7335
− 70°	30	172.51	92.50	2.1736
40°	30	92.50	66.25	2.3873
0°	40	66.25	29.87	1.1272
+ 25	25	21.87	17.62	2.5296
Case b : 315 minutes u.v. time irradiation				
−196°	0	—	3830	0.00
−163°	33	3830	2919	2.3093
−128°	35	2919	1943	1.9017
−100°	28	1943	1378	2.5328
− 70°	30	1378	846	2.0463
− 40°	30	846	580	2.2223
− 0°	40	580	332	1.4310
+ 25	25	332	217	2.6144

Conditions : $F = 3205$ G; Sc : 500 G/10 min; L = 100; $R = 2$;
Att = 15 dB; untreated Vycor rod.
(Sample was kept for ten minutes at each temperature).

Note : $\Delta = \frac{\text{col } 2 - \text{col } 3}{\text{col } 2}$

An increase in the initial methyl radical concentration by increasing the u. v. light irradiation time (up to 315 minutes) from the value usually used as reference (337 arbitrary units for the ESR signal at − 196°) up to 3830 arbitrary units, leads to a more prominent decay at temperatures below − 100° and diminishes this decay at higher temperatures (− 100° to + 25°).

Influence of the chemical treatment on the methyl radical lifetime. Attempts were made to increase the stability of the methyl radicals into the Vycor glass pores by means of pretreatment with aqueous solutions (of different concentrations) of sodium tetraborate and hydrogen fluoride (treatment using Teflon provided no satisfactory results). Treatment with aqueous solutions of sodium tetraborate of various concentrations followed by a fifteen minutes u.v. time irradiation, produced the methyl radical amounts tabulated in Table 5.

The treatment with aqueous solutions of sodium tetraborate (0.1% — 0.2%) provided an increase of methyl radical concentration (compared

Table 5

Influence of treatment with sodium tetraborate (aq.sol) and the corresponding temperature decay

Sodium tetraborate (aq.sol) %	Signal intensity as function of temperature (a.u.).				
	$-196°$	$-130°$	$-65°$	$0°$	$+25°$
2.00	183.00	91.00	45.00	23.00	7.00
0.20	410.00	88.00	38.00	27.00	15.00
0.10	572.00	275.00	114.00	40.00	29.00
0.05	126.00	81.00	37.00	14.00	9.00
untreated Vycor as reference sample	337.00	162.00	64.00	21.00	10.00

Conditions : $F = 3205$ G; Sc = 500 G/10 min
Att = 10 dB (15 dB for 0.2%)
$L = 100$; Md = 400; R = 2
u.v. time = 15 min; untreated Vycor rod.
(Sample was kept for 60 minutes at each temperature).

with methyl radical concentration on untreated Vycor glass) and also a more rapid diminution of methyl radicals concentration as temperature rose (Fig.5).

Table 6

Influence of treatment with hydrogen fluoride (aq.sol) and corresponding temperature decay

Hydrogen fluoride (aq.sol) %	Signal intensity as function of temperature (a.u.).				
	$-196°$	$-130°$	$-65°$	$0°$	$+25°$
0.50	220	96	44	15	7
0.35	440	203	89	25	15
0.25	309	167	72	25	14
0.10	241	118	53	16	10
untreated Vycor rod as reference	337	162	64	21	10

Conditions : $F = 3205$ G; Sc = 500 G/10 min;
Att = 10 dB; Md = 400; $R = 2$;
$L = 100$; u.v. time = 15 min
(sample was kept for 60 minutes at eaoh temperature).

The treatment with aqueous solutions of hydrogen fluoride solutions produced the folowing quantities of free methyl radicals tabulated in Table 6 and plotted in Fig. 6.

Thus, the treatment of Vycor rods with 0.35% H F aqueous solution produced the largest quantity of methyl radicals. The decay curves for the

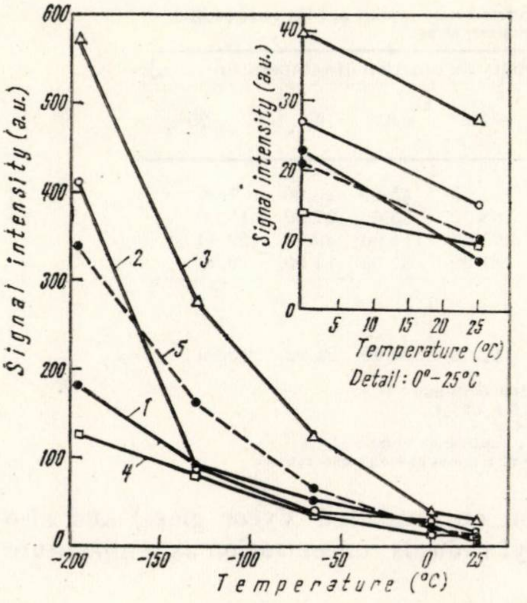

Fig. 5. — Decay curves of methyl radicals after sodium tetraborate treatment.

1, $Na_2B_4O_7$ sol. 2.00%; *2*, $Na_2B_4O_7$ sol. 0.20%; *3*, $Na_2B_4O_7$ sol. 0.10%; *4*, $Na_2B_4O_7$ sol. 0.05%; *5*, dotted line = untreated Vycor rod.

Fig. 6. — Decay curves of methyl radicals after hydrogen fluoride treatment.

1, hydrogen fluoride sol. 0.50%; *2*, hydrogen fluoride sol. 0.35%; *3*, hydrogen fluoride sol. 0.25%; *4*, hydrogen fluoride sol. 0.10%; *5*, dotted line: untreated Vycor rod.

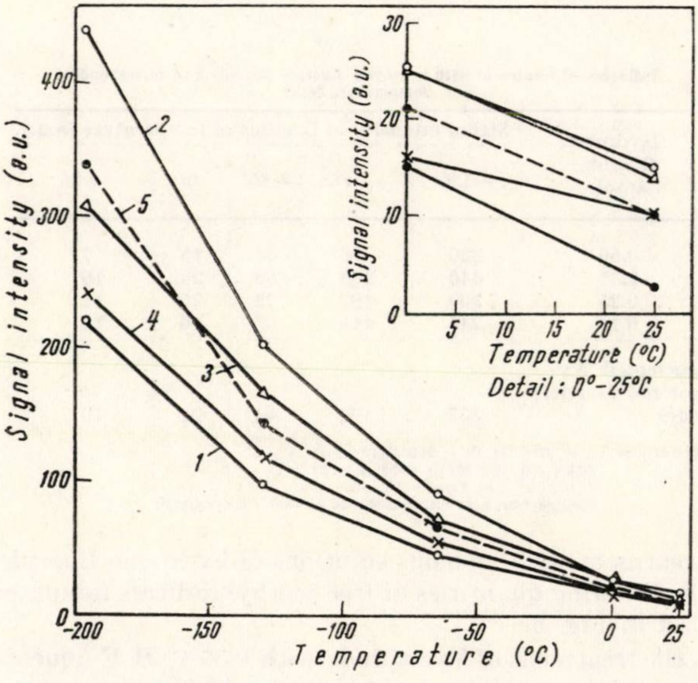

Table 7

Time decay of methyl radicals obtained by γ-rays irradiation

Temperature °C	Time for thermal equilibrium (min.)	Signal intensity (a.u.)
−196°	10	84.50
−160°	10	23.60
−125°	10	12.90
−100°	10	7.46
− 70°	10	4.43
− 40°	10	signal disappeared

Conditions: **F = 3205 G; Sc = 500 G/10 min; Att = 15 dB; R = 2; L = 100; γ-rays irradiation time = 12 hrs at liquid nitrogen temperature; untreated Vycor rod.**

methyl radicals concentrations on treated Vycor rods are similar and exhibit a broad maximum between −130 °C and 0°C (Fig. 5 and Fig. 6).

Methyl iodide irradiated for 24 hours at liquid nitrogen temperature with γ-rays from a Co^{60} source gave a ESR signal of 86 arbitrary units. The lifetime decay of the methyl radicals during this experiment is illustrated on Table 7.

Methyl bromide was found to be a poorer source of methyl radicals (compared with methyl iodide) giving a signal of 42 arbitrary units where the methyl iodide gave a signal of 572 arbitrary units (under the same experimental conditions).

Attempts to get methyl radicals directly captured on Vycor glass from methane gas using electrical discharges gave no satisfactory results.

Revue Roumaine de Chimie, **18**, *4*, 549–556 (1973)

KINETICS AND MECHANISM OF THE THERMAL DECOMPOSITION OF AZIBENZYL. I

DECOMPOSITION IN BENZENE SOLUTION

M. CONTINEANU*, TATIANA ONCESCU* and R. N. SCHINDLER**

* Department of Physical Chemistry, University of
Bucharest, Bd. Republicii 13, Romania
** Institut für Physikalische Chemie
der Kernforschungsanlage Jülich GmbH

Received September 9, 1972

The thermal decomposition of azibenzyl in benzene solution was studied by gas chromatographic determination of the N_2 evolved during the reaction and by following the change in azibenzyl absorption at $\lambda = 320$ nm. Kinetic evaluation of the data indicate that the decomposition can be described as a unimolecular process with an activation energy of 26.5 Kcal/mole. A pre-exponential coefficient $A \approx 10^{14}$ sec^{-1} and an activation entropy $\Delta S^* = 3$ e.u. are calculated for the process.

INTRODUCTION

The present paper deals with the decomposition kinetics of azibenzyl (known also as Phenyl-benzoyl-diazomethane or Diazodesoxybenzoine) in the inert solvent benzene. The kinetic parameters were determined by means of the spectrophotometric as well as chromatographic technique. They permitted to evaluate the reaction mechanism of this thermal decomposition.

Numerous papers have dealt with the study of the reactivity of diazocarbene compounds in different media.[1-9] The high reactivity of this group of substances has been found useful both in preparative organic chemistry and in the development of theoretical interpretations of reactions in which these compounds occur.

---

[1] B. EISTERT, "Neure Methoden der präparativen organischen Chemie", Bd. I. Verlag Georg Thieme Stuttgart, 1968, p. 473.

[2] R. HUISGEN, *Angew. Chem.* **67**, 439 (1955).

[3] V. FRANZEN, *Chem. Ztg.*, **81**, 359 (1957).

[4] R. HUISGEN, *Angew. Chem.*, **75**, 604 (1963).

[5] R. HUISGEN. H. KÖNIG, G. BINSCH and H. J. STURM, *Angew Chem.*, **73**, 368 (1961).

[6] R. HUISGEN, G. BINSCH and L. GHOSEZ, *Chem. Ber.*, **97**, 2628 (1964).

[7] R. HUISGEN, G. BINSCH and H. KÖNIG, *Chem. Ber.*, **97**, 2868, 2884 (1964).

[8] G. BINSCH, HUISGEN and H. KÖNIG, *Chem. Ber.*, 97, 2893 (1964).

[9] E. FAHR, K. H. KEIL, H.LIND and F. SCHECKENBACH, *Z. Naturforsch.*, **206**, 526 (1965).

The formation of diphenylketene by heating a benzene solution of azibenzyl to 60° was long ago mentioned by Schröter.[10]

The reaction mechanism is known as Wolff's rearrangement.[11]

The thermolytic, photolytic and catalytic (with copper powder or silver ions) decomposition cause the elimination of N_2 from the azibenzyl molecule with the formation of the intermediate α-ketocarbenic radical. This intermediate forms diphenylketene through an intermolecular rearrangement when the reaction takes place in inert solvents.[10,12] Under these conditions the diphenylketene can be isolated. There is a competition between the rearrangement and different capture processes when working in solvents which capture the α-ketocarbenic radical.[13]

EXPERIMENTAL

Azibenzyl was prepared by oxidizing the corresponding hydrazone.[14]

1st Technique : The thermal decomposition of azibenzyl in benzene was carried out in a cell as shown in figure 1.

The cell containing 5 ml solution (3×10^{-2} m/l) under investigation was introduced into liquid N_2 and a stream of helium was passed through, to remove the air from the installation. After this, the tap R_2 in figure 1 is turned so that helium under a pressure of 1.2 atm flows as carrier gas to a Perkin Elmer F_6 Chromatograph and the four-way tap R_1 is turned to separate cell and chromatograph.

The cell was introduced into a thermostat and the N_2 evolved in the reaction was measured chromatographically as function of reaction time. Experiments were carried out for the temperatures in the 55° – 32.5° range.

The value of the rate constants obtained in this way shows errors which increase with temperature. Consequently we adopted another technique.

2nd Technique : In this case the cell shown in figure 2a was used.

5 ml of azibenzyl solution were introduced at *A* into the cell, which was then cooled to −193° and evacuated through joint *A*.

At the point marked I in figure 2a, the cell was sealed off by flame melting. The cell thus evacuated was placed in the thermostat at the working temperature for a certain time. Through the joints *S* and *S'*, the cell was connected to the same chromatograph tap R_2, as can be seen from figure 2b.

The cell tap was washed with helium, brought from outside, then R_2 was turned so that the carrier gas helium could flow through the cell tap.

From the beginning two short iron bars (*M*, *M'*) were introduced into the cell (figure 2a), which can be actioned from outside by a magnet in order to break the two pointed ends *P* and *P'* of the cell. In this way, the connection with the rest of the cell is achieved. The working temperatures for these experiments were 40°, 50°, 60° and 70°, respectively.

For the two chromatographic techniques we used a column made in laboratory of 1.5 m and $\Phi_i = 5$ mm, filled with molecular sieve of 5 Å.

---

[10] G. SCHROETER, *Ber. dtsch. chem. Ges.*, **47**, 2336 (1909) ; **49**, 2704 (1916).

[11] L. WOLFF, *Liebigs Ann. Chem.*, **394**, 23 (1912).

[12] P. YATES and T. J. CLARK, *Tetrahedron Letters*, **13**, 435 (1961).

[13] W. JUGELT and D. SCHMIDT, *Tetrahedron*, **25**, 969 (1969).

[14] C. D. NENIŢESCU and E. SOLOMONICA, Organic Syntheses Coll., vol. 2, Wiley, New York, 1955, p. 496.

In order to check the results obtained by the chromatographic technique, spectrophotometric experiments were also carried out. A spectrophotometer Pye-Unicam SP 1800 was used

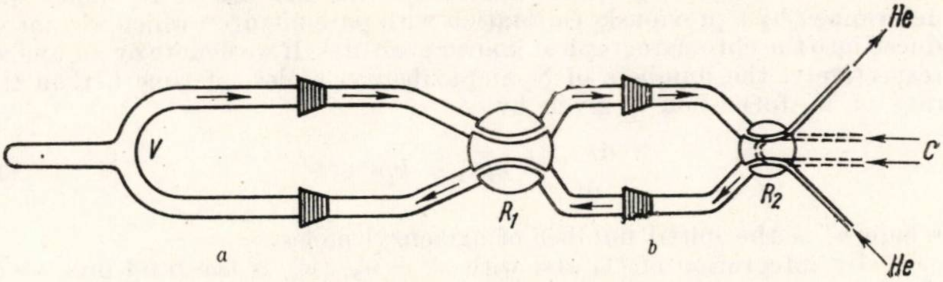

Fig. 1. – Reaction cell V, connected to chromatograph C, (1st technique). R_1, R_2, four-way taps.

a) before the measurement of N_2; b) during the measurement of N_2.

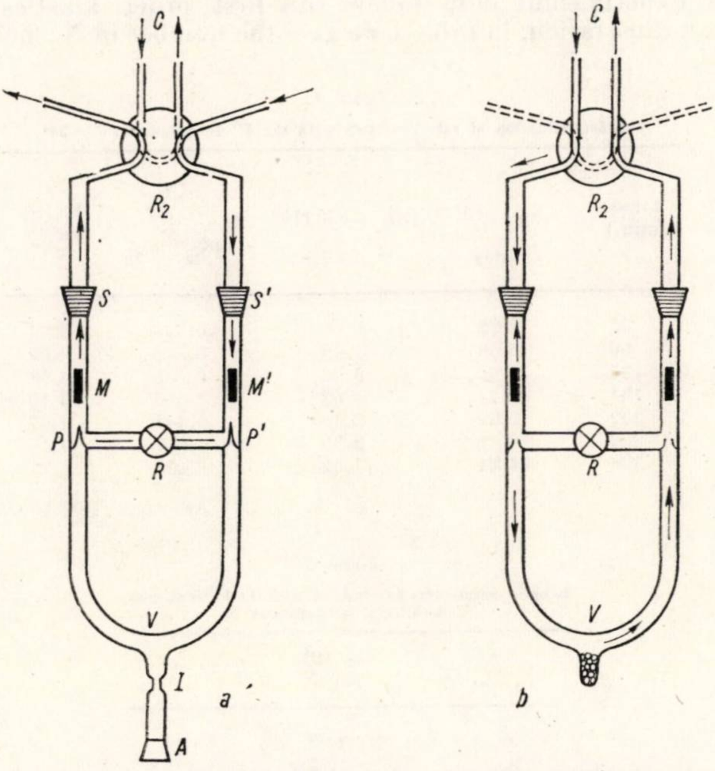

Fig. 2. – Reaction cell connected to chromatograph *C* (2nd technique) *A*, *S*, *S'* joints; *P*, *P'*, glass pointed ends; *M*, *M'*, iron bars; *R*, tap, R_2 fours-way tap;

a) during the reaction; b) after the stopping of reaction, during the measurement of N_2.

to study the decomposition of azibenzyl in benzene solution at temperatures of 40°, 50°, 60° and 70°, respectively.

RESULTS

In the chromatographic experiments the number of N_2 moles was determined by a previously calibration with pure nitrogen which was introduced into the chromatograph at known pressures. If we denote by n_{N_2} and n_A respectively, the numbers of N_2 and azibenzyl moles, at time t, then the rate of N_2 formation is given by

$$\frac{dn_{N_2}}{dt} = k_1 n_A = k_1 n_A^0 e^{-k_1 t} \qquad (1)$$

where n_A^0 is the initial number of azibenzyl moles.

By integration of (1) and with $n_A^0 = n_{N_2}^0$ ($n_{N_2}^0$ is the total number of N_2 moles at complete decomposition) equation (2) is obtained

$$k_1 = (2.303/t) \cdot \lg (n_{N_2}^0 / n_{N_2}^0 - n_{N_2}) \qquad (2)$$

Our experimental data follow this first order kinetics equation. As an illustration, in table 1 we give the number of N_2 moles and the rate constants for a working temperature of 50° and a $3 \cdot 10^{-2}$ mole/l azibenzyl concentration.

Table 1

The determination of rate constants with the 1st technique at $T = 50°$

Time (min.)	$n_{N_2} \cdot 10^5$ moles	$(n_{N_2}^0 - n_{N_2})10^5$	$\ln \frac{n_{N_2}^0}{n_{N_2}^0 - n_{N_2}}$	$k_1 \cdot 10^4$ sec^{-1}
55	3.72	9.03	0.345	1.04
90	5.68	7.08	0.589	1.09
122	7.00	5.76	0.795	1.08
154	8.14	4.62	1.016	1.10
202	9.29	3.46	1.304	1.07
252	10.37	2.39	1.677	1.10
308	11.24	1.52	2.128	1.15

Average: $1.05 \cdot 10^{-4}$

Table 2

Kinetic parameters determined with the 1st technique at several temperatures

$T°$ °C	$k_1 \cdot 10^4$ sec^{-1}	lg A
55	1.92	13.95
50	1.05	13.98
45	0.464	13.90
40	0.246	13.92
32.75	0.090	13.96

Average: 13.94

Further data obtained by this technique are evaluated in table 2.

Table 3

Kinetic parameters determined with the 2nd technique at several temperatures

T °C	$n_{N_2}\cdot 10^5$ moles	$(n^0_{N_2} - n_{N_2})\,10^5$	$\ln \dfrac{n^0_{N_2}}{n^0_{N_2} - n_{N_2}}$	$k_1\cdot 10^4$ sec.$^{-1}$	lg A
70	13.43	1.566	2.269	12.61	14.00
65	13.878	1.107	2.606	6.21	13.94
60	12.589	2.411	1.830	3.05	13.89
50	12.525	2.475	1.801	0.97	13.96
40	11.964	3.036	0.6708	0.266	13.95
				Average :	13.95

The values of the rate constants determined by the second chromatographic technique are given in table 3.

The rate constants from spectrophotometric measurements were calculated with equation (3)

$$k_1 = (2.303/t)\,.\,\lg(\varepsilon_0/\varepsilon_t) \tag{3}$$

where ε_0 and ε_t are the optical densities of the initial solution and after a reaction time t, respectively. These were measured at $\lambda = 320$ nm at which wavelength the azibenzyl has an absorption maximum and the reaction product is not absorbing.

Table 4

Spectrophotometric determination of rate constants at $T = 50°$

Time (min)	ε	$\lg \dfrac{\varepsilon_0}{\varepsilon_t}$	$k_1\cdot 10^4$ sec^{-1}
0	1.95	—	—
12	1.84	0.0253	0.808
30	1.64	0.0751	0.959
60	1.28	0.1826	1.16
90	1.15	0.2291	0.975
120	0.97	0.3032	0.926
150	0.81	0.3815	0.975
205	0.58	0.5265	0.984
285	0.38	0.7102	0.955
360	0.23	0.9282	0.988
420	0.16	1.0859	0.991
495	0.1	1.29	0.99

Average : $k_1 = 0.974\cdot 10^{-4}$

As an illustration the rate constants for a temperature of 50° of a solution of $4\cdot 10^{-3}$ mole/l are given in table 4.

It was found that the rate constant satisfies quite well equation (3) and its mean values come close to that calculated from the determinations of N_2 by the chromatographic technique.

The values of the rate constants for a whole range of temperatures are given in table 5.

Table 5

Kinetic parameters determined spectrophotometrically at several temperatures

T °C	$k_1 \cdot 10^4$ sec^{-1}	lg A
40	0.262	13.93
50	0.974	13.96
60	3.12	13.90
65	6.01	13.93
70	9.24	13.87

Average: 13.91

DISCUSSION

The first order kinetics verified by our experimental data both by relation to the N_2 evolved from the reaction and to the azibenzyl decomposed, suggests the following mechanism also mentioned in literature.[4,10]

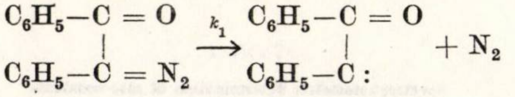

$$\begin{array}{c} C_6H_5-C=O \\ | \\ C_6H_5-C=N_2 \end{array} \xrightarrow{k_1} \begin{array}{c} C_6H_5-C=O \\ | \\ C_6H_5-C: \end{array} + N_2 \qquad (4)$$

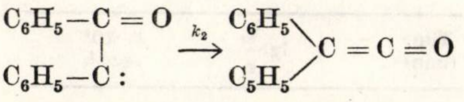

$$\begin{array}{c} C_6H_5-C=O \\ | \\ C_6H_5-C: \end{array} \xrightarrow{k_2} \begin{array}{c} C_6H_5 \\ C_5H_5 \end{array}\!\!\!>C=C=O \qquad (5)$$

The number of the N_2 moles measured at the end of the reaction corresponds quantitavely to the theoretical value according to the stoichiometry of reaction (4). This excludes the possibility of a secondary reaction between the intermediate radical and a molecule which is not decomposed, with the formation of the corresponding ketazene as it is reported in the thermal decomposition of diphenyldiazomethane.[15]

A reaction with the solvent is not likely to occur because the latter is inert.

The formation of diphenylketene could not be studied quantitatively by the spectrophotometric technique, as it presents an absorption maximum[16] at $\lambda = 409$ nm (the molar extinction coefficient $K = 270$) and the azibenzyl, having an absorption maximum at $\lambda = 435$ nm, absorbs well at $\lambda = 409$ nm ($K = 103$).

---

[15] T. Oncescu, M. Contineanu and G. Bălăceanu, *Rev. Roumaine Chim.*, **17**, 213 (1972)

[16] G. Lardy, *J. Chim. phys.*, **21**, 281 (1932).

But in this case in the absorption spectra of azibenzyl solutions for different reaction times shown in figure 3, a shifting of the absorption maximum from 435 nm to 409 nm can be noticed, accompanied by an increase of the absorption. This proves the formation of diphenylketene at the expense of azibenzyl.

Mention must be made of the fact that if the heating of the solution is continued, the absorption begins to decrease at a certain moment, which indicates that a transformation of diphenylketene takes place too.

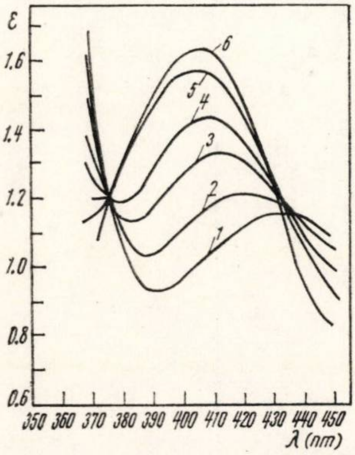

Fig. 3. — Absorption curves watching the diphenylketene formation at $T = 60°$ during the reaction.

1 – 6 various reaction moments between 0 – 60 minutes.

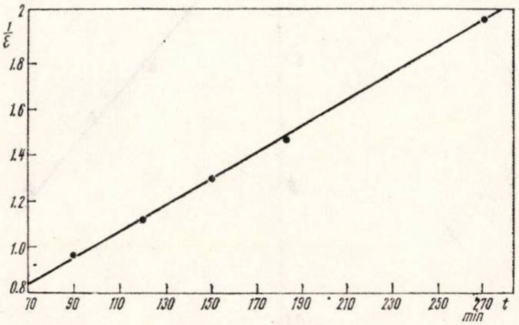

Fig. 4. — Plotting reciprocal values of diphenylketene absorption $\frac{1}{\varepsilon}$ *versus* time at $T = 60°$.

Plotting $1/\varepsilon$ measured at $\lambda = 409$ nm as function of time, a straight line is obtained, characteristic of the reaction :

$$2A \rightarrow B$$

suggesting the disappearance of diphenylketene from the system through dimerization.

It is known from literature that diphenylketene forms dimers, as can be also seen from our experimental data.

Figure 5 shows the values of log k versus $1/T$, obtained from the three techniques we used. From the slope of the straight line an activation energy of 26.5 Kcal/mole was calculated, whose value agrees quite well, with the values typical of unimolecular processes.

Using this energy the pre-exponential coefficients were calculated for all the working temperatures in the three techniques used, and they are given in tables 2, 3, 5. They agree each other leading to a mean value of log $A = 13.93$.

This points to a pre-exponential coefficient of about 10^{14} $\sec^{-1}$. With the aid of equation (6) the activation entropy $\Delta S^* = 3$ e.u. was calculated.[17]

$$A = \frac{e k T_m}{h} e^{\Delta S^*/R} \tag{6}$$

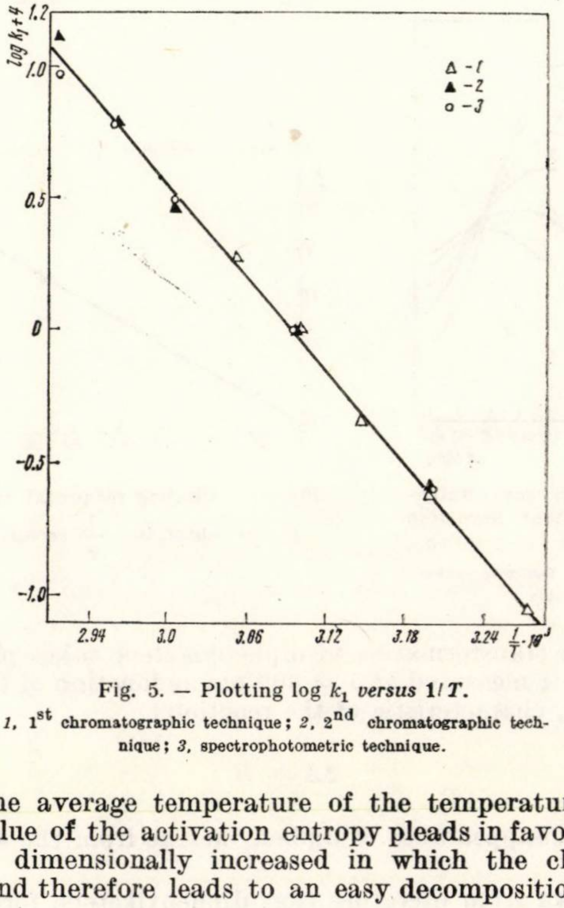

Fig. 5. — Plotting log k_1 *versus* 1/*T*.

1, 1st chromatographic technique; *2*, 2nd chromatographic technique; *3*, spectrophotometric technique.

where T_m is the average temperature of the temperature range used. The positive value of the activation entropy pleads in favour of an activated complex, dimensionally increased in which the chemical bonds are weakened and therefore leads to an easy decomposition of azibenzyl.

---

[17] SIDNEY W. BENSON "Thermochemical kinetics, Methods for the estimation of thermochemical data and rate parameters", John Wiley Sons. Inc., New York, London, Sydney, 1968, p. 66.

Revue Roumaine de Chimie, 18, 4, 557–567 (1973)

ON THE EQUILIBRIUM CONSTANT OF THE SIDE REACTION IN THE CONCENTRATION CELL IN DILUTE Cd–Pb LIQUID SOLUTIONS

Z. MOSER, K. FITZNER, L. ZABDYR

Institute for Metal Research, Polish Academy of Sciences,
Kraków, Reymonta 25, Poland

Received September, 9, 1972

Researches on dilute liquid cadmium solutions in lead carried out by means of emf measurements of concentration cells : Cd | $CdCl_2$ in LiCl-KCl | Cd–Pb resulted in determination of thermodynamic properties in the form of Wagner equation : $\ln \gamma_{Cd} = \ln\gamma^0_{Cd} + X_{Cd}\,\varepsilon^{Cd}_{Cd}$. On the basis of the known thermodynamic data of liquid metal and salt phases the equilibrium constant of side reaction : $Pb + CdCl_2 = Cd + PbCl_2$ occurring in the concentration cell has been determined. Also the curve of equilibrium compositions was obtained and the range of compositions and temperature in application to Cd – Pb system has been considered.

In the investigations on dilute zinc solutions with $X_{Zn} = 0.01-0.1$ molar fraction in the systems Zn–Cd[1] and Zn–In,[2] using the emf method of the concentration cells, it has been found that the results for $X_{Zn} = 0.01$ show considerable errors. They are caused by the side reactions which occur between $ZnCl_2$ from the electrolyte and the components of alloy electrode, especially when they are placed near the zinc in the electromotive series.

Hence we may conclude that the occurring of side reactions may be combined with the difference in standard free energy of the formation of chlorides appearing in electrolyte and of the alloy component. Wagner [3] informs that if the absolute value of the difference $\Delta F^0_{ZnCl_2} - \Delta F^0_{MCl_2}$ (where M = the alloy component) is greater than 7000 cal then the side reaction does not take place at all or its effect is negligible.

As a result of side reactions for the molar fraction $X_{Zn} = 0.01$, especially at higher temperatures, the amount of alloy component is being reduced and thus the increase of the electromotive force with temperature is smaller, which as a consequence leads to higher values of the activity coefficients. This is evident from Fig. 1 in which the results of the investigations on the dilute Zn—Pb[4] Zn—Cd[1] and Zn—In[2] and Cd—Pb solutions described in the present paper, are enclosed. As

---

[1] Z. Moser, *Bull. Acad. Polon. Sci. Ser. Sci. Techn.*, 5, 27 (1969).

[2] Z. Moser *ibid*, 6, 51 (1970).

[3] C. Wagner in "The physical chemistry of metallic solutions and intermetallic compounds", vol. 1, paper 1 B, London 1959, p. 16.

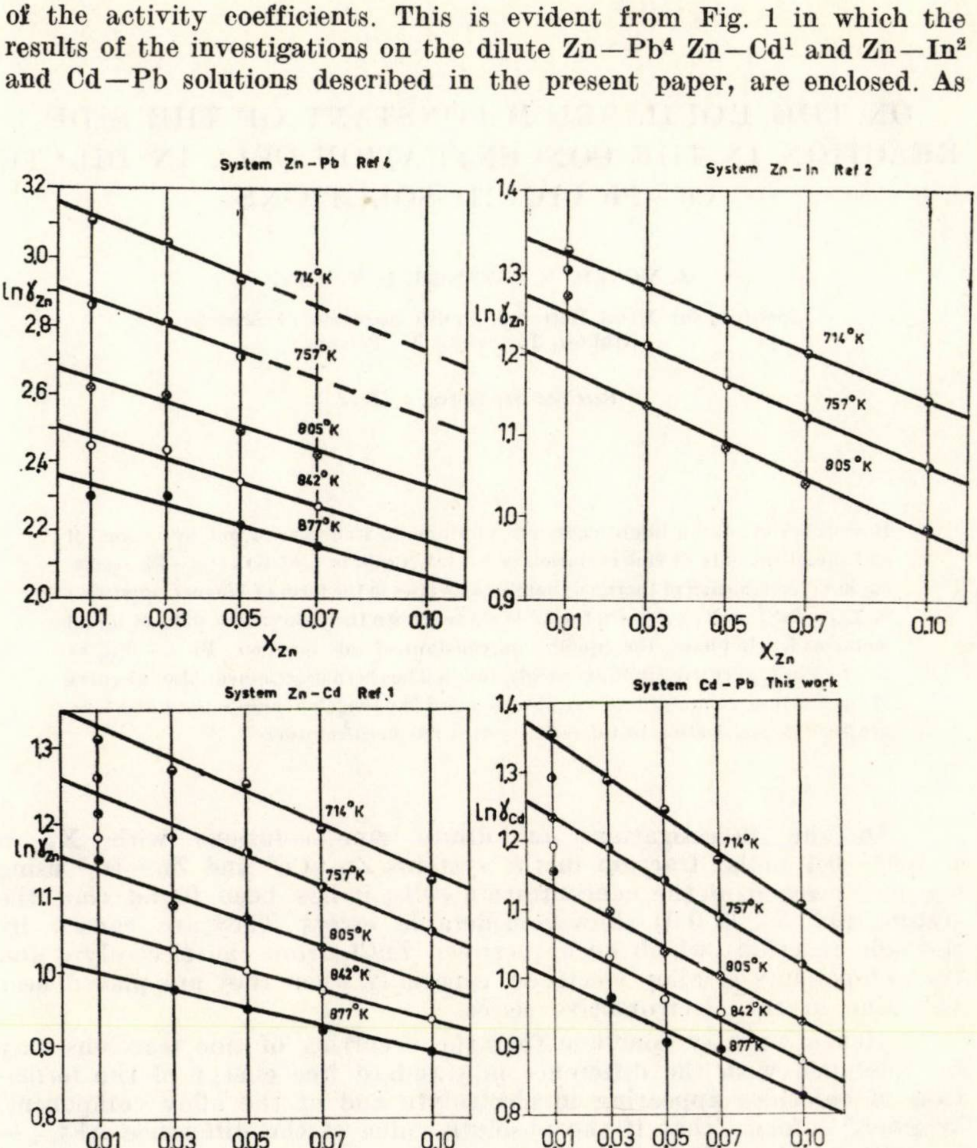

Fig. 1. — Dependence of $\ln \gamma_{Zn}$ *vs* X_{Zn} in the systems Zn—Pb,[4] Zn—Cd,[1] Zn—In[2] and $\ln \gamma_{Cd}$ *vs* X_{Cd} obtained in this paper for Cd—Pb liquid dilute solutions.

can be seen from Fig. 1 only in the investigations on dilute Zn—Pb solutions the side reaction does not affect the experimental results of the electromotive forces.

---

[4] Z. Moser, *Arch. Hutn.*, **4**, 385 (1969).

In paper[5] the side reaction is discussed which occurs in the investigations of zinc-cadmium dilute solutions

$$ZnCl_2 + Cd = Zn + CdCl_2 \tag{1}$$

and the equilibrium constant of this reaction has been determined on the basis of the thermodynamic properties of the dilute Zn–Cd, $ZnCl_2$ and $CdCl_2$ solutions in the eutectic LiCl–KCl.

The present paper discusses the side reaction

$$Pb + CdCl_2 = Cd + PbCl_2 \tag{2}$$

which occurs in the investigations on the dilute solutions of cadmium in lead when applying the method of the electromotive forces of concentration cells as a result of the similar electrochemical properties of cadmium and lead. For this purpose the thermodynamic properties of the dilute Cd–Pb solutions have been determined, which in connection with the previously carried out investigations on the activity of $CdCl_2$[5] and $PbCl_2$[6] in the eutectic LiCl–KCl will help to define the equilibrium constant of the reaction (2) and relate it to the alloy composition and temperature above which this reaction takes place.

THERMODYNAMIC PROPERTIES OF THE DILUTE Cd–Pb SOLUTIONS

Applying the emf method of the concentration cells with liquid electrodes and liquid electrolyte the cells have been arranged according to the following scheme :

$$Cd \mid CdCl_2 \text{ in the eutectic } LiCl - KCl \mid Cd{-}Pb \tag{3}$$

The way of preparing the electrolyte and its dehydration have been described in one of the previous papers.[1,2,4] The purity of the metals used for preparing the alloys was not less than 99.99%. The measurements were made at temperatures from 680–840 K in the concentration range of cadmium $X_{Cd} = 0.01-0.1$ molar fraction. The obtained values of the electromotive forces depending on temperature are shown in Fig. 2. Using the least squares method their mean values have been found, and from the obtained linear equations the values of the electromotive forces at the temperatures : 714, 757, 805, 842 and 877 K have been determined, and these again were used for further calculations. In

---

[5] Z. Moser and K. Fitzner, Paper presented on the 23rd Meeting of International Society of Electrochemistry, Stockholm, 27.8–2.9.1972.

[6] L. Yang and R. Hudson, *Trans. of AIME*, **215**, 589 (1959).

Table 1 are given the linear equations from which the E_{mV} values for the temperatures 714–877 K were calculated, and these were next used to obtain the values of the activity coefficient for cadmium from the dependence

$$\gamma_{Cd} = \frac{1}{X_{Cd}} e^{\frac{-nEF}{RT}} \tag{4}$$

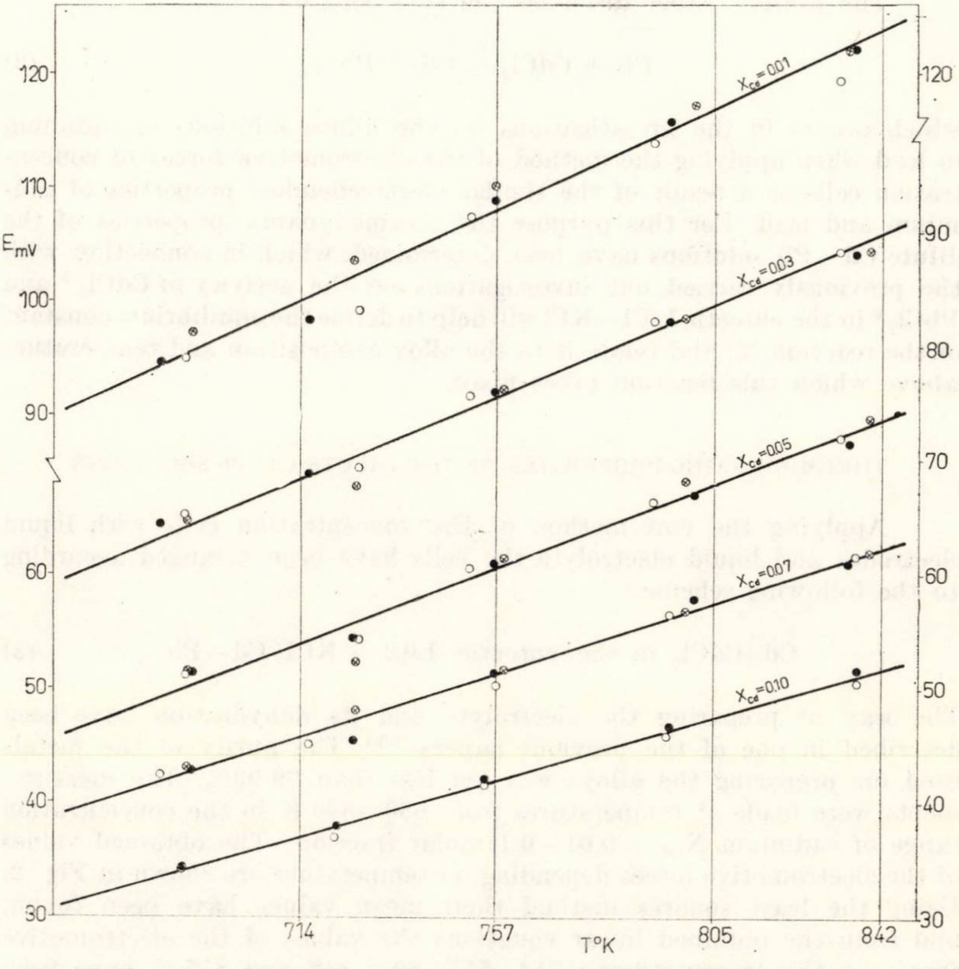

Fig. 2. – Dependence of E_{mV} on temperature in liquid dilute Cd–Pb solutions.

where γ_{Cd} – activity coefficient of cadmium,
X_{Cd} – concentration of cadmium in molar fractions,
n – valence, ($n = 2$),
E – electromotive force,
F – Faraday's constant (23066 cal/volt).

On the basis of the obtained results, a diagram (Fig. 1) showing the dependence of ln γ_{Cd} *vs* X_{Cd} for the temperature range 714–877 K has been plotted. As can be seen from Fig. 1 due to the side reaction (2) higher values of ln γ_{Cd} for $X_{Cd} = 0.01$ are obtained when compared with the results given for the other concentrations, especially at higher temperatures. From the above diagram it is possible to determine the interaction parameters derived by Wagner[7] using the least squares method from the dependence

Table 1

Experimental results in dilute Cd–Pb solutions

X_{Cd}	Linear equations obtained by the least squares method	$\ln\gamma_{Cd}$					$T°K$	$\ln \overset{\circ}{\gamma}_{Cd}$	ε_{Cd}^{Cd}
		714°	757°	805°	842°	877°			
0.01	$E = -32.405 + 0.18544\ T$	1.348	1.236	1.132	1.060	0.998	714	1.376	−2.79
0.03	$E = -52.372 + 0.16900\ T$	1.292	1.187	1.088	1.020	0.960	757	1.261	−2.45
0.05	$E = -55.875 + 0.15375\ T$	1.236	1.138	1.044	0.979	0.922	805	1.155	−2.21
0.07	$E = -46.226 + 0.12882\ T$	1.181	1.090	1.000	0.938	0.884	842	1.081	−2.04
0.10	$E = -45.376 + 0.11531\ T$	1.097	1.016	0.934	0.877	0.827	877	1.017	−1.90

$$\varepsilon_{Cd}^{Cd} = \left(\frac{\partial \ln \gamma_{Cd}}{\partial X_{Cd}}\right)_{X_{Cd}=0} \tag{5}$$

To establish the slope for the temperature 714° the values of ln γ_{Cd} were taken for all concentrations, whereas for all the other temperatures only the values starting from $X_{Cd} = 0.03$. The values ε_{Cd}^{Cd} given in Table 1 were used to establish the dependence of ε_{Cd}^{Cd} on temperature. For this purpose the Fig. 3, ε_{Cd}^{Cd} *vs* $\frac{1}{T}\ 10^3$ was plotted, from which the following relation was derived

$$\varepsilon_{Cd}^{Cd} = -\frac{3273}{T} + 1.827 \tag{6}$$

In a similar way from the limiting values of the activity coefficients $\ln \gamma_{Cd}^{0}$ in Table 1 the dependence on temperature has been established and the following formula obtained

$$\ln \gamma_{Cd}^{0} = \frac{1385}{T} - 0.504 \tag{7}$$

Making use of formulae (6) and (7) it is possible to establish, in accordance with Wagner,[7] relation for the activity coefficient of cadmium in the dilute liquid solutions in lead as a function of the composition of the solution

---

[7] C. Wagner, "Thermodynamic of alloys", Cambridge Massachusets, 1952.

$$\ln \gamma_{Cd} = \ln \gamma^0_{Cd} + X_{Cd}\, \varepsilon^{Cd}_{Cd} \tag{8}$$

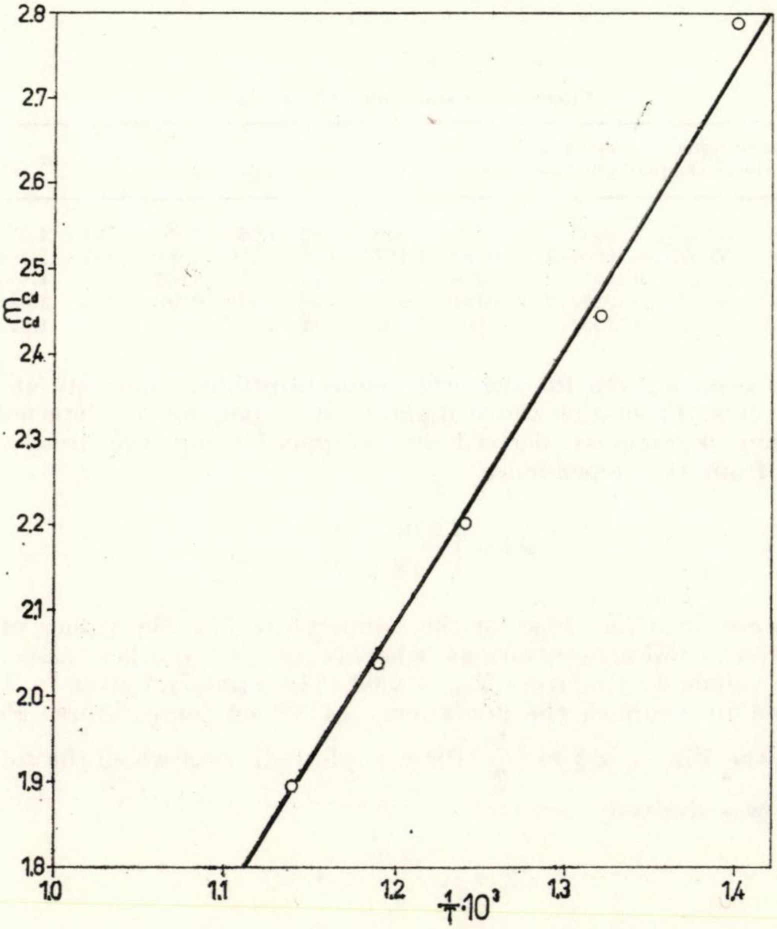

Fig. 3. — Dependence of self-interaction parameter ε^{Cd}_{Cd} *vs* $\frac{1}{T} \cdot 10^3$ in liquid dilute Cd—Pb solutions.

Formula (8) may be successfully applied for the concentration range $X_{Cd} = 0.01-0.1$ molar fraction. To calculate the equilibrium constant of the side reaction (2) the data obtained from Eq. (7) are used.

THE EQUILIBRIUM CONSTANT OF REACTION (2) IN THE CONCENTRATION CELL

The reaction occurring between the lead of the alloy electrode and the cadmium chloride in the salts may be considered from the point of view of the equilibrium between the salt and the metal phase. Considering the fact that both cadmium in lead in the metal phase as well as $CdCl_2$ and $PbCl_2$ in the solution with LiCl–KCl in the salt phase are dilute solutions, the equilibrium constant of reaction (2) may be presented as follows

$$K = \left(\frac{1 - X_{CdCl_2}}{X_{CdCl_2}}\right)\cdot\left(\frac{X_{Cd}}{1 - X_{Cd}}\right)\cdot\frac{\gamma^0_{PbCl_2}}{\gamma^0_{CdCl_2}}\cdot\gamma^0_{Cd} \tag{9}$$

assuming that $X_{CdCl_2} + X_{PbCl_2} \cong 1$; $X_{Cd} + X_{Pb} \cong 1$ and $\gamma_{Pb} \cong 1$. In Eq. (9):

γ^0_{Cd} – limiting activity coefficient of cadmium in lead when $X_{Cd} = 0$,

$\gamma^0_{CdCl_2}$ – limiting activity coefficient of $CdCl_2$ in LiCl – KCl when $X_{CdCl_2} = 0$,

$\gamma^0_{PbCl_2}$ – limiting activity coefficient of $PbCl_2$ in LiCl – KCl when $X_{PbCl_2} = 0$.

When assuming Eq. (9) at the assumption that the metal and the salt phases behave like ideal solutions, the following dependence has been obtained

$$X_{CdCl_2} = \frac{1}{(1 - K) + \dfrac{K}{X_{Cd}}} \tag{10}$$

whereas in the case of real solutions

$$X_{CdCl_2} = \frac{1}{(1 - K') + \dfrac{K'}{X_{Cd}}} \tag{11}$$

$$\text{where}: K' = \left(\frac{K}{\gamma^0_{Cd}}\right)\cdot\left(\frac{\gamma^0_{CdCl_2}}{\gamma^0_{PbCl_2}}\right) \tag{12}$$

what makes possible the calculation of the equilibrium compositions of reaction (2). It follows from Eqs. (10) and (12) that for this purpose it is necessary to know:

1. the equilibrium constant K of reaction (2) which can be calculated from the free energy change ΔF^0_T of the reaction (2),

2. the value γ^0_{Cd}, which can be defined from the thermodynamic properties of the dilute Cd–Pb solutions,

3. the values $\gamma^0_{CdCl_2}$ and $\gamma^0_{PbCl_2}$, which can be defined from the thermodynamic properties of the dilute $CdCl_2$–LiCl–KCl and $PbCl_2$–LiCl–KCl solutions.

THE DETERMINATION OF THE EQUILIBRIUM CONSTANT K

In the previous paper[5] a formula has been derived for the mean value of $E^0_{CdCl_2} = 1.6990 - 0.000599\ T°$. (13)

On the basis of the works by Lorenz and Velde[8], Lantratow andAłabyszew,[9] Wachter and Hildebrandt[10] the mean value of $E^0_{PbCl_2}$ has been established

$$E^0_{PbCl_2} = 1.5766 - 0.000602\ T° \tag{14}$$

The change in the standard free energy ΔF^0_T of reaction (2) can be calculated from the Eq.

$$\Delta F^0_T = -2F(E^0_{PbCl_2} - E^0_{CdCl_2}) \tag{15}$$

which in connection with the known dependence

$$\Delta F^0_T = -RT \ln K$$

allowed to determine the value K of reaction (2) at the temperatures 773, 823 and 873 K.

THE DETERMINATION OF THE $\gamma^0_{PbCl_2}$ and $\gamma^0_{CdCl_2}$ VALUES

In paper,[5] $\gamma^0_{CdCl_2}$ values have been defined by constructing the cells of formation of $CdCl_2$ with chlorine electrode. The activity measurements of $CdCl_2$ carried out in the range of dilute solutions ($X_{CdCl_2} = 0.010 - 0.073$) in the eutectic LiCl—KCl allowed the extrapolation of the values $\ln \gamma_{CdCl_2}$ to $\ln \gamma^0_{CdCl_2}$ when $X_{CdCl_2} = 0$. This was possible due to the linear dependence of $\ln \gamma_{CdCl_2}$ *vs* X_{CdCl_2} obtained for the dilute $CdCl_2$ solutions. Similarly $\gamma^0_{PbCl_2}$ has been defined basing on the work of Yang and Hudson[6] by extrapolating the obtained values of electromotive forces of the cell Pb | $PbCl_2$—LiCl—KCl | Cl_2 to the temperatures 773, 823, 873 K; and next from plots $\ln \gamma_{PbCl_2}$ *vs.* X_{PbCl_2} the dependence of $\ln \gamma^0_{PbCl_2}$ on temperature has been defined by the Eq.

$$\ln \gamma^0_{PbCl_2} = -\frac{175}{T} - 0.655 \tag{16}$$

from which the values of $\gamma^0_{PbCl_2}$ (when $X_{PbCl_2} = 0$) have been obtained.

The corresponding values of γ^0_{Cd} have been calculated from (7). The obtained values are given in Table 2.

---

[8] R. Lorenz and H. Velde, *Z. anorg. Chem.*, **183**, 81 (1929).

[9] M. F. Lantratow and A. F. Ałabyszew, *Zhur. priklad. Khim.*, **3**, 263 (1953).

[10] W. Wachter and J. Hildebrandt, *J. Amer. Chem. Soc.*, **54**, 4655 (1930).

Table 2

The values of equilibrium constant of side reaction (2) and the terms in Eq. (9)

$T° K$	ΔF°_T	K	$\overset{\circ}{\gamma}_{Cd}$	$\overset{\circ}{\gamma}_{CdCl_2} \cdot 10^2$	$\overset{\circ}{\gamma}_{PbCl_2} \cdot 10^2$	K'
773	5716	0.024	3.41	4.54	41.41	0.00078
823	5720	0.030	2.06	5.59	41.98	0.00130
873	5730	0.037	2.78	6.73	42.50	0.00209

Basing on the data given in Table 2 and Eqs. (10), (11) the equilibrium compositions of reaction (2) have been determined and compared with the experimental data obtained by Lorenz, Frenkel and Silberstein [11] and by Jellinek and Hewsky [12]. The comparison is shown in Fig. 4.

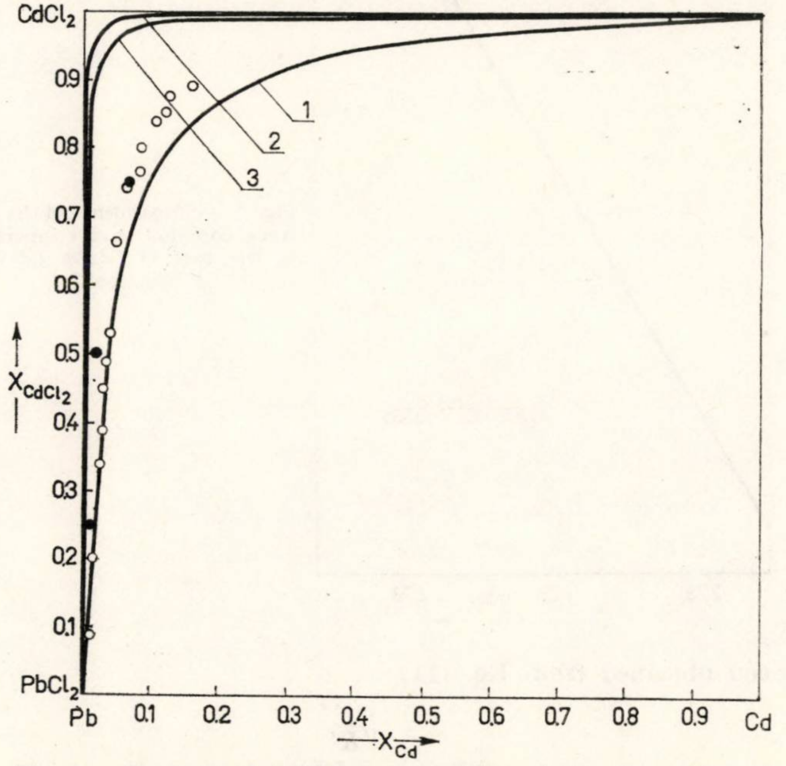

Fig. 4. — The curve of equilibrium compositions of the side reaction (2) in comparison with ideal solutions and the data obtained from literature.

1, correspond to ideal solutions at temperature 873 K; *2*, *3*, correspond to real solutions calculated respectively at temperatures 773 K (line 2) and 873 K (line 3);

○ — data of Lorenz, Frenkel and Silberstein [11] at 873 K,

● — data of Jellinek and Hewsky [12] at 873 K.

---

[11] R. Lorenz, W. Frenkel and F. Silberstein, *Z. anorg. Chem.*, **131**, 247 (1923).

[12] K. Jellinek and D. Hewsky, *Z. Elektrochem.*, **39**, 444 (1933).

Assuming that the beginning of the side reaction in the cell corresponds to a point on the equilibrium curve when

$$\frac{dX_{CdCl_2}}{dX_{Cd}} = 1 \tag{17}$$

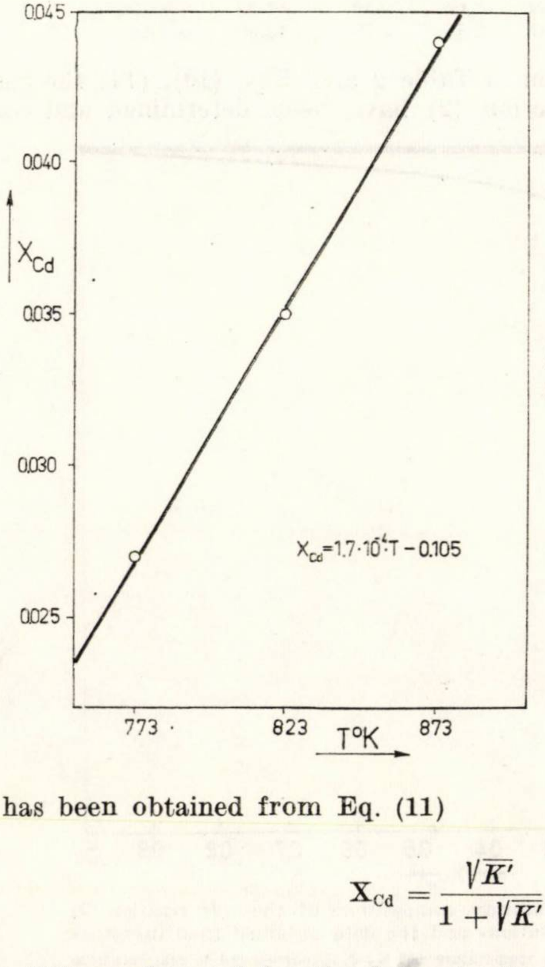

Fig. 5. — Dependence of the electrode composition on temperature in the case of liquid Cd — Pb solutions.

it has been obtained from Eq. (11)

$$X_{Cd} = \frac{\sqrt{K'}}{1+\sqrt{K'}} \tag{18}$$

Eq. (18) can be used for the determination of the composition of alloy electrode depending on temperature. The obtained results are defined by the formula

$$X_{Cd} = 1.7\cdot10^{-4}\cdot T - 0.105 \tag{19}$$

which is plotted in Fig. 5. It is easy to calculate that the composition $X_{Cd} = 0.01$ is attained by the electrode already at 677 K and $X_{Cd} = 0.03$ at 793 K. Fig. 1 confirms the deviation of the points caused by reaction (2) at 757 K for $X_{Cd} = 0.01$ and for $X_{Cd} = 0.03$ at 805 K.

DISCUSSION AND CONCLUSIONS

In the present paper the equilibrium constant of a side reaction occurring in the concentration cell when investigating liquid solutions of cadmium in lead has been defined. It has been found that the condition 7000 cal given by Wagner and the difference between the standard free energy of forming of the respective chlorides is confirmed not only when zinc forms the reference electrode and $ZnCl_2$ is present in electrolyte, but also when investigations deals with cadmium in lead solutions.

A detailed discussion on the subject of applying the metal-salt equilibrium dependences for defining the equilibrium of the side reaction in the cell is to be found in.[5] In reference to the $Cd-Pb-CdCl_2-PbCl_2$ system the identical phenomenon of divergence between the experimental data [11,12] and the curve calculated from (11) is observed. This phenomenon is caused by the presence of the eutectic LiCl$-$KCl when defining the experimental values of $\gamma^0_{CdCl_2}$ and $\gamma^0_{PbCl_2}$. Similarly as in [5] the eutectic is not a neutral medium when the thermodynamic properties of $CdCl_2$ and $PbCl_2$ in the $CdCl_2-LiCl_2-KCl$ and $PbCl_2-LiCl-KCl$ solutions are being determined.

The observed discrepancy between the calculated temperatures at the beginning of the side reaction and the corresponding temperatures resulting from Fig. 2 for the assumed compositions: $X_{Cd} = 0.01$ and $X_{Cd} = 0.03$ is due to the combination of the investigation results carried out independently on the Cd$-$Pb system in the concentration range $X_{Cd} = 0.1-0.9$ and $X_{Cd} = 0.01-0.07$.

When the points for $X_{Cd} = 0.1$ are disregarded and the results obtained only for low concentrations taken into account the agreement is considerably better. This may have some connection with the fact that, in practice, $PbCl_2$ is always formed, though not any amount of it distorts the e.m.f. measurements. Therefore, as the composition of the beginning of the side reaction there should be considered such amount of $PbCl_2$ in the solution which would distort the e.m.f. measurement. For the composition $X_{Cd} = 0.1$ in the solution there is some amount of $PbCl_2$ (Fig. 1), which unavoidably affects the measurement result but does not distort it i.e. reaction (2) does not occur yet. It causes probably the shifting of the points for $X_{Cd} = 0.1$ (Fig. 1) in relation to the points obtained in the concentration range $X_{Cd} = 0.01-0.07$ when the $PbCl_2$ content is increasing. This remark suggests that the formula defining the thermodynamic properties of metal solutions based on the data obtained by the e.m.f. method should be determined on the basis of experimental data from the concentration range $X_{Cd} = 0.9-0.5$, where the amount of the formed $PbCl_2$ is possibly small.

Revue Roumaine de Chimie, 18, 4, 569–573 (1973)

ВЛИЯНИЕ ДОБАВОК И ВОССТАНОВИТЕЛЬНОЙ СРЕДЫ НА ФОРМИРОВАНИЕ ФАЗОВОГО СОСТАВА В КАТАЛИЗАТОРЕ ДЛЯ НИЗКОТЕМПЕРАТУРНОЙ КОНВЕРСИИ ОКИСИ УГЛЕРОДА

П. ПУТАНОВ, Ж. ЙОВАНОВИЧ и Р. ХЕРАК

Технологический факультет Университета, Нови Сад
Институт химии, технологии и металлургии, Белград
Институт ядерных наук « Борис Кидрич », Белград

Получена 26 сентября 1972

Предметом настоящей работы является исследование фазового состава катализатора, к которому с целью улучшения термических свойств добавлены марганец и алюминий. Образцы одинакового основного состава подвергнуты рентгеноструктурному анализу при комнатной температуре и при повышенных температурах, в атмосфере водорода, окиси углерода или их смеси. Полученные результаты показывают, что улучшение активности и термической устойчивости катализатора с добавкой марганца можно объяснить полным восстановлением окиси меди до элементарной меди с повышенной кристалличностью присутствием закиси меди в большом количестве. Присутствие алюминия, который проявляет ингибирующее действие на активность катализаторов, препятствует образованию кристаллических структур основных компонентов, а также восстановлению окиси меди до элементарной меди и закиси меди.

В нашей предыдущей работе [1] показаны результаты рентгенофазового анализа катализатора для низкотемпературной конверсии окиси углерода, синтетизированного в нашей лаборатории, основные компоненты которых показаны последовательно по количественному присутствию: цинк-медь-хром. В отсутствии добавок, при температуре 180—250°, этот катализатор способствует конверсии окиси углерода в выходном газе до 0,2%, но при температурах больше 250° он теряет свою каталитическую активность. Рентгеноструктурным анализом в атмосфере воздуха при комнатной температуре и высокотемпературной рентгеновой дифракцией в атмосфере водорода, окиси углерода и воздуха, мы установили, что образцы этого катализатора, которые отличаются высокой активностью, характеризуются выделением элементарной меди при относительно низких температурах, присутствием закиси меди в измерительных количествах и хорошим формированием кристаллической решетки окиси цинка. После прокалки при температурах свыше 500° в катализаторе этого состава замечено появление цинкохромового шпинеля.

---

[1] P. Putanov, Ž. Jovanović i R. Herak, *Hem. ind.*, *Beograd*, sdano k pečati, 1972.

Задачей этой работы является определение фазового состава катализатора, к которому, с целью улучшения термических свойств, добавляли марганец и алюминий. Наши предыдущие исследования влияния большого числа добавок [2] показали, что окиси этих двух металлов, добавленые одновременным осаждением с основными компонентами, приводят к значительному изменению активности катализатора. Присутствие марганца улучшает каталитическую активность и термическую устойчивость катализатора, в тоже время алюминий проявляет заметное тормозящее действие.

Для утверждения способа действия этих добавок интересным является результат, полученный методом термического анализа [3], где в интервалах температур, при которых каталитическая активность изменялась, происходили фазовые трансформации, зарегистрированные в образцах с добавками и без добавок.

В этой работе использовался метод рентгеноструктурного анализа при комнатной температуре в атмосфере воздуха и рентгеновская дифракция при повышенной температуре в атмосферах водорода и окиси углерода, а также и в их смеси, образцов того же основного состава, к которым добавлены марганец или алюминий в количестве до 0,2%.

Результаты исследования фазового состава при комнатной температуре, до и после активирования образцов с добавками, показаны на рисунках 1 и 2.

На рисунке 1 представлена рентгенограмма образца катализатора с добавкой марганца, который отличается высокой активностью, до 0,2% окиси углерода в выходном газе и хорошей термической устойчивостью до 400°. На рисунке видны пики окислов металлов, представленных в образце до исследования его активности (1) и после исследования активности, [2] при условиях составе газовой смеси, объемной скорости и температуре, которые способствуют промышленному применению. На рисунке 2 показана рентгенограмма образца с добавкой алюминия, который характеризуется значительно меньшей активностью, до 5,2% окиси углерода в выходном газе. И в этом случае рентгенограммы получены при 20° в атмосфере воздуха до [1] и после [2] исследования активности, проведенного в тех же самых условиях, как и в случае исследования катализатора без добавок и с добавками марганца.

Сопоставление рентгенограммы образцов с добавками между собой и с результатами, полученными исследованием без добавок [1], можно отметить полную аналогию разниц в активности и в фазовом составе. Образец с добавкой марганца [1] характеризуется до исследования активности присутствием окиси цинка и окиси меди в кристаллическом виде, а окись хрома находится в аморфном состоянии. После активирования [2] в этом образце, наряду с хорошо формированной решеткой окиси цинка, появляются и четкие дифракционные линии элементарной меди и очень нечеткие и «размытие» линии окиси меди. Эта рентгенограмма отличается от рентгенограммы образца без добавок [1], отсутствием измерительных количеств окиси меди, что указывает на ускорение превращения этой фазы в присутствии добавленного марганца.

---

[2] P. Putanov i Ž. Jovanović, *Bull. soc. chem., Beograd*, **35**, 279 (1970).

[3] P. Putanov, Ž. Jovanović i Bj. Aleksić, *Bull. soc. chem. Beograd*, **35**, 285 (1970).

Катализатор с добавкой алюминия, показан на рисунке 2, имеет до и после активирования фазового состава подобен менее активному катализатору без добавок [1]. До восстановления в этом образце плохо сформирована кристаллическая решетка окиси цинка и окиси меди, а окись хрома в аморфном состоянии; после восстановления появляются очень небольшие количества закиси меди.

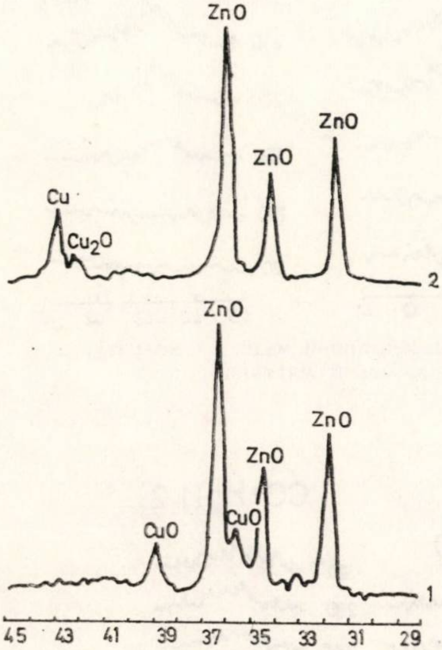

Рис. 1. — Характерные пики рентгенограммы катализатора с добавкой марганца до (1) и после (2) исследования активности.

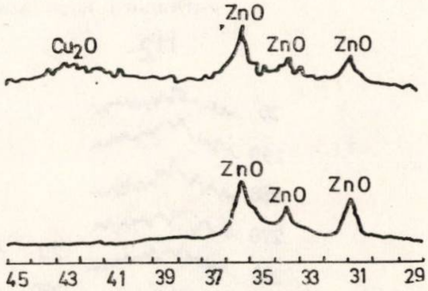

Рис. 2. — Характерные пики рентгенограммы катализатора с добавкой алюминия до (1) и после (2) исследования активности.

Следовательно, улучшение активности и термической устойчивости, которое выражает катализатор с добавкой марганца, можно объяснить выделением элементарной меди с большой степенью кристалличности, присутствием закиси меди в больших количествах и полным восстановлением окиси меди. В присутствии алюминия заметно ограничено формирование кристаллической структуры основных компонентов: окиси цинка и окиси хрома, а также восстановление окиси меди в элементарную медь и закись меди.

Ни у одного из двух образцов с добавками не замечено появление шпинельной структуры в интервале до 400°, марганец и алюминий не могли быть обнаружены, имея в виду чувствительность метода при количествах 2%.

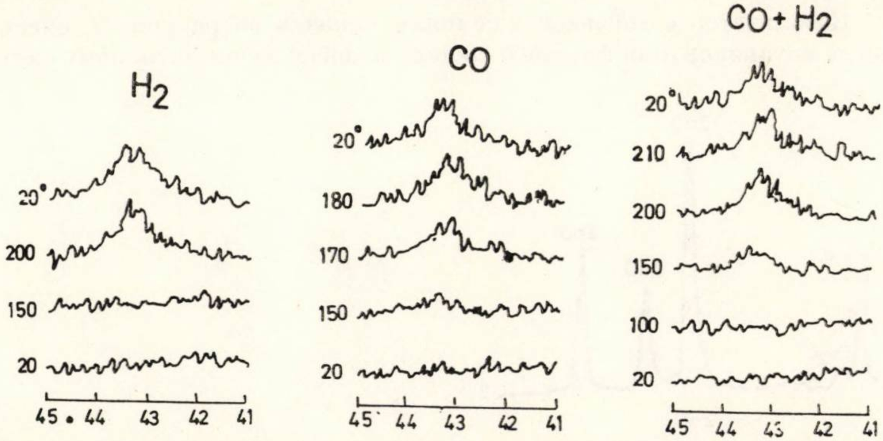

Рис. 3. — Характерные пики появления элементарной меди с температурой у активного катализатора с добавкой марганца.

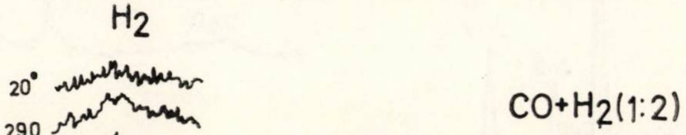

Рис. 4. — Характерные пики появления элементарной меди с температурой у менее активного катализатора с добавкой алюминия.

Результаты исследований влияния температуры на выделение элементарной меди в различных восстановительных средах показаны на рисунках 3 и 4.

На рисунке 3 показаны пики элементарной меди, замеченные с помощью высокотемпературной рентгеновой камеры при исследовании образца с добавкой марганца в атмосферах водорода, окиси углерода и в смеси этих двух газов в соотношении 1 : 1.

Как видно на рисунке, элементарная медь появляется уже при температуре около 170°, независимо от газовой среды. При 200° количество формированной меди значительно, оно потом замечается и на охлажденном катализаторе (20°).

На рисунке 4 показаны аналогические результаты, полученные для образца с добавкой алюминия. У этого катализатора образование меди начинается только при температуре 200°; замечается, что линии очень слабые и размытые. При более высоких температурах (300—400°) во всех образцах замечено появление закиси меди.

Улучшение качеств катализатора с добавкой марганца, которые отражаются как на активность, так и на термическую устойчивость этого образца, можно объяснить влиянием марганца на формирование кристаллической структуры компонентов и полным восстановлением окиси меди в элементарную медь. В тоже время можно сделать вывод, что алюминий в синтетизированном катализаторе препятствует формированию кристаллической структуры основных компонентов, а также формированию активного компонента — элементарной меди, в чем и выражается его ингибирующее действие.

На основании этих фазовых исследований можно заключить, что при синтезе катализаторов для низкотемпературной конверсии окиси углерода водяным паром состава цинк-медь-хром, необходимо добавлять марганец, совместным осаждением с основными компонентами, в качестве промотора.

Revue Roumaine de Chimie, 18, 4, 575–581 (1973)

INVESTIGATION OF SOME PROPERTIES OF THE AMMONIA SYNTHESIS CATALYSTS OBTAINED BY MELTING NATURAL MAGNETITE

BOJANA D. ALEKSIĆ and ANA TERLECKI-BARIČEVIĆ

Institute for Chemistry, Technology and Metallurgy,
Department for Catalysis, Beograd, Yugoslavia

Received September 26, 1972

Within the framework of systematic studying of ammonia synthesis catalyst properties and functions, investigations of correlations between the promotor addition procedure and physico-chemical properties and activity of catalysts obtained by fusion natural magnetite have been conducted. In addition to the determination of structural and textural characteristics of catalysts, measurements of electrical conductivity of unreduced catalysts, to which the same promotors have been added by two different procedures, were performed. Simultaneously, an industrial catalyst of similar type and a natural magnetite without promotors have been investigated. The results obtained have shown that the manner of addition the promotor affects to a large extent the investigated properties and catalyst activity in the reaction of ammonia synthesis.

Under the conditions of ammonia catalyst synthesis by high temperature melting, distribution of promotors in catalysts as well as their phase compositions depend, *inter alia*, on the procedure of promotors addition-sequence of addition, the nature of added promotor compound and relative concentrations of some of promotors.

Within the framework of ammonia synthesis catalyst properties and functions, investigations of correlations between promotor addition procedure and physico-chemical properties and activity of catalysts obtained by melting natural magnetite have been conducted.

EXPERIMENTAL

Natural magnetite from Yugoslav deposits of the "Ibarski rudnici" mine was purified by successive dry and wet separations.

Catalyst samples were synthetized by melting purified natural magnetite in electric-arc vacuum furnace with a wolfram electrode, in argon. [1] After melting the samples were cooled fast.

---

[1] B. D. ALEKSIĆ and Dj. I. MILOSAVLJEVIĆ, "Proceedings of the Ist National Congress on Chemical Engineering", June 1971, Beograd, Yugoslavia, p. 291.

Two different procedures of promotor addition were applied. Following the first, a mixture of magnetite and magnesium oxide powders has been soaked in aluminium nitrate solution, and ammonia hydroxide was added by dropping and permanent mixing; after washing and filtration, the slurry was mixed with lime, dried at 140° and soaked with alcoholic solution of potassium hydroxide; after elimination of alcohol by evaporation in vacuum, the sample was heated for 4 hours at 600° in air, and then subjected to melting. This sample was marked as MB—1.

By the second procedure, promotors under the form of aluminium, calcium and magnesium oxides and potassium carbonate, *p.a.* grade, were added to the powdered magnetite, and before melting, the mixture was homogenized in the rotated mixer for twelve hours. The sample was marked with MB—2.

Sample microstructure was investigated by metallographic microscope. Samples were ground with grinding papers and polished on the cloth with γ-alumina.

Specific surfaces determinations were performed by means of Perkin Elmer Shell, model 212 D, sorptometer.

The pore distribution was determined by the method of mercury porosimetry.

An attempt was made to investigate the distribution of promotors in a catalyst grain, by electron microprobe. Measurements were performed on the device type SEM—2, AEI—Manchester *. Radiations of potassium are detected only.

The electric conductivity changes of the synthetized samples were observed in vacuum, in nitrogen and in air in a temperature range of 100 to 450°. The measurement cycle in different atmosphere was identical for all synthetized samples and it consisted of heating the tablets in vacuum up to 450°, keeping at this temperature until constant resistance had been reached and then cooling with permanent evacuation. This cycle was repeated twice, the resistance being registered at every 50°, then a steam of nitrogen was passed over the tablet cooled to the room temperature and the resistance recorded during heating and cooling. The tablet was then evacuated for 30 minutes and conductivity measured during heating and cooling in air. In all cases the tablet was kept for about 30 minutes at 450° for resistance stabilization.

Within the framework of investigation of changes occurring during melting in natural magnetite as the catalyst base, the electric conductivity of natural magnetite without promotors was measured before and after melting. After outgasing the sample surface and stabilizing its electric conductivity in vacuum, the resistances were measured on heating and cooling in air, the cycle being repeated.

Measurement of catalytic activity, in reaction of ammonia synthesis were performed in the differential reactor at pressure of 280 at, the space velocities of the stoichiometric mixture of hydrogen, nitrogen and 5 % of inert gas being 10, 25 and 50.000 h^{-1} and temperatures up to 550°. Reduction was made *in situ*, with space velocities 25.000 h^{-1}. Granulation of the samples was of 4 — 6 mm, volume of catalyst bed 30 ml **.

RESULTS AND DISCUSSION

In Table 1, chemical compositions of natural magnetite, two synthetized samples and one commercial sample of industrial catalyst used for comparison, are listed.

---

* Measurements were performed at the Institute of Nuclear Sciences, Vinča, Beograd.

** Authors wish to express their thanks to ing. L. Sokol for the catalyst activity measurements in the laboratory of Chemical Works, Zaluži u Mostu, ČSSR.

For its rich content of magnetite fraction the selected magnetite was very convenient as a base for ammonia synthesis catalyst. Sulphur and phosphor being eliminated by evaporation during the melting process, the remaining ingredients in magnetite are in tolerant limits regarding their influence on catalyst activity.[2] The only disadvantage is a somewhat higher content of silica.

Table 1

Chemical composition of natural magnetite and investigated catalyst samples

Component sample	Natural magnetite	MB – 1	MB – 2	Industrial catalyst (D)
Magnetite fraction	96.59	—	—	—
Fe — total	69.40	61.40	63.72	67.89
Fe^{+2}	23.13	24.44	32.21	27.64
Fe^{+2}/Fe^{+3}	0.50	0.66	1.02	0.40
SiO_2	2.54	3.00	2.70	1.30
Al_2O_3	0.20	4.10	3.50	1.82
CaO	none	1.39	1.75	1.36
MgO	0.65	0.81	1.15	0.77
K_2O	—	0.75	1.54	0.32
S	0.60	none	none	none
P_2O_5	0.04	none	none	none
MnO	0.03	—	—	—
Na_2O+K_2O	0.12	—	—	—

According to the chemical analysis results, the conclusion might be drawn that less potassium evaporation from the surface occurred with the melted sample that contained potassium carbonate than with that one in which potassium hydroxide solution was poured.

The different way of promotors deposition on the catalyst surface may have protective effects on the shift of iron oxidation state during melting in an inert atmosphere, which resulted in the difference of Fe^{+2}/Fe^{+3} ratio in the MB-1 and MB-2 samples.

Microstructure of the natural magnetite, melted without promotors and two synthetized catalyst samples, is shown in Fig. 1 (a—c).

Presence of promotors in the MB-1 and MB-2 samples resulted, *inter alia*, in occurrence of finer, more developed dendrites and smaller pores.

Specific surfaces were of order 10^{-1} m²/g for natural magnetite and unreduced samples MB-1 and MB-2, sample granulation being $-1.02 + + 2$ mm, but the results obtained prevented drawing a definite conclusion concerning the dependence of the specific surface on the mode of catalyst synthesis.

---

[2] J. Beneš and J. Šuša *Chem. průmysl.*, 10/35, **9**, 453 (1960).

The cumulative pore volume against pore radius in synthetized samples is shown in Fig. 2. Besides the evident difference in cumulative pore volumes, the size of pores and shape of their relative distribution curves are similar for both samples.

Table 2

Activation energies of electrical conductivity for samples obtained by melting magnetite

Sample	E, eV		
	Vacuum	Nitrogen	Air
MB−1	0.32(100−350°) 0.42(350−450°)	0.25(100−350°) 0.52(350−450°)	0.38(100−200°) 0.68(200−450°)
MB−2	0.29(150−250°) 0.80(250−450°)	0.48(150−300°) 1.22(300−450°)	0.67(150−280°) 1.44(280−450°)
D	0.42(215−300°) 1.10(300−425°)	0.57(215−350°) 1.24(350−425°)	0.41(125−260°) 1.54(260−425°)
Melted magnetite	0.60(200−450°)	0.95(250−450°)	0.61(150−300°) 0.85(300−450°)

Higher porosity of MB-2 sample may be the result of a more effective porous structure regulation during the cooling process in the presence of promotors in the form of powdered oxides.

Distribution of promotors in catalyst grain investigated by electron microprobe is shown in Figs. 3 and 4 (a−b).

On the electronic picture of the chosen part of MB-2 sample surface, shown in Fig. 3, bright surfaces are visible surrounded by dark ones, like a network; inside the bright areas there are dark points corresponding to various concentrations of the promotor in the holes or grain boundaries, concentration of potassium being greater in the dark areas. A cross-section is chosen along which a distribution of potassium K_α radiation was further investigated (Figs. 4a and 4b).

On the basis of the results obtained, conclusions can be drawn that the segregation of potassium takes place in distinct points of grain boundaries in amounts about 8−10 times greater than on the grain surface.

Lg σ dependencies on reciprocal absolute temperature during cooling in various atmospheres obtained for natural magnetite after melting, for two synthetized catalysts on magnetite basis to which promotors were added by different methods (MB-1 and MB-2) and for one commercial sample of industrial catalyst (D), are shown in Fig. 5 (a, b, c and d).

The electric conductivity of all tested samples did not change uniformly with temperature. Two regions with different activation energies were observed. Calculated activation energies for intervals of lg σ linear dependence on $1/T$ in vacuum, nitrogen and air, are shown in Table 2.

Fig. 1. — Optical micrographs of investigated samples unetched, visible light, × 150

a, natural magnetite without promotors after melting; *b*, synthetized sample MB – 1; *c*, synthetized sample MB – 2.

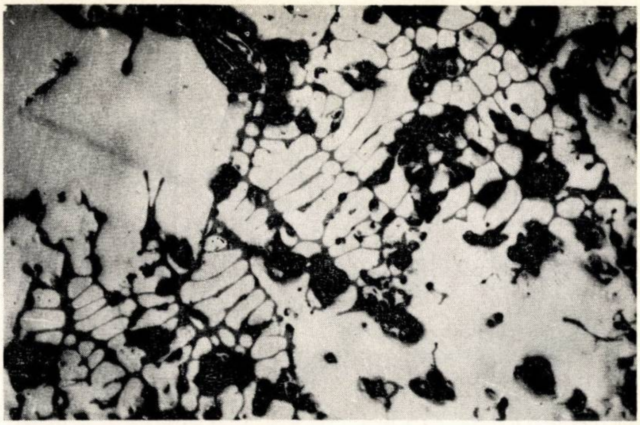

a

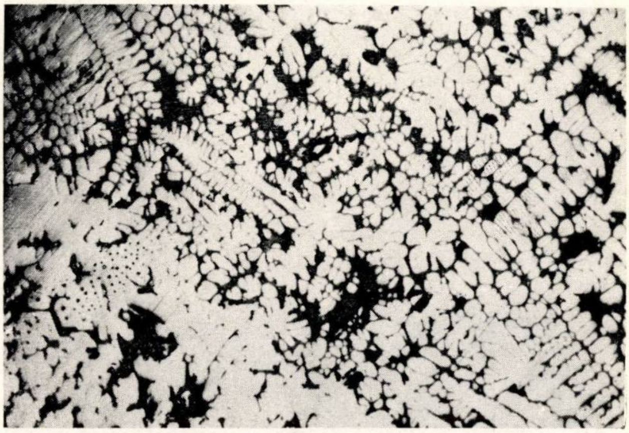

b

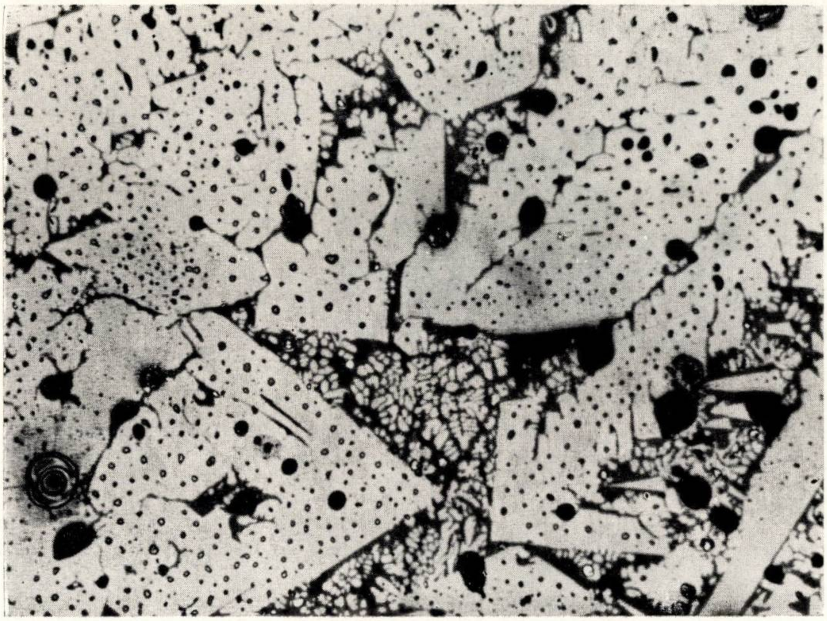

c

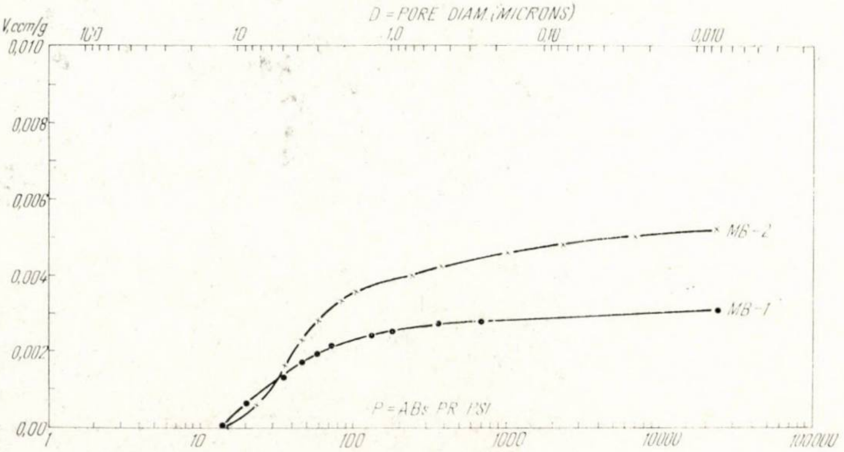

Fig. 2. — Total pore volume distribution *vs* pore radius of unreduced synthetized samples.

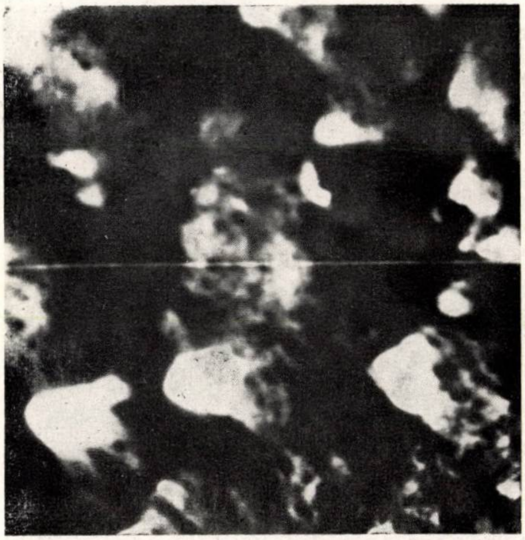

Fig. 3. — Electronic picture of MB—2 surface (with the marked line), × 280.

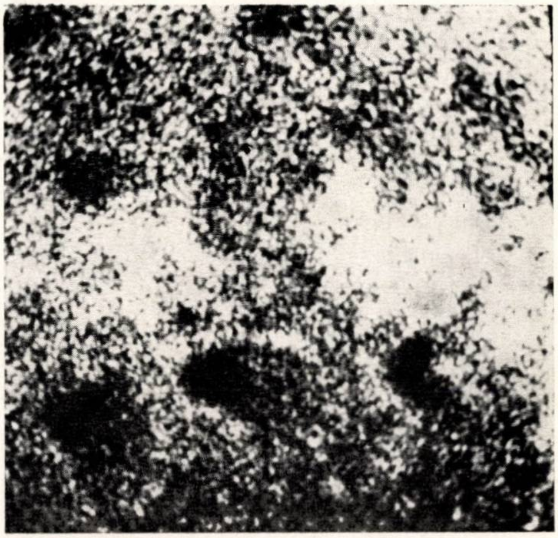

a

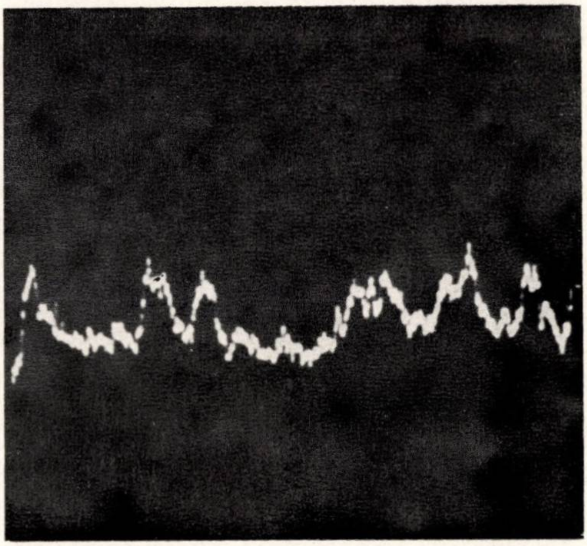

b

Fig. 4. — *a*, Electron microprobe exposure showing distribution of potassium; density of light spots proportional to concentration. b, Relative intensity of K_α radiation of potassium along the line marked on Figs. 3 and 4, proportional to concentration.

Differences in activation energies undoubtedly indicate that in lower temperature intervals predominates conductivity which, according to activation energy, corresponds to the surface conductivity of additives.[3] At higher temperatures, activation of defects in the magnetite mass with more consumption of energy and simultaneous diffusion of these defects over the surface of catalyst, takes place.

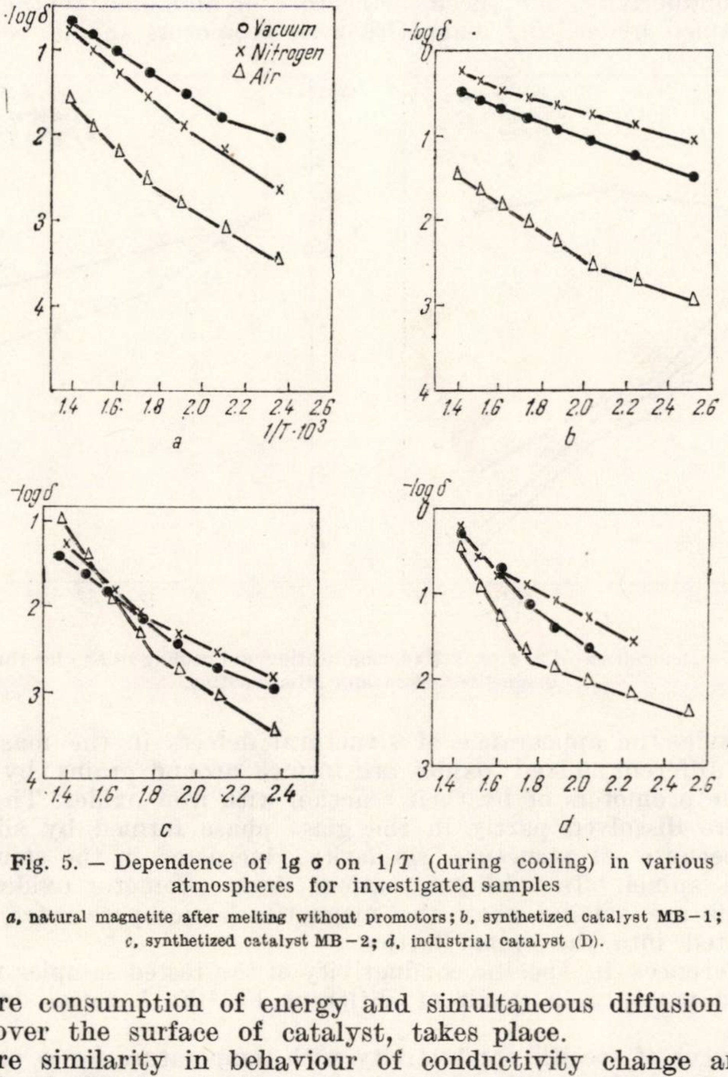

Fig. 5. — Dependence of lg σ on $1/T$ (during cooling) in various atmospheres for investigated samples

a, natural magnetite after melting without promotors; *b*, synthetized catalyst MB – 1; *c*, synthetized catalyst MB – 2; *d*, industrial catalyst (D).

More similarity in behaviour of conductivity change and closer values of calculated activation energies, in the lower and higher temperature intervals for the sample MB-2 and D catalyst, can be ascribed to the effect of similar procedure of promotor addition during catalyst synthesis. The effect was also manifested in higher activation energies in comparison with the MB-1 sample, to which promotors were added in another way.

---

[3] V. I. SPICYN, B. V. EROFEEV and I. V. MIHAJLENKO, *Izvest. Akad. Nauk S.S.S.R. Otdel. khim. Nauk*, **10**, 2117 (1969).

While explaining the effect of the mode of promotor addition on electric conductivity, the specific structure of ammonia synthesis catalysts obtained by melting magnetite with promotors should be kept in mind. Besides the appearance of structural defects in the mass during melting, different mixed oxides are formed around grains by interaction of the promotors or by their reaction with iron oxides. These compounds are dissolved partly in the glass phase formed by silica and, partly, because of structure similarity, incrusted in the structure of magnetite spinel.[4] In addition, cations from promotor oxides, whose ionic radia are smaller than the magnetite lattice parameter, can be incorporated into the spinel lattice.

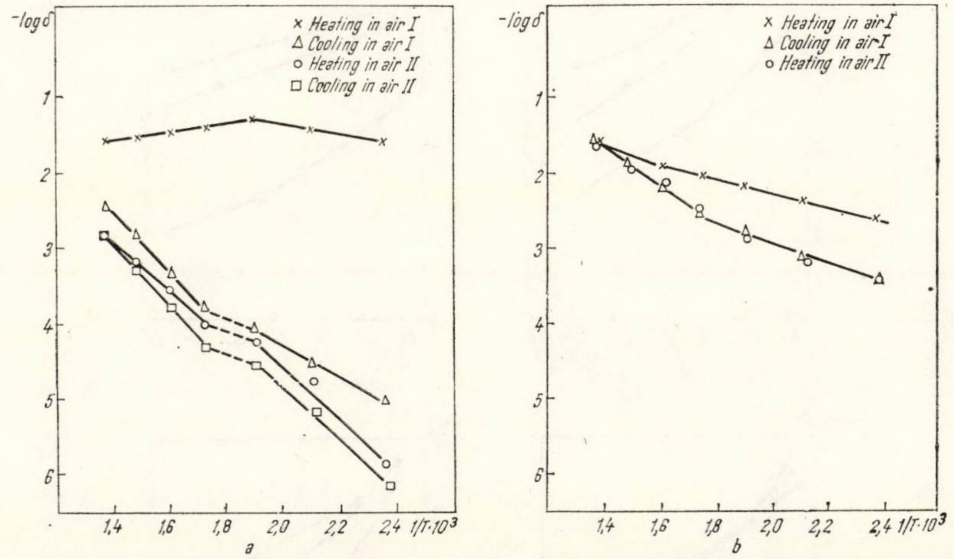

Fig. 6. — Dependence of lg σ on $1/T$ (during heating and cooling in air) for the natural magnetite before and after melting.

Differences in specific conductivity of the tested samples might be considered partly as a result of different Fe^{+2}/Fe^{+3} ratios in melted catalysts.

Changes of specific conductivity with temperature for a nonmelted and melted sample of natural magnetite are shown in Fig. 6.

Nonmelted natural magnetite shows characteristic behaviour of conductivity during heating. The conductivity decrease at temperature over 250°, which is not observed in melted magnetite, may be ascribed to the surface oxidation of magnetite grains, which takes place in air within this temperature range. Comparison of the first and the second cycle of heating in air shows that, in contrast with melted magnetite, the conductivity in the natural magnetite was not stabilized during the first cycle of heating.

---

[4] R. Hosemann, *Chem. Ind. Techn.*, **42**, 21, 1325 (1970).

Activities of synthetized catalysts samples and a commercial sample of industrial catalyst, expressed by rate constant of ammonia synthesis reaction are listed in Table 3.

Table 3

Results of catalyst activity determination. Rate constant, k, of the reaction of ammonia synthesis (for Temkin-equation coefficient $\alpha = 0.75$)

t°C	Catalyst sample		
	MB–1	MB–2	*D*
400	—	0.01	0.05
425	—	—	0.16
450	0.08	0.25	0.48
475	—	0.51	1.38
500	1.11	0.90	3.07
525	—	—	4.95
550	3.76	3.28	6.40

The catalyst activity of the MB–1 sample was somewhat higher as compared to MB–2, which could be expected according to its more favorable Fe^{+2}/Fe^{+3} ratio, as well as to more convenient binding of promotors to the magnetite catalyst base. The lower activity of the synthetized samples in comparison with that one of the most active industrial catalysts, resulted partly from the technology of laboratory sample synthesis which could not completely simulate the industrial catalyst production conditions, and partly from the higher content of silica in natural magnetite.

CONCLUSIONS

Promotors addition procedure has various effects on the investigated physico-chemical, textural and structural properties of unreduced catalysts for ammonia synthesis.

The applied methods have shown that those effects are more pronounced in the microstructure formation, than in the development of the specific surface and in the character of porous structure of unreduced samples.

The mode of promotor addition was reflected on electric conductivity changes and activation energies of conduction in investigated conditions, too.

Results obtained for the catalytic activity of reduced synthetized samples are in agreement with the conclusions concerning the effect of promotor addition procedure on the properties of unreduced catalysts.

Revue Roumaine de Chimie, **18**, *4*, 575–581 (1973)

Revue Roumaine de Chimie. **18**, *4*, 583–588 (1973)

POLAROGRAPHIC BEHAVIOUR OF BISMUTH (III) IN ACID PERCHLORATE SOLUTIONS

C. DRĂGULESCU, ANA NIMARĂ, I. JULEAN and D. MARANDIUC

Chemical Research Center
Bd. Mihai Viteazul 24, Timişoara, Romania

Received November 4, 1972

The polarographic behaviour and the kinetics of Bi (III) reduction in acid solutions, pH 0–2, were investigated. A scheme of the electrode reaction is proposed consisting in the participating of species $BiOH^{2+}$ in the slow stage. The heterogenous rate constant of the electrode process and the activation energy for both waves at different pH were determined.

Kinetics of electrode processes and determination of electroactive species for hydrolyzing metallic ions are complex phenomena.

The great influence exerted by pH on reduction processes of some metals in acid solutions pointed out the importance of hydrolyzed species in these processes.

In order to elucidate the dependence of kinetics of the electrode processes on the pH of the solution, the influence of acidity on reduction rate of bismuth ions have been studied using the dropping mercury electrode and the hanging mercury drop electrode.

Taking into account the great hydrolyzing tendency manifested by bismuth (III) even in acid solution, we thought interesting to study the behaviour of hydrolyzed species in the electrode process.

Polarographic determinations depending on pH show the existence of two waves, that denote the establishment of some equilibria in solution. pH-metric data [1,2] and the spectrophotometric as well cyclic voltametric data [3] show the existence of the following hydrolyzed species within the pH range of 0–2 :

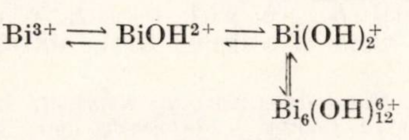

$$\begin{tikzcd} Bi^{3+} \arrow[r, leftrightharpoons] & BiOH^{2+} \arrow[r, leftrightharpoons] & Bi(OH)_2^{+} \arrow[d, leftrightharpoons] \\ & & Bi_6(OH)_{12}^{6+} \end{tikzcd}$$

---

[1] A. Olin, *Acta Chem. Scand.*, **11**, 1445 (1957).

[2] R. S. Tobias, *J. Amer. Chem. Soc.*, **82**, 1070 (1960).

[3] C. Drăgulescu, A. Nimară and I. Julean, *Chem. Analit.*, **17**, 631 (1972).

As to the species reduced on the electrode the conclusions drawn in the literature are still questionable. Losev and Gorodetki[4] consider that at pH 0—2 the reduced species is $BiOH^{2+}$, resulted both through Bi^{3+} hydrolysis and hexamer dissociation.

The later results obtained by Moorhead and Lipscey[5] show that the first wave represents the reduction of both Bi^{3+} and $BiOH^{2+}$, while for the second wave they are ready to accept Goward's hypothesis[6] that this wave is due to the reduction of $Bi(OH)_2^+$ in rapid equilibria with the hexamer $Bi_6(OH)_{12}^{6+}$.

The present work deals with the investigation of the electrode process mechanism in order to obtain information about the nature of reducing species and, indirectly, about the hydrolyzed species existent in the solution. This was obtained by determining the kinetic parameters k^0, αn function of pH, and the temperature — then, out of the rate constant values, the activation energy was determined knowing this to be a direct measure of the energy required by structural changes of the reacting particle.[7]

EXPERIMENTAL

Measurements have been carried on PO4 polarograph and PHM 25 pH-meter.

The capillary had the following characteristics : $h = 58$ cm, $t = 3.5$ s, $m = 2.09$ mgS^{-1} in $HClO_4 + NaClO_4$ 1 M solution, open circuit. A slow cyclic polarization technique was applied using 0.8 V.p.m. potential change rate.

The ionic strength has been maintained constant with sodium perchlorate at 1.0 mol l^{-1}.

RESULTS AND DISCUSSION

Polarographic and cyclic voltametric curves show that the electrode process is irreversible, and that in the process hydrogen ions are taking part, since the half-wave potential becomes more negative with the increase of pH.

The kinetics of the electrode process was followed by analysis according to the method given by Meites and Israel[8] by means of the following relation

$$E = \frac{0.0591}{\alpha n_a} \log \frac{1.349\, k^0 t^{1/2}}{D^{1/2}} - \frac{0.0542}{\alpha n_a} \log \frac{I}{I_d - I}$$

where k^0 is the heterogeneous rate constant of the electrode process at an arbitrary potential $E' = 0$, with respect to the saturated calomel electrode; t is life time of a drop; D, the diffusion constant of the depolarizer ; α, the electron transfer coefficient ; n_a, the number of electrons participating in the slow stage of the process ; I is the maximum current at a potential E and I_d is the diffusion current. From the slope of the plot of E *vs*.log $[I/(I_d - I)]$ the value of αn_a is obtained and the intercept having the meaning of the half-wave potential, yields the constant k^0.

---

[4] V. V. Losev and V. V. Gorodeţki, *Zhur. fiz. Khim.*, **37**, 842 (1963).

[5] E. D. Moorhead and S. Lipscey, *J. Electroanalyt. Chem.*, **26**, 27 (1970).

[6] G. W. Goward, Ph. D. Thesis, Princeton Univ. 1954 conf. *J. Electroanalyt. Chem.*, **26**, 27 (1970).

[7] A. A. Vlcek, *Coll. Czech. Chem. Comm.*, **24**, 3538 (1959).

[8] L. Meites and J. Israel, *J. Amer. Chem. Soc.*, **83**, 4903 (1961).

By the method suggested by Nicholson[9] from cyclic voltammetric curves by means of relation

$$\psi = \gamma K_S / \sqrt{\pi a D}$$

where ψ = kinetic parameter tabulated *vs* experimental ΔE_p

$$\gamma = \left[\frac{Da}{D_R}\right]^{1/2} \cong 1$$

$$a = \frac{nFv}{RT}$$

v = potential change rate V_{sec}^{-1}

Values of rate constants for the two mentioned waves are presented in table 1.

Table 1

Dependence of the heterogeneous rate constant on pH ; $C_{Bi}^{3+} = 1 \cdot 10^{-3}$M 1 M NaClO$_4$; 25°C

pH	First wave		Cyclic voltammetry	Second wave	
	Polarographic			Polarographic	
	k^0	αn	k^0	k^0	αn
0	$4.49 \cdot 10^{-4}$	0.797	$6.5 \cdot 10^{-4}$	—	—
1	$1.39 \cdot 10^{-3}$	0.757	$2.26 \cdot 10^{-3}$	—	—
1.12	$3.76 \cdot 10^{-3}$	1.77	$2.38 \cdot 10^{-3}$	$1.36 \cdot 10^{-4}$	0.786
1.30	$4.56 \cdot 10^{-3}$	1.77	$2.87 \cdot 10^{-3}$	$8.92 \cdot 10^{-5}$	0.786
1.50	$2.22 \cdot 10^{-3}$	1.475	$1.87 \cdot 10^{-3}$	$6.31 \cdot 10^{-5}$	0.786
1.90	$1.49 \cdot 10^{-3}$	1.44	$1.00 \cdot 10^{-3}$	$3.24 \cdot 10^{-5}$	0.786

Data in table 1 show that in the pH range 0—1.3 the increase of pH brings about the increase of the cathodic process rate. This can be accounted for by presuming the existence of a chemical reaction preceding the discharge phase and consisting in Bi^{3+} ions passing into hydrolyzed ions.

The increase of the rate constant with pH confirms the De Maeyer and Kustin's hypothesis[10] by which cation reduction is easier when water molecules in the hydrated shell of the metallic ion are replaced by OH^- ions, which act as a catalyst, accelerating the electron transition between the electrode surface and the particle in discharge.

---

[9] R. S. Nicholson, *Analyt. Chem.*, **37,** 1351 (1965).

[10] L. De Mayer and K. Kustin, *Ann. Rev. Phys. Chem.*, **14,** 12 (1963).

When pH is beyond 1.3, formation of polymeric species $Bi_6(OH)_{12}^{6+}$ takes place in solution and as its concentration increases, the rate constant decreases, probably due to diminution of $BiOH^{2+}$ concentration. For the second wave also a decrease of rate constant is established with increase of pH, then the process irreversibility increases, which is confirmed also by voltammograms shape.

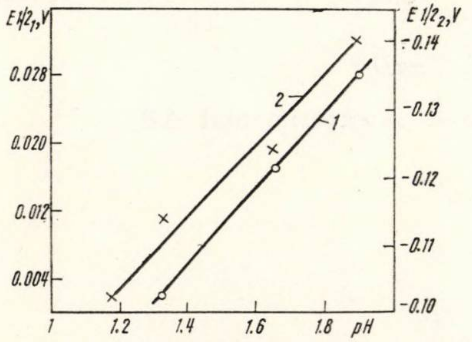

Fig. 1. — The change in the half-wave potential on variation of the pH of the solution. 1.0×10^{-3} M Bi^{3+} ; 1 M $NaClO_4$.

1, First wave; *2*, Second wave.

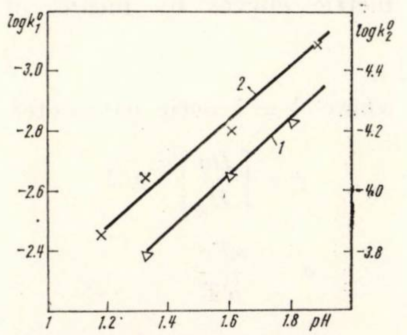

Fig. 2. — The change in the heterogeneous rate constant on pH of the solution. 1.0×10^{-3} M Bi^{3+} ; 1 M $NaClO_4$.

1, First wave; *2*, Second wave.

The change in the half-wave potential and the constant k^0 on variation of the pH of the solution are plotted in figs. 1 and 2 and show that hydrogen ions are participating in the slow stage of the electrode process. By inserting the slopes obtained corresponding to these straight lines into the following relation

$$\frac{\Delta E\,1/2}{\Delta \mathrm{pH}} = \frac{0.0591}{\alpha n_a} \qquad \frac{\log k^0}{\Delta \mathrm{pH}} = \frac{0.0591}{\alpha n_a}\,\mathrm{p}$$

we could determine the number of hydrogen ions that take part in the process, and for both waves, values very close to unity were obtained. This means that in the slow stage of the process only one electron is taking part. The resulting value of $p = 1$ leads to the conclusion that the slow electrode process involves only one hydrogen ion. The probable electrode process is occurring according to the following scheme

$$BiOH^{2+} + H^+ + e^- \rightleftharpoons Bi^{2+} + H_2O$$

$$Bi^{2+} + 2e \rightleftharpoons Bi$$

Taking into account that the rate constant corresponding to the second wave is proportional to $[H^+]^1$ concentration we can presume the species $BiOH^{2+}$ for the second wave to result from reaction

$$Bi(OH)_2^+ + H^+ \rightleftharpoons BiOH^{2+} + H_2O$$

The scheme given above is in a good agreement with the one suggested by Lovrecek and Mekjavic,[11] who from galvanostatic determinations draw the conclusion that the slow stage of the electrode process is represented by the elimination of the first electron.

Confirmation of the above mentioned has been obtained studying the dependence of the rate constant on the temperature at different pH values, corresponding to different hydrolysis stages and determining the activation energy.

For the first wave, determinations were carried out at pH 0 and 1, results being given in figs. 3 and 4.

For a Bi^{3+} solution of pH 0 (fig. 3) it has been ascertained that within the range of 25–35°, the rate constant varies slightly. This being a proof that up to 35° the hydrolysis process develops very slowly. At temperatures higher than 35°, hydrolysis makes progress and consequently rate constant increases. Activation energy, determined from the slope, is of 3.07 kcal/mol for temperatures of 25–35°. This value is close to that of the activation energy for diffusion of metallic ions in water which, according to literature, is about 4 kcal/mol.[12] So, we are entitled to consider that at pH 0, the reduced species is the simple unhydrolyzed Bi^{3+} ion. For the range of 40–50° a value of 17.7 kcal/mo for the activation energy is obtained.

Carrying out the same determinations with a solution of pH 11 (fig. 4), when both Bi^{3+} and $BiOH^{2+}$ are present, it was found that up to 40° the rate constant increases and then remains approximately constant. This shows that over 40° bismuth is totally hydrolyzed, the value of activation energy being also of 17.5 kcal/mol.

The same determinations were carried out for the second wave at pH 1.60. The rate constant increases in this case, also with the increase of the temperature (fig. 5).

Temperature increase causes the two waves to fuse into a single one with a half wave potential of −0.05 V (SCE) that means that under the influence of temperature $Bi(OH)_2^+$ passes into $BiOH^{2+}$, the latter species participating in the reduction process. This is confirmed also by the slope, which gives a value of 17.3 kcal/mol, approximately identical in all the three cases.

---

[11] B. Lovrecek and I. Mekjavic, *Electrochim. Acta*, **14**, 301 (1969).

[12] R. Parsons, "Handbook of electrochemical constants", Butterworths, London, 1959, p. 79.

In conclusion, the study of the mechanism of the electrode process allowed the identification of species formed at bismuth hydrolysis. Bi^{3+} species is present and reduced only in solution with pH=0. At a greater pH than 1 there appear the mononuclear species $BiOH^{2+}$ and $Bi(OH)_2^+$. The latter polymerizing rapidly in hexamer, the reduced species on the electrode being $BiOH^{2+}$. So, these hydrolyzed species behave as a series of successive complex compounds, only one of them being reduced on the electrode.

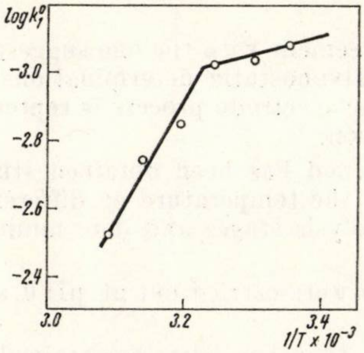

Fig. 3. — Dependence of the rate constant on the temperature at pH 0 (first wave).

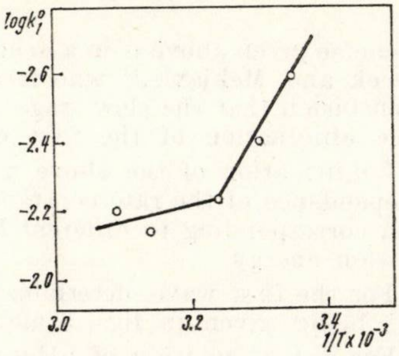

Fig. 4. — Dependence of the rate constant on the temperature at pH 1 (first wave).

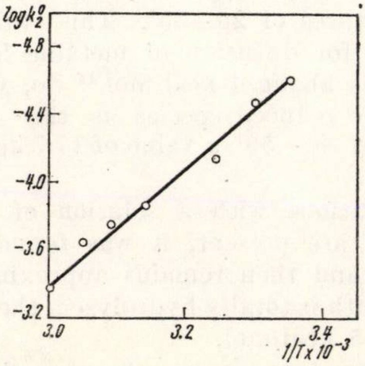

Fig. 5. — Dependence of the rate constant on the temperature at pH 1.60 (second wave).

Revue Roumaine de Chimie, **18**, 4, 589–598 (1973)

NEW COMPOUNDS OF YTTRIUM AND LANTHANIDES WITH N,N'-ETHYLENEDIANTHRANILIC ACID (EDAN)*

P. SPACU and EUGENIA IVAN

Center of Physical Chemistry, Dumbrava Roşie, 23
Bucharest – 9, Romania

Received October 20, 1972

A new series of lanthanide compounds with a ligand containing nitrogen, ethylenedianthranilic acid (EDAN) were prepared. The compounds have the general formula $Ln_2(EDAN)_3$ (Ln = La, Ce, Pr, Nd, Sm, Eu, Gd, Tb, Dy, Ho, Er, Yb and Y) and contain 1 – 2 water molecules. The new synthetized compounds were characterized by their electronic spectra in UV and visible ranges as well as by IR spectra and X-ray Debyegrams which gave informations about their structural formula.

In these last years, the affinity of the lanthanide ions towards a wide variety of donor atoms was intensively investigated. It has been generally observed that the lanthanide ions have a marked preference to form chemical bonds with those ligands containing oxygen as the donor atom.[1]

Nevertheless, the possibility of chemical bond formation with ligands containing nitrogen as donor atom is not excluded. The case of the aminopolycarboxilic acids, whose geometry allows the aliphatic nitrogen atoms be tightly bound to the lanthanide ion and which is invoked by many authors,[2–6] is an example of interaction between nitrogen and the lanthanide ions.

The aim of the present note is to demonstrate the existence of this interaction in the lanthanide complexes containing N,N'-ethylenedianthranilic acid (EDAN) as coordinated ligand.

---

*The present paper was presented at the 3rd National Conference on Pure and Applied Chemical Physics, 3 – 7 September 1972, Bucharest.

[1] G. Schwarzenbach, *Adv. Inorg. Chem. Radiochem.*, **3**, 257 (1961).

[2] L. C. Thompson, *J. Inorg. Nuclear Chem.*, **24**, 1083 (1962).

[3] M. Cefola, *Inorg. Chem.*, **1**, 290 (1962).

[4] Th. Moeller, *Inorg. Chem.*, **1**, 49 (1962).

[5] L. C. Thompson, *Inorg. Chem.*, **2**, 89 (1963).

[6] L. C. Thompson, *Inorg. Chem.*, **3**, 1015, 1319 (1964).

EXPERIMENTAL

REAGENTS

— Lanthanide chlorides and nitrates were prepared from lanthanide oxides (Johnson-Matthey — 99.9% purity, except for Eu_2O_3 — 98%) treated with diluted 1 : 1 hydrochloric acid and nitric acid, respectively.

— N, N′-ethylenedianthranilic acid (EDAN) molecular formula ($C_{16}H_{16}N_2O_4$) was prepared using the modified Frankel and Spero method [7] as well as the Sweet and Harris indications, [8] as follows : 4 moles of methyl anthranilate and 1 mole of ethylenebromide are refluxed for 6 hours at 140—150° on the oil bath. One must take care to keep the indicated temperature interval, otherwise at higher temperatures (over 160°) the products decompose and the reaction yield tends to zero. The product is cooled on ice and treated with 2n HCl to solve the excess of anthranilic acid, the insoluble dianthranilic ester being afterwards crystallized from ethanol as thin needles with mp = **117°**.

The esther is refluxed with 20% alcohol solution of KOH for 12 hours (pH = 8 — 9). The crystallized potassium salt is filtered, solved in water and treated with acetic acid (1 : 10 in water) up to pH=3, when the ethylenedianthranilic acid precipitates. The recrystallization is made from a 20% KOH alcohol solution (1 : 4 alcohol and water, respectively) by precipitation with acetic acid. Its melting point is 222—223°.

SYNTHESIS OF LANTHANIDE COMPOUNDS

4.5 g of EDAN are solved in 50 ml 2N NH_4OH, slightly heated to remove the excess of ammonia, diluted in 200 ml of water and then filtered. Alcohol is added to the filtrate up to 500 ml, to obtain a 0.03 M (pH = 7.5) solution. The lanthanides and yttrium react quantitatively with EDAN in the following way : 0.01 M (pH = 4.5—5) solution of lanthanide chloride is precipitated by the reagent prepared as shown above. One must take care that a slight excess of cation solution should be present, to assure the complete reaction. The precipitates are immediately formed in a few minutes at the room temperature, the pH being maintained at 5. The solid products are left to stay for 24 hours, then filtered, washed with water and absolute ethanol and dried in the air at the room temperature.

ELEMENTAL ANALYSIS

The lanthanide elements were estimated from their oxides obtained by the direct combustion of the compounds. Nitrogen, carbon and hydrogen were determined by microanalysis. The results of the chemical analysis are given in table 1.

The electronic spectra in UV were recorded for EDAN and all its synthetized compounds in 10^{-4} M absolute methanol or DMF solutions, as well as by reflectance on the solid state in MgO pellets (1 : 10 or 1 : 20). The absorption in the visible range was determined as reflectance spectra only for all the compounds obtained, as well as for hexahydrated lanthanide nitrates taken as standards.

---

[7] J. Frankel and K. Spero, Ber. dtsch. chem. Ges., **28**, 1686 (1895).

[8] R. Sweet and F. Harris, *J. Phys. Chem.*, **61**, 694 (1957).

Table 1

The results of the chemical analysis

Compound	Ln %		N%		C%		H%	
	Calc.	*Found*	*Calc.*	*Found*	*Calc.*	*Found*	*Calc.*	*Found*
$La_2.EDAN_3.H_2O$	23.33	23.40	7.06	6.95	48.42	47.86	3.72	4.26
$Ce_2.EDAN_3.2H_2O$	23.14	23.11	6.94	6.73	47.60	46.80	3.83	4.08
$Pr_2.EDAN_3.2H_2O$	23.24	23.18	6.93	6.91	47.54	46.62	3.82	4.56
$Nd_2.EDAN_3.2H_2O$	23.66	23.61	6.89	6.75	47.28	46.49	3.80	4.41
$Sm_2.EDAN_3.2H_2O$	24.42	24.45	6.82	6.91	46.81	46.30	3.76	4.52
$Eu_2.EDAN_3.H_2O$	24.98	25.04	6.91	6.87	47.38	46.14	3.64	4.38
$Gd_2.EDAN_3.2H_2O$	25.25	25.17	6.75	6.74	46.29	45.05	3.72	4.32
$Tb_2.EDAN_3.H_2O$	25.83	25.61	6.83	6.73	46.84	45.44	3.60	4.57
$Dy_2.EDAN_3.H_2O$	26.26	26.33	6.79	6.76	46.57	45.03	3.42	4.21
$Ho_2.EDAN_3.H_2O$	26.54	26.51	6.76	6.89	46.39	45.21	3.57	4.30
$Er_2.EDAN_3.2H_2O$	26.44	26.40	6.64	6.73	45.56	44.30	3.66	4.37
$Yb_2.EDAN_3.H_2O$	27.49	27.47	6.67	6.51	45.79	44.83	3.52	4.12
$Y_2.EDAN_3.H_2O$	16.30	16.51	7.71	7.66	52.85	51.90	4.07	4.89

The spectral measurements on solutions were carried out using a Zeiss VSU–2 spectrophotometer and those on the solid state using a Zeiss VSU–1 spectrophotometer with the corresponding attached reflectance device.

IR spectra were recorded for the solid EDAN and neodymium compound using pellets of KBr in suitable dilutions.

The IR spectra within 4 000 – 400 cm^{-1} range were recorded using a UR–10 spectrophotometer.

X – Ray Debyegrams were recorded on powders by means of the Debye-Scherrer method for EDAN and all synthetized compounds, using a TUR–M 60 equipment and the following radiations and filters :

– Cr $K\alpha_1$ ($\lambda = 2.28962$ Å) radiation and V filter for La, Ce, Pr, Nd compounds ;

– Fe $K\alpha_1$ ($\lambda = 1.93597$ Å) radiation and Mn filter for the Sm compound ;

– Co $K\alpha_1$ ($\lambda = 1.78892$ Å) radiation and Fe filter for Eu and Gd compounds ;

– Ni $K\alpha_1$ ($\lambda = 1.65784$ Å) radiation and Co filter for Tb and Dy compounds ;

– Cu $K\alpha_1$ ($\lambda = 1.54051$ Å) radiation and Ni filter for EDAN and Y, Ho, Er and Yb compounds.

The films were recorded using a microphotometer with photocell Carl Zeiss with automatic recording.

The diffractograms for EDAN and ytterbium compound were recorded using a HZG–1 (DDR) diffractometer, $CuK\alpha_1$ radiation and Ni filter. θ angles were transformed into d(Å) using the A. J. Rose standard tables.

RESULTS AND DISCUSSION

As results from the chemical analysis (table 1), the chemical formula of the synthetized compounds corresponds to $2Ln.3EDAN.nH_2O$ ($n = 1, 2$). The presence of water in such compounds influences the analytical results, especially the data concerning carbon and hydrogen, as happens in the case of the metal compounds containing aminobenzoic acids with substituted rings.[9] Usually, the water molecules are inserted within the crystalline lattice, the complexes occasionally containing one or more moles of water.

All the synthetized compounds are solid and very stable, their melting points being over 300°. Except the europium compound which is intense yellow-coloured, all the compounds of the lanthanides series are cream-coloured.

The solubility of these compounds is reduced and it does not exceed 10^{-4} M for the majority of ordinary organic solvents : ethanol, methanol, acetone, acetophenone, dioxane, chloroform, benzene, carbontetrachloride, methyl ethylcetone and no more than 10^{-3} M in dimethylformamide or dimethylsulfoxide. The insolubility of the synthetized compounds makes difficult the recording of the absorption spectra on solutions. Like the bisanthranilates of bivalent metals,[10] the scarce solubility in different solvents, a polymeric structure could be proposed in our compounds.

The absorption electronic spectra in UV of all the new compounds are similar to each other, either in shape or intensity log ε (solution) or 100-R (solid).

Fig. 1 shows, for this reason, the absorption spectra of EDAN and its compounds with La and Yb only, recorded on solutions of 10^{-4} M in methanol and DMF. Fig. 2 shows the same spectra recorded on the solid state, using pellets of MgO at the ratio 1 : 20. For other compounds, the two absorption spectra are summarized in table 2.

The absorption maxima occurring in the UV range are ascribed to the π electron system of the ligand.

As may be seen in figs. 1–2, EDAN presents the same absorption curve both in absolute methanol or DMF, while the corresponding absorption maxima of the compounds have exactly the same position in both solvents, but in DMF a marked increase in their intensity should be observed.

The reflectance spectra have the same two absorption maxima shifted with 10–15 nm towards higher wavenumbers, the shifts being probably due to the interaction between ligand (compound) and the crystalline lattice. The almost perfect identity between the absorption spectra recorded for the solid state and solution would indicate the lack of any structural changes of the compounds in solution or solid state.

---

[9] J. S. Decker and Frye Herchel, *Z. Naturforsch*, **21**, 522 (1966).

[10] S. Sandhu, S. Manhas, R. Mittal and S. Parnar, *Indian J. Chem.*, **7** 1051 (1969).

As may be seen in table 2, the absorption maxima of the coordinated ligand occurring in the reflectance or solution spectra are shifted towards higher wave numbers if they compared with those of the free ligand.

The shift of the maximum appearing at 260 nm is small (~5 nm), but nevertheless it becomes evident for heavier lanthanide ions. The other shift of the absorption maximum at 350 nm is more pronounced (10—12 nm) and it is maintained in all the series of compounds. The bandshifts mentioned above could be ascribed to the interruption of the "π" conjugation between the carboxylic group and the phenyl ring, as a consequence of nonplanarity between them, caused by the coordination requirements. The above assumption agrees with the chemical results and the X-Ray data which would indicate a polymeric structure.

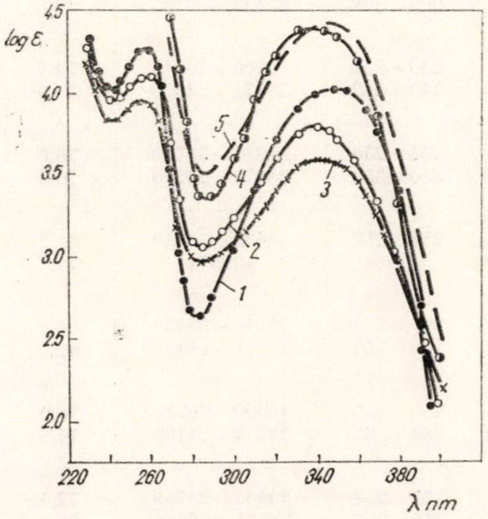

Fig. 1. — Absorption spectra in UV of 10^{-4} M solution.

1, EDAN in methanol and DMF
2, $La_2EDAN_3.H_2O$ } in methanol
3, $Yb_2EDAN_3.H_2O$
4, $La_2EDAN_3.H_2O$ } in DMF
5, $Yb_2EDAN_3.H_2O$

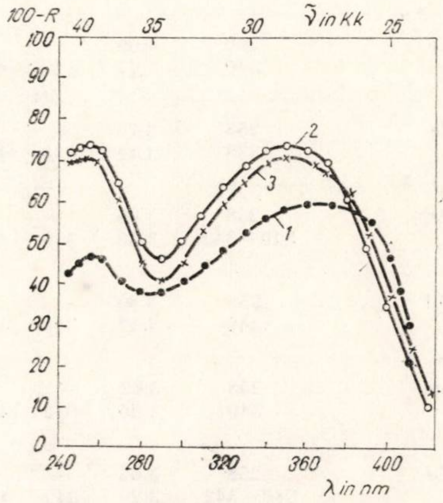

Fig. 2. — Reflexion spectra in UV in 1 : 20 dilution with MgO for :

1, EDAN
2, $La_2EDAN_3.H_2O$
3, $Yb_2EDAN_3.H_2O$

As far as the electronic spectra are concerned, the absorption bands occurring in the visible range could be assigned to the internal transitions between the spectral terms of the central metal ion.

The absorption bands of ethylendianthranilates with Pr, Nd, Dy, Ho and Er have been compared with the maxima occurring in the corresponding hexahydrated nitrates taken as reference.

As may be observed from table 3 the almost all absorption bands are shifted towards smaller wavenumbers (red shift).

Table 2

The maximum of absorption for EDAN and $Ln_2 \cdot EDAN_3 \cdot nH_2O$ compounds

Compound	Solutions 10^{-4} M				Solid state		
	Methanol		DMF		λnm	$\bar{\nu}$ cm^{-1}	100 − R
	λnm	lgε	λnm	lg ε			
EDAN	260	4.28	—	—	258	38759	46.5
	349	4.03	349	4.0	366 − 368	27322 − 27133	59.5
La	260	4.09	—		250 − 255	40000 − 39215	72.5
	340	3.77	340	4.40	350 − 352	28571 − 28409	73.0
Ce	258	3.76	—		255 − 258	39215 − 38759	76.0
	338	3.42	340	4.43	350 − 354	28571 − 28248	76.5
Pr	258	3.66	—		252 − 257	39682 − 38910	81.0
	340 − 342	3.30	340	4.43	350	28571	79.0
Nd	258	3.80	—		255 − 258	39215 − 38759	81.5
	340	3.42	340	4.44	350 − 355	28571 − 28169	82.0
Sm	258	3.62	—		250 − 255	40000 − 39215	76.0
	340	3.25	342	4.44	354 − 355	28248 − 28169	75.5
Eu	258	3.62	—		252 − 258	39682 − 38759	77.5
	340 − 342	3.29	342	4.41	350 − 355	28571 − 28169	76.0
Gd	260	3.70	—		255	39215	67.5
	340	3.36	342	4.42	352 − 354	28409 − 28248	69.1
Tb	256	3.71	—		254 − 256	39370 − 39062	65.5
	340	3.36	342	4.40	354	28248	66.8
Dy	255	3.67	—		253 − 257	39525 − 38910	72.5
	342	3.31	342	4.41	350 − 356	28571 − 28089	73.5
Ho	256	3.77	—		250 − 257	40000 − 38910	67.0
	342	3.44	342	4.41	352 − 355	28409 − 28169	68.8
Er	256	3.77	—		255 − 258	39215 − 38759	73.5
	342	3.43	342	4.42	350 − 356	28571 − 28089	75.0
Yb	256	3.95	—		253 − 257	39525 − 38910	70.0
	342 − 344	3.61	344	4.43	354 − 355	28248 − 28169	71.0
Y	256	3.84	—		256 − 257	39062 − 38910	68.8
	342	3.50	342	4.41	354 − 355	28248 − 28169	71.0

The shifts were used to evaluate the mean covalency degree of the chemical bonds by means of the formula :

$$\delta' = \frac{1-\beta'}{\beta'} \cdot 100,^{11} \text{ where } \beta' - \text{is the nephelauxetic ratio,}$$

$$\beta' = \frac{\beta_{\text{complex}}}{\beta_{\text{aquo ion}}} = \frac{\tilde{\nu}_{\text{complex}}}{\tilde{\nu}_{\text{aquo ion}}}, \text{ and } \tilde{\nu}$$

are the wavenumbers of the same transition in the aquo ion taken as standard and complex.

The quantity δ′ represents a measure of the covalency degree of the metal-ligand chemical bond.

Table 3

The electronic spectra in visible range

Excitet state	$\bar{\nu}_{aq}$ cm^{-1}	$\bar{\nu}_c$ cm^{-1}	β′	δ′
Pr_2. $EDAN_3.2H_2O$				
${}^3P_2$	22675	22522	0.99325	0.68
${}^3P_1$	21459	21276	0.99147	0.86
${}^3P_0$	20833	20746	0.99582	0.42
${}^1D_2$	17006	16949	0.99664	0.34
$Nd_2.EDAN_3.2H_2O$				
${}^4G_{9/2}$	19723	19607	0.99411	0.59
${}^4G_{7/2}$, ${}^2K_{13/2}$	19230	19138	0.99521	0.48
${}^4G_{5/2}$, ${}^2G_{7/2}$	17391	17241	0.99137	0.87
${}^4I_{9/2} \rightarrow {}^4F_{5/2}$ ${}^2H_{9/2}$	14925	14814	0.99256	0.75
${}^4F_{5/2}$ ${}^4S_{3/2}$	13698	13605	0.99321	0.68
${}^2H_{9/2}$ ${}^4F_{5/2}$	12738	12658	0.99371	0.63
$Dy_2.EDAN_3.H_2O$	13333	13333	1	0
$Ho_2.EDAN_3.H_2O$				
${}^5F_1$	22271	22222	0.99779	0.22
${}^5F_3$	20790	20746	0.99788	0.21
${}^5F_4$	18691	18691	1	0
$Er_2.EDAN_3.2H_2O$				
${}^4F_{7/2}$	20661	20576	0.99588	0.41
${}^2H_{11/2}$	19305	19230	0.99611	0.39
	12738	12658	0.99371	0.63

The assignments of spectral terms were made consulting the literature. [12,13]

As may be seen from table 3, the δ′ parameter assumes positive values for the majority of absorption bands, which indicates that the chemical bonds, with the oxygen atoms of carboxylic groups are more covalent than those with the water molecules.

---

[11] S. P. Sinha, *Spectrochim. Acta*, **22**, 57 (1966).

[12] N. K. Dutt and S. Gupta *J. Inorg. Nuclear Chem*, **33**, 4188 (1971).

[13] T. H. Siddall and N. E. Stewart, *J. Inorg. Nuclear Chem.*, **32**, 1147 (1970).

It should be mentioned that the bands are differently shifted, and hence different δ' are estimated. This could be explained by the fact that the "*f*" orbitals are differently involved in the chemical bonding, function of the stereochemistry of the complex.

It should be also noted that the covalency degree δ' assumes higher values for Pr(f^2) and Nd (f^3), lower for Er (f^{11}), zero or negative values for Dy(f^9) or Ho(f^{10}) ethylenedianthranilates.

This fact should be explained by the lowering of the bond covalency due to the gradual filling with electrons of the "*f*" orbitals, which renders difficult the possibility of their participation to the chemical bond formation. The IR spectra of EDAN and its compounds with lanthanides were analyzed comparing to vibration frequencies characteristic to the groups able to coordinate. The assignment was empirically made using the data [14,15] for similar amino acids.

The intensity changes of the carboxylic and CN frequencies going from the free ligand to the coordinated one constitute an obvious indication of complex formation. If the vibration frequency which occurs at 1670 – 1650 cm^{-1} is characteristic for the anthranilic acids with internal hydrogen bonds, the frequencies at 1610 and 1555 cm^{-1} in neodymium compound correspond to the antisymmetric vibrations of the ionized carboxylic group. Moreover, the vibration $\nu_{C=O}$ of the unionized carboxylic group does not occur in the IR spectra of the compound. The existence of these changes proves the coordination of carboxylic groups to the lanthanide ion.

The intense and narrow band at 1420 cm^{-1} has been ascribed to the symmetric vibration ν_S(CCN) of the aliphatic group, moved by coordination at 1400–1395 cm^{-1}, and at the same time increased in intensity, due to the presence in the same region of the symmetric vibration of COO$^-$.

Besides oxygen coordination, the changes in the C–N frequencies prove also the nitrogen coordination to the central metal ion.

The vibration characteristic to the NH group appears in EDAN as a narrow and intense band at 3375 cm^{-1} and in the coordination compounds at 3370–3340 cm^{-1}, broadened (due probably to the polymeric associations by the intermolecular hydrogen bonds).

The X-ray diffraction for EDAN leads to similar Debyegrams and diffractograms. Table 4 shows the d expressed in [Å] for the main diffraction lines of diffractograms.

The röentgenograms recorded for all the synthetized ethylenedianthranilates do not present any diffraction line, proving the amorphous state and high molecular weight.

The Debyegrams recorded for La, Ce, Pr, Nd, Sm, Eu, Gd, Dy, Er, Yb and Y compounds present two halos within 1.5–2.5 [Å] and 2.5–6.3 [Å]. The first halo is less obvious for the first lanthanides but

---

[14] L. J. BELLAMY, "The infrared spectra of complex molecules", London Methuen et Co. Ltd. New York, John Wiley et sons, INC, 1959.

[15] K. NAKAMOTO, "Infrared spectra of inorganic and coordination compounds", John Wiley et sons. INC, New York, Izdatelsvo "Mir" — Moscova 1966.

Table 4

The main diffraction lines for EDAN

d [Å]	I/I_0	d [Å]	I/I_0
6.35	52.5	3.61	92.0
6.03	17.0	3.58	100.0
5.32	15.0	3.46	52.0
4.96	37.0	2.95	50.5
4.76	22.5	2.79	35.0
4.53	77.5	2.74	17.0
4.16	32.5	2.67	12.0
3.92	67.5	1.78	17.0

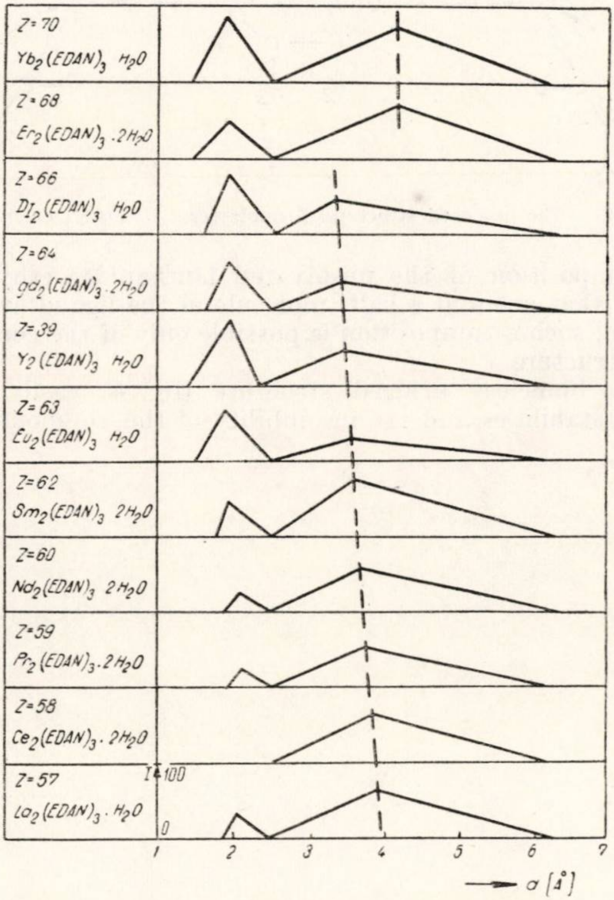

Fig. 3. – Debyegrams of $Ln_2EDAN_3.nH_2O$ compounds.

increases in intensity for heavier ones. The maximum of the second halo at 3.4–4.2 [Å] varies linearly with *Z* in the sequences La–Dy (including *Y*) and Er–Yb, as shown in figure 3.

Like the organic polymers, the halo-shape of the diffraction effects appearing in Debyegrams shows the amorphous and polymeric structure of the synthetized compounds, different from the roëntgenograms of the former lanthanides salts and original EDAN.

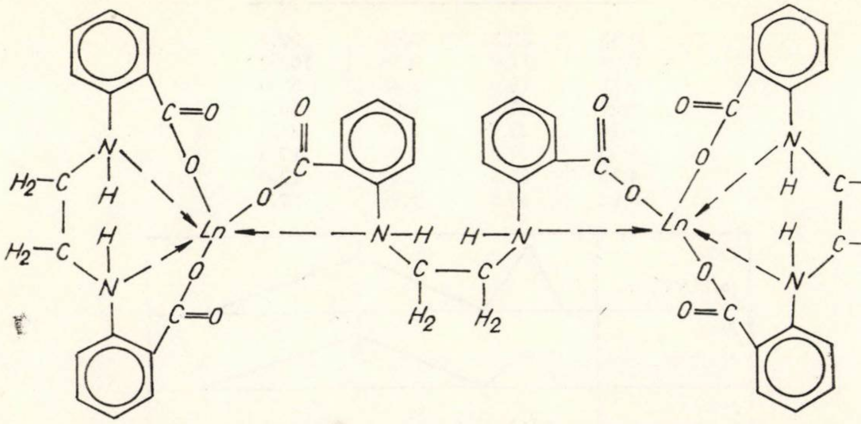

Fig. 4. – The proposed structural formula for Ln_2EDAN_3 compounds.

The composition of the unsolvated lanthanides ethylenedianthranilates shows that one and a half molecule of the ligand are attached to a metal atom; such a composition is possible only if the compounds have a dimeric structure.

Such a binuclear bridged structure (fig. 4) easily explains the high thermal stabilities and the insolubility of the compounds in organic solvents.

Revue Roumaine de Chimie, 18, 4, 599 - 608 (1973)

CONTRIBUTIONS TO THE STUDY OF LANTHANIDES WITH BIGUANIDE DERIVATIVES. V[1-4]

LANTHANIDE COMPOUNDS WITH HYDROCHLORIC PALUDRINE

ILEANA ALBESCU

Center of Physical Chemistry, str. Dumbrava Roşie 23,
Bucharest, Romania

Received September 28, 1972

The present paper describes the syntheses used to obtain some new compounds of lanthanides with hydrochloric paludrine, pald. HCl, compounds of the type: $(\text{pald. HCl})_n\ \text{LnCl}_3$, where $\text{Ln} = \text{Nd}-\text{Y}_b$. The new combinations were structurally characterized by means of their electronic absorption spectra.

In the previous papers [1-4] we have studied the effect of paludrine basis upon the lanthanide halides. Later on we directed our works also on the hydrochloric paludrine, pald. HCl, and on the thiocyanic paludrine, pald. HSCN, in order to obtain new types of combinations.

The aim of the present paper is the study of the systems:

$$\text{pald HCl}-\text{LnCl}_3 \qquad \text{Ln} = \text{Nd} - \text{Yb}$$

$$\text{and} \quad \text{pald HSCN}-\text{Ln(SCN)}_3 \qquad \text{Ln} = \text{Nd,Sm.Tb}$$

as regarding their syntheses, their physico-chemical properties and the analyses of their electronic spectra in order to establish their bond types.

There are two possibilities to synthetize the new compounds:

1) syntheses carried out in solution, using anhydrous reagents, in anhydrous solvents and in inert gas medium.

2) syntheses carried out in the first stage in molten salts followed by an extraction, refluxing with THF and then the concentration and the removal of the solvent; in this case hydrated salts were initially used, the subsequent working operations being made in inert gas medium too.

In an intermediate stage Ln(SCN)_3 was obtained in order to be used in the preparation of the new compounds with thiocyanic paludrine.

---

[1] P. Spacu and I. Albescu, *Z. Chem*, **10**, 470 (1970).

[2] P. Spacu and I. Albescu, *Rev. Roumaine Chim.*, **16**, 1503 (1971).

[3] I. Albescu, *Rev. Roumaine Chim*, **10**, (1972).

[4] I. Albescu, *Rev. Roumaine Chim.*, **11**, (1972).

EXPERIMENTAL

1. *pald $HCl.LnCl_3$* Ln = Nd, Sm, Eu, Gd, Dy, Ho, Yb.

A mixture of anhydrous $LnCl_3$ or adduct, $LnCl_3$.xTHF, and pald. HCl in a molar ratio 1 : 3 is refluxed in a minimum amount of anhydrous methanol for two hours. The solution is evaporated under vacuum on P_4O_{10} till the complete removal of the solvent and the crystals thus obtained are refluxed for 10 minutes with a minimum quantity of THF. The solution is rapidly filtered at heat; from the filtrate a precipitate can immediately be separated as a gel which by stirring becomes crystalline and is coloured according to the nature of the metal ion.

All the working operations are made in inert gas medium as we have mentioned in the previous paper. [1-4] The chemical analysis of the compound corresponds to the above mentioned formula.

2. *(pald $HCl)_nLnCl_3$* n = 2 Ln = Nd, Sm, Eu, Yb

n = 3 Ln = Gd, Dy, Ho.

Besides the compound we have mentioned at point 1° as a main product and with a high efficiency one obtains in the filtrate, after 3—6 days concentration under vacuum crystals coloured in yellow (Sm), violet (ND, Yb), pink (Eu, Dy), cream (Dy). All the compounds thus synthetized are unstable in air, soluble in alcohol, acetone, THF whereas the compounds of general formula pald. $HCl.LnCl_3$ are more stable.

With a view of preparing compounds of the general formula (pald. $HCl)_nLnCl_3$ in a more varied series and with a better efficiency our observations led us to a second method: in a first stage the synthesis is carried out in molten salts, then it is continued in solution by extraction with solvent. The general development of the synthesis runs as follows:

3. *(pald $HCl)_n.LnCl_3$* n = 2 Ln = Yb

n = 3 Ln = Nd, Eu, Dy, Ho.

n = 4 Ln = Sm

n = 5 Ln = Gd

A mixture of $LnCl_3.nH_2O$ and pald. HCl in a ratio 1 : 3 is carefully melted in a China crucible lest the temperature should exceed 210°, then all the quantity becomes a homogeneous paste, it is treated with 25 ml anhydrous methanol or THF; the operation being now made in nitrogen atmosphere. The extract is stirred and left to settle the unsoluble part as a secondary product which contains the oxychloride of lanthanide. After 6—8 hours it is filtered and the extract is refluxed in a nitrogen atmosphere for two hours. During the refluxing the colour of the solution becomes more intense according to the nature of the metal ion: intense yellow (Sm, Ho), light yellow (Gd, Eu), violet (Nd), pink yellow (Dy), violet yellow intense (Yb). After refluxing the solution is concentrated under vacuum on P_4O_{10}; after 2—3 days the glue obtained becomes crystalline. The above mentioned compounds have been identified at the chemical analysis. The compounds thus prepared as well as the compounds which were synthetized at point 2° are unstable in air, soluble in alcohol, acetone, THF.

4. *(pald $HCl).3LnCl_3$* Ln = Dy, Ho

In this case after refluxing, the solution extracted from melting with THF deposits a white crystalline precipitate, before it is concentrated under vacuum in order to lead to compounds of type (pald $HCl)_3.LnCl_3$; the precipitate is separated by filtration, washed with THF and dried under vacuum. The chemical analysis of the compound thus obtained leads to the combination of general form, pald. $HCl.3LnCl_3$

These new combinations are stable only in the absence of humidity ; they are kept in nitrogen atmosphere. They are unsoluble in alcohol, acetone and THF. Table 1 shows the chemical analysis of the new compounds

PSEUDOHALOGENO-COMPOUNDS

To obtain these combinations the anhydrous thiocyanates of lanthanides, used in the syntheses, have been prepared in an intermediary stage.

5. *pald* $HSCN.Ln(SCN)_3$ Ln = Nd, Sm, Tb

In the exchange reaction between $LnCl_3$ and KSCN in a methanol solution, $Ln(SCN)_3$ is obtained after the filtration of KCl ; a solution of pald HCl in methanol in ratio 1 : 3 is added and then the solution is refluxed for two hours in nitrogen atmosphere. After the removal of the solvent by evaporation under vacuum on P_4O_{10}, a crystalline mass is obtained, which is passed in a schlenk with frit G_3 and then it is extracted by refluxing with THF. The excess of pald HCl remains on the frit and the solution is concentrated under vacuum ; after 6–8 days a microcrystalline paste is obtained, which becomes crystalline in time.

For the syntheses the following ratios were used : 0.777 g $NdCl_3$ in 10 ml methanol with 0.914 g KSCN in 5 ml methanol. After the quantitative titration of KCl, supposing that in the solution there are 0.986 g $Nd(SCN)_3$ this solution is treated with 2.699 g pald HCl in 10 ml methanol which would correspond to the 1 : 3 salt-ligand ratio.

For the respective compound of Sm there were used : 0.5306 g $SmCl_3.1^{1/2}$ THF,0.4242 g KSCN and 1.266 g pald HCl respectively, keeping the proportion of the solvents.

For the compound with Tb we worked with : 0.5842 g $TbCl_3$, 0.6421 g KSCN and 1.917 g pald HCl recommending the respective proportions of solvent.

As regarding the refluxing with THF, 25–30 ml is the maximum quantity of solvent we recommend, for working with the best concentration of solution.

The compounds are coloured in : intense violet (Nd), dark yellow (Sm), pink yellow(Tb). They are not stable in air, decompose with water, are soluble in alcohol and THF.

6. (*pald* $HSCN)_3.Ln(SCN)_3$ Ln = Nd, Sm, Tb.

In this case the working operations are the same as those in the above mentioned syntheses till in the last stage of preparation a compound in the form of a glue is obtained. The latter is treated in ice with a minimum quantity of water till a precipitate appears. The chemical analysis shows the above mentioned combination.

The compounds are coloured in violet-brown (Nd), yellow (Sm), intense yellow towards pink (Tb) ; they are unstable in air, pass into glue if they lose water, are soluble in ethanol, THF, are kept in nitrogen.

The analytical results are given in table 2.

The electronic absorption spectra have been recorded in order to establish the structure of these compounds.

Table 1

Analytical results on the lanthanide compounds with pald HCl

Compound	Ln % *calc.- found*	N % *calc.- found*	C % *calc.- found*	H % *calc.- found*	Cl % *calc.- found*	Colour	m.p. °C
pald $HCl.NdCl_3$	26.68 25.68	12.95 12.88	24.43 23.64	3.18 3.42	26.23 25.92	light-violet	205
pald $HCl.SmCl_3$	27.49 26.89	12.81 12.06	24.15 25.00	3.14 3.05	25.93 25.10	white-yellow	207
pald $HCl.GdCl_3$	28.55 25.69	12.72 11.19	23.98 21.26	3.11 3.31	25.61 22.10	white	218
pald $HCl.EuCl_3$	27.71 27.03	12.77 11.99	24.08 23.85	3.12 3.65	25.85 25.50	white-yellow	219
pald $HCl.DyCl_3$	29.07 27.98	12.53 12.05	23.63 22.30	3.06 3.20	25.37 24.35	white	218
pald $HCl.HoCl_3$	29.38 28.58	12.47 11.95	23.53 22.55	3.05 4.01	25.26 24.70	white-yellow	218
pald $HCl.YbCl_3$	30.38 30.00	12.30 12.05	23.19 22.88	3.00 3.18	24.90 24.55	white	219
2 pald $HCl.NdCl_3$	17.36 17.38	16.85 16.65	31.89 30.54	4.12 5.00		light-yellow	210
2 pald. $HCl.SmCl_3$	16.54 16.00	15.41 15.05	34.34 33.10	4.65 5.00	19.50 17.98	white-yellow	188
2 pald $HCl.EuCl_3$ 2THF	15.46 14.94	14.25 14.03	36.65. 35.77	5.13 4.95	18.04 16.96	cream	192
2 pald $HCl.YbCl_3$	20.13 19.42	16.29 15.98	30.73 30.05	3.85 4.00	20.62 19.82	pink-violet	186
3 pald $HCl.NdCl_3$	11.34 11.24	16.38 16.61	39.91 39.40	5.18 6.00		orange-violet	180
3 pald $HCl.EuCl_3$	13.46 12.40	18.61 17.15	35.10 32.43	4.55 4.15	18.84 18.19	yellow	180
3. pald $HCl.GdCl_3$ 2/3 THF	12.58 12.62	16.83 16.55	42.27 42.30	5.88 6.00	17.02 16.82	yellow	180
3 pald $HCl.DyCl_3$	14.25 14.98	18.43 18.10	34.76 34.20	4.51 4.22	18.66 18.22	cream-pink	182
3 pald $HCl.HoCl_3$	14.44 14.00	18.40 18.00	34.70 34.20	4.52 4.20	18.63 18.29	grey-green	180
4 pald $HCl.SmCl_3$	10.60 10.35	19.75 19.60	37.36 36.36	4.83 4.96	17.50 17.44	cream	180
5 pald $HCl.GdCl_3$	9.17 9.19	20.42 20.39	38.52 38.17	4.99 5.00	16.54 16.43	orange	186
pald $HCl.3DyCl_3$	44.44 44.39	6.38 6.15	12.04 12.10	1.56 1.68	32.32 32.27	white-yellow	256
pald $HCl.3HoCl_3$	44.82 44.78	6.34 6.28	11.97 11.89	1.57 1.64	32.12 32.00	white-yellow	252

Table 2

Analytical results on the lanthanide compounds with pald SCNH

Compound	Ln % *calc.-found*	N % *calc.-found*	C % *calc.-found*	H % *calc.-found*	Colour
pald $HSCN\cdot Nd(SCN)_3\cdot THF$	20.51 20.05	17.91 17.75	32.44 32.02	3.58 3.72	dark-violet
pald $HSCN\cdot Sm(SCN)_3\cdot THF$	21.19 20.99	17.76 17.23	32.16 31.94	3.55 3.65	yellow
pald $HSCN\cdot Tb(SCN)_3\cdot THF$	21.63 20.86	17.55 16.98	31.78 30.95	3.50 3.75	yellow-pink
(pald $HSCN)_3\cdot Nd(SCN)_3$	11.48 11.02	23.40 23.88	37.26 38.00	4.09 4.25	violet-brown
(pald $HSCN)_3\cdot Sm(SCN)_3$	11.90 10.95	23.29 23.30	37.09 37.07	4.07 5.00	yellow
(pald $HSCN)_3\cdot Tb(SCN)_3$	11.46 11.56	23.40 23.26	37.26 37.25	4.09 4.84	yellow-pink

GENERAL DISCUSSIONS

The preparation of the new lanthanide compounds with pald HCl in the series of the studied elements strongly depends on two factors :

— the concentration of the initial components ; the concentration must be as much as possible near to the value of the molar concentration and it must be kept constant during the reaction. The observation is in concordance also with our studies in solution on the $MX\text{-}LnCl_3$, $M = Na$, K, Rb, Cs systems when we worked at the molar concentrations,[5-7] as well as with those in meltings concerning the existence and the stability of the $[LnX_n]^{n-3}$ ion.

— the second main factor refers to the difference of solubility in THF between paludrine basis and hydrochloride paludrine , the latter being unsoluble, as well as the difference of solubility between the compounds of general formulas, pald HCl. $LnCl_3$, and those of the type (pald $HCl)_n.LnCl_3$; the first ones precipitate and are separated from the THF

---

[5] P, Spacu, I. Albescu and E. Dragomir, *Rev. Roumaine Chim.*, **8**, 31 (1963).

[6] P, Spacu, and. I. Albescu, *Rev. Roumaine Chim.*, **12**, 667 (1967).

[7] P, Spacu, I. Albescu and E. Ivan, *Rev. Roumaine Chim.*, **13**, 425 (1968).

solution making possible the preparation of the latter ones in the crystalline form.

We remark that in the syntheses carried out in the first stage in meltings, hydrated halides are used because the anhydrous halides melt over 600° which does not allow their melting together with the ligand which

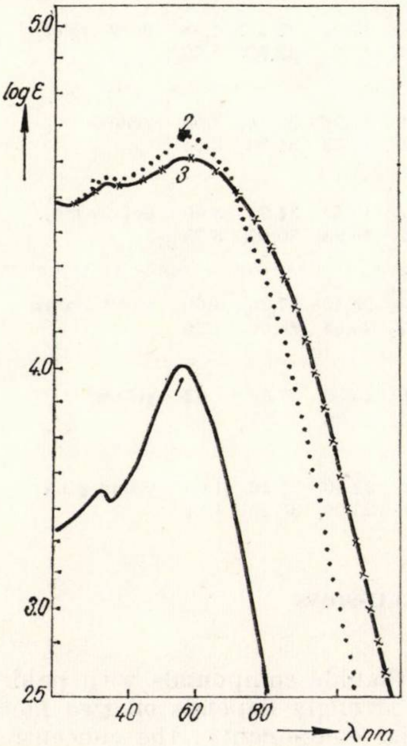

Fig. 1. – UV spectra of the Ho compounds. *1*, pald HCl ; *2*, pald HCl. $HoCl_3$; *3*, (pald HCl)$_3$.$HoCl_3$.

has the melting point at 212° ; through melting the situation of the anhydrous salts is somehow reached.

Since the compounds are not stable in air and are soluble in alcohol, their electronic spectra have been recorded on solution.

The combination pald HCl.$LnCl_3$ is the most stable from the whole series of compounds and it has permitted also the recording of its spectra on pellets.

Figs. 1,2 and 3 show the absorption spectra in UV and visible range of Ho and Dy compounds, against the corresponding aquo ions and anhydrous chlorides.

Unlike the compounds obtained with paludrine basis with the same elements,[1–4] the new combinations have, besides the characteristic band at 260 nm, proper to the benzene ring, a second absorption band at 233 nm of the pald HCl, slightly shifted towards smaller wavenumbers in the corresponding compounds.

To estimate the covalency degree of the chemical bands one evaluates the mean nephelauxetic ratio of the absorption band shifts reported to the absorption bands of the corresponding complex, $[Ln(H_2O)_6]^{3+}$.

The forbidden spin frequencies for the f^n configuration of the central ion are shifted by coordination.

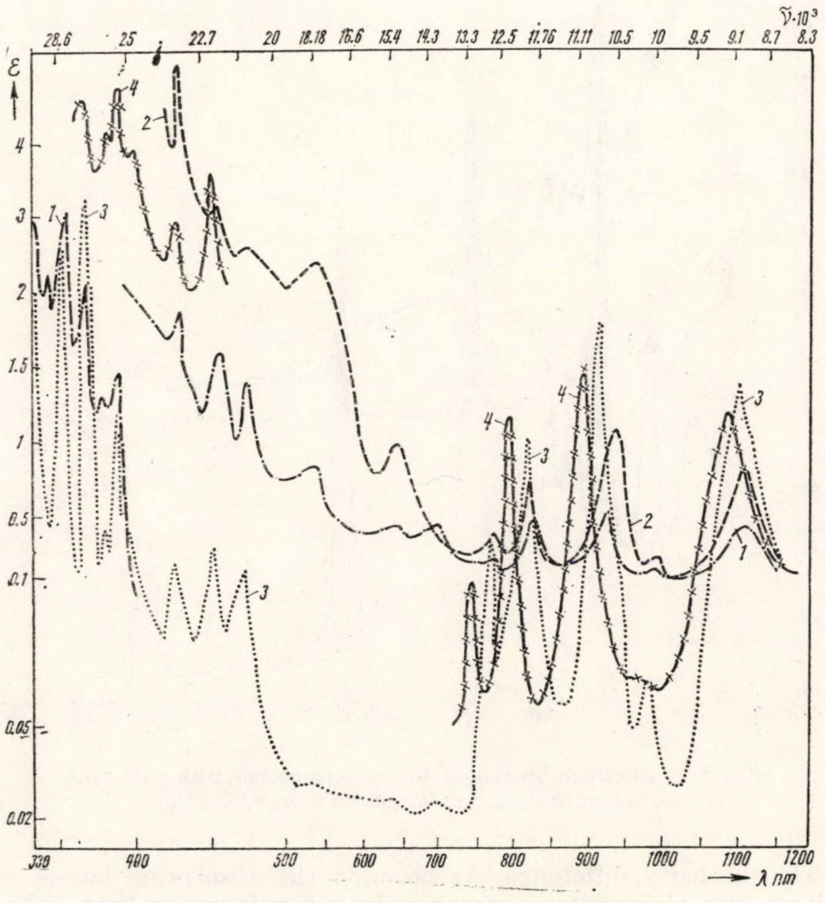

Fig. 2. — Electronic spectra of the Dy compounds with pald HCl.
1, pald HCl.$DyCl_3$; *2*, (pald HCl)$_3$.$DyCl_3$ *3*, $[Dy(H_2O)_6][NO_3]_3$ *4*, $DyCl_3$.

Like in the paludrine complexes the shifts assume low values in the present compounds. For each complex the δ_m parameter was calculated.

The most probable assignment of the absorption bands and of the corresponding transitions of the metal ion has been established like for the paludrine compounds. That is why table 3 presents the illustrative data only for Nd complexes.

As may be seen, δ_m values show a higher covalency degree of the chemical bands in our complexes than in the corresponding aquaion.

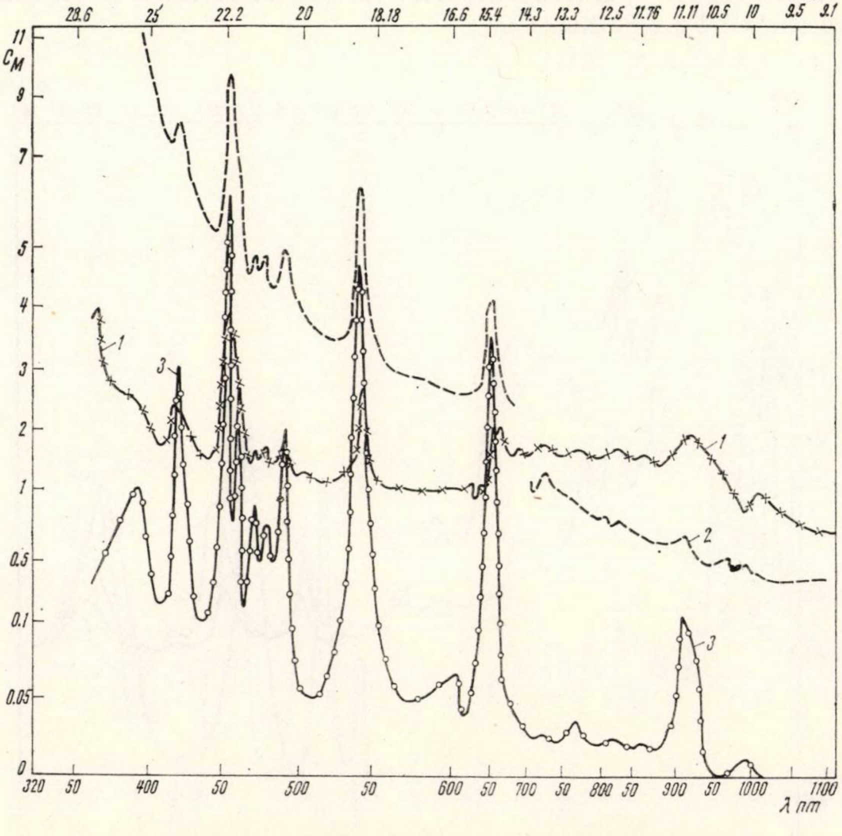

Fig. 3. — Electronic spectra of the Ho compounds with pald HCl.
1, pald HCl. $HoCl_3$; *2*, (pald HCl)$_3$.$HoCl_3$; *3*, $[Ho(H_2O)_6][NO_3]_3$.

The intensity difference $\Delta\varepsilon$ between the absorption bands of our complexes and those of the corresponding aquaions has been calculated by means of the simple formula :

$$\Delta\varepsilon = \varepsilon_{\text{mol complex}} - \varepsilon_{\text{mol aquaion}}$$

As may be seen from the data presented in Tables 5—6, the highest intensity differences which are noticed with δ_m parameter assume the highest values too.

The fact proves once more the coordination of the ligand to the rare earth metal ion.

Further researches on this line will follow in forthcoming papers.

Table 3

Energy levels of the Nd^{3+} ion observed with the Nd compounds, taking $[Nd(H_2O)_6]^{3+}$ as standard

Ground state Nd = $^4I_{9/2}$ δ = covalency degree

Excited levels	$Nd(H_2O)_6$ $[NO_3]_3$		pald HCl·$NdCl_3$		δ	(pald HSCN)$_3$·$NdCl_3$		δ
	$\tilde{\nu}_{max}$ cm^{-1}	λ_{max} nm	$\tilde{\nu}_{max}$ cm^{-1}	λ_{max} nm		$\tilde{\nu}_{max}$ cm^{-1}	λ_{max} nm	
$^4F_{3/2}$	11695	855	11627	860	0.5	11627	860	0.5
$^2H_{9/2}$	12739	785	12658	790	0.64	12658	790	0.64
$^4F_{7/2}$	13699	730	13513	740	1.37	13513	740	1.37
$^4F_{9/2}$	14925	670	14705	680	1.49	14925	670	0
$^2H_{11/2}$	16129	620	16000	625	0.86	—	—	—
$^4G_{5/2}$	17391	575	17241	580	0.87	17241	579	0.87
$^4G_{7/2}$	19231	520	19047	527	0.97	19120	523	0.53
$^2G_{9/2}$	19802	505	19607	510	0.99	—	—	—
$^4G_{9/2}$	21277	470	20920	478	1.78	—	—	—
$^4G_{11/2}$	21882	457	—	—	—	21643	462	1.1
					δ_m=1.06			δ_m=0.83

Table 4

Mean covalency degree

Complex compound	Values δ_m
pald HCl.$NdCl_3$	1.06
(pald HSCN)$_3$. $Nd(SCN)_3$	0.83
pald HCl.$DyCl_3$	0.58
(pald HCl)$_3$.$DyCl_3$	1.19
pald HCl.$HoCl_3$	0.71
(pald HCl)$_3$. $HoCl_3$	0.94

Table 5

Characteristic band intensities of the Dy^{3+} ion in its compounds, compared with those of $Dy(H_2O)_6]^{3+}$ taken as reference

$[Dy(H_2O)_6]$ $[NO_3]_3$		pald HCl·$DyCl_3$		$\Delta\varepsilon_1$	(pald HCl)$_3$·$DyCl_3$		$\Delta\varepsilon_2$
λ_{max} nm	ε_M	λ_{max} nm	ε_M		λ_{max} nm	ε_M	
350	2.622	352	2.768	+0.146	—	—	—
366	3.220	365	2.183	−1.04	—	—	—
379	0.430	378	1.328	+0.898	—	—	—
387.5	1.197	387	1.455	+0.258	—	—	—
397.5	0.367	—	—	—	—	—	—
427.5	0.174	427	1.874	+1.70	427.5	5.07	+4.90
452.5	0.314	455	1.612	+1.298	452.5	3.169	+2.855
472.5	0.138	473	1.417	+1.279	472.5	2.535	+2.397
540	0.034	540	0.824	+0.790	545	2.358	+2.324
640	0.027	640	0.449	+0.422	640	1.114	+0.987
690	0.026	695	0.449	+0.423	—	—	—
770	0.368	775	0.228	−0.139	775	0.392	+0.024
820	1.205	825	0.473	−0.733	820	0.783	−0.422
920	1.814	925	0.548	−1.266	940	1.116	−0.698
980	0.066	990	0.149	+0.084	990	0.213	+0.147
1100	1.442	1100	0.449	−0.992	1100	0.855	−0.587

Table 6

Characteristic band intensities of the Ho^{3+} ion in its compounds, compared with those of $[Ho(H_2O)_6]^{3+}$ taken as reference

$[Ho(H_2O)_6][NO_3]_3$		pald $HCl \cdot HoCl_3$		$\Delta\varepsilon_1$	$(pald\ HCl)_3 \cdot HoCl_3$		$\Delta\varepsilon_2$
λ_{max} nm	ε_M	λ_{max} nm	ε_M		λ_{max} nm	ε_M	
390	1.106	—	—	—	—	—	—
415	3.303	417	2.483	−0.82	417	8.271	4.968
450	6.142	452	3.935	−2.207	450	9.918	3.776
455	2.882	—	—	—	—	—	—
467	0.967	468	1.663	0.696	468	4.940	3.973
475	0.767	474	1.701	0.935	474	4.965	4.198
485	2.231	485	1.850	−3.810	485	5.027	2.796
535	4.710	536	2.756	−1.954	536	6.125	1.413
645	3.576	650	2.160	−1.416	645	4.217	0.641
720	0.026	720	1.788	1.762	720	2.420	2.394
760	0.037	760	1.663	1.626	—	—	—
810	0.002	815	1.713	1.711	800	0.820	0.817
900	0.194	910	2.073	1.879	900	0.725	0.531
990	0.011	1000	1.043	1.032	990	0.522	0.510

Revue Roumaine de Chimie, 18, 4, 609–621 (1973)

CONTRIBUTION À L'ÉTUDE DE L'HYDROLYSE DE L'ION UO_2^{2+} EN MILIEU PERCHLORIQUE

MARIA MAVRODIN-TĂRĂBÎC
Centre de Chimie Physique — Bucarest,
31, str. Galați

Reçu le 5 juillet 1972

On détermine, par la méthode de la « fonction de formation » et la méthode « core + links », la nature des espèces ioniques formées par l'hydrolyse de l'uranium (VI). On tire la conclusion que, si jusqu'au pH = 2,5, le seul ion d'uranium (VI) qui se forme dans la solution est l'ion UO_2^{2+}, à des valeurs de pH>2,5, l'ion UO_2^{2+} hydrolyse par une suite de réactions qui mènent, même dans des solutions très diluées, à la formation des complexes polynucléaires du type « core + links », caractérisés par la formule générale $UO_2[(OH)_2UO_2]_n^{2+}$.

Tel qu'il résulte de l'analyse des travaux, souvent contradictoires, effectués ces derniers temps,[1–16] l'étude de la nature des espèces ioniques qui se forment par l'hydrolyse de l'uranium (VI) représente un domaine de recherche très important et très actuel.

Vu la grande complexité des réactions d'hydrolyse de l'uranium (VI), pour pouvoir déterminer exactement la nature et la stabilité des espèces ioniques qui se forment dans la solution, nos études sur le système perchlorate d'uranyle-eau, effectuées dans un autre travail [17] par voie spectrophotométrique et par l'analyse mathématique différentielle des courbes pH-métriques, ont été vérifiées et complétées dans ce travail, par *la mé-*

---

[1] S. Hietanen, *Acta Chem. Scand.*, **8**, 1607 (1954).
[2] J. Faucherre, *Compt. rend.*, **227**, 1367 (1948).
[3] J. Sutton, *J. Chem. Soc.*, **1949**, 275.
[4] S. Hietanen et L. G. Sillen, *Acta Chem. Scand.*, **13**, 1828 (1959).
[5] J. A. Hearne, *J. Chem. Soc.*, **1957**, 2168.
[6] D. Cole, *J. phys. Chem.*, **71**, 2771 (1967).
[7] A. Patterson, *J. Amer. Chem. Soc.*, **74**, 4056 (1952).
[8] J. Faucherre, *Compt. rend.*, **227**, 1367 (1948).
[9] S. Ahrland, S. Hietanen et L. G. Sillen, *Acta Chem. Scand.*, **9**, 1907 (1954).
[10] L. G. Sillen, *Acta Chem. Scand.*, **8**, 299 (1954).
[11] S. Hietanen et L. G. Sillen, *Acta. Chem. Scand.*, **13**, 1828 (1959).
[12] S. Hietanen et L. G. Sillen, *Acta Chem. Scand.*, **11**, 526 (1959).
[13] H. S. Dunsmore, S. Hietanen et L. G. Sillen, *Acta Chem. Scand.*, **17**, 2644 (1963).
[14] U. Schedin et M. Frydman, *Acta Chem. Scand.*, **22**, 115 (1968).
[15] A. Robert, *Acta Chem. Scand.*, **22**, (1968).
[16] C. Drăgulescu et I. Julean, *Studii și Cercetări Chimice Timișoara*, **6**, 3–4, 33 (1959).
[17] M. Mavrodin-Tărăbîc, *Rev. Roumaine Chim.* (à paraître).

thode de la «fonction de formation», élaborée par Bjerrum[18] — pour le cas général des complexes en solution — et adaptée par Ahrland[19] — pour le cas spécial des réactions d'hydrolyse et par la méthode «*core + links*», élaborée par Sillen[20] pour l'étude des complexes polynucléaires.

L'étude des équilibres hydrolytiques par une méthode générale utilisée pour les complexes en solution est justifiée par le fait que les réactions d'hydrolyse peuvent être considérées comme des réactions de formation des complexes, dans le cas de l'ion UO_2^{2+} — en qualité d'ion central — avec les ions OH^- — en qualité de ligand —, l'ion d'uranyle représentant une constellation d'atomes parfaitement stable dans toutes les conditions du milieu de réaction.

PARTIE EXPÉRIMENTALE

RÉACTIFS

Perchlorate d'uranyle, $UO_2(ClO_4)_2\ 6\ H_2O$ (*p.a.* Th. Schuchardt). On a préparé une solution «stock» approximativement 0,1 N, dont on a obtenu, en diluant avec de l'eau bidistillée, les solutions de perchlorate d'uranyle de différentes concentrations : 0,02 N, 0,05 N, 0,01 N, 0,001 N.

Les concentrations de ces solutions ont été vérifiées par voie gravimétrique (évaporation et calcination à l'état d'oxyde U_3O_8).

Perchlorate de sodium, $NaClO_4$ (*purum,* Merck). Il a été utilisé après trois recristallisations et séchage à 110°C.

Hydroxyde de sodium (*p. a.* Merck). Les solutions utilisées ont été préparées en diluant une solution «stock» approximativement 0,1 N. La concentration des solutions de NaOH a été établie avec du phtalate acide de kalium.

Acide perchlorique, $HCl\ O_4$, (*p.a.* Merck) de concentration d'environ 75%. On a utilisé des solutions approximativement 0,1 N, analysées par titrage alcalimétrique.

APPAREILS

On a utilisé un pH-mètre Radiometer — Copenhagen (électrodes de verre et calomel). Les déterminations ont été faites dans une installation fermée, spécialement construite.

MODE DE TRAVAIL

Les déterminations pH-métriques ont été effectuées en titrant les solutions de perchlorate d'uranyle dans lesquelles on a ajouté auparavant une quantité d'acide perchlorique ; les titrages ont été faits en utilisant une solution de NaOH 0,1 M, le domaine de pH étudié étant compris entre 1,6 ÷ 4,5. Pour tirer des conclusions sur l'influence de la concentration sur la nature des espèces ioniques qui se forment par l'hydrolyse, on a travaillé avec des solutions de perchlorate d'uranyle de différentes concentrations, comprises entre 0,1 ÷ 0,001 M.

---

[18] N. Bjerrum, Thèse, Copenhaga (1948).

[19] S. Ahrland, *Acta Chem. Scand.*, **3**, 374 (1949).

[20] L. G. Sillen, *Acta Chem. Scand.*, **9**, 179 (1955).

L'influence de la force ionique a été évaluée en effectuant des déterminations pour chaque concentration, à quatre forces ioniques : $I = 0,5$; 1 ; 1,5 et 2, réalisées avec du $NaClO_4$.

(À mentionner que tous les titrages ont été répétés trois fois, les valeurs du pH représentées graphiquement et utilisées dans le calcul étant les valeurs moyennes. Les valeurs d'équilibre ont été obtenues après 60 secondes d'agitation continue.)

RÉSULTATS ET DISCUSSIONS

1. L'ÉTUDE DU SYSTÈME PERCHLORATE D'URANYLE – EAU PAR LA MÉTHODE DE LA « FONCTION DE FORMATION »

Si l'on élimine, conformément aux déterminations spectrophotométriques, la formation des polymères $(UO_2)_2$, $(UO_2)_3 \ldots (UO_2)_n$, dans les solutions aqueuses du perchlorate d'uranyle il existe — théoriquement — la possibilité de la formation des séries de complexes suivantes :

— mononucléaires MA, MA_2, MA_3 . . . .

— binucléaires M_2A, M_2A_2, M_2A_3 . . . .

— *m*- nucléaires M_mA, M_mA_2, M_mA_3 . . . .

La sélection des espèces ioniques qui se forment réellement dans la solution a été faite conformément à la méthode de Bjerrum en calculant $\bar{n}$, le nombre moyen de ligands OH^- liés à l'ion central d'uranyle et en analysant les courbes de la fonction de formation du système pour les différentes concentrations de l'ion UO_2^{2+}.

Les relations fondamentales utilisées dans le calcul ont été les suivantes :

$$\bar{n} = \frac{C_A - (A)}{C_M} \tag{1}$$

dans laquelle :

— C_A = la concentration totale du ligand (OH^-), connue dès les données initiales du travail :

$$C_A = (A) + (MA) + 2(MA_2) + \ldots + (M_2A) + 2(M_2A_2) + \ldots$$
$$\ldots + (M_mA) + 2(M_mA_2) + \ldots \tag{2}$$

— C_M = la concentration de l'ion central (UO_2^{2+}) également connue dès les données initiales du travail :

$$C_M = (M) + (MA) + (MA_2) + \ldots + 2(M_2A) + (M_2A_2) + \ldots$$
$$\ldots + m((M_mA) + (M_mA_2) + \ldots) + \ldots \tag{3}$$

— A = la concentration du ligand « libre » déterminée par la méthode pH-métrique.

La courbe de la fonction de formation du système a été obtenue en représentant $\overline{n}$ en fonction de (A) et est définie par l'équation :

$$\overline{n} = \frac{\beta_1'(A) + 2\beta_2'(A)^2 + 3\beta_3'(A)^3 + \ldots + (M)\,\beta_1''(A) +}{1 + \beta_1'(A) + \beta_2'(A)^2 + \beta_3'(A)^3 + \ldots + 2(M)(\beta_1''(A) +}$$
$$\frac{+\, 2\beta_2''(A)^2 + \ldots + (M)^{m-1}(\beta_1^{(m)}(A) + 2\beta_2^{(m)}(A)^2 + \ldots}{+\, \beta_2''(A)^2 + \ldots + m(M)^{m-1}(\beta_1^{(m)}(A) + \beta_2^{(m)}(A)^2 \ldots} \qquad (4)$$

L'équation (4) a été obtenue en remplaçant, dans l'équation (1), C_A et C_M par leurs valeurs déduites de la relation (2) et, respectivement (3) ; les concentrations des différentes espèces ioniques ont été, de même, remplacées, par leurs expressions déterminées par la relation générale :

$$(M_m A_n) = \beta_n^{(m)} (M)^m (A)^n \qquad (5)$$

Lorsque dans la solution du sel d'uranyle il ne se forme que des complexes mononucléaires, les constantes β'', β''', … β^m … $= 0$ et — ainsi qu'on peut le constater de l'analyse de la relation (4) — $\overline{n}$ dépend seulement de (A) et ne dépend pas de (M).

Dans ce cas on obtient graphiquement, pour les différentes concentrations du C_M, des courbes $n = f(A)$, coïncidentes.

Lorsque dans le système il se forme aussi des complexes polynucléaires, les constantes β'', β''' … $\neq 0$, et $\overline{n}$ dépend tant de (A) que de (M), ce qui se traduit graphiquement par l'obtention des courbes $\overline{n}$ en fonction de (A), à de différentes valeurs du C_M, parallèles.

Compte tenu que les données déterminées expérimentalement ont été obtenues par la méthode pH-métrique et se rapportent au ligand « libre » $(A) = (\mathrm{OH}^-)$ d'une manière indirecte, la quantité mesurée directement étant la concentration des ions H^+, liée à (OH^-) par la relation : $(\mathrm{OH}^-) = K_w/(\mathrm{H}^+)$, l'expression mathématique de la fonction de formation devient :

$$\overline{n} = \frac{1}{(\mathrm{H}^+)} = \frac{\left(x_1' + \frac{2x_2'}{(\mathrm{H}^+)} + \frac{3x'}{(\mathrm{H}^+)^2} + \ldots\right) + (M)\left(x_1'' + \frac{2x_2''}{(H^+)} + \right.}{\left(1 + \frac{x_1'}{(\mathrm{H}^+)_{(m)}} + \frac{x_2'}{(\mathrm{H}^+)^2} + \ldots\right) + 2(\mathrm{M})\left(\frac{x_1''}{(\mathrm{H}^+)} + \frac{x_1''}{(\mathrm{H}^+)^2} + \right.}$$
$$\frac{\left. + \frac{3x_3''}{(\mathrm{H}^+)^2} + \ldots\right) + (M)^{(m-1)} \frac{p x_p}{(\mathrm{H}^+)^{p-1}} + \frac{(p+1)\, x_{p+1}^{(m)}}{(\mathrm{H}^+)^p} +}{+ \frac{x_3''}{(\mathrm{H}^+)^3} + \ldots + m(M)^{m-1} \frac{x_p^{(m)}}{(\mathrm{H}^+)^p} + \frac{x_{p+1}^{(m)}}{(\mathrm{H}^+)^{p+1}} +}$$
$$\frac{\left. + \frac{(p+2)\, x_{p+2}^{(m)}}{(\mathrm{H}^+)^{p+1}} + \ldots\right) + \ldots}{\left. + \frac{x_{p+2}^{(m)}}{(\mathrm{H}^+)^{p+2}} + \ldots\right) + \ldots} \qquad (6)$$

L'équation (6) a été obtenue en remplaçant, dans la relation (4), les valeurs de $A = (OH^-)$ par $K_w/(H^+)$ et en réunissant les constantes β et K_w dans de nouvelles constantes x, conformément à la relation :

$$(M_mA_n) = (M_m(OH)_n) = \beta_n^{(m)}(M)^m(OH^-)^n =$$

$$= \beta_n^{(m)} + K_w^n + \frac{(N)^m}{(H^+)^n} = x_n^{(m)} + \frac{(N)^m}{(H^+)^n} \tag{7}$$

Ainsi qu'on peut observer de l'équation (6), $\bar{n}$, le nombre moyen de ligands OH^- liés à l'ion central de UO_2^{2+}, dépend seulement de (H^+), si dans le système il ne se forme que des complexes mononucléaires ; $\bar{n}$ dépend tant de (H^+) que de (M), lorsque dans le système il se forme aussi des complexes polynucléaires.

Le calcul de la concentration des ions OH^- consommés pour la formation des complexes, à un moment donné du titrage, C_{OH}, a été fait compte tenu du fait que la quantité de NaOH qui correspond au premier point d'inflexion des courbes pH-métriques équivaut à la quantité d'acide présente dans la solution au moment initial.

En corrigeant, dans les calculs, la concentration des solutions en fonction du volume, $\bar{n}$ peut être déterminé à l'aide de la relation :

$$\bar{n} = \frac{C_{OH}}{C_M} \tag{8}$$

Les données expérimentales et les résultats obtenus par le calcul pour les solutions de perchlorate d'uranyle de différentes concentrations et forces ioniques sont présentés dans les tableaux 1–16.

Tableau 1

Nombre moyen des ligands, caractéristique pour la solution de perchlorate d'uranyle 0,0765 M, à I = 0,5

V_B ml	pH	C_{OH} 10^{-3} moles/l	C_M 10^{-3} moles/l	$\bar{n}$
5,4	2,95	2,02	37,50	0,05
6,0	3,22	4,40	36,40	0,12
6,5	3,35	6,34	35,60	0,17
7,0	3,47	8,43	34,80	0,24
7,5	3,59	10,35	34,00	0,30
8,0	3,65	12,22	33,20	0,36
8,5	3,72	14,09	32,50	0,43
9,0	3,80	15,75	31,90	0,49
9,5	3,88	17,33	31,20	0,55
10,0	3,95	19,11	30,60	0,62
10,5	4,03	20,59	30,00	0,68
11,0	4,10	21,97	29,40	0,74
11,5	4,17	23,46	28,80	0,81
12,0	4,23	24,85	28,30	0,87
13,0	4,39	27,54	27,30	1,00

Tableau 2

Nombre moyen des ligands, caractéristique pour la solution de perchlorate d'uranyle 0,0765 M, à I = 1

V_B ml	pH	C_{OH} 10^{-3} moles/l	C_M 10^{-3} moles/l	$\bar{n}$
5,5	3,01	1,92	37,50	0,05
6,0	3,22	4,40	36,40	0,12
7,0	3,50	8,41	34,80	0,24
8,0	3,66	12,21	33,20	0,36
9,0	3,84	15,76	31,90	0,49
10,0	3,99	19,10	30,60	0,62
11,0	4,12	21,97	29,40	0,74
13,0	4,40	27,53	27,30	1,00

Tableau 3

Nombre moyen des ligands, caractéristique pour la solution de perchlorate d'uranyle 0,0765 M, à I = 1,5

V_B ml	pH	C_{OH} 10^{-3} moles/l	C_M 10^{-3} moles/l	$\bar{n}$
6,0	3,20	3,92	36,4	0,10
7,0	3,47	7,938	34,8	0,22
8,0	3,69	11,80	33,20	0,35
9,0	3,88	15,37	31,90	0,48
10,0	4,00	18,75	30,60	0,61
11,0	4,12	21,07	29,40	0,70
12,0	4,25	24,45	28,30	0,86
13,0	4,40	27,13	27,30	0,99
14,0	4,60	29,52	26,40	1,11

Tableau 4

Nombre moyen des ligands, caractéristique pour la solution de perchlorate d'uranyle 0,0765 M, à I = 2

V_B ml	pH	C_{OH} 10^{-3} moles/l	C_M 10^{-3} moles/l	$\bar{n}$
6,0	3,16	4,50	36,40	0,11
7,0	3,39	8,29	34,80	0,23
8,0	3,70	12,00	33,20	0,36
9,0	3,82	15,35	31,90	0,48
11,0	3,90	21,12	29,40	0,71
12,0	4,05	24,48	28,30	0,86
13,0	4,15	27,17	27,30	0,99
14,0	4,35	29,54	26,40	1,11

Tableau 5

Nombre moyen des ligands, caractéristique pour la solution de perchlorate d'uranyle 0,0255 M, à I = 0,5

V_B ml	pH	C_{OH} 10^{-3} moles/l	C_M 10^{-3} moles/l	$\bar{n}$
5,4	3,27	1,90	12,5	0,15
5,6	3,47	2,43	12,3	0,19
5,8	3,59	3,13	12,2	0,25
6,0	3,70	4,55	12,1	0,37
6,2	3,78	4,89	12,0	0,40
6,4	3,85	5,66	11,9	0,47
7,0	4,10	8,179	11,6	0,70

Tableau 6

Nombre moyen des ligands, caractéristique pour la solution de perchlorate d'uranyle 0,0255 M, à I = 1

V_B ml	pH	C_{OH} 10^{-3} moles/l	C_M 10^{-3} moles/l	$\bar{n}$
5,4	3,27	1,43	12,5	0,11
5,6	3,47	2,23	12,3	0,18
5,8	3,60	3,05	12,2	0,25
6,2	3,76	4,87	12,0	0,40
6,4	3,85	5,64	11,9	0,47
6,8	4,00	7,40	11,7	0,63

Tableau 7

Nombre moyen des ligands, caractéristique pour la solution de perchlorate d'uranyle 0,0255 M, à I = 1,5

V_B ml	pH	C_{OH} 10^{-3} moles/l	C_M 10^{-3} moles/l	$\bar{n}$
5,4	3,20	1,52	12,5	0,12
5,6	3,40	2,29	12,3	0,18
5,8	3,52	3,10	12,2	0,25
6,0	3,65	4,52	12,1	0,37
6,4	3,69	5,70	11,9	0,47
6,6	3,85	5,84	11,8	0,49
7,0	3,97	8,20	11,6	0,70
7,6	4,20	10,56	11,2	0,94

Tableau 8

Nombre moyen des ligands, caractéristique pour la solution de perchlorate d'uranyle 0,0255 M, à I = 2

V_B ml	pH	C_{OH} 10^{-3} moles/l	C_M 10^{-3} moles/l	$\bar{n}$
5,4	3,16	1,59	12,5	0,12
5,6	3,40	2,29	12,3	0,18
5,8	3,55	3,08	12,2	0,25
6,0	3,65	4,52	12,1	0,37
6,4	3,80	5,65	11,9	0,47
7,0	3,95	8,21	11,6	0,72
7,6	4,20	10,56	11,2	0,94
8,0	4,36	12,04	11,0	1,09
8,4	4,52	13,33	10,9	1,22

Tableau 9

Nombre moyen des ligands, caractéristique pour la solution de perchlorate d'uranyle 0,0153 M, à I = 0,5

V_B ml	pH	C_{OH} 10^{-3} moles/l	C_M 10^{-3} moles/l	$\bar{n}$
5,0	3,47	0,80	7,65	0,10
5,2	3,70	1,69	7,58	0,22
5,4	3,87	2,53	7,50	0,33
5,6	3,99	3,40	7,43	0,45
5,8	4,12	4,27	7,36	0,58
6,2	4,31	6,14	7,22	0,85
6,6	4,55	7,72	7,09	1,08
6,8	4,65	8,62	7,02	1,22

Tableau 10

Nombre moyen des ligands, caractéristique pour la solutionde perchlorate d'uranyle 0,0153 M, à I = 1

V_B ml	pH	C_{OH} 10^{-3} moles/l	C_M 10^{-3} moles/l	$\bar{n}$
5,0	3,47	0,80	7,65	0,10
5,2	3,69	1,70	7,58	0,22
5,4	3,83	2,54	7,50	0,33
5,6	3,94	3,41	7,43	0,45
5,8	4,10	4,27	7,36	0,58
6,0	4,20	5,76	7,29	0,79
6,2	4,30	6,15	7,22	0,85
6,4	4,40	6,93	7,15	0,97
6,6	4,52	7,73	7,09	1,09

Tableau 11

Nombre moyen des ligands, caractéristique pour la solution de perchlorate d'uranyle 0,0153 M, à I = 1,5

V_B ml	pH	C_{OH} 10^{-3} moles/l	C_M 10^{-3} moles/l	$\bar{n}$
5,0	3,00	1,47	7,65	0,19
5,8	3,57	4,46	7,36	0,60
6,4	3,85	7,04	7,15	0,90
6,6	3,92	7,82	7,09	1,10
6,8	3,98	8,64	7,02	1,23
7,4	4,12	11,07	6,83	1,62
8,0	4,34	13,34	6,65	2,00

Tableau 12

Nombre moyen des ligands, caractéristique pour la solution de perchlorate d'uranyle 0,0153 M, à I = 2

V_B ml	pH	C_{OH} 10^{-3} moles/l	C_M 10^{-3} moles/l	$\bar{n}$
5,0	3,37	0,89	7,65	0,11
5,2	5,70	1,69	7,58	0,22
5,4	3,82	2,55	7,50	0,34
5,6	3,93	3,41	7,43	0,45
5,8	4,10	4,279	7,36	0,58
6,0	4,17	5,567	7,29	0,76
6,6	4,32	7,747	7,09	1,09
7,0	4,59	9,65	6,95	1,38

Tableau 13

Nombre moyen des ligands, caractéristique pour la solution de perchlorate d'uranyle 0,0076 M, à I = 0,5

V_B ml	pH	C_{OH} 10^{-3} moles/l	C_M 10^{-3} moles/l	$\bar{n}$
4,8	3,53	0,79	3,86	0,20
5,0	3,94	1,61	3,82	0,42
5,2	4,28	2,45	3,78	0,64
5,4	4,44	3,43	3,75	0,91
5,6	4,62	4,32	3,71	1,16
5,8	4,90	5,21	3,67	1,41
6,0	5,26	6,60	3,64	1,81

Tableau 14

Nombre moyen des ligands, caractéristique pour la solution de perchlorate d'uranyle 0,0076 M, à I = 1

V_B ml	pH	C_{OH} 10^{-3} moles/l	C_M 10^{-3} moles/l	$\bar{n}$
4,8	3,61	0,74	3,86	0,19
5,0	3,96	1,60	3,82	0,41
5,2	4,21	2,46	3,78	0,65
5,4	4,45	3,34	3,75	0,91
5,6	4,57	4,32	3,71	1,16
5,6	4,77	5,21	3,67	1,41
6,00	5,12	6,60	3,64	1,81

Tableau 15

Nombre moyen des ligands, caractéristique pour la solution de perchlorate d'uranyle 0,0076 M, à I = 1,5

V_B ml	pH	C_{OH} 10^{-3} moles/l	C_M 10^{-3} moles/l	$\bar{n}$
4,8	3,34	0,95	3,86	0,24
5,0	3,70	1,69	3,82	0,44
5,2	4,00	2,56	3,78	0,67
5,4	4,14	3,47	3,75	0,92
5,6	4,30	4,35	3,71	1,17
5,8	4,63	5,22	3,67	1,42
6,0	4,86	6,61	3,64	1,81

Tableau 16

Nombre moyen des ligands, caractéristique pour la solution de perchlorate d'uranyle 0,0076 M, à I = 2

V_B ml	pH	C_{OH} 10^{-3} moles/l	C_M 10^{-3} moles/l	$\bar{n}$
4,8	3,52	0,80	3,86	0,20
5,0	3,90	1,62	3,82	0,42
5,2	4,10	2,47	3,78	0,65
5,4	4,26	3,45	3,75	0,92
5,6	4,47	4,33	3,71	1,16
5,8	4,50	5,23	3,67	1,42
6,0	4,85	6,61	3,64	1,81

La détermination de la nature des espèces ioniques formées par l'hydrolyse a été faite par l'analyse du diagramme 1.

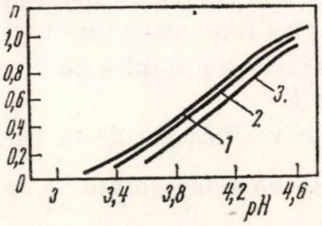

Fig. 1. — Courbes de formation déterminées pour les différentes concentrations des solutions de perchlorate d'uranyle, à I = 0,5.

C = 0,05 M (courbe *1*) ; C = 0,02 M (courbe *2*) ; C = 0,01 M (courbe *3*).

De l'analyse de la figure 1 on constate que les courbes $\overline{n} = f(\mathrm{pH})$ ne coïncident ni même pour les moindres valeurs de C_M ; on tire la conclusion que l'hydrolyse de l'ion UO_2^{2+} implique la formation des complexes polynucléaires, cette tendance se manifestant même à des dilutions très grandes.

La tendance de l'ion UO_2^{2+} de former, dans la solution, des complexes polynucléaires est analogue à celle de tous les métaux du groupe VI qui, en état d'ions hexavalents, apparaissent sous forme d'ions complexes avec de l'oxygène (CrO_4^{2-}), MoO_4^{2-} et WO_4^{2-}) et ont une tendance très marquée à l'agrégation.

2. L'ÉTUDE DU SYSTÈME PERCHLORATE D'URANYLE-EAU PAR LA MÉTHODE « CORE + LINKS »

Conformément à la méthode « core + links », considérée à présent, la méthode la plus efficace pour l'étude des complexes polynucléaires, la déduction de la nature et de la formule générale des espèces ioniques formées par l'hydrolyse est basée sur l'analyse des courbes $Z(\log h)_M$, analogues aux courbes $n(\log h)_M$, obtenues en représentant les valeurs de Z en fonction de $\log h$ et en réunissant tous les points qui se caractérisent par M constant.

(A mentionner que : Z représente le nombre moyen d'ions OH^- liés à l'ion central d'uranyle ; h = la concentration des ions d'hydrogène « libres » ; M = la concentration totale des ions UO_2^{2+} libres ou liés dans les complexes.)

Lorsque les courbes $Z(\log h)_M$ coïncident, dans le système il ne se forme que des complexes mononucléaires, caractérisés par la formule générale $Me(OH)_n$; si les courbes $Z(\log h)_M$, obtenues pour les différentes valeurs de M, sont parallèles, la distance entre elles, $\Delta\log h$, étant proportionnelle à $\Delta\log M$, on peut écrire la relation :

$$\left[\frac{\partial \log M}{\partial \log h}\right]_Z = -R = t = \text{constant}. \tag{9}$$

Dans le cas où la concentration des ions UO_2^{2+}, « libres » (m) est négligeable en comparaison de la concentration totale de l'ion $UO_2^{2+}(M)$, les complexes formés dans le système peuvent être considérés de type « core + links » et caractérisés par la formule générale $Me[(OH)_t Me]_n$, dans laquelle « t » est une constante déterminée graphiquement en utilisant la relation (9) et « n » représente une variable non déterminée.

Ainsi qu'il résulte de l'équation (9), Z est fonction de $X = \log M - t \log h$.

La vérification de la valeur déterminée graphiquement pour « t » a été faite en représentant $Y = \frac{Z}{t}$ en fonction de $X = \log M - t \log h$.

Dans le cas où « t » a été correctement calculé, on obtient, pour toutes les valeurs de M, une seule courbe $Y = f(X)$.

Après avoir établi la formule générale des complexes résultés de l'hydrolyse, il faut déterminer les valeurs de « n » et la nature des réactions qui ont lieu dans le système.

En considérant que, dans le système perchlorate d'uranyle-eau, il se forme des complexes « core + links », le type général de réaction qui doit être analysée est :

$$UO_2^{2+} + tnH_2O + nUO_2^{2+} \rightleftarrows UO_2[(OH)_tUO_2)]_n^{2+} + tn\ H^+$$

En ce qui concerne la valeur de « n », on obtient des indications en analysant l'allure des courbes $Y(X)$.

Du fait que les courbes $Z\ (\log h)_M$ obtenues pour les solutions aqueuses de perchlorate d'uranyle sont parallèles, on tire la conclusion que l'ion UO_2^{2+} hydrolyse avec la formation des ions complexes polynucléaires du type « core + links » caractérisés par la formule générale $UO_2\,[(OH)_t\,UO_2]_n^{2+}$.

La valeur de « t » $\left(t = -R = \frac{\log M}{\log h}\right)$ a été établie à l'aide du diagramme 2, qui représente $\log M = f(\log h)_{Z=\text{ct}}$.

Tel qu'on le voit dans la figure 2 les droites $\log M = f\ (\log h)_{Z=\text{ct}}$ sont parallèles et se caractérisent par une pente $\frac{\log M}{\log h} = 2$, ce qui mène à la conclusion que $t = -R = 2$, Z étant fonction de $X = \log M - 2 \log h$.

Pour confirmer la valeur $t = 2$, les données expérimentales ont été recalculées et représentées dans le système de coordonnées $Y = Z/2$, en fonction de X (fig. 3).

Ainsi qu'on le constate de la figure 3, les courbes $Y = f(X)$ obtenues pour deux solutions de perchlorate d'uranyle (0,033 M et 0,02 M) se superposent, ce qui confirme que $t = 2$ et les ions formés par l'hydrolyse se caractérisent par la formule générale : $UO_2[(OH)_2UO_2]_n^{2+}$.

En ce qui concerne le nombre des complexes qui résultent de l'hydrolyse on a obtenu des indications en analysant l'allure des courbes $Y(X)$.

Du fait que, dans le domaine de concentration et du pH étudié, la courbe qui représente la variation du nombre des ions OH^-/UO_2^{2+} croît continuellement à mesure que la valeur de X augmente, on peut déduire que, par l'hydrolyse de l'ion UO_2^{2+}, il se forme une série illimitée de complexes polynucléaires du type $UO_2[(OH)_2\ UO_2]_n^{2+}$.

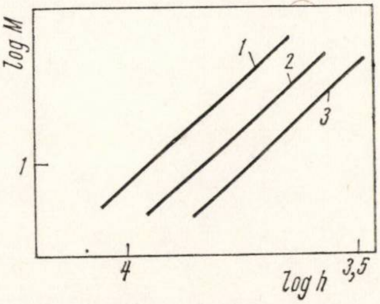

Fig. 2. — Détermination de la valeur « t » de la formule : $UO_2[(OH)_tUO_2]_n^{2+}$ ($Z=0,2(1)$; $0,3(2)$ et $0,4(3)$)

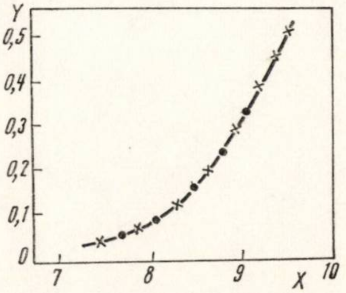

Fig. 3. — Vérification de la valeur « t » à l'aide de la courbe $Y = f(X)$.

CONCLUSIONS

L'application de la méthode de la « fonction de formation » et « core + links » à l'étude de l'hydrolyse de l'ion UO_2^{2+} en milieu perchlorique, tenant compte de toutes les espèces ioniques qui peuvent résulter de la réaction, a démontré que l'hydrolyse de l'uranium (VI) a lieu par une suite de réactions qui mènent, même dans le cas des solutions très diluées, à la formation d'une série illimitée de complexes polynucléaires du type $UO_2[(OH)_2\ UO_2]_n^{2+}$.

Ce comportement est analogue à celui de certains autres ions métalliques qui contiennent de l'oxygène et qui font partie du même groupe du système périodique : CrO_4^{2-}, MoO_4^{2-}, WO_4^{2-}.

Revue Roumaine de Chimie, 18, 4, 609–621 (1973)

Revue Roumaine de Chimie, **18**, *4*, 623 – 634 (1973)

THE ROLE OF CLINKER AND OF CALCIUM CHLORIDE IN THE HARDENING PROCESS OF SOME SILICATE SLAGS

I. TEOREANU and MARIA GEORGESCU

Polytechnic Institute
Laboratory of Technology of Silicates
and Oxide Compounds
Str. Polizu 1
Bucharest, Romania

Received October 25, 1972

The present paper studies the hardening processes of some silicate slags corresponding to wollastonite and rankinite and the manner in which they are influenced by adding Portland cement clinker and calcium chloride, single or together. Additions of 15 % Portland cement clinker, 2 % calcium chloride or 15 % clinker + 2 % calcium chloride, activate the hardening process of wollastonite and rankinite slags. The intensity of the activating effect varies with respect to the nature of the additions and to the basicity of the silicate slag. The mixed addition of 15 % Portland cement clinker + 2 % calcium chloride proved to be most efficient. The activating action of clinker or calcium chloride additions is manifested both by the intensification of the hydration processes of slags and by the increased crystallinity of the hydrated phases and, possibly, change of their basicity.

1. The reduced basicity of calcium silicates existing in high furnace slags accounts for the insignificant rate at which hydration processes are manifestly intensified by adding basic substances (introducing calcium hydroxide into the system), either calcium sulphate or calcium chloride — single or together.

The activating action of calcium hydroxide generating additions upon the hardening processes of calcium silicates in C_2S, C_3S_2, CS * slags is certainly ascertained; however, different opinions are expressed with regard to the nature of this action — as to whether the calcium hydroxide introduced into the system participates or not in the chemical reaction of hydrosilicates formation. Thus, while a number of researchers [1-4] consider that the role of $Ca(OH)_2$ is to provide a certain basicity of the medium, permitting thus a relatively high-speed formation of hydrosilicates which would condition the hardening of the system (without direct participating in the chemical formation process of those compounds), others [5] consider that the silicate slag, in the process of hydration, binds the calcium hydroxide resulting from basic additions. Smolczyk [6] relates the nature of calcium hydroxide action to the water/solid ratio of the system : in the case of β-C_2S pastes or mortars, calcium hydroxide introduced into the system by a basic addition, adheres to the silicate being hydrated, having, however, an indirect action in suspensions, since it influences the rate of the hydration processes without direct participating in them.

---

* $C_2S = 2CaO.SiO_2$; $C_3S_2 = 3CaO.2SiO_2$; $CS = CaO.SiO_2$

[1] Iu. M. Butt, O. M. Astreeva and Z. S. Krasnoslobodskaia, *Tsement*, **3**, 8 (1960).

[2] H. Kühl, "Zement-Chemie", 2. Bd., Verlag VEB, Berlin 1958.

[3] F. Keil, "Hochofenschlacke", Berlin 1949.

[4] J. D'Ans and H. Eick, *Zement-Kalk-Gips*, **7**, 449 (1954).

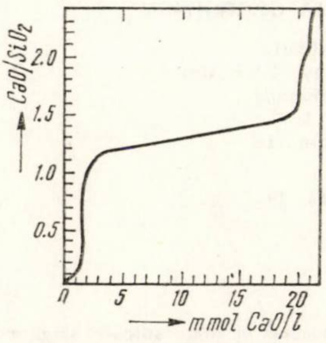

Fig. 1. — Dependence of CaO/SiO_2 ratio of the solid phase formed by hydration of calcium silicates on CaO concentration of the solution.

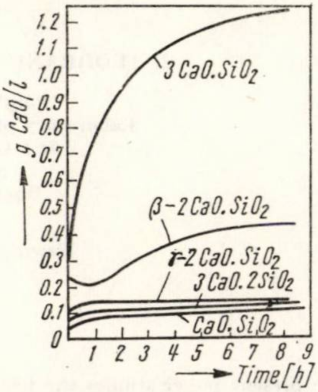

Fig. 2. — Variation of the CaO concentration in solution in the hydration of calcium silicates.

A unitary point of view may be reached in this sense, considering the equilibrium conditions that are being established in the calcium silicate — water system (figs. 1 and 2)

If the presence of the basic addition induces in the silicate — water system a higher CaO concentration than the equilibrium concentration, corresponding to the CaO/SiO_2 ratio of the hydrosilicate, formed by hydration of the silicate slag, it will bind calcium oxide in solution; in the opposite case, CaO will not be consumed in the hydration process or will be consumed only in small amounts.

2. Our present investigations concentrated on the effect of the Portland cement clinker and calcium chloride additions — single or together — upon the hydration of some silicate slags and the nature of hydrated phases formed under these conditions. Slags corresponding to rankinite ($3\,CaO.2SiO_2$) and wollastonite ($CaO.SiO_2$) * were synthesized to this end by melt-

---

[5] H. G. Schmidt, *Zement-Kalk-Gips*, **16**, 321 (1963).

[6] H. G. Smolczyk, "4-ii Mezhdunarodnyi congres po khimii tsementa", Izd. lit. po stroit., Moskva, 1964, p. 227.

* Bicalcium silicate, another constituent of furnace slags, has formed the object of numerous previous investigations.

ling stoichiometric mixtures of chemically pure oxides in an oxiacetylene flame and granulating in water.

Determinations of bound water (table 1) made according to the method described by Butt [7] and roentgenographic and derivatographic investigations made on paste with a 0.4 water/binder ratio, point out the fact that the higher basicity of the medium resulting from a 15% clinker addition significantly intensifies the hydration of wollastonite and rankinite, compared to clinker — free systems.

Table 1

Hydration degree of some silicate slags

Compound	Activating addition (%)		Amount of water bound in hydration (%) after :			
	Clinker	$CaCl_2$	28 days	90 days	180 days	360 days
$CaO \cdot SiO_2$	—	—	2.619	2.860	3.266	2.483
	—	2	3.128	4.080	5.576	6.903
	—	3.5	3.757	5.205	7.051	—
	—	5	4.125	8.311	7.981	7.408
	—	10	5.553	8.324	10.065	9.382
	—	20	7.715	11.065	12.080	17.220
	15	—	7.573	10.680	9.873	11.505
	15	2	10.576	12.360	11.937	13.336
$3CaO \cdot 2SiO_2$	—	—	2.930	6.290	7.281	11.574
	—	2	3.180	10.500	9.833	11.554
	15	—	11.500	11.800	9.980	10.614
	15	2	11.050	10.880	12.113	13.830

The increased hydration rate in the presence of an addition of 15% clinker, after 28 days could not be explained even if assuming the total hydration of the clinker (an unworkable phenomenon in fact), without also considering the acceleration of the hydration-hydrolysis processes of silicate slags in the presence of clinker.

Pure *wollastonite* does not form roentgenographically detectable hydrated phases, even after a period of 360 days. The endothermic effects appearing at temperature ranges of 150 . . . 220° and 600 . . .780° on the differential thermal analysis curves presented in figure 3, indicate the existence of certain amounts of hydro-compounds of the tobermorite hydrosilicates type.[8–10] Their preponderant gelic nature makes roentgenographic detection difficult.

It has been found that calcium hydrosilicates of CSH(I) type are formed in the presence of Portland cement clinker, even after short periods of time. They are revealed roentgenographically by interferences 3.03—3.05 (3.02)Å, 2.74—2.81 (2.78)Å and 1.79—1.82 (1.81)Å and thermographically by the endothermic effects from 140 ...150° and 660 . . . 750° (fig.4).

---

[7] Iu. M. Butt, "Practicum po technologhii vyazhuschikh veschestv i izdelii iz nih", izd. 2, Promstroizdat, Moskva, 1953, p. 320.

[8] H. F. W. Taylor, "The chemistry of cements", vol. 2, Academic Press, London and New York, 1962.

[9] V. S. Gorschov, "Termografia stroit. materialov", Izd. lit po stroit., Moskva, 1968.

[10] Iu. M. Butt and L. N. Raschovich, "Hardening of binders at high temperatures", Ed. Tehnică, Bucharest, 1969 (translated from Russian).

All investigated wollastonite samples reveal the presence of an exothermic effect at temperatures of 840.. .850°. The higher amplitude of this effect for the anhydrous wollastonite or for wollastonite hydrated without additions causes us to assume that it is determined by the devitrification of the wollastonite slag.

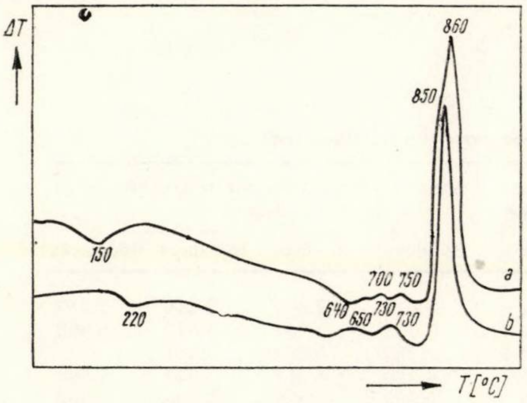

Fig. 3. — ATD curves of slag with a $CaO.SiO_2$ composition, hydrated for :
a — 90 days; b — 180 days.

Fig. 4. — ATD curves of slag with a $CaO.SiO_2$ composition, with 15% Portland cement clinker addition, hydrated for :
a, 90 days; b, 180 days.

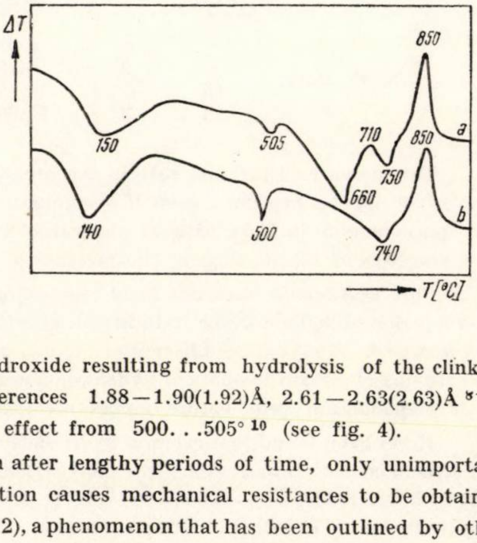

The existence of the free calcium hydroxide resulting from hydrolysis of the clinker, is expressed roentgenographically by interferences 1.88 — 1.90(1.92)Å, 2.61 — 2.63(2.63)Å [8-10] and thermographically by the endothermic effect from 500. . .505° [10] (see fig. 4).

While pure wollastonite acquires, even after lengthy periods of time, only unimportant mechanical resistances, a 15% clinker addition causes mechanical resistances to be obtained as early as after 7 days of hardening (table 2), a phenomenon that has been outlined by other researchers as well. [11-13]

The mechanical resistances obtained must be attributed, in the first place, to the hardening of clinker and also to the activated slag. This statement is also supported by the fact, for instance, that mechanical resistance obtained for wollastonite and enstatite ($MgO.SiO_2$) [14]

---

[11] P. P. Budnikov and V. L. Pankratov, *Doklady Akad. Nauk SSSR*, **146**, 156 (1962).

[12] P. P. Budnikov, V. S. Gorschov and T.A. Hmelevskaia, *Stroit. materialy*, **5**, 30 (1960).

[13] V. S. Gorschov, *Zhur. priklad. Khim.*, **38**, 3448 (1966).

[14] I. Teoreanu and M. Georgescu, unpublished data.

Table 2

Mechanical resistances of slag with a $CaO.SiO_2$ composition

Activating additon (%)		Compressive strength * (daN/cm^2), after :				Tensile strength * (daN/cm^2), after :			
Clinker	$CaCl_2$	7 days	28 days	90 days	180 days	7 days	28 days	90 days	180 days
—	—	0	0	10	10	0	0	10.2	12.5
15	—	25	72.5	90	111	16	32.5	56.8	57.1
—	2	0	5	10	10	0	3.6	4.5	7.1
—	5	0	0	0	0	0	0	0	0
—	10	0	0	0	0	0	0	0	0
—	20	0	0	20	—	0	0	15.4	—
15	2	35.5	90	132.5	150	29.4	50.1	77.7	83.4
10	7	55	80	100	100	24.5	40.8	50.2	49.8
7	10	10	45	100	90	21.6	43.5	53.5	67.8

* Mechanical resistances were determined on Kühl microsamples, manufactured of mortar with a 1 : 3 binder/aggregate ratio. They were calculated by relation : $R_c = F/S = F/2$ (daN/cm^2) ; $R_t = 6.F.l/a.b^2 = 60.F$ (daN/cm^2), where :

R_c – the compressive strength (daN/cm^2) ;
R_t – tensile strength (daN/cm^2) ;
F – breaking stress (daN) ;
S – cross-section area of the sample (cm^2) ;
l – length of the arm of the apparatus (cm) ;
a – width of the prism (cm) ;
b – thickness of the prism (cm).

with a similar clinker addition, has different values. In addition to this, significantly different mechanical resistances were obtained by replacing the slag in slag + clinker mortar by sand having a similar fineness (table 3).

Table 3

Mechanical resistances of additions used as activators

Composition of the binder (%)			Compressive strength (daN/cm^2), after :		Tensile strength (daN/cm^2), after :	
Fine sand	Clinker	$CaCl_2$	7 days	28 days	7 days	28 days
85	15	—	6.5	15.0	7.8	8.8
83	15	2	8.0	16.5	7.8	9.0
83	10	7	4.5	7.5	0	0
83	7	10	4.0	5.0	0	0

Calcium chloride does not exert an intensifying action upon wollastonite hydration (see table 1). The possible roentgenographic detection of some hydrated compounds of the tobermorite calcium hydrosilicates-type, even after 7 days of hydration, must be looked upon as a result of their more pronounced crystallization degree, compared to hydro-compounds formed by hydration of the pure wollastonite.

The fact that even in the case of big amounts of calcium chloride (up to 20 %), its binding and the formation of chlorinated complex combinations has not been reflected by roentgenographic and thermographic approaches, or by chemical analysis, makes us consider that

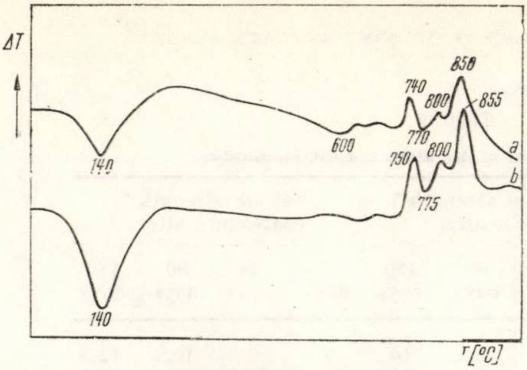

Fig. 5. — ATD curves of slag with a $CaO.SiO_2$ composition, with 2% $CaCl_2$ addition, hydrated for : *a*, 90 days; *b*, 180 days.

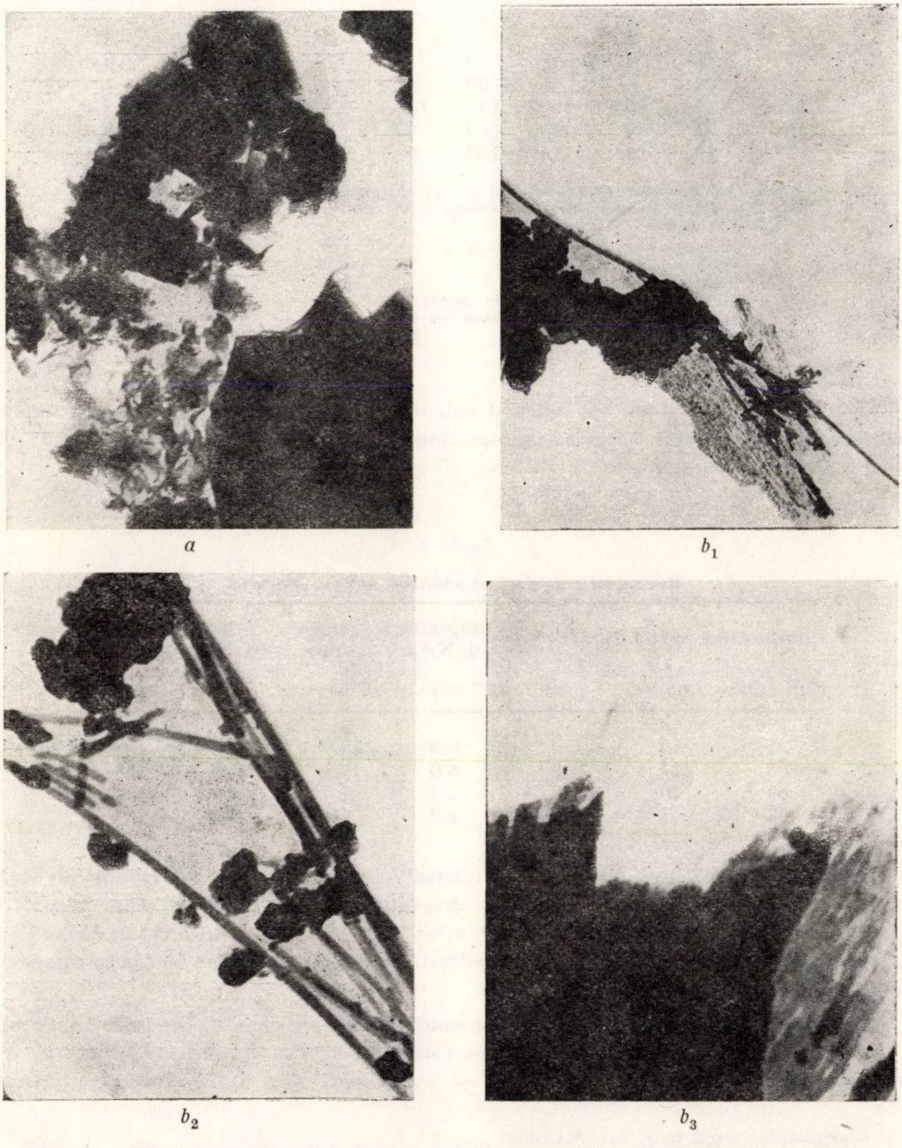

a

b_1

b_2

b_3

Fig. 6. — Electronomicroscopic images of the slag with a $CaO.SiO_2$ composition, hydrated for 90 days :
a – in pure state; b_1 – b_3 – with 2% $CaCl_2$.

its action of intensifying wollastonite hydration (visible particularly after long periods of time) is a consequence of changes which it determines in the ionic equilibrium of the silicate-water system (especially from the viewpoint of its saturation),[15] withtout a direct participation in the chemical reactions involving the formation of hydrocompounds.

It is however possible to assume that chlorine ions introduced by calcium chloride are "built-in" in the calcium hydrosilicates lattice (this phenomenon was reported by Richartz[16] for the hydration of tricalcium silicate in the presence of calcium chloride) entailing consequences for morphology of the formed hydrosilicates. Such a phenomenon may induce the occurrence of an intense exotermic effect at 740...750° on the thermograms (fig. 5) owing to the displacement of the effect corresponding to tobermorite hydrosilicates towards lower temperatures.

Fig. 7. — ATD curves of slag with a $CaO.SiO_2$ composition, hydrated in the presence of 15% Portland cement clinker + 2% $CaCl_2$, for:
a, 90 days; *b*, 180 days.

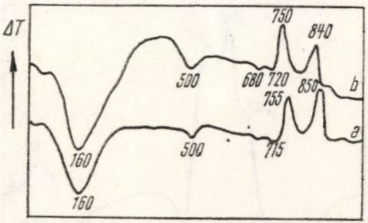

At the same time, the electronomicroscopic images of wollastonite hydrated for 90 days in the presence of 2% $CaCl_2$ (fig.6) reveal the fibrous aspect of the hydrated phases (different from those noticed in pure wollastonite). This aspect is similar to that reported by other research workers[8,17,18] for stronger basic hydrosilicates, formed in chlorine-free systems.

The influence of calcium chloride on wollastonite hydration and hardening processes is however insignificant, particularly if we take into account the values of mechanical resistances obtained in the $CaO.SiO_2$ system ; we must consider, in the first place, the accelerating action exerted by calcium chloride on clinker hydration-hydrolysis processes, especially in short intervals of time, with consequences upon wollastonite hydration. The activating action of clinker on the hydration of monocalcium silicate is, in fact, intensified in this way. An important increase in the hydration rate is subsequently observed, materialized both by a higher amount of bound water after 28 days (see table 1) and by a significant reduction of the amount of nonhydrated wollastonite (as indicated by the amplitude of the devitrification effect from 840...850° — fig. 7) compared to the sample activated by the clinker alone (see fig.4). The endothermic effect from 500° — more reduced in amplitude as against the same effect on the thermograme, if wollastonite hydrated in the presence of clinker (see fig. 4) — ascertains the more intense hydration of monocalcium silicate, with $Ca(OH)_2$ binding under the conditions of a mixed addition of 15% clinker and 2% calcium chloride.

Tobermorite-type calcium hydrosilicates — CSH(I) — are identified as the main hydrated phases, in this case too. They have a more pronounced crystalline character reveling a higher number and intensity of roentgenographic interferences. Chlorinated complex combinations are not reported this time either. The strong exothermic effect from 750...755° (see fig. 7), ampler than for wollastonite hydrated in the presence of 2% $CaCl_2$ may be explained by the possible "built-in" of chlorine in the calcium hydrosilicates lattice.

---

[15] I. Teoreanu, Paper presented at the 36-th Congress of Chemical Engineering, Bucharest, 1970.

[16] W. Richartz, *Zement-Kalk-Gips*, **22**, 447 (1969).

[17] A. Van Bemst, *Silicates Industriels*, **22**, 213 (1957).

[18] P. I. Bojenov and G. F. Suvorova, *Tsement*, **8**, 23 (1957).

Owing to an increased hydration rate and to a certain proportion being established between gelic and crystalline hydrated formations, wollastonite with a 15 % clinker + 2 % $CaCl_2$ addition presents, after hardening, significantly higher mechanical resistances than in the case of another addition (see table 2).

By using mixed additions, in which the proportion of calcium chloride was higher (correspondingly reducing that of the clinker) we found that resistance-wise the optimum addition for the hardened binder consists of 15% clinker + 2% $CaCl_2$.

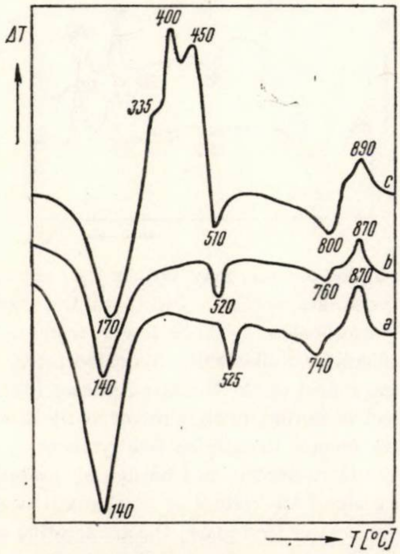

Fig. 8. — ATD curves of slag with a $3CaO.2SiO_2$ composition, hydrated in the presence of 15% Portland cement clinker, for :
a, 28 days ; *b*, 90 days ; *c*, 180 days.

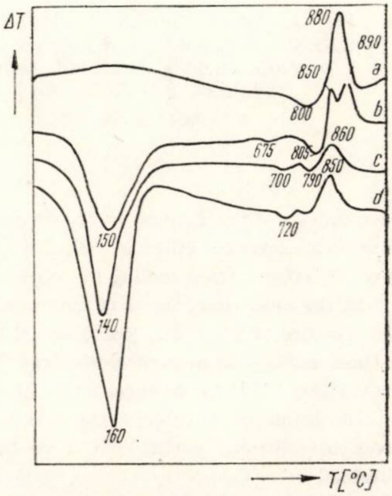

Fig. 9.— ATD curves of slag with a $3CaO.2SiO_2$ composition :
a, anhydrous ; *b*, hydrated for 28 days ; *c*, hydrated for 90 days ; *d*, hydrated for 180 days.

In the case of slags having the composition of *rankinite*, characterized by a stronger basicity than wollastonite and which, even in pure state hydrates more intensely than wollastonite, the intensity of the activating action of clinker and calcium chloride — single or together — undergoes some changes : if in the case of calcium chloride, the hardening processes of rankinite slag are intensified to a larger extent, addition of clinker or clinker + calcium chloride induces changes, particularly in the nature of the hydrated products being formed.

Pure rankinite forms by hydration, weakly basic tobermorite calcium hydrosilicates— CSH (I), as main products. The presence of a 15% clinker addition in the system determines also the formation of some more basic hydrosilicates. The diminution in time of the endothermic effect characterizing calcium hydroxide (fig. 8) and the occurrence on the debyegrame of some specific interferences — 1.99—2.03 (2.0)Å, 1.51—1.52 (1.56)Å ascertain the formation of some CSH(II)-type compounds too.

The amount of hydrated, mostly gelic formations is much larger in the presence of clinker in the system and significantly increases after 180 days, which explains the appearence on the thermogram of the exotermic effect group from 335...460°[19] (fig. 8), effects that are not reported for pure rankinite hydrated over a similar period of time (fig. 9).

---

[19] A. V. Volzhenskii, Iu. S. Burov, B. N. Vinogradov and K. V. Gladkih, "Betony i izdelia schlakovykh i zolinykh materialov", Izd. lit. po stroit., Moskva, 1969.

In the presence of calcium chloride, vitrous rankinite behaves more actively with respect to water than wollastonite. This is reflected both by the higher hydration rate – particularly in long periods of time (see table 1) – and by the higher values of mechanical resistances – particularly after periods of time involving more than 28 days (table 4).

Table 4

Mechanical resistances of slags with a $3CaO.2SiO_2$ composition

Activating addition (%)		Compressive strength (daN/cm^2), after :				Tensile strength (daN/cm^2), after :			
Clinker	$CaCl_2$	7 days	28 days	90 days	180 days	7 days	28 days	90 days	180 days
—	—	0	21	40	—	0	6.9	—	—
15	—	22.5	62.5	85	—	18.8	31.0	—	—
—	2	40.0	115.0	126.0	—	26.4	41.5	—	—

Since, for a period of 28 days, calcium chloride does not change the hydration rate of rankinite, the relatively high mechanical resistances, acquired after this interval, must be due especially to the intensification of the crystallization processes of the hydrated products. Roentgenographic and electronomicroscopic investigations confirm the change in the crystallinity of the hydration products of rankinite, in the presence of calcium chloride. The more crystalline character of the hydrated phases in samples of rankinite with calcium chlorite is evident if comparing the electronomicroscopic images of pure rankinite with those of rankinite with 2% calcium chloride addition (fig. 10).

In the case of rankinite with calcium chloride addition, the curves ATD (fig.11) outline the displacement of the exothermic effect characteristic for weakly basic hydrosilicates, towards lower temperatures (746...810°). The probable explanation is the same as in the case of wollastonite.

The results of the chemical analyses carried out on rankinite suspensions with a calcium chloride addition, and with a water/binder $=50$ ratio of 50, show that not even in the case of large addition of calcium chloride (up to 20%) do we find formations of chlorinated complex combinations.

The simultaneous presence of clinker and calcium chloride in the rankinite-water system provides it with a more active character due to the intensification of hydration-hydrolysis processes of the clinker by calcium chloride, in the first place, and also to the activated hardening of the slag.

The more improved behaviour of the hardening system of C_3S_2-(clinker + $CaCl_2$)-water, versus the C_3S_2-clinker-water system, is likely to be largely determined by the better crystallization of hydrated formations (reflected in increased intensitites of roentgen interferences) and in a lesser degree by larger amounts of hydrocompounds. The hydration rate increases significantly, with the formation of increased amounts of hydrocompounds (however, preponderantly gelic on the whole) only after longer periods of time (180 days). The group of exothermic effects from 350...490° (fig. 12) and the amount of bound water beyond this interval (see table 1) reflects this phenomenon.

The diminution in time of the exothermic effect from 505...530° indicate the intensification of rankinite hydration, with the binding of calcium hydroxide liberated by hydrolysis of

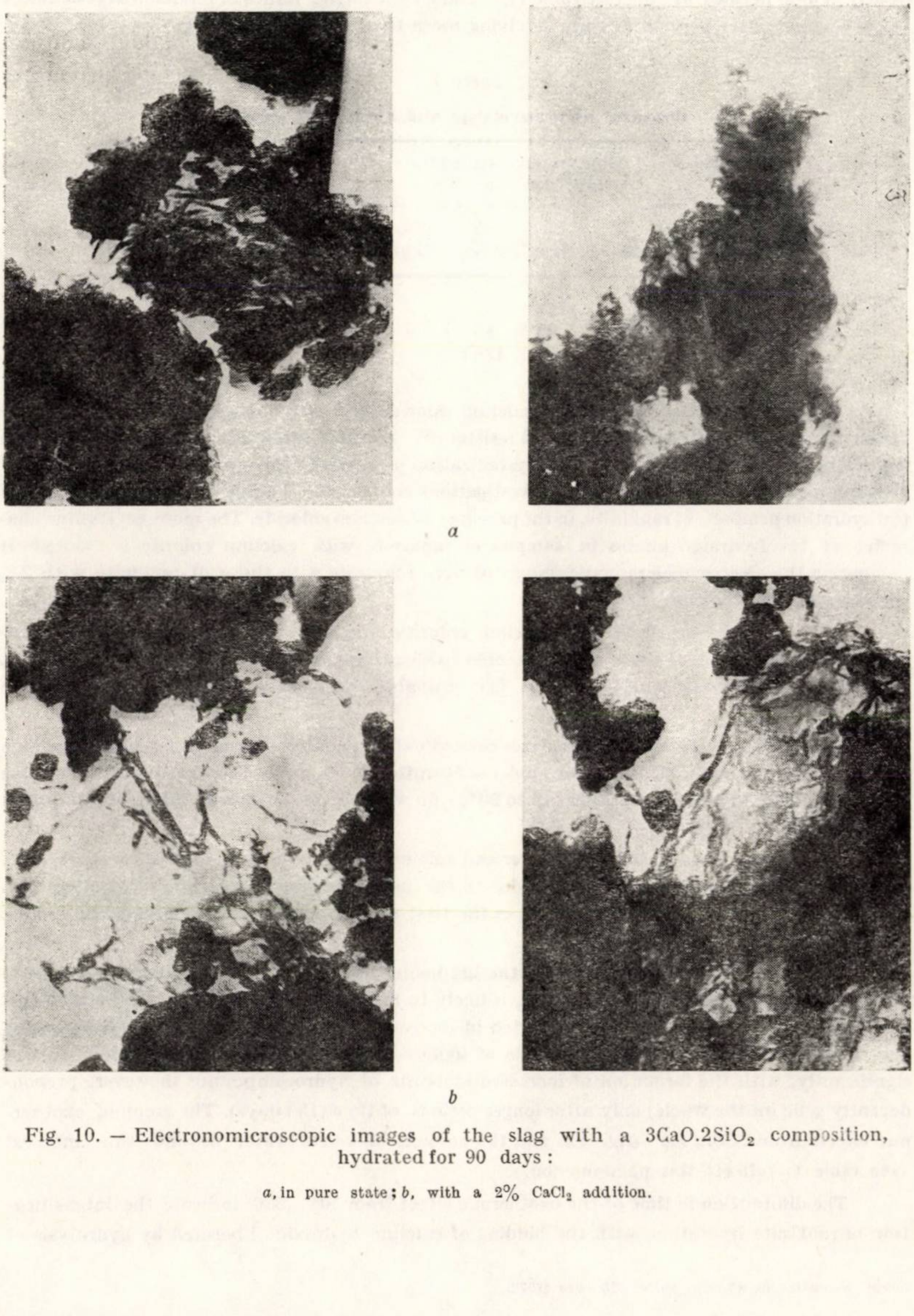

Fig. 10. — Electronomicroscopic images of the slag with a $3CaO.2SiO_2$ composition, hydrated for 90 days :

a, in pure state; *b*, with a 2% $CaCl_2$ addition.

the clinker. The reduced amplitude of this effect, compared to that of the similar effect on the thermogram of rankinite with an addition of clinker, must be considered as a confirmation of a more intense activation of rankinite by the mixed addition of clinker and calcium chloride.

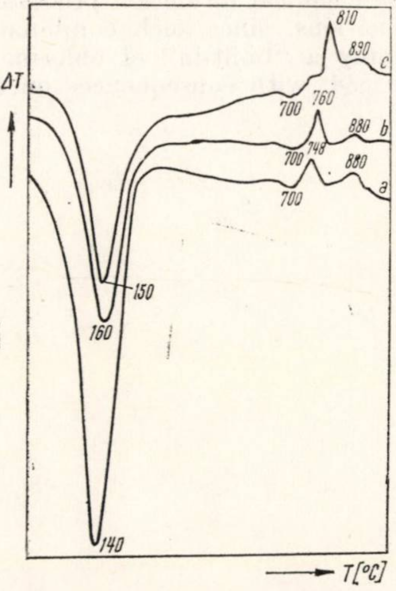

Fig. 11. — ATD curves of the slag with a $3CaO.2SiO_2$ composition, hydrated in the presence of 2 % $CaCl_2$, for : *a*, 28 days; *b*, 90 days; *c*, 180 days.

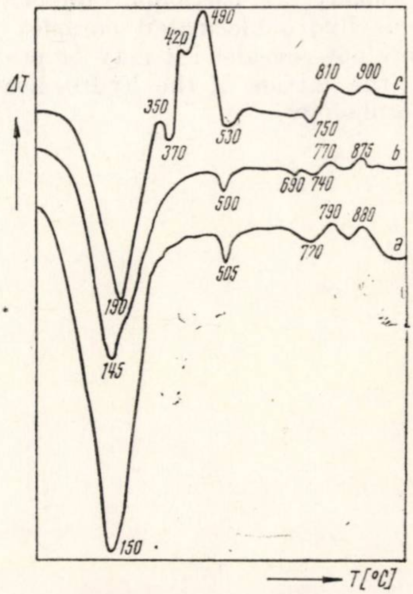

Fig. 12. — ATD curves of the slag with a $3CaO.2SiO_2$ composition, hydrated in the presence of 15 % Portland cement clinker + 2 % $CaCl_2$, for : *a*, 28 days; *b*, 90 days; *c*, 180 days.

3. Based on the results obtained with regard to the behaviour of calcium silicates in the presence of some activators, we may conclude that the action of additions used is manifested both by an intensified hydration rate of silicate slags and by an increased crystallinity of hydrated formations and the change of their basicity.

The existence of a parallelism between the behaviour of pure compounds and that in the presence of calcium chloride is also outlined.

The effect of calcium chloride varies in relation to the basicity of the silicates. By corroborating the present results with results obtained from other papers [15] we may say that, in the series of calcium silicates, the activating action of calcium chloride decreases in intensity in the following order :

$$3CaO.SiO_2 \rightarrow 2CaO.SiO_2 \rightarrow 3CaO.2SiO_2 \rightarrow CaO.SiO_2$$

Considering the fact that the reactivity of calcium silicates, even in pure state, increases as the basicity is increased, it may assumed that the intensified crystallization of the formed hydrated compounds is the prime determining element in the activation action of calcium chloride on those compounds.

With regard to the nature of the action of calcium chloride, it does obviously not participate directly in the chemical formation processes of some hydrochlorinated complex combinations, since such combinations were not revealed; it may be possible only a "built-in" of chlorine ion in the lattice of the hydrosilicates formed, with consequences on their morphology.

Revue Roumaine de Chimie, **18**, *4*, 635–653 (1973)

CHEMICAL GRAPHS. XVIII[1]

GRAPHS OF DEGREES FOUR OR LESS, ISOMERS OF ANNULENES, AND NOMENCLATURE OF BRIDGED POLYCYCLIC STRUCTURES

ALEXANDRU T. BALABAN

Institute of Atomic Physics, P. O. Box 35, Bucharest, Romania

Received November 23, 1972

Tables of graphs with degrees 2 — 4 and orders (number of points) 1 — 5 are presented and a recurrent procedure for the construction of such graphs is developed. The use of these tables is illustrated by a procedure for finding all possible isomers of annulenes, with explicit solutions for [4]-and [6]annulene: there are 217 possible graphs corresponding to formula C_6H_6, from which 58, including the five valence isomers $(CH)_6$, are not too unduly strained so as to preclude their existence as stable chemical compounds. Bridged polycyclic structures have topologies that are completely described by the same types of graphs, which could therefore find applications in coding and/or nomenclature. Several ways of improving the Baeyer system for the nomenclature of bridged polycyclics are briefly discussed. An exhaustive table of bi-, tri- and tetracyclic topologies is presented.

INTRODUCTION

In previous papers of this series, a recurrent procedure was presented for the construction of trivalent multigraphs (i.e. regular graphs where each point (vertex) has degree 3, i.e. is incident to three lines (edges), and two points may be joined by simple or multiple edges),[2] or trivalent general graphs (where a point may also be joined to itself by a loop which is counted twice in the degree). [3] Tables were presented, enumerating all possible trivalent multigraphs [2] or general graphs [3] with 10 points or less ; from larger graphs, only planar * multigraphs with 12 points were enumerated.[5]

---

* For graph terminology see previous parts and ref. [4]

[1] Part. XVII, A. T. Balaban, *Rev. Roumaine Chim.*, **17**, 1531 (1972).

[2] A. T. Balaban, *Rev. Roumaine Chim.*, **11**, 1097 (1966).

[3] A. T. Balaban, *Rev. Roumaine Chim.*, **15**, 463 (1970).

[4] F. Harary, „Graph Theory" Addison-Wesley, Reading, Mass. 1969.

[5] A. T. Balaban, *Rev. Roumaine Chim.*, **17**, 865 (1972).

The tables with all possible trivalent multigraphs are useful for an exhaustive search of valence isomers of annulenes since each point can be considered to represent a CH group, and each line one covalent bond. Tables of trivalent general graphs can, in addition, provide an exhaustive list of chemical structures which possess also divalent groups, such as valence isomers of 5- or 7-membered heterocyclic compounds; in this case a loop with the vertex to which it is attached is considered to represent the divalent group of atoms.[3]

Organic chemical structures can, however, possess quaternary carbon atoms which would correspond to points of degree 4 in the graph. In the project of devising an algorithm for the generation of all isomers corresponding to a given molecular formula, Lederberg [6,7] tried to avoid this complication by replacing vertices of degree four by vertices of degree three. This can be done either (i) by inserting an edge [6,7] resulting in the replacement of one vertex of degree four by two vertices of degree three or (ii) by replacing the vertex of degree four by the four intersections of lines emerging from this vertex with a small circuit around the vertex.[8] However, these procedures are not free from ambiguities, as indicated by figure 1 which proves that one and the same graph with a point of degree 4 can give rise to more than one trivalent graph in both procedures (i) and (ii).

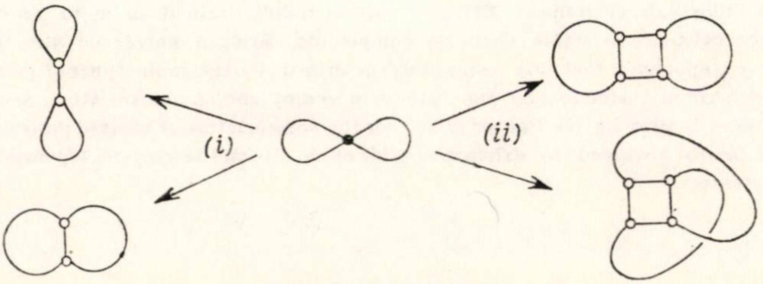

Fig. 1. — Replacement of a vertex of degree four in the unique graph of degree 4 and order 1 with two loaps by (i) two or (ii) four vertices of degree three.

In the present paper we will present a recurrent procedure for enumerating "head-on" [7] all given graphs with degrees equal to, or less than, four. Unlike previous cases, the degrees of the points will not be required to be all equal, i.e. the multigraphs will no longer be regular except where stated. It can be easily proved that in a graph the number of vertices with odd degree must be even.[4] All the following discussion will concern only connected graphs, i.e. graphs where any two vertices are connected by a path.

---

[6] J. Lederberg, *Proc. Natl. Acad. Sci.*, **53**, 134 (1965).

[7] J. Lederberg, in "The Mathematical Sciences", The MIT Press, Cambridge, Mass. 1969, p. 37.

[8] O. Ore, "The Four-Colour Problem", Academic Press, New York, 1967, p. 117.

MULTIGRAPHS AND GENERAL GRAPHS OF DEGREE FOUR OR LESS

The construction of regular graphs of degree 3, including multigraphs and general graphs, was presented earlier.[2,3] Regular graphs of degree 2 are simple circuits with the required number of points. Graphs of degrees 3 and 2 (noted 3/2) and order p can be obtained from loop-graphs of degree 3 and order $p + 2k$ which do not have "geminal" loops, i.e. two loops bonded to the same point, by deleting the k loops and their lines of attachment. Alternatively, they can be obtained from trivalent graphs of order $p-1$ by inserting a point of degree 2 on each non-equivalent line.

The construction of regular graphs of degree 4 proceeds from the simplest circuit without any point, by intersecting it with itself and forming thus one point and the unique graph of degree 4 and order 1 with two loops. By repeating the procedure with this graph the intersection can be made within a loop or between the two loops, resulting in the two possible regular graphs of degree 4 with two points. The same process gradually builds or up all regular graphs of degree 4. Graphs of degrees 4/2 can be obtained from the latter by inserting a point of degree 2 on each non-equivalent edge or loop. Graphs of degrees 3/4 can be obtained from regular graphs of degree 4 by deleting one edge at a time, if it connected two vertices of degree four. Graphs of degree 4/3/2 are obtained from the last graphs by inserting points of degree 2 on each of their non-equivalent edges or loops.

Figure 2 presents the exhaustive list of connected multigraphs and general graphs with 1 through 5 vertices of degrees 2, 3 and/or 4. The numbers of these graphs are indicated in table 1 according to the parameters : total number of points p, number of loops λ, degrees, and partition of points according to their degree. As examples for points of degree 2,3 and 4, table 1 lists CH_2, CH and C groups, respectively ; in figure 2, black circles indicate points (vertices) of degree four and open circles of degree three ; no special symbol is used for vertices of degree 2. The outlay of figure 2 follows that of table 1. Excepting the complete graph K_5 with five points (5-clique)[4], all graphs presented here are planar, according to Kuratowsky's theorem ;[9] to emphasize their planarity, all planar graphs are drawn so that no line crosses.

By the procedure outlined above, figure 2 can be continued to orders $p > 5$ when necessary.

ISOMERS OF HYDROCARBONS

In their comprehensive search for the automation of inductive inference in organic chemistry, Lederberg and co-workers developed the DENDRAL program which can compute the isomers of acyclic organic compounds and match them against mass and NMR spectral data for struc-

---

[9] K. KURATOWSKY, *Fund. Math.*, **15**, 271 (1930).

Ta-

Number of general graphs

Degree(s) :		2	3/2		3		4/2
Number of points of each degree :		p	$2, p-2$	$4, p-4$	p	$1, p-1$	$2, p-2$
Order p	Nº of loops λ	E.g. $(CH_2)_p$	E.g. $(CH)_2(CH_2)_{p-2}$	E.g. $(CH)_4(CH_2)_{p-4}$	E.g. $(CH)_p$	E.g. $C(CH_2)_{p-1}$	E.g. $C_2(CH_2)_{p-2}$
1	0	0	—	—	—	—	—
	1	1					
	2	0					
2	0	1	—	—	1	0	—
	1	0			0	1	
	2	0			1	0	
3	0	1	1	—	—	1	1
	1	0	1			1	1
	2	0	1			0	1
	3	0	0			0	0
4	0	1	3	—	2	1	3
	1	0	2		1	1	2
	2	0	1		1	0	2
	3	0	0		1	0	0
	4	0	0		0	0	0
5	0	1	5	4	—	2	5
	1	0	3	4		1	4
	2	0	1	3		0	2
	3	0	0	1		0	0
	4	0	0	0		0	0
	5	0	0	0		0	0

tural identification with a minimal amount of manpower. [10] Cyclic structures, however, have not yet been included into this program.

Generally, for a structure formed from p_i atoms of valence $i (1 \leqslant i \leqslant 4)$ represented by a graph in which only vertices with $2 \leqslant i \leqslant 4$ are shown, the number q of edges is given by

$$2q = 4p_4 + 3p_3 + 2p_2 - p_1 \tag{1}$$

In the case of hydrocarbons with $p_4 = p$ carbon atoms and $p_1 = h$ hydrogens, represented by a graph showing only the C—C bonds, we have the number of edges according to (1),

$$q = (4p - h)/2 \tag{2}$$

---

[10] G. SCHROLL, A. M. DUFFIELD, C. DJERASSI, B. G. BUCHANAN, G. L. SUTHERLAND and J. LEDERBERG, *J. Amer. Chem. Soc.*, **91**, 7440 (1969) and previous papers in the series.

ble 1

with degrees four or less

		4/3/2		4/3		4
$3,\ p-3$	$4,\ p-4$	$1,\ 2,\ p-3$	$2,\ 2,\ p-4$	$p-2,\ 2$	$p-4,\ 4$	p
E.g. $C_3(CH_2)_{p-3}$	E.g. $C_4(CH_2)_{p-4}$	E.g. $C(CH)_2(CH_2)_{p-3}$	E.g. $C_2(CH)_2(CH_2)_{p-4}$	E.g. $C_{p-2}(CH)_2$	E.g. $C_{p-4}(CH)_4$	E.g. C_p
—	—	—	—	—	—	0 0 1
—	—	—	—	—	—	1 0 1
—	—	—	—	1 2 1 1	—	1 1 1 1
2 3 2 1 0	—	4 5 4 1 0	—	5 6 7 3 1	—	3 2 3 1 1
7 9 6 2 0 0	8 9 9 4 1 0	12 17 9 2 0 0	20 30 25 10 2 0	14 27 24 14 5 1	6 10 8 4 2 0	6 7 7 5 2 1

The cyclomatic number μ of the graph indicates the number of its cycles, and for a connected graph is

$$\mu = q - p + 1 \tag{3}$$

Indeed, saturated alkanes, with $h = 2p + 2$, have according to (2) $q = p - 1$, hence $\mu = 0$. For hydrocarbons C_pH_h, by eliminating q between relationships (2) and (3), the number of cycles or double bonds is found to be

$$\mu = (2p - h + 2)/2 \tag{4}$$

Indeed, the same value results as half the difference between the number of hydrogens in an alkane with the same number of carbon atoms, $2p + 2$, and the actual number h of hydrogens.

Finding all isomers of a hydrocarbon is equivalent to finding all graphs according to partitions of $2q$ among the degrees of the points of the graph,[4] i.e. in the case of a hydrocarbon C_pH_h, partitioning $2q = 4p - h$ into p positive integers equal to, or smaller than, four. Alternatively, the h hydrogens must be partitioned into p non-negative integers equal to, or smaller than, three. These two partitions are in one-to-one correspondence since each of the pairs of p integers add up to four. The former partition gives smaller numbers for alkanes where $2q<h$; for cycloalkanes or monoolefins $2q = h$, hence the two groups of partitions are equal; for all other hydrocarbons, the latter partition is the simplest.

In such a case, the partitions of h into p non-negative integers 0, 1, 2, or 3, can be easily found from the table of partitions of h into at most p terms * by deleting all those partitions containing numbers greater than 3.

Having found all possible partitions of $2q$ or of h into p integers, one must then construct for each partition all possible graphs corresponding to that partition. Such graphs corresponding to one partition are *per definitionem* [2,3] valence isomeric structures.

ISOMERS OF ANNULENES

Annulenes C_pH_p have a long history with benzene, and a more recent one with cyclobutadiene, cyclooctatetraene, cyclodecapentaene, and the large annulenes which were intensely studied in the last years.[12] In order to obtain a complete list of all isomers ** of a given annulene, we divide the points of the graph corresponding to its structural formula according to their degrees $(C)_a\,(CH)_b\,(CH_2)_c\,(CH_3)_d$, and write the two balance equations for the carbon and hydrogen atoms, which must be solved in integers; a, b, c, and d are, respectively, number of points of degree 4, 3, 2 and 1 (points of degree one will be treated differently in the following).

$$a + b + c + d = b + 2c + 3d = p$$

By assigning to b various values $0 \leqslant b \leqslant p$, the second equation becomes a Diophantic one and can be easily solved in terms of integer c and d values. Then the first equation gives the value of a.

Alternatively, the following equivalences can be employed sequentially starting with $(CH)_p$ to yield all other isomeric partitions

$$(CH)_2 = C + (CH_2)$$

$$(CH)_3 = C_2 + (CH_3)$$

---

* The number of these partitions can be found in table 2 of ref. [11] or in references cited therein.

** Only topological (structural) factors are considered, geometrical or sterical isomerism is disregarded.

[11] A. T. Balaban, *Rev. Roumaine Chim.*, **17**, 9 (1972).

[12] F. Sondheimer, *Accounts Chem. Res.*, **5**, 81 (1972); *Pure Appl. Chem.*, **28**, 331 (1971).

For illustration the isomers of cyclobutadiene and of benzene are presented in figures 3 and 4, respectively. For C_4H_4 there are four classes of valence isomers, * corresponding to the four possible partitions of 4 into four non-negative integers smaller than, or equal to 3. There are 11 possible graphs corresponding to molecular formula C_4H_4, namely two valence isomers $(CH)_4$ i.e. cyclobutadiene and tetrahedrane which are cubic (trivalent) graphs of order 4, four isomers $C(CH)_2(CH_2)$, three isomers $C_2(CH_2)_2$ and two isomers $C_2(CH)(CH_3)$. These partitions of carbons and hydrogens result also by assigning integer non-negative values to variables k and j in the formula $(CH_3)_{1-k}(CH_2)_{2k-j}(CH)_{2j-k+1}(C)_{2-j}$.

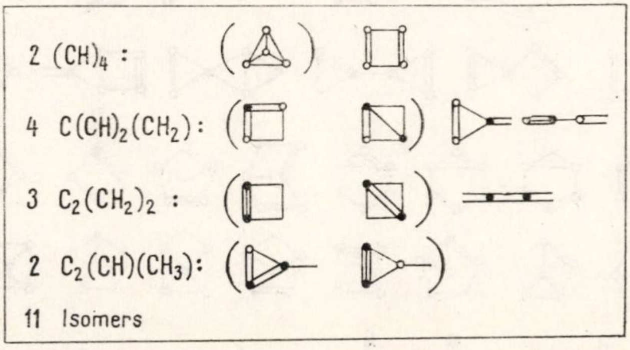

Fig. 3. — Isomers of C_4H_4.

All but the last group are to be found in the table of graphs of order 4 without loops. The last isomers with methyl groups corresponding to points of degree one will be treated differently, i.e. the methyl group will be considered together with the point to which it is attached; this point will accordingly have a degree lower by one and the whole graph an order lower by one if the methyl group is ignored. Hence the last group of isomers are found by attaching a point of degree 1 (a path of length one, i.e. a methyl group) to a point of degree 3 in graphs $C(CH)_2$, or to a point of degree 2 in graphs $C_2(CH_2)$. Alternatively, the last group (class) of isomers with methyl result from graphs $C_2(CH)_2$ with four vertices and one loop on a vertex of degree three, by replacing the loop with a methyl.

Owing to steric and electronic factors, only vinylacetylene and allene are stable compounds. Cyclobutadiene [13] and methylenecyclopropene [14-16] are unstable but have stable substituted derivatives : thus annelated naph-

---

* Valence isomers correspond to connected graphs with the same partition of the degrees of their vertices, [2-4] when only atoms of valence higher than one are considered.

[13] P. Reeves, T. Devon and R. Pettit, *J. Amer. Chem. Soc.*, **91**, 5890 (1969).

[14] G. Binsch, E. Heilbronner and J. N. Murrell, *Mol. Phys.*, **11**, 355 (1966).

[15] I. J. Miller, *Tetrahedron*, **25**, 1349 (1969).

[16] N. C. Baird and M. J. S. Dewar, *J. Chem. Phys.* **50**, 1262 (1969); *J. Amer. Chem. Soc.*, **89**, 3966 (1967).

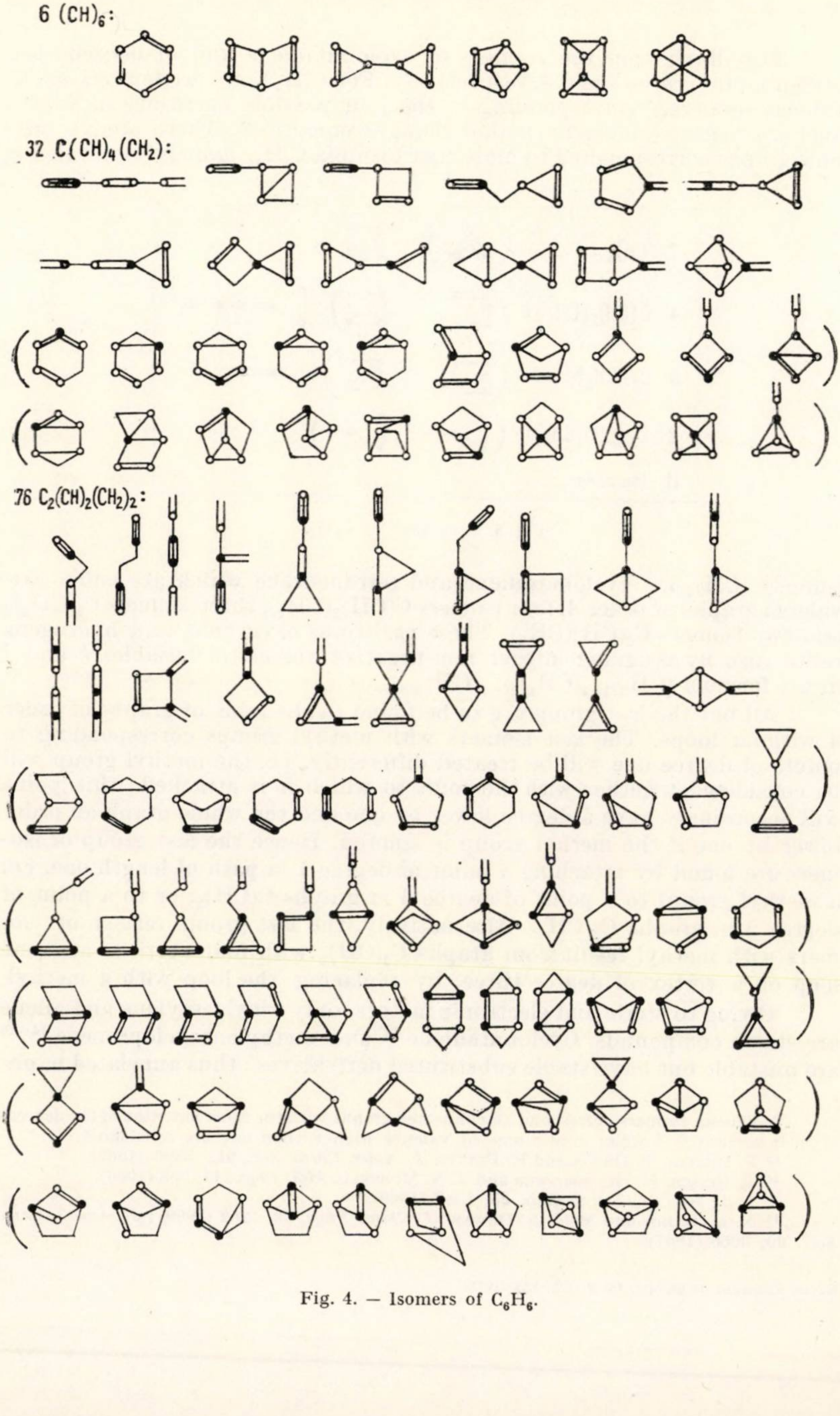
6 $(CH)_6$:
32 $C(CH)_4(CH_2)$:
76 $C_2(CH)_2(CH_2)_2$:

Fig. 4. — Isomers of C_6H_6.

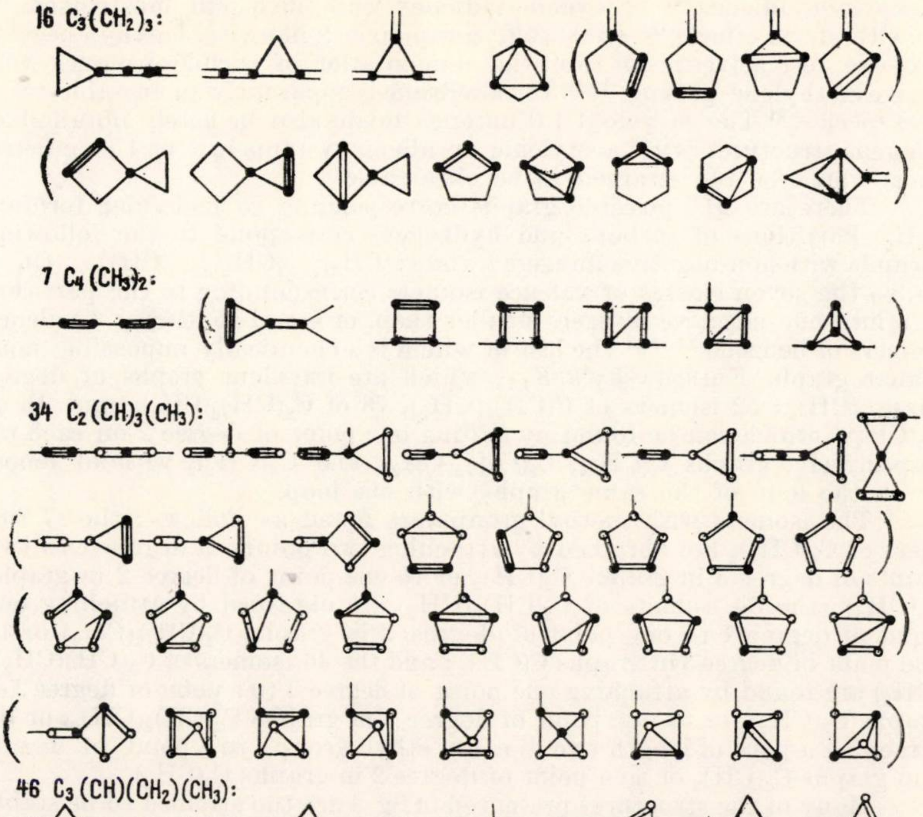
16 $C_3(CH_2)_3$:
7 $C_4(CH_3)_2$:
34 $C_2(CH)_3(CH_3)$:
46 $C_3(CH)(CH_2)(CH_3)$:

Fig. 4 (continued)

thocyclobutadienes,[17] or cyclobutadienes with push-pull substituents[18a] or with steric effects[18b] are stable compounds; likewise, methylenecylopropene derivatives result from the condensation of cyclopropenones with active methylene groups.[19,20] Tetrahedrane is apparently an unstable reactive species.[21] The bicyclo[1.1.0]butenes might also be barely obtainable, whereas structures with acetylenic or allenic systems in 3- or 4-membered rings would be too strained to be obtainable.

There are 217 possible graphs corresponding to molecular formula C_6H_6. Partitions of carbons and hydrogens correspond to the following formula with non-negative integers k and j : $(CH_3)_{2-k}(CH_2)_{2k-j}(CH)_{2j-k}(C)_{4-j}$, i.e. to the seven classes of valence isomers corresponding to the partition of 6 into non-negative integers smaller than, or equal to, three : 6 valence isomers of benzene[2,5,22,23] the last of which is a chemically impossible non-planar graph, Kuratowsky's $K_{3,3}$, which are trivalent graphs of degree three, $(CH)_6$; 32 isomers of $C(CH)_4(CH_2)$, 76 of $C_2(CH)_2(CH_2)_2$ and 16 of $C_3(CH_2)_3$, which can be found by adding one point of degree 2 on each of, respectively, graphs $C(CH)_4$, $C_2(CH)_2(CH_2)$, and $C_3(CH_2)_2$ without loops, or on the loop of the same graphs with one loop.

The isomers with methyl groups are found as follows : the 7 isomers of $C_4(CH_3)_2$ are obtained by attaching two points of degree 1 to two points of degree 3 in graphs $C_2(CH)_2$ or to one point of degree 2 in graphs $C_3(CH_2)$; the 34 isomers of $C_2(CH)_3(CH_3)$ are obtained by attaching one point of degree 1 to one point of degree 2 in graphs $C_2(CH)_2(CH_2)$ or to one point of degree 3 in graphs $C(CH)_4$; and the 46 isomers of $C_3(CH)(CH_2)(CH_3)$ are found by attaching one point of degree 1 to a point of degree 2 of graphs $C_3(CH_2)_2$ or to one point of degree 3 of graphs $C_2(CH)_2(CH)_2$, or by attaching a path of length two (i.e. an ethyl group) to a point of degree 3 in graphs $C_2(CH)_2$ or to a point of degree 2 in graphs $C_3(CH_2)$.

Many of the structures presented in fig. 4 are too strained to be stable compounds (e. g. non-planar graphs, structures containing triple or cumulated double bonds in small rings, structures which do not obey Bredt's rule, derivatives of cyclobutadiene or tetrahedrane which are elusive molecules, or structures with all four valences of a carbon atom being coplanar or nearly coplanar);[24] the remaining 58 structures (all 15 acyclic ones in agreement with literature data,[25] fulvene, dimethylenecyclobutene, trimethylenecyclopropane, cyclopropenylallene, spirocompounds, etc.) should be obtainable and several of these are known. Isomerizations and valence isomerizations can occur : thermochemical and photochemical rearrangements of valence isomers of benzene $(CH)_6$ are known[2,5,12,23] and in addition to these, other thermal isomerizations are known, e.g. dimethylenecyclobutene, fulvene and benzene are formed on heating 1,5-hexadiyne to 300°.[26]

---

[17] M. P. Cava and M. J. Mitchell, "Cyclobutadiene and Related Compounds", Academic Press, New York, 1967.

[18a] R. Gompper and G. Seybold, in "Aromaticity, Pseudo-Aromaticity and Anti-Aromaticy ", Israel Acad. Sci. Humanities. Jerusalem, 1971, p. 215.

[18b] H. Kimling and A. Krebs, *Angew. Chem.*, **84**, 592 (1972).

[19] H. U. Wagner, R. Seidl and H. Fauss, *Tetrahedron Letters*, **1972**, 3383.

[20] T. Eicher and T. Pfister, *Tetrahedron Letters*, **1972**, 3969.

[21] P. B. Shevlin and A. P. Wolf, *J. Amer. Chem. Soc.* **92**, 406, 3523, 5291.

[22] L. T. Scott and M. Jones Jr., *Chem. Revs.*, **72**, 181 (1972).

[23] E. E. van Tamelen, *Accounts Chem. Res.*, **5**, 186 (1972).

[24] R. Hoffmann, *Pure Appl. Chem.* **28** 181 (1971).

[25] J. Lederberg, G. I. Sutherland, B. G. Buchanan, E. A. Feigenbaum, A. V. Robertson, A. M. Duffield and C. Djerassi, *J. Amer. Chem. Soc.*, **91**, 2973 (1969).

The number of isomers of C_pH_p increases exponentially with increasing p, but that of structures able to exist as stable compounds increases less rapidly. On the other hand, in hydrocarbons which are richer in hydrogen than annulenes, the difference between the number of possible isomers and of structures able of existence is smaller. Thus taking the C_5H_8 as an example, the possible 26 isomers which include isoprene, cyclopentene or pentyne are all strain-free and able of existence (fig. 5). For C_5H_8 there are six classes of valence isomers corresponding to the 6 partitions of 8 into at most 5 non-negative integers equal to, or smaller than, three : $3 + 3 + 2$, $3 + 3 + 1 + 1$, $3 + 2 + 2 + 1$, $2 + 2 + 2 + 2$, $3 + 2 + 1 + 1 + 1$, and $2 + 2 + 2 + 1 + 1$. They can be found as bicyclic structures (cf. next paragraph) from graphs without loops of figure 2, with degrees 3/2 or 4/2 and 3, 4 or 5 points possessing side-chains of 2, 1 or 0 carbon atoms, respectively ; with degree 3 and 2 points, possessing side-chains of 3 carbon atoms. These partitions correspond to formula $(CH_3)_{2-k}(CH_2)_{2k-j+1}(CH)_{2j-k}(C)_{2-j}$ with integer non-negative variables j and k.

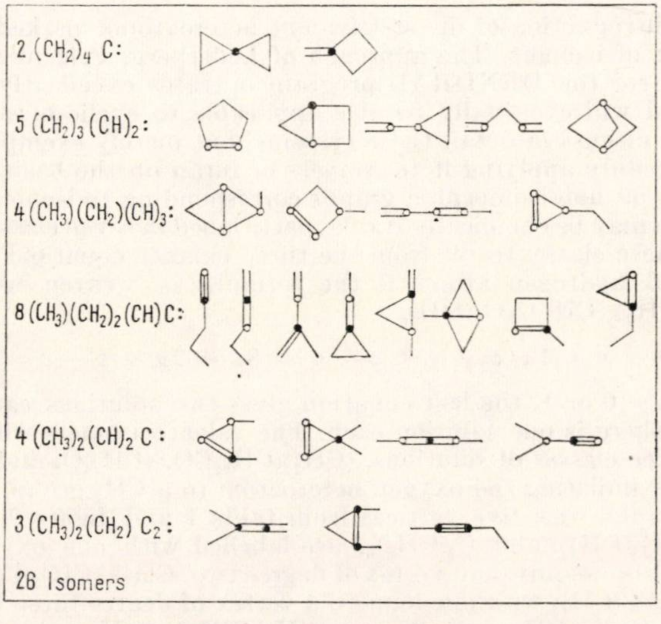

Fig. 5. — Isomers of C_5H_8.

---

[26] B. A. W. Coller, M. L. Heffernan and A. J. Jones, *Austral. J. Chem.*, **21**, 1807 (1968) ; A. T. Blomquist and P. M. Maitlis, *Proc. Chem. Soc.*, **1961**, 332.

Similarly, saturated alkanes[27a] C_nH_{2n+2} can be partitioned into classes according to formula $(CH_3)_{2+k}(CH_2)_{n-2k+j-2}(CH)_{k-2j}(C)_j$, with integers $0 \leqslant k \leqslant (2n-4)/3$ and $0 \leqslant j \leqslant (n-2)/3$: these classes correspond to partitioning $2q = 2p - 2$ into p positive integers $\leqslant 4$. Most of these are strain-free, hence stable molecules.

ISOMERS OF SYSTEMS WITH HETEROATOMS

The introduction of di- or trivalent heteroatoms markedly increases the number of isomers. The approach of Lederberg, Feigenbaum and coworkers[27b] *via* the DENDRAL program operates excellently for acyclic systems and will eventually be also applicable to cyclic ones. Therefore, we will not discuss in detail these systems, but merely exemplify the preceding procedure applying it to isomers of furan on the basis of figure 2. There exist 59 non-isomorphic graphs corresponding to isomers of C_4H_4O- (23 of which may be chemically stable) partitioned in seven classes of valence isomers. These classes result from the three balance equations for oxygen, carbon, and hydrogen atoms if the formula is written as $C_4H_4O \equiv \equiv (CH_3)_x(CH_2)_y(CH)_zC_wO_u(OH)_v$:

$$u + v = 1; \quad x + y + z + w = 3x + 2y + z + v = 4.$$

For $z = 0$ or 1, the last equation gives two solutions each, for $z =$ 2, 3, or 4, there is one solution each. The valence isomers within each of the last three classes of solutions, $(CH_2)(CH)_2CO$, $(CH)_4O$, and $(CH_2)_2C_2O$, result by assimilating the oxygen heteroatom to a CH_2 group. The corresponding graphs with five vertices from table 1 and figure 2, i.e. $C(CH)_2$-$(CH_2)_2$, $(CH)_4(CH)_2$, and $C_2(CH_2)_3$, are labelled with one oxygen heteroatom at each non-equivalent vertex of degree two. Class $(CH)_3\,C(OH)$ results from graphs $C(CH)_4$ with one loop on a vertex of degree three by replacing this loop with an OH group. Classes $(CH_2)\,(CH)\,C_2(OH)$ and $(CH_3)(CH)C_2O$ result similarly from graphs $C_2(CH)_2(CH_2)$ with one loop, by replacing the loop with an OH or a CH_3 group, respectively. Class $(CH_3)\,C_3(OH)$ results from graphs $C_2(CH)_3$ with two loops on vertices of degree three, by replacing them with one methyl and hydroxyl group. The resulting 59 isomers are presented in figure 6 ; the unstable chemical species are enclosed in brackets.

BRIDGED POLYCYCLIC COMPOUNDS

According to the IUPAC nomenclature rules[28] based on the Baeyer system[29] (also adopted by Chemical Abstracts and by the Ring Index[30]) a compound is termed "μ-cyclic" if it can be converted into an acyclic structure (a tree) by deleting μ bonds, suitably selected.[31]

[27a] H. R. Henze and C. M. Blair, *J. Amer. Chem. Soc.*, **53**, 3077 (1931).

[27b] A. Buchs, A. B. Delfino, A. M. Duffield, C. Djerassi, B. G. Buchanan, E. A. Feigenbaum and J. Lederberg, *Helv. Chim. Acta*, **53**, 1394 (1970) and previous papers in the series.

[28] IUPAC, "Nomenclature Rules for Organic Chemistry", Butterworths, London, 1965.

[29] A. Baeyer, *Ber. dtsch. chem. Ges.*, **33**, 3771 (1900).

[30] A. M. Patterson, L. T. Capell, and D. F. Walker, "The Ring Index", 2nd Ed., Amer. Chem. Soc. Washington, D. C., 1960.

[31] M. Frèrejaque, *Bull. Soc. Chim. France*, **6**, 1008 (1939).

According to this convention, tetrahedrane is a tricyclic compound, and cubane a pentacyclic one, at variance with the polyhedra they represent ; even in condensed or bridged bicyclic compounds, there are three possible circuits. This causes some confusion, [23] but strict adherence to the convention can overcome this difficulty.

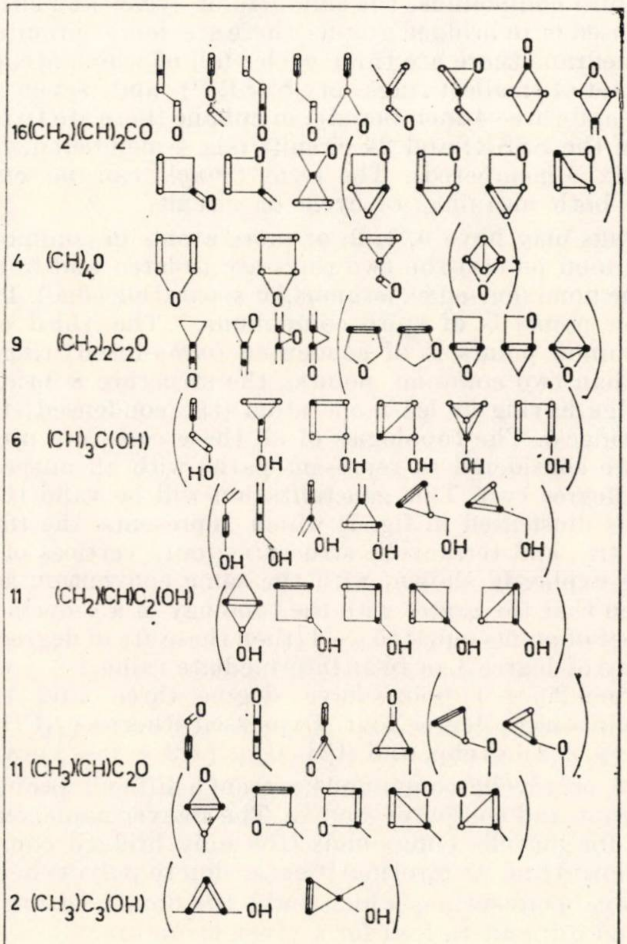

Fig. 6. — Isomers of C_4H_4O.

It is deemed advisable to maintain this convention since it is consistent with assimilating the number of cycles with the cyclomatic number μ (or nullity, or cycle rank) of a graph, $\mu = q - p + c$, where q, p and c are the numbers of edges, points and components of the graph. There have been several attempts to accomodate six rings in cubane, by defining fundamental [32] and real rings, [33] but they involve elaborate definitions and algorithms. One must take into account, however, that in condensed or bridged rings, deletion of one edge removes two circuits. Therefore, one should make a distinction between *cycles* (their number is given by the cyclomatic number) and *circuits* (which can include smaller cycles, but must not pass twice through the same edge or point). In separable graphs with isolated rings or in spiro compounds, the numbers of cycles and circuits are equal, but in condensed or in bridged graphs there are more circuits than cycles; e.g. in tetrahedrane there are three cycles (all of which are 3-membered in the smallest set of smallest rings or SSSR [34]) and seven circuits (four 3-membered and three 4-membered); in cubane there are five cycles (all 4-membered in the SSSR) and 24 circuits (six 4-membered, twelve 6-membered and six 8-membered). The term "*ring*" can be employed more loosely with both meanings of cycle or circuit.

Two rings may have 0, 1, 2, or more atoms in common. In the first case (no common points) the two rings are isolated and linked by a path of at least one bond (cut-edge, isthmus, or separating edge). The second case (one common point) is of spiro compounds. * The third case with two adjacent common points is of condensed (*ortho*-fused) rings. In the last case (more than two common points), the structure is bridged, with the shortest bridge having at least one atom (the condensed structures have zero-atom bridges). The topologies of all these cases are present in figure 2, if edges are considered to represent paths with an unspecified number of points of degree two. This generalization will be valid throughout this section and is illustrated in fig. 7, which represents the topologies of all possible bi-, tri-, and tetracyclic structures (only vertices of degrees three and four are explicitly shown, with the same convention as in figure 2). It can be seen that the graph with the topology of a μ-cyclic structure can have a number of points equal to $\mu-1$ (then these are of degree 4), to $2(\mu-1)$, when these are of degree 3, or to an intermediate value $\mu + j$ with $j = 0,1,2,.\ldots, \mu-3$, when $2(j + 1)$ points have degree three and the remaining $\mu - j - 2$ points have degree four. Expressed otherwise, $(CH)_p$ is $(p/2+1)$-cyclic, C_p is $(p + 1)$- cyclic, and $(CH)_xC_y$ is $(x/2 + j + 1)$-cyclic.

Bridged polycyclic compounds present a difficult problem for nomenclature, notation and computer storage. The Baeyer nomenclature system[29] was devised for bicyclic compounds (the only bridged compounds which were then known) and its informal [35] extension to polycyclic systems introduces additional conventions which make the nomenclature cumbersome redundant and difficult to find for a given structure.

Cumbersome: for more than three bridged rings, the Baeyer system name becomes very long. Therefore, trivial names are coined for such structures, e.g. for the newly discovered valence isomers of annulenes. In fact long systematic names are even funny.[36] Considerable confusion exists when trivial and semisystematic names coexist, as for example in the case of pentacyclo[$4.4.0.0^{2,5}.0^{3,8}.0^{4,7}$]dec-9-ene.[37,38] It was first synthetized by Masamune *et al.*[39] who gave it the trivial name "basketene" (and an erroneous Baeyer system name), and it was named by other workers 1,2-teheno-1, 2-secocubane[40] (but the structure was different because of an unexpected silver-ion catalyst effect).

---

* Larger spiro rings may have two or more common points, but these are not adjacent.

[32] R. Fugmann, U. Dolling and H. Nickelsen, *Angew. Chem.*, **79**, 802 (1967); *Angew. Chem. Internat. Edit.* **6**, 733 (1967).

[33] E. J. Corey and W. T. Wipke, *Science*, **166**, 178 (1969).

[34] M. Plotkin, *J. Chem. Docum.* **11**, 60 (1971).

[35] J. Meinwald and J. K. Crandall, *J. Amer. Chem. Soc.*, **88**, 1292 and especially pag. 1300 (1669).

Redundant : two informations are given twice each in the Baeyer name : the number of cycles (both as the prefix "μ-cyclo", and as the number of dots in the bracket, separting the numbers of atoms indicating the bridges) and the total number of atoms (both as a Greek numeral following the bracket, and as the sum of all bridge atom numbers within the brackets, plus two for the main bridgehead atoms).

Difficult : finding the corrected systematic name for a given structure is a tedious job, even for tricyclic structures ; for more than three bridged cycles, either a computer program must be employed,[41] or a long systematic approach must be followed.[38] There are many examples of incorrect names assigned to newly discovered bridged structures. Only two of these will be mentioned, namely (i) the tricyclo [$2.1.0.0^{2,5}$] pentane skeleton[35] to which *three incorrect* names were given by all three groups having prepared it (in turn, this has led to the failure of recognizing that one and the same structure had been obtained, which is irritating because chemistry is the best documented science), and (ii) the longer list given by Conrow[41] for erroneous and corrected * names.

At the same time, it must be recognized that the correct Baeyer system names are widely used, are unambiguous and allow an easy conversion into structural formulas.

In describing the computer program for generating correct Baeyer system names of bridged structures, Conrow[41] considered bi- to tetracyclic bridged structures. In figure 3 of his paper, Conrow lists the possible tricyclic and tetracyclic skeletons. These are in fact all cubic multigraphs without loops with 4 and 6 points, respectively (with the observation that Conrow's strucures *b* and *c* are isomorphic, therefore one of them should be deleted, and that the non-planar $K_{3,3}$ graph should be added to the list to make it complete).

The present list (fig.6) is complete because it contains also quaternary ring atoms (points of degree four). Together with the other lists of multigraphs without loops,[2,3] it could be used for expanding Conrow's program.

---

* One of the corrected names has a typographical error ;[41] instead of tetracyclo [$4.4.0.0^{2,4}.0^{3,6}$] decane one should read : tetracyclo[$4.4.0.0^{2,4}.0^{3,7}$]decane.

[36] *Nachr. Chem. Techn.*, **17**, 26, 62 (1969).
[37] W. G. Dauben and G. L. Whalen, *Tetrahedron Letters*, **1966**, 3743.
[38] D. R. Eckroth, *J. Org. Chem.*, **32**, 3362 (1967).
[39] S. Masamune, H. Cuts and M. G. Hogben, *Tetrahedron Letters*, **1966**, 1017.
[40] R. Furstoss and J. M. Lehn, *Bull. Soc. Chim. France*, **1966**, 2497.
[41] K. Conrow, *J. Chem. Docum.*, **6**, 206 (1966).

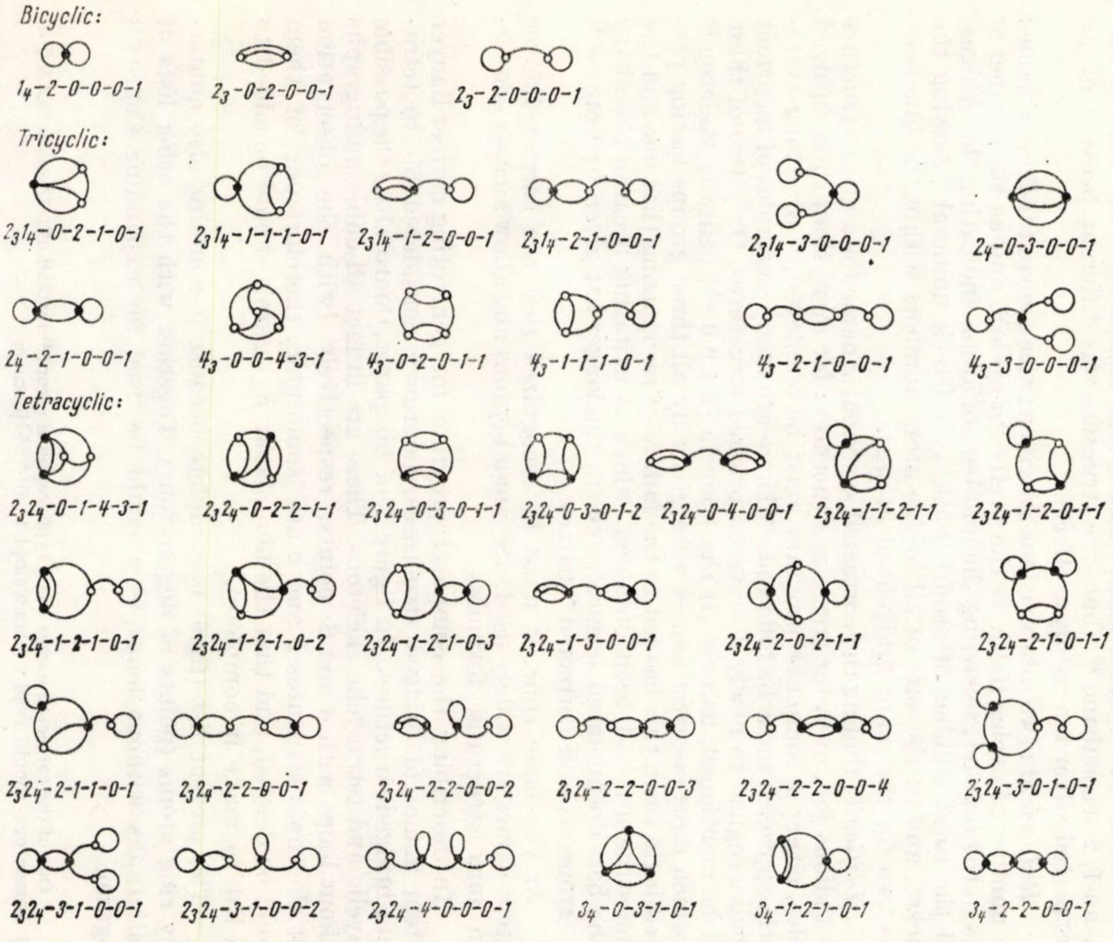
Bicyclic:
1_4-2-0-0-0-1
2_3-0-2-0-0-1
2_3-2-0-0-0-1
Tricyclic:
2_31_4-0-2-1-0-1
2_31_4-1-1-1-0-1
2_31_4-1-2-0-0-1
2_31_4-2-1-0-0-1
2_31_4-3-0-0-0-1
2_4-0-3-0-0-1
2_4-2-1-0-0-1
4_3-0-0-4-3-1
4_3-0-2-0-1-1
4_3-1-1-1-0-1
4_3-2-1-0-0-1
4_3-3-0-0-0-1
Tetracyclic:
2_32_4-0-1-4-3-1
2_32_4-0-2-2-1-1
2_32_4-0-3-0-1-1
2_32_4-0-3-0-1-2
2_32_4-0-4-0-0-1
2_32_4-1-1-2-1-1
2_32_4-1-2-0-1-1
2_32_4-1-2-1-0-1
2_32_4-1-2-1-0-2
2_32_4-1-2-1-0-3
2_32_4-1-3-0-0-1
2_32_4-2-0-2-1-1
2_32_4-2-1-0-1-1
2_32_4-2-1-1-0-1
2_32_4-2-2-0-0-1
2_32_4-2-2-0-0-2
2_32_4-2-2-0-0-3
2_32_4-2-2-0-0-4
2_32_4-3-0-1-0-1
2_32_4-3-1-0-0-1
2_32_4-3-1-0-0-2
2_32_4-4-0-0-0-1
3_4-0-3-1-0-1
3_4-1-2-1-0-1
3_4-2-2-0-0-1

Fig. 7. — Topologies of polycyclic systems (completing and correcting data from references [41] and [42]): bi- tri-, and tetracyclic systems.

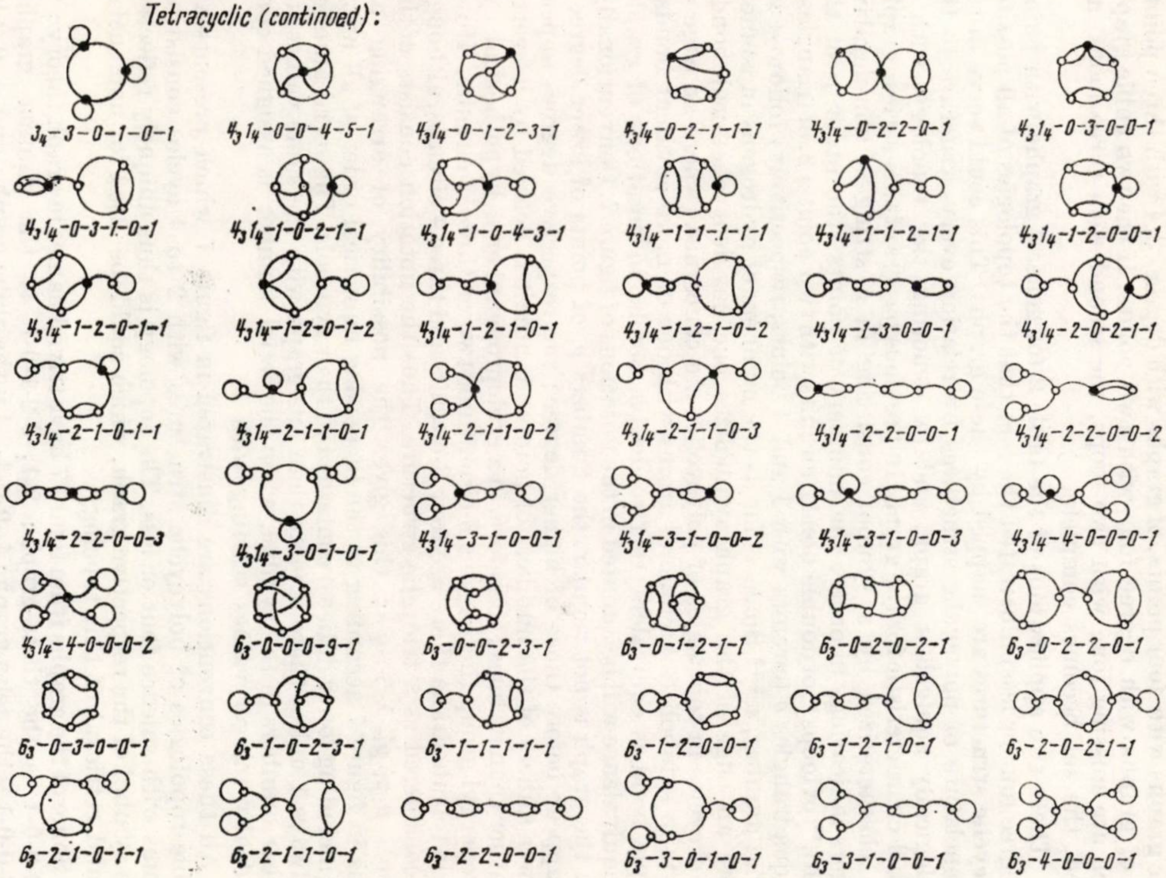
Tetracyclic (continued):
3_4-3-0-1-0-1
4_31_4-0-0-4-5-1
4_31_4-0-1-2-3-1
4_31_4-0-2-1-1-1
4_31_4-0-2-2-0-1
4_31_4-0-3-0-0-1
4_31_4-0-3-1-0-1
4_31_4-1-0-2-1-1
4_31_4-1-0-4-3-1
4_31_4-1-1-1-1-1
4_31_4-1-1-2-1-1
4_31_4-1-2-0-0-1
4_31_4-1-2-0-1-1
4_31_4-1-2-0-1-2
4_31_4-1-2-1-0-1
4_31_4-1-2-1-0-2
4_31_4-1-3-0-0-1
4_31_4-2-0-2-1-1
4_31_4-2-1-0-1-1
4_31_4-2-1-1-0-1
4_31_4-2-1-1-0-2
4_31_4-2-1-1-0-3
4_31_4-2-2-0-0-1
4_31_4-2-2-0-0-2
4_31_4-2-2-0-0-3
4_31_4-3-0-1-0-1
4_31_4-3-1-0-0-1
4_31_4-3-1-0-0-2
4_31_4-3-1-0-0-3
4_31_4-4-0-0-0-1
4_31_4-4-0-0-0-2
6_3-0-0-0-9-1
6_3-0-0-2-3-1
6_3-0-1-2-1-1
6_3-0-2-0-2-1
6_3-0-2-2-0-1
6_3-0-3-0-0-1
6_3-1-0-2-3-1
6_3-1-1-1-1-1
6_3-1-2-0-0-1
6_3-1-2-1-0-1
6_3-2-0-2-1-1
6_3-2-1-0-1-1
6_3-2-1-1-0-1
6_3-2-2-0-0-1
6_3-3-0-1-0-1
6_3-3-1-0-0-1
6_3-4-0-0-0-1

Fig. 7 (continued).

The present list (fig. 7) is also more comprehensive than the set of tricyclic graphs of degrees 3 and 4 presented in their figure 2 by Whitlock and Siefken. [42] * That set of ten graphs is essentially the list of cubic graphs with four points, of graphs with degrees 3/4 with three points, and of graphs with degree four with two points. If the two cubic graphs which are missing (one with two loops, the second with three loops) are added, the set becomes complete.

These two applications of the table 2 (of general graphs with points of degree four or less) illustrated the fact that the topologies of all possible polycyclic structures are mapped by these graphs. This could serve in the nomenclature of polycyclic structures by relating every structure to the topologically equivalent graph, and by denoting the topology with a symbol characteristic for the graph. In previous papers of this series, graphs were characterized by a symbol consisting in a string of non-negative integers indicating, in order, the numbers of points (the order p of the graph),** of loops λ, of double bonds (circuits with two points) β, of triangles t, and quadrangles q (circuits with 3 and 4 points, respectively) followed by a serial number, s. [2,3,5] Since as far as the numbers of hydrogens in isomers (where an edge of the graph symbolizes one covalent chemical bond), and of cycles in topologies of polycyclics are concerned (where an edge of the graph symbolizes a chain of atoms with one or more covalent bonds), a triple bond is equivalent to two double bonds, in notations of graphs this equivalence will be adopted in the notations of figure 7. Conventionally, when the graph is not regular, the numbers p_i of points of lower degree i will appear before those of higher degree; the respective degrees appear as lower indices of the numbers of points. A circuit is defined by its vertices rather than its lines; therefore, in a cyclopropenyl or a hypothetical cyclopropargyl group there is one 3-circuit not two or three 3-circuits. However, in tetrahedrane there are four 3-circuits and three 4-circuits, although it is considered as a tricyclic structure. Thus the notation consists of the symbols $p_i p'_{i'} p''_{i''}$-λ-β-t-q-s; this gives the possibility of arranging all graphs in figure 7 according to the increasing numerical order of all numbers (including lower indices) contained in their symbols. The serial number s is always 1 unless there is more than one graph with the same values for all other numbers in the symbol, when the serial number is assigned conventionally integer values starting with 1.

All these conventions are illustrated in figure 7 which presents all possible topologies of polycyclic structures with 2 to 4 cycles consisting of atoms with valence four or less. The topology is thus uniquely reflected in the symbol of the respective graph, which could be used for nomenclature and retrieval of this topology.

Some of the graphs from figure 7 have trivial names in graph theory; [43] 2_3-0-2-0-0-1 is the theta-graph; $2_3 1_4$ -0-2-1-0-1 is the gamma graph; 2_4-0-3-0-0-1 is the delta graph; 4_3-0-0-4-3-1 is the alpha graph; and 4_3-0-2-0-

---

* Cf. footnote [4] of that paper [42] for another critical remark concerning the Baeyer nomenclature system.

** Using subscripts for degrees, one should indicate the number of points of each degree.

[42] H. W. Whitlock Jr., and M. W. Siefken, *J. Amer. Chem. Soc.*, **90**, 4929 (1968).

[43] J. W. Essam and M. E. Fisher, *Rev. Mod. Phys*, **42**, Suppl., 271 (1970).

-1-1 is the beta graph. These are all the graphs without loops with cyclomatic numbers μ equal to two or three.

A previous list of graphs classified according to their cyclomatic number was compiled by Foster for electrical circuits.[44] The aim was different, therefore that list is at the same time more comprehensive (including also disconnected graphs and vertices of any degree) and less comprehensive (excluding loop-graphs and omitting some of the other graphs).

Alternatively, another approach might be used, namely a completely new proposal for the nomenclature of bridged systems. One such possibility rests on the facts that trees may be coded unambiguously starting from their centre [45,46] * or from their centroid [25,47] ** (both of these may be either one point, or two adjacent points [4,48,49]), and that μ cuts in a μ-cyclic bridged structure convert it into a tree. One could propose a convention for an unambiguous selection of cuts in order to convert a graph into a tree, e.g. the shortest bridges should be cut in order next to a bridgehead atom to lead to the longest non-branched chain); the μ cycles would result from specifying μ connections between pairs of points in the tree. One can take advantage of the existence of algorithms for finding the smallest set of smallest rings in a graph, [34] whose number equals the cyclomatic number of the graph, in these conventions for cuts.

---

* The centre of a tree [4,43] consists in the point(s) of minimum eccentricity, i.e. yielding minimal longest paths to any endpoint of the tree.

** The centroid or mass centre of a tree [4,43] (which may or may not coincide with its centre) consists in the point(s) of minimum weight, i.e. yielding the smallest maximum number of lines in any branch starting from it (them).

[44] R. M. Foster, *Trans. Amer. Inst. Electr. Engrs.*, **51**, 309 (1932).

[45] R. C. Read, "The coding of trees and tree-like graphs", Univ. of the West Indies, Jamaica (Report, 1969).

[46] R. C. Read and R. S. Milner, "A new system for the designation of chemical compounds for the purposes of data retrieval. I. Acyclic compounds", Univ. of the West Indies, Jamaica (Report, 1969).

[47] B. G. Buchanan, A. M. Duffield and A. V. Robertson, "Mass Spectrometry. Techniques and Applications", editor G. W. A. Milne, Wiley-Interscience, New York, 1971, p. 121.

[48] C. Jordan, *J. reine angew. Math.*, **70**, 185 (1869).

[49] J. J. Sylvester, *Proc. Roy. Inst. Gt. Brit.* **7**, 179 (1873–1875); *J. Hopkins Univ. Circulars*, I, 202 (1882).

Revue Roumaine de Chimie, 18, 4, 655 – 665 (1973)

MATRIZIELLE CHARAKTERISIERUNG DER STRUKTUR UND TOPOLOGIE DER ORGANISCHEN VERBINDUNGEN. III[1,2]

KONFORMATION, CHIRALE KONFORMEREN

FRANCISC KEREK und IOAN MOȚOC

Organisch-chemisches Laboratorium des Polytechnischen Instituts „Traian Vuia",
Postfach 103 Timişoara, Romania

Eingegangen am 13. Oktober 1972

Es wurde eine matrizielle Ausdrucksweise der topologischen Beziehungen der chiralen Konformeren angestrebt. Zuerst werden die einfacheren Fälle der axialen Chiralität behandelt und nachher jene Fälle, in denen die die Achse bestimmenden Atome oder die von ihnen abzweigenden Liganden chiral sind. Die analytische Form des Chiralitätsoperatoren wurde sowohl für den allgemeinen Fall als auch für Sonderfälle abgeleitet.

1. EINLEITUNG

In den vorhergehenden Arbeiten [1,2] wurde eine matrizielle Charakterisierung der Konstitution und der Konfiguration der organischen Verbindungen, sowie der mit der zentralen Chiralität der Molekülarten zusammenhängenden Beziehungen versucht. So wie das in der zweiten Arbeit[2] klargelegt wurde, haben wir uns in erster Reihe mit den topologischen Aspekten der behandelten Probleme beschäftigt, wobei wir die Betrachtungen, soweit es möglich war, auf jene Strukturelemente beschränkten, die eine wesentliche Rolle in der Festlegung des Chiralitätssinnes einer sterischen Formation haben, was auch für die folgenden Diskussionen gültig bleibt.

2. AXIALE CHIRALITÄT, KONFORMATION

Die Existenz der axialen Chiralität setzt bidimensionelle Unterscheidungen bezüglich einer internuklearn Achse [3] voraus. Der Chiralitätssinn

---

[1] F. Kerek und I. Moțoc *Rev. Roumaine Chim.* **18**, 285 (1973).

[2] I. Moțoc und F. Kerek, *Rev. Roumaine Chim.* **18**, 291 (1973).

[3] R. S. Cahn, C. K. Ingold und V. Prelog, *Angew. Chem.*, **78**, 413 (1968).

kann auch konfigurativ spezifiziert werden, es ist aber angebrachter, dies konformativ zu tun, wobei die Bezeichnungen (+); P oder (−); M verwendet werden.

Um eine allgemein gültige Behandlung zu erreichen, die von den Kriterien zur Unterscheidung der konfigurativen und konformativen Aspekte der Molekülstruktur [4,5,6] unabhängig ist, werden in dieser Arbeit alle Fälle der axialen Chiralität einheitlich als konformative behandelt.[*]

2.1. DIE MATRIZIELLE CHARAKTERISIERUNG DER MOLEKULAREN KONFORMATIONEN

Indem wir die Bezeichnungen der vorhergehenden Arbeit [2] beibehalten, erhalten die Liganden die von den Achsenenden abzweigen die Symbole ψ_i, wobei $1 \leqslant i \leqslant n$; $(n = 2, \ldots, 8)$.[**]

Es ist gleichfalls bekannt, daß die Liganden mit Hilfe der dem Liganden ψ_i zugeordneten Matrix matriziell beschrieben werden können.

Im Einklang mit der Cahn-Ingold-Prelog-Konvention [3,4] kann der Sinn einer axialen Chiralität eindeutig durch die relative räumliche Anordnung zweier Bezugsliganden ψ_α und ψ_β (je ein Ligand von jedem Achsenende) festgelegt werden. Die Bezugsliganden werden ihrerseits nach einfachen, allgemein anwendbaren Kriterien gewählt. Im Einklang mit den in den vorhergehenden Arbeiten veröffentlichten Ideen, können diese Bezugsliganden mit Hilfe der Matrizen M_α und M_β beschrieben werden.

Die Liganden ψ_i können unendlich viele räumliche Anordnungen in Bezug auf eine Torsionsachse einnehmen. Mathematisch ausgedrückt lautet dies wie folgt:

Die möglichen Konformationen in Bezug auf eine Torsionsachse bilden eine unendliche, unzählbare Menge K. Die Menge K kann in Abhängigkeit von dem axialen Chiralitätssinn in zwei Untermengen K_+ und K_- geteilt werden:

$$\begin{aligned} K_+ \cup K_- &= K \\ K_+ \cap K_- &= K_0 \end{aligned} \tag{1}$$

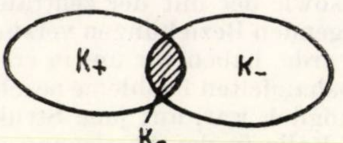

wo mit K_0 die Menge der achiralen Konformere bezeichnet wurde.

---

[*] Die Konformationen sind gemäß[3] die verschiedenen Varianten der räumlichen Anordnung der Atome im Molekülraum, welche Varianten sich eine von der anderen durch die Torsionsbewegung um eine internukleare Bindungsgerade unterscheiden.

[**] Bei Wasserstoffperoxyd $n = 2$, bei H_2N-OH $n = 3$, bei Äthylen $n = 4$, bei HC_3-CHO $n = 5$, bei Äthanabkömmlingen $n = 6$, bei organischen Phosphorverbindungen sind auch Fälle mit $n = 7$ oder $n = 8$ möglich.

[4] IUPAC Tentative Rules for the Nomenclature of Organic Chemistry Section E. Fundamental Stereochemistry; *J. Org. Chem.*, **35**, 2849 (1970).

[5] * * *, *Nachr. Chem. Techn.*, **17**, 443 (1969).

[6] G. Ostrogovich und F. Kerek (noch unveröffentlicht).

Einige Elemente der Menge K, d.h. besondere Konformationen, zeichnen sich durch Symmetrieeigenschaften oder durch die Inflexionspunkte in dem Enthalpiegehalt/Torsionswinkel (τ) - Diagramm aus. Die Abbildung 1 widerspiegelt solche Konformationen, die nach der relativen Anordnung der Bezugsliganden (ψ_α und ψ_β) bezeichnet wurden.

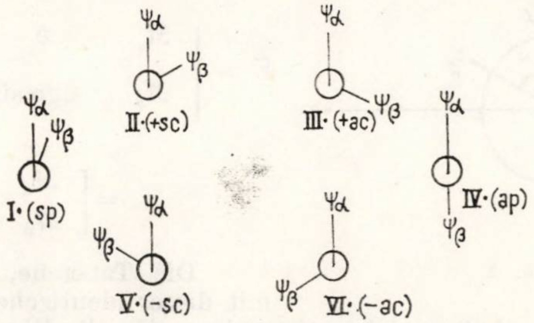

Abb. 1

Es kann leicht festgestellt werden, daß folgende Beziehungen wahr sind :

$$\text{II, III} \in \mathrm{K}_+ ; \quad \text{V, VI} \in K_- ; \quad \text{I, IV} \in K_0$$

Für den „Chiralitätssinn" spielt der Zahlenwert des Torsionwinkels τ eine zweitrangige Bedeutung. Also ist der Chiralitätssinn ein und derselbe für alle Werte* von τ die größer als Null und kleiner als π sind, d.h. + (Plus).

Genauso definieren negative Werte des Torsionwinkels einen negativen Sinn der axialen Chiralität, unabhängig von dem Zahlenwert von τ.

Für die topologische Charakterisierung der räumlichen Anordnung in Bezug auf eine Achse werden die Matrizen V' verwendet, die man von dem allgemeinen Matrizentyp V ableitet :

$$V = \begin{bmatrix} M_\alpha & 0 \\ M_\beta & \text{sign} \ \sin \tau \end{bmatrix} \qquad (2)$$

wobei M_α und M_β die konfigurativen Matrizen der Bezugsliganden ψ_α beziehungsweise ψ_β sind.

Das Element Null (0) aus der Stellung (12) zeigt übereinkunftsgemäß an, daß das Element aus derselben Reihe, d.h. ψ_α den dem Beobachter nahegelegenen Liganden darstellt.

---

* Bekanntlich spricht man von dem positiven Sinn, wenn der von dem Torsionswinkel zwischen ψ_α und ψ_β bestimmte Schraubsinn (vom Beobachter aus) nach rechts ist ; im Gegenfall handelt es sich um den negativen Sinn. Der Winkel τ wird hier im trigonometrischen Sinn betrachtet so daß sign sin τ den den Konformationen zugeordneten + oder – Zeichen entpricht.

Das Element aus der Stellung (22), d.h. sign sinτ legt den Sinn der Chiralität fest, wobei τ der von ψ_α und ψ_β gebildete Torsionswinkel ist.

Für den konkreten Fall des Beispiels, das in Abb. 1 mit II bezeichnet wurde, hat die Matrix V' folgende Form, die mit V'_{II} bezeichnet wird:

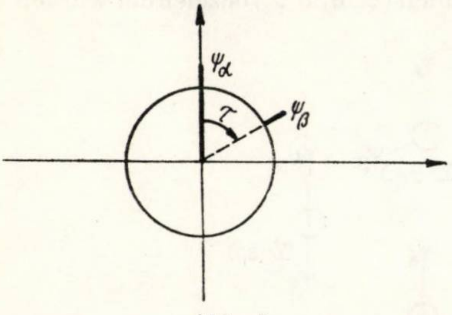

Abb. 2

$$V = \begin{bmatrix} \mathbf{M}_\alpha & 0 \\ M_\beta & \text{sign}\sin\dfrac{\pi}{3} \end{bmatrix} = V'_{\mathrm{II}} = \begin{bmatrix} M_\alpha & 0 \\ M_\beta & + \end{bmatrix} \tag{3}$$

Die Tatsache, daß man eine mit dieser identische Matrix V' auch für den Fall III erhält und im allgemeinen, für alle Werte $0° < \tau < \pi$ des Moleküls aus Abb. 1, weist auf die topologische Gleichwertigkeit dieser räumlichen Anordnung was ihren Chiralitätssinn anbelangt hin.

Für die achiralen Fälle I und IV aus Abb. 1 wird die konformationelle Matrix V' die Form V'_{I}, bzw V'_{IV} haben:

$$V'_{\mathrm{I}} = \begin{bmatrix} M_\alpha & 0 \\ M_\beta & \text{sign}\sin 0° \end{bmatrix} = V'_{\mathrm{IV}} = \begin{bmatrix} M_\alpha & 0 \\ M_\beta & \text{sign}\sin\pi \end{bmatrix} = \begin{bmatrix} M_\alpha & 0 \\ M_\beta & 0 \end{bmatrix} \tag{4}$$

Für den Zweck einer möglichst volkommenen matriziellen Beschreibung ist es notwending neben (i) *rein konformationellen Informationen* auch Daten bezüglich der:
(ii) *Konstitution und Konfiguration der Liganden* die von der betreffenden Achse abzweigen und
(iii) *der Konfiguration der die Achse bestimmenden Atome* miteinzuschließen.

Den Beobachtungen aus den vorhergehenden Arbeiten gemäß [1,2], wird die Konfiguration und damit auch die Konstitution durch Matrizen vom Typ M_i ($i = 1, \ldots, n$) wiedergegeben.

In dem Falle aus Abb. 3, in welcher $\psi_1, \ldots, \psi_6$ die Liganden sind, die von den die Achse bestimmenden Atome X und Y abzweigen, wird die Konfiguration des Atoms X bzw Y durch die Matrizen M_X bzw M_Y beschrieben, in deren Aufbau (siehe Beziehung 5) die den Liganden $\psi_1, \ldots, \psi_6$ entsprechenden Matrizen $M_1, \ldots, M_6$ eingegliedert sind.

$$M_X = \begin{bmatrix} M_1 & M_2 \\ \psi_Y & M_3 \end{bmatrix}; \quad M_Y = \begin{bmatrix} M_4 & \psi_X \\ M_5 & M_6 \end{bmatrix} \tag{5}$$

wobei ψ_Y (siehe Abb. 3) die Matrix 2×2 des Molekülteils darstellt, der an das Atom X durch das Atom Y angegliedert ist.

Genauso stellt ψ_X die Matrix des anderen Molekülteils dar, der durch das Atom Y an des Atom X gebunden ist.

Dies kann matriziell durch folgende Beziehungen ausgedrückt werden :

$$\psi_Y = M_Y = \begin{bmatrix} 0 & \psi_X \\ 0 & 0 \end{bmatrix} \tag{6}$$

$$\psi_X = M_X = \begin{bmatrix} 0 & 0 \\ \psi_X & 0 \end{bmatrix} \tag{7}$$

Vom Standpunkt des Moleküls als Gesamtheit können die Daten bezüglich der Konfiguration (und somit auch der Konstitution) der Liganden, sowie auch der der Atome vom Ende der Bezugsachsen in einer Matrix 2×1 gemäß der Beziehung (8)

$$W = \begin{bmatrix} M_X \\ M_Y \end{bmatrix} \tag{8}$$

zusammengefaßt werden.

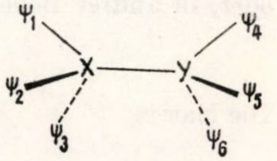

Abb. 3

Folglich wurden Matrizen folgenden Typs definiert :

1° V, die die Konformation der betreffenden Achse topologisch charakterisieren (i)

2° W, die die Konfiguration der Liganden, die von der Achse abzweigen matriziell beschreibt, einschließlich die Konfiguration der die Achse bestimmenden Atome.

Für das gleichzeitige Umfassen der durch W und V ausgedrückten Aspekte ist es angebracht, eine Matrix $\mathcal{W}$ zu verwenden, die wie folgt aufgebaut wird :

$$\mathcal{W} = \begin{bmatrix} W \\ V \end{bmatrix} \tag{9}$$

In dem nun Folgenden wird die Möglichkeit, die verschiedenen Beziehungen der konformativen Isomerie matriziell auszudrücken untersucht

Zuerst werden die einfachsten „rein konformationellen" Aspekte analysiert, das heißt jene Informationen die in den Matrizen V enthalten sind.

2.2. MOLEKÜLE, DIE NUR AXIALE CHIRALITÄT AUFWEISEN

Die Natur und die relative Anordnung der Liganden in Bezug auf eine Torsionsachse führt häufig zu einer chiralen Struktur.

Für zwei äußerst einfache Beispiele wie dies II und V aus Abb. 1 sind, kann man folgende rein konformationelle Matrizen V'_{II} und V'_{V} schreiben:

$$V'_{\mathrm{II}} = \begin{bmatrix} M_\alpha & 0 \\ M_\beta & + \end{bmatrix}; \quad V'_{\mathrm{V}} = \begin{bmatrix} M_\alpha & 0 \\ M_\beta & - \end{bmatrix} \tag{10}$$

Von matriziellem Standpunkt aus besteht folgende Beziehung zwischen V'_{II} und V'_{V}:

$$\begin{bmatrix} M_\alpha & 0 \\ M_\beta & + \end{bmatrix} \cdot \begin{bmatrix} 1 & 0 \\ 0 & - \end{bmatrix} = \begin{bmatrix} M_\alpha & 0 \\ M_\beta & - \end{bmatrix} \tag{11}$$

oder, in andrer Benennung:

$$V'_{\mathrm{II}} \cdot F_a = V'_V \tag{11'}$$

Die Matrix

$$F_a = \begin{bmatrix} 1 & 0 \\ 0 & - \end{bmatrix}$$

die den Übergang von V'_{II} zu V'_V verwirklicht, weist folgende Eigenschaft auf:

$$F_a^2 \cdot V' = V' \tag{11''}$$

wo: $F_a^2 = F_a \cdot F_a$; V' ist jedwelche konformative Matrix. Mit anderen Worten entspricht F_a der Widerspiegelung bei beschränktem konformationellen Niveau, während F_a^2 zwei aufeinanderfolgenden Widerspiegelungen, ebenfalls in beschränktem konformationellem Sinn, entspricht.

Man bemerkt, daß zwischen den Konformeren II und V eine Beziehung der Enantiomerie besteht, deren matrizielle Ausdrucksweise durch die Gleichung (11) erreicht wird.

Folgender allgemeiner Satz kann ausgesagt werden: Ein Konformer ist chiral dann und nur dann, wenn die Beziehung

$$V \cdot F \neq V \tag{12}$$

besteht.

Man kann nämlich feststellen, daß für die Beispiele aus Abb. 1 die Matrizen V'_{I} und V'_{IV} wie folgt geschrieben werden können:

$$V'_{\mathrm{I}} \cdot F = V'_{\mathrm{I}}; \quad V'_{\mathrm{IV}} \cdot F = V'_{\mathrm{IV}} \tag{13}$$

Vergleicht man nun die Beziehungen (13) mit (12), so folgt daraus, daß sie achiral sind.

Die Beispiele II, III, V, VI sind der Beziehung (12) gemäß chiral.

2.3. AXIALE CHIRALITÄT IN GEGENWART ANDERER CHIRALITÄTSELEMENTE

Für einen möglichst allgemeinen Fall ist es notwendig auch die konfigurativen Aspekte zu behandeln, sowohl jene der Liganden, als auch jene der die Achse bestimmenden Atome, d.h. die Matrizen W und V zu verwenden. Im Sinne der Beziehung (9) bedeutet dies, die Matrix $\mathcal{W}$ zu verwenden.

Es sei nun $\overline{\mathcal{W}}$ die Matrix, die das Enantiomer des durch $\mathcal{W}$ charakterisierten Moleküls darstellt.

In dem nun Folgenden wird die Beziehung $\mathcal{R}$ bestimmt, die zwischen den zwei Matrizen besteht. Das heißt:

$$\mathcal{W}\mathcal{R}\overline{\mathcal{W}}$$

Wir bezwecken die Beziehung $\mathcal{R}$ so zu bestimmen, daß

$$\mathcal{W}\mathcal{R}\overline{\mathcal{W}} \Leftrightarrow \overline{\mathcal{W}}\mathcal{R}\mathcal{W} \tag{14'}$$

das heißt, man wird eine symmetrische Beziehung $\mathcal{R}$ suchen. Selbstverständlich wird $\mathcal{R}$ nicht reflexiv sein

$$\nexists\, \mathcal{W}\mathcal{R}\overline{\mathcal{W}}\,;\ \nexists\, \overline{\mathcal{W}}\mathcal{R}\mathcal{W} \tag{14''}$$

Zur Behauptung (14'') gelangen wir durch Analogie mit der Beziehung (12). Aus dem nun Folgenden wird man feststellen, daß (14'') wahr ist.

Die allgemeine Beziehung (14'') wird als (14) wie folgt neu geschrieben:

$$\mathcal{F}\mathcal{W} = \overline{\mathcal{W}} \Leftrightarrow \mathcal{F}\overline{\mathcal{W}} = \mathcal{W} \tag{14}$$

Zur Ableitung der analytischen Form des Operatoren $\mathcal{F}$, der eine Widerspiegelung des Moleküls in seiner Gesamtheit verwirklichen muß, ist folgende Bemerkung wichtig, die aus der Beziehung (14) hervorgeht:

Der Operator $\mathcal{F}$ hat einen umgekehrten Operator $\mathcal{F}^{-1}$ und zwar:

$$\mathcal{F}^{-1} = \mathcal{F}$$

Also besteht die Beziehung: $\mathcal{F}^{-1}\cdot\mathcal{F} = \mathcal{F}\cdot\mathcal{F} = \mathcal{F}^2 = E = \begin{bmatrix} 1 & 0 \\ 0 & 1 \end{bmatrix}$. Das heißt, man sucht einen Operator, der eine Matrix 2×2 ist. Hier wurden die Ergebnisse von Kapitel 2.2 wieder aufgegriffen. Also ist die

Widerspiegelung eines Moleküls, die durch die Matrix $\mathcal{W}$ beschrieben wird, bei rein konformationellem Niveau, durch folgende Beziehung definiert :

$$\begin{bmatrix} 1 & 0 \\ 0 & F_a \end{bmatrix} \mathcal{W} = \begin{bmatrix} 1 & 0 \\ 0 & F_a \end{bmatrix} \cdot \begin{bmatrix} W \\ V \end{bmatrix} = \begin{bmatrix} W \\ F_a\, V \end{bmatrix} \tag{15}$$

Vergleicht man nun (15) mit (11′), so stellt man fest, daß in $\mathcal{W}$, durch die Anwendung des Operatoren $\begin{bmatrix} 1 & 0 \\ 0 & F_a \end{bmatrix}$ nur eine rein konformationelle Widerspiegelung verwirklicht wurde.

Es ist nützlich, in Anbetracht des nun Folgenden, auf zwei Eigenschaften des Operatoren F_a hinzuweisen :

$$\begin{aligned} F_a^{2k} &= F_a^2 \qquad (k = 1,\ 2,\ \ldots) \\ F_a^{2k+1} &= F_a \qquad (k = 1,\ 2,\ \ldots) \end{aligned} \tag{16}$$

Die Widerspiegelung der Konfiguration der die Achse bestimmenden Atome wird durch die Anwendung des Operatoren $\begin{bmatrix} F_{XY} & 0 \\ 0 & F_a^2 \end{bmatrix}$ gemäß folgender Beziehung erzielt :

$$\begin{bmatrix} F_{XY} & 0 \\ 0 & F_a^2 \end{bmatrix} \cdot \begin{bmatrix} W \\ V \end{bmatrix} = \begin{bmatrix} F_{XY} W \\ V \end{bmatrix} \tag{17}$$

In (17) wurde auch die Beziehung (11″) beachtet. Mit F_{XY} wurde der Operator bezeichnet, der durch folgende Beziehung definiert wird :

$$F_{XY} = \begin{bmatrix} \delta & 0 \\ 0 & \delta \end{bmatrix} \tag{18}$$

in welcher δ auf das Ausführen der Transponierung der Matrix hinweist :

$$\delta [a_{ij}] = [a_{ij}] \delta = [a_{ij}]^T \tag{19}$$

Also :

$$F_{XY} \cdot W = \begin{bmatrix} \delta & 0 \\ 0 & \delta \end{bmatrix} \cdot \begin{bmatrix} M_X \\ M_Y \end{bmatrix} = \begin{bmatrix} \delta M_X \\ \delta M_Y \end{bmatrix} = \begin{bmatrix} M_X^T \\ M_Y^T \end{bmatrix} \tag{20}$$

Zieht man die Ergebnisse der vorhergehenden Arbeit in Betracht, so stellt man wirklich fest, daß die Anwendung des Operatoren F_{XY} einer Widerspiegelung der Konfiguration der die Achse bestimmenden Atome gleichkommt. (ii)

Folgende Beziehung ist offensichtlich :

$$F_{XY}\cdot F_{XY} = F_{XY}^2 \sim E = \begin{bmatrix}1 & 0\\ 0 & 1\end{bmatrix} \qquad (20')$$

Also $F_{XY}^2\cdot W = W$, unabhängig davon, welches die durch (8) definierte Matrix ist.

Die Widerspiegelung der Konfiguration der Liganden (iii) wird durch folgende Beziehung definiert :

$$\begin{bmatrix}F_n & 0\\ 0 & F_a^2\end{bmatrix}\cdot\begin{bmatrix}W\\ V\end{bmatrix} = \begin{bmatrix}F_n W\\ V\end{bmatrix} \qquad (21)$$

Bei der Ableitung der Beziehung (21) wurde auch die Beziehung (11') beachtet. F_n ist der Operator, der durch folgende Matrix definiert wird :

$$F_n = \begin{bmatrix}F & 0\\ 0 & F\end{bmatrix},\ \text{wo}: F = \begin{bmatrix}\delta & 0\\ 0 & \delta\end{bmatrix}$$

Also : $F \equiv F_{XY}$

Führt man das Produkt $F_n.W$ aus, so erhält man :

$$F_n\cdot W = \begin{bmatrix}F & 0\\ 0 & F\end{bmatrix}\cdot\begin{bmatrix}M_X\\ M_Y\end{bmatrix} = \begin{bmatrix}FM_X\\ FM_Y\end{bmatrix}$$

Da M_X und M_Y Matrizen 2×2 sind, während $[m]$ Glieder aus M_X order/und M_Y darstellen, bemerkt man, daß die Glieder in FM_X und FM_Y $[m]^T$ sein werden. Indem wir von neuem von den Ergebnissen der vorhergehenden Arbeit[2] Gebrauch machen, stellt man fest, daß sich in den Matrizen FM_X und FM_Y Liganden befinden, die auch in den Matrizen M_X und M_Y vorkommen, aber mit widerspiegelten Konfigurationen.

Für den Operator F_n sind folgende Beziehungen wahr :

$$F_n\cdot F_n = F_n^2 \sim E = \begin{bmatrix}1 & 0\\ 0 & 1\end{bmatrix} \qquad (22)$$

$F_n^2\cdot W = W$ für jedwelche durch die Beziehung (8) definierte Matrix W.

Um die analytische Form des Operatoren F_n zu bestimmen, ist die Anwendung folgender Bemerkungen notwendig :
Man führt mit einem System, in unserem Fall mit einem organischen Molekül, eine Reihe von Widerspiegelungsoperationen aus. Man stellt fest, daß das Ergebnis der Anwendung des gesamten Widerspiegelungsoperatoren $\mathcal{F}$ der Anwendung des Produkts der mit F_a, F_{XY} und F_n gebildeten Operator-Matrizen gleichwertig ist :

$$\mathcal{F} = \begin{bmatrix}1 & 0\\ 0 & F_a\end{bmatrix}\cdot\begin{bmatrix}F_{XY} & 1\\ 0 & F_a^2\end{bmatrix}\cdot\begin{bmatrix}F_n & 0\\ 0 & F_a^2\end{bmatrix} \qquad (23)$$

Aus der physikalischen Natur des gestellten Problems kann man feststellen, daß $\mathcal{F}$, der durch die Beziehung (23) definiert wird, invariant in Bezug auf die Permutationen der Faktoren von der rechten Seite ist. Also ist :

$$\mathcal{F} = \begin{bmatrix} F_{XY} \cdot F_n & 0 \\ 0 & F_a \end{bmatrix} \tag{24}$$

die Form des gesuchten Operatoren. Die Beziehung (24) wurde unter Beachtung der Beziehung (16) festgelegt, wonach :

$$F_a^5 = F_a$$

Man kann nun die Tatsache überprüfen, daß der durch die Beziehung (24) definierte Operator $\mathcal{F}$ die Beziehung $\mathcal{R}$, die durch (14′) definiert wird, darstellt, und zwar folgendermaßen :

$$\mathcal{F} \cdot \mathcal{W} = \begin{bmatrix} F_n \cdot F_{XY} \cdot W \\ F_a \cdot V \end{bmatrix} = \overline{\mathcal{W}} \tag{25}$$

Beachtet man die Definition der Enantiomerie, so stellt man fest, daß die Beziehung (25) wahr ist. Durch die Beziehung (25) wurde ein Sinn aus der Beziehung (14) klargelegt. Ein zweiter Sinn wird gezeigt, indem man beweist, daß die Beziehung (25) symmetrisch ist, wie dies aus (26) folgt :

$$\mathcal{F}\mathcal{W} = \overline{\mathcal{W}} \,|\, \mathcal{F}$$

$$\mathcal{F} \cdot \mathcal{F}\mathcal{W} = \mathcal{F}\overline{\mathcal{W}} \tag{26}$$

Verwendet man die Beziehungen (16), (20′), (22), so findet man :

$$\mathcal{F} \cdot \mathcal{F} = \mathcal{F}^2 = \begin{bmatrix} F_n \cdot F_{XY}^2 & 1 \\ 0 & F_a^2 \end{bmatrix} = \begin{bmatrix} 1 & 0 \\ 0 & 1 \end{bmatrix}$$

Aber : $\mathcal{F}^2 \mathcal{W} = E \cdot \mathcal{W} = \mathcal{W}$ (27)

Mit Hilfe von (27) wird die Beziehung (26) :

$$\mathcal{W} = \mathcal{F}\overline{\mathcal{W}}$$

Also wurde gezeigt, daß :

$$\mathcal{F}\mathcal{W} = \overline{\mathcal{W}} \Leftrightarrow \mathcal{W} = \mathcal{F}\overline{\mathcal{W}}$$

das heißt die Beziehung (14) erfüllt ist.

$\mathcal{F}$ erfüllt offensichtlich die Beziehungen (14″) Unter Beachtung des vorhergehend Behandelten kann man den folgenden Satz behaupten :

Gegeben sei ein organisches Molekül, das durch die Matrix $\mathcal{W}$ beschrieben wird. Dieses Molekül ist achiral auf allen Niveaus (i, ii, iii) dann und nur dann, wenn :

$$\mathcal{F}\mathcal{W} = \mathcal{W} \tag{28}$$

Um Beziehungen der Diastereoisomerie zu erhalten, genügt es den Operatoren $\mathcal{F}$ mit einigen der hier definierten Operatoren zu bilden (F_a, F_n, F_{XY}), die entsprechend der gegebenen Situation gewählt werden.

SCHLUSSFOLGERUNG

Die Verwendung der matriziellen Schreibweise für die Charakterisierung der axialen konformationellen Chiralität erlaubt eine mathematische Ausdrucksweise der chiralen Beziehungen zwischen den Konformeren. Gleichfalls wurde die analytische Form des Operatoren der Widerspiegelung für verschiedene Charakterisierungsniveaus der Struktur der Konformeren abgeleitet, das heißt bei rein konformationellem Niveau, beziehungsweise beim Niveau, in dem auch die Konfiguration der die Achse bestimmenden Atome oder auch die Konfigurationen der von der Achse abzweigenden Liganden eingeschlossen wurden.

Revue Roumaine de Chimie, 18, 4, 655–665 (1973)

Revue Roumaine de Chimie, 18, 4, 667 – 676 (1973)

HETEROCYCLIC ORGANOBORON COMPOUNDS. XV*

BORONIUM CHELATE SALTS AND BERYLLIUM CHELATES OF 1,3-KETOENOLS WITH DISTURBED RESONANCE IN THE CHELATE RING

ELENA IŞFAN and A. BARABÁS

Institute of Atomic Physics, P. O. Box 35, Bucharest

Received November 9, 1972

Chelate complexes of the $(L_2B)^+X^-$ and L_2Be types, in which L = ethyl acetoacetate, 2-acetylcyclohexanone, 2′-hydroxy-acetophenone (2-acetyl-phenol) or 2′-hydroxy-5′-methyl-acetophenone (2-acetyl-4-methylphenol), $X^- = SbCl_6$, ClO_4 or $FeCl_4$, were prepared and characterized by UV, IR ^1H- and ^{11}B-nmr spectra. The influence of factors disturbing the electron delocalization in the chelate ring on the properties of these chelates is discussed.

INTRODUCTION

In previous papers in this series [1-3] and related works [4-6] various investigations were reported on $(L_2B)^+X^-$ and L_2Be complexes, having 1,3-diketones of different structures as chelating ligands, LH. From these studies several conclusions could be drawn concerning the dependence between structure and properties of these chelate complexes. A brief summary of these will be given below.

1. In all chelates there are six electrons delocalized on the 1,5-oxa-oxonia-pentadienic system of the ligand, in the sense of the formulae I – III. Thus $R' = R'' = CH_3$ groups appear in ^1H-nmr

---

* Preceding part in the series is I. Bally and A. T. Balaban, *Rev. Roumaine Chim.*, **16**, 739 (1971).

[1] A. Barabás, E. Işfan, M. Roman, M. Paraschiv, E. Romaş and A. T. Balaban, *Tetrahedron*, **24**, 1133 (1968).

[2] A. Barabás, E. Işfan, E. Romaş and A. Trestianu, *Rev. Roumaine Chim.*, **14**, 253 (1969).

[3] E. Işfan, A. Barabás, J. C. Hammel and J. A. S. Smith, *Tetrahedron*, **26**, 5057 (1970).

[4] A. Trestianu, H. Niculescu-Majewska, I. Bally, A. Barabás and A. T. Balaban, *Tetrahedron*, **24**, 2499 (1968).

[5] J. C. Hammel and J. A. S. Smith, *J. Chem. Soc. A*, **1970**, 1855, and previous papers cited therein.

[6] J. C. Hammel, R. J. Lynch, J. A. S. Smith, A. Barabás and E. Işfan, *J. Chem. Soc. A.*, **1970**, 3000.

spectra as magnetically equivalent.

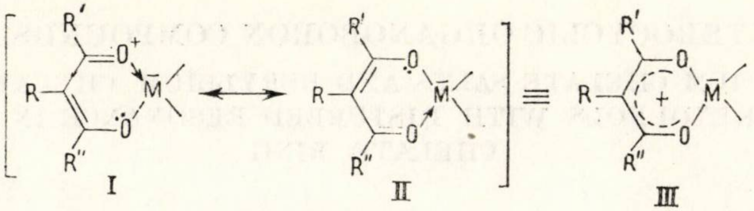

2. Aromatic R', R'' substituents decrease the excitation energy (π→π * transition) of the delocalized electronic system of the chelate ring by conjugation. As ^{1}H-nmr evidence indicates, these groups are coplanar with the chelate ring. Inductive effects of the R', R'' groups (e.g. R' = CF_3) seem to have no significant influence on the above mentioned electronic trasition.

3. π-Electrons of the R = C_6H_5, $COCH_3$, COC_6H_5 substituents are not conjugated with the delocalized system of the chelate ring, having a minor influence on its excitation energy. ^{1}H-nmr data suggest that the two π systems are non-coplanar. Inductive effects of R groups seem to lower the π→π * transition energy in the chelate ring.

In this work compounds are studied, whose R, R', R'' substituents perturb the chelate ring resonance. Complexes of structurally analogous ligands, but without perturbed resonance, are used as reference : acetylacetone for ethyl acetoacetate and 2-acetyl-cyclohexanone for 2-acetylphenol.

For convenience, the following abbrevations will be used for chelating ligands referred to in this work :

ethyl acetoacetate — acacoetH
2-acetyl-cyclohexanone — acyhexH
2'-hydroxy-acetophenone (2-acetyl-phenol) — acphoH
2'-hydroxy-5'methyl-acetophenone (2-acetyl-4-methylphenol) — — meacphoH
2,4-pentanedione (acetylacetone) — acacH
3-methyl-2,4-pentanedione (methylacetylacetone) — meacacH.

EXPERIMENTAL

1. Syntheses of ligands : Commercial acetoacetic ester was distilled before use. 2-Acetylcyclohexanone was prepared by BF_3-catalyzed acetylation of cyclohexanone.[7] 2-Acetyl-phenol and 2-acetyl-4-methylphenol were obtained by Fries transposition [8] of the appropriated esters.[9]

2. *Syntheses of the boronium chelate salts.* 20 mmoles of chelating ligand (LH) were dissolved in 5 ml of dry dichloromethane and 2.8 ml (2.2 g, 10 mmoles) of tri-(n-butyl)-borate were added.

---

[7] J. T. Adams and C. R. Hauser, *J. Amer. Chem. Soc.*, **67**, 284 (1945).
[8] K. W. Rosenmund and W. Shnurr, *Liebig's Ann. Chem.*, **460**, 56 (1928).
[9] A. Spassow, *Chem. Ber.*, **75**, 779 (1942).

This mixture was cooled to − 40° and dry HCl gas was bubbled through for ca. 30 min. A solution of the corresponding chelated complex boronium chloride, $(L_2B)^+Cl^-$ resulted this way. Isolable salts were prepared by adding an appropriate anion-forming component in dichloromethane solution : 1.3 ml (3.0 g, 10 mmoles) of $SbCl_5$, 1.6 g (10 mmoles) of $FeCl_3$ or 10 mmoles of anhydrous $HClO_4$ in dichloromethane. These salts were isolated by concentration and recrystallized as shown in Table 1.

3. *Syntheses of the beryllium chelates.* The free ligand, LH, (20 mmoles) was dissolved in 5 ml of ethyl acetate. This solution was heated to reflux and a solution of 0.8 g (10 mmoles) of dry $BeCl_2$ in 25 ml of ethyl acetate was dropped into. The refluxing was continued for several hours, till the evolution of HCl ceased. The solvent was then evaporated *in vacuo*, and the complex purified by recrystallization, as indicated in Table 1.

bis-(Ethyl acetoacetato)-beryllium was prepared also in aqueous medium : 1.8 g (10 mmoles) of $BeSO_4.4H_2O$ were added to 5 ml of saturated sodium acetate solution and this mixture was shaken with 2.6 ml (*ca.* 2.6 g, 20 mmoles) of ethyl acetoacetate. The emulsion resulted was extracted with benzene and the organic layer fractionated to give a 10% yield of product. Non-reacted beryllium ion can be recovered from the aqueous phase with acetylacetone.

bis-(Ethyl acetoacetato)-beryllium was reported in literature, [10] *bis*-(2-acetyl-phenolato)-beryllium was prepared earlier in our laboratory. [11] *bis*-(2-Acetyl-cyclohexanonato)-beryllium was studied potentiometrically [12] but not isolated as pure substance.

4. *Analyses and spectra.* Elementary analyses for carbon and hydrogen were effected by standard combustion. Chlorine was determined by argentometric titration. Electronic spectra were recorded in 1,2-dichloroethane solution by a CF−4 Optica-Milano double-beam recording spectrophotometer. Infrared spectra were taken on a Carl Zeiss-Jena UR−10 instrument. Nuclear magnetic resonance spectra were recorded by Perkin Elmer R 10 and R 12 instruments. ^{11}B-nmr spectra were taken at a frequency of 19.2519 MHz with external $BF_3.Et_2O$ as reference.

RESULTS AND DISCUSSION

Electronic spectra of the studied complexes, the free ligands and of some analogous complexes used as reference compounds are shown in tables 2−4. Based on previous studies,[1−3] the absorption maxima in the column labelled with Z were attributed to the $\pi\to\pi^*$ transition in the chelate ring. The wavelength of this absorption is inversely proportional to the excitation energy of the delocalized electrons in the chelate ring, which in turn is inversely proportional to the resonance energy of this delocalized system. The wavelength in question will measure thus the extent of delocalization of the π electrons of the chelate ring.

As may be seen from table 2, an $R' = OC_2H_5$ substituent produces a hypsochromic shift of the $\pi\to\pi^*$ transition compared to the reference compound with $R' = CH_3$. The value $d\lambda$ of this shift is measured as the wavelength difference for the $\pi\to\pi^*$ transition (Z) in the studied compound

---

[10] C. Weygand and H. Forkel, *Chem. Ber.*, **59**, 2243 (1926).

[11] A. Barabás, *Rev. Roumaine Chim.*, **11**, 751 (1966).

[12] E. S. Prjevalskii and L. M. Moiseeva, *Vestn. Mosk. Univ., ser. mat., mekh., astron., fiz., khim.*, **14**, No. 1, 203 (1959).

Table 1

Boronium chelate salts and beryllium chelates

Compound no.	Formula Ligand LH	Anion, X^-	m.p. °C	Recrystallized from	Analyses					
					C		H		Cl	
					found	calc.	found	calc.	found	calc.
	boronium compounds $L_2B^+X^-$									
1	ethyl acetoacetate	$SbCl_6$	135	CH_2Cl_2	23.33	23.87	3.38	3.00	35.41[a]	35.25
2	2-acetyl- -cyclohexanone	$SbCl_6$	110	CH_2Cl_2	30.26	30.81	3.50	3.56	34.0	34.22
3		ClO_4	195	CH_2Cl_2	49.10	49.45	5.89	5.71	—	—
4	2-acetyl -phenol	$SbCl_6$	162	$C_2H_4Cl_2$	30.75	31.21	2.41	2.30	34.5	34.56
5		ClO_4	259	CH_3CN	50.80	50.60	4.28	3.71	—	—
6	2-acetyl-4- -methylphenol	$SbCl_6$	163	$C_2H_4Cl_2$	32.99	33.59	3.35	2.82	33.3	33.05
7		$FeCl_4$	dec.	none	b,	42.65	4.01	3.58	27.9	27.99
	beryllium compounds, L_2Be								Be[d],	
8	ethyl acetoacetate	—	59[c],	$n\text{-}C_7H_{16}$						
9	2-acetyl-cyclohexanone	—	134	$n\text{-}C_7H_{16}$	67.12	66.88	7.61	7.72	3.32	3.13
10	2-acetyl-phenol	—	172[e],	C_6H_6						

a, from combustion; b, incorrect; c, lit. [10] m.p. 63°; d, combustion residue taken as BeO; e, ref. 11.

Table 2

Electronic absorption spectra of the ethyl acetoacetate complexes and of the analogous acethylacetone compounds[1]

Compound	λ_{max} (nm) ϵ(l/mole·cm) Z	dλ (nm)^{a}	Λ (nm)^{b}
acacoetH IV	244 —	−29	0
acacoet$_2$Be V	272 30200	−22	28
acacoet$_2$B$^+$SbCl$_6^-$ VI	272 43000	−24	28
acacH VII	273 —	0	0
acac$_2$Be VIII	294 36700	0	21
acac$_2$B$^+$SbCl$_6^-$ IX	296 17300	0	23

a, compared to the corresponding acetylacetone compound; b, compared to the free ligand.

Table 3

Electronic absorption spectra of the 2-acetyl-phenol-complexes

Compound	λ_{max} (nm)/ϵ (l/mole·cm)			dλ (nm)^{a}	Λ (nm)
acphoH X		252 10400	327 3700	−38	0
acpho$_2$Be XI	261(s) 19500	269 22000	380 9500	−44	17
acpho$_2$B$^+$SbCl$_6^-$ XII		303 44000	388 8000	−11	51
meacphoH XIII		254 7000	339 2600	−36	0
meacpho$_2$B$^+$SnCl$_6^-$ XIV		294 44000	406 7800	−20	40

a, compared to the corresponding acetyl-cyclohexanone compound, Table 4

Table 4

Electronic absorption spectra of the acetyl-cyclohexanone complexes and of the analogous methyl-acetylacetone compounds [2]

Compound	λ_{max} (nm) ε (l/mole·cm) Z		dλ (nm)[a],	Λ (nm)
acyhexH XV		290 8000	1	0
acyhex$_2$Be XVI	258(s) 2250	313 29000	2	23
acyhex$_2$B$^+$SbCl$_6^-$ XVII	274(s) 11800	314 22300	4	24
acyhex$_2$B$^+$ClO$_4^-$ XVIII	269(s) —	314 —	2	24
meacacH XIX		289 —	0	0
meacac$_2$Be XX		311 —	0	22
meacac$_2$B$^+$SbCl$_6^-$ XXI	273(s) —	310 —	0	21
meacac$_2$B$^+$ClO$_4^-$ XXII	268(s) —	312 —	0	23

a, compared to the corresponding methyl-acetylacetone compound.

(ethyl acetoacetate derivatives in Table 2) and the analogous compound chosen as reference (acetylacetone derivatives in Table 2). The negative dλ values obtained mean less resonance energy, restricted delocalization in the chelate ring produced by the $R' = OC_2H_5$ substituent. $R', R'' = C_6H_5$ substituents, conjugated with the chelate ring, produced[1] large positive dλ shifts against the same reference compounds (VII – IX), having $R', R'' = CH_3$.

Similarly, the benzo- R—R′ substituent in the 2-acetyl-phenolcompounds (Table 3), produces a hypsochromic shift of the $\pi \rightarrow \pi^*$ transition, compared to the saturated analogues, the 2-acetyl-cyclohexanone compounds (Table 4), having tetramethylene R—R′ substituent. As the respective dλ values are also negative, it can be assumed, that the benzo- R—R′ substituent reduces the extent of delocalization in the chelate ring compared to the reference. This hypsochromic effect on the $\pi \rightarrow \pi^*$ transition in the chelate ring due to the benzene ring condensed to it is of electronic (mesomeric) rather than of steric or any other nature. The saturated acetyl-cyclohexanone compounds chosen as reference behave "normally", giving no significant shifts compared to the analogous compounds of methyl-acetylacetone, (Table 4), having $R, R', R'' = CH_3$ substituents to which no mesomeric and only very small inductive or steric effects could be attributed.

Consequently, it must be admitted that both structural elements (an $R'=OC_2H_5$ substituent and a condensed benzene ring) perturb the resonance in the chelate ring. This perturbation in chelates of ethyl acetoacetate and of 2-acyl-phenols may be performed as shown in formulae XXIII–XXV and XXVI – XXVIII, respectively, where the limiting structures XXIV and XXVII, respectively, prevail in the resonance hybrid.

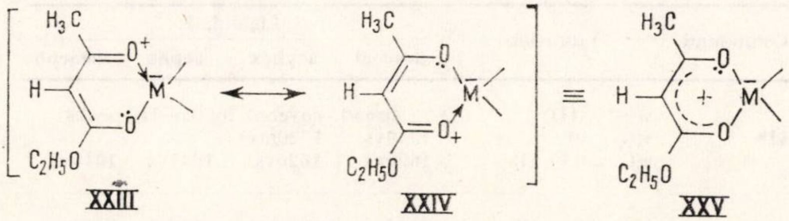

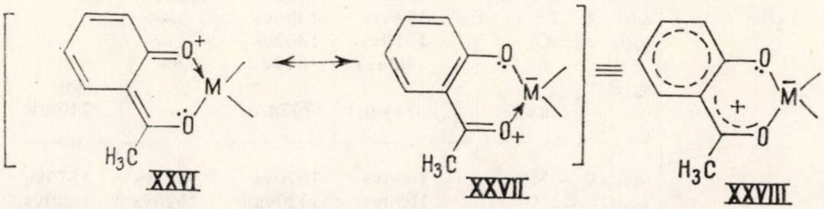

Unlike I and II, the canonical structures XXIII and XXIV, respectively XXVI and XXVII, are energetically non-equivalent, which means in terms of the valence bond theory less resonance energy. The MO method will express this as less extended delocalization of the chelate ring conjugated system in the sense of formulae XXV or XXVIII, compared to formula III. Structure XXIII will have a higher energy content than its counterpart XXIV, because the strong donor OC_2H_5 substituent will favour the apparition of the positive charge at the oxygen atom of the adiacent carbonyl group, as in XXIV. Structure XXVI will be of higher energy than XXVII due to its *o*-chinoidic nature.

Complexation to Be or B causes throughout a bathochromic shift of the $\pi\rightarrow\pi^*$ transition, that is complexation will favour delocalization in the chelate ring, compared to the free ligand, LH. This is shown in Tables 2–4 as the difference Λ between the wavelengths Z for the complex in question and the free ligand. As may be seen, Λ values are non-negative for all complexes.

Infrared spectra of the studied compounds deserve some comment. Most of the observed intense absorption peaks could be attributed to individual vibrations by an empirical procedure, using results of previous work[1-3] and of some studies on similar compounds[13,14]. Some of these peaks are shown in Table 5. The broad (2500–3300 cm^{-1}) absorption of

---

[13] H. Musso and H. Junge, *Tetrahedron Letters*, **1966**, 4003, 4009.

[14] E. Funck, *Ber. Bunsenges. Physik. Chem.*, **68**, 617 (1964); **71**, 170 (1967).

the hydrogen-bonded OH in the free ligands LH is missing in the complexes. The stretching frequency of the non-coordinated C=O groups, appearing in ethyl acetoacetate and in 2-acetyl-cyclohexanone is also non-existent in the spectra of their complexes. Carbonyl groups in 2-acetyl-phenols are completely hydrogen-bonded .[15] The frequencies of coordinated C=O groups in complexes ($C \cdots O \rightarrow M$) are lower than in the free ligands ($C \cdots O \rightarrow H$), reinforcing the conclusion drawn above, that complexation of either Be or B implies stronger coordinative bonds than those to hydrogen. For attribution of metal-ligand absorption frequencies, the analysis of Funck [14] was followed. Two vibrations of the BeO_4 tetrahedron appear as absorption bands. They were attributed as antisymmetric stretching vibrations degenerated into two components : one perpendicular (*n*) and the other parallel (*ax*) to the symmetry axis of the molecule. (Rigorously speaking, there is no symmetry axis in these complexes with $R' \neq R''$; they consist of a racemic mixture of two enantiomers. In this discussion the symmetry axis considering $R' = R''$ is meant). The same vibrations appear for the BO_4 tetrahedron, but with a further splitting due to the isotopes ^{10}B and ^{11}B.

Table 5

Some characteristic IR absorption frequencies (cm^{-1}) of the free ligands, LH, their beryllium complexes, L_2Be and boronium chelate salts, $L_2B^+SbCl_6^-$ in KBr pellets

Compound	Vibration	Ligand, L			
		acacoet	acyhex	acpho	meacpho
$LH^{a,}$	$\nu(O \cdots H)$	broad, covered by (C—H) peaks			
	$\nu(C = O)$	1740vs	1720ms	—	—
	$\nu(C \cdots O \rightarrow H)$	1650vs	1620vs	1647vs	1645vs
L_2Be	$\nu(C \cdots O \rightarrow M)$	1620s	1580vs	1587vs	1580vs
	$\nu_{as}(C \cdots C \cdots C)$	1520vs	1485vs	1535vs	1535vs
	$\omega(O \cdots C \cdots C \cdots C \cdots O)$	1385vs	1390vs	—	—
	$\nu_s(C \cdots C \cdots C)$	1310vs	1302vs	—	—
	$\nu_{as}BeO_4$ n	860ms	840vs	920s	920
					890^s
	$\nu_{as}BeO_4$ ax	748m	757mw	—	740mw
$L_2B^+ SbCl_6$	$\nu(C \cdots O \rightarrow M)$	1600vs	1570vs	1575vs	1575vs
	$\nu_{as}(C \cdots C \cdots C)$	1530vs	1520vs	1525vs	1530vs
	$\omega(O \cdots C \cdots C \cdots C \cdots O)$	—	1405vs	—	—
	$\nu_s(C \cdots C \cdots C)$	—	1298s	—	—
	$\nu_{as}BO_4$ n ^{10}B	1120shs	1090s	1135ms	1175shma
	$\nu_{as}BO_4$ n ^{11}B	1098vs	1068vs	1105vs	1140vs
	$\nu_{as}BO_4$ ax ^{10}B	—	—	895m	—
	$\nu_{as}BO_4$ ax ^{11}B	—	—	875ms	—

a, in CCl_4 solution.

---

[15] S. BĂDILESCU and I. BĂDILESCU, *Rev. Roumaine Chim.*, **10**, 103 (1965).

Some nuclear magnetic resonance frequencies of the studied compounds are shown in Table 6. The effect of the $R' = OC_2H_5$ substituent on the proton chemical shifts may be treated in similar terms as electronic spectra were discussed above. The chemical shift differences dδ between ethyl acetoacetate compounds ($R' = OC_2H_5$) and acetylacetone compounds ($R' = CH_3$) are shown for the $R'' = CH_3$ and $R = H$ protons. The throughout negative dδ values show that an $R' = OC_2H_5$ group produces an upfield shift (i.e. more screening) of the protons considered. This may be explained with less delocalization in the chelate ring compared to the reference compound. This explanation is supported by the observation that (absolute) dδ values are an order of magnitude greater for the $R = H$ proton attached directly to the chelate ring, than for the $R'' = CH_3$ protons. The chemical shift differences Δ between complexes and their free ligands are positive, suggesting that delocalization in the chelate ring is more advanced in the metal complexes. This applies for Be complexes only, because in boronium salts the overall positive charge in the complex cation produces large positive Δ shifts. In this connection it is most interesting to note that Δ values near to zero were observed for the boronium salts of the 2-acyl-phenols (see Table 6).

Table 6

Nuclear magnetic resonance frequencies of some complexes and their free ligands
(δ, dδ and Δ values are given in ppm)

Compound	Solvent	^{1}H-resonance						^{11}B-resonance
		$R'' = CH_3$			$R = H$			δ
		δ	dδ[a],	Δ	δ	dδ[a],	Δ	
acacoetH[b],	$CDCl_3$	1.95	−0.05	0	5.04	−0.36	0	—
$acacoet_2Be$	$CDCl_3$	2.02	−0.07	0.07	5.09	−0.54	0.05	—
$acacoet_2B^+ SbCl_6^-$	$CDCl_3$	2.40	−0.04	0.45	5.88	−0.72	0.84	4.7
acphoH	CCl_4	2.46	—	0	—			—
$acpho_2 B^+ SbCl_6^-$	$CDCl_3$	2.56	—	0.10	—			3.2[c],
$acpho_2 B^+ ClO_4^-$	$CDCl_3$	2.51	—	0.05	—			3.5[c],
meacphoH	CCl_4	2.52	—	0	—			—
$meacpho_2B^+ SbCl_4^-$	$CDCl_3$	2.46	—	−0.06	—			3.6[c].

a, compared to the corresponding acetylacetone derivative; b. enoe form; c. in CH_3CN

^{11}B-chemical shifts are similar to those observed for boronium complex salts of other 1,3-ketoenols, and they are shown here only as proof for the assigned structure. ^{11}B-resonance in boron 1,3-diketonates will be discussed elsewhere.[16]

From the discussion of the results outlined in this work a further point may be added to the conclusions concerning structure — properties relationships in 1,3-diketone chelates, quoted in the introduction :

---

[16] J. C. HAMMEL, J. A. S. SMITH, A. BARABÁS and E. IȘFAN, to be published.

4. Substituents like $R' = OC_2H_5$ or a benzene nucleus condensed to the chelate ring as $R - R'$ substituent, by their electronic effect interfere with the delocalization in the chelate ring, favouring one limiting structure, as shown by electronic and ^1H-nmr spectra.

Acknowledgements. The authors are indebted to Prof. A. T. Balaban for helpful criticism. Thanks are expressed to Mrs. M. Roman for elementary analyses and to Mrs M. Paraschiv, Mrs. E. Romaş and Dr. J. C. Hammel for recording the spectra.

Revue Roumaine de Chimie, **18**, *4*, 677–683 (1973)

ELECTRONIC SPECTRA AND ACIDITY CONSTANTS OF SOME 2-AMINO-5-SUBSTITUTED THIAZOLES

DAN SUCIU

Oncological Institute, Str. Republicii nr. 34–36, Cluj, Romania

Received July 17, 1972

The ultraviolet data and acid dissociation constants of some 2-amino-5-substituted thiazoles support the assumption that between the electron-donating group 2-amino and an electron-attracting 5-substituted group a charge polarization should be possible. Evidence is presented about the common feature of this effect with the intramolecular charge-transfer which occurs in *para*-substituted anilines.

The highly unsymmetrical aromatic compounds of the type (*X*) where (*D*) group is an electron-donating substituent (amino or alkyl substituted amino) and the (*A*) group is an electron-attracting substituent (nitroso, nitro, aldehyde, acetyl, carboxyl etc.) have two absorptions in ultraviolet. The stronger absorption found in the near ultraviolet region has been assigned to a transition which was qualitatively represented as being from the ground state (*X*) to the excited state (*Y*).[1,2] In the present work we report some ultraviolet data which support the assumption that in the 2-amino-thiazole series almost similar transitions with those of the type (*X*↔*Y*) may be possible.

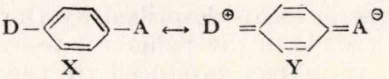

X Y

The electronic spectra in ethanol of some 2-amino-4-methyl-5-acylthiazoles (Table 1) show strong absorptions in the region 325–345 nm and weaker absorptions between 220–262 nm, from this point of view the spectra being similar with those reported for *para*-substituted anilines[1,2].

Taking into account the unsymmetrical distribution of the charge density in the 2-aminothiazole molecule,[3] a restriction of the charge polarization between the 2-amino group and an electron-attracting substituent located in the 4 or 5 positions of the ring should be excepted. On the

---

[1] W. D. Kumler, *J. Amer. Chem. Soc.*, **68**, 1184 (1946).

[2] G. Yamaguri, Y. Kakinoki and H. Tsumbura, *Bull. Chem. Soc. Japan.*, **40**, 526 (1967).

[3] J. Sandström, *Acta Chem. Scand.*, **18**, 871 (1964).

Table 1

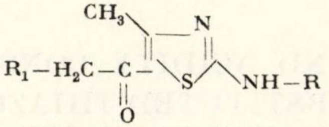

Ultraviolet maxima of some 2-amino-5-acylthiazoles

Compound	R	R_1	Ethanol		0.1N−HCl solution	
			λ (nm)	log ε	λ (nm)	log ε
1	H	H	225 325	3.49 4.15	246 295	3.32 4.05
2	$CH_2-CH=$ CH_2	H	226 330	4.07 4.36	248 300	3.60 4.12
3	$CH_2-CHBr-$ $-CH_2Br$	H	231 332	3.52 4.15	242 297	2.95 4.15
4	H	Br	220 328	3.45 3.95	295	4.01
5	$CH_2-CH=$ CH_2	Br	262 345	3.47 3.80	303	4.13
6	CH_2-CHBr $-CH_2Br-$	Br	239 345	3.53 4.02	305	4.00

basis of the limit mesomeric forms described by Dorn *et al.* [4] for 2-aminothiazole an attempt was made in the Scheme 1 to explain, with the aid of similar representations, the effect produced by the presence of the keto group on the charge distribution in the 2-amino-4-methyl-5-acetylthiazole molecule. The mesomeric forms (b−d) show the charge distribution of the amidine system, and the structures (e−h) the charge polarization along the long axis of the molecule. Both effects could be qualitatively emphasized on the basis of ultraviolet spectra.

The protonation of 2-aminothiazoles takes place at the endocyclic nitrogen atom. [4] Compounds **10**−**15** (Table 2) exhibit quite similar spectra in neutral and acid media. On the contrary, for the 2-amino-5-substituted thiazoles **1**−**6** (Table 1) and **8**, **9** (Table 2) the near ultraviolet absorption band is shifted to shorter wavelengths in acid solution. The ammonium salt of *p*-aminoacetophenone (**7**) also absorbs at a shorter wave length than the corresponding free base (Table 2). All these compounds (**1**−**15**) are protonated in 0.1 N−HCl solution, but the blue shift of the near ultraviolet absorption band could be observed only for *p*-amino-acetophenone and 2-amino-5-substituted thiazoles carrying a strong electron-attracting group (phenyl or acetyl) in the 5 position of the ring. This could

---

[4] H. DORN, G. HILGETAG and A. RIECHE, *Angew. Chem.*, **16**, 560 (1961).

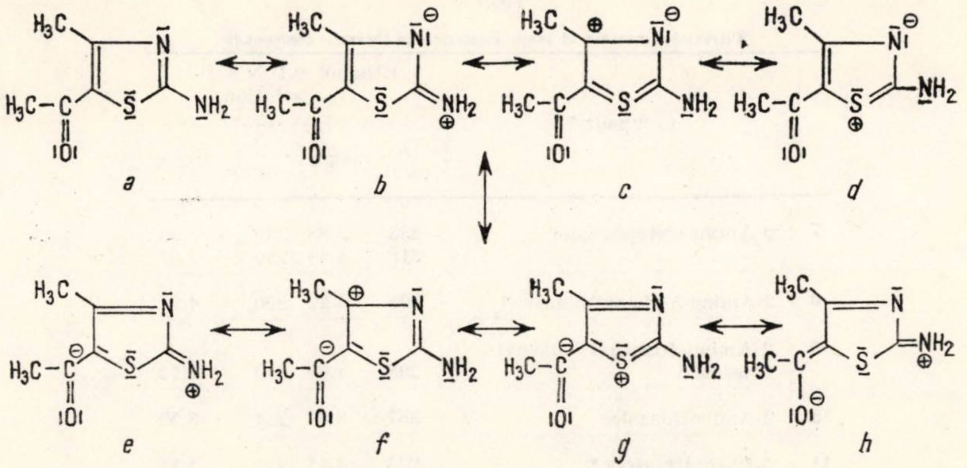

Scheme 1. Mesomeric forms of 2-amino-4-methyl-5-acetyl-thiazole.

be explained assuming that protonation prevents the intramolecular charge transfer of the type (*a* ⟷ *h*) or (*X* ⟷ *Y*).

2-Amino-4-phenylthiazole **(18)** and 2-allylamino-4-acetyl-thiazole **(19)** also exhibit two absorptions in ultraviolet. However, the bands which appear in the near ultraviolet region have lower intensities as compared with those produced in the blue region of the spectra, in contrast with *para*-substituted anilines [1,2] and 2-amino-5-substituted thiazoles (Table 1 and 2). This effect is probably due to the position of the electron attracting group (acetyl or phenyl) which does not favour the transmission of the mesomeric effect through the molecule, similarly as in the *meta*-substituted aromatic compounds.

The ultraviolet data lead to the conclusion that an intramolecular charge transfer nearly similar to that produced in molecules like *para*-substituted anilines may be possible in the 2-amino-thiazole series only for 2-amino-5-substituted thiazoles, when the 5-substituted group has strong electron attracting properties. The charge polarization is highly probably facilitated along the $-\overline{\underline{S}}-$ bridge as it is emphasized in the mesomeric structures (*e* — *h*) (Scheme 1).

Accordingly, for molecules of the 2-amino (5,4′)-2′-amino-bithiazole type **(19—21)** in the 2-amino-5-substituted thiazole group a similar charge polarization should be excepted, the electron attracting substituent being the 4′-thiazolyl group. The mesomeric structure (*W′*) indicates the stabilization tendency by resonance of this excited molecular state. The assumption made above is qualitatively supported by the ultraviolet spectra of these compounds, because the near ultraviolet absorption band found

Table 2

Ultraviolet maxima of some aromatic and thiazolic compounds

	Compound	Ethanol		0.1 N−HCl solution	
		λ (nm)	log ε	λ (nm)	log ε
7	p-Aminoacetophenone	233 318	3.88 4.43	239 280	3.95 3.07
8	2-Amino-5-phenylthiazole *	308	4.22	290	4.21
9	2-Amino-4-methyl-5-phenylthiazole *	293	4.05	280	4.12
10	2-Aminothiazole	257	3.87	254	3.52
11	5-Phenylthiazole *	275	4.11	275	4.11
12	2-Amino-4-methyl-5-(α-hydroxy)-ethylthiazole	273	3.82	270	3.74
13	2-Acetylamino-4-methyl-5-acetylthiazole	229 305	3.95 4.14	229** 303	3.79 4.16
14	2-(N-allyl, N-acetyl) amino-4-methyl-5-acetylthiazole	229 304	4.11 4.23	230** 307	3.99 4.29
15	p-Acetylaminoacetophenone	287	4.40	287**	4.41
16	4-Phenylthiazole*	252	4.14	252	4.14
17	2-Amino-4-phenylthiazole*	228 284	4.36 3.90	 265	 4.22
18	2-Allylamino-5-acetylthiazole	229 315	4.05 3.45	 255	 3.93

* Data reported by Wilson and Woodger[5] (The spectra have been recorded in ethanol and ethanol-HCl solution).

** Spectra recorded in ethanolic 0.1 N−HCl solution.

Table 3

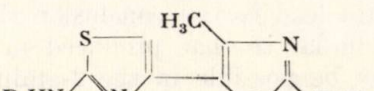

Ultraviolet maxima of 2-amino-(5,4′)-2′-aminobithiazoles

Compound	R	R_1	Ethanol		0.1N−HCl solution	
			λ (nm)	log ε	λ (nm)	log ε
19	H	H	262 313	4.08 4.20	266	4.21
20	$CH_2-CH=CH_2$	H	268 320	3.89 3.95	269	3.96
21	$CH_2-CHBr-CH_2Br$	H	244 316	4.20 4.00	271	4.14

---

[5] W. Wilson and R. Woodger, *J. Chem. Soc.*, **1955**, 2943.

in the spectra recorded in ethanol is absent in the spectra recorded in 0.1 N—HCl solution (Table 3).

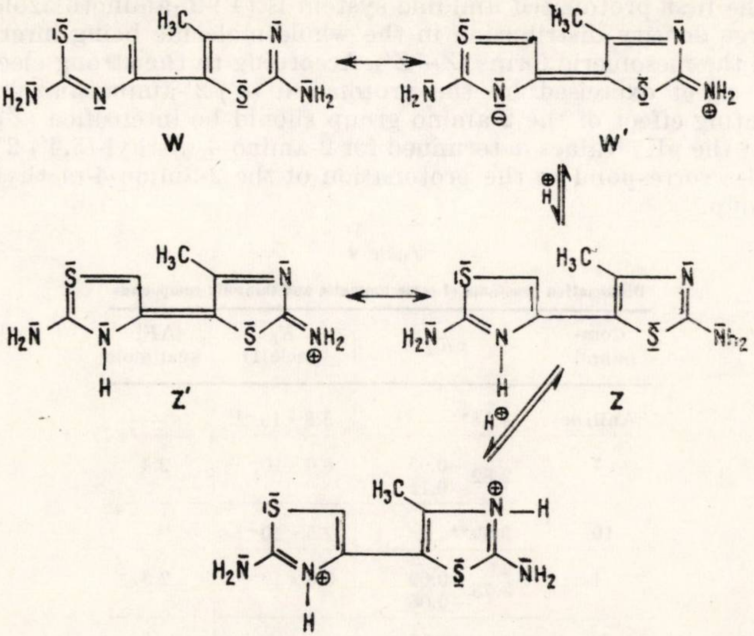

Quantitative data regarding the intramolecular charge transfer which occurs in molecules like *p*-aminoacetophenone or 2-amino-5-substituted thiazoles were obtained on the basis of the acid dissociation constants (Table 4). The pK_a values of *p*-aminoacetophenone as well as those of 2-amino-5-substituted thiazoles are lower than those determined for aniline and 2-aminothiazole respectively, according to the charge deficit induced in the ring by the electron-attracting groups (acetyl or 4′-thiazolyl). The conjugation energy $|\Delta F|$ (Table 4) required for the charge polarization between the donating and the accepting group was calculated following the relation :

$$\Delta F = -RT \ln \frac{K_1}{K_2}$$

K_1 = basicity constants of aniline and 2-aminothiazole, respectively,

K_2 = basicity constants of *p*-aminoacetophenone, 2-amino-5-acetylthiazoles and 2-amino-(5,4′)-2′-aminobithiazoles.

The $|\Delta F|$ values corresponding to *p*-aminoacetophenone and 2-amino-5-acetylthiazoles were estimated to be about 2.5 kcal/mole (Table 4).

For bithiazoles the $|\Delta F|$ values are significantly higher (about 3.5 kcal/mole), probably because in these compounds there are two amidine systems which are protonated at different hydrogen ion concentrations. Very likely, the first protonated amidine system is (4′)-2′-aminothiazole group, the charge density distribution in the whole molecule being intermediate between the mesomeric forms ($Z \leftrightarrow Z'$). According to the strong electron-attracting effect exercised by the protonated (4′)-2′-aminothiazole group, the donating effect of the 2-amino group should be intensified (Z). It follows that the pK_a values determined for 2-amino-4-methyl-(5,4′)-2′-aminobithiazoles correspond to the protonation of the 2-amino-4-methyl-5-thiazolyl group.

Table 4

Dissociation constants of some aromatic and thiazolic compounds

Compound	pK_a	K_b (mole/1)	$\|\Delta F\|$ kcal/mole
Aniline	4.58*	3.8×10^{-10}	—
7	$2.82^{+0.05}_{-0.11}$	6.6×10^{-12}	2.4
10	5.39**	2.5×10^{-9}	—
1	$3.75^{+0.09}_{-0.06}$	5.6×10^{-11}	2.3
2	$3.49^{+0.04}_{-0.08}$	3.1×10^{-11}	2.6
19	$3.05^{+0.07}_{-0.11}$	1.1×10^{-11}	3.2
20	$2.99^{+0.03}_{-0.06}$	9.7×10^{-12}	3.3
21	$2.86^{+0.12}_{-0.15}$	7.2×10^{-12}	3.5

*) and **) Data reported by [6] and, [4] respectively.

EXPERIMENTAL

The compounds employed were partially obtained from commercial sources (**7, 9**) and the others were synthesized as previously described : **1, 13** ; [7] **2, 14** ; [8] **3, 5, 6, 20, 21** ; [9] **4, 19** ; [10] **12** ;[11] **15** ;[12] **18**.[13]

[6] C. D. Neniţescu, "Chimie organică", vol. I., ed. VI, Editura Tehnică Bucureşti, 1966.

[7] P. M. Kochergin, *Zhur. obschei. Khim.*, **26**, 2897 (1957).

[8] F. Gagiu, G. Csávássy and G. Todor, *Arch. Pharmaz.*, **11**, 964 (1967).

[9] D. Suciu, *Arch. Pharmaz.*, **306**, 152 (1973).

[10] D. Suciu, *Studia Univ. Babeş-Bolyai Cluj/Ser. Chem./*, **XV (2)**, 123 (1970).

[11] D. Suciu, *J. prakt. Chem.*, **314**, 961 (1972).

[12] J. Heilborn and H. M. Bunbury, "Dictionary of organic compounds", vol. I, London, 1946.

[13] F. Gagiu, G. Csávássy and G. Valau, *Bull. Soc. chim. France*, **2**, 686 (1966).

The ultraviolet spectra were recorded with a VSU–2P (Carl Zeiss Jena) spectrophotometer.

The acid dissociation constants were determined in glycine-HCl buffer solution with the standard spectrophotometric technique utilizing the large hipsochromic shifts on ionization. The pK_a data (Table 4) represent the mean values of 4–6 determinations carried out near the pH of equivalence (25°).

Acknowledgement. I wish to thank Professor Dr. V. Fărcăşan, for advice and encouragement.

Revue Roumaine de Chimie, 18, 4, 685–694 (1973)

CONTRIBUTIONS TO THE STUDY OF HETEROCYCLES. XXIV *

A STUDY OF INTERMEDIATES IN THE HANTZSCH REACTION. A NEW METHOD TO OBTAIN 5-ACETYLTHIAZOLE DERIVATIVES

I. SIMITI, MIOARA COMAN, I. SCHWARTZ

Institute of Medicine and Pharmacy, Laboratory of Organic Chemistry
Str. V. Babeş 41, Cluj, Romania

Received November 12, 1971

The present paper investigates the chemical and physico-chemical properties of intermediates resulted in Hantzsch reaction. A new method is proposed to obtain some 2-aryl-4-R-5-acetylthiazoles.

In previous publications we investigated the condensation of symmetrical dichloroacetone with aryl-thioamides, N-arylthiourea and thiosemicarbazones under different conditions. [1–3]

We noted that in acetone solutions at room temperature these reactions occur differently depending on the thioamidic component. Aryl-thioamides unlike N-aryl-thiourea and thiosemicarbazones do not give the appropriate thiazoles, but intermediate ones. These intermediates if neutralized with ammonia or bicarbonate or by simple washing with water, yield the corresponding bases. On heating them in alcoholic solution or in contact with concentrated sulphuric acid, thionylchloride or alkaline hydroxides at room temperature they yield the corresponding 2-aryl-4-chlormethylthiazoles. Contrary to the corresponding alkyl derivatives, the aryl compounds are stable.

Since an influence of the halocarbonylic component could be also invoked, we investigated various halocarbonylic components. The reaction mechanism was the same in all cases. Hooper and Johnson [4] considered these intermediates as iminothioether-hydrochlorides /*A*/. Later, however,

---

* Note XXIII. I. Simiti and E. Chindriş., *Arch. Pharm.*, **305**, 509 (1972).

[1] Al. Silberg, I. Simiti and H. Mantsch, *Chem. Ber.*, **94**, 2287 (1961).
[2] I. Simiti, M. Farkas and S. Silberg, *Chem. Ber.*, **95**, 2672 (1962).
[3] I. Simiti and M. Coman, *Bull. Soc. chim. France*, **1969**, 3276.
[4] W. Hooper and T. B. Johnson, *J. Amer. Chem. Soc.*, **65**, 1967 (1943).

Metzger *et al.*[5] who was investigating the intermediate resulted from the reaction of thioacetamide with symmetrical dichloracetone, assigned a 4-hydroxy-Δ_2-thiazoline /B/ structure to it.

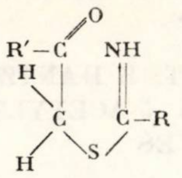

/A/.

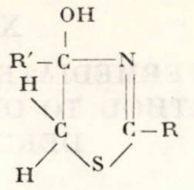

/B/.

In order to elucidate the mechanism of the Hantzsch reaction we undertook a physico-chemical and kinetic study of these intermediates.

The IR and UV spectra of such intermediates, hydrochlorides, bases and the corresponding thiazoles are given in table 1. The I.R. spectra were recorded as KBr pellets with an IR 27 G Shimadzu-spectrometer, the UV spectra in methanol with a VSU–2 Zeiss-Jena Spectrophotometer.

The IR data show that both the hydrochlorides and bases give a band between 1590–1620 cm^{-1} which can be assigned to the endocyclic $C = N$ bond (the exocyclic $C = N$ appears generally above 1630 cm^{-1}; for the substance XVI it appears at 1660 cm^{-1}).[6] The intermediate hydrochlorides and bases give always a band between 3080 and 3100 cm^{-1} which usually can be attributed to the hydroxyl. Such bands appear also in the case of thiazoles unsubstituted in position 5, but are missing in the substituted thiazoles.[7] Since this band appears also in thiazolines which are unsubstituted in position 5, and without a hydroxyl group in 4, it cannot be assigned with certainty to the hydroxyl group.[8] However, since Metzger confirmed the presence of the hydroxyl group in 2-methyl-4-hydroxy-4-chloromethyl-Δ_2-thiazoline by NMR measurements the mentioned band could be due to the hydroxy group.

The UV spectra of these intermediates, show a single absorption band at 242–255 nm contrary to the 2-phenyl-, 2-aniline- and 2-hydrazonothiazole derivatives which give two bands (Table 1).

Since under the influence of concentrated sulphuric acid or of sodium hydroxide the intermediates obtained in the condensation of phenyl-thioamide with symmetrical dichloracetone yield thiazoles, we investigated the influence of the pH for the range 0.5–10 on this process.

In the acid range (pH = 3.2) the absorption band of the substance, as seen in Fig. 1., is identical with that obtained in methanol, suggesting that it corresponds to the unprotonated form. The changes observed in

---

[5] A. Babadjamian, M. Chanon and J. Metzger, *Compte rend.*, **267**, 918 (1968).

[6] L. J. Bellamy, "The infrared spectra of complex molecules", Methuen, London, 1954, p. 114.

[7] Al. Silberg, E. Hamburg, Z. Frenkel and L. Cormos, *Rev. Roumaine Chim.*, **9**, 215 (1964).

[8] G. F. Bolsaev and E. A. Glebovskaia, "Tablitsy tsastost infrakrasnyh spektrov heteroorganitscheskich soedinenii", Khimia, Leningrad, 1968.

Table 1

Characteristic absorption bands: UV in methanol and IR in KBr tablets

Derivatives	IR	UV	
	$\nu_{C=N}$	λ_{max} (nm)	ε
(I) 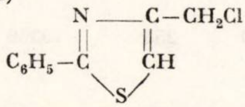 c)	1610	290 218	11100 9000
(II) 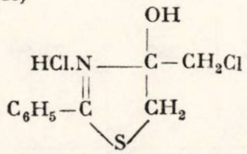	1595	244	75000
(III) 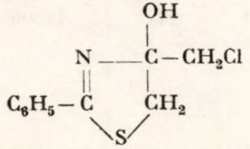 d)	1590	242	20700
(IV) 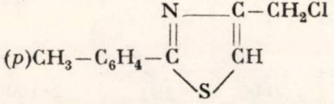 c)	1620	290 218	15600 13000
(V) 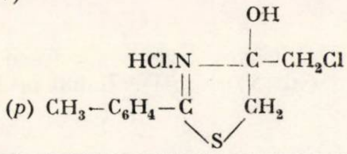	1590	253	20000
(VI) 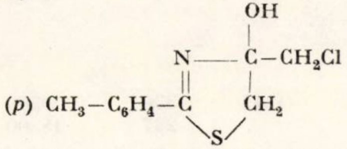	1590	255	9400
(VII) 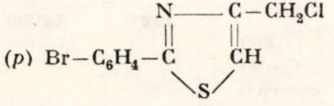 c)	1595	295 220	15900 12900

Table 1 (continued)

Derivatives	IR	UV	
	$\nu_{C=N}$	λ_{max} (nm)	ε
(VIII) 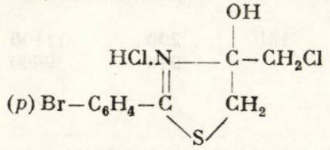	1590	255	19300
(IX) 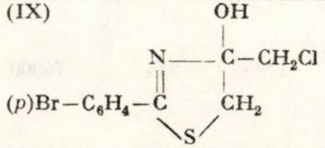	1595	255	22000
(X) 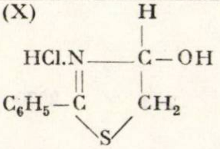	1580	242	14600
(XI) 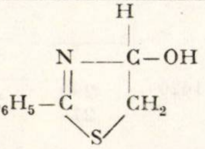	1590	244	13900
(XII) 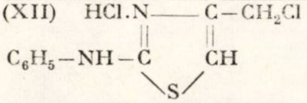 a)	1600 ($\nu C=N$)	292	28100
(XIII) 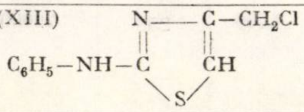 a)	1595 ($\nu C=N$)	290 245–7	19600 infl. point
(XIV) 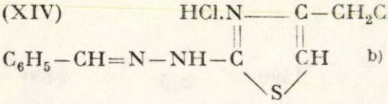 b)	1610	330	19100
(XV) 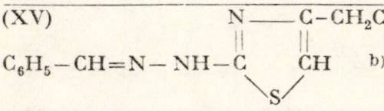 b)	1615	330 237	20200 18300
(XV I) 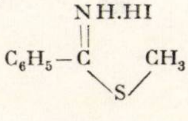	1660 ($\nu C=N$) exo-cicl.	222	11000

a) = (2); b) = (3); c) = (10); d = (13).

the UV spectra at subsequent lower pH values (2.5 ; 2.0 ; 1.8) indicate a partially protonation which is complete at pH = 1.5. (The spectrum is identical with that observed at pH = 0.5).

Increasing the pH values in the opposite direction from 0.5 to 3.2, the same absorption curves were obtained which demonstrates the reversible character of this process (Fig. 1). This excludes a possible conversion of the intermediate into 2-phenyl-4-chlormethyl-thiazole. On the other hand, the spectrophotometrically[9] determined basicity constant of III ($pK_{BH^+} = 1.48$) is different from that of 2-phenyl-4-chlormetyl thiazole which is 0.96.[10]

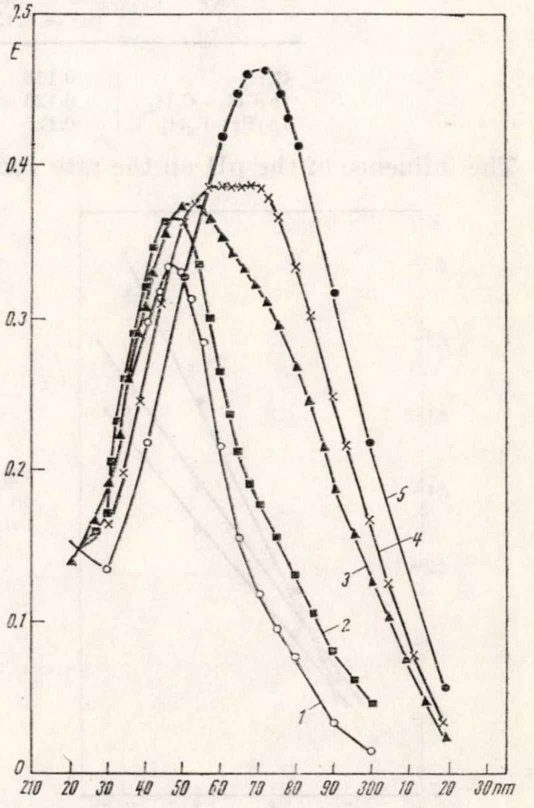

Fig. 1. — UV spectra of thiazolines in the pH range 1.5–3.2.

1, pH =3.2; *2*, pH=2.5; *3*, pH=2.0 *4*, pH=1.8; *5*, pH = 1.5.

The changes of the UV spectra within the basic pH range are even more evident. Thus, the bands in the 238–246 nm region belonging to the thiazoline disappear and others appear at 292–296 nm which are characteristic of the Ar-thiazole system (See table 1).

---

[9] P. Masoni, *Bull. Soc. chim. France*, **1964**, 519.

[10] I. Schwartz, Dissertation, Babeş-Bolyai University Cluj, 1970.

These experiments were carried out for the following pH values: 7.15; 7.65; 8.95. The processes occur according to the first order reactions. The rate constants determined at 25±0.2° are given in table 2.

Table 2

Rate constants for different pH-s

Ar	Rate constant 1/mol·min		
	pH = 7.15	pH=7.65	pH=8.95
C_6H_5	0.156	0.247	0.411
$(p)CH_3-C_6H_4$	0.126	0.218	0.300
$(p)Br-C_6H_4$	0.125	0.274	0.518

The influence of the pH on the rate constant is given in Fig. 2.

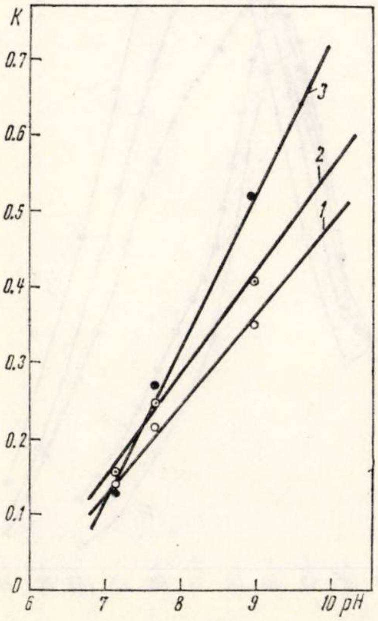

Fig. 2.—Dependence of the rate constant on the pH in the transformation of thiazolines into the corresponding thiazoles; *1*, x = $-CH_3$; *2*, x = $-H$; *3*, x = $-Br$.

A linear dependence can be observed. The influence of the substituents on the first order rate constant, as seen in table 2, at pH = 7.65 and 8.95, shows that the *p*-bromine accelerates the reaction, while the p-CH_3 group has an opposite effect in comparison with the unsubstituted derivative.

From our studies we can conclude that the presence of an $-NH-$ group in position 2 favours the formation of the thiazole but we were not able to isolate an intermediate. With phenyl and alkyl substituents in the same position and under certain conditions the intermediates could be isolated.

The appearance of these intermediates supposes apparently a simultaneous attack of both sulphur and nitrogen. Considering the difference in their nucleophylicity, we consider that sulphur is to attack first, followed immediately by the attack of the nitrogen. Our attempts to demonstrate the initial attack in a condensation reaction between a halocarbonylic and thioamidic component were unsuccessful.

By reacting the 2,4-dinitrophenyl-hydrazone of the symm. dichloracetone with thiobenzamide, a very stable cyclization product was obtained. The latter remained unchanged even after extended boiling in alcohol (10 h) or alcoholic solution of concentrated HCl (10–12 h).

According to the spectral data and kinetic studies we suppose that the isolable intermediates from a reaction between aryl-thioamide and different alfa-halocarbonyls are 4-hydroxy-Δ_2-thiazolines.

The chemical behaviour of these compounds supports such a presumption since they do not react with typical reagents of the $C = O$ group (2,4 DFH) which should be the case if iminothioethers were present. Furthermore, the $C = O$ absorbtion band is absent in the IR spectra.

Investigating comparatively the desulphuration reaction of thiazole, thiazoline and S-methyl-thioamide, evident differences can be observed.

At room temperature 2-phenyl-4-hydroxyl-4-chloromethyl-Δ_2-thiazoline with NaOH easily gives 2-phenyl-4-hydroxyl-methyl thiazole while 2-phenyl-4-chloromethyl thiazole yields the corresponding alcohol only under special conditions.

Since these intermediates easily undergo a cyclization at room temperature under the influence of conc. suplhuric acid we investigated their behaviour towards other dehydrating agents like acetic anhydride. Both 2-aryl-4-chloromethyl-4-hydroxy-Δ_2-thiazolines and 2-phenyl-4-hydroxy-Δ_2-thiazoline, after a short boiling with acetic anhydride give solid products with high melting points showing the characteristic reactions for the carbonyl group (2,4 dinitrophenylhydrazones ; oxymes and the corresponding 2-aryl-thiazoles). On reduction with Zn in HCl they yield 2-phenyl-4-methyl-5-acetyl thiazoles which we obtained also by other route. The compound XVII is identical with the product obtained by Kochetkov [11] in a condensation reaction and by Eiichi Haruki [12] in an oxidation process.

In conclusion, under the influence of acetic anhydride a dehydration reaction and the acetylation of position 5 occur simultaneously. This represents a new method to obtain 5-acetyl thiazoles *via* the corresponding thiazolines.

It is interesting to mention that this reaction occurs much easier with the corresponding thiazoline hydrochlorides. Investigating the action of acetic anhydride on 2-phenyl-4-chloromethyl thiazole hydrochloride and on 2-phenyl-4-chloromethyl thiazole regardless of the boiling time no modifications could be observed. This confirms the presumption that only hydroxythiazolines undergo simultaneous dehydration and acetylation reactions.

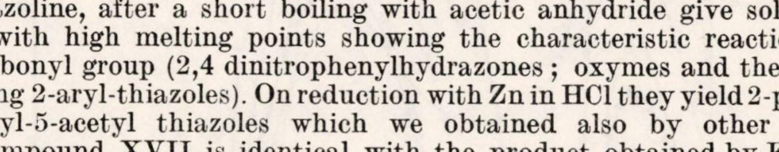

[11] N. K. Kochetkov, E. E. Nifontiev and Molodstov, *Zhur. obschei. Khim.*, **29**, 2330 (1959).

[12] Eiichi Haruki, Shoichi Izumita and Eiyi Imito, *Chem. Abstr.*, **65**, 13688 a (1966).

[13] K. Brown, R. A. Newberry, *Quart. Reps., Sulphur. Chem.*, **3**, 4 (1969).

All ketones were submitted to the haloform reaction and transformed into the corresponding acids. The acid obtained by the haloform reaction of 2-phenyl-5-acetyl thiazoles is identical with that mentioned in the literature.[11,12]

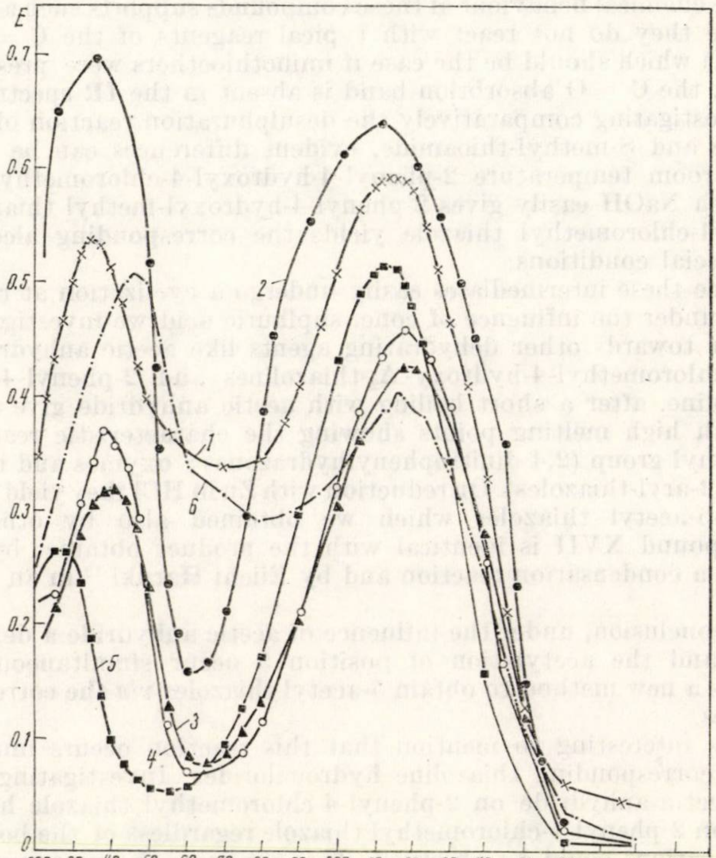

Fig. 3. — UV spectra of 5-acetyl thiazole derivatives.

1, 2-phenyl-4-methyl-5-acetylthiazole ; *2*, 2 -phenyl-4-chloromethyl-5-acetyl thiazole ; *3*, 2-p-tolyl-4-chloromethyl-5-acetyl-thiazole ; *4*, 2-*m*-tolyl-4-chloromethyl-5-acetyl thiazole ; *5*, 2-phenyl-5-acetyl thiazole ; *6*, 2-*p*-brom-phenyl-4-chloromethyl-5-acetyl-thiazole.

The structure of the 2-acetyl derivatives is supported also by their IR and UV spectra (Fig. 3). The mass-spectrum of 2-phenyl-4-chloromethyl-5-acetyl thiazole is also conclusive.

Table 3

UV and IR spectra of 5-acetyl thiazoles

Derivatives		IR C=O	UV λ max (nm)	UV ε
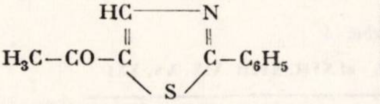	(XVII)	1650	312 227	22739 11744
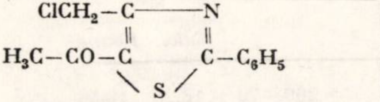	(XVIII)	1670	316 238	37164 27481
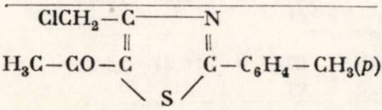	(XIX)	1665	318 241	18370 13596
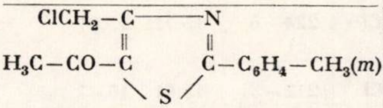	(XX)	1665	318 238	19586 15416
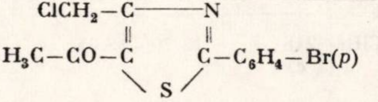	(XXI)	1670	316 247	25691 32385

EXPERIMENTAL

2-Phenyl-4-chloromethyl-5-acetyl thiazole (XVIII) :

On boiling 0.2 g of 2-phenyl-4-chloromethyl-4-hydroxy-Δ_2-thiazolinechlorohydrate for 1 minute with acetic anhydride leads to XVIII which after repeated recrystallizations from alcohol has a melting point of 111–112°. The substances XVII, XVIII, XIX, XX, XXI were obtained by the same method. These substances are presented in Table 4.

Table 4

2-Aryl-4-R-5-acetyl th iazole

Derivatives	Formula	m.p.°	N% Calc.	N% Found
(XVII)	$C_{11}H_9OSN$	149–50 a	6.90	7.27
(XVIII)	$C_{12}H_{10}SNOCl$	111–12 b	5.57	5.56
(XIX)	$C_{13}H_{12}NOSCl$	108–9 b	5.25	5.11
(XX)	$C_{13}H_{12}ONSCl$	84–85 a)	5.27	5.24
(XXI)	$C_{12}H_9ONSClBr$	118–20 b	4.24	4.22

The 2,4-dinitro-phenylhydrazones of XVII, XVIII, XIX, XX, XXI are presented in Table 5.

2-Phenyl-4-chloromethyl-5-carboxy thiazole (XXIII)

0.25 g (0.01 M) of 2-phenyl-4-chloromethyl-5-acetyl thiazole is shaked with sodium, hypobromite solution (50 ml 5 % NaOH and 0.4 ml Br_2) for 3 h. The filtrate is diluted with water, treated with Na bisulphite, ice-cooled and slightly acidified. The acid obtained after filtration and recrystallization from aqueous alcohol has a melting point of 192−193°. The substances XXII, XXIV, XXV, XXVI were obtained similarly. These substances are presented in Table 6.

Table 5

2,4-Dinitro-phenylhydrazones of XVII, XVIII, XIX, XX, XXI

Derivatives	Formula	m.p.°	N %	
			Calc.	*Found*
(XVII)a	$C_{17}H_{13}O_4N_5S$	269−70 c)	18.28	18.54
(XVIII)a	$C_{18}H_{14}O_4N_5SCl$	214−5 c)	16.31	16.22
(XIX)a	$C_{19}H_{16}O_4N_5SCl$	224−5 c)	15.71	15.67
(XX)a	$C_{19}H_{16}O_4N_5SCl$	212−3 c)	15.61	15.67
(XXI)a	$C_{18}H_{13}O_4N_5SClBr$	218 c)	13.70	13.65

Table 6

2-Aryl-4-R-5-carboxy-thiazole (XXIII)

Derivatives		Formula	m.p.°	N %	
R	Ar			*Calc.*	*Found*
(XXII) H	C_6H_5	$C_{10}H_7O_2NSCl$	192−3 a	6.82	6.94
(XXIII) $ClCH_2$	C_6H_5	$C_{11}H_8O_2NSCl$	193−4 a	5.27	5.49
(XXIV) $ClCH_2$	$C_6H_4-CH_3(p)$	$C_{12}H_{10}O_2NSCl$	221−2 a	5.23	5.62
(XXV) $ClCH_2$	$C_6H_4-CH_3(m)$	$C_{12}H_{10}O_2NSCl$	190−2 a	5.23	5.36
(XXVI) $ClCH_2$	$C_6H_4-Br(p)$	$C_{11}H_7O_2NSClBr$	224−5 a	4.21	4.30

a) Recrystallization from aqueous ethanol;
b) Recrystallization from ethanol;
c) Recrystallization from acetic acid;

Revue Roumaine de Chimie, 18, 4, 695–715 (1973)

STUDIES IN THE POLYETHYLENE FIELD. VI[1]

PRESSURE-VOLUME-TEMPERATURE-CRYSTALLINITY RELATIONSHIP IN HIGH-PRESSURE ADDITIVE-CONTAINING POLYETHYLENE*

D. A. ISĂCESCU, I. V. IONESCU, FLORIADA GULUȚĂ

Institute for Macromolecular Chemistry "P. Poni",
Str. Dumbrava Roșie 18, Bucharest, Romania

and

C. RONCEA, D. MIHĂIȚĂ

Petrochemical Industrial Group, Ploiești, Romania

Received Octomber 6, 1972

In this work the specific volume-pressure-temperature relationship was studied in high-pressure additive-containing polyethylene of the ROPOL type, obtained by the I. C. I. process. From experimental data obtained under isothermal and isobaric conditions, were calculated the specific volume, the coefficients of isothermal compressibility (β_T), the ratio $\Delta V/V_{23^\circ}$ and the coefficients of thermal expansion (α), as well as the variation of the degree of crystallinity with the temperature, pressure and time.

The obtained data are in good accordance with prior results obtained with polyethylene types.

INTRODUCTION

The studies presented in this work belong to the field of supermolecular morphology and high polymer properties, a field we began to deal with in 1958, by the research made on low-pressure polyethylene (PE) obtained by amyl-sodium catalysis.[2–4]

---

* Presented at the second Meeting for General and Applied Physical Chemistry, Bucharest, 1–4 Sept. 1970.

[1] Part. V. : D. A. Isăcescu, I. V. Ionescu, M. Leca, C. Roncea, D. Mihăiță and E. Rizescu, *European Polymer J.*, **7**, 913 (1971).

[2] D. A. Isăcescu and I. V. Ionescu, *Rev. Roumaine Chim.*, **7**, 257 (1962).

[3] D. A. Isăcescu, I. V. Ionescu, V. Ursu and C. Vass, *Rev. Roumaine Chim.*, **8**, 959 (1962).

[4] I. V. Ionescu, V. Kenyereș-Ursu, C. Vass, I. Petruș and D. A. Isăcescu, *J. Chim. phys.*, **65**, 1232 (1968).

In the period following 1960, and especially after 1964–1965, the specialists of many developed countries, Japan, USA, USSR and Germany arrived at the conclusion that the two most important problems of economy – the quality of the finished product and the production rate – can no more be solved in the case of polymers by the old method of repeated experiments, but only on the basis of the relations between the manufacturing processes and the inside morphology of the polymer.

The interest for the new direction of research has so much increased that, in a short time, it has become one of the modern spheres of research in polymers on world-wide scale, proving that supermolecular morphology is the fundamental problem for the study of the synthesis and processing of polymers.

In this sphere, we first studied – in a prior work [1] – the relationship pressure-volume-temperature-total induced crystallinity in high-pressure, no-additive-containing P.E. (grades 121, 322 and 721), manufactured at the Petrochemical Industrial Group – Ploieşti. In that work, a part of the literature known until 1968 was cited. Then, in the present work, the literature up to 1971 is cited with regard to the behaviour of polyolefines crystallizable from the melt in general, and especially of PE, in the pressure-volume-temperature relationship. As regards the measuring of the specific volume under pressure and of compressibility of PE and of other polymers, the works [5–17] are cited, of which [11–16] relate to other polymers than PE.

About melting and crystallization of PE and of other polyolefines under variable pressures from 1 to 30,000 at and temperatures up to 270°, the works [18–35] are known too.

---

[5] I. F. Kanavets and L. G. Batalova, *Plast. Massy*, **1965**, 50.

[6] G. Menges and E. Giegerich , *Plastverarbeiter*, **21**, XVI–1 (1970).

[7] H. Wilsky, *Kunststoffe*, **54**, 90 (1964).

[8] M. G. Sharma and V. Mc. Carty, *High Speed Testing*, **5**, 201 (1965).

[9] C. C. Surland, *J. Appl. Polymer Sci.*, **12**, 1423 (1968).

[10] C. D. Armeniades and E. Baer, *J. Macromol. Sci.-Phys.*, B **1**, 309 (1967).

[11] U. Bianchi, A. Turrturo and G. Basile, *J. Phys. Chem.*, **71**, 3555 (1967).

[12] B. E. Eichinger and P. J. Flory, *Macromolecules*, **1**, 285 (1968).

[13] T. Ishinabe and K. Ishikawa, *Jap. J. Appl. Phys.*, **7**, 462 (1968).

[14] D. A. Grindstaff and R. A. Griskey, *J. Appl. Polymer Sci.*, **12**, 1986 (1968).

[15] R. W. Warfield, *Makromol. Chem.*, **116**, 78 (1968).

[16] A. V. Chebanov and A. M. Ariev, *Ukrain. fiz. Zhur.*, **13**, 445 (1968).

[17] T. W. Huseby and S. Matsuoka, *Mod. Plastics*, **42**, 117 (1964).

[18] Th. Davidson, *U. S. Govt. Res. Develop Rep.*, **68**, 103 (1968) ; *Chem. Abstr.*, **70**, 38.219 (1969).

[19] B. Wunderlich, *Chemistry*, **39**, 8 (1966).

[20] J. Osugi and K. Hara, *Rev. Phys. Chem. Japan*, **36**, 28 (1966).

[21] J. M. G. Fatou, *Rev. Plast . Mod.* (*Madrid*), **17**, 346 (1966) ; **17**, 430 (1966).

[22] J. L. Kardoş, *Univ. Microfilms*, (*Ann. Arbor, Mich.*) Order No. 66–14, 299 ; *Diss. Abstr. B*, **27** 2335 (1967).

[23] J. Osugi and K. Hara, *Nipon, Kagaku Zasshi*, **88**, 33 (1967) ; *Chem. Abstr.*, **67**, 3292 (1967).

[24] Th. Davidson, *Univ. Microfilms* (*Ann. Arbor, Mich.*) Order No. 69–2457 : *Diss. Abstr. B*, **30**, 151 (1969) : *Chem. Abstr.*, **72**, 101187 (1970).

[25] P. D. Cavlèrt and D. R. Uhlmann, *J. Polymer Sci., Part B, Polymer Letters*, **8**, 1965 (1970).

[26] S. Matsuoka, *J. Appl. Polymer Sci.*, **4**, 115 (1960).

In the works,[36-40] the morphology of PE crystallized under high pressures is particularly discussed, and in [41] the problem of PE hardening under pressure is treated.

To determine the degree of total crystallinity from calorimetric and specific volume data, the works [42,43] are important. From the above cited literature and from that mentioned in our prior work,[1] it does not clearly result if the studies have been carried out on additive — or nonadditive — containing polymers.

Therefore, we first studied nonadditive-containing PE,[1] and in the present work we present the results obtained with the same polyethylene, but containing additives, thus pointing out the role played by additives in thebehaviour of high-presure PE, manufactured at the Petrochemical Industrial Group-Ploieşti, in the pressure-volume-temperature-crystallinity relationship.

EXPERIMENTAL

The research has been carried out on high-pressure additive-containing PE, grades 121 A and 322 A, characterized by data given in Table 1. The molecular structure of the two grades of PE is characterized by a chain with many short branches : formed of methyl groups ($-CH_3$) arranged at random along the chain, a group at about 35 to 40 carbon atoms in the chain direction.

To study the two PE grades, plates of about 35 mm thickness have been compression moulded, from which have been processed (by mechanical cutting parallel to the PE plate thickness) cyclinders of 13±0,02 mm diameter and 30 mm length under the conditions described in the experimental part of the prior work.[1]

---

[27] J. M. Lupton, *Trans. Soc. Plastics Eng.*, **1**, 105 (1961).

[28] A. Van Valkenburg and J. Powers, *J. Appl. Phys.*, **34**, 2433 (1963).

[29] B. Wunderlich, *J. Polymer Sci. Part A—1 Polymer Chemistry*, **1**, 1245 (1963).

[30] T. Arakawa and. B. Wunderlich, *J. Polymer Sci. Part A—2, Polymer Phys.*, **4**, 53 53 (1966).

[31] J. L. Kardos, E. Baer, P. H. Geil and J. L. Koenig, *Kolloid—Z.*, **204**, 1 (1965).

[32] E. Baer and J. L. Kardos, *J. Polymer Sci. Part A, General Papers*, **3**, 2827 (1965).

[33] R. A. Baltenas and L. A. Igonin, *Doklady Akad. Nauk. S.S.S.R.*, **163**, 917 (1965).

[34] B. Wunderlich and Th. Davidson, *J. Polymer Sci. Part A—2, Polymer Phys.*, **7**, 2043 (1969).

[35] R. B. Prime and B. Wunderlich, *J. Polymer Sci. Part A—2, Polymer Phys.*, **7**, 2061 (1969).

[36] P. H. Geil, F. R. Anderson, B. Wunderlich and T. Arkawa, *J. Polym. Sci. Part A—2 Polymer Phys.*, **8**, 3707 (1964).

[37] Th. Davidson and B. Wunderlich, *J. Polymer Sci. Part A—2, Polymer Phys.*, **7**, 2051 (1969).

[38] B. Wunderlich and T. Arakawa, *J. Polymer Sci. Part A—2, Polymer Phys.*, **8** 3697 (1964).

[39] P. J. Holdsworth and A. Keller, *J. Macromol. Sci. Phys.*, **B 1**, 595 (1967).

[40] P. J. Holsworth and A. Keller, J. Macromol. Sci-Phys., **B**, **1**, 595 (1967).

[41] Ch. L. Gruner, B. Wunderlich and R. C. Bopp, *J. Polymper Sci. Part A—2, Polymer Phy s.*, **7**, 2099 (1969).

[42] H. Hendus and K. H. Illers, *Kunststoffe*, **17**, 193 (1967).

[43] H. Hendus and K. H. Illers, *Faserforsch. Textiltechn.*, **18**, 169 (1967).

Table 1

Physico-chemical properties of additive-containing polyethylene*

Property	Units of measure	322 A	121 A
Additives Antioxidant	ppm	0.053	250
Additives Antiblocking agent	,,	0.212	—
Sliding agent	,,	0.105	—
Density (d^{20}_{4})		0.919	0.922
Weight-average molecular weight (tetraline 130°)	—	32.103	$43 \cdot 10^3$
Flow point	°C	103	106.5
Crystallinity*	%	28	27.8

*) Trade-mark ROPOL

**) Calculated from the density (d_4^{25})of cylindrical PE specimen processed from a plate by mechanical cutting.

It has to be mentioned that during the granulation, additive introducing and plate compression moulding operations, the morphological structure is continuously modified when passing from the synthesized polyethylenes to the cylinders that have been submitted to the study, during which study they will have to suffer new changes, especially in crystallinity, according to the working conditions.

The study of the pressure-volume-temperature relationship has been performed on an improved equipment, the description and working method of which have been published in our prior work. [1]

The equipment is characterized by maintaining constant the temperature during the whole working interval with an accuracy of ± 0,25°, and by a perfect tightness of the compression chamber to avoid polymer loesses.

We mention that in works accomplished by other authors, these two characteristics have not been sufficiently taken into consideration, and this led to results that are not comparable for the same polymer. To this, the fact must be added that many of the prior works have been effected on narrow temperature and pressure ranges, and not on a large range so as to gain a complete knowledge about the phenomenon.

The present study has been carried out on a value range comprised between 23° and 300° and between 1o and 1800 at. The choice of these ranges was based on the fact that they include the usual values used in the polyethylene processing machines to obtain finished products.

PROCEDURE

For measurements, the PE specimen, previously degreased with analytical benzene, was weighed to the nearest fourth decimal and measured with an accurecy of ± 0,01 mm then it was introduced very slowly, under a slight compression, into the compression chamber through its lower part, after the upper piston had first been introduced.

In this way, the possibility of including air in the compression chamber is eliminated, taking into account the fact that the specimen diameter is by about 0.3 to 0.4 mm larger than the diameter of the compression chamber. After mould closing and its fitting on the general purpose machine for mechanical tests, the necessary temperature and pressure are attained, according to the desired working conditions.

Heating and cooling of the specimens were performed, as a function of isobaric conditions $(\partial V/\partial T)_{P=\mathrm{const}}$ or of isothermal conditions $(\partial V/\partial P)_{T=\mathrm{const}}$, according to the diagrams in Figures 2 and 3 of the work.[1]

In both measurement types, the changes of specific volume have been achieved with a constant rate of 0,10% volume changes per minute. The other experimental conditions were described in the same work.[1]

After compression, the polyethylene specimens were cooled under pressure down to 25°, then again measured and weighed.

Table 2

The influence of the time of maintining PE at constant T and P upon the degree of crystallinity (X) and its evolution with time

Presure * P, at	Time of maintaining at $T=100°$, min	Temperature (T), °C	Degree of crystallinity (X) in % after hours:				
			0	1	24	48	504
800	20	100	61.90	61.89	61.90	61.97	—
800	40	100	62.10	61.94	61.97	62.1	63.2
800	60	100	62.57	62.50	62.40	62.5	62.8
800	120	100	61.68	61.72	61.80	61.9	62.8

* The presure of 800 at represents the level to which pressure was raised after reaching the temperature of 100°.

The degree of crystallinity was determined at atmospheric pressure by the densimetric method[44,45] using for the specific volume of the completely amorphous phase (V_a^{25}) the value of 1.1165 ml/g and for the specific volume of the 100% crystalline phase (V_{cr}^{25}) the value of 1.0262 ml/g.[46]

Before effecting the thermodynamic study our researches were directed to checking the time interval in which the thermal equilibrium is reached.

The time required for reaching the equilibrium and eliminating the thermal gradients is comprised according to literature[1,30] between 15 and 60 minutes. Prolonging this time, for the same temperature, pressure and cooling rate conditions, we established the influence exerted by the time of maintaining at the equilibrium upon the variation of the specific volume and of the degree of crystallinity. The results are given in Table 2.

They show that by maintaining PE at the temperature of 100° and pressure of 800 at (parameters characterizing the lower limit of the range within which the crystallinity induced by pressure manifests itself) a time of 20 minutes is sufficient to attain the thermal equilibrium. The prolongation of the time to 120 minutes has only a slight influence upon the specific volume and the degree of crystallinity. Above this period of time, there is observed a tendency of diminishing the degree of crystallinity.

From data presented in the same table (columns 6 to 8), it may furthermore be seen that, after withdrawal of the PE specimens from the mould and allowing them to stand at normal room temperature and pressure, no substantial change in the degree of crystallinity will be found any more with time, this meaning that the induced crystallization process does not continue with time after taking off the pressure in the case of high-pressure additive-containing PE, as this is the case with other polyethylenes, such as the low-pressure AS polyethylene.[2]

[44] P. Heydeman and H. D. Guicking, *Kolloid—Z*, **193**, 16 (1963).

[45] I. Diaconescu, V. Dobrescu and M. Costin, *Materiale Plast.* (*Romania*), **3**, 270 (1966).

[46] T. Shibukawa, V. D. Gupta, R. Turner, J. H. Dillon and A. V. Tobolsky, *Textile Res. J.*, **1962**, 810; **1962**, 1008.

THE EXPERIMENTAL RESULTS AND THEIR INTERPRETATION

The study of compressibility and crystallinity in high-pressure PE presumes the previous-knowledge of a very important parameter, the total specific volume, as well as of the variation of this parameter both with the pressure and with temperature under the conditions shown in the experimental part. For this purpose, first the *variation of the specific volume without outside action* was studied, that is the free volume expansibility.

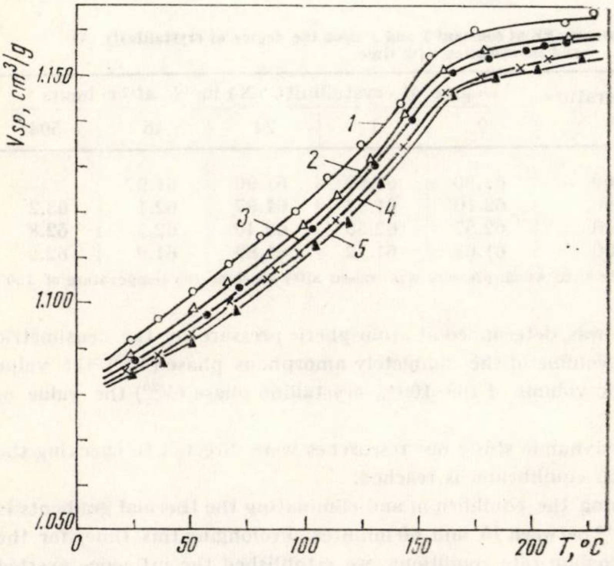

Fig. 1. — Variation of the **polyethylene** specific volume **without outside action.**

***1,* Polyethylene 721 N**: *2,* **Polyethylene 322 N**: *3,* Polyethylene 121 N: ***4,* Polyethylene 322 A**: *5,* Polyethylene 121:

A=Aditive-containing polyethylene; **N =NO-Aditive-co** taining polyethylen .

The specimens with and without additive, prepared and submitted to melting in the mentioned equipment, showed a variation of the specific volume which is presented in Figure 1.

It will be seen that independent of the fact that PE contains or not an additive, the general behaviour of the polymer will be the same. However, it will be noted that the specific volumes of the no-additive-containing polymers are a little greater than those of polymers containing additives, owing to the volatilization of the antioxidant and respectively of the sliding agent.

The common phenomenon in these processes is the transition of the polymer from the solid to the liquid state, which represents the melting of the polymer. From Figure 2, it may be seen that during melting the pressure increases with time up to 200 minutes, and from Figure 3, the increase of pressure with the temperature can be observed up to 160°, above which the pressure tends toward a constant value.

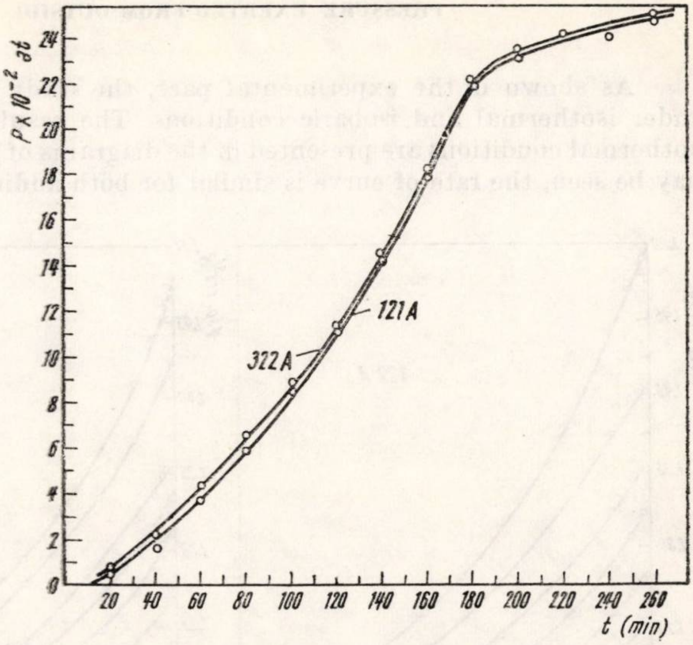

Fig. 2. — Variation of the polyethylene pressure with time during melting without outside action.

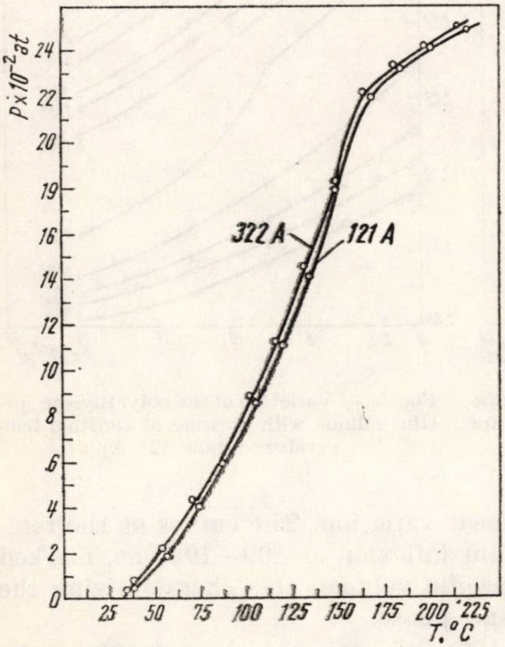

Fig. 3. — Variation of the polyethylene pressure with temperature during melting without outside action.

THE VARIATION OF THE SPECIFIC VOLUME UNDER THE EFFECT OF HYDROSTATIC PRESSURE EXERTED FROM OUTSIDE

As shown in the experimental part, the study has been performed under isothermal and isobaric conditions. The results obtained under isothermal conditions are presented in the diagrams of Figures 4 and 5. As may be seen, the rate of curve is similar for both additive-containing grades and is characterized by a nonlinear variation. The curves at the temperature of 130° present an important inflexion at 800–1000 at, marked by a sudden diminishing of the specific volume, this characterizing the complete melting of the crystalline phase.

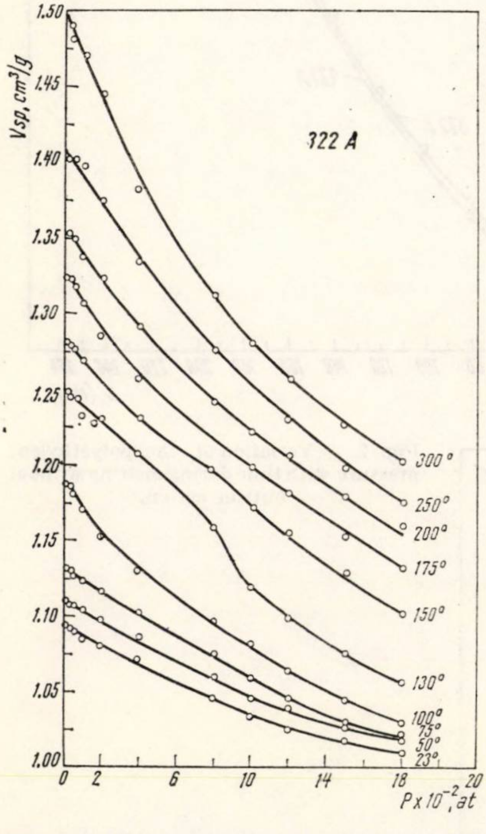

Fig. 4. — Variation of the polyethylene specific volume with pressure at constant temperature (grade 322 A).

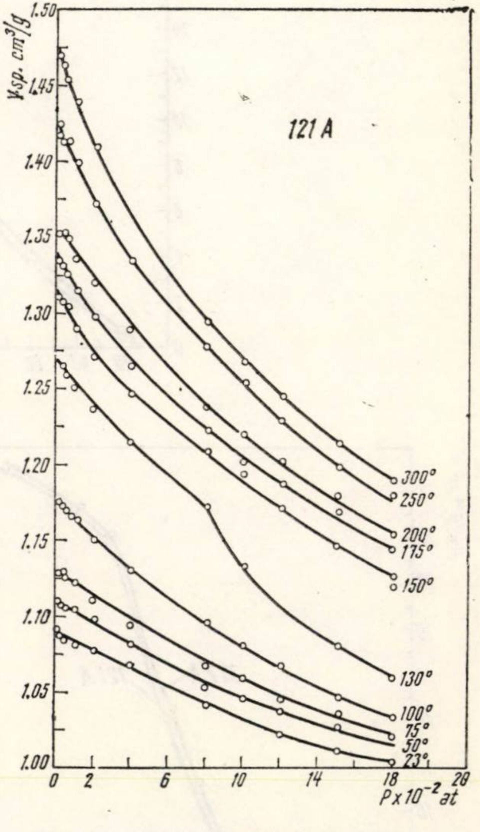

Fig. 5. — Variation of the polyethylene specific volume with pressure at constant temperature (grade 121 A).

At temperatures higher than 130° and pressures above 1 000 at, the specific volume of the melt tends to diminish nearly linear as the pressure increases.

The results obtained under isobaric conditions are represented in Figures 6 and 7.

Under these conditions too, the general rate of the curves is the same for both grades.

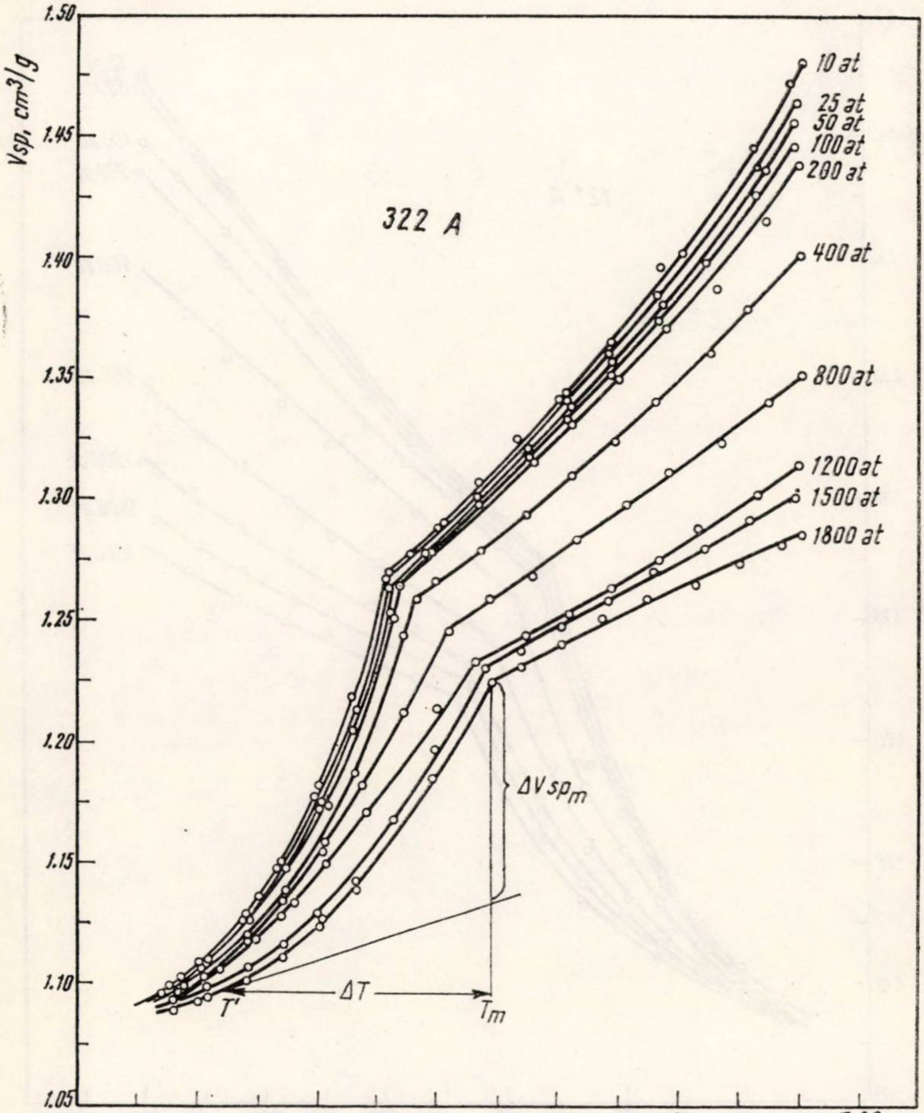

Fig. 6. — Variation of the polyethylene specific volume with temperatures at constant pressure (grade 322 A).

If the curves in Figure 6 are considered, and their slope is compared, calculated from the tangent of the angle made by the linear portion with a parallel to the abscissa represented in Table 3, it is found that it decreases from a value of about 11 for the pressure of 10 at to 5.2 (4.4) for 180 at, that is: as the pressure is increased, the slope of the isobaric curves diminishes.

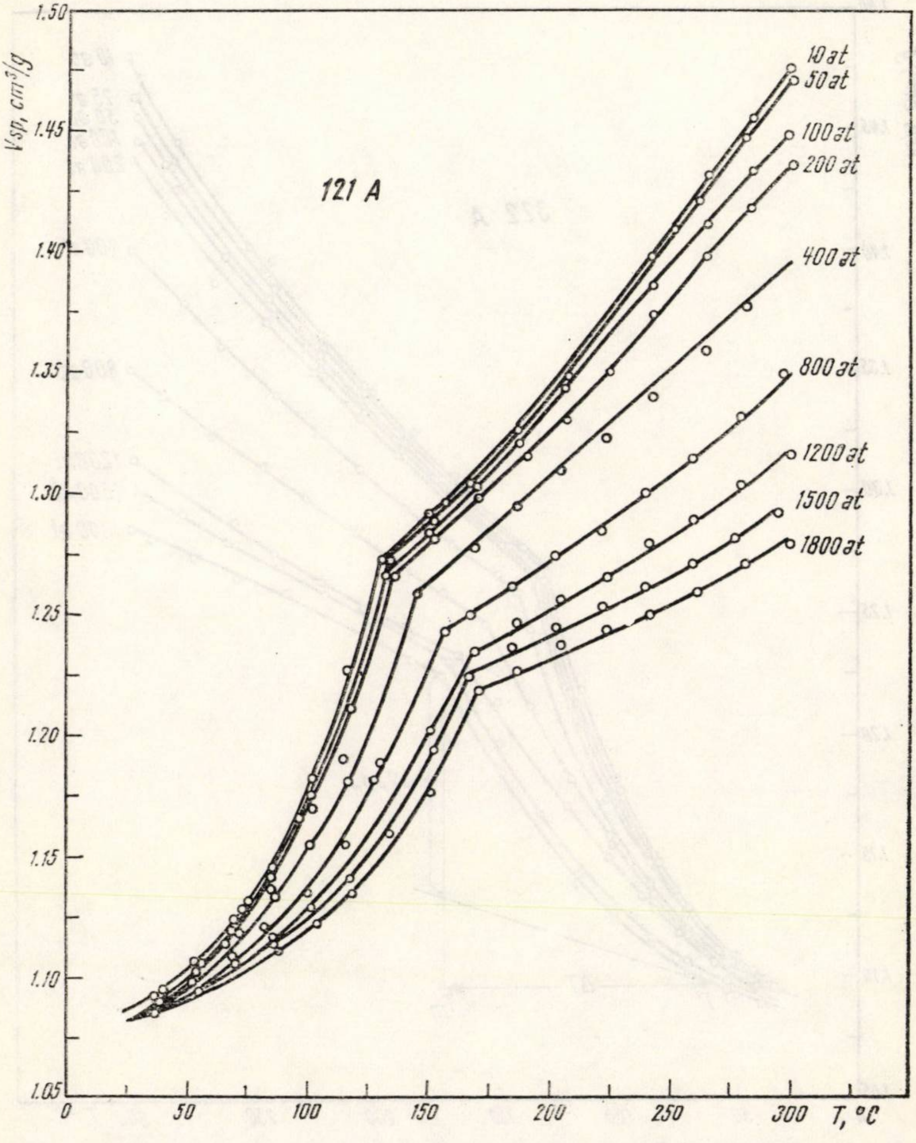

Fig. 7. — Variation of the polyethylene specific volume with temperature at constant pressure (trade 121 A).

This is explained by the forcing of chains to approach each other, giving the possibility of creating interchain cohesive forces with a specific molecular attraction of 1 kcal/mol, which by partially annihialating the effect of temperature lead to the pressure induced crystallization.

From Table 3 it also results that the additives increase the slope of the lines in comparison with the slope of lines obtained with the same grades but without additive. [1] This increase corresponds to greater specific volumes in additive-containing polymers, owing to the partial volatilization of the antioxidants and sliding agents.

Table 3

The slope of the line $(\partial V/\partial T)_p$ in the linear zone as a function of pressure

Pressure (P) at	Slope of line × 10^4	
	322 A*)	121 A**)
10	11.7	11.8
25	12.0	11.5
50	11.2	11.2
100	11.0	10.8
200	10.4	10.0
400	8.8	9.4
800	6.6	6.8
1200	6.0	5.8
1500	5.8	5.4
1800	5.2	4.4

*) Data in Figure 6.
**) Data in Figure 7.

In grade 322, the slope of the curves is somewhat greater owing to higher volatilization of the sliding agent.

At the same time as the increase of pressure, a rise of the melting temperature (T_m) is established, as can be seen from Figure 8.

The rise of the melting temperature, considered at the point where the sudden change of volume occurs, has a linear behaviour only up to 1200 at, above this value being established a tendency of approaching of the lines and of their remaining on the same level of about 170°.

This is due to the additives which by the fact that they interpose themselves between the chains, weaken the Van der Waals forces, increasing the rate of melting.

The linear variation of the melting point with pressure may be expressed by a simple empirical relationship of the form :

$$T = a + b \,.\, P \tag{1}$$

wherein the a and b coefficients have the values 130 and 0.0320 for the PE grade 121 A and 127.8 and, respectively, 0.0321 for grade 322 A.

It was been calculated from Fig. 8 that T_m increases in the linear zone with 3.2×10^{-2}°/at for grade 322 A and with 3.5×10^{-2}°/at for grade 121 A. This rate of melting point rises with the pressure in additive-containing polymers is about 0.7 to 1×10^{-2}°/at higher than that of the corresponding polymers without additive,[1] this being explained by the presence of the additives which facilitate the melting process.

The rise in temperature T_m in polyethylene ROPOL with the pressure within the range of 10 to 1200 at is in good concordance with the data

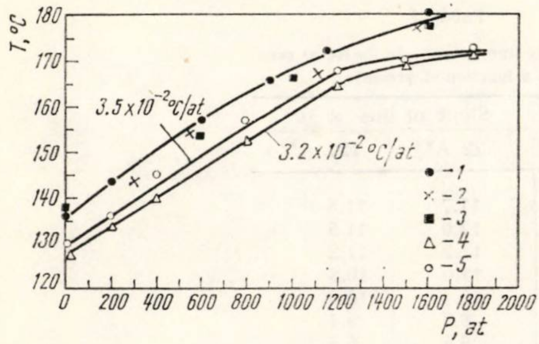

Fig. 8. – Plot melting point *vs.* presure.

1, Baer [32]: *2*, Matsuoka[49] *3*, Huseby[17]: *4*, Polyethylene 322A: *5*, Polyethylene 121 A;

of E. Baer and of L. Kardos [32] and is with 0,012 to 0.015°/at higher than the values obtained in [26,29] and[47,48].

The volume of the melt in type ROPOL PE (ΔV_{sp_m}) has been determined on the graph (Figures 6 and 7) by the difference between the volume of the melt at the temperature T_m at the beginning of the linear portion of the isobar and the volume of solid PE extrapolated at T_m. The interval of temperature between T_m and T' has been considered as in other similar works[10], as the melting interval (ΔT) of PE at the considered pressure.

The values T', T_m, ΔT and ΔV_{sp_m} are given in Table 4.

Table 4

The effect of pressure upon the extending of the melting interval and the melt volume

Polyethylene grade	Pressure (*P*), at	T_m, °C	T′, °C	ΔT, °C	$\Delta V_{sp_m} \times 10^2$ cc/g
322 A	10	128	37	91	11.50
	200	133	43	90	11.25
	400	141	44	97	10.10
	800	155	53	102	8.15
	1200	165	54	111	7.25
	1800	172	55	117	6.80
121 A	10	130	36	94	12.65
	200	135	38	97	11.45
	400	143	38	105	11.20
	800	155	42	112	10.75
	1200	167.5	43.5	124	9.80
	1800	170	44	126	9.45

---

[47] W. Parks and R. B. Richards, *Trans. Faraday Soc.*, **45**, 203 (1949).

[48] C. E. Weir, *J. Res. Nat. Bur. Stand.*, **53**, 245 (1954).

When analysing these data, it can be observed that as pressure increases, a widening of the interval of melting (ΔT) and a rise of the melting temperature (T_m) occur.

At the same time a diminishing of the volume of the melt (ΔV_{sp_m}) occurs.

These phenomena are similar to those already observed [10,32,49] in polyethylene and other polymers, but with the difference, in comparison to the mentioned researches, that in the ROPOL PE the interval of melting is situated in a higher range of temperature. The average molecular weight (within the range $32 \cdot 10^3$ to $43 \cdot 10^3$) does not sensibly influence the interval (ΔT) nor the volume of the melt (ΔV_{sp_m}) under the conditions of the present work.

It has been suggested [32,50] that these phenomena could be attributed to the polydispersion of the molecular weights of PE as well as to the relaxation phenomena occurring in the crystalline polymer before melting.

THE VARIATION OF THE COEFFICIENTS OF THERMAL EXPANSION AND ISOTHERMAL COMPRESSIBILITY

The variation of the specific volume of high-pressure PE with the temperature at constant pressure being known, the coefficient of thermal expansion (α) has been calculated, utilizing the curve $V_{sp} = f(T)$, at the pressure $P = 100$ at.

The obtained results are presented in Table 5.

Table 5

The variation of the coefficient of thermal expansion α(°C^{-1}) with the temperature*

Polyethylene grade	αX 10^4							
	Temperature, °C							
	50	75	100	130	150	200	250	300
322 A	6.41	8.1	10.8	12.1	14.1	12.92	12.56	12.7
121 A	6.12	7.95	11.2	13.2	14.9	13.5	13.1	13.0

* Calculated from the curve $V_{sp} = f(T)$ at $P = 100$ at (figs. 6and 7).

Up to the temperature range of 130° to 150°, corresponding to the melting zone, the coefficient of thermal expansion increases with the temperature. Above the melting range, the coefficient remains practically constant in the interval 12—13°, $^{-1}$, this showing that the temperature exerts a relatively little influence upon the coefficient of thermal expansion in PE in the melted state.

---

[49] S. Matsuoka, *J. Polymer Sci.*, **57**, 569 (1962).
[50] M. Takayanagi, *Mem. Fac. Eng. Kyushu Univ.*, **23**, 72 (1963).

Further, the compressibility expressed by the coefficient of isothermal compressibility (β_T) has also been calculated by the relative variation of the total specific volume with pressure.

From the specific data volume-pressure-temperature, under constant temperature conditions, the relative variation of the volume with pressure was calculated, tracing the curves of compressibility of Matsuoka type.[51]

$$(\Delta V/V_{23^\circ})_T = f(P)$$

shown in Figures 9 and 10.

By analysis of the curves presented in these figures, it will be seen that in the additive-containing polyethylenes (322 A and 121 A), the variation of the volume $(\Delta V/V_{23^\circ})_T$ takes place with a much slower rate than in the case of polyethylenes of the same type containing no additive.[1]. Thus, for example, in Table 6 limit values of the ratio $(\Delta V/V_{23^\circ})_T$ at 1800 at and different temperatures are given for the grades with and without additive.

Table 6

The variations of the ratio $\Delta V/V_{23^\circ}$ with temperature at the pressure of 1800 at

P at	T, °C	$(\Delta V/V_{23^\circ})\times 10^{-2}$			
		Polyethylenewithout additives		Additive-containing polyethylene	
		322 N	121 N	322 A	121 A
1800	23	6.12	6.35	7.60	7.70
	50	7.10	6.80	8.45	8.70
	75	7.70	7.90	10.10	9.80
	100	10.10	10.30	14.30	13.60
	150	11.20	12.80	17.70	16.80
	200	14.00	14.15	—	20.55
	250	16.10	16.75	21.10	26.75
	300	19.70	20.00	26.80	30.75

Remarks The data in the columns 3 and 4 are from our prior work,[1] The data from tne columns 5 and 6 are represented in the Figures 9 and lo,

From this table, it will be observed that the values obtained for the additive-containing PE are always higher than those for the polymer without additive and the difference is higher as the temperature is nearer to 300°. This means that the additives exert an influence upon the compressibility of the polymer and namely the compressibility of the additive-containing PE is always higher than that of the polymer without additive, as a consequence — probably — of the influence exerted by the sliding and plasticizing agent which facilitates the sliding and rearrangement of the chains. The fact will be noted that in additive-containing PE there has no more been observed in the evalution of the ratio $(\Delta V/V_{23^\circ})_T$ the sudden changes in the slope, within the range 150—175°, as is the case in similar grades without additive. This could explained in that the process of crystal-

---

[51] S. Matsuoka and B. Maxwell, *J. Polymer Sci.*, **32**, 131 (1958).

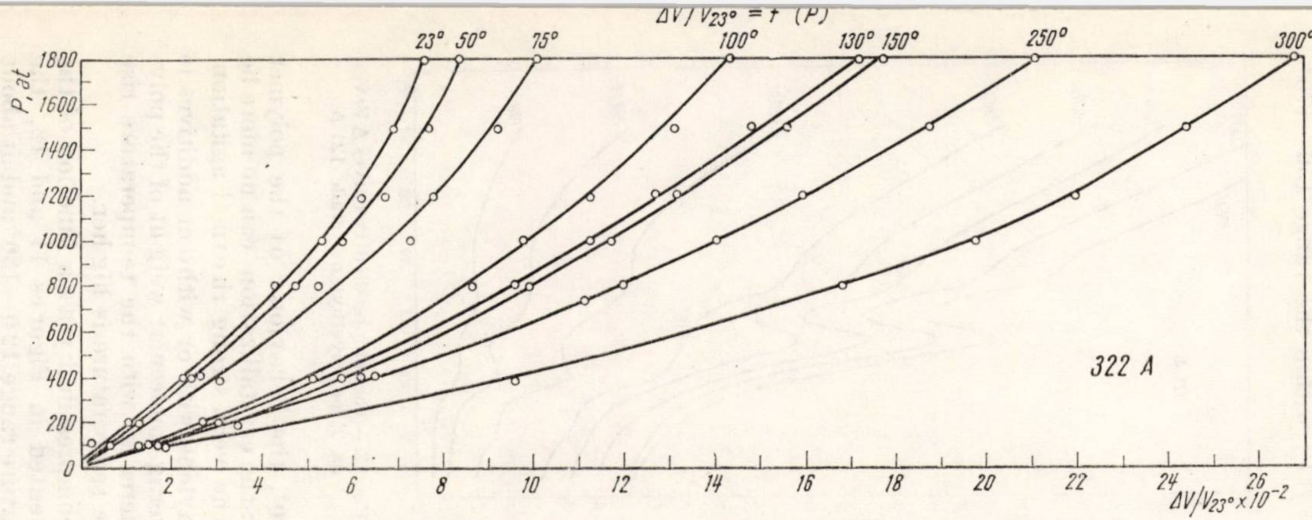

Fig. 9. — The compressibility curves $\Delta V/V_{23°}$ *vs* *P* according to Matsuoka [51] (grade 322 A)

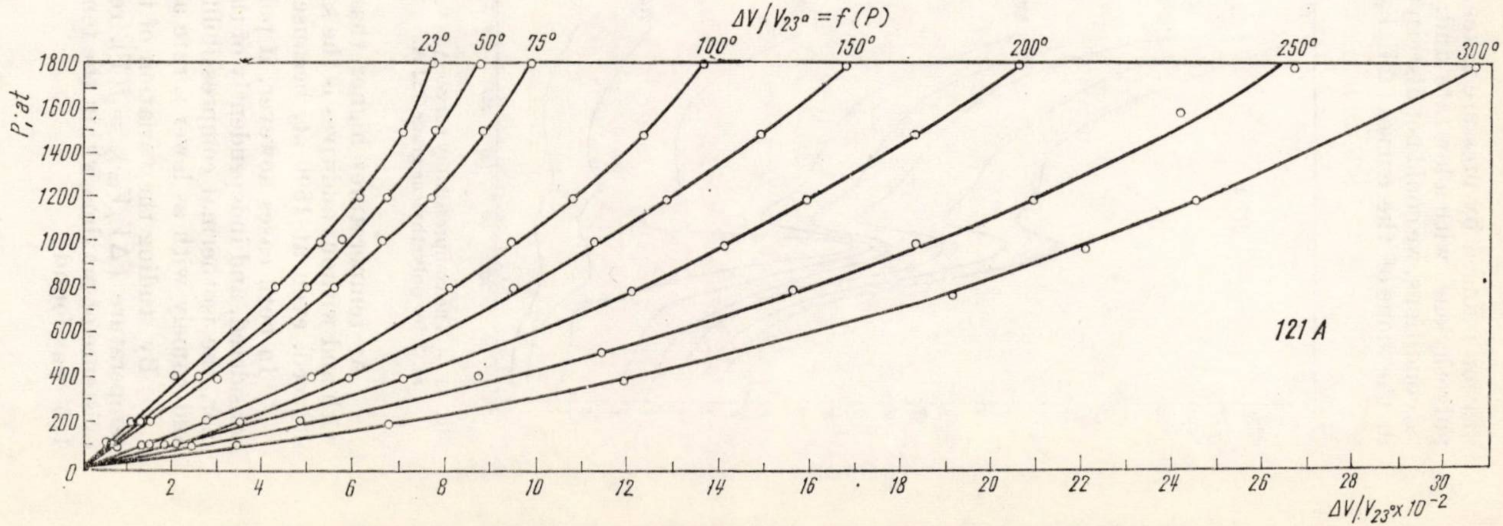

Fig. 10. — The compressibility curves Δ $V/V_{23°}$ *sv.* *P.* according to Matsuoka [15] (grade 121 A).

lization induced by pressure takes place, in the case of additive-containing polyethylene, with a low rate and, therefore, at least under our experimental conditions, we could not discern the jump, respectively the sudden change in the slope of the curves $(\Delta V/V_{23^\circ})_T = f(P)$ within the range 150—175°.

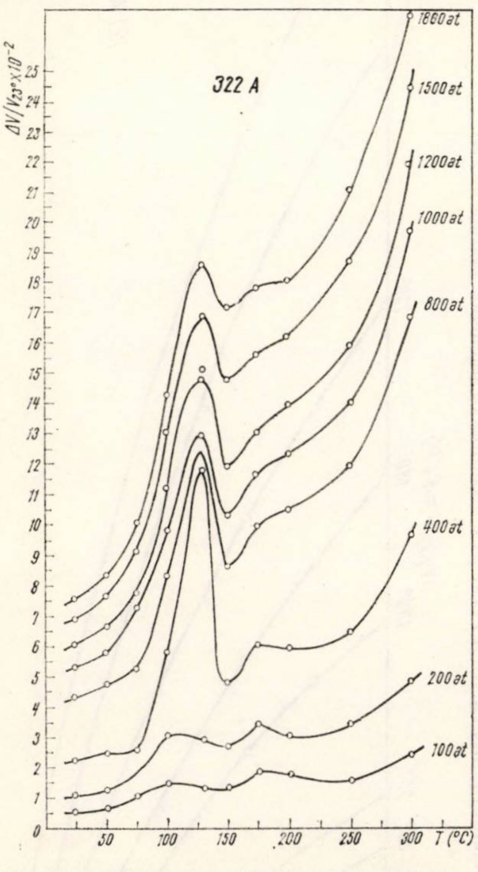

Fig. 11. — The compressibility curves $\Delta V/V_{23^\circ}$ *vs.* T for polyethylene grade 322 A.

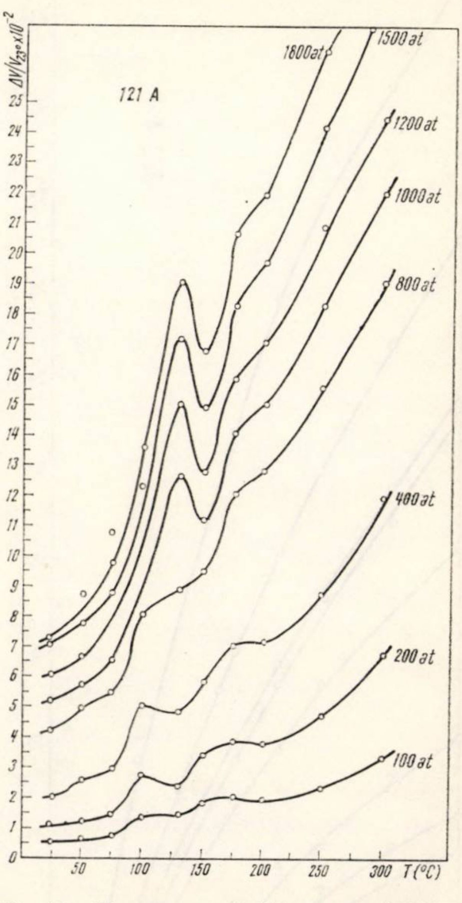

Fig. 12. — The compressibility curves $\Delta V/V_{23^\circ}$ *vs.* T for polyethylene grade 121 A.

At temperatures higher than 200°, the behaviour of the polymer with and without additives is the same : the crystallization can no more be induced, even at 1800 at, because of the very strong thermal agitation.

In both cases however, if polyethylene with or without additives is considered, and independently of the average molecular weight of the polymer, the isothermal compressibility increases with the temperature rise and namely with as lower a rate as the temperature is higher.

By studing the variation of the compressibility as a function of the temperature $(\Delta V/V_{23^\circ})_P = f(T)$, represented in Figures 11 and 12, the existence of maxima within the temperature range 120—130° and at about 175° was found.

The maxima at 130° appear at 100 at and grown in height with increasing pressure within the studied range. The heights of the maxima do not differ much for the two grades of PE especially at pressure higher than 800 at. This similarity can be explained according to [52] by the degrees of crystallinity being very little differentiated one from another, which is experimentally verified, as will be shown later on.

At 175°, the second maximum of compressibility appears at 100 at too, but its height gradually diminishes up to 1 000 at, after which it practically disappears.

The existence of a second maximum at 175° can be explained by the apparition of supercrystalline structure having high melting point, determined by the process of crystallization induced by pressure and by existence in PE of *alien* crystallization centres (the additives). These structures determine the appearance of the second phase transition.

From the experimental data pressure-volume-temperature, with the aid of the known relationship (2) : [1]

$$\beta_T = -\frac{1}{V}\left(\frac{\partial V}{\partial P}\right)_T \tag{2}$$

the coefficient of isothermal compressibility (β_T) has been calculated, the variation with temperature of which is represented in Figures 13 and 14.

It is found that the value (β_T) is increasing with temperature and attains a maximum at approximately 130—150° corresponding to the rapid melting of the crystalline phase, after which the compressibility increases slowly with temperature at $P \geqslant 800$ at.

In grade 322 A (Fig. 13), with a lower average molecular weight, the compressibility is more rapid within a narrower temperature range too than in the grade 121 A, the molecular weight of which is higher with about 10^4 than that of PE 322 A. The existence of a second maximum of compressibility at $P \leqslant 400$ at and temperature of about 175° is also to be noted, which is probably due — as already shown — to the presence of supercrystalline structures generated by the presence of additives (antiblocking agents). The decrease of (β_T) with increasing pressure must be pointed out, due to the diminishing of interchain distances, respectively of the free volume,with the tendency of arrangement of the macromolecules in the melt when only their compression is achieved, this permitting the crystallization of the polymer at high temperature.

At pressures above 400 at, it may be estimated that β_T presents (within the range 150—300°) an approximately linear increase with temperature as in PE without additives [1], at pressures $P \geqslant 800$ at.

---

[52] M. M. MARTYNYUK and V. K. SEMENCHENKO, *Kolloid. Zhur.*, **25**, 190 (1963).

As can be seen by comparison of the diagrams in Figures 11–12 with those in Figs. 13–14, the two maxima with the transition range 130–150°, respectively 175, found at the variation of the ratio $(\Delta V/V_{23°})_P = f(T)$ will be also found in the case of the variation of β_T with the temperature.

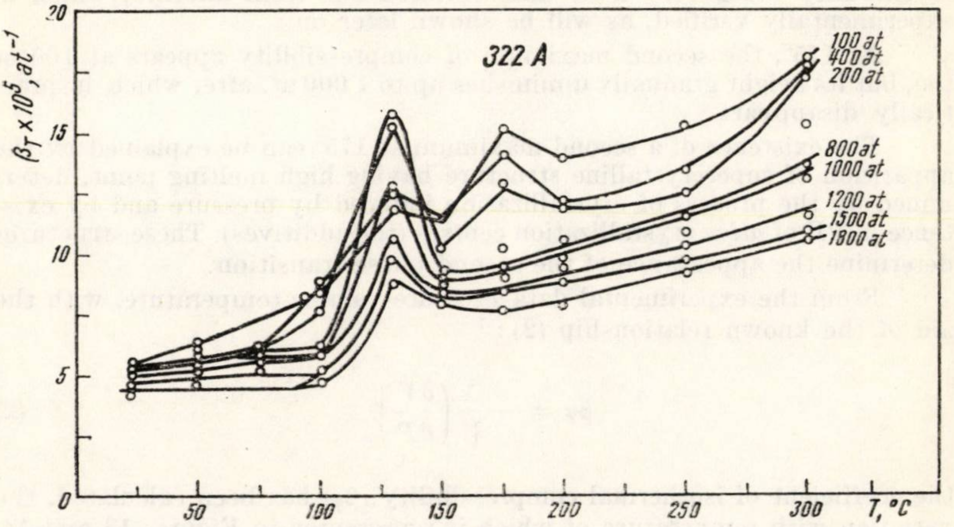

Fig. 13. – Plot of the polyethylene isothermal compressibility variation *vs.* temperature at constant pressure, both for the solid and liquid phase (grade 322 A).

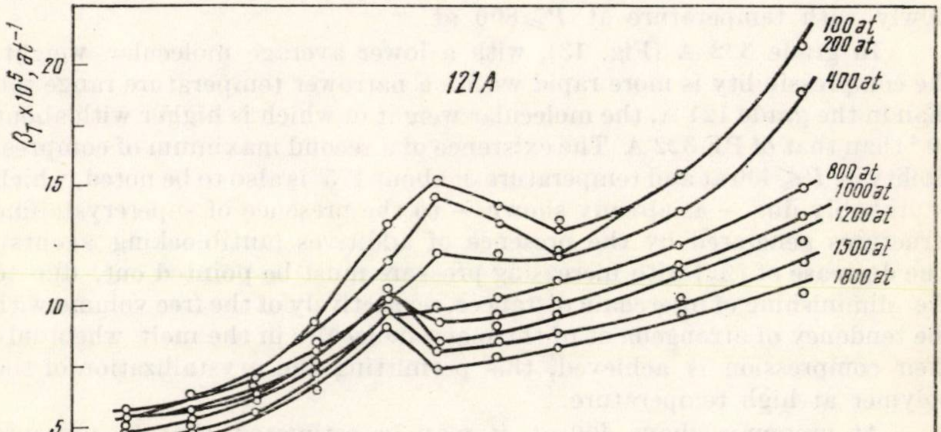

Fig.14. – Plot of the polyethylene compressibility variation *vs.* temperature at constant pressure, both for the solid and liquid phase (grade 121 A).

THE VARIATION OF THE DEGREE OF CRYSTALLINITY WITH TEMPERATURE AND PRESSURE

The compression moulding of the two PE grades under isothermal and isobaric conditions reported in Table 7 results in the arrangement of the macromolecular chains and their compaction, with the partial inducing of PE nucleating and crystallization.

Table 7

The variation of the degree of crystallinity with pressure and temperature

P at	*T* °C	322A		121 A		*T* °C	*P* at	322 A		121 A	
		d_4	X, %	d_4^{25}	X, %			d_4^{24}	X, %	d_4^{25}	X, %
			isobaric conditions					isothermal conditions			
10		0.9257	60.6	0.9250	60.2	23		0.9273	62.1	0.9282	62.7
25		0.9254	60.4	0.9253	60.1	50		0.9282	62.7	0.9279	62.4
50		0.9260	60.9	0.9247	59.9	75		0.9282	62.7	0.9308	64.9
100	300	0.9261	61.0	0.9263	61.2	100	1800	0.9291	63.5	0.9292	63.6
200	↑	0.9260	60.9	0.9285	63.4	130	↑	0.9285	63.0	0.9288	63.3
400	23	0.9263	61.2	0.9257	60.6	150	10	0.9280	62.8	0.9272	62.0
800		0.9265	61.3	0.9260	60.9	175		0.9266	61.4	0.9265	61.3
1200		0.9258	60.7	0.9259	60.8	200		0.9262	61.1	0.9265	61.3
1500		0.9261	61.0	0.9256	60.0	250		0.9262	61.1	0.9265	61.3
1800		0.9262	61.1	0.9256	60.6	300		0.9265	61.0	0.9262	61.1

The consequence of these structural changes is the increase of density. From the values of the density determined at 25° on PE specimens compression moulded under isothermal or isobaric conditions (Figures 4–5, respectively 6–7), and then cooled to 25° under the maximum pressure corresponding to each isobar or isotherm, the V_{sp} was calculated and on its basis the total degree of crystallinity (X) was deduced, expressed in percentages according to the known relationship (3):

$$X = (V_{sp} - V_a)/(V_{cr} - V_a) \tag{3}$$

wherein

V_{sp} = total specific volume
V_a = specific volume of the 100% amorphous phase
V_{cr} = specific volume of the 100% crystalline phase

From the results presented in Table 7, it can be seen that the degree of crystallinity of both PE grades increases both after the isobaric treatment and after the isothermal treatment in comparison with that of the initial material. The degree of crystallinity increases however, relatively, very little within the studied limits of the temperature and pressure ranges. This behaviour has been noticed in low pressure PE too even at pressures above 2 000. at [38,53]

---

[53] S. Matsuoka, *J. Appl. Polymer Sci.*, **4**, 115 (1960).

Thus in the isothermally treated polymers X increases from about 28% at 23° to 63.0–63.6% at 100–130° and then decreases to 61% at 300°. Both grades present a maximum at 130° within the limits of experimental errors.

The increase of the degree of crystallinity up to 130° is owed to the increase of the nucleating rate under the influence of the high hydrostatic pressure.

The heating and cooling of the polymer under pressure, near the melting point, allows the reorganization of the initial fold of the crystalline chain into a fold with greater length.

The increase of the degree of crystallinity much above 60% is however not possible, because of the great number of $-CH_3$ groups in the chains, which hinder their arrangement and compaction, even if the time of maintaining the specimen at the equilibrium is prolonged 6 times, as it has been shown in the experimental part (Table 2).

To this, the length of the chain brings its contribution too, respectively the molecular weight of PE which, being not high enough, puts a limit to the increase of the crystal size in the chain direction. The total degree of crystallinity (X) does not show differences between the two polymer grades, although the 121 A grade contain only an antioxidant in a large amount, and the 322 A contains, besides a little antioxidant, a sliding agent and an antiblocking agent too.

The differences that have been previously established undoubtedly result from the fineness of the crystalline structure, coming from the dimensions, number and perfection of the spherulites, which are forming during crystallization and post-crystallization.

The antiblocking agent increases the number of nucleating centres during crystallization, and the small amounts of sliding agent increases the number of nucleating centres during post-crystallization.

In isobar treated PE, the increase in crystallinity (measured after traversing the temperature range 23 to 300 at different constant pressures within the range of 10 to 1800 at) (Table 7) is somewhat lower than in the case of isothermal treated PE and is comprised within the same order of magnitude of about 60%. This behaviour is normal, taking into account that under isobaric conditions the thermal equilibrium has not been reached.

CONCLUSION

The high-pressure additive-containing polyethylenes present in comparison to the same grades without additives a similar behaviour from the point of view of the volume-pressure-temperature relationship, this leading at first sight to the conclusion that the used additives do not cause any essential change in the structural properties.

Although the rate of the curves is approximately the same, the values V_{sp}, β_T and α in the grades with additives are in general somewhat higher than those in the grades without additives, due to the influence of the additives.

The sliding and antiblocking agents exert a greater influence upon the additive-containing polymers than the antioxidant. The antiblocking agent (SiO_2) increases the number of nucleating centres during crystallization, and the sliding agent increases the number of nucleating centres during post-crystallization, this explaining why the 322 A grade presents a relatively higher increase of the degree of crystallinity as against the 322 grade without additive, in comparison with the 121 A grade, under the same temperature, pressure and time conditions, as can be seen in Table 8.

Table 8

Comparison of the average degree of crystallinity in polyethylene with and without additives

PE grade	Degree of crystallinity (X), %				
	initial	after isobaric treatment		after isothermal treatment	
		Polymer without additive	Additive-containing polymer	Polymer without additive	Additive-containing polymer
322	28.0	59.9	60.9	60.5	62.2
121	27.8	60.5	60.8	61.2	62.5

Note: The values in columns 3 and 5 represent the arithmetic mean of the data obtained in our prior work [1]. The values in columns 4 and 6 represent the arithmetic mean of the data comprised in Table 7 of the present work.

The presented conclusions have immediate practical consequences, namely:

At high pressure (750 to 1 000 at) the temperature interval between 130 and 175° constitutes the optimum range for achieving pressure induced crystallization with the attaining of a higher or lower degree of crystallinity, according to the working conditions.

Above 180°, it is no more possible to induce crystallization, as high as the hydrostatic pressures is raised.

Pressure-induced crystallization, postcrystallization, surfusion, cooling rate and the contraction of the finished product impose a rigorous temperature control, the making of judiciously designed moulds and the strict observing of the temperature and pressure history, the more so when a high quality level and least variation of dimensional properties are required. From the interplay of these parameters, the necessary conditions can be created to turn to profit one or the other of the desired properties.

The stirring and [illegible] of complete [illegible] from the [illegible]. The [illegible] increases the number of [illegible] centres during crystallization, and the [illegible] increases the number of [illegible] centres during [illegible] crystallization, [illegible] a more [illegible] degree, [illegible] the [illegible] under the same temperature, pressure and [illegible] (Table 2).

TABLE 2

[illegible]

[illegible]	[illegible]	[illegible]	[illegible]	[illegible]	[illegible]
22	250	560	55.9	60.3	62.3
[illegible]	375	565	60.8	61.2	62.5

[illegible]

The present conclusions have immediate practical consequences, namely:

a) High pressure (750 to 1 000 at) the temperature interval between 650 and 670 constitutes the optimum range for achieving pressure induced crystallization with the obtaining of a higher or lower degree of crystallization, according to the working conditions.

b) About 1000, it is no more possible to induce recrystallization, as high as the hydrostatic pressure is raised.

c) Besides [illegible] crystallization, [illegible] recrystallization, the [illegible] cooling rate and the contraction of the finished product impose a rigorous temperature control, the making of judiciously designed moulds and the strict observing of the temperature and pressure history, the more so when a high quality level and a set variation of dimensional properties are required. From the interplay of these parameters, the necessary conditions can be selected to favour one or the other of the desired properties.

Revue Roumaine de Chimie, **18**, *4*, 717 – 722 (1973)

ZERO CURRENT BIPOTENTIOMETRIC INDICATION WITH PRETREATED ELECTRODES. I

OXIDIMETRIC TITRATION OF Fe(II) USING PLATINUM ELECTRODES

L. KÉKEDY* and F. MAKKAY **

* Department of Analytical Chemistry "Babeş-Bolyai" University,
Str. Arany J. 11, Cluj, Romania

** Central Institute for Training Teaching Staff, "Babeş-Bolyai" University, Cluj, Romania

Received July 29, 1972

Details are presented concerning the new zero current bipotentiometric indication with differently pretreated platinum electrodes of the Fe(II) titration with oxidants ($Ce(SO_4)_2$, $K_2Cr_2O_7$ and $KMnO_4$).

The role of the surface state of the solid indicator electrodes in many electroanalytical techniques is well recognized now, e.g. in potentiometry, bipotentiometry, polarography, coulometry, amperometry, biamperometry and chronopotentiometry.[1,2] In an early short communication[3] we have reported on a new bipotentiometric indication technique, called zero current bipotentiometry, based on the determination of the potential difference setting in during a titration between two identical but differently pretreated indicator electrodes. The potential difference appears owing to differences in kinetic parameters (reversibility) of the respective electrode reactions, i.e. to differences in the rates with which the dissimilar electrodes approach equilibrium. The potential difference will show a sudden change at the end point allowing its location. The purpose of this paper and of some other following ones is to present details concerning the performance of this method in the case of different titration systems. At present the performance characteristics of the redox titration of Fe(II) with the most common oxidants,[4] $Ce(SO_4)_2$, $K_2Cr_2O_7$, $KMnO_4$, are reported.

[1] L. Kékedy and F. Makkay, *Rev. Roumaine Chim.*, **13**, 739 (1968).

[2] L. Kékedy and F. Makkay, *Stud. Univ. Babeş-Bolyai, Chem.* **1969**, 95.

[3] L. Kékedy and F. Makkay, *Talanta*, **16**, 1212 (1969).

[4] R. Belcher and A. J. Nutten, "Qualitative inorganic analysis", London, 3rd Ed. Butterworth, 1970.

EXPERIMENTAL

A conventional potentiometric titration assembly was used consisting of a tall beaker of 50 ml, a 10 ml semi-microburret and an electromagnetic stirrer. Two identical rectangular platinum indicator electrodes were used with an apparent geometric area of 0.93 cm^2 each. The platinum electrodes were connected directly to the RADIOMETER Type TTT1 pH-meter which served as a potential measuring device. The very small current drain of the apparatus, 10^{-12} A, is negligible as far as its polarizing effect is concerned. Before use, the platinum electrodes were subjected to the pretreatment procedures indicated in our previous paper. [1] For replicate titrations the following pretreatment procedure was chosen. Both electrodes were subjected for 1 minute to an anodic-cathodic cyclization in 1N H_2SO_4 using 2 VA.C. from the mains, in order to eliminate the adsorbed impurities. After that, one of the electrodes was dipped in KI to obtain a bare surface, the other (always the same) was heated for a short time in natural methane gas flame. The titration curves of the potential difference between the platinum electrodes vs. volume of the titrant added were recorded in the usual way. 5 ml 0.01 N $FeSO_4$ diluted to 30 ml with 1N H_2SO_4 were titrated with 0.01 N $Ce(SO_4)_2$, $K_2Cr_2O_7$ or $KMnO_4$. Analytical grade chemicals and doubly distilled water were used.

RESULTS AND DISCUSSION

First of all different pretreatment combinations were investigated in order to select the most suitable electrode pair for routine work. It has been found that the shape of the zero current bipotentiometric titration curves depends on the titrant used as well as on the pretreatments applied to the electrodes. Some representative curves are shown in Fig. 1. One can see that the same electrode pair exhibited completely different titration curves according to the titrant used (curves *A*, *B*, *C*) in spite of the fact that in all cases the same redox system, Fe(III)/Fe(II), was present before the e.p. This fact emphasizes newly that the surface state of the electrodes depends on the nature of the adsorbed ions too, in this case on the reduced formes of the titrants used, namely Ce(III), Cr(III) and Mn(II), respectively. Using the same titrant but different pretreatment combinations, completely different titration curves have been obtained (compare curves *A* and *D* or *B* and *E*, respectively), accentuating the role of the oxidation state of the platinum surface. It is apparent from Fig. 1. that the bipotentiometric titration curves can be divided, according to their shape, into three categories : first derivative curves, second derivative curves of an usual potentiometric titration curve and/or some intermediate forms. Their appearance has been explained earlier. [3]

From all the titrations performed, the following can be concluded : 1) The shape of both potentiometric and bipotentiometric titration curves differs according to the pretreatments applied as well as the electrode pair combination used. 2) The potentiometric equivalence values showed slight oscillations depending on the pretreatment as well as on the titrant used. The oscillations were smaller in the case of titrations with dichromate (number of titrations $n = 34$, variance $s^2 = 0.0010$) and were slightly greater using $KMnO_4$ as titrant ($n = 28$, $s^2 = 0.0022$). As expected, the bipotentiometric equivalence volumes showed smaller fluctuations ($n = 17$ and

$s^2 = 0.0004$ in the case of dichromate, and $n = 14$, $s^2 = 0.0011$ in the case of $KMnO_4$) than the potentiometric ones. 3) Using dichromate as titrant, the mean of equivalence volumes obtained potentiometrically was equal with the bipotentiometric mean, $\overline{v} = 4.52$ ml. Titrating with $KMnO_4$, the potentiometric mean, $\overline{v} = 4.52$ ml, differed slightly from the bipotentiometric one ($\overline{v} = 4.54$ ml). 4) The potential break near the e.p. $(\Delta E)_{\pm 10\%}$ also varies with the pretreatment. Using $KMnO_4$, this break was always smaller than by titrating with $K_2Cr_2O_7$. 5) In order to obtain well-shaped bipotentiometric signals, one of the electrodes must be more reversible than the other. 6) At the beginning, the indicator electrodes were immersed in the Fe(II) solution. As expected, the strong reducing medium has modified the initial surface state of the electrodes, reducing the oxide film on their surface. Consequently, before the e.p. the oxidized electrodes behaved like the reduced ones. 7) The equivalence signal and the shape of the titration curves are also determined by the action of the excess of titrant on the electrodes. The more different this action on each electrode is, the more pronounced will be the equivalence signal, a fact which depends on the pretreatment. In accordance with our earlier findings,[1] it was observed, this time too, that the bare electrode is easier oxidized than the previously reduced one. Therefore, making a choice of a proper electrode pair for a given titration, one must also take into account the possible action of both titrate and excess of titrant on the electrodes.

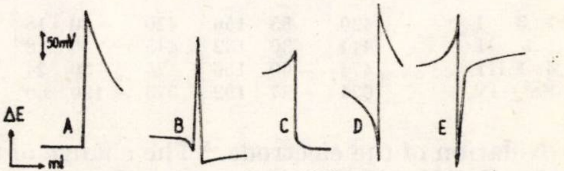

Fig. 1. — Zero current bipotentiometric titration curves of Fe (II) with different titrants using dissimilarly pretreated platinum electrode pairs.

Titrants: A) Ce (IV), B) $KMnO_4$, C) $K_2Cr_2O_7$. One electrode oxidized at + 1500 mV (vs. S.C.E.), the other reduced at − 300 mV. Titrant: D) Ce (IV), E) $KMnO_4$. One electrode was bare, the other reduced at − 300 mV.

In order to ascertain the most suitable pretreatment, the problems of time response and reproducibility of measurements have been also investigated. For this purpose, the potentials in 1N H_2SO_4 solutions containing different Fe(III) : Fe(II) ratios have been recorded as a function of time in stirred solutions. Some illustrative data are given in Table 1. ΔE and Δt represent the potential drift and, respectively, the time elapsed till the constant electrode potentials (E) have been obtained, after dipping the electrodes in the respective solutions. The reduced (R) and bare (B) electrodes are apparently free of surface oxides, the oxidized (O) and heated (H) ones are at least partially covered with oxide. The rest potentials observed on oxide-free surfaces are apparently identical (R I—III), (B I—II) but slower than those observed on oxidized surfaces (0 I—II), (H I—II). In the solution III all the surfaces investigated exhibited the same redox potential, owing rather to a strong Fe(III)-ion adsorption than to a surface

Table 1

Rest potentials of pretreated platinum electrodes (vs.S C.E.) in Fe(III)/Fe (II) solutions

Fe (III)/(II) ratio	Symbol	Pretreatments											
		Reduced (R)			Bare (B)			Oxidized (0)			Heated (H)		
		E mV	ΔE mV	Δt s	E mV	ΔE mV	Δt s	E mV	ΔE mV	Δt s	E mV	ΔE mV	Δt s
1 : 3	I	420	−55	156	420	−30	18	430	−115	180	433	−36	168
1 :1	II	444	−30	132	445	−40	18	460	−53	180	453	−36	168
3 : 1	III	474	−50	156	475	−30	24	472	−180	132	474	−35	120
Fe^{3+}	IV	624	+37	192	575	+120	60	665	−343	528	627	+27	84

oxidation of the electrode. [5] The change of the redox potential values with the Fe(III) : Fe(II) ratio generally corresponds to the theoretical value (28.2 mV) within the experimental errors, denoting that the redox potentials observed were equilibrium potentials (excepting of course solution IV). Nevertheless, on oxidized surfaces these changes were always significantly less, than the theoretical values and decreased with the increase of oxygen coverage of the electrodes. The observed potential values in this case were mixed potentials determined by the surface oxide layer

$$\mathrm{Pt} + 2\mathrm{H_2O} = \mathrm{Pt(OH)_2} + 2\mathrm{H^+} \qquad \mathrm{E_0} = 0.98\ \mathrm{V}.$$

According to Vetter, [6] the potentials of oxide electrodes with electron conducting oxide layers are given by the expression

$$E = \frac{\mathrm{d}\,[\Delta G\,(n)]}{2F\cdot \mathrm{d}n} - \frac{RT}{F}\ln a_{H^+} \tag{1}$$

where n represents the degree of oxidation of the electrode, and ΔG the free enthalpy of formation of the oxide. Consequently, if the degree of oxidation of the electrode varies continuously (at constant pH) during an experiment, E will vary similarly, according to the variation of $\Delta G(n)$. This is one of the causes of the potential drifts observed in oxidizing media. Inversely, the reduction of oxide film in reducing media will cause negative potential drifts. [7] The sign of the potential drifts reported in Table 1 has the same explanation.

It was to be expected that such potential drifts will appear during the bipotentiometric measurements too. Indeed, a slow stabilization of the potential difference has been observed at higher redox potentials, mainly if the electrodes used were poorly oxidized ones. The bipotentiometric technique is superior also from this point of view to the conventional potentiometry with one working electrode, the potential drift of the electrodes being partially compensated.

---

[5] S. Gilman, "The anodic film on platinum electrodes", in A. J. Bard editor, "Electroanalytical Chemistry", vol. 2. New York, E. Arnold and M. Dekker, 1967, p. 111.

[6] K. J. Vetter, *Z. Elektrochem.*, **66**, 577 (1962).

[7] C. B. Roy and S. C. Das, *Indian J. Chem.*, **8**, 833 (1970).

Other kinds of potential drifts were also observed. By stopping the stirring of the solution sometimes rapid potential increase took place. It has been proved that this phenomenon is due to the oxygen oxidation of Fe(II) ions on catalytically active electrode surfaces. Potential drifts of this kind never occurred in the absence of dissolved oxygen or Fe(II) ions, neither when both electrodes were reduced ones.

The most suitable electrode pair for routine work has been also investigated. For this purpose the electrode pretreatment procedure given in the experimental part was applied. Using the same electrode-pair combination, a great number of replicate titrations have been performed in order to test the reproducibility of the procedure. Although the same electrode pair was always used, different titration curves have been obtained in this case too, according to the titrant used. Using $Ce(SO_4)_2$ the curves were of B and D type (Fig. 1), the equivalence volumes being identified as the abscissa of a characteristic peak on the curve. Titrating with $K_2Cr_2O_7$ the titration curves were of *A* type (Fig. 1). With $KMnO_4$ *B* type curves have been obtained with very sharp peak, enabling us the exact location of the e.p. For comparison, usual potentiometric titration curves have been also registered, the e.p. being evaluated according to Hosteller and Roberts.[8] The comparative data are given in Table 2.

Table 2

Comparsion of potentiometric and bipotentiometric titration data

Method / Titrant	$Ce(SO_4)_2$		$K_2Cr_2O_7$		$KMnO_4$	
	n	$s^2 \cdot 10^6$	n	$s^2 \cdot 10^6$	n	$s^2 \cdot 10^6$
Potentiometric	14	152	12	327	8	77
Bipotentiometric	25	179	26	340	11	50

The electrode potentials observed were mixed potentials acquiring steady state values only after some time, when the sum of the currents of all cathodic processes equals to the sum of all anodic currents [9]

$$\sum k^0_{0x,i}\,[0x, i] \exp\left[\frac{-\alpha_i n_i F}{RT}\,E\right] = \sum k^0_{\text{red},i}\,[\text{red}, i] \exp\left[\frac{\beta_i n_i F}{RT} E\right] \quad (2)$$

The value of this constant potential is given by the equation

$$E = \frac{RT}{\sum \alpha_i n_i + \sum \beta_i n_i} \ln \frac{\sum k^0_{0x,i}}{\sum k^0_{\text{red},i}} + \frac{RT}{\sum \alpha_i n_i + \sum \beta_i n_i} \ln \frac{\sum[0x, i]}{\sum[\text{red}, i]} \quad (3)$$

---

[8] J. C. Hosteller and H. S. Roberts, *J. Amer. Soc.*, **41**, 1337 (1919).

[9] M. S. Zaharevskii, "Oxredmetriia", Leningrad, Himiia, 1967.

Equation (3) indicates that the value of the individual electrode potentials depends, besides the concentrations, also on the values of the rate constants (k^0) and the electrochemical transfer coefficients (α, β) of each cathodic and anodic process, being highly dependent on the surface state of the electrode. The fluctuations observed in the bipotentiometric equivalence values are mainly due to this phenomenon. Nevertheless, the bipotentiometric technique is superior to the usual potentiometric one, the time dependence of the potential values observed being less pronounced.

Non-equilibrium steady state of the mixed potentials have been observed by others too[10] at the potentiometric titration of Fe(II) with oxidants like $S_2O_8^{2-}$, H_2O_2 and $K_2Cr_2O_7$.

Using the above mentioned pretreatment procedure, Fe (II) solutions down to 10^{-3} molar concentrations could be titrated with good results.

---

[10] L. M. Pozin, I. E. Flis and V. L. Heifetz, *Zhur. priklad. Khim.*, **44**, 1784 (1971).

Revue Roumaine de Chimie, **18**, *4*, 723–732 (1973)

THE SYNTHESIS AND SPECTROPHOTOMETRIC STUDIES ON BENZOYL CYANIDE PHENYLHYDRAZONES

LUCIA BEU and JANA RUSSU
Institute of Chemical and Pharmaceutical Research
Str. Fabricii 126, Cluj, Romania

Received March 8, 1972

Some phenylhydrazones of benzoyl cyanide substituted with the acetyl group have been prepared and their dissociation and rate constants have been determined.

The most controversial problem about the structure of phenylhydrazones is that concerning their existence in normal form (I) or in two tautomer forms : azo (II) or enehydrazine form (III), respectively.[1]

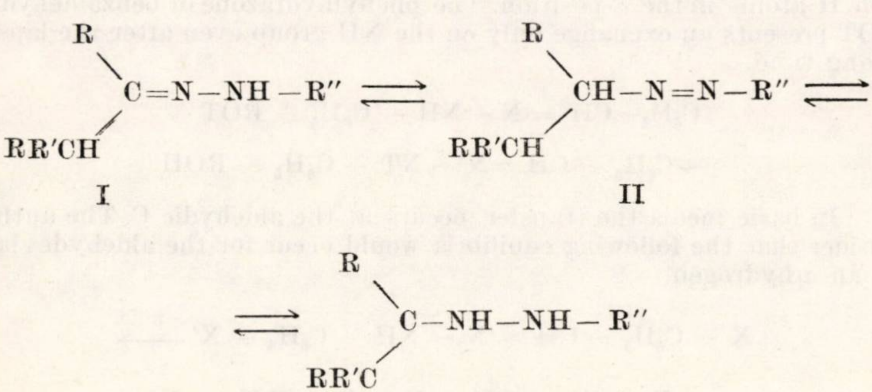

I

II

III

The discussions especially dealt with O' Connor's [2–4] affirmation who considered these substances as existing only in the azo form. The doubts were generated by the existence of azo-peroxides (IV), which are obtained from the phenylhydrazones of aldehydes, and whose spectra are very similar to those of the compounds (II).

---

[1] J. Buckingham, *Quart Rev.*, **25**, 37 (1969).
[2] R. O'Connor, *J. Org. Chem.*, **26**, 4375 (1961).
[3] R. O'Connor and W. Rosenbrook, *J. Org. Chem.*, **26**, 5208 (1961).
[4] R. O'Connor and G. Henderson, *Chem. and Ind.*, **1965**, 850.

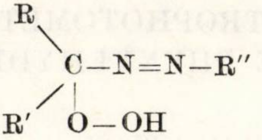

IV (R′=H)

It has been shown that spectra of these substances recorded cautiously (fast and avoiding oxygen) are different from those recorded without special care. [5–7]

O'Connor's assumption, which assigns the yellow colour of the phenylhydrazone solutions in the presence of air to a mixture of azo-compounds (II), was strongly opposed by many authors. By means of spectrophotometry, [5,8,9] labelling,[10] polarography [11] and other methods it has been proved that the phenylhydrazones cannot exhibit tautomerism in neutral solution.

These facts are worth discussing as the results of the above mentioned workers were obtained in neutral solutions at room temperature. In more vigorous conditions, e. g. in acid or basic media, the equilibrium may vary favouring the azo form; the result obtained with one class of hydrazones should not be generalized to another class.

Studying various hydrazones, semicarbazones and oximes in *T* labelled ethanol solutions, Simon and Moldenhauer[10] have found by tritiating the C atoms that the II ⇌ I equilibrium is indicated in the case of aldehydes and a II ⇌ III equilibrium in the case of the aldehydes and ketones with H atoms in the α-position. The phenylhydrazone of benzaldehyde in EtOT presents an exchange only on the NH group even after the lapse of a long time.

$$C_6H_5{-}CH = N - NH - C_6H_5 + ROT \rightarrow$$

$$\rightarrow C_6H_5 - CH = N - NT - C_6H_5 + ROH$$

In basic media the transfer occurs at the aldehydic C. The authors consider that the following equilibria would occur for the aldehydes lacking an α-hydrogen.

$$X - C_6H_4 - CH = N - NH - C_6H_4 - X' \xrightarrow{-H^{(+)}}$$

$$\longrightarrow X{-}C_6H_4 - \overset{(-)}{C}H - N = N - C_6H_4 - X'$$

$$\upharpoonleft\!\downharpoonright$$

$$X - C_6H_4 - CH = N - \overset{(-)}{N} - C_6H_4 - X'$$

---

[5] H. Yao and P. Resnick, *J. Am. Chem. Soc.*, **84**, 3514 (1962); *J. Org. Chem.*, **30**, 2832 (1965).

[6] H. Yao, *J. Org. Chem.*, **29**, 2959 (1964).

[7] A. Bellamy and R. Guthirie, *J. Chem. Soc.*, **1965**, 2788; **1966**, 1989; **1968**, 2090.

[8] C. Reichard and W. Grahm, *Chem. Ber.*, **103**, 1065 (1970).

[9] L. Beu and A. Balog, *Rev. Chim. Analitică (Buc.)*, **2**, 154 (1972).

[10] H. Simon and W. Moldenhauer, *Chem. Ber.*, **100**, 1949 (1967).

[11] L. Kitaev and T. Tropolskaya, *Doklady. Akad. Nauk. S.S.S.R.*, **1963**, 465.

The H→T exchange depends on the structure of the aldehyde and is largely proportional with the concentration of the base. The tritium appears in the aldehydic C atom and the transfer is mediated by the azo compound.

Yao and Resnik, [5,6] studying the spectra of phenylhydrazones of the above mentioned type, assign to these the band at 230−240 nm and a more intense one beyond 320 nm, and to the azo derivatives a maximum at 270−280 nm.

Iffland and co-workers [12] studying the spectra of di-, tri- and tetrasubstituted phenylhydrazones with the general formula : 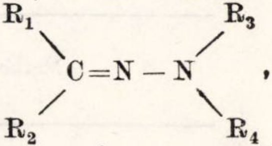 ,

having at least one H atom on the carbon or nitrogen of the 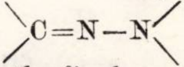 chromophore, present, in the case of an aryl substitution on the final carbon or nitrogen atom, three absorption bands about 340 nm (maximum absorption), 300 nm (shoulder) and 230 nm (absorption of medium value). The difference between the spectra of the phenylhydrazone of benzaldehyde and that of the substituted compounds on the terminal C or N atom is minimal.

In our spectrophotometric studies we have investigated the trisubstituted phenylhydrazones of the $R_1R_2C{=}N{-}NH{-}C_6H_4{-}Z$ type, where $R_1{=}C_6H_5$; $R_2 = CN$; and $Z{=}H$, $CO{-}CH_3$ (*o*, *m*, *p*), as they possess an increased stability compared to the hydrazones used by Iffland [12] and, on the other hand, in order to establish a comparison between our compounds and those used by Iffland and Simon in their studies.

In order to obtain suitable compounds, we have prepared these phenylhydrazones by coupling the mono substituted diazonium salts with nitriles having an α-acylated methyne group :

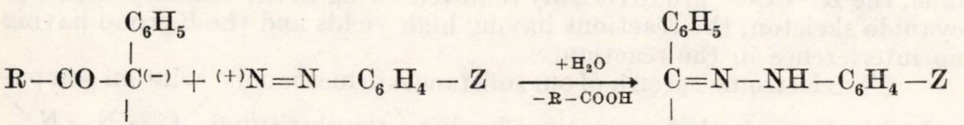

$$R{-}CO{-}\underset{CN}{\overset{C_6H_5}{C^{(-)}}} + {}^{(+)}N{=}N{-}C_6H_4{-}Z \xrightarrow[-R-COOH]{+H_2O} \underset{CN}{\overset{C_6H_5}{C}}{=}N{-}NH{-}C_6H_4{-}Z$$

where

$Z{=}H$; $CO{-}CH_3$ (*o*, *m*, *p*) and $R{=}H$; CH_3 ; $CH_3{-}CH_2$;

$CH_3{-}CH{-}CH_3$; OC_2H_5 ; $COOC_2H_5$; C_6H_5 ; $CH_2 - C_6H_5$.

As the reactivity of the active methylene in benzyl cyanide is much reduced, the product cannot react directly with the diazonium salt and, therefore, the benzoyl cyanide phenylhydrazone (the only known compound in table 1) was prepared by the Japp-Klingemann reaction.[13-15] We used the same reaction, the methynic compound being the α-acyl benzyl cyanide. The results of the coupling reaction are summarized in table 1.

---

[12] D. Iffland, Mc. Aneny and D. Weber, *J. Chem. Soc.*, (C), **1969**, 1703.

Table 1

Benzoylcyanide phenylhydrazones

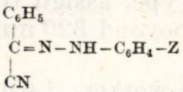

$$\begin{array}{l} C_6H_5 \\ | \\ C=N-NH-C_6H_4-Z \\ | \\ CN \end{array}$$

Z	Method	Yield %	m. p°C (solvent)	Formula (M.W.)	Analysis *Calc/Found* C	H	N
H	a	97	148–149 (EtOH)	$C_{14}H_{11}N_3$ (221.2)			
$o-CO-CH_3$	b	95	"A"128–129 (toluol) "B"183–185 (AcOH)	$C_{16}H_{13}N_3O$ (263.3) ,,	72.98 73.00	4.97 5.12	15.95 15.75
$m-CO-CH_3$	b	75	184–186 (AcOH)	,,	72.98 73.02	4.97 5.30	15.95 15.70
$p-CO-CH_3$	a, c	67	208–209 (Toluol)	,,	72.98 72.91	4.97 5.02	15.95 15.90

The splitting of R—CO— group, following a Japp-Klingemann reaction, was performed on eight acylated derivatives of benzyl cyanide, where R may be quite different. The splitting reaction, which may be also a decarboxylation ($R = COOC_2H_5$), develops spontaneously at room temperature at different pH values. In nine of these cases the azoic intermediate was isolated and we observed in all described reactions the same behaviour as in the case of α-acetyl benzyl cyanide, the same phenylhydrazone being isolated with very similar yields.

We may draw the conclusion that in the case of α-acetyl benzyl cyanide, the R—CO— group is easily removed owing to the stability of benzyl cyanide skeleton, the reactions having high yields and the R group having no interference in the reaction.

The electronic spectra of our substances in methanolic solution compared with those of other derivatives having a trisubstituted 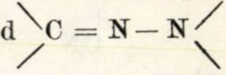 chrompohore show a very high resemblance.

For the di- and trisubstituted hydrazones the chromophore may be represented as a hybrid having the following structure :

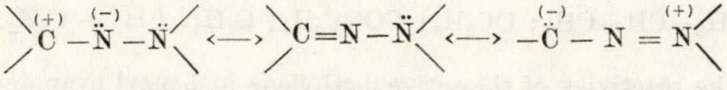

The compounds given in table 1 have unchanged spectra in methanol and acids. We shall try to establish the actual interaction between the nitro-

---

[13] R. Phillips, "Organic reaction", vol. 10, ed. John Wiley, New York, 1959, p. 143.

[14] J. Thesing and D. Witzel, *Chem. Ber.*, **88**, 119 (1955).

[15] K. Walker, *J. Chem. Soc.*, **125**, 1622 (1924).

Table 2

U.V. spectra of hydrazones $C_6H_5-\overset{R_1}{\overset{|}{C}}=N-NH-C_6H_4-Z$

R_1	Z		λ_{max} nm (ε_{max})			lit
H	H		237(14300)	302(11100)	344(24100)	12
CH_3	H		232(12850)	302(13750)	330(19900)	—
C_6H_5	H		237(18600)	298(11400)	340(20600)	—
$COCH_3$	H		240(13500)	285(7710)	364(19800)	9
CN	H		240(19900)	290(3400)	370(24000)	—
CN	$o-COCH_3$	"A"	230(23900)		390(27500)	—
		"B"		320(9700)	395(13250)	—
CN	$m-COCH_3$		240(26600)		370(24600)	—
CN	$p-COCH_3$		240(16750)	280(6750)	374(37300)	—

gen and the C=N group, as well as their dependence upon the aryl rest substitution. In fig. 1 the spectra of these substances in methanol : water are represented.

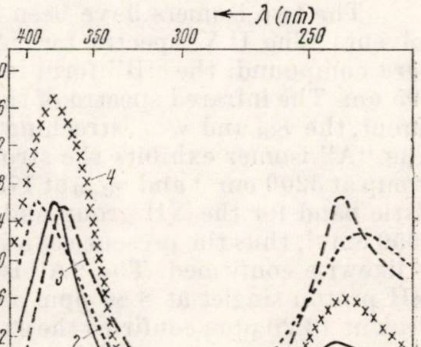

Fig. 1. — The U.V. spectra of benzoyl cyanide phenylhydrazones in $MeOH/H_2O$

1, $C_6H_5-\underset{\underset{CN}{|}}{C}=N-NH-C_6H_4-Z$; Z=H *2*, Z=$o$-$COCH_3$

3, Z=m-$COCH_3$ *4*, Z=p-$COCH_3$

The *para* substitution ($Z=COCH_3$) exerts a bathochromic shift of the 360 nm band. This may be assigned to the electromer action of the $CO-CH_3$ rest, suggesting the following conjugated structure :

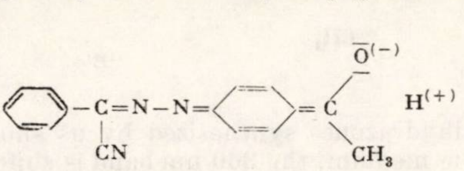

The *meta* derivative has no shoulder at 280 nm but the intensity of the 360 nm band is strongly decreased. The existence of two different *ortho* derivatives : one with m.p. 128–129° and another with m.p. 183–185 °, having different U.V., I.R. and N.M.R. spectra allow us to consider two geometric isomers "A" and "B".

Table 3

I.R. and N.M.R. spectra of phenylhydrazones $CN-C(C_6H_5)=N-NH-C_6H_4-Z$

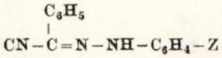

$CN-\overset{C_6H_5}{\overset{|}{C}}=N-NH-C_6H_4-Z$

Z	I.R cm^{-1}					N.M.R. ppm	
	ν_{NH}	$\nu_{C=N}$	$\nu_{C=O}$	$\nu_{C=N}$	$\nu_{C=C/arom}$	$=N-NH$	$COCH_3$
H	3245 vs	2215 vs	—	1645 w	1605 vs	8.77	
o-$CO-CH_3$							
"A"	3200	2215 vs	1730 vs	1630 s	1580 s	8.80	2.68
"B"	—	2210 s	1650 s	1605 m	1580 s	13.20	2.70
m-$CO-CH_3$	3250 vs	2210 s	1680 vs	1610 s	1591 s	8.87	2.67
p-$CO-CH_3$	3245 s	2210 s	1720 vs	1615 s	1590 s	8.88	2.57

The two isomers have been isolated by crystallization from different solvents. The U.V. spectra for "A" form are very similar to those of the *para* compound, the "B" form having a weak maximum at 320 nm and 395 nm. The infrared spectra of the two isomers "A" and "B" are quite different, the ν_{NH} and $\nu_{C=O}$, streching frequencies differ for the two substances. The "A" isomer exhibits the strong and characteristic maxima of the ν_{NH} group at 3200 cm^{-1} and $\nu_{C=O}$ at 1730 cm^{-1}. The "B" isomer has no characteristic band for the NH group and the C = O group frequency is shifted to 1650 cm^{-1}, thus the presence of a hydrogen bond seen in the N.M.R. spectra is likewise confirmed. The "A" isomer presents in the N.M.R. spectra the NH proton singlet at 8.80 ppm and, as to the "B" isomer, the shift of the peak at 13.20 ppm confirms the existence of the hydrogen bond.

These facts suggest the following two formulas for the isomers :

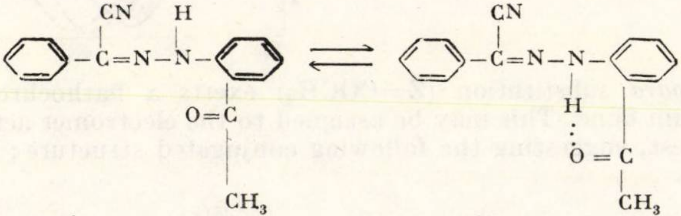

"A" "B"

All the phenylhydrazones synthesized by us show a strong bathochromic shift in basic medium, the 360 nm band is shifted to 460 nm, and the 290 nm shoulder appears in all derivatives. The recording of the U.V.-visible spectra in KOH (methanol-water 1 : 1) of different concentrations demonstrates that the shifts and intensity of the bands vary with the hydroxide

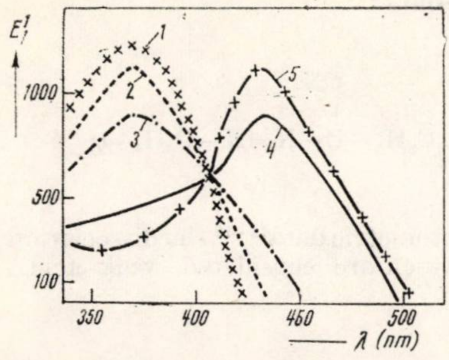

Fig. 2. – The U.V. spectra of benzoyl cyanide phenylhydrazone in various KOH concentrations, in aqueous methanolic solution 1: 1

(*1*, aqueous methanolic solution; *2*, 0.01 M KOH; *3*, 0.05 M KOH; *4*, 0.2 M KOH; *5*, 0.5 M KOH)

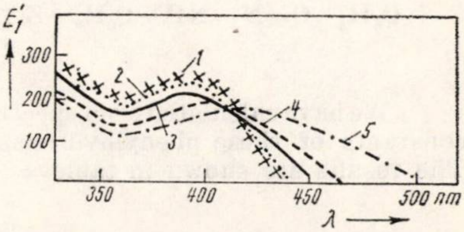

Fig. 3. – The U.V. spectra of benzoyl cyanide *ortho*-$COCH_3$ phenylhydrazone in various KOH solutions in aqueous methanolic solutions 1 : 1

(*1*, aqueous methanolic solution; *2*, 0.05 M KOH; *3*, 0.1 M KOH; *4*, 0.2 M KOH; *5*, 0.5 M KOH)

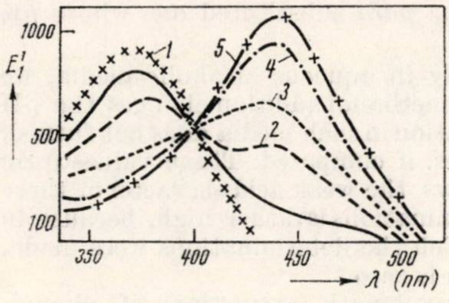

Fig. 4. – The U.V. spectra of benzoyl cyanide *meta*-$COCH_3$ phenylhydrazone in various KOH concentrations in aqueous methanolic solutions 1 : 1

(*1*, aqueous methanolic solution; 0.01 M KOH; *2*, 0.05 M KOH; *3*, 0.1 M KOH; *4*, 0.2 M KOH; *5*, 0.5 M KOH)

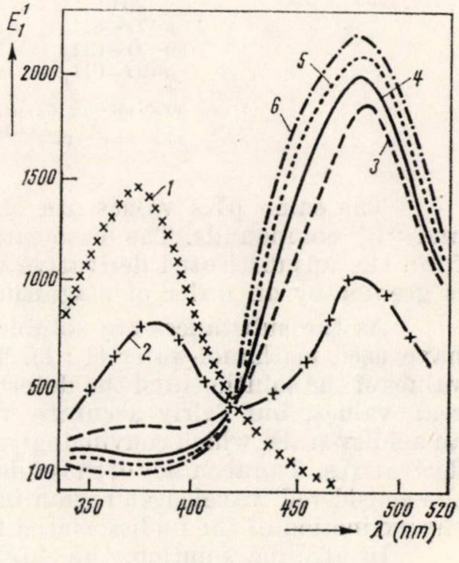

Fig. 5. – The U.V. spectra of benzoyl cyanide *para*-$COCH_3$ phenylhydrazone in various KOH concentrations in aqueous methanolic solutions, 1 : 1

(*1*, aqueous methanolic solution; *2*, 0.01 M KOH; *3*, 0.05 M KOH; *4*, 0.1 M KOH; *5*, 0.2 M KOH; *6*, 0.5 M KOH).

concentration. Two isosbestic points are present in the 300–500 nm region, suggesting the following equilibrium :

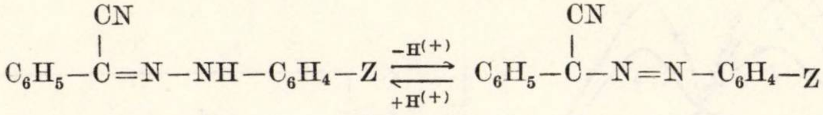

$$C_6H_5-\overset{\overset{CN}{|}}{C}=N-NH-C_6H_4-Z \underset{+H^{(+)}}{\overset{-H^{(+)}}{\rightleftharpoons}} C_6H_5-\overset{\overset{CN}{|}}{C}-N=N-C_6H_4-Z$$

We have calculated from spectrophotometric data[16-19] the dissociation constants of these phenylhydrazones which are considered weak acids. The results are shown in table 4.

Table 4

pKs values of the benzoylcyanide phenylhydrazones

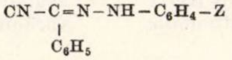

$$CN-\underset{\underset{C_6H_5}{|}}{C}=N-NH-C_6H_4-Z$$

Z	pKs	Δ_{pKs}
H	12.72	
o-CO–CH_3	12.33	−0.30
m-CO–CH_3	12.28	−0.44
p-CO–CH_3	11.71	−1.00

$pKs = pH - \log E_{ned}/(E_{dis} - E_{ned})$

$pKs = pKs^{Z} - pKs^{Z=H}$

The same pKs values are obtained for the *ortho* substituted "A" and "B" compounds. The dissociation constants increase as it is expected from the unsubstituted derivative to the *para* substituted one whose pK is greater by an order of magnitude.

As the substances are soluble only in aqueous alcoholic media, we have used methanol-water (1 : 1). The methanol addition changes the pH values of the solutions and the determination in such media does not furnish real values, but fairly accurate values, if compared. These values form an acidity scale, which convincingly shows the weak acid character of these derivatives. The accuracy of these determinations is rather high, because in the considered wavelength region in which the determinations were made, the extinction of the undissociated form is zero.

In alkaline solution, the high wavelength extinctions of phenylhydrazones decrease with the time, while those in the low region slowly increase. In order to clear up this effect, we have performed extinction measurements, at fixed intervals, of an aqueous alcoholic KOH 0.5 n solution.

---

[16] B. EISTERT and M. REGITZ, *Liebigs Ann. Chem.*, **666**, 97 (1963).

[17] C. REICHARD and W. GRAHM, *Chem. Ber.*, **103**, 1072 (1970).

[18] F. VLACIL, *Coll. Czech. Chem. Comm.*, **32**, 3183 (1967).

[19] J. SOCHA and M. VECERA, *Coll. Czech. Chem. Comm.*, **34**, 3740 (1969).

The presence of air oxygen has no influence upon the results, so that we do not consider that the derivative with the following formula :

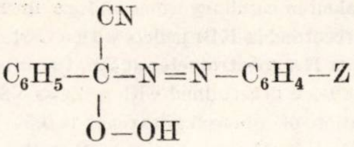

$$C_6H_5-\overset{\overset{CN}{|}}{\underset{\underset{O-OH}{|}}{C}}-N=N-C_6H_4-Z$$

described by Yao, [6] could be present.

The decrease of the extinction in the 430–360 nm region suggests the following transition of the chromophore.

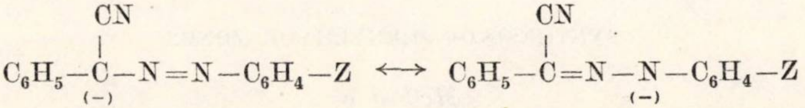

$$C_6H_5-\overset{\overset{CN}{|}}{\underset{(-)}{C}}-N=N-C_6H_4-Z \longleftrightarrow C_6H_5-\overset{\overset{CN}{|}}{C}=N-\underset{(-)}{N}-C_6H_4-Z$$

The rate constants of the assumed reaction are given in table 5.

Table 5

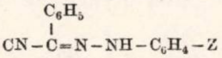

Rate constants of phenylhydrazones $CN-\overset{\overset{C_6H_5}{|}}{C}=N-NH-C_6H_4-Z$

Z	time in minutes	ln Ao/(Ao−x)	k_{det} min^{-1}	$(k \pm s^1)\cdot 10^3$ min^{-1}
H	500	1.30	2.50×10^{-3}	2.58±0.06
	1000	2.57	2.58×10^{-3}	
	1485	3.85	2.59×10^{-3}	
o-$CO-CH_3$	45	0.29	6.44×10^{-3}	6.45±0.02
	70	0.45	6.43×10^{-3}	
	118	0.76	6.48×10^{-3}	
m-$CO-CH$	620	0.44	7.00×10^{-4}	0.70±0.05
	1760	1.20	7.10×10^{-4}	
	3000	2.12	7.05×10^{-4}	
p-$CO-CH_3$	700	0.11	1.57×10^{-4}	0.15±0.01
	1800	0.28	1.55×10^{-4}	
	3000	0.50	1.56×10^{-4}	

$k = 1/t \ln Ao/(Ao-x)$

The extinction decrease in alkaline media is reversible. Acid treating of these solutions restores the initial spectra in acid solution.

In conclusion, the new phenylhydrazones we have prepared are weak acids presenting a chromophore group, sensitive only to alkali and not to the presence of oxygen. The dissociation and rate constants are varying with the substitution in the ring.

EXPERIMENTAL

Melting points were taken in capillary tubes and are uncorrected.

Infrared spectra were recorded in KBr pellets with a Carl Zeiss UR – 10 spectrophotometer and the N.M.R. spectra with a HA spectrometer at 20°, the solvent being $DCCl_3$.

The U.V. spectra have been determined with a Zeiss VSU-1 spectrophotometer, with 1 cm silica cells. The concentration of phenylhydrazones is $0.5-2 \cdot 10^{-5}$ M/l. The solutions were made up with methanol, methanol – H_2O 1 : 1, and methanolic aqueous solution (1 : 1) of KOH or HCl $0.5-5 \cdot 10^{-4}$ M/l. The dissociation constants were determined at 25° and the rate constants at 20°. The extinctions were determined at every 2 nm. The ionic strength was made 0.5 with KCl. The values of the dissociation constants were corrected to 0 time, the necessary correction being however very small.

SYNTHESIS OF PHENYLHYDRAZONES

Method a

0.01 moles of derivative possessing an active methyne group are suspended in 10 ml AcOH and 5 ml $B(OCH_3)_3$. To this solution at 0°, 0.01 moles of Z-phenyldyazonium fluoroborate are added under stirring. After 15 minutes 3 g AcOK, dissolved in 10 ml AcOH, are added. The reaction mixture is left until next day, then poured over 300 ml of water. The precipitate which is formed is filtered off. After drying the product is isolated from the solvents indicated in table 1.

Method b

0.01 moles Z-phenylamine hydrochloride are dissolved in 25 ml AcOH and 2 ml HCl. The mixture is diazotized at 0° with 0.01 butyl nitrite. The diazotized solution is poured dropwise over a mixture formed by 0.01 moles derivative with an active methine group, 30 ml AcOH and 3 g AcOK. After 24 hours the hydrazone is isolated by pouring over 300 ml water. The precipitate which is formed is filtered off. After drying, the product is isolated from the solvents indicated in table 1.

Method c

0.01 moles of derivative possessing an active methyne group are dissolved in 30 ml acetonitrile. To this solution, 0.01 moles of Z-phenyldiazonium fluoroborate are added at 0° and 3 ml triethylamine are dropped under stirring. The solution is maintained for 3 hours at 0°, then the hydrazone is isolated by pouring on 300 ml water. The precipitate formed is filtered off. The product is crystallized from the solvents indicated in table 1.

Revue Roumaine de Chimie, **18**, *4*, 733 (1973)

COMPTE RENDU

Gel permeation chromatography, Marcel Dekker Inc., New York, 1971, Ed. by K.H. ALTGELD and LEON SEGAL

The Symposium of the American Chemical Society held in February 1970 offered an opportunity to quite a number of important papers on theoretical basis, dealing with the experimental technique and the field of practical application of gel permeation chromatography, to be submitted.

Altgeld and Segal, two research workers with an important and long activity in the domain of polymers reference, have selected and systematized these papers in a volume offering to specialists a possibility to acquire a good knowledge of this method.

The book has 646 pages and classifies 43 papers into 4 chapters. The scientific status of the authors and the numerous fields approached ensure a high scientific level to the whole work.

The first chapter aims to inform the reader on the present problems connected to the appliance of this method to the chemistry of polymers, as well as on the separation possibilities and the limits of chromatography on permeable gel.

Chapter II deals with "Theories and methods of chromatography on permeable gel", discussing the theoretical interpretation of the collected data. The opportunity is used to present the methods of interpreting the data thus obtained, the calibration methods and the way of estimating the gel chromatograms.

Chapter III, "New developments of permeable gel chromatography" presents certain characteristic features of the method (the interpenetration effect, the dispersion effect), their theoretical interpretation, as well as the corrections to be applied to avoid them. Some new experimental proceedings (elution by recycling, rapid elution) ensuring an increase of the method efficiency, are meanwhile suggested.

Chapter IV, "The application of permeable gel chromatography in polymer chemistry and petrochemistry" presents the fields in which this method may be used. The chapter examines the numerous possibilities offered by this method to the synthetic and natural polymers, to identify the materials added in the polymerization processes, as well as the use of this method to characterize the mixtures made of small molecules.

The theroretical interpretation, the experimental data, the great number of fields approached, as well as the scientific status of the authors, confer to the whole work a high scientific level and gives it an essential character for specialists dealing with polymer- or petro-chemistry.

The graphical aspect and the way in which the material is presented permits an easy assimilation of all problems dealt with.

C. V. Uglea

ORSZÁGOS MŰSZAKI KÖNYVTÁR ÉS DOKUMENTÁCIÓS KÖZPONT 83

NOTE POUR LES AUTEURS

La *Revue Roumaine de Chimie* publie des articles en anglais, français, russe, allemand ou espagnol. Les auteurs sont priés d'envoyer des articles, notes communications et comptes rendus inédits.

Les manuscrits seront dactylographiés à deux intervalles. Les tableaux seront dactylographiés sur feuilles séparées, de même que la légende des figures. Les diagrammes seront tracés à l'encre de Chine sur papier calque. Les tableaux et les figures seront numérotés par des chiffres arabes, en nombre strictement nécessaire. Prière de ne pas inscrire les mêmes données dans les tableaux et les figures. Les formules chimiques seront incluses dans le texte ; en outre, elles seront transcrites sur des feuilles séparées. Les auteurs sont priés d'indiquer les caractères italiques (en soulignant les lettres au crayon), ainsi que tout autre caractère spécial. L'ordre des références bibliographiques sera celui de leur mention dans le texte ; le nom de l'auteur sera précédé de l'initiale du prénom ; les publications périodiques seront présentées suivant les prescriptions internationales. Les références seront ajoutées à la fin de l'article ; elles paraîtront comme des notes, au bas de la page. Le texte sera précédé d'un résumé, comprenant 15 lignes au maximum.

L'entière responsabilité du contenu des articles appartient aux auteurs. On publie des articles dus aux collaborateurs roumains ou étrangers. Les auteurs recevront 50 tirés à part.

ORSZÁGOS MŰSZAKI KÖNYVTÁR ÉS DOKUMENTÁCIÓS KÖZPONT
1883

PRINTED IN ROMANIA

TRAVAUX PARUS AUX ÉDITIONS DE L'ACADÉMIE DE LA RÉPUBLIQUE SOCIALISTE DE ROUMANIE

P. BALTĂ et E. BALTĂ, **Introducere in chimia fizică a stării vitroase** (Introduction à la chimie physique de l'état vitreux), 1971, 240, 15,50 lei.

LYDIA-MARIA VAICUM, **Biodegrabilitatea detergenților** (La biodégrabilité des détergents), 1971, 254 p., 16 lei.

TIBERIU NĂSCUȚIU, **Metode radiometrice de analiză** (Méthodes radiométriques d'analyse), 1971, 346 p., 19,50 lei.

I. ZUGRĂVESCU et L. STOICESCU-CRIVETZ, **Polimeri heterociclici** (Polymères hétérocycliques), 1971, 190 p., 9,50 lei.

CRISTOFOR SIMIONESCU et C. V. UGLEA, **Fracționarea compușilor macromoleculari** (Fractionnement des composés macromoléculaires), 1962, 292 p., 18,50 lei.

I. MAXIM, **Materiale nucleare** (Matériaux nucléaires), 1969, 444 p., 30 lei.

CRISTOFOR SIMIONESCU et CLEOPATRA VASILIU-OPREA, **Mecanochimia compușilor macromoleculari** (La mécanochimie des composés macromoléculaires), 1967, 344 p., 23,50 lei.

CORNEL BODEA et collab., **Tratat de biochimie vegetală**, partea I, **Fitochimie** (Traité de biochimie végétale, Ire partie, Phytochimie), Ier vol., 1964, 747 p. + 4 annexes + 2 pl., 41 lei ; IIe vol., 1965, 1262 p., 1 pl., 56 lei ; IIIe vol., 1967, 773 p., 35 lei.

V. GHEȚIE et V. MICUȘAN, **Analiza imunochimică. Teorie și practică** (Analyse immunochimique. Théorie et pratique), 1966, 369 p., 28 lei.

R. PORTOCALĂ et L. POPA, **Acizii ribonucleici celulari și virali** (Les acides ribonucléiques cellulaires et viraux), 1966, 375 p., 8 pl., 26 lei.

I.P.I. – c. 2639

43 426

Lei 25.–

F1103

[illegible]

REVUE ROUMAINE DE CHIMIE

TOME 18
Nº 5
Mai 1973

RRCHAX, 18, *5*, 735–918 (1973)

ÉDITIONS DE L'ACADÉMIE DE LA RÉPUBLIQUE SOCIALISTE DE ROUMANIE

Rev. Roumaine Chim.

18, *5*, p. 735–918 (1973), Bucarest

COMITÉ DE RÉDACTION

Rédacteur en chef :

I. G. MURGULESCU, membre de l'Académie de la République Socialiste de Roumanie

Rédacteurs en chef adjoints :

A.T. BALABAN et V. EM. SAHINI, membres correspondants de l'Académie de la République Socialiste de Roumanie

Collège de rédaction :

C. DRĂGULESCU, RALUCA RIPAN, CR. SIMIONESCU, membres de l'Académie de la République Socialiste de Roumanie ; EM. BRATU, ECATERINA CIORĂNESCU-NENITZESCU, P. SPACU, membres correspondants de l'Académie de la République Socialiste de Roumanie ; MARGARETA AVRAM, D. I. MARCHIDAN, G. NIAC et D. SĂNDULESCU

La Revue Roumaine de Chimie paraît 12 fois par an. Toute commande de l'étranger (fascicules ou abonnements) sera adressée à **Intreprinderea Rompresfilatelia, Boîte Postale 2001, telex 011631, Bucarest, Roumanie.**

Les manuscrits, les livres **et** les **revues** proposés en **échange, ainsi** que toute correspondance seront envoyés à la rédaction

REVUE ROUMAINE DE CHIMIE

23, Str. Dumbrava Roşie, Bucarest, Roumanie

ÉDITIONS DE L'ACADÉMIE DE LA RÉPUBLIQUE SOCIALISTE DE ROUMANIE
3 bis, str. Gutenberg, Bucarest

ORSZÁGOS MŰSZAKI KÖNYVTÁR ÉS DOKUMENTÁCIÓS KÖZPONT

REVUE ROUMAINE
DE
CHIMIE

Tome 18, N° 5 Mai 1973

Page

I. G. MURGULESCU and LUDMILA POPESCU, Diffusion potentials in molten salts · · · 737–752 t

M. CONTINEANU, TATIANA ONCESCU and R.N. SCHINDLER, Kinetics and mechanism of the thermal decomposition of azibenzil. II. Studies in the absence of a solvent · · · 753–760

M. CONTINEANU, C. PODINĂ and V. CONSTANTIN, Mass spectrum of diphenyldiazomethane · · · 761–765

O. RADOVICI, MARIA MAVRODIN-TĂRĂBÎC, IOANA ONACA et I. SOLACOLU, Contribution à l'étude de la source chimique de courant Zn/MOH/O_2. I. L'efficacité électrochimique d'une pile à cathode activée avec de l'argent · · · 767–776 R

SHYAMA P. SINHA, Simple HMO-calculations on some N-heterocyclic ligands of analytical importance · · · 777–787

LIGIA SINGUREL and G. SINGUREL, On the oscillation spectrum of dimethyl sulphoxide (DMSO) in solution · · · 789–795

J. VODNÁR, The study of the decomposition of organic hydroperoxides on cation exchangers. II. Decomposition of cumene hydroperoxide on fine granulated Vionit CS-1 in static conditions · · · 797–802 R

AL. FRUMA, D. CIOMÂRTAN, I. BRAȘOVEANU und I.V. NICOLESCU, Die Struktur des mit Lithium und Titan dotiertem Aluminiumoxyd · · · 803–808

N. S. BIRADAR, V. B. MAHALE and V. H. KULKARNI, Titanium (IV) chloride complexes with cobalt (II) chelates of tetradentate Schiff bases · · · 809–814

IRSHAD A KHAN and ANWAR H. HASHMI, Studies on coordination compounds. Thiourea and phosphine complexes of Ni(II) and Co(II) · · · 815–821

C. VÁRHELYI, I. GĂNESCU, und M. PREDA, Über α-Dioximinkomplexe der Übergangsmetalle. XXXVI. Neue Dimethylglyoximin-Chelate des Kobalts (III) mit α,α'-Dipyridyl und *o*-Phenanthrolin · · · 823–828

ILEANA ALBESCU, Contributions to the study of lanthanides with biguanide derivatives. VI. Halogeno- and pseudohalogeno-compounds of lanthanides 829–840

ALEXANDRU T. BALABAN, Chemical graphs. XVI. Intramolecular isomerizations of octahedral complexes with six different ligands. · · · 841–854

ALEXANDRU T. BALABAN, Chemical graphs. XIX. Intramolecular isomerizations of trigonal-bipyramidal structures with five different ligands · · · 855–862

Rev. Roumaine Chim. **18**, *5*, p. 735–918 (1973), Bucarest

Page

MARGARETA AVRAM, I. G. DINULESCU, F. CHIRALEU and C. D. NENITZESCU, Investigations in the cyclobutane series. XXXII. The addition of bromine to derivatives of *exo.exo*-tetracyclo[4.4.2.$0^{2.5}$.$0^{7.10}$]dodeca-3.11-diene 863–872

N. BĂRBULESCU, M. MORARU and D. ŞOTCĂ, Bicyclo[3.3.1]nonane. The acid-catalyzed reactions of a bicyclic epoxide 873–881

M. IOVU et G. CÎMPEANU, Tris-éthers. I. La condensation du bis (chlorométhyle) éther avec les phénoxyde, méthyle- et diméthyle-phénoxydes de sodium 883–888

C. TĂRĂBĂŞANU-MIHĂILĂ, L. FLORU, EUGENIA BALTĂ and A. PREDESCU, Heterocyclic derivatives with thiazolic rings. I. Synthesis of 6-aminothiazolo[4,5-f]indazole 889–898

A. M. EL-ABBADY, M. A. OMARA and N. G. KANDIL, γ-keto acids in the Pfitzinger reaction 899–905

D. S. VASILESCU, MARIA ŞTEFĂNESCU and AL. BĂLĂNESCU, The polymerization of N-vinylcarbazole by the systems acrylonitrile-$ZnCl_2$ and acrylonitrile-$HgCl_2$ . . . . 907–912 R

D. COSTACHE and S. SASU, Kinetic determination of vanadium by the reaction between pyrogallol bromine red and potassium bromate . . . . 913–917 R

Revue Roumaine de Chimie, **18**, *5*, 737–752 (1973)

DIFFUSION POTENTIALS IN MOLTEN SALTS

I. G. MURGULESCU and LUDMILA POPESCU
Centre of Physical Chemistry
Str. Galaţi 31, Bucharest, Romania

Received December 25, 1972

The diffusion potentials, ε_D in concentration cells of the type :

$$\mathrm{Ag}(s)\left|\begin{array}{l}\mathrm{AgX}(l),\ x^{\mathrm{I}}_{\mathrm{AgX}}\\ \mathrm{MeX}(l),\ x^{\mathrm{I}}_{\mathrm{MeX}}\end{array}\right\|\begin{array}{l}\mathrm{AgX}(l),\ x^{\mathrm{II}}_{\mathrm{AgX}}\\ \mathrm{MeX}(l),\ x^{\mathrm{II}}_{\mathrm{MeX}}\end{array}\left|\mathrm{Ag}(s)\right.$$

where X = Cl, Br and Me = Na, K, Rb, Cs have been determined as function of mole fraction and temperature. A quartz cell without diaphragm, the contact of the salts being achieved directly through a twisted capillary, has been used. A theoretical evaluation of the diffusion potential was attempted by considering the diffusion layer as a Henderson type one ; in some systems good agreement was obtained.

In molten salts the diffusion or junction potentials exist at the contact between two different mixtures of the salts.

The mixtures may have different concentrations of the active component as in the example :

$$\mathrm{Cu}(s)\left|\begin{array}{l}\mathrm{CuCl}(l),\ c_1\\ \mathrm{KCl}(l)\end{array}\right\|\begin{array}{l}\mathrm{CuCl}(l),\ c_2\\ \mathrm{KCl}(l)\end{array}\left|\mathrm{Cu}(s)\right. \qquad \text{(A)}$$

$$\mathrm{Ag}(s)\left|\begin{array}{l}\mathrm{AgCl}(l),\ x^{\mathrm{I}}_{\mathrm{AgCl}}\\ \mathrm{KCl}(l),\ x^{\mathrm{I}}_{\mathrm{KCl}}\end{array}\right\|\begin{array}{ll}\mathrm{AgCl}(l), & x^{\mathrm{II}}_{\mathrm{AgCl}}\\ \mathrm{KCl}(l), & x^{\mathrm{II}}_{\mathrm{KCl}}\end{array}\left|\mathrm{Ag}(s)\right. \qquad \text{(B)}$$

where c_1 and c_2 are the volume concentrations, x_{AgCl} and x_{KCl} the mole fractions. If in the cell (B), the molar fraction $x^{\mathrm{I}}_{\mathrm{AgCl}}$ is equal to one, the following asymmetric concentration cell results :

$$\mathrm{Ag}(s)\left|\ \mathrm{AgCl}(l)\ \right\|\begin{array}{l}\mathrm{AgCl}(l),\ x_{\mathrm{AgCl}}\\ \mathrm{KCl}(l),\ \ \ x_{\mathrm{KCl}}\end{array}\left|\mathrm{Ag}(s)\right. \qquad \text{(C)}$$

which is also met with in the study of molten salts by concentration cells with transport.

The mixtures of molten salts may differ with respect to the nature of their components as in the case of Daniell pyrogalvanic cells :

$$\mathrm{Zn}(l)\,|\,\mathrm{ZnCl_2}(l)\,||\,\mathrm{PbCl_2}(l)\,|\,\mathrm{Pb}(l) \qquad \text{(D)}$$

As in the electrolyte solutions, the diffusion potentials are also caused in molten salts by the difference in ionic mobilities of mixtures and are expressed by the same general equation :

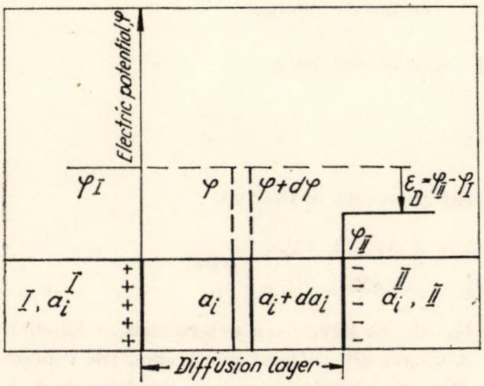

Fig. 1. — The diffusion layer and the corresponding diffusion potential.

$$\varepsilon_D = -\frac{RT}{F}\int_{\mathrm{I}}^{\mathrm{II}} \sum_i \frac{t_i}{z_i}\,\mathrm{dln}\,a_i \qquad (1)$$

where I and II represent the two compartments of the cell with transport which form the diffusion layer (Fig. 1). The other symbols have well-known meanings. The integration of equation (1) presents the same difficulties as in the case of electrolyte solutions.

That is why equation (1) may be successfully exploited only in the case of simple systems as those represented by concentration cells with transport of type (A), (B) and (C).

The concentration cells of type (A) are comparable to those formed in electrolyte solutions, the solvent being a molten salt, potassium chloride. At lower concentrations c_1 and c_2, the transport of current is effected by the ions of molten salts (KCl, NaCl, $\mathrm{NaNO_3}$) which play the role of a solvent ; the transport of the solute ions becomes zero and so does the diffusion potential.

This behaviour of (A) type cells has been confirmed by Gordon,[1] Sackur, [2] Blickslager, [3] Laity, [4] Blander and co-workers [5] and Bakès, [6]

---

[1] C. M. Gordon, *Z. phys. Chem.*, **28**, 302 (1899).

[2] O. Sackur, *Z. phys. Chem.*, **83**, 297 (1913).

[3] H. J. Blickslager, *Rec. Trav. chim.*, **46**, 305 (1927) ; Dissertation, Amsterdam, 1927.

[4] R. W. Laity, *J. Amer. Chem. Soc.*, **79**, 1849 (1957).

[5] M. Blander, F. F. Blankenship and R. F. Newton, *J. Phys. Chem.*, **63**, 1259 (1959).

[6] M. Bakès, *Ber. Bunsengesellschaft Phys. Chem.*, **70** 581 (1966).

The (C) type concentration cells formed the object of numerous researches. Since 1934, Grube and Rau [7] showed that cells as :

$$Pb(l)\,|\,PbCl_2(l)\,||\,PbCl_2(l),\ x_{PbCl_2} + KCl(l),\ x_{KCl}\,|\,Pb(l)$$

possess a diffusion potential of 30−40 mV.

After 1950, many works on diffusion potentials of (C) type concentration cells have been published, the results being remarkably contradictory. Thus, Murgulescu and Marchidan, [8] Terpiłowski and Josiak, [9] Langevin and co-workers [10] have obtained diffusion potentials of some milivolts, values which do not exceed the experimental errors. Concomitantly, in other mixtures, Bloom and Easteal[11], Behl and Egan [12] evidenced important values, up to 20 − 30 mV.

The present work deals only with the diffusion potentials of concentration cells with transport of (B) type.

The following cell of this type :

$$Ag(s)\left|\begin{array}{c} AgNO_3(l),\ x_1^I \\ NaNO_3(l),\ x_2^I \end{array}\right|\left|\begin{array}{c} AgNO_3(l),\ x_1^{II} \\ NaNO_3(l),\ x_2^{II} \end{array}\right| Ag(s)$$

was studied by Laity [4] who found a zero junction potential.

It is easily shown that in binary mixtures of molten salts with common anion, the diffusion potentials are zero if the transport number of the cations are proportional to the corresponding mole fractions.

Actually, admitting that the activity of the common anion which has the same mole fraction in both compartments of the cell, does not change with electrolyte composition (which may be not rigorously exact), the equation (1) for the former cell becomes

$$\varepsilon_D = -\frac{RT}{F}\int_{x_1}^{x_2}(t_{Ag^+} + \mathrm{dln}\, a_{Ag^+} + t_{K^+}\,\mathrm{dln}\, a_{K^+})$$

Taking into account Gibbs' equation,

$$x_{KCl}\,\mathrm{dln}\, a_{K^+} + x_{AgCl}\,\mathrm{dln}\, a_{Ag^+} = 0$$

the preceding equation becomes

$$\varepsilon_D = -\frac{RT}{F}\int_{x_1}^{x_2}\frac{x_{KCl}\, t_{Ag^+} - x_{AgCl}\, t_{K^+}}{x_{KCl}}\,\mathrm{dln}\, a_{Ag^+}$$

which gives immediately the condition that diffusion potential ε_D equals zero

$$x_{KCl}\, t_{Ag^+} - x_{AgCl}\, t_{K^+} = 0$$

---

[7] G. GRUBE and E. A. RAU, *Z. Electrochem.*, **40**, 352 (1934).

[8] I. G. MURGULESCU and D. I. MARCHIDAN, *Rev. Chim. Acad. R.P.R.*, **3**, 69 (1958); **5**, 17, 299 (1960); *Zhur fiz, Khim.*, **34**, 2534 (1960).

[9] J. TERPIŁOWSKI and J. JOSIAK, *Roczniki Chem.*, **38**, 97 (1964); **39**, 805, 1777 (1965); **40**, 1833 (1966); **42**, 219 (1968).

[10] B. LANGEVIN, A. BERLIN and G. DIRIAN, *J. Chim. phys.*, **66**, 167 (1969).

[11] H. BLOOM and A. J. EASTEAL, *Austral. J. Chem.*, **18**, 2039 (1965).

[12] W. K. BEHL and J. J. EGAN, *J. Phys. Chem.*, **71**, 1764 (1967).

that is

$$\frac{t_{Ag^+}}{t_{K^+}} = \frac{x_{AgCl}}{x_{KCl}}$$

The system studied by Laity could, by chance, accomplish this condition.

EXPERIMENTAL

The cell we used is represented in Fig. 2. Entirely made of quartz, the cell consisted of a test tube A (25 mm diameter, 250 mm length) containig the tube B which had at the end the twisted capillary C (1 mm internal diameter, 110 mm length). In the test tube, which was one of the compartments of the cell, one of the mixtures was introduced while in the capillary which was the second compartment, the other mixture was introduced. The junction between the electrolytes in the two compartments was so directly established through the corresponding diffusion layer.

Keeping the same level of the salts in both compartments, the twisted capillary (C) reduced the mechanical mixing to an acceptable extent and the diffusion layer formed within the capillary was of approximately 1 — 2 mm thick (which was observed by the difference in colour of the two mixtures).

Since the stability and reproducibility of emf of the cell depended on the way the diffusion layer is formed at the contact of the two mixtures, the following procedure has been used : the mixture for the tube (B) with capillary was prepared separately in another furnace at a temperature slightly higher than that of the main furnace, with the test tube A. Then, the B tube was filled with the mixture so prepared. The gas bubbles which could have formed in the capillary (and break the liquid column) were removed by forcing the mixture through the capillary and refilling it. The volume of the mixture in the test tube (approximately 10 cm^3) was previously calculated so as the open end of the capillary to be tangent to the level of the mixture in the test tube.

In addition, the working furnace was provided with an optical system formed of a prism with total reflexion and an ocular. This system allows the adjusting of capillary height depending on the mixture level so that the junction to be achieved through a thin layer.

A vertical furnace with a Kanthal resistance was used (Fig. 3). To lower the temperature gradient along the cell, ceramic discs were disposed around the cell in the inner tube of the furnace. Water running through copper tube coils disposed around the sheath of furnace was used for cooling.

Since the mixtures of silver halides and alkali halides corrode the silica walls, the cell has been washed after each run with diluted hydroflouric acid, so that the inner diameter of the capillary should not have been sensibly altered.

In order to check if the cell had an asymmetry potential, pure silver chloride has been introduced in both compartments together with two identical silver electrodes ; in the cell utilized in our experiments no asymmetry potential was evidenced.

The two silver electrodes were of silver wire of 99.9 % purity (3 mm diameter, 400 length). To avoid contact potentials, the silver electrodes were welded at two thinner silver wires which connected the cell to the meter. The silver electrodes were introduced in silica protection sheath, *D*.

Before every run the silver crystals formed during the previous run have been cleared out from the electrode and its thinned portions cut away.

The emf's have been measured with 0.1 mV precision; use has been made of a Solartron (type LM 1440.2) digital voltmeter of $2 \times 10^{10}\ \Omega$ internal resistance.

Fig. 2. — Experimental cell.

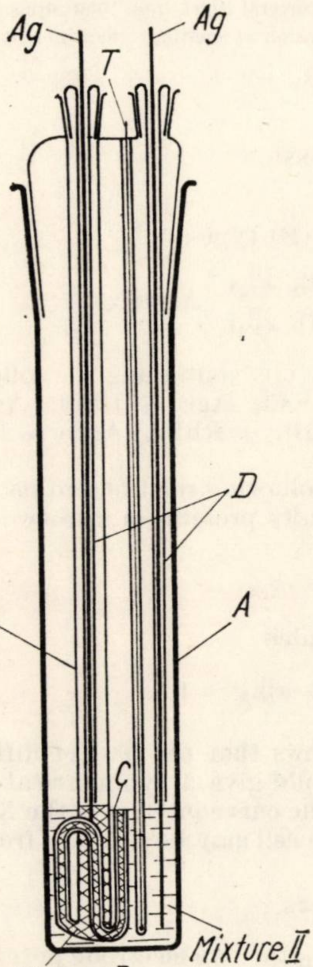

Fig. 3. — The furnace:

1 – experimental cell; *2* – silver electrodes; *3* – twisted capillary; *4* – ceramic discs; *5* – visualization device (*a*, light source; *b*, *c*, total reflexion prism with the possibility of adjusting the position; *d* – ocular); *6* – water cooling coils.

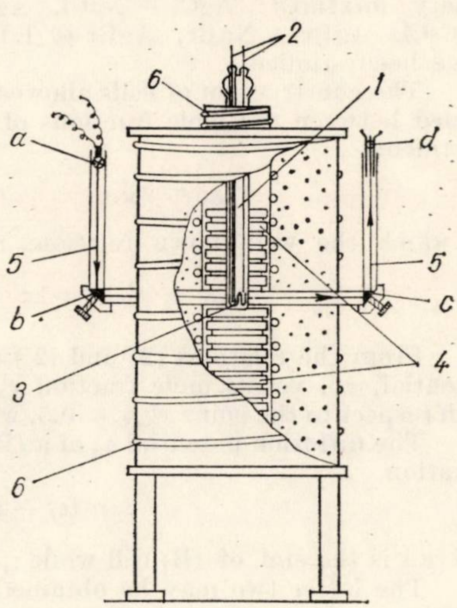

The temperature has been measured with a calibrated Pt/Pt 13% Rh thermocouple introduced directly into the mixture in the test tube; its emf was measured with a Feussner bridge.

Runs have been performed at each 10 degrees either increasing or decreasing temperatures and plots $\varepsilon_t = f(t^\circ)$ drawn for each mole fraction.

Junction between mixtures quickly established and the electrodes have been connected immediately to the meter.

Silver halides were prepared by precipitation of *p.a.*silver nitrate with *p.a.* corresponding hydro-acids; the precipitate was then dried, melted and purified by electrolysis (until silver traces were completely removed).

P.a. alkali halides have been purified by melting and bubbling with the corresponding gaseous hydro-acids; they have been preserved in desiccators.

Rubidium and cessium halides were recrystallized several times from their aqueous solutions in order to remove impurities appearing as suspension at melting; then melted in HCl or HBr gaseous stream.

RESULTS AND DISCUSSION

Concentration cells with transport of (B) type:

$$\mathrm{Ag}(s)\left|\begin{matrix}\mathrm{AgX}(l),\ x^{\mathrm{I}}_{\mathrm{AgX}}\\ \mathrm{MeX}(l),\ x^{\mathrm{I}}_{\mathrm{MeX}}\end{matrix}\right\|\begin{matrix}\mathrm{AgX}(l),\ x^{\mathrm{II}}_{\mathrm{AgX}}\\ \mathrm{MeX}(l),\ x^{\mathrm{II}}_{\mathrm{MeX}}\end{matrix}\left|\mathrm{Ag}(s)\right. \qquad \text{(B)}$$

where X = Cl, Br and Me = Na, K, Rb, Cs (i. e. containing the following binary mixtures: AgCl + NaCl, AgCl + KCl, AgCl + RbCl, AgCl + + CsCl, AgBr + NaBr, AgBr + KBr, AgBr + RbBr, AgBr + CsBr), have been studied.

The construction of cells allowed the following relations to be maintained between the mole fractions of the salts present in the two compartments

$$x^{\mathrm{I}}_{\mathrm{AgX}} = x^{\mathrm{II}}_{\mathrm{MeX}}; \qquad x^{\mathrm{I}}_{\mathrm{MeX}} = x^{\mathrm{II}}_{\mathrm{AgX}} \qquad (2)$$

to which the well-known relations are added

$$x^{\mathrm{I}}_{\mathrm{AgX}} + x^{\mathrm{I}}_{\mathrm{MeX}} = 1; \quad x^{\mathrm{II}}_{\mathrm{AgX}} + x^{\mathrm{II}}_{\mathrm{MeX}} = 1 \qquad (2')$$

From the relations (2) and (2′) it follows that the plot of diffusion potential, ε_D, versus mole fraction $x^{\mathrm{I}}_{\mathrm{AgX}}$ should give a symmetrical curve with respect to the point $x^{\mathrm{I}}_{\mathrm{AgX}} = 0.5$, where the curve intercepts the X axis.

The diffusion potential ε_D of a (B) type cell may be deduced from the equation

$$\varepsilon = (\varepsilon_{\mathrm{I}} - \varepsilon_{\mathrm{II}}) + \varepsilon_D \qquad (3)$$

where ε is the emf of (B) cell while ε_{I} and $\varepsilon_{\mathrm{II}}$ the two electrode potentials.

The latter two may be obtained from the corresponding formation cells:

$$\mathrm{Ag}(s)\left|\begin{matrix}\mathrm{AgX}(l),\ x^{\mathrm{I}}_{\mathrm{AgX}}\\ \mathrm{MeX}(l),\ x^{\mathrm{I}}_{\mathrm{MeX}}\end{matrix}\right|\mathrm{C(graphite)},\ \mathrm{X}_2\ (g,\ 1\ \mathrm{at})$$

$$\mathrm{Ag}(s)\left|\begin{matrix}\mathrm{AgX}(l),\ x^{\mathrm{II}}_{\mathrm{AgX}}\\ \mathrm{MeX}(l)\ \ x^{\mathrm{II}}_{\mathrm{MeX}}\end{matrix}\right|\mathrm{C(graphite)},\ \mathrm{X}_2\ (g,\ 1\ \mathrm{at})$$

It is easily seen that the difference between the emf's of the two formation cells equals $\varepsilon_{\mathrm{I}} - \varepsilon_{\mathrm{II}}$ from equation (3).

If the emf of (B) type cells are measured and the emf's of the suitable formation cells known we possess enough data to use equation (3) and calculate ε_D :

$$\varepsilon_D = \varepsilon - (\varepsilon_I - \varepsilon_{II}) \tag{4}$$

The emf's of formation cells have been available in literature; thus for AgCl + NaCl mixture, the emf was taken from Sternberg and Gheorghiu, [13] for AgBr + NaBr, AgBr + KBr and AgBr + RbBr from Salstrom, [14] for AgCl + KCl from Murgulescu and Sternberg [15] and for AgCl + RbCl and AgCl + CsCl from Pelton and Flengas. [16] Data for AgBr + + CsBr have been available in our own work. [17]

Activity coefficients deduced from the regular solutions equation:

$$RT \ln \gamma = \mathrm{B}\, x^2_{\mathrm{MeX}}$$

have been used in Nernst's equation to calculate emf's at mole fractions for which no data had been available, the binary mixtures under consideration having a regular behaviour.

In Tables 1 – 8 are listed the experimental results obtained in the cell we studied. In the last but one column, the values of diffusion potentials as deduced by equation (4) are listed.

Examination of tables shows that in (B) type concentration cells with transport, important diffusion potentials appear and their value may reach ± 20 mV. As expected, the larger are the composition differences between the compartments of the cells the higher the diffusion potentials.

The diffusion potentials also show a slight increase with temperature.

The dependence of diffusion potentials on silver halide concentration $x^{\mathrm{I}}_{\mathrm{AgX}}$ is drawn on Fig. 4 which refers to AgCl (l)+ KCl(l) cell (Table 2), for $T = 700°$.

A different behaviour is shown by the cells containing sodium salts. In these systems the change of diffusion potentials is more complicated, as comes out from Fig. 5 which represents data for AgCl(l) + NaCl(l) cell (Table 1), for $T = 700°$.

It is finally worth mentioning the relatively low values of diffusion potentials in cells with rubidium and cessium halides, especially at lower temperatures. This could be due to the inaccuracy of data for corresponding formation cells. Resuming the study of these cells is very indicated.

To compare the diffusion potentials in the above tables (last but one column) with the theoretical values given by equation (1), this equation should be integrated.

---

[13] S. Sternberg and S. Gheorghiu, *Studii şi Cercetări Chim. Acad. R. P.R.*, **7**, 107 (1959)

[14] E. J. Salstrom, *J. Chem. Soc.*, **53**, 1794, 3385 (1931); **54**, 4252, 4257 (1932).

[15] I. G. Murgulescu and S. Sternberg, *Rev. Chim. Acad. R.P.R.*, **2**, 251 (1957).

[16] A. D. Pelton and S. N. Flengas, *J. Electrochem. Soc.*, **117**, 1130 (1970).

[17] I. G. Murgulescu and L. Popescu, *Rev. Roumaine Chim.*, **17**, 1287 (1972).

Table 1

$$\text{The cell : Ag}(s)\left|\begin{array}{l}\text{AgCl}(l),\ x^{\text{I}}_{\text{AgCl}}\\ \text{NaCl}(l),\ x^{\text{I}}_{\text{NaCl}}\end{array}\right\|\begin{array}{l}\text{AgCl}(l),\ x^{\text{II}}_{\text{AgCl}}\\ \text{NaCl}(l),\ x^{\text{II}}_{\text{NaCl}}\end{array}\left|\text{Ag}(s)\right.$$

$x^{\text{I}}_{\text{AgCl}}$	ε (mV)	$\varepsilon_{\text{I}} - \varepsilon_{\text{II}}$ (mV)	ε_D (mV)	
			found	*calc.*
$T = 700°$ $\lambda_{\text{AgCl}} = 138.8$ $\lambda_{\text{NaCl}} = 116.06$				
0.3	−61.4	−51.4	−10.0	−6.0
0.4	−21.0	−24.2	+ 3.2	−3.0
0.5	0.0	0.0	0.0	0.0
0.6	+21.6	+24.2	− 2.6	+3.0
0.7	+63.4	+51.4	+12.0	+6.0
$T = 750°$ $\lambda_{\text{AgCl}} = 143.2$ $\lambda_{\text{NaCl}} = 125.17$				
0.3	−67.0	−55.0	−12.0	−4.7
0.4	−23.4	−25.9	+ 2.5	−2.4
0.5	0.0	0.0	0.0	0.0
0.6	+25.0	+25.9	− 0.9	+2.4
0.7	+69.0	+55.0	+14.0	+4.7
$T = 800°$ $\lambda_{\text{AgCl}} = 147.2$ $\lambda_{\text{NaCl}} = 134.03$				
0.3	−72.2	−56.2	−16.0	−3.5
0.4	−25.7	−27.7	+ 2.0	−1.7
0.5	0.0	0.0	0.0	0.0
0.6	+28.5	+27.7	+ 0.8	+1.7
0.7	+74.5	+56.2	+18.3	+3.5

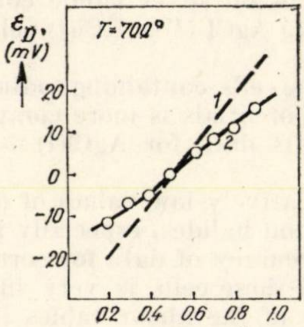

Fig. 4. — The diffusion potential ε_D versus mole fraction $x^{\text{I}}_{\text{AgCl}}$ in the concentration cell :

$$\text{Ag}(s)\left|\begin{array}{l}\text{AgCl}(l),\ x^{\text{I}}_{\text{AgCl}}\\ \text{KCl}(l),\ \ \ x^{\text{I}}_{\text{KCl}}\end{array}\right\|\begin{array}{l}\text{AgCl}(l),\ x^{\text{II}}_{\text{AgCl}}\\ \text{KCl}(l),\ \ \ x^{\text{II}}_{\text{KCl}}\end{array}\left|\text{Ag}(s)\right.$$

1, Experimental

2, Calculated according to eq (10).

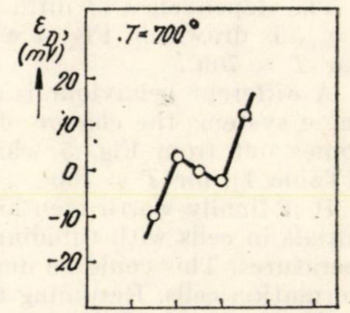

Fig. 5. — The diffusion potential ε_D versus mole fraction $x^{\text{I}}_{\text{AgCl}}$ in the concentration cell:

$$\text{Ag}(s)\left|\begin{array}{l}\text{AgCl}(l),\ x^{\text{I}}_{\text{AgCl}}\\ \text{NaCl}(l),\ x^{\text{I}}_{\text{NaCl}}\end{array}\right\|\begin{array}{l}\text{AgCl}(l),\ x^{\text{II}}_{\text{AgCl}}\\ \text{NaCl}(l),\ x^{\text{II}}_{\text{NaCl}}\end{array}\left|\text{Ag}(s)\right.$$

Table 2

$$\text{The cell : } Ag(s) \left| \begin{matrix} AgCl(l), & x^{I}_{AgCl} \\ KC(l), & x^{I}_{KCl} \end{matrix} \right\| \begin{matrix} AgCl(l), & x^{II}_{AgCl} \\ KCl(l), & x^{II}_{KCl} \end{matrix} \left| \, Ag(s) \right.$$

x^{I}_{AgCl}	ε (mV)	$\varepsilon_I - \varepsilon_{II}$ (mV)	ε_D (mV)	
			found	*calc.*
$T = 700°$ $\lambda_{AgCl} = 138.8$ $\lambda_{KCl} = 93.74$				
0.2	−170.0	−158.8	−11.2	−19.6
0.3	−104.6	− 97.2	− 7.4	−13.0
0·4	− 50.6	− 45.1	− 5.5	− 6.5
0.5	0.0	0.0	0.0	0.0
0.6	+ 50.5	+ 45.1	+ 5.4	+ 6.5
0.7	+105.5	+ 97.2	+ 8.3	+13.0
0.8	+170.0	+158.8	+11.2	+19.6
0.9	+251.5	+235.5	+16.0	+26.2
$T = 750°$ $\lambda_{AgCl} = 143.2$ $\lambda_{KCl} = 102.2$				
0.2	−178.5	−165.0	−13.5	−17.7
0.3	−110.5	−100.9	− 9.6	−11.8
0.4	− 53.2	− 46.9	− 6.3	− 5.9
0.5	0.0	0.0	0.0	0.0
0.6	+ 53.0	+ 46.9	+ 6.1	+ 5.9
0.7	+111.5	+100.9	+10.6	+11.8
0.8	+178.0	+165.0	+13.0	+17.7
0.9	+263.0	+245.0	+18.0	+23.7
$T = 800°$ $\lambda_{AgCl} = 147.2$ $\lambda_{KCl} = 110.5$				
0.2	−183.0	−168.7	−14.3	−15.8
0.3	−116.0	−105.3	−10.7	−10.5
0.4	− 56.0	− 51.0	− 5.0	− 5.3
0.5	0.0	0.0	0.0	0.0
0.6	+ 56.0	+ 51.0	+ 5.0	+ 5.3
0.7	+117.0	+105.3	+11.7	+10.5
0.8	+183.5	+168.7	+14.8	+15.8
0.9	+277.0	+257.1	+19.9	+21.2

An exact integration is not possible since the individual activities a_i of the ions are not available. Approximate results may be obtained, as for electrolyte solutions, by making use of non-thermodynamic simplifying assumptions.

That is what we try in the following. Firstly, not to uselessly make intricate calculations we limit the treatment to common anion binary mixtures of the type $AC_1 + AC_2$, C_1^+ and C_2^+ representing the two cations Ag^+ and Me^+ with Me = Na, K, Rb, Cs and A^-, the common anion $X^-(X = Cl, Br)$.

Since the mole fraction of the anion is the same in both compartments of the studied cell, we assume that the activity remains approximately constant.

Table 3

$$\text{The cell : Ag}(s)\left|\begin{array}{l}\text{AgCl }(l),\ x^{\text{I}}_{\text{AgCl}}\\ \text{RbCl }(l),\ x^{\text{I}}_{\text{RbCl}}\end{array}\right\|\begin{array}{l}\text{AgCl}(l), x^{\text{II}}_{\text{AgCl}}\\ \text{RbCl}(l),\ x^{\text{II}}_{\text{RbCl}}\end{array}\left|\ \text{Ag}(s)\right.$$

$x^{\text{I}}_{\text{AgCl}}$	ε(mV)	$\varepsilon_{\text{I}} - \varepsilon_{\text{II}}$(mV)	ε_D (mV)	
			found	*calc.*
	$T = 600°$	$\lambda_{\text{AgCl}} = 129.1$	$\lambda_{\text{RbCl}} = 59.70$	
0.3	−115.2	−113.2	− 2.0	−22.3
0.4	− 55.5	− 55.0	− 0.5	−10.9
0.5	0.0	0.0	0.0	0.0
0.6	+ 56.0	+ 55.0	+ 1.0	+10.9
0.7	+115.2	+113.2	+ 2.0	+22.3
	$T = 650°$	$\lambda_{\text{AgCl}} = 134.1$	$\lambda_{\text{RbCl}} = 68.49$	
0.3	−120.0	−116.7	− 3.3	−20.7
0.4	− 59.0	− 57.5	− 1.5	−10.3
0.5	0.0	0.0	0.0	0.0
0.6	+ 59.0	+ 57.5	+ 1.5	+10.3
0.7	+120.0	+116.7	+ 3.3	+20.7
	$T = 700°$	$\lambda_{\text{AgCl}} = 138.8$	$\lambda_{\text{RbCl}} = 77.48$	
0.3	−125.0	−120.0	− 5.0	−19.1
0.4	− 62.0	− 60.0	− 2.0	− 9.5
0.5	0.0	0.0	0.0	0.0
0.6	+ 62.0	+ 60.0	+ 2.0	+ 9.5
0.7	+126.0	+120.0	+ 6.0	+19.1

Equation (1) takes then the form

$$\varepsilon_D = -\frac{RT}{F}\int_{\text{I}}^{\text{II}} (t_{\text{C}_1}\,\text{dln}\,a_{\text{C}_1} + t_{\text{C}_2}\,\text{dln}\,a_{\text{C}_2}) \qquad (5)$$

t_{C_1}, t_{C_2} and a_{C_1}, a_{C_2} being the transport numbers, respectively the activities of the cations C_1^+ and C_2^+.

The second hypothesis which we introduce regards the structure of diffusion layer. We assume that the diffusion layer has a structure analogous to that proposed by Henderson[18] for aqueous electrolytic solutions. In molten salts, this structure may be described by the following relations

$$a_{\text{C}_1} = a^{\text{I}}_{\text{C}_1} + (a^{\text{II}}_{\text{C}_1} - a^{\text{I}}_{\text{C}_1})x\,; \qquad a_{\text{C}_2} = a^{\text{I}}_{\text{C}_2} + (a^{\text{II}}_{\text{C}_2} - a^{\text{I}}_{\text{C}_2})x \qquad (6)$$

$$x_{\text{AC}_1} = x^{\text{I}}_{\text{AC}_1} + (x^{\text{II}}_{\text{AC}_1} - x^{\text{I}}_{\text{AC}_1})x\,; \qquad x_{\text{AC}_2} = x^{\text{I}}_{\text{AC}_2} + (x^{\text{II}}_{\text{AC}_2} - x^{\text{I}}_{\text{AC}_2})x \qquad (7)$$

---

[18] P. Henderson, *Z. phys. Chem.*, **50**, 118 (1907); **63**, 325 (1908).

Table 4

$$\text{The cell : Ag}(s)\left|\begin{matrix}\text{AgCl}(l).\ x^{\text{I}}_{\text{AgCl}}\\ \text{CsCl}\ (l),\ x^{\text{II}}_{\text{CsCl}}\end{matrix}\right\|\begin{matrix}\text{AgCl}(l),\ x^{\text{II}}_{\text{AgCl}}\\ \text{CsCl}(l)\ \ x^{\text{II}}_{\text{CsCl}}\end{matrix}\left|\text{Ag}(s)\right.$$

$x^{\text{I}}_{\text{AgCl}}$	ε(mV)	$\varepsilon_{\text{I}} - \varepsilon_{\text{II}}$(mV)	ε_D (mV)	
			found	*calc.*
T = 600°	λ_{AgCl} = 129.1	λ_{CsCl} = 57.98		
0.3	−146.0	−136.0	−10.0	−23.1
0.4	− 71.0	− 69.0	− 2.0	−11.5
0.5	0.0	0.0	0.0	0.0
0.6	+ 72.0	+ 69.0	+ 3.0	+11.5
0.7	+145.0	+136.0	+ 9.0	+23.1
T = 650°	λ_{AgCl} = 134.1	λ_{CsCl} = 68.01		
0.3	−151.0	−138.5	−12.5	−20.9
0.4	− 73.0	− 69.5	− 3.5	−10.4
0.5	0.0	0.0	0.0	0.0
0.6	+ 76.0	+ 69.5	+ 6.5	+10.4
0.7	+150.5	+138.5	+12.0	+20.9
T = 700°	λ_{AgCl} = 138.8	λ_{CsCl} = 78.47		
0.3	−158.0	−140.5	−17.5	−18.7
0.4	− 75.0	− 70.0	− 5.0	− 9.5
0.5	0.0	0.0	0.0	0.0
0.6	+ 79.0	+ 70.0	+ 9.0	+ 9.5
0.7	+156.0	+140.5	+15.5	+18.7

The I and II denote as before the compartments of the cell to which the activities and mole fractions refer, and $0 < x < 1$. The transport numbers t_{C_1} and t_{C_2} become

$$t_{\text{C}_1} = \frac{x_{\text{C}_1}u_{\text{C}_1}}{x_{\text{C}_1}u_{\text{C}_1} + x_{\text{C}_2}u_{\text{C}_2} + x_{\text{A}}u_{\text{A}}}; \qquad t_{\text{C}_2} = \frac{x_{\text{C}_2}u_{\text{C}_2}}{x_{\text{C}_1}u_{\text{C}_1} + x_{\text{C}_2}u_{\text{C}_2} + x_{\text{A}}u_{\text{A}}}$$

u_{C_1}, u_{C_2} and u_{A} being the mobilities, while x_{C_1}, x_{C_2} and x_{A} the concentrations (molar fractions) of the ions indicated by subscript.

As $x_{\text{A}} = x_{\text{C}_1} + x_{\text{C}_2}$ the transport numbers become

$$t_{\text{C}_1} = \frac{x_{\text{C}_1}u_{\text{C}_1}}{x_{\text{C}_1}(u_{\text{C}_1} + u_{\text{A}}) + x_{\text{C}_2}(u_{\text{C}_2} + u_{\text{A}})}; \qquad t_{\text{C}_2} = \frac{x_{\text{C}_2}u_{\text{C}_2}}{x_{\text{C}_1}(u_{\text{C}_1} + u_{\text{A}}) + x_{\text{C}_2}(u_{\text{C}_2} + u_{\text{A}})}$$

However, $u_{\text{C}_1} + u_{\text{A}} = \lambda_{\text{AC}_1}$, $u_{\text{C}_2} + u_{\text{A}} = \lambda_{\text{AC}_2}$, λ_{AC_1} and λ_{AC_2} being the equivalent conductivities of the two salts AC_1 and AC_2. It is easy to notice that

Table 5

$$\text{The cell : Ag}(s) \left| \begin{matrix} \text{AgBr}(l),\ x^{\mathrm{I}}_{\mathrm{AgBr}} \\ \text{NaBr}(l),\ x^{\mathrm{I}}_{\mathrm{NaBr}} \end{matrix} \right\| \begin{matrix} \text{AgBr}(l),\ x^{\mathrm{II}}_{\mathrm{AgBr}} \\ \text{NaBr}(l),\ x^{\mathrm{II}}_{\mathrm{NaBr}} \end{matrix} \right| \text{Ag}(s)$$

$x^{\mathrm{I}}_{\mathrm{AgBr}}$	ε (mV)	$\varepsilon_{\mathrm{I}} - \varepsilon_{\mathrm{II}}$ (mV)	ε_D (mV)	
			found	*calc.*
$T = 700°$ $\lambda_{\mathrm{AgBr}} = 118.8$ $\lambda_{\mathrm{NaBr}} = 117.3$				
0.3	−64.8	−52.8	−12.0	−0.4
0.4	−23.0	−24.9	+ 1.9	−0.2
0.5	56.0	0.0	0.0	0.0
0.6	+22.0	+24.9	− 2.9	+0.2
0.7	+66.7	+52.8	+13.9	+0.4
$T = 750°$ $\lambda_{\mathrm{AgBr}} = 122.1$ $\lambda_{\mathrm{NaBr}} = 127.3$				
0.3	−70.0	−56.5	−13.5	+1.5
0.4	−25.7	−26.7	+ 1.0	+0.7
0.5	0.0	0.0	0.0	0.0
0.6	+24.0	+26.7	− 2.7	−0.7
0.7	+71.0	+56.5	+14.5	−1.5
$T = 800°$ $\lambda_{\mathrm{AgBr}} = 128.2$ $\lambda_{\mathrm{NaBr}} = 137.1$				
0.3	−76.2	−60.2	−16.0	+2.5
0.4	−28.5	−28.6	+ 0.1	+1.2
0.5	0.0	0.0	0.0	0.0
0.6	+27.0	+28.6	− 1.6	−1.2
0.7	+75.2	+60.2	+15.0	−2.5

$x_{\mathrm{C}_1} = \dfrac{x_{\mathrm{AC}_1}}{2}$ and $x_{\mathrm{C}_2} = \dfrac{x_{\mathrm{AC}_2}}{2}$ in which case the transport numbers take the form

$$t_{\mathrm{C}_1} = \frac{x_{\mathrm{AC}_1} u_{\mathrm{C}_1}}{x_{\mathrm{AC}_1}\lambda_{\mathrm{AC}_1} + x_{\mathrm{AC}_2}\lambda_{\mathrm{AC}_2}}; \qquad t_{\mathrm{C}_2} = \frac{x_{\mathrm{AC}_2} u_{\mathrm{C}_2}}{x_{\mathrm{AC}_1}\lambda_{\mathrm{AC}_1} + x_{\mathrm{AC}_2}\lambda_{\mathrm{AC}_2}}$$

Taking into account (2) and (7) one finally obtains

$$\left.\begin{aligned} t_{\mathrm{C}_1} &= \frac{[x^{\mathrm{I}}_{\mathrm{AC}_1} + (x^{\mathrm{II}}_{\mathrm{AC}_1} - x^{\mathrm{I}}_{\mathrm{AC}_1})x]u_{\mathrm{C}_1}}{x^{\mathrm{I}}_{\mathrm{AC}_1}\lambda_{\mathrm{AC}_1} + x^{\mathrm{I}}_{\mathrm{AC}_2}\lambda_{\mathrm{AC}_2} + (\lambda_{\mathrm{AC}_1} - \lambda_{\mathrm{AC}_2})(x^{\mathrm{II}}_{\mathrm{AC}_1} - x^{\mathrm{I}}_{\mathrm{AC}_1})x} \\ t_{\mathrm{C}_2} &= \frac{[x^{\mathrm{I}}_{\mathrm{AC}_2} + (x^{\mathrm{II}}_{\mathrm{AC}_2} - x^{\mathrm{I}}_{\mathrm{AC}_2})x]u_{\mathrm{C}_2}}{x^{\mathrm{I}}_{\mathrm{AC}_1}\lambda_{\mathrm{AC}_1} + x^{\mathrm{I}}_{\mathrm{AC}_2}\lambda_{\mathrm{AC}_2} + (\lambda_{\mathrm{AC}_1} - \lambda_{\mathrm{AC}_2})(x^{\mathrm{II}}_{\mathrm{AC}_1} - x^{\mathrm{I}}_{\mathrm{AC}_1})x} \end{aligned}\right\} \quad (8)$$

The equations (5), (6) and (8) give

$$\varepsilon_D = -\frac{RT}{F}\int_0^1 \frac{[x^{\mathrm{I}}_{\mathrm{AC}_1} + (x^{\mathrm{II}}_{\mathrm{AC}_1} - x^{\mathrm{I}}_{\mathrm{AC}_1})x]u_{\mathrm{C}_1}}{x^{\mathrm{I}}_{\mathrm{AC}_1}\lambda_{\mathrm{AC}_1} + x^{\mathrm{I}}_{\mathrm{AC}_2}\lambda_{\mathrm{AC}_2} + (\lambda_{\mathrm{AC}_1} - \lambda_{\mathrm{AC}_2})(x^{\mathrm{II}}_{\mathrm{AC}_1} - x^{\mathrm{I}}_{\mathrm{AC}_1})x} \cdot \frac{a^{\mathrm{II}}_{\mathrm{C}_1} - a^{\mathrm{I}}_{\mathrm{C}_1}}{a^{\mathrm{I}}_{\mathrm{C}_1} + (a^{\mathrm{II}}_{\mathrm{C}_1} - a^{\mathrm{I}}_{\mathrm{C}_1})x}\,\mathrm{d}x -$$

$$-\frac{RT}{F}\int_0^1 \frac{[x^{\mathrm{I}}_{\mathrm{AC}_2} + (x^{\mathrm{II}}_{\mathrm{AC}_2} - x^{\mathrm{I}}_{\mathrm{AC}_2})x]u_{\mathrm{C}_2}}{x^{\mathrm{I}}_{\mathrm{AC}_1}\lambda_{\mathrm{AC}_1} + x^{\mathrm{I}}_{\mathrm{AC}_2}\lambda_{\mathrm{AC}_2} + (\lambda_{\mathrm{AC}_1} - \lambda_{\mathrm{AC}_2})(x^{\mathrm{II}}_{\mathrm{AC}_1} - x^{\mathrm{I}}_{\mathrm{AC}_1})x} \cdot \frac{a^{\mathrm{II}}_{\mathrm{C}_2} - a^{\mathrm{I}}_{\mathrm{C}_2}}{a^{\mathrm{I}}_{\mathrm{C}_2} + (a^{\mathrm{II}}_{\mathrm{C}_2} - a^{\mathrm{I}}_{\mathrm{C}_2})x}\,\mathrm{d}x$$

If the activity coefficients $f^{\mathrm{I}}_{\mathrm{C}_1}$, $f^{\mathrm{II}}_{\mathrm{C}_1}$ and $f^{\mathrm{I}}_{\mathrm{C}_2}$ and $f^{\mathrm{II}}_{\mathrm{C}_2}$ are introduced the equation becomes

$$\varepsilon_D = -\frac{RT}{F}\int_0^1 \frac{[x^{\mathrm{I}}_{\mathrm{AC}_1} + (x^{\mathrm{II}}_{\mathrm{AC}_1} - x^{\mathrm{I}}_{\mathrm{AC}_1})x]u_{\mathrm{C}_1}}{x^{\mathrm{I}}_{\mathrm{AC}_1}\lambda_{\mathrm{AC}_1} + x^{\mathrm{I}}_{\mathrm{AC}_2}\lambda_{\mathrm{AC}_2} + (\lambda_{\mathrm{AC}_1} - \lambda_{\mathrm{AC}_2})(x^{\mathrm{II}}_{\mathrm{AC}_1} - x^{\mathrm{I}}_{\mathrm{AC}_1})x} \times$$

$$\times \frac{f^{\mathrm{II}}_{\mathrm{C}_1}x^{\mathrm{II}}_{\mathrm{AC}_1} - f^{\mathrm{I}}_{\mathrm{C}_1}x^{\mathrm{I}}_{\mathrm{AC}_1}}{f^{\mathrm{I}}_{\mathrm{C}_1}x^{\mathrm{I}}_{\mathrm{AC}_1} + (f^{\mathrm{II}}_{\mathrm{C}_1}x^{\mathrm{II}}_{\mathrm{AC}_1} - f^{\mathrm{I}}_{\mathrm{C}_1}x^{\mathrm{I}}_{\mathrm{AC}_1})x}\,\mathrm{d}x -$$

$$-\frac{RT}{F}\int_0^1 \frac{[x^{\mathrm{I}}_{\mathrm{AC}_2} + (x^{\mathrm{II}}_{\mathrm{AC}_2} - x^{\mathrm{I}}_{\mathrm{AC}_2})x]u_{\mathrm{C}_2}}{x^{\mathrm{I}}_{\mathrm{AC}_1}\lambda_{\mathrm{AC}_1} + x^{\mathrm{I}}_{\mathrm{AC}_2}\lambda_{\mathrm{AC}_2} + (\lambda_{\mathrm{AC}_1} - \lambda_{\mathrm{AC}_2})(x^{\mathrm{II}}_{\mathrm{AC}_1} - x^{\mathrm{I}}_{\mathrm{AC}_1})x} \times$$

$$\times \frac{f^{\mathrm{II}}_{\mathrm{C}_2}x^{\mathrm{II}}_{\mathrm{AC}_2} - f^{\mathrm{I}}_{\mathrm{C}_2}x^{\mathrm{I}}_{\mathrm{AC}_2}}{f^{\mathrm{I}}_{\mathrm{C}_2}x^{\mathrm{I}}_{\mathrm{AC}_2} + (f^{\mathrm{II}}_{\mathrm{C}_2}x^{\mathrm{II}}_{\mathrm{AC}_2} - f^{\mathrm{I}}_{\mathrm{C}_2}x^{\mathrm{I}}_{\mathrm{AC}_2})x}\,\mathrm{d}x$$

Since the expressions of the individual activity coefficients (versus mole fractions x_{AC_1} and x_{AC_2}) are not accessible, the exact value of the integrals cannot be determined. To get approximate results and simplify the calculations we set

$$f^{\mathrm{I}}_{\mathrm{C}_1} \sim f^{\mathrm{II}}_{\mathrm{C}_1} \text{ and } f^{\mathrm{I}}_{\mathrm{C}_2} \sim f^{\mathrm{II}}_{\mathrm{C}_2} \tag{8'}$$

This is rough approximation which holds only for $x^{\mathrm{I}}_{\mathrm{AC}_1} \sim x^{\mathrm{II}}_{\mathrm{AC}_1}$ and $x^{\mathrm{I}}_{\mathrm{AC}_2} \sim x^{\mathrm{II}}_{\mathrm{AC}_2}$. For very different compositions in the two compartments of the cell a satisfactory agreement between the diffusion potentials so calculated and those deduced from formation cells is not to be expected.

On the basis of the above simplifying assumption, the diffusion potential becomes

$$\varepsilon_D = -\frac{RT}{F}[(x^{\mathrm{II}}_{\mathrm{AC}_1} - x^{\mathrm{I}}_{\mathrm{AC}_1})u_{\mathrm{C}_1} + (x^{\mathrm{II}}_{\mathrm{AC}_2} - x^{\mathrm{I}}_{\mathrm{AC}_2})u_{\mathrm{C}_2}] \times$$

$$\times \int_0^1 \frac{\mathrm{d}x}{x^{\mathrm{I}}_{\mathrm{AC}_1}\lambda_{\mathrm{AC}_1} + x^{\mathrm{I}}_{\mathrm{AC}_2}\lambda_{\mathrm{AC}_2} + (\lambda_{\mathrm{AC}_1} - \lambda_{\mathrm{AC}_2})(x^{\mathrm{II}}_{\mathrm{AC}_1} - x^{\mathrm{I}}_{\mathrm{AC}_1})x}$$

Equation (2) and the condition $u_{\mathrm{C}_1} - u_{\mathrm{C}_2} = \lambda_{\mathrm{AC}_1} - \lambda_{\mathrm{AC}_2}$ lead to the following expression for diffusion potential

$$\varepsilon_D = -\frac{RT}{F}(x^{\mathrm{II}}_{\mathrm{AC}_1} - x^{\mathrm{I}}_{\mathrm{AC}_1})(\lambda_{\mathrm{AC}_1} - \lambda_{\mathrm{AC}_2}) \times$$

$$\times \int_0^1 \frac{\mathrm{d}x}{x^{\mathrm{I}}_{\mathrm{AC}_1}\lambda_{\mathrm{AC}_1} + x^{\mathrm{I}}_{\mathrm{AC}_2}\lambda_{\mathrm{AC}_2} + (\lambda_{\mathrm{AC}_1} - \lambda_{\mathrm{AC}_2})(x^{\mathrm{II}}_{\mathrm{AC}_1} - x^{\mathrm{I}}_{\mathrm{AC}_1})x} \tag{9}$$

Table 6

The cell : Ag(s) | AgBr (*l*) $x^{\mathrm{I}}_{\mathrm{AgBr}}$, KBr (*l*), $x^{\mathrm{I}}_{\mathrm{KBr}}$ || AgBr(*l*), $x^{\mathrm{II}}_{\mathrm{AgBr}}$, KBr (*l*), $x^{\mathrm{II}}_{\mathrm{KBr}}$ | Ag(*s*)

$x^{\mathrm{I}}_{\mathrm{AgBr}}$	ε (mV)	$\varepsilon_{\mathrm{I}}-\varepsilon_{\mathrm{II}}$ (mV)	ε_D (mV) *found*	ε_D (mV) *calc.*
$T = 700°$	$\lambda_{\mathrm{AgBr}} = 118.8$	$\lambda_{\mathrm{KBr}} = 85.17$		
0.1	−249.0	−234.5	−14.5	−22.2
0.2	−167.0	−155.4	−11.6	−16.6
0.3	−105.5	− 96.8	− 8.7	−11.1
0.4	− 51.5	− 46.7	− 4.8	− 5.5
0.5	0.0	0.0	0.0	0.0
0.6	+ 52.3	+ 46.7	+ 5.6	+ 5.5
0.7	+106.0	+ 96.8	+ 9.2	+11.1
0.8	+166.4	+155.4	+11.0	+16.6
0.9	+249.5	+234.5	+15.0	+22.2
$T = 750°$	$\lambda_{\mathrm{AgBr}} = 122.1$	$\lambda_{\mathrm{KBr}} = 93.62$		
0.1	−262.0	−245.0	−17.0	−18.7
0.2	−175.0	−160.9	−14.1	−14.0
0.3	−110.5	−100.3	−10.2	− 9.3
0.4	− 54.0	−48.1	− 5.9	− 4.7
0.5	0.0	0.0	0.0	0.0
0.6	+ 54.0	+ 48.1	+ 5.9	+ 4.7
0.7	+112.0	+100.3	+11.7	+ 9.3
0.8	+174.6	+160.9	+13.7	+14.0
0.9	+262.0	+245.0	+17.0	+18.7
$T = 800°$	$\lambda_{\mathrm{AgBr}} = 125.3$	$\lambda_{\mathrm{KBr}} = 102.0$		
0.1	−273.0	−254.5	−18.5	−15.2
0.2	−183.0	−166.7	−16.3	−11.4
0.3	−118.0	−104.0	−14.0	− 7.6
0.4	− 56.0	− 50.3	− 5.7	− 3.8
0.5	0.0	0.0	0.0	0.0
0.6	+ 56.5	+ 50.3	+ 6.2	+ 3.8
0.7	+118.0	+104.0	+14.0	+ 7.6
0.8	+183.5	+166.7	+16.8	+11.4
0.9	+273.5	+254.5	+19.0	+15.2

Integration and calculations lead to the following simple expression of ε_D

$$\varepsilon_D = -\frac{RT}{F}\ln\frac{x^{\mathrm{II}}_{\mathrm{AC}_1}\lambda_{\mathrm{AC}_1} + x^{\mathrm{II}}_{\mathrm{AC}_2}\lambda_{\mathrm{AC}_2}}{x^{\mathrm{I}}_{\mathrm{AC}_1}\lambda_{\mathrm{AC}_1} + x^{\mathrm{I}}_{\mathrm{AC}_2}\lambda_{\mathrm{AC}_2}} \tag{10}$$

Equation (10) represents a generalization of Lewis-Sargent [19] equation for binary mixtures. The diffusion potentials given in the last column of tables 1—8 have been calculated by equation (10).

---

[19] G. N. Lewis and L. W. Sargent, *J. Amer. Chem. Soc.*, **31**, 363 (1909).

Table 7

$$\text{The cell}: \mathrm{Ag}(s) \left| \begin{array}{l} \mathrm{AgBr}(l),\ x^{\mathrm{I}}_{\mathrm{AgBr}} \\ \mathrm{RbBr}(l),\ x^{\mathrm{I}}_{\mathrm{RbBr}} \end{array} \right\| \begin{array}{l} \mathrm{AgBr}(l),\ x^{\mathrm{II}}_{\mathrm{AgBr}} \\ \mathrm{RbBr}(l),\ x^{\mathrm{II}}_{\mathrm{RbBr}} \end{array} \left| \mathrm{Ag}(s) \right.$$

$x^{\mathrm{I}}_{\mathrm{AgBr}}$	ε(mV)	$\varepsilon_{\mathrm{I}} - \varepsilon_{\mathrm{II}}$(mV)	ε_D (mV)	
			found	*calc.*
$T = 600°$		$\lambda_{\mathrm{AgBr}} = 111.26$	$\lambda_{\mathrm{RbBr}} = 55.24$	
0.2	−176.8	−170.9	− 5.9	−30.8
0.3	−113.8	−108.5	− 5.3	−20.4
0.4	− 56.5	− 52.8	− 3.7	−10.1
0.5	0.0	0.0	0.0	0.0
0.6	+ 57.0	+ 52.8	+ 4.2	+10.1
0.7	+114.0	+108.5	+ 5.5	+20.4
0.8	+177.0	+170.9	+ 6.1	+30.8
$T = 650°$		$\lambda_{\mathrm{AgBr}} = 115.16$	$\lambda_{\mathrm{RbBr}} = 62.91$	
0.2	−185.0	−177.4	− 7.6	−28.3
0.3	−118.5	−112.2	− 6.3	−18.7
0.4	− 59.0	− 54.6	− 4.4	− 9.3
0.5	0.0	0.0	0.0	0.0
0.6	+ 59.0	+ 54.6	+ 4.4	+ 9.3
0.7	+118.5	+112.2	+ 6.3	+18.7
0.8	+185.4	+177.4	+ 8.0	+28.3
$T = 700°$		$\lambda_{\mathrm{AgBr}} = 118.8$	$\lambda_{\mathrm{RbBr}} = 70.715$	
0.2	−193.0	−183.3	− 9.7	−25.7
0.3	−124.0	−116.8	− 7.2	−17.1
0.4	− 61.5	− 56.4	− 5.1	− 8.5
0.5	0.0	0.0	0.0	0.0
0.6	+ 61.0	+ 56.4	+ 4.6	+ 8.5
0.7	+123.0	+116.8	+ 6.2	+17.1
0.8	+193.0	+183.3	+ 9.7	+25.7
$T = 750°$		$\lambda_{\mathrm{AgBr}} = 122.1$	$\lambda_{\mathrm{RbBr}} = 78.57$	
0.2	−200.0	−189.3	−10.7	−23.1
0.3	−128.5	−119.5	− 9.0	−15.4
0.4	− 62.5	− 58.5	− 4.0	− 7.6
0.5	0.0	0.0	0.0	0.0
0.6	+ 63.0	+ 58.5	+ 4.5	+ 7.6
0.7	+129.0	+119.5	+ 9.5	+15.4
0.8	+201.0	+189.3	+11.7	+23.1

For the equivalent conductivity which we needed, use has been made of the equation given in a well-known Janz's work[20].

In Figure 4 are given the diffusion potentials, both experimental and calculated by equations (10), for the same system and temperature.

---

[20] G. Janz, "Molten Salts Handbook", Academic Press, New York, London, 1967, p. 287.

Table 8

$$\text{The cell: Ag}(s)\left|\begin{array}{l}\text{AgBr}(l),\ x^{\text{I}}_{\text{AgBr}}\\ \text{CsBr}\ (l),\ x^{\text{I}}_{\text{CsBr}}\end{array}\right\|\left.\begin{array}{l}\text{AgBr}\ (l),\ x^{\text{II}}_{\text{AgBr}}\\ \text{CsBr}(l),\ x^{\text{II}}_{\text{CsBr}}\end{array}\right|\ \text{Ag}(s)$$

$x^{\text{I}}_{\text{AgBr}}$	ε(mV)	$\varepsilon_{\text{I}} - \varepsilon_{\text{II}}$ (mV)	ε_D (mV)	
			found	*calc.*
$T = 600°$	$\lambda_{\text{AgBr}} = 111.26$		$\lambda_{\text{CsBr}} = 48.20$	
0.3	−114.0	−106.0	− 8.0	−24.0
0.4	− 51.0	− 47.0	− 4.0	−12.0
0.5	0.0	0.0	0.0	0.0
0.6	+ 52.0	+ 47.0	+ 5.0	+12.0
0.7	+114.0	+106.0	+ 8.0	+24.0
$T = 650°$	$\lambda_{\text{AgBr}} = 115.16$		$\lambda_{\text{CsBr}} = 57.29$	
0.3	−119.0	−109.5	− 9.5	−21.5
0.4	− 55.0	− 48.0	− 7.0	−10.7
0.5	0.0	0.0	0.0	0.0
0.6	+ 55.0	+ 48.0	+ 7.0	+10.7
0.7	+119.0	+109.5	+ 9.5	+21.5
$T = 750°$	$\lambda_{\text{AgBr}} = 118.8$		$\lambda_{\text{CsBr}} = 66.89$	
0.3	−127.0	−113.0	−14.0	−18.8
0.4	− 58.0	− 49.0	− 9.0	− 9.4
0.5	0.0	0.0	0.0	0.0
0.6	+ 59.0	+ 49.0	+10.0	+ 9.4
0.7	+125.5	+113.0	+12.5	+18.8

Comparison of the last two columns in Tables 1 — 8 shows that equation (10) gives only a qualitative description of diffusion potentials in cells with transport except for cells in which sodium salts are present. When the compositions in the two compartments of the cell are not too different, the values of diffusion potentials, calculated according to equation (10), come very close to the experimental ones as expected. Similarly, with the increase of temperature, the differences between the theoretical and experimental values are smaller. The phenomenon is evident in AgCl + + KCl system; at 800° the difference is within experimental errors. It looks like as the temperature increases, the structure of the diffusion layer in cells, in given experimental conditions, is close to the structure given by Henderson.

We finally mention that equation (10) could be reached by introducing in equation (1) the activity coefficients and replacing the logarithm of products by sums of logarithms.

For mixtures of $AC_1 + AC_2$ we get:

$$\varepsilon_D = -\frac{RT}{F}\int_{\text{I}}^{\text{II}} (t_{C_1}\,\text{dln}\ C_1 + t_{C_2}\,\text{dln}\ C_2) - \frac{RT}{F}\int_{\text{I}}^{\text{II}} (t_{C_1}\,\text{dln}\ f_{C_1} + t_{C_2}\,\text{dln}\ f_{C_2})$$

Neglecting the second term and processing the first one as above we find again equation (10). The present approximation of activity coefficients proves to be equivalent to that introduced above by conditions (8′).

Revue Roumaine de Chimie, 18, 5, 753 – 760 (1973)

KINETICS AND MECHANISM OF THE THERMAL DECOMPOSITION OF AZIBENZIL. II[1]

STUDIES IN THE ABSENCE OF A SOLVENT

M. CONTINEANU *, TATIANA ONCESCU * and R. N. SCHINDLER **

* Physical Chemistry Laboratory, University of Bucharest,
Bd. Republicii 13, Romania
** Institut für Physikalische Chemie, Kernforschungsanlage
Jülich GmBH, Jülich, BRD

Received November 17, 1972

The kinetics and the mechanism of the thermal decomposition of azibenzil was studied below and above the melting point. The data obtained, following the rate of N_2 evolution during the reaction, indicate that the decomposition follows a first order kinetics in the absence of a solvent.

The spectrophotometric analysis of the products, at different reaction times, reveal that in addition to diphenylketene at least one other product is formed in the reaction.

INTRODUCTION

This paper describes the kinetics of the thermal decomposition of solid and molten azibenzil, respectively. No previous investigation on the decomposition of this compound, in the absence of a solvent, has been reported in the literature.

Our own preliminary experiments, carried out previously, indicated that the decomposition rate of molten azibenzil is comparatively high and from here arises a series of experimental difficulties.

EXPERIMENTAL

The rate of decomposition of molten azibenzil was directly followed in vacuum, recording the pressure of nitrogen evolved in the course of the reaction. The kinetics was studied at seven different temperatures in the range 80 – 102°. The experimental set-up is similar to that one described in a previous paper.[2]

---

[1] Part I, M. Contineanu, T. Oncescu and R. N. Schindler, *Rev. Roumaine Chim.*, in print (1973).

[2] M. Contineanu, T. Oncescu and R. N. Schindler, *Z. phys. Chem.* (Frankfurt), in print (1972).

The precision pressuremeter (Baratron-MKS) was part of the experimental arrangement. Using the same notation, the following volumes were determined : cell $V_c = 111.75$ cm^3 ; Inlet system $V_x = 232.11$ cm^3. It was established that the recorder deflection d (mm) was a linear function of N_2 pressure p (torr). A calibration constant of

$$p/d = \beta = 2.42 \times 10^{-2} \text{ Torr/mm}$$

was obtained for our set-up.

Applying first order treatment, straight lines were obtained when the time, at which a marked increase in N_2-production occurred was taken as start for the reaction.

The decomposition of solid azibenzil, i.e. below the melting point, was carried out at 60°, 65° and 75°, respectively. The reaction was again followed by measuring the N_2 pressure evolved with the Baratron Pressure Meter in a similar set-up as above. In this arrangement the following values for the volumes were measured :

Cell : $V_c = 102.3$ cm^3, Inlet System : $V_x = 198.55$ cm^3

In parallel experiments, spectrophotometric analyses were carried out with a Pye Unicam SP 1800 spectrophotometer. Data were obtained for the decomposition of solid azibenzil only.

After known reaction times t, the samples were suddenly cooled. Measurements were carried out in benzene solution at $\lambda = 320$ nm and $\lambda = 409$ nm, at which wavelengths the azibenzil and the diphenylketene, respectively, possess an absorption maximum.

RESULTS AND DISCUSSION

The pressure changes obtained as function of reaction time in the decomposition of azibenzil at temperatures above the melting point are given in fig. 1. Since the working temperature of the thermostat is not instantaneously reached by the sample, sigmoid shaped curves for the N_2 yield are registered in all experiments.

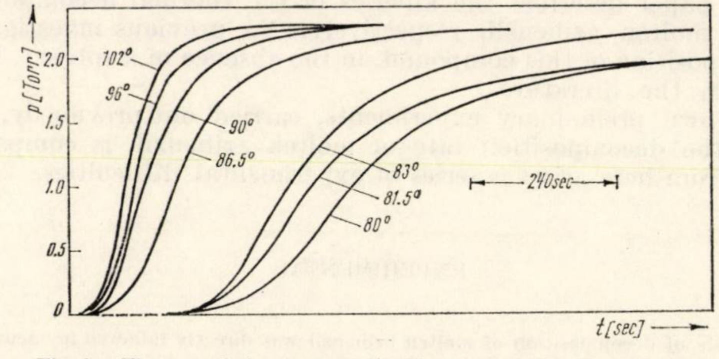

Fig. 1.—The recorded curves of the N_2 pressure function of time

We have, therefore, considered as the starting point of the reaction the moment at which a marked increase of the N_2 pressure could be noticed. The results given in figure 1 clearly demonstrate that the same plateau is reached for all temperatures. This suggests that the reaction is carried out in all experiments to total decomposition according to the equation (A) as in solution.

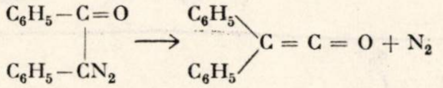

(A)

Separate experiments were undertaken to establish this assumption by quantitative determination of the total amount of N_2 formed. The same technique was applied as in a previous paper.[2] The average of the results obtained lead to 4.32×10^{-5} moles N_2, which agrees well with the theoretical value of 4.5×10^{-5} moles.

With n_{N2} and n_A describing the number of moles N_2 and azibenzil, respectively, at time t, the formation rate of N_2 is given by

$$\frac{dn_{N2}}{dt} = k_1 n_A = k_1 n_A^0 \cdot e^{-k_1 t} \tag{1}$$

where n_A^0 is the initial number of azibenzil moles. From reaction (A) we obtain $n_A^0 = n_{N2}^0$ if n_{N2}^0 is the number of N_2 moles at total decomposition of azibenzil. Integration of equation (1) yields (2)

$$k_1 = \frac{2.303}{t} \lg \frac{n_{N2}^0}{n_{N2}^0 - n_{N2}} \tag{2}$$

Since the rate of N_2—production is directly proportional to the measured deflection of the pressure meter, equation (2) can be written in the form (3)

$$k_1 = \frac{2.303}{t} \lg \frac{d_\infty}{d_\infty - d_t} \tag{3}$$

In this equation d_∞ denotes the deflection at total decomposition, i.e. at time ∞ and d_t the deflection at time t.

The registered curves given in figure 1 have been evaluated according to (3). Straight lines were obtained for all temperatures (fig. 2) showing that the evolution of N_2 follows a first order kinetics after the sample has reached thermal equilibrium.

As mentioned, a clear deviation is observed for the initial part of the reaction. As examples are given in figure 2 the temperatures 83° and 86°.

From the slope of the straight lines denoted as tg α the rate constants for the individual temperatures were calculated as follows

$$\operatorname{tg} \alpha = 1/(t_1 - t_2) \times \left(\lg \frac{d_\infty}{d_\infty - dt_1} - \lg \frac{d_\infty}{d_\infty - dt_2} \right) \tag{4}$$

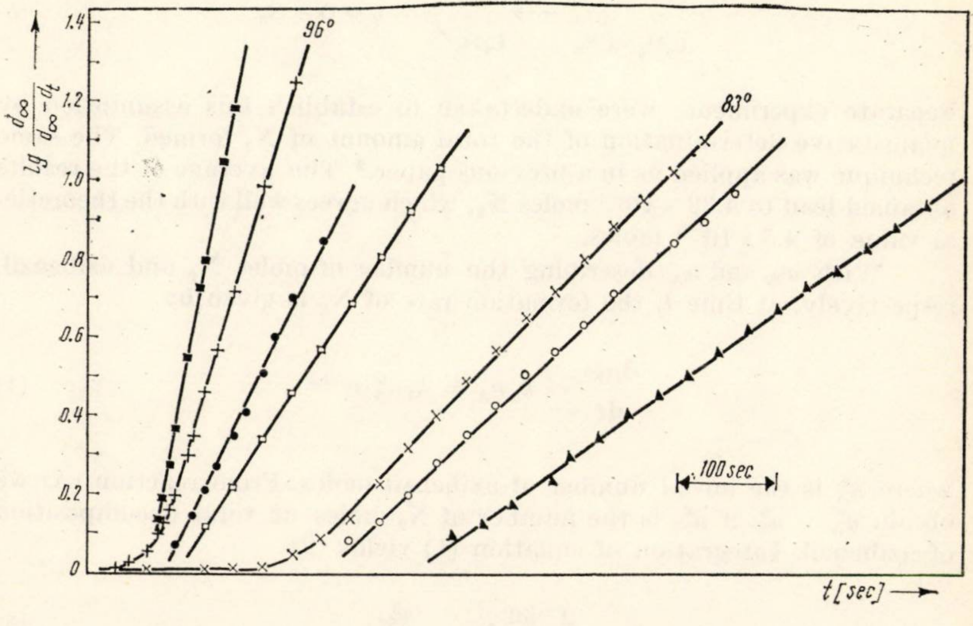

Fig. 2. — The plotting of $\lg \dfrac{d_\infty}{d_\infty - d_t}$ versus time (sec).

The rate constant k_1 is then obtained as

$$k_1 = 2.303 \operatorname{tg} \alpha \tag{5}$$

Table 1

Kinetic parameters of the azibenzil decomposition above its melting point

T	$\frac{1}{T} \times 10^3$ K^{-1}	$(\mathrm{tg}\alpha)_m \times 10^3$	$(k_1)_m \times 10^3$ sec^{-1}	$\lg A$
80	2.8329	1.85	4.24	13.65
81.5	2.8209	2.313	5.34	13.68
83	2.8089	2.62	6.02	13.85
86.5	2.7816	3.95	9.1	13.68
90	2.7549	5.53	12.74	13.69
96	2.7100	8.6	19.83	13.79

$(\lg A)_a = 13.74$

The data taken from figure 2 are summarized in table 1. The k-valnes given in the fourth column are average values from several recordings.

The preexponential factors listed in the last column show good constancy. The average value obtained is lg $A = 13.74$.

A plot of log k_1 versus $1/T$ for the decomposition of azibenzil above the melting point is given in figure 3.

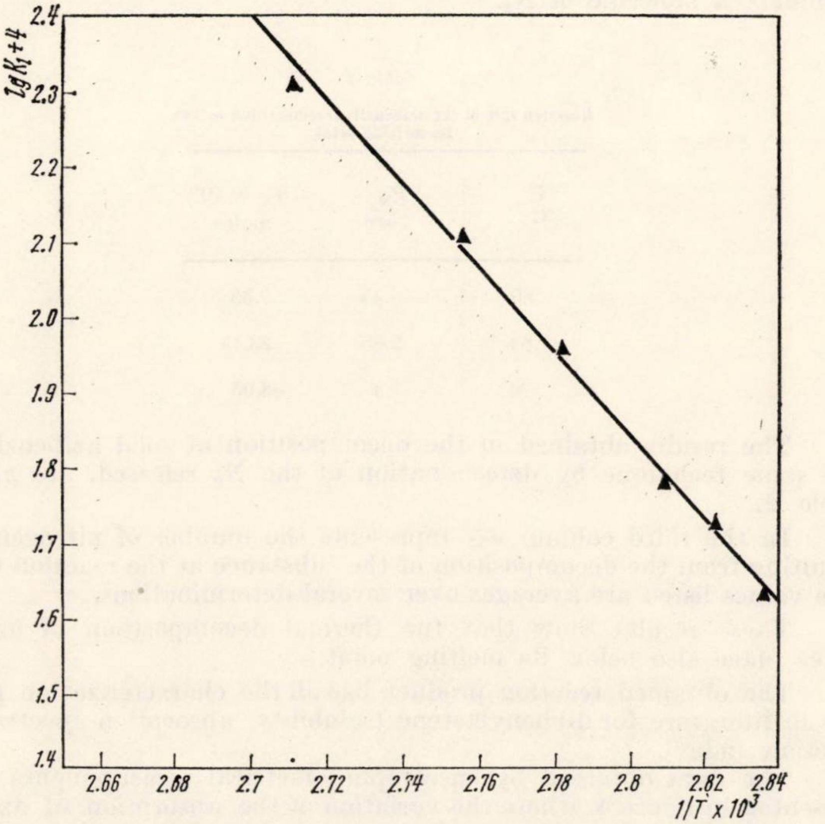

Fig. 3. – The plotting lg k_1 versus $1/T$.

An activation energy $E_A = 25.9$ kcal/mole was obtained from the slope of this line. This value is practically identical with the activation energy of azibenzil decomposition in benzene solution.[1] This result clearly indicates that benzene is an inert solvent, for the azibenzil decomposition, which does not modify the mechanism of the reaction. The activation energy refers thus to the monomolecular decomposition process.

It is of interest to speculate about the reason for the difference in the activation energy for azibenzil and diphenyldiazomethane decomposition for which compound $E_A = 22.3$ kcal/mole has been obtained.[3] The main difference between these two diazoic compounds appears to be the stabilizing effect of the carbonyl group in the azibenzil. Since the $>C=O$—electrons participate in the mesomeric system,[4] the extended charge delocalization in the parent azibenzil brings about a higher stability than in the diphenyldiazomethane. Thus, more energy is required to eliminate a molecule of N_2.

---

[3] T. Oncescu, M. Contineanu and G. Bălăceanu, *Rev. Roumaine Chim.*, **17**, 213 (1973).

Table 2

Reaction rate of the azibenzil decomposition below its melting point

T °C	P_{N_2} Torr	$n_{N_2} \times 10^6$ moles
60	0.45	7.33
65	2.85	23.15
70	5.4	88.05

The results obtained in the decomposition of solid azibenzil, with the same technique by determination of the N_2 released, are given in table 2.

In the third column n_{N_2} represents the number of nitrogen moles resulting from the decomposition of the substance at the reaction times t. The values listed are averages over several determinations.

These results show that the thermal decomposition of azibenzil takes place also below its melting point.

The obtained reaction product has all the characterization pointed out in literature for diphenylketene (solubility, absorption spectrum, refraction index).

The data obtained by spectrophotometrical measurements are represented in figure 4, where the variation of the absorption of azibenzil, at $\lambda = 320$ nm (curve 1) and of the preponderant final product diphenylketene (curve 2) at $\lambda = 409$ nm ($k_A = 103$, $k_{DK} = 270$) are plotted versus reaction time for the temperature of 60°.

Three regions can be discerned on curve I. On the first (0—120′) the absorption is kept practically constant, which shows that the substance has not decomposed. In the second region (120 — 360′), the absorption suddenly decreases, while it is again kept constant in the third region.

We must mention the fact that during the heating of the substance a change of its aggregation state is observed. On the first part the substance is solid, on the second it gets softer and on the last part it is practically in liquid state as the pure diphenylketene is.

It therefore results that the sudden decrease of the absorption and thus the decomposition of azibenzil coincides with the formation of liquid diphenylketene in this system.

---

[4] W. JUGELT and D. SCHMIDT, *Tetrahedron*, **25**, 969 (1969).

Curve 2 in figure 4 shows that the sudden decrease of the absorption at $\lambda = 320$ nm is accompanied by a sudden increase of absorption at $\lambda = 409$ nm. This proves that while the substance decomposes the diphenylketene is formed on account of the azibenzil.

In the third region the system becomes liquid due to diphenylketene, the dominant reaction product, which is liquid at that temperature.

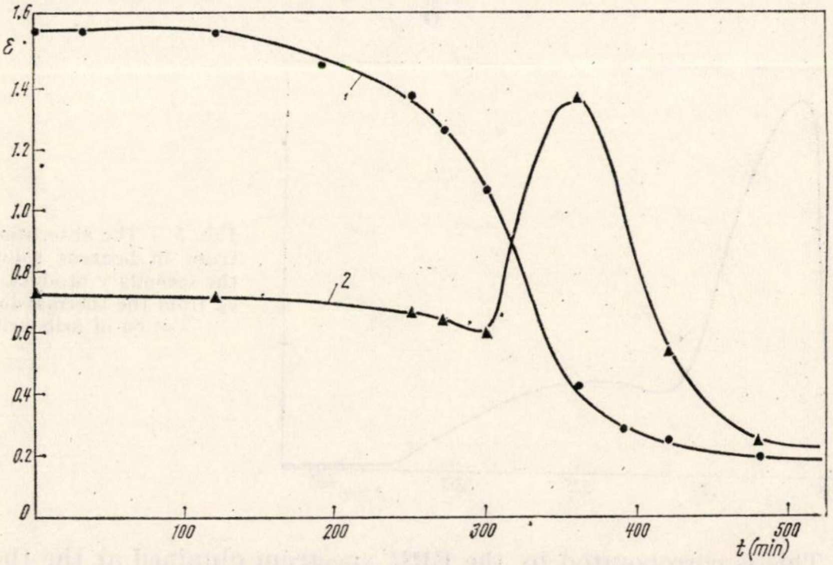

Fig. 4. – The variation of the absorption during the thermal decomposition
1 of azibenzil at $\lambda = 320$ nm
2 of diphenylketene at $\lambda = 409$ nm

In this region the absorption should have decreased to nil (if the final reaction product was only diphenylketene) as it does not absorb at $\lambda = 320$ nm, but we notice that the absorption keeps practically constant, around 0.2. This is due to the absorption of another final reaction product which appears at the same time.

Indeed, especially for low degree decomposition (room temperature), there appears, besides diphenylketene, a colourless substance. This separates from the ketene, being insoluble in hexane, and a melting point could be determined for it at 159°. The chemical analysis has lead to 82.5% C, 5.95% H, which has not allowed us to assign it an exact formula. The possibility of the presence of the corresponding ketazine is out because the nitrogen is not dosed by chemical analysis. This result is in agreement with the one obtained by Curtius. [5] The respective substance can be a dimer type one [6,7]

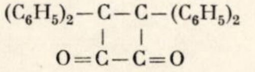

$$\begin{array}{c}(C_6H_5)_2-\underset{|}{C}-\underset{|}{C}-(C_6H_5)_2\\ O=C-C=O\end{array}$$

---

[5] Th. Curtius and H. Lang, *J. prakt. Chem.*, **44**, 544 (1891).
[6] G. Schröter, *Ber. dtsch. chem. Ges.*, **42**, 2346 (1909).
[7] H. Staudinger, *Ber. dtsch. chem. Ges.*, **40**, 1148 (1907).

or an oxygen compound of type[8] :

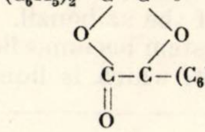

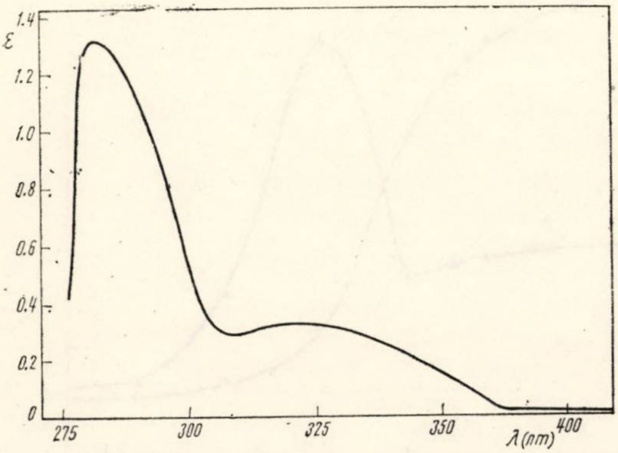

Fig. 5 – The absorption spectrum in benzene solution of the secondary product resulted from the thermal decomposition of azibenzil.

This is corroborated by the EPR spectrum obtained at the thermal decomposition of azibenzil, [9] when a signal is originated by a radical strongly influenced by the presence of O_2. This can be only the intermediate species leading towards such an oxygenated compound.

The absorption spectrum of this substance in benzene is given in figure 5, where it can be seen that it presents enough absorption at $\lambda = 320$ mm.

To conclude, we may state that from the kinetic data obtained

– only the formation of N_2 can reflect the kinetics of the unimolecular process of the azibenzil thermal decomposition;

– the diphenylketene formation, the main reaction product can not serve for this purpose, because as one can see from figure 4 (the descendent side of curve 2) it transforms chemically too :

– one can also establish that, besides diphenylketene, undoubtedly at least one more substance is formed and identified by its melting point, its absorption spectrum and its chemical analysis.

---

[8] H. Staudinger, *Liebigs Ann. Chem.*, **236**, 51 (1907).

[9] O. Constantinescu and M. Contineanu, to be published.

Revue Roumaine de Chimie, 18, 5, 761–765 (1973)

MASS SPECTRUM OF DIPHENYLDIAZOMETHANE

M. CONTINEANU, C. PODINĂ and V. CONSTANTIN

University of Bucharest, Department of
Physical Chemistry, Bd. Republicii 13, Romania

Received August 21, 1972

The mass spectrum of diphenyldiazomethane was recorded at 70 eV. The formation mechanism of the ions corresponding to the main peaks of the spectrum are proposed. The relative stability of ions *m/e*= 165 and *m/e* = 166 as function of electrons energy is discussed.

The photochemical and thermal decomposition of solid diphenyldiazomethane has been studied in former works.[1,2] In both cases a nitrogen molecule is eliminated through the absorption of thermal energy or of radiation and the diphenylcarbene appears as an intermediate species (reaction 1):

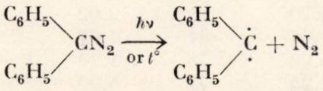

(1)

Aiming to establish the possible correlations with the thermal and photochemical decomposition we have studied the ionic species formed through electronic bombardment (much higher energies than those of the above mentioned agents) of diphenyldiazomethane. The mass spectrum of this compound was studied by Schumann and co-workers.[3] They have studied comparatively the influence of $\rangle C=Y$ ($Y= 0$, S and N_2) groups bounded in some aromatic compounds with more phenyl rings, upon the main fragmentation processes.

EXPERIMENTAL

The diphenyldiazomethane was obtained by oxidizing the corresponding hydrazone.[4] The mass spectra were recorded at room temperature by means of an M.I.1305 type mass spectrometer. The sample to be analysed was introduced and vaporized directly at the

---

[1] T. Oncescu, D. Bogdan, M. Contineanu and G. Bălăceanu, *Ber. Bunsen Ges. phys. Chem.*, **72**, 274 (1968).

[2] T. Oncescu, M. Contineanu and G. Bălăceanu *Rev. Roumaine Chim.*, **17**, 213 (1972).

[3] D. Schumann, E. Frese and A. Schönberg, *Chem, Ber.*, **102**, 3192 (1969).

[4] C. D. Nenițescu and E. Solomonica, Organic Syntheses, Coll. Vol. 2, New York, 1946, p. 496.

ion source of the device. The working parameters were as follows : emission current 1.5 mA, ionization voltage 70 V, acceleration voltage 4kV, pressure at the ion source $5 \cdot 10^{-6}$ mm Hg.

RESULTS AND DISCUSSIONS

Table 1 gives the relative intensities corresponding to ions with higher peaks than 1% of the basic peak's height ($m/e = 165$).

Table 1

Mass spectrum of diphenyldiazomethane at 70 eV

m/e	Ion abundance	*m/e*	Ion abundance	*m/e*	Ion abundance
194	0.81	113	3.07	76	2.55
182	1.56	105	4.38	75	3.28
168	1.98	99	1.09	74	4.07
167	10.95	98	1.56	65	1.67
166	62.50	89	4.17	64	1.41
165	100.00	88	2.19	63	8.71
164	13.90	87	4.69	62	4.37
163	11.00	86	3.13	53	2.31
162	1.77	83	4.38	52	1.61
152	1.25	82.5	9.36	51	8.15
140	1.25	82	6.57	50	4.68
139	9.70	81.5	3.02	39	7.20
138	1.04	81	1.67	38	1.67
115	5.63	78	1.20	28	2.08
114	1.25	77	5.00	27	2.24

The most intense ions of the spectrum are those having a 165 and 166 specific mass.

As could be expected, taking into account the strength of the C —N and N ≡ N bonds, the main primary fragmentation process of the molecular ion is the elimination of an N_2 molecule with the formation of the ion-radical $(C_6H_5)_2C^+$ according to reaction :

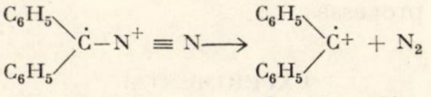

$$(C_6H_5)_2\dot{C}-N^+\equiv N \longrightarrow (C_6H_5)_2\dot{C}^+ + N_2 \qquad (2)$$

a, *m/e* = 194 **b**, *m/e* = 166

Under this aspect the phenomenon is like the thermal and photochemical decomposition.

Informations about the structure of the ion-radical $(C_6H_5)_2\dot{C}^+$ may be inferred from the E.S.R. studies on the diphenylcarbene [5–8]

---

[5] A. M. Trozzolo and W. A. Gibbons, *J. Amer. Chem. Soc.*, **89**, 239 (1967).

[6] R. M. Etter, H. S. Skovronek and P. S. Skell, *J. Amer. Chem. Soc.*, **81**, 1009 (1959).

[7] A. M. Trozzolo, *Accounts Chem. Res.*, **1968**, 329.

[8] E. Wasserman, A. M. Trozzolo and W. A. Yager, *J. Chem. Phys.*, **40**, 2408 (1964).

$(C_6H_5)_2\dot{C}$. This is a radical in triplet state in which the two phenyls are in the same plane and are placed at an approximately 140 — 150° degree one another. The odd electrons are each to be found in a *p* orbital. Taking into account the structure of the diphenylcarbene we may state that the ion-radical $(C_6H_5)_2\dot{C}^+$ is similar to it, the only difference being the inexistence of a *p* orbital.

The **b**, $m/e = 166$ ion being less stable because of the impar electron it contains, tends to stabilize through a re-setting process with the formation of a cycle of five.

The mechanism of this process is displayed according to reaction (3). One of the hydrogen atoms of α or α' positions is eliminated, while the other is transferred to the carbon atom carrying positive charges with the formation of the fluorenyl (**c**, $m/e = 165$) cation. [3]

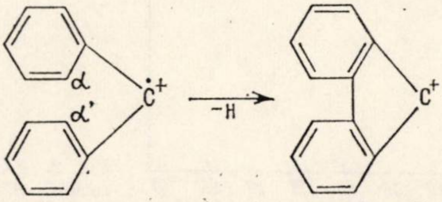

b, m/e = 166 **c**, m/e = 165 (3)

The latter, unlike the diphenylcarbene ion, does not possess an uncoupled electron and shall, therefore, have a higher stability, which explains the fact that the corresponding peak is the most intensive of the spectrum (the basic peak).

It is interesting to point out that the intensities of the $m/e = 166$ and $m/e = 165$ ions vary differentily according to the energy of the ionizing electrons.

Figure 1 gives the dependence of the ratio R, between the intensity of the $m/e = 165$ ion and that of the $m/e = 166$ ion, versus the acceleration potential of the electrons.

One notices that for higher energies than 50 eV this ratio is > 1 and maintains a practically constant value (1.7). For energies lower than 50 eV the value of this ratio decreases perceptibly becoming 1 between 29 — 30 eV, and then rapidly decreasing parallelly to the energy. This means that concomitantly to the decrease of the ionizing electrons energy, the probability of the process represented by reaction (3) also decreases considerably. Reaction (3) is, therefore, conditioned by the electronic excitation energy possessed by the diphenylcarbenic ion-radical ($m/e = 166$). When this excitation energy is small, the $m/e = 166$ ion-radical does no longer undergo the re-setting process in the fluorenyl cation. This is in agreement with the results formerly obtained by thermic and photochemical decomposition, when the energy received by the molecule is much lower than the value of the appearance potential of the ion-radical $m/e = 166$ and, therefore, only the diphenylcarbene in triplet state is formed.

The group of double charged ions from $m/e=183$ up to $m/e=81$ with a relatively high intensity proves that parallelly to the formation of the fluorenyl cation (process (3)) there also takes place an elimination of the contained odd electron, leading to the appearance of doubly charged ions. This would be one more argument in favour of the radical structure of the diphenylcarbene ion.

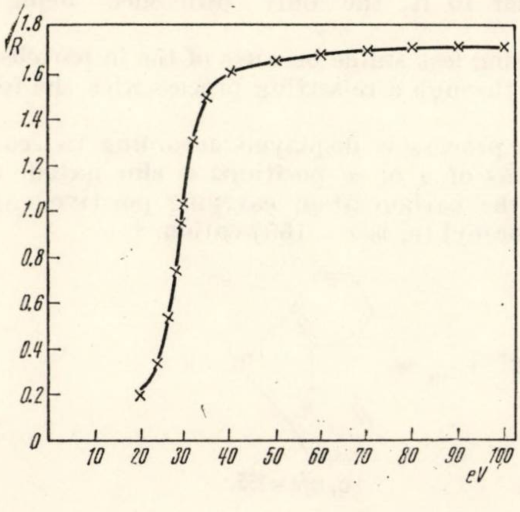

Fig. 1. — Variation of the ratio between the intensities of ions *c* and *b* versus the energy of the ionizing electrons.

Fig. 2. — Curve of the ionization efficiency of the molecular ion.

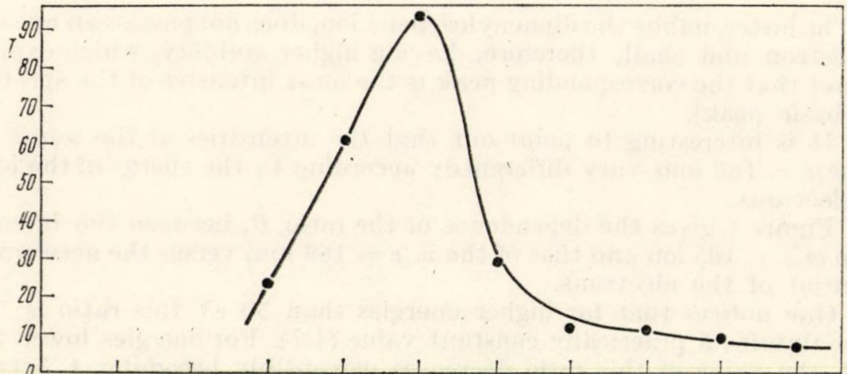

The molecular ion is to be found at $m/e = 194$ and is of small intensity (<1 %), which shows the instability of the diphenyldiazomethane molecules at electronic impact. This intensity depends on the energy of the ionizing electrons and presents a marked maximum around 50 eV (figure 2).

The peaks at $m/e = 167$ and m/e 168 are isotopic peaks of the ions with specific masses m/e 165 and m/e 166. The peaks at $m/e = 164$ and m/e 163 are evidently formed through successive hydrogen losses from m/e 165.

The ion $m/e = 139$ also results from the ion m/e 165 through the breaking of a benzenic cycle and the elimination of a neutral acetylene molecule. The process is confirmed by the existence in the spectrum of a metastable ion found at $m/e = 117.2$ (by calculation 117.1).

One also notices the existence of a group of doubly charged ions around the specific mass of 69.5, the intensity of which, compared to basic peak, is $< 1\%$ but they represent approximately 4% of the $m/e=$ 139 ion's intensity. It can be thus inferred that the $m/e = 139$ ion has also a radical structure.

The breaking up of the benzenic cycle of the $m/e = 166$ ion leads to the formation of the $m/e = 115$ and $m/e = 51$ ions. This process is justified by the existence of the metastable ion at $m/e = 79.8$ (by calculation 79.7), corresponding to the keeping of the charge on the $m/e= 115$ fragment. The structure of these ions may be represented by :

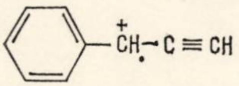

$m/e = 115$

$CH \equiv C - CH = CH^{+}$ $m/e = 51$

By comparing the intensities of the respective peaks, we may state that the repartition of the positive charge in this breaking up process takes place approximately with the same probability on both fragments.

The smaller intensity of the $m/e = 115$ ion, compared to the $m/e =$ 51 ion, is explained by the fact that it can further eliminate a neutral acetylene molecule forming the $m/e = 89$ ion. The latter can lose two and three hydrogen atoms passing into the $m/e=87$ and, respectively, $m/e=$ 86 ions.

Through the elimination of a neutral radical $C_4H_3^{\cdot}$ of the $m/e = 139$ ion, the $m/e = 88$ ion is formed. In this breaking up process, a metastable ion also appears at $m/e = 55.5$ (by calculation 55.7). By the breaking of the fluorenyl radical and elimination of $C_4H_4^{\cdot}$, the $m/e = 113$ ion is formed.

In the recorded mass spectrum there have also been rendered evident more abundent ions at $m/e < 78$, ions appearing in the spectra of aromatic hydrocarbons and evidently having their origin in the breaking up of the benzene ring.[9]

---

[9] J. H. Beynon "Mas-Spectrometria i eio primenenie v organicheskoi khimii", Izd. Mir, Moskow, 1964, p. 330 – 351.

Revue Roumaine de Chimie, **18**, *5*, 767–776 (1973)

CONTRIBUTION À L'ÉTUDE DE LA SOURCE CHIMIQUE DE COURANT $Zn/MOH/O_2$. I

L'EFFICACITÉ ÉLECTROCHIMIQUE D'UNE PILE À CATHODE ACTIVÉE AVEC DE L'ARGENT

O. RADOVICI, MARIA MAVRODIN-TĂRĂBÎC, IOANA ONACA et I. SOLACOLU
Centre de Chimie Physique, Bucarest, 31, str. Galaţi

Reçu le 12 juillet 1972

On a réalisé une source chimique de courant du type zinc-oxygène à cathode, poreuse activée avec de l'argent. Les données thermodynamiques de la réaction, ainsi que les courbes V-i, ont permis le calcul du rendement thermodynamique, électrique et total réalisé dans la conversion de l'énergie chimique en énergie électrique.

La pile du type métal-air représente une source chimique de courant, dont le rôle est de transformer directement l'énergie chimique du combustible en énergie électrique ; ce type de pile peut être considéré comme une combinaison entre une source chimique primaire classique (anode métallique) et une pile à combustible (cathode alimentée dynamiquement avec de l'oxydant). Parmi les piles métal-air ce sont surtout les sources chimiques Zn/électrolyte alcalin /O_2 (air) [1,2] qui se remarquent par leur efficacité.

La réaction chimique se trouvant à la base de l'obtention du courant électrique est l'électrooxydation du zinc en milieu alcalin concentré, ayant pour résultat la formation de l'ion $Zn(OH)_4^{2-}$. [3,4]

Tout comme dans le cas des piles à combustible, la rendement de la conversion de l'énergie chimique en énergie électrique réalisé dans les piles du type métal-air est élevé et nettement supérieur aux rendements réalisés dans le cas des machines thermiques classiques, ce qui démontre que ce type de sources chimiques de courant représente un procédé avantageux pour l'obtention de l'énergie électrique. Le rendement de la conversion de l'énergie dépend tant du rendement thermodynamique de la

---

[1] M. Eisenberg, « Physical Chemistry, vol. IXB, Electrochemistry ». Academic Press, New York, 1970, p. 777.

[2] O. Radovici, M. Mavrodin-Tărăbîc, I. Onaca et I. Solacolu, *Studii şi Cercetări Chim. Acad. Bucureşti* **21**, 37 (1973).

[3] J. P. G. Farr et N. A. Hampson, *J. Electroanalyt. Chem.*, **13**, 433 (1967).

[4] H. Landsberg, *Z. phys. Chem. (Leipzig)*, **206**, 291 (1957).

réaction chimique qui est à la base de l'obtention du courant électrique dans les conditions pratiques de fonctionnement, que du rendement électrique de la pile, dont la valeur varie selon la grandeur des pertes énergétiques irréversibles (polarisation de transfert de charge, de concentration et de résistance ohmique, pertes ohmiques dans les conducteurs).[5]

Etant donné que les applications pratiques des sources chimiques du type métal-air sont limitées aux domaines où elles ne sont pas concurrencées par le prix de revient relativement réduit de l'énergie électrique obtenue par les procédés classiques et que le rendement de la conversion de l'énergie constitue une caractéristique déterminante de la grandeur du prix de revient de l'énergie électrique, les études concernant l'amélioration du rendement énergétique de ces sources de courant présentent un intérêt considérable.

Dans ce travail nous nous sommes proposé de réaliser une étude détaillée du rendement thermodynamique et électrique d'une pile zinc-oxygène que nous avons construite dans notre laboratoire, et d'établir la valeur du rendement d'une telle source chimique de courant dans les conditions de l'obtention, en circuit ouvert, d'une puissance maximale.

PARTIE EXPÉRIMENTALE

1. LA RÉALISATION DE LA SOURCE CHIMIQUE DU TYPE MÉTAL-AIR

On a réalisé, dans notre laboratoire, une pile métal-air, du type :

(−) $Zn/KOH\ 5\ N/O_2(Ag)$ (+)

Pour la réalisation de cette pile on a utilisé :

— une anode de zinc (pureté 99,9 %),

— une cathode — électrode à gaz du type DSK (« Doppel Skelet Katalyst ») avec une porosité globale de 45 %, activée avec de l'argent, obtenue et caractérisée, ainsi que nous l'avons montré dans un travail antérieur,[6]

— un électrolyte KOH *p.a.* 5 N,

— un dépolariseur cathodique — oxygène, à des surpressions de 300 et de 400 mm Hg.

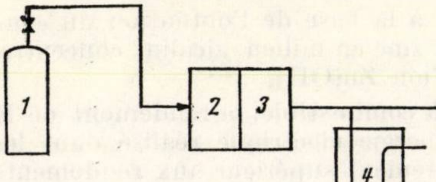

Fig. 1. — Schéma de l'installation pour l'alimentation avec de l'oxygène, à surpression constante, de la cathode de la pile zinc-oxygène.

1, bouteille à oxygène, *2*, réducteur, *3*, réducteur de réglage fin, *4*, manomètre à mercure, *5*, vers la cathode de la pile.

L'alimentation de la cathode avec de l'oxygène, à surpression constante, a été réalisée à l'aide de l'installation représentée dans la figure 1. La température de travail a été d'environ 25° et la cellule, ayant les dimensions 120 × 72 × 56 mm, a été confectionnée en polystyrène.

---

[5] M. Mavrodin-Tărăbîc, I. Onaca et I. Solacolu, *Studii şi Cercetări Chim. Acad. Bucureşti* **21**, 335 (1973).

[6] O. Radovici, M. Mavrodin-Tărăbîc, I. Onaca et I. Solacolu, *Rev. Roumaine Chim.*, **17**, 1153 (1972).

2. LES MESURES ÉLECTRIQUES

En vue de déterminer les courbes de décharge V-i de la pile zinc-oxygène réalisée dans notre laboratoire, à différentes surpressions de l'oxygène, la source chimique de courant a été déchargée, tout en variant la résistance, dans le montage représenté dans la figure 2, en utilisant un millivoltmètre électronique Radiometer 22 (précision ± 1 mV), un milliampèremètre de classe 0,5, une boîte à résistances (précision ± 0,1 Ω).

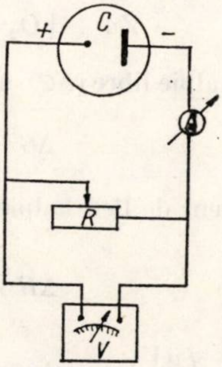

Fig. 2. — Schéma du montage utilisé pour la décharge de la pile zinc-oxygène.

C — la cellule, *A* — milliampèremètre, *V* — millivoltmètre électronique, *R* — résistance décadique.

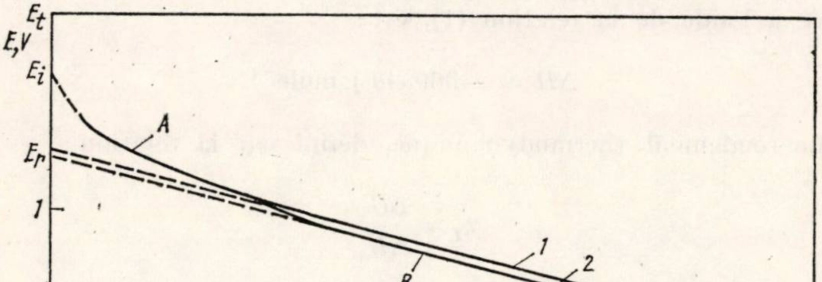

Fig. 3. — Les courbes de décharge de la pile zinc-oxygène.
1 — ΔP_{O_2} = 400 mm Hg, 2 — ΔP_{O_2} = 300 mm Hg.

Les courbes V-i, obtenues pour la pile zinc-oxygène réalisée dans notre laboratoire, sont représentées dans la figure 3.

LE CALCUL DU RENDEMENT DE LA CONVERSION DE L'ÉNERGIE

1. LE RENDEMENT THERMODYNAMIQUE

La réaction chimique caractéristique pour la production du courant dans la pile zinc-oxygène est :

$$\mathrm{Zn} + \tfrac{1}{2}\,\mathrm{O_2} + 2\mathrm{OH^-} \rightarrow \mathrm{ZnO_2^{2-}} + \mathrm{H_2O}$$

L'enthalpie libre (ΔG), à la température de 25°,a, dans cette réaction, la valeur

$$\Delta G = -311410 \text{ j. mole}^{-1}$$

La valeur de l'enthalpie (ΔH) peut être calculée à l'aide de la relation :

$$\Delta H = \Delta G + zF\,T\left(\frac{\partial V}{\partial T}\right)_p \qquad (1)$$

dans laquelle $\left(\frac{\partial V}{\partial T}\right)_p$ représente le coefficient de température de la tension électrique, dont la valeur, pour la réaction analogue $\mathrm{Zn} + 2\mathrm{OH^-} \rightarrow \mathrm{Zn(OH)_2} + 2\mathrm{e^-}$ est de $-1{,}002.10^{-3}$ V. deg.$^{-1}$; la même valeur peut être utilisée, avec une bonne approximation, dans le cas de la pile zinc-oxygène, réalisée dans notre laboratoire. La valeur de l'enthalpie, calculée à l'aide de la relation (1), est :

$$\Delta H = -369040 \text{ j. mole}^{-1}$$

Le rendement thermodynamique, défini par la relation :

$$\eta_T = \frac{\Delta G}{\Delta H} \qquad (2)$$

est de 0,8439 pour la réaction chimique caractéristique à la pile zinc-oxygène, à une température de 25°.

2. LE RENDEMENT ÉLECTRIQUE

Les courbes de décharge V-i, représentées dans la figure 3, offrent une image des phénomènes qui ont lieu pendant le fonctionnement de la pile zinc-oxygène ; l'analyse de ces courbes permet de tirer une série de conclusions intéressantes concernant le rendement de la conversion de l'énergie chimique en énergie électrique. On peut distinguer sur les courbes V-i trois zones :

— *la zone A*, des courants faibles, dans laquelle la courbe V-i présente un décroissement non linéaire, la tangente de la courbe ayant la pente ($-r$),

— *la zone B*, qui présente de l'intérêt pour l'exploitation, dans laquelle la courbe de décharge manifeste un décroissement, généralement linéaire, sa tangente ayant la pente égale à (—R), et

— *la zone C*, des courants à grande intensité, dans laquelle la tension électrique de la pile décroît brusquement avec l'augmentation de l'intensité du courant, zone qui n'intéresse pas l'exploitation.

Sur l'ordonnée des courbes V-i (fig. 3) on peut distinguer les valeurs suivantes de la tension électrique :

— *la tension électrique totale*, E_t, obtenue par l'addition des potentiels des électrodes qui constituent la pile,

— *la tension électrique idéale*, E_i, l'ordonnée à l'origine de la zone *A* des courbes de décharge, tension électrique que l'on obtient lorsque l'intensité du courant est égale à zero, et

— *le tension électrique réelle*, E_r, l'ordonnée à l'origine de la zone *B* des courbes de décharge, tension électrique maximale qui peut être obtenue dans les conditions d'exploitation de la pile.

Entre ces tensions, pendant l'exploitation, s'établissent les pertes suivantes :

— *la perte thermodynamique*, $\Delta E_u = E_t - E_i$, résultée de la transformation incomplète de l'énergie chimique en énergie électrique dans les conditions de fonctionnement (pression, température) de la pile, et

— *la perte électrique*, $\Delta E_p = E_i - E_r$, résultée de l'apparition des phénomènes de polarisation survenus pendant le fonctionnement de la pile.

Entre les données thermodynamiques de la réaction caractéristique pour la production du courant dans la pile zinc-oxygène et ses caractéristiques électriques, il y a les relations suivantes :

$$E_t = -\frac{\Delta H}{zF} \tag{3}$$

$$E_i = -\frac{\Delta G}{zF} \tag{4}$$

$$E_u = E_t - E_i = \frac{\Delta H - \Delta G}{zF} = -\frac{T\Delta S}{zF} \tag{5}$$

Les valeurs calculées pour E_t, E_i et ΔE_u, dans le cas de la pile zinc-oxygène, sont respectivement 1,912, 1,614 et 0,298 V.

On peut définir un facteur thermodynamique (ν) :

$$\nu = \frac{\Delta E_u}{E_t} = \frac{T\Delta S}{\Delta H} \tag{6}$$

qui, dans le cas de la pile zinc-oxygène, a la valeur de 0,1561. Entre ce facteur thermodynamique, le rendement thermodynamique (2) et les tensions électriques E_i et E_t il y a la relation :

$$\eta_T = 1 - \nu = \frac{E_i}{E_t} \tag{7}$$

Dans la zone B des courbes de décharge, zone qui intéresse l'exploitation, la tension varie linéairement en fonction de l'intensité du courant, la pente de cette droite ayant la valeur $(-R)$; l'ordonnée à l'origine (E_r) — la tension électrique en circuit ouvert — dans certaines conditions de pression et de température, lorsque l'intensité du courant tend à zéro — est :

$$E_r = E_i - \Delta E_p \tag{8}$$

et a la valeur de 1,285 V et de 1,260 V, à des surpressions de l'oxygène de 400 et, respectivement, de 300 mm Hg.

De l'équation (8) on peut calculer la perte électrique (ΔE_p), dont la valeur est de 0,329 V et, respectivement, de 0,354 V, dans les conditions mentionnées ci-dessus.

On peut définir un facteur de polarisation (μ) :

$$\mu = \frac{\Delta E_p}{E_i} \tag{9}$$

qui a les valeurs de 0,2037 et, respectivement, de 0,2193.

Le rendement électrique maximal $(\varepsilon_{\max})$ de la pile zinc-oxygène, lorsque l'intensité du courant tend à zéro, est :

$$\varepsilon_{\max} = \frac{E_r}{E_i} = \frac{E_i - \Delta E_p}{E_i} = 1 - \mu \tag{10}$$

et a la valeur de 0,7963 et, respectivement, de 0,7807.

L'intensité maximale du courant produit par la pile — l'abscisse à l'origine de la zone B des courbes de décharge représentées dans la figure 3 — est :

$$I_{\max} = (1 - \mu)\frac{E_i}{R} \tag{11}$$

dans laquelle R représente la pente de la zone B des courbes (fig. 3) et a la valeur de 2,2. Les valeurs de l'intensité maximale des courants produits par la pile réalisée dans notre laboratoire sont de 0,5842 A/cm^2 et de 0,5728 A/cm^2 (rapportées à la surface géométrique de la cathode poreuse), dans le cas de la surpression de l'oxygène de 400 et, respectivement, de 300 mm Hg.

Dans les conditions réelles d'exploitation, on peut considérer, avec une bonne approximation, que l'on obtient un courant :

$$I_{\text{moyen}} = \tfrac{1}{2} I_{\max} \tag{12}$$

qui a la valeur de 0,2921 A/cm² et, respectivement, de 0,2864 A/cm² et, la pile présente un rendement électrique moyen :

$$\varepsilon_{\text{moyen}} = \tfrac{1}{2} \varepsilon_{\max} = \tfrac{1}{2}(1 - \mu) \tag{13}$$

dont la valeur est de 0,3982 et, respectivement, de 0,3904.

Dans les conditions de fonctionnement, la puissance électrique maximale qui peut être fournie dans le circuit extérieur, peut être calculée à l'aide de la relation :

$$P_{\max} = I^2_{\text{moyen}} R = \tfrac{1}{4}(1 - \mu)^2 \frac{E_i^2}{R} \tag{14}$$

et a la valeur de 0,1877 w/cm² et, respectivement, de 0,1805 w/cm².

La tension électrique (E) fournie par la pile zinc-oxygène réalisée dans notre laboratoire, dans les conditions définies par la zone B des courbes (fig. 3), est :

$$E = E_t - \Delta E_u - \Delta E_p - RI \tag{15}$$

dans laquelle E_t représente la tension électrique totale définie par l'équation (3), ΔE_u—la perte de potentiel entropique définie par l'équation (5) et ΔE_p — les pertes par polarisation.

Si l'on définit un coefficient σ qui exprime les pertes par polarisation :

$$\sigma = \frac{\Delta E_p}{E_t} \tag{16}$$

dont la valeur est de 0,172 et, respectivement, de 0,185, pour la pile réalisée dans notre laboratoire ; la valeur du rendement de la conversion de l'énergie chimique en énergie électrique peut être calculée à l'aide de la relation :

$$\eta = \frac{E}{E_t} = 1 - \nu - \sigma - \frac{RI}{E_t} \tag{17}$$

et présente une valeur maximale lorsque l'intensité du courant produit est égale à zéro[5] :

$$\eta_{\max} = 1 - \nu - \sigma = (1 - \nu)(1 - \mu) \tag{18}$$

La valeur du rendement maximal de la conversion de l'énergie dans la pile zinc-oxygène construite dans notre laboratoire est de 0,6719 et de 0,6589, pour des surpressions de l'oxygène de 400 et, respectivement, de 300 mm Hg.

Le rendement de la conversion de l'énergie chimique en énergie électrique est égal au produit obtenu par la multiplication du rendement thermodynamique de la réaction chimique avec le rendement électrique, dans les conditions de fonctionnement :

$$\eta = \eta_T \cdot \varepsilon \tag{19}$$

LE RENDEMENT DE LA CONVERSION DE L'ÉNERGIE DANS LES CONDITIONS DE L'OBTENTION D'UNE PUISSANCE MAXIMALE DANS LE CIRCUIT EXTÉRIEUR

Le décroissement des performances de la pile — effet des polarisations qui apparaissent pendant le fonctionnement de la pile—se manifeste par l'obtention, dans le circuit extérieur, d'un courant réduit par un facteur i :

$$i = \frac{R}{E_i} I \tag{20}$$

relation dans laquelle I est $I_{\max}$ de l'équation (11) lorsque $\mu = 0$. Pour la pile construite dans notre laboratoire, ce facteur de réduction de l'intensité a les valeurs de 0,40 et de 0,39, pour des surpressions de l'oxygène de 400 et, respectivement, de 300 mm Hg.

A ce facteur de réduction du courant correspond un facteur de réduction de la puissance p :

$$p = \frac{4R}{E_i^2} P \tag{21}$$

relation dans laquelle P est $P_{\max}$ de l'équation (14), pour $\mu = 0$.

Entre les facteurs p et i il y a la relation [5] :

$$p = 4i(1 - \mu - i) \tag{22}$$

qui démontre que p est une fonction parabolique de i.

La représentation graphique de cette fonction (fig. 4) nous montre que la valeur minimale du facteur de puissance ($p = 0$) s'enregistre pour les valeurs $i = 0$ et $i_{\max} = 1 - \mu$. La valeur maximale du facteur de puissance ($p_{\max}$), correspondant à la puissance maximale dans le circuit extérieur, est :

$$p_{\max} = (1 - \mu)^2 \tag{23}$$

et a les valeurs de 0,634 et, respectivement, de 0,610 pour la pile zinc-oxygène construite dans notre laboratoire. A ce facteur de puissance ($p_{\max}$) correspond un i moyen :

$$i_{\text{moyen}} = \tfrac{1}{2}(1 - \mu) = \tfrac{1}{2} i_{\max} \tag{24}$$

qui a les valeurs calculées par la relation (20).

Tableau

Caractéristiques thermodynamiques et électriques de la pile

Pile du type	ΔH	ΔG	$T\Delta S$	$E_t = -\frac{\Delta H}{zF}$	$\Delta E_u = -\frac{T\Delta S}{zF}$	$E_i = -\frac{\Delta G}{zF}$
	j. mole^{-1}	j. mole^{-1}	j. mole^{-1}	V	V	V
1. zinc-oxygène (ΔP_{O_2}=400 mm Hg)	−369040	−311410	−57630	1,912	0,298	1,614
2. zinc-oxygène (ΔP_{O_2}=300 mm Hg)						

Dans les conditions de fonctionnement, la pile zinc-oxygène fournira une tension électrique (E), dont l'expression est représentée par l'équation (15) et a les valeurs de 0,642 V et, respectivement, de 0,630 V.

Etant donné les pertes par polarisation, le rendement réel de la conversion de l'énergie réalisé dans la pile construite dans notre laboratoire, dans les conditions de fonctionnement, peut être calculé à l'aide de la relation :

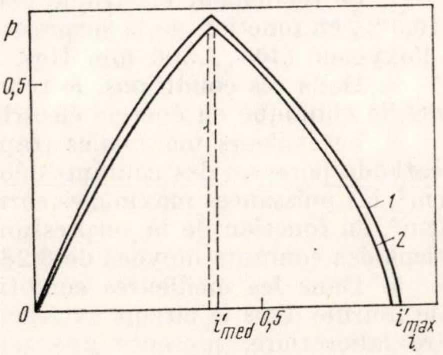

Fig. 4. — La représentation graphique de la fonction parabolique $p = (f)i$ pour la pile zinc-oxygène.
1 – $\Delta P_{O_2} = 400$ mm Hg, 2 – $\Delta P_{O_2} = 300$ mm Hg.

$$\eta_{\text{réel}} = (1 - \nu)(1 - \mu - i) \tag{25}$$

et a les valeurs de 0,3355 et de 0,3298, pour les surpressions de l'oxygène de 400 et, respectivement, de 300 mm Hg.

Le rendement élevé de la conversion de l'énergie chimique réalisé dans la pile zinc-oxygène construite dans notre laboratoire est comparable aux données de la littérature de spécialité pour les piles à combustible et est supérieur au rendement de la conversion de l'énergie réalisée dans les sources classiques de courant.

Les données thermodynamiques et électriques qui caractérisent la pile zinc-oxygène construite dans notre laboratoire sont présentées dans le tableau 1.

du type zinc-oxygène, à une température de 25°

E_r	$\Delta E_p = E_i - E_r$	$\nu = \frac{\Delta E_u}{E_t}$	$\eta_T = 1 - \nu$	$\mu = \frac{\Delta E_p}{E_i}$	$\varepsilon = 1 - \mu$	$\sigma = \frac{\Delta E_p}{E_t}$	$\eta_{\max} = \eta_T \cdot \varepsilon$	$\eta_{\text{réel}} = (1-\nu)(1-\mu-i)$
V	V	—	—	—	—	—	—	—
1,285	0,329	0,1561	0,8439	0,2037	0,7963	0,172	0,6719	0,3355
1,260	0,354			0,2139	0,7807	0,185	0,6589	0,3298

CONCLUSIONS

1. Le rendement thermodynamique de la pile du type zinc-oxygène, construite dans notre laboratoire, à cathode poreuse du type DSK activée avec de l'argent, est de 84,39%.

2. Le rendement électrique maximal de la pile est compris entre 78 et 79,6%, en fonction de la surpression d'alimentation de la cathode avec de l'oxygène (400...300 mm Hg).

3. Dans ces conditions, le rendement maximal de la conversion de l'énergie chimique en énergie électrique est compris entre 66 et 67%.

4. Les valeurs maximales (rapportées à la surface géométrique de la cathode poreuse) des courants débités sont comprises entre 0,57 et 0,58 A/cm², les puissances maximales correspondantes étant de 0,18 et de 0,19 W/cm², en fonction de la surpression de l'oxygène. Dans la pratique, on obtient des courants moyens de 0,28 et de 0,30 A/cm².

5. Dans les meilleures conditions d'exploitation (puissance maximale fournie dans le circuit extérieur), la pile zinc-oxygène réalisée dans notre laboratoire, présente une tension électrique de 0,63...0,64 V. Dans ces conditions, le rendement électrique présente la valeur de 40% et la pile zinc-oxygène réalise une conversion de l'énergie chimique en énergie électrique avec un rendement de 33...34%.

Revue Roumaine de Chimie, 18, 5, 777 – 787 (1973)

SIMPLE HMO-CALCULATIONS ON SOME N-HETEROCYCLIC LIGANDS OF ANALYTICAL IMPORTANCE*

SHYAMA P. SINHA

Department of Chemistry, University of Malaya
Kuala Lumpur, Malaysia

Received September 7, 1972

Simple Hückel Molecular Orbital calculations were performed on a number of N-heterocyclic ligands of analytical importance, i.e., six isomeric dipyridyls and three phenylpyridines. The effect of variation of α_N on the first $\pi \rightarrow \pi^*$ transition energy has been investigated. The best value of h_N for each compound was obtained by comparing the observed transition energy (ν_{obs}) of the compound with that calculated (ν_{calc}) by assuming various values of h_N. A linear correlation between ν_{obs} and ν_{calc} was obtained.

The dipyridyls, in particular, the 2,2′-isomer form complexes with a variety of metal ions.[1–3] The analytical uses of 2,2′-dipyridyl and its derivatives are well known.[4] We are currently investigating the 1,10-phenanthroline and dipyridyl complexes of the lanthanides by NMR spectroscopy.[5] We have observed high field shift of all protons of phenanthroline and both high and low field shifts for 2,2′-dipyridyl[6] due to complexation of these ligands with lanthanide ions. In an attempt to understand these shifts, it is thought that an analysis of the charge density on various atoms of the ligand might be useful. Often the chemical shifts of protons can be correlated to the charge densities on the carbon atoms to which they are bounded.[7] With this in mind we started simple Hückel MO-calculations on the six isomeric dipyridyls and the related phenylpyridines (Fig. 1).

---

* Presented at the 3rd National Conference of Pure and Applied Physical Chemistry organized by the Ministry of Education and the Center of Physical Chemistry, University of Bucharest, Romania, September 4 – 7 (1972).

[1] W. W. Brandt, F. P. Dwyer and E. C. Gyarfas, *Chem. Rev.*, *54*, 959 (1954).

[2] S. P. Sinha, "Complexes of the Rare Earths", Pergamon Press, Oxford, 1966.

[3] S. P. Sinha, *Z. Chem.*, *4* 150(1964) ; *Indian J. Chem.*, *8*, 82 (1970).

[4] A. A. Schilt, "Analytical Applications of 1,10-Phenanthroline and Related Compounds", Pergamon Press, Oxford, 1969.

[5] S. P. Sinha and R. D. Green, *Spectrosc. Letters*, *4*, 399 (1971).

[6] S. P. Sinha, to be published.

[7] H. Rosenberger, M. Pettig, K. Madeja, G. Engelhardt and R. Radeglia, *Ber. Bunsengesell. phys. Chem.*, **73**, 662 (1969).

ISOMERIC DIPYRIDYLS

Like biphenyl, all isomeric dipyridyls present a 12 π-electron system, each N-atom like the CH-group contributing one π-electron to the aromatic ring. In the HMO method, the heteroatoms (here nitrogen) may be treated by appropriate change in the empirical α and β parameters associated with each atom and bound in the secular determinant $|H_{ij} - S_{ij}| = 0$ as:

$$\alpha_N = \alpha_0 + h_N\beta_0 \tag{1}$$

and

$$\beta_{CN} = k_{CN}\beta_0 \tag{2}$$

where α_0 and β_0 are the Coulomb integrals and the resonance integrals of (usually) benzene, respectively, and the other symbols have their usual meaning. It remains now to choose the values of h_N and k_{CN} and solve the secular determinant for energies and orbital coefficients and to calculate the charge densities bond order etc.

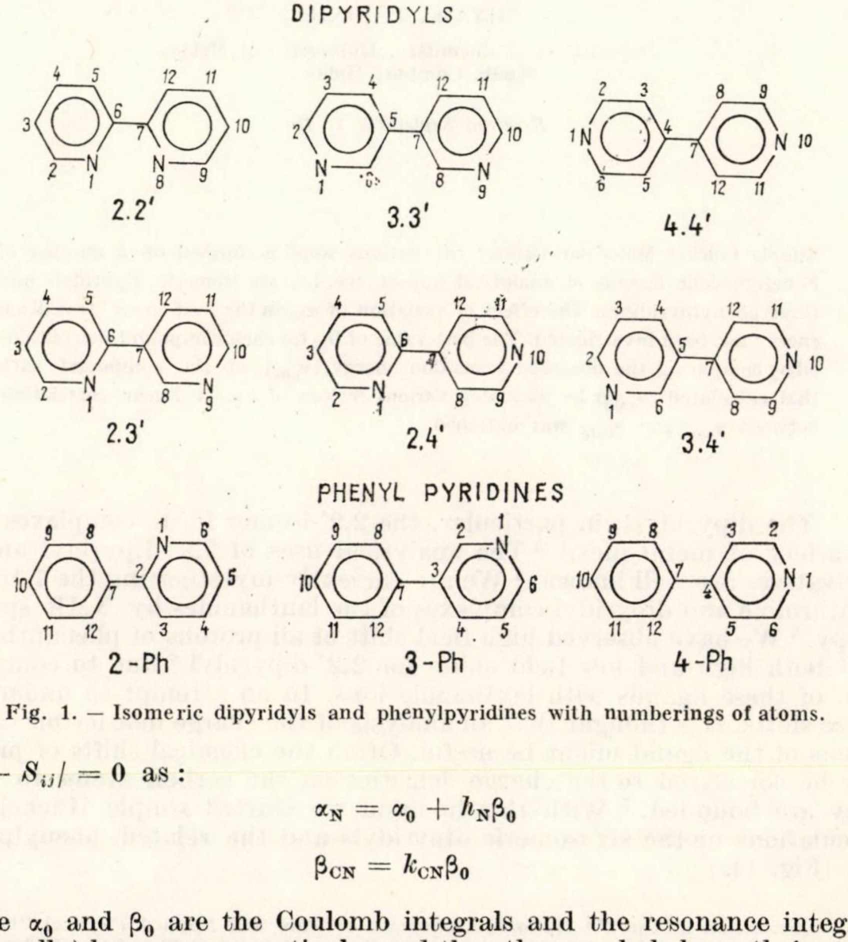

Fig. 1. — Isomeric dipyridyls and phenylpyridines with numberings of atoms.

The values of the parameters h_N and k_{CN} are usually assigned as "inteligent guesses" from studies on variety of similar compounds. It is commonly assumed that the value of k_{CN} is 1 or very near to 1 and the calculated charge distribution is rather insensitive to small variation in this parameter.[7] Throughout this study we have used $k_{CN} = 1$.

A survey of the parameter h_N, however, shows a wide variation of the values adopted for various compounds by various authors. Brown and coworkers[8-10] prefer to use $h_N = 0.5$ (for N contributing a core charge of $+1$) and $h_N = 2.0$ (for N contributing a core charge of $+2$) for neutral and protonated pyridine systems, while Mason[11] obtained good correlation by using $h_N = 0.6$. Yet, other values of h_N ranging between 0.9 and 1.2 have been used by other authors.[12-14]

Table 1

The calculated $\pi \to \pi^*$ transition energies from the highest occupied orbital (HOO) to the lowest unoccupied orbital (LUO) for the isomeric dipyridyls for a set of h_N values

h_N	2,2′	3,3′	4,4′	2,3′	2,4′	3,4′
0.1	1.4064	1.4085	1.4093	1.4077	1.4075	1.4086
0.2	1.3985	1.4068	1.4097	1.4034	1.4027	1.4070
0.3	1.3865	1.4036	1.4101	1.3964	1.3949	1.4043
0.4	1.3697	1.3993	1.4107	1.3871	1.3844	1.4007
0.5	1.3503	1.3935	1.4115	1.3769	1.3719	1.3962
0.6	1.3288	1.3862	1.4123	1.3631	1.3576	1.3908
0.7	1.3059	1.3776	1.4130	1.3491	1.3491	1.3848
0.8	1.2822	1.3675	1.4136	1.3344	1.3252	1.3782
0.9	1.2581	1.3562	1.4139	1.3192	1.3082	1.3710
1.0	1.2341	1.3440	1.4142	1.3039	1.2906	1.3634
1.2	1.1872	1.3174	1.3661	1.2734	1.2558	1.3477
1.4	1.1426	1.2893	1.3219	1.2441	1.2217	1.3315
1.5	1.1216	1.2754	1.3012	1.2302	1.2054	1.3233
1.6	1.1013	1.2651	1.2814	1.2168	1.1895	1.3153
1.8	1.0634	1.2345	1.2444	1.1913	1.1594	1.2995
2.0	1.0289	1.2089	1.2107	1.1680	1.1314	1.2845

All energies are in terms of β-units. The HOO → LUO transition in biphenyl has been calculated to be 1.4092 β, and $\nu_{obs} = 40000\ cm^{-1}$.

The first objective of our study was to determine the best value of the parameter h_N for the dipyridyl systems and to see if there exists a unique value of the parameter for all isomeric dipyridyls.

The orbital coefficients, energies, electron densities and bond orders for all six isomeric dipyridyls were calculated[15] for a wide range of values (0.1 — 2.0) of the parameter h_N. In Table 1, the calculated energies for the first $\pi \to \pi^*$ transition from the highest occupied orbital (HOO) to the lowest unoccupied orbital (LUO) for a set of h_N values are presented,

---

[8] R. D. Brown and R. D. Harcourt, *J. Chem. Soc.*, **1959**, 3451.

[9] R. D. Brown and A. Penfold, *Trans Faraday Soc.*, *53*, 397 (1957).

[10] R. D. Brown and M. L. Hefferman, *Austral. J. Chem.*, *10*, 211 (1957) and *ibid.*, *12* 319 (1959).

[11] S. F. Mason, *J. Chem. Soc.*, *1958*, 674.

[12] F. A. Matsen, *J. Amer. Chem. Soc.*, *72*, 5243 (1950).

[13] J. N. Murrell, *Mol. Phys.*, *1*, 384 (1958).

[14] D. Peters, *J. Chem. Soc.*, *1957*, 1993.

[15] The program used is an adaptation of the MO calculation (K.B. Wiberg, "Physical Organic Chemistry", Wiley, 1964, p. 577). All calculations were carried out in an IBM 1130 computer.

and these data are plotted in Fig. 2. Except for the case of 4,4′-isomer, the calculated transition energy is a monotonic function of the parameter h_N (Fig. 2). At lower values of h_N, the transition energies approached (Fig. 2) that of biphenyl (1.4092β).

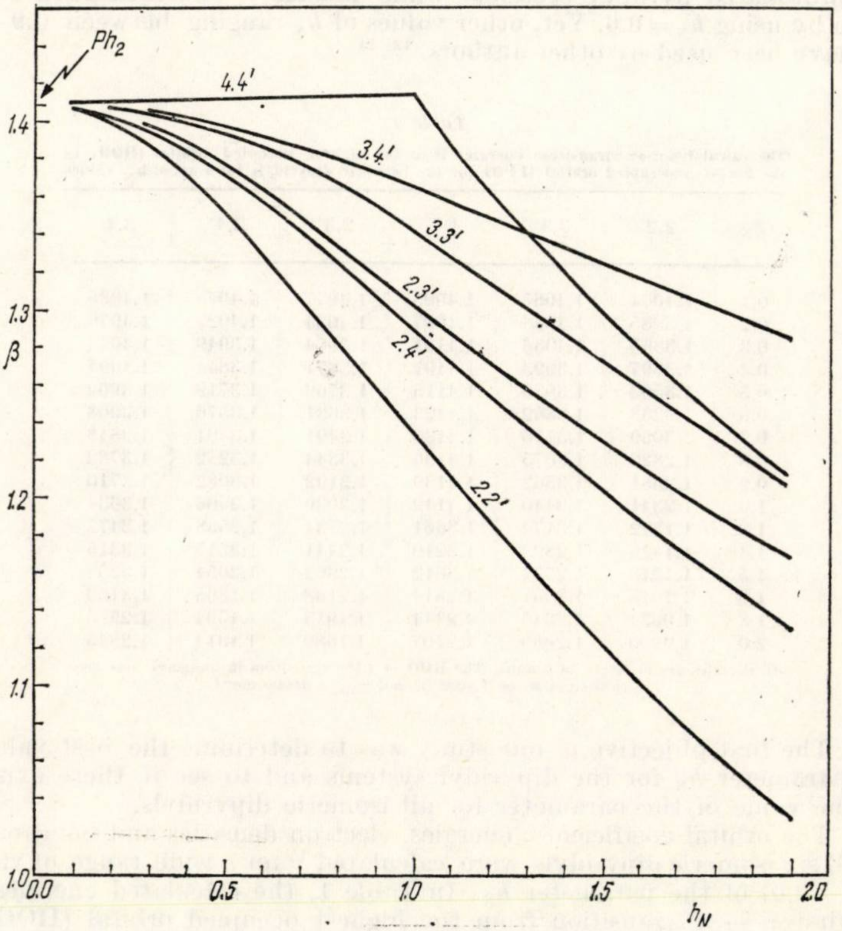

Fig. 2. — The variation of the calculated HOO → LUO energies with h_N.

Studies on aromatic hydrocarbons show [16] a good linear correlation between the observed first π→π* transition energy and the calculated HMO energy difference (E in β units between HOO and LUO :

$$\nu_{obs}\,(\mathrm{cm}^{-1}) = 19020\ (E\beta) + 10520 \qquad (3)$$

At least for one heterocyclic ligand [17] (i.e. 8-hydroxyquinoline) this equation was assumed to be valid. A correlation of the experimentally

---

[16] A. Streitwieser, "Molecular Orbital Theory", Wiley, New York, 1961, Chapter 8, pp. 217.

[17] R. E. Burton and W. J. Davis, *J. Chem. Soc., 1964*, 1766.

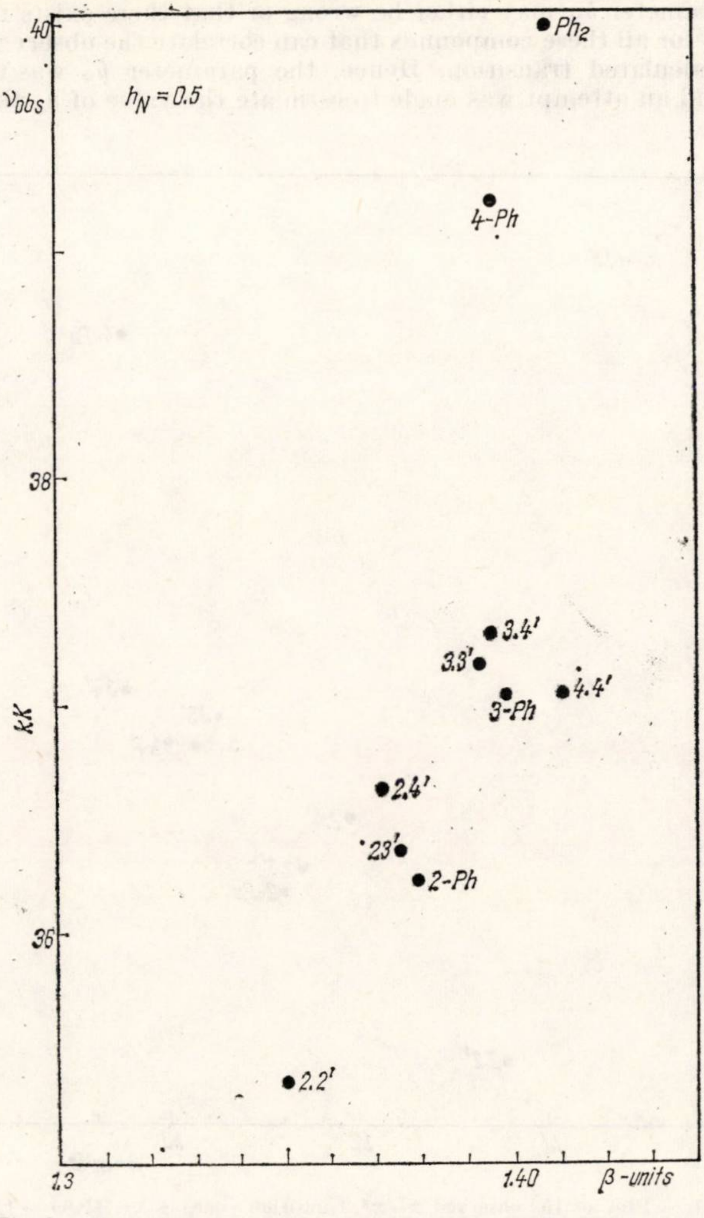

Fig. 3. — Plot of the observed $\pi \rightarrow \pi^*$ transition energies vs. HOO→LUO energies for a value $h_N = 0.5$.

observed first transition (ν_{obs}) and E for the six isomeric dipyridyl and three phenylpyridines using selected values of h_N (i. e. 0.5, 1.0, 1.5) does show wide scatter (Figs. 3 — 5). It is assumed that the choice of the values for the parameter h_N may either be wrong or that there exists no unique value of h_N for all these compounds that can correlate the observed spectra and the calculated transition. Hence, the parameter h_N was treated as variable and an attempt was made to estimate the value of h_N that would

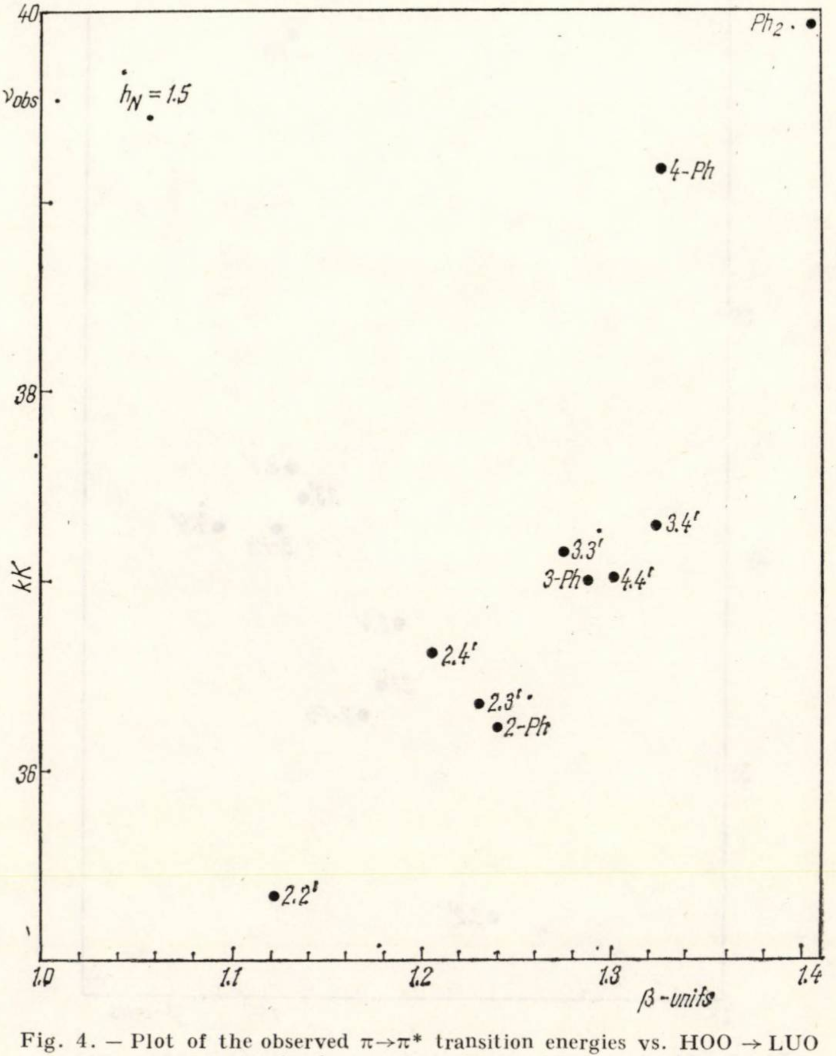

Fig. 4. — Plot of the observed $\pi \rightarrow \pi^*$ transition energies vs. HOO → LUO energies for a value of $h_N = 1.0$.

give the best fit for the observed spectrum of a compound. The following approach was made.

The dipyridyls and phenylpyridines were considered to be ring-substituted biphenyl, which was taken as the reference compound. It was further assumed that the two N-atoms in each dipyridyl were equivalent and could be represented by the same h_N parameter. The dimensionless quantity $(E_b - E_d)/E_b$, where E_b = the HOO→LUO transition in biphenyl (1.4092 β) and E_d is the corresponding transition in dipyridyls and phenylpyridines, was calculated for each value of h_N and a plot was made for each compound. Next the shift of the observed transition[18] for the compound with respect to biphenyl $(\nu_b - \nu_d)/\nu_b$ (ν_b = transition in biphenyl = 40000 cm^{-1}) was calculated. The value of the parameter h_N was then read off the plot, where the value of $(\nu_b - \nu_d)/\nu_b$ corresponds to that of

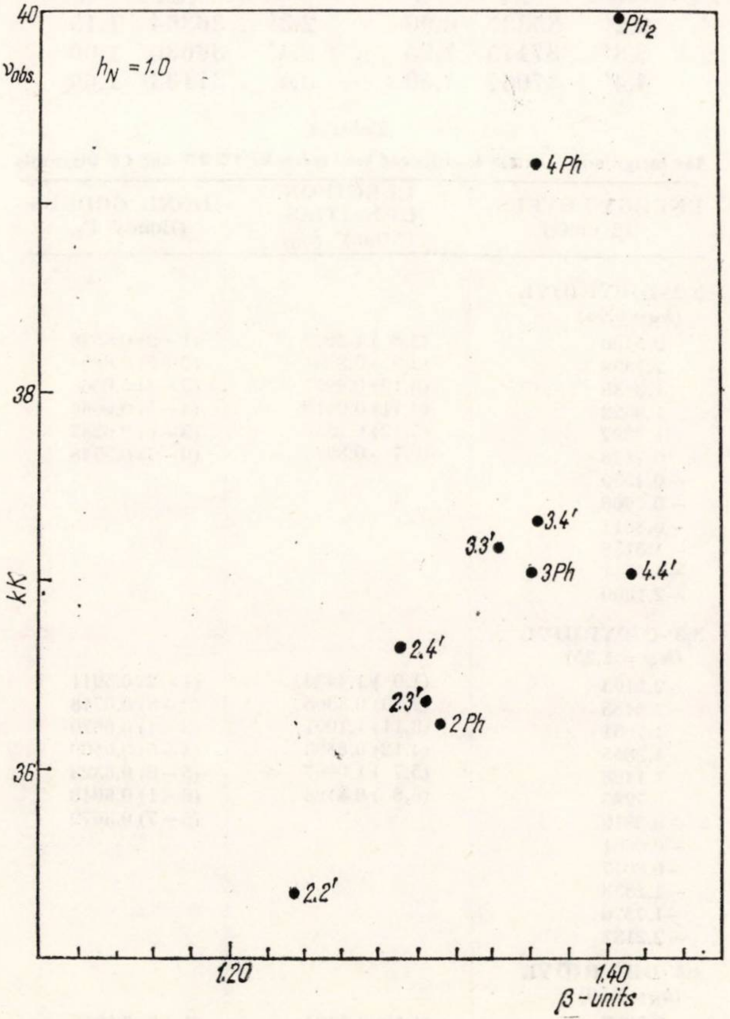

Fig. 5. — Plot of the observed π→π* transition energies vs. HOO→LUO energies for a value of $h_N = 1.5$.

---

[18] P. KRUMHOLZ, *J. Amer. Chem. Soc.* 73, 3487 (1961).

$(E_b - E_d)/E_b$. In this way, the following h_N values for the dipyridyls were obtained :

Dipyridyl isomers	ν_{obs}	h_N	Dipyridyl isomers	ν_{obs}	h_N
2,2′	35335	0.96	2,3′	36364	1.15
3,3′	37175	1.25	2,4′	36630	1.00
4,4′	37037	1.50	3,4′	37133	1.60

Table 2

The energy levels, electron densities and bond orders for 2,2′ 3,3′ and 4,4′ Dipyridyls

ENERGY LEVELS (β units)	ELECTRON DENSITIES (Atom)* π_{ED}	BOND ORDERS (Bond)* P_{rs}
2,2′-DIPYRIDYL		
(h_N=0.96)		
2.5180	(1,8) 1.3622	(1−2) 0.6328
2.1398	(2,9) 0.8531	(2−3) 0.6654
1.3435	(3,10) 0.9973	(3−4) 0.6568
1.3022	(4,11) 0.9919	(4−5) 0.6666
1.2397	(5,12) 0.9836	(5−6) 0.6287
0.7878	(6,7) 0.8917	(6−7) 0.3748
−0.4559		
−0.7960		
−0.8811		
−1.3138		
−1.8041		
−2.1600		
3,3′-DIPYRIDYL		
(h_N = 1.25)		
2.5163	(1,9) 1.4433	(1−2) 0.5911
2.3485	(2,10) 0.8305	(2−3) 0.6748
1.7051	(3,11) 1.1001	(3−4) 0.6670
1.2855	(4,12) 0.8893	(4−5) 0.6109
1.1498	(5,7) 1.0067	(5−6) 0.6323
0.7285	(6,8) 0.8198	(6−1) 0.6048
−0.5819		(5−7) 0.3672
−0.6661		
−0.8017		
−1.2333		
−1.7376		
−2.2132		
4,4′-DIPYRIDYL		
(h_N=1.50)		
2.5887	(1,10) 1.5104	(1−2) 0.5675
2.5056	(2,11) 0.8049	(2−3) 0.6913
1.8999	(3,12) 0.9953	(3−4) 0.6088
1.1089	(4,7) 0.8889	(4−5) 0.6088
1.0000	(5,8) 0.9953	(5−6) 0.6913
1.0000	(6,9) 0.8049	(6−1) 0.5675
−0.3012		(4−7) 0.3665
−0.8895		
−1.0000		
−1.0000		
−1.6875		
−2.2250		

For numbering of atoms see Fig. 1.

Using these values of h_N, the orbital coefficients, energies, electron densities and the bond orders for the isomeric dipyridyls have been recalculated (Tables 2 and 3). The new calculated energies (in β units) for the HOO → LUO transition for the dipyridyls were then plotted against the observed

Table 3

The energy levels, electron densities and bond orders for 2,3′ 2,4′ and 3,4′ -Diypyridyls

ENERGY LEVELS (β units)	ELECTRON DENSITIES (Atom)* π_{ED}	BOND ORDERS (Bond)* P_{rs}
2,3′-DIPYRIDYL		
($h_N = 1.15$)		
2.5353	(1) 1.4376	(1– 2) 0.6055
2.2732	(2) 0.8343	(2– 3) 0.6780
1.5015	(3) 1.0144	(3– 4) 0.6484
1.3525	(4) 0.8984	(4– 5) 0.6716
1.1704	(5) 1.0050	(5– 6) 0.6265
0.7660	(6) 0.8613	(6– 1) 0.5571
–0.5149	(7) 1.0174	(6– 7) 0.3824
–0.7047	(8) 0.8067	(7– 8) 0.6265
–0.8558	(9) 1.4145	(8– 9) 0.6163
–1.2681	(10) 0.8238	(9–10) 0.5985
–1.7747	(11) 1.0104	(10–11) 0.6695
–2.1809	(12) 0.8756	(11–12) 0.6695
		(12– 7) 0.6064
2,4′-DIPYRIDYL		
($h_N = 1.0$)		
2.4742	(1) 1.3766	(1– 2) 0.6283
2.2138	(2) 0.8481	(2– 3) 0.6667
1.5243	(3) 0.9986	(3– 4) 0.6564
1.3098	(4) 0.9082	(4– 5) 0.6662
1.0000	(5) 0.9861	(5– 6) 0.6299
0.8620	(6) 0.8823	(6– 1) 0.5721
–0.4286	(7) 0.9258	(6– 7) 0.3719
–0.8143	(8) 0.9942	(7– 8) 0.6127
–1.0000	(9) 0.8590	(8– 9) 0.6837
–1.1672	(10) 1.3670	(9–10) 0.6137
–1.7768	(11) 0.8590	(10–11) 0.6137
–2.1972	(12) 0.9942	(11–12) 0.6837
		(12– 7) 0.6127
3,4′-DIPYRIDYL		
($h_N = 1.60$)		
2.6501	(1) 1.5348	(1– 2) 0.5550
2.5620	(2) 0.7762	(2– 3) 0.6807
1.8670	(3) 1.0125	(3– 4) 0.6638
1.2981	(4) 0.8421	(4– 5) 0.6009
1.0000	(5) 1.0153	(5– 6) 0.6345
0.8860	(6) 0.7553	(6– 1) 0.5716
–0.4293	(7) 0.8758	(5– 7) 0.3804
–0.6139	(8) 1.0180	(7– 8) 0.6009
1.0000	(9) 0.8011	(8– 9) 0.7049
–1.1057	(10) 1.5492	(9–10) 0.5485
–1.7008	(11) 0.8001	(10–11) 0.5485
–2.2135	(12) 1.0180	(11–12) 0.7049
		(12– 7) 0.6009

For numbering of atoms, see Fig. 1

Table 4

Parameters for isomeric phenyl pyridines

Isomer	ν_{obs} (cm^{-1})	$(\nu_b - \nu_d)/\nu_b$	h_N	Calculated E_β	E_β predicted from eq .4
2-Ph	36232	0.0942	1.25	1.2745	1.276
3-Ph	37037	0.0741	1.40	1.3026	1.304
4-Ph	39216	0.0196	0.75	1.3820	1.380

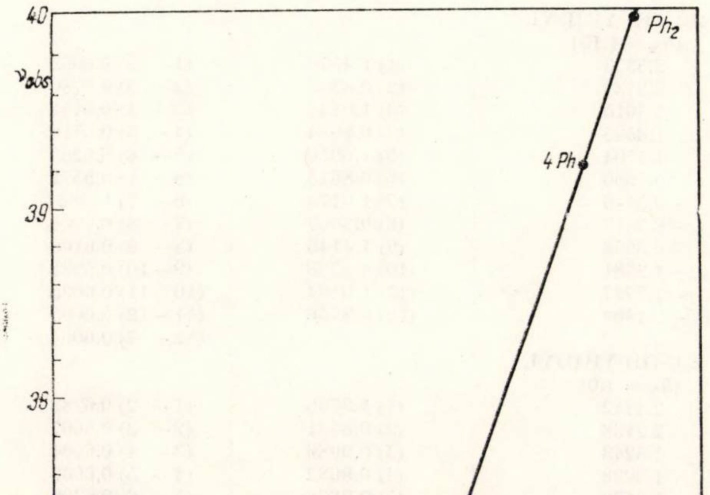

Fig. 6. — Correlation between the observed $\pi \rightarrow \pi^*$ transition energies and the calculated (see text) HOO → LUO energies for isomeric dipyridyls and phenylpyridines.

energy (ν_{obs}) which yields a linear correlation and the least square line is best described by:

$$\nu_{obs}(\mathrm{cm}^{-1}) = 28597\ (E_{\beta}) - 262 \qquad (4)$$

PHENYLPYRIDINES

An approach similar to the isomeric dipyridyls was made for the three phenylpyridines (Fig. 1). The h_N values and the calculated E values are reported in Table 4. It was of interest to test the validity of eq. 4, in the case of phenylpyridines. The predicted HOO→LUO transition energies for the phenylpyridines agree very closely (Table 4) to those calculated by using the derived h_N parameters.

A final correlation between ν_{obs} and calculated HOO→LUO transitions for all nine compounds resulted in a linear plot (Fig. 6) described by the following least square equation:

$$\nu_{obs}(\mathrm{cm}^{-1}) = 28400\ (\mathrm{E}_{\beta}) - 2.9 \qquad (5)$$

The average deviation between ν_{obs} and ν_{calc} values for all nine compounds is of only 34 cm^{-1}. It is gratifying to see that biphenyl also falls on this linear plot.

In conclusion we annotate that the very imprecise nature of the parameter h_N does not warrant the use of any specific value for the correction of the Coulomb parameter, at least in the case of the dipyridyl and phenylpyridine systems. In specific correlations (as with UV spectral data presented here) it is advisable to adjust the value of h_N for best fit.

Acknowledgement. My thanks are due to Dr. R.J. Fereday for his keen interest in this work and for various enlightenments that were needed from time to time.

[illegible], which yields [illegible] and the best square line is described by

[illegible]

[illegible]

[illegible] and the calculated [illegible] values [illegible]

[illegible] the following [illegible] function:

[illegible]

The average deviation [illegible] compounds is only [illegible]. It is gratifying to see that [illegible] on this [illegible] point.

In conclusion we [illegible] that the [illegible] nature of the [illegible] does not warrant [illegible] any specific value for the [illegible] of the Coulomb [illegible], at least in the case of [illegible] diatomic and [illegible]. In specific [illegible] spectral data [illegible] the values of [illegible].

Acknowledgment. My thanks are due to Dr. [illegible] for [illegible] interest in the work and [illegible] encouragement [illegible]

Revue Roumaine de Chimie, **18**, 5, 789–795 (1973)

ON THE OSCILLATION SPECTRUM OF DIMETHYL SULPHOXIDE (DMSO) IN SOLUTION

LIGIA SINGUREL and G. SINGUREL
Spectroscopy Laboratory, "Al. I. Cuza" University,
Iaşi, str. 23 August 11, Romania

Received July 3, 1972

Raman lines parameters of DMSO in carbon tetrachloride, chloroform, water, phenol, acetic and chloroacetic acid were studied. The parameter variation was interpreted as the manifestation of molecular interactions which appear in the studied solutions. For the active solvents a Raman line appeared in close vicinity of the Raman line belonging to the S = O-oscillation which has been assigned to the complex formed by the hydrogen bond. In order to verify the proposed interaction type, IR spectra of DMSO in solvents containing hydroxylic group were recorded. Besides the OH-free oscillation band there appeared a large band with smaller frequency, characteristic of the complex formed by the hydrogen bond. The interaction energy was calculated and a linear relationship between the acidity constants of the used solvents and $\Delta\nu_{OH}$ and $\Delta\nu_{S=O}$ shifts was established.

INTRODUCTION

The Raman spectrum of DMSO was first investigated by Vogel-Hogler.[1] This work contains some data in connection with the degree of depolarization ρ, but because the method of their determination is not described, it is not clear if these represent the real values of ρ. The data on the structure of these molecules, as well as the theoretical investigation of their oscillations are given in,[2] where the IR-spectrum of DMSO-molecule is also presented.

The solvent effect on the band of S = O-oscillation has been studied in the IR-domain in several works.[3–10] In,[11] Selvarajan has investigated the Raman spectra of DMSO mixtures with some liquids, using the method of photographical recording, which did not allow to study the variation of all Raman line parameters. Likewise, in this work, only the changes in the S = O-frequency of DMSO in used solvents are given.

---

[1] R. Vogel – Hogler, *Acta Phys. Austriaca*, **1**, 311 (1948).

[2] W. D. Horrocks and F. A. Cotton, *Spectrochim. Acta*, **17**, 134 (1961).

[3] L. J. Bellamy and R. L. Williams, *Trans. Faraday Soc.*, **55**, 14 (1959).

[4] L. J. Bellamy, C. P. Conduit, R. J. Pace and R. L. Willams, *Trans. Faraday Soc.*, **55**, 1677 (1959).

[5] M. Tamres, S. Searles, *J. Amer. Chem. Soc.*, **81**, 2100 (1959).

[6] T. Gramstad, *Spectrochim. Acta*, **19**, 829 (1963).

[7] P. Klaxbae, *Acta Chem. Scand.*, **18**, 27 (1964).

[8] P. Biscarini and G. Gersetti, *Gazz. chim. Ital.*, **92**, 61 (1962).

[9] H. Hadži and N. Kobilarov, *J. Chem. Soc. (A)*, **1966**, 439.

[10] M. T. Forel and M. Tranquille, *Spectrochim. Acta*, **26A**, 1023 (1970).

[11] A. Selvarajan, *Proc. Indian Acad. Sci.*, **64A**, 44 (1966).

In this work, the results of the change in line parameters for DMSO in carbon tetrachloride, chloroform, water, phenol, acetic and chloroacetic acid solutions with different concentrations, as well as the variations occurred in the OH-oscillation domain of IR-absorption of the DMSO mixtures with compounds containing hydroxylic group (alcohol, water, phenol, and cresol) are presented.

EXPERIMENTAL

Raman line shape was recorded photoelectrically with a grating spectrometer having a dispersion of 6.7Å/mm. As exciting source, a Hg-low pressure lamp was used. The exciting line was of 4368 Å. Accuracy in the frequency determination was of ± 1 cm^{-1}. Integral intensity (I_∞) was measured with a planimeter which gave the area of the spectral line contour. The comparison was made with the band 802 cm^{-1} of the cyclohexane, the integral intensity of which was considered equal to 500 units, while the intensity in maximum was taken equal to 250 units.[12] In the case of solutions, the integral intensity was taken per mol and was expressed in the relative units, where the intensity of the Raman-band of the pure DMSO was considered equal to 100 units. In this case, for the intensity of the bands, the corrections determined by the refraction index variations were introduced. The concentration of the solutions is given as the ratio between the numbers of molecules of DMSO and numbers of the molecules of the solvent. During the recording of spectra the temperature was 25°. The error in the measurement of the integral intensity varied between 5 and 15%, depending on the line character. The line width was corrected by the errors caused by the apparatus split or exciting line. The error in line width determination was of 5%. The degree of depolarization was measured by using the method described by Edssall and Wilson.[13] Using the gauge graph, real values of ρ were obtained.

IR — absorption spectra were obtained by using the IKS-14 spectrophotometer; because only the range of the OH-oscillation was studied, LiF prisms were used. The error in determination was of 3 — 5 cm^{-1} for the narrow bands and of 5 — 15 cm^{-1} for wide bands, including here the error in the calibration curve.

RESULTS AND DISCUSSION

In order to measure the modifications in the Raman line parameters of DMSO under the influence of molecular interaction forces, frequencies, widths, integral intensities, intensities in maximum and the depolarization degree of the Raman lines for DMSO were measured. Their values are given in Table 1.

---

[12] G. S. Landsberg, P. A. Bajulin and M. M. Suscinski, "Osnovnie parametry spectrov combinatyonogo rascianya uglevodorodov", Ed. A.N. S.S.S.R., Moscow, 1956.

[13] J. T. Edssall and E. B. Wilson, *J. Chem. Phys.*, **6**, 124 (1938).

Table 1

Raman lines parameters of DMSO

ν cm^{-1}	Assignment	δ cm^{-1}	I_0	I_∞	ρ
			(relative units)		
304	C-S-C	16	69	283	0.71
332	C-S-O	13	120	446	0.7
385	C-S-O	11	40	125	0.34
668	C-S	10	363	1 164	0.3
699	C-S	18	205	643	0.76
1 042	S=O	36	78	648	0.64
1 420	C-H	23	83	443	0.77
2 915	C-H	8	—	—	0.06
3 000	C-H	22	—	—	0.8

By passing DMSO in solved state, the changes in the Raman line parameters depend on the solvent nature and the type of the oscillation. These changes may by seen in Table 2. As was to be expected, frequency and line width modifications are more prominent when the solvent is more active. The changes in the parameters of the line 1042 cm^{-1} belonging to S = O valence oscillation are taken into account. These changes have a maximum value for all solvents thus indicating that S = O group in DMSO molecule is the group most influenced by the solvent molecules. It should be pointed out that for this line the wave number increases when DMSO solves in CCl_4. This modification is, probably, caused by the fact that the DMSO molecules interact and by solving in CCl_4 pass in the monomer. Large width of the 1042 cm^{-1} and 3000 cm^{-1} in pure DMSO and the narrowing of the width of these lines for the solution of the DMSO in CCl_4 come in support of this supposition. The integral intensity of the DMSO bands in the solutions changes very little. This indicates that the tensor of the polarization derivative of the molecule of DMSO is not strongly modified when the DMSO solves.

As the solvent acidity increases, the complex formation between DMSO and solvent leads to a stronger modification in frequency of S=O-oscillation. Thus in solutions of DMSO with chloroform and water this line is shifted to the larger wave number, the shift being three times larger in water than in chloroform. Because in chloroform and water the Raman line splitting was not observed, it is supposed that the interaction has a dipole — dipole and partly ionic character.

In stronger solvents, as acetic and chloroacetic acids, the line of 1042 cm^{-1} is split in two components of 1015 cm^{-1} and 1050 cm^{-1}. Investigations about the concentration variations show that by the decrease in DMSO content the first line intensity increases and the second one decreases (Fig. 1). This effect shows that 1015 cm^{-1} line belongs to the S = O-oscillation of the DMSO molecule bound in the complex with solvent molecule. Line of 1050 cm^{-1} belongs to the free DMSO molecules, a fact which comes in favour of the supposition concerning the association of DMSO molecules between themselves. In the last case, at the interaction of the DMSO molecules with acetic and chloroacetic acids, DMSO com-

Table 2

Raman line frequency, width and integral intensity of DMSO in solution

Solvent	ν cm^{-1} $(CH_3)_2S{=}O$	Concentration	ν cm^{-1} $(CH_3)_2S{=}O$ in sol	δ cm^{-1}	I_∞
CCl_4	668	1 : 1	664	10	99
	669	1 : 1	695	18	92
	1 042	1 : 1	1 050	29	89
	2 915	1 : 1	2 917	8	100
	3 000	1 : 1	2 998	17	94
$CHCl_2$	304	1 : 1	306	14	100
	332	1 : 1	337	13	92
	385	1 : 1	390	13	100
	1 042	1 : 1	1 036	42	114
	1 420	1 : 1	1 419	21	90
	2 915	1 : 1	2 918	8	105
H_2O	304	1 : 4	308	15	97
	332	1 : 4	335	15	93
	385	1 : 4	385	16	91
	668	1 : 4	677	11	95
	699	1 : 4	708	15	100
	1 042	1 : 4	1 022	40	84
	1 420	1 : 4	1 418	21	100
	2 915	1 : 4	2 925	15	98
	3 000	1 : 4	3 010	21	85
C_6H_5OH	668	1 : 1	671	12	
	699	1 : 1	703	18	
	2 915	1 : 1	2 917	7	
	3 000	1 : 1	3 000	14	
CH_3COOH	304	1 : 1	292	11	90
	332	1 : 1	334	15	59
			306	12	
	385	1 : 1	390	20	110
	668	1 : 1	675	11	100
	699	1 : 1	698	6	80
			710	16	
	1 042	1 : 1	1 053	25	40
			1 016	40	
	2 915	1 : 1	2 922	10	104
	3 000	1 : 1	2 991	20	71
$ClCH_2COOH$	304	1 : 1	280	7	
	332	1 : 1	332	13	
			294	15	
	385	1 : 1	385	9	
	668	1 : 1	668	13	
	699	1 : 1	699	16	
			713	7	
	1 042	1 : 1	1 049	25	
			1 013	21	
	2 915	1 : 1	2 915	9	
	3 000	1 : 1	3 000	18	

plex unbinds, fact spectrally manifested by the appearance of Raman line of 1050 cm^{-1} belonging to the S=O free oscillation. In DMSO solutions with acetic and chloroacetic acids, the lines 332 cm^{-1} and 699 cm^{-1} are also splitting. Thus, in the solution of DMSO with acetic acid the line of 306 cm^{-1} appear while with chloroacetic acid that of 294 cm^{-1} appear. The stronger decrease in frequency in the last case indicates an increase in the interaction.

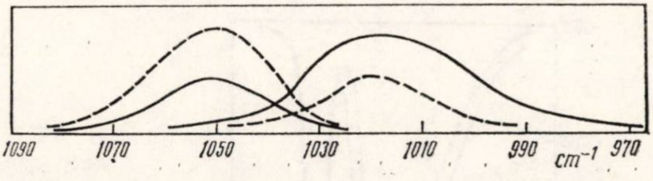

Fig. 1. — The intensity variation of lines belonging to S = O-oscillation of DMSO and the formed complex with acetic acid function of DMSO concentration in acid.

In both cases the appearance of new lines is caused by the complex formation. It should be emphasized that the position change of the S = O and C — S = O lines in solution is similar, indicating that these groups are to the same extent affected by intermolecular forces. As for the solvent, in the last two cases it interacts by the hydroxylic group, because it is more active and an interaction of hydrogen bond type takes place :

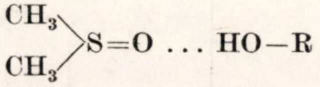

$$\begin{matrix} CH_3 \\ CH_3 \end{matrix}\!\!> S=O \ldots HO-R$$

The verification of this supposition was done by the investigations in the IR-absorption range of the DMSO solutions containing hydroxylic compounds. The change in line parameters for the OH-oscillation range in the solutions of DMSO with the butyl-, *n*-propyl-, ethyl-, methyl alcohol, water *ortho*-cresol, *para*-cresol and phenol were studied. The investigations were carried out in the ternary solutions, a solvent being inert, in order to permit the alcohol dissociation in monomers. The hydroxylic compound concentration was smaller than 10^{-2} mol/l, thus assuring the presence of the alcohol molecule in the monomer form. This effect was spectrally verified (the appearance of a narrow band of wave number 3600 cm^{-1}). When, in the above mixture, DMSO is present in very small quantities (10^{-2} mol/l), a very broad and intense band appears in the spectral region with small wave numbers. It belongs to the complex formed between hydroxylic compound and DMSO. This fact can be confirmed if we maintain the hydroxylic compound concentration constant and modify the DMSO concentration; then the intensity of the broad band decreases and the monomer band intensity increases. This is very well illustrated in Fig. 2. The complex band position and intensity depend on the interaction intensity between DMSO and the compound containing OH-group. In Table 3 are indicated the frequency values of monomer and complex for DMSO solutions in various substances. The values of

$\Delta\nu_{OH}$, being experimentally measured and using the linear relation between $\left(\frac{\Delta\nu}{\nu}\right)_{OH}$ and interaction energy E: $\left(\frac{\Delta\nu}{\nu}\right)_{OH} = kE$, experimentally found by Badger-Bauer [14] and theoretically verified by Sokolov, [15] the interaction energy was calculated. The constant k was taken after Sokolov of 1.6×10^{-2}mol/kcal. The obtained values of the interaction energy are presented in Table 3 and are in agreement with those given in [16] obtained by calorimetrically determinations. These values indicate the presence of hydrogen bond.

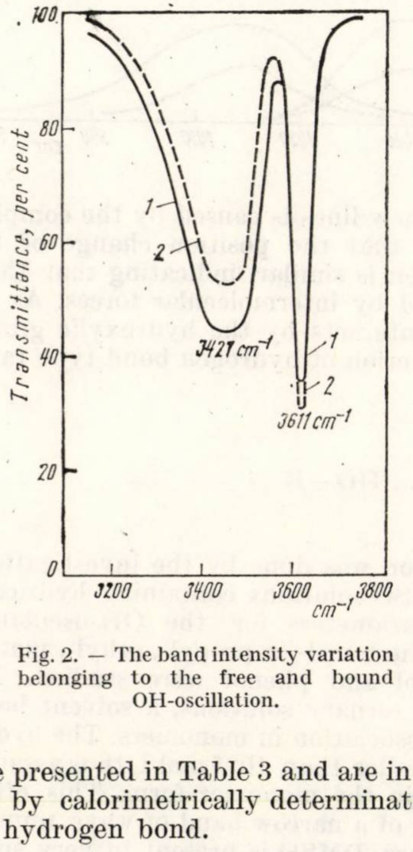

Fig. 2. — The band intensity variation belonging to the free and bound OH-oscillation.

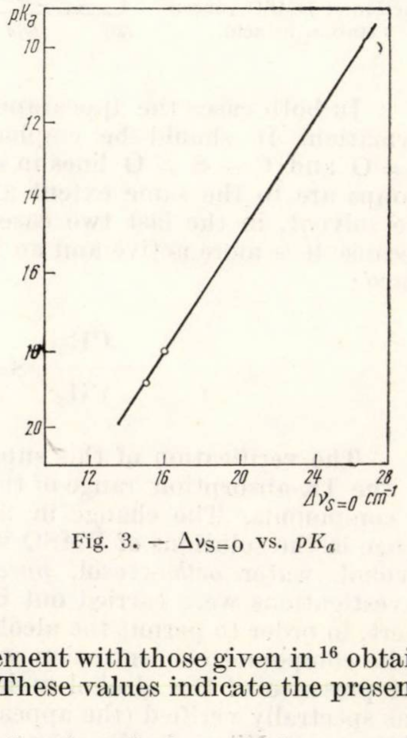

Fig. 3. — $\Delta\nu_{S=O}$ vs. pK_a

In the present work we searched for the relation which may exist between $\Delta\nu_{OH}$ and acidity constant K_a of the solvents:

$$pK_a = -\lg K_a = -\lg \frac{A^+H^-}{AH}$$

The results of these measurements are presented in Table 3. As was already stated, there exists a linear relation between $\Delta\nu_{OH}$ and pK_a, which,

---

[14] R. M. Badger and S. H. Bauer, *J. Chem. Phys.*, **5**, 839 (1937).

[15] N. D. Sokolov, "Vodorodnaya sviazy", Ed. Nauca, Moscow, 1964, p. 7.

[16] R. S. Drago, N. O'Bryan and G. C. Vogel, *J. Amer. Chem. Soc.*, **92**, 3924 (1970).

Table 3

Interaction between DMSO and the compounds containing OH-group

Solvent	pK_a	ν^{mon} cm^{-1}	ν^{com} cm^{-1}	$\Delta\nu cm^{-1}$	E Kcal/mol
butyl alcohol	19	3 635	3 440	195	3.4
n-propyl alcohol	18	3 630	3 440	190	3.3
ethyl alcohol	18	3 640	3 435	205	3.7
methyl alcohol	16	3 655	3 445	210	3.8
water	14	3 687	3 437	250	4.2
o-cresol	10.28	3 620	3 284	336	5.8
p-cresol	10.19	3 620	3 280	340	6
phenol	9.95	3 614	3 264	350	6

generally, may be used for pK_a determination by spectroscopic methods. Likewise, we wanted to find out if the correlation is valid for the band shift S = O of DMSO in various solvents containing OH-groups. The results are presented in fig. 3.

Revue Roumaine de Chimie, **18**, *5*, 797–802 (1973)

THE STUDY OF THE DECOMPOSITION OF ORGANIC HYDROPEROXIDES ON CATION EXCHANGERS. II[1]

DECOMPOSITION OF CUMENE HYDROPEROXIDE ON FINE GRANULATED VIONIT CS-1 IN STATIC CONDITIONS

J. VODNÁR

Babeş-Bolyai University, Department of Chemical Technology,
str. Arany János, 11, Cluj, Romania

Received March 11, 1972

The paper presents experimental results, obtained by the decomposition of cumene hydroperoxide into phenol and acetone by acidic catalysis, in static conditions. Fine granulated Vionit CS-1 cation exchanger has been used as catalyst; its chemical and some physical properties were described in a previous paper.[1] The cation exchanger, as catalyst, was activated by a method patented by the author.[2] This catalyst proved to be very efficient. The highest conversion of cumene hydroperoxide into phenol (96 – 99 %) can be obtained on low temperature, with a low concentration of hydroperoxide in the samples subjected to decomposition.

The experimental results described in this paper are concerned with the catalytic decomposition of cumene hydroperoxide by using activated,[2] fine granulated Vionit CS-1 cation exchanger. As reaction products phenol and acetone were obtained. This is, actually, the best method of producing these substances in high quantities.

In a previous paper[1] the data obtained by the decomposition of cumene hydroperoxide on the same cation exchanger were discussed, but this was used in its original (industrially realized) granulation, at temperatures higher than 25°. On the basis of these conclusions it seemed important to study the decomposition process on fine granulated catalyst, at lower temperatures.

EXPERIMENTAL

In the paper there are presented the results obtained on the decomposition of cumene hydroperoxide on activated, fine granulated Vionit CS-1 cation exchanger. The granulation of the catalyst is 0.25 – 0.50 mm; its chemical characteristics were described in another paper.[1]

---

[1] J. Vodnár, *Rev. Chim.*, Bucureşti, **22**, 394 (1971).

[2] J. Vodnár and G. J. Kulcsár, Romanian Patent, **49.842** (1967).

Experiments have been carried out in static conditions, using 0.1 g of catalyst and 20 ml of hydroperoxide samples. The reaction mixture was stirred vigorously. Temperature was maintained constant by means of a Wobser U_8 ultrathermostat. Tests for dosing hydroperoxide and phenol are periodically taken from the reaction mixture. The applied analytical methods are described in a printed paper. [3]

RESULTS AND DISCUSSION

Decomposition of cumene hydroperoxide has been studied depending on the following parameters : temperature, hydroperoxide content of the samples, quantity of the catalyst, water content of the reaction mixture and the generated heat (using different hydroperoxide content of the samples). Kinetic curves are designed at six temperatures, between 11.8 and 22.5°.

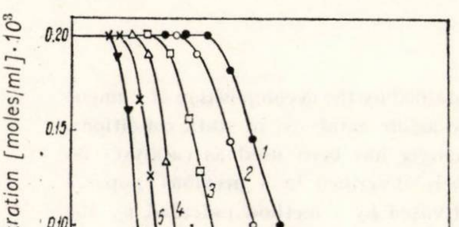

Fig. 1. – Kinetic curves at different temperatures. Quantity of the catalyst, 0.1 g :

1, 11.8°; *2*, 13.5°; *3*, 15.25°; *4*, 17.5° *5*, 20.5°; *6*, 22.5°.

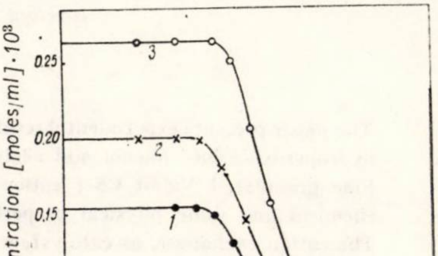

Fig. 2. – Kinetic curves by different initial hydroperoxide concentrations. Temperature, 11.8° :

1, 0.1546 (mole/ml)·10³; *2*, 0.200 (mole/ml)·10³; *3*, 0.2633 (mole/ml)·10³.

The experimental results are illustrated in figures 1 – 8.

The curves of figure 1 illustrate the results obtained by the decomposition of cumene hydroperoxide in accordance with the reaction time, at different temperatures. The time, necessary for total decomposition at 22.5° is no more than 28 minutes, but it increases much if the temperature is 11.8°, when the total decomposition is realized in about 95 minutes.

The process has an autocatalytic character at all temperatures.

Figure 2 contains the graphs designed on the basis of results obtained by the decomposition of samples with different initial hydroperoxide contents : 0.1546 ; 0.200 and 0.2633 mol·l^{-1}. Temperature was maintained constant at 11.8°. The curves of figure 2 show that the decomposition has a long induction period (about 40 minutes). The time necessary for the decomposition of cumene hydroperoxide is nearly equal in all cases (95 – 100 minutes).

---

[3] J. Vodnár, *Rev. Roumaine Chim.*, **15**, 1947 (1970).

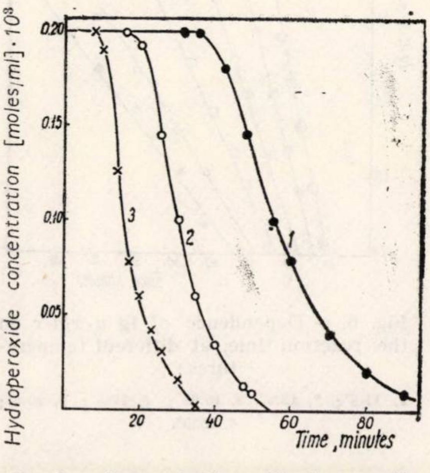

Fig. 3. – Concentration of hydroperoxide in accordance with the reaction time, using different quantities of catalyst. Temperature 11.8°.

1, 0.1 g; 2, 0.2 g; *3*, 0.3 g.

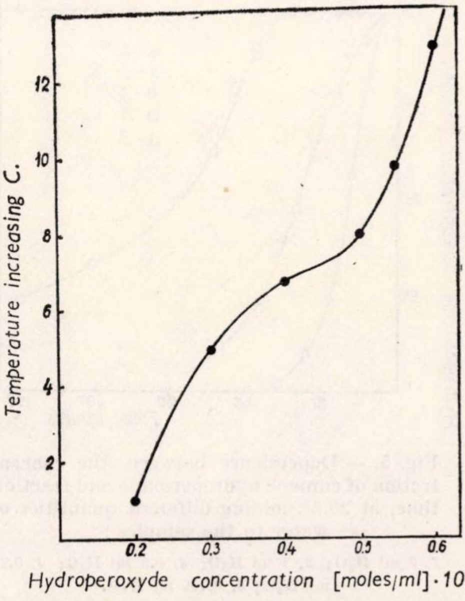

Fig. 4. – Dependence between the increases of the temperature and initial hydroperoxide content of the samples. Temperature 39.8° and the quantity of the catalyst 0.5 g.

In the following experiments the temperature was 11.8° and the quantity of the used catalyst was as follows : 0.1 ; 0.2 and 0.3 g. The results are illustrated in figure 3 ; we can observe that the induction period decreases quickly with the quantity of the catalyst, from 35 min by 0.1 g to 8 min by 0.3 g catalyst.

The decomposition process is exotermic and the heat of the reaction can overheat the mixture to the boiling point of acetone, which troubles the process. With a view to determine the increase of the temperature in the decomposition of the samples, with different cumene hydroperoxide content, there were made a series of experiments illustrated in figure 4. The temperature was 39.8°.

In figure 4 there are represented the increases of temperature in accordance with initial cumene hydroperoxide content of the samples. Temperature increases suddenly when the hydroperoxide content of the samples is more than 0.45 mol·l^{-1}. Consequently, the initial hydroperoxide concentration could not exceed this value. In other case, the condensation of phenol with acetone occurs, yielding resinous substances.

In the last series of experiments, the effect of the water on the activity of the catalyst was studied. We can state that when we work at 20.5°, 1 ml of water causes a total inactivation of 0.2 g catalyst (see figure 5), but a quantity of 0.25 ml water permits decomposition to take place with enough high rate.

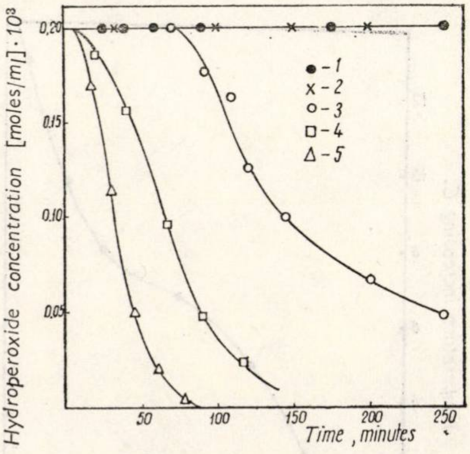

Fig. 5. — Dependence between the concentration of cumene hydroperoxide and reaction time, at 20.5°, adding different quantities of water to the samples :

1, 2 ml H_2O; *2*, 1 ml H_2O; *3*, 0.5 ml H_2O; *4*, 0.25 ml H_2O; *5*, 0.125 ml H_2O.

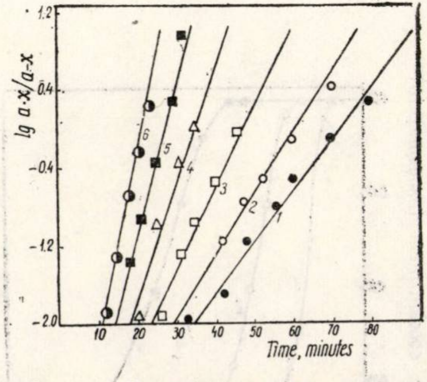

Fig. 6. — Dependence of lg $a \cdot x/a\text{-}x$ on the reaction time, at different temperatures :

1, 11.8°; *2*, 13.5° *3*, 15.25°; *4*, 17.5°; *5*, 20.5°; *6*, 22.5°.

This is a technologically important statement, because it makes possible the reactivation of the catalyst by washing it with the mixture obtained by decomposition.

On the basis of the experimental results obtained, the activation energy, enthalpy, entropy and the activation free enthalpy were determined.

The kinetics of the decomposition process can be designed by the following relation

$$\frac{dx}{dt} = k(a - x)x$$

The integrated form of this relation

$$k \cdot t = \frac{1}{a} \cdot \ln a \cdot x/a - x$$

made possible the linearization of the kinetic curves and the calculation of k values (see figure 6) by representing the values of $\lg a \cdot x/a\text{-}x$ in accordance with the reaction time.

The apparent activation energy of the decomposition process, as deduced from pairs of lg k and $1/T$ values, corresponding to six temperatures (see figure 7) becomes 21 kcal/mole.

Applying the k values, some other kinetic data ($\Delta H^{\ddagger}$; $\Delta S^{\ddagger}$ and $\Delta G^{\ddagger}$), were calculated by representing the pairs of lg k/T and $1/T$ (see figure 8), using the relation

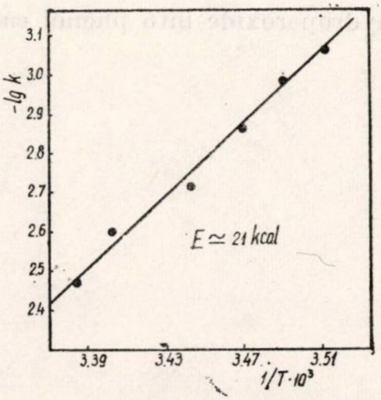

Fig. 7. – Dependence of lg k values on $1/T$.

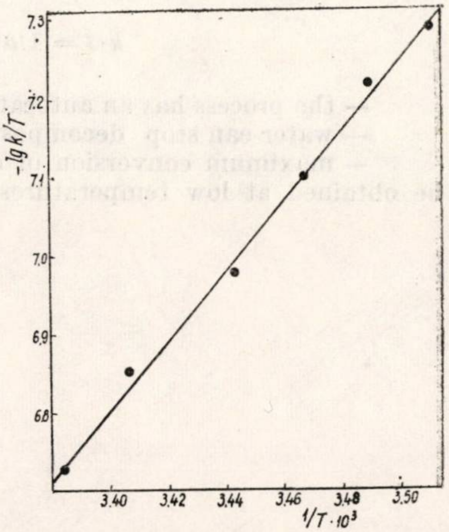

Fig. 8. – Dependence of lg k/T values on $1/T$.

$$\lg\frac{k}{T} = \lg\frac{k}{h} + \frac{\Delta S^{\ddagger}}{2.303\cdot R} - \frac{\Delta H^{\ddagger}}{2.303\cdot R\cdot T}$$

The calculated data are:

$$\Delta H^{\ddagger} = 20.57 \text{ kcal/mole}$$

$$\Delta S^{\ddagger} = -8.37 \text{ cal/K°}$$

$$\Delta G^{\ddagger} = 22.98 \text{ kcal/mole}$$

CONCLUSIONS

Decomposition of cumene hydroperoxide on cation exchanger Vionit CS-1 (fine granulated and activated [2]) has been studied in order to obtain phenol and acetone. We can state that:

— the catalyst used is perfectly fit to decomposition of cumene hydroperoxide;

— the kinetics of the process can be designed by the relation:

$$k \cdot t = 1/a \cdot \ln a \cdot x/a - x;$$

— the process has an autocatalytic character;

— water can stop decomposition;

— maximum conversion of cumene hydroperoxide into phenol can be obtained at low temperatures.

Revue Roumaine de Chimie, **18**, 5, 803–808 (1973)

DIE STRUKTUR DES MIT LITHIUM UND TITAN DOTIERTEM ALUMINIUMOXYD

AL. FRUMA, D. CIOMÂRTAN, I. BRAŞOVEANU und
I. V. NICOLESCU

Institut für physikalische Chemie
Bukarest, str. Dumbrava Roşie 23

Eingegangen am 7. November, 1972

Es werden die röntgenographischen Diffraktogramme einiger mit Lithium und Titanionen dotierten Aluminiumoxyde im Vergleich zum Aluminiumoxyd besprochen. Bei dem mit Lithiumionen dotiertem Aluminiumoxyd wurde ein Aluminat vom $LiAl_5O_8$-Typ festgestellt, für den die Strukturformel $Al[Li_x\square_{0.5-x}Al_{1.5}]O_4$, in der in die rechteckigen Klammern die oktaedrischen Plätze bezeichnet wurden, vorgeschlagen. Im Fall des Titan-dotiertem Aluminiumoxyds, befindet sich das Titan fein dispergiert auf die Oberfläche. Die Größe der Aluminiumoxyd-Kristalliten, befindet sich sowohl bei dem dotierten, als auch beim reinen Aluminiumoxyd zwischen 40 – 50 Å.

1. EINLEITUNG

Die weitgehende Benützung der aktiven Aluminium oxyde (γ oder η) als Träger bei der Herstellung von industriellen Katalysatoren bedingte umfangreiche Forschungen über die Möglichkeiten der Änderung der Struktureigenschaften durch Dotierung mit Fremdionen mit einer größeren oder kleineren Wertigkeit als die des Al^{3+}. [1–9]

Derartige Strukturänderungen haben manchmal einen bedeutenden Einfluß auf die katalytischen Eigenschaften des Aluminiumoxyds. Sowohl das Verständnis dieser Erscheinungen, als auch die Bestimmung der gegenseitigen Abhängigkeit zwischen den durch Dotierung verursachten Änderungen und der Besonderheit der Oberflächenreaktionen, bedingten

---

[1] G. M. Schwab, J. Block, W. Müller und D. Schultze, *Naturwiss.*, **44**, 582 (1959).
[2] G. M. Schwab, A. Beer und J. Foitzig, *Z. angew. Physik*, **14**, 763 (1962).
[3] G. M. Schwab und H. Derleth, *Z. phys. Chem. (Frankfurt)*, **53**, 1 (1962).
[4] V. A. Fomichev, *Fizica Tverdovo Tela*, **8**, 2892 (1966).
[5] P. J. Harrop, *Brit. J. Appl. Phys.*, **16**, 729 (1965).
[6] H. Pscheidl und H. Witzmann, *Z. phys. Chem. (Leipzig)*, **240**, 161 (1969).
[7] J. Cohen, *Bull. Amer. Ceram. Soc.*, **38**, 441 (1959).
[8] W. Pfeil, *Z. phys. Chem. (Leipzig)*, **243**, 51 (1970).
[9] G. M. Schwab und G. Mutzbauer, *Z. phys. Chem. (Frankfurt)*, **32**, 367 (1962).

Röntgendiffraktionsbestimmungen und kristallographische Untersuchungen bezüglich der Lage der Dotierungsionen in Kristallgitter des Aluminiumoxyds.

Aus diesem Grunde haben wir das vorliegende Studium unternommen, in dem wir die Ergebnisse der Untersuchung der Röntgendiffraktogramme des mit Lithium- und Titanionen, in verschiedenen Konzentrationen dotiertem Aluminiumoxyds mitteilen.

2. HERSTELLUNG DER PROBEN UND MESSTECHNIK

Die untersuchten Proben wurden folgendermaßen hergestellt : Das aus Aluminiumchlorid bei einem pH = 8,5 ergebene Aluminiumhydroxyd wurde nach waschen, filtrieren und austrocknen bei 260°, mit Titannitrat- oder Lithiumkarbonatlösung von verschiedener Konzentration impregniert. Die nach dem Austrocknen gewonnene Masse wurde während 6 Stunden bei 800° ausgeheitzt. Unter diesen Herstellungsbedingungen wurden die in Tabelle 1 aufgezählten Proben erhalten.

Tabelle 1

Die spezifische Oberfläche „S" der Aluminiumoxydproben

Nr.	Atom % im Al_2O_3		S
	Li	Ti	m^2/g
1	—	—	152
2	0,5	—	158
3	2,0	—	146
4	4,0	—	139
5	—	0,5	149
6	—	2,0	138
7	—	4,0	124

Aus Tabelle 1 ist ersichtlich, daß sowohl bei dem mit Lithium als auch bei dem mit Titan dotiertem Aluminiumoxid die spezifische Oberfläche mit dem Ansteigen der Konzentration des Dotierkomponents fällt.

Für die Untersuchung mittels der Röntgenstrahlen Diffraktion, wurden die Proben vorerst eine halbe Stunde in einer Agatkapsel gerieben. Mit Hilfe des Diffraktometers TUR-M-61 wurde dann das Beugungsspektrum der einzelnen Proben aufgenommen. Die Diffraktogramme wurden auf Grund der Cu K α Strahlung ermittelt. Die Monochromatisierung erfolgte durch einen Nickel-Filter. Es wurden folgende Arbeitsbedingungen angewendet :

- Hochspannung : 30 kV
- Anodenstrom : 16 mA
- Detektor : Zähler, Typ Geiger-Müller
- Skala : $1{,}8.10^3$ Impuls/s

3. ERGEBNISSE UND DISKUSSION

Die Ergebnisse der Berechnung der interplanären Abstände und der Bestimmung der Intensitäten für die mit Lithium und Titan dotierten Aluminiumoxydproben und für die Probe mit reinem Aluminiumoxyd, sind aus Tabelle 2 ersichtlich. Die Intensitäten der Linien wurden im Verhältnis zu ihrer Oberfläche gemessen, wobei die Linie bei 1,40 Å mit Oberfläche 100 betrachtet wurde.

Nach dem Vergleich der für unsere Proben erhaltenen Daten der Röntgenstrahlendiffraktion, mit den ASTM - Karten und mit anderen veröffentlichten Arbeiten[10] können wir behaupten, daß das untersuchte Aluminiumoxyd einer Mischstruktur von γ und μ Aluminiumoxyd entspricht, wobei die γ Form vorherrscht. Das mit Lithium dotierte Aluminiumoxyd zeigt im Beugungsspektrum auch die charakteristischen Linien des Lithiumaluminats $LiAl_5O_8$, Form I und II auf. Zu diesem Schluß gelangten wir durch die Vergleichung der Beugungshöchstwerte bei d = 2,809 Å; 1,40 Å und 1,96 – 1,99 Å. Es ist ersichtlich, daß der für die Form I und II spezifische Höhepunkt bei 2,809 Å schmal ist und mit der Vergrößerung der Lithiumkonzentration in Intensität zunimmt. Die flache Form des Höhepunkts bei d = 2,30 Å und 1,40 Å deutet auf eine geringere Gitterordnung in den betreffenden Kristallebenen, wo ein größerer Beitrag der Aluminium- und Sauerstoffatomen als der Lithiumatomen vorhanden ist.

Die mittlere Partikelgröße des Al_2O_3 wurde auf Grund Scherrers Gleichung

$$D_{hkl} = \frac{k\lambda}{\beta_{hkl} \cdot \cos \theta_{hkl}}$$

aus der Beugungslinie bei 1,40Å berechnet und betrug 40 – 50 Å.

Nach der Dotierung mit Lithium blieb die Lage, Form und Breite dieser Linie unverändert, was auf dieselbe mittlere Größe der Al_2/O_3 und $LiAl_5O_3$ Partikeln deutet.

Wir betrachten für das $LiAl_5O_8$ ein gleichartiges Kristallsystem wie für das γ Al_2O_3, und zwar kubisch Fd3m. Aus den mehr unten angegebenen Abbildungen ist ersichtlich, daß die Li^+ Ionen nur oktaedrische Plätze besetzen können, und zwar die mit a′, b′ und c′ in der Abbildung 2 bezeichneten Plätze.

Nur diese Plätze können zu einer so bedeutenden Vergrößerung der Intensität, wie die experimentell bei den Höhepunkten 2,809 (220) und 1,99 (400) beobachtete Vegrgrößerung führen. Die Tatsache daß der Höhepunkt (440) bei 1,40 Å nach der Dotierung mit Lithium nicht verändert wird, beweist daß diese Linie durch den Beitrag der Aluminiumionen aus den oktaedrischen Plätzen und der umgebenden Sauerstoffatomen gebildet wird.

---

[10] B. C. Lippens und Y. Y. Steggerda, „Physical and Chemical Aspects of Adsorbents and Catalysts" Ed. B. C. Linsen, Acad. Press. London, New York, 1970, S. 187.

Tabelle 2

Die interplanären Abstände und die Intensitäten der Linien für reines Aluminiumoxyd dotierte Aluminiumoxyde und Etalons

Probe	Experimentelle Ergebnisse									
Al_2O_3+ 4 Atom % Li	d	3,24	2,809	2,40	2,28	1,988	1,978	1,624	1,409	1,260
	I	5	80	80	20	70	80	5	100	10
Al_2O_3 + 2 Atom % Li	d	3,24	2,812	2,41	2,28	1,991	1,976	1,626	1,401	1,260
	I	3	65	80	20	60	80	5	100	10
Al_2O_3+ 0,5 Atom % Li	d	3,24	2,808	2,40	2,28	1,987	1,979	1,619	1,402	1,262
	I	3	50	80	20	50	80	5	100	5
Nicht dotiertes Al_2O_3	d	—	2,81	2,40	2,28	1,993	1,961	—	1,392	—
	I	—	20	60	20	80	60	—	100	—
γAl_2O_3 Lippens [10]	d	—	2,77	2,397	2,284	1,990	1,956	—	1,407	—
	I	—	25	60	30	65	65	—	100	—
ηAl_2O_3 Lippens [10]	d	—	2,76	2,39	2,28	1,980	—	—	1,396	—
	I	—	36	70	36	80	—	—	100	—
$LiAl_5O_8$ Form I ASTM 17–5731	d	3,55	2,81	2,39	2,29	—	1,98	1,62	1,40	—
	I	10	80	100	—	—	70	—	100	—
$LiAl_5O_8$ Form II ASTM 17–4971I	I	3,22	2,79	2,38	2,28	—	1,97	1,52	1,40	—
	d	10	80	100	—	—	60	—	70	—
Al_2O_3+ 4Atom % Ti	d	—	2,81	2,39	2,28	1,980	—	—	1,392	—
	I	—	10	60	20	80	—	—	100	—
Al_2O_3+ 2 Atom % Ti	d	—	2,81	2,39	2,28	1,973	—	—	1,394	—
	I	—	10	60	20	80	—	—	100	—
Al_2O_3+ 0,5 % Atom T	d	—	2,80	2,39	2,28	1,970	—	—	1,398	—
	I	—	10	60	30	80	—	—	100	—

Die Li^+ Ionen haben einen größeren Radius als die Al^{3+} Ionen, respektiv 0,80 Å und 0,57 Å. Die durch den Beitrag der Al^{3+} Ionen gebildeten Beugungslinien sind wegen der Vibration dieser Ionen in den von ihnen besetzten tetraedrischen und oktaedrischen Plätze sehr erweitert.

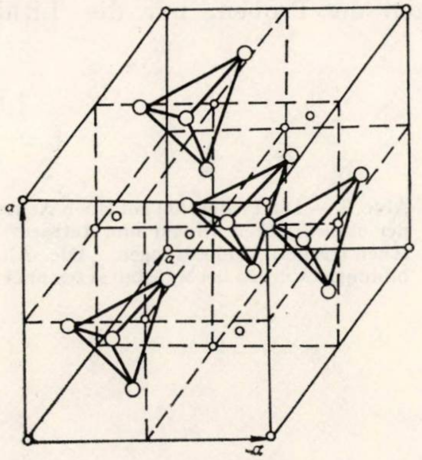

Abb. 1. — Kristallgitter des γ Al_2O_3 aus dem kubischen System Fd3m (227). Parameter a = 7,9Å. Die kleinen Kreise bedeuten tetraedrische Plätze, die größeren Kreise bedeuten oktaedrische Plätze.

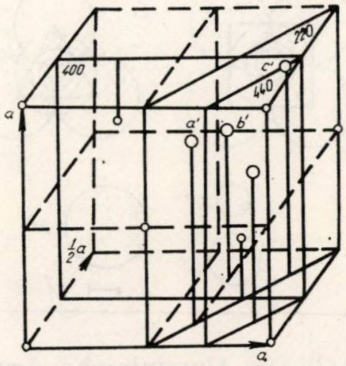

Abb. 2. — Die Hälfe der Elementarzelle des γ Al_2O_3 oder $LiAl_5O_8$. Die kleinen Kreise bedeuten tetraedrische Plätze, die größeren Kreise bedeuten oktaedrische Plätze.

Die Beugungslinien die durch den Beitrag der Li^+ erhalten wurden sind schärfer, da das Li^+ eine geringere Vibrationsmöglichkeit in der oktaedrischen Umkreisung hat, wie aus Abb. 3 ersichtlich ist.

Die Änderung der Intensitäten der Linie bei d = 2,809 Å mit der Konzentration der Li^+ Ionen weist daraufhin, daß das Lithiumaluminat freie oktaedrische Plätze besitzt, die durch Dotierung allmählich mit den Li^+Ionen von $Al[Li_x\square_{0,5-x}Al_{1,5}]O_4$ bis $Al[Li_{0,5}Al_{1,5}]O_4$, wo $0 < x < 0,5$, besetzt werden. Die Elementarzelle enthält 8 solche Strukturformeln. Diese Annahme ist in Übereinstimmung mit Brauns,[11] Jerweys[12] und Jagodzinskys[13] Arbeiten.

Im Zusammenhang zu den mit Titan dotierten Proben, machen wir folgende Bemerkungen : In den Beugungsspektren kommt nur das Bild des Aluminiumoxyds vor, wobei eine Stabilisierung der η Form erscheint. Es wurde eine mittlere Kristallitgröße von etwa 40 Å berechnet. Man bemerkt außerdem, daß die Anwesenheit des Titans bei jedwelcher Konzentration den Höhepunkt bei 1,990 Å nicht ändert. Zum Unterschied zu der Dotierung mit Lithium, befindet sich das Titan fein dispergiert auf die Oberfläche der Aluminiumoxydpartikeln.

---

[11] P. D. Braun, *Nature*, **170**, 1123 (1959).

[12] E. S. W. Jerwey, *Z. Krist.*, **91**, 317 (1935).

[13] H. Jagodzinsky und H. S. Saalfeld, *Z. Krist.*, **110**, 197 (1958).

4. SCHLUSSFOLGERUNG

Infolge der Untersuchung der Röntgenstrahlen Diffraktogramme des dotierten und reinen Aluminiumoxyds, kamen wir zur Schlußfolgerung, daß inunseren Herstellungsbedingungen der Proben, nur die Lithiumionen völlig im Aluminiumoxydgitter eingedrungen sind und das Aluminat mit der wahrscheinlichen Grenzstruktur $Al[Li_{0.5}Al_{1.5}]O_4$, in der in den geraden Klammern die oktaedrischen Plätze bezeichnet wurden, bildeten.

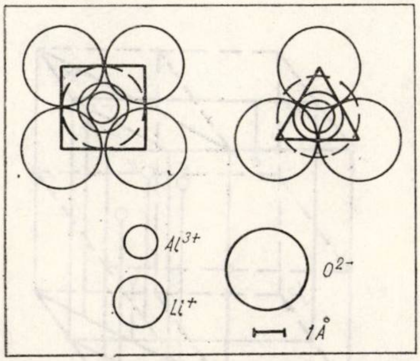

Abb. 3. — Die Projektion auf einer Achse der oktaedrischen (links) und tetraedrischen (rechts) Umkreisungen. Die Abbildungen wurden bei Maßstab gezeichnet.

In unseren Herstellungsbedingungen dringen die Ti^{4+} Ionen im Kristallgitter des Aluminiumoxyds nicht ein.

Revue Roumaine de Chimie, 18, 5, 809–814 (1973)

TITANIUM (IV) CHLORIDE COMPLEXES WITH COBALT (II) CHELATES OF TETRADENTATE SCHIFF BASES

N. S. BIRADAR*, V. B. MAHALE and V. H. KULKARNI
Department of Chemistry, Karnatak University, Dharwar – 3

Received November 7, 1972

The square planar cobalt (II) Schiff base complexes react with titanium (IV) chloride in chloroform medium to form complexes of 1 :1 stoichiometry. The characterization of these bimetallic complexes using magnetic and visible spectral data shows that cobalt (II) has changed its configuration from square planar to tetrahedral on reaction with $TiCl_4$. The i.r. data show that one of the two chelate rings is ruptured during the reaction. The probable structures have been suggested for these bimetallic complexes depending on the available evidences.

INTRODUCTION

The ability of some Schiff base complexes to function as neutral ligands under certain conditions has been the subject matter of a good number of publications.[1–3] They have used X-ray crystallographic information, i.e., n.m.r. and Moessbauer spectral data to characterize the complexes. Hobday and Smith[4–5] have shown that N, N′-ethylene-*bis* (salicylidene-aminato) cobalt (II) reacts with PCl_3 and $AsCl_3$ to yield cyclic derivatives and the square-planar stereochemistry of cobalt (II) changes to tetrahedral, while the complexation of $SnCl_4$ with $[M^{II}$ (Salen)] does not change the square-planar stereochemistry of M(II). Kogan and co-workers[6] have demonstrated that the reaction of titanium (IV) chloride with transition metal complexes of bidentate Schiff bases leads to the formation of substitution complexes. However, the literature records no attempts on the synthesis of titanium (IV) complexes with cobalt (II) tetradentate Schiff base complexes.

---

* To whom all the correspondence should be addressed.

[1] E. SINN and C. M. HARRIS, *Coord. Chem. Rev.*, **4**, 391 (1969).

[2] E. N. BAKER, D. HALL and T. N. WATERS, *J. Chem. Soc.*, (*A*), **1970**, 400.

[3] P. A. YEATS, J. R. SAMS and F. AUBKE, *Inorg. Chem.*, **9**, 740 (1970) ; M. F. FARONA and J. G. GRASSELLI, *Inorg. Chem.*, **6**, 1675 (1967).

[4] M. D. HOBDAY and T. D. SMITH, *J. Chem. Soc., (A)*, **1970**, 1085.

[5] M. D. HOBDAY and T. D. SMITH, *J. Chem. Soc., (A)*, **1971**, 1453.

[6] V. A. KOGAN, V. P. SOKOLOV, O. A. OSIPOV and V. N. EVREEV, *Zhur. neorg. Khim.*, **15**, 778 (1970).

In the present paper we wish to report titanium (IV) complexes with tetradentate Schiff base complexes of cobalt (II). The complexes of 1 :1 stoichiometry are formed and observations are consistent with the tetrahedral stereochemistry about cobalt (II).

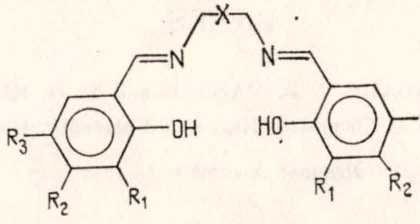

R	R_2	R_3	X	
			E_n	P_n
H	H	H	I	VI
CH_3	H	H	II	VII
H	CH_3	H	III	VIII
H	H	CH_3	IV	IX
H	H	Cl	V	X

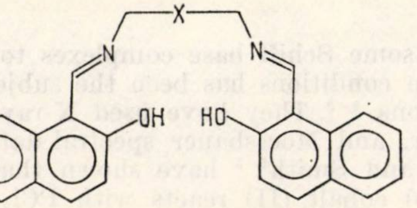

XI X = En
XII X = Pn

EXPERIMENTAL

The chemicals used in preparing the complexes were of reagent grade. The substituted salicylaldehydes were prepared by the Duff method.[7]

Schiff bases of ethylenediamine and propylenediamine with substituted salicylaldehydes were prepared according to the method reported elsewhere.[8]

Cobalt (II) complexes with the Schiff bases I–XII were prepared in ethanol medium[9] and dried in vacuum over fused calcium chloride.

---

[7] J. C. Duff, *J. Chem. Soc.*, **1941**, 547.

[8] N. S. Biradar and V. H. Kulkarni, *Rev. Roumaine Chim.*, **15**, 1993 (1970).

[9] R. H. Bails and M. Calvin, *J. Amer. Chem. Soc.*, **69**, 1886 (1947).

GENERAL METHOD FOR PREPARING TITANIUM (IV) COMPLEXES

Cobalt (II) complex prepared as above was dissolved in chloroform and treated with titanium (IV) chloride in 1 :1 molar proportion, with vigorous shaking, and left to stand for several hours at room temperature with occasional shaking. The resulting precipitate of bimetal complex was filtered off and washed with chloroform and dried *in vacuo.*

ELEMENTAL ANALYSIS

In all the complexes titanium was precipitated as hydroxide, filtered, weighed as TiO_2 after ignition. Cobalt in the complexes was estimated gravimetrically as 8-hydroxy-quinolinate. Chloride was determined as AgCl and nitrogen by the Kjeldahl method. The results of the elemental analysis are shown in Table 1.

Table 1

Elemental analysis of the complexes *

S. Nº	Complex	%Ti	%Co	%N	%Cl
1	Co(Salen)$TiCl_4$	9.30 (9.30)	10.74 (11.45)	5.20 (5.44)	26.81 (27.57)
2	Co(3-Me-Salen)$TiCl_4$	8.32 (8.82)	9.65 (10.85)	4.74 (5.16)	25.89 (26.15)
3	Co(4-Me-Salen)$TiCl_4$	8.40 (8.82)	10.79 (10.85)	5.06 (5.16)	26.01 (26.15)
4	Co(5-Me-Salen)$TiCl_4$	8.50 (8.82)	10.37 (10.85)	4.93 (5.16)	26.00 (26.15)
5	Co(5-Cl-Salen)$TiCl_4$	7.90 (8.20)	9.53 (10.01)	4.60 (4.79)	23.78 (24.15)
6	Co(2-OH-Naphthalen)$TiCl_4$	7.52 (7.78)	10.36 (9.58)	4.30 (4.55)	22.91 (23.09)
7	Co(Salpn)$TiCl_4$	8.72 (9.05)	11.00 (11.14)	4.82 (5.29)	26.00 (26.84)
8	Co(3-Me-Salpn)$TiCl_4$	8.23 (8.59)	10.25 (10.58)	4.95 (5.03)	25.00 (25.50)
9	Co(4-Me-Salpn)$TiCl_4$	8.18 (8.59)	10.30 (10.58)	4.85 (5.03)	24.78 (25.50)
10	Co(5-Me-Salpn)$TiCl_4$	8.26 (8.59)	9.96 (10.58)	5.09 (5.03)	25.17 (25.50)
11	Co(5-Cl-Salpn)$TiCl_4$	7.95 (8.00)	9.64 (9.85)	4.50 (4.68)	23.61 (23.74)
12	Co(2-OH-Naphthalpn)$TiCl_4$	7.23 (7.61)	8.92 (7.37)	4.18 (4.45)	22.25 (22.57)

* The values in the parentheses are the calculated values.

PHYSICAL MEASUREMENTS

Infrared spectra of the complexes in nujol mulls were recorded on a Beckman IR-20 spectrophotometer in the 4000 – 250 cm^{-1} region.

Visible spectra were obtained on a Unicam S.P. 700 A recording spectrophotometer. The samples were prepared in nujol mulls. The solution spectra were taken on a Hilger

UVISPEK H-700 using 2 cm glass cells in the region 550 — 750 mμ. The samples were dissolved in DMF (A.R. grade) and diluted to the required strength.

The magnetic measurements were made at room temperature on a Gouy balance with glass tube calibrated for diamagnetism.

The molar conductance measurements of the complexes in DMF were made with an ELICO conductivity bridge having a cell of cell-constant 0.829 cm^{-1} manufactured by Electronic Industrial Instruments Co. Hyderabad.

RESULTS AND DISCUSSION

All the complexes are green in colour, amorphous and soluble in DMF. The elemental analysis (Table 1) shows that titanium (IV) chloride forms complexes of 1 :1 stoichiometry with square-planar cobalt (II) Schiff base complexes of the ligands I—XII.

The molar conductance values in DMF at the concentration 10^{-3} M show that all these complexes are non-electrolytes in DMF.

MAGNETIC PROPERTIES

The magnetic moments obtained at room temperature for the cobalt (II) complexes show μ_{eff} in the range of 2.23—2.58 BM indicating that these all possess a low-spin square-planar configuration. The bimetal complexes formed as a result of reaction of titanium (IV) chloride with cobalt (II) Schiff base complexes exhibit μ_{eff} around 4.5 BM, showing that cobalt (II) has changed its configuration from square-planar to tetrahedral as a result of complexation with titanium (IV) chloride. This finds additional support in the study of visible spectra.

VISIBLE SPECTRA

The visible spectra of the complexes have been studied with a view to establish the configuration of the bimetal complexes and to find further proof in support of the above conclusion. The square-planar cobalt (II) complexes show a band maximum around 1175 mμ. This is the characteristic band for the low-spin square-planar cobalt (II) complexes. This band is not observed in bimetal complexes of titanium (IV). Hence it may be concluded that cobalt (II) has lost its square-planar configuration in bimetal complexes.

In all the spectra, we observe an intense multicomponent band in the region 600 — 750 mμ. It is known that cobalt (II) complexes having tetrahedral configuration possess a characteristic intense multicomponent band associated with $^4A_2 \rightarrow {}^4T_1$ (P) transition in the region 600 — 800 mμ.[10,11] The multicomponent band observed in these bimetal com-

---

[10] R. H. Holm and F. A. Cotton, *J. Amer. Chem. Soc.*, **82**, 2979 (1960).

[11] M. Goodgame, *J. Chem. Soc., (A).*, **1966**, 63.

plexes, therefore, may be attributed to the $^4A_2 \rightarrow {}^4T_1(P)$ transition. Our observations agree well with the known tetrahedral cobalt (II) complexes.[12]

The complexes are soluble in DMT and solutions are green in colour. The visible spectra in the region 550 — 750 mμ exhibit two intense bands around 610 mμ and 675 mμ with an inflexion at 650 mμ. This multicomponent band is attributed to $^4A_2 \rightarrow {}^4T_1(P)$ transition and indicates that cobalt (II) maintains its tetrahedral stereochemistry even in the solutions. Unlike the bimetal complexes of tin (IV) which undergo change in DMF and give rise to tin (IV) Schiff base complexes,[5] these do not show any change in colour even after standing for several hours. Our observations agree well with those of Balmfield.[13]

INFRARED SPECTRA

The formation of cobalt (II) complexes with the tetradentate Schiff bases is indicated by the shift of an intense band in the region 1640 — 1620 cm^{-1} of the base, attributable to the C=N stretch, to the lower

Table 2

Infrared frequncies (in cm^{-1}) of titanium (IV) bimetallic complexes and their assignments

	ν (Co-N)	ν (Ti-Cl)	ν (Co-Cl)
1	545 m	350 m	295 m
	465 m	—	—
2	540 m	350 m	305 m
	455 m	—	—
3	530 br.m.	350 m	305 m
	450 br.m.	—	—
4	550 m	355 m	310 m
	465 m	—	—
5	550 s	360 m	290 s
	470 s	—	—
6	555 m	350 m	295 m
	490 m	—	—
7	530 br.m.	350 w	310 m
	470 br.m.	—	—
8	520 m	350 m	290 m
	450 m	—	—
9	530 br.	350 w	305 m
	470 br.m.	—	—
10	545m	350 m	310 m
	450 m	—	—
11	540 m	350 m	320 m
	470 m	—	—
12	550 s	350 m	295 m
	470 s	—	—

---

[12] C. K. Jorgensen, *Acta Chem. Scand.*, **8**, 1495 (1954).

[13] P. Bamfield, *J. Chem. Soc., (A)*, **1967**, 804.

frequency 1620—1600 cm^{-1}. The phenolic C—O vibration around 1280 cm^{-1} of the base is found in the region 1340—1310 cm^{-1} in the cobalt (II) complexes.

In the bimetallic complexes with titanium (IV) chloride, we observe an intense band around 1650 cm^{-1}, and the phenolic C—O stretch is found around 1280 cm^{-1}.

The bands around 590 and 520 cm^{-1} assignable to ν(Co—N) vibrations[14] are much altered in the bimetallic complexes.

The cobalt (II) Schiff base complexes do not show any absorption around 310 cm^{-1} attributable to ν(Co—Cl) vibration,[15] whereas the bimetallic complexes show an intense band around 310 cm^{-1} and may be attributed to ν (Co—Cl) vibration. This provides an evidence that Co—Cl bond is formed when titanium (IV) chloride has reacted with cobalt (II) complexes.

All these observations together with magnetic and electronic spectral evidences establish that the square planar coordination around cobalt (II) ion is disrupted on reaction of titanium (IV) chloride with tetradentate Schiff base cobalt (II) complexes. Similar observations have been made by Hobday and Smith.[4]

Taking into consideration all the above experimental evidences, we propose the following structure for these bimetallic complexes.

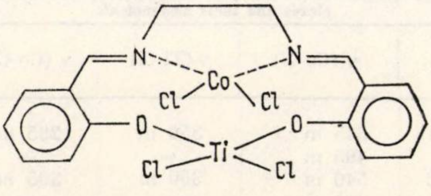

Acknowledgement. Authors wish to thank Prof. C.C. Patel, I.I. Sc., Bangalore, for the facilities provided for magnetic and spectral measurements.

---

[14] K. Ueno and A. E. Martell, *J. Phys. Chem.*, **60**, 1270 (1956); J. R. Durig, B. R. Mitchell, D. W. Sink, J. N. Willis, and A. S. Wilson, *Spectrochim. Acta*, **23 A**, 1121 (1967); C. P. Prabhakaran and C. C. Patel *J. Inorg. Nuclear Chem.*, **31**, 3316 (1969); B. C. Sharma and C. C. Patel, *Indian J. Chem.*, **8**, 747 (1970).

[15] R. J. H. Clark, *Spectrochim. Acta*, **21**, 955 (1965).

Revue Roumaine de Chimie, 18, 5, 815–821 (1973)

STUDIES ON COORDINATION COMPOUNDS
THIOUREA AND PHOSPHINE COMPLEXES OF Ni(II) AND Co(II)

IRSHAD A. KHAN and ANWAR H. HASHMI,

Department of Chemistry,
University of Karachi,
Karachi: — 32

Received August 2, 1972

The work described here consists of synthesis, chemical and spectral studies of some new transition metal complexes containing mixed ligands and bearing the general formula $(ML_4 \cdot 2H_2O)\ X_2$ (where M = Ni or Co ; L = thiourea or triphenyl phosphine ; X = Cl, Br or CN). The spectra of $Co\ (Thio)_5\ (NO_3)_2$ shows that at least one nitro group is forming coordination linkage with metal atom.

Coordination compounds of ligands containing more than one donor group, have been of great interest during recent years. The preferential bonding of one of the groups have been the subject of discussion in many cases.[1,2] Amino acids, amides and dithiocarbamates are some such ligands, but the compounds containing water molecules along with thiourea or triphenyl phosphine are rare.

In the present work we have tried to prepare such aqua complexes in which water molecules are coordinated to metal atom with other simple ligands and both the ligands are situated within the coordination sphere. The general formula for the complexes is proposed to be $(ML_4 \cdot 2H_2O)X_2$. The metals to be tried are nickel and cobalt, anions under consideration are chloride, bromide and cyanide. The ligands thiourea and triphenyl phosphine have been introduced.

Dipole-moment of thiourea indicates a resonance hybrid with 20 – 30% contribution of highly polar structure of thiourea.[3] Electrographic studies [4] of high temperature phase of thiourea shows the intermediate character of C—S bond between a single and double bond, whereas the value of C—M bond comes out to be 1.33 A, which proved the structure of thiourea highly polar.

---

[1] C. L. ROLLIFSON and R. G. WHITE, *Inorg. Chem.*, **1**, 281 (1962).

[2] R. E. PENLAND, S. MIZUCHLIMA, C. CURRAN and J. V. QUAGLINANO, *J. Amer. Chem. Soc.*, **79**, 1575 (1957).

[3] W. D. KULMAR and G. M. FOHLER, *J. Amer. Chem. Soc.*, **64**, 1944 (1942).

[4] V. F. DORYANKIN and B. K. VAINSHTEIN, *Kristallografiya*, **5**, 589 (1960).

RESULTS AND DISCUSSION

All the compounds described here are new except [Ni(Thio)$_6$]Br$_2$ and [Ni(ThiO)$_6$](NO$_3$)$_2$ which have been reported by other[5,6,7] workers. However, the methods of preparation of these two adopted here are original in itself and different from those already reported. Although triphenyl phosphine has been commonly used as ligand, however, the compound containing this ligand, obtained here is new and has not been reported anywhere else. Analysis and other characteristics of these compounds have been tabulated in Table 1.

Table 1

Analysis, melting point and state of the complexes

Compound	Metal %		S%	N %	C%	H%	M.P.C°.	Colour
[Ni(Thio)$_4$2H$_2$O]Cl$_2$	Found	12.49	27.25	23.84	10.22	4.26	192(d)	Yellow
	Calcd	12.22	27.84	23.18	9.69	3.54		
[Ni(Thio)$_4$2H$_2$O]Br$_2$	Found	10.51	22.57	21.10	8.76	3.69	204(d)	Brownish
	Calcd	10.57	22.92	20.05	8.59	3.58		Yellow
[Ni(Thio)$_6$]Br$_2$	Found	8.64	28.35	24.80	11.32	3.44	181(d)	Green
	Calcd	8.70	28.46	24.91	10.68	3.55		
[Ni(Thio)$_6$](NO$_3$)$_2$	Found	9.31	29.99	30.99	11.15	3.50	162	Green
	Calcd	9.22	30.15	30.78	11.31	3.76		
Co(Thio)$_5$(NO$_3$)$_2$	Found	10.46	27.64	30.00	10.69	3.82	118	Dark Brown
	Calcd	10.48	28.42	29.84	10.66	3.55		
[Co(Thio)$_4$2H$_2$O]Cl$_2$	Found	13.00	27.90	33.13	10.33	3.82	135(d)	Dark blue
	Calcd	12.55	27.24	23.83	10.21	4.20		
[Ni(PH$_3$P)$_4$.2H$_2$O](CN)$_2$	Found	5.10	—	2.51	74.35	5.09	224(d)	Yellow
	Calcd	4.94	—	2.34	74.32	5.36		

Spectra observed for free thiourea in the 700 – 2000 cm^{-1} range agree well with those reported by other workers.[8,9,10] But the band observed at about 2685 cm^{-1} in this work which was not reported by Yamaguchi,[11] it is assigned to N—H bonds. This conclusion is also supported by Ollif's idea, as it will be discussed later in the case of complexes. Absorption at 1613 cm^{-1} has been assigned to NH$_2$ bonding vibrations. Yamaguchi[11] observed a splitting in this region and reported two bands at 1610 cm^{-1} and 1625 cm^{-1} corresponding to two symmetries A and B, respectively. This type of splitting, however, has not been observed in this work.

The band observed at 1983 cm^{-1} corresponds to NH$_2$ rocking modes and indicates the coincidence of A$_1$(a$_1$) and B$_1$(b$_2$) NH$_2$ rocking modes.

---

[5] J. Rosenheim and W. Meyer, *Z. anorg. Chem.*, **49**, 13 (1906).

[6] A. V. Babaeva and Pei-Ta-Yang, *Zhur. neorg. Khim.*, **5**, 2735 (1960).

[7] L. A. Salsheheva, M. I. Usanovich and T. N. Smarokva, *Zhur. strukt. Khim.*, **16** *3*, 19 (1966).

[8] W. Stewart, *J. Chem. Phys.*, **26**, 248 (1957).

[9] E. E. Eynsley and W. A. Compbell, *J. Chem. Soc.*, **1958**, 3290.

[10] R. W. Ollif, *J. Chem. Soc.*, **1965**, 2036.

[11] A. Yamaguchi, R. H. Penland and S. Mizuchima, *J. Amer. Chem. Soc.*, **80**, 527 (1958).

Calculation of Yamaguchi[11] shows that they should be distinct. Ollif,[10] however, observed a broader and weaker band at 1200 cm^{-1}, which was completely absent in the complexes.

The absorptions in 3400...3200 cm^{-1} region may conveniently be assigned to the N—H bonds, that does not seem to be shifted significantly by coordination. This region of spectrum can thus be used to determine the donor atom in a given complex. The band observed by Ollif[10] at about 3400 cm^{-1} corresponding to N—H bonds has not been observed in free thiourea or in any of the complexes. These bands are broader and this nature is most probably due to the hydrogen bonding in free thiourea.

Table 2

Infrared absorption frequencies for thiourea and its complexes

(Range 650—4000 cm^{-1})

$SC(NH_2)_2$	$[Ni(Thio)_4.2H_2O]Cl_2$	$[Ni(Thio)_4.2H_2O]Br_2$	$[Co(Thio)_4.2H_2O]Cl_2$	$Co(Thio)_5(NO_3)_2$
	3442 S	3445 S	3459 S	
3377 S	3368 S	3364 S	3380 S	3376 S
3274 S	3280 S	3280 S	3280 m	3275 S
3178 S	3180 S	3182 S	3184 S	3180 S
2685 m	2700 S	2695 W	2710 W.b.	2700 W.b.
				1754 V.S.
1613 S	1605 S	1602 S	1620 W	1635 S.b.
		1608 Sh.	1606 S	1625 S.
1464 m	1474 S	1480 S	1476 S	1494 S
	1435 W	1440 Sh.	1418 Sh.	
1410 S	1393 S	1390 S	1397 S	1388 S
1083 S	1088 m	1090 S	1090 S	1110 W
	720 Sh.	722 Sh.	717 Sh.	825 m
729 Sh.	713 S	717 S.	706 S	703 S

The infrared absorption spectra of the compounds $[Ni(Thio)_4 2H_2O]X_2 (X=Cl$ or Br) proved that water is coordinated to a metal atom. Tibor Sramko[12] prepared $[Ni(Thio)_6]Br_2$ and $[Ni(Thio)_6](NO_3)_2$ by dissolving nickel nitrate, hexahydrate and lithium bromide dihydrate in acetone and adding thiourea during constant mixing, molar ratio (Ni : Thio = 1 : 9) and the latter one in acetone media, taking molar proportion (1: 6). Whereas, in the present work, these compounds are prepared by simple methods and with high yields.

The absorptions in the infrared region of new complexes are tabulated in Table 2.

Bonds observed in 3 u region at 3368, 3280, 3180 cm^{-1} for $[Ni(Thio)_4 .2H_2O]Cl_2$, 3364, 3280, 3182 cm^{-1} for $[Ni(Thio)_4.2H_2O]Br_2$ are undoubtedly assigned to the N—H stretching vibrations. These bands are broader in nature. This broader nature of these bands is assigned to considerable hydrogen bonding but not as much as in thiourea. Though Yamaguchi[11] observed the sharpening of these bands for $Ni(Thio)_2(NSC)_2$ and discussed the complete absence of hydrogen bonding. However, this sharpening is restricted only to the said compound and has not been observed for any other complex. This hydrogen bonding is similar to that described by Cavalca [13] for the compounds like $[Ni(Thio)_6]Br_2$ i.e., (Br. . .H—N). The absorptions at 3442 and 3445 cm^{-1} may conveniently be assigned to O—H stretching, indicating the presence of water in the coordination sphere. N—H bonds of the ligand thiourea gave the absorptions at 2700 and 2695 cm^{-1}. This band is not shifted appreciably on coordination which is intensive to the bonding through sulphur. Stewart [8] assigned the band as a combination of C=S and S—C—N stretching vibrations. Such a combination must be sensitive to the complex formations. That does not happen further more. These bands are not appreciably shifted from their positions. This supports the idea that these bands are due to N—H bonds.

---

[12] S. Tibor, *Chem. Zvesti*, **15**, 271 (1961).

Bands observed at 1474 and 1480 cm^{-1} (for chloride and bromide complexes, respectively) correspond to B_1 type N—C—H stretching mode, found at 1464 cm^{-1} in free thiourea. It should be sensitive to coordination through sulphur, and it increases its electron demand and thereby the double bond character of C = S decreases, whereas, the double bond character of C—N bond increases, resulting in an increase in frequency. The absorptions at 1410, 1083 and 729 cm^{-1} in free thiourea have previously been assigned to three A_1 modes, i.e. C≡S stretching, N—C—N stretching and NH_2 rocking. As it has been stated above, coordination will lead to a decrease in the C = S stretching frequency and an increase in N—C—N stretching frequency. Observed frequency will result from "hybrids" of these three modes and the effect of coordination on the frequency will depend on their relative weightings in each hybrid. . .

On coordination through sulphur, the nature of vibration is changed slightly causing a change in 1410 cm^{-1} band of thiourea (i. e. 1393 and 1390 cm^{-1}) but the presence of other absorption bands in this region makes interpretation difficult. However, the decrease has been observed. Peculiar result has been obtained in the region of 1100 cm^{-1}. Yamaguchi[11] observed that the intensity of a strong band at 1083 cm^{-1} of free thiourea is extremely weakened or disappears on complex formation. He explained that, since N—C—N stretching vibration (A_1) which increases on complex formation, cannot contribute much to the intensity in the 1100 cm^{-1} region and the major contribution which is due to C=S stretching decrease, hence the intensity of this band has decreased. We observed that this decrease is not as great as stated by Yamaguchi, but instead there is a broadening in the band, which certainly cannot be due to the relative increase or decrease of "weighting" in the "hybrid", which can produce only shift and not broadening.

For these complexes the intensity has not been decreased appreciably. The bands observed at 713 and 1717 cm^{-1} for chloride and bromide complexes correspond to 729 cm^{-1} band for free thiourea. The decrease in frequency on coordination is attributed to the decrease in double bond character of C = S bond. A similar but smaller effect of broadening the band in 1100 cm^{-1} region has been observed, which is most probably the effect of coordination.

---

[13] L. Cavalca, M. Nardelli and A. Baribenti, *Gazz. chim. Ital.*, **86**, 942 (1956).

Two new cobalt complexes $[Co(Thio)_4 2H_2O]Cl_2$ and $Co(Thio)_5(NO_3)_2$ have been prepared in alcoholic media. Except the band observed at 3459 cm^{-1} which corresponds to the coordinated water, spectra of both complexes are identical in 3 u region. The observations at 3380, 3280, 3184 and 3376, 3275, 3180 for chloride and nitrate complexes, respectively, in 3 u region are assigned to NH_2 bonds. Coordination of thiourea through nitrogen causes a splitting of these bands into groups and the decrease in their intensity.[10] None of these effects has been observed. This proves that the bonding is through sulphur, moreover, these bands are little sharper than those in thiourea which shows that hydrogen bonding is decreased up to some extent.

A weak broad band observed in the region at 2700 cm^{-1} corresponds to 2685 cm^{-1} band of thiourea assigned to N—H bonds, contrary to Yamagachi [11] who assigned it to C = S bonds. Since coordination through sulphur must bring about some changes in the double bond character of C=S bond and this must bring a shift in the position of the band, which is not the case, thus the idea that this band is due to N—H bonds seems to be more true.

In the spectra of thiourea we have assigned the band at 1613 cm^{-1} as due to NH_2 deformation. On complex formation this has been observed to split up and actually two bands have been observed in the complexes as it is obvious from Table 3, corresponding to two symmetries A_1 and B_1. This result supports Yamaguchi's analysis whereas it is quite contrary to Stewart [8] who did not observe this splitting.

Bands observed at about 1476 and 1494 cm^{-1} in these complexes correspond respectively, to 1464 cm^{-1} band of free thiourea and, due to N—C—N stretching, they are sensitive to bonding through sulphur. Absorptions at about 1400 cm^{-1} region, 1100 cm^{-1} region and 700 region have already been assigned to the bonding through sulphur and have been appreciably shifted from their positions.

Absorption at 1110 cm^{-1} for $Co(Thio)_5(NO_3)_2$ is very weak and agrees with the idea that for this complex, the chance of hydrogen bonding is least. [11] Bands observed at 825 and 1754 cm^{-1} are assigned to nitrate groups. The former one has not been shifted from its position for ionic nitrates, whereas, that at 1754 cm^{-1} has gone out of range and thus shows coordination of at least one nitrate group. Hence, the compound is better formulated as $[Co(Thio)_5(NO_3)]NO_3$. Brown [14] studied a number of nitrate esters and observed that coordinated nitrate shows a sharp peak in the range 1610—1652 cm^{-1}. Similar type of shift has been observed by Beattle[15] for nitrate compounds, when the group goes into the coordination sphere. The band observed at 717 cm^{-1} for $[Co(Thio)_4 2H_2O]Cl_2$ corresponds to chlorine and there is no considerable shift from its normal position for ionic chlorides.

---

[14] J. F. Brown, *J. Amer. Chem. Soc.*, **77**, 6341 (1955).

[15] I. R. Beattic and H. J. V. Tyrrelli, *J. Chem. Soc.*, **1956**, 2849.

Yellow coloured plates, obtained by the reaction of nickel cyanide with triphenyl phosphine, were found quite stable under nitrogen and ether vapours. Whereas, it readily decomposes in air. The formula assigned to this new compound is $[Ni(Ph_3P)_4.2H_2O](CN)_2$. Its infrared spectra are listed parallel to the spectra observed for pure triphenyl phosphine, in Table 3.

Table 3

Infrared absorptions frequencies in 650–4000 cm^{-1} region

Ph_3P	$[Ni(Ph_3P)_4.2H_2O](CN)_2$	
696 s	708 s	H–C out of plane deformation
743 vs	862 s	
998 m	1013 m	
1027 vs	1040 sh	
1071 s	1051 s	H–C in plane deformation
1090 s	1104 s	
—	1110 sh	
1180 w	1195 m	
1280 m	—	
1365 sh	1380 s	
1434 vs	—	P–C Stretching
1580 vs	—	
—	2132 vs	C–N-Stretching
3030 s	—	C=C Stretching
—	3374 s	O–H Stretching

The strong band observed at 3374 cm^{-1} may conveniently be assigned to C–H stretching, supporting the presence of water in the coordination sphere. The reported bands of triphenyl phosphine at 3030 cm^{-1} and 1580 cm^{-1} have disappeared in the complex, attributed to –CH=CH-stretching. Coordination of phosphorus to metal which may cause an electron attraction thereby producing hinderance in the delocalization of electrons, may be the reason of disappearance.

Absorption at 1434 cm^{-1} observed for triphenyl phosphine is however eliminated in the complex. This band is assigned to P–C stretching and may be due to ring vibrations. However, the 1434 cm^{-1} band is not shown in many of the spectra and there is no reason to suppose that this is not a reliable and useful correlation for P-phenyl group.[16] Dassch and Smith[17] found bands in the region 1005–995 cm^{-1} in their work attributed to P-aryl group. The band observed in this work at 1051, 1040 and 1013 cm^{-1} have quite close relation to the work mentioned above. The shifting of the absorption may be due to the coordination of phosphorus to nickel.

---

[16] D. E. C. Cobridge, *J. Appl. Chem.*, **6**, 456 (1956).

[17] L. W. Dassch and D. C. Smith, *Analyl. Chem.*, **23**, 853 (1951).

The absorption at 1104 cm^{-1} for the complex corresponds to 1090 cm^{-1} band of triphenyl phosphine and is assigned to an in-plane C—H deformation mode.[18] Generally, these bands for mono-substituted aromatic ring are found in the region 1050—1190 cm^{-1}. Peaks observed at 708 cm^{-1} and 862 cm^{-1} correspond to 696 and 743 cm^{-1} bands of triphenyl phosphine, and may be attributed to aromatic carbon hydrogen out of plane deformation. All these shifts in the bands indicate the coordination of triphenyl phosphine, in the complex, whereas the frequencies at 3374 and 2132 cm^{-1} support the coordination of water and ionic nature of CN group.

EXPERIMENTAL

$[Ni(Thio)_4.2H_2O]Cl_2$ — A mixture of thiourea and partly dehydrated nickel chloride (molar proportion, 4 : 1) in anhydrous methanol was refluxed for 20 minutes. The resulting green solution gave yellow crystals which are recrystallized in methanol. Yield : 58.24 %. Stable in air and unstable in water.

$[Ni(Thio)_4.2H_2O]Br_2$— The same procedure was adopted as mentioned above, having the refluxing time 45 minutes. Brownish yellow crystals were obtained from the resulting solution, which were recrystallized in methanol. Yield : 52 %. Stable in air and unstable in water.

$[Ni(Thio)_6]Br_2$— Procedure adopted was the same as described above with 30 minutes refluxing time. The resulting green solution was concentrated and 5 ml of dry ether was mixed with it and left overnight. Green crystalline material crystallized out. It was washed and recrystallized in methanol. Yield : 94 %. Stable in air and unstable in water.

$[Ni(Thio)_6](NO_3)_2$— Above mentioned procedure was adopted for the preparation. The compound obtained was crystalline. Yield : 95.3 %. Stable in air and unstable in water.

$[Co(Thio)_4 2H_2O]Cl_2$ — A mixture of thiourea and partly dehydrated cobalt chloride (molar proportion 4 : 1) in anhydrous methanol was refluxed for one hour. The resulting blue solution was concentrated and mixed with 10 ml dry ether. Next day, dark blue crystals were separated and recrystallized in methanol. Yield : 62.9 %.

$Co(Thio)_5(NO_3)_2$— Above mentioned procedure was adopted having the refluxing time of 30 minutes. Dark brown crystals were obtained from the resulting solution which were recrystallized in methanol; Yield : 58 %.

$[Ni(Ph_3P)_4.2H_2O]\ (CN)_2$— To the refluxing solution of triphenyl phosphine in anhydrous methanol, nickel cyanide (molar proportion 4 : 1) was added in small portions. The mixture was refluxed for one hour. The volume of the resulting yellow solution was reduced and mixed with dry ether and placed at —5° for 7 — 10 days in air tight flask. Yellow crystals (plates) were obtained. They were recrystallized in the same solvent. Unstable in air and water, stable in dry ether, dry methanol and dry nitrogen. Yield : 10 %.

---

[18] J. Chatt and D.M.P. Mingos, *J. Chem. Soc.*, (A), **1969**, 1770.

Revue Roumaine de Chimie, **18**, *5*, 823–828 (1973)

ÜBER α-DIOXIMINKOMPLEXE DER ÜBERGANGSMETALLE. XXXVI *

NEUE DIMETHYLGLYOXIMIN-CHELATE DES KOBALTS (III) MIT α, α'-DIPYRIDYL UND *o*-PHENANTHROLIN

CSABA VÁRHELYI, ION GĂNESCU und MIRCEA PREDA

Aus der Chemischen Fakultät der Universität, Craiova,
Calea Bucureşti 165

Eingegangen am 4. Oktober 1972

Es wurde die Oxydation von Kobalt (II) Salz-Lösung in Anwesenheit von Dimethylglyoxim und heterocyclischen N-Basen untersucht und 25 Salze der $[Co(DH)_2Dipy]^+$ und $[Co(DH)_2(o\text{-phen})]^+$-Katione durch doppelte Umsetzungsreaktionen erhalten. Diese Annahme wurde auch durch U.R. spektroskopische Untersuchung behauptet.

Wie aus präparativen und IR-spektroskopischen Untersuchungen hervorgeht, gehören die meisten, bis heute erhaltene bis-Dimethylglyoximin-Chelate des Kobalts(III) vom Typ: $[Co(DH)_2AB]$ mit zwei einzähnigen Liganden (A und B) zu der *trans*-Reihe. Die zwei sehr kurzen, in diesen Verbindungen auftretenden O-H..O Wasserstoffbindungen stabilisieren die $Co(DH)_2$..-Gruppe, bzw. die *trans* geometrische Konfiguration der $[Co(DH)_2AB]$-Komplexe.[1-3] (DH= das deprotonierte Dimethylglyoxim).

Bis-dimethylglyoximin-kobalt(III)-Chelate mit cis geometrischer Konfiguration entstehen in Anwesenheit von zweizähnigen Liganden, wie aliphatischen Diamine (en, pn,), α-Aminosäuren (Alanin, Glycocoll) und zweibasische Säuren, wie Oxalsäure, Kohlensäure.[4-6]

In dieser Arbeit haben wir die Oxydation von Kobalt(II) salz Lösungen in Gegenwart von Dimethylglyoxim und der zweizähnigen heterocyclischen Diaminen: α, α'-Dipyridyl und *ortho*-Phenanthrolin untersucht.

---

* Part. XXXV: I. Gănescu, Cs. Várhelyi und A. Man, *Monatsh*, im Druck.

[1] K. Nakahara, *Bull. Chem. Soc. Japan*, **28**, 473 (1955).

[2] R. Ripan, Cs, Várhelyi und E. Hamburg, *Studii şi Cercetări Şti. Chim. Fil. Cluj*, **14**, 27 (1963).

[3] R. Ripan, Cs. Várhelyi und F. Hamburg, *Stud. Univ. Babeş Bolyai, Chem.*, **9** (2), 33 (1964).

[4] R. Ripan und Cs. Várhelyi, *Rev. Roumaine Chim.*, **17**, 259 (1972).

[5] A. V. Ablov, N. M. Samus und O. A. Bologa, *Zhur. neorg., Khim.*, **8**, 860 (1963).

[6] A. V. Ablov, O. A. Bologa und N. M. Samus, *Zhur. neorg. Khim.*, **11**, 2632 (1966).

Die ersten Bis-dimethylglyoximin-Chelate des Kobalts mit Dipyridyl und *o*-Phenanthrolin wurden von Pagglia[7] durch Wechselwirkung von $H[Co(DH)_2Br_2]$ mit den obenerwähnten Chelatbildnern erhalten.

Die Struktur der von Pagglia beschriebenen nicht wohldefinierten Substanzen: $Co(DH)(Dipy)_{2.25}.Br_2.3\ H_2O$, $CoDH_2.Br_2.o\text{-Phen}$, bzw. $CoD_2(DH)_2(o\text{-Phen})_3.4H_2O$ wurde bis heute nicht aufgeklärt.

Die obenerwähnten heterocyclischen Diamine treten leicht in die innere Koordinationssphäre der Kobalt(III)-dioximine:

$$2Co^{2+} + 4DH_2 + 2Dipy + 1/2O_2 = 2[Co(DH)_2Dipy]^+ + H_2O + 2H^+$$

$$2Co^{2+} + 4DH_2 + 2o\text{-Phen} + 1/2O_2 = 2[Co(DH)_2(o\text{-Phen})]^+ + H_2O + 2H^+$$

Die entstehenden $[Co(DH)_2Dipy]\ X$ und $[Co(DH)_2(o\text{-Phen})]\ X$ sind im allgemeinen leicht lösliche Chelate zweiter Ordnung und können aus verdünnten alkoholischen Lösungen durch doppelten Umsetzungsreaktionen ausgeschieden werden. Die $[Co(DH)_2Dipy]\ X$ und $[Co(DH)_2(o\text{-Phen})]\ X$-Salze lösen sich viel leichter im Wasser oder in verd. Alkohl, als die analogen Derivate: $[Co(DH)_2(Amin)_2]\ X$ mit aromatischen Aminen in der inneren Koordinationssphäre.

Für die doppelten Umsetzungsreaktionen haben wir insbesonders Komplexsalze mit voluminösen Komplexanionen $[Co(NH_3)_2(NO_2)_4]^-$, $[Cr(NCS)_6]^{3-}$, $[Cr(NCS)_4(Amin)_2]^-$, verwendet.

Es wurden 25 neue Komplexsalze im festen Zustand isoliert und charakterisiert. (Siehe Tabelle 1 und 2)

Es ist bemerkenswert, daß, in $[Co(DH)_2Dipy]^+$ und $[Co(DH)_2(o\text{-Phen})]^+$ Gegensatz zu den Kationen $[Co(DH)_2(Amin)_2]^+$ mit aromatischen und heterocyclischen Aminen, für die Bildung von binären Komplexsalzen vom Typ: $[Co(DH)_2\ (Amin)_2 \cdot [Co(DH)_2X_2]$ nicht geeignet sind.

$Co(DH)_2Dipy]^+$ und $[Co(DH)_2(o\text{-Phen})]^+$ sind tricyclische Chelate mit asymmetrischer Struktur, wie $[Co(en)_3]^{3+}$, $[Co(Dipy)_3]^{3+}$, $[Co(o\text{-Phen})_3]^{3+}$ und das Nichtelektrolyt $[Co(DH)_3]$[8].

Die $[Co(DH)_2Dipy]^+$, $[Co(DH)_2(o\text{-Phen})]^+$ und $[Co(DH)_3]$ sind nicht wegen sterischen Hindernissen von kurzen intramolekularen O-H..O-Wasserstoffbrückenbindungen stabilisiert.

Wie aus unseren UR-spektroskopischen Untersuchungen hervorgeht, fehlen die schwachen, für die Wasserstoffbindungen charakteristische Banden um 1680 – 1740 cm^{-1} bei den obenewähnten Komplexen. Die zwei Dimethylglyoximin-Reste besetzen also nicht den Äquatorialplan des Oktaedermodels.

In den UR-Spektren der $[Co(DH)_2\ Dipy]ClO_4$ und $[Co(DH)_2(o\text{-Phen})]\ ClO_4$ treten neben den Absorptionsbanden der Dioximligande auch jene des Dipyridyls und Phenanthrolins und deshalb haben wie auch die Spektren des $[Co(Dipy)_3]\ (ClO_4)_3$ und $[Co(o\text{-Phen})_3]\ (ClO_4)_3$ aufgenommen und verglichen.

---

[7] E. Pagglia. *Gazz. chim. Ital.*, **87**, 1133 (1957).

[8] A. Nakahara und R. Tschuchida, *J. Amer. Chem. Soc.*, **76** 3103 (1954).

Tabelle 1

Neue Komplexsalze des Typs: $[Co(DH)_2Dipy]X$

Formel	Ausb. (% d. Th)	Charakteristik	Analyse		
				Ber.	Gef.
$[Co(DH)_2Dipy]ClO_4$	55	Braune kleine Krist.	Co N	10,78 15,36	10,66 15,20
$[Co(DH)_2Dipy]I$	60	Braun-violette mikrokrist.Masse	N Co	14,63 10,26	14,55 10,12
$[Co(DH)_2Dipy]NCS$	50	Braune mikrokrist. Masse	Co N	11,67 19,40	11,60 19,19
$[Co(DH)_2Dipy]NCSe$	40	Aggregate aus kleinen braunen Krist.	Co N	10,67 17,75	10,58 17,62
$[Co(DH)Dipy]Picrat.H_2O$	60	Gelbbraune, kleine Krist.	Co N	8,50 18,17	8,41 18,00
$[Co(DH)_2Dipy]$. $[Co(NH_3)_2(NO_2)_4]$	60	Braune mikrokrist.Masse	Co N	12,93 23,19	12,88 22,88
$[Co(DH_2)$ Dipy]. $[Cr(NCS)_4(Pyridin)_2]$	70	Rotbraune, mikrokrist. Masse	Co+Cr S	12,47 14,42	12,29 14,33
$[Co(DH_2)Dipy]$. $[Cr(NCS)_4(Dipy)]$	70	Rotbraune, mikrokrist. Masse	Co+Cr N	12,51 18,92	12,52 19,11
$[Co(DH_2)Dipy]$. $[Cr(NCS)_4(o\text{-}Phen]$	70	Rotbraune, kleine rhomb, Prismen	Co+Cr N S	12,16 18,39 14,04	12,05 18,22 13,89
$[Co(DH_2)Dipy]$. $[Cr(NCS)_4(p\text{-}Phenetidin)_2]$	66	Rotbraune unregelmäßige Platten	Co+Cr N S	11,04 16,70 12,79	11,00 16,35 12,49
$[Co(DH)_2Dipy]$. $[Cr(NVS)_4(p\text{-}Anisidin)_2]$	72	Rotbraune große Tafeln	Co+Cr N S	11,35 17,18 13,12	11,30 17,00 13,20
$[Co(DH)_2Dipy]$. $[Cr(NCS)_4(Anilin)_2]$	70	Rotbraune Nadeln	Co+Cr N S	12,09 17,76 13,57	11,92 17,69 13,50
$[Co(DH)_2Dipy]$. $[Cr(NCS)_4(p\text{-}Toluidin_2]$	75	Rotbraune, dünne Platten	Co+Cr N S	11,74 17,76 13,57	11,60 17,69 13,50
$[Co(DH)_2Dipy]$ $[Cr(NCS)_4(NH_3)_2].2H_2O$	70	Rotbraune, mikrokrist. Masse	Co+Cr N S	14,39 21,49 16,41	14,29 21,24 16,19
$[Co(DH)_2Dipy]_3$. $[Cr(NCS)_3]H_2O$	80	Gelbbraune, mikrokrist. Masse	3Co+Cr S	13,00 10,94	12,83 10,71

Tabelle 2

Neue Komplexsalze des Typs: $[Co(DH)_2(o\text{-}Phen)]X$

Formel	Ausb. (% d. Th)	Charakteristik	Analyse		
				Ber.	Gef.
$[Co(DH)_2(o\text{-}Phen)ClO_4$	60	Braune, mikrokrist. Masse	Co N	10,29 14,67	10,33 14,44
$[Co(DH)_2(o\text{-}Phen)I$	45	Braunviolette, rechtanguläre Prismen	Co N	9,82 14,00	9,71 13,82
$[Co(DH)_2(o\text{-}Phen)]NCS$	40	Gelbraune kleine Kristalle	Co N	11,09 18,45	11,20 18,12
$[Co(DH)_2(o\text{-}Phen)NCSe$	50	Braune, dünne Plättchen	Co N	10,19 16,95	10,22 16,49
$[Co(DH)_2(o\text{-}Phen)]. [Co(NH_3)_2(NO_2)_4]$	55	Aggregate aus kleinen, braunen Krist.	Co N	15,72 22,40	15,59 21,90
$[Co(DH)_2(o\text{-}Phen)]. [Cr(NCS)_4(Pyridin)_2]$	80	Rotbraune mikrokrist. Masse	Co+Cr N S	12,12 18,35 14,01	12,03 18,18 14,12
$[Co(DH)_2(o\text{-}Phen)]. [Cr(NCS)_4(Dipy)]$	82	Rotbraune rechtanguläre Prismen	Co+Cr N S	11,79 18,25 13,94	12,00 18,20 14,00
$[Co(DH)_2(o\text{-}Phen)]. [Cr(NCS)_4(o\text{-}Phen)]$	70	Rotbraune hexagonale Plättchen	Co+Cr N S	11,91 17,88 13,65	11,76 17,66 13,44
$[Co(DH)_2(o\text{-}Phen)]. [Cr(NCS)_4(p\text{-}Phenetidin)_2]$	70	Rotbraune, große Tafeln	Co+Cr N S	10,76 16,28 12,43	10,65 16,20 12,20
$[Co(DH)_2(o\text{-}Phen)]. [Cr(NCS)_4(p\text{-}Anisidin)_2]$	72	Rotbraune, dünne unregelmäßige Platten	Co+Cr N S	11,06 16,73 12,78	11,16 16,39 12,60

Die komplizierten $\nu_{C\equiv N}$, $\nu_{C=N}$ Valenz- und Deformationsschwingungen und Skelettschwingungen des Dipy und *o*-Phen erschweren die Auswertung der UR-Spektren der obenerwähnten gemischen Chelaten. [9–11]

Die wichtigsten, identifizierten Ur-Schwingungsfrequenzen der untersuchten Chelate sind in der Tabelle 3 zusammengestellt.

Für die koordinierten Dimethylglyoximligande charakteristische $\nu_{C=N}$ und ν_{N-O} Banden liegen in diesen Fällen um 1530 cm^{-1} (s.), 1240 (m) und 1100 cm^{-1} (s.) von den Dipy und *o*-Phen-Frequenzen stark beeinflußt. Die ν_{Co-N} Frequenzen erschienen, wie im Falle der klassischen Kobalt (III)-aminen, bei 500—510 cm^{-1} (s.).

---

[9] A. Schilt und R. C. Taylor, *J. Inorg. Nuclear Chem.*, **9**, 211 (1959).

[10] A. Schilt, *J. Amer. Chem. Soc.*, **81**, 2966 (1959).

[11] R. Blinc und D. Hadzi, *J. Chem. Soc.*, **1958**, 4536.

In allen untersuchten Spektren treten die Valenzschwingungsfrequenzen $\nu_{C=N}$ und $\nu_{C=C}$ der heterocyclischen Amine um 1600 und 1300 cm^{-1}.

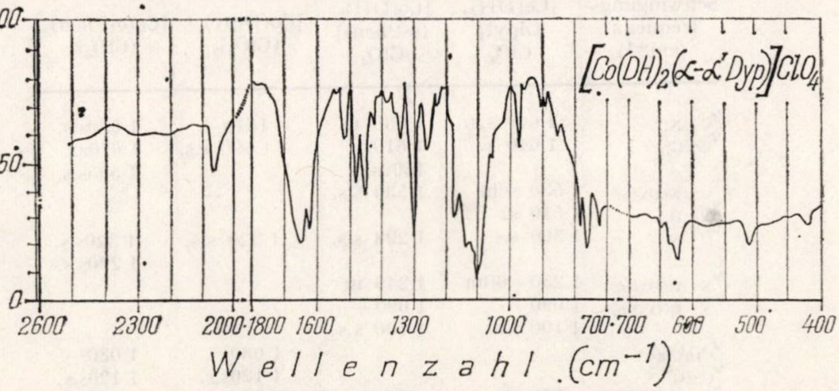

Abb. 1. – Ultrarotspektrum von [Co(DH)$_2$(α-α'Dyp)]ClO$_4$.

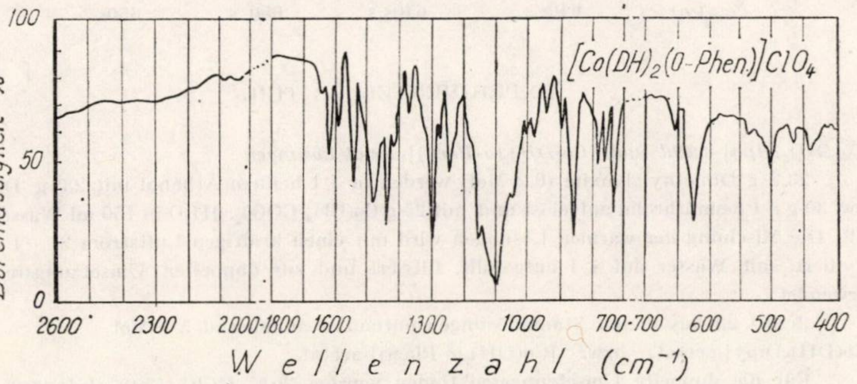

Abb. 2. – Ultrarotspektrum von [Co(DH)$_2$(o-Phen)]ClO$_4$.

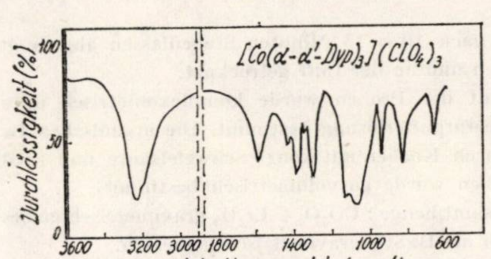

Abb. 3. – Ultrarotspektrum von [Co(α-α'-Dyp)$_3$](ClO$_4$)$_3$.

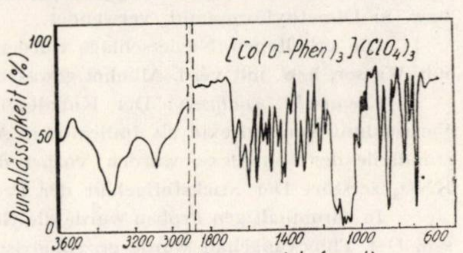

Abb. 4. – Ultrarotspektrum von [Co(o-Phen)$_3$](ClO$_4$)$_3$.

Die Lage der $\nu_{C=N}$, ν_{N-O} und ν_{Co-N} UR-Absorptionsbanden bestätigen den kovalenten Charakter der Co-Ligand-Bindungen.

Revue Roumaine de Chimie, 18, 5, 823–828 (1973)

Tabelle 3

IR-Absorptionsbanden einiger Komplexeverbindungen mit Dipy und *o*-Phen

Schwingungs-frequenz (cm^{-1})	$[Co(DH)_2$ Dipyl] ClO_4	$[Co(DH)_2$ (*o*-Phen)] ClO_4	$[Co(Dipy)_3]$ $(ClO_4)_3$	[Co(*o*-Phen)$_3$] $(ClO_4)_3$
$\nu_{C=N}$	1 640 s.s.	1 630 m.	1610–	1 630s.s.
$\nu_{C=C}$	1 610 s.	1 610s.	1 590 s.s.	1 610s.
		1590s.		1 595s.s.
$\nu_{C=N(Oxim)}$	1 530 sch.	1 530 s.s.	—	—
$\nu_{C=H}$	1 510 s.			
$\nu_{C=N}$	1 300 s.s.	1 298 s.s.	1 320 s.s.	1 320s.s.
				1 290s.s.
$\nu_{N—O(Oxim)}$	1 250–60m	1 240 m		
$\nu_{N-O(Oxim)}$	1 090–	1 090–		
	1 100 s.s.	1 100 s.s.		
$\nu_{C10}(\nu_3)$			1 080–	1 080–
$\nu_{C=C^4}$			1 120s.s.	1 120s.s.
$\delta_{C—H}$	850 m	850s.s.	840s.s.	855s.s.
$\nu_{Co—N}$	505m	510 m		
$\nu_{C10_4}(\nu_4)$	640s.s.	640s.s.	650 s.	650s.

EXPERIMENTELLER TEIL

$[Co(DH)_2Dipy]$-acetat und $[Co(DH)_2$(o-Phen)]-acetat-Lösungen

23,2 g Dimethylglyoxim (0,2 Mol) werden in 1 l heißem Äthanol mit 23 g Dipyridyl, bzw. 30 g *o*-Phenanthrolin aufgelöst und mit 25 g $Co(CH_3\text{-}COO)_2 \cdot 4H_2O$ in 150 ml Wasser behandelt. Die Mischung der warmen Lösungen wird mit einen kräftigen Luftstrom 3 – 4 Stunden oxydiert, mit Wasser auf 1 l aufgefüllt, filtriert und zur doppelten Umsetzungsreaktionen verwendet.

Je 50 ml aus diesen Stammlösungen enthalten annähernd 5 mMol $[Co(DH)_2Dipy]$-acetat, bzw. $[Co(DH)_2$(*o*-Phen)]-acetat.

Für die doppelte Umsetzungsreaktionen wurden 20% $HClO_4$, 20% KI, 20% KCNS, 20% KCNSe, 2% $NH_4[Co(NH_3)_2(NO_2)_4]$ und 2 – 3%-ige Reineckesalzanaloga in Äthanol, bzw. in Dimethylformamid. verwendet.

Die erhaltenen Niederschläge wurden nach 10 – 15 Minuten Stehenlassen abgesaugt, mit Wasser, bzw. mit verd. Alkohol gewaschen und an der Luft getrocknet.

Chemische Analysen: Der Kobaltgehalt der Proben wurde komplexometrisch unter Verwendung von Murexid als Indicator in Acetatpufferlösung bestimmt. Die organischen Bestandteile der Komplexe wurden vorher durch Kochen mit konz. Schwefelsäure und krist. KNO_3 zerstört Der Stickstoffgehalt der Proben wurde gasvolumetrisch bestimmt.

In chromhaltigen Proben wurde die Gesamtmenge : $CO_3O_4 + Cr_2O_3$ gravimetrisch gemessen. Der Thiocyangehalt wurde gravimetrisch als $BaSO_4$ gravimetrisch gemessen.

Die Ultrarotspektra der obenerwähnten Verbindungen wurden mit einem UR 10 Spektrophotometer (Carl Zeiss, Jena) in KBr-Presslingen untersucht.

Revue Roumaine de Chimie, 18, 5, 829–840 (1973)

CONTRIBUTIONS TO THE STUDY OF LANTHANIDES WITH BIGUANIDE DERIVATIVES. VI[1]

HALOGENO- AND PSEUDOHALOGENO-COMPOUNDS OF LANTHANIDES

ILEANA ALBESCU

Center of Physical Chemistry
str. Dumbrava Roșie 23, Bucharest
Romania

Received October 30, 1972

The present paper continues the study of the vibration spectra and of the thermograms of lanthanides compounds with paludrine. HCl and paludrine. HSCN, compounds whose synthesis has been presented in a previous note. The interpretation of the chemical and physico-chemical results led us to elucidate the structure of the new combinations and to formulate them as acido-complexes.

In a previous paper[1] we presented the syntheses of some new lanthanides compounds with paludrine. HCl and pald. HSCN*, compounds of the general type:

(pald.HCl).$LnCl_3$	Ln = Nd, Sm, Eu, Gd, Dy, Ho, Yb
$(pald.HCl)_2.LnCl_3$	Ln = Nd, Sm, Eu, Yb
$(pald.HCl)_3.LnCl_3$	Ln = Nd, Sm, Eu, Gd, Dy, Ho
$(pald.HCl)_4.LnCl_3$	Ln = Sm
$(pald.HCl)_5.LnCl_3$	Ln = Gd
(pald.HCl).$3LnCl_3$	Ln = Dy, Ho
(pald.HSCN).$Ln(SCN)_3$	Ln = Nd, Sm, Tb
$(pald.HSCN)_3.Ln(SCN)_3$	Ln = Nd, Sm, Tb

In order to establish the bonding type, the absorption spectra in UV and visible were analysed. The covalency parameter δ_m assumes higher values in the new compounds than in the corresponding aquo ions. Great intensity differences have resulted from the comparison between the intensities of the absorption bands in the complexes and in the corresponding aquoions; the differences are noticed especially with those compounds for which the δ_m parameter assumes high values too.

---

* paludrine will be abridged to pald.

[1] I. Albescu, *Rev. Roumaine Chim.*, (under press).

The fact proves once more the coordination and therefore a relative covalency degree of the new synthetized compounds.

In order to establish the chemical structure of the new compounds synthetized with pald. HCl and pald. HSCN, the vibration spectra in the domain 3800 — 220 cm^{-1} have been studied. The results are presented in Table 1 and Figs. 1 — 2.

For the other compounds the IR bands (in cm^{-1}) are summarized as follows :

$pald.HCl.GdCl_3$: 3400 (v. broad) ; 2980 (m) ; 2940(w) ; 1660(v.w) ; 1550(w) ; 1510(s) ; 1480 (m) ; 1430 (v.s) ; 1390 (s) ; 1300 (s) ; 1265 (v.s) ; 1190 (vs) ; 1135 (s) ; 1100 (v.s) ; 1020 (v.s) ; 980 (v.w) ; 850 (w) ; 835 (v.s) ; 730 (s).

$(pald.HCl)_3GdCl_3$: 3300(v. broad) ; 2980 (v.w) ; 2935 (s) ; 2875 (s) ; 1600(v.w) ; 1550(w); 1510 (s) ; 1480 (m) ; 1435 (s) ; 1390 (m) ; 1300 (m) ; 1265 (s) ; 1185 (s) ; 1100 (v.s) ; 1020 (s) ; 835 (v.s) ; 730 (m).

$(pald.\ HCl)_5GdCl_3$: 3400—3200 (v. broad) ; 2985 (m) ; 1670—1620 (broad) ; 1565 (v.w) ; 1550 (w) ; 1510 (m) ; 1430(m); 1390 (w) ; 1300(w) ; 1265 (s) ; 1185 (v.s) ; 1140 (w) ; 1100 (s) ; 1020 (s) ; 835 (v.s) ; 730 (m).

$(pald.HCl.DyCl_3$: 3316 (m) ; 3208 (w) ; 3016 (w) ; 1643 (s) ; 1595 (m) ; 1536 (v.s) 1500 (v.s) ; 1465 (v.w) ; 1411 (s) ; 1383 (s) ; 1289 (m) ; 1250 (s) ; 1180 (s) ; 1132 (w) ; 1091 (s) ; 1011 (s) ; 844 (m) ; 827 (v.s) ; 722 (s).

$(pald.\ HCl)_3.DyCl_3$: 3316 (m) ; 3208 (w) ; 3016 (w) ; 1643 (s) ; 1595 (w) ; 1536 (v.s); 1500 (v.s) ;1411 (s) ; 1383 (v.w) ; 1289 (m) ; 1250 (s) ; 1180 (v.s) ; 1132 (m) ; 1091 (v.s) ; 1011 (v.s) ; 844 (m) ; 827 (v.s) ; 722(s).

$(pald.\ HCl.HoCl_3$: 3316 (v.s) ; 3208(m) ; 3016 (s) ; 1643 (m) ; 1615 (v.w) ; 1595 ((w) ; 1536 (v.s) ; 1500 (v.s) ; 1465 (w) ; 1411 (v.s) ; 1383 (s) ; 1289 (s) ; 1250 (v.s) ; 1180 (v.s) ; 1132 (m) ; 1091 (v.s) ; 1011(v.s); 844 (m) ; 827 (v.s) ; 722 (v.s).

$(pald.HCl)_3.HoCl_3$: 3316 (m) ; 3208 (v.w) ; 3016 (v.w) ; 1643 (w) ;1595 (v.w) ; 1536 (s) ; 1500 (s) ; 1411 (m) ; 1289 (v.w) ; 1250 (m) ; 1180 (m) ; 1132 (m) ; 1091 (s) ; 1011(m) ; 827 (m).

$(pald.\ HCl)_2.YbCl_3$: 3316 (v.w) ; 3208 (v.w) ; 3016 (v.w) ; 1643 (m) ; 1591 (v.w) ; 1536 (s) ; 1500 (s) ; 1411 (m) ; 1289 (v.w) ; 1250 (w) ; 1180 (m) ; 1132 (v.w) ; 1091 (m) ; 1011(m) ; 827 (m) ; 722 (v.w).

(w. = weak ; m. = medium ; s. = strong ; v. w. = very weak ; v.s. = = very strong).

Whereas for the compounds obtained with paludrine great differences were noticed between the spectrum of the ligand and those of its com

Table 1

IR spectra 200–3500 cm^{-1}

pald.HCl 1 max. cm^{-1}	pald. HCl. $EuCl_3$ 2 max. cm^{-1}	(pald. HCl)$_2$$EuCl_3$ 3 max. cm^{-1}	(pald. HCl)$_3$ $EuCl_3$ 4 max. cm^{-1}	pald. HCl. $NdCl_3$ 5 max. cm^{-1}	(pald.HCl)$_2$$SmCl_3$ 6 max.cm^{-1}	(pald. HCl)$_4$ $SmCl_3$ 7 max. cm^{-1}
	3450–3300	3450–3370	3 380–3 320	3 360–3 380		
3316(s)	3250–3190		3 240–3 190	3 230(w)	3 316(m)	3 316(s)
3 208-(s)						3 208(m)
3 190					3 016(m)	3 016(m)
2 990(w)	2 980(s)	2 980(m)	2 980(m)	2 990(m)		
2 980(m)		2 950(w)		2 970		
2 880(m)						
		2 180(s)	2 185(m)			
1 890(m)						
	1 670–1 600	1 650(m)	1 660–1 600			
1 643(m)					1 643(s)	1 643(s)
1 629(v.w)				1 620(m)		
1 615(w)						
1 591(w)				1 590(w)	1 595(v.w)	1 595(m)
				1 580(v.w)		
1 560(v.w)	1 570(v.w)		1 570(v.w)	1 560(v.w)		
1 550(v.w)	1 550(w)	1 550(m)	1 560(m)	1 540(m)	1 536(s)	1 536(v.s)
1 530(w)						
1 500(v.s)	1 510(s)	1 510(m)	1 510(m)	1 500(v.s)	1 500(s)	1 500(v.s)
	1 480(v.w)			1470(m)		

Revue Roumaine de Chim'e, 18, 5, 829–840 (1973)

Table 1 (continued)

pald.HCl 1 max. cm^{-1}	pald. HCl. $EuCl_3$ 2 max. cm^{-1}	(pald. $HCl)_2EuCl_3$ 3 max. cm^{-1}	(pald. $HCl)_3$ $EuCl_3$ 4 max. cm^{-1}	pald. HCl. $NdCl_3$ 5 max. cm^{-1}	(pald. $HCl)_2$ $SmCl_3$ 6 max. cm^{-1}	(pald. $HCl)_4$ $SmCl_3$ 7 max. cm^{-1}
1 465(m)	1 430(s)	1 430(m)	1 430(m)	1 420(s)		
1 411(s)					1 411(s)	1 411(s)
1 380(m)	1 390(s)	1 400(w)	1 390(v.w)	1 390(s)		1 383(s)
1 290(m)	1 300(s)	1 350(v.w)	1 300(w)	1 300(s)		
						1 286(s)
1 260(s)	1 265(v.s)	1 270(m)	1 265(s)	1 260(v.s)	1 260(s)	1 250(v.s)
1 190(s)	1 190(v.s)	1 185(m)	1 190(s)	1 185(v.s)	1 180(s)	1 180(v.s)
1 135(m)	1 135(w)		1 140(w)	1 135(w)	1 132(v.w)	1 132(m)
1 100(s)	1 100(s)	1 100(s)	1 100(s)	1 100(v.s)	1 091(s)	1 091(v.s)
1 020 (s)	1 020 (s)	1 025 (m)	1 020 (s)	1 015(v.s)	1 011(m)	1 011(v.s)
980 (v.w)	975(w)			970(m)		
850(m)	850(s)		835(v.s.)	840(m)		844(v.w)
835(v.s.)	835(v.s)			830(v.s)	816	827(v.s)
					801	
730(m)	730(s)	740(v.s)	740(s)		722(broad)	722(s)
580(w)		510—				
548(v.s)	490(v.s)	470(v.s)	480(s)	570(m)		
490(s)						
422(w)				480(s)		
397(w)						
353(m)						
264(v.s)	250—240(s)	250—240(s)	250—40(s)	250—40(s)		
243(s)						

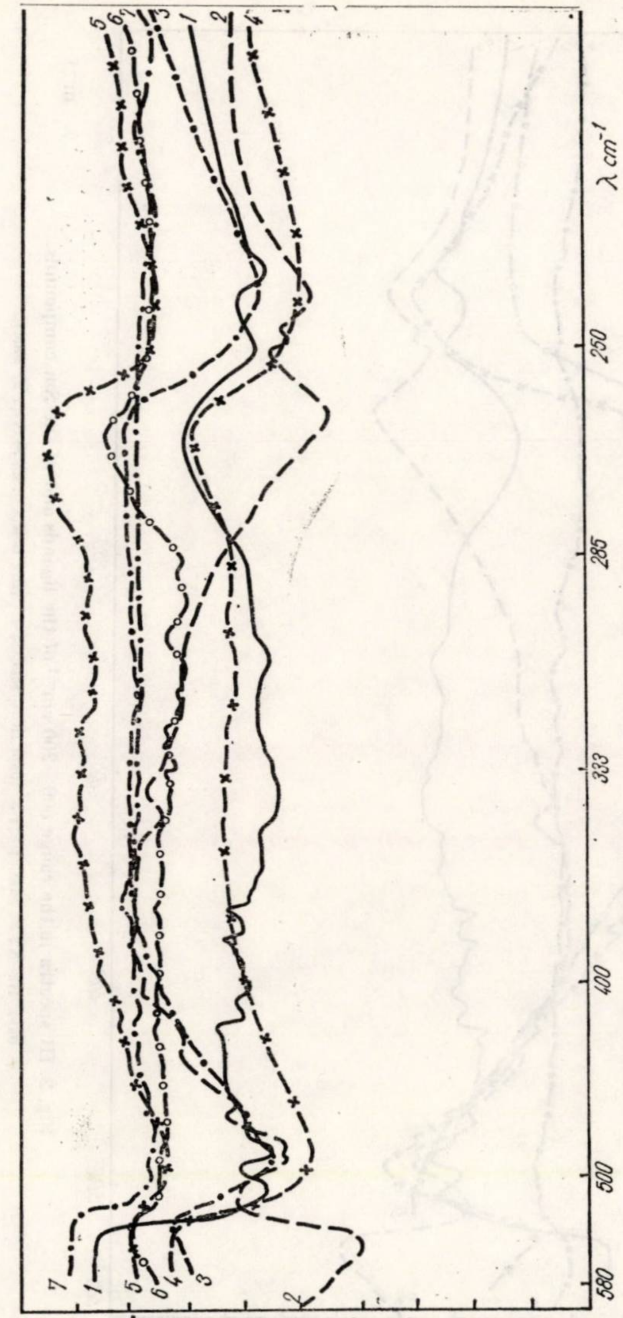

Fig. 1. — IR spectra in the range 600—200 cm^{-1} of the ligands and of the Nd and Tb compounds.

1, pald.HSCN; *2*, pald. HCl; *3*, pald.HCl.NdCl$_3$; *4*, (pald.HCl)$_2$.NdCl$_3$; *5*, (pald.HCl)$_3$.NdCl$_3$; *6*, (pald.HSCN)$_3$.Nd(SCN)$_3$; *7*, (pald.HSCN)$_3$.Tb(SCN)$_3$.

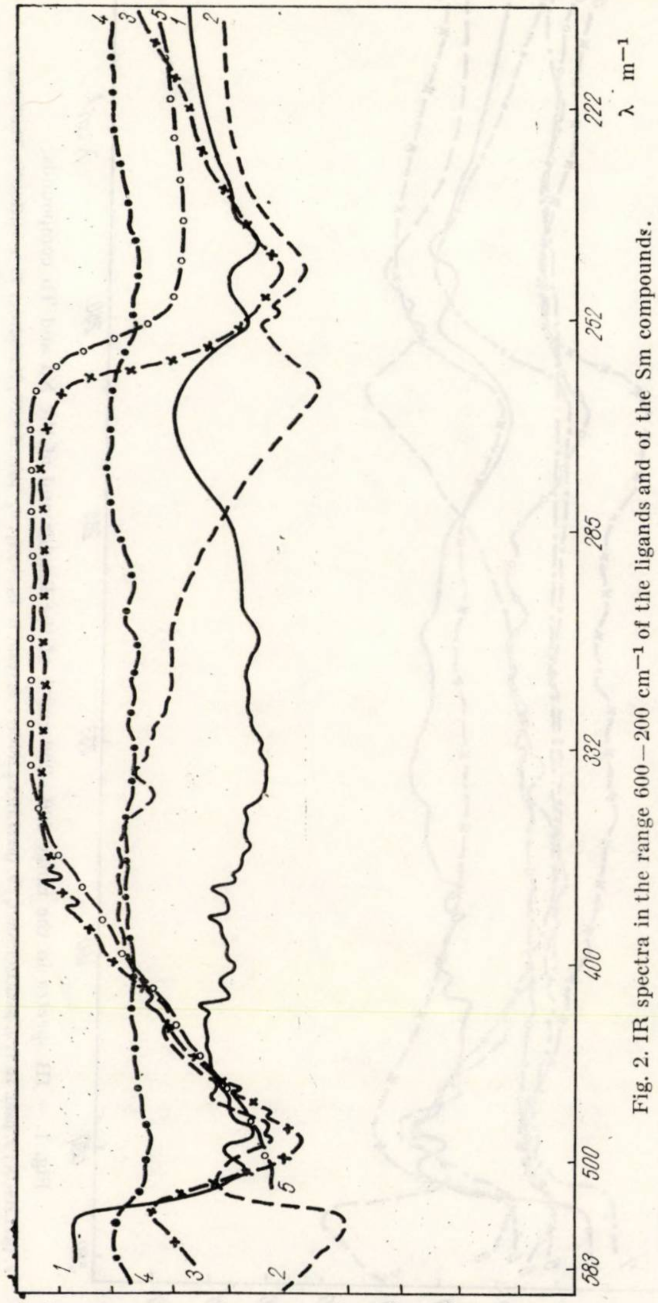

Fig. 2. IR spectra in the range 600 − 200 cm^{-1} of the ligands and of the Sm compounds.

1, pald. HSCN; *2*, pald. HCl; *3*, (pald.HCl)$_3$.SmCl$_3$; *4*, (pald.HSCN)$_3$.Sm(SCN)$_3$; *5*, SmCl$_3$.

pounds with lanthanides, [2-4] in the case of the combinations with pald. HCl and pald.HSCN the spectra ligand-compounds are very much similar, especially in the domain 3800 – 600 cm^{-1}.

Slight differences, in the sense of some shifts (730 cm^{-1}, 1260 cm^{-1}, 1380 cm^{-1}), disappearances (2990 – 1890 cm^{-1}, 1629 cm^{-1}, 1465 cm^{-1}, 980 cm^{-1}, 850 cm^{-1}) and intensifications of some bands (1411 cm^{-1}, 1550 cm^{-1}, 730 cm^{-1}) can be noticed; generally no regularity is remarked when going from an element to another of the same series of compounds.

For the compounds of the same element the more increases the quantity of ligand the wider some bands become till they completely disappear, great changes taking place at the frequencies 740 cm^{-1} and 833 cm^{-1}.

In the domain 600 – 220 cm^{-1}, pald.HCl presents bands at 243 cm^{-1}, 264 cm^{-1}, 353 cm^{-1}, 397 cm^{-1}, 422 cm^{-1}, 490 cm^{-1} and 497 cm^{-1} as well as at 532 cm^{-1}; pald.HSCN has marked bands at the frequencies : 240 cm^{-1}, 251 cm^{-1}, 321 cm^{-1}, 336 – 350 cm^{-1}, 485 cm^{-1} and 500 cm^{-1}.

Differences between the ligands spectrum and that of the compounds appear in this domain, too; in the series of the combinations with pald. HCl there are obvious changes around the frequencies 480 – 580 cm^{-1}, the bands which are in pald.HCl at 490 cm^{-1}, 497 cm^{-1} and 532 cm^{-1} appear in the compounds merged into a single band at 490 cm^{-1} which gradually widens and sometimes are shifted towards higher frequencies, when the quantity of ligand increases. The observation is valid in the region 240 – 260 cm^{-1} too : the characteristic frequencies 243, 249, 264 cm^{-1} in pald. HCl appear in the compound merged into one band, wide enough at 240 – 250 cm^{-1}; generally the greater the volume of the cation the stronger is the deformation.

The combinations with pald.HSCN mark in these regions differences between the ligand spectrum and that of the compounds, too. The characteristic bands in pald.HSCN at 485 cm^{-1} and 500 cm^{-1} appear as a single band, wide enough, at 490 cm^{-1} and those at 240 cm^{-1} and 251 cm^{-1} almost disappear, when the mass of ligand is augmented.

Because the lanthanide halides have in this region characteristic bands at almost the same values with those of the ligand it is difficult to appreciate whether the Ln-X or Ln-N bond is influenced.

From the analysis of the absorption spectra in UV and visible and of the IR spectra we shall try to hypothetically appreciate the structure of the new lanthanides combinations with pald.HCl and pald.HSCN.

As mentioned in a previous paper [4] using the data reported in the literature, [5] one showed that the band at 233 cm^{-1} in UV, which is obvious in pald.HCl, is characteristic of the conjugated system $=N-C=N-$; this band can be found in all the compounds with the above mentioned ligand, sometimes is shifted towards lower frequencies [1]; this means that the system of double conjugated bonds did not disappear but only a perturbation of the system of electrons π has occurred in the newly formed compound.

---

[2] P. Spacu and I. Albescu, *Rev. Roumaine Chim.*, **16**, 1503 (1971).

[3] I. Albescu, *Rev. Roumaine Chim.*, **10** . . . . . .(1972).

[4] I. Albescu, *Rev. Roumaine Chim.*, **11** . . . . .(1972).

[5] R. C. Hirt and R. G. Schmidt, *Spectrochim. Acta*, **12**, 127 (1958).

As in the case of the compounds with paludrine, if we consider the ligand :

$$Cl-C_6H_4-NH-C(=NH)-NH-C(=NH)-NH-C_3H_7.HCl$$

the appearance of the system of double conjugated bonds may be explained when admitting the ligand is of the form of a quaternary salt :

$$Cl-C_6H_4-\underset{H}{\overset{\oplus}{N}}=C(NH_2)-N=C(NH_2)-NH-C_3H_7$$

or :

$$Cl-C_6H_4-NH-C(=NH)-N=C(NH_2)-\overset{\oplus}{N}H_2-C_3H_7$$

which should appear on N_1 close to *p*-Cl-phenyl, also affecting the bands at 710, 750, 831 cm^{-1}, characteristic of the *p*-Cl-phenyl, but also of the N_5 close to the isopropyl group, the affected band in this case being around the frequencies at 820 cm^{-1} and 750 cm^{-1}.

Because the IR spectra of the compounds are similar in the range 3800 – 600 cm^{-1} with that of pald.HCl, with marked changes especially at the characteristic vibrations of *p*-Cl-phenyl group (the same bands are maintained as in the free ligand slightly shifted in their frequencies), the cation formation appears more probably on the nitrogen atom (N_1) close to the above mentioned radical.

The fact led us to assume that the halogeno- and pseudohalogeno-complexes of lanthanides with pald.HCl and pald.HSCN could be considered as paludronium salts which behave as monoprotonated biguanide derivatives, of the type :

$$[\text{Hpald}]_n\,[\text{LnX}_m]$$

$$\text{Ln} = \text{Nd}-\text{Yb}\,; \qquad X=Cl^-,\ SCN^-$$

$$n = 1-5\,;\ m = 4-8 \quad (X=Cl^-)$$

$$n = 1\,;3 \quad m = 4\,;6 \quad (X=SCN^-)$$

That is to say :

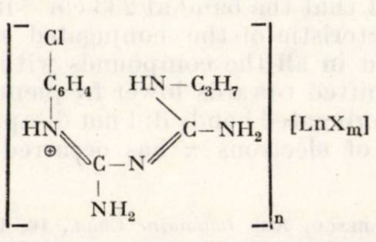

Unlike the lanthanides compounds with paludrine, whose structure has been explained by a system of double conjugated bonds which appear during an internal mechanism of a limit structure created in special conditions, the compounds of acido-complex type are formed admitting a quaternary salt with the same system of double bonds but differently placed in the ligand molecule.

The formulas:

$$[\mathrm{Hpald}]_3[\mathrm{LnX}_6];\quad [\mathrm{Hpald}]_2[\mathrm{LnX}_5];\quad [\mathrm{Hpald}][\mathrm{LnX}_4]$$

are suggested, that is to say the coordination numbers 6, 5, 4, the latter compound being the most stable.

For the compounds with a high content of pald.HCl, ex. $[\mathrm{Hpald}]_4[\mathrm{SmCl}_7]$ and $[\mathrm{Hpald}]_5[\mathrm{GdCl}_8]$ the coordination numbers 7 and 8 are admitted, which is possible for the lanthanides but the compounds are less stable.

In our paper dealing with the study in aqueous solution and through the refractometrical method [6-10] of some systems of the type:

$$\mathrm{MX-LnX_3}\qquad \begin{array}{l} \mathrm{M = Na, K, Rb, Cs} \\ \mathrm{X = Cl, Br} \\ \mathrm{Ln = Ce-Yb} \end{array}$$

we proved the existence of the $[\mathrm{LnX}_n]^{n-3}$ ion regarding the possibility of formation of lanthanides combinations of acido-complex type and of a superior order. The conclusions of these researches have been greatly in agreement with those derived from the works [11-12] about meltings.

At Dy and Ho, compounds of general form $\mathrm{KLn_3Cl_{10}}$ have been noticed in solution; they correspond to those mentioned in literature, in meltings at the same elements.

It is interesting that in the series of compounds synthetized with pald HCl, combinations with a high content of $\mathrm{LnCl_3}$ and of the form: pald $\mathrm{H.Dy_3Cl_{10}}$ and pald $\mathrm{H.HO_3Cl_{10}}$ have been found at Dy and Ho too; they are similar with those studied in solutions and meltings but they have a different cation.

These combinations have the formula:

$$[\mathrm{Hpald}][\mathrm{LnCl_4}].2\mathrm{LnCl_3}\qquad \mathrm{Ln = Dy, Ho}$$

and

$$\mathrm{K[LnCl_4].2LnCl_3}\qquad \mathrm{Ln = Dy, Ho,\ respectively}$$

Their existence can be explained by the fact that the lanthanide ionic radius has reached the borderline of the possibility to form compounds with high content of $\mathrm{LnCl_3}$ by the addition of two molecules of $\mathrm{LnCl_3}$ to the most stable compound $[\mathrm{Hpald}][\mathrm{LnCl_4}]$ or $\mathrm{K[LnCl_4]}$.

We also observed that the combinations rich in pald.HCl are obtained in all the elements up to Gd; this tendency increases in the elements after Sm, that is to say, in Eu and Gd, and then it decreases; like that in Yb only compounds 1 : 1 and 1 : 2 are obtained.

---

[6] P. Spacu, I. Albescu and E. Dragomir, *Rev. Roumaine Chim.*, **8**, 31 (1963).

[7] P. Spacu and I. Albescu, *Rev. Roumaine Chim.*, **11**, 79 (1966).

[8] P. Spacu and I. Albescu, *Rev. Roumaine Chim.*, **11**, 1073 (1966).

[9] P. Spacu and I. Albescu, *Rev. Roumaine Chim.*, **12**, 667 (1967).

[10] P. Spacu, I. Albescu and E. Ivan *Rev. Roumaine Chim.*, **13**, 425 (1968).

[11] Sun-Ju-Ciju and I. S. Morozov, *Zhur. neorg. Khim.*, **3**, 1914 (1958).

[12] B. G. Corshunov and D. V. Drobot, *Zhur. neorg. Khim.*, **10**, 939 (1965).

In conclusion, through a chemical synthesis using biguanide derivatives as ligand, the $[LnX_n]^{n-3}$ becomes stable leading to the obtention of solid crystalline combinations.

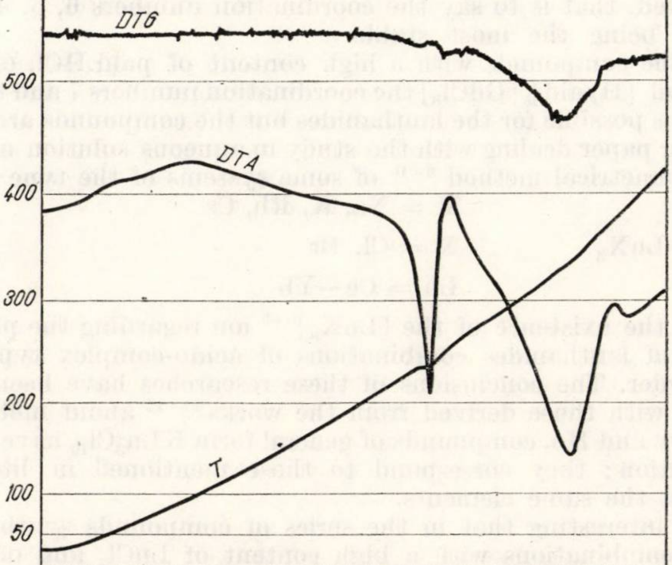

Fig. 3. — Thermal decomposition of pald.HCl.

When the new compounds were studied it obviously appeared a perfect parallelism between them and the same type of combinations studied through other methods and with different cations.

The thermal and thermodifferential analyses have been carried out by studying physico-chemically these compounds. Only the data for the combination $[Hpald]_3$ $[HoCl_6]$ are discussed because for the other compounds the results can be generalized.

The substance begins to decompose at 160° with the elimination of the ligand, operation highly marked by three steps and equivalent to the losing of 76% of weight against 76.2% theoretically calculated.

It is difficult to establish the intermediate products which could appear during the elimination of the ligand, because the processes overlap.

At about 540° $HoCl_3$ is obtained corresponding to a 23% quantity; through heating later on the anhydrous chloride passes into HoOCl, corresponding to a 18.3% quantity. Finally the latter decomposes with the appearance of Ho_2O_3, the process being marked by the last step at 700° corresponding to a 16% quantity as compared to 16.5% theoretically calculated.

The thermodifferential analysis clearly underlines the decomposition processes of the ligand and of the compound (Figs. 3 and 5).

The beginning of the decomposition process of the ligand is noticed at 150° — 160° to which an endothermal effect corresponds with the maximum at 240°. A second endothermal process of smaller intensity follows at 280° and it is hidden by the third endothermal process represented by a peak with a maximum at 340°.

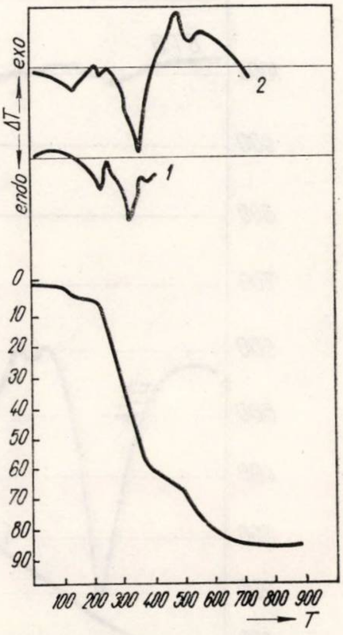

Fig. 4. — Thermal decomposition of the ligand and of the $(pald.HCl)_3HoCl_3$.

For the compound a first decomposition with the maximal speed at 150° is noticed; the process may correspond to the elimination of the absorbed water. The decomposition of the compound with the elimination of the ligand in three definite stages occurs at 225° and is represented by an endothermal process with the maximal speed at 240°, too; like in the free ligand, but the effect is smaller. The second process of decomposition of the ligand has the highest speed at 290° compared to 280° in the free ligand; the second process is also of a reduced intensity and it is hidden by the last endothermal process with a peak at 360° in comparison with 340° in the free ligand.

The two exothermal processes, the former placed within 400°—500° with a maximum at 490°, probably due to the elimination of the last residuum produced by the ligand decomposition, and the latter which begins at 540° when $HoCl_3$ occurred with a maximal speed corresponding to a peak at 570°.

If the DTA curve for pald.HCl is compared with the DTA curve of the compound, the similarity in the sense of the existence of both endothermal processes with very close maxima is also observed.

We find once more the conclusions in concordance with those found in spectral studies.

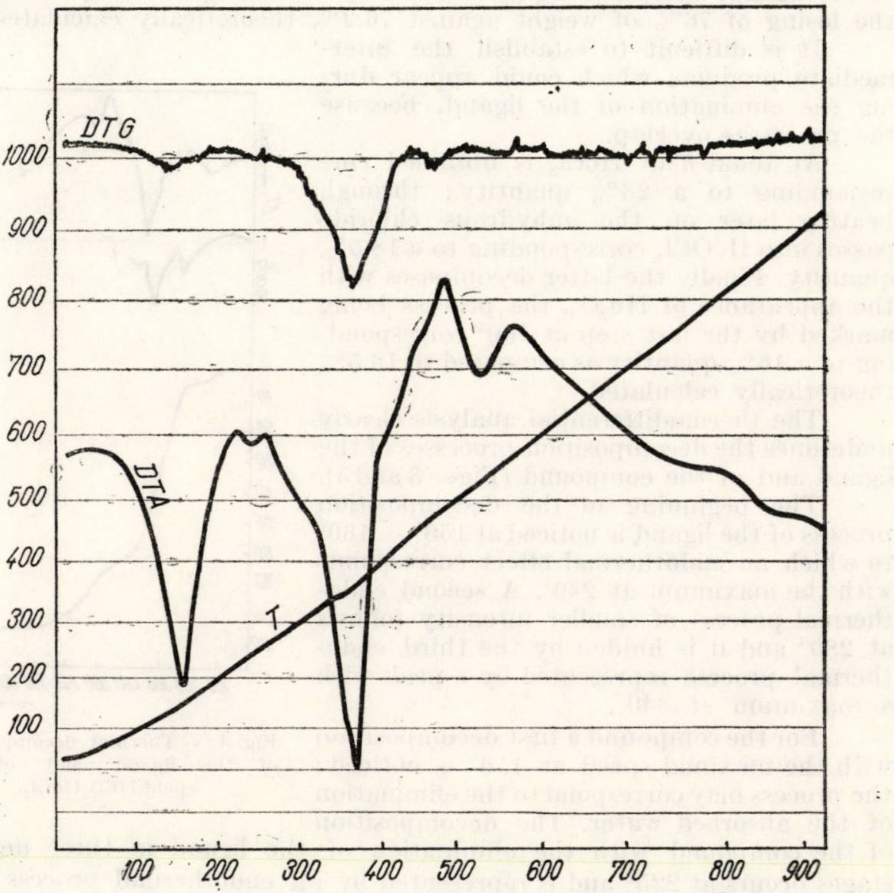

Fig. 5. — DTA for $(pald.HCl)_3HoCl_3$.

The ligand maintains its structure in the newly formed compounds with rare earth ions, hence the analogy between the spectra and the DTA curves of the compounds and those of the free ligand.

The fact that the DTA curve for pald.HCl-compounds is different from the DTA curve of the paludrine complexes and of the paludrine itself shows that the newly formed compounds have different structures than with those of the compounds reported in our previous papers.

Revue Roumaine de Chimie. **18**, *5*, 841–854 (1973)

CHEMICAL GRAPHS. XVI[1]
INTRAMOLECULAR ISOMERIZATIONS OF OCTAHEDRAL COMPLEXES WITH SIX DIFFERENT LIGANDS*

A. T. BALABAN

Institute of Atomic Physics, P.O.B. 35, Bucharest, Romania

Received December 13, 1972

Intramolecular isomerizations of octahedral complexes *via* digonal, trigonal or rhombic twists are tetra-, tri- or diligostatic processes, whose topology can be represented by regular graphs. A 15-vertex graph of degree six and a 30-vertex graph of degree twelve are presented for processes *via* digonal twists, and a 30-vertex graph of degree eight is shown for the other processes, displaying Hamiltonian circuits. The symmetry of the graph can be used for achieving a self-consistent notation of the isomers.

INTRODUCTION

Six-coordinate complexes ML_6 with octahedral geometry can give rise to $6!/24 = 30$ isomers when the six ligands L are different, i.e. to 15 pairs of enantiomers.[2] They may become interconverted through non-bond rupture mechanisms in several ways, as presented systematically by Gielen[3]; (i) Bailar trigonal twist[4]; (ii) Ray-Dutt rhombic twist,[5] or Springer-Sievers process[6]; (i) and (ii) are equivalent and can be represented by a regular graph of degree eight[7]; (iii) digonal twist,[8,9] and other mechanisms.[10] We will examine more closely cases (i) or (ii), and (iii), starting with the last one.

---

* Presented at the First International Symposium on Dynamic Organometallic Stereochemistry held in Brussels on 30 May-1 June 1972.

[1] Part XV, A. T. Balaban, *Rev. Roumaine Chim.* **17**, 883 (1972).

[2] E. L. Muetterties, *J. Amer. Chem. Soc.*, **91**, 1636 (1969).

[3] M. Gielen, Med. *Vlaam. Chem. Ver.*, **31**, 201 (1969); M. Gielen, in "Chemical Applications of Graph Theory" (ed. A. T. Balaban), Academic Press, London (under print).

[4] J. C. Bailar, *J. Inorg. Nuclear Chem.*, **8**, 165 (1958).

[5] P. Ray and N. K. Dutt, *J. Indian Chem. Soc.*, **20**, 81 (1943).

[6] C. S. Springer and T. E. Sievers, *Inorg. Chem.*, **6**, 852 (1967).

[7] E. L. Muetterties, *J. Amer. Chem. Soc.*, **90**, 5097 (1968).

[8] M. Gielen, *Bull. Soc. chim. belges*, **78**, 351 (1969).

[9] E. L. Muetterties, *J. Amer. Chem. Soc.*, **91**, 4115 (1969).

[10] M. Gielen and N. Vanlautem, *Bull. Soc. chim. belges*, **79**, 679 (1970); J. I. Musher, *Inorg. Chem.*, **11**, 2335 (1972).

Two ligands *cis* to one another may interchange by a ligand metathesis, while the other four ligands conserve their positions. Such a tetraligostatic process [11] (iii) is less favoured energetically than the triligostatic process (i), or than the diligostatic process (ii), but is an interesting theoretical possibility. Process (iii) has the property that each of the 30 isomers, having twelve *cis*-ligand pairs and three *trans*-ligand pairs, and totalling as required $\binom{6}{2} = 15$ pairs, leads by *cis*-ligand metathesis to 12 different isomers forming six pairs of enantiomers. Thus, every ligand metathesis results in complete loss of chirality, which will allow a significant simplification of the problem.

The notation of the 30 isomers follows previously adopted rules.[12,13] Gielen's simplification of the six-digit notation to a two-digit notation will be adopted, remarking that the two digits determine unambiguously one pair of enantiomers. Indeed, the first digit indicates the ligand *trans* to substituent 1, whereas the second digit indicates the ligand *trans* to substituent 2, unless substituent 2 is *trans* to substituent 1, when the second digit indicates the ligand *trans* to substituent 3 (therefore, ligand 1 never appears in the notation and from all arrangements of two digits out of five, i. e. out of digits 2 through 6, arrangements 23, 32, 42, 52 or 62 never appear as notations). The third pair of ligands follows by difference. The two enantiomers are distinguished in Gielen's notation by a bar, i. e. as 24 and $\overline{24}$ (in a similar case an asterisk was used earlier [14]).

It was shown by Ruch [15] that the homochirality criterion does not apply to octahedral complexes. Therefore, the assignment of any such complex to an enantiomeric series is conventional. It will be shown in this paper that the symmetry of the graphs can be used for a consistent conventional assignment.

The 30 octahedral isomers are presented with their notations in figure 1.

REQUIREMENTS FOR TOPOLOGICAL REPRESENTATIONS OF INTRAMOLECULAR ISOMERIZATIONS

The graph representing the topology of intramolecular isomerizations consists of vertices symbolizing the isomers; two isomers which can become interconverted by an allowed elementary process are adjacent, i. e. are connected by a line.

Since the process can start from any isomer, the resulting graph must be vertex-transitive. In some cases, [14] higher symmetry is attained (s-unitransitive graphs [16] or s-regular graphs[17]).

---

[11] D. C. Garwood and D. J. Cram, *J. Amer. Chem. Soc.*, **92**, 4575 (1970).

[12] E. L. Muetterties and C. M. Wright, *Quart. Rev.*, **21** 179 (1967).

[13] M. Gielen and C. Depasse-Delit, *Theor. Chim. Acta.*, **14**, 212 (1969).

[14] A. T. Balaban, *Rev. Roumaine Math. Pures Appl.*, **17**, 3 (1972).

[15] E. Ruch, *Accounts Chem. Res.*, **5**, 49 (1972).

[16] F. Harary, "Graph Theory", Addison-Wesley, Reading, Mass. 1969. p. 174.

[17] W. T. Tutte, "Connectivity in Graphs", Univ. of Toronto Press, 1966, p. 62.

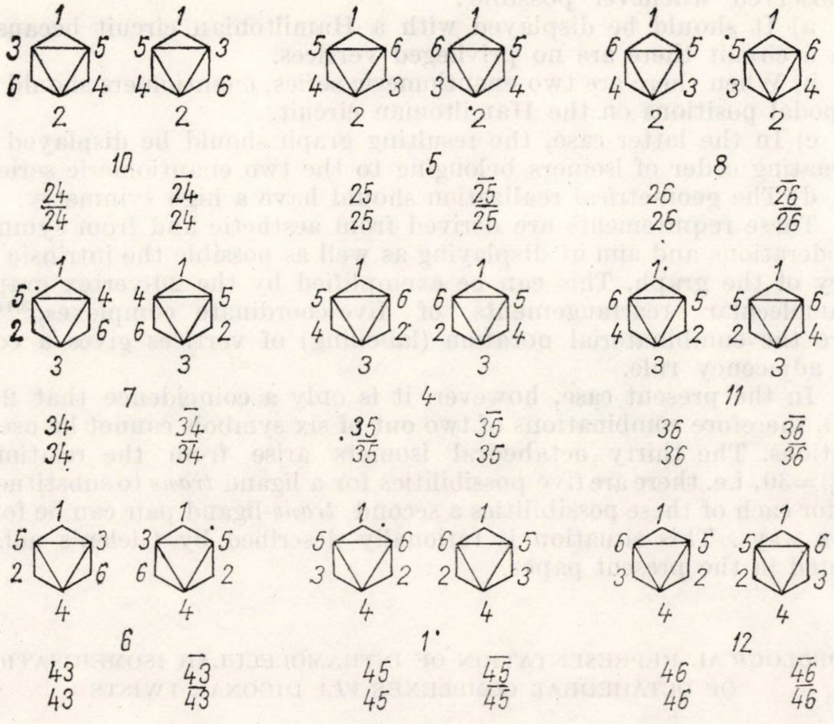
10
24
$\overline{24}$
$\overline{24}$
24
5
25
$\overline{25}$
25
$\overline{25}$
8
26
$\overline{26}$
26
$\overline{26}$
7
34
$\overline{34}$
34
$\overline{34}$
4
35
$\overline{35}$
$\overline{35}$
35
11
36
$\overline{36}$
36
$\overline{36}$
6
43
$\overline{43}$
43
$\overline{43}$
1
45
$\overline{45}$
45
$\overline{45}$
12
46
$\overline{46}$
46
$\overline{46}$
9
53
$\overline{53}$
$\overline{53}$
53
13
54
$\overline{54}$
54
$\overline{54}$
0
56
$\overline{56}$
56
$\overline{56}$
3
63
$\overline{63}$
63
$\overline{63}$
2
64
$\overline{64}$
64
$\overline{64}$
14
65
$\overline{65}$
65
$\overline{65}$

Fig. 1. — The 30 octahedral isomers (15 enantiomeric pairs) with their notations: upper line as in ref. 10; middle line as in ref. 3 and figures 4 and 5 of the present paper; lower line, proposed assignments as in fig. 9 and 10.

The following requirements for the presentation of the graph should be observed whenever possible:

a) It should be displayed with a Hamiltonian circuit because on such a circuit there are no privileged vertices.

b) When there are two enantiomeric series, enantiomers should have antipodal positions on the Hamiltonian circuit.

c) In the latter case, the resulting graph should be displayed with alternating order of isomers belonging to the two enantiomeric series.

d) The geometrical realization should have a high symmetry.

These requirements are derived from aesthetic and from symmetry considerations and aim at displaying as well as possible the intrinsic symmetry of the graph. This can be exemplified by the 20-vertex graph of intramolecular rearrangements of five-coordinate complexes,[3,14,18–23] where the combinatorial notation (labelling) of vertices gives a consistent adjacency rule.

In the present case, however, it is only a coincidence that $2\binom{6}{2} = 30$, therefore combinations of two out of six symbols cannot be used for notations. The thirty octahedral isomers arise from the relationship $\binom{5}{1}\cdot\binom{4}{2}=30$, i.e. there are five possibilities for a ligand *trans* to substituent 1, and for each of these possibilities a second *trans*-ligand pair can be formed in six ways. This situation is rationally described by Gielen's notation adopted in the present paper.

TOPOLOGICAL REPRESENTATION OF INTRAMOLECULAR ISOMERIZATIONS OF OCTAHEDRAL COMPLEXES *VIA* DIGONAL TWISTS

In the tetraligostatic process (iii) involving digonal twists, i.e. interchange of two *cis*-ligands, each isomer can be converted into six pairs of enantiomers with loss of chirality. Disregarding enantiomerism, we need therefore consider only a 15-vertex graph of degree six; in the notation of each isomer the presence or absence of a bar can be disregarded.

Inspecting the adjacency table presented in detail by Gielen,[10] and converting it into the present notation, the following adjacency rules between vertices emerge for an isomer represented by a vertex with notation AB, which is a common vertex of three 3-circuits (denoting by Y and Z two digits from the set 4, 5 and 6 which are different from B):

1. For A = 2 (therefore, B = 4, 5, or 6), the three 3-circuits are:
   AB–AY–AZ, AB–YZ–ZY, AB–3B–B3
2. For A = 3 (therefore, B = 4, 5, or 6), they are:
   AB–AY–AZ, AB–YB–ZB, AB–2B–BA

---

[18] M. Gielen, J. Brocas, M. De Clercq, G. Mayence and J. Topart, "Proc. 3rd Symp. on Coordination Chemistry" held in Debrecen, vol. 1. Akademiai Kiado, Budapest, 1970, p. 495.

[19] K. Mislow, *Accounts Chem. Res.*, **3**, 321 (1970).

[20] A. T. Balaban, D. Fărcaşiu and R. Bănică, *Rev. Roumaine Chim.*, **11**, 1205 (1966).

[21] P. Gillespie, P. Hoffmann, H. Klusacek, D. Marquarding, S. Pfohl, F. Ramirez, E. A. Tsolis and I. Ugi, *Angew. Chem.*, **83**, 691 (1971); *Angew. Chem. Internat. Edit.*, **10**, 687 (1971).

[22] M. Gielen and J. Nasielski, *Bull. Soc. chim. belges*, **78**, 339 (1969)

[23] M. Gielen, *Med. Vlaam. Chem. Ver.*, **31**, 185 (1969).

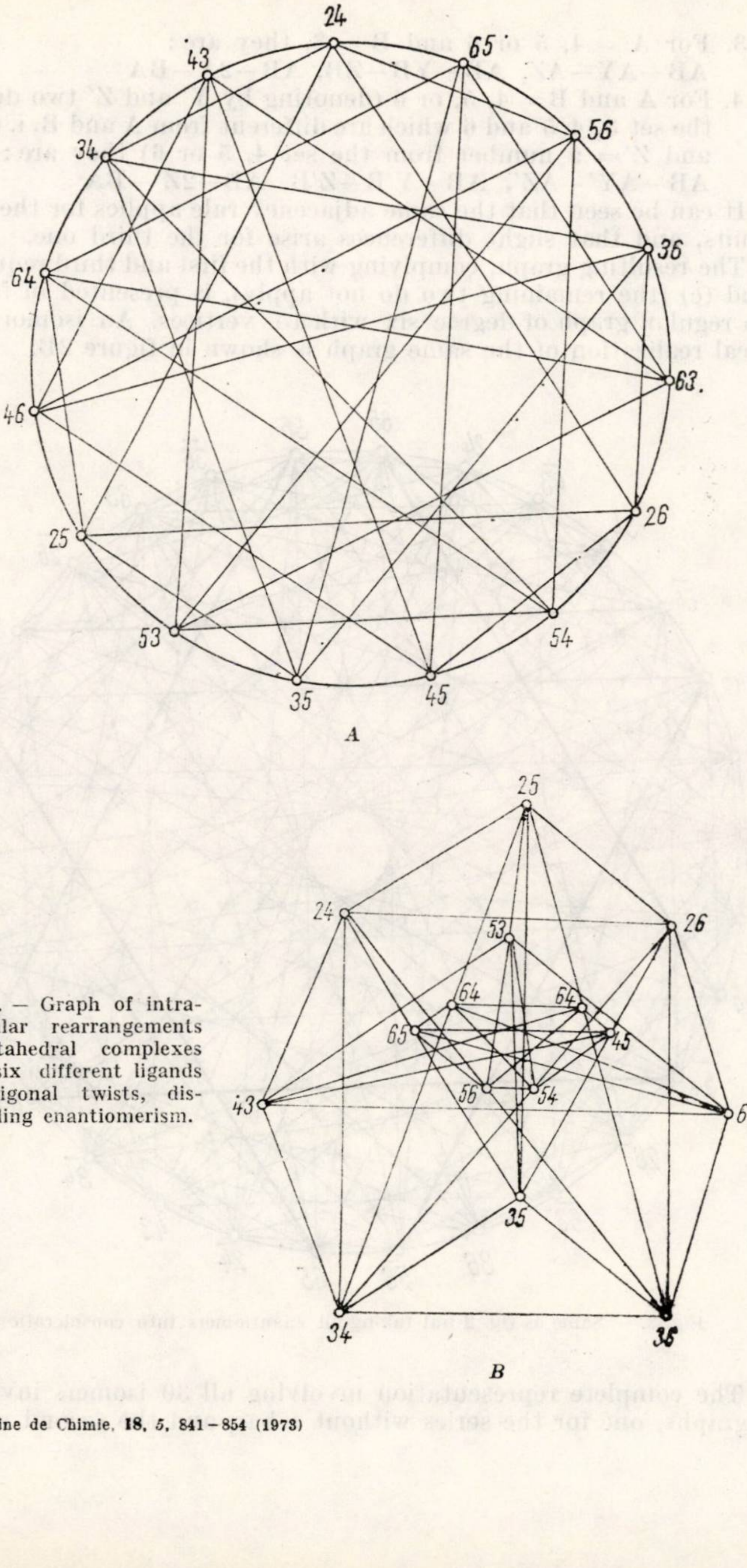
24
43
65
56
34
36
64
63.
46
26
25
53
54
35
45
A
25
24
26
53
64
64
65
45
43
56
54
63
35
34
36
B

Fig. 2. — Graph of intramolecular rearrangements of octahedral complexes with six different ligands *via* digonal twists, disregarding enantiomerism.

3. For $A = 4$, 5 or 6 and $B = 3$, they are:
   $AB-AY-AZ$, $AB-YB-ZB$, $AB-2A-BA$
4. For A and $B = 4$, 5, or 6 (denoting by Y' and Z' two digits from the set 3, 4, 5 and 6 which are different from A and B, i. e. $Y' = 3$, and $Z' =$ a number from the set 4, 5 or 6) they are:
   $AB-AY'-AZ'$, $AB-Y'B-Z'B$, $AB-2Z'-BA$

It can be seen that the same adjacency rule applies for the first two 3-circuits, and that slight differences arise for the third one.

The resulting graph, complying with the first and third requirements (a) and (c) (the remaining two do not apply), is presented in figure 2A. It is a regular graph of degree six with 15 vertices. An isomorphic geometrical realization of the same graph is shown in figure 2B.

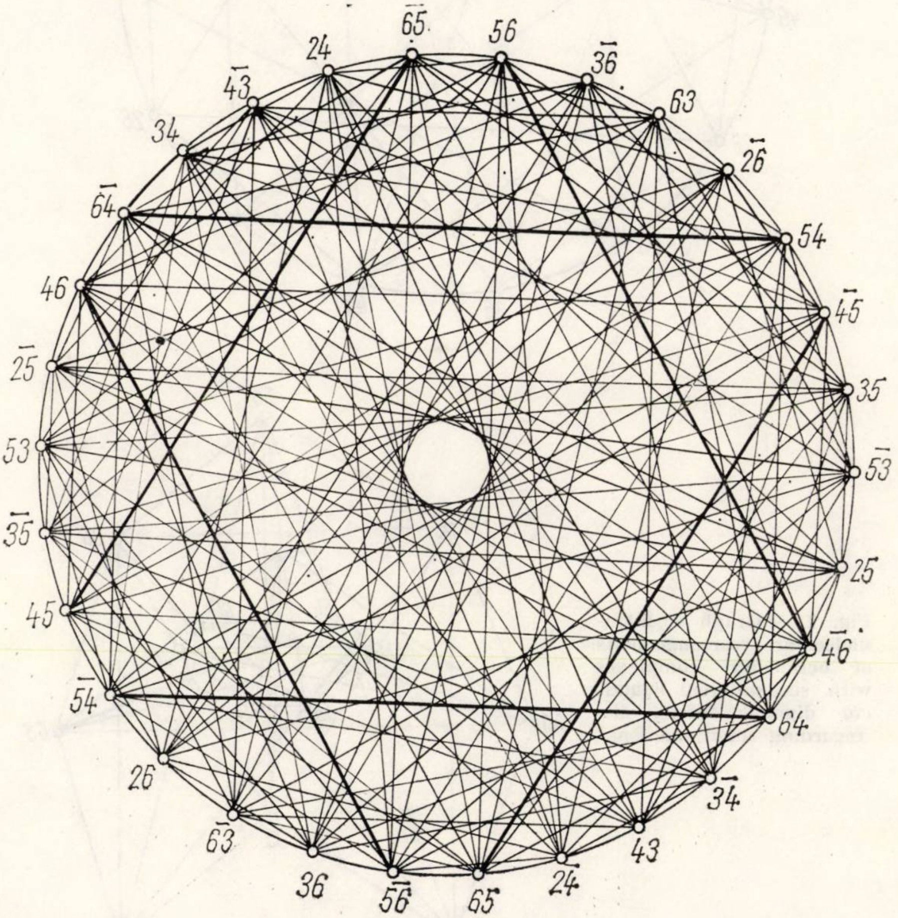

$\overline{65}$
56
$\overline{36}$
63
$\overline{26}$
54
$\overline{45}$
35
$\overline{53}$
25
$\overline{46}$
64
$\overline{34}$
43
$\overline{24}$
65
$\overline{56}$
36
$\overline{63}$
26
$\overline{54}$
45
$\overline{35}$
53
$\overline{25}$
46
$\overline{64}$
34
$\overline{43}$
24

Fig. 3. — Same as fig. 2 but taking all enantiomers into consideration.

The complete representation involving all 30 isomers involves two such graphs, one for the series without a bar, and the second with a bar over the notation of each vertex. The two graphs are linked by lines connecting each point from one graph with six other points from the other graph, according to the above adjacency rules. Alternatively, the graph presented in fig. 3, complying with all four requirements (a)-(d), includes all 30 isomers. This graph has the same sequence of vertices as that of figure 2, but repeated twice. Since the adjacency rules do not take into account the assignment of any isomer into a particular enantiomeric series, any change of the assignment is permitted without affecting the graphs presented in figures 2 and 3.

TOPOLOGICAL REPRESENTATION OF INTRAMOLECULAR ISOMERIZATIONS OF OCTAHEDRAL COMPLEXES *VIA* TRIGONAL OR RHOMBIC TWISTS

The result of either the triligostatic process (i) involving trigonal twists, or of the diligostatic process (ii) involving rhombic twists is the same : each isomer can be converted into eight isomers.

Considering the adjacency table presented in detail by Gielen, [3] the following adjacency rules emerge (conserving the previous conventions and disregarding the presence or absence of a bar)

1) For A = 2, the four 3-circuits are : *
AB–BY–Z3, AB–BZ–Y3, AB–YB–3Z, AB–ZB–3Y
2) For A = 3, they are :
AB–BY–YA, AB–BZ–ZA, AB–YZ–2Z, AB–ZY–2Y
3) For A = 4, 5 or 6 and B = 3 they are :
AB–BY–YA, AB–BZ–ZA, AB–YZ–2Y, AB–ZY–2Z
4) For A and B = 4, 5 or 6, they are :
AB–BY′–Y′A, AB–BZ′–Z′A, AB–Y′Z′–2B, AB–Z′Y′–2A

There is, however, no regularity whatever when the bar is considered, and this is apparently due to the fact that the assignement of isomers to the two enantiomeric series denoted by the presence or absence of a bar is not self-consistent.

Conserving Gielen's notations, the 30-vertex graph complying with the first requirement (a) is presented in fig. 4. This representation has a trigonal symmetry but does not satisfy requirements (b) or (c).

To satisfy requirement (b), this graph can be rearranged as shown in fig. 5 or 6. No rearrangement, however, can fulfil requirement (c) because four points, namely 45, $\overline{45}$, 54 and $\overline{54}$, are not adjacent to at least two points of the opposite enantiomeric series.

The minimal change in Gielen's notations and adjacency table allowing also requirement (c) to become satisfied [is] the reversal of assignments for 25 and $\overline{25}$. With this reversal, the resulting graph complying with the first three requirements, (a)—(c) is presented in figure 7. Since this last graph does not reveal a high symmetry, it is likely that more than one reversal of enantiomer notations is necessary in Gielen's adjacency table.

---

* The cuboöctahedron, and the graphs presented in figures 2, 4–9 and 3, form a series of regular graphs of degrees 4, 6, 8 and 12, respectively, where 2, 3, 4 or 6 three-circuits respectively, with no common edge, meet at each vertex.

To find out which reversals end up in a highly symmetric graph fulfiling all three requirements (a)—(c), an indirect approach was employed. Starting from the observation that the adjacency rules for digonal twists are complementary to those for trigonal or rhombic twists, the complementary graph of the 15-vertex graph from fig. 2 was constructed by linking all its pairs of disconnected vertices and removing all original lines from that graph. Thus the graph from fig. 8 was obtained.* By repeating

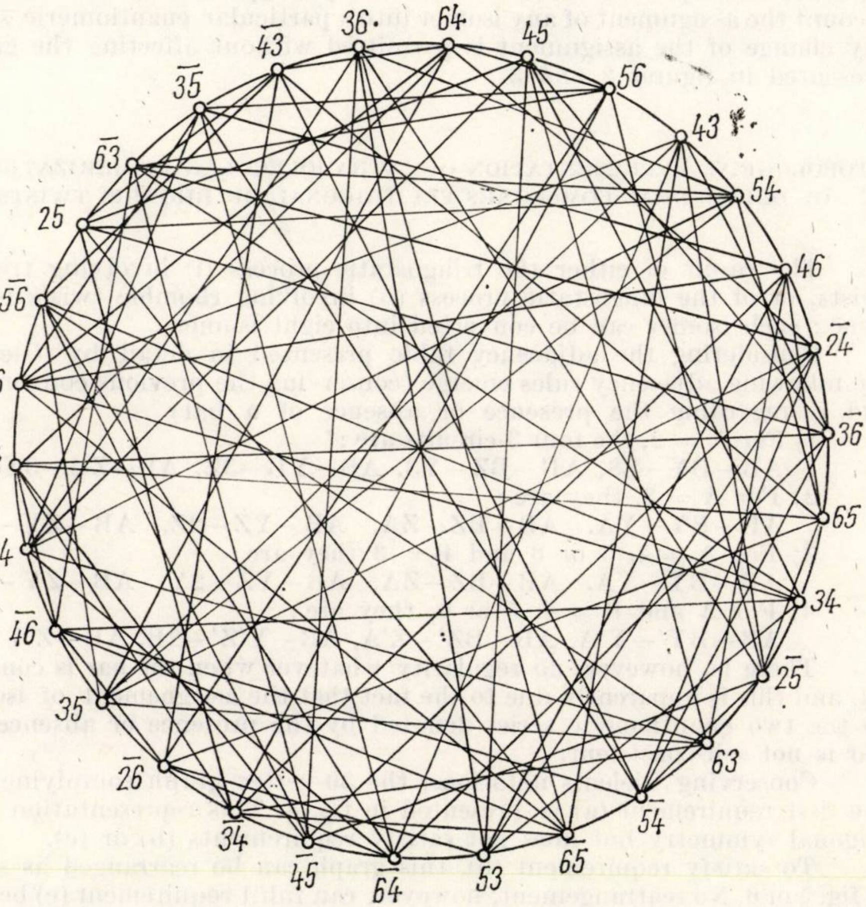
$\overline{43}$
36
64
45
56
$\overline{35}$
43
$\overline{63}$
54
25
46
$\overline{56}$
$\overline{24}$
26
$\overline{36}$
$\overline{53}$
65
24
34
$\overline{46}$
$\overline{25}$
35
63
$\overline{26}$
$\overline{54}$
$\overline{34}$
$\overline{65}$
$\overline{45}$
$\overline{64}$
53

Fig. 4. — Graph of intramolecular rearrangements of octahedral complexes with six different ligands *via* trigonal or rhombic twists, using Gielen's assignment (middle line of notations in fig. 1).

---

* There are 132 symmetrical hamiltonian circuits which result from fig. 8, leading to different assignment reversals but to similar completed adjacency rules. The reversal of four vertex notations presented here seems to be one of the simplest.

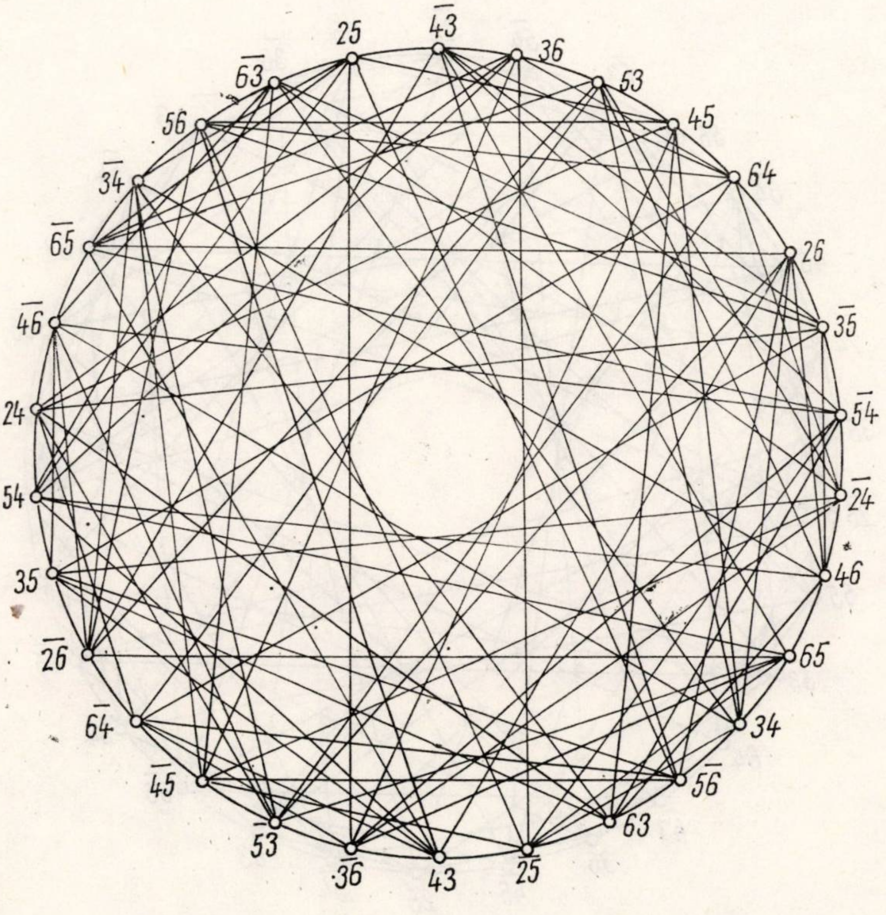
25
$\overline{43}$
36
53
45
64
26
$\overline{35}$
$\overline{54}$
$\overline{24}$
46
65
34
$\overline{56}$
63
$\overline{25}$
43
$\overline{36}$
$\overline{53}$
$\overline{45}$
$\overline{64}$
$\overline{26}$
35
54
24
$\overline{46}$
$\overline{65}$
$\overline{34}$
56
$\overline{63}$

Fig. 5. – Same as fig. 4, in a different geometric realization.

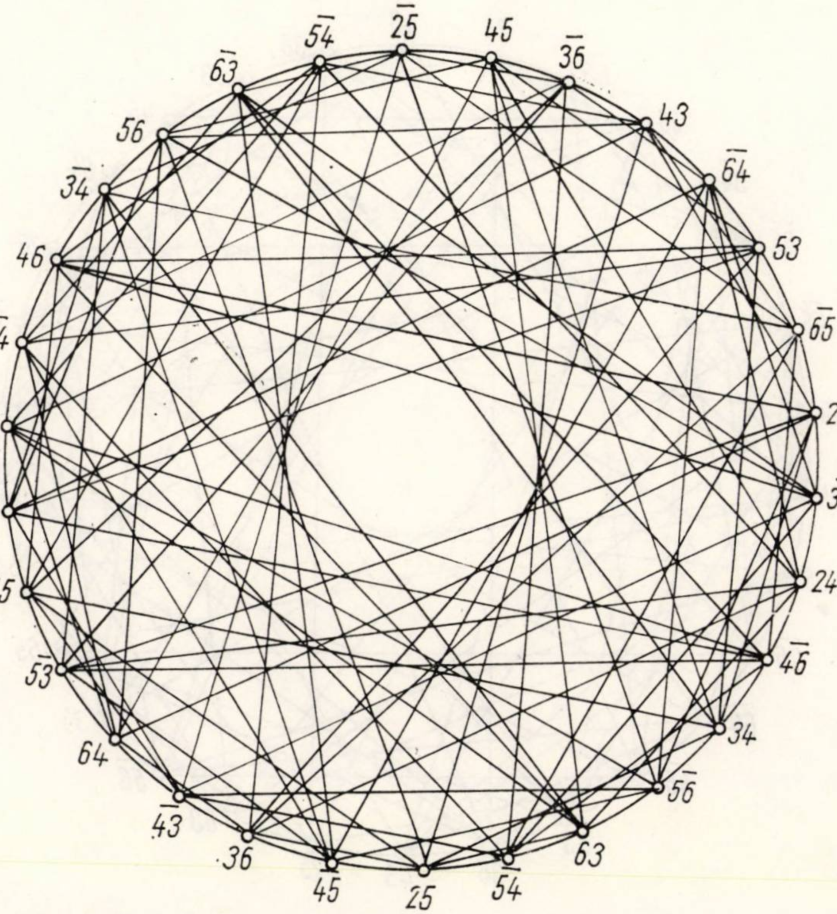
$\overline{54}$
$\overline{25}$
45
$\overline{36}$
43
$\overline{64}$
53
$\overline{65}$
26
$\overline{35}$
24
$\overline{46}$
34
$\overline{56}$
63
$\overline{54}$
25
$\overline{45}$
36
$\overline{43}$
64
$\overline{53}$
65
$\overline{26}$
35
$\overline{24}$
46
$\overline{34}$
56
$\overline{63}$

Fig. 6. – Graph of intramolecular rearrangements of octahedral complexes with six different ligands *via* trigonal or rhombic twists. Notations of the enantiomeric pair 25 are reversed relatively to Gielen's assignment.

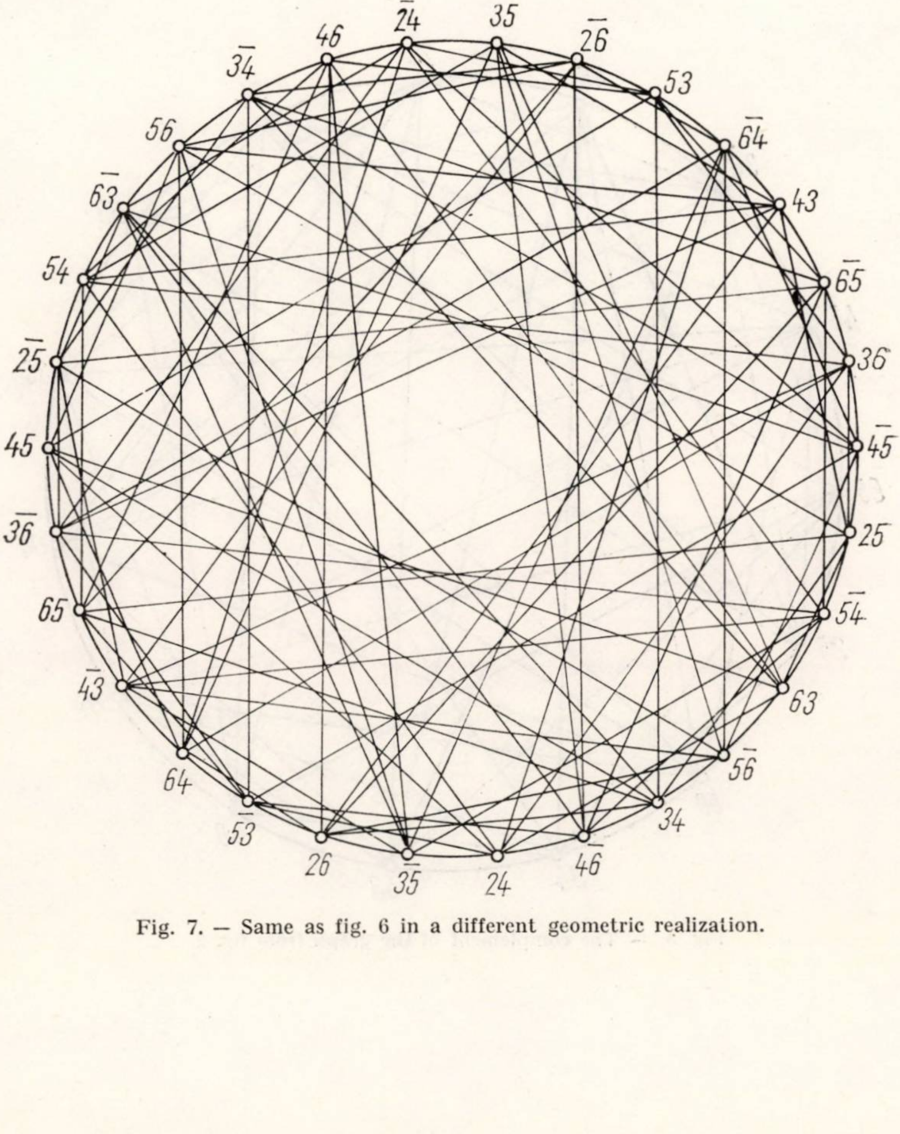
46
$\overline{24}$
35
$\overline{26}$
53
$\overline{64}$
43
$\overline{65}$
36
$\overline{45}$
25
$\overline{54}$
63
$\overline{56}$
34
$\overline{46}$
24
$\overline{35}$
26
$\overline{53}$
64
$\overline{43}$
65
$\overline{36}$
45
$\overline{25}$
54
$\overline{63}$
56
$\overline{34}$

Fig. 7. – Same as fig. 6 in a different geometric realization.

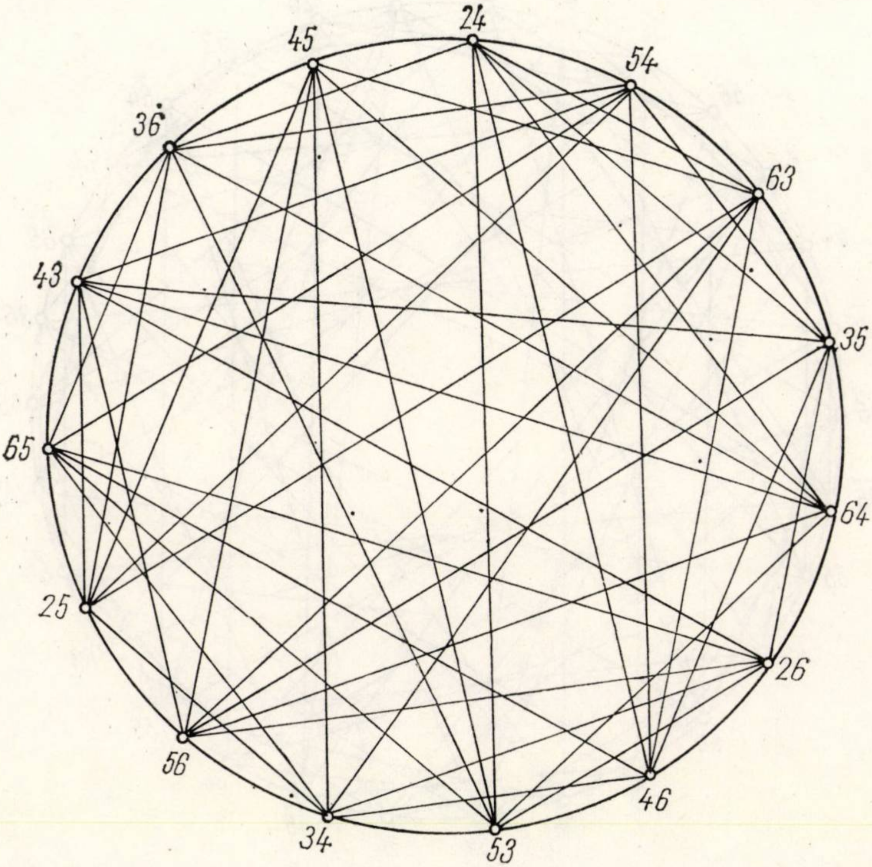
24
45
54
36
63
43
35
65
64
25
26
56
46
34
53

Fig. 8. — The complement of the graph from fig. 2.

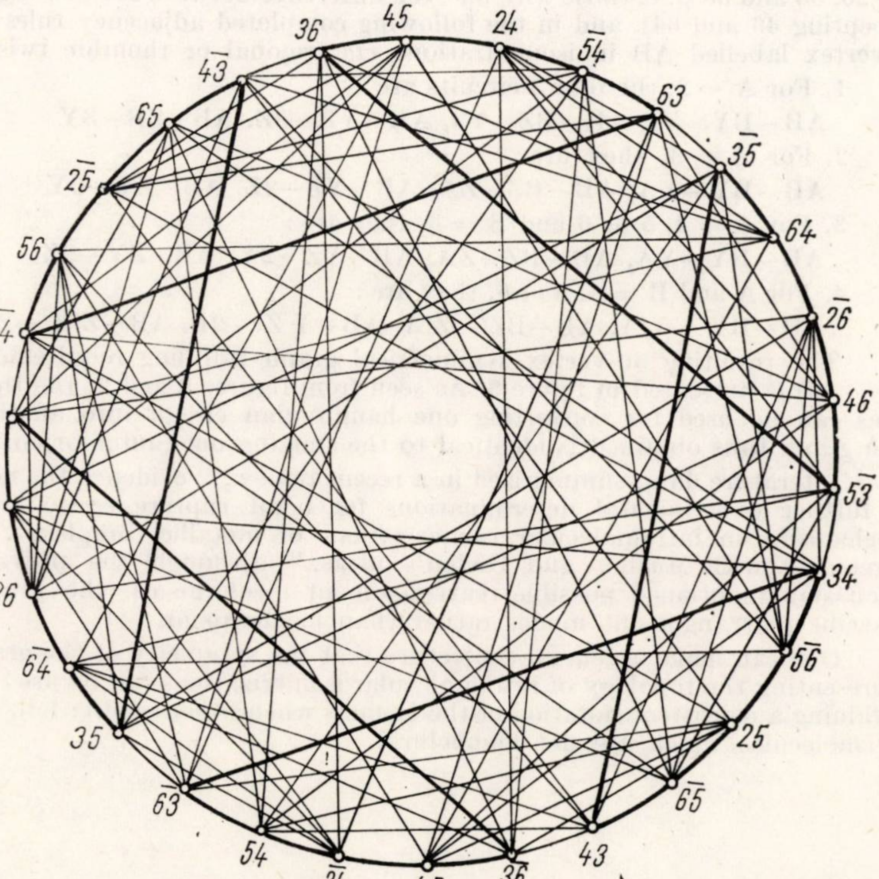
$\overline{45}$
36
24
$\overline{54}$
43
63
65
$\overline{35}$
$\overline{25}$
64
56
$\overline{26}$
$\overline{34}$
46
53
$\overline{53}$
$\overline{46}$
34
26
$\overline{56}$
$\overline{64}$
25
35
$\overline{65}$
$\overline{63}$
54
43
$\overline{24}$
45
$\overline{36}$

Fig. 9. – Graph of intramolecular rearrangements of octahedral complexes with six different ligands *via* trigonal or rhombic twists. The newly proposed assignments of isomers are used (lower line of notations in fig. 1).

its sequence of vertices twice on a 30-vertex Hamiltonian circuit, the perimeter of the graph presented in fig. 9 was obtained. Starting from vertex 24 and labelling it $\overline{24}$, one adds bars alternately over the labels of the vertices. This procedure results in the reversals of assignements relatively to Gielen's original notations for the following four pairs of enantiomers: 24, 26, 35 and 53 (i. e. those with an even difference between the two digits, excepting 46 and 64), and in the following completed adjacency rules for a vertex labelled AB in isomerizations *via* trigonal or rhombic twists:

1. For A = 2, the four 3-circuits are:
$\mathrm{AB}-\overline{\mathrm{BY}}-\overline{\mathrm{Z3}}$, $\mathrm{AB}-\mathrm{BZ}-\overline{\mathrm{Y3}}$, $\mathrm{AB}-\overline{\mathrm{YB}}-\overline{\mathrm{3Z}}$, $\mathrm{AB}-\mathrm{ZB}-\overline{\mathrm{3Y}}$
2. For A = 3, they are:
$\mathrm{AB}-\mathrm{BY}-\overline{\mathrm{YA}}$, $\mathrm{AB}-\overline{\mathrm{BZ}}-\overline{\mathrm{ZA}}$, $\mathrm{AB}-\overline{\mathrm{YZ}}-\overline{\mathrm{2Z}}$, $\mathrm{AB}-\mathrm{ZY}-\overline{\mathrm{2Y}}$
3. For A = 4, 5 or 6 and B = 3, they are:
$\mathrm{AB}-\overline{\mathrm{BY}}-\mathrm{YA}$, $\mathrm{AB}-\overline{\mathrm{BZ}}-\overline{\mathrm{ZA}}$, $\mathrm{AB}-\mathrm{YZ}-\overline{\mathrm{2Y}}$, $\mathrm{AB}-\overline{\mathrm{ZY}}-\overline{\mathrm{2Z}}$
4. For A and B = 4, 5 or 6, they are:
$\mathrm{AB}-\overline{\mathrm{BY'}}-\mathrm{Y'A}$, $\mathrm{AB}-\mathrm{BZ'}-\mathrm{Z'A}$, $\mathrm{AB}-\overline{\mathrm{Y'Z'}}-\mathrm{2B}$, $\mathrm{AB}-\mathrm{Z'Y'}-\overline{\mathrm{2A}}$.

The resulting 30-vertex symmetrical graph fulfilling requirements (a) – (d) is presented in figure 9. As seen from figures 3 and 9, the thick lines can be used for converting one hamiltonian circuit into another. The graph thus obtained is identical to the starting one (automorphism).

Literature data, summarized in a recent review, [24] evidence the need of further experimental determinations for bond rupture *versus* twist mechanisms in intramolecular isomerizations of metallic complexes. In agreement with Musher and Gielen's ideas, [10] although the previous discussion mentioned possible rearrangement mechanisms, the graphs describe rearrangement modes rather than mechanisms.

One can make a general conjecture that the symmetry of the graph representing the topology of intramolecular isomerizations can be used for obtaining a consistent notation of the isomers when other criteria fail, e.g. for molecules which are not homochiral.

---

[24] J. J. Fortman and R. E. Sievers, *Coordin. Chem. Rev.* **6**, 331 (1971).

Revue Roumaine de Chimie, **18**, *5*, 855–862 (1973)

CHEMICAL GRAPHS. XIX[1]

INTRAMOLECULAR ISOMERIZATIONS OF TRIGONAL-BIPYRAMIDAL STRUCTURES WITH FIVE DIFFERENT LIGANDS

ALEXANDRU T. BALABAN

Institute of Atomic Physics, P. O. Box 35, Bucharest, Romania

Received December 29, 1972

In order that in the topological representation of intramolecular isomerizations presented by pentacoördinated TBP structures *via* BPR or TR mechanisms, which is a bipartite graph with 20 vertices, the two sets of vertices be assigned to isomers from the two enantiomeric series, a simple change in the notation of TBP stereoisomers currently in use is necessary. Topological representations are given all for possible modes of rearrangement of TBP structures with five different ligands.

Many pentacoördinated phosphorus compounds and organometallic complexes possess a trigonal-bipyramidal (TBP) geometry. [2] The order of the rotation group is in this case 6, so that there are $5!/6 = 20$ isomers when all five ligands are different. [3] Their intramolecular isomerization was first discussed by Berry who devised a pseudorotation mechanism (BPR), [4] and more recently by Ugi and Ramirez who advocated that a turnstile rotation (TR) mechanism could take place in some cases.[5–9] The complete set of all possible intramolecular isomerizations was considered by Musher,[10] reformulating earlier ideas of Muetterties,[11-13] Gielen, Nasielski and Brocas.[14,15] Thus, both the BPR and TR mechanisms are denoted by Musher[10] as mode $M_1(3)$, where the subscript indicates the number of ligands conserving their positions,* and the number in parentheses indicates how many isomers can be formed in one step from a given structure (i. e. the degree of the graph representing topologically the rearrangement).

---

[1] Preceding part in the series, A. T. Balaban, *Rev. Roumaine Chim.* **18**, 635 (1973).

[2] E. L. Muetterties and R. A. Schumm, *Quart. Rev.*, **20**, 245 (1966); P. Meakin, E. L. Muetterties and J. P. Jesson, *J. Amer. Chem. Soc.*, **94**, 5271 (1972); R. H. Holmes, *Accounts Chem. Res.*, **5**, 296 (1972); F. Ramirez, *ibid.*, **1**, 168 (1968); *Trans. N. Y. Acad. Sci.*, **30**, 410 (1968); F. H. Westheimer, *Accounts Chem. Res.*, **1**, 70 (1968); R. Schmutzler, *Angew. Chem.*, **77**, 530 (1965); *Angew Chem. Internat. Edit.*, **4**, 496 (1965); "Halogen Chemistry" (V. Gutmann, editor), vol. 2, p. 31, Academic Press, New York, 1967.

[3] D. H. McDaniel, *Inorg. Chem.*, **56**, 2678 (1972).

[4] R. S. Berry, *J. Chem. Phys.*, **32**, 933 (1960).

[5] I. Ugi, D. Marquarding, H. Klusacek, G. Gokel and P. Gillespie, *Angew. Chem.*, **82**, 741 (1970); I. Ugi, G. Gokel, P. Gillespie, H. Klusacek and D. Marquarding, *Angew. Chem. Internat. Edit.*, **9**, 703 (1970).

[6] I. Ugi, D. Marquarding, H. Klusacek, P. Gillespie and F. Ramirez, *Accounts Chem. Res.*, **4**, 288 (1971).

[7] F. Ramirez, S. Pfohl, E. A. Tsolis, J. F. Pilot, C. P. Smith, I. Ugi, D. Marquarding, P. Gillepsie and P. Hoffmann, *Phosphorus*, **1**, 1 (1971).

[8] P. Gillespie, P. Hoffmann, H. Klusacek, D. Marquarding, S. Pfohl, F. Ramirez, E. A. Tsolis and I. Ugi. *Angew. Chem.*, **83**, 691 (1971); *Angew. Chem. Internat. Edit.*, **10**, 687 (1971).

[9] F. Ramirez and I. Ugi, *Adv. Phys. Org. Chem.*, **9**, 25 (1971), V. Gold (ed.).

Musher made a specific call for generalizing the topological representations to cover all possible rearrangement modes listed by him. This is done in the present paper.

Theoretical calculations favour the BPR mechanism in normal cases but do not rule out a TR mechanism in cases when steric factors cause two *cis*-ligands to be closely associated.[18]

Irrespective of which of these two mechanisms (which are the most favourable energetically) is actually operating, the complete chart of reactions linking the 20 isomers is the same, since both the BPR and the TR mechanisms can convert one isomer into three other ones. In a topological representation[13,15,19,20] where a chemical species (one isomer) is represented by a point (vertex) and where a chemical reaction (one-step isomerization) is represented by a line (edge), this complete chart is a 20-vertex regular graph where each vertex has degree three (i.e. a cubic or trivalent graph).

This graph is isomorphic with the Desargues-Levi graph which was used for a first chemical application in rationalizing the rearrangements of carbonium ions.[20]

The Desargues-Levi graph was shown[21] to be a particular case of regular combination graphs: for each odd integer $n \geqslant 3$, a graph with two sets of $\binom{n}{(n-1)/2)}$ vertices of degree $\frac{n+1}{2}$ is defined. Each vertex in one set is labelled with groups of $(n-1)/2$ unordered symbols out of n symbols (these symbols can be the first n natural numbers), and the two sets are distinguished by placing a bar over the notation of vertices from one set. Two vertices are adjacent if they belong to different sets and if they have no common symbol. For $n = 5$, the Desargues-Levi graph results (figure 1). It is a bipartite or bicolourable graph by the adjacency rule, and the vertex notation with barred and non-barred symbols agrees with the bipartite character of the graph. It is not possible to obtain a hamiltonian circuit with enantiomers * in antipodal positions (requirement b of the preceding paper [22]). Figure 1 presents several isomorphic

---

* The BPR and TR mechanisms are monoligostatic proceses, using Cram's nomenclature.[16,17]

[10] J. I. Musher, *J. Amer. Chem. Soc.*, **94**, 5662 (1972).

[11] E. L. Muetterties, *J. Amer. Chem. Soc.*, **91**, 1636 (1969).

[12] E. L. Muetterties and C. M. Wright, *Quart. Rev.*, **21**, 109, 179 (1967).

[13] E. L. Muetterties, *Inorg. Chem.*, **6**, 635 (1967); *J. Amer. Chem. Soc.*, **91**, 4115 (1969).

[14] M. Gielen, in "Chemical Applications of Graph Theory" (A. T. Balaban, editor), Academic Press, London, in print.

[15] M. Gielen and J. Nasielski, *Bull. Soc. Chim. Belges*, **78**, 339 (1969); J. Nasielski, *Pure Appl. Chem.*, **30**, 449 (1972); J. Brocas, *Fortschr. Chem. Forsch.*, **32**, 43 (1972).

[16] D. C. Garwood and D. J. Cram, *J. Amer. Chem. Soc.*, **92**, 4575 (1970).

[17] D. J. Cram and J. M. Cram, *Fortschr. Chem. Forsch.*, **31**, 1 (1972).

[18] R. Hoffmann, J. M. Howell and E. L. Muetterties, *J. Amer. Chem. Soc.*, **94**, 3047 (1972).

[19] W. G. Klemperer, *J. Chem. Phys.*, **56**, 5478 (1972); *Inorg. Chem.*, **11**, 2669 (1972); *J. Amer. Chem. Soc.*, **94**, 6940 (1972); E. L. Muetterties, *Record Chem. Progr.*, **31**, 51 (1970).

[20] A. T. Balaban, D. Fărcaşiu and R. Bănică, *Rev. Roumaine Chim.*, **11**, 1205 (1966).

[21] A. T. Balaban, *Rev. Roumaine Math. Pures Appl.*, **17**, 3 (1972).

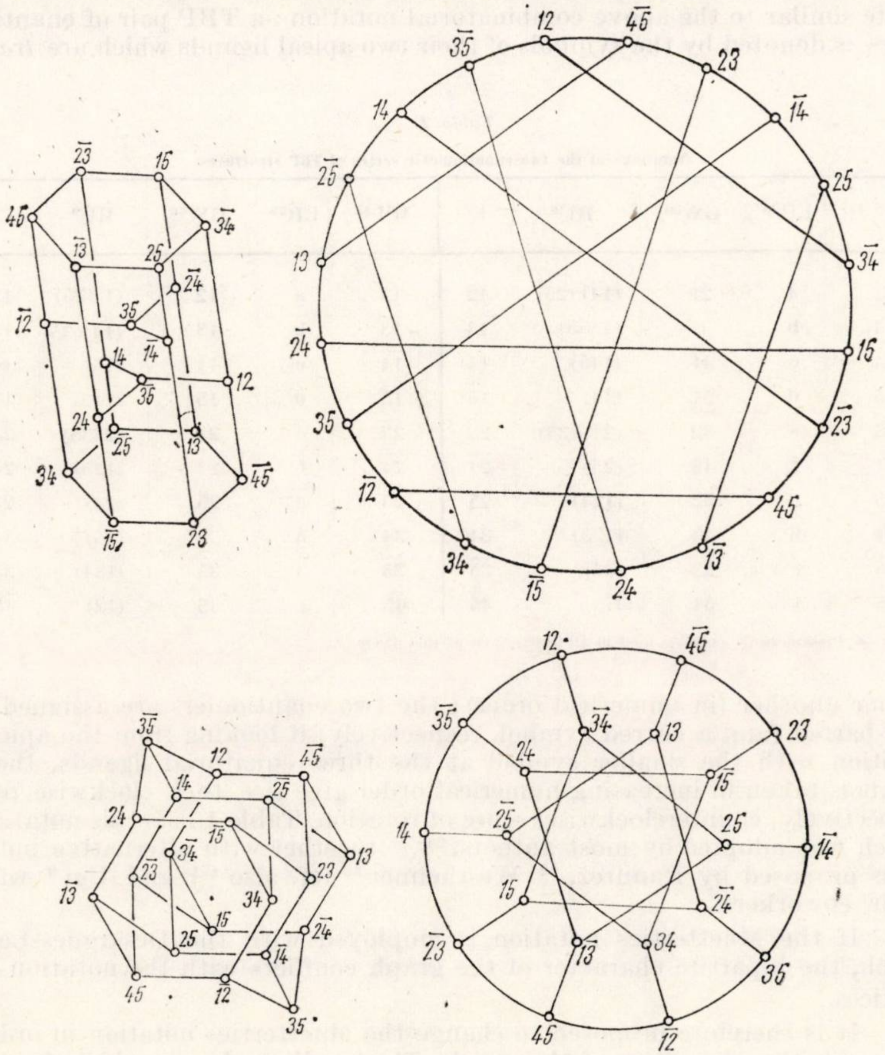

Fig. 1. — The Desargues-Levi graph in several geometric realizations with combinatorial notation of vertices.

---

* Two enantiomers will be shown to correspond to the same numerical symbol, and to differ by the presence of a bar over the symbol.

[22] A. T. Balaban, part XVI, preceding paper.

geometrical realizations of this 20-vertex graph. Its girth (smallest circuit) is six.

The notation proposed for TBP complexes by Muetterties [11,12] is quite similar to the above combinatorial notation : a TBP pair of enantiomers is denoted by the symbols of their two apical ligands which are *trans* to one another (in numerical order) ; the two enantiomers are assigned a non-barred (and a barred symbol, respectively) if looking from the apical position with the smaller symbol at the three equatorial ligands, their symbols taken in increasing numerical order give rise to a clockwise (or, respectively, counterclockwise) sense of rotation. Table 1 lists this notation which was adopted by most authors, [23–28] together with alternative notations proposed by Ramirez, [29] Westheimer [30] (cf. also [17]) and Ugi [9] with their coworkers.

Table 1

Notations of the two enantiomeric series of TBP structures

$M^{11,12}$	LR^{29}	GW^{30}	RU^{9}	C^{a}	$M^{11,12}$	LR^{29}	GW^{30}	RU^{9}	C^{a}
12	a	21	(14) (25)	12	$\overline{12}$	$\overline{a}$	12	(1 425)	$\overline{12}$
13	b	31	(1435)	$\overline{13}$	$\overline{13}$	$\overline{b}$	13	(14)(35)	13
14	c	41	(145)	14	$\overline{14}$	$\overline{c}$	14	(15)	$\overline{14}$
15	d	51	(14)	$\overline{15}$	$\overline{15}$	$\overline{d}$	15	(142)	15
23	e	32	(24) (35)	23	$\overline{23}$	$\overline{e}$	23	(2435)	$\overline{23}$
24	f	42	(25)	$\overline{24}$	$\overline{24}$	$\overline{f}$	24	(125)	24
25	g	52	(124)	25	$\overline{25}$	$\overline{g}$	25	(24)	$\overline{25}$
34	h	43	(135)	34	$\overline{34}$	$\overline{h}$	34	(35)	$\overline{34}$
35	i	53	(34)	$\overline{35}$	$\overline{35}$	$\overline{i}$	35	(134)	35
45	j	54	E	45	$\overline{45}$	$\overline{j}$	45	(12)	$\overline{45}$

[a] Present work, notation used in all illustrations of this paper.

If the Muetterties notation is employed with the Desargues-Levi graph, the bipartite character of the graph conflicts with the notation of vertices.

It is therefore proposed to change the Muetterties notation in order to match the properties of the graph. The smallest change which brings about this matching consists in *reverting the assignment into the two enantio-*

---

[23] K. E. DeBruin, K. Naumann, G. Zon, and K. Mislow, *J. Amer. Chem, Soc.*, **91**, 7031 (1969).

[24] K. Mislow, *Accounts Chem. Res.*, **3**, 321 (1970).

[25] J. Heller, *Chimia* (*Aarau*), **23**, 351 (1969).

[26] M. Gielen, M. de Clercq and J. Nasielski, *J. Organometal. Chem.*, **18**, 217 (1969).

[27] J. Brocas and M. Gielen, *Bull. Soc. Chim. Belges*, **80**, 207 (1971).

[28] M. Gielen, *Med. Vlaam. Chem. Ver.*, **31**, 185 (1969).

[29] P. C. Lauterbur and F. Ramirez, *J. Amer. Chem. Soc.*, **90**, 6722 (1968).

[30] D. Gorenstein and F. H. Westheimer, *J. Amer. Chem. Soc.*, **92**, 634 (1970).

meric series whenever the difference between the two apical symbols is an even number. Unlike the case of octahedral complexes discussed previously, [22] which had many hamiltonian circuits, the present smallest change is unique. It results in the notation presented in column C (for combinatorial) of table 1. With this change, the permutational notation proposed by Ramirez and Ugi [9] becomes closely related to the new combinatorial notation, in that now every barred symbol in the combinatorial notation corresponds to one permutation of an even number of vertices in the permutational notation.

$$
\begin{array}{c|cccccccccccccccccccc|}
 & 12 & 13 & 14 & 15 & 23 & 24 & 25 & 34 & 35 & 45 & \overline{12} & \overline{13} & \overline{14} & \overline{15} & \overline{23} & \overline{24} & \overline{25} & \overline{34} & \overline{35} & \overline{45} \\
\hline
12 & & & & & & & & & & & & & & & & & & 1 & 1 & 1 \\
13 & & & & & & & & & & & & & & & & 1 & 1 & & & 1 \\
14 & & & & & & & & & & & & & & & 1 & & 1 & & 1 & \\
15 & & & & & & & & & & & & & & & 1 & 1 & & 1 & & \\
23 & & & & & & & & & & & & & 1 & 1 & & & & & & 1 \\
24 & & & & & & & & & & & & 1 & & 1 & & & & & & 1 \\
25 & & & & & & & & & & & & 1 & 1 & & & & & & 1 & \\
34 & & & & & & & & & & & 1 & & & 1 & & & & 1 & & \\
35 & & & & & & & & & & & 1 & & 1 & & & & 1 & & & \\
45 & & & & & & & & & & & 1 & 1 & & & & 1 & & & & \\
\overline{12} & & & & & & & & 1 & 1 & 1 & & & & & & & & & & \\
\overline{13} & & & & & & 1 & 1 & & & 1 & & & & & & & & & & \\
\overline{14} & & & & & 1 & & 1 & & 1 & & & & & & & & & & & \\
\overline{15} & & & & & 1 & 1 & & 1 & & & & & & & & & & & & \\
\overline{23} & & & 1 & 1 & & & & & & 1 & & & & & & & & & & \\
\overline{24} & & 1 & & 1 & & & & & & 1 & & & & & & & & & & \\
\overline{25} & & 1 & 1 & & & & & & 1 & & & & & & & & & & & \\
\overline{34} & 1 & & & 1 & & & & 1 & & & & & & & & & & & & \\
\overline{35} & 1 & & 1 & & & & 1 & & & & & & & & & & & & & \\
\overline{45} & 1 & 1 & & & & 1 & & & & & & & & & & & & & & \\
\hline
\end{array}
$$

Fig. 2. — Adjacency matrix of the Desargues-Levi graph.

With the new combinatorial notation, figure 1 is at the same time a topological representation of intramolecular isomerizations in TBP complexes with five different ligands *via* BPR or TR mechanisms. The adcency matrix of the Desargues-Levi graph for the new combinatorial anotation of vertices is presented in full in figure 2 : digit 1 indicates adjacency, void stands for zero, i.e. non-adjacency. Figure 3 presents a reduced form of the previous matrix, where a minus sign indicates that two vertices from opposite sets are adjacent (e.g. 12 with $\overline{34}$; conversely, a plus sign would indicate adjacency of vertices from the same set).

If the signs in the adjacency matrix of the above graph are changed, one obtains the adjacency matrix of the topological representation of

Musher's M_5 (3) mode of rearrangement.[10] Since in the new combinatorial notation the two sets now become disjoint, the representation consists in two Peterson graphs,[21,22,31] one for each enantiomeric series: the girth is five, and the high symmetry of the Petersen graph is reflected in its identification with the 5-cage.[32]

	12	13	14	15	23	24	25	34	35	45
12								—	—	—
13						—	—			—
14					—		—		—	
15					—	—		—		
23			—	—						—
24		—		—						—
25		—	—						—	
34	—			—				—		
35	—		—				—			
45	—	—				—				

Fig. 3. — Reduced form of the matrix presented in figure 2.

By working out the adjacency table for Musher's $M_2(6)$ process,[10] one obtains in the new combinatorial notation another bipartite graph, which is now of degree six and whose adjacency matrix is presented in figure 4 in reduced form. One can see that the matrices from figures 3 and 4 are complementary, because minus signs and zeroes are reversed. The resulting graph is presented in figure 5. It has girth four. By following the hamiltonian circuit $12-\overline{23}-13-\overline{14}-45-\overline{15}-14-\overline{24}-23-\overline{34}-24-\overline{25}-15-\overline{12}-25-\overline{35}-34-\overline{45}-35-\overline{13}-12$ this graph is converted into a different isomorphic geometrical realization.

	12	13	14	15	23	24	25	34	35	45
12	—	—	—	—	—	—	—			
13	—	—	—	—	—			—	—	
14	—	—	—	—		—		—		—
15	—	—	—	—			—		—	—
23	—	—			—	—	—	—	—	
24	—		—		—	—	—	—	—	
25	—			—	—	—	—	—		—
34		—	—		—	—	—		—	—
35		—		—	—	—		—	—	—
45			—	—	—		—	—	—	—

Fig. 4. — Reduced form of the adjacency matrix representing rearrangement mode $M_2(6)$ with combinatorial notation of isomers.

---

[31] J. D. Dunitz and V. Prelog, *Angew. Chem.*, **80**, 700 (1968); *Angew. Chem. Internat. Edit.*, **7**, 725 (1968).

[32] W. T. Tutte, "Connectivity in Graphs", University of Toronto Press, p. 74 (1966); F. Harary, "Graph Theory", Addison-Wesley, Reading, Mass., p. 89, 175 (1969).

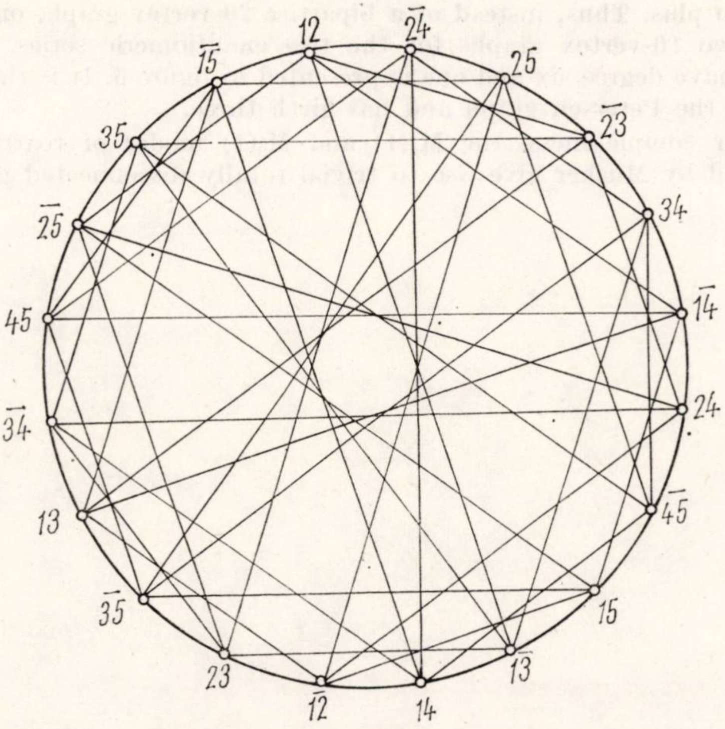
12
$\overline{24}$
$\overline{15}$
25
35
$\overline{23}$
$\overline{25}$
34
45
$\overline{14}$
$\overline{34}$
24
13
$\overline{45}$
$\overline{35}$
15
23
$\overline{13}$
$\overline{12}$
14

Fig. 5. — Graph representing topologically rearrangement mode $M_2(6)$.

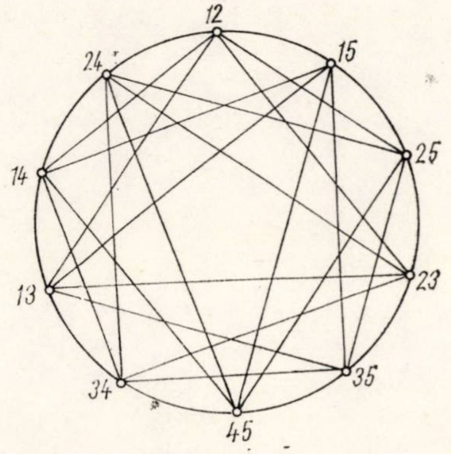
12
24
15
14
25
13
23
34
35
45

Fig. 6. — One of the two identical graphs representing topologically rearrangement mode $M_4(6)$ with combinatorial notation of isomers.

Musher's $M_4(6)$ mode bears the same relationship to $M_2(6)$ as $M_5(3)$ to $M_1(3)$, i.e. all signs in the reduced adjacency matrix are changed from minus to plus. Thus, instead of a bipartite 20-vertex graph, one obtains again two 10-vertex graphs for the two enantiomeric series. Now the graphs have degree six and one is presented in figure 6. It is the complement of the Petersen graph and has girth three.

For completeness, the $M_0(1)$ and $M_3(1)$ modes of rearrangement presented by Musher give rise to trivial totally disconnected graphs.

Revue Roumaine de Chimie, **18**, 5, 863–872 (1973)

INVESTIGATIONS IN THE CYCLOBUTANE SERIES. XXXII[1]

THE ADDITION OF BROMINE TO DERIVATIVES OF *exo.exo*-TETRACYCLO[$4.4.2.0^{2.5}.0^{7.10}$]DODECA-3.11-DIENE

MARGARETA AVRAM, ILIE G. DINULESCU, FILIP CHIRALEU
and COSTIN D. NENITZESCU *

Institute of Organic Chemistry, Bucharest, Spl. Independenţei 202B

Received December 4, 1972

exo, exo-Tetracyclo-dodeca-3,11-diene derivatives were synthesized and the behaviour toward bromine was studied. The structure of the reaction products is elucidated.

It was previously observed in the case of derivatives of hydrocarbon $(CH)_{10}$ with tricyclo [$4.2.2.0^{2.5}$] decadienic skeleton **1** that the C_3-C_4 double bond of the cyclobutene ring is conveniently located for through-space interactions with the median bridge bond[2,3]. In the course of configurational and structural studies of tricyclodecadiene **1**, the ability of this kind of bonds to form stable complexes with transitional metals, of **2** type, was shown.[4]

Investigating the halogen addition, a through-space π participation of the C_9-C_{10} bond, leading to semicage systems (**3** or **4**), was demonstrated.[2]

Photochemically induced cycloaddition reactions leading to cage systems (**5**) are also well-known.[5] As a continuation of our interest concerning through-space π-p participation in the course of halogen addition, it seemed attracting to study the behaviour of some derivatives of a $(CH)_{12}$ hydrocarbon[6] with tetracyclo [$4.4.2.0^{2.5}.0^{7.10}$] dodeca-3,11-dienic skeleton (**6**), namely the cyclobutanic homolog of Nenitzescu's hydrocarbon (**7**).[7]

---

* Deceased July 28, 1970.

[1] Part XXXI: M. Avram, L. Enescu, I. G. Dinulescu, F. Chiraleu and C. D. Nenitzescu, *Rev. Roumaine Chim.*, **16**, 1783 (1971).

[2] M. Avram, G. D. Mateescu and C. D. Nenitzescu, *Liebigs Ann. Chem.*, **636**, 174 (1960).

[3] G. D. Mateescu, M. Avram and C. D. Nenitzescu, *Studii şi cercetări Chim., Acad. R.P.R.*, **10**, 65 (1962.)

[4] M. Avram, E. Sliam and C. D. Nenitzescu, *Liebigs Ann. Chem.*, **636**, 184 (1960).

[5] S. Masamune, H. Cuts and M. G. Hogben, *Tetrahedron Letters*, **1966**, 1017; W. G. Dauben and D. L. Whalen, *Tetrahedron Letters*, **1966**, 3743.

[6] L. A. Paquette and J. C. Stowell, *J. Amer. Chem. Soc.*, **93**, 5735 (1971).

[7] C. D. Nenitzescu, M. Avram, I. Pogany, G. D. Mateescu and M. Fărcaşiu, *Studii şi Cercetări Chim., Acad. R.P.R.*, **11**, 7 (1963).

In the present paper we report the synthesis and some reactions of this system.

For the preparation of the tetracyclodecadiene (**6**) derivatives, the acyloine condensation was used.[8] By treating **1** with sodium, in the presence

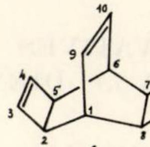

1

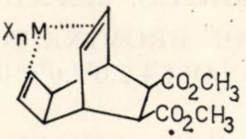

2

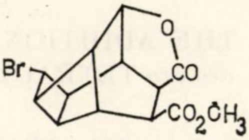

3

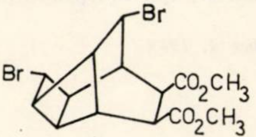

4

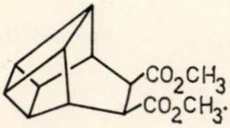

5

of trimethylchlorosilane, the bis-silyloxyderivative **8** was obtained. The hydrolysis of the latter, in acetone solution, afforded acyloin **9**. On treatment with bromine, **8** yielded diketone **10**.

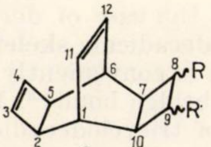

6

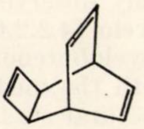

7

The choice between the two possible configurations for acyloin, **9** and **9a**, was made on the basis of IR and NMR data and also on chemical grounds.

IR spectrum shows νCO at 1795 cm^{-1} and νOH at 3590 and 3612 cm^{-1}. On dilution the 3590 cm^{-1} band remained unchanged, indicating intramolecular hydrogen bonds. Such bonds are possible in the case of configuration **9**, where the OH group is near the double bond, which makes possible an O-H...π association. The shoulder at 3612 cm^{-1}, due to free OH, indicates a shift Δν 22 cm^{-1}. The small value of Δν, as compared with other systems,[9] could be attributed to the larger distance between the median bridge ($C_{11} - C_{12}$) and the cyclobutanolone ring. Usually, cyclic acyloins with five or six-membered rings show νOH absorptions at 3300 — — 3500 cm^{-1}, indicating intermolecular associations of OH groups.[10]

---

[8] J. J. Bloomfield, *Tetrahedron Letters*, **1968**, 587; J. M. Conia and J. P. Barnier, *Tetrahedron Letters*, in press.

[9] M. Avram and G. D. Mateescu, "Infrared Spectroscopy. Applications in Organic Chemistry", Wiley, London, 1972, p. 252.

[10] J. C. Sheehan, R. C. O'Neil and M. A. White, *J. Amer. Chem. Soc.*, **72**, 3376 (1950); J. C. Sheehan and R. C. O'Neil, *J. Amer. Chem. Soc.*, **72**, 4614 (1950).

In the NMR spectrum, the proton adjacent to the OH group forms a quartet at δ 4.7 ppm with $J_{9,10} = 9$ Hz and $J_{7,9} = 4$ Hz. In cyclobutanic systems, the vicinal J_{cis} is 8.7 – 9.7 Hz and $J_{1,2\text{-}trans}$ is 6,4 – 8.2 Hz.[11]

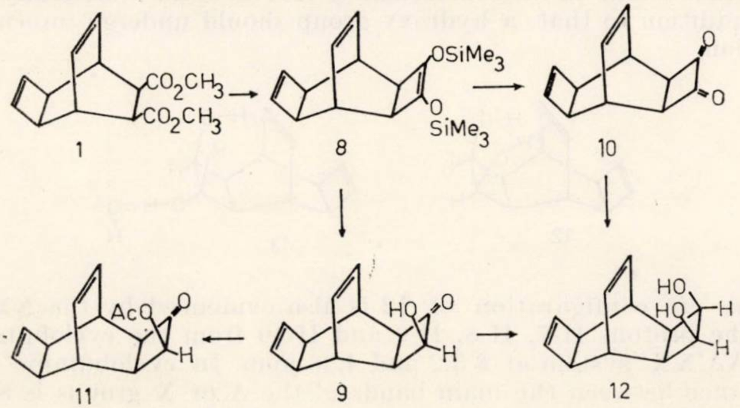

For the $J_{1,3}$ coupling 0.5 – 2.0 Hz values are indicated. This long-range coupling can have higher values under specific steric conditions.[12] Literature [13] gives a value of 3.5 Hz for the $J_{1,3\text{-}cis}$ in a cyclobutane ring belonging to a strained and distorted bicyclic system. A 4 Hz coupling would correspond to a distorted ring, in our case due to the carbonyl group.

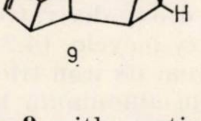

9

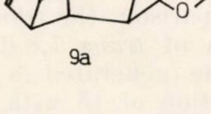

9a

By treating **9** with acetic anhydride an acetyl-derivative **11** was obtained. The NMR spectrum of **11** shows for the proton adjacent to the acetoxy group, a characteristic quartet at δ 5.6 ppm ($J_{9,10} = 9$ Hz, $J_{7,9} =$ $= 4$ Hz).

Reducing **9** with sodium borohydride, a dihydroxy-derivative **12** was obtained. The IR spectrum of **12** presents two ν OH bands at 3545 and 3615 cm^{-1}. The existence of the 3545 cm^{-1} band, unchanged by dilution, indicates an intramolecular hydrogen bond. The high value of the shift, $\Delta\nu = 70$ cm^{-1}, is in accordance with a hydrogen bond O-H. . . O, which is possible only for a *cis* configuration of the two hydroxy groups. In a *trans* derivative **13**, the hydrogen bond O-H. . .π would give a smaller shift (of the same order of magnitude as those observed for acyloin **9**); on the other hand, an intramolecular O-H. . .O bond is sterically impossible. In addition to that, a hydroxy group should undergo intermolecular association.

---

[11] B. Braillon, J. Salaün, J. Gore and J. M. Conia, *Bull. Soc. chim. France*, **1964**, 1981.

[12] S. Sternhell, *Quart. Rev.*, **23**, 236 (1969).

[13] J. W. Hanifin and G. O. Morton, *Tetrahedron Letters*, **1967**, 2307.

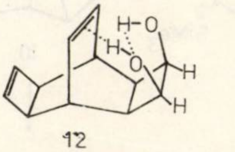

12

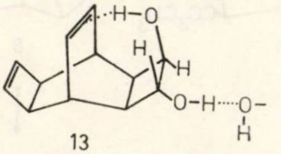

13

The *cis* configuration of **12** is also evidenced by the NMR spectrum. The protons H-7, H-8, H-9 and H-10 from the cyclobutanic ring form a AA'XX' system at δ 3.2 and 4.38 ppm. In cyclobutanic systems, the distance between the main bands of the A or X groups is 8–10 Hz for the *cis* and 4 – 5 Hz for the *trans* isomer. [14]

In the spectrum of **12** the distance between the main bands of the multiplet due to protons H-7, H-10 (H-8, H-9) is 8 Hz, which corresponds to *cis* orientation of the four protons.

The *cis*-dihydroxy-derivative **12** was also obtained by reducing diketone **10** with lithium aluminium hydride. In this case, the hydride ion attack is stereospecific, being directed from the unhindered part of the molecule, according to the general rule of *exo* attack in polycyclic systems. [15]

The treatment of **12** with acetic anhydride afforded the *cis*-diacetate **14**. Its NMR spectrum shows a multiplet centered at δ 5.25 ppm, due to H-8, H-9 protons.

For the comparison, the *trans*-dihydroxy-derivative **13** was synthesized, by reaction of *trans* 7,8-diacetoxy-bicyclo [4.2.0] octa-2,4-diene with cyclobutadiene (generated *in situ* from its iron-tricarbonyl complex) followed by reduction of **15** with lithium aluminium hydride.

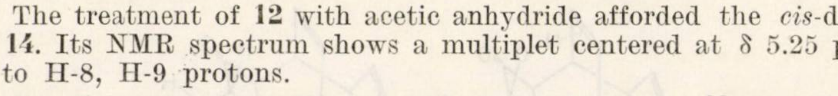

IR spectrum of **13** presents a band due to associated OH at 3300 cm^{-1}. In the NMR spectrum, the false triplet of the olefinic protons of the bridge is broader for **13** than for **12**, which indicates [6,16] *trans* configuration of the two OH groups.

---

[14] R. Steinmetz, W. Hartmann and G. O. Schenck, *Chem. Ber.*, **92**, 3854 (1965); V. Georgian, L. Georgian and A. V. Robertson, *Tetrahedron*, **19**, 1219 (1963).

[15] E. L. Eliel, "Stereochemistry of Carbon Compounds", McGraw-Hill Book Company, Inc., New York, 1962, p. 303.

[16] J. P. Snyder and D. G. Farnum, *J. Org. Chem.*, **31**, 1699 (1966).

By catalitic hydrogenation of **9** only the double bond from the cyclobutenic ring was reduced, yielding the dihydro-derivative **16**; the double bond of the median bridge ($C_{11} - C_{12}$), sterically shielded, is unaffected under these conditions. The same dihydro compound was also obtained by acyloinic condensation of the dihydro-ester **17**.[2]

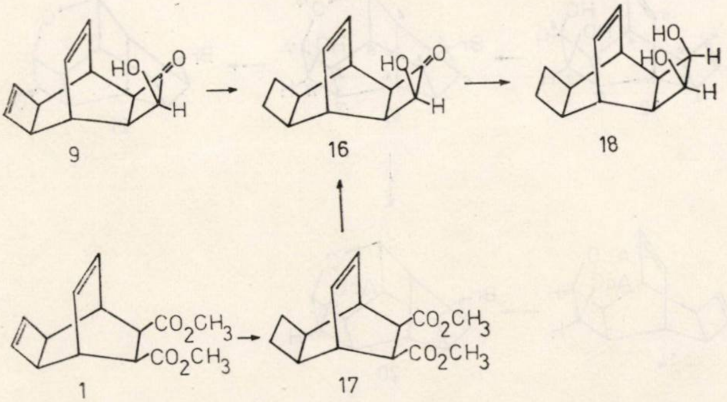

The IR spectrum of **16**, has νCO at 1795 cm^{-1} and νOH at 3600 cm^{-1}, unchanged on dilution. In the NMR spectrum, the proton H-9, adjacent to OH group, forms a quartet centered at δ 4.65 ppm ($J = 9$ Hz and $J = 4$ Hz), which is characteristic for such a system.

The treatment of **16** with sodium borohydride yielded the dihydroxy-derivative **18**.

By treating **12** with one mole of bromine in methylene chloride solution, the reaction mixture became instantly colourless and hydrobromic acid was evolved. By working up a bromohydroxy-ether $C_{12}H_{13}BrO_2$ was obtained, to which the structure **19** was attributed.

The OH group from **19**, with νOH at 3560 cm^{-1}, unchanged on dilution, is intramolecularly associated with the ethereal oxygen. In the NMR and IR spectra there are no characteristic bands of the double bonds.

With acetic anhydride, **19** underwent acetylation yielding **20**. The same acetoxy-derivative **20** was obtained by treating the diacetate **14** with one mole of bromine.

Oxidation of **19** led to ketone **21**; in the IR spectrum, of the latter, the ν CO absorption appears at 1780 cm^{-1}, in good agreement with the literature value for cyclobutanones.[17] In the NMR spectrum the proton H-12, coupled with H-9, gives a doublet centered at δ 6.07 ppm ($J = 3.25$ Hz). By irradiation of H-9, the signal of H-12 appears as singlet at δ 6.01 ppm.

---

[17] Cf. 9, p. 361.

The synthesis of ether **19** and **20** from **12**, respectively **14**, and bromine, involves the long range participation, during bromine addition, of the double bond ($C_{11}-C_{12}$) electrons and of the oxygen p electrons.

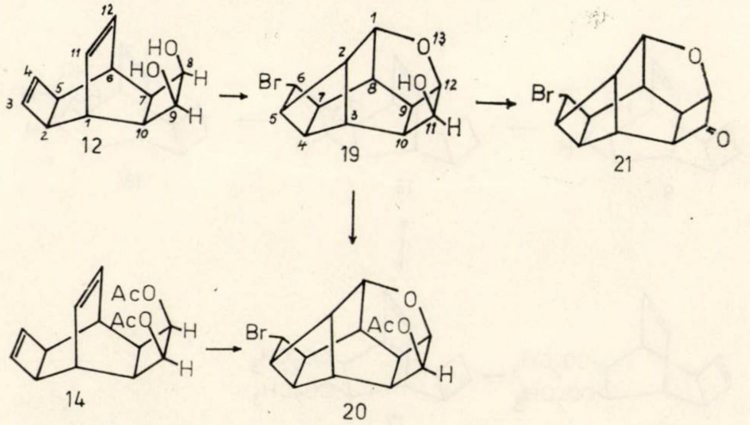
12
11
4
5
HO
HO
6
8
H
3
7
9
H
1
10
2
12
1
O
13
2
Br
6
7
HO
8
12
5
9
3
11
H
4
10
19
Br
O
O
21
AcO
AcO
H
H
14
Br
O
AcO
H
20

Initially, the bromine attacks the cyclobutenic double bond C_3-C_4, which is more reactive and sterically accessible.

To fill in the free orbital of the cation **22**, the π electrons of the nearby $C_{11}-C_{12}$ double bond participate preferentially, leading to the cation **23**. In cation **23** the charge is very near the oxygen of the OH or OAc group. These interactions lead to the ions **24** and **25**, respectively ; by elimination of a proton, or the acetylium ion, respectively, they give rise to the ethers **19** and **20**.

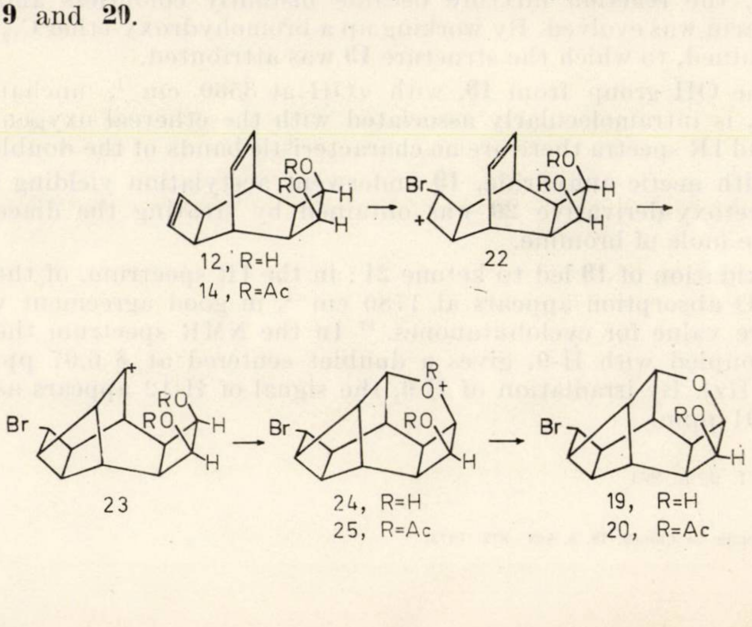
RO
RO
H
H
12, R=H
14, R=Ac
Br
+
RO
RO
H
H
22
+
RO
Br
RO
H
H
23
R
O+
Br
RO
H
24, R=H
25, R=Ac
O
Br
RO
H
19, R=H
20, R=Ac

A nonclassical ion like **26** would produce the same ethers **19** and **20** through formation of a bond between C_3-C_{11}. The formation of a bond between C_3-C_{12} is sterically unfavoured.

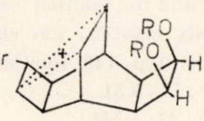

26

Other aspects of the same subject are presently under investigation.

EXPERIMENTAL

NMR spectra were measured at 60 MHz with a Varian A60-A spectrometer. $(CH_3)_4Si$ was used as an internal standard. Chemical shifts are expressed in ppm on a δ scale. IR spectra were determined with a double beam Jena UR 20 spectrophotometer.

8,9-BIS-TRIMETHYLSILYLOXY-*exo*, *exo*-TETRACYCLO [4.4.2.0^{2,5}.0^{7,10}]DODECA-3,8,11-TRIENE (**8**)

A solution of 15 g (0.06 moles) **1** and 40 ml trimethylchlorosilane in 30 ml xylene was added dropwise over a period of 1.5 hr to a suspension of 8 g (0.35 moles) sodium in 70 ml xylene heated at 40° (in argon atmosphere). The temperature was raised at 60° in 2 hr (an exothermic reaction occured and the mixture turned violet), then the reaction mixture was heated at 80° for 6 hr. The mixture was cooled, filtered, the filtrate was evaporated in vacuo and the residue (15.5 g) distilled, yielding 12.5 g (62%) **8**, b.p. 155°/1 mm.

$C_{18}H_{28}O_2Si_2$ *Calcd*: C, 65.00; H, 8.49; Si, 16.89
Found: C, 65.88; H, 8.75; Si, 16.70

NMR (CCl_4): δ 0.16 (s, 18 H, two methyl groups bonded to Si), 2.25–2.66 (m, 6H, H-1, H-2, H-5, H-6, H-7, H-10), 5.70 (m centered, 2 olefinic H. H-11, H-12), 5.81 (s, 2 olefinic H, H-3, H-4).

exo, *exo*-TETRACYCLO[4.4.2.0^{2,5}.0^{7,10}]DODECA-3,11-DIEN-9-*exo*-OL-8-ONE (**9**)

Into a solution of 7.5 g (22.5 mmoles) **8** in 15 ml acetone, 0.9 ml (50 mmoles) water was added and the homogeneous mixture kept for 24 hr at room temperature. After solvent evaporation and crystallization of residue from methanol 3.8 g (90%) **9** was obtained; m.p. 136°.

$C_{12}H_{12}O_2$ *Calcd*: C, 76.58, H, 6.42
Found: C, 76.02; H, 6.64.

IR (CH_2Cl_2): 1795(CO), 3590, 3612 cm^{-1} (OH).

NMR $(CDCl_3)$: δ 2.66–3.36 (m, 6H, H-1, H-2, H-5, H-6, H-7, H-10), 4.7 (quartet, 1 H near OH group, J=4Hz and 9 Hz), 5.80–6.15 (m, 4 olefinic H; a singlet at 5.88 was evidenced, 2 olefinic H from cyclobutene ring).

exo, exo-TETRACYCLO[4.4.2.$0^{2,5}$.$0^{7,10}$]DODECA-3,11-DIEN-8.9-DIONE (**10**)

Into a solution of 3.1400 g (9.5 mmoles) **8** in 25 ml methylene chloride was added slowly a solution of 1.50 g (0.480ml, 9.5 mmoles) bromine in 25 ml methylene chloride. The colour of bromine disappeared instantaneously and the solution became orange. After 10 min the solvent was evaporated, and the residue, oily crystals, was chromatographied on Al_2O_3 with ether, yielding 0.65 g (37%) **10**, red crystals, m.p. 148° (methanol).

$C_{12}H_{10}O_2$ *Calcd* : C, 77.40 ; H, 5.51
Found : C, 76,70 ; H, 5.55

IR(CCl_4) : 1780, 1813 (CO), 3060 (=C–H) cm^{-1}.

NMR ($CDCl_3$) ; δ 2.75(s, 2 H, H-1, H-6), 3.30 (s, 4 H, H-2, H-5, H-7, H-10), 5.87 (m, 4 olefinic H, H-3, H-4, H-11, H-12).

exo-9-ACETOXY-*exo, exo*-TETRACYCLO[4.4.2.$0^{2,5}$.$0^{7,10}$]
DODECA-3,11-DIEN-8-ONE (**11**)

A solution of 1.0 g (5.3 mmoles) **9** in 20 ml acetic anhydride was treated with 3 drops of pyridine and kept at room temperature for 24 hr. Water was then added and the mixture was extracted with methylene chloride. The organic extract was washed with 5% natrium bicarbonate until complete removal of acetic acid. Evaporation of the dried solution and recrystallization of residue from methanol yielded 0.80 g (65%) **11**, m.p. 105°.

$C_{14}H_{14}O_3$ *Calcd* : C, 73.02 ; H, 6.12
Found : C, 73.05 ; H, 6.31

IR(CCl_4) : 1760(CO from ester), 1810(CO fromcyclobutanic ketone), 3055 cm^{-1} (=C–H).

NMR ($CDCl_3$) : δ 2.1 (s, 3H, CH_3 from acetyl group), 2.6–3.5 (complex 6 H, H-1, H-2, H-5, H-6, H-7, H-10), 5.6 (quartet, 1H near acetyl group, J = 4 Hz and 9 Hz), 5.8 – 6.0 (complex, 4 olefinic H, H-2, H-4, H-11, H-12 ; a singlet at 5.88 was evidenced, 2 olefinic H from cyclobutene ring).

exo, cis-8.9-DIHYDROXI-*exo, exo*-TETRACYCLO[4.4.2.$0^{2,5}$.$0^{7,10}$]
DODECA-3,11-DIENE (**12**)

A solution of 1.0 g (5.3 mmoles) **9** in 20 ml ether and 20 ml methanol was treated, portionwise, with a solution of 1.0 g sodium borohydride in 20 ml methanol and 2 ml water. After 24 hr crystals which separated were filtered and recrystallized from diluted methanol, yielding 0.8 g (80%) **12**, m.p. 176°.

$C_{12}H_{14}O_2$ *Calcd* : C, 75.76 ; H, 7.41
Found : C, 75.84 ; H, 7.69

IR (CH_2Cl_2) : 3545, 3615 cm^{-1} (OH).

NMR ($CD_3.CO.CD_3$) : δ 6.03 (t, 2 olefinic H, H-11, H-12), 5.78 (s, 2 olefinic H, H-3, H-4), 4.38 (broad signal, 2 H near OH groups, H-8, H-9), 3.2 (m of A type from AA′XX′ system, 2 saturated H), 2.6 (broad s, 4 saturated H).

The same dihydroxy-derivative **12** was obtained in 66% yield by reduction of diketone **10** with lithium aluminium hydride in ethereal solution.

exo-cis-DIACETOXY-*exo, exo*-TETRACYCLO[4.4.2.$0^{2,5}$.$0^{7,10}$]
DODECA-3,11-DIENE (**14**)

Into a solution of 1.0 g (5.25 mmoles) **12** in 15 ml acetic anhydride were added 3 drops of pyridine and the solution was left at room temperature for 24 hr. After working up 1.0 g (72%) **14** was obtained ; m.p. 95° (methanol).

$C_{16}H_{18}O_4$ *Calcd*: C, 70.05; H, 6.61
Found: C, 70.10, H, 6.79

IR(CCl_4): 1760 (CO), 3060 cm^{-1} (=C−H).

NMR ($CDCl_3$): δ 5.80 (s, 2 olefinic H, H-3, H-4), 5.86 (m, 2 olefinic H, H-11, H-12), 5.25 (m, 2 H near acetoxy groups), 2.5-2.8 (m, 6H, H-1, H-2, H-5, H-6, H-7, H-10), 2.05 (s, 6H from acetyl groups).

trans-8,9-DIHYDROXY-*exo*, *exo*-TETRACYCLO[4.4.2.$0^{2,5}$.$0^{7,10}$] DODECA-3,11-DIENE (13)

Into a stirred solution of 1.97 g (10 mmoles) cyclobutadiene-iron tricarbonyl complex and 2.00 g (9 mmoles) *trans*-7.8-diacetoxy-bicyclo [4.4.0] octa-2.4-diene in 30 ml acetone, 7g cerium (IV)-ammonium nitrate was added protionwise over 1 hr. After 1 hr water was added, the mixture was extracted with ether and the dried solution was evaporated in vacuo yielding an oily product. The latter was chromatographied on Al_2O_3 with petroleum ether-ether (8 : 2). A fraction was obtained, which was mainly diacetoxy-derivative **15**, as shown by IR and NMR spectra. It was reduced with lithium aluminium hydride in ethereal solution, yielding 0.17 g (10%) **13**, m.p. 138°.

$C_{12}H_{14}O_2$ *Calcd*: C, 75.76, H, 7.41
Found: C, 75.45, H, 7.80

exo, *exo*-TETRACYCLO[4.4.2.$0^{2,5}$.$0^{7,10}$]DODECA-11-EN-9-*exo*-OL-8-ONE (16)

Treating a solution of 0.5 g (2.66 mmoles) **9** in 25ml methanol with hydrogen in the presence of Pd/C, 70 ml gas were absorbed. After working up, 0.4 g (80%) **16**, m.p. 136° (methanol), was obtained.

$C_{12}H_{14}O_2$ *Calcd*: C, 75.76; H, 7.41
Found: C, 75.80; H, 7.65

IR (CCl_4): 1795 (CO), 3600 cm^{-1} (OH).

NMR(CCl_4): δ 1.3−3.2 (m, 10 H, H-1, H-2, H-3, H-4, H-5, H-6, H-7, H-10), 4.65 (quartet, 1H, H-9, J = 4 Hz and 9 Hz), 6.38 (m, 2 olefinic H, H-11, H-12).

The same acyloin **16** (IR and NMR spectra are identical) was obtained by treating, as above, **17** with sodium and trimethyl-chlorosilane. The acethyl-derivative was obtained by treating **16** with acetic anhydride; m.p. 137° (methanol).

$C_{14}H_{16}O_3$ *Calcd*: C, 72.38; H, 6.94
Found: C, 72.04; H, 7.13

exo, *cis*-8,9-DIHYDROXY-*exo*, *exo*-TETRACYCLO[4.4.2.$0^{2,5}$.$0^{7,10}$] DODECA-11-ENE (18)

Reduction of acyloin **16** with sodium borohydride, as above, yielded **18**, m.p. 137° (methanol).

$C_{12}H_{16}O_2$ *Calcd*: C, 74.94; H, 8.39
Found: C. 73.81; H, 8.92

endo-6-BROMO-*exo*-11-HYDROXY-13-OXA-HEXACYCLO[$6.5.0^{2,5}.0^{3,10}.0^{4,7}.0^{9,12}$] TRIDECANE (**19**)

Into a suspension of 0.5 g (2.63 mmoles) **12** in 30 ml methylene chloride was added a solution of 0.42 g (0.134 ml, 2.63 mmoles) bromine in 30 ml methylene chloride; the colour of bromine disappeared practically instantaneously and hydrogen bromide was evolved. Evaporation of solvent in vacuo and recrystallization of residue from methanol yielded 0.45 g (63%) **19**, m.p. 162°.

$C_{12}H_{13}BrO_2$ *Calcd* : C, 53.55 ; H, 4.87 ; Br 29.69

Found : C, 53.35 ; H, 4.94 ; Br 29.96

IR (CCl_4) : 3560 cm^{-1} (OH).

NMR ($CDCl_3$) : δ 4.85 (quartet, 1H, H-12, J = 4 Hz, J = 4 Hz, J = 4.5 Hz), 4.66 (quartet, 1 H, H-1, J = 2 Hz, J = 7 Hz), 4.33 (octet 1H, H-11, J = 7 Hz, J = 4.5 Hz, J = 2 Hz), 3.93 (s, 1H, H-6), 3.25 (broad signal, 1H, H-8, more deshielded due to the neighbouring oxygen); other protons such as H-3, H-4, H-5, H-7, H-9, H-10 and OH give signals between 2.0–2.9.

endo-6-BROMO-*exo*-11-ACETOXY-13-OXA-HEXACYCLO[$6.5.0.0^{2,5}.0^{3,10}.0^{4,7}.0^{9,12}$] TRIDECANE (**20**)

A solution of 0.27 g (1 mmoles) **14** in 10 ml methylene chloride was treated with a solution of 0.16 g (0.05 ml, 1 mmole) bromine in 10 ml methylene chloride. The solvent was evaporated in vacuo and the residue was chromatographied on Al_2O_3 with ether, yielding 0.25 g (80%) **20**, m.p. 106° (methanol).

$C_{14}H_{15}BrO_3$ *Calcd.* : C, 54.03 ; H, 4.86 ; Br, 25.63

Found : C, 53.66 ; H, 4.93 ; Br, 26.41

IR (CCl_4) : 1758 cm^{-1} (CO).

NMR ($CDCl_3$) : δ 5.00 (m, A group from a A_2X_2 system, 2H, H-12, H-11), 4.61 (quartet, 1H, H-1, J= 7Hz, J = 2.5 Hz), 3.90 (s, 1 H, H-6), 3.28 (m, 1H, H-8), 2.0–3.0 (m, 6H, H-3, H-4, H-5, H-7, H-9, H-10), 2.1 (s, 3H from acetyl group).

The same compound **20** was obtained by treating the hydroxyderivative **19** with acetic anhydride and a drop of pyridine.

endo-6-BROMO-13-OXA-HEXACYCLO[$6.5.0.0^{2,5}.0^{3,10}.0^{4,7}.0^{9,12}$]TRIDECAN-11-ONE (**21**)

A solution of 0.5 g (1.87 mmoles) **19** in 10 ml methylene chloride was treated with a solution of CrO_3.py (from 1.10 g, 1.1 mmoles CrO_3 and 1.5 ml pyridine) in 50 ml methylene chloride, and the mixture was stirred for 2 hrs at room temperature. Water was added, the solution was washed, dried and evaporated, yielding 0.26 g (52%) **21**, m.p. 161° (methanol).

$C_{12}H_{11}BrO_2$ *Calcd* : C, 53.96 ; H, 4.15 ; Br, 33.50

Found : C, 51.85 ; H, 4.48 ; Br, 31.45

IR (CCl_4): 1780 cm^{-1} (CO).

NMR ($CDCl_3$) : δ 2.40 – 3.40 (m, 7H, H-3, H-4, H-5, H-7, H-8, H-9, H-10), 4.00 (s, 1 H, H-6), 4.40 (broad d, 1H, H-1, J = 7 Hz), 6.07 (d, 1H, H-12, J = 3.25 Hz).

Revue Roumaine de Chimie, **18**, *5*, 873–881 (1973)

BICYCLO [3.3.1] NONANE
THE ACID-CATALYZED REACTIONS OF A BICYCLIC EPOXIDE

N. BĂRBULESCU, M. MORARU and D. ŞOTCĂ

Department of Organic Chemistry,
University of Bucharest, Spl. Independenţei 89,
Bucharest, Romania

Received November 29, 1972

The paper describes the synthesis and some acid-catalyzed reactions of the bicyclic epoxide **4**. The rigid conformation and the presence of a phenyl group attached to the epoxide ring are shown to be the structural factors which determine the course of all reactions under study. The stereochemistry of all new bicyclic compounds was established by chemical and spectroscopic methods.

INTRODUCTION

The cleavage of the epoxides with electrophylic reagents is a problem of current interest to organic chemists. [1] The particular course the reaction assumes depends on the nature of the epoxide, catalyst and solvent. For cyclic epoxides the structural features are generally separated into a stereoelectronic and a conformational factor, but actually, it is difficult to estimate their relative contribution. Because of their rigidity, the bicyclic epoxides are models of choice for such studies.[1–4]

We report here some results concerning the stereochemistry of the acid-catalyzed reactions of *anti*-2β, 3β-epoxy-2α-phenylbicyclo [3.3.1] nonan-9-ol (**4**); these results support and supplement those obtained by Palazzo and Baiocchi for a structurally similar epoxide.[4]

RESULTS AND DISCUSSION

The bicyclic epoxide **4** was prepared as shown in Scheme 1. The cyclisation of the diketone **1** gave the bicyclic unsaturated ketone **2**,[5] which was reduced with $LiAlH_4$ in ether to a mixture of epimeric enols

---

[1] I. I. Schiketanz and F. Badea, *Studii şi Cercetări Chim. Acad. R.S.R.*, **18**, 567 (1970).

[2] R. A. Appleton, J. R. Dixon, J. M. Evans and S. H. Graham, *Tetrahedron*, **23**, 805 (1967).

[3] E. N. Marvell, J. Seubert, D. Sturmer and W. Frederici, *J. Org. Chem.*, **35**, 396 (1970).

[4] G. Palazzo and L. Baiocchi, *Gazz. chim. Ital.*, **99**, 1068 (1969).

[5] A. C. Cope and E. C. Hermann, *J Amer. Chem. Soc.*, **72**, 3405 (1950).

3a and **3b**. The NMR-spectra of the acetate or benzoate of the crude alcohol indicated that the major isomer **3a** represents 73 – 81%. The

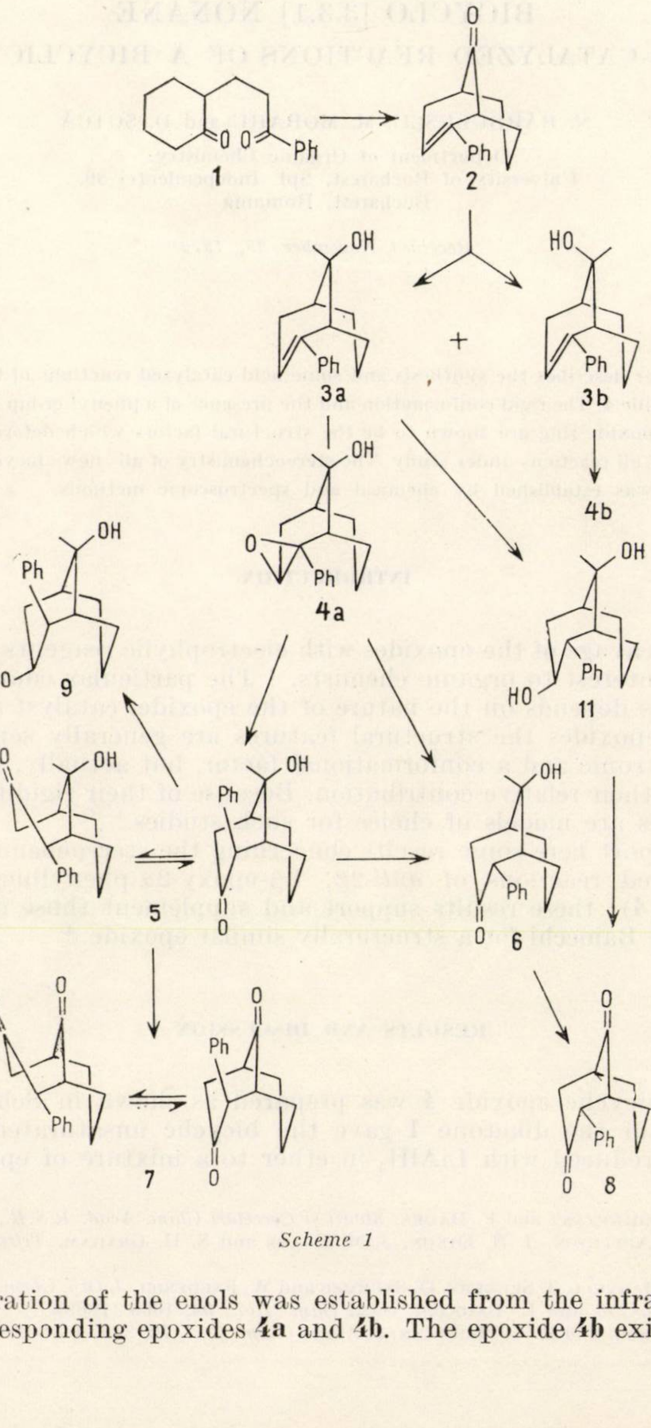

Scheme 1

C-9 configuration of the enols was established from the infrared spectra of their corresponding epoxides **4a** and **4b**. The epoxide **4b** exibited intramolecular hydrogen bond between the C-9 hydroxy group and the epoxy oxygen, so it has the *sin* configuration.[6] Hence the major enol **3a** has *anti* C-9 configuration.

The course of $LiAlH_4$ reduction indicates different steric requirements to the attack from the two sides, the *anti* approach being more hindered by two axial hydrogen atoms. Several recrystallizations of the crude enol from ethanol gave a pure sample of **3a**. Epoxidation of this compound with perbenzoic acid afforded the epoxide **4a** with exo-oriented epoxy ring (Scheme 1).

The exo-attack at the double bond is a normal trend for the bicyclo [3.3.1] nonane alkenes, being encountered in the hydrogenation[5] and hydroboration of bicyclo [3.3.1] non-2-ene.

The NMR spectrum of epoxide **4a** exhibited a doublet ($J = 4$ Hz) at $\delta = 3.54$ ppm, corresponding to the oxiranic proton H-3. The doublet appearance of this proton supports the previous configurational assignment. The doublet is actually a quartet resulting from the coupling of H-3 with H-4α and a small (unresolved) coupling of about 1 Hz with H-4β. From the simplified Karplus relation $J = 5.1 \cos^2\theta$, established for steroidal epoxides,[7] a value of 27° was calculated for the dihedral angle H-3 ; H-4α. This value corresponds to a "L" half-chair conformation of the epoxide **4a**.[8]

Treatment of the epoxide **4a** with $BF_3.Et_2O$ in benzene at 20° afforded a rearranged product whose structure proved to be **5**, on the basis of chemical and spectral evidences. The infrared spectrum in KBr pellet shows peaks at 1683 cm^{-1} (carbonyl group) and 3450 cm^{-1} (OH). The NMR spectrum shows a singlet at $\delta = 3.68$ ppm due to the C-2 proton, and a triplet at $\delta = 4.30$ ppm, due to the C-9 proton. The small coupling between H-2 and the bridgehead proton H-1 (less than 1.5 Hz) is consistent with a β-configuration at C-2 (exo phenyl group).

The infrared spectrum in KBr pellet exhibits peaks at 3450 cm^{-1} (hydroxyl group) and 1683 cm^{-1} (carbonyl, but at a very low frequency). It is noteworthy that **5** shows in solution two carbonyl stretching bands at 1681 cm^{-1} and 1710 cm^{-1}. A similar splitting was recorded for 2β-phenylbicyclo [3.3.1] nonan-3-one.[4] On the other hand, the epimeric hydroxyketone **6** (see below) shows no splitting at all.

Initially, a hydrogen bond was suggested to explain this splitting, but this suggestion was rejected by a careful study of the ν(OH) region. As a matter of fact, the above explanation does not apply to 2β-phenyl bicyclo [3.3.1] nonan-3-one. The presence in solution of two different conformers could also account for such a splitting. The assumption of two conformations of comparable stability for **5** is a realistic one.

Bicyclo [3.3.1] nonane, the parent hydrocarbon, is known to occur in a double-chair conformation, but the free energy difference between this conformation and the chair-boat one is much less than in the case of cyclohexane. [9-12] ($\Delta G^0_{25} = 2.7$ kcal/mol, respectively 6.8 kcal/mol [13]). This comes mainly from a considerable repulsion between C-3 and C-7 endo protons in the double-chair conformation.

---

[6] R. A. Appleton, K. H. Baggaley, C. Egan, J. M. Davies, S. H. Graham and D. O. Lewis, *J. Chem. Soc.* (*C*), **1968**, 2035.

[7] K. Tori, T. Komeno and T. Nakagawa, *J. Org. Chem.*, **29** 1136 (1964).

[8] M. P. Hartshorn and D. N. Kirk, *Tetrahedron*, **21**, 1547 (1965).

A carbonyl group at C-3 removes the unfavourable transannular interaction, but also decreases the diference between chair and boat by at least 1.5 kcal/mol. This value, calculated for C_s-boat form of cyclohexanone, [14,15] is equally good for the bicyclic ketone which could assume but such a boat conformation. Consequently, the double-chair and chair-boat conformations of bicyclo [3.3.1] nonan-3-one could differ by 2.5-3.5 kcal/mol and both could be populated at the normal temperature (the barrier to inversion is low for all cyclohexanones [15]). Some recent reports, on the equivalence of all protons α to the carbonyl group in bicyclo [3.3.1] nonan-3-one [16,17] support these considerations.

An exo phenyl group at C-2 introduces severe 1,3-diaxial repulsions with C-4 and C-9 protons in the double-chair conformation. The corresponding free energy gain could be assimilated with the conformational energy of phenyl in 2-phenylcyclohexanone. Calculations [18] and direct determinations of conformational energy [19] for a free rotating phenyl group give $\Delta G^0_{25} = 2 - 3.1$ kcal/mol. Thus the difference in energy between double-chair and chair-boat conformations of **5** becomes negligible and both forms are to be found in solution.

The absence of splitting for the infrared spectrum in pellet corresponds to a single fixed conformation.

Reduction of **5** with $LiAlH_4$ in ether afforded the diol **9** with an equatorial hydroxy group at C-3. The infrared spectrum of **9** exhibits the characteristic absorption bands for equatorial OH (1060 cm^{-1} and 1068 cm^{-1}). The NMR coupling constants, $J_{12} = 1.8$ Hz and $J_{23} = 6.5$ Hz, are also consistent with a β-configuration at C-3.

The diol **9** could result only by the attack of the complex hydride on the carbonyl group in the chair-boat conformation of the hydroxy-ketone **5**. For the other conformation the product would be the axial alcohol **10**. In this case the molecule would be forced in a chair-boat conformation with coupling constants $J_{12} \approx 1$ Hz and $J_{23} \approx 10$ Hz. [9]

---

[9] R. A. Appleton, C. Egan, J. M. Evans, S. H. Graham and J. R. Dixon, *J. Chem. Soc. (C)*, **1968**, 1110.

[10] E. N. Marvell, G. J. Gleicher, D. Sturmer and K. Salisbury, *J. Org. Chem.*, **33**, 3393 (1968).

[11] E. N. Marvell and R. S. Knutson, *J. Org. Chem.*, **35**, 388 (1970).

[12] M. Fisch, S. Smallcombe, J. C. Gramain, M. A. McKervey and J. E. Anderson, *J. Org. Chem.*, **35**, 1886 (1970).

[13] E. L. Eliel, N. L. Allinger, S. J. Angyal and G. A. Morrison, "Conformational Analysis, Interscience Publishers, New York, 1966, p. 140.

[14] N. L. Allinger, M. T. Tribble and M. A. Miller, *Tetrahedron*, **28**, 1173 (1972).

[15] N. L. Allinger, H. M. Blatter, L. A. Freiberg and F. M. Karkowski, *J. Amer. Chem. Soc.*, **88**, 2999 (1966).

[16] A. Caragheorgheopol, U. Gräfe, M. Hartmann, V. E. Sahini and K. Wermann, *Tetrahedron Letters*, **1970**, 3035.

[17] M. R. Vegar and R. J. Wells, *Tetrahedron Letters*, **1971**, 2847.

[18] N. L. Allinger and M. T. Tribble, *Tetrahedron Letters*, **1971**, 3259.

[19] N. L. Allinger and E. L. Eliel "Topics in Stereochemistry", vol. 1, Wiley-Interscience, New York, 1967, p. 207.

Treatment of hydroxy-ketone **5** with HBr 47% gave the epimeric compound **6**. This was also produced by the cleavage of the epoxide **4a** with HBr 47%. The α-configuration at C-2 was confirmed by the NMR spectrum which shows a doublet ($J_{12} = 4.7$ Hz) at $\delta = 3.70$ ppm, due to the H-2 proton. The magnitude of J_{12} is normal for an axial-equatorial coupling.

Table 1

NMR-and IR-data for compounds 5–8

	Chemical shift (δppm)				J_{12}	$\nu(C=O)cm^{-1}$	
	H−1	H−2	H−4	H−9		KBr pellet	CS_2
5	—	3.70	2.55	4.30	1	1 683	1680, 1 710
6	—	3,68	2.58	4.34	4.7	1 706	1 711
7	3.08	4.01	2.80	—	0.8	1 725	1 720
8	2.73	4.03	2.88	—	5	1 723	1 724

Noteworthy is the coincidence of chemical shifts of C-2 protons in the NMR spectra of the epimeric compounds **5** and **6**. This coincidence is also consistent with a chair-boat conformation of **5**, which has the same geometry of the $C_2 - C_3$ fragment as compound **6** in the chair-chair conformation.

The hydroxy-ketones **5** and **6** were treated with Jones reagent to afford the epimeric 1,4-diketones **7** and **8**. In their NMR spectra the H-2 proton occurs as a singlet, respectively as a doublet, in agreement with the previous assigned configuration (See Table 1).

The hydroboration of the enol **3a** furnished a chemical proof of the stereochemistry of compounds **5** – **8**. When oxidized with Jones reagent, the hydroboration product **11** gave the diketone **8**. Hydroboration of the enol **3a** led to the diol **11** with a $2\alpha, 3\beta$ configuration. This assignment was supported by the NMR spectrum ($J_{12} = 3.8$ Hz and $J_{23} = 11$ Hz), the intramolecular hydrogen bond between OH and phenyl ($\Delta\nu_{OH} = 48$ cm^{-1}) and the ν(C−OH) stretching bands (1052 cm^{-1} and 1062 cm^{-1}).

The isomerisation of the epoxides to ketones by treatment with BF_3 is a well-known process.[4,20–24] The reaction involves the cleavage of the epoxy ring by the electrophilic catalyst, followed or concerted with a 1,2-hydride shift. The inversion of configuration for substituted epoxides was considered as an argument for the concerted mechanism.

Which carbon-oxigen bond is broken depends upon the electronic and conformational factors. In the case of the epoxide **4a** both are respons-

---

[20] R. C. Cookson and J. Hudec, *Proc. Chem. Soc.*, **1957**, 24.

[21] G. Berti, F. Bottari, B. Macchia, and F. Macchia, *Tetrahedron*, **22**, 189 (1966).

[22] G. Berti, B. Macchia and F. Macchia, *Tetrahedron*, **24**, 1735 (1968).

[23] P. L. Barili, G. Berti, B. Macchia, F. Macchia and L. Monti, *J. Chem. Soc. (C)*, **1970**, 1168.

[24] G. Berti, B. Macchia, F. Macchia and L. Monti, *J. Chem. Soc. (C)*, **1971**, 3371.

ible for the breaking of the C_2-O bond. The equatorial cleavage, accompanied by a 1,2-hydride shift, is the usual path for "L"-conformers.[8] On the other side the scission of the C_2-O bond produces the stable benzylic carbocation.

As it was pointed out, some other aryl-substituted epoxides with a fixed conformation, i.e *cis*- and *trans*-1-phenyl 4-t-butyl-cyclohexen-1, 2-oxides, give not only 1,2-hydride shift products but also ring contracted componds.[23] The absence of such ring contracted products in the reaction of **4a** is unexpected on mechanistic grounds. The concerted, 1,2-hydride shift mechanism cannot account for this result as the reaction of the alcohol **13** with BF_3 Et_2O (a process with a well established nonconcerted mechanism) affords only the hydroxy-ketone **5** (see Scheme 2).

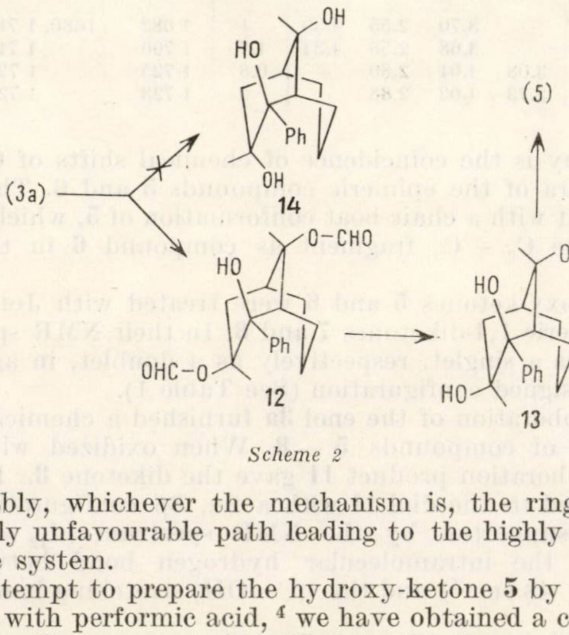

Scheme 2

Presumably, whichever the mechanism is, the ring contraction is an energetically unfavourable path leading to the highly strained bicyclo [3.2.1] octane system.

In an attempt to prepare the hydroxy-ketone **5** by the epoxidation of the enol **3a** with performic acid,[4] we have obtained a complex mixture of formic esters (five products identified by thin layer chromatographiy). The main product (30 – 40%) is the formic diester **12**.

The IR spectrum of 12 has the characteristic peaks at 1191 cm^{-1} and 1728 cm^{-1}. The NMR spectrum exhibits two doublets (J = 1 Hz) at $\delta = 7.90$ ppm and $\delta = 8.12$ ppm, corresponding to formic esters of secondary hydroxy groups, two triplets at $\delta = 6.29$ ppm (J = 8.5 Hz) and $\delta = 5.77$ ppm (J = 2.5 Hz), due to C-3 and C-9 protons, and a singlet at $\delta = 2.74$ ppm, due to the tertiary hydroxyl. These NMR data agree with a β-configuration at C-3 (equatorial OCHO).

Reduction of the formic ester **12** with $LiAlH_4$ gave the triol **13** (Scheme 2), whose NMR spectrum exhibited a triplet at $\delta = 4.83$ ppm (J = 8.2 Hz), in agreement with a β-configuration at C-3.

The same triol **13** was prepared by *cis*-hydroxylation of the enol **3a** with osmium tetroxide. The well established stereochemistry of this reaction prompted us to assign the β-configuration at C-2 (axial tertiary OH).

The configuration of the formolysis products **12** is in total disagreement with the well known rule of diaxial opening of the epoxides. For the epoxide **4a** this rule would require the scission of C_3-O bond and the formation of the 2β, 3α-triol **14**.

The infringement of the rule is another consequence of the preferential formation of a stabilized benzylic carbocation.

The developing or solvent-protected carbocation would collapse with a solvent molecule from the exo-side, to yield the unstable tertiary formic ester **16**. This intermediate probably undergoes an axial-equatorial formyl shift [22] to give the normal diester **12**. (Scheme 3)

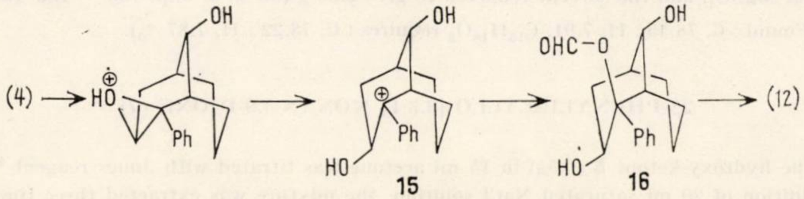

Scheme 3

EXPERIMENTAL

Infrared spectra were determined on a UR-20 spectrophotometer for solutions in CCl_4 and CS_2, or in KBr pellets.

NMR spectra were recorded on a Varian A-60 A spectrometer in CCl_4, $CDCl_3$ and DMSO-d_6 solutions, with TMS as internal standard. The hydroxy groups were assigned by exchange with D_2O. Coupling constants were measured at 250 Hz S.W.

Melting points were determined with a Boetius apparatus and are uncorrected.

2-PHENYLBICYCLO [3.3.1] NON-2-EN-9-0L (3)

To 10 g $LiAlH_4$ in 500 ml dry ether a solution of 106 g unsaturated ketone **2**,[5] in 500 ml ether was added for 2 h. The reduction was completed by heating 10 h at reflux. Excess $LiAlH_4$ was destroyed and the product worked up as usually to afford 98 g crude alcohol, b.p. 184 – 185° at 3 mm Hg.

The *anti*-alcohol **3a** was obtained by repeated recrystallization of the crude alcohol from ethanol.

2β, 3β-EPOXY-2α-PHENYLBICYCLO [3.3.1] NONAN-9-0L (4a)

To a solution of 15 g perbenzoic acid in 250 ml chloroform at 0°, were added dropwise 21.4 g **3a** in 50 ml chloroform, and the solution was kept overnight in a refrigerator. An iodometric titration gave 1.53 g excess peracid (the calculated excess).

The chloroformic solution was washed with saturated $NaHCO_3$ solution, water, then dried over anhydrous $MgSO_4$. The solvent was removed to give 21.8 g crude epoxide (95 %), m.p. 138-150°.

After recrystallization from acetone-water, m.p.154 — 155°.
(Found : C, 78.35 : H, 7.71. $C_{15}H_{18}O_2$ requires : C, 78.22 : H, 7.87 %).

2β-PHENYLBICYCLO [3.3.1] NONAN-9-OL-3-ONE (5)

A solution of 2.67 g epoxide **4a** in 300 ml dry benzene was stirred with 2 ml $BF_3.Et_2O$ for 2 minutes, then quenched with $NaHCO_3$ solution. The organic layer was washed with water, dried over $MgSO_4$, and the solvent removed to give 2.36 g (88 %) **5**, m.p. 155 — 156° (benzene)
(Found : C, 78.45 : H, 7.91. $C_{15}H_{18}O_2$ requires : C, 78.22 : H, 7.87 %).

2β-PHENYLBICYCLO [3.3.1] NONAN-3,9-DIONE (7)

The hydroxy-ketone **5** (0.5g) in 15 ml acetone was titrated with Jones reagent [25] at 0°. After addition of 20 ml saturated NaCl solution, the mixture was extracted three times with 50 ml ether, the extracts were washed with $NaHCO_3$ solution, water, dried over $MgSO_4$ anh. and the ether distilled to give 0.37 g (64 %) diketone **7**, m.p. 97—99° (from ethanol 80 %).
(Found: C, 78.75 : H, 7.11. $C_{15}H_{16}O_2$ requires : C, 78.92 : H, 7.06 %).

2α-PHENYLBICYCLO [3.3.1] NONAN-9-OL-3-ONE (6)

a) The epoxide **4a** (4.28 g) was heated at 60° in 30 ml HBr 47 % for 15 minutes. Addition of water to the clear violet solution gave 3.96 g **6** as needles, m.p. 144—145°.

b) By the same procedure compound **5** (0.5 g) gave 0.36 g **6**. The two products have the same IR spectrum and their mixed m.p. shows no depression.
(Found: C, 78.09: H, 8.01. $C_{15}H_{18}O_2$ requires: C, 78.22: H, 7.87 %).

2α-PHENYLBICYCLO [3.3.1] NONAN-3,9-DIONE (8)

a) The hydroxyketone **6** (0.22 g), treated with Jones reagent and worked up as above, produced 0.207 g oil, which was chromatographed in pentane over alumina to give 0.157 g **8**, m.p. 160—162°.

b) The oxidation of diol **11** (0.43 g) with Jones reagent as described, gave 0.39 g **8** as white crystals, m.p. 161 — 162°.
(Found : C, 78.91 : H, 7.28. $C_{15}H_{16}O_2$ requires : C, 78.92 : H, 7.06 %).

2α-PHENYLBICYCLO [3.3.1] NONAN-3β,9-DIOL (11)

A solution of 1 ml freshly distilled $BF_3.Et_2O$ in 5 ml dimethoxyethane was added dropwise, under nitrogen, to 2.14 g **3a** in 30 ml diglyme. The borane was decomposed at 40—50° with H_2O_2 30 % and NaOH 3N, the mixture was saturated with NaCl and extracted with 500 ml benzene. Evaporation of solvent left 1.95 g **11**, m.p. 178—179° (from ethyl acetate-petroleum ether).

---

[25] R. G. Curtis, I. Heilbron, E. R. H. Jones and G. F. Woods, *J. Chem. Soc.*, **1953**, 457.

(Found : C, 77.63 : H, 8.31. $C_{15}H_{20}O_2$ requires : C, 77.55 : H, 8.68 %).

2β-PHENYLBICYCLO [3.3.1] NONAN-3β, 9-DIOL (9)

The ketol **5** (0.943 g) was reduced with 0.5 g $LiAlH_4$ in 250 ml ether for 5 hr, at reflux. Excess $LiAlH_4$ was destroyed, the separated alumina washed with ether, and the combined etheric solutions were washed with water and dried. After removal of ether, the solid compound **9** (0.933 g) was obtained. M.p. 103 — 105° from AcOEt-petroleum ether.

(Found : C, 77.93 ; H, 8.33. $C_{15}H_{20}O_2$ requires : C, 77.55 : H, 8.68 %).

2α-PHENYLBICYCLO [3.3.1] NONAN-2β, 3β, 9-TRIOL (13)

a) To a stirred suspension of 10 g **3a** in 500 ml HCOOH 98 % at 50 — 60° was added H_2O_2 30 % (5 ml), stirring was continued for 1 hr to obtain a clear solution, then the mixture was poured into 300 ml ice water. The product was thoroughly extracted with chloroform, the organic layer was washed with diluted brine, water and dried over $MgSO_4$. Removal of the solvent left 11.3 g oil which was taken with a small amount of warm ethanol. The solution set aside overnight in a refrigerator separated 3 — 4 g of a product, melting at 161 — 162° (from benzene), which is the formic diester **12**.

(Found : C, 67.00 : H, 6.89. $C_{17}H_{20}O_5$ requires : C, 67.09 : H, 6.62 %).

The formic ester **12** (0.82 g) was reduced with $LiAlH_4$ (1 g) in ether to give 0.51 g **13**, m.p. 182 — 183° (from AcOEt-petroleum ether).

b) *cis*-Hydroxylation of **3a** with OsO_4.

The enol **3a** (0.84 g) in 10 ml dry ether was treated with OsO_4 (1 g) and dry pyridine (2ml) at 0°. The solution was set aside overnight, then the brown precipitate was filtered and washed with ether.

The osmic complex (2.21 g, 92 %) was treated with 3 g mannitol in 30 ml KOH 10 % to afford 0.71 g **13**, m.p. 180 — 183°.

(Found : C, 72.66 : H, 8.17. $C_{15}H_{20}O_3$ requires : C, 72.55 : H, 8.10 %).

REACTION OF 13 WITH $BF_3.ET_2O$

The triol **13** (0.15 g) in 100 ml benzene was treated with $BF_3.Et_2O$ (1ml) at room temperature for 5 minutes, then quenched with saturated $NaHCO_3$. On work-up as described we obtained an oil (97 mg), which was chromatographed on alumina to give 55 mg **5**, m. p. 154 — 155°.

We are indebted to D. Pop for performing IR-spectra and to F. Chiraleu for performing NMR-spectra.

Revue Roumaine de Chimie, **18**, 5, 883–888 (1973)

TRIS-ÉTHERS. I

LA CONDENSATION DU BIS(CHLOROMÉTHYLE) ÉTHER AVEC LES PHÉNOXYDE, MÉTHYLE- ET DIMÉTHYLE-PHÉNOXYDES DE SODIUM

M. IOVU et G. CÎMPEANU

Faculté de Chimie, Université de Bucarest
Splaiul Independenţei, 89, Bucarest

Reçu le 11 Septembre 1972

Dans les articles antérieurs,[1–4] on a montré la possibilité de la polycondensation des dérivés dichlorométhylés aromatiques avec des phénoxydes alcalins, qui, contrairement à la réaction Ullmann, a lieu à des températures basses (moins de 65°) dans le solvant et sans catalyseur (cuivre métallique). Les phénoxydes alcalins anhydres ont été obtenus par la distillation azéotrope de l'eau. Dans les conditions similaires à celles mentionnées a aussi lieu la condensation du bis(chlorométhyle) éther avec les phénoxydes alcalins. Il résulte des tris-éthers dont la formule générale est : $Ar\text{-}O\text{-}CH_2\text{-}O\text{-}CH_2\text{-}O\text{-}Ar$ où le radical aromatique peut être substitué. Dans les tris-éthers obtenus on trouve une fonction éther aliphatique et deux fonctions mixtes aliphatiques-aromatiques, fait mis en évidence par analyse spectrale en UV et IR.

Les bons résultats obtenus dans l'étude de la condensation des phénoxydes alcalins avec des dérivés dichlorométhylés aromatique,[1–4] selon un nouveau procédé, nous ont déterminés à l'étendre aussi à la condensation du bis(chlorométhyle) éther avec les phénoxydes alcalins. Conformément au nouveau procédé les phénoxydes alcalins anhydres sont obtenus par la réaction du phénol avec l'hydroxyde alcalin en milieu d'éthanol-benzène (1 :1 en volumes) suivie par l'élimination de l'eau de réaction en distillant un mélange azéotrope eau-éthanol-benzène.

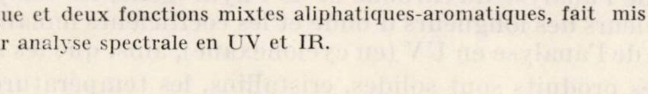

---

[1] M. Iovu, *Rev. Roumaine Chim.*, **16**, 1223 (1971).

[2] M. Iovu et N. Nicolau, *Rev. Roumaine Chim.*, **16**, 1919, (1971).

[3] M. Iovu, *Rev. Roumaine Chim.*, **17**, 1261 (1972).

[4] M. Iovu, N. Miclovici et S. Creţu, *Rev. Roumaine Chim.*, **17**, 1417 (1972).

On ajoute au phénoyxde alcalin se trouvant en mélange de benzène et d'alcool qui n'a pas été distillé, le bis(chlorométhyle) éther

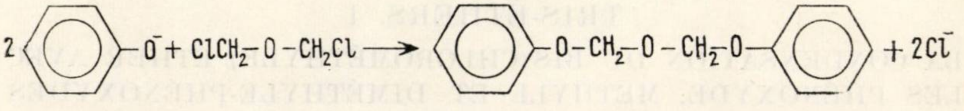

Il résulte le tris-éther correspondant et le chlorure de sodium qui précipitent ensemble. Le précipité est isolé des solvants contenant de petites quantités de matières premières n'ayant pas réagit et éventuellement des produits secondairs de réaction, par filtration. La chlorure de sodium est ensuite éliminé en lavant le précipité sur le filtre avec de l'eau. Le produit de réaction, séché, est cristallisé de nouveau toujours du mélange d'éthanol-benzène en proportions différentes.

Selon ce procédé on a condensé le bis(chlorométhyle) éther avec les sels de sodium du phénol, des crésols et des xylénols en obtenant dix tris-éthers qui n'ont pas été décrits jusqu'à présent dans la littérature, dont la formule générale est Ar-O-CH_2-O-CH_2-O-Ar où Ar est un phényle, un crésyle ou un xylénile. La fonction éther se trouve trois fois dans la molécule : une fois comme éther aliphatique et deux fois comme éther mixte, aromatique et aliphatique.

RÉSULTATS ET DISCUSSIONS

Sur le tableau 1 on trouve les formules des tris-éthers synthétisés, les résultats de l'analyse du carbone et de l'hydrogène, les températures de fusion, les valeurs des longueurs d'onde et les coefficients molaires d'extinction obtenus de l'analyse en UV (en cyclohexane), ainsi que les rendements.

Tous les produits sont solides, cristallins, les températures de fusion étant influencées par les positions des radicaux méthyle sur les noyaux benzéniques. Ces températures sont inférieures aux températures de fusion des bis-éthers synthétisés antérieurement[1-3] ceux-ci se faisant remarquer des tris-éthers par l'existence d'un noyau benzénique au lieu de l'atome d'oxygène médian et ayant la formule générale Ar-O-CH_2-Ar-CH_2-O-Ar.

Les rendements peuvent dépasser 90%. La différence relativement grande entre les rendements dont on obtient les différents éthers synthétisés est plutôt due à leur solubilité différente dans le milieu de réaction (alcool-benzène) d'où ils cristallisent. La concentration a été maintenue la même.

L'analyse spectrale en IR fait ressortir l'existence des bandes d'absorption caractéristiques des fonctions éther aliphatique -CH_2-O-CH_2- et mixte Ph-O-CH_2-. Les groupements méthylène appartiennent à deux fonctions éther -O-CH_2-O-CH_2-O-. Celles-ci conduisent à des spectres IR différents de ceux des bis-éthers synthétisés antérieurement.[1-4] On en trouve pour ν_{asym} C-O-C entre 1200 – 1115 cm^{-1} deux bandes intenses d'absorption, une due à la fonction éther aliphatique-aromatique (figure 1). La bande de 1160 à 1190 cm^{-1} est attribuée à la vibration des éthers mixtes.

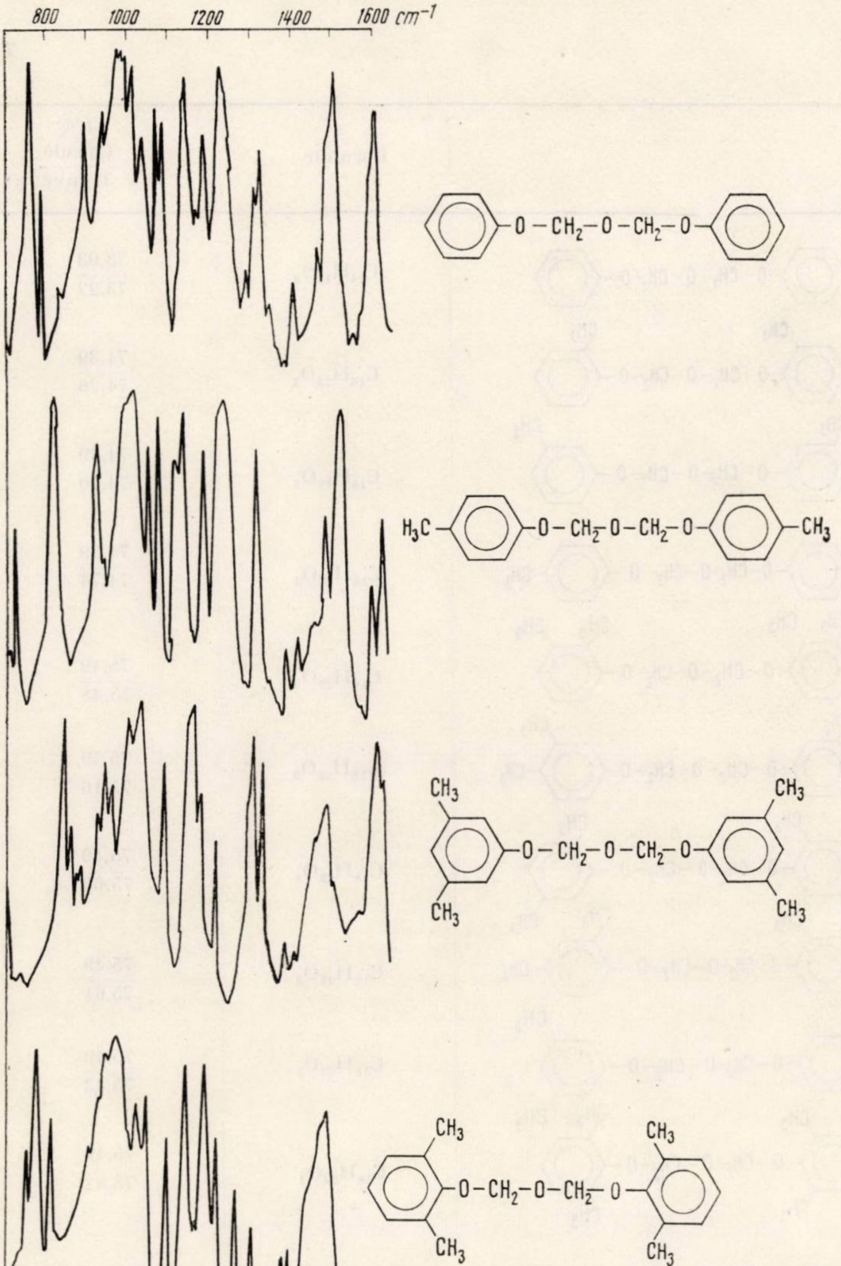

Fig. 1. — Spectres IR du bis(phenoxyméthyle) éther, bis(4-méthylphenoxyméthyl) éther, bis (3,4-diméthylphenoxyméthyl) éther et du bis (2,6-diméthylphenoxyméthyle) éther.

Tableau

TRIS-

	Formule	C % Calculé / Trouvé
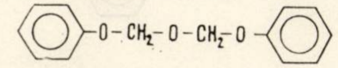	$C_{14}H_{14}O_3$	$\frac{73,03}{73,22}$
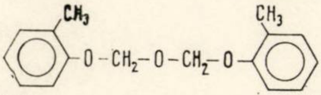	$C_{16}H_{18}O_3$	$\frac{74,39}{74,26}$
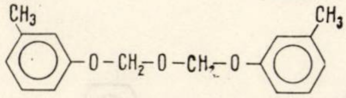	$C_{16}H_{18}O_3$	$\frac{74,39}{74,70}$
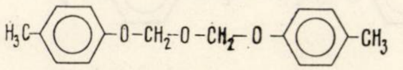	$C_{16}H_{18}O_3$	$\frac{74,39}{74,74}$
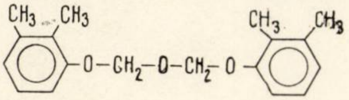	$C_{18}H_{22}O_3$	$\frac{75,49}{75,48}$
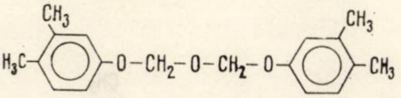	$C_{18}H_{22}O_3$	$\frac{75,49}{75,16}$
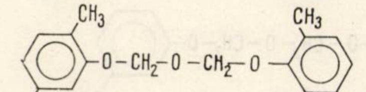	$C_{18}H_{22}O_3$	$\frac{75,49}{75,63}$
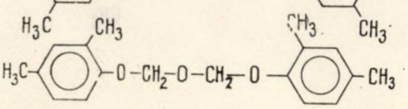	$C_{18}H_{22}O_3$	$\frac{75,49}{75,61}$
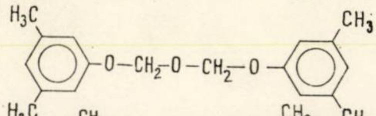	$C_{18}H_{22}O_3$	$\frac{75,49}{75,43}$
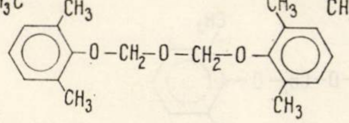	$C_{18}H_{22}O_3$	$\frac{75,49}{75,82}$

De même, pour ν_{sym} C—O—C, il existe pour la plupart des éthers appartenant à ce groupe, deux bandes entre 940 — 920 cm^{-1}.

Les tris-éthers synthétisés, absorbent en UV dans la région de 260 à 280 mμ caractéristique des composés benzéniques. La substitution du noyau benzénique par des radicaux méthyle déplace les bandes d'absorption par rapport à la position des radicaux vers des longueurs d'ondes plus grandes (tableau 1) de 10 à 20 mμ.

1

ÉTHERS

H % Calculé / Trouvé	Point de fusion °C	λ_{max} mμ	ε_{max}	Rend %
6,12 / 6,07	81–83	261,2 268 274,5	1 700 2 700 2 300	85,0
7,02 / 6,80	73–75	262 269 275,2	1 850 2 700 2 400	78,6
7,02 / 6,97	34,5–35,5	364,4 270 274,5	1 800 2 750 2 650	60,1
7,02 / 7,14	86	267 273 275 282	2 200 2 700 3 150 2 700	90,1
7,74 / 7,79	79,5–80,5	264 268 271 276,8	1 350 1 510 1 560 1 840	94,0
7,74 / 7,96	90	267 272 275 281,5	2 000 2 650 2 750 2 500	71,4
7,74 / 7,99	83–84	265,3 270 273 279	2 000 2 700 2 900 2 800	71,4
7,74 / 7,82	64	268 273 276 281,5	2 100 2 580 2 800 2 550	59,3
7,74 / 8,15	85–86	263 270 273 278	1 300 1 800 1 600 2 000	73,6
7,74 / 7,47	89,5–90,5	261 264 267 272	1 250 1 300 1 260 1 050	65,5

Lorsque le radical méthyle est substitué en position *para*, le déplacement est plus grand que pour les positions *meta* et *ortho*. Les bandes d'absorption sont déplacées vers des longueurs d'ondes plus grandes (approximativement 10 mμ) et dû aux groupements $-O-CH_2-$, liés au noyau aromatique.

Les coefficients d'extinction ayant des valeurs de l'ordre 2000 correspondent aux absorptions caractéristiques des composés aromatiques de la même classe.

L'analyse thermogravimétrique des tris-éthers étudiés ne fait pas ressortir un processus de décomposition ou de réarrangement à des températures inférieures à celle d'ébullition.

PARTIE EXPÉRIMENTALE

Le bis(chlorométhyle) éther a été obtenu en passant un puissant courant d'acide chlorhydrique sur le paraformaldéhyde suspendu en acide sulfurique concentré.

Le phénol utilisé a été un produit commercial « Reactivul », l'-*o*-crésol un produit UCB, le *m*-crésol Toskat et le *p*-crésol Riedel de Haen. Le 2,3-, 2,5- et 2,6-xylénol un produit BDH, le 3,4-xylénol UCB et le 3,5-xylénol Loba Chemie-Wien.

Les spectres IR ont été obtenus en tablettes de KBr à l'aide d'un appareil UR-20, Karl Zeiss Jéna.

Les spectres UV ont été obtenus en solution de cyclohexane en utilisant un apareil CF Optica, Milano.

L'analyse thermogravimétrique a été effectuée à l'aide d'un dérivatographe de type Pauly.

LA SYNTHÈSE DU BIS(PHENOXYMÉTHYLE) ÉTHER

Dans un ballon de 50 ml, ayant deux cols, muni d'un réfrigérant ascendant et d'un thermomètre sont introduits, 3,765 g (1/25 moles) phénol, 1,660 g NaOH (1/25 moles) et 30 ml d'un mélange composé d'alcool-benzène (1 : 1 en volume). On chauffe au reflux jusqu'à la formation totale du phénoxyde de sodium et on distille 15 ml de mélange azéotrope d'alcool-eau-benzène.

On ajoute au phénoxyde de sodium anhydre, se trouvant dans le ballon, 2,300 g bis(chlorométhyle) éther et on chauffe pendant 3 heures au reflux. On laisse le mélange de réaction refroidir à la température ambiante. Le tris-éther formé est cristallisé. Le produit solide, comprenant aussi du chlorure de sodium, est séparé de la part liquide, par filtration. Le précipité déposé sur le filtre est lavé plusieurs fois avec de l'eau afin d'éliminer le NaCl et ensuite avec 1 ml d'alcool et séché. Il résulte 3,2 g. Le rendement est de 85%. Après deux recristallisations du mélange alcools-benzène (1 : 1 en volume) la température de fusion du bis(phénoxyméthyle) éther est $T_f = 81 - 83°$.

La synthèse des autres produits a eu lieu dans des conditions identiques.

Revue Roumaine de Chimie, **18**, *5*, 889–898 (1973)

HETEROCYCLIC DERIVATIVES WITH THIAZOLIC RINGS. I

SYNTHESIS OF 6-AMINOTHIAZOLO[4,5-f]INDAZOLE

C. TĂRĂBĂŞANU-MIHĂILĂ, L. FLORU, EUGENIA BALTĂ*) and
A. PREDESCU

**Laboratory for the Technology of Aromatic Intermediates
and Organic Dyes, Polytechnic Institute, Bucharest,
Calea Victoriei 149
and
* Laboratory for Analytical Chemistry, Polytechnic
Institute, Bucharest, Str. Polizu, 1**

Received November 28, 1972

A new possibility for obtaining 6-aminothiazolo [4,5-f] indazole and some derivated cationic and dispersion dyes has been investigated.

1. INTRODUCTION

In recent years, there has been an increasing trend toward introducing heterocyclic systems in the structure of cationic and dispersion dyes. Derivative dyes of benzothiazole, indazole and triazole have found large commercial applications because of their remarkable tinctorial properties.

The presence of the benzodithiazole systems I and II, studied by Kiprianov and Mihailenko, [1] confers special qualities and colours on the cationic dyes.

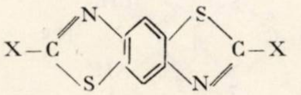

I

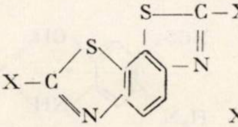

II

X= N=N−Ar

---

[1] A. I. Kiprianov and F. A. Michailenko, *Khim. geterotsikl. Soedinenyi* **2**, 270 (1967); *Chem. Abstr.*, **70**, 1269a (1969).

Based on these findings, we intend to obtain other heterocyclic systems III and IV which may be included in the structure of cationic and dispersion dyes

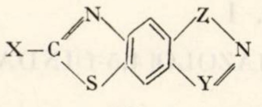
III

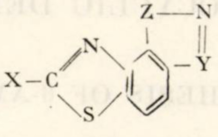
IV

where : $X = NH_2$, SH or substituted aryl
$Y = N$, CH, CHCl, CHBr
$Z = NH$, O, S

The present paper reports on the results of our experimental investigations regarding the synthesis of 6-aminothiazolo [4,5-f] indazole IV (III ; $Y = N$, $Z = CH_2$; $X = NH_2$), a compound which was obtained by Bellavita [2] in 1968 for pharmaceutical purposes ; it also suggests some possibilities for including this compound in the structure of the dyes.

2. RESULTS AND DISCUSSIONS

2.1. SYNTHESIS OF 6-AMINOTHIAZOLO[4,5-f]INDAZOLE

The compound was synthesized according to the following reaction sequence :

(1)
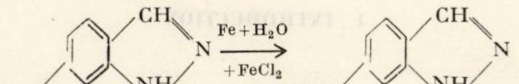

6-Nitroindazole was prepared by the method described by Meunier [3] (m.p. = 179 — 180°). Its reduction (1) to 6-aminoindazole occurred in aqueous medium with iron in the presence of iron chloride as electrolyte.

(2)
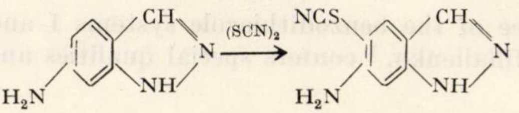

(3)
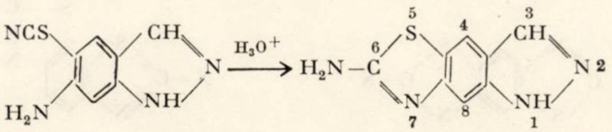

IV

---

[2] C. Bellavita, N. Martani and F. A. Amaldo, *Ann.Chim.* (*Ital.*), **58**, 823 (1968).
[3] J. Meunier, *Bull. Soc. chim. France*, **31**, 641 (1904).

The following reaction was used [2] as a dithiocyanate source :

$$2NH_4SCN + Br_2 = 2NH_4Br + (SCN)_2 \tag{4}$$

It is known [4] that reaction (4) is more rapid than the bromination reaction. For this reason, no bromination process occurs in synthesis making use of reaction (4) at a NH_4SCN to Br_2 molar ratio of over 3 : 1.

Bromination may appear in the case of a lower ratio between reactants. Thus, 3-bromo-6-aminothiazolo [4,5-f] indazole appears as a reaction (2) product at a 6-aminoindazole : NH_4SCN : Br_2 molar ratio of 1 : 2.5 : 6. Its presence is explicable since indazole as such brominates more readily in position 3 than in the benzene nucleus.[5]

Copper thiocyanate used as a dithiocyanate source,[6] or the reaction between alkaline thiocyanate and sulphuryl chloride[7] also gave favourable results.

This method for 6-aminothiazolo [4,5-f] indazole synthesis is not mentioned in literature. We point out the fact that high-purity products have been obtained by using copper thiocyanate without running the risk of bromination.

$$2Cu(SCN)_2 \rightarrow 2CuSCN + (SCN)_2 \tag{5}$$

2.2. IR SPECTRA OF 6-NITRO- AND 6-AMINOINDAZOLE

Spectroscopic studies carried out by O'Sullivan [8] on type V compounds show that the variation of substitutes :

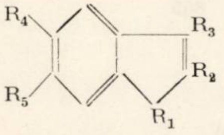

V

where : R_1, R_2, R_3 may be CH_2 NH, O, CO, SO_2, CH, N.

R_4 and R_5 produce hardly noticeable changes in the overall aspect of spectra, except for the appearance of their characteristic bands. Bands situated around 1600, 1460, 1390, 1310, 1270, 1250, 1200, 1160, 1100, 1060, 1020, 950, 890, 850, 800 and 750 cm^{-1} seem to be characteristic of the type V heterocyclic systems.[9]

[4] M. F. Randvere (American Cyanamid Co.), F. Pat. 1502178 (1967).
[5] H. Sanielevici, *Coloristica*, **13**, 9 (1969).
[6] W. Kaufmann, *Ber. dtsch. hem. Ges.*, **67**, 946 (1934).
[7] J. Hunter, *J. Chem. Soc.*, **1926**, 1399.
[8] D. G. O'Sullivan and J. Sadler, *J. Org. Chem.*, **22**, 283 (1957).
[9] D. G. O'Sullivan, *J. Chem. Soc.*, **8**, 3278 (1960).

Table 1

Infrared bands of the compounds IV, V and thiazole

1. 6-nitroindazole (V ; $R_1 = NH$; $R_2 = N$; $R_3 = CH$; $R_4 = H$; $R_5 = NO_2$)
2. 6-aminoindazole (V ; $R_1 = NH$; $R_2 = N$; $R_3 = CH$; $R_4 = H$; $R_5 = NH_2$)
3. 6-aminothiazolo-[4,5-f] indazole (IV)
4. 2-aminobenzothiazole [13,15,16] (V ; $R_1 = S$; $R_2 = C-NH_2$; $R_3 = N$; $R_4 = R_5$ H) ; a part of the bands
5. thiazole [14] ; a part of the bands

1.			3160m	3075m	2920m	2995w	2935m	2850m				1620m
2.	3440m	3360m	3130–2980m									1620s
3.	3380 s	3315s	3160m	3065m		3030m	2935m	2885m	2805s	2765m	1632s	
4.											1632	
5.												

1.	1562w	1532s	1529s		1503m	1455s	1425w	1392s	1352s	1320m	1303m	1245m
2.					1490m	1455s		1390s		1330m	1310m	1248m
3.	1580w	1540m		1510m			1420w	1390s		1330m		1245m
4.	1590	1540		1510						1340		1250
5.								1375				

1.	1208m	1130w	1090m	1072s		960s			880w		878s	860s	850s
2.	1212m	1132w	1110w	1070s		958s			890w				850s
3.	1210m	1132m	1098m	1075s	1032m	952s	982m	920s		855m			848s
4.		1126	1107				980	921	890	855			
5.		1160					980	930		855			

1.	816w	794s	777s	745w		686s			
2.		785m		745w					
3.	826w	795m	775m	745w	720w	690w	658w	630m	620 m
4.				742	721	706	660	632	624
5.			770		730				

The spectrum of 6-nitroindazole (V ; R = NH ; R = N ; R = CH ; R = H ; R $=NO_2$) reveals bands at 1620, 1455, 1392, 1245, 1208, 1130, 1090, 1972, 960 and 850 cm^{-1} (table 1), which may be identified as distinctive for the type V heterocyclic system.

---

[10] C. N. R. Rao and R. Venkataraghavan, *Canad. J. Chem.*, **42**, 43 (1964).

[11] W. Lüttke and M. Klessinger, *Chem. Ber.*, **97**, 2342 (1964).

[12] J. Weinstein and G. M. Wymann, *J. Amer. Chem. Soc.*, **78**, 2387 (1956).

[13] K. S. Suresh, J. Ramachandran and G. N. R. Rao, *J. Sci. Ind. Res., India*, **20B**, 203 (1961).

[14] J. M. Bonnier, M. Gelus and B. Papoz, *Bull. Soc. chim. France*, **9**, 2485 (1965).

[15] A. Taurins, J. G. E. Fenyes and R. N. Jones, *Canad. J. Chem.*, **35**, 423 (1957).

[16] E. Baltă, *Rev. Roumaine Chim.*, **17**, 1241 (1972).

They also appear in the case of 6-aminoindazole (V; $R_1 = NH$; $R_2 = N$; $R_3 = CH$; $R_4 = H$; $R_5 = NH_2$) with minor changes (table 1).

Indazole derivatives may exist under two tautomeric forms: VI and VII.

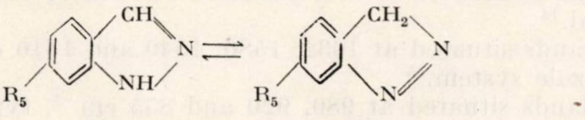

VI VII

Since no accurate spectral differentiation can be made between C=N and N=N frequencies [10] the IR spectra analysis did not establish — in the case of these compounds — the tautomeric form which contributes most significantly to the overall mesomerism of the molecule. This band is situated at 1620 cm^{-1} for compounds VI and VII (table 1).

The presence of ν_{CH} at 2920 cm^{-1} in the case of 6-nitroindazole (an imperceptible band for 6-aminoindazole being probably included in the large band at 3130–2980 cm^{-1}) supports the structure VI which we consider as being the most probable.

In the structure of compounds VI, $N-H\ldots N$ hydrogen bonds make an important contribution. [9] The presence of the above mentioned large band certifies the involvement of NH group in strong intermolecular hydrogen bonds. They are stronger in the case of 6-aminoindazole than in that of 6-nitroindazole where ν_{NH} is certainly situated at 3160 cm^{-1}. This value is lower than in the case of the indigo itself ($\nu_{NH} = 3246\ cm^{-1}$),[11] a molecule in which the contribution of hydrogen bridges is considerable.[12]

The position of $\nu_{NO_2\ sym.}$ at 1352 and $\nu_{NO_2\ asym.}$ at 1532 cm^{-1} — therefore at normal frequencies [9] — suggests that these groups are not involved in hydrogen bonds.

Amino groups were also revealed for 6-aminoindazole by vibrations $\nu_{NH_2\ sym.}$ at 3360 cm^{-1} and $\nu_{NH_2\ asym.}$ at 3440 cm^{-1}.

Since the substituted indazoles are sparingly soluble in the usual solvents, a detailed study of the association by means of the hydrogen bonds was not possible.

2.3. IR SPECTRUM OF 6-AMINOTHIAZOLO[4,5,-f]INDAZOLE. IV

Considering O'Sullivan's[8,9] findings with regard to compounds V it may be assumed that the spectrum of 6-aminothiazolo-[4,5-f]indazole must retain the typical 2-aminobenzothiazole bands and those of the indazole cycle unless substitutes R_4 and R_5 cause major changes in the spectrum. Table 1 presents the spectral data established by Surish and coworkers for 2-aminobenzothiazole, [13] by Bonnier and coworkers, for benzothiazole[14] and the IR spectrum determined by us for compound IV.

By comparing these data it may be seen that above assumption is a real one.

The following bands have been assigned in the spectrum of compound IV :

1. Bands situated at 658, 630 and 620 cm^{-1}, corresponding to the C$-$S bond.[13]

2. Bands situated at 1632, 1580, 1540 and 1510 cm^{-1}, typical of the benzothiazole system.[15]

3. Bands situated at 980, 920 and 855 cm^{-1}, typical of the thiazole system.[6]

4. All the bands typical of the indazole system : $\nu_{NH} = 3160\ cm^{-1}$, $\nu_{CH}=3065\ cm^{-1}$ and 2935 cm^{-1} and also all the bands situated within the 1380 $-$ 1071 and 850 $-$ 720 cm^{-1} ranges.

5. Bands $\nu_{NH_2\ asym.}$ at 3380 cm^{-1} and $\nu_{NH_2\ sym.}$ at 3315 cm^{-1}, which confirms the presence of amino groups.

The fact that the IR spectrum of compound IV obeys O'Sullivan's findings, proves that even if type V heterocycles are included in compactly-condensed heterocyclic systems, they will keep their individuality, from IR absorption viewpoint.

3. DERIVATIVE DYES OF SYSTEM IV

3.1. DISPERSION DYES

These compounds were obtained by the following reaction sequence :

(6)

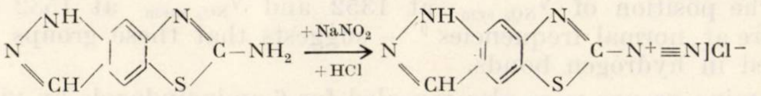

(7)

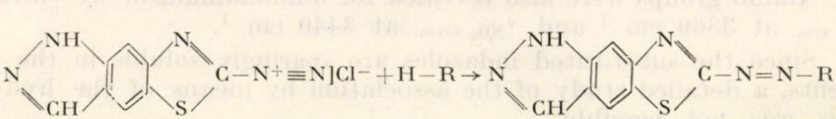

VIII

R = substituted aromatic or heterocyclic residue.

Type VIII products proved to be dispersion dyes with remarkable properties, used for dyeing of polyester fibres and cellulosis acetate.

Table 2 lists data concerning the synthesis and the tinctorial properties of these compounds.

3.2. CATIONIC DYES

All type VIII structures will become cationic dyes by methylation at one of the nitrogen atoms included in the heterocycle and may be used for dyeing of polyacrylonitrile fibres.

Table 2

Data concerning the synthesis and tinctorial properties of the compounds VIII with R = p – C_6H_4 – NXY or with T =

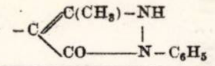

$-C\langle\begin{smallmatrix}C(CH_3)-NH\\ |\\ CO\text{———}N-C_6H_5\end{smallmatrix}$

X	Y	Obtaining of the diazonium salt of the compound IV					Coupling reaction				Tinctorial results	
		Comp. IV g	Solvent (ml)	$NaNO_2$ g	Temp. °	Time hrs	R – H g	Solvent (ml)	Temp. °	%	Colour on cellulose acetate	Colour on polyester fibres
H	CH_3	10	H_2SO_4 (35)	2.6	0	4	4.2	CH_3COOH 70 %(60)	0	70	blue-red	red
CH_3	CH_3	10	H_3PO_4 (25)	2.6	–15	2.5	4.5	CH_3COOH 70 %(60)	0	75	red	red
H	C_2H_5	10	H_2SO_4 (35)	2.6	0	4	4.5	CH_3COOH 70 %(80)	0	65	blue-red	blue-red
C_2H_5	C_2H_5	10	HCl 15 % (25)	2.6	–5	4	5	H_2O (200)	0	70	red	red
C_2H_5	C_2H_4OH	10	H_3PO_4 (25)	2.4	–15	2.5	8.2	H_2O (200)	0	70	black-red	black-red
T		10	H_3PO_4 (25)	2.4	–15	16	15	$HCON(CH_3)_2$ (40)	–5	80	yellow	yellow

Methylation has been carried out with dimethylsulfate in an aqueous medium at 65 — 70°.

Although there are three possible methylations (the nitrogen atoms from positions 1, 2 and 4), the reaction results in a unitary product; this fact was proved by paper chromatography analysis.

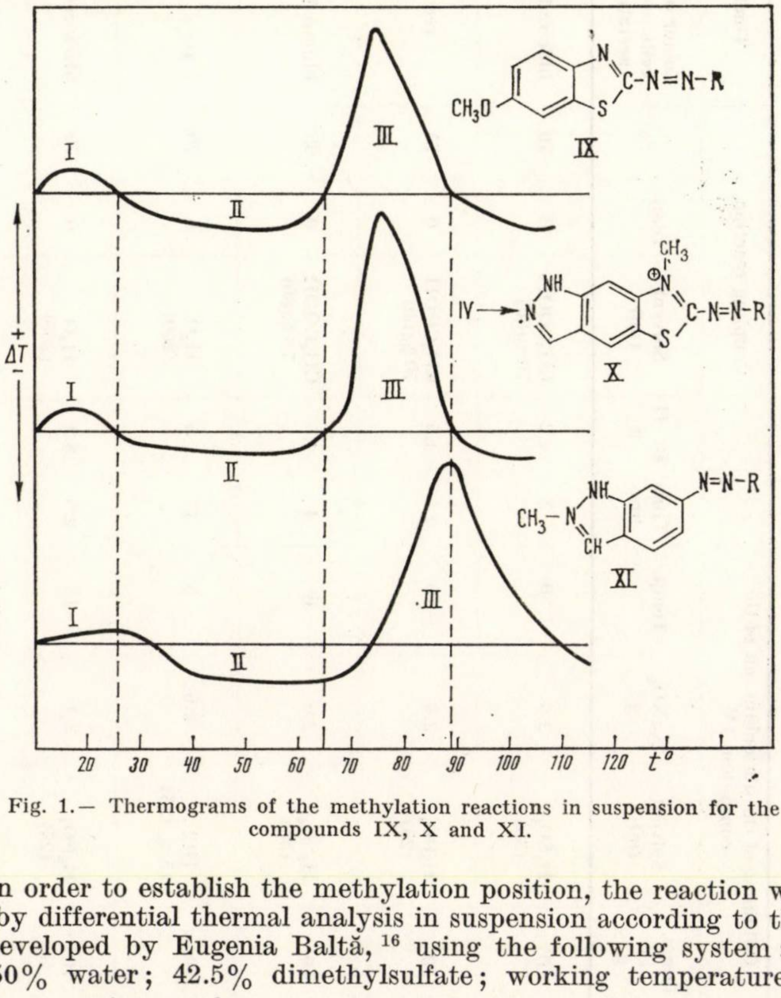

Fig. 1.— Thermograms of the methylation reactions in suspension for the compounds IX, X and XI.

In order to establish the methylation position, the reaction was followed by differential thermal analysis in suspension according to the method developed by Eugenia Baltă, [16] using the following system: 7.5% dye; 50% water; 42.5% dimethylsulfate; working temperature: 70°.

Comparative results are presented in figure 1 for compounds IX, IV and XI.

As reflected by the charts, a great similarity has been found between the methylation thermogram of compounds IX and X and also a clear-cut difference with respect to pigment XI.

The three common effects—two exo- and one endothermal—may be assigned as follows: [16]

I. A solvation exothermal effect of the pigment in water or dimethylsulfate;

II. An endothermal effect due to the decomposition of the transition product typical of the SN-2 mechanism.

III. An exothermal effect due exclusively to the hydrolysis of dimethylsulfate.

The beginning of the fourth thermal effect (endothermal) suggests the appearance of protonation at one of the protonation centers existing in the molecule.

Table 3

Tinctorial properties of the compounds X with $R = p-C_6H_5-NXy$

X	Y	Colour on polyacrylonitrile fibres
H	CH_3	blue-red
CH_3	CH_3	blue
H	C_2H_5	blue-red
C_2H_5	C_2H_5	blue
C_2H_5	C_2H_4OH	blue-violet

The perfect overlapping of the temperature ranges including the three effects for compounds IX and IV leads us to assign the structure X to the methylated compound, in which the quaternary group is localized on the thiazole cycle.

Table 3 shows the results obtained by dyeing of polyacrylonitrile fibres with type X products. The synthesis conditions are identical with those required for the differential thermal analysis in suspension.

4. EXPERIMENTAL

SYNTHESIS OF 6-AMINOTHIAZOLO[4,5-f]INDAZOLE

Introduce 620 ml glacial acetic acid into a 2.5 liter 3-neck flask equipped with stirrer, reflux refrigerator and thermometer, having the possibility to cool to 10° and add thereafter 121.6 ammonium sulfocyanide with stirring until a fine suspension results. Subsequent addition of 200.4 g crystallized copper sulfate gives a black coloured precipitate, $Cu(SCN)_2$. Add 20 g 6-aminoindazole at the same temperature. Continue stirring for 90 minutes at 10° after adding the reactants and increase the temperature to 40° over the next 90 minutes. Keep the reaction mass at this temperature for 6 hours with stirring. The mass turns yellowish-brown when the reaction is completed.

Dilute it then with 1500 ml water heated to 80°, keep under stirring for another 15 minutes. The reaction mass takes the aspect of a yellow suspension and is filtered. Stirr the filtrate with 6 g animal charcoal, heat it to 80° and filter it. After cooling to 20°, the filtrate is alkalinised with solid $NaHCO_3$ up to pH 8.5. Filter the resulting precipitate and wash with cold water until a neutral pH is obtained. One obtains 14 – 17 g of product V. Yield 60 – 70 %; melting point above 300°.

The elementary analysis for $C_8H_6N_4S$: C % :*calc.* : 50.53 ; *found* : 50.18 ; H % : *calc.* : 2.63 ; *found* :2.07 ; N % : *calc.* : 29.47 ; *found* : 29.80 ; S % : *calc.* :16.84 ; *found* : 16.75.

IR spectra were taken in a KBr disk using a UR-10 spectrophotometer.

5. CONCLUSIONS

1. A new method was established for the synthesis of 6-aminothiazolo [4,5-f] indazole by using copper sulfocyanide as a dithiocyanate source.

2. The introduction of this heterocycle in the structure of dispersion and cationic azo-dyes results in products with remarkable tinctorial properties which may be used for dyeing of hydrophobe synthetic fibres. They have not been reported in the literature so far.

Revue Roumaine de Chimie, **18**, *5*, 899–905 (1973)

γ-KETO ACIDS IN THE PFITZINGER REACTION

A. M. EL-ABBADY*, M. A. OMARA and N. G. KANDIL

Department of Chemistry, University College for Girls
A'in Shams University, Cairo, Egypt

Received July 26, 1972

β-Aroylpropionic acids (I, R = H, CH_3, Cl) are condensed with isatin under Pfitzinger conditions to give the corresponding 2-aryl-3-carboxymethyl cinchoninic acids (II). These are esterified with diazomethane to give the corresponding dimethyl esters (III). Acetyl chloride gives with (II) the anhydrides (IV), but acetic anhydride and fused sodium acetate give (IV), together with 5-acetoxybenz (c) acridines (V). The acids (II) on heating in vacuum just above their melting points give 5,6-dihydro-5-oxo-benz(c) acridines (VI), but on treatment with boiling nitrobenzene they give 2-aryl-3-methyl cinchononic acids (VII). The structure of all the products is inferred from their analytical data, infrared spectra and chemical properties.

As far as we are aware only α-keto acids and α-keto esters as pyruvic acid, substituted pyruvates [1] and oxaloacetic esters [2] have been tried to react with isatin and substituted isatin under the conditions of Pfitzinger reaction. [3]

In the present investigation the Pfitzinger reaction between γ-keto acids and isatin is reported. β-Aroylpropionic acids namely β-benzoylpropionic acids (I, R = H), β-toloylpropionic acid (I, R = CH_3) and β-p-chlorobenzoylpropionic acid (I, R = Cl) are condensed with isatin in the presence of alcoholic potassium hydroxide solution (33%). Good yields of 2-aryl-3-carboxymethylcinchoninic acids (II, R = H, $-CH_3$, Cl) were obtained by this treatment. These dibasic acids were found to exist as zwitterions as indicated from their infrared spectra [4] which revealed absorption bands at : 3400–3100 cm^{-1} characteristic of the stretching frequency of the OH of the dimeric carboxyl groups ; 1720, 1630, 1500 cm^{-1} characteristic of the stretching frequencies of carbonyl of the carboxyl groups, of the aromatic rings skeleton, and of the antisymmetrical carboxylate anion respectively; 950, 830, 770, 740 and 690 cm^{-1} characteristic of the out-of-plane bending frequencies of OH for the carboxyl groups and of two, four and five adjacent aromatic hydrogen atoms respectively; 725cm^{-1} characteristic of the stretching frequency for the carbon chlorine bond.

---

* Present address : Head of the Chemistry Department, Faculty of Science at Tanta Egypt.

[1] Th. S. Work, *J. Chem. Soc.*, **1942**, 426.

[2] J. Halberkann, *Ber. dtsch. chem. Ges.*, **54**, 3079 (1921).

[3] W. Pfitzinger, *J. prakt. Chem.*, **33**, 100 (1886).

[4] L. J. Bellamy, "The Infrared Spectra of Complex Molecules", Methuen, London, 1958.

Usual methods of esterification of these dicarboxylic acids using methanol and concentrated sulphuric acid or hydrogen chloride gas were found to give unsatisfactory results. Treatment of the acid chlorides with methanol also failed to react.

Esterification was, however, carried out using diazomethane [5] where the diesters, methyl 3-carbomethoxymethyl-2-arylcinchoninates (III) were obtained in good yield. The structure of these diesters was inferred from their analytical data, and from their infrared absorption spectra which showed the following bands: 1745, 1735, 1600, 1580, 1500, 830, 770, 750, 700 and 725 cm^{-1}, characteristic of ν C=O of saturated and aromatic esters, of the aromatic ring skeleton, of the aromatic γ-CH of two, four and five adjacent hydrogen atoms, and of the ν C—Cl respectively.

3-Carboxymethyl-2-aryl-cinchoninic acids (II, R = H, CH$_3$) were converted into their anhydrides (IV, R = H, CH$_3$) by refluxing with acetyl chloride, but 3-carboxymethyl-2-*p*-chlorophenyl-cinchoninic acid (II, R = Cl) required treatment with acetic anhydride at room temperature to be converted to its anhydride (IV, R = Cl).

The infrared spectra of these anhydrides show the doublet stretching frequencies of the carbonyl at 1740 and 1660 cm^{-1} besides the rest of the usual bands. Although these doublets have lower stretching frequencies than those for six-membered ring anhydrides [6] which absorb at 1821 and 1774 cm^{-1}, yet they are similar to those of homophthalic anhydride which showed doublet at 1760 and 1680 cm^{-1}.

Treatment of the dibasic acids (II) with sodium acetate in acetic anhydride [7] yielded 5-acetoxy-benz (c) acridine or its 3-methyl-or 3-chloroderivatives (V) contaminated with the corresponding anhydrides (IV). The structure of acridines (V) was inferred from their analytical data; and infrared spectra which showed the characteristic bands of ν C = O and ν C — O of the acetoxy group at 1740, 1730, 1240 and 1150 cm^{-1} respectively.

Decarboxylation of the dibasic acids (II) was carried out by thre methods:

(a) Heating just above their melting points under reduced pressure,[8] whereupon 5,6-dihydro-5-oxo-benz (c)acridine and its derivatives (VI) were obtained. The structure of these acridines was inferred from: i — Their analytical data. ii — Their stability in hot sodium hydroxide solution. iii — Their infrared spectra which showed two bands at 1750 and 1660 cm^{-1} characteristic of the stretching frequencies of ketonic carbonyl group and aromatic ring skeleton respectively.

(b) Heating in nitrobenzene [9] gave 2-aryl-3-methylcinchoninic acids (VII). The structure of these monobasic acids was confirmed from

---

[5] V. Pechmann, *Ber. dtsch. chem. Ges.*, **28**, 856 (1895).

[6] J. C. P. Shwartez, "Physical Methods in Organic Chemistry", 1965, p. 64.

[7] A. M. El-Abbady and L. S. El-Assal, *J. Chem. Soc.*, **1959**, 1024.

[8] J. T. Raunhaldz and F. G. Mann, *J. Chem. Soc.*, **1958**, 3368.

[9] J. Renshaw and D. Friedman, *J. Chem. Soc.*, **61**, 3320 (1939).

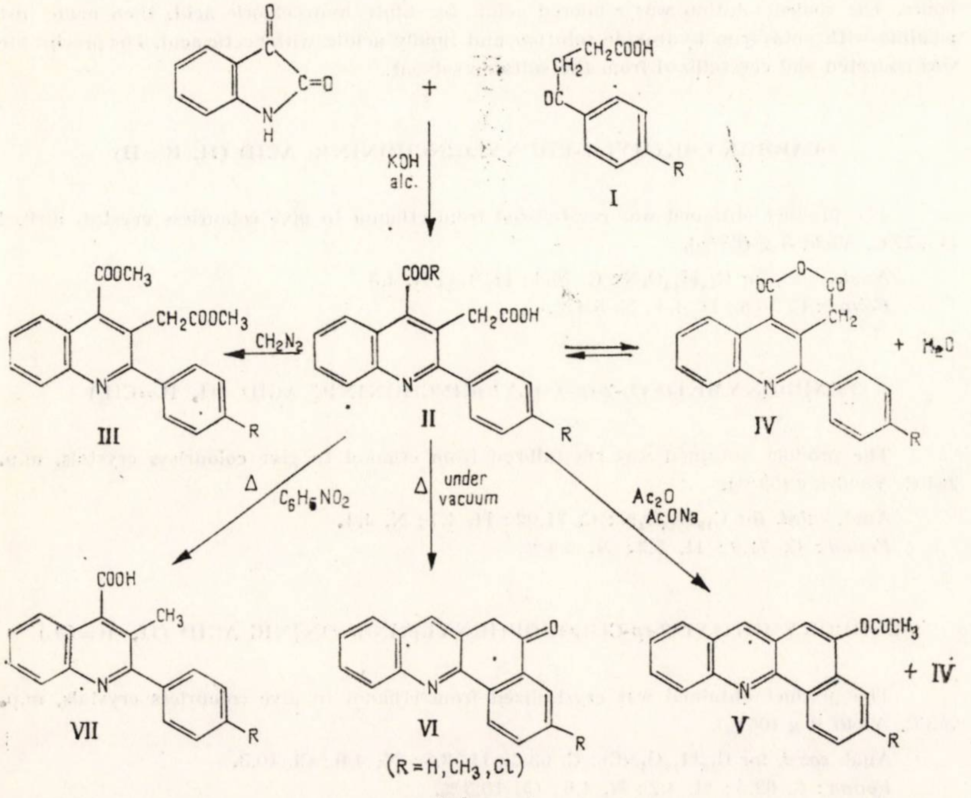

KOH alc.
I
COOCH3
CH2COOCH3
CH2N2
COOR
CH2COOH
III
II
IV
+ H2O
Δ
C6H5NO2
Δ under vacuum
Ac2O AcONa
COOH
CH3
VII
VI
V
OCOCH3
+ IV
(R=H, CH3, Cl)

Scheme 1

their analytical data and their infrared spectra which showed bands at 3400 (br) and 1620 cm^{-1} with a broad base, (1700–1550 cm^{-1}) characteristic of stretching frequencies of hydroxyl and carbonyl groups of dimeric carboxylic acids.

Furthermore, 3-methyl-2-phenylcinchoninic acid (VII; R = H) was prepared authentically [10] and was decarboxylated by the first method to 3-methyl-2-phenylquinoline. [10,11]

(c) Heating with copper-bronze [7] in quinoline or with sodalime gave unsatisfactory results.

EXPERIMENTAL[12]

Pfitzinger reaction between isatin and β-aroylpropionic acids. General Procedure:

β-Aroylpropionic acids (0.04 mole) was added to a solution of isatin (0.04 mole) in 33% ethanolic potassium hydroxide solution (100 ml) and the mixture was refluxed for about 12 hours. The cooled solution was rendered acidic by dilute hydrochloric acid, then made just alkaline with potassium hydroxide solution and finally acidic with acetic acid. The precipitate was collected and crystallized from the suitable solvent.

---

[10] V. Braun and L. Braun, *Ber. dtsch. chem. Ges.*, **60**, 1256 (1927).

[11] V. Miller, J. Kinkelin, *Ber. dtsch. chem. Ges.*, **19**, 527 (1886).

[12] Melting points are not corrected. Infrared spectra were measured on infrared spectrophotometer UNICUM SP 200G.

3-CARBOXYMETHYL-2-PHENYLCINCHONINIC ACID (II, R=H)

The product obtained was crystallized from ethanol to give colourless crystals melted at 277°C. Yield 8 g (65 %).

Anal. *calcd.* for $C_{18}H_{13}O_4N$: C, 70.4 ; H, 4.3 ; N, 4.5
Found : C, 70.8 ; H, 4.4 ; N, 5.4 %.

3-CARBOXYMETHYL-2-(*p*-TOLYL)CINCHONINIC ACID (II, R=CH$_3$)

The product obtained was crystallized from ethanol to give colourless crystals, m.p. 264°C. Yield 8 g (53 %).

Anal. *calcd.* for $C_{19}H_{15}O_4N$: C, 71.02 ; H, 4.7 ; N, 4.4.
Found : C, 71.9 ; H, 5.3 ; N, 4.4 %.

3-CARBOXYMETHYL-2-(*p*-CHLOROPHENYL)CINCHONINIC ACID (II, R=CL)

The product obtained was crystallized from ethanol to give colourless crystals, m.p. 255°C. Yield 9 g (66 %).

Anal. *calcd.* for $C_{18}H_{12}O_4NCl$: C, 63.2 ; H, 3.5 ; N, 4.0 ; Cl, 10.3.
Found : C, 62.5 ; H, 4.2 ; N, 4.6 ; Cl, 10.3 %.

Esterification of 3-carboxymethyl-2-arylcinchoninic acids (II) General procedure:

The diacid (1g) was treated with diazomethane (from 10 g nitrosomethyl urea) in ether (250 ml). The ethereal solution was left overnight in an ice chest, washed with aqueous sodium carbonate, dried over anhydrous sodium sulphate, filtered and evaporated nearly to dryness. The residual product obtained was crystallized from the suitable solvent.

METHYL 3-CARBOXYMETHYL-2-PHENYLCINCHONINATE (III, R=H)

The product obtained was crystallized from petroleum ether (b.p.60 – 80°) in colourless crystals, m.p. 100–101°C. Yield 0.8 g (73 %).

Anal. *calcd.* for $C_{20}H_{17}O_4N$: C, 71.6 ; H,5.1 ; N, 4.1.
Found : C, 70.9 ; H, 5.1 ; N, 3.7 %.

METHYL 3-CARBOMETHOXYMETHYL-2-(*p*-TOLYL)CINCHONINATE (III, R=CH$_3$)

The product obtained was crystallized from ethanol in glittering colourless crystals, m.p. 105 – 106°C. Yield 0.8 g (73.6 %).

Anal. *calcd.* for $C_{21}H_{19}O_4N$: C, 72.2 ; H, 5.4 ; N, 4.0.
Found : C, 71.9 ; H, 5.7 ; N, 4.0 %.

METHYL 3-CARBOMETHOXYMETHYL-2-(*p*-CHLOROPHENYL)CINCHONINATE (III, R=Cl)

The product obtained was crystallized from petroleum ether (b.p.60 – 80°) in colourless needles, m.p. 99 – 100°C. Yield 0.8 g (73.9 %).

Anal. *calcd.* for $C_{20}H_{16}O_4NCl$: C, 64.9 ; H, 4.3 ; N, 3.7 ; Cl, 9.6.
Found : C, 64.0 ; H, 4.8 ; N, 4.5 ; Cl, 9.6 %.

ACTION OF ACETYL CHLORIDE ON THE 3-CARBOMETHOXYMETHYL-2-ARYLCINCHONINIC ACIDS

General procedure :

The diacid (1 g) was treated with acetyl chloride or acetic anhydride (10 ml). After evaporation, the residue was dissolved in ether and the ethereal solution washed with sodium carbonate solution then dried over anhydrous sodium sulphate. The product obtained was crystallized from the suitable solvent.

3-CARBOXYMETHYL-2-PHENYLCINCHONINIC ACID ANHYDRIDE (IV, R = H)

The diacid (II, R = H) was refluxed with acetyl chloride for 5 hours. The product obtained was crystallized from benzene/petroleum ether (b.p. 40 – 60°) as yellow needles, m.p. 170°. Yield 0.6 g (66 %).

Anal. *calcd.* for $C_{18}H_{11}O_3N$: N, 4.8.
Found : N, 5.1 %

3-CARBOXYMETHYL-2-(*p*-TOLYL)CINCHONINIC ACID ANHYDRIDE (IV, R=CH_3)

The diacid (II, R = CH_3) was refluxed with acetyl chloride for 1 hour. The product so obtained was crystallized from petroleum ether (b.p. 80 – 100°), in yellow needles, m.p. 170 – 171°. Yield 0.85 g (94 %).

Anal. *calcd.* for $C_{19}H_{13}O_3N$: C, 75.24 ; H, 4.3 ; N, 4.6.
Found : C, 75.6 ; H, 4.9 ; N, 4.8 %.

3-CARBOXYMETHYL-2-(*p*-CHLOROPHENYL)CINCHONINIC ACID ANHYDRIDE (V, R = Cl)

The diacid (II, R = Cl) was dissolved in cold acetic anhydride and left at a room temperature for 2 days. The product obtained was crystallized from benzene/petroleum ether (b. p. 40 – 60°), as a yellow powder, m.p. 173 – 74°C. Yield 0.05 g (5 %).

Anal. *calcd.* for $C_{18}H_{10}NO_3Cl$: N, 4.4.
Found : N, 4.4 %.

Hydrolysis of the anhydrides (IV, R = H, CH_3 and Cl) with 10 % aqueous potassium hydroxide solution gave back the diacids (II, R = H, CH_3 and Cl), mixed m.p. undepressed.

CYCLISATION OF THE 3-CARBOXYMETHYL-2-ARYLCINCHONINIC ACIDS

General procedure :

A mixture of the diacid (0.02 mole), fused sodium acetate (2 g) and acetic anhydride (25 ml) was refluxed for 5 hours. After removal of acetic anhydride under reduced pressure water was added. The solid formed was digested with ether. The ethereal solution was dried over anhydrous sodium sulphate, and evaporated to give the anhydrides (IV, R = H, CH_3, Cl). This was proved by melting and mixed m.p. with the anhydrides obtained by treating the dibasic acids (II) with acetyl chloride or acetic anhydride.

The ether insoluble fraction was crystallized from the suitable solvent.

5-ACETOXYBENZ(c)ACRIDINE (V, R =H)

The product obtained was crystallized from benzene as yellow needles, m.p.300°. Yield 2.5 g (47%).

Anal. *calcd.* for $C_{19}H_{13}NO_2$: C, 79.4 ; H, 4.5 ; N, 4.8.

Found : C, 79.9 ; H, 4.1 ; N, 4.5%.

5-ACETOXY-3-METHYLBENZ(c)ACRIDINE (V, R = CH_3)

The product insoluble in ether was crystallized from bezene as yellow crystals, m.p. above 312°C. Yield 2.8 g (40%).

Anal. *calcd.* for $C_{20}H_{15}NO_2$: C, 79.7 ; H, 5.0 ; N, 4.7.

Found : C, 80.6 ; H, 4.4 ; N, 4.9%.

5-ACETOXY-3-CHLOROBENZ(C)ACRIDINE (V, R=Cl)

The product insoluble in ether was crystallized from benzene as yellow needles, m.p. 280°C. Yield 2.8 g (46%).

Anal. *calcd.* for $C_{19}H_{12}NClO_2$: C, 70.9 ; H, 3.7 ; N, 4.4 ; Cl, 11.

Found : C, 71.8 ; H. 3.6 ; N, 4.9 ; Cl, 11.8%.

PYROLYSIS OF 3-CARBOXYMETHYL-2-ARYLCINCHONINIC ACIDS

General procedure :

The diacid (1 g), placed in a test tube fitted with a cold finger, was heated at about 20° above its m.p. under diminished pressure (10 mm/Hg). The compound melted, evolution of gases was observed and a dark redish-brown liquid was formed. This liquid was kept under these conditions for about half an hour. The solid obtained on cooling was extracted with ether. The ethereal solution was washed with sodium carbonate solution, dried over anhydrous sodium sulphate, and filtered. After removal of the solvent the residue was crystallized from the suitable solvent.

5,6-DIHYDRO-5-OXOBENZ(C)ACRIDINE (VI, R=H)

The product was crystallized from petroleum ether (b.p. 40 – 60°) in pale brown crystals ; m.p. 172 – 74°. Yield 0.6 g (85%).

Anal. *calcd.* for $C_{17}H_{11}NO$: C, 83.3 ; H, 4.5.

Found : C, 84.1 ; H, 4.6%.

5,6-DIHYDRO-3-METHYL-5-OXOBENZ(c)ACRIDINE (VI, R= CH_3)

The product obtained was crystallized from benzene in yellow balls, m.p. 202°C. Yield 0.6 g (75%).

Anal. *calcd.* for $C_{18}H_{13}NO$: C, 83.3 ; H, 5.0 ; N, 5.4.
Found : C, 83.8 ; H, 5.1 ; N, 5.7%.

3-CHLORO-5,6-DIHYDRO-5-OXOBENZ(c)ACRIDINE (VI, R=Cl)

The product obtained was crystallized from benzene/petroleum ether (b.p. 40 – 60°), as brown powder, m.p. 226 – 27°C. Yield 0.6 g (75%).

Anal. *calcd.* for $C_{17}H_{10}NOCl$: 72.9 ; H, 3.5 ; N, 5.0 ; Cl, 12.3.
Found : C, 72.7, H, 3.7 ; N, 5.0 ; Cl, 12.7%.

ACTION OF BOILING NITROBENZENE ON 3-CARBOXYMETHYLCINCHONINIC ACIDS

General procedure :

The diacid (1 g) was refluxed in nitrobenzene (20 ml) for 1 hour. The solid separated on cooling to room temperature was filtered off and crystallized from a suitable solvent.

3-METHYL-2-PHENYLCINCHONINIC ACID[10] (VII, R = H)

The product obtained was crystallized from ethanol to give colourless needles, m.p. 299°. [10] Yield 0.4 g (50%).

A sample of the product was decarboxylated by heating under vacuum to give the known 3-methyl-2-phenylquinoline, m.p. 50° from benzene/petroleum ether, b.p. 40 – 60° (ref. [10] m.p. 52 – 53° (43°).

Picrate derivative, m.p. 205° (from benzene). [11]

3-METHYL-2-(*p*-TOLYL)CINCHONINIC ACID (VII, R=CH_3)

The product obtained was crystallized from benzene to give colourless needles, m.p 295°C. Yield 0.5.g (62%).

Anal. *calcd.* for $C_{18}H_{15}NO_2$: C, 77.9 ; H, 5.4 ; N, 5.0.
Found : C, 78.0 ; H, 5.5 ; N, 5.3%.

2-(*p*-CHLOROPHENYL)-3-METHYLCINCHONINIC ACID (VII, R=Cl)

The product obtained was crystallized from ethanol to give colourless crystals, m.p. 310°. Yield 0.4 g (50%).

Anal. *calcd.* for $C_{17}H_{12}NO_2$: N, 4.6 ; Cl, 11.9.
Found : N, 4.5 ; Cl, 11.2%.

[illegible]

The product obtained was crystallized from benzene [illegible]

Anal. calcd. for [illegible]

Found: [illegible]

[illegible]

The product obtained was crystallized from [illegible]

Anal. calcd. for [illegible]

Found: [illegible]

ACTION OF [illegible] ACIDS

Crude product.

[illegible]

[illegible]

The product obtained was crystallized from [illegible]

A sample of the product [illegible]

[illegible]

[illegible]

The product obtained was crystallized from [illegible]

Anal. calcd. for [illegible]

Found: [illegible]

[illegible]

The product obtained was crystallized from [illegible]

Anal. calcd. for [illegible]

Found: [illegible]

[illegible]

Revue Roumaine de Chimie, 18, 5, 907–912 (1973)

THE POLYMERIZATION OF N-VINYLCARBAZOLE BY THE SYSTEMS ACRYLONITRILE-$ZnCl_2$ AND ACRYLONITRILE-$HgCl_2$

D. S. VASILESCU, MARIA ŞTEFĂNESCU and AL. BĂLĂNESCU

Laboratory of Macromolecular Chemistry, Polytechnic Institute, Bucharest, Romania

Received September 21, 1972

The polymerization of N-vinylcarbazole in the presence of the acrylonitrile-$ZnCl_2$ complex or acrylonitrile-$HgCl_2$ homogeneous mixture was studied. The polymerization occurs very fast; no alternating copolymers were obtained. The process is cationic.

1. INTRODUCTION

The complexes of acrylonitrile or methyl methacrylate with $ZnCl_2$ were obtained first by Imoto. [1] The influence of metal salts on the reactivity of vinyl monomers has been studied extensively by a great number of investigators in recent years. [2–4]

Several authors have found that some complexes may be polymerized to obtain stereoregular polymers [2]; on the other hand other authors have prepared alternating copolymers of high regularity by copolymerization of complexed monomers with electron-donating monomers.[3–4] Gaylord and his co-workers [5] reported data, in order to elucidate the behaviour of these systems.

The complex from a vinyl monomer (containing nitrile or ester groups) and a metal salt (such as $ZnCl_2$, $Et_{1.5}AlCl_{1.5}$, $SnCl_4$, $AlCl_3$) acts generally as an electron acceptor. The polymerization of N-vinylcarbazole by electron acceptors is well known [6]; Plesch and his co-workers, [7] have studied the polymerization of N-vinylcarbazole (NVC) by $HgCl_2$ using chlorobenzene as solvent.

---

[1] M. Imoto, T. Otsu and S. Shimizu, *Makromol. Chem.*, **65**, 174 (1963); M. Imoto, T. Otsu and K. Nakabayashi, *Makromol, Chem.*, **65**, 194 (1963).

[2] V. A. Kargin, V. A. Kabanov and V. P. Zubov, *Vysokomol. Soedineniya*, **2**, 765 (1962); H. Hirai and T. Ikegami, *J. Polymer Sci.*, A-1, **8**, 2407 (1970) and references therein.

[3] M. Hirooka, H. Yabuuchi, S. Morita, S. Kawasumi and K. Nakaguchi, *J. Polymer Sci.*, B, **5**, 47 (1967); M. Hirooka, H. Yabuuchi, J. Iseki and Y. Nakai, *J. Polymer. Sci.*, A-1, **6**, 1381 (1968).

[4] S. Yabumoto, K. Ishii and K. Arita, *J. Polymer. Sci.*, A-1, **7**, 1577 (1969); idem, A-1, **8**, 295 (1970).

[5] N. G. Gaylord, *J. Polymer Sci.*, D, **4**, 183 (1970); O. F. Solomon and D. S. Vasilescu, *Materiale Plastice (Romania)*, **7**, 112 and 221 (1970).

In this work we present results concerning the polymerization of NVC by the acrylonitrile-$ZnCl_2$ and acrylonitrile-$HgCl_2$ systems.

2. EXPERIMENTAL

a. MATERIALS

NVC "FLUKA" was three times recrystallized from *n*-hexane and dried in vacuum at 30°, 48 h (m.p. = 64.2°).

$ZnCl_2$ was dried in vacuum at 200°; $HgCl_2$ was sublimated in vacuum. Acrylonitrile (AN) was distilled, dried over calcium hydride and recondensed in vacuum over dried $ZnCl_2$ (or $HgCl_2$). The complexes were prepared according to the procedures reported by Imoto [1] and put in ampoules; the presence of moisture was avoided.

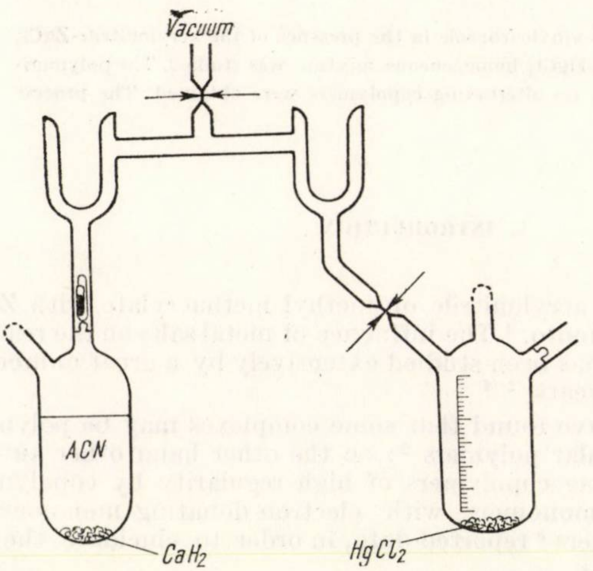

Fig. 1. — Installation for the catalyst solution.

For the determination of the salt concentration in AN, analytic methods were used.

An amount of $HgCl_2$-AN solution was evaporated in vacuum, AN condensing in a trape frozen in liquid nitrogen; the solid product consists in $HgCl_2$, fact demonstrated by performed analyses (melting point, cryoscopic molecular weight in dioxane).

Toluene (T), chlorobenzene (CB), dioxane (D), dimethylformamide (DMF). acetonitrile, styrene (S), *n*-butylvinylether (NBVE) and *t*-butylvinylether (TBVE) were purified by distillation and dried by conventional ways; methanol was used without special purification.

---

[6] O. F. SOLOMON, N. COBIANU, D. S. VASILESCU and C. BOGHINĂ, *J. Polymer Sci.*, B, 6, 551 (1968).

[7] M. A. HAMID, M. NOWAKOWSKA and P. H. PLESCH, *Makromol. Chem.*, 132, 1 (1970).

b. POLYMERIZATION PROCEDURE

The polymerizations were carried out in a vacuum-dilatometer with two charging arms and pressure-compensator, whose construction and operation way have been described.[8] Other tests were carried out in test tubes with two arms too, which were connected to a short vacuum assembly. The glass ampoules (or dilatometer's tube) were frozen in liquid nitrogen, degassed several times and sealed under vacuum. The tubes were put at the desired temperature in a thermostated bath; the polymerization may begin with the mixing. After an appropriate time of polymerization the tube (or dilatometer) was opened and the polymer was precipitated by pouring the solution into a large amount of cold methanol. After filtration, polymers were reprecipitated, dried and weighed.

c. ANALYSES OF POLYMERS

Molecular weights (MW) of these products were determined by viscosimetric ways[9] using an Ubbelohde viscometer; IR absorption spectra (recorded on a UR-10 spectrophotometer) and nitrogen contents (micro-Dumas method), confirm all methanol-reprecipitated products as poly-N-vinylcarbazole.[10]

3. RESULTS AND DISCUSSION

We carried out the polymerization of N-vinylcarbazole in toluene or other solvents using a complex AN-$ZnCl_2$ (molar ratio AN/$ZnCl_2$ = = 20, analytic determination).

Table 1

NVC polymerization by the complex AN-$ZnCl_2$

No	$\frac{Zn}{NVC}\,10^2$	NVC mole/l	Solvent	Temp. (°)	Time (min)	Yield (%)	[η] (dl/g)	M.W.
1	2	0.2	T	0	15	14.4	—	—
2	3	0.2	T	0	15	24.8	0.418	246 000
3	5	0.2	T	0	15	38.6	0.375	170 000
4	10	0.2	T	0	15	64.3	0.454	289 000
5	10	0.5	DMF	0	240	traces	—	—
6	5	1.0	CB	0	15	62.5	0.545	398 000
7	10	1.0	D	15	60	traces	—	—

As one can see from data given in Table 1, polymerization rates are fast and polymers are obtained in high yields with a remarkable molecular weight; the dependence of molecular weight on concentrations or conversion is negligibly small. It may be seen that the polymerization rate increases proportionally with the AN-$ZnCl_2$ complex concentration.

---

[8] D. S. Vasilescu and I. Negru, *Materiale Plastice* (*Romania*), **8**, 317 (1971).

[9] G. Sitaramaiah and D. Jakobs, *Polymer*, **11**, 165 (1970).

[10] O. F. Solomon, I. Z. Ciută and N. Cobianu, *J. Polymer Sci.*, B, **2**, 311 (1964).

When the complex acetonitrile-$ZnCl_2$ was used in equivalent concentrations no polymerization occurred; $ZnCl_2$, only, in equivalent concentrations too, produced nonfiltrable traces of polymer.

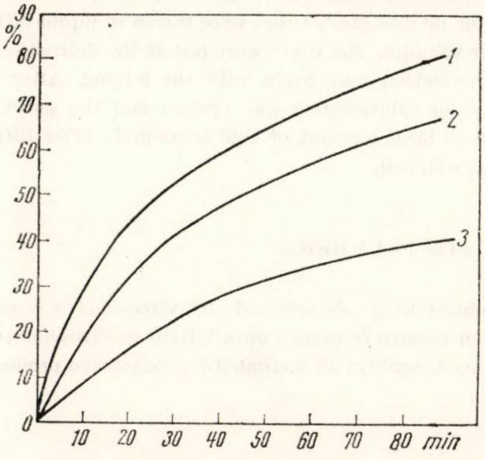

Fig. 2. — Conversion against time for the NVC polymerization by the complex AN-$ZnCl_2$; [NVC] = 0.2 mole/l; t = 0°; solvent, toluene;

1, $[ZnCl_2]/[NVC] = 5 \times 10^{-2}$; *2*, $[ZnCl_2]/[NVC] = 3 \times 10^{-2}$; *3*, $[ZnCl_2]/[NVC] = 2 \times 10^{-2}$.

The data from Table 1, and the tests with acetonitrile-$ZnCl_2$ or only with $ZnCl_2$, show that the effective catalyst is the complex AN-$ZnCl_2$.

The same behaviour can be seen in the presence of other electron-donating monomers.

Table 2

Polymerization of NVC in the presence of various comonomers (All polymerizations were made with the complex $AN/ZnCl_2 = 20$, in toluene at 0°; $ZnCl_2/NVC = 5 \times 10^{-2}$)

No	NVC mole/l	Comonomer mole/l		Time (min)	Yield (%)	[η] (dl/g)	M.W.
8	0.2	S	0.8	60	27.0	0.336	186 000
9	0.2	S	0.8	120	40.7	0.362	239 000
10	0.5	S	0.5	120	71.5	0.532	380 000
11	0.2	NBVE	0.8	60	traces	—	—
12	0.5	TBVE	0.5	120	28.5	—	—

All products are poly-N-vinylcarbazole. When a mixture of $HgCl_2$-AN is evaporated in vacuum, the obtained solid product is $HgCl_2$. This shows that either no complex was formed between $HgCl_2$ and AN, or that the complex formation has an equilibrium character. The adding of a concentrated $HgCl_2$ solution in AN over a toluene solution of NVC leads to the very fast polymerization of NVC.

We therefore used a small ratio of $HgCl_2$/AN (1/500) and an experimental technique in which the contact with moisture was avoided. Since the great disponibility of NVC towards cationic polymerization is known, we carried out tests (Table 3) to verify if the effective agent of initiation is AN, $HgCl_2$ or their mixture.

The product isolated in experiment 16 does not contain styrene units and consists only in poly-N-vinylcarbazole ; in the presence of AN, without $HgCl_2$, at 0°, no polymer formation could be observed (17-th exp.).

Table 3

Polymerization of NVC in various solvents, in argon medium ; monomer concentration : 0.5 mole/l; temperature : 0°

No	Solvent	$HgCl_2$/NVC	Time (min)	Yield (%)	Obs.
13	DMF	10^{-2}	60	0	—
14	CB	10^{-2}	15	57	—
15	T	5×10^{-3}	15	17	a
16	T	5×10^{-3}	15	32	b
17	T	0	15	0	c

a) The test was carried out in the absence of AN ; $HgCl_2$ was put on the wall of tube from acetone solution.

b) The mixture are containing styrene, (S)=0.5 mole/l, which does not polymerize.

c) The test was made in the absence of AN-$HgCl_2$ mixture, by adding only the corresponding quantity of AN (AN/NVC = 2.5).

These data permit us to affirm that $HgCl_2$ is implied in polymerization and the formed cation, which is not strong, may initiate the polymerization of NVC, but not that of styrene ; this fact is demonstrated also by the inhibition of the process in DMF, in spite of the fact that polymerizations of NVC in DMF under the influence of slight Lewis acids [6] are known.

Table 4

NVC polymerization in toluene at 0° ; monomer concentration = 0.5 mole/l; time 15 min ; $HgCl_2$/AN=1/500

No	$HgCl_2$/NVC	Conversion (%)	M.W.
18	$1\cdot10^{-3}$	2.0	—
19	$3\cdot10^{-3}$	18.2	101 200
20	$5\cdot10^{-3}$	62.0	41 300
21	$7\cdot10^{-3}$	71.5	18 600

Probably, the role of AN is only that of $HgCl_2$ solubilizer with the result of a homogeneous system ; this fact is also proved by the tests presented in Table 4.

The effect of AN results form the comparison between test 15 and 20 ; when the system is homogeneous the conversion increases. Molecular weights decrease and the yield increases with the $HgCl_2$ content as shown in Table 4.

In figure 3 are given typical conversion-time curves (dilatometric method) for the NVC polymerization by the $HgCl_2$-AN mixture. The rate constant of reaction is similar to that reported by Plesch.[7] This fact is another argument to say $HgCl_2$ is the effective catalyst of the process. $CdCl_2$ is not soluble in AN.

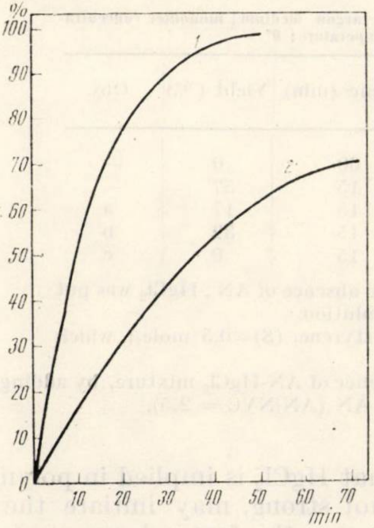

Fig. 3. — Conversion-time curves for NVC polymerization at 0°; [NVC]=0.5 mole/l; solvent, toluene; $[HgCl_2]/[AN]=1/500$;

1, $[HgCl_2]=2.5 mole/l \times 10^{-3}$; *2*, $[HgCl_2]=1.0 mole/l \times 10^{-3}$.

CONCLUSION

When $ZnCl_2$—AN complex was used, no alternate copolymerization occurred, probably due to a reaction rate of the pseudo-cationic polymerization of NVC greater than that of the copolymerization. This seems to be facilitated by the large cationic reactivity of NVC to the electron-donor nitrogen and the high stability of the cation, due to the conjugated carbazole ring.

Mercuric chloride does not form a stable complex with AN, but its solutions in AN may initiate the NVC polymerization, by a mechanism of cationic nature.

Revue Roumaine de Chimie, **18**, *5*, 913–917 (1973)

KINETIC DETERMINATION OF VANADIUM BY THE REACTION BETWEEN PYROGALLOL BROMINE RED AND POTASSIUM BROMATE

D. COSTACHE and S. SASU

University of Bucharest, Faculty of Chemistry
Chair of Analytical Chemistry and
State Committee of Planning
Bucharest, Romania

Received August 21, 1972

The reaction between pyrogallol bromine red and potassium bromate in acid medium, catalysed by vanadium ions, and the influence of the amounts of reagents, pH, wavelength and temperature on the reaction rate are investigated. A quantitative method for the determination of vanadium is given. The influence of other ions is studied and the main examined parameters are calculated.

The rate of a chemical reaction depends on the concentration of reagents, temperature, reaction medium (ionic strength, dielectric constant) and the presence of some substances called catalysts, as it results from the following reaction :

$$V = f\,(\text{conc., } t, \text{ medium, catalysts}) \qquad (1)$$

According to the classical definition of catalysts, these are substances, the presence of which, accelerates the reaction, and are again found complete at the end of the reaction. This definition can be accepted today only accompanied by the statement that their presence is active, and alters elementary processes.

The catalysts open new ways, energetically more advantageous, by means of some new transition stages, energetically poorer.

The action of the catalysts is selective in many cases, i. e. they increase the reaction rate of certain chemical processes. It is on these characteristics of the catalytic action that the determination of some ion traces is based. [1-9]

---

[1] K. B. Iatsimirski and V. E. Kalinina, *Zhur. analit. Khim.*, **24**, 390 (1969).

[2] A. I. Lazarev and V. I. Lazareva, *Zhur. analit. Khim.*, **24**, 395 (1969).

[3] J. Bognar and O. Jellinek, *Mikrochim. Acta*, **318** (1969).

[4] D. Costache, *Rev. Roumaine Chim.*, **16**, 849 (1971).

[5] D. Costache and S. Sasu, *Rev. Roumaine Chim.*, **16**, 1211 (1971).

[6] D. Costache, *Chimie analitică*, **4**, 198 (1971).

[7] D. Costache, *Anal. Univ. București*, **XX**, 2 (1972).

[8] S. Sasu and D. Costache, *Rev. Roum. Chim. (București)*, **23**, 4, 223 (1972).

[9] D. Costache and S. Sasu, *Works of the IIIrd National Conference on Analytical Chemistry*, Brașov, 1971, vol. 4, p. 455.

The present work investigate the reaction between pyrogallol bromine red and potassium bromate in acetic acid medium. The rate constants are calculated, the variation of these constants with the temperature is investigated, and the activation energies and pre-exponential factors are calculated.

On the basis of these studies an analytical method for the determination of vanadium traces in the range 6.16×10^{-10} gV/cm^3 – 6.16×10^{-9} gV/cm^3 is given.

EXPERIMENTAL

REAGENTS

Pyrogallol bromine red, concentration 5.20×10^{-4} g/cm^3 in ethyl alcohol.
Potassium bromide solution : 1.85×10^{-2} g/cm^3.
Reaction medium : acetic acid solution.
Vanadate solution : concentration 1.54×10^{-7} gV/cm^3
Bi-distilled water was used for all solutions.

PROCEDURE

The reaction mixture was prepared in 25 cm^3 flasks, in the following order : pyrogallol bromine red, acetic acid, potassium bromate and various amounts of ammonium vanadate. It is brought to the mark with twice distilled water. The timer is started and the flask content is stirred for 1 minute, then being passed into the spectrophotometer vat. Since after reaction the initially coloured solution decolorates, water is poured into the blind vat.

The concentrations of solutions in the vat are as follows

Pyrogallol bromine red	2.08×10^{-5} g/cm^3
Potassium bromate	7.40×10^{-4} g/cm^3
Vanadium ions	$6.16 \times 10^{-10} - 6.16 \times 10^{-9}$ gV/cm^3.

APPARATUS

The work was carried out with the horizontal Pulfrich Zeiss, Jena spectrophotometer and V.S.U.-1, and the wavelengths at which the method was set up, was $\lambda = 533$ nm.

DISCUSSIONS

The kinetic study of the reaction between pyrogallol bromine red and potassium bromate led to the conclusion that the reaction rate does not change with the time, which shows that we are dealing with an order zero reaction.

The expression of the rate in this case is :

$$-\frac{\mathrm{d}(a-x)}{\mathrm{d}t}=k \tag{2}$$

If we take into account the fact that the reaction takes place even in the absence of vanadium ions, but at a low rate, the expression of the rate should be written as follows :

$$-\frac{{}^{\mathrm{d}C}\text{pyrogallol bromine red}}{\mathrm{d}t}=k'C\text{ pyrogallol bromine red}=kCk^{C}\text{ pyrogallol bromine red}+k_c\cdot C_v\cdot C\text{ pyrogallol bromine red} \tag{3}$$

where :

k' = global rate constant
k = rate constant for the non-catalysed reaction
k_c = catalyst contribution to the increase of the rate reaction
C = pyrogallol bromine red = the reagent concentration
C_v = vanadium concentration.

Table 1 gives the values of the global rate constants for various catalyst concentrations.

Table 1

Values of the rate constants k for various concentrations of the catalyst

Conc. of V ($\mathrm{g/cm^3} \times 10^{-9}$)	$k \times 10^{-2}$ ($\mathrm{mol \cdot min^{-1}}$)
—	0.36
0.61	0.85
1.23	1.16
1.85	1.80
2.46	2.25
3.08	2.70
3.69	3.10
4.31	3.60
4.93	4.00
5.54	4.50
6.16	5.20

As it results from relation (1) the reaction rate is function of the reagent concentration, visible chiefly for the variation of the oxidant concentration ($KBrO_3$). Figure 1 shows the influence of the concentration of potassium bromate on the reaction rate.

By ΔD we have denoted the differences between the optical densities read after 10 and 12 minutes of the samples to which other amounts of bromates are added, the concentrations of other components being constant.

The figure shows that the reaction rate increases with the potassium bromate concentration and presents a relative stability in the concentration range $3.70 \times 10^{-4} - 14.80 \times 10^{-4}$ g $KBrO_3/cm^3$.

The reaction medium greatly influences the reaction rate.

If hydrochloric acid is used in the reaction, the reaction rate differs for each concentration of the acid, no matter how slightly this changes.

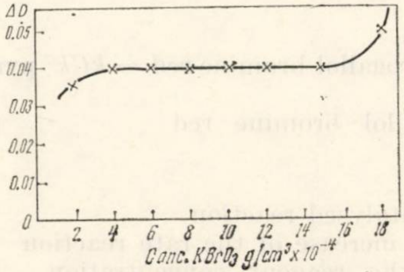

Fig. 1. — Influence of $KBrO_3$ concentration on the reaction rate.

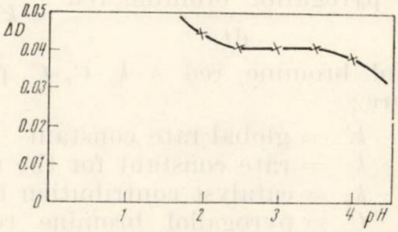

Fig. 2. — Influence of pH on the reaction rate.

If acetic acid is used there exists a range where the reaction rate remains constant. This range lies within pH 2.5—3.5, as may be observed from figure 2.

From relation (1) it also results that the reaction rate is influenced by the temperature. This influence is shown in table 2. The values of the rate constants are those corresponding to the catalytic reaction with vanadium concentration in the sample of 1.23×10^{-9} gV/cm³.

Table 2

Values of the rate constant k K, *vs* temperature (catalyst conc. 1.23×10^{-9} g/cm³)

$T°$	288	293	298	303	308
$k \times 10^{-2}$ ($mol \cdot min^{-1}$)	0.90	1.16	1.70	2.50	3.90
$\log k$	−2.055	−1.935	−1.770	−1.602	−1.409
$1/T \times 10^{-3}$	3.47	3.41	3.38	3.30	3.24

Figure 3 shows the values of the optical density *vs* the vanadium concentration. It should be noted that the readings after 10 and 12 minutes are listed. For the calibration graph we took into account the values read at minute 12.

Further on, the influence of alien ions was investigated. We have concluded that the determination of vanadium by the kinetic method, by means of the reaction between pyrogallol bromine red and potassium bromate in acetic acid medium, is disturbed by the Fe^{2+} and Fe^{3+} ions if the

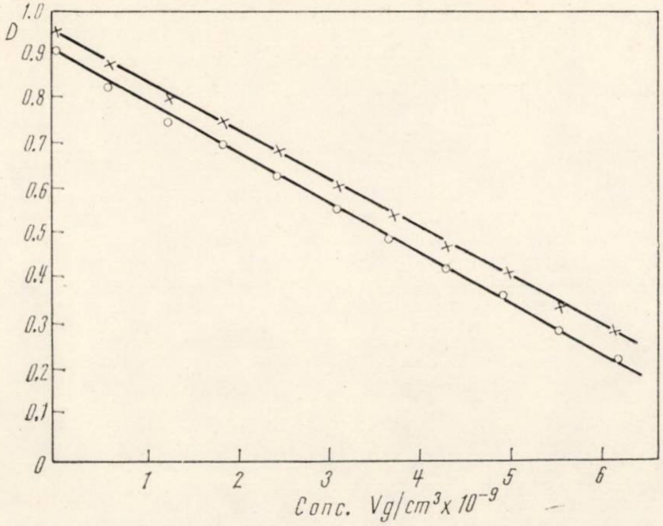

Fig. 3. — Variation in time of the D value.

ratios Fe^{2+}/V^{5+} and Fe^{3+}/V^{5+} exceed the value 100 : 1 and if the ratio Ti^{4+}/V^{5+} exceeds 1000 :1.

Table 3 shows a statistical processing of the results. The dispersions of selection around the points, the dispersions of selection around the calibration line and the range of dispersion are calculated.

Table 3

Main parameters of the statistical processing

Conc. of V g/cm³ × 10⁻⁹	$\bar{D}_{exp}$	$\bar{D}_{calcd}$	s^2 point 10^{-4}	A_0	A_1	$s^2 \times 10^{-4}$	$2ts$
0.61	0.811	0.819	5.434				
1.23	0.735	0.751	5.513				
1.85	0.692	0.683	8.300				
2.46	0.610	0.616	6.150				
3.08	0.539	0.547	5.147				
3.69	0.458	0.480	11.297				
4.31	0.401	0.412	9.989				
4.93	0.345	0.344	7.842				
5.54	0.274	0.277	5.626				
6.16	0.209	0.209	9.065				
				0.886	−0.110	10.96	0.284

To conclude we may say that with the aid of this method, vanadium can be determined in the range of concentrations between 6.16×10^{-10} gV/cm³ and 6.16×10^{-9} gV/cm³.

Revue Roumaine de Chimie, 18, 5, 913–917 (1973)

ORSZÁGOS MŰSZAKI KÖNYVTÁR ÉS DOKUMENTÁCIÓS KÖZPONT 1883

NOTE POUR LES AUTEURS

La *Revue Roumaine de Chimie* publie des articles en anglais, français, russe, allemand ou espagnol. Les auteurs sont priés d'envoyer des articles, notes, communications et comptes rendus inédits.

Les manuscrits seront dactylographiés à deux intervalles. Les tableaux seront dactylographiés sur feuilles séparées, de même que la légende des figures. Les diagrammes seront tracés à l'encre de Chine sur papier calque. Les tableaux et les figures seront numérotés par des chiffres arabes, en nombre strictement nécessaire. Prière de ne pas inscrire les mêmes données dans les tableaux et les figures. Les formules chimiques seront incluses dans le texte ; en outre, elles seront transcrites sur des feuilles séparées. Les auteurs sont priés d'indiquer les caractères italiques (en soulignant les lettres au crayon), ainsi que tout autre caractère spécial. L'ordre des références bibliographiques sera celui de leur mention dans le texte ; le nom de l'auteur sera précédé de l'initiale du prénom ; les publications périodiques seront présentées suivant les prescriptions internationales. Les références seront ajoutées à la fin de l'article ; elles paraîtront comme des notes, au bas de la page. Le texte sera précédé d'un résumé, comprenant 15 lignes au maximum.

L'entière responsabilité du contenu des articles appartient aux auteurs. On publie des articles dus aux collaborateurs roumains ou étrangers. Les auteurs recevront 50 tirés à part.

PRINTED IN ROMANIA

1973 JUL 2

TRAVAUX PARUS AUX ÉDITIONS DE L'ACADÉMIE DE LA RÉPUBLIQUE SOCIALISTE DE ROUMANIE

P. BALTĂ et E. BALTĂ, **Introducere în chimia fizică a stării vitroase** (Introduction à la chimie physique de l'état vitreux), 1971, 240 p., 15,50 lei.

LYDIA-MARIA VAICUM, **Biodegrabilitatea detergenţilor** (La biodégrabilité des détergents), 1971, 254 p., 16 lei.

TIBERIU NĂŞCUŢIU, **Metode radiometrice de analiză** (Méthodes radiométriques d'analyse), 1971, 346 p., 19,50 lei.

I. ZUGRĂVESCU et. L. STOICESCU-CRIVETZ, **Polimeri heterociclici** (Polymères hétérocycliques), 1971, 190 p., 9,50 lei.

I. MAXIM, **Materiale nucleare** (Matériaux nucléaires), 1969, 444 p., 30 lei.

CORNEL BODEA et collab., **Tratat de biochimie vegetală**, partea I, **Fitochimie** (Traité de biochimie végétale, Ire partie, Phytochimie), Ier vol., 1964, 747 p. + 4 annexes + 2 pl., 41 lei ; IIe vol., 1965, 1962 p., 1 pl., 56 lei ; IIIe vol., 1967, 773 p., 35 lei.

CRISTOFOR SIMIONESCU, C. V. UGLEA, **Fracţionarea compuşilor macromoleculari** (Fractionnement des composés macromoléculaires), 1969, 292 p., 18,50 lei.

CRISTOFOR SIMIONESCU et CLEOPATRA VASILIU-OPREA, **Mecanochimia compuşilor macromoleculari** (La mécanochimie des composés macromoléculaires), 1967, 344 p., 23,50 lei.

V. GHEŢIE et V. MICUŞAN, **Analiza imunochimică. Teorie şi practică** (Analyse immunochimique. Théorie et pratique), 1966, 369 p., 28 lei.

R. PORTOCALĂ et L. POPA, **Acizii ribonucleici celulari şi virali** (Les acides ribonucléiques cellulaires et viraux), 1966, 375 p., 8 pl., 26 lei.

I.P.I. – c. 2782

43 426

Lei 25.–

F 1103

R

PETSPALVA

REVUE ROUMAINE DE CHIMIE

TOME 18
N° 6
Juin 1973

RRCHAX, **18**, *6*, 919–1102 (1973)

ÉDITIONS DE L'ACADÉMIE DE LA RÉPUBLIQUE SOCIALISTE DE ROUMANIE

Rev. Roumaine Chim. **18**, *6*, p. 919–1102 (1973), Bucarest

COMITÉ DE RÉDACTION

Rédacteur en chef :

I. G. MURGULESCU, membre de l'Académie de la République Socialiste de Roumanie

Rédacteurs en chef adjoints :

A.T. BALABAN et V. EM. SAHINI, membres correspondants de l'Académie de la République Socialiste de Roumanie

Collège de rédaction :

C. DRĂGULESCU, RALUCA RIPAN, CR. SIMIONESCU, membres de l'Académie de la République Socialiste de Roumanie ; EM. BRATU, ECATERINA CIORĂNESCU-NENITZESCU, P. SPACU, membres correspondants de l'Académie de la République Socialiste de Roumanie ; MARGARETA AVRAM, D. I. MARCHIDAN, G. NIAC et D. SĂNDULESCU

La Revue Roumaine de Chimie paraît 12 fois par an. Toute commande de l'étranger (fascicules ou abonnements) sera adressée à Întreprinderea Rompresfilatelia, Boîte Postale 2001, telex 011631, Bucarest, Roumanie.

Les manuscrits, les livres et les revues proposés en échange, ainsi que toute correspondance seront envoyés à la rédaction

REVUE ROUMAINE DE CHIMIE

23, str. Dumbrava Roşie, Bucarest, Roumanie

ÉDITIONS DE L'ACADÉMIE DE LA RÉPUBLIQUE SOCIALISTE DE ROUMANIE
3 bis, str. Gutenberg, Bucarest

REVUE ROUMAINE
DE
CHIMIE

Tome 18, Nº 6 Juin 1973

Page

MARIANA DOBRESCU-CIUREANU and V. E. SAHINI, A perturbation treatment of molecular complexes. III. Iodine complexes with five-membered heteroaromatics 921–930

P. G. PERKINS, The electronic structure of some ladder polymers. I. Band structure of polyacenes and nitrogen substituted polyacenes 931–943

S. STERNBERG and IUDITA ADORIAN, Thermodynamic excess properties of molten LiCl + KCl, LiCl + RbCl, NaCl + RbCl and NaCl + CsCl mixtures 945–952

I. V. NICOLESCU und AL. FRUMA, Die Chemisorption von Wasserstoff, Benzol und Cyclohexan auf mit Lithium und Titan dotiertem Aluminiumoxyd. I. Adsorptionsisothermen . . . . 953–969 R

P. SPACU and SILVIA PLOŞTINARU, Spectral study of some mixed ligand compounds of lanthanides 971–977

F. GAYMARD, R. GUEDJ et A. VERMEGLIO, Sur la chloration et l'oxychloration spécifiques des cycloheptène et cyclopentène . . . . 979–993 R

N. NEGOIȚĂ, R. BAICAN, F. DOMŞA and A. T. BALABAN, Use of ESR spectrum simulator for determining precisely hyperfine coupling constants of stable nitrogen free radicals 995–1004

M. RĂILEANU and ILEANA RADULIAN, Reaction of amines with phenothiazinium cation. I. Synthesis and properties of 3H-phenothiazine-3-[potassium 4-anilsulphonate], 3H-phenothiazine-3-[potassium 3-anilsulphonate] and 3H-phenothiazine-3-[potassium 2-anilsulphonate]. . . . . 1005–1011 R

M. CÎRJE, Über 1,2,3,4-Tetrahydroakridin-9-Carboxyl-Säure-Derivate. I. Amide 1013–1018 R

F. URSEANU, C. DRĂGHICI, RODICA VINTILĂ and ELVIRA ŞLIAM, New syntheses of naphth[2,3-c]acridan-5,8,14-trionic dyes 1019–1032

M. ARSHAD, A. BEG and M. A. HASHMI, Correlation of the physical properties of organosulphur compounds. II. Effective electronegativity of the molecules and their physical properties 1033–1040

I. IONESCU, Quelques remarques sur les propriétés des bétons aux résines synthétiques et aux liants minéraux 1041–1065

FL. POPESCU, SIMONA PERCEC, IG. POINESCU et I. PETRARIU, La phosphorylation des copolymères ternaires macroporeux . . . . 1067–1074 R

Rev. Roumaine Chim. **18**, *6*, 919–1102 (1973), Bucarest

Page

J. PRASHAD, Studies of the Joshi effect in halogens and oxygen. Influence of intersleeve exposure to brushes from a d.c. and various a.c. high tension sources 1075–1086

L. CAMPANELLA and P. L. CIGNINI, X-ray powder spectra of pyridinemonocarboxylic acids and their use for the qualitative analysis of a mixture of these acids. 1087–1091

IOVANCA HAIDUC, DOINA DĂNILĂ and C. LITEANU, Influence of indicating electrode pretreatment on potentiometric titration parameters. V. Gold pretreated electrode in potentiometric titration of $Cr_2O_7^{2-}$ with Fe^{2+} . 1093–1100

COMPTE RENDU 1101–1102

Revue Roumaine de Chimie, **18**, *6*, 921–930 (1973)

A PERTURBATION TREATMENT OF MOLECULAR COMPLEXES. III.[1]

IODINE COMPLEXES WITH FIVE-MEMBERED HETEROAROMATICS

MARIANA DOBRESCU-CIUREANU and V. E. SAHINI
Physical Chemistry Laboratory, University of Bucharest,
Bd. Republicii 13, Romania

Received December 28, 1972

A perturbation treatment described in a previous paper [1a] is applied to give a quantum mechanical description of the electronic structure of molecular complexes formed by iodine with several five-membered heteroaromatic molecules. The stable geometrical configuration of the complexes in the ground state is predicted by means of the stabilization energies calculated for various relative orientations between the donor and the acceptor. The charge distributions changes occurring by complex formation and the dipole moments of the complexes are calculated and discussed. The CT spectra are calculated and compared with the experimental data.

INTRODUCTION

The electronic structure of molecular complexes has already been the subject of numerous theoretical treatments aiming at constructing a satisfactory model which would describe their ground and excited state properties.[1–11] There are, however, some problems still open, which claim for further study :

---

[1] Part I, M. Dobrescu, *Rev. Roumaine Chim.*, a) **16**, 1825 (1971) ; b) **16**, 1841 (1972).

[2] R. S. Mulliken, *J. Amer. Chem. Soc.*, **72**, 600 (1950) ; *J. Phys. Chem.* 801 (1952) ; *J. Amer. Chem. Soc.*, **74**, 811 (1952).

[3] G. Briegleb "Electronen Donator-Acceptor Komplexe", Springer Verlag, Berlin, 1961.

[4] H. Yada, J. Tanaka and S. Nagakura, *Bull. Chem. Soc. Japan*, **33**, 1660 (1960).

[5] R. S. Mulliken and W. Person, "Molecular Complexes", Wiley Interscience, New York, N.Y., 1969.

[6] J. N. Murrell, *Quart Rev.*, **15**, 191 (1961) ; *J. Amer. Chem. Soc.*, **81**, 5037 (1959).

[7] H. Kuroda, J. Ikemoto and H. Akamatu, *Bull. Chem. Soc. Japan*, **39**, 1842 (1966).

[8] a) S. Iwata, J. Tanaka, and S. Nagakura, *J. Amer. Chem. Soc.*, **88**, 894 (1966). b) ibid **89**, 2813 (1967).

[9] J. R. Le Fèvre, D. V. Randford and P. J. Stiles, *J. Chem. Soc. B*, **1968**, 1297.

[10] H. Kuroda, J. B. Kunii, S. Hiruna and H. Akamatu, *J. Mol. Spectrosccopy*, **22**, 60 (1967).

[11] M. Ciureanu, *Studii şi Cercetări Chim. Acad. Bucureşti*, **20**, 1217 (1972).

a) the relative contributions of polarization and charge transfer in determining the ground state properties: stabilization energy, dipole moment, infrared spectra, etc.;

b) The possibility to calculate the energy contour maps and thus to predict the equilibrium geometrical configuration of a complex;

c) the evaluation of the charge displacements occurring both in the donor and the acceptor by reciprocal polarization and electron transfer;

d) the assignment of CT transitions and their relationship with the molecular structure of the parent molecules.

Our purpose was to examine these points in the particular case of complexes formed by pyrrole, furan and thiophene with iodine, applying a perturbation treatment described in a previous paper.[1a]

These complexes were already experimentally studied by Lang.[12]

On the basis of his results it seems to be clear that these complexes are of the $\pi-\sigma$ type, that is, the donor action is spread over the π electronic system of the heteroaromatic molecule.

1. METHOD OF CALCULATION

The general features of the present treatment are those presented in paper I.[1a] The SCF MO's for the heterocyclic molecules, used as a starting point in our calculation, were those calculated by Solony, Birss and Greenshields.[13]

As all complexes were considered to be of a $\pi-\sigma$ type, we assumed in all cases a model which allowed the $5p\sigma$ orbitals of iodine molecule to overlap with the donor's $2p\pi$ orbitals.

In calculating the energy contour maps, a great number of geometrical configurations were taken into account under the following limitations:

a) The halogen molecule was kept at right angles to the plane of the heterocyclic ring.

b) The donor-acceptor distance was 3.5 Å in all cases.*

We considered that only the $5p\sigma_u$ and $5p\sigma_g$, from the valence orbitals of the iodine molecule, participated in forming the molecular complex. Thus, the charge transfer takes place from the occupied π orbitals of the heterocycle to the strongly antibonding $5p\sigma_u$ orbital of the iodine molecule.

Choice of parameters. In calculating the energy of the CT states we used the vertical ionization potentials of the heterocyclic molecules, experimentally determined from electron impact data.[14]

$$I_p^{\text{pyrrole}} = 8.20 \text{ eV} : I_p^{\text{furan}} = 8.89 \text{ eV} \quad I_p^{\text{thiophene}} = 8.99 \text{ eV}$$

* This is the value experimentally determined for benzene-I_2.

---

[12] J. P. Lang, *J. Amer. Chem. Soc.*, **84**, 4438 (1962).

[13] N. Solony, F. W. Birss and J. B. Greenshields, *Canad, J. Chem.*, **43**, 1569 (1965).

[14] a) R. W. Kiser "Introduction to Mass Spectrometry and its Applications",Prentice Hall, Inc., 1965; b) K. Watanabe and T. Naguyama, *J. Chem. Phys.*, **29**, 48 (1958); c) W. C. Price and A. D. Walsh, *Quart Rev.*, **2**, 73 (1948); *Proc. Roy. Soc. (London) Ser. A*, **179**, 201 (1941).

The upper ionization potentials were determined from these data by assuming that the difference between two ionization potentials is equal to the difference in the corresponding SCF orbital energies.

The electron affinity of the iodine molecule was taken to be 2 eV.[1b]

The semiempirical parameters used in our calculations were calculated as follows. The intermolecular resonance integrals $\beta_{\delta\rho}$ were calculated using Mullikans'formula

$$\beta_{\delta\rho} = \frac{1 + Scc}{1 + S_{\delta\rho}} \cdot \frac{S_{\delta\rho}}{Scc}\ \beta cc \tag{1}$$

$S_{\delta\rho}$ is the overlap integral between the atomic orbital φ_δ of the donor and the atomic orbital φ_ρ of the acceptor. In order to calculate these overlap integrals, the atomic orbitals of the basic system were decomposed into a σ and π part, as shown in fig. 1.

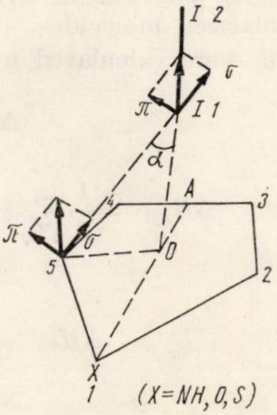

Fig. 1. — Iodine complexes with five-membered heteroaromatics.

Thus

$$S_{\delta\rho} = S^{\pi}_{\delta\rho} \sin^2 \alpha + S^{\sigma}_{\delta\rho} \cos^2 \alpha \tag{2}$$

The $S^{\pi}_{\delta\rho}$ and $S^{\sigma}_{\delta\rho}$ integrals were calculated according to Mulliken, Orloff and Orloff.[15] The $S^{\pi}_{\delta\rho}$ integrals have proved to be negligible, so that

$$S_{\delta\rho} \cong S^{\sigma}_{\delta\rho} \cos^2 \alpha \tag{3}$$

In order to simplify the calculation we made the assumption of formal neglect of differential overlap.

The bielectronic repulsion integrals $(\delta\delta/\rho\rho)$ were calculated using Klopmans' formula.[16]

---

[15] R. S. Mulliken, C. A. Rieke, D. Orloff and H. Orloff, *J. Chem. Phys.*, **17**, 1248 (1949).

[16] G. Klopman, *J. Amer. Chem. Soc.*, **86**, 4550 (1964).

2. RESULTS AND DISCUSSIONS

2.1. STABILIZATION ENERGY

The stabilization energy of a donor-acceptor complex can be partitioned in several parts

$$\Delta H = \Delta H_{\text{coul}} + \Delta H_{\text{pol}} + \Delta H_{\text{CT}} + \Delta H_{\text{CT pol}} + \dots$$

In this formula ΔH_{coul} and ΔH_{pol} are due to the Coulomb- and polarization-type electrostatic interactions between the donor and the acceptor; ΔH_{CT} is due to the intermolecular resonance, therefore to the interaction between the ground and CT states. The last term, which was called "the charge transfer polarization term" appears because the resonance occurs between polarized molecules.

These terms were calculated as follows

$$\Delta H_{\text{coul}} = 0 \tag{4}$$

$$\Delta H_{\text{pol}} = \frac{1}{2} \sum_{\delta < \varphi} \left[\pi_{\rho\rho} \, (\Delta\alpha_\rho)^2 + 2\pi_{\rho\varphi} \, \Delta\alpha_\rho \, \Delta\alpha_\varphi\right] \tag{5}$$

$$\Delta H_{\text{CT}} = \sum_{i_d}^{\text{occ}} \frac{\left(\sum\limits_{\delta,\rho} c^{\delta}_{i_d} \, c^{\rho}_{j'_a} \, \beta_{\delta\rho}\right)^2}{E_{N_0} - E_{E, id \to j'_a}} \tag{6}$$

$$\Delta H_{\text{CT pol}} = \sum_{i_d}^{\text{occ}} \frac{\left\{\sum\limits_{\delta,\rho} 2\sqrt{2}\left[\sqrt{2}\,\eta^{E_n}_{l_d \to i_d} \, c^{\delta}_{l_d} \, c^{\rho}_{j'_a} + \xi^{N_0}_{j_a \to j'_a} \, c^{\delta}_{i_d} \, c^{\rho}_{j_a}\right] \beta_{\delta\rho}\right\} \sum\limits_{\delta,\rho} c^{\delta}_{i_d} \, c^{\rho}_{j'_a} \, \beta_{\delta\rho}}{E_{N_0} - E_{E, id \to j'_a}} \tag{7}$$

An important problem to be solved is to determine the stable geometrical configuration of the complex in the ground state; to do that, stabilization energies were calculated for a great number of geometrical configurations; the energy contour map was obtained by plotting the stabilization energies against the position of the I—I bond projection in the plane of the heterocycle (O). All complexes show an energy minimum located in the symmetry plane of the ring. As an example, the energy contour map of pyrrole—I_2 is presented in fig. 2. The stable geometrical structures predicted by the present theoretical considerations are presented in table 1.

Another point to solve is to establish the relative importance of Coulomb, CT, polarization and CT polarization terms in determining the stability of the complexes.

The results calculated by (4)–(7) for the equilibrium configuration of the three complexes are presented in table 2 together with those previously obtained for some molecular complexes of aromatic hydrocarbons.[1b]

Table 1

Predicted equilibrium geometrical configuration for iodine complexes with five-membered heteroaromatics

Donor	OX (Å)	OA (Å)
pyrrole	1.7	0.42
furan	1.8	0.33
thiophene	1.4	0.62

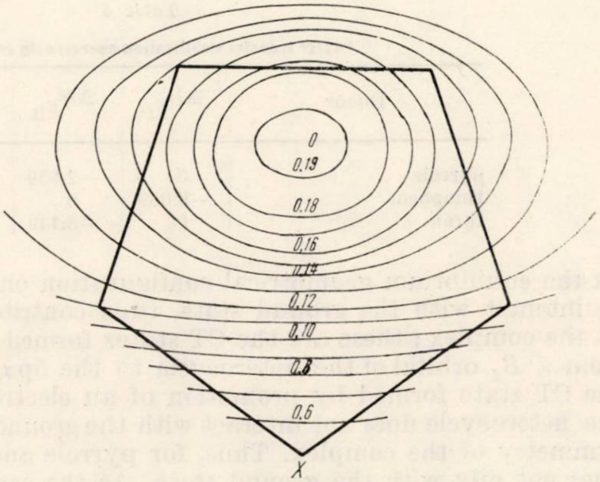

Fig. 2. – The energy contour map of pyrrole-I_2 complex (the energies are expressed in eV).

Table 2

Stabilization energies of iodine complexes with aromatic and heteroaromatic donors (in *k*cal/mol)

Donor	ΔH_{coul}	ΔH_{pol}	ΔH_{CT}	$\Delta H_{CT\ pol}$	ΔH_{tot}
pyrrole	0	−0.0004	−4.377	+0.050	−4.327
thiophene	0	−0.0001	−3.972	+0.001	−3.971
furan	0	−0.0003	−3.804	+0.036	−3.768
benzene	0	0	−4.78	0	−4.78
naphthalene	0	0	−4.39	−0.48	−4.87
phenanthrene	0	0	−4.75	−0.15	−4.90

As shown in table 2 the Coulomb term is zero in all cases, whereas the polarization term is zero only for hydrocarbon complexes; in the case of the complexes formed by iodine with five membered heteroaromatics this term is different from zero, but negligibly small, and thus it plays no role in determining the binding energy. The main contribution to the complex stabilization is given in all cases by the CT term *. $\Delta H_{\mathrm{CT\ pol}}$ takes small (but not negligible), positive or negative values (see for example the naphthalene-I_2 complex); thus, this term has to be taken into account in a complete evaluation of the stabilization energy. According to the data presented here, we are able to predict the following order of the terms contributing to the binding energy of a molecular complex :

$$\Delta H_{\mathrm{CT}} \gg \Delta H_{\mathrm{CT\ pol}} \gg \Delta H_{\mathrm{pol}}$$

The contribution of the three CT states to the binding energy of the complex is shown in table 3.

Table 3

Charge transfer stabilization energies (in kcal/mol)

Donor	$\Delta H_{E_{\mathrm{I}}}$	$\Delta H_{E_{\mathrm{II}}}$	$\Delta H_{E_{\mathrm{III}}}$	ΔH_{CT}
pyrrole	0	−2.659	−1.718	−4.377
thiophene	−0.039	0	−3.933	−3.972
furan	0	−3.149	−0.655	−3.804

In the equilibrium geometrical configuration only two CT states are able to interact with the ground state, thus contributing to the stabilization of the complex; these are the CT states formed by promoting an electron from a B_2 orbital of the heterocycle to the $5p\sigma_u$ orbital of the complex; the CT state formed by promotion of an electron from the A_2 orbital of the heterocycle does not interact with the ground state owing to the overall symmetry of the complex. Thus, for pyrrole and furan the first CT state does not mix with the ground state. As the same thing happened in the case of halogen-aromatic hydrocarbon complexes (except for phenanthrene-I_2), we can infer that there is generally no direct correlation between the stabilization energy and the ionization potential of the donor.

As shown in table 3, the contributions of the two CT states are generally of a comparable order of magnitude. Thus, it should be noted that all CT states should be taken into account in calculating the stabilization energy of a complex, not only the lower ones.

2.2. THE CHARGE DISPLACEMENTS AND DIPOLE MOMENTS

The charge densities of the donor atoms, in the ground state of the complex, can be expressed as :

$$q_{\delta}^{\mathfrak{N}_0} = \frac{1}{1 + a_{E_1}^2 + a_{E_2}^2}\left[p_{\delta\delta}^{N_0} + a_{E_1}^2 p_{\delta\delta}^{E_1} + a_{E_2}^2 p_{\delta\delta}^{E_2} + 2a_{E_1} a_{E_2} c_{i_d}^{\delta} c_{l_d}^{\delta}\right] \qquad (8)$$

---

* This is why, in calculating the energy contour maps we took into consideration only the CT stabilization energy.

where the two CT states interacting with the ground state were noted by E_1 and E_2; these states occurred by the promotion of an electron from the occupied MO's of the donor (φ_{i_d} and φ_{i_d} respectively) to the empty one of the acceptor ($\varphi_{j_a'}$). The $p_{\delta\delta}^{E_1}$ and $p_{\delta\delta}^{E_2}$ were calculated according to eqs. (43)—(44) of part I.[1a]

The charge densities of the acceptor atoms are calculated following the formula

$$q_\rho^{\mathcal{N}_0} = \frac{1}{1 + a_{E_1}^2 + a_{E_2}^2} \left[p_{\rho\rho}^{N_0} + a_{E_1}^2 \, p_{\rho\rho}^{E_1} + a_{E_2}^2 \, p_{\rho\rho}^{E_2}\right] \tag{9}$$

In calculating $q_\delta^{N_0}$ and $q_\rho^{N_0}$ we found out that a_{E_1} and a_{E_2} can be satisfactorily approximated as

$$a_{E_1} = \frac{H_{N_0 E_1}}{W_{N_0} - W_{E_1}} \cong \frac{\sqrt{2} \sum\limits_{\delta,\rho} c_{i_d}^{\delta} \, c_{j_a'}^{\rho} \, \beta_{\delta\rho}}{W_{N_0} - W_{E_1}} \equiv a_1 \tag{10}$$

$$a_{E_2} = \frac{H_{N_0 E_2}}{W_{N_0} - W_{E_2}} \cong \frac{\sqrt{2} \sum\limits_{\delta,\rho} c_{i_d}^{\delta} \, c_{j_a'}^{\rho} \, \beta_{\delta\rho}}{W_{N_0} - W_{E_2}} \equiv a_2 \tag{11}$$

Thus, $\Delta q_{\rho,\delta} = q_{\delta,\rho}^{\mathcal{N}_0} - q_{\delta,\rho}$ can be partitioned in the following form

$$\Delta q = \Delta q^{\mathrm{CT}} + \Delta q^{\mathrm{pol}} + \Delta q^{\mathrm{CT\,pol}} \tag{12}$$

The terms in (12) were calculated for the acceptor atoms using the formulae

$$\Delta q_\rho^{\mathrm{CT}} = \frac{(a_1^2 + a_2^2)\,(c_{j_a'}^{\rho})^2}{1 + a_1^2 + a_2^2} \tag{13}$$

$$\Delta q_\rho^{\mathrm{pol}} = \frac{2\sqrt{2}}{1 + a_1^2 + a_2^2} \, \xi_{j_a \to j_a'}^{N_0} \, c_{j_a}^{\rho} \, c_{j_a'}^{\rho} \tag{14}$$

$$\Delta q_\rho^{\mathrm{CT\,pol}} = \frac{2\,(a_1^2 + a_2^2)}{1 + a_1^2 + a_2^2} \, \xi_{j_a \to j_a'}^{E_1, E_2} \, c_{j_a}^{\rho} \, c_{j_a'}^{\rho} \tag{15}$$

The results obtained using these formulae are presented in table 4 together with the total amount of charge transfer.

$$\Delta Q = \sum_\rho \Delta q_\rho = - \sum_\delta \Delta q_\delta \tag{16}$$

As seen from table 4, the main contribution to Δq_{N_0} is given by Δq^{CT}. The Δq^{pol} and $\Delta q^{\mathrm{CTpol}}$ have small, positive or negative values, thus determining the polarization of the halogen molecule.

Table 4

Amount of charge transferred to the acceptor atoms in the ground state of the complex (in − e units)

Donor	ρ	$\Delta q_\rho^{\mathrm{CT}}$	$\Delta q_\rho^{\mathrm{pol}}$	$\Delta q_\rho^{\mathrm{CTpol}}$	Δq_ρ	ΔQ
pyrrole	1	+0.0202	−0.0016	+0.0033	+0.0219	0.0404
	2	+0.0202	+0.0016	−0.0033	+0.0185	
furan	1	+0.0145	−0.0008	+0.0024	+0.0161	0.0290
	2	+0.0145	+0.0008	−0.0024	+0.0129	
thiophene	1	+0.0124	−0.0013	+0.0023	+0.0134	0.0248
	2	+0.0124	+0.0013	−0.0023	+0.0114	

Similar formulae were derived to calculate the Δq_δ for the donor atoms. As in all cases $\Delta q_\delta^{\mathrm{pol}}$ are zero and $\Delta q_\delta^{\mathrm{CTpol}}$ are negligibly small, the only significant contribution to be considered was Δq^{CT}

$$\Delta q_\delta^{\mathrm{CT}} = -\frac{(a_1\, c_{i_d}^{\delta} - a_2\, c_{i_d}^{\delta})^2}{1 + a_1^2 + a_2^2} \tag{17}$$

The charge distribution changes after complexing are presented in fig. 3; they can be discussed in terms of the electronic structure of the donor molecules. In fact, one can observe a gradual diminution of the heteroatom capacity to donate electrons to aromatic conjugation in the pyrrole-furan-thiophene series. For iodine complexes formed by these donors one can note several changes occurring in the same order:

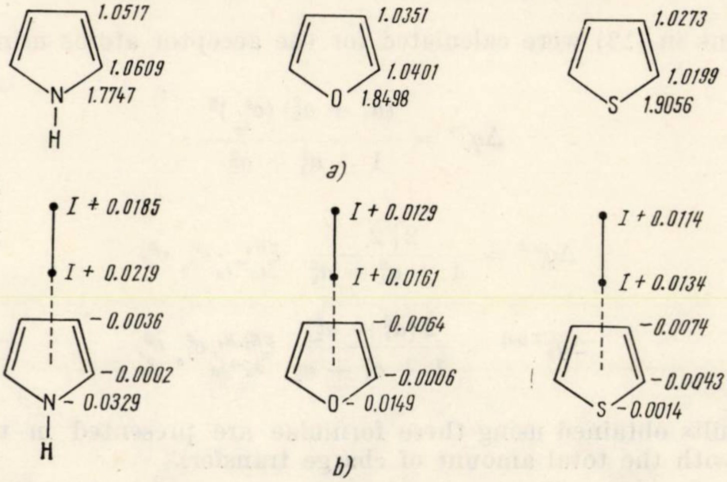
1.0517
1.0609
1.7747
N
H
1.0351
1.0401
1.8498
O
1.0273
1.0199
1.9056
S
a)
I + 0.0185
I + 0.0219
− 0.0036
−0.0002
N − 0.0329
H
I + 0.0129
I + 0.0161
−0.0064
−0.0006
O − 0.0149
I + 0.0114
I + 0.0134
−0.0074
−0.0043
S −0.0014
b)

Fig. 3. — Charge densities of uncomplexed donors (*a*) and charge displacements occurring by complex formation (*b*) (in − e units).

a) The gradual diminution of the heteroatom donor power and the enhancement of the donating capacity of the positions 2,5 and 3,4. As seen from fig. 3, in pyrrole-I_2 almost the whole positive charge due to complex formation is located on nitrogen, whereas in furan-I_2 this charge is distributed between oxygen and the C_3-C_4 positions. In thiophene-I_2 complex the charge transfer occurs predominantly from the C_2-C_5 and C_3-C_4 positions.

These charge displacements are in accordance with the predicted changes in the geometry of the complex.

b) The lowering of the total amount of charge transfer.

c) The gradual diminution of iodine molecule polarization.

The dipole moments of these complexes can be expressed as

$$\vec{\mu}^{\text{complex}} = \vec{\mu}^{\circ} + \vec{\mu}^{\text{CT}} + \vec{\mu}^{\text{pol}} + \vec{\mu}^{\text{CT pol}} \tag{18}$$

A comment should be made with respect to $\vec{\mu}^{\text{CT}}$. $\vec{\mu}^{\text{CT}}$ is obtained as a vectorial sum of two components

$$\vec{\mu}^{\text{CT}} = \vec{\mu}_{\parallel}^{\text{CT}} + \vec{\mu}_{\perp}^{\text{CT}}$$

where the subscripts indicate the orientation to the ring plane, $\vec{\mu}_{\parallel}^{\text{CT}}$ can be either parallel or antiparallel to the the permanent dipole moment $\vec{\mu}_0$. As seen from table 5, in the case of pyrrole-I_2 and thiophene-I_2 complexes, $\vec{\mu}_{\parallel}^{\text{CT}}$ is parallel, whereas for furan-I_2 $\vec{\mu}_{\parallel}^{\text{CT}}$ is antiparallel to $\vec{\mu}^{\circ}$. Thus, for the latter, $\vec{\mu}_{\parallel}^{\text{CT}}$ causes a lowering of the in-plane dipole moment μ° * The results are presented in table 5.

Table 5

Calculated dipole moments in the ground state* (in Debye)

Donor	$\mu^{\circ 19}$	$\mu_{\parallel}^{*\text{CT}}$	$\mu_{\perp}=\mu_{\perp}^{\text{CT}}+\mu^{\text{pol}}+\mu^{\text{CTpol}}$	μ^{complex}
pyrrole	1.8 ↓	0.254 ↓	0.915	2.27
furan	0.7 ↑	0.115 ↓	0.652	0.87
thiophene	0.56 ↑	0.017 ↑	0.564	0.80

* The arrows indicate the orientation of the in-plane dipole moments against the heteroatom.

2.3. CHARGE TRANSFER SPECTRA

The CT spectra calculated for the three complexes are presented in table 6 together with the experimental data.

---

* We suppose that in other cases this lowering might be large enough to determine a diminution of the overall moment of the complex compared with the moment of the parent molecule (For example the dipole moment of uncomplexed nitrobenzene is 4.22 D, whereas it is 3.73 D for the naphthalene complex). Such cases were considered so far to be a proof of the determining role of polarization forces.[17,18]

[17] M. J. Mantione *Theor. Chim. Acta,* **11,** 119 (1968).

[18] J. P. Malrieu and P. Claverie, *J. chim. phys,* **65,** 735 (1968).

[18] H. Kofod, L. E. Sutton and J. Jackson, *J. Chem. Soc.,* **1952,** 1476.

For pyrrole and furan complexes the theory predicts the existence of two CT bands, which are in agreement with the experimental ones. For thiophene-I_2 complex the theory predicts two superimposed bands, whereas the experiment reveals the existence of a single large CT band. We suppose that the observed band is due to a superposition of the first two CT transitions, a fact which is supported by the broadening of this band *.

Table 6

Experimental and calculated CT spectra

Donor	$\lambda_{\text{calc (nm)}}$	$\lambda^{12}_{\text{exp (nm)}}$
pyrrole	360.3	360
	318.7	285
furan	301.8	317
	233.2	240
thiophene	289.5	295 large
	289.0	

It should be noticed that, both for pyrrole and furan complexes, the first CT state, which is responsible for the apearance of the first CT band, does not interact with the ground state. Thus, ground state properties like : dipole moment, infrared spectra and stabilization energy should not be related to the CT transition energy. This idea is supported by our previous results on halogen-aromatic hydrocarbon complexes.[1b]

* This idea was also formulated by Lang.[12]

Revue Roumaine de Chimie, 18, 6, 931–943 (1973)

THE ELECTRONIC STRUCTURE OF SOME LADDER POLYMERS. I

BAND STRUCTURE OF POLYACENES AND NITROGEN SUBSTITUTED POLYACENES

PETER G. PERKINS

Department of Pure and Applied Chemistry,
University of Strathclyde, Glasgow C. 1., Scotland

Received January 15, 1973

The fused ring polyacene, polypyrazine, and polypyridine have been studied by the extended Hückel tight bonding solid state method. It is found that some band overlap occurs between valence σ and conduction π^* bands but the density of states in these regions are not high enough to confer metallic conductivity. Moreover the direct band gap at $k = \pi/a$ is, in effect, increased by the low density of states at the top of the π valence band.

There is presently considerable interest in the electrical properties of organic polymers related to the polyacenes (Figure 1*a*). Recent experimental studies on paracyanogen [1] ('polypyrazine') (Figure 1*b*), directed towards determining the valence-conduction band gap for this material and comparing its semi-conducting properties with those of the related polyacenes,[2] have shown that substitution of two nitrogen atoms for two carbons in each unit of the structure only marginally increases the band gap ΔE.

In order to throw light on these findings, to ascertain to what extent the polypyridine structure (Figure 1*c*) are related electronically, and to try and rationalise other aspects of the electronic behaviour of the series of compounds*, we have calculated the electronic band structures in the solid state of several series of these compounds. In the cases chosen, the approach which has been adopted is that of the extended Hückel procedure, couched in the solid-state formalism, and including all valence orbitals (both σ and π type) in the basis set. This treatment was carried through so as to ascertain the ordering of the bands, and their character, on both sides of the valence-conduction energy gap. As a consequence we are able to reveal the important features of the energy spectrum (*i, e.* the bands near the gap) and in future work will examine the states more closely and in a more sophisticated manner. This is important because until recently it has been assumed that planar molecules, on which the polymers are based, have energy level patterns in which π type orbitals alone are juxtaposed to the bonding-antibonding energy gap. However, theoretical work [3] on several such molecules (*e.g.* on ethylene) has shown this supposition to be untrue and there are a number of levels of σ symmetry in this energy region. That this was not known until recently is not surprising since their existence is not readily shown up by experiment : in general, optical excitations from, or to, σ levels are either forbidden or only weakly polarised out of the molecular plane. Hence one of the problems we tackle here is to establish how the σ and π levels are situated with respect to the wave vector k in the $E(k)$ *vs* k diagram.

---

[1] T. Graham and D. I. Packham, *Polymer*, **10**, 645 (1969).

[2] Y. Okamoto and W. Brenner, 'Organic Semiconductors', Reinhold, New York, 1964, p. 42–45; I. A. Misurkin and A. A. Ovchinnikov, *Theoret. Chim. Acta*, **13**, 115 (1969).

* For example, only polyacenes with up to seven rings in the molecule are known[2] and hence there must be some uncertainty with respect to the degree of polymerisation of materials such as paracyanogen.

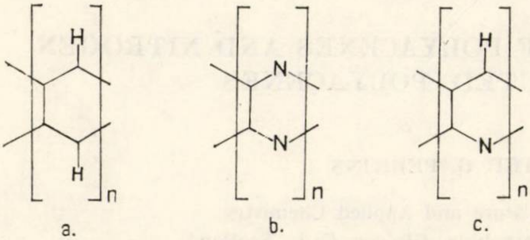

Fig. 1. — Structures of (*a*) polyacenes (*b*) polypyrazines and (*c*) polypyridine.

CALCULATIONAL METHOD

EXTENDED HÜCKEL THEORY FOR THE SOLID STATE

We write a crystal wave function thus,

$$\Psi_i(k) = \sum_{r=1}^{n} c_{ir}(k)\, b_r(k)$$

where $b_r(k)$ is a Bloch wave function

$$b_r(k) = \frac{1}{\sqrt{N}} \sum_{R_i(i=1)}^{N} e^{ikR_i}\, a_r(R - R_i)$$

---

[3] M. B. Robin and R. R. Hart, *Theoret. chim. Acta*, **3**, 375 (1965) ; *ibid.* and N. A. Kuebler, *J. Chem. Phys.*, **44**, 1803 (1966).

k is the wave vector and $a_r(R - R_i)$ is an atomic orbital situated at a vector distance R_i from the origin.

Use of the one-electron crystal wave functions leads to the problem of solving the set of simultaneous equations

$$\sum_{r=1}^{n} c_{ir}(k)\,[\mathrm{H}_{sr} - E_i(k)\,S_{sr}(k)] = 0$$

where

$$\mathrm{H}_{sr} = < b_s(k)^* \,|\mathrm{H}|\, b_r(k) >$$

and

$$S_{sr} = < b_s(k)^* \,|\, b_r(k) >$$

These equations may be considered in determinantal form in the usual way, thus

$$\begin{vmatrix} \mathrm{H}_{11} - E\mathrm{S}_{11} & \mathrm{H}_{12} - E\mathrm{S}_{12} \ldots\ldots \\ \mathrm{H}_{21} - E\mathrm{S}_{21} & \mathrm{H}_{22} - E\mathrm{S}_{22} \ldots\ldots \\ \cdot & \\ \cdot & \\ \cdot & \\ \cdot & \\ \mathrm{H}_{n1} - E\mathrm{S}_{n1} \ldots & \mathrm{H}_{nn} - E\mathrm{S}_{nn} \end{vmatrix} = 0$$

The fact that $\mathrm{S}_{ii} \neq 0$ is troublesome. Unlike Hückel theory for molecules (where $\mathrm{H}_{rr} = \alpha$) the diagonal element H_{rr} is represented.

$$\mathrm{H}_{rr} = < b_r(k)^* \,|\mathrm{H}|\, b_r(k) >$$

In expanding this term all non-neighbour interactions are neglected. There are N cases where $i = j$, *i.e.*, $R_i - R_j = 0$. We refer to these $\mathrm{H}_{rr}(R_0)$. Similarly, there are N terms where $a_r(R - R_i)$ and $a_r(R - R_j)$ are functions situated on neighbouring atoms, *i.e.*, $R_i - R_j = R_1$, and a further N terms where $R_i - R_j = -R_1$. These are designated R_1 and R_{-1} respectively. Hence, we have

$$\mathrm{H}_{rr}(R_0) = < a_r(R_0)^* \,|\mathrm{H}|\, a_r(R_0) > = -I_r$$

$$\mathrm{H}_{rr}(R_1) = \mathrm{e}^{ik\cdot R_1} < a_r(R_0)^* \,|\mathrm{H}|\, a_r(R_1) >$$

I_r is the valence state ionisation potential $< a_r(R_0) \,|\mathrm{H}|\, a_r(R_1) >$ represents the interaction energy of orbitals a_r in neighbouring unit cells.

These terms may be evaluated by the Mulliken-Wolfsberg-Helmholtz expression [4]

$$< a_r (R_0)^* |\mathrm{H}| a_r (R_1) > = 0.5 \times A \times S_{rr} (R_1) [-I_r + (-I_r)]$$

A is constant which is generally given a value between 1.0 and 2.0 (see later). $S_{rr}(R_1)$ is the usual interorbital overlap integral. Now, $\mathrm{H}_{rr}(R_{-1})$ may be evaluated by substituting R_{-1} for R_1 in the expression for $\mathrm{H}_{rr}(R_1)$.

Hence we have,

$$\mathrm{H}_{rr} (R_1) = \mathrm{e}^{ik \cdot R_1} \times A \times 0.5 \times S_{rr} (R_1) [-2\mathrm{I}_r]$$

$\mathrm{H}_{rr} (R_{-1})$ is obtained by substituting R_{-1} for R_1

Thus,

$$\mathrm{H}_{rr} = -I_r + 2 \cos (k \cdot R_1) \times A \times S_{rr} (R_1) [-I_r]$$

The H_{rr} may thus be calculated for any particular value of k.

The off-diagonal elements H_{sr} may now be derived in a similar way and is

$$\mathrm{H}_{rs} = \mathrm{H}_{rs} (R_0) + \cos (k \cdot R_1) [\mathrm{H}_{rs}(R_1) + \mathrm{H}_{rs} (R_{-1})] +$$
$$+ i \sin (k \cdot R_1) [\mathrm{H}_{rs} (R_1) - \mathrm{H}_{rs} R_{-1}]$$

Now, the determinant to be evaluated contains terms S_{ij}, which are not equal to zero, and so heavy transformations of the type

$$\begin{vmatrix} \mathrm{H}_{11} - E\mathrm{S}_{11} \cdot \cdot \cdot \cdot & \cdot \\ \mathrm{H}_{21} - E\mathrm{S}_{21} & \cdot \\ \cdot & \cdot \\ \cdot & \cdot \\ \cdot & \cdot \\ \cdot & \cdot \\ \cdot \cdot \cdot \cdot & \mathrm{H}_{nn} - E\mathrm{S}_{nn} \end{vmatrix} \rightarrow \begin{vmatrix} \dfrac{\mathrm{H}_{11}}{\mathrm{S}_{11}} - E \cdot \cdot \cdot \cdot \cdot & \cdot \\ [\mathrm{S}_{11}\mathrm{S}_{22}]^{-1/2}\mathrm{H}_{21} - E\mathrm{S}_{21} & \cdot \\ \cdot & \cdot \\ \cdot & \cdot \\ \cdot & \cdot \\ \cdot \cdot \cdot \cdot \cdot \cdot \cdot & \dfrac{\mathrm{H}_{nn}}{\mathrm{S}_{nn}} - \mathrm{E} \end{vmatrix} = 0$$

$$\mathrm{S}_{11} \neq 1, \; \mathrm{S}_{22} \neq 1 \; \ldots\ldots \; \mathrm{S}_{nn} \neq 1$$

---

[4] R. S. MULLIKEN, *J. Phys. Chem.*, **56**, 295 (1952); M. WOLFSBERG and L. HELMHOLTZ, *J. Chem. Phys.*, **20**, 837 (1952).

are required to bring it into a suitable form for diagonalisation of the corresponding matrix.[5] Moreover, the eigenvectors of the matrix must be back-transformed thus

$$(C_{kj,1}\ C_{kj,2} \cdots C_{kj,n}) \to (C'_{kj,1}\ C'_{kj,2} \cdots C'_{kj,n}) \left| \begin{array}{cccc} S_{11}^{-\frac{1}{2}} & 0 & \cdots & 0 \\ 0 & S_{22}^{-\frac{1}{2}} & & \\ \vdots & & \ddots & \\ 0 & \cdots & \cdots & S_{nn}^{-\frac{1}{2}} \end{array} \right|$$

A simple way out of this problem is found by setting the Bloch overlap integrals, $S_{ij} = \delta_{ij}$. This is in keeping with the zero differential overlap approximation and reduces the eigenvalue problem considerably.

In the present work the atomic parameters (α) were accorded the values given in Table 1.

Table 1

Hückel α parameters (eV)

Carbon	$2s$	-19.44
	$2p$	-10.67
Hydrogen		
	$1s$	-13.06
Nitrogen	$2s$	-25.58
	$2p$	-13.19

The elements $<a_r (R - R_i)^* \,|\mathrm{H}|\, a_r (R - R_j)>$ which occur in the Hückel matrix were obtained by the arithmetic Mulliken-Wolfsberg-Helmholtz expression.[4] Bond lengths were those for anthracene, pyridine, and pyrazine.[6]

---

[5] A. Imamura, *J. Chem. Phys.*, **52**, 3168 (1970).

[6] * * * 'Tables of Interatomic Distances in Molecules and Ions', *Chem. Soc. Special Publ.*, London, No. 11, 1958.

RESULTS AND DISCUSSION

1. ENERGY BAND STRUCTURE

Figures 2—6 illustrate the $E(k)$ *vs* k curves for polyacene, polypyrazine, and polypyridine. In the first two cases two separate values for A (1.0 and 2.0) were used in the series of calculations. This was done so as to check the sensitivity of the results of the calculation in the important regions (*e.g.*, around the band gap) so as to be sure that the conclusions drawn would not stem from artefacts of the calculational method. A full discussion of the effects of the change of this A factor, in the context of a more sophisticated method, has been given previously with regard to polyethylene [7] and, in that work, it was pointed out that the main changes in band structure due to the change of A occurs in the high-energy bands, whilst leaving the picture relatively unchanged around the band gap. It was further concluded that an A factor close to 2.0 is appropriate for calculations of this type. This has been confirmed by a comparison of Extended Hückel and CNDO-type calculations on the linear phosphite polymer. [8,9] Hence for polypyridine only one calculation, with $A = 2.0$ was performed.

Polyacene has 18 bands, polypyridine 17, and polypyrazine, 16, and so for clarity in figures 2—6 some of the electronic bands have been excluded: those remaining are restricted to featuring (*a*) the π bands, which are expected to be important in electron delocalisation phenomena and (*b*) the σ bands which border the band gap.

It is immediately obvious in all the systems that, contrary to the usual assumptions, π or π^* bands are not the only ones to border the band gap and the electronic properties depend somewhat on high lying σ and low lying σ^* levels. However what is important is that the pattern for $A = 1.0$ and $A = 2.0$ is similar in this region for the first two cases. We therefore assume that this situation will also obtain for polypyridine.

It is interesting and significant that, in all three cases, there is no real band gap and indirect overlap between the valence and conduction bands appears. (Table 2) The parallel with the situation in graphite,[10] where band overlap is also believed to occur, is quite marked.

In all cases the conduction bands are of π^* type and the width of these are also listed in Table 2.

Remarkably, the band gaps between the $\pi \rightarrow \pi^*$ bands are unaffected by changing A from 1.0 to 2.0 whilst both the band widths and the band overlaps are approximately doubled.
Another effect of A is to shift the position of the band gap in the energy scale. Because of the latter features, we do not really know what is the 'correct' A factor and so we should not take the calculated band widths

---

[7] B. J. McAloon and P. G. Perkins, *J. Chem. Soc.*, Faraday II, **68**, 1121 (1972).

[8] B. J. McAloon, Ph. D. Thesis, University of Strathclyde, 1972.

[9] B. J. McAloon and P. G. Perkins, *J. Chem. Soc.*, Faraday II, **68**, 1833 (1972).

[10] C. A. Coulson, *Nature*, **159**, 265 (1941).

too seriously (although clearly they are broad). However, we may safely compare changes over the series of systems. It is interesting that, in all characteristics, both the polyacene and polypyrazine exhibit propensity to electron delocalisation which is greater than in polypyridine. However, because the conduction bands of all the systems are wide, the polypyridine

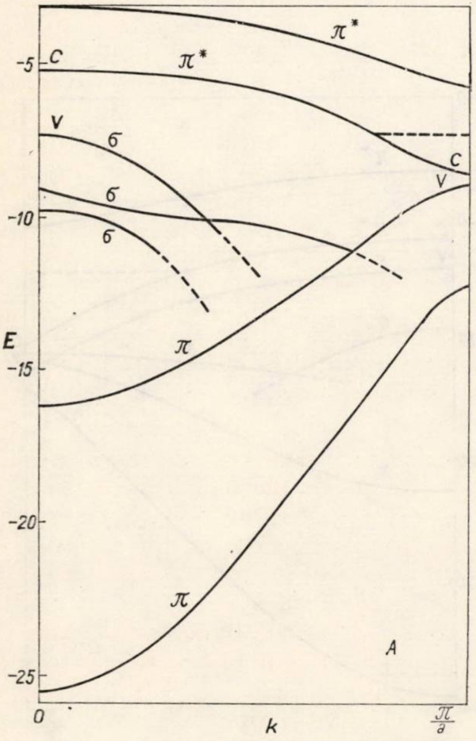

Fig. 2. — Band structure for polyacene $A = 1.0$.

Fig. 3 — Band structure for polyacene $A = 2.0$.

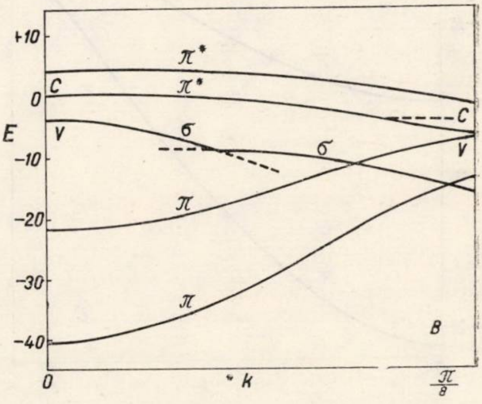

Table 2

Calculated Properties for Ladder Polymers (eV)

	Polyacene		Polypyrazine		Polypyridine
	$A = 1.0$	$A = 2.0$	$A = 1.0$	$A = 2.0$	$A = 2.0$
$\pi - \pi^*$ band gap	0.3	0.3	1.0	1.0	4.1
$\pi^* - \sigma$ band overlap	1.2	2.7	2.5	6.0	1.7
π^* band width	3.3	6.8	4.0	8.5	5.7
π band width	16.8	33.5	14.8	28.4	28.2

should not be a poorer conductor of electricity. Experimentally, polyacrylonitrile has been found [11] to exhibit a conductivity which varies with the degree of further heat treatment of the material but which, in all cases, is symptomatic of a good electrical conductor.

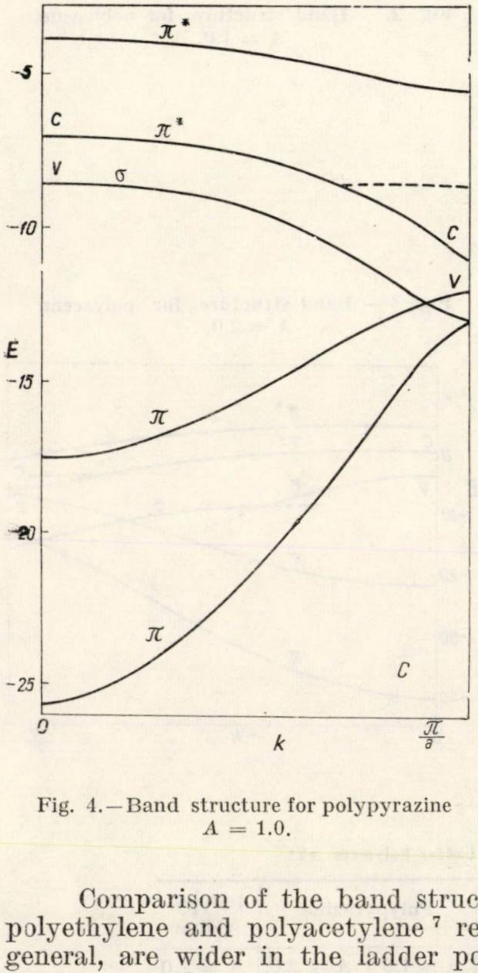

Fig. 4.—Band structure for polypyrazine $A = 1.0$.

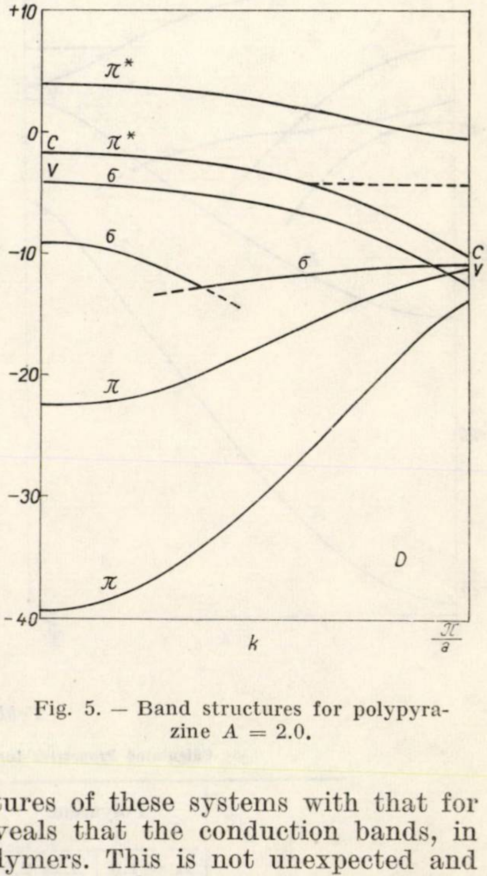

Fig. 5. — Band structures for polypyrazine $A = 2.0$.

Comparison of the band structures of these systems with that for polyethylene and polyacetylene [7] reveals that the conduction bands, in general, are wider in the ladder polymers. This is not unexpected and stems partly from the fact that the ladder polymer can be regarded as being built from two coupled polyacetylene units, thus

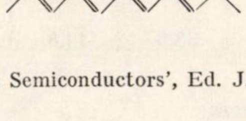

---

[11] J. J. Brophy in 'Organic Semiconductors', Ed. J. J. Brophy and J. Buttrey, Macmillan, New York, 1962, p. 169.

In the polymer studied here, there are essentially no barriers to electron delocalisation in the excited states such as are inherent in molecular crystals such as anthracene. Hence exciton states are essentially buried in the conduction states and the widths of both valence and conduction bands ensure that both the electron and hole pair are fully delocalised. The effective mass of the electrons and holes are those of the free carriers, again on account of the band widths.[12] Hence, both should be efficient carriers. The valence and conduction bands overlap indirectly in each case and the basic conduction properties of the material are expected to be enhanced by this. However, an additional cogent affective factor is the density of states in the region of the direct band gap at $k = \pi/a$ in each case. This will affect the absolute conductance, since at any particular temperature this quantity is governed by the number of electrons

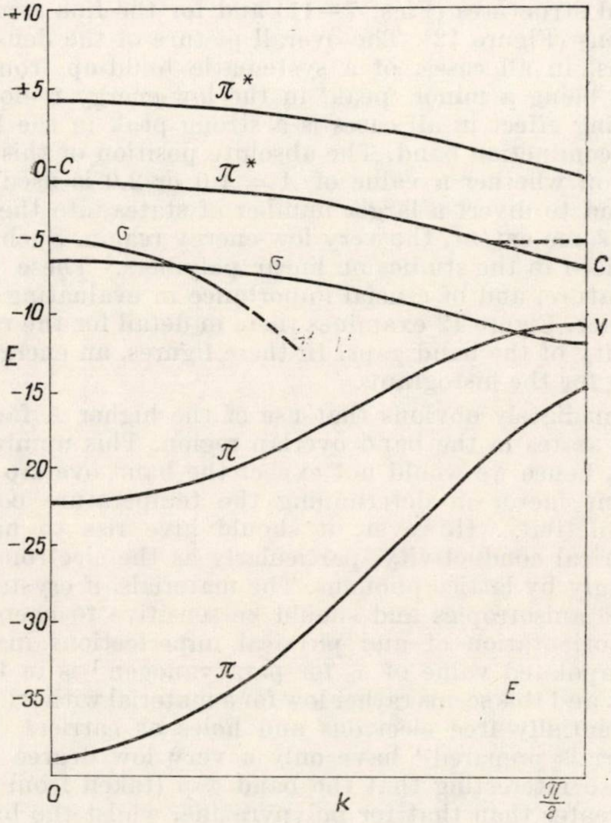

Fig. 6. — Band structure for polypyridine $A = 2.0$.

---

[12] W. Shockley, 'Electrons and Holes in Semiconductors', Van Nostrand, Princeton, N.J., 1950, p. 398.

in the conduction band, which in turn depends critically on the number energetically available in the valence levels. Hence, it is important to consider the *effective band gap*, *i.e.*, the energy gap which is bordered by levels having high densities of states. This leads to an *effective band width* for the π valence band.

The density of states functions are shown histogrammatically for the whole band structures (Figs. 7—11) and for the fine structure in the band gap regions (Figure 12). The overall picture of the density of states (Figs. 7—11) is, in all cases, of a systematic build-up from the lowest energies, there being a minor 'peak' in the low-energy region. However, the most striking effect in all cases is a strong peak in the lower energy regions of the conduction band. The absolute position of this latter sharp peak depends on whether a value of $A = 1.0$ or 2.0 is used. The higher values of A tend to divert a larger number of states into the high-energy region and, to some extent, the very low-energy region. Such effects were previously noticed in the studies on linear polymers.[7] These peaks are an outstanding feature, and of crucial importance in evaluating the physical properties. Hence, Figure 12 examines them in detail for the regions which lie in the vicinity of the band gaps. In these figures, an energy interval of 2eV was taken for the histograms.

It is immediately obvious that use of the higher A factor depletes the number of states in the band overlap region. This number is, in any case, not large, hence we would not expect the band overlap to be a crucially important factor in determining the temperature coefficient for electrical conductivity. However, it should give rise to high absolute values of electrical conductivity, particularly as the electrons will not be scattered strongly by lattice phonons. The materials, if crystalline, should also show large anisotropies and should be sensitive to chemical impurities, and the orientation of and physical imperfections in the crystal. Now, the extrapolated value of σ_0 for paracyanogen [1] is in the region of $10^{-2}\ \Omega^{-1}\ \mathrm{cm}^{-1}$, and this seems rather low for a material with wide electronics bands and essentially free electrons and holes as carriers. This implies that the materials prepared [1] have only a very low degree of polymerisation. It is also interesting that the band gap (taken from Table 2) for polyacene is greater than that for polypyrazine, whilst the band overlaps fall in the reverse order. It we correlate this band overlap with σ_0, the situation is remarkably similar to that found experimentally by Graham and Packham [1] for certain polymers where ΔE shows a good inverse linear correlation with absolute conductance, σ_0. By our calculation this relation does not, however, extend to polypyridine, and Eley [13] has also reported breakdown in this relation.

The temperature coefficient and activation energy for the materials will be determined essentially by the *effective* band gap and, in this context, it is significant from Figure 11 that in no case is there a high density of states lying immediately below the $\pi - \pi^*$ band gap at $k = \pi/a$. Hence, we should expect the effective band gaps for each material to be of the order of 2—4 eV, *i.e.*, somewhat in excess of the measured gaps. The effect-

---

[13] D. D. Eley and M. R. Willis, in 'Electrical Conductivity in Organic Solids', Ed. H. Kallmann and M. Silver, Interscience, New York, 1961, p. 257.

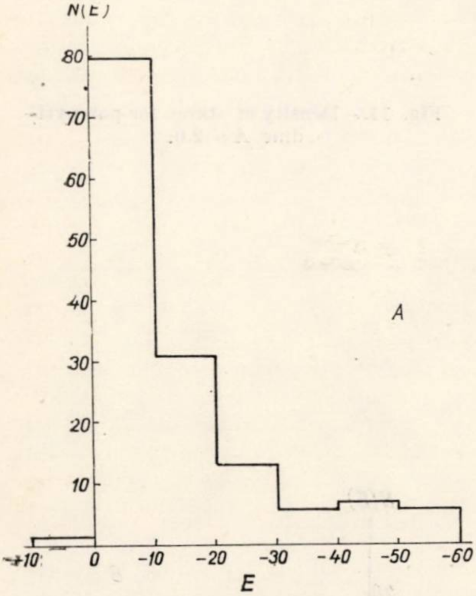

Fig. 7.—Density of states for polyacene $A = 1.0$.

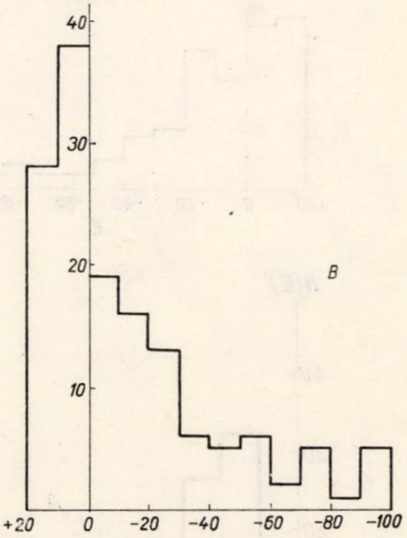

Fig. 8.—Density of states for polyacene $A = 2.0$.

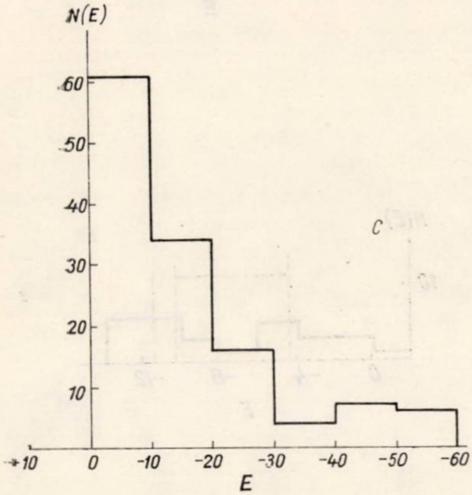

Fig. 9.—Density of states for polypyrazine $A = 1.0$.

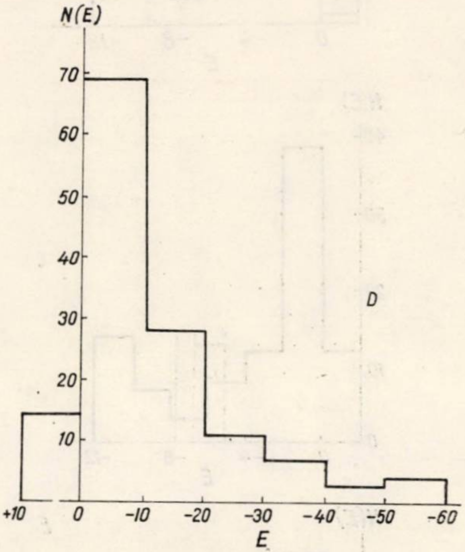

Fig. 10.—Density of states for polypyrazine $A = 2.0$.

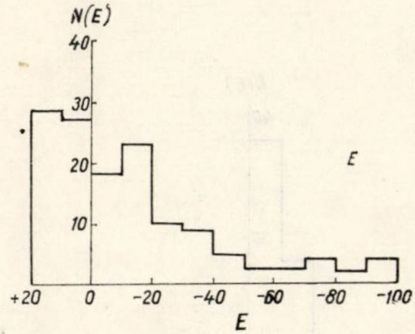

Fig. 11.—Density of states for polypyridine $A = 2.0$.

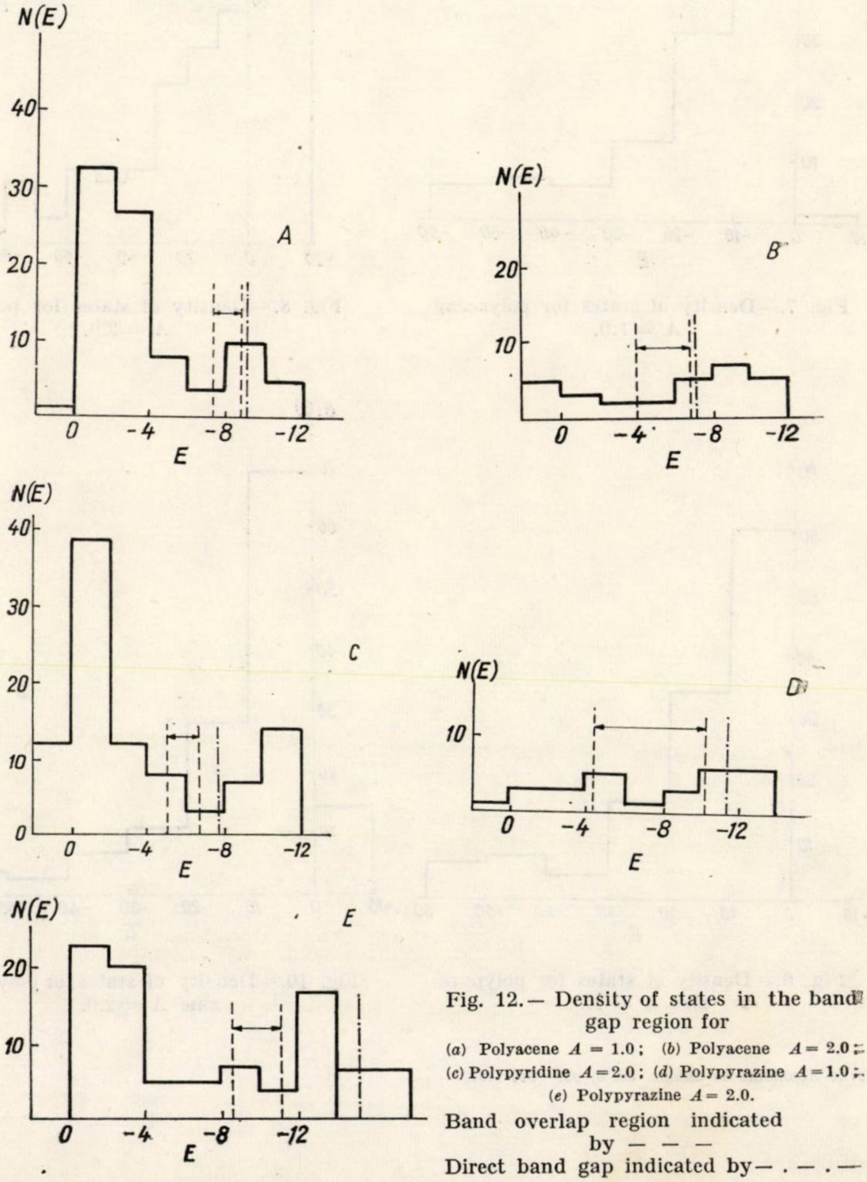

Fig. 12.— Density of states in the band gap region for

(*a*) Polyacene $A = 1.0$; (*b*) Polyacene $A = 2.0$; (*c*) Polypyridine $A = 2.0$; (*d*) Polypyrazine $A = 1.0$; (*e*) Polypyrazine $A = 2.0$.

Band overlap region indicated by — — —

Direct band gap indicated by— . — . —

ive band gap itself may not, however, constitute the thermal excitation energy reported, since (i) by taking the direct $\pi-\pi^*$ band gap we are ignoring the correction which would result from the introduction of configuration interaction in the excited states, (ii) no distinction between excited singlet and triplet states is made in Hückel theory.

Hence, in the next stage of this work we propose to calculate the excited states of some polyacenes, polypyrazines, and the polypyridines in order-firstly, to gauge the effect on the excited states of increasing the number of rings and secondly, to discover what correction to the band gaps the inclusion of electronic interaction brings about.

Revue Roumaine de Chimie, **18**, *6*, 945–952 (1973)

THERMODYNAMIC EXCESS PROPERTIES OF MOLTEN LiCl + KCl, LiCl + RbCl, NaCl + RbCl AND NaCl + CsCl MIXTURES

S. STERNBERG and IUDITA ADORIAN

Polytechnic Institute,
Str. Polizu 1, Bucureşti, Romania

Received December 7, 1972

Partial molar thermodynamic excess functions of the components in molten LiCl+KCl, LiCl+RbCl, NaCl+RbCl and NaCl+CsCl mixtures have been calculated, from cryoscopic and calorimetric data. Equations for thermodynamic activities, excess enthalpies, free enthalpies and entropies of the components in the mixtures mentioned above are established. A statistical interpretation is given to the negative excess entropy of the said mixtures.

Binary mixtures of molten salts that do not yield compounds of definite composition on solidification, have been treated in a first approximation as regular solutions. Their departures from ideality were attributed to the existence of an energy of mixing, the excess entropy has been considered zero.[1]

The appearance of new experimental data that permitted a comparison of the heat of mixing with the free energy of mixing of the same mixture, pointed out the existence of negative excess entropies in a large number of mixtures.[2]

In the present paper partial molar thermodynamic excess functions are calculated for the LiCl+KCl, LiCl+RbCl, NaCl+RbCl, and NaCl+CsCl systems, based on cryoscopic measurements presented in an earlier paper [3] and on calorimetric measurements of Hersh and Kleppa, [4] concerning the same systems.

Thermodynamic activity a_1 of the "solvent" at temperature T has been calculated by the Schroeder-van Laar equation as

$$\ln a_1 = \frac{\Delta H_{T_0}}{R}\left(\frac{1}{T}-\frac{1}{T_0}\right)+\frac{\Delta C_p}{R}\left(\ln\frac{T_0}{T}-\frac{T_0-T}{T}\right) \qquad (1)$$

---

[1] I. G. Murgulescu and S. Sternberg, *Discuss. Faraday Soc.*, **32**, 107 (1962).

[2] S. Sternberg and I. Adorian, *Electrochim. Acta*, **13**, 1647 (1968).

[3] I. G. Murgulescu and S. Sternberg, *Z. phys. Chem.* (*Leipzig*), **219**, 114 (1962).

[4] L. S. Hersh and O. J. Kleppa, *J. Chem. Phys.*, **42**, 1309 (1965).

ΔH_{T_0} is the molar heat of solidification of the pure solvent at its melting point T_0, T the temperature of the first separation of the solvent on cooling the solution, and $C_p = C_p(s) - C_p(l)$ is the difference, regarded as constant, between the molar heat capacities of the solvent in solid and liquid state, respectively.

Partial molar free enthalpies are calculated as

$$\overline{G}_1^E = RT \ln \gamma_1 \tag{2}$$

the subscript 1 being used for the "solvent".

Based on equation (1) and using thermochemical data indicated by Kubaschewski, Evans and Alcock,[5] presented in table 1, we have

Table 1

Thermochemical data

Salt	Temp	ΔH_f kcal/mole	$C_p(s)$ cal/mole deg	$C_p(l)$ cal/mole deg
CsCl	645	4.9 ± 0.1[6]	$0.805 + 17.64 \times 10^{-3} T - 0.89 \times 10^5 T^{-2}$ [6]	$13.86 + 4.2810^{-5} T$[6]
LiCl	610	4.75 ± 0.1[7]	$11 + 3.40 \times 10^{-3} T$[8]	
NaCl	801	6.7 ± 0.1[7]	$10.98 + 3.90 \times 10^{-3} T$[8]	16[8]
RbCl	715	4.4[9]	$11.50 + 2.49 \times 10^{-3} T$[8]	15.3[8]
KCl	772	6.35 ± 0.1[7]	$9.89 + 5.20 \times 10^{-3} T + 0.77 \times 10^5 T^{-2}$ [8]	16[8]

established the following equations for the thermodynamic activities of alkali chlorides:

(ΔC_p of LiCl has been approximated as 1 cal/mole deg)

$$\log a_{\mathrm{LiCl}} = -845.43\ \mathrm{T}^{-1} + 0.5031 \log T - 0.5247 \tag{3}$$

$$\log a_{\mathrm{NaCl}} = -1267.1\ T^{-1} + 0.4182 \log T - 0.0877 \tag{4}$$

$$\log a_{\mathrm{KCl}} = -1249.05\ T^{-1} + 0.3069 \log T + 0.2701 \tag{5}$$

$$\log a_{\mathrm{RbCl}} = -950.1\ T^{-1} + 0.67418 \log T - 1.0573 \tag{6}$$

$$\log a_{\mathrm{CsCl}} = -934.796\ T^{-1} + 0.3421 \log T + 0.00465 \tag{7}$$

The thermodynamic activities of the components in the investigated mixtures, calculated with equations (3) – (7), and the partial molar excess free enthalpies calculated with equation (2) are presented in columns 4 and 5 of tables 2,3,4 and 5.

Kleppa and Hersh [4] have determined the heat of mixing of the systems mentioned above and have given the following equation for the integral heat of mixing

---

[5] O. Kubaschewski, E. L. Evans and C. B. Alcock, "Metallurgical Thermochemistry", Pergamon Press, Oxford — London, 1967.

[6] C. E. Kaylor, G. E. Wolden and N. F. Smith, *J. Phys. Chem.*, **64**, 276 (1960); *J. Amer. Chem. Soc.*, **81**, 4172 (1959).

[7] A. S. Dworkin and M. A. Bredig, *J. Phys. Chem.*, **64**, 269 (1960); **67**, 697, 2499 (1963).

[8] K. K. Kelley, *Bull. U.S. Bur. Mines*, **1935**, *384*.

[9] L. Brewer, *Natl. Nuclear Sci. Ser. Div. IV.*, **19.B** p. 193.

$$H^E = \Delta H_m = x_1 x_2 (a + b x_1 + c x_1 x_2) \tag{8}$$

where x_1 is the mole fraction of the salt with the smaller cation while, a, b and c are constants for any given mixture.

Table 2

Thermodynamic excess functions of the components in the molten LiCl + KCl mixture (T_m = 1013 K)

LiCl

X_{LiCl}	T K	a_{LiCl}	$\overline{G}^E_{LiCl}$ cal/mole	$\overline{H}^E_{LiCl}$ cal/mole	S^E_{LiCl} cal/mole deg	$\overline{G}^E_{T_m(LiCl)}$ cal/mole
1	883	1	0	0	0	0
0.90	846	0.889	− 21	− 44	−0.027	− 16
0.80	769	0.673	−265	−174	+0.118	−285
0.65	684	0.463	−461	−529	−0.099	−428
0.60	638	0.364	−633	−689	−0.088	−600
0.595	632	0.344	−688	−706	−0.03	−677
0.50	580	—	−900*	−1073	−0.3	−770

KCl

X_{KCl}	T K	a_{KCl}	$\overline{G}^E_{KCl}$ cal/mole	$\overline{H}^E_{KCl}$ cal/mole	$\overline{S}^E_{KCl}$ cal/mole deg	$\overline{G}^E_{T_m(KCl)}$ cal/mole
1	1044	1	0	0	0	0
0.90	1006	0.891	−20	−41	−0.02	−20
0.83	975	0.806	−57	−120	−0.064	−55
0.698	894	0.601	−266	−380	−0.127	−251
0.550	777	0.355	−678	−849	−0.220	−626
0.500	722	0.262	−930	−1050	−0.16	−863
0.450	659	0.174	−1246	−1273	−0.04	−1232
0.405	632	0.142	−1313	−1493	−0.28	−1206

* extrapolated values.

Based on the Gibbs-Duhem equation, the partial molar enthalpies of the components may be calculated from the integral heat of mixing by means of equations

$$\overline{H}_1^E = H^E + (1 - x_1) \frac{\mathrm{d}H^E}{\mathrm{d}x_1} \tag{9}$$

and

$$\overline{H}_2^E = H^E + (1 - x_2) \frac{\mathrm{d}H^E}{\mathrm{d}x_2} \tag{10}$$

Table 3

Thermodynamic excess functions of the components in the molten LiCl + RbCl mixture
(T_m = 1013 K)

LiCl

X_{LiCl}	T K	a_{LiCl}	$\overline{G}^E_{\mathrm{LiCl}}$ cal/mole	$\overline{H}^E_{\mathrm{liCl}}$ cal/mole	$\overline{S}^E_{\mathrm{LiCl}}$ cal/mole deg	$\overline{G}^E_{T_m(\mathrm{LiCl})}$ cal/mole
1	883	1	0	0	0	0
0.85	811	0.788	−122	−130	−0.01	−120
0.70	699	0.498	−474	−523	−0.07	−452
0.55	585	0.264	−851	−1158	−0.52	−628
0.50	550	—	−1050*	−1414	−0.66	−744

RbCl

X_{RbCl}	T K	a_{RbCl}	$\overline{G}^E_{\mathrm{RbCl}}$ cal/mole	$\overline{H}^E_{\mathrm{RbCl}}$ cal/mole	$\overline{S}^E_{\mathrm{RbCl}}$ cal/mole deg	$\overline{G}^E_{T_m(\mathrm{RbCl})}$ cal/mole
1	988	1	0	0	0	0
0.85	923	0.817	− 72	− 68	0.004	− 72
0.70	826	0.574	−325	−337	−0.014	− 322
0.55	691	0.303	−816	−878	−0.09	− 787
0.50	634	0.215	−1060	−1127	−0.105	−1020
0.45	575	0.142	−1321	−1411	−0.156	−1253

Table 4

Thermodynamic excess functions of the components in the molten NaCl + RbCl mixture
(T_m = 1083 K)

NaCl

X_{NaCl}	T K	a_{NaCl}	$\overline{G}^E_{\mathrm{NaCl}}$ cal/mole	$\overline{H}^E_{\mathrm{NaCl}}$ cal/mole	$\overline{S}^E_{\mathrm{NaCl}}$ cal/mole deg	$\overline{G}^E_{T_m(\mathrm{NaCl})}$ cal/mole
1	1074	1	0	0	0	0
0.9	1045	0.917	38	− 9	−0.04	39.5
0.8	995	0.781	− 48	− 36	−0.01	−49
0.7	954	0.676	− 65	− 79	−0.015	−63
0.6	908	0.567	−100.7	−139	−0.042	−93
0.5	839	0.421	−285	−213	0.09	−306

RbCl

X_{RbCl}	T K	a_{RbCl}	$\overline{G}^E_{\mathrm{RbCl}}$ cal/mole	$\overline{H}^E_{\mathrm{RbCl}}$ cal/mole	$\overline{S}^E_{\mathrm{RbCl}}$ cal/mole deg	$\overline{G}^E_{T_m(\mathrm{RbCl})}$ cal/mole
1	988	1	0	0	0	0
0.846	937	0.856	20	−17	−0.04	25.8
0.773	910	0.783	22	−37	−0.064	33
0.616	840	0.607	−23	−111	−0.105	2.5
0.50	800	—	−50*	−193	−0.179	0.65

On the basis of equations (9) and (10) and using the values a, b and c as determined by Kleppa, we have established for the partial molar enthalpies of the components equations of the type :

$$\overline{H}^{E}_{\mathrm{Mex}} = A + Bx + Cx^2 + Dx^3 + Ex^4 \tag{11}$$

Table 5

Thermodynamic excess functions of the components in the molten NaCl + CsCl mixture (T_m = 1083 K)

NaCl

X_{NaCl}	T K	a_{NaCl}	$\overline{G}^{E}_{\mathrm{NaCl}}$ cal/mole	$\overline{H}^{E}_{\mathrm{NaCl}}$ cal/mole	$\overline{S}^{E}_{\mathrm{NaCl}}$ cal/mole deg	$\overline{G}^{E}_{T_m\,(\mathrm{NaCl})}$ cal/mole
1	1074	1	0	0	0	0
0.75	978	0.737	− 35	−55	−0.02	−32.9
0.50	854	0.451	−174	−233	−0.069	−158
0.40	794	0.338	−265	−342	−0.097	−237
0.35	762	0.285	−312	−406	−0.123	−273

CsCl

X_{CsCl}	T K	a_{CsCl}	$\overline{G}^{E}_{\mathrm{CsCl}}$ cal/mole	$\overline{H}^{E}_{\mathrm{CsCl}}$ cal/mole	$\overline{S}^{E}_{\mathrm{CsCl}}$ cal/mole deg	$\overline{G}^{E}_{T_m\,(\mathrm{CsCl})}$ cal/mole
1	918	1	0	0	0	0
0.85	860	0.835	−31	−25	−0.007	− 32
0.75	820	0.727	−51	−67.5	−0.020	− 46
0.65	764	0.603	−113	−130	−0.022	−106
0.50	700	—	−210*	−258	−0.068	−184

where x is the mole fraction of the MeX component, and the numeric coefficients A, B, C, D and E are given in table 6. Partial molar excess free enthalpies calculated with equation (11) are given in column 5 of tables 2—5.

In the next column of these tables, the partial molar excess entropies are presented as

$$\overline{S}^{E}_{1} = \frac{\overline{H}^{E}_{1} - \overline{G}^{E}_{1}}{T}, \tag{12}$$

where T is the temperature at which the $\overline{G}^{E}_{1}$ free enthalpy is determined. Each of the investigated systems exhibits negative excess entropies. Considering in a first approximation that the molar heat capacities do not change on mixing ($\Delta C_{p_m} = 0$), $\overline{S}^{E}_{\mathrm{Mex}}$ and $\overline{H}^{E}_{\mathrm{Mex}}$ may be considered independent of temperature. Using the values of excess entropies, excess free enthalpies have been recalculated for the temperatures at which the heats of mixing were measured, i.e. 1013°K and 1083°K, respectively. These values calculated as $\overline{G}^E_{1(T_m)} = \overline{G}^E_1 - \overline{S}^E_1 (T_m - T)$ are presented in the last columns of tables 2—5. The partial molar excess free enthalpies are negative, and present departures from the Hildebrand relation for regular solutions: $\overline{G}^E_1 = \beta x_2^2$. The concentration dependence of the $\overline{G}^E_{1(T_m)}$ in the concentration range investigated follows equations of the type

Table 6

Coefficients in equations (11) for partial molar excess enthalpies

Salt	*A* cal/mole	*B* cal/mole	*C* cal/mole	*D* cal/mole	*E* cal/mole
LiCl (in LiCl+KCl)	−4200	8270	−3840	− 180	0
KCl (in LiCl+KCl)	−4290	8760	−4650	180	0
LiCl (in LiCl+RbCl)	−4270	4340	6980	−9900	2850
RbCl (in LiCl+RbCl)	−5420	11240	−3370	−5380	2850
NaCl (in NaCl+RbCl)	− 770	1380	− 450	− 160	0
RbCl (in NaCl+RbCl)	− 850	1860	−1170	160	0
NaCl (in NaCl+CsCl)	−1030	2260	−1430	200	0
CsCl (in NaCl+CsCl)	− 930	1660	− 530	− 200	0

$$\frac{\overline{G}^E_1}{x_2^2} = \beta + \gamma x_2 + \delta x_2^2 \qquad (13)$$

where the values of coefficients β, γ and δ have been established by the least square method and are given in table 7.

Table 7

Coefficients in equation (13) for partial molare excess free enthalpies

Salt	β cal/mole	γ cal/mole	δ cal/mole
LiCl (in LiCl + KCl)	−3456	− 267	− 941
KCl (in LiCl + KCl)	−1375	−4621	1070
LiCl (in LiCl + RbCl)	−5019	−5269	20809
RbCl (in LiCl + RbCl)	−2786	−2405	286
NaCl (in NaCl + RbCl)	−3499	16450	−23360
RbCl (in NaCl + RbCl)	2737	−12434	13680
NaCl (in NaCl + CsCl)	307	−1081	858
CsCl (in NaCl + CsCl)	−2395	8511	−10524

The existence of negative excess entropies can be explained by the existence of a certain degree of order in the mixture, due to a departure from random distribution of the two species of cations in the mixture.[2]

Degree of order σ increases with increases in the energy of mixing. Following a model proposed by Wasastjerna [10] for solid solutions, the degree of order in an equimoleculare solution can be calculated from interaction parameter β by means of relation

---

[10] I. A. Wasastjerna, *Soc. Sci. Fennica. Com. Phys. Math.*, **14**, 3 (1948).

$$\ln \frac{1+\sigma}{1-\sigma} = -\frac{\beta}{2RT} \tag{14}$$

The significance of parameter β is : $\beta = zNw$, where z is the number of next neighbours, N is the Avogadro number and $w = \varepsilon_{1,2} - \frac{1}{2}\varepsilon_1 - \frac{1}{2}\varepsilon_2$ is the change of interaction energy when a mixed ionic group is formed in the mixture. In regular solutions, β is related to the heat of mixing as : $\Delta H_m = \beta\, x_1 x_2$.

For calculating the degree of order in the studied systems, we used values of β calculated in a previous work,[11] based on Lumsden's [12] theory, from the energy of polarization of the anion and the variation of the London forces during mixing. Lumsden's theory accounts well for the behaviour of salt mixtures with a sizeable difference between the cation radii. At the formation of binary molten salt mixtures the vibrational entropy can be considered as constant. The excess entropy that appears is mostly a configurational entropy due to the effect of ordering : $S^E = S^E_{\text{ord}}$.

For the entropy of mixing on solid solutions, Hovi[13] gives the following relation

$$S_m = R\,(x_1 \ln x_1 + x_2 \ln x_2) - R\,(\varkappa \ln \varkappa + \lambda \ln \lambda + \mu \ln \mu + \nu \ln \nu) \tag{15}$$

where $\varkappa$, λ, μ and ν are the probabilities of the formation of a mixed or unmixed ionic triplet, that depend on mole fractions x_1 and x_2 and on the

Table 8

Degree of order and excess entropy in equimolecular molten mixtures

System	T K	cal/mole	σ	$S^E_{x_1=x_2=0.5}$ cal/mole deg	
				calculated	experimental
LiCl + KCl	1013	−4000	0.461	−0.22	−0.23
LiCl + RbCl	1013	−4974	0.550	−0.32	−0.38
NaCl + RbCl	1083	−1270	0.146	−0.02	−0.04
NaCl + CsCl	1083	−2063	0.235	−0.06	−0.07

---

[11] S. Sternberg and Constanța Herdlicka, *Rev. Roumaine Chim.*, **13**, 13 (1968).

[12] J. Lumsden, *Discuss. Faraday Soc.*, **32**, 138 (1961).

[13] V. Hovi, *Soc. Sci. Fennica Com. Phys. Math.*, **15**, 7 (1950).

degree of order σ. Equation (15) applied to a binary mixture of molten salts yields the following relation for the excess entropy

$$S^E = 2R\,(x_1 \ln x_1 + x_2 \ln x_2) - R\,(\varkappa \ln \varkappa + \lambda \ln \lambda + \mu \ln \mu + \nu \ln \nu) \quad (16)$$

The values of the degrees of order calculated with equation (13) and the excess entropies of equimolecular mixtures calculated by equation (15) are presented in table 8. In the last column, the experimental values of the integral excess entropies, calculated as: $S^E = x_1\bar{S}_1^E + x_2\bar{S}_2^E$ are presented for equimolecular mixtures. There is a satisfactory agreement between experimental and calculated values.

Revue Roumaine de Chimie, 18, 6, 953–969 (1973)

DIE CHEMISORPTION VON WASSERSTOFF, BENZOL UND CYCLOHEXAN AUF MIT LITHIUM UND TITAN DOTIERTEM ALUMINIUMOXYD. I

ADSORPTIONSISOTHERMEN

I. V. NICOLESCU und AL. FRUMA

Institut für physikalische Chemie
str. Dumbrava Roşie 23, Bukarest, Romania

Eingegangen am 24. November 1972

Es wurde die Chemisorption von Wasserstoff, Benzol und Cyclohexan auf einer Reihe von sechs, mit 0,5 ; 2 und 4 Atom % Li respektiv Ti dotierten Aluminiumoxyde, in einem Gleichgewichtsdruckbereich zwischen 0,5 und 20 Torr, bei der Temperatur von 25 und 250° für den Wasserstoff und 100 und 250° für das Benzol und Cyclohexan untersucht. Die chemisorptive Kapazität der Aluminiumoxyde für den Wasserstoff hängt von der Natur und Konzentration des Dotierstoffs ab, und vermindert sich in folgender Reihenfolge : Aluminiumoxyd dotiert mit 4 ; 2 und 0,5 Atome % Ti, reines Aluminiumoxyd, Aluminiumoxyd dotiert mit 0,5 ; 2 und 4 Atome % Li. Auf Grund der Ergebnisse der Wasserstoffchemisorption, die mit Röntgenstrahl-Beugungsmessungen korreliert wurden, wird je ein Strukturmodell für die mit Lithium und Titan dotierten Aluminiumoxyde vorgeschlagen. Die für das in Oxydform auf der Aluminiumoxydoberfläche befindliche Titan berechnete Oberfläche betrug 1,11 ; 2,94 und 5,4 m^2/g für die Proben mit 0,5 ; 2 bzw. 4 Atom % Ti. Anhand der Darstellung Langmuirs, Temkins und Freundlichs Isothermengleichungen für die Chemisorption des Wasserstoffs, Benzols und Cyclohexans, werden Schlüsse über die Heterogenität der Oberflächen gezogen. Diese Schlüsse sind in Übereinstimmung mit den Röntgenstrahl-Beugungsuntersuchungen.

1. EINLEITUNG

Bei dem Audrücken der Aktivität der Katalysatoren wird nur die Gesamtaktivität der Oberflächen-, Volumen- und Masseneinheit des Katalysators in Betracht genommen. Die Hinweise über die Aktivität der einzelnen Komponente, die von besonderer Wichtigkeit für die Klärung einiger theoretischen Probleme der heterogenen Katalyse und für die praktische Benützung der Katalysatoren sind, kommen sehr selten vor.

Für die Berechnung der spezifischen Aktivität ist es nötig die Gesamtaktivität des Katalysators und seine aktive Oberfläche zu kennen. Bei nicht aufgetragenen Katalysatoren, wie z.B. auf Metalloyxden und Metallpulvern, bei denen die ganze Oberfläche aktiv sein kann, wird diese Oberfläche leicht mit der BET Methode bestimmt. Viel schwieriger ist die

Bestimmung der aktiven Oberfläche bei Katalysatoren mit mehreren Komponenten, bei denen die aktive Oberfläche viel kleiner als die Gesamtoberfläche des Katalysators ist. Wegen der Spezifizität die die Chemisorptionsmethode kennzeichnet, wird die Methode der Gas- und Dampfchemisorption mit Erfolg für die Charakterisierung der aktiven Oberfläche der Katalysatoren, sowohl hinsichtlich der spezifischen Oberfläche und Dispersion als auch der Heterogenität verwendet. [1–3]

Boreskov[4] zeigte schon im Jahre 1952, daß für die Berechnung der spezifischen Oberfläche bei aufgetragenen Platinkatalysatoren, die Bestimmungen sowohl auf dem Katalysator, als auch auf dem Träger nötig sind. In diesem Sinn erschienen nachher zahlreiche Arbeiten [5–8] über die Wasserstoffchemisorption auf Katalysatoren vom Pt/Al_2O_3-Typ, in denen die Gasadsorption separat auf dem Träger und dem Katalysator mit verschiedener Platinkonzentration untersucht wurde. Die Anzahl der Arbeiten über die katalytischen Eigenschaften der Platinkatalysatoren, die auf Grund von mit Fremdionen dotierten Aluminiumoxyde hergestellt wurden ist gering. [9–11] Das Studium der chemisorptiven Eigenschaften dieser Katalysatoren wurde aber gänzlich vernachlässigt, so daß es heutzutage noch keine Arbeit gibt die die Frage inwiefern die Gas- und Dampfchemisorption auf Katalysatoren vom Pt/Al_2O_3-Typ von dem durch Dotierung veränderten Halbleitercharakter des Trägers abhängig ist, beantwortet.

In der vorliegenden Arbeit nahmen wir uns vor, die Ergebnisse der Wasserstoff, Benzol und Cyclohexanchemisorption auf einer Reihe von 6 mit Lithium und Titan dotierten Aluminiumoxyde und auf reinem Aluminiumoxyd das in denselben Bedingungen wie die dotierten Aluminiumoxyde hergestellt wurde, vorzustellen. Diese Aluminiumoxyde benützten wir als Träger für eine Reihe Katalysatoren vom Pt/Al_2O_3-Typ, über deren chemisorptiven und strukturellen Eigenschaften wir später berichten werden.

2. EXPERIMENTELLES

Es wurde eine vorher beschriebene [12] Hochvakuumanlage benützt, mit welcher die Chemisorption des Wasserstoffs, Benzols und Cyclohexans im Druckbereich 0,5 bis 20 Torr bei Temperaturen zwischen 25 und 250° untersucht wurde. Die Druckänderungen im Arbeitsraum wurden mit Hilfe einer Theromröhre und mit einem differenziellem Ölmanometer gemessen.

---

[1] I. Müller, *Rev. Pure and Appl. Chem.*, **19**, 151 (1969).

[2] Al. Fruma, *Studii și Cercetări Chim. Acad. București*, **19**, 1115 (1971).

[3] Al. Fruma, *Studii și Cercetări Chim. Acad. București*, **20**, 100 (1972).

[4] G. K. Boreskov und A. P. Karnaukhov, *Zhur. fiz. Khim.*, **26**, 1814 (1952).

[5] L. Spenadel und M. Boudart, *J. Phys. Chem*, **64**, 204 (1960).

[6] H. S. Gruber, *J. Phys. Chem.*, **66**, 68 (1961).

[7] J. Benson und M. Boudart, *J. Catalysis*, **4**, 704 (1965).

[8] N. N. Zaidman, V. A. Dzisko, A. P. Karnaukhov, N. P. Krasilenko, N. G. Koroleva und G. P. Vishnarkova, *Kinetika i Kataliz*, **9**, 863 (1965).

[9] O. M. Schwab, A. Beer und J. Foitzig, *Z. angew. Physik*, **14**, 763 (1962).

[10] H. Pscheidl und H. Witzmann, *Z. phys. Chem. (Leipzig)*, **240**, 161 (1969).

[11] W. Pfeil, *Z. phys. Chem. (Leipzig)*, **243**, 52 (1970).

[12] I. V. Nicolescu, Al. Fruma und I. Suciu, *Rev. Roumaine Chim.*, **16**, 91 (1971).

Es wurden folgende 7 Aluminiumoxydproben benützt: Aluminiumoxyd dotiert mit 0,5; 2 und 4 Atom % Li, Aluminiumoxyd dotiert mit 0,5; 2 und 4 Atom % Ti und eine Etalonprobe mit reinem Aluminiumoxyd. Die Herstellungsweise dieser Aluminiumoxyde wurde vorher berichtet.[13] Die spezifischen Oberflächen wurden auf Grund der Stickstoffadsorption berechnet und betrugen 158, 146, 139, 149, 138 und 124 m^2/g für das Aluminiumoxyd dotiert mit respektiv 0,5; 2; 4 Atom % Li und 0,5; 2 und 4 Atom % Ti, während die spezifische Oberfläche des reinen Aluminiumoxyds 152 m^2/g betrug. Bei den Chemisorptionsmessungen wurden 2 g Proben benützt. Der Wasserstoff wurde durch selektive Absorption und Desorption auf sprödem Palladium[14] gereinigt, während das Benzol und Cyclohexan komerzielle „Merck PA" Ware war, die weiter durch Vakuumverdampfung gereinigt wurde. All diese Reinigungsprozesse wurden in der Anlage, gleich vor den Bestimmungen vorgenommen, so daß die gereinigten Stoffe nicht mehr in Kontakt mit der Atmosphäre zu kommen konnten.

Die während 5 Stunden unter einem Vakuum von 5.10^{-6} Torr bei 500° entgaste Proben, wurden nach der Kühlung den Chemisorptionsbestimmungen bei der vorbestimmten Temperatur und Druck ausgesetzt.

3. ERGEBNISSE UND DISKUSSION

3.1. WASSERSTOFFCHEMISORPTION

Da die Anzahl der experimentellen Ergebnisse die wir uns zu berichten und zu besprechen vornehmen groß ist, beginnen wir mit der Wasserstoffchemisorption auf den Proben mit dotiertem Aluminiumoxyd und reinem Aluminiumoxyd um dann, in den nächsten Abschnitten die Benzol- und Cyclohexanchemisorption zu besprechen.

Die Wasserstoffchemisorption bei der Temperatur von 25° und 250°, in dem Druckbereich 0,5 bis 20 Torr auf 1 g Probe ist in Abb. 1 und respektiv Abb. 2 dargestellt. Aus diesen Abbildungen ergibt sich sofort der große Unterschied zwischen den Wasserstoffchemisorptionsisothermen auf dem mit Titan dotiertem Aluminiumoxyd und dem mit Litium dotiertem oder reinem Aluminiumoxyd. Während die bei Sättigung chemisorbierte Wasserstoffmenge bei 25°, 9,1 μ mol H_2/g auf dem mit 4 Atom % dotiertem Aluminiumoxyd beträgt, ist sie 2,6 μ mol H_2/g auf dem reinen Aluminiumoxyd und nur 1,8 μ mol H_2/g auf dem mit 4 Atom % dotiertem Aluminiumoxyd. Dieser bedeutende Unterschied im chemisorptiven Verhalten der Aluminiumoxyde kann auf keinem Fall den Änderungen der spezifischen Oberflächen nach der Dotierung zugeschrieben werden, da diese Änderungen, wie wir vorher zeigten,[15] nur höchstens 25% betragen. Die große Affinität des Wasserstoffs für die mit Titan dotierten Aluminiumoxyde kann an zwei Ursachen zugeschrieben werden: Änderung der Konzentration und Stärke der aktiven Zentren, oder Übergang von schwachen, der physikalischen Adsorption eigenen Bindungen, zu stärkeren Chemisorptionsbindungen, die zu einem hohen Bedeckungsgrad führen.

---

[13] Al. Fruma, D. Ciomârtan, I. Brașoveanu und I. V. Nicolescu, *Rev. Roumaine Chim.*, **18**, 803 (1973).

[14] D. Cismaru und Al. Fruma, *Rev. Roumaine Chim.*, **13**, 139 (1968).

[15] I. V. Nicolescu und Al. Fruma, Mitteilung bei der III. Rep. Konf, für phys. Chem., Bukarest, 1972.

Für die erste dieser Möglichkeiten spricht die beobachtete fast geradlinige Änderung der Sättigungsadsorption mit der Titankonzentration.

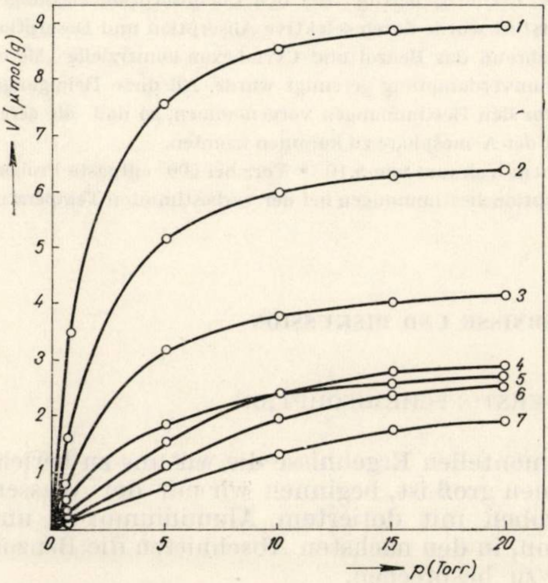

Abb. 1. — Isothermen der Wasserstoffchemisorption bei 25° auf folgenden dotierten Aluminiumoxyden:

4 Atom % Ti (*1*); 2 Atom % Ti (*2*); 0,5 Atom % Ti (*3*); 0,5 Atom % Li (*4*); reines Aluminiumoxyd (*5*); 2 Atom % Li (*6*) und 4 Atom % Li (*7*).

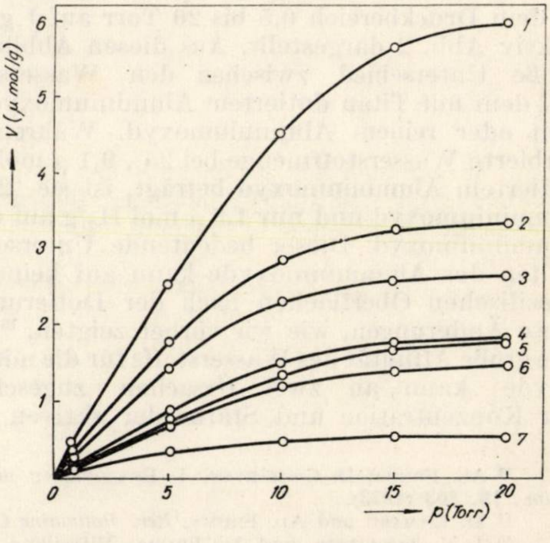

Abb. 2. — Isothermen der Wasserstoffchemisorption bei 250° auf folgenden dotierten Aluminiumoxyden:

4 Atom % Ti (*1*); 2 Atom % Ti (*2*); 0,5 Atom % Ti (*3*); reines Aluminiumoxyd (*4*); 0,5 Atom % Li (*5*); 2 Atom % Li (*6*) und 4 Atom % Li (*7*).

Dieses weist daraufhin, daß sich die Adsorptionszentren mit großer Affinität für Wasserstoff allmählich mit der Titanmenge im Aluminiumoxyd bilden. Da die Wasserstoffchemisorption auf diesen Aluminiumoxyden eine Oberflächenerscheinung ist, ergibt sich die Schlußfolgerung, daß sich das Titan größtenteils auf die Oberfläche lagert und demnach nicht in die Aluminiumoxydmasse eindringt. Zum gleichen Schluß kamen wir auch infolge der Besprechung der Röntgenstrahlen-Diffraktogramme, die wir für diese Proben ausführten [13]. Es ist ersichtlich, daß in den Beugungsspektren nur das Bild des Al_2O_3 vorkommt, das weite Höchstwerte aufweist. Diese Tatsache und die Bemerkung, daß sich die interplanären Abstände des mit Titan dotierten Aluminiumoxyds gegenüber dem reinen Aluminiumoxyd nur betrefflich der Spaltung des Höhepunkts bei 1,99 Å änderten,[16] führten zur Schlußfolgerung, daß sich das Titanoxyd fein dispergiert auf der Oberfläche der Al_2O_3 Partikeln befindet. In dieser Weise stimmen die Ergebnisse der Chemisorption mit den durch Röntgenstrahlenbeugung erhaltenen Strukturbetrachtungen.

Die zweite Möglichkeit und zwar die Änderung infolge der Dotierung der Bindungsweise zwischen der adsorbierten Phase und dem Aluminiumoxyd, kann die beobachteten Unterschiede nicht erklären, da es gut bekannt ist, [17–19] daß die Temperatur von 25° die geeigneteste Temperatur für die Wasserstoffchemisorptionsmessungen ist. Bei dieser Temperatur ist bei der Sättigung eine Höchstbedeckung der Oberfläche mit einer chemisorbierten Wasserstoffschicht gesichert, was sich auch aus der Form der Isothermen, die schon bei Drücken unter 20 Torr einem Gleichwert streben, ergibt.

Unsere Schlüsse bezüglich der Struktur der mit Titan dotierten Aluminiumoxyde müssen sich in den Gleichungen der Adsorptionsisothermen die den Heterogenitätszustand der Oberfläche angeben unvermittelt widerspiegeln. In Abb. 3–5 stellen wir die experimentellen Ergebnisse in Koordinaten entsprechend der Langmuir-, Temkin- und Freundlich--Adsorptionsisothermengleichung dar. Langmuirs Gleichung, die eine homogene Oberfläche voraussetzt, ist von keinem System bestätigt. Temkins Gleichung, die einer „gleichmäßig nichthomogener" Oberfläche, wie sie Roghinski [20] nennt, entspricht, wird durch die Wasserstoffchemisorption auf das reine Aluminiumoxyd, auf allen mit Lithium dotierten Aluminiumoxyden und auf das mit 0,5 Atom % Ti dotiertem Aluminiumoxyd bestätigt, während Freundlichs Gleichung, die der Chemisorption auf einer sehr heterogenen Oberfläche entspricht, von der Wasserstoffchemisorption auf mit Titan dotierten Aluminiumoxyde bestätigt wird. Das Auftragen des Titans auf der Oberfläche der Aluminiumoxydpartikeln ist die Ursache der besonderen Heterogenität dieses Aluminiumoxydtyps. Infolge einer größeren Anzahl von Titanatomen ist die chemisorptive

---

[16] B. C. Lippens und Y. Y. Steggerda „Physical and Chemical Aspects of Adsorbents and Catalysts", Ed. B. C. Linsen, Acad. Press, London, New York, 1970, S. 18.

[17] S. F. Adler und J. Keavney, *J. Phys. Chem.*, **64**, 208 (1960).

[18] D. Cismaru und Al. Fruma, *Rev. Roumaine Chim.*, **14**, 1489 (1969).

[19] D. Cismaru und Al. Fruma, *Rev. Roumaine Chim.*, **13**, 679 (1968).

[20] S. Z. Roghinski „Adsorbtsia i Kataliz na neodnorodnikh povernostiakh", Verlag Akad. Nauk, Moskau, Leningrad, 1948.

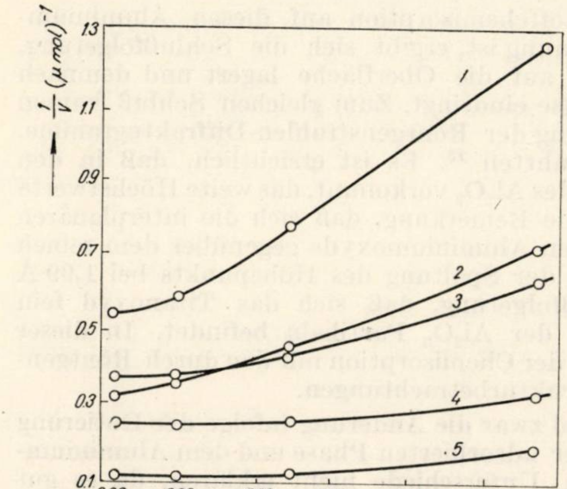

Abb. 3. — Darstellung der Langmuir Isothermgleichung für die Wasserstoffchemisorption bei 25° auf folgenden dotierten Aluminiumoxyden :

4 Atom % Li (*1*) ; 0,5 Atom % Li (*2*) ; reines Aluminiumoxyd (*3*) ; 0,5 Atom % Ti (*4*) und 4 Atom % Ti (*5*).

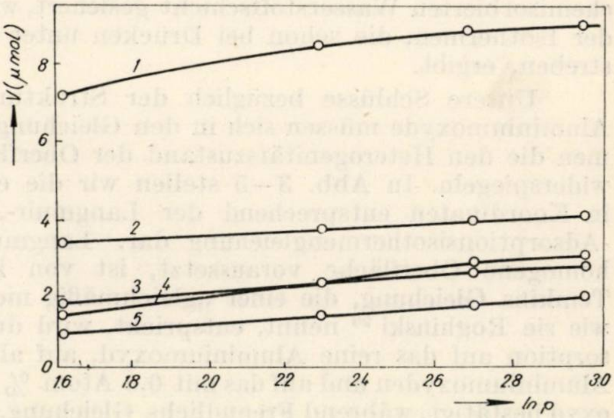

Abb. 4. — Darstellung der Temkin Isothermgleichung für die Wasserstoffchemisorption bei 25° auf folgenden dotierten Aluminiumoxyden :

4 Atom % Ti (*1*) ; 0,5 Atom % Ti (*2*) ; reines Aluminiumoxyd (*3*) ; 0,5 Atom % Li (*4*) und 4 Atom % Li (*5*).

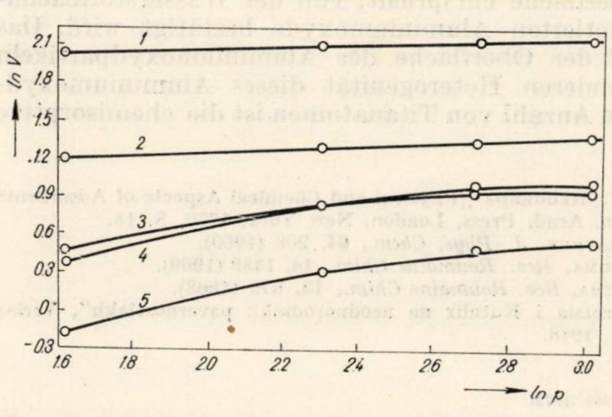

Abb. 5. — Darstellung der Freundlich Isothermgleichung für die Wasserstoffchemisorption bei 25° auf folgenden dotierten Aluminiumoxyden :

4 Atom % Ti (*1*) ; 0,5 Atom % Ti(*2*) ; reines Aluminiumoxyd (*3*) ; 0,5 Atom % Li (*4*) und 4 Atom % Li (*5*).

Kapazität der dotierten Aluminiumoxyde entsprechend größer, aber der Mechanismus der gegenseitigen Wirkung bleibt unverändert.

Gegenüber dem Wasserstoff weisen die mit Lithium dotierten Aluminumioxyde ein gänzlich verschiedenes Verhalten als die titandotierten Aluminiumoxyde auf, und zwar mit dem Ansteigen der Lithiumkonzentration in den Proben, fällt die chemisorptive Kapazität. Bei der Temperatur von 25° sind die Unterschiede zwischen den Sättigungschemisorptionen der mit 0,5 ; 2 und 4 Atom % Li dotierten Aluminiumoxyde und dem reinen Aluminiumoxyd gering und übertreffen nur wenig die Genauigkeit der experimentellen Methode. Auch bei dieser Temperatur bemerkt man eine Verminderung der Adsorption in der Reihenfolge : 0,5 ; 2 und 4 Atom % Li. Bei höherer Temperatur bleibt die Reihenfolge unverändert und die Chemisorption ist im ganzen Druckbereich geringer als die auf dem reinen Aluminiumoxyd. Dieses Verhalten der lithiumdotierten Aluminiumoxyde, wie auch die Tatsache, daß sich Temkin's Gleichung, die einer „gleichmäßig nichthomogener" Oberfläche entspricht, bewährt, weist daraufhin, daß das Lithium im Gitter des Aluminiumoxyds eindringt und ein bei der Wasserstoffchemisorption nicht aktives Aluminat bildet, dessen Konzentration im Aluminiumoxyd mit der Dotierungsmasse wächst.

Für die Prüfung dieser Voraussetzung führten wir auch die Röntgenstrahlendiffraktogramme der mit Lithium dotierten Aluminiumoxyde aus. Zum Unterschied zu den mit Titan dotiertem Aluminiumoxyd, weist das mit Litium dotierte Aluminiumoxyd im Diffraktionsspektrum die charakteristischen Linien des Litiumaluminats $LiAl_5O_8$ Form I und II auf. Zu diesem Schluß gelangten wir durch das Vergleichen der Beugungshöchstwerte bei 2,809 Å, 1,40 und 1,96—1,99 Å.[13] Es ist ersichtlich, daß der für die Form I und II spezifische Höhepunkt bei 2,809 Å schmal ist und mit der Vergrößerung der Lithiumkonzentration zunimmt. Die flache Form des Höhepunkts bei 2,30 Å und 1,40 Å deutet auf eine größere Gitterordnung in den betreffenden Kristallebenen, wo ein größerer Beitrag der Aluminium und Sauerstoffatomen als der Lithiumatomen vorhanden ist. Wir zeigten, [13] daß die Änderung der Intensitäten der Linie bei 2,809 Å mit der Konzentration der Li^+ Ionen daraufhin deutet, daß das Lithiumaluminat freie oktaedrische Plätze besitzt, die durch Dotierung allmählich mit den Li^+ Ionen von $Al\,[Li\square_{0,5-x}\,Al_{1,5}]\,O_4$ bis $Al\,[Li_{0,5}\,Al_{1,5}]\,O_4$, wo $0 < x < 0,5$, besetzt werden.

Da wir bewiesen, [13] daß in unseren Herstellungsbedingungen das Titan nicht im Aluminiumoxydgitter eindringt, sondern sich in Form von dispergiertem Oxyd auf der Oberfläche befindet, versuchten wir auf Grund unserer Wasserstoffchemisorption Ergebnisse, eine Dispersionsberechnung für diese Proben vorzunehmen. Wir unternahmen darum einige Wasserstoffchemisorptionmessungen auf einer TiO_2 Etalonprobe, die aus $Ti(NO_3)_4$ in denselben Bedingungen wie das mit Titan dotierte Aluminiumoxyd hergestellt wurde. Das Titanoxyd kommt in Rutilform (tetragonal, a=4,59 Å, c=2,95 Å) vor. Bei 25° betrug seine Sättigungschemisorption 6,8 μ mol H_2/g für eine spezifische Oberfläche von 5,4 m^2/g. Da es experimentell unmöglich ist einige Daten zu ermitteln, wie z.B. die Oberflächendichte des Titanoxyds aus unseren Proben, das Verhältnis, aus der Gesamtmenge, das sich auf der Aluminiumoxydoberfläche befindet und die Anzahl der chemisorbierten Wasserstoffatome die einem Oberflächengebilde TiO_2 entspricht, könnten wir eine vollständige Berechnung der Dispersion, wie sie gewöhnlich bei der Bestimmung der Partikelgröße bei aufgetragenen Metallkatalysatoren ausgeführt wird, nicht vollbringen. Auf Grund der Daten die wir besitzen ist es möglich Wellers [21] Berechnungsmethode anzuwenden. Diese Methode gestattet das gegenseitige Vergleichen der Dispersion des TiO_2 aus den entsprechenden Proben und führt zur Ermittelung der Oberfläche die dem TiO_2 aus der Gesamtoberfläche der Probe ankommt, ohne aber als Endresultat eine Partikelgröße anzugeben. Im Folgenden werden wir diese Berechnung unternehmen.

Aus den in Abb. 1 dargestellten Chemisorptionisthermen wird durch Subtraktion die chemisorbierte Wasserstoffmenge des auf der Oberfläche befindlichen Titanoxyds ermittelt. Bei den Proben mit 4;2 und 0,5 Atom % Ti beträgt diese Menge respektiv 6,4; 3,7 und 1,4 μ mol H_2/g Probe. Auf einem Gramm TiO_2 bezogen ist die chemisorbierte Wasserstoffmenge respektiv 102, 118 und 178μ mol $H_2/g\ TiO_2$. Angenommen, daß sowohl auf dem dotierten Aluminiumoxyd als auch auf die Etalonprobe der Mechanismus derselbe ist, wird 1 g TiO_2 aus den dotierten Aluminiumoxyden um 102/6,8 = 15, 0; 118/6,8 = 17,35 und 178/6,8 = 26,2 mehr Wasserstoff als 1 g TiO_2 aus der Etalonprobe adsorbieren. Es ergibt sich dadurch, daß das auf der Oberfläche des Aluminiumoxyds befindliche TiO_2 im Vergleich zu der Etalonprobe 15,0; 17,35 und 26,2 mal dispergierter, bei den mit 4; 2 und 0,5 Atom % Ti dotierten Proben, vorkommt. Mit der Zunahme der Konzentration des Dotierstoffs, wird die Dispersion vermindert. Diese Erscheinung war zu erwarten, da größere Oberflächenkonzentrationen das Wachstum im Volumen der Oberflächenkristalliten fördert.

Die Berechnung der Oberfläche die dem TiO_2 aus dem dotierten Aluminiumoxyd ankommt kann nur in der Annahme, daß sich die Gesamtmenge des TiO_2 auf der Oberfläche befindet, ausgeführt werden. Diese Annahme kann nicht geprüft werden, aber für sie plädieren die Chemisorptionsmessungen und Röntgenstrahlenbestimmungen die wir mehr oben besprachen. Wenn 6,8 μ mol H_2 auf 5,4 m^2 der Etalonprobe chemisorbiert werden, dann werden sich 6,4; 3,7 und 1,4 μ mol H_2 auf 5,10; 2,94 und 1,11 m^2 auf den mit respektiv 4; 2 und 0,5 Atom % Ti dotierten Aluminiumoxyde chemisorbieren. Im Vergleich zu der über 100 m^2 großen Gesamtoberfläche der dotierten Aluminiumoxyde, ist die Oberfläche die dem Titan ankommt klein. Dieses könnte eine Ursache für das Fehlen der charakteristischen Linien des Rutils im Diffraktionspektrum der mit Titan dotierten Aluminiumoxyde sein.

3.2. BENZOLADSORPTION

Wir untersuchten die Adsorption der Benzoldämpfe bei der Temperatur von 100° in dem Druckbereich 0,5 bis 20 Torr. In Abb. 6 und

---

[21] S. Weller und S. E. Voltz, *J. Amer. Chem. Soc.*, **75**, 5227 (1953).

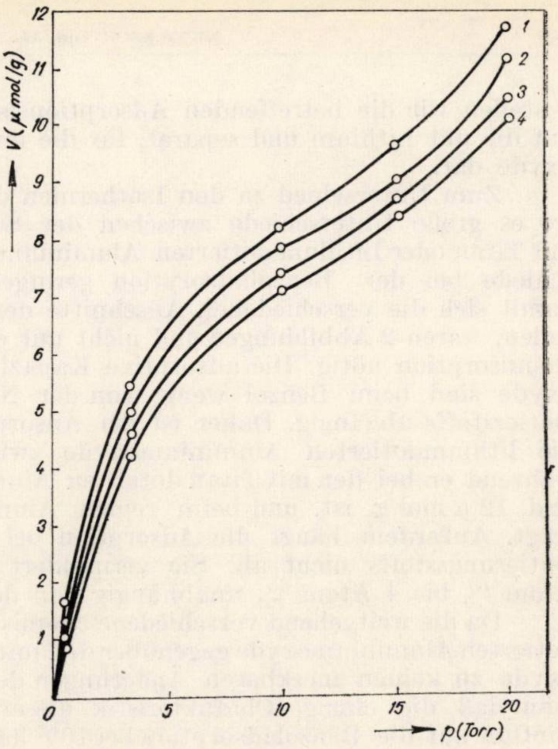

Abb. 6. — Isothermen der Benzoladsorption bei 100° auf folgenden dotierten Aluminiumoxyden :

0,5 Atom% Li (*1*) ; reines Aluminiumoxyd (*2*) ; 2 Atom% Li (*3*) und 4 Atom % Li (*4*)

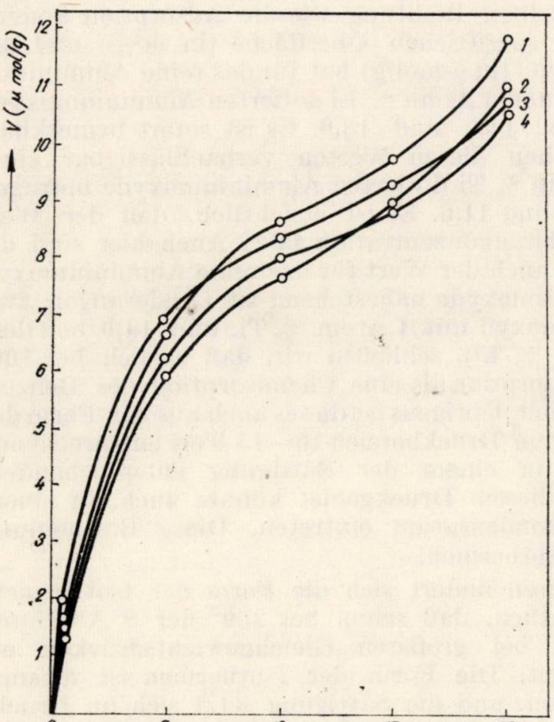

Abb. 7. — Isothermen der Benzoladsorption bei 100° auf folgenden dotierten Aluminiumoxyden :

0,5 Atom% Ti (*1*) ; reines Aluminiumoxyd (*2*) ; 2 Atom % Ti (*3*) 4 Atom % Ti (*4*).

7 stellen wir die betreffenden Adsorptionsisothermen für die Adsorption auf die mit Lithium und separat, für die mit Titan dotierten Aluminiumoxyde dar.

Zum Unterschied zu den Isothermen der Wasserstoffchemisorption, wo es große Unterschiede zwischen der Sättigungsadsorption auf den mit Titan oder Lithium dotierten Aluminiumoxyde gab, sind diese Unterschiede bei der Benzoladsorption geringer. Aus diesem Grund und damit sich die verschiedenen Abschnitte der Isothermen nicht schneiden sollen, waren 2 Abbildungen und nicht nur eine, wie bei der Wasserstoffchemisorption nötig. Die adsorptive Kapazität der dotierten Aluminiumoxyde sind beim Benzol wenig von der Natur und Konzentration des Dotierstoffs abhängig. Daher ist der Adsorptionsbereich bei 20 Torr für die lithiumdotierten Aluminiumoxyde zwischen 10 und 11,7 μ mol/g, während er bei den mit Titan dotierten Aluminiumoxyden zwischen 10,7 und 12 μ mol/g ist, und beim reinen Aluminiumoxyd 11,2 μ mol/g beträgt. Außerdem hängt die Adsorption bei 20 Torr von der Natur des Dotierungsstoffs nicht ab. Sie vermindert sich bei Dotierung von 0,5 Atom % bis 4 Atom %, unabhängig von der Natur des Dotierungsions.

Da die weitgehend verschiedene chemische Struktur der mit Lithium dotierten Aluminiumoxyde gegenüber den mit Titan dotierten Aluminiumoxyde zu keinen merkbaren Änderungen der Adsorption führt, schließt man, daß die einzige Charakteristik dieser Aluminiumoxyde die einen Einfluß auf die Benzoladsorption bei 100° hat, die spezifische Oberfläche ist, die sich genau in der selben Richtung wie die Adsorption ändert. Das Verhältnis zwischen der spezifischen Oberfläche (in m^2/g) und der Adsorption bei 20 Torr und 100° (in μ mol/g) hat für das reine Aluminiumoxyd und für die mit 0,5 ; 2 und 4 Atom % Li dotierten Aluminiumoxyde folgende Werte : 13,7 ; 13,5 ; 14,0 und 13,9. Es ist sofort bemerkbar, daß die Unterschiede zwischen diesen Werten vernachlässigbar sind. Für die mit 0,5 ; 2 und 4 Atom % Ti dotierten Aluminiumoxyde betrugen diese Verhältnisse 12,5 ; 12,5 und 11,6. Es ist ersichtlich, daß der Wert dieser Verhältnisse mit der Titankonzentration fällt. Auch hier sind die Unterschiede sehr gering. Da auch der Wert für das reine Aluminiumoxyd und für die dotierten Aluminiumoxyde nahestehend ist (Änderungen zwischen 11,6 bei dem Aluminiumoxyd mit 4 Atom % Ti, und 14,0 bei dem Aluminiumoxyd mit 2 Atom % Li), schließen wir, daß es sich bei 100° eher um eine physikalische Adsorption als eine Chemisorption des Benzols auf dem Aluminiumoxyd handelt. Übrigens ist dieses auch aus der Form der Isothermen ersichtlich. Der dem Druckbereich 10—15 Torr entsprechende Isothermenteil steigt, statt in einem der Sättigung entsprechendem Gleichwert überzugehen. In diesem Druckgebiet könnte auch, in einem gewissen Maß die Kapillarkondensation eintreten. Diese Erscheinung verursacht meistens S-Typ Isothermen.

Bei höheren Temperaturen ändert sich die Form der Isothermen. Aus Abb. 8 und 9 ist ersichtlich, daß schon bei 250° der S Abschnitt der Isothermen, der bei 100° bei größeren Gleichgewichtsdrücken erscheint, nicht mehr vorkommt. Die Form der Isothermen ist diesmal klassisch für die Chemisorption, und die Sättigung setzt sich im Druckbereich 15—20 Torr für alle Proben ein. Die Reihenfolge der Sättigungsadsorptionen ist der bei 20 Torr und 100° verschieden. Zum Unterschied zu der Adsorption bei 100°, wo die Sättigungswerte nur von der spezifischen Oberfläche abhängen, was die physikalische Adsorption bei dieser Temperatur charakterisierte, ist die Benzolchemisorption bei 250° sowohl von der spezifischen Oberfläche, als auch von der Natur des Dotierstoffs

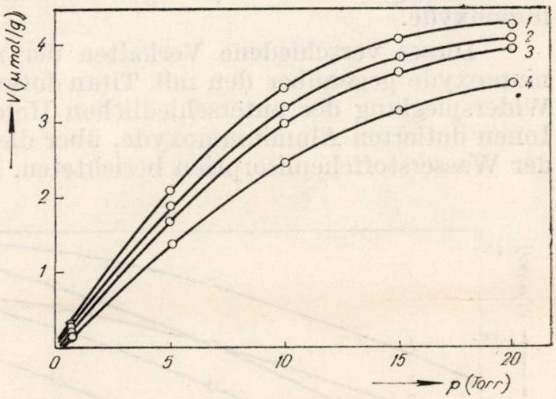

Abb. 8. – Isothermen der Benzoladsorption bei 250° auf folgenden dotierten Aluminuimoxyden :

0,5 Atom % Li (*1*) ; 2 Atom % Li (*2*) ; reines Aluminiumoxyd (*3*) und 4 Atom % Li (*4*).

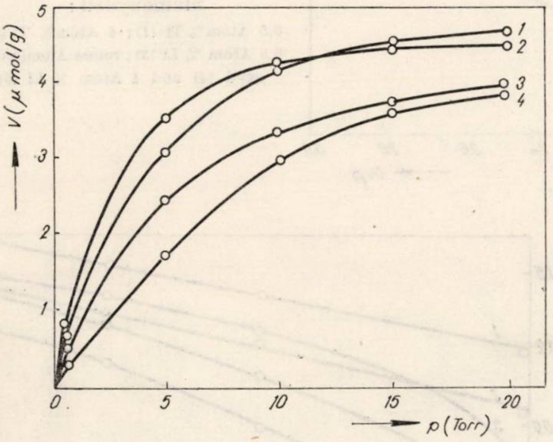

Abb. 9. – Isothermen der Benzoladsorption bei 250° auf folgenden dotierten Aluminiumoxyden :

0,5 Atom % Ti (*1*) ; 2 Atom % Ti (*2*) ; 4 Atom % Ti (*3*) und reines Aluminiumoxyd (*4*).

abhängig. Für die mit Titan dotierten Aluminiumoxyde ist die Sättigungsadsorption immer größer als die des reinen Aluminiumoxyds. Die Tatsache, daß die Sättigungschemisorption bei dem 0,5 Atom % Ti dotiertem Aluminiumoxyd größer ist als die bei dem 4 Atom % Ti dotiertem Aluminiumoxyd kann sowohl mit der größeren spezifischen Oberfläche, als auch mit der höheren Dispersion bei der Probe mit 0,5 Atom % Ti in Verbindung gesetzt werden.

Die größten Unterschiede zwischen der auf dem reinen Aluminiumoxyd entsprechenden Isotherme und die Chemisorptionisothermen auf den dotierten Aluminiumoxyde kommen bei Gleichgewichtsdrücken zwischen 0,5 und 5 Torr vor, demnach im Gebiet der geringen Bedeckungsgraden. Dieses weist auf die Tendenz der mit Titan dotierten

Aluminiumoxyde sich schneller als das reine Aluminiumoxyd zu sättigen, was durch den ersten stark steigenden Abschnitt der Isothermen zum Vorschein kommt. Dadurch wird auch die Schneidung der Isothermen der mit 0,5 und 2 Atom % Ti dotierten Aluminiumoxyde bedingt. All diese Erscheinungen sind viel geringer bei den mit Lithium dotierten Aluminiumoxyde.

Dieses verschiedene Verhalten der mit Lithium dotierten Aluminiumoxyde gegenüber den mit Titan dotierten Aluminiumoxyden ist eine Widerspieglung der unterschiedlichen Heterogenität der mit verschiedenen Ionen dotierten Aluminiumoxyde, über die wir mehr bei der Besprechung der Wasserstoffchemisorption berichteten. In Abb. 10 und 11 bringen wir die Adsorptionsisothermen des Benzols bei 250° auf den dotierten Aluminiumoxyden und dem reinen Aluminiumoxyd in Koordinaten entsprechend Temkins und Freundlichs Isothermengleichung dar. Wie erwartet, sind die Ergebnisse der Benzoladsorption in guter Übereinstimmung mit denen die wir über die Heterogenität der Oberfläche bei der Wasserstoffchemisorption besprochen haben. Aus Abb. 10 ist ersichtlich, daß sich Temkins Adsorptionsisotherm, die eine gleichmäßig nichthomogene Oberfläche

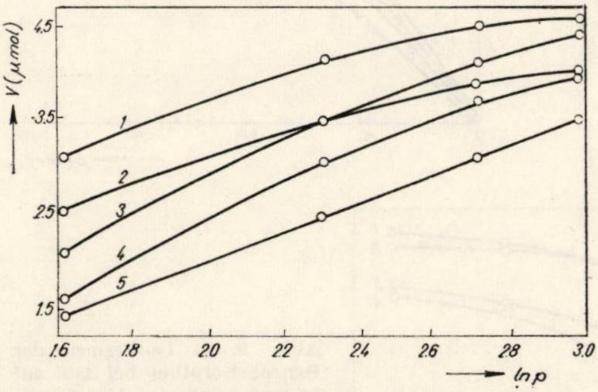

Abb. 10. — Darstellung der Temkin Isothermgleichung für die Benzoladsorption bei 250° auf folgenden dotierten Aluminiumoxyden:

0,5 Atom% Ti (*1*); 4 Atom% Ti (*2*); 0,5 Atom % Li (*3*); reines Aluminiumoxyd (*4*) und 4 Atom % Li (*5*).

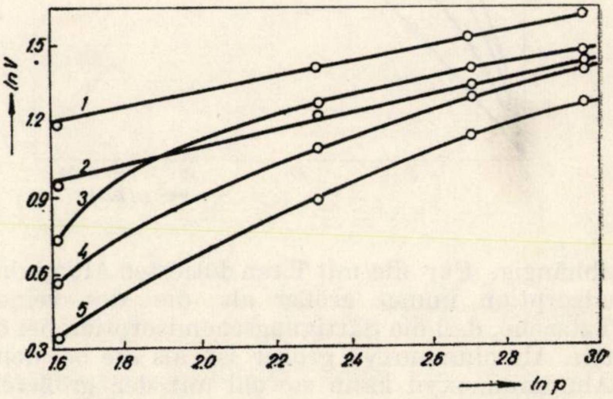

Abb. 11. — Darstellung der Freundlich Isothermgleichung für die Benzoladsorption bei 250° auf folgenden dotierten Aluminiumoxyden:

0,5 Atom% Ti (*1*); 4 Atom % Ti (*2*); 0,5 Atom % Li (*3*); reines Aluminiumoxyd (*4*) und 4 Atom % Li (*5*).

voraussetzt, dem mit 4 Atom % Li dotiertem Aluminiumoxyd vortrefflich, und dem mit 0,5 Atom % Li dotiertem Aluminiumoxyd ziemlich gut anpaßt. Die anderen Aluminiumoxyde, die eine weitgehende Heterogenität besitzen, bestätigen nicht Temkins Gleichung, sondern Freundlichs Gleichung, wie aus Abb. 11 ersichtlich ist. All diese Ergebnisse sind in guter Übereinstimmung mit den Strukturbetrachtungen die wir auf Grund der Besprechung der Röntgenstrahlen Diffraktogramme, wie wir auch bei der Wasserstoffchemisorption zeigten, vorführten.

Da die adsorptiven Eigenschaften der dotierten Aluminiumoxyde für das Benzol nur wenig von der chemischen Natur dieser Aluminiumoxyde abhängig sind, und demnach nicht spezifisch sind, ist eine Dispersionsbestimmung oder die Schätzung der Oberfläche eines Komponents, ähnlich wie bei der Wasserstoffchemisorption, nicht möglich.

3.3. CYCLOHEXANADSORPTION

Die Adsorption des Cyclohexans wurde im Temperaturbereich 100—250° bei Gleichgewichtsdrücken zwischen 0,5 und 20 Torr untersucht. Da bei 100° die Adsorptionsisothermen ähnlich denen des Benzols sind, stellten wir nur die Isothermen des Cyclohexans bei 250° dar, wo das Verhalten des Cyclohexans ganz verschieden wie das des Benzols ist. Auch bei 100° kommen aber einige Unterschiede gegenüber den Benzoladsorptionsisothermen vor, und zwar defindet sich die bei 20 Torr adsorbierte Menge zwischen 6 und 8μ mol Cyclohexan/g, d.h. weniger als beim Benzol, und der S Abschnitt der Isothermen, der die physikalische Adsorption und die kapillare Kondensation charakterisierte, erscheint beim Cyclohexan, wahrscheinlich wegen der größeren Volatilität, nicht mehr. Bei der Cyclohexanadsorption bei 100° sind die Unterschiede zwischen dem adsorptiven Verhalten den mit Lithium dotierten, gegenüber den mit Titan dotierten Aluminiumoxyde.gering. Dieses weist daraufhin, daß bei dieser Temperatur der Effekt der spezifischen Oberfläche und nicht die chemische Natur maßgebend ist. Es ist demnach ein Gebiet der physikalischen Adsorption das für besondere Auslegungen nicht geeignet ist.

In Abb. 12 stellten wir die Isothermen der Cyclohexanchemisorption auf den dotierten Aluminiumoxyden und auf dem reinen Aluminiumoxyd vor. Von Anfang an bemerkt man einen deutlichen Unterschied gegenüber den Isothermen des Benzols auf diesen Aluminiumoxyden, bei derselben Temperatur. Die dem reinen Aluminiumoxyd entsprechende Isotherme hat eine mittlere Lage zwischen den Isothermen die dem mit Lithium und Titan dotierten Aluminiumoxyd entsprechen. Dieses ist dem Verhalten bei der Wasserstoffchemisorption sehr ähnlich und dem bei der Benzolchemisorption beobachteten Verhalten entgegengesetzt. Der Effekt der spezifischen Oberfläche ist vernachlässigbar, da die Sättigungsadsorptionen nur von der chemischen Natur der Aluminiumoxyde und von der Konzentration des Dotierstoffs abhängen. Die Werte der Sättigungsadsorptionen ändern sich in der Reihenfolge: Aluminiumoxyd dotiert mit 4 Atom % Ti — 2 Atom % Ti — 0,5 Atom % Ti — reines

Aluminiumoxyd — Aluminiumoxyd dotiert mit 0,5 Atom % Li — 2 Atom % Li — 4 Atom % Li, von 5 bis 2,5 μ mol/g. In Vergleich zu der Wasserstoffchemisorption bleibt bei dieser Temperatur die Reihenfolge unverändert, aber der Wertebereich ist viel geringer.

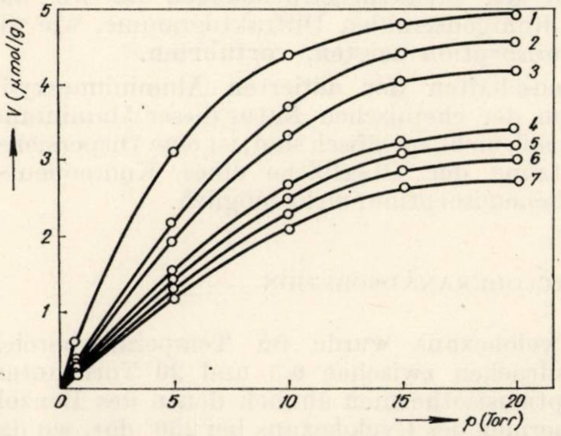

Abb. 12. — Isothermen der Cyclohexanadsorption bei 250° auf folgenden dotierten Aluminiumoxyden :

4 Atom % Ti (*1*) ; 2 Atom % Ti (*2*) ; 0.5 Atom % Ti (*3*) ; reines Aluminiumoxyd (*4*) ; 0.5 Atom % Li (*5*) 2 Atom % Li (*6*) und 4 Atom % Li (*7*).

Auf Grund der Isothermgleichung der Cyclohexanadsorption werden wir einige Schlüsse über die Heterogenität des dotierten und reinen Aluminiumoxyds ziehen. Unsere Aufgabe ist festzustellen in welchem Maße die Chemisorption des Cyclohexans die Ergebnisse der Wasserstoff- und Benzolchemisorption bezüglich der Prüfung der Temkin und Freundlich Gleichung bestätigt.

In Abb. 13 und 14 stellten wir die Resultate der Cyclohexanchemisorption bei 250° in Koordinaten entsprechend Temkins und Freundlichs Isothermengleichung dar. Es ist ersichtlich, daß die Schlüsse die wir bei der Wasserstoff und Benzolchemisorption über die fortgeschrittene Heterogenität der titandotierten Aluminiumoxyde feststellten, auch von diesen experimentellen Ergebnissen bestätigt werden. Man bemerkt bei den beiden Darstellungen, daß sich die Punkte die dem Druck von 20 Torr entsprechen, nicht auf den Geraden befinden, sondern gegen geringere Werte der Adsorption verschoben sind. Diese Tatsache ist der Sättigung der Oberfläche bei Drücken unter 20 Torr zu verdanken, wie aus Abb. 12 ersichtlich ist. Da bei den anderen Gleichgewichtsdrücken die experimentellen Punkte auf den Geraden gut angepaßt sind, und zwar für die Chemisorption des Cyclohexans auf mit Titan dotiertem Aluminiumoxyd die Freundlich Gleichung, während für das mit Lithium dotierte Aluminiumoxyd die Temkin Gleichung bestätigt wird, bleiben unsere Schlüsse gültig.

Auf Grund der Struktur der mit Titan dotierten Aluminiumoxyde die wir vorher besprachen, wir auch wegen den Unterschieden zwischen der Chemisorption auf die Titan dotierten gegenüber den Lithium dotierten Aluminiumoxyde, versuchten wir die Oberfläche die dem Cyclohexan bei 250° auf das Titanoxyd, das sich auf der Aluminiumoxydoberfläche befindet, ankommt zu ermitteln. Zum Unterschied zu der Berechnung die

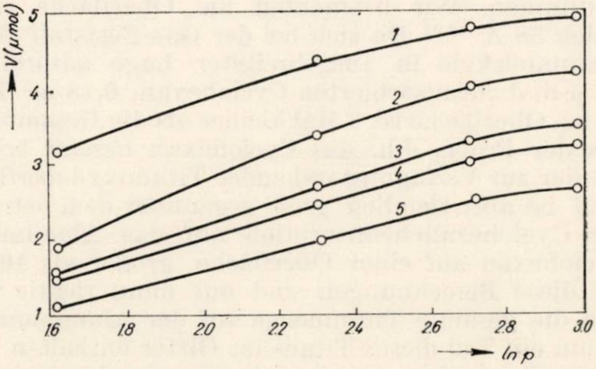

Abb. 13. – Darstellung der Temkin Isothermgleichung für die Cyclohexanadsorption bei 250° auf folgenden dotierten Aluminiumoxyden : 4 Atom % Ti (*1*) ; 0,5 Atom% Ti (*2*) ; reines Aluminiumoxyd (*3*) ; 0,5 Atom% Li (*4*) und 4 Atom % Li (*5*).

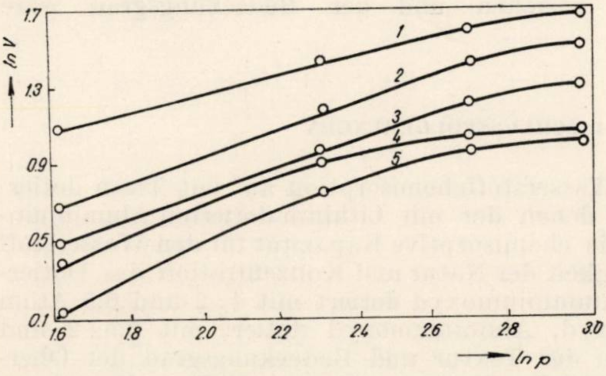

Abb. 14. – Darstellung der Freundlich Isothermgleichung für die Cyclohexanadsorption bei 250° auf folgenden dotierten Aluminiumoxyden : 4 Atom % Ti (*1*) ; 0,5 Atom % Ti (*2*): reines Aluminiumoxyd (*3*) ;0,5 Atom%. Li (*4*) und 4 Atom % Li (*5*).

wir bei der Wasserstoffchemisorption ausführten erscheinen bei der Cyclohexanchemisorption einige Schwierigkeiten die mit dem Gleichgewicht Gas-Feststoff verbunden sind. Die Temperatur von 250°, für die wir die Berechnung ausführen, ist hoch genug damit neben der eigentlichen Adsorption auch in einem gewissen Maße die Desorption einwirkt· Dieses kommt durch die ständige Verminderung der Sättigungsadsorption mit der Temperatur zum Vorschein. Die Adsorption bei der von uns gewählten Temperatur ist dadurch nur ein mittlerer Wert zwischen der großen, bei tieferer Temperatur, physikalisch und chemisch adsorbierten Menge, und der geringen chemisorbierten Menge bei höherer Temperatur wo die Desorption maßgebend sein kann und der Bedeckungsgrad klein ist. Da wir nur die gesamtadsorbierte Dampfmenge bestimmen, d.h. die Summe der Adsorptionen auf dem Titanoxyd und dem Aluminiumoxyd, können wir nicht deuten in welchem Maße die Desorption, die bei 250° erscheint den Bedeckungsgrad des Titanoxyds gegenüber dem Aluminiumoxyd beeinflußt. Durch das Abziehen der Cyclohexanmenge das auf dem Aluminiumoxyd chemisorbiert wurde aus der Gesamtmenge des auf der Probe, z.B. mit 0,5 Atom % Ti, chemisorbierten Cyclohexans, kann man die Cyclohexanmenge die auf dem Titanoxyd bei 250° chemisorbiert wurde berechnen, ohne aber behaupten zu können, daß die Gesamtoberfläche des Titanoxyds bedeckt wurde. Da wir aber anhand der Wasserstoffchemisorption berechneten, daß diese Oberfläche 111 m^2/g für das mit 0,5 Atom % Ti dotierte Aluminiumoxyd beträgt, können wir den Teil aus dieser Oberfläche der bei 250° mit Cyclohexan bedeckt ist bestimmen. Wir betrachten die Oberfläche eines Cyclohexanmoleküls gleich 38 $\mathring{A}^2$[22,23] Da sich bei der Gas-Feststoff Wechselwirkung die Cyclohexanmoleküle in ausgebreiteter Lage adsorbieren,[24] entsprechen dem 0,8 μ mol chemisorbierten Cyclohexan, 0,18 m^2 Titanoxyd aus der Probe. Diese Oberfläche ist 6 Mal kleiner als die Gesamtoberfläche des Titanoxyds aus der Probe, d.h. das Cyclohexan besetzt bei Sättigung bei 250° nur 1/6 der zur Verfügung stehender Titanoxydoberfläche. Dieser Bedeckungsgrad ist aber ziemlich groß gegenüber dem betreffenden Bedeckungsgrad der Cyclohexanchemisorption auf das Aluminiumoxyd, wobei 3,4 μ mol Cyclohexan auf einer Oberfläche größer als 100 m^2 adsorbiert werden. All diese Berechnungen sind nur dann richtig wenn man annimmt, daß sich die gesamte Titanmenge auf der Aluminiumoxydoberfläche befindet. Wenn ein Teil dieses Titans im Gitter enthalten und der Adsorption nicht zugänglich wäre, würde sich die adsorbierte Cyclohexanmenge auf eine geringere Titanoberfläche beziehen und der Bedeckungsgrad wäre größer als 1/6.

4. SCHLUSSFOLGERUNGEN

Die Isothermen der Wasserstoffchemisorption auf mit Titan dotierten Aluminiumoxyde sind denen der mit Lithium dotierten Aluminiumoxyde sehr verschieden. Die chemisorptive Kapazität für den Wasserstoff vermindert sich in Abhängigkeit der Natur und Konzentration des Dotierstoffs in der Reihenfolge : Aluminiumoxyd dotiert mit 4 ; 2 und 0,5 Atom % Ti, reines Aluminiumoxyd, Aluminiumoxyd dotiert mit 0,5 ; 2 und 4 Atom % Li. Sie ist von der Textur und Bedeckungsgrad der Oberfläche unabhängig. Auf Grund der Bestätigung Freundlichs Adsorptionsisothermgleichung von den mit Titan dotierten Aluminiumoxyde wurden Schlüsse über die Heterogenität der Oberfläche dieser Aluminiumoxyde gezogen. Diese Schlüsse, zusammen mit den röntgenographischen diffraktometrischen Untersuchungen, gestatteten die Ausführung eines Strukturmodells für die mit Titan dotierten Aluminiumoxyde, gemäß dem sich der größte Teil der durch Dotierung eingeführten Titanionen, in Form von TiO_2 auf der Aluminiumoxydoberfläche wiederfinden. Durch den Vergleich der Ergebnisse der Wasserstoffchemisorption auf den dotierten Aluminiumoxyde gegenüber einer TiO_2 Etalonprobe, berechneten wir, daß in den 0,5 ; 2 und 4 Atom % Ti dotierten Aluminiumoxyde, das TiO_2 respektiv 1,11 ; 2,94 und 5,4 m^2/g beträgt. Für die mit Lithium dotierten Aluminiumoxyde sind wir der Ansicht, daß die Oberflächen gleichmäßig nichthomogen sind, und daß die Homogenität mit dem Lithium-

---

[22] R. N. Smith, C. Pierce und H. Cordes, *J. Amer. Chem. Soc.*, **72**, 5595 (1950).
[23] J. S. Mardaschew, *Uchenie Zapiski*, **464**, 12 (1971).
[24] K. V. Topchieva, *Zhur. fiz. Khim.*, **27**, 411 (1953).

gehalt wächst. Das Lithium dringt im Aluminiumoxydgitter ein und bildet folgendes Aluminat $Al\,[Li_x\square_{0,5-x}Al_{1,5}]O_4$.

Aus den Isothermen der Benzoladsorption auf den dotierten Aluminiumoxyden ergab sich die Unabhängigkeit der Sättigungsadsorption von der Natur des Dotierstoffs und die maßgebende Rolle der spezifischen Oberfläche. Wegen der Nichtspezifizität der Benzoladsorption konnte eine Dispersionsberechnung nicht unternommen werden. Die Schlüsse der Röntgenstrahlen Diffraktogramme und Wasserstoffchemisorption über die Heterogenität der Oberflächen werden auf Grund der Darstellung der experimentellen Ergebnisse in Koordinaten entsprechend Temkins und Freundlichs Adsorptionsisothermen bestätigt.

Die Chemisorption des Cyclohexans auf den dotierten Aluminiumoxyde weist eine ähnliche Spezifizität wie bei der Wasserstoffchemisorption beobachtete auf. Die Reihenfolge der Verminderung der chemisorptiven Kapazität ist von den titandotierten zu den lithiumdotierten Aluminiumoxyde dieselbe wie bei der Wasserstoffchemisorption. Man schätzte, daß bei 250° der Bedeckungsgrad mit Cyclohexan des Titanoxyds auf der Oberfläche des mit 0,5 Atom % Ti dotierten Aluminiumoxyds, etwa 16,2 % beträgt. Die vorherigen Schlüsse über die Heterogenität der Oberfläche werden auch von der Chemisorption des Cyclohexans bestätigt.

Wir sind der Ansicht, daß die Entwicklung dieser Forschung zu einer besseren Kenntnis der Beziehungen zwischen der Oberflächenchemie, des Gas-Feststoff Gleichgewichts und Heterogenität, im Verhältnis zu der Struktur der Moleküle die adsorbiert werden und zu den Herstellungsbedingungen der dotierten Aluminiumoxyde führen kann.

Revue Roumaine de Chimie, 18, 6, 971–977 (1973)

SPECTRAL STUDY OF SOME MIXED LIGAND COMPOUNDS OF LANTHANIDES

P. SPACU and SILVIA PLOŞTINARU

Institute of Physical Chemistry, Dumbrava Roşie, 23, Bucharest, Romania

Received December 15, 1972

A series of ternary compounds with a general formula LnL_2X_3 (where Ln=La, Ce, Pr, Nd, Sm, Eu, Tb, Dy, Er; X=bromomandelic and chlorosalicylic acid and L=-*o*-phenanthroline and 5,6-dimethylphenantroline) were synthetized and studied. The type of coordination of the ligands was established by the study of their IR spectra. The electronic visible spectra inform us on the hypersensitivity and allow us to calculate the nephelauxetic ratio and the covalency degree of the Pr(III) and Nd(III) compounds.

Carrying further our studies[1] on new compounds of lanthanide carboxylates with nitrogen donor atom organic bases, we have obtained and studied a new series of coordination compounds of lanthanide bromomandelates and chlorosalicylates with *o*-phenanthroline and 5,6-dimethylphenanthroline.

The new compounds obtained have the general formula:

LnL_2X_3 where: Ln = La, Ce, Pr, Nd, Sm, Eu, Tb, Dy, Er.
X = bromomandelic acid (BrMand)
$Br-C_6H_4-CHOH-COOH$
5–chlorosalicylic acid (ClSal)
$HO-C_6H_3-Cl-COOH$
L = *o*-phenanthroline (phen)
5,6-dimethylphenanthroline (DMPh)

RESULTS AND DISCUSSIONS

A spectral study was carried out on the new synthetized compounds in order to establish the character of the chemical bonding and ability of "f" orbitals to participate to the chemical bond formation. To this purpose we have therefore studied the UV and visible electronic spectra as well as the IR spectra.

---

[1] P. Spacu and S. Ploştinaru, *Rev. Roumaine Chim.*, **17**, 697 (1972).

The UV spectra recorded in ethanol and methanol solutions ($C = 10^{-5}M$) are practically identical to the spectra of the free ligands. The characteristic maxima of phenanthroline and 5,6-dimethylphenanthroline appear in all the complexes. The high values of the extinction molar coefficients of the compounds (table 1) are in good agreement with the fact that two basic molecules enter into the composition of the complexes. The absorption bands of the chlorosalicylic acid at 233 and 314 nm are covered by the more intense bands of the *o*-phenanthroline and, respectively, 5,6-dimethylphenanthroline.

Table 1

Absorption maxima in UV for free ligand and its lanthanide compounds

λ nm	$\varepsilon \times 10^{-4}$	Ln (phen)$_2$(BrMand)$_3$			Ln(phen)$_2$(ClSal)$_3$	
		$\varepsilon \times 10^{-4}$			$\varepsilon \times 10^{-4}$	
	phen	Ce	Eu	Nd	Nd	Eu
230	3.48	8.28	8.68	8.63	9.41	9.35
264	3.28	4.36	4.56	4.48	6.03	5.80

The electronic spectra in the visible range recorded on the solid state as well as on DMF and benzene solutions are practically identical. This shows that in the solution too there prevail the same species as in the solid state. The specific bands of the central metal ion which appear, are due to the transition of the electrons from the ground level to the "J" excited levels. The visible spectra of these complexes give us informations on two important factors: the hypersensitivity and nephelauxetic ratio. These factors are determined by the changes due to the coordination which are taking place in the absorption spectrum of the free ion. These changes were experimentally observed by comparing the absorption spectrum of the aquo-ion to the absorption spectrum of the respective complex (figure 1).

No significant changes are generally observed in the intensity or frequency of the absorption bands of the complexes compared to the aqua-ion, which shows a weak participation of the 4*f* orbitals to the formation of the chemical bonds. We may nevertheless mention some *f*—*f* transitions which seem to be intensified by coordination (table 2).

The table 2 shows an increase in the intensity of the absorption bands of the complexes compared to the aquo-ion; there also appears an increase of these band intensities for the complexes with a substituted ligand compared to those with an unsubstituted ligand. This latter is due to the increase of the electronic density around the nitrogen atoms, brought about by the electro-donor influence of the methyl groups, leading to the strengthening of the chemical nitrogen-metal bonds.

Table 2
Hypersensitive transitions

Ln^{3+}	Transition	$\tilde{\nu}$ (10^{-3}) cm^{-1}	ε_1	ε_2	ε_3	ε_4
Nd^{3+}	$^4I_{9/2} \rightarrow {}^4G_{5/2}$	17.3	7.08	15.92	16.62	18.29
	$\rightarrow {}^4G_{7/2}$	19.2	3.58	5.68	6.77	8.36
Pr^{3+}	$^3H_4 \rightarrow {}^3P_2$	22.5	9.04	10.60	11.34	13.02
Er^{3+}	$^5I_{15/2} \rightarrow {}^2H_{11/2}$	19.2	5.60	13.42	14.23	17.05

ε_1 = molar extinction coefficients for aquo ion.
ε_2 = molar extinction coefficients for $Ln(phen)_2\ (ClSal)_3$.
ε_3 = molar extinction coefficients for $Ln(phen)_2\ (BrMand)_3$.
ε_4 = molar extinction coefficients for $Ln(DMPh)_2\ (BrMand)_3$.

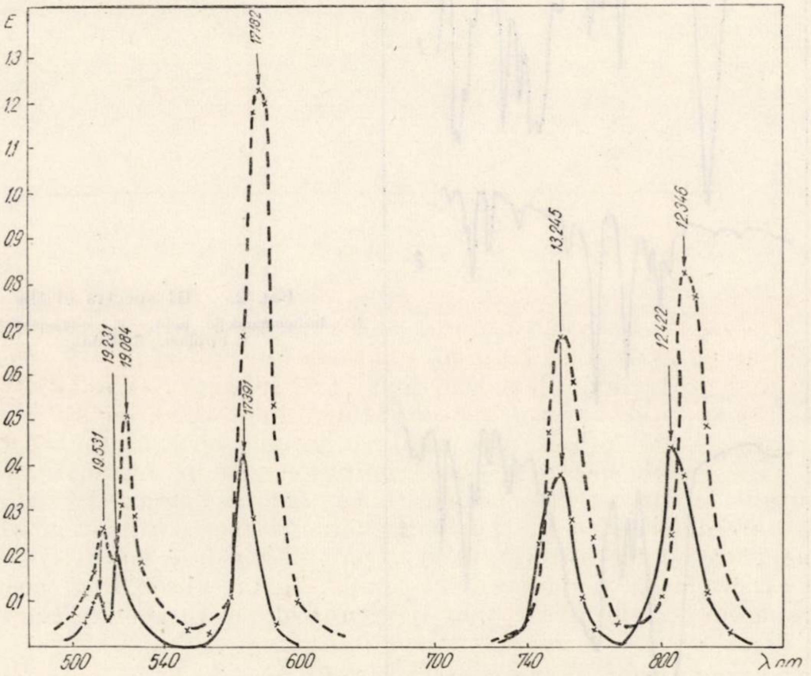

Fig. 1. – The visible absorption spectra of the ——— aquo ion ; – – – $Nd(phen)_2\ (BrMand)_3$.

The shifts taking place in the position of the absorption bands, though small, have nevertheless permitted us to calculate the parameter β (the nephelauxetic ratio)[2] and the covalency degree δ.[3] These were calculated for Pr(III) and Nd(III) complexes and are of the same order of magnitude as in the case of complexes with chloromandelic acid.[1] In the case of erbium there appear no shifts of the absorption bands, but only their intensification.

---

[2] C. K. Jørgensen, *Progr. Inorg. Chem.*, **4**, 73(1962).
[3] S. P. Sinha, *Spectrochim. Acta*, **22**, 57 (1966).

IR SPECTRA

We have examined the IR spectra of the studied ternary complexes to determine the way in which the anions and the bases coordinate with the central metal ion. These spectra are rather complicated, and their interpretation is somewhat difficult due to the overlapping of the frequencies of the coordinate *o*-phenanthrolines on those of the coordinate oxyacids. To study them, we have recorded the IR spectra of the respective oxyacids, of the free bases and of the ternary complexes (figure 2, table 3). For a better comparison, in some cases, we have also determined the spectrum of the corresponding simple salt. By analysing these spectra we have observed a series of changes in the spectrum of the complexes *vs.* the spectrum of the free ligands, changes appearing owing to the coordina-

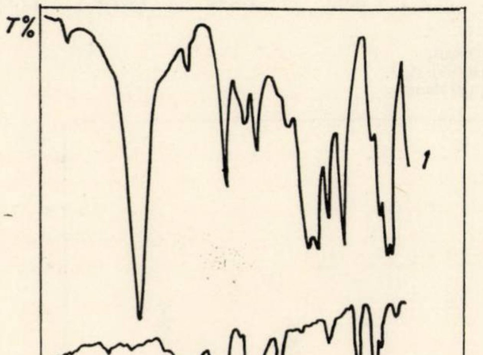

Fig. 2. — IR spectra of the *1*, bromomandelic acid. *2*, *o*-phenanthroline. *3*, $Pr(phen)_2(BrMand)_3$.

tion. Strong bands were identified in the 700–1750 cm^{-1} range, but most important to watch are the bands in the 1350–1750 cm^{-1} range, where the C = N, C = C vibrations of the *o*-phenanthroline ring appear, as well as the OCO vibration frequencies of the respective acids.

The monobasic aliphatic acids show a strong absorption of the carbonyl group between 1705–1720 cm^{-1}.[4] The substitution by a halogen or CN^- group, results in the shift of the absorption range of the carbonyl group towards higher frequencies[5]; thus for bromomandelic acid, the frequency of the carbonyl group appear at 1735 cm^{-1}. This frequency is moved by coordination and appears in the complexes under the form of two bands corresponding to the asymmetric vibration OCO ($\nu_{as} \approx 1610$ cm^{-1}) and the symmetric vibration OCO ($\nu_s \approx 1400$ cm^{-1}). The strong band at 1600–1610 cm^{-1} appears to be very broad owing to the overlapping with the triplet of the coordinate phenanthroline (1600 cm^{-1}). Also the bands of the free phenanthroline spectrum at 1425 and 1500 cm^{-1} appear to be moved towards higher frequencies as a consequence of the coordination.

In the case of 5-chlorosalicylic acid, which can form intermolecular hydrogen bonds stabilized through a chelatic conjugation, the frequency of the carbonyl group decreases, appearing at 1670 cm^{-1}. As for compounds with bromomandelic acid we find intense bands in two frequency ranges :

Table 3

IR spectral data

Free phen	ClSal acid	Nd $(ClSal)_3$	$Nd(phen)_2(ClSal)_3$	Er $(phen)_2(ClSal)_3$
1628 w	1670 vs		1620 s	1620 s
1600 m	1605 m			
	1570 vw	1550 sh.s	1580 sh.s	1580 sh.s
1513 s			1525 m	1525 m
	1470 s	1465 s	1470 s	1470 s
	1440 s	1435 s	1440 s	1440 s
1425 s			1430 s	1435 s
1340 w	1360 m	1365 s	1370 s	1370 s
	1290 s	1290 m	1290 m	1290 m
	1240 vs			
	1230 vs	1240 s	1250 s	1250 s
	1205 m			
1145 w	1155 m	1155 m	1150 m	1150 m
1100 m	1110 w	1115 m	1110 m	1110 m
850 s	830 s	830 s	850 s	850 s
820 vw			835 s	830 s
774 m			780 m	780 m
740 s			735 s	735 s

s = strong, m = medium, w = weak, sh = shoulder.

---

[4] J. FLETT, *J. Chem. Soc.*, **1951**, 962.

[5] L. J. BELLAMY, "The Infra-red Spectra of Complex Molecules", Methuen, London, 1962.

1. — 1600 — 1500 cm^{-1} where the C=C,C=N frequencies of phenanthroline appear (1620 cm^{-1} şi 1525 cm^{-1}) as well as the asymmetric OCO stretching vibration of the chlorosalicylic acid (1580 cm^{-1}). In the Nd(III) chlorsalicylate ν_{as} appears at a lower value (1550 cm^{-1}) as in the case of ternary complexes. The higher value of the ν_{as} frequency in this case may be interpreted as showing a higher covalency degree as for the simple neodimium salt.

2. — 1450 — 1360 cm^{-1}, bands of the coordinate *o*-phenanthroline (1435 cm^{-1}) as well as the band corresponding to the OCO symmetric vibration frequency (1370 cm^{-1}) of the chlorosalicylic acid.

The same changes also appear in the complexes with 5,6-dimethylphenanthroline, which show the fact that the ligands do participate in the coordination with the central metal ion.

EXPERIMENTAL

The ternary complexes were obtained from an aqueous solution by the same methods as in the former paper.[1]

The analytical data and the chemical formulas of the new compounds obtained are systematized on table 4.

The compounds thus obtained are solid anhydrous substances and very stable in time. They are difficult to solve in most of the usual organic solvents, but easy enough to solve in dimethylformamide and dimethylsulphoxide, and the compounds with chlorosalicylic acid

Table 4

Analytical data

Formula of the compound	Ln		C		H		N	
	Calc.	*Found*	*Calc.*	*Found*	*Calc.*	*Found*	*Calc.*	*Found*
$La(phen)_2(BrMand)_3$	11.60	11.42	48.44	48.15	2.86	3.12	4.71	4.96
$Ce(phen)_2(BrMand)_3$	11.77	11.98	48.40	48.10	2.85	3.10	4.70	4.85
$Pr(phen)_2(BrMand)_3$	11.84	11.96	48.38	48.16	2.84	3.18	4.70	4.95
$Nd(phen)_2(BrMand)_3$	12.14	12.40	48.25	47.96	2.84	3.09	4.69	4.90
$Eu(phen)_2(BrMand)_3$	12.64	12.72	48.32	48.06	2.82	3.21	4.66	4.83
$Tb(phen)_2(BrMand)_3$	13.26	13.45	48.08	47.72	2.81	3.15	4.65	4.73
$Dy(phen)_2(BrMand)_3$	13.32	13.48	47.53	47.21	2.80	2.98	4.62	4.82
$Er(phen)_2(BrMand)_3$	13.76	13.91	47.29	46.98	2.79	3.05	4.56	4.81
$Pr(phen)_2(ClSal)_3$	13.88	14.06	53.20	52.96	2.75	3.29	5.51	5.62
$Nd(phen)_2(ClSal)_3$	14.17	14.38	53.18	52.89	2.75	2.98	5.50	5.74
$Eu(phen)_2(ClSal)_3$	14.96	14.80	53.15	53.13	2.73	3.01	5.51	5.96
$Tb(phen)_2(ClSal)_3$	15.14	14.89	52.27	51.98	2.71	3.13	5.42	5.53
$Dy(phen)_2(ClSal)_3$	15.59	15.64	52.13	51.87	2.70	3.09	5.40	5.45
$Er(phen)_2(ClSal)_3$	16.09	16.30	51.87	51.52	2.69	3.02	5.38	5.61
$Pr(DMPh)_2(BrMand)_3$	11.38	11.06	49.92	49.78	3.68	3.96	4.00	4.37
$Nd(DMPh)_2(BrMand)_3$	11.50	11.36	49.75	49.60	3.66	3.84	4.48	5.06
$Eu(DMPh)_2(BrMand)_3$	12.05	12.42	49.68	49.29	3.64	3.98	4.43	4.78
$Er(DMPh)_2(BrMand)_3$	13.13	13.34	48.83	48.62	3.59	3.93	4.38	4.48

are soluble in benzene and chloroform. A qualitative study of the solubility of these compounds in different solvents show that it changes according to the oxycarboxylic acid in the molecule, in the following order :

Chlorosalicylic > *Chloromandelic* > *Bromomandelic*

Also, as the radius of the lanthanide ion decreases, the solubility decreases too, so that the Dy(III) and Er(III) complexes with bromomandelic acid are very hard to solve even in DMF.

Measurements of molar conductivity in anhydrous methanol and DMF give values within $8-11\ \Omega^{-1}\ cm^2 mol^{-1}$ in the case of methanol solutions and between $18-20\ \Omega^{-1}\ cm^2\ mol^{-1}$ in the DMF solution. The values for the obtained molar conductivity show, according to the data from literature,[6] that in these solvents none of the compounds undergoes practically any noticeable dissociation, behaving as non-electrolytes.

Reagents. The following reagents were used : oxides (Ln_2O_3) of spectral purity (Matthey and Johnson) ; $Ce(NO_3)_3$ (E. Merck-puriss) ; *o*-phenanthroline E. Merck p.a.) ; 5,6-dimethylphenanthroline (Fluka AG-Switzerland) ; bromo-mandelic acid (Fluka AG-Switzerland) ; Chlorsalicylic acid (BDH).

Apparatus. IR spectra of the free ligands and its metal complexes were recorded on a UR-10 spectrophotometer in the $4000-700\ cm^{-1}$ range. UV and visible spectra in DMF and benzene solutions were recorded using an VSU$-$2 spectrophotometer. Concentration of the solutions were $\approx 10^{-5}$ M in the case of UV and $\approx 10^{-2}$ M in the case of visible spectra. The reflectance spectra at room temperature were recorded on a spectrophotometer VSU$-$1 using MgO as a standard. Electric conductivity of the complexes was determined with OK$-$102/1 conductometer on solutions of absolute methanol and DMF.

Acknowledgement. We express our thanks to Mrs. M. Popa for the carbon, hydrogen and nitrogen microanalyses.

---

[6] W. J. Geary, *Coord. Chem. Rev.*, **1**, 81 (1971).

Revue Roumaine de Chimie, **18**, *6*, 979–993 (1973)

SUR LA CHLORATION ET L'OXYCHLORATION SPÉCIFIQUES DES CYCLOHEPTÈNE ET CYCLOPENTÈNE

FRANÇOIS GAYMARD, ROGER GUEDJ et ANDRÉ VERMEGLIO

Laboratoire de Chimie Structurale Organique — Université de Nice —
U.E.R.M.S.T. — Campus Valrose — 06 Nice 02

Reçu le 25 novembre 1972

La chloration et l'oxychloration ménagées du cyclopentène et du cycloheptène sont étudiées en système dynamique en phase gazeuse, avec recyclage des produits transformés. L'obtention en quantité prépondérante de dérivés *trans*-Dichlorés 1,2 (plus de 90 % pour les deux cycloalcènes) est remarquable dans la réaction de chloration. L'oxychloration est caractérisée par la faible réactivité et même la non-réactivité de l'oxygène vis-à-vis de ces deux alcènes. La comparaison des résultats de l'oxydation, de la chloration et de l'oxychloration des cyclopentène, cycloheptène et cyclohexène montre le comportement différent du chlore et de l'oxygène, et permet de préciser les mécanismes proposés dans le cas de ce dernier hydrocarbure. Plus particulièrement, la stéréochimie permet de comprendre la différence de réactivité du chlore et de l'oxygène vis-à-vis de chaque alcène.

L'oxydation, notamment par l'oxygène moléculaire, des matières organiques constitue une importante technique industrielle de synthèse.

On peut cependant noter, à travers les résultats bibliographiques fort nombreux, que l'oxydation en phase gazeuse d'hydrocarbures aliphatiques, cycliques ou alicycliques, est caractérisée par le manque de sélectivité.

A titre d'exemple, signalons que Fisch et Brown[1] dans l'oxydation du méthyl-2 hexadécane à 300° décomptent près de 160 produits ! !

Cette absence de sélectivité justifie les interprétations très divergentes constatées dans la littérature. On peut néanmoins dégager quatre axes qui correspondent aux analyses les plus vraisemblables des mécanismes d'oxydation : l'isomérisation de Semenov,[2] l'isomérisation de Shtern,[3] la théorie d'Yenikolopyan,[4] la théorie oléfinique de Knox.[5]

---

[1] D. M. Brown et A. Fisch, *Proc. Roy. Soc.*, **A 308**, 547 (1968).

[2] N. M. Semenov, «Problèmes de cinétique chimique et mécanismes réactionnels», Akad. Nauk. S.S.S.R, Khim. Otled Nauk. Moscou, 1954, p. 95.

[3] V. Ya. Shtern, «The Gas Phase Oxidation of Hydrocarbons», Pergamon Press, 1964, p. 106.

[4] N. S. Yenikolopyan, *Zhur. fiz. Khim.*, **32**, 2224 (1958).

[5] M. A. Knox, *Chem. Comm.*, **1965**, 108.

En réalisant la chloration et l'oxychloration des cyclopentène, cyclohexène[6] et cycloheptène, nous pensions apporter une contribution à l'étude des mécanismes attachés à ces processus radicalaires. Cette « série » s'adaptait, semble-t-il, parfaitement aux problèmes posés dans la mesure où les différences de structures pouvaient rendre compte de la compétition entre le chlore et l'oxygène vis-à-vis de ces alcènes.

La variation de paramètre tels que la température du réacteur et le rapport O_2/Cl_2 nous semblait être un moyen d'atteindre d'une part cet objectif et d'autre part de rendre dans une certaine mesure les réactions plus sélectives.

PARTIE EXPÉRIMENTALE

Le choix des conditions expérimentales a été dicté essentiellement par une double exigence : Nécessité d'obtenir de forts rendements et de fortes concentrations en produits transformés : Nécessité de diminuer la possibilité de participation à un deuxième étage de réaction des produits initialement transformés.

Le dispositif déjà décrit [7,8] permet l'oxydation ou la chloration ménagée en système dynamique avec extraction en continue des « produits lourds » ; il est donc assez bien adapté à cette double exigence.

Les conditions expérimentales correspondent à celles du mémoire précédent.[6]

ANALYSE. La quasi-totalité des produits de réaction a été identifiée selon les techniques usuelles : distillation du mélange brut de réaction — chromatographie des fractions ainsi obtenues — récupération en C.P.P.V. — vérification de leur pureté sur une colonne analytique apolaire et sur une colonne analytique polaire — identification par spectrométrie de Masse, I.R., R.M.N. — enfin, synthèse des différents isomères dans les cas douteux où les méthodes physiques ne sont pas suffisantes.

Les divers résultats analytiques et quantitatifs (les pourcentages pondéraux ont été corrigés après étalonnage par C.P.V.) sont indiqués dans les tableaux 1 (chloration) et 2 (oxychloration).

DISCUSSION

MÉCANISMES DE LA CHLORATION

Dans une précédente publication,[6] nous avions discuté en particulier les mécanismes de dichloration et proposé la première partie du schéma 1 pour expliquer la stéréosélectivité de la réaction (obtention de 85% de *trans*-Dichloro-1,2 cyclohexane).

En ce qui concerne la chloration du cyclopentène et du cycloheptène, la stéréospécificité est encore plus caractéristique. Dans les deux cas, les pourcentages de produits dichlorés sont supérieurs à 90%. Les *trans*-

---

[6] F. GAYMARD, R. GUEDJ et A. VERMEGLIO, *Bull. Soc. chim. France*, 3282 (1971).

[7] R. GUEDJ et J. JULLIEN, *Bull. Soc. chim. France*, **1964**, 1501.

[8] R. GUEDJ, Thèse, Orsay, 1966.

Dichloro-1,2 cyclopentane et *trans*-Dichloro-1,2 cycloheptane peuvent être justifiés par une attaque en deux étapes par le chlore, mécanisme analogue à celui proposé dans le cas du cyclohexène (schéma 1).

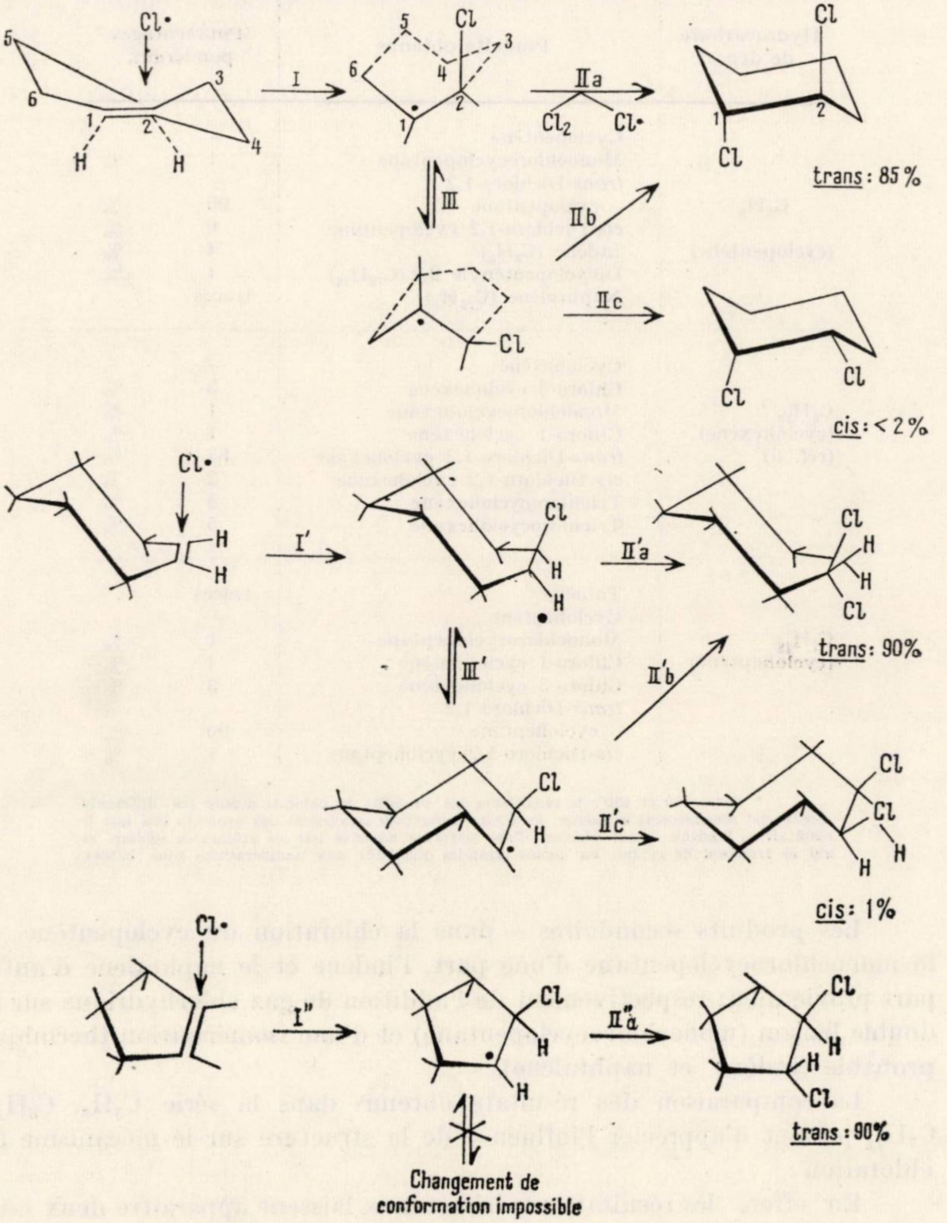
Cl•
5
6
1
2
3
4
H
H
I
5
Cl
3
6
4
1
2
IIa
Cl₂
Cl•
Cl
1
2
Cl
trans : 85 %
III
IIb
IIc
Cl
Cl
Cl
cis : < 2 %
Cl•
H
H
I′
Cl
H
H
II′a
Cl
H
H
Cl
trans : 90%
III′
II′b
Cl
H
II′c
Cl
Cl
H
H
cis : 1%
Cl•
I″
Cl
H
H
II″a
Cl
H
H
Cl
trans : 90%
Changement de conformation impossible

Schéma 1.

Influence de la stéréochimie dans la chloration ménagée en phase vapeur de la série cyclique $C_5H_8 - C_7H_{12}$ (à 450°).

Tableau 1

Résultats analytiques de la Chloration à 450°C* de la série C_6H_8 . . . C_7H_{12} avec un rapport molaire alcène/Cl_2 = 14

Hydrocarbure de départ	Produits obtenus	Pourcentages pondéraux
C_5H_8 (cyclopentène)	Cyclopentène	—
	Monochlorocyclopentane	1 %
	trans-Dichloro-1,2 cyclopentane	90 %
	cis-Dichloro-1,2 cyclopentane	0 %
	Indène (C_9H_8)	4 %
	Dicyclopentényle 2,2′($C_{10}H_{14}$)	4 %
	Naphtalène ($C_{10}H_8$)	traces
C_6H_{10} (cyclohexène) (réf. 6)	Cyclohexène	—
	Chloro-3 cyclohexène	3 %
	Monochlorocyclohexane	1 %
	Chloro-1 cyclohexène	1 %
	trans-Dichloro-1,2 cyclohexane	85 %
	cis-Dichloro-1,2 cyclohexane	2 %
	Trichlorocyclohexène	3 %
	Trichlorocyclohexane	5 %
C_7H_{12} (cycloheptène)	Toluène	traces
	Cycloheptène	—
	Monochlorocycloheptane	1 %
	Chloro-1 cycloheptène	4 %
	Chloro-3 cycloheptène	3 %
	trans-Dichloro-1,2 cycloheptane	90 %
	cis-Dichloro-1,2 cycloheptane	1 %

* Entre 250 et 450°, la répartition des produits de chloration pour ces différents alcènes est sensiblement la même : les seules différences concernent des produits tels que le naphtalène, l'indène... qui dérivent d'une pyrolyse amorcée par les atomes de chlore et qui se trouvent de ce fait en moins grandes quantités aux températures plus basses.

Les produits secondaires — dans la chloration du cyclopentène — le monochlorocyclopentane d'une part, l'indène et le naphtalène d'autre part proviennent respectivement de l'addition de gaz chlorhydrique sur la double liaison (monochlorocyclopentane) et d'une isomérisation thermique probable (indène et naphtalène).

La comparaison des résultats obtenus dans la série C_5H_8, C_6H_{10}, C_7H_{12} permet d'apprécier l'influence de la structure sur le mécanisme de chloration :

En effet, les résultats expérimentaux laissent apparaître deux faits importants :

— primo, sélectivité de la réaction qui se traduit par l'apparition prépondérante de *trans*-Dichloro-1,2 cycloalcanes,

Tableau 2

A – Oxychloration du cyclopentène

Hydrocarbure de départ	Produits obtenus	Pourcentages pondéraux à 450°C	Remarques
C_5H_8 (cyclopentène)	C_5H_8 cyclopentène C_5H_9 Cl monochlorocyclopentane $C_5H_8Cl_2$ *trans*-dichloro 1,2 cyclopentane	non évalué 4 % 96 %	Réaction très sélective dans un large domaine de température

B – Oxychloration du cyclohexène

Hydrocarbure de départ	Produits / O_2/Cl_2	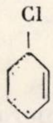	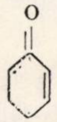	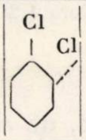	Autres produits
C_6H_{10} Cyclohexène (cf. réf. 6)	$O_2/Cl_2=0$	2,5 %	0 %	85 %	13 % Chloro-1 cyclohexène 1 % Monochlorocyclohexane 1,5 % *Cis*-Dichloro-1,2 cyclohexane 1,5 % Trichloro-cyclohexanes 8,5 %
	$O_2/Cl_2=1/2$	23 %	traces	77 %	environ 0 %
	$O_2/Cl_2=1$	45 %	8 %	47 %	environ 0 %
	$O_2/Cl_2=2$	35 %	20 %	45 %	traces de Toluène
	$O_2/Cl_2=3$	22 %	28 %	11 %	39 % Cyclohexène-3, 01 22 % Cyclohexanone 22 % Toluène 8 % non identifiés 9 %
	Oxydation pure (réf. 33)	0 %	20 %	0 %	65 % Cyclohexadiène 14 % Benzène 11 % Allyl-3 cyclohexène 12 % Cyclohexanone 5 % Cyclohexène-4 one 5 % Cyclohexanol 11 % Cyclopentène-carboxaldéhyde 5 %

Tableau 2 (suite)

C – Oxychloration du cycloheptène

Hydrocarbure de départ	Produits obtenus	Pourcentages pondéraux	
		$O_2/Cl_2 = 1$	$O_2/Cl_2 = 2$
C_7H_{12} Cycloheptène	C_7H_8 Toluène	traces	traces
	C_7H_{12} Cycloheptène	non évalué	non évalué
	X	traces	traces
	$C_7H_{12}O$ Cycloheptanone	traces	1 %
	$C_7H_{10}O$ Cycloheptène-2 one	5 %	9 %
	$C_7H_{11}Cl$ monochloro-cycloheptène	0,5 %	3,5 %
	$C_7H_{12}Cl_2$ *trans*-Dichloro 1,2 cycloheptane	92,5 %	84 %
	$C_7H_{12}Cl_2$ *cis*-Dichloro 1,2 cycloheptane	1 %	1,5 %

— secundo, présence, certes faible, de *cis*-Dichloro-1,2 cyclohexane et de *cis*-Dichloro-1,2 cycloheptane comparée à l'absence totale de *cis*-Dichloro-1,2 cyclopentane.*

Les pourcentages de *trans*-Dichloro-1,2 cycloalcanes dans les trois cas suggèrent une réactivité très prononcée de la double liaison, liée à l'accès facile de cette dernière par le chlore radicalaire.

En effet, dans les cas des cyclopentène, cyclohexène et cycloheptène, la géométrie de ces molécules montre clairement qu'il n'y a aucun empêchement stérique à l'approche de la double liaison par le chlore radicalaire.

L'absence de *cis*-Dichloro-1,2 cyclopentane comparée à la présence des homologues supérieurs présente sur la plan théorique un intérêt non négligeable, bien que ces composés soient très peu abondants dans nos mélanges réactionnels (1,5 % et 1 %).

Ces différences peuvent justifier les mécanismes avancés pour expliquer la formation des *trans* dichloro-cycloalcanes. Le schéma 1 montre clairement que les radicaux chloro-2 cyclohexyle et chloro-2 cycloheptyle, formés dans une première étape, sont susceptibles de changer de conformation ; une nouvelle attaque du chlore peut alors conduire aux composés *trans* et aux composés *cis* (voie II *b* et II *c*). Par contre, il n'est pas possible, compte tenu de la rigidité du cycle en C_5, d'envisager une inversion de conformation pour le radical chloro-2 cyclopentyle. La nouvelle attaque du chlore, qui se fait sur la face la plus accessible, conduira seulement au *trans*-Dichloro-1,2 cyclopentane.

On peut dégager un deuxième aspect théorique important lié à l'absence de *cis*-Dichloro-1,2 cyclopentane. En effet, il n'était pas déraisonnable de penser que l'attaque de la double liaison puisse se faire par le chlore moléculaire suivant un mécanisme concerté (schéma 2).

---

* L'absence de *cis*-Dichloro-1,2 cyclopentane a pu être vérifiée par comparaison des temps de rétention d'un échantillon authentique et de ceux des produits de la fraction brute.

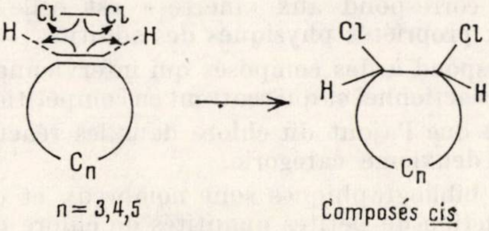

Schéma 2.
Attaque de la double liaison par le chlore moléculaire selon un mécanisme concerté.

Cette hypothèse pouvait à la rigueur être retenue dans le cas du cycloheptène et du cyclohexène, avec, somme toute, une contribution très faible pour expliquer les dérivés dichlorés *cis* 1,2 du cycloheptane et du cyclohexane. Du fait de l'absence de *cis*-Dichloro-1,2 cyclopentane on ne peut en tout état de cause, l'avancer pour justifier l'obtention de ces produits : l'approche de la double liaison par le chlore pouvant se faire dans les trois cas de façon identique.

Remarquons que Ashton et Tedder dans deux récentes publications,[9,10] en étudiant la chloration en phase gazeuse des chlorocyclohexane et chlorocyclopentane, envisagent les mêmes intermédiaires que nous-mêmes (les radicaux chloro-2 cycloalykles) et expliquent le grand rapport *trans/cis* des produits dichlorés (12/1 dans le cas du C_6 et 16/1 dans le cas du C_5) par une interaction entre l'orbitale π à moitié remplie des radicaux chloro-2 cycloalkyles et l'orbitale atomique 3 p_z du chlore. Cette théorie n'est pas du tout contradictoire avec les voies IIb et IIc de notre schéma 1.

MÉCANISMES DE L'OXYCHLORATION

A – POSITION DU PROBLÈME :

De nombreux auteurs [11 à 19] ont étudié l'influence d'additifs dans les réactions d'oxydation. A quelles fins ? Probablement pour initier et pour orienter dans une certaine mesure les réactions d'oxydations caractérisées par leur manque de sélectivité.

[9] D. S. Ashton et J. M. Tedder, *J. Chem. Soc.* (B), **1970**, 1031.

[10] D. S. Ashton et J. M. Tedder, *J. Chem. Soc.* (B), **1971**, 1719.

[11] L. Audier, F. Gaymard, R. Guedj et J. Jullien, *Bull. Soc. chim. France*, 1192 (1969).

[12] F. Gaymard, *Compte rend*, C. **269**, 1660 (1969).

[13] F. Gaymard, R. Guedj et J. Jullien, *Bull. Soc. chim. France*, **1970**, 1864.

[14] F. Gaymard, R. Guedj et J. Jullien, *Bull. Soc. chim. France*, **1971**, 1101.

[15] F. Gaymard, Thèse, Nice, 1970.

[16] H. Amadei, Thèse de spécialité, Nice, 1970.

[15] J. Bizongwako, Mémoire, Université libre de Bruxelles, 1970.

[18] G. Huybrechts, J. Olbregts et K. Thomas, *Trans. Faraday Soc.*, **63**, 1647 (1967),

[19] P. Goldfinger, G. Huybrechts, G. Martens, L. Meyers et J. Olbreghts, *Trans. Faraday Soc.*, **61**, 1933 (1965).

Les additifs sont en première approximation classées selon leur nature en deux catégories :

— la première qui correspond aux «inertes» est celle qui est associée essentiellement aux propriétés physiques des additifs,

— la seconde correspond à des composés qui interviennent véritablement dans le processus réactionnel et qui rentrent en compétition avec l'oxygène.

Il est évident que l'ajout du chlore dans les réactions d'oxydation se place dans cette deuxième catégorie.

Les résultats bibliographiques sont nombreux et concernent essentiellement l'introduction de petites quantités de chlore dans les réactions d'oxydation [19] et des petites quantités d'oxygène dans les réactions de chloration [20] — sans faire une analyse exhaustive de ces résultats bibliographiques il est possible de faire apparaître deux idées maîtresses sur lesquelles s'accordent ces auteurs :

Premièrement : l'addition d'oxygène dans les réactions radicalaires de chloration inhibe ces dernières.[20,21,22,23]

Deuxièmement : l'addition de chlore dans les réactions d'oxydation en phase gazeuse ou liquide diminue la période d'amorçage et abaisse le seuil thermique de l'oxydation.

Cette généralisation nous paraissait de prime abord surprenante parce qu'il était raisonnable de penser que les résultats dépendaient des appareillages utilisés, de la température, de la *structure* des composés étudiés, des *groupements fonctionnels* et des rapports O_2/Cl_2 mis en jeu...

Les résultats obtenus au laboratoire,[16] confirmaient ces présomptions. Cette généralisation, bien que discutable, avait toutefois le mérite de schématiser des processus complexes. Et, dans la mesure où nous la refusions, il était indispensable de trouver une explication raisonnable et aussi générale que possible à des résultats contradictoires sur les effets compétitifs de l'oxygène et du chore dans les réactions d'oxychloration.

Une réponse, qui va dans le sens de nos résultats, a été apportée récemment par Bizongwako et Huybrechts.[17,18] En effet, ces auteurs ont montré que le caractère « inhibiteur » de l'oxygène dans les réactions radicalaires de chloration dépend étroitement de la stabilité de radicaux peroxydiques formés. Plus particulièrement, ces auteurs ont étudié l'effet de l'oxygène sur les photochlorations en phase gazeuse de l'éthane, des tri et tétrachloréthylènes et du pentachloréthane. Ces études ont fourni de précieux renseignements sur l'effet « inhibiteur » de l'oxygène. En effet, le pentachloréthane, les tri et tétrachloréthylènes ont un comportement fort semblable tant au point de vue de la photochloration influencée par l'oxygène que du point de vue de l'oxydation photosensibilisée par le chlore. Par contre, l'éthane est beaucoup plus sensible à l'effet inhibiteur de l'oxygène lors de la photochloration. Il apparaît ainsi que les différences de comportement observées correspondent aux différentes structures des radicaux intervenant dans ces réactions.

[20] A. Pichler, Thèse, Strasbourg, 1964.

[21] S. Yuster et L. H. Reyerson, *J. Phys. Chem.*, **39**, 859 (1935).

[22] S. Yuster et L. H. Reyerson, J. Phys. Chem., **39**, 1111 (1935).

[23] A. M. Chaikin « Candidate's dissertation », Moscou, State University, 1955.

1 — Dans le cas de l'oxychloration du cyclohexène,[6] *nous avions nous-même proposé le mécanisme concerté suivant:*

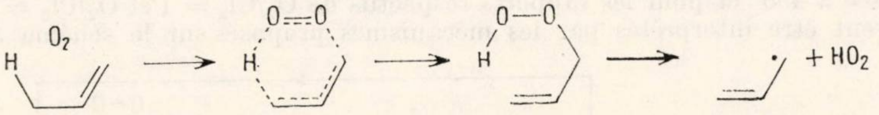

Un certain nombre de faits expérimentaux semblent corroborer ce genre de mécanisme (cf. réf. 6). En particulier, lorsque l'on analyse, au cours du temps, les produits transformés, on remarque (figure 1) que le pourcentage (chloro-3 cyclohexène + cyclohexénone) par rapport à celui du *trans*-Dichloro-1,2 cyclohexane ne cesse d'augmenter pour se stabiliser vers la sixième heure. Ce résultat est compatible avec le temps d'initiation des réactions d'oxydation (beaucoup plus long que celui des réactions de chloration) et semble indiquer que le radical cyclohexène-3 yle provient de la seule action de l'oxygène sur le cyclohexène.

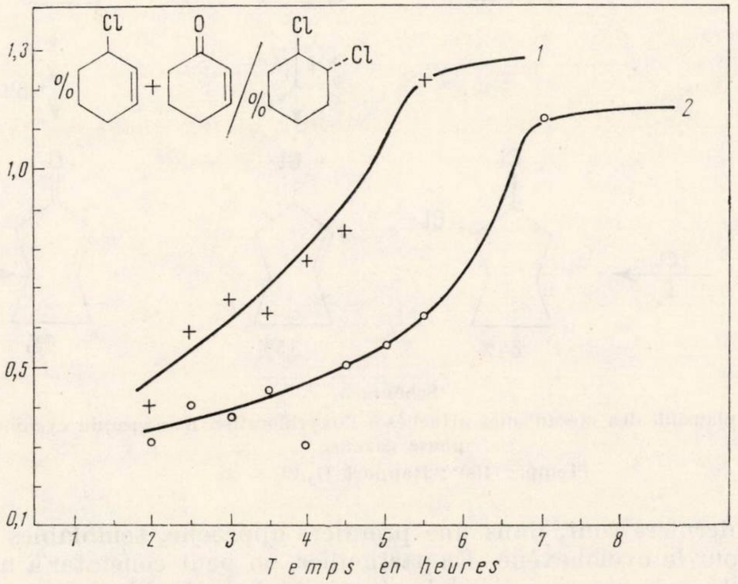

Fig. 1. — *Evolution au cours du temps du rapport* :
(% chloro-3 cyclohexène + % cyclohexénone) / (% *trans*-Dichloro-1,2 cyclohexane).
Courbe *1* : rapport $O_2/Cl_2 = 2$; courbe *2* : rapport $O_2/Cl_2 = 1$.

Ce radical est ensuite piégé soit par le chlore, soit par l'oxygène pour aboutir respectivement au chloro-3 cyclohexène ou à la cyclohexènone conjuguée.

2 — *Mécanismes d'oxychloration du cycloheptène*

Les résultats expérimentaux [24] de l'oxychloration du cycloheptène réalisée à 450° et pour les rapports respectifs de $O_2/Cl_2 = 1$ et $O_2/Cl_2 = 2$ peuvent être interprétés par les mécanismes proposés sur le schéma 3.

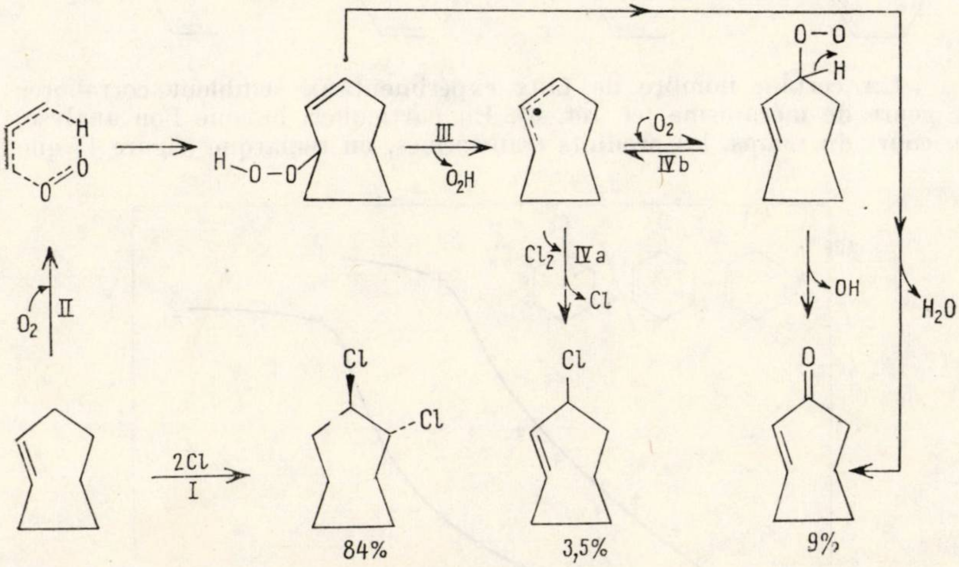

Schéma 3.
Description plausible des mécanismes attachés à l'oxychloration ménagée du cycloheptane en phase gazeuse
(Temp. : 450° ; Rapport $O_2/Cl_2 = 2$)

Ces derniers sont, dans une première approche, semblables à ceux avancés pour le cyclohexène. En particulier, on peut constater à nouveau la sélectivité de la réaction, liée à la réactivité de la double liaison vis-à-vis du chlore, réactivité qui se traduit par l'obtention presque quantitative de *trans*-Dichloro-1,2 cycloheptane. On peut noter là aussi des produits dérivant du radical cycloheptène-2 yle, c'est-à-dire, le chloro-3 cycloheptène et la cycloheptène-2 one. L'apparition de ces composés est liée à la présence de l'oxygène dans le milieu réactionnel. En effet, les pourcentages de ces produits augmentent lorsque le rapport O_2/Cl_2 croît. Comme dans le cas du cyclohexène, l'obtention de chloro-3 cycloheptène et cycloheptène-2 one montre une fois encore la compétition, au niveau du radical cycloheptène-2 yle, du chlore et de l'oxygène. Il faut cependant remarquer les faibles pourcentages des produits dérivant du radical cycloheptène-2 yle comparés à ceux obtenus dans le cas du cyclohexène, ce qui implique une plus faible réactivité de la position en α de la double liaison dans le cas du cycloheptène. On voit là l'influence de la géométrie qui sera développée ultérieurement.

---

[24] A. VERMEGLIO, Thèse de spécialité, Nice, 1971.

3 — *Mécanismes d'oxychloration du cyclopentène*

L'analyse comparée des résultats de la réaction pour les cycloalcènes en C_6 et C_7 laissait apparaître une diminution de la réactivité de la position en α de la double liaison dans le cas du cycloheptène. Cette tendance s'accentue et se cristallise dans le cas du cyclopentène, caractérisé par l'absence de tout produit dérivant du radical allylique : cyclopentène-2 yle. En conséquence, la réaction d'oxychloration du cyclopentène est sélective, la sélectivité se manifestant par l'obtention de 96% de *trans* dichloro-1,2 cyclopentane.

B – INFLUENCE DE LA STRUCTURE SUR LE MÉCANISME D'OXYCHLORATION

Les données bibliographiques accessibles, ainsi que nos propres données expérimentales peuvent nous permettre de répondre à deux questions.

Premièrement : Comment peut-on expliquer les différences qui apparaissent dans la série C_5 à C_7 en ce qui concerne l'attaque en α de la double liaison ?

Deuxièmement : Si ce processus est possible, comment peut-on justifier la répartition entre les produits chlorés et les produits oxydés pour cette position particulière (en α de la double liaison) ?

Nous avions déjà noté les différences, fondamentales semble-t-il sur le plan théorique dans la « série » cyclopentène, cyclohexène, cycloheptène. On remarque (tableau 3) et note à nouveau que l'attaque en α

Tableau 3

Étude comparée de la réactivité de la double liaison et de la position en α de celle-ci

% Alcènes	Pourcentages d'attaque en α de la double liaison	Pourcentages d'attaque du chlore sur la double liaison
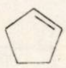	0 %	96 %
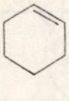	47 %	53 %
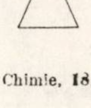	5,5 %	92,5 %

de la double liaison est importante dans le cas du cyclohexène, beaucoup plus faible dans celui du cycloheptène, et inexistante en ce qui concerne le cyclopentène.

Ces différences montrent que la formation du radical allylique, lorsqu'elle est possible, ne correspond pas à un simple arrachement de l'hydrogène en α de la double liaison par l'oxygène selon la réaction : $(-CH_2-CH{=}CH- + O_2 \rightarrow -\underset{\cdots\cdots}{CH-CH-CH}- + .O_2H)$. On comprend mal, en effet, l'influence de la structure si l'on admet un tel processus.

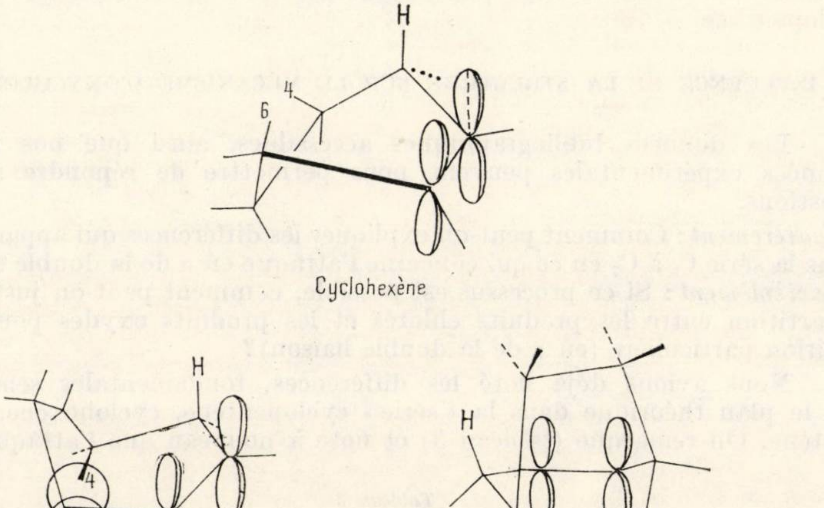
H
4
6
Cyclohexène
H
4
7
H
4
7
Cycloheptène
NAUGE II (3 électrons)
5
4
3
2
1
H_4
6
H_6
Interaction faible
Interaction forte
5
6
4
3
2
1
H_4
7
H_7
Radical cyclohexène – 2 yle
Radical cycloheptène – 2 yle

Schéma 4.

Interactions de non liaison associées :

- aux molécules de cyclohexène et cycloheptène
- aux radicaux cyclohexène-2 yle et cycloheptène-2 yle

Ainsi le mécanisme avancé dans le cas du cyclohexène, pour justifier la formation du radical cyclohexène-2 yle et suivant lequel l'oxygène réagissait par un processus concerté à six centres, prend, à nos yeux, plus de poids. Il est possible, dès lors, de justifier les différences qui apparaissent dans l'oxychloration de la série des cycloalcènes en C_5, C_6, C_7.

En effet, pour qu'un tel mécanisme puisse avoir lieu entre l'oxygène moléculaire et l'alcène, il est nécessaire que les liaisons C—H des hydrogènes vicinaux à la double liaison puissent se placer parallèlement aux orbitales π de cette dernière.[25,26,27,28]

On comprend, dans ces conditions, qu'il n'y ait pas de produits dérivant d'une attaque en α dans le cas du C_5 (cycle rigide).

De plus, le schéma 4 permet d'expliquer les différences notables de pourcentages d'attaque en α entre le cyclohexène et le cycloheptène. En effet, si l'on considère ces deux molécules dans la conformation permettant un mécanisme concerté, on constate que les interactions entre les hydrogènes 4 et 6 (du cyclohexène) sont nettement plus faibles que celles qui existent entre les hydrogènes 4 et 7 (du cycloheptène).

La conformation impliquant un mécanisme concerté pour le cyclohexène est donc plus favorisée que celle du cycloheptène.

Ainsi l'addition du chlore sur la double liaison, plus importante dans le cas du cycloheptène et du cyclopentène que dans celui du cyclohexène, ne paraît pas devoir être attribuée à une réactivité spéciale de la double liaison, mais plutôt au manque de réactivité des hydrogènes en α de celle-ci.

C — RÉPARTITION DES PRODUITS CHLORÉS ET OXYDÉS

Le problème de la répartition des produits chlorés et oxydés à partir d'un radical peut être posé d'une manière explicite à travers les trois séries de réactions concernant l'oxychloration du cyclohexane, * du cyclohexène et du cycloheptène réalisées au laboratoire.[24]

— On constate que, dans le cas de l'oxychloration du cyclohexane,[11] la compétition entre le chlore et l'oxygène vis-à-vis du radical cyclohexyle se traduit par l'absence de monochlorocyclohexane. La formation de dérivé monochloré est donc inhibée par la présence d'oxygène, et il est important de remarquer que de nombreux auteurs [21 à 23] systématisent ce type d'inhibition.

— Deuxièmement, en ce qui concerne les résultats obtenus pour le cyclohexène et le cycloheptène, on peut noter, d'une part, l'apparition de produits monochlorés, d'autre part, signaler que les pourcentages des produits oxydés dans le cas du cycloheptène sont supérieurs à ceux des produits chlorés, alors que la situation est inversée pour le cyclohexène.

Remarquons que l'oxychloration du cyclohexène conduit à près de 45% de chloro-3 cyclohexène.

---

[25] N. A. Khan, *J. Chem. Phys.*, **22**, 2090 (1954).
[26] N. A. Khan, *Canad. J. Chem.*, **32**, 1149 (1954).
[27] E. H. Farmer, *Trans. Faraday Soc.*, **42**, 228 (1946).
[28] K. U. Ingold, *Chem. Rev.*, **61**, 563 (1961).

* Les résultats sont très semblables dans le cas du cyclopentane et du cycloheptane.

Ces résultats, déroutants à première vue, mettent toutefois en évidence le fait que l'oxygène n'est pas nécessairement un inhibiteur ; ils s'insèrent d'ailleurs parfaitement dans l'ensemble développé ci-dessous.

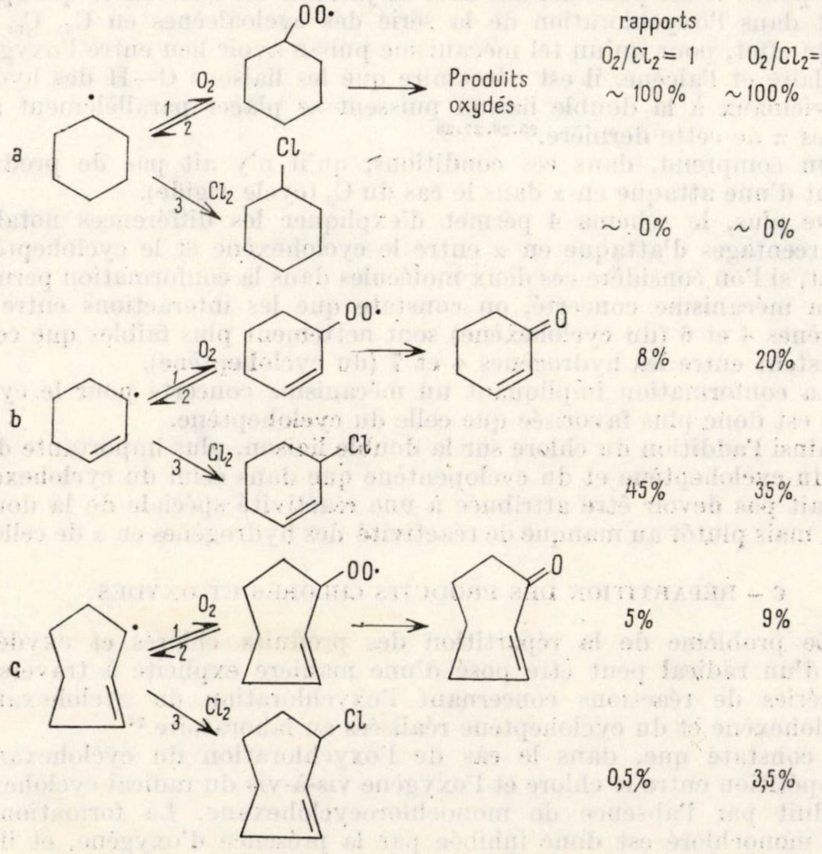

Pour expliquer les données contradictoires qui résultent de la compétition entre le chlore et l'oxygène, il faut semble-t-il, tenir compte de la stabilité des radicaux alkoyles obtenus. Dans le cas du cyclohexane (a), l'équilibre est déplacé dans le sens 1 car le radical cyclohexyle est peu stable. Par contre, les radicaux allylique cyclohexène-2 yle et cycloheptène-2 yle étant relativement stables, la réaction R. + $O_2 \underset{2}{\overset{1}{\rightleftharpoons}} RO_2$. (b et c) n'est que partielle. Il s'ensuit une accumulation de ces deux radicaux allyliques, évacués sous forme de chloro-3 cycloalcènes, selon la réaction R. + Cl → RCl.

Pour justifier la différence de pourcentages des produits monochlorés et oxydés dans les cas respectifs du cyclohexène et du cycloheptène, il suffit de noter la différence de stabilité des deux types de radicaux allyliques : le radical cycloheptène-2 yle étant moins stable que son homologue inférieur du fait des interactions de non-liaison. L'équilibre $R. + O_2 \underset{2}{\overset{1}{\rightleftharpoons}} ROO.$

est, de ce fait, plus fortement déplacé dans le sens 2 dans le cas du cyclohexène que dans celui du cycloheptène. Les travaux de Bizongwako [17] et Huybrechts [18] confirment ce point de vue. En effet, ces auteurs ont réalisé la photooxychloration des dérivés chlorés de l'éthane et ont montré que la fixation de l'atome de chlore ou de l'oxygène sur les radicaux dépendait étroitement de leur stabilité. Le radical éthyle, en présence de chlore et d'oxygène, conduit essentiellement aux produits oxydés, tandis que le radical plus stable dérivant du pentachloréthane réagit essentiellement avec le chlore.

CONCLUSION

L'analyse des résultats de la chloration des cyclopentène, cyclohexène et cycloheptène à 250° et 450° (pour un rapport alcènes/$Cl_2=14$) et de ceux de l'oxychloration en phase vapeur de ces mêmes hydrocarbures nous a permis de mettre en relief un certain nombre de points fondamentaux consignés ci-dessous :

— Le phénomène de chloration :

Les réactions de chloration, dans nos conditions expérimentales, se traduisent par l'obtention presque quantitative de *trans*-Dichloro-1,2 cycloalcanes (respectivement 90 %, 85 %, 90 % pour le C_5H_8, C_6H_{10}, C_7H_{12}). Cette stéréospécificité peut être aisément justifiées par une attaque en deux étapes de la double liaison de l'alcène par le chlore radicalaire.

— Le phénomène d'oxychloration :

Nous avons pu mettre en évidence les réactivités différentes de l'oxygène et du chlore vis-à-vis de l'alcène : elles se manifestent par l'obtention de cyclénones, de chloro-3 cycloalcènes et de *trans*-Dichloro 1,2 cycloalcanes. En effet, l'oxygène est à l'origine du radical allylique vraisemblablement par un mécanisme concerté à six centres, tandis que le chlore se fixe préférentiellement sur la double liaison ou en α de celle-ci si le radical allylique est initialement formé par l'action de l'oxygène.

— Influence de la structure :

Dans le cas de la chloration, l'influence de la structure se traduit à travers l'absence ou l'obtention de *cis*-Dichloro-1,2 cycloalcanes. Plus particulièrement, l'absence de *cis*-Dichloro-1,2 cyclopentane permet d'exclure un mécanisme impliquant une attaque du chlore moléculaire sur la double liaison.

En ce qui concerne l'oxychloration, les différences notables, observées dans les séries C_5, C_6 et C_7, concernent en particulier l'attaque en α de la double liaison par l'oxygène et la répartition entre les produits chlorés et oxydés pour cette position particulière. Ces différences corroborent l'hypothèse d'un processus concerté à six centres entre l'oxygène et l'alcène. Celui-ci permet en outre de mieux comprendre la répartition entre produits oxydés et chlorés, répartition liée à la stabilité des radicaux allyliques formés. Ces résultats soulignent le caractère gratuit d'une généralisation de l'effet inhibiteur de l'oxygène sur les réactions radicalaires de chloration. Il est clair que la compétition du chlore et de l'oxygène dépend du substrat qui leur est offert, et plus particulièrement de la stabilité des radicaux intermédiaires.

Revue Roumaine de Chimie, **18**, *6*, 995–1004 (1973)

USE OF ESR SPECTRUM SIMULATOR FOR DETERMINING PRECISELY HYPERFINE COUPLING CONSTANTS OF STABLE NITROGEN FREE RADICALS

N. NEGOIȚĂ, R. BAICAN, F. DOMȘA and A. T. BALABAN

Institute of Atomic Physics, P.O. Box 35, Bucharest, Romania

Received February 14, 1973

By means of an ESR spectrum simulator, the hyperfine coupling constants of arenesulphonyl-phenyl-nitroxides (I), aryl-nitroso-nitroxides (II–IV) and 1-benzenesulphonyl-2,2-diphenylhydrazyl (V) were determined with a precision of ±0.05 Gauss.

In a preceding paper,[1] a method was described for determining in a first order approximation isotropic hyperfine coupling constants of organic stable free radicals in solution from experimentally obtained electron spin resonance (ESR) spectra. Even though this method was expanded into a computer program,[2] it is limited by the assumption that coupling constants are integer multiples of a smallest unit. To overcome this limitation either a spectrum simulator, or a more complex program [3] must be employed. The present paper exemplifies the former alternative.

The factors which limit the precision of data determined from an ESR spectrum depend on the ESR spectrometer and on the sample. Among these factors, the most important are the following ones :[4–9]

— limited sensitivity of the spectrometer ;

— non-linearity of the static magnetic field in the sweeped range ;

— non-optimized amplitude of the magnetic field modulating the static magnetic field ;

— distortions induced by the sweep rate, attenuation and other recording conditions ;

---

[1] A. T. Balaban, *Rev. Roumaine Chim.*, **17**, 9 (1972).

[2] C. Pomponiu and A. T. Balaban, *ibid.*, **18**, Nr. 7 (1973).

[3] F. Schneider and M. Plato, "Elektronenspin-Resonanz. Experimentelle Technik", Thiemig, München, 1971, p. 182.

[4] S. A. Altshuler and B. M. Kozyrev, "Electron Paramagnetic Resonance", Academic Press, New York, 1964.

[5] I. Ursu, "La résonance paramagnétique électronique", Dunod, Paris, 1968.

[6] R. S. Alger, "Electron Paramagnetic Resonance", Interscience, New York, 1968.

[7] C. P. Poole Jr., "Electron Spin Resonance", Interscience, New York, 1967.

[8] D. J. E. Ingram, "Spectroscopy at Radio and Microwave Frequencies", Butterworths, London, 1967.

[9] F. Gerson, "High Resolution ESR Spectroscopy", Wiley–Verlag Chemie, Weinheim, 1970.

— instability of the free radical;

— polarity of the solvent, influencing the quality factor of the cavity;

— paramagnetic impurities in the solution, including oxygen left by an incomplete degassing of the sample;

— interactions with other paramagnetic centres owing to the finite dilution of the solution.

Nevertheless, even under standard conditions without special precautions, data concerning the g-factor, the spin-spin relaxation time, line widths and hyperfine coupling constants cover a wide informational area which characterizes completely a free radical. The last two parameters can be determined with a high precision by employing an ESR spectrum simulator.

Free radicals whose odd electron interacts with more than two non-equivalent nuclear spins have a fairly large number of lines which are usually partly overlapped. Therefore the number and intensities of peaks do not allow a straightforward determination of hyperfine coupling constants. Rather, an assumed set of coupling constants and line widths is used to simulate an ESR spectrum which is then visually compared with the experimental one.

In the present paper the coupling constants of five free radicals are determined with a precision of ±0.05 Gauss using a SPECTROSYSTEM-100 data processing system consisting of a VARIAN Data 620/i computer connected ON-LINE with an ESR VARIAN E-12 spectrometer. The block scheme of the data processing system is represented in figure 1.[10]

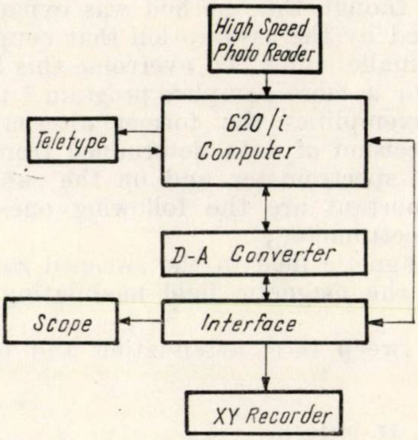

Fig. 1. — Block scheme of the data processing system.

EXPERIMENTAL

The simulation is carried out on the basis of a standard program provided by the producer, through which the following parameters of the ESR spectrum are controlled:

1) range of magnetic field over which the spectrum extends, having a maximum extension of 1000 Gs;

---

[10] Prospect SPECTROSYSTEM 100 VARIAN.

2) position of spectrum on this range;

3) total number of interacting non-equivalent nuclei (i.e., coupling constants); limited to seven;

4) number of equivalent nuclei (i.e. possessing the same coupling constant); limited to 19;

5) nuclear spins;

6) shape of lines, assumed to be linear combinations of purely lorentzian and purely gaussian line shapes;

7) line width calculation is based on

Lorentzian line = $(\sqrt{3}/2)\ \Delta H$

Gaussian line = $(\sqrt{2 \ln 2/2})\ \Delta H$

where H is the peak-to-peak first-derivative linewidth.

8) coupling constants;

9) oscilloscope display, recorder operation for graphical representation, or punched tape output.

The program contains routines allowing the pairwise combination of three spectra from the three buffers.

ESR spectra of the five free radicals which are either nitroxides (aminyloxides), or hydrazyls with an acceptor and a donor group attached to the nitrogen atom,[11] were experimentally determined with the VARIAN E–12 spectrometer at room temperature and recorded graphically. From these spectra, the magnetic field range, line widths, numbers, and positions of lines were measured. First-order approximations for coupling constants and relative intensities were determined as described previously.[1,2]

RESULTS AND DISCUSSION

On the basis of the program, and ESR spectrum is computed and stored in the memory using a first-order approximation for calculating line positions. The first step consists in generating a list of line positions and relative intensities. Starting from one line of unit intensity in position zero each set of n equivalent nuclei of nuclear spin I_x coupled with the unpaired electron splits this line into $2nI_x + 1$ lines with a spacing equal to the coupling constant a_x, and so on for every other set.

Comparing the experimental spectrum with the simulated one, line widths and coupling constants are modified in order to result in a new simulated spectrum matching more closely the experimental one. Especially relative peak intensities are very sensitive to small variations of these two parameters.

I. *Arenesulphonyl-phenyl-nitroxides* * (*I*) (Ar = phenyl, *p*-tolyl or *p*-bromophenyl) afford practically identical ESR spectra with 27 lines grouped in three components of nine lines each.[12] A first-order approximation yields the following coupling constants

$$a_N = 11.5 \text{ Gauss};\ a_{o,p-H} = 1.48 \text{ Gs};\ a_{m-H} = 0.74 \text{ Gs}$$

* Nitroxides are more correctly named aminyloxides.

---

[11] A. T. Balaban, *Rev. Roumaine Chim.*, **16**, 725 (1971).

[12] A. T. Balaban and N. Negoiță, *Rev. Roumaine Chim.*, **17**, 1227 (1972).

assuming the *meta*-hydrogens to have coupling constants half as large as the other phenyl protons, and the arenesulphonyl protons to have unresolved couplings. The component of a triplet should therefore have the following line intensities : 1 : 2 : 4 : 6 : 6 : 6 : 4 : 2 : 1. Actually the central line is weaker (fig. 2) and this is due to the fact that the ratio $a_{o,p-H}/a_{m-H}$ is not exactly 2. Since a_N and a_{m-H} can be measured directly from the spectrum (as the distance between components of the triplet, and the leftmost interval within a triplet, respectively), $a_{o,p-H}$ was varied systematically until with the value 1.68 Gs the simulated spectrum matched the experimental one (fig. 2). The components of the triplet in the experimental spectrum are unequal because the radical decomposes partly during the recording of the spectrum.

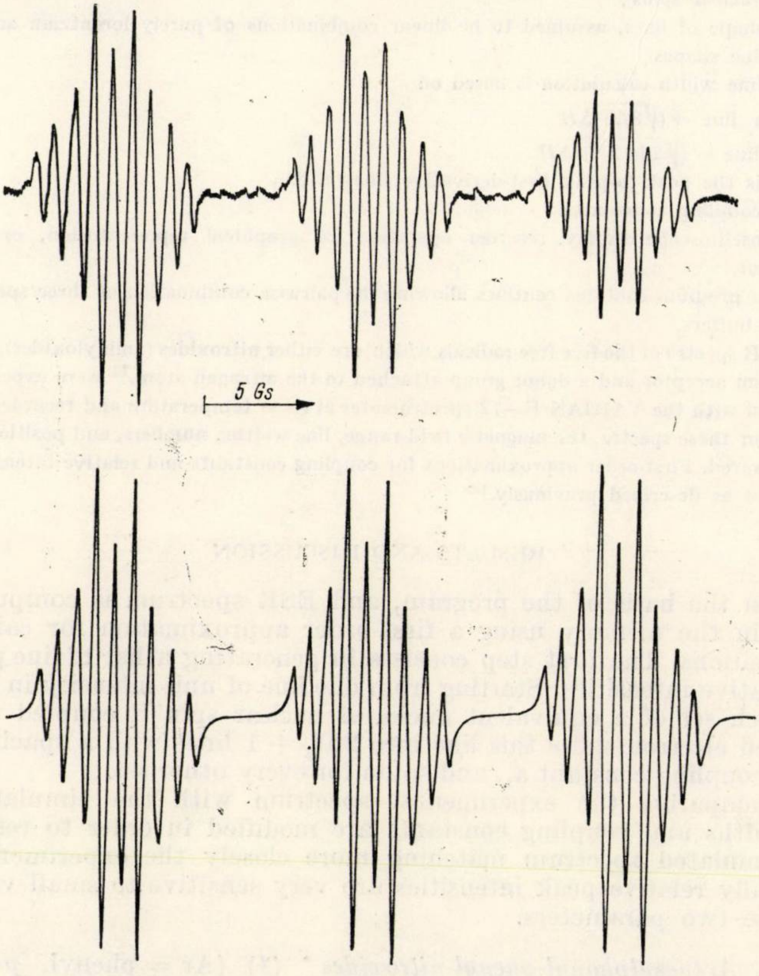

Fig. 2. — Experimental (in 1,4-dioxane) and simulated ESR spectra of benzenesulphonyl-phenyl-aminyloxide (I). Scan time : 3 minutes.

In the next cases, more than one variable must be modified in the search.

II. *N-Nitroso-N-phenyl-nitroxide* (II) was obtained by three independent reactions: decomposition of the preceding radical (I),[12] oxidation of cupferron or of N-nitroso-N-phenylhydroxylamine,[13,14] and spin trapping of nitric oxide by nitrosobenzene.[13] The ESR spectrum was analyzed[1] and yielded the following first-approximation coupling constants listed in the first part of table 1. The large a_{N-O} coupling constant can be measured directly on the spectrum, leaving three coupling constants to be varied systematically. We have chosen to leave unchanged the intermediate coupling constant which corresponds to the *ortho* and *para* protons of the phenyl ring, and to test the effect of varying the other two constants. The result (table 1 and figure 3) is a fairly good matching of experimental and simulated spectra.

Table 1

Coupling constants (in Gauss) used for simulating ESR spectra of nitroxides

Radical	Initial values (ref. 1)						Best values obtained in simulation					
	a_{N-O}	$a_{N=O}$	a_{o-H}	a_{p-H}	a_{m-H}	$\Delta H_{1/2}$	a_{N-O}	$a_{N=O}$	a_{o-H}	a_{p-H}	a_{m-H}	$\Delta H_{1/2}$
I	11.5	—	1.48	1.48	0.74	0.5	11.5	—	1.68	1.68	0.74	0.30
II	10.34	3.74	2.8	2.8	0.95	0.5	10.34	3.78	2.80	2.80	1.98	0.45
III	10.2	3.7	2.8	2.8 (3H)	0.93	0.5	10.20	3.80	2.80	2.95 (3H)	0.88	0.48
IV	10.3	3.43	3.43	—	0.5	1.2	10.30	3.43	2.30	—	0.50	1.00

III. *N-Nitroso-N-p-tolyl-nitroxide* (*III*), i.e. the *p*-methyl homologue of the preceding radical, gives an ESR spectrum presenting 48 peaks which were analyzed in terms of four coupling constants[1,14] (the proton coupling constants for the *ortho* phenyl protons and the *p*-methyl group having the same value).[1,14] Proceeding similarly to the preceding case, i.e. leaving unchanged the large a_{N-O} constant and the a_H constant for the *ortho* phenyl protons, the remaining three coupling constants were varied systematically affording the results presented in table 1 and figure 4. The *ortho*-hydrogens and the *para*-methyl hydrogens no longer appear to have the same coupling constant.

---

[13] A. T. Balaban, N. Negoiţă and I. Pascaru, *Rev. Roumaine Chim.*, **16**, 721 (1971).

[14] A. T. Balaban, N. Negoiţă and R. Baican, *J. Magn. Resonance*, **9**, 1 (1973).

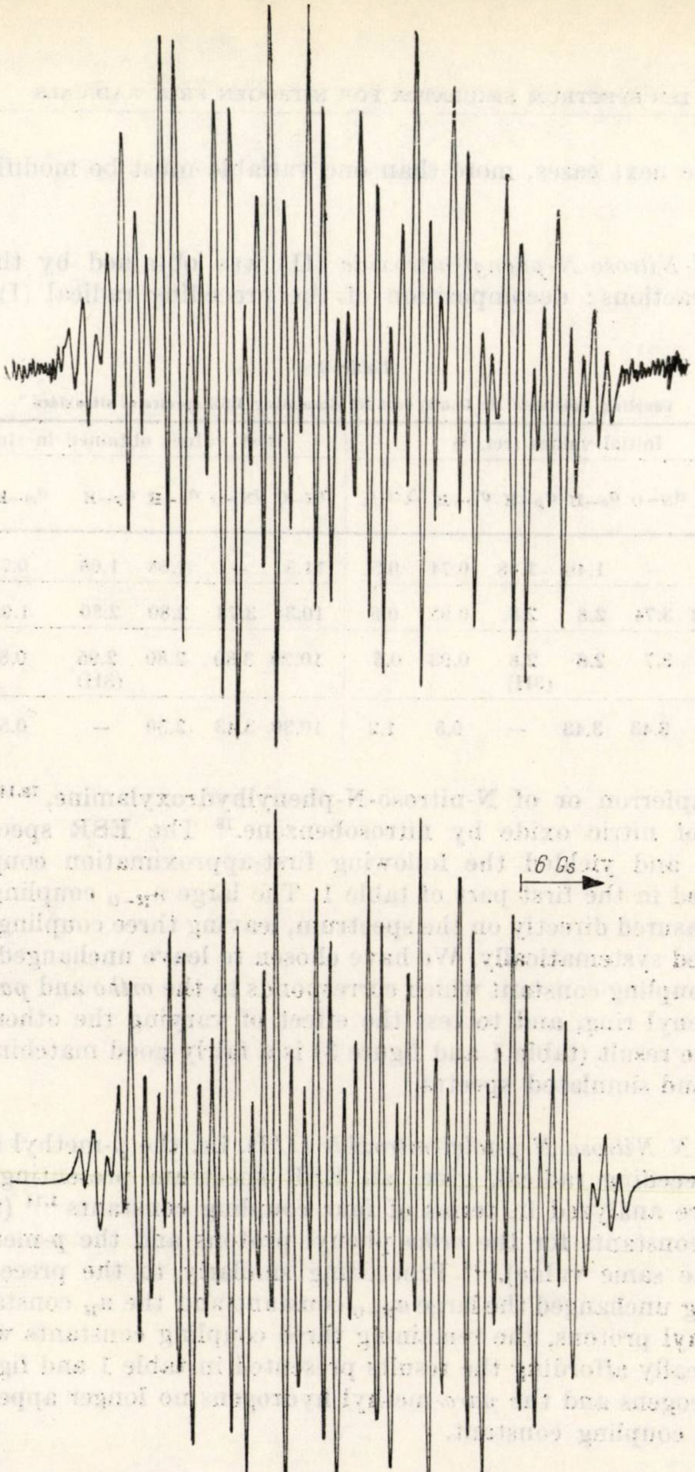

Fig. 3. — Experimental (in 1,4-dioxane) and simulated left half of the first-derivative spectra of N-nitroso-N-phenyl-aminyloxide (II).

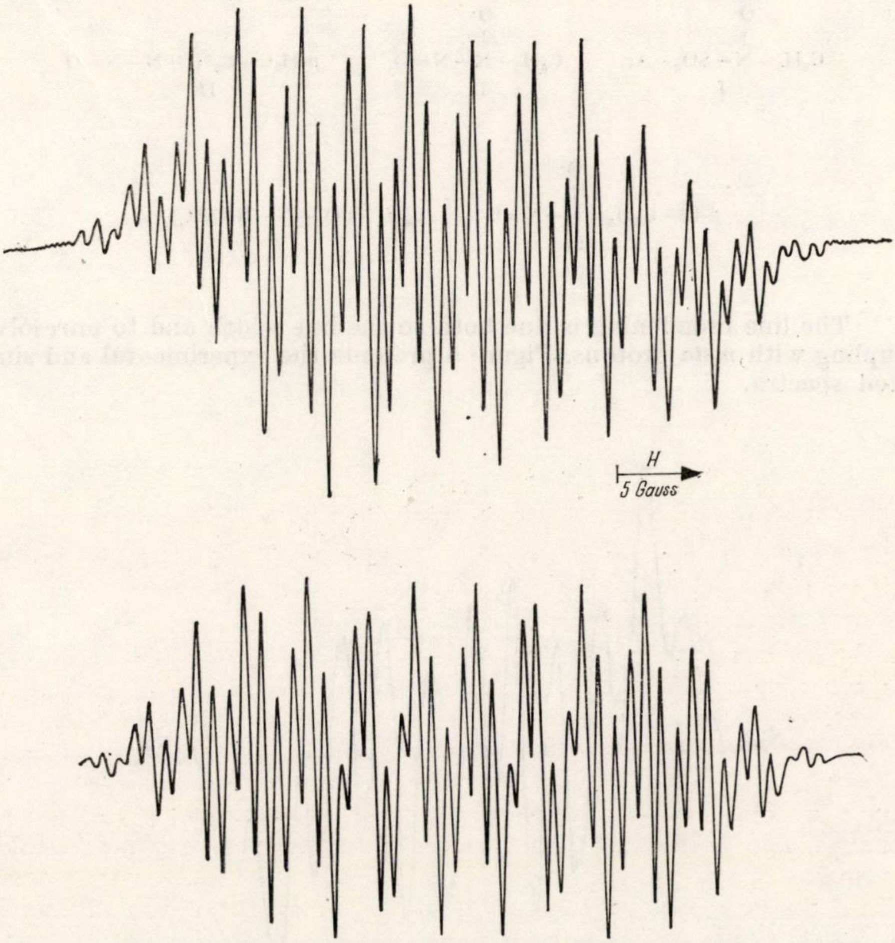

Fig. 4. — Experimental (in dioxane) and simulated ESR first-derivative spectra of N-nitroso-N-*p*-tolyl-aminyloxide (III).

IV. *N-(p-Chlorophenyl)-N-nitroso-nitroxide* (IV) presents eleven peaks (additional splittings due to the *meta* protons might be discerned but are poorly resolved).[14] An interesting feature of the spectrum is that the envelope of the peaks (the lines connecting the tops and bottoms of individual peaks) evidences a triplet. To reproduce this spectrum starting from the initial assumption that $3a_{o-H} = 3a_{N=O} = a_{N-O}$, one coupling constant (a_{o-H}) was varied systematically keeping the other two fixed. At the same time, in recording the simulated ESR spectrum, the a_{N-O} value was fed from buffer 1 with amplitude A_i and $a_{N-O} = a_{o-H}$ from buffers 2 and 3 with amplitudes A_j. The ratio A_i/A_j was measured from the experimental spectrum, A_i corresponding to the envelope and A_j to individual splittings of the spectrum. The total amplitude $A = A_i + A_j$ can be chosen as convenient (in our case, $A = 100\%$).

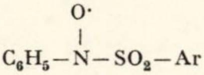

$C_6H_5-\overset{\overset{O^{\cdot}}{|}}{N}-SO_2-Ar$

I

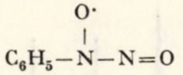

$C_6H_5-\overset{\overset{O^{\cdot}}{|}}{N}-N{=}O$

II

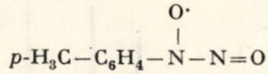

$p\text{-}H_3C-C_6H_4-\overset{\overset{O^{\cdot}}{|}}{N}-N{=}O$

III

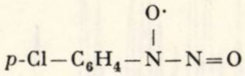

$p\text{-}Cl-C_6H_4-\overset{\overset{O^{\cdot}}{|}}{N}-N{=}O$

IV

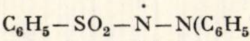

$C_6H_5-SO_2-\dot{N}-N(C_6H_5)_2$

V

The line broadening is due both to the line width and to unresolved coupling with *meta* protons. Figure 5 presents the experimental and simulated spectra.

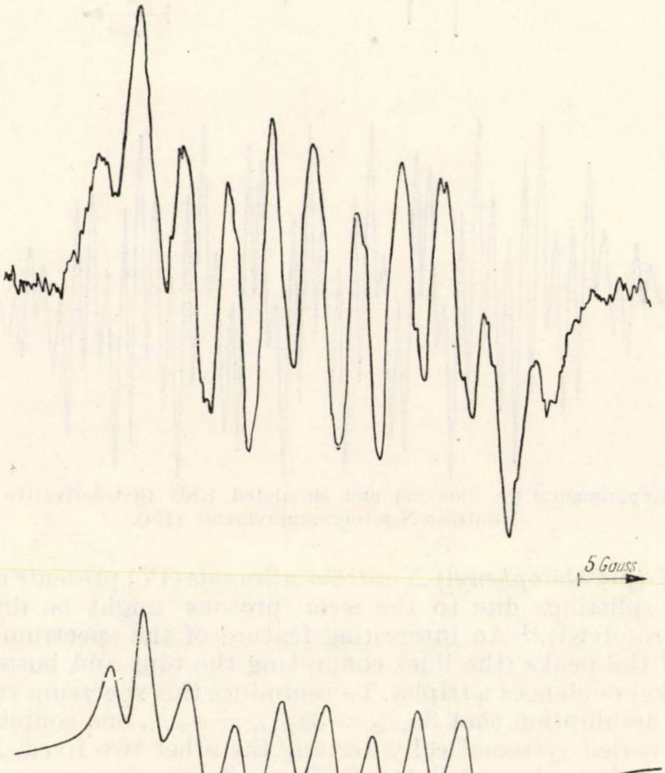

Fig. 5. — Experimental (in dioxane) and simulated ESR first-derivative spectra of N-(p-chlorophenyl)-N-nitroso-aminyloxide (IV).

V. *1-Arenesulphonyl-2,2-diphenylhydrazyls* (*V*) where the aryl group is phenyl or *p*-tolyl present identical ESR spectra.[12] Their analysis [1] indicates that the two phenyl groups appear to be non-equivalent, that the two nitrogens have approximately the same coupling constant and that the arenesulphonyl group does not couple. Owing to the large number of independent variables, the simulation is less precise in this case. Also, as in the preceding case, the envelope of the spectrum presents five maxima which can be reproduced by using two buffers, one for the two nitrogen coupling constants and the second for the remaining ones. The five-peak envelope with amplitude A_i due to the two nitrogens modulates the spectrum (fig. 6). The resulting comparison between experimental and simulated spectra can be seen in figure 7 and table 2.

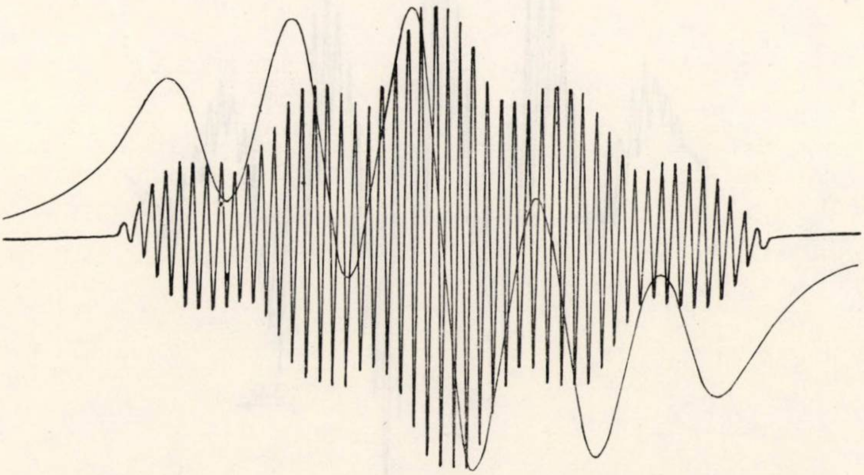

Fig. 6. — Simulated spectra which on overlapping will result in fig. 7 : five-peak spectrum from buffer 1 is due to the two nitrogens of V ; it modulates the second spectrum from buffer 2 due to couplings with nitrogen and hydrogen nuclei.

Table 2

Coupling constants (in Gauss) used for simulating ESR spectra of 1-benzenesulphonyl-2,2-diphenylhydrazyl (V)

	a_{N1}	a_{N2}	Phenyl a_{o-H}	Phenyl a_{p-H}	Phenyl a_{o-H}	Phenyl a_{m-H}	Phenyl a_{p-H}	$\Delta H_{1/2}$	A_i/A_j
Initial values (ref.[1])	9.4	9.4	1.0	1.0	2.1	1.0	4.2	0.5	—
Best values	9.40	9.25	1.0	1.0	2.1	1.0	4.2	0.38	0.7/0.3

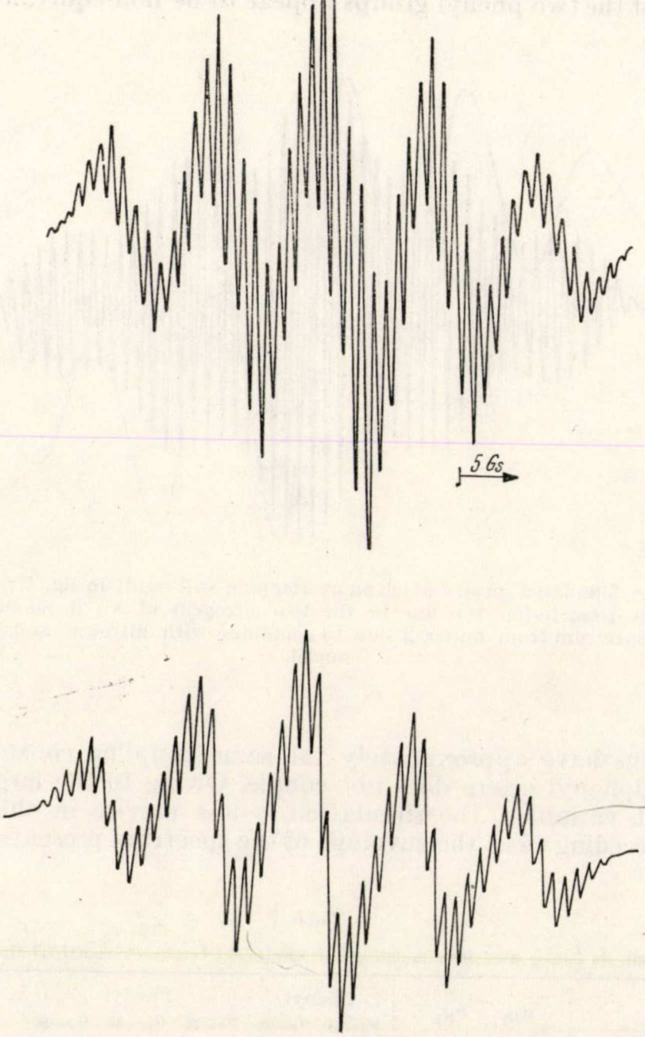

Fig. 7. — Experimental (in dioxane) and simulated ESR first derivative spectra of 1-benzenesulphonyl-2,2-diphenylhydrazyl (V).

Revue Roumaine de Chimie, **18**, *6*, 1005 – 1011 (1973)

REACTION OF AMINES WITH PHENOTHIAZINIUM CATION. I

SYNTHESIS AND PROPERTIES OF 3H-PHENOTHIAZINE-3-[POTASSIUM 4-ANILSULPHONATE], 3H-PHENOTHIAZINE-3-[POTASSIUM 3-ANILSULPHONATE] AND 3H-PHENOTHIAZINE-3-[POTASSIUM 2-ANILSULPHONATE]

M. RĂILEANU and ILEANA RADULIAN

Chair of Organic Chemistry,
University of Craiova,
Str. Al. I. Cuza, 13, Romania

Received August 28, 1972

By oxidizing phenothiazine with ferric chloride in the presence of the potassium salts of sulphanilic, metanilic and orthanilic acid, we obtained respectively 3H-phenothiazine-3-[potassium 4-anilsulphonate](Ia), 3H-phenothiazine-3-[potassium 3-anilsulphonate] (Ib) and 3H-phenothiazine-3-[potassium 2-anilsulphonate] (Ic). These three isomeric compounds are soluble in water, have two protonation stages with corresponding colour changes, and may be used as neutralization indicators.

In 1902 Kehrmann and Vesely[1] have obtained 3-anil-3H-phenothiazine by oxidizing with ferric chloride a mixture of phenothiazine and aniline hydrochloride.

The reaction mechanism of phenothiazine with nucleophilic reactants in the presence of ferric chloride was recently described by Daneke and Wanzlick.[2] These authors consider that nucleophilic reactants add in position 3 to the phenothiazinium cation, that appears intermediately.

By analogy to 3-anil-3H-phenothiazine, we have synthetized and studied in the present paper 3H-phenothiazine-3-[potassium 4-anilsulphonate] (Ia), 3H-phenothiazine-3-[potassium 3-anilsulphonate] (Ib) and 3H-phenothiazine-3-[potassium-2-anilsulphonate](Ic) in view of their use as neutralization indicators.

---

[1] F. Kehrmann and O. Vesely, *Liebigs, Ann. Chem.*, **322**, 41 (1902).
[2] J. Daneke and H. W. Wanzlick, *Liebigs, Ann. Chem.*, **740**, 52 (1970).

The isomeric compounds Ia, Ib and Ic are obtained and purified extremely easily, as shown in the experimental part. They are salts of sulphonic acids and, therefore, dissolve in water even at room temperature with the formation of blue solutions.

The substances Ia, Ib and Ic are coloured in violet-pink in a basic medium, and in blue or green in an acid medium, according to the acid concentration. Owing to the double colour change as function of the pH, these dyes were named correspondingly : chameleon blue I(Ia), chameleon blue II(Ib) and chameleon blue III(Ic).

The colour change of chameleon blue I, II and III versus the pH is reversible and is due to a gradual protonation reaction. Indeed, substances Ia, Ib and Ic have unshared electrons at the iminic nitrogen atom in position 3 and at the heterocyclic nitrogen atom in position 10. This fact explains the basic character of chameleon blue I, II and III, as well as the ease with which these are protonated when dissolved in water :

$$I + H_2O \rightleftarrows IH^+ + OH^-$$

In the first phase, their protonation takes place at the iminic nitrogen atom, and, in the second, at the heterocyclic nitrogen atom.

The protonation in the second stage (IH_2^{2+}) is achieved only in concentrated acids, as the positive charge in the monoprotonated cation(IH^+), that appeared intermediately, strongly blocks the unshared electrons of the heterocyclic nitrogen atom.

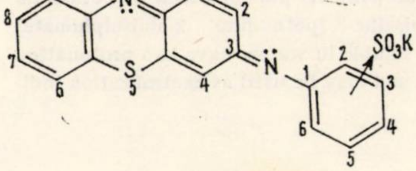

$Ia: -SO_3K(4)$
$Ib: -SO_3K(3)$
$Ic: -SO_3K(2)$

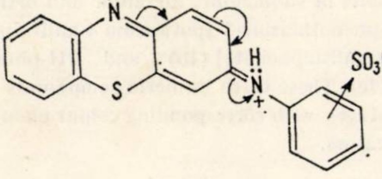

$IaH^+: -SO_3K(4)$
$IbH^+: -SO_3K(3)$
$IcH^+: -SO_3K(2)$

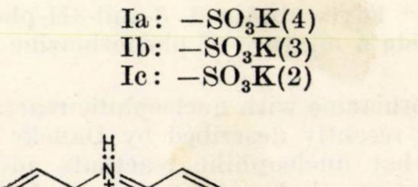

$IaH_2^{2+}: -SO_3K(4)$
$IbH_2^{2+}: -SO_3K(3)$
$IcH_2^{2+}: -SO_3K(2)$

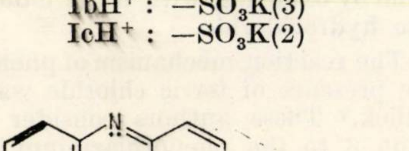

II

The protonation of the heterocyclic nitrogen atom in the presence of acids was also demonstrated recently in the case of some 3H-phenothiazinones(3).[3]

By analogy to chameleon blue I, II and III, another substance synthetized by us, 3-[*m*-nitroanil]-3H-phenothiazine (II), is also protonized in two stages; it is violet in an alkaline medium, blue in the monoprotonated form (IIH^+) and green in the diprotonated form (IIH_2^{2+}). It therefore results that at the dissolution of chameleon blue I, II and III in concentrated acids, the appearing green colour, is indeed due to the protonation of the heterocyclic nitrogen atom, and not to an eventual protonation of the sulphonic anion

$$(-SO_3^- + H^+ \rightleftarrows -SO_3H).$$

The two forms, basic and monoprotonated, of chameleon blue I, II and III, were studied spectrophotometrically at 21°, using 1.60×10^{-5}M solutions for chameleon blue I and III, and 1.25×10^{-5} M solutions for chameleon blue II, which is less soluble.

The absorption spectra, presented in figures 1–3, point out the coexistence of the two forms, acid and basic, of chameleon blue I, II and III for certain pH values, as the absorption curves pass through an isosbestic point.

The diprotonated form (IH_2^{2+}) coloured in green, appears in more concentrated acids, as can be seen in the absorption spectra given in figures 4–6.

Indeed, if in 1.2N H_2SO_4 the monoprotonated form prevails in 11N H_2SO_4 chameleon blue I, II and III appear entirely diprotonated; but in 5.5N H_2SO_4 the equilibrium between the two stages is evident.

The fact that the three absorption curves do not pass in this case through an isosbestic point is due to the appearance in the system of a new species, which, in concentrated acids, could be the diprotonated form of the dye with undissociated sulphonic group ($-SO_3^- + H^+ \rightarrow -SO_3H$).

The absorption maxima, extinctions and molar absorption coefficients for the basic and monoprotonated form (IH^+) are given in tables 1–3.

Table 1

Absorption maxima, extinctions and molar absorption coefficients for chameleon blue I in its basic and monoprotonated form (for a 1.6×10^{-5} M solution at 21°)

pH = 11 Basic form	$\lambda_{max(1)} = 560$ nm	$E_{560} = 0.4380$	$\varepsilon_{560} = 27.370$
	$\lambda_{max(2)} = 294$ nm	$E_{294} = 0.6020$	$\varepsilon_{294} = 37.620$
pH = 2.2 Acid form	$\lambda_{max(1)} = 660$ nm	$E_{660} = 0.8100$	$\varepsilon_{660} = 50.620$
	$\lambda_{max(2)} = 308$	$E_{308} = 0.6780$	$\varepsilon_{308} = 42.370$

---

[3] M. Răileanu, I. Radulian, O. Duliu, and S. Radu, *Collection Czechoslov. Chem. Commun.*, **37**, 478 (1972).

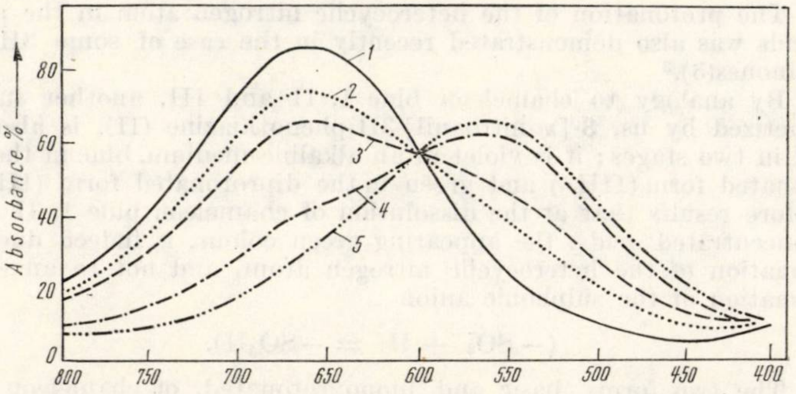

Fig. 1. — Absorption curves of chameleon blue I for certain values of pH.

pH : 6.1 (*1*) ; 7.4(*2*) ; 7.7(*3*) ; 8.3(*4*) ; 8.6(*5*).

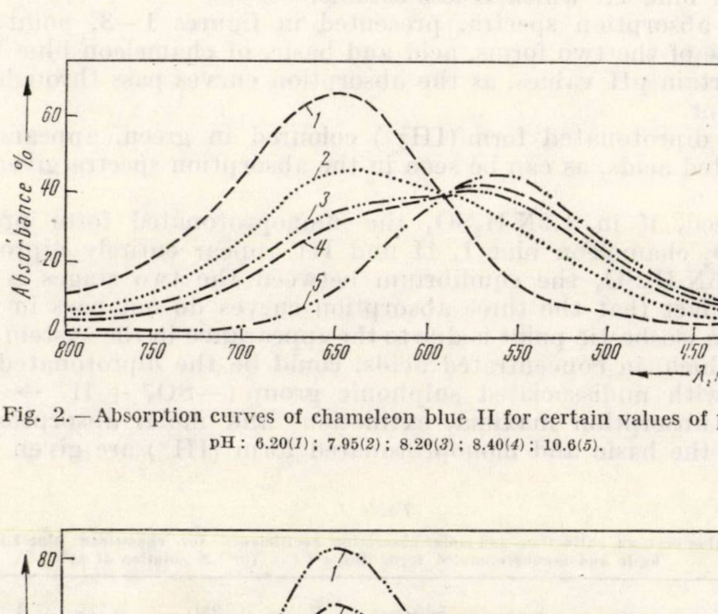

Fig. 2. — Absorption curves of chameleon blue II for certain values of pH.

pH : 6.20(*1*) ; 7.95(*2*) ; 8.20(*3*) ; 8.40(*4*) ; 10.6(*5*).

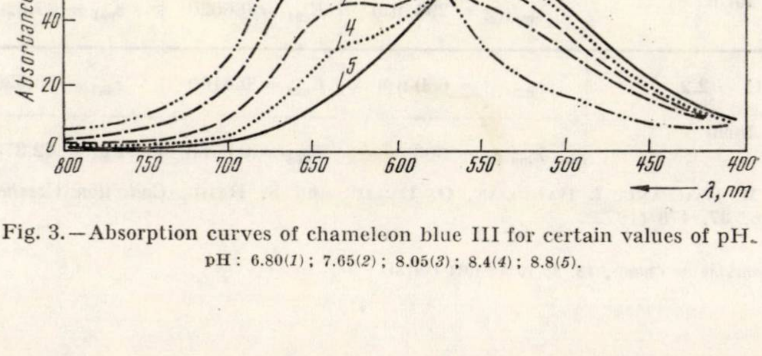

Fig. 3. — Absorption curves of chameleon blue III for certain values of pH.

pH : 6.80(*1*) ; 7.65(*2*) ; 8.05(*3*) ; 8.4(*4*) ; 8.8(*5*).

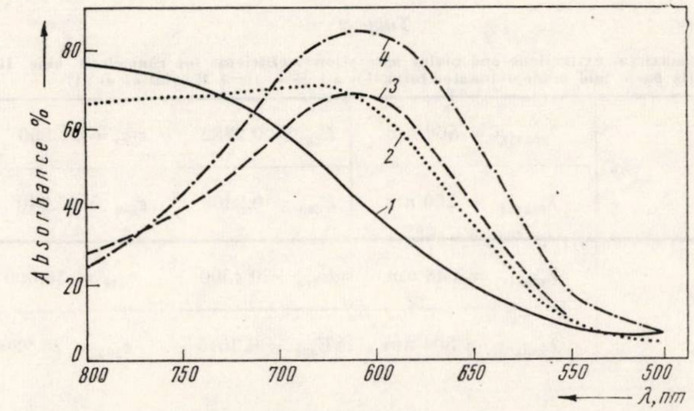

Fig. 4. — Absorption of chameleon blue I in concentrated acids.
11 N H_2SO_4 (*1*) ; 5.5 N (*2*) ; 2.9 N (*3*) ; 1.2 N (*4*).

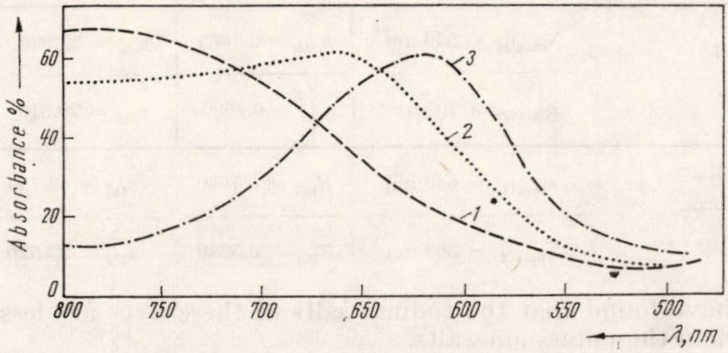

Fig. 5. — Absorption of chameleon blue II in concentrated acids.
11 N H_2SO_4 (*1*) ; 5.5 N (*2*) ; 1.2 N (*3*).

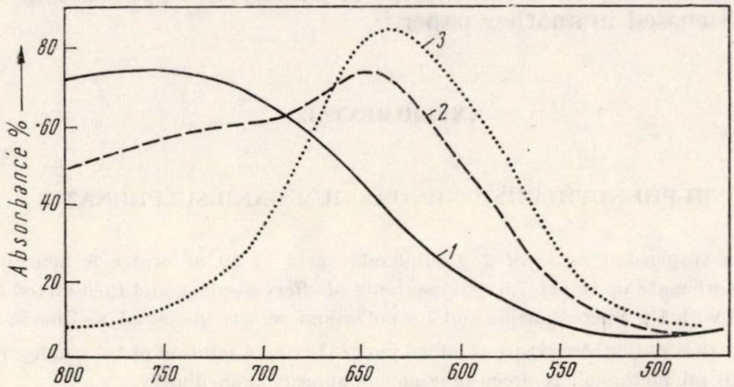

Fig. 6. — Absorption of chameleon blue III in concentrated acids.
11 N H_2SO_4 (*1*) ; 5.5 N (*2*) ; 1.2 N (*3*).

Table 2

Absorption maxima, extinctions and molar absorption cœfficients for chameleon blue II in its basic and monoprotonated form (for a 1.25 × 10^{-5} M solution at 21°)

pH = 11 Basic form	$\lambda_{max(1)} = 560$ nm	$E_{560} = 0.2882$	$\varepsilon_{560} = 23.050$
	$\lambda_{max(2)} = 290$ nm	$E_{290} = 0.3468$	$\varepsilon_{290} = 27.740$
pH = 6 Acid form	$\lambda_{max(1)} = 648$ nm	$E_{648} = 0.4500$	$\varepsilon_{648} = 36.000$
	$\lambda_{max(2)} = 304$ nm	$E_{304} = 0.3615$	$\varepsilon_{304} = 28.920$

Table 3

Absorption maxima, extinctions and molar absorption coefficients for chameleon blue III in its basic and monoprotonated form (for a 1.6 × 10^{-5} M solution at 21°)

pH = 11 Basic form	$\lambda_{max(1)} = 546$ nm	$E_{546} = 0.3665$	$\varepsilon_{546} = 22.900$
	$\lambda_{max(2)} = 290$ nm	$E_{290} = 0.4690$	$\varepsilon_{290} = 29.310$
pH = 3 Acid form	$\lambda_{max(1)} = 640$ nm	$E_{640} = 0.7960$	$\varepsilon_{640} = 49.750$
	$\lambda_{max(2)} = 304$ nm	$E_{304} = 0.5380$	$\varepsilon_{304} = 33.620$

We have found that the sodium salts of these dyes are less soluble in water than the potassium salts.

Owing to their solubility in water, and the ability to change their colour according to pH, chameleon blue I, II and III may be used with good results as acid-basic indicators. The analytical applications of these dyes are discussed in another paper.[4]

EXPERIMENTAL

1) 3H-PHENOTHIAZINE-3-[POTASSIUM 4-ANILSULPHONATE]

(*Ia*). A suspension made of 2 g sulphanilic acid in 10 ml water is neutralized with potassium bicarbonate up to pH 7.5 (disapearance of effervescence), and then mixed to a solution obtained with 1 g phenothiazine and 1 g potassium acetate in 100 ml methanol.

To the thus obtained mixture is added under stirring a solution of 1.8 g anhydrous ferric chloride in 10 ml methanol. A green-blue colour appears immediately.

The precipitate formed after about 12 hours, was filtered, washed with methanol, and recrystallized from 75 % methanol.

---

[4] M. Răileanu, I. Radulian and H. Krauss, *Rev. Roumaine Chim.* (under press).

When the solution was cooled a precipitate of overpassed blue needles was formed, which was filtered, washed with a little 75 % methanol and then dried at 140°. Yield 0.74 g *Calcd.* for $C_{18}H_{11}N_2O_3S_2K$: N 6.89 ; S 15.78 ; *Found* : N 7.02 ; S 15.56.

3H-Phenothiazine-3-[potassium 4-anilsulphonate](Ia) does not melt up to 360° and burns with extreme difficulty.

2) 3H-PHENOTHIAZINE-3-[POTASSIUM 3-ANILSULPHONATE](Ib).

The proceeding is the same as in 1) but 2 g of metanilic acid are introduced into reaction.

There results 0.7 g of dye in the form of blue needle-shaped crystalls grouped together like a hedgehog. *Calcd.* for $C_{18}H_{11}N_2O_3S_2K$: N 6.89 ; S 15.78 ; *found* : N 6.63 ; S 15.51.

3H-Phenothiazine-3-[potassium 3-anilsulphonate](Ib) is less soluble in water than 3H-phenothiazine-3-[potassium 4-anilsulphonate] (Ia). This salt does not melt till 360° and burns with great difficulty.

3) 3H-PHENOTHIAZINE-3-[POTASSIUM 2-ANILSULPHONATE] (Ic).

The proceedings are the same as in 1), but 2 g of 2-aminobenzensulphonic acid (orthanilic acid) were used. The deposited precipitate was recrystallized in this case from 85 % methanol.

There results 0.23 g of dye in the form of needle-shaped crystalls grouped in the form of a hedgehog. *Calcd.* for $C_{18}H_{11}N_2O_3S_2K$: N 6.89 ; S 15.78 ; *found* : N 6.77 ; S 15.59.

3H-Phenothiazine-3-[potassium 2-anilsulphonate](Ic) does not melt till 360° and burns with great difficulty.

The buffer solutions with different values of pH were obtained after Sörensen and Mc. Ilvain. The pH of the buffer solutions was continuously controlled with a pH-meter.

For the spectral absorption study 1.6×10^{-5} M solutions of chameleon blue I and III and 1.25×10^{-5} M solutions of chameleon blue II, were used and the spectra were recorded with a Beckman model DB spectrophotometer at 21°.

Revue Roumaine de Chimie, 18, 6, 1013–1018 (1973)

ÜBER 1,2,3, 4-TETRAHYDROAKRIDIN-9-CARBOXYLSÄURE-DERIVATE. I

AMIDE

M. CÎRJE

Physiologisches Institut „D. Danielopolu'',
Bd. 1 Mai nr. 11, Bukarest,

Eingegangen am 7. Dezember 1972

Es wurde die Synthese einiger Amid-Derivate der im Titel angegebenen Säure bezüglich ihrer Wirkung auf das Nervensystem vorgenommen. Anylin, *p*-Chloranylin und *p*-Anisidin reagiert mit Chloralhydrat und Hydroxylamin, wobei die entsprechenden Isonitrosoazetanylide entstehen, die in Gegenwart der Schwefelsäure zur Ringverbindung der Isatine führen. Letztere reagieren mit Cyklohexanon in alkalischem Milieu, wobei 7–R–1,2,3,4-Tetrahydroakridin-9-Carboxyl-Säure (R = H, Cl, OCH_3) entsteht. Unter der Einwirkung von PCl_5 kommt das entsprechende Säurechlorid zustande, das sowohl mit NH_3, als auch mit den nachstehenden Aminen reagiert : $HN(C_2H_5)_2$, $HN(C_2O_4OH)_2$, $HN(C_2H_4)_2O$. Die neuen Amide werden auch durch IR-Spektra charakterisiert.

Die Einführung der Akridine in der Therapie führte zur Synthese einer breiten Serie von Verbindungen und damit zum Studium ihrer pharmakodynamischen Eigenschaften. Neben ihren bakteriziden Wirkungen, mit denen sie erstmalig auftraten, wurden noch weitere antimalarische, antivirale, krebsbekämpfende, Traquillizer, enzyminhibierende u.a. Eigenschaften beschrieben. Die Bildung komplexer Verbindungen zwischen Akridinen und Nukleinsäuren oder Proteinen führte zu einem tieferen Verständnis ihres pharmakodynamischen Wirkungsmechanismus.

Pharmaka mit Akridinstruktur und Einwirkung auf das Nervensystem — als Analeptika — weisen einen teilweise oder vollständig H-gesättigten Ring auf, z.B. Tetrophan (1,2-Dihidro-3,4-Benzakridin-9-Carboylsäure) oder Takrin(1,2,3,4-Tetrahydro-9-Aminoakridin). Der Anlaß zum Studium einiger Akridinderivate mit H-gesättigtem Ring war für uns eben diese Wirkung zu verfolgen.

Wir nahmen uns vor, wobei wir von der 1,2,3,4-Tetrahydroakridin-9-Carboxylsäure (THA-Säure) ausgingen, einige Abkömmlinge mit biologisch aktiver Funktion zu synthetisieren. In der vorliegenden Arbeit führen wir die Synthese einiger Amidderivate der THA-Säure vor, die je eine Chlor oder Methoxy-Gruppe in Position 7 aufwiesen, die so im Atebrinmolekül aktive Gruppen bilden.

Die Synthese dieser Derivate wurde dem nachstehenden Schema gemäß vorgenommen :

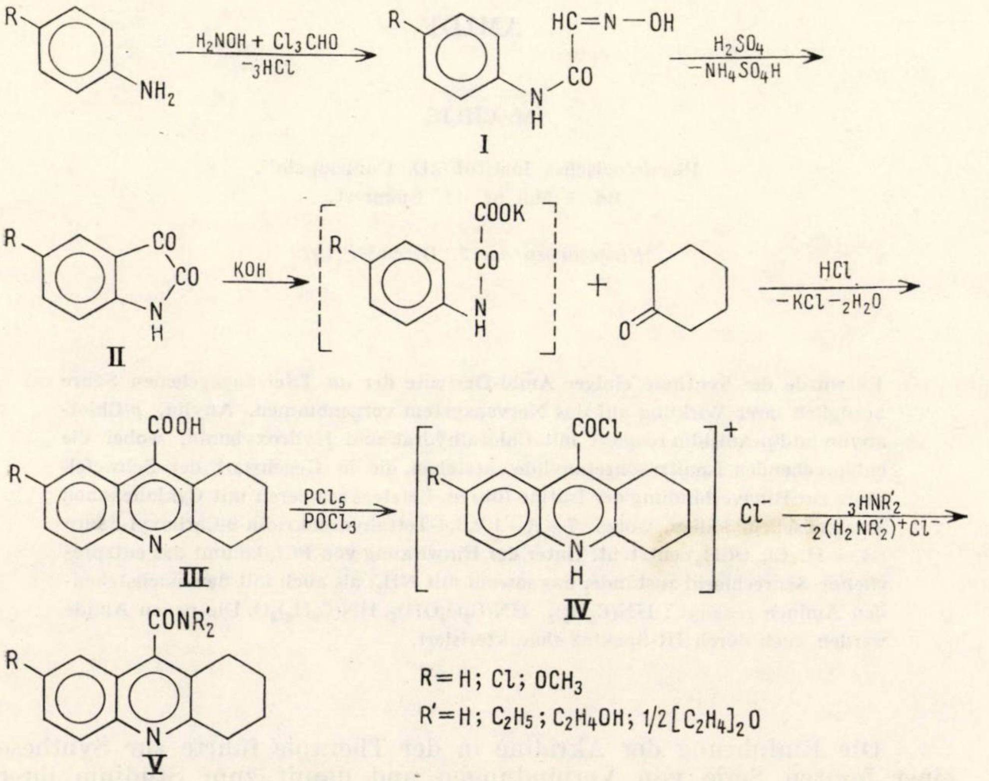
R
NH$_2$
H$_2$NOH + Cl$_3$CHO
−3HCl
HC=N—OH
CO
N
H
I
H$_2$SO$_4$
−NH$_4$SO$_4$H
CO
CO
II
KOH
COOK
+
O
HCl
−KCl−$_2$H$_2$O
COOH
III
PCl$_5$
POCl$_3$
COCl
IV
Cl$^-$
$_3$HNR$'_2$
−2(H$_2$NR$'_2$)$^+$Cl$^-$
CONR$'_2$
V

R=H; Cl; OCH$_3$

R′=H; C$_2$H$_5$; C$_2$H$_4$OH; 1/2[C$_2$H$_4$]$_2$O

Von dem entsprechenden Amin ausgehend, gelangt man durch eine Sandmeyersche,[1] nachträglich modifizierte Reaktion[2] unter zufriedenstellenden Bedingungen zum entsprechenden Isonitrosoazetanylid (I). Dieses bildet in Gegenwart der Schwefelsäure, nach den von Pietra[3] festgesetzten Bedingungen einen Ring, wobei das entsprechende Isatin zustandekommt (II). Durch eine Pfitzinger-Borsche-Reaktion[4,5] reagiert Isatin in alkalischem Milieu mit Cyklohexanon, woraus sich die THA-Säure ergibt (III). Wir machen darauf aufmerksam, daß 7-Methoxi-THA-Säure im Schrifttum nicht verzeichnet ist. Zum Erhalten des Säurechlorids verfügen wir über einen einzigen Hinweis,[6] der besagt, daß die Umwandlung der THA-Säure in Säurechlorid, sowohl in Gegenwart des Phosphopentachlorids, als auch der des Phosphooxychlorids möglich ist, während für die andern Säuren kein Hinweis vorliegt. Die Ergebnisse dieser Umwandlung waren wenig zufriedenstellend: die Ausbeute ist gering, etwa 30%, die Methode nicht reproduzierbar. Die Frage wurde gelöst, durch die Umwandlung der betreffenden Säure in Chlorhydrat, — eine kristalline Substanz, die dann in Benzen-Milieu und unter reproduzierbaren Bedingungen, mit Phosphorpentachlorid zu den Säurechloriden mit guter Ausbeute (80—90%) führte. Von den entwickelten Amiden, wird bloß für das Diethylamid der THA-Säure in der Literatur [6] der Schmelzpunkt angegeben, wobei jedoch nichts über die Bedingungen unter denen seine Synthese erfolgt, bekannt gegeben wird. Die Amydierung wurde in Azetonmilieu vorgenommen, das sowohl die Bedingung als Reaktionsmilieu zu dienen erfüllt und zugleich keine Verbindung mit dem Säurechlorid eingeht. Die synthetisierten Amide, die von der THA-Säure ausgehen, sind in Tab. 1 angezeigt.

---

[1] T. Sandmeyer, *Helv. Chim. Acta*, **2**, 234 (1919).

[2] „Organic Synthesis" coll. vol. I., J. Wiley, New York, 1958, S. 327.

[3] S. Pietra, *Farmaco*, **13**, 75 (1958).

[4] A. Albert, „The Acridines", E. Arnold, London, 1951, S. 66.

[5] Bun-Hoi und P. Cagniant, *Bull. Soc. chim. France*, **11**, 343 (1944).

Zur Charakterisierung der Substanzen und zur Identifizierung der verschiedenen Funktionsgruppen wurden die Infrarot-Spektren der neu synthetisierten Amide bestimmt.

Die dabei erhaltenen Werte verhielten sich innerhalb der im Schrifttum [7] angegebenen Werte, sowohl für die Amid I-Schleifen als auch für die Amid II — Schleifen und die Ausdehunungsfrequenzen N—H. Die den aetherischen Funktionen charakteristischen Frequenzen bewegten sich in der Zone 1226—1230 cm^{-1} für die Aryl-Alkyl-Aethere und in der Zone 1110—1113 cm^{-1} für Morpholin-Derivate.[8]

Die Charakterisierung des teilweise gesättigten Ringes,[9] erfolgt mit Hilfe der Ausdehnungs- und Deformierungs-Frequenzen der CH_2-Gruppe. Bei den in der Seitenkette Alkilgruppen enthaltenden Derivaten erschienen, selbstverständlich Schleifenübergriffe. Es wurde keine Schleifenzuordnung versucht; in Tab. 2 werden bloß sämtliche Maxima in den charakteristischen Zonen angezeigt.

EXPERIMENTELLER TEIL

Isonitrosoazetanylide I: In einer aus 0,65 Mol. Chloralhydrat in 2400 ml Wasser bestehenden Lösung werden 690 g wasserfreies Natriumsulfat aufgelöst. Es wird in dünnem Fluß, unter ständigem Rühren eine aus 0,6 Mol. des betreffenden Amins (Anylin, *p*-Chloranylin oder *p*-Anisidin) in 360 ml Wasser und 52 ml Konz. Salzsäure bestehende Lösung beigefügt. Eine aus 0,96 Mol. Hydroxylaminchlorhydrat bestehenden Lösung in 300 ml Wasser wird zu

---

[6] O. Yu. Magidson und A. I. Travin, *Zhur. obshchei Khim.*, **7**, 842 (1937); *Chem. Abstr.*, **31**, 5800 (1937).

[7] L. J. Bellmay, „The Infrared Spectra of Complex Molecules", Methuen, London, 1960.

[8] A. D. Cross, „Introduction to Practical Infrared Spectroscopy", Butterworts, London, 1960.

[9] C. N. Rao, „Chemical Applications of Infrared Spectroscopy", Academic Press, New York, 1963.

Tabelle

Charakteristika der

Nr.	Benennung	R	R′
1	THA-säureamid	H	NH_2
2	THA-chlorsäureamid	Cl	NH_2
3	THA-methoxysäureamid	OCH_3	NH_2
4	THA-säurediaethylamid	H	$N(C_2H_5)_2$
5	THA-chlorsäurediaethylamid	Cl	$N(C_2H_5)_2$
6	THA-methoxysäurediaethylamid	OCH_3	$N(C_2H_5)_2$
7	THA-säurediaethanolamid	H	$N(C_2H_4OH)_2$
8	THA-chlorsäurediaethanolamid	Cl	$N(C_2H_4OH)_2$
9	THA-methoxysäurediaethanolamid	OCH_3	$N(C_2H_4OH)_2$
10	THA-säurediaethyleneoxyamid	H	$N(C_2H_4)_2O$
11	THA-chlorsäurediaethylene-oxyamid	Cl_3	$N(C_2H_4)_2O$
12	THA-metosysäurediethyleneoxyxdamid	OCH_3	$N(C_2H_4)_2O$

Die Schm.p. wurden nicht korrigiert.

der schon erhaltenen Lösung hinzugefügt. Unter ständigem Rühren wird erwärmt, so daß es innerhalb 50—60 Min. zum Sieden kommt. Dieser Zustand wird 1—2 Minuten aufrechterhalten. Dann läßt man abkühlen; am nächsten Tag werden die gebildeten Kristalle filtriert und mit Wasser gespült. Die Ausbeute ist 85—95%; die entsprechenden Isonitrosoazetanylide weisen jeweils die nachstehenden Siedepunkte auf; R = H, Cl, OCH_3, 175°, 165°, 184°.

Isatine II: Bei 3,6 Mol. Schwefelsäure d = 1,81, bei einer Temperatur von 72°, unter energischem Rühren, wird in Teilen von je 0,3 Mol. das betreffende fein zerstoßene Isonitrosoazetanylid im Laufe von 8—10 Minuten hinzugegeben. Hierbei wird die ganze Zeit und noch weitere 5 Minuten eine Temperatur von 75—78° aufrechterhalten. Anschließend wird die Reaktionslösung gekühlt und über zerstoßenes Eis gegossen. Nach 30 Minuten wird filtriert und mit Wasser gewaschen. Die entsprechenden Isatine weisen nachstehende Schmelzpunkte auf: R = H, Cl, OCH_3: 195—8°, 246—7°, 192—5°; die Ausbeuten sind jeweils: 75—78%; 85—90%; 55—65%.

THA-Chlorhydrat-Säure III: 0,1 Mol. Isatin wird in 0,3 Mol. KOH (30%-ige Lösung) und 100 ml Aethanol aufgelöst. Anschließend werden unter Rühren 0,3 Mol. Cyclohexanon hinzugegeben. Die Reaktionsmasse blieb 12 Stunden lang unter Aufrühren und Rückfluß. Nach Abkühlen wird die jeweilige THA-Säure mit 0,34—0,4 Mol. 50%-iger Essigsäure abgesetzt. (Im Falle des H- und Cl-Derivats wird die Reaktionsmasse vor der Neutralisierung durch Destillation von 50 ml derselben unter niederem Druck konzentriert). Am nächsten Tag wird filtriert, mit Aethanol und Aethyläther gewaschen. Die erhaltenen Säuren weisen folgende

1

erhaltenen Amide

Schmp. p.	Ausbeute %	N % Berechnet	N % Gefunden	Rekrystallisierungsflüssigkeit
259–61	94	12,38	12,09	Dioxan
236–38	92	10,75	10,71	Azeton
244–46	90	10,93	11,71	Dioxan
103–5	74	9,92	10,10	Azeton + Ligroin
119–21	85	8,84	8,56	Azeton
84–86	81	8,97	9,12	Essigsäure Aethylester
192–94	83	8,91	8,89	Dioxan
193–95	80	8,03	8,17	Azeton
198–200	87	8,13	8,10	Azeton + Aethanol
193–94	83	9,45	9,30	Ligroin
169–71	85	8,47	8,49	Azeton + Ligroin
163–65	84	8,58	8,70	Azeton

Schmelzpunkte und Ausbeuten auf : R = H, Cl, OCH_3 : 295–8°, 80–90 % ; 285–7°, 85–90 % ; 312–14°, 60–70 %.

Erhalten des Chlorhydrats : Zu einer heißen aus 40 ml Aethanol, 20 ml konz. Salzsäure und 20 ml Wasser bestehenden Lösung werden 10 g fein zerstoßener jeweiliger THA-Säure und ein wenig entfärbende Kohle hinzugegeben. Es wird 20–30 Min. lang rückgeflossen und nachträglich heiß filtriert. Nach einer Stunde werden die erhaltenen Kristalle filtriert, die dann mit Azeton und Aether gewaschen werden. Es ergeben sich Chlorhydrate mit den nachstehenden Schmelzpunkten und Ausbeuten : R = H, Cl, OCH_3 : 262–4°, 80–85 % ; 258–60°, 75–80 % ; 255–7°, 80–90 %.

Säurechlorid der THA-Säure IV : Zu 0,05 Mol. jeweiliger HCl-THA-Säure in 75 ml wasserfreiem Benzol werden unter Rühren 0,06 Mol. Phosphorpentachlorid hinzugegeben. Es wird eine Stunde lang in Trockenluft schwach zürückgeflossen. Nach einer Abkühlung von ungefähr einer Stunde werden die sich ergebenden Kristalle filtriert, sie werden dann mit Benzol gespült. Die Chlorhydrate der Säurechloride der THA-Säure werden mit folgenden Schmelzpunkten und Ausbeuten erhalten : R = H, Cl, OCH_3 : 202–205°, 80–87 % ; 188–190°, 78–86 % ; 210–212°, 83–93 %.

Die Amide der THA-Säure V : Zu 0,01 Mol. Chlorhydrat des entsprechenden Säurechlorids in 10 ml Azeton, kommen unter Aufschütteln 0,04 Mol des entsprechenden in 5 ml Azeton aufgelösten Amins hinzu. Die Reaktionsmasse wird 10 Min. lang erwärmt. Nach Abkühlung

Tabelle 2

Infrarot Spektren

Nr. der Verbind.	Spektrum	Amid. Schleife		Aethere Methoxy			Die Vibrationen der CH_2 – Gruppe		
		I	II	N–H	C–O	C–H	C–H asym.	C–H sym.	C–H
1	1646	1652	1625	3302 3149	—	—	2940 2954	2882	1460 1425
2	1689	1665	1621	3347 3162	—	—	2938	2866	1458 1436
3	1719	1670	1624	3302 3130	1230	2832	2941	2871	1470 1434
4	1675	1635	—	—	—	—	2938	2869	1474 1462 1439
5	1690	1623	—	—	—	—	2950 2938	2864	1462 1453 1441
6	1720	1625	—	—	1227	2834	2934	2868	1479 1458 1434
7	1676	1618	—	—	—	—	2950	2862	1473 1442
8	1697	1634	—	—	—	—	2941	2868	1473 1432
9	1721	1629	—	—	1227	2831	2940	2867	1478 1428
10	1677	1642	—	—	1113	—	2960 2932	2866	1464 1442
11	1699	1638	—	—	1110	—	2947 2929	2849	1468 1442
12	1722	1643	—	—	1226 1113	2835	2929 2920	2858 2920	1472 1453 1434

Spektrophotometer UR 10, Carl Zeiss-Jena, pastilliert mit KBr.
Alle Frequenzen sind in cm^{-1} ausgedrückt.

werden 100 ml Wasser hinzugegeben. Das entsprechende Amid wird filtriert und mit Wasser gespült. Es wird über Chlorhydrat gereinigt. Die sich ergebenden Amide sind in Tab. 1 aufgezeichnet.

Die elementaren Stickstoffanalysen wurden im Onkologischen Institut Bukarest von E. Tărnăuceanu durchgefürt, und die IR-Spektren wurden von V. Feyns entwickelt. Wir bringen ihnen auch auf diesem Wege unseren besten Dank.

Revue Roumaine de Chimie, **18**, *6*, 1019–1032 (1973)

NEW SYNTHESES OF NAPHTH [2,3-c]ACRIDAN-5,8,14-TRIONIC DYES

F. URSEANU *), C. DRĂGHICI **), RODICA VINTILĂ ***) and ELVIRA ŞLIAM **)

*) Laboratory of Chemistry and Technology of Aromatic Intermediates and Dyes, Polytechnic Institute, Bucharest, Calea Victoriei 149

**) Center of Organic Chemistry, Bucharest, Splaiul Independenţei 202–B

***) Central Laboratory of the Ministry of Light Industry, Bucharest, Str. Siret 95

Received October 19, 1972

New syntheses and experimental procedures for the preparation of 6-aminonaphth [2,3-c]acridan-5,8,14-trione dyes are described.

1. INTRODUCTION

The first naphth[2,3-c]acridan-5,8,14-trionic dyes**** were discovered and manufactured in 1909–1911 by Ullmann [1-4] and were utilized as vat dyes for dyeing cotton. They showed good light and hypochlorite fastness, but were rather sensible to hot alkaline solutions. Comparatively, few anthraquinoneacridonic dyes were used as acid dyes for dyeing wool, namely those possessing a solubilizing sulphonic acid group in the molecule. Later on disperse dyes were prepared,[5-7] for dyeing polyester fibres, with excellent light and sublimation fastness.

****) According to the older nomenclature: anthraquinoneacridonic dyes.

[1] F. Ullmann, Ger. Pat. 221 853, March 3, 1909; *Frd.*, **10**, 703.

[2] F. Ullmann, *Ber. dtsch. chem. Ges.*, **43**, 536 (1910).

[3] F. Ullmann and M. Sonne, *Liebigs Ann. Chem.*, **380**, 336 (1911).

[4] F. Ullmann and P. Ochsner, *Liebigs Ann. Chem.*, **381**, 1 (1911).

[5] D. C. Eaton and F. Irving, Brit. Pat. 944 513, Nov. 1, 1960; *Chem. Abstr.*, **60**, 10 846 (1964).

[6] D. C. Raton, Brit. Pat. 944 722, Dec. 6, 1960; *Chem. Abstr.*, **60**, 10 846 e (1964).

[7] Thoms River Chemical Corp., Brit. Pat. 1 027 576, Sept. 27, 1963; *Chem. Abstr.*, **65**, 2,392 (1966).

Among the three possible isomeric structures

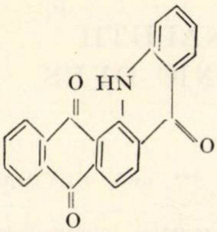

naphth[2,3-c]acridan-5,8,14-trione

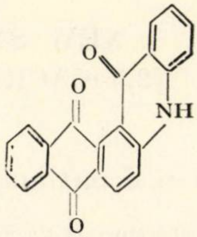

naphth[2,3-a]acridan-8,13,14-trione

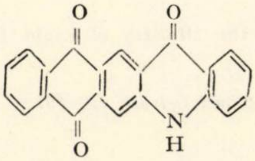

naphth[2,3-b]acridan-7,12,14-trione

only the naphth[2,3-c]acridan-5,8,14-trione derivatives present a technological and tinctorial interest; the derivatives of -trione and naphth[2,3-a] acridan-8,13,14-naphth[2,3-b]acridan-7,12,14-trione show a rather low affinity in vat for textile fibres, and are rather sensible to the action of alkalis.

The first syntheses of anthraquinoneacridonic dyes were aimed at varying the aromatic moiety of the molecule, leading thus to benzene[1], naphthalene,[8,4] antraquinone,[9] anthraquinonediacridone,[10] carbazole[11] derivatives.

By substituting these in various ways a great number of dyes were obtained, with interesting shades and tinctorial properties. For instance, an amino group in the 6-position of the anthraquinone moiety shifts the shade towards blue,[12,13] while the substitution of the amino group (with aryl,[14] benzoyl[15] or heterocycle groups[16]) deepens even more the shade (bathrochromic effect), improving at the same time the affinity in vat for cotton. To the same purpose were synthesized compounds in which the

---

[8] BIOS Final Rep., nr. 1 493, p. 41.

[9] Badische Anilin und Sodafabrik, Ger. Pat. 279 867, Sept. 4, 1913; *Frd.*, **12**, 445.

[10] BIOS Final Rep., nr. 1 493, p. 51.

[11] W. Bauer and B. Bollweg, U. S. Pat. 2 238 209, Apr. 15, 1940; *Chem. Abstr.*, **35**, 4 968 (1941).

[12] M. Lucius, Ger. Pat. 243 586, Nov. 2, 1909; *Frd.*, **10**, 716.

[13] F. Ullmann and G. Billig, *Liebigs Ann. Chem.*, **381**, 24 (1911).

[14] M. Lucius, Ger. Pat. 239 543, Nov. 2, 1909; *Frd.*, **10**, 716.

[15] FIAT Final Rep., nr. 1 313, vol. 2, p. 143.

[16] BIOS Final Rep., nr. 1 493, p. 56.

aromatic moiety of the acridonic structure was substituted with chlorine [17–20] or trifluoromethyl group.[21]

In view of the fact that most of the earlier dyes, with simple structures, were later on used as mere intermediates for the manufacture of substituted compounds with improved tinctorial properties, in the present work we undertook the synthesis of derivatives of 6-aminonaphth[2,3-c] acridan-5,8,14-trione with the following general formula

$X = H$, $Y = H$ (V)

$X = H$, $Y = PCH_3$ (VII)

$X = 11-NO_2$ $Y = H$ (X)

$X = 11-NO_2$ $Y = OCH_3$ (XII)

$X = 10-Br$, $Y = H$ (XIV)

$X = H$, $Y = CONH_2$ (XVII)

$X = 10-Br$, $Y = CONH_2$ (XIX)

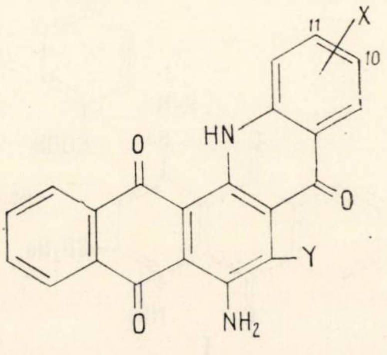

We hoped to find them useful as vat dyes for cotton, similarly to the well-known anthraquinoneacridonic dyes, but, at the same time, they seemed promising as disperse dyes for polyester fibres and as starting materials for the manufacture of new cationic dyes for polyacrylonitrile fibres and of new disperse dyes for polyester fibres. By using the above-shown substituents X and Y we hoped to attain the main required properties of disperse dyes, namely light and sublimation fastness and affinity to fibre.[22,23]

2. SYNTHESIS OF 6-AMINONAPHTH(2,3-c)ACRIDAN-5,8,14-TRIONE DERIVATIVES

The starting material for all syntheses was 1-amino-4-bromoanthraquinone-2-sulphonic acid (bromamine acid [24]), which is an excellent anthraquinonic intermediate for the preparation of many dyes. The great number of dyes deriving from the bromoaminic acid is explained first by the relatively facile substitution of bromine by various amines, under the conditions of the Ullmann reaction [1–4] (due to the activating effect of the

[17] Badische Anilin und Sodafabrik, Ger. Pat. 287 615, Jun 11, 1914; *Frd.*, **12**, 478.

[18] B. S. Ioshi, *Bombay Technologist*, **2**, 78 (1952); *Chem. Abstr.*, **48**, 1 688 (1954).

[19] H. Schlichenmaier and L. Berlin, Ger. Pat. 693 610, Jun 20, 1940; *Chem. Abstr.*, **35**, 4 968 (1941).

[20] B. S. Ioshi, B. D. Tilak and K. Venkataraman, *Proc. Indian Acad. Sci.*, **32 A**, 201 (1950).

[21] W. W. Groves, Brit. Pat. 495 375, May 5, 1937; *Chem. Abstr.*, **33**, 3 170 (1939).

[22] J. Reichel, "Tehnologia coloranţilor antrachinonici", Ed. Academiei, Bucharest, 1961, p. 108.

[23] C. Călin, *Bul. Inform. Laborat. Centr. Coloristic*, **7**, 23 (1967).

[24] Badische Anilin und Sodafabrik, Ger. Pat. 263 395, Jan. 13, 1911; *Frd.*, **11**, 555.

neighbouring carbonyl and sulphonic acid group) and then to the numerous possibilities of replacement of the sulphonic acid group after the replacement of bromine.

2.1. CONDENSATION OF BROMAMINE ACID WITH ANTHRANILIC AND SUBSTITUTED ANTHRANILIC ACID

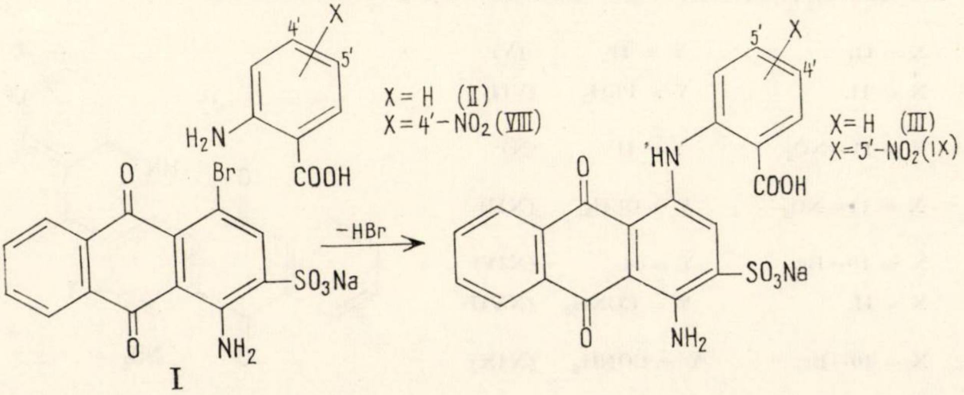

4'
X
5'
H_2N
COOH
Br
O
SO_3Na
O
NH_2
I
X = H (II)
X = 4'−NO_2 (VIII)
−HBr
5'
X
4'
HN
COOH
O
SO_3Na
O
NH_2
X = H (III)
X = 5'−NO_2 (IX)

The condensation is carried out under the conditions of the Ullmann reaction [1–4]: refluxing in aqueous alkaline solution (sodium acetate) in the presence of copper powder as catalyst. 4-Amino-1-anilinoanthraquinone-3-sulphonic-2′-carboxylic acids (III, IX) are thus obtained.

As compared to literature,[15] the reaction time was shortened from 5 to 3 hours by introducing solid anthranilic acid to a hot alkaline solution of bromoaminic acid (higher reagent concentrations were thus used).

2.2. REPLACEMENT OF THE SULPHONIC ACID GROUP FROM 4-AMINO-1-ANILINOANTHRAQUINONE-3-SULPHONIC-2′-CARBOXYLIC ACIDS

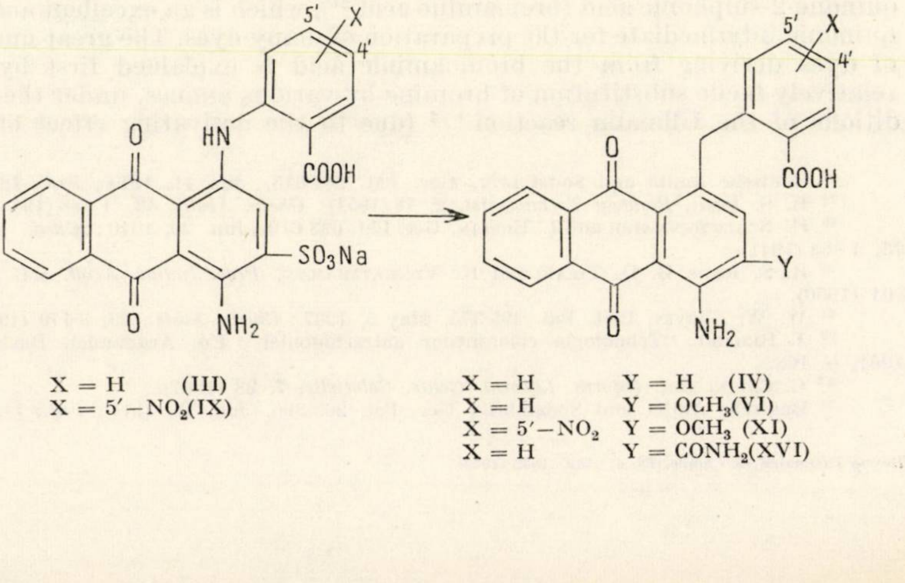

5'
X
4'
O
HN
COOH
SO_3Na
O
NH_2
5'
X
4'
O
COOH
Y
O
NH_2

X = H (III)
X = 5′−NO_2(IX)

X = H Y = H (IV)
X = H Y = OCH_3(VI)
X = 5′−NO_2 Y = OCH_3 (XI)
X = H Y = $CONH_2$(XVI)

2.2.1. *Replacement of the sulphonic acid group by hydrogen (Y=H)*

The sulphonic acid group of compound III was eliminated by refluxing in aqueous solution with glucose and NaOH.[25] The method indicated in the literature [17] for similar compounds, namely heating with $Na_2S_2O_4$ and NaOH, was not used since it led to considerable loss of substance because of overreduction to leuco compound.

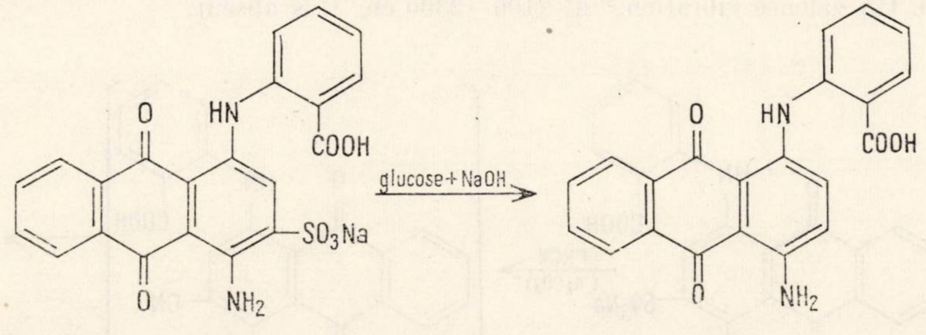

III

VI

Compound IV was thus obtained in a new way, starting from bromamine acid (the literature [20] indicates the condensation of 1-chloro-4-aminoanthraquinone with anthranilic acid).

2.2.2. *Replacement of the sulphonic acid group by methoxy group ($Y=OCH_3$)*

The reaction was carried out by refluxing compounds III, IX, in a $KOH-CH_3OH$ solution, according to a literature procedure.[26]

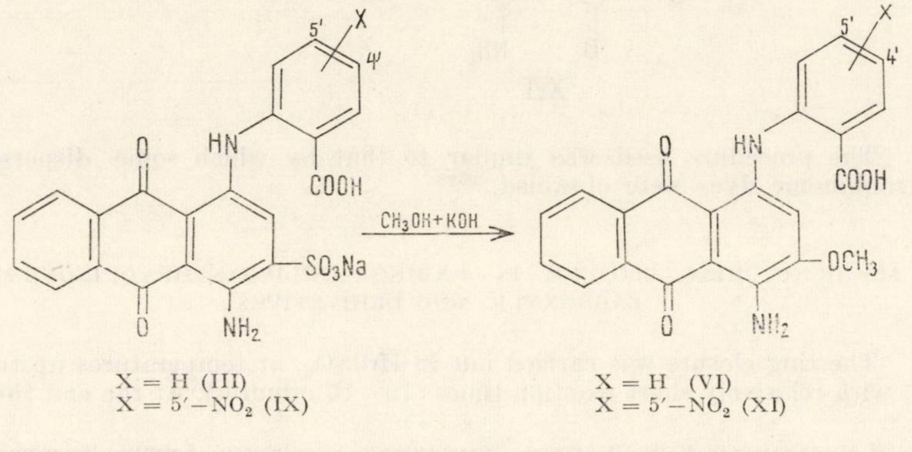

X = H (III)
X = 5'$-NO_2$ (IX)

X = H (VI)
X = 5'$-NO_2$ (XI)

---

[25] R. N. Heslop, F. Irving and A. Livingston, Brit. Pat., 586 999 Apr. 10, 1947; *Chem. Abstr.*, *4*, 7 601 (1948).

[26] FIAT Final Rep., nr. 1 313, vol. 2, p. 202.

2.2.3. *Replacement of the sulphonic acid group by carbamoyl group ($Y=CONH_2$)*

The sulphonic acid group of compound III was replaced by a carbamoyl group on treatment with KCN and K_2CO_3, in aqueous solution, at 130° and 3 atm. The CN group of the intermediate XV is totally hydrolized to $CONH_2$, as shown by the IR spectrum of the reaction product in which the CN valence vibration,[27] at 2100–2300 cm^{-1}, is absent.

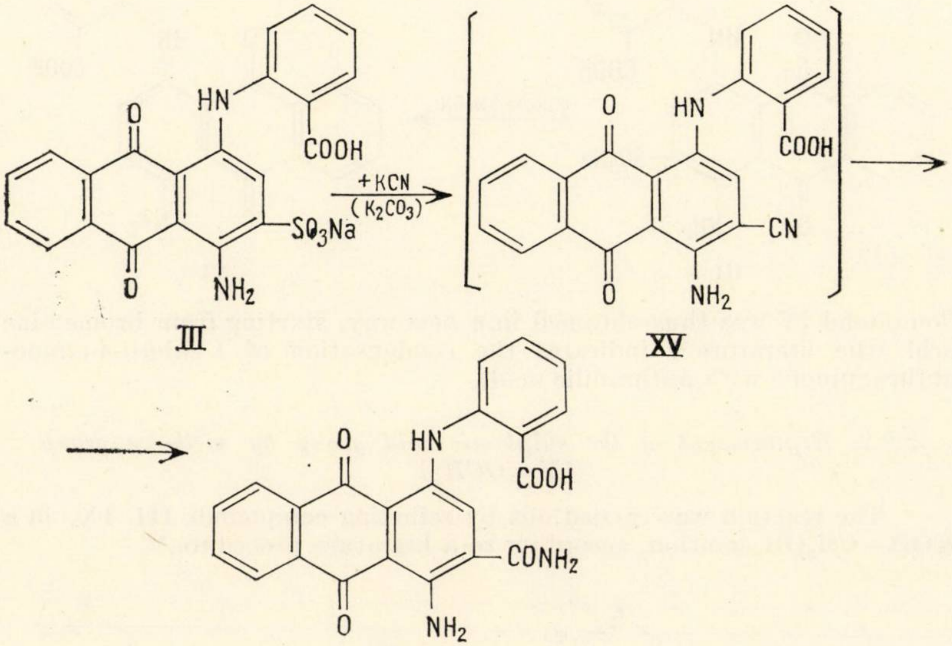

The procedure used was similar to that by which some disperse antraquinonic dyes were obtained. [28,29]

2.3. ACRIDONIC RING CLOSURE IN 4-AMINO-1-ANILINOANTHRAQUINONE-2'-CARBOXYLIC ACID DERIVATIVES

The ring closure was carried out in $HClSO_3$, at temperatures up to 40°, with relatively short reaction times (10–15 minutes). At the end the mixture was poured on ice in order to decompose the excess chlorosulphonic acid and to precipitate the acridonic products.

---

[27] M. Avram and G. D. Mateescu, "Spectroscopia în infraroșu. Aplcații în chimia organică", Ed. tehnică, Bucharest, 1966, p. 508.

[28] H. Sanielevici and L. Floru, "Sinteza intermediarilor aromatici și a coloranților", ed. 2, Ed. didactică și pedagogică, Bucharest, 1971, p. 308.

[29] BIOS Final Rep., nr. 1 484, p. 56.

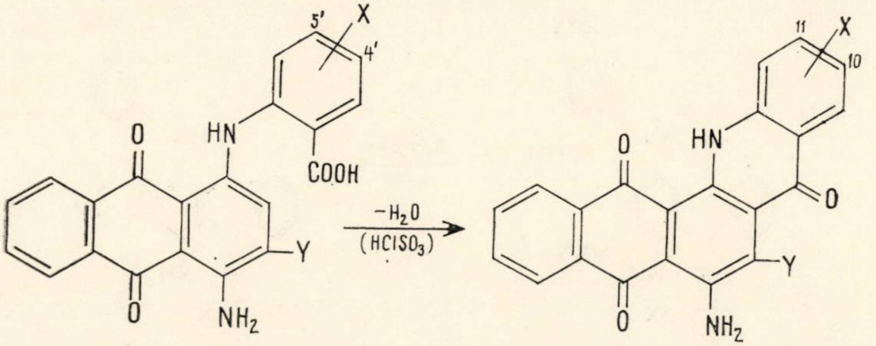

$X = H$ $Y = H$ (IV)
$X = H$ $Y = OCH_3$ (VI)
$X = 5'-NO_2$ $Y = OCH_3$ (XI)
$Xx = H$ $Y = CONH_2$ (XVI)

$X = H$ $Y = H$ (V)
$X = H$ $Y = OCH_3$ (VII)
$X = 11-NO_2 Y = OCH_3$ (XII)
$X = H$ $Y = CONH_2$ (XVII)

The direct conversion of III to V was attempted by using concentrated H_2SO_4, according to literature procedures,[21,30] but the results were not satisfactory, as the product was rather impure, because of the facile sulphonation of the benzene ring of acridone, in the 5′ position.[1,17]

According to the literature,[5,6] 7-alkoxynaphth[2,3-c] acridan-5,8,14-trione compounds are prepared by treating the corresponding 7-bromo-naphth[2,3-c]acridan-5,8,14-trione derivatives with alcohol in alkaline medium. In the present work, compound VII was synthesized in a new way: replacement of the sulphonic acid group of compound III by the methoxy group, on treatment with $KOH-CH_3OH$, followed by ring closure, in $HClSO_3$, of the intermediate VI.

For the synthesis of compound XVII the literature [7] indicates the treatment of the corresponding 7-bromo-naphth[2,3-c] acridan-5,8,14-trione derivatives with cuprous cianide; the intermediate 3-CN compound is then hydrolized with 89% H_2SO_4 to the 3-carbamoyl compound. In the present work, compound XVII was prepared by a new procedure, involving the treatment of III with KCN and K_2CO_3, as in similar cases,[28,29] then hydrolysis to the carbamoyl derivative and finally ring closure, in $HClSO_3$, of the intermediate XVI.

2.4. SYNTHESIS OF 6-AMINO-11-NITRONAPHTH[2,3-c]ACRIDAN-5,8,14-TRIONE (X)

The transformation of compound IX to X, by ring closure accompanied by desulphonation, was carried out by heating with concentrated H_2SO_4 at 90−95°, according to literature procedures.[21,30]

---

[30] Farbenfabriken Bayer, Brit. Pat. 775 802, May 29, 1957; *Chem. Abstr.*, **51**, 15 142 (1957).

The possibility of secondary sulphonation of the benzene ring of acridone was eliminated due to the presence of the nitro group.

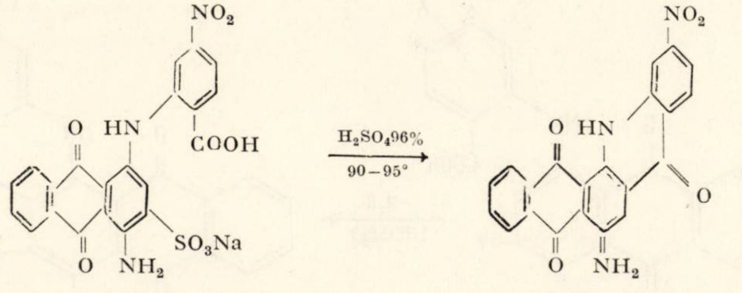
NO$_2$
O HN
COOH
SO$_3$Na
O NH$_2$
H$_2$SO$_4$96%
90–95°
NO$_2$
O HN
O
O NH$_2$

IX X

2.5. SYNTHESIS OF 6-AMINO-10-BROMONAPHTH[2,3-c]ACRIDAN-5,8,14-TRIONE DERIVATIVES (XIV, XIX)

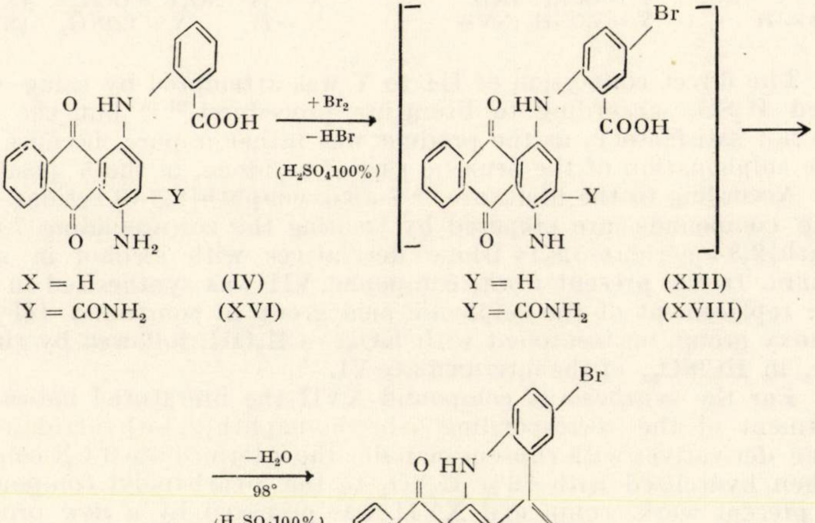
O HN
COOH
–Y
O NH$_2$
+Br$_2$
–HBr
(H$_2$SO$_4$100%)
Br
O HN
COOH
–Y
O NH

X = H (IV) Y = H (XIII)
Y = CONH$_2$ (XVI) Y = CONH$_2$ (XVIII)

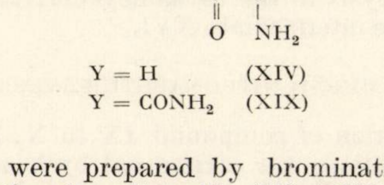
–H$_2$O
98°
(H$_2$SO$_4$100%)
Br
O HN
O
O NH$_2$

Y = H (XIV)
Y = CONH$_2$ (XIX)

The compounds were prepared by bromination of the 4-amino-1-anilinoanthraquinone-2′-carboxylic acids (IV, XVI) with the theoretical amount of bromine, in 100% H_2SO_4, followed by heating at 98° in order to close the acridonic ring. This constitutes a modification of the literature method,[17,30] which indicates bromination of the sulphonic derivative III, ollowed by ring closure and desulphonation on heating.

3. EXPERIMENTAL

3.1. A mixture of 40.4 g (0.1 mol) bromamine acid (I), 34.6 g $CH_3COONa.3H_2O$ and 0.99 g copper powder in 450 ml water is heated to 85—90° until the bromamine acid is completely dissolved; 14.4 g (0.105 mol) anthranilic acid (II) and 0.5 g copper powder are then added and the temperature is then raised to 95—98° for 2.5—3 hours. The colour of the reaction mixture turns gradually from red to blue. The conversion of bromamine acid to product II is followed by means of paper chromatography (eluent E^1 : BuOH :EtOH :water :25% NH_3 = 100 :20 :44 :1 in volumes).

Finally, when the reaction ends and the product separates as blue needles, 58.5 ml 30% HCl are added and the mixture is heated at 80° for 0.5 hours. The crystals are filtered, washed with 300 ml 1% HCl at 60°, then with cold water until the filtrate turns from purple to pale blue, showing that the product III is being dissolved. After drying at 75—80°, 45 g III are obtained (97.8% yield).

3.2. 41.4 g (0.09 mol) compound III is dissolved in a solution of 14 g NaOH in 450 ml water at 85—90°, then the solution resulted is added dropwise, for 15 minutes, to a warm solution of 29.6 g glucose in 60 ml water.

The reaction is completed by heating at 95° for 1 hour; the mixture is then cooled to 20°, neutralized with concentrated HCl to pH = 6 — 6.5 and filtered. The purple precipitate is washed with 600 ml water and dried at 75—80°, yielding 31.6 g product IV (92.2% yield).

3.3. 30 g (0.084 mol) compound IV are dissolved in 110 ml $HClSO_3$ and the violet-red solution is heated for 10 minutes at 35—40° when the colour turns to orange. The mixture is poured over 400 g crushed ice, the blue-green precipitate is filtered, washed with water until the filtrate is neutral and dried at 75—80°. 25.6 g product V are obtained (89.8% yield).

3.4. To a solution of 138 g KOH in 374 ml CH_3OH, 45 g (0.1 mol) compound III are added, for 0.5 hour, at 50—60°. The mixture is heated at 85—90°, for 4.5—5 hours, until the compound III disappears, as checked by means of chromatography; the colour turns from blue to violet. When the reaction ends 400 ml water are added, then the alcohol is distilled until the temperature of the distillate reaches 100°. The mixture is poured over 1 l cold water and neutralized with concentrated HCl, at 20—30°, in an ice bath. The precipitate formed is filtered, washed with 2.5 kg water and dried at 75—80°.34.5 g product VI are obtained (89% yield).

3.5. 34.5 g (0.089 mol) compound VI are dissolved in 110 ml $HClSO_3$ at 10° and stirred at this temperature for 15—20 minutes, when the colour turns from purple to red-yellow. The mixture is poured over 400 g crushed ice, the blue-green precipitate is filtered, washed with water until the filtrate is neutral and dried at 75—80°, yielding 30.6 g VII (93% yield).

3.6. A mixture of 60.6 g (0.15 mol) bromamine acid (I), 51.9 g $CH_3COONa.3H_2O$ and 1.48 g copper powder in 675 ml water is heated to 85—90° until dissolution of I: 28.6 g (0.157 mol) 4-nitroanthranilic acid (VII) and 1 g copper powder are then added, the temperature is raised to 95—98° and maintained for nearly 3 hours up to the completion of the reaction. The latter is determined by means of paper chromatography (eluent E^1). 86.5 ml 30% HCl are added to the mixture, which is then heated to 80° for 0.5 hour and filtered hot. The precipitate is washed with 450 ml 1% HCl at 60°, then with cold water until the colour of the filtrate turns from purple to pale blue. After drying at 75—80°, 72.8 g product IX are obtained (96% yield).

3.7. 50.5 g (0.1 mol) compound IX is dissolved in 270 ml 96% H_2SO_4 for 1.5 hours and the resulted solution is heated for 2 hours at 90—95°. (A drop from the mixture, decomposed with water, forms a blue-green precipitate). The mixture is cooled to 20°, poured over 1.2 kg crushed ice, filtered and the precipitate is washed with water until the filtrate is neutral and colourless, dried at 75—80°, affording 34.5 g X (89.7% yield).

3.8. To a solution of 138 g KOH in 410 ml CH_3OH, 50.5 g (0.1 mol) compound IX are added or 40 minutes at 50—60°; the mixture is refluxed ($t^\circ \approx 90^\circ$) for nearly 5 hours until compound IX disappears, as shown by paper chromatography of a sample (eluent E^2), when the colour of the mixture turns from blue to violet. After the completion of reaction the alcohol is vapour--distilled with 500 ml water, then the mixture is poured over 1.2 l water, neutralized with concentrated HCl at 20—30° (external ice-cooling) and filtered. The precipitate is washed with 3 l water and dried at 75—80°, affording 38.2 g XI (92.6% yield).

3.9. 38.1 g (0.088 mol) compound XI are dissolved in 125 ml $HClSO_3$ at 30—40° and stirred at this temperature for 10—15 minutes; the colour turns from violet to dark orange. The mixture is poured over 450 g crushed ice, the blue-green precipitate is filtered, washed with water until the filtrate is neutral and colourless and dried at 75—80°, affording 33.8 g XII (92.6% yield).

3.10. 35.8 g (0.1 mol) compound IV are added to a solution of 5.6 ml (17.6 g; 0.11 mol) Br_2 in 190 ml H_2SO_4 100% for 1 hour, at 5—8°. The solution is stirred for 6 hours raising slowly the temperature up to 30°, then is heated for 3 hours at 95—98°. The mixture is cooled to 0°C and poured over 850 g ice; the blue-green suspension is filtered, the precipitate is washed with water until neutral and dried at 75—80°, yielding 38.9 g product XIV (92.8% yield).

3.11. A stainless steel autoclave equipped with a thermometer, a mechanical stirrer and an oil heating mantle, is charged with 750 ml water and 20.7 g (0.15 mol) K_2CO_3; the solution is heated at 60—70°, then 46 g (0.1 mol) compound III are added, stirring until the latter dissolves completely. After the pH is checked (it should be alkaline), 37 g (0.57 mol) KCN are added. The mixture is stirred for 6 hours at 130° ($p \approx 3$ atm), then cooled at 20—25°. The autoclave is opened and the solubility of the product is checked (a sample on filter paper must present a colourless aura; if a slight solubility is noticed, the product is precipitated by adding KCl). The precipitate is filtered, washed with 25% KCl solution (about 3 l) to remove traces of cyanide and dried at 75—80°. 45 g product XVI (containing KCl) are thus obtained.

3.12. 45 g product XVI (containing KCl) are dissolved in 170 ml $HClSO_3$ and the solution is stirred during 10—15 minutes at 35—40°, the colour turning from brown to dark yellow. The mixture is poured over 600 g ice, the green precipitate is filtered, washed with water until neutral and dried at 75—80°.27.6 g product XVII are obtained (72.1% yield).

3.13. 43.9 g (0.1 mol) compound XVI are added to a solution of 5.6 ml (17.6 g; 0.11 mol) Br_2 in 200 ml 100% H_2SO_4, for 1 hour, at 5—8°. The mixture is stirred for 6 hours raising slowly the temperature up to 30°, then for 3 hours at 95—98°. The mixture is cooled to 0° and poured over 900 g ice; the green precipitate is filtered, washed with water until the filtrate is neutral and colourless and dried at 75—80°, affording 40.7 g product XIX (88% yield).

4. ANALYSES

The compounds analyzed were previously purified by recrystallization from an appropiate solvent: glacial acetic acid, nitrobenzene or *ortho*-dichlorobenzene (see table 1).

Melting points could not be determined for some compounds since they decomposed over 300°.

The purified compounds were subjected to elemental, chromatographic, spectral and tinctorial analyses.

4.1. ELEMENTAL ANALYSIS

Microcombustions were carried out, determining the nitrogen after the micro-Dumas method, while carbon, hydrogen and bromine were analyzed according to the modified Pregl method. The results are presented in table 1.

Table 1

Characteristic of compounds and elemental analysis

Compound	Empirical formula	Molecular weight	Solvent for recrystallization	MP °C	C% *Calc.* *Found*	H% *Calc.* *Found*	N% *Calc.* *Found*	Br% *Calc.* *Found*
IV	$C_{21}H_{14}O_4N_2$	358.356	CH_3COOH	263	70.39 70.11	3.94 4.06	7.82 7.78	— —
V	$C_{21}H_{12}O_3N_2$	340.340	nitrobenzene	>300	74.11 73.91	3.56 3.72	8.23 8.26	— —
VI	$C_{22}H_{16}O_5N_2$	388.382	CH_3COOH	274	68.03 67.74	4.15 4.18	7.21 7.52	— —
VII	$C_{22}H_{14}O_4N_2$	370.367	nitrobenzene	>300	71.34 71.11	3.81 3.89	7.56 7.61	— —
X	$C_{21}H_{11}O_5N_3$	385.338	nitrobenzene	>300	65.45 65.17	2.87 3.18	10.90 10.61	— —
XI	$C_{22}H_{15}O_7N_3$	433.380	CH_3COOH	271	60.97 60.88	3.49 3.42	9.69 9.63	— —
XII	$C_{22}H_{12}O_6N_3$	415.364	*o*-dichlorobenzene	>300	63.61 63.72	3.15 3.17	10.11 10.14	— —
XIV	$C_{21}H_{11}O_3N_2Br$	419.241	nitrobenzene	>300	60.16 60.44	2.64 2.93	6.68 6.81	19.06 18.75
XVII	$C_{22}H_{13}O_4N_3$	383.365	*o*-dichlorobenzene	>300	68.92 68.78	3.42 3.40	10.96 10.88	— —
XIX	$C_{22}H_{12}O_4N_3Br$	462.266	*o*-dichlorobenzene	>300	57.16 57.41	2.62 2.89	9.09 9.32	17.28 16.99

4.2. CHROMATOGRAPHY

Chromatographic analyses were carried out on Whatman paper no. 1 in ascendent system, at 25°, in order to follow the reactions and to check the purity of recrystallized compounds, The results are presented in table 2.

Table 2

Paper chromatography

Compound	I	III	IV	V		VI	VII		IX
Solvent	water	water	CH_3COOH	DMF		CH_3COOH	DMF		water
Eluent	E^1	E^2	E^2	E^2	E^3	E^2	E^2	E^3	E^1
R_f	0.91	0.78	0.67	0.19	0.56	0.89	0.36	0.74	0.68

Compound	X		XI	XII		XIV		XVI	XVII		XIX	
Solvent	DMF		CH_3COOH	DMF		DMF		CH_3COOH	DMF		DMF	
Eluent	E^2	E^3	E^2	E^2	E^3	E^2	E^3	E^2	E^2	E^3	E^2	E^3
R_f	0.15	0.48	0.74	0.24	0.52	0.15	0.38	0.61	0.17	0.53	0.14	0.34

DMF = N,N′-dimethylformamide

E^1 = BuOH : EtOH : water : 25% NH_3 = 100 : 20 : 44 : 1 (in volumes)

E^2 = $CH_3COOH : H_2O$ = 20 : 4 (in volumes)

E^3 = $HCOOH : H_2O$ = 20 : 0.5 (in volumes)

In the case of eluents E^2 and E^3, the chromatography paper was impregnated with a 10% solution of 1-bromonaphthalene in ethanol.

4.3. SPECTRAL ANALYSIS

Infrared and visible absorption spectra of products were recorded.

IR spectra were recorded using a UR—10 spectrophotometer, in pellet KBr. Characteristic vibration frequences :

Compound IV : 731 m ; 752 m ; 1178 s ; 1228 v.s ; 1242 v.s ; 1575 v.s ; 1630 m ; 1655 m ; 1690 m ; 3310 m ; 3428 m.
Compound V : 731 m ; 748 m ; 760 m ; 1589 v.s ; 1618 v.s ; 1632 m ; 3310 s ; 3421 s ;
Compound VI : 731 s ; 1125 s ; 1280 v.s ; 1585 v.s ; 1615 v.s ; 1677 v.s ; 1700 m ; 2200—3300 ; 3275 m ; 3480 s ;
Compound VII : 728 s ; 745 v.s ; 771 s ; 945 s ; 1158 s ; 1550 v.s ; 1570 v.s ; 1620 v.s ; 1660 v.s ; 3320 s ; 3483 s ;
Compound X : 731 w ; 745 w ; 1245 s ; 1268 s ; 1287 s ; 1350 s ; 1529 s ; 1608 m ; 1620 s ; 1632 s ; 3320 m ; 3430 m ;
Compound XII : 1285 m ; 1350 m ; 1480 w ; 1520 m ; 1590 s ; 1615 s ;
Compound XIV : 735 w ; 758 w ; 1495 s ; 1570 s ; 1585 s ; 1610 s ; 1640 m ; 3300 m ; 3425 m ;
Compound XVI : 731 m ; 752 s ; 1578 s ; 1700 m ;
Compound XVII : 731 m ; 745 m ; 755 m ; 1590 v.s ; 1619 v.s ; 1631 s ; 3315 m ; 3420 m ;
Compound XIX : 732 m ; 742 m ; 1585 v.s ; 1611 s ; 1638 s ; 3315 w ; 3430 w.
(w = weak ; m = medium ; s = strong ; v.s. = very strong)

Visible spectra were determined with a Specord apparatus. The qualitative determinations were carried out in dimethylformamide ; for compound V the extinction coefficient was calculated : $\varepsilon_{max}^{DMF} = 12{,}200\ l \cdot mol^{-1}.cm^{-1}$. The characteristic absorption maxima are presented in table 3.

When substituents are introduced into the benzene ring of acridone ($X = 11-NO_2$, $10-Br$) or into the 7-position of the anthraquinone moiety ($Y = OCH_3$, $CONH_2$), the absorption maxima do not change appreciably ($\lambda_{max} \approx 670$ nm ; compounds VII, X, XIV, XVII, XIX) the corresponding products possessing similar colours, namely various shades of blue green.

If the compound has a methoxy group ($Y = OCH_3$) in the 7-position of the anthraquinone moiety and, at the same time, a nitro group ($X = 11-NO_2$) on the benzene ring of acridone, the strongest absorption maximum is shifted towards lower wavelengths ($\lambda_{max}^{XII} = 610$ nm) ; the greenish grey colour of the respective compound, different from the colours shown by the other anthraquinoneacridonic derivatives, is explained by the presence of two additional absorption maxima, less intense, in the visible spectrum ($\lambda = 380-390$ nm and $\lambda_{shoulder} = 589$ nm).

5. UTILIZATION OF THE PRODUCTS

The 6-aminonaphth[2,3-c]acridan-5,8,14-trione compounds synthesized were used as disperse dyes for polyester fibres and also as starting materials for the preparation of new disperse dyes with pyrazoleanthroneacridone structure [31] and of new cationic dyes[32,33] for polyacrylonitrile fibres.

---

[31] H. Sanielevici, I. Zugrăvescu and F. Urseanu, Patent claim submitted to OSIM, 66 381, March 25, 1971.

[32] F. Urseanu, R. Vintilă and M. Preoteasa, Patent claim submitted to OSIM, 70 055, March 9, 1972.

[33] F. Urseanu and R. Vintilă, Patent claim submitted to OSIM, 70 142, March 16, 1972.

Table 3

Maxima absorption and determinations with dyed polyester fibres

Compound	DMF λ_{max} [nm]	Polyester fibres dyeing						
		Colour	Fastness					Coloristic yield*) %
			Light	Washing at 40°	Sweat		Thermo-fixation 200°; 30 sec	
					acid pH = 5.5	alkaline pH = 8.4		
V	672	greenish blue 15–40	5–6	4–5/4–5/4–5	5/4–5/4–5	5/4–5/4–5	4–5/5	90
VII	670	greenish blue 15	5	5/5/5	5/5/5	5/5/5	5/5	100
X	674	greenish blue 16	7	4–5/4–5/4–5	5/5/5	5/5/5	4–5/4–5	65
XII	380–390 589 shoulder 610	greenish grey 46–47	6–7	5/5/5	5/5/5	5/5/5	4–5/4–5	50
XIV	675	bluish green 16–17	7	5/5/5	5/5/5	5/5/5	4–5/5	70
XVII	668	greenish blue 16–15	7–8	5/5/5	5/5/5	5/5/5	4–5/5	100
XIX	625	greenish blue 15–39	7–8	5/5/5	5/5/5	5/5/5	4–5/5	80

* The polyester fibres were dyed with solutions of the same concentration (3 g/l) in order to estimate the affinity of dyes as coloristic yield.

The results of the determinations carried out with "Terom" polyester fibres dyed are presented in table 3. The colours were defined according to C.I. Hue Chart.[34] A good agreement is observed between the colours seen and the values of the absorption maxima.[35]

They show compounds XVII, VII, XIV, XIX, X have better qualities as dyes for polyester fibres.

---

[34] C. I. HUE, Indication Chart, American Association of Textile Chemists and Colourists, Lowell Institute, Lowell Massachussets, USA.

[35] C. D. NENIȚESCU, "Chimie Organică", vol. 2, ed. 6, Ed. didactică şi pedagogică, Bucharest, 1968, p. 520.

Revue Roumaine de Chimie, **18**, *6*, 1033–1040 (1973)

CORRELATION OF THE PHYSICAL PROPERTIES OF ORGANOSULPHUR COMPOUNDS. II[1]

EFFECTIVE ELECTRONEGATIVITY OF THE MOLECULES AND THEIR PHYSICAL PROPERTIES

M. ARSHAD A. BEG and M. A. HASHMI

P.C.S.I.R. Laboratories, Karachi — 39, Pakistan

Received March 27, 1972

Molecular electronegativity which is the arithmetic mean of the electronegativities of the central atom and of the substituents is shown to be related to the macro-physical properties like boiling point, density and refractivity. While correlation with boiling point and density separates the sulphides and mercaptans into different classes depending on the substituents the plot of Mn_D *vs* χ_M gives a single straight line which has been made use of in calculating the electronegativity of other groups.

The previous paper[1] has described a correlation of the physical properties of the organosulphur compounds. In our earlier papers[2,3,4] a new parameter effective electronegativity χ effective was described and was correlated with the basicity of the phosphines and also with the vibrational frequencies of the various groups *viz* C—H, P=O, M—CH_3 and M—C_6H_5. The effective electronegativity of a molecule MABC, where *M* is the central atom and *A*, *B* and *C* are substituents, is calculated from equation (A)

$$\chi_{MABC} = \frac{\chi_M}{2} + \frac{1}{6}[\chi_A + \chi_B + \chi_C] \cdots (A)$$

where χ_M, χ_A, χ_B and χ_C are the electronegativities of *M*, *A*, *B* and *C*. The effective electronegativity has been shown to influence the basicity of phosphines since this depends on the electronic environment of these molecules which in turn changes with the electronegativity of the substituents. It is, therefore, of interest to see if $\chi_{\text{effective}}$ would also be able to correlate the various properties like their boiling point, density and refractivity which were found to be interrelated through various parameters like M_ρ^2 and Mn_D^1.

---

[1] Part I. M.A.A. Beg and M. A. Hashmi, *Rev. Roumaine Chim.*, **16**, 1435 (1971).

[2] M.A.A. Beg, *Scientist Pakistan*, **7**, 37 (1964).

[3] M.A.A. Beg, *Pakistan J. Sci. Ind. Res.*, **11**, 345 (1968).

[4] M.A.A. Beg, *Pakistan J. Sci. Ind. Res.*, **12**, 16 (1969).

The concept of the relation between the effective electronegativity of a molecule and its electronic environment can be visualized by considering the formation of a molecule from atoms with different atomic electronegativities. The atoms adjust themselves so as to satisfy the demands of electron attraction and repulsion by the atom with higher electronegativity attracting and the lower one donating its electronic charge. A new electrical system with a lower energy content appears as a result of the demand by the electron acceptors or donors. This new system has a different ionization potential and electron affinity and thus a different electron density. Electronegativity depends on the first two properties and hence its relationship with compactness of the molecule is obvious. Physical properties which are related to the intermolecular forces and are dependent on the electronic compactness should, therefore, be related to the electronegativity of the system. It is the purpose of this paper to correlate the physical properties of organosulphur compounds viz. the mercaptans and the sulphides with their effective electronegativity.

RESULTS AND DISCUSSION

The macrophysical properties discussed here are for the same compounds which have been listed in Tables 1 and 2 of the previous paper.[1] It is found that the electronegativity differences among the homologous series of compounds is very minor. $\chi_{\text{effective}}$ has, therefore, been multiplied with the molecular weight to obtain χ_M. The plot of χ_M *vs* boiling point, M_ρ^2 and Mn_D for the mercaptans and sulphides are presented in Figs. 1 – 6.

CORRELATION WITH BOILING POINT

It might be noted from Fig. 1 that on the basis of boiling point alone, the mercaptans can be divided into two classes as obtained with T_b *vs* M_ρ^2 and Mn_D which shows that the molecular electronegativity is related to the intermolecular forces as much as the cohesive energy given by M_ρ^2 or the molar refractivity given by Mn_D. It is indeed expected to be so because in each case the macro-physical property depends on the overall electronic environment.

For the sulphides also a similar pattern as obtained in earlier correlations has been noted in Fig. 2. On the basis of χ_M, the compounds are again divided into the same number of groups *viz.* **(1)** (n-alkyl)S, **(2)** n-alkyl-branched-chain-alkyl like i-Pr-S-Me and **(3)** branched alkyls like $(i\text{-Pr})_2S$. We have mentioned earlier [1] that boiling point is also dependent on how closely the molecules are interpenetrated into one another. Interaction of this type gives a higher boiling point and hence it has been

Table 1

Equations correlating χ_M and boiling points	
(1) *n*-Alkyl Mercaptans	$\chi_M = 1.308\ \mathrm{Tb} - 273.3$
(2) Branched Alkyl Mercaptans	$\chi_M = 1.295\ \mathrm{Tb} - 249.1$
(3) *n*-Alkyl Sulphides	$\chi_M = 1.311\ \mathrm{Tb} - 261.6$
(4) *iso*-Alkyl Sulphides	$\chi_M = 1.491\ \mathrm{Tb} - 322.2$
(5) *sec*-Alkyl Sulphides	$\chi_M = 1.44\ \mathrm{Tb} - 285.3$
(6) Alkenyl Sulphides	$\chi_M = 1.304\ \mathrm{Tb} - 266.1$

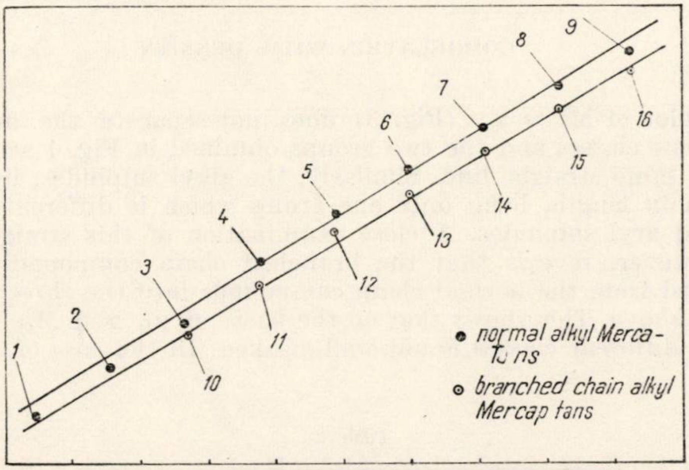

Fig. 1. — Correlation of boiling points of mercaptans with their electronegativities.

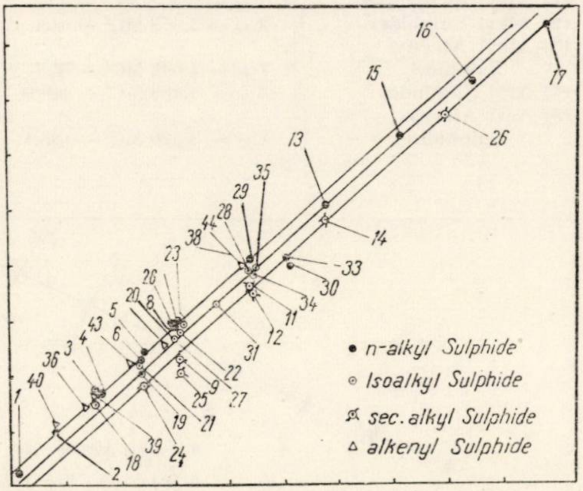

Fig. 2. — Correlation of boiling points of sulphides with their electronegativities.

concluded that normal chain analogues with chains longer than four have higher boiling point than their branched chain analogues, which could be attributed to the flexibility of the chain in the former. The relation with electronegativity has also some bearing with this phenomenon. It may be noticed from Table 4 that with a lengthening of the chain the electronegativity difference is less marked, which can easily be attributed to the attenuation of the electronic effect by the intervening methylene groups. Such an electronic environment would therefore be dominated by electrostatic effects such as those of interpenetration.

CORRELATION WITH DENSITY

The plot of M_ρ^2 *vs* χ_M (Fig. 3) does not separate the mercaptans into different classes and the two groups obtained in Fig. 1 are found to fall on the same straight line. Similarly, the alkyl sulphides, irrespective of their chain length, form only one group which is different from the alkenyl and aryl sulphides. A close examination of this straight line in Fig. 4, however, reveals that the branched chain compounds can also be separated from the normal chain compounds into the three classes as mentioned above. This shows that on the basis of χ_M and M_ρ^2, the separation into different classes is not well-marked. In the case of *n*-alkyl-S-

Table 2

Equations correlating χ_M and MC^2	
(1) Alkyl mercaptans	$\chi_M = 3.278\ MC^2 + 75$
(2) Alkyl Sulphides	$\chi_M = 3.473\ MC^2 - 4.4$
(3) Alkyl Alkenyl Sulphide	$\chi_M = 4.043\ MC^2 - 78.7$
(4) Aryl Sulphides	$\chi_M = 4.489\ MC^2 - 240.9$
(5) Aryl Alkenyl Sulphides	$\chi_M = 3.526\ MC^2 - 183.1$

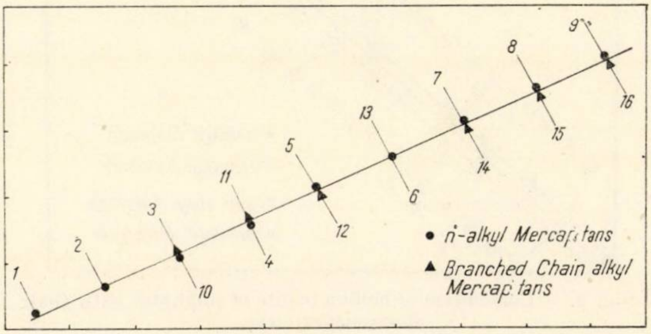

Fig. 3. — Correlation of densities of mercaptans with their electronegativities.

-aryl and branched-chain-alkyl-S-aryl compounds, however, the classification is quite distinct. This supports the above conclusion that if the electronegativity differences are not large enough the intermolecular forces become more marked. Since density depends on these forces it would be able to classify only such compounds which show variations in their electronegativity. Thus, the aryl compounds, by virtue of a different electronic environment, would form a different class from the various alkyl and alkenyl sulphides. Similarly, the branched chain compounds have also a different electronegativity and hence would give a different slope for the straight line.

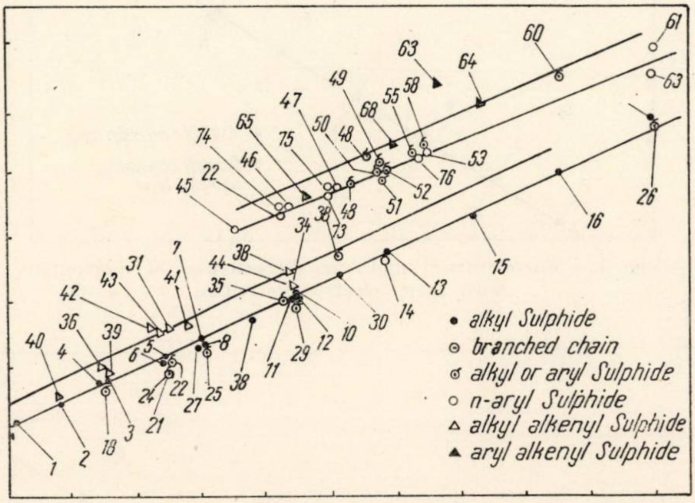

Fig. 4. — Correlation of densities of sulphides with their electronegativities.

REFRACTIVITY

On the basis of molar refractivity and electronegativity there is no separation into further groups with respect to the nature of the substituents or chains. There is only one straight line governing the various classes whether aromatic or aliphatic (Fig. 5,6). Based on this finding, it is possible to derive the molar electronegativity of compounds for which the evaluation of this property is difficult. We have thus obtained the χ_M of the alkenyl and aryl compounds. In fact the χ_M values obtained in this manner have been plotted against the boiling point and M_ρ^2 and the expected different classifications have been obtained.

Table 3

Equations correlating χ_M	and Mn_D
(1) Alkyl Mercaptans	$\chi_M = 1.606\ Mn_D + 4.1$
(2) Organo-Sulphides	$\chi_M = 1.646\ Mn_D + 2.7$

It might at first, seem surprising for the falling of all the sulphides on the same straight line. The noted indifference may be related to the nature of these two properties in that both of them are additive, whereas boiling point and density are both additive and constitutive. It may, therefore, be generalized that if a clear separation into different classes is desired, the properties should also be different. This explains why the straight lines for density are closer than those observed for the boiling

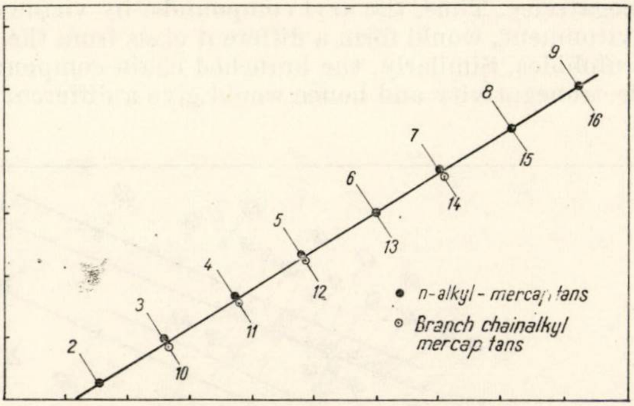

Fig. 5. — Correlation of molecular refractivities of mercaptans with their electronegativities.

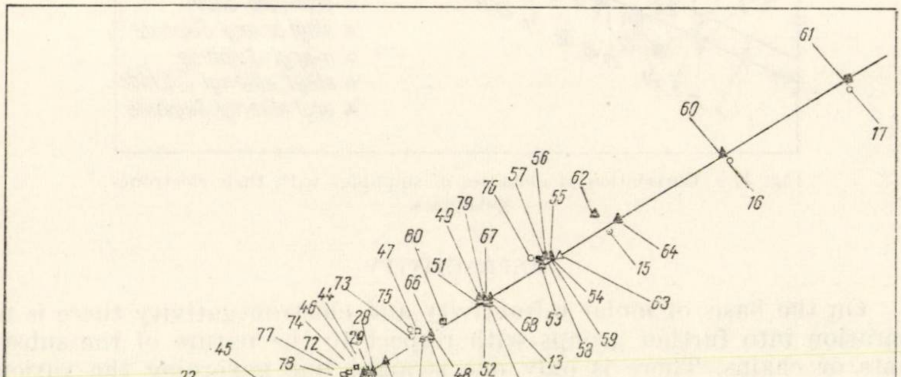

Fig. 6. — Correlation of molecular refractivities of sulphides with their electronegativities.

point. $M\rho^2$ has both additive and constitutive nature and hence the separation here would not be so marked as for T_b. The additivity of $M\rho^2$ has already been demonstrated in the earlier paper and that of χ_M is shown by Table 4.

Table 4

Calculated molecular electronegativities of various bonds

Bond	......	χ_M
S—H	......	37.65
S—CH_2	......	34.3
S—methyl	......	74.4
S—ethyl	......	108.5
S—propyl	......	142.8
S—*iso*-propyl	......	143.55
S—butyl	......	177.25
S—*iso*-butyl	......	176.85
S—*sec*-butyl	......	177.75
S—amyl	......	211.3
S—*iso*-amyl	......	210.5
S—hexyl	......	245.35
S—heptyl	......	279.3
S—octyl	......	313.3
S—nonyl	......	347.2
S—decyl	......	385.65
S—phenyl	......	241.85
S—totyl	......	266.8
S—benzyl	......	272.5
S—vinyl	......	106.2
S—allyl	......	142.5
S—crotyl	......	176.5
S—cyclopentyl	......	223.15
S—cyclohexyl	......	258.15

One of the main advantages of this correlation has, therefore, been the calculation of the electronegativity of various groups for which the same was either unknown or had a different value. Table 5 lists these electronegativities which are quite close to the values obtained by other methods. Thus, the phenyl group has an electronegativity of 2.70, obtained from chemical shift data, whereas by this correlation it is 2.65. The derivation of the electronegativity is also simple since one needs only to know the refractive index and by the use of equation (A), the desired value can be obtained. If the refractive index is not known, it may be calculated from the additivity principle using the parameters recorded earlier. Since there is a linear relationship between the molar refractivity and molecular electronegativity, there is a logical justification for the correlation of the physical properties by the use of the effective electronic environment given by χ_M. This paper has established the usefulness of the molecular effective electronegativity parameter. It has been shown that the simple physical picture presented by it is related in a simple manner with the macrophysical properties.

Table 5

Group electronegativities		
Methyl	······	2.3^{+}
Ethyl	······	2.33^{+}
Propyl	······	2.34^{+}
Butyl	······	2.34^{+}
iso-propyl	······	2.36^{+}
iso-Butyl	······	2.34^{+}
sec-Butyl	······	2.37^{+}
t-Butyl	······	2.4^{+}
Amyl	······	2.34^{+}
iso-Amyl	······	2.34^{+}
sec-Amyl	······	2.37^{+}
Hexyl	······	2.34^{+}
Octyl	······	2.34^{+}
Sec-Octyl	······	2.37^{+}
Nonyl	······	2.34^{+}
Decyl	······	2.34^{+}
Phenyl	······	2.7^{+}, 2.82^{*}
Tolyl	·····	2.5
Benzyl	······	2.76^{+}
Vinyl	······	2.36^{+}
Allyl	······	2.272^{+}
Crotyl	······	2.36^{+}
Cyclopentyl	······	2.66^{+}
Cyclohexyl	······	2.62^{+}

* Calculated from equation: $\chi_M = m(\mathrm{Mn}_D) + C$

+ Calculated from equation (A) in the text

Revue Roumaine de Chimie, **18**, *6*, 1041–1065 (1973)

QUELQUES REMARQUES SUR LES PROPRIÉTÉS DES BÉTONS AUX RÉSINES SYNTHÉTIQUES ET AUX LIANTS MINÉRAUX

ION IONESCU

Laboratoires des Bétons, Mortiers et Armatures
pour Bétons — I.C.M.P.C. — Bucarest,
Şos. Giurgiului, 507 — Roumanie

Reçu le 1er août 1972

On présente les résultats des recherches sur l'influence de certaines propriétés physiques et chimiques des différents types de résines synthétiques, du taux de résine employé comme addition et des facteurs de composition sur les principales propriétés structurales et physiques-chimiques des bétons à liants minéraux et résines synthétiques.

1. ASPECTS GÉNÉRAUX ET MATÉRIAUX UTILISÉS POUR LES RECHERCHES ET EXPÉRIENCES. MÉTHODE DE TRAVAIL

Pour les bétons aux résines synthétiques et aux liants minéraux, il n'existe pas encore de classification ou de terminologie acceptées par la plupart des chercheurs qui travaillent dans ce domaine, aussi trouve-t-on ce type de béton dans les revues spécialisées diversement dénommé et répertorié. L'une des classifications utilisées le plus fréquemment est celle qui indique le type de résine utilisé comme adjuvant, par exemple : bétons avec addition d'acétate de polyvinyle, bétons avec addition de résines acryliques, bétons avec addition de latex de caoutchouc naturel ou synthétique, etc.[1–10]

---

[1] J. Brocard et R. Cirodde, *Rev. Annales de l'Institut Technique du Bâtiment et des Travaux Publics*, **1960**, 1355.

[2] P. Dutron et Y. Collet «Les résines de synthèse dans le Construction», 1er vol., International Symposium — RILEM — Ed. Eyrolles, Paris, 1970, p. 80.

[3] I. Ionescu «Studii de Geotehnică, Fundaţii şi Construcţii Hidrotehnice» Vol. 5, ISCH, Bucarest, 1962, p. 31.

[4] I. Ionescu et M. Goldstein, «Studii de Geotehnică, Fundaţii şi Construcţii Hidrotehnice», 6e vol., ISCH, Bucarest, 1963, p. 103.

[5] I. Ionescu et M. Enculescu, «Întrebuinţarea maselor plastice pentru impermeabilizarea şi protecţia anticorozivă a construcţiilor hidrotehnice», Chp. IV et V, ISCH, Bucarest, 1964.

[6] I. Ionescu, M. Enculescu, P. Ghinescu et D. Nedelcu, *Rev. Materiale Plastice*, **1966**, 146.

[7] I. Ionescu et M. Enculescu, «Les Résines de Synthèse dans La Construction», vol. 1er, International Symposium, RILEM, Ed. Eyrolles, Paris, 1970, p. 380.

[8] P. C. Kreijger, *Rev. Matériaux de Construction* (*Bulletin RILEM*), **1968**, p. 187.

[9] S. Solacolu, «Chimia fizică a silicaţilor tehnici», Ed. tehnică, Bucarest, 1968.

[10] O. Solomon, I. Ionescu, M. Enculescu et I. Mihai, «Compuşi macromoleculari în construcţii hidrotehnice şi lucrări speciale», chap. II—III, Ed. tehnică, Bucarest, 1966.

Les bétons aux résines synthétiques et aux liants minéraux ne sont, en général, qu'un complément du béton de ciment, suscité par le besoin d'adjuvants susceptibles de pallier, totalement ou partiellement, quelques-uns des désavantages des bétons de ciment, tels que : résistance réduite à la traction, faible plasticité, fissurabilité sous charge, perméabilité relativement élevée, faible résistance à l'agression chimique, résistance relativement faible aux actions mécaniques abrasives et à l'action gel-dégel répétée, faible adhérence du béton frais au béton ancien, etc. La plupart des auteurs admettent que les matériaux suivants qui composent les bétons aux résines synthétiques et liants minéraux : agrégat minéral, liant minéral (ciment) et eau, doivent satisfaire aux mêmes exigences de qualité que dans le cas du béton de ciment.

Les rapports entre les matériaux composant les bétons aux résines synthétiques et liants minéraux sont établis en fonction des matériaux disponibles à l'emploi, du but poursuivi et de la destination de l'élément de construction qui en résultera. Généralement, la composition est calculée comme pour un béton de ciment, et c'est ensuite qu'on ajoute une quantité de résine exprimée en pourcentage du poids du ciment, compte tenu des variations du dosage de celui-ci. Les critères généraux auxquels doivent répondre les résines synthétiques, pour être utilisées comme adjuvants dans les bétons de ciment, sont d'ordinaire les suivants[3—10] :

— être compatibles avec le liant minéral et avec la manière de préparer le béton, condition essentielle qui fait supposer les conditions supplémentaires suivantes :

— les résines livrées sous forme d'émulsion aqueuse ou les résines solubles dans l'eau, qui peuvent être ajoutées directement à l'eau de gâchage, paraissent être les plus indiquées ;

— l'émulsion aqueuse de résine ou la résine dissoute utilisée doit garantir la conservation d'un pH = 7 pour l'eau de gâchage et, si possible, elle ne doit pas contenir d'éléments ou de substances qui puissent contrarier la prise et le durcissement du ciment ;

— l'émulsion de résine doit être stable pendant une période assez prolongée, afin qu'elle puisse être utilisée dans des conditions parfaitement sûres et, de même, il ne doit pas se produire de coagulation après qu'on l'ait mélangée au ciment ;

— incorporée au mélange frais de béton, la résine doit, si possible, durcir dans des conditions de durcissement qui conviennent au béton, afin que les propriétés des deux types de liants utilisés soient ainsi, au maximum, mises en valeur (il faut remarquer qu'on ne peut satisfaire pleinement cette condition avec les résines que l'industrie chimique nous fournit actuellement) ;

— la résine doit posséder des résistances propres très élévées et une très bonne adhérence à l'agrégat et au liant minéral utilisé, de sorte qu'elle contribue à réduire les inconvénients présentés par le béton de ciment et entraîne l'amélioration effective de ses propriétés, surtout l'augmentation de la résistance à la traction ;

— les résines synthétiques ne sont pas de simples adjuvants du béton de ciment, au sens habituel de la terminologie, mais des liants organiques supplémentaires qui, par leurs propriétés, influencent sensiblement celles du béton de ciment frais et durci et, avec le liant minéral (ciment), constituent alors un liant mixte ou complexe.

Lorsqu'on a élaboré le programme de travail et la liste des résines synthétiques qui devaient constituer l'objet des recherches pour l'obtention de bétons aux résines synthétiques et liants minéraux, entre les résines produites en Roumanie, ont été retenus pour la première phase de l'étude :

a) L'acétate de polyvinyle (PVA)

— des émulsions non plastifiées de type E 50 et Ec ;

— des émulsions plastifiées à 25 et 50% de diphtalate de butyle, type EP 25 et EP 50;

— le copolymère DIA (obtenu par la copolymérisation de l'acétate de vinyle avec le métacrylate de métyle, produit expérimental).

b) Dans le groupe des résines acryliques : quatre produits expérimentaux.

c) Dans la deuxième phase des études, on a utilisé comme adjuvants supplémentaires (au PVA), des résines urée-formaldéhydes du type Urélite R (UR), Urélite R modifié à la mélanine (URM) et la résine mélamine-formaldéhyde de type mélamine modifiée au méthanole (MM), produits par voie industrielle ou expérimentale.

d) Les liants minéraux utilisés sont 9 types de ciments portland ou portland avec adjuvants, produits par voie industrielle ou semi-industrielle par les fabriques de ciment des types : P 400 et P 500, B.S.S., RIM 200 et RIM 400, Blanc, PZ 400 et PZ 500, MPA 400, dont les caractéristiques physiques, mécaniques et chimiques sont comprises dans les limites prévues par les normes en vigueur. Il est à remarquer que le choix des ciments a été effectué en partant de l'idée d'inclure, autant que possible, dans le programme d'études, les variations normales de la composition chimique et minéralogique des ciments. Ainsi, selon les analyses chimiques et les calculs effectués, pour les ciments sans addition, le taux de C_3S variait de 46 à 74%, et le taux de C_2S de 1 à 24%. Le taux de scories basiques de haut fourneau, utilisées comme adjuvant lors du broyage du ciment PZ et MPA, était de 15%.

e) L'agrégat minéral était constitué de sable et de gravier, fourni par les ballastières de la rivière Argeş, et de criblures d'andésite basaltique de Malnaş livrée couramment pour les travaux routiers. Les agrégats ont été lavés et soumis à un nouveau tri dans le laboratoire, afin d'utiliser des matériaux correspondant aux conditions de qualité prévues par les normes en vigueur pour les bétons de ciments. Dans certains travaux expérimentaux, on a aussi utilisé l'agrégat quartzeux lavé, à plus de 98 % de SiO_2, provenant de la carrière Glatna, arrondissement du Timiş, comme sable normal polygranulaire 0 à 2 mm (STAS 7727—71) ou comme sable à bétons 0 à 3 mm.

f) L'eau de gâchage était de l'eau potable.

g) Les recherches ont été effectuées sur des bétons préparés avec : les ciments cités en d), les dosages en ciment variant entre 1 : 3 et 1 : 6,5 (ou 500 à 270 kg de ciment par m^3 de béton) ; des agrégats de carrière ou de concassage à composition granulométrique variable entre 0 à 2 et 0 à 15 mm ; des rapports eau/ciment = 0,50 à 0,75 et des rapports résine (solide)/ciment entre 0 et 50%.

h) La méthodologie de travail a été celle recommandée par les normes nationales et internationales relatives à la détermination des propriétés du béton (frais et durci) et du ciment, auxquelles ont été ajoutées certaines précisions, afin de mieux rendre compte des propriétés du nouveau type de bétons. Le milieu de conservation des éprouvettes faisait intervenir différents régimes, tels que : conservation à l'air humide les 24 premières heures après la coulée et conservation ultérieure à l'air, en laboratoire ; conservation à l'air humide, avec une humidité relative de 95 à 100% pendant l'intervalle de temps coulée — essai ; conservation dans l'eau ou conservation à l'air et dans l'eau, etc., afin de déterminer les conditions optimales de durcissement.

2. SÉLECTION DES RÉSINES SUSCEPTIBLES D'ÊTRE UTILISÉES DANS LA PRÉPARATION DES BÉTONS AUX LIANTS MINÉRAUX

a) *Etude de l'influence de l'addition de résine synthétique sur la prise et sur la constance volumétrique du ciment.* Les résultats des recherches effectuées avec la pâte de ciment à consistance normale et avec addition de résine de 0 à 30% ont montré essentiellement les faits suivants :

— les résines vinyliques, les 4 émulsions PVA utilisées (E 50, Ec, EP 25 et EP 50), retardant le début de prise de 10 à 255 minutes et prolongeant l'intervalle entre le début et la fin de la prise des ciments de 50 à 390 minutes, le temps de prise des ciments augmente, en général, avec le taux de résine ajoutée à la pâte de consistance normale. Le copolymère DIA accélère sensiblement la prise des ciments (de même que les additions de chlorure de calcium) l'effet d'accélérateur dépendant directement du taux de l'addition. Le temps du début de prise a été réduit à 2 minutes et celui de la fin de prise à 10 minutes.

Les résines acryliques accélèrent fortement la prise du ciment, de telle sorte que, dans certains cas, la pâte à consistance normale commençait sa prise dès le gâchage (moins de 3′). On a donc dû renoncer à l'étude de l'utilisation de ces résines comme adjuvants.

Quant à la constance volumétrique des ciments, les 4 émulsions PVA et le copolymère DIA agissent de manière différente, le ciment gardant sa constance volumétrique jusqu'aux taux suivants de résine utilisée : E 50 jusqu'à 30% ; Ec jusqu'à 10% ; EP 25 jusqu'à 10 à 15% ; EP 50 jusqu'à 10% ; DIA jusqu'à 5 et 10%.

b) *Etude de l'influence du type de résine et du taux d'addition sur les propriétés du béton frais.* Les recherches préliminaires effectuées ont indiqué que les additions d'émulsions PVA et de copolymère DIA influencent les propriétés du béton frais dans les sens suivants :

— Réduction du poids apparent — qui diffère selon le type de résine et le taux d'addition — due au volume d'air occlus dans le béton, grâce surtout au fait que les cinq résines utilisées agissent comme entraîneurs d'air (fig. 1 *a*). L'effet d'entraînement le plus fort est enregistré avec le copolymère DIA et l'émulsion non plastifiée PVA, type E 50. Dans les bétons avec addition d'émulsion PVA plastifiées du type EP 25 et EP 50, la réduction du poids apparent du béton due au volume d'air, entraîné dans sa masse, est moins importante, car les additions de diphtalate de butyle, utilisées comme plastifiant externe dans la fabrication de ces émulsions à partir des résines E 50, jouent dans le béton le rôle d'agents désaérateurs, manifesté de façon concrète par la réduction moins accentuée du poids du béton (réduction du taux d'air occlus dans la masse du béton) avec l'augmentation du taux de plastifiant dans l'émulsion et du taux d'émulsion dans le mélange. Il apparaît que le même rôle est rempli par les adjuvants utilisés dans la préparation de l'émulsion Ec. Il est à remarquer que le type de ciment exerce une influence assez réduite (pratiquement insignifiante) sur le taux d'air occlus et sur la réduction de poids du béton, ce qui prouve que l'hypothèse que « l'effet des entraîneurs d'air n'est pas influencé d'une façon appréciable par la nature minéralogique des ciments, mais essentiellement par la nature de l'entraîneur et par la proportion de celui-ci dans le mélange », est aussi valable dans le cas de l'utilisation des résines synthétiques comme adjuvants dans les bétons de ciment ;

— Amélioration de l'ouvrabilité du béton (déterminée par le tassement et par la diffusion) grâce aux propriétés rhéologiques des émulsions et à l'effet d'entraînement d'air.

c) *Etude de l'influence du type de résine et du taux d'addition sur les propriétés du béton fin durci.* Cette étude a conduit, dans la phase préliminaire des études, aux conclusions suivantes : les additions d'émulsions PVA et de copolymère DIA contribuent à la réduction, différente selon le type de résine utilisé, de l'adsorption d'eau des éprouvettes en béton fin, réduction pratiquement proportionnelle au taux de résine utilisé (fig. 1b), l'adsorption d'eau la plus faible étant enregistrée pour les éprouvettes avec addition d'émulsion non plastifiée E 50.

La réduction de l'adsorption d'eau des éprouvettes proportionnellement au taux d'addition de résine s'explique par le fait que les résines synthétiques qui obturent les canaux capillaires du béton, contribuent à la réduction de l'adsorption. C'est dans le même sens qu'agit aussi l'alcool polyvinylique utilisé dans la préparation des émulsions de PVA, à un taux d'environ 3%, comme émulsifiant et stabilisateur et qui, en présence de l'eau a la propriété d'augmenter de volume, de sorte que les pellicules de résine gonflent facilement, exerçant le rôle d'agents d'imperméabilisation et de colmatage.

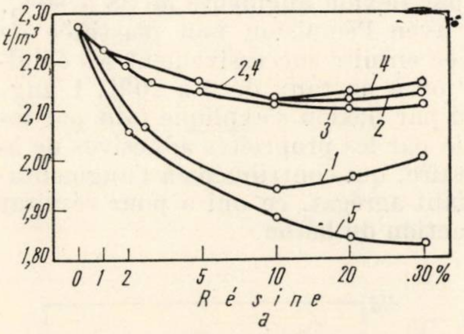

Fig. 1*a*. — Variation de la densité apparente des bétons fins 1 : 3 de ciment P 400 en fonction du type et du pourcentage de résine vinylique PVA et de copolymère DIA (substance sèche).

1, Bétons E 50 ; *2*, Bétons EC ; *3*, Bétons EP 25 ; *4*, Bétons EP 50 ; *5*, Bétons à copolymère DIA.

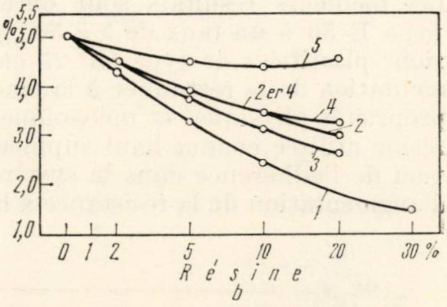

Fig. 1*b*. — Variation de l'adsorption d'eau lors de l'immersion pendant 3 jours pour les bétons fins 1 :3 de ciment P 400 en fonction du type et du pourcentage de résine vinylique PVA et de copolymère DIA (substance sèche).

1, Bétons E 50 ; *2*, Bétons EC ; *3*, Bétons EP 25 ; *4*, Bétons EP 50 ; *5*, Bétons à copolymère DIA.

Quant aux résistances mécaniques, l'influence des additions de résines utilisées dans la préparation des bétons fins s'est manifestée de la façon suivante (fig. 2*a*) : par une réduction des résistances à la compression différente selon le type et le taux de résine, exception faite pour les compositions à taux très élevés : 30 à 50% de résine de l'émulsion non plastifiée E 50, qui augmentent la résistance à la compression. La réduction de la résistance à la compression des bétons avec addition de résine synthétique s'explique, essentiellement, par l'augmentation de l'élasticité avec le taux de résine et par la réduction de la densité du béton due à l'air entraîné et occlus dans sa masse. Mais il faut remarquer que pour les bétons aux résines synthétiques et liants minéraux l'augmentation sensible de la résistance à la traction a une influence favorable sur la réduction de la résistance à la compression, au moins pour les compositions avec plus de 5% de résine et où celle-ci, par sa propre résistance, compense partiellement (en vertu de ses propriétés physico-chimiques) le relâchement de la structure du béton dû à l'air occlus dans sa masse, et que la réduction des résistances est moindre que dans la cas des bétons de ciment sans additions de résines synthétiques (fig. 2 *a*).

La résistance à la traction par flexion des bétons fins augmente selon le type de résine et le type de ciment utilisés, les différences étant sensibles surtout pour les taux élevés de résine ; par exemple pour 20% d'addition, la résistance à la traction par flexion augmente de 38 à 80%. Les meilleurs résultats sont obtenus avec l'émulsion non plastifiée de type E 50 à un taux de 5 à 50 %, avec ensuite successivement les émulsions plastifiées de type EP 25 et EP 50 à un taux de 5 à 20%. L'augmentation de la résistance à la traction par flexion s'explique tant par les propriétés physiques et mécaniques que par les propriétés adhésives de la résine utilisée comme liant supplémentaire, qui contribuent à l'augmentation de l'adhérence dans le système liant-agrégat, ce qui a pour résultat l'augmentation de la résistance à la traction du béton.

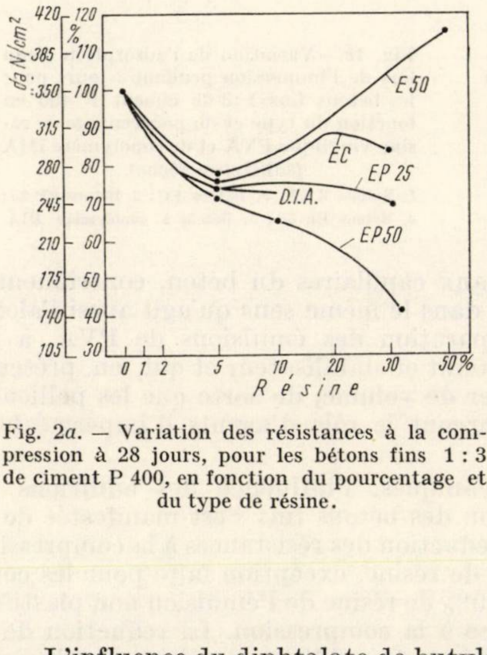

Fig. 2*a*. — Variation des résistances à la compression à 28 jours, pour les bétons fins 1 : 3 de ciment P 400, en fonction du pourcentage et du type de résine.

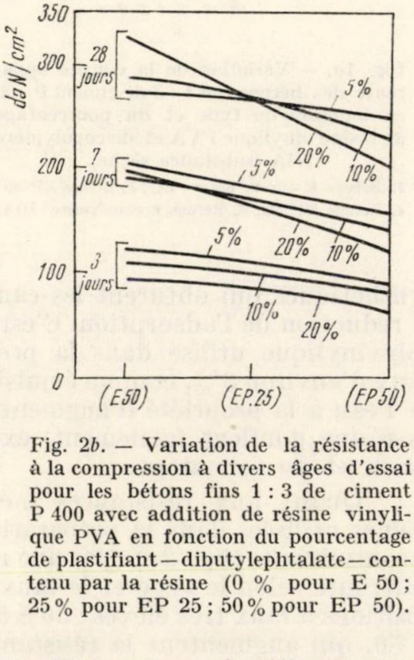

Fig. 2*b*. — Variation de la résistance à la compression à divers âges d'essai pour les bétons fins 1 : 3 de ciment P 400 avec addition de résine vinylique PVA en fonction du pourcentage de plastifiant—dibutylephtalate—contenu par la résine (0 % pour E 50 ; 25 % pour EP 25 ; 50 % pour EP 50).

L'influence du diphtalate de butyle (utilisé comme plastifiant externe dans la fabrication des résines) se manifeste par des résistances à la compression et à la traction par flexion beaucoup plus faibles, pour des taux égaux de résine, qué celles obtenues avec l'émulsion non plastifiée E 50. Les réductions de résistance sont sensibles au-delà de 5% de résine et d'autant plus qu'augmentent l'âge d'essai et le pourcentage de résine, donc en fonction du temps et du taux de diphtalate de butyle dans le mélange (fig. 2b).

d) *Influence des variations des dimensions des particules de résine dans les émulsions utilisées.* Les recherches effectuées sur les variations des dimensions des particules de résine dans les limites des possibilités de fabrication ont prouvé que les meilleurs résultats concernant les résistances mécaniques sont obtenus avec des émulsions PVA où plus de 70 % des particules de résine ont un diamètre compris entre 2 et 5 μ ; les autres propriétés du béton étant pratiquement dans les mêmes limites, quelle que soit la grosseur des particules.

e) *Quelques remarques sur la formation des propriétés structurales des bétons aux résines synthétiques et aux liants minéraux.* Les recherches effectuées pendant plusieurs années sur des bétons avec addition d'émulsion PVA, sur des pellicules de résine sans ciment ou avec ciment portland, ou encore avec hydroxyde de calcium, ont conduit aux conclusions suivantes. Les résistances mécaniques des pellicules d'émulsion de PVA, y compris l'adhérence au béton, à la pierre naturelle et à d'autres matériaux classiques de construction, sont améliorées par le mélange au ciment portland dans certaines proportions, ce qui prouve que les émulsions de PVA ont une bonne adhérence tant à l'agrégat minéral qu'aux ciments du type portland utilisés dans la préparation des bétons. Cette propriété se traduit par l'augmentation sensible de la résistance à la traction du béton modifié au PVA et de l'adhérence des bétons de ce type aux bétons sans addition. Les réactions du ciment et la formation de sa structure durcie dans le béton additionné de résine ne sont pas sensiblement influencées de façon négative par les résines vinyliques et les émulsions de PVA similaires au type E 50 ou à taux réduit de plastifiant, tel que le type EP 25 utilisé jusqu'à 20 % de résine.

Le processus de durcissement des résines vinyliques — émulsions du type PVA, mélangées au ciment — est essentiellement un processus physique, celui du passage en phase solide de la résine (polymère) émulsionnée en raison de la perte de l'eau de constitution et de l'eau apportée par l'émulsion. La réduction de la résistance à la compression du béton avec certaines résines est due essentiellement à la réduction de la densité apparente du béton en raison de l'air occlus dans le mélange (fig. 1*a*) et de l'augmentation de l'élasticité grâce à l'addition de résine. Les observations effectuées ont montré que les émulsions de PVA — E 50 et EP 25 — sont complètement dispersées dans l'eau après une légère agitation d'environ une minute. Les émulsions ainsi obtenues ont une bonne stabilité, et ne coagulent pas lors du mélange avec le ciment. Les particules de résine de l'émulsion diluée par l'eau de gâchage ont généralement des dimensions entre à peu près 0,5 et 5 μ ; d'autre part, en raison des rapports e/c importants (de 0,40 à 0,60 au lieu d'environ 0,25 à 0,30 habituellement nécessaires) peu après le gâchage apparaissent des pores capillaires — outre ceux qui naissent dans les gels —, produits par l'ascension de l'eau en excès dans la pâte de ciment qui commence à durcir, ainsi que des pores à plus fortes dimensions et même certains vides sous les granulats à côté des pores formés par les inclusions d'air pendant le gâchage : il s'ensuit que la résine dispersée dans l'eau de gâchage, qui remplit momentanément les pores et les vides du béton frais, se dépose sous forme de pellicules minces, continues ou discontinues selon la quantité de résine du mélange, sur les parois des pores et des vides du béton. L'évaporation de l'eau laisse durcir la pellicule de résine, et il en résulte une meilleure adhérence entre l'agrégat minéral et la pierre de ciment, ce qui contribue à l'augmentation de la résistance à la traction du béton, selon l'épaisseur de la pellicule, donc selon le taux de résine et les caractéristiques propres de résistance de celle-ci. Ainsi, la résistance du béton modifié à des taux réduits de résine (au-dessous de 5 %) est due à la structure continue rigide formée par le liant minéral et durcie par la pellicule de résine. Si le taux de résine augmente, jusqu'à 10 ou 20 %, l'épaisseur de la pellicule s'accroît bien que la structure formée par le liant minéral soit encore continue (mais la résine peut remplir la plupart des vides du béton) ; dans ces conditions, la résistance de la pellicule de résine augmente considérablement et ceci se manifeste par l'accroissement de la densité du béton additionné de E 50 (fig. 1 *a*), par l'importante augmentation de la résistance du béton à la traction, à la compression (il s'agit du béton préparé avec l'émulsion non plastifiée) (fig. 2*a*, 3 et 4 *ab*), ainsi que par l'augmentation sensible du retrait lorsque ce béton est conservé à l'air faiblement humide et par un gonflement accentué à l'immersion dans l'eau (fig. 5*a*, *b* et 6, *a*, *b*, *c*).

Pour des taux de résine dans le mélange dépassant 20%, on peut supposer la formation de deux structures continues dans le béton et, selon le dosage du ciment et le rapport résine/ciment l'influence exercée sur les propriétés du béton sera tout à fait différente. Ainsi, pour d'importants taux de résine, il est possible que la structure rigide continue, formée habituellement par le liant minéral et par les agrégats, soit interrompue en certains points par la structure continue de la résine, et que la structure rigide du béton s'articule (par l'adhérence entre le ciment ou l'agrégat et la résine) avec la structure élastique continue formée par la résine synthétique. Il est alors évident que les propriétés du béton sont considérablement affectées par l'addition de résine et par les propriétés de celle-ci.

3. QUELQUES RÉSULTATS DES RECHERCHES SUR LES PRINCIPALES PROPRIÉTÉS DES BÉTONS AUX RÉSINES SYNTHÉTIQUES ET AUX LIANTS MINÉRAUX ET LES FACTEURS QUI LES MODIFIENT

a) *Influence de la nature et du type de ciment, du dosage, de la granulométrie, de la nature des agrégats et du rapport eau/ciment.* Les données qu'on trouve dans la littérature spécialisée ont comme point de départ l'idée que « la résine synthétique doit être compatible avec le liant minéral dans n'importe quelles conditions » et que « l'agrégat minéral doit satisfaire les mêmes conditions que dans le cas des bétons de ciment ». Les recherches effectuées par l'auteur dans cette voie, avec pour liants minéraux 8 ciments différents et comme adjuvants l'émulsion non plastifiée — PVA — E 50, ainsi que différentes compositions d'agregats, ont abouti aux conclusions suivantes : le poids apparent du béton frais et l'adsorption de l'eau par les éprouvettes durcies de béton additionné de résine synthétique ne varient sensiblement pas selon le type de ciment utilisé.

Pour des taux égaux de résine dans le mélange et de forts dosages en ciment (1/3), les meilleurs résultats d'essai à la compression à 28 jours sont obtenus avec les ciments RIM 200 et Pz 400, et, pour les bétons à dosages moyens en ciment (1 : 4), avec les ciments Pz 400, MPA 400 et blanc (fig. 3, 4*a*). Pour de faibles dosages de ciment (1 : 6,5), on obtient de très bons résultats avec les ciments Pz 400, moins bons avec les ciments RIM 400, B.S.S. et Pz 500. Ainsi, l'influence du type de ciment utilisé (dans des conditions identiques de préparation du béton) dépend du dosage en ciment par mètre cube de béton et s'exprime par des écarts, par rapport à la moyenne des résistances à la compression, de 5 à 10% pour des dosages élevés (1 : 3) et de 3 à 7% pour des dosages moyens (1 : 4).

Pour des taux égaux de résine dans le mélange et de forts dosages en ciment (1 : 3), les meilleurs résultats d'essai de traction par flexion à 28 jours sont obtenus avec les ciments P 500, Pz 400, MPA 400 et RIM 200, et, pour les bétons à dosages moyens et faibles en ciment (1 : 4 et 1 : 6,5), avec le ciment RIM 400, Pz 400 et MPA 400 (fig. 4*b*). De résultats moins satisfaisants sont obtenus avec les ciments B.S.S. et Pz 500. L'influence du type de ciment utilisé sur la résistance à la traction par flexion dépend elle aussi du dosage en ciment et s'exprime par des écarts, par rapport à la moyenne des résistances, de 5 à 20% pour des dosages élevés en ciment (1 : 3) et de 4 à 12 % pour des dosages moyens (1 : 4).

L'influence de la granulométrie et de la nature des agrégats se manifeste par les faits suivants : pour les bétons fins à agrégats 0—2 mm et de dosage 1 : 3, la résistance à la compression à 28 jours diminue pour une addition de résine inférieure à 5% ; et elle augmente fortement avec le taux de résine de 5 à 30% (fig. 3). Pour les bétons à agrégats 0 à 7 mm et de dosage 1 : 4 la résistance à la compression diminue pour moins de 5% de résine et augmente avec le taux de résine de 5 à 30%. Pour les bétons 1 : 4 à agrégats 0 à 15 mm (fig. 4 *a*), la résistance à la compression diminue

Fig. 3. — Variation de la résistance à la compression à 28 jours, pour les bétons fins 1 : 3 à agrégats 0 à 2 mm et avec différents ciments, en fonction du pourcentage de résine E 50.

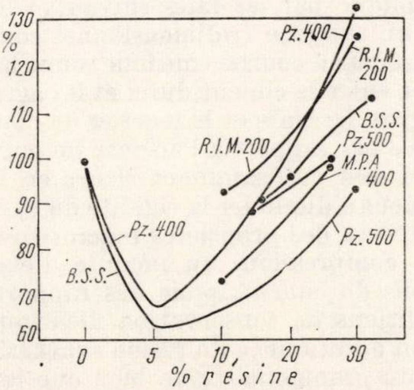

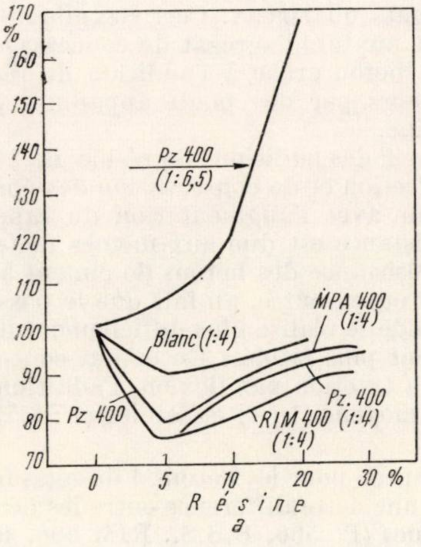

Fig. 4*a*. — a) Variation de la résistance à la compression à 28 jours ;

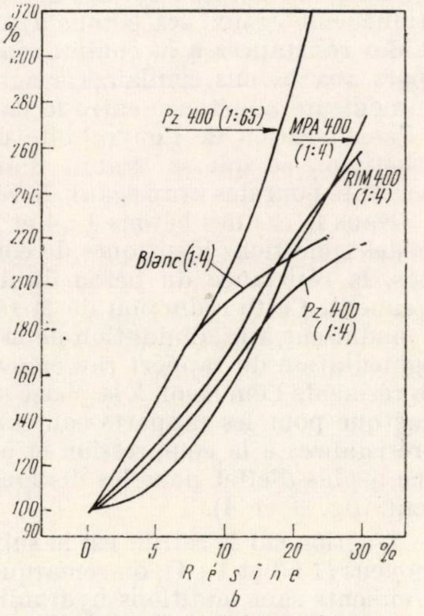

4*b*. — Variation de la résistance à la traction par flexion à 28 jours pour les bétons 1 : 4 et 1 : 6,5 à agrégats 0—15 mm et avec différents ciments, en fonction du pourcentage de résine.

également pour moins de 5% de résine mais l'augmentation de la résistance avec le taux de résine (5 à 20% E 50) est ici un peu plus lente, et si l'on augmente le taux de résine jusqu'à 30%, les résistances à la compression n'augmentent plus, mais au contraire elles manifestent une tendance à diminuer. Ce comportement différent du béton à gros agrégats 0 à 15 mm s'explique par les faits suivants : le béton à gros agrégats est constitué par un système tridimensionnel complexe, composé d'un squelette rigide d'agrégats à courbe continue, dont la configuration rigide résulte de l'adhérence entre le ciment durci et les agrégats et du remplissage des vides entre les gros agrégats et le mortier de ciment, matériaux à rigidité relativement élevée par rapport à l'acétate de polyvinyle. Quand le mortier et le ciment durci sont suffisamment riches en PVA, ils gagnent en élasticité et contribuent à diminuer la rigidité du système tridimensionnel, ce qui se traduit au niveau des propriétés macroscopiques par la réduction de la résistance à la compression, du module d'élasticité, etc. Comme dans le cas des bétons de ciment, pour des rapports eau/ciment, une ouvrabilité et des conditions de conservation identiques, la résistance à la compression du béton additionnée de résine synthétique augmente avec l'élargissement du fuseau granulométrique bien que le dosage en ciment diminue de 500 kg à 430 kg/m³ de béton. Pour des dosages en ciment et des additions de résine pratiquement égaux, les bétons ayant un agrégat de concassage fournissent des résistances à la compression de 20 à 40% plus importantes par rapport aux bétons similaires à agrégats quartzeux. Ceci s'explique par une meilleure adhérence entre le liant mixte et l'agrégat de concassage et par l'amélioration de l'ouvrabilité du béton grâce à l'addition de résine synthétique, ce qui se traduit d'ailleurs par des poids apparents plus importants pour des taux égaux de résine.

Dans le cas des bétons 1 : 4 et pour des additions de résine de 20%, dans des conditions identiques de confection et de conservation des éprouvettes, la résistance du béton diminue avec l'augmentation du rapport eau/ciment. Cette réduction de la résistance est due aux mêmes facteurs qui conduisent à la diminution de la résistance des bétons de ciment avec l'augmentation du rapport eau/ciment et, en outre, au fait que le passage de la résine de l'émulsion à la phase solide se réalise plus difficilement dans ce cas que pour les rapports eau/ciment plus faibles. En ce qui concerne les résistances à la compression et à la traction par flexion, l'addition de résine a plus d'effet pour les dosages moyens (1 : 4) et faibles (1 : 6,5) de ciment (fig. 3 et 4).

L'action sur le retrait est la suivante : pour les bétons à dosages forts et moyens (1 : 3 et 1 : 4), on remarque une nette différence entre les bétons aux ciments sans additions hydrauliques (P 500, B.S.S., RIM 200, RIM 400 et blanc), qui montrent ordinairement des retraits plus faibles que ceux subis par les ciments à additions hydrauliques (Pz 400, Pt 500, MPA 400), en général plus importants en valeur absolue, et qui augmentent plus fortement avec le taux de résine, par rapport aux retraits des bétons préparés avec le même type de ciment, mais sans addition de résine (fig. 5 *a* et *b*). Ainsi, dans le cas des bétons fins 1 : 3 préparés avec des ciments sans additions hydrauliques et avec 10 à 20% de résine le retrait est 2 à 3 fois plus faible que pour les bétons à même taux de résine, mais préparés avec des ciments à additions hydrauliques (fig. 5*a* et *b*). Pour un dosage 1 : 4, les différences entre les retraits des bétons de ciments à additions hydrauliques et les bétons de ciments sans additions hydrauliques sont un peu plus faibles, ce qui s'explique par la réduction du dosage en ciment de 1 : 3 à 1 : 4 et la réduction correspondante de la quantité de résine, ce qui a pour résultat d'atténuer, dans une certaine mesure, le retrait (fig. 5*b*). Les données représentées graphiquement dans la fig. 5*a* et *b* indiquent l'influence sensible des types et de la composition des ciments sur le retrait des bétons aux résines synthétiques et aux liants minéraux, surtout pour des taux supérieurs à 10% de résine, les retraits les plus forts étant constatés dans les bétons où le volume relatif de gel dans la phase hydratée du ciment durci est plus grand (ciments à additions hydrauliques du type Pz et MPA), tandis que les bétons à ciments riches en silicate tricalcique RIM 400, P 500, B.S.S., RIM 200 et Blanc, où le volume relatif du gel est plus faible, ont un retrait moindre. Le retrait des bétons à addition de PVA — émulsion non plastifiée — E 50 — diminue avec la réduction du dosage en ciment. Ce qui explique, d'une part, comme dans le cas des bétons classiques le fait que la réduction du dosage en ciment entraîne une diminution du volume relatif du ciment durci, en l'occurrence du gel et, d'autre part, le fait que le volume correspondant de résine synthétique dont l'addition est exprimée comme un pourcentage du ciment, diminue avec la réduction du dosage de ce dernier. Dans des conditions identiques de préparation, de conservation des éprouvettes et d'essai, le retrait des bétons à liants minéraux et à résines synthétiques augmente avec le rapport eau/ciment, ce qui s'explique par la diminution de la compacité du béton avec l'augmentation du rapport eau/ciment.

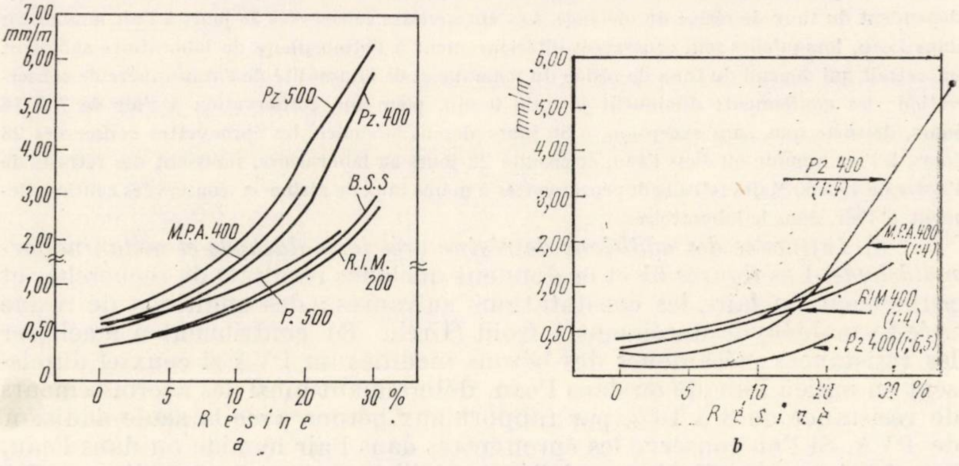

Fig. 5. — Variation des retraits à 28 jours en fonction du type de ciment et du pourcentage de résine ;

a) bétons fins 1 : 3 à agrégats 0 à 2 mm ; b) bétons 1 : 4 et 1 : 6,5 à agrégats 0 à 15 mm.

b) *Influence de la forme et des dimensions des éprouvettes et du milieu de conservation.* Les recherches effectuées ont conduit aux conclusions suivantes : la résistance des bétons additionnés de PVA diminue avec l'augmentation des dimensions des éprouvettes. En effet, pour des éprouvettes de dimensions importantes (10 × 10 × 55 cm ou 10 × 10 × 10 cm), le passage de la résine de l'émulsion à la phase solide (liée à l'évaporation de l'eau) se fait plus difficilement dans le même délai, ce qui empêche d'atteindre les résistances obtenues lors des essais avec les éprouvettes de faibles dimensions (4 × 4 × 16 cm). A l'essai de compression, en raison de l'augmentation des surfaces et de la hauteur des éprouvettes, l'influence exercée par le frottement entre les plateaux de la presse et les surfaces des éprouvettes est quelque peu réduite.

L'augmentation de l'humidité du milieu de conservation des éprouvettes a un effet considérable sur les résistances mécaniques des bétons additionnés de PVA (émulsion non plastifiée E 50) entraînant une diminution accentuée de la résistance à la compression avec le taux de résine du mélange, diminution qui se situe entre 28 et 63 % par rapport aux éprouvettes sans addition de résine. Les diminutions de résistance à la traction par flexion sont de l'ordre de 10 à 39 %. Les éprouvettes avec 5 à 20 % PVA — E 50, conservées d'abord dans l'air humide ou immergées dans l'eau durant 1 à 28 jours, lorsqu'elles sont ensuite conservées à l'ambiance du laboratoire, à une humidité relative de 50 à 70 %, atteignent en 15 à 24 jours approximativement les mêmes résistances (±10 %) que les éprouvettes de même composition conservées continuellement à l'atmosphère du laboratoire, ce qui prouve que le phénomène est, dans une certaine mesure, réversible. Des diminutions de résistance de l'ordre de 10 à 40 % ont été remarquées aussi lors de l'immersion dans l'eau d'éprouvettes conservées d'abord 28 à 90 jours à l'atmosphère du laboratoire, ce qui prouve que leur comportement est meilleur. Conservés dans l'air humide ou immergés dans l'eau, les bétons additionnés de PVA — E 50 enregistrent des gonflements importants qui augmentent avec le taux de résine. Ainsi, pour 20 % de résine, les bétons fins 1 : 3 subissent, à l'immersion dans l'eau, des gonflements de 2,88 mm/m, et les bétons 1 : 4 à agrégats 0—15 mm, des gonflements de 1,78 mm/m (fig. 6*a*). Si l'on conserve ultérieurement à l'air humide ou dans l'eau les éprouvettes en béton additionné de résine, placées les 28 premiers jours dans l'atmosphère du laboratoire, on enregistre des gonflements qui dépendent du taux de résine du mélange. Les éprouvettes conservées 28 jours à l'air humide ou dans l'eau, lorsqu'elles sont conservées ultérieurement à l'atmosphère du laboratoire subissent un retrait qui dépend du taux de résine du mélange et de l'humidité de l'atmosphère de conservation ; les gonflements diminuent jusqu'à 0 mm pour une conservation à l'air de 7 à 18 jours, de sorte que, sans exception, à 56 jours depuis la coulée, les éprouvettes conservées 28 jours à l'air humide ou dans l'eau, et ensuite 28 jours au laboratoire, subissent des retraits de l'ordre de 40 à 80 % des retraits des éprouvettes à même taux de résine et conservées continuellement à l'air, dans le laboratoire.

c) *Influence des additions de résine urée-formaldéhyde et mélanine-formaldéhyde.* Les figures 6*b* et 6*c* donnent quelques résultats de recherches et permettent de faire les constatations suivantes : des additions de résine urée-formaldéhyde durcissant à froid (Urélit R) contribuent à améliorer les résistances mécaniques des bétons modifiés au PVA si ceux-ci durcissent en milieu humide ou dans l'eau, déterminant ainsi des accroissements de résistance de 8 à 16 % par rapport aux bétons avec la seule addition de PVA. Si l'on conserve les éprouvettes dans l'air humide ou dans l'eau, les additions de mélanine modifiée au méthanol contribuent elles aussi à l'accroissement des résistances mécaniques de 2 à 41 % par rapport aux éprouvettes sans addition de ce type et à la réduction de 6 à 30 % des gonflements des éprouvettes.

L'accroissement de la résistance et du gonflement des éprouvettes par additions de résine urée-formaldéhyde (Urélit R et Urélit R modifiée à la mélamine), lorsqu'elles sont conservées dans l'air humide ou immergées, s'explique par les propriétés des deux résines de durcir et de gonfler

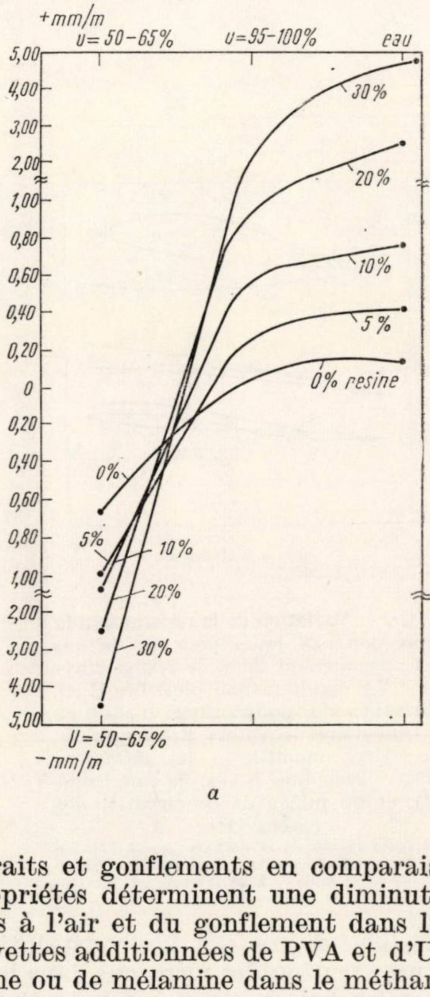

Fig. 6*a*. — Variation des retraits et des gonflements à 28 jours pour les bétons fins 1 : 3 en fonction de l'humidité du milieu de conservation des éprouvettes (u) et du pourcentage de résine vinylique PVA, émulsion non plastifiée E 50.

en présence de l'eau. L'accroissement de résistance des éprouvettes additionnées de mélamine dans le méthanol, et conservées dans l'atmosphère du laboratoire, l'air humide ou l'eau, s'explique par les propriétés des résines mélamine-formaldéhydes, qui durcissent dans les trois milieux de conservation, avec de faibles retraits et gonflements en comparaison d'autres résines, etc. Ces mêmes propriétés déterminent une diminution du retrait des éprouvettes conservées à l'air et du gonflement dans l'air humide ou dans l'eau. Pour les éprouvettes additionnées de PVA et d'Urélit R, Urélit R modifiée à la mélamine ou de mélamine dans le méthanol, qui ont été conservées 28 jours à l'ambiance du laboratoire puis immergées de 3 à 15 jours dans l'eau, on enregistre des réductions de résistance mécanique de 20 à 40%, selon le type et le taux de résine utilisée comme addition supplémentaire. La réduction des résistances mécaniques est, dans une certaine mesure, réversible lors d'une conservation ultérieure à l'air ambiant, la plupart des éprouvettes retrouvant leurs résistances initiales dans un délai de 7 à 14 jours. Les meilleurs résultats ont été obtenus aussi avec les additions de mélamine dans le méthanol de d'Urélit modifié à la mélamine à un taux d'environ 10% du poids du PVA (émulsion E 50).

d) *Influence des additions de PVA sur la vitesse de propagation des ultrasons, sur la relation vitesse de propagation — résistance et sur le module d'élasticité dynamique.* Les constatations suivantes ont été faites : la vitesse de propagation des ultrasons dans le béton aux résines synthétiques diminue selon le taux de résine du mélange, le dosage du ciment, la granulométrie, la compacité du béton, et selon l'âge des éprouvettes au moment de l'essai. La variation des paramètres cités détermine des valeurs différentes de vitesse de propagation pour des résistances mécaniques égales ou de même ordre de grandeur. Ces différences de vitesse de propagation des ultrasons dans les bétons 1 : 4, de rapport eau/ciment 0,50 et modifiés aux résines synthétiques s'expliquent ainsi : généralement, la diminution de la vitesse de propagation est causée par un volume supplémentaire d'air occlus lors de la préparation du béton et dû à l'addition de résine, par la diminution de la compacité, et par le fait que dans la composition

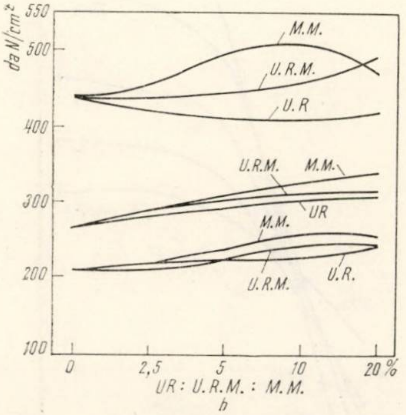

Fig. 6*b*. — Variation de la résistance à la compression à 28 jours pour les bétons fins 1 : 3 contenant 20% de résine vinylique PVA émulsion non plastifiée E 50, en fonction du pourcentage d'addition supplémentaire de résine uréoformaldéhyde (UR), modifiée à la mélamine (URM) : mélamine dans le méthanol (MM), et du milieu de conservation des éprouvettes :

α = à l'atmosphère du laboratoire ; β = à l'air humide ; γ = immersion dans l'eau pendant l'intervalle 1 à 28 jours.

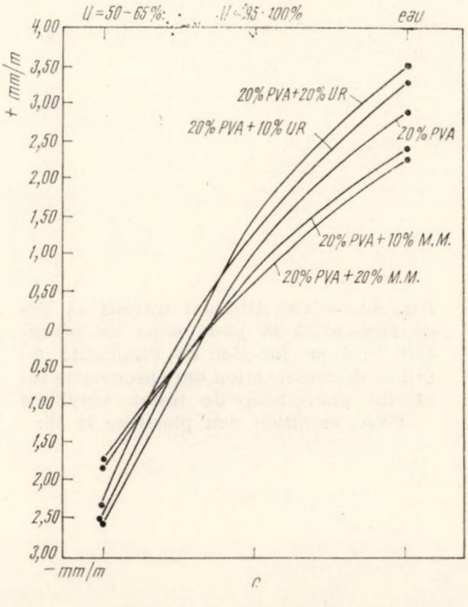

Fig. 6*c*. — Variation des retraits et de gonflements à 28 jours pour les bétons 1 : 3 contenant 20% de résine vinylique PVA, émulsion non plastifiée E 50, en fonction de l'humidité du milieu de conservation des éprouvettes (u) et de l'addition supplémentaire de résine uréo u-formaldéhyde (UR) ou mélamine modifiée au méthanol (MM).

du béton est introduit, dans certaines proportions, un matériau beaucoup moins rigide que les matériaux de base des éprouvettes témoins (ciment durci et agrégats). La diminution de la vitesse de propagation, à de jeunes âges d'essai, avec l'augmentation du taux de résine dans le mélange, jusqu'à 40 à 70% de la vitesse pour les éprouvettes étalon, s'explique par la plus forte proportion dans le mélange d'un matériau de très faible rigidité et doué d'une forte capacité de rétention d'eau, qui devient ensuite rigide, consolidant la structure du béton par la perte graduelle de son eau de constitution (ou de l'eau supplémentaire ajoutée pendant le gâchage) (fig. 7*a*); ceci se traduit par l'augmentation relativement lente dans la période initiale des résistances mécaniques des bétons additionnés de PVA. Entre 28 et 365 jours, la vitesse de propagation varie de 88 à 98% des valeurs obtenues avec les éprouvettes étalon, les différences étant dues au degré différent de consolidation de la structure du béton selon le taux de résine utilisé. Un taux plus important de résine, par la perte graduelle de l'eau et par le durcissement, rend la structure plus rigide, d'où une augmentation sensible de la vitesse de propagation des ultrasons dans le béton 1 : 4 avec des taux de 20 à 40% (fig. 7*a*).

Pour des dosages de ciment de 1 : 6,5 et pour des rapports eau/ciment de 0,75 ou 0,70, la vitesse de propagation diminue avec le taux de résine entre 1 et 3 jours ; on enregistre ensuite des différences de vitesse avec un agrégat de 0 à 7 mm et un rapport eau/ciment = = 0,75 par rapport aux bétons à agrégat de 0 à 15 mm et un rapport eau/ciment = 0,70, — pour les bétons 1 : 6,5 à agrégats de 0 à 7 mm et une compacité plus faible ($\gamma_a = 2{,}23 - 1{,}93$ t/m^3), la vitesse de propagation diminue avec une addition de 10% de résine à tous les âges d'essai entre 7 et 365 jours par rapport aux éprouvettes sans addition, ce qui s'explique par la réduction sensible de la compacité du béton et par le fait que le faible taux de résine utilisé forme une pellicule assez mince sur les parois des vides et des pores du béton, qui ne peut que partiellement compenser la réduction sensible de la compacité du béton et par le fait que le faible taux de résine utilisé forme une pellicule assez mince sur les parois des vides et des pores du béton, qui ne peut que partiellement compenser la réduction de la compacité du béton, en raison de l'important volume d'air entraîné. Tandis que, pour un taux de résine de 20% dans le mélange, la pellicule de résine étant plus épaisse, elle consolide mieux la structure et compense la réduction de la compacité du béton entre 28 et 365 jours.

La représentation graphique des données des recherches qui concernent la relation entre la résistance du béton et la vitesse de propagation des ultrasons conduit à des courbes assez distinctes pour les bétons avec et sans résine (fig. 7*b*). La forme des diagrammes est affectée par les facteurs cités antérieurement, indiquant même une importante variation de la vitesse de propagation entre 1 et 3 jours dans les bétons aux résines synthétiques, période où la vitesse diminue généralement selon le taux de résine du mélange pour un certain type de béton, de sorte qu'à des résistances mécaniques du même ordre de grandeur correspondent des valeurs sensiblement différentes de la vitesse de propagation.

Les recherches, les expériences et les calculs effectués pour déterminer le module d'élasticité statique et dynamique des bétons aux résines synthétiques ont indiqué que leurs valeurs sont sensiblement affectées par le taux, le type et les propriétés de la résine utilisée, par le dosage en ciment, par la granulométrie, par la compacité du béton, par l'âge des éprouvettes, etc. Ainsi, pour des dosages de ciment 1 : 4, un rapport eau/ciment = 0,50 constant (fig. 8), si l'essai est effectué à 1, 3 ou 7 jours, le module dynamique d'élasticité des bétons modifiés diminue en général avec le taux de résine. La réduction du module d'élasticité dynamique

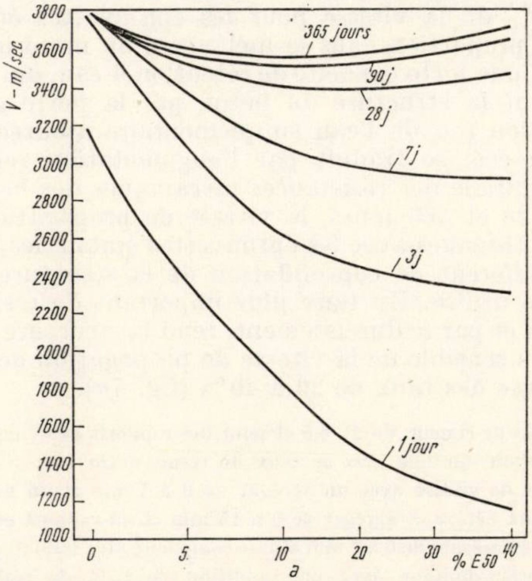

Fig. 7*a*. — Variation de la vitesse de propagation des ultrasons dans le béton, à différents âges d'essais, en fonction du pourcentage de résine vinylique PVA, émulsion non plastifiée E 50, pour les bétons 1 : 4 de ciment Pz 400, agrégats 0 à 15 mm, e/c = 0,50.

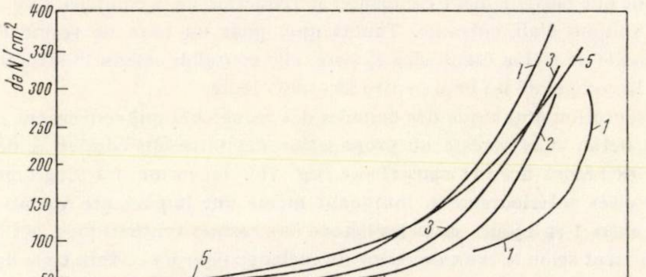

Fig. 7*b*. — Variation de la relation résistance à la compression-vitesse de propagation des ultrasons pour les bétons 1 : 4 d'agrégats 0 à 15 mm, ciment Pz 400, e/c = 0,50 et différents pourcentages de résine vinylique PVA, émulsion non plastifiée E 50 (1 = 0% de résine ; 2 = 5% ; 3 = 10% ; 4 = 20% ; 5 = 40%).

pour les bétons à agrégats 0 à 7 mm à 1 jour est maximale pour des compositions à 20% de résine et représente environ 21% du module d'élasticité des bétons témoins. Pour les bétons à agrégats 0 à 15 mm, la réduction maximale du module d'élasticité est enregistrée pour les compositions à 40% de résine et représente environ 11% du module d'élasticité des bétons non modifiés. Aux essais à un âge plus avancé (28 à 365 jours), les modules d'élasticité dynamiques des bétons 1 : 4 aux résines synthétiques représentent, au maximum, 88% des modules d'élasticité des bétons témoins. Pour les bétons 1 : 4 à agrégats 0 à 7 additionnés de 5 à 20% de résine, si les valeurs du module d'élasticité sont bien distinctes, elles ne s'écartent de la moyenne que d'environ ±2 à 5%. Pour les bétons 1 : 4 à agrégats 0 à 7 mm à 40% de résine, le module d'élasticité augmente fortement entre 28 et 365 jours, soit dans l'année environ 88% de la valeur du module dynamique d'élasticité des bétons non modifiés. Les modules dynamiques d'élasticité pour les bétons aux liants minéraux et aux résines synthétiques ont les valeurs suivantes exprimées en pourcentage, par rapport aux modules du béton témoin :

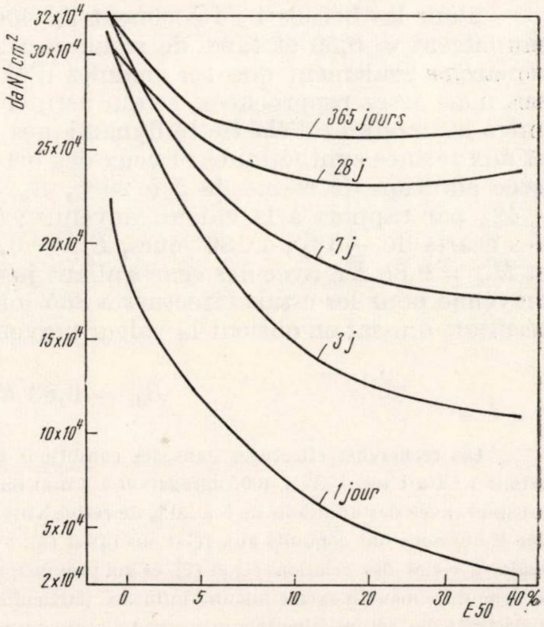

Fig. 8. — Variation du module d'élasticité dynamique E_d, à différents âges d'essais, en fonction du pourcentage de résine vinylique PVA, émulsion non plastifiée E 50 pour les bétons 1 : 4 de ciment Pz 400, agrégats 0 à 15 mm, e/c=0,50.

A 28 jours, pour des additions de résine de 5 à 20%, $E_{\mathrm{dr}} = 0{,}70\, E_{\mathrm{do}}$, avec un écart de ±4% par rapport à la valeur moyenne ; à 90 jours, $E_{\mathrm{dr}}=0{,}72\, E_{\mathrm{do}}$, avec des écarts de ±3% par rapport à la valeur moyenne ; à 180 jours, $E_{\mathrm{dr}} =0{,}72\, E_{\mathrm{do}}$, avec des écarts de ±2% par rapport à la valeur moyenne ; et à 365 jours, $E_{\mathrm{dr}}=0{,}75\, E_{\mathrm{do}}$, avec des écarts allant jusqu'à ±3% par rapport à la valeur moyenne.

Par le calcul statistique des résultats des essais effectués entre 28 et 365 jours, on obtient une valeur moyenne (1) du module dynamique d'élasticité des bétons 1 : 4 à ciment Pz 400, agrégats 0 à 7 mm, rapport eau/ciment = 0,50 et résine 5 à 20% :

$$E_{\mathrm{dr}} = 0{,}72\ E_{\mathrm{do}} \tag{1}$$

Pour les bétons 1 : 4 à ciment Pz 400, agrégats 0 à 15 mm, rapport eau/ciment = 0,50 et taux de résine 5 à 20%, entre 28 et 365 jours, on remarque également que les modules d'élasticité ont des valeurs distinctes, mais assez rapprochées, ce qui permet d'établir les relations suivantes entre les modules d'élasticité dynamiques des bétons aux liants minéraux et aux résines synthétiques et ceux des bétons témoins (fig. 8) : à 28 jours, avec addition de résine de 5 à 20%, $E_{\mathrm{dr}} = 0{,}82\ E_{\mathrm{do}}$, les écarts étant de ±4% par rapport à la valeur moyenne ; à 90 jours, $E_{\mathrm{dr}} = 0{,}84\ E_{\mathrm{do}}$ avec des écarts de ±3% ; à 180 jours, $E_{\mathrm{dr}} = 0{,}83\ E_{\mathrm{do}}$ avec des écarts de ±2% et $E_{\mathrm{dr}} = 0{,}85\ E_{\mathrm{do}}$ avec des écarts allant jusqu'à 4% par rapport à la valeur moyenne pour les essais effectués à 365 jours. Par le calcul statistique des résultats d'essai on obtient la valeur moyenne (2) :

$$E_{\mathrm{dr}} = 0{,}83\ E_{\mathrm{do}} \tag{2}$$

Les recherches effectuées dans des conditions identiques entre 28 et 365 jours sur des bétons 1 : 4 à ciment RIM 400, agrégats 0 à 7 mm ou 0 à 15 mm, rapport eau/ciment = 0,50 constant, avec des additions de 5 à 20% de résine vinylique du type PVA (émulsion non plastifiée E 50) nous ont conduits aux relations (3) et (4), avec des valeurs moyennes pratiquement égales à celles des relations (1) et (2), ce qui prouve qu'à des âges plus avancés (28 à 365 jours), le type du ciment n'exerce aucune influence particulière sur les valeurs du module dynamique d'élasticité des bétons à liants minéraux et à résines synthétiques :

— bétons 1 : 4 à agrégats 0 à 7 mm : $E_{\mathrm{dr}} = 0{,}72\ E_{\mathrm{do}}$ (3), avec des écarts maximaux de ±5% par rapport à la valeur moyenne ;

— bétons 1 : 4 à agrégats 0 à 15 mm : $E_{\mathrm{dr}} = 0{,}82\ E_{\mathrm{do}}$ (4), avec des écarts maximaux de ±4%.

Les recherches effectuées entre 28 et 365 jours, sur des séries de 6 éprouvettes (confectionnées et conservées dans des conditions identiques) de béton 1 : 4 ciment RIM 400, agrégats 0 à 7 mm, rapport eau/ciment = 0,50 et addition de 20% de résine vinylique du type PVA (émulsion non plastifiée E 50) pour déterminer le module d'élasticité statique à des charges de 0,20 à 0,67 de la charge de rupture et le module d'élasticité dynamique ont donné les résultats moyens suivants :

$$E_{\mathrm{do}} = 354\,000\ \mathrm{daN/cm^2}$$

$$E_{\mathrm{dr}} = 251\,000\ \mathrm{daN/cm^2}$$

$$E_{\mathrm{str}\,0.20} = 218\,000\ \mathrm{daN/cm^2} \ldots \alpha = 0{,}87$$

$$E_{\mathrm{str}\,0.33} = 194\,000\ \mathrm{daN/cm^2} \ldots \alpha = 0{,}77$$

$$E_{\mathrm{str}\,0.50} = 178\,000\ \mathrm{daN/cm^2} \ldots \alpha = 0{,}71$$

$$E_{\mathrm{str}\,0.67} = 158\,000\ \mathrm{daN/cm^2} \ldots \alpha = 0{,}63$$

Les résultats ci-dessus montrent que, pour la corrélation de E_{statique} avec $E_{\text{dynamique}}$, il n'y a pas de coefficient α unique, mais qu'au contraire ses valeurs sont sensiblement affectées par la charge pour laquelle on vient de déterminer E_{statique}. Comme en pratique on utilise généralement la valeur de E_{statique} pour des charges égales à environ 1/3 de la charge de rupture, les recherches se sont poursuivies sur des bétons 1 : 4 à ciment Pz 400, agrégats 0 à 7 mm et rapport eau/ciment = 0,50 avec 10 à 20% de résine PVA (émulsion E 50), avec les résultats suivants :

— bétons avec 10% de résine : α moyen = 0,74

— bétons avec 20% de résine : α moyen = 0,76

c'est-à-dire des valeurs très rapprochées de la valeur de α moyen = 0,77 obtenue pour les bétons à ciment RIM 400 ; il en résulte que pour les bétons 1 : 4 on peut prendre avec assez de précision $\alpha_{\text{moyen}} = 0{,}75$ (les écarts étant dans les limites $\pm 5\%$), ce qui conduit à la relation (5) :

$$E_{\text{str}} = \alpha\, E_{\text{dr}}$$

ou, pour les bétons 1 : 4 avec 5 à 20% de résine ;

$$E_{\text{str}} \cdot 0{,}33 = 0{,}75\ E_{\text{dr}} \tag{5}$$

Les recherches sur des bétons 1 : 4 à ciment RIM 400, avec comme addition la résine vinylique du type PVA : émulsion plastifiée EP 25, ont indiqué que, tant pour les vitesses de propagation des ultrasons que pour les modules d'élasticité, on obtient des valeurs sensiblement différentes avec le taux de résine du mélange à tous les âges d'essai (jusqu'à 365 jours), de sorte qu'il n'est pas possible d'établir une relation unique pour les bétons à différents taux de résine plastifiée. Les recherches sur des bétons à agrégats 0 à 7 mm, effectuées entre 28 et 365 jours, ont conduit aux relations suivantes (valeurs moyennes) :

— pour 5% d'addition de EP 25, $E_{\text{dr}} = 0{,}92\, E_{\text{do}}$ (6′)

— pour 10% d'addition de EP 25, $E_{\text{dr}} = 0{,}78\, E_{\text{do}}$ (6″)

— pour 20% d'addition de EP 25, $E_{\text{dr}} = 0{,}67\, E_{\text{do}}$ (6‴)

Les valeurs sensiblement différentes des modules d'élasticité des bétons avec addition d'émulsion plastifiée EP 25 confirment les faits cités antérieurement concernant l'influence de l'addition d'émulsions plastifiées de diphtalate de butyle sur les principales propriétés physiques et mécaniques des bétons.

Les recherches effectuées sur des éprouvettes de béton 1 : 5,5 ont conduit aux résultats suivants : pour les bétons à agrégats 0 à 7 mm, où la densité varie sensiblement avec l'addition de résine : (γ_a = 2,23 — 1,93 t/m^3), le module d'élasticité dynamique des éprouvettes avec addition de résine est plus faible à tous les âges d'essai. On notera que, dans le cas des bétons 1 : 6,5 qui ont des dosages plus faibles en ciment, avec 20 % de résine (pour mieux consolider la structure du béton), on obtient, à partir des essais effectués à 7 jours, des valeurs nettement supérieures à celles obtenues avec des bétons à 10 % de résine. Ainsi, au cours des essais effectués entre 7 et 365 jours, les valeurs du rapport E_{dr}/E_{do} varient sensiblement selon le taux de résine du mélange : pour l'addition de 10 % de résine, $E_{dr} = 0{,}66\ E_{do}$ à 7 jours, 0,77 à 28 jours et 0,81 à 365 jours ; pour les bétons avec 20 % de résine, $E_{dr} = 0{,}81\ E_{do}$ à 7 jours, 0,93 à 28 jours et 0,93 à 365 jours.

Pour les bétons à agrégats 0 à 15 mm, où l'addition de résine modifie la densité du mélange dans des limites plus restreintes ($\gamma_a = 2{,}33$ à $2{,}19\ t/m^3$), le module d'élasticité dynamique n'est plus faible qu'à un âge d'essai inférieur à 10 jours ; entre 10 et 365 jours il est plus important que celui des éprouvettes témoin. L'augmentation du module d'élasticité pour les bétons 1 : 6,5 varie selon le taux de résine, de sorte que pour 10 % de résine $E_{dr} = 0{,}87\,E_{do}$ à 7 jours ; 1,05 à 28 jours et 1,10 à 365 jours. Pour les bétons avec 20 % de résine $E_{dr} = 0{,}95\ E_{do}$ à 7 jours ; 1,15 à 28 jours et 1,17 à 365 jours. Ainsi, pour les bétons 1 : 6,5 avec 10 à 20 % de résine, il résulte, des essais entre 28 et 365 jours, les valeurs moyennes suivantes du rapport E_{dr}/E_{do} (7 et 8) :

$$\text{— bétons à agrégats 0 à 7 mm, } E_{dr} = 0{,}85\ E_{do} \tag{7}$$

avec des écarts de ±8 % par rapport à la valeur moyenne ;

$$\text{— bétons à agrégats 0 à 15 mm, } E_{dr} = 1{,}11\ E_{do} \tag{8}$$

avec des écarts de ±6 % par rapport à la valeur moyenne.

e) *Influence des additions de PVA sur la résistance à l'usure, la résistance au choc mécanique, l'adhérence entre le béton et l'armature, la perméabilité et la résistance au gel-dégel.* Les recherches effectuées ont mis en évidence les faits suivants : la résistance à l'usure des bétons additionnés de PVA est sensiblement affectée par le dosage en ciment, le taux et le type de la résine, le fuseau granulométrique, le degré de compactage des éprouvettes et leur milieu de conservation durant la période confection-essai (fig. 9*a* et *b*), ainsi :

— la résistance à l'usure augmente avec le taux de résine, le taux optimal d'addition étant d'environ 10 à 20 % ;

— la résistance à l'usure des bétons aux résines synthétiques augmente elle aussi, dans certaines limites, avec le dosage en ciment.

Pour les dosages égaux en ciment (plus de 400 kg/m³) et des taux égaux de résine dans le mélange, les bétons à agrégats quarzeux à granulation plus fine ont des résistances à l'usure plus grandes. Ceci s'explique par le fait que la résistance à l'usure du ciment durci additionné de résine (matériau beaucoup plus élastique) est plus grande que celle des gros éléments de l'agrégat quartzeux, qui sont plus facilement polis par abrasion.

Le milieu de conservation des éprouvettes pendant l'intervalle confection-essai exerce une influence considérable sur la résistance à l'usure des bétons aux résines synthétiques (fig. 9*b*), car si elle augmente de 1,5 à 10 fois lorsqu'ils sont conservés dans l'air à une humidité relative de 50 à 70%, non seulement elle n'augmente plus mais elle peut être réduite de 5 à 10% par rapport aux bétons étalon, lorsque les éprouvettes sont conservées dans l'air humide pendant 28 jours, et de 10 à 25% lorsqu'elles sont conservées dans l'eau. Dans un milieu de forte humidité, en effet, la résistance des bétons modifiés augmente beaucoup plus lentement, car la résine synthétique utilisée comme liant supplémentaire a des difficultés à passer de l'émulsion aqueuse à la phase solide et à conférer ainsi au béton des qualités supérieures. Il est à remarquer qu'après immersion dans l'eau durant 3 à 15 jours, précédée d'une conservation initiale de 28 jours dans l'air à faible humidité, les éprouvettes avec résine synthétique ont des résistances à l'usure égales, ou inférieures de 10 à 40%, aux résistances des éprouvettes témoin. Les éprouvettes qui, outre 10 à 15% de PVA renferment aussi de 0,75 à 1% de mélamine modifiée au méthanol (5 à 10% de l'addition de PVA) ou d'urée-formaldéhyde modifiée à la mélamine, ont, lors d'une immersion prolongée dans l'eau (après le durcissement initial de 28 jours dans l'air à la température normale), une résistance à l'usure plus grande d'au moins 1,5 à 2 fois que les éprouvettes témoin.

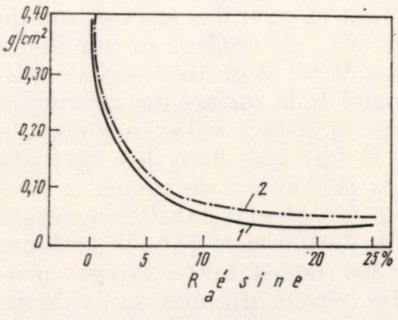

Fig. 9*a*. — Variation de l'usure pour les bétons fins 1 : 3 de ciment Pz 400, agrégats 0 à 3 mm, e/c = 0,50, à 28 jours d'âge, pour différents pourcentages de résine vinylique.

1, éprouvettes additionnées d'émulsion non plastifiée E 50; *2*, éprouvettes additionnées d'émulsion plastifiée EP 25.

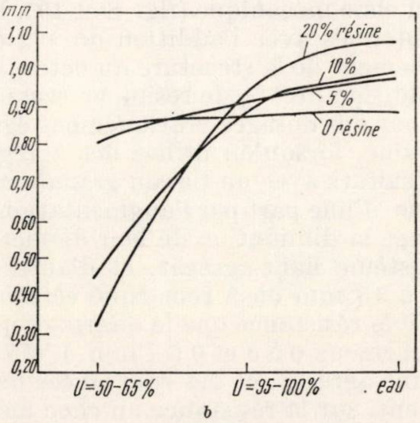

Fig. 9*b*. — Variation de la résistance à l'usure à 28 jours d'âge pour les bétons 1 : 4 de ciment RIM 400, agrégats quartzeux 0 à 7 mm, e/c = 0,50, avec différents pourcentages de résine vinylique PVA E 50, en fonction de l'humidité du milieu de conservation des éprouvettes (u).

La résistance au choc mécanique des bétons avec addition de PVA est affectée par le type et le taux de résine, la rugosité des surfaces et les résistances mécaniques de l'agrégat, le dosage en ciment, le milieu de conservation des éprouvettes, etc. Ainsi, (fig. 10), conservés dans un milieu d'humidité relative peu élevée, les bétons modifiés par 10 à 20% de PVA (E 50) enregistrent à 28 jours, par rapport aux éprouvettes témoin des augmentations de résistance de l'ordre de 120 à 300%, qui continuent à se développer notablement jusqu'à 90 jours, tandis que la résistance des non modifiés reste pratiquement aux alentours des valeurs obtenues à 7 jours. Cette augmentation de la résistance au choc s'explique par une plus grande adhérence dans le système liant — agrégat et par la transformation du béton en un matériau moins dur (plus élastique) grâce aux additions de PVA, ce qui se traduit, au niveau des propriétés mesurables, par la baisse du module d'élasticité et par l'augmentation de la résistance au choc mécanique (fig. 8 et 10). Les résistances au choc mécanique faibles obtenues avec l'addition de 5% de PVA confirment donc qu'il y a relâchement de la structure du béton, dû à l'air entraîné, et au fait que la faible addition de 5% de résine ne réussit pas à la consolider de façon suffisante. Pour des dosages pratiquement égaux en ciment et pour des taux égaux de résine, lorsqu'on utilise des agrégats de carrière, on obtient de meilleurs résultats avec un fuseau granulométrique plus étroit (fig. 10). Ceci s'explique d'une part par l'augmentation de la rugosité de la surface des granulats avec la diminution de leur diamètre, d'où une meilleure adhérence dans le système liant-agrégat, et d'autre part par le fait que dans les agrégats 7 à 15 mm on a remarqué certains éléments provenant de roches à plus faible résistance que le quartz et qui n'ont pas été décelés dans les agrégats quartzeux 0 à 3 et 0 à 7 mm. L'effet marqué de l'adhérence dans le système liant-agrégat, et des résistances mécaniques des roches dont l'agrégat provient, sur la résistance au choc mécanique des bétons, est mise en évidence par le fait que, dans des conditions identiques de préparation, de conservation et d'essai des éprouvettes, et pour un même taux de résine, les bétons à andésite basaltique concassée ont des résistances au choc de 30 à 60% plus fortes que ceux à agrégats quartzeux (fig. 10). L'humidité du milieu de conservation des bétons avec addition de PVA affecte aussi leur résistance au choc, observation également explicable si nous tenons compte du fait que la résine introduite comme liant supplémentaire se trouve alors empêchée de passer de l'état d'émulsion à la phase solide.

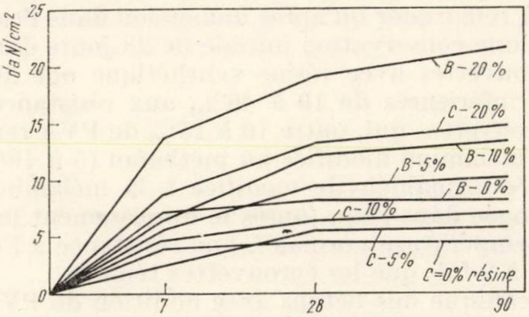

Fig. 10. — Variation de la résistance au choc mécanique dans le temps pour différents pourcentages de résine vinylique PVA, émulsion non plastifiée E 50 pour les bétons 1 : 4 de ciment RIM 400, agrégats 0 à 15 mm, e/c = 0,50. C — agrégats quartzeux 0—15 mm ; B = agrégats quartzeux 0 à 1 mm + andésite basaltique de Malnaş 1à 15mm.

Les recherches sur l'adhérence entre le béton modifié au PVA et le béton de ciment ont abouti aux conclusions suivantes.

Pour réaliser une bonne adhérence au béton ancien, une addition de 10 à 20% de résine vinylique PVA émulsion non plastifiée du type E 50 est nécessaire. L'adhérence déterminée par des essais à la traction axiale est alors, à 28 jours, de 36,5 à 52,0 daN/cm² pour le béton fin avec 10% de

E 50 et de 40,5 à 62,0 daN/cm^2 pour le béton fin avec 20% de E 50, c'est-à-dire 4 à 10 fois plus grande que l'adhérence du béton non modifié. Avec des taux plus faibles de résine, de 5 à 8%, la rupture se fait par les joints, ou en partie par les joints et par le matériau de base, surtout lorsque les surfaces de départ sont lisses. L'état hygroscopique de la surface de béton de ciment sur laquelle doit être appliqué le béton aux résines synthétiques n'exerce une influence sensible sur l'adhérence (avec conservation des éprouvettes dans l'ambiance de laboratoire) qu'aux jeunes âges d'essai, généralement jusqu'à 5 jours. Aux essais à 7 et à 28 jours, les différences enregistrées en plus ou en moins sont de l'ordre des erreurs expérimentales, même si le béton de ciment, au moment de la coulée du béton modifié, a conservé son humidité naturelle, s'il est saturé par une immersion préalable durant 24 heures, ou s'il a été amené à une humidité constante par séchage à l'étuve à 70 à 80° pendant 4 à 5 heures. Le milieu de conservation des éprouvettes, depuis la coulée du béton additionné de résine jusqu'à l'essai, affecte les résultats, les meilleurs étant obtenus avec les éprouvettes conservées à l'atmosphère du laboratoire, la conservation en milieu humide et dans l'eau donne respectivement des résultats moins bons et mauvais, si bien que dans ce dernier cas les éprouvettes pour la détermination de l'adhérence peuvent être rompues à la main assez facilement. L'état de surface du béton ancien, recouvert de couches à faible adhérence, telles que tache d'huile ou de peinture, influence sensiblement les résultats des essais : si des moitiés d'éprouvettes sont immergées dans l'huile minérale, ne serait-ce que 5 à 10 minutes, puis collées à du béton avec addition de résine, l'adhérence est pratiquement nulle ; les matériaux durcissent séparément et se détachent facilement. L'adhérence est d'autant meilleure et le taux de résine à ajouter sera d'autant plus faible que la rugosité de la surface qui reçoit le béton modifié est plus grande. En général, avec des taux de 12 à 15 % de résine, l'état de surface n'exerce pratiquement plus d'influence négative sur l'adhérence qui, par contre, se révèle sensible à la consistance du béton modifié. Les meilleurs résultats ont été obtenus avec des bétons plastiques (tassement de 8 à 10 cm à l'essai normalisé), et un compactage par tassement léger. Dans les cas de matériaux de consistance assez forte (tassement de 1 à 5 cm au cône normalisé, ou moyenne pour garantir l'adhérence, il a été nécessaire d'exercer des pressions de 0,2 à 5,0 daN/cm^2.

Les résultats des essais à la flexion, à la traction, au cissaillement et à la compression sont sensiblement influencés par la manière dont est appliqué l'effort par rapport au joint entre le béton de ciment et le béton modifié, ainsi que par la résistance du matériau de base.

Les recherches sur l'adhérence à l'armature (fig. 11) ont mis en évidence les fait suivants : l'adhérence entre le béton et l'armature tend à diminuer pour de faibles taux de résine, insuffisants pour consolider la structure affaiblie par le surcroît d'air entraîné au moment de la coulée, tandis qu'avec des taux de 10 à 20%, l'adhérence augmente fortement, non seulement du fait de la consolidation de la structure, mais aussi, probablement, grâce aux propriétés adhésives de la résine qui renforcent à un très haut degré la liaison ciment durci-armature. Avec 30 à 40%

de résine dans les bétons 1 : 4, l'augmentation de l'adhérence entre le béton et l'armature est relativement insignifiante par rapport à la consommation importante de résine. Donc là aussi, le taux optimal de résine vinylique du type émulsion non plastifiée E 50 se situe entre 10 et 20%. On retiendra que l'addition de résine favorise de meilleurs résultats avec de plus faibles dosages en ciment.

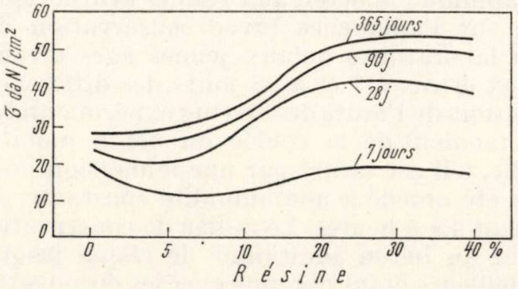

Fig. 11. — Variation de l'adhérence aux armatures des bétons 1 : 4 de ciment Pz 400, agrégats 0 à 7 mm, e/c = 0,50, pour différents pourcentages de résine vinylique PVA, émulsion non plastifiée E 50, à différents âges.

L'émulsion de résine a un effet favorable par la plus grande imperméabilité qu'elle détermine du fait de la fermeture partielle ou totale des pores du béton par la résine utilisée comme addition lors du gâchage.

Les recherches sur la résistance aux alternances gel-dégel ont prouvé que les bétons avec 10 et 15% d'additions ont perdu 2 à 5% de leur poids initial et 3 à 6% de leur résistance, par rapport aux éprouvettes témoins, après avoir subi 50 cycles de gel-dégel ; on peut donc considérer qu'elles ont subi l'épreuve de façon satisfaisante. Les éprouvettes avec 20% de résine voient leur poids augmenter de 2 à 4% (elles n'ont probablement pas perdu intégralement l'eau absorbée pendant les déterminations) et leur résistance diminue de 6 à 10% par rapport aux éprouvettes témoins, ce qui met encore une fois en évidence l'action négative à la longue de l'eau sur les bétons modifiés, et limite par conséquent leur domaine d'application.

f) *Variation de quelques propriétés, dans diverses conditions de conservation des éprouvettes, et comportement dans le temps de certaines réalisations expérimentales.* Les bétons avec addition de PVA — E 50 à un taux de 5 à 20%, conservés, dans la période de coulage-décoffrage, à l'air à une humidité relative de 50 à 65%, montrent de faibles retraits, de l'ordre de 0,003 à 0,02 mm/m, comme les bétons de ciment. Mais, avec une ventilation forcée de la surface de l'éprouvette, le retrait initial peut atteindre, pour les bétons de ciment 4 à 7 mm/m et, pour le béton aux résines synthétiques, de 2 à 10 mm/m, ce qui entraîne dans certains cas l'apparition de fissures à la surface des éprouvettes (pour des taux élevés d'addition de résine, de 20 à 40%). Au cours des 24 premières heures de la conservation des éprouvettes à l'air humide, le retrait initial est égal à zéro, quel que soit le taux de résine. Ainsi, à partir de mesures, de remarques et d'essais, on a établi que, afin d'éviter le retrait initial, il est préférable de conserver les éprouvettes dans l'air humide les 24 premières heures et, ensuite, afin d'atteindre les propriétés maximales de résistance, à l'air à faible humidité relative, 50 à 60%. Les travaux expérimentaux réalisés au cours des années 1961 à 1968 et qui ont donné lieu à diverses applications : revêtements de sols d'ateliers, réparation de revêtements de béton routiers, réparation de divers éléments de construction préfabriqués, protection pour hydrocyclones, revêtements de canaux d'irrigation et protection anticorrosive du canal collecteur d'un combinat chimique, montrent pratiquement dans tous les cas un bon comportement à l'usage, même dans un milieu humide ou dans l'eau, ce qui révèle une concordance satisfaisante avec les résultats de laboratoire et démontre leur possibilité de développement, si l'on observe les conditions imposées par les caractéristiques des bétons avec addition de résine synthétique, en fonction de chaque mise en œuvre.

Revue Roumaine de Chimie, 18, 6, 1041–1065 (1973)

Revue Roumaine de Chimie, **18**, *6*, 1067–1074 (1973)

LA PHOSPHORYLATION DES COPOLYMÈRES TERNAIRES MACROPOREUX

FL. POPESCU, SIMONA PERCEC, IG. POINESCU et I. PETRARIU

Institut de Chimie macromoléculaire « Petru Poni »,
41 A, Aleea Gr. Ghica Vodă, Jassy, Roumanie

Reçu le 7 novembre 1972

Par la phosphorylation des perles des copolymères ternaires macroporeux, styrène-divinylbenzène-acrylonitrile, méthacrylate de méthyle, méthacrylate d'éthyle ou de butyle, on obtient des échangeurs d'ions ayant une bonne résistance mécanique. On constate une réticulation supplémentaire, par le phosphore, des copolymères phosphorylés. Les résultats sont comparés avec les données obtenues dans le cas des copolymères de type gel.

Les études concernant la synthèse des résines macroporeuses sont relativement récentes.[1] Les échangeurs d'ions macroporeux ont été obtenus en partant des copolymères binaires styrène-divinylbenzène.[2-6]

Les ionites poreux ou macroporeux ont un très grand nombre de canaux microscopiques (pores) par lesquels la surface de contact avec le milieu augmente par quelques dizaines de fois et même par quelques centaines de fois comparativement aux résines de type gel.[7]

L'introduction d'un troisième comonomère, dans une proportion de 1 à 20%, dans les copolymères macroporeux, augmente plusieurs fois la porosité du copolymère, comparativement aux copolymères macroporeux binaires styrène-divinylbenzène.[8] En utilisant le squelette macroporeux styrène-divinylbenzène-acrilonitrile, les propriétés physiques et chimiques des échangeurs d'ions sulphoniques s'améliorent.[9]

---

[1] H. Knall et I. Gres, *Mat. Plast.*, **5**, 182 (1968).

[2] K. Dusek, J. Seidl et J. Malinsky, *Coll. Czech. Chem. Comm.*, **31**, 3979 (1966).

[3] I. N. Gribanova, I. D. Kholkina et A. V. Nikolaev, *Doklady Akad. Nauk S.S.S.R.*, **179**, 1336 (1968).

[4] A. V. Nikolaev, I. N. Gribanova, I. D. Kholkina et N. I. Yakovleva, *Izvest. Sib. Otd. Akad. Nauk S.S.S.R. Ser. Khim. Nauk*, **1967**, (3) 86 ; *Chem. Abstr.*, **68**, 30523 (1968).

[5] A. V. Nikolaev, I. N. Gribanova et I. D. Kholkina, *Izvest. Sib. Otd. Akad. Nauk S.S.S.R. Ser. Khim. Nauk.*, **1967**, (3) 91 ; *Chem. Abstr.*, **68**, 30518 (1968).

[6] W. Busse et E. Schmidt, Ger. Pat., 1 569 285, 6 Mai 1970 ; *Chem. Abstr.*, **73**, 26244 (1970).

[7] R. Kumin, E. Meitzner, J. Oline, S. Fischer et N. Frisch, *Ind. Eng. Chem.*, **54**, 78 (1962).

[8] Ig. Poinescu, Stela Drăgan, Steliana Maxim et A. Dima, Rev. Roumaine Chim. (à paraître).

Dans le présent travail on a étudié la phosphorylation des copolymères ternaires styrène-divinylbenzène (DVB) — acrylonitrile (AN), méthacrylate de méthyle (MAM), méthacrylate d'éthyle (MAEt) ou méthacrylate de butyle (MABu) par le trichlorure de phosphore en présence du trichlorure d'aluminium.

Le trichlorure de phosphore, étant aussi réactant et milieu de réaction, est utilisé en excès. Les autres paramètres de la synthèse : la durée de la synthèse, la quantité de trichlorure d'aluminium, la quantité de DVB et le troisième composant du copolymère (AN, MAM, MAEt et MABu) ont été modifiés séparément, dans le but d'établir les conditions de la réaction. La température a été maintenue à 78° pendant toute la durée de la synthèse.

La synthèse a été conduite de la même manière que la phosphorylation des copolymères styrène-DVB de type gel.[10] On obtient des copolymères phosphorylés qui contiennent des groupes P—Cl dans lesquels le phosphore est lié par des liaisons C—P à la chaîne. Les groupes P—Cl sont transformés en groupes P—OH par immersion dans l'eau glacée.

La porosité des copolymères de type gel est très petite.[11,12] Le transport des ions aux groupes actifs est réalisé par la diffusion et non par les pores, phénomène caractéristique de l'état gel. Si l'agent de réticulation est le divinylbenzène la croissance du degré de réticulation conduit à une surtension croissante dans le réseau tridimensionnel, qui produit des destructions et conduit à la formation des microfissures. La capacité d'adaptation à des variations de volume, dans le cas des copolymères gel étant petite, l'hydrolyse du trichlorure de phosphore absorbé dans la perle de copolymère et des groupes $-PCl_2$, phénomène qui est accompagné par le dégagement d'acide chlorhydrique, conduit à la destruction des perles.

Tels effets négatifs ne sont pas enregistrés au cas des copolymères macroporeux utilisés, du fait que, à cause de leur structure poreuse, ils supportent bien les dégagements de gaz résultés pendant la purification des produits obtenus par synthèse Friedel-Crafts. Après la phosphorylation ils peuvent être introduits directement dans l'eau sans dégradation des perles.

Dans la figure 1 sont montrés les photos comparatives d'un copolymère styrène-divinylbenzène gel et d'un copolymère ternaire macroporeux phosphorylés, auxquels l'hydrolyse des groupes $-PCl_2$ de la chaîne et du trichlorure de phosphore absorbé dans le copolymère a été réalisée dans des conditions identiques, par immersion dans l'eau glacée.

Dans la figure 2 sont données les variations de volume de gonflement dans le trichlorure de phosphore des copolymères ternaires macroporeux comparativement aux copolymères de type gel.

---

[9] Fr. Wolf, R. Bachmann, H. Reuter, G. Schwachula, D. Warnecke, W. Wehlend et U. Krauss, Brit. Pat. 1 020 907, 23 Fev 1966 ; *Chem. Abstr.*, **64**, 14374 (1966).

[10] Fl. Popescu, *Rev. Roumaine Chim.*, **13**, 977 (1968).

[11] A. A. Tager, M. V. Tsilipotkina, E. B. Makovskaya, A. B. Pashkov, E. I. Lustgarten et M. A. Pechenkina, *Visokomol. Soedineniya.*, **10**, 1065 (1968).

[12] A. A. Tager, M. V. Tsilipotkina, A. V. Passchkov et N. I. Bykova, *Visokomol. Soedineniya*, **2**, 997 (1960).

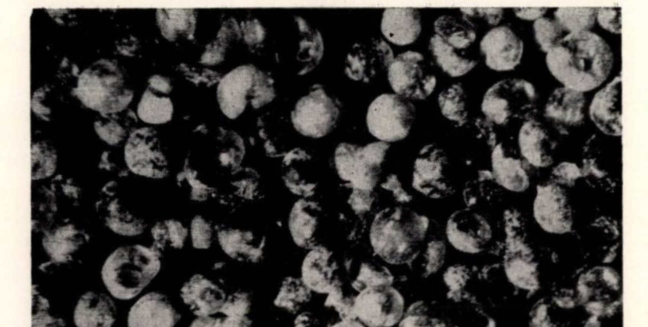

Fig. 1. — Aspect des perles des copolymères phosphorylés par synthèse Friedel-Crafts après leur immersion dans l'eau.

1, Copolymère gel styrène-DVB (8%) ; *2*, Copolymère macroporeux styrène (80,9%) – DVB (16,1%) – MAM (3%). Diamètre des perles 0,5 à 0,75 mm.

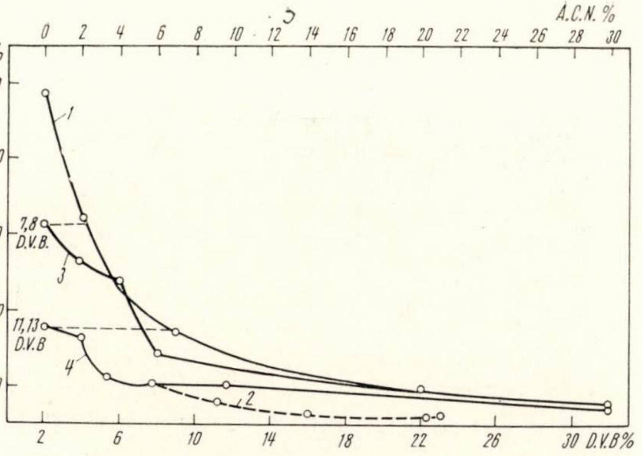

Fig. 2. — Variation du degré de gonflement dans le trichlorure de phosphore, des perles non phosphorylé de copolymère.
(Diamètre des perles = 0,5—0,75 mm).
En fonction du contenu de DVB :
1, Copolymère gel styrène-DVB ; *2*, Copolymère macroporeux styrène-DVB-MAM (10%). En fonction du contenu en AN : *3*, Copolymère macroporeux styrène-DVB (7 8%)-AN ; *4*, Copolymère macroporeux styrène-DVB (11,1%)-AN.

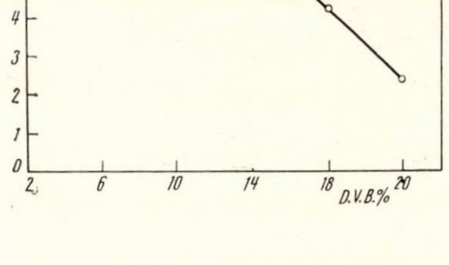

Fig. 3. — Variation de la teneur en phosphore en fonction du contenu de DVB.
1, Copolymère gel styrène-DVB ; *2*, Copolymère macroporeux styrène-DVB-MABu (10%).

On constate dans le cas des copolymères macroporeux une variation apparente de volume, en fonction de la teneur en divinylbenzène, qui diffère du comportement des copolymères de type gel.

Les inflexions visibles sur les courbes représentant la variation du volume des perles de copolymère, en fonction de la quantité en troisième comonomère, sont dues aux différences des porosités.

La croissance de la porosité conduit à un amincissement du volume apparent de gonflement dans le trichlorure de phosphore, le gonflement étant réalisé aussi par l'amincissement du volume interstitiel.

Bien que la porosité croît avec la teneur en divinylbenzène ou avec le contenu dans le troisième comonomère (AN, MAM MAEt, MABu), elle dépend aussi du mode dont la synthèse des copolymères a été conduite, la somme des effets de tous les paramètres (diluant, agitation, température...) menant à des variations de la porosité.

La variation de la teneur en phosphore en fonction de la quantité de DVB est représentée dans la figure 3.

On constate que la croissance de la quantité de divinylbenzène conduit à une réduction du contenu en phosphore dans le cas des copolymères de type gel fait expliqué par la réduction de la perméabilité des perles. Le gonflement dans le trichlorure de phosphore baisse en fonction de la quantité de DVB (figure 2), tandis que dans le cas des perles macroporeux la teneur en phosphore subit des variations irrégulières, la pénetration du complexe réactant dans la perle étant favorisée par la porosité (tableau 1 et figure 3).

La teneur en phosphore croît en fonction de la durée de la synthèse. A une durée dépassant 6 heures, la croissance s'arrête. On peut expliquer ainsi l'arrêt de la phosphorylation : 1) Par la phosphorylation de la perle se fixent sur la chaîne des substituents volumineux ($-PCl_2$, $AlCl_3$)[13]; 2) La prolongation de la durée de synthèse conduit à un pontage supplémentaire des chaînes par le phosphore[9] (visible en IR, figure 6). En conséquence la perméabilité de la perle de copolymère décroît.

Les perles chlorméthylées fixent une quantité supérieure de phosphore, mais aussi dans ce cas, la croissance du contenu en phosphore est limitée de la même manière (figure 4).

Des quantités croissantes de trichlorure d'aluminium déterminent une croissance de la quantité de phosphore fixée. De 2,2 à 3,2 moles de trichlorure d'aluminium pour un mole d'unité structurelle de copolymère la croissance est lente. Elle s'arrête si on utilise plus de 3,2 moles de trichlorure d'aluminium (figure 5, courbe *2*).

En comparant les données des figures 3,4 et 5 on constate que, en général la teneur en phosphore, fixée sur les copolymères ternaires macroporeux, est plus réduite que dans le cas des copolymères styrène-divinylbenzène de type gel. Le fait est dû à l'amincissement du contenu de styrène des copolymères (tableau 1, colonne 5).

---

[13] Houben-Weyi, «Methoden der organischen Chemie», vol. 12/1, 1re éd., G. Thieme Verlag, Stuttgart, 1963, p. 314.

La porosité présente une importance de premier ordre dans le processus de phosphorylation. En variant le contenu de divinylbenzène et en gardant constant le contenu de la troisième composante (tableau 1) on constate que la valeur du contenu de phosphore est fortement influencée par la porosité qui facilite la phosphorylation à l'intérieur des perles.

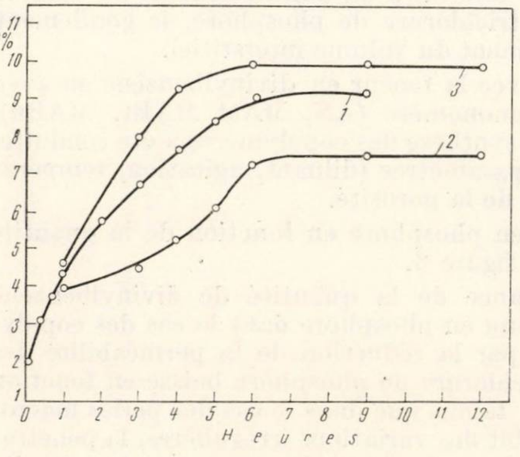

Fig. 4. — Variation de la teneur en phosphore, en fonction de la durée de la synthèse.

1, Copolymère gel styrène-DVB (8%) ; *2*, Copolymère macroporeux styrène-DVB (16,1%)-MAM (3%) ; *3*, Copolymère chlorométhylé macroporeux (10,50%) Cl), styrène-DVB (7,8%)-MAEt (3%).

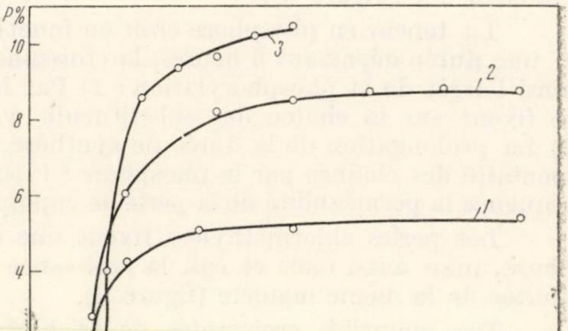

Fig. 5. — Variation du contenu en phosphore en fonction de la quantité de trichlorure d'aluminium.

1, Copolymère macroporeux styrène-DVB (16,1%)-MAEt (3%). Durée de la synthèse 3 heures. *2*, Copolymère macroporeux styrène-DVB (16,1%)-MAEt (3%) ; Durée de la synthèse 6 heures. *3*, Copolymère gel styrène-DVB (8%). Durée de la synthèse 6 heures.

Le contenu en phosphore est fortement influencé par la teneur en DVB, dans le cas des copolymères de type gel (figure 3). Cette dépendance est beaucoup plus limitée dans le cas des copolymères ternaires. C'est ainsi que, dans les exemples 4—10 du tableau 1, on constate qu'on peut obtenir une teneur en phosphore relativement élevée, si la porosité est bonne, même à un contenu de DVB plus grand que 16%. Des exemples 1—3 du tableau 1, on constate que la variation quantitative de la troisième composante (MAM dans le cas exemplifié) n'est pas accompagnée — dans certaines limites — des modifications significatives du contenu de phosphore. La croissance de la quantité de comonomère qui ne se phosphoryle pas, par synthèse Friedel-Crafts, est compensée dans le cas illustré (MAM) par une croissance marquée de la porosité.

Pour suivre le comportement thermique des copolymères phosphorylés les épreuves ont étés soumises à l'analyse thermogravimétrique(TG) et à l'analyse thermique différentielle (ATD).

Tableau 1

La teneur en phosphore des copolymères ternaires en fonction de la porosité et de la valeur en pour cent de comonomère-styrène Rapport des réactants, copolymère : $AlCl_3$: PCl_3 = =1 : 1,2 : 10 (moles)

N°	Durée de phosphorylation (heures)	La 3e composante Nom	%	DVB	Styrène	Porosité %	P %
0	1	2	3	4	5	6	7
1	5	méthacrylate de méthyle	3	16,1	80,9	29,74	6,7
2	5		5	16,1	78,9	29,9	6,5
3	5		10	16,1	73,9	32,6	6,2
4	5	méthacrylate d'éthyle	3	7,8	89,2	0,6	6,1
5	5		3	11,1	85,9	19,81	5,8
6	5		3	16,1	80,9	32,6	6,81
7	5	,,	3	21,5	75,5	28,6	7,71
8	4	méthacrylate de butyle	3	7,8	89,2	0,6	5,4
9	4		3	11,1	85,9	25,9	5,9
10	4		3	16,1	80,9	2,6	4,7

On constate que le témoin est totalement décomposé à 615°, tandis que le produit phosphorylé subit une décomposition limité (figure 6).

Dans le cas illustré, le copolymère styrène (80,9%)—DVB (16,1%)—AN (3%) contenant 6,3% de phosphore a perdu 73% de son poids à 870°.

Sur la courbe TG du copolymère phosphorylé on constate une première perte en poids à environ 100° (figure 6), phénomène endotherme dû à l'élimination de l'eau entre deux groupes de P—OH avec formation [14] des liaisons P—O—P. Suit une periode stationnaire comprise entre 170 à 375° pendant laquelle le polymère perd en poids. Dans cet intervalle ont lieu des transformations chimiques de nature exotherme (ATD, figure 7, courbe *2*). Le maximum est atteint à 370°, ensuite le polymère se décompose et perd en poids en deux étapes séparées par un palier situé à approximativement 420°.

La décomposition thermique du copolymère non phosphorylé diffère par la position des paliers, la première période de décomposition étant aussi la plus importante.

---

[14] Fl. Popescu, *Rev. Roumaine Chim.*, **16**, 285 (1971).

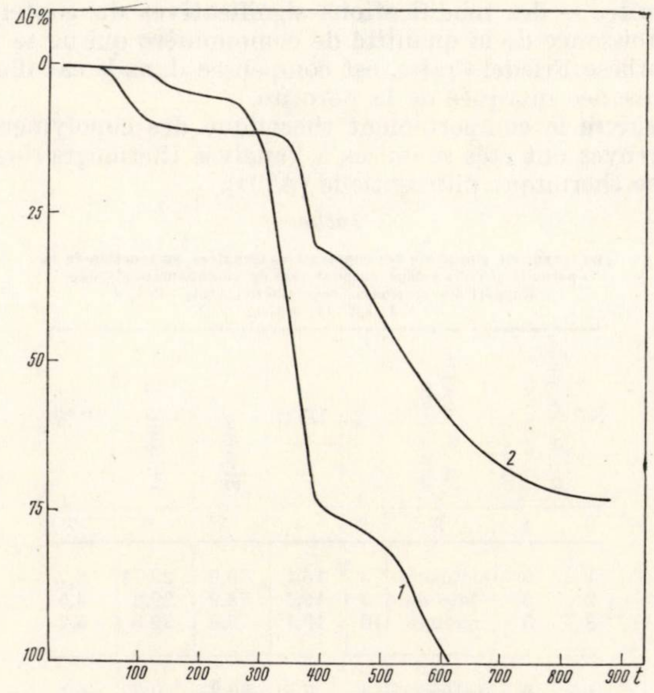

Fig. 6. — Analyse thermogravimétrique (TG).

1, Copolymère macroporeux styrène-DVB (16,1%)-MAM (3%) ; *2*, Le même copolymère phosphorylé (6,3%P).

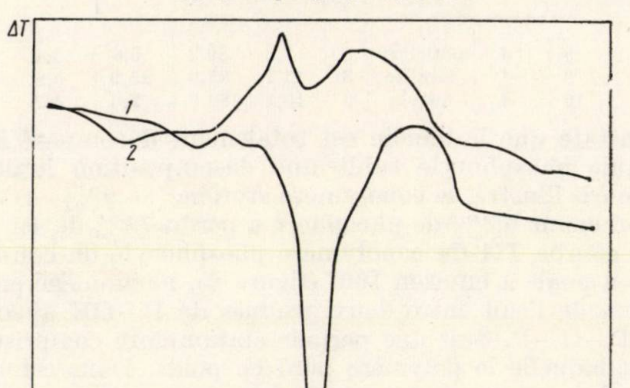

Fig. 7. — Analyse thermodifférentielle (ATD).

1, Copolymère macroporeux styrène-DVB(16,1%)-MAM (3%) ; *2*, Le même copolymère phosphorylé (6,3%P).

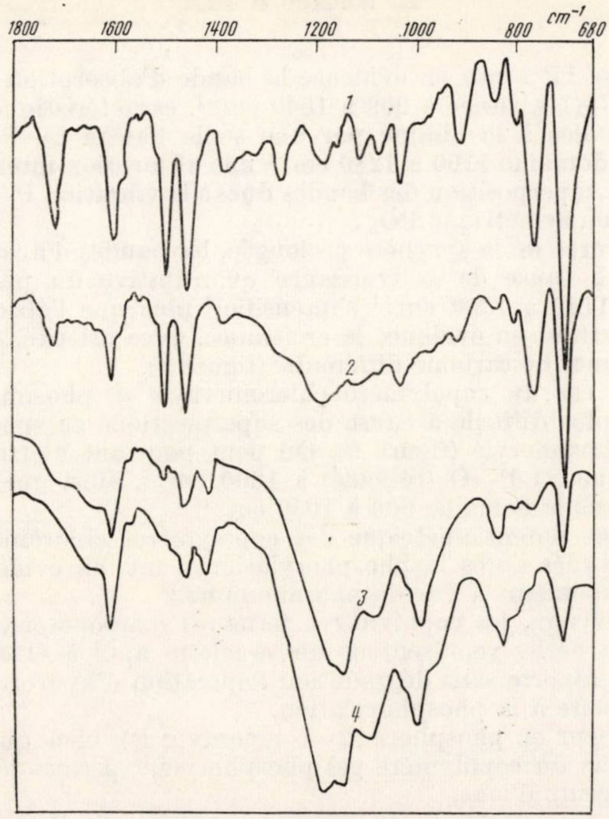

Fig. 8. — Spectres en IR.

1, Témoin, copolymère macroporeux styrène-DVB (16,1)-MAEt (3%); 2, Le même copolymère phosphorylé (1,6%P). Durée de la synthèse 3 heures. 3, Le même copolymère phosphorylé (5,6%P). Durée de la synthèse 4 heures. 4, Le même copolymère phosphorylé (6,8%P). Durée de la synthèse 6 heures.

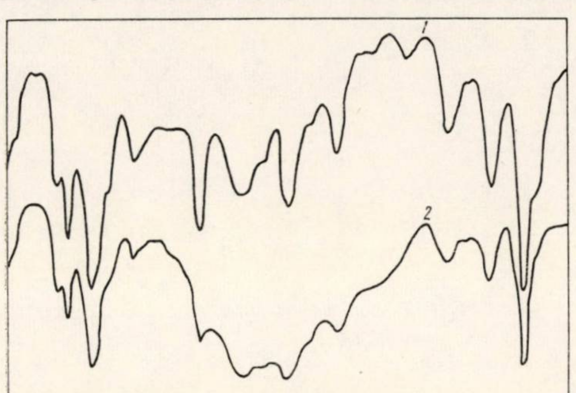

Fig. 9. — Spectres IR des copolymères macroporeux chlorométhylés.

1, Témoin, copolymère macroporeux chlorométhylé (9,72%Cl) styrène-DVB (16,1%)-MAEt (10%); 2, Le même copolymère phosphorylé (2,9%P).

L'analyse IR a mis en évidence la bande d'absorption due au groupement P—O—(H), située à 909 à 1040 cm^{-1}, caractéristique des groupes du phosphore liés à la chaîne par une seule liaison C—P.

Dans le domaine 1100 à 1230 cm^{-1} une absorption intense est visible résultée par la superposition des bandes dues à la vibration $P \rightarrow O$ (réticulée) et à la vibration symétrique PO_2^-.

A une durée de la synthèse prolongée, les bandes d'absorption citées s'intensifient à cause de la croissance quantitative du phosphore fixé. L'absorption 1100 à 1300 cm^{-1} s'intensifie[15] plus que l'absorption 909 à 1040 cm^{-1} mettant en évidence la croissance, avec priorité, du phosphore lié à deux atomes de carbone différents (figure 8).

Dans le cas du copolymère chlorométhylé α phosphorylé l'interprétation est plus difficile à cause des superpositions au spectre du copolymère non phosphorylé (figure 9). On peut pourtant mettre en évidence l'absorption due au $P \rightarrow O$ (réticulé) à 1200 cm^{-1}, ainsi que celle due au P—O—(H) dans le domaine 900 à 1040 cm^{-1}.

Le titrage potentiométrique des copolymères chlorométhylés phosphorylés et oxydés après la phosphorylation a mis en évidence deux inflexions correspondant à l'acide phosphonique.[10]

En conclusion, les copolymères ternaires macroporeux, polymérisés sous forme de perles représentent un squelette apte à être phosphorylé du fait qu'il supporte sans dégradation l'opération d'hydrolyse et la purification ultérieure à la phosphorylation.

Leur teneur en phosphore (2—5 méquiv/g P), bien que plus petite que dans le cas du copolymère gel phosphorylé,[16] permet leur utilisation comme échangeurs d'ions.

---

[15] Fl. Popescu, *Rev. Roumaine Chim.*, **14**, 1525 (1969).

[16] E. V. Trostianskaia, Lu-Sian-Jao, A. S. Tevlina et I. P. Losev, *Vysokomol. Soedineniya*, **3**, 41 (1961).

Revue Roumaine de Chimie, **18**, *6*, 1075–1086 (1973)

STUDIES OF THE JOSHI EFFECT IN HALOGENS AND OXYGEN

INFLUENCE OF INTERSLEEVE EXPOSURE TO BRUSHES FROM d.c. AND VARIOUS a.c. HIGH TENSION SOURCES

JAGDISH PRASHAD

Department of Chemistry, Meerut College, Meerut, U.P. (INDIA)

Received March 27, 1972

Influence on Joshi effect ($\mp \Delta i$) of exposure to brushes from a (i) 20 kilocycle, (ii) 500 cycle, (iii) 50 cycle and (iv) direct current potentials was studied at 30° and 90° in chlorine, bromine, iodine and oxygen confined in glass tube under sleeve excitation. The high tension pointed electrode connected to each of the sources was moved to-and-fro for 5 minutes over the portion of the tube between the sleeves wound at 30 mm apart. $(V-i)_{D.L}$ characteristics observed with 50 cycle after and before the exposure indicated an increase of the threshold potential (V_m) by 7–55%. Generally, after an exposure, the discharge current ($i_{D.L}$) decreased by 10–60%. Due to exposure, the magnitude of the maximum relative negative Joshi effect ($-\%\Delta i$) decreased by 19–80% and that of relative positive Joshi effect ($+\%\Delta i$) increased to a very large extent. The influence on increasing V_m, on decreasing $i_{D.L}$ and $-\%\Delta i$ varied in the order :

20 kilocycle > 500 cycle > 50 cycle and d.c.

The effect of exposure on $-\%\Delta i$ was negligible at 90° as compared with that at 30°. The results showed that the recovery to the pre-exposure conditions as a result of rest was quicker in halogens than in oxygen, especially at 30°. The results have been explained on the basis of the desorption occurring under high frequency exposure and Joshi's theory for the phenomenon ($\mp \Delta i$).

INTRODUCTION

Investigations have established[1] that short duration of aging favours the inception and numerical magnitude of $-\%\,\Delta i$; prolonged aging, however, exerts the opposite influence; and that $-\%\,\Delta i$ is disfavoured more, the larger the magnitude of the frequency of the exciting potential. The major seat of $-\Delta i$ has been attributed to the adsorption-like boundary or wall-layer formed under discharge.[2] The higher frequency (500 and 20 kilocycle) brushes may disturb the above boundary-layer and therefore the magnitude of $-\Delta i$. The object of the work reported in this communication was, therefore, to extend the study of the author,[1] to a few electronegative gases confined in non-degassed tubes at 90° at which the probability of attenuation of space charge and denaturing of the surface by the desorption of electrode layer is more as compared with that at 30°.

---

[1] P. Jagdish, Ph. D. Thesis, 1961, Banaras Hindu University.

EXPERIMENTAL

The tubes used for this work were all Siemens type (glass) ozonizers used as sleeve tubes (Fig. 1). Prior to the present investigations, these tubes were in use for various studies in aging. After a rest period of a couple of years, two sleeves of bright copper wire, 30 mm apart, were wound tightly on each of the four — $S_1(Cl_2)$, $S_2(Br_2)$, $S_3(I_2)$ and $S_4(O_2)$ tubes.

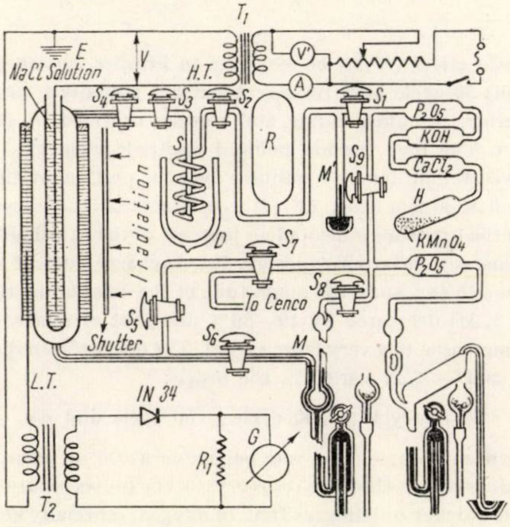

Fig. 1. — Joshi effect in oxygen.

The pointed high tension electrodes fed by (i) the localized high frequency brushes (20 kc/s) from a Tesla leak tester, (ii) 500 c/s obtained from a converter, (iii) 50 c/s obtained from the mains supply and (iv) the cathode of the direct current, at about 4 kV obtained by rectifying the stepped-up 50 c/s with the help of the thermionic valves arranged in the d. c. unit, were moved up and down along the surface between the sleeves of the discharge tube for 5 minutes. This is referred to as "exposure" hereafter. Before giving any exposure the tubes were disconnected from the exciting electrical circuit. $(V-i)_{D,L}$ characteristics were observed with 50 c/s before and after exposure at 30° and 90° (Figs.2 to 9). Before observing the $(V-i)_{D.L}$ characteristics at 90°, the tubes were heated for 2 hours at this temperature in the asbestos lined heating chamber.

---

[2] S. S. Joshi, *Curr. Sci.*, **13**, 253 (1944).

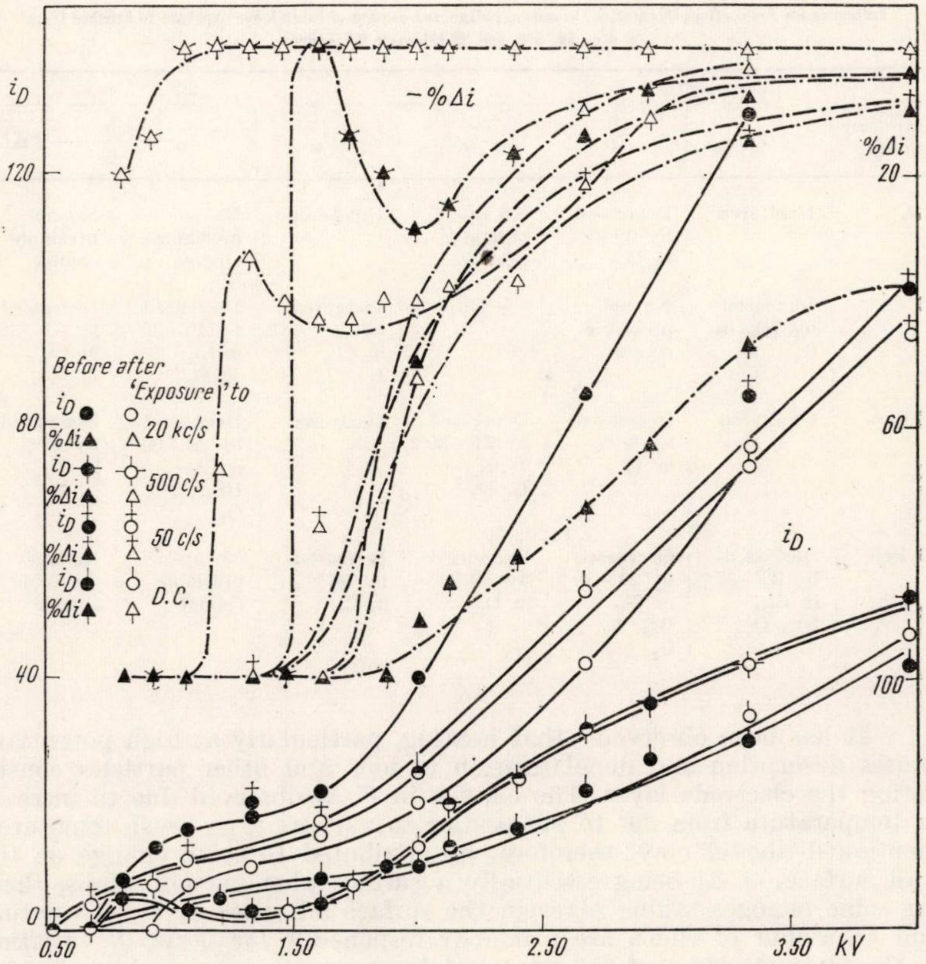

Fig. 2. – Influence on i_D and $-\%\Delta i$ in chlorine at 30° of "Exposure" to 20 kc/s, 500 c/s, 50 c/s and d.c.

RESULTS AND DISCUSSION

The variation of V_m, i_D and $-\%\Delta i$ with the frequency of h.t. exciting field of exposure is summarized in table 1.

Table 1

Influence on Joshi effect in chlorine, bromine, iodine and oxygen of intersleeve exposure to brushes from a d.c., 50, 500 and 20 kilocycle h.t. source

	Temperature °C 30°			90°		
Exposure to h.t.	V_m	i_D	$-\%\Delta i$	V_m	i_D	$-\%\Delta i$
d.c.	Unaltered	Decreased by 30% in O_2	No appreciable change	Unaltered	No appreciable change	No appreciable change
50 c/s	Increased by 7% in O_2	No appreciable change	—Do—	Increased by 20–40% in Cl_2, I_2	Decreased by 10–30% in Cl_2, I_2, O_2	Decreased by 37–38% in Cl_2, I_2
500 c/s	Unaltered	Decreased by 30% in I_2	Decreased by 21–80% in Cl_2, I_2, O_2	Unaltered	Decreased by 20–60% in Cl_2 Br_2, I_2, O_2	Decreased by 19% in Cl_2
20 kc/s	Increased by 22–32% in Cl_2, Br_2, O_2	Decreased by 20–40% in Cl_2, Br_2, I_2, O_2	Decreased by 73% in O_2	Increased by 55% in Cl_2	No appreciable change	No appreciable change

It has been observed [3] that heating, particularly at high potentials, causes desorption and depolarization of ions and other particles constituting the electrode layer. The change in $\mp \Delta i$ observed due to increase in temperature from 30° to 90° and/or to various type brush exposures, mentioned above, may, therefore, be attributed to some change on the wall surface, $\mp \Delta i$ being essentially a surface phenomenon. Thus, there are some changes taking place in the surface adsorbed layer, the nature and behaviour of which are primarily responsible for $\mp \Delta i$. A variation in the characteristics of the adsorbed layer due to heating depends also on the type of adsorption. In the van der Waals type of adsorption, an increase in temperature decreases the magnitude of adsorption, and this is also characterized by instability at high temperature resulting in its annulment [4] but as the temperature is once again decreased, van der Waals adsorption being instantaneous and reversible, there should be no change in $\mp \Delta i$, if it is assumed that the adsorbed layer is the only determinant, and other parameters are constant. The present results, therefore, indicate that the surface layer is not purely a physical or van der Waals layer. Since changes in $\mp \Delta i$ are observed due to exposure at 30° and 90° and particularly under a.c. and d.c., it is likely that chemisorption, requiring activation energy which is supplied by the electric field, takes place on the glass walls.[5] Although the increase in $-\Delta i$ due to aging[1] and the decrease due to rest and heating of the system,[1] favour chemisorption at the surface, the residual $\mp \Delta i$ associated with any system and the production of $+\Delta i$ below V_m, its enhancement with temperature and diminution with continuous exposure to discharge at $V > V_m$, would

---

[3] S. S. Joshi, *Curr. Sci.*, **16**, 19 (1947).

[4] S. Glasstone, "A Textbook of Physical Chemistry", Mc Millan & Co., 1951, p. 1202.

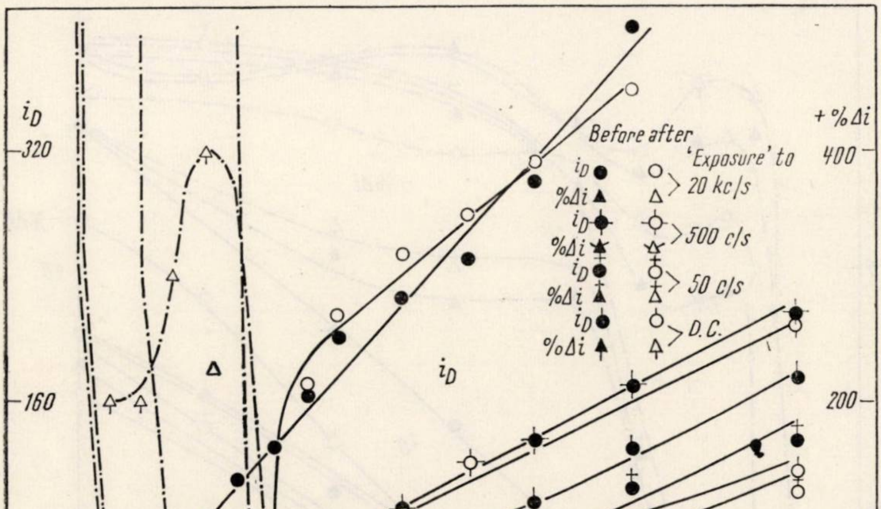

Fig. 3. — Influence on i_D and $\mp$ %Δi in bromine at 30° of "Exposure" to 20 kc/s, 500 c/s, 50 c/s and d.c.

---

[5] H. S. Taylor, *Nature*, **121**, 708 (1928).

indicate that van der Waals or physical adsorption is also partly responsible for the observed characteristics of the adsorbed layer. This has led a number of workers to the conclusion that on the adsorbent-adsorbate

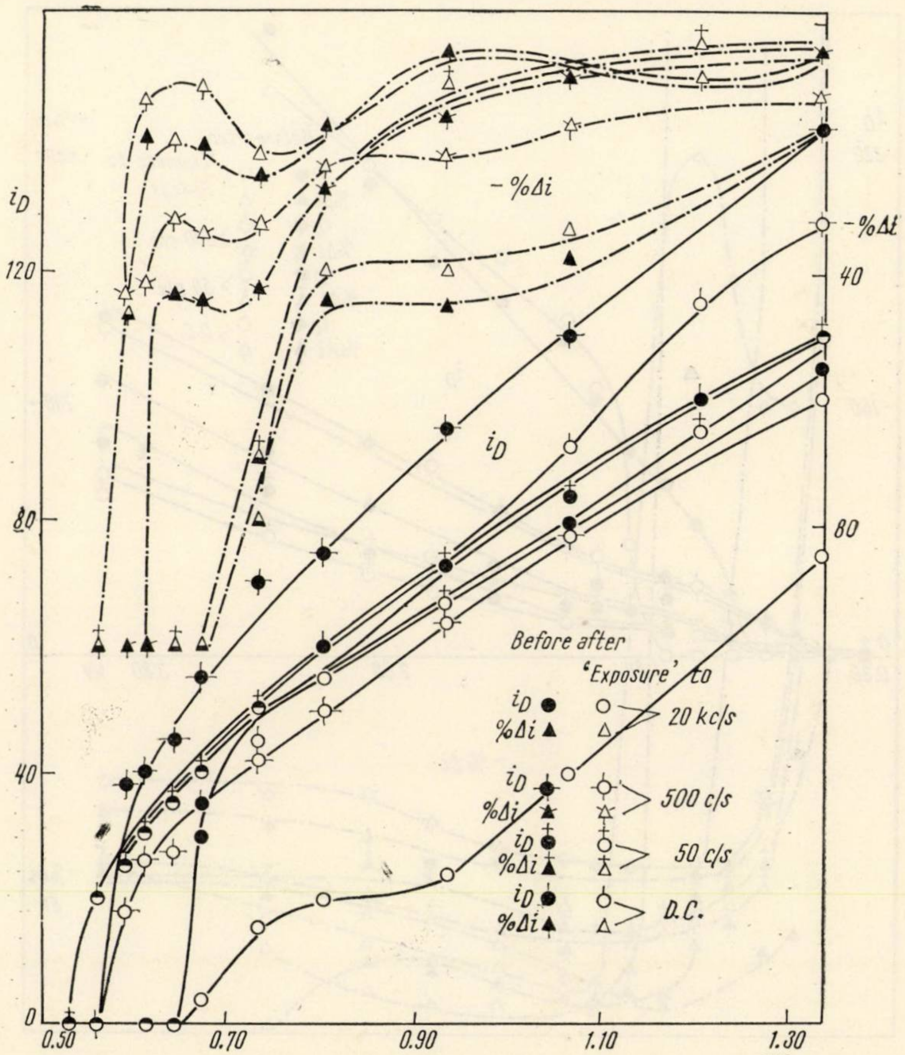

Fig. 4. — Influence on i_D — $\%\Delta i$ in iodine at 30° of "Exposure" to 20 kc/s, 500 c/s, 50 c/s and d.c.

complex layers both van der Waals adsorption and chemisorption take place simultaneously as well as independently.

It is well known that reactive gases like halogens have a chemical affinity for the walls of the discharge tube. It is natural that the equilibrium set up between the adsorbent and adsorbate can be disturbed to a marked extent by but a limited disturbance of physical conditions. For an equilibrium of chemisorption type, a small rise in temperature would

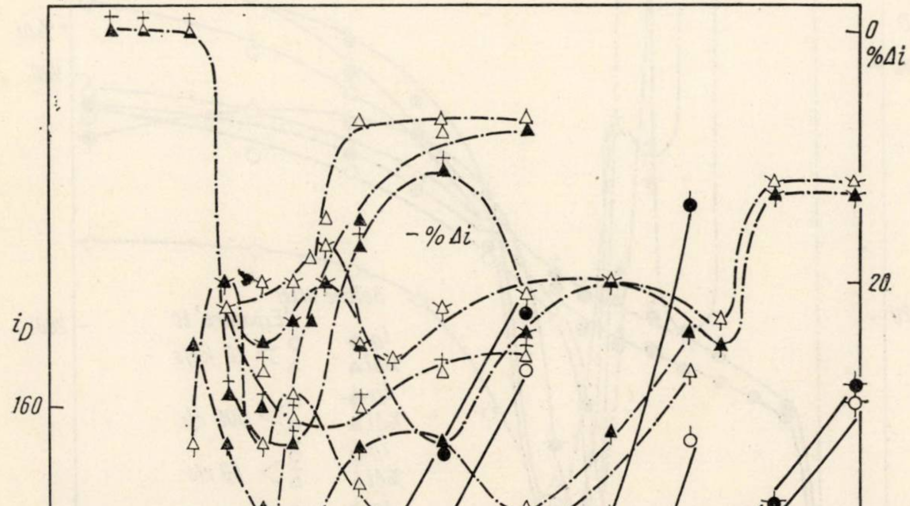

Fig. 5. — Influence on i_D and $-\%\,\Delta i$ in oxygen at 30° of "Exposure" to 20 k-c/s, 500 c/s, 50 c/s and d.c.

result only in a small decrease of $-\Delta i$, but almost complete annulment of $-\Delta i$, observed especially in the case of oxygen, goes to prove that the adsorption forces are of physical origin too.

The formation of surface compounds, when halogens enclosed in glass are subjected to discharge, is well known.[6,7,8,9] Thus, the results cited herein follow from the electrolytic nature of conduction of electricity through glass. The formation of the compounds in glass vessels is attributed to the union of atoms like Cl, Br and I with the Na^+ ions accessible at the glass electrodes.

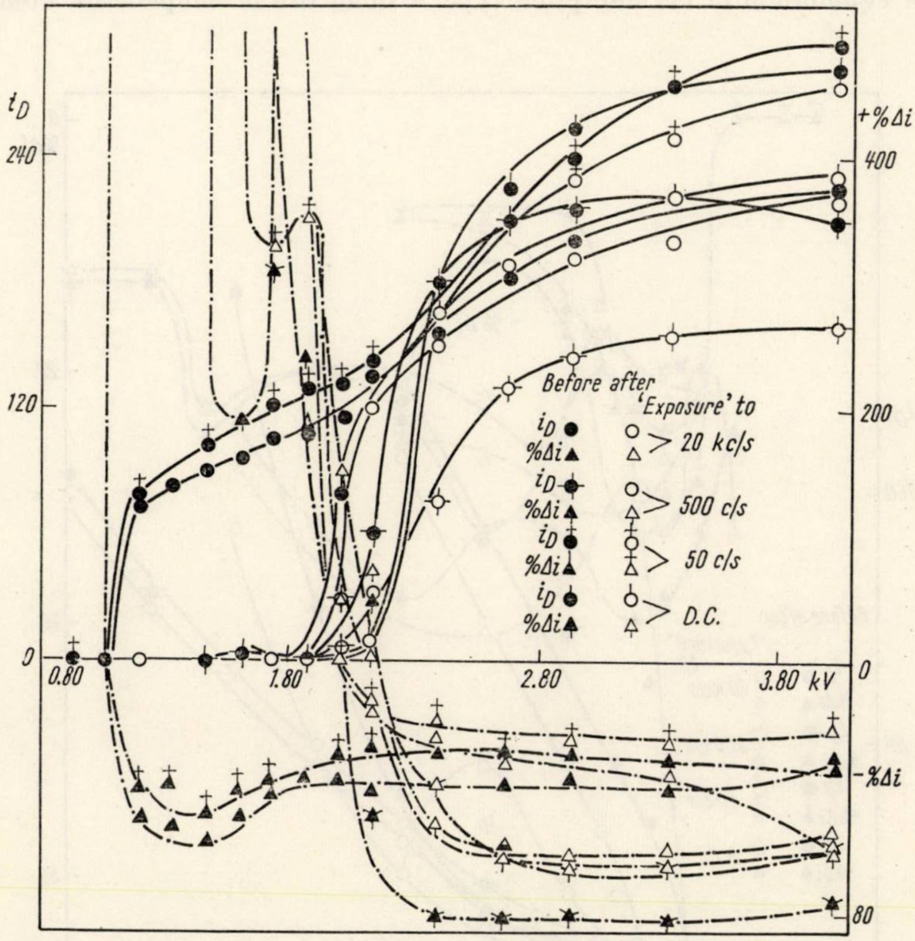

Fig. 6. — Influence on i_D and $\mp\%\Delta i$ in chlorine at 90° of "Exposure" to 20 kc/s, 500 c/s, 50 c/s and d.c.

---

[6] H. Kellner, *Z. Electrochem.*, **8**, 500 (1902).

[7] A. Ludeking, *Chem. News.*, **61**, 1 (1890).

[8] W. H. Rodebush and W. C. Klingelhoeffer Jr., *J. Amer. Chem. Soc.*, **55**, 130 (1933).

[9] G. W. Morey, "Properties of Glass", Reinhold Publishing Corp., New York, 1948.

At ordinary temperatures, irrespective of the influence of light, one molecular layer of bromine became attached to the glass and three times as much at high temperature.[10,11] The rate of adsorption is proportional to the amount of water adsorbed on the glass and the adsorption of bromine on glass may proceed through interaction with adsorbed water on the surface.[10] The observed changes in $\mp \Delta i$ at 30° and 90° due to the various brush exposures might, therefore, be due partly to a difference in the nature and thickness of the adsorbed layer.

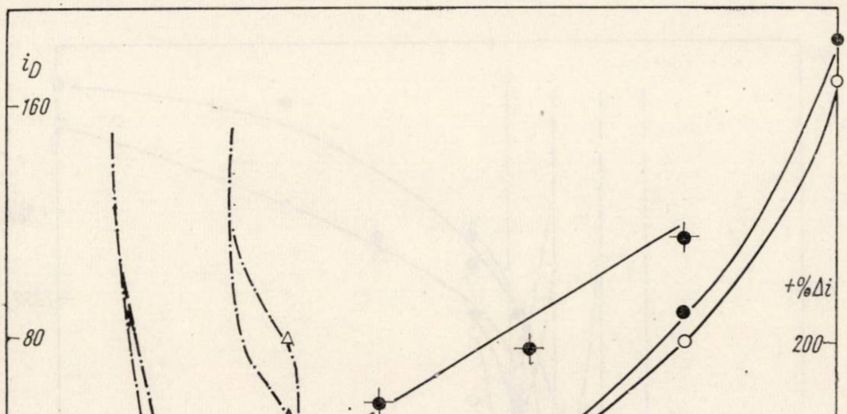

Fig. 7. — Influence on i_D and $\mp \% \Delta i$ in bromine at 90° of "Exposure" to 20 kc/s, 500 c/s, 50 c/s and d.c.

---

[10] W. C. Johnstone, Ph. D. Thesis, 1952, Wisconsin University.
[11] H. B. Willard, *J. Phys. Chem.*, **57**, 129 (1953).

At low applied electric fields of low frequency a.c. like 50 c/s, when the temperature is increased, desorption of van der Waals layer takes place besides the formation of a chemisorbed layer. As a result the surface work function decreases first and then increases with temperature up to a critical limit. This limit is reached when an equilibrium

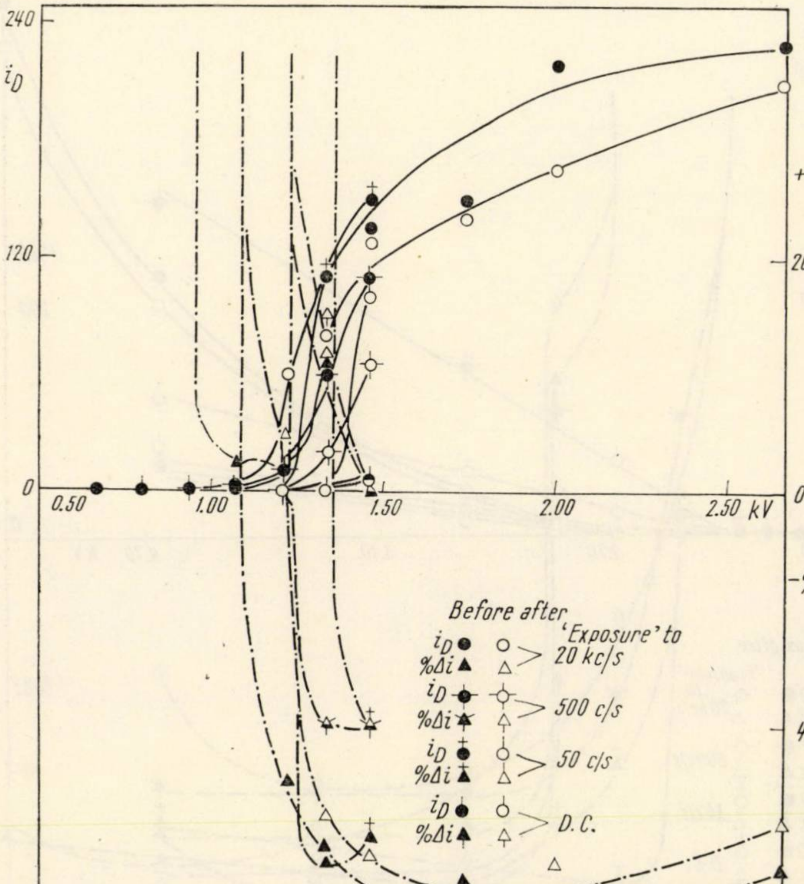

Fig. 8. — Influence on i_D and $\mp \% \Delta i$ in iodine at 90° of "Exposure" to 20 kc/s, 500 c/s, 50 c/s and d.c.

is set up on the chemisorbed surface, since the effect of a low electrical field is to create more and more active centres or patches for adsorption, that of temperature is to destroy their adsorbability. This limit is, therefore, dependent on the magnitude and frequency of the applied potential and temperature.[1] Beyond this critical limit desorption takes place due to further enhancement in frequency, in applied potential or in temperature.

By brush exposure to h.t. 20 kc/s at 30°, the adsorbed gases come out into the volume.[12,13] This results in the increase of the threshold potential and consequently the discharge current at any applied potential decreases as observed in the present investigation. The formation of an adsorption-like electrode-layer is essential for the manifestation of $\mp \Delta i$,[14] a disruption of which by the methods employed here explains the decrease in $-\% \Delta i$. During rest the desorption or strain caused by the brush exposure is relaxed and the pre-exposure conditions are retraced partially or/and completely depending upon the mutual affinity between the adsorbate and adsorbent. Halogens, in general, having more affinity for glass, recover the pre-exposure conditions quickly. After h.t. 20 kc/s, brush exposure in bromine at 30°, $-\% \Delta i$ at 2.00 kV decreased from 82 to 75 when it was observed just after, i.e., after about $^1/_4$ minute of the brush exposure. It recovered almost its pre-exposure value when the full $(V\text{-}i)_{D,L}$

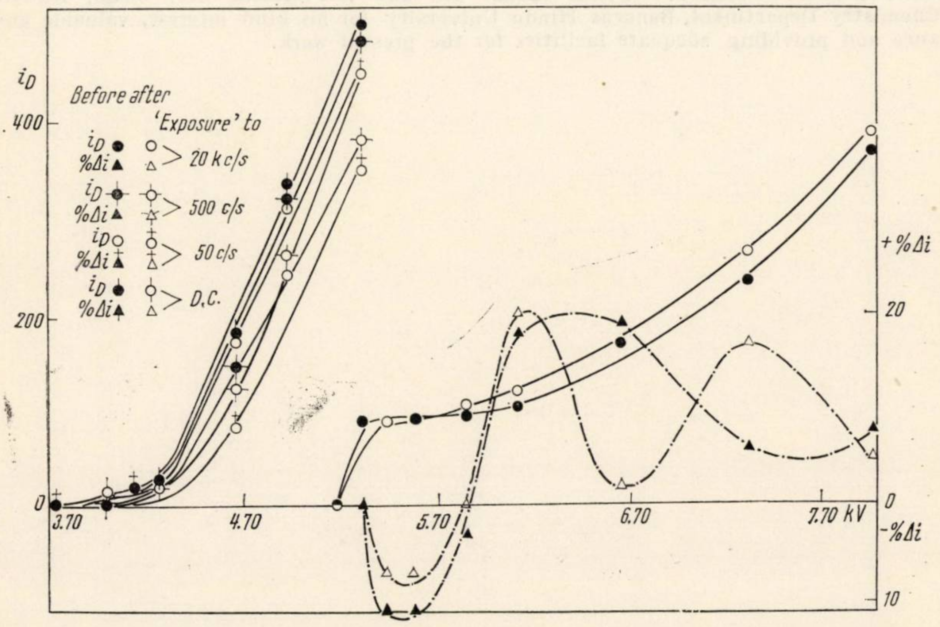

Fig. 9. — Influence on i_D and $\mp \% \Delta i$ in oxygen at 90° of "Exposure" to 20 kc/s, 500 c/s, 50 c/s and d.c.

---

[12] C. H. Bachman, "Techniques in Experimental Electronics", 1948, p. 104.

[13] M. Pirani, *Z. Physik*, **9**, 327 (1922).

[14] S. S. Joshi, *Proc. Indian Sci. Cong.*, **1946**, Part III, Phys. Sec. Abstr., 26.

characteristics were observed after about 1 minute. No appreciable change in $-\%\,\Delta i$ due to h.t. 20 kc/s brush exposure in halogens at 30° seems to be due to their quick recovery during the time that ela psed between putting off the exposure and the commencement of the $(V-i)_{D.L}$ characteristics especially at a potential where maximum $-\%\,\Delta i$ was observed. This is substantiated by the corresponding data of brush exposures with lower frequencies (0—50 c/s) and at 90° when the adsorption or recovery was retarded by the thermal vibrations.

ACKNOWLEDGEMENT. Grateful thanks are due to Professor S.S. Joshi, Ex-Head Chemistry Department, Banaras Hindu University for his kind interest, valuable guidance and providing adequate facilities for the present work.

Revue Roumaine de Chimie, **18**, *6*, 1087–1091 (1973)

X-RAY POWDER SPECTRA OF PYRIDINEMONOCARBOXYLIC ACIDS AND THEIR USE FOR THE QUALITATIVE ANALYSIS OF A MIXTURE OF THESE ACIDS*

LUIGI CAMPANELLA and PIER LUIGI CIGNINI

Institute of Analytical Chemistry, University, Rome, Italy

Received October 4, 1972

The X-ray powder method is proposed for the identification of the components of a mixture of pyridinemonocarboxylic acids. The d_{hkl} key values for each one of the three considered acids are given.

The identification of the pyridinemonocarboxylic acids in mixture is generally performed by paper and thin layer chromatographic methods.[1–12] In facing the same problem we obtained satisfactory results by the application of the X-ray powder method directly on the solid sample to be analyzed. The method is non-destructive, does not require long time and can be easily adapted to a routine analysis.

EXPERIMENTAL

Materials. Pyridinemonocarboxylic acids (picolinic or 2-, nicotinic or 3-, isonicotinic or 4-) produced by Aldrich Chemicals Co., purified by crystallization and controlled for the purity by their spectra and melting points.

Procedure. X-ray analysis was performed in a Debye-Scherrer camera of diameter 114.8 mm with monochromatized CuKα_1 and FeKα_1 radiations. The examined samples, if mixtures, were carefully homogenized.

---

* Work carried out with the aid of the Italian National Research Council (C.N.R.).

[1] D. Jerchel and W. Jacobs, *Angew, Chem.*, **65**, 342 (1953).
[2] F. Kuffner and N. Faderi, *Monatsh.*, **86**, 955 (1955).
[3] J. K. Chakrabarti and A. K. Guha, *Nature*, **178**, 538 (1956).
[4] R. D. Hartley and G. J. Lawson, *J. Chromatog.*, **7**, 69 (1962).
[5] F. Schindler and F. Kuffner, *Monatsh.*, **94**, 252 (1963).
[6] A. Gutowaska, *Chem. Analit.*, **9**, 597 (1964).
[7] V. Carunchio and A. Marino, *J. Chromatog.*, **31**, 601 (1967).
[8] J. Lopez Gorgé, M. Monteoliva and F. Mayor, *Anales real Soc. espan. Fis. Quim.*, **63 B**, 465 (1967).
[9] E. M. Diamont, *Analyt. Biochem.*, **21**, 46 (1967).
[10] I. Morimoto and K. Furuta, *Analyt. Chem.*, **34**, 1033 (1962).
[11] I. Morimoto, K. Furuta and H. Oida, *Japan Analyst.*, **10**, 664 (1961).
[12] V. Anger, *Mickrochim. Acta*, **1968**, 350.

Table 1

X-ray powder patterns data of picolinic (a), nicotinic (b) and isonicotinic (c) acid. Visual intensity degrees: S = strong; MS = middle-strong; M = middle; MW = middle-weak; W = weak

d (Å)	I (visual)	d (Å)	I (visual)	d (Å)	I (visual)	d (Å)	I (visual)
10.10	M	1.78	W	5.74	S	2.00	W
6.63	MW	1.74	W	4.37	M	1.86	W
5.06	MS	1.70	W	4.19	M	1.81	W
4.79	MS	1.68	W	3.72	W	1.78	MW
3.68	M	1.65	MW	3.59	MS	1.75	W
3.55	M	1.62	W	3.43	MS	1.67	W
3.35	S	1.58	W	3.31	S	1.63	W
3.18	S	1.55	W	3.18	MS	1.58	W
2.95	W	1.51	W	3.05	W	1.54	W
2.88	W	1.46	W	2.88	W	1.51	W
2.79	W	1.43	W	2.76	W	1.45	W
2.65	W	1.40	W	2.63	MW	1.42	W
2.47	W	1.33	W	2.51	MW	1.39	W
2.42	W	1.29	W	2.35	MW	1.31	W
2.36	W	1.28	W	2.29	W	1.26	W
2.30	W	1.24	W	2.25	W	1.20	W
2.21	MW	1.19	W	2.19	M	1.17	W
2.12	W	1.18	W	2.15	W	1.15	W
2.00	W	1.16	W	2.08	W		
1.93	W	1.15	W				
1.90	W	1.12	W				
1.84	W						
	(a)					(b)	

d (Å)	I (visual)	d (Å)	I (visual)
6.20	MW	1.84	W
5.73	MW	1.82	W
5.31	S	1.79	W
4.49	MW	1.76	W
4.07	MW	1.72	W
3.61	MW	1.62	W
3.39	S	1.52	W
3.17	MS	1.49	W
2.91	W	1.45	W
2.72	W	1.41	W
2.64	W	1.37	W
2.52	W	1.35	W
2.46	W	1.32	W
2.39	M	1.27	W
2.29	W	1.24	W
2.23	MS	1.21	W
2.09	MW	1.20	W
2.01	W	1.17	W
1.98	W	1.15	W
1.91	W	1,12	W
1.88	W		

(c)

RESULTS

As the X-ray powder spectra of pyridinemonocarboxylic acids were almost completely unknown, only being possible to get from ASTM[13] the values of the d_{hkl} of the most intense lines of nicotinic acid, we started to record the powder spectra of the pure acids (table 1, fig. 1). Then we passed to several mixtures both binary (table 2 and 3, fig. 2) and ternary (table 4, fig. 3), at varying compositions.

Table 2

X-ray powder patterns of mixtures of picolinic – nicotinic acid (1 : 1 by weight) (a), picolinic – isonicotinic acids (1 : 1 by weight) (b), nicotinic – isonicotinic acids (1 : 1 by weight) (c). The letter in brackets refers all the effects to the spectra of the pure acids : p = picolinic, n = nicotinic, i = isonicotinic

d (Å)	d (Å)	d (Å)	d (Å)	d (Å)	d (Å)
10.10 (p)	2.00 (n, p)	10.10 (p)	2.09 (i)	6.20 (i)	1.85 (i, n)
6.63 (p)	1.93 (p)	6.63 (p)	1.99 (p, i)	5.73 (i, n)	1.81 (i, n)
5.73 (n)	1.90 (p)	6.20 (i)	1.94 (p)	5.31 (i)	1.79 (i, n)
5.08 (p)	1.84 (n, p)	5.73 (i)	1.90 (p, i)	4.37 (n)	1.76 (i, n)
4.79 (p)	1.78 (n, p)	5.31 (i)	1.84 (p, i)	4.19 (n)	1.72 (i)
4.37 (n)	1.74 (n, p)	5.06 (p)	1.79 (p, i)	4.06 (i)	1.67 (n)
4.20 (n)	1.70 (p)	4.79 (p)	1.76 (p, i)	3.72 (n)	1.63(i, n)
3.69 (p)	1.68 (p)	4.49 (i)	1.72 (p, i)	3.60 (i, n)	1.58 (n)
3.57 (n, p)	1.66 (n)	4.07 (i)	1.65 (p)	3.40 (i, n)	1.55 (n)
3.36 (n, p)	1.62 (n, p)	3.68 (p)	1.62 (p, i)	3.31 (n)	1.52 (n, i)
3.18 (n, p)	1.58 (n, p)	3.55 (p)	1.58 (p)	3.18 (i, n)	1.49 (i)
2.95 (p)	1.55 (n, p)	3.38 (i, p)	1.55 (p)	3.05 (n)	1.46 (i, n)
2.88 (n, p)	1.51 (n, p)	3.18 (p, i)	1.52 (p, i)	2.90 (i, n)	1.42 (i, n)
2.80 (n, p)	1.47 (p)	2.95 (p)	1.47 (p, i)	2.76 (n)	1.40 (n)
2.65 (p)	1.40 (n, p)	2.88 (p, i)	1.35 (p, i)	2.64 (i, n)	1.37 (i)
2.51 (n, p)	1.32 (n, p)	2.80 (p)	1.32 (p, i)	2.52 (i, n)	1.35 (i)
2.42 (p)	1.29 (p)	2.65 (p, i)	1.30 (p)	2.39 (i)	1.33 (i)
2.36 (n, p)	1.27 (n, p)	2.52 (i)	1.27 (p, i)	2.35 (n)	1.31 (n)
2.30 (n, p)	1.21 (n, p)	2.46 (p, i)	1.24 (p, i)	2.29 (i, n)	1.27 (i)
2.26 (n)	1.17 (n, p)	2.39 (p, i)	1.20 (p, i)	2.24 (i, n)	1.25 (i, n)
2.21 (n, p)	1.12 (p)	2.30 (p, i)	1.18 (p, i)	2.19 (n)	1.22 (i)
2.11 (n, p)		2.22 (p, i)	1.15 (p, i)	2.09 (i, n)	1.20 (i, n)
			1.12 (p, i)	1.99 (i, n)	1.17 (i, n)
				1.91 (i)	1.15 (i, n)
				1.88 (i)	1.12 (i)
(a)		(b)		(c)	

DISCUSSION

By the analysis of the recorded spectra it can be said that :

1) the effects with $d < 3.31$ Å, being very numerous, close to each other and common to all the three acids are of no help in the identification of any of the considered acids in the presence of the others ;

---

[13] "Powder Diffraction File (Organic)", A.S.T.M., Philadelphia, 1963.

Table 3

X-ray powder patterns data of mixtures of picolinic – nicotinic acids (9: 1 by weight) (a), picolinic – nicotinic acids (1: 9 by weight) (b), picolinic – isonicotinic acids (9: 1 by weight) (c), picolinic – isonicotinic acids (1: 9 by weight) (d), nicotinc – isonicotinic acids (9: 1 by weight) (e), nicotinic – isonicotinic acids (1: 9 by weight) (f). The reported values are the most important from the analytical point of view

d (Å)	d (Å)	d (Å)	d (Å)	d (Å)	d (Å)
10.10 (p)	10.10 (p)	10.10 (p)	10.10 (p)	6.20 (i)	6.20 (i)
6.63 (p)	6.63 (p)	6.63 (p)	6.63 (p)	5.73 (i, n)	5.74 (n, i)
5.74 (n)	5.74 (n)	6.20 (i)	6.20 (i)	5.31 (i)	5.31 (i)
5.06 (p)	5.06 (p)	5.31 (i)	5.74 (i)	4.37 (n)	4.37 (n)
4.79 (p)	4.79 (p)	5.06 (p)	5.30 (i)	4.07 (i)	4.19 (n)
4.37 (n)	4.37 (n)	4.79 (p)	5.06 (p)	3.72 (n)	3.72 (n)
3.68 (p, n)	4.19 (n)	4.49 (i)	4.79 (p)	3.61 (i, n)	3.59 (n, i)
3.55 (p, n)	3.68 (p, n)	4.07 (i)	4.49 (i)	3.39 (i, n)	3.43 (n, i)
4.43 (n)	3.59 (n, p)	3.68 (p)	4.07 (i)	3.31 (n)	3.31 (n)
3.35 (p)	3.43 (n)	3.55 (p, i)	3.60 (i)	3.17 (i, n)	3.18 (n, i)
3.18 (p, n)	3.35 (p)	3.35 (p)	3.39 (i)		
	3.31 (n)	3.18 (p, i)	3.18 (i, p)		
	3.18 (n, p)				
(a)	(b)	(c)	(d)	(e)	(f)

Table 4

X-ray powder patterns data of ternary mixtures of picolini – nicotinic – isonicotinic acids (1: 1: 1 by weight) (a), picolinic – nicotinic – isonicotinic acids (1: 1: 8 by weight) (b), (1: 8: 1 by weight) (c), (8: 1: 1 by weight) (d). For the last three spectra only the most analytically important lines are reported

d (Å)	d (Å)	d (Å)	d (Å)	d (Å)
	1.95 (p, i)	10.10 (p)	10.10 (p)	10.10 (p)
10.10 (p)	1.91 (p, i)	6.63 (p)	6.63 (p)	6.63 (p)
6.63 (p)	1.84 (n, p, i)	6.20 (i)	6.20 (i)	6.20 (i)
6.20 (i)	1.79 (n, p, i)	5.73 (n, i)	5.74 (n, i)	5.74 (n, i)
5.73 (i, n)	1.76 (n, p, i)	5.31 (i)	5.31 (i)	5.31 (i)
5.31 (i)	1.72 (n, p, i)	5.06 (p)	5.06 (p)	5.06 (p)
5.05 (p)	1.68 (n, p)	4.79 (p)	4.79 (p)	4.79 (p)
4.79 (p)	1.66 (n, p)	4.49 (i)	4.37 (n)	4.37 (n)
4.38 (n)	1.62 (n, p, i)	4.37 (n)		
4.19 (n)	1.59 (n, p)	4.07 (i)	4.19 (n)	4.07 (i)
4.08 (i)	1.55 (n, p)	3.59 (n, p)	3.59 (n, p)	3.68 (p)
3.68 (p)	1.53 (n, p, i)	3.39 (n, i)	3.43 (n, i)	3.55 (n, p)
3.55 (n, p)	1.49 (i)	3.31 (n)	3.31 (n)	3.43 (n, i)
3.38 (n, p, i)	1.47 (n, p,i)	3.18 (i, p, n)	3.18 (n, p, i)	3.35 (p)
3.18 (n, p, i)	1.42 (n, p, i)			3.18 (p, n, i)
3.06 (n)	1.37 (n, i)			
2.96 (p)	1.32 (n, p, i)			
2.88 (n, p, i)	1.30 (n, p)			
2.79 (n, p)	1.27 (n, p, i)			
2.65 (n, p, i)	1.24 (p, i)			
2.50 (n, p, i)	1.21 (n, i)			
2.39 (n, p, i)	1.19 (p)			
2.30 (n, p, i)	1.18 (p)			
2.23 (n, p, i)	1.17 (n, i)			
2.18 (n, p)	1.15 (n, p, i)			
2.09 (n, p, i)	1.12 (p, i)			
1.99 (n, p, i)				
(a)		(b)	(c)	(d)

2′

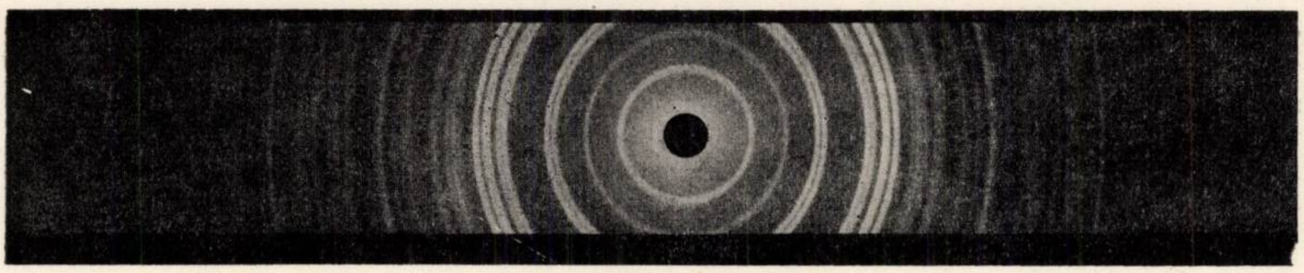

Picolinic acid

2″

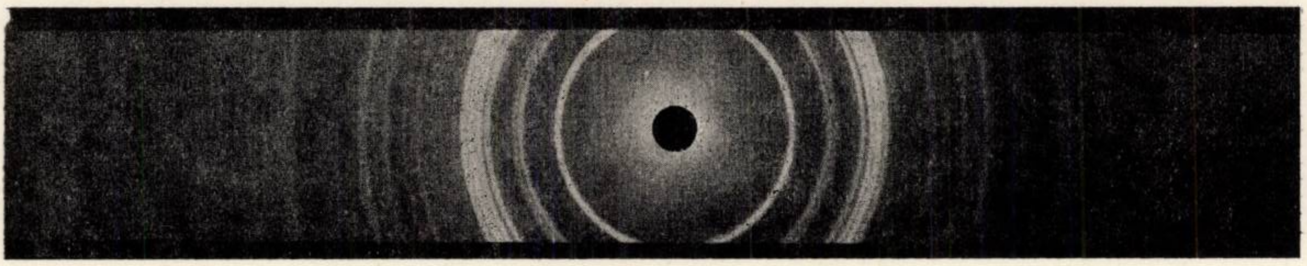

Nicotinic acid

2‴

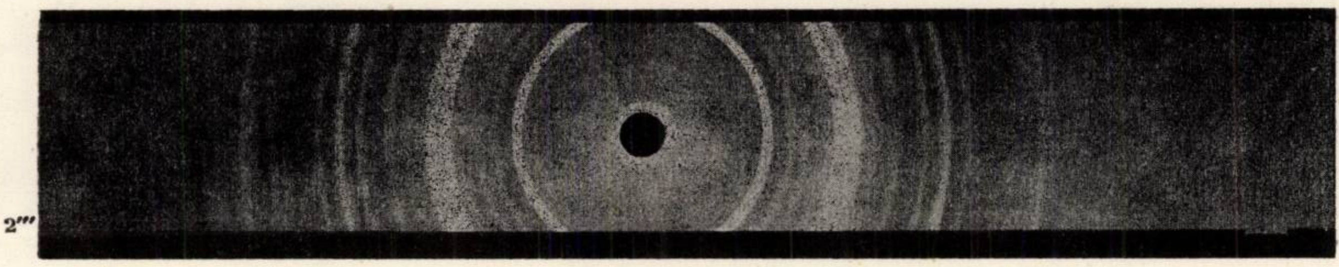

Isonicotinic acid

Fig. 1. — X-ray spectra of picolinic, nicotinic and isonicotinic acid.

1′

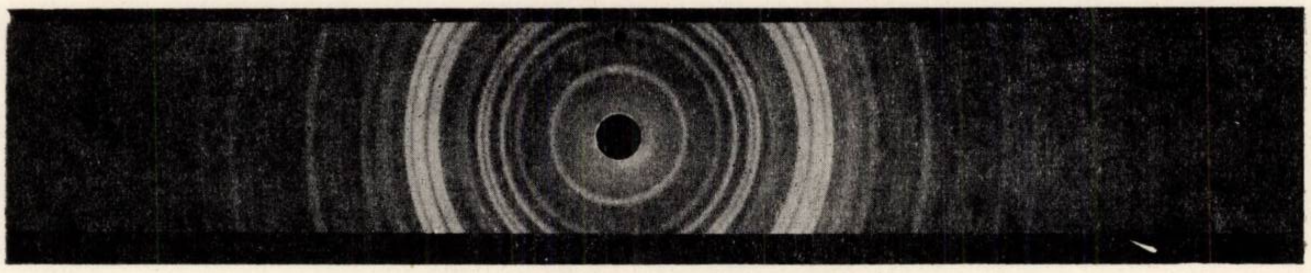

Mixture of picolinic and nicotinic acid (1:1)

1″

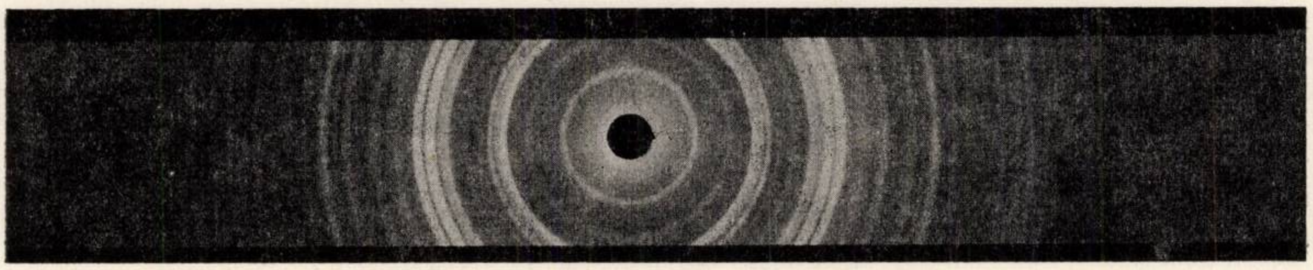

Mixture of picolinic and isonicotinic acid (1:1)

1‴

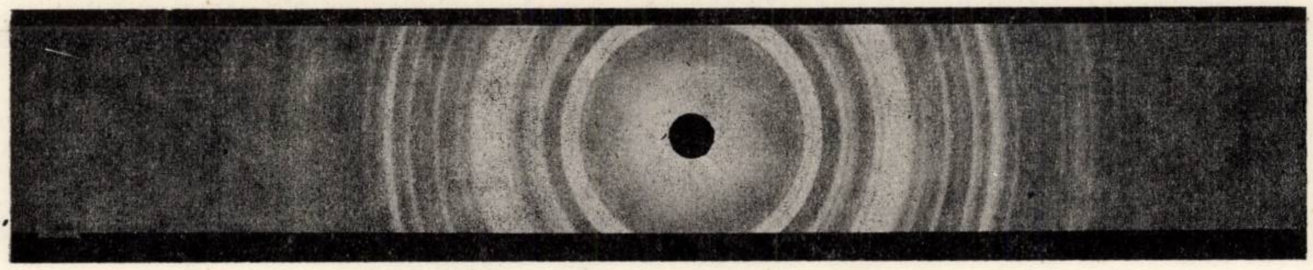

Mixture of nicotinic and isonicotinic acid (1:1)

Fig. 2. — X-ray powder spectra of mixtures of: picolinic and nicotinic, picolinic and isonicotinic, nicotinic and isonicotinic acids all the mixtures are 1 : 1.

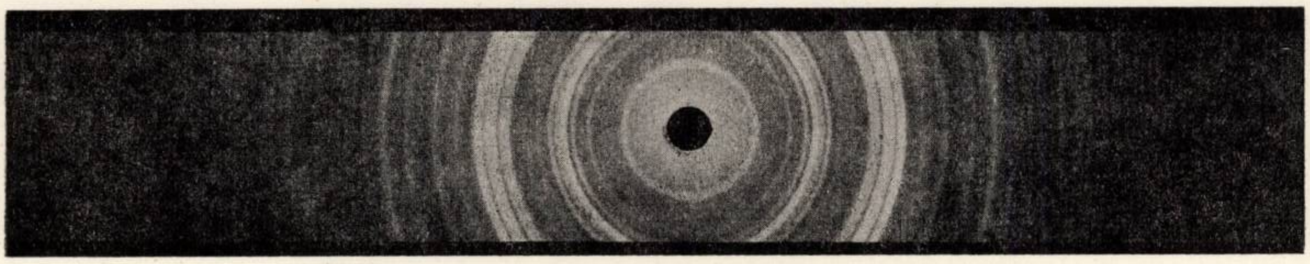

Mixture of picolinic, nicotinic and isonicotinic acid (1: 1: 1)

Fig. 3. — X-ray powder spectrum of a mixture (1 : 1 : 1) of picolinic, nicotinic and isonicotinic acid.

2) the d_{hkl} values which result to be fundamental in the resolution of a mixture of picolinic, nicotinic and isonicotinic acids are 10.10, 6.63, 5.06 and 4.79 Å for picolinic, 4.37, 4.19, 3.43 and 3.31 Å for nicotinic, 6.20, 5.31, 4.49 and 4.07 Å for isonicotinic;

3) only for nicotinic acid at very low concentration (~5%) some difficulties of identification can be found;

4) the reproducibility of the d_{hkl} measurements varied with the interested region of the spectrum, but generally did not exceed ± 0.01 Å.

Revue Roumaine de Chimie, **18**, *6*, 1093–1100 (1973)

INFLUENCE OF INDICATING ELECTRODE PRETREATMENT ON POTENTIOMETRIC TITRATION PARAMETERS. V *

GOLD PRETREATED ELECTRODE IN POTENTIOMETRIC TITRATION OF $Cr_2O_7^{2-}$ WITH Fe^{2+}

IOVANCA HAIDUC, DOINA DĂNILA and CANDIN LITEANU

Department of Analytical Chemistry, University of Cluj, Romania

Received October 30, 1972

The behaviour of a pretreated gold electrode as indicating electrode in the potentiometric titration of $Cr_2O_7^{2-}$ with Fe^{2+} was investigated. The electrode preanodized at 1.25–1.75 V can be used as indicating electrode, since the potential variation around the equivalence point is 200 mV larger than the value obtained with the untreated electrode. The electrode preanodized at $E = 1.75$ V for a longer time ($t > 5$ min) cannot be used as indicating electrode in potentiometric titration because it induces the shifting of the inflexion volume of titration. This shift is due to the reduction of Au_2O_3 from the electrode surface with Fe^{2+}. The gold oxide Au_2O_3 formed on the electrode surface functions at the titration as an auxiliary redox system sensibilizing the titration under certain conditions.

INTRODUCTION

One of the most serious problems in solid electrode methodology is the real surface and its influence on the electrode process.[1] The "inert metal" concept was used with the assumption that platinum, gold or other noble metals participate in the electrode transfer reaction only as conducting materials.

For many years, the chemists have seriously thought that platinum, gold, rhodium, iridium or ruthenium are "noble metals" not subjected to oxidation, when they are used as electrodes in potentiometric titration or voltametry. The metal – metal oxide thermodynamic potential suggests that oxidation of these metals is possible. Recent studies confirmed this and showed that the oxidation of the electrode surface cannot be ignored.

---

* Partea IV, C. Liteanu and I. Haiduc, III Conf. Naţională Chim. Anal., Braşov, Sept. 1971, vol. I, p. 93.

[1] R. N. Adams, "Electrochemistry of Solid Electrodes", Marcel Dekker, Inc., New York, 1969, p. 187.

Gold is the first on the scale of thermodynamical nobility established by Pourbaix [2] and the fourth on the scale of practical nobility. The gold metal can be oxidized either anodically [3-9] or chemically.[10-11] The gold electrode, subjected to anodic oxidation at $E > 1.2$ V (vs. NHE) in acidic medium, ends up as an Au/Au_2O_3 system, and behaves as a metal-metal oxide electrode with a standard potential $E_0 = 1.36$ V[6,12] according to the following equilibrium:

$$2\ Au + 3\ H_2O \rightleftarrows Au_2O_3 + 6\ H^+ + 6e\,; \qquad E_0 = 1.36\ V$$

Other gold oxides containing Au(I)[13] or higher oxides [14] were suggested in the literature, but these are unstable and finally are converted to Au_2O_3.

There are very few analytical applications of the gold electrode with known state of its surface. Some electrochemical reactions of organic compounds [15-17] on gold electrode were described, and some applications in redox and acid-base titration [18] were mentioned.

The present paper reports some data concerning the potentiometric titration of $Cr_2O_7^{2-}$ with Fe^{2+} by using a pretreated gold electrode.

EXPERIMENTAL

A gold plate of 0.5 cm² surface area, sealed in glass tube was used as electrode.

The pretreatment conditions of the gold electrode are summarized in table 1. The varied factors were the pretreatment potential, the duration and solution medium. The solutions were prepared from analytical grade reagents in doubly distilled water. Direct ($E - V$) or derivative potential-volume ($dE/dV - V$) curves were recorded with a Radelkis R—OH 102 polarograph and an automatic burette with a flow rate of 3 ml/min. The saturated calomel electrode (SCE) was used as reference, and the potentials were then recalculated and are given with respect to the normal hydrogen electrode (NHE) in the same solution.

---

[2] M. J. N. Pourbaix, "Atlas of Electrochemical Equilibria Aqueous Solutions", Pergamon Press Ltd., London, 1966, p. 80, 358.

[3] F. Bauman and I. Shain, *Analyt. Chem.*, **29**, 303 (1957).

[4] D.A.J. Rand and R. Woods, *J. Electroanalyt. Chem.*, **35**, 209 (1972).

[5] D. E. Icenhower, H. B. Urbach and J. H. Harrison, *J. Electrochem. Soc.*, **117**, 1500 (1970).

[6] A. Hickling, *Trans. Faraday Soc.*, **42**, 518 (1946).

[7] K. J. Vetter and D. Berndt, *Z. Electrochem.*, **62**, 378 (1958).

[8] J. P. Hoare, *J. Electrochem. Soc.*, **110**, 245 (1963).

[9] F. Will and C. Knorr, *Z. Electrochem.*, **64**, 258 (1960).

[10] J. K. Lee, Ph. thesis, Princeton Univ., Princeton N. I., 1955.

[11] S. Uneri and M. Kabasakaloglu, *Comm. Fac. Sci. Univ. Ankara*, **16 B**, 1 (1969).

[12] J. P. Hoare, *Electrochimica Acta*, **11**, 203 (1966).

[13] G. Grüneberg, *Electrochimica Acta*, **10**, 339 (1965).

[14] A. I. Tsinman, *Ukrai. khim. Zhur.*, **26**, 454 (1960).

[15] T. I. Gerisek and A. I. Pripelina, "Elektrokhim. Protsessy Elektoosazhdenii Anodnom Rastvorenii Metalov", 9, 162 (1969).

[16] U. Eisner and E. Gileadi, *J. Elektroanalyt. Chem.*, **28**, 81 (1970).

[17] J. P. Claude, *Compt. rend.*, **27**, 272 (1971).

[18] J. P. Schwing, *Compt. rend.*, **24**, 266 (1968).

Table 1

Electrode pretreatment

Type of pretreatment	Duration (min)	Potential (V)	Medium
Anodic	1	1.25	H_2SO_4 1 N
	5		
	10		
	20		
	1	1.50	H_2SO_4 1 N
	5		
	10		
	20		
	1	1.70	H_2SO_4 1 N
	5		
	10		
	20		
	10	2.00	$K_2Cr_2O_7$ 1 N
	5		
	1	2.00	H_2SO_4 1 N
	5		
	20		
Cathodic	20		H_2SO_4 1 N
	60		
	10		ascorbic acid
	20		

RESULTS AND DISCUSSION

The chemical and electrochemical oxidation of the gold electrode can be readily followed with the aid of current-potential or potential-time ($E-t$) curves. The occurrence of plateaus and the corresponding potential values are connected with the presence of various gold oxides on the pretreated electrode surface. Fig. 1 shows the $E-t$ curves for a preanodized gold electrode, dipped in $K_2Cr_2O_7$ solution (the solution to be titrated). Curves 1—3 are for gold electrodes, pretreated in 1 N H_2SO_4, for 20 min at 1.2, 1.5, and 2.0 V, respectively. Curve 4 is recorded with an untreated electrode.

The potential shown immediately after pretreatment (1300 mV) indicates the presence of the Au/Au_2O_3 system. The decrease of the potential in time, even when the electrode is dipped in the solution of an oxidizing reagent, shows the instability of the oxide even under these conditions. The potential between 1050—1100 mV is the potential of the Cr(VI)/Cr(III) system (in our practical condition) and is the same as for the untreated electrode (fig. 1, curve 4). Therefore, the oxide Au_2O_3 (the most stable oxide of gold) remains for some time on the electrode surface. Its life time depends on the pretreatment potential and duration.

If the electrode pretreated anodically is dipped in the $FeSO_4$ solution the curves shown in fig. 2 are obtained. The curves 1–4 were obtained with gold electrodes subjected to anodic pretreatment in 1 N H_2SO_4 solution, for 20 min at 1.2, 1.5, 1.7 and 2.0 V and then introduced in 0.1 $FeSO_4$ solution.

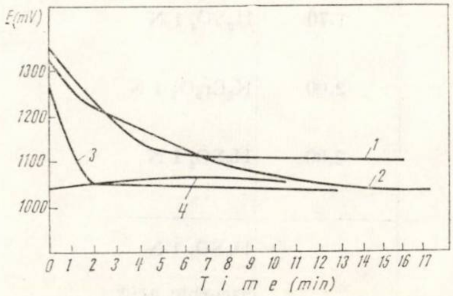

Fig. 1. — The potential-time variation of a preanodized electrode introduced into 0.1 N $K_2Cr_2O_7$.

1, Au anodized for 20 min in H_2SO_4 1 N at 1.2 V; 2, Au anodized for 20 min in H_2SO_4 1 N at 1.5 V; 3, Au anodized for 20 min in H_2SO_4 1 N at 2.0 V; 4, Au untreated.

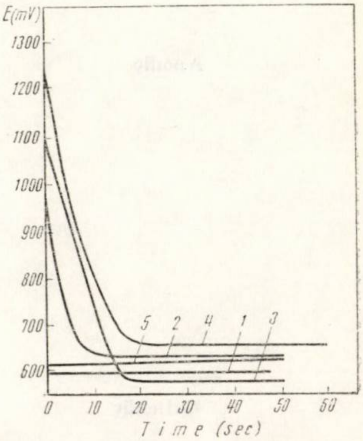

Fig. 2. — The potential-time variation of a preanodized electrode introduced into 0.1 N $FeSO_4$.

1, Au anodized for 20 min in 1 N H_2SO_4 at 1.2 V; 2, Au anodized for 20 min in 1N H_2SO_4 at 1.5 V; 3. Au anodized for 20 min in 1 N H_2SO_4 at 1.7 V; 4, Au anodized for 20 min in 1 N H_2SO_4 at 2.0 V; 5, Au untreated.

The rapid decrease of the potential (5–15 seconds) is due to the reduction of the gold oxide by Fe(II):

$$Au_2O_3 + 6\,Fe^{2+} + 6H^+ \rightleftharpoons 2\,Au + 6\,Fe^{3+} + 3\,H_2O$$

The final potential of 600–700 mV is that of an untreated gold electrode dipped into a Fe^{2+}/Fe^{3+} system (fig. 3, curve 5).

THE TITRATION OF $Cr_2O_7^{2-}$ WITH Fe^{2+}

The untreated gold electrode. For comparative purposes a 0.1 N $K_2Cr_2O_7$ solution was titrated with 0.1 N $FeSO_4$ by using an untreated gold electrode. The titration curve is given in fig. 3, curve 1. The potential variation at the equivalence point is *ca.* 200 mV.

The preanodized gold electrode. The first anodizations were done at 1.25 V in 1 N H_2SO_4 for 1 min and 10 min, and the titration curves recorded with these electrodes are shown in fig. 3, curves 2 and 3, respectively. The potential shown by the electrode in $K_2Cr_2O_7$ solution, at the beginning of the titration was *ca.* 1150 mV. This suggests that no Au_2O_3 was formed on the electrode surface. However, the potential variation at the equivalence point was 400 mV (fig. 3, curbe 3), therefore the use of preanodized electrode improves the precision of the titration, as compared to the untreated electrode.

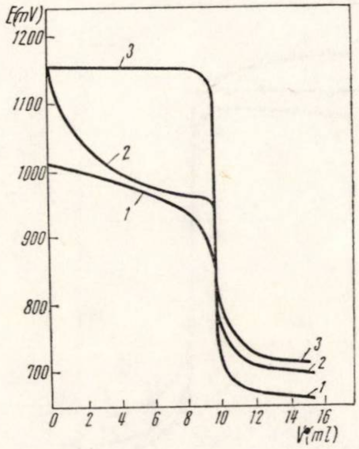

Fig. 3. — Potentiometric titration of 0.1 N $Cr_2O_7^{2-}$ with 0.1 M Fe^{2+}.
1, Au untreated, *2*, Au anodized for 1 min at 1.25 V in 1 NH_2SO_4; *3*, Au anodized for 10 min at 1.25 V in 1 N H_2SO_4.

The gold electrode preanodized at 1.5 V for 20 min in 1 N H_2SO_4, used in titration, gives the titration curve shown in fig. 4, curve 4. The potential of the gold electrode, at the beginning of the titration was 1200 mV, thus showing no Au_2O_3 on the surface. The potential difference around the equivalence point ($\Delta E_{\pm 1\%}$) is *ca.* 400 mV, and thus the titration is again more precise.

A more drastic anodic pretreatment of the gold electrode results in the formation of an Au_2O_3 layer on its surface. Thus the electrode preanodized in 1 N H_2SO_4 at 1.7 V, after dipping in 0.1 N $K_2Cr_2O_7$, shows a potential approaching the potential of the Au/Au_2O_3 system (fig. 5). After longer anodic pretreatments in 1 N H_2SO_4, e.g. 20 min (fig. 5, curve 1) or 10 min (fig. 5, curve 2) the amount of oxygen or Au_2O_3 on the surface is larger and this results in a modification in the shape of the titration curve. This can be explained in the following way. The Fe^{2+} ion reduces the $Cr_2O_7^{2-}$ ions in a fast reaction, but it reacts also with Au_2O_3 on the surfaces :

$$Au_2O_3 + 6\,Fe^{2+} + 6\,H^+ \rightleftharpoons 2\,Au + 6\,Fe^{3+} + 3\,H_2O$$

The rate of this reaction is, however, slow and therefore Au_2O_3 remains on the surface until after the equivalence point, when all the dichromate from the solution was consumed. Depending on the anodization potential and duration, the precision and exactity of the titration will be affected.

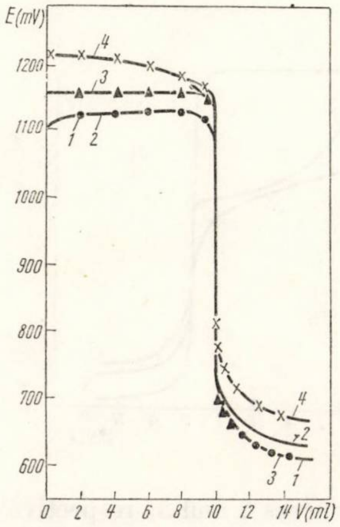

Fig. 4. — Potentiometric titration of 0.1 N $Cr_2O_7^{2-}$ with 0.1 M Fe^{2+}

1, Au anodized for 1 min at 1.5 V in 1 N H_2SO_4; *2*, Au anodized for 5 min at 1.5 V in 1N H_2SO_4; *3*, Au anodized for 10 min at 1.5 V in 1 N H_2SO_4; *4*, Au anodized for 20 min at 1.5 V in 1 N H_2SO_4.

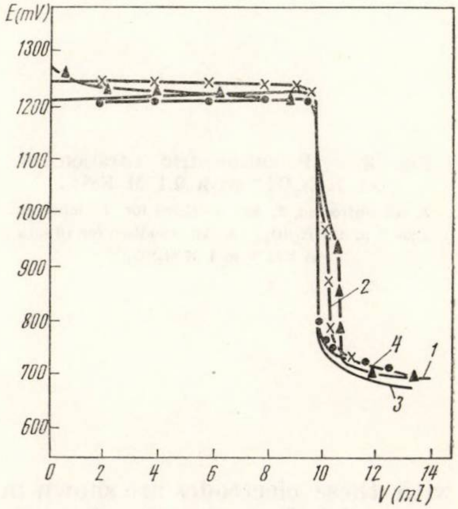

Fig. 5. — Potentiometric titration of 0.1 N $Cr_2O_7^{2-}$ with 0.1 M Fe^{2+}.

1, Au anodized for 20 min at 1.7 V in 1 N H_2SO_4; *2*, Au anodized for 10 min at 1.7 V in 1 N H_2SO_4; *3*, Au anodized for 5 min at 1.7 V in 1 N H_2SO_4; *4*, Au anodized for 1 min at 1.7 V in 1 N H_2SO_4.

If the amount of the Au_2O_3 was large (after drastic anodization e.g. 5 min at 2.0 V in 1 N H_2SO_4), the equivalence volume is shifted (fig. 6, curve 3). This shift shows the influence of the auxiliary redox system (Au/Au_2O_3) in the end point indication.[19]

It follows from our data that the surface Au_2O_3 can be "titrated" with the reducing reagent ($FeSO_4$). To follow this titration a gold electrode was subjected to a severe anodic pretreatment, namely 10 min at 2.0 V in $K_2Cr_2O_7$ 0.1 N and then it was used in successive titrations shown in fig. 7.

Curve 1, fig. 7, shows clearly the "titration" of Au_2O_3, after the dichromate was titrated. The first inflexion is the titration of dichromate and the second inflexion corresponds to the "titration" of Au_2O_3. The magnitude of the equivalence point shift due to the titration of Au_2O_3 is evident from data shown in table 2.

---

[19] C. LITEANU and I. HAIDUC, *Talanta*, **19**, 1009 (1972).

Fig. 6. — Potentiometric titration of 0.1 N $Cr_2O_7^{2-}$ with 0.1M Fe^{2+}.

1, Pt untreated; *2*, Au untreated; *3*, Au anodized for 5 min at 2.0 V in 1 N H_2SO_4; *4*, Au washed after curve 3; *5*, Au washed after curve 4.

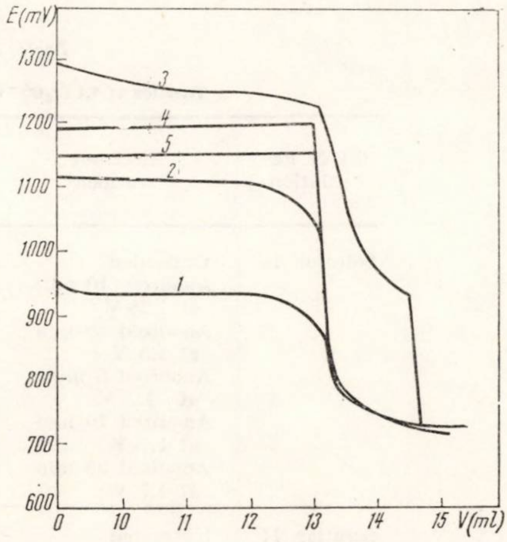

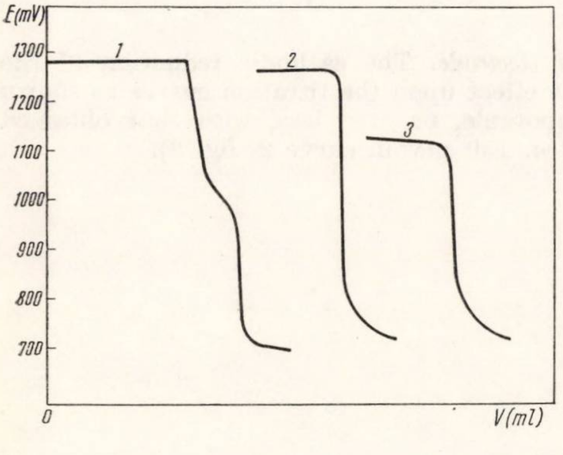

Fig. 7. — Successive potentiometric titration of 0.1 N $Cr_2O_7^{2-}$ with 0.1 M Fe^{2+}.

1, Au anodized for 10 min at 2.0 V in 0.1 N $K_2Cr_2O_7$; *2*, Au washed after curve 1; *3*, Au washed after curve 2.

Fig. 8. — Potentiometric titration of 0.1 N $Cr_2O_7^{2-}$ with 0.1 M Fe^{2+}.

1, Au cathodically reduced for 25 min in ascorbic acid; *2*, Au cathodically reduced for 40 min in ascorbic acid.

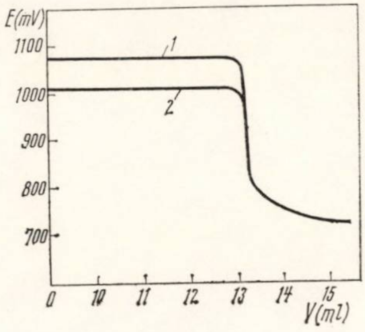

Table 2

Titration of 0.1 $Cr_2O_7^{2-}$ with 0.1 M Fe^{2+}

0.1 N Fe^{2+} solution	Electrode treatment	Volume of titrant added at inflexion point (ml)
Solution I	Untreated	10.00
	Anodized 10 min at 1.25 V	10.00
	Anodized 20 min at 1.5 V	10.01
	Anodized 5 min at 1.7 V	10.01
	Anodized 10 min at 1.7 V	10.30
	Anodized 20 min at 1.7 V	10.43
Solution II	Untreated	13.20
	Anodized 3 min at 2.0 V	14.60

Cathodically reduced gold electrode. The cathodic reduction of the gold electrode surface has little effect upon the titration curves as shown in fig. 8. The precision is comparable, or even less, with that obtained with an untreated electrode (*ca.* 150 mV in curve 2, fig. 8).

D. DAVIDESCU und VELICICA DAVIDESCU „Chimizarea agriculturii ; Testarea stării de fertilitate prin plantă şi sol" (Die Chemisierung der Landwirtschaft ; Untersuchung des Fertilitätszustandes durch Pflanze und Boden), Ed. Academiei, Bukarest, 1972, 497 S.

Das Betreiben der Landwirtschaft ist sicher eine der ältesten Beschäftigungen der Menschen. Während der Jahrtausende entwickelte sich die Technik der landwirtschaftlichen Arbeiten fortwährend, so daß heutzutage die intensive Landwirtschaft eine feste theoretische Grundlage benötigt. In diesem Sinn gliedern wir auch die Theorie über die Leitung der vegetativen Faktoren und die Kontrolle des Fertilitätszustandes, die, in Praxis angewandt, ein Mittel für die Lenkung der Nährung der Pflanzen und der wirtschaftlichen Benützung der Düngemittel darstellt.

In der vorliegenden Arbeit stellten sich die Verfasser vor, den Fachmännern eine Gesamtheit von Methoden zur Untersuchung des Fertilitätszustandes vorzubringen, damit der Fachmann der auf dem Gebiete der vegetalen Landwirtschaft arbeitet, den Nährungszustand der Kulturpflanzen bestimmen soll und das Düngerungssystem in Höchstwirtschaftlichkeit gliedern kann.

Die Arbeit besteht aus 20 Abschnitten. Aus diesen behandeln die ersten vier die spezifischen Probleme der Agronomie, und zwar darunter : die Pflanzen und ihre Karenzzustände, die unterschiedliche Diagnostizierung der Ursachen die negativ auf dem Wachstum und Entwicklung der Pflanzen einwirken, die Faktoren die den Nährungszustand ändern und Ratschläge über die Benützung der Düngemittel und Amendamenten, wie auch über die Praxis der Kontrolle des Fertilitätszustandes für die richtige Anwendung der Düngemittel.

In den nächsten sechszehn Abschnitten werden die eigentlichen chemischen Analysen besprochen. In den Abschnitten 5—8 stellen die Verfasser Methoden für die Bestimmung der Fertilität durch die chemische Analyse der vegetalen Teile vor. Es werden eingehend die allgemeinen Prinzipen über die Sammlung und Vorbereitung der Proben für die Analyse, die Ausführung der Analysen, die Auswertung der Ergebnisse der chemischen Analyse der Pflanzen, die Anwendung der Foliardiagnose bei den wichtigsten Kulturpflanzen und die Untersuchung der grünen Gewebe besprochen.

Der Schwerpunkt der Arbeit befaßt sich aber mit der Untersuchung des Fertilitätszustandes durch die chemische Analyse des Bodens. Dieses Problem wird in Abschnitten 9—20 behandelt. In diesen Abschnitten werden folgende Hauptprobleme eingehend besprochen : Allgemeines über die chemische Untersuchung des Bodens, die Sammlung der Bodenproben und ihre Vorbereitung für die Analyse, die genauesten und die schnellsten Methoden der Analyse des Bodens, die Prinzipien die den Methoden der Bestimmung des Gehalts des Bodens an Nährstoffen zu Grunde liegen, die Auswertung der Ergebnisse der chemischen Analyse des Bodens, das pH und der Kaliumbedarf des Bodens, die Bestimmung der wechselbaren und löslichen Kationen, die Bestimmung der löslichen Salze des Bodens, die schnelle Untersuchung der Nährstoffe des Bodens, landwirtschaftliche Anzeichen die bei der Untersuchung der Fertilität des Bodens benützt werden und die Herstellung der verschiedenen Reagenzen die bei den Analysen benötigt werden.

Zum Schluß bringen die Verfasser ein reiches Literaturverzeichnis auf diesem Gebiet vor. Die Behandlung eines so umfangreichen Materials wird sehr systematisch und klar ausgeführt. Die Gliederung der Arbeit in 20 Abschnitten und fast 500 Unterabschnitten erleichtert wesentlich die praktische Arbeit für die schnelle Dokumentierung über eine Methode der Analyse des Bodens oder über eine Bestimmungsmethode des Nährungszustandes der Pflanzen. Die Arbeit setzt keine besondere Chemie- oder Landwirtschaftskenntnisse voraus und wird daher einem weiten Kreis von Studenten, Technikern und Spezialisten empfohlen.

Al. Fruma
Centrul de Chimie Fizică
Bucureşti, str. Dumbrava Roşie 23

CORRIGENDUM

Chemical Graphs. XVI. Intramolecular isomerizations of octahedral complexes with six different ligands, by A. T. Balaban.

Rev. Roumaine Chim., **18**, 841 (1973)

On page 843, in figure 1, right-hand corner, the notations should be:

$$\begin{array}{ccc} & 8 & \\ 26 & & \overline{26} \\ \overline{26} & & 26 \end{array}$$

KÖNYVTÁRA

NOTE POUR LES AUTEURS

La *Revue Roumaine de Chimie* publie des articles en anglais, français, russe, allemand ou espagnol. Les auteurs sont priés d'envoyer des articles, notes, communications et comptes rendus inédits.

Les manuscrits seront dactylographiés à deux intervalles. Les tableaux seront dactylographiés sur feuilles séparées, de même que la légende des figures. Les diagrammes seront tracés à l'encre de Chine sur papier calque. Les tableaux et les figures seront numérotés par des chiffres arabes, en nombre strictement nécessaire. Prière de ne pas inscrire les mêmes données dans les tableaux et les figures. Les formules chimiques seront incluses dans le texte ; en outre, elles seront transcrites sur des feuilles séparées. Les auteurs sont priés d'indiquer les caractères italiques (en soulignant les lettres au crayon), ainsi que tout autre caractère spécial. L'ordre des références bibliographiques sera celui de leur mention dans le texte ; le nom de l'auteur sera précédé de l'initiale du prénom ; les publications périodiques seront présentées suivant les prescriptions internationales. Les références seront ajoutées à la fin de l'article ; elles paraîtront comme des notes, au bas de la page. Le texte sera précédé d'un résumé, comprenant 15 lignes au maximum.

L'entière responsabilité du contenu des articles appartient aux auteurs. On publie des articles dus aux collaborateurs roumains ou étrangers. Les auteurs recevront 50 tirés à part.

PRINTED IN ROMANIA

1973 AUG 16

TRAVAUX PARUS AUX ÉDITIONS DE L'ACADÉMIE DE LA RÉPUBLIQUE SOCIALISTE DE ROUMANIE

P. BALTĂ et E. BALTĂ, **Introducere în chimia fizică a stării vitroase** (Introduction à la chimie physique de l'état vitreux), 1971, 240 p., 15,50 lei.

LYDIA-MARIA VAICUM, **Biodegrabilitatea detergenților** (La biodégrabilité des détergents), 1971, 254 p., 16 lei.

TIBERIU NĂSCUȚIU, **Metode radiometrice de analiză** (Méthodes radiométriques d'analyse), 1971, 346 p., 19,50 lei.

I. ZUGRĂVESCU et L. STOICESCU-CRIVETZ, **Polimeri heterociclici** (Polymères hétérocycliques), 1971, 190 p., 9,50 lei.

I. MAXIM, **Materiale nucleare** (Matériaux nucléaires), 1969, 444 p., 30 lei.

CRISTOFOR SIMIONESCU et C. V. UGLEA, **Fracționarea compușilor macromoleculari** (Fractionnement des composés macromoléculaires), 1962, 292 p, 18,50 lei.

CRISTOFOR SIMIONESCU et CLEOPATRA VASILIU-OPREA, **Mecanochimia compușilor macromoleculari** (La mécanochimie des composés macromoléculaires), 1967, 344 p., 23,50 lei.

CORNEL BODEA et collab., **Tratat de biochimie vegetală**, partea I, **Fitochimie** (Traité de biochimie végétale, Ire partie, Phytochimie), Ier vol., 1964, 747 p. + 4 annexes + 2 pl., 41 lei ; IIe vol., 1965, 1262 p., 1 pl., 56 lei ; IIIe vol., 1967, 773 p., 35 lei.

V. GHEȚIE et V. MICUȘAN, **Analiza imunochimică. Teorie și practică** (Analyse immunochimique. Théorie et pratique), 1966, 369 p., 28 lei.

R. PORTOCALĂ et L. POPA, **Acizii ribonucleici celulari și virali** (Les acides ribonucléiques cellulaires et viraux), 1966, 375 p., 8 pl., 26 lei.

D. PURDELEA et R. VÎLCEANU, **Chimia compușilor organici ai fosforului și ai acizilor lui** (La chimie des composés organiques du phosphore et de ses acides), 1965, 540 p., 37 lei.

I.P.I.—c. 2859

43 426

Lei 25.—

F 1103

R

REVUE ROUMAINE DE CHIMIE

REZERVA

TOME 18
N° 7
Juillet 1973
RRCHAX, 18, 7, 1103–1280 (1973)

ÉDITIONS DE L'ACADÉMIE DE LA RÉPUBLIQUE SOCIALISTE DE ROUMANIE

Rev. Roumaine Chim. 18, 7, p. 1103–1280 (1973), Bucarest

COMITÉ DE RÉDACTION

Rédacteur en chef:

I. G. MURGULESCU, membre de l'Académie de la République Socialiste de Roumanie

Rédacteurs en chef adjoints:

A. T. BALABAN et V. EM. SAHINI, membres correspondants de l'Académie de la République Socialiste de Roumanie

Collège de rédaction:

C. DRĂGULESCU, RALUCA RIPAN, CR. SIMIONESCU, membres de l'Académie de la République Socialiste de Roumanie; EM. BRATU, ECATERINA CIORĂNESCU-NENITZESCU, P. ŞPACU, membres correspondants de l'Académie de la République Socialiste de Roumanie; MARGARETA AVRAM, D. I. MARCHIDAN, G. NIAC et D. SĂNDULESCU

La Revue Roumaine de Chimie paraît 12 fois par an. Toute commande de l'étranger (fascicules ou abonnements) sera adressée à Intreprinderea Rompresfilatelia, Boîte Postale 2001, telex 011631, Bucarest, Roumanie

Les manuscrits, les livres et les revues proposés en échange, ainsi que toute correspondance seront envoyés à la rédaction

REVUE ROUMAINE DE CHIMIE

23, Str. Dumbrava Roşie, Bucarest, Roumanie

ÉDITIONS DE L'ACADÉMIE DE LA RÉPUBLIQUE SOCIALISTE DE ROUMANIE
3 bis, Str. Gutenberg, Bucarest

REVUE ROUMAINE DE CHIMIE

ORSZÁGOS MŰSZAKI KÖNYVTÁR ÉS DOKUMENTÁCIÓS KÖZPONT
1833

Tome 18, N° 7 Juillet 1973

Page

O. RADOVICI and CECILIA VASS, Kinetics of copper electrocrystallization from pyrophosphate electrolytes . . . . 1105—1109 R

P. G. PERKINS, The electronic structure of ladder polymers. II. Excited states of *cata*-condensed benzenes, pyrazines and pyridines . . . . 1111—1119

MARIA MAVRODIN-TĂRĂBÎC, IOANA ONACA et I. SOLACOLU, L'étude de la réaction d'oxydation de l'hydrogène sur les électrodes poreuses en nickel . . . . 1121—1129 R

AL. FRUMA und I. V. NICOLESCU, Die Chemisorption von Wasserstoff, Benzol und Cyclohexan auf mit Lithium und Titan dotiertem Aluminiumoxyd. II. Adsorptionswärmen . . . . 1131—1142 R

P. SPACU, A. C. BANCIU and C. I. LEPĂDATU, Co(II) and Ni(II) chelates with ligands containing donor nitrogen atoms . . . . 1143—1153 R

A. V. BOTAR und T.J.R. WEAKLEY, Heteropolywolframate des Th(IV) . . 1155—1157 R

IULIA I. GEORGESCU, D. CIOMÂRTAN, G. TEODORESCU, MARIA HLEVCA and MARIA ZAHARESCU, Complexes of isonicotinic acid hydrazide with Fe(II) and thiocyan, $(INAH)_2 Fe(NCS)_2 . H_2O$ . . . . . 1159—1172

C. POMPONIU and A. T. BALABAN, Computing program for interpreting ESR spectra of organic free radicals . . . . 1173—1209 Bef

F. URSEANU and I. ZUGRĂVESCU, New disperse dyes with naphth[2,3-c] acridan[5,6-cd]pyrazol-4,10(2H)-dione structure . . . . 1211—1224

R. VÎLCEANU, B. D. BADER, MARIA RĂDULESCU und MARIA MARINESCU, Neue organische Pigmente — Isatinderivate. IV. Thermisches Verhalten . . . . 1225—1231

ELENA IȘFAN, CORNELIA UNCUȚA and A. BARABÁS, Beryllium-(3-acyl-2,4-pentanedionates) . . . . 1233—1241

M. RĂILEANU, ILEANA RADULIAN, MARINA OLTENEANU and MARIA CONSTANTIN, Donor-acceptor complexes. III. Charge transfer complexes of 1,3,6,8-tetranitrocarbazole . . . . 1243—1248 R

Rev. Roumaine Chim. **18**, 7, 1103—1280 (1973), Bucarest

E. POP, L. KLASINC and N. TRINAJSTIĆ, Theoretical studies of some furocoumarin isomers 1249–1257
TEODORA PANEA, V. FĂRCĂŞAN and C. BODEA, Hydroxy-phenothiazine-5,5-dioxides. I. 1,7,9-trichloro-3-hydroxy-5,5-dioxi-phenothiazine 1259–1262
ЮЛИЯ КОВАЧ и БЕЛЛА ТОКЕШ, Полярографическое исследование комплексообразования этилксантогената калия с ионами H^{2+} . . 1263–1268
L. CAMPANELLA, P. CIGNINI and G. DE ANGELIS, Polarographic, oscillopolarographic and chronopotentiometric behaviour and determination of nicotinic acid 1269–1272
R A. CONSTANTINESCU and C. LITEANU, Ionophoresis with flow gradient . 1273–1279

Revue Roumaine de Chimie, **18**, 7, 1105–1109 (1973)

KINETICS OF COPPER ELECTROCRYSTALLIZATION FROM PYROPHOSPHATE ELECTROLYTES

O. RADOVICI and CECILIA VASS

Centre of Physical Chemistry, str. Galaţi 31, Bucharest 13, Romania

Received January 23, 1972

The kinetic parameters of copper electrocrystallization from pyrophosphate electrolytes have been determined by a galvanostatic method in the presence of Na_2SO_4 up to a concentration of 1.5 M. The influence of Cu^{2+} concentration on the electrodeposition process was studied. A Tafel type equation was found in the current density range up to 10 $mA \cdot cm^{-2}$ for the reaction overpotential and the transfer coefficients and current exchange densities were calculated.

INTRODUCTION

Although the high solubility and stability of the complex anion $Cu^{2+}-P_2O_7^{4-}$ have been well known for a long time, which recommended it for copper deposition from alkaline media, only recently has this system been given a practical importance. [1] It was demonstrated [2] that in the pH range 7–9.5 the main complex has the form $Cu(P_2O_7)_2^{6-}$ according to reactions

$$\begin{aligned} Cu^{2+} + P_2O_7^{4-} &\rightarrow Cu_2P_2O_7 \\ Cu_2P_2O_7 + {}_3P_2O_7^{4-} &\rightleftharpoons {}_2Cu(P_2O_7)_2^{6-} \end{aligned} \tag{1}$$

while in very diluted solutions, complexes may be formed in which the $Cu : P_2O_7$ ratio may have the value 2 : 1 or 4 : 1. The pyrophosphate copper plating baths have proved their advantages over the cyanide ones due to their high cathodic efficiency, chemical stability, low cost and nontoxicity and these are the reasons for the special attention given to establish their optimal operating conditions. [3,4] The use of kalium pyrophosphate was recommended [5,6] instead of the natrium compound because of its higher electrical conductivity and solubility. The studies were mainly directed towards establishing the influence of different additions,[7-10] the effect of different parameters on the cathodic efficiency[11] and the structure of deposits.[12] It has also been proved[13,14] that the permitted current density and hence the deposition rate is considerably increased by applying reversible current and by using ultrasounds.

---

[1] F. Passal, *Plating*, **46**, 628 (1959).

[2] J. Waters and A. Aaron, *J. Amer. Chem. Soc.*, **75**, 611 (1953).

[3] T. L. Rama Char, *Bull. India Sect. Electrochem. Soc.*, **6**, 69 (1957).

[4] V. I. Lainer, "Teoriya i praktica blestiashchykh galvanopokrytii", Gosudarstvennoe Izdatel'stvo Politicheskoi i Nauchnoi Literatury Litovskoi S S R, Vilnius, 1963, p. 255.

[5] T. L. Rama Char, *J. Sci. Ind. Res., India*, **A19**, 265 (1960).

[6] B. L. Reizin and V. I. Lainer, *Zashchita Metallov*, **2**, 339 (1966).

A particular importance was given to obtaining bright deposits from these baths, either by using large numbers of brightening additives or by a convenient anodic treatment.[15,16]

There are few theoretical studies concerning the electrodeposition process of copper from pyrophosphate solutions which aim at determining the equilibrium potential of copper electrode[17] and the influence of different parameters on the copper polarization,[18] with some attempts to elucidate the reaction mechanism.[19] Recently,[20-22] for the same purpose, Faraday impedance and oscillographic measurements have been carried out.

In the present paper the influence of Cu^{2+} concentration on the copper electrocrystallization process from pyrophosphate electrolytes was studied and the kinetic parameters of the corresponding electrode reaction were determined.

EXPERIMENTAL

The cell, electric circuits and electronics were described in a previous paper.[23] The measurements have been made with and without compensation of ohmic polarization.

The concentration of Cu^{2+} solutions was in the $1.10^{-2}-2.5\times10^{-1}$ M range; the excess of $K_4P_2O_7$ corresponding to the mole ratio 2.5 : 1 was added to them. To each solution, Na_2SO_4 was added as support electrolyte, till total concentration of 1.5 M was reached. The preparation of the solution and working method were previously described.[23] Before measurements on each electrode, copper was deposited from solution at the current density of 10 $mA \cdot cm^{-2}$ for 30 min.

The experiments have been carried out at 60° the precision of the temperature readings being ± 0.1°.

---

[7] C. J. Owen, H. Jackson and E. R. York, *Plating*, **54**, 821 (1967).

[8] T. H. Irvine, *Plating*, **54**, 1251 (1967).

[9] B. M. Dikova and N. T. Kudryavtsev, *Zashchita Metallov*, **4**, 110 (1968).

[10] N. T. Kudryavtsev and B. M. Dikova, *Zashchita Metallov*, **5**, 177 (1969).

[11] J. W. Dini, H. R. Johnson and J. R. Helms, *Plating*, **54**, 1337 (1967).

[12] E. Z. Napuch and E. A. Nechaev, *Zashchita Metallov*, **6**, 710 (1970).

[13] V. Gurylev, *Zhur. priklad. Khim*, **37**, 1053 (1964).

[14] L. Domnikov, *Metal Finish.*, **67**, 59 (1969).

[15] A. T. Vagramyan and V. N. Titova, *Oberflaeche-Surface*, **9**, 169 (1969).

[16] J. Glayman, *Galvano*, **37**, 819 (1968).

[17] E. K. Yastrebova and A. T. Vagramyan, *Zhur. fiz. Khim.*, **38**, 1551 (1964).

[18] E. K. Yastrebova and A. T. Vagramyan, *Zhur. fiz. Khim.*, **38**, 2503 (1964).

[19] A. T. Vagramyan and E. K. Yastrebova, *Zhur. fiz. Khim.*, **39**, 865 (1965).

[20] Yu. M. Loshkarev, *Khim. Tekhnol.*, **1967**, 67.

[21] E. A. Necheaev, E. Z. Napuch and N. T. Kudryavtsev, *Elektrokhimiya*, **3**, 1493 (1967).

[22] Yu. M. Loshkarev, V. N. Kovtun and Yu. M. Ivanchenco-Urskii, *Elektrokhimiya*, **5**, 560 (1969).

[23] O. Radovici and C. Vass, *Rev. Roumaine Chim.*, **14**, 1099 (1969).

RESULTS AND DISCUSSIONS

Current pulses of $5 \times 10^{-3} - 1 \times 10^{-2}$ sec have been used, current density being in the $6 \times 10^{-1} - 50$ mA·cm^{-2} range (considering 1 cm^2 of the geometrical area of the copper deposited before the run). Steady-state overpotential values were obtained and from semilogarithmic plots of the overpotential versus current density straight lines resulted for overpotential values greater than 40 mV. In fig. 1 this Tafel type dependence is presented for the solution of 5×10^{-2} M Cu^{2+} concentration at 60°. By extrapolating linear portion the exchange current density value i_0 was calculated.

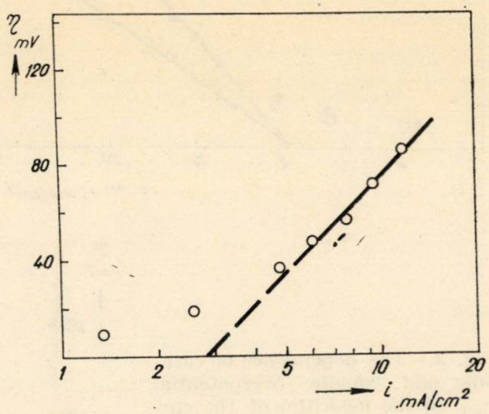

Fig. 1.—The dependence of cathodic overpotential η_{mv} on the logarithm of the current density i_{mA/cm^2}. $C_{Cu^+} = 5 \times 10^{-2}$ M.

Before each cathodic pulse an equal size anodic pulse was applied and a similar linear dependence between $\eta - \log i$ was obtained. In figures 2 and 3, cathodic and anodic curves for 2.5×10^{-1} and 1×10^{-1} M Cu^{2+} solutions are presented. The extrapolation of linear fragments for zero overpotential gives common values for the exchange current density, which allows us to state that the rate of both reactions is determined by the same process.

The dependence of cathodic overpotential on the logarithm of current density is described by a Tafel relationship up to values of the current density not higher than the limit of 10 mA·cm^{-2}. This fact leads us to the conclusion that, within this range the rate determining step of the entire reaction is the charge transfer.

The slopes of cathodic and anodic curves in this region take values, within the 100—130 mV range, approximately equal to the 2.3 RT/F ratio, which shows that a monovalent ion takes part in the reaction.

From the Tafel equation used for cathodic and anodic curves the values of the transfer coefficients α_c and α_a for the corresponding processes were calculated. In table 1 the values of the cathodic and anodic transfer coefficients α_c and α_a, respectively, and of the exchange current density i_0 are presented for the studied concentrations at 60°.

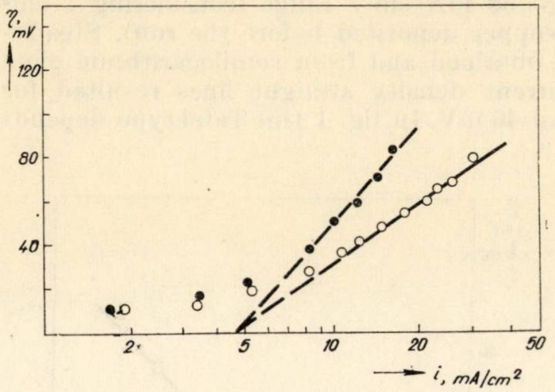

Fig. 2. — The dependence of cathodic and anodic overpotential η_{mv} on the logarithm of the current density $i_{mA/cm^2} \cdot C_{Cu^{2+}} = 2.5 \times 10^{-1}$.

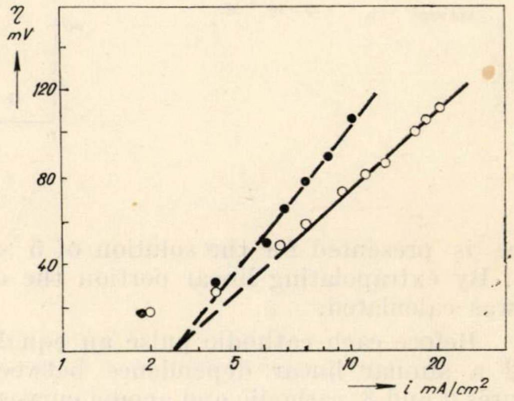

Fig. 3. — The dependence of cathodic and anodic overpotential η_{mv} on the logarithm of the current density $i_{mA/cm^2} \cdot C_{Cu^{2+}} = 1 \cdot 10^{-1}$ M.

Table 1

Kinetic parameters of copper electrodeposition from pyrophosphate electrolyte of different concentrations in Cu^{2+} at 60°

$C_{Cu^{2+}, M}$	$i_{0\,mA \cdot cm^{-2}}$	α_c	α_a
1×10^{-2}	2.45	0.39	0.55
5×10^{-2}	2.8	0.36	0.88
1×10^{-1}	3	0.38	0.82
2.5×10^{-1}	4.6	0.47	0.77

One can see from the table that the sum of cathodic and anodic transfer coefficients is approximately equal to 1.

From the plots of values η_{Ω} versus current density a straight line is obtained, which corresponds to the Ohm law, and from which the resistance of the layer between the working electrode and Luggin capillary,

R_Ω, is calculated. This value is constant for all the current density range used and depends only on the solution composition and working temperature (figure 4).

From the linearity of η versus $\log i$ for the studied solutions and from the commun values of i_0 of the two processes it comes out that the rate determining step of Cu^{2+} discharge reaction is the charge transfer.

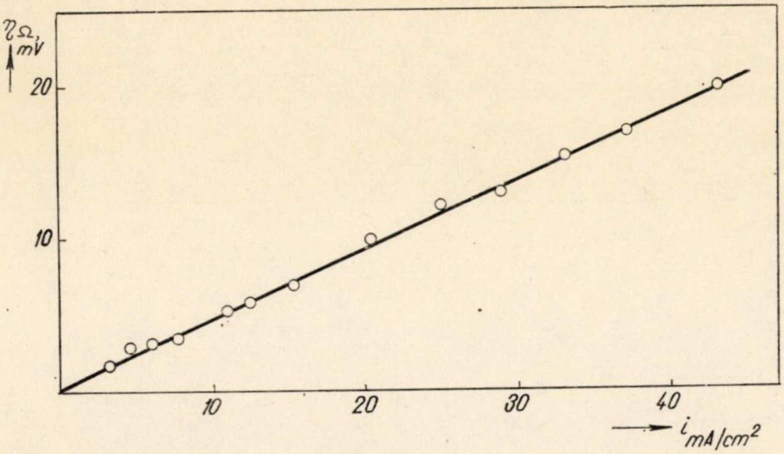

Fig. 4. — The dependence of ohmic overpotential $\eta_{\Omega mV}$ on the logarithm of the current density $i_{mA/cm^2} \cdot R_\Omega = 0.45\Omega \cdot cm^{-2}$.

Taking into account the difference between the slopes of the $\eta - \log i$ plots for cathodic and anodic processes, b_c and b_a, it may be considered that the rate determining step of the transfer process is the $Cu^{2+} \rightarrow Cu^+$ conversion, which is in good agreement with the results obtained at the copper electrodeposition from sulphate solutions. [24,25]

The R_Ω values and the proportionality between R_Ω and the distance capillary-working electrode for constant current density show that, as the current increases no oxide or hydroxide layers are formed, the electrode surface being identical to the initial one.

---

[24] J. O'M. Bockris and E. Mattson, *Trans. Faraday Soc.*, **55**, 1586 (1959).
[25] O. Radovici and C. Vass, *Rev. Roumaine Chim.*, **12**, 1181 (1967).

Revue Roumaine de Chimie, **18**, 7, 1111–1119 (1973)

THE ELECTRONIC STRUCTURE OF LADDER POLYMERS. II

EXCITED STATES OF *CATA*-CONDENSED BENZENES, PYRAZINES AND PYRIDINES

PETER G. PERKINS

Department of Pure and Applied Chemistry
University of Strathclyde
Glasgow, C. 1, Scotland

Received January 17, 1973

Studies are made, by the Pariser-Parr-Pople method, of the electronic states of a number of linear polyacenes, polypyrazines, and polypyridines. It is found that the first excited-state energies tend to a limit for each series and the extrapolated values agree well with the experimental activation energies for dark conductivity. Valence and conduction π bands of $\sim$ 8eV width are calculated. It is further found that the π energy per ring also tends to a limit as the number of rings in the molecule increases.

INTRODUCTION

An earlier paper[1] has dealt with the electronic band structures of some ladder polymers based on benzene, pyrazine, and pyridine. All valence electrons were considered in the treatment and, from the electronic bands and computed densities of states, it was concluded that, although band overlap occurs for all the systems at the zone edge near $\mathbf{k} = \pi/a$, there will be an effective band gap width. Furthermore, the states situated at either side of the latter are mainly of π and π^* type. Experimentally it is known[2] that the absolute electrical conductances of these materials are sizeable, although they do appear to possess a band gap of *ca.* 1eV.

In the present work we have followed up the previous treatment by studying the important π states in a more sophisticated manner. This was so as to take account of the configuration interaction in the excited levels and also so as to interdistinguish the singlet and triplet excited states. Neither of these features were included in the previous study. A further aim in the work was to investigate how the "band gap" between the ground and any set of excited states varies as one increases the length (*i.e.*, the number of rings) in a *cata*-condensed system. Some years ago, Peacock and Wilkinson [3] carried through calculations similar to ours on the first nine members of the polyacene series and concluded that, with increasing chain length, the first excited singlet states would converge to a limit of ~ 18000 cm^{-1}. These calculations were repeated here, firstly to try and improve agreement with experiment and, secondly, so as to erect a scheme consistent with extended calculations on nitrogen-containing systems.

---

[1] P. G. Perkins, *Rev. Roumaine Chim.*, in press.
[2] J. Graham and D. I. Packham, *Polymer*, **10**, 645 (1969).

In all the calculations we used the Pariser-Parr-Pople approach, [4] since it is a well-established and reliable method for molecules in which $\sigma-\pi$ interaction should not be strong The calculational method is too well known to require discussion here. Bond lengths were abstracted from Ref. [5] and, for the higher series members, the bond lengths for anthracene were employed. Spectral energy predictions fortunately do not rely very heavily on these geometrical parameters. The diagonal core Hamiltonian and the electron repulsion matrix elements are given in table 1.

Table 1

Input data (eV)

	C	N
$H_{\mu\mu}$	-11.16	-11.95
$\gamma_{\mu\mu}$	9.76	11.07

In calculating the energies of the excited states, all possible transitions between the three highest-bonding and the three lowest-antibonding levels were taken into account, with all configuration interaction between the nine singlet and nine triplet states.

RESULTS AND DISCUSSION

The results are most usefully presented under three heads.

POLYACENES

a. *Excited States*

Calculations on the polyacene series have previously been performed by both a self-consistent field method [3] and by a configuration interaction treatment [6] for the ground and excited states.

---

[3] T. E. Peacock and P. T. Wilkinson, *Proc. Phys. Soc.*, London, **83**, 525 (1964).

[4] R. Pariser and R. G. Parr, *J. Chem. Phys.*, **21**, 446 (1953); J. A. Pople, *Trans. Farad. Soc.*, **49**, 1375 (1953).

[5] "Interatomic Distances in Molecules and Ions", *Chem. Soc. Special Publ.*, London, **1958**, 11.

[6] R. Pariser, *J. Chem. Phys.*, **24**, 250 (1956).

Our calculated energies are generally in good agreement with both the work cited above and with experimental data (quoted in Pariser's paper [6]). For brevity, we shall not reproduce all our calculated energies here but quote only relevant results for naphthalene and anthracene (table 2). The essential conclusion from table 2 is that our results agree at least as well with experiment as those of the previous workers.

Table 2

Excited states for naphthalene and anthracene

	Symmetry	Energy (eV)	f	Experimental results
Naphthalene	$^{1}B_{3\mu}^{-}$	4.11	0	3.97^{d} $f \sim 0^{c}$
		4.39^{a}	0	
		4.02^{b}	0	
	$^{1}B_{2\mu}^{+}$	4.42	0.16	4.33^{d} $f = 0.18^{c}$
		4.39^{a}	0.21	
		4.49^{b}	0.26	
	$^{3}B_{3\mu}^{+}$	4.19	0	3.7^{c}
		4.04^{a}	0	
		3.64^{b}	0	
	$^{3}B_{2\mu}^{+}$	2.97	0	2.63^{e}
		2.57^{a}	0	
		2.18^{b}	0	
Anthracene	$^{1}B_{2\mu}^{+}$	3.40	0.30	3.28^{d} $f = 0.10^{c}$
		3.56^{a}	0.37	
		3.65^{b}	0.39	
	$^{1}B_{3\mu}^{-}$	4.12	0	4.88^{d} v. intense
		4.11^{a}	0	
		3.72^{b}	0	
	$^{3}B_{2\mu}^{+}$	2.13	0	1.85^{f}
		1.78^{a}	0	
		1.66^{b}	0	

[a] data taken from ref. [3]: the authors give calculated energies in wave numbers ($\bar{\nu}$). These have been converted to eV and rounded to two decimal places.

[b] data taken from ref. [6] and rounded to two decimal places.

[c] experimental data quoted in ref. [6] (although not measured by the author of that paper).

[d] taken from "Theory and Applications of Ultraviolet Spectroscopy", H. H. Jaffé and D. M. Orchin, Wiley, New York, 1962, p. 303, 316.

[e] H. Shull, *J. Chem. Phys.*, **17**, 295 (1949).

[f] S. P. McGlynn, M. R. Padhye, and M. Kasha, *J. Chem. Phys.*, **23**, 593 (1955).

For pyrazine and pyridine the results are also in satisfactory agreement with experiment.

b. *Energy Gaps*

Figure 1 is a plot of the first excited singlet and triplet state energies and the orbital energy gaps for the polyacenes *vs.* the number of rings in the polymer.

It is clear immediately that, for the polyacenes, the energies of all the above quantities are initially rapidly decreased as the number of rings in the system increases. A levelling-out effect is evident, however, when the latter number exceeds five or six. Further extrapolation of the curve suggests that a limiting value near 1.0 eV would be expected for a long-chain polyacene polymer. Now the energy gap; ΔE, calculated from the change in dark conductivity with temperature for hexacene, using the expression,

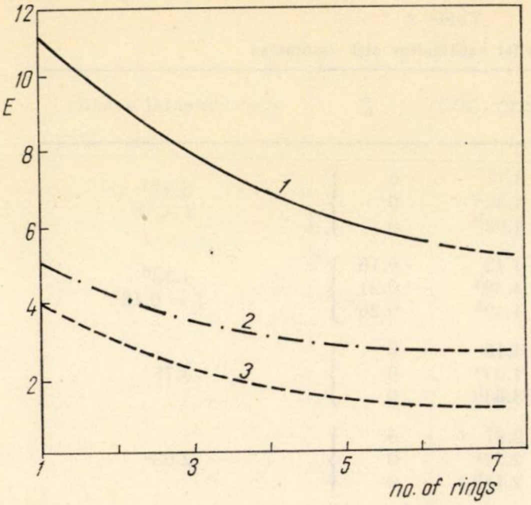

Fig. 1. — Calculated energies vs chain length for polyacenes. *1*, bonding-antibonding gap; *2*, singlet state energies; *3*, triplet state energies.

$$\sigma = \sigma_0 \exp\left(-\Delta E/2kT\right)$$

has variously been reported as 1.14 [7] and 1.3 eV [8] and, moreover, it has been suggested that the same value would be appropriate for a long-chain polymer. [7] Whichever of the known values is the best, from figure 1, clearly the energies of both the first excited singlet and the bonding-antibonding orbital gap are too large to account satisfactorily for the semiconductivity observed.

The limiting energy of the first singlet-triplet excitation is, however, in good agreement with the experimental value. It has been argued[9a] that the triplet state of a single molecule in a crystal is non-conducting since the excited electron is correlated with the hole. Moreover the energy of excitation to the triplet state will be different from that of a conduction state where electron and hole are widely separated and independent. However for polymers of the type considered here the electron and hole can be well physically separated in the triplet state purely by the form of the eigenvectors in the depopulated and excited orbital. Hence we would expect that hopping of electrons and holes to adjacent molecules would be facilitated by increasing the chain length of the molecule. Eley and Willis[9b] have postulated a model for a series of such transfers through an intermolecular barrier. The initial step they postulate involves the separation of hole and electron after excitation of the latter.

---

[7] Y. Okamoto and W. Brenner, "Organic Semi-Conductors", Reinhold, New York, 1964, p. 42—45.

[8] D. C. Northrop, *Proc. Phys. Soc.*, London, **74**, 756 (1959).

[9a] H. Kallmann and M. Silver, "Electrical Conductivity of Organic Solids", Interscience, New York, 1961, p. 243; [b], p. 257.

Figure 2 shows the singlet, triplet and bonding-antibonding gaps for condensed pyrazines. Again, it is clear that only the triplet states are

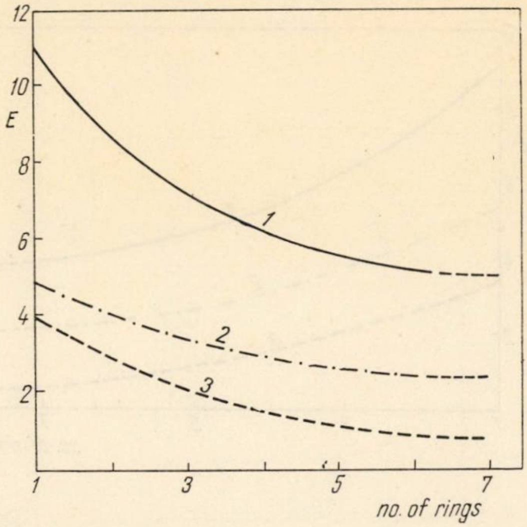

Fig. 2. — Calculated energies vs chain length for pyrazines. *1*, bonding-antibonding gap ; *2*, singlet state energies ; *3*, triplet state energies.

of low enough energy to correlate with the observed activation energy (1.18eV) for paracyanogen. [2] Extrapolation of the triplet state energies leads to a limiting value of 1.18eV.

In order to study the behaviour of intermediate molecules, the *cata*-condensed pyridines were also studied. Here there are two regular isomers in which the nitrogen atoms are on the same side of the ladder or where they alternate thus :

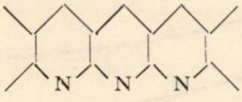

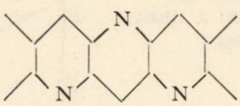

Again, a similar series of calculations was carried through for systems of both types and we find that the change in energy, with increase in chain length (figures 3 and 4), shows similar behaviour to the polyacene and polypyrazine cases. Hence, we would predict that a polyacrylonitrile of the form

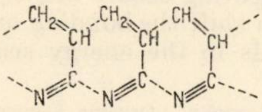

would show a band gap near 0.5 eV and, moreover, alternation of the nitrogen atoms would have little or no effect on this property. It has been found [10] that polyacrylonitrile pyrolysed under various conditions leads to a material with a forbidden gap of ~ 0.2eV.

The diminution in the band gap for the nitrogen-containing compounds as against the polyacenes stems from the participation of nitrogen in the highest bonding and lowest virtual orbitals. In a long-chain polypyridine, nitrogen is heavily weighted in both the above orbitals, whilst in a polypyrazine this weighting occurs heavily only in the bonding level. The effect of nitrogen is to shift the bonding orbital upwards and the antibonding orbital downwards in the energy scale.

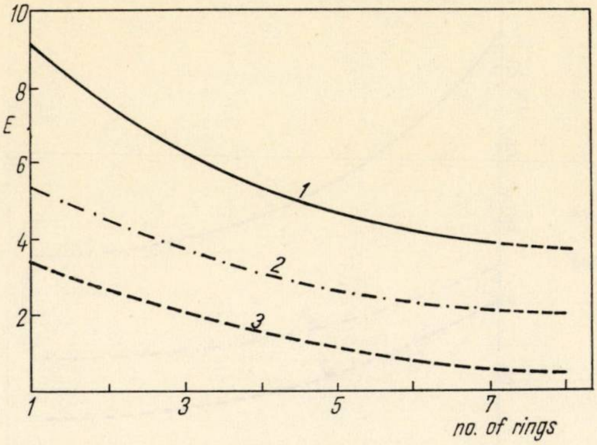

Fig. 3. — Calculated energies vs chain length for pyridines.
1, bonding-antibonding gap ; *2*, singlet state energies ; *3*, triplet state energies.

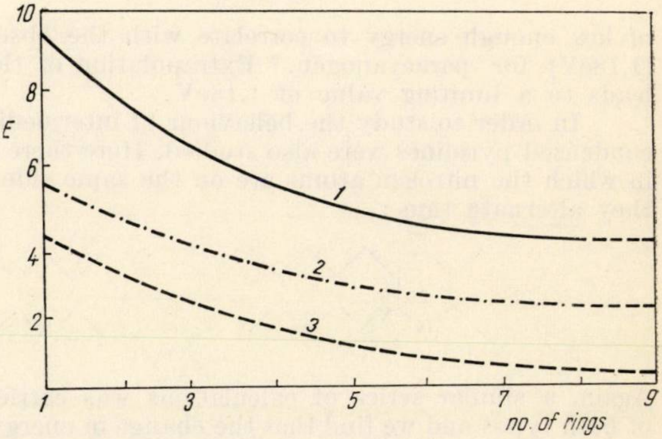

Fig. 4. — Calculated energies vs chain length for altering pyridines.
1, bonding-antibonding gap, *2*, singlet state energies; *3*, triplet state energies.

---

[10] J. J. BROPHY and J. BUTTREY, "Organic Semiconductors", MacMillan, New York, 1962, p. 169.

c. *Band Widths*

Figure 5 shows how the one-electron orbital energies are spread in the polyacenes as the number of rings increases. (In this context we use energy levels rather than states, as we have not calculated sufficient states for them to be truly representative of the molecules.) Clearly, the spread of levels is limited and rapidly converges on valence and conduction bands with widths of just less and just greater than 8eV, respectively. For polypyrazine and the two polypyridines, the effects are quantitatively similar and need not be expanded on here.

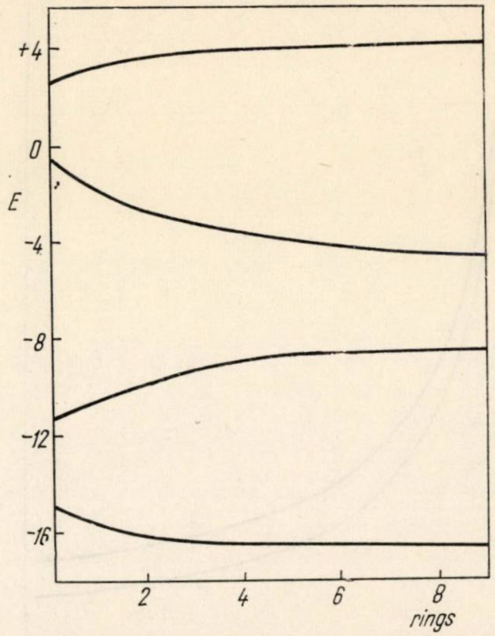

Fig. 5. — Band widths for polyacenes.

These may be compared with the results found from the band-structure calculations of the previous work,[1] where the overall π band widths *in toto* were found to be much greater (between 17 and 30eV). The π^* bands are much more comparable : by the solid-state method we obtain band widths between 3 and 8 eV for the different materials.

When one looks at the region where most of the bonding states lie, then the band widths calculated by the two methods are much closer. This is particularly true for the solid-state calculations in which the MWH factor, $A = 1$ since, in the SCF calculations, in effect we are using the same scaling factor.

The width of the bands here leads to low effective mass for both hole and electron just as we found in the solid-state calculations. This correlates with the high mobility observed [10] in the experiments on pyrolysed polyacrylonitrile.

d. *Electronic π Energy of the Polymers*

Figure 6 shows the change in π energy per ring as a function of the number of rings. The polyacene systems (curve *A*) retain greater energy at all stages than do the polypyrazines (curve *B*). Polypyridines behave almost identically to polypyrazines. It is interesting that the stabilizing ring delocalization energy falls off so rapidly with chain length, and this feature is consistent with the experimental observation that polyacenes containing more than seven rings are unstable.[11]

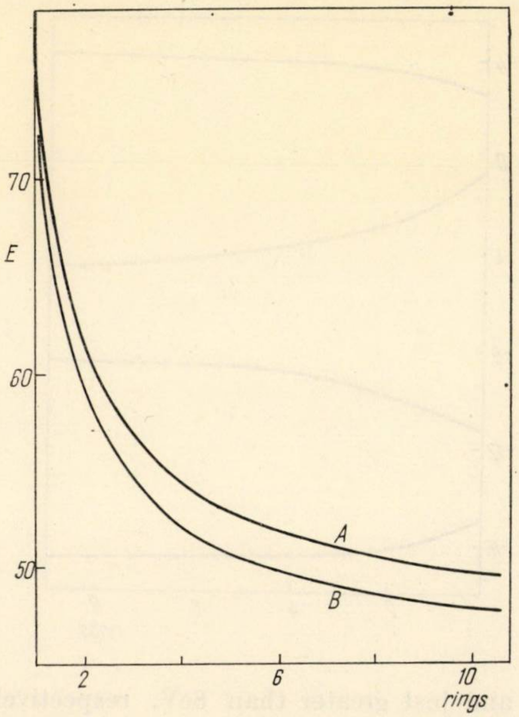

Fig. 6. — Electronic π energy for *cata*-condensed systems.
A, polyacenes; B, polypyrazines.

e. *Physical Properties*

The total conductance at any given temperature depends on the number of charge carriers in the activated state, their nature and their mobility. Firstly, the number of charge carriers depends (to first order) on the activation energy for the system; in our cases, we suggest that this is essentially the first triplet energy. Secondly, the mobility of the charge carriers depends on the forces opposing their movement in the crystal. In the "infinite" ladder polymers, we may suppose that the latter forces are "small" and, hence, a high absolute conductance should be observed.

---

[11] I. A. Misurkin and A. A. Ovchinnikov, *Theoret. chim. Acta*, **13**, 115 (1969).

However, for molecules such as anthracene, electrons have to leave one molecule under the influence of the applied potential and drift to another. This clearly involves passing through energy barriers between pairs of molecules.

Eley [9b] has considered this problem in related systems in terms of the crystal forming a number of linked potential wells in a cascade: here the steepness of the cascade is a function of the applied voltage. The electrons are then supposed to tunnel from the excited states of one molecule to another under the influence of the potential.

In considering how this situation determines σ_0, then it would seem reasonable that σ_0 would vary in a way dependent on the number of intermolecular barriers per unit length. Thus we should, in general, find an increase in σ_0 with chain length for crystals of *cata*-condensed hydrocarbons, since with increase in chain length a greater proportion of the unit cell is given over to molecular "path". Experiment does in fact confirm this. [4]

A further interesting aspect of the calculated data is the fact that convergence on the measured ΔE is achieved with *only a relatively short chain length* ($\sim$ 10 rings). This means that in a solid material, only *short-range* order appears to be required for the substance to exhibit the conductance temperature coefficient of the infinite ordered polymer (although the σ_0 value might well be different). This has interesting implications for the electrical properties of amorphous materials, where there may be regions of short-range order chemically bonded through randomised areas to each other.

However, for much of the work it is true that, electrons have to move from [illegible] under the influence of the applied potential and tend to [illegible] [illegible] a [illegible] through energy barrier between pairs of molecules.

[illegible] has considered this problem in crystal systems in terms of the model forming a number of [illegible] potential wells in a [illegible] form; the [illegible] of the electrode is a function of the applied voltage. The electrons are then supposed to tunnel from the excited states of one molecule to another under the influence of the potential.

In considering how the activation energy, ϵ, [illegible] then it would seem reasonable that ϵ would vary in a way dependent on the number of [illegible] between [illegible] length. Thus we should, in general, find a decrease in ϵ with chain length for crystals of a [illegible] order [illegible], i.e. with increase in chain length a greater proportion of the unit cell is given over to molecular "spots". Experiment does in fact confirm this.

A further interesting aspect of the calculated data is the fact that convergence on the [illegible] ΔE is achieved with only a relatively short chain length (~ 10 rings). This means that in a solid material, only short-range order appears to be required for the substance to exhibit the conductance properties characteristic of the highly ordered polymer, although the ϵ value might well be different. This has interesting implications for the electrical properties of amorphous materials, where there may be regions of short-range order chemically bonded through conjugated atoms to each other.

Revue Roumaine de Chimie, **18**, 7, 1121−1129 (1973)

L'ÉTUDE DE LA RÉACTION D'OXYDATION DE L'HYDROGÈNE SUR LES ÉLECTRODES POREUSES EN NICKEL

MARIA MAVRODIN-TĂRĂBÎC, IOANA ONACA et I. SOLACOLU

Centre de Chimie physique, Bucharest, 31, str. Galaţi

Reçu le 6 janvier 1973

On a réalisé une série d'électrodes poreuses en nickel de type MSK (« Mono Skelet Katalyst ») à petits pores, de type MSK à grands pores et de type DSK (« Doppel Skelet Katalyst »), caractérisées par des porosités comprises entre 57 et 68 %. Les électrodes ont été caractérisées au point de vue structural, par examen microscopique. On a étudié la cinétique de la réaction d'oxydation de l'hydrogène, en utilisant la technique potentiostatique et on a calculé les valeurs des constantes Tafel, pour chaque type d'électrode, à différentes surpressions de l'hydrogène.

Pour réaliser des systèmes de piles à combustible à grande efficacité et à un prix de revient relativement bas, on a étudié, ces dernières années, un grand nombre de systèmes d'électrodes en nickel, chose illustrée aussi par les nombreux travaux publiés dans ce domaine après 1960. Les électrodes poreuses en nickel se caractérisent par des propriétés catalytiques supérieures et par une résistance chimique et mécanique élevée. Parmi les électrodes en nickel que l'on a étudiées, ce sont les types suivants qui présentent le plus d'efficacité : les électrodes poreuses en nickel poreux frittées, [1−14] les électrodes en nickel Raney [15−19] et les électrodes à base de borure de nickel. [20,21]

---

[1] V. A. Tracy et N. J. Williams, *Electrochem. Technol.*, **3**, 17 (1965).

[2] J. Jasinski, U. S. Pat. 3 183 124, 11 mai 1965 ; *Chem. Abstr.*, **63**, 5244b (1965).

[3] V. A. Tracy, *Powder Met.*, **8**, 241 (1965).

[4] I. Przyluski, *Przemysl. Chem.*, **44**, 679 (1965) ; *Chem. Abstr.*, **64**, 7670c (1966).

[5] H. Scheibe, Ger. Pat. (Est) 47 212, 5 avril 1966 ; *Chem. Abstr.*, **64**, 11771b (1966).

[6] A. Rogers, U. S. Pat. 3 287 169, 22 novembre 1966 ; *Chem. Abstr.*, **66**, 25477 m (1967).

[7] H. Oswin, U. S. Pat. 3 291 643, 13 décembre 1966 ; *Chem. Abstr.*, **66**, 34274v (1967).

[8] R. L. Lambert, U. S. Pat. 3 323 915, 6 juin 1967 ; *Chem. Abstr.*, **67**, 60346k (1967).

[9] G. Sandstede, U. S. Pat. 3 382 067, 7 mai 1968 ; *Chem. Abstr.*, **69**, 32525r (1968).

[10] E. P. Weber, U. S. Pat. 3 409 473, 5 novembre 1968 ; *Chem. Abstr.*, **70**, 16647x(1969).

[11] F. Roberts, U. S. Pat. 3 471 287, 7 octobre 1969 ; *Chem. Abstr.*, **71**, 118992u (1969).

[12] D. Pouli et T. L. Larson, Ger. Pat. 1 812 736, 21 août 1969 ; *Chem. Abstr.*, **71**, 87181x (1969).

[13] Brown Boveri, A.-G., Fr. Pat. 1 553 750, janvier 1969 ; *Chem. Abstr.*, **72**, 17904g (1970).

L'oxydation de l'hydrogène dans les électrodes poreuses, en milieu alcalin, à des températures inférieures à 90° C, a lieu selon l'équation générale :

$$H_2 + 2\,OH^- \rightleftarrows 2\,H_2O + 2e^-$$

en deux étapes [22] : dans la première étape l'hydrogène est adsorbé à l'intérieur du réseau catalytique actif de l'électrode où, dans la deuxième étape, a lieu la réaction avec le radical OH^- :

$$H_{2\,(ads)} \rightarrow 2H_{(ads)}$$

$$2H_{(ads)} + 2\,OH^- \rightarrow 2H_2O + 2e^-$$

Le développement de la réaction d'oxydation électrochimique de l'hydrogène dans les électrodes à gaz comprend trois étapes lentes : le transport de l'hydrogène dissous dans l'électrolyte vers la surface active de l'électrode (dans la zone triphasique de réaction), la conversion électrochimique de l'hydrogène moléculaire en ions d'hydrogène et le transport des ions d'hydrogène de l'intérieur de l'électrode vers l'électrolyte. Dans ce mécanisme de réaction on considère que le transport de l'hydrogène gazeux à la surface du liquide et sa dissolution dans l'électrolyte est un processus rapide, la concentration de l'hydrogène à la surface du liquide restant constante.

La vitesse totale du processus d'oxydation de l'hydrogène est contrôlée par ces étapes lentes (un processus électrochimique entre deux processus de transport). En conséquence, la vitesse de la réaction est sensiblement influencée par l'activité du catalyseur et par la géométrie de l'électrode à gaz.

★

Dans ce travail nous nous sommes proposé d'étudier la réaction d'oxydation de l'hydrogène sur une série d'électrodes poreuses en nickel, de structure et de porosité différentes et de déterminer la corrélation entre les performances électrochimiques et la structure des électrodes.

[14] M. Lang et R. Pasquale, Ger. Pat. 1 942 111, 26 fevrier 1970 ; *Chem. Abstr.*, **73**, 51648g (1971).

[15] A. Winsel et E. Justi, U. S. Pat. 3 150 011, 22 septembre 1964 ; *Chem. Abstr.*, **61**, 14193a (1964).

[16] E. Justi et K. H. Friese, U. S. Pat. 3 126 273, 24 mai 1964 ; *Chem. Abstr.*, **60**, 14129c (1964).

[17] E. Justi, K. H. Friese et A. Winsel, U. S. Pat. 3 201 282, 17 août 1965 ; *Chem. Abstr.*, **71**, 66736s (1969).

[18] A. Winsel, Ger. Pat. 1 280 362, 17 octobre 1968 ; *Chem. Abstr.*, **70**, 16748y (1969).

[19] E. Justi, H. J. Thuy et A. Winsel, Ger. Pat. 957 491, 7 fevrier 1957 ; *Chem. Abstr.*, **53**, 13844f (1960).

[20] R. J. Jasinski, *Electrochem. Technol.*, **3**, 40 (1965).

[21] R. J. Jasinski, *Electrochem. Technol.*, **3**, 129 (1965).

[22] A. B. Hart et G. J. Womack, « Fuel Cells. Theory and Applications », Chapman and Hall Ltd., Londres, 1967, p. 86.

PARTIE EXPÉRIMENTALE

1. ÉLECTRODES

Les électrodes ont été obtenues par homogénéisation d'un mélange de nickel carbonyle, de carbonate de nickel et de deux types de poroformateurs (bicarbonate d'ammonium et chlorure de sodium).

Le carbonate de nickel a été préparé par précipitation, en utilisant du chlorure de nickel et du carbonate de sodium. (Toutes les substances utilisées ont été de pureté *p.a.*)

Pour obtenir la structure désirée, les constituants des mélanges ont eu la granulation suivante : nickel carbonyle — au-dessous de 5 microns, carbonate de nickel — au-dessous de 5 microns, bicarbonate d'ammonium et chlorure de sodium — environ 40 à 60 microns.

Les mélanges ont été homogénéisés, par voie sèche, pendant 4 heures et par voie humide en agitant avec du benzène, en sédimentant, en décantant et en séchant.

Des quantités prélevées sur ces mélanges ont été pressées dans des matrices en acier inoxydable, à une pression de $2{,}8.10^8$ N/m^2.

Les électrodes obtenues, de forme cylindrique, à un diamètre de 10 mm et à une épaisseur de 3 mm, ont été soumises à un traitement thermique pour former la structure poreuse, à l'activation et au frittage en chauffant à 700°, dans une atmosphère d'hydrogène.

Pendant le traitement thermique, les poroformateurs se décomposent, avec la formation dans la masse du matériel de certains pores à petits diamètres (le carbonate de nickel) et à grands diamètres (le bicarbonate d'ammonium). Le chlorure de sodium a été utilisé en vue d'une réduction des contractions des électrodes. Après le frittage, le chlorure de sodium a été éloigné en maintenant les électrodes dans de l'eau, à 90°, pendant 10 heures.

2. L'ÉTUDE DE LA STRUCTURE DES ÉLECTRODES

Les électrodes ont été caractérisées au point de vue structural par :

— l'étude de la répartition des pores par un examen microscopique à l'aide d'un microscope métallographique de réflexion de type MIM-7 ;

— des déterminations de la porosité totale, en pesant les échantillons avant et après l'imprégnation avec du toluène.

3. LES MESURES ÉLECTROCHIMIQUES

L'étude de la cinétique de la réaction d'oxydation de l'hydrogène a été effectuée par technique potentiométrique, à l'aide d'un montage classique, en utilisant un potentiostat Tacussel de type PRT 500 LC, un millivoltmètre électronique Radiometer 22 (précision ± 1 mV), un milliampèremètre (classe de précision 0,5).

Comme électrode de référence on a utilisé un électrode de calomel saturé.

On a appliqué des niveaux de potentiel de 10 à 50 mV, à un intervalle de temps de 5 minutes, jusqu'à la valeur finale.

La cellule de travail (dimensions 120 × 72 × 56 mm) a été confectionnée en polystyrène.

Comme électrode auxiliaire on a utilisé une spirale de nickel de grande pureté.

L'alimentation des électrodes avec de l'hydrogène, à pression constante, a été réalisée à l'aide d'une installation classique. [23]

Les courbes de polarisation $\eta - i$ ont été déterminées pour différentes surpressions de l'hydrogène comprises entre 100 et 600 mm Hg.

Les déterminations ont été effectuées à la température ordinaire, en utilisant comme électrolyte une solution de KOH 5N.

RÉSULTATS ET DISCUSSIONS

1. CARACTÉRISATION DES ÉLECTRODES AU POINT DE VUE STRUCTURAL

En établissant les différentes compositions des mélanges (tableau 1) on a obtenu des électrodes à gaz caractérisées par des structures différentes :

— structure de type MSK («Mono Skelet Katalyst»), avec un seul type de pores : les électrodes A_1 et A_2 (à petits pores) et les électrodes A_3 et A_4 (à grands pores) ;

— structure de type DSK («Doppel Skelet Katalyst»), les électrodes A_5 et A_6 (à grands et à petits pores).

En variant le rapport entre la substance active et les poroformateurs, on a obtenu des électrodes caractérisées par des porosités très variées. Les valeurs de la porosité totale, présentées dans le tableau 1, ont été comprises entre 57% (l'électrode A_3) et 68% (l'électrode A_1).

L'examen microscopique a démontré, ainsi qu'on le voit dans les microphotographies présentées dans les figures 1 et 2, que les pores, petits et grands, sont uniformément répartis dans la masse de l'électrode.

2. LE COMPORTEMENT DES ÉLECTRODES DANS LA RÉACTION D'OXYDATION DE L'HYDROGÈNE

En vue d'établir une corrélation entre la structure des électrodes et leur comportement dans la réaction d'oxydation de l'hydrogène, on a fait des études, par la technique potentiostatique, à des surpressions de l'hydrogène comprises entre 100 et 600 mm Hg. Les courbes $\eta - i$ déterminées sont représentées dans les figures 3 à 8. (Les valeurs des densités du courant sont rapportées à la surface géométrique de l'électrode.)

On constate que, dans le cas de toutes les structures et des valeurs de la porosité des électrodes, l'augmentation de la surpression de l'hydrogène a un effet favorable sur la réaction, en déplaçant les courbes de polarisation vers des valeurs plus négatives. Il y a une surpression optimale, située entre la surpression de « bullage » et la surpression de « noyage », à laquelle la surtension atteint sa moindre valeur ; la valeur de cette surpression est de 400 mm Hg dans le cas des électrodes A_1 et A_3 et de 200 mm

---

[23] O. Radovici, M. Mavrodin-Tărăbîc, I. Onaca et I. Solacolu, *Rev. Roumaine Chim.*, **17**, 1153 (1972).

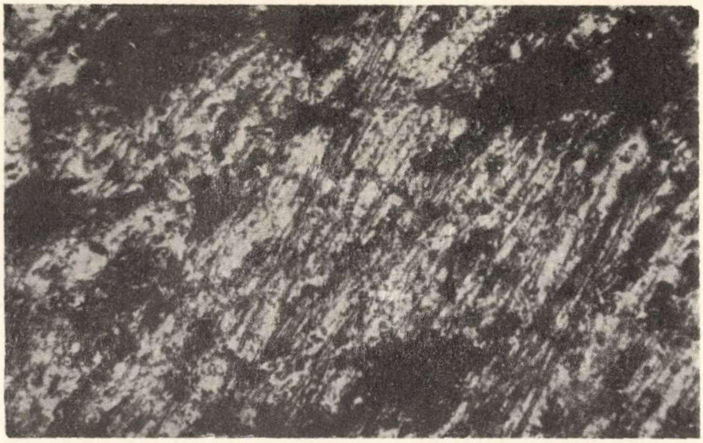

Fig. 1. — La structure de l'électrode A_4 de type MSK à grands pores. Microphotographie, 500 ×.

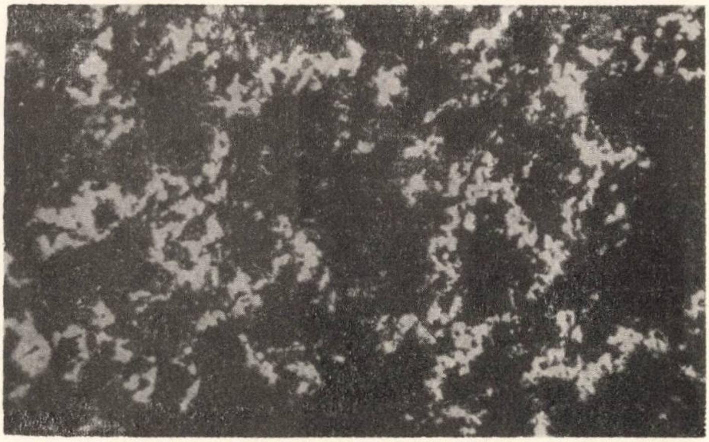

Fig. 2. — La structure de l'électrode A_6 de type DSK. Microphotographie, 500 ×.

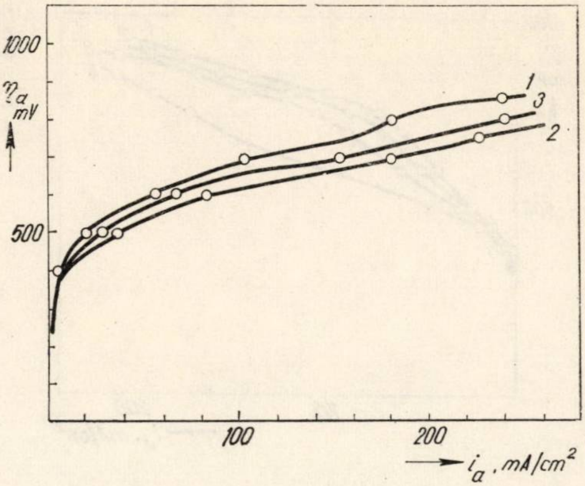

Fig. 3. — Courbes de polarisation $\eta - i$ caractéristiques pour la réaction d'oxydation de l'hydrogène sur l'électrode à gaz A_1.
1, ΔP_{H_2} = 300 mm Hg; 2, ΔP_{H_2} = = 400 mm Hg; 3, ΔP_{H_2} = 500 mm Hg.

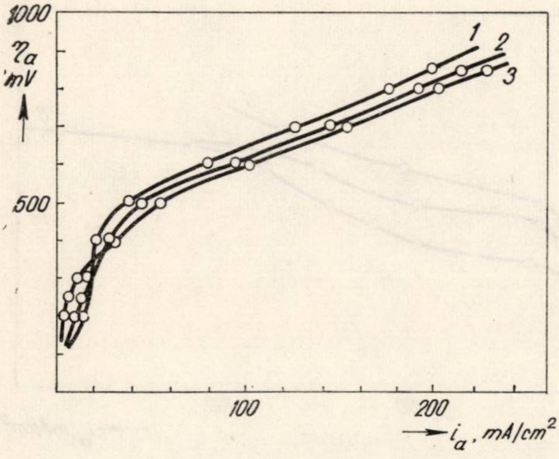

Fig. 4. — Courbes de polarisation $\eta - i$ caractéristiques pour la réaction d'oxydation de l'hydrogène sur l'électrode à gaz A_2.
1, ΔP_{H_2} = 250 mm Hg; 2, ΔP_{H_2} = = 400 mm Hg; 3, ΔP_{H_2} = 550 mm Hg.

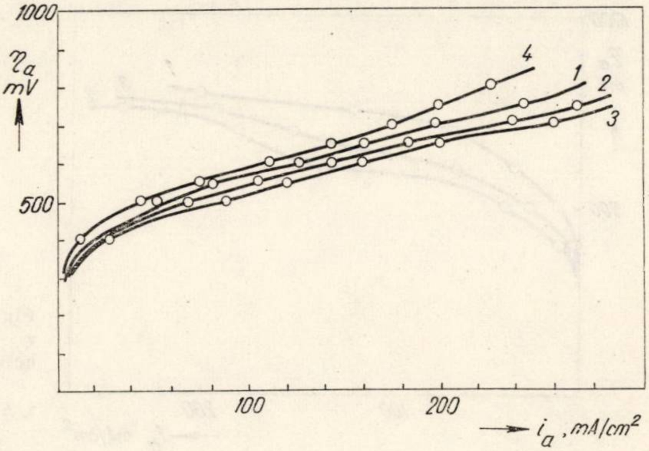

Fig. 5. — Courbes de polarisation $\eta - i$ caractéristiques pour la réaction d'oxydation de l'hydrogène sur l'électrode à gaz A_3.
1, ΔP_{H_2} = 100 mm Hg; 2, ΔP_{H_2} = = 300 mm Hg; 3, ΔP_{H_2} = 400 mm Hg; 4, ΔP_{H_2} = 500 mm Hg.

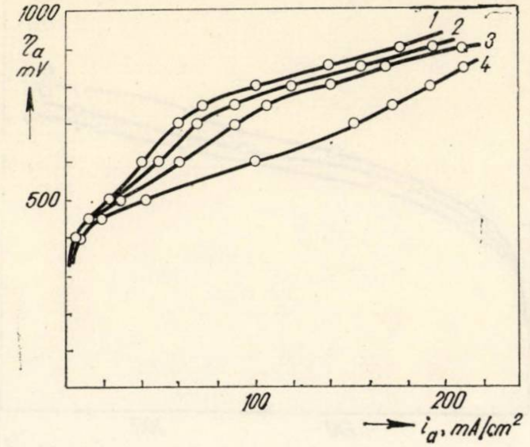

Fig. 6. — Courbes de polarisation $\eta - i$ caractéristiques pour la réaction d'oxydation de l'hydrogène sur l'électrode à gaz A_4.
1, ΔP_{H_2} = 100 mm Hg; 2, ΔP_{H_2} = = 200 mm Hg; 3, ΔP_{H_2} = 300 mm Hg; 4, ΔP_{H_2} = 400 mm Hg.

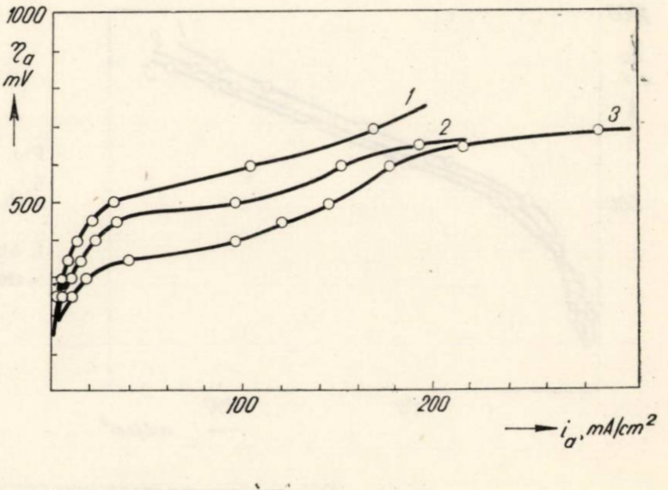

Fig. 7. — Courbes de polarisation $\eta - i$ caractéristiques pour la réaction d'oxydation de l'hydrogène sur l'électrode à gaz A_5.
1, ΔP_{H_2} = 100 mm Hg; 2, ΔP_{H_2} = = 200 mm Hg; 3, ΔP_{H_2} = 300 mg Hg.

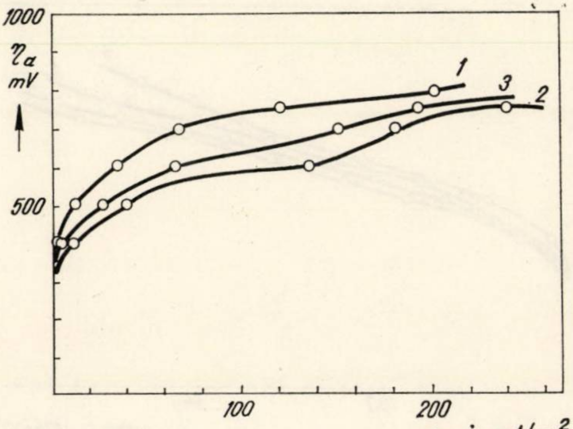

Fig. 8. — Courbes de polarisation $\eta - i$ caractéristiques pour la réaction d'oxydation de l'hydrogène sur l'électrode à gaz A_6.
1, ΔP_{H_2} = 100 mm Hg; 2, ΔP_{H_2} =200 mm Hg; 3, ΔP_{H_2} = 300 mm Hg.

Hg, dans le cas de l'électrode A_6 (du type DSK). Dans le cas des électrodes A_2, A_4 et A_5, la surpression optimale ne se trouve pas dans le domaine étudié.

Les résultats obtenus indiquent l'effet favorable de la structure de type DSK sur la réaction d'oxydation de l'hydrogène : ainsi, par les courbes de polarisation $\eta - i$, on constate qu'à une densité de courant de 100 mA/cm^2 et à une surpression de l'hydrogène de 300 mm Hg, la surtension a une valeur de 400 mV, dans le cas de l'électrode A_6 (du type DSK), par rapport aux valeurs de 700 mV et de 580 mV, correspondant aux électrodes A_1 (du type MSK à petits pores) et, respectivement, A_3 (du type MSK à grands pores).

Les courbes de polarisation $\eta - \log i$ indiquent l'applicabilité de la relation Tafel ; on a calculé les valeurs des constantes Tafel (*b*) pour chaque électrode et pour chaque surpression de l'hydrogène (tableau 1).

Tableau 1

Caractéristiques structurales et performances électrochimiques des électrodes poreuses en nickel,

Electrode	Type de structure	Composition du mélange initial, %				Porosité %	Surtension de l'hydrogène, mm Hg	Valeur de la constante Tafel (*b*), V
		Ni	$NiCO_3$	NH_4HCO_3	NaCl			
A_1	MSK à petits pores	30,0	70,0	—	—	68,04	300 400 500	0,150 0,153 0,158
A_2	MSK à petits pores	50,0	50,0	—	—	61,97	250 400 550	0,17 0,17 0,17
A_3	MSK à grands pores	66,6	—	33,4	—	57,00	100 300 400 500	0,148 0,162 0,145 0,161
A_4	MSK à grands pores	66,6	—	—	33,4	67,07	100 200 300 400	0,182 0,184 0,180 0,180
A_5	DSK	33,3	33,3	16,7	16,7	59,98	100 200 300	0,147 0,143 0,159
A_6	DSK	45,5	45,5	—	9,0	64,03	100 200 300	0,170 0,165 0,165

Des données obtenues pour les constantes Tafel (*b*) il résulte que ces valeurs varient entre 0,14 et 0,18 V.

Les valeurs les plus élevées obtenues pour les constantes Tafel dans le cas des électrodes contenant du chlorure de sodium (électrode A_4), indiquent que la modalité de former la structure poreuse par la dissolution du chlorure de sodium, après avoir fritté les électrodes dans une atmosphère d'hydrogène, ne favorise pas l'obtention des pores à surfaces de réaction actives. Les mêmes observations sont valables aussi pour l'électrode A_6, de type DSK, obtenue dans des conditions identiques.

Les moindres valeurs de la constante Tafel (approximativement 0,14 V) ont été obtenues pour l'électrode A_5 (de type DSK), que l'on a obtenue en utilisant comme poroformateur, le bicarbonate d'ammonium.

On sait que la cinétique de l'électrode poreuse à gaz est différente par rapport à celle de l'électrode non poreuse : une électrode poreuse à gaz peut présenter une tension de polarisation deux fois plus grande qu'une électrode non poreuse, et la constante Tafel peut atteindre, pour la réaction d'oxydation de l'hydrogène, la valeur maximale de 0,22 V. (Dans le cas des électrodes poreuses, la surtension totale de l'électrode représente la somme des polarisations de transfert de charge et de diffusion. [24])

La comparaison des valeurs des constantes Tafel caractéristiques aux électrodes A_5 et A_6, avec le même type de structure (DSK) et avec des porosités à peu près égales, démontre l'effet favorable de la formation de la structure poreuse de l'électrode avant le frittage dans une atmosphère d'hydrogène. La différence de 0,02 V entre les valeurs des constantes Tafel, pour une surpression de l'hydrogène de 200 mm Hg, démontre l'effet du traitement thermique sur l'augmentation de l'activité de la surface intérieure de l'électrode.

Les performances supérieures des électrodes de type DSK sont dues à la présence, dans l'électrode, des grands pores où est localisée la zone triphasique de réaction et des petits pores qui assurent l'alimentation de la zone de réaction avec de l'électrolyte et l'élimination des produits de réaction, en facilitant la diffusion des espèces ioniques vers la zone triphasique de réaction.

CONCLUSIONS

1. On a réalisé une série d'électrodes poreuses en nickel de type MSK à petits pores, de type MSK à grands pores et de type DSK, avec des porosités comprises entre 57 et 68%, en utilisant comme poroformateurs le carbonate de nickel, le bicarbonate d'ammonium et le chlorure de sodium.

2. La réaction d'oxydation de l'hydrogène est favorisée par l'augmentation de la surpression du gaz ; pour quelques-unes de ces électrodes on a déterminé une surpression optimale, située entre la surpression de bullage et la surpression de noyage, à laquelle la surtension est minimale.

3. La formation de la structure poreuse avant le frittage dans une atmosphère d'hydrogène a mené à l'obtention des électrodes à gaz carac-

---

[24] W. MITCHELL, « Fuel Cells », Ier vol., Academic Press, New York—Londres, 1963, p. 98.

térisées par des performances supérieures, en démontrant l'effet favorable du traitement thermique sur l'activité de la surface intérieure des électrodes.

4. Les meilleures performances dans la réaction d'oxydation de l'hydrogène ont été obtenues dans les cas des électrodes de type DSK, ce qui démontre que cette structure est la plus favorable à la réaction ; la présence des petits pores (à diamètres inférieurs à 5 microns) à côté des grands pores (où est localisée la zone triphasique de réaction) facilite la diffusion des espèces ioniques vers la zone de réaction.

Revue Roumaine de Chimie, **18**, 7, 1121–1129 (1973)

Revue Roumaine de Chimie, **18**, 7, 1131–1142 (1973)

DIE CHEMISORPTION VON WASSERSTOFF, BENZOL UND CYCLOHEXAN AUF MIT LITHIUM UND TITAN DOTIERTEM ALUMINIUMOXYD. II *

ADSORPTIONSWÄRMEN

AL. FRUMA und I. V. NICOLESCU

Institut für physikalische Chemie
Bukarest, str. Dumbrava Roşie 23

Eingegangen am 23. Dezember 1972

Es wird die Änderung der isostherischen Adsorptionswärme des Wasserstoffs, Benzols und Cyclohexans auf das mit Lithium und Titanionen dotierte Aluminiumoxyd, in Abhängigkeit von chemischer Natur der Oberfläche und Konzentration des Dotierstoffs, bei sechs verschiedenen Bedeckungsgraden der Oberfläche besprochen. Bei dem mit Titan dotiertem Aluminiumoxyd wird ein Ansteigen der Adsorptionswärme mit der Konzentration des Titans nachgewiesen, während bei dem lithiumdotierten Aluminiumoxyd, unter gleichen Bedingungen, eine Verminderung bemerkbar wird. Dieses Verhalten kann auf Grund der verschiedenen chemischen Natur der Oberfläche der dotierten Aluminiumoxyde, die mittels der Röntgenstrahl-Beugung untersucht wurde, erklärt werden. Bei allen Systemen fällt die Adsorptionswärme liniär oder logarithmisch mit dem Bedeckungsgrad, was auf die verschiedenartige Heterogenität der Oberflächen zurückzuführen ist.

1. EINLEITUNG

Die Gasadsorption auf festen Oberflächen ist von thermischen exothermen Effekten begleitet, die sich allmählich mit dem Ansteigen des Bedeckungsgrades vermindern. Das Studium dieser Erscheinung ist für die heterogene Katalyse dadurch von Bedeutung, da es Auskünfte über die Reaktivität der adsorbierten Partikeln gibt, in Abhängigkeit von denjenigen Eigenschaften die die Chemie der Oberfläche des Katalysators kennzeichnen, und die von der chemischen Natur und Herstellungsbedingungen abhängig sind. Aus diesem Gesichtspunkt hielten wir es für interessant die Adsorption des Wasserstoffs und einiger Kohlenwasserstoffe mit verschiedener Struktur auf aktivem, mit Kationen deren Wertigkeit kleiner oder größer ist als die des Aluminiums, dotiertem Aluminiumoxyd zu untersuchen.

---

* I. Teil: I. V. Nicolescu und Al. Fruma *Rev. Roumaine Chim.*, **18**, 953 (1973).

Die vielseitige Verwendung des aktiven Aluminiumoxyds als Träger bei der Herstellung von industriellen Katalysatoren, bedingte zahlreiche Forschungen über die Möglichkeiten der Änderung der Struktureigenschaften des Aluminiumoxyds durch Dotierung mit Fremdionen. Diese Arbeiten[1–3] wie auch andere elektrische[4–6] und optische[6,7] Untersuchungen bestätigten die geringe Konzentration der Ladungsträger im Aluminiumoxyd. Für das, mit Ionen deren Wertigkeit größer als drei ist, dotierte γ Aluminiumoxyd erhält man eine schwache «n»-Typ Leitfähigkeit, während, wegen der geringen Konzentration der freien Ladungsträger, führen schwache Dotierungen mit Fremdionen kleinerer Wertigkeit zu «p»-Typ Leitfähigkeit. Diese Änderungen üben manchmal einen bedeutenden Einfluß auf die katalytischen Eigenschaften des Aluminiumoxyds aus.[8,9]

Die Deutung der Änderung der Adsorptionswärme mit dem Bedeckungsgrad der Oberfläche bildete den Gegenstand zahlreicher Forschungen.[10] Diese befaßten sich insbesondere mit der Wechselwirkung der Gasen mit Metallen. Einige der Ergebnisse können erweitert werden um auch die Gas-Oxyd Wechselwirkungen zu erfassen. Zwischen den zahlreichen Ursachen die die Änderung der Adsorptionswärme mit dem Bedeckungsgrad bedingen, besprechen wir in der vorliegenden Arbeit nur die Ansicht nach der die Verminderung der Adsorptionswärme mit dem Bedeckungsgrad auf die Heterogenität der Oberfläche zurückzuführen ist, wobei die verschiedenen Zentren in der Reihenfolge der Verminderung ihrer Aktivität besetzt werden.

2. EXPERIMENTELLES

Für die Untersuchung der Asdorption von Wasserstoff, Benzol und Cyclohexan wurde eine Hochvakuumanlage benützt, die in einer vorherigen Arbeit beschrieben wurde.[11] Dei Adsorptionsisothermen von sechs mit 0,5; 2 und 4 Atom % Lithium bzw. Titan dotierten Aluminiumoxydprobe wurden festgestellt. Sowohl die Herstellung dieser Aluminiumoxyde als auch ihre Struktur-, Textur- und Adsorptionseigenschaften wurden früher besprochen.[12,13] Auf Grund dieser experimentellen Ergebnisse berechneten wir die isostherischen Adsorptionswärmen aus der Darstellung Clausius-Clapeyrons Gleichung. Die Berechnung erfolgte für einen Temperaturbereich zwischen 100 und 400°, und zwar von 50 zu 50°, bei sechs von uns willkürlich auserwählten Bedeckungsgraden. Im Fall des Wasserstoffs wurden Untersuchungen auch bei der Temperatur von 25° unternommen. In diesem Temperaturbereich waren die Schwankungen der Adsorptionswärme gering genug um einen Mittelwert in betracht zu nehmen.

---

[1] G. M. Schwab, J. Block, W. Müller und D. Schultze, *Naturwiss.*, **44**, 582 (1959).
[2] G. M. Schwab, A. Beer und J. Foitzig, *Z. anegw. Physik*, **14**, 763 (1962).
[3] G. M. Schwab und H. Derleth, *Z. phys. Chem. (Frankfurt)*, **53**, 1 (1967).
[4] H. Pscheidl und H. Witzmann, *Z. phys. Chem. (Leipzig)*, **240**, 161 (1969).
[5] J. Cohen, *Bull. Amer. Ceram. Soc.*, **38**, 441 (1959).
[6] P. J. Harrop, *Brit. J. Appl. Phys.*, **16**, 729 (1965).
[7] V. A. Fomichev, *Fizica Tverdovao Tela*, **8**, 2892 (1966).
[8] W. Pfeil, *Z. phys. Chem. (Leipzig)*, **243**, 51 (1970).
[9] G. M. Schwab und G. Mutzbauer, *Z. phys. Chem. (Frankfurt)*, **32**, 367 (1962).
[10] E. I. Segal, *Studii şi Cercetări Chim. Acad. Bucureşti*, **17**, 25 (1969).
[11] I. V. Nicolescu, Al. Fruma und I. Suciu, *Rev. Roumaine Chim.*, **16**, 91 (1971).
[12] Al. Fruma, D. Ciomârtan, I. Braşoveanu und I. V. Nicolescu, *Rev. Roumaine Chim.*, **18**, 803 (1973).
[13] I. V. Nicolescu und Al. Fruma, *Rev. Roumaine Chim.*, im **18**, 953 (1973).

3. ERGEBNISSE UND DISKUSSION

3.1. ISOSTHERISCHE ADSORPTIONSWÄRMEN

Der Bedeckungsgrad kann in drei verschiedenen Arten definiert werden und zwar durch das Verhältnis zwischen der Anzahl der infolge der Adsorption besetzten Zentren und der Gesamtanzahl der verfügbaren Zentren, oder wenn die Zentrenanzahl unbekannt und nur die Gesamtoberfläche bekannt ist, kann der Bedeckungsgrad als das Verhältnis zwischen der besetzten Oberfläche und der Gesamtoberfläche ausgedrückt werden. Eine dritte Möglichkeit den Bedeckungsgrad auszudrücken besteht im Verhältnis zwischen dem bei einem bestimmten Druck und Temperatur adsorbierten Gasvolumen und dem Höchstvolumen der bei Sättigungsbedingungen der Oberfläche adsorbiert werden kann. Für die Adsorption von einfachen Gasen (O_2, H_2) auf Metallen geben die drei Ausdrücksmöglichkeiten des Bedeckungsgrades gleiche Ergebnisse, aber für die Adsorption von Molekülen mit großer Oberfläche (Benzol, Cyclohexan) sind die Werte verschieden, aber die Änderungen sind immer in derselben Richtung. In der vorliegenden Arbeit haben wir diese letztere Ausdrucksmöglichkeit für den Bedeckungsgrad vorgezogen.

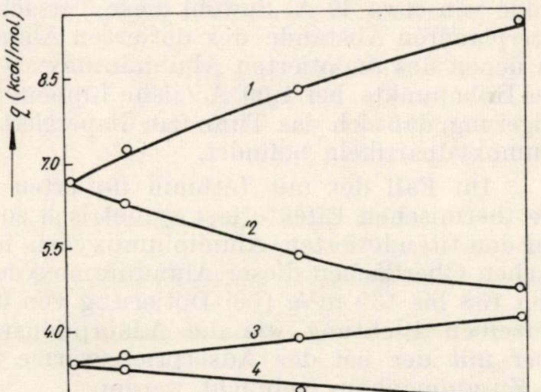

Abb. 1. — Die Adsorptionswärmen des Benzols auf mit Lithium (1) und Titan (2) dotierten Aluminiumoxyde und des Cyclohexans auf mit Lithium (3) und Titan (4) dotierten Aluminiumoxyde.

In Abb. 1 wird die Änderung der Adsorptionswärme des Benzols und Cyclohexans mit der Konzentration des Dotierstoffs für einen kleinen, der Adsorption von $V = 1\mu$ mol/g entsprechenden Bedeckungsgrad dargestellt. Für die anderen fünf Bedeckungsgraden, die der Adsorption von $V = 1{,}5$; 2 ; 2,5 ; 3 ; und 3,5 μ mol/g entsprechen, werden andere fünf gleichartige Darstellungen erhalten. Man bemerkt erstens die viel größeren Adsorptionswärmen des Benzols als die des Cyclohexans. Während die thermischen Effekte der Benzoladsorption bis 10 kcal/mol erreichen, sind bei der Cyclohexanadsorption die thermischen Effekte viel kleiner, und befinden sich zwischen 2 —4 kcal/mol. Für uns ist aber die Änderung der Adsorptionswärme für dieselben adsorbierten Gase auf mit Titan oder Lithium dotiertem Aluminiumoxid interessanter. Aus der Abbildung ist ersichtlich, daß sowohl die Benzol, als auch die Cyclohexanadsorption auf dem mit Titan dotiertem Aluminiumoxyd einen größeren, von der Titankonzentration abhängigen thermischen Effekt ergibt.

Das undotierte Aluminiumoxyd weist eine Adsorptionswärme des Benzols von 6,7 kcal/mol. Für eine Konzentration von nur 0,5 Atom % Ti wächst die Adsorptionswärme bis 7,5 kcal/mol, um bei dem mit 4 Atom % Ti dotiertem Aluminiumoxyd fast 10 kcal/mol zu erreichen. Dieses Ansteigen der Adsorptionswärme geschieht in den Verhältnissen in denen die spezifische Oberfläche [12] von 152 m^2/g (reines Aluminiumoxyd) bis 124 m^2/g (mit 4 Atom % Ti dotiertem Aluminiumoxyd) vermindert wird. Der thermische Effekt kann daher mit der Änderung der spezifischen Oberfläche nicht in Zusammenhang gebracht werden. Das Ansteigen der Adsorptionswärme kann, in diesen Bedingungen nur der Änderung der Konzentration und Stärke der aktiven Zentren zugeschrieben werden.

Die Röntgenstrahl-Beugungsspektren für das mit Titan dotierte Aluminiumoxyd enthalten nur das Beugungsbild des Aluminiumoxyds, wobei din η Form stabilisiert wird. Es ergab sich eine mittlere Kristallitgröße von etwa 40 Å. Sowohl diese Tatsache, als auch diejenige, daß die interplanären Abstände des dotierten Aluminiumoxyds sich im Vergleich zu denen des undotierten Aluminiumoxyds nur hinsichtlich der Spaltung des Höhepunkts bei 1,99 Å (siehe Lippens [14]) änderten, führt zur Schlußfolgerung, daß sich das Titan fein dispergiert auf der Oberfläche der Aluminiumoxydpartikeln befindet.

Im Fall der mit Lithium dotierten Aluminiumoxyde ändern sich die thermischen Effekte fast symetrisch zu denen die bei der Adsorption auf den titandotierten Aluminiumoxyden festgestellt wurden. Die spezifischen Oberflächen dieser Aluminiumoxyde ändern sich ziemlich wenig, von 158 bis 139 m^2/g (bei Dotierung von 0,5 bis 4 Atom % Li), aber in derselben Richtung wie die Adsorptionswärme. Diese Änderung kann aber mit der bei der Adsorptionswärme festgestellten Änderung nicht in Zusammenhang gebracht werden.

Die Röntgenstrahl-Diffraktogramme wiesen daraufhin, daß das mit Lithium dotierte Aluminiumoxyd auch die charakteristischen Linien des Lithiumaluminats $LiAl_5O_8$, Form I und II im Diffraktionsspektrum aufweisen. Der für das Lithiumaluminat spezifische Höhepunkt bei 2,809 Å ist schmal und nimmt in Intensität mit dem Ansteigen der Lithiumkonzentration zu. Die flache Form des Höhepunkts bei 2,30 Å und 1,40 Å deutet auf eine geringere Gitterordnung in den betreffenden Kristallebenen, wo ein größerer Beitrag der Aluminium- und Sauerstoffatome als der Lithiumatome vorhanden ist. Die Verminderung der Adsorptionswärme mit dem Ansteigen der Lithiumkonzentration kann daher der Bildung des unaktiven Lithiumaluminats zugeschrieben werden, dessen Konzentration mit der Dotierungsmenge wächst.

---

[14] B. C. Lippens und Y. Y. Steggerda, „Physical and Chemical Aspects of Adsorbants and Catalysts", Ed. B. C. Linsen, Acad. Press, London, New York, 1970, S. 18.

Die Adsorptionswärme des Wasserstoffs konnte nur für die mit Titan dotierten Aluminiumoxyde bestimmt werden, da die thermischen Effekte bei der Wasserstoffadsorption auf den lithiumdotierten Aluminiumoyxden vernachlässigbar sind. Die isostherischen Adsorptionswärmen des Wasserstoffs auf den mit Titan dotierten Aluminiumoyxden befinden sich zwischen 2 und 6,4 kcal/mol und hängen sowohl von der Titankonzentration der Aluminiumoxyde, als auch von dem Bedeckungsgrad ab. Die erste dieser Ursachen wird, in gleicher Weise wie bei der Adsorption des Benzols und Cyclohexans, von der spezifischen Struktur der mit Titan dotierten Aluminiumoxyde bestimmt, während die zweite Ursache, die Änderung der Adsorptionswärme mit dem Bedeckungsgrad, im folgenden Abschnitt besprochen wird.

3.2. DIE ÄNDERUNG DER ISOSTHERISCHEN ADSORPTIONSWÄRME MIT DEM BEDECKUNGSGRAD DER OBERFLÄCHE

Die Adsorptionswärmen wurden für sechs verschiedene Bedeckungsgrade der Oberfläche berechnet, und zwar entsprechend einer Adsorption von 1 ; 1,5 ; 2 ; 2,5 ; 3 und 3,5 μ mol/g. Die adsorbierten Gasmengen hängen von der Natur des Systems, der Konzentration des Dotierstoffs und Temperatur ab, und befinden sich zwischen 1 und 12 μ mol/g.[13] Es ergibt sich, daß sich die Werte für den Bedeckungsgrad der den von uns ausgewählten Adsorptionen entspricht, im Gebiet der geringen oder mittleren Bedeckungsgraden befindet.

Aus Abb. 2 ist ersichtlich, daß für die Adsorptionswärme des Wasserstoffs auf den mit Titan dotierten Aluminiumoxyden, eine stetige Verminderung der Adsorptionswärme mit dem Bedeckungsgrad bemerkbar ist. Diese Verminderung ist von der Titankonzentration abhängig. Während bei dem mit 0,5 Atom % Ti dotiertem Aluminiumoxyd diese Verminderung praktisch liniär vor sich geht, wird sie bei den Aluminiumoxyden mit einer größeren Dotierstoffkonzentration allmählich krummlinig.

Auf dieser Weise ist die Schätzung der Adsorptionswärme bei der Bedeckung Null nur für die Adsorption auf dem mit 0,5 Atom % Ti dotiertem Aluminiumoxyd möglich, wo die entsprechende Gerade extrapolierbar ist. Um aber doch ein entsprechendes System zu finden, das zu charakteristischen Geraden führen soll, versuchten wir verschiedene andere Darstellungsweisen. Nach mehreren Versuchen fanden wir, daß das System „Adsorptionswärme in Abhängigkeit vom Logarithmus der Adsorption'' zu einer Darstellung führt, bei der sich die Punkte entsprechend auf den Geraden anpassen, wie aus Abb. 3 ersichtlich ist. Dem System H_2/Al_2O_3 + 0,5 Atom % Ti das auch von einer einfachen Darstellung $q - V$ charakterisiert werden kann, entspricht wegen der geringen Änderung der Adsorptionswärme auch die Darstellung $q - \ln V$.

Die Adsorptionswärme des Benzols auf den mit Titan und Lithium dotiertem Aluminiumoxyd, vermindert sich bei der Bedeckung der Oberfläche, wie aus Abb. 4 und 5 ersichtlich ist. Für das System Benzol/Al_2O_3 + 0,5 −4 Atom % Ti wie auch für das nicht dotierte Aluminiumoxyd ist diese Verminderung nicht liniär, während sie für das System Benzol/Al_2O_3 + 0,5 −4 Atom % Li liniär ist. Hinsichtlich der Adsorption des Benzols auf den mit Titan dotierten Aluminiumoxyde kommt dieselbe Erscheinung wie bei der Wasserstoffadsorption vor, wo ebenfalls eine halblogarithmische Darstellung nötig war, um Liniarität zu erzielen. Eine derartige Änderung der Adsorptionswärme mit der adsorbierten Gasmenge (oder mit dem Bedeckungsgrad der Oberfläche) charakterisiert sehr unhomogene Oberflächen, zum Unterschied zur liniären Änderung, die bei den mit Lithium dotierten Aluminiumoxyden vorkommt, und die

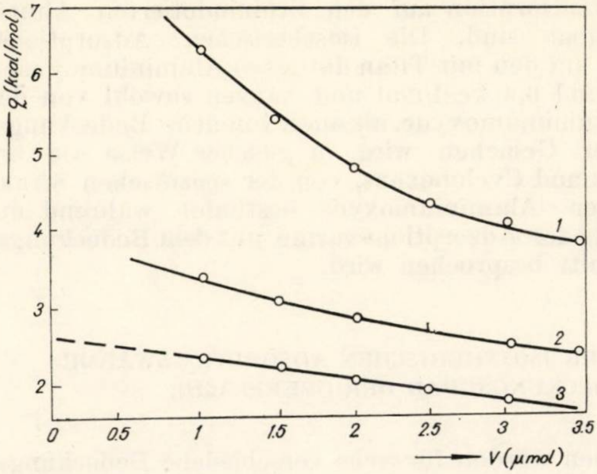

Abb. 2. — Die Änderung der Adsorptionswärme des Wasserstoffs mit der adsorbierten Menge für das mit 4 Atom % Ti (1) ; 2 Atom % Ti (2) und 0,5 Atom % Ti (3) dotierte Aluminiumoxyd.

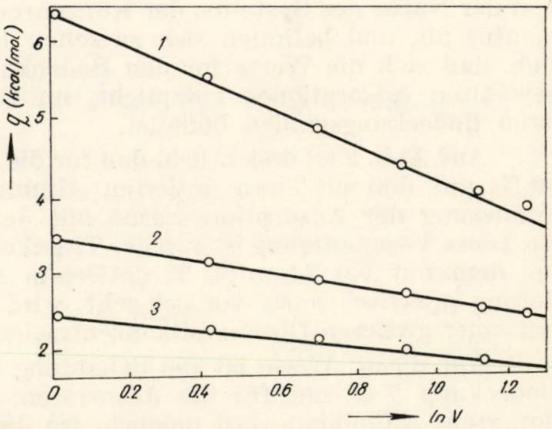

Abb. 3. — Die halblogarithmische Darstellung der Änderung der Adsorptionswärme des Wasserstoffs mit der adsorbierten Menge für das mit 4 Atom % Ti (1) ; 2 Atom % Ti (2) und 0,5 Atom % Ti (3) dotierte Aluminiumoxyd.

Oberflächen mit einer geringeren Heterogenität gekennzeichnet. In dieser Weise sind die Schlüsse die sich aus der Untersuchung der Änderung der Adsorptionswärme mit dem Bedeckungsgrad ergeben, in guter Übereinstimmung zur chemischen Struktur dieser Aluminumoxyde. Zum

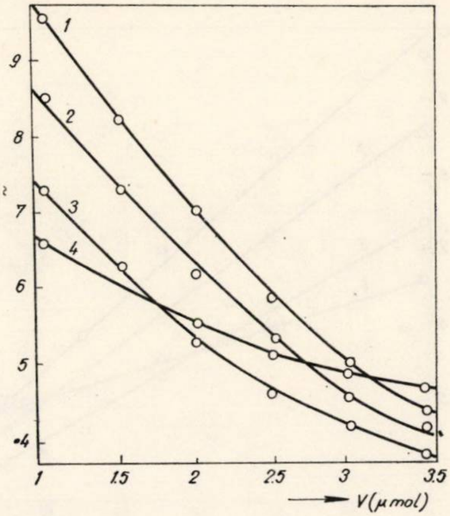

Abb. 4. — Die Änderung der Adsorptionswärme des Benzols mit der adsorbierten Menge für das mit 4 Atom % Ti (1); 2 Atom % Ti (2); 0,5 Atom % Ti (3) dotierte und undotiertes (4) Aluminiumoxyd.

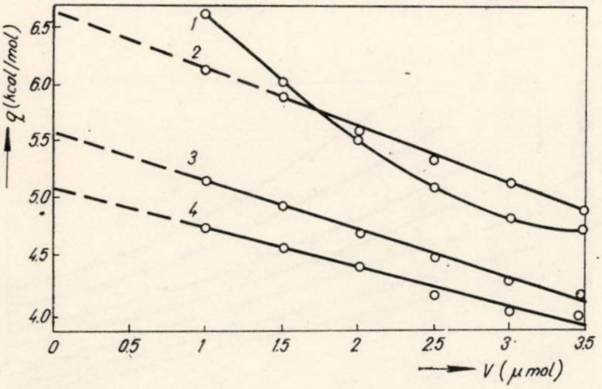

Abb. 5. — Die Änderung der Adsorptionswärme des Benzols mit der adsorbierten Menge für undotiertes (1), mit 0,5 Atom % Li (2); 2 Atom % Li (3) und 4 Atom % Li (4) dotiertes Aluminiumoxyd.

Unterschied von Lithium, das durch Eindringen im Gitter dieses stabilisiert, leiht das Titan der Oberfläche eine bedeutende Heterogenität, da es im Gitter des Aluminiumoxyds nicht eindringt, und auf der Oberfläche bleibt.

Während die Kurve der Änderung der Adsorptionswärme des Benzols mit dem Bedeckungsgrad der Oberfläche des nicht dotierten Aluminiumoxyds gegen größere Bedeckungsgrade die entsprechenden Kurven der mit Titan und 0,5 Atom % Li dotierten Aluminiumoxyde schneidet, und die Werte der Adsorptionswärme sind, wenigstens bei größeren Bedeckungsgraden, unabhängig von der Natur des Dotierstoffs, bleibt bei der Adsorption des Cyclohexans auf den dotierten und undotierten Aluminiumoxyden eine gewisse Reihenfolge im ganzen Gebiet der Bedeckungsgraden bestehen. Die eigenen Änderungen der Adsorptionswärme hängen aber eher von der Natur des Dotierstoffs als vom Bedeckungsgrad ab. Im ganzen Gebiet ist die Reihenfolge der Verminderung der thermischen Effekte die gleiche die auch bei den experimentellen, vorher beschriebenen ^{13} Adsorptionsisothermen vorkam. Obwohl sich für die mit Titan dotierten Aluminiumoxyde eine halblogarithmische Darstellung, für Erzielung der Liniarität als nötig erwies, gilt im Gebiet der kleineren Bedeckungsgraden (Werte für die Adsorption zwischen

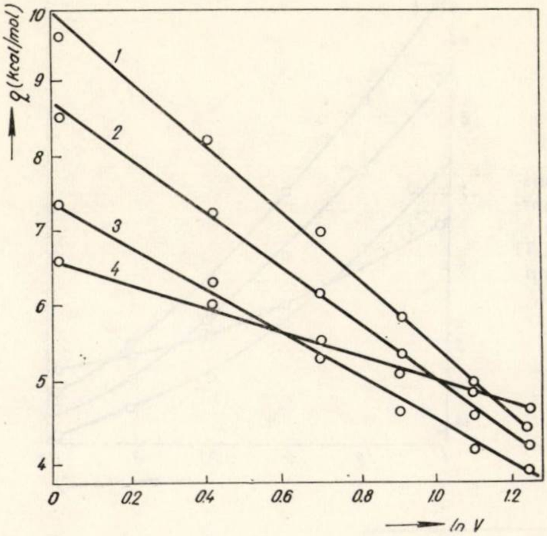

Abb. 6. – Die halblogarithmische Darstellung der Änderung der Adsorptionswärme des Benzols mit der adsorbierten Menge für das mit 4 Atom % Ti (1) ; 2 Atom % Ti (2) ; 0,5 Atom % Ti (3) dotierte und undotiertes (4) Aluminiumoxyd.

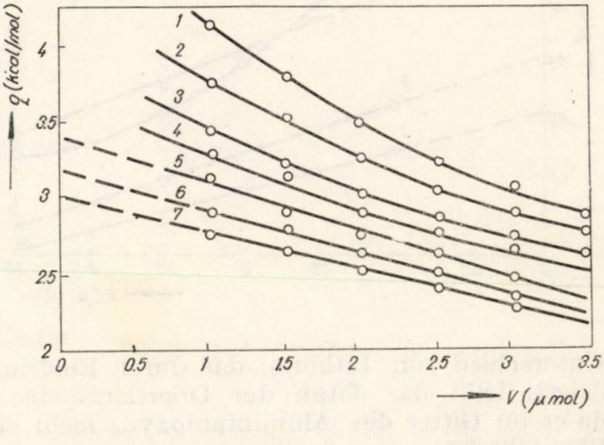

Abb. 7. – Die Änderung der Adsorptionswärme des Cyclohexans mit der adsorbierten Menge für das mit 4 Atom % Ti (1) ; 2 Atom % Ti (2) ; 0,5 Atom % Ti (3) ; 0,5 Atom % Li (5) ; 2 Atom % Li (6) ; 4 Atom % Li (7) dotierte und undotiertes (5) Aluminiumoxyd.

1–2 μ mol/g) auch die einfache Darstellung $q - V$, die ebenfalls zu Liniarität führt. Die Tatsache, daß die Änderungen der Adsorptionswärme beim Cyclohexan kleiner als beim Benzol sind, deutet auf eine verschiedene Spezifizitätt der Adsorptionszentren für das Cyclohexan und für das Benzol.

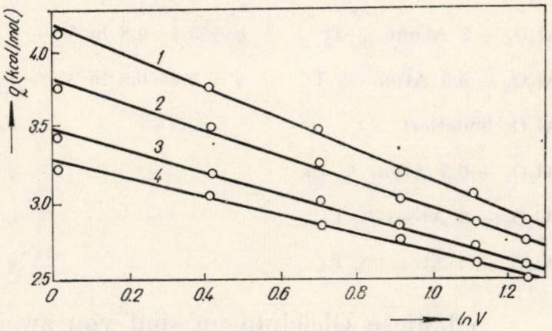

Abb. 8. — Die hablogarithmische Darstellung der Änderung der Adsorptionswärme des Cyclohexans mit der adsorbierten Menge für das mit 4 Atom % Ti (1) ; 2 Atom % Ti (2) ; 0,5 Atom % Ti (3) dotierte und undotiertes (4) Aluminiumoxyd.

3.3. ZUSAMMENHANG ZWISCHEN DER ÄNDERUNG DER ADSORPTIONSWÄRME UND DER GLEICHUNG DER ADSORPTIONSISOTHERMEN

In Untersuchungen dieser Art gibt es drei verschiedene Möglichkeiten : 1. Die Adsorptionswärme ändert sich mit dem Bedeckungsgrad nicht. In diesem Fall ist die Adsorption von einer Langmuir Gleichung charakterisiert, d.h. die Adsorptionszentren sind äquivalent, und es fehlt jede Wechselwirkung zwischen den adsorbierten Molekülen. Keines der von uns untersuchten Systeme befindet sich in diesem Fall, folglich ist keine der experimentell erhaltenen Isothermen vom Langmuir-Typ. 2. Die Adsorptionswärme kann liniär mit dem Bedeckungsgrad fallen. Es ist der Fall der von Roghinski [15] sogenannten „gleichförmig nichthomogenen" Oberflächen, und stellt eine zwischen Homogenität und Heterogenität intermediären Zustand dar, in dem sich die thermischen Effekte gleichmäßig mit dem Bedeckungsgrad der Oberfläche ändern. In diesem Fall befindet sich die Adsorption auf den mit Lithium dotierten Aluminiumoxyden. 3. Die dritte Möglichkeit besteht in einer exponentiellen oder logarithmischen Änderung der Adsorptionswärme mit dem Bedeckungsgrad. In diesem Fall, der typisch für Oberflächen mit bedeutender Heterogenität ist, befinden sich die Oberflächen der mit Titan dotierten Aluminiumoxyde.

Aus den dargestellten Abbildungen erhält man gleich die Gleichungen der Geraden die die Änderung der Adsorptionswärme mit dem Bedeckungsgrad kennzeichnen. Es ergeben sich die in Tabelle 1 ersichtlichen Gleichungen.

---

[15] S. Z. Roghinski, „Adsorbtsia i kataliz na neodnorodnykh povernostiak, Ed. Akad. Nauk, Moskau, Leningrad, 1948.

Tabelle 1

Die Gleichungen der Änderungen der Adsorptionswärme mit der adsorbierten Menge

Probe	Wasserstoff	Benzol	Cyclohexan
Al_2O_3 + 4 Atom % Ti	$q = 6{,}4-2{,}3 \ln V$	$q = 9{,}8-4{,}4 \ln V$	$q = 4{,}2-\ln V$
Al_2O_3 + 2 Atom % Ti	$q = 3{,}4-0{,}8 \ln V$	$q = 8{,}7-3{,}6 \ln V$	$q = 3{,}8-0{,}8 \ln V$
Al_2O_3 + 0,5 Atom % Ti	$q = 2{,}4-0{,}5 \ln V$	$q = 7{,}4-2{,}8 \ln V$	$q = 3{,}5-0{,}7 \ln V$
Al_2O_3 undotiert	—	$q = 6{,}7-1{,}7 \ln V$	$q = 3{,}3-0{,}6 \ln V$
Al_2O_3 + 0,5 Atom % Li	—	$q = 6{,}7-0{,}5\ V$	$q = 3{,}4-0{,}3\ V$
Al_2O_3 + 2 Atom % Li	—	$q = 5{,}5-0{,}4\ V$	$q = 3{,}2-0{,}3\ V$
Al_2O_3 + 4 Atom % Li	—	$q = 5{,}1-0{,}3\ V$	$q = 3{,}0-0{,}2\ V$

All diese Gleichungen sind von zwei Typen:

$$q = a - bV \tag{1}$$

$$q = m - n \ln V \tag{2}$$

Die Gleichung (1) ist für die Adsorption auf den mit Lithium dotierten Aluminiumoxyden charakteristisch, während die Gleichung (2) die titandotierten Aluminiumoxyde kennzeichnet. Im Folgenden werden wir unseren Ergebnissen Brunauer und Mitarb. [16] Berechnungsmethode anwenden, um charakteristische Gleichungen für die Adsorptionsisothermen zu gewinnen.

Wir betrachten darum die Gesamtoberfläche in einer Anzahl Oberflächenelemente „dS'' aufgeteilt, wobei jedes einzelne Element von einem bestimmten konstanten Bedeckungsgrad charakterisiert wird. In diesem Fall kann man jedem einzelnen Element eine Gleichung der Langmuirisotherme anpassen:

$$\theta_S = \frac{a_0 p e^{q/\mathrm{RT}}}{1 + a_0 p e^{q/\mathrm{RT}}}. \tag{3}$$

Die verschiedenen Bezeichungen sind bekannt. Für die Gesamtoberfläche erhält man den Bedeckungsgrad durch Integration:

$$\theta_S = \int \theta_S \, \mathrm{d}S. \tag{4}$$

Wir sahen daß q liniär mit der adsorbierten Menge, d.h. mit dem Bedeckungsgrad fällt, so daß auch

$$q = c\,(1 - gS) \tag{5}$$

wobei c und g konstant sind.

---

[16] S. Brunauer, K. S. Love und R. G. Keenan, *J. Amer. Chem. Soc.*, **64**, 751 (1942).

Durch Einführung von (4) und (5) in (3) erhalten wir:

$$\theta = \int_0^1 \frac{A_0 p \, e^{-cgS/RT}}{1 + A_0 p \, e^{-cgS/RT}} \, dS \qquad (6)$$

wo $A_0 = a_0 e^{c/RT}$. Die Gesamtoberfläche wurde als 1 betrachtet. Gleichung (6) kann leicht integriert werden und es ergibt sich:

$$\theta = \frac{RT}{cg} \ln \frac{1 + A_0 p}{1 + A_0 p \, e^{-cg/RT}} \qquad (7)$$

Dieses ist eine Gleichung vom Temkin-Typ. Da $\theta = V/V_m$, wo $V_m =$ konstant ist, haben wir auf diesem Wege den Gleichungstyp

$$V = C' \ln p + C''$$

wiedergefunden, den wir experimentell für die Adsorption auf den mit Lithium dotierten Aluminiumoxyde erhalten haben.[13]

Im Fall der Adsorption auf den mit Titan dotierten Aluminiumoxyde ist Zeldovichs[17] Methode geeignet, um von der Gleichung der Änderung der Adsorptionswärme mit dem Bedeckungsgrad zu den charakteristischen Gleichungen der Adsorptionsisothermen überzugehen. Durch Einführung von Gleichung (2) in einer Langmuirgleichung ergibt sich ein nichtintegrierbarer Ausdruck. Für die ziemlich geringen Bedeckungsgrade bei denen wir die Adsorptionswärme berechneten, entspricht jedoch dem Integrall eine Lösung vom Typ:

$$\ln \theta = RT/C \ln p + B \qquad (8)$$

Wir erkennen in (8) eine Gleichung vom Freundlich Typ, die der Gleichung

$$\ln V = A' \ln p + A''$$

die wir bei der Adsorption auf den mit Titan dotierten und undotierten Aluminiumoxyde erhalten haben, gleich ist.

Ausgehend von der Änderung der Adsorptionswärme mit dem Bedeckungsgrad, kamen wir auf dieser Weise zu den experimentellen Isothermengleichungen. Da die isostherischen Adsorptionswärmen ebenfalls aus den Isothermen berechnet wurden, stellten die vorliegenden Berechnungen eine Bestätigung für die bei verschiedenen Bedeckungsgraden berechneten Adsorptionswärmen dar.

---

[17] J. ZERDOVICH, *Acta Physicochim.*, URSS, **1**, 961 (1934).

4. SCHLUSSFOLGERUNG

Die Adsorptionswärme des Wasserstoffs auf den mit Titan dotierten Aluminiumoxyde befinden sich zwischen 2 und 6,4 kcal/mol und nehmen mit der Titankonzentration der Aluminiumoxyde zu. Bei der Adsorption des Benzols und Cyclohexans steigen die thermischen Effekte mit der Titankonzentration und fallen mit der Lithiumkonzentration. Diese Erscheinung ist der Struktur des mit Titan dotierten Aluminiumoxyds zuzuschreiben, bei welcher das Titan nicht im Gitter eindringt, sondern auf der Oberfläche verbleibt, bezüglich die Struktur des mit Lithium dotierten Aluminiumoxyds, wo das Lithium im Gitter des Aluminiumoxyds, vorzüglich in den oktaedrischen Plätzen eindringt, um ein unaktives Aluminat $LiAl_5O_8$ zu bilden.

Die Adsorptionswärme fällt bei allen Systemen mit dem Ansteigen des Bedeckungsgrades der Oberfläche. Diese Tatsache kann auf Grund der allmählich, während der Adsorption, verminderten Zentrenzahl in Reihenfolge ihrer Aktivitätsverminderung erklärt werden. Bei den mit Lithium dotierten Aluminiumoxyden fällt die Adsorptionswärme liniär mit dem Bedeckungsgrad, wobei sie bei den mit Titan dotierten Aluminiumoxyde logarithmisch fällt. Die Gleichungen der Änderung der Adsorptionswärme mit dem Bedeckungsgrad führen zu Gleichungen der Adsorptionsisothermen vom Temkin Typ für die mit Lithium, und vom Freundlich Typ für die mit Titan dotierten Aluminiumoxyde. In dieser Weise werden die vorherigen Ergebnisse über die Heterogenität der Oberfläche bestätigt.

Die Entwicklung von Forschungen dieser Art führt zu einer besseren Kenntnis der Beziehungen zwischen der chemischen Natur der Oberfläche, Heterogenität und adsorptive Kapazität, im Zusammenhang zu der Struktur der Moleküle die adsorbiert werden und des energetischen Potentials der Oberfläche.

Revue Roumaine de Chimie, 18, 7, 1143–1153 (1973)

Co(II) AND Ni(II) CHELATES WITH LIGANDS CONTAINING DONOR NITROGEN ATOMS

P. SPACU, A. C. BANCIU and C. I. LEPĂDATU

Center of Chemical Physics, Dumbrava Roşie, 23,
Bucharest-9, Romania

Received December 28, 1972

New ligands from the class of substituted glyoxalanil-arylhydrazones were prepared, and with one of these, 1-methyl-2-carbethoxy-glyoxalanil-(1)-phenylhydrazone-(2), chelates of Co (II) and Ni(II) were synthetized. Depending on the preparation method, two different Ni(II) chelates were obtained, one of these having the anil group substituted by an imino group. The elemental analysis data as well as the magnetic measurements, molar conductivities and the absorption/reflectance spectra show that all the compounds behave as nonelectrolyte, four-coordinate, the spatial arrangement being high spin tetrahedral for Co(II) and low spin square planar for Ni(II) complexes.

In the last ten years, Co (II), Ni(II) and Cu(II) complexes with ligands from the class of substituted glyoxalanilarylhydrazones have been reported, [1–5] the ligands being prepared starting often from acetylacetone and benzoylacetone. All these complexes have been roughly characterized only by their melting points, elemental analysis data and absorption spectra, recorded but not interpreted in terms of the current theories concerning the molecular electronic structure. Due to the variety of the possible substituents attached to these ligands, as well as of the numerous transition-metal ions which may coordinate them, the class of compounds becomes very large, and the lack of any chemical bond studies make them interesting and relevant.

It should be pointed out that among the above mentioned ligands, only one containing carbethoxy group, $COOC_2H_5$, is known in the literature, [3] their obtention being much more difficult than those having ceto group, i.e. CH_3CO or C_6H_5CO, due to the low values assumed by the reaction yields. [3] This is the reason why the preparation of new ligands from the class of 1-methyl-2-carbethoxy-glyoxalanil-(1)-arylhydrazones-(2)

---

[1] B. Hirsch and A. Bassl, *Z. Chem.*, **2**, 115 (1962).
[2] B. Hirsch and E. Förster, *Z. Chem.*, **2**, 150 (1962).
[3] B. Hirsch and A. Bassl, *Z. Chem.*, **2**, 276 (1962).
[4] B. Hirsch and A. Bassl, *Z. Chem.*, **2**, 340 (1962).
[5] B. Hirsch and J. A. Singh, *Chimia* (*Basel*), **21**, 27 (1967).

substituted to the phenyl radical of the hydrazone group, as well as chelates with transition metal ions will be reported in a series of papers. The present note deals with Co(II) and Ni(II) chelates obtained from 1-methyl-2-carbethoxy-glyoxalanil-(1)-phenylhydrazone-(2) (I, Y = H).

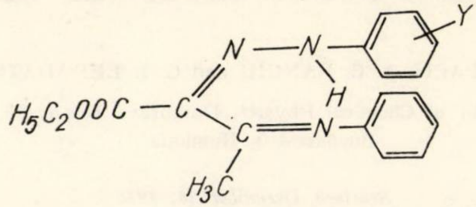

(I)

EXPERIMENTAL

Reagents. Acetylacetic ester (Merck, reagent for synthesis, min. content 98%), aniline (tridistilled), *p*-toluidine (Carlo Erba, min. content 99%), *p*-anisidine (VEB Berlin-Chemie, *p.a.*), *p*-nitroaniline (B.D.H., *p.a.*), *p*-chloraniline (Fluka, puriss.), *p*-bromaniline (Ferak, Berlin, reinst), triethylamine (Merck, min. content 99.5%), anhydrous $NaCH_3COO$ (Austranal, *p.a.*), $NiCl_2 \cdot 6H_2O$ (Reactivul, Bucharest, *p.a.*), $CoCl_2 \cdot 6H_2O$ (Reactivul, Bucharest, *p.a.*), $NaNO_2$ (Reactivul, Bucharest, *p.a.*), NH_3 25% – solution (Reactivul, Bucharest, *p.a.*).

Preparation of ligands. The preparation starts with the acetylacetic ester, by condensation with aniline; the ligands are prepared from the obtained anil[6] by azoic coupling reaction[1,3] with solutions of diazonium salts of the aromatic amines, freshly prepared and buffered up to pH = 3, the reaction yield being of about 15–25%. The ligands were recrystallized from absolute ethanol on charcoal, the operation is once more repeated and the products are dried under vacuum on di-P_2O_5. Some of the ligands thus prepared are systematized in table 1.

Preparation of chelates. Chelates of Ni(II) were prepared by means of a method earlier reported,[1,2] refluxing alcoholic solutions, containing amounts of 1/100 m ligand and 1/200 m $NiCl_2 \cdot 6H_2O$, plus a slight excess of 15% from theoretical value of the last reagent, in order to assure the completeness of the reaction. Chelate of type (IIa) is obtained in the presence of triethylamine (ca. 1 ccm), and of type (IIb) if concentrated NH_3 *ca.* 20 ccm) is present, which causes the splitting of the anil group[4] and its substitution by the imino group, NH, in the ligand molecule.

The crystalline products were repeatedly washed with 3% acetic acid, until the washing solutions did not contain Ni(II) ions any more, and then washed repeatedly with warm absolute ethanol to remove the traces of ligand or its degradation products. The Ni(II) chelates are microcrystalls, intensely coloured in dark violet, very unsoluble in methanol, ethanol, little soluble in acetone, chloroform and DMF. The attempts to obtain the Co(II) chelate, of type (IIa), using the indicated method[2] have failed. This chelate has been however prepared using the above mentioned preparation way, in the presence of triethylamine, which shows that the manifested care[2] with regard to the fact that in the presence of basic reagents excepting sodium acetate, the Co(II) ion, would tend towards a higher than four coordination, coordinating other ligands (in this case triethylamine) from the reaction medium is unjustified. The purification was performed through repeated washing with 3% warm acetic acid, followed in this case by recrystallization from absolute ethanol on charcoal, due to the higher solubility of the compound in ethanol, in comparison with the other Ni(II) chelates. Big crystals of dark blue-violet colour with metallic glistening are obtained. The compound has been finally dried on di-P_2O_5.

---

[6] L. Knorr, *Ber. dtsch. chem Ges.*, **20**, 1397 (1887).

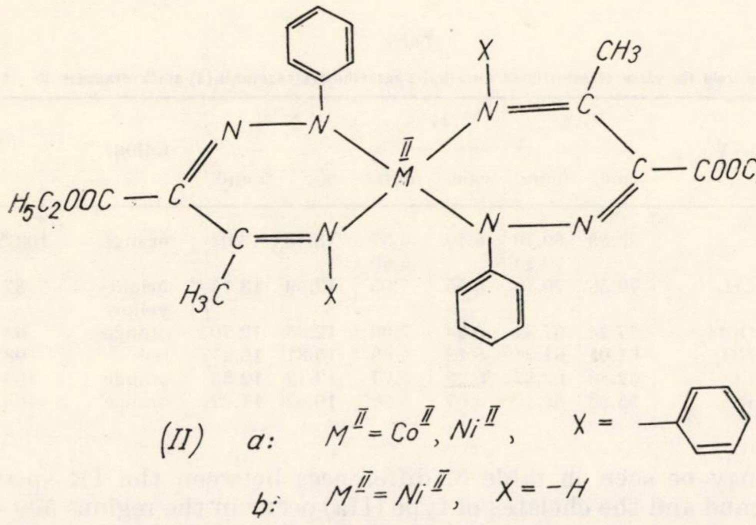

The elemental analyses of C, H and N were made by microcombustion. The metal amount was measured by disintegration with H_2SO_4 and H_2O_2, and the Ni(II) determined with dimethylglyoxime and Co (II) as $Co(C_5H_5N)_4(SCN)_2$, after the Spacu's method.[7]

The absorption spectra of compounds were recorded with a VSU-2 Carl Zeiss (Jena) spectrophotometer on solutions in absolute ethanol of $0.5-2.5 \times 10^{-4}$ m/l concentration for UV measurements and of $2.5-5 \times 10^{-4}$ m/l concentration for visible and near IR range.

The reflectance spectra of chelates were recorded on a VSU-1 Carl Zeiss (Jena) spectrophotometer using MgO as standard.

The IR spectra of the compounds were recorded within $400-4000\ \mathrm{cm}^{-1}$ range by means of a Perkin-Elmer 621 spectrophotometer, using KBr pellets.

The electric conductivity of the chelates was determined with a OK-102/1 conductometer on solutions of absolute ethanol of 2.5×10^{-4} m/l.

The magnetic susceptibilities were measured at the room temperature according to the Faraday method, using $Hg[Co(NCS)_4]$ as standard. The magnetic moment was calculated from $\mu = 2.828\ (\chi'_M \cdot T)^{1/2}$, where $\chi'_M = \chi_M - \chi_{dia}$ is the corrected molar susceptibility. The following diamagnetic corrections were used $\chi_{dia} = -250 \times 10^{-6}$ for Ni(II) chelate of type (IIb) and $\chi_{dia} = -340 \times 10^{-6}$ (c.g.s.u.) for the other two chelates.

RESULTS AND DISCUSSIONS

The analytical data for ligands, given in table 1, agree with the formula (I).

---

[7] G. Spacu and I. Dick, *Z. analyt. Chem.*, **71**, 97 (1927).

Analytical data for Co(II) and Ni(II) chelates, summarized in table 2, lead to the structural formulas (II a and b).

Differences between the free ligands and the coordinated ones were put in evidence by means of the IR spectra as shown in table 3.

Table 1

Ligands from the class of substituted 1-methyl-2-carbethoxy-glyoxalanil-(1)-arylhydrazones-(2) (I)

$-C_6H_4-Y$	C %		H %		N %		Colour	m.p. °C
	calc.	found	calc.	found	calc.	found		
$-C_6H_5$	69.88	69.70 70.24	6.19	6.37 6.60	13.58	13.64	orange	103,5 − 105.5
$-C_6H_4-p-CH_3$	70.56	70.76	6.55	7.05	12.99	13.15	bright-yellow	87 − 89
$-C_6H_4-p-OCH_3$	67.24	67.62	6.24	7.00	12.38	12.79	orange	88 − 90.5
$-C_6H_4-p-NO_2$	61.01	61.21	5.12	5.69	15.81	16.27	red	98 − 100
$-C_6H_4-p-Cl$	62.88	62.87	5.28	5.77	12.12	12.53	orange	103 − 107
$-C_6H_4-p-Br$	55.68	56.10	4.67	5.28	10.82	11.02	orange	103 − 106

As may be seen in table 3, differences between the IR spectra of the free ligand and the chelates of type (IIa) occur in the regions 500 − 615 ; 680 − 730 ; 890 − 1020 ; 1220 − 1270 ; 1320 − 1370 and 1480 − 1520 cm^{-1}, the more pronounced being observed at 1320 − 1370 cm^{-1}, where instead of the weak bands of the ligand, very intense and broad absorption bands of the chelated ligand occur as a consequence of the changes due to the coordination.

Table 2

Analytical data for Co(II) and Ni(II) chelates

Chelate type	M %		C %		H %		N %		m.p. °C
	calc.	found	calc.	found	calc.	found	calc.	found	
IIa $M^{II} = Co^{II}$	8.72	8.40	64.00	63.88	5.37	6.02	12.44	12.89	175 − 176,5
IIa $M^{II} = Ni^{II}$	8.69	8.22	64.02	63.83	5.37	5.98	12.44	12.96	148 − 150.5
IIb $M^{II} = Ni^{II}$	11.22	10.91	55.09	54.74	5.39	5.86	16.06	12.28 16.42	239 − 242

The IR spectra of the two Ni(II) chelates are obviously different, a further intense band at 3280 cm^{-1}, appearing only in the spectrum of the chelate (IIb), may be ascribed according to the related literature as being proper to the imino group frequency. The above observation agrees with the chemical data which tell us that the coordinated ligand in this case does not contain the anil group, but imino group in accord with our structural formulation.

The very low values assumed by the molar conductivities for the chelates in absolute ethanol, of about 0.6 $ohm^{-1}\,cm^2\,mol^{-1}$ for Ni(II) chelate (IIb) and of 1.4 and 1.8 $ohm^{-1}cm^2mol^{-1}$ for Co(II) and Ni(II) chelates of the type (IIa) show that all the chelates behave as nonelectrolyte.

Table 3

The IR spectra of the free ligand and chelates (cm^{-1})

Ligand (I) (Y=H)	Chelate (IIa) $M^{II} = Co^{II}$	Chelate (IIa) $M^{II} = Ni^{II}$	Chelate (IIb) $M^{II} = Ni^{II}$
		420 vw	
		440 vw	450 w
480 w		470 w	
500 w	500 w, v broad		520 w
550 vw			
	590 m	580 m	580 s
			590 s
620 w		615 w	615 w
680 s	685 s	690 vs	685 vs
695 s			700 vs
730 m	730 s	730 s	740 w
750 vs	755 vs	750 vs	755 vs
	770 vw	770 vw	770 m
810 m	820 m	820 w	830 m, broad
			885 w
890 w	905 w	910 w	910 vw
	940 w		960 vw
	990 m	990 w	
	1020 w		1020 w
1070 vs	1070 vs	1070 vs	1080 vs
1150 s	1155 vs	1160 s	1160 vs
			1175 vs
1180 vs	1200 vs, v. broad	1190 vs	1180 vs
1220 w			
1270 w	1285 sh		1280 sh
1320 w	1330 vs		1310 vs
1360 w	1360 vs	1350 vs, v broad	
1370 w			1385 vs, v broad
	1430 m	1430 s	1430 w
			1450 m
1480 s	1480 m	1480 m	1480 w
1510 s	1510 m, broad	1520 m, broad	1550 m
1570 m	1580 m	1580 m	1580 w
1680 vs	1700 vs	1680 vs	1860 vs
	2930 vw	2940 vw	2950 vw, v broad
2980 vw			
			3280 vs

vs – very strong; s – strong; m – medium; w – weak; sh – shoulder.

The insignificative differences between the electronic absorption bands of the chelates, measured either on absolute ethanol solutions or on the solid state, show that no structural changes occurred during the dissolution, and the same molecular species are therefore present in both solution and solid state.

ELECTRONIC SPECTRA AND MAGNETIC PROPERTIES
$[Ni(II)L_2)$ and $[Ni(II)L'_2]$

Both compounds are diamagnetic, and namely :

$$[Ni(II)L_2] \quad \mu_{eff} = 0.6 \pm 0.7 \text{ BM}$$

and

$$[Ni(II)L'_2] \quad \mu_{eff} = 0.2 \pm 0.3 \text{ BM}$$

the determined magnetic moments being characteristic for a low spin square planar d^8 configuration. (L means the ordinary ligand of type (I, Y = H), and L′ the ligand containing the imino group, NH, instead of the anil group into the molecule).

The electronic spectra in the visible range recorded on solutions (absolute ethanol) are plotted in figure 1.

Besides the maxima proper to the coordinated ligands (within 220 – 400 nm), in the visible range, two further intense absorption bands occur, as follows :

$$[Ni(II)L_2]: 625 \text{ nm } (16{,}000 \text{ cm}^{-1}; \ \varepsilon_{mol} \approx 270)$$
$$510 \text{ nm } (19{,}600 \text{ cm}^{-1}; \ \varepsilon_{mol} = 5000)$$

$$[Ni(II)L'_2]: 575 \text{ nm } (17{,}300 \text{ cm}^{-1}; \ \varepsilon_{mol} \approx 330)$$
$$475 \text{ nm } (21{,}000 \text{ cm}^{-1}; \ \varepsilon_{mol} = 6400).$$

The very high intensity of the absorption bands at 510 and 475 nm, respectively, indicate a charge transfer (CT) nature of these transitions. According to Jørgensen's expression [8a,b]

$$\nu_{CT} \approx 30{,}000 \ (\mathcal{X}_N - \mathcal{X}_{Ni}) \text{ cm}^{-1}$$

where [8a] $\mathcal{X}_{Ni(square\ planar)} = 2.2$ and [8b] $\mathcal{X}_N = 3.2$ are the optical electronegativities, it follows that the ligand→metal CT bands must occur at approximately 330 nm (30,000 cm^{-1}). It may be concluded that the two absorption maxima are not due to a ligand → metal CT mechanism, the only remained alternative is to ascribe them to CT metal → ligand transitions, and namely from the filled MO's of the coordination bonds to the empty antibonding MO's of the organic ligand.

The other weaker bands ($\varepsilon_{mol} \approx 300$) occurring as shoulders of the CT bands at 625 and 575 nm may undoubtedly be assigned to spin allowed $d - d$ transitions.

[8a] A. B. P. Lever, "Inorganic Electronic Spectroscopy", Chapt. 8 – 9, Elsevier Publishing Company, Amsterdam – London – New York, 1968.

[8b] C. K. Jørgensen, "Electron Transfer Spectra", in "Progress in Inorganic Chemistry", vol. 12, Interscience Publishers, New York – London – Sydney – Toronto, 1970, p. 101 – 158.

The energetic expressions of the spin allowed transitions for low spin square planar d^8 configuration obtained in a strong field coupling are [8a]:

$$^1A_{1g}(e_g^4\,b_{2g}^2\,a_{1g}^2) \rightarrow {}^1B_{1g}\,(e_g^4\,b_{2g}^2\,a_{1g}^1 b_{1g}^1)\,;\;\; \Delta_1 - C$$

$$^1A_{1g}(e_g^4\,b_{2g}^2\,a_{1g}^2) \rightarrow {}^1E_g\,(e_g^3\,b_{2g}^2\,a_{1g}^2\,b_{1g}^1)\,;\;\; \Delta_1 + \Delta_2 + \Delta_3 - 3B - C$$

$$^1A_{1g}\,(e_g^4\,b_{2g}^2\,a_{1g}^2) \rightarrow {}^1A_{2g}\,(e_g^4\,b_{2g}^1\,a_{1g}^2\,b_{1g}^1)\,;\;\; \Delta_1 + \Delta_2 - C$$

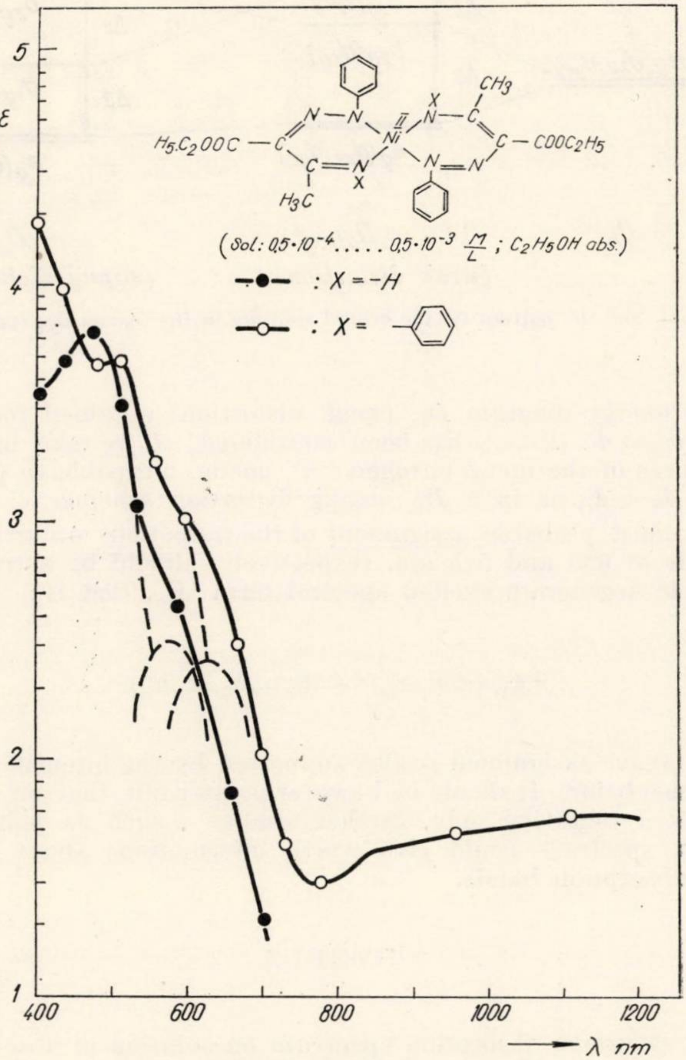

Fig. 1. — The absorption spectra of the Ni(II) chelates in absolute ethanol.

where B and C are the Racah parameters for the interelectronic repulsion energies, and Δ_1, Δ_2, Δ_3 the orbital energies as represented in the most probable MO pattern valid for our chelates (see fig. 2).

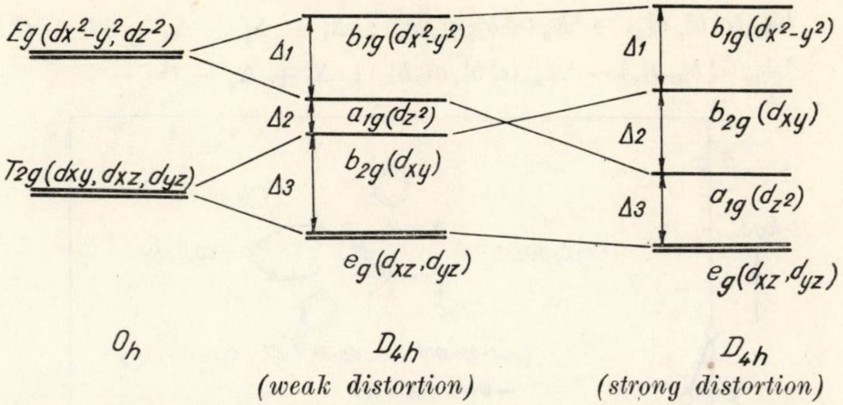

Fig. 2. – The MO pattern for the orbital splitting in the O_h and D_{4h} symmetries.

The energy diagram D_{4h} (weak distortion) obtained for the order d_{xz}, $d_{yz} < d_{xy} < d_{z^2} < d_{x^2-y^2}$ has been considered, if we take into account the weakness of the metal-nitrogen "π" bonds, incapable to produce the inversion $d_{z^2} < d_{xy}$ as in a D_{4h} strong distortion scheme.

The most probable assignment of the transitions occurring in both compounds at 625 and 575 nm, respectively, should be a transition up to a double degenerate excited spectral term ${}^1E_g$, that is :

$$ {}^1A_{1g}\,(e_g^4\,b_{2g}^2\,a_{1g}^2) \rightarrow {}^1E_g\,(e_g^3\,b_{2g}^2\,a_{1g}^2\,b_{1g}^1). $$

The above assignment is also supported by the intensity arguments as mentioned before. It should be however pointed out, that our assignment constitutes a tentative only, further studies – such as polarized light absorption spectra – could give worth informations about the nature of these absorption bands.

$[Co(II)L_2]$

The electronic absorption spectrum on solution of absolute ethano is plotted in figure 3.

The absorption bands at 560 nm (17,850 cm^{-1}) and at ≈ 1000 nm (10,000 cm^{-1}) which could be ascribed to $d-d$ transitions for high spin tetrahedral d^7 configuration[8a] are important to characterize the metal-ligand chemical bonds. Their high intensity is explained, on the one hand, by the lack of molecular center of inversion in the tetrahedral arrangement of the ligands, which make the electric dipole transition be Laporte allowed, without further molecular distorsions through a vibronic coupling, and, on the other hand, to the noticeable covalency of the metal-ligand bonds which may increase the oscillator strength.

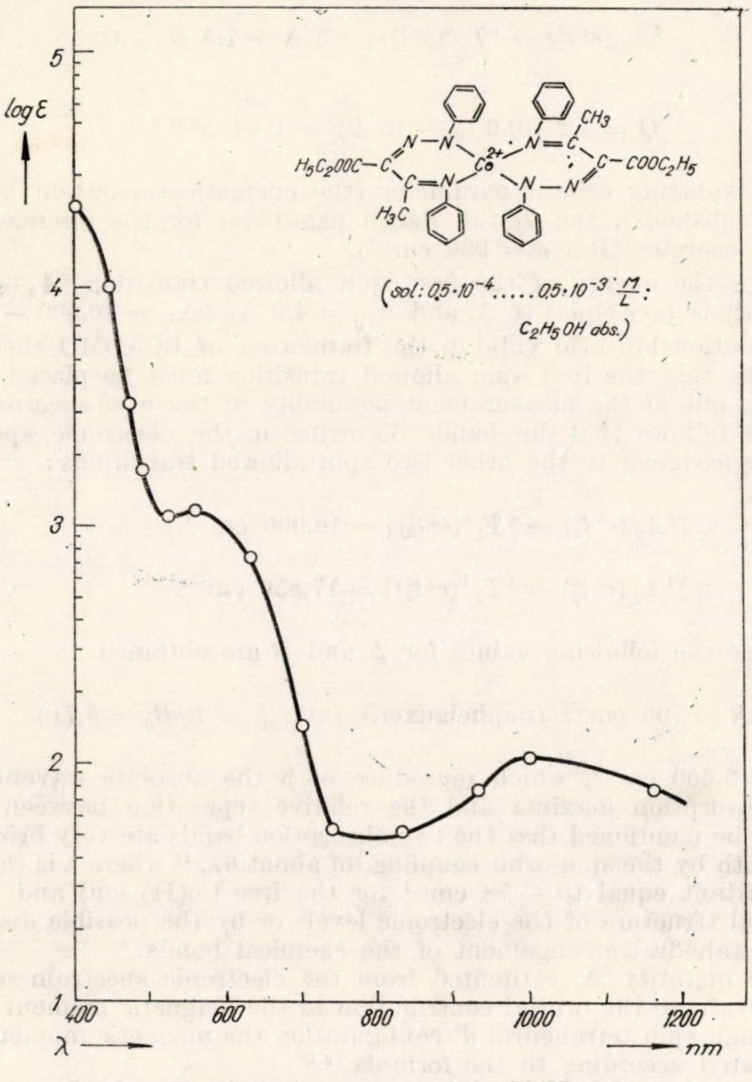

Fig. 3. — The absorption spectrum of the CO(II) chelate.

The energetic expressions for the spin allowed transitions of $d^7\,(T_d)$ configuration obtained in the assumption of a weak field coupling are as follows [8–10]:

$$^4A_2\,(e^4\,t_2^3) \to {}^4T_2\,(e^3\,t_2^4)\,;\ \Delta$$

$$^4A_2\,(e^4\,t_2^3) \to {}^4T_1{}^a(e^3\,t_2^4)\,;\ 1.5\ \Delta + 7.5\ B - Q$$

$$^4A_2\,(e^4\,t_2^3) \to {}^4T_1{}^b(e^3\,t_2^4)\,;\ 1.5\ \Delta + 7.5\ B + Q$$

where

$$Q = 1/2\ [(0.6\ \Delta - 15\ B)^2 + 0.64\ \Delta^2]^{1/2},$$

Δ is the splitting orbital parameter (the energetic separation between t_2 and e subshells), and B the Racah parameter for the interelectronic repulsion energies ($B_{\mathrm{CO(II)}} = 980$ cm^{-1}).

Since the energy of the first spin allowed transition $^4A_2\,(e^4\,t_2^3) \to {}^4T_2\,(e^3t_2^4)$ is just equal to Δ, and $\Delta_{T_d} = 4/9\ \Delta_{0_h}$ ($\Delta_{0_h} = 10{,}000 - 15{,}000$ cm^{-1}) (relationship also valid in the framework of LCAOMO theory [11]), this means that the first spin allowed transition must be placed in the IR range, out of the measurement possibility of the used spectrophotometer. It follows that the bands occurring in the electronic spectrum should be assigned to the other two spin allowed transitions:

$$\nu_2\ [^4A_2\,(e^4\,t_2^3) \to {}^4T_1{}^a(e^3\,t_2^4)] = 10{,}000\ \mathrm{cm}^{-1}$$

$$\nu_3\ [^4A_2\,(e^4\,t_2^3) \to {}^4T_1{}^b(e^3\,t_2^4)] = 17{,}850\ \mathrm{cm}^{-1}$$

and thence the following values for Δ and B are obtained

$$B \approx 700\ \mathrm{cm}^{-1}\ \text{(nephelauxetic ratio } \beta = B/B_0 = 0.71)$$

and $\Delta = 5{,}600$ cm^{-1}, which reproduce both the absolute wavenumbers of the absorption maxima and the relative separation between them. It should be mentioned that the two absorption bands are very broadened caused both by the spin-orbit coupling (of about 6λ, [12] where λ is the spin-orbit constant equal to -78 cm^{-1} for the free Co(II) ion) and by the vibrational structure of the electronic levels or by the possible distortion of the tetrahedral arrangement of the chemical bonds. [8a]

The quantity Δ, estimated from the electronic spectrum may be used to evaluate the orbital contribution to the magnetic moment value. For the high spin tetrahedral d^7 configuration the magnetic moment may be calculated according to the formula [12,13]

$$\mu = (\mu_S - 15.59\ \lambda/\Delta)\ \mathrm{BM}$$

---

[9] Y. Tanabe and S. Sugano, *J. Phys. Soc. Japan.*, **9**, 753 (1954).

[10] E. König, *Struct. and Bonding*, **9**, 175 (1971).

[11] H. H. Schmidtke, *Z. Naturforsch.*, **19a**, 1502 (1964).

[12] R. Stahl-Broda and W. Low, *Phys. Rev.*, **113**, 775 (1959).

[13] F. A. Cotton and M. Goodgame, *J. Amer. Chem. Soc.*, **83**, 1777 (1961).

where $\lambda = -178\ \mathrm{cm^{-1}}$ is the spin-orbit constant, Δ the splitting orbital parameter and $\mu_S = 3.89$ BM the pure spin value of the magnetic moment. Using the spectral value $\Delta = 5{,}600\ \mathrm{cm^{-1}}$ one obtains $\mu = 4.385$ BM, a value very close to that experimentally found

$$\mu = 4.44 \pm 0.05\ \mathrm{BM}$$

The very good agreement between the spectral and magnetic properties allows us to assign a preponderant tetrahedral symmetry for $[\mathrm{Co(II)L_2}]$.

The high value taken by Δ is due, on the one hand, to the weak "π" bonding between the "d" metal orbitals and nitrogen orbitals and, on the other hand, to the strong "σ" interaction, both effects leading to a higher energetic separation between t_2 ("σ" antibonding) and e_2 ("π" antibonding) sublevels.

The noticeable covalency of the "σ" bonds results from the low value assumed by the nephelauxetic ratio $\beta = 0.71$, approximately equal[13] to that of the tetrahedral complex $[\mathrm{Co(II)Cl_4}]^{2-}$, even though in the last case the "π" metal-ligand bonds contribute, to a higher extent, to the lowering of Racah parameters.

Acknowledgement. We express our thanks to Mr. V. Mincu from the University of Bucharest for the magnetic susceptibility measurements.

Revue Roumaine de Chimie, **18**, 7, 1155–1157 (1973)

HETEROPOLYWOLFRAMATE DES Th(IV)

A. V. BOTAR und T. J. R. WEAKLEY *

Chemie-Institut des Unterrichtsministeriums Cluj, str. Donath 65–103
* Dundee-Universität, Chemie-Department, Dundee DD 1 4 HN, Scotland.

Eingangen am 24. November 1972

Es wurde das Natriumsalz des $\mathrm{Thw_{10}O_{35}^{6-}}$ -Anions isoliert und die vorhergehende Formulierung als $\mathrm{ThW_8O_{28}^{4-}}$ revidiert. Das untersuchte Heteropolyanion ist stabil im pH-Bereich von 5,5–8,0; die Lösung der freien Säure zersetzt sich mit der Zeit. Das $\mathrm{Th^{4+}}$-Ion reagiert schnell mit den ungesättigten Heteropolyanioneu und gibt Komplexe des Typs $\mathrm{ThL_2}$, wo $\mathrm{L = SiW_{11}O_{39}^{8-}}$, $\mathrm{PW_{11}O_{39}^{7-}}$ unde $\mathrm{P_2W_{17}O_{61}^{10-}}$. Das Kaliumsalz des Typs $\mathrm{ThL_2}$ wurde isoliert und untersucht.

In einer vorhergehenden Arbeit [1] haben wir die Th(IV)-Oktowolframate sowie die entsprechende Säure synthetisiert und untersucht. Wir haben die Th(IV)-Heteropolywolframate wieder untersucht und haben von neuem das Natriumsalz und die freie Säure dargestellt und das Verbindungsverhältnis (Th/W) = 1/10 gefunden und nicht 1/8 so wie vorher berichtet wurde.

Gleichfalls haben wir die Reaktion zwischen dem $\mathrm{Th^{4+}}$-Ion und den $\mathrm{SiW_{11}O_{39}^{8-}}$, $\mathrm{PW_{11}O_{39}^{7-}}$ und $\mathrm{P_2W_{17}O_{61}^{10-}}$-Heteropolyanionen, die bei der teilweisen Zersetzung der Heteropolyanionen des Typs $\mathrm{SiW_{12}O_{40}^{4-}}$, $\mathrm{PW_{12}O_{40}^{3-}}$ und $\mathrm{P_2W_{18}O_{62}^{6-}}$ bei einem in der Nähe des Neutralwertes gelegenen pH-Wert entstehen, untersucht.

In der Fachliteratur ist bekannt, daß diese „ungesättigten'' Heteropolyanionen mit einer Reihe von zwei-, drei- und vierwertigen Kationen reagieren und eine Reihe von Heteropolyanionen [2–11] bilden. Wir haben festgestellt, daß das Th(II)-Ion Komplexe des Typs $\mathrm{ThL_2}$ bildet, wo $\mathrm{L = SiW_{11}O_{39}^{8-}}$, $\mathrm{PW_{11}O_{39}^{7-}}$ unde $\mathrm{P_2W_{17}O_{61}^{10-}}$.

[1] GH. MARCU, I. TODORUȚ und A. BOTAR, *Rev. Roumaine Chim.*, **16**, 1335 (1971).

[2] T. J. R. WEAKLEY und S. A. MALIK, *J. Inorg. Nuclear Chem.*, **29**, 2935 (1967).

[3] L. C. W. BAKER und J. S. FIGGIS, *J. Amer. Chem. Soc.*, **92**, 3794 (1970).

[4] L. C. W. BAKER, V. S. BAKER, K. ERIKS, M. T. POPE, M. SHIBATA, O. W. ROLLINS, J. H. FANG und L. L. KOH, *J. Amer. Chem. Soc.*, **88**, 2329 (1966).

[5] C. M. TOURNE, *Compt. rend.*, Seria C **266**, 702 (1968).

[6] C. M. TOURNE und G. TOURNE, *Bull. Soc. chim. France*, **1124** (1969).

[7] S. A. MALIK und T. J. R. WEAKLEY, *J. Chem. Soc.* (A), **2647** (1968).

[8] C. M. TOURNE, G. TOURNE, S. A. MALIK und T. J. R. WEAKLEY, *J. Inorg. Nuclear Chem.*, **32**, 3875 (1970).

[9] S. A. MALIK und T. J. R. WEAKLEY, *Chem. Comm.*, **1094** (1967).

[10] R. D. PEACOCK und T. J. R. WEAKLEY, *J. Chem. Soc.* (A), **1836** (1971).

[11] V. E. SIMMONS, PH. D. THESIS, Boston University, 1963.

EXPERIMENTELLES

10-Th(IV)-Wolframat. Die allgemeine Arbeitsmethode wurde in einem vorhergehenden Bericht[1] beschrieben. Einer Natriumwolframat-Lösung, die zum Sieden gebracht wurde und deren pH-Wert mit Eisessig auf 7,3—7,5 gebracht wurde, wurde tropfenweise und unter stündigem Rühren eine heiße Thoriumnitrat-Lösung zugefügt. Das Reaktionsgemisch wird filtriert und plötzlich auf 5° abgekühlt. Aus der Lösung scheiden sich schnell weiße Kristalle mit gut gebildeten Flächen ab. Die erhaltene Substanz wurde dreimal aus warmem Wasser (70°) durch plötzliches Abkühlen bis 5° umkristallisiert.

Komplexe mit ungesättigten Heteropolyanionen. Diese Komplexe wurden nach der allgemeinen Synthesemethode der Heteropolyanionen-Typs [2,7–10] erhalten. Da die Kaliumsalze der synthetisierten Heteropolyanionen in Wasser sogar bei Kälte eine große Löslichkeit aufweisen, wurde 1,4-Dioxan für ihre Trennung verwendet. In allen Fällen sind sie synthetisierten Salze feine Kristalle von weißer Farbe. Der Versuch, das Ammoniumsalz zu trennen, ausgehend von $(NH_4)_{10}P_2W_{17}O_{61} \cdot xH_2O$ und dem Th(IV)-Ion, war nicht von Erfolg gekrönt. Die durchgeführten chemischen Analysen zeigen, daß es sich in diesem Fall um ein Gemisch von Heteropolyanionen handelt.

ARBEITSMETHODEN UND CHEMISCHE ANALYSE

— Die Analyse der synthetisierten Th(IV) Heteropolywolframate wurde nach der bekannten Methode[11] durchgeführt. Thorium wurde durch Fällen mit Oxalsäure[12] bestimmt. Es waren zwei Wiederausfällungen nötig, um den Wolframspuren los zu werden, sonst hätten wir von neuem das Verbindungsverhältnis Th/W = 1/8 gefunden. Die andern im System enthaltenen Elemente wurden, so wie in den vorhergehenden Arbeiten[2,7–11] gezeigt wurde, bestimmt.

— Die Bestimmung der Basizität der Salze, beziehungsweise der freien Säuren (erhalten beim Durchfluß wäßriger Lösungen der synthetisierten Salze durch eine Austauscherkolonne Zeocarb 226 in H-Form, wurde durch Zersetzung mit NaOH und der Retitration des Basenausschusses mit HCl in Gegenwart von Phenolphtalein als Indikator durchgeführt.

— Die i.r.-Spektren wurden mit einem Spektrophotometer des Typs Perkin-Elmer 521 in KCl und Paraffinöl bestimmt.

Die kalorimetrischen Bestimmungen wurden mit einem Differentialkalorimeter des Typs Perkin-Elmer DSC-1B durchgeführt. Die Diffraktionsmessungen mit X-Strahlen wurden mittels eines Phillips 1050/25-Apparates vorgenommen.

— Die Ergebnisse der chemischen Analysen sind in Tabelle 1 angeführt.

Tabelle 1

Chemische Analyse der Th(IV)-Heteropolywolframate*

Verbindung	Elemente, %					
	Na	K	Th	W	P	Si
$Na_6ThW_{10}O_{35} \cdot 27H_2O$	4,2(4.1)	—	7,0(6,9)	55,5(54,8)	—	—
$K_{12}Th(SiW_{11}O_{39})_2 \cdot 27H_2O$	—	7,3(7,1)	3,3(3,4)	61,9(61,0)	—	0,8(0,8)
$K_{10}Th(PW_{11}O_{39})_2 \cdot 36H_2O$	—	5,9(5,7)	3,4(3,3)	60,1(58,4)	0,9(0,9)	—
$K_{16}Th(P_2W_{17}O_{61})_2 \cdot 45H_2O$	—	6,6(6,3)	2,3(2,3)	62,8(63,5)	1,4(1,2)	—

* Die berechneten Werte sind in Klammern angegeben.

---

[12] A. I. Vogel, „Quantitative Inorganic Analysis", 3th Ed., 1961, p. 541.

ERGEBNISSE UND DISKUSSIONEN

So wie die durchgeführten chemischen Analysen, die in Tabelle 1 angeführt sind, zeigen, ist das Verbindungsverhältnis Th/W im Falle des Th(IV) Wolframates 1/10. Die vorher veröffentlichten Ergebnisse [1] erklären wir dadurch, daß die Th(IV)-Heteropolywolframate in einer Form von ungenügend reinen Makrokristallen erhalten wurden und andererseits wegen den bei der Thoriumbestimmung als ThO_2 vorhandenen Wolframspuren.

Das Studium der Reaktion zwischen Natriumwolframat und den Th(IV)-Ce(III)-beziehungsweise Ce(IV) [13]-Ionen mittels der Papierelektrophorese zeigt, daß es sich um eine einzige Ionenart handelt.

Wenn die Summe der elektrophoretischen Mobilitäten der untersuchten Heteropolyanionen in Abhängigkeit des pH-Wertes der Wolframatlösung graphisch dargestellt wird, erhält man eine Kurve in „S"-Form, die charakteristisch für die Bildung einer einzigen Ionenart ist. Eigentlich weisen die i.r. Spektren der Ce(III)—Ce(IV)- und Th(IV)-Heteropolywolframate im Gebiet 300—1000 cm^{-1} große Ähnlichkeiten auf.

Die röntgenographische Untersuchung der kristallinen Pulver zeigte, paß sich die erhaltenen Heteropolysalze in Form kleiner Kristalle vorfinden. Mikroskopisch scheinen die Natriumsalze der Ce(VI), -und Th(IV)-Heteropolyanionen isomorph. Wir nehmen an, da die Zelleneinheit monoklin ist, doch können kleine Abweichungen der Werte a, b, c, und eine bemerkenswerte Veränderung der Pulverdiagramme hervorrufen.

Schlußfolgernd kann aufgrund der chemischen Analysen (Tabelle 1), sowie der Bestimmung der Basizität sowohl für das Natriumsalz des Th(IV)-Heteropolywolframates als auch für die freie Säure, das Thoriumheteropolywolframat als $ThW_{10}O_{35}^{6-}$ formuliert werden. Wir unterstreichen, daß es in diesem Fall sehr schwer ist, des Kaliumsalz dieses Heteropolyanions zu erhalten. Durch Wechselreaktion zersetzt sich das Th(IV)-Heteropoliowolframat sehr leicht und geht in Kaliumparawolframate über, die viel stabiler sind.

Die in Tabelle 1 angeführten analyitschen Ergebnisse bezüglich den Th(IV). Verbindungen mit den untersuchten, „ungesättigten" Heteropolyanionen stehen im Einklang mit unsern Vermutungen, wenn die Ähnlichkeit zwischen den chemischen Eigenschaften des Th(IV) mit denen des Ce(III), beziehungsweise des Ce(IV), in Betracht gezogen wird. Wir unterstreichen, daß diese Heteropolyanionen Säuren und Basen gegenüber viel stabiler sind als das Heteropolyanion $ThW_{10}O_{85}^{10}.^{-}$

Fragen im Zusammenhang mit der Struktur dieser Heteropolywolframat-Typen wurden in einer anderen Arbeit [11] behandelt.

Wir erwähnen, daß die thermogravimetrische Analyse aller getrennten Salze auf keine festgebundenen Wassermoleküle deutet. Die untersuchten Salze sind bei 200° vollkommen dehydriert.

---

[13] Gh. Marcu, I. Todoruţ und A. Botar, *Rev. Roumaine Chim.*, **16**, 829 (1971).

Revue Roumaine de Chimie, 18, 7, 1159–1172 (1973)

COMPLEXES OF ISONICOTINIC ACID HYDRAZIDE WITH Fe(II) AND THIOCYAN, $(INAH)_2Fe(NCS)_2 . H_2O$

IULIA I. GEORGESCU *), D. CIOMÂRTAN **), G. TEODORESCU ***)
MARIA HLEVCA *) and MARIA ZAHARESCU **)

*) Polytechnical Institute, Faculty of Chemical Engineering, Bucharest, Str. Polizu, 1 Romania
**) Institute of Physical Chemistry, Str. Galaţi 31, Bucharest, Romania
***) Polytechnical Institute, Faculty of Energetics, Bucharest, Romania

Received September 21, 1972

A number of physical analyses : thermogravimetric, polarized light microscopy, infrared molecular spectra, ultraviolet reflexion spectra, X-ray diffraction as well as electron microscopy have been carried out, in order to prove the possible existence of the *cis-trans* isomerism of the isonicotinic acid hydrazide complex with iron (II) and thiocyan $(INAH)_2Fe(NCS)_2 \cdot H_2O$. The existence of the yellow stable *cis*-form complex below 85° and of the brown reddish *trans*-form complex above this temperature has been proved.

INTRODUCTION

Complex compounds of the isonicotinic acid hydrazide (INAH) with metallic ions belonging to the first group of transition elements were prepared in 1958. [1] The chelate formation with a 5-atoms cycle – the metal-ligand ratio being 1 : 1, in an acid medium and 1 : 2 in a pH 7 medium – was revealed by the same authors, together with the increase of their "in vivo" antitubercular activities in the presence of metals. On the other hand, in the case of hydrazide tetracycline complexes, only the phenolic β-diketone group in the molecule proved to be responsible for chelate formation with metallic ions. [2]

This paper intends to provide some experimental cases in support of the existence of two *cis-trans* isomers, but in particular in the case of the INAH complex with Fe(II) and thiocyan in which the thiocyan acts as a strongly negative biased group, favouring the INAH addition to the iron. We point out that the existence of the $(INAH)_2Fe(NCS)_2.H_2O$ *cis-trans* isomers was proved for the first time in 1971, by the Mössbauer effect. [3]

---

[1] W. O. Foye and R. N. Duvall, *J. Amer. Pharm. Assoc.*, **47**, 285 (1958).

[2] M. Ishidate, T. Sakaguohi, K. Taguchi and S. Kanao, *Helv. Chim. Acta*, **22**, 457 (1960).

EXPERIMENTAL

SYNTHESES OF THE $(INAH)_2Fe(NCS)_2 \cdot H_2O$ COMPLEX [3–5]

An aqueous solution of ferrous sulphate was first run in an INAH aqueous solution and then treated with stoichiometric amounts of ammonium thiocyanate at room temperature and with a slightly alkaline pH, resulting in a light yellow precipitate which became reddish yellow by heating in the forming solution. Two syntheses were made in parallel : the first at room temperature, yielding a yellow precipitate which we called the (*a*) compound and the second at 80–90°, yielding a reddish precipitate referred to as the (*b*) precipitate (compound). These precipitates were filtered separately through a vacuum pump, washed in cold distilled water and in alcohol and subsequently dried on a porous porcelain plate. Both the (*a*) yellow and (*b*) reddish compounds are in an incipient microcrystalline state, stable and insoluble in water, alcohol, ether, chloroform, benzene. The elementary analyses of the complexes led to the rough formula $(INAH)_2Fe(NCS)_2 \cdot H_2O$ for both the (*a*) yellow and (*b*) reddish forms with the following errors compared to theoretical values : 0.8 % for Fe ; 0.27 % for N and 0.15 %for the NCS group.

Taking into account the remarks made in [1] stating that the solubility of the chelates in aqueous solutions decreases, that they form coloured combinations and that the elementary analyses agree, within the limits of the experimental errors, with the theoretical values of the chelate structure, and also considering the tautomeric equilibrium observed in the case of $Co(INAH)_2$ and $Fe(INAH)_2$, having the structures I and II, we propose formulae III and

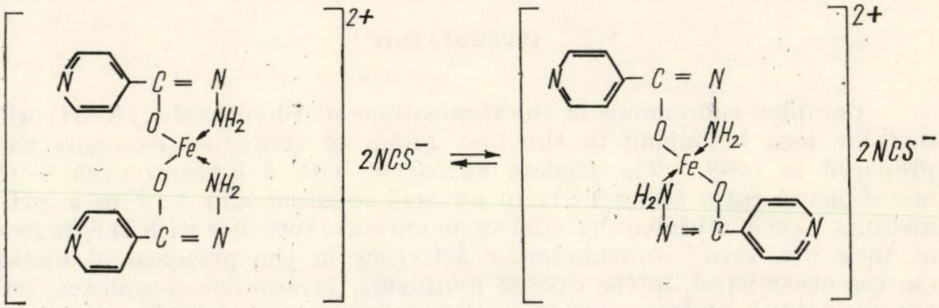

I-form II-form

---

[3] I. I. Georgescu, M. Hlevca, D. Barb, M. Morariu and D. Tarina, "Proceedings of the Conference on Mössbauer Spectrometry", vol. 2, Dresda, 1971, p. 470.

[4] M. Hlevca, *Studii şi Cercetări Chim. Acad. Bucureşti*, **3**, 547 (1961).

[5] I. Grecu and E. Ciurea, *Studii şi Cercetări Chim. Acad. R.S. România*, Fil. Cluj, **13**, 29 (1962).

IV for the thiocyan complex:

But by plotting *cis* and *trans* forms in this manner, since hydrazide is a bidentate ligand, the Fe(II) will be found in an octahedral complex with a bond of the d^2sp^3 high spin type.

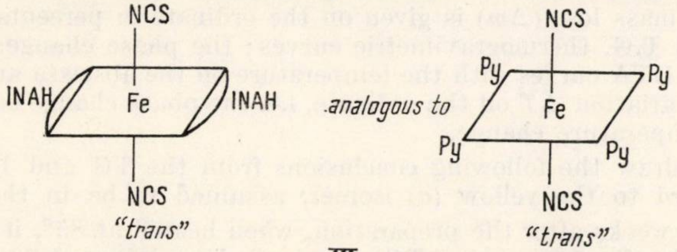

III

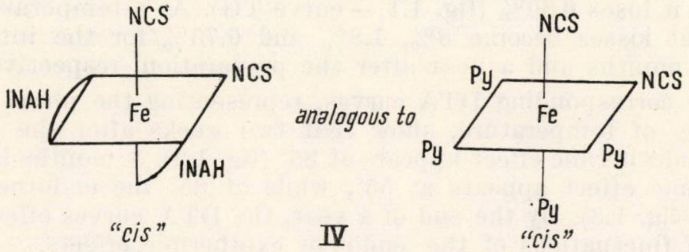

IV

STRUCTURAL ANALYSES BY PHYSICAL METHODS

We chose physical methods for the structural analyses of our compounds, because the chemical ones are limited by the fact that some complex combinations give substitution reactions with structural changes which sometimes lead to an uncertain interpretation of the results.[6]

The following physical analyses were carried out:

- thermogravimetric; thermodifferential;
- polarized light microscopy;
- IR molecular spectra;
- ultraviolet reflexion spectra;
- X-ray diffraction by the Debye-Scherrer powder method;
- electron diffraction by electron microscope.

The thermogravimetric analyses were made by means of an OD-102 derivatograph with a 1 deg/min heating rate, the standard substance being the aluminum oxide Al_2O_3 (alumina). The substances were heated in the air up to 180°.

The yellow (*a*) compound was analysed three times: the first time directly after its preparation (approx. after two weeks), the second time

[6] P. Spacu and M. Brezeanu, "Chimia Combinaţiilor Complexe", Ed. didactică şi pedagogică, Bucharest, 1969.

after a five months interval and the third time a year after the preparation; the analysed substance was taken each time from the same initial synthesis. The results of these analyses are given in figure 1.

The temperature is marked in Celsius degrees on the abscissa, while the mass loss (Δm) is given on the ordinate in percentages for the considered T.G. thermogravimetric curves; the phase changes are represented by DTA curves with the temperature on the abscissa and the temperature variation ΔT on the ordinate, i.e. the phase change as a function of the temperature change.

We draw the following conclusions from the TG and DTA curves with regard to the yellow (*a*) isomer, assumed to be in the *cis*-form:

Two weeks after the preparation, when heated at 85°, it loses 3.3% of its weight (fig. 1.2 — curve TG); 5 months later it loses 1.5% (fig. 1.3 — curve TG) and a year after its preparation, when heated at the same temperature, it loses 0.30% (fig. 1.1 — curve TG). At a temperature of 100°, the weight losses become 6%, 1.8% and 0.75% for the intervals of 2 weeks, 5 months and a year after the preparation, respectively.

The corresponding DTA curves, representing the phase changes as a function of temperature, show that two weeks after the preparation a weak endothermic effect appears at 85° (fig. 1.2), 5 months later a weak endothermic effect appears at 55°, while at 85° the endothermic effect vanishes (fig. 1.3). By the end of a year, the DTA curves offer a stability devoid of fluctuations of the endo- or exothermic effects.

The DTA curves, after two weeks and a year, present a minimum at 150° under the base line (slightly shifted after 5 months to 140°). Further, the curves show the melting (or possibly the decomposition) of the substance (fig. 1.1, 1.2 and 1.3).

The DTA curve in figure 1.3, read five months after the preparation of the complex, indicates an unstable state of rearrangement similar to the phase changes occurring in the silica gel; the molecules are rearranged in a crystal structure, tending toward the stable equilibrium state. [7]

We attributed the endothermic effect appearing at 85° in the yellow (*a*) form assumed to be *cis*, to the absorption of caloric energy for passing from the *cis* into the *trans* form (this phenomenon will be further described when dealing with the UV reflexion spectrum).

Polarized light microscopy study. The samples were examined by an oil-immersion objective both in polarized and in natural light at a 300 × magnification.

Fig. 1. — The thermogravimetric curves (T.G) together with the differential thermic analysis, curves (D.T.A), of the yellow (*a*) form of $(INAH)_2Fe(NCS)_2 \cdot H_2O$ samples between 25—145°, carried out one year (fig. 1.1), two weeks (fig. 1.2) and five months (fig. 1.3) after the preparation.

---

[7] M. Cerchez, private communication and thesis, Bucharest, (1972).

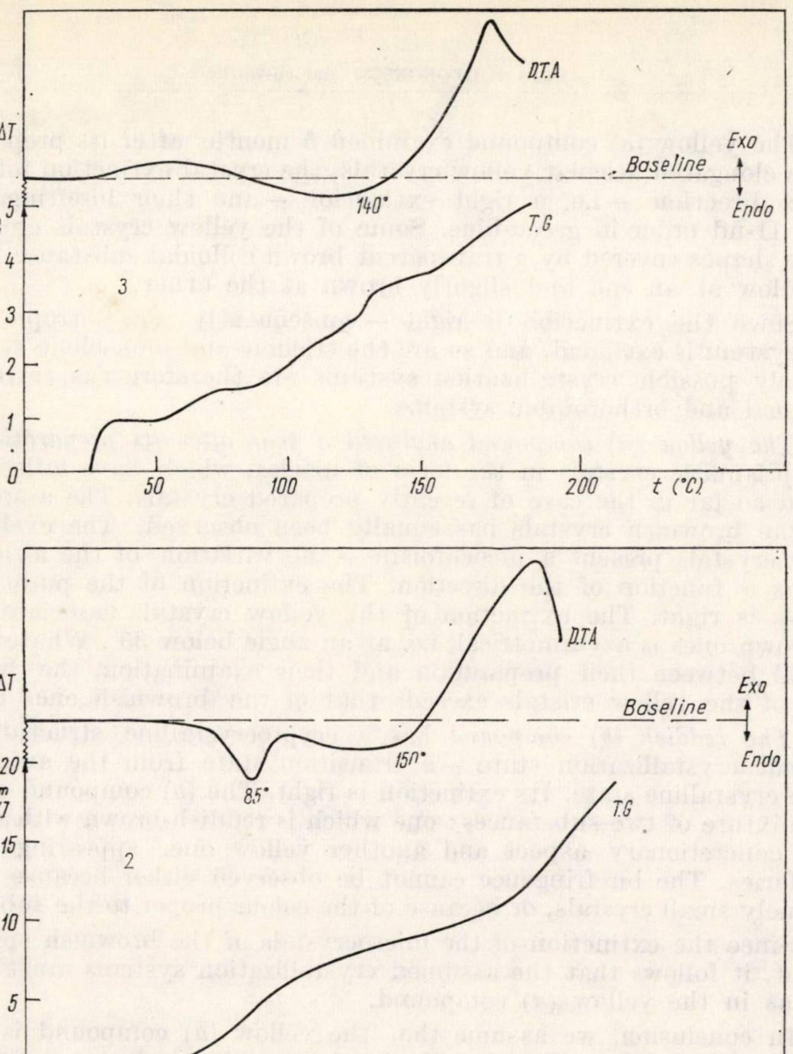

Fig. 1

Revue Roumaine de Chimie **18**, 7, 1159–1172 (1973)

The yellow (*a*) compound examined 5 months after its preparation reveals elongated acicular yellow crystals, the crystal extinction following the $n\alpha$ direction — i.e. a right extinction — and their birefringence is of the II-nd order in green-blue. Some of the yellow crystals cluster in rosette shapes covered by a transparent brown colloidal substance, others are yellow at an end and slightly brown at the other.

Since the extinction is right — consequently non-isotropic — the cubic system is excluded, and so are the triclinic and monoclinic systems. The only possible crystallization systems are therefore the tetragonal, hexagonal and orthorombic systems.

The yellow (*a*) *compound analysed a year after its preparation* has short prismatic crystals in the form of macles, which have failed to be noticed so far in the case of recently prepared crystals. The association with the brownish crystals has equally been observed. The exclusively yellow crystals present a pleochroism — the variation of the absorption light as a function of the direction. The extinction of the pure yellow crystals is right. The extinction of the yellow crystals associated with the brown ones is asymmetrical, i.e. at an angle below 35°. Whatever the interval between their preparation and their examination, the birefringence of the yellow cristals exceeds that of the brownish ones by $\lambda/4$.

The reddish (*b*) *compound* has a cryptocrystalline structure — an incipient crystallization state — a transition state from the amorphous to the crystalline state. Its extinction is right. The (*b*) compound consists of a mixture of two substances : one which is reddish-brown with a spherulitic concretionary aspect and another yellow one, appearing on the boundaries. The birefringence cannot be observed either because of the extremely small crystals, or because of the colour proper to the substance.

Since the extinction of the microcrystals of the brownish spherules is right, it follows that the assumed crystallization systems must be the same as in the yellow (*a*) compound.

In conclusion, we assume that the yellow (*a*) compound is stable at room temperature and takes the *cis*-form with maximum asymmetry when the atomic orbitals are adequately overlapping each other enabling the most stable combination, while the brownish (*b*) compound which is always associated with yellow crystals would represent the *trans* unstable form. The two isomers cannot be completely separated from each other, since the brownish isomer occurs even at room temperature during synthesis by local overheatings resulting from the formation chemical reaction, when the necessary rotation energy of the cycle in the *trans*-position can be absorbed. The concentration of the brownish crystals in the (*b*) compound is approx. 90% out the total amount of crystals, approx. 10% being yellow (*a*) crystals. For the yellow (*a*) compound, the ratio is about 85—90% yellow crystals, the remainder being conglomerates of reddish-brownish crystal spherules.

On the other hand, the possibility is not excluded of a slow modification of some small amounts of the yellow (*a*) form assumed to be *cis*, into brownish (*b*) crystals of the *trans* form reaching the equilibrium form of macles.

Infrared molecular spectra. Although molecular spectra are not always edifying for drawing conclusions on the *cis-trans* isomerism, we took them in order to prove the purity of the ligands and to explain how they are bound to the central atom of Fe(II).

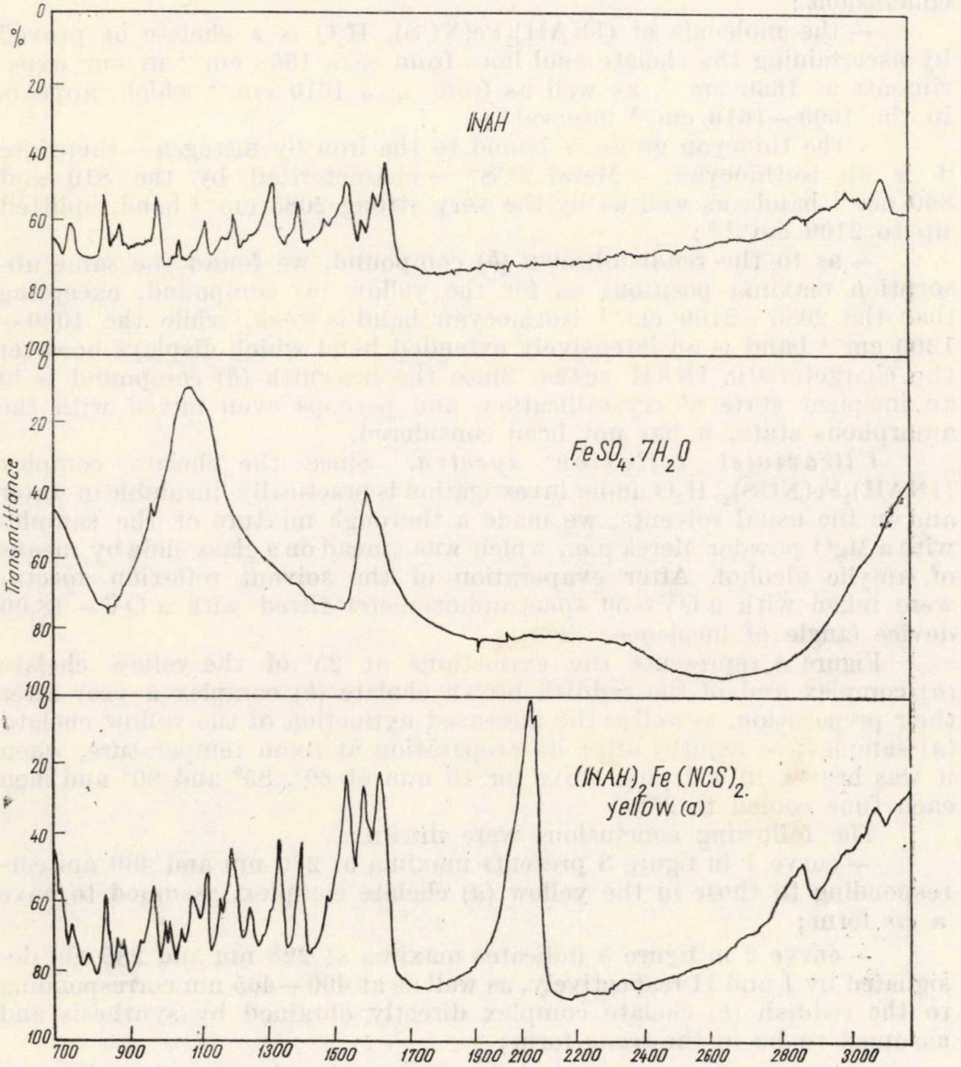

Fig. 2. — Infrared spectra of the $(INAH)_2Fe(NCS)_2 \cdot H_2O$ chelate yellow (*a*) form compared with the ligands INAH and $FeSO_4 \cdot 7H_2O$ in a kalium bromide medium.

A UR-20 spectrometer was used between 545 and 3500 cm^{-1}, with a recording rate of 160 cm^{-1}/min. From 400 –700 cm^{-1} we used the KBr prism, from 700 –1800 cm^{-1}, the NaCl prism and from 1800 –3500 cm^{-1}, the LiF one. Figure 2 represents the spectra of the INAH, of the $FeSO_4.7\,H_2O$ and of the yellow (*a*) compound. Fig. 2 gives their absorption bands.

The study of the infrared spectra resulted in the following positive conclusions :

– the molecule of $(INAH)_2Fe(NCS)_2.H_2O$ is a chelate as proved by ascertaining the chelate enol lines from $\nu_{C=O}$ 1668 cm^{-1} in our experiments at 1660 cm^{-1}, as well as from $\nu_{C=O}$ 1610 cm^{-1} which appears in the 1600 –1616 cm^{-1} interval[8];

– the thiocyan group is bound to the iron by nitrogen – therefore it is an isothiocyan, – Metal-NCS^{-} – characterized by the 810 and 860 cm^{-1} bands as well as by the very strong 2085 cm^{-1} band, splitted up to 2100 cm^{-1}[9];

– as to the reddish-brown (*b*) compound, we found the same absorption maxima positions as for the yellow (*a*) compound, excepting that the 2085 –2100 cm^{-1} isothiocyan band is weak, while the 1000 – 1200 cm^{-1} band is an intensively extended band which displays however the characteristic INAH peaks. Since the brownish (*b*) compound is in an incipient state of crystallization, and perhaps even mixed with the amorphous state, it has not been considered.

Ultraviolet reflexion spectra. Since the chelate complex $(INAH)_2Fe(NCS)_2.H_2O$ under investigation is practically insoluble in water and in the usual solvents, we made a thorough mixture of the samples with a MgO powder Merck *p.a.*, which was spread on a glass slide by means of amylic alcohol. After evaporation of the solvent reflexion spectra were taken with a QV–50 spectrophotometer fitted with a QV – 18.00 device (angle of incidence : 30°).

Figure 3 represents the extinctions at 25° of the yellow chelate (*a*) complex and of the reddish brown chelate (*b*) complex a year after their preparation, as well as the increased extinction of the yellow chelate (*a*) sample five months after its preparation at room temperature, when it was heated in a drying stove for 10 min at 80°, 85° and 90° and then each time cooled to 25°.

The following conclusions were drawn :

– curve 1 in figure 3 presents maxima at 270 nm and 460 nm corresponding to those in the yellow (*a*) chelate complex, assumed to have a *cis* form ;

– curve 2 in figure 3 indicates maxima at 228 nm and 285 nm designated by I and II respectively, as well as at 460 –465 nm corresponding to the reddish (*b*) chelate complex directly obtained by synthesis and assumed to be in the *trans* form ;

– two maxima appear in the spectrum when heating the yellow (*a*) sample at 80 –85°, compared to the unheated sample, namely at 228 and 285 nm, corresponding to maxima I and II of the reddish (*b*) sample spectrum ;

---

[8] M. Avram and Gh. D. Mateescu, "Spectroscopie infrarouge. Applications en Chimie Organique", Ed. Dunod, Paris, 1970.

[9] A. Turco and L. Pecile, *Nature*, **191**, 66 (1961).

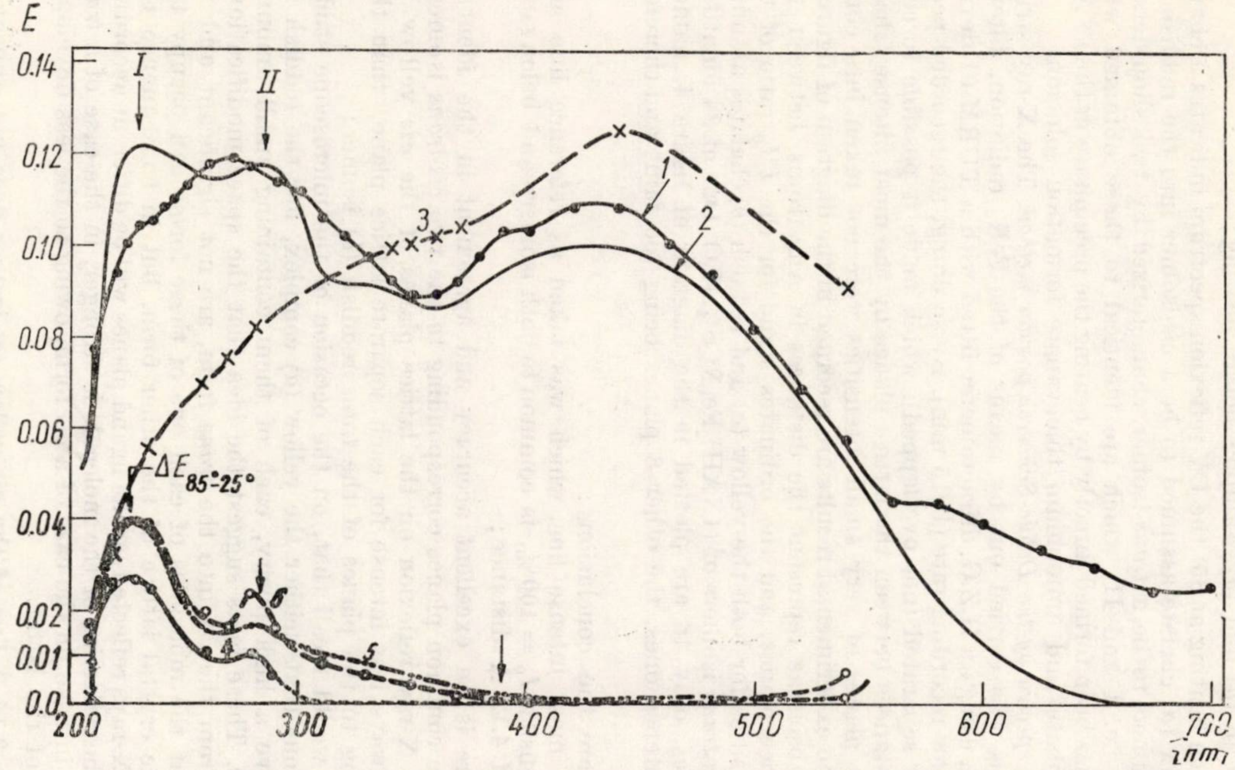

Fig. 3. — Reflexion spectra of the $(INAH)_2Fe(NCS)_2 \cdot H_2O$ yellow (*a*) chelate sample (curve *1*), reddish (*b*) chelate sample (curve *2*) one year after the preparation taken at 25°; the yellow (*a*) form five months after the preparation (curve *3*) taken at 25° and the same sample after heating at 80°, 85° and 90° for ten minutes and then cooled at 25° (*4,5,6* : extinction curves). All reflexion spectra were taken with samples incorporated in MgO.

— before heating, the spectrum of the sample (*a*) showed only a shoulder in UV at 270 nm, the maximum situated at 460—465 nm being also present in (*a*) and (*b*) samples before heating;

— when heating at 85° the UV reflexion spectrum indicates a change of the yellow (*a*) chelate assumed to be a *cis*-isomer into the reddish (*b*) chelate assumed to be a *trans*-isomer, characterized by two shoulders in ultraviolet, i.e. I and II, which are identical to those obtained when chelate (*b*) has been formed directly by heating the precipitate in the INAH, ferrous sulphate and ammonium thiocyanate formation solution.

X-ray spectra by the Debye-Scherrer powder method. The X-ray structure analysis was carried out by means of the FeK_{α} radiation, filtered through Mn, using an H.Z.G. difractometer fitted with a TURM-61 device, at a very slow recording rate (1°/15 min). By so doing, the recorded peaks were widely separated (not overlapped), which made it possible to compute the distances between the lattice planes by the most intense (sharp) lines. Other planes of very small intensities were not taken into consideration. The experimental results are recorded in the diagram of figure 4, where the abscissae represent the distances in Angströms between the various lattice planes, and the ordinates stand for the I/I_0 ratio of the X-ray intensities for both the yellow (*a*) and reddish (*b*) chelates assumed to be the *cis-trans* isomers of $(INAH)_2Fe(NCS)_2.H_2O$. Out of 24 identified lattice planes, only 16 are plotted in the diagram of figure 4, namely the more intense ones, the other 8 planes being too faint and therefore uncertain.

Here are the conclusions:

— the most intense line, which was taken as reference line and has the intensity $I_0 = 100\%$, is common to both isomers and belongs to the plane of 4.12 Å distance;

— there is an excellent accuracy and agreement in the identification of the common planes corresponding to the two *cis-trans* isomers;

— the X-ray reflexion on the lattice planes of the *cis* yellow (*a*) isomer is always less intense for each separate lattice plane, than that corresponding to the planes of the *trans* reddish (*b*) isomer;

— we would recall that, on the occasion of the microscope study, we pointed out that neither the yellow (*a*) complex, nor the reddish (*b*) complex have a high purity, each of them containing small amounts of the other. These facts suggest the idea that the space modifications, in passing from the *cis* into the *trans* form, are not significant and we conclude that the molecules of each one of these forms can occupy the points of the crystal lattice of the other form, but in consequence the intensity of X-rays reflected on the ligand planes will be different according to whether the reflection of the molecule is stronger, in the case of a *trans* form or less intense, in the case of a *cis* form, owing to the less developed space form of the latter.

— The 3.14 Å line of the *cis* yellow (*a*) isomer does not appear in the case of the *trans* reddish (*b*) form. This is due to an impurity that, however, does not at all affect our interpretation of the results.

We emphasize that a similar study was made by a member of our

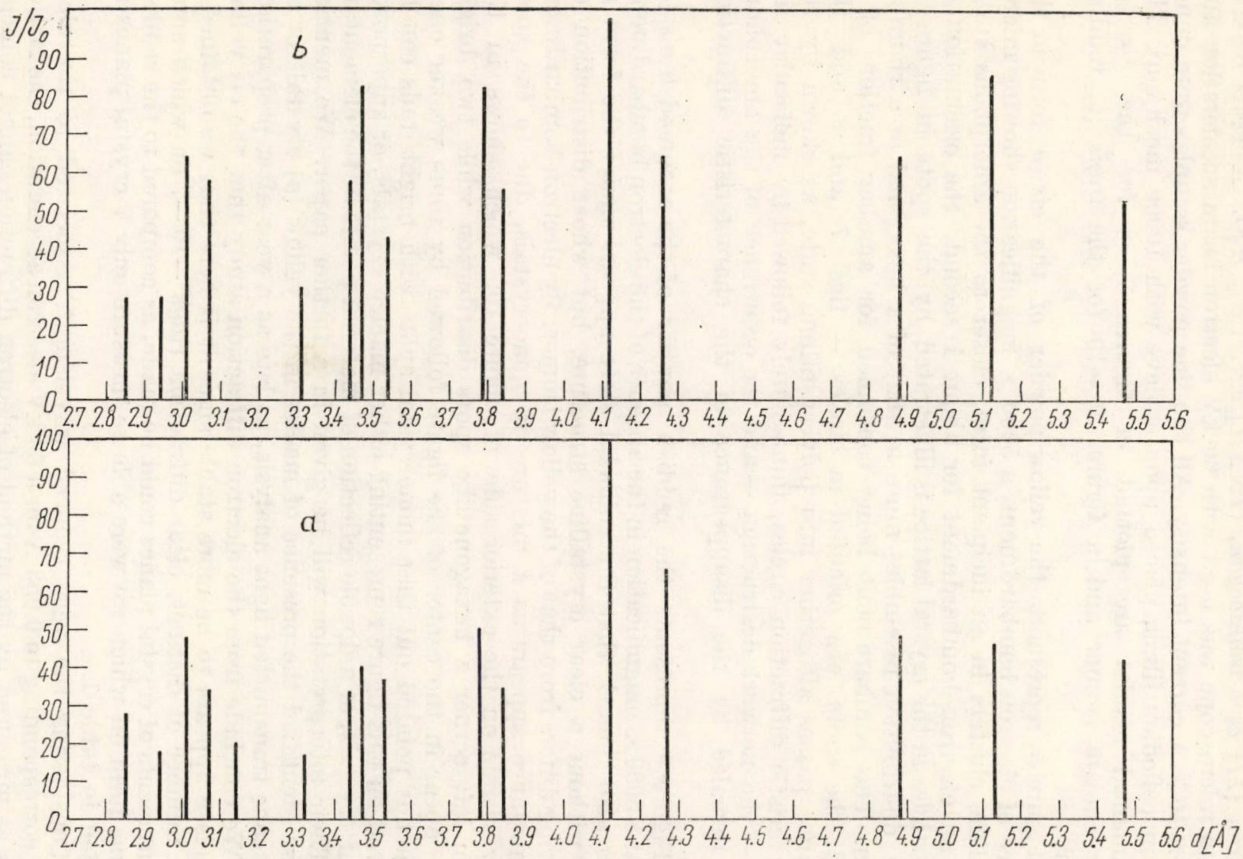

Fig. 4. — Diagram representing the d(Å) distances of lattice planes versus I/I_0 in $(INAH)_2$ $Fe(NCS)_2 \cdot H_2O$ yellow (*a*) *cis* form and reddish (*b*) *trans* form chelates.

team, on the yellow and violet form of $Py_4Fe(NCS)_2$, by X-ray diffraction [10] as well.

Electron diffraction analysis of the isonicotinic acid hydrazide chelate with iron (*II*) *and isothiocyan*, $(INAH)_2Fe(NCS)_2.H_2O$. A Tesla BS-242 electron microscope was used with 60 kV electron beam acceleration and a 1.5×10^{-7} A current intensity. All the fine powder samples were deposited on collodion films, placed upon a sieve with 10000 mesh/cm^2. The experimental results are plotted in figures 5 —8 for the *cis* (*a*) yellow chelate isomer and in figures 9 —10 for the *trans* (*b*) reddish isomer.

Figure 5 represents the yellow powder of the *cis* (*a*) form in the absence of electron bombardment, a 5000 × magnification showing microcrystalline clusters in an incipient form, closer to the amorphous state. After an electron bombardment for about 1 second, the orientation of the particles in the crystal lattice is illustrated by the spots in figure 6, whose distribution resembles more to that of a hexagonal or a rhombic system. The bombardment being continued for another fraction of a second, the spots are oriented in circles — figs. 7 and 8 and the substance passes altogether into polycrystalline state, as shown by the characteristic diffraction circles, immediately followed by molecular disorder — the network destruction — and the occurrence of the amorphous state revealed by the disappearance of the characteristic diffraction circles.

Figure 9 represents the reddish powder of the assumed *trans* (*b*) form at a 5000 × magnification in the absence of the electron bombardment. Let us also remark that the colloidal state appears under the form of spots without a clear crystalline structure, but whose distribution or clustering differs from that of the yellow isomer. By electron bombardment the substance appears as a mixture of monocrystals, due to the spots clearly visible on the exterior side of figure 10, which shows in the bottom left corner a hexagone-like spots distribution while two bright rings appear in the center of the figure followed by some weaker ones. The fact is pointed out that monocrystal spots with bright tails can be observed on this figure representing either macled crystals, or superposed rows of crystals, or a double reflection of material points of the elementary cell. Their interpretation will be given in a further paper. We mention that we identified the presence of macles in the yellow (*a*) crystals or by microscope transmitted light analysis, as late as a year after preparation.

We conclude from the electron diffraction study that the *cis* yellow (*a*) chelate appears to be more stable since it is here that we obtained a larger number of distinct, clear diffraction rings —10 —, on which some measurements of crystal planes could be made, as compared to the reddish (*b*) *trans* form on which we were able to measure only 7 crystal planes as recorded in table 1.

Considering the very reduced wavelength associated to the electrons, corresponding to 0.053 Å for a 60 kV electron acceleration, the lattice planes as measured by the method of electron diffraction cannot coincide with those measured by X-ray diffraction. Since the experimented organic

---

[10] P. Spacu, D. Ciomârtan and M. Teodorescu, *Z. Chem.*, **8**, 233 (1968).

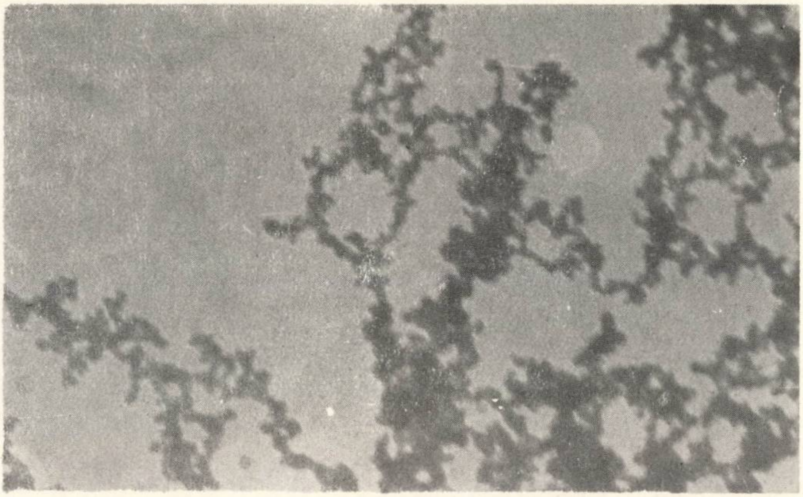

Fig. 5. — Yellow (*a*) *cis* chelate under 5000 × magnification without electron bombardment, shows microcrystalline conglomerates in an incipient state.

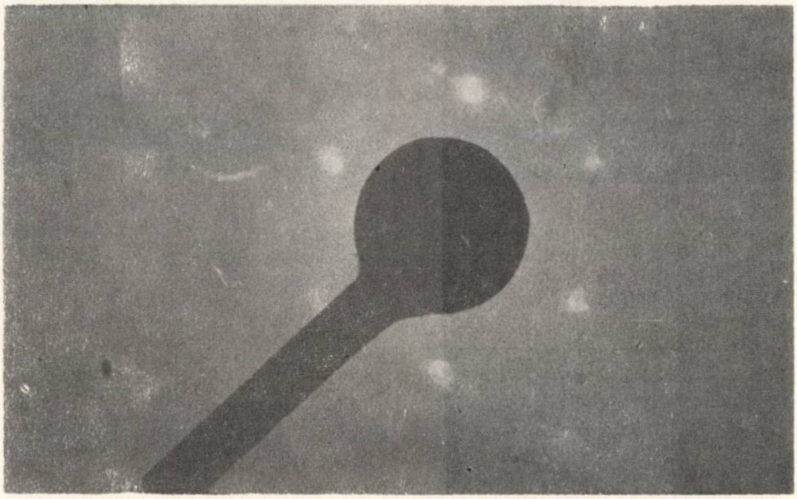

Fig. 6. — Yellow (*a*) *cis* chelate under electron bombardment for one second. The spots are oriented in a hexagonal or rhombic system.

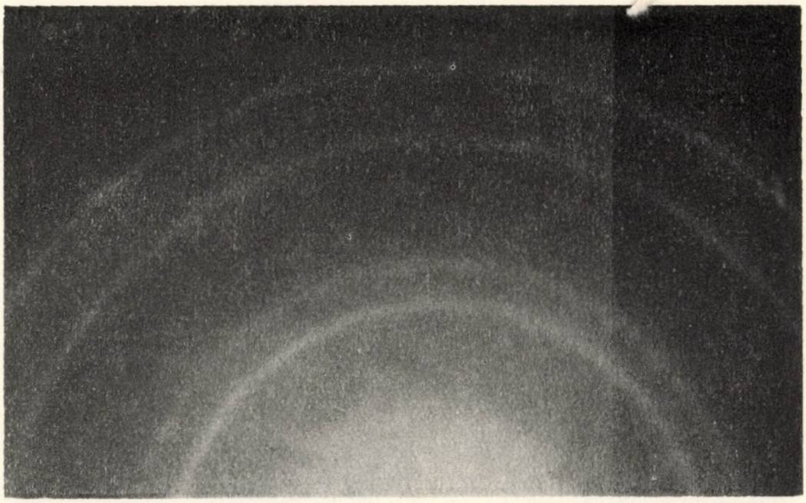

Fig. 7. — Yellow (*a*) *cis* chelate after about 2 seconds of electron bombardment shows monocrystalline spots lattice oriented on diffraction circles of polycrystalline state.

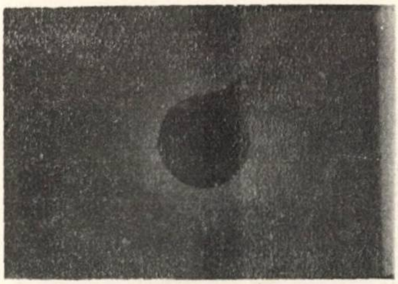

Fig. 8. — Yellow (*a*) *cis* chelate, under continued electron bombardment, the polycrystalline state is destroyed (disappearance of the diffraction circles) and the amorphous state appears.

Fig. 9. — Reddish (*b*) *trans* chelate under a 5000 × magnification without electron bombardment shows colloidal stains.

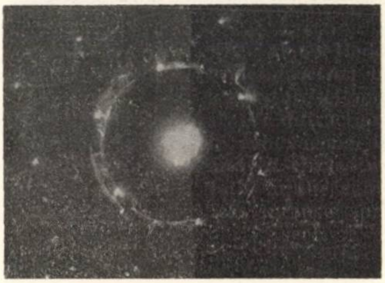

Fig. 10. — Reddish (*b*) *trans* chelate under electron bombardment passes into a mixture of mono and polycrystalline state; diffraction spots are distributed in a hexagonal form bottom left corner and in circles with spots with bright tails in the center of the figure. Other less intense spots with tails can be seen all over the figure.

Table 1

Results of the electronograms obtained for $(INAH)_2Fe(NCS)_2 \cdot H_2O$, carried out under 60 kV electron beam and 1.5×10^{-7} A current

	$(INAH)_2Fe(NCS)_2 \cdot H_2O$			
N°	yellow (*a*)	*cis*-form	reddish-brown (*b*)	*trans*-form
	d (Å)	I/I_0	*d* (Å)	I/I_0
1	3.58	5	—	—
2	3.05	40	—	—
3	—	—	2.67	50
4	2.34	100	—	—
5	2.21	60	2.16	100
6	1.98	50	2.09	60
7	1.77	70	1.87	50
8	—	—	1.30	70
9	1.19	70	1.185	60
10	—	—	1.13	70
11	0.95	40	—	—
12	0.91	30	—	—
13	0.85	10	—	—

chelate is easily destroyed, we estimate that the results obtained by X-ray diffraction on the distances between the lattice planes are more conclusive while the distribution of the spots obtained by electron diffraction provide us with valuable information on : the crystallization system, the macles, the stratification of the compound under study (traces of bright tails in the reddish (*b*) chelate).

CONCLUSIONS

The following conclusions can be drawn from the combined chemical and physical analysis of the isonicotinic acid hydrazide with iron (II) sulphate and ammonium-sulphocyanide synthesis :

1. The formula of the compound obtained corresponds to $(INAH)_2Fe(NCS)_2.H_2O$, where the iron (II) is bound in an octahedral surrounding of the d^2sp^3 high spin type with a *cis-trans* isomerism possibility.

2. It results from the IR spectra that the SCN group is bound to the Fe(II) complex through N, this being a isothiocyan bond, i.e. $Fe-NCS^-$, which is generally observed in the case of the elements of the first transition group, comprising also the iron.

3. The complex is a chelate as proved by the IR spectrum whose 1500–1700 cm^{-1} bands are much wider than those of the pure ligand – the hydrazide – in the same interval ; by the cryptocrystalline rather amorphous state – as revealed by the microscope analysis in natural transmitted light, which is characteristic of the colloidal state, consisting of the insolubility in water and in the usual solvents and the absence of the electrical conductivity ; by the tendency of the molecules to rearrange

in a more orderly crystalline structure in time, as proved by the ADT curve of the complex on which a weak exothermal effect is observed, due to the loss of water and to the tendency to recrystallize, as in the case of the silica gel.

4. At room temperature, the most stable form is the yellow (*a*) — *cis* one since it has always been obtained in the largest amounts during the synthesis, though it has not always reached a high purity, the yellow crystals being accompanied by reddish brown (*b*) cryptocrystalline formations that appear by local heating at 80—85° during the synthesis.

The evidence that on heating the yellow (*a*) *cis* form changes into the *trans* reddish (*b*) isomer resulted from the study of the ultraviolet reflexion spectrum. The unheated yellow (*a*) form shows a single shoulder at 220 nm, while by heating at 80—85° two shoulders appear in the same sample at 220 nm and 240 nm, which are identical to the maxima on the ultraviolet reflexion spectrum of the *trans*-reddish (*b*) isomer obtained by heating below 100° the complex formed in the synthesis solution.

5. The X-ray diffraction spectra obtained by the powder method by means of the FeK_α radiation filtered through Mn, led to the identification of over 16 intense lattice planes, common to both chelate isomers of the isonicotinic acid hydrazide with iron (II) and isothiocyan.

A most important remark which attests the existence of the two *cis-trans* isomers, is that the intensity of all the lattice planes homologous of the *trans* form is much higher than that of the *cis* form planes.

6. The electron diffraction on the two chelate isomers of $(INAH)_2Fe(II)(NCS)_2 . H_2O$ reveal initially a colloidal phase, followed by an orderly distribution of the matter with a crystalline lattice belonging to the hexagonal, trigonal or rhombic systems. This remark is also suported by the fact that in the polarized light extinction takes place on $n\alpha$. We point out again that the birefringence of the yellow (*a*) *cis* chelate exceeds by $\lambda/4$ that of the reddish (*b*) *trans* chelate. The *cis* yellow (*a*) form is more stable under electron bombardment, since it provides electronograms with several distinctive rings, in opposition to the *trans* reddish (*b*) one that shows a smaller number of rings which disappear very quickly under an electron bombardment.

The *trans* reddish (*b*) form presents both macles and a stratification of reticular planes as proved by the bright short tails of the spots in the mixture of mono- and polycrystalline phase of the reddish (*b*) *trans* chelate.

7. In order to prove that the $(INAH)_2Fe(II)(NCS)_2 . H_2O$ is stable at room and higher temperatures — and that no chemical degradation occurs especially at 80—100°, the behaviour of this complex chelates was investigated in paper. [3] The conclusion was that the two *cis* and *trans* isomers are stable between —194 and 145° by Mössbauer effect, the yellow (*a*) *cis* form having a smaller quadrupolar ΔQ splitting of Fe(II) than the ΔQ of *trans* reddish (*b*) form, while the δ isomeric shift keeps a constant value for both isomers, which means that the electron vicinity of the iron (II) nucleus is the same.

Acknowledgements. The authors are indebted to Dr. M. Cerchez of the Institute for Physical Chemistry, Bucharest, for the support in carrying out the thermogravimetric curves of the samples under study.

Revue Roumaine de Chimie, 18, 7, 1173–1209 (1973)

COMPUTING PROGRAM FOR INTERPRETING ESR SPECTRA OF ORGANIC FREE RADICALS

C. POMPONIU and A. T. BALABAN

Institute of Atomic Physics, Bucharest, Romania

Received January 5, 1973

A computer program was developed for interpreting ESR spectra of organic free radicals possessing atoms of nuclear spin 1/2 and 1. It is based on the assumption that coupling constants can be expressed in terms of integers, leading to the solving of a diophantine equation. Input data are numbers of coupling atoms with their nuclear spins, numbers of equidistant lines in the spectrum (even if lines are not equidistant, the spectrum can be accomodated by including zero-intensity lines at points separated by the smallest equidistance λ), experimentally measured intensities of all lines except the two marginal ones, and relative errors in determining intensities. The program output gives the theoretical intensities and the number of atoms of spin 1/2 and 1 with their coupling constants expressed in terms of λ. These solutions can then be refined with a spectrum simulator, removing the restriction that all coupling constants must be multiples of λ.

1. INTRODUCTION

In a previous paper [1] a method was presented for interpreting the hyperfine structure of electron spin resonance (ESR) spectra of organic free radicals, in particular of nitrogen free radicals. Since ESR spectrometers do not have infinite resolution, and since line broadening effects are always present in experimental recordings of ESR spectra, these frequently consist in a large number of more or less equidistant lines with various intensities. The problem of deducing from a given ESR spectrum the coupling constants of the nuclei responsible for the splitting of the energy levels of the odd electron is often a complicated one. In some cases more than one solution is compatible with the experimental data. Frequently, the large number of lines makes very difficult the initial guess of approximated coupling constants, which could then be refined by a spectrum simulator through visual comparison of experimental and simulated spectra.

---

[1] A. T. BALABAN, *Rev. Roumaine Chim.*, **17**, 9 (1972).

The informations presented by the experimental spectrum are the number $(N+1)$ and the relative intensities I_i of lines, and the distances between them. In the following, we postulate that there exists a minimal equidistance λ which allows the abscissas of all lines to be presented as multiples of λ.

The method[1] consisted in assuming known values for the numbers χ_1 and χ_2 of nuclei with nuclear spin 1/2 and 1, respectively, which cause the hyperfine structure of the ESR spectrum. These numbers must obey the relationship $2^{\chi_1} \cdot 3^{\chi_2} = \sum_i I_i$. The initial postulate is equivalent to assuming that all coupling constants can be expressed as integer multiples of λ. By partitioning χ_1 into m_i nuclei with coupling constant a_i $(\chi_1 = \sum_i m_i)$, and χ_2 into n_i nuclei with coupling constant a_i $(\chi_2 = \sum_i n_i)$, the following diophantine equation results

$$N = \sum_i m_i\, a_i + 2 \sum_i n_i\, a_i$$

By considering all partitions of N, sets of coupling constants a_i are found, which correspond to various distributions of intensities I_i. From these sets, those which are compatible with the experimental ESR spectrum are selected. For a number of lines lower than 10, a complete table of all possible equidistant line ESR spectra (with no missing line in between) can be compiled.[1,*] However, for larger numbers of lines the method becomes impracticable. Therefore a computer program was devised. It is based on the same postulate and accepts as input data the numbers of coupling nuclei with their spins, the numbers of equidistant lines with their experimentally determined (non-normalized and non-symmetric) intensities (possibly also lines with zero-intensity, which gives the possibility to include non-equidistant line ESR spectra in this treatment), and the relative errors in determining intensities. Since the intensities of the two marginal lines are most affected by the noise, these two intensities are ignored.

The solutions compatible with these data are found by the program which gives as output the theoretical intensities, and the numbers of atoms with nuclear spin 1/2 and 1, together with their coupling constants (as multiples of λ). Usually more than one solution is compatible with the experimental data, therefore all solutions are printed. A unique final solution must then be found on the basis of chemical intuition and/or of a spectrum simulator, by removing the restriction that all coupling constants are multiples of λ.

2. THE SPIN 1/2 CASE

In this section we shall suppose that the atoms responsible for the ESR spectrum have the same nuclear spin, namely 1/2. The discussion of the spin 1 case, as well as the mixed case (atoms of spins 1/2 and 1) will be deferred to the next sections.

---

[*] A table for larger N values will be published in a future paper.

Specifically, let us have χ_1 atoms of spin 1/2, such that m_1 of them have coupling constant λ, m_2 of them have coupling constant $2 \cdot \lambda$, and so on. (Here, m_1, m_2, ... stand for non-negative integers; zero value is also allowed for). Then we have:

$$\chi_1 = \sum_{i=1}^{p} m_i \tag{2.1}$$

If we denote by a_1, a_2, ..., a_{χ_1} the coupling constants which correspond to these atoms, ordered so that

$$a_1 \geqslant a_2 \geqslant a_3 \geqslant \ldots \geqslant a_{\chi_1}$$

then one can choose the abscissas of the intensities of the spectrum in the following way: denote by x_0 the leftmost of the abscissas and, moving to the right, x_1, x_2, ... the next abscissas. Then, as can be easily verified,

$$\begin{aligned}
x_0 &= (-a_1 - a_2 - \ldots - a_{\chi_1-2} - a_{\chi_1-1} - a_{\chi_1})/2 \\
x_1 &= (-a_1 - a_2 - \ldots \ - a_{\chi_1-2} - a_{\chi_1-1} + a_{\chi_1})/2 \\
x_2 &= (-a_1 - a_2 - \ldots - a_{\chi_1-2} + a_{\chi_1-1} - a_{\chi_1})/2 \\
x_3 &= (-a_1 - a_2 - \ldots - a_{\chi_1-2} + a_{\chi_1-1} + a_{\chi_1})/2 \\
x_4 &= (-a_1 - a_2 - \ldots + a_{\chi_1-2} + a_{\chi_1-1} - a_{\chi_1})/2 \qquad (2.2) \\
x_5 &= (-a_1 - a_2 - \ldots + a_{\chi_1-2} - a_{\chi_1-1} + a_{\chi_1})/2 \\
x_6 &= (-a_1 - a_2 - \ldots + a_{\chi_1-2} + a_{\chi_1-1} - a_{\chi_1})/2 \\
x_7 &= (-a_1 - a_2 - \ldots + a_{\chi_1-2} + a_{\chi_1-1} + a_{\chi_1})/2 \\
&\ldots\ldots\ldots\ldots\ldots\ldots\ldots\ldots\ldots\ldots\ldots
\end{aligned}$$

These are all possible abscissas (of intensities) which can be obtained with χ_1 atoms, each of nuclear spin 1/2. All these intensities are normed to unity and we shall call them elementary intensities. Their number is equal to the number of abscissas, which is obviously 2^{χ_1}. It is the superposition of these elementary intensities, due to the coincidence of their abscissas, that leads to the observed intensities: I_0, I_1, I_2, ..., I_N whose values (after a suitable normalization, choosing $I_0 = 1$) are integer numbers (multiples of unity).

The sum of the observed intensities must then be equal to the sum of the elementary intensities

$$\sum_{i=0}^{N} I_i = \sum_{k=0}^{2^{\chi_1}-1} i_k$$

But since $i_k = 1\,(k = 0, 1, \ldots)$, we have:

$$\sum_{i=0}^{N} I_i = 2^{\chi_1} \tag{2.3}$$

This is one necessary condition which must be observed by the intensities of the investigated spectrum, if this spectrum is to be produced by χ_1 atoms each of spin 1/2. A second necessary condition is obtained when one looks at the symmetry of the relations (2.2) with respect to the origin $x = 0$. This imposes on the observed intensities the symmetry relations

$$\begin{aligned} I_0 &= I_N \\ I_1 &= I_{N-1} \\ I_2 &= I_{N-2} \\ &\ldots \end{aligned} \tag{2.4}$$

Thus, given a spectrum $(I_0, \ldots, I_N)$, and a number χ_1 of atoms of nuclear spin 1/2 that supposedly generate it, and given that the intensities satisfy (2.3) and (2.4), one looks for the partition numbers of the total number χ_1:

m_1 atoms of coupling constant λ

m_2 atoms of coupling constant $2\cdot\lambda$

. . . .

Once the partition numbers are found it is easy to compute the actual value of λ from the well-known relation

$$N = \sum_{i=1}^{p} m_i \cdot \lambda_i = \sum_{i=1}^{p} m_i \cdot i \cdot \lambda = \lambda \sum_{i=1}^{p} i \cdot m_i$$

wherefrom

$$\lambda = N / \sum_{i=1}^{p} i \cdot m_i \tag{2.5}$$

Here N is the number of the intervals between the intensities (there are $N + 1$ intensities, hence N intervals). The relations (2.2) lead to the following remarks :

1. There is no abscissa x_i $(i \neq 0)$ which can coincide with x_0; indeed, coincidence would mean

$$\sum_{k=p}^{q} = a_k = 0,$$

which is impossible for *positive* integers $a_p, \ a_{p+1}, \ \ldots, \ a_q$. Hence I_0 is always equal to 1.

2. The nearest neighbour to x_0 will be that intensity with the lowest number of plus signs and with the lowest value of the terms which have plus sign. This implies that to I_1 will contribute only terms with $a_i = \lambda$ (the lowest value of the coupling constant) and in such combination that only *one* of all of the a_i $(i = 1, \ldots, m_1)$ has plus sign. The total number of elementary intensities which contribute to I_1, will then be represented by the diagram (only the signs are shown ; the last m_1 terms have equal coupling constants, namely, λ) :

$$\begin{array}{l}
- - - \;\ldots\ldots\; \overbrace{- - - \;\ldots\ldots\; - - - +}^{m_1} \\
- - - \;\ldots\ldots\; - - - \;\ldots\ldots\; - - + - \\
- - - \;\ldots\ldots\; - - - \;\ldots\ldots\; - + - - \\
- - - \;\ldots\ldots\; - - - \;\ldots\ldots\; + - - - \\
\ldots\ldots\ldots\ldots\ldots\ldots\ldots\ldots\ldots\ldots \\
- - - \;\ldots\ldots\; - - + \;\ldots\ldots\; - - - \\
- - - \;\ldots\ldots\; - + - \;\ldots\ldots\; - - - - \\
- - - \;\ldots\ldots\; + - - \;\ldots\ldots\; - - - -
\end{array}$$

Of course, there are $\binom{m_1}{1} = C_{m_1}^{1}$ such terms, so that

$$I_1 = C_{m_1}^{1} = m_1 \tag{2.6}$$

Now it is easy to investigate the other intensities. To the next but one neighbour of x_0, I_2, will contribute single terms from the group of coupling constant $2 \cdot \lambda$, or double terms from the group of coupling constant λ, that is, in units of λ (the smallest interval between two lines)

$$2 = 2z_2 + z_1, \tag{2.7}$$

where z_2 is the number of terms from the group of coupling constant $2 . \lambda$, z_1 being the number of terms from the group of coupling constant λ. To every possible solution of (2.7), (z_2, z_1), corresponds a number of elementary intensities

$$n\,(z_2, z_1) = C^{z_2}_{m_1} \cdot C^{z_1}_{m_1} \tag{2.8}$$

The sum of all these numbers must give the observed intensity value (normed in such a way as to have $I_0 = 1$)

$$I_2 = \sum_{\substack{z_2, z_1 \\ (2 = 2z_2 + z_1)}} C^{z_2}_{m_2} \cdot C^{z_1}_{m_1}$$

In the same manner one would obtain for I_3 the expression

$$I_3 = \sum_{\substack{z_3,\, z_2,\, z_1 \\ (3 = 3z_3 + 2z_2 + z_1)}} C^{z_3}_{m_3} \cdot C^{z_2}_{m_2} \cdot C^{z_1}_{m_1}$$

and so on.

These considerations allow for the construction of an algorithm. Namely, given $I_0, I_1, I_2, \ldots, I_N$ which observe (2.3) and (2.4), one has

$$m_1 = I_1 \text{ (the relation (2.6))} \tag{2.9}$$

Then I_2 has to be *at least* equal to $C^2_{m_1} : I_2 \geqslant C^2_{m_1}$

1) If equality holds it follows that $m_2 = 0$, there is no atom with coupling constant $2 \cdot \lambda$ and one proceeds to I_3.

2) If strict inequality is obeyed, there must be a group of m_2 atoms of coupling constant $2 \cdot \lambda$ to account for the discrepancy, namely

$$m_2 \equiv I_2 - C^2_{m_1} \tag{2.10}$$

Now I_3 has to be *at least* $\sum\limits_{\substack{z_2,\, z_1 \\ (3 = 2z_2 + z_1)}} C^{z_2}_{m_2} \cdot C^{z_1}_{m_1}$, i.e.

$$I_3 \geqslant \sum_{\substack{z_2,\, z_1 \\ (3 = 2z_2 + z_1)}} C^{z_2}_{m_2} \cdot C^{z_1}_{m_1}$$

Then define

$$m_3 \equiv I_3 - \sum_{\substack{z_2,\, z_1 \\ (3 = 2z_2 + z_1)}} C_{m_2}^{z_2} \cdot C_{m_1}^{z_1} \tag{2.11}$$

where m_3 has to be non-negative; proceed further

$$m_4 \equiv I_4 - \sum_{\substack{z_3,\, z_2,\, z_1 \\ (4 = 3z_3 + 2z_2 + z_1)}} C_{m_3}^{z_3} \cdot C_{m_2}^{z_2} \cdot C_{m_1}^{z_1}$$

and so on.

The process will stop at the stage p, when

$$\sum_{i=1}^{p} m_i = \chi_1.$$

The other intensities (if there are such) must coincide with the predicted expressions, i.e.:

$$m_i = 0 \ (i = p + 1,\ p + 2,\ \ldots,\ N). \tag{2.12}$$

The violation of at least one of the equations (2.12) means that the given spectrum cannot be generated by χ_1 atoms of spin 1/2, so that the process terminates. The same thing happens whenever one of the previously found m_i terms turns out to be less than zero.

3. THE SPIN 1 CASE

The considerations outlined in the preceding section concerning the superposition of the elementary intensities to give the observed intensity value, can also be applied to the case of χ_2 atoms, each of nuclear spin 1. Suppose the sought partition numbers are in this case: n_1, n_2, ... i.e. we have:

n_1 atoms of coupling constant λ,

n_2 atoms of coupling constant $2 \cdot \lambda$,

. . . .

and so on.

However, it must be remembered that an atom of coupling constant λ and spin 1 can give rise to two new lines besides the old line, so that we are left with three equally spaced lines. Taking the leftmost of these lines as the origin we have, with respect to it, one line at a distance λ and *a second line* at a distance $2 \cdot \lambda$.

When speaking about the intensity I_1 (the nearest to the left margin I_0), the only contributors will be the atoms from the group of coupling constant λ, with only one of the lines they generate, and namely that one which is nearest (at a distance λ) to the left end I_0.

Therefore, we shall have as above

$$I_1 = C^1_{n_1} = n_1. \tag{3.1}$$

But, to the line I_2 there will be the following types of contributions :

a) single atoms of coupling constant $2 \cdot \lambda$, with their first line, that one situated at a distance $2 \cdot \lambda$ from I_0.

b) pairs of atoms of coupling constant λ, with their first line.

c) single atoms of coupling constant λ, with their second line, that one situated at a distance $2 \cdot \lambda$ from I_0.

The difference from the spin 1/2 case studied in section 2 consists in the presence of the c) type contribution.

Let us introduce the notation :

x_i = fraction of atoms of coupling constant $i \cdot \lambda$, contributing their second line, situated at a distance $2 \cdot i \cdot \lambda$

y_i = fraction of atoms of coupling constant $i \cdot \lambda$, contributing their first line, situated at a distance $i \cdot \lambda$.

Then to the I_2 line will contribute those atoms for which

$$2 = 2 \cdot (2 \cdot x_2 + y_2) + 1 \cdot (2 \cdot x_1 + y_1) \tag{3.2}$$

Here : y_2 accounts for the a) type contribution,

y_1 accounts for the b) type contribution,

x_1 accounts for the c) type contribution

Observation. It can be easily seen that for the I_1 line, one would obtain for the partition of atoms, the equation

$1 = 1 \cdot (2x_1 + y_1)$ —this having contribution from y_1 only.

(The only solution in non-negative integers for the above equation is $x_1 = 0$; $y_1 = 1$).

To a given solution (x_2, y_2, x_1, y_1) of the equation (3.2) corresponds a number of coincident elementary intensities $n\,(x_2, y_2, x_1, y_1)$ equal to

$$n\,(x_2, y_2, x_1, y_1) = \frac{A^{x_2+y_2}_{n_2}}{x_2!\; y_2!} \cdot \frac{A^{x_1+y_1}_{n_1}}{x_1!\; y_1!} \tag{3.3}$$

which is nothing but the number of different ways of disposing two groups of objects $x_2 + y_2$ and $x_1 + y_1$ in two sets of n_2 or n_1 cells, respectively (here it is assumed that all x_2 objects are identical, all y_2 objects are identical but not the same as x_2 objects and so on).

The intensity I_2 will then be equal to the sum of the numbers $n(x_2, y_2, x_1, y_1)$ corresponding to *all* possible solutions of the equation (3.2)

$$I_2 = \sum_{\substack{x_2,\, y_2,\, x_1,\, y_1 \\ (2=2(2x_2+y_2)+2x_1+y_1)}} \frac{A_{n_2}^{x_2+y_2}}{x_2!\; y_2!} \cdot \frac{A_{n_1}^{x_1+y_1}}{x_1!\; y_1!}$$

In just the same way one would obtain for the third intensity I_3, the expression

$$I_3 = \sum_{\substack{x_3,\, y_3,\, x_2,\, y_2,\, x_1,\, y_1 \\ (3=3(2x_3+y_3)+2(2x_2+y_2)+2x_1+y_1)}} \frac{A_{n_3}^{x_3+y_3}}{x_3!\; y_3!} \cdot \frac{A_{n_2}^{x_2+y_2}}{x_2!\; y_2!} \cdot \frac{A_{n_1}^{x_1+y_1}}{x_1!\; y_1!}$$

and so on.

Again, the algorithm for finding the partition numbers: $n_1, n_2, \ldots, n_p$ of the total number of atoms χ_2, can be summed up in the following way

$$n_1 = I_1$$

$$n_2 = I_2 - \sum_{\substack{x_1,\, y_1 \\ (2x=2x_1+y_1)}} \frac{A_{n_1}^{x_1+y_1}}{x_1!\; y_1!}$$

$$n_3 = I_3 - \sum_{\substack{x_2,\, y_2,\, x_1,\, y_1 \\ (3=2(2x_2+y_2)+2x_1+y_1)}} \frac{A_{n_2}^{x_2+y_2}}{x_2!\; y_2!} \cdot \frac{A_{n_1}^{x_1+y_1}}{x_1!\; y_1!}$$

and so on.

The compatibility conditions are the same.

4. THE MIXED CASE (SPIN 1/2 AND SPIN 1)

We are given χ_1 atoms of nuclear spin 1/2 and χ_2 atoms of spin 1, which presumably give rise to a spectrum of intensities: $I_0, I_1, \ldots, I_N$. The intensities should obey the conditions

$$\begin{aligned} I_0 &= I_N \\ I_1 &= I_{N-1} \qquad (2.4) \\ &\cdot\;\cdot\;\cdot\;\cdot\;\cdot \end{aligned}$$

and a generalized form of the conservation relation (2.3), namely

$$\sum_{i=0}^{N} I_i = 2^{\chi_1} \cdot 3^{\chi_2} \tag{4.1}$$

Let us denote by

$$m_1, m_2, \ldots, m_p$$

the partition numbers of the χ_1 atoms of spin 1/2 and by

$$n_1, n_2, \ldots, n_q$$

the partition numbers of the χ_2 atoms of spin 1.

Then the same type of reasoning as that employed in the sections 2 and 3, tells us that the intensities of the given spectrum will have the following expression

$$\begin{aligned} I_1 &= \sum_{\substack{x_1,\, y_1,\, z_1 \\ (1=2x_1+y_1+z_1)}} \frac{A_{n_1}^{x_1+y_1}}{x_1!\, y_1!} \cdot \frac{A_{m_1}^{z_1}}{z_1!} \\ I_2 &= \sum_{\substack{x_2,\, y_2,\, z_2,\, x_1,\, y_1,\, z_1 \\ (2=2(2x_2+y_2+z_2)+2x_1+y_1+z_1)}} \frac{A_{n_2}^{x_2+y_2}}{x_2!\, y_2!} \frac{A_{m_2}^{z_2}}{z_2!} \frac{A_{n_1}^{x_1+y_1}}{x_1!\, y_1!} \frac{A_{m_1}^{z_1}}{z_1!} \end{aligned} \tag{4.2}$$

and so on. (Note that $\frac{A_{m_1}^{z_1}}{z_1!} \equiv C_{m_1}^{z_1} \equiv \binom{m_1}{z_1}$).

Let us write explicitly the terms contributing to I_1.

The diophantine equation

$$1 = 2x_1 + y_1 + z_1$$

has obviously only two solutions

$$x_1 = 0, \quad y_1 = 1, \quad z_1 = 0$$

and

$$x_1 = 0, \quad y_1 = 0, \quad z_1 = 1,$$

for non-negative integers x_1, y_1, z_1.

Then we get for I_1

$$I_1 = \frac{A^1_{n_1}}{0!\,1!} \cdot \frac{A^0_{m_1}}{0!} + \frac{A^0_{n_1}}{0!\,0!} \cdot \frac{A^1_{m_1}}{1!} = n_1 + m_1$$

(we use the convention $0! = 1$).

Thus, in the case of mixtures, one can no longer find the partition numbers corresponding to the lowest coupling constant solely in terms of the first intensity. Instead, one is given only *the sum* of the first partition numbers

$$m_1 + n_1 = I_1 \tag{4.3}$$

so that one can make (at this stage) any choice compatible with the condition (4.3) and with the restrictions

$$0 \leqslant m_1 \leqslant \chi_1 ; \quad 0 \leqslant n_1 \leqslant \chi_2$$

As soon as a suitable set (m_1, n_1) is selected, one can pass to the analysis of the second relation (4.2), which upon writing explicitly the solution of the diophantine equation corresponding to at least one of x_1, y_2, z_2, being non zero, has the following expression

$$I_2 = \frac{A^1_{n_2}}{0!\,1!} \cdot \frac{A^0_{m_2}}{0!} \cdot \frac{A^0_{n_1}}{0!\,0!} \cdot \frac{A^0_{m_1}}{0!} + \frac{A^0_{n_2}}{0!\,0!} \cdot \frac{A^1_{m_2}}{1!} \cdot \frac{A^0_{n_1}}{0!\,0!} \cdot \frac{A^0_{m_1}}{0!} +$$

$$+ \sum_{\substack{x_1,\, y_1,\, z_1 \\ (2 = 2x_1 + y_1 + z_1)}} \frac{A^{x_1+y_1}_{n_1}}{x_1!\, y_1!} \cdot \frac{A^{z_1}_{m_1}}{z_1!}$$

But the first two terms on the right hand side are exactly n_2, respectively m_2, so that we get a relation for their *sum* in terms of the second intensity I_2 and the previously chosen m_1, n_1

$$m_2 + n_2 = I_2 - \sum_{\substack{x_1,\, y_1,\, z_1 \\ (2 = 2x_1 + y_1 + z_1)}} \frac{A^{x_1+y_1}_{n_1}}{x_1!\, y_1!} \cdot \frac{A^{z_1}_{m_1}}{z_1!} \tag{4.4}$$

We have again the problem of making a choice for m_2 and n_2, compatible with (4.4) and with the inequalities

$$0 \leqslant m_2 \leqslant \chi_1 - m_1$$

$$0 \leqslant n_2 \leqslant \chi_2 - n_1.$$

Then, in the same way we shall obtain a relation for $m_3 + n_3$ in terms of the third intensity I_3 and of m_2, n_2, m_1, n_1, we shall have to make a new choice and so forth.

The compatibility conditions mentioned at the end of the section 2 might forbid some combinations of the partition numbers (m_i, n_i), but in general we are left with a non-unique solution to the posed problem: there are several sets of partition numbers giving rise to the same spectrum. This is a characteristic feature of the mixed case which has been frequently encountered.

5. NON-EQUIDISTANT SPECTRA

If the given intensities are not equidistant, then choosing as a unit length the smallest distance, we obtain an equidistant spectrum equivalent to the given one by putting zero intensities in appropriate places. This case, with some of the intensities equal to zero, can be treated by the same methods as above; one must only put zero there, where the diophantine equation has no solutions.

6. SPECTRA WITH ERRORS

The real spectra, experimentally found, do not satisfy exactly either the symmetry condition *

$$\begin{aligned} T_0 &= T_N \\ T_1 &= T_{N-1} \\ &\cdots \end{aligned} \tag{2.4}$$

or the conservation relation

$$\sum_{i=0}^{N} T_i = 2^{\chi_1} \cdot 3^{\chi_2} \tag{4.1}$$

The remedy for (4.1) is immediate: one has to renormalize the spectrum by passing to a new set of intensities $z_0, z_1, \ldots, z_N$ defined by

$$\begin{aligned} z_0 &= 2^{\chi_1} \cdot 3^{\chi_2} \frac{T_0}{\sum_{i=0}^{N} T_i} \\ z_1 &= 2^{\chi_1} \cdot 3^{\chi_2} \frac{T_1}{\sum_{i=0}^{N} T_i} \end{aligned} \tag{6.1}$$

---

* Integer intensities are denoted by I_i, experimentally found (possibly non-integer) intensities are denoted by T_i.

and so on. We have obviously

$$\sum_{i=0}^{N} z_i = 2^{\chi_1}\cdot 3^{\chi_2}$$

The trouble now is that z_i are neither integers nor do they satisfy a symmetry relation of type (2.4). Nevertheless the situation is not as hopeless as it seems, for the original intensities $T_0, \ldots, T_N$ are never exact. If they were, they would have certainly obeyed (2.4) and $\{z_i\}$ would be then integers and everything would then be simple : apply the general algorithm outlined in section 4, and find all possible sets of coupling constants (partitions) compatible with the given spectrum. Actually one is provided not only with the numbers χ_1, χ_2 and the set of measured intensities $T_0, \ldots, T_N$, but also with their relative errors :

$$\varepsilon_0,\ \varepsilon_1,\ \varepsilon_2,\ \ldots,\ \varepsilon_N$$

Then one can compute the absolute errors for z_1 in the standard way :

$$\Delta z_i = 2^{\chi_1}\cdot 3^{\chi_2}\frac{(\sum_j T_j)\cdot \Delta T_i + T_i\cdot(\sum_j \Delta T_j)}{(\sum_j T_j)^2}$$

and replacing ΔT_i by $\varepsilon_i\cdot T_i$, one is led to

$$\Delta Z_i = 2^{\chi_1}\cdot 3^{\chi_2}\left[\frac{\varepsilon_i\cdot T_i}{\sum_j T_j} + \frac{T_i}{\sum_j T_j}\,\frac{\sum_j \varepsilon_j\cdot T_j}{\sum_j T_j}\right]$$

which can be written also, as

$$\Delta z_i = z_i\left[\varepsilon_i + \frac{\varepsilon_0\cdot T_0 + \ldots + \varepsilon_N\cdot T_N}{T_0 + \ldots + T_N}\right] \tag{6.2}$$

The relation (6.2) simply tells us that the relative error of z_i is greater than the corresponding relative error of T_i by a constant quantity $\bar{\varepsilon}$

$$\bar{\varepsilon} \equiv \frac{\varepsilon_0\, T_0 + \ldots + \varepsilon_N\, T_N}{T_0 + \ldots + T_N}$$

After computing the renormalized intensities z_i and their absolute errors Δz_i, one must find a set of $N-1$ *integers* $I_1, \ldots I_{N-1}$ with the properties *

$$\sum_{i=1}^{N} I_i = 2^{\chi_1} \cdot 3^{\chi_2} - 2$$

$$I_1 = I_{N-1} \tag{6.3}$$

$$I_2 = I_{N-2}$$

$$\cdot \quad \cdot \quad \cdot \quad \cdot \quad \cdot$$

and

$$|z_i - I_i| \leqslant \Delta z_i \ (i = 1, 2, 3, \ldots, N-1)$$

Once the set $I_1, \ldots, I_{N-1}$ satisfying (6.3) is found, the problem is within reach for the general algorithm of section 4.

The symmetry condition imposes further restriction on the admissible range of I_i. Indeed, from the $N-1$ inequalities of (6.3) we have in particular

$$z_1 - \Delta z_1 \leqslant I_1 \leqslant z_1 + \Delta z_1$$

$$z_{N-1} - \Delta z_{N-1} \leqslant I_{N-1} \leqslant z_{N-1} + \Delta z_{N-1}$$

But the symmetry conditions tell us that $I_1 = I_{N-1}$ so that

$$\max(z_1 - \Delta z_1, z_{N-1} - \Delta z_{N-1}) \leqslant I_1 = I_{N-1} \leqslant \min(z_1 + \Delta z_1, z_{N-1} + \Delta z_{N-1})$$

---

* As outlined in section 2, we take the first and last lines I_0 and I_N to be normalized to unity, and all other intensities in units of I_0 ad I_N. Then we have

$$I_0 = I_N = 1$$

and

$$\sum_{i=1}^{N-1} I_i = 2^{\chi_1} . 3^{\chi_2} - 2.$$

This is the condition we shall work with henceforth.

We get similar shrinkage of the intervals for the remaining intensities. If we denote by

$$A_i \equiv \max\,(z_i - \Delta z_i,\; z_{N-i} - \Delta z_{N-i})$$

$$B_i \equiv \min\,(z_i + \Delta z_i,\; z_{N-i} + \Delta z_{N-i})$$

$i = 1, 2, \dots [(N-1)/2]$ (here by $[(N-1)/2]$ is denoted the integer part of the number $(N-1)/2$), then the problem of spectrum fit can be stated as follows.

Find *all* solutions of the diophantine equation

$$2^{\chi_1}\cdot 3^{\chi_2} - 2 = 2\cdot(I_1 + I_2 + \dots + I_{[(N-1)/2]}) + \left(N - 1 - 2\cdot\left[\frac{N-1}{2}\right]\right) I_{\left[\frac{N-1}{2}\right]+1} \tag{6.4}$$

subject to conditions

$$A_p \leqslant I_p \leqslant B_p \qquad p = 1, 2, \dots [(N-1)/2]; \tag{6.5}$$

(the equality holds if and only if either A_p or B_p are integers).

Even stated in this form, where use has been made of the symmetry to halve the number of the variables, the equation still has a tremendous number of solutions for large N and for the usual error magnitudes, 15–20%. Every solution has then to undergo the search for a suitable set of coupling constants. Most of these solutions turn out to be incompatible (they cannot be generated by χ_1 atoms of spin 1/2 and χ_2 atoms of spin 1) and all this procedure ends up in a substantial computer time waste. Thus it would not be worth while providing the user with a computer program of this type, even though for the *exact spectra* the algorithm presented above is very efficient, doing its job in a matter of seconds. One of the reasons for writing this paper at all is that the proposed algorithm, when used in a sensible way, can do away with the difficulty of scanning *all* possible solutions of the diophantine equation (6.4) that obey (6.5) : the point is that the bounds A_p, B_p entering (6.5) can be substantially sharpened. In fact computing the partition numbers for every intensity imposes restrictions on the permissible range for all other intensities, that can then be used to sharpen (6.5) eliminating thus a great many solutions of (6.4) incompatible with our given numbers of atoms χ_1 and χ_2.

As we have shown in sections 2 and 3 for every intensity I_p the relationship (6.6) holds

$$n_p + m_p = I_p - \sum_{\substack{x_{p-1},\, y_{p-1},\, z_{p-1}, \dots x_1,\, y_1,\, z_1 \\ (p=(p-1)\,(2x_{p-1}+y_{p-1}+z_{p-1}+\dots+ \\ +2x_1+y_1+z_1)}} \frac{A_{n_{p-1}}^{x_{p-1}+y_{p-1}}\; A_{m_{p-1}}^{z_{p-1}}}{x_{p-1}!\, y_{p-1}!\, z_{p-1}!} \cdot \dots \tag{6.6}$$

$$\dots \cdot \frac{A_{n_1}^{x_1+y_1}\, A_{m_1}^{z_1}}{x_1!\, y_1!\, z_1!}$$

(the straightforward generalization of relation (4.4)). If we denote the sum by

$$\mathrm{MINI}\,(n_1, m_1, \dots, n_{p-1}, \; m_{p-1}),$$

we can rewrite the relation (6.6) in the form

$$n_p + m_p = I_p - \mathrm{MINI}\,(n_1, m_1, \dots, n_{p-1}, m_{p-1}). \tag{6.7}$$

Now, n_p and m_p must obviously satisfy the inequalities

$$0 \leqslant m_p \leqslant \chi_1 - \sum_{k=1}^{p-1} m_k$$

$$0 \leqslant n_p \leqslant \chi_2 - \sum_{k=1}^{p-1} n_k$$

which give for the sum $n_p + m_p$ the condition

$$0 \leqslant n_p + m_p \leqslant \chi_2 - \sum_{k=1}^{p-1} n_k + \chi_1 - \sum_{k=1}^{p-1} m_k$$

Using (6.7) we obtain in terms of I_p

$$\mathrm{MINI}\,(n_1, m_1, \dots, n_{p-1}, m_{p-1}) \leqslant I_p \leqslant \mathrm{MINI}\,(n_1, m_1, \dots, n_{p-1}, m_{p-1}) +$$

$$+ \chi_2 - \sum_{k=1}^{p-1} n_k + \chi_1 - \sum_{k=1}^{p-1} m_k \tag{6.8}$$

Comparing (6.8) with the condition (6.5) we arrive at the sharpened inequalities

$$\max\,(A_p, \mathrm{MINI}\,(n_1, \ldots, m_{p-1})) \leqslant I_p \leqslant \tag{6.9}$$

$$\leqslant \min\left(B_p, \mathrm{MINI}\,(n_1, \ldots, m_{p-1}) + \chi_2 - \sum_{k=1}^{p-1} n_k + \chi_1 - \sum_{k=1}^{p-1} m_k\right)$$

It is apparent that (6.9) is much more efficient than (6.5) in disposing of the non-physical solutions. Indeed, in (6.5) the difference between B_p and A_p increases as p increases (until $p = [(N-1)/2)]$), as for relative errors of the same magnitude, the absolute error is bigger for larger intensities, that are usually around the center of the spectrum, and $B_p - A_p$ is just twice the absolute error. With (6.9) the things are different: when p increases, $\chi_2 - \sum n_k + \chi_1 - \sum m_k$ diminishes until zero, so that the upper bound becomes MINI $(n_1, \ldots, m_{p-1})$ (since $B_p \geqslant$ MINI $(n_1, \ldots, \ldots, m_{p-1})$) and the lower bound becomes also MINI $(n_1, \ldots, m_{p-1})$ so that there is a unique choice for $I_p : I_p =$ MINI $(n_1, \ldots, m_{p-1})$, as it should be.

7. DESCRIPTION OF THE PROGRAM

The program consists of six blocks depicted in figure 1.

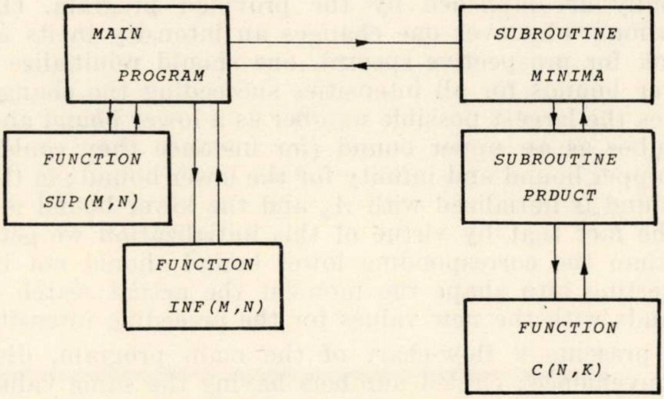

Fig. 1. — Block diagram of the program.

The program is written in FORTRAN language (the FORTRAN IV, or FULL FORTRAN version).

The main program works according to the procedure presented in Section 6.

However, let us take a closer look at the relation (6.9). It simply says that given the first $p-1$ intensities, $I_1, I_2, \ldots, I_{p-1}$, and a choice compatible with these intensities being made for the partition numbers $n_1, m_1, n_2, m_2, \ldots, n_{p-1}, m_{p-1}$, the next intensity I_p should be located qetween a lower bound : $\max(A_p, \mathrm{MINI}\,(n_1, m_1, n_2, m_2, \ldots, n_{p-1}, m_{p-1}))$ and an upper bound : $\min(B_p, \mathrm{MINI}\,(n_1, m_1, n_2, m_2, \ldots, n_{p-1}, m_{p-1}) + \chi_1 - \sum_{k=1}^{p-1} m_k + \chi_2 - \sum_{k=1}^{p-1} n_k)$. Now to make these bounds independent on the particular choice of the partition numbers, for we distinguish spectra according to their intensities only, we have to take the least lower bound and the largest upper bound with respect to all partitions compatible with our first $p-1$ intensities found, i.e.

$$\min_{\substack{(n_1,\, m_1,\, \ldots\, n_{p-1},\, m_{p-1}) \\ I_1=C_1,\, I_2=C_2 \,\ldots\, I_{p-1}=C_{p-1}}} [\max(A_p, \mathrm{MINI}\,(n_1, m_1, n_2, m_2, \ldots, n_{p-1}, m_{p-1}))]$$

$$\max_{\substack{(n_1,\, m_1,\, \ldots\, n_{p-1},\, m_{p-1}) \\ I_1=C_1,\, I_2=C_2,\, \ldots\, I_{p-1}=C_{p-1}}} \left[\min(B_p, \mathrm{MINI}\left(n_1, m_1, n_2, m_2, \ldots, n_{p-1}, m_{p-1}) + \right.\right.$$

$$\left.\left. + \chi_1 - \sum_{k=1}^{p-1} m_k + \chi_2 - \sum_{k=1}^{p-1} n_k\right)\right]$$

This is what must be done at every stage of investigation of a spectrum and is actually accomplished by the provided program. One further word of caution : whenever one changes an intensity in its allowed interval to look for prospective spectra, one should reinitialize the upper and the lower bounds for all intensities succeeding the changed one, in that one takes the largest possible number as a lower bound and the least possible number as an upper bound (for instance they could be taken zero for the upper bound and infinity for the lower bound ; in the program the upper bound is initialized with A_p and the lower bound is initialized with B_p. The fact that by virtue of this initialization we get an upper bound less than the corresponding lower bound should not bother us : things are getting into shape the moment the actual search begins for the best bounds with the new values for the preceding intensities.

Fig. 2 presents a flow-chart of the main program, divided into blocks for convenience ; circled numbers having the same value are connecting the flow control.

The subroutine MINIMA together with its auxiliary subprograms, PRDUCT and C (N, K), computes the quantity MINI $(n_1, m_1, \ldots, n_{p-1}, m_{p-1})$ defined by relations (6.6) and (6.7), for each value of p. The sub-

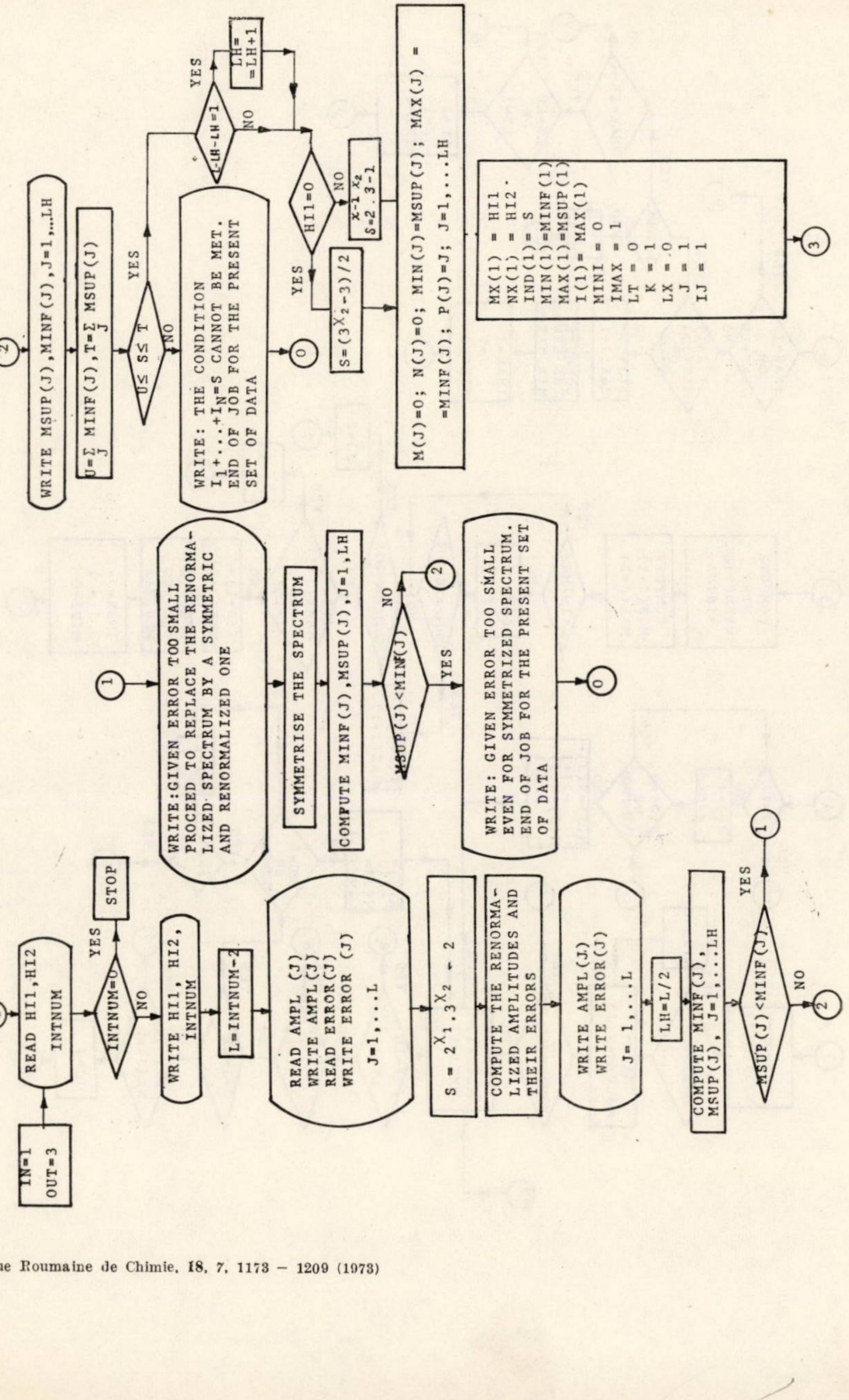
IN=1
OUT=3
0
READ HI1,HI2
INTNUM
INTNUM=0
YES
STOP
NO
WRITE HI1, HI2,
INTNUM
L=INTNUM-2
READ AMPL (J)
WRITE AMPL(J)
READ ERROR(J)
WRITE ERROR (J)
J=1,...L
$S = 2^{X_1},3^{X_2} - 2$
COMPUTE THE RENORMALIZED AMPLITUDES AND THEIR ERRORS
WRITE AMPL(J)
WRITE ERROR(J)
J= 1,...L
LH=L/2
COMPUTE MINF(J), MSUP(J), J=1,...LH
MSUP(J)<MINF(J)
YES
1
NO
2
1
WRITE:GIVEN ERROR TOO SMALL PROCEED TO REPLACE THE RENORMALIZED SPECTRUM BY A SYMMETRIC AND RENORMALIZED ONE
SYMMETRISE THE SPECTRUM
COMPUTE MINF(J),MSUP(J),J=1,LH
MSUP(J)<MINF(J)
NO
2
YES
WRITE: GIVEN ERROR TOO SMALL EVEN FOR SYMMETRIZED SPECTRUM. END OF JOB FOR THE PRESENT SET OF DATA
0
2
WRITE MSUP(J),MINF(J),J=1,...LH
$U=\sum_J MINF(J), T=\sum_J MSUP(J)$
$U\leq S\leq T$
YES
NO
WRITE: THE CONDITION $I_1+\ldots+I_N=S$ CANNOT BE MET. END OF JOB FOR THE PRESENT SET OF DATA
0
L-LH-LH=1
YES
LH= =LH+1
NO
HI1=0
YES
NO
$S=(3^{X_2}-3)/2$
$S=2^{X_1-1}.3^{X_2}-1$
M(J)=0; N(J)=0; MIN(J)=MSUP(J); MAX(J) = =MINF(J); P(J)=J; J=1,...LH
MX(1) = HI1
NX(1) = HI2
IND(1)= S
MIN(1)=MINF(1)
MAX(1)=MSUP(1)
I(1)= MAX(1)
MINI = 0
IMAX = 1
LT = 0
K = 1
LX = 0
J = 1
IJ = 1
3

Fig. 2. — Flow-chart of the main program.

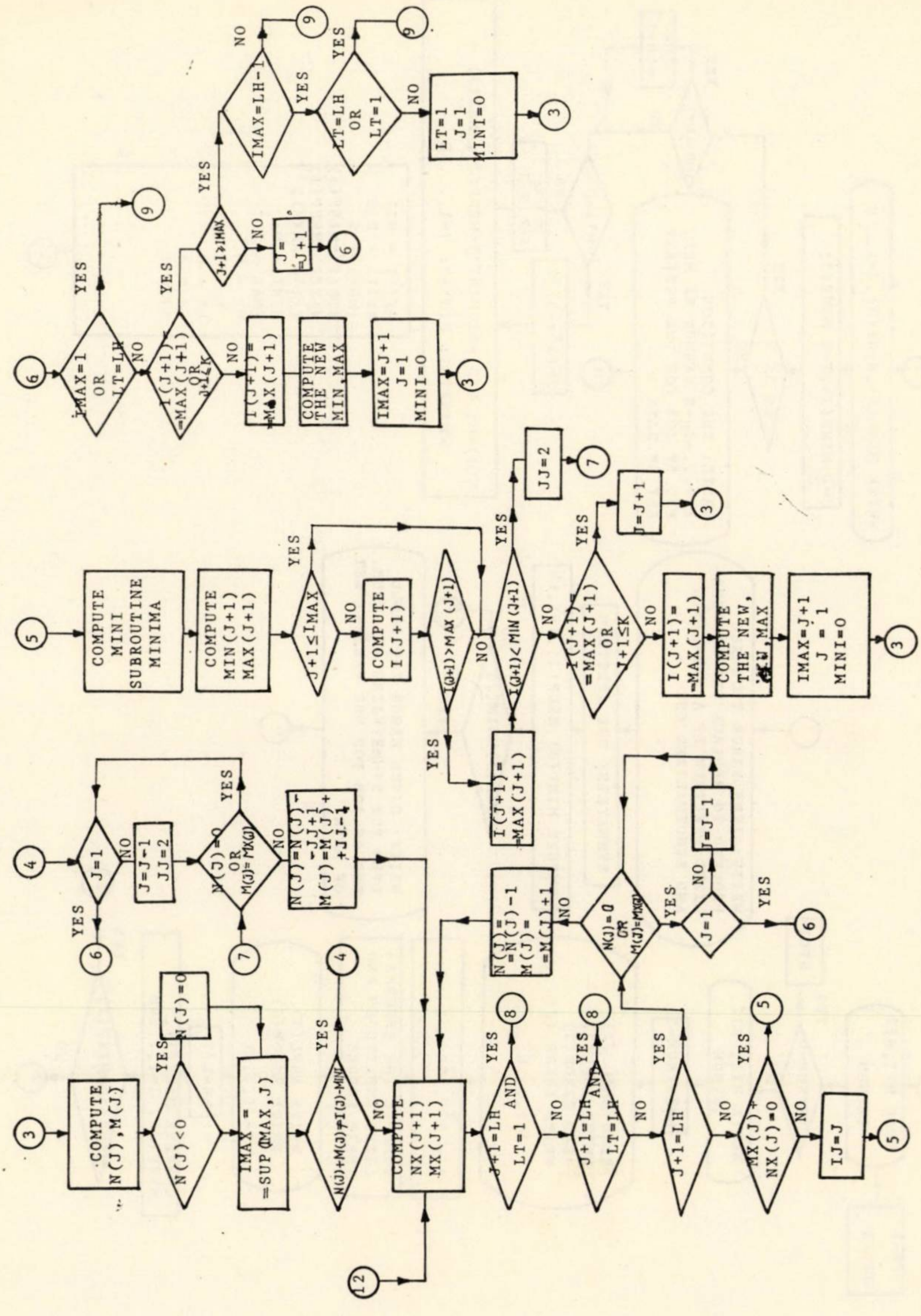
3
COMPUTE N(J),M(J)
N(J)<0
YES
N(J)=0
IMAX = SUP (IMAX,J)
N(J)+M(J)=I(J)-MINI
YES
4
NO
COMPUTE NX(J+1) MX(J+1)
12
J+1=LH AND LT=1
YES
8
NO
J+1=LH AND LT=LH
YES
8
NO
J+1=LH
YES
NO
MX(J)+NX(J)=0
YES
5
NO
IJ=J
5
4
J=1
YES
6
NO
J=J-1 JJ=2
N(J)=0 OR M(J)=MX(J)
YES
7
NO
N(J)=N(J)-JJ+1 M(J)=M(J)+JJ-1
N(J)=N(J)-1 M(J)=M(J)+1
NO
N(J)=0 OR M(J)=MX(J)
YES
J=1
NO
J=J-1
YES
6
5
COMPUTE MINI SUBROUTINE MINIMA
COMPUTE MIN(J+1) MAX(J+1)
J+1≤IMAX
YES
NO
COMPUTE I(J+1)
I(J+1)>MAX(J+1)
YES
I(J+1)=MAX(J+1)
NO
I(J+1)<MIN(J+1)
YES
JJ=2
7
NO
I(J+1)=MAX(J+1) OR J+1≤K
YES
J=J+1
3
NO
I(J+1)=MAX(J+1)
COMPUTE THE NEW MIN,MAX
IMAX=J+1 J=1 MINI=0
3
6
IMAX=1 OR LT=LH
YES
9
NO
I(J+1)=MAX(J+1) OR J+1<K
YES
J+1≥IMAX
YES
NO
J=J+1
6
NO
I(J+1)=MAX(J+1)
COMPUTE THE NEW MIN,MAX
IMAX=J+1 J=1 MINI=0
3
IMAX=LH-1
NO
9
YES
LT=LH OR LT=1
YES
9
NO
LT=1 J=1 MINI=0
3

Fig. 2. (continued).

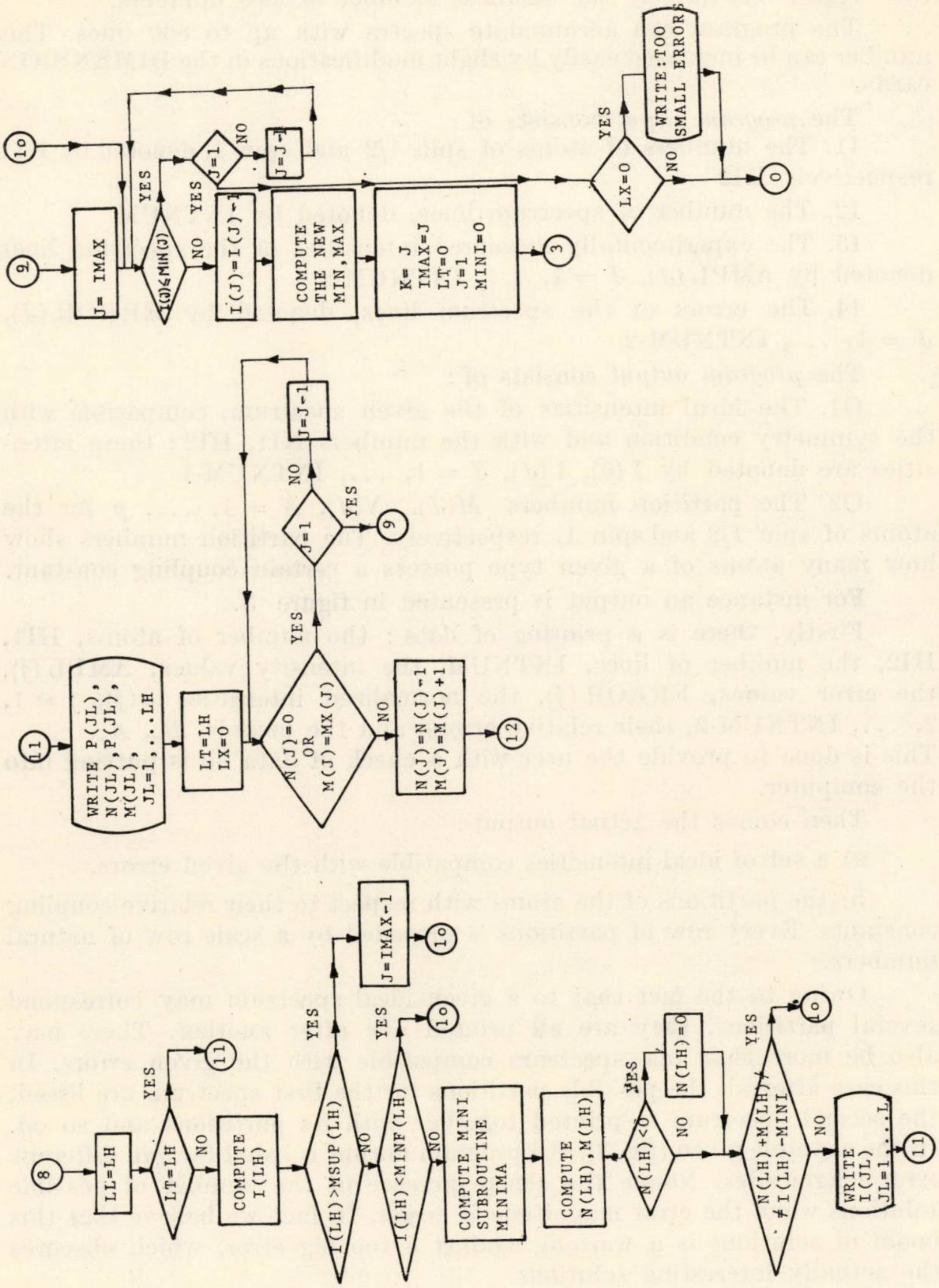

1o
2
J= IMAX
I(J)≤MIN(J)
YES
NO
J=1
J=J-1
I(J)=I(J)-1
COMPUTE THE NEW MIN,MAX
K= J
IMAX=J
LT=0
J=1
MINI=0
3
LX=0
YES
NO
WRITE:TOO SMALL ERRORS
0
11
WRITE P(JL), N(JL),P(JL), M(JL), JL=1,...LH
LT=LH
LX=0
N(J)=0 OR M(J)=MX(J)
YES
NO
N(J)=N(J)-1
M(J)=M(J)+1
12
J=1
YES
NO
J=J-1
9
8
LL=LH
LT=LH
YES
NO
11
COMPUTE I(LH)
I(LH)>MSUP(LH)
YES
NO
J=IMAX-1
1o
I(LH)<MINF(LH)
YES
NO
1o
COMPUTE MINI SUBROUTINE MINIMA
COMPUTE N(LH),M(LH)
N(LH)<0
YES
NO
N(LH)=0
N(LH)+M(LH)≠I(LH)-MINI
YES
NO
1o
WRITE I(JL) JL=1...L
11

Fig. 2. — (continued).

programs SUP (M, N) and INF (M, N) yield, as their names suggest, the biggest respectively the smallest member of two numbers.

The program can accomodate spectra with up to 800 lines. This number can be increased easily by slight modifications in the DIMENSION cards.

The *program input* consists of :

I1. The numbers of atoms of spin 1/2 and spin 1, denoted by HI1 respectively HI2

I2. The number of spectrum lines, denoted by INTNUM

I3. The experimentally measured intensities of the spectrum lines denoted by AMPL (J), $J = 1, \ldots,$ INTNUM-2

I4. The errors of the spectrum lines, denoted by ERROR (J), $J = 1, \ldots,$ INTNUM-2

The *program output* consists of :

O1. The ideal intensities of the given spectrum, compatible with the symmetry condition and with the numbers HI1, HI2 ; these intensities are denoted by I (0), I (J), $J = 1, \ldots,$ INTNUM-1

O2. The partition numbers $M(J)$, $N(J)$, $N = 1, \ldots, p$ for the atoms of spin 1/2 and spin 1, respectively. The partition numbers show how many atoms of a given type possess a certain coupling constant.

For instance an output is presented in figure 3.

Firstly, there is a printing of data : the number of atoms, HI1, HI2, the number of lines, INTNUM, the intensity values, AMPL (j), the error values, ERROR (j), the normalized intensities $z(j)$, $j = 1, 2, \ldots,$ INTNUM-2, their relative errors, and the bounds, B_p, A_p. This is done to provide the user with a check of data he is putting into the computer.

Then comes the actual output :

a) a set of ideal intensities compatible with the given errors.

b) the partitions of the atoms with respect to their relative coupling constants. Every row of partitions is preceded by a scale row of natural numbers.

Owing to the fact that to a given ideal spectrum may correspond several partitions, they are all printed one after another. There may also be more than one spectrum compatible with the given errors. In this case after all the possible partitions for the first spectrum are listed, the second spectrum is printed together with its partitions and so on. In the example given (fig. 3), the program output is listed for two different error magnitudes. Notice the sharp increase of the number of possible solutions when the error magnitude is larger. In fact we believe that this boom of solutions is a warning against a too big error, which obscures the actually interesting solutions.

The last card in the set of data must be blank. Then the program stops. Fig. 4 presents the listing of the program.

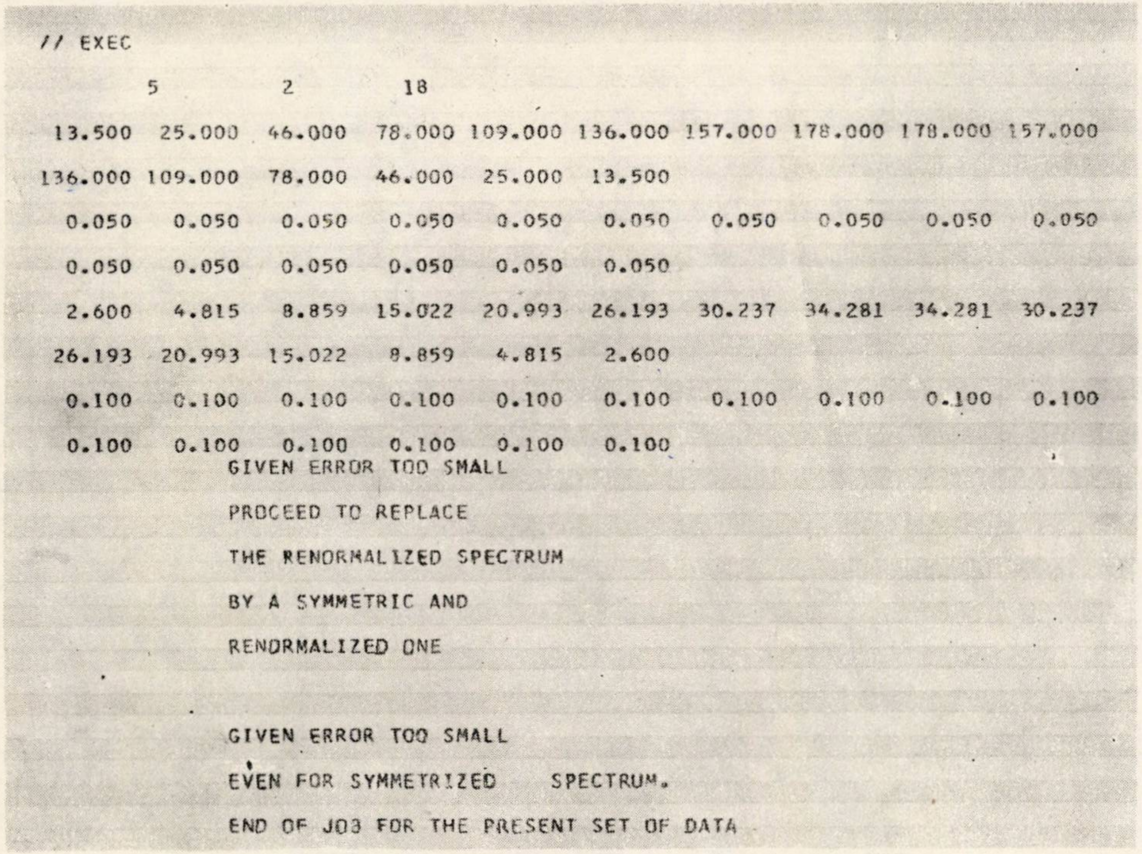

```
// EXEC

       5         2         18

 13.500   25.000   46.000   78.000 109.000 136.000 157.000 178.000 178.000 157.000

136.000  109.000   78.000   46.000  25.000  13.500

  0.050    0.050    0.050    0.050   0.050   0.050   0.050   0.050   0.050   0.050

  0.050    0.050    0.050    0.050   0.050   0.050

  2.600    4.815    8.859   15.022  20.993  26.193  30.237  34.281  34.281  30.237

 26.193   20.993   15.022    8.859   4.815   2.600

  0.100    0.100    0.100    0.100   0.100   0.100   0.100   0.100   0.100   0.100

  0.100    0.100    0.100    0.100   0.100   0.100
                  GIVEN ERROR TOO SMALL

                  PROCEED TO REPLACE

                  THE RENORMALIZED SPECTRUM

                  BY A SYMMETRIC AND

                  RENORMALIZED ONE


                  GIVEN ERROR TOO SMALL

                  EVEN FOR SYMMETRIZED    SPECTRUM.

                  END OF JOB FOR THE PRESENT SET OF DATA
```

Fig. 3a. — Example with errors 5, 10, and 20%.

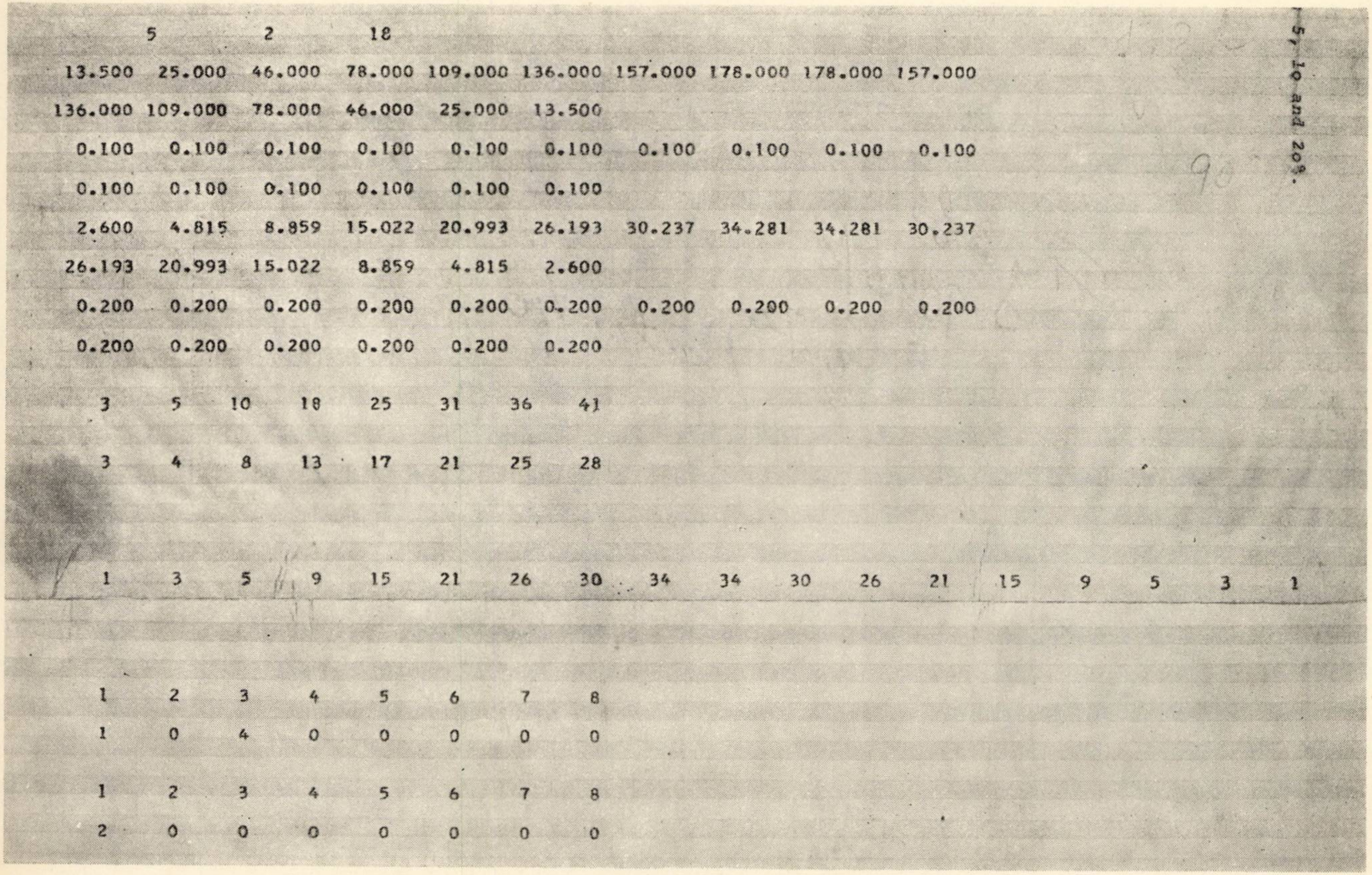

```
5, 1o and 2o%.
```

90

```
      5        2        18
 13.500   25.000   46.000   78.000  109.000  136.000  157.000  178.000  178.000  157.000
136.000  109.000   78.000   46.000   25.000   13.500
  0.100    0.100    0.100    0.100    0.100    0.100    0.100    0.100    0.100    0.100
  0.100    0.100    0.100    0.100    0.100    0.100
  2.600    4.815    8.859   15.022   20.993   26.193   30.237   34.281   34.281   30.237
 26.193   20.993   15.022    8.859    4.815    2.600
  0.200    0.200    0.200    0.200    0.200    0.200    0.200    0.200    0.200    0.200
  0.200    0.200    0.200    0.200    0.200    0.200

    3      5     10     18     25     31     36     41

    3      4      8     13     17     21     25     28


    1      3      5      9     15     21     26     30     34     34     30     26     21     15      9      5      3      1


    1      2      3      4      5      6      7      8
    1      0      4      0      0      0      0      0

    1      2      3      4      5      6      7      8
    2      0      0      0      0      0      0      0
```

Fig. 3b.

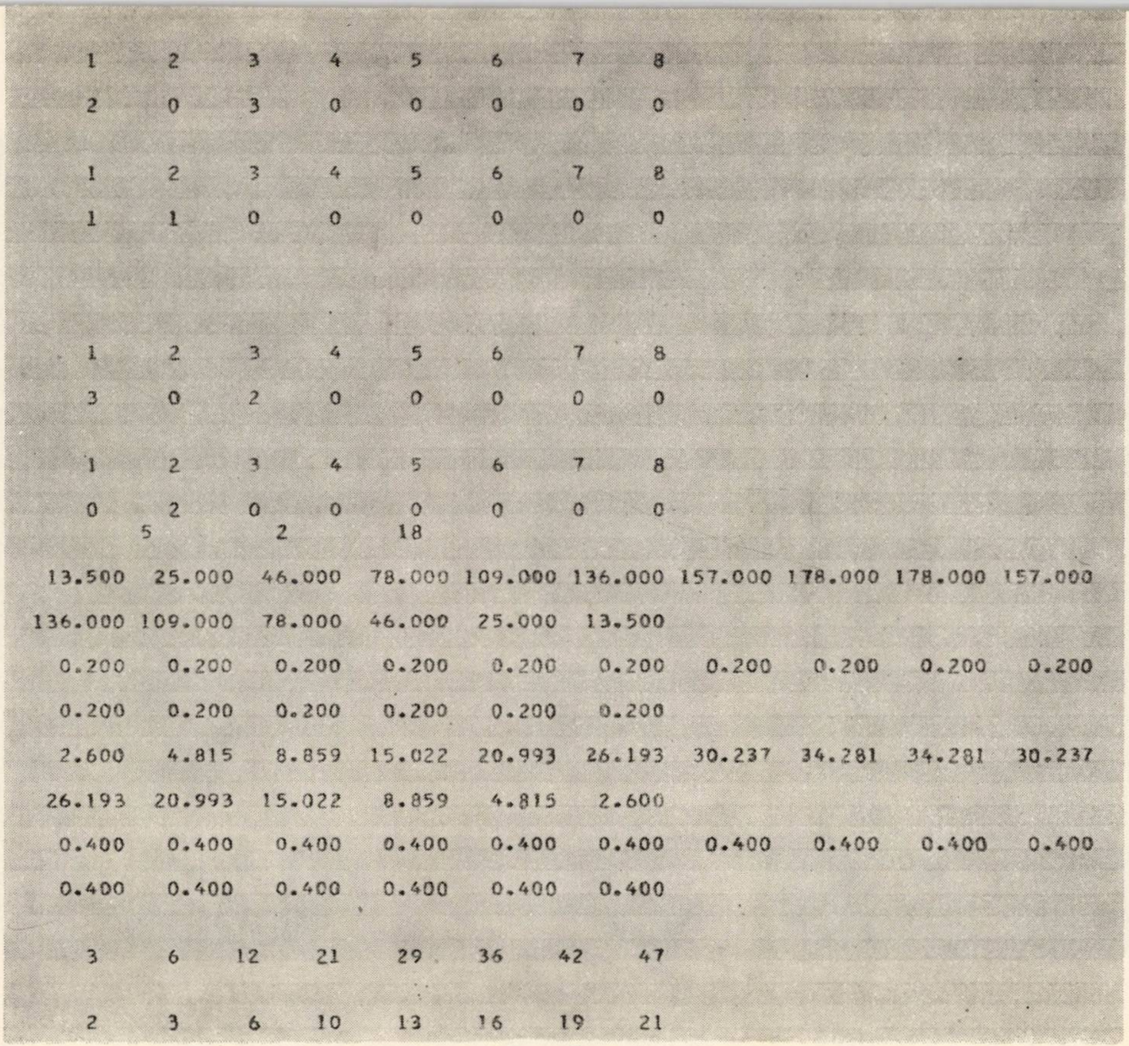

```
      1       2       3       4       5       6       7       8
      2       0       3       0       0       0       0       0

      1       2       3       4       5       6       7       8
      1       1       0       0       0       0       0       0


      1       2       3       4       5       6       7       8
      3       0       2       0       0       0       0       0

      1       2       3       4       5       6       7       8
      0       2       0       0       0       0       0       0
          5          2          18
 13.500  25.000  46.000  78.000 109.000 136.000 157.000 178.000 178.000 157.000
136.000 109.000  78.000  46.000  25.000  13.500
  0.200   0.200   0.200   0.200   0.200   0.200   0.200   0.200   0.200   0.200
  0.200   0.200   0.200   0.200   0.200   0.200
  2.600   4.815   8.859  15.022  20.993  26.193  30.237  34.281  34.281  30.237
 26.193  20.993  15.022   8.859   4.815   2.600
  0.400   0.400   0.400   0.400   0.400   0.400   0.400   0.400   0.400   0.400
  0.400   0.400   0.400   0.400   0.400   0.400

      3       6      12      21      29      36      42      47

      2       3       6      10      13      16      19      21
```

Fig. 3c.

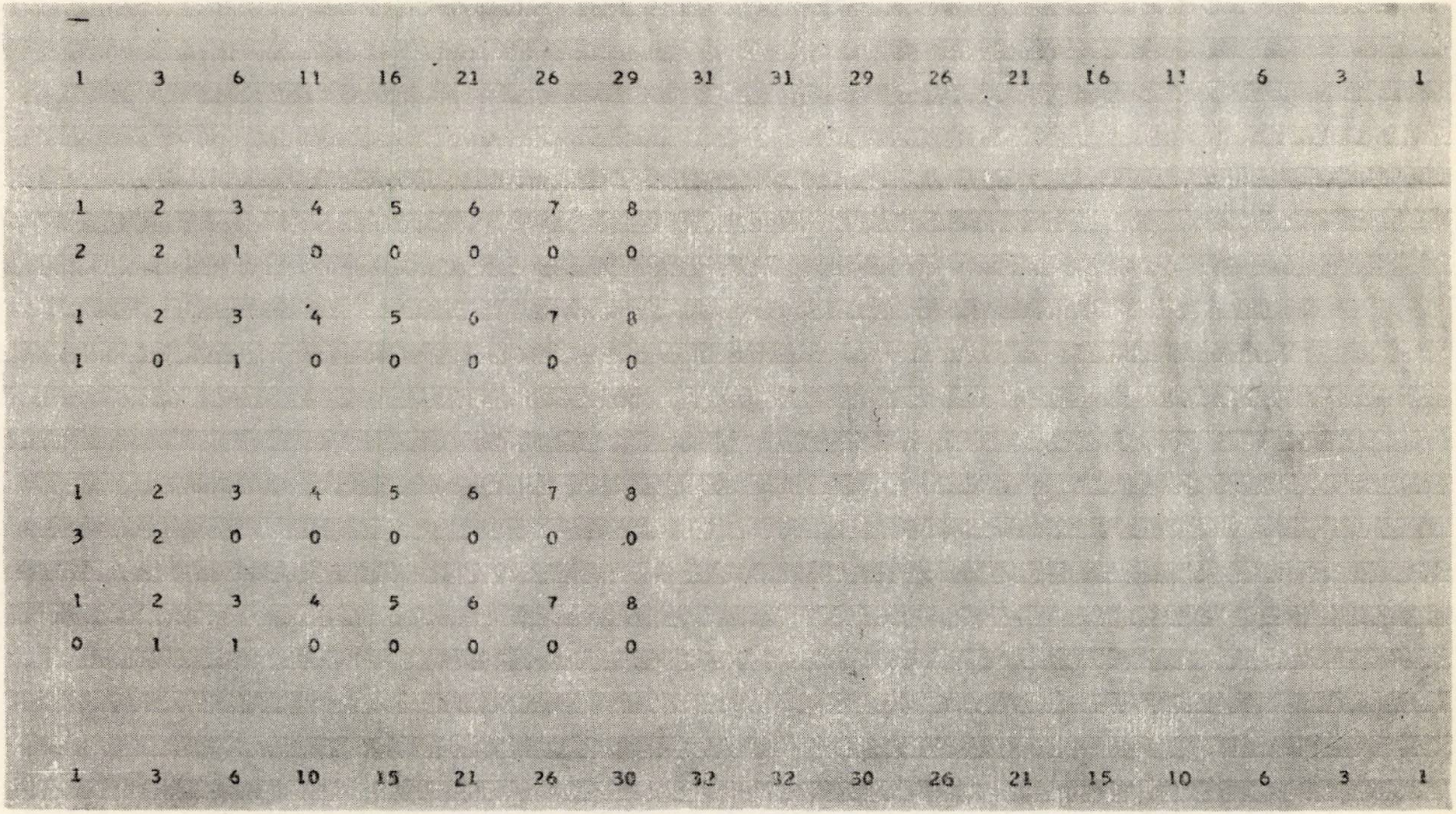

```
—
1    3    6   11   16   21   26   29   31   31   29   26   21   16   11    6    3    1

1    2    3    4    5    6    7    8
2    2    1    0    0    0    0    0

1    2    3   '4    5    6    7    8
1    0    1    0    0    0    0    0


1    2    3    4    5    6    7    8
3    2    0    0    0    0    0   .0

1    2    3    4    5    6    7    8
0    1    1    0    0    0    0    0


1    3    6   10   15   21   26   30   32   32   30   26   21   15   10    6    3    1
```

Fig. 3d.

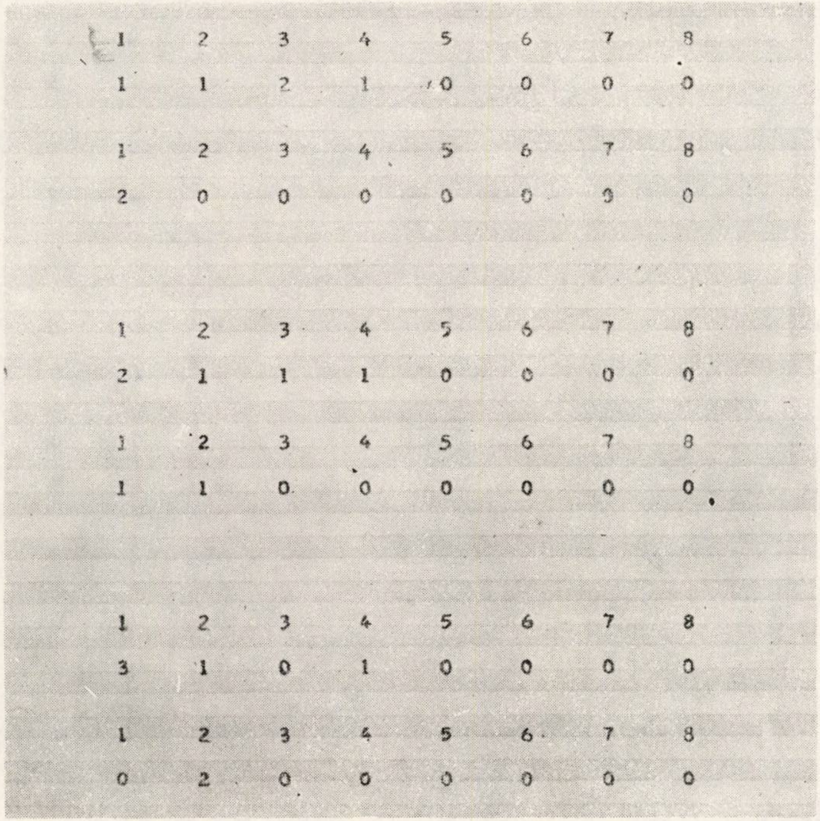

```
1  2  3  4  5  6  7  8
1  1  2  1  0  0  0  0

1  2  3  4  5  6  7  8
2  0  0  0  0  0  0  0


1  2  3  4  5  6  7  8
2  1  1  1  0  0  0  0

1  2  3  4  5  6  7  8
1  1  0  0  0  0  0  0


1  2  3  4  5  6  7  8
3  1  0  1  0  0  0  0

1  2  3  4  5  6  7  8
0  2  0  0  0  0  0  0
```

Fig. 3e.

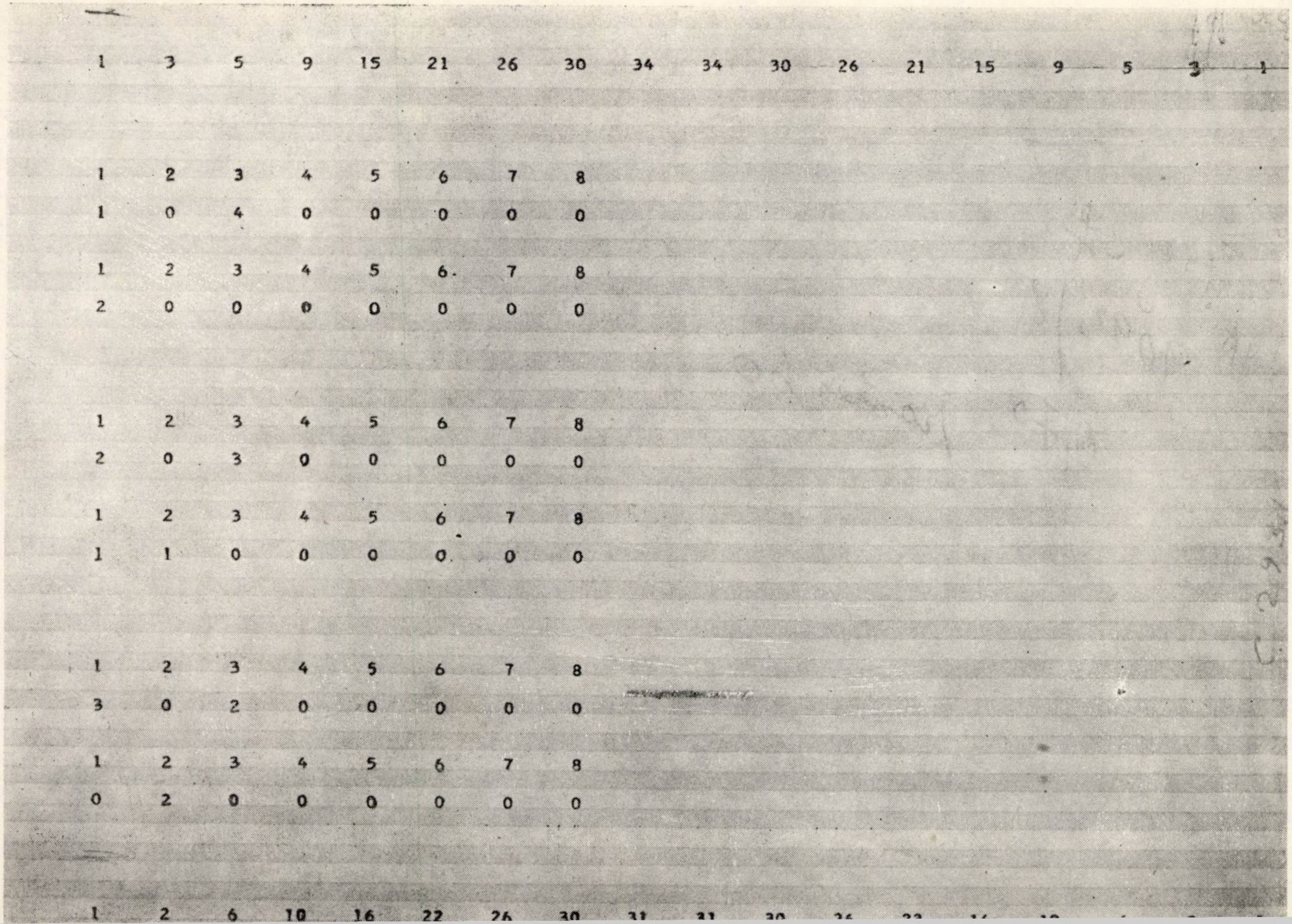

```
1   3   5   9   15  21  26  30  34  34  30  26  21  15  9   5   3   1


1   2   3   4   5   6   7   8
1   0   4   0   0   0   0   0

1   2   3   4   5   6.  7   8
2   0   0   0   0   0   0   0



1   2   3   4   5   6   7   8
2   0   3   0   0   0   0   0

1   2   3   4   5   6   7   8
1   1   0   0   0   0.  0   0



1   2   3   4   5   6   7   8
3   0   2   0   0   0   0   0

1   2   3   4   5   6   7   8
0   2   0   0   0   0   0   0



1   2   6   10  16  22  26  30  31  31  30  26  22
```

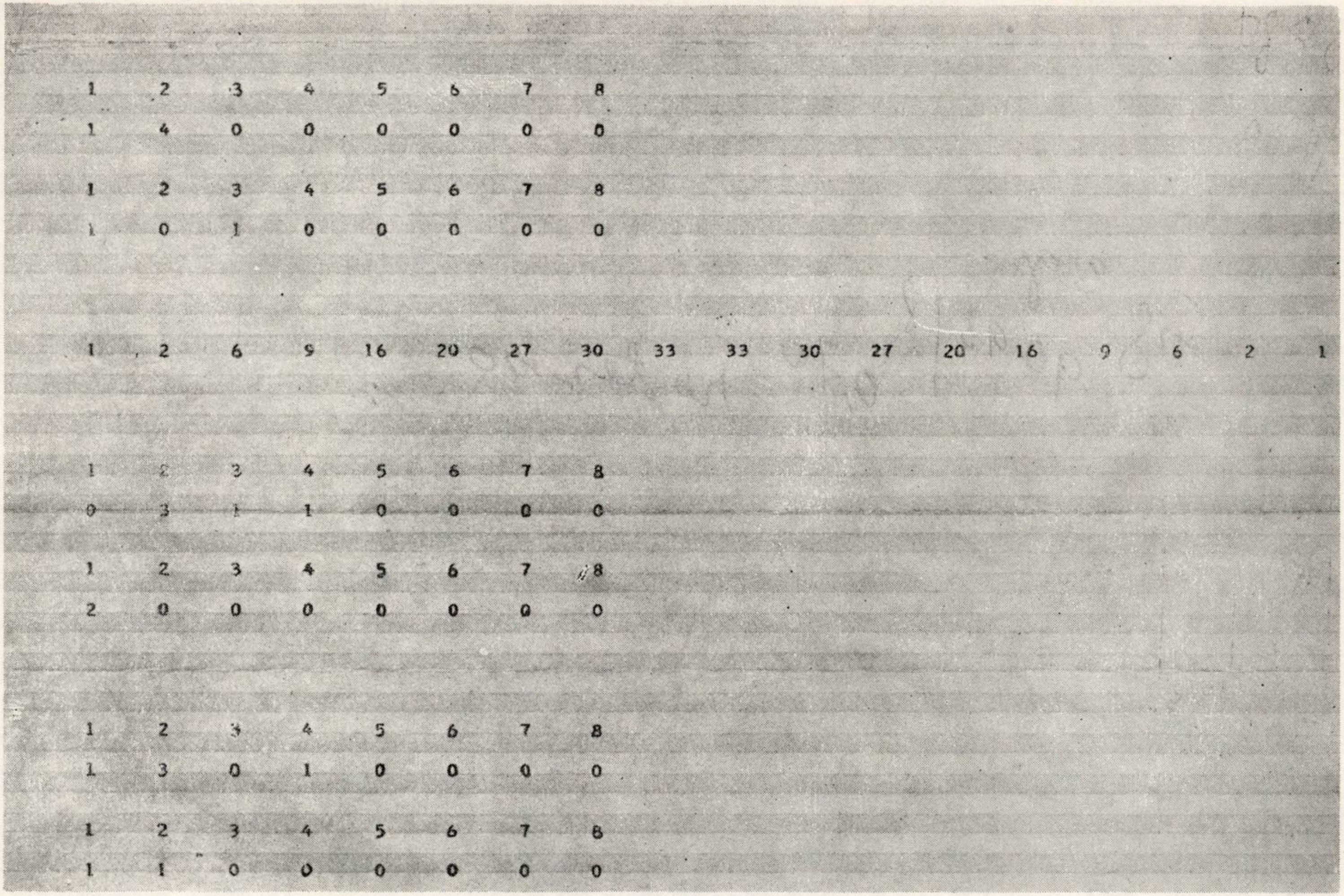

```
1   2   3   4   5   6   7   8
1   4   0   0   0   0   0   0

1   2   3   4   5   6   7   8
1   0   1   0   0   0   0   0



1   2   6   9   16  20  27  30  33  33  30  27  20  16  9   6   2   1



1   2   3   4   5   6   7   8
0   3   1   1   0   0   0   0

1   2   3   4   5   6   7   8
2   0   0   0   0   0   0   0



1   2   3   4   5   6   7   8
1   3   0   1   0   0   0   0

1   2   3   4   5   6   7   8
1   1   0   0   0   0   0   0
```

Fig. 3g.

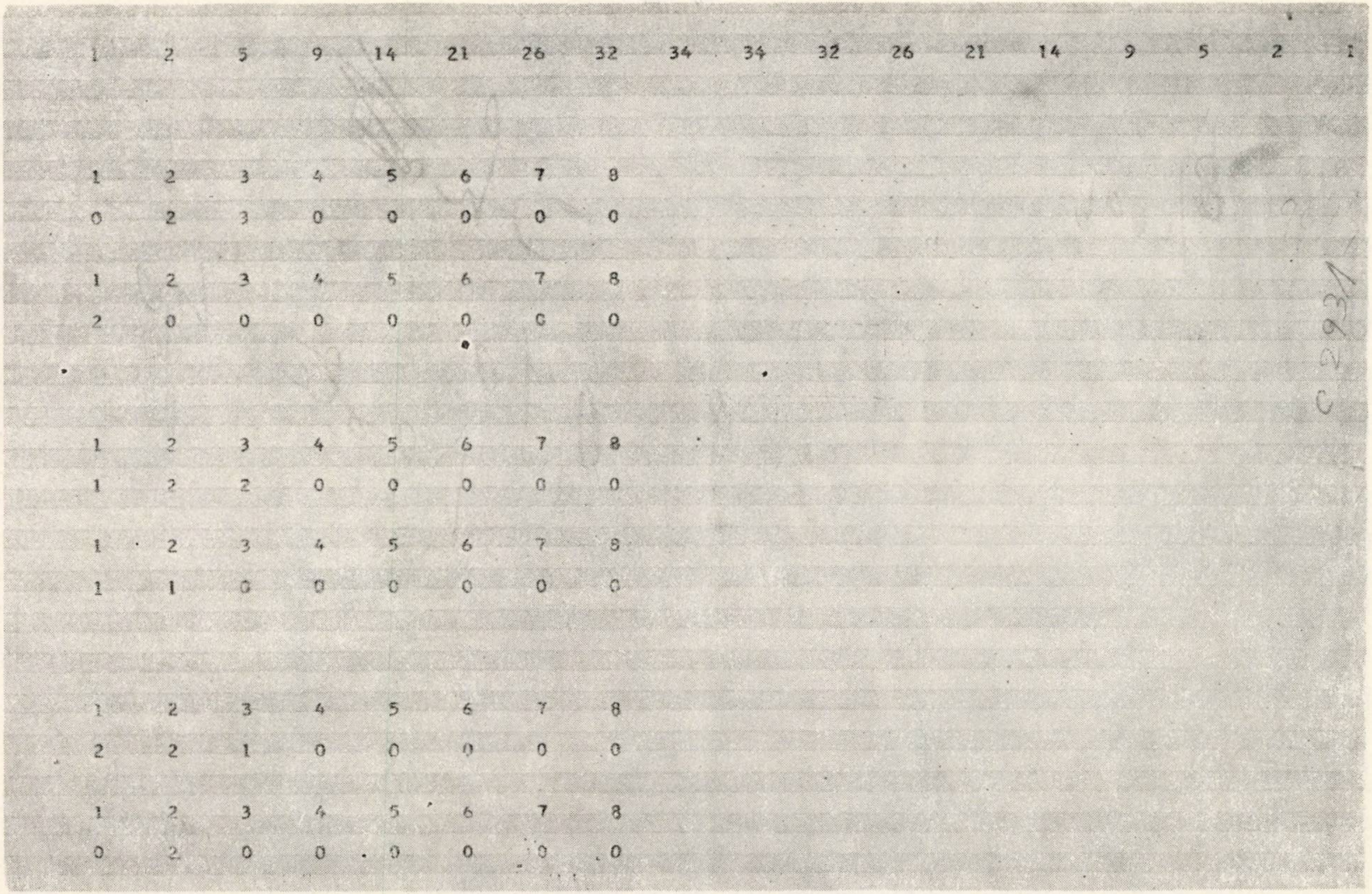

```
  1    2    5    9   14   21   26   32   34   34   32   26   21   14    9    5    2    1


  1    2    3    4    5    6    7    8
  0    2    3    0    0    0    0    0

  1    2    3    4    5    6    7    8
  2    0    0    0    0    0    0    0


  1    2    3    4    5    6    7    8
  1    2    2    0    0    0    0    0

  1    2    3    4    5    6    7    8
  1    1    0    0    0    0    0    0


  1    2    3    4    5    6    7    8
  2    2    1    0    0    0    0    0

  1    2    3    4    5    6    7    8
  0    2    0    0    0    0    0    0
```

Fig. 3h.

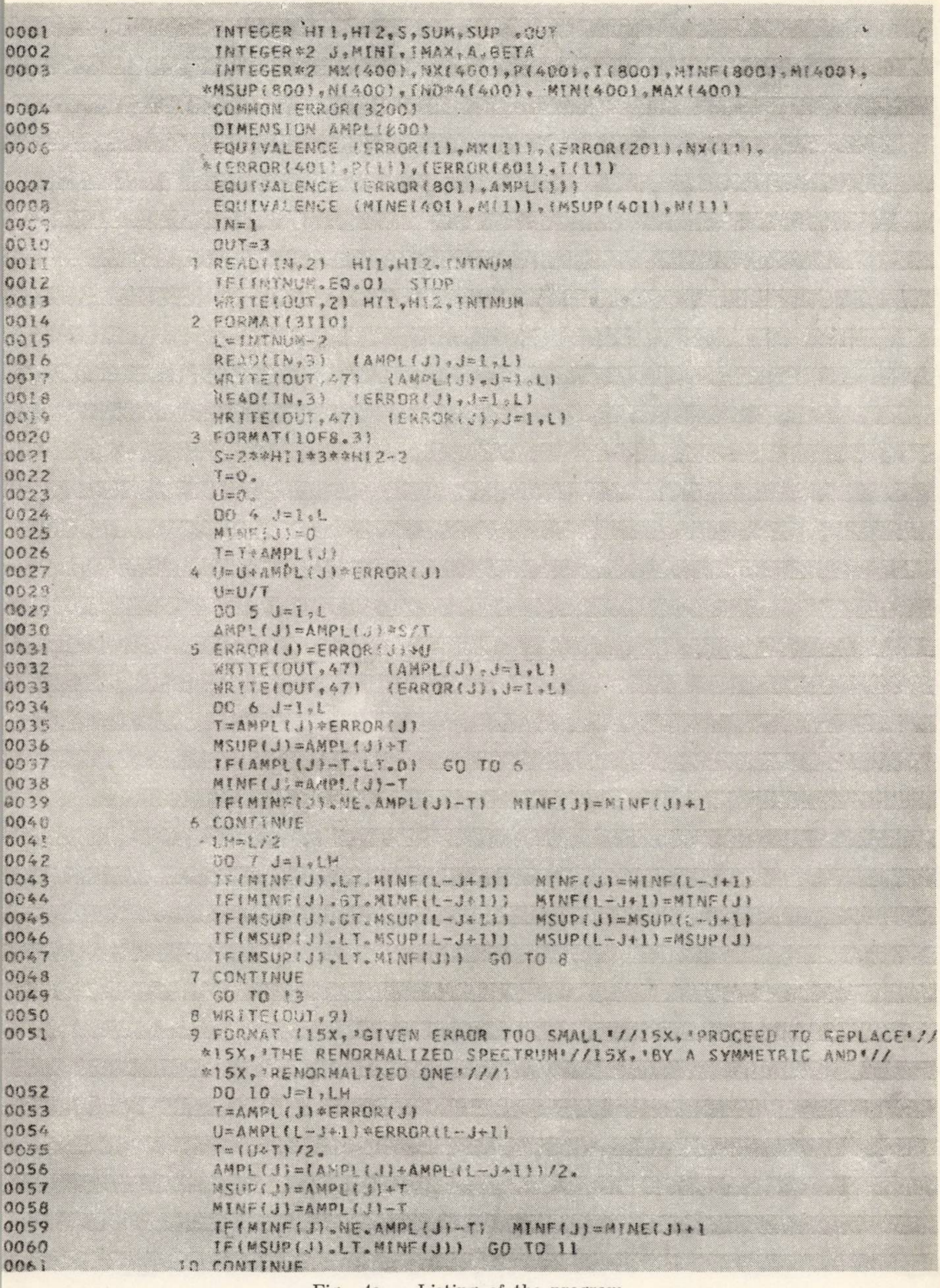

```
      INTEGER HI1,HI2,S,SUM,SUP ,OUT
      INTEGER*2 J,MINI,IMAX,A,BETA
      INTEGER*2 MX(400),NX(400),P(400),I(800),MINF(800),M(400),
     *MSUP(800),N(400),IND*4(400). MIN(400),MAX(400)
      COMMON ERROR(3200)
      DIMENSION AMPL(800)
      EQUIVALENCE (ERROR(1),MX(1)),(ERROR(201),NX(1)),
     *(ERROR(401),P(1)),(ERROR(601),I(1))
      EQUIVALENCE (ERROR(801),AMPL(1))
      EQUIVALENCE (MINE(401),M(1)),(MSUP(401),N(1))
      IN=1
      OUT=3
    1 READ(IN,2)  HI1,HI2,INTNUM
      IF(INTNUM.EQ.0)  STOP
      WRITE(OUT,2) HI1,HI2,INTNUM
    2 FORMAT(3I10)
      L=INTNUM-2
      READ(IN,3)  (AMPL(J),J=1,L)
      WRITE(OUT,47)  (AMPL(J),J=1,L)
      READ(IN,3)  (ERROR(J),J=1,L)
      WRITE(OUT,47)  (ERROR(J),J=1,L)
    3 FORMAT(10F8.3)
      S=2**HI1*3**HI2-2
      T=0.
      U=0.
      DO 4 J=1,L
      MINF(J)=0
      T=T+AMPL(J)
    4 U=U+AMPL(J)*ERROR(J)
      U=U/T
      DO 5 J=1,L
      AMPL(J)=AMPL(J)*S/T
    5 ERROR(J)=ERROR(J)*U
      WRITE(OUT,47)  (AMPL(J),J=1,L)
      WRITE(OUT,47)  (ERROR(J),J=1,L)
      DO 6 J=1,L
      T=AMPL(J)*ERROR(J)
      MSUP(J)=AMPL(J)+T
      IF(AMPL(J)-T.LT.0)  GO TO 6
      MINF(J)=AMPL(J)-T
      IF(MINF(J).NE.AMPL(J)-T)  MINF(J)=MINF(J)+1
    6 CONTINUE
      LH=L/2
      DO 7 J=1,LH
      IF(MINF(J).LT.MINF(L-J+1))  MINF(J)=MINF(L-J+1)
      IF(MINF(J).GT.MINF(L-J+1))  MINF(L-J+1)=MINF(J)
      IF(MSUP(J).GT.MSUP(L-J+1))  MSUP(J)=MSUP(L-J+1)
      IF(MSUP(J).LT.MSUP(L-J+1))  MSUP(L-J+1)=MSUP(J)
      IF(MSUP(J).LT.MINF(J))  GO TO 8
    7 CONTINUE
      GO TO 13
    8 WRITE(OUT,9)
    9 FORMAT (15X,'GIVEN ERROR TOO SMALL'//15X,'PROCEED TO REPLACE'//
     *15X,'THE RENORMALIZED SPECTRUM'//15X,'BY A SYMMETRIC AND'//
     *15X,'RENORMALIZED ONE'///)
      DO 10 J=1,LH
      T=AMPL(J)*ERROR(J)
      U=AMPL(L-J+1)*ERROR(L-J+1)
      T=(U+T)/2.
      AMPL(J)=(AMPL(J)+AMPL(L-J+1))/2.
      MSUP(J)=AMPL(J)+T
      MINF(J)=AMPL(J)-T
      IF(MINF(J).NE.AMPL(J)-T)  MINF(J)=MINE(J)+1
      IF(MSUP(J).LT.MINF(J))  GO TO 11
   10 CONTINUE
```

Fig. 4a. — Listing of the program.

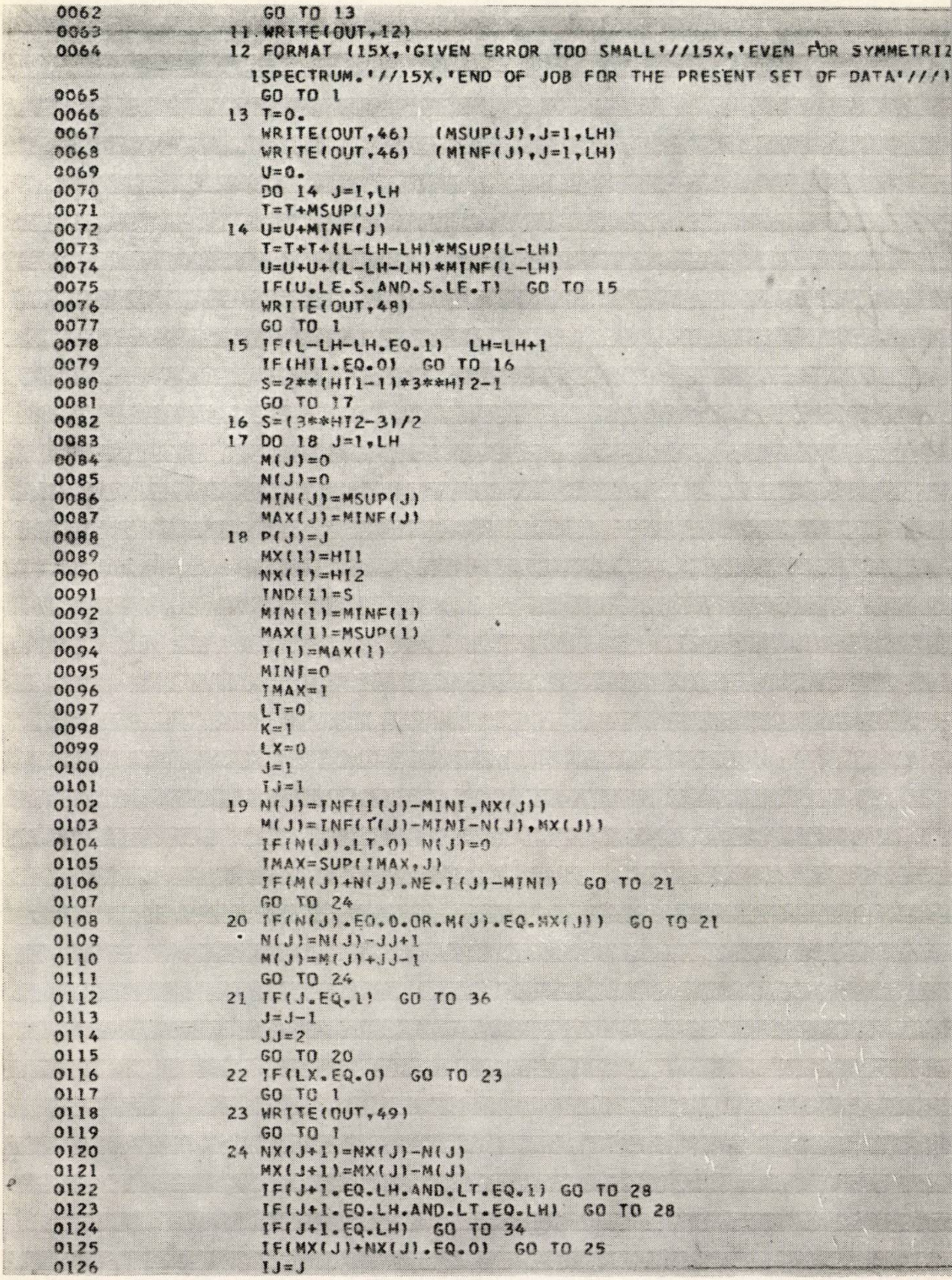

```
      GO TO 13
   11 WRITE(OUT,12)
   12 FORMAT (15X,'GIVEN ERROR TOO SMALL'//15X,'EVEN FOR SYMMETRIZ
     1SPECTRUM.'//15X,'END OF JOB FOR THE PRESENT SET OF DATA'///)
      GO TO 1
   13 T=0.
      WRITE(OUT,46)  (MSUP(J),J=1,LH)
      WRITE(OUT,46)  (MINF(J),J=1,LH)
      U=0.
      DO 14 J=1,LH
      T=T+MSUP(J)
   14 U=U+MINF(J)
      T=T+T+(L-LH-LH)*MSUP(L-LH)
      U=U+U+(L-LH-LH)*MINF(L-LH)
      IF(U.LE.S.AND.S.LE.T)  GO TO 15
      WRITE(OUT,48)
      GO TO 1
   15 IF(L-LH-LH.EQ.1)  LH=LH+1
      IF(HI1.EQ.0)  GO TO 16
      S=2**(HI1-1)*3**HI2-1
      GO TO 17
   16 S=(3**HI2-3)/2
   17 DO 18 J=1,LH
      M(J)=0
      N(J)=0
      MIN(J)=MSUP(J)
      MAX(J)=MINF(J)
   18 P(J)=J
      MX(1)=HI1
      NX(1)=HI2
      IND(1)=S
      MIN(1)=MINF(1)
      MAX(1)=MSUP(1)
      I(1)=MAX(1)
      MINI=0
      IMAX=1
      LT=0
      K=1
      LX=0
      J=1
      JJ=1
   19 N(J)=INF(I(J)-MINI,NX(J))
      M(J)=INF(I(J)-MINI-N(J),MX(J))
      IF(N(J).LT.0) N(J)=0
      IMAX=SUP(IMAX,J)
      IF(M(J)+N(J).NE.I(J)-MINI)  GO TO 21
      GO TO 24
   20 IF(N(J).EQ.0.OR.M(J).EQ.MX(J))  GO TO 21
      N(J)=N(J)-JJ+1
      M(J)=M(J)+JJ-1
      GO TO 24
   21 IF(J.EQ.1)  GO TO 36
      J=J-1
      JJ=2
      GO TO 20
   22 IF(LX.EQ.0)  GO TO 23
      GO TO 1
   23 WRITE(OUT,49)
      GO TO 1
   24 NX(J+1)=NX(J)-N(J)
      MX(J+1)=MX(J)-M(J)
      IF(J+1.EQ.LH.AND.LT.EQ.1) GO TO 28
      IF(J+1.EQ.LH.AND.LT.EQ.LH)  GO TO 28
      IF(J+1.EQ.LH)  GO TO 34
      IF(MX(J)+NX(J).EQ.0)  GO TO 25
      IJ=J
```

Fig. 4b.

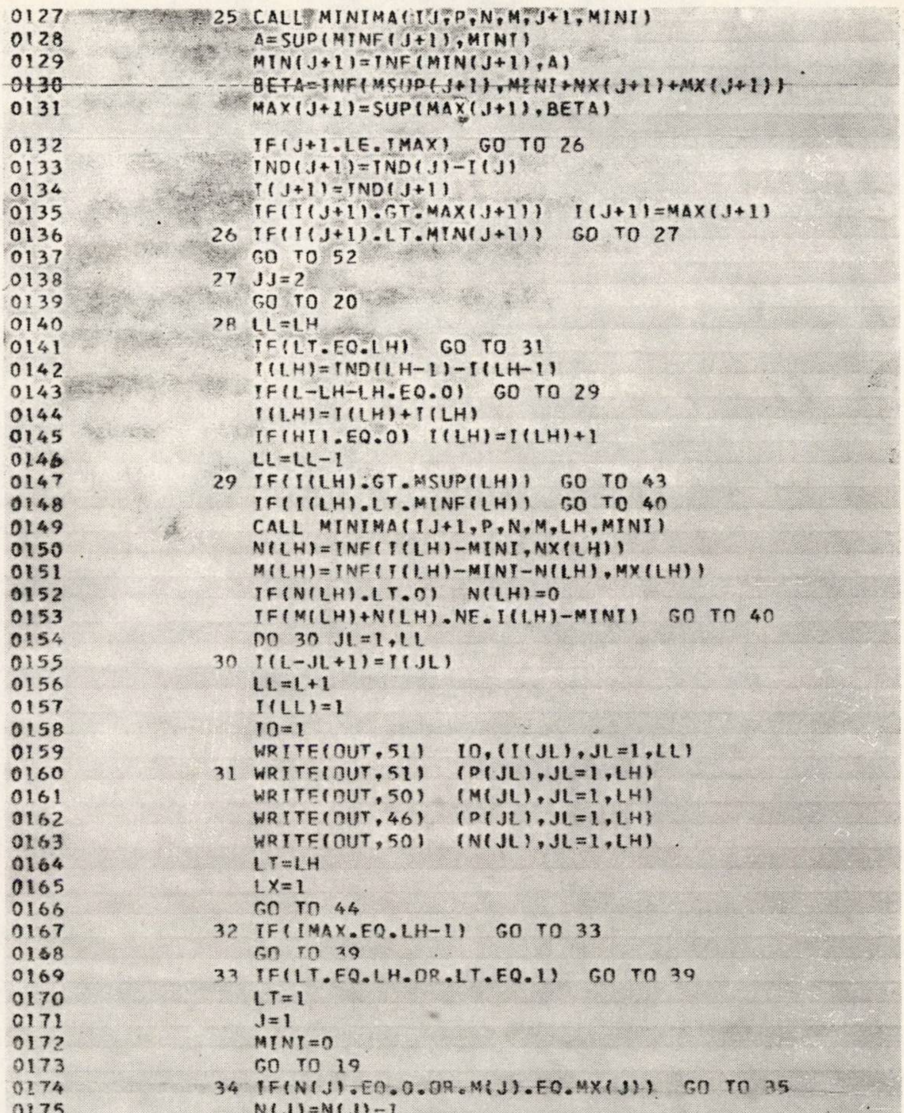

```
   25 CALL MINIMA(IJ,P,N,M,J+1,MINI)
      A=SUP(MINF(J+1),MINI)
      MIN(J+1)=INF(MIN(J+1),A)
      BETA=INF(MSUP(J+1),MINI+NX(J+1)+MX(J+1))
      MAX(J+1)=SUP(MAX(J+1),BETA)
      IF(J+1.LE.IMAX)  GO TO 26
      IND(J+1)=IND(J)-I(J)
      I(J+1)=IND(J+1)
      IF(I(J+1).GT.MAX(J+1))  I(J+1)=MAX(J+1)
   26 IF(I(J+1).LT.MIN(J+1))  GO TO 27
      GO TO 52
   27 JJ=2
      GO TO 20
   28 LL=LH
      IF(LT.EQ.LH)  GO TO 31
      I(LH)=IND(LH-1)-I(LH-1)
      IF(L-LH-LH.EQ.0)  GO TO 29
      I(LH)=I(LH)+I(LH)
      IF(HI1.EQ.0) I(LH)=I(LH)+1
      LL=LL-1
   29 IF(I(LH).GT.MSUP(LH))  GO TO 43
      IF(I(LH).LT.MINF(LH))  GO TO 40
      CALL MINIMA(IJ+1,P,N,M,LH,MINI)
      N(LH)=INF(I(LH)-MINI,NX(LH))
      M(LH)=INF(I(LH)-MINI-N(LH),MX(LH))
      IF(N(LH).LT.0)  N(LH)=0
      IF(M(LH)+N(LH).NE.I(LH)-MINI)  GO TO 40
      DO 30 JL=1,LL
   30 I(L-JL+1)=I(JL)
      LL=L+1
      I(LL)=1
      IO=1
      WRITE(OUT,51)  IO,(I(JL),JL=1,LL)
   31 WRITE(OUT,51)  (P(JL),JL=1,LH)
      WRITE(OUT,50)  (M(JL),JL=1,LH)
      WRITE(OUT,46)  (P(JL),JL=1,LH)
      WRITE(OUT,50)  (N(JL),JL=1,LH)
      LT=LH
      LX=1
      GO TO 44
   32 IF(IMAX.EQ.LH-1)  GO TO 33
      GO TO 39
   33 IF(LT.EQ.LH.OR.LT.EQ.1)  GO TO 39
      LT=1
      J=1
      MINI=0
      GO TO 19
   34 IF(N(J).EQ.0.OR.M(J).EQ.MX(J))  GO TO 35
      N(J)=N(J)-1
      M(J)=M(J)+1
      GO TO 24
   35 IF(J.EQ.1)  GO TO 36
      J=J-1
      GO TO 34
   36 IF(IMAX.EQ.1.OR.LT.EQ.LH)  GO TO 39
      IF(I(J+1).EQ.MAX(J+1).OR.J+1.LE.K)  GO TO 38
      I(J+1)=MAX(J+1)
      LT=J+2
      DO 37 JL=LT,IMAX
      MIN(JL)=MSUP(JL)
   37 MAX(JL)=MINF(JL)
      IMAX=J+1
      J=1
      MINI=0
      GO TO 19
```

Fig. 4c.

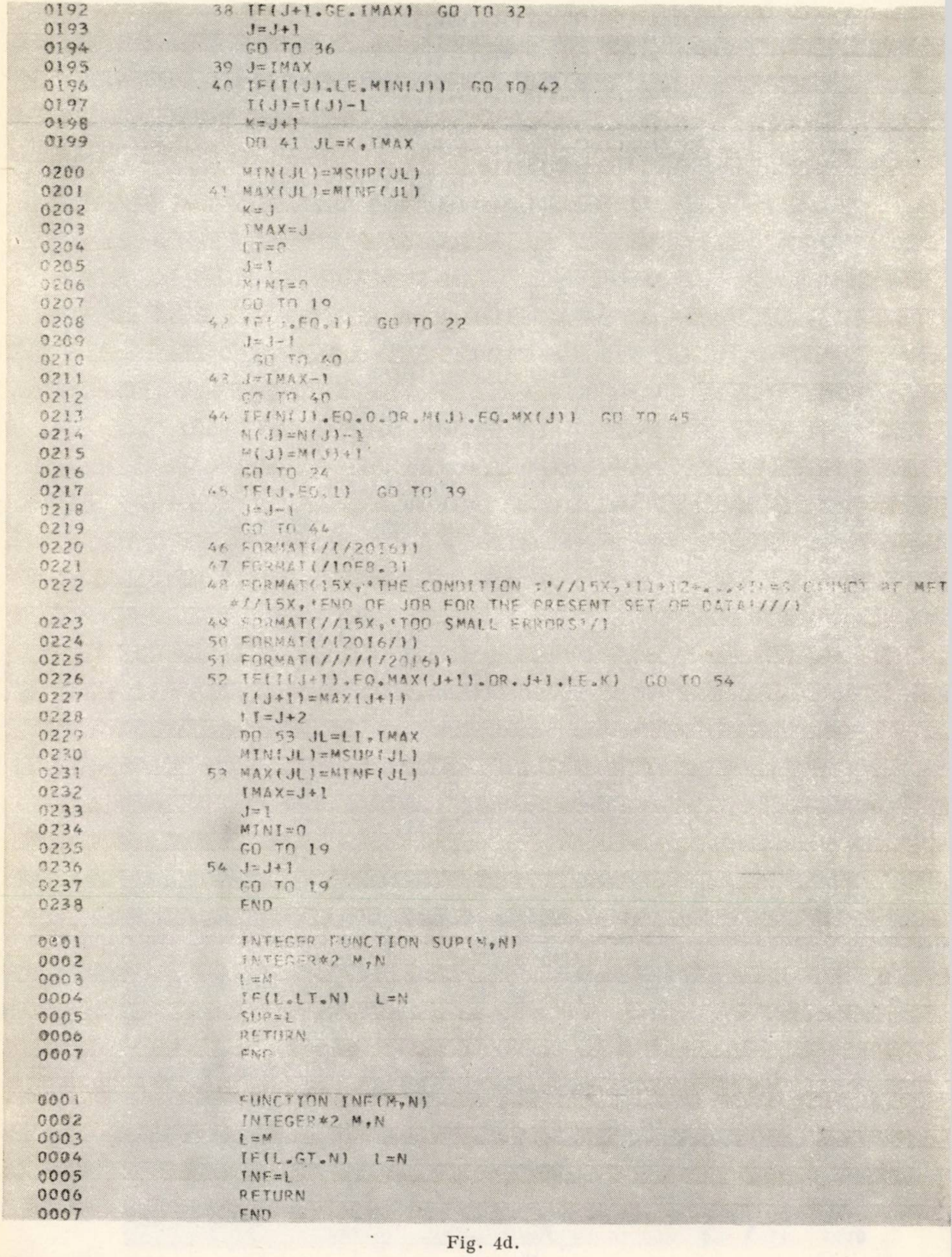

```
   38 IF(J+1.GE.IMAX)  GO TO 32
      J=J+1
      GO TO 36
   39 J=IMAX
   40 IF(I(J).LE.MIN(J))  GO TO 42
      I(J)=I(J)-1
      K=J+1
      DO 41 JL=K,IMAX
      MIN(JL)=MSUP(JL)
   41 MAX(JL)=MINF(JL)
      K=J
      IMAX=J
      LT=0
      J=1
      MINI=0
      GO TO 19
   42 IF(J.EQ.1)  GO TO 22
      J=J-1
       GO TO 40
   43 J=IMAX-1
      GO TO 40
   44 IF(N(J).EQ.0.OR.M(J).EQ.MX(J))  GO TO 45
      N(J)=N(J)-1
      M(J)=M(J)+1
      GO TO 24
   45 IF(J.EQ.1)  GO TO 39
      J=J-1
      GO TO 44
   46 FORMAT(/(/20I6))
   47 FORMAT(/10F8.3)
   48 FORMAT(15X,'THE CONDITION :'//15X,'I1+I2+...+IL=S CANNOT BE MET
     *//15X,'END OF JOB FOR THE PRESENT SET OF DATA'///)
   49 FORMAT(//15X,'TOO SMALL ERRORS'/)
   50 FORMAT(/(20I6/))
   51 FORMAT(////(/20I6))
   52 IF(I(J+1).EQ.MAX(J+1).OR.J+1.LE.K)  GO TO 54
      I(J+1)=MAX(J+1)
      LI=J+2
      DO 53 JL=LI,IMAX
      MIN(JL)=MSUP(JL)
   53 MAX(JL)=MINF(JL)
      IMAX=J+1
      J=1
      MINI=0
      GO TO 19
   54 J=J+1
      GO TO 19
      END

      INTEGER FUNCTION SUP(M,N)
      INTEGER*2 M,N
      L=M
      IF(L.LT.N)  L=N
      SUP=L
      RETURN
      END

      FUNCTION INF(M,N)
      INTEGER*2 M,N
      L=M
      IF(L.GT.N)  L=N
      INF=L
      RETURN
      END
```

Fig. 4d.

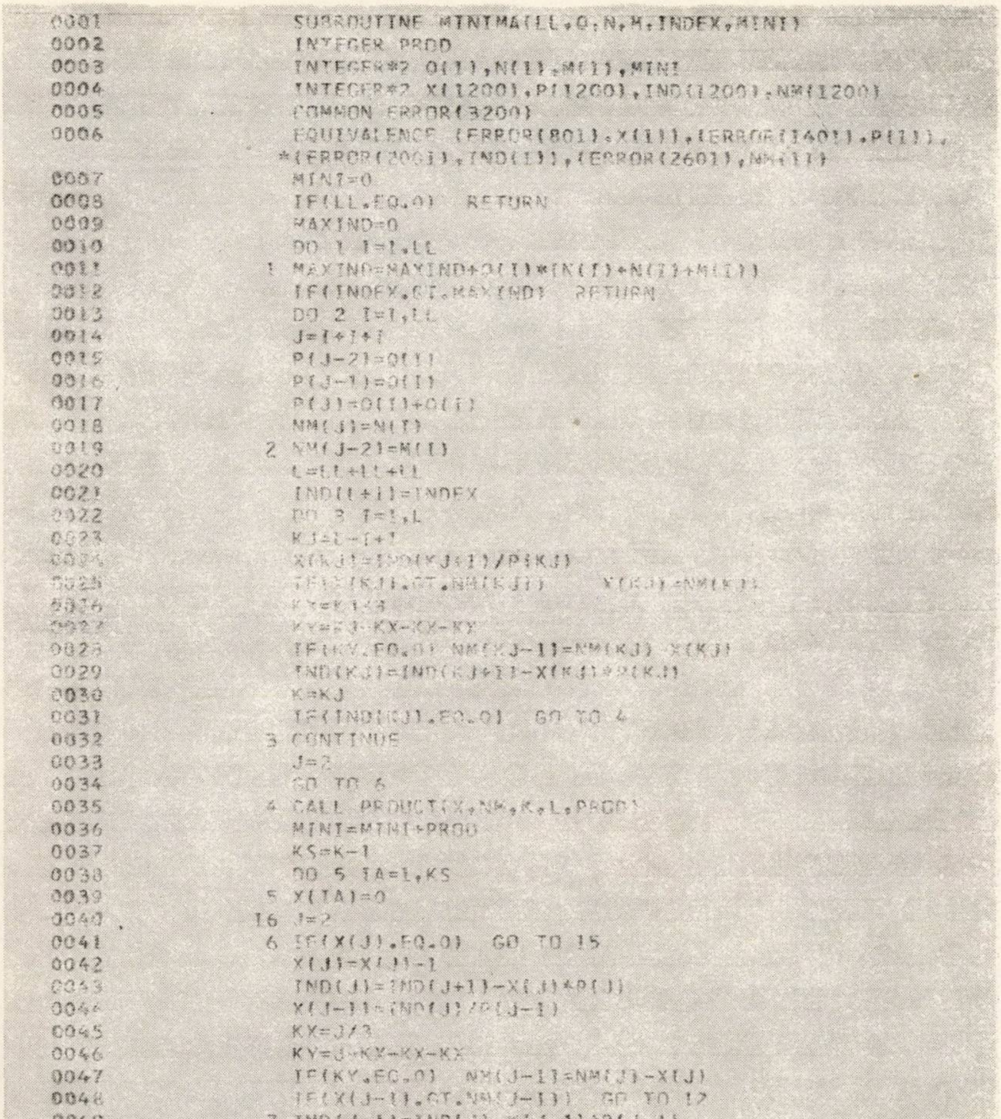

```
      SUBROUTINE MINIMA(LL,O,N,M,INDEX,MINI)
      INTEGER PROD
      INTEGER*2 O(1),N(1),M(1),MINI
      INTEGER*2 X(1200),P(1200),IND(1200),NM(1200)
      COMMON ERROR(3200)
      EQUIVALENCE (ERROR(801),X(1)),(ERROR(1401),P(1)),
     *(ERROR(2001),IND(1)),(ERROR(2601),NM(1))
      MINI=0
      IF(LL.EQ.0)  RETURN
      MAXIND=0
      DO 1 I=1,LL
    1 MAXIND=MAXIND+O(I)*(N(I)+N(I)+M(I))
      IF(INDEX.GT.MAXIND)  RETURN
      DO 2 I=1,LL
      J=I+I+I
      P(J-2)=O(I)
      P(J-1)=O(I)
      P(J)=O(I)+O(I)
      NM(J)=N(I)
    2 NM(J-2)=M(I)
      L=LL+LL+LL
      IND(L+1)=INDEX
      DO 3 I=1,L
      KJ=L-I+1
      X(KJ)=IND(KJ+1)/P(KJ)
      IF(X(KJ).GT.NM(KJ))     X(KJ)=NM(KJ)
      KX=KJ/3
      KY=KJ-KX-KX-KX
      IF(KY.EQ.0) NM(KJ-1)=NM(KJ)-X(KJ)
      IND(KJ)=IND(KJ+1)-X(KJ)*P(KJ)
      K=KJ
      IF(IND(KJ).EQ.0)  GO TO 4
    3 CONTINUE
      J=2
      GO TO 6
    4 CALL PRODUCT(X,NM,K,L,PROD)
      MINI=MINI+PROD
      KS=K-1
      DO 5 IA=1,KS
    5 X(IA)=0
   16 J=2
    6 IF(X(J).EQ.0)  GO TO 15
      X(J)=X(J)-1
      IND(J)=IND(J+1)-X(J)*P(J)
      X(J-1)=IND(J)/P(J-1)
      KX=J/3
      KY=J-KX-KX-KX
      IF(KY.EQ.0)  NM(J-1)=NM(J)-X(J)
      IF(X(J-1).GT.NM(J-1))  GO TO 10
    7 IND(J-1)=IND(J)-X(J-1)*P(J-1)
      IF(IND(J-1).EQ.0)  GO TO 13
      KL=J-2
      IF(KL.EQ.0) GO TO 6
      DO 9 K2=1,KL
      K3=KL-K2+1
      X(K3)=IND(K3+1)/P(K3)
      KX=(K3+1)/3
      KY=K3+1-KX-KX-KX
      IF(KY.EQ.0)     NM(K3)=NM(K3+1)-X(K3+1)
      IF(X(K3).GT.NM(K3))  GO TO 11
    8 IND(K3)=IND(K3+1)-X(K3)*P(K3)
      IF(IND(K3).EQ.0)  GO TO 14
    9 CONTINUE
      GO TO 16
   10 J=J-1
      GO TO 6
```

Fig. 4e.

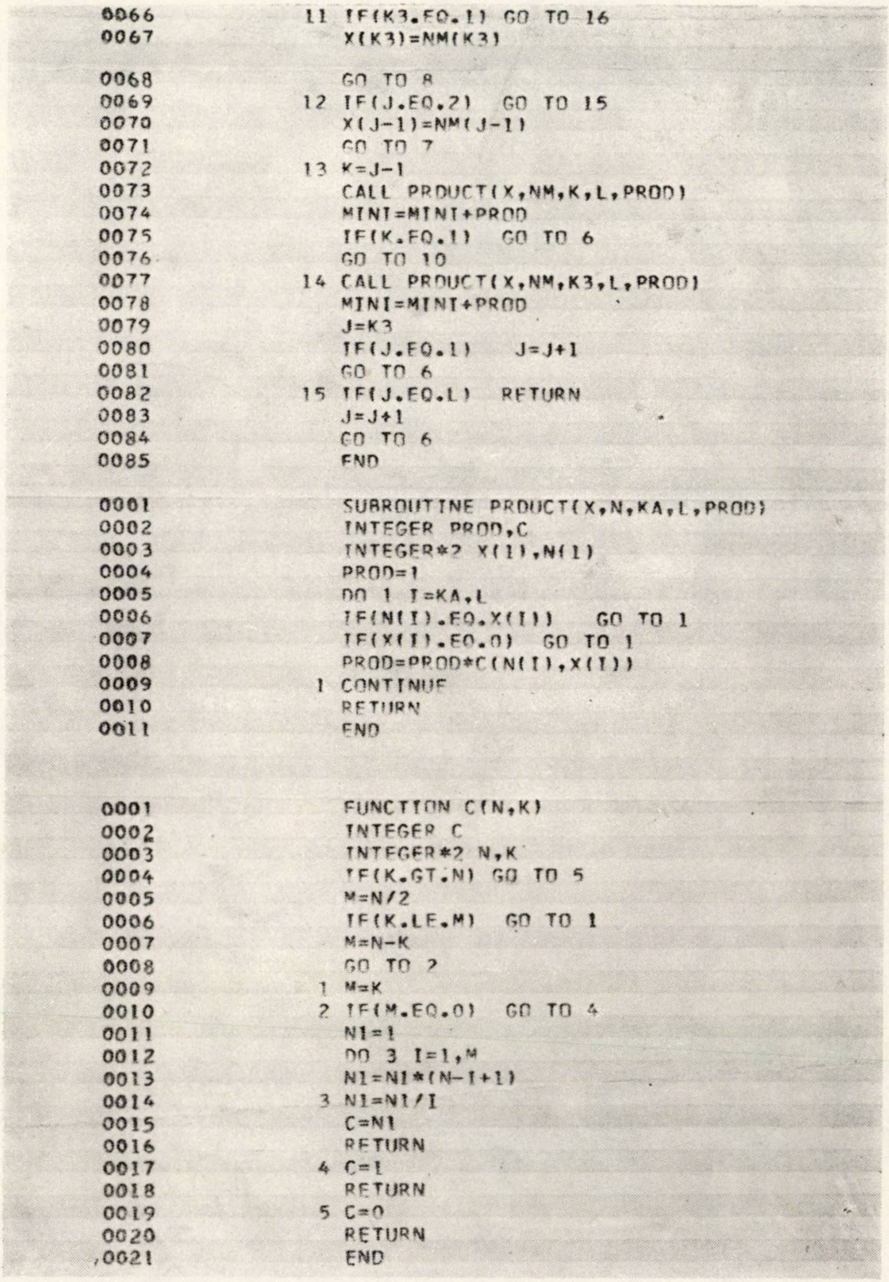

```
   11 IF(K3.EQ.1) GO TO 16
      X(K3)=NM(K3)

      GO TO 8
   12 IF(J.EQ.2)  GO TO 15
      X(J-1)=NM(J-1)
      GO TO 7
   13 K=J-1
      CALL PRDUCT(X,NM,K,L,PROD)
      MINI=MINI+PROD
      IF(K.EQ.1)  GO TO 6
      GO TO 10
   14 CALL PRDUCT(X,NM,K3,L,PROD)
      MINI=MINI+PROD
      J=K3
      IF(J.EQ.1)   J=J+1
      GO TO 6
   15 IF(J.EQ.L)  RETURN
      J=J+1
      GO TO 6
      END

      SUBROUTINE PRDUCT(X,N,KA,L,PROD)
      INTEGER PROD,C
      INTEGER*2 X(1),N(1)
      PROD=1
      DO 1 I=KA,L
      IF(N(I).EQ.X(I))   GO TO 1
      IF(X(I).EQ.0)  GO TO 1
      PROD=PROD*C(N(I),X(I))
    1 CONTINUE
      RETURN
      END


      FUNCTION C(N,K)
      INTEGER C
      INTEGER*2 N,K
      IF(K.GT.N) GO TO 5
      M=N/2
      IF(K.LE.M)  GO TO 1
      M=N-K
      GO TO 2
    1 M=K
    2 IF(M.EQ.0)  GO TO 4
      N1=1
      DO 3 I=1,M
      N1=N1*(N-I+1)
    3 N1=N1/I
      C=N1
      RETURN
    4 C=1
      RETURN
    5 C=0
      RETURN
      END
```

Fig. 4f.

8. POSSIBLE GENERALIZATIONS AND CONCLUSIONS

The algorithm outlined in sections 2, 3 and 4 can obviously be adapted to the case of spin higher than 1. For instance, if we have a mixture of atoms of spin 1/2, 1 and 3/2, then by the same argument that led to (4.2), one can write

$$I_1 = \sum_{\substack{\alpha_1, \beta_1, \gamma_1, \delta_1, \varepsilon_1 \zeta_1 \\ (1 = 3\alpha_1 + 2\beta_1 + \gamma_1 + 2\delta_1 + \varepsilon_1 + \zeta_1)}} \frac{A_{p_1}^{\alpha_1+\beta_1+\gamma_1}}{\alpha_1!\,\beta_1!\,\gamma_1!} \frac{A_{n_1}^{\delta_1+\varepsilon_1}}{\delta_1!\,\varepsilon_1!} \frac{A_{m_1}^{\zeta_1}}{\zeta_1!} \tag{8.1}$$

and in the same manner for I_2, and the rest of spectrum. Of course the ambiguity problem mentioned at the end of section 4, turns from bad to worse, for now one has relations for the sum of *three* quantities p_k, n_k, m_k, namely

$$\begin{aligned} p_1 + n_1 + m_1 &= I_1 \\ p_2 + n_2 + m_2 &= I_2 - \mathrm{MINI}\,(p_1, n_1, m_1) \qquad (8.2) \\ p_3 + n_3 + m_3 &= I_3 - \mathrm{MINI}\,(p_1, n_1, m_1, p_2, n_2, m_2) \\ &\ldots\ldots\ldots\ldots\ldots\ldots \end{aligned}$$

Nevertheless not every possible choice of p_k, n_k, m_k will be compatible with a given spectrum, so by introducing a selector in the program one can keep only the "good" solutions. There is no difficulty in designing a computer program for this case. The problem that will arise concerns solely the computer memory and the time needed to perform the exhaustion of the various possibilities.

Existing programs for the analysis of ESR spectra employ usually an initial guess which then is sharpened by various mathematical methods. [2] The present program, which provides an initial guess, would then be useful in conjunction with either such a program, or a spectrum simulator.

To conclude, we proposed a simple and efficient algorithm to analyse ESR spectra of various complexity, ideal as well as real ones (with errors), equidistant or not. We wrote a FORTRAN program for the case when only two types of atoms (spin 1/2 and spin 1) are present. The program was tested on several examples and proved the efficiency of the algorithm in eliminating the enormous amount of solutions to be considered.

---

[2] F. Schneider and M. Plato, "Elektronenspin – Resonanz. Experimentelle Technik" Thiemig, München, 1971, p. 182.

Revue Roumaine de Chimie, **18**, 7, 1211–1224 (1973)

NEW DISPERSE DYES WITH NAPHTH[2,3-c]ACRIDAN [5,6-cd]PYRAZOL-4,10(2H)-DIONE STRUCTURE

F. URSEANU [*] and I. ZUGRĂVESCU [**]

[*] Laboratory of Chemistry and Technology of Aromatic Intermediates and Dyes, Polytechnic Institute, Calea Victoriei 149, Bucharest, Romania

[**] Laboratory of Organic Chemistry, University "Al. I. Cuza", Str. 23 August, 11 Iassy, Romania

Received November 28, 1972

Syntheses for the preparation of new dyes with naphth [2,3-c] acridan[5,6-cd] pyrazol-4,10(2H)-dione structure[***] are described.

1. INTRODUCTION

The continuous development of synthetic fibre industry makes it necessary to study and find new classes of dyes. The fact that the structure and chemical properties of synthetic fibres differ from those of natural ones should be taken into account; hence, most of the new created dyes should differ from the classic products.

Disperse dyes, [1] products almost insoluble in water (the solubility varies between 0.1 –10 mg/l at 80°), that have been initially used to dye the first hydrophobic fibres (silk cellulose acetate), later on used to dye new textile fibres (polyester, polyamide, polyacrylonitrile fibres), are organic substances of various structures (azoic, [2] anthraquinonic, [3] anthraquinoneacridonic [4–6] structures) which are applied from finely dispersed aqueous suspensions. [7–9]

[***] Trivial, less correct nomenclature : pyrazoleanthroneacridone structure.

[1] C. CĂLIN, *Bul. Inform. Laborat. Centr. Coloristic*, **7**, 23 (1967).

[2] J. REICHEL, "Chimia și tehnologia coloranților azoici", Ed. Academiei R.P.R., București, 1955, p. 324.

[3] J. REICHEL, "Tehnologia coloranţilor antrachinonici", Ed. Academiei R.P.R., Bucureşti, 1961, p. 108.

[4] D. C. EATON and F. IRVING, Brit. Pat. 944 513, Nov. 1, 1960 ; *Chem. Abstr.*, **60**, 10 846 a (1964).

[5] D. C. RATON, Brit. Pat. 914 722, Dec. 6, 1960: *Chem. Abstr.* **60**, 10 846e (1964).

[6] Thoms River Chemical Corp., Brit. Pat. 1 027 576, Sept. 27, 1963 ; *Chem. Abstr.*, **65**, 2 392 d (1966).

[7] K. H. MEYER, C. SCHUSTER and W. BULLOW, *Melliands Text. Ber.*, **6**, 757 (1925).

[8] C. L. BIRD, *Tinctoria*, **61**, 529 (1964).

[9] B. CAMPBELL, *J. Soc. Dyers and Colourists*, **82**, 8 and 303 (1966).

The conditions a new synthesized disperse dye should observe in order to be applied to dyeing synthetic fibres are, on the one hand, its affinity with the fibre (this is determined by its chemical structure and the possibility of finely dispersing the product by mechanical grinding, dissolving in a solvent and fine reprecipitation in water in the presence of a dispersion agent, etc.) and, on the other hand, its dyeing fastness at light, thermofixation, wet treatment, etc. These conditions are determined by the chemical structure of the dyes, the functional groups grafted on the simple system in which the chromophore is included being most important.

In the present work we undertook the synthesis of new disperse dyes with condensed naphth [2,3-c] acridan[5,6-cd]pyrazol-4,10(2H)-dione structure [10] with the following general formula :

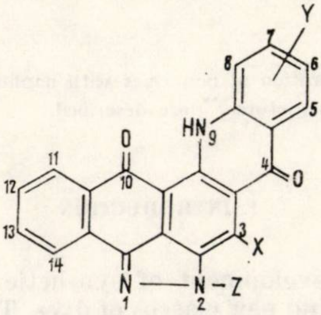

in which : $X = \mathrm{H}, \mathrm{OCH_3}, \mathrm{CONH_2}$
$Y = \mathrm{H}, \text{7-NO}_2, \text{7-NH}_2, \text{6-Br}$
$Z = \mathrm{H}, \mathrm{CH_3}, \mathrm{COCH_3}, \mathrm{COC_6H_5}$

taking into account the fact that naphth[2,3-c]acridan-5,8,14-trione [11,12] and anthra[1,9-cd]pyrazol-6(2H)-one [13] structure dyes are known :

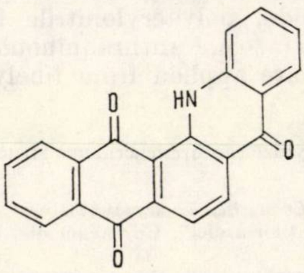

naphth[2,3-c]acridan-5,8,14-trione

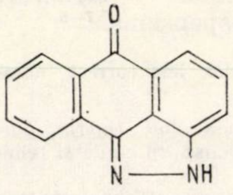

anthra[1,9-cd]pyrazol-6(2H)-one

The new synthesized dyes include both structures in their molecules.

---

[10] H. SANIELEVICI, I. ZUGRĂVESCU and F. URSEANU, R.S.R. Pat. 54 972, March 25, 1971.

[11] F. ULLMANN, Ger. Pat. 221 853, March 3, 1909 ; *Frd.*, **10**, 703.

[12] F. ULLMANN, *Ber. dtsch. chem. Ges.*, **43**, 536 (1910).

[13] Farbenfabriken vorm Friedrich Bayer Co. in Elberfeld, Ger. Pat. 171 293, Aug. 31, 1904 ; *Frd.*, **8**, 304.

2. SYNTHESIS OF NAPHTH[2,3-c] ACRIDAN [5,6-cd]PYRAZOL-4,10(2H)-DIONE DERIVATIVES

Naphth[2,3-c]acridan[5,6-cd]pyrazol-4,10(2H)-dione dyes have been synthesized by a method similar to the one used to obtain anthra[1,9-cd] pyrazol-6(2H)-one [13-16]: diazotation of the corresponding 6-amino-naphth [2,3-c]acridan-5,8,14-trione [17] with nitrosylsulphuric acid in concentrated sulphuric acid at a temperature between 30–35°; reduction of diazonium salts with sodium sulphite resulting in sodium hydrazinedisulphonic salts and their cycling by heating in concentrated sulphuric acid at moderate temperatures (40–50°).

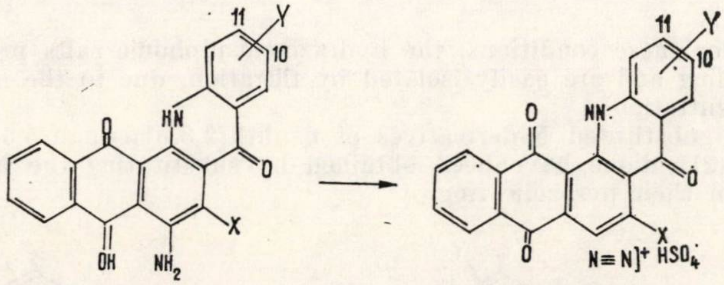

X=H, Y=H **(1)**
$X=OCH_3$, Y=H **(8)**
X=H, $Y=11\text{-}NO_2$ **(15)**
$X=OCH_3$, $Y=11\text{-}NO_2$ **(22)**
X=H, Y=10-Br **(29)**
$X=CONH_2$, Y=H **(36)**
$X=CONH_2$, Y=10-Br **(43)**

X=H, Y=H **(2)**
$X=OCH_3$, Y=H **(9)**
X=H, $Y=11\text{-}NO_2$ **(16)**
$X=OCH_3$, $Y=11\text{-}NO_2$ **(23)**
X=H, Y=10-Br **(30)**
$X=CONH_2$, Y=H **(37)**
$X=CONH_2$, Y=10-Br **(44)**

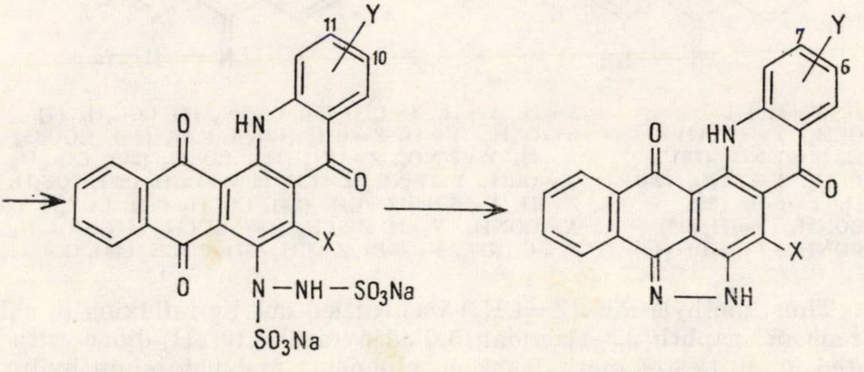

X=H, Y=H **(3)**
$X=OCH_3$, Y=H **(10)**
X=H, $Y=11\text{-}NO_2$ **(17)**
$X=OCH_3$, $Y=11\text{-}NO_2$ **(24)**
X=H, Y=10-Br **(31)**
$X=CONH_2$, Y=H **(38)**
$X=CONH_2$, Y=10-Br **(45)**

X=H, Y=H **(4)**
$X=OCH_3$, Y=H **(11)**
X=H, $Y=7\text{-}NO_2$ **(18)**
$X=OCH_3$, $Y=7\text{-}NO_2$ **(25)**
X=H, Y=6-Br **(32)**
$X=CONH_2$, Y=H **(39)**
$X=CONH_2$, Y=6-Br **(46)**

---

[14] Farbenfabriken vorm Friedrich Bayer Co in Elberfeld, Ger. Pat. 163 447, Aug. 18, 1904; *Frd.*, **8**, 301.

[15] R. Möhlau, *Ber. dtsch. chem. Ges.*, **45**, 2 233 (1912).

[16] T. Maki, T. Akamatsu and M. Maezawa, *J. Chem. Soc. Japan*, **54**, 244 (1951); *Chem. Abstr.*, **47**, 2 490 f (1953).

[17] F. Urseanu, C. Drăghici, R. Vintilă and E. Sliam, *Rev. Roumaine Chim.*, (under print).

As compared to the literature method [14] referring to obtaining anthra[1,9-cd]pyrazol-6(2H)-one, we have used a greater quantity of sodium sulphite when reducing the diazonium salts; towards the end of the reduction we added some sodium disulphite to the mixture, to make sure that no azosulphonic salt remained in the final product:

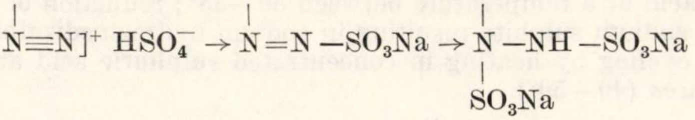

$$N{\equiv}N]^+\,HSO_4^- \rightarrow N{=}N-SO_3Na \rightarrow \underset{SO_3Na}{N}-NH-SO_3Na$$

Under these conditions, the hydrazinedisulphonic salts precipitate when cooling and are easily isolated by filtration, due to the increased salt concentration.

The substituted N-derivatives of naphth[2,3-c]acridan[5,6-cd]pyrazol-4,10(2H)-dione have been obtained by substituting the hydrogen atom from their pyrazolic ring.

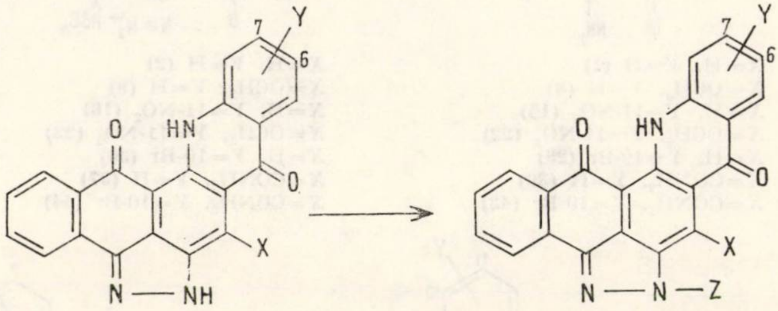

$X=H$, $Y=H$ **(4)** $X=H$, $Y=H$, $Z=CH_3$ **(5)**, $COCH_3$ **(6)** COC_6H_5 **(7)**
$X=OCH_3$, $Y=H$ **(11)** $X=OCH_3$, $Y=H$, $Z=CH_3$ **(12)**, $COCH_3$ **(13)**, COC_6H_5 **(14)**.
$X=H$, $Y=7\text{-}NO_2$ **(18)** $X=H$, $Y=7\text{-}NO_2$, $Z=CH_3$ **(19)**, $COCH_3$ **(20)**, COC_6H_5 **(21)**.
$X=OCH_3$, $Y=7\text{-}NO_2$ **(25)** $X=OCH_3$, $Y=7\text{-}NO_2$, $Z=CH_3$ **(26)**, $COCH_3$ **(27)**, COC_6H_5 **(28)**.
$X=H$, $Y=6\text{-}Br$ **(32)** $X=H$, $Y=6\text{-}Br$, $Z=CH_3$ **(33)**, $COCH_3$ **(34)**, COC_6H_5 **(35)**.
$X=CONH_2$, $Y=H$ **(39)** $X=CONH_2$, $Y=H$, $Z=CH_3$ **(40)**, $COCH_3$ **(41)**, COC_6H_5 **(42)**.
$X=CONH_2$, $Y=6\text{-}Br$ **(46)** $X=CONH_2$, $Y=6\text{-}Br$, $Z=CH_3$ **(47)**, $COCH_3$ **(48)**, COC_6H_5 **(49)**.

Thus, methylation ($Z=CH_3$) was carried out by refluxing in chlorobenzene of naphth[2,3-c]acridan[5,6-cd]pyrazol-4,10(2H)-dione with calculated quantities of methylbenzenesulphonate and potassium hydroxide (necessary to neutralize the free acid formed during the reaction). Acetylation ($Z=COCH_3$) was carried out by refluxing in acetic anhydride of naphth[2,3-c]acridan[5,6-cd]pyrazol-4,10(2H)-dione, adding sulphuric acid as catalyst.

Benzoylation ($Z=COC_6H_5$) was carried out by refluxing in *ortho*-dichlorobenzene of naphth[2,3-c] acridan[5,6-cd]pyrazol-4,10 (2H)-dione with benzoyl chloride, adding pyridine during the reaction to neutralize the hydrogen chloride formed.

Note. 7-aminonaphth[2,3-c] acridan [5,6-cd] pyrazol-4,10(2H)-dione derivatives have been obtained by reduction with saturated aqueous solution of ammonia sulphide in N,N-dimethylformamide of the corresponding 7-nitronaphth[2,3-c]acridan[5,6-cd]pyrazol-4,10(2H)-dione derivatives :

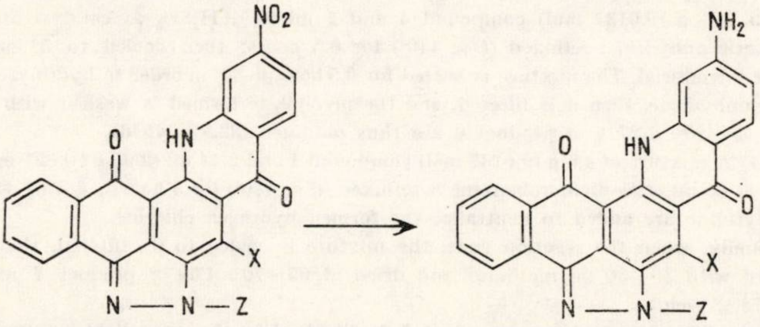

X=H, *Z*=H (**18**), CH_3 (**19**), $COCH_3$ (**20**), COC_6H_5 (**21**).
X=OCH_3, *Z*=H (**25**), CH_3 (**26**), $COCH_3$ (**27**), COC_6H_5 (**28**).

X=H, *Z*=H (**50**), CH_3 (**51**), $COCH_3$ (**52**), COC_6H_5 (**53**).
X=OCH_3, *Z*=H (**54**), CH_3 (**55**), $COCH_3$ (**56**), COC_6H_5 (**57**).

The reduction of the **18**, **19**, **25** and **26** derivatives was carried out at 80° ; the reduction of the **20**, **21**, **27** and **28** derivatives was carried out at lower temperatures (45 –50°), in order to avoid the hydrolysis of the acyl group, but the reaction time was longer, as shown by the experiment.

3. EXPERIMENTAL

3.1. To a solution of nitrosylsulphuric acid, obtained from 6.8 g dry $NaNO_2$ and 150 ml 96 % H_2SO_4, 20.4 g (0.06 mol) compound **1** is added for 1.5 hours,at 15–20°. The diazotation reaction is completed by heating at 30–35° for 3.5 hours. The mixture is poured over 600 g crushed ice under 20°, in an ice bath ; the orange precipitate formed is filtered and washed with 22 % NaCl solution (about 1 l).

The diazonium salt (**2**) thus obtained is added to a solution of 47 g Na_2SO_3 in 400 ml water and stirred for 10 hours at 25–30° ; in the meanwhile the reaction medium pH is maintained slightly alkaline (pH $\approx$ 7.5) by adding concentrated NaOH solution. Then, 9 g $NaHSO_3$ are added and heated for 5 hours at 70–75°. The mixture is cooled at 10–15°, the blue precipitate of product **3** is filtered, washed with 200 ml 22 % NaCl solution until the filtrate is colourless and dried at 30–40°, and p = 10 mmHg.

Compound **3** thus obtained is dissolved in 110 ml 96 % H_2SO_4 at 30–40° and the solution is heated for 1.5 hours at 50°. The mixture is poured over 400 g crushed ice, and the red precipitate is filtered, washed with cold water until the filtrate is neutral and dried at 75–80°. 14 g product **4** are obtained (9.3 % yield).

3.2. A mixture of 4.6 g (0.0137 m) compound **4**, 2.4 ml (3.06 g ; 0.0178 mol) $C_6H_5SO_3CH_3$ and 0.77 g (0.0137 mol) KOH in 65 ml chlorobenzene is refluxed ($t° \approx 132°$) for 9 hours. The mixture is cooled to 0°, filtered, and the precipitate is washed with 15–20 ml cold chlorobenzene and 25–30 ml ethanol, dried at 80°, yielding 3.28 g product **5** (68.4% yield).

Note. A quantity of product **5** is dissolved in the chlorobenzene filtrate and it may be recovered by precipitation with ethanol, filtration, washing with ethanol and drying.

3.3. 4.6 g (0.0137 mol) compound **4** and 1 ml 96% H_2SO_4 as catalyst are added to 65 ml acetic anhydride, refluxed ($t° \approx 140°$) for 6.5 hours, then cooled to 5° and 150 ml water are introduced. The mixture is heated for 0.5 hour at 80° in order to hydrolyze the excess of acetic anhydride, then it is filtered, and the precipitate formed is washed with water and dried at 75–80°. 4.27 g of product **6** are thus obtained (82.5% yield).

3.4. A mixture of 4.6 g (0.0137 mol) compound **4** and 2.44 ml (2.95 g; 0.021 mol) benzoyl chloride in 65 ml *ortho*-dichlorobenzene is refluxed ($t° \approx 180°$) for 5 hours; during the reaction 1.1 ml pyridine are added to neutralize the formed hydrogen chloride.

Finally, when the reaction ends, the mixture is cooled to 0°, filtered, the precipitate is washed with 25–30 ml methanol and dried at 65–70°. 4.69 g product **7** are thus obtained (78% yield).

Note. Since a quantity of product **7** is dissolved in the *ortho*-dichlorobenzene filtrate, it may be recovered by precipitation with methanol, filtration, washing with methanol and drying.

Syntheses of other naphth[2,3-c]acridan[5,6-cd]pyrazol-4,10(2H)-dione derivatives, in which X ≠ H and Y ≠ H, were carried out under conditions similar to those described above. The results are presented in table 1.

Table 1

Results of the syntheses of naphth[2,3-c] acridan [5,6-cd] pyrazol-4,10(2H) -dione derivatives

Synthesis	Starting material	Procedure	Product	Yield %
3.5	**8**	3.1	**11**	68,2
3.6	**11**	3.2	**12**	74
3.7	**11**	3.3	**13**	80
3.8	**11**	3.4	**14**	81
3.9	**15**	3.1	**18**	75
3.10	**18**	3.2	**19**	77.1
3.11	**18**	3.3	**20**	84,6
3.12	**18**	3.4	**21**	76
3.13	**22**	3.1	**25**	74,5
3.14	**25**	3.2	**26**	71.3
3.15	**25**	3.3	**27**	81.1
3.16	**25**	3.4	**28**	77
3.17	**29**	3.1	**32**	71
3.18	**32**	3.2	**33**	67
3.19	**32**	3.3	**34**	84.9
3.20	**32**	3.4	**35**	74.1
3.21	**36**	3.1	**39**	67
3.22	**39**	3.2	**40**	72
3.23	**39**	3.3	**41**	79
3.24	**39**	3.4	**42**	76
3.25	**43**	3.1	**46**	64
3.26	**46**	3.2	**47**	66
3.27	**46**	3.3	**48**	79.5
3.28	**46**	3.4	**49**	68

3.29. 3.82 g (0.01 mol) compound **18** is dissolved in 100 ml N.N-dimethylformamide at 80°, then 70 ml saturated solution of $(NH_4)_2S$ are added dropwise to the resulting solution for 2 hours. The reaction is completed by heating at 80° for 2.5 hours. The mass colour turns from orange to brownish red. The formation of the amino group by reducing the nitro group is determined by the colour characteristic reaction by the Erlich reactive.

Then, 100 ml distilled water are added, the mixture is cooled at 3—5°, the formed precipitate is filtered, washed with distilled water until the filtrate is neutral and colourless, and dried at 60—70°, yielding 2.1 g product **50** (60% yield).

Note. A quantity of product **(50)** is dissolved in the filtrate and it may be recovered by precipitation with concentrated HCl at pH = 7, filtering, washing with water and drying.

The compounds **51**, **54**, **55** are obtained in conditions similar to those described for the 3.29 synthesis of the corresponding derivatives **19**, **25**, **26**. The results are presented in table 2.

3.30. The compounds **52**, **53**, **56** and **57** are obtained by reducing the corresponding derivatives **20**, **21**, **27** and **28** in conditions slightly different from those described at the 3.29 synthesis, namely the reaction temperature is lower (45—50°) and its completing time is longer (4 hours).

The results are presented in table 2.

Table 2

Results of the syntheses of 7-aminonaphth [2,3-c] acridan [5,6-cd] pyrazol-4,10(2H)-dione derivatives

Synthesis	Starting material	Procedure	Product	Yield %
3.30	**19**	3.29	**51**	61
3.31	**20**	3.30	**52**	61.4
3.32	**21**	3.30	**53**	62
3.33	**25**	3.29	**54**	60.4
3.34	**26**	3.29	**55**	60.6
3,35	**27**	3.30	**56**	63
3.36	**28**	3.30	**57**	62.2

4. ANALYSES

The compounds analysed were previously purified by recrystallization from an appropiate solvent: nitrobenzene, glacial acetic acid, acetic anhydride, *ortho*-dichlorobenzene, N.N-dimethylformamide (see table 3).

The melting points of the compounds could not be determined since they decompose over 300°.

The purified compounds were subjected to elemental, chromatographic, spectral and tinctorial analyses.

4.1. ELEMENTAL ANALYSIS

Microcombustions were carried out, determining the nitrogen after the micro-Dumas method, while carbon, hydrogen and bromine were analysed according to the modified Pregl method. The results are presented in table 3.

Table 3

Elemental analysis

Compound	Empirical formula	Solvent for recrystallization	C % *Calc.* *Found*	H % *Calc.* *Found*	N % *Calc.* *Found*	Br % *Calc.* *Found*
4	$C_{21}H_{11}O_2N_3$	nitrobenzene	74.77 74.57	3.29 3.32	12.45 12.63	— —
5	$C_{22}H_{13}O_2N_3$	nitrobenzene	75.20 74.86	3.73 3.46	11.95 12.22	— —
6	$C_{23}H_{13}O_3N_3$	nitrobenzene	72.81 72.58	3.45 3.58	11.07 11.20	— —
7	$C_{28}H_{15}O_3N_3$	nitrobenzene	76.18 76.49	3.42 3.61	9.51 9.78	— —
11	$C_{22}H_{13}O_3N_3$	glacial acetic acid	71.92 71.62	3.56 3.47	11.43 11.32	— —
12	$C_{23}H_{15}O_3N_3$	glacial acetic acid	72.43 72.15	3.96 3.91	11.01 11.12	— —
13	$C_{24}H_{15}O_4N_3$	glacial acetic acid	70.41 70.12	3.69 3.56	10.26 10.32	— —
14	$C_{29}H_{17}O_4N_3$	glacial acetic acid	73.87 73.86	3.63 3.64	8.91 8.98	— —
20	$C_{23}H_{12}O_5N_4$	glacial acetic acid	65.09 64.81	2.85 2.76	13.20 13.31	— —
21	$C_{28}H_{14}O_5N_4$	glacial acetic acid	69.13 68.86	2.90 2.79	11.51 11.63	— —
26	$C_{23}H_{14}O_5N_4$	nitrobenzene	64.78 64.49	3.31 3.17	13.13 13.07	— —
27	$C_{24}H_{14}O_6N_4$	glacial acetic acid	63.43 63.14	3.10 3.06	12.32 12.25	— —
28	$C_{29}H_{16}O_6N_4$	*ortho*-dichlorobenzene	67.44 67.73	3.12 3.08	10.84 10.74	— —
32	$C_{21}H_{10}O_2N_4Br$	*ortho*-dichlorobenzene	60.59 60.38	2.42 2.68	10.09 10.27	19.19 18.88
34	$C_{23}H_{12}O_3N_3Br$	acetic anhydride	60.29 60.45	2.64 2.73	9.17 9.19	17.43 17.24
39	$C_{22}H_{12}O_3N_3$	*ortho*-dichlorobenzene	69.47 69.17	3.18 3.06	14.72 14.68	— —
41	$C_{24}H_{14}O_4N_4$	acetic anhydride	68.24 68.11	3.34 3.19	13.26 13.39	— —
48	$C_{24}H_{13}O_4N_4Br$	acetic anhydride	57.50 57.32	2.61 2.70	11.17 11.29	15.94 15.60

4.2. CHROMATOGRAPHY

Chromatographic analyses were carried out on Whatman paper n°. 1 in ascendent system, at 25°, in order to follow the reactions and to check the purity of recrystallized compounds. The results are presented in table 4.

Table 4

Paper chromatography

Compound	Eluent	R_f	Elution time [min]	Compound	Eluent	R_f	Elution time [min]	Compound	Eluent	R_f	Elution time [min]
4	E^1	0.598	90	**25**	E^4	0.303	40	**46**	E^4	0.119	60
5	E^1	0.525	90	**26**	E^4	0.182	40	**47**	E^4	0.156	60
6	E^1	0.226	90	**27**	E^4	0.167	40	**48**	E^4	0.171	60
7	E^1	0.088	90	**28**	E^4	0.106	40	**49**	E^4	0.134	60
11	E^2	0.290	60	**32**	E^5	0.257	60	**50**	E^1	0.727	40
12	E^2	0.374	60	**33**	E^5	0.244	60	**51**	E^1	0.763	40
13	E^2	0.313	60	**34**	E^5	0.214	60	**52**	E^1	0.708	40
14	E^2	0.343	60	**35**	E^5	0.167	60	**53**	E^1	0.692	40
18	E^3	0.366	60	**39**	E^1	0.335	90	**54**	E^1	0.312	40
19	E^3	0.360	60	**40**	E^1	0.289	90	**55**	E^1	0.180	40
20	E^3	0.106	60	**41**	E^1	0.051	90	**56**	E^1	0.104	40
21	E^3	0.037	60	**42**	E^1	0.028	90	**57**	E^1	0.076	40

E^1 = HCOOH; E^2 = CH_3COOH 90%; E^3 = HCOOH 95%; E^4 = CH_3COOH 80%; E^5 = HCOOH : CH_3COOH = 1 : 1 (in volumes).

The chromatography papers were impregnated with a 10% solution of 1-bromonaphthalene in ethanol.

4.3. SPECTRAL ANALYSIS

Infrared and visible absorption spectra of the products were recorded. *IR spectra* were recorded using a UR-10 spectrophotometer, in pellet KBr. Characteristic vibration frequencies ν [cm^{-1}]:

Compound **4**: 1260 s; 1565 s; 1595 s; 1625 v.s.; 1685 s; 3250 s.

Compound **5**: 1255 s; 1345 m; 1480 s; 1565 s; 1600 s; 1625 v.s.; 1675 s; 3272 s.

Compound **6**: 1270 v.s.; 1545 v.s.; 1590 v.s.; 1620 v.s.; 1660 s; 1725 v.s.; 3270 s.

Compound **7**: 1275 v.s.; 1545 v.s.; 1590 v.s.; 1625 v.s.; 1661 v.s.; 1690 s; 3270 s.

Compound **11**: 1005 s; 1280 v.s.; 1590 v.s.; 1611 v.s.; 1670 s; 3265 s.

Compound **12**: 1005 s; 1280 v.s.; 1360 s; 1485 s; 1590 v.s.; 1611 v.s.; 1670 s; 3265 s.

Compound **13**: 1005 m; 1280 v.s.; 1590 s; 1611 v.s.; 1670 s; 1720 s; 3265 s.

Compound **14**: 1021 s; 1050 s; 1080 s; 1110 v.s.; 1125 v.s.; 1210 s; 1270 v.s; 1280 v.s; 1450 s; 1480 s; 1526 v.s; 1595 v.s; 1611 v.s; 1660 v.s; 1680 s; 3265 s.

Compound **18**: 1350 v.s; 1535 v.s; 1585 v.s; 1615 v.s; 1660 s; 3265 s.

Compound **19**: 1345 v.s; 1380 s; 1470 s; 1535 v.s; 1600 v.s; 1610 v.s; 1640 s; 1660 s; 3270 s.

Compound **20**: 1350 v.s; 1535 v.s; 1585 s; 1610 v.s; 1680 s; 1720 s; 3270 s.

Compound **21**: 1345 v.s; 1535 v.s; 1585 v.s; 1610 v.s; 1660 s; 1690 s; 3270 s.

Compound **25**: 1005 w; 1290 m; 1330 m; 1550 m; 1610 s; 1675 m; 3265 m.

Compound **26**: 1005 m; 1290 s; 1330 s; 1370 m; 1490 s; 1550 s; 1610 v.s; 1675 m; 3265 m.

Compound **27**: 1005 m; 1280 s; 1330 s; 1540 s; 1620 v.s; 1675 s; 1720 s; 3265 m.

Compound **28**: 1005 m; 1275 s; 1330 s; 1520 s; 1630 v.s; 1675 s; 1690 m; 3265 m.

Compound **32**: 1060 m; 1245 m; 1265 m; 1545 m; 1570 m; 1620 s; 1660 m; 3245 m.

Compound **33**: 1270 s; 1380 m; 1480 s; 1500 s; 1580 s; 1615 s; 1660 s; 3250 m.

Compound **34**: 1280 s; 1590 s; 1610 s; 1660 s; 1725 s; 3250 m.

Compound **35**: 1265 s; 1590 s; 1615 s; 1665 m; 1690 m; 3250 m.

Compound **39**: 1250 s; 1555 s; 1588 s; 1618 s; 1630 m; 1660 m; 3265 m.

Compound **40**: 1250 v.s; 1275 v.s; 1335 s; 1470 s; 1550 v.s; 1595 v. s; 1620 v.s; 1630 s; 1660 s; 3270 s.

Compound **41**: 1280 v.s; 1335 v.s; 1545 v.s; 1592 v.s; 1615 v.s; 1628 v.s; 1660 v.s; 1723 v.s; 3270 s.

Compound **42**: 1250 s; 1275 s; 1590 v.s; 1615 v.s; 1635 s; 1662 s; 1685 s; 3270 s.

Compound **46**: 1245 s; 1550 s; 1580 v.s; 1620 v.s; 1630 s; 1660 s; 3265 s.

Compound **47**: 1250 s; 1275 v.s; 1380 s; 1465 s; 1580 v.s; 1615 v.s; 1630 s; 1675 s; 3270 s.

Compound **48**: 1270 s; 1590 s; 1615 s; 1630 s; 1665 s; 1720 s; 3270 m.

Compound **49**: 1270 s; 1590 s; 1620 s; 1665 m; 1685 m; 3270 m.

Compound **50**: 1293 v.s; 1550 v.s; 1571 v.s; 1622 v.s; 1640 s; 1675 s; 3220 s; 3330 s.

Compound **51**: 1345 m; 1480 s; 1575 m; 1640 s; 1672 m; 3220 m; 3330 m.

Compound **52**: 1580 s; 1640 v.s; 1670 s; 1715 m; 3220 s; 3320 s.

Compound **53**: 1580 s; 1640 v.s; 1674 s; 1685 s; 3220 s; 3320 s.

Compound **54**: 1010 m; 1290 s; 1620 s; 1680 m; 3220 m; 3340 m.

Compound **55**: 1008 s; 1290 v.s; 1365 s; 1490 v.s; 1620 v.s; 1630 s; 1680 s; 3220 s; 3340 s.

Compound **56**: 1008 s; 1280 s; 1620 s; 1630 s; 1680 s; 1720 m; 3220 s; 3330 s.

Compound **57** : 1008 s; 1280 v.s; 1620 v.s; 1660 s; 1680 s; 3220 s; 3330 s.

(w = weak; m = medium; s = strong; v.s = very strong).

Visible spectra were determined with a Specord apparatus. The qualitative determinations were carried out in N.N-dimethylformamide; for compounds **4**, **5**, **6** and **7** the extinction coefficient was calculated:

$$\varepsilon^4_{\max} = 20\,380\ \mathrm{l \cdot mol^{-1} \cdot cm^{-1}}; \qquad \varepsilon^5_{\max} = 17\,550\ \mathrm{l \cdot mol^{-1} \cdot cm^{-1}};$$

$$\varepsilon^6_{\max} = 15\,320\ \mathrm{l \cdot mol^{-1} \cdot cm^{-1}}; \qquad \varepsilon^7_{\max} = 26\,930\ \mathrm{l \cdot mol^{-1} \cdot cm^{-1}}.$$

The characteristic absorption maxima are presented in table 5.

4.4. TINCTORIAL ANALYSIS

The naphth[2,3-c]acridan[5,6-cd]pyrazol-4,10(2H)-dione derivatives were used as disperse dyes for "Terom" polyester fibres. The results of the determinations are presented in table 5. The colours were defined according to C.I. Hue Chart. [18]

4.4.1. *Analysis of dyeing fastness.* The analysis of light and thermofixation fastness shows that the general relation between the structure (the nature of the grafted substituents) and the tinctorial properties of the dyes is observed.

Thus, the dyes including electronacceptor groups in their molecule ($X=CONH_2$, $Y=7\text{-}NO_2$, 6-Br) have a good light fastness (=7 –8); those including electrondonor groups in their molecule $X=OCH_3$, ($Y=7\text{-}NH_2$) have a lower light fastness. A slight influence of the Z substituent is observed, namely the methyl group favours the light fastness less than the acyl groups.

The best values of the thermofixation fastness belong to the compounds including electrondonor groups in their molecule: $X=OCH_3$, $Y=7\text{-}NH_2$, $Z=CH_3$. (In this case the substituents have an effect opposite to the one regarding the light fastness).

The other kinds of fastness – washing, sweating and equalization – have good and very good values.

4.4.2. *Dyes affinity.* From the analysis of the dyed samples (expressed in colour yield) we may draw the following conclusions:

a) The best affinity for polyester fibres belongs to the compounds possessing dispersion favouring groups in their molecule: $CONH_2$, OCH_3 NH_2.

---

[18] C. I. Hue, Indication Chart, American Association of Textile Chemists and Colourists, Lowell Institute, Lowell Massachussets, USA.

Table 5

Maxima absorption and determinations with dyed polyester fibres *

Compound	DMF λmax [nm]	Polyester fibres dyeing							
			Fastness						Coloristic yield %
					Sweat				
		Colour	Light	Washing at 40°	acid pH = 5.5	alkaline pH = 8.4	Thermofixation 200° 30 sec	Equalization	
4	397 504	bluish pink 51	5–6	4–5/5/5	4–5/5/5	4–5/5/5	4–5/5	4–5	55
5	398 506	bluish pink 50–51	5	4–5/5/5	4–5/5/5	4–5/5/5	5/5	4–5	60
6	397 503	yellowish pink 48–49	6	5/5/5	4–5/5/5	4–5/5/5	4–5/5	4	50
7	397 502	yellowish pink 48	6	5/5/5	5/5/5	4–5/5/5	4–5/5	4	45
11	500 595	bluish violet 13–38	5	4–5/5/5	4-5/4-5/4-5	4-5/4-5/4-5	5/5	4–5	98
12	500 595	bluish violet 12	4–5	5/5/5	4–5/5/5	4–5/5/5	5/5	4–5	65
13	502	bluish red 51–27	5	4–5/5/5	4-5/4-5/4-5	4-5/4-5/4-5	5/5	4	80
14	505	bluish pink 51–50	5	5/5/5	4-5/4-5/4-5	4-5/4-5/4-5	5/5	4	50
18	518	bluish pink (dull) 51	7–8	5/5/5	5/5/5	5/5/5	4/4–5	4–5	15
19	520 540	reddish violet 11	7–8	4–5/5/5	4-5/4-5/4-5	4-5/4-5/5	4-5/4-5	4	70
20	500	bluish red 27–51	8	4–5/5/5	4–5/5/5	4–5/5/5	4/4–5	4	55
21	500	bluish pink (dull) 51–10	8	4–5/5/5	4–5/5/5	4–5/5/5	4/4–5	4	60
25	480 595	brown 24–25	7	4–5/5/5	4–5/5/5	4–5/5/5	4–5/5	4–5	55
26	490	yellowish red 48	6–7	5/5/5	5/5/5	5/5/5	4–5/5	4	35
27	495	yellowish red (dull) 48–26	7	5/5/5	5/5/5	5/5/5	4–5/5	4	40
28	508	bluish pink (dull) 48–7	7	5/5/5	5/5/5	5/5/5	4–5/5	4	50
32	510	bluish pink 50–9	7	5/5/5	5/5/5	5/5/5	4–5/5	4–5	55
33	545	bluish pink 10–51	6–7	4-5/4-4 /5	4-5/4-5/4-5	4-5/4-5/4-5	5/5	4	90

Table 5 (continued)

Compound	DMF λ_{max} [nm]	Polyester fibres dyeing							
			Fastness						Coloristic yield %
					Sweat				
		Colour	Light	Washing at 40°	acid ph=5.5	alkaline pH=8.4	Thermofixation 200° 30 sec	Equalization	
34	500	yellowish red 48−26	7−8	4−5/5/5	4−5/5/5	4−5/5/5	4−5/5	4	70
35	495	yellowish red (bright) 48−26	7−8	4−5/4−5/5	4-5/4-5/4-5	4-5/4-5/4-5	4−5/5	4	80
39	510	bluish red 9−51	7−8	5/5/5	5/5/5	5/5/5	4−5/5	4−5	50
40	515	bluish pink 51−10	7	4−5/5/5	4−5/5/5	4−5/5/5	5/5	4−5	80
41	502	bluish pink 27−51	7−8	4−5/5/5	4−5/5/5	4−5/5/5	4−5/5	4−5	75
42	500	brownish orange 7−25	7−8	4-5/4-5/4-5	4-5/4-5/4-5	4-5/4-5/4-5	4−5/5	4−5	100
46	516	bluish pink 51−10	8	5/5/5	5/5/5	5/5/5	4−5/5	4−5	50
47	520	bluish pink 51−50	7−8	5/5/5	5/5/5	5/5/5	5/5	4−5	10
48	500	bluish pink 51−9	8	5/5/5	5/5/5	5/5/5	4−5/5	4−5	25
49	505	bluish pink 9−50	8	4−5/5/5	4−5/5/5	4−5/5/5	4−5/5	4	95
50	508 627 790	brown (dull) 32−44	4−5	5/5/5	5/5/5	5/5/5	5/5	4−5	50
51	512 730 827	reddish brown 48−26	4	5/5/5	5/5/5	5/5/5	5/5	4−5	65
52	508 742 795	brown 32−44	4−5	4−5/5/5	4−5/5/5	4−5/5/5	5/5	5	92
53	507 734 800	reddish brown (dull) 26	4−5	5/5/5	5/5/5	5/5/5	5/5	5	75
54	548 775	yellowish brown 31	4−5	4−5/4−5/5	4−5/4−5/5	4−5/4−5/5	5/5	4	80
55	490 785	yellowish brown 23	4−5	4−5/4−5/5	4−5/5/5	4−5/5/5	5/5	4−5	40
56	505 755	brownish orange 24	5	4−5/5/5	5/5/5	5/5/5	5/5	4−5	45
57	505 745	brown (dull) 25	5	5/5/5	5/5/5	5/5/5	5/5	4−5	10

* The polyester fibres were dyed with solutions of the same concentration (1 g/l) in order to estimate the affinity of dyes as coloristic yield ;the most intense sample (42) was noted 100% and was considered the comparison standard. DMF=N.N−dimethylformamide.

Note. The compounds possessing both groups X=OCH_3 and Y=7-NH_2 **(25, 26, 27, 28)** have a low affinity, probably because of the increase of the molecule polarity which confers an increased solubility in the dyeing bath; thus, the diffusion speed of the dyes in the fibre decreases.

b) The unfavourable effect of the nitro group on the dyes may be clearly observed in the compounds **25, 26, 27** and **28.**

The tinctorial analysis shows that the products **6, 7, 11, 18, 32, 33, 39, 40, 41, 42, 47** and **49** have the best qualities for applying to polyester fibres dyeing.

4.4.3. *The relation between molecular structure and colour.* The determination of the absorption visible maxima of the dyes permitted an analysis of their colours, corresponding to the relation which must exist between the absorbed and the seen colour. [19] Thus, for compound **4**, $\lambda_{max} = 504$ nm. This means that it absorbs green light, and the seen colour must be a red shade; indeed, the analysis of the dyed samples established according to C. I. Hue Chart [18] "bluish pink 51" colour. Compound **4** may be considered a standard from the colour point of view.

For compound **5** a very slight displacement of the bathochromic absorption maximum is observed ($\lambda^5_{max} = 506$ nm); the colour established according to C. I. Hue Chart [18] is "bluish pink 50–51".

For compounds **6** and **7** a very slight displacement of the hypsochromic absorption maximum is observed: $\lambda^6_{max} = 503$ nm and $\lambda^7_{max} = 502$ nm. The colours established for the two compounds are "yellowish pink 48–49", respectively "yellowish pink 48".

The analysis of the other compounds, made on the basis of their maximum absorption characteristics in visible spectra, shows also the correspondence existing between their molecular structure and colour.

---

[19] C. D. Nenițescu, "Chimie Organică", vol. 2, 6th edition, Ed. didactică și pedagogică, Bucharest, 1968, p. 520.

Revue Roumaine de Chimie, **18**, 7, 1225–1231 (1973)

NEUE ORGANISCHE PIGMENTE – ISATINDERIVATE. IV[1]

THERMISCHES VERHALTEN

R. VÎLCEANU *, B. D. BADER **, MARIA RĂDULESCU **
und MARIA MARINESCU **

* Zentrum für Chemische Forschungen, Timişoara, B-dul Mihai Viteazul, 24

** Forschungslaboratorium der Industriellen Gruppe für Petrochemie, Piteşti, Şos. Giurgiului, 127, Rumänien.

Eingegangen am 3. Nov. 1972

Durch Thermogravimetrie und Differential-Thermoanalyse wird das thermische Verhalten einiger Kondensationsprodukte des Isatins sowie des 5,7-Dichlorisatins im Vergleich zu anderen organischen heterozyklischen Pigmenten studiert.

EINLEITUNG

Die thermische Stabilität von organischen Pigmenten welche für die Einfärbung von Kunststoffen eingesetzt werden, stellt eine der wichtigsten Bedingungen zu ihrer Einsatzmöglichkeit dar.

Mit dem Kunststoff muß das Pigment gleichzeitig den ganzen Verarbeitungsprozeß durchgehen, wo hauptsächlich im Falle der Verarbeitung von Polyolefinen, Polystyrol und PVC sehr harte Bedingungen vorliegen. Temperaturen von 200–300 °C während der Verarbeitung setzen erhöhte Thermostabilität voraus, welche praktisch nur von heterozyklischen organischen Pigmenten aus den Klassen der Phthalocyanine, Chinacridone, Perylene, Dioxazine und Tetrachlorisoindolinone erfüllt wird.[2]

In früheren Arbeiten [3,4] haben wir über die Synthese von neuen Derivaten des Isatins (I) berichtet, welche mit guten Ergebnissen als Pigmente für Kunststoffe eingesetzt werden können.

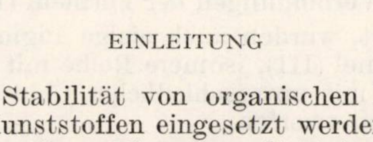

(I)

---

[1] R. Bacaloglu und B. D. Bader, *Rev. Roumaine Chim.*, **18**, *2*, 275 (1973).

[2] B. D. Bader, *Studii şi cercetări chim. (Bucureşti)*, **20** (1972), 553.

[3] J. Reichel, B. D. Bader und R. Vîlceanu, *Rev. Roumaine Chim.*, **17**, *11*, 1889 (1972).

[4] B. D. Bader und R. Vîlceanu, *Rev. Roumaine Chim.*, **17**, *12*, 1991 (1972).

Um die Anwendungsmöglichkeit dieser Verbindungen zu prüfen, haben wir ein Studium durch Differential-Thermoanalyse und Thermogravimetrie unternommen, wobei ihr thermisches Verhalten in einer gewissen Zeitspanne und in weiten Temperaturgrenzen verfolgt wurde.

Gleichzeitig haben wir in den gleichen wie schon früher berichteten Bedingungen [3,4] einige Vertreter einer neuen Reihe von Verbindungen der Strukturformel (II), welche vom 5,7-Dichlorisatin abstammen, synthetisiert.

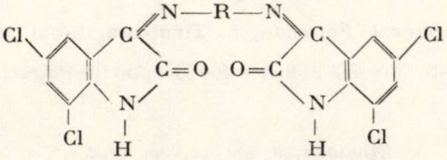
(II)

Durch thermogravimetrische Analyse dieser Verbindungen, wurde versucht den Einfluß zu ermitteln, welchen die Substitution der an den Enden des Systems gelegenen Benzolringe auf die Thermostabilitët der Verbindungen ausüben könnte. Desgleichen wurde der Einfluß auf die thermischen Eigenschaften der Verbindungen beobachtet, welchen die Natur des in der Synthese verwendeten Diamins, das heißt die Abänderung von *R* in den Verbindungen der Formeln (I) und (II), ermöglicht.

In der selben Art, wurden auch einige Pigmente der Isoindolinon-Reihe der Strukturformel (III), isomere Reihe mit denjenigen der Isatinderivate (I) und (II), mit unterschiedlicher Chlorsubstitution, der thermischen Zersetzung unterworfen.

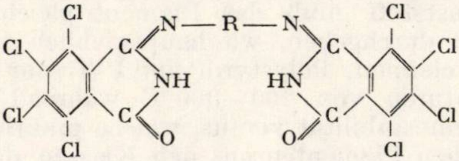
(III)

Zum Vergleich wurden auch zwei organische Pigmente aus den mit hoher Wärmeechtheit bekannten Klassen, und zwar ein Dioxazin- und ein Phthalocyaninpigment, dem gleichen Studium unterzogen.

ERGEBNISSE UND DISKUSSIONEN

In Tabelle 1 werden die Ergebnisse der thermogravimetrischen Analyse der vom Isatin abstammenden Reihe von Pigmenten wiedergegeben. Es wurden bestimmt: Temperaturbereich in welchem die thermische Zersetzung stattfindet, Gewichtsverlust während der Zersetzung, beziehungsweise Rückstand, bei einer Temperaturgrenze von 500 – 600° und Maximum der Zersetzungsgeschwindigkeit (DTG-Kurve).

Die Untersuchungsbedingungen waren für alle Fälle die gleichen und zwar: Gewicht der untersuchten Probe 15 – 30 mg., in statischer

Tabelle 1

Ergebnisse der thermogavimetrischen Analyse der Isatinderivate der Formel (I)

Diamin entsprechend *R* aus Formel (I)	Zerzetzungsbereich, °C	Gewichtsverlust, %	Rückstand bei 600 °C, %	Temp. bei DTG-Maximum, °C	Kritische Temp., °C
(IV) 1,4-Phenylendiamin	286–621	98,2	1,8	470	320
(V) 2,4-Toluylendiamin	290–590	96,3	3,7	488	312
(VI) Benzidin	313–592	95,6	4,4	460	335
(VII) *o*-Tolidin	295–537	95,3	4,7	470	332
(VIII) *o*-Dianisidin	305–506	90,3	9,7	475	327
(IX) 3,3-Dichlorbenzidin	316–525	96,1	3,9	468	340
(X) 4,4′-Diaminodiphenylsulfon	292–590	96,3	3,7	484 556	327
(XI) 4,4′-Diaminodiphenyläther	290–542	97,8	2,2	468	320
(XII) 4,4′-Diaminodiphenylmethan	312–570	96,8	3,2	480	337

Luft bei einer Aufheizgeschwindigkeit von 4°/Min. Die Messungen wurden mit einer Mettler- Thermowaage ausgeführt.

Aus den obengezeigten Ergebnissen kann man bemerken, daß die Natur des Diamins kaum einen Einfluß auf die den Verbindungen entsprechende Anfangstemperatur der Zersetzung sowie auf die Temperatur der maximalen Zersetzungsgeschwindigkeit ausübt. Die Werte für alle untersuchten Verbindungen liegen zwischen 290 –310° entsprechend der Anfangstemperatur der Zersetzung und bei 460 –490° für die Temperatur der maximalen Zersetzungsgeschwindigkeit.

Aus dem Verlauf der thermischen Zersetzungskurven der Verbindungen (IV) –(XII), welche in Figur 1 und 2 dargestellt werden, sowie auch aus einigen auf einem Dioxazin-Pigment ausgeführten Versuchen, in Hinblick auf die thermische Zersetzung bei konstanter Temperatur in größeren Zeitspannen (wobei für die Temperatur jener Wert gewählt wurde, bei welchem bei normaler Aufheizung 4 –8% der Substanz zersetzt wird) und durch Färbeversuche auf Polyäthylen bei der gleichen Temperatur mit Beobachtung des Verhaltens des Pigmentes, konnten wir die Schlußfolgerung ziehen, daß die kritische Temperatur bei welcher sich ein Pigment noch für die Einfärbung eines Kunststoffes durch einen Verarbeitungsprozeß eignet etwas höher liegt als die Anfangstemperatur der Zersetzung. Die kritische Temperatur liegt im allgemeinen bei organischen Pigmenten in jenem Bereich, bei welchem bei konstanter Aufheizgeschwindigkeit sich 4% des Pigmentes zersetzen. Dieser Hilfsparameter wurde für alle untersuchten Verbindungen bestimmt und in Tabelle 1 aufgeführt. Aus dem Vergleich dieser Werte kann man ersehen, daß für jene Verbindungen die von kernsubstituierten Diaminen abstammen ein leichtes Absinken der kritischen Temperatur zu verzeichnen ist.

Das thermische Verhalten der Derivate des 5,7-Dichlorisatins (XIII)–(XV) wird aus den Ergebnissen der thermischen Analyse ersichtlich, welche in Tabelle 2 wiedergegeben werden. Der Verlauf der Zersetzungskurven der Verbindungen ist in Figur 3 aufgezeichnet. Wie bei der vorher besprochenen Isatin-Reihe kann man bemerken, daß weder die Natur des Diamins noch dessen Substitution im Kern einen bedeutenden Einfluß auf das thermische Verhalten der Verbindungen ausübt.

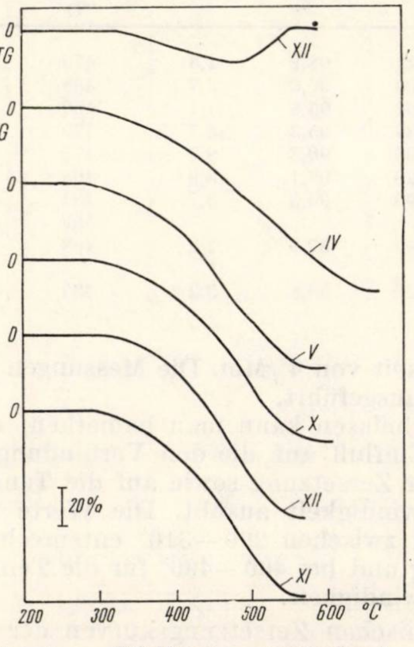

Abb. 1. — TG-Kurven entsprechend den Verbindungen der Isatin-Reihe (IV), (V), (X)—(XII) und DTG-Kurve der Verbindung (XII).

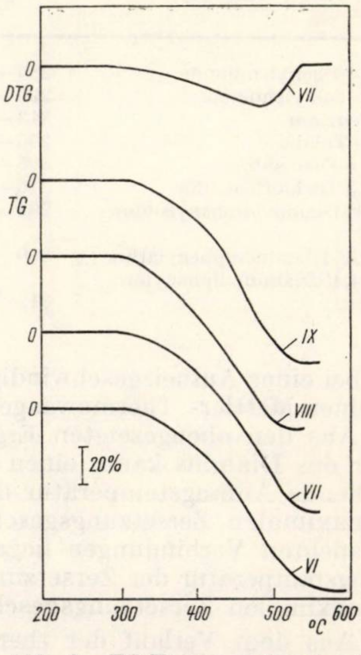

Abb. 2.—TG-Kurven enstprechend den Verbindungen der Isatin-Reihe (VI)—(IX) und DTG-Kurve der Verbindung (VII).

Tabelle 2

Ergebnisse der thermogravimetrischen Analyse der 5,7-Dichlorisatinderivate der Formel (II)

Diamin entsprechend *R* aus Formel (II)	Zersetzungs-bereich, °C	Gewichts-verlust, %	Rück-stand bei 600 °C, %	Temp. bei DTG-Maximum, °C	Kritische Temp., °C
(XIII) 2,4-Toluylendiamin	310—558	92,6	7,4	494	362
(XIV) Benzidin	322—630	91,3	8,7	434 595	350
(XV) *o*-Tolidin	320—531	93,8	6,2	492	355

Werden aber die Ergebnisse der thermischen Analyse der Verbindungen der Isatin-Reihe (V)—(VII) einerseits mit denen der Verbindungen des 5,7-Dichlorisatins (XIII)—(XV) anderseits untereinander verglichen, so kann man ein allgemeines Ansteigen der charakteristischen Werte feststellen, welches durch die Chlorsubstitution im Heterozyklus hervorgerufen wird, wie ersichtlich : Anfangszersetzungstemperatur 310—

320° statt 290 –310°, Temperatur entsprechend maximaler Zersetzungsgeschwindigkeit 490 –495° statt 460 –480° und kritische Temperatur der thermischen Stabilität 350 –360° statt 312 –332°.

Ähnliche Ergebnisse werden auch in der Isoindolinon-Reihe (III) erhalten, wobei die Unterschiede noch größer sind. Die Verbindungen die vom unsubstituierten Phthalimid abstammen weisen wesentlich kleinere Werte als die der Isatin-Reihe auf. Durch totale Chlorsubstitution des Phthalimidabschnittes wurde eine neue und sehr wichtige Reihe von Pigmenten aufgefunden (Irgazin). Die Werte die das thermische Verhalten der Verbindungen kennzeichnen, werden hier um vieles verbessert. Die in Tabelle 3 angeführten Ergebnisse ergeben für die Anfangstemperatur der Zersetzung 298 –328°, für die Temperatur entsprechend der maximalen Zersetzungsgeschwindigkeit liegen zwei Werte vor welche zwischen 393 –414° und 478 –516° schwanken, während für die kritische Temperatur Werte zwischen 345 –400° kennzeichnend sind.

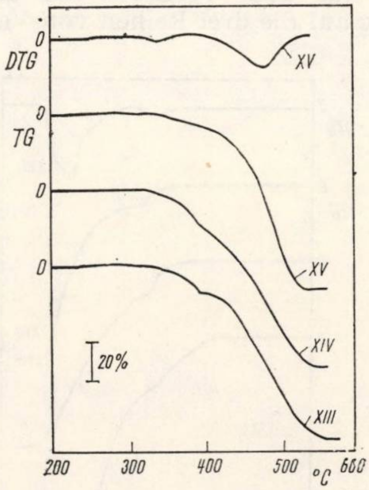

Abb. 3. – TG-Kurven entsprechend den Verbindungen der 5,7-Dichlorisatin-Reihe (XIII)–(XV) und DTG-Kurve der Verbindung (XV).

Tabelle 3

Ergebnisse der thermogravimetrischen Analyse der Tetrachlorisoindolinonderivate der Formel (III)

Diamin entsprechend *R* aus Formel (III)	Zersetzungsbereich, °C	Gewichtsverlust, %	Rückstand bei 600 °C, %	Temp. bei DTG-Maximum, °C	Kritische Temp., °C
(XVI) 2,4-Toluylendiamin	298–410	17,8	1,3	405	390
	410–555	80,9		500	
(XVII) Benzidin	328–426	11,3	7,4	414	400
	426–545	81,3		516	
(XVIII) *o*-Tolidin	308–401	23,8	4,5	393	345
	401–492	71,7		478	

Das Vorhandensein zweier Maxima der Zersetzungsgeschwindigkeit wird auch aus dem Verlauf der in Figur 4 gezeigten TG-Zersetzungs-Kurven ersichtlich.

Wie in den beiden Reihen der Isatinderivate wird auch hier kein besonderer Einfluß der Natur des Diamins auf das thermische Verhalten der Verbindungen verzeichnet.

Aus dem Vergleich der Ergebnisse der thermischen Analyse in Bezug auf die drei Reihen von Verbindungen (I), (II) und (III) kann man die Schlußfolgerung ziehen, daß ihr thermisches Verhalten hauptsächlich durch die Halogensubstitution im Heterozyklus beeinflußt wird, während es von der Natur des in der Synthese verwendeten Diamins praktisch unabhängig ist.

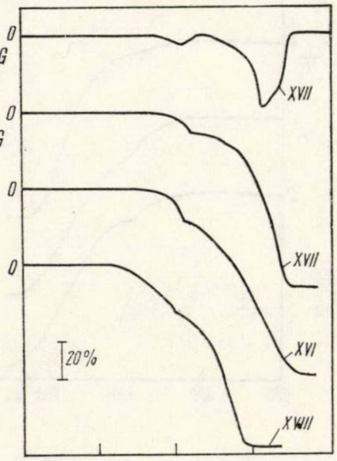

Abb. 4. – TG-Kurven entsprechend den Verbindungen der Tetrachlorisoindolinon-Reihe (XVI) – (XVIII) und DTG-Kurve der Verbindung (XVII).

Noch muß gezeigt werden, daß neben den durch thermogravimetrischer Analyse bestimmten Temperaturen welche in Tabelle 1–3 aufgeführt werden, auch die dem DTA-Maximum entsprechende Temperatur bestimmt wurde. In allen Fällen liegt diese jedoch der Temperatur der maximalen Zersetzungsgeschwindigkeit DTG sehr nahe, so daß man sie für die Charakterisierung des thermischen Verhaltens der Verbin-

Tabelle 4

Ergebnisse der thermogravimetrischen Analyse einiger organischen heterozyklischen Pigmente

Hochwertige Pigmente	Zersetzungsbereich, °C	Gewichtsverlust, %	Rückstand bei 600 °C, %	Temp. bei DTG-Maximum, °C	Kritische Temp., °C
Echt-Blau PV (Hoechst) (Cu-Phthalocyanin)	361–470	83,9	16,1	413	375
Echt-Violet PV-BL (Hoechst) (Dioxazin)	240–492	96,1	3,9	438 462	325

dungen von minderer Bedeutung betrachten kann und wurde deshalb auch nicht in die Tabellen eingeschlossen.

Aus dem Vergleich des thermischen Verhaltens der Verbindungen der Isatin- und 5,7-Dichlorisatin-Reihe mit dem der Tetrachlorisoindolinon-Reihe sowie mit dem eines Dioxazin-Pigmentes (XIX) oder Phthalocyanin-Pigmentes (XX) dessen Werte in Tabelle 4 zusammengefaßt werden, kann man abschließend behaupten, daß die untersuchten Verbindungen sich thermisch sehr ähnlich mit den Pigmenten höchster Wärmeechtheit verhalten und daß sie daher im größten Maße die während der Einfärbung von Kunststoffen auf Verarbeitungsmaschinen geforderten Bedingungen erfüllen.

Revue Roumaine de Chimie, 18, 7, 1225–1231 (1973)

Revue Roumaine de Chimie, **18**, 7, 1233–1241 (1973)

BERYLLIUM-(3-ACYL-2,4-PENTANEDIONATES)

ELENA IŞFAN, CORNELIA UNCUŢA and A. BARABÁS

Institute of Atomic Physics, P.O. Box 35,
Bucharest, Romania

Received January 27, 1973

The beryllium complexes of 3-formyl-, 3-acetyl- and 3-benzoyl-2,4-pentanedione were synthetized and characterized by UV, IR and ^{1}H-nmr spectra. Preferential chelation through acetyl groups was found for each ligand. *bis*-(3-Acetyl-2,4-pentanedionato)-beryllium was prepared from *bis*-(2,4-pentanedionato)-beryllium by acylation with acetic anhydride.

INTRODUCTION

A number of papers concerning boron and beryllium chelates of various 1,3-ketoenols were published by our laboratory. [1–7] Beryllium-1,3-ketoenolates were intensely studied; a now somewhat outdated literature survey [8] was published by one of the authors in 1966. In connection to this former work, it seemed of interest to examine *beta*-triketones (I–III) as chelating agents for beryllium.

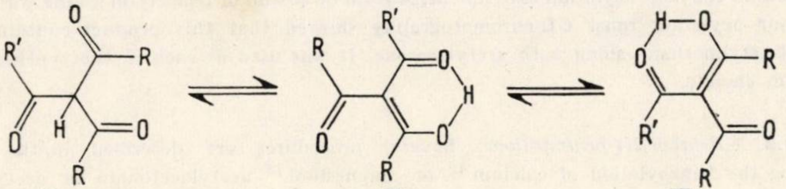

---

[1] A. Barabás, E. Işfan, M. Roman, M. Paraschiv, E. Romaş and A. T. Balaban, *Tetrahedron*, **24**, 1133(1968); and previous work cited therein.

[2] A. Barabás, E. Işfan, E. Romaş and A. Trestianu, *Rev. Roumaine Chim.*, **14**, 253 (1969).

[3] E. Işfan, A. Barabás, J. C. Hammel and J. A. S. Smith, *Tetrahedron*, **26**, 5057(1970).

[4] A. Trestianu, H. Niculescu-Majewska, I. Bally, A. Barabás and A. T. Balaban, *Tetrahedron*, **24**, 2499(1968).

[5] A. Barabás, *Rev. Roumaine Chim.*, **11**, 751(1966).

[6] A. Barabás, *Rev. Roumaine Chim.*, 1972, in press.

[7] E. Işfan and A. Barabás, *Rev. Roumaine Chim.*, 1973, in press.

[8] A. Barabás, *Studii şi Cercetări Chim. Acad.* Bucureşti, **14**, 87(1966).

The elucidation of two points was followed : (i) the possible isomerism between derivatives of the two different enols II and III ; (ii) the nature of interaction between the chelate ring and the unchelated acyl substituent.

For convenience, the following abbreviations will be used for the triketones dealt with in this work :

3-formyl-2,4-pentanedione : facH ;
3-acetyl-2,4-pentanedione : aacH ;
3-benzoyl-2,4-pentanedione : bacH.

EXPERIMENTAL PART

1. SYNTHESES OF 3-ACYL-2,4-PENTANEDIONES

1.1. *3-Formyl-2,4-pentanedione.* [9] 17 ml of acetylacetone (16.6 g, 0.166 moles), 27 ml (*ca.* 25 g, 0.166 moles) of ethyl orthoformate and 32 ml (*ca.* 34 g, 0.332 moles) of acetic anhydride were refluxed for 40 min. Ethyl acetate, acetic acid and unreacted starting materials were distilled quickly at atmospheric pressure and the residue fractionated *in vacuo.* The fraction boiling between 80 – 90°/5 mm was collected as product. Yield 5 g (16 mmoles, 10 %). This product was converted into its copper salt by stirring it with a solution of 2 g (8 mmoles) of copper acetate, filtering off the precipitate formed, washing it with water and petroleum ether. The solid product was suspended in ether and shaken with 5 % H_2SO_4 aq. in excess, till all precipitate was dissolved. The ethereal layer was dried over Na_2SO_4 and fractionated collecting 2.5 g of 3-formyl-2,4-pentanedione at 100°/20 mm.

1.2. *3-Acetyl-2,4-pentanedione* (*triacetylmethane*).[10] Ketene generated [11] from 500 ml of acetone by the usual "ketene lamp" was bubbled through 500 ml acetylacetone for 8 – 14 hours. The resulting mixture was fractionated *in vacuo* collecting a forerun which consisted mainly of unconverted acetylacetone (distilled up to 60°/5 mm) and the triacetylmethane product, distilled at 68 – 69°/5 mm. The forerun was completed with fresh acetylacetone and used again in the next acylation experiment. A total of 204 ml of triacetylmethane was obtained after four acylation runs. GL-chromatography showed that this product contained about 80 % triacetylmethane along with acetylacetone. It was used as such in the synthesis of the beryllium chelate.

1.3. *3-Benzoyl-2,4-pentanedione.* Several procedures are described in the literature involving the benzoylation of calcium [12] or magnesium [13] acetylacetonate or acetylation of benzoylacetone with ketene. [13] After some attempts, the benzoylation of *bis*-(acetylacetonato)-Mg was followed : 2.0 g (88 mmoles) of Mg were suspended in 20 ml of boiling absolute ethanol. 15 ml of acetylacetone (1.48 g, 148 mmoles) dissolved in 100 ml of absolute ethanol were dropped into, under continuous refluxing and stirring. After the addition of acetylacetone was concluded (*ca.* 30 min), the reaction mixture was stirred and refluxed for further 2 h. The boilinghot solution was filtered and cooled to yield the crystalline chelate (10 g, 60%), m.p. 270° (dec.). 9 g (40 mmoles) of *bis*-(acetylacetonato)-Mg were dissolved in 125 ml of hot diglyme, 500 ml of dry benzene were added and 10 ml (*ca.* 12 g, 85 mmoles) of benzoyl chloride diluted with 20 ml of dry benzene were dropped into this mixture. The solution was kept at room temperature for 24 h; thereafter, it was transferred into a separatory funnel and shaken with 500 ml of HCl 1 N. From the organic layer the triketone was extracted with NaOH 2 N. This alkaline solution was neutralized with HCl 1 N and the triketone extracted with ether. After evaporation of the ether, 12 g (60%) of product were obtained, m.p. 30−32°. This triketone undergoes slow deacetylation on standing, yielding benzoylacetone. The use of an older preparate may lead to puzzling results as it happened at one moment during this work.

---

[9] L. Claisen, *Liebig's Ann. Chem.*, **297**, 20 (1897).

[10] J. P. Collman, R. L. Marshall, W. L. Young, III, and C. T. Sears, Jr., *J. Org. Chem.*, **28**, 1449 (1963).

[11] J. W. Williams and C. D. Hurd, *J. Org. Chem.*, **5**, 122 (1940).

[12] S. S. Sabnis, K. D. Kulkarni and C. D. Deliwala, J. *Sci. and Ind. Research*, **17A**, 421 (1958).

[13] M. M. Coombs and R. P. Houghton, *J. Chem. Soc.*, **1961**, 5015.

2. SYNTHESES OF THE BERYLLIUM TRIKETONATES

Beryllium chelates of the triketones were prepared by both procedures currently used in our laboratory:

2.1. *In aqueous solution.* 20 mmoles of ligand were dissolved in 10 ml of ethanol and added dropwise into a stirred solution of 1.77 g (10 mmoles) of $BeSO_4 \cdot 4H_2O$ (or $Be(NO_3)_2 \cdot 4H_2O$) and 2.5 g of sodium acetate. The precipitate deposited on continued stirring was left overnight, filtered off and dried in air.

2.2. *In organic solvent.* 20 mmoles of ligand were dissolved in 10 ml of ethyl acetate and a solution of 0.8 g (10 mmoles) of dry $BeCl_2$ in 10 ml of ethyl acetate was added. The mixture was refluxed till evolution of HCl ceased. The product was obtained by evaporating the solvent to dryness.

The chelates obtained using both procedures were purified by recrystallization from benzene-*n*-heptane.

3. ACYLATION OF BIS-(ACETYLACETONATO)-BERYLLIUM

2.1 g (10 mmoles) of beryllium acetylacetonate were dissolved in 20 ml of dry benzene, 5 g of $NaHCO_3$ and 5 ml of acetic anhydride added, the mixture refluxed for 10 h and left overnight. The solution was filtered from excess sodium hydrogen carbonate and evaporated to dryness. The residue was recrystallized from benzene-*n*-heptane giving pure *bis*-(triacetylmethanato)-beryllium, as proved by mixed m.p., IR and ^1H-nmr spectra.

4. ANALYSES AND SPECTRA

Elementary analyses for C and H were effected by standard combustion procedure. Beryllium was determined from the combustion residue taken as BeO. Results are displayed in table 1. Electronic spectra were recorded in 1,2-dichloroethane solution with an Optica Milano CF 4 double-beam recording spectrophotometer, IR spectra with a Carl Zeiss-Jena UR-10 instrument. Proton magnetic resonance spectra were recorded at 60 MHz by a Varian A60A instrument or at 80 MHz by a Tesla BS-487-B nmr spectrometer.

Table 1

Beryllium-(3-acyl-2,4-pentanedionates), L_2Be

Ligand, LH	m.p. °C	Analyses, %					
		C		H		Be	
		found	*calcd.*	*found*	*calcd.*	*found*	*calcd.*
$CH_3-CO-\underset{\overset{\mid}{CHO}}{CH}-CO-CH_3$	117–120	incorrect	54.75	5.24	5.36	3.58	3.42
$CH_3-CO-\underset{\overset{\mid}{CO-CH_3}}{CH}-CO-CH_3$	157	57.66	57.72	6.25	6.23	3.38	3.08
$CH_3-CO-\underset{\overset{\mid}{CO-C_6H_5}}{CH}-CO-CH_3$	205	69.86	69.38	4.97	5.34	2.38	2.17

RESULTS AND DISCUSSION

Results obtained by UV, IR and ^1H-nmr spectroscopy on the beryllium triketonates are shown in tables 2, 3 and 4, respectively. They are used in the discussion of the two points proposed to be elucidated in the introduction.

(i) ISOMERISM OF THE TRIACYLMETHANE CHELATES

3-Acyl-2,4-pentanediones can form with metals two kinds of chelate rings, IV or V derived from the enols II or III, where *n* is the number of chelating ligands per central atom in the complex.

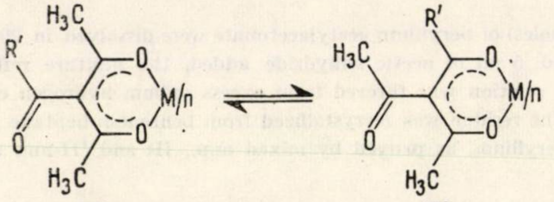

IV V

Combination of these two different chelate rings can afford $n + 1$ isomeric complex compounds if additional possibilities of stereoisomerism are disregarded.

Electronic absorption spectra of the prepared complexes are interpreted as follows. The band at longer wavelength, labelled with *Z* (table 2) is attributed to the $\pi \rightarrow \pi^*$ transition in the chelate ring, in accordance with earlier results on 1,3-diketone complexes.$^{1-3}$ The other absorption band at shorter wavelength, which is missing in the spectrum of beryllium acetylacetonate, may be a $\pi \rightarrow \pi^*$ transition in the free carbonyl group. (Acetophenone absorbs[14] at 245 nm (ε=12000), (*K*-band) and at 280 nm (ε = 1300 l/mole·s), (*B*-band)). The dλ values in table 2 are defined as the difference between wavelengths of band *Z* in the compound under consideration and of beryllium acetylacetonate; thus they will reflect the influence of the R′CO substituent on the delocalization in the chelate ring. This problem will be discussed in more detail under point (ii); here we shall only mention that the very small $d\lambda$ value observed for *bis*-(3-benzoyl-2,4-pentanedionato)-beryllium, bac$_2$Be, suggests that this compound consists mostly of IV-type chelate rings, derived from acetylacetone. Chelate rings of type V derived from benzoylacetone should show large positive $d\lambda$ values as *bis*-(benzoylacetonato)-beryllium has its band *Z* at 329 nm, $d\lambda$ = 35 nm. This conclusion is supported by IR spectroscopic evidence : bac$_2$Be shows its only non-chelated carbonyl absorption band at 1665 cm^{-1} (acetophenone absorbs at 1670 cm^{-1}), whereas the non-chelated acetyl group in aac$_2$Be absorbs at 1690 cm^{-1} (see table 3). No significant changes in the carbonyl absorption region could be detected in IR spectra recorded in CCl$_4$ solution.

Table 2

Electronic absorption spectra of the beryllium triketonates in 1,2-dichloroethane solution

R′ (formulae IV, V)	λ_{max} (nm) ε, (1/mole · s)	*Z*	$d\lambda^a$ (nm)
H	245 9100	297 19500	+3
CH$_3$	245 30500	287 22800	−7
C$_6$H$_5$	250 23800	295 25600	+1

[a] relating to *bis*-(2,4-pentanedionato)-beryllium.

Proton magnetic resonance spectra allow a quantitative determination of the IV $\rightleftharpoons$V equilibrium concentrations (table 4). ^{1}H-nmr studies on the keto-enol tautomerism of the 1,3-dicarbonyl compounds[15,16] revealed that the protons of a non-chelated CH$_3$CO group (as in V) resonate at a lower field than those of a chelated CH$_3$CO (as in IV). This difference was attributed to the magnetic anisotropy of the carbonyl double bond : the electron density (double bond character) at the chelated carbonyl band is diminished by the chelate ring resonance, consequently the chelated carbonyl group will exhibit less anisotropic deshielding effect at the adjacent methyl group, than a non-chelated carbonyl group. The methyl resonance signals of the chelated and free acetyl groups in aac_2Be were identified according to these considerations. In the same solvent ($CDCl_3$) bac_2Be showed a single methyl signal, corresponding to a IV-type ring. Two methyl and two HCO signals appeared however in the spectrum of fac_2Be; based on their chemical shifts and relative intensities a content of 78% in IV-type rings was calculated. The spectra of these beryllium

---

[14] P. GRAMMATIKATIS, *Bull. Soc. chim. France*, **20**, 865(1953).

[15] J. L. BURDETT and M. T. ROGERS, *J. Amer. Chem. Soc.*, **86**, 2105(1964).

[16] R. L. LINTVEDT and H. F. HOLTZCLAW, JR., *Inorg. Chem.*, **5**, 239(1966); *J. Amer. Chem. Soc.*, **88**, 2713(1966).

Table 3

Some assigned IR absorption frequencies (cm^{-1}) of the beryllium triketonates in KBr pellets

R′ Assignment	—[a]	CH_3	C_6H_5	H
ν(C−H), chelater ing	3110w	—	—	—
ν(C−H), phenyl group	—	—	3080w	—
	3000w	3010w	3012w	3015w
ν(C−H), methyl groups	2930w	2930w	2930w	2930w
ν(C−H), H−C=O	—	—	—	2790m
ν(C=O), non-chelated	—	1690vs	1665vs	1680vs
ν(C=O−M), chelated	1570vs	1580vs	1590vs	1590vs
ν_{as}(C⋯C⋯C), chelate ring	1504vs	1540vs	—	1540vs
ν(C=C), phenyl group	—	—	1470 vs	—
ω(O⋯C⋯C⋯C⋯O)	1400vs	1390vs	1390vs	1390vs
ν_s(C⋯C⋯C), chelate ring	1310m	1311m	1330ms	1308m
δ(C−H), in-plane	1198w	1190w	1188w	1190shw
CH_3−rocking	1045m	1045m 1020	1020s	1040s 1015vs
ν_{as}, BeO_4 (n)	830s	840s	850vs	870vs
ν_{as}, BeO_4 (ax)	752m	769m	762w	759mw
δ(C−H) out-of-plane, C_6H_5	—	—	710s	—

[a] *bis*-(acetylacetonato)-beryllium, ref. [1].

Table 4

Proton magnetic resonance spectra of the beryllium triketonates at 60 or 80 MHz

R′ (formulae IV, V)	Chemical shifts, δ, (ppm)					Content in IV-type rings %	Solvent
	IV-type ring		V-type ring				
	CH_3	R′	CH_3 (chelated)	CH_3 (free)	R′		
—[a]	2.09	—	—	—	—	—	$CDCl_3$
CH_3	2.22	2.42	2.22	2.42	2.22	—	$CDCl_3$
	2.66	2.85	2.66	2.85	2.66	—	$Cl_2C=CCl_2$
C_6H_5	2.09	X[b]	—	—	—	100	$CDCl_3$
	2.47		—	—	—	100	$Cl_2C=CCl_2$
H	2.12	10.15	2.12	2.37	9.10	78	$CDCl_3$
		10.58			9.45	75	$Cl_2C=CCl_2$

[a] *bis*-(acetylacetonato)-beryllium, ref. [1]; [b] multiplet.

triketonates were recorded also in tetrachloroethylene solution at 30 and 130° respectively. Except for an overall low-field shift of 0.35 – 0.45 ppm due to this latter solvent, no change was detected related to the spectra in $CDCl_3$: there seems to be no rapid isomerization between rings of type IV and those of type V. Ligand redistribution was shown [17,18] to be a slow process in beryllium 1,3-diketonates. One-end dissociation was suggested for the crucial first step towards redistribution, as it was found in other chelate complexes. [19–22] The isomerization IV $\rightleftharpoons$ V should be most probably an intramolecular process performed also *via* one-end dissociation. The fact that no rapid isomerization could be detected supports the conclusion that one-end dissociation is a slow process in these compounds, and probably rate-determining in the ligand redistribution.

From the results presented it can be seen that the triketones studied chelate preferentially through acetyl groups. This seems rather surprising for bacH, where a V-type ring should be more stable than a IV-type ring, owing to the conjugation between the chelate ring and the phenyl group in V. The reasons for the observed order of stability (IV $\rightleftharpoons$ V) are most probably steric: repulsion between the substituents of the chelate ring must be more powerful in V than in IV. Models showed a minimum distance between two nuclei of an $R' = C_6H_5$ substituent in V (taken coplanar to the chelate ring) and the non-chelated $COCH_3$ group (considered as being situated in a plane perpendicular to the chelate ring) amounting to 1.6 Å. On the other hand, the minimum distance between the CH_3 substituents of the chelate ring and the non-chelated benzoyl group in IV (considered perpendicular to the plane of the chelate ring) was found to be of 2.3 Å.

(ii) INTERACTION BETWEEN THE CHELATE RING AND THE UNCHELATED ACYL SUBSTITUENT

A substituent Y (formula VI) may interact with the chelate ring or its other substituents X in several ways: conjugation of its mobile electrons with the delocalized system of the chelate ring; inductive effect on the delocalized system of the chelate ring; electronic shielding – de-

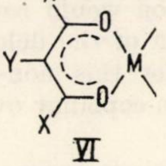

VI

---

[17] A. Barabás, *Inorg & Nucl. Chem. Letters*, **6**, 775 (1970).

[18] A. Barabás, *J. Coord. Chem.*, 1973, in press.

[19] C. A. Bunton, J. H. Carter, D. R. Llewellyn, C. O. Connor, A. L. Odell, S. Y. Yih and R. W. Oliff, *J. Chem. Soc.*, **1964**, 4615, 4627.

[20] K. Saito and K. Masuda, *Bull. Chem. Soc. Japan*, **41**, 384(1968); **43**, 119(1970).

[21] K. Saito and M. Takahashi, *Bull. Chem. Soc. Japan*, **42**, 3462(1969).

[22] R. C. Fay, A. Y. Girgis and U. Klabunde, *J. Amer. Chem. Soc.*, **92**, 7056, 7061(1970).

shielding of nuclei in the X substituents *via* its above mentioned electronic effects on the chelate ring or directly through space by its magnetic anisotropy; steric effects. Some of these will be discussed below.

Substituents $Y = CH_3$ (ref. [2]) or Cl (ref. [3]) both were found to extend delocalization in the chelate ring ($d\lambda = 17$ nm for $Y = CH_3$; $d\lambda = 22$ nm for $Y = Cl$) relatively to $Y = H$. These two substituents also deshield the $X = CH_3$ protons relatively to $Y = H$ ($d\delta_X = 0.06$ ppm for $Y = CH_3$ and $d\delta_X = 0.25$ ppm for $Y = Cl$). There is some difficulty to attribute these effects to a given cause. Both groups are expected to exhibit only small steric effects, and it is difficult to explain how steric effects would achieve the observed results, especially the deshielding of the X substituent. Electron-attracting inductive effects (and perhaps through-space anisotropic effects for $Y = Cl$) would account both for observed $d\lambda$ and $d\delta_X$ values; but CH_3 is known as an electron-repelling group, compared to H. We should retain the idea that electron-attracting inductive effects would cause more delocalization in the chelate ring (positive $d\lambda$ values) and deshielding of the $X = CH_3$ protons (positive $d\delta_X$ values).

We shall consider now the above effects due to an $Y = C_6H_5$ substituent, which causes a positive $d\lambda = 13$ nm, but a negative $d\delta_X = -0.17$ ppm value [2] ($X = CH_3$). Its electron-attracting inductive effect would account for the observed $d\lambda$. Its mesomeric effect (conjugation) cannot be effective because of its non-coplanarity with the chelate ring. The observed negative $d\delta_X$ value must be attributed to a direct interaction between the Y and X substituents. The magnetic anisotropy of the $Y =$ phenyl group (due to its ring current) will explain the observed $d\delta_X$ value if assumed that the plane of the phenyl group is nearly perpendicular to that of the chelate ring (the X substituents being contained in the latter). Using the tables of Haigh and Mallion [23] and standard molecular geometry, a value of $d\delta_X = -0.14$ ppm was estimated for the $X = CH_3$ protons in their nearest possible position to the center of the $Y = C_6H_5$ ring, assuming the two ring systems to be perpendicular to each other.

The way, acyl Y substituents interact with the chelate ring could not be fully cleared up from our results, but the small $d\lambda$ values related to beryllium acetylacetonate, observed for all triketonates suggest that there is no conjugation between the non-chelated carbonyl group and the chelate ring. Such conjugation would cause a bathochromic shift of the band *Z*, due to the extension of the delocalized electronic system of the chelate ring. The reasons for this non-conjugation are most probably steric: the two units are non-coplanar owing to steric hindrance as verified on models.

The inductive effect of these groups would still be expected to cause some extra delocalization in the chelate ring: however, this is not observed experimentally.

Like a $Y = C_6H_5$ group, acyl substituents should influence the chemical shift of the $X = CH_3$ protons by two antagonistic effects; a deshielding *via* the chelate ring due to their inductive effect and a through-space shielding due to the magnetic anisotropy of the carbonyl double bond. The neat effect is deshielding (positive $d\delta_X$) for $Y = HCO$ and especially for $Y = CH_3CO$ (see table 4); it becomes nil for $Y = C_6H_5CO$ in which there are two anisotropic components causing shielding at $X = CH_3$.

---

[23] C. W. Haigh and R. B. Mallion, *Org. Magn. Resonance*, **4**, 203 (1972).

Acknowledgements. Thanks are expressed to Dr. F. Chiraleu and Dr. M. Elian from the Institute of Organic Chemistry, Bucharest, for recording part of the nmr spectra and helpful discussions. The authors are most indebted to Prof. A. T. Balaban who initiated and stimulated their studies on metal chelates.

Revue Roumaine de Chimie, **18**, 7, 1243 – 1248 (1973)

DONOR-ACCEPTOR COMPLEXES. III[1,2]

CHARGE TRANSFER COMPLEXES OF 1,3,6,8-TETRANITROCARBAZOLE

M. RĂILEANU *, ILEANA RADULIAN *, MARINA OLTENEANU **
and MARIA CONSTANTIN ***

* University of Craiova, Chair of Organic Chemistry, Str. A. I. Cuza 31, Craiova, Romania

** Institute of Physical Chemistry, Str. Galaţi 31, Bucharest, Romania

*** Institute of Atomic Physics, P. O. Box 35 Bucharest, Romania

Received June 2, 1972

A series of charge transfer complexes of 1,3,6,8-tetranitrocarbazole (for short TNC) were synthetized using for donors carbazole, anthracene, phenanthrene, benzidine, diphenylamine, phenothiazine, α- and β-naphtol and piperazine. In solid state, the compounds obtained are stable, having high melting or decomposition points.

A series of charges transfer complexes were obtained as shown in former papers, [1,2] using 1,3,7,9-tetranitrophenothiazine-5-oxide and 1,3,7,9-tetranitrophenothiazine-5,5-dioxide as acceptor.

To investigate further the acceptor characteristics of other polynitro heterocyclic compounds, some charge transfer complexes were synthetized using 1,3,6,8-tetranitrocarbazole (TNC) as acceptor and various donors, such as carbazole, anthracene, phenanthrene, benzidine, diphenylamine, phenothiazine, α- and β-naphthol and piperazine.

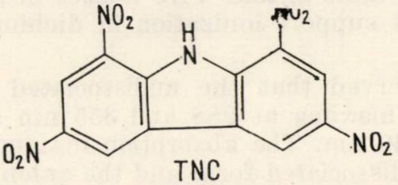

TNC

All the obtained complexes are well crystallized and stable, having high enough melting and decomposition points. The combining donor-

[1] Part I: M. Răileanu, M. Olteneanu, I. Radulian, C. Volanschi, A. Turcu and H. Căldăraru, *Rev. Roumaine Chim.*, **16**, 1269 (1971).

[2] Part II: M. Răileanu, C. Volanschi, I. Radulian, M. Olteneanu and H. Căldăraru, *Rev. Roumaine Chim.*, **16**, 1613 (1971).

acceptor ratio at the complexing of TNC with these donors is 1 : 1, excepting benzidine where this ratio is 1 : 2.

But unlike 1,3,7,9-tetranitrophenothiazine-5-oxide and 1,3,7,9-tetranitrophenothiazine-5,5-dioxide, forming stable complexes with ammonia,[3] TNC forms an unstable complex with ammonia, easily decomposing when dried at a 100° temperature.

The complexes obtained by the reaction between TNC and the above mentioned donors are insoluble in nonpolar organic solvents and split entirely into their components, a fact pointed out by the absence of the transfer band of the absorption spectrum.

Actually, the presence in the TNC molecule of four nitro-groups in *ortho* and *para* positions towards the heterocyclic nitrogen atom, lends to the substance an acid character, besides the quality of acceptor.

Because of this acid character, TNC ionizes in polar solvents, while the resulting anion, having a negative charge, loses the quality of acceptor, and thus the decomposition of the TNC complexes into polar solvents appears as a natural phenomenon.

The acid character of the acceptor is pointed out if its absorption in different solvents is studied, as shown in table 1.

Table 1

Absorption of the TNC acceptor in solution

Solvent	Absorption maxima in nm		
	In UV		In visible
Methanol	**290**	**330**	**430 (inflexion)**
Methanol + KOH	**—**	**330**	**428**
Methanol+HCl	**290**	**330**	**—**
Acetonitrile	**288**	**335**	**440**
Acetonitrile+KOH	**—**	**335**	**440**
Acetonitrile+HCl	**288**	**335**	**—**
Dichloromethane	**285**	**328**	**—**

It results from table 1, that TNC ionizes in methanol and in acetonitrile, but does not support ionization in dichloromethane, which is a nonpolar solvent.

It is also observed that the undissociated form of the acceptor presents absorption maxima at 288 and 355 nm and the corresponding anion at 335 and 440 nm. The absorption maximum at 335 nm equaly characterizes the undissociated form and the anion. This results from the absorption spectrum of the substance in acetonitrile, to which hydrochloric acid or potassium hydroxide is added.

Table 1 shows also small differences for the values of the absorption maxima corresponding to the undissociated form and the anion, owing to the interaction of these two species with the solvent.

---

[3] A. TURCU and M. RĂILEANU, *Rev. Roumaine Chim.*, **14**, 1579 (1969).

As the anion presents only a single visible absorption maximum it results that it cannot exist in tautomeric forms I and II with a localized negative charge. This anion has evidently a structure intermediary between the two limit electronic structures.

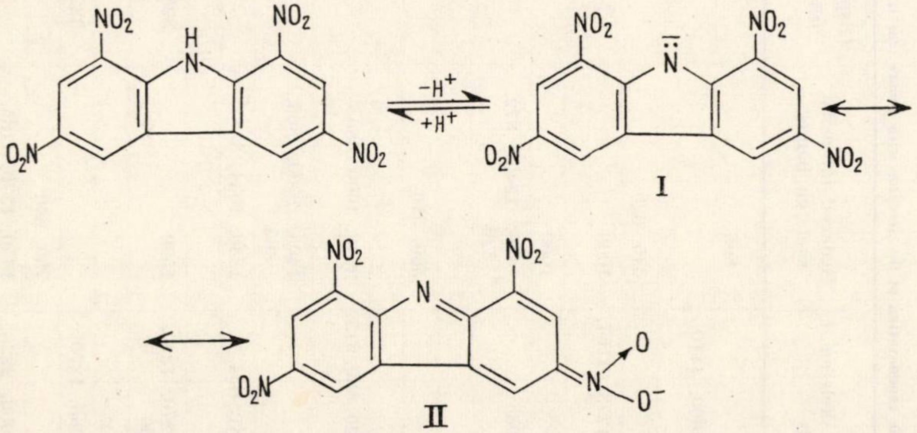

A spectral IR study was carried out to establish the localization of coordination centers which appear in the acceptor and donor by complexation. The IR spectra of the acceptor, donors and of the corresponding complexes were therefore registered and compared, and a series of data, shown in table 2, were obtained.

Table 2 shows that for the complexes formed by TNC with benzidine, diphenylamine, phenothiazine, piperazine or α- and β-naphtol, the donor-acceptor bond appears practically localized.

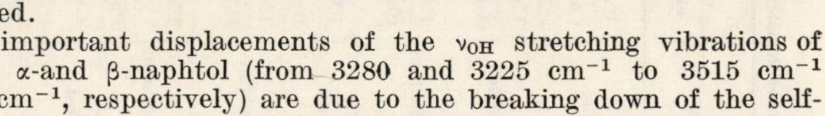

For these complexes a marked displacement of the ν_{NH} stretching vibration of the acceptor as well as important displacements of the ν_{NH} and ν_{OH} stretching vibrations of the donors (excepting diphenylamine) are recorded.

The important displacements of the ν_{OH} stretching vibrations of complexed α-and β-naphtol (from 3280 and 3225 cm^{-1} to 3515 cm^{-1} and 3500 cm^{-1}, respectively) are due to the breaking down of the self-association of the α-, respectively β-naphtol molecules during complexation (intermolecular hydrogen bonds OH-electrons of the ring) and to the appearance of the bands corresponding to free OH vibrations. The important changes in the region of the skeleton vibrations may be assigned to the rearrangement of the electronic cloud after the breaking down of the hydrogen bonds and his orientation toward the acceptor center of the TNC.

Table 2

Displaced IR absorption bands, disappeared or with smaller intensity following the complexation of the acceptor with donors (cm^{-1})

N°	Complex	Complexed donor or acceptor	Displacement of ν_{NH} stretching band	Disappeared skeleton bands	Reduced intensity skeleton bands	Displacement of ν_{OH} stretehing band
1	TNC-carbazole	TNC	3455 → 3455	1600, 1565	865	
		Carbazole	3420 → 3420	1600, 1585, 1600, 1110, 997, 885		
2	TNC-anthracene	TNC	3455 → 3455	1265, 1215	645, 620	
		Anthracene		3077, 1399, 1273, 1167, 737	1000	
3	TNC-phenanthrene	TNC	3455 → 3455	1565, 1135	1000	
		Phenanthrene		3058, 1200, 1038	1456, 1245, 872, 820	
4	TNC-benzidine	TNC	3455 → 3440			
		Benzidine	3335 → 3380		550, 510	
5	TNC-diphenylamine	TNC	3455 → 3445	1565		
		Diphenylamine	3385 → 3398	1465, 1248, 1020, 880, 615, 495	3048, 1600, 680	
6	TNC-phenothiazine	TNC	3455 → shoulder		1405, 1000, 865, 805	
		Phenothiazine	3345 → 3410	1240, 1115, 881, 654	1380, 1034, 858	
7	TNC-α-naphtol	TNC	3455 → 3425	1565, 865		
		α-Naphtol		1455, 1305, 1270, 1240, 959, 861, 766	1590	3280 → 3515
8	TNC-β-naphtol	TNC	3455 → 3430	1260		
		β-Naphtol		1575, 1460, 1265, 1270		3225 → 3500
9	TNC-piperazine	TNC	3455 → 3440	1405, 1215	750, 640	
		Piperazine	3210 → 3305	2990, 2959, 2900, 2220, 1200, 885, 820, 600, 505	1450, 1370, 1185	

In the case of piperazine, which is a strong base, the participation of the lone pair electrons of the nitrogen into the donor-acceptor bond will considerably influence the skeleton vibrations as the nitrogen is directly bound to the ring. Conversely in the complexes formed by TNC with carbazole, anthracene and phenanthrene, the donor-acceptor bond appears not to be strictly localized. In the TNC-carbazole complex, the ν_{NH} stretching bands of TNC and carbazole have no shifts, while the skeleton vibrations of the acceptor and of the donor undergo substantial changes. The important changes observed in the spectra of complexed anthracene, and phenanthrene seem to point out a displacement of the electronic cloud towards the NH group of the acceptor, a fact influencing the skeleton vibrations.

EXPERIMENTAL

1) *TNC complex with carbazole.* A solution of 0.5 g TNC in 40 ml glacial acetic acid is mixed with 1 g of carbazole solved in 25 ml of the same solvent. The mixture of the two solutions is brought to the boiling point. It immediately deposits a voluminous precipitate, formed by crystals which have the appearance of small yellow-orange sticks. The precipitate is filtered at 70°, then washed with acetic acid and dried at 120°. There result 0.45 g of complex, which is stable up to a 300° temperature. *Calcd.* for $C_{12}H_5N_5O_8$: C 56.06 ; H 2.72 ; N 16.33 ; *Found* : C 56.10 ; H 2.56 ; N 16.02.

2) *TNC complex with anthracene.* 0.5 g of TNC are suspended in 20 ml of xylene and mixed with 1 g of anthracene dissolved in xylene (solution saturated at room temperature). The mixture is brought to a boiling point and then left to cool. In a short time a precipitate of yellow-orange crystals will appear. After filtration the precipitate is washed with xylene and methylic alcohol to remove the donor excess, and then dried at 120°. There result 0.45 g of complex, which darkens in colour over 250°, shrinks gradually and then melts between 275 and 280°. *Calcd.* for $C_{26}H_{15}N_5O_8$: N 13.32 ; *Found* : N 13.00.

3) *TNC complex with phenanthrene.* 0.5 g of TNC are dissolved under heating in 24 ml glacial acetic acid, and the obtained solution is mixed with 1 g of phenanthrene, also dissolved in acetic acid. When the two solutions are mixed, a yellow-orange precipitate immediately appears. The mixture is heated up to the boiling point, then cooled at 60° and filtered. The precipitate is washed on the filter with warm acetic acid and dried at 120°. There result 0.4 g of a complex with a clear melting point at 270°. *Calcd.* for $C_{36}H_{22}N_{12}O_{16}$: C 49.24 ; H 2.53 ; N 19.13 ; *Found* : C 49.50 ; H 2.56 ; N 18.91.

4) *TNC complex with benzidine.* 0.5 g of TNC suspended at room temperature in 5 ml of methyl alcohol is added to a solution of 3 g benzidine in the same solvent saturated at room temperature. The mixture is boiled for ten minutes and left at cool overnight. It deposits a dark brown crystalline precipitate, which is filtered, washed with methyl alcohol and dried at 110°. There result 0.4 g of complex which gradually shrinks in the 150–190° interval. According to analytical data the donor-acceptor ratio is 1 : 2. *Calcd.* for $C_{36}H_{22}N_{12}O_{16}$: C 49.24 ; H 2.53 ; N 19.13 ; *Found* : C 49.50 ; H 2.56 ; N 18.91.

5) *TNC complex with diphenylamine.* 0.5 g of TNC suspended in 5 ml of xylene are added to a solution of 1.5 g diphenylamine in the same solvent saturated at room temperature. The mixture is boiled for 10 minutes, then left at cool overnight. The obtained precipitate,

Revue Roumaine de Chimie, **18**, 7, 1243–1248 (1973)

formed of small brown-grey pearls, is filtered, well washed with xylene and then dried at 120°. There result 0.5 g of a complex with a shrinking point in the interval 208–230°. *Calcd.* for $C_{24}H_{16}N_6O_8$: C 55.81 ; H 3.12 ; N 16.27 ; *Found* : C 55.60 ; H 3.22 ; N 16.56.

6) *TNC complex with phenothiazine.* 0.5 g of TNC are added to a solution, saturated at room temperature, of 1.5 g phenothiazine in toluene. The mixture is boiled for 10 minutes and is filtered when hot to remove the unreacted acceptor. After 4 hours staying, it deposits a black precipitate formed by needleshaped crystals, which are filtered, washed with xylene and dried at 120°. There result 0.45 g of complex with a clear melting point at 225°. *Calcd.* for $C_{24}H_{14}N_6O_8S$: N 15.38 ; *Found* : N 15.09.

7) *TNC complex with α-naphtol.* 0.5 g of TNC are added to a hot solution of 2 g α-naphtol in 20 ml xylene, and the mixture is boiled for 10 minutes. The solution is filtered when still hot to remove the unreacted TNC. After cooling for one hour, the deposited precipitate is filtered, thoroughly washed with xylene and dried at 120°. There result 0.3 g of complex, which melts and decomposes at 225° (stretching in the tube). *Calcd.* for $C_{22}H_{13}N_5O_9$: C 53.74 ; H 2.66 ; N 14.25 ; *Found* : C 53.61 ; H 2.82 ; N 14.50.

8) *TNC complex with β-naphtol.* 2 g of β-naphtol and 0.5 g of TNC are made to react in the same conditions as in experiment 7. Thus, there result 0.4 g of a brownish complex formed of wing-shaped crystals. The substance shrinks at 205° and decomposes at 215° (stretching in the tube). *Calcd.* for $C_{22}H_{13}N_5O_9$: C 53.77 ; H 2.66 ; N 14.25 ; *Found* : C 53.44 ; H 2.67 ; N 14.11.

9) *TNC complex with piperazine.* 0.5 g of well-ground TNC are added to a solution of 0.6 g piperazine in 15 ml methyl alcohol, and the mixture is boiled for 10 minutes. After an hour cooling, the precipitate formed of reddish-brown coloured sticks is filtered, washed in alcohol and dried at 120°. The complex has a clear melting point at 203–204°. Yield 0.45 g. *Calcd.* for $C_{16}H_{15}N_7O_8$: C 44.34 ; H 3.49 ; N 22.63 ; *Found* : C 44.23 ; H 3.41 ; N 22.29.

The TNC used for the synthesis of the complexes was obtained by direct nitration of the carbazole according to Graebe and Adlerskron's method. [4]

The absorption spectra were recorded by means of a Beckman DK 2 spectrophotometer.

The IR spectra were recorded by means of a UR 10 Zeiss Jena spectrophotometer with KBr pellets.

---

[4] C. Graebe and B. Adlerskron, *Liebigs Ann. Chem.*, **202**, 23 (1880).

Revue Roumaine de Chimie, **18**, 7, 1249–1257 (1973)

THEORETICAL STUDIES OF SOME FUROCOUMARIN ISOMERS

E. POP *, L. KLASINC and N. TRINAJSTIĆ**

* Chemical-Pharmaceutical Research Institute, str. Fabricii 126, Cluj, Romania
** "Rugjer Bošković" Institute, P.O.B. 1016, 41001 Zagreb, Croatia, Yugoslavia

Received November 22, 1972

Molecular orbital calculations using the Pariser-Parr and Hückel methods are reported for some furocoumarin isomers.

The annelation of coumarin (benzopyran) and furan leads to various isomeric furocoumarins, [1] which fall distinctly in two topologically different groups depending on where the annelation on the 5-membered ring occurs. If the annelation occurs at the short (2,3) bond the resulting isomeric furocoumarins are stable compounds. These molecules : 7H-furo [3,2-g][1]-benzopyran-7-one (psoralen, I), 6H-furo [2,3-g][1]-benzopyran-6-one (pseudopsoralen, II), 2H-furo [2,3-h][1]-benzopyran-2-one (isopsoralen, III), 8H-furo [3,2-h][1]-benzopyran-8-one (pseudoisopsoralen, IV), 7H-furo [2,3-f][1]-benzopyran-7-one (V), and 7H-furo [3,2-f][1]-benzopyran-7-one (isopseudopsoralen, VI), respectively, are presented in fig. 1. Some of these compounds occur naturally in many plants (e.g. figs, carrots, celery, parsley, many fruits of the citrus family), [1,2] others can be obtained by synthetic methods. [3] On the other hand, if the annelation occurs at the long (3,4) bond of furan ring the resulting isomeric furocoumarins (see fig. 2) are predicted to be unstable. As a matter of fact, these furocoumarins are not reported yet.

Since, the isomeric furocoumarins (see figs. 1 and 2) really differ only in the position of the furanic oxygen, they belong to the class of compounds named positional isomers. [4] The main characteristic of the positional isomers is that they can be always divided in two groups differing considerably in their properties and stabilities.

---

[1] S. M. Sethna and N. M. Shah, *Chem. Rev.*, **36**, 1 (1945).

[2] W. L. Stanley and S. H. Vannier, *J. Amer. Chem. Soc.*, **79**, 3488 (1957).

[3] E. C. Horning and D. B. Reisner, *J. Amer. Chem. Soc.*, **72**, 1514 (1950); D. N. Shah and N. M. Shah, *J. Indian Chem. Soc.*, **17**, 41 (1940); K. D. Kaufman, J. F. W. Keana, R. C. Kelly, D. W. Mc Bride and G. Slomp, *J. Org. Chem.*, **27**, 2567 (1962).

[4] N. Trinajstić, *Record. Chem. Progress*, **32**, 85 (1971).

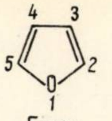

Furan

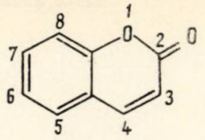

Coumarin

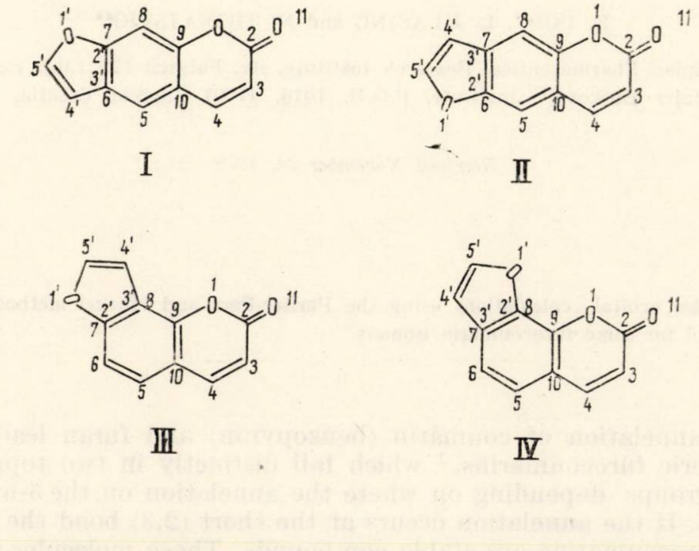
I
II
III
IV
V
VI

Fig. 1. — Stable furocoumarin isomers.

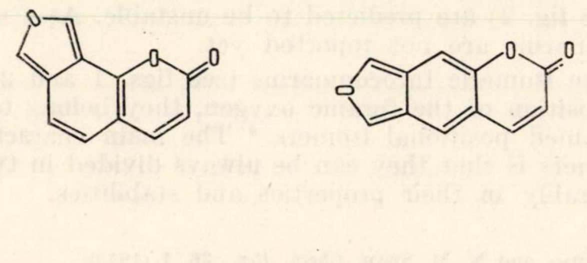

Fig. 2. — Unstable furocoumarin isomers.

Previously we have studied several groups of positional isomers; benzothiophenes,[5,6] benzofurans,[6,7] benzopyrroles,[6,7] thienylfurans,[8] benzodifurans,[8a] benzodithiophenes,[8a] thienobenzofurans.[8a] The same conclusion was reached in all cases: ***the properties and stabilities of positional isomers greatly depend on the position of the heteroatom.***

In the present communication we report the Pariser-Parr (PP) calculations[9] for the stable furocoumarin isomers (see fig. 1) in order to predict the lower singlet-singlet transitions. The standard version of the PP method is used.[10] The electronic transition energies and oscillator strengths have been calculated by a limited configuration interaction (LCI) procedure. The parameter set used is given in table 1. All electronic repulsion integrals have been treated semiempirically. The two-centre repulsion integrals have been evaluated in the Mataga-Nishimoto manner.[11]

Table 1

Parameters used in P–P calculations

Atom (r)	W_r(eV)	(rr/rr) (eV)	Bond $(r-s)$	β^{c}_{rs} (eV)
C	11.16	11.13	C–C	–2.39
>O	32.90	21.53	C–O–	–2.12
=O	17.70	15.23	C=O	–3.00

The calculated transition energies (ΔE) and oscillator strengths (f) are reported in table 2. Only lower transitions are recorded. In table 2 we also give the weights (in %) of the most important configurations in LCI procedure. The available experimental data are very limited. UV spectra (see references[12] in table 3) are only available for psoralen (I) and isopsoralen (III) and their derivatives. The experimental data are given in table 3. The agreement between the experimental data and calculated values is reasonable. The slope of the least-squares line (1.096) is nearly equal to the theoretical value of unity, the correlation coefficient being 0.998 and the standard deviation 0.07 eV.

It can be seen (table 2) that the long wavelength absorption band in psoralen can mainly be described by the excitation from the highest

---

[5] M. J. S. Dewar and N. Trinajstić, *J. Amer. Chem. Soc.*, **92**, 1453 (1970).

[6] L. Klasinc, E. Pop, N. Trinajstić and J. V. Knop, *Tetrahedron*, **28** 3465 (1972).

[7] M. J. S. Dewar, A. J. Harget, N. Trinajstić and S. D. Worley, *Tetrahedron*, **26**, 4505 (1970).

[8] L. Klasinc and N. Trinajstić, *Tetrahedron*, **27**, 4045 (1971).

[8a] L. Klasinc and J. V. Knop, *Z. Naturforsch.*, **26b**, 1235 (1971).

[9] R. Pariser and R. G. Parr, *J. Chem. Phys.*, **21**, 466, 767 (1953).

[10] J. N. Murrell, "The Theory of the Electronic Spectra of Organic Molecules", Methuen, London, 1963, see Appendix.

[11] N. Mataga and K. Nishimoto, *Z. phys. Chem. (Frankfurt)*, **13**, 140 (1957).

[12] see references in table 3.

Table 2

Calculated singlet-singlet transition energies (ΔE), oscillator strengths (f) and weight (in %) of the most important configurations; only transitions with ΔE below 6 eV are recorded

Molecule	ΔE (eV)	f	Weight of configurations	
I	3.881	0.144	Φ_8^9, Φ_7^{10}	71, 11
	4.334	0.690	Φ_7^9	85
	4.939	0.795	Φ_8^9, Φ_8^{10}, Φ_7^{10}	13, 39, 35
	5.184	0.461	Φ_8^{10}, Φ_7^{10}	53, 31
	5.710	0.100	Φ_8^{11}, Φ_6^9	30, 51
	5.984	0.058	Φ_8^{11}, Φ_7^{11}, Φ_6^9, Φ_5^9	25, 27, 17, 25
II	3.930	0.623	Φ_8^9, Φ_7^9	39, 50
	4.076	0.496	Φ_8^9, Φ_7^9	57, 30
	5.080	0.208	Φ_8^{10}, Φ_8^{11}, Φ_7^9, Φ_6^9	31, 23, 17, 14
	5.491	0.002	Φ_8^{10}, Φ_8^{11}, Φ_7^{10}, Φ_6^9	22, 28, 30, 14
	5.559	0.023	Φ_8^{10}, Φ_6^9	25, 44
	5.951	0.894	Φ_7^{10}, Φ_7^{11}	38, 45
III	3.917	0.279	Φ_8^9	82
	4.415	0.357	Φ_8^{10}, Φ_7^9	20, 62
	4.949	0.648	Φ_7^{10}	67
	5.117	0.574	Φ_8^{10}, Φ_7^9	74, 30
	5.725	0.264	Φ_8^{11}, Φ_6^9	72, 15
IV	3.865	0.502	Φ_8^9	86
	4.312	0.258	Φ_8^9, Φ_8^{10}, Φ_7^9	10, 20, 59
	5.278	0.549	Φ_8^{10}, Φ_8^{11}, Φ_7^{10}, Φ_6^9	18, 17, 36, 24
	5.325	0.533	Φ_8^{10}, Φ_7^9	53, 27
	5.445	0.112	Φ_8^{11}, Φ_6^9	19, 58
	5.910	0.674	Φ_8^{11}, Φ_7^{10}	47, 40
V	3.881	0.414	Φ_8^9	84
	4.278	0.323	Φ_8^9, Φ_8^{10}, Φ_7^9	12, 14, 60
	5.101	1.010	Φ_8^{10}, Φ_7^9, Φ_7^{10}	59, 14, 12
	5.351	0.114	Φ_8^{10}, Φ_7^{10}, Φ_6^9	14, 20, 53
	5.404	0.009	Φ_8^{11}, Φ_7^9, Φ_7^{10}, Φ_6^9	30, 14, 20, 28
	5.865	0.199	Φ_8^{11}, Φ_7^{10}	40, 38
VI	3.869	0.859	Φ_8^9	92
	4.129	0.115	Φ_8^{10}, Φ_7^9	13, 70
	5.164	0.253	Φ_8^{10}, Φ_7^9	57, 22
	5.374	0.000	Φ_8^{10}, Φ_8^{11}, Φ_6^9	16, 41, 36
	5.775	0.169	Φ_8^{11}, Φ_7^{10}, Φ_6^9	23, 28, 35
	5.909	0.509	Φ_8^{11}, Φ_7^{10}	14, 53

Table 3

Experimental singlet-singlet transition energies of isomeric furocoumarins

Molecule	Solvent	Transition energy (eV) and log ε (in parentheses)					Reference[12]
Psoralen (I)	EtOH	3.76 (3.8)			5.10 (4.4)		a
	Dioxan	3.70 (3.8)	4,28 (4.0)	4.96 (4.3)	5.06 (4.3)		b
	EtOH	3.65 (3.9)	4.20 (4.0)		5.06 (4.5)		c
		3.65 (3.8)	4.28 (4.0)	4.96 (4.4)			d
	average ΔE	3.69	4.25	4.96	5.07		
Isopsoralen (III)	Dioxan	3.76 (3.6)	4.13 (3.9)	4.90 (4.3)			b
	MeOH		4.18 (4.0)	4.96 (4.4)			e
			4.13 (4.0)		5.17 (4.4)	5.64 (4.2)	d
	EtOH		4.13 (4.03)	5.00 (4.45)			f
	EtOH		4.13 (3.67)	4.98 (4.13)		5.44 (3.67)	g
	average ΔE	3.76	4.14	4.96	5.17	5.54	

a E. C. Horning, D. B. Reisner, *J. Amer. Chem. Soc.*, **72**, 1514 (1950).
b F. Wessely, J. Kotlan, *Monatsh.*, **86**, 430 (1955).
c W. L. Stanley, S. H. Vannier, *J. Amer. Chem. Soc.*, **79**, 3488 (1957).
d A. Rodighiero, V. Capellini, *Gazz. Chim. Ital.*, **91**, 103 (1961).
e H. Böhme, T. Severin, *Arch. Pharm.*, **290**, 486 (1957).
f T. Nakabayashi, *J. Chem. Soc. Japan.*, **83**, 182 (1962).
g M. Mitsukashi, T. Itoh, *Chem. Pharm. Bull. (Japan)*, **10**, 514 (1962).

occupied MO to the lowest unoccupied MO (8 —9 transition). A small contribution from the 7 —10 excitation belongs also to this band. The second band appears to be predominantly due to the 7 —9 excitation, whereas the third is a combination of 8 —9, 8 —10, and 7 —10 excitations. Finally, the shortest wavelength band is a combination of 8 —10 and 7 —10 excitations. The long wavelength absorption band in isopsoralen can be associated mostly with 8 —9 excitation, i.e. with the jump of an electron from the highest occupied MO to the lowest unoccupied MO level. The second band appears to be predominantly due to the 7 —9 excitation, whereas the third band has the major contribution from the 7 —10 excitation. The next two bands have major contributions from the 8 —10 and 8 —11 excitations, respectively. The UV spectra of both compounds (I and III) show a great similarity indeed.

It is interesting to note the clear resemblance between tricyclic aromatic molecules and psoralenes, i.e. : anthracene and psoralen, and phenanthrene and isopsoralen, respectively. Anthracene has two distinct bands (*p*-, β-) at 3.31 eV (log ε : 3.87) and at 4.92 eV (log ε : 5.29)[13]; *p*-band having a fine vibronic structure. In psoralen both bands are shifted bathochromically (at 3.69 eV (log ε : 0≃3.8) and at 5.06 (log ε : ∼ 4.5)). Phenanthrene has four distinct bands (α-, *p*-, β-, and β′-) at 3.59 eV (log ε : 3.46), 4.23 eV (log ε : 4.30), 4.94 eV (log ε : 4.78), and 5.91 eV (log ε : 4.44),[14] respectively ; α- and *p*- bands having a fine vibronic

---

[13] E. Clar, "Polycyclic Hydrocarbons", Volume 1, Academic Press, New York, 1964, p. 291.

[14] Reference 13, p. 228.

Table 4

π-Electron charge densities

Molecule	Method	1	2	3	4	5	6	7	8	9	10	11	1′	4′	5′
I	a	1.771	0.703	1.066	0.835	0.985	1.046	0.960	1.080	0.927	1.037	1.723	1.771	1.145	0.951
	b	1.805	0.770	1.022	0.938	0.978	1.035	1.012	1.064	0.993	1.044	1.459	1.784	1.065	1.033
II	a	1.773	0.705	1.066	0.840	1.100	0.987	1.015	1.068	0.939	1.031	1.724	1.776	1.123	0.942
	b	1.805	0.770	1.018	0.942	1.012	1.037	1.011	1.032	1.011	1.037	1.450	1.786	1.068	1.022
III	a	1.754	0.715	1.071	0.843	1.000	1.049	0.958	1.077	0.893	1.046	1.732	1.763	1.108	0.986
	b	1.794	0.775	1.022	0.940	0.992	1.035	1.019	1.055	0.979	1.048	1.464	1.777	1.067	1.033
IV	a	1.763	0.715	1.070	0.846	1.010	1.032	1.021	1.060	0.915	1.040	1.732	1.760	1.137	0.931
	b	1.803	0.775	1.022	0.938	1.001	1.005	1.015	1.060	1.007	1.040	1.465	1.781	1.063	1.025
V	a	1.764	0.714	1.073	0.843	0.957	1.068	0.962	1.068	0.906	1.051	1.732	1.760	1.113	0.989
	b	1.794	0.775	1.020	0.951	1.022	1.038	0.970	1.042	0.985	1.060	1.463	1.776	1.062	1.038
VI	a	1.765	0.717	1.072	0.849	1.026	1.016	0.979	1.060	0.914	1.039	1.733	1.761	1.136	0.933
	b	1.799	0.775	1.021	0.941	1.020	1.042	1.003	1.033	0.993	1.037	1.466	1.778	1.067	1.025

a. HMO
b. P−P

Table 5

Bond orders [a]

Molecule	Method	1−2	2−3	3−4	4−10	5−6	7−8	8−9	4′−5′	6−7	4′−6	4′−7	4′−8
I	b	0.424	0.535	0.758	0.494	0.617	0.632	0.654	0.821		0.474		
	c	0.364	0.382	0.854	0.408	0.605	0.615	0.669	0.850				
II	b	0.423	0.537	0.755	0.500	0.653	0.593	0.608	0.817			0.491	
	c	0.366	0.381	0.853	0.412	0.632	0.591	0.677	0.844				
III	b	0.425	0.547	0.748	0.510	0.733		0.549	0.822	0.572			0.488
	c	0.365	0.390	0.846	0.422	0.734		0.543	0.842	0.573			
IV	b	0.425	0.547	0.745	0.513	0.747		0.585	0.798	0.540		0.503	
	c	0.363	0.391	0.844	0.424	0.744		0.570	0.839	0.544			
V	b	0.424	0.548	0.744	0.518		0.714	0.600	0.825	0.558			
	c	0.365	0.389	0.843	0.430		0.729	0.590	0.843	0.596			
VI	b	0.424	0.550	0.739	0.527		0.699	0.604	0.793	0.596			
	c	0.366	0.391	0.841	0.434		0.717	0.591	0.834	0.581			

a, only important bond orders are reported; b, HMO; c, P−P.

structure. The UV spectrum of isopsoralen shows similar features : 3.76 eV (log ε : $\sim$3.6), 4.14 eV (log ε : $\sim$4.0), 5.17 eV (log ε : $\sim$4.4), and 5.54 eV (log ε : $\sim$4.0), respectively.

We report the π-electron densities and the relevant bond orders in tables 4 and 5, respectively. In both tables we report the results obtained from the PP calculations and also the results obtained from HMO calculations. In the Hückel calculations the parameter set recommended by Pullmans[15] is used: $\alpha_{-O-} = \alpha_C + 2\beta_{CC}$; $\alpha_{=O} = \alpha_C + 1.2\ \beta_{CC}$; $\beta_{C-O-} = 0.9\ \beta_{CC}$; and $\beta_{C=O} = 2.0\ \beta_{CC}$, respectively.

The π-electron charge densities can serve within the isolated molecule approximation[16] for predicting the most reactive positions on each molecule towards electrophilic and nucleophilic attack. This is, of course, a very approximate approach but useful for qualitative predictions.[17,18] Using this approach we predict the position 4′ in all isomers to be the most reactive site for electrophilic attack. Similarly, the position 4 is predicted to be the most reactive site for nucleophilic attack.

The addition reactions will most probably happen at bonds with the highest values of bond orders. Thus, the 3—4 (pyronic) and 4′—5′ (furanic) bonds are predicted to be the most reactive in all cases.

The most reactive positions towards the radical attack were obtained by considering the free valence indices (see table 6). On these grounds we predict the positions 5 and 5′ in I and positions 5′ in isomers II—VI to be the most reactive sites for radical attack.

Table 6

Free valence indices

Molecule	3	4	5	6	7	8	9	10	4′	5′	11
I	0.439	0.488	0.510	0.098	0.198	0.446	0.209	0.100	0.437	0.505	1.150
II	0.440	0.478	0.486	0.176	0.112	0.474	0.202	0.167	0.423	0.522	1.151
III	0.437	0.474	0.456	0.427	0.187	0.117	0.243	0.103	0.422	0.520	1.161
IV	0.440	0.474	0.445	0.446	0.104	0.210	0.227	0.108	0.431	0.501	1.161
V	0.440	0.471	0.220	0.103	0.460	0.418	0.211	0.123	0.423	0.518	1.161
VI	0.443	0.447	0.133	0.143	0.431	0.429	0.205	0.137	0.425	0.507	1.163

Yeargers and Augenstein[19] correlated the free valence index with the photosensitizing ability of a number of psoralen derivatives. On the other hand, recent studies of Song and co-workers[18] have shown that the photosensitizing properties of furocoumarins should be really correlated with reactivity indices of the excited states. It is interesting to note that the bond order of the furanic 4′—5′ bond remains of the same magnitude in the singlet (0.76)[20] and in the triplet (0.76)[20] state and is not very different from the corresponding value (0.85) in the ground state. On the other hand, the bond order of the pyronic 3 – 4 bond is strongly reduced in the triplet state (0.46)[20] in comparison with the value (0.72)[20] in the singlet state. This reduction is nearly 50% when compared with the value in the ground state (0.85).

---

[15] B. Pullman and A. Pullman, "Quantum Biochemistry", Interscience, New York, 1963.

[16] J. N. Murell, S. F. A. Kettle and J. M. Tedder, "Valence Theory", Wiley, London, 1965, p. 317.

[17] R. Daudel, "Advances in Quantum Chemistry", (Edited by P. O. Löwdin), Volume 3, Academic Press, New York, 1967, p. 161.

[18] R. Zahradnik, "Aspects de la chimie quantique contemporaine", Colloque internationaux de CNRS organisé par R. Daudel and A. Pullman, Menton, 8—13 Juillet 1970, p. 108.

[19] E. Yeargers and L. Augenstein, *Nature*, **212**, 251 (1966).

Finally, it is interesting to compare the predictions concerning the positions of the electrophilic and nucleophilic attack in the ground (a), singlet (b), and triplet (c) states based on the calculations of Song and co-workers,[20] and our calculations of charge densities. The most reactive positions for electrophilic (E) and nucleophilic (N) attacks are indicated bellow :

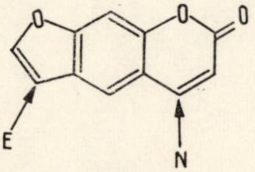

(a)

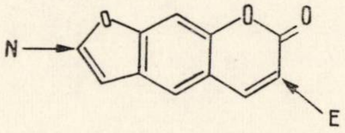

(b)

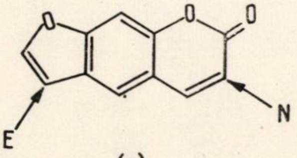

(c)

---

[20] P. S. Song, M. L. Harter, T. A. Moore and W. C. Herndon, *Photochem. Photobiol.*, **14**, 521 (1971).

Revue Roumaine de Chimie, 18, 7, 1259–1262 (1973)

HYDROXY-PHENOTHIAZINE-5,5-DIOXIDES. I

1,7,9-TRICHLORO-3-HYDROXY-5,5-DIOXI-PHENOTHIAZINE

TEODORA PANEA, VALER FĂRCĂŞAN and C. BODEA

Ministry of Education, Institute of Chemistry, str. Donath 65—103, Cluj,
Romania

Received January 19, 1973

The obtention of 1,7,9 tricholoro-3 hydroxy-5,5-dioxi-phenothiazine (I) by the oxidation ol 1, 7, 9, -trichloro-3-hydroxy-phenothiazine (III) with PBA, without protecting the hydroxy group, was demonstrated, using chemical and physical methods.

In a previous work[1] we reported the obtention of 1,7,9-trichloro-3-hydroxy-5,5-dioxi-phenothiazine (I) by hydrolysis of 3-(1,7,9-trichloro-5,5-dioxi-phenothiazinyl)-β-D-2,3,4,6-tetra-0-acetyl-glucopyranoside (II).

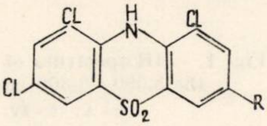

I : R = OH

II : R =

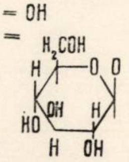

IV : R = OCH_3

VI : R = $OCOCH_3$

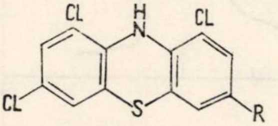

III : R = OH

V : R = $OCOCH_3$

VII : R = OCH_3

We considered of interest from many points of view to attempt the direct obtention of I, by reacting 1,7,9-trichloro-3-hydroxy-phenothiazine (III) with perbenzoic acid (PBA). But in these conditions, in addition to 5,5-dioxide, other derivatives may be formed. Indeed, the phenothiazines are easily oxidized to phenothiazones[2]; on the other hand, the building-up of a quinone-system using PBA was reported.[3] Also, a cleavage of the heterocycle cannot be excluded.[4] Therefore, an elaborated examination of the oxidation product (A) of III is required.

The IR spectrum of *A* registered in chlorbenzene shows two bands at 3387 and 3565 cm^{-1}, assigned to N—H respectively to O—H vibrations (fig. 1.a). The last one is absent in the spectrum of 1,7,9-trichloro-3-

---

[1] C. Bodea, T. Panea and V. Fărcăşan, *Rev. Roumaine Chim.*, **15**, 1923 (1970).

[2] C. Bodea and I. Silberg, "Advances in Heterocyclic Chemistry", vol. 9, Editor A. R. Katritzky, Academic Press, New York and London, 1968, p. 321.

[3] H. Fernholz, *Chem. Ber.*, **84**, 110 (1951).

[4] E. Ochiai, "Aromatic Amine Oxides", Elsevier publishing company Amsterdam, London, New York, 1967, p. 39.

methoxy-5,5-dioxi-phenothiazine (IV) (fig. 1.b). The absorptions corresponding to the symmetrical and asymmetrical SO_2 vibrations, observable at 1152 and 1399 cm^{-1}, are present in the range reported for other 5,5-dioxi-phenothiazines.[5]

The presence of the NH and OH groups in compound *A* is pointed out also in the NMR spectrum by the two signals, at 8.8 and 10.9 ppm; the disappearance of one of them, at 10.9 ppm, when *A* is transformed in IV permits the attribution of this signal to the OH group. As an additional proof could be mentioned the absence of this last signal in the spectrum of *A* if trifluoroacetic acid is added.

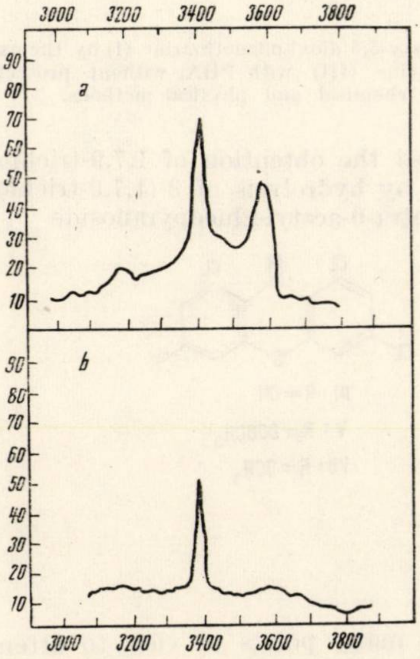

Fig. 1. — IR spectrum of *A* and IV in the 3,000–3,800 cm^{-1} range
a=A; *b*=IV.

The electronic spectrum of *A* shows four bands in the 220–400 nm region, distinctive for 5,5-dioxi-phenothiazines,[6] and the bathochromic shift of all the four bands, if KOH is added to the methanolic solution,[1] is manifest.

In the mass spectrum of *A*, a peak at 350 m/e corresponding to the parent ion from I is observed.

This demonstrates that no cleavage of the heterocycle occurred during oxidation. Thus product *A* has the structure I.

We prepared 1,7,9-trichloro-3-hydroxy-5,5-dioxi-phenothiazine (I) also by another method precluding an oxidation which would involve the OH group. Namely, we reacted 1,7,9-trichloro-3-acetoxy-phenothiazine

---

[5] S. K. Jain and R. L. Mital, *J. Chem. Soc. (B)*, **1970**, 1456.

[6] R. J. Warren, J. B. Eisdorfer, W. E. Thompson and J. E. Zarembo, *J. Pharm. Sci.*, **55**, 144 (1966).

(V) with PBA, and hydrolyzed the thus obtained 1,7,9-trichloro-7-acetoxy-5,5-dioxi-phenothiazine (VI). The m.p. and IR spectrum of the product proved to be identical with those of compound I.

By reacting I with acetic anhydride, VI was obtained.

The above data show that the use of PBA presents a suitable method to transform III into I, by selective oxidation, without protecting the hydroxy group.

The behaviour of III under these conditions agrees with that observed in the case of some hydroxy-sulfides when reacted with hydrogen peroxide in glacial acetic acid.[7]

It is worth mentioning that only two papers[8,9] claimed the obtention of hydroxy-5,5-dioxi-phenothiazines so far, but their structure was presumed considering only the elemental analyses and some analogies. Taking into account the big molecular weight of the products, these data are not sufficient to support the coexistence of a hydroxy and a 5,5-dioxy group.

Some preliminary tests indicate that the above described selective oxidation with PBA is not restricted to the case of III but can be extended to another hydroxy-phenothiazines.

Future papers will be devoted to these topics.

EXPERIMENTAL *

1,7,9-Trichloro-3-hydroxy- 5,5-dioxi-phenothiazine (I)

a) From III[10] in the conditions described in[11] I was obtained. M.p. 280–281°.

IR ν_{SO_2} 1150 1299 cm^{-1} (in KBr) and
ν_{OH} 3560 cm^{-1} ν_{NH} 3389 cm^{-1} (in chlorobenzene)
UV λ_{max} 352, 320, 281, 227 nm (methanol)
372, 337, 298, 229.5 nm (in methanol + KOH).
$C_{12}H_6Cl_3NO_3S$ (350.62)
Calcd : C, 41.10 ; H, 1.73 ; N, 4.00
Found : C, 41.23 ; H, 2,03 ; N, 4.18.

---

* The m.p. were determined in capillaries and are uncorrected.

For the recording of IR spectra, a double beam spectrophotometer Carl Zeiss Jena type UR-10 was used ; the substances were prepared as KBr pellets or dissolved in chlorobenzene.

The electronic spectra were recorded in methanol solution on a DK-2A Beckmann spectrophotometer.

The NMR spectra were recorded on a Varian A 60 apparatus in $DMSOd_6$, TMS as internal reference.

The mass spectrum was determined on a C.I.C. 21110 B mass spectrometer, with ionizing voltage 70 eV and the compound was introduced using the direct insertion lock.

[7] A. O. Pedersen, G. Schrotl, S. O. Lavesson, W. A. Laurie and R. I. Reed, *Tetrahedron*, **26**, 4449 (1970).

[8] T. Urbánski, K. Gzyc-Lewánska and P. Kalinowski, *Bull. Acad. polon. Sci., Ser. Sci. chim.*, **7**, 147 (1959).

[9] H. Wunderlich and A. Stark, *Pharmazie*, **21**, 56 (1966).

[10] C. Bodea and M. Răileanu, *Liebigs Ann. Chem.*, **614**, 171 (1958).

[11] T. Panea and C. Bodea, *Rom. pat.* 60238, 14 June, **1969**.

b) 1 g VI and 10 ml $n/10$ sodium methoxide in 10 ml anhydrous methanol were boiled for 15 min. After cooling, the precipitate ($R = 98\,\%$) was filtered and recrystallized from methanol-water.

M.p. 281°

IR ν_{SO_2} 1150 1299 cm^{-1} (in KBr) and
ν_{OH} 3560 cm^{-1} ν_{NH} 3389 cm^{-1} (in chlorobenzene)

UV λ_{max} 352, 320, 281, 227 nm (methanol)
372, 337, 298, 229.5 nm (in methanol + KOH).

$C_{12}H_6Cl_3NO_3S$ (350.62)
Calcd: C 41.10 ; H 1.73 ; N 4.00
Found: C 41.20 ; H 1.86 ; N 4.09

1,7,9-trichloro-3-acetoxy-5,5-dioxi-phenothiazine (VI)

a) From V [12] in the conditions given in,[11] VI was obtained. After recrystallization from dimethylformamide-water, m.p. 211°.

IR ν_{SO_2} 1162 cm^{-1} 1317 cm^{-1}.
ν_{CO} 1787 cm^{-1} (in KBr)
$C_{14}H_8Cl_3NO_4S$ (392.65)
Calcd: C 42.82 ; H 2.06 ; N 3.57
Found: C 42.75 ; H 2.00 ; N 3.30

b) 0.2 g I in 6 ml acetic anhydride were boiled for 30 min. After cooling, the precipitate was filtered and washed with glacial acetic acid and finally with water. The white rhombic crystals ($R = 92\,\%$) melt at 210°. After recrystallization from dimethylformamide-water, m.p. 211°.

IR ν_{SO_2} 1162 cm^{-1} 1317 cm^{-1}
ν_{CO} 1787 cm^{-1} (in KBr)
$C_{14}H_8Cl_3NO_4S$ (392.65)
Calcd: C 42.82 ; H 2.06 ; N 3.57
Found: C 42.63 ; H 2.10 ; N 3.48

1,7,9-trichloro-3-methoxy-5,5-dioxi-phenothiazine (IV)

From 1,7,9-trichloro-3-methoxy-phenothiazine (VII), [12] IV was obtained. After recrystallization from chlorobenzene m.p. 173–174°.

IR ν_{SO_2} 1309 cm^{-1} 1162 cm^{-1} (in KBr)
ν_{NH} 3361 cm^{-1}
$C_{13}H_8Cl_3NO_3S$ (364.62).
Calcd: C 42.78 ; H 2.19 ; N 3.84
Found: C 42.69 ; H 2.20 ; N 3.81

Acknowledgement. The authors thank for the possibility to record the NMR and mass spectra to Prof. F. Winternitz of L'École Nationale Supérieure de Chimie de Montpellier.

---

[12] C. Bodea and V. Fărcășan, *Studii și Cercetări Chim., Acad. R.P.R., Fil. Cluj*, **11**, 121 (1960).

Revue Roumaine de Chimie, 18, 7, 1263–1268 (1973)

ПОЛЯРОГРАФИЧЕСКОЕ ИССЛЕДОВАНИЕ КОМПЛЕКСО-ОБРАЗОВАНИЯ ЭТИЛКСАНТОГЕНАТА КАЛИЯ С ИОНАМИ Hg^{2+}

ЮЛИЯ КОВАЧ и БЭЛА ТОКЕШ

Лаборатория биохимии и физической химии
Медико-фармацевтический Институт
Тыргу-Муреш, улица Г. Маринеску, 38

Получена 17 ноября 1972 г.

Изучались условия образования комплекса $[Hg(S_2COC_2H_5)_3]^-$ на основе анодного растворения ртутного электрода в присутствии этилксантогената калия. Определялись число лигандов, константа устойчивости и другие термодинамические параметры комплексо-образования. Соотношение между константой устойчивости и температурой можно выразить через следующее уравнение:

$$lg\ \beta_3 = 12{,}48 \cdot 10^3 \frac{1}{T} + 3{,}0$$

Термодинамические данные реакции равны: $\Delta \overline{H} = -5{,}71.10^4$ кал/моль, $\Delta G_{298} = -6{,}11.10^4$ кал/моль, $\Delta S_{298} = 13{,}43$ э.ед.

Исследования, произведенные в последние годы цоказали, что малорастворимые металлические соли ксантогенатов растворяются при избытке ксантогената, образуя комплексы. Так были выявлены полярографическим путем комплексы этилксантогената калия с ионами Cd^{2+}, Zn^{2+},[1–4] Ti^{3+},[5] Co^{3+},[6] Pt^{2+}, Pd^{2+}, Ni^{2+}, Cr^{3+}.[7] Была определена спектрофотометрическим методом стехиометрия реакции образования и константа устойчивости комплексов двухвалентной ртути со смешанными лигандами CN^-

---

[1] H. Kodama и K. Hayashi, *J. Electroanalyt. Chem.*, **14**, 209 (1967).

[2] T. Yamasaki и M. Nanjo, *Chem. Ind.* (*London*), **36**, 1530 (1966).

[3] K. Hayashi, Y. Sasaki и H. Nojima, *Bunseki Kagaku*, **19**, 3 (1970); *Chem. Abstr.*, **73**, 21020d (1970).

[4] M. Nanjo и T. Yamasaki, *Sci. Rep. Res. Inst. Tohoku Univ. Ser. A.*, **21**, *Chem. Abstr.* **33** (1969); **71**, 97727 (1969).

[5] R. S. P. Coutts, P. C. Wailes и J. V. Kingston, *Austral. J. Chem.*, **23**, 469 (1970).

[6] I. M. Korenman, F. R. Sheyanova и S. A. Ryabova, *Zhur. neorg. Khim.*, **2**, 65 (1957).

[7] G. W. Watt и B. J. McCormick, *J. Inorg. Nuclear. Chem.*, **27**, 898 (1965).

и метил-, этил-, бутил-, гексилксантогенатов.[8,9] При анализе разных ксантогенатов полярографическим методом, В. Сихо[10] отмечает четыре анодной волны, из которых одна отвечает анодному растворению ртути. Ввиду того, что ни процесс растворения, ни химическая природа образованного продукта между растворенной ртутью и ионами ксантогената не были изучены, мы решили рассмотреть эти проблемы, важные с аналитической точки зрения.

ТЕОРЕТИЧЕСКАЯ ЧАСТЬ

Предполагая, что при избытке ксантогената образуется комплексное соединение, то эту реакцию можно выразить уравнением:

$$\mathrm{Hg}^{2+} + nEX^- \overset{\beta_n}{\rightleftharpoons} [\mathrm{Hg}(EX)_n]^{-n+2} \tag{I}$$

где β_n обозначает незнакомую константу устойчивости. Чтобы определить ее величину, мы опирались на следующие соображения.

В условиях обыкновенного полярографирования, вследствие анодного растворения ртутного капельного электрода, при достаточном уровне положительных потенциалов, раствор всегда содержит ионы Hg_2^{2+} и Hg^{2+}. Имея в виду, что константа равновесия процесса:

$$\mathrm{Hg} + \mathrm{Hg}^{2+} \rightleftharpoons \mathrm{Hg}_2^{2+} \tag{II}$$

имеет величину К $= 1{,}6.10^2$, при отсутствии комплексообразующих реагентов, в растворе находятся практически только ионы Hg_2^{2+}. Напротив, если анодное окисление ртути имеет место в присутствии таких веществ, равновесие отодвигается в направление возникновения ионов Hg^{2+}, так как они образуют более устойчивые комплексы, чем ионы Hg_2^{2+}. В результате реакции образования комплекса, поляризационные кривые ток — напряжение сдвигаются в сторону более отрицательных потенциалов, а из величины отодвижения возможно вычислить параметры изучаемого равновесия. Потенциал ртутного электрода выражается следующим уравнением:

$$E = E^0_{\mathrm{Hg}^{2+}} + \frac{RT}{2F} \ln \frac{[\,[\mathrm{Hg}\,(EX)_n]^{-n+2}]_0}{\beta_n\,[EX^-]_0^n} \tag{1}$$

то есть

$$E = E_{\mathrm{Hg}^{2+}} + \frac{RT}{2F} \ln \frac{\varkappa_{EX}^n}{\varkappa_{\mathrm{Hg}(EX)_n}} \cdot \frac{-i}{(i - I_d)^n} \cdot \frac{1}{\beta_n} \tag{2}$$

---

[8] K. G. Ashurst и N. M. Rice, *Nat. Inst. Met. Repub. S. Afr. Rep.*, **1970**, 56; *Chem. Abstr.*, **74**, 91817p (1971).

[9] K. G. Ashurtst, L. A. Goold и N. M. Rice, *Nat. Inst. Met. Repub. S. Afr. Rep.*, **1970**, 14; *Chem. Abstr.*, **74**, 91828t (1971).

[10] V. Sicho, Sbornik vysoka skola Chem.-technol. Prague, **1957**, 7.

где $\varkappa$ обозначает константу уравнения Илковича, i — анодный ток, I_d — предельный анодный ток. Потенциал полуволны равен:

$$E_{1/2} = E^0_{\mathrm{Hg}^{2+}} + \frac{RT}{2F} \ln \frac{\varkappa^n_{EX}}{\varkappa_{\mathrm{Hg}(EX)_n}} \cdot \frac{1}{\left(\frac{I_d}{2}\right)^{n-1}} \cdot \frac{1}{\beta_n} \qquad (3)$$

или

$$E_{1/2} = E^0_{\mathrm{Hg}^{2+}} + \frac{RT}{2F} \ln \frac{D^{1/2}_{EX}}{D^{1/2}_{\mathrm{Hg}(EX)_n}} \cdot \frac{2^{n-1}}{n\,\beta_n\,[EX^-]^{n-1}} \qquad (4)$$

РЕЗУЛЬТАТЫ И ИХ ОБСУЖДЕНИЕ

Экспериментальные результаты приведены в табл. 1.

Таблица 1.

Изменение потенциала полуволны ($-E_{1/2}$, в, н.к.э.) в зависимости от концентрации лиганда и температуры, и средние значения $\lg \beta_3$

T (°K) / $[EX^-]$ (M)	298	303	308	313	318
0,1	0,660	0,660	0,657	0,657	0,650
0,3	0,683	0,680	0,682	0,688	0,691
0,6	0,693	0,697	0,695	0,699	0,694
0,8	0,713	0,710	0,709	0,707	0,699
$\lg \beta_3$	44,83	44,30	43,58	43,01	42,18

Предполагая, что $D_{EX} \approx D_{\mathrm{Hg}(EX)_n}$ и подставляя численное значение нормального потенциала ($E^0_{\mathrm{Hg}^{2+}} = 0{,}854$ в относительно н.в.э. и $E^0_{\mathrm{Hg}^{2+}} = 0{,}610$ в относительно н.к.э., при T=298°K), получается следующее соотношение:

$$E_{1/2} = 0{,}610 - 0{,}030 \lg n\ \beta_n - (n-1)\,0{,}030 \lg \frac{[EX^-]}{2} \qquad (5)$$

Оно дает возможность вычислить число лигандов n и константу устойчивости β_n. С этой целью следует зарегистрировать полярографические кривые при разных концентрациях лиганда EX^-. Уравнение регрессионной линии, полученное в результате обработки экспериментальных данных при T = 298°K, соответствует статистически достоверной линейной корреляции между $E_{1/2}$ и $[EX^-]$:

$$E_{1/2} = -(0{,}7303 \pm 0{,}0089) - (0{,}0560 \pm 0{,}0105) \lg \frac{[EX^-]}{2} \tag{6}$$

$$r = -0{,}984, \ s_0 = \pm 0{,}0071 \text{ в},$$

где r обозначает корреляционный коэффициент, s_0 —стандартная ошибка. Из уравнения (6) получается:

$$n = 2{,}88 \approx 3 \text{ и } \lg \beta_3 = 44{,}83$$

Надо иметь в виду однако и возможность образования малорастворимой соли ионов EX^- с ионами, которые образуются при анодном растворении ртути. Среди двух ионов ртути особенно ион Hg_2^{2+} образует многочисленные малорастворимые соли, а соответствующая анодная волна в некоторой степени подобна волне, зарегистрированной при комплексообразовании. Потенциал ртутного электрода определяется уравнением:

$$E = E^0_{Hg_2^{2+}} + \frac{RT}{2F} \ln L - \frac{RT}{F} \ln [EX^-], \tag{7}$$

то есть

$$E = E^0_{Hg_2^{2+}} + \frac{RT}{2F} \ln L - \frac{RT}{F} \ln \frac{i - I_d}{\varkappa_{EX}}, \tag{8}$$

где $L = [Hg_2^{2+}]\,[EX^-]^2$ и обозначает произведение растворимости соли $Hg_2(EX)_2$. Из соотношения потенциала полуволны

$$E_{1/2} = E^0_{Hg_2^{2+}} + \frac{RT}{2F} \ln L - \frac{RT}{F} \ln \frac{[EX^-]}{2}, \tag{9}$$

употребляемого для определения величины L, видно, что в то время, как при образовании комплекса наклон прямой $\left(\lg \frac{[EX^-]}{2}, E_{1/2}\right)$ зависит от n (см. уравнение (4)), в этом случае наклон постоянный при данной температуре. Это различие между угловыми коэффициентами можно употреблять для распознования типа процесса. Однако, при $n=3$ оба наклона равны, значит упомянутый критерий непригоден. Предполагая временно, что процесс, определяющий анодную кривую, является образование малорастворимой соли и подставляя для нормального потенциала $E^0_{Hg_2^{2+}} = 0{,}798$ в (н.в.э.), т.е. $E^0_{Hg_2^{2+}} = 0{,}554$ в (н.к.э.) при $T = 298°$К, значение произведения растворимости было бы равным $\mathrm{p}L = 43{,}38$. Проблема разграничения изученных процессов была разрешена определением произведения растворимости при помощи одного независимого метода, потенциометрически, и сравнивая его значения с гипотетической величиной, полученной полярографическим путем. Среднее значение данных нескольких определений, исполненных с помощью элемента:

$$^{(+)}\mathrm{Hg}\,\left|\,\mathrm{Hg_2Cl_2}, \text{нас. раств. } \mathrm{KCl}\,\right|\,\begin{matrix}\text{агар-агар}\\ \text{нас. раств.}\\ \mathrm{KNO_3}\end{matrix}\,\left|\,\text{раств.}\mathrm{KNO_3}, EX^-, \mathrm{Hg}(EX)_2\,\right|\,\mathrm{Hg}^{(-)}$$

равно $pL = 34{,}81 \pm 0{,}20$, т.е. $L = 1{,}5 \cdot 10^{-35}$. Этот результат, который, впрочем, соответствует литературным данным,[11] убедительно показывает, что комплексообразование является тем процессом, который определяет форму экспериментальной полярографической кривой. Те же выводы можно делать при сравнении полярограммы (Рис. 1) с графической картиной обеих рассмотренных уравнений, (2) и (8). Уравнение (2) выражает, что при $i \to 0$, $E \to -\infty$, а при $i \to I_d$, $E \to +\infty$. Напротив, из выражения (8) вытекает, что при $i \to I_d$ $E \to +\infty$, а при $i \to 0$ E имеет постоянное значение. Наши экспериментальные данные заметно соответствуют первому случаю.

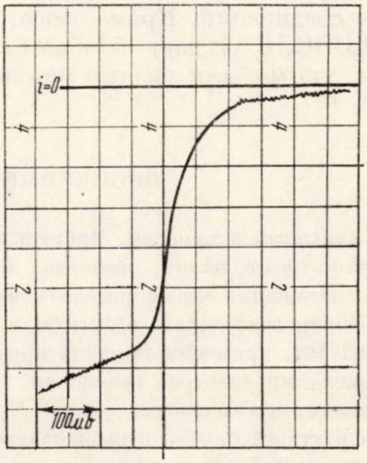

Рис. 1. — Кривая анодного растворения ртути в растворе 0,3 М этилксантогената калия и 0,7 М нитрата калия при $T = 298$°К.

Термодинамические параметры комплексообразования были определены на основе отличной линейной корреляции (r=0,996) между $\lg \beta_3$ и $1/T$, в интервале температур между 298 и 318°К:

$$\lg \beta_3 = (12{,}48 \pm 0{,}62)\, 10^3 \frac{1}{T} + (3{,}0 \pm 2{,}0). \qquad (10)$$

$$s_0 = \pm\, 0{,}10.$$

Из этого соотношения следует, что изменение энталпии реакции, которое считается постоянным в интервале экспериментальных температур, имеет значение $\Delta\overline{H}=-5{,}71.10^4$ кал/моль. Изменения свободной энталпии и энтропии при $T=298°$К равны:

---

[11] S. Mukai и T. Wakamatsu, *J. Mining metallurg. Inst. Japan*, 79, 12 (1963).

$$\Delta G_{298} = -6{,}11.10^4 \text{ кал/моль}$$

и

$$\Delta S_{298} = 13{,}43 \text{ э.ед.}$$

Знак изменения энтропии соответствует ожиданию, если учесть, что имеет место частичная нейтрализация электрических зарядов в процессе комплексообразования, а так же и освобождение молекул воды из гидратной сферы иона Hg^{2+} в этой реакции.

Глубокое знание процесса анодного растворения ртути в присутствии ксантогената расширяет круг полярографических данных об этом классе соединений. Кроме этого, особенно большая прочность комплекса $[Hg(S_2COC_2H_5)_3]^-$ дает-большие возможности применения в аналитической химии, употребляя разные методы установления конечной точки определений. [12]

ЭКСПЕРИМЕНТАЛЬНАЯ ЧАСТЬ

Реактивы и приборы. Чистота всех применяемых веществ была порядка *p.a.* (этилксантогенат калия, желатин, нитрат калия). Концентрация раствора этилксантогената калия была определена титриметрически, по методу Караиванова и сотр.[13]

Полярографические волны были зарегистрированы полярографом «Раделкис», типа OH 102, применяя термостатированный сосудик для электролиза, формы «H», и каломельный электрод сравнения. Постоянство температуры обеспечивалось ультратермостатом с точностью ±0,05°. Чувствительность регистрации была 4.10^{-8} а/мм. Высота ртутного столба поддерживалась на 47 см, а константа капиляра равнялась $m^{2/3}t_1^{1/6} = 1{,}67$ мг$^{2/3}$ сек$^{-1/2}$.

Ход работы. Зарегистрировались полярографические кривые, соответствующие анодному растворению ртути в растворах с разными концентрациями этилксантогената калия (0,1; 0,3; 0,4; 0,5; 0,6; 0,8 и 1,0 M), ионная сила которых поддерживалась на постоянном уровне, 1,0 добавлением нитрата калия. Из параметров этих кривых вычислялись число лигандов и константа устойчивости образующегося комплекса. Термодинамические параметры были вычислены из данных полярограмм, полученных при разных температурах между 298 и 318°К.

Удаление растворенного кислорода во всех случаях производилось пропусканием метана, полученного из светильного газа, через раствор в течение 15 минут до начала определения.

Фоновой раствор содержил в минимальном количестве желатин (0,01 %) для подавления максимумов.

---

[12] H. Wojahn, *Pharm. Zentralhalle*, **85**, 99 (1944).

[13] St. Karaivanov, D. Dimitrov и Su. Magaeva, *Z. analyt. Chem.*, **244**, 319 (1969).

Revue Roumaine de Chimie, **18**, 7, 1269–1272 (1973)

POLAROGRAPHIC, OSCILLOPOLAROGRAPHIC AND CHRONOPOTENTIOMETRIC BEHAVIOUR AND DETERMINATION OF NICOTINIC ACID*

LUIGI CAMPANELLA, PIERLUIGI CIGNINI and GIORGIO DE ANGELIS

Institute of Analytical Chemistry, University, of Rome, Italy

Received August 10, 1972

By polarography (working potential no more negative than −1.15 V vs SCE), oscillopolarography (at about −1.30 V) and chronopotentiometry (electrolysis current = 1μ A) nicotinic acid can be quantitatively determined in the concentration range $10^{-4}-10^{-2}$ M with satisfactory precision and accuracy (1 %).

In previous papers [1-4] we dealt with the polarographic behaviour of heterocyclic compounds containing an N atom in their molecule. Particularly for pyridinemonocarboxylic acids, by the analysis of the obtained results, it can be deduced that among the species under which these acids can exist in aqueous solution the protonated cationic one determines the polarographic behaviour of the acids both by a process of direct reduction and by a kinetic process of equilibrium with the other species. We want now to point out the analytical interest of polarography and other voltametric techniques, if applied to the quantitative determination of nicotinic acid. In literature two papers with the same aim can be found,[5,6] but both refer to polarography only, utilize very negative working potentials, so that the influence of possible interfering agents is felt, and require very rigorous experimental conditions of pH and ionic strength. Here we propose the application of polarography, oscillopolarography and chronopotentiometry to the determination of nicotinic acid in largely varying operating conditions.

---

* Work carried out with the aid of the Italian National Researches Council (C.N.R.).

[1] L. Campanella and G. De Angelis, *Rev. Roumaine Chim.*, **16**, 545 (1971).

[2] L. Campanella, E. Chiacchierini and M. Palchetti, *Rev. Roumaine Chim.*, **17**, 647 (1972).

[3] L. Campanella and G. De Angelis, "IUPAC International Congress on Analytical Chemistry", Kyoto, 3–7 april, 1972.

[4] L. Campanella, P. L. Cignini and G. De Angelis, "23rd Meeting of International Society of Electrochemistry", Stockholm, 27 august–2 september, 1972.

[5] T. Komnova and B. Ermakova, *Vay Vitan.*, **19**, 61 (1960).

[6] P. C. Tompkins and L. A. Schmidt, *Pub. Physiol.*, **8**, 221 (1943).

EXPERIMENTAL

Materials. Nicotinic acid supplied by the Aldrich Chemical Co. was purified by recrystallization from water and controlled by melting point determination and by potentiometric titration.

Procedure. The study was carried out at 25.0 ± 0.5° in aqueous solutions, whose free acidity was varied from very high values (~ 2 M $HClO_4$) up to pH 10, with $NaClO_4$ as supporting electrolyte and citric buffer as buffering agent. For the experiments at high acidity, ionic strength was buffered at 2.0 M with $HClO_4$ and $NaClO_4$. The solutions were prepared by dissolving in distilled water weighed amounts of the anhydrous acid (dried at 115°) in order to have a concentration of about 10^{-3} M. Citric buffer was prepared as usually. As surface active agent, Merck gelatin was used. All chemicals used were analytically pure.

Apparatus. AMEL (Milan, Italy) polarograph (mod. 461) with pen recording and with a dropping mercury electrode having at open circuit the following characteristics $m = 0.865$ mg sec^{-1}, $t = 3.00$ sec (obtained by a hammer), $r = 0.050$ mm.

Saturated calomel electrode (SCE) was always employed as reference electrode connected to the measurement cell by means of an agar KNO_3 conductivity bridge. Oscillopolarograph AMEL mod. 448, dropping time 8 sec, waiting time 6 sec, measurement time 2 sec.

pH meter Electroscan Beckman 30 equipped with usual electrodes and agar KNO_3 bridges. The scanning rate of the potential in the polarographic experiments was 0.2 V/min, in the oscillopolarographic ones it was varied in the 0.25 V/sec—25.0 V/sec range, generally fixed at 1.0 V/sec.

Chronopotentiometry was performed by means of Electroscan and a stationary working electrode formed by a Hg drop of volume 4 l (surface = 0.12 cm^2).

The solutions for the analysis were deaerated by N_2, deoxygenated and suitably humified.

AMEL Corrograph mod. 561 ; Spectrophotometer Beckman DU ; Spectrophotometer IR Perkin Elmer Infracord.

RESULTS AND DISCUSSION

The polarographic behaviour of nicotinic acid is characterized by the presence of four waves. The first one, with less negative half-wave potential, is present in the whole acidity range where nicotinic acid is polarographically active ($\log [H^+] > -0.5$; $1 < pH < 7$). The height of this wave, constant in the range of pH 1.5 — 5.7, decreases for pH > 5.7 ; $E_{1/2}$ is a linear function of pH with two break points at pH 1.8 and 4.3 corresponding to the pK values of the acid ; for pH lower than 1.8 respectively, falling in the range 1.8÷4.3 and higher than 4.3 the slopes $\Delta E_{1/2}/\Delta pH$ are 0, 60 and 120 mV/pH. For pH < 2 a second wave appears ; it is much more evident and well defined in very acid solutions. $E_{1/2}$ of this wave (about —1.150 V vs SCE) is about 100 mV more negative than $E_{1/2}$ of the first wave. Two other waves with $E_{1/2}$ $-1.54 \div -1.57$ and $-1.71 \div -1.73$ V vs SCE can be recorded but in our experimental conditions they cannot be correctly studied because of the influence exerted by the discharge of the cation of the supporting electrolyte.

Through the results of different experiments, all agreeing that no consumption of organic acids takes place during the polarographic electrolysis — such as the perfect identity between polarographic curves and u.v. spectra, recorded before and after electrolysis performed for prolonged times on mercury pool — all the reduction processes can be assumed as not interesting directly the acids which must be considered only as catalyzing agents for the hydrogen discharge.

The nature of the first two waves was also investigated. By the value obtained for the Kheifets slope,[7] temperature coefficient of the limiting currents, shift of the electrocapillary maximum in the presence of nicotinic acid and by the observation that, if the concentration of nicotinic acid is increased beyond 10^{-4} M, the first wave is transformed into two waves, of which one has constant height, it can be concluded that the first wave is an adsorption one, while the second is diffusion controlled. The first two waves follow Ilkovich equation in the concentration range $10^{-2}-10^{-4}$ M and can be profitably employed for the quantitative determination of the acid; particularly the first wave is to be preferred when the pH of the test solution is in the 2—6 range, the second one when pH is lower. The accuracy and reproducibility of the measurements are quite satisfactory (about 1%).

The oscillopolarographic peaks corresponding to the polarographic waves can be recorded. The first peak is well developed up to pH 5.5, where it assumes the shape of a step; its potential of peak (E_p) — about —1.24 V vs SCE — is depending on the potential scanning rate and on pH, not on acid concentration. The peak current increases with the potential scanning rate and is proportional to the concentration of the studied acid (Randles-Sevcik equation: $I_p = Kn^{3/2} m^{2/3} t^{2/3} D^{1/2} V^x C = K'C$), giving thus the possibility of quantitatively determining nicotinic acid. This first peak is characterized by a partially kinetic nature clearly evidenced a) by its above said very similar looking to a polarographic step, particularly at pH > 5 for which the free acidity concentration is so low to markedly reduce the rate of the recombination reaction between the not completely protonated species of the acid and the hydrogen ions [1,3] and b) by the value of x in the Randles-Sevcik equation depending on pH (table 1), but in any case lower than the theoretical characteristic value (=0.5) of the diffusion controlled processes.

Table 1

Values of x in the Randles-Sevcik equation as function of pH

pH	x
1.6	0.40
2.5	0.40
3.2	0.42
4.8	0.30
5.5	0.26

---

[7] L. Ya. Kheifets, *Zhur. analit. Khim.*, **20**, 855 (1965).

The second peak is formed nearby the first when pH of the solution is lower than 2.5. As the corresponding wave this peak too is particularly developed in very acid solutions where, being its height proportional to the acid concentration, it can be utilized for analytical purposes. Accuracy and precision are of the same order as for polarographic determination.

The peaks at the most negative potentials can be hardly studied, because they feel the influence of the supporting electrolyte discharge.

About the chronopotentiometric measurements can be said that the results are markedly affected by the choice of the value of the electrolysis current; when this is 1 μA the transition time can be measured with satisfactory precision and Sand equation ($i^{1/2} = kC$) results are followed, giving another chance of quantitative analysis of nicotinic acid.

Revue Roumaine de Chimie, **18**, 7, 1273 – 1279 (1973)

IONOPHORESIS WITH FLOW GRADIENT*

A. CONSTANTINESCU and C. LITEANU

"Babeş-Bolyai" University, Cluj, Str. Arany János, 11, Romania

Received November 11, 1972

The effciency of some ionophoretic separations was increased by associating, for the first time, a flow gradient brought about by the form of the used ionophoregram, to the tension gradient. The separation of a $Cu^{2+} + Ni^{2+}$ mixture, which could not be achieved by classical ionophoresis, in the same working conditions, was thus obtained.

Among the chromatographic methods so much used nowadays to separate and concentrate small quantities of substance, we also find the electrophoresis on paper, though the principle of electrophoretic separation is markedly different from that of chromatographic separations.

Chromatography and electrophoresis on paper (ionophoresis in the case of ion separation) are similar by the use of the same filter paper as migration support, as well as by numerous technical details, such as the same way of charging the chromatogram and the electrophoregram, the same way of interpreting qualitatively and quantitatively the results of the chromatographic and electrophoretic separation.

Differing from the chromatographic separation, the electrophoretic separation is based on the difference of the migration rates of the ions, the charged particles, colloidal or in suspension, towards the electrodes with a contrary sign, under the influence of an electric field, created inside of the respective solution.

If the substance in the solution is pure, its particles will migrate with the same velocity, so that they will be found on the same spot on the electrophoregram.

If, on the contrary, there are different species of ions in the solution, as they migrate with different velocities, we shall obtain as many spots on the electrophoregram as many species of ions are in the analysed solution.

---

* The paper was read at the Symposium of "Gradient Chromatography", Cluj, Sept. 1972.

Based on the theory of electromigration, we have established the equation of zonal separation

$$l = \frac{\mu t I}{Ks} \tag{1}$$

where l is the covered way ; μ — the mobility of the ions ; t — the migration time interval; I — the intensity of the electric current, s — the cross-section of the support, and K a constant.

Considering that there are two ions, A and B, and that the distances covered by them are l_A and l_B, the equation of the zonal separation becomes

$$\Delta l = l_A - l_B = (\mu_A - \mu_B)\frac{tI}{Ks} \tag{2}$$

The distance l, covered by anion or charged particle, depends thus on the migration time t, the intensity of the electric current I, the cross-section s of the crossed column, as well as on the form and dimension of the particle, through the magnitude μ.

The success of many researches in chromatography are due to the improvement of the chromatographic separations by introducing the gradient technique [1-6] and among the new methods we must mention the use of gradient association. [7-8]

We therefore propose to extend the gradient technique also to ionophoresis on paper, applying it especially to the separation of those ion mixtures which do not take place in conditions of classical ionophoresis.

EXPERIMENTAL

We have used in our experiments an electrophoresis apparatus adapted to the vertical technique. This device is made up of a rectifier and the migration cell, containing the vats for the buffer solution and the support of the electrophoregrams (ionophoregrams). The apparatus has a tension adjustable between 0 and 500 V and the intensity is also adjustable between 0 and 25 mA. We have tried a series of electrolytes, solutions of mineral and organic acids, at different pH (from pH = 5 to pH = 1). No satisfactory results were obtained with mineral acid solutions in the studied cases of ion mixtures and, besides, their use presents numerous disadvantages.

We have preferred to use organic acids (acetic and formic) as electrolytes, as they are volatile enough, and therefore rapidly eliminated when the ionoforegrams are dried.

Using acetic acid solutions (from pH = 5 to pH = 2.5) we have noticed that the spots are better marked around pH = 2.5.

[1] C. Liteanu and C. Gocan, *Bull. Soc. chim. France*, **1967**, 3836.

[2] C. Liteanu and C. Gocan, *Talanta*, **17**, 1115 (1970).

[3] W. Mathias, *Naturwiss.*, **38**, 18 (1954).

[4] M. Lederer, *Nature*, **172**, 727 (1953).

[5] H. Hesse and H. Engelhardt, *J. Chromatog.*, **21**, 228 (1966).

[6] C. G. Honegger, *Helv. Chim. Acta*, **47**, 2385.

[7] C. G. Honegger, *Bull. Soc. chim. France*, **1970**, 4527.

[8] C. Liteanu and A. Constantinescu, Lucrările celei de a III-a Conferinţe Naţionale de Chimie Analitică, Braşov, vol. IV, 1971, p. 127–131.

The best results were obtained using a formic acid 2*n* solution, with pH = 1.5 (formic acid : water 9.2 : 100 v/v) as electrolyte.

The tension used during the experiment varied between 250–400 V.

Continuous electrophoretic bands (Schleicher-Schiil 2040 a paper strips of 26 cm length and 3 cm breadth) as well as electrophoretic bands provided with 1–3 baffles were used as support for the electrophoretic migration.

The loading of the ionoforegram was carried out spreading 0.02 ml of the 1 % solutions and their mixtures on the nil line, parallel to the paper strip breadth and placed on the middle of the strip.

After the migration has taken place, the ionophoregrams were dried in a drying chamber at 80°, and the reactives used to develop the spots were sprayed.

Taking into account the influence of physico-chemical factors on the migration of the ions, we have varied the potential gradient, the migration time period and the concentration of the electrolyte to obtain clear separations.

IONOPHORESIS OF THE $UO_2^{2+} + Ni^2$ MIXTURE

This was preceded by a study of the electrophoretic behaviour of each ion, separately. The obtained data are given in table 1.

We notice that the migration of the ions is proportional to the applied tension and that the clearest separations are obtained at higher tensions.

Table 1

Migration of UO_2^{2+} and Ni^{2+} ions versus potential gradient

Tension (V)	Potential gradient (v/cm)	Time (minutes)	Distance covered (mm)	
			UO_2^{2+}	Ni^{2+}
200	7.7	30	2	6
300	11.5	30	4	12
400	15.4	30	6	16

Studying also the migration of these two ions versus time we have noticed that their migration is proportional to the time factor, and that the separation possibilities increase in time, especially for larger potential gradients (table 2).

Table 2

Migration of UO_2^{2+} and Ni^{2+} ions versus time for a potential gradient of 11.5 V/cm

Electrolyte : formic acid 2*n*
Tension : 400 V

Time (minutes)	Covered distance (mm)	
	UO_2^{2+}	Ni^{2+}
15	3	9
30	6	16
60	12	32

Submitting to ionophoresis, in the same working conditions, a solution of the mixture : aqueous $NiCl_2$ solution 1% + aqueous $(CH_3-COO)_2.UO_2$ 1% solution, in equal quantities, no change in the migration distance could be traced, either for UO_2^{2+} or for Ni^{2+}.

MIGRATION ON AN IONOPHOREGRAM WITH BAFFLES

Besides the physico-chemical factors, the influence of which is commonly studied in ionophoresis, we have studied for the first time the influence of a new factor, the form of the ionophoregram in the process of electrophoretic migration, by means of ionophoregrams provided with one, two and three baffles.

The role of the baffles and the influence of the number of baffles on the electrophoregram in the electrophoresis of the studied mixtures is obvious (table 3).

Table 3

Migration of UO_2^{2+} + Ni^{2+} mixture versus the number of baffles on the ionophoregram

Tension : 400 V
Potential gradient : 15.4 V/cm
Intensity : 7 mA
Migration time : 30 minutes

Distance covered by the ionophoregram (mm)											
No baffles		l	1 baffle		l	2 baffles		l	3 baffles		l
UO_2^{2+}	Ni^2		UO_2^{2+}	Ni^{2+}		UO_2^{2+}	Ni^{2+}		UO_2^{2+}	Ni^{2+}	
6	16	10	8	25	17	22	49	27	30	63	33

For the same 15.4 V/cm tension gradient and the same 30 minutes migration time, the use of an ionophoregram with one baffle, compared to the ionophoregram with a continuous strip, brings about a distance difference of:

$$\Delta l = l_{Ni^{2+}} - l_{UO_2^{2+}} = 7 \text{ mm}.$$

This distance Δl grows to 17 mm and 23 mm for ionophoregrams with two, and respectively three baffles (figure 1).

This proves the efficiency increase of separations by ionophoresis on filter paper cut up with baffles.

IONOPHORESIS OF THE Cu^{2+} + Ni^{2+} MIXTURE

The migration of Cu^{2+} and Ni^{2+} ions was also studied separately for the solution of each ion apart, as well as for the mixture of both ions solutions (aqueous 1% $CuCl_2$ solution + aqueous 1% $NiCl_2$ solution, in equal volumes).

Using the same electrolyte, 2*n* formic acid solution, 400 V tension and a 15.4 V potential gradient, for a 30 minutes migration time, on ionophoregrams of continuous strips (without baffles) we have obtained very near migration distances. Thus, for Cu^{2+} we had 14 mm and for Ni^{2+} 16 mm.

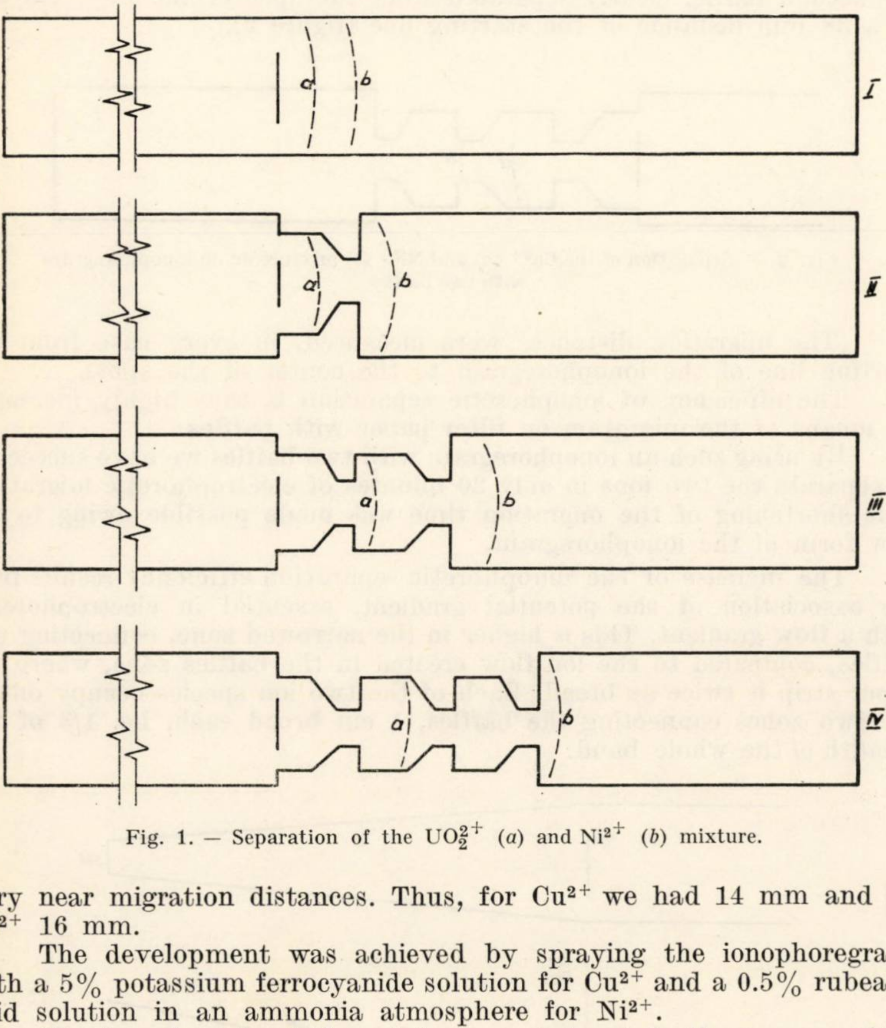

Fig. 1. — Separation of the UO_2^{2+} (*a*) and Ni^{2+} (*b*) mixture.

The development was achieved by spraying the ionophoregrams with a 5% potassium ferrocyanide solution for Cu^{2+} and a 0.5% rubeanic acid solution in an ammonia atmosphere for Ni^{2+}.

The ionophoresis of the mixture, carried out in the same working conditions, lets us obtain two spots with poorly marked limits, and partially overlapping.

To achieve the separation of these two ions mixture we have tried to carry out the ionophoresis on Schleicher-Schüll 2040 a, paper strips with two baffles, the other working conditions being the same.

The Cu^{2+} and Ni^{2+} ions were thus separated, and the development of the ionophoregram with a 5% potassium ferrocyanide solution showed the Cu^{2+} ion as a well-marked greenish spot, in the zone of the second baffle at a distance of 27 mm of the starting line.

The Ni^{2+} ion, by developing with 5% rubeanic acid in an ammonia atmosphere, appears as a violet-blue, well-marked spot, at the end of the second baffle, clearly separated from the spot of the Cu^{2+} ion and at a 38 mm distance of the starting line (figure 2).

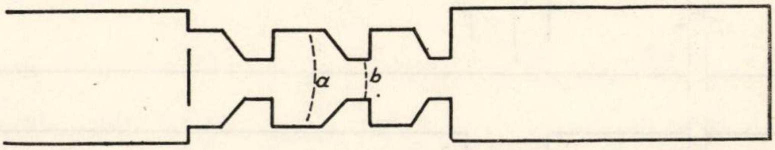

Fig. 2. — Separation of the Cu^{2+} (*a*) and Ni^{2+} (*b*) mixture on an ionophoregram with two baffles.

(The migration distances were measured, in every case from the starting line of the ionophoregram to the center of the spot).

The efficiency of ionophoretic separation is thus highly increased by means of the migration on filter paper with baffles.

By using such an ionophoregram with two baffles we have succeeded to separate the two ions in only 20 minutes of electrophoretic migration. This shortening of the migration time was made possible owing to the new form of the ionophoregram.

The increase of the ionophoretic separation efficiency results from the association of the potential gradient, essential in electrophoresis, with a flow gradient. This is higher in the narrowed zone, connecting two baffles, compared to the ion flow created in the baffles zone, where the paper strip is twice as broad. Each of the two ion species occupy one of the two zones connecting the baffles, 1 cm broad each, i.e. 1/3 of the breadth of the whole band.

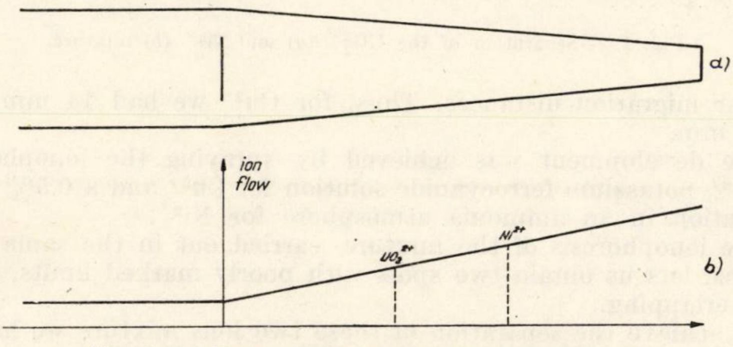

Fig. 3. — a. Progressive narrowing ionophoregram.
b. Corresponding variation of the ionic flow.

An increase of the ion flow, three times bigger than in the migration zone on continuous paper, and twice bigger than in the baffle zone, is thus achieved in this region.

Using two ionoforegrams of the form shown in figure 3a, we have noticed that, when separating the $UO_2^{2+} + Ni^{2+}$ mixture, the respective spots show a Δl 30 mm interval only after 90 minutes of migration.

With the baffle ionophoregram, a 33 mm interval between the spots of the UO_2^{2+} and Ni^{2+} is obtained, as shown, after 30 minutes only.

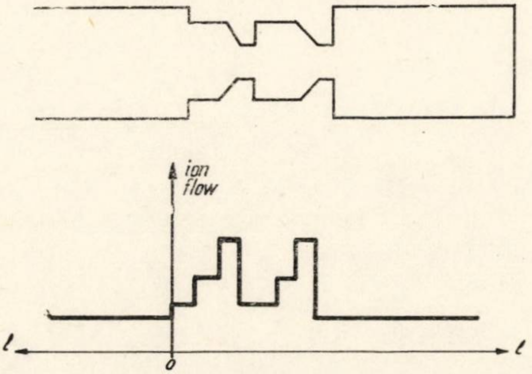

Fig. 4. — Complex flow gradient in the case of an ionophoregram with two baffles.

These experimental data show that while a simple flow gradient (figure 3 b) corresponds to the ionophoregram with progressive narrowing (figure 3 a), a complex flow gradient (figure 4) appears in the case of ionophoregrams with baffles, which favours a differentiated migration of the ions.

CONCLUSIONS

The ionophoregram with baffles brings about an increase of the ion flow in the connecting zones of the baffles. This determines a supplementary increase of the potential gradient, which in turn increases the efficiency of ionophoretic separations.

ORSZÁGOS MŰSZAKI KÖNYVTÁR ÉS DOKUMENTÁCIÓS KÖZPONT

Revue Roumaine de Chimie, 18, 7, 1273–1279 (1973)

NOTE POUR LES AUTEURS

La *Revue Roumanie de Chimie* publie des articles en anglais, français, russe, allemand ou espagnol. Les auteurs sont priés d'envoyer des articles, notes, communications et comptes rendus inédits.

Les manuscrits seront dactylographiés à deux intervalles. Les tableaux seront dactylographiés sur feuilles séparées, de même que la légende des figures. Les diagrammes seront tracés à l'encre de Chine sur papier calque. Les tableaux et les figures seront numérotés par des chiffres arabes, en nombre strictement nécessaire. Prière de ne pas inscrire les mêmes données dans les tableaux et les figures. Les formules chimiques seront incluses dans le texte; en outre, elles seront transcrites sur des feuilles séparées. Les auteurs sont priés d'indiquer les caractères italiques (en soulignant les lettres au crayon), ainsi que tout autre caractère spécial. L'ordre des références bibliographiques sera celui de leur mention dans le texte; le nom de l'auteur sera précédé de l'initiale du prénom; les publications périodiques seront présentées suivant les prescriptions internationales. Les références seront ajoutées à la fin de l'article; elles paraîtront comme des notes, au bas de la page. Le texte sera précédé d'un résumé comprenant 15 lignes au maximum.

L'entière responsabilité du contenu des articles appartient aux auteurs. On publie des articles dus aux collaborateurs roumains ou étrangers. Les auteurs recevront 50 tirés à part.

PRINTED IN ROMANIA

1973 OKT 17

TRAVAUX PARUS AUX ÉDITIONS DE L'ACADÉMIE DE LA RÉPUBLIQUE SOCIALISTE DE ROUMANIE

MARIA FITI, **Dozimetria chimică a radiaţiilor ionizante** (La dosimétrie chimique des radiations ionisantes), 1973, 240 p., 13,50 lei.

MIHAI FLORESCU, **Eficienţa economică a cercetării ştiinţifice** (L'efficience économique de la recherche scientifique), 1972, 115 p., 15 lei.

GEORGETA LĂZĂRESCU, **Sistematizarea informaţiilor în chimia organică** (La systématisation des informations dans la chimie organique), 1972, 242 p., 10,50 lei.

P. BALTĂ et E. BALTĂ, **Introducere în chimia fizică a stării vitroase** (Introduction à la chimie physique de l'état vitreux), 1971, 240 p., 15,50 lei.

LYDIA-MARIA VAICUM, **Biodegrabilitatea detergenţilor** (La biodégrabilité des détergents), 1971, 346 p., 19,50 lei.

I. ZUGRĂVESCU et L. STOICESCU-CRIVETZ, **Polimeri heterociclici** (Polymères hétérocycliques), 1971, 190 p., 9,50 lei.

I. V. MAXIM, **Materiale nucleare** (Matériaux nucléaires), 1969, 444 p., 30 lei.

CORNEL BODEA et collab., **Tratat de biochimie vegetală**, partea I, **Fitochimie** (Traité de biochimie végétale, Ire partie, Phytochimie), Ier vol., 1964, 747 p. + 4 annexes + 2 pl., 41 lei; IIe vol., 1965, 1962 p., 1 pl., 56 lei; IIIe vol., 1967, 773 p., 35 lei.

CRISTOFOR SIMIONESCU et CLEOPATRA VASILIU-OPREA, **Mecanochimia compuşilor macromoleculari** (La méchanochimie des composés macromoléculaires), 1967, 344 p., 23,50 lei.

V. GHEŢIE et V. MICUŞAN, **Analiza imunochimică. Teorie şi practică** (Analyse immunochimique. Théorie et pratique), 1966, 369 p., 28 lei.

R. PORTOCALĂ et L. POPA, **Acizii ribonucleici celulari şi virali** (Les acides ribonucléiques cellulaires et viraux), 1966, 375 p., 8 pl., 26 lei.

I.P.I. – c. 2931

43 426

Lei 25.–

F 1103

R

REFERÁLNA

REVUE ROUMAINE DE CHIMIE

TOME 18
N° 8
Août 1973
RRCHAX, 18, 8, 1281–1490 (1973)

ÉDITIONS DE L'ACADÉMIE DE LA RÉPUBLIQUE SOCIALISTE DE ROUMANIE

Rev. Roumaine Chim. 18, 8, p. 1281–1490 (1973), Bucarest

COMITÉ DE RÉDACTION

Rédacteur en chef:

I. G. MURGULESCU, membre de l'Académie de la République Socialiste de Roumanie

Rédacteurs en chef adjoints:

A. T. BALABAN et V. EM. SAHINI, membres correspondants de l'Académie de la République Socialiste de Roumanie

Collège de rédaction:

C. DRĂGULESCU, RALUCA RIPAN, CR. SIMIONESCU, membres de l'Académie de la République Socialiste de Roumanie; EM. BRATU, ECATERINA CIORĂNESCU-NENITZESCU, P. SPACU, membres correspondants de l'Académie de la République Socialiste de Roumanie; MARGARETA AVRAM, D. I. MARCHIDAN, G. NIAC et D. SĂNDULESCU

La Revue Roumaine de Chimie paraît 12 fois par an. Toute commande de l'étranger (fascicules ou abonnements) sera adressée à Intreprinderea Rompresfilatelia, Boîte Postale 2001, telex 011631, Bucarest, Roumanie

Les manuscrits, les livres et les revues proposés en échange, ainsi que toute correspondance seront envoyés à la rédaction

REVUE ROUMAINE DE CHIMIE

23, str. Dumbrava Roşie, Bucarest, Roumanie

ÉDITIONS DE L'ACADÉMIE DE LA RÉPUBLIQUE SOCIALISTE DE ROUMANIE
3 bis, str. Gutenberg, Bucarest

REVUE ROUMAINE DE CHIMIE

Tome 18, N° 8 Août 1973

Page

V. E. SAHINI, C. PODINĂ et MIRIAM STRUL, L'étude des isomères de la nitroaniline par spectrométrie de masse 1283–1288
P. G. PERKINS, The electronic structures of some molecules and ions containing carbon, silicon, oxygen and sulphur. II. CO, SiO, CS, SiS and COS. 1289–1294
D. I. MARCHIDAN and LAURA VASU, Heat of melting for eutectics formed in binary systems of $AgNO_3$ with KNO_3, $RbNO_3$, $CsNO_3$, AgCl and AgBr 1295–1299
RODICA VÎLCU and B. COMAN, Caloric capacities of vapours of organic liquids. I. A flow calorimeter 1301–1310
C D. TOPOR, Transference numbers and mobilities in molten univalent nitrates 1311–1317
S. STERNBERG and MARIANA TERZI, Surface tension of the reciprocal molten salt pairs (K, Ag; Cl, Br) 1319–1324
A O. RADOVICI, CECILIA VASS and I. SOLACOLU, Electroplating of copper from pyrophosphate baths. I. The effect of electrolyte pH 1325–1331
T. CHIRULESCU, CORNELIA CIOBANU and GH. ŞERBAN, Kinetic study on the reduction of nickel catalysts 1333–1338
N. DUŞOIU, Magnetic dispersion and magnetic absorption of some ferrimagnetic compounds in the domain of centimetre waves. I. Li–Fe–Be and Ni–Fe–Be 1339–1344
G. D. CISMARU and P. SPACU, Electrical conductivity of intermetallic compounds of the cerium–thallium system 1345–1351
R. VÎLCEANU, Z. SIMON and A. CHIRIAC, Stability of three-membered heterocycles. I. Considerations concerning thermodynamic stability and conservation of orbital symmetry 1353–1359
LILIANA PETROVA und EUGENIA COMANIŢĂ, Über die Synthese einiger quartären Pyridiniumsalze 1361–1365
GEORGETA CSOMONTANYI, MARIŢA NETTA et MAGDALENA BALMEZ, Hydrogénation catalytique de l'acétophénone 1367–1372
V. P. KUDESIA, Kinetics of oxidation of butan-2-ol by peroxydisulphate catalyzed by Ag (I) ion 1373–1377
S. MAGER and E. L. ELIEL, Synthesis and configurational equilibrium of 2-isopropyl-5-acetyl-1,3-dioxane 1379–1387
V. V. BADIGER and S. C. BENNUR, Pyrimidine. IV. Synthesis of N-aryl-N'-4-(2-methylthio-5-bromopyrimidoyl) ureas and -thiourea. 1389–1393
M. ARSHAD A. BEG and I. A. KHAN, Correlation of the physical properties of organosilicon compounds. III. Electronegativity of molecules and their boiling point, refractivity and density 1395–1407

Rev. Roumaine Chim. **18**, *8*, p. 1281–1490 (1973), Bucarest

Page

V. TĂMAŞ, VICTORIA CIURDARU and C. BODEA, Azlactones of carotenoids. I. Synthesis and properties of azlactones of β-apo-carotenals and of diapo-carotenedials 1409–1417

I. MOŢOC, Die mathematische Darstellung der Homologie und der homologen Serien 1419–1426

FL. POPESCU et SIMONA PERCEC, La chlorophosphonation du polychlorure de vinyle et de l'alcool polyvinylique 1427–1439

E. CHIACCHIERINI and RENATA COCCHIERI, Behaviour of Cr(III)-poly(aminocarboxylate) ligands solutions at the dropping-mercury electrode (DME) 1441–1450

I. C. POPESCU, C. LITEANU and L. SAVICI, Characterization of ceramic ion-selective membrane-electrodes. V. Ag_2S, S^{2-}-selective membrane-electrode 1451–1457

I. C. POPESCU, V. CIOVÎRNACHE, L. SAVICI and C. LITEANU, Characterization of ceramic ion-selective membrane-electrodes. VI. Selectivity of the Ag^+/S^{2-}-selective Ag_2S membrane-electrode 1459–1466

C. LITEANU, I. C. POPESCU and A. MOCANU, Characterization of ceramic ion-selective membrane-electrodes. VII. The $AgI-Ag_2S$, CN^--selective membrane electrode 1467–1473

V. ARMEANU and ELENA DRĂGUŞIN, Spectrophotometric study of cadmium complex with benzthiazolylazo-2,4-dichlorophenol reagent 1475–1482

IULIA KOVÁCS and L. KÉKEDY, Polarographic investigation of the cadmium and zinc ethyl xanthate complexes 1483–1487

COMPTE RENDU 1489

MŰSZAKI KÖNYVTÁR

Revue Roumaine de Chimie, **18**, *8*, 1283–1288 (1973)

L'ÉTUDE DES ISOMÈRES DE LA NITROANILINE PAR SPECTROMÉTRIE DE MASSE

V. E. SAHINI, C. PODINĂ, MIRIAM STRUL *

Laboratoire de Chimie Physique de
l'Université de Bucarest, 13
Bd. Republicii, Bucarest
* Centre de Chimie Physique 31, str. Galați,
Bucarest, Roumanie

Reçu le 14 mars 1973

Les spectres de masse des isomères de la nitroaniline ont été étudiés, ainsi que les mécanismes de formation de ions correspondants. Les résultats ont été mis en corrélation avec les diagrammes moléculaires en approximation HMO.

Le mécanisme de fragmentation sous l'impact électronique des molécules organiques présente une importance particulière pour établir une corrélation entre le spectre de masse et la structure moléculaire.

Les spectres de masse des dérivés benzéniques sont caractérisés, en général, par l'intensité remarquable du maximum correspondant à l'ion moléculaire, dû à la possibilité de localisation de la charge positive sur le noyau aromatique[1]. Ce maximum est souvent le plus intense du spectre. Pour les benzènes substitués, les principaux processus de fragmentation sont déterminés par la nature des substituants. Dans le cas des dérivés disubstitués, la nature des substituants est importante de même que leur position relative; ainsi, le spectre de masse reflète, le plus souvent, l'effet de l'isomérie.[2,3]

Nous présentons dans cet ouvrage les mécanismes de dissociation des isomères de la nitroaniline sous l'influence du bombardement électronique.

PARTIE EXPÉRIMENTALE

Les spectres ont été obtenus à l'aide d'un spectromètre de masse de type MI−1305, en utilisant les paramètres suivants : courant d'ionisation : 1,5 mA; tension d'ionisation : 70 V ; potentiel d'accélération : 4 kV. Les nitroanilines utilisées ont été purifiées par recristallisations répétées. Les résultats expérimentaux sont présentés dans le tableau 1, qui contient seulement les pics dont l'intensité dépasse 1 % de l'abondance ionique totale. On a observé aussi des métastables aux masses apparentes suivantes : 106,2 ; 69,5 ; 61,3 ; 59,3 ; 46,4 ; 35,2 ; 23,4.

---

[1] G. Spiteller et M. Spiteller-Friedmann, *Monatsh.*, **93**, 1395 (1962).

[2] I. Howe et D. H. Williams, *J. Amer. Chem. Soc.*, **91**, 7137 (1969).

[3] I. Howe, D. H. Williams et R. G. Cooks, *Org. Mass. Spectrom.*, **2**, 137 (1967).

Les diagrammes moléculaires en approximation de Hückel ont été calculés en utilisant les paramètres suivants[4] :

$$\alpha_N = \alpha_C + \beta \qquad \beta_{CN} = 0{,}7$$

$$\alpha_O = \alpha_C + \beta \qquad \beta_{NO} = 1{,}2$$

$$\beta_{C-C} = -2{,}8 \text{ eV}$$

DISCUSSION DES RÉSULTATS

Nos résultats prouvent que les molécules des isomères de la nitroaniline sont relativement stables à l'impact électronique. Les maximums principaux dans les spectres correspondent aux ions de m/e : 138 (l'ion moléculaire), 92, 80, 65, 39. Les maximums des ions moléculaires sont intenses, mais ils ne constituent pas les maximums de base des spectres (tableau 1).

Tableau 1

Les spectres de masse des nitroanilines

m/e	*orthc*-nitroaniline	*meta*-nitroaniline	*para*-nitroaniline
138	13,6	12,13	10,94
122	0,42	0,11	0,56
121	0,73	—	—
108	3,61	1,48	9,70
92	10,8	15,7	9,70
91	1,89	1,20	1,03
80	4,80	3,58	3,65
65	15,93	18,30	15,9
64	2,7	2,16	2,01
63	3,42	2,94	2,9
62	1,29	1,32	1,38
53	1,71	1,28	1,88
52	4,11	2,61	2,82
51	1,75	1,03	1,28
39	6,42	6,84	6,34

Les spectres de masse de plusieurs dérivés nitroaromatiques prouvent que les processus primaires de dissociation des ions moléculaires sont déterminés essentiellement par le groupement NO_2. Les dissociations avec élimination de fragments NO, O ou NO_2 sont caractéristiques ; l'intensité des maximums correspondants dépend des voies de stabilisation des ions fragmentaires (résonance, effets inductifs, hyperconjugaison, mésomerie, etc.[5–8]).

---

[4] V. E. Sahini, F. Keplinger et M. Hillebrand, *Rev. Roumaine Chim.*, **12**, 361 (1967).

Le rapprochement du groupement NO_2 d'un groupement fonctionnel qui contient des atomes d'hydrogène rend possible l'élimination du radical OH (par « l'effet ortho »).[9]

Le mécanisme de fragmentation proposé pour les isomères de la nitroaniline est présenté dans le schéma 1.

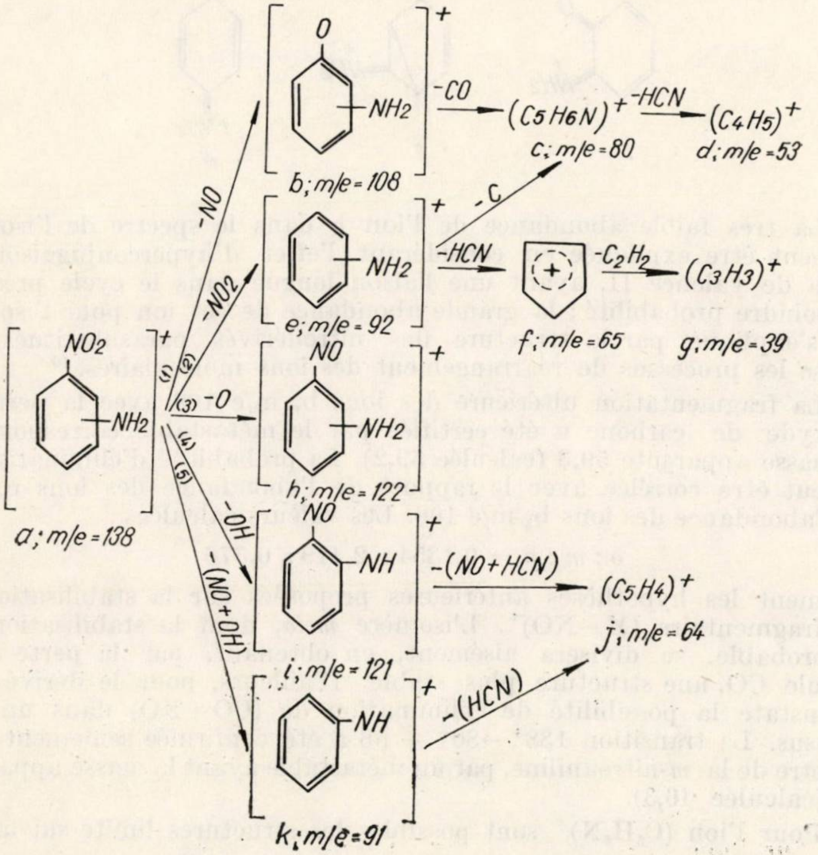

NO2
NH2
a; m/e = 138
(1) -NO
(2) -NO2
(3) -O
(4) -OH
(5) -(NO+OH)
O
NH2
b; m/e = 108
-CO
(C5H6N)+
c; m/e = 80
-HCN
(C4H5)+
d; m/e = 53
-C
NH2
e; m/e = 92
-HCN
(+)
f; m/e = 65
-C2H2
(C3H3)+
g; m/e = 39
NO
NH2
h; m/e = 122
NO
NH
i; m/e = 121
-(NO+HCN)
(C5H4)+
j; m/e = 64
NH
k; m/e = 91
-(HCN)

Schéma 1. — Le mécanisme de dissociation de l'ion moléculaire de la nitroaniline.

L'élimination du groupement NO (réaction 1, schéma 1) est une réaction favorisée par la mince entropie du processus de formation de la

---

[5] J. H. Beynon, „Mass spectrometria i eio primennenie v organicheskoi khimii", Izd. Mir, Moskva, 1964, p. 275.

[6] R. H. Shapiro et J. W. Serum, *Org. Mass. Spectrom.*, **2**, 533 (1969).

[7] F. W. Mc. Lafferty, *Analyt. Chem.*, **31**, 477 (1959).

[8] F. W. Mc. Lafferty, „Uspekhi mass spetrometrii", Izd. Inostrannoi Literatury, Moskva, 1963, p. 349.

[9] F. Benoit et J. L. Holmes, *Org. Mass Spectrom.*, **3**, 993 (1970).

molécule neutre de monoxyde d'azote et par la possibilité de stabilisation de la charge positive sur l'ion formé. Ce processus implique comme étape intermédiaire, le réarrangement de l'ion moléculaire. Après l'élimination de la molécule NO, l'ion fragmentaire résulté (l'ion b ; m/e 108) peut être assigné à l'une des formes limite :

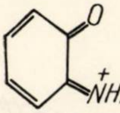
I

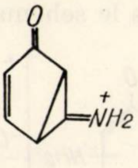
II

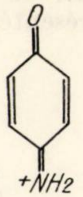
III

La très faible abondance de l'ion b dans le spectre de l'isomère *meta* peut être expliquée en considérant l'effet d'hyperconjugaison : le schéma de valence II, ayant une liaison longue dans le cycle présente une moindre probabilité ; la grande abondance de cet ion pour l'isomère *para* s'explique par la structure des nitrodérivés parasubstitués qui favorise les processus de réarrangement des ions moléculaires. [10]

La fragmentation ultérieure des ions b, m/e 108 avec la perte de monoxyde de carbone a été certifiée par le métastable correspondant à la masse apparente 59,3 (calculée 59,2). La probabilité d'élimination de CO peut être corrélée avec le rapport de l'abondance des ions c, m/e 80 à l'abondance des ions b, m/e 108. Les valeurs calculées :

$$o : m : p = 0{,}1354 \,;\; 2{,}419 \,;\; 0{,}376$$

confirment les hypothèses antérieures proposées sur la stabilisation de l'ion fragmentaire $(M-NO)^+$. L'isomère *meta*, dont la stabilisation est peu probable, se divisera aisément, en obtenant, par la perte de la molécule CO, une structure plus stable. D'ailleurs, pour le dérivé *meta* on constate la possibilité de l'élimination de (CO+NO) dans un seul processus. La transition $138^+ \rightarrow 80^+ + 58$ a été confirmée seulement dans le spectre de la *m*-nitroaniline, par un métastable ayant la masse apparente 46,4 (calculée 46,3).

Pour l'ion $(C_5H_6N)^+$ sont possibles les structures limite suivantes :

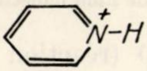
I

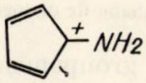
II

la plus stable étant celle de l'ion pyridinium (I), dû à la stabilité accordée par la conjugaison des liaisons. [1]

La supposition que l'étape suivante de fragmentation est l'élimination de l'acide cyanhydrique, processus spécifique pour les amines, a été confirmée par le métastable $m^* = 35{,}2$ (calculée 35,1).

---

[10] M. M. Bursey, *Org. Mass. Spectrom.*, **2**, 907 (1969).

La réaction 2 de formation de l'ion fragmentaire $(M-NO_2)^+$ a lieu par la simple fragmentation de la chaîne C—N, le réarrangement préalable de l'ion moléculaire n'étant plus nécessaire. Ainsi, les résultats concernant les ordres de liaison de la molécule neutre peuvent être utilisés dans une première approximation à l'évaluation de la probabilité de rupture de cette liaison. La probabilité d'élimination du groupement nitro, expérimentalement déterminée par la valeur du rapport $(M-NO_2)^+/M^+$ est en concordance avec les valeurs calculées pour les indices de liaison p_{C-N};

$$(M-NO_2)^+/M^+ \quad o:m:p = 0{,}795\,;\ 1{,}3\,;\ 0{,}888$$

$$p_{C-N} \quad o:m:p = 0{,}276\,;\ 0{,}259\,;\ 0{,}269$$

Les deux séries de valeurs mènent au même ordre de probabilité de fragmentation : $m > p > o$.

Le processus d'élimination de la molécule neutre NO_2 de l'ion moléculaire a été attesté par les métastables de masse apparente 61,3 (valeur calculée : 61,3), mis en évidence dans tous les spectres.

L'ion le plus abondant dans les spectres de la nitroaniline est l'ion cyclopentadiényl, f, m/e 65, formé le plus probable, par le processus secondaire d'élimination d'une molécule HCN de l'ion $(C_6H_4NH_2)^+$ réarrangé sous la forme[11] :

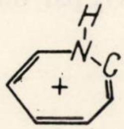

La transition suivante proposée $(C_5H_5)^+ \rightarrow (C_3H_3)^+ + 26$ a été confirmée par le métastable $m^* = 23{,}4$ (calculée 23,4) mis en évidence dans tous les spectres.

Une réaction peu commune est le processus $92^+ \rightarrow 80^+ + 12$. La perte d'un atome de carbone de l'ion $(M-NO_2)^+$ s'explique par la structure stable de l'ion c, m/e 80 (l'ion pyridinium). La transition a été proposée après l'identification dans tous les spectres du pic métastable de masse apparente 69,5 (calculée 69,5).

Un autre processus caractéristique pour le substituant nitro est la fragmentation de l'ion moléculaire par l'élimination d'un atome d'oxygène. La probabilité d'élimination d'oxygène peut être aussi déterminée par les valeurs pour les ordres de liaison $p_{N-}O$.

$$p_{N-}O : o:m:p : = 0{,}674\,;\ 0{,}679\,;\ 0{,}670$$

La croissance de la probabilité de rupture de l'oxygène du groupement NO_2 dans l'ordre $p > o > m$ correspond aux résultats expérimentaux, le rapport de l'abondance des ions $(M-O)^+/M$ ayant les valeurs : $o\,;\ m\,;\ p\,; = 0{,}0308\,;\ 0{,}0091\,;\ 0{,}0512$.

---

[11] N. UCELLA, I. HOWE et D. H. WILLIAMS, *Org. Mass. Spectrom.*, **6**, 229 (1972).

Le rapprochement des groupements fonctionnels dans l'orthonitroaniline permet le développement des processus spécifiques uniquement pour cet isomère.

Le maximum *i*, m/e 121 (réaction 4) qui correspond à la perte d'un radical OH de l'ion moléculaire apparaît seulement dans le spectre de l'orthonitroaniline. (Les intensités pour les dérivés *meta* et *para* sont négligeables.) La réaction 4 d'élimination du radical OH par effet *ortho* est confirmée par le métastable $m^* = 106{,}2$ (calculée 106), identifié seulement dans le spectre de l'isomère *ortho*. Il est probable quel'ion *i*, m/e 121, reçoit une structure stable par l'élimination de (NO+HCN) en formant l'ion *j*, m/e 64.

L'apparition des ions 91^+ dans les spectres de masse de nitroanilines peut être expliquée soit par la perte d'un atome d'hydrogène de l'ion e, m/e 92, soit, quand il s'agit d'ortho-dérivé, par l'élimination du groupement HNO_2, comme (OH+NO), de l'ion moléculaire regroupé ou non (réaction 5). L'intensité plus grande du maximum 91^+ dans le spectre de l'orthonitroaniline confirme la possibilité de développement de ce deuxième mécanisme proposé.

L'étude des nitroanilines par spectrométrie de masse prouve que dans les processus primaires de leur dissociation est impliqué de préférence le substituant le plus électronégatif (le groupement NO_2). Les réactions spécifiques pour les amines apparaissent comme des fragmentations ultérieures à l'élimination de NO_2 par différents mécanismes.

Revue Roumaine de Chimie, **18**, *8*, 1289–1294 (1973)

THE ELECTRONIC STRUCTURES OF SOME MOLECULES AND IONS CONTAINING CARBON, SILICON, OXYGEN AND SULPHUR. II[1] CO, SiO, CS, SiS and COS

PETER G. PERKINS

Department of Pure and Applied Chemistry,
University of Strathclyde,
Glasgow, C. 1, Scotland

Received January 15, 1973

The valence electronic structures of molecular CO, SiO, CS, SiS, and COS have been studied by a self-consistent molecular orbital method. The results for CO and SiO compare satisfactorily with those of *ab initio* treatments. The calculated properties of the species are consistent with their chemical properties. The electronic structures of SiS and CS suggest that these molecules may complex with transition metal ions.

INTRODUCTION

In Part I[1] we discussed the differences in electronic structure between some neutral and anionic species containing the Si—O and the C—O bonds. In that paper, we concluded that the silicon 3*d* orbitals played a role in stabilising the bonding orbitals in such systems.

We now discuss the electronic properties of molecules generated by changing from oxygen to sulphur and here present results for the systems CO, CS, SiO, and SiS. Both CO and SiO have been studied by *ab initio* techniques and, hence, provide a convenient standard against which to check the validity of our results, calculated by a CNDO-based method.

The calculational method was identical to that employed previously.[1] For silicon, both the diffuse and the "contracted" *d* orbitals were used in the case of SiO : the latter are considered to be more realistic[1] for a situation where Si is directly bonded to an electronegative atom like oxygen. For sulphur, "diffuse" *d* orbitals were employed throughout with parameters computed in earlier work, [2] whilst in SiS the diffuse *d* orbitals were employed for Si.

[1] P. G. Perkins, *Rev. Roumaine Chim.*, **17**, 773 (1972).

[2] K. A. Levison and P. G. Perkins, *Theor. chim. Acta.*, **14**, 206 (1969).

Bond lengths were abstracted from standard compilations [3] and are given in table 1.

Table 1

Geometrical data (Å)

C–O	1.1282
Si – O	1.509
Si – S	1.928
C – S	1.534
C – S (in COS)	1.560
C – O (in COS)	1.161

RESULTS AND DISCUSSION

COMPARISON WITH *AB INITIO* CALCULATIONS

There have been many previous calculations on carbon monoxide by a variety of *ab initio* methods [4] with extensive basis sets. Table 2 sets out the results of the present work next to those of the *ab initio* work of McLean and Yoshimine. [4] We see that, for CO, our eigenvalues are consistently $\sim 1.5-2$ eV higher than those of the *ab initio* calculation. However, we obtain an identical ground-state configuration to the *ab initio* method. There are three points which should be made here, however, *a* corresponding eigenvalues from different *ab initio* calculations frequently differ by 2 eV or more. [4] Hence one might regard 2 eV as the "tolerance" of such a calculation *b* the experimental ionization potential of CO lies between 20 and 23 eV[4a] and the fit of the *ab initio* eigenvalues to this quantity is little better than that of the present work. (This value of I.P. does involve also some generation of excited oxygen atoms). *c* if we alter the k value in the equation for off-diagonal matrix elements to 1.1 then the lower eigenvalues become better fitted whilst the higher energy levels remain little affected. The charge distribution for all types of calculation reveals an essentially neutral molecule.

Several *ab initio* calculations are reported for SiO.[4] The present work (table 1) shows good agreement with these results. Those for "contracted" $3d$ orbitals on silicon do not differ significantly except that the polarity is Si$+0.09$, O-0.09. For brevity the eigenvalues are not listed here. There is, however, an interesting point of discrepancy; in our calculations a number of antibonding levels appear between 2 and 3 eV. Three of these interact with the molecular π and σ systems whilst the

---

[3] "Interatomic Distances in Molecules and Ions", Chem. Soc. Special Publ. N° 11, London, 1958.

[4] A. D. McLean and M. Yoshimine, "Tables of Linear Molecules Wave Functions", Supplement to Paper, "Computation of Molecular Properties and Structure" I.B.M. Journal of Research and Development, Nov. 1967.

[4a] "Electron Impact Phenomena", F. H. Field and J. L. Franklin, Academic Press, New York, 1957, p. 247.

Table 2

Electronic properties of carbon monoxide, carbon monosulphide, silicon monoxide and silicon monosulphide

CO

Eigenvalues			Charge distribution	
$1\Sigma^+$	−39.52	41.38^{+}	C 2*s*	1.59
$2\ \Sigma^+$	−20.25	21.86	$2p_\sigma$	1.14
1π	−15.17	17.40	$2p_\pi$	1.22
$3\Sigma^+$	−12.22	15.08	Nett charge on C	+0.05
$2\ \pi$	5.03	3.45	O 2*s*	1.64
$4\ \Sigma^+$	10.65	7.49	$2p_\sigma$	1.64
			$2p_\pi$	2.77
			Nett charge on O	--0.05

CS

	a		*b*		*a*	*b*
$1\Sigma^+$	−29.08		−29.50	C 2*s*	1.59	1.56
$2\Sigma^+$	−18.02		--18.40	$2p_\sigma$	1.33	1.22
$1\ \pi$	−12.51		−13.00	$2p_\pi$	1.08	1.20
$3\Sigma^+$	−10.30		−10.68	Nett charge on C	+0.00	+0.02
$2\ \pi$	3.90		1.90	S 3*s*	1.67	1.67
	— —	1Δ	3.55	$3p_\sigma$	1.42	1.45
	— —	$4\Sigma^+$	4.03	$3p_\pi$	2.92	2.71
	— —	3π	5.39	$3d_\sigma$	— —	0.10
$4\ \Sigma^+$	8.21	5Σ	8.03	$3d_\pi$	— —	0.09
				Nett charge on S	−0.00	−0.02

SiO

	a		*b*			*a*	*b*
$1\Sigma^+$	−34.46		−34.55	−34.78^{+}	Si 3*s*	1.71	1.71
$2\Sigma^+$	−17.12		−17.15	−16.60	$3p_\sigma$	0.80	0.81
$1\ \pi$	−11.84		−12.00	−13.23	$3p_\pi$	1.30	1.26
$3\ \Sigma^+$	−10.49		−10.53	−11.82	$3d_\sigma$	— —	0.01
	a		*b*			*a*	*b*
2π	1.85		1.51	1.40	$3d_\pi$	— —	0.03
	— —	1Δ	2.33		Nett charge on Si	+0.19	+0.18
	— —	$4\Sigma^+$	2.39		O 2*s*	1.72	1.72
	— —	3π	2.64		$2p_\sigma$	1.77	1.75
$4\Sigma^+$	4.72	$5\Sigma^+$	4.70	4.71	$2p_\pi$	2.70	2.71
					Nett charge on O	−0.19	−0.18

SiS

	a		*b*		*a*	*b*
$1\Sigma^+$	−25.60		−26.27	Si 3*s*	1.67	1.62
$2\Sigma^+$	−16.33		−16.96	$3p_\sigma$	1.12	1.03
1π	−11.57		−12.35	$3p_\pi$	1.20	1.22
$3\Sigma^+$	−8.87		−9.68	$3d_\sigma$	— —	0.05
2π	1.54		−0.04	$3d_\pi$	— —	0.06
	— —	1Δ	1.29	Nett charge on Si	+0.01	+0.02
	— —	$4\Sigma^+$	1.82	S 3*s*	1.67	1.66
	— —	3π	2.12	$3p_\sigma$	1.54	1.52
	— —	2Δ	3.63	$3p_\pi$	2.80	2.62
	— —	$5\Sigma^+$	3.67	$3d_\sigma$	— —	0.12
	— —	4π	4.31	$3d_\pi$	— —	0.10
$4\Sigma^+$	5.37	$6\Sigma^+$	5.06	Nett charge on S	−0.01	−0.02

$^{+}$ **eigenvalues abstracted from Ref. [4].**

Table 3

Electronic properties of carbonyl sulphide

COS	*a*		*b*
$1\Sigma^+$	−40.30		−40.95
$2\Sigma^+$	−28.66		−28.77
$3\Sigma^+$	−17.60		−17.92
1π	−17.38		−17.84
$4\Sigma^+$	−11.90		−12.08
2π	−10.07		−10.17
3π	− 3.59		2.29
	— —	1Δ	3.91
	— —	$5\Sigma^+$	3.93
	— —	4π	5.23
$5\Sigma^+$	6.62	$6\Sigma^+$	6.87
$6\Sigma^+$	9.69	$7\Sigma^+$	9.43

	a	*b*
C $2s$	1.14	1.14
$2p_\sigma$	0.94	0.93
$2p_\pi$	1.56	1.58
Nett charge on C	+0.36	+0.35
O $2s$	1.64	1.64
$2p_\sigma$	1.41	1.42
$2p_\pi$	3.12	3.08
Nett charge on O	−0.17	−0.14
S $3s$	1.67	1.67
$3p_\sigma$	1.19	1.19
$3p_\pi$	3.33	3.27
$3d_\sigma$	— —	0.02
$3d_\pi$	— —	0.06
Nett charge on S	−0.19	−0.21

other constitutes the essentially non-bonding silicon d_{xy} and $d_{x^2-y^2}$ orbitals which have δ symmetry. None of these levels appear in the *ab initio* calculations for SiO although a form of *d* orbital was included in the calculation. This would be consistent with the use, in the *ab initio* method of polarization functions instead of a complete set of *d* orbitals.

The charge distribution shows a more polar molecule than CO: this is as would be expected and agrees with the trend given by the *ab initio* results. One valuable criterion for judging semiempirical against *ab initio* results is whether one would draw different conclusions about the chemistry from them. In the cases quoted here essentially the same meaning would be inferred from both sets of results.

EFFECT OF *d* ORBITALS IN THE BONDING

Firstly, the 3*d* orbitals take part to some extent in the bonding of all the silicon and sulphur systems. Because of the linear symmetry of all the species studied there is true separability into σ, π and δ bonding. The *d* orbitals can partake in all three and, indeed, only *d* orbitals can be involved in the latter. In CS, SiO, and COS there must be a pair of non-bonding δ type orbitals on the second-row atom. Under the axis definition used these are the d_{xy} and $d_{x^2-y^2}$ orbitals. Inclusion of *d* orbitals lowers the molecular energy to a small extent *i.e*, SiO, 0.07%; SiS 0.8%; CS 0.4%; and COS 0.1%. This is remarkably small and ties up with the population of the *d* orbitals (in no case > 0.3e). The *d* electron density generally resides in σ and π type orbitals and only in SiS can the δ-type orbitals become occupied. In practice the latter pair of orbitals do not enter the bonding scheme and hence their resultant population is zero.

The molecular one electron energy levels are all displaced to lower energies by *d* orbital inclusion and this factor raises the ionization potentials of the systems. The charge distribution over the systems reflects the classical electro-negativity principle : thus the most polar molecule is SiO > CO > CS ~ SiS. Surprisingly in COS both oxygen and sulphur remove electrons from carbon whereas one might have expected a drift from sulphur to oxygen across the molecule leaving carbon virtually neutral.

For brevity, the bond order data will not be given here as it is possible to generalise the results. Essentially, the *d* orbitals all undergo mutually weak interactions and only affect the overall bonding through mixing with the 3*s* and 3*p* levels. In fact the main effects are manifest on the σ systems of the molecules.

THEORETICAL INTER-RELATIONSHIPS OF THE MOLECULES SiO and CO

It is instructive to compare CO and SiO together with their oxidation products CO_2 and SiO_2. CO is a stable species whilst SiO is short-lived and we hope to elucidate the reasons for this from the calculations. Perhaps the most striking differences between the computed results lie in the eigenvalues : here the highest bonding levels in SiO are less energetic than they are in CO and are hence more prone to electron loss. Moreover, the electron-acceptor orbitals (*i, e.* the first antibonding) are very much more stable (by ~ 3 eV) in SiO than in CO. Hence SiO should also more readily accept electrons than CO.

On comparing the energy levels of the two systems with those of their oxidation products [1] CO_2 and molecular SiO it is seen that the energy levels of CO gain little stability by attachment of a second oxygen. Furthermore the CO molecule has little tendency to gain or lose electrons and hence it is hardly surprising that the compound is a neutral generally non-reactive gas.

With SiO marked changes in electronic structure occur when we pass to the SiO_2 molecule. In the latter the new π bond formed lies at similar energy to the one already existing in SiO but the stable first σ level in SiO becomes much less stable in SiO_2. Hence we would expect that SiO, although more susceptible to both loss and gain of electrons than CO, would gain little stabilizing energy by forming SiO_2 molecules but would readily be oxidized to the condensed phase (*i.e.* SiO_2 solid).

The $3\sigma^+$ bonding orbital in CO is 60% (*ab, initio* [4] 62%) composed of a mixture carbon 2*s* and $2p_z$ orbitals (an *sp* hybrid) carbon whilst in SiO the proportion is 62% (*ab initio* [4] 63%) a minor portion occupying the d_{z^2} orbital. In the first antibonding orbitals (2π) of CO each component of the degenerate pair is 70% centred on C and in SiO this localization is nearly 80% of which ~ 20% is in the d_π orbitals.

It is therefore expected that SiO should be a σ donor and π acceptor like CO but because of its lower ionization potential should give electrons more readily whilst accepting efficiently from elements having available electrons in orbitals at energies around +1 −2 eV. The polarity of SiO compared with CO may, of course, militate against its efficacy as an electron donor to a transition element as these are frequently positive centres themselves. The difficulty would be lessened in an organometallic compound, however.

CO and CS, SiO and SiS

The energy level characteristics of CS are very similar to those of SiO. Hence it would also be expected to lose and gain electrons readily and be a reactive species. This is, in fact, the case. However, whereas we do not expect SiO to yield *molecular* SiO_2, both molecular CS_2 and the intermediate, COS, are known. It is noticeable that COS exhibits stable energy levels comparable with those of CO_2[1] (table 3). Hence CS should be stabilized by addition of an oxygen atom. Addition of a further sulphur atom however leads to quite different theoretical results. In CS_2 the *bonding* π_g, π_u and σ_u^+ are comparable with those of CO_2 and COS although somewhat more labile.[5] The first π_u level is however very well disposed energetically for accepting electrons. There are, moreover, a number of low-lying levels stemming from the *d* orbitals of sulphur which can also accept electrons. This is consistent with the known chemical reactivity of CS_2, (the compound which is endothermic with respect to its elements and is entropy-stabilized).

By comparison with CO, CS and SiO and using the same criteria SiS is predicted to be the most labile of this series of diatomic molecules.

It is interesting to speculate on the possibility of stabilizing SiS, or CS by coordination to a transition metal. Firstly, neither of these molecules is predicted to be polar (unlike SiO). Their highest bonding levels are again built partly from *sp* hybrids on C or Si (SiS 53%; CS, 50%) but the electrons are less concentrated on Si and C in this donor orbital. This is because the sulphur d_{z^2} orbital tends to remove some of the electronic charge. The first antibonding acceptor orbitals in CS are very strongly weighted with respect to sulphur whilst in SiS they are more strongly weighted with respect to Si. Coupled with the low energies of this orbital pair this means that it might be possible to form SiS stabilized by a low oxidation state transition metal ion. Further, CS might also be stabilized by a transition metal ion and because of the polarity of the donor and acceptor orbitals could perhaps be attached as —SC rather than CS.

COS

As aforestated, we find that COS should have intermediate stability between CO_2 and CS_2. Now it is interesting that CO_2 does not form coordination complexes with transition metal ions whereas CS_2 has been shown to give such complexes with Pt.[6] From table 3 it can be seen that the electrons in the bonding π level of COS are more readily available than are those in the π_g level of CO_2.[1] Moreover, the acceptor π orbitals of COS is more favourably disposed than is the π_u level of CO_2. Hence, we should expect to form transition metal π complexes of COS. In these the molecule might be angular.

---

[5] P. G. Perkins, to be published.

[6] M. Baird, G. Hartwell, R. Mason, A.I.M. Rae and G. Wilkinson, *Chem. Comm.*, **1967**, 92.

Revue Roumaine de Chimie, **18**, *8*, 1295–1299 (1973)

HEAT OF MELTING FOR EUTECTICS FORMED IN BINARY SYSTEMS OF $AgNO_3$ WITH KNO_3, $RbNO_3$, $CsNO_3$, AgCl AND AgBr

D. I. MARCHIDAN and LAURA VASU

Centre of Physical Chemistry
str. Galaţi 31, Bucharest, Romania

Received March 31, 1973

By means of a differential calorimetric method the heats of melting in the binary eutectic mixtures of $AgNO_3$ with KNO_3, $RbNO_3$, $CsNO_3$, AgCl and AgBr were determined. The results are explained on the basis of a thermodynamic cycle.

In this work, we have extended the differential calorimetric studies [1,2] on heats of melting to binary mixtures with eutectic and distectic compositions. We have worked on some binary mixtures with silver salts. The purpose of this study is twofold : to extend the performance of the differential calorimeter and to obtain heat of melting values for some eutectic mixtures.

EXPERIMENTAL

The results were obtained with a differential calorimeter similar to that used in a previous work,[1] except that the sensitivity was increased three times by using four thermocouple beads symmetrically disposed on the bottom of the cell. To calibrate the calorimeter we have used the method already reported.[1] Runs were carried out at a heating rate of 2.7°/min.

The pure chemicals used for calibration were $AgNO_3$, KNO_3, $NaNO_3$, AgCl and AgBr. The pure salts were dried and melted in the respectiv acid atmosphere and the eutectic mixtures were prepared by melting the components together and pouring the melt into the cell, in the dark.

---

[1] D. I. Marchidan and L. Vasu, *Rev. Roumaine Chim.*, **17**, 1649 (1972).

[2] D. I. Marchidan and M. Gambino, *Bull. Soc. chim. France*, **6**, 1954 (1966).

RESULTS AND DISCUSSIONS

The systems we have studied are: $AgNO_3 + KNO_3$, $AgNO_3 + RbNO_3$, $AgNO_3 + CsNO_3$, $AgNO_3 + AgCl$, $AgNO_3 + AgBr$. Phase diagrams of these systems (figs. 1 and 2) were taken from literature [3-6] and verified by the differential calorimetric curves.

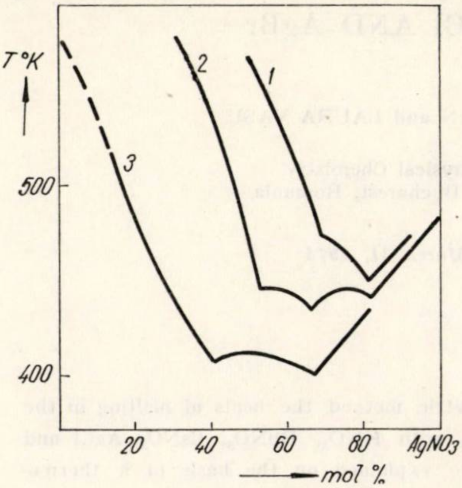

Fig. 1. — Phase diagrams for the systems: $AgNO_3 + AgCl$ (*1*), $AgNO_3 + CsNO_3$ (*2*) and $AgNO_3 + RbNO_3$ (*3*).

Fig. 2. — Phase diagrams for the systems: $AgNO_3 + AgBr$ (*1*) and $AgNO_3 + KNO_3$ (*2*).

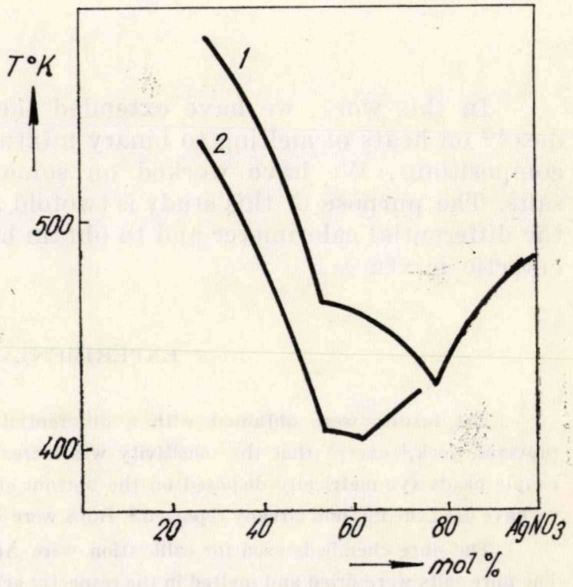

---

[3] M. K. Voskresenskaya "Spravochnik po plavkosti sistem iz bezvonjkh neorganicheskikh solei", vol. 1, Izv. Nauk SSSR, Moscow, 1961, p. 50, 51, 57, 581 and 585.

[4] G. M. Lifshitz, *Zhur. obshchei Khim.*, **26**, 19 (1956).

[5] P. V. Clark "Data Cumulation: Fused Salt Mixtures. Eutectic Compositions and Melting Points", Albuquerque USA, 1961, p. A 40, A 45 and A 216.

[6] P. Franzosini and C. Sinistri, *Ric. Sci. Rend.* Sez. A **3**, 439 (1963).

In table 1, the heats of transition for pure salts are given (the first four salts have been used for calibration).

Table 2 contains the heats of melting for the eutectics and distectics and the values we have obtained for eutectic compositions. We have determined the eutectic and distectic compositions from the extreme points on the melting temperature-composition curve and also by requiring the shape of the differential temperature-time curve recorded to be the same as for a pure salt. The peak of the differential temperature-time curve for an eutectic is very narrow (the transition takes place at a certain temperature). The shape of the recorded curve is very sensitive to the "departure" from eutectic. This way, we found the eutectic composition for $AgNO_3 + AgBr$ mixture at 78% mol $AgNO_3$ and for $AgNO_3 + CsNO_3$ mixture at 66% mol $AgNO_3(E_1)$, while the references [3] give the values 76.5%, and 67.5%, respectively.

Table 1

Heats of transition and heats of melting for pure salts

Salt	T_{tr} K	ΔH_{tr} j/mol	$\Sigma\Delta H_{tr}$ j/mol	Salt	T_{tr} K	ΔH_{tr} j/mol	$\Sigma\Delta H_{tr}$ j/mol
$AgNO_3$	432	2430[7]		$RbNO_3$	448	4390	
	484*	12570[7]	15000		501	3110	
KNO_3	401	5570[7]			548	800	
	608*	9830[1]	15400		580*	4305**	12650
AgCl	728*	12970[1,8]	12970	$CsNO_3$	429	5020	
AgBr	695*	9200[1,8]	9200		679*	13810**	18830

* melting point; ** values given by Janz in ref.[9] are 4640, respectively 14100 j/mol (in this paper 1 cal = 4.184 joules).

As one can see from table 2, the eutectic melting heats are smaller than a ponderal value including all transitions before melting, and the melting values for pure salts.

Let us consider a binary eutectic $A + B$, whose components have no transition before melting (more precisely, between the melting point of the eutectic and the melting points of the pure components) and draw

---

[7] T. Ozawa, H. Isozaki and A. Nagishi, *Thermochimica Acta*, **1**, 549 (1970).

[8] O. Kubachevskii and E. Evans "La thermochimie en métallurgie", Dunod, Paris, 1964, p. 272.

[9] G. J. Janz "Molten Salts Handbook", Academic Press, N.Y., 1967, p. 184.

Table 2

Heats of melting for the binary mixtures

Mixture $A + B$	mol % A	T_m K	ΔH_E^{exp} j/mol	ΔH_m^{id} j/mol	Transition***	$\frac{\Delta H_E^{\text{exp}} - \Delta H_m^{\text{id}}}{\Delta H_m^{\text{id}}}$ (%)
(E)* $AgNO_3+KNO_3$	62	405	13600	(15150)	A_I, A_m, B_I, B_m	− 10.3
(E) $AgNO_3 + AgCl$	81.5	449	10550	(12650)	A_m,B$_m$	− 8.8
(E) $AgNO_3 + AgBr$	78	428	13000	(13720)	$A_I . A_m, B_m$	− 5.2
(E_1) $AgNO_3 \cdot RbNO_3+AgNO_3$	65	401	13390	14240	A_m, B_I, B_m	− 6.6
(E_2) $AgNO_3 \cdot RbNO_3+RbNO_3$	80	410	13100	(13720)	A_m, B_I, B_{II}, B_{III}, B_m	− 4.5
(E_1) $3AgNO_3 \cdot CsNO_3+AgNO_3$	72	440	13850	14520	A_m, B_I, B_m	− 4.6
(E_2) $3AgNO_3 \cdot CsNO_3+CsNO_3$	88	436	14430	(14890)	A_m, B_I, B_m	− 3.1
(D)** $AgNO_3 \cdot RbNO_3$	50	413	13970	13990	A_I, A_m, B_I, B_{II} B_{III}, B_m	
(D) $3AgNO_3 \cdot CsNO_3$	75	445	14350	15950	A_I, A_m, B_I, B_m	

* eutectic: ** distectic; *** transitions included in the calculated H_m^{id}.

the following cycle:

$$\begin{tikzcd}
A_S + B_S(T_E) \arrow[r] & A_S + B_S(T_A) \arrow[r] & A_L + B_S(T_A) \arrow[d] \\
 & & A_L + B_S(T_B) \arrow[d] \\
(A + B)_L \text{ mix } (T_E) \arrow[uu, "\Delta H_E"] & (A+B)_L \text{ mix } (T_B) \arrow[l] & A_L + B_L(T_B) \arrow[l]
\end{tikzcd}$$

where the subscript S refers to solid, L — to liquid, mix — to mixture and T_A, T_B, T_E are the melting temperatures of the components and of the eutectic ($T_B > T_A$).

So, we can write for a binary eutectic

$$\Delta H_E = x_A \Delta H_A + x_B \Delta H_B + \Delta H^L_{\text{mix}}(T_B) + [x_A Cp^S_A + x_B Cp^S_B](T_A - T_E) +$$
$$+ [x_A Cp^L_A + x_B Cp^S_B](T_B - T_A) - Cp^L_{A+B}(T_B - T_E) \qquad (1)$$

where

x_A, x_B = molar fractions of the pure components in the eutectic.

ΔH_A, ΔH_B, ΔH_E = heats of melting for the pure components and for the eutectic.

$\Delta H^L_{\text{mix}}(T_B)$ = heat of mixing of the components A_L and B_L at the temperature T_B.

Cp^S_A, Cp^L_A, Cp^L_{A+B} ... = molar heat capacities for the pure components in the solid and liquid state and for the liquid mixture.

If there are transitions before melting in the pure salts (in the ranges $T_E - T_A$ and $T_E - T_B$) we have

$$\Delta H^{\text{calc}}_E = \Delta H^{\text{id}}_m + \Delta H^L_{\text{mix}}(T_B) + \Delta H(Cp) \qquad (2)$$

where

$$\Delta H^{\text{id}}_m = x_A \sum_i \Delta H_{Ai} + x_B \sum_j \Delta H_{Bj}$$

ΔH_{Ai}, ΔH_{Bj} = heat of the i—th and respectively j—th transition of the components A and B, respectively.

$\Delta H(Cp)$ = excess heat due to the differences in heat capacities for all temperature ranges between transitions and heat capacity of the liquid.

The magnitude and the sign of the difference

$$\Delta H^E_E = \Delta H^{\text{exp}}_E - \Delta H^{\text{id}}_m \qquad (\Delta H^{\text{exp}}_E = \Delta H_E \text{ experimental})$$

depends on the sum $\Delta H^L_{\text{mix}}(T_B) + \Delta H(Cp)$.

For binary mixtures with silver ions (nitrates or nitrate-halide) the experimental heats of mixing are, in the most cases, negative [9–11] so that, in our case, the sign of the ΔH^E_E is more likely to be negative. Unfortunately, we can refer only to two eutectic mixtures, *i.e.* $AgNO_3 + AgNO_3 \cdot RbNO_3$ and $AgNO_3 + 3AgNO_3 \cdot CsNO_3$, the others being complicated by the instability of the distectic or by the presence of a peritectic (In table 2, the brackets signify that one component is not the right one to be taken into account).

For binary mixtures forming solid solutions, the "excess" heat of melting is given by

$$\Delta H^L_{\text{mix}} - \Delta H_{S \cdot S} + \Delta H(Cp),$$

where $\Delta H_{S \cdot S}$ is the heat of formation of the solid solution.

It may be noticed that ΔH^E_E is not what is usually taken as an excess quantity; an excess heat of melting would be the difference $\Delta H^{\text{exp}}_E - \Delta H^{\text{calc}}_E$, where ΔH^{calc}_E is defined by eq. (2).

To conclude, it is necessary to do a systematic study on simple one-eutectic binary mixtures and on solid solutions.

---

[10] G. J. Janz "Molten Salts Handbook", Academic Press, N.Y., 1967, p. 194.

[11] J. Lumsden "Thermodynamics of Molten Salt Mixtures", Academic Press,N. Y., 1966, p. 122 and 130.

Revue Roumaine de Chimie, **18**, *8*, 1301–1310 (1973)

CALORIC CAPACITIES OF VAPOURS OF ORGANIC LIQUIDS. I

A FLOW CALORIMETER

RODICA VÎLCU and B. COMAN

Chair of Chemical Thermodynamics and Electrochemistry,
University of Bucharest, Bd.Republicii 13, Romania

Received January 17, 1973

The construction and the way a flow calorimeter functions for fixing the caloric capacities of organic fluids in the vapour phase, at a constant pressure and a large temperature range (25–150°) are described. The device, previously tested with argon, was gauged with benzene vapours and checked with acetone and methanol vapours. The obtained results were in good agreement with the caloric capacities published for these substances.

INTRODUCTION

Though we have many experimental data on the caloric capacities of organic fluids, mainly at average temperatures, when systematizing them, we find in most cases considerable gaps for temperatures higher than those of the boiling point of the liquids.

The absence of these thermal quantities can be supplied by the data calculated by acknowledged methods, of which some are empirical, others based on statistical calculus. Besides the empiric and semiempiric methods, such as the structural similarity method[1] and the group contribution method[2–5], we notice rigorous statistical methods developed by Rossini and Pitzes[6], with modifications suggested by Mecke[7] and applied to the calculus of the caloric capacities of organic vapours by Bennewitz and Rossner[8].

---

[1] G. S. PARKS and H. M. HUFFMAN, "The Free Energies of Some Organic Compounds", *A. Chem. Soc. monograph.*, N°. 60, Chemical catalogue, Co. New York (**1932**).

[2] J. W. ANDERSON, G. H. BEYER and K. M. WATSON, *Natl. Petrol. News*, **36**, R 476 (1944).

[3] J. L. FRANKLIN, *Ind. Eng. Chem.*, **41**, 1070 (1949).

[4] M. SANDERS, C. S. MATTHEWS and C. O. HURD, *Ind. Eng. Chem.*, **41**, 1037, 1048 (1949).

[5] D. W. VAN KREVELEN and H.A.G. CHERMIN, *Chem. Eng. Sci.*, **1**, 66 (1951).

[6] F. D. ROSSINI, K. S. PITZER, R. L. ARNET, R. M. BRAURE and G. C. PIMENTEL, "Selected Values of Physical and Thermodynamic Properties of Hydrocarbons and Related Compounds", Am. Petroleum Inst. Project 44 (Pittsburgh), 1953.

[7] H. MECKE, *Z. phys. Chem.*, **B 16**, 409, 421 (1932).

[8] K. BENNEWITZ and W. ROSSNER, *Z. phys. Chem.*, **B 39**, 126 (1938).

Variants of such equations improve the calculated values of the caloric capacities [9,10].

Among the experimental methods applied to determine the caloric capacities, based on various types of measurements (propagation velocity of ultrasonic waves, adiabatic expansion, the hot wire method, interferometric and chromatographic methods, calorimetry, etc.), we have chosen for the gas phase in dynamic conditions, [11] a calorimetric method adapted by us to direct determinations of caloric capacities under constant pressure for vapours produced by organic liquids.

EXPERIMENTAL

The model on which the construction of the flow calorimeter is based, for determining the heat capacities of organic vapours, is an electric calorimeter, experimented by Sokolov [11] on gases, which works based on an elementary calorimetry principle : a given energy Q supplied to a given quantity m of gas, determines a given temperature increase Δt, as a function of the nature of the chosen system, so that the heat capacity of the gas is

$$C_p = Q/\Delta T \tag{1}$$

The differences in the thermal behaviour of the vapours, studied in comparison with the particularities of the gases studied by means of the Sokolov calorimeter, imposed some structural adaptations, as well as the introduction of some additional elements into our original device, the usefulness of which is shown in a minute description of the calorimeter :

The general equipment for determining the heat capacities of organic vapours is represented in the block diagram in figure 1.

It consists of the following main parts :

1. **Preheater, P**
2. **Vapour generator, G**
3. **Calorimetric cell, C**
4. **Measuring device for temperature differences, T**
5. **Thermostatic system, S_T**
6. **Condensation system, S_C**
7. **Vacuum device, A**

1. *The preheater* (P) (fig. 2) consists of a Pyrex glass tube, on which the electric resistance R_1 of 75 Ω, 750 w, is wound fed by the electric network through the agency of an autotransformer.

The temperature of the liquid in the preheater is measured with a mercury thermometer.

The temperature value should not exceed the boiling point. The temperature can be controlled by means of the autotransformer's rheostat.

---

[9] P. Fugassie and C.E. Rudy, *Ind. Eng. Chem.*, **30**, 1020, 1029 (1938).

[10] C. J. Dobratz, *Ind. Eng. Chem.*, **33**, 759 (1941).

[11] S. N. Sokolov, *Izvest. V. U. Z. Fiz.*, **5**, 179 (1963).

2. *The vapour generator* (*G*) coupled with the preheater (fig. 2) is made of Pyrex glass with double walls, between which flows the thermostatic liquid, refluxed from a thermostat.

It is meant to grant, as far as possible, a constant vapour flow, without carrying away the liquid droplets.

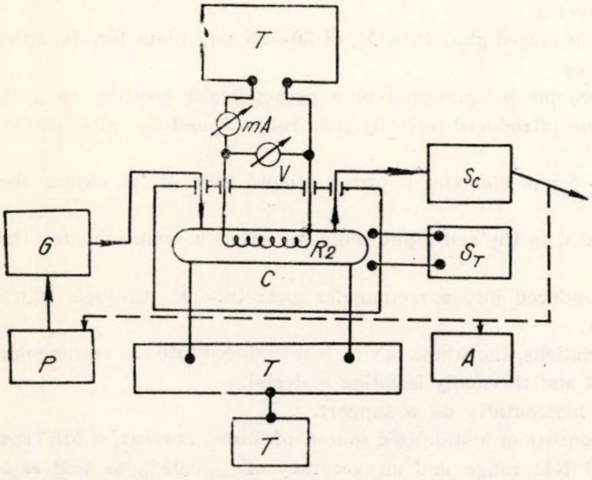

Fig. 1. — The general layout of the calorimeter device.

P — Preheater; *G* — Vapour generator; *C* — Calorimetric cell; *T* — Measuring device for temperature differences; S_T — Thermostatic system; S_C — Condensation system; *A* — Vacuum device.

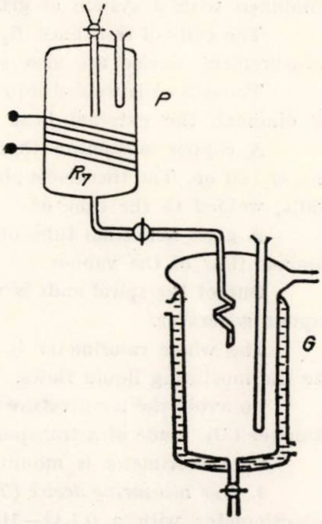

Fig. 2. — The general scheme of the preheater and of the boiler.

P — Preheater; R_1 — Electric resistance; *G* — Vapour generator.

The temperature of the liquid in the generator, as well as of the generated vapours, is constantly measured.

3. *The calorimeter* (*C*) (fig. 3) is made of Pyrex glass: it consists of a glass cell (ab) of 260 mm length and of 8 mm inner diameter; the thickness of its wall should not

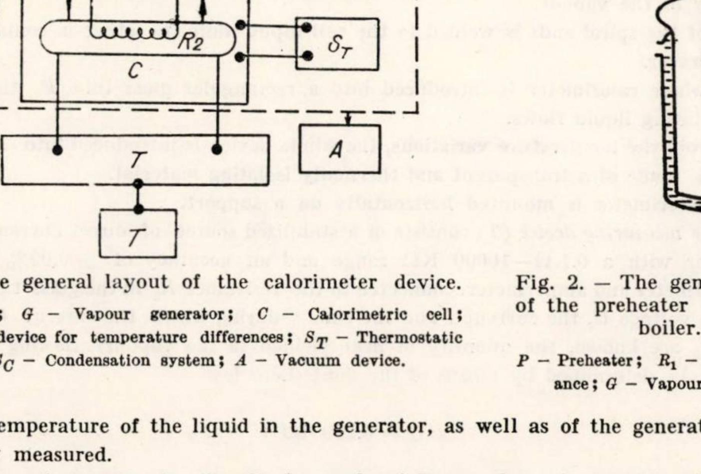

Fig. 3. — The principal elements of the calorimeter.

C — Calorimetric cell; *a,b* — glass cell; *M,E* — glass jacket; *S* — glass helicoidal; *D* — rectangular chamber; t_i — hole for thermometer; *F,V* — Refrigerator; S_c — Condensation system.

exceed 0.2–0.5 mm, so as to allow the thermal equilibrium to be established in a short time. A resistance (R_2), of 15–20 Ω, made of platinum or constantan is introduced into the cell.

The resistance R_2 is removable, to be easily replaced in case of deterioration, without affecting the rest of the installation. It is fitted into cell *ab* by means of thin cowal tubes, combined with a system of grinding stopper.

The ends of resistance R_2 are bound on the outside to rings to which the wires of the measurement device are also connected.

The cell *ab* is welded into a vacumized glass tube M, of 30–35 mm diameter, in order to diminish the external heat losses.

A copper-constantan thermocouple is connected in a perpendicular position to each end of cell *ab*. The thermocouples are introduced into the glass tubes d_1 and d_2, with double walls, welded to the tube *ab*.

A glass helicoidal tube of 4–5 mm diameter is placed around tube M, to ensure the laminar flow of the vapour.

One of the spiral ends is welded to the cell input while the other is connected to the vapour generator.

The whole calorimeter is introduced into a rectangular glass tube E, through which the thermostating liquid flows.

To avoid the temperature variations, the whole device is introduced into a rectangular chamber (D), made of a transparent and thermally isolating material.

The calorimeter is mounted horizontally on a support.

4. *The measuring device* (T) consists of a stabilized source of direct current, a METRA potentiometer with a 0.1 Ω–10000 KΩ range and an accuracy of ± 0.02% as well as a class 0.5, voltmeter and ampermeter, connected to the resistance R_2 in the glass tube *ab* (fig. 1).

If the voltage U, the current I and the time τ during which the current flows through resistance R_2 are known, the quantity of heat yielded to the vapours flowing through the tube *ab* may be determined by means of the Joule-Lenz law

$$Q = 0.239\ UI\ \tau \qquad (2)$$

By means of the two thermocouples, differentially connected, we read on the FEA type E 36 electronic recorder, automatically compensated with a ± 0.5% regulating accuracy and a sensitivity of 0.1%, the temperature difference (ΔT) of the vapour between the input and output of the calorimeter.

The ΔT temperature difference should not exceed 10–15° so as to avoid high temperature gradients disturbing the determinations.

5. *The thermostatic system* (S_T) forms an important element of the equipment since it conditions the vapour temperature of the calorimeter input.

In most cases, the errors in determining the caloric capacities are due to deficiencies of the thermostatic system.

When the determinations are carried out at temperatures higher than the boiling point of the liquid in the vapour generator, the thermostat shall be connected with the calorimeter through tubes that are themselves under the influence of the thermostat, thus avoiding the vapour condensation. The thermostatic effect was ensured for the temperature range of 25–150°, the thermostating liquid being paraffin.

The vapour temperature in the circuit should not exceed by more than ± 0.1° the temperature of the calorimeter thermostat, so as to avoid temperature gradients, which disturb the measurements.

The thermostat device should ensure a ± 0.01° accuracy.

6. *The condensation system* (S_c) attached to the calorimeter (fig. 3) is composed of the refrigerator F and the Dewar type vessel V, vertically set. The conduct of refrigerator F leads into vessel V, which contains a refrigerent mixture (ice with salt, or liquid nitrogen) to ensure the condensing of the vapour.

The condensate thus obtained is collected in a graduated tube. The quantity of vapour flowing in time τ through the calorimeter is equivalent to the quantity of condensate collected in the graduated glass, which is accurately read and measured by means of two marks.

Before introducing the studied vapours into the installation, the air is evacuated by means of a vacuum device A.

The installation is washed by means of the vapours of the substance under study, for 5 minutes before the determination.

The measurements are not to be made during the washing. The temperature in the vapour generator shall be maintained all the time at the value necessary for the liquid vaporization.

PROCEDURE

After washing the installation, one awaits the stabilization of the temperature at the boiling point of the substance to be experimented.

Then, the liquid is poured into the preheater P, the temperature of which is beneath the boiling point, and approximately 5–10 min later, the substance is flown into the vapour generator (G).

After about 5 min, till the thermal equilibrium is established, resistance R_2 is connected into the electric circuit and the voltage (U) and the current (I) are set at the chosen values. At rigorously recorded time intervals (*e.g.* every 5 min), the values ΔT, U, I as well as the mass of the condensed liquid are read.

The vapour flow may be measured in volume units, or in mass units per time unit.

The calorimeter was gauged for the temperature range within which the determinations were carried out. For the gauging, benzene with a known heat capacity is used, the determination being made as described above. The total heat capacity of the $(C_{p\,\mathrm{tot}})_B$ system is thus obtained

$$(C_{p\,\mathrm{tot}})_B = C_{p\,B} + K \tag{3}$$

being composed of the caloric capacity (constant) of the apparatus (K), and the caloric capacity ($C_{p\,B}$) of the benzene. From the measured quantity $(C_{p\,\mathrm{tot}})_B$, and $C_{p\,B}$ being a known quantity, the apparatus constant is easily calculated.

When experimenting with organic vapours with an unknown heat capacity ($C_{p\,x}$), the total heat capacity of the new system $(C_{p\,\mathrm{tot}})_x$ is measured, from which the unknown thermal quantity is deduced

$$C_{p_x} = (C_{p_{\mathrm{tot}}})_x - K \tag{4}$$

By means of equation (1), the heat capacities are easily computed according to the measured quantities. The electric energy, transformed into the heat quantity (Q) absorbed by the vapours, is computed by means of equation (2); ΔT, with the given significance, is directly measured, while the vapour mass (m) — on the assumption of their ideal behaviour — is expressed as a function of the state parameters system (volume V of the condensed substance in (1) atmospheric pressure P in 1 atm/mol deg and the molecular mass of the substance under study) as follows

$$m = M(PV/RT)$$

The heat capacity takes generally the form

$$C_p = 0.239\ RTUI\tau/PV\,(\Delta T) \tag{5}$$

where : $T = 273.16 + t$, with

$$t = t_1 + (\Delta t/2)$$

where : t_1 — is the vapour temperature at the cell C input. It results that the complete calculation formula of the heat capacity (C_p) is

$$C_{p_x} = 0.239\ RTUI\tau/PV\,(\Delta T) - K \tag{6}$$

The above described apparatus has not only the qualities of a calorimeter for experiments in the gaseous phase, but also a construction specially adapted to the calorimetric study of the organic vapours. These particularities are required by the necessity of purifying the organic substances, in certain thermal conditions imposed by the working conditions at high temperatures for maintaining the substance in the vapour phase, and of preventing any noxious effects when experimenting with corrosive vapours, etc.

Such requirements led to special precautions to avoid thermal losses by providing the calorimeter with isolating linings and thermostatic tube coils (the coil (*s*) and the calorimeter play the role of an equalizer making the vapour flow at a constant speed).

Evidently, the vapour generator (*G*) of an original construction is a specific element of the calorimeter for thermal studies of vapours.

The way of setting the resistance R_2 in the calorimeter circuit is achieved according to an original conception, the various construction details, apparently unimportant, yet leading to efficient results. For instance, the perpendicular placing of the thermocouples, with regard to the vapour flow and to the position of resistance R_2, allows a correct reading of the temperature difference (ΔT) at the vapour input and output of the calorimeter.

In literature, a common direction of the thermocouples and of resistance R_2 is given, which we found inadequate.

RESULTS AND DISCUSSIONS

Tables 1, 2, 3 record the experimental values of the caloric capacities of benzene, acetone and methanol, supplied by the installation described in this paper.

The substances used came from SERVA (Federal Republic of Germany); WIENFISCHAMEND (Austria) and REACTIVUL — Bucharest.

The experimental determinations were carried out at the atmospheric pressure, in the temperature range between 150° and the boiling points of the liquids.

Table 1

The heat capacities of benzene in the gas phase

Experimental data							C_p cal	C_p cal	C_p cal
T K	U(v)	I(A)	τ(s)	V(l)	ΔT	K	mole°K calcd.	mole°K lit.	mole°K lit.
358	6.1	0.35	120	0.085	285.6	58.60	24.28	—	—
363	6.2	0.35	120	0.086	285.6	59.50	24.90	—	—
368	6.33	0.35	120	0.088	285.6	60.10	25.30	—	—
370	6.4	0.36	120	0.091	285.6	60.60	25.64	25.43[12]	25.10
373	6.4	0.36	120	0.091	285.6	61.01	25.92	25.722[14]	—
								25.74[13]	—
378	6.45	0.37	120	0.094	285.6	62.21	26.21	—	—
383	6.6	0.37	120	0.096	285.6	63.23	26.50	—	—
388	6.8	0.38	120	0.101	285.6	64.85	26.72	—	—
393	6.9	0.38	120	0.102	285.6	67.54	26.94	26.50[13]	26.40
								26.70[8]	—
398	7.00	0.39	120	0.106	285.6	70.78	27.16	—	—
403	7.35	0.41	120	0.109	285.6	75.10	25.45	27.52[13]	—
410	7.6	0.42	120	0.112	285.6	80.08	27.90	27.81[12]	27.60

Table 2

The heat capacities of acetone in the gas phase

Experimental data							C_p cal/mole °K Calcd.	C_p cal/mole °K lit.
TK	U(v)	I(A)	τ(s)	V(l)	ΔT	K		
333	4.85	0.27	120	0.049	285.6	54.72	20.02	19.97[8]
338	5.05	0.28	120	0.053	285.6	55.30	20.28	20.40[8]
343	5.21	0.29	120	0.057	285.6	56.00	20.46	—
348	5.40	0.30	120	0.061	285.6	56.85	20.60	—
353	5.60	0.32	120	0.068	285.6	57.75	20.80	—
358	5.95	0.33	120	0.074	285.6	58.57	20.98	—
363	6.30	0.34	120	0.081	285.6	29.32	21.05	—
368	6.20	0.35	120	0.082	285.6	60.24	21.25	—
373	6.50	0.36	120	0.088	285.6	61.10	21.35	—
376	6.51	0.37	120	0.088	285.6	61.70	21.46	21.30[8]

The comparative analysis of the experimental results, with regard to the published data, [8,12–17] shows a good agreement of the values thus obtained with the existing ones; the differences between the values of the two series do not exceed 0.3 % of the caloric capacity values of the vapours.

---

[12] J. B. Montgamery and T. De Vries, *J. Amer. Chem. Soc.*, **64**, 2372, 2375 (1942).

[13] D. W. Scott, G. Waddington, J. C. Smith and H. M. Huffman, *J. Chem. Phys.*, **15**, 565 (1947).

[14] J. L. Hales, J. D. Cox and F. B. Lees, *Trans. Faraday Soc.*, **59**, 1544 (1963).

[15] E. Strönsöe, H. G. Rönne and A. Lydersen, *J. Chem. and Eng. Data*, **15**, 286 (1970).

[16] G. S. Sinke, T. De Vries, *J. Amer. Chem. Soc.*, **75**, 1815 (1953).

[17] T. De Vries, and B. T. Collins, *J. Amer. Chem. Soc.*, **63**, 1343 (1941).

Table 3

The heat capacities of methanol in the gas phase

	Experimental data						C_p cal	C_p cal
T °K	U(v)	I(A)	τ(s)	V(l)	ΔT	K	mole °K calcd.	mole °K lit.
343	7.00	0.39	240	0.205	285.6	56.30	20.33	20.76[15]
348	7.10	0.40	240	0.219	285.6	56.90	18.79	
356	7.30	0.40	240	0.232	285.6	58.50	16.35	15.92[15]
373	7.70	0.43	240	0.278	285.6	61.20	13.22	13.43[15]
378	7.90	0.44	240	0.293	285.6	62.20	12.92	—
383	8.10	0.45	240	0.307	285.6	63.27	12.87	—
388	8.30	0.46	240	0.318	285.6	64.80	12.78	—
398	8.86	0.50	240	0.354	285.6	70.67	12.87	12.66[15]
								12.94[15]
403	9.40	0.52	240	0.370	285.6	75.87	13.10	12.96[17]
								13.03[16]
408	9.60	0.53	240	0.386	285.6	77.99	13.20	—
413	9.80	0.54	240	0.386	285.6	81.44	13.25	—

The graphic representations show more intuitively the dependence between the temperature and the data of the molar caloric capacities.

In the cases under study, they are represented in figures 4, 5, 6.

We notice that while the existing data concern caloric capacity values of vapours studied at disparate temperatures, our determinations aim at a systematic evaluation of these thermal quantities at small enough temperature intervals, for instance at every 5°. It was thus possible to plot the representative curve of $C_p = C_p(T)$, with absolute certainty. The representative points of the studied dependence, taken from the available bibliographical sources, [8,13-17] were placed on the same graphical representations.

The examination of the graphs in figures 4, 5 and 6 point out a $C_p = C_p(T)$ dependence of the same nature of the benzene and acetone vapours, though the behaviour of methanol is different from this standpoint.

CONCLUSIONS

The above calorimetric method offers the advantage of supplying directly exact data on caloric capacities for every temperature. The method can also be extended to the determination of variable pressures, although the significance of the data obtained under these conditions do not equal the practical importance of tne caloric capacity values at various temperatures.

It is also to be remarked that, the recorded heat capacity values could be dissimilar only in the case of large pressure variations.

The method is based on a robust device, of a simple enough construction, easy to operate and offering a quick response.

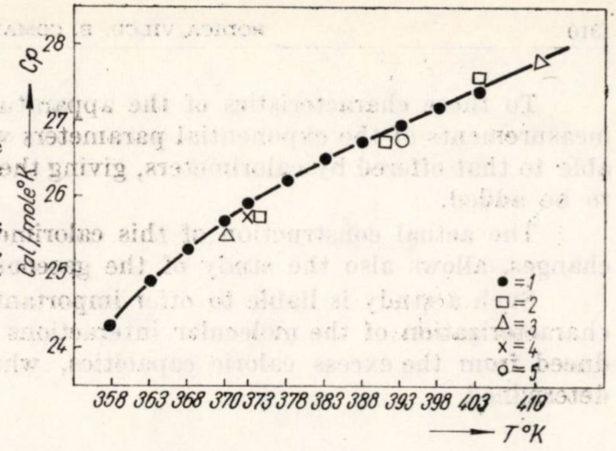

Fig. 4. — Correlation between the heat capacities of benzene in the gas and the temperature:

1, our data; *2*, Scott, Smith and Hyffman[13]; *3*, Montgomery and De Vries[12]; *4*, Hales, Cox and Lees[14]; *5*, Benewitz and Rossner.[8]

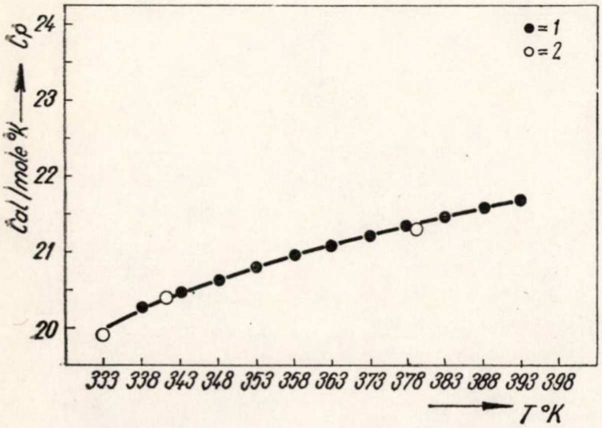

Fig. 5. — Correlation between the heat capacities of acetone in the gas and the temperature:

1, our data; *2*, Benewitz and Rossner.[8]

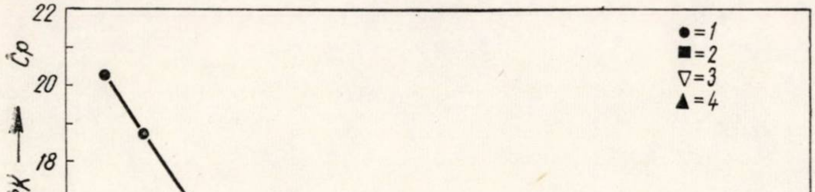

Fig. 6. — Correlation between the heat capacities of methanol in the gas and the temperature:

1, our data; *2*, Strömsoe, Rönne and Lydersen[15]; *3*, De Vries and Collins[17]; *4*, Sinche and De Vries[16].

To these characteristics of the apparatus, the possibility of exact measurements of the exponential parameters with an accuracy comparable to that offered by calorimeters, giving the best performances [8,12–17] is to be added.

The actual construction of this calorimeter, only with unessential changes, allows also the study of the gaseous mixtures.

Such a study is liable to offer important prospects concerning the characterization of the molecular interactions in the vapour phase, deduced from the excess caloric capacities, which could thus be directly determined.

Revue Roumaine de Chimie, **18**, *8*, 1311–1317 (1973)

TRANSFERENCE NUMBERS AND MOBILITIES IN MOLTEN UNIVALENT NITRATES

DUMITRU TOPOR

Centre of Physical Chemistry,
Str. Galaţi 31, Bucharest, Romania

Received February 24, 1973

The behaviour of the electrical transport properties of molten nitrates was described in connection with the specific structure of these fused salts. The electrical mobility and the transference numbers were measured by electromigration and with a modified Hittorf method using radioactive tracers. Transference data for univalent cations follow a simple mass relation and the Nernst-Einstein relation for alkali nitrates and silver nitrate. The mobilities of nine of the first and second group cations in fused Na, K, Rb and Cs nitrates can be in a close correlation with the volume changes on fusion of these peculiar melts.

INTRODUCTION

Various studies on the transport processes in the ionic liquids have established, besides the temperature dependence of these processes, a close correlation with their structure but no theoretical interpretation has yet been made about them. For the solid state and the ideal gas a fairly good precision has been obtained in the calculation of the macroscopic properties from a rather common microscopic model. For liquids, particulary molten salts, the prediction of macroscopic properties has not been possible since the type and strength of the local interactions as well as the actual structure are still obscure. The interparticle potential in the ionic liquids is prevailing Coulombian, like in ionic crystals and many authors have considered the two systems very near with regard to their structure and particle motions. Thus, the strong interactions between ions lead to correlated motion of the particles and this statement was lately confirmed by molecular dynamics calculation of self-diffusion coefficients of solid and molten LiCl, NaCl and KCl by Woodcook.[1] The self-diffusion coefficients (D_+ and D_-) were calculated from the limiting slopes of the mean square displacement versus time curves and the results for NaCl and KCl are fairly close to experimental values derived from isotopic tracer measurements.[2]

---

[1] L. Woodcook, *Chem. Phys. Lett.*, **10**, 257 (1971).

[2] J. O' M. Bockris, S. Nanis and N. Richards, *J. Phys. Chem.*, **69**, 1627 (1965).

This paper is concerned with some results on the electric charge transport in the molten univalent nitrates which could be related to properties which are descriptive for these melts. These correlations are only qualitative because of the complex structure with local asymmetry of molten nitrates and the derivative character of measured properties. The structure of these melts has been recently reviewed [3] but in the past few years important achievements[4-6] have been made towards clearing it up on the basis of aggregate formation or clustering of the type $(MeNO_3)_n$.

EXPERIMENTAL

The cation transference number determinations in molten nitrates were carried out with a modified Hittorf method using radioactive tracers.[7] Some simplifications of the cell were made which are allowed by the use of radioactive tracers so that the experimental quantities supply reliable data for transference number calculation.[8]

For the electrolysis of molten $TlNO_3$, platinum electrodes were used and the samples prepared for counting were formed by both the salt and the separated metal contained in the catholyte.[9] For molten Rb and Cs nitrates the $Ag/AgCl/AgNO_3$ cathode was isolated by placing it in a tube attached through a capillary constriction to the cathodic compartment. Thus, the radioactivity of the catholyte was measured only for the salt contained in this compartment.[10,11] Details of the cell construction and procedure were described elsewhere.[8]

The cation mobilities were determined by a cell with a cylindrical zone of migration (a glass tube 3 mm in diameter filled with SiO_2 powder particles 0.1 mm in size and a nitrate melt) along whose an uniform potential gradient was established. Thus, through a long zone (about 15 cm) formed by a molten alkali nitrate (Na, K, Rb, or Cs) a small zone with the "foreign" cation (Li^+, Na^+, K^+, Rb^+, Cs^+, Ag^+, Tl^+, Sr^{++} and Ba^{++}) was moved towards cathode by electromigration. The apparent distance covered in a fixed time by these small zones was corrected with a labyrinth factor for each alkali nitrate (1.35 for $NaNO_3$ to 1.30 for $CsNO_3$) following the method of Berlin, Forcheri, Langevin and Wagner.[12] Other experimental details were previously described.[8]

RESULTS AND DISCUSSION

Transference numbers in molten nitrates

The experimental values for the transference numbers of the Rb^+, Cs^+ and Tl^+ ions in their own nitrates are expressed as an average of at least ten independent determinations as follows:

---

[3] D. Topor, *Studii și Cercetări Chim. Acad. București*, **20**, 673 (1972).

[4] G. Pollard, N. Smyrl and P. Delvin, *J. Phys. Chem.*, **76**, 1826 (1972).

[5] L. Woodcook, *Nature*, **232**, 63 (1971).

[6] P. Spedding, *J. Phys. Chem.*, **76**, 1348 (1972).

[7] F. Duke and A. Bowman, *J. Electrochem. Soc.*, **106**, 626 (1959).

[8] D. Topor, Thesis, University of Bucharest, 1971.

[9] I. G. Murgulescu and D. Topor, *Z. phys. Chem. (Leipzig)*, **219**, 134 (1962).

[10] I. G. Murgulescu and D. Topor, *Z. phys. Chem. (Leipzig)*, **221**, 39 (1962).

[11] I. G. Murgulescu and D. Topor, *Rev. Roumaine Chim.*, **13**, 3 (1968).

[12] A. Berlin, S. Forcheri, B. Langevin and V. Wagner, Report EUR-2954e (1966).

$$t_{Rb^+} = 0{,}376 \pm 0{,}003$$

$$t_{Cs^+} = 0{,}398 \pm 0{,}0015$$

$$t_{Tl^+} = 0{,}306 \pm 0{,}003$$

In table 1 the values of these transference numbers are given together with the most reliable data of other authors[13-16] for univalent cations in molten nitrates.

Table 1

Cation transference numbers in molten nitrates

Nitrate	t_+	Author
$LiNO_3$	0.84	F. Duke and R. Laity[13]
$NaNO_3$	0.71	F. Duke and B. Owens[14]
KNO_3	0.60	F. Duke and B. Owens[14,15]
$RbNO_3$	0.38	our data
$CsNO_3$	0.40	our data
$AgNO_3$	0.75	H. Bloom and D. James[16]
$TlNO_3$	0.31	our data

The simplest correlations between transference numbers and ionic properties were predicted by Mulcahy and Heymann[17] and by Sundheim.[18] The former authors have inferred a radius dependence, *i.e.* $t_+ = r_-/(r_+ + r_-)$, while the latter author has shown that the mass dependence, *i.e.* $t_+ = m_-/(m_+ + m_-)$, is of significance in pure molten salts. For the calculation of transference numbers with the relation of Mulcahy and Heymann the ionic radii in the nitrate melts must be known. However, these values are doubtful or dissimilar[19] since many authors have accepted the ionic crystalline radii which were given by Pauling.[20] Recently, Shannon and Prewitt[21] in a critical review on published ionic radii of most of the elements have proposed new values particulary for Rb^+ and Cs^+ ions. In table 2 three series of values as well as the chosen values are presented.

Although the mass and radius relations for transference number calculation are based on models and interactions borrowed from the theory of aqueous electrolytes or the momentum balance, a comparison

---

[13] F. Duke and R. Laity, *J. Phys. Chem.*, **59**, 549 (1955).

[14] F. Duke and B. Owens, *J. Electrochem. Soc.*, **105**, 548 (1958).

[15] S. Forcheri and C. Monfrini, *J. Phys. Chem.*, **67**, 1566 (1963).

[16] H. Bloom and D. James, *J. Phys. Chem.*, **63**, 757 (1959).

[17] M. Mulkahy and E. Heymann, *J. Phys. Chem.*, **47**, 485 (1943).

[18] B. Sundheim, *J. Phys. Chem.*, **60**, 1381 (1956).

[19] O. Kleppa and L. Hersh, *J. Chem. Phys.* **34**, 351 (1961); *Discuss. Faraday Soc.*, **32**, 157 (1962).

[20] L. Pauling, "The Nature of the Chemical Bond", Cornell University Press, Ithaca, 1960, p. 514.

[21] R. Shannon and C. Prewitt, *Acta Cryst.*, **25B**, 925 (1969); **26B**, 1046 (1970).

Table 2

Ionic radii (in 10^{-8} cm) in molten nitrates

Ion	Ionic radii			
	Traditional	Pauling	Shannon	Selected
Li^+	0.60–0.70	0.60	0.74	0.68
Na^+	0.95–0.98	0.95	1.02	0.96
K^+	1.33	1.33	1.38	1.33
Rb^+	1.48–1.49	1.48	1.66	1.66
Cs^+	1.65–1.69	1.69	1.82	1.82
Tl^+	1.50–1.90	1.59	1.50	1.60
Ag^+	1.02–1.44	1.29	1.15	1.26
$r_{NO_3^-}$	1.89–2.19	—	—	1.90

with experimental data can be relevant for the controlling factor in the electrical charge transport in molten nitrates. Table 3 lists the experimental transference numbers and the values calculated from the relations mentioned above.

Table 3

Experimental and calculated cation transference numbers for nitrates

Nitrate	t_{exp}	$t = r_- / (r_+ + r_-)$	$t = m_- / (m_+ + m_-)$
	Light nitrates		
$LiNO_3$	0.84	0.74	0.90
$NaNO_3$	0.71	0.66	0.73
KNO_3	0.60	0.59	0.61
	Heavy nitrates		
$RbNO_3$	0.38	0.53	0.42
$CsNO_3$	0.40	0.51	0.32
$TlNO_3$	0.31	0.54	0.23
	Coordination nitrate		
$AgNO_3$	0.75	0.60	0.36

The agreement of the experimental transference numbers with those calculated is good, except for t_{Ag^+} in silver nitrate. The mass relation agrees quite well even for "heavy nitrates", so that the ionic mass seems to play a prominent part. The radius relation can also be improved if the ionic polarizability P (having the meaning of electric configuration distorsion measure in the field of neighbouring ions of unlike charge) is used as correction factor for ionic radii. Thus, r_+ can be replaced by $r_+(P_+/P_-)^{1/3}$ and using the experimental values for P_+ and P_- reported by Tesman, Khan and Shokley [22] for $P_{NO_3^-} = 2{,}23$ (Å)^3 and by Pirenne and Kartheuser [23] for $P_{Cs^+} = 3{,}335$ (Å)^3 and $P_{Tl^+} = 3{,}88$ (Å)^3 the new values are : $t_{Cs^+} = 0{,}46$ and $t_{Tl^+} = 0{,}49$.

---

[22] J. Tesman, A. Khan and W. Shokley, *Phys. Rev.*, **92**, 890 (1953).

Additional informations can be acquired by applying the Nernst-Einstein equation to the case of univalent nitrates, [24] *i.e.*

$$t_+ = 1/2 + (F^2/2RT\Lambda)(z_+D_+ + z_-D_-)$$

where Λ is the equivalent conductivity of pure molten nitrate, D_+ and D_- are the self-diffusion coefficients of cation and anion, respectively, and $z_+ = z_- = 1$. In table 4 the experimental and calculated transference numbers are included.

Table 4

Nernst-Einstein relation for univalent nitrates, $t_+ = 1/2 + (F^2/2RT\Lambda)(D_+ + D_-)$*

Nitrate	D_+	D_-	t_+^{exp}	t_+^{calc}	Δt %
	cm^2 s^{-1}				
		Light nitrates			
LiNO$_3$	5.40	2.35	0.84	0.80	5.0
NaNO$_3$	4.84	2.49	0.74	0.74	0.0
KNO$_3$	2.81	2.36	0.60	0.56	6.7
		Heavy nitrates			
RbNO$_3$	1.57	2.87	0.38	0.35	8.2
CsNO$_3$	1.97	2.28	0.40	0.43	7.0
TlNO$_3$	3.22	3.70	0.31	0.44	29.5
		Coordination nitrate			
AgNO$_3$	4.95	2.79	0.75	0.70	7.1

* Λ, D_+ and D_- at $T = 723$ K

The self-diffusion coefficients were reported by Nagarajan and Bockris,[25] Dworkin, Escue and van Artsdalen,[26] Bhen and Sjöblom, [27] Forcheri and Wagner [28] and Kwak [29] and D_- for TlNO$_3$ was estimated to 3.7×10^{-4} cm^2 s^{-1} in agreement with Sundheim and Berlin [30] who have noticed that $D_{NO_3^-}$ in TlNO$_3$ must be greater then in molten silver nitrate. The conductivity data were calculated from the measurements reported by de Nooijer. [31] All the data are valid for 723 K.

From table 4 only the data for TlNO$_3$ are inconsistent with a small mean deviation (about 6 per cent) from Nernst-Einstein relation.

---

[23] J. Pirenne and E. Kartheuser, *Physica*, **30**, 2005 (1964).

[24] R. Laity, *Discuss. Faraday Soc.*, **32**, 172 (1962).

[25] M. Nagarajan and J. O'M. Bockris, *J. Phys. Chem.*, **70**, 1857 (1968).

[26] A. Dworkin, R. Escue and E. van Artsdalen, *J. Phys. Chem.*, **64**, 872 (1960).

[27] A. Behn and C. Sjöblom, *Z. Naturforsch.*, **24a**, 464 (1969).

[28] S. Forcheri and V. Wagner, *Z. Naturforsch.*, **22a**, 1171 (1967).

[29] J. Kwak, Thesis, University of Amsterdam, 1967.

[30] B. Sundheim and A. Berlin, *J. Phys. Chem.*, **68**, 1266 (1964).

[31] B. de Nooijer, Thesis, University of Amsterdam, 1965.

Thus, it appears that the transport numbers reported here support the application of the Nernst-Einstein relation to univalent nitrates too.

Cationic mobilities in molten alkali nitrates.

The mobilities of nine cations in alkali nitrates ($LiNO_3$ excluded) are given in table 5.

Table 5

Cationic mobilities (in 10^4 cm^2 s^{-1}) in molten nitrates at 723 K

Nitrate	Migrating ion								
	Li^+	Na^+	K^+	Rb^+	Cs^+	Ag^+	Tl^+	Sr^{++}	Ba^{++}
$NaNO_3$	4.58	—	4.71	4.45	4.43	4.98	4.73	4.70	4.86
KNO_3	3.59	4.78	—	2.81	2.60	4.92	3.20	3.83	3.80
$RbNO_3$	1.70	2.10	2.69	—	1.47	4.37	2.02	—	—
$CsNO_3$	1.45	1.77	1.45	1.86	—	2.24	1.95	1.51	1.56

Some remarks are suggested by these data. Firstly, the mobility of "foreign" cation decreases with the increasing mass of alkali cation of the nitrate which formed the migration zone (Ag^+ not included). Some minor features can be noticed in connection with the similarity of ionic size or mass of the pair of cations involved in an electromigration experiment. Secondly, the mobility values are remarkably well grouped together for all cations (again Ag^+ not included) in molten $NaNO_3$ and $CsNO_3$ and scattered for KNO_3 and $RbNO_3$. Thus, the average mobility of "foreign" cations is roughly 4.6×10^{-4} cm^{2}s^{-1} in molten $NaNO_3$ close to Na^+ mobility and 1.7×10^{-4} cm^{2}s^{-1} in molten $CsNO_3$ close to Cs^+ mobility. This behaviour can be correlated with the volume changes ΔV on melting of the alkali nitrates, [32] namely the large ΔV for $NaNO_3$ and $CsNO_3$ (4.32 cm^3 mole^{-1} and 7.48 cm^{3}mole^{-1}, respectively) and the very small or negative ΔV for KNO_3 and $RbNO_3$. If we assume that the volume change on melting is equivalent to an introduction into the melt structure of an important number of holes [33,34] the migration of cations is no longer determined in $NaNO_3$ and $CsNO_3$ exclusively by cation-anion interaction. On the other hand, in molten KNO_3 and $RbNO_3$ the prevailing interactions remain those between cations and anions so that each cation seems to preserve its mobility as in the proper nitrate.

In table 6 are listed the experimental mobilities of univalent cations in molten nitrates and the calculated mobilities using our transference data through the simple relation $\mu_+ = \Lambda t_+/F$, where for Λ use was made of de Nooijer's data. [31]

The deviations are within 10 per cent which may be reasonable for this type of determinations.

The above mentioned correlations between the transference numbers, cationic mobilities and some structural properties of univalent nitrates emphasize the complex character of the charge transport and new ideas could be tried for further improvements in the knowledge of this class of liquids. For instance, from the applicability of Nernst-Einstein equation is evident, at present, that the mass and charge transport requires the participation of the same entities but the actual nature of the transport mechanism is open. Woodcook [35] has suggested in his works on computer generated structure of some molten salts that the "pairing of unlike ions and further clustering together of pairs is complemented by large vacancies. There remains in these voids a strong Coulombic force field". But more computations should be made "to furnish informations regarding lifetimes of the pairs and clusters which are essential in clearing up the mechanism of the transport processes". In a certain sense the Spedding's[6] ideas meet the conclusion inferred by Woodcook from molecular dynamics calculations. Thus, to the individual ions as charge carriers the agglomerate carriers (which are a structural entity) are added for which a Grotthus-Clausius type mechanism is proposed. Our data support the model drawn by Spedding but adequate experimental methods are needed to define it more accurately.

---

[32] H. Schinke and F. Sauerwald, *Z. anorg. Chem.*, **304**, 25 (1960).

[33] R. Fürth, *Proc. Cambridge Phil. Soc.*, **37**, 252 (1941).

[34] J. O'M. Bockris and N. Richards, *Proc. Roy. Soc.*, **241 A**, 441 (1957).

Table 6

Experimental and calculated cation mobilities in molten nitrates at 723 K

Nitrate	$\mu_+ \times 10^4$ cm^2 s^{-1}	
	experimental	calculated
$LiNO_3$	—	6.62
$NaNO_3$	5.03	5.64
KNO_3	3.10	3.45
$RbNO_3$	2.32	2.08
$CsNO_3$	2.00	1.79
$TlNO_3$	—	1.91
$AgNO_3$	—	6.62

---

[35] L. Woodcook, *Proc. Roy. Soc.*, **328A**, 83 (1972).

Revue Roumaine de Chimie, **18**, *8*, 1319–1324 (1973)

SURFACE TENSION OF THE RECIPROCAL MOLTEN SALT PAIRS (K, Ag ; Cl, Br)

S. STERNBERG and MARIANA TERZI

Institute of Physical Chemistry
Str. Galaţi 31, Bucharest, Romania

Received November 25, 1972

The surface tensions of the reciprocal molten $KCl + AgBr$, and $KBr + AgCl$ mixtures have been measured versus temperature and composition by a detachment method. The surface tension isotherms for both mixtures show large negative deviations from the ideal behaviour. The experimental isotherms of surface tension, at 800°, were compared with those calculated according to Eberhart equation that has been derived for the binary mixtures.

In a previous paper[1] the results of surface tension measurements in the reciprocal molten salt pairs (Na, Ag ; Cl, Br) were reported. These reciprocal mixtures present large negative deviations from ideality. In the present paper similar results for the reciprocal $KCl+AgBr$ and $KBr+AgCl$ mixtures are presented.

EXPERIMENTAL

The surface tension measurements were carried out by a detachment method previously described.[2,3] Use has been made of a platinum pin calibrated at 20° in organic liquids. The temperature was maintained within ±0.5°. Chemically pure KCl and KBr, recrystallized and premelted in a stream of pure dry gaseous HCl or HBr, were used. The silver halides were prepared from chemically pure $AgNO_3$ and HCl or HBr solution and also premelted.

The experimental results were reproducible within 1 per cent.

RESULTS AND DISCUSSIONS

The surface tensions for the simple salts KCl, KBr, AgCl, AgBr and for the reciprocal salt pairs $KCl + AgBr$, $KBr + AgCl$ were determined as a function of temperature and composition. For all simple salts and mixtures studied a linear dependence of surface tension on temperature holds

---

[1] S. Sternberg and M. Terzi, *Rev. Roumaine Chim.*, **17**, 1147 (1972).
[2] S. Sternberg and M. Terzi, *Rev. Roumaine Chim.*, **15**, 527 (1970).
[3] G. I. Janz and M. R. Lorenz, *Rev. Sci. Instr.*, **31**, 18 (1960).

$$\delta = a - bt \tag{1}$$

within a temperature range of 200° above the melting point.

The values of *a* and *b* constants derived by the least squares method for both mixtures are given în tables 1 and 2.

Table 1

Temperature variation of surface tension of the reciprocal KCl + AgBr mixture at mole fraction of AgBr

x(AgBr)	a dyne cm^{-1}	$-b \cdot 10^2$ dyne cm^{-1} $degree^{-1}$	Temperature range, °C
1.000	178.0	3.99	453 – 728
0.900	165.87	5.05	408 – 648
0.700	157.33	5.96	408 – 629
0.600	157.95	6.79	490 – 689
0.500	154.43	6.60	556 – 757
0.400	154.16	6.87	601 – 795
0.300	155.16	7.42	712 – 824
0.200	155.55	7.50	729 – 851
0.100	161.03	8.37	800 – 871
0.000	153.00	7.10	790 – 910

Table 2

Temperature variation of surface tension of the reciprocal KBr + AgCl mixture at mole fraction of AgCl

x(AgCl)	a dyne cm^{-1}	$-b \cdot 10^2$ dyne cm^{-1} $degree^{-1}$	Temperature range, °C
1.000	209.2	5.64	460 – 706
0.900	182.63	5.73	447 – 599
0.800	176.33	6.72	415 – 601
0.700	168.00	6.62	402 – 599
0.649	163.08	6.46	435 – 634
0.500	149.65	5.93	535 – 728
0.400	159.12	7.89	630 – 758
0.300	149.69	7.05	663 – 815
0.200	145.04	6.82	720 – 867
0.100	147.46	7.34	764 – 854
0.000	147.33	7.53	752 – 875

Our values of surface tension for KBr are the same as those of Bertozzi[4] obtained by the Wilhelmy plate method and are 1 – 3% higher than those of Boardman[5] and Bloom[6], obtained by the maximum bubble pressure method.

---

[4] G. Bertozzi, *J. Phys. Chem.*, **69**, 2606 (1965).

The dependence on composition of surface tension for the reciprocal salt pairs (K, Ag ; Cl, Br), at 800°, is plotted in figure 1 (curves 2 and 4). The ideal isotherms of surface tension for both reciprocal mixtures are represented by the curves 1 and 3 in figure 1. The ideal isotherms were calculated according to equation

$$\delta_0 = x_{Ag^+}x_{Cl^-}\delta_{AgCl} + x_{Ag^+}x_{Br^-}\delta_{AgBr} + x_{K^+}x_{Cl^-}\delta_{KCl} + x_{K^+}x_{Br^-}\delta_{KBr} \quad (2)$$

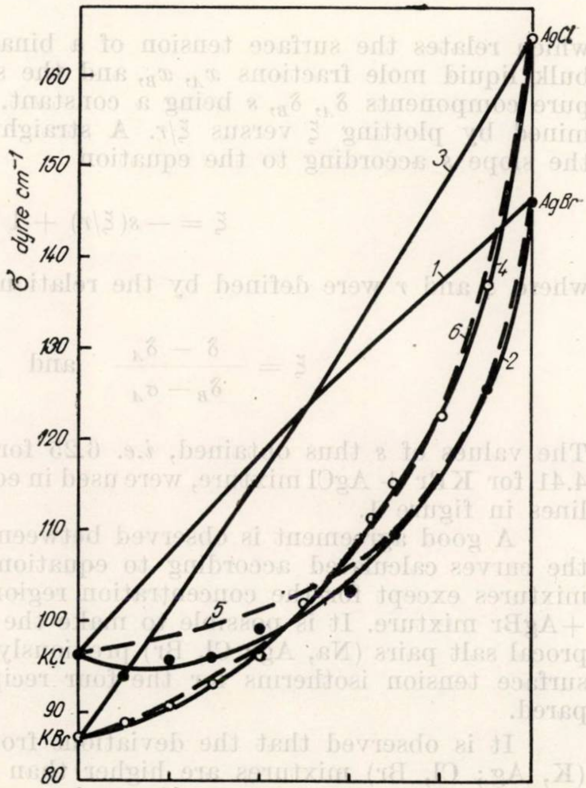

Fig. 1. — The surface tension isotherms at 800° for the reciprocal KCl + AgBr and KBr + AgCl mixtures.

1,2 — The ideal and experimental isotherms for KCl + AgBr mixture ; *3,4* — The ideal and experimental isotherms for KBr + AgCl mixture ; *5,6* — The curves calculated according to equation (3) for KCl + AgBr and KBr + AgCl mixtures.

where x_{Me^+} represents the cationic fraction, x_{X^-} the anionic fraction, δ_{MeX} the surface tension for pure salts and δ_0 the surface tension of an ideal reciprocal mixture (K^+, Ag^+ ; Cl^-, Br^-).

---

[5] N. K. Boardman, A. R. Palmer and E. Heymann, *Trans. Faraday Soc.*, **51**, 277 (1955).

[6] H. Bloom, F. G. Davis and D. W. James, *Trans. Faraday Soc.*, **56**, 1179 (1960).

The large negative deviations from the ideal isotherms are visible for both reciprocal mixtures.

It is observed also, that the experimental values of surface tension are equal (100 dyne cm^{-1}) for both reciprocal mixtures at the mole fraction $x(\mathrm{AgX}) = x(\mathrm{KX}) = 0.5$.

The curves 5 and 6 in figure 1 represent the surface tension isotherms calculated according to Eberhart[7] equation

$$\delta = \frac{sx_{AA} + x_{BB}}{sx_A + x_B} \tag{3}$$

which relates the surface tension of a binary liquid mixture with the bulk liquid mole fractions x_A, x_B, and the surface tensions of the two pure components δ_A, δ_B, s being a constant. The s constant was determined by plotting ξ versus ξ/r. A straight line was obtained having the slope s according to the equation

$$\xi = -\, s(\xi/r) + 1 \tag{4}$$

where ξ and r were defined by the relations

$$\xi = \frac{\delta - \delta_A}{\delta_B - \sigma_A} \quad \text{and} \quad r = \frac{x_B}{x_A} \tag{5}$$

The values of s thus obtained, *i.e.* 6.25 for $\mathrm{KCl} + \mathrm{AgBr}$ mixture, and 4.41 for $\mathrm{KBr} + \mathrm{AgCl}$ mixture, were used in eq. (3) and lead to the dashed lines in figure 1.

A good agreement is observed between the experimental data and the curves calculated according to equation (3) for the two reciprocal mixtures except for the concentration region rich in KCl of the $\mathrm{KCl} + \mathrm{AgBr}$ mixture. It is possible to make the same remarks for the reciprocal salt pairs (Na, Ag; Cl, Br) previously studied[1]. The experimental surface tension isotherms for the four reciprocal salt pairs were compared.

It is observed that the deviations from ideality of the reciprocal (K, Ag; Cl, Br) mixtures are higher than those of the mixtures with Na. The deviations of the calculated curves (Eberhart) from the experimental curves for the reciprocal mixture with K are higher than those with Na.

The significance of constant s for reciprocal mixtures cannot be the same with that of binary mixtures, where s is the extent of surface layer enrichment in the lower surface tension component ($s = x_A^{\delta} . x_B / x_B^{\delta} . x_A$). For instance at the mixture of the mole fraction $x_A = x_B = 0.5$, the two reciprocal mixtures should have the same extent of surface enrichment, that is the same surface layer composition. This results from the experimental data, where the surface tensions of the two reciprocal mixtures of the equimolecular composition are practically equal. In these conditions, *s* has the significance of an empirical constant, and the Eberhart relation may be used as an empirical equation which allows the correlation of the surface tension for the reciprocal mixture with the surface tension of the components.

---

[7] J. G. Eberhart, *J. Phys. Chem.*, **70**, 1183 (1966).

From the experimental data of the surface tension and its thermal coefficient, other surface thermodynamic quantities have been calculated. Thus, we calculated the surface entropy and enthalpy per unit area, according to equations

$$S^{\delta}/A^{\delta} = -\,\mathrm{d}\delta/\mathrm{d}T, \tag{6}$$

$$H^{\delta}/A^{\delta} = \delta - T\,\mathrm{d}\delta/\mathrm{d}T, \tag{7}$$

where A^{δ} is the surface area. The calculated values of the surface entropy and enthalpy for the reciprocal salts pairs (Na, Ag; Cl, Br) and (K, Ag; Cl, Br) are given in tables 3 and 4.

Table 3

Surface thermodynamic quantities for the reciprocal NaCl + AgBr and NaBr + AgCl mixtures

NaCl + AgBr mixture

x(AgX)	$-(S^{\delta}/A^{\delta}).10^2$ erg·cm^{-2} degree^{-1}	H^{δ}/A^{δ} erg·cm^{-2}
1.000	3.99	188.9
0.900	7.36	211.9
0.800	7.54	207.1
0.700	7.51	204.2
0.500	6.68	189.8
0.300	7.11	190.3
0.200	9.08	212.1
0.100	8.63	206.4
0.000	9.00	211.5

NaBr + AgCl mixture

x(AgX)	$-(S^{\delta}/A^{\delta}).10^2$ erg·cm^{-2} degree^{-1}	H^{δ}/A^{δ} erg·cm^{-2}
1.000	5.64	224.6
0.900	5.90	213.3
0.800	6.03	204.7
0.700	7.35	208.8
0.500	7.93	203.3
0.300	6.83	181.9
0.100	7.66	184.7
0.000	6.82	173.5

Table 4

Surface thermodynamic quantities for the reciprocal KCl + AgBr and KBr + AgCl mixtures

KCl + AgBr mixture

x(AgX)	$-(S^s/A^s)\cdot 10^2$ erg cm^{-2} degree^{-1}	H^s/A^s erg$\cdot$cm^{-2}
1.000	3.99	188.9
0.900	5.05	179.7
0.700	5.96	173.6
0.600	6.79	176.5
0.500	6.60	172.4
0.400	6.87	172.9
0.300	7.42	175.4
0.200	7.50	176.1
0.100	8.37	183.8
0.000	7.10	172.4

KBr + AgCl mixture

x(AgX)	$-(S^s/A^s)\cdot 10^2$ erg cm^{-2} degree^{-1}	H^s/A^s erg$\cdot$cm^{-2}
1.000	5.64	215.8
0.900	5.79	198.9
0.800	6.72	194.7
0.700	6.62	186.0
0.649	6.46	180.7
0.500	5.92	165.8
0.400	7.89	180.6
0.300	7.05	168.9
0.200	6.82	163.7
0.100	7.34	167.5
0.000	7.53	167.9

Revue Roumaine de Chimie, **18**, *8*, 1325 – 1331 (1973)

K

ELECTROPLATING OF COPPER FROM PYROPHOSPHATE BATHS. I

THE EFFECT OF ELECTROLYTE pH

O. RADOVICI, CECILIA VASS and I. SOLACOLU

Centre of Physical Chemistry
str. Galaţi 31, Bucharest 13, Romania

Received December 28, 1972

The influence of copper plating electrolyte, based on pyrophosphate corresponding to a weight ratio $P_2O_7^{4-}/Cu^{2+} = 7 \cdots 7.5$, upon electrodeposition process is studied. Use has been made of the potentiostatic technique and the cathodic and anodic polarization curves plotted for pH values between 5.5 and 9.5 ; the cathodic copper deposits have been microscopically studied. The results lead to establishing the optimum pH regime for the studied electrolyte.

The outstanding interest shown during the last 20 years to procedures of obtaining copper galvanic deposits, from alkali pyrophosphate baths, is understandable given the advantages offered by them from which we quote : high cathodic efficiency, good chemical stability, low cost and non-toxicity.

According to Waters and Aaron [1] within the 7 – 9.5 pH range the copper ion exists as complex anion predominantly as $[Cu(P_2O_7)_2]^{6-}$ especially in concentrated solutions; in diluted solutions, complexes may exist whose $P_2O_7^{4-}/Cu^{2+}$ ratio is 2/1 or 4/1. This complex anion is very stable under working conditions and copper electrodeposition in such an electrolyte presents all advantages connected to using complexing baths.

In order to clear up the electrochemical processes occurring in copper deposition from these nontoxic electrolytes, theoretical studies as well as applied research have been carried out. The theoretical studies aimed at either determining the equilibrium potential of copper electrode,[2] the influence of different factors on its polarization [3] or elucidating the copper electrocrystallization mechanism by measuring the kinetic parameters of this reaction[4–8]. The applied research has been trying to establish the characteristics of pyrophosphate complex electrolyte,[9] the role played by different additives,[10,11] as well as the effect of different factors upon the structure of deposits and the cathodic efficiency of the process.[12–15]

---

[1] J. Waters and A. Aaron, *J. Amer. Chem. Soc.*, **75**, 611 (1953).
[2] E. K. Yastrebova and A. T. Vagramyan, *Zhur. fiz. Khim.*, **38**, 1551 (1964).
[3] E. K. Yastrebova and A. T. Vagramyan, *Zhur. fiz. Khim.*, **38**, 2503 (1964).

An outstanding advantage of pyrophosphate baths over the other modern replacements for cyanide based classic baths, *e.g.* sulphate or fluoroborate, is the possibility of making good deposits on metallic supports easily attacked by acids as zinc alloys.[14]

To apply this method on industrial scale, studies have been carried out as regards copper cathodic deposition on steel, brass and zinc alloys from pyrophosphate baths. To establish the optimum conditions of pyrophosphate bath functioning we have studied the influence of its various parameters (pH, temperature, stirring, brightening additive) upon the development of electrochemical process and the quality of copper deposits.

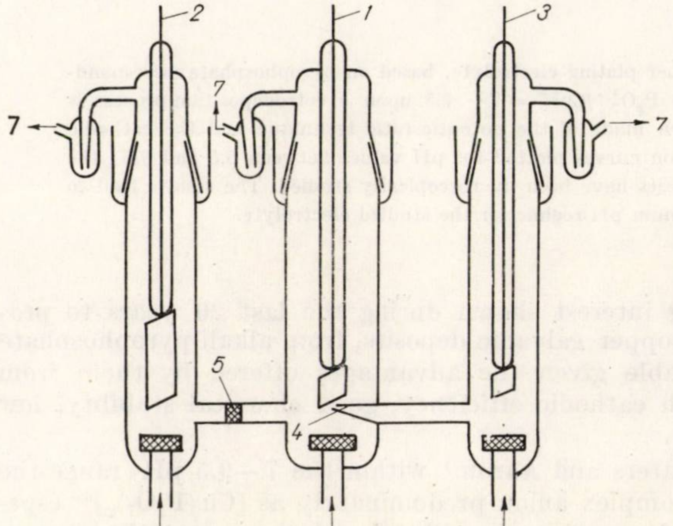

Fig. 1. — Working cell.

1, working electrode, *2*, auxiliary electrode, *3*, reference electrode, *4*, Luggin capillary, *5*, porous glass, *6*, gas inlet, *7*, gas outlet valve.

---

[4] A. T. Vagramyan and E. K. Yastrebova, *Zhur. fiz. Khim.*, **39**, 865 (1965).

[5] E. A. Necheaev. E. Z. Napukh and N. T. Kudryavtsev, *Elektrokhimiya*, **3**, 1493 (1967).

[6] Yu. M. Loshkarev, V. N. Kovtun and Yu. M. Ivanchenko-Urskii, *Elektrokhimiya*, **5**, 560 (1969).

[7] O. Radovici and C. Vass, *Rev. Roumaine Chim.*, *18*, 1105 (1973).

[8] A. Zh. Kadyrbekova, M. M. Yarlykov and N. T. Kudryavtsev, *Elektrokhimiya*, **7**, 1588 (1971).

[9] B. M. Dikova and N. T. Kudryavtsev, *Khim. Ind. (Sofia)*, **1970**, 307.

[10] T. H. Irvine, *Plating*, **54**, 1251 (1967).

[11] N. T. Kudryavtsev and B. M. Dikova, *Zashch. Metal.*, **5**, 177 (1969).

[12] E. Z. Napukh and E. A. Necheaev, *Zashch. Metal.*, **6**, 710 (1970).

[13] J. W. Dini, H. R. Johnson and J. R. Helms, *Plating*, **54**, 1337 (1967).

[14] O. Radovici, C. Vass and I. Solacolu, *Rev. Coroz.*, in press.

[15] R. Yu. Bek and G. M. Sorkin, *Izv. Sib. Otd. Akad. Nauk S.S.S.R., Ser. Khim. Nauk*, **1971**, 117 ; *Chem. Abstr.*, **76**, 120695w (1972).

1. EXPERIMENTAL

1.1. POLARIZATION MEASUREMENTS

The working cell, presented in figure 1, consists of two compartments, anodic and cathodic, separated by a porous glass ; the two compartments are separately stirred by bubbling.

The working electrode, a platinum plate of 1 cm² surface area on which a copper layer was deposited before each run for 20 minutes at 20 mA/cm².

The auxiliary electrode, of platinum, 4 cm², similarly prepared.

The reference electrode, identical with the working electrode.

To draw the polarization curves a Wenking type potentiostat was used. Potential steps of 10–50 mV were applied each minute and the value of the current corresponding to each step was measured with a 0.2 class microampermeter.

1.2. DETERMINATION OF CURRENT EFFICIENCY AND STRUCTURE OF DEPOSITS

The electrolysis cell, cylindrical, of 250 cm³ capacity, was provided with a device for gas bubbling.

The anodes – made of 99.9% pure electrolytic copper foils – were degreased before runs in trichlorethylene.

The cathodes were made of a zinc alloy (Zamak) in order to study the structure of deposits and the cathodic efficiency of the process under the least favourable conditions from the point of view of the support. The cathodic prisms of 4 cm² surface area were successively polished on metallographic paper and felt soaked in alumina suspension. After degreasing in trichlorethylene, cathodes were chemically degreased for 5 minutes at 60° in a solution of Na_2CO_3 40, NaOH 5, Na_3PO_4 15 and Na_2SiO_3 15 g/l ; then washed in water and electrochemically degreased for 1 minute at 60° and with a current of 40 mA/cm² in an electrolyte of the following composition : NaOH 40, Na_2CO_3 50 and sodium gluconate 40 g/l. After washing, a 10 g/l H_2SO_4 solution was used to etch the cathodes ; etching lasted 10 seconds at 25° and was followed by washing in water and drying at room temperature.

In order to ensure the experiment with the needed current range (20–80 mA/cm²) a classic intensiostatic polarization scheme, consisting of a stabilized power supply (Orion EMG 1832/C) and a variable resistor, was used.

The current efficiency was gravimetrically determined by dividing to the quantity theoretically deposited.

The structure of deposits was studied by the MIM-7 type (500× magnification) metallographic reflexion electron microscope.

1.3. COPPER PLATING ELECTROLYTE

The electrolyte. Solutions of copper plating with the $Cu(P_2O_7)_2^{6-}$ complex, characterized by a weight ratio $P_2O_7^{4-}/Cu^{2+} = 7.0...7.5$, were used. The electrolyte was prepared by well-known methods from *p.a.* chemicals.

The pH of the bath was kept constant during runs (within 5.5–9.5) by ammonia addition and its value controlled by a Radiometer PHM-22r type pH-meter.

The temperature during runs was maintained at 60° ± 0.1 ; an U10 thermostat was used.

The stirring was ensured by bubbling pure nitrogen at a constant overpressure of 20 mm Hg.

2. RESULTS AND DISCUSSION

2.1. THE EFFECT OF pH UPON ELECTRODE POLARIZATION

The anodic and cathodic polarization curves in potentiostatic conditions at 60° for electrolyte solutions of 5.5—9.5 pH values are given in figure 2.

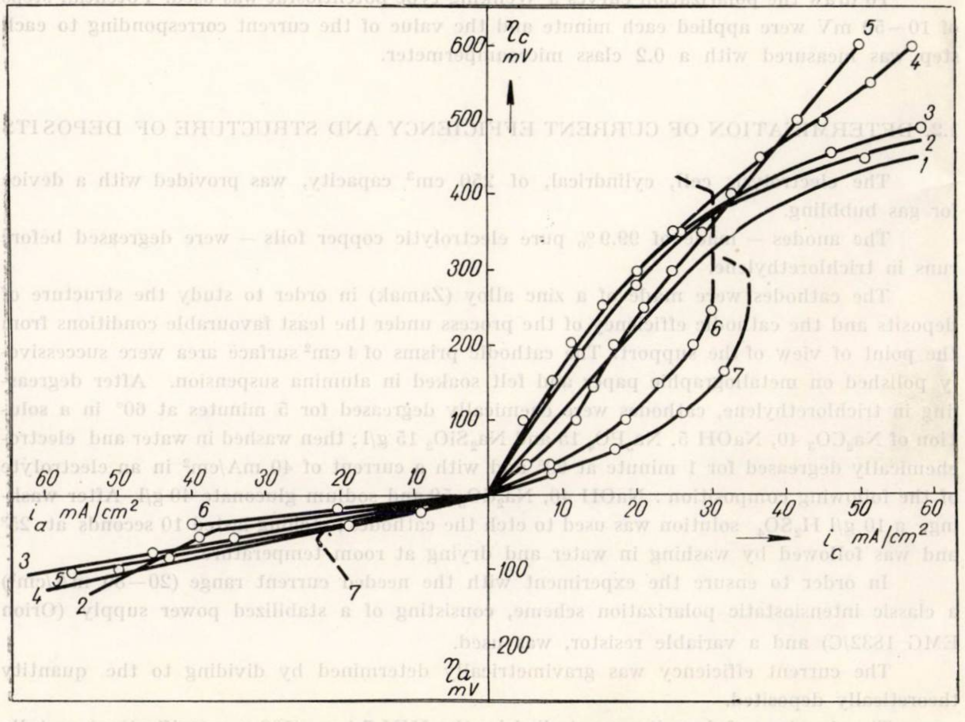

Fig. 2.—Cathodic and anodic polarization curves drawn for different pH values at 60°.

1, 9.5, *2*, 9.0, *3*, 8.5, *4*, 7.0, *5*, 6.5, *6*, 6.0, *7*, 5.5.

The figure shows that the pH value is critical in determining the electrochemical processes. So, within the 7.0—9.5 pH range, the pH decrease produces a shift of the working electrode potential towards more negative values while within the 6.5—5.5 range the effect is opposite.

Within the applied current density range, the processes take place at important rate within the 6.5—9.5 pH range, while for 6.0 and 5.5 values, limit currents of 30 mA/cm² and 35 mA/cm², respectively, are established.

This behaviour clearly shows that the pH range between 5.5 and 6.0 does not offer good working conditions of pyrophosphate electrolyte since on this range the $[Cu(P_2O_7)_2]^{6-}$ complex is unstable and in the presence of H^+ the following equilibrium is established

$$[Cu(P_2O_7)_2]^{6-} + 2H^+ \rightleftharpoons [CuP_2O_7]^{2-} + H_2P_2O_7^{2-}$$

with insoluble copper pyrophosphate ($Cu_2P_2O_7$) formation in the anodic compartment.

This limitation of the process is shown on the curves of anodic polarization (*6* and *7* in fig. 2) which indicate the stability of limit anodic currents whose value is 40 mA/cm² and 20 mA/cm², respectively.

The influence of the electrolyte pH on the polarization of electrodes is better illustrated on the curves which represent the cathodic (fig. 3) and anodic (fig. 4) overpotential *versus* the pH of the electrolyte at different current densities.

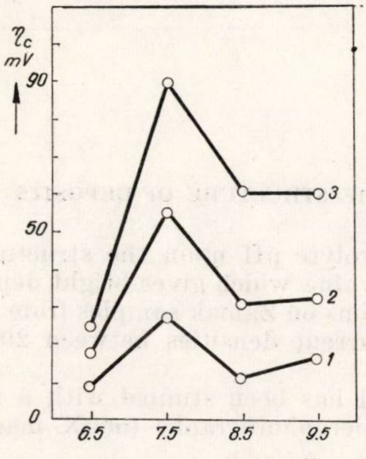

Fig. 3. — The change of cathodic polarization versus electrolyte pH for different current density values.

1, 10 mA/cm², *2*, 20 mA/cm², *3*, 30 mA/cm².

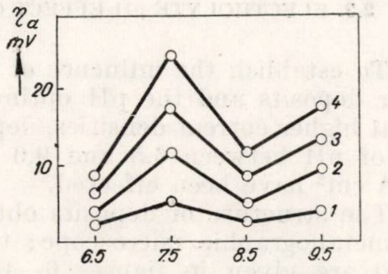

Fig. 4. — The change of anodic polarization versus electrolyte pH for different current density values.

1, 5 mA/cm², *2*, 10 mA/cm², *3*, 15 mA/cm², *4*, 20 mA/cm².

Examination of curves in figures 3 and 4 shows that the minimum value of polarization for both processes corresponds to a 8.5 pH value of the electrolyte.

2.2. THE ELECTROLYTE pH INFLUENCE UPON CATHODIC EFFICIENCY

In order to determine the pH range corresponding to a maximum current efficiency, the values of this efficiency for the 7.2—9.3 pH range and current densities of 20—40 mA/cm² (fig. 5) have been calculated.

The efficiencies range there is between 97.5–99.5%, 95–99% and 86–98.5% for current densities of 20, 30 and 40 mA/cm², respectively, and presents a maximum value within 8.2–8.6 pH range.

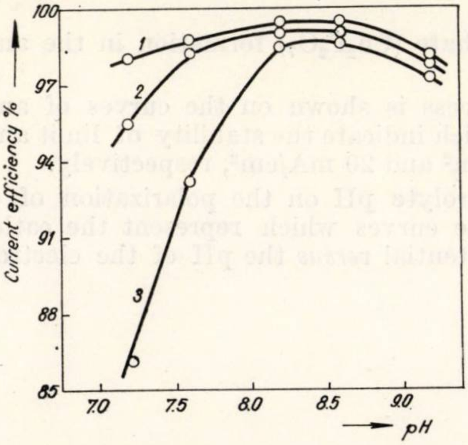

Fig. 5. – The effect of electrolyte pH on the current efficiency for different current density values.

1, 20 mA/cm², *2*, 30 mA/mA/cm², *3*, 40 mA/cm².

2.3. ELECTROLYTE pH EFFECT ON THE STRUCTURE OF DEPOSITS

To establish the influence of electrolyte pH upon the structure of copper deposits and the pH optimum value which gives bright deposits even at higher current densities, depositions on Zamak samples from solutions of pH between 6.5 and 9.0 at current densities between 20 and 50 mA/cm² have been effected.

The structure of deposits obtained has been studied with a reflexion metallographic microscope; the microphotographs (500X magnification) are given in figures 6–14.

Examination of microphotographs in figures 10–12 shows the effect of current density increase upon the structure of deposits. So, with the 7.5 pH electrolyte, fine and bright structures are obtained at 20 mA/cm² current density (fig. 10) while at 30 mA/cm² only semibright structures are deposited (fig. 11). With increasing current densities, up to 40 mA/cm², the crystallites, visible in figure 11, sensitively increase, the aspect of deposits becoming mat (fig. 12). At higher values of current densities (40 mA/cm²) one can notice some larger spherical formations spread over the whole surface area of the support (fig. 12).

The microphotographs in figs. 13 and 14 prove that good quality deposits are impossible to be obtained from solutions with pH lower than 7.0 due to the instability of the $[Cu(P_2O_7)]^{6-}$ complex in these conditions. Thus, even at low current density (20 mA/cm²) the deposits do not have a fine structure (fig. 13) while the deposits at the same current density but at a pH of the electrolyte of 7.5 (fig. 10) are bright.

Evidently, the copper deposition electrolyte based on pyrophosphate may work in good conditions within a pH range of 7.0–9.5. All over

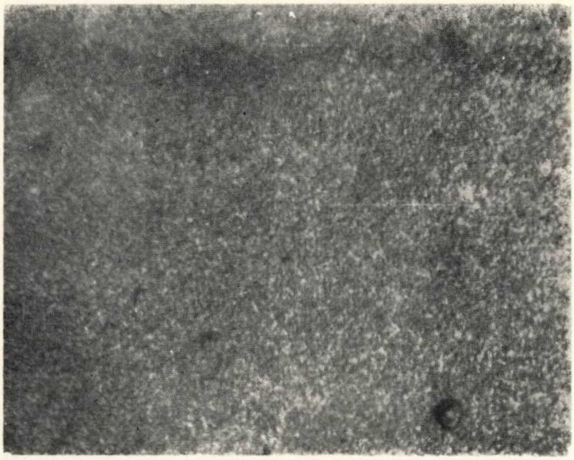

Fig. 6. — The structure of the copper deposit on Zamak, pH = = 9.0, i_c = 20 mA/cm². Microphotograph, 500 ×.

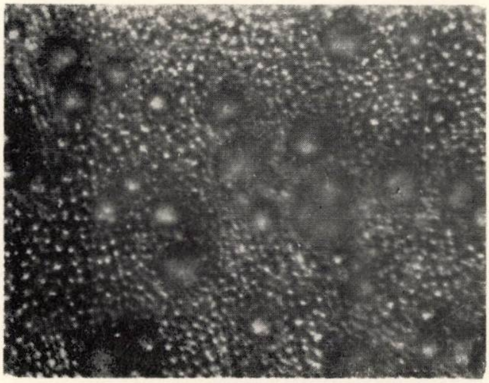

Fig. 7. — The structure of the copper deposit on Zamak, pH = = 9.0, i_c = 30 mA/cm². Microphotograph, 500 ×.

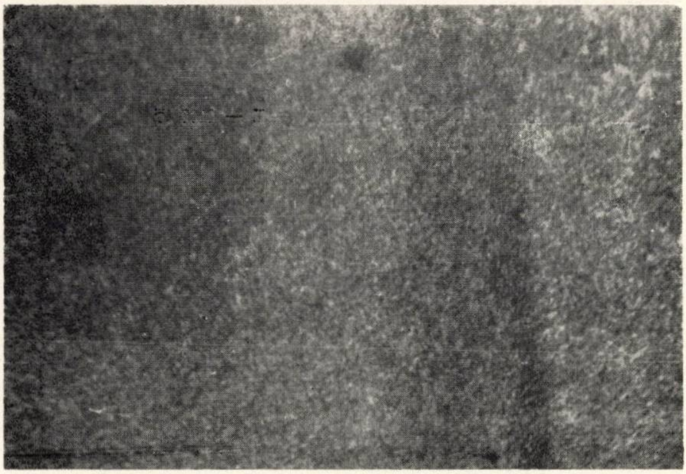

Fig. 8. — The structure of the copper deposit on Zamak, pH = 8.5, i_c = 20 mA/cm². Microphotograph, 500 ×.

Fig. 9. — The structure of the copper deposit on Zamak, pH = 8.5, i_c = 30 mA/cm². Microphotograph, 500 ×.

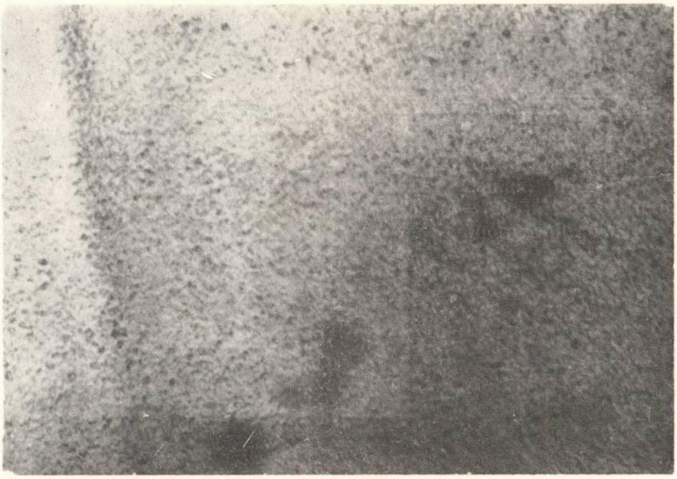

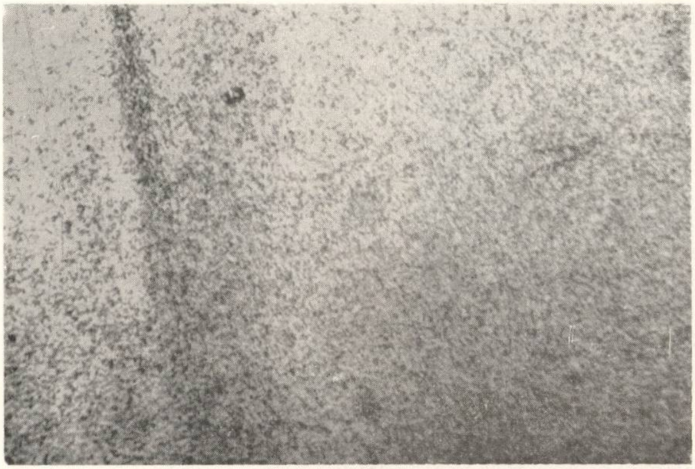

Fig. 10.— The structure of the copper deposit on Zamak, pH = 7,5, i_c = 20 mA/cm². Microphotograph, 500 ×.

Fig. 11. —The structure of the copper deposit on Zamak, pH = 7.5, i_c = 30 mA/cm². Microphotograph, 500 ×.

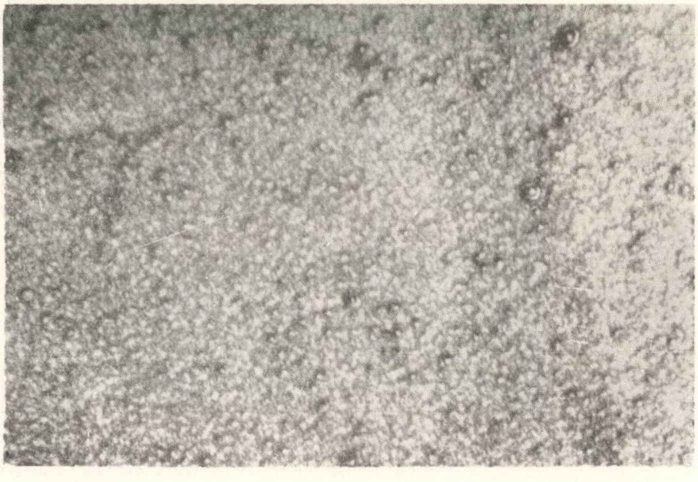

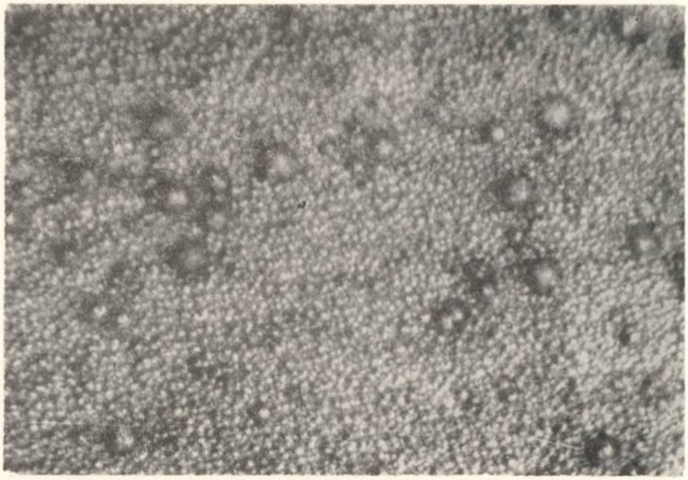

Fig. 12. —The structure of the copper deposit on Zamak, pH = 7.5, i_c = 40 mA/cm². Microphotograph, 500 ×.

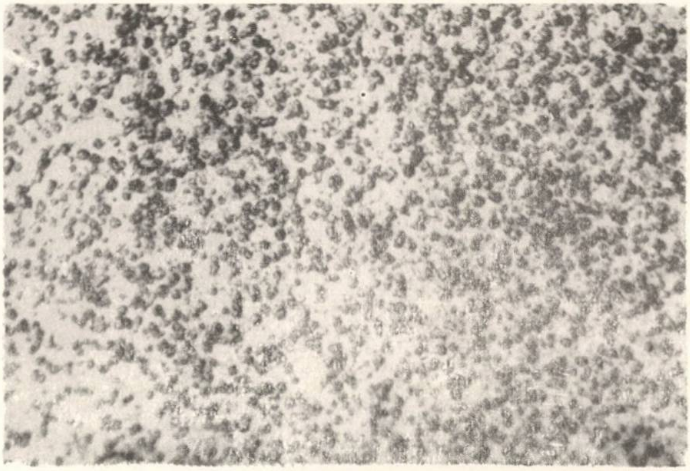

Fig. 13. —The structure of the copper deposit on Zamak, pH = 6.5, i_c = 20 mA/cm². Microphotograph, 500 ×.

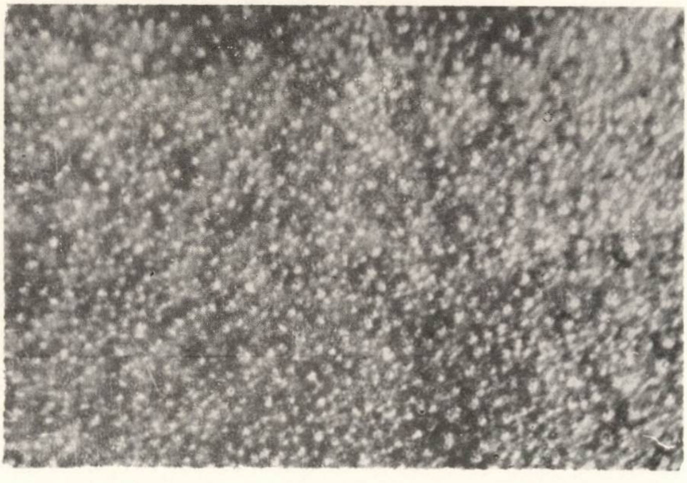

Fig. 14. —The structure of the copper deposit on Zamak, pH = 6.5, i_c = 30 mA/cm². Microphotograph, 500 ×.

this pH range at current densities relatively low (20 mA/cm^2) bright deposits with fine structure have been obtained (figs. 6, 8 and 10).
with fine structure have been obtained (figs. 6, 8 and 10).

At higher current densities (30 mA/cm^2) bright deposits have been obtained only in solutions of pH 8.5 (fig. 9), while in solutions of pH 7.5 the deposits have been semibright (fig. 11) and in solutions of 0.9, mat and rough (fig. 7).

The variation of the domain within which bright deposits are obtained versus the value of the pH is plotted in figure 15.

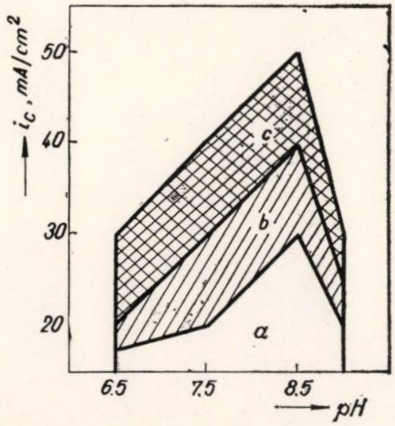

Fig. 15. – The extension of the bright deposits domain versus electrolyte pH.

a, bright deposits, *b*, semibright deposits, *c*, mat deposits.

The data presented above clearly show that the structure of deposit from the electrolyte under study agrees with the works on the electrolyte pH influence upon the electrode polarization and cathode efficiency. The optium results come out when the pyrophosphate electrolyte pH stands about 8.5.

3. CONCLUSIONS

1. The copper plating electrolyte based on pyrophosphates characterized by a $P_2O_7^{4-}/Cu^{2+}$ ratio = 7.0–7.5 may work in good conditions (high efficiency, fine structure deposits) within a 7.0–9.5 pH range.

2. Within this range the decrease of the pH produces a shift of cathode potential towards more negative values, the process taking place at considerably high speed.

3. The study of cathodic and anodic overpotential change versus pH has shown that the minimum polarization for both processes is obtained at a pH of 8.5.

4. The cathodic efficiency of the process is high, as high as 99.5–99% for a pH range of 8.2–8.6 and current density 20 and 30 mA/cm^2, respectively.

5. Within the pH range 7.0–9.5 the deposits have a fine structure and are bright for a current density value of 20 mA/cm^2. At pH = 8.5 the current density may be as high as 30 mA/cm^2 without having any unfavourable effect upon the aspect of deposits.

this pH range at current densities relatively low (20 mA/cm²) bright deposits with fine structure have been obtained (figs. 6, 8 and 10), with fine structure have been obtained (figs. 6, 8 and 10).

At higher current densities (30 mA/cm²) bright deposits have been obtained only in solutions of pH 8.5 (fig. 9), while in solutions of pH 7.5 the deposits have been semibright (fig. 11) and in solutions of 6.9, mat and rough (fig. 7).

The variation of the domain within which bright deposits are obtained versus the value of the pH is plotted in figure 15.

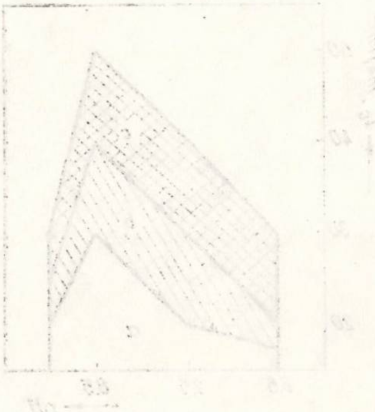

Fig. 15. — The extension of the bright deposits domain versus electrolyte pH.

a, bright deposits; b, semibright deposits; c, mat deposits.

The data presented above clearly show that the structure of deposit from the electrolyte under study agrees with the works on the electrolyte pH influence upon the electrode polarization and cathode efficiency. The optimum results come out when the pyrophosphate electrolyte pH stands about 8.5.

3. CONCLUSIONS

1. The copper plating electrolyte based on pyrophosphates characterized by a $P_2O_7^{4-}$: Cu^{2+} ratio = 7.0–7.5 may work in good conditions (high efficiency, fine structure deposits) within a 7.0–8.5 pH range.

2. Within this range the decrease of the pH produces a shift of cathode potential towards more negative values, the process taking place at considerably high speed.

3. The study of cathode and anodic overpotential change versus pH has shown that the minimum polarization for both processes is obtained at a pH of 8.5.

4. The cathodic efficiency of the process is high, as high as 98.5–99.8%, for a pH range of 8.2–8.5 and current density 20 and 30 mA/cm², respectively.

5. Within the pH range 7.0–8.5 the deposits have a fine structure and are bright for a current density value of 20 mA/cm². At pH = 8.5 the current density may be as high as 30 mA/cm² without having any unfavourable effect upon the aspect of deposits.

Revue Roumaine de Chimie, **18**, *8*, 1333–1338 (1973)

KINETIC STUDY ON THE REDUCTION OF NICKEL CATALYSTS

T. CHIRULESCU*, CORNELIA CIOBANU** and GH. ŞERBAN**

* Institute of Physical Chemistry, str. Dumbrava Roşie 23, Bucharest, Romania

** Petrochim Institute, Bd. Republicii 291, Ploieşti, Romania

Received February 22, 1973

The magnetic reduction isotherms of nickel-kieselguhr catalysts at 517–607 K were obtained. The reduction degree of nickel oxide was expressed by : $\ln f = n \ln t - B/T$, where f is the reduction degree, t – reduction time, T – absolute reduction temperature, while n and B are two constants determined from the magnetic reduction isotherms. The apparent activation energy of reduction was estimated in the case of two assumptions : zero-, and 1/2-order kinetics. However, experimental data support the 1/2-order kinetics, which corresponds to diffusion processes.

Supported metal catalysts are characterized by some specific properties, particularly, by a very high degree of dispersion of the metal.[1–4] These properties can largely be influenced by the preparation method of catalysts.[5,6]

During the preparation of nickel-kieselguhr catalysts an essential step consists in the reduction of NiO-kieselguhr system in a hydrogen flow, according to reaction :

$$\text{NiO-kieselguhr} + H_2 \rightarrow \text{Ni-kieselguhr} + H_2O$$

The study of the kinetics of this reaction allows to determine the order of reaction and the activation energy, which presents some interest regarding the energy consumption during the reduction process.

This paper deals with the kinetic study of the reduction of five catalyst samples in a hydrogen flow. Metallic nickel content in all the samples

---

[1] J. L. Carter and J. H. Sinfelt, *J. Phys. Chem.*, **70**, 3003 (1966).

[2] R. C. Adams, H. A. Benesi, R. M. Curtis and R. G. Meisenheimer, *J. Catalysis*, **1**, 336 (1962).

[3] L. Spenadel and M. Baudart, *J. Phys. Chem.*, **64**, 204 (1960).

[4] J. J. F. Scholten and A. van Montfoort, *J. Catalysis*, **1**, 85 (1962).

[5] W. Heukelom, J. J. Broeder and L. L. van Reijen, *J. Chim. phys.*, **54**, 474 (1954).

[6] K. Umemura, *Nippon Kagaku Zasshi*, **81**, 863 (1960).

was 55 per cent. From the magnetic reduction isotherms, the reduction degree as function of reduction time and temperature was determined and some considerations on the reaction order were made. Ultimately, the activation energy was obtained.

EXPERIMENTAL

Materials. A series of catalyst samples was prepared by thermal decomposition and reduction of basic nickel carbonate supported on kieselguhr. All samples contain 55 % by weight of metallic nickel; each sample is characterized by a certain degree of initial reduction.

Apparatus and procedure. The gas circulating open system and the a.c. permeameter [7] and procedure were previously described.[8] All reductions were performed at a temperature ranging from 517 to 607 K, at a hydrogen flow rate of 117.5 $cm^3 min^{-1}$.

RESULTS AND DISCUSSION

Kinetic law. The reduction degree of nickel oxide was previously defined as [8]

$$f = 0.55 \frac{m_{Ni}}{m_{Ni} + m_{NiO}} \qquad (1)$$

where m_{Ni} is the mass of metallic nickel in the catalyst, m_{NiO} represents the mass of nickel oxide, and 0.55 is the maximum metallic concentration in the catalyst. The following expression for the reduction degree was also assumed

$$\ln f = n \ln t - B/T \qquad (2)$$

where t and T represent time in minutes and absolute temperature, respectively, and n and B are two constants depending on the catalyst sample.

Figure 1 gives the logarithmic plot of the magnetic reduction isotherms in the case of sample n° 1, T being considered as a parameter.

We can observe that these magnetic reduction isotherms are parallel straight lines. The common slope of these isotherms is equal to the value of constant n in eq. (2), and from the free terms of these isotherms the value of constant B can be obtained. Similar magnetic reduction isotherms were obtained for the other catalyst samples.

The average values of n, B, and f_0 (initial value of the reduction degree) are given in table 1.

---

[7] T. Chirulescu, *Rev. Roumaine Chim.*, **16**, 507 (1971).

[8] T. Chirulescu, C. Ciobanu and Gh. Şerban, *Rev. Roumaine Chim.*, **17**, 1507 (1972).

The examination of table 1 leads to the following remarks :
1° when the reduction temperature is constant, sample nº. 5 ($n = 0.280$) is the most difficult to reduce ;

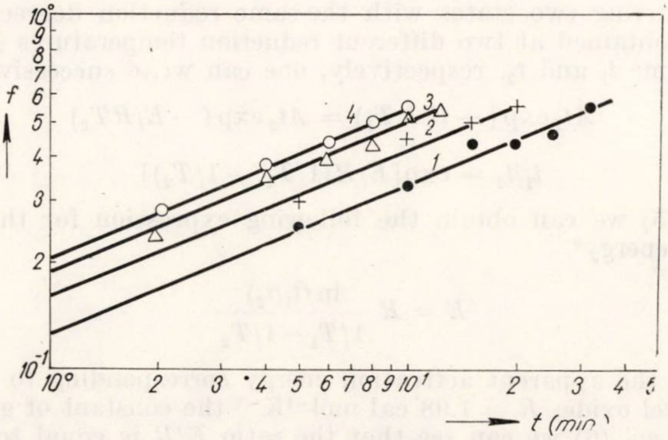

Fig. 1. — Magnetic reduction isotherms in the case of the sample nº 1 ; reduction temperature : *1*, 517 K, *2*, 546 K, *3*, 563 K, and 4, 607 K.

Table 1

Characteristic data of catalyst samples

Sample nº	$\bar{n}$	$\bar{B}$(K)	$\bar{f}$o*
1	0.419 ± 0.010	980 ± 15.4	0.320 ± 0.012
2	0.295 ± 0.022	880 ± 15.3	0.270 ± 0.010
3	0.308 ± 0.013	961 ± 19.3	0.290 ± 0.090
4	0.280 ± 0.016	849 ± 8.1	0.370 ± 0.090
5	0.450 ± 0.058	1140 ± 44.5	0.370 ± 0.010

* from eq. (1) we can see that f is ranging from 0 to 0.55.

2° when the reduction time is constant, the reduction kinetics of sample nº 5 is the most influenced by temperature ;
3° sample nº 2 presents the lowest value of f_0, while samples nº 4 and nº 5, the highest ones.

Activation energy. The apparent activation energy of the reduction of catalyst samples was estimated in the case of two assumptions :

a) if we assume a zero-order kinetics, we can write the following equation

$$\frac{\mathrm{d}x}{\mathrm{d}t} = k \tag{3}$$

where x is the decrement of the nickel oxide amount, and k represents the kinetic constant. By integrating Eq. (3) we obtain

$$x = kt + a$$

or

$$x - a = kt = At \exp(-E/RT) \tag{4}$$

where the kinetic constant was expressed by means of the Arrhenius law.

Considering two states with the same reduction degree ($x_1 - a = x_2 - a$) obtained at two different reduction temperatures T_1 and T_2, after the time t_1 and t_2, respectively, one can write successively

$$At_1 \exp(-E/RT_1) = At_2 \exp(-E/RT_2)$$

or

$$t_1/t_2 = \exp[E/R(1/T_1 - 1/T_2)] \tag{5}$$

From eq. (5) we can obtain the following expression for the apparent activation energy[9]

$$E = R\,\frac{\ln(t_1/t_2)}{1/T_1 - 1/T_2} \tag{6}$$

where E is the apparent activation energy corresponding to the reduction of nickel oxide, $R = 1.98$ cal mol^{-1}K^{-1} the constant of gases.

From eq. (6) we can see that the ratio E/R is equal to the slope of the Arrhenius plotting, $\ln t = f(1/T)$, where the reduction degree is constant.

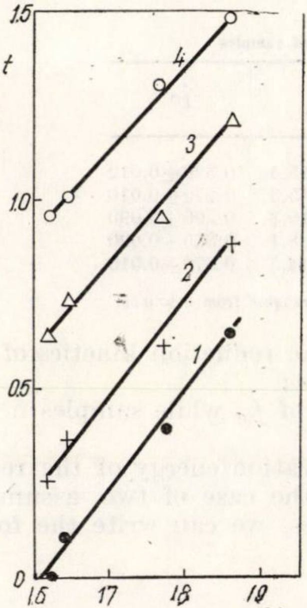

Fig. 2. — Arrhenius plottings, lg t *vs.* $1/T$, in the case of the sample n° 2; reduction degree : *1*, 0.25, *2*, 0.30, *3*, 0.40, and *4*, 0.50.

Figure 2 shows the ln t *vs.* $1/T$ plotting for the sample n° 2. We can observe that the Arrhenius dependence is verified indeed. Similar plottings were found for the other samples.

---

[9] D. Barb, M. Morariu, M. Răsvanţă and E. Weissmann, *Rev. Roumaine Phys.*, **10**, 927 (1965).

Table 2 gives the values of the activation energy obtained from the slopes of the Arrhenius plotting. From this table one can observe that the sample n° 5 is the most difficult to reduce, while the sample n° 3 is the easiest one; the large value of the activation energy in case of the sample n° 5 may be correlated with the high value of the constant *B*, in table 1.

Table 2

Activation energy

Sample n⁰	$\overline{E}$(kcal/mol)[a]	$\overline{E}$(kcal/mol)[b]
1	7.80±2.75	1.97
2	6.42±2.02	1.77
3	5.10±0.77	1.92
4	8.00±0.64	1.72
5	12.00±0.03	2.30

a activation energy calculated for the zero-order kinetics.
b activation energy calculated for the 1/2-order kinetics.

b) if we assume a 1/2-order kinetics, one can write

$$\frac{\mathrm{d}x}{\mathrm{d}t} = kt^{-0.5} \tag{7}$$

By integrating eq. (7), one obtains

$$x - a = (1/2)\,kt^{0.5} \tag{8}$$

Eq. (8) is a typical one for diffusion processes, [10,11] but if we express *k* by means of the Arrhenius law, it results

$$\ln(x - a) = (1/2)\ \ln t - E/RT - \ln A - \ln 2 \tag{9}$$

but as *A* is small, eq (9) may be written as follows

$$\ln(x - a) = (1/2)\ \ln t - E/RT \tag{10}$$

Eq. (10) is just eq. (2) where

$$f = x - a\,;\ n = 1/2\,;\ \text{and, } E/R = B \tag{11}$$

One can see that the experimental values for n (ranging from 0.45 to 0.28) are close enough to the theoretical value of 0.5. Also, we can remark the proportionality between E and B.

---

[10] K. J. Laidler, *Chem. Kinetics*, **1**, 316 (1965).
[11] C. H. Bomford, *Chem. Kinetics*, **2**, 406 (1969).

The values of the activation energy calculated by means of the last relation in eq. (11) are also given in table 2.
We observe that these values are smaller than the similar values obtained for zero-order kinetics.

CONCLUSIONS

Some conclusions on the reduction kinetics of nickel oxide-kieselguhr catalysts may be summed up as follows :
1° the reduction kinetics satisfies an Arrhenius type law,
2° diffusion processes play an important part in the reduction process.

Acknowledgements. The authors wish to express their deep gratitude to Professor I. G. Murgulescu for many useful discussions and comments.

Revue Roumaine de Chimie, **18**, *8*, 1339–1344 (1973)

MAGNETIC DISPERSION AND MAGNETIC ABSORPTION OF SOME FERRIMAGNETIC COMPOUNDS IN THE DOMAIN OF CENTIMETRE WAVES. I
Li—Fe—Be AND Ni—Fe—Be

N. DUŞOIU

Centre of Physical Chemistry, Str. Galaţi 31, Bucharest-9, Romania

Received November 9, 1972

One presents the experimental method utilized for the study of magnetic dispersion and absorption in the X-band frequency. We have studied compounds Li–Fe–Be (LFB) and Ni–Fe–Be (NFB).

1. INTRODUCTION

In the domain of radio frequencies and microwaves, the magnetic susceptibility $\varkappa$ is a complex quantity. The real component $\varkappa'$ is associated to the dispersion phenomenon while the imaginary component $\varkappa''$ is associated to the absorption phenomenon.

Measurement of the magnetic dynamical susceptibility components, in the microwaves domain, has constituted the object of numerous papers (see[1–3]). From the recent papers we quote : Cogan and Lemaire[4], Bodi and Baican[5], Patton[6], Patton and Kohane[7].

For the simultaneous measurement of the components $\varkappa'$ and $\varkappa''$ of magnetic susceptibility, function of field and temperature, in the present paper we have utilized a parallelepipedal resonant cavity, operating by reflection and utilized in the ESR measurements. Inside of the cavity the temperature can be changed between $-150 - +200°$.

---

[1] H. P. Y. Wijn, "Handbuch der Physik – Ferromagnetismus", **18**/2, Springer-Verlag, Berlin, 1966, p. 220–239.

[2] A. E. Pannenborg, "Handbuch der Physik – Electrische Instrumente", Springer-Verlag, vol. 23, Berlin, 1967, p. 131–156.

[3] L. Silber, "Handbook of Microwave Measurements – Intrinsic Properties of Ferrites", vol. 2, Ed. M. Sucher and J. Fox, Polyt. Press. of the Polyt. Inst. of Brooklin, 1963, p. 777–801.

[4] V. Cogan and B. Lemaire, "Proceedings of the 12th Colloque Ampère Bordeaux, 1963", Ed. R. Servant and A. Charru, Bordeaux, North-Holland Publishing Comp., Amsterdam, 1964, p. 517.

[5] A. Bodi and R. Baican, *Rev. Roumaine Phys.*, **3**, 174 (1968).

[6] C. E. Patton, *J. Appl. Phys.*, **41**, 1637 (1970).

[7] C. E. Patton and T. Kohane, *Rev. Sci. Instr.*, **43**, 76 (1972).

The experimental method is based on the principle of the perturbation of the resonance parameters in the presence of the studied sample.[3,5]

Using this method we have obtained the dispersion and absorption curves of ferrimagnetic compounds Li—Fe—Be (LFB) and Ni—Fe—Be (NFB). Also we have plotted the curves of the temperature dependence of the components $\varkappa'$ and $\varkappa''$ in the range 0—200°, for different values of continuous magnetic fields. Some of the standard parameters are determined from the experimental curves.

The magnetic loss factor studied is tg δ, definite as ratio of the diagonal components of the permeability tensor and not the standard parameter α, because the curves tg δ (H_0) present a high sensibility in the range where the measurements are more precise.

The geometrical parameters for the cavity and the sample and the values of the resonance parameters are indicated in table 1.

Table 1

Geometrical parameters

Sample	a mm	b mm	l mm	f_0 Mc/s	Q_0
Empty cavity for determinations (H_0)	22.86	10.16	45.21	9 388	3 380
Empty cavity for determinations (T)	—	—	—	9 154	3 300
Sample LFB, for (H_0)	1	1	2	—	—
Sample LFB, for (T)	1	1	15	—	—
Sample NFB, for (H_0)	1	1	2.3	—	—
Sample NFB, for (T)	1	1	15.4	—	—

For the absolute measurement utilising the resonant cavity of the type TE_{102}, with the values contained in table 1, on the base of Silber's computation schema we have obtained:

$$\text{LFB}\begin{cases}\chi(\mathrm{H}_0) & \left|\begin{array}{l}\chi' = -0.5466\ \Delta f\\ \chi'' = 3.035\ \Delta Q/Q\end{array}\right.\\[2ex] \chi(T) & \left|\begin{array}{l}\chi' = -0.0785\ \Delta f\\ \chi'' = 0.4311\ \Delta Q/Q\end{array}\right.\end{cases}$$

$$\text{NFB}\begin{cases}\chi(\mathrm{H}_0) & \left|\begin{array}{l}\chi' = -0.4793\ \Delta f\\ \chi'' = 2.665\ \Delta Q/Q\end{array}\right.\\[2ex] \chi(\mathrm{T}) & \left|\begin{array}{l}\chi' = -0.766\ \Delta f\\ \chi'' = 0.3939\ \Delta Q/Q\end{array}\right.\end{cases} \qquad \text{(I)}$$

where Q is the quality factor and Δf is the frequency variation, measured in Mc/S. The numerical factors from the system of equations (I) contain also the values of the resonance parameters of the empty cavity f_0 and Q_0.

2. EXPERIMENTAL METHOD

The numerical factors from the equations system (I) represent the proportionality constants, for which the exactly values are not important. For this reason we have determined the χ' and χ'' components variations function of H_0 and T.

The experimental technique must give the values of Δf and Q under the conditions of variation of the parameters H and T.

We have used an apparatus consisting of the microwaves unit from ESR equipment, of type JES—3B. The measurements were made to read directly the signal position and the form of the resonance on the synchroscope.

The measurement of the frequency was made with the wavemeter of the equipment which gives the values of the wavelength with four decimal fractions.

The procedure of measurement of the quality factor consists in : one reads the value of the resonance frequency f_0, the frequency f_s with the signal of the measure shifted to the left at 0.7 L and the frequency f_d with the signal shifted to the right at the same height. The quality factor is determined from the classical relation

$$Q = \beta \frac{f_0}{f_s - f_d} \tag{II}$$

in which we have considered $\beta = 1$. During the measurements, the attenuator is maintained in a fixed position. The precision of the measurements is conditioned of the precision taken for the position 0.7 L.

To avoid other sources of errors we have taken the following precautions :

1. The sample was fixed in the center of the resonant cavity being introduced inside of a test glass tube with the internal diameter of 1.5 mm and with a known length.

2. The fastening of the empty test tube at $E = 0$ and $H = H_{\max}$ was made by its shifting in the position of the minimum dispersion. The values f_0 and Q_0 were measured when the empty test tube was inside the resonant cavity.

3. The sample was fastened inside of the cavity for the direction of the continuous magnetic field H_0 to be perpendicular on the surface of the sample contained in the plane XOZ.

4. The effects of the electric dispersion and absorption generated by the inexactitude of the fastening of the sample in $E = 0$, give errors only at $H_0 = 0$, because the dielectric constant is independent of H_0. The introduced errors are insignificant.

5. The test glass tube was set rigidly on the metallic support of the cavity to avoid vibrations.

6. The measurement of the field H_0 and variation of the temperature T was made with a good accuracy using the adjustment of the ESR equipment. Since temperature variations inside of the empty cavity determine changes of the resonance frequency, the measured values in the presence of the sample were corrected taking into account the values in table 2.

3. EXPERIMENTAL RESULTS

The used samples were obtained from the Institute of Physics, Bucharest. The curves $\chi(H_0)$, $\chi(T)$ and tg $\delta(T)$ were plotted. The porosity degree of samples was approximatively 16%. The magnetic effects of the pores was neglected. We have assumed that the dependence of the gyromagnetic ratio γ on the field $\overline{H}_0$ can be neglected. The following experimental results were obtained :

1°. The saturation magnetization, $4\pi M_s$, is 5.9 kGs for the sample LFB and 4.7 kGs for the sample NFB. These values were determined by comparison on the samples in bar and sphere form.

Table 2

Correction values of temperatures

T °C	f Mc/s
20	—
25	—
50	+0.24
75	+0.40
100	+0.56
125	+0.75
150	+0.86
175	+1.03
200	+1.19

2°. Curves of the dispersion $\chi'(H_0)$ and absorption $\chi''(H_0)$ and the magnetic loss factor tg δ ($\overline{H}_0$) for the sample LFB are given in fig. 1. The maximum absorption is obtained for the field $\overline{H}_0 = 2.75$ kOe and the maximum dispersion at the resonance field gives a shifting of the frequency of ~ 10 Mcfs. The sign changes of the component χ' determined of the spin transitions $(-)\rightarrow(+)$ (which generate the rotation plane of the polarization) of the electrons 3d from the Fe, take place at $\overline{H}_0 = 3.35$ kOe. The line width of the resonance is $\Delta H = 290$ Oe and the region of the marked dispersion is extended on a range of 1.25 kOe. The absorption curve can be approximate as being of a Lorentzian form.

The magnetic loss factor tg $\delta(H_0)$ has a maximum value at $H_0 = 3.75$ kOe and a minimum value at $H_0 = 4.5$ kOe, what gives convenient conditions of the measurement of the parameters f and Q in the study of some processes in the dynamical regime.

3°. The same curves as in fig. 1 but for sample NFB are given in fig. 2. The resonance is obtained at $H_0 = 1.9$ kOe. The maximum dispersion for the field $H_0 = 1.4$ kOe determines a shifting 1.25 Mc/s of the frequency. The minimum dispersion at the resonance field generates a shifting frequency of 2.47 Mc/s. The sign changes resulted from the spin transitions take place at $H_0 = 1.8$ kOe. The linewidth of the resonance is $\Delta H = 360$ Oe and the range of the extension of the marked dispersion is 0.7 kOe.

The form of the resonance line is the same with the line of the polycrystalline substances having the microcrystals with the rhombohedral symmetry. The magnetic losses have maximum values at the resonance.

4°. The gyromagnetic ratio computed are: for the sample LFB, $\gamma = 2.92$ Mc/S. Oe and for the sample NFB $\gamma = 3.35$ Mc/s. Oe

5°. The temperature dependence, in the range 0 – 200° of the components χ' and χ'' is presented in fig. 3, for the sample LFB and in fig. 4 for the sample NFB. Data written in the diagrams represent the relative variations taking into account values for 20°. The temperature dependence of the components $\chi'(T)$ and $\chi''(T)$ was determined at initial different magnetization due to the fact that the temperature changes give variations of the internal magnetic field.

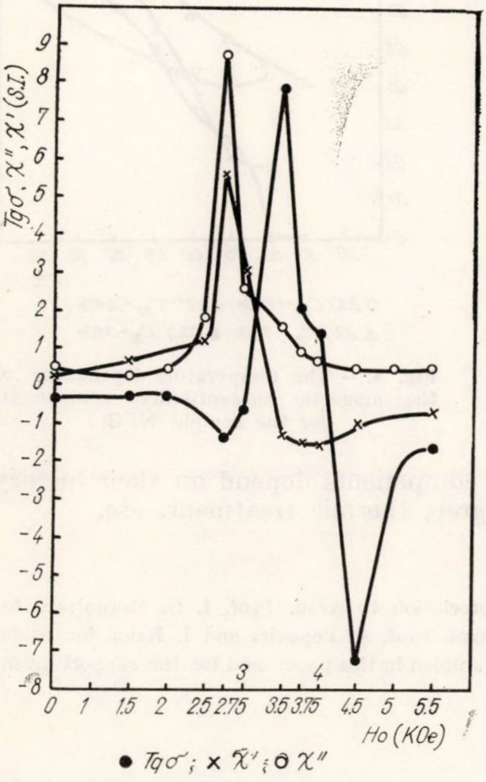

Fig. 1. — The experimental curves $\chi(H_0)$ and tg $\delta(H_0)$ for the sample LFB.

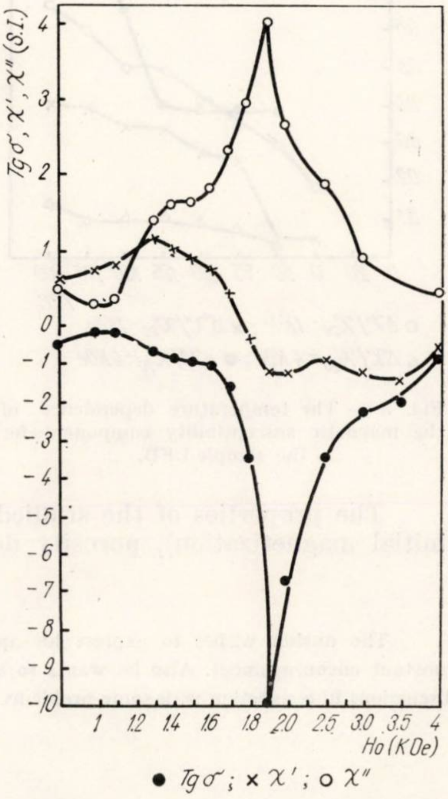

Fig. 2. — The experimental curves $\chi'(H_0)$, $\chi''(H_0)$ and tg $\delta(H_0)$ for the sample NFB.

The curves plotted in fig. 3 describe different behaviours of the components $\chi'(T)$ and $\chi''(T)$ for the fields 1 kOe and 4 kOe. The medium slopes of the two curves have different values. A marked decreasing of the magnetic susceptibility is observed from 125°. The same fact is observed for the sample NFB, fig. 4, for which the measurements were made at 1.3 kOe and 3kOe. The transitions to the paramagnetism begin at 75°.

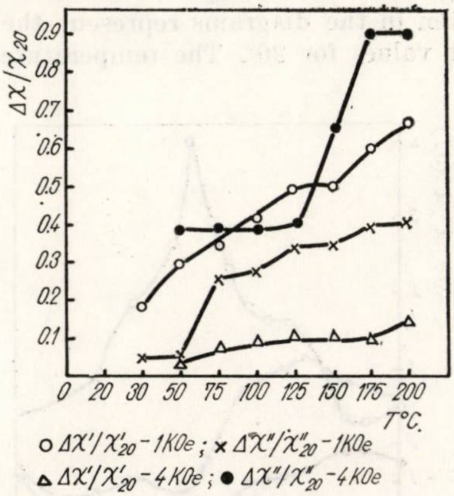

Fig. 3. — The temperature dependence of the magnetic susceptibility components for the sample LFB.

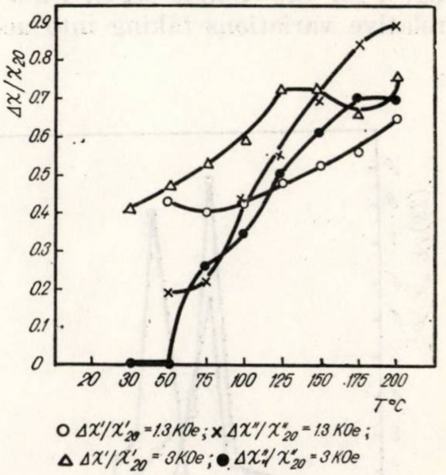

Fig. 4. — The temperature dependence of the magnetic susceptibility components for the sample NFB.

The properties of the studied components depend on their history (initial magnetization), porosity degree, thermic treatment, etc.

The author wishes to express his appreciation to Acad. Prof. I. G. Murgulescu for constant encouragement. Also he wants to thank Prof. A. Popovici and I. Raicu for useful discussions in connection with some problems studied in this paper and for the support given.

Revue Roumaine de Chimie, **18**, *8*, 1345 – 1351 (1973)

ELECTRICAL CONDUCTIVITY OF INTERMETALLIC COMPOUNDS OF THE CERIUM–THALLIUM SYSTEM

G. D. CISMARU and P. SPACU

Centre of Physical Chemistry,
Str. Dumbrava Roșie 23, Bucharest, Romania

Received December 1, 1972

The electrical conductivity of intermetallic compounds of the Ce – Tl system was studied. An exponential increase of conductivity was observed on increasing the atomic fraction of Tl. The conductivity variation within the system confirmed the formation of Ce_5Tl_3, CeTl and $CeTl_3$ compounds and infirmed the existence of the Ce_2Tl compound. Values of $N_{ef}^{2/3}\,l$ product for each compound of Drude's corrected equation were determined.

INTRODUCTION

The first compound studied by Iandelli[1] using X-ray methods was CeTl. As far as the cerium-thallium phase diagram is concerned, Vogel and Heumann[2] report the existance of three compounds : Ce_2Tl, CeTl and $CeTl_3$.

The crystal structures of intermetallic compounds given in this system, have been investigated by Iandelli and co-workers.[1,3–7] Thus Iandelli[1,3,4] and Palenzona[3,5] show for CeTl the CsCl type structure with lattice constant value $a = 3.893$ Å and for $CeTl_3$ the $AuCu_3$ type structure, with lattice constant value $a = 4.767$ Å. The same research in a study referring to MX_2 compounds[6] (where M = rare earth metals and X = Tl or IB, IIB and IIIB group elements) found that no intermetallic compounds of this type exist in the Ce-Tl system.

From the X-ray studies, Franceschi and Palenzona[7] found that a new compound Ce_5Tl_3 was formed. This belongs to a tetragonal W_5Si_3

---

[1] A. Iandelli, "Atti X Congr. Intern. Chim.", 2, Roma, 1938, p. 688 – 694.

[2] R. Vogel and T. Heumann, *Z. Metallk.*, **35**, 29 (1943).

[3] A. Iandelli and A. Palenzona, *J. Less-Common Metals*, **9**, 1 (1965).

[4] A. Iandelli, "Proceedings of the 9th Symposium of the NPL Physical Chemistry of Metals and Alloys", 3F, (1958).

[5] A. Palenzona, *J. Less Common Metals*, **10**, 290 (1966).

[6] A. Iandelli and A. Palenzona, *J. Less Common Metals*, **15**, 273 (1968).

[7] E. Franceschi and A. Palenzona, *J. Less Common Metals*, **18**, 93 (1969).

type structure, with lattice constants values $a = 12.642$ Å, $c = 6.192$ Å and the cube root unit formula $R = 6.278$ Å. But, in this case, it is necessary to revise the possibility of the Ce_2Tl compound existence.

In order to examine the intermetallic compounds, that may be formed within the Ce—Tl system and to establish the variation criterion of some properties in the compounds series, a study on the conductivity of these compounds was carried out.

EXPERIMENTAL

The metals used for preparing the intermetallic compounds, were Ce with a purity of 99.9 % produced by Johnson Matthey & Co. Ltd. England, and Tl with a purity of 99.9 % supplied by the Serva Heidelberg, R.F.G.

Melting of metals introduced into tantalum nacelles was performed in a pure argon atmosphere in a Vacutherm. Reichert installation, modified with a tantalum heating element. The installation design was presented in a previous paper.[8]

Samples were heated to 400°, for 4 hours, then the temperature was increased to 1300°, for about 30 minutes. The feeding tension was then suddenly dropped to 0 with final current stopping, bringing about a rapid low temperature to 200°, followed by a slower cooling down to 25° (it is due to the installation thermal inertia).

Besides the samples for compounds, other eight samples were prepared, where the ratio ranged from 2.3 : 1 to 1 : 4. These samples were chosen so that, on either side of the supposed compounds, two alloys with similar proportions might exist.

Samples of each alloy were examined metallographically in order to verify the homogeneity.

For conductivity determinations, prisms of 10 × 2 × 2 mm were prepared from samples. The electrical conductivity was determined at 25° by means of the Thomson method, using an R-329 bridge (U.S.S.R.).

The samples of intermetallic compounds and alloys were kept in paraffin oil, because they present a pronounced corrosion in air.

RESULTS AND DISCUSSION

From conductivity measurements on samples, three singular points resulted from the concentration interval studied. Peaks observed on the conductivity-composition diagram, correspond to Ce_5Tl_3, CeTl and $CeTl_3$ intermetallic compounds. As concerns the Ce_2Tl compound, indicated by Vogel and Heumann [2], the lack of a minimum conductivity at ratio 2 : 1, compared to alloys conductivity in the interval where the atomic ratio Ce : Tl changes from 2.3 : 1 to 1.8 : 1 does not confirm the formation of a compound.

The values obtained show that the criterion of conductivity exponential variation is applied to intermetallic compounds of the Ce—Tl system, the same was also observed with La—Tl,[8] Pr—Tl[9] and Nd—Tl[10] systems previously studied by the authors.

---

[8] P. Spacu and G. D. Cismaru, *Studii și Cercetări Chim. Acad. R.P.R.*, **1963**, 399.

The increasing of conductivity values in the serie of compounds occurring in the Ce—Tl system, were produced with the increasing of the atomic fraction of the hyperelectronic element — thallium — according to the following equation

$$\sigma = A\,\mathrm{e}^{Kc_B} \tag{1}$$

where σ is the electrical conductivity; A is the preexponential coefficient with a constant value for each temperature; K is a constant whose value is given by the line slope and c_B is the concentration of Tl hyperelectronic element, expressed by its atomic fraction.

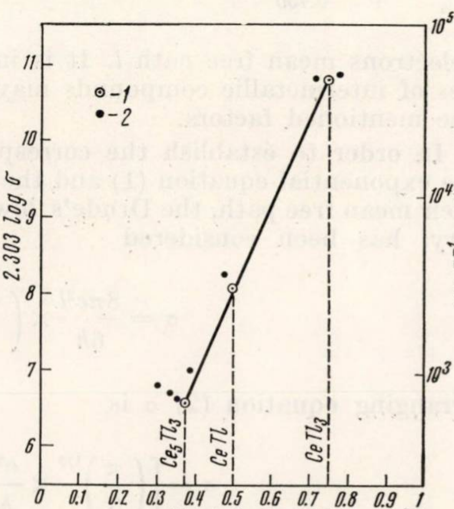

Fig. 1. — Exponential variation of conductivity in intermetallic compounds within Ce—Tl system.

1, values corresponding to intermetallic compounds; *2*, values corresponding to any alloys in the zones between compounds.

The diagram ln $\sigma - c_B$ (fig. 1), obtained by introduction of the experimental values in the logarithmated equation (1), gives the possibility to find the values of A and K. The values of the compounds conductivity and of A and K for 25° were presented in table 1.

In the binary intermetallic compounds, formed between a hypoelectronic and hyperelectronic elements according to Pauling's theory[11] on metallic bond, strong bonds occur due to the participation of valence electrons. This leads to the formation of a more compact crystal lattice, by reduction of the interatomic distances in compounds, which reflect on

---

[9] P. Spacu and G. D. Cismaru, *Rev. Roumaine Chim.*, **17**, 1723 (1972).

[10] P. Spacu and G. D. Cismaru, Paper presented at the Second Republican Conference of Chemistry, Iași, Romania (May 1964).

[11] L. Pauling, "The Nature of Chemical Bond", 3rd ed., Cornell University Press, New York, 1960, p. 431—432.

Table 1

Values σ, A and K of equation (1) for intermetallic compounds at 25°

Intermetallic compound	Atomic fraction of Tl c_B	A $[\Omega^{-1}-\mathrm{cm}^{-1}]$	K	σ $[\Omega^{-1}-\mathrm{cm}^{-1}]$ experimental σ_e	calculated σ_c	$\frac{\sigma_e}{\sigma_c}$
Ce_5Tl_3	0.375			7.10×10^2	7.42×10^2	0.957
Ce Tl	0.500	11.23	11.17	3.13×10^3	3.00×10^3	1.042
Ce Tl_3	0.750			4.69×10^4	4.90×10^4	0.957

the electrons mean free path l. It is in that way that the conductivity values of intermetallic compounds may be explained by the correlation of the mentioned factors.

In order to establish the correspondence between the coefficients of the exponential equation (1) and the number of free electrons, as well as their mean free path, the Drude's low, corrected according to quantum theory, has been considered

$$\sigma = \frac{8\pi e^2 l}{6h} \times \left(\frac{3N_{\mathrm{ef}}}{8\pi}\right)^{2/3} \tag{2}$$

Rearranging equation (2) σ is

$$\sigma = \left[\left(\frac{\pi}{3}\right)^{1/3} \times \frac{\mathrm{e}^2}{h}\right] \times N_{\mathrm{ef}}{}^{2/3}\, l \tag{3}$$

where σ is the electrical conductivity; e — the electron charge in abs. esu; l — the mean free path in cm; N_{ef} — the real number of free electrons in 1 cm³ and h — Planck constant in erg-sec.

Because the product of the first two ratios (right patantheses) is a constant, it is noted

$$\frac{1}{C} = \left(\frac{\pi}{3}\right)^{1/3} \times \frac{e^2}{h} \tag{4}$$

It results $C = 2.8293 \times 10^{-8}$ erg-sec/(esu)² or by multiplication of this value by 9×10^{11} an equivalent value in ohm, necessary for calculation was thus obtained. Therefore, $C = 2.54637 \times 10^4\ \Omega$.

Equation (3) becomes

$$\sigma = \frac{1}{C}\ N_{\mathrm{ef}}{}^{2/3}\, l \tag{5}$$

From equations (1) and (5) we have

$$\frac{1}{C} N_{ef}^{2/3} l = A e^{K c_B} \tag{6}$$

or rearranging equation (6), $N_{ef}^{2/3} l$ is

$$N_{ef}^{2/3} l = A C e^{K c_B} \tag{7}$$

Therefore, the product $N_{ef}^{2/3} l$ varies exponentially with the atomic fraction c_B of the hyperelectronic element.

The values of this product, which characterize the intermetallic compounds, occurring in the Ce–Tl system, were presented in table 2.

Table 2

Values of $N_{ef}^{2/3}$ l product and of C constant from equations (5) and (7) for intermetallic compounds at 25°

Intermetallic compound	Atomic fraction of Tl c_B	$A \times C$ [cm^{-1}]	$N_{ef}^{2/3}$ l [cm^{-1}] from eq.5*	from eq. 7
Ce_5Tl_3	0.375		1.808×10^7	1.889×10^7
CeTl	0.500	2.86×10^5	7.970×10^7	7.637×10^7
$CeTl_3$	0.750		1.194×10^9	1.248×10^9

* Values σ_e from table 1 were used in calculation.

For a clearer image on the percentage of valence electrons leading the electric current, the value n_{ef} representing the number of free electrons that correspond to 1 atom, was used instead of N_{ef}. The following relation exists between these two values

$$N_{ef} = n_{ef} N_a \tag{8}$$

and

$$N_a = \frac{N D n_a}{M} \tag{9}$$

where N_a is the number of atoms included in 1 cm³ ; M – molecular weight of the compound in grams ; N – Avogadro's number 6.0235×10^{23}; D – compound density in gm/cm³ and n_a – number of atoms in the compound formula.

Replacing N_{ef} in equation (5) with $n_{\text{ef}}N_a$ product, according to the equation (8) for n_{ef}, the following expression is obtained

$$n_{\text{ef}} = \left(\frac{\sigma_e C}{N_a{}^{2/3}\, l}\right)^{3/2} \tag{10}$$

where σ_e = experimental conductivity.

If, within the first approximation, the mean free path l is considered equal to the distance between the plans of crystal lattice, then we may use the value $R = 6.278$Å (cube root of unit formula volume) for Ce_5Tl_3, and the lattice constants for the other compounds, that is 3.893 Å for CeTl and 4.767 Å for $CeTl_3$. In the case of these values chosen for l, n_{ef} is 0.21 for Ce_3Tl_5, 2.65 for CeTl and 77.50 for $CeTl_3$. Thus, these are too low values for Ce_5Tl_3 or too high values $CeTl_3$, that is impossible in reality.

The limits within which n_{ef} may vary should be considered for determining the possible values of l.

For this purpose, we may take into consideration the indications of magnetic studies which show that in metallic state, cerium is partly trivalent and partly tetravalent, due to the transfer of the last 4f electron in the 5d conduction band, for any part of the atoms. Because it is possible to produce a partial or total transition in the intermetallic compounds too, it has been considered that n_{ef} may take vlaues in the intervals from 3 to 3.6 electrons/atom for Ce_5Tl_3, from 3 to 3.5 for CeTl and from 3 to 3.25 for $CeTl_3$.

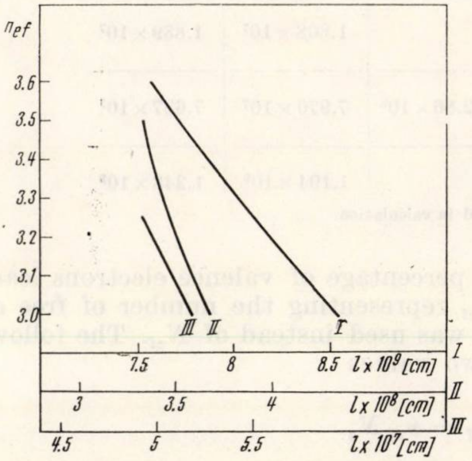

Fig. 2. – The diagrams $l = f(n_{\text{ef}})$ for intermetallic compounds of the Ce–Tl system.

I – Ce_5Tl_3; II – CeTl; III – $CeTl_3$.

In order to know these possible limits, the diagrams $l = f(n_{\text{ef}})$ have been marked, using the relationship

$$l = \frac{\sigma_e C}{(n_{\text{ef}} N_a)^{2/3}} \tag{11}$$

The curves for the three compounds are shown in fig. 2.

These curves will permit the direct determination of the mean free path of electron using the data concerning the value of n_{ef} obtainable from the studies of magnetic properties of intermetallic compounds.

The cases studied so far show that the mean free path is more than the crystalline lattice constants for CeTl and $CeTl_3$ compounds. This may by explained, on the one side, by the fact that collectivized electrons are moving according to the laws of wave mechanics and, on the other side, by the deforming contribution on crystal potential periodicity in the real structure.

CONCLUSIONS

1. In the Ce—Tl system, the intermetallic compounds Ce_5Tl_3, CeTl and $CeTl_3$ were identified by means of conductivity. No conductivity minimum has been noticed for the Ce_2Tl composition, which infirms the occurrence of this compound.

2. The electrical conductivity variation follows an exponential law $\sigma = Ae^{Kc_B}$, which was found valid in the La—Tl, Pr—Tl and Nd—Tl systems.

The increase in the conductivity value is observed in the series of intermetallic compounds from Ce_5Tl_3 to $CeTl_3$.

3. The product $\mathrm{N}_{\mathrm{ef}}^{2/3}\, l$ has a similar exponential variation as the conductivity has, depending on the atomic fraction of the hyperelectronic element : $N_{\mathrm{ef}}^{2/3}\, l = ACe^{Kc_B}$.

The value of $N_{\mathrm{ef}}^{2/3}\, l$ was determined from this equation, as well as the mean free path l of compounds for different N_{ef} values, with the purpose of orientation on its size order.

4. The diagrams $l = f(n_{\mathrm{ef}})$ were marked for the three compounds, having in view the limits of the n_{ef} change due to the possibility of 4f electron transition in the conduction band.

Revue Roumaine de Chimie, 18, *8*, 1345—1351 (1973)

Revue Roumaine de Chimie, **18**, *8*, 1353–1359 (1973)

STABILITY OF THREE-MEMBERED HETEROCYCLES. I

CONSIDERATIONS CONCERNING THERMODYNAMIC STABILITY AND CONSERVATION OF ORBITAL SYMMETRY

R. VÎLCEANU, Z. SIMON and A. CHIRIAC
Department of Chemistry, University of Timişoara, Bd. V. Pârvan 4, Romania

Received April 20, 1972

The thermodynamic stability against decyclization of the $\overline{\mathrm{CH_2CH_2X}}$ cycles ($X = CH_2$, O, NH, S, PH, PH_3) is predicted at the hand of the bond strengths. The real stability of these cycles must be due to the high activation energies required for the bond angle deformations in the transition states of the exothermic decyclization pathways. Woodward-Hoffmann correlation diagrams indicate that the $C_2H_2 + PH_3 \rightarrow$ cyclo $- C_2H_4PH$ reaction should be possible in the ground state, while the $C_2H_4 + PH_3 \rightarrow$ cyclo $- C_2H_4PH_3$ reaction should be possible by photochemical $3\,sp^2 \rightarrow 3\,d$ excitation of PH_3.

The synthesis and stability of three-membered heterocycles is of great interest for organic chemistry both from the theoretical and practical point of view. From the general class (I) representatives for $X = CH_2$, O, S, NH [1] as well as for $X = PH$ [2a,b,c] are known, but not for a pentavalent P-atom as X.

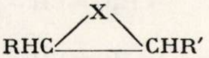

I

As obviously known, the stability of heterocycles depends on their size (maximum for five- and six-membered rings), on their nature (on X) and on the substituents R, R′. The possibility to synthesize such rings depends not only on the stability against the possible decyclization reactions, but also on the absence of energy barriers (*i.e.* activation energies) for the thermodynamically possible cyclization reactions. These stabilities can be predicted from bond energy arguments, while considerations concerning the conservation of orbital symmetry should be able to predict the existence or absence of such energy barriers. Correlations of occupied bonding orbitals in the reactant with unoccupied ones in the products produce an energy increase in the activated complex, *i.e.* give rise to an energy barrier in the reaction path.

---

[1] A. R. Katritzky and J. M. Lagowski, "The Principles of Heterocycles Chemistry", Methuen & Co. Ltd., London, 1967, p. 159.

[2a] R. I. Wagner, U.S.A. Pat. 3 086 053, 1963; *Chem. Abstr.*, **59**, 10124 (1963).

[2b] R. I. Wagner, L. D. Freedman, H. Goldwhite and D G. Rowsell, *J. Amer. Chem. Soc.*, **89**, 1102 (1969).

[2c] J. Chan, *Tetrahedron*, **25**, 1097 (1969).

In this note, we calculate the enthalpies, ΔH, for the various decyclization reactions possible for a cycle given by the general formula (I) and discuss the applicability of orbital symmetry conservation rules to the prediction of energy barriers for such reactions.

Thermodynamic considerations. The possible decyclization reactions which were taken into account for the type (I) heterocycles are listed below (1—11):

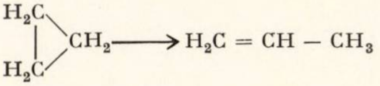
(1)

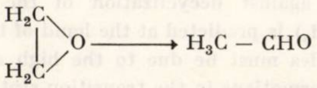
(2)

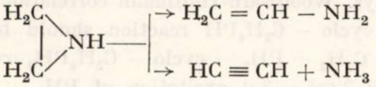
(3)
(4)

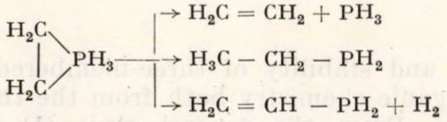
(5)
(6)
(7)

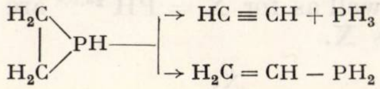
(8)
(9)

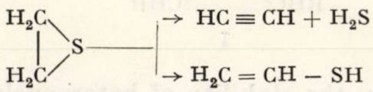
(10)
(11)

The reaction enthalpies, H, for these reactions were calculated out of the bond energies, ε_i, according to the well-known additive formula[3]

$$H_k = \sum_i \nu_{ik}\varepsilon_i - T_3 ; \quad k = 1,2, \ldots 11 \qquad (12)$$

The sum refers to the bonds broken and formed in the reaction k. The pertinent bond energies are given in table 1, according to Cotton and Wilkinson.[4] T_3 is the bond angle deformation energy for triatomic cycles, taken as equal to 27.6 kcal/mol for all cycles (as for cyclopropane[5]) as there are no available data for the heterocycles (I). The errors in calculating the ΔH_k's are probably of about ±5 kcal/mol. The ΔH_k values calculated according to equation (12) are listed in table 2. According to these values the stability of our three-membered heterocycles against the similar reactions (1), (2), (3), (7), (9), (11) is highest for the phosphoranic cycle ($X = PH_3$) and lowest for ethylene oxide. For the other decyclization paths ΔH_k is always endothermic.

---

[3] D. R. Stull, E. F. Westrum Jr. and G. C. Sinke, "The Chemical Thermodynamics of Organic Compounds", J. Wiley & Sons, Inc., New York, 1969, p. 78.

Table 1

Bond energies, kcal/mol (according to (4))

ε_{C-C}	$\varepsilon_{C=C}$	$\varepsilon_{C\equiv C}$	ε_{C-H}	ε_{C-O}	$\varepsilon_{C=O}$	ε_{C-N}
83	148	194	99	82	169	70

ε_{P-C}	ε_{P-H}	ε_{C-S}	ε_{H-S}	ε_{H-H}	ε_{N-H}
63	76	62	81	102.6	93

Table 2

Calculated reaction enthalpies (kcal/mol) for decyclization reactions

Reaction n°	ΔH kcal/mol	Reaction n°	ΔH kcal/mol
1	− 9.6	7	42.8
2	−32.6	8	23.4
3	−17.6	9	− 6.6
4	13.4	10	21.4
5	33.4	11	−12.6
6	12.4		

The phosphiranic cycle ($X = PH$) should be less stable than the phosphoranic ($X = PH_3$) one. The most favourable decyclization path seems to be that one in which the lowest degree of unsaturation is obtained. Exothermicity obtained for reactions (1), (2), (3), (9) together with the existence of the respective cycles indicates rather high energy barriers in these reaction paths.

---

[4] F. A. Cotton and G. Wilkinson, "Advanced Inorganic Chemistry", Interscience Publishers. A Division of J. Wiley & Sons, New York-London-Sydney, 1966, p. 121.

[5] J. March, "Advanced Organic Chemistry. Reactions, Mechanisms and Structure", McGraw-Hill Inc., New York, 1968, p. 120.

Conservation of orbital symmetry. Energy level correlations by the Woodward-Hoffmann rules,[6] require synchronous reactions and at least one symmetry element common for reactants, products and all intermediate nuclear configurations, at least for idealized molecules ($R=R'=H$. in our case). For the reaction paths (1), (2), (3), (7), (9), (11) no such common symmetry element can be found. For example, in cyclopropane, the most symmetric heterocycle, the transition state for path (1):

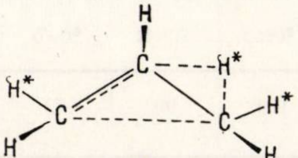

II

is completely asymmetric (*atom below the molecular plane). (Therefore, the bonding molecular orbitals of the reactant will be correlated only with the bonding ones in the product and the same is true for antibonding molecular orbitals). According to the Woodward-Hoffmann rules no energy barrier should appear by the conservation of orbital symmetry-effect. Nevertheless, such decyclization reactions have considerable activation energies : 65 kcal/mol for the decyclization of cyclopropane[7] (which proceeds *via* a biradical[8]; the activation energy for the molecular decyclization must be higher than this figure), 57 kcal/mol for the decyclization of ethylene oxide[9].

An inspection of the transition state (II) indicates that it requires a very strong deformation of a HCC angle and torsion of the methylenic group. Such bond angle deformations must be responsibe for the existence of the energy barriers in the reactions paths (1), (2), (3), (7), (9) (11). For the reaction paths (4), (5), (8) and (10) the molecular plane σ_M and $\sigma_\perp$ (figure 1) may be considered if the group, X, is idealized to higher symmetry. These reaction paths are endothermic for decyclization but may be perhaps used in the synthesis of such cycles. Especially the phosphorus-tricycles ($X = PH, PH_3$) which should be very sensitive against various reagents, especially oxydizing ones, could perhaps be synthesized by the reverse reactions (5), (8) if there are no energy barriers. The symmetry elements and the correlation of molecular orbitals for the reversed reaction (5) are given in figure 1.

An energy barrier should appear in this reaction, as the nonbonding occupied $3\,sp^2 - P$ orbital of PH_3 is symmetric to $\sigma_\perp$ and correlates with the symmetric combination of the two antibonding $P-C$ molecular orbitals, while the unoccupied $3\,d_{xz} - P$ orbital of PH_3 is antisymmetric to $\sigma_\perp$ and correlates with the antisymmetric combination of the two bonding P—C molecular orbitals. In this respect, a trivalent phosphorus derivative, as for example POCl, should be similar to a double bond, with the 3 sp^2 — P lone pair in the role of the bonding π-orbital and the 3 d — P orbital in the role of the antibonding one. The photochemical reaction with a 3 $sp^2 \rightarrow 3d$ excited PH_3 molecule should be possible according to this diagram.

---

[6] R. B. Woodward and R. Hoffmann, "The Conservation of Orbital Symmetry", Weinheim, 1970.

[7] T. C. Chambers and G. B. Kistiakowsky, *J. Amer. Chem. Soc.*, **56**, 399 (1934).

[8] B. S. Rabinovitch, E. W. Schlag and K. B. Wiberg, *J. Chem. Phys.*, **29**, 235 (1958).

[9] S. W. Benson, *J. Chem. Phys.*, **40**, 105 (1964).

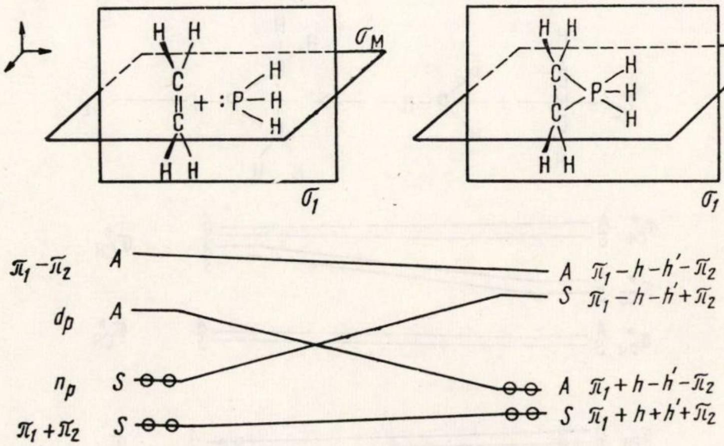

Fig. 1. — Correlation diagram for the hypothetic reaction:

$$H_2C = CH_2 + PH_3 \rightarrow \underbrace{CH_2CH_2PH_3}_{}$$

Substitution by more electronegative groups of the H atoms in PH_3 will decrease the energy of both P-orbitals and, to a lower extent, also the energy of the intersection point in the correlation diagram (figure 1). The activation energy for the thermal cycloaddition should thus be increased by such substitutions and the one of the thermal decomposition (inverse reaction 5) decreased. The photochemical cycloaddition should be disfavoured by such substitutions : less energy will be released as the 3d electron in the excited PH_3 molecule passes on the A-symmetry P—C bonding orbital of the resulting cycle.

The symmetry elements and correlation of molecular orbitals for the reversed reaction (8) are given in figure 2. The symmetry element common to all nuclear configurations is a median C_2-axis. Two C—H bonds, two P—H bonds and the two π_{C-C} bonds in the reactants as well as the four C—H bonds and two P—C bonds in the product must be taken into account. As seen from fig. 2, all binding molecular orbitals of the reactants can be correlated with binding molecular orbitals of the products. No energy barrier should appear and the hypothetical $C_2H_2 + PH_3 \rightarrow$ cyclo-C_2H_4PH reaction should be possible. Linear addition of PH_3 to the ethylenic double bond takes place by usual mechanisms : radical-initiated thermal[10] or photochemical [11,12] mechanism, acidic or bazic catalysis. [12] These reactions may be explained by the relatively low dissociation energy of the P-H bond (radicalic reactions with the $PH_2^{\bullet}$-radical), by the low basicity of PH_3, which is not protonated while the ethylene derivative gives a carbocation (acidic catalysis) and respectively by the formation of a PH_2^--anion in basic catalysis. These linear addition reactions require rather drastic conditions and it may be hoped that corresponding substituents may allow the photochemical cycloaddition to take place.

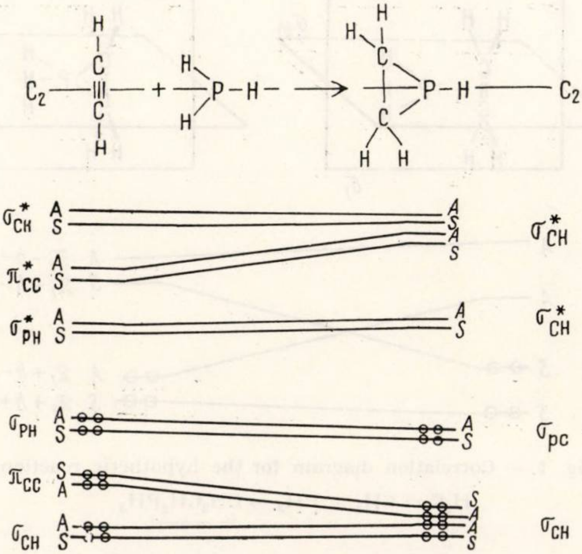

Fig. 2. — Correlation diagram for the hypothetic reaction.

$$HC \equiv CH + PH_3 \rightarrow \underbrace{CH_2CH_2PH}$$

Substitutions in our compounds (R, R′ ≠ H) may change essentially the possible reaction paths and the stability of the substituted cycles. For example, if R and the substituent of X have different electronegativities, so as to favour a charge separation in the transition state, various conrotatory decyclization reactions become possible according to the Woodward-Hoffmann rules, as demonstrated for example by Scherr [13] and Huisgen[14] for compounds of the type:

---

[10] M. M. Rauhut, H. A. Currier, A. M. Semsel and V. P. Wystrach, *J. Org. Chem.*, **26**, 5138 (1961).

[11] G. M. Burch, H. Goldwhite and R. N. Haszeldine, *J. Chem. Soc.*, **1963**, 1083.

[12] E. Fluck and V. Novobilsky, *Fortschr. Chem. Forschg.*, **13**, 125 (1969).

[13] W. Scherr, Dissertation, München, 1968.

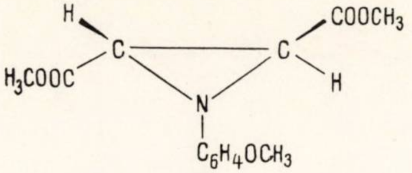

III

CONCLUSIONS

Reaction enthalpy evaluations based on bond strengths indicate that the stability of several three-membered heterocycles against spontaneous decyclization must be due to the existence of energy barriers. These energy barriers are not due to conservation of orbital symmetry effects as no common symmetry element can be found for all pertinent nuclear configurations. The high deformation of bond angles in the hypothetical transition states must be responsible for these barriers. Common symmetry elements appear in endothermal decyclization which produce highly unsaturated compounds.

In future notes we intend to perform systematic experimental and theoretical studies on the stability and synthesis of certain aziridinic and phosphirinic cycles.

---

[14] R. Huisgen, W. Scherr and H. Huber, *J. Amer. Chem. Soc.*, **89**, 1753 (1967).

Revue Roumaine de Chimie, **18**, *8*, 1361–1365 (1973)

ÜBER DIE SYNTHESE EINIGER QUARTÄREN PYRIDINIUMSALZE

LILIANA PETROVA und EUGENIA COMANIȚĂ

Lehrstuhl für Organische Chemie, Polytechnisches Institut Jassy, Calea 23 August, Nr. 11, Jassy, Rumänien

Eingegangen am 27. November 1972

Pyridinderivate mit unterschiedlichen funktionellen Gruppen wurden der Alkylierung zu quartären Salzen nach der Methode von Menschutkin unterworfen. Die meisten quartären Verbindungen wurden aus 2- und 4-Pyridinmethanolen mit Alkylhalogeniden erhalten. Es wurden auch Alkylierungsversuche einiger Zwischenprodukte, Derivate der Carbaminsäureester und des Pyridylacetamids durchgeführt.

1. EINFÜHRUNG

Unter den quartären Ammoniumverbindungen zeichnen sich die Salze des Pyridins und seiner Derivate als Stoffe mit technischer und biologischer Bedeutung aus. Sie werden nach der von Menschutkin erarbeiteten Methode synthetisiert, die auf der Reaktion der tertiären Amine mit Alkylhalogeniden in Lösungsmitteln beruht :[1]

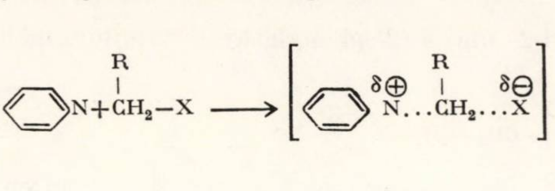

Der Vorgang der Substitution wird von elektronischen und sterischen Effekten der im Pyridinmolekül vorhandenen Substituenten beeinflußt, aber auch von der Art des zur N-Alkylierung verwendeten Alkyhalogenids. [2-8] Auch die Rolle des Lösungsmittels darf nicht übersehen werden.

---

[1] N. Menschutkin, *Journ. russ. phys.-chem. Ges.*, **34**, 411–22, 26/5, (1901); *Chem. Zentr.*, **2**, 86 (1902).

2. ERGEBNISSE UND DISKUSSIONEN

Die vorliegende Arbeit hat das Ziel, die Synthese einiger quartärer Pyridiniumsalze mit verschiedenen an den Heterozyklus gebundenen funktionellen Gruppen zu realisieren. Zu diesem Zweck wurden mehrere Arten von Pyridinderivaten verwendet:

a) 2- und 4-Hydroxymethylpyridine
b) 2- und 4-(2'-Phenyläthyl)-pyridine
c) N-*p*-Cl-Phenylcarbaminsäure-2-pyridylmethylester
d) N-*p*-Cl-Phenyl-2-pyridylacetamid

Die beiden letzten Zwischenprodukte wurden neuerlich aus 2-Pyridylmethanol und 2-Picolin durch Addition an *p*-Cl-Phenylisocyanat hergestellt. Folgende Alkylhalogenide wurden verwendet: Propyljodid, Isopropyljodid, *n*-Butyljodid, tert-Butyljodid, Allylbromid und Allylchlorid.

Die N-Alkylierung wurde in absolutem Methanol bei 75 –80° unter Druck geführt. Die Reaktionsdauer beträgt bis zu 10 Stunden. Die erhaltenen Ausbeuten liegen zwischen 50 und 80%. Die Reinigung der quartären Salze wurde durch Auflösen in Methanol bei Zimmertemperatur und Ausfällung mit Äthyläther verwirklicht. Nach dieser Methode wurden aus den oben erwähnten Zwischenprodukten vier Arten von quartären Salzen erhalten:

1) N-Alkyl-2- und 4-hydroxymethylpyridiniumhalogenide mit Struktur I und II.

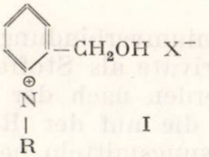

I

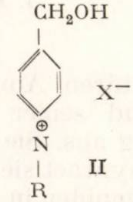

II

2) N-Alkyl-2- und 4-(2'-phenyläthyl)-pyridiniumhalogenide III, IV

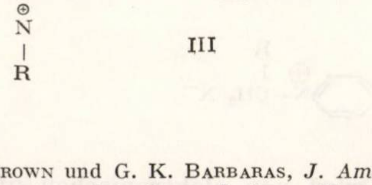

III

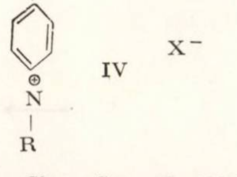

IV

---

[2] H. C. Brown und G. K. Barbaras, *J. Amer. Chem. Soc.*, **69**, 1137 (1947).
[3] H. C. Brown und A. Cahn, *J. Amer. Chem. Soc.*, **77**, 1715 (1955).
[4] H. C. Brown und R. Horowitz, *J. Amer. Chem. Soc.*, **77**, 1733 (1955).
[5] H. C. Brown und R. Holms, *J. Amer. Chem. Soc.*, **77**, 1727 (1955).
[6] M. M. Markowitz, *J. Org. Chem.*, **22**, 983 (1957).
[7] I. G. Chumakov, „Piridinovje Osnovanie“, Ed. tehn. Kiev, 1965.
[8] M. Avramoff und Y. Sprinzak, *J. Amer. Chem. Soc.*, **78**, 4090 (1956).

3) N-Alkyl-2-(*p*-Cl-phenyl-carbamoyl-oxymethyl)-pyridiniumhalogenide V.

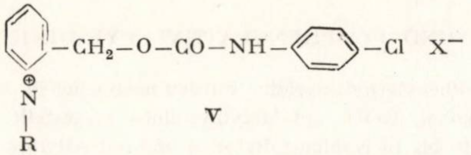

V

4) N-Allyl-2-(*p*-Cl-phenyl-carbamoylmethyl)-pyridiniumhalogenide VI.

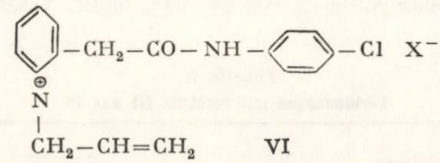

VI

Das N-*p*-(chlorphenyl)-2-pyridylacetamid, der Ausgangsprodukt der letzten Synthese, wurde durch Anlagerung des 2-Picolins an das *p*-Cl-Phenylisocyanat erhalten.

3. EXPERIMENTELLER TEIL

1) N-ALKYL-2- UND 4-HYDROXYMETHYL-PYRIDINIUMHALOGENIDE

Äquivalente Mengen der 2- oder 4-Hydroxymethylpyridine und der Alkylhalogenide wurden in Glasampullen (1/3 gefüllt) 10 Stunden auf ca 80° erhitzt. Die Ausbeuten der nachstehenden Produkte schwanken zwischen 60—75% (Tab. 1)

Tabelle 1

Verbindungen mit Struktur I und II

R	X	Schmp. °C	Summenformel		Analysen % C	H	N
			a) *N-Alkyl-2-hydroxymethyl-pyridiniumhalogenide*				
C_3H_7	I	87	$C_9H_{14}NOI$	Ber.	38,70	5,01	5,01
				Gef.	39,00	5,39	5,08
C_3H_7	Br	114	$C_9H_{14}NOBr$	Ber.	46,55	6,03	6,03
				Gef.	46,57	6,45	6,30
i-C_3H_7	Br	122	$C_9H_{14}NOBr$	Ber.	46,55	6,03	6,03
				Gef.	46,32	6,20	6,33
C_3H_5	Br	110	$C_9H_{12}NOBr$	Ber.	46,95	5,21	6,08
				Gef.	46,65	5,50	6,42
			b) *N-Alkyl-4-hydroxymethyl-pyridiniumhalogenide*				
C_3H_7	I	98	$C_9H_{14}NOI$	Ber.	38,70	5,01	5,01
				Gef.	38,90	5,20	5,33
C_3H_7	Br	107	$C_9H_{14}NOBr$	Ber.	46,55	6,03	6,03
				Gef.	46,30	6,29	6,45
i-C_3H_7	Br	119	$C_9H_{14}NOBr$	Ber.	46,55	6,03	6,03
				Gef.	46,38	6,42	6,38
C_3H_5	Br	111	$C_9H_{12}NOBr$	Ber.	46,95	5,21	6,08
				Gef.	46,80	5,51	6,23

Das t-Butylbromid bildet anstatt des quartären Salzes das Bromhydrat des 2- oder 4-Pyridylmethanols.

2) N-ALKYL-2- UND 4-(2'-PHENYLÄTHYL)-PYRIDINIUMHALOGENIDE

Die 2- und 4-(2'-Phenyläthyl)-pyridine wurden nach einer in der Literatur angegebenen Methode aus Benzylalkohol, KOH und Metylpyridinen hergestellt. Die Alkylierung wurde mit Alkylhalogeniden (10 bis 16 Kohlenstoffatome) und mit Allylbromid bei 75—80° durchgeführt. Im Fall des 2-(Phenyläthyl)-pyridins dauert die Reaktion 5 Stunden; die Ausbeute beträgt 80—85%. Das 4-substituierte Isomere benötigt eine 10 stundige Erhitzung, wobei sich das Endprodukt in einer Ausbeute von 50—60% bildet. Tabelle 2 zeigt die quartären Salze die erhalten wurden.

Tabelle 2

Verbindungen mit Struktur III und IV

R	X	Schmp. °C	Summenformel		Analysen %		
					C	H	N
			a) *N-Alkyl-2-(2'-phenyläthyl)-pyridiniumhalogenide*				
$C_{10}H_{21}$	I	80	$C_{23}H_{34}NI$	Ber.	61,19	7,53	3,10
				Gef.	61,30	7,57	3,17
$C_{12}H_{25}$	I	70	$C_{25}H_{38}NI$	Ber.	62,63	7,91	2,92
				Gef.	62,35	7,80	3,00
$C_{16}H_{33}$	I	86	$C_{29}H_{46}NI$	Ber.	65,46	8,59	2,61
				Gef.	65,60	8,65	2,85
C_3H_5	Br	152	$C_{16}H_{18}NBr$	Ber.	63,15	5,92	4,60
				Gef.	63,35	5,88	4,87
			b) *N-Alkyl-4-(2'-phenyläthyl)-pyridiniumhalogenide*				
$C_{12}H_{25}$	I	69	$C_{25}H_{38}NI$	Ber.	62,63	7,91	2,92
				Gef.	62,90	8,70	3,10
$C_{16}H_{33}$	I	67	$C_{29}H_{46}NI$	Ber.	65,46	8,59	2,61
				Gef.	65,20	8,37	2,90
$C_{18}H_{37}$	I	69	$C_{31}H_{50}NI$	Ber.	66,07	8,88	2,48
				Gef.	66,25	8,53	2,75

3) N-ALKYL-2-(*p*-Cl-PHENYL-CARBAMOYLOXYMETHYL)-PYRIDINIUM-HALOGENIDE

Die Reaktion des 2-Pyridylmethanols mit *p*-Cl-Phenylisocyanat hat zum N-*p*-Cl-phenylsubstituierter-carbaminsäure-2-pyridyl-methylester geführt, der der Alkylierung mit Alkylhalogeniden unterworfen wurde; die synthetisierten Verbindungen sind in Tab. 3 dargestellt.

Tabelle 3

Verbindungen mit Struktur V

R	X	Schamp. °C	Summenformel		Analysen %		
					C	H	N
C_3H_5	Cl	114	$C_{16}H_{16}N_2O_2Cl_2$	Ber.	—	—	8,25
				Gef.	—	—	8,26
C_3H_7	Br	109	$C_{16}H_{18}N_2O_2BrCl$	Ber.	—	—	7,26
				Gef.	—	—	7,63
C_3H_5	Br	119	$C_{16}H_{16}N_2O_2BrCl$	Ber.	—	—	7,30
				Gef.	—	—	7,70

4) N-ALLYL-2-(*p*-CHLORPHENYL-CARBAMOYLMETHYL)-PYRIDINIUM-HALOGENIDE

Aus N-(*p*-Chlorphenyl)-pyridylacetamid und Allylchlorid wurde ein quartäres Salz hergestellt. (Tab. 4)

Tabelle 4

Verbindungen mit Struktur VI

R	X	Schmp. °C	Summenformel		Analysen %		
					C	H	N
C_3H_5	Cl	118	$C_{16}H_{16}N_2OCl_2$	Ber.	59,44	4,95	8,66
				Gef.	59,35	5,05	8,82

Die Reaktionsbedingungen sind ähnlich denen, die bei den vorhergehenden Verbindungen angegeben wurden.

Revue Roumaine de Chimie, **18**, *8*, 1367 – 1372 (1973)

HYDROGÉNATION CATALYTIQUE DE L'ACÉTOPHÉNONE

GEORGETA CSOMONTANYI, MARIȚA NETTA et MAGDALENA BALMEZ

Institut PETROCHIM
Ploiești, 291, B-dul Republicii, Roumanie

Reçu le 9 octobre 1972

La réaction de réduction de l'acétophénone à l'état de méthylphénylcarbinol et respectivement d'éthylbenzène est caractérisée du point de vue thermodynamique. On présente les résultats de l'étude cinétique de l'hydrogénation sélective de la chaîne de l'acétophénone, en présence d'un catalyseur de type Adkins. En vertu des données expérimentales est déterminée l'énergie apparente d'activation de la première étape d'hydrogénation : acétophénone → méthylphénylcarbinol, $E_1 = 10\ 500$ cal/mole, et de la seconde étape : méthylphénylcarbinol → éthylbenzène, $E_2 = 24\ 080$ cal/mole.

L'acétophénone, produit intermédiaire de la synthèse du styrène par le procédé indirect, peut être valorisée comme telle en cosmétique, ou bien transformée en monomères vinyliques, tels que le styrène ou le vinylcyclohexane. Dans ce dernier cas il doit être réduit au carbinol correspondant.

Une série d'auteurs ont étudié la réduction catalytique de l'acétophénone, soit sélectivement, en agissant par l'hydrogénation de la chaîne latérale, avec obtention de méthylphénylcarbinol ou d'éthylbenzène, — soit par hydrogénation de la chaîne et du noyau obtenant du cyclohexylcarbinol ou même de l'éthylcyclohexane.[1–5]

Mushenko et ses collaborateurs[2,3] étudient la réduction de l'acétophénone sur catalyseurs à base de chromite de cuivre ou Ni-Cr, à l'état de méthylcyclohexylcarbinol, dans des conditions de pression de 300 atmosphères et à une température de 100 à 200°.

Barinov et ses collaborateurs[4,5] étudient la réduction de l'acétophénone à des pressions élevées (300 at.) et à une température de 200°, en présence de catalyseurs de ruthénium et rhodium déposés sur l'alumine.

---

[1] N. S. Barinov, D. V. Mușhenko et E. H. Lebedev, *Doklady Akad. Nauk S S.S.R.*, **127**, 1109 (1967).

[2] D. V. Mushenko et E. H. Lebedev, *Zhur. priklad. Khim.*, **39**, 2769 (1966).

[3] D. V. Mushenko et E. H. Lebedev, *Zhur. priklad. Khim.*, **39**, 2596 (1966).

[4] N. S. Barinov, D. V. Mushenko et E. H. Lebedev, *Zhur. priklad. Khim.*, **39**, 1884 (1966).

[5] N. S. Barinov, D. V. Mushenko et E. H. Lebedev, *Zhur. priklad. Khim.*, **39**, 2599, (1966).

Dans le présent ouvrage on a étudié la thermodynamique et la cinétique de la réaction d'hydrogénation sélective de l'acétophénone, en phase liquide, sur un catalyseur de type chromite de cuivre et d'additions sous forme de poudre, en suspension.

CONSIDÉRATIONS THÉORIQUES

La réaction d'hydrogénation de l'acétophénone (AcF) se déroulant conformément au schéma :

$$\mathrm{AcF} \xrightarrow{H_2} \mathrm{MFC} \xrightarrow{H_2} \mathrm{EB} + H_2O$$

par l'étape intermédiaire de méthylphénylcarbinol (MFC) jusqu'à l'éthylbenzène (EB) est caractérisée au point de vue thermodynamique par les fonctions présentées dans le tableau 1.

Tableau 1

Fonctions thermodynamiques pour la réaction d'hydrogénation de l'acétophénone

I. $\mathrm{AcF(1)} + H_2(g) \rightarrow \mathrm{MFC(1)}$

II. $\mathrm{MFC(1)} + H_2(g) \rightarrow \mathrm{EB(l)} + H_2O(1)$

T, °K		298	373	393	413	433	453	473
ΔH_r cal/mole	I	−16446,8	−16566,8	−16598,8	−16630,8	−16662,8	−16694,8	−16726,8
	II	−21754,6	−21244,6	−21108,6	−20972,6	−20836,6	−20700,6	−20564,6
ΔG_r cal/mole	I	−5031,3	−2858,2	−2267,8	−1652,8	−1055,9	−448,3	−170,2
	II	−18677,1	−17160,4	−16771,7	−16390,9	−16010,8	−15635,3	−15264,0
log K_p	I	3,69	1,67	1,26	0,87	0,533	0,216	0,078
	II	13,71	10,06	9,33	8,68	8,09	7,55	7,06
K_p	I	$4{,}9.10^3$	$4{,}68.10^1$	$1{,}82.10^1$	7,42	3,41	1,64	1,19
	II	$5{,}13.10^{13}$	$1{,}15.10^{10}$	$2{,}14.10^9$	$4{,}78.10^8$	$1{,}23.10^8$	$3{,}57.10^7$	$1{,}15.10^7$
α (p= 1 atm)	I	98,6	85,53	77,2	65,5	52,4	38,6	32,4
	II	→ ∼ 99,9 ←						
α (p= 50 atm)	I	99,8	97,9	96,7	94,8	92,4	89,0	87,1
	II	→ ∼ 99,9 ←						

Dans des conditions standard les deux étapes de la réaction peuvent être considérées irréversibles, c'est-à-dire que les valeurs des constantes à l'équilibre sont élevées, et les conversions à l'équilibre dépassent 90% mole.

Les valeurs de l'enthalpie de réaction $\Delta H_r^{298} = -16\,446{,}8$ cal/mole pour la première étape d'hydrogénation et $\Delta H_r^{298} = 21\,754{,}6$ cal/mole pour la seconde étape de la réaction indiquent le caractère exotherme de la transformation, plus prononcé pour la formation de l'éthylbenzène.

L'effet défavorable de la température sur la réaction résulte de la variation de ΔH_r avec la température (tableau 1). En même temps la pression agit favorablement sur la réaction d'hydrogénation de l'acétophénone pour arriver au méthylphénylcarbinol, ainsi qu'il résulte de la figure 1, dans laquelle la variation de la conversion à l'équilibre avec la température est rendue pour différentes pressions (p — est la pression totale du système).

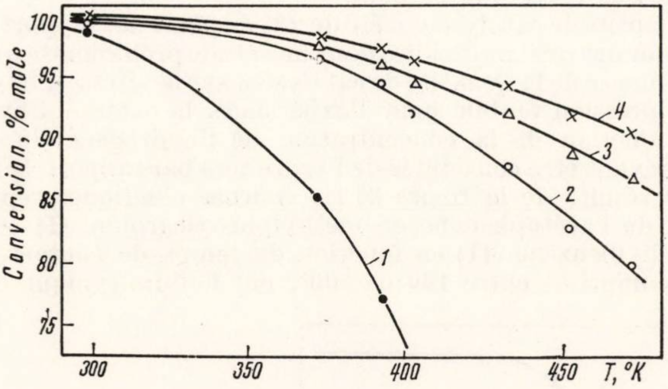

Fig. 1.— Variation de la conversion avec la température, à diverses pressions pour la réaction: AcF $\xrightarrow{H_2}$ MFC.
1, p = 1 atm; 2, p = 20 atm; 3, p = 50 atm; 4, p = 100 atm.

PARTIE EXPÉRIMENTALE

L'étude cinétique a été effectuée dans un appareil métallique sous pression, en système discontinu, en phase liquide, avec le catalyseur maintenu en suspension par agitation mécanique (au-dessus de 500 tours/minutes).

De l'acétophénone et du méthylphénylcarbinol d'une pureté au-dessus de 99 % ont été employés pour l'expérience.

Le catalyseur étudié a été constitué de chromite de cuivre et d'additions sous forme de poudre de dimensions au-dessous de 60 μ, catalyseur utilisé à l'échelle industrielle.

La matière première et les produits de réaction ont été analysés en utilisant un chromatographe de type Willy Giede à double flamme d'ionisation et à température programmée, sur une colonne d'une longueur de 1 m, remplie de cellite C_{22} imprégnée de l'Igepal CO 880 (3 %).

RÉSULTATS ET DISCUSSION

On a considéré la réaction AcF$\xrightarrow{k_1}$MFC$\xrightarrow{k_2}$EB pseudo-monomoléculaire, irréversible et on a déterminé les constantes apparentes de vitesse k_1 et k_2 et les énergies apparentes d'activation E_1 et E_2 pour les deux étapes d'hydrogénation.

L'étude a été effectuée à une pression de 50 atm et des températures comprises entre 140 et 200°.

La quantité de catalyseur a été de 2 % en poids par rapport à la matière première pour des raisons établies dans une étude préliminaire qui s'est occupée de l'influence de la quantité de catalyseur sur la vitesse d'hydrogénation.

A la pression établie pour l'expérience, la vitesse d'hydrogénation n'est pas fonction de la concentration de l'hydrogène du système, la réaction pouvant être considérée de l'ordre zéro par rapport à l'hydrogène. Ainsi qu'il résulte de la figure 3, les courbes cinétiques représentant la conversion de l'acétophénone en méthylphénylcarbinol (I) et respectivement en éthylbenzène (II) en fonction du temps de contact, à des températures comprises entre 140 et 200°, ont l'allure typique des réactions

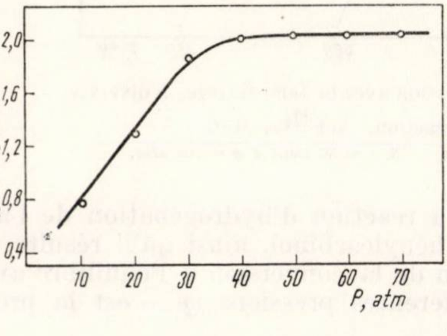

Fig. 2. — Variation de la vitesse d'hydrogénation avec la pression (t =140° C, Cu-Cr 2 %g).

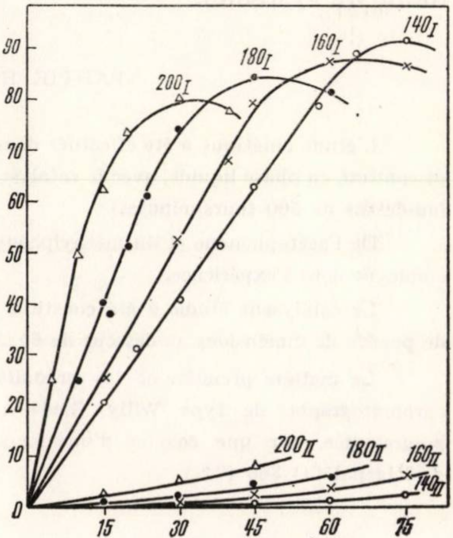

Fig. 3. — Isothermes pour la transformation AcF$\xrightarrow{H_2}$MFC (courbes I) et MFC $\xrightarrow{H_2}$ EB (courbes II). (p = 50 atm, Cu-Cr 2 % g).

consécutives partant de l'acétophénone vers l'éthylbenzène, par l'étape intermédiaire du carbinol.

L'ordre de réaction rapporté à l'acétophénone a été zéro pour des concentrations d'acétophénone de 100 à 20 % mole, intervalle au cours duquel la vitesse d'hydrogénation ne dépend pas de la concentration du produit intermédiaire de réaction, le méthylphénylcarbinol.

Pour des valeurs de conversion de l'acétophénone au méthylphénylcarbinol dépassant 80% mole, l'éthylbenzène se forme dans le produit de réaction (résultat de la seconde étape d'hydrogénation) la vitesse de formation de celui-ci dépendant de la concentration du produit intermédiaire de la réaction, ce qui confirme le caractère consécutif des deux réactions d'hydrogénation.

Les vitesses de réaction des deux étapes d'hydrogénation sont très différentes, la vitesse de formation de l'éthylbenzène étant beaucoup inférieure à celle de formation du méthylphénylcarbinol, dû certainement au catalyseur et aux conditions expérimentales choisies.

Les isothermes conversion—temps de contact pour la transformation de l'AcF en MFC (figure 4) et MFC en EB (figure 6) nous ont permis de déterminer les valeurs de l'énergie apparentes d'activation $E_1 = 10.500$ cal/mole (figure 5) pour la première étape d'hydrogénation et $E_2 = 24\,080$ cal/mole (figure 7) pour la formation de l'éthylbenzène à partir du méthylphénylcarbinol.

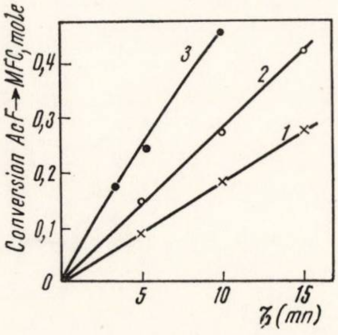

Fig. 4. — Isothermes conversion = $f(\tau)$ pour la réaction : AcF $\xrightarrow{H_2}$ MFC(1)—160° ; (2)—180° ; (3)—200°.

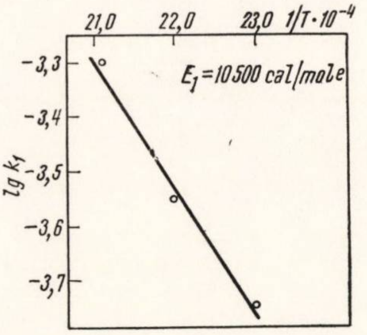

Fig. 5. — Variation de la fonction lg $k_1 = f(1/T)$ pour la réaction : AcF $\xrightarrow{H_2}$ MFC.

Les valeurs trouvées pour les énergies apparentes d'activation indiquent le fait que la constante de vitesse de formation de l'éthylbenzène à partir de méthylphénylcarbinol est plus influencée par la température que la constante de vitesse de la première étape de la réaction.

Etant donné que notre but était d'établir les conditions dans lesquelles l'hydrogénation de l'acétophénone découle sélectivement pour le carbinol correspondant, nous avons établi, en conclusion de l'étude cinétique, le fait que, en conduisant la réaction à la pression de 50 atm

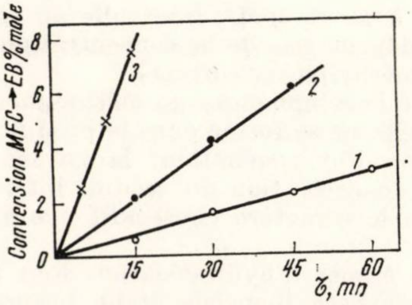

Fig. 6. — Isothermes de 160°(1), 180° (2), 200°(3) pour la réaction : MFC$\xrightarrow{H_2}$EB+ + H_2O.

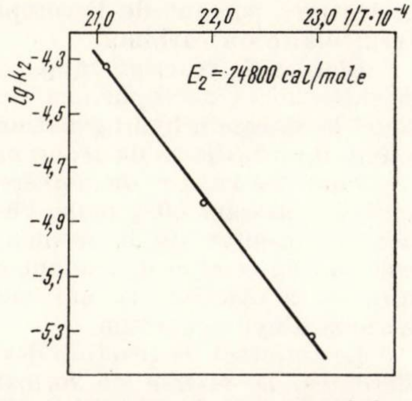

Fig. 7. — Variation de la fonction lg $k_2 = f(1/T)$ pour la réaction : MFC$\xrightarrow{H_2}$ EB + + H_2O.

en phase liquide, en présence de 2% en poids de poudre de catalyseur à base de chromite de cuivre et d'additions, on réussit dans l'intervalle de température 140–160° la transformation sélective de l'acétophénone en méthylphénylcarbinol, avec des vitesses négligeables pour la réaction secondaire de formation de l'éthylbenzène.

Revue Roumaine de Chimie, **18**, *8*, 1373–1377 (1973)

KINETICS OF OXIDATION OF BUTANE-2-ol BY PEROXYDISULPHATE CATALYZED BY Ag(I) ION

V. P. KUDESIA

Department of Chemistry, D. N. Post-Graduate College, Meerut, U.P., INDIA

Received June 5, 1972

The Ag (I) catalyzed oxidation of butane-2-ol by potassium peroxydisulphate in 50% acetic acid medium has been found to be first order with respect to peroxydisulphate. The first order rate constant increases with increasing concentration of alcohol in the concentration range 0.0628 – 0.3 M and above 0.3 M the reaction is independent of the initial alcohol concentration. The order with respect to (Ag^+) has been found to be 0.5. It is found that the allyl acetate inhibits the reaction to a large extent. A free radical mechanism involving Ag (II) ion as active oxidizing species has been suggested.

INTRODUCTION

The kinetics of peroxydisulphate oxidation of organic compounds has been studied quite extensively. The characteristic feature of these oxidations is the free radical formation of SO_4^- : The Ag (I) ion catalyzed oxidation of butane-2-ol has not been thoroughly investigated. In this paper the peroxydisulphate oxidation of this substrate catalyzed by Ag (I) is reported.

MATERIALS AND METHODS

Butane-2-ol (AR) was purified by distillation from an all glass apparatus. Large head and tail fractions were rejected.

Acetic acid was purified by usual procedures. Potassium peroxydisulphate (AR) was used.

Kinetic procedure. The thermostat was controlled within ± 0.05°C. The oxidation has been carried out in binary solvent mixtures of acetic acid (50%) and water (50%) at constant ionic strength 0.2 by the addition of sodium perchlorate. The rate of reaction was followed by estimating unreacted peroxydisulphate by the iodometric procedure. The experiments were performed in black coloured bottles to avoid photochemical complications.

RESULTS AND DISCUSSION

The reaction is of the first order with respect to $(S_2O_8^{2-})$ in the concentration range .0055∼0.04 M (table 1). The plot of log k_1 *versus* log (ROH) gives a straight line with a slope = 0.5 indicating a one-half order dependence on alcohol in the concentration range .0628 M∼0.3M and above 0.3 M the reaction is found to be independent of the initial alcohol concentration (table 2). The order with respect to Ag (I) ion has also been found to be 0.5 (table 3). Thus, the rate equation may be written as

$$\frac{-\,d(S_2O_8^{2-})}{dt} = k_1'[S_2O_8^{2-}][Ag^+]^{1/2} \qquad \text{(at concentrations } >.3\text{M)}$$

and

$$\frac{-\,d(S_2O_8^{2-})}{dt} = k_1''[S_2O_8^{2-}]\,[Ag^+]^{1/2}\,[ROH]^{1/2} \qquad \text{(at concentrations } < .3\text{M)}$$

$$\text{where } k_1' = k_1 \,|\, [Ag^+]^{1/2} \qquad \text{(at concentrations } > .3\text{M)}$$

and

$$k_1'' = k_1 \,|\, [Ag^+]^{1/2}[ROH]^{1/2} \qquad \text{(at concentrations } < .3\text{M)}$$

Table 1

Dependence of oxidation rate on concentration of peroxydisulphate at 35°C
(Butane-2-ol) = 0.0628M; [Ag(I)] = 1.188 × 10^{-3}M
Solvent : 50% HOAc

$(S_2O_8^{2-})$ M	$k_1 \times 10^4$ sec^{-1}	$\frac{k_1}{(S_2O_8^{2-})} \times 10^3$
0.0055	.449	8.16
.0073	.599	8.19
.0085	.694	8.17
.0096	.784	8.16
.0141	1.15	8.16
.0211	1.72	8.16
.0285	2.32	8.16
.0400	3.27	8.16

Table 2

Dependence of oxidation rate on concentration of (Ag+) at 35°C
(Butane-2-ol) = 0.0628M; $(S_2O_8^{2-})$ = .0055M;
Solvent : 50% HOAc

[Ag(I)] × 10^3 M	$k_1 \times 10^4$ sec^{-1}	$k_1 \times 10^3/[\text{Ag(I)}]^{\frac{1}{2}}$
1.188	0.449	1.30
2.345	.629	1.30
4.445	.866	1.30
6.550	1.05	1.30
8.530	1.20	1.30
9.221	1.25	1.30
14.20	1.55	1.30

Table 3

Dependence of oxidation rate on concentration of butane-2-ol at 35°C

$(S_2O_8^{2-})$ = 0.0055M; [Ag(I)] = 1.188 × 10^{-3}M; Solvent: 50% HOAc

Butane-2-ol M	$k_1 \times 10^4$ sec^{-1}	$k_1 \times 10^4/(\text{Butane-2-ol})^{\frac{1}{2}}$
0.0628	0.449	1.79
.0815	.511	1.79
.1510	.696	1.79
.1820	.763	1.79
.2431	.882	1.79
.3000	.981	1.79
	independent of alcohol concentration	
.4000	1.13	
.5112	1.14	
.6105	1.16	
.7225	1.15	
.8100	1.16	
.9112	1.16	
1.312	1.16	
2.412	1.16	

Table 4

Effect of added allyl acetate on oxidation rate at 35°C

$(S_2O_8^{2-})$ = 0.0055M; [Ag(I)] = 1.188 × 10^{-3}M; (Butane-2-ol) = .0628M; Solvent: 50% HOAc

(Allyl acetate) M	$k_1 \times 10^4$ sec^{-1}
.04	2.24
.06	2.20
.08	2.16
.20	2.10
.25	2.02

Table 5

Effect of varying temperature on the rate of oxidation of butane-2-ol at 35°C

(Butane-2-ol) = 0.0628M; $(S_2O_8^{2-})$ = = .0055M, [Ag(I)] = 1.188 × 10^{-3}M; Solvent: 50% HOAc

Temp. °C	k_2''
35°	0.945
40°	1.43
45°	2.41
50°	3.65

$k_1'' = k_1/(\text{Ag}^+)^{\frac{1}{2}}(\text{ROH})^{\frac{1}{2}}(S_2O_8^{2-})$

Effect of addition of allyl acetate. It is observed that the reaction is strongly inhibited by allyl acetate which is efficient scavenger for the sulphate radical ion $SO_4^{-\cdot}$. It is further observed that the inhibited reaction proceeds at a faster rate than the Ag (I) catalyzed oxidation of water by $S_2O_8^{2-}$ under similar conditions (table 4).

Effect of ionic strength. The effect of adding different concentrations of sodium perchlorate solution on the reaction rate has been studied. The results indicate that there is a decrease in the values of k_1 with an increase in ionic strength. When a graph is plotted between log k_1 and the square root of the ionic strength, a slope of 0.5 is obtained, indicating a rate determining step between ions of opposite charges.

Effect of adding some salts. The influence of some salts on the reaction rate has been studied at constant ionic strength of 0.2. The difference in the rate constants of the reaction in the presence of the salt from that in the absence of salt shows the influence of the salt used. The result shows that silver, copper, zinc, calcium, barium, nickel, cobalt and iron chlorides accelerate the reaction.

Temperature dependence. In table 5, the variation of the rate constant k_1'' with temperature is shown. The plot of log k_1'' versus $1/T$ exhibits an Arrhenius dependence. From slope of the line, the energy of activation is found to be 16.9 kcal/mole.

Mechanism. The oxidation of butane-2-ol by peroxydisulphate catalyzed by Ag (I) ion is found to be of the first order, half and half with respect to peroxydisulphate, alcohol and Ag (I) ion. The rate is found to be independent of alcohol concentration above 0.3M. The reaction is strongly inhibited by the allyl acetate. It is also observed that the inhibited reaction still proceeds at a faster rate than the silver (1) catalyzed oxidation of water by peroxydisulphate in the same conditions. The results obtained with the change of ionic strength also indicate that the rate determining step involves ions of opposite charges.

These all results are indicative of the operation of a chain mechanism involving the $SO_4^{-\cdot}$ and other free radicals. The kinetic studies in this paper, however, do not yield any information regarding the nature of silver species. Recently,[1] it has been discovered that in aqueous acid solutions Ag (II) ions exist rather than Ag (III) ions. According to Allen and his associates,[1] the equilibrium

$$2Ag^{2+} \rightleftharpoons Ag^+ + Ag^{3+}$$

lies far to the left.

The experimental finding that allyl acetate inhibits the oxidation but reaction still proceeds faster than Ag (I) ion clearly shows that the intermediate which attacks the reducing agents is formed in the rate determining step. This is probably Ag (II) or $SO_4^{-\cdot}$. The intermediates like $OH^\cdot$ radicals or radicals obtained from the organic reductant will also be responsible for chain propagation steps. Probably the free radical mechanism proceeds *via* Ag (II) ion.

Case I. The mechanism when alcohol concentration is > 0.3M.

$$Ag^+ + S_2O_8^{2-} \xrightarrow{k_1} Ag^{2+} + SO_4^{-\cdot} + SO_4^{2-}$$

$$Ag^{2+} + C_2H_5CHOHCH_3 \xrightarrow{k_2} Ag^+ + C_2H_5\dot{C}OHCH_3 + H +$$

$$C_2H_5\dot{C}OHCH_3 + S_2O_8^{2-} \xrightarrow{k_3} C_2H_5COCH_3 + HSO_4^- + SO_4^{-\cdot}$$

$$Ag^+ + SO_4^{-\cdot} \xrightarrow{k_4} Ag^{2+} + SO_4^{2-}$$

---

[1] T. L. Allen, H. N. Po and J. H. Swinehart, *Inorg. Chem.*, **7**, 244 (1968).

$$SO_4^{-\cdot} + H_2O \xrightarrow{k_6} HSO_4^- + OH^\cdot$$

$$OH^\cdot + C_2H_5CHOHCH_3 \xrightarrow{k_7} C_2H_5\dot{C}OHCH_3 + H_2O$$

and finally

$$C_2H_5\dot{C}OHCH_3 + SO_4^{-\cdot} \xrightarrow{k_8} C_2H_5COCH_3 + HSO_4^-$$

Case II. The mechanism when alcohol concentration is $<.3M$

$$Ag^+ + S_2O_8^{2-} \xrightarrow{k_1} Ag^{2+} + SO_4^{-\cdot} + SO_4^{2-}$$

$$Ag^{2+} + C_2H_5CHOHCH_3 \xrightarrow{k_2} Ag^+ + C_2H_5\dot{C}OHCH_3 + H^+$$

$$C_2H_5\dot{C}OHCH_3 + S_2O_8^{2-} \xrightarrow{k_3} C_2H_5COCH_3 + SO_4^{-\cdot} + HSO_4^-$$

$$Ag^+ + SO_4^{-\cdot} \xrightarrow{k_4} Ag^{2+} + SO_4^{2-}$$

$$S_4^{-\cdot} + C_2H_5CHOHCH_3 \xrightarrow{k_5} C_2H_5\dot{C}OHCH_3 + HSO_4^-$$

$$C_2H_5\dot{C}OHCH_3 + SO_4^{-\cdot} \xrightarrow{k_8} C_2H_5COCH_3 + HSO_4^-$$

Acknowledgement. The author is thankful to Dr. S. P. Gupta, Professor and Head of Chemistry Department for his valuable suggestions.

Revue Roumaine de Chimie, 18, *8*, 1373–1377 (1973)

$$SO_4^{-} + H_2O \rightarrow HSO_4^{-} + OH$$

$$OH + C_6H_5CHOHCH_3 \xrightarrow{k} C_6H_5\dot{C}OHCH_3 + H_2O$$

was finally

$$C_6H_5\dot{C}OHCH_3 + SO_4^{-} \rightarrow C_6H_5COCH_3 + HSO_4^{-}$$

Case 1b. The introduction when alcohol concentration is [illegible]

$$Ag^{+} + S_2O_8^{2-} \rightarrow Ag^{2+} + SO_4^{-} + SO_4^{2-}$$

$$Ag^{2+} + C_6H_5CHOHCH_3 \rightarrow Ag^{+} + C_6H_5\dot{C}OHCH_3 + H^{+}$$

$$C_6H_5\dot{C}OHCH_3 + S_2O_8^{2-} \rightarrow C_6H_5COCH_3 + SO_4^{-} + HSO_4^{-}$$

$$Ag^{+} + SO_4^{-} \rightarrow Ag^{2+} + SO_4^{2-}$$

$$SO_4^{-} + C_6H_5CHOHCH_3 \rightarrow C_6H_5\dot{C}OHCH_3 + HSO_4^{-}$$

$$C_6H_5\dot{C}OHCH_3 + SO_4^{-} \rightarrow C_6H_5COCH_3 + HSO_4^{-}$$

Acknowledgements. The author is thankful to Dr. S. P. Gupta, Professor and Head of Chemistry Department, for his valuable suggestions.

Revue Roumaine de Chimie, **18**, *8*, 1379–1387 (1973)

SYNTHESIS AND CONFIGURATIONAL EQUILIBRIUM OF 2-ISOPROPYL-5-ACETYL-1,3-DIOXANE

SORIN MAGER* and ERNEST L. ELIEL**

Department of Chemistry, University of Notre Dame, Notre Dame, Indiana, U.S.A.

Received December 1, 1972

2-Isopropyl-5-acetyl-1,3-dioxane was synthesized and the position of configurational equilibrum for *cis*- and *trans*-isomers was established in several solvents using different acidic and basic catalysts. The configurational preference varies with the polarity of the solvent from 72% to 58% in favour of the *trans*-isomer, corresponding to a free energy difference, ΔG°_{25}, between 0.56 and 0.19 kcal/mol.

In order to develop studies concerning the stereochemistry of 1,3-dioxane derivatives, 2-isopropyl-5-acetyl-1,3-dioxane was synthesized using as starting materials both malonic ester and acetoacetic ester, following the reaction sequences depicted in figure 1.

The configurational assignments of the two isomers (figure 2) are based on N.M.R. data, dipole moment measurements and chemical correlation with the known isomers of 2-isopropyl-5-carbomethoxy-1,3-dioxane.[1] Focussing on the chemical shifts of the protons belonging to the acetyl group, the sharp singlet at $\delta = 2.06$ ppm represents the peak for the equatorial group (*trans*-isomer) while the peak at $\delta = 2.26$ ppm represents the more deshielded protons of the axial group (closer to the oxygen of the ring).

The dipole moment measurements confirm the above tentative configurational assignment, with the higher dipole moment, $\mu = 3.09$ D, clearly being that of the *cis*-isomer and the smaller one ($\mu = 1.94$ D) that of the *trans*-isomer, in accord with the relative orientation of the ring and substituent dipoles (figure 2). The different polarity of the two isomers is also reflected in the higher retention time of the *cis*-isomer in the gas-liquid partition chromatogram as shown in table 1 for different temperatures, using a 3-m Carbowax 20 M 20% on Chromosorb *A* (60/80 mesh) column with a 60 ml/min He flow.

---

* Permanent address : Catedra de chimie organică, Universitatea Babeş-Bolyai, Cluj, Romania.

** Present address : Department of Chemistry, University of North Carolina at Chapel Hill, 27514 U.S.A.

[1] E. L. Eliel and H. D. Banks, *J. Amer. Chem. Soc.*, **94**, 171 (1972).

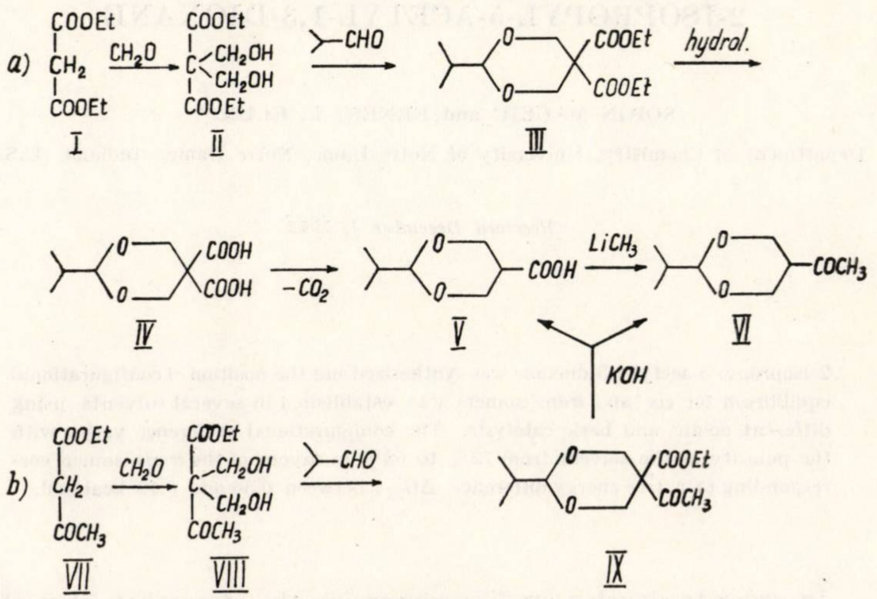
a)
CH₂O
CHO
hydrol.
−CO₂
LiCH₃
KOH
b)
CH₂O
CHO
I
II
III
IV
V
VI
VII
VIII
IX

Fig. 1. — Reaction sequence for synthesis of the 2-isopropyl-5-acetyl-1,3-dioxane.

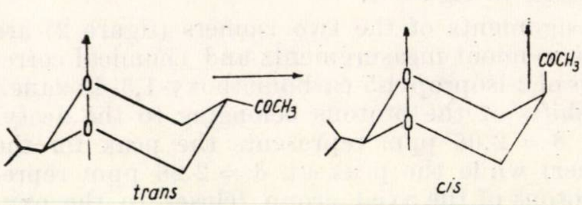
trans
μ = 1.94 D
δ = 2.06 ppm
cis
μ = 3.09 D
δ = 2.26 ppm

Fig. 2. — *Cis*- and *trans*-isomers of 2-isopropyl-5-acetyl-1,3-dioxane.

Table 1

Retention times of *trans*- and *cis*-isomers as a function of temperature

Temperature	Retention time	
	trans-isomer	*cis*-isomer
101°	12′40″	17′20″
105°	11′	16′
110°	8′	11′20″
130°	3′	4′10″

Concerning chemical correlation evidence, the *cis*-acid V (m.p.= = 127°), from which *cis*-2-isopropyl-5-acetyl-1,3-dioxane was formed, gave with diazomethane the known *cis*-2-isopropyl-5-carbomethoxy-1,3-dioxane identified by its m.p = 72.[1] (The *trans*-isomer is a liquid with b.p. = 50°/0.45 mm).

The configurational equilibrium $A \rightleftharpoons B$ shown in figure 3 was measured by gas chromatography, using acidic and basic catalysts for isomerization. ΔG° values were calculated by means of equation.

$$\Delta G^\circ = -RT\ln K = -RT\ln\frac{[trans]}{[cis]}$$

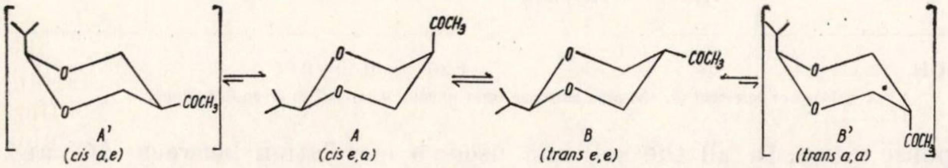

Fig. 3. — Configurations and conformations of 2-isopropyl-5-acetyl-1,3-dioxane.

The diaxial intermediate B', as well as the intermediate A' with the axial isopropyl group, may be disregarded because of the very large ΔG°-value of the 2-isopropyl group (−4.2 kcal/mol)[2] which is therefore acting as a "holding group"; the twist-boat forms may also be neglected because of their high enrgy. [3,4]

As acidic catalyst (acting as shown in figure 4) Amberlyst-15 (beaded polystyrenesulphonic acid) was used and as basic catalyst tetramethyl-ammonium hydroxide (TMAH), sodium methoxide or potassium hydroxide (acting as shown in figure 5).

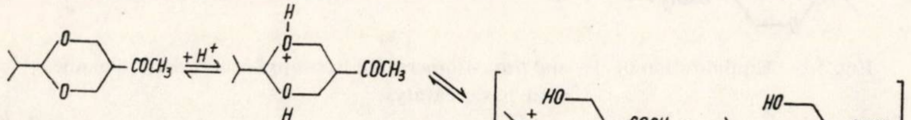

Fig. 4. — Equilibration of *cis*- and *trans*- isomers of 2-isopropyl-5-acetyl-1,3-dioxane with acidic catalyst.

Equilibrium composition was determined by gas-liquid chromatography using pure *cis*- and *trans*-isomers for establishing the area re-

---

[2] F. W. Nader and E. L. Eliel, *J. Amer. Chem. Soc.*, **92**, 3050 (1970).

[3] K. Pihlaja, *Acta Chem. Scand.*, **22**, 716, 2401 (1968).

[4] E. L. Eliel, *Acc'ts Chem. Research*, **3**, 1 (1970).

Table

Variations of K and $-\Delta G^\circ_{25}$ values as a

Catalysts and solvents	Me OH		Et OH		Me CN	
	K	$-\Delta G^\circ$	K	$-\Delta G^\circ$	K	$-\Delta G^\circ$
Amberlyst	1.48	0.23 ± 0.05	—	—	1.61	0.28 ± 0.06
TMAH	1.47	0.23 ± 0.06	—	—	—	—
CH_3ONa	1.46	0.22 ± 0.06	—	—	—	—
KOH	—	—	1.36	0.19 ± 0.06	—	—

* K values are corrected for the area response ratio (0.966 ± 0.04) ΔG° is given in kcal/mol.

sponse ratios. In all the solvents used, a correlation between ΔG° and the polarity of the solvent was observed, the position of equilibrium being governed by the normal polar and steric interactions. The different values for K and $-\Delta G^\circ$ at 25° in several solvents are given in table 2, and the correlation between $-\Delta G^\circ$ and the empirical parameters E_T of the polarity of solvents (determined by Dimroth and Reichardt[5,6] and summarized by Reichardt[7]) is presented in figure 6. As shown in table 2, in all solvents the preferred configuration has the acetyl group in the equatorial position, unlike in the case of the hydroxy, fluoro, nitro, sulfoxide and sulfone groups which all prefer the axial orientation.[8,9,10] However, the $-\Delta G^\circ$ values for the 5-acetyl-substituted 1,3-dioxane in

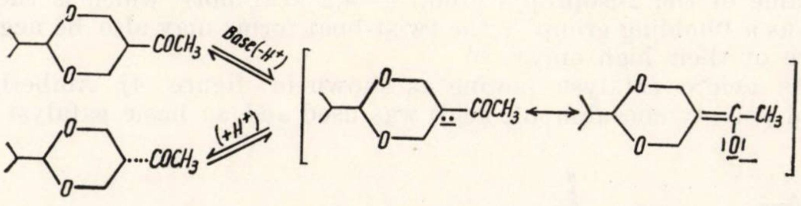

Fig. 5. — Equilibration of *cis*- and *trans*-isomers of 2-isopropyl-5-acetyl-1,3-dioxane with basic catalyst.

---

[5] K. Dimroth and C. Reichardt, *Palette* No. **11**, p. 28 (1962). Publication by Sandoz AG. (Basel), Switzerland.

[6] H. Dimroth, C. Reichardt, T. Siepman and F. Bohlman, *Liebigs Ann. Chem.*, **661**, 1 (1963).

[7] C. Reichardt, *Angew. Chem. Internat. Edit.*, **4**, 29 (1965).

[8] E. L. Eliel and M. K. Kaloustian, J. Chem. Soc., *Chem. Comm.*, **1970**, 290.

[9] R. J. Abraham, H. D. Banks, E. L. Eliel, O. Hofer and M. K. Kaloustian, *J. Amer. Chem. Soc.*, **94**, 1913 (1972).

[10] E. L. Eliel and S. A. Evans, *J. Amer. Chem. Soc.*, **94**, 0000 (1972).

function of catalysts and solvents

Et_2O		C_6H_6		*n*-Hexane	
K	$-\Delta G°$	*K*	$-\Delta G°$	*K*	$-\Delta G°$
2.40	0.52 ± 0.05	2.01	0.41 ± 0.06	2.40	0.52 ± 0.06
2.46	0.54 ± 0.02	2.08	0.44 ± 0.04	2.54	0.56 ± 0.06
—	—	—	—	—	—
—	—	—	—	—	—

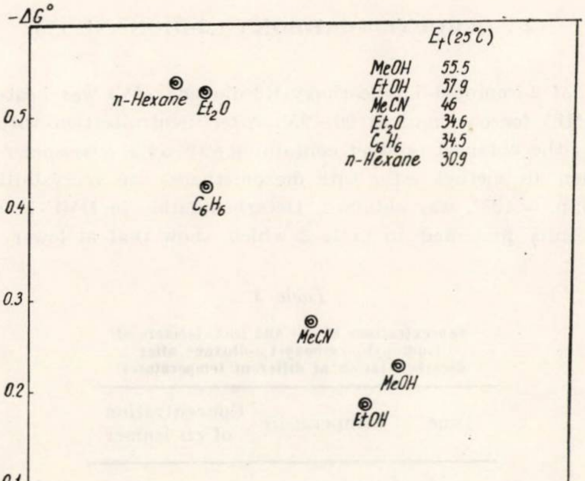

Fig. 6. — Correlation between $-\Delta G^0_{25}$ and the empirical parameter F_T of the polarity of the solvents.

the entire range of solvents (0.19—0.56 kcal/mol) are *substantially* lower than $-\Delta G°$ for acetyl-cyclohexane (1.52 kcal/mol[11]). While this may be ascribed primarily to steric causes [12] [absence of *syn* axial hydrogen atoms at positions 1 and 3 in the axial (*cis*) dioxane], the diminution in

---

[11] E. L. Eliel and M. C. Reese, *J. Amer. Chem. Soc.*, **90**, 1560 (1968).

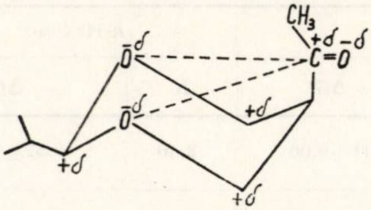

Fig. 7. — Attractive electrostatic interactions in 2-isopropyl-5-acetyl-1,3-dioxane.

$-\Delta G^\circ$ (1 —1.3 kcal/mol) is so large that an attractive electrostatic interaction between the $\delta_O^- = \delta_C^+ - CH_3$ group and $\delta_O^- - \delta_C^+$ of the ring (figure 7) may also be involved (cf.[10]).

EXPERIMENTAL

2-ISOPROPYL-5-CARBOXY-1,3-DIOXANE (V)

a) One gram of 2-isopropyl-5,5-dicarboxy-1,3-dioxane (IV) was heated in 50 ml dimethylformamide (DMF) for one hour at 90—95°. After neutralization with conc. HCl (dropwise under cooling) the obtained product containing 89 % axial (*cis*) isomer (analysed by g.l.c after transformation to methyl ester with diazomethane) was recrystallized from hexane. Pure *cis*-isomer, m.p. = 127°, was obtained. Decarboxylation in DMF at different temperatures gave the results presented in table 3 which show that at lower temperature more *cis*-isomer seems to be formed (possibly because of the greater extent of intramolecular H-bonds at low temperature).

Table 3

Concentrations of *cis*- and *trans*-isomers of 2-isopropyl-5-carboxy-1,3-dioxane after decarboxylation at different temperatures

Time	Temperature	Concentration of *cis*-isomer
1 h	90—95°	89 %
2 h	125°	84 %
2 h	153°	76 %

b) Decarboxylation without solvent by heating the diacid IV for 2 hours at 145—150° gave a mixture of 67 % *trans*-isomer and 33 % *cis*-isomer. The reaction product was dissolved in 10 %KOH and the acid (after filtering the basic solution with charcoal) was precipitated with conc. HCl (cooling) yielding the *trans*-isomer, m.p. = 138° (the *cis*-isomer is more soluble and remained in the mother liquid mixed with some amount of the *trans*-acid).

c) Hydrolysis of 2-isopropyl-5-acetyl-5-carbethoxy-1,3-dioxane (IX) with KOH led also to the formation of the acid (see below).

---

[12] E. L. Eliel and M. C. Knoeber, *J. Amer. Chem. Soc.*, **90**, 3444 (1968).

Anal. *Calcd.* for $C_8H_{14}O_4$: C, 55.16 ; H, 8.10. *Found* : *cis*-isomer, C, 55.35 ; H, 8.22, *trans*-isomer, C, 55.32 ; H, 8.15.

2-ISOPROPYL-5-ACETYL-1,3-DIOXANE (VI)

According to the general procedure[13], 17.4 g 2-isopropyl-5-carboxy-1,3-dioxane was dissolved in 300 ml anhydrous ether and 4.6 g $LiCH_3$ (130 ml 1.66 M ethereal solution + 100 ml ether) were dropped in (with stirring) as quickly as normal reflux allowed. After 15′ the mixture was cooled at 10° and water was added dropwise. Immediately, the etheral layer was separated and washed with water (1/2 of the amount of ether) three times, dried, concentrated and the residue distilled ; thus 11.6 g (67.4 % yield) of ketone was obtained, b.p. = = 48°/0.2 mm. The two isomers were separated with a 4.5 m Carbowax 20 M 20 % on Chromosorb *A* (45/60 mesh) Column, at 185°, with a 330 ml/min He flow ; retention time for the *trans*-isomer, 22′24″ and for the *cis*-isomer, 28′24″. The ratio of the two isomers was about the same as that of the starting acids if the etheral layer was immediately separated from the alkaline solution (which brings about equilibration). Starting, for instance, from pure *trans*-acid (m.p. = 138°) the pure *trans*-ketone (only 1.6 % *cis*-isomer) was obtained in 67% yield. In the separation of the *cis*- isomer it was not possible to remove small amounts of carbinol (formed as side product) whose retention time lies between those of *trans*- and *cis*-isomers such that the *cis*-isomer was always contaminated with traces of carbinol. The pure *cis*-isomer was therefore obtained from pure *trans*-isomer after equilibration. The limit of separation of the two isomers was *trans*-isomer containing 1.2 % of *cis* and *cis*-isomer with 4 % of *trans*.

Physical constants of 2-isopropyl-5-acetyl-1,3-dioxane are tabulated in table 4.

Table 4

Physical constants of the *cis*- and *trans*-isomers of 2-isopropyl-5-acetyl-1, 3-dioxane

Physical constants		*cis*-isomer	*trans*-isomer
IR bands for C=O group (neat)		1710 cm^{-1}	1710 cm^{-1}
UV bands	$n - \pi^*$ transition	$\lambda_{max} = 274$ nm ; $\lambda_{max} = 26$	$\lambda_{max} = 280$ nm $\varepsilon_{max} = 23$
	$\pi - \pi^*$ transition	$\lambda_{max} = 185{,}8$ nm $\varepsilon_{max} = 1490$	$\lambda_{max} = 186$ nm $\varepsilon_{max} = 1413$
NMR chemical shift for $-COCH_3$ protons		$\delta = 2.26$ ppm (s)	$\delta = 2.06$ ppm(s)
Dipole moment		$\mu = 3.09$ D	$\mu = 1.94$ D
Refractive index		$n_D^{20} = 1.4480$	$n_D^{20} = 1.4447$
Semicarbazone, melting point		178°	191°

---

[13] C. Tegner, *Acta Chim. Scand.*, **6**, 282 (1952).

Anal. *Calcd.* for $C_9H_{16}O_3$: C, 62.77 ; H, 9.36. *Found* : *cis*-isomer, C, 63.20 ; H, 9.50 ; *trans*-isomer, C, 63.09 ; H 9.40.

2-ISOPROPYL-5-ACETYL-5-CARBETHOXY-1,3-DIOXANE (IX)

A mixture of 172 g ethyl 2-dihydroxymethylacetoacetate[14] (VIII), 20 g isobutyraldehyde and 3.2 g *p*-toluenesulphonic acid were refluxed (with stirring) in 100 ml Skellysolve *F* (petroleum ether, b.p.→60°) until no more water was separated in the Dean-Stark trap. After cooling, 1.5 g sodium acetate was added, the mixture was again stirred, and after filtration and concentration the residue was distilled ; b.p.=91°/0.4 mm. Chemical pure material (mixture of the two stereo-isomers) was obtained in 58 % yield ; $n_D^{20} = 1.4470$.

Anal. *Calcd.* for $C_{12}H_{20}O_5$: C, 59 ; H, 8.25. *Found* : C, 59.18 ; H, 8.32.

HYDROLYSIS OF 2-ISOPROPYL-5-ACETYL-5-CARBETHOXY-1,3-DIOXANE

a) Fifty grams of ester (IX) were poured into KOH solution (25 g KOH in 500 ml 95 % ethanol) and kept at room temperature for 24 hours. The solution was concentrated vacuum at 40° to a volume of 70 ml, diluted with 400 ml water, extracted with 3×200 ml ether, washed with 2×100 ml water, dried, concentrated and distilled at reduced pressure with a small Vigreux column to yield 8.3 g (25 %) of ketone. The alkaline solution was neutralized with 20 % HCl leading to precipitation of 14 g (40 % yield) *trans*-2-isopropyl-5-carboxy-1,3-dioxane (m.p. = 138°). The acidic solution was extracted with ether and, after evaporation, 6.4 g mixture of *cis*- and *trans*-acids were obtained (4.2 g *cis* and 2.2 g *trans*, by analysis of methyl esters). Total yield in the hydrolysis : 25 % ketone (14 % *trans*, 11 % *cis*), 58 % acid (46 % *trans*, 12 % *cis*). This method provided the possibility of directly obtaining the pure *cis*-isomer by g.l.c., since the problem of carbinol contamination (see above) did not arise.

b) The ester (1 g) was dissolved in boiling ethanol (10 ml) and to this boiling solution, ethanolic 5 % KOH solution (10 ml) was added dropwise, over two hours. The reaction mixture was processed as above but no ketone was obtained (only resinification product in the distillation flask) ; the acid was obtained in about the same yield as above.

EQUILIBRATION TFCHNIQUE

Equilibrations were effected at 25°. Basic solutions 0.05 M CH_3ONa in methanol and 0.05 M KOH in 95% ethanol were used. A suspension of tetramethylammonium hydroxide in different solvents was also employed. Amberlyst-15 was used as an acid catalyst.

Ten microlitres *cis*- and *trans*- isomers in 100 microlitres solvent were sealed with the catalyst in small ampoules. After equilibrium was reached (12 –24 hours) the solutions were neutralized : the Ch_3ONa and KOH solutions by treatment with acetic acid ; the samples with TMAH by similar treatment but after separation from the catalyst. The samples equilibrated with Amberlyst were separated from the catalyst, kept 2 –3 minutes with K_2CO_3 and separated again. (No equilibration occurs with K_2CO_3 under these conditions). All analytical determinations were effected at 110° with a 3 m Carbowax 20 M 20% on Chromosorb *A* (60/80 mesh) column using 60 ml/min He flow. The mean of *K* values was calculated using 3 –6 different injections. Area response ratio at the same temperature was 0.966 ± 0.004.

---

[14] H. Gault, *Bull. Soc. Chim. France*, **5**, 5, 385 (1938).

U. V. MEASUREMENTS

For spectral analysis cyclohexane was used as solvent in 1 cm cells. The purity of the isomers was : *trans* with 1.4% *cis*-isomer and *cis* with 4% *trans*-isomer. Concentration for the *n*-transition was $3.075 . 10^{-2}$ for the *trans*-isomer 280 nm and $3.06 \cdot 10^{-2}$ mol/1 for the *cis*-isomer (274 nm).

For the $\pi - \pi^*$ transition (186 nm and 185.8 nm) concentrations were $1.68 . 10^{-4}$ mol/1 and $1.56 \cdot 10^{-4}$ mol/1, respectively. The Cary 15 Spectrophotometer was flushed with nitrogen while measurements for the $\pi - \pi^*$ transition were effected.

DIPOLE MOMENT MEASUREMENTS

Dipole moments were determined with a DM 01 Dipolemeter using a DFL2/D cell. Cyclohexane (spectrograde) was used as solvent; the temperature was 20°. Equation

$$\mu^2 = \frac{27\, kT}{4\pi N_L} \cdot \frac{M}{d_1(\varepsilon_1 + 2)^2} \cdot (a_\varepsilon - a_n)$$

was used for calculations, where k = Boltzman constant, N_L = Loschmidt's number, d_1 = density of the solvent, M = molecular weight of the compound, ε_1 = dielectric constant of the solvent, a_ε = slope of the curve $(\varepsilon_{\text{soln}} - \varepsilon_1) = f(w)$ and a_n = slope of the curve $n^2_{\text{soln}} - n^2_1 = f'(w)$; ($n$ = refractive index). Calibration of the dipolemeter gave the factor $7.21 \cdot 10^{-4}$ (for $\Delta\varepsilon / \Delta S$) which was used in calculation (with this factor the value $\mu = 1.580$ was found for chlorobenzene as a standard).

This work was supported in part by an NSF postdoctoral fellowship (to S.M.) and in part under NSF grant GP-24910.

Revue Roumaine de Chimie, **18**, *8*, 1379 – 1387 (1973)

Revue Roumaine de Chimie, **18**, *8*, 1389 – 1393 (1973)

PYRIMIDINE. IV

SYNTHESIS OF N-ARYL-N′-4-(2-METHYLTHIO-5-BROMOPYRIMIDOYL) UREAS AND -THIOUREA

V. V. BADIGER and S. C. BENNUR

Department of Chemistry, Karnatak University, Dharwar-580003, India

Received January 5, 1973

Synthesis of some new N-aryl-N′-4-(2-methylthio-5-bromopyrimidoyl)ureas and -thiourea of pharmacological interest is described.

In recent years a number of 2-pyrimidinylureas were tested for immunosuppression in sheep, erythrocyte assay in mice and antiviral activity against *Coxsackie virus* infection in mice.[1] The preparation of various N,N′-substituted-thiourea [2] and N-aryl-N′-2-pyrimidylthioureas possessing antitubercular activity was described by Deliwala and co-workers.[3] Astwood *et al* [4] reported antithyroid activity in a class of pyrimidine compounds and arrived at the conclusion that $-N=C=X$ was the unit necessary for the antithyroid activity where X stands for N, S or O. Recently, N-carbamoylpyrazinecarboxamides of the general structure (I) have been reported by Hanifin and co-workers [5] as diuretic agents. The antidiuretic activity has also been demonstrated by a number of heterocyclic compounds like 5-pyrazolone derivatives [6,7] and various thiadiazoles containing —N = C = N— grouping were described as herbicides in pre- and post-emergent applications.[8,9,10]

---

[1] C. J. Paget, C. W. Ashbrook, R. L. Stones and D. C. De Long, *J. Med. Chem.*, **12**, 1097 (1969).

[2] C. V. Gheorghiu, L. Stoicescu-Crivetz, C. Budeanu, El. Budeanu, M. Alexa-Petrovanu, L. Mandasescu, N. Constantinescu, A. Toma and Gr. Stavri, *Rev. Chim. Acad. R.P.R.* **1**, 97 (1956); *Chem. Abs.*, **52**, 17502d (1958).

[3] B. S. Rathore, Z. Mulziani and C. V. Deliwala, *J. Sci. Ind. Res. (India)*, **20 c**, 266 (1961).

[4] E. B. Astwood, A. Bissel and A. M. Hughes, *Endocrinology*, **37**, 456 (1945); *Chem. Abstrs.*, **40**, 3827° (1946).

[5] J. W. Hanifin, R. Capuzzi and E. Cohen, *J. Med. Chem.*, **12**, 1102 (1969).

[6] A. Robelet, F. Guerrin, F. Debrayneand and J. Bizard, *Therapie*, **17**, 569 (1962); *Chem. Abstr.*, **61**, 16673e (1964).

[7] C. Sunkel and N. Gomez, *J. Med. Chem.*, **12**, 726 (1969).

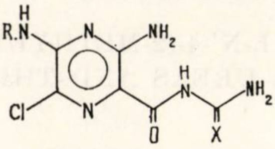

X = 0 or S

I

Based on these observations, it was considered worthwhile to prepare N-aryl-N′-4-(2-methylthio-5-bromopyrimidoyl) ureas and -thiourea and to examine their pharmacological properties. The pyrimidine nucleus was chosen because of its biological importance.

During the present work, arylureas, urea and thiourea were converted to the monosodium derivative (II) with sodium hydride in dimethylformamide. To this was added methyl 2-methylthio-5-bromo-4-pyrimidine-4-carboxylate (III). The temperature of the reaction mixture was maintained below zero during the reaction. The reaction product was made slightly acidic to get the desired product (IV). These compounds are described in table 1. The characteristic vibrations in the IR spectra of compounds are listed in table 2 along with their pertinent assignments.

Table 1

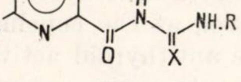

Sl. N°	R	X	Formula	Yield %	m.p.°C	Analysis					
						Calculated %			Found %		
						C	H	N	C	H	N
1	H	0	$C_7H_7N_4O_2SBr$	40	243—44	28.87	2.41	19.24	29.24	2.11	18.78
2	*p*-Tolyl	0	$C_{14}H_{13}N_4O_2SBr$	50	157—58	44.10	3.41	14.70	43.97	3.01	14.47
3	*p*-Methoxy-phenyl	0	$C_{14}H_{13}N_4O_3SBr$	50	195—96	42.32	3.27	14.10	42.83	2.98	13.71
4	*p*-Ethoxy-phenyl	0	$C_{15}H_{15}N_4O_3SBr$	57	180—81	48.80	3.65	13.62	49.20	4.10	13.92
5	H	S	$C_7H_7N_4OS_2Br$	50	228—29(d)	27.36	2.28	18.24	27.83	2.71	18.51

All compounds were crystallized from a mixture of rectified spirit and dioxane.

---

[8] P. R. Driscoll, Ger. Pat., 2017842 ; *Chem. Abstr.*, **74**, 13158k (1971).

[9] C. Metzger, L. Euec and H. Haak, Ger. Pat., 1816568 ; *Chem. Abstr.*, **74**, 13162g (1971).

[10] K. Hoegerle, P. R. Rathgeb, H. J. Cellarius and J. Rumpf, Ger. Pat., 1816696; *Chem. Abstr.*, **72**, 12734s (1970).

Table 2

Infrared spectral data of pyrimidoylureas and thiourea

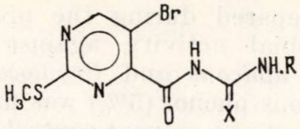

S1 N^0	R	X	ν_{max} cm^{-1}	Assignment
1	H	O	3440 m, 3380m, 3340w, 1700s 1540m	— NH — —C = O aromatic C = C and C = N vibrations
2	*p*-Tolyl	O	3360s 1730s 1600m, 1555m, 1540m.	— NH — — C = O aromatic C = C and C=N vibrations
3	*p*-Methoxyphenyl	O	3360m 1730s 1610m, 1570m, 1545m, 1520m 1255s, 1235s, 1215s 1040m	— NH — — C = O aromatic C = C and C = N vibrations asymmetric stretching of C — O — C asymmetric stretching of C — O — C
4	1-Ethoxyphenyl	O	3340m 1725s 1600m, 1550m, 1510m 1240s, 1220s 1050s	— NH — C = O aromatic C = C and C = N vibrations asymmetric stretching of C — O — C symmetric stretching of C — O — C
5	H	S	3330m 1710m 1605m, 1540m, 1480s C = N vibrations 1205s, 1150m, 1035m	NH — C = O aromatic C = C and C = N vibrations C = S.

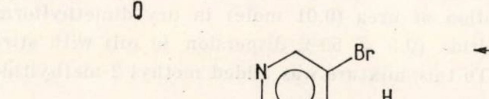

$$H_2N{-}\underset{\underset{X}{\|}}{C}{-}NH.R \xrightarrow[DMF]{NaH} \overset{\oplus\,\ominus}{Na.NH}{-}\underset{\underset{X}{\|}}{C}{-}NH.R$$

II

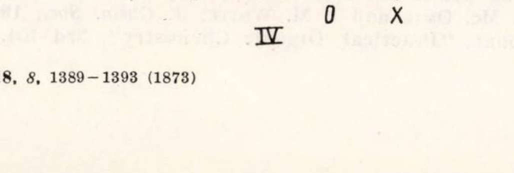

IV

R = H, *p*-tolyl, *p*-methoxyphenyl, *p*-ethoxyphenyl, and X = 0 and S.

The compounds prepared during the present investigation were evaluated for antimicrobial activity against *Staphyllococcus aureus*, *Escherchia coli*, *Candida albicans* and *Cryptococcus neoformans* by the cup-plate method. Aqueous phenol (5%) was used as a positive control. Dimethylformamide was put as a solvent control. No growth of microorganisms was observed in solvent. None of the compounds tested showed any promising antimicrobial activity.

EXPERIMENTAL [11]

2-Methylthio-5-bromopyrimidine-4-carboxylic acid was prepared according to the method described by McOmie and White.[12] Urea and thiourea used in the reaction were B.D.H. samples. *p*-Tolylurea, *p*-methoxyphenylurea and *p*-ethoxyphenylurea were prepared according to the literature method.[13]

METHYL 2-METHYLTHIO-5-BROMOPYRIMIDINE-4-CARBOXYLATE

2-Methylthio-5-bromopyrimidine-4-carboxylic acid (2 g.) was dissolved in magnesium dried methanol (20 ml) and cooled in a freezing mixture. Dry hydrogen chloride gas was passed into the above solution until the weight increased to about 14 g. The resulting reaction mixture was heated under reflux on a water bath for 3–4 hours. After cooling, the reaction mixture was poured over crushed ice and neutralized with 10 percent sodium carbonate solution. The precipitated solid was collected, dried and crystallized from aqueous ethanol as straw coloured needles, m.p. 61–62° ; yield, 1.5 g.

IR ν_{max} cm^{-1}, 1750s C=0 ; 154w, 1514w, aromatic C = C and C = N vibrations ; 1290s, 1220s, 1200m, asymmetric stretching vibrations of C-O-C ; 1030 m, symmetric stretching vibrations of C-O-C.

Analysis $C_7H_7N_2O_2$ SBr
Calculated : C, 31.94 ; H, 2.66 ; N,10.54%.
Found : C, 32.00 ; H, 3.01 ; N, 10.49%.

N-ARYL-N′-4-(2-METHYLTHIO-5-BROMOPYRIMIDOYL)UREAS

The synthesis of N-aryl-N′-4-(2-methylthio-5-bromopyrimidoyl)ureas is exemplified by condensing urea with methyl 2-methylthio-5-bromopyrimidine-4-carboxylate.

To a cooled solution of urea (0.01 mole) in dry dimethylformamide (15 ml) at 15°, was added sodium hydride (0.5 g, 50% dispersion in oil) with stirring. The stirring was continued for an hour. To this mixture was added methyl 2-methylthio-5-bromopyrimidine-4-

---

[11] All melting points are taken in capillary and are uncorrected.

[12] J. F. W. Mc. Omie and I. M. White, *J. Chem. Soc.*, **1953**, 3129.

[13] A. I. Vogel, "Practical Organic Chemistry", 3rd Ed., 1956, p. 646.

carboxylate (2g) and stirred for 2 hours. The reaction mixture was then poured over ice-water and made slightly acidic with acetic acid. The yellow precipitate was collected, dried and crystallized from a mixture of dioxane and ethanol in yellow needles; m.p. 243–44°., yield, 1 g.

The same general procedure was employed for condensing thiourea.

Acknowledgement. We thank Dr. S. Siddappa, Professor and Head of the Department of Chemistry for his interest in this work. We also thank Professor M. Sirsi, Department of Pharmacology and Microbiology, Indian Institute of Science, Bangalore, for providing facilities to undertake antimicrobial testing and his valuable guidance. We thank V.A Desai and G.S. Gadaginmath for recording the analytical data, and Dr. L. D. Basanagoudar for recording IR data. One of us (S.C.B) is grateful to University Grants Commission, New Delhi, for providing fellowship.

Revue Roumaine de Chimie, **18**, *8*, 1389–1393 (1973)

Revue Roumaine de Chimie, **18**, *8*, 1395–1407 (1973)

CORRELATION OF THE PHYSICAL PROPERTIES OF ORGANOSILICON COMPOUNDS. III[1]

ELECTRONEGATIVITY OF MOLECULES AND THEIR BOILING POINT, REFRACTIVITY AND DENSITY

M. ARSHAD A. BEG * and IRSHAD A. KHAN **

* P.C.S.I.R. Laboratories, Karachi — 39, Pakistan
** Department of Chemistry, University of Karachi, Karachi — 32, Pakistan

Received August 17, 1972

The effective electronegativity χ_M of the molecules is shown to be directly related with the boiling point T_b, refractivity Mn_D and density given by $M\rho^2$ of a series of organosilicon compounds like the alkyl silanes, haloalkyl and alkyl halosilanes, alkoxy, isocyanato and isothiocyanato silanes. On the basis of T_b and χ_M and $M\rho^2$ and χ_M the molecules of certain classes fall into different groups, but the correlation of Mn_D with χ_M gives a smooth relationship. This is attributed to the similarity, *i.e.* additivity of these properties. Moreover, since polarizability is related to molar refractivity, the linear relationship suggests that χ_M is a good measure of polarizability.

INTRODUCTION

In our previous publications [1,2] we have correlated the physical properties like boiling point, density and refractivity of the organosilicon compounds. It was also shown that electronegative groups bring about maximum deviations in the properties of these compounds. The electronegativity of different series of compounds has been calculated and has been related to the basicity and vibrational frequency. [3,4,5] It was, therefore, of interest to see if the effective electronegativity of the molecules can be correlated with these properties and a neat correlation being described herein shows that the earlier observation is valid. Such a correlation has recently been demonstrated for organosulphur compounds. [6]

---

[1] M. A. A. Beg and I. A. Khan, *Rev. Roumaine Chim.* (under publication).
[2] M. A. A. Beg and I. A. Khan, *Rev. Roumaine Chim.* (under publication).
[3] M. A. A. Beg, *Scientist Pakistan*, **7**, 37 (1964).
[4] M. A. A. Beg, *Pakistan J. Sci. Ind. Res.*, **11**, 345 (1968).
[5] M. A. A. Beg, *Pakistan J. Sci. Ind. Res.*, **12**, 16 (1969).
[6] M. A. A. Beg and M.A. Hashmi, *Rev. Roumaine Chim.* (submitted for publication).

Effective electronegativity χ_{MXYZ} of molecules is an arithmetic mean of the electronegativity of the central atom and of the substituents. Thus the χ_{MXYZ} of the molecule MXYZ, where M is the central atom and X, Y and Z are the substituents, is obtained from equation (A).

$$\chi_{MXYZ} = \frac{1}{2}\chi_M + \frac{1}{6}[\chi_X + \chi_Y + \chi_Z] \quad \ldots (A)$$

Since electronegativity is the power to attract an electron and this power varies with the change of substituents on the central atom, it is logical to explore the dependence of the physical properties on the overall change in the electronic environment as given by the effective electronegativity of molecules.

RESULTS AND DISCUSSION

The different physical properties have already been listed in Parts I and II of this series. The electronegativity of the different groups are listed in table 1 and the bond parameters in table 2.

Table 1

Electronegativity of the groups

N°	Group	Electronegativity
1	Methyl	2.30
2	Ethyl	2.333
3	*n*-Propyl	2.337
4	*i*-Propyl	2.367
5	*n*-Butyl	2.34
6	*i*-Butyl	2.361
7	*t*-Butyl	2.40
8	*s*-Butyl	2.72
9	*n*-Pentyl	2.34
10	Benzyl	2.45
11	Methoxy	2.90
12	Ethoxy	2.915
13	Propoxy	2.917
14	Butoxy	2.92
15	Phenyl	2.70
16	Hydroxy	3.51
17	Cyanide	2.52
18	Isocyanate	3.00
19	Isothiocyanate	2.75
20	Cyanate	3.125
21	Chloromethyl	2.45
22	Iodomethyl	2.367
23	Dichloromethyl	2.60
24	Chloroethyl	2.483

In correlating the physical properties like the boiling point, etc., with the effective electronegativity, it is observed that there is a very minor change in the latter property as the chain length is increased.

However, when $\chi_{effective}$ was multiplied with the molecular weight, a neat correlation of these properties was observed. Consequently, the term molar effective electronegativity χ_M has been found to be more appropriate here. In discussing the properties with respect to the molecular electronegativity of the molecules the pattern adopted is similar to that in earlier papers.

Table 2

χ_M Values of Si-X bonds

N⁰	Groups	χ_M Coefficient
1	$Si-CH_3$	45.146
2	$Si-C_2H_5$	74.386
3	$Si-C_3H_7$	103.472
4	$Si-C_4H_9$	132.527
5	$Si-C_5H_{11}$	161.507
6	$Si-C_6H_{13}$	189.437
7	$Si-C_7H_{15}$	218.207
8	$Si-C_8H_{17}$	246.977
9	$Si-C_{10}H_{21}$	304.517
10	$Si-C_{12}H_{25}$	362.057
11	$Si-C_{14}H_{29}$	419.597
12	$Si-C_6H_5$	50.298
13	$Si-CH_2C_6H_5$	204.064
14	$Si-OCH_3$	85.753
15	$Si-OC_2H_5$	114.252
16	$Si-OC_4H_9$	175.367
17	$Si-H$	13.223
18	$Si-F$	80.045
19	$Si-Cl$	90.573
20	$Si-Br$	187.772
21	$Si-CH_2Cl$	118.104
22	$Si-CH_2I$	304.953
23	$Si-(OCN)$	90.202
24	$Si-(NCO)$	117.654
25	$Si-(NCS)$	148.068

Correlation with boiling points. Tetra-alkyls and aryls. From fig. 1 it will appear that the division into different classes as obtained earlier is less well marked and all the points may be represented by the same straight line and are governed by equation 1.

However, a closer examination suggests that this class may be further subdivided into three groups (1) the trimethyl alkyl silanes, (2) the dimethyl dialkyl silanes and (3) triethyl alkyl silanes each governed by equations 1a, 1b and 1c. The grouping of all these compounds into three classes is significant in that, their molecular electronegativity is found to change with a change in the substituent, although as stated above the effective electronegativity attenuates with increasing chain length. The dependence noted here shows that the overall electronic atmosphere is appreciably altered. The boiling point depends not only on the molecular weight but also on the intermolecular forces and hence a linear relationship here suggests that the combination of molecular weight and effective electronegativity is a good measure of the intermolecular forces.

The subdivision into three classes is similar to that noted earlier in the correlation of boiling point with refractivity. The triethyl alkyl silanes have slightly higher χ_M and also higher boiling points. The compounds with similar molecular weight like 5 and 23 ; 7 and 24, etc. are also separated here. It may also be noted that a similar difference exists for the dimethyl dialkyl silanes and among the tetraethyl, propyl, butyl and pentyl silanes which assume a different slope given by equation 1d. These differences are obviously a result of a different electronic environment as given by their χ_M.

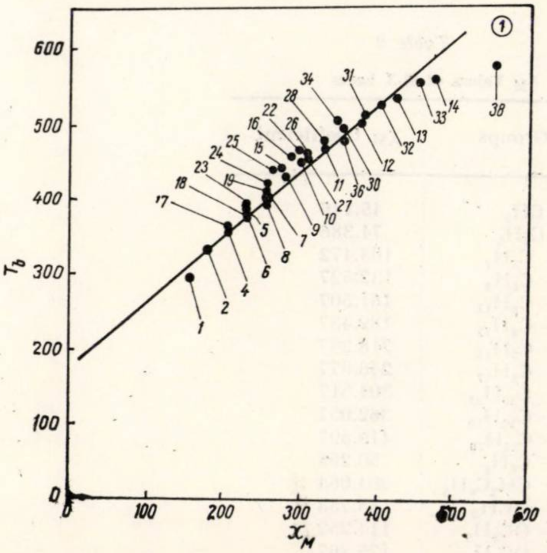

Fig. 1. — Correlation of molecular electronegativity and boiling points of tetra-alkyl and aryl silanes.

Haloalkyl and alkyl halosilanes. Some of the chloroalkyl trimethylsilanes and the monofluorosilanes fall on the same straight line in fig. 2 given by equation 2. The difluoro- and trifluorosilanes fall, respectively, on different lines given by equations 3 and 4. These have also been noted previously to form separate groups. The separation here is quite well-defined and this might be attributed to the larger difference in the values of the fluorides.

Similarly, the mono-, di- and trichlorosilanes are also distinctly separated into two groups (fig. 3) following the equations 5, 6 and 7. The anomalies noted in the correlation of boiling point with $M\rho^2$ are not found here and the di- and trichlorides are at their predicted positions.

Alkoxy silanes. Among alkoxy silanes the differentiation on the basis of boiling point and effective electronegativity is less marked compared with the earlier correlations. However, the trialkoxy silanes occupy the lower portion of the straight line (fig. 4) given by equation 8. The

Table 3

Equations correlating the molecular electronegativity and boiling point of organosilanes

N⁰	Compounds	Equations
1	Tetra-alkyl and aryl silanes	$\chi_M = 0.7885\ \mathrm{Tb} + 171.019$
1a	Trimethyl alkyl silanes	$\chi_M = 0.7783\ \mathrm{Tb} + 177.366$
1b	Dimethyl dialkyl silanes	$\chi_M = 0.7171\ \mathrm{Tb} + 197.517$
1c	Triethyl alkyl silanes	$\chi_M = 0.6197\ \mathrm{Tb} + 245.728$
1d	Tetraethyl, propyl, butyl and pentyl silanes	$\chi_M = 0.4566\ \mathrm{Tb} + 296.024$
2	Chloroalkyl trimethyl silanes and monofluoro silanes	$\chi_M = 0.4878\ \mathrm{Tb} + 252 - 102$
3	Difluoro silanes	$\chi_M = 0.5662\ \mathrm{Tb} + 176.162$
4	Trifluoro silanes	$\chi_M = 0.6618\ \mathrm{Tb} + 75.737$
5	Mono-trichloro silanes	$\chi_M = 0.9211\ \mathrm{Tb} + 78.641$
6	Di-trichloro silanes	$\chi_M = 0.5406\ \mathrm{Tb} + 204.878$
7	Tri-trichloro silanes	$\chi_M = 0.5172\ \mathrm{Tb} + 183.157$
8	Trialkoxy silanes	$\chi_M = 0.5672\ \mathrm{Tb} + 204.750$
9	Di- and mono-isocyanato silanes	$\chi_M = 0.6410\ \mathrm{Tb} + 206.353$
10	Tri-isocyanato silanes	$\chi_M = 0.7355\ \mathrm{Tb} + 128.693$
11	Halo isocyanato silanes	$\chi_M = 1.1460\ \mathrm{Tb} - 109.491$
12	Di-isothiocyanato silanes	$\chi_M = 0.5327\ \mathrm{Tb} + 289.654$
13	Tri-isothiocyanato silanes	$\chi_M = 0.4840\ \mathrm{Tb} + 282.836$

rise in boiling point with respect to electronegativity is quite gradual and the slope is similar to the alkyl silanes. This shows that the electronic environment is not very much altered in spite of the presence of the intervening electronegative oxygen. The difference arising out of the variation in intermolecular forces due to the replacement of alkyl by alkoxy group is seen here to be nicely represented by the χ_M values.

Isocyanato and isothiocyanato silanes. The correlation of the isocyanato and isothiocyanato silanes (figs. 5 and 6 and equations 9 –13) is similar to that noted for the halides, i.e. the separation occurs with regard to the number of groups which shows that the isocyanato and isothiocyanato groups are present as an electronegative moiety like the halides and not like the alkoxy groups. This would explain the difference noted in the last two classes. It may also be noted from the correlation (table 3) that the slopes in the two cases are similar. The differentiation is thus better understood in terms of the molecular electronegativity rather than intermolecular forces alone.

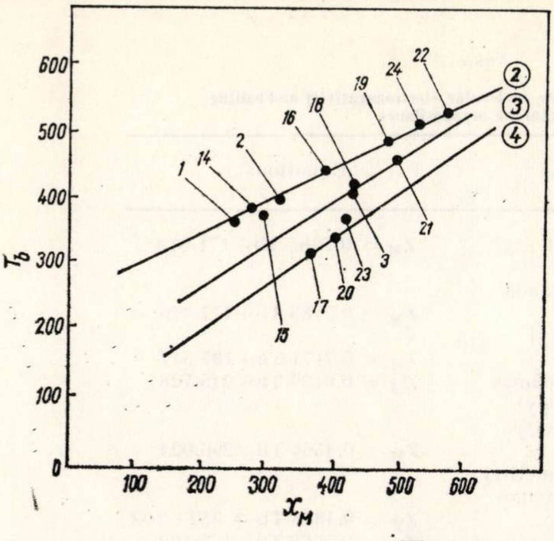

Fig. 2. — Correlation of molecular electronegativity and boiling point of haloalkyl silanes.

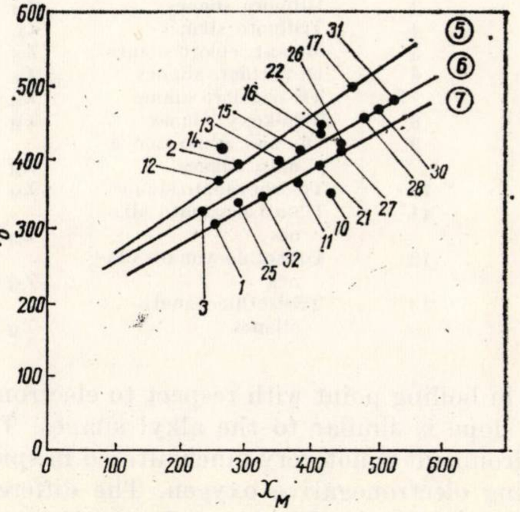

Fig. 3. — Correlation of molecular electronegativity and boiling point of alkyl halo silanes.

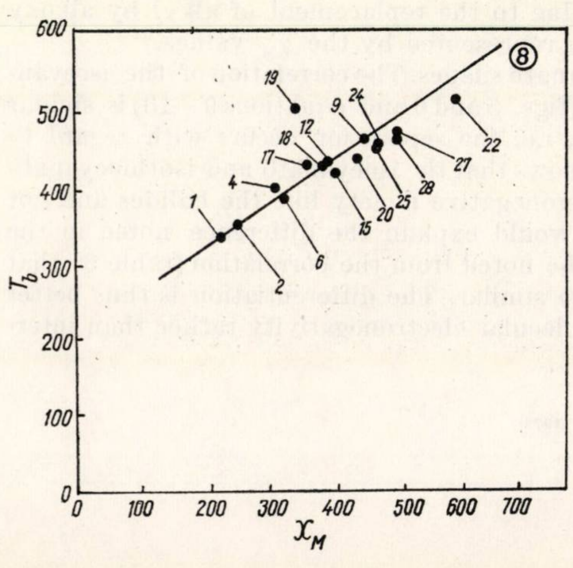

Fig. 4. — Correlation of molecular electronegativity and boiling point of alkoxy silanes.

Correlation with density. On the basis of $M\rho^2$ and molecular electronegativity the tetra-alkyl and alkyl aryl silanes are distributed into three groups in fig. 7 : (1) trimethylalkyl silanes, (2) dimethyl dialkyl silanes and (3) trialkyl phenyl silanes. These three classes follow equations 1—3 in table 4. It may be noted that the slopes of the first two lines are quite similar. It may also be noted that the classification of the first two groups is similar to those obtained in correlating T_b and Mn_D and $M\rho^2$ and Mn_D *i.e.* whether the methyl group is directly attached to the silicon atom or there is an intervening methylene group. This similarity is directly related to the additive nature of the three properties *viz*. $M\rho^2$,

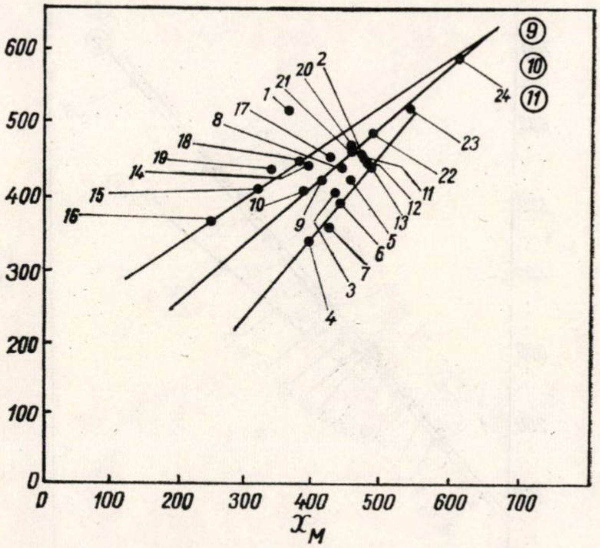

Fig. 5. — Correlation of molecular electronegativity and boiling point of isocyanato silanes.

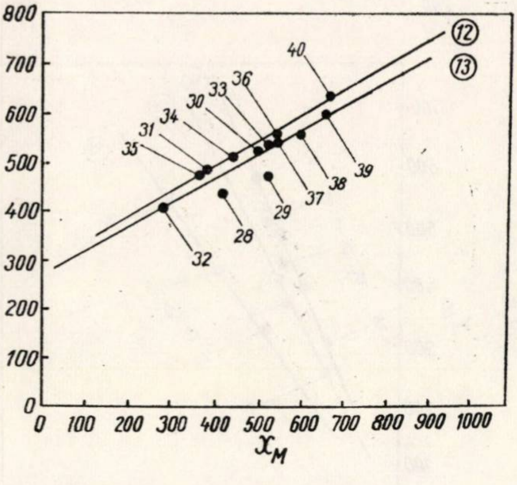

Fig. 6. — Correlation of molecular electronegativity and boiling point of isothiocyanato silanes.

Mn_D and χ. The slight difference noted in the case of T_b is due to its being additive as well as constitutive. The additive nature of χ_M may be noted from table 2 which lists the χ_M of various bonds.

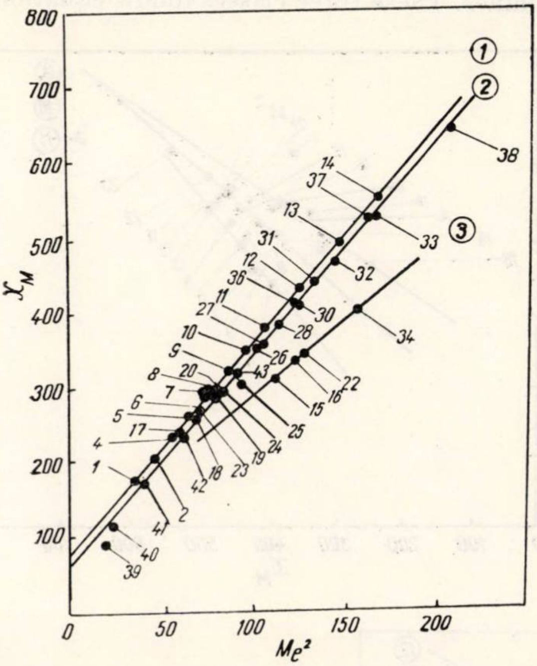

Fig. 7. — Correlation of molecular electronegativity and density of tetra-alkyl and aryl silanes.

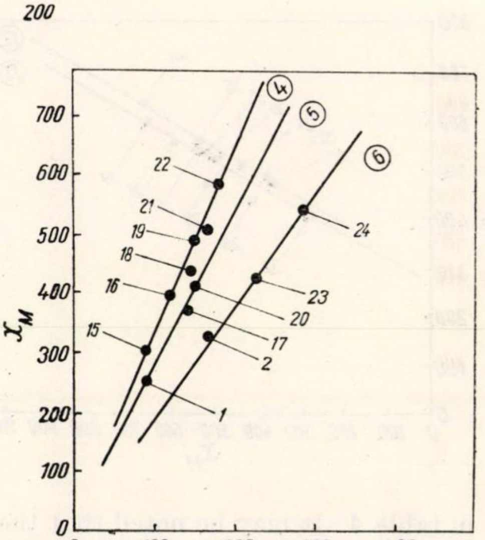

Fig. 8. — Correlation of molecular electronegativity and density of haloalkyl silanes.

Among the alkyl or aryl fluoro silanes, a better classification is obtained in the present case than obtained earlier. The mono-, di- and trifluoro silanes form different groups while the phenyl fluoro silanes are separated from the alkyls (fig. 8, equations 4, 5 and 6). This is related to the larger differences in electronegativity obtained for the fluorides. The nonlinear effects of fluorine have been pointed out earlier in correlating electronegativity with the C—H stretching frequency of the methyl and methylene halides.[5] Here also, the displacement of the charge cloud would be towards the more electronegative fluorine. The high electronegativity of fluorine would be differently compensated in each class of alkyl or aryl fluoro-silanes by the hybrid function of the alkyl silane moiety. The prediction in the previous case is found to hold in the present group of compounds. This compensation by the hybrid function was also taken as a criterion for the validity of the electronegativity parameter.[5]

Table 4

Equations correlating the molecular electronegativity and density of organosilanes

N°	Compounds	Equations
1	Trimethyl alkyl silanes	$\chi_M = 2.8672\ M\rho^2 + 75.191$
2	Dimethyl dialkyl silanes	$\chi_M = 2.8361\ M\rho^2 + 60.500$
3	Trialkyl phenyl silanes	$\chi_M = 1.9915\ M\rho^2 + 91.545$
4	Mono-fluoro-silanes	$\chi_M = 3.1432\ M\rho^2 + 13.738$
5	Difluoro-silanes	$\chi_M = 2.7266\ M\rho^2 + 4.\ 665$
6	Trifluoro-silanes	$\chi_M = 1.9214\ M\rho^2 - 16.651$
7	Alkyl-dichloro-silanes	$\chi_M = 1.5892\ M\rho^2 + 105.716$
8	Alkyl-aryl-dichloro-silanes or alkyl-trichloro-silanes	$\chi_M = 1.3990\ M\rho^2 + 81.834$
9	Alkoxy silanes	$\chi_M = 2.4770\ M\rho^2 + 130.000$
10	Methyl and methoxy isocyanato silanes	$\chi_M = 0.8325\ M\rho^2 + 234.080$
11	Ethyl and ethoxy isocyanato silanes	$\chi_M = 0.8213\ M\rho^2 + 139.448$
12	Alkyl isothiocyanato silanes	$\chi_M = 1.0900\ M\rho^2 + 152.304$

The alkyl-chloro-silanes are also similarly divided into three groups depending on the number of chlorine atoms (fig. 9). The first group given by equation (7) consists of dichloro-silanes. The second consists of alkyl-aryl-dichloro-silanes or alkyl-trichloro-silanes given by equation 8. The alkyl-dichloro-silanes 1, 2, 25 as also dimethyl-dichloro-silane fall in the second group. Here again the higher electronegativity of chlorine should be responsible for the withdrawal of electron density from the hybrid function representing the 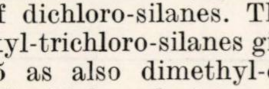 $\text{(Alkyl)(H)}\rangle\text{Si}$ or $\text{(Me)}_2\rangle\text{Si}$ groups. Thus, the electronegativity parameter explains the grouping better than in the previous cases.

The alkoxy silanes, fig. 10, are correlated by equation 9 and like the case of T_b *vs.* χ_M the differences among the various groups is less marked. This may be attributed to the modification of the electronic

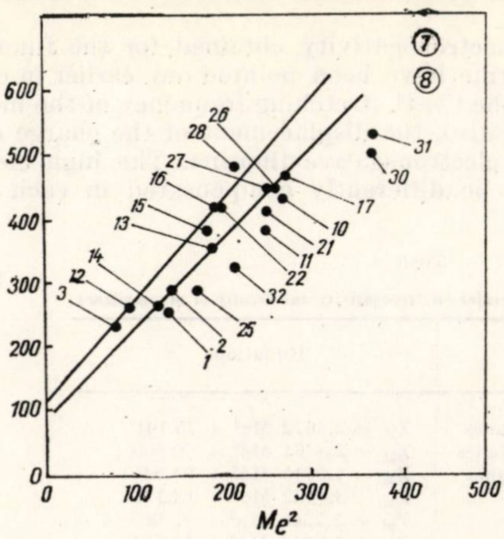

Fig. 9. — Correlation of molecular electronegativity and density of alkyl halo-silanes.

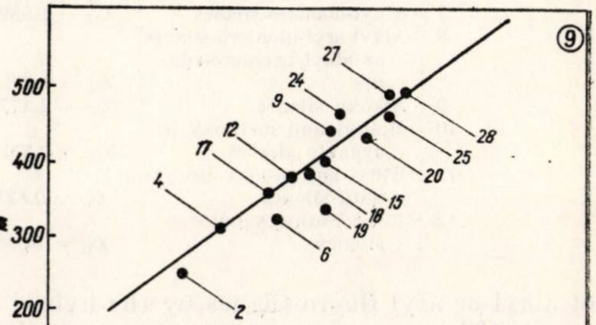

Fig. 10. — Correlation of molecular electronegativity and density of alkoxy silanes.

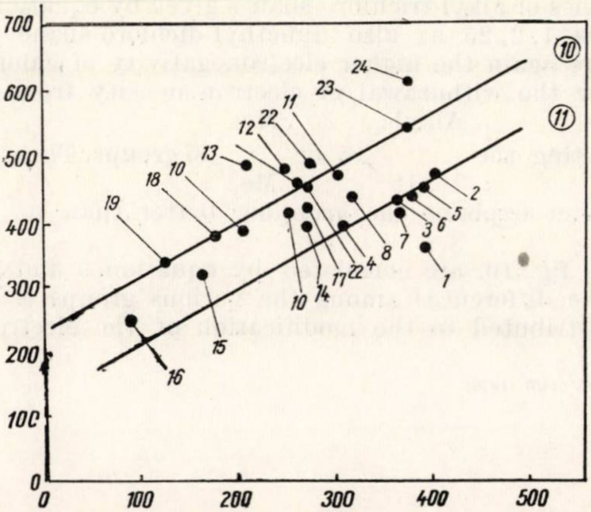

Fig. 11. — Correlation of molecular electronegativity and density of isocyanato silanes.

environment of oxygen by the alkyl groups attached to it on the one hand and by the hybrid function of the alkyl silyl group on the other. Consequently the oxygen is no longer as much electron withdrawing as a halogen and hence a smooth relationship of the two properties.

The isocyanato silanes form one group represented by equation 10 in fig. 11. The alkyl and alkoxy isocyanato silanes form the second group and are given by equation 11. The formation of these groups is again in conformity with the electronegativity of the hybrid function acting nonlinearly and with the displacement of charge towards the isocyanato group. Here again the alkoxy group is not acting as an electronegative group in which case they might have been classed with the halogens. On the other hand, the methoxy isocyanato silanes and the methyl isocyanato silanes 8, 9, 10 and 14, 15, 16 fall on the same straight line given by equation 10. The ethyl and ethoxy isocyanato silanes fall on a separate line given by equation 11. The isothiocyanates listed in table 5 (part I) form only one class given by equation 12, fig. 12. It may be noticed that these are mainly the alkyl isothiocyanates which by analogy with the isocyanates should form one group.

Correlation with refractivity. The tetra-alkyl or alkylaryl silanes all form one class given by equation 1 in table 5, fig. 13. It has been noted in the case of sulphides and mercaptans also (6) that although there are two or three subgroups on the basis of T_b *vs* χ_M and Mρ^2 *vs* χ_M there is only one group in correlating the Mn$_D$ with χ_M, (Fig. 13). This has been attributed to the strictly additive nature of both Mn$_D$ and χ_M. Thus, compounds having the same electronic environment like the tetra-alkyl and trialkylaryl silanes and some haloalkyl silanes have the same slope. The alkoxy alkyl silanes and some haloalkyl silanes and also the isocyanato and isothiocyanato silanes fall on a different line given by equation 2. Because of the additivity of these properties the differentiation among the alkyl groups as seen in T_b *vs* χ_M is not so marked.

Table 5

Equations correlating the molecular electronegativity and refractivity of organosilanes

N°.	Compounds	Equations
1	Tetra-alkyl and aryl silanes	$\chi_M = 1.6750\ \mathrm{Mn}_D - 22.780$
2	Alkyl halo alkoxy, isocyanato and isothiocyanato silanes	$\chi_M = 1.3997\ \mathrm{Mn}_D + 12.182$

It may be remarked that refractivity being related to polarizability, *i.e.* the deformability of the electronic cloud of the molecule should be directly related to the arithmetic mean of the electronegativity of the central atom and substituents as given by χ_M. A smooth relationship

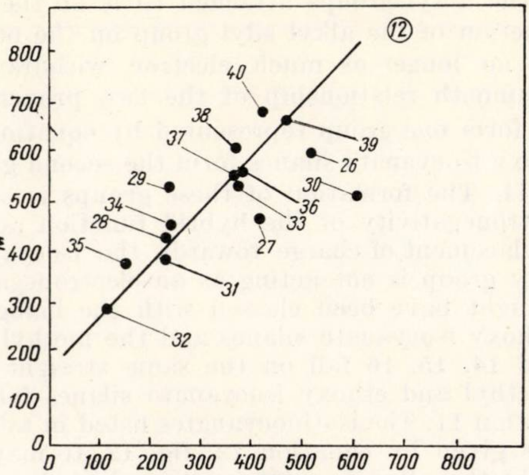

Fig. 12. — Correlation of molecular electronegativity and density of isothiocyanato silanes.

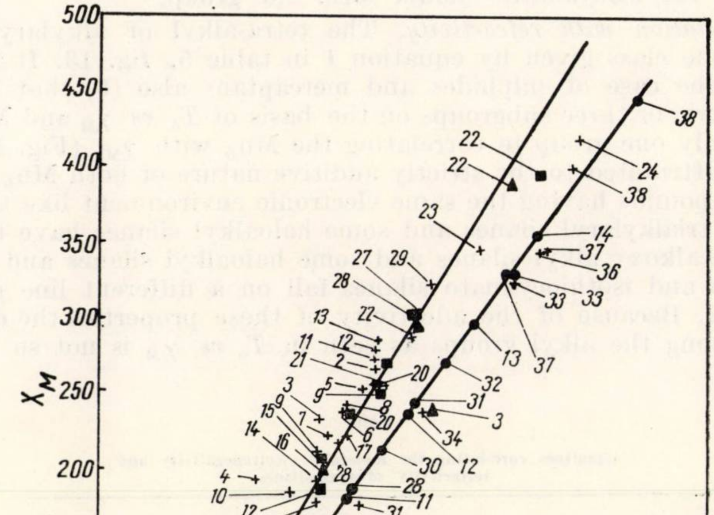

Fig. 13. — Correlation of molecular electronegativity and refractivity of organosilicon compounds.

in the case of the molar refractivity shows that the χ_M is a good measure of the polarizability of the molecules. This correlation can be used for estimating the electronegativity of the molecules wherefrom the group electronegativity can be estimated. Table 1 lists some of these values which are quite close to those obtained by other methods.

In developing these correlations it is now possible to obtain the data on the physical properties of molecules by a simple method of calculation. From the electronegativity data it is also possible to estimate the polarizability of the molecules and this will be the subject of a future discussion.

Revue Roumaine de Chimie, **18**, *8*, 1395 – 1407 (1973)

Revue Roumaine de Chimie, **18**, *8*, 1409–1417 (1973)

AZLACTONES OF CAROTENOIDS. I

SYNTHESIS AND PROPERTIES OF AZLACTONES OF β-APO-CAROTENALS AND OF DIAPO-CAROTENEDIALS

V. TĂMAŞ, VICTORIA CIURDARU and C. BODEA

Department of Chemistry, Institute of Agronomy,
str. Mănăştur 3, Cluj, Romania

Received January 3, 1973

The reaction of several β-apo-carotenals and diapo-carotenedials with hippuric acid resulted in the formation of azlactones. The reaction is characteristic for carotenoid-aldehydes and can serve for their identification. The absorption spectra in visible light and the i.r. spectra of the azlactones were recorded and discussed.

It is known that in plant and animal tissues occur numerous apo-carotenoids, usually aldehydes, methyl ketones or carboxylic acids. The aldehydes, termed apo-carotenals, are oxidation products formed by oxidative fission of a certain double bond of the polyene chain.[1,2] In living organisms the apo-carotenals and the diapo-carotenedials are mainly intermediary steps in the degradation of various carotenoids, especially in the transformation of provitamins A into vitamin A[3] or into other products with a skeleton less than 20 carbon atoms.[4] The most important natural apo-carotinals contain a β-ionone ring, being therefore designated as β-apo-carotenals. They occur frequently in nature but always in small quantities and they are acting as provitamins A.

The identification of β-apo-carotenals was in previous decades a difficult task because of their occurrence in small amounts and the lack of pure authentic samples. Today we dispose of some physical and chemical methods for their identification and quantitative determination.[5] The physical methods include absorption spectra in ultraviolet and visible light,[6] IR-spectra,[7,8] proton magnetic resonance spectra[7,8] and high-resolution mass spectra.[7,8,9] Chemical methods available are reduction of

---

[1] O. Isler and M. Montavon, *Chimia (Basel)*, **12**, 1 (1958).

[2] H. Glover and E. R. Redfearm, *Biochem. J.*, **58**, 15 (1954).

[3] J. Glover, *Vitamins and Hormons*, **18**, 371 (1962).

[4] H. Yokoyama and M. J. White, *Phytochemistry*, **7**, 1031 (1968).

[5] N. Arpin, J. L. Fiasson and Ph. Lebreton, *Prod. et probl. Pharm.*, **24**, 1 (1969).

[6] L.S. Jensen and A. Jensen, *Progr. Chem.*, **8**, 129 (1965).

[7] V. Tămaş, *Studii şi Cercetări Chim.*, Bucureşti, **18**, 137 (1970).

[8] O. Isler, "Carotenoids", Birkhäuser Verlag, Basel-Stuttgard, 1971, p. 202–265.

[9] C. R. Enzell, G. W. Francisc and S. Liaaen-Jensen, *Acta Chem. Scand.*, **23**, 727 (1969).

the aldehyde group to hydroxy group [10] or oxidation to carboxylic group [11] or condensation with rhodanine, [12] hydroxyl-amine [13] and diphenyl-acetyl-2-indandione-1,3-hydrazone. [14] Except the reaction with rhodanine, all the other reactions are common to the aldehyde and keto group.

Taking into account that carbonyl functions form azlactones by condensation with hippuric acid, we have examined the behaviour of

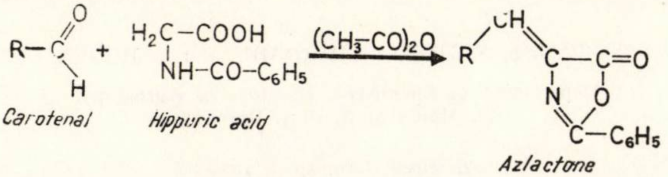

Fig. 1. — Formation of azlactones starting from carotenals and hippuric acid.

various aldehyde and keto carotenoids toward this reagent. Only the aldehyde carotenoids react with hippuric acid.

To prepare azlactones of carotenoids we have chosen the method of Erlenmeyer-Plöchl, [15,16,17] according to which the reaction is carried out in the presence of acetic anhydride and sodium acetate as catalyst. The reaction takes place according to the mechanism shown in fig. 1.

Reactions have been carried out with various apo-carotenals at temperatures between 75 and 150°. The best yields have been obtained at 85° and a reaction time of 1 1/2 —3 1/2 hours. Under these conditions the yield in azlactones was 60—90%. From diapocarotinals mono- as well as di-azlactones have been obtained.

In table 1 are given the apo-carotenals used to synthesize azlactones and in figs. 2 and 3 the structure of the isolated azlactones.

Table 1

Apo-carotenals and diapo-carotenedials used for condensation with hippuric acid

β-Apo- 8′-carotenal	β-Citraurin
β-Apo-10′-carotenal	C_{30}-Diapo-carotenedial
β-Apo-12′-carotenal	C_{24}-Diapo-carotenedial

Figs. 2 and 3 show that monoazlactones have been obtained from cyclic and acyclic apo-carotenals and diazlactones from acyclic apo-carotenals.

The obtained azlactones are dark violet crystalline products with rather high m.p. They are generally little soluble in less polar solvents

---

[10] S. L. Jensen, *Acta Chem. Scand.*, **17**, 489 (1963).

[11] Kuhn and H. H. Roth, *Ber. dtsch. chem. Ges.*, **66**, 1274 (1933).

[12] A. Winterstein and B. Hegedus, *Chimia (Basel)*, **14**, 18 (1960).

[13] A. J. Aasen and L. S. Jensen, *Acta Chem. Scand.*, **21**, 2185 (1967).

[14] H. Thommen and O. Wiss, *Z. Ernährungswissenschaft*, **3**, 18 (1963).

[15] E. Erlenmeyer, *Liebigs Ann. Chem.*, **275**, 1 (1893).

[16] J. Plöchl, *Ber. dtsch. chem. Ges.*, **16**, 2815 (1883).

[17] C. Bodea, V. Fărcăşan and I. Oprean, *Rev. Roumaine Chim.*, **10**, 11 (1965).

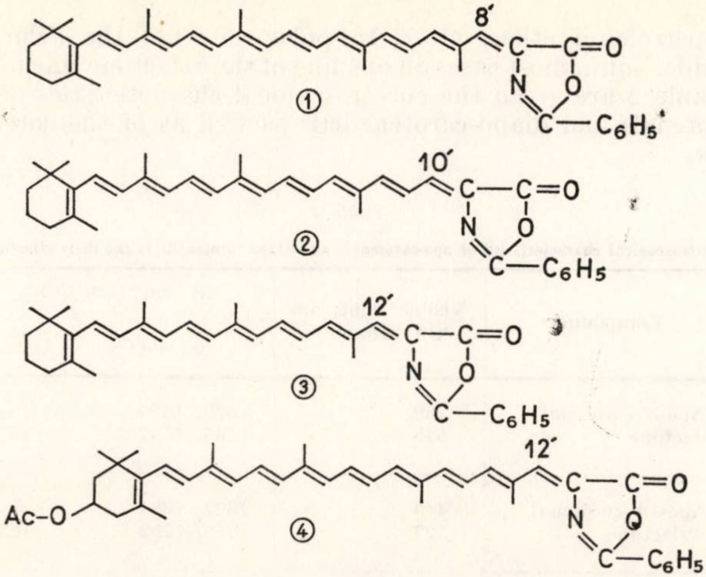
8′
①
10′
②
12′
③
12′
Ac–O
④
C=O
N
O
C–C₆H₅

Fig. 2. — Monoazlactones with cyclic structures.

1, Azlactone of β-apo-8′-carotenal; *2*, Azlactone of β-apo-10′-carotenal; *3*, Azlactone of β-apo-12′-carotenal; *4*, Azlactone of β-citraurin.

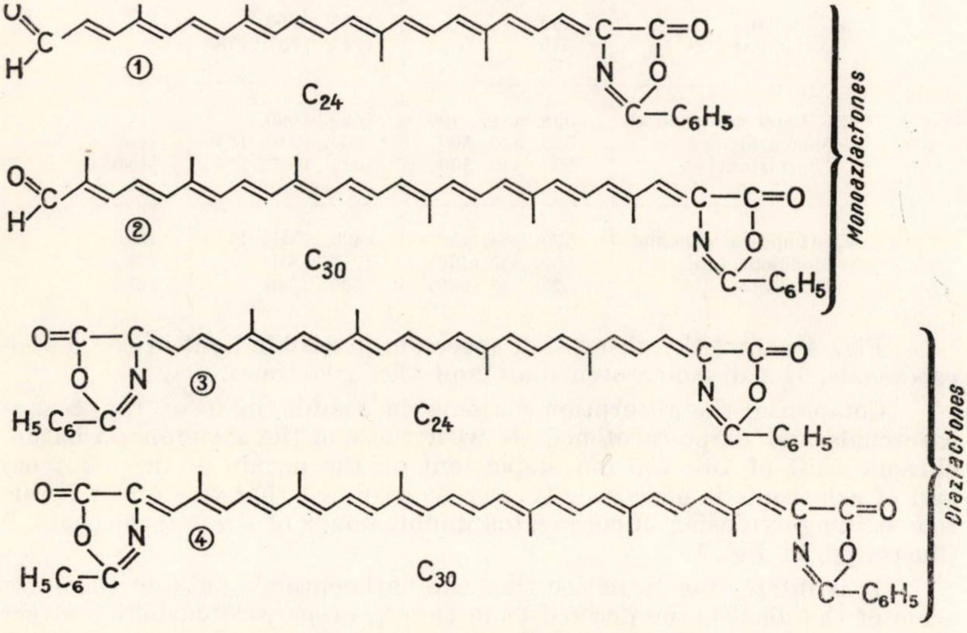
O
H
①
C24
②
C30
③
C24
④
C30
H5C6
C=O
N
O
C–C6H5
Monoazlactones
Diazlactones

Fig. 3. — Monoazlactones and diazlactones with acyclic structures.

1, Monoazlactone of C_{24}-diapo-carotenedial; *2*, Monoazlactone of C_{30}-diapo-carotenedial; *3*, Diazlactone of C_{24}-diapo-carotenedial; *4*, Diazlactone of C_{30}-diapo-carotenedial.

(hexane, petroleum ether, etc.). In polar solvents the azlactones are easily soluble, but in most cases an opening of the azlactone ring takes place.

In table 2 are given the spectroscopical characteristics of the used β-apo-carotenals and diapo-carotenedials as well as of the correspondent azlactones.

Table 2

Spectroscopical characteristics of apo-carotenals and diapo-carotenedials and their azlactones

Compound	Visible light, nm (in benzene)	IR, cm^{-1} (in CCl_4)	
		$\nu C = O$	$\nu C = N$
β-Apo-8′-carotenal	469	1620, 1680	—
Azlactone	545	1735, 1787	1635
β-Apo-10′-carotenal	449	1622, 1684	—
Azlactone	527	1740, 1792	1635
β-Apo-12′-carotenal	430	1618, 1680	—
Azlactone	516	1744, 1797	1640
β-Citraurin	469	1615, 1680	—
Azlactone	545	1715, 1737, 1788	—
C_{30}-Diapo-carotenedial	538, 4517, 490	1620, 1660	—
Monoazlactone	545, 530, 500	1660, 1740, 1840	1680
Diazlactone	565, 545, 500	1690, 1715, 1740	1680
C_{24}-Diapo-carotenedial	520, 484, 458	1820, 1715, 1740	1680
Monoazlactone	550, 535 (498)	1740, 1840	1680
Diazlactone	575, 556 (535)	1690, 1740	1680

Fig. 4 shows the absorption spectrum in visible light of the β-apo-carotenals, the diapo-carotenedials and the azlactones.

Comparing the absorption maxima in visible light of the β-apo-carotenals and diapo-carotenedials with those of the azlactones a bathochromic shift of 76—155 nm, dependent on the nature of the carotenal and of azlactone, is observed. It may be assumed that this effect is due to a striking extension of conjugated double bonds of the polyene chain, [18] illustrated in fig. 5.

It is interesting to notice that the bathochromic shift in the spectrum of the diazlactone derived from the C_{24}-diapo-carotenedial is larger than in the case of the diazlactone derived of the C_{30}-diapo-carotenedial.

In the i.r. spectra of all carotenal azlactones a strong band is observed in the 1730—1800 cm^{-1} region, attributed to the azlactonic carbonyl vibration. This strong absorption at such high wavelengths is characteristic for unsaturated azlactones. Characteristic is also the band at 1635 cm^{-1} due to the $C = N$ vibration. A parallelism can be observed

---

[18] D. A. Bassi, V. Deulofeu and F.A.F. Ortega, *J. Amer. Chem. Soc.*, **75**, 171 (1953).

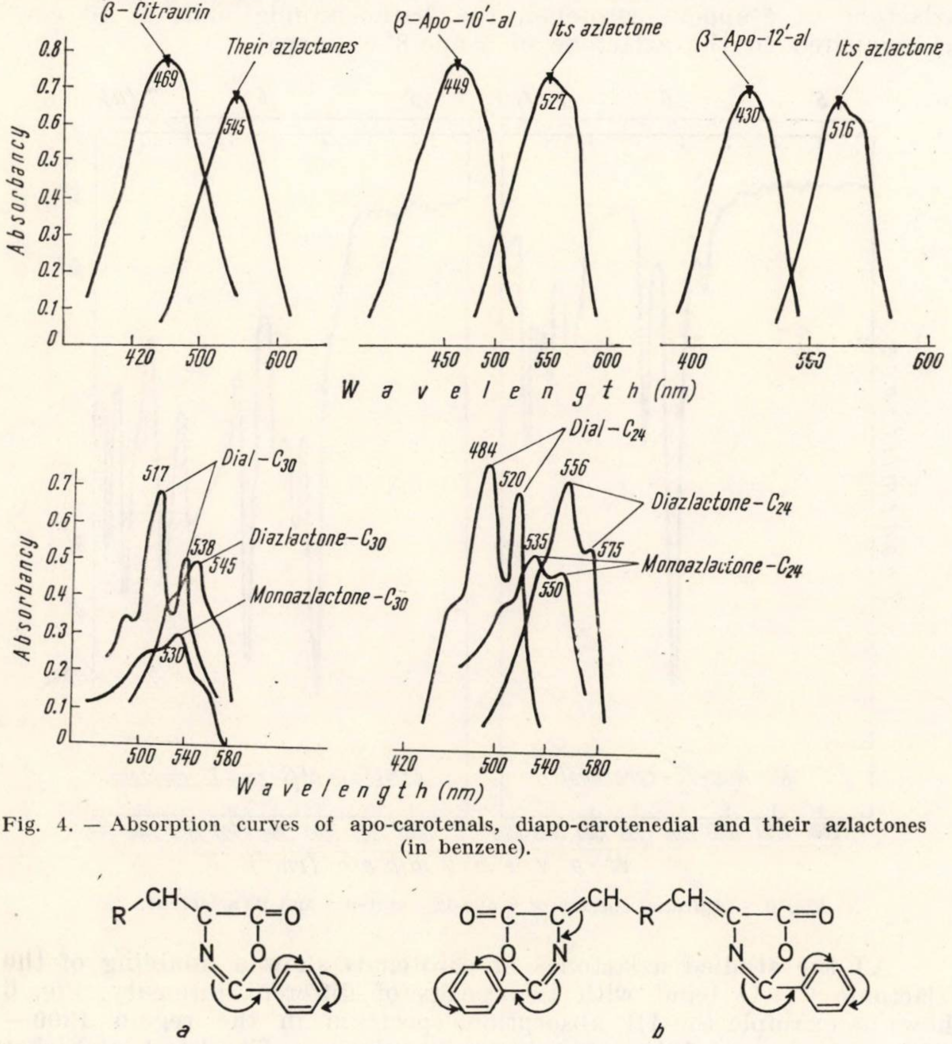

Fig. 4. — Absorption curves of apo-carotenals, diapo-carotenedial and their azlactones (in benzene).

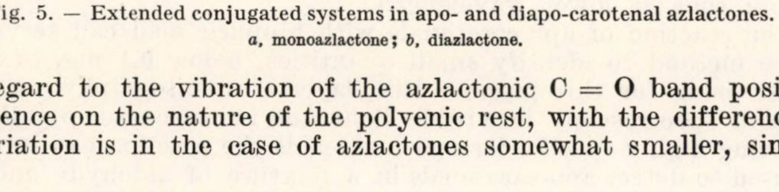

Fig. 5. — Extended conjugated systems in apo- and diapo-carotenal azlactones.
a, monoazlactone; *b*, diazlactone.

with regard to the vibration of the azlactonic $C = O$ band position in dependence on the nature of the polyenic rest, with the difference that the variation is in the case of azlactones somewhat smaller, since the carbonyl grouping in azlactones is separated from the isoprenoid rest by a C = C grouping. Furthermore, it is to be noticed that the shorter the conjugated polyene chain the larger is the shifting of the azlactonic C =O band towards higher wavelengths. For example, in the case of the azlactone of β-apo-12′-carotenal, the bathochromic shift is 10 cm^{-1} as compared to the azlactone of β-apo-8′-carotenal.

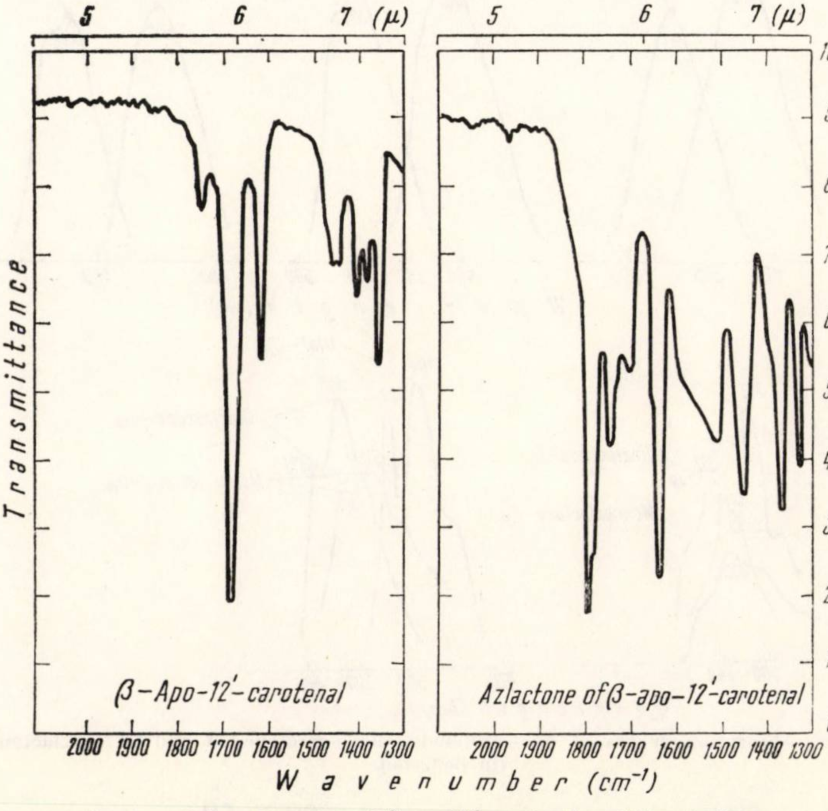

Fig. 6. — Infrared spectra of β-apo-12′-carotenal and its azlactone.

All the studied azlactones of carotenals show a doubling of the azlactonic C =O band with two peaks of different intensity. Fig. 6 shows as example the IR absorption spectrum in the region 1300—2000 cm^{-1} of β-apo-12′-carotenal and its azlactone. The band at higher wavelength and stronger intensity is more influenced by the polyenic rest than that at lower wavelength.

The reaction of apo-carotenals with hippuric acid can serve as an effective method to identify small quantities, below 0.1 mg, of apo-carotenals, using for this purpose thin layer chromatography as well as absorption spectroscopy in visible light and i.r. spectroscopy. Furthermore, being highly specific for apo-carotenals the reaction can be successfully used to detect apo-carotenals in a mixture of aldehyde and keto-carotenoids.

Further investigations should illustrate the possibility to convert the azlactones of carotenals into N-acyl-carotenoic acids or other derivatives, especially by opening the azlactone ring.

EXPERIMENTAL

The carotenals used in the condensation reactions with hippuric acid were synthetic products from Hoffmann-La Roche, Basel.

Electronic spectra were recorded on a spectrophotometer Zeiss VSU-1 and i.r. spectra on an Unicam SP. 200 G.

Azlactone of β-apo-8′-carotenal. β-Apo-8′-carotenal (0.2 g), hippuric acid (0.17 g) and anhyd. sodium acetate (0.15 g) were well mixed and acetic anhydride (0.8 cm^3) added. The reaction mixture was kept for 1 1/2 hour at 85°. After cooling, the reaction product was twice washed with petroleum ether (10 cm^3) in the reaction vessel. From the residue the pigments were extracted till colourless with benzene and the extracts filtered. The dark benzenic solution was concentrated to a small volume (2–3 cm^3) and on adding petroleum ether (40–50 cm^3) precipitation of the azlactone took place. After decantation, the adding of petroleum ether was repeated to remove completely unreacted β-apo-8′-carotenal. The remaining azlactone is a dark powder. Yields about 80 %.

Thin layer chromatography with silicagel G was used to obtain highly purified azlactone. The development was carried out with a mixture of petroleum ether-benzene (1 : 1 volumes). The R_f values are shown in table 3.

After elution of zone *A* with ether and evaporation of the solution, violet crystals of azlactone were obtained, m.p. 212°. Yields 60–65 %.

$C_{39}H_{46}N$(560) *Calcd* : C 83.60 ; H 8.70 :; N 2.50 ;
Found : C 83.00 ; H 7.96 ; N 2.72

The azlactone of β-apo-8′-carotenal is easily soluble in ether, benzene and CCl_4, less soluble in petroleum ether. By treatement with polar solvents, opening of the azlactone ring takes place.

The absorption spectra in visibile light and i.r. are shown in table 2 and fig. 4.

Azlactone of β-apo-10′-carotenal. A mixture of β-apo-10′-carotenal (20 mg), hippuric acid (15 mg), sodium acetate (15 mg) and acetic anhydride (0.3 cm^3) was treated as shown above.

The distribution of the pigments in the chromatogram was the same as shown in table 3. The purified azlactone was obtained with 70 % yield. Violet crystals, m.p. 210°, show the same solubilities as the above described azlactone.

By lack of larger quantities of starting material, no microanalyses were carried out.

Table 2 and fig. 4 show visible light and i.r. absorption spectra.

Azlactone of β-apo-12′-carotenal. A mixture of β-apo-12′-carotenal (10 mg), hippuric acid (10 mg) and acetic anhydride (0.2 cm^3) was worked up as before.

From zone A (see table 3) the azlactone was obtained with 75 % yield. Violet crystals, m.p. 240°, show the same solubility as the other azlactones of carotenals. (For absorption spectra in visible light and i.r. see table 2 and fig. 4).

Azlactone of β-citraurin. A mixture of β-citraurin (10 mg), hippuric acid (10 mg), sodium acetate (10 mg) and acetic anhydride were worked up as above. The thin layer

Table 3

Thin-layer chromatography; zones and R_f values

Starting apocarotenal	Zones		R_f
	colour	compound	
β-Apo-8′-carotenal	violet	azlactone (A)	0.84
	orange	*cis-trans*-β-apo-8′-carotenal	0.66
	orange	all-*trans*-β-apo-8′-carotenal	0.59
	violet-pink	unidentified	0.50
	violet	unidentified	0.32
β-Apo-10′-carotenal	violet	azlactone (A)	0.86
	orange	*cis-trans*-β-apo-10′-carotenal	0.68
	orange	all-*trans*-β-apo-10′-carotenal	0.62
	ochre	unidentified	0.52
β-Apo-12′-carotenal	violet	azlactone (A)	0.89
	orange	*cis-trans*-β-apo-12′-carotenal	0.71
	orange	all-*trans*-β-apo-12′-carotenal	0.65
	ochre	unidentified	0.55
β-Citraurin	violet	azlactone (A)	0.76
	orange	*cis-trans*-β-citraurin-acetate	0.54
	orange	all-*trans*-β-citraurin-acetate	0.50
	ochre	unidentified	0.28
C_{30}-Diapo-carotenedial	blue	diazlactone (A)	0.70
	violet	monoazlactone (B)	0.65
	pink	C_{30}-diapo-carotenedial	0.35
C_{24}-Diapo-carotenedial	blue	diazlactone (A)	0.75
	violet	monoazlactone (B)	0.68
	pink	C_{24}-diapo-carotenedial	0.37

chromatogram showed zones as those illustrated in table 3. Yield of the azlactone 60%. Violet crystals, m.p. 85–90°.

Easily soluble in benzene, ether, CCl_4 and even in petroleum ether. The electronic spectrum maxima and i.r. band are shown in table 2 and fig. 4.

Azlactones of C_{30}-diapo-dialdehyde. A mixture of C_{30}-diapo-dialdehyde (25 mg), hippuric acid (25 mg), sodium acetate (25 mg) and acetic anhydride (0.35 cm^3) was heated at 85° for 3 1/2 hours and worked up as above. A mono- and a diazlactone were obtained.

Monoazlactone. The pigment of zone *B* (see table 3) was eluated with ether. After evaporation of the ether, violet crystals (7–8 mg), m.p. 170°, soluble in benzene, ether, CCl_4, less soluble in petroleum ether. The electronic spectrum (benzene) with diminished fine structure (see fig. 4).

Diazlactone. The pigment of zone *A* (see table 3) was eluated like that of zone *B*. Violet crystals (10 mg), m. p. 160°, soluble in benzene, ether, CCl_4, less soluble in petroleum ether.

The electronic spectrum shows diminished fine structure, with maxima at 500, 545, 565 nm (see fig. 4). In the i.r. spectrum (CCl_4) peaks at 1680 cm^{-1} (C = N) and 1715, 1745 cm^{-1} (azlactone C = O).

Azlactones of C_{24}-diapo-dialdehyde. Working with the same quantities of reagents as in the case of C_{30}-diapo-dialdehyde a mono- and diazlactone were obtained with similar yields.

Monoazlactone. Violet crystals, m.p. 172°. Spectroscopical characteristics are shown in table 2 and the R_f values in table 3.

Diazlactone. Violet crystals, m.p. 167°. Solubilities of both azlactones similar to those of azlactones of C_{30}-diapo-dialdehyde. See also tables 2 and 3.

Use of hippuric acid reaction for identification of carotenals

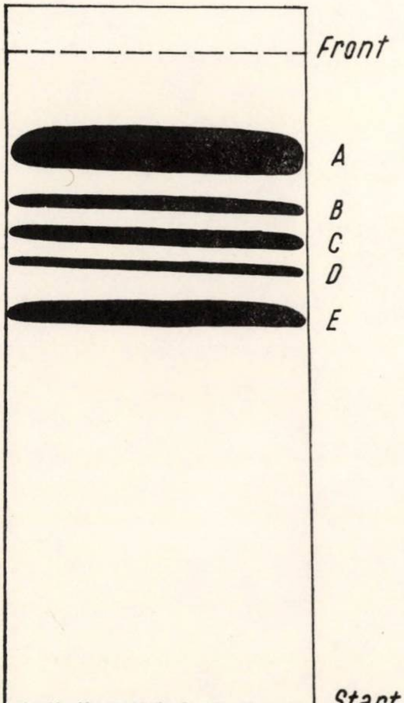

Fig. 7. — Thin-layer chromatogram of a mixture containing:

A, azlactone of β-apo-8′-carotenal (violet); B and C, *cis-trans* and all-*trans* β-carotene (orange); D, β-apo-8′-carotenal (orange)′; E, canthaxanthin (blood-red).

A mixture of β-carotene (0.1 mg), canthaxanthin (0.1 mg) and β-apo-8′-carotenal (0.1mg) was worked up as in the case of carotenals.

After developing with a mixture of petroleum ether and benzene (1 : 1) the chromatogram shown in fig. 7 was obtained.

Acknowledgements. We are grateful to Dr. Otto Isler and to Dr. Hans Thommen from Hoffmann-La Roche, Basel, for providing us with samples of apo-carotenals.

Revue Roumaine de Chimie, **18**, *8*, 1419–1426 (1973)

DIE MATHEMATISCHE DARSTELLUNG DER HOMOLOGIE UND DER HOMOLOGEN SERIEN

I. MOŢOC

Fakultät für Industriechemie, Polytechnisches Institut Timişoara, Postfach 103, Timişoara, Rumänien

Eingegangen am 8. Dezember 1972

Diese Arbeit ist ein Versuch, die Beziehung der Homologie in einem abstrakteren Rahmen darzustellen. Damit entlehnt man einen allgemeineren Formalismus zur Behandlung dieses Problems und erhält eine allgemeinere Definition der Homologie und der homologen Serien.

1. EINLEITUNG

Die immer häufiger werdenden Versuche, die verschiedensten Aspekte der organischen Chemie mathematisch zu formulieren, bezwecken die Definition, Systematisierung, Nomenklatur, das Aufzählen der chemischen Entitäten.

Beachtenswerte Ergebnisse erzielte man durch die Anwendung der Graphentheorie,[1-6] der Permutationsgruppen,[7,8] algebraischer Polynome.[9,10] Es wurde auch die matrizielle Behandlung einiger Aspekte der Stereochemie versucht.[11-14]

In dieser Arbeit wird eine genauere mathematische Analyse der Beziehung der Homologie und der homologen Serien versucht. Es wer-

---

[1] A. Cayley, Phil. Mag., **67**, 444 (1874); *Mathematical Papers* (Cambridge), **9**, 202 (1895).

[2] A. T. Balaban, *Rev. Roumaine Chim.*, **11**, 1097 (1966).

[3] A. T. Balaban, *Tetrahedron*, **27**, 6115 (1971).

[4] A. T. Balaban und F. Harary, *Rev. Roumaine Chim.*, **12**, 1511 (1967).

[5] A. T. Balaban, *Rev. Roumaine Math. Pures Appl.*, **17**, 9 (1972).

[6] A. T. Balaban, *Rev. Roumaine Chim.*, **17**, 000 (1972).

[7] I. Ugi, D. Marquarding, H. Klusacek, G. Gokel und P. Gillespie, *Angew. Chem.*, **82**, 741 (1970).

[8] P. Gillespie, P. Hoffmann, H. Klusacek, D. Marquarding, S. Pfohl, F. Ramirez, E. Tsolis und I. Ugi, *Angew. Chem.*, **83**, 691 (1971).

[9] E. Ruch und A. Schonhofer, *Theor. Chim. Acta*, **19**, 225 (1970).

[10] E. Ruch und A. Schonhofer, *Theor. chim.* Acta, **10**, 91 (1968).

[11] F. Kerek und I. Moţoc, *Rev. Roumaine Chim.*, **18**, 000 (1973).

[12] I. Moţoc und F. Kerek, *Rev. Roumaine Chim.*, **18**, 000 (1973).

[13] F. Kerek und I. Moţoc, *Rev. Roumaine Chim.*, **18**, 000 (1973).

[14] I. Moţoc und F. Kerek, *Rev. Roumaine Chim.*, **18**, 000 (1973).

den bestimmte Begriffe aus der Mengenlehre und allgemeine Begriffe des matriziellen Rechnens angewendet.[15–19]

Man erzielt die Aussage mehrerer Definitionen für homologe Serien. Diese Definitionen sind abstrakter als die gewöhnlichen. Gleichfalls wird gezeigt, dass die Homologie eine liniare Beziehung ist.

2. HOMOLOGE SERIEN

In dem nun Folgenden wird mit $\wedge$ eine binäre Beziehung bezeichnet, mit S_j und S_0 Mengen chemischer Entitäten, die weiter unten definiert werden. A, B, C werden beliebige Mengen symbolisieren. I, J werden die Index-Mengen sein.

Betrachten wir eine Menge von Objekten (chemische Entitäten) s_{ji}, die mit dem Index i, der eine Index-Menge I durchläuft, bezeichnet werden. Man stellt fest, daß $I \subseteq N$, wobei N die Menge der natürlichen Zahlen ist. Also stellt die Bezeichnung der Elemente s_j mit Indizien eine isomorphe Anwendung der Menge $\{ \underset{i \in I}{U} s_{ji}\} = S_j$ auf die Menge I dar:

$$S_j \cong I \tag{1}$$

In dem nun Folgenden wird gezeigt, dass die Behauptung (1) wahr ist. Die so aufgebaute Menge ist aber nicht von besonderem Nutzen, da wir nicht genügend Informationen bezüglich ihrer Elemente besitzen. Wir werden der Menge S_j auch folgende Bedingung stellen:

$$S_j = \{ \in_j : s_{ji} \}_{i \in I} \tag{2}$$

$$\text{mit: } \in_j = \{ \in_{j1}, \in_{j2}, \ldots \} \tag{3}$$

Das heisst also, dass die Beziehung (2) anzeigt, dass die Menge S_j mit der Eigenschaft $\in_j$ ausgerüstet ist.

Durch die Beziehung (3) wird gezeigt, dass $\in_j$ eine Menge, und zwar eine Menge von Charakteristiken ist. Zum Beispiel:

$\in_1$ = {Verbindungen bestehend nur aus C und H, enthalten nur σ-Bindungen, enthalten keine Ringe}

Dann erkennt man in $S_1 = \{ \in_1 : s_{1i} \}_{i \in N}$ die Serie der Alkane.

In Zusammenhang mit $\in_j$ wird folgendes noch gezeigt: Bezeichnet man mit $|\in_j|$ den Rang der Menge $\in_j$ und mit S die Menge aller organischer Verbindungen, dann besteht die Beziehung:

$$S_j = \{ S \cap \{ s_{ji} / \in_j \}_{i \in I} \} \tag{4}$$

---

[15] E. BOREL, ,,Eléments de la théorie des ensembles", Albin Michel.

[16] N. BOURBAKI, ,,Eléments de mathématique", Livre I et Livre III, Hermann, Paris, 1958.

[17] R. FAURE, A. KAUFMANN und M. DENIS-PAPIN, ,,Mathématiques nouvelles", Dunod, Paris, 1964.

[18] CL. CHEVALLEY, ,,Fundamental Concepts of Algebra", Academic Press, Enc., New York, 1956.

[19] H. SCHWEDTFEGER, ,,Introduction to Liniar Algebra and The Theory of Matrices", Noordhoff, Groningen, 1950.

Auf Grund der Beziehung (4) haben wir folgende:

Definition 1. Eine homologe Serie ist durch folgende Bedingung definiert:

$$|\in_j| = \text{MAX}, \ |I| = \infty$$

Mit $|I|$ wurde der Rang der Index-Menge bezeichnet, von der schon gezeigt wurde, dass sie zählbar ist. $\in_j$ führt zur Bezeichnung mit einem Index j, der die zählbare Menge J durchläuft.

Man kann annehmen, dass $J \equiv N$. Theoretisch ist $|J| = \infty$, praktisch ist $|J|$ sehr gross.

Wenn die Bezeichnung richtig gemacht wurde, kann man voraussetzen, dass für zwei nahegelegene Werte m und n, S_m und S_n sich nicht viel voneinander unterscheiden und dass es eine chemische Reaktion χ gibt, die die Interkonversion:

$$S_m \underset{\chi^{-1}}{\overset{\chi}{\rightleftarrows}} S_n$$

darstellt.

3. DIE HOMOLOGIEBEZIEHUNG

Man betrachtet die Mengen A, B, C, die distinkt oder nicht distinkt sind. Das kartesische Produkt der Mengen A und B, mit $A \times B$ bezeichnet, ist die Menge der Paare:

$$\{(x, y)/x \in A, y \in B\}$$

Das Produkt $A \times B \times C$ ist analog die Menge:

$$\{(x, y, z)/x \in A, \ y \in B, \ z \in C\}$$

Man kann auch verallgemeinern für die Mengen $A_1, A_2, \ldots, A_i, \ldots$ In diesem Fall haben wir:

$$\underset{i}{X} A_i = \{(x_1, x_2, \ldots, x_i, \ldots)/x_1 \in A_1, \ldots, x_i \in A_i, \ldots\}$$

Eine unäre Beziehung ist eine Untermenge $R_1 \subset A$.

Eine binäre Beziehung ist eine Untermenge $R_2 \subset A \times B$ u.s.w.

In dem nun Folgenden werden wir unäre und binäre Beziehungen verwenden.

Mit der Definition 1. gleichwertig ist folgende:

Definition 2. Eine homologe Serie ist eine unäre Beziehung auf S, die von jenen Elementen aus S erfüllt wird, für die $|\in_j| = \text{MAX} \Rightarrow |I| = \infty$.

Es sei nun s_{j1} jenes Element, welches das Minor der Menge $\{\mathcal{M}(s_{ji})\}_{i\in I}$ darstellt, das heisst:

$$\mathcal{M}(s_{j1}) \leqslant \{\mathcal{M}(s_{ji})\}_{i\in I\cap\{1\}}$$

Mit $\mathcal{M}(s_{ji})$ wurde die Masse der chemischen Verbindung s_{ij} bezeichnet.

Wir bezeichnen mit S_0 die Menge:

$$S_0 = \{s_0, s_1, 2s_1, \ldots, n_1s_1, \ldots\} = \{s_0, ns_1\},\ n = 2,\ 3, \ldots$$

s_0 zeigt an, dass S_0 mit keinem Element s_1 beginnt; s_1 stellt das Methylen-Radikal CH_2 dar.

Man definiert die binäre Beziehung:

$R_2 \subset \{s_{j1}\}\times S_0$ folgendermassen:

$$s_{j1} \wedge s_0 = s_{j1} \in R_2 \tag{5}$$

$$s_{j1} \wedge ms_1 = s_{1,\,m+1} \in R \tag{6}$$

Man kann also sagen, dass s_{jp} homolog mit $s_{.q}$ ist, wenn:

$$s_{j1} \wedge qs_1 = s_{jq} = s_{.q}$$

Zur Verallgemeinerung kann man annehmen, dass:

$$s_{jp} \wedge (-n)\, s_1 = s_{j,\,p-n} \tag{7}$$

$n,\ p \in N$, mit der Bedingung, dass $p - 1 \geqslant 1$.

Bemerkung: In Paragraph 4 wird die Verwendung der Beziehung (7) nicht notwendig sein.

Die weiter oben festgelegten Begriffe erlauben die Aussage der:

Definition 3. Die Homologie ist eine binäre Beziehung.

Mit den Beziehungen (5), (6), (7) kann man folgende Eigenschaften der Homologiebeziehung festlegen:

i.) Reflexivität: Tatsächlich besteht laut (5) die Beziehung:

$$s_{ji} \wedge s_0 = s_{ji}$$

ii.) Symmetrie: Tatsächlich, gemäss (7) ist:

$$s_{jp} \wedge ns_1 = s_{jq} \Rightarrow s_{jq} \wedge (-n)s_1 = s_{jp}$$

Offensichtlich wurde vorausgesetzt, dass $p + n = q$.

iii.) Transitivität :

Es seien $s_{jx}, s_{jy}, s_{jz} \in S_j$. Ohne die Allgemeingültigkeit zu beeinträchtigen, kann man voraussetzen, dass :

$$\mathcal{M}(s_{jx}) < \mathcal{M}(s_{jy}) < \mathcal{M}(s_{jz})$$

(mit $\mathcal{M}(\ )$ wurde die Masse des Gliedes ( ) bezeichnet).
Wenn :

$$s_{jx} \wedge n s_1 = s_{jy}\,; \quad s_{jy} \wedge m s_1 = s_{jz}$$

dann ist : $s_{jx} \wedge (n + m)\, s_1 = s_{jz}$
Offensichtlich wurde vorausgesetzt, dass $x + n = y,\ y + m = z$.

4. DER AUFBAU EINER HOMOLOGEN SERIE

Es wird nun gezeigt, dass folgende Beziehung existiert :

$$s_{jp} \wedge s_{jq} = s_{jq} \wedge s_{jp} \tag{8}$$

Tatsächlich :

$$s_{jp} \wedge s_{jq} = s_{j,\,p+q} \tag{8'}$$

Aber der Gruppoid (N, +) ist kommutativ, das heisst :

$$p + q = q + p\,; \quad p, q \in N.$$

Daraus folgt, dass :

$$s_{j,p+q} = s_{j,q+p} = s_{jq} \wedge s_{jp} \tag{8''}$$

Also wurde mit Hilfe von (8′) und (8″) die Beziehung (8) wiedergefunden :

$$s_{j,p} \wedge s_{jq} = s_{jq} \wedge s_{jp}$$

Wir machen folgende Bemerkung : Den Index j setzt man fest, indem man $\in_j$ für verschiedene j vergleicht. Der zweite Index p (oder q usw.) bezeichnet die Anzahl der Kohlenstoffatome, die die Kette bilden. Z.B. für die Alkane, die mit S_1 bezeichnet werden, versteht man unter $s_{11} \in S_1$ Methan CH_4. Das Glied $s_{\alpha 1} \in S_\alpha$ (die Reihe der gesättigten acyklischen aliphatischen Fettsäuren) stellt HCOOH dar, usw.

In dem nun Folgenden bezwecken wir, eine Methode zu entwerfen, mit der irgendeine homologe Reihe gebildet werden kann. Man wird einen matriziellen Formalismus entwerfen. Die Beziehungen (5) und (6) werden benützt.

Mit den Elementen s_{j1}, s_1, s_0 baut man die Matrix:

$$M(j) = \begin{bmatrix} s_{j1} \\ s_1 \\ s_0 \end{bmatrix} \tag{9}$$

auf. Die Matrix (9) wird die charakteristische Matrix für die Serie sein, die wir aufbauen wollen. Der Ausdruck „charakteristisch'' ist angebracht, da die Matrix das Element s_{j1} enthält, was den Aufbau der Reihe S_j miteinbegreifen wird.

Die Matrix:

$$P(\lambda) = \begin{bmatrix} s_0 & 0 & 0 \\ 0 & \lambda & 0 \\ 0 & 0 & s_0 \end{bmatrix} \tag{10}$$

wird die Indexierungsmatrix darstellen, da man durch die Werte des Parameters λ, $\lambda = 0, 1, \ldots$, die Glieder der homologen Serie erhält und indexiert.

Und schliesslich wird die Matrix:

$$0 = [s_0 \ s_0 \ s_0]$$

die Homologiematrix sein, da sie, wie das weiterhin gezeigt wird, allen homologen Reihen eigen ist, also die Homologie charakterisiert.

Mit $\odot$ werden wir die Multiplikation zweier Matrizen, die, wie oben gezeigt, definiert werden, bezeichnen. Die Multiplikation $\odot$ unterscheidet sich ein wenig von der gewöhnlichen. Es wird nun anhand eines effektiven Rechnens gezeigt, wie eine $\odot$ Multiplikation durchgeführt wird.

Das Einführen der Beziehung:

$$0 \,.\, s_{ji} = s_0 \tag{11}$$

hat auch eine anschauliche Begründung.

Wir führen folgendes Produkt aus:

$$\begin{aligned} [s_0 s_0 s_0] \odot \left(\begin{bmatrix} s_0 & 0 & 0 \\ 0 & \lambda & 0 \\ 0 & 0 & s_0 \end{bmatrix} \odot \begin{bmatrix} s_{j1} \\ s_1 \\ s_0 \end{bmatrix} \right) &= [s_0 s_0 s_0] \odot \begin{bmatrix} s_0 \wedge s_{j1} \wedge s_0 \wedge s_0 \\ s_0 \wedge \lambda s_1 \wedge s_0 \\ s_0 \wedge s_0 \wedge s_0 \end{bmatrix} = \\ = [s_0 s_0 s_0] \odot \begin{bmatrix} s_{j1} \\ \lambda s_1 \\ s_0 \end{bmatrix} = [s_0 \wedge s_{j1} \wedge \lambda s_1 \wedge s_0] &= [s_{j1} \wedge \lambda s_1] = [s_{j,\lambda+1}] = s_{j,\lambda+1} \in S_j \end{aligned} \tag{12}$$

Beim Ausführen des obigen Produkts wurde neben der Beziehung (5), (6) auch (11) beachtet.

Das Ergebnis führt zur Schlussfolgerung, dass, um dieses Glied $s_{jp} \in S_j$ zu erhalten, es notwendig und hinreichend ist, dass $\lambda = p - 1$.

Nun können wir beweisen, dass die Beziehung (1) wahr ist. Damit $S_j \cong I$ ist es notwendig und hinreichend, dass wenn:

$$\begin{gathered} m \to s_{jm} \\ n \to s_{jn} \end{gathered} \tag{13}$$

auch:

$$m + n \to s_{jm} \wedge s_{jn}$$

Es ist leicht zu erkennen, dass:

$$s_{j,m+n} = s_{jm} \wedge s_{jn}$$

Aber: $m + n \to s_{j,m+n} = s_{jm} \wedge s_{jn}$
Also: $m + n \to s_{jm} \wedge s_{jn}$, was zu beweisen war.

Abschliessend wollen wir beweisen, dass die Matrix **0** tatsächlich die Beziehung der Homologie charakterisiert.

Die Menge aller organischen Verbindungen kann als:

$$S = \underset{j \in J}{U} S_j \tag{14}$$

geschrieben werden.

Die Beziehung (13) kann auch in der Form:

$$S = \underset{j \in J}{U} \underset{i \in I}{U} s_{ji} \tag{15}$$

geschrieben werden.

Aber die Beziehung (15) wird gemäss (12) zu:

$$S = \underset{j \in J}{U} \underset{\lambda \in N}{U} \mathbf{0} \odot (P(\lambda) \odot M(j)) = \mathbf{0} \bigcirc \underset{j \in J}{U} \underset{\lambda \in N}{U} P(\lambda) \odot M(j) \tag{16}$$

Da die Matrix **0** vor dem Zeichen U steht, bedeutet es, dass **0** den allgemeinen Aspekt der Beziehung der Homologie darstellt.

5. DIE DEFINITION DER HOMOLOGIE IN DER MENGENLEHRE

Es wird hier gezeigt, dass man die Homologie in einer kompakten Art und Weise definieren kann, wobei wir den Rahmen der Mengenlehre nicht überschreiten.

Revue Roumaine de Chimie, 18, 8, 1419–1426 (1973)

Gegeben sei die Abbildung:

$$f : A \rightarrow B, \text{ wo } B = \bigcup_{\sigma \in \Sigma} B_\sigma$$

Die Menge $M\{A \rightarrow B\}$ der Abbildungen mit dem Bereich in A und Cobereich in B wird mit HOM(A, B) bezeichnet.

Setzt man $A = S$ und $B_\sigma = S_j$ gleich, gelangt man zur:

Definition 4. Die Homologie ist eine Beziehung vom Typ HOM(S, S_j).

6. SCHLUSSFOLGERUNGEN

Unter Anwendung des allgemeinen Notierungssystems aus der Algebra und Mengenlehre war es möglich, einen abstrakteren und kompakteren Formalismus zur Behandlung der Homologie aufzubauen.

Dadurch wurde unseres Erachtens nach der Sinn und Bereich der Begriffe Homologie und homologe Reihe besser klargelegt.

Für die homologen Reihen wurde eine Definition mit Hilfe des algebraischen Formalismus und eine andere mit Hilfe des Formalismus der Mengenlehre (Definition 2, bzw. 1) aufgestellt.

Ähnlich ging man auch im Falle des Begriffes der Homologie vor.

Gleichfalls wurde ein Verfahren angegeben, um alle Glieder einer homologen Reihe zu erhalten.

Im Einklang mit Voraussagungen [20,21] ist es wahrscheinlich, dass die Anzahl jener Probleme der Chemie, in deren Beziehungen der mathematische Formalismus (Graphen usw.) verwendet wird, stark ansteigen wird.

---

[20] A. GEWIRTZ, A Call for Interdisciplinary Relationships, in International Conference on Combinatorial Mathematics, Ann. N.Y. Acad. Sci., **175**, 5 (1970).

[21] A. T. BALABAN, ,,Multidisziplinäre und Interdisziplinäre Forschungen. Ihre Herkunft, Entwicklung und Perspektiven'', Verlag der Akademie, Rumänien, Bukarest, 1972, Seite 203.

Revue Roumaine de Chimie, **18**, *8*, 1427–1439 (1973)

LA CHLOROPHOSPHONATION DU POLYCHLORURE DE VINYLE ET DE L'ALCOOL POLYVINYLIQUE

FL. POPESCU et SIMONA PERCEC
Institut de Chimie macromoléculaire «Petru Poni», 41 A, Aleea Gr. Ghica Vodă, Jassy, Roumanie

Reçu le 17 septembre 1972

Le polychlorure de vinyle et l'alcool polyvinylique peuvent être phosphorylés par chlorophosphonation oxydative, avec du trichlorure de phosphore en présence d'oxygène. L'hydrogène lié à l'atome de carbone est substitué par le phosphore. Dans le cas du polychlorure de vinyle la présence du chlore sur la chaîne fait plus difficile la fixation du phosphore. Les produits phosphorylés sont colorés, fait attribué à la formation des doubles liaisons conjuguées, sur la chaîne.

Le polyéthylène [1] entre facilement en réaction avec le trichlorure de phosphore et l'oxygène, avec formation des groupes dichlorophosphoniques fixés sur la chaîne. En traitant les produits de réaction avec de l'eau, des alcools ou des amines, on obtient des acides phosphoniques, des esters ou leurs amides.

La phosphorylation du polypropylène [2] avec du trichlorure de phosphore et de l'oxygène, ainsi que des copolymères d'éthylène-propylène [3], a lieu à l'atome de carbone tertiaire.

Le polyvinylacétate [4,5] a été phosphorylé de la même manière. Dans le cas du polyvinylacétate sont possibles les voies suivantes : formation des liaisons P–C à l'atome de carbone tertiaire, à l'atome de carbone secondaire ou à l'atome de carbone primaire de l'acétate.

Laszkievicz,[5] en hydrolysant avec l'hydroxyde de sodium le polyacétate de vinyle phosphorylé, arrive à la conclusion que le phosphore peut se fixer tout aussi bien à l'atome de carbone secondaire qu'à l'atome de carbone tertiaire de la chaîne.

Par la chlorophosphonation de la chaîne de polystyrène déjà phosphorylé au noyau,[6] la quantité de phosphore fixé peut être accrue appréciablement. La chlorophosphonation du polyisobutylène, du polyméthacrylate et du polystyrène conduit à la dégradation avancée de la chaîne.

---

[1] J. P. Schroeder et W. P. Sopchak, *J. Polymer Sci.*, **47**, 417 (1960).

[2] D. Bellus, Z. Manasek et M. Lazăr, *Vysokomol. Soedineniya*, **5**, 145 (1963).

[3] E. C. Leonard Jr., W.E. Loeb, J. H. Mason et J. A. Stenstrom, ,,Memorandum Report'' Res. Dept. Union Carbide, New Jersey, 1961, p. 1–40.

[4] S. R. Raficov, G. N. Chelnokova et Yu. V. Artemova, *Vysokomol. Soedineniya*, **7**, 1612 (1965).

[5] B. Laszkiewicz, *Polimery*, **15**, 447 (1970).

[6] Fl. Popescu, *Rev. Roumaine Chim.*, **16**, 894 (1971).

Les groupes phosphoniques fixés par cette voie confèrent aux polymères indiqués plus haut des propriétés d'échange ionique, thermorésistance ou même non-inflammabilité. Une quantité de 0,9 –1,0% phosphore seulement modifie favorablement les propriétés mécaniques, en principal l'élasticité.[3]

Le contenu en phosphore peut dépasser 7% dans le cas du polypropylène,[2] 12% dans le cas du polyvinylacétate[4,5] et arriver à 16% dans le cas du polyéthylène.

MODE DE TRAVAIL

On a utilisé un polychlorure de vinyle Kw 79,5 et un alcool polyvinylique Kw 50 ayant 2% groupes acétate.

Le polychlorure de vinyle purifié a été séché sous vide et gardé sur chlorure de calcium. L'oxygène utilisé a été séché avec de l'hydroxyde de potassium.

On utilise pour la synthèse un ballon rond prévu d'un réfrigérant ascendant et d'un tube barboteur. Les gaz éliminés sont captés à la partie supérieure du réfrigérant et éliminés. On introduit successivement dans le ballon 1,5 g de polychlorure de vinyle, 30 ml de trichlorure de phosphore et ensuite on fait passer par le tube un courant d'oxygène avec une vitesse constante (1–5 litres/heure).

La durée de la synthèse a varié d'une heure jusqu'à douze heures. Pendant la synthèse, la température du ballon croît spontanément, se maintient un temps à 48–55° en fonction du débit d'oxygène et ensuite décroît lentement.

Le polychlorure de vinyle, initialement insoluble dans le trichlorure de phosphore, se dissout lentement pendant la synthèse et on obtient une solution visqueuse qui fait plus difficile le barbotage de l'oxygène.

Après l'intervalle de temps établi pour la synthèse on filtre pour séparer le produit solubilisé du produit resté insoluble. On lave le produit avec du trichlorure de phosphore. Les produits insolubles et les produits dissous dans le trichlorure de phosphore sont traités séparément avec de l'eau et de la glace. Les produits dissous précipitent. On lave avec de l'eau jusqu'à neutralité.

La phosphorylation de l'alcool polyvinylique a été réalisée de la même manière. L'alcool polyvinylique ne se dissout pas dans le trichlorure de phosphore pendant la synthèse.

Dans les deux cas on a effectué aussi une série de synthèses, en chauffant les ballons sur un bain d'huile pour maintenir une température constante.

RÉSULTATS ET DISCUSSIONS

Dans la figure 1 sont données les variations de la température dues à l'échauffement spontané du milieu de réaction, en fonction de la durée de synthèse.

On constate dans le cas du polychlorure de vinyle l'abaissement rapide de la température, causé par la croissance de la viscosité de la solution, qui empêche la ventilation uniforme par l'oxygène.

Les données du tableau 1 montrent que les valeurs moyennes du contenu en phosphore sont de 2 à 3%. On peut dépasser 5%P dans le cas des synthèses dans lesquelles on maintient la température à 55°.

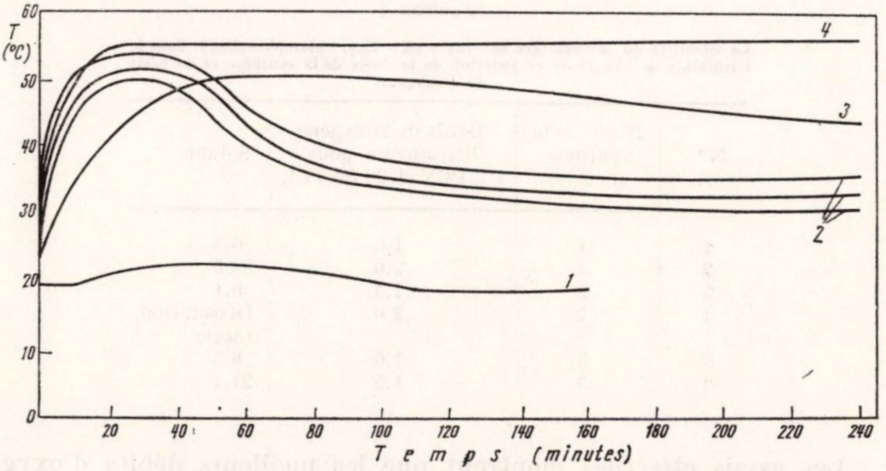

Fig. 1. — Variation de la température du milieu de réaction (Débit de l'oxygène = =2 litres/ heure pour un gramme de polychlorure de vinyle).

A. Variations spontanées :

1, Témoin, polychlorure de vinyle dissous dans le diméthylformamide. *2*, Polychlorure de vinyle suspendu dans le trichlorure de phosphore. *3*, Alcool polyvinylique suspendu dans le trichlorure de phosphore.

B. Synthèses à une température constante :

(polychlorure de vinyle ou alcool polyvinylique) (*4*).

Tableau 1

Le contenu en phosphore du polychlorure de vinyle chlorophosphoné en fonction de la durée de synthèse

N°	Durée de synthèse (heures)	Débit d'oxygène (+)	Température maximale	P % Soluble	P % Insoluble	Chauffage (*)
1	1	1,5	45°,0°	1,48	0,46	—
2	2	1,3	41,2°	1,54	0,816	—
3	2	2,0	51,0°	3,00	—	—
4	3	1,5	43,2°	1,60	0,96	—
5	3	1,8	48,2°	1,65	0,98	—
6	3	2,0	52,8°	3,20	—	—
7	4	2,0	50,1°	3,50	—	—
8	6	2,0	50,5°	3,80	—	—
9	6	2,0	55,0°	5,28	—	*
10	12	1,8	48,2°	4,10	—	—
11	3	(++)	23,0°	—	1,12	—
12	3	—	76,0°	—	1,10	*

+ Debit d'oxygène : litres/heure pour 1 g de substance et 20 ml de PCl_3
++ Air sec : 2 litres/h.

Le débit d'oxygène influence la vitesse de dissolution du polychlorure de vinyle dans le trichlorure de phosphore et modifie la température de réaction (tableaux 1 et 2).

Tableau 2

La solubilité du polychlorure de vinyle (Kw 79,5) chlorophosphoné, dans le trichlorure de phosphore en fonction de la durée de la synthèse et du débit de l'oxygène

N°	Durée de la synthèse (heures)	Débit de l'oxygène litres/heure pour 1 g PCV et 20 ml PCl_3	Soluble %
1	1	1,5	6,5
2	1	2,0	26,5
3	2	1,3	6,1
4	2	2,0	Dissolution totale
5	3	1,0	6,5
6	3	1,5	21,1

Les essais effectués montrent que les meilleurs débits d'oxygène sont situés entre 1 à 2,5 litres pour 1 g de polychlorure de vinyle ou de polyvinylalcool, suspendus dans 20 ml de trichlorure de phosphore.

L'accroissement du rapport 1 g polychlorure de vinyle/20 ml trichlorure de phosphore, par l'abaissement de la quantité de trichlorure de phosphore, a comme résultat la formation des solutions fortement visqueuses qui empêchent le barbotage par l'oxygène.

Au commencement de la phosphorylation le milieu de la réaction est incolore. Après la dissolution du polychlorure de vinyle, la solution se colore progressivement en jaune et ensuite en vert. Après l'hydrolyse avec formation des liaisons P—OH le polychlorure de vinyle phosphorylé ne se dissout plus dans le trichlorure de phosphore. Le polychlorure de vinyle phosphorylé contenant des liaisons P—OH se dissout dans le diméthylformamide et le tétrahydrofuranne. Il se gélifie dans : acétone, éther éthylique, éther de pétrole, benzène et chloroforme.

Dans le cas dans lequel pendant la synthèse, la température est maintenue constante au moyen d'une source de chauffage extérieure (à 55° dans les cas illustrés — fig. 1, courbe *4*), le contenu en phosphore croît (tableau 1).

Le témoin — polychlorure de vinyle dissous dans le diméthylformamide — n'a pas présenté des variations significatives de température pendant le barbotage par l'oxygène. La solution ne se colore pas pendant la synthèse et après la précipitation par l'eau on obtient une poudre blanche de polychlorure de vinyle. Son spectre IR ne diffère pas du spectre IR initial.

L'analyse du chlore effectuée avant et après la phosphorylation (tableau 3) indique que l'abaissement de la valeur du chlore en pour cent des produits phosphorylés dépasse la valeur calculée en partant de la quantité des groupes $-P(O)(OH)_2$ fixés sur la chaîne.

On constate donc une déshydrochloration qui est aussi responsable de la légère coloration du produit final (brun jusqu'à gris). Les épreuves témoins effectuées dans le tétrahydrofurane ont mis aussi en évidence une perte réduite en chlore sans la coloration du produit, même en l'absence de la réaction de chlorophosphonation. La perte ne produit pas des modifications [7] en UV pour le cas des épreuves témoins.

Tableau 3

Le contenu en chlore du polychlorure de vinyle. Débit d'oxygène = 2 litres/heure pour 1 g de PCV et 20 ml de PC^{l}

N°	Nature du produit	Chlore initial (a)	Chlore final (b)	Perte apparente en chlore (a−b)	P %	Chlore calculé (c)	Différence en chlore comparativement à valeur calculée (c−b)
1	témoin	54,4	—	—	—	56,8	2,4
2	phosphorylé 6 heures à 55°	54,4	40,5	13,9	5,28	46,9	6,4
3	phosphorylé 6 heures (variation spontanée de la température)	54,4	42,0	12,4	3,80	49,0	7,0
4	chauffé 6 heures à 55° en diméthylformamide	52,31	50,8	—	—	52,31	1,51
5	— le même — sans chauffage	52,31	50,0	—	—	52,31	2,31
6	chauffé à 76° pendant 6 heures en l'absence de l'oxygène	54,4	48,75	5,65	1,65	52,05	3,3

Les spectres UV des épreuves de polychlorure de vinyle chlorophosphoné, dissous dans le tétrahydrofuranne, ont mis en évidence l'apparition d'une zone d'absorption intense dans l'intervalle 230 à 400 mμ avec un maximum à 275 mμ, tandis que le spectre témoin — polychlorure de vinyle non traité — dans les mêmes conditions d'enregistrement (concentration en tétrahydrofurane, = M/200, Spectrophotomètre UNICAM SP 800) a présenté une ligne parallèle avec l'abscisse dans le domaine indiqué plus haut.

Si on remplace l'oxygène par l'air, la teneur en phosphore reste petite (tableau 1) et les produits obtenus sont insolubles dans le trichlorure de phosphore.

Dans le cas dans lequel on porte à l'ébullition une suspension de polychlorure de vinyle dans le trichlorure de phosphore (point d'ébullition 76°) en l'absence de l'oxygène, on constate la présence d'une petite quantité de phosphore fixé sur la chaîne (tableau 1). On constate aussi une perte en chlore, comparativement à la valeur calculée (tableau 4), causée par la déshydrochloration. Vu que l'ébullition à 76° à lieu en l'absence de l'oxygène on peut tirer la conclusion que dans ce cas a lieu une addition de trichlorure de phosphore à la double liaison.[8,9]

---

[7] J. E. Campbell et W. H. Rauscher, *J. Polymer Sci.*, **18**, 461 (1955).

Pendant l'ébullition ont lieu de dégradations : de petites quantités de polychlorure de vinyle se dissolvent dans le milieu de réaction en le colorant.

Le contenu en phosphore des fractions solubilisées est petit variant entre 0,4 à 0,9%.

Si on traite le produit contenant des groupes $0 \leftarrow PCl_2$ avec de l'alcool éthylique anhydre mélangé avec de la pyridine [10] on obtient l'ester blanc du polychlorure de vinyle phosphorylé.

Le produit estérifié se dissout partiellement dans des solvants organiques, fait qui indique une estérification non uniforme (tableau 4).

Tableau 4

La solubilité du polychlorure de vinyle chlorophosphoné et estérifié avec de l'alcool éthylique, ayant un contenu en phosphore de 1,76%

N°	Le solvant	Solubilité %
1	Benzène	3
2	Dioxanne	0,8
3	Ether éthylique	6
4	Dichloréthane	5
5	Trichlorure de phosphore	1,3

Les spectres IR présentent à 1050 cm^{-1} l'absorption caractéristique pour la liaison $P-O-C_2H_5$.

Dans le cas de l'alcool polyvinylique phosphorylé, la croissance de la teneur en phosphore en fonction du temps est sensible et arrive (dans le cas des synthèses dans lesquelles on chauffe le ballon) à 10%P pour un intervalle de synthèse de 6 heures (tableau 5). Les produits sont colorés en brun ou violet.

Tableau 5

Le contenu en phosphore de l'alcool polyvinylique chlorophosphoné

N°	Durée de la synthèse (heures)	Débit d'oxygène litres/h pour 1 g de substance et 20 ml de PCl_3	Conditions de synthèse P	%
1	3	2	sans chauffage	3,0
2	5	2	sans chauffage	5,5
3	6	2	sans chauffage	6,2
4	6	2	chauffage à 55°	10,0
5	6	2,5	chauffage à 65°	10,5

---

[8] Yu. M. Zinoviev, T. G. Spiridonova et L. Z. Soborovskii, *Zhur. obshchei Khim.*, **29**, 3594 (1959).

[9] L. Z. Soborovskii, Yu. M. Zinoviev et L. I. Muler, *Zhur. obshchei Khim.*, **29**, 3947 (1959).

[10] Fl. Popescu, «39 Congrès international de Chimie Industrielle» 7—11 sept. 1970, vol. 4, p. 12/144.

L'alcool polyvinylique chlorophosphoné est insoluble, aussi bien sous la forme P—Cl que sous la forme P—OH. Il se gonfle fortement dans les solutions alcalines.

L'insolubilité de l'alcool polyvinylique a été constatée par Daul et Reid [11] après phosphorylation par estérification avec de l'acide orthophosphorique et attribuée à un pontage des chaînes par le phosphore. On peut supposer, que dans le cas présent à lieu aussi une réticulation partielle par le phosphore.

Keith [12] a obtenu des esters phosphoriques de l'alcool polyvinylique en refluxant avec du PCl_3, $PhCl_2$ et Ph_2PCl.

Dans le présent travail on a chauffé l'alcool polyvinylique chlorophosphoné, avec de l'hydroxyde de sodium 4M à 80° pendant 6 heures et on a constaté un abaissement de son contenu en phosphore de 10,1% à 8,1% dans le cas étudié. On arrive à la conclusion que pendant la chlorophosphonation a lieu aussi une fixation de phosphore par liaisons estériques. La présence dans le spectre IR des absorptions caractéristiques des liaisons P—O—C n'a pas été mise en évidence dans le cas de l'alcool polyvinylique.

Les spectres IR ont permis les observations suivantes : Les absorptions du spectre du polychlorure de vinyle témoin [13,14] baissent en intensité après la fixation du phosphore à la chaîne. La présence des groupes —OH de l'acide phosphonique est visible en IR à 3500 cm^{-1}. Dans le domaine 900 à 1400 cm^{-1} le spectre du polychlorure de vinyle est partiellement couvert par les bandes d'absorption attribuées aux groupes P—O—H (909—1040 cm^{-1}) et $(C)-P \rightarrow O$ (1350 cm^{-1}).

Si le contenu en phosphore s'approche de 5%, les absorptions caractéristiques du polychlorure de vinyle, du domaine 900 à 1200 cm^{-1}, ne sont plus visibles (fig. 2).

La différence en chlore calculée en partant de la valeur théorique et la mince coloration des produits phosphorylés mènent à la conclusion de l'existence d'une déshydrochloruration avec formation des doubles liaisons conjuguées. Dans le spectre n'est pas visible la liaison $C = C$ conjuguée (1585 cm^{-1}), ni même le C—H du $-CH = CH-$ conjuguée (1005 cm^{-1}), à cause de la superposition des bandes d'absorption.

Dans le cas de l'alcool polyvinylique phosphorylé, les bandes d'absorption en IR caractéristiques pour l'acide phosphonique couvrent partiellement — ou même totalement si le contenu en phosphore s'approche de 10% — le spectre de l'alcool polyvinylique témoin, dans le domaine 900 à 1400 cm^{-1} (fig. 3 courbe 1). Le spectre tout entier subit des modifications profondes causées par la diminution des absorptions caractéristiques de l'alcool polyvinylique, à l'exception d'une absorption intense à 3000 à 3650 cm^{-1} (νOH) qui se maintient (fig. 3, courbes *2* et *3*).

---

[11] G. C. Daul, J. D. Reid et R. M. Reinhardt, *Ind. Eng. Chem.*, **46**, 1042 (1954).

[12] K. G. Allum et R. D. Hancock, Ger. Pat., 2 003 293, 10 déc. 1970 ; *Chem. Abstr.*, **74**, 54627 (1971).

[13] S. Krimm et C. Y. Liang, *J. Polymer Sci.*, **22**, 95 (1956).

[14] S. Narita, S. Ichinohe et S. Enunato, *J. Polymer Sci.*, **37**, 273 (1959).

L'étude comparative du comportement thermique du polychlorure de vinyle modifié par la chlorophosphonation et du polychlorure de vinyle non modifié a montré les choses suivantes :

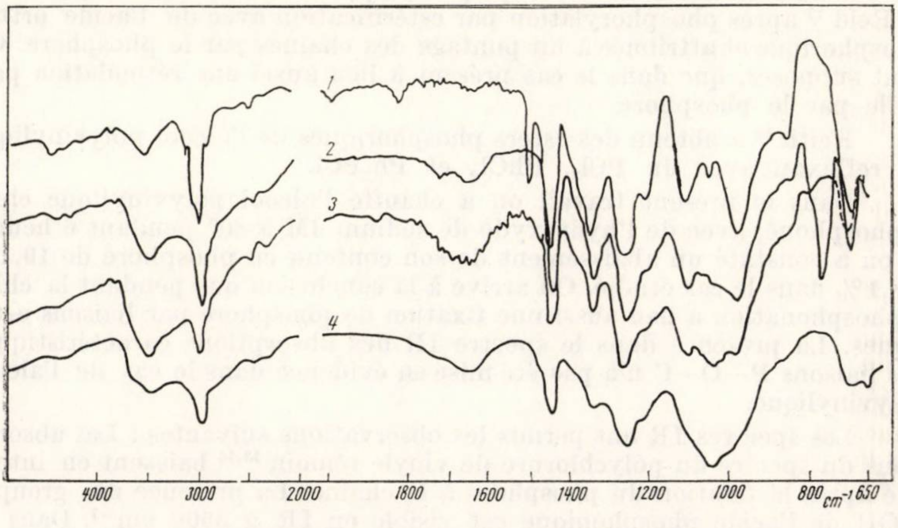

Fig. 2. — Spectres IR du polychlorure de vinyle chlorophosphoné :

1, polychlorure de vinyle témoin; *2*, avec 1,48%P; *3*, avec 3,20%P; *4*, avec 5,28%P.

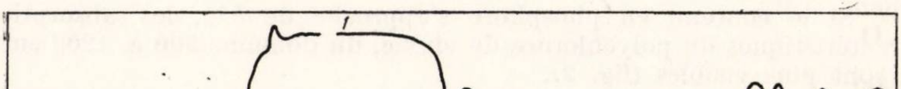

Fig. 3. — Les spectres IR de l'alcool polyvinylique chlorophosphoné :

1, alcool polivynylique témoin; *2*, avec 4,20%P; *3*, avec 10,00%P.

La déshydrochloruration thermique du polychlorure de vinyle a lieu avec une vitesse appréciable à $\simeq 200°$. On peut distinguer trois domaines sur la courbe représentant la perte en poids en fonction de la température (fig. 4). Le premier domaine correspond à un premier maximum de dégradation, pendant lequel a lieu la déshydrochloration. Dans le domaine entre 300 à 350° la perte en poids est très petite à cause du dégagement de l'acide chlorhydrique qui ralentit progressivement. Enfin au-dessus de 350° la perte en poids est importante. Au-dessus de 350° on ne constate pas l'élimination d'acide, mais la libération de l'hydrogène, du méthane et d'autres hydrocarbures[15].

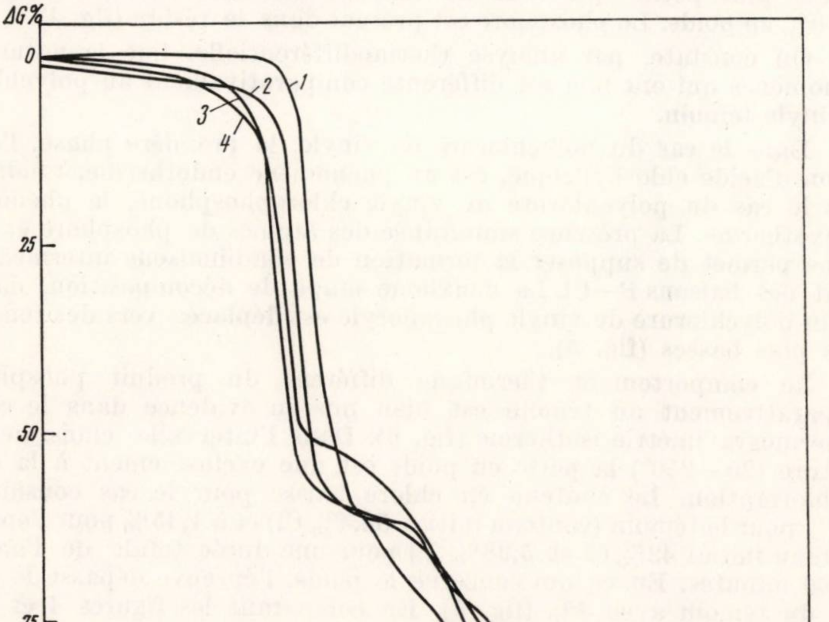

Fig. 4. — La perte en poids du polychlorure de vinyle chlorophosphoné en fonction de la température :
1, polychlorure de vinyle non modifié; *2*, avec 0,96%P; *3*, avec 3,80%P; *4*, avec 5,28%P.

De l'analyse des courbes concernant la perte en poids en fonction de la température, on constate que la thermostabilité définie comme la température la plus petite à laquelle la dégradation se manifeste est plus basse dans le cas du polychlorure de vinyle chlorophosphoné, les différences de température allant jusqu'à 50°. Avec la croissance de la température la perte en poids du polychlorure de vinyle chlorophosphoné devient plus petite que celle du témoin. Les différences, représentent 8 –10% en poids. Le phosphore est présent dans le résidu (fig. 4).

---

[15] V. J. Kasatotkine, A. A. Berlin, R. M. Aseeva, Z. S. Smutkina, Y. G. Arseev et G. B. Finkelstein, *Izvest. Akad. Nauk S S S R., Otdel. khim. Nauk*, **6**, 1003 (1965).

On constate, par analyse thermodifférentielle, que la nature des phénomènes qui ont lieu est différente comparativement au polychlorure de vinyle témoin.

Dans le cas du polychlorure de vinyle, la première phase, l'élimination d'acide chlorhydrique, est un phénomène endotherme, tandis que dans le cas du polychlorure de vinyle chlorophosphoné, le phénomène est exotherme. La présence simultanée des atomes de phosphore et d'halogène permet de supposer la formation de combinaisons intermédiaires ayant des liaisons P—Cl. La deuxième étape de décomposition, dans le cas du polychlorure de vinyle phosphorylé est déplacée vers des températures plus basses (fig. 5).

Le comportement thermique différent du produit phosphorylé comparativement au témoin est bien mis en évidence dans le cas de la thermogravimétrie isotherme (fig. 6). Dans l'intervalle choisi de température (20 –250°) la perte en poids est due exclusivement à la déhydrochloruration. Le contenu en chlore baisse pour le cas considéré à 2,59% pour le témoin (contenu initial 54,4% Cl) et à 1,45% pour l'épreuve (contenu initial 42% Cl et 5,28% P) pour une durée totale de l'analyse de 160 minutes. En ce qui concerne le poids, l'épreuve dépasse le poids final du témoin avec 4% (fig. 6). En comparant les figures 4 et 6 on constate que la chlorophosphonation n'améliore pas le comportement thermique du polychlorure de vinyle.

L'alcool polyvinylique chlorophosphoné soumis à l'analyse thermique montre un abaissement de la stabilité thermique de $\simeq 50°$. Avec la prolongation de la durée de l'analyse et à des températures plus hautes, la perte en poids est comparativement plus petite. Dans le cas présenté dans la figure 7 l'épreuve perd 70% de son poids à 700°, tandis que le témoin perd 98% de son poids à la même température.

L'étude des viscosités dans le tétrahydrofuranne des solutions de polychlorure de vinyle chlorophosphoné (fig. 8) a montré que dans des solutions auxquelles on n'a pas ajouté d'acides ou de bases, les valeurs obtenues pour l'épreuve diffèrent bien peu des valeurs obtenues pour le témoin. La différence peut être attribuée aux groupements contenant du phosphore attachés à la chaîne.

Les différences non significatives constatées entre les viscosités du polychlorure de vinyle initial et phosphorylé (fig. 8) montrent que pendant la chlorophosphonation oxydative n'ont pas lieu des dégradations de la chaîne.

Dans le cas des solutions acides, on constate une croissance marquée de la viscosité du produit phosphorylé comparativement au témoin. Dans le cas des solutions alcalines le rapport η_{sp}/c présente de grandes variations. Il croît fortement avec la croissance de la concentration.

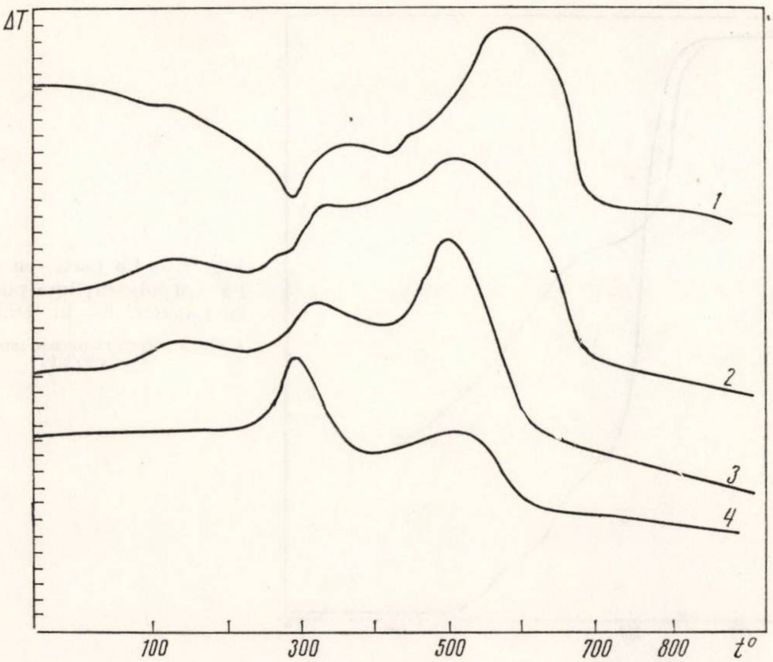

Fig. 5. — Analyse thermodifférentielle du polychlorure de vinyle chlorophosphoné : 1, polychlorure de vinyle non modifié, 2, avec 0,96%P; 3, avec 3,80%P; 4, avec 5,28%P.

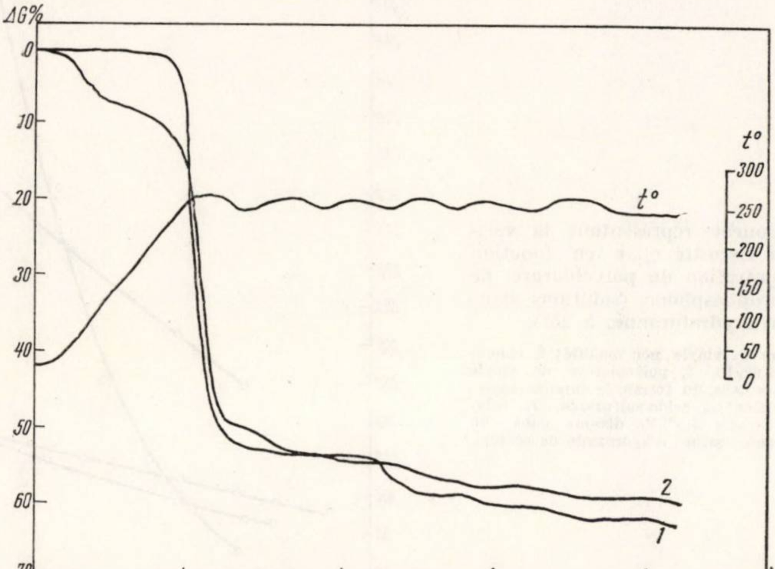

Fig. 6. — La perte en poids du polychlorure de vinyle chlorophosphoné, dans l'intervalle 20 à 250° ; 1, polychlorure de vinyle non modifié; 2, avec 4,20%P.

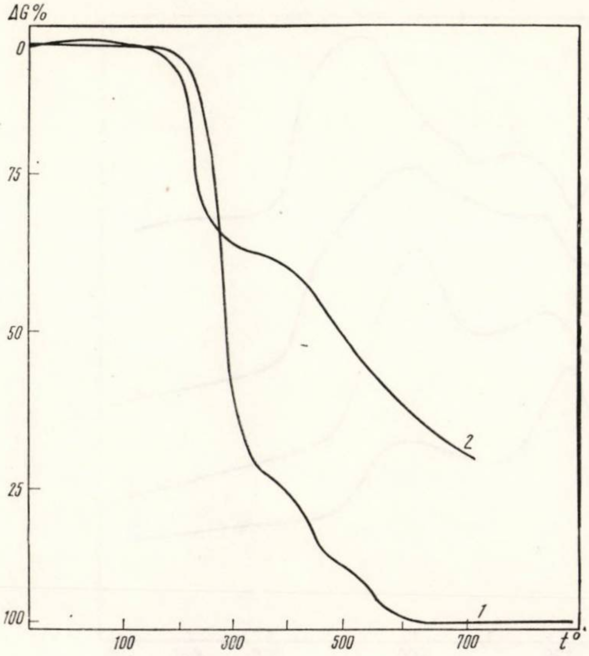

Fig. 7. — La perte en poids de l'alcool polyvinylique phosphorylé, en fonction de la température :

1, alcool polyvinylique non modifié ; *2*, avec 4,20%P.

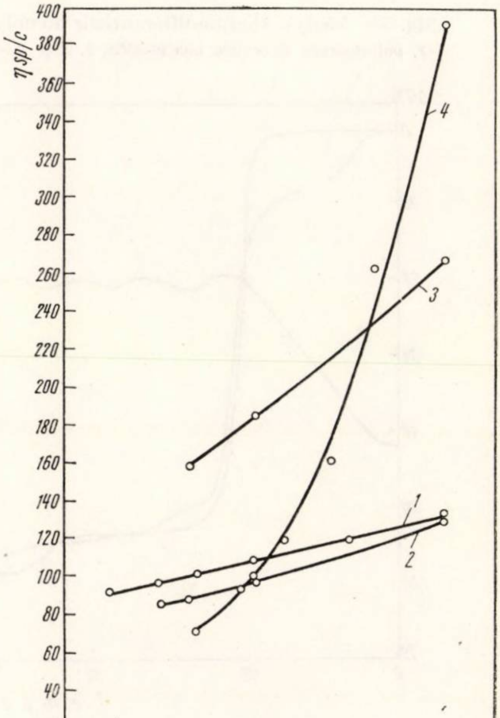

Fig. 8. — Courbes représentant la variation de la viscosité η_{sp}/c en fonction de la concentration du polychlorure de vinyle chlorophosphoné (solutions dans le tétrahydrofuranne, à 25°),

1, polychlorure de vinyle non modifié ; *2*, chlorophosphoné (5,3%P), *3*, polychlorure de vinyle (5,3%P) dissous dans du tétrahydrofuranne contenant 26 m. moles ‰ acide sulfurique, *4*, polychlorure de vinyle (5,3%P) dissous dans du tétrahydrofuranne saturé d'hydroxyde de sodium.

La capacité d'échange statique déterminée dans une solution aqueuse de chlorure de sodium avec une solution d'hydroxyde de sodium n/50 en excès est 98% de la valeur théorique pour le polychlorure de vinyle chlorophosphoné et l'alcool polyvinylique chlorophosphoné.

CONCLUSIONS

Par la chlorophosphonation oxydative du polychlorure de vinyle et de l'alcool polyvinylique on peut obtenir les structures suivantes :

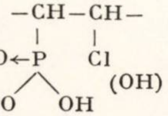

I

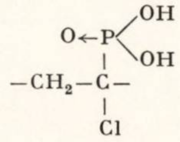

II

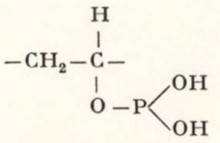

III

La structure III est possible pour l'alcool polyvinylique seulement.

En comparant les deux polymères phosphorylés on constate que la chlorophosphonation du polychlorure de vinyle est plus limitée, à cause de l'atome de chlore qui fait la substitution plus difficile. La chlorophosphonation est accompagnée d'une déhydrochlororation de petites proportions, qui représente un facteur d'instabilité sur la chaîne.

La croissance de l'instabilité thermique dans les deux cas étudiés, phénomène contraire au comportement des polymères phosphorylés[16] plaide pour l'existence de la structure II, vu que la présence du carbone tertiaire à côté des doubles liaisons formées sur la chaîne est une cause[17] de l'abaissement de la température de décomposition.

L'étude comparative des viscosités du polychlorure de vinyle chlorophosphoné et du témoin a mis en évidence des modifications évidentes du rapport η_{sp}/c dans des solutions acides et alcalines.

---

[16] A. F. Childs et H. Coates, *Kunststoffe*, **59**, 501 (1964).

[17] M. Bert, « Étude de la stabilité thermique de polychlorures de vinyle semi-cristallins » — Thèse — Ed AGEL Lyon, 1968, p. 4—44.

Revue Roumaine de Chimie, 18, 8, 1427—1439 (1973)

Revue Roumaine de Chimie, **18**, *8*, 1441–1450 (1973)

BEHAVIOUR OF Cr(III)-POLY(AMINOCARBOXYLATE) LIGANDS SOLUTIONS AT THE DROPPING-MERCURY ELECTRODE (DME)*

ERNESTO CHIACCHIERINI and RENATA COCCHIERI

Institute of Analytical Chemistry, University of Rome, Italy

Received September 11, 1972

The polarographic behaviour of Cr(III) and some complexones (EDTA, CyDTA, DTPA, HEDTA and EGTA) has been investigated as function of the temperature of reaction, the nature of supporting electrolyte and ligand. A possible general mechanism of reaction of Cr(III) with poly(aminocarboxylate) ligands is suggested.

Chelate formation between Cr(III) and various poly(aminocarboxylate) ligands (complexones) has been subject of numerous investigations, but polarographic data are reported only for CyDTA,[1] EDTA[2-5] and EGTA.[6]

The present work was undertaken for a systematic polarographic and oscillopolarographic investigation of the Cr(III)-complexones solutions as function of the experimental work conditions (reaction temperature, presence of various electrolytes, molar excess of metal or ligand, nature of the ligand and acidity of the solutions) to explain the mechanism of reaction.

The considered ligands are : EDTA (ethylenediaminetetracetic acid), CyDTA (cyclohexanediaminetetracetic acid), HEDTA (N-Hydroxyethylenediaminetriacetic acid), DTPA (diethylenetriaminepentacetic acid) and EGTA (ethylenglycolbis (β-aminoethyl)-tetracetic acid).

---

* The work was carried out with the aid of the Italian National Research Council (CNR) and was presented at the IInd National Conference of Pure and Applied Physical Chemistry, Bucharest, 1–4 September, 1970.

[1] R. Pribil, Z. Zoubal and E. Svatex, *Coll. Czech. Comm.*, **18**, 43 (1953).
[2] J. H. Walsh and J. E. Earley, *Inorg. Chem.*, **3**, 343 (1964).
[3] N. Tanaka and H. Ogino, *J. Electroanalyt. Chem.*, **7**, 332 (1964).
[4] N. Tanaka and K. Ebata, *J. Electroanalyt. Chem.*, **8**. 120 (1964).
[5] E. Chiacchierini, *Ann. Chim. (Ital.)*, **56**, 1405 (1966).
[6] E. Chiacchierini, *Ricerca Sci.*, **36**, 1016 (1966).

EXPERIMENTAL

MATERIALS

All chemicals used were analytically pure.

Cr(III) stock solutions : aqueous chromium nitrate and chloride solutions were prepared by respective salts (Merck) ; the hydrolysis of Cr(III) was avoided keeping the acidity of solutions not less than 10^{-3} M. Chromium perchlorate solutions were obtained by reduction of CrO_3 with H_2O_2 in perchloric acid medium. The standardization of Cr(III) was made by iodometric titration after oxidation of Cr(III) to Cr(VI).

Complexones stock solutions : as reported previously.[5]

Supporting electrolytes : 0.11 M aqueous solutions of $KClO_4$, KNO_3 and KCl.

APPARATUS AND PROCEDURE

Apparatus as reported previously.[7]

The polarographic and oscillopolarographic measurements were performed on two general types of solutions :

Type A : solutions obtained by mixing components at 25±0.2° and quickly examined at 25.0±0.2° ; in our experimental conditions and for all examined ligands the resulting solutions were little pale-violet or pale-green coloured ;

Type B : solutions obtained by mixing and boiling components, cooled at 25.0±0.2° and examined at 25.0±0.2° ; in our experimental conditions and for all examined ligands the resulting solutions were deep red-violet coloured.

Acidity control. Acidity was adjusted by dilute acid (chloride, perchloric or nitric) and dilute potassium hydroxide ; no buffers were used in order to avoid competitive reactions or catalytic effects and only the acid medium was investigated ; the acidity is expressed by $-\log [H^+]$. All solutions were 0.1 M in supporting electrolyte if not otherwise mentioned. The solutions to be tested were deaerated by N_2, deoxygenated on vanadous chloride solutions and opportunely humidified. All measurements were carried out at 25.0±0.2°.

RESULTS

TEMPERATURE OF THE REACTION

The investigation as function of temperature was carried out by polarography of the two types of the mentioned solutions (see Experimental). The polarograms of the solutions of metal (M) and ligand (L) in the molar ratio 1 :1 show in both cases two waves or two peaks of reduction : the second wave or peak is sometimes complicated by reduction of hydrogen ions. The half-wave potentials of the reduction waves in the two above mentioned solutions agree each other and also with the values reported by Walsh and Earley [2] ; the results in 0.1 M $KClO_4$ as supporting electrolyte are reported in table 1. The peak-potentials values for the first and the second peak are reported in table 2. The limiting current and the maximum peak current do not differ for the two types of solutions.

---

[7] L. Campanella, E. Chiacchierini, M. Palchetti, *Rev. Roumaine, Chim.*, **17**, 647 (1972).

Table 1

E 1/2 (V *vs.* S.C.E.) of the first reduction wave for Cr (III)-complexones solutions; supporting electrolyte $KClO_4$ 0.1 M; $T = 25.0 \pm 0.2°$; $-\log [H^+] = 3.50$. The tabulated values are means of at least 4 values

Ligand	E 1/2 (V *vs.* S.C.E.)	
	Type *A* solutions	Type *B* solutions
EDTA	−1.24[a]	−1.22[a]; −1.22[c]
CyDTA	−1.24[a]	−1.23[a]; −1.20[d]
HEDTA	−1.20[a]	−1.20[a]
DTPA	−1.16[a]	−1.16[a]
EGTA	−0.94[b]	−1.02[b]; −1.15[a]

a mononuclear[5] species.
b binuclear[6] species.
c at pH = 3.0 cf. reference[2]
d at pH 4.6 buffer 0.4 M acetic acid, 0.4 M sodium acetate cf. reference[1]

Table 2

Ep(V *vs.* S.C.E.) for the Cr(III)-complexones solutions; supporting electrolyte $KClO_4$ 0.1 M; $T = 25.0 \pm 0.2°$; $-\log (H^+] = 3.50$; V/sec = 1.0. The tabulated values are means of at least 4 values

Ligand	Type *A* solutions		Type *B* solutions	
	Ep_1	Ep_2	Ep_1	Ep_2
EDTA	−1.33[a]; −1.25[c]	−1.65[a]	−1.30[a]	−1.64[a]
CyDTA	−1.32[a]	−1.63[a]	−1.28[a]	−1.62[a]
HEDTA	−1.30[a]	−1.75[a]	−1.29[a]	−1.73[a]
DTPA	−1.24[a]	−1.66[a]	−1.25[a]	−1.68[a]
EGTA	−1.12[a]; −1.07[b]	−1.63[a]	−1.08[a]	−1.57[a]

a mononuclear[5] species.
b binuclear[6] species.
c cf. reference[3].

SUPPORTING ELECTROLYTES

Potassium perchlorate, nitrate or chloride as supporting electrolytes were used. The half-wave potentials as well as the peak-potentials of Cr(III)-complexones solutions agree well for the used supporting electrolytes; in table 3 the half-wave potential values (*V vs.* S.C.E.) for the first reduction wave of type *A* solutions (L/M = 1/1) are reported. The limiting current, as well as the maximum peak current, has the same values when $KClO_4$ or KCl are used as supporting electrolytes but values higher than the previous ones are found when nitrate ions (from Cr(III) salt or from the supporting electrolyte) are present in the solution (fig. 1 and 2).

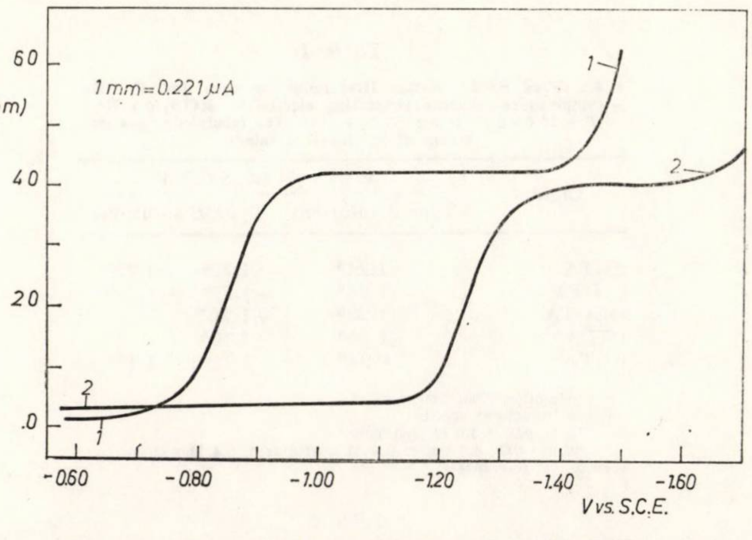

Fig. 1. — Polarograms of the Cr(III)-perchlorate and Cr(III)-EDTA solutions; type *A* solutions; supporting electrolyte $KClO_4$ at concentrations of 0.1 M; $T = 25.0 \pm 0.2°$; $C_M = 3.07.10^{-3}$ M; $-\log[H^+] = 3.50$.
Curves: *1*, metal; *2*, metal and ligand ($C_L/C_M = 10$).

NATURE OF THE LIGAND

The polarographic and oscillopolarographic behaviour of Cr(III)-complexones solutions at dropping mercury electrode is similar for all the examined ligands except for the EGTA; in fact the polarograms of metal and poly(aminocarboxylate) ligands show two reduction steps for all ligands with the exception of the Cr(III)-EGTA systems which can present a third wave or peak (fig. 3).

METAL EXCESS

In the case of the polarography of the solutions with metal excess ($L/M \leqslant 2/3$) for solutions of type *A*, it occurs a shift of the half-wave potential or peak potential of the metal towards more positive potential values for the first reduction step. This behaviour is the same for all examined complexones with the exception of the EGTA; in this case, as for solutions of type *B*, the shift is always towards more negative potential values (*V vs.* S.C.E.).

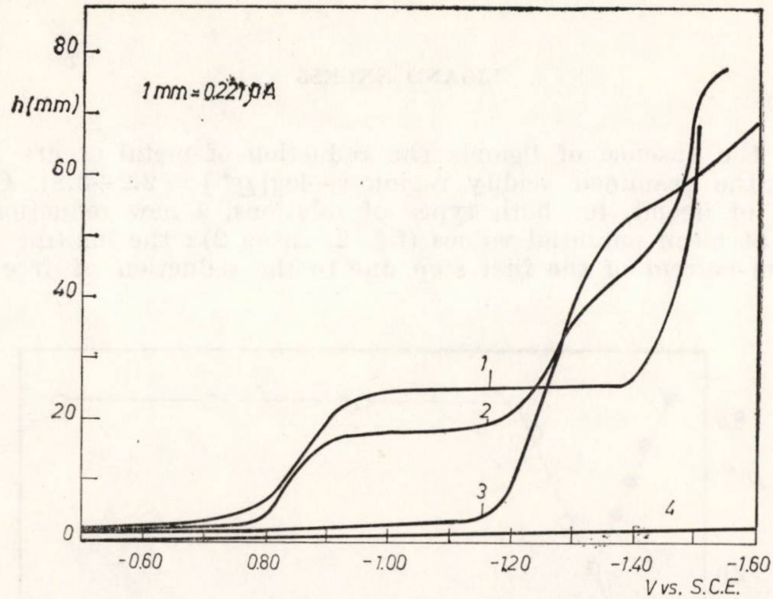

Fig. 2. — Polarograms of the Cr(III)-nitrate and Cr(III)-EDTA solutions; type *A* solutions; $T = 25.0 \pm 0.2°$; supporting electrolyte $KClO_4$ at concentration of 0.1 M; $C_M = 1.07 . 10^{-3}$ M; $- \log [H^+] = 3.50$.

Curves: *1*, metal; *2*, metal and ligand ($C_L/C_M = 0.25$); *3*, metal and ligand ($C_L/C_M = 10$); *4*, $KClO_4$ 0.1 M.

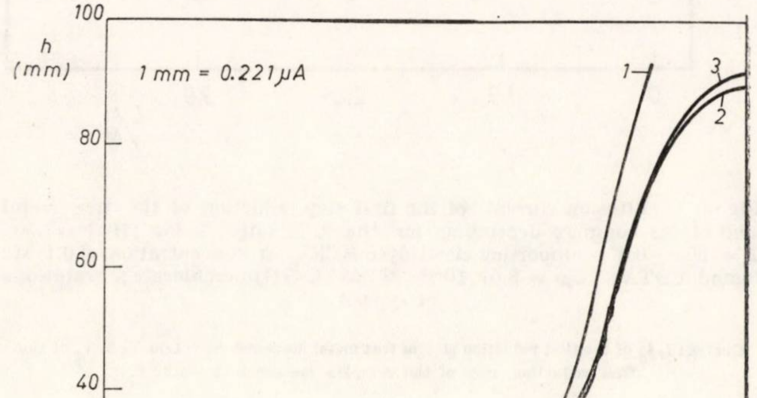

Fig.3. — Polarograms of the Cr(III)-nitrate and Cr(III)-EGTA solutions; type *A* solutions; $T = 25.0 \pm 0.2°$; supporting electrolyte $KClO_4$ at concentration of 0.1 M; $C_M = 2.00 . 10^{-3}$ M; $-\log [H^+] = 3.50$.

Curves: 1, metal; 2, metal and ligand ($C_L/C_M = 5$); 3, metal and ligand ($C_L/C_M = 10$).

LIGAND EXCESS

In the absence of ligands the reduction of metal occurs in two steps in the examined acidity region ($-\log[H^+] = 2.2 \div 3.8$). On the addition of ligand, for both types of solutions, a new reduction step appears at mean potential values (fig. 2, curve 2): the limiting or the maximum current of the first step due to the reduction of free metal ion decreases linearly with the ligand concentration and disappears for the ratio L :M = 1 :1, whereas the new step increases linearly up to the same L/M molar ratio (fig. 4). For type *B* solutions in the presence of nitrate ions as supporting electrolyte, the limiting or maximum current increases with the excess of ligand. The addition of ligand to type *B* solutions in the ratio M :L = 1 :1, previously prepared, causes a surfactant action in all cases examined. In the case of EGTA as ligand[6], for both types of solutions, with increasing ligand excess, the first reduction step of the complex breaks into two steps as high as the first (fig. 3,

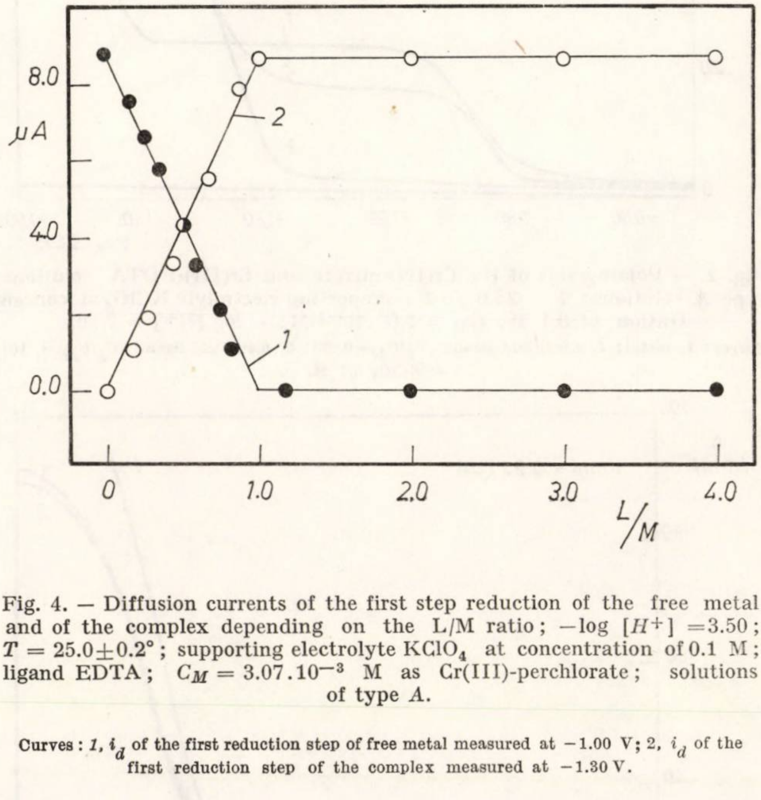

Fig. 4. — Diffusion currents of the first step reduction of the free metal and of the complex depending on the L/M ratio; $-\log[H^+] = 3.50$; $T = 25.0 \pm 0.2°$; supporting electrolyte $KClO_4$ at concentration of 0.1 M; ligand EDTA; $C_M = 3.07 \cdot 10^{-3}$ M as Cr(III)-perchlorate; solutions of type *A*.

Curves: *1*, i_d of the first reduction step of free metal measured at −1.00 V; 2, i_d of the first reduction step of the complex measured at −1.30 V.

curves *2* and *3*); when the molar ratio M :L is higher than 10 the step at more positive half-potential disappears.[6]

The half-wave potential or the peak-potential of the reduction step of the various complexes is constant increasing concentration for both types of tested solutions.

ACIDITY

For the solutions of the type *A* at $-\log[H^+]$ lower than 1.5 no differences were observed in respect of the polarogram of the Cr(III) alone at the same acidity; decreasing acidity in the case of the solutions with ratio as L :M = 1 :1 a shift of the $E_{1/2}$ or E_p towards more negative values occurs [2] for both types of solutions. In the case of the EGTA as ligand decreasing acidity the first reduction step of the complex changes in two steps as in the case of ligand excess.

DISCUSSION AND CONCLUSION

The reported results are very useful for the interpretation of the reaction of Cr(III) with poly(aminocarboxylate) ligands; as a matter of fact, the reduction of the complexes at DME occurs in the same way for both types of the tested solutions. The first reduction step of the Cr(III)-complexes with poly(aminocarboxylate) is assigned to the following equilibrium (the charge of the complexes and the bound water molecules are omitted):

$$\mathrm{Cr^{III}L} + \mathrm{e} \rightarrow \mathrm{Cr^{II}L}$$

in fact, plots of log $i/(i_d - i)$ *vs.* the applied potential were linear with an average slope near -60 mV with a provisional indication of polarographic reversibility (one electron change); the second wave of the complex was complicated by reduction of hydrogen ion [2]. The limiting current of the first wave, at each L :M molar ratio, is proportional to the square root of the height of the mercury column (diffusion controlled) and the $E_{1/2}$ and E_p for both types of solutions are very near (tables 1 and 2). It means that the complexing reaction of Cr(III) with poly(aminocarboxylate) ligands occurs firstly through a "chemical-inert" species (ion-pairs)[8,9] little pale-violet or pale green[10] coloured which changes slowly (quickly with the help of temperature or catalysts) into the final stable and deep red-violet coloured compound.[5,6,11,12] Therefore, the reaction formation of the "outer-sphere" complex according to the proposed general dissociative mechanism of Eigen[9] can be represented by the scheme:

$$Cr(H_2O)_6^{3+} + H_2L^{2-} \overset{k_1}{\rightleftharpoons} Cr(H_2O)_6^{3+} \ldots H_2L^{2-} \xrightarrow{k_2} Cr(H_2O)_5^{3+} \ldots H_2L^{2-} +$$

$$+ H_2O \longrightarrow Cr\,(H_2O)_5H_2L^{+} \qquad (C)$$

where

k_1 = the diffusion-controlled equilibrium constant for the formation of the "outer-sphere" complex:

$$Cr(H_2O)_6^{3+} \ldots H_2L^{2-}$$

k_2 = the rate constant for metal-water bond breaking. Therefore, the first loss of a coordinated water molecule from the metal ion in the "outer-sphere" complex represents the rate-determining step; the subsequent bonding steps are usually rapid and in the region of examined acidity [13] occurs with the formation of a quinquedentate chelate:

$$Cr(H_2O)_5H_2L^{+} \xrightarrow{k_{ML}} Cr(H_2O)L^{-} + 2H^{+} + 4H_2O \qquad (D)$$

where k'_{ML} = rate-constant for metal-ligand bond formation. In support of the outlined mechanism our experimental results can be mentioned: in fact, the formation of the "outer-sphere" complex according to equilibria reported in (C) comes without variation of acidity of the solution, which is weakly coloured in pale-violet or pale-green as a consequence of the metal-carboxylic oxygen donor atom bond[5,11,14] initially more probable than the metal-nitrogen donor atom bond greatly hindered; successively, the complexing reaction of the final compound occurs with the increase of the acidity of the solution in agreement with the proposed equilibrium reported in (D). The reaction rate of Cr(III) with poly (aminocarboxylate) ligands can be appreciably increased with the help of temperature or catalysts; the most important catalysts are Cr(II)

---

[8] D. Banerjea and P. Chaudhuri, *J. Inorg. Nuclear Chem.*, **30**, 3259 (1968).

[9] M. Eigen in "Advances in the Chemistry of the Coordination Compounds", S. Kirschner, Ed., The MacMillan Co., New York, N.Y., 1961, p. 373.

[10] I. Crişan and C. Liteanu, *Studia Univ. Babeş-Bolyai*, **10**, 113 (1965).

[11] R. E. Hamm, *J. Amer. Chem. Soc.*, **75**, 5670 (1953).

[12] N. M. Dyatlova, B. I. Bikhman and R. P. Lastovskiv, *Zhur. Neorg. Khim.*, **10**, 237 (1965); Chem. Abstr. **62**, 7355 (1965).

[13] C. Furlani, G. Morpurgo and G. Sartori, *Z. anorg. Chem.*, **303**, 1 (1960).

[14] L. Treindl and P. Hrdlovic, *Chem. Zvesti*, **16**, 593 (1962); *Chem. Abstr.*, **59**, 13600 (1963).

ions,[2,3,4,15,16] acetate ions,[10,17,18] bicarbonate ions,[19,20,21] and hydrogen ions.[11] In our experimental conditions an electron-transfer catalysis of Cr(II) for the formation of Cr(III)-complexes can be supported; in fact the amperometry is more useful than other physical techniques[5,12] in order to perform analytical determination of Cr(III) with poly(aminocarboxylate) ligands at room temperature. The proposed mechanism of reaction between Cr(III) and poly (aminocarboxylate) ligands is moreover confirmed by results in the presence of nitrate ions; in fact, the presence of nitrate ions (coming from Cr(III)-salt or from supporting electrolyte) causes an enhancement of *id* or *ip* of the reduction step of the Cr(III)-complexes for both types of solutions examined. According to Tanaka[22] mechanism, nitrate ions react chemically in the vicinity of the mercury drop of the electrode with the Cr(II)-L species which comes from the reduction at DME of Cr(III)-L. New formed Cr(III)-L is reduced again at DME (together with some intermediate products of nitrate ions) causing, consequently, an enhancement of the *id* or *ip*. The following equilibria take place at DME:

$$\mathrm{Cr^{III}} + \mathrm{L} \rightarrow \mathrm{Cr^{III}\,L} \tag{E}$$

$$\mathrm{Cr^{III}\,L} + \mathrm{e} \rightarrow \mathrm{Cr^{II}\,L} \tag{F}$$

$$\mathrm{Cr^{II}\,L} + \text{nitrate} \rightarrow \mathrm{Cr^{III}\,L} + \text{reduction product of nitrate} \tag{G}$$

with the result that the chemically produced $\mathrm{Cr^{III}\,L}$ is reduced again at DME according to equilibrium (F). Nevertheless, the nature of the ligand influences the rate of reaction of nitrate with the $\mathrm{Cr^{II}\,L}$ complex: at $25.0 \pm 0.2°$ the rate is high for DTPA, EDTA and HEDTA, but low for CyDTA and EGTA. In addition, for type *B* solutions the nitrate ions are able to react chemically upon the boiling of the solutions, equally with ligand excess; the intermediate nitrate products react at DME having as a result an enhancement of *id* or *ip* of the first reduction step of the Cr(III)-complexes; also, in this case, the rate of reaction is function of the ligand: in fact, the oxidative action of nitrate ions on the ligands is evident for the EDTA, DTPA and HEDTA but negligible for EGTA and CyDTA. The oxidation of complexones from other oxidative agents, such as Cr(VI), had already been pointed out by other authors.[23,24,25]

[15] R. Pribil and J. Klubalova, *Coll. Czech. Comm.*, **15**, 42 (1950).

[16] J. B. Hunt and J. E. Earley, *J. Amer. Chem. Soc.*, **82**, 5312 (1960).

[17] H.M.N.H. Irving and W.R. Tomlinson, *Chemist — Analyst*, **55**, 14 (1966); *Chem. Abstr.*, 13371 (1966).

[18] E. Fischerova, O. Draoka and M. Meloun, *Coll. Czech. Chem. Comm.*, **33**, 473 (1968).

[19] V. K. Rao, D. S. Sundar and M. N. Sastri, *Chemist — Analyst*, **54**, 86 (1965).

[20] T. R. Bhat and G. M. Phatak, *J. Inorg. Nuclear Chem.*, **28**, 3058 (1966).

[21] G. M. Phatak, T. R. Bhat and J. Shanhar, *J. Inorg. Nuclear Chem.*, **32**, 1305 (1970).

[22] N. Tanaka and T. Ito, *Bull. Chem. Soc. Japan*, **39**, 1043 (1966).

[23] D.B. Rorabacher, T. S. Turan, J. A. Defever and W. G. Nickels, *Inorg. Chem.*, **8**, 1498 (1969).

[24] P. N. Palei, N.I. Udal'tsova, *Zhur. analyt. Khim.*, **15**, 761 (1960).

[25] P. Fouchecourt and P. Berlin, *Compt. rend. C.*, **262**, 605 (1966).

Table 3

$E_{1/2}$ (*V vs.* S.C.E.) of the first reduction wave for the Cr(III)-complexones solutions in different supporting electrolytes; $T = 25.0 \pm 0.2°$; $-\log [H^+] = 3.50$; type *A* solutions. The tabulated values are means of at least 4 values

Ligand	$E_{1/2}$		
	$KClO_4$	KNO_3	KCl
EDTA	−1.22[a]	−1.20[a]	−1.20[a] ; −1.23[c]
CyDTA	−1.24[a]	−1.22[a]	−1.23[a]
HEDTA	−1.20[a]	−1.18[a]	−1.19[a]
DTPA	−1.16[a]	−1.18[a]	−1.16[a]
EGTA	−1.94[b]	−0.96[b]	−0.96[b]

a mononulclear[5] species;
b binuclear[6] species;
c cf. reference [27] (anodic half-potential for Cr(II)-EDTA).

The anomalous $E_{1/2}$ and E_p values for the first reduction step of free metal in the case of type *A* solutions with metal excess (L :M = 2 :3) can be ascribed to the changes in the viscosity and in the degree of polymerization of the Cr(III) solution adding ligands [2,26]. The reduction of the Cr(III)-EGTA solutions is particularly a consequence of the complexing of Cr(III) by EGTA which occurs with two complexes[6] in the molar ratios L : M = 1 : 2 and L : M = 1 : 1 while all other poly(aminocarboxylate) ligands give with Cr(III) complexes[5] in the molar ratio L : M = 1 : 1. The polynuclear complex of Cr(III)-EGTA is reduced at a more positive potential value in respect of the mononuclear complex (tables 1, 2 and 3).

[26] I. Filipovic, I. Piljac, A. Neodved, S. Savic, A. Bujak, B. Bach-Dragutinovic and B. Mayer, *Croatica Chim. Acta*, **40**, 131 (1968).

[27] R. L. Pecskok, L. D. Shields and W. P. Schaefer, *Inorg. Chem.*, **3**, 114 (1964).

Revue Roumaine de Chimie, **18**, *8*, 1451–1457 (1973)

CHARACTERIZATION OF CERAMIC ION-SELECTIVE MEMBRANE-ELECTRODES. V*

Ag_2S, S^{2-}-SELECTIVE MEMBRANE-ELECTRODE

I. C. POPESCU, C. LITEANU and L. SAVICI

"Babeş-Bolyai" University, Str. Arany János 11, Cluj, Romania

Received, December 13, 1972

A new type of S^{2-}-selective membrane-electrode is studied and used. The electrode presents a nernstian answer in the concentration range $pS \in [1-7]$ at $pH = 14$. The influence of the pH and temperature on the electrode function E-pS is estimated. At $pS \geqslant 6$ the response time is 10 minutes. The electrode was used in the automatic potentiometric titration of Na_2S with $AgNO_3$ up to 10^{-4} M. The results of the titration are compared statistically to those obtained with an Ag/Ag_2S electrode.

A series of studies were published on the use of ion selective membrane-electrodes (ISME) in the S^{2-} determination. What is most common to all these is that all are made of silver sulphide, as active electrochemical material. This is used either in the form of a monocrystal,[1] or as a precipitate included in an inert binding material. [2]

It being a well-known fact that the feats of the homogeneous ISME are superior to the heterogeneous ones, [3] we have dealt in a former paper [4] with the way to obtain an Ag_2S homogeneous membrane-electrode by a simpler method than that of obtaining monocrystalls.[5] In the present paper we have studied some of the characteristics of this electrode, implied in the determination of the S^{2-} anion.

---

* Part IV. I. C. Popescu, C. Liteanu and V. Ciovîrnache, *Rev. Roumaine Chim.*, **18**, 145 (1972).

[1] J. W. Ross and M.S. Frant, Paper presented at Eastern Analytical Symposium, New York, November 8–10, 1967.

[2] E. Pungor, *Analyt. Chem.*, **39** (13), 28A (1967).

[3] N. Bottazzini and V. Crespi, *Chim. Ind.*, **52**, 866 (1970).

[4] I. C. Popescu, C. Liteanu and V. Ciovîrnache, *Rev. Roumaine Chim.*, **18**, 145 (1972).

[5] C. Liteanu, I. C. Popescu and S. B. Domşa, Romanian Patent N° 67066 (1971).

EXPERIMENTAL AND RESULTS

Apparatus and reactants. An electronic registering millvoltmeter (Radelkis OH-102) was used to trace the E-pS electrode functions, to measure the response rate and to carry out the usual potentiometric titrations. The automatic titrations at a pre-established final potential were carried out by means of an autotitrator Radiometer TTT lc. in the setting in figure 1.

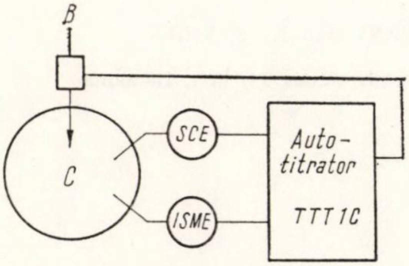

Fig. 1. – The schematic diagram of the device used for automatic titrations.
V – magnetic valve, B – burette, C – cell.

The membrane-electrode used, made by us, was identical to that described previously.[6] The Ag/Ag_2S was obtained by anodizing a metallic silver thread in a Na_2S 1 M solution.

The potential of the membrane-electrode was estimated by measuring the cell's e.m.f.

$$\text{Pt, Hg} \;\Big|\; \begin{matrix}\text{Ag}_2\text{S}\\ \text{membrane}\end{matrix} \;\Big|\; \begin{matrix}\text{Test}\\ \text{solution}\end{matrix} \;\Big\|\; \begin{matrix}\text{Salt bridge}\\ \text{of KNO}_3\text{ 0.1 M}\\ \text{agar-agar}\end{matrix} \;\Big\|\; \text{S.C.E.} \qquad (1)$$

The test solution was thermostated and stirred magnetically.

All reactives used were of *p.a.* purity and were used without any previous purification.

RESULTS

E-pS electrode function. Using test solutions of Na_2S 10^{-1}–10^{-8} M in NaOH (pH = 14) with ascorbic acid (1 g/l) as anti-oxidating agent, we have measured the cell's e.m.f. (1). The results of the measurements are given in figure 2, curve 1. For the sake of comparison we have also presented the results of the E-pS measurements for the Ag/Ag_2S electrode (figure 2, curve 2).

Dependence of the electrode potential on pH. Two series of measurements were undertaken to establish the way in which the potential of the electrode depends on the pH of the adjacent solution. In the first case, the pH of the test solutions used to trace the electrode function E-pS was adjusted at pH = 13.4 (by adding H_2SO_4). The obtained electrode function E-pS is represented in figure 2, curve 3.

---

[6] I. C. Popescu and C. Liteanu, *Rev. Roumaine Chim.*, **17**, 1622 (1972).

In the second case, we have worked at a constant pS (pS = 3) for the pH range between 12 and 13. The results obtained are plotted in figure 3.

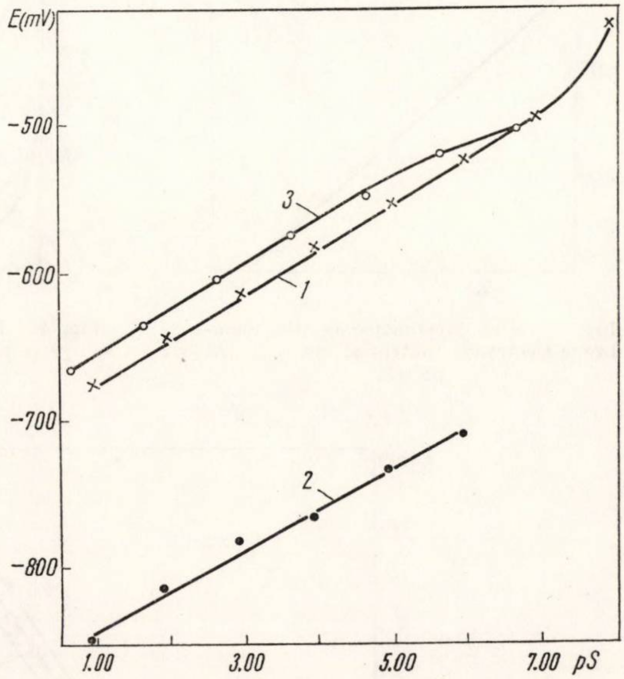

Fig. 2. – The E-pS electrode function.

1, ISME at pH = 4;
2, Ag/Ag_2S at pH = 14;
3, ISME at pH = 13.4.

Response rate. By plunging the membrane-electrode in sodium sulphide solutions (pH = 14, with antioxidant) of different concentrations, we have recorded the variation in time of the electrode potential. Up to pS = 6 the response of the electrode is practically instantaneous. The $E-t$ curves represented in figure 4 show that the electrode reaches the equilibrium potential in maximum 10 minutes up to pS = 7.

Influence of the temperature. The electrode functions E-pS were plotted at 20°, 30° and 40° (±0.1°) by measuring the potential of the cell (1) at different temperatures for different values of pS (pH = 14, with antioxidant).

Potentiometric titrations. We have carried out the titration of some Na_2S solutions with a concentration between 1 M and 10^{-4} M with $AgNO_3$ using a membrane-electrode as indicator electrode. The same titrations were carried out with an Ag/Ag_2S electrode for comparison. The obtained titration curves were represented in figures 6 and 7.

Automatic potentiometric titrations. Using the device shown in figure 1, we have carried out automatic potentiometric titrations at a pre-esta-

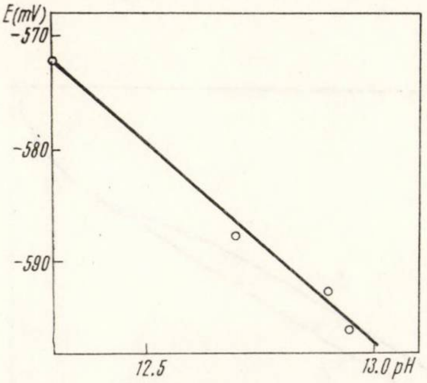

Fig. 3. — The dependence of the membrane-electrode potential on pH, at pS = 3.

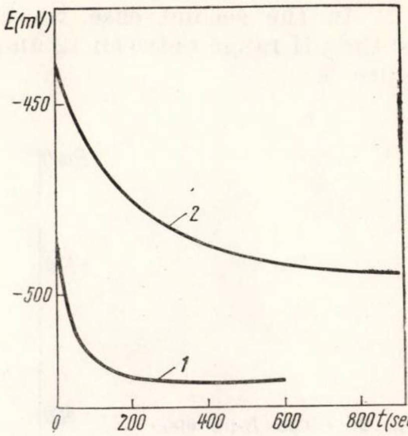

Fig. 4. — The response rate of the ISME at pS = 6(1) and pS = 7(2).

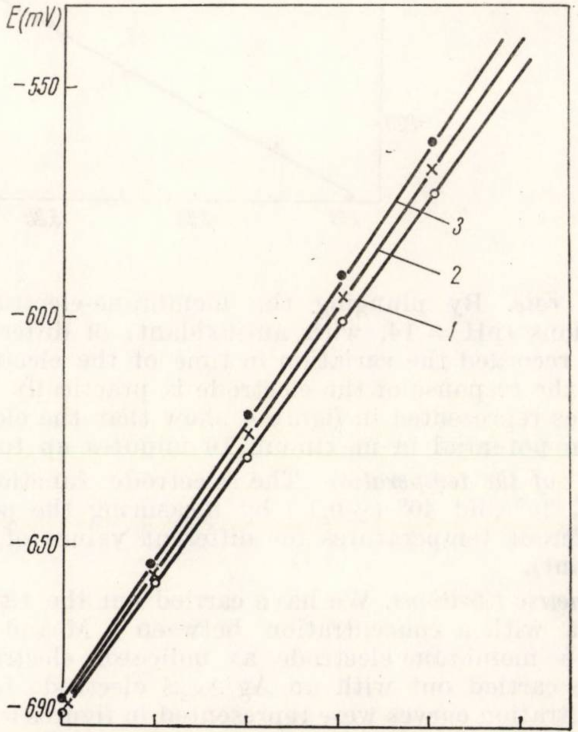

Fig. 5. — The temperature influence of the electrode function *E*-pS.

1, 20° C; *2*, 30° C; *3*, 40° C

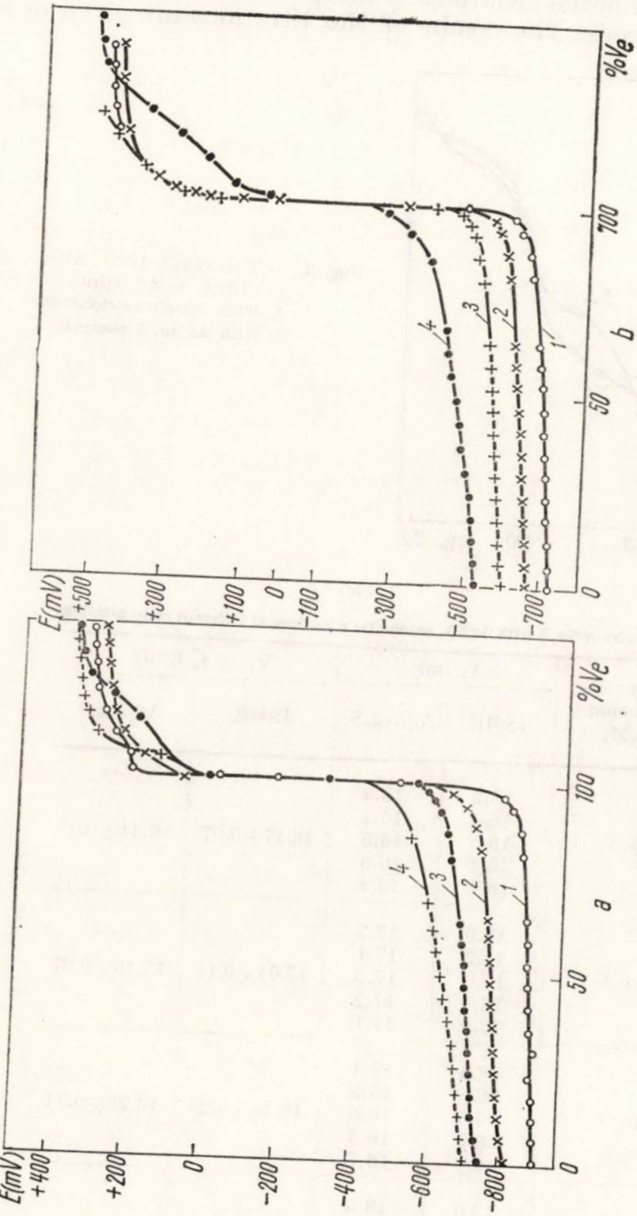

Fig. 6. — The Na_2S with $AgNO_3$ titration.

1, Na_2S 1 M + $AgNO_3$ 1 M;
2, Na_2S 10^{-1} M + $AgNO_3$ 10^{-1} M;
3, Na_2S 10^{-2} M + $AgNO_3$ 10^{-2} M;
4, Na_2S 10^{-3} M + $AgNO_3$ 10^{-3}.

blished final potential, determined by means of the titration curves in figures 6 and 7. Two series of titrations were carried out by comparison : one using the membrane-electrode as indicator electrode, the other using the Ag/Ag_2S electrode. The results of the titrations are given in table 1.

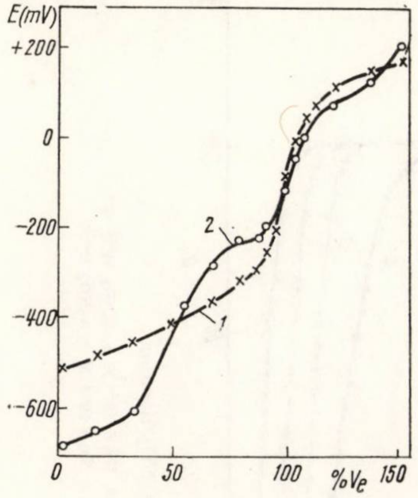

Fig. 7. – The Na_2S 10^{-4} with $AgNO_3$ 10^{-4} M titration.
1, With membrane-electrode;
2, With Ag/Ag_2S electrode.

Table 1

The results of Na_2S with $AgNO_3$ automatic titrations at different concentrations

Concentration (M)	V_e (ml)		$\overline{V}_e \pm s_v^* t$(ml)	
	ISME	Ag/Ag_2S	ISME	Ag/Ag_2S
10^{-1}	16.2 16.5 16.5 16.4 16.4	16.4 16.4 16.5 16.5 16.4	16.47±0.07	16.44±0.07
10^{-2}	17.0 17.2 17.0 17.0 17.0	17.2 17.1 17.2 17.2 17.1	17.04±0.11	17.16±0.07
10^{-3}	16.3 16.5 16.8 16.2 16.4	16.1 16.2 16.0 16.3 16.7	16.44±0.29	16.26±0.34
10^{-4}	12.6 12.1 11.9 11.4 11.6	13.0 12.0 11.9 12.4 11.3	11.92±0.58	12.12±0.77

* $\alpha = 0.95$
$k = 4$

The two series of titrations were compared statistically using the criteria "*F*" and "*t*", and obtaining the results included in table 2.

Table 2

The statistic comparison of the automatic titration results

Concentration (M)	"F"* *calc.*	"F"* tab.	"t"* *calc.*	"t"* tab.
10^{-1}	1.16	6.39	0.13	2.31
10^{-2}	2.66	6.39	0.71	2.31
10^{-3}	1.38	6.39	0.57	2.31
10^{-4}	1.83	6.39	0.42	2.31

*$\alpha = 0.95$
$k = 4$

DISCUSSIONS

The tested S_2^{2-} selective membrane-electrode shows a linear response in the $pS \in [1-7]$ range at $pH = 14$. The slope of the electrode function of 30.3 mV/ΔpS, determined by means of the least square method, is in good agreement with the theoretical value (29 mV/pS).

The optimum working pH is 14. The linearity range of the electrode function *E*-pS narrows at $pH \leqslant 14$. The slope of the line in figure 3, calculated by means of the least squares method, is near to the theoretical value 27.7 mV/ΔpH against 29 mV/ΔpH.[7]

The influence of temperature on the electrode potential is shown through the change of the slope of the function *E*-pS (the least squares method):
a) 28 mV/ΔpS at 20°, b) 29 mV/ΔpS at 30° and c) 30 mV/ΔpS at 40°. Similar results were obtained with the Ag_2S monocrystal membrane-electrode.[8]

The response rate of the studied membrane-electrode is higher than that given by the similar monocrystal electrode.[9]

The shape of the $E-t$ curves corresponds to an exponential relationship.

To conclude, the Ag_2S ceramic membrane-electrode behaves perfectly as an S^{2-}-selective electrode. It can be used with results similar to those of the Ag/Ag_2S electrode for the titration of the S^{2-} anion with Ag^+ in the concentration range of 1 M 10^{-4} M.

---

[7] T. M. Hseu and G. A. Rechnitz, *Analyt. Chem.*, **40**, 1054 (1968).
[8] R. Bock and H. J. Puff, *Z. analyt. Chem.*, **240**, 381 (1968).
[9] E. Pungor and K. Toth, *Hung. Sci. Instr.*, **18**, 1 (1970).

Revue Roumaine de Chimie, **18**, *8*, 1459 – 1466 (1973)

CHARACTERIZATION OF CERAMIC ION-SELECTIVE MEMBRANE-ELECTRODES. VI *

SELECTIVITY OF THE Ag^+/S^{2-}-SELECTIVE Ag_2S MEMBRANE-ELECTRODE

I. C. POPESCU, V. CIOVÎRNACHE, L. SAVICI and C. LITEANU

"Babeş-Bolyai" University, Str. Arany J., 11, Cluj, Romania

Received December 13, 1972

The results of the quantitative estimation of the ceramic Ag_2S membrane-electrode are given for different interfering anions and cations. The Pungor method is used to calculate the selectivity ratios. The obtained values are compared to those corresponding to the Ag_2S membrane-electrode embedded in silicone rubber and to the theoretical forecast. It was established that the Ag_2S ceramic membrane-electrode is an Ag^+/S^{2-}-selective electrode.

In a former paper,[1] the Ag_2S ceramic membrane-electrode was used with good results as S^{2-} selective electrode. Taking also into account the results [2-4] previously obtained with this electrode, we may state that like the monocrystal Ag_2S membrane-electrode, the above electrode is an Ag^+/S^{2-}-selective electrode. This is quantitatively corroborated in the present paper by determining the selectivity ratios corresponding to the different tested interfering cations and anions.

EXPERIMENTAL

Apparatus. **An electronic millivoltmeter "Radiometer" (type TTTlc) or "Carl Zeiss" (type G1B1) was used to measure the potential of the membrane-electrode, in a usual assembling.**

The membrane-electrode of our own device[5] was used in the previously described[3] type of assembling. The e.m.f. of the cell :

$$\text{Pt, Hg} \,|\, \text{Membrane} \,|\, \text{Test solution} \,\|\, \begin{matrix}\text{Salt bridge}\\ KNO_3\ 0.1\ M\\ \text{agar-agar}\end{matrix} \,\|\, \text{SCE} \qquad (1)$$

---

* Part V : I. C. Popescu, C. Liteanu and L. Savici, *Rev. Roumaine Chim.*, **18**, 1451 (1973).

[1] I. C. Popescu, C. Liteanu and L. Savici, *Rev. Roumaine Chim.*, **18**, (1973).

[2] C. Liteanu, I. C. Popescu and V. Ciovîrnache, *Talanta*, **19**, 985 (1972).

[3] C. Liteanu and I. C. Popescu, *Rev. Roumaine Chim.*, **17**, 1629 (1972).

[4] I. C. Popescu, C. Liteanu and V. Ciovîrnache, *Rev. Roumaine Chim.*, **18**, 145 (1973).

[5] C. Liteanu, I. C. Popescu and S. B. Domşa, Roumanian Patent, N° 67.066/1971.

was considered identical to the potential of the studied membrane-electrode. The test solution was stirred magnetically and thermostated at 25±0.1°.

Reactants. The reactants used were of *p.a.* purity, without any previous purification. The Na_2S solutions was standardized by potentiometric titration with $AgNO_3$, using an Ag/Ag_2S electrode as indicator electrode. The other solutions were obtained by weighing.

Procedure. There are two, in principle, different possible methods to determine the selectivity ratios of an ion-selective membrane-electrode.

1. by test solutions containing only a single ionic species for which the electrode is sensitive [6,7]

2. by test solutions containing the interfering ion [7-10] besides the ion for which the electrode is selective.

Though the studies carried out so far do not permit us to draw a definite conclusion, we incline however towards the second method. The conditions in which the selectivity of the electrode is estimated by means of the second method, are indeed nearer to those in which the same electrode may be used. On the other hand, one of this method variants, suggested and used by Pungor *et al.*, [8-12] allows the estimation of the selectivity ratios even in the case of some very slight interferences, which is otherwise impossible. Therefore, this variant of the second method was also used in the present paper.

Thus, to determine the selectivity ratios for anions we have titrated the binary mixtures of $S^{2-}+X^{z-}$(where X^{z-} is the interfering anion) with $AgNO_3$, and for cations, we have analogously titrated different $Ag^{+}+M^{z+}$(M^{z+}being the interfering cation) binary mixtures with Na_2S. According to the hypothesis of the authors[9] of the method, the moment in which the coprecipitation phenomenon is put into evidence on the titration curve $E-V$ coincides with the installation of the interference. The selectivity ratio was directly calculated, knowing the value of the ion concentration at which the electrode is selective, from the calibration curve of the electrode.

The accuracy of the obtained results is evidently very much influenced by an eventual discrepancy between the conditions in which the calibration was achieved and the actual working conditions. We have therefore measured the pH of the titrated solutions the very moment the coprecipitation appears, to carry out the pH correction necessary to determine the real value of pS of the solution.

EXPERIMENTAL RESULTS

Interfering anions. Using the membrane-electrode placed in cell (1) in which the test solution was formed by 10 ml Na_2S $2\cdot10^{-2}$ M and 10 ml $2\cdot10^{-2}$N solution of a Na or K salt of the interfering anion, we have carried out 2 potentiometric titrations for each interfering anion. An Ag/Ag_2S indicator electrode was used simultaneously for comparison. The results of the titration are plotted as titration curves in figures 1—5.

---

[6] G. Eisenman, *Biophys., J.*, **2**, part 2, 259 (1962).

[7] G. A. Rechnitz and K. Srinivasan, *Analyt. Chem.*, **41**, 1203 (1969).

[8] E. Pungor, *Analyt. Chem.*, **39** (11), 28A (1967).

[9] E. Pungor and K. Toth, *Analyt. Chim. Acta*, **47**, 291 (1969).

[10] E. Pungor and K. Toth, *Analyst*, **95**, 625 (1970).

[11] Z. Puhony, K. Toth and E. Pungor, *Magyar Kém. Folyóirat*, **76**, 206 (1970).

[12] Z. Puhony, K. Toth and E. Pungor, *Acta Chim. Acad. Sci. Hung.*, **68**, 177 (1971).

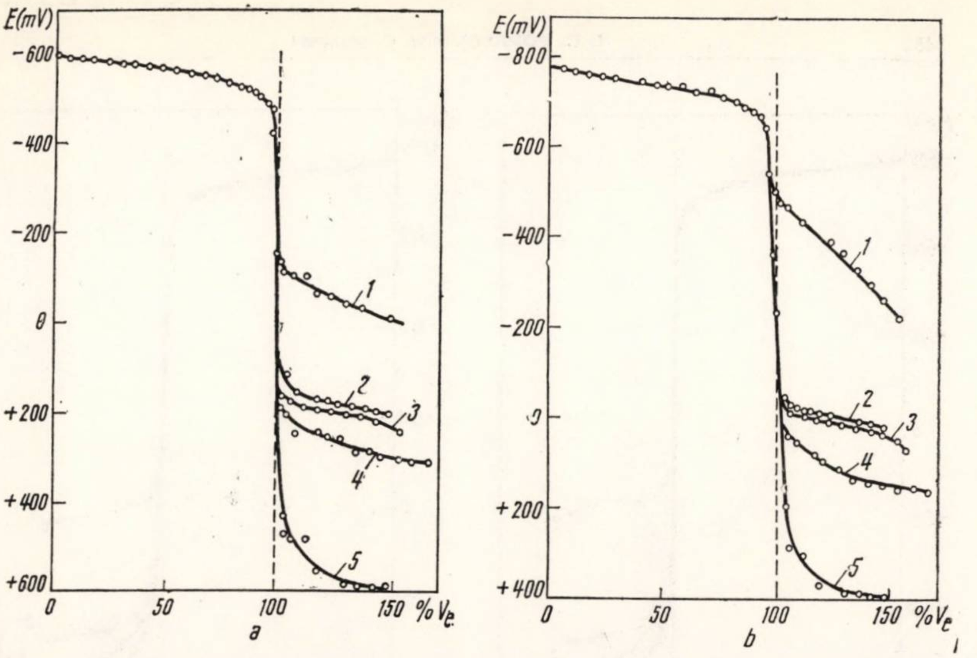

Fig. 1.—The 10^{-2} Na_2S with $AgNO_3$ titration using membrane-electrode (a) and Ag/Ag_2S) electrode (b) in the presence of :

1, I^- 10^{-2}M; *2*, Br^- 10^{-2} M; *3*, SCN^- 10^{-2} M; *4*, Cl^- 10^{-2} M; *5*, without interfering anion.

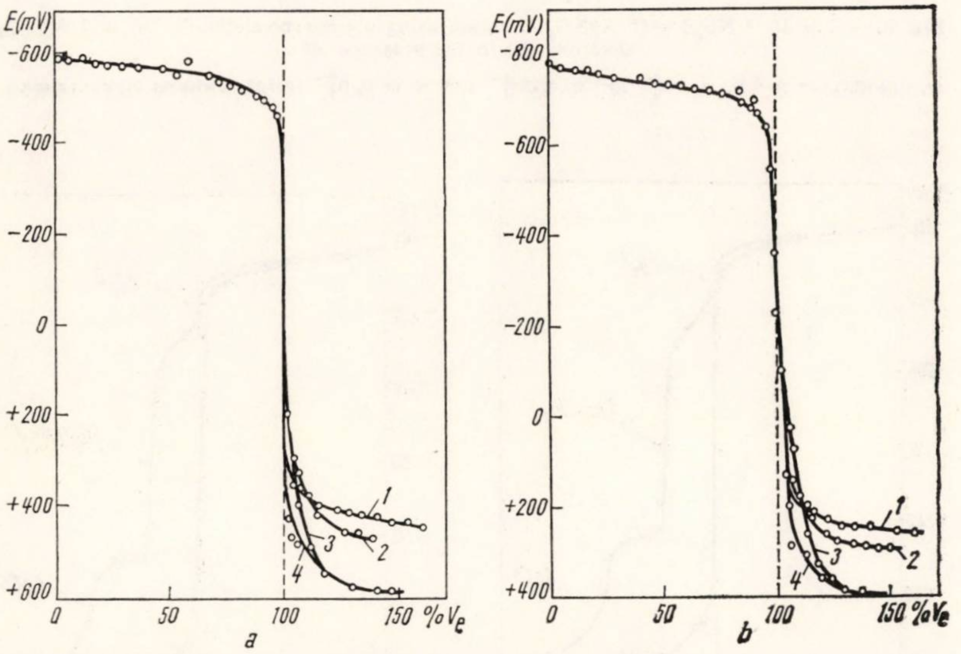

Fig. 2. — The $10^{-2}Na_2S$ with $AgNO_3$ titration using membrane-electrode (a) and Ag/Ag_2S electrode (b) in the presence of :

1, OH^- 10^{-2} M; *2*, SO_3^{2-} 10^{-2} N, *3*, SO_4^{2-} 10^{-2} N; *4*, without interfering anion.

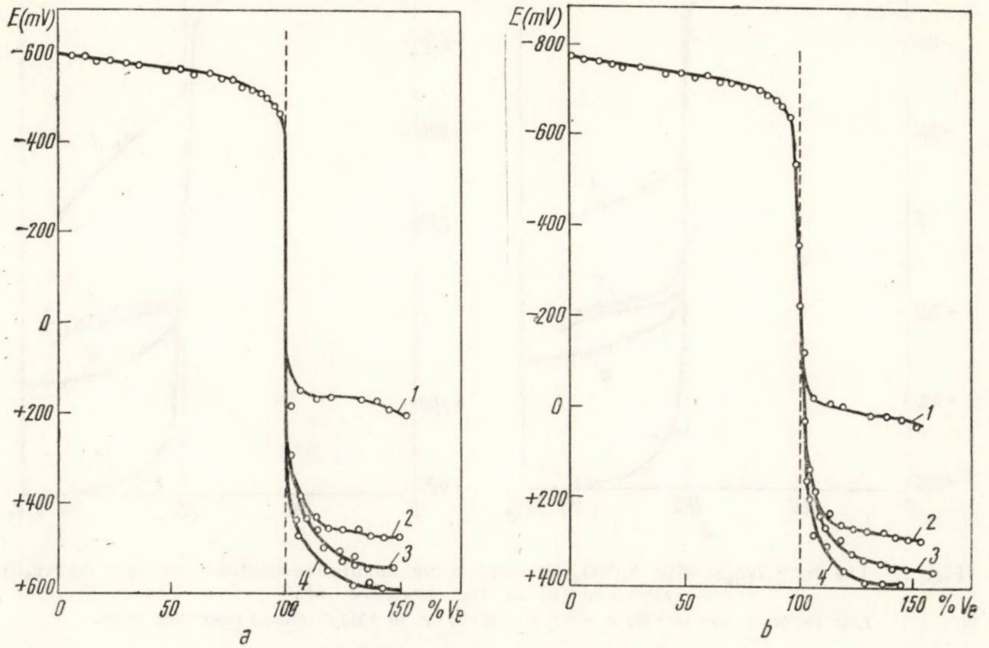

Fig. 3. — The 10^{-2} Na_2S with $AgNO_3$ titration using membrane-electrode (a) and Ag/Ag_2S electrode (b) in the presence of :

1, $[Fe(CN)_6]^{4-}$ 10^{-2} N, *2,* PO_4^{3-} 10^{-2} M, *3,* CO_3^{2-} 10^{-2} N or $C_2O_4^{2-}$ 10^{-2} N, *4,* without interfering anion.

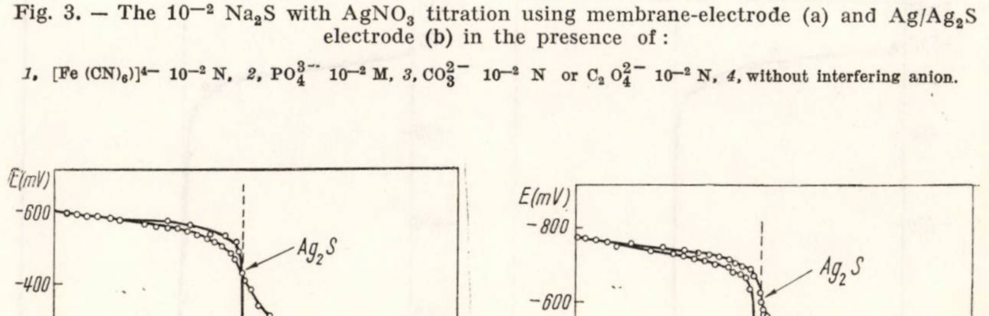

Fig. 4. — The 10^{-2} Na_2S with $AgNO_2$ titration using membrane-electrode (a) and Ag/Ag_2S electrode (b) in the presence of 10^{-2} M KCN.

Interfering cations. We have proceeded as in the case of interfering anions, but titrating 10 ml of a $AgNO_3$ 2.10^{-2}M solution containing different interfering cations with a 2.10^{-2}M Na_2S solution. An Ag/Ag_2S electrode was used simultaneously for comparison. The $E - \%V_e$ titration curves are represented in figures 6–8.

To estimate the experimental selectivity ratios we have considered the following precipitation equilibria [13]:

– for interfering anions

$$\frac{1}{2} Ag_2S + \frac{1}{z} X^{z-} \rightleftarrows \frac{1}{z} Ag_zX + \frac{1}{2} S^{2-} \tag{2}$$

– for interfering cations.

$$Ag_2S + \frac{2}{z} M^{z+} \rightleftarrows \frac{1}{z} M_2S_z + 2Ag^+ \tag{3}$$

The equilibrium constants corresponding to reactions (2) and (3), defined by relations [13]

$$K_{S,X} = \frac{a_{S^{2-}}^{1/2}}{a_{X^{z-}}^{1/z}} \tag{4}$$

$$K_{Ag,M} = \frac{a_{Ag^+}^{2}}{a_{M^{z+}}^{2/z}} \tag{5}$$

were calculated, taking into account the fact that the equations of the calibration lines E-pS, respectively E-pAg are

$$E = -704.5 + 30.3 \text{ pS} \pm 4.1 \text{ (mV/ESC) (pH} = 14, 25°\text{C)} \tag{6}$$

$$E = +726.1 - 58.0 \text{ pAG} \pm 21.8 \text{ (mV/ESC) (}25°\text{C)} \tag{7}$$

The same equilibrium constants may be estimated by calculus according to the relations

$$K_{S,X} = \frac{S_{Ag_2S}^{1/2}}{S_{Ag_zX}^{1/z}} \tag{8}$$

$$K_{Ag,M} = \frac{S_{Ag_2S}}{S_{M_2S_z}^{1/z}} \tag{9}$$

---

[13] E. Schmidt and E. Pungor, Proc. 2nd Conf. Appl. Phys. Chem., Veszprém, 1971. I. Buzás (ed.), Akad. Kiadó, Budapest (1971), p. 615.

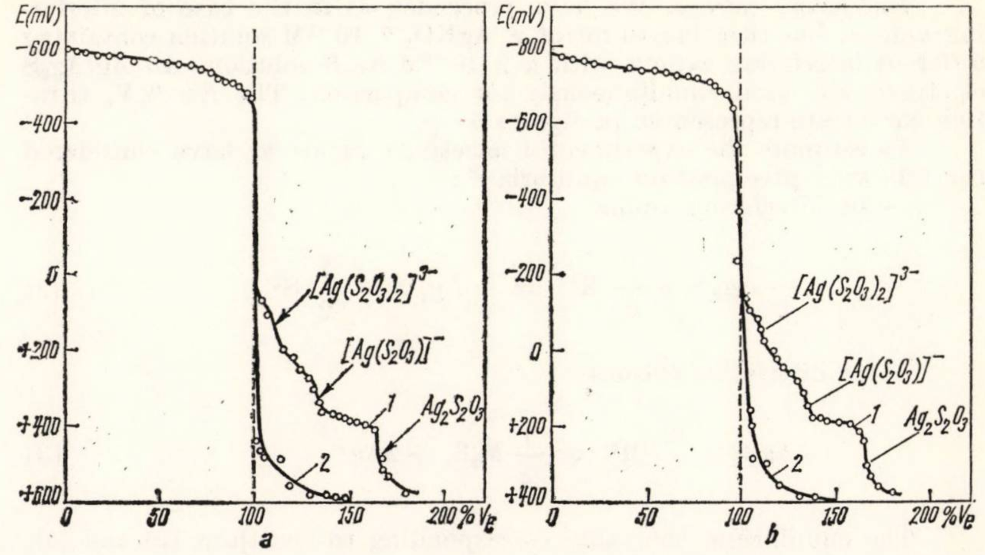

Fig. 5. — The 10^{-2}M Na_2S titration with $AgNO_3$, using membrane-electrode (a) and Ag/Ag_2S electrode (b) in the presence of 10^{-2}N $Na_2S_2O_3$.

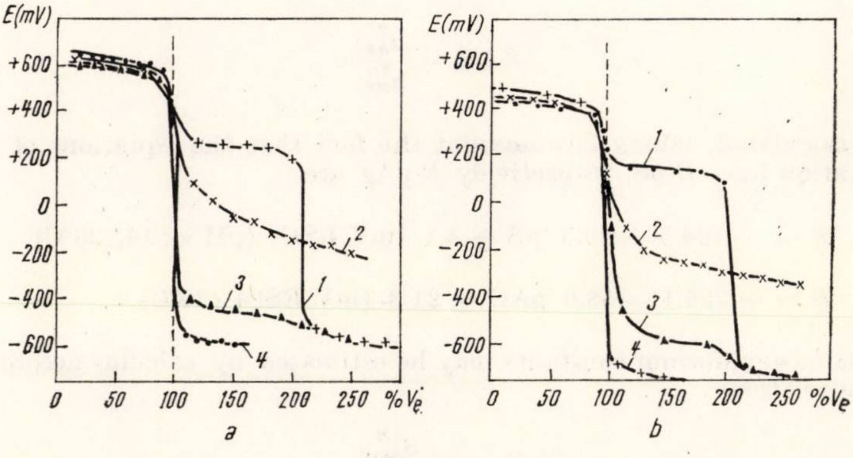

Fig. 6. — The 2.10^{-2} M $AgNO_3$ titration with Na_2S using membrane-electrode (a) ana Ag/Ag_2S electrode (b) in the presence of: 1, Cu^{2+} 10^{-2}M, 2, Tl^+ 10^{-2} M, 3, Mn^{2+} 10^{-2} M, 4, without interfering cation.

where S_{Ag_2S}, S_{Ag_zX}, $S_{M_2S_z}$ are the solubility products of the Ag_2S, Ag_zX and M_2S_z precipitates.

The experimental and the calculated results for the membrane-electrode and the Ag/Ag_2S electrode are given in tables 1 and 2, together

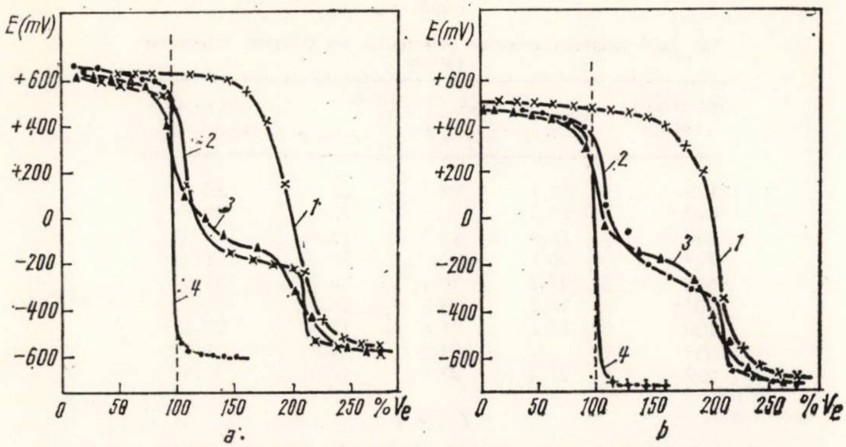

Fig. 7. — The $2\cdot10^{-2}$ M $AgNO_3$ titration with Na_2S using membrane-electrode (a) and Ag/Ag_2 S electrode (b) in the presence of : *1*, Hg^{2+} 10^{-2}M, *2*, Ni^{2+} 10^{-2}M, *3*, Co^{2+} 10^{-2} M, *4*, without interfering cation.

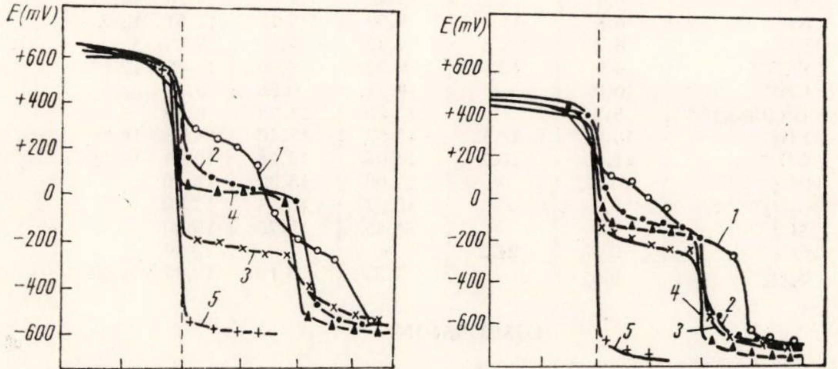

Fig. 8. — The $2\cdot10^{-2}$M $AgNO_3$ titration with Na_2S using membrane-electrode (a) and Ag/Ag_2 S electrode (b) in the presence of : *1*, Pb^{2+} 10^{-2} M. *2*, Zn^{2+}, 10^{-2} M, *3*, Fe^{2+} 10^{-2} M, *4*, Cd^{2+} 10^{-2} M, *5*, without interfering cation.

with the corresponding ones obtained by Pungor *et al.* for the membrane-electrode of Ag_2S embedded in silicone rubber.[13–15]

[14] E. Schmidt and E. Pungor, *Magyar Kém. Folyóirat*, **77**, 397 (1971).

[15] E. Schmidt and E. Pungor, *Analyt. Lett.*, **4**, 641 (1971).

Table 1

The Ag_2S membrane-electrode selectivity for different interfering cations

Interfering cation	$pK_{Ag,Y}$ measured			$pK_{Ag,Y}$ calculated
	ISME	Ref.[13]	Ag/Ag_2S	
Cd^{2+}	22.4	22.4	23.2	23.1
Co^{2+}	25.5	—	23.6	28.8
Cu^{2+}	13.8	13.7	12.3	14.0
Fe^{2+}	29.1	31.0	27.2	31.9
Mn^{2+}	37.2	36.2	39.7	39.6
Ni^{2+}	28.2	23.3	26.0	30.7
Pb^{2+}	13.4	21.8	15.5	22.6
Tl^{+}	—	24.2	24.8	28.9
Zn^{2+}	21.4	27.9	18.5	27.6

Table 2

The Ag_2S ceramic membrane-electrode selectivity for different interfering anions

Interfering anion	pH for coprecipitation	$pK^{pot}_{S^{2-},X}$ measured			$pK^{pot}_{S^{2-},X}$ calculated
		Ref.[13]	ISME	Ag/Ag_2S	
Cl^-	6.4	14.2	10.43	11.37	14.10–14.50
Br^-	6.8	11.6	9.00	9.42	11.51–12.09
I^-	6.7	7.8	4.32	0.56	7.85–8.60
SCN^-	6.5	12.1	9.24	9.80	11.86–12.13
CN^-	10.0	—	0.71	0.98	3.30–5.98
$[Fe(CN)_6]^{4-}$	6.7	—	13.95	11.08	8.30
PO_4^{3-}	10.6	16.1	16.52	17.46	14.75–18.45
OH^-	11.5	16.2	14.95	16.58	16.00–16.73
CO_3^{2-}	10.2	—	17.00	18.35	12.70
$C_2O_4^{2-}$	6.6	—	15.37	16.53	12.70
SO_3^{2-}	7.1	—	14.45	15.70	15.00
SO_4^{2-}	6.45	21.2	—	—	22.00
$S_2O_3^{2-}$	6.5	—	7.73	8.12	10.47–11.40

DISCUSSIONS

The experimental results obtained for the anionic interferences as well as for the cationic ones are in good qualitative agreement with the theory suggested by Pungor and Toth.[9] Among the possible reasons for the observed discrepancies between the two types of electrodes, two must be mainly taken into consideration :

a) the adsorption at the membrane-solution interface and

b) the diffusion in the mass of the membrane. It is to be expected that these phenomena should be encountered in a higher proportion at ceramic membrane-electrodes because of the increase of the interface surface and, on the other hand, because of the increase of the membrane porosity.

To conclude, the Ag_2S ceramic membrane-electrode behaves like a typical Ag^+/S^{2-} selective electrode. The main interfering anions are the CN^- and I^- ions, and the Hg^{2+} (Hg_2^{2+}) and H^+ ions are the main interfering cations.

Revue Roumaine de Chimie, **18**, *8*, 1467–1473 (1973)

CHARACTERIZATION OF CERAMIC ION-SELECTIVE MEMBRANE-ELECTRODES. VII *

THE AgI-Ag_2S, CN^--SELECTIVE MEMBRANE-ELECTRODE

C. LITEANU, I. C. POPESCU and A. MOCANU

"Babeş-Bolyai" University, Str. Arany J. 11, Cluj, Romania

Received December 13, 1972

Some features and a few uses of the AgI–Ag_2S, CN^-, selective ceramic membrane-electrode are investigated. The linearity range of the electrode function $\in[2-6]$ was determined. The optimum working pH, the influence of some interfering anions and cations, as well as the response rate of the electrode, were also stated. The electrode is used with good results in different potentiometric titrations by precipitation and by complex formation.

Very different methods are being used to determine the CN^- ion. Among these, the potentiometric methods occupy a special place due to their simplicity and rapidity and also owing to their low cost and the possibility of an immediate automatization. But, up to a few years ago, the interpretation problems, unavoidably arising with the use of conventional CN^--sensitive electrodes (of Au, Hg, amalgam, Ag, etc.) reduced the competitiveness of potentiometric determinations.

The first step towards their reactivation was undertaken by Gerchman and Rechnitz,[1] who use an Ag^+ sensitive glass indicator electrode to titrate the CN^- ion with $AgNO_3$. Later, Pungor *et al.*[2–4] studying the characteristics of the membrane-electrode from AgI embedded in silicone rubber, show that this electrode can work with good results as CN^--selective membrane-electrode. This is the first CN^- selective membrane-electrode. On the other hand, Ross and Frant[5,6] obtain by pressing a Ag_2S-AgI mixture, an I^--selective membrane-electrode which can also be perfectly used as CN^--selective electrode.

---

* Part VI. I. C. Popescu, V. Ciovîrnache, L. Savici and C. Liteanu, *Rev. Roumaine Chim.*, **18**, 1459 (1973).

[1] L. Gerchman and G. A. Rechnitz, *Z. analyt. Chem.*, **230**, 265 (1967).

[2] J. Havas, K. Toth, J. Szabó and E. Pungor, Proc. Physico-Chemical Methods of Analysis Conference, Budapest, 1966, Akad. Kiadó, p. 159.

[3] J. Havas, M. Huber, J. Szabó and E. Pungor, *Hung. Sci. Instr.*, **9**, 19 (1967).

[4] K. Toth and E. Pungor, *Analyt. Chim. Acta*, **51**, 221 (1970).

[5] J. W. Ross, Jr., in "Ion Selective Electrodes", R. A. Durst (ed.), N.B.S. Spec. Publ. N°. 314, Washington, 1969, p. 78.

[6] Orion Research Inc., Britain Patent I, 150.698 (1969).

Thus, two types of CN^--selective membrane-electrode are known and used, both of the solid heterogeneous membrane-electrodes class.[7] The first type, the one suggested by Pungor *et al.*, uses an inert matrix of silicone rubber, and the second one, worked out by Frant and Ross resorts to a matrix of silver sulphide. Silver iodide is used in both cases as active electrochemical material (table 1).

Table 1

The characteristics of comercial CN^--selective membrane-electrodes

Firm	Range	Optimum pH	Interferences
Radelkis[a]	$10^{-2}-10^{-6}$	12	S^{2-} must be absent; $I^-=CN^-/10$
Orion[b]	$10^{-2}-10^{-6}$	13	S^{2-} must be absent; $I^-=CN^-/10$
Corning -EEL[b]	$1-5\times10^{-8}$	—	S^{2-} must be absent; $K_{CN.I}=0.4$
Philips[b]	$10^{-1}-10^{-6}$	—	S^{2-} must be absent; $K_{CN.I}=3.0$
Crytur[b]	$10^{-2}-5\times10^{-6}$	11	S^{2-} must be absent; I^- idem.

[b] Ag_2S matrix; [a]silicone rubber matrix.

In the present paper we investigate the behaviour of an Ag_2S-AgI ceramic membrane-electrode as CN^--selective electrode. The electrode was obtained in our laboratory according to the Frant-Ross's method.

EXPERIMENTAL

Apparatus and reagents. All potential measurements of the tested membrane-electrode were carried out with an electronic pH-meter (Clamann Grahnert MV-11). To estimate the response rate we have used a recording electronic milivoltmeter (Radelkis OH-102). The potential of the membrane-electrode combined by us, and obtained as formerly described,[8] was identified with the e.m.f. of the cell:

$$\text{SCE} \,||\, \text{Test solution} \,|\, \text{membrane } AgI-Ag_2S \,|\, \text{Hg, Pt} \qquad (1)$$

in which the test solution was thermostated (25±0.1°) and stirred magnetically.

The standard cyanide solutions were prepared by diluting from a KCN 1 M stock solution obtained by weighing. All used reactants were of *p.a.* purity and were not previously purified. Their solutions were obtained by weighing.

EXPERIMENTAL RESULTS

The E-pCN electrode function. Using KCN ($10^{-1}-5\times10^{-7}$M) test solutions, we have measured the e.m.f. of cell (1) in the presence (fig.1) and absence of NaOH (figure 2). By means of the least squares method we have calculated the equations of the calibration curves.

---

[7] C. Liteanu and I. C. Popescu, *Stud. Cerc. Chim.*, **20**, 73 (1969).

[8] C. Liteanu and I. C. Popescu, *Rev. Roumaine Chim.*, **17**, 1629 (1972).

— at pH = 10 (figure 1 a, curve 1)

$$E = -315.9 + 63.5 \text{ pCN} \pm 17.6 \tag{2}$$

— at pH = 12 (figure 1 a, curve 2)

$$E = -256.8 + 53.6 \text{ pCN} \pm 21.3 \tag{3}$$

— at pH = 13 (figure 1b, curve 1)

$$E = -278.3 + 60.5 \text{ pCN} \pm 5.1 \tag{4}$$

— at pH = 14 (figure 1b, curve 2)

$$E = -258.5 + 55.2 \text{ pCN} \pm 11.6 \tag{5}$$

— Without NaOH (J = var., figure 2 curve 1)

$$E = -324.9 + 81.4 \text{ pCN} \pm 22.7 \tag{6}$$

— Without NaOH ($J = 10^{-2}$ M, added KNO_3, figure 2, curve 2)

$$E = -381.0 + 83.3 \text{ pCN} + 33.2 \tag{7}$$

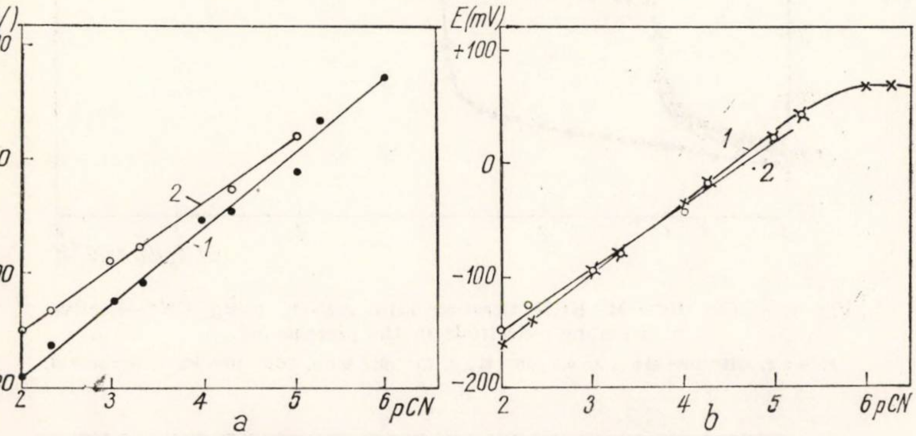

Fig. 1. — The E-pCN electrode function in the presence of NaOH.
a) *1*, pH = 10; *2*, pH = 12; b) *1*, pH = 13; *2*, pH = 14.

Response rate. Using the method of plunging the membrane-electrode into KCN (10^{-2}—5×10^{-5} M) solutions of pH = 12 we have plotted the E—t curves in figure 3.

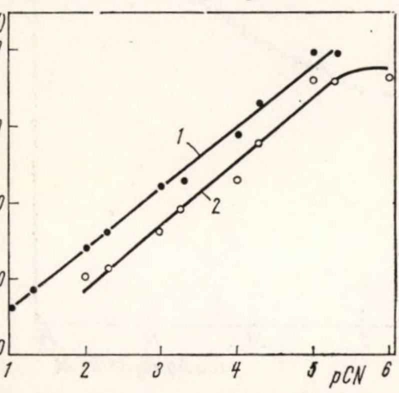

Fig. 2. — The E-pCN electrode function in the absence of NaOH.
1, J = var.; *2*, $J = 10^{-2}$ M.

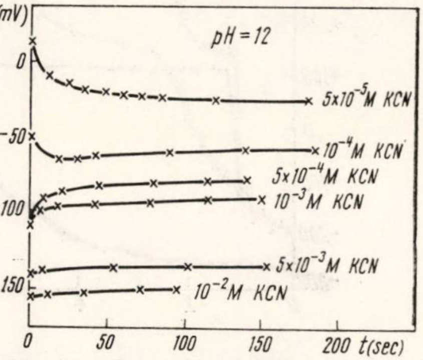

Fig. 3. — The response rate of membrane-electrode.

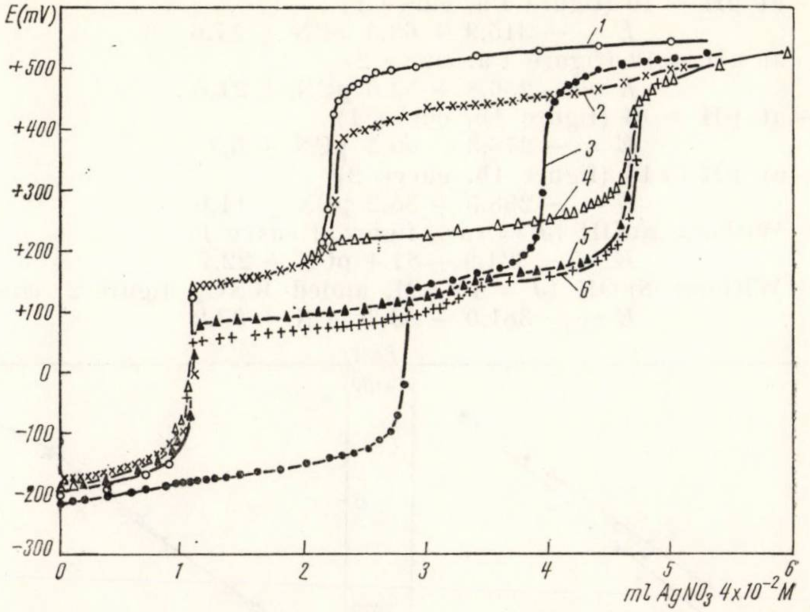

Fig. 4. — The 10^{-2} M KCN titration with $AgNO_3$ using CN^--selective membrane-electrode in the presence of :

1, — ; *2*, OH^- 10^{-2} M; *3*, I^- 6.5×10^{-3} M; *4*, Cl^- 10^{-2} M; *5*, SCN^- 10^{-2} M; *6*, Br^- 10^{-2} M.

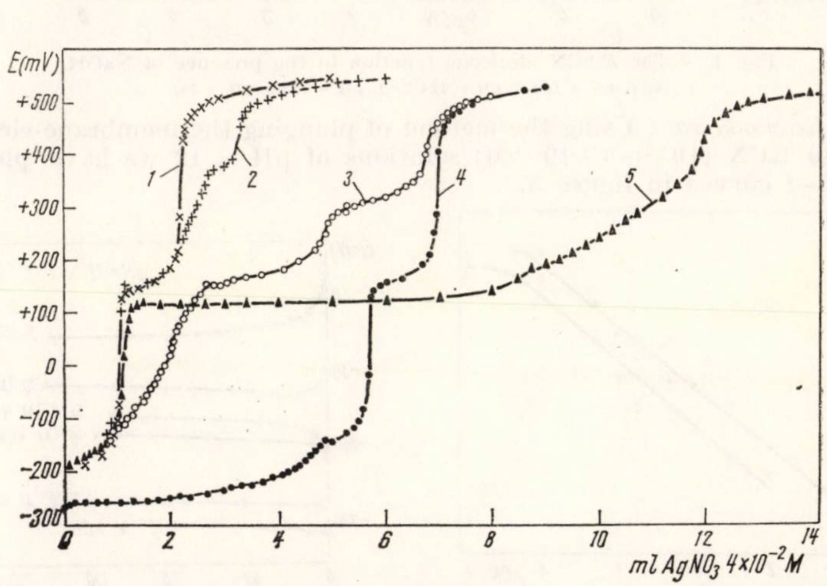

Fig. 5. — The 10^{-2} M KCN titration with $AgNO_3$ using CN^--selective membrane-electrode in the presence of :

1, — ; *2*, SO_3^{2-} 2×10^{-3} M; *3*, $S_2O_3^{2-}$ 10^{-2} M; *4*, S^{2-} 10^{-2} M; *5*, $[Fe(CN)_6]^{4-}$ 10^{-2} M.

Selectivity. By means of the method described by Pungor and Toth,[9] we have determined the selectivity ratio corresponding to the different tested interfering anions (figures 4,5, table 2).

Table 2

The selectivity ratios for different tested anions

Interfering anion	E_{copp} (mV)	pX_{copp}	pCN_{copp}	$pK_{CN,X}$	
				calcd.	measured
OH^-	+ 400	2.1	—	3.6*	4.0
SO_3^{2-}	+ 225	2.8	—	2.2*	2.3
Cl^-	+ 220	2.1	—	1.9*	1.5
$[Fe(CN)_6]^{4-}$	+ 116	2.1	5.4	6.2	4.9
SCN^-	+ 80	2.1	5.0	3.8	2.9
Br^-	+ 50	2.1	4.6	3.5	2.5
$S_2O_3^{2-}$	− 120	2.1	2.5	2.9	1.5
I^-	− 175	2.1	1.8	− 0.3	− 0.9
S^{2-}	− 140	6.0	2.2	− 4.5	− 0.8

* $pK_{Ag(CN)_2^-, X^-}$; $pK_{CN^-, Ag(CN)_2^-} = 8.7$.

Uses. The Ag_2S-AgI membrane-electrode was used in the titration of KCN with $AgNO_3$ in the concentration field 10^{-2}—10^{-5} (figure 6). The results of the titrations carried out (average of 3 titrations) are given in table 3.

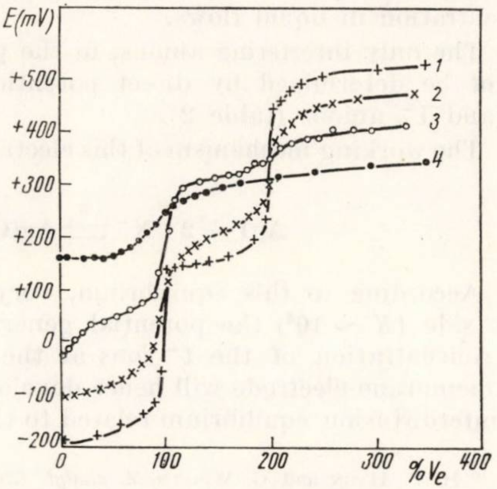

Fig. 6. — The KCN with $AgNO_3$ titration using $AgI-Ag_2S$ membrane-electrode as indicator electrode.

1, KCN 10^{-2} M + $AgNO_3$ 10^{-2} M; *2,* KCN 10^{-3} M + $AgNO_3$ 10^{-3} M; *3,* KCN 10^{-4} M + $AgNO_3$ 10^{-4} M; *4,* KCN 10^{-5} M + $AgNO_3$ 10^{-5} M.

---

[9] E. Pungor and K. Toth, *Analyt. Chim. Acta*, **47**, 291 (1969).

Table 3

The KCN with $AgNO_3$ titration results using the AgI-Ag_2S membrane-electrode

N°	KCN concentration	V_i^* (ml)	$\overline{V}_i \pm s^{**}\overline{V}_i$ (ml)	$s_{\overline{V}_i}/\overline{V}_i$ (%)	$(\overline{\Delta E})$ ±1%
1	10^{-2}	1.01	1.02±0.005	0.5	17.7
2		1.03			
3		1.02			
1	10^{-3}	0.77	0.77±0.004	0.6	5.0
2		0.78			
3		0.77			
1	10^{-4}	0.67	0.68±0.007	1.0	7.8
2		0.69			
3		0.67			
1	10^{-5}	0.61	0.62±0.005	0.8	1.6
2		0.62			
3		0.62			

* calculated with the Hahn-Weiler method.[10]
** standard deviation of the mean.

DISCUSSIONS

As a result of the obtained experimental results we note that the Ag_2S-AgI membrane-electrode behaves like a typical CN^--sensitive electrode. At $pH = 13$, the linearity range of the electrode function E-pCN is 10^{-2}—10^{-6}M (figure 1b, curve 1). These results are in good agreement with the data in literature[11] (table 1, second line).

The response rate of the tested electrode is sufficiently high (at $pCN = 4.3$ $t_{1/2} \sim 1$ minute) to be used in the control of the cyanide concentration in liquid flows.

The only interfering anions, in the presence of which the CN^- ion cannot be determined by direct potentiometric measurements are the S^{2-} and I^- anions (table 2).

The working mechanism of this electrode is based on the reaction.[4,12]

$$AgI + 2\,CN^- \overset{K}{\rightleftharpoons} Ag(CN)_2^- + I^- \qquad (8)$$

According to this equilibrium, very much displaced towards the right side ($K \sim 10^4$) the potential generating process is controlled by the concentration of the I^- ions at the membrane-solution interface. The membrane-electrode will hence develop a stable potential only when the interdiffusion equilibrium related to the I^- and CN^- is achieved.[13,14]

---

[10] H. F. Hahn and G. Weiler, *Z. analyt. Chem.*, **69**, 417 (1926).

[11] Instruction Manual for Cyanide Activity Electrode Model 94—96, Orion Research Inc.

[12] J. W. Ross, Jr., in "Ion Selective Electrodes", R. A. Durst (ed), N.B.S. Spec. Publ. N° 314, Washington, 1969, p. 84.

[13] B. Fleet and H. von Storp, *Analyt. Chem.*, **43**, 1575 (1971).

[14] D. H. Evans, *Analyt. Chem.*, **44**, 875 (1972).

Knowing that the Ag_2S—AgI membrane-electrode is an I^--selective electrode

$$E = E_0' - \frac{RT}{F} \ln a_{I^-} \tag{9}$$

and taking into account equation (8) we immediately obtain

$$E = E_0'' - \frac{RT}{F} \ln \frac{a^2_{CN^-}}{a_{Ag(CN)_2^-}} \tag{10}$$

where

$$E_0'' = E_0' - \frac{RT}{F} \ln K$$

as meanwhile $a_{Ag(CN)_2^-} = \frac{a_{CN^-}}{2}$, we finally obtain

$$E = E_0 - \frac{RT}{F} \ln a_{CN^-} \tag{11}$$

a relationship expressing the dependence of the electrode potential on the activity of the cyanide ions.

The CN^--selective membrane-electrode has already been used in a series of appliances, such as :

— determination of the stability constants[15]

— determination of the CN^- in fodders.[16,17]

The titrations carried out by us point out, besides a good reproducibility, a high sensitivity of the membrane-electrode towards the CN^- ion (table 3).

To conclude, according to the experimental results obtained we can state that the working parameters, such as the CN^--selective electrode of the Ag_2S—AgI membrane-electrode worked out by us, are at the same level as all actually known CN^--selective electrodes.

---

[15] E. PUNGOR and K. TOTH *Hung. Sci. Instr.*, **14**, 15 (1968).

[16] B. GYÖRGY, L. ANDRE and E. PUNGOR, *Analyt. Chim. Acta*, **46**, 318 (1969).

[17] W. J. BLAEDEL, D. B. EASTY, L. ANDERSON and T. R. FARRELL, *Analyt. Chem.*, **43**, 890 (1971).

Revue Roumaine de Chimie, 18, 8, 1475–1482 (1973)

SPECTROPHOTOMETRIC STUDY OF CADMIUM COMPLEX WITH BENZTHIAZOLYLAZO-2,4-DICHLOROPHENOL REAGENT*

V. ARMEANU** and ELENA DRĂGUȘIN

Academy of Economic Studies, Chair of Chemistry and Physics, Piața Romană 6,
Bucharest, Romania
Petrochemical Industrial Trust, Șos. Giurgiului 117 Pitești, Romania

Received November 17, 1972

The paper deals with the qualitative and quantitative spectrophotometric study of the cadmium benzthiazolylazo-2,4-dichlorophenol system. The structure and stability of the complex combination formed, and also the optimum working conditions are determined.

In a previous paper[1] we have presented a spectrophotometric study of the cadmium-thiazolylazo systems, in which the benzthiazolic component was coupled to chromotropic acid or 2-naphthol-3,6-disulphonic acid (R acid). In this case, the formed complexes presented a combination ratio of R : Me = 2 : 1.

The study of the absorbance variation *versus* the pH in different buffer solutions has brought us to the conclusion that these latter change the absorbance of the reagents as well as that of the complexes, because the reagents are also acid-basic indicators, having a red colour in an acid medium and a blue one in an alkaline medium. The spectrophotometric study was therefore carried out in nonbuffered neutral solutions.

In the present paper a new benzthiazolylazo-reagent was studied, which presents the principal advantage, in comparison with the previous series of benzthiazolylazoic reagents, in the fact that it forms a chelate with Cd(II) in an acid medium, with a maximum of absorption at pH = 5. It is one of the few organic reagents which forms with the Cd(II) element a complex with the maximum of absorption in an acid medium. The reactive colour at pH = 5 is reddish-violet, and that of the complex with cadmium is yellow.

---

* Presented at the third National Conference of Pure and Applied Physical Chemistry 4–7 September 1972, Bucharest.

[1] V. Armeanu and E. Drăgușin, *Rev. Roumaine Chim.*, 16, 1357 (1971).

The structure of the reagent is benzthiazolylazo-2,4-dichlorophenol.

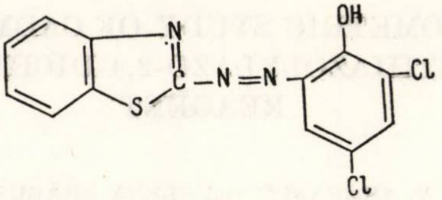

The appearance of the reagent is that of a reddish-brown powder.

EXPERIMENTAL

The reagent benzthiazolylazo-2,4-dichlorophenol was synthetized starting from the respective intermediate, obtained according to the method in the literature, [2] and was then dinitrated using nitrosylsulphuric acid and coupled with 2,4-dichlorophenol in a weakly acid medium.

The composition of the reagent was checked up by the elementary analysis method, and the IR analysis method.

By the elementary analysis method we obtained:

Anal. *Calcd.* for $C_{13}H_6N_3OSCl_2$: C, 44.06; H, 1.69; N, 11.86; 0, 4.51; S, 9.05; Cl 2.00%. *Found.*: C, 45.44; H, 1.76; N, 12.02 %.

By the IR method: 3,430–3,440 cm^{-1} (ν–OH); 3,100 cm^{-1} (δ O–H); 1,185 cm^{-1} (ν C–O); 730 cm^{-1} (ν C–Cl).

Buffer solutions with definite pH were prepared by attentively mixing 0.1M citric acid and 0.2 M disodium hydrogen phosphate solutions.

The spectrophotometric study of the Cd reagent system was carried out by means of a spectrophotocolorimeter SPEKOL, using 10 mm vats. The study was carried out in water-acetone solutions. The concentration of the solutions of reagents and Cd^{2+} was of 1×10^{-3} M

To establish optimum working conditions we have first carried out a qualitative study of the Cd-reagent system. We have observed by spectrophotometry the variation of the absorption of the reagent as compared to that of the complex, versus the wavelength and the pH.

The quantitative study of the system was meant to establish the combination ratio and the dissociation degree and constant.

1. ABSORPTION SPECTRA

Fig. 1 presents the absorption spectrum in the visible range $\lambda = 430 - 700$ nm of the reagent and complex with Cd in 90% water-acetone solution at neutral pH. The colour of the complex is green and the reagent is yellow.

---

[2] S. Skraup, *Liebigs Ann. Chem.*, **419**, 65 (1919).

In figure 2, are given the absorption spectra in the visible range $\lambda = 430 - 640$ nm of the reagent and of the complex with Cd^{2+} in water-acetone (85%) solution, at pH = 5 (buffer: citric acid and disodium hydrogenphosphate solutions). In this case the colour of the reagent is red-violet and that of the complex is yellow.

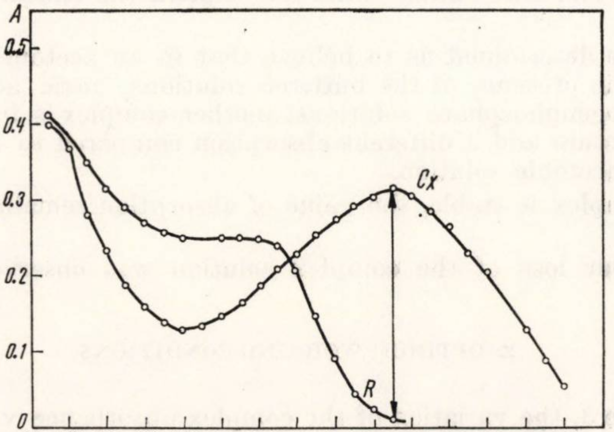

Fig. 1. — Absorption spectra of the Cd complex (Cx) and of the reagent (R) in water acetone 90% solution.

As shown in figs 1 and 2, the absorption spectra of the reagent as well as that of the complex changes much, according to the acidity of the medium.

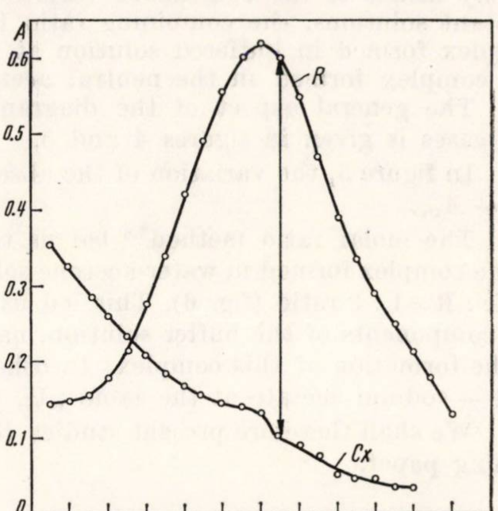

Fig. 2. — Absorption spectra of the Cd complex (Cx) and of the reagent (R) in water-acetone 85% solution at pH = 5 (buffer solution of citric acid and disodium hydrogen-phosphate).

It is very interesting to note the fact that for the same pH = 5, but in the presence of other buffered solutions e.g. acetic acid and sodium acetate, the complex is not formed. This has also been observed by F Kai[3] in the case of the complex formed by Hg(II) and *o*-(2-thiazolylazo)-2,4-dichlorophenol (TADC), in dioxane-water solution in the pH-range of 3.8 – 5.0. The author could not explain the reason of this phenomenon.

This has determined us to believe that in an acetone medium, at pH = 5, in the presence of the buffered solutions, citric acid with disodium hydrogenphosphate solutions, another complex is formed, with a different structure and a different absorption compared to its formation in a neutral acetonic solution.

The complex is stable, the value of absorption remaining constant in time.

No colour loss of the complex solution was observed for 24 h.

2. OPTIMUM WORKING CONDITIONS

In figure 3, the variation of the complex absorbance versus the pH is given for the 85% water-acetone solution. It is easy to establish that the maximum absorption of the complex is achieved at pH = 5.

3. STRUCTURE OF THE CADMIUM COMPLEXES

In accordance with a quantitative study of the systems, carried out by means of the continuous variation method,[4] with equimolecular reactant solutions, the combining ratio R : Cd = 1 : 1 in the case of the complex formed in buffered solution at pH = 5, and R : Cd = 2 : 1, for the complex formed in the neutral acetone solution.

The general aspect of the diagrams $A = f(C_{\mathrm{Cd}}/C_{\mathrm{R}} + C_{\mathrm{Cd}})$ in these two cases is given in figures 4 and 5.

In figure 5, the variation of the absorbance is calculated as $\Delta A' = A_{\mathrm{R}} - A_{\mathrm{Cx}}$.

The molar ratio method[5,6] led us to the same results in the case of the complex formed in water-acetone solutions at pH = 5, respectively a Me : R = 1 : 1 ratio (fig. 6). This led us to the conclusion that one of the components of the buffer solution, namely the citric acid takes part in the formation of this complex. In other buffered solutions, *e.g.* acetic acid – sodium acetate at the same pH, the complex cannot be formed.

We shall therefore present studies to confirm this fact in a forthcoming paper.

---

[3] F. Kai, *Bull. Chem. Soc. Japan*, **43**, 759 (1970).

[4] P. Job, *Ann. Chim. (France)*, **9**, 113 (1928).

[5] Y. A. Yoe and L. A. Jones, *Ind. Eng. Chem. Analyl. Ed.*, **16**, 111 (1944).

[6] Y. A. Yoe and A. E. Harvey, *J. Amer. Chem. Soc.*, **70**, 648 (1943).

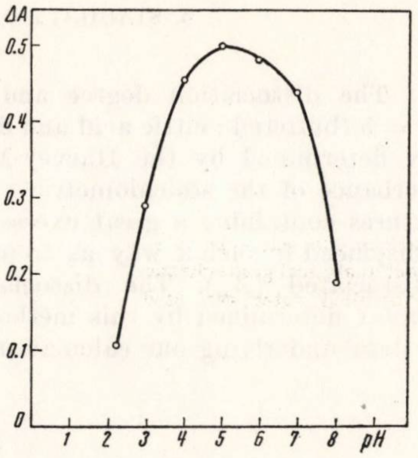

Fig. 3. — Variation of the absorbance of the complex *versus* the pH in water-acetone 85 % solution ; $\lambda = 550$ nm ; $\Delta A = A_{RCD} - A_R$.

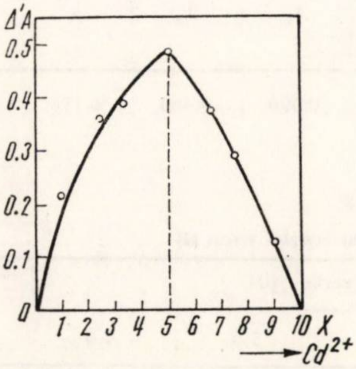

Fig. 4. — $A = f(C_{Cd}/C_R + C_{Cd})$ curve to establish the combining ratio according to Job ; 85 % acetone in water solution ; pH=5 ; $\lambda=550$ nm.

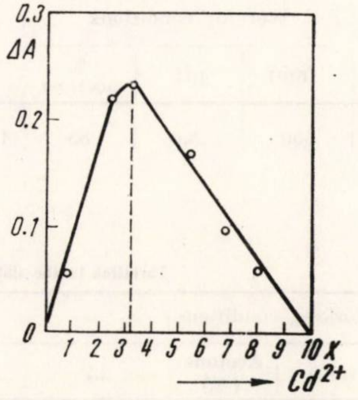

Fig. 5. — $A = f(C_{Cd}/C_R + C_{Cd})$ curve to establish the combining ratio according to Job ; 90 % acetone in water solution ; neutral pH ; $\lambda = 610$ nm.

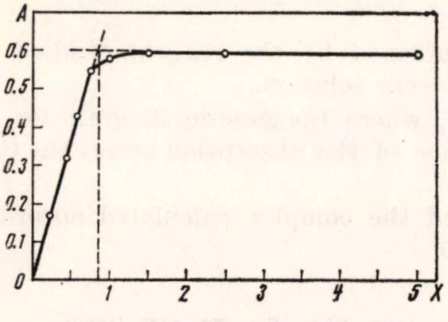

Fig. 6. — Establishing of the combining ratio by the molar ratio method. Concentration of the reactive : 4×10^{-5}M ; 85 % acetone in water solution ; pH = = 5 ; $\lambda = 550$ nm.

4. STABILITY OF THE COMPLEXES

The dissociation degree and constant of the complex formed at pH = 5 (buffered : citric acid and disodium hydrogenphosphate solutions) were determined by the Harvey-Manning method,[7,8] by measuring the absorbance of the stoichiometric mixtures of reactants (A_s) and of those mixtures containing a great excess of Cd^{2+} ions so that the equilibrium be displaced in such a way as to make the formed compound practically undissociated (A_m). The dissociation degree and constants of the complex determined by this method are given in table 1, together with the data underlying our calculations.

Table 1

Dissociation degree and constant of the complex

Nº	Working conditions			C mol/l	A_m	A_s	α	K
	(nm)	pH	% acetone					
1	550	5.0	85	4×10^{-5}	0.590	0.485	0.178	1.54×10^{-8}

Table 2

Variation in the stability of the complex versus pH

Nº	Working conditions		K versus pH				8.0
	(nm)	Acetone (%)	2.2	4.0	5.0	7.0	
1	550	85	2.0×10^{-6}	1.4×10^{-6}	1.54×10^{-8}	1.13×10^{-5}	1.8×10^{-5}

5. SPECTROPHOTOMETRIC DETERMINATION OF Cd^{2+}

The Lambert-Beer law is confirmed by the reagent studied for amounts up to 114 μg Cd^{2+} for 25 ccm solution.

This can be noticed in figure 7, where the gauging diagram for the checking up of the linear dependence of the absorption *versus* the Cd^{2+} content is given.

The molar absorbance value of the complex calculated according to the diagram in figure 7 is 38,800.

---

[7] A. E. Harvey and D. L. Manning, *J. Amer. Chem. Soc.*, **72**, 4448 (1950).

[8] A. E. Harvey and D. L. Manning, *J. Amer. Chem. Soc.*, **74**, 4744 (1952).

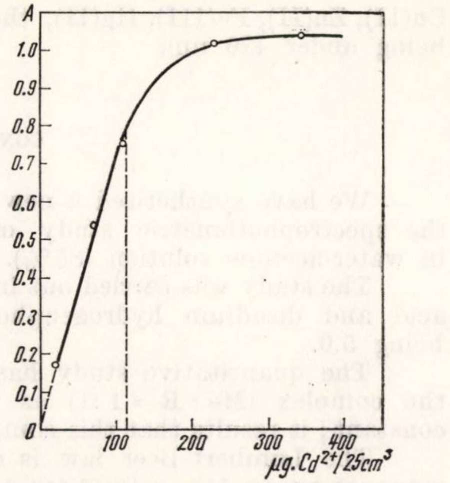

Fig. 7. — Checking of the Lambert-Beer law in an 85 % acetone-water solution.

6. SELECTIVITY OF REAGENTS

The reagent studied does not present an outstanding selectivity for the Cd^{2+} ion, giving also colour reactives in the conditions of determining Cd(II) with a whole series of other elements, such as : Ba(II), Ca(II), Hg(II), Zn(II), Fe(III), Co(II), Cu(II), and Pb(II).

In figure 8 are given absorption spectra of the complexes formed by the reagent benzthiazolylazo-2,4-dichlorophenol with the elements : Ba(II),

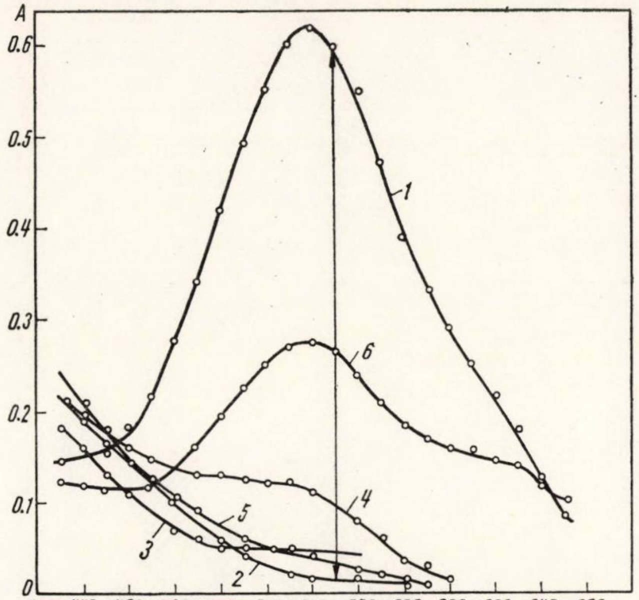

Fig. 8. — Absorption curves of the reagent (*1*) and of Ba^{2+}(*2*), Cu^{2+}(*3*), Zn^{2+}(*4*), Fe^{3+}(*5*), Hg^{2+}(*6*) ions in 85 % acetone-water solution.

Cu(II), Zn(II), Fe(III), Hg(II), the maximum of absorption for the 4 ions being under 430 nm.

CONCLUSIONS

We have synthetized a new thiazolylazoic reagent and carried out the spectrophotometric study of the complexes with the Cd element in water-acetone solution (85%).

The study was carried out in buffered solution prepared with citric acid and disodium hydrogenphosphate, the optimum value of pH being 5.0.

The quantitative study has established the combination ratio of the complex (Me : R = 1 :1) as well as the value of the dissociation constant; it results that this complex has a great stability.

The Lambert-Beer law is confirmed by the studied reagent for amounts up to 114μg Cd^{2+} for a 25 ccm solution.

Revue Roumaine de Chimie, **18**, *8*, 1483–1487 (1973)

POLAROGRAPHIC INVESTIGATION OF THE CADMIUM AND ZINC ETHYL XANTHATE COMPLEXES

IULIA KOVÁCS* and L. KÉKEDY**

* Medical and Pharmaceutical Institute, Str. G. Marinescu 38, Tîrgu Mureş, Romania

** Department of Analytical Chemistry, "Babeş-Bolyai" University, Str. Arany J. 11, Cluj, Romania

Received November 2, 1972

Chemical and electrochemical parameters of the complexing reaction of cadmium and zinc ions with potassium ethyl xanthate have been determined polarographically. The following data have been obtained : a) for the cadmium complex $[Cd\ (Ex)_4]^{2-}$ coordination index $p = 4$, overall formation constant $\beta_4 = 5.27 \times 10^{11}$, enthalpy, entropy and free enthalpy of the complexing reaction $\Delta H = -14.3$ kcal/mol, $\Delta S = -12.5$ e.u., $\Delta G = -14.85$ kcal/mol, respectively. The parameters of the quasi-reversible electrochemical reduction of the complex are : heterogeneous rate constant $k^\circ = 1.22 \times 10^{-2}$ cm/sec, electrochemical transfer coefficient $\alpha_{Cd} = 0.36$; $\Delta G^{\neq} = 9.72$ kcal/mol ; $\Delta H^{\neq} = 7.88$ kcal/mol and $\Delta S^{\neq} = -6.14$ e.u. ; b) for the zinc complex $[Zn(Ex)_3]^-$ coordination index $p = 3$; overall formation constant $\beta_3 = 2.38 \times 10^5$; enthalpy, entropy and free enthalpy of the complexing reaction are : $\Delta H = -10.65$ kcal/mol $\Delta G = -6.80$ kcal/mol and $\Delta S = -11.21$ e.u., respectively. The parameters of the quasi-reversible electrochemical reduction of the zinc complex are : heterogeneous rate constant $k^\circ = 7.31 \times 10^{-3}$ cm/sec, electrochemical transfer coefficient $\alpha_{Zn} = 0.47$; $\Delta G^{\neq} = 9.93$ kcal/mol ; $\Delta H^{\neq} = 5.18$ kcal/mol and $\Delta S^{\neq} = -15.57$ e.u., respectively.

The sparingly-soluble precipitates of cadmium and zinc ethyl xanthates dissolve in the presence of excess xanthate forming water-soluble complexes.[1,2,3,4] The aim of the present study is to investigate by the polarographic method the nature of the complexes formed, to estimate the overall formation constants, the thermodynamic constants of the complexing reaction, as well as the kinetic constants of the electrode reaction.

---

[1] T. Yamasaki and M. Nanjo, *Chem. Ind.*, **36**, 1530 (1966).

[2] H. Kodama and K. Hayashi, *J. Electroanalyt. Chem.*, **14**, 209 (1967).

[3] M. Nanjo and T. Yamasaki, *Sci. Reports Res. Inst. Tohoku Univ. Ser. A.*, **21**, 33, (1969) ; *Chem. Abstr.*, **71**, 97727 n (1969).

[4] H. Hayashi, Y. Sasaki and H. Nojima, *Bunseki Kagaku*, **19**, 325 (1970) ; *Chem. Abstr.*, **73**, 21020 d (1970).

EXPERIMENTAL

A *H* cell was used with a saturated calomel electrode as reference electrode. The test solution was deaerated by bubbling with purified methane gas from the pipe for 20 minutes before each experiment. The polarographic waves were recorded with a RADELKIS Type OH 102 polarograph. Cadmium complexes have been investigated using a 5×10^{-4} M cadmium nitrate stock solution and 0.1 to 0.4 M potassium ethyl xanthate solutions. Experiments with the zinc complex were performed with a 5×10^{-4} M zinc nitrate solution and 0.06 to 0.4 M potassium ethyl xanthate solutions. In both cases the ionic strength was kept to 1.0 by addition of the requisite amount of potassium nitrate. Throughout analytical grade chemicals (K ethyl xanthate Loba Chemie, Austranal, Wien) and doubly distilled water were used. The experiments were carried out at 25 ± 0.1 °C and, respectively at the temperatures indicated in the text.

RESULTS AND DISCUSSION

The plots of log $i/(i_d - i)$ against potential shown in figs. 1 and 2 (full lines) indicate that the polarographic reduction both of cadmium

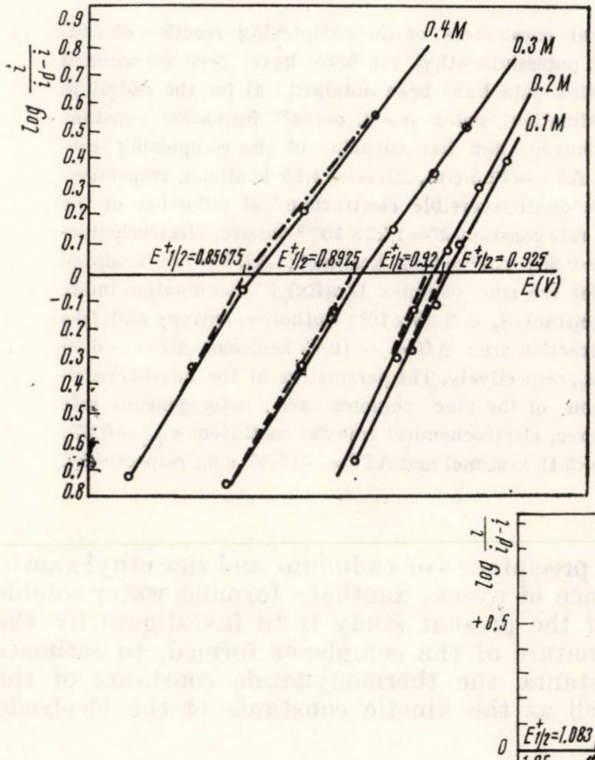

Fig. 1. — Plot of log $i/(i_d - i)$ *vs.* *E* for the reduction of the cadmium complex. The xanthate concentrations are indicated on the lines.

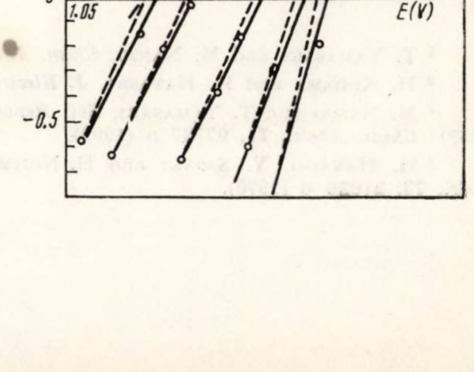

Fig. 2. — Plot of log $i/(i_d - i)$ *vs.* *E* for the reduction of the zinc complex. The xanthate concentrations are indicated on the lines.

and zinc in the presence of xanthate is quasi-reversible.[5] From these graphs the polarographic half-wave potentials have been evaluated using the Matsuda-Ayabe equation,[6] the intersection of the lower asymptote (dotted lines) with the X-axis being considered. From the slope of the asymptote to the upper part of the plots the electrochemical transfer coefficient of the electrode reactions has been computed, obtaining $\alpha_{Cd} = 0.36$ and $\alpha_{Zn} = 0.47$, respectively. The plots of the log xanthate concentrations against the half-wave potentials show a linear relationship (figs. 3 and 4) suggesting that in both cases only one species is reduced. From the slopes of the straight lines in figs. 3 and 4 the number of ligands associated with the Cd^{2+} and Zn^{2+} ions, respectively, have been calculated using the equation [7]

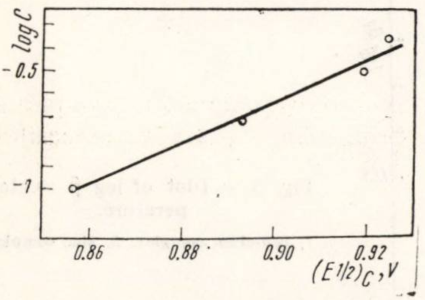

Fig. 3. – Plot of log xanthate concentration *vs.* $(E_{\frac{1}{2}})_c$ for the cadmium complex.

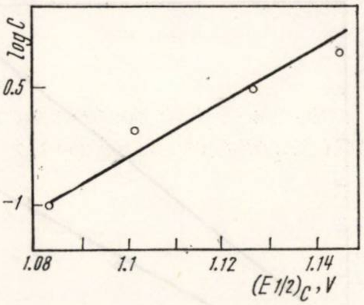

Fig. 4. – Plot of log xanthate concentration *vs.* $(E_{\frac{1}{2}})_c$ for the zinc complex.

$$p = -\frac{\Delta(E_{\frac{1}{2}})_c}{d\log[\mathrm{KEx}]} \Big/ \frac{RT}{0.4343\, nF}$$

The following values have been obtained : $\Delta(E_{\frac{1}{2}})_c / \Delta \log C = 0.0685/0.57 = 0.120$; $p = 0.120/0.0295 = 4.06 \approx 4$ for cadmium and $\Delta(E_{\frac{1}{2}})_c / \Delta\log C = 0.064/0.68 = 0.941$; $p = 0.941/0.0295 = 3.18 \approx 3$ for zinc, respectively. Using the known expression

$$\Delta E_{\frac{1}{2}} = (E_{\frac{1}{2}})_c - (E_{\frac{1}{2}})_s = -0.059/n \log \beta - 0.059/n.p \log [\mathrm{KEx}]$$

the overall formation constants have been computed obtaining $\beta_4 = 5.27 \times 10^{11}$ for the $[Cd(Ex)_4]^{2-}$ complex and $\beta_3 = 2.38 \times 10^5$ for the $[Zn(Ex)_3]^{-}$ complex in accordance with earlier determinations.[1,2,3,4,8]

---

[5] P. Delahay, *J. Amer. Chem. Soc.*, **75**, 1430 (1953).

[6] H. Matsuda and Y. Ayabe, *Z. Elektrochem.*, **63**, 1164 (1959).

[7] D. D. DeFord and D. Hume, see in *J. Electroanalyt. Chem.*, **14**, 209 (1967).

[8] V. U. Shulman, S. V. Larionov and L. A. Podolskaia, *Izvest. Sibirsk. otdel. Akad. Nauk, Ser. khim. Nauk*, **1967**, 154.

The temperature dependence of the overall formation constants has also been investigated. The log β — $1/T^3$ relationship yields the straight lines given in fig. 5. Considering the slopes of the lines and using the van't Hoff equation

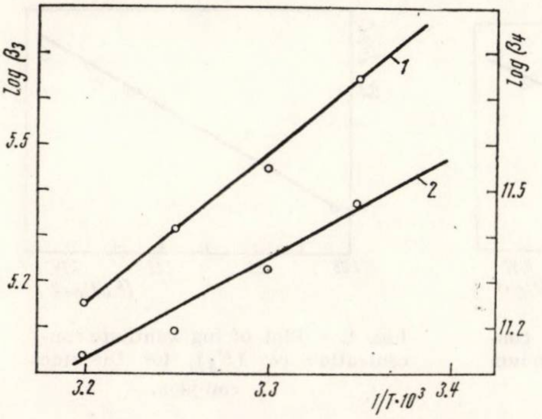

Fig. 5. — Plot of log β *vs.* temperature.

1, cadmium complex, *2*, zinc complex.

$$\frac{\mathrm{d}\log\beta}{\mathrm{d}T} = -\frac{\Delta H}{RT^2} \text{ and } \frac{\mathrm{d}\log\beta}{\mathrm{d}(1/T\cdot 10^3)} = -\frac{\Delta H}{2.303\,R}, \text{ respectively,}$$

the enthalpies of formation have been calculated obtaining $\Delta H = -14.3$ kcal/mol for the cadmium complex and $\Delta_H = -10.65$ kcal/mol for the zinc complex, respectively. From the overall formation constants the free enthalpy-change $\Delta G = -RT \ln \beta$ of the complexing reaction was calculated yielding —14.85 kcal/mol for the cadmium complex and **—6.80** kcal/mol for the zinc complex. The entropy change of formation of the cadmium complex is —12.5 e.u. and that of the zinc complex is —11.21 e.u. Further, using the graphs in figures 1 and 2 the rate constants ($k°$) of the electrode reactions were estimated according to Koryta.[9] At the electrode potential $E = E^r_{\frac{1}{2}}$, the following expression is valuable

$$k^\circ = i'/(i_d - 2i')\cdot D^{\frac{1}{2}}/0.886\, t^{\frac{1}{2}} \tag{1}$$

From the plot of log $i'/(i_d - i')$ against E the value of the log $i'/(i_d - i') = $ = a term is obtained at $E = E^r_{\frac{1}{2}}$. Denoting antilog $a = b$ and considering that $i' = b(i_d - i') = bi_d - bi'$ one obtains $i' = bi_d/1 + b$ and

$$i'/(i_d - 2i') = b/1 - b \tag{2}$$

Introducing (2) in (1) one obtains

$$k^\circ = \frac{b}{1-b}\cdot\frac{D^{\frac{1}{2}}}{0.866\, t^{\frac{1}{2}}} \tag{3}$$

'. KORYTA, *Elektrochim. Acta*, **6**, 67 (1962).

Using equation (3), the rate constant of the electro-reduction of the cadmium complex was calculated, a value of 1.22×10^{-2} cm/sec being obtained. For the zinc complex the same value was 7.31×10^{-3} cm/sec.

The rate constant values have been also determined as function of temperature. The plots of pk° values against $1/T \cdot 10^3$ represented in figures 6 and 7 enabled us to calculate the thermodynamic parameters of the respective electrode reactions: the heat of activation (Q°), the enthalpy ($\Delta H^{\neq}$), entropy ($\Delta S^{\neq}$) and the free enthalpy change ($\Delta G^{\neq}$). For this purpose the equations of Leffler and Grunwald,[10] Leidler[11] and Delahay[12] have been used as follows: $pk^\circ = \log A^\circ - Q^\circ/RT$, where Q° is the heat of activation of the electrode process. This can be obtained from the slope of the plots represented in figures 6 and 7:

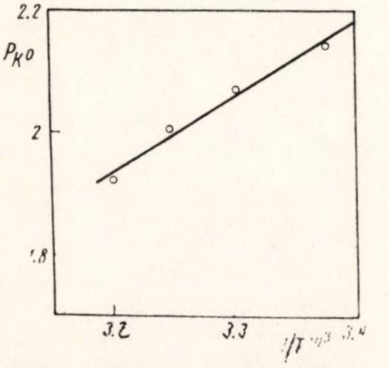

Fig. 6.—pk° vs. temperature for the cadmium complex.

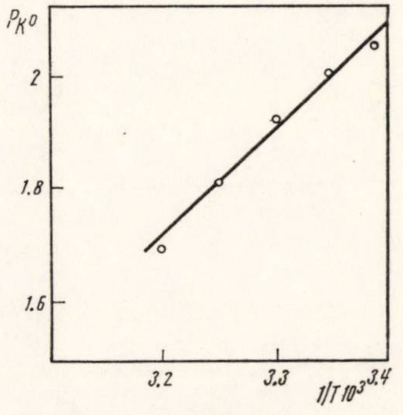

Fig. 7.—pk° vs. temperature for the zinc complex.

$$Q^\circ = 2.3\,R\,\frac{\Delta pk^\circ}{\Delta 1/T \cdot 10^3} = 4.57 \cdot \frac{\Delta pk^\circ}{\Delta 1/T \cdot 10^3}$$

The log A° term is used to calculate the entropy of the electrode process: $\Delta S^{\neq} = 4.575\,(\log A^\circ - 5.521)$. The enthalpy of the process was calculated using equation: $\Delta H^{\neq} = Q^\circ - 595.5$, and equation $\Delta G^{\neq} = \Delta H^{\neq} - T\Delta S^{\neq}$ for computing the free enthalpy. The following values have been obtained: a) for the reduction of the cadmium complex: $Q^\circ = 8.48$ kcal/mol, $\log A^\circ = 4.18$; $\Delta S^{\neq} = -6.14$ e.u.; $\Delta H^{\neq} = 7.88$ kcal/mol and $\Delta G^{\neq} = 9.72$ kcal/mol. b) for the reduction of the zinc complex: $Q^\circ = 5.77$ kcal/mol, $\log A^\circ = 6.35$; $\Delta S^{\neq} = -15.57$ e.u.; $\Delta H^{\neq} = 5.18$ kcal/mol and $\Delta G^{\neq} = 9.93$ kcal/mol.

---

[10] J. E. Leffler and E. Grunwald, "Rates and Equilibria of Organic Reactions". New York, London, J. Wiley, 1963, p. 71.

[11] K. J. Leidler, "Kinetika organicheskhi reaktsii" Moskva, Mir, 1966, p. 90.

[12] P. Delahay, "Novye pribory i metody v elektrokhimii", Moskva, Innostr. Literatura, 1957, p. 58.

Revue Roumaine de Chimie, 18, 8, 1489 (1973)

COMPTE RENDU

P. FRANZOSINI, P. FERLONI and G. SPINOLO, *Molten Salts with Organic Anions. An Atlas of Phase Diagrams.* Ed. Istituto di Chimica Fisica, Pavia, Italy, 1973.

Available literature data regarding molten salt systems containing at least one organic anion are presented in the form of an atlas.

Three hundred and six binary, additive ternary or reciprocal ternary systems are taken into account. Such information is reported as data on the pure components, the coordinates of the invariant points, the liquidus curve or the map of the liquidus area, etc. This XXVIII/306 pages brochure, including 226 diagrams, might be useful to investigators working in the molten salt area.

The atlas, printed with the financial support of the Italian National Research Council (Rome), is not for sale. However, free of charge copies are available from the Istituto di Chimica Fisica della Università, Via Taramelli 16, 27100 Pavia, Italy.

D. I. Marchidan

NOTE POUR LES AUTEURS

La *Revue Roumanie de Chimie* publie des articles en anglais, français, russe, allemand ou espagnol. Les auteurs sont priés d'envoyer des articles, notes, communications et comptes rendus inédits.

Les manuscrits seront dactylographiés à deux intervalles. Les tableaux seront dactylographiés sur feuilles séparées, de même que la légende des figures. Les diagrammes seront tracés à l'encre de Chine sur papier calque. Les tableaux et les figures seront numérotés par des chiffres arabes, en nombre strictement nécessaire. Prière de ne pas inscrire les mêmes données dans les tableaux et les figures. Les formules chimiques seront incluses dans le texte ; en outre, elles seront transcrites sur des feuilles séparées. Les auteurs sont priés d'indiquer les caractères italiques (en soulignant les lettres au crayon), ainsi que tout autre caractère spécial. L'ordre des références bibliographiques sera celui de leur mention dans le texte ; le nom de l'auteur sera précédé de l'initiale du prénom ; les publications périodiques seront présentées suivant les prescriptions internationales. Les références seront ajoutées à la fin de l'article ; elles paraîtront comme des notes, au bas de la page. Le texte sera précédé d'un résumé comprenant 15 lignes au maximum.

L'entière responsabilité du contenu des articles appartient aux auteurs. On publie des articles dus aux collaborateurs roumains ou étrangers. Les auteurs recevront 50 tirés à part.

AGOS MŰSZAKI KÖNYVT

PRINTED IN ROMANIA

1973 OKT 24

TRAVAUX PARUS AUX ÉDITIONS DE L'ACADÉMIE DE LA RÉPUBLIQUE SOCIALISTE DE ROUMANIE

MARIA FIFI, **Dozimetria chimică aradiaţiilor ionizante** (La dosimétrie chimique des radiations ionisantes), 1973, 240 p ., 13,50 lei.

MIHAI FLORESCU, **Eficienţa economică a cercetării ştiinţifice** (L'effcience économique de la recherche scientifique), 1972, 115, p., 15 lei.

GEORGETA LĂZĂRESCU, **Sistematizarea informaţiilor în Chimia organică** (La systématisation des informations dans la chimie organique), 1972, 242 p., 10,15 lei.

P. BALTĂ et E. BALTĂ, **Introducere în chimia fizică a stării vitroase** (Introduction à la chimie physique de l'état vitreux), 1971, 240 p., 15,50 lei.

LYDIA-MARIA VAICUM, **Biodegrabilitatea detergenţilor** (La biodégrabilité des détergents), 1971, 254 p., 16 lei.

TIBERIU NĂSCUŢIU, **Metode radiometrice de analiză** (Méthodes radiométriques d'analyse), 1971, 346 p., 19,50 lei.

I. ZUGRĂVESCU et L. STOICESCU-CRIVETZ, **Polimeri heterociclici** (Polymères hétérocycliques), 1971, 190 p., 9,50 lei.

I. MAXIM, **Materiale nucleare** (Matériaux nucléaires), 1969, 444 p., 30 lei.

CRISTOFOR SIMIONESCU et C. V. UGLEA, **Fracţionarea compuşilor macromoleculari** (Fractionnement des composés macromoléculaires), 1969, 292 p , 18,50 lei.

CRISTOFOR SIMIONESCU et CLEOPATRA VASILIU-OPREA, **Mecanochimia compuşilor macromoleculari** (La mécanochimie des composés macromoléculaires), 1967, 344 p., 23,50 lei.

CORNEL BODEA et collab., **Tratat de biochimie vegetală**, partea I, **Fitochimie** (Traité de biochimie végétale, Ire partie, Phytochimie), Ier vol., 1964, 747 p. + 4 annexes + 2 pl., 41 lei ; IIe vol., 1965, 1262 p., 1 pl., 56 lei ; IIIe vol., 1967, 773 p., 35 lei.

V. GHEŢIE et V. MICUŞAN, **Analiza imunochimică. Teorie şi practică** (Analyse immunochimique. Théorie et pratique), 1966, 369 p., 28 lei.

R. PORTOCALĂ et L. POPA, **Acizii ribonucleici celulari şi virali** (Les acides ribonucléiques cellulaires et viraux), 1966, 375 p., 8 pl., 26 lei.

D. PURDELEA et R. VÎLCEANU, **Chimia compuşilor organici ai fosforului şi ai acizilor lui** (La chimie des composés organiques du phosphore et de ses acides), 1965, 540 p., 37 lei.

I.P.I. – c. 3043

43 426

Lei 25.—

F1103

R

REFERALVA

Ádám olt

REVUE ROUMAINE DE CHIMIE

TOME 18
N° 9
Septembre 1973

RRCHAX, 18, *9*, 1491–1664 (1973)

ÉDITIONS DE L'ACADÉMIE DE LA RÉPUBLIQUE SOCIALISTE DE ROUMANIE

Rev. Roumaine Chim. 18, *9*, p. 1491–1664 (1973), Bucarest

COMITÉ DE RÉDACTION

Rédacteur en chef :

I. G. MURGULESCU, membre de l'Académie de la République Socialiste de Roumanie

Rédacteurs en chef adjoints :

A. T. BALABAN et V. EM. SAHINI, membres correspondants de l'Académie de la République Socialiste de Roumanie

Collège de rédaction :

C. DRĂGULESCU, RALUCA RIPAN, CR. SIMIONESCU, membres de l'Académie de la République Socialiste de Roumanie ; EM. BRATU, ECATERINA CIORĂNESCU-NENITZESCU, P. SPACU, membres correspondants de l'Académie de la République Socialiste de Roumanie ; MARGARETA AVRAM, D. I. MARCHIDAN, G. NIAC et D. SĂNDULESCU

La Revue Roumaine de Chimie paraît 12 fois par an. Toute commande de l'étranger (fascicules ou abonnements) sera adressée à Întreprinderea Rompresfilatelia, Boîte Postale 2001, telex 011631, Bucarest, Roumanie

Les manuscrits, les livres et les revues proposés en échange, ainsi que toute correspondance seront envoyés à la rédaction :

REVUE ROUMAINE DE CHIMIE
23, Str. Dumbrava Roșie, Bucarest

ÉDITIONS DE L'ACADÉMIE DE LA RÉPUBLIQUE SOCIALISTE DE ROUMANIE
3 bis, str. Gutenberg, Bucarest, Roumanie

REVUE ROUMAINE
DE
CHIMIE

ORSZÁGOS MŰSZAKI KÖNYVTÁR DOKUMENTÁCIÓS
18
INT

Tome 18, N° 9 Septembre 1973

Page

V. E. SAHINI and JOSETTE WEINBERG, Xylidine isomers. II. The influence of isomerism on dipole moments . . . . 1493–1496 Rf

AGNETA CARAGHEORGHEOPOL, H. CĂLDĂRARU and V. E. SAHINI, Assignment of proton hyperfine splitting constants in cyclic α-keto-iminoxy radicals 1497–1500

P. G. PERKINS, The electronic strucure of some molecules and ions containing carbon, silicon, oxygen and sulphur. III. Anions formed by carbon, silicon and sulphur 1501–1512

J. CHANU et M. E. WEILL, Chaleurs de transfert en milieux ioniques : application aux solutions aqueuses de KCl et HCl à 25° et 35°C 1513–1519

G. PETIT, Les analyses cryométriques dans la recherche de la structure des substances dissoutes en milieu salin électrolyte fort 1521–1529

RODICA VÎLCU and ŞT. PERIŞANU, Application of the Allen-Skinner bond energy scheme to benzenoid polynuclear hydrocarbons 1531–1535

I. SĂLĂGEANU, DOMNINA TRESTIANU and E. SEGAL, Study of the thermal decomposition of ammonium molybdate supported on alumina . 1537–1546 Rf

MARIA TOMOAIA, ZENO ANDREI et EMIL CHIFU, Tension interfaciale dans le système solution benzénique de tributylphosphate/solution aqueuse de nitrate cuivrique 1547–1554

E. SEGAL, Méthodes non isothermiques utilisées pour la détermination des paramètres cinétiques des réactions hétérogènes décrites par des équations cinétiques non encadrées dans le modèle de l'ordre de réaction. 1555–1576

I. MIHALCEA and R. R. HENTZ, Transient species from the reaction of the hydrated electron with hexacyanocobaltate. III 1577–1580

RENÉE STERNBERG, Contribution à l'étude de l'alcoolyse alcaline du chlorure de *n*-butyle 1581–1585

MIHAELA CONSTANTINESCU and E. SEGAL, Successive chemisorption of gases on semiconductor thin films in the dark and under irradiation. I. The oxygen, carbon monoxide and hydrogen on zinc oxide system . . . 1587–1594 Rf

N. VOICULESCU, I. POPESCU and LUCIA ROMAN, Reactions of coordinated ligands. II.[1] Reaction of triphenylaluminium with nickel, palladium and copper bisdimethylglyoximates 1595–1600

N. VOICULESCU, I. POPESCU and N. LUCHIAN, Reactions of coordinated ligands. III.[1] Aluminium-organic compounds of coordinated salicylaldoxime 1601–1608

ALEXANDRU T. BALABAN, Reaction of pyrylium salts with nucleophiles. X[1]. N(12)-substituted 11,13-dimethyl-[9](2,6)-pyridinophanium perchlorates 1609–1612

N. BĂRBULESCU und F. POTMISCHIL, Darstellung und Untersuchung der Hydroacridine. XI.[1] Der sterische Ablauf der Quaternierung von N-methyl-α-perhydroacridin und N-methyl-β-perhydroacridin mit Trideuteromethyljodid 1613–1616

I. NICULESCU-DUVĂZ, MARIA ROTARU, V. FEYNS and O. MAIOR, Potential anticancer agents. VIII.[1–4] New aromatic and heteroaromatic nitrogen mustards 1617–1626

E. VARGHA, A. BALOG, F. GÖNCZY, D. BREAZU and LUCIA BEU, Peptides. XIV[1]. The synthesis of several peptide sequences related to the Glu^5- and Asp^5-eledoisins 1627–1635

MARIA MIOȘCU, ELENA HOPÎRTEAN and C. LITEANU, Liquid membrane-electrodes. II. The *n*-butanol-frit electrode in acid-base potentiometric titration 1637–1641

C. LITEANU, ELENA HOPÎRTEAN and MARIA MIOȘCU, Liquid membrane-electrodes. III. Electrodes with water-immiscible organic liquids in frit. Applications in potentiometric acid-base titrations. 1643–1647

L. CAMPANELLA, P. L. CIGNINI and G. DE ANGELIS, Polarographic behaviour of isocinchomeronic acid 1649–1657

L. M. BĂLOIU, Spectrophotometric determination of the partition constant using variable amounts of solvent 1659–1662

COMPTES RENDUS 1663–1664

Revue Roumaine de Chimie, 18, 9, 1493–1496 (1973)

XYLIDINE ISOMERS. II[1]
THE INFLUENCE OF ISOMERISM ON DIPOLE MOMENTS

V. E. SAHINI and JOSETTE WEINBERG

Centre of Physical Chemistry, Str. Galaţi 31, Bucarest, Romania

Received March 22, 1973

The conformation of xylidine isomers is discussed in terms of their dipole moment. Nonpolar solvents evidence a correlation between the isomerism of xylidine molecules and their dipole moments.

In a previous paper[1] the xylidine isomers were studied in order to correlate their electronic structure with the basicity constants.

The aim of the present paper is to relate the conformation of xylidine isomers with their dipole moments.

The solvent effect upon the dipole moment of xylidine molecules was taken into account using nonpolar solvents only.

1. MEASUREMENT OF THE DIPOLE MOMENT

Dipole moments were determined by the Guggenheim's method.[2] The measurements were carried out in the concentration range $3.10^{-4}-1.10^{-3}$ moles of xylidine per cc of solution, at 25° ± 0.05°. A-solvents, we used benzene, carbon tetrachloride and *n*-hexane of spectroscopic purity.

In order to calculate the electric dipole moments of the compunds in solutions of nonpolar solvents, we used a FORTRAN IV program woitten by Gilli and Pulidori.[3]

2. CALCULATION OF THEORETICAL DIPOLE MOMENTS

The distribution of π net charge over the xylidine atoms was determined by the SCF-MO-PPP method.

---

[1] Previous paper: V. E. Sahini and J. Weinberg, *Analele Universităţii Bucureşti*, **20**, 2 (1971).

[2] E. A. Guggenheim, *Trans. Faraday Soc.*, **45**, 714 (1949).

[3] G. Gilli and F. Pulidori, *Annali Dell'Universita di Ferrara*, **3**, 1 (1969).

The parameter values used initially are given in table 1.

Table 1

Parameter values used in the SCF – MO – PPP method

Integral	R (in Å)	Value (eV)	Observations	Refs.
(CC/CC)	0	10.53	—	4
(CC/CC)	0	9.35	carbon atom adjacent to the methyl group	5
(C_1C_1/C_2C_2)	1.40	7.28	calcd.	
(C_1C_1/C_3C_3)	2.43	5.40	,,	
(C_1C_1/C_4C_4)	2.80	4.87	,,	6
(NN/NN)	0	14.09		
(NN/C_1C_1)	1.35	9.85	calcd.	
(NN/C_2C_2)	2.38	6.18	,,	
(NN/C_3C_3)	3.65	3.35	,,	
(NN/C_4C_4)	4.15	2.94	,,	4
IP_{C+}	0	-11.22		
IP_{C+}	0	-10.04	carbon atom adjacent to the methyl group	5
IP_{N+}	0	-27.53		6
β_{CC}	1.40	-2.39		4
β_{CN}	1.35	-2.74		7

The σ dipole moment of xylidine was obtained by vector addition of bond moments (cf. table 2).

Table 2

Bond moments used in calculating the theoretical dipole moments[8]

Bond	Moment bond (D)
N–N	1.31
$C_{ar}-N$	1.15
$C_{ar}-H$	0.40

The presence of the methyl group is taken into account by an inductive effect over π net charge of adjacent atom of carbon only.[9]

---

[4] R. Pariser and R. G. Parr, *J. Chem. Phys.*, **21**, 767 (1953).

[5] Huy Le-Khac and W. Forst, *Theor. Chim. Acta*, **16**, 393 (1970).

[6] M. J. S. Dewar and L. Paoloni, *Trans. Faraday Soc.*, **53**, 261 (1957).

[7] I. Fischer–Hjalmars, *Arkiv Fysik*, **21**, 123 (1962).

[8] R. Daudel, R. Lefebvre and C. Moser, "Quantum Chemistry, Methods and Applications", Interscience Publishers, Inc., New York, 1965, p. 206.

[9] L. E. Sutton, "Determination of Organic Structures by Physical Methods", vol. 1, E. A. Braude, F. C. Nachod eds., Academic Press Inc. Publishers, New York. 1955, p. 380, 399.

Therefore, in order to obtain the total dipole moment, we considered the σ dipole moment of aniline added with the π dipole moment of each isomer.

Since the NH_2 group of aniline is not in the same plane with the benzene ring,[10-14] we considered, according to Klessinger [11], an angle of 43° between the plane of NH_2 group and the benzene plane.

3. RESULTS AND DISCUSSION

3.1. THE INFLUENCE OF THE ISOMERISM

Table 3 shows the angle between the two N—H bonds of NH_2 group for each isomer.

Table 3

HNH angle values

Isomer	The angle HNH	Theoretical dipole moment (*D*)	Experimental dipole moment in benzene (*D*)
2,6-xylidine	95°	1.67	1.62
2,3-xylidine	100°	1.58	1.51
2,5-xylidine	100°	1.53	—
2,4-xylidine	113°	1.41	1.40 (Ref. [12])
3,5-xylidine	113°	1.40	1.37
3,4-xylidine	115°	1.28	1.31

The following conclusions can be drawn :

— For the 2,6-xylidine isomer, in which the methyl groups are in the *ortho*-positions, so that they are closest to the NH_2 group, the HNH angle has the smallest value (95°).

— The HNH angle value is 100°, for both 2,3- and 2,5-xylidine isomers, owing to position similarities.

— For the 2,4-xylidine isomer, in which one methyl group is distant from the NH_2 group, the HNH angle is 113°.

— The same fact is observed in the case of 3,5-xylidine, in which both methyl groups are in the *meta*-positions.

---

[10] M. Aroney, *J. Chem. Soc.*, **1965**, 2775.

[11] M. Klessinger, *Theor. Chim. Acta.*, **5**, 236 (1966).

[12] A. L. Mc Clellan, "Tables of Experimental Dipole Moments", W. F. Freeman ed., San Francisco, 1963, p. 300.

[13] M. J. Mantione, *Theor. Chim. Acta.*, **11**, 119 (1968).

[14] L. N. Ferguson, "The Modern Structural Theory of Organic Chemistry", Prentice-Hall, Inc. Englewood Cliffs, New Jersey, 1964, p. 206.

— The 3,4-xylidine isomer, in which one methyl group is in the *meta*-, and another in the *para*-positions (both methyl groups being the most distant from the NH_2 group), has the greatest value of the HNH angle (115°).

3.2. THE SOLVENT EFFECT

The experimental data, concerning the solvent effect for some xylidine isomers, are presented in table 4.

Table 4

Solvent effect

Isomer	Experimental dipole moment in :		
	Benzene	CCl_4	*n*-Hexane
2,6-xylidine	1.62	1.63	1.62
2,3-xylidine	1.51	1.55	1.45
3,4-xylidine	1.31	1.19	1.17

We emphasize that 2,6-xylidine, with both methyl groups in *ortho*-position, has the greatest steric hindrance and therefore the solvent effect is hardly noticeable.

In the case of 2,3-xylidine, the solvent effect is of the same order of magnitude in both benzene and carbon tetrachloride.

The steric hindrance of only one methyl group is much weaker than in the case of 2,6-xylidine, but still noticeable.

For 3,4-xylidine, the solvent effect could be better estimated.

The fact that the dipole moment, measured in benzene, has a significant larger value than in *n*-hexane could be explained by the formation of a $\pi-\pi$ complex between 3,4-xylidine and benzene.

In this "sandwich" complex, where the components are almost overlapped in parallel planes, the vectorial addition [13] of a certain charge transfer dipole moment, with the dipole moment of 3,4-xylidine, leads possibly to a larger resulting dipole moment as compared to the initial one.

The solvent effect of carbon tetrachloride is very weak with respect to that of benzene, due to the fact that carbon tetrachloride forms very weak bridges ; in this case a hardly noticeable charge transfer is possibly involved.

Revue Roumaine de Chimie, 18, 9, 1497–1500 (1973)

ASSIGNMENT OF PROTON HYPERFINE SPLITTING CONSTANTS IN CYCLIC α-KETO-IMINOXY RADICALS

AG NETA CARAGHEORGHEOPOL, H. CĂLDĂRARU and V. E. SAHINI

Centre of Physical Chemistry, Str. Galaţi 31, Bucharest 13, Romania

Received April 11, 1973

Hydrogen atoms lying anti to the iminoxy group oxygen in (*Z*)-α-keto-iminoxy radicals were found to be involved in the hyperfine interaction unlike previous assignments.

In an earlier paper Fox, Mc Rae and Symons [1] have studied the ESR spectra of a large number of α-keto-iminoxy radicals. They assigned the proton hyperfine splittings (hfs) of radical *Z*—I to hydrogen atoms syn to the iminoxy oxygen (see the formula), as observed for other iminoxy radicals. [2,3]

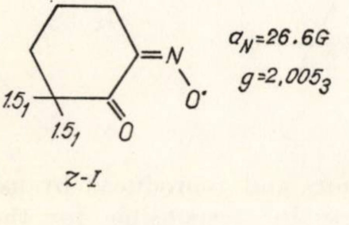

Z-I

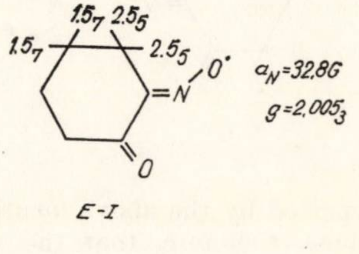

E-I

We intended to use radical *Z*—I as a model compound for the assignment of the hfs in a series of radicals having the general formulae *Z*—II and *Z*—III. However, the interpretation of all our spectra leads to the idea that in fact the two anti protons are involved in the hf interaction.

---

[1] W. M. Fox, J. A. Mc Rae and M.C.R. Symons, *J. Chem. Soc.* (*A*), **1967**, 1773.

[2] M. Bethoux, H. Lemaire and A. Rassat, *Bull. Soc. chim. France*, **1964**, 1985.

[3] R.O.C. Norman and B. C. Gilbert, *J. Phys. Chem.*, **71**, 14 (1967).

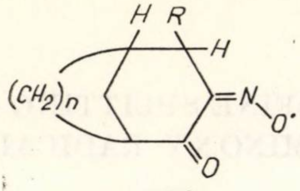
H
R
H
(CH2)n
=N
O·
O

Z-II

n=2,3
R=H, Me, Ph

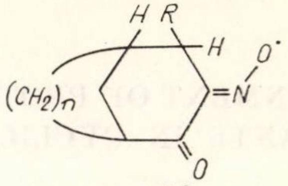
H
R
H
O·
(CH2)n
=N
O

E-II

n=2,3
R=H, Me, Ph

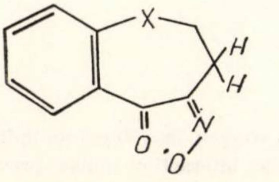

Z-III

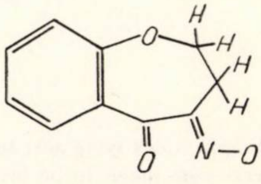

E-III

In order to check up this supposition, the radical $Z-IV$ has been prepared.* Its esr spectrum is entirely identical to that of radical $Z-I$,

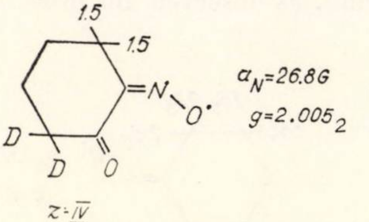
1.5
1.5
=N
O·
D
D
O
aN=26.8G
g=2.0052

Z-IV

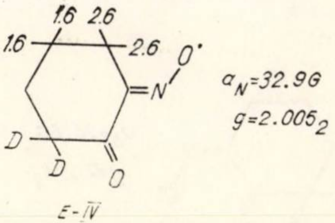
1.6
2.6
1.6
2.6
O·
=N
D
D
O
aN=32.9G
g=2.0052

E-IV

as reported by the above mentioned authors and reproduced by us. We conclude, therefore, that the protons actually responsible for the hfs in the radicals $Z-I$ and $Z-IV$ are those anti to the iminoxy oxygen, the same being true for the type $Z-II$ and $Z-III$ radicals.

The spectrum of the deuterated radical $E-IV$ supports the assignments of Fox, Mc Rae and Symons for the radical $E-I$. It follows that in radicals $E-$I, $E-$II, $E-$III and $E-$IV the protons involved in the hf interaction are those syn to the iminoxy group oxygen, as usually in iminoxy radicals.

---

* The radical was obtained by reacting deuterated ketone with nitrogen dioxide. Cyclohexanone was deuterated by refluxing with deuterium oxide and sodium hydrogen carbonate, and distilling off the ketone. After three succesive treatments, the pmr spectrum showed that replacements of the four α-protons by deuterium was of about 90%.

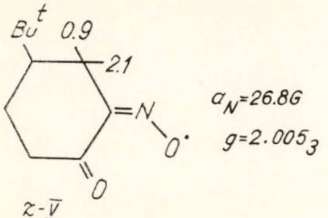

Z-V

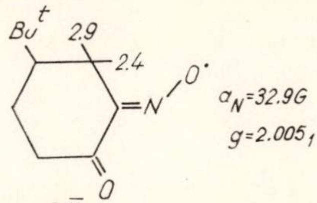

E-V

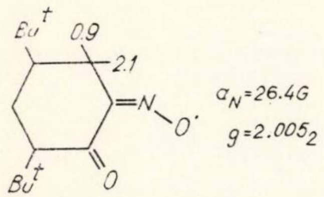

Z-VI

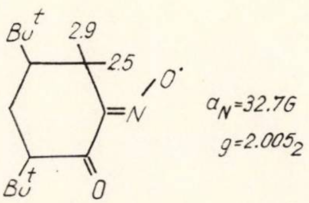

E-VI

The radicals I and IV have not a rigid conformation, but are rapidly interconverting between limiting structures, as indicated by the equivalence of the hfs for geminal protons. In order to be compared with the bicyclic radicals II, radicals V and VI with more rigid conformations were chosen. As expected, in these radicals the geminal protons are no longer equivalent.

We look forward to using these data in the assignment of the hfs in the type II and III bicyclic radicals.

Revue Roumaine de Chimie, **18**, 9, 1501–1512 (1973)

THE ELECTRONIC STRUCTURE OF SOME MOLECULES AND IONS CONTAINING CARBON, SILICON, OXYGEN, AND SULPHUR. III

ANIONS FORMED BY CARBON, SILICON AND SULPHUR

PETER G. PERKINS

Department of Pure and Applied Chemistry, University of Strathclyde, Glasgow C.1., Scotland

Received February 13, 1973

The electronic structure of the systems CS_2, SiS_2, H_2CS_3, CS_3^{2-}, SiS_3^{2-}, CS_4^{4-}, and SiS_4^{4-} are studied by the self-consistent molecular orbital method. For the first two molecules both linear and angular geometries are considered particularly with regard to the possible formation of transition metal complexes. The results are consistent with the known chemical properties of the systems.

The unknown ions SiS_3^{2-}, and SiS_4^{4-} may well be stable : although they possess a number of unstable energy levels it should be possible to shift these adequately by the attractive ligand field of appropriate cations.

H_2CS_3 is shown to be a stable molecule and the position of its eigenvalues in the energy scale highlights the "reverse crystal field effect" in the CS_3^{2-} ion.

INTRODUCTION

In two previous papers[1,2] we have discussed the correlation of the chemistry of some species containing, Carbon, Silicon, Oxygen, and Sulphur with their electronic structure. The present paper continues the discussion with reference to CS_2, SiS_2, and the ions CS_3^{2-}, SiS_3^{2-}, CS_4^{4-}, and SiS_4^{4-}. It is of interest to enquire whether attachment of sulphur to the central atom is likely to enhance or detract from the stability of such species. *e.g.* in Part I[1] we rationalised the non-existence of the CO_4^{4-} ion but could produce no reason for the *intrinsic* instability of SiO_3^{2-}.

Of the species listed, CS_2 is well known and is endothermic with respect to its elements. The CS_3^{2-} ion has been prepared both in salts and in the parent acid form.[3] The CS_4^{n-} ion is known[3] but like CO_4^{3-} is almost certainly a perthiosalt *i.e.*

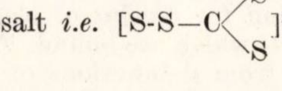

.

---

[1] P. G. Perkins, *Rev. Roumaine Chim.*, **17**, 773 (1972).

[2] Part II. P. G. Perkins, *Rev. Roumaine Chim.*, submitted for publication.

[3] "Interatomic Distances in Molecules and Ions", *Chem. Soc. Special Publ.*, London, N⁰ 11, 1958.

Neither of the ions in which silicon is the central atom seems to have been prepared although there has been little experimental work in the area as a whole and it is by no means certain *a priori* that *e.g.* SiS_4^{4-} would not form an analogous series of salts to those of SiO_4^{4-}. SiS_2 is known in the solid state[4] as a linearly polymeric material in which each silicon is tetrahedrally surrounded by four sulphur atoms.

RESULTS AND DISCUSSION

The calculational method and its parameterisation was identical to that employed previously.[1,2] As before *d* orbitals were included on both silicon and sulphur. Because of the similarity in electronegativity between these atoms, "diffuse" *d* orbitals were considered to be appropriate. The geometrical data are not available for any of the species studied apart from CS_2 and so interpolated and extrapolated values for bond lengths were assumed. The symmetries of the ionic entities were assumed to be the same as those for the analogous CO_3^{2-}, SiO_4^{2-} ; SiS_2 (molecular) was assumed linear like CS_2. Table 1 lists the values employed for bond lengths.

Table 1

Bond distances, X–S (nm)

CS_2	0.1554*		
SiS_2	0.214		
CS_3^{2-}	0.178	scaled from CO_3, CO_2, and CO	
SiS_3^{2-}	0.234	scaled from CO_2, CS_2, and CS_3^{2-}	
CS_4^{4-}	0.205	extrapolated from CS, CS_2 and CS_3^{2-}	
SiS_4^{4-}	0.240	assumed	
SiOS	Si-O,	0.141	SiS, 0.214

ref.[3]

CS_2 *and* SiS_2

The results of calculations on these two molecules are in tables 2 and 3. The most striking feature of the eigenvalues for these two systems is that, in both, all electrons are quite strongly bonding. The chemical reactivity of the molecules will hence be governed almost completely by their high polarisability. The strong bathochromic shift from the corresponding oxygen compounds induced by the sulphur energy levels is clearly marked and since light absorption in CS_2 is known to occur in the visible region then we would predict that molecular SiS_2 would also be coloured. The solid form of SiS_2 is a polymer and crystallizes as white needles[4] : the blue shift in the electronic spectrum is clearly due to the scission of the π bonds. In both cases a large number of excited levels lie in an energetically favourable position for receipt of electrons. Indeed, linear SiS_2 possesses antibonding levels which are bound. For both systems the latter orbitals are built largely from *d* functions on both sulphur and silicon. Thus, using the arguments of the previous paper, [2] SiS_2 could well form

---

[4] "Nouveau Traité de Chimie Minerale", vol. 8, Ed. P. PASCAL, Masson et Cie, Paris, 1968, p. 850, 851.

Table 2

Electronic properties of carbon disulphide

Eigenvalues (eV)				Charge distribution		
	a		*b*		*a*	*b*
1 Σ_g^+	−33.41		−34.21	C 2*ps*	1.15	1.13
1 Σ_u^+	−25.56		−26.06	2_σ	1.05	1.00
2 Σ_g^+	−16.07		−16.67	2 p_π	1.54	1.60
1 π_u	−15.82		−16.45	Nett charge on C	+0.26	+0.27
2 Σ_u^+	−10.93		−11.32			
1 π_g	− 9.25		−9.51	S 3*s*	1.67	1.65
2 π_u	2.87		0.97	$3p_\sigma$	1.23	1.24
	—	1 Δ_g	2.92	$3p_\pi$	3.23	3.10
	—	3 Σ_g^+	3.35	$3d_\sigma$	—	0.04
	—	3 Σ_u^+	3.65	$3d_\pi$	—	0.11
	—	2 Δ_g	3.81	Nett charge on S	−0.13	−0.14
	—	1 π_g	4.04			
	—	3 π_u	4.90			
3 Σ_g^+	6.14	4 Σ_g^+	6.39			
Σ_u^+	7.64	4 Σ_u^+	7.47			

Table 3

Electronic properties of silicon disulphide

Eigenvalues				Charge distribution		
	a		*b*		*a*	*b*
1 Σ_g^+	−24.96		−26.04	Si 3*s*	1.33	1.24
1 Σ_u^+	−24.05		−25.01	$3p_\sigma$	0.90	0.82
2 Σ_g^+	−15.72		−17.03	$3p_\pi$	1.44	1.50
1 π_u	−12.82		−13.78	$3d_\sigma$	—	0.05
2 Σ_u^+	−10.00		−11.02	$3d_\pi$		0.35
1 π_g	−9.02		−10.32	$3d_\delta$		0.02
				Nett charge on Si	+0.33	+0.02
2 π_u	0.66		−0.86	S 3*s*	1.75	1.73
		1 Δ_g	0.01	$3p_\sigma$	1.13	1.17
		3 Σ_g^+	0.83	$3p_\pi$	3.28	3.00
		2 π_g	1.04	$3d_\sigma$	—	0.02
3 Σ_g^+	2.78	4 Σ_g^+	1.19	$3d_\pi$	—	0.08
		1 Δ_u	3.38	$3d_\delta$	—	0.01
		2 Δ_g	3.39	Nett charge on S	−0.16	−0.01
		3 Σ_u^+	3.53			
		3 π_g	3.64			
		3 π_u	4.20			
		5 Σ_g^+	4.32			
3 Σ_u^+	5.28	4 Σ_u^+	4.58			

"π type" complexes with transition metals. As in the CS_2 complexes,[5] these would most likely incorporate SiS_2 as a bent moiety. In this context, it is interesting, therefore, to study theoretically the angular forms of both CS_2 and SiS_2 in order to try and understand the nature of the bonding in the complexes. Table 4 lists the computed data for the angular models of SiS_2 and CS_2.

Table 4

Electronic properties of angular CS_2 and SiS_2

CS_2	Eigenvalues (eV)	Charge Distribution	SiS_2	Eigenvalues (eV)	Charge distribution
a_1	−33.40	C 2s 1.22	a_1	−26.28	Si 3s 1.26
b_1	−25.05	2p 2.52	b_1	−24.79	3p 2.29
a_1	−17.48	Nett charge on C +0.26	a_1	−16.99	3d 0.41
b_2	−15.94		b_2	−13.79	
a_1	−15.13	S 3s 1.70	a_1	−13.77	Nett charge on Si +0.03
b_1	−11.78	3p 4.27	b_1	−11.01	S 3s 1.73
a_2	− 9.46	3d 0.16	a_2	−10.27	3p 4.17
b_1	− 9.01	Nett charge on S −0.13	b_1	−10.20	3d 0.11
a_1	0.29		a_1	− 1.12	Nett charge on S −0.01
b_2	0.70		b_2	− 0.90	
a_1	2.95		a_1	0.15	
b_2	2.96		b_2	0.18	
a_1	3.42		a_1	0.92	
b_1	3.77		b_1	1.03	
a_2	3.90		a_2	1.03	
b_1	3.92		a_1	1.55	
b_1	4.10		b_2	3.35	
a_2	4.14		a_1	3.36	
a_1	4.44		b_1	3.42	
b_2	4.77		a_2	3.44	
a_1	6.43		b_1	3.57	
b_1	6.84		b_1	3.63	
			a_2	3.71	
			a_1	4.06	
			b_2	4.21	
			a_1	4.48	
			b_1	4.55	

Although the CS_2 molecule does not possess equivalent C−S bonds in the platinum complex, we took it to have C_{2v} symmetry for the purposes of our calculation. This was so the orbitals would be easier to correlate. For both bonds we took $C-S = 0.172$ nm and $S\text{-}C\text{-}S = 136°$ as in the platinum complex.[5] Combination and interpretation of the data given in tables 3 and 4 lead to a most interesting situation with respect to the complexes of CS_2. Since the metal atoms involved (Pt, Pd) lie at the right-hand end of the transition block, then we would expect the bonding between the metal and CS_2 to be of the σ-π synergic type and, hence, it is cogent to inspect the disposition and nature of the orbitals which will constitute σ donors and π acceptors. We take CS_2 as our example for analysis and later, drawing on this, suggest what differences should be expected for SiS_2. Firstly, as a donor CS_2 should not be compared with ethylene since, in the latter system, the π bonding orbital lies at the top of the filled sequence.[6] In linear CS_2 the bonding $1\ \pi_u$ orbitals lie much lower in the energy scale and are not strongly involved in the bonding of the molecule to a transition metal atom.

---

[5] M. BAIRD, G. HARTWELL Jr., R. MASON, A.I.M. RAE and G. WILKINSON, *Chem. Comm.*, **92** (1967); R. MCWEENY, R. MASON and A.D.C. TOWL, *Discuss. Farad. Soc.*, **47**, 20 (1969).

It is instructive to study the changes which are likely to take place on forming such a complex. We suppose, formally, that the CS_2 molecule bends as it approaches the Pt centre and so interaction governed by symmetry takes place. Figure 1 shows how the linear molecule levels correlate with those of the bent C_{2v} molecule. The interesting levels are those deriving from the bonding $2\sigma_u^+$, $1\pi_g$ and the antibonding $2\pi_u$ orbitals. Despite symmetry lowering the b_1 orbital derived from $1\pi_g$ retains a large electron population in the p_y, p_z orbitals of sulphur (~ 1 electron). Hence, for CS_2 to be a σ donor, electron donation to the central metal atom must involve either one sulphur atom only or two widely separated ones. The latter situation is obviously not reasonable, since the molecule is 0.311 nm long and, at a guessed reasonable Pt-C distance of ~ 0.25 nm, would produce donor-acceptor bonds 0.29 nm long. This would clearly

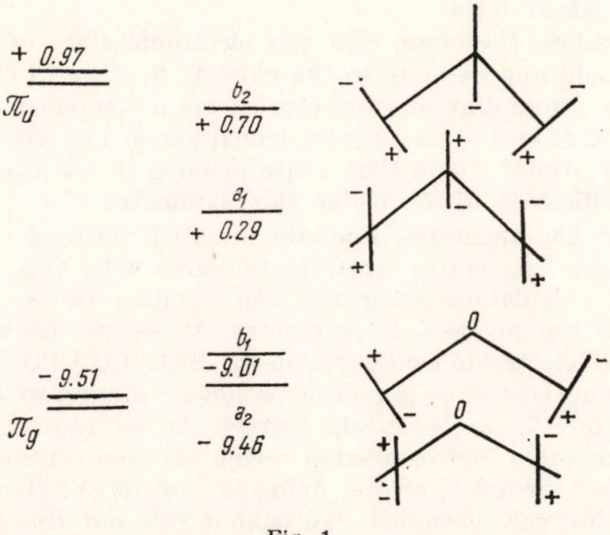

Fig. 1

---

[6] M. B. Robin and R. R. Hart, *Theor. Chim. Acta*, **3**, 375 (1965); M. B. Robin and N. A., Kuebler, *J. Chem. Phys.*, **44**, 1803 (1966).

not lead to any degree of stable bonding. Hence, it is not surprising to find that the molecule is asymmetrically attached to the Pt or Pd atom. If we now study the make-up of the first a_1 antibonding orbital (Fig. 1) it can be seen how further stability can be achieved. This orbital, empty in bent CS_2, has wave function amplitude on the carbon atom (p_z and s) as well as on the sulphur (p_z) : it arises from the p_π antibonding in-plane orbitals of linear CS_2. Its energy is drastically lowered on going from the planar to the bent form and so it is well situated to accept electron density from the central transition metal. The fascinating point here is that it is both a σ donor and a σ acceptor, because the $2\ \pi_u$ orbital from which it derives becomes σ type on bending the molecule. Acceptance of electrons into this orbital does, of course, weaken the bonding force of the original $1\pi_u$ pair and so the C-S bond is lengthened. Moreover, the neutralisation of π_u bonding plus nuclear repulsion between central atom and sulphur will bend the molecule away from the transition metal. Acceptance of electron density onto the carbon will render the molecule less polar than it is in the linear form.

We predict, therefore, that the electronic state of CS_2 in such a complex should approximate to the excited B_1 state of CS_2. This would be formed by promotion of an electron from a component of $1\ \pi_g$ in one plane to another of $2\pi_u$ in the orthogonal plane. The antibonding nature of the latter orbital would then cause bending in the excited state and, hence, classification of B_1 under this symmetry.

Mason[5] has suggested that the excited state of the molecule is similar to the $^3A_2$ state. In order to agree with this, it necessitates that in our calculation either the top bonding or the lowest virtual orbital pairs are reversed in symmetry. It should be noted that our predictions of electronic configuration for SiO,[2] CO,[2] CO_2,[1] and COS,[3] do not differ from those of *ab initio* calculations.[7,8] Hence, we believe that the eigenvalues for CS_2 are probably correct. An alternative explanation is that, *in the complex*, better overlap occurs between central atom orbitals and the *second* virtual b_2 orbital, lying at $+\ 0.70$ eV. Hence, this orbital might be selectively occupied. We cannot rule out this possibility, but if it did happen (and with particular elements, it might be more favoured or it might depend on other attached ligands), the nature of the b_2 orbital involved is such that the distribution of electrons would be similar and the C-S π bond weakening would be brought about in a complementary way. It would be interesting to devise experiments to distinguish between the two kinds of bonding.

It should, moreover, be remembered that the first A_2 state of CS_2 differs from the b_1 only in that the complementary components of the $1\pi_g$ and $2\pi_u$ orbitals are involved.

---

[7] E. Clementi, *J. Chem. Phys.*, **36**, 750 (1962).

[8] A. D. McLean and M. Yoshimine, "Table of Linear Molecule Wave Functions" Supplement to Paper, "Computation of Molecular Properties and Structure" I.B.M. Journal of Research and Development, Nov., 1967.

It is interesting to speculate on whether complexes of the type

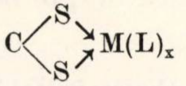

could be formed where CS_2 is bent symmetrically. Sterically, only two coordination positions on M would be required as before but one difference would be that the σ reverse electron transfer would be inhibited by the long C-M distance. Complexes of this kind would, therefore, appear to gain nothing in energy by bending and would more likely be linear in the CS_2 moiety.

In the case of SiS_2 the eigenvalues are not nearly as strongly affected by bending as they are in CS_2. (figure 2). Perhaps the most striking difference is that the d functions on silicon play a part in both the b_1 and a_1 orbitals which border the bonding-antibonding gap. Thus, we would expect to get the same type of bonding mechanism with transition metals since (a) the first antibonding orbitals are favourably situated for occupation and (b) the incorporation of some d character on the central atom causes the molecular orbitals to diffuse out towards the transition metal.

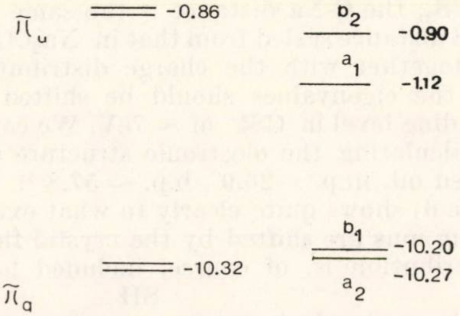

Both CS_2 and SiS_2 appear to be more stable than molecular SiO_2[1] and, whereas SiO_2 in the vapour phase was predicted to be less stable than SiO (it does, in fact, dissociate to SiO and oxygen above 2000°[4]), SiS_2 should be more stable than SiS.[1] This is, in fact, the case[4] and at high temperature, SiS decomposes.

$$2SiS \rightarrow SiS_2 + Si$$

The solid form of SiS_2 is "less" polymerised than is SiO_2 and consists of linear chains, thus

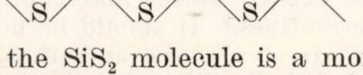

This would argue that the SiS_2 molecule is a more thermodynamically stable entity than in SiO_2. In the solid state the latter acquires stability only as a three-dimensional net.

The differential polarity of CS_2 and SiS_2 is remarkable in that one would perhaps have expected SiS_2 to be the more polar, whereas it is virtually neutral.

CS_3^{2-} *and* SiS_2^{3-}

The principal results are shown in table 5. For both these systems, it will be seen immediately that certain of the bonding levels correspond to positive eigenvalues. This feature was also encountered in the calculations on the oxyanions [1] and it was shown there that this was due to the "reverse crystal field effect". The eigenvalue sequence may be shifted downwards in the energy scale by the application of the field of the neutralising cations. Unfortunately we do not know the appropriate anion-cation distances for salts of either of the above species and moreover, there is no accurate guide from the crystal structures of similar compounds. Considering for the moment CS_3^{2-}, we can assume that, in the Na^+ salt, Na_2CS_3, the C-Na distance is the same as that taken from Na_2CO_3. [1] The Na-S distance scaled from that in Na_2CO_3 is then 0.272 nm. Using this value together with the charge distribution of table 5, we calculate that all the eigenvalues should be shifted by $\sim$ 10 eV. This gives a highest bonding level in CS_3^{2-} of $\sim$ 7eV. We can check our reasoning roughly by calculating the electronic structure of the known compound H_2CS_3 (a red oil, m.p. $-26.9°$, b.p. $\sim 57.8°$[4]). The calculation for this molecule (table 6) shows quite clearly to what extent the eigenvalues of the corresponding ions are shifted by the crystal field of two H^+ ions. The covalent contribution is, of course, included here and, moreover, the geometry of the molecule is 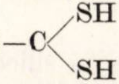 $S{-}C(SH)_2$ (C_{2v}) with the H^+ ions close to two of the sulphurs rather than occupying positions above and below the CS_3^{2-} plane. However, the result is instructive and lends quantitative support to the suggested mode of correcting the eigenvalues of an anion.

The 3*d* orbitals of sulphur are fairly strongly occupied in CS_3^{2-}, and about half of the electron population resides in π type orbitals. The ion is more polar than is CO_3^{2-1}. One particularly striking feature is that the energy gap between bonding and antibonding orbitals is reduced by sulphur *d* orbital participation. Thus, whilst in CO_3^{2-} the gap is $\sim$ 14 eV, [1] in CS_3^{2-} it is $\sim$ 9 eV. This correlates with experiment, since carbonates are colourless in general (unless the colour is conferred by a central metal ion) whilst Na_2CS_3 is yellow.[3] Of course the orbital gap is not the correct quantity to compare with spectra and it should be corrected by configuration interaction terms. Such a calculation on the excited states of CS_3^{2-} would almost certainly reduce this energy gap of $\sim$ 9 eV down to 4 or 5 eV, in better agreement with experiment. A future paper will be concerned with the excited states and configuration interaction in these ions and their derivatives.[9] It should be noted that the first antibonding orbital of CS_3^{2-} is of π^* type and of a_2'' symmetry. In CS_3^{2-}, when *d* orbitals are included, the first virtual a_2'' orbital is very strongly localised on the sulphur atoms. Thus, a transition from the first bonding

---

[9] P. G. Perkins, to be published.

Table 5

Electronic properties of CS_3^{2-} and SiS_3^{2-}

CS_3^2	Eigenvalues (eV)			Charge distribution		
	a		*b*		*a*	*b*
$1a'_1$	-19.85		-21.72	C $2s$	1.07	1.05
$1e'$	-9.97		-11.49	$2p\sigma$	2.09	1.96
$2a'_1$	-2.49		-4.03	$2p\pi$	0.58	0.66
$1a''_2$	-2.10		-3.52	Nett charge on C	$+0.26$	$+0.33$
$2e'$	-0.66		-1.58	S $3s$	1.75	1.70
$1e_1''$	3.52		2.73	$3p\sigma$	3.20	3.08
$1a_2'$	4.25		2.81	$3p\pi$	1.81	1.68
$3e'$	4.42		3.39	$3d\sigma$	—	0.21
				$3d\pi$	—	0.11
$2a''_2$	15.85		12.23	Nett charge on S	-0.76	-0.78
	—	$3a'_1$	13.12			
	—	$2e''$	13.67			
	—	$4a'_1$	14.09			
	—	$4e'$	14.43			
	—	$5e'$	14.57			
	—	$6e'$	14.80			
	—	$3e''$	14.82			
	— —	$1a_1''$	15.09			
	—	$2a'_2$	15.25			
	—	$3a_2''$	16.50			
$3a'_1$	18.41	$5a'_1$	18.07			
$4e'$	19.33	$7e'$	18.74			
SiS_3^2 ca CS_3^2				Si $3s$	1.29	1.12
$1a'_1$	-12.97	$1a'_1$	-14.43	$3p_\sigma$	1.92	1.66
$1e'$	-10.39	$1e'$	-12.24	$3p_\pi$	0.71	0.80
$2a'_1$	-4.05	$2a'_1$	-5.73	$3d_\sigma$	—	0.45
$1a''_2$	-1.56	$1a''_2$	-3.04	$3d_\pi$	—	0.72
$2e'$	-0.72	$2e'$	-2.79	Nett charge on Si	$+0.08$	-0.75
		$1a_2'$	0.34			
$1a_2'$	1.77	$1e''$	0.75	S $3s$	1.79	1.74
$1e''$	2.22	$3e'$	1.08	$3p_\sigma$	3.53	3.11
$3e$	2.86	$3a'_1$	8.73	$3p_\pi$	1.37	1.39
$2a_2''$	11.61	$2a_2''$	9.42	$3d_\sigma$	—	0.10
		$4e'$	9.52	$3d_\pi$	—	0.08
		$5e'$	9.62	Nett charge on S	-0.69	-0.42
		$4a'_1$	11.20			
		$6e'$	12.00			
		$2e''$	12.20			
		$5a'_1$	12.21			
		$7e'$	12.70			
		$8e'$	12.84			
		$3e''$	12.87			
		$3a_2''$	12.96			
		$2a'_2$	13.09			
		$4a''_2$	13.84			
$3a'_1$	14.03	$6a'_1$	14.52			
$4e'$	15.28	$9e'$	14.72			

Table 6

Electronic properties of H_2CO_3 and H_2CS_3

Eigenvalues (eV)			Charge distribution		
H_2CO_3					
	$1a_1$	-44.50	C	$2s$	1.04
	$1b_1$	-37.64		$2p$	2.55
	$2a_1$	-34.14	Nett charge on C		$+0.41$
	$3a_1$	-19.69			
	$1b_2$	-17.78	O(H)	$2s$	1.51
	$4a_1$	-16.60		$2p$	4.76
	$2b_1$	-16.49	Nett charge on O(H)		-0.27
	$3b_1$	-13.41			
	$1a_2$	-13.21	O(C)	$2s$	1.68
	$4b_1$	-10.72		$2p$	4.57
	$5a_1$	-10.56	Nett charge on O(C)		-0.25
	$2b_2$	-10.19			
	$3b_2$	4.84	H	$1s$	0.81
	$6a_1$	7.39	Nett charge on H		$+0.19$
	$5b_1$	8.93			
	$7a_1$	9.90			
	$6b_1$	10.18			
	$8a_1$	10.54			
H_2CS_3			C	$2s$	1.04
				$2p$	2.69
	$1a_1$	-35.79	Nett charge on C		$+0.27$
	$1b_1$	-28.77	S(C)	$3s$	1.70
	$2a_1$	-25.46		$3p$	4.31
	$3a_1$	-21.18		 $3d$	0.20 -0.21
	$1b_2$	-17.02	Nett charge		
	$2b_1$	-15.29	on S(C)		
	$4a_1$	-15.29	S(H)	$3s$	1.49
	$3b_1$	-13.62		$3p$	4.44
	$1a_2$	-11.25		$3d$	0.25
	$5a_1$	-10.05	Nett charge		
	$2b_2$	-9.51	on S(H)		-0.18
	$4b_1$	-9.15	H	$1s$	0.85
	$3b_2$	0.36	Nett charge on H		$+0.15$
	$6a_1$	1.70			
	$7a_1$	2.14			
12 eigenvalues ranging from 2.29−4.19 eV. $(4b_1 + 3a_1 + 2b_2 + 3a_2)$					
	$6b_2$	4.54			
	$11a_1$	5.06			
	$9b_1$	5.73			
	$12a_1$	6.39			
	$10b_1$	7.57			
	$13a_1$	7.62			

level would give rise to a state of symmetry $e' \times a_2'' = e''$. Transitions to this state are forbidden and, hence, would give rise to only weak colour induced vibronically. The next level down in the energy scale is of a_2' symmetry and would give an A_1'' state – again forbidden. It is not until one considers the third highest bonding orbital that we would observe an allowed transition. This would be ${}^1A_1' \rightarrow {}^1E'$ and would be strongly polarised in the horizontal plane. There are a number of states which are in the same energy region due to sulphur *d* orbital participation and these should aggregate to produce the observed colour.

The uncorrected energy levels for SiS_3^{2-} are of comparable stability to those of CS_3^{2-} and of CO_3^{2-} and, on this basis, one would expect the ion to be of similar stability. We include the crystal field of, *eg.*, a Na^+ cation by taking the Na-Si distance to be scaled from the Na-C distance

Table 7

Electronic properties of CS_4 and SiS_4^{4-}

CS_4^{4-}	Eigenvalues			Charge distribution			
	a		*b*			*a*	*b*
1*a*	−6.65	1*a*	−9.26	C	2*s*	1.06	1.05
1*t*	2.24	1*t*	0.14		2*p*	2.70	2.61
2*a*	7.48	2*a*	6.13	Nett charge on C		+0.24	+0.34
2*t*	9.49	2*t*	8.14	S	3*s*	1.84	1.78
1*e*	11.91	1*e*	10.62		3*p*	5.22	4.89
3*t*	13.93	3*t*	12.22		3*d*	—	0.41
4*t*	14.73	4*t*	13.40	Nett charge on S		−1.06	−1.08
		5*t*	21.90				
		3*a*	22.57				
		2*e*	22.89				
		6*t*	23.27				
		7*t*	23.31				
		3*e*	23.50				
		8*t*	23.72				
		9*t*	24.00				
3*a*	26.75	4*a*	26.48				
5*t*	28.15	10*t*	27.40				
SiS_4^{4-}				Si	3*s*	1.18	0.95
1*a*	−3.80		−5.54		3*p*	2.73	2.29
1*t*	0.13		−2.50		3*d*	—	2.28
2*a*	5.92		3.76	Nett charge on Si		+0.09	−1.52
2*t*	8.46		5.88	S	3*s*	1.78	1.72
1*e*	10.74		7.90		3*p*	5.25	4.62
3*t*	11.65		10.11		3*d*	—	0.28
4*t*	12.95		10.61	Nett charge on S		−1.03	−0.62
5*t*	—		16.97				
2*e*	—		17.32				
6*t*	—		19.32				
3*a*	—		19.35				
3*e*	—		19.86				
7*t*	—		19.91				
8*t*	—		20.51				
4*e*	—		20.54				
9*t*	—		20.62				
10*t*	—		20.84				
3*a*, 11*t*	24.03		23.82				
5*t*, 4*a*	24.61		24.43				

in the Si-S : C-S ratio (*i.e.* 0.27 nm) together with trigonal geometry as for Na_2CO_3 and Na_2CS_3. Using the charge distribution from table 5 we conclude that the highest bonding level in SiS_3^{2-} lies at ~ −10eV. Because of our assumed geometry this figure will only be accurate to at best ±20%, However, it does show that the SiS_3^{2-} ion ought to be intrinsically stable in simple salts.

CS_4^{4-} *and* SiS_4^{4-}

Again (table 7) one finds that a number of positive eigenvalues appear in both these systems.

We first assume a geometry for the sodium salts Na_4XS_4 based, as before, on a cube and for simplicity assume that $Na-C = S-C = 0.205$ nm and $Na-Si = S = Si = 0.240$ nm. The energy shifts to be imposed, based on the calculated charge distributions are ~ 12 eV for CS_4^{4-} and ~ 47 eV for SiS_4^{4-}. This means that, whereas all the eigenvalues of the latter become bonding, the former is left, after correction, with a significant number of levels which have positive energies. This parallels the situation previously found[1] for the CO_4^{4-}, SiO_4^{4-} ions.

Revue Roumaine de Chimie, **18**, *9*, 1513–1519 (1973)

CHALEURS DE TRANSFERT EN MILIEUX IONIQUES: APPLICATION AUX SOLUTIONS AQUEUSES DE KCl ET HCl À 25° ET 35°C

J. CHANU et M. E. WEILL

Laboratoire de Thermodynamique des Milieux Ioniques et Biologiques — Université PARIS VII Tour 33—2, Place Jussieu, Paris 5ème —75

Reçu le 28 juin 1972

Après avoir brièvement rappelé les bases théoriques de la Thermodiffusion, on décrit le montage ayant servi à déterminer les chaleurs de transfert. Une interprétation qualitative des résultats est donnée, ainsi qu'une application au calcul des coefficients d'activité.

La thermodiffusion ou l'effet SORET consiste en la création d'un gradient de concentration sous l'effet d'un gradient de température. Ce phénomène ne peut s'interpréter que dans le cadre de la Thermodynamique des Phénomènes Irréversibles (T.P.I.). En effet, celle-ci prévoit théoriquement des « effets croisés » tel que l'effet SORET ou son opposé, l'effet DUFOUR (création d'un gradient de température sous l'action d'un gradient de concentration.

L'importance du phénomène de thermodiffusion, pour un mélange donné, ne dépend que du gradient de température imposé. Dans des conditions expérimentales favorables, il est possible de mesurer la séparation des constituants. Pour un mélange binaire, cette séparation peut se décrire par un coefficient dit coefficient SORET tel que

$$S_T = -\frac{1}{N_1 N_2}\left(\frac{\mathrm{d}N_1}{\mathrm{d}t}\right)_{t\to\infty} = -\frac{1}{m}\left(\frac{\mathrm{d}m}{\mathrm{d}T}\right)_{t\to\infty} \tag{1}$$

suivant que le titre du mélange est repéré en fractions molaires ou en molalité.

L'application de l'approximation linéaire de la T.P.I. (Relations de Onsager[1] permet de prévoir, grâce au théorème du minimum d'entropie, dû à Prigogine,[2] l'évolution du phénomène. Le mélange macroscopique, initialement homogène, évoluera au cours du temps vers un état stationnaire de non-équilibre indépendant du temps. Dans cet état, le gradient de température étant toujours maintenu uniforme, la production d'entropie sera minimum. Physiquement, il y a compensation entre la séparation créée sous l'action du gradient de température et la diffusion pure qui tend continuellement à homogénéiser le mélange.

---

[1] L. Onsager, *Phys. Rev.*, **37**, 405 (1931) ; **38**, 2265 (1931).

[2] Cf. par exemple — I. Prigogine, « Introduction à la Thermodynamique des Processus Irréversibles » (trad. J. Chanu), Dunod, Paris, 1968.

Parmi les quantités de transport introduites par la thermodynamique, on peut relever la chaleur de transfert, reliée au coefficient SORET par

$$S_T \ m \left(\frac{\partial \mu}{\partial m} \right)_T = \frac{Q^*}{T} = S^* \tag{2}$$

dans le cas d'un mélange binaire soluté-solvant (μ : potentiel chimique du soluté, Q^* : chaleur de transfert du soluté, S^* : entropie de transfert du soluté).

Dans le cas où le soluté est un élecyrolyte dissocié en ν_+ cations et ν_- anions de chaleurs de transfert Q^*_+ et Q^*_-, on a

$$\nu R T^2 S_T \left[1 + \frac{\partial \log f^\pm}{\partial \log m} \right] = \nu_+ Q^*_+ + \nu_- Q^*_- = Q^* \tag{3}$$

où $\nu = \nu_+ + \nu_-$ et $f^\pm$ est le coefficient d'activité molal de l'électrolyte.

Nous voyons donc que des mesures expérimentales fourniront non seulement la valeur des coefficients SORET mais surtout celle des chaleurs et entropies de transfert. Rappelons que le transport d'ions dans un solvant fait intervenir, quelle que soit la concentration, des interactions ion-solvant que l'on peut, en thermodynamique, représenter de manière imagée par les chaleurs de transfert ionique, Q_k^{*}[3,4], de sorte que la densité de flux de chaleur J_q s'écrit

$$J_q = \sum_k (h_k + Q_k^*) J_k, \tag{4}$$

J_k : densité de flux de diffusion du constituant k ;
h_k : enthalpie spécifique partielle du constituant k.

Les chaleurs de transfert de HCl et KCl à 25° et 35° ont été mesurées dans le montage suivant.

MONTAGE EXPÉRIMENTAL

Nous avons utilisé la méthode qui consiste à imposer un gradient de température vertical à la solution comprise entre deux plaques horizontales. On peut espérer dans ce cas s'affranchir de la convection qui fausserait la mesure puisqu'on doit obtenir une stratification

---

[3] E. D. Eastman, *J. Amer. Chem. Soc.*, **50**, 283 (1928).

[4] J.N. Agar, »Advances in Electrochemistry and Electrochemical Engineering », vol. 3, Paul Delahay, 1963.

de la solution. Cette méthode ne convient qu'aux sels de coefficient SORET positif, c'est-à-dire ceux pour lesquels la thermodiffusion se traduit par une augmentation de densité dans la partie inférieure de la cellule. La mesure elle-même consiste alors dans la comparaison des concentrations de la solution à deux niveaux différents. Pour cela nous avons employé conjointement deux méthodes.

MÉTHODE INTERFÉROMÉTRIQUE

L'indice de réfraction varie avec la concentration d'une solution à une température donnée. Nous envoyons un faisceau lumineux sur la solution et à la sortie de la cellule nous plaçons des fentes d'Young ; il y a formation de franges d'interférences. Un dispositif optique permet de localiser les franges sur un photomultiplicateur (fig.1). Quand la concentration varie par thermodiffusion (∇T constant et uniforme), le déplacement des franges est détecté et enregistré par l'intermédiaire du P.M. Si l'on connaît $(\partial n/\partial m)_T$ de la solution, on peut relier la variation de concentration au nombre de franges ayant défilé, donc connaître le coefficient SORET par

$$S_T = -\frac{1}{m}\,\frac{1}{(\partial n/\partial m)_T}\,\frac{\partial n/\partial z}{\partial T/\partial z} \tag{5}$$

MÉTHODE POTENTIOMÉTRIQUE

On place à l'intérieur de la solution deux électrodes à anion réversible à deux niveaux différents ; nous obtenons alors une différence de potentiel (d.d.p.) due à :

– la différence de température entre les deux niveaux ;

– la différence de concentration due à la thermodiffusion.

En l'absence de courant, la d.d.p. ψ engendrée dans le milieu par les différences de température et de concentration s'écrit

$$\mathrm{grad}\ \psi = -\frac{1}{\mathcal{F}}\left[\sum_j \frac{t_j}{z_j}\frac{Q_j^*}{T}\,\mathrm{grad}\ T + \sum_j \frac{t_j}{z_j}\,(\mathrm{grad}\ \mu_j)_{p,T}\right] \tag{6}$$

Le deuxième terme du deuxième membre de (6) correspond au potentiel créé par thermodiffusion. Il faut y ajouter, puisque l'on utilise des électrodes de seconde espèce, la d.d.p. de Nernst, soit $-\nabla\mu/\mathcal{F}$, pour obtenir la variation de potentiel, grad $\varnothing$, détectée au cours de l'expérience. Celle-ci s'écrira en tenant compte de ce que $\nu_j = \mp z_j$ [5]

$$\mathrm{grad}\ \varnothing = -\frac{1}{\mathcal{F}}\,\frac{t_+}{\nu_+\,\nu_-}\sum_j \nu_j\,(\mathrm{grad}\ \mu_j)_{p,T} \tag{7}$$

[5] G. Milazzo and J. Chanu, « True Temperature Coefficients of the Electric Tension of Individual Electrodes », *Z. Phys. Chem. (Frankfurt)*, **68**, 250 (1969).

D'autre part, à l'état stationnaire ($t \to \infty$), l'annulation des flux de diffusion entraîne

$$\sum_j \nu_j (\text{grad } \mu_j)_{p,T} = - \frac{\text{grad } T}{T} Q^* \tag{8}$$

Si on remarque que le premier terme du deuxième membrane de (6) ne varie plus à partir de l'instant $t = 0$ où le gradient de température est établi jusqu'à la fin du phénomène, la valeur du potentiel Ø à l'état stationnaire s'obtient simplement en tenant compte dans (7) de la condition (8), soit

$$\left(\frac{d\text{Ø}}{dT}\right) = \frac{t_+ Q^*}{\mathfrak{F}\,\mathrm{T}} \tag{9}$$

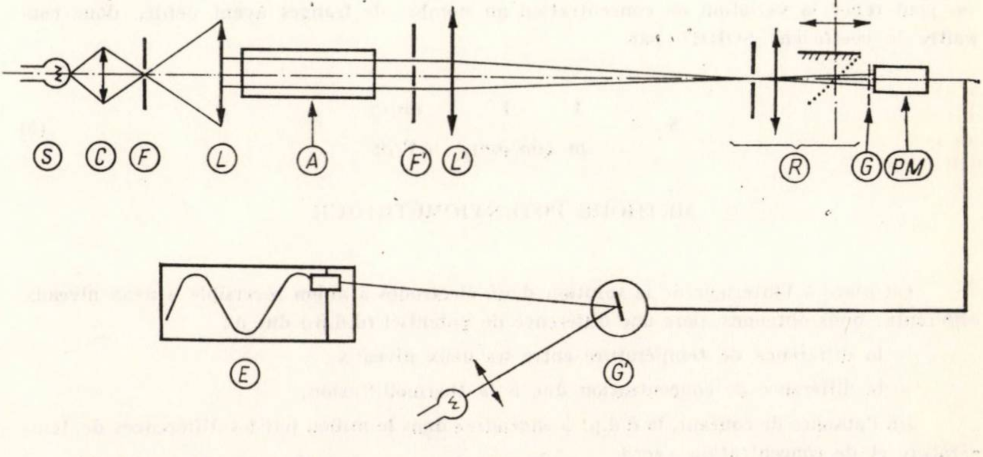

Fig. 1. — S :Source ; C :condenseur ; F : Diaphragme ; L : lentille collimatrice ; A : cellule de mesure ; F' : fente ; L' : lentille de champ ; R : chambre réflexe ; G : grille ; PM : photomultiplicateur ; G' : galvanomètre ; E : enregistreur.

LES PROBLÈMES CONVECTIFS

Il est évident que les mesures de thermodiffusion statique sont faussées ou même impossibles dès que la convection apparait*. En particulier, en dessous d'une certaine concentration variable suivant les sels, il a été expérimentalement impossible jusqu'ici d'obtenir un état stationnaire, la convection s'introduisant pendant l'évolution du phénomène vers cet état. Ceci avait déjà été remarqué par Agar[6] qui disposait d'un appareillage différent du nôtre et mesurait les chaleurs de transfert par conductimétrie.

---

* Les appareils à thermogravitation au contraire créent la convection afin d'obtenir une séparation plus importante des constituants. Mais les coefficients SORET obtenus par cette méthode sont plus difficiles à évaluer de manière précise.

[6] J. N. Agar et J.C.R. Turner, *Proc. Roy. Soc., A*, **255**, 307 (1960).

Les travaux récents de Prigogine et Glansdorff[7] sur les instabilités ont montré que dans notre cas -gradient de température direct, gradient de concentration adverse- la convection ne doit pas s'introduire « spontanément ». Mais il est certain que ces calculs ne prennent en compte pour l'instant que des conditions expérimentales idéales réalisées dans une cellule pour laquelle les surfaces seraient parfaitement planes et horizontales et le gradient de température uniforme, constant et vertical. Or, comme le remarque AGAR, dans l'évolution vers l'état stationnaire une petite perturbation du gradient de température va retentir de manière importante sur la répartition des concentrations (le coefficient de diffusion est environ cent fois plus grand que le coefficient de diffusivité thermique). Dans ces conditions des divergences notables peuvent apparaître entre, par exemple, les valeurs des coefficients SORET obtenues pour l'état stationnaire et celles calculées dès le début du phénomène.

Grossièrement, on peut dire que la convection s'introduit d'autant plus facilement que la solution est diluée et, à concentration égale, que la variation de densité est plus faible en fonction de la concentration : $BaCl_2$ plus stable que KCl, par exemple.

RÉSULTATS

Ils sont résumés dans les graphes ci-après :

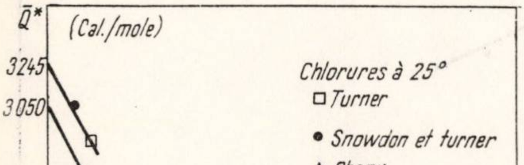

Fig. 2. — Chaleurs de transfert à 25°C de HCl, NaCl, KCl en fonction de la racine carrée de la molalité.

---

[7] P. Glansdorff et I. Progogine, « Structure, Stabilité et Fluctuations », Masson 1971, Paris.

Ces courbes montrent d'abord une nette similitude entre elles, sauf pour HCl pour lequel nous n'avons pu faire d'expériences à concentration élevée. La forme des courbes peut s'interpréter, au moins qualitativement, à partir du modèle de l'ion hydraté de Franck et Wen[8].

Rappelons que ces auteurs estiment que l'ion est entouré de trois zones d'eau : une couche *A*, très fortement liée à l'ion, une zone *B*, dite de structure brisée, dans laquelle les molécules sont soumises contradictoirement à l'influence de l'ion et à celle de la région *C* d'eau libre. Quand la concentration s'élève (partie à la gauche du minimum) la décroissance sensiblement linéaire viendrait de la diminution de la région *C* d'eau libre. La concentration continuant à augmenter, l'espace contrôlé par chaque ion diminuerait de sorte qu'au minimum la région *C* aurait pratiquement disparu.

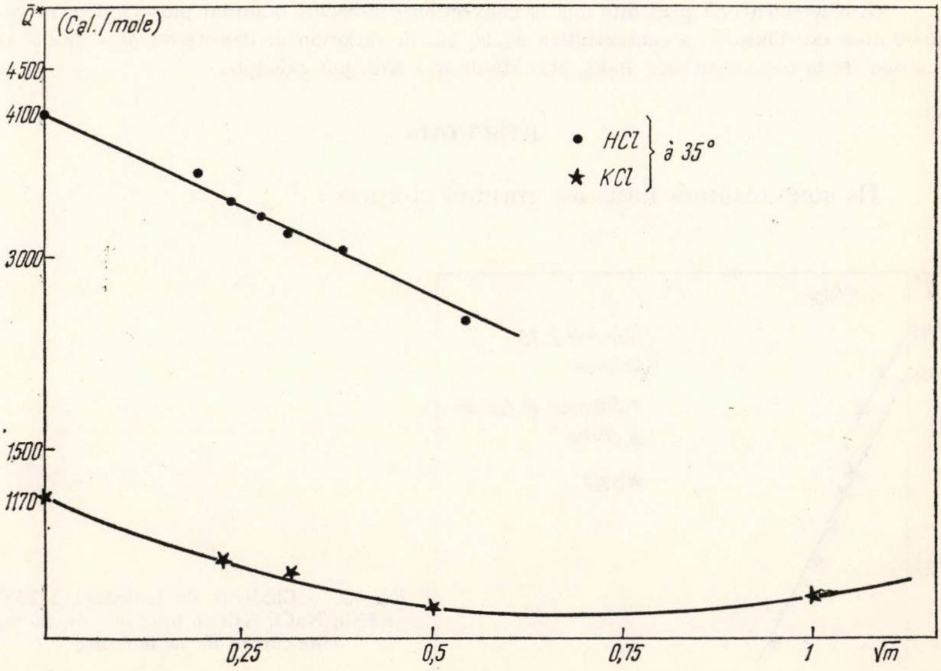

Fig. 3. — Chaleurs de transfert à 35°C de HCl, KCl en fonction de la racine carrée de la molalité.

On constate d'autre part un décalage des minima des courbes suivant les différents sels. Le minimum de la courbe de KCl se situe à une concentration plus élevée que celui de NaCl. Or le rayon de K^+ est supérieur à celui de Na^+ pour une charge égale. Il y aura donc à priori moins de molécules d'eau autour de K^+ qu'autour de Na^+, donc, à concentrations égales, une région *C* d'eau libre plus importante pour K^+ que pour Na^+, ce qui expliquerait le décalage des minima. Le même raisonnement peut se tenir si l'on compare les courbes représentatives de HCl et KCl, à condition de considérer H^+ en solution aqueuse sous la forme H_3O^+, ce qui est habituellement admis.

---

[8] H. S. Franck et Y. W. Wen, *Discuss. Faraday Soc.*, **24**, 133 (1957).

On notera aussi la valeur élevée de la chaleur de transfert d'HCl qui serait à rapprocher des mécanismes de transport particuliers proposés pour l'ion H^+, et la linéarité très grande de sa courbe représentative qui pourrait être une conséquence du rôle joué par l'encombrement stérique dans le mécanisme du phénomène.

Si l'on considère la courbe au-delà du minimum, l'interprétation devient nettement moins aisée faute d'une théorie satisfaisante en solution concentrée. Disons seulement qu'une liaison avec un modèle de type cristallin serait à tenter.

Nous voyons donc déjà par cette approche encore qualitative l'intérêt de la mesure des chaleurs de transfert, directement liées à la structure des ions en solutions.

APPLICATION AUX COEFFICIENTS D'ACTIVITÉ

Milazzo a montré récemment[5] que l'on pouvait chercher à atteindre le coefficient d'activité ionique individuel à l'aide de piles thermiques avec transport, à condition de connaître les chaleurs de transfert individuelles des ions. Malheureusement l'expérience ne peut fournir que les chaleurs globales $Q^* = \nu_+ Q^*_+ + \nu_- Q^*_-$ et non Q^*_+ et Q^*_-. Néanmoins, si l'on connaît Q^* pour différents sels, il est possible d'admettre un partage entre Q^*_+ et Q^*_-. Par exemple, pour KCl, une valeur de départ correcte serait $Q^*_{K^+} =$ $= Q^*_{Cl^-} = \frac{1}{2} Q^*_{KCl}$. Il est alors possible de déterminer les chaleurs individuelles limites de tous les ions. Bien entendu, le calcul montre pour certains ions que la partition n'est pas valable, d'où modification de la partition formelle initiale. Il sera donc possible, par approximations successives, de découvrir les valeurs individuelles réelles de Q^*_+ et Q^*_- à concentration nulle et donc les coefficients d'activité ionique individuels. Encore une fois apparaît la nécessité, pour mener ces calculs à bien, d'obtenir des valeurs précises de Q^* pour de nombreux sels.

Revue Roumaine de Chimie, **18**, *9*, 1521–1529, (1973)

LES ANALYSES CRYOMÉTRIQUES DANS LA RECHERCHE DE LA STRUCTURE DES SUBSTANCES DISSOUTES EN MILIEU SALIN ÉLECTROLYTE FORT

GEORGES PETIT

Université Paris VI, Laboratoire de Thermodynamique du Liquide Salin, 9, Quai St. Bernard, Paris 5^{e}

Reçu le 7 mars 1973

Cet exposé, qui montre l'élucidation de la structure des substances dissoutes à l'aide de l'analyse cryométrique, se divise en deux parties : 1) la numération est valable dans les solutions hautement diluées ; 2) l'interprétation, la traduction de ces nombres globaux de particules conduit à caractériser la nature des substances dissoutes.

1ère PARTIE

INTERPRÉTATION EN ANALYSE CRYOMÉTRIQUE DE L'ACTIVITÉ EN MILIEU SALIN ÉLECTROLYTE FORT (CAS DES FLUOSELS)

Nous avons, depuis de nombreuses années [1,2] basé l'interprétation de nos travaux cryométriques sur l'hypothèse suivant laquelle en milieu salin électrolyte fort, *et en milieu hautement dilué*, le regroupement particulaire suivant Arrhénius est pratiquement le seul facteur cryométriquement détectable avec nos méthodes de mesure, hypothèse basée essentiellement sur les données expérimentales. En effet dans le cas de décroissances de la courbe de Raoult nous observons fréquemment à haute dilution un quasi-palier correspondant à un nombre de particules dont l'interprétation chimique est toujours acceptable.

La solution est donc idéale pour le complexe formé. Ceci nous a amené à définir une solution idéale pour un soluté donné comme une solution dans laquelle tous les facteurs entropiques et d'interaction énergétique à distance disparaissent (indépendamment des réactions chimiques antérieures qui ont donné naissance au soluté actuel), et où la numération reste donc seule pratiquement valable.

---

[1] G. Petit, « La cryométrie à haute température et ses applications », Mason Editeurs, Paris, 1965.

[2] G. Petit et Chr. Bourlange, *Compt. rend.*, **237**, 497 (1953).

La résolution de ce problème s'est beaucoup précisée à la suite d'une remarque de Doucet[3] qui a montré que l'on pouvait écrire :

$$(\theta/m_s)/(\theta/m_s)_{m_s} = 0 = \nu_s^{(m)}/\nu_s^{(0)} - (\nu_S/\nu_s^{(0)})(\ln\ \gamma_S\ .1000/m_s M_S)$$

où :

(θ/m_s) = dépression thermique molaire,
ν_s = nombre de particules étrangères dissoutes,
$\nu_s^{(0)}$ = nombre de particules étrangères dissoutes à la dilution infinie,
ν_S = nombre de particules de solvant,
m_s = molarité du corps dissous,
$\nu_s^{(m)}$ = nombre de particules étrangères dissoutes à la molarité m,
M_S = masse molaire du solvant,
γ_S = coefficient d'activité du solvant.

La solution idéale étant une solution qui donne une numération correcte des particules dissoutes, le terme logarithmique apparaît dans cette expression comme un facteur correctif dans la numération. C'est donc essentiellement une fonction d'énergie d'interaction à distance et d'entropie d'ordre (et de dimension), indépendamment de toute théorie d'Arrhénius. Ce terme sera donc évalué pour une structure déterminée, à une molarité donnée du corps dissous, par exemple à un quasi-palier de la courbe cryométrique, indépendamment de tout phénomène antérieur.

La théorie d'Arrhénius peut être considérée comme seule *techniquement* vérifiable lorsque nous avons :

$$(\theta/m_s)/(\theta/m_s)_{m=0} \# \nu_s^{(m)}/\nu_{(s)}^0$$

ou

$$(\nu_S\ /\nu_{(s)}^m)(\ln\ \gamma_S \cdot 10^3/m_s\ M_S) \leqslant 4\,\%$$

4 % étant la précision de nos expériences.

Cette relation nous permet d'évaluer $\ln\gamma_S$ étant connu la valeur de la molarité du corps dissous, au-delà de laquelle notre hypothèse n'est plus expérimentalement valable.

CALCUL DE $\ln\gamma_S$

a) *Facteur entropique*

Nous ne parlerons point ici de ce facteur qui ne peut guère se manifester qu'à grande concentration. Quoique discernable dans ces conditions dans les mélanges d'halogénures alcalins[4] il n'intervient que peu chez de gros ions à symétrie sphérique (cas de F_6AlNa_3 dans FNa[5] et Doucet et son école[6]). (Voir cependant Cantor[7]).

---

[3] Y. Doucet, Communication privée.

[4] A. Lumsden, « Thermodynamics of Molten Salt Mixtures », Academic Press, Londres, 1966.

b) Facteur enthalpique

Nous nous sommes limité aux systèmes formés d'un solvant de particules A, B, C, en nombre ν_A, ν_B, ν_C, par molécule et d'un soluté formé de particules P, Q, R (en nombre ν_P, ν_Q, etc.).

Nous avons évalué $\ln\gamma_S$ par la méthode de Hildebrand et Salström[8] suivant les principes de Flood[9] (voir l'exposé de Lumsden[4] et la symbolique de Temkin[10] et Haase[11]).

Dans la théorie de Flood nous ne devons considérer que les interactions entre particules de signes contraires. L'activité est donc fonction du facteur entropique d'ordre et de dimension d'une part et de l'énergétique des interactions $+-$ d'autre part. Celles-ci se dissocient en deux groupes : 1) les interactions du type A entre voisins immédiats $A^- C^+$ par exemple ; 2) les interactions du type B entre ions de même signe séparés par une particule de l'autre signe $A^-C^+A^-$ par exemple.

Pour M_S molécules de solvant et M_d de corps dissous, les fonctions énergétiques s'écriront par exemple :

$$M_S\, \nu_{A^-}\, (M_S\, \nu_{C^+}/\Sigma^+)\, \O_{AC} \text{ pour } A^-\, C^+ \text{ et}$$

$$M_S\, \nu_{A^-} (M_S\, \nu_{C^+}/\Sigma^+)(M_S\, \nu_{B^-}/\Sigma^-)\, \O_{A^-C^+A^-} \text{ pour } A^-\, C^+\, A^-,$$

où Σ^+ et Σ^- sont les nombres totaux de cations et d'anions :

$$\Sigma^+ = M_S\, \nu^+_{\theta S} + M_d\, \nu^+_{\theta d}\,;\ \Sigma^- = M_S\, \nu^-_{\theta S} + M_d\, \nu^-_{\theta d}\,.$$

Dans le cas d'ions monovalents on a $\Sigma^+ = \Sigma^-$. Ci-dessus ν_θ sont les nombres totaux d'ions par molécule, $\O_{A^-C^+}$ est l'enthalpie de A^-C^+ et $\O_{A^-C^+B^-}$ est le facteur d'interaction énergétique de Hildebrand pour le système $A^-\, C^+$ dans B^-C^+.

Type A. En écrivant toutes les interactions concevables, on obtient après avoir divisé par deux, éliminé avec Flood [4] les interactions propres au solvant et dérivé par rapport à M_S, la relation pour le facteur enthalpique A seul :

$$RT\ln \gamma_S = [M_d^2\, \nu_{\theta d}/(M_S\, \nu_{\theta s} + M_d\, \nu_{\theta d})^2]\, (\nu_A \nu'_R\, \O_{AR} + \nu_B\, \nu'_R\, \O_{BR} +$$
$$+ \nu_C\, \nu'_P\, \O_{CP} + \nu_C\, \nu'_Q\, \O_{CQ}).$$

---

[5] K. Grjotheim, *Kgl. Norske Videnskab. Selskabs, Skrifter*, **1956**, N° 5.

[6] Y. Doucet et M. Bizouard, *Compt. rend.*, **242**, 2137 (1956) ; **246**, 719 (1958).
Y. Doucet et J. Leduc, *Compt. rend.*, **237**, 52 (1953) ; **238**, 1018 (1955).
Y. Doucet, J. Leduc et G. Pannetier, *Compt. rend.*, **236**, 1018 (1953).

[7] S. Cantor et W. Ward, *J. Chem. Phys.*, **67**, 2766 (1963).

[8] J. Hildebrand et E. Salstrom, *J. Amer. Chem. Soc.*, **54**, 4257 (1932).

[9] H. Flood, T. Förland et K. Grjotheim, « The Physical Chemistry of Melts », Institution of Mining and Metallurgy, Londres, 1953, p. 46.

[10] M. Temkin, *Acta Physicochim.*, **20**, 411 (1945).

[11] R. Haase, *Z. Naturforsch.*, **8**, 380 (1953).

Type B. En opérant d'une façon identique pour le type B on obtient finalement pour le terme énergétique (N sont les fractions particulaires : N_d du corps dissous, N_S du solvant) :

$$\mathrm{RT}\ln\gamma_S = N_d^2\,[N_S\,[2\,\nu^{\pm}_{\theta d}\,(S_5) - \nu^{\pm}_{\theta s}\,(S_6)]]$$

où les $\nu^{\pm}_{\theta d}$ et $\nu^{\pm}_{\theta s}$ sont les nombres totaux d'anions (ou de cations) dans le corps dissous et le solvant et où :

$$S_5 = (\nu_{\mathrm{A}}\,\nu_{\mathrm{B}}\,\nu'_{\mathrm{R}}\,\varnothing_{\mathrm{ARB}} + \nu_{\mathrm{A}}\,\nu_{\mathrm{C}}\,\nu'_{\mathrm{P}}\,\varnothing_{\mathrm{ACP}} + \nu_{\mathrm{A}}\,\nu_{\mathrm{C}}\,\nu'_{\mathrm{Q}}\,\varnothing_{\mathrm{ACQ}} + \nu_{\mathrm{B}}\,\nu_{\mathrm{C}}\,\nu'_{\mathrm{P}}\,\varnothing_{\mathrm{BCP}} +$$

$$+ \nu_{\mathrm{B}}\,\nu_{\mathrm{C}}\,\nu'_{\mathrm{Q}}\,\varnothing_{\mathrm{BCQ}} + \nu_{\mathrm{C}}\,\nu_{\mathrm{A}}\,\nu'_{\mathrm{R}}\,\varnothing_{\mathrm{CAR}} + \nu_{\mathrm{C}}\,\nu_{\mathrm{B}}\,\nu'_{\mathrm{R}}\,\varnothing_{\mathrm{CBR}}),$$

$$S_6 = (\nu_{\mathrm{A}}\,\nu'_{\mathrm{R}}\,\nu'_{\mathrm{P}}\,\varnothing_{\mathrm{ARP}} + \nu_{\mathrm{A}}\,\nu'_{\mathrm{R}}\,\nu'_{\mathrm{Q}}\,\varnothing_{\mathrm{ARQ}} + \nu_{\mathrm{B}}\,\nu'_{\mathrm{R}}\,\nu'_{\mathrm{P}}\,\varnothing_{\mathrm{BRP}} + \nu_{\mathrm{B}}\,\nu'_{\mathrm{R}}\,\nu'_{\mathrm{Q}}\,\varnothing_{\mathrm{BRQ}} +$$

$$+ \nu_{\mathrm{C}}\,\nu'_{\mathrm{P}}\,\nu'_{\mathrm{R}}\,\varnothing_{\mathrm{CPR}} + \nu_{\mathrm{P}}\,\nu'_{\mathrm{C}}\,\nu'_{\mathrm{Q}}\,\varnothing_{\mathrm{PCQ}} + \nu_{\mathrm{C}}\,\nu'_{\mathrm{Q}}\,\nu'_{\mathrm{R}}\,\varnothing_{\mathrm{CQR}}).$$

Note. Ces termes se simplifient si les cations sont communs ($C = R$). Il reste alors après élimination des nouvelles interactions devenues caractéristiques des substances pures :

$$S_5 = \nu_{\mathrm{A}}\,\nu_{\mathrm{C}}\,\nu'_{\mathrm{P}}\varnothing_{\mathrm{ACP}} + \nu_{\mathrm{A}}\,\nu_{\mathrm{C}}\,\nu'_{\mathrm{Q}}\varnothing_{\mathrm{ACQ}} + \nu_{\mathrm{B}}\,\nu_{\mathrm{C}}\,\nu'_{\mathrm{P}}\varnothing_{\mathrm{BCP}} + \nu_{\mathrm{B}}\,\nu_{\mathrm{C}}\,\nu'_{\mathrm{Q}}\varnothing_{\mathrm{BCQ}}$$

$$S_6 = \nu_{\mathrm{A}}\,\nu'_{\mathrm{R}}\,\nu'_{\mathrm{P}}\varnothing_{\mathrm{ACP}} + \nu_{\mathrm{A}}\,\nu'_{\mathrm{R}}\,\nu'_{\mathrm{Q}}\varnothing_{\mathrm{ACQ}} + \nu_{\mathrm{B}}\,\nu'_{\mathrm{R}}\,\nu'_{\mathrm{P}}\varnothing_{\mathrm{BCP}} + \nu_{\mathrm{B}}\,\nu'_{\mathrm{R}}\,\nu'_{\mathrm{Q}}\varnothing_{\mathrm{BCQ}}$$

Nous avons alors étudié les cas suivants :

CRYOLITHE DANS ClNa

$$\nu_{\mathrm{A}} = 0, \quad \nu_{\mathrm{B}} = 1, \quad \nu_{\mathrm{C}} = 1, \; \nu'_{\mathrm{P}} = 1, \; \nu'_{\mathrm{Q}} = 2, \; \nu'_{\mathrm{R}} = 3$$

$(C = B)$.

Après élimination des interactions devenues celles des substances pures, il reste :

$$S_5 = \varnothing_{\mathrm{BCP}} + 2\varnothing_{\mathrm{BCQ}}$$

$$S_6 = 3\varnothing_{\mathrm{BCP}} + 6\varnothing_{\mathrm{BCQ}}$$

$$\Sigma^+ = \Sigma^- = M_S + 3M_d.$$

On a :

$$RT\ln\gamma_S = M_d^2/(M_S + 3M_d)^3\,[M_S(3\varnothing_{\mathrm{BCP}} + 6\varnothing_{\mathrm{BCQ}}) +$$

$$+ M_d(9\varnothing_{\mathrm{BCP}} + 18\varnothing_{\mathrm{BCQ}})] = M_d^2/(M_S + 3M_d)^2\,(3\varnothing_{\mathrm{BCP}} +$$

$$+ 6\varnothing_{\mathrm{BCQ}}) = N^2_{(\mathrm{F_4Al})^-}\,[(3\varnothing_{\mathrm{Cl^-Na^+(F_4Al)^-}} + 6\varnothing_{\mathrm{Cl^-Na^+F^-}})].$$

Mais $\varnothing_{\mathrm{Cl^-Na^+F^-}} = 0$ (ref.[4] p. 155).

CRYOLITHE DANS FNa

Pour la cryolithe dans FNa on a :

$$RT\ln\gamma_S = N^2_{(\mathrm{F_4Al})^-}3\varnothing_{\mathrm{F^-Na^+(F_4A\ )^-}})$$

Mais Grjotheim[5] a montré que la solution est idéale, tout au moins dans la branche FNa, de telle sorte que $\varnothing_{\mathrm{F^-Na^+(F_4Al)^-}} = 0$. FNa donnant une solution idéale avec ClNa et avec $(\mathrm{F_4Al})^-\mathrm{Na}^+$, on peut penser que ces deux substances (puisque donnent une telle solution avec FNa) donnent une solution de même type entre elles, donc $\varnothing_{\mathrm{Cl^-Na^+(F_4Al)^-}} \sim 0$ et la solution de cryolithe dans ClNa est donc idéale avec le sens restreint que nous avons donné au début de cet exposé. Ces résultats peuvent être généralisés et nous dirons que la solution d'un complexe imparfait, par exemple un halogéno-métallate alcalin, dissous dans une molécule tronçon (l'halogénure alcalin correspondant) doit donner suivant notre concept une solution ne différant de l'idéalité que par le facteur entropique, c'est-à-dire que la numération des particules étrangères au solvant (Stortenbecker) données par ce complexe dissous dans une molécule tronçon n'est pas perturbée par les interactions énergétiques à distance. Cette idéalité est trouvée expérimentalement dans le cas des systèmes chlorés ($\mathrm{TiCl_3 + ClNa}$)[12], ($\mathrm{FeCl_3 + FNa}$)[13] et fluorés ($\mathrm{AlF_3 + FNa}$)[5], la non-idéalité trouvée par Cantor[7] est donc d'origine entropique. De même ce résultat montre que les numérations effectuées par nous de fluosels dans les chlorures sont valables.[14]

ALUMINE DANS FNa ET LA CRYOLITHE

a) C'est une solution d'oxyfluorure d'aluminium dans la cryolithe. Nous avons la réaction [15] :

$$(2/3)(\mathrm{Al_2O_3} + \mathrm{F_6AlNa_3}) \rightarrow (\mathrm{Al_2O_2F_2}) + 2\mathrm{F}^- + 2\mathrm{Na}^+.$$

---

[12] E. Kamenetskii, *Tsvetnye Metally*, **31**.

[13] C. Cook Jr. et W. Dum Jr., *J. Phys. Chem.*, **1505** (1961).

[14] G. Petit et Chr. Bourlange, *Compt. rend.*, **237**, 457 (1961).

[15] G. Petit et Chr. Bourlange, *Compt. rend.*, **270**, 937 (1970).

Donc ce mélange dans FNa doit donner une solution ne différant de l'idéalité que par le facteur entropique.

b) Dans la cryolithe étudions le système :

	(A)	(B)	(C)
solvant :	$(F_4Al)^-$	$2F^-$	$3Na^+$
	(P)	(Q)	(R)
corps dissous :	$Al_2O_2F_2$	$2F^-$	$2Na^+$

Un examen de ce schéma montre que la seule interaction provocant une « réalité » est l'interaction $(F_4Al)^- \longleftrightarrow (Al_2O_2F_2)^\circ$ justiciable du type A puisque l'oxyfluorure n'est pas chargé, or l'enthalpie de liaison ne peut être que faible donc là aussi la solution ne doit différer de l'idéalité que par le facteur entropique.

Ainsi ces solutions de molécules oxymétalliques sont en solution diluée extrêmement voisines de l'idéalité, ce qui explique dans le cas d'oxyfluorures métalliques dissous dans les halogénures alcalins la valeur élevée des molarités où existe encore le palier cryométrique.[16]

Ces conclusions sont loin naturellement d'être généralisables chaque cas demandant une étude particulière. Mais cependant les valeurs des paramètres énergétiques données dans le livre de Lumsden[4] dans divers types de mélanges d'halogénures métalliques suggèrent que notre hypothèse suivant laquelle en milieu hautement dilué, l'influence des fonctions d'excès des solutions régulières est très faible (de telle sorte que le regroupement particulaire suivant Arrhénius est observé pratiquement seul), est vérifié dans la très grande majorité des cas pour une molarité de 1/10 et qu'ainsi une analyse cryométrique structurale en milieu hautement dilué est valable.

2ème PARTIE

RELATIONS EN MILIEU IONISÉ LIQUIDE ENTRE LES NOMBRES DE PARTICULES ET LEUR COMPOSITION

Cette note a pour but de montrer que les numérations « atypiques » de la cryométrie, non spécifiques de la nature de particules qu'elle ne peuvent a priori que dénombrer, sont cependant susceptibles de nous révéler, en milieu ionique et grâce aux multiples conditions chimiques et arithmétiques qui leur sont associées, la composition d'ensembles complexes en solution, c'est-à-dire qu'il existe une relation entre un nombre de particules et les natures de celles-ci. Nous avons voulu ainsi répondre à la critique fondamentale faite aux numérations quant à leur valeur descriptive « les particules sont comptées certes, mais que sont-elles » en montrant que les modes de traduction de leurs nombres en leur composition ne sont pas arbitraires, mais obéissent à des règles très acceptables que nous avons voulu exposer brièvement.

---

[16] G. PETIT et CHR. BOURLANGE, *Compt. rend.*, **273**, 1069 (1971).

Nous avons déjà, dans de précédentes publications, étudié les réactions chimiques intervenant entre les diverses espèces particulaires issues de mélange salins en solution.[1-3]

Nous avons envisagé ici le cas général d'un mélange $pM + qO$ (p et q étant les nombres de particules M et O susceptibles de s'unir entre elles). Nous pouvons ainsi observer à priori plusieurs éventualités.

A) Tout d'abord, suivant que les particules O ou M sont en excès, le système final, dans le cas le plus général peut donner soit :

$$pM + qO \rightarrow (m_1/n_1)\ [(M_{x_1}\, O_{y_1})n_1] + (q - m_1 y_1)O$$

soit

$$pM + qO \rightarrow (m_2/n_2)[(M_{x_2}\, O_{y_2})n_2] + (p - m_2 x_2)M,$$

où n_2 et n_2 sont les degrés de polymérisation, m_1 et m_2 le nombre de particules complexe.

Le problème de leur caractérisation et de la composition des complexes formés a été résolu dans les travaux antérieurs,[4-6] et dont les principes sont ici immédiatement applicables.

Rappelons que ces systèmes se détectent cryométriquement par le fait que la particule en excès :

a) n'est évidemment pas captée par le système lors d'une addition ultérieure de celle-ci,

b) que dissoute dans un solvant la contenant elle devient cryométriquement « inactive » (théorème de Stortenbecker). Le nombre de particules dans un solvant qui ne contient pas la particule en excès étant évidemment plus grand que dans un solvant qui la contient (théorème de Stortenbecker).

B) Considérons maintenant le cas où ni O ni M ne sont en excès et sont donc acceptés par le système lors de leur addition.

Notons incidemment que cette captation, cryométriquement décelable, contrastant avec la non captation, révélatrice elle des états a) et b) est un test de discrimination d'états qui peuvent éventuellement donner certes un même nombre global de particules mais se différencient alors par des propriétés chimiques différentes.[7]

---

[1] G. Petit et Ch. Bourlange, *Compt. rend.*, **261**, 5132 (1965).

[2] G. Petit et Ch. Bourlange, *Compt. rend.*, **264**, 1437 (1967).

[3] G. Petit et Ch. Bourlange, *Rev. Hautes Temp. Réfract.*, **6**, 121 (1969).

[4] G. Petit et Ch. Bourlange, *Compte rend.*, **269**, 657 (1969).

[5] G. Petit et Ch. Bourlange, *Compt. rend.*, **270**, 937 (1970).

[6] G. Petit et Ch. Bourlange, *Compt. rend.*, **273**, 1065 (1971).

[7] G. Petit, ,,La cryométrie à haute température et ses applications, Masson Editeur, Paris, 1965, p. 38.

Il est alors nécessaire d'étudier le mode de répartition des particules O sur les particules M.

Nous nous appuierons sur les postulats suivants :

A) En milieu liquide salin homogène, les réactions de particules à liaison très ionique doivent être réversibles. *La structure finale, indépendante du mode d'introduction de particules est uniquement fonction des seules quantités relatives des ions en présence*, c'est-à-dire que l'état créé par les additions successives de $1, 2 \ldots q$ particules O sur les p particules M sera identique à celui qu'eut donné le système $p\mathrm{M} + q\mathrm{O}$ dissous en une seule opération. Nous pouvons donc raisonner sur les systèmes obtenus par additions successives.

B) Si nous partons d'un état initial formé de particules identiques, par exemple de structure $\mathrm{M}_x\mathrm{O}_y$ l'addition d'une particule à ce système formera deux types de particules par exemple $\mathrm{M}_x\mathrm{O}_y$ et $\mathrm{M}_x\mathrm{O}_{y+1}$mais l'addition d'une seconde particule O n'initiera pas $\mathrm{M}_x\mathrm{O}_{y+2}$ et $\mathrm{M}_x\mathrm{O}_y$, car il est difficile d'admettre qu'un complexe ayant déjà capté la particule O puisse encore en capter une autre au détriment du complexe initial ne l'ayant pas encore accepté.

Cela sous-entend par exemple que nous devons toujours observer une réaction chimique (décelable par cryométrie entre une particule MO_{y+n} et MO_y, $n > 1$). Effectivement $\mathrm{SiO}_2 + \mathrm{Si}^{4+} \rightarrow 2(\mathrm{SiO})^{++}$ par exemple.[1,3]

Lors des additions successives des particules O toutes les particules préexistantes tendent vers un état final commun. *Dans un stade transitoire dû a un apport insuffisant de particules O il ne peut se former que deux états correspondant l'un à l'état préexistant, l'autre à l'état suivant l'addition.*

C) Dans le cas le plus général nous écrirons :

$$p\mathrm{M} + q\mathrm{O} \rightarrow (m_1/n_1)[(M_{x_1}\,\mathrm{O}_{y_1})n_1] + (m_2/n_2)(\mathrm{M}_{x_2}\,\mathrm{O}_{y_2})n_2\,.$$

Ce système est indéterminé, quoique cependant, existent les conditions supplémentaires suivant lesquelles tous les paramètres sont des nombres entiers positifs.

Il existe un cas cependant (heureusement le plus fréquemment rencontré) où $\nu_\theta = p (p < q)$, ν_θ étant le nombre total de particules. Alors en notant que $m_1x_1 + m_2x_2 = p$, de la relation :

$$\nu_\theta = m_1/n_1 + m_2/n_2 = m_1x_1 + m_2x_2$$

découlent les conditions $n_1 = n_2 = 1$ et $x_2 = x_1 = 1$. Le système se réduit donc à :

$$p\mathrm{M} + q\mathrm{O} \rightarrow m_1\,(\mathrm{MO}_{y_1}) + m_2\,(\mathrm{MO}_y).$$

D'après ce que nous avons vu plus haut y_1 doit être le plus voisin possible de y, donc $y_1 = y + 1$, avec les conditions $m_2 < p$ et y = nombre entier, cet ensemble de conditions donne y.

Nous voyons donc que la seule détermination du nombre de particules complexes nous permet de connaître leurs compositions et que la traduction d'un nombre de particules en structures n'est pas purement arbitraire comme on peut le penser. Le schéma est imposé par la coexistence de diverses conditions aisément acceptables, qui doivent être satisfaites simultanément et qui sont :

a) cryométriques (nombre global de particules),

b) de répartition des particules entre elles (principes de moindre différenciation) et

c) d'arithmétrique chimique (les paramètres sont des entiers positifs).

Nous avons ainsi précisé la nature des particules complexes (M_xO_y). Si nous rappelons que nous savons étudier cryométriquement leurs solvatations,[2,4] nous voyons que partant du système initial $pM + qO + rX$ nous déterminons le complexe final $M_xO_yX_z$. A ce titre les numérations cryométriques peuvent sans doute être considérées dans l'étude des milieux polyparticulaires que sont les liquides salins, comme un aspect nouveau d'une chimie analytique originale.

Il nous a paru nécessaire de fixer ces données aisément acceptables pour préciser la valeur structurale des numérations cryométriques qui peuvent peut-être parfois sembler comporter une certaine incertitude dans leurs interprétations.

Ainsi, partant uniquement de la connaissance d'un ensemble de dépressions thermiques, nous arrivons à donner une image de la nature des substances en solution.

Ces données représentent donc un appoint souvent irremplaçable dans la connaissance des solutions salines.

En terminant nous remercions vivement Monsieur D. Topor ainsi que la rédaction pour leur amabilité et l'aide qu'ils ont voulu nous apporter.

Revue Roumaine de Chimie, **18**, *9*, 1531–1535 (1973)

APPLICATION OF THE ALLEN-SKINNER BOND ENERGY SCHEME TO BENZENOID POLYNUCLEAR HYDROCARBONS

RODICA VÎLCU and ŞT. PERIŞANU

Chair of Chemical Thermodynamics, Electrochemistry and Macromolecules, University of Bucharest, Bd. Republicii 13, Bucharest, Romania

Received December 25, 1972

The heats of atomization of benzenoid polycyclic hydrocarbons in the gaseous and liquid states were calculated by means of the Allen-Skinner bond energy scheme. A correction was introduced, which answers satisfactorily for the influence of the molecular shape on its energetic content.

In a previous paper [1] the heats of atomization of amines, alkylbenzenes and alkylnapthalenes were calculated by means of the Allen-Skinner bond energy scheme. For the amines we could obtain a mean difference between experimental and calculated values of ±0.42 kcal/mole, if the new experimental data of Good and co-workers[2-4] were taken into account and if a correction of 0.85 kcal/mole was introduced for every two amine groups bonded to neighbouring carbon atoms. If the compounds containing the ethyl radical were not considered in the calculation of the above mentioned difference, this became only ±0.24 kcal/mole.

The purpose of this work is to extend the calculation to other benzenoid hydrocarbons. Unfortunately we found very few data referring to the ideal gas state heats of formation of benzenoid hydrocarbons, except the alkylbenzenes and alkylnaphthalenes. The tabulated data refer for most substances to the solid and liquid states. The schemes based on additivity cannot be applied to the solid state, but this is possible for the liquid state, because the heats of vaporization can be calculated additively.

The only estimated parameters of the Allen-Skinner scheme for the liquid state were those of Kalb, Chung and Allen [5] for paraffins. Using them we could calculate the specific parameters for the benzenoid hydrocarbons (see table 1). For a better comparison with the results for the ideal gas state, we recalculated the parameters for this state, using the parameters for paraffins of the authors [5] (in another work, [1] the calculation was made by use of Skinner's [6] parameters).

---

[1] R. Vîlcu and St. Perişanu, *Rev. Roumaine Chim.*, **17**, 447 (1972).

[2] N. K. Smith and W. D. Good, *J. Chem. Eng. Data*, **12**, 572 (1967).

[3] W. D. Good and R. T. Moore, *J. Chem. Eng. Data.*, **15**, 150 (1970).

[4] W. D. Good, *J. Chem. Eng. Data*, **17**, 28 (1972).

[5] A. J. Kalb, A. L. H. Chung and T. L. Allen, *J. Amer. Chem. Soc.*,**88**, 2938 (1966).

Table 1

The interaction parameters used in the calculation of the heats of atomization of the benzenoid hydrocarbons (kcal/mole)

Parameter	The value for the liquid state (parameters for the paraffins given by Kalb *et al.*[5])	The value for the ideal gas state (parameters for the paraffins given by Kalb *et al*[5].)	The value for the ideal gas state (parameters for the paraffins given by Skinner[6])
B_{CC}	79.27	78.84	78.81
B_{CH}	99.65	99.305	99.29
Γ_{CCC}	2.73	2.67	2.58
Δ	−1.05	−0.82	−0.55
$B_{\mathrm{C}^a\mathrm{C}^a}$	109.80	105.385	102.61
$B_{\mathrm{C}^a\mathrm{H}}$	109.685	110.93	112.86
$B_{\mathrm{C}^a\mathrm{C}}$	91.575	90.31	91.16
$\Gamma_{\mathrm{C}^a\mathrm{C}^a\mathrm{C}^a}$	1.74	3.555	4.23
$\Gamma_{\mathrm{C}^a\mathrm{C}^a\mathrm{C}}$	2.07	3.26	3.68
$\Gamma_{\mathrm{C}^a\mathrm{CC}}$	2.40	2.965	3.13
ε	—	−0.5	−0.5
η	3.8	−0.75	—
Ø	−7	−7	—

For the alkylbenzenes the results are in very close agreement with the first ones and with the experimental values, the mean difference between experimental and calculated values being of ±0.62 kcal/mole and of only ±0.25 kcal/mole if the compounds containing the radicals ethyl and isopropyl were not taken into account.

In table 2 a comparison is given between the experimental and calculated heats of atomization of some benzenoid hydrocarbons with more cycles, in the ideal gas state. Westrum and Wong [7] have suggested that in benzenoid polynuclear hydrocarbons with condensed cycles, the resonance is promoted by a disk-like shape of the molecule, that is by the greater compactness of the molecule. We introduced in our correlation a parameter Ø which must be multiplied $D-d/d$, where D is the maximum linear dimension of the molecule and d the dimension in the perpendicular direction in the plane of the molecule, to answer for the influence of the shape of the benzenoid molecule on its energy. We had to introduce also a corrective parameter η for the interaction of two benzenoid cycles bonded at the same carbon atom, and another (ε) for two alkyl radicals substituted in neighbouring positions at a benzenoid cycle (see table 1). The use of parameter Ø does not lead to a close agreement between experimental and calculated heats of atomization for the molecules with a star-like shape (e.g. perylene).

---

[6] H. A. SKINNER, *J. Chem. Soc.*, **1962**, 4396.

[7] E. F. WESTRUM JR. and S. W. WONG, U. S. At. Energy Comm. COO 1149—92.

We accounted for the deviation observed for triphenylmethane taking into account that the respective molecule is highly perturbed. This fact is proved by the abnormal stability of the triphenylmethyl radical. The great deviations for biphenyl and 1,3,5, triphenylbenzene were expected too, their aromatic character being diminished by the non-planarity of the molecule ought to the repulsion of the hydrogen atoms from the positions neighbouring the bond between cycles.

Table 2

Experimental and calculated heats of atomization of some benzenoid polycyclic hydrocarbons in the ideal gas state

Hydrocarbons	H^{at}_{exp} (kcal/mole)	H^{at}_{calcd} (kcal/mole)	$H^{at}_{exp} - H^{at}_{calcd}$
Benzene	1318.18	1318.17	0.01
Naphthalene	2089.72	2089.70	0.02
Anthracene	2858.43	2859.19	−0.76
Phenanthrene	2864.14	2863.88	0.26
Pyrene	3203.10	3203.12	−0.02
Perylene	3967.55*	3978.71	−11.16
α-Methylnaphthalene	2372.97	2372.69	0.28
β-Methylnaphthalene	2373.15	2372.69	0.46
Diphenylmethane	2804.36*	2804.36	0.00
Triphenylmethane	4002.49*	4006.80	−4.31
1,2-Diphenylethane	3090.04*	3088.46	1.58
Biphenyl	2528.28	2532.44	−4.16
1,3,5-Triphenylbenzene	4956.35*	4965.54	9.19

* The values with asterisk are uncertain.

In table 3, the experimental atomization heats of some phenylalkanes in liquid state are given together with the calculated ones. The agreement is somewhat less satisfactory than that for the ideal gas state.

Table 3

Experimental and calculated heats of atomization of some alkylaromatics in liquid state

Hydrocarbons	H^{at}_{exp} (kcal/mole)	H^{at}_{calcd} (kcal/mole)	$H^{at}_{exp} - H^{at}_{calcd}$
Benzene	1326.30	1326.30	0.00
Toluene	1610.23	1610.23	0.00
Ethylbenzene	1891.18	1891.20	−0.02
Propylbenzene	2172.48	2172.50	−0.02
Isopropylbenzene	2173.15	2173.52	−0.37
n-Butylbenzene	2453.68	2453.80	−0.12
Diphenylmethane	2825.65	2825.66	−0.01
Triphenylmethane	4041−4042	4043.84	−1.84 −2.84
Tetraphenylmethane	5256.70	5261.62	−4.92
1,1-Diphenylmethane	3110.30	3109.03	1.27
1,2-Diphenylethane	3109.69	3105.23	4.46
1,1,2-Triphenylethane	4324.90	4323.06	1.84
1,1-Diphenylpropane	3390.3	3390.33	−0.03
1,2-Diphenylpropane	3390.3	3388.93	1.37
1,3-Diphenylpropane	3385.3	3386.53	−1.23

The greatest deviations are noticed for tri- and tetraphenylmethanes for the above-mentioned reasons, and for dibenzyl. This deviation could not be explained. Again a corrective parameter η was introduced for more benzenoid cycles bonded at the same carbon atom.

We must use the difference between the experimental atomization heats in solid state and the calculated heats of atomization in liquid state for the benzenoid polynuclear hydrocarbons because of the lack of experimental values of the heats of formation in liquid state for most of these substances. This difference was compared with the latent heat of fusion, if the latter was known. We noticed that the value of the corrective parameter Ø, which is a measure of the influence of the degree of compactness of the molecule, is equal with that for the ideal gas state.

The agreement between the above mentioned difference and the latent heat of fusion is on the whole quite good. For a very accurate calculation of the heat of atomization of a substance in liquid state, $H^{at}_{exp}(s) - H^{at}_{calcd.}(l)$ must be smaller than $\Delta\, {}^{t}H$ by some tenths of kcal/mole, as in the case of benzene.

The same reasons as in the case of the deviations noticed in the ideal gas state are responsible for the negative values of the difference under consideration for biphenyl and 1,3,5 triphenylbenzene. The significant nonplanarity of the molecule is the cause of the difference of -4.55 kcal/mole for 9,9′—bianthryl too. The same difference $H^{at}_{exp}(s) - H^{at}_{calcd.}(l)$ seems to have a normal value for 9,9′ biphenanthryl, the nonplanarity of which must be much smaller, because of the existence of repulsive interactions between fewer hydrogen atoms.

Our correlation answers only partially for the isomeric variations between the benzenoid hydrocarbons with 4 cycles. We could not explain the difference between the heats of atomization of benz [1, 2] anthracene and chrysene. The values of $H^{at}_{exp}(s) - H^{at}_{calcd.}(l)$ are plausible for tetracene and chrysene, but the negative value for benz [1, 2] anthracene is due in part to the imperfection of our method and in part to some experimental values which must be revised.

The differences between the calculated heats of atomization of the above mentioned isomers are in agreement, to a certain measure, with the differences between the resonance energies calculated by the molecular orbitals method. Thus, the difference between the values for tetracene and benz [1, 2] anthracene is about two times (0.169 β units) the difference between benz [1, 2] anthracene and chrysene (0.089 β units). As regards the benz [3, 4] phenanthracene, the value -7.44 of the difference under consideration is due, at least in part, to the bent shape of the molecule, which implies a significant strain.

CONCLUSIONS

We did not notice unusual deviations for the compounds in the liquid state, which contain the radicals ethyl and isopropyl, as we did for the same compounds in the ideal gas state.

We subscribe to the fact that the concept of bond energy is inadequate for the benzenoid molecules because of the delocalization of electrons.

There is no correspondence between the energetic parameters characteristic for the benzenoid hydrocarbons for the liquid and gaseous states, in contrast with those characteristic for the saturated molecules. For this reason the former should be regarded as simple calculation increments.

Table 4

Heats of atomization of some polycyclic benzenoid hydrocarbons in condensed states

Hydrocarbons	$H^{at}_{exp}(s)$	$H^{at}_{calcd}(l)$	$H^{at}_{exp}(s)-H^{at}_{calcd}(l)$	Δt_H
Benzene	1328.55	1326.30	2.25	2.35
Naphthalene	2107.14	2102.43	4.71	4.53
Anthracene	2882.75	2876.53	6.22	6.88
Phenanthrene	2885.84	2881.22	4.62	4.45
Tetracene	3663.40	3650.70	12.70	
Benz[1,2]anthracene	3660.50	3662.81	−2.31	
Chrysene	3666.60	3662.81	3.79	
Benz[3,4]phenanthrene	3657.10	3664.54	−7.44	
Pyrene	3227.99	3222.36	5.63	
Perylene	3999.54	4002.54	−3.00	
Biphenyl	2547.78	2547.89	−0.11	4.46
1,3,5-Triphenylbenzene	4987.10	4995.27	−8.17	
9,9′-Bianthryl	5644.9	5648.35	−4.55	
9,9′-Biphenanthryl	5672.0	5657.73	14.27	

The expression $D-d/d$ introduced by us is an adequate measure of the degree of compactness of the polycyclic benzenoid hydrocarbons, this fact being confirmed by the concordance of the values of Ø for the liquid and gaseous states.

As for the saturated molecules, the deviations of the calculated heats of atomization from the experimental values give information about special energetic contributions like : resonance, steric effects, strain, interactions between high order neighbour atoms (this is true of course when the deviations are not due to the lack of accuracy of the experimental data).

The experimental data used in this paper were taken from the book of Stull, Westrum and Sinke,[8] from the Landolt–Börnstein tables and from a paper of Tatevski.[9]

---

[8] D. R. Stull, E. F. Westrum Jr. and G. C. Sinke, "The Chemical Thermodinamics of Organic Compounds", Wiley, Inc., New York, 1969, p. 634–769.

[9] V. M. Tatevski, *Doklady Akad. Nauk S.S.S.R.*, **74**, 743 (1950).

Revue Roumaine de Chimie, **18**, *9*, 1537–1546 (1973)

STUDY OF THE THERMAL DECOMPOSITION OF AMMONIUM MOLYBDATE SUPPORTED ON ALUMINA

I. SĂLĂGEANU, DOMNINA TRESTIANU and E. SEGAL

Chair of Kinetic Theory of Matter and of Chemical Kinetics, University of Bucharest,
Bd. Republicii 13, Bucharest, Romania

Received January 15, 1973

The kinetic parameters of the decomposition reactions of ammonium molybdate supported on alumina in different concentrations were determined. The reactions were performed in nonisothermal conditions with linear heating programme. Activation energies and preexponential factors values are correlated with molybdate concentrations on alumina. The support influence on the decomposition reactions is discussed.

INTRODUCTION

The molybdenum oxide supported on alumina is much used as a catalyst in dehydrogenation and dehydrosulphuration processes.[1,2] This catalyst is prepared by thermal decomposition of the ammonium molybdate $(NH_4)_6Mo_7O_{24}.4H_2O$ impregnated on alumina in required concentrations. The intermediate stages of the pure ammonium molybdate thermal decomposition are known [3]

$$(NH_4)_6Mo_7O_{24}.4H_2O \rightarrow (NH_4)_4Mo_5O_{17} \quad (I)$$

$$(NH_4)_4Mo_5O_{17} \longrightarrow (NH_4)_2Mo_4O_{13} \quad (II)$$

$$(NH_4)_2Mo_4O_{13} \longrightarrow MoO_3 \quad (III)$$

Till now, data about the supported ammonium molybdate decomposition and the kinetic parameters of decomposition reactions, both for pure and supported state, do not exist.

---

[1] R. A. Fashutdinov and M. A. Tanatarov, *Kinetika i Kataliz*, **12**, 239 (1971).

[2] E. M. Davydova and A. V. Mashkina, *Kinetika i Kataliz*, **12**, 652 (1971).

[3] C. Duval, "Inorganic Thermogravimetric Analysis", Elsevier Publishing Company, Amsterdam, New York, London, 1963, p. 462.

It is also interesting to study the support influence on the different stages of the molybdate decomposition, the support effect being observed in the case of supported chromium oxide decomposition.[4] This effect consists in the dependence of the chromium oxide decomposition kinetic parameters from the concentration on the support.

In this work, a kinetic study of the alumina supported ammonium molybdate decomposition in nonisothermal conditions with linear heating programme and a correlation between the kinetic parameters and the molybdate concentrations on the support are presented.

EXPERIMENTAL

Four samples of alumina supported ammonium molybdate with different concentrations (14%, 20%, 29% and 40%) were prepared by impregnating B.D.H. alumina with $(NH_4)_6Mo_7O_{24} \cdot 4H_2O$ *p.a.* solutions of adequate concentrations and evaporating under continuous stirring. Then the concentrations were checked by the samples thermal decomposition.

For the study of the thermal decomposition under nonisothermal conditions with a heating rate of 10°/min, a derivatograph M.O.M. Budapest type Paulik, Paulik, Erdey was used. The experiments were performed in the air, with a sensitivity of 20 mg.

The kinetic parameters of the decomposition reactions were calculated by means of the Freeman-Carroll and Coats-Redfern methods.[5,6]

RESULTS

The thermal decomposition of the pure ammonium molybdate takes place according to the above mentioned stoichiometry, the same temperature intervals of the intermediate compounds thermal stability being found (fig. 1). In case of supported molybdate, the same intermediates have been evidenced, but with much smaller stability intervals. In all cases, the temperatures corresponding to the maximums of the decomposition rates remained constant and equal to those corresponding to the pure molybdate decomposition: 125—127° for the first process, 242—244° for the second process and 352—355° for the third one.

The kinetic parameters of the reactions I, II and III were calculated. For the unsupported molybdate, using the Freeman-Carroll method, the value of the reaction order has been found equal to 2 for the reactions I and II and equal to 1 for the reaction III. Figure 2 shows the case of reaction II. The same reaction orders correspond to the stages of supported molybdate decomposition for all the concentrations. This fact was checked using the Coats-Redfern method corresponding to the values 2 and 1 of the reaction orders at the relevant processes.

Reactions I and II. To establish the kinetic parameters of these reactions, the Coats-Redfern method corresponding to a reaction order equal to 2 was used. The Freeman-Carroll method could not be applied

---

[4] A. Bencovski, A. Caraman, D. Fătu, E. Pop, E. Segal and G. Şerban, *J. Thermal Analysis* (in print).

[5] A. W. Coats and J. P. Redfern, *Nature*, **201**, 68 (1964).

[6] E. S. Freeman and B. J. Carroll, *J. Phys. Chem.*, **62**, 394 (1958).

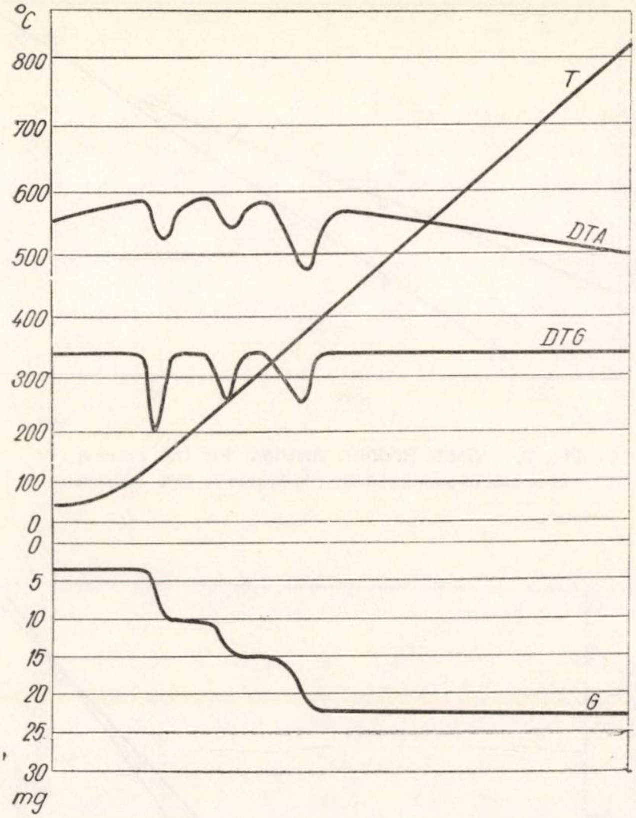

Fig. 1. — Complete thermoanalytical curves for $(NH_4)_6Mo_7O_{24}.H_2O$.

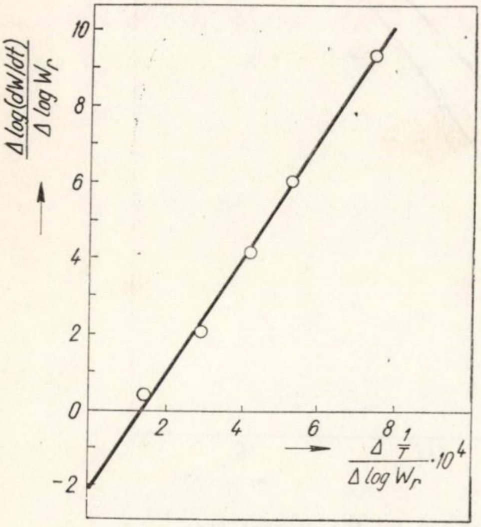

Fig. 2. — Freemann-Carroll method for the process II in case of pure molybdate.

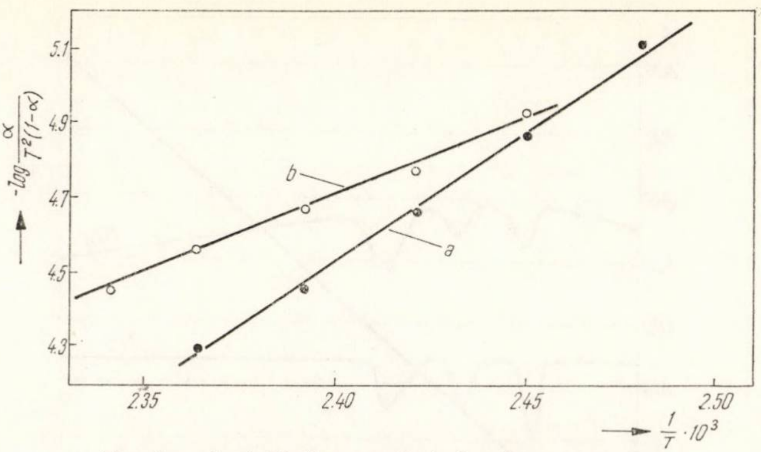

Fig. 3. — Coats-Redfern method for the process I:
a) in case of pure molybdate; *b*) in case of 20% molybdate.

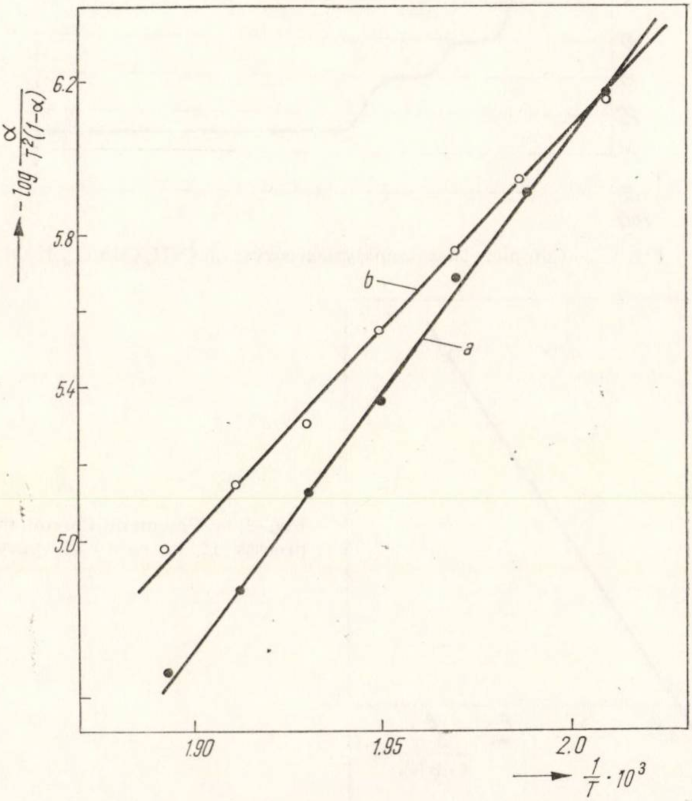

Fig. 4. — Coats-Redfern method for the process II:
a) in case of pure molybdate; *b*) in case of 29% molybdate.

to the supported molybdates because the DTG line did not turn back to the baseline at the end of a process and also due to the short temperature interval of the reactions.

The following equation was applied

$$\frac{\alpha}{1-\alpha}\cdot\frac{1}{T^2}=\frac{AR}{aE}\left(1-\frac{2RT}{E}\right)\cdot\exp\,(-\,E/RT)$$

where the following notations have been used

α — conversion degree, T — absolute temperature, A — preexponential factor, R — gas constant, a — heating rate, E — activation energy. By plotting $\log\left(\frac{\alpha}{1-\alpha}\cdot\frac{1}{T^2}\right)$ *versus* $1/T$, a straight line was obtained, whose slope allowed to determine the activation energy, while the preexponential factor was calculated from the intercept. The calculation of these parameters was carried out by means of the least squares method. The above mentioned straight lines corresponding to the first process are represented in figures 3a and 3b (fig. 3a — 100% molybdate, fig. 3b — — 20% molybdate) and those corresponding to the second process in figures 4a and 4b (fig. 4a — 100% molybdate, fig. 4b — 29% molybdate). The values obtained for the activation energies and the preexponential factors in case of the processes I and II are shown in tables 1 and 2.

Reaction III. The Coats-Redfern method corresponding to a reaction order equal to 1 was used to determine the kinetic parameters

Table 1

Values of the activation parameters of the process I for different ammonium molybdate concentrations

Concentration %	Activation energy kcal/mol	Preexponential factor s^{-1}
14	15	2.5×10^{6}
20	18	1×10^{8}
29	20	1×10^{9}
40	23	5.7×10^{10}
100	31.5	2.4×10^{15}

Table 2

Values of the activation parameters of the process II for different ammonium molybdate concentrations

Concentration %	Activation energy kcal/mol	Preexponential factor s^{-1}
14	37.4	7×10^{13}
20	45.5	3×10^{17}
29	48.2	4×10^{18}
40	54.3	3×10^{21}
100	63	1.4×10^{25}

for the same reasons as in the case of reactions I and II. The following equation was applied

$$-\frac{\ln(1-\alpha)}{T^2}=\frac{AR}{aE}\left(1-\frac{2RT}{E}\right)\exp(-E/RT)$$

where the different notations have the same meaning as above. The activation energy was determined from the slope of the straight line

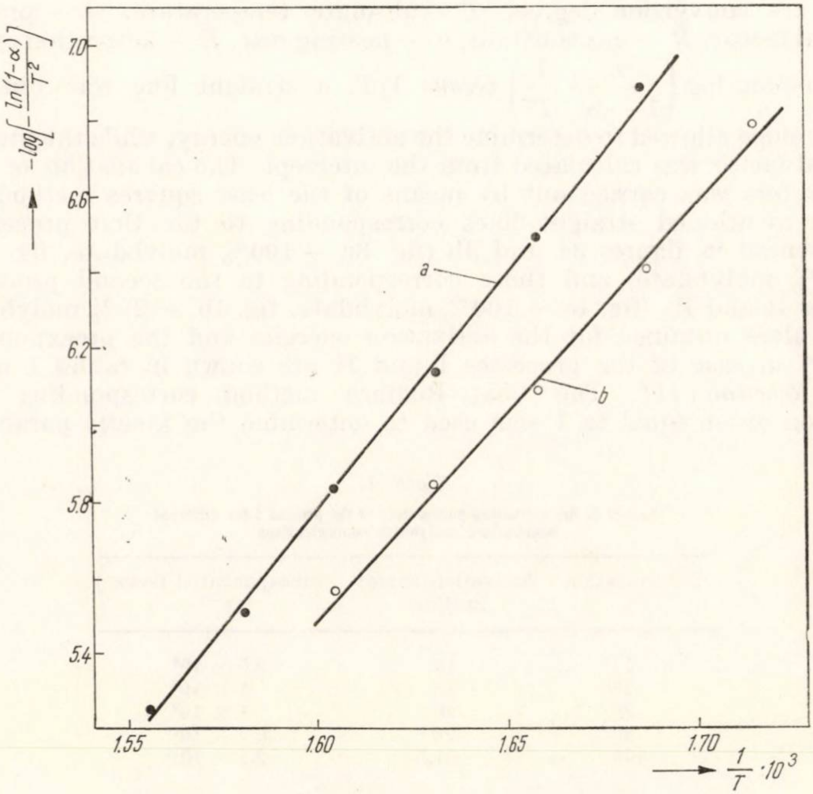

Fig. 5. — Coats-Redfern method for the process III: *a*) in case of pure molybdate; *b*) in case of 29% molybdate.

obtained by plotting $\log\left[-\frac{\ln(1-\alpha)}{T^2}\right]$ *versus* $1/T$; the preexponential factor was calculated from the intercept. This calculation was also carried out by means of the least squares method. The straight line corresponding to unsupported molybdate is represented in fig. 5a, while that corresponding to a 29% supported molybdate concentration is represented in fig. 5b.

The values obtained for the activation parameters of the reaction III are shown in table 3.

Table 3

Values of the activation parameters of the process III for different ammonium molybdate concentrations

Concentration %	Activation energy kcal/mol	Preexponential factor s^{-1}
14	45.5	7×10^{13}
20	50.6	7×10^{15}
29	51.8	1.7×10^{16}
40	54.2	1×10^{17}
100	56	3×10^{17}

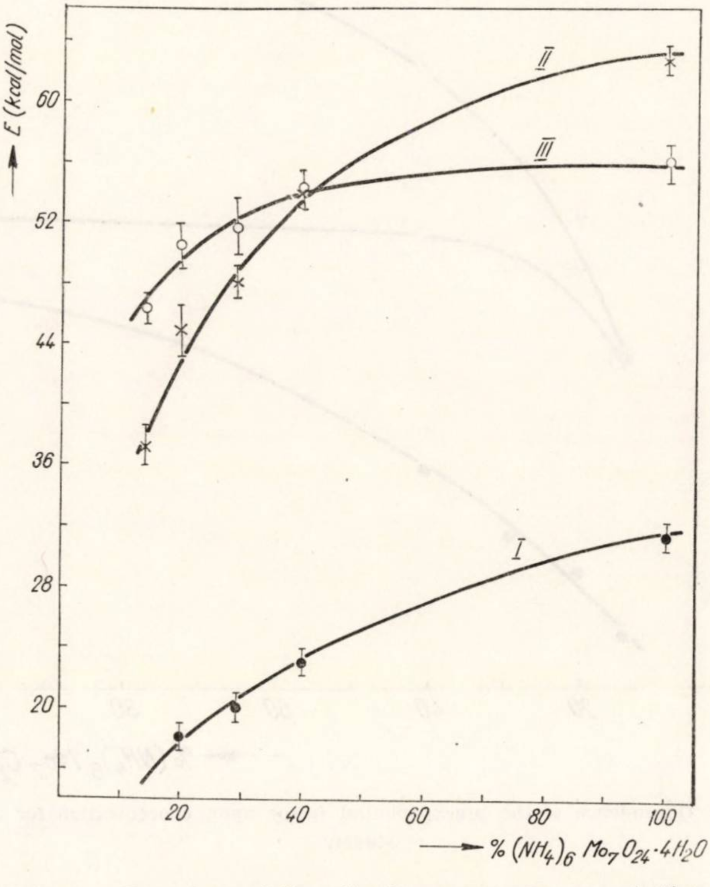

Fig. 6. — Dependence of the activation energy upon concentration for all three stages.

DISCUSSIONS

1. The value 2 of the reaction order in cases of reactions I and II has a formal significance. The value 1 of the reaction order corresponding to the reaction III could be an indication that it is the chemical process which is the rate-limiting step. This is very probable, because it is the last stage of the decomposition, when the initial compact structure of the molybdate lattice is practically destroyed by the successive elimination of water and ammonia during the two previous stages.

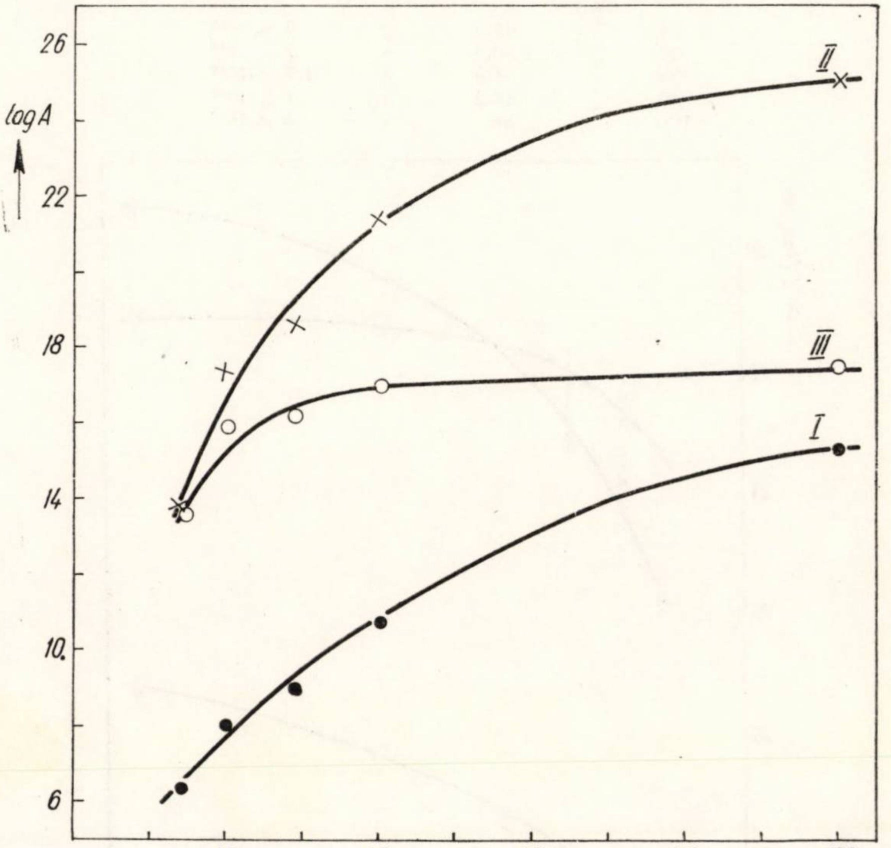

Fig. 7. — Dependence of the preexponential factor upon concentration for all three stages.

2. The dependences upon concentration for both activation energy (fig. 6) and preexponential factor (fig. 7) are evidenced for all the three stages. This dependence may be due to the support effect.

The support can act on the development of a chemical reaction in two ways:

a. by shortening the induction period of the reaction due to the reactant dispersion on the support;

b. the temperature gradients are smaller for supported molybdate decomposition than for the unsupported one, most of the heat transfer occurring in the first case through the support.

At the same time, the preexponential factor decreases, as a compensation of the activation energy decrease. The decrease of the preexponential factor, as a consequence of the activation entropy, may be due to a strong distortion of the activated complex by the crystalline lattice in case of unsupported molybdate. This distortion is weaker in case of supported molybdates.

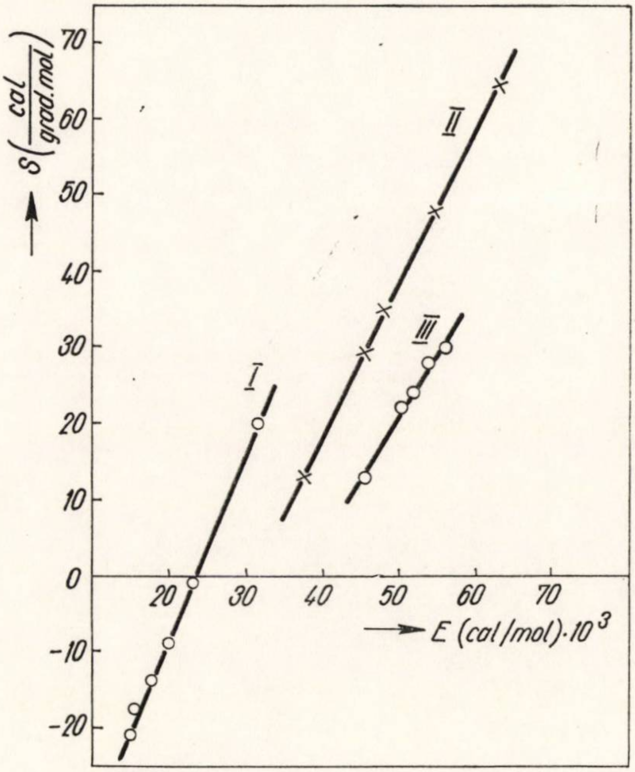

Fig. 8. — Linear dependence between activation energy and activation entropy, for different concentrations for all three stages.

On the other hand, it can be supposed that the molybdate decomposition mechanism, both supported and unsupported, is the same. This hypothesis seems to be right if we take into account the mainteinance of the same stoichiometry and reaction orders for the three decomposition stages, irrespective of concentration. We may draw the conclusion that the support does not modify the number of decomposition intermediate stages, the free energy of the activated complexes formation being not considerably influenced. This fact leads to the dependence of the activation energy upon the activation entropy, namely that the activation energy decrease must be accompanied by the activation entropy decrease.

A linear dependence between activation energy and entropy, for different concentrations for the same reaction, is observed (fig. 8). For each reaction, an isokinetic temperature can be determined.

Revue Roumaine de Chimie, 18, 9, 1547–1554 (1973)

TENSION INTERFACIALE DANS LE SYSTÈME SOLUTION BENZÉNIQUE DE TRIBUTYLPHOSPHATE/SOLUTION AQUEUSE DE NITRATE CUIVRIQUE

MARIA TOMOAIA, ZENO ANDREI et EMIL CHIFU

Université de Cluj, Chaire de Chimie Physique, 11, str. Arany János, Cluj

Reçu le 27 février 1973

On a étudié, par mesures de tension interfaciale, l'interaction entre le tributylphosphate (TBP) et le nitrate cuivrique dans le système TBP-benzène/nitrate-eau à divers rapports molaires r = [TBP]/[nitrate], dans le domaine de concentrations 0,0–0,3 M. Les valeurs extrêmes (minima ou points d'inflexion à tangente horizontale) de la tension interfaciale situées autour du rapport r = 3/1 attestent la formation d'un associé moléculaire 3 TBP/1 $Cu(NO_3)_2$ plus superficiellement actif que le TBP tout seul. C'est dans ce sens que plaide aussi l'augmentation de l'aire moléculaire du TBP en présence du nitrate (114 Å^2) vis-à-vis de l'aire en son absence (97 Å^2).

INTRODUCTION

La tension interfaciale joue un rôle important dans l'extraction liquide-liquide. Les variations de tension interfaciale qui accompagnent les phénomènes d'extraction sont relativement peu étudiées.[1–4] Parmi les divers stades du phénomène d'extraction on peut distinguer aussi celui de la formation, à l'interface liquide-liquide, d'un complexe entre l'agent extractif et l'espèce moléculaire que l'on extrait.[5–6]

Le tributylphosphate est utilisé couramment à l'extraction de nombreux composés, surtout des nitrates [7], de leurs solutions aqueuses.

Dans un travail antérieur, nous avons étudié la tension interfaciale dans le système extractif solution hexanique de TBP/solution aqueuse de nitrate de lithium [3]. On a montré que la formation de l'associé $LiNO_3 . 2$ TBP était accompagnée d'une diminution de la tension interfaciale, l'associé étant l'espèce la plus superficiellement active.

[1] G. T. Frumin, M. V. Ostrovski et A. A. Abramzon, *Zhur. priklad. Khim.*, **40**, 1328 (1967).

[2] V. B. Lazarev et Y. A. Tsylov, *Zhur. neorg. Khim.*, **10**, 22 (1965).

[3] E. Chifu et G. Gabrielli, *Gazz. chim. Ital.*, **98**, 1213 (1968).

[4] M. Kugo et Y. Kumakowa, *Hokkaido Daigaku Kogakubu Kenkyu Hokoku*, **47**, 75 (1968).

[5] D. R. Olander, *Nucl. Sci. Eng.*, **15**, 354 (1963).

[6] H. T. Hahn, *J. Amer. Chem. Soc.*, **79**, 4625 (1957).

[7] Y. Marcus, *Chem. Rev.*, **63**, 139 (1963).

Nous présentons, dans ce travail, des données concernant la tension interfaciale dans le système solution benzénique de TBP/solution aqueuse de nitrate cuivrique, en conditions supposées d'équilibre*.

PARTIE EXPÉRIMENTALE

On a utilisé des réactifs à pureté adéquate : du TBP *p.a.* Schuchardt-München, du benzène *p.a.* Reactivul-Bucarest, du nitrate cuivrique *p.a.* Reactivul-Bucarest. Les solutions de nitrate ont été préparées avec de l'eau doublement distillée ; le dosage du Cu(II) a été fait avec de l'EDTA.

Les tensions interfaciales σ dyn/cm ont été mesurées à $25° \pm 0{,}2$ par la méthode de l'anneau (Lecompte du Noüy), avec un tensiomètre bifilaire. Toutes les mesures ont été effectuées 30 minutes après la formation de l'interface benzène — eau. Les données obtenues sont représentées en isothermes tension interfaciale — composition, sur les figures 1—5. Chaque valeur de la tension interfaciale est la moyenne de dix lectures, affectée d'une erreur de $\pm$ 0,05 dyn/cm

RÉSULTATS EXPÉRIMENTAUX. DISCUSSIONS

Pour pouvoir décider sur la variation de la tension interfaciale avec la composition dans le système TBP-benzène/nitrate-eau, on a déterminé, au préalable, les isothermes tension interfaciale — concentration pour les deux systèmes TBP-benzène /eau et benzène/nitrate-eau, respectivement (voir fig. 1). On peut observer que le TBP est une substance suffisamment superfiellement active à l'interface eau/benzène (isotherme *a*) ; il n'en est pas de même avec le nitrate cuivrique, qui s'avère superficiellement inactif à l'interface en question (isotherme *b*). On constate en même temps que les deux isothermes ne présentent ni des valeurs extrêmes de la tension interfaciale, ni d'autres anomalies.[8]

L'étude de la tension interfaciale dans le système TBP—benzène/nitrate-eau a été faite, au commencement, sur des mélanges isomolaires hétérogènes, dans lesquels l'addition des concentrations du TBP en benzène aux concentrations du nitrate en eau totalisait une valeur constante.

La fig. 2 représente un exemple d'isotherme tension interfaciale (σ) — rapport molaire [TBP]/[nitrate] (r). Elle se réfère aux mélanges isomolaires [TBP] + [nitrate] à concentration totale 0,133 M et relève l'existence d'un minimum au rapport molaire r égal à 3,7.

Dans une seconde série de mesures, on a maintenu constante la concentration du nitrate cuivrique dans la phase aqueuse, en variant seulement la concentration du TBP dans la phase benzénique.

---

* Données présentées à la IIIe Conférence républicaine de Chimie physique, Bucarest, 4—7 septembre 1972.

[8] R. Defay, J. Prigogine, A. Bellemans et D. H. Everett, « Surface Tension and Adsorption », Longmans, Green, Londres, 1966, p. 114—132.

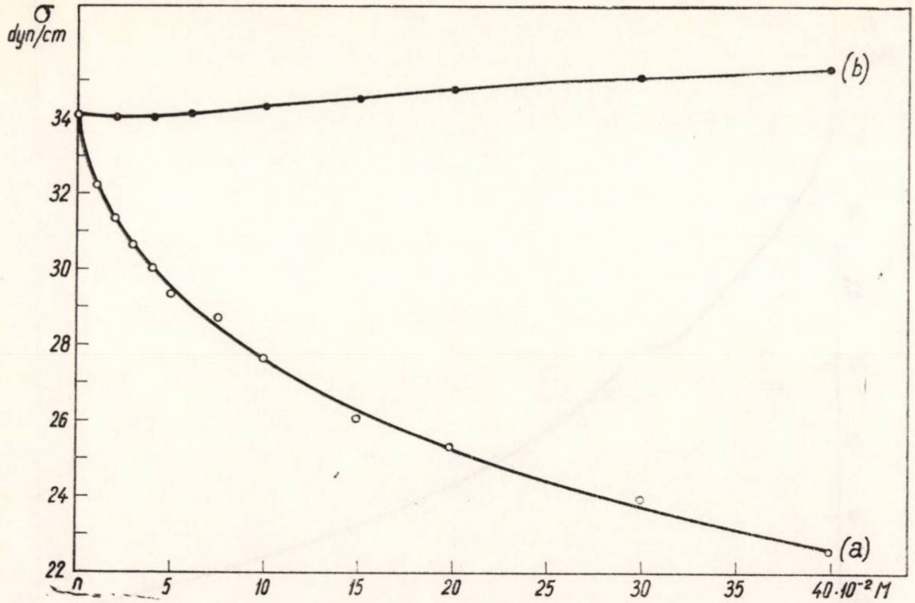

Fig. 1. — Isothermes tension interfaciale-concentration pour les systèmes TBP-benzène/ /eau (*a*) et benzène/nitrate-eau (*b*).

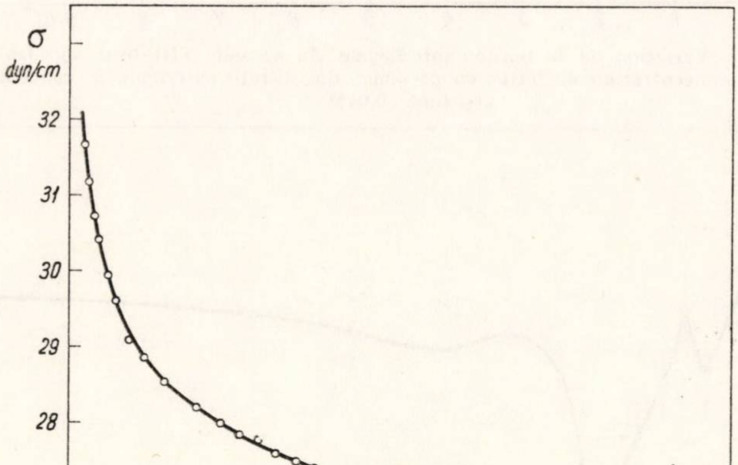

Fig. 2. — Isotherme tension interfaciale-rapport molaire **r** = [TBP]/ /[nitrate] pour les mélanges isomolaires hétérogènes TBP-benzène/ /nitrate-eau aux concentrations totales [TBP] + [nitrate] égales à 0,133 M.

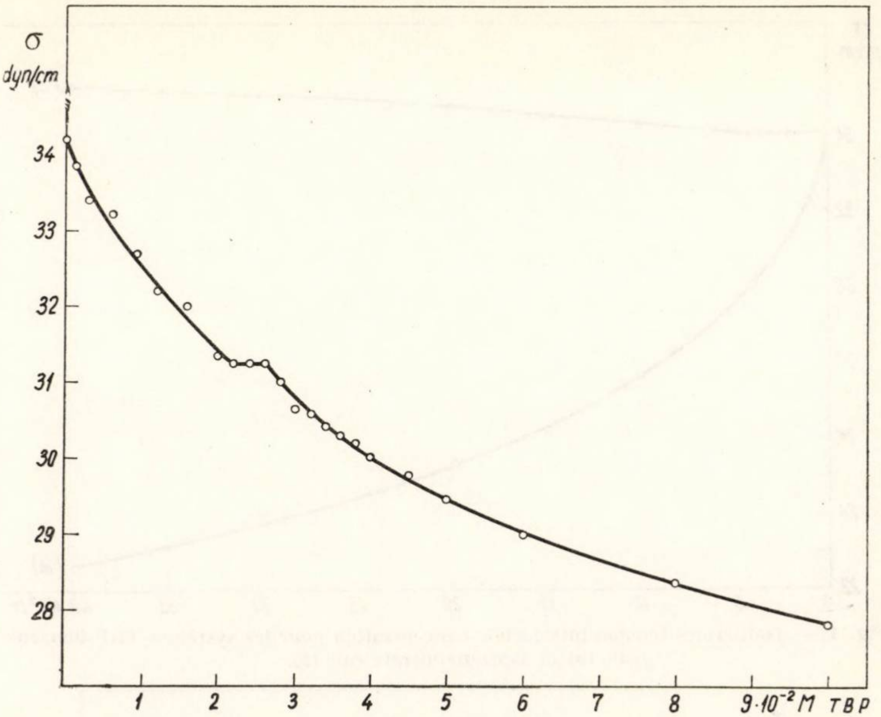

Fig. 3. — Variation de la tension interfaciale du système TBP-benzène/nitrate-eau, avec la concentration du TBP, en présence du nitrate cuivrique à concentration constante 0,01M.

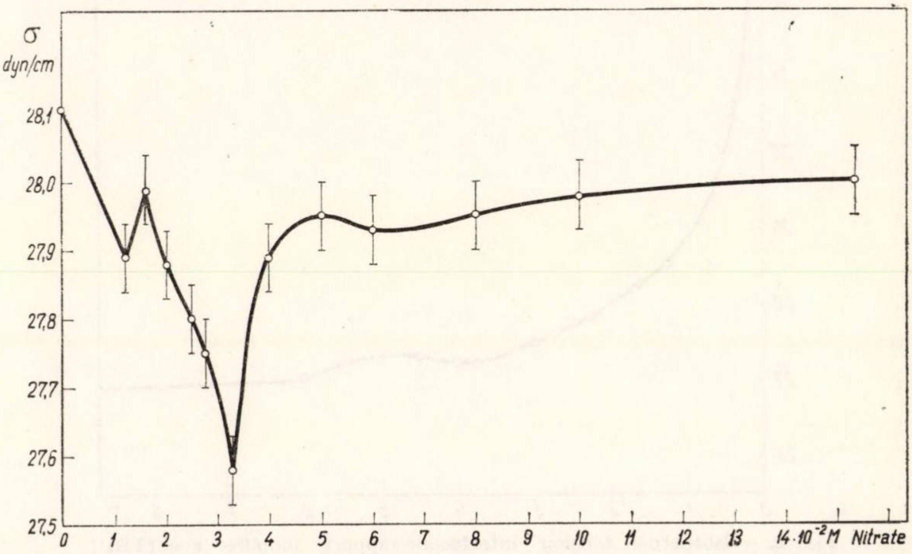

Fig. 4. — Variation de la tension interfaciale, du système TBP-benzène/nitrate—eau, avec la concentration du nitrate cuivrique, en présence du TBP à concentration constante 0,1 M.

La fig. 3 présente les résultats obtenus dans le cas où la concentration constante du nitrate était 0,01 M et celle du TBP variait dans l'intervalle 0,00 à 0,10 M. On constate l'existence d'un point d'inflexion à tangente horizontale au rapport molaire [TBP]/[nitrate] égal à 2,6. Une autre série de mesures a été faite en maintenant constante la concentration du TBP en benzène et en variant seulement celle du nitrate cuivrique en phase aqueuse.

Sur la fig. 4 on a représenté les données obtenues quand la concentration du TBP était 0,1 M et celle du nitrate variait entre 0,00 et 0,15 M. On observe l'apparition d'un minimum net au rapport molaire [TBP]/[nitrate] égal à 3,0.

En utilisant en tant que solvant du TBP l'hexane (Merck—Darmstadt) au lieu du benzène et en opérant dans les conditions indiquées sur le diagramme 4, nous retrouvons un minimum de la tension interfaciale au même rapport molaire TBP/nitrate égal à 3,0.[9]

Les minima de tension interfaciale aussi bien que les points d'inflexion à tangente horizontale s'incluent dans la catégorie des extréma de tension interfaciale (superficielle), dans toutes les deux situations la dérivée première de la tension interfaciale en rapport avec la composition étant nulle.[8]

Nous mettons en liaison les valeurs extrêmes de la tension interfaciale en fonction de la composition, relevées par les isothermes antérieurs, avec l'interaction du TBP avec le nitrate cuivrique.

Conformément à nos données, le rapport d'interaction TBP/nitrate oscille autour de la valeur 3 : 1 à savoir de 2,6 : 1 à 3,7 : 1. Une explication complète de ces faits ne peut pas être donnée pour le moment. Nous mentionnons cependant que Healy et McKay [10] admettent le rapport 2,7 : 1, tandis que Sevcenko, Shilin et Jdanov[11] trouvent des rapports situés dans l'intervalle 2 : 1 jusqu'à 5 : 1, en se basant sur des mesures de coefficients de répartition. Ces derniers auteurs expliquent la variation du rapport TBP/nitrate, déterminé expérimentalement, tant par des déviations à l'idéalité, que par de possibles réactions successives.

ESTIMATIONS DE L'AIRE MOLÉCULAIRE

En vue d'obtenir des informations supplémentaires concernant l'interaction du TBP avec le nitrate cuivrique à l'interface eau/benzène, on a tenté l'évaluation de l'aire moléculaire du TBP en l'absence et puis en présence du nitrate cuivrique, moyennant des mesures de tension interfaciale.

Ainsi en utilisant l'isotherme (*a*) de la fig. 1, remaniée conformément à l'équation de Gibbs, nous avons évalué les adsorptions Γ du TBP à l'interface eau/benzène.

---

[9] M. Tomoaia, Z. Andrei et E. Chifu (données non publiées).

[10] T. V. Healy et H.A.C. McKay, *Trans. Faraday Soc.*, **52**, 633 (1956).

[11] V. B. Shevcenko, I. V. Shilin et Y. F. Jhdanov, *Zhur. neorg. Khim.*, **5**, 1366 (1960).

Nous avons fait aussi des mesures de tension interfaciale pour le même intervalle de concentrations en TBP que celui utilisé dans le diagramme 1(*a*). Mais cette fois-ci dans la phase aqueuse il y avait de plus le nitrate cuivrique, dont la concentration a été établie de façon à réaliser dans chaque échantillon le rapport molaire [TBP]/[nitrate] égal à 3,0. On tient compte ainsi de l'existence du complexe 3 : 1. Les résultats sont portés sur la fig. 5. On a évalué, aussi dans ce cas, les adsorptions Γ.

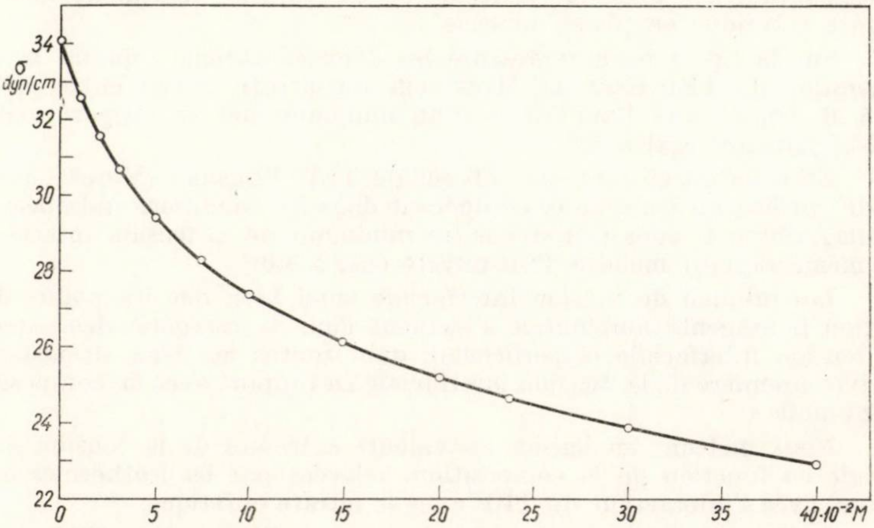

Fig. 5. — Isotherme tension interfaciale—concentration du TBP en benzène, en présence du nitrate cuivrique en eau, au rapport molaire constant, r= [TBP]/[nitrate]=3/1.

On a déterminé, de la manière indiquée, les isothermes d'adsorption $\Gamma = \Gamma(c)$ dans les deux situations correspondant aux diagrammes 1(*a*) et 5. En admettant que l'équation de Langmuir soit valable pour le film interfacial de TBP, les pentes des droites $c/\Gamma = f(c)$ représentées sur la fig. 6 (et calculées par la méthode des moindres carrés) nous ont permis d'évaluer les adsorptions maximales, respectivement les aires moléculaires du TBP en l'absence et en présence du nitrate cuivrique.

Dans le tableau 1 nous présentons les valeurs de ces aires, que nous avons déterminées à l'interface eau/benzène, à côté d'autres valeurs, rapportées dans la littérature,[12] pour la surface eau/air (film monomoléculaire). On peut constater, des données du tableau, qu'à l'interface eau/benzène si bien qu'à la surface eau/air apparaît un incrément de l'aire moléculaire du TBP en présence du nitrate cuivrique. Cet incrément plaide en faveur de l'interaction TBP-nitrate cuivrique.

---

[12] E. Ferroni et A. Ficalbi, *Acad. Naz. Lincei*, **28**, 207 (1960).

En ce qui concerne l'aire moléculaire du TBP à l'interface eau/benzène, elle est de 27 Å² plus grande qu'à la surface eau/air. Le fait est plausible, parce que, en général, les films à l'interface eau/huile sont plus étendus, dû à la pénétration des molécules d'« huile » entre les chaînes d'hydrocarbure du film.[13]

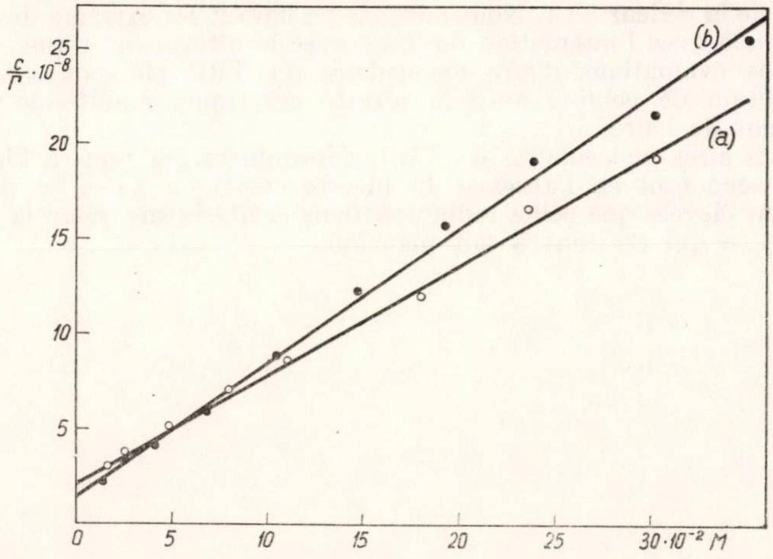

Fig. 6. — Les droites concentration/adsorption — concentration du TBP à l'interface benzène/eau en l'absence (*a*) et en présence (*b*) du nitrate cuivrique.

Tableau 1

Aires moléculaires du TBP en absence et en présence du nitrate cuivrique, à l'interface eau/benzène et à la surface eau/air

Film de TBP à l'interface eau/benzène (présent travail)		Film de TBP à la surface eau/air (littérature[12])	
phase aqueuse	aire moléculaire Å²	support	aire moléculaire Å²
eau doublement distillée	97±2	eau doublement distillée	70
eau-nitrate	114±3	eau-nitrate	76

On observe aussi que l'incrément d'aire déterminé par la présence du nitrate cuivrique est 17 Å² à l'interface eau/benzène, tandis que la littérature[12] consigne 6 Å² pour la surface eau/air.

---

[13] J. T. DAVIES et E. K. RIDEAL, « Interfacial Phenomena », Academic Press, New York — Londres, 1963, p. 227.

En conclusion, les mesures de tension interfaciale dans le système solution aqueuse de nitrate cuivrique/solution benzénique de TBP attestent l'existence des valeurs extrêmes — minimales ou points d'inflexion à tangente horizontale — pour des rapports molaires TBP/nitrate oscillant autour de la valeur 3 : 1. Nous mettons en liaison les extréma de tension interfaciale avec l'interaction du TBP avec le nitrate cuivrique.

Les évaluations d'aire moléculaire du TBP plaident aussi pour l'interaction de celui-ci avec le nitrate cuivrique, manifestée par un incrément de l'aire.

Les aires moléculaires du TBP, déterminées par nous à l'interface eau/benzène tant en l'absence du nitrate cuivrique qu'en sa présence, sont plus élevées que celles indiquées dans la littérature pour la surface eau/air, ce qui est tout à fait plausible.

Revue Roumaine de Chimie, **18**, 9, 1555–1576 (1973)

MÉTHODES NON ISOTHERMIQUES UTILISÉES POUR LA DÉTERMINATION DES PARAMÈTRES CINÉTIQUES DES RÉACTIONS HÉTÉROGÈNES DÉCRITES PAR DES ÉQUATIONS CINÉTIQUES NON ENCADRÉES DANS LE MODÈLE DE L'ORDRE DE RÉACTION

E. SEGAL

Chaire de « Théorie cinétique de la matière et de cinétique chimique »
Faculté de Chimie, Université de Bucarest, 13, B^{bul} Republicii

Reçu le 6 Septembre 1972

On présente quelques principes généraux destinés à élaborer des procédés non isothermiques pour la détermination des paramètres cinétiques des réactions hétérogènes , dans le cas où leur comportement cinétique est décrit par des lois qui ne peuvent être encadrées dans le modèle de l'ordre de réaction.

1. INTRODUCTION

Les méthodes non isothermiques utilisées pour la détermination des paramètres cinétiques sont de plus en plus largement appliquées dans les plus divers domaines de la chimie. Un nombre croissant de chercheurs utilisent ces méthodes pour étudier la décomposition des substances inorganiques, la destruction thermique des polymères, la thermolyse du charbon, etc.

La majorité de ces études traite des processus hétérogènes de forme

$$A(s) \rightarrow B(s) + C(g), \qquad \text{I}$$

dont la cinétique isothermique est considérée décrite par l'équation différentielle[1-3]

$$\frac{\mathrm{d}\alpha}{\mathrm{d}t} = k(1-\alpha)^n \qquad (1)$$

---

[1] T. Ozawa, *Bull. Chem. Soc. Japan*, **38**, 1881 (1965).
[2] J. H. Flynn et L. A. Wall, *J. Res. Nat. Bur. Stand.*, **A 70**, 487 (1966).
[3] I. G. Murgulescu, D. Fătu et E. Segal, *J. Thermal Analys.*, **1**, 98 (1969).

où α représente le degré de conversion au moment t, k — la constante cinétique et n — l'ordre de réaction qui, pour des processus hétérogènes, peut avoir aussi des valeurs moindres que l'unité.

La relation (1), vérifiée expérimentalement pour plusieurs cas, représente en fait la généralisation d'une équation utilisée dans la cinétique homogène, pour des processus hétérogènes. Il est important de noter qu'on peut obtenir une description cinétique fidèle des processus hétérogènes en tenant compte de certaines de leurs caractéristiques. Ainsi, par exemple, Jacobs et Tompkins[4] ont proposé une méthode cinétique générale de traitement des réactions de type I, en rapportant celles-ci à la formation et la croissance des germes de la nouvelle phase. La particularisation d'une formule générale, pour différentes lois cinétiques de formation et de croissance des germes, conduit à un important nombre d'équations cinétiques dont seulement une partie sont de type (1).

Pour exprimer correctement la cinétique des réactions hétérogènes, il est donc nécessaire d'utiliser une équation cinétique plus générale.

$$\frac{\mathrm{d}\alpha}{\mathrm{d}t} = kf(\alpha) \qquad (2)$$

où $f(\alpha)$ est une fonction quelconque du degré de conversion; c'est pourquoi on la nommera plus loin « fonction de conversion ». Dans cette forme, l'équation cinétique différentielle (2) peut être appliquée non seulement aux réactions de décomposition dans les systèmes solide-gaz, mais aussi à d'autres processus hétérogènes comme, par exemple, les réactions dans les systèmes solide-solide décrites par des lois cinétiques dont la forme diffère de (1).

Dans ce qui suit, on se propose d'analyser la possibilité d'adapter les méthodes non isothermiques thermogravimétriques et thermodifférentielles pour évaluer les paramètres cinétiques des processus hétérogènes pour lesquels, dans l'équation (2), $f(\alpha) \neq (1 - \alpha)^n$.

Dans ce but, on considère que le système analysé est échauffé avec une vitesse constante, a,

$$\frac{\mathrm{d}T}{\mathrm{d}t} = a \qquad (3)$$

et on tient compte du fait que la relation entre la constante k de l'équation cinétique différentielle (2) et la température est exprimée par la loi d'Arrhénius

$$k = A\,\mathrm{e}^{-E/RT} \qquad (4)$$

où A représente le facteur préexponentiel, E — l'énergie d'activation, R — la constante des gaz et T — la température absolue.

---

[4] P. Jacobs et F. Tompkins, « Khimia Tverdogo Sostoiania », V. Garneva, Izdatelstvo inostrannoi literatury, Moscou, 1961, p. 245.

En introduisant dans l'équation (2) les relations (3) et (4) et en séparant les variables, celle-ci devient :

$$\frac{d\alpha}{f(\alpha)} = \frac{A}{a} e^{-E/RT} \, dT \tag{5}$$

Les méthodes différentielles d'évaluation des paramètres cinétiques sont basées sur les équations (2) et (5).

Si on effectue l'intégration dans l'équation (5), on obtiendra :

$$-\int_0^{\alpha} \frac{d\alpha}{f(\alpha)} = \frac{A}{a} \int_0^{T} e^{-E/RT} \, dT \tag{6}$$

L'intégrale du premier membre de l'égalité (6) s'appelle « intégrale de conversion » et sera notée plus loin $F(\alpha)$, tandis que l'intégrale du second membre est dénommée « intégrale de température ». Cette dernière ne pouvant être effectuée avec exactitude, on a élaboré divers procédés permettant de la résoudre approximativement.[2,5] Dans ce but, on utilise le changement de variable, $x = -\frac{E}{RT}$, et la relation (6) devient :

$$F(\alpha) = \frac{AE}{aR} p\,(x) \tag{7}$$

La fonction $p(x)$ peut être évaluée approximativement en utilisant différents développements en série.[6-8]

Une résolution exacte du problème peut être obtenue en utilisant un programme non linéaire d'échauffement. Ainsi, par exemple, dans le cas d'un programme hyperbolique d'échauffement,[9,10] pour lequel

$$\frac{dT}{dt} = bT^2 \tag{8}$$

l'intégrale de température s'effectue exactement et l'équation cinétique intégrale devient :

$$F(\alpha) = \frac{AR}{bE} e^{-E/RT} \tag{9}$$

---

[5] D. Fătu, *Studii și Cerc. Chim. Acad. București.* **19**, 849 (1971).

[6] E. Jahnke, F. Loesch et F. Ende, « Tables of Higher Functions », ed. 6, Mc. Graw Hill Book Co., New York, 1960, p. 18.

[7] O. Schlömilch, « Vorlesungen über höheren Analysen », Bruenschweig, 1874, p. 266.

[8] C. D. Doyle, *J. Appl. Polymer Sci.*, *6*, 639 (1962).

[9] D. Fătu et E. Segal, *Rev. Roumaine Chim.*, **16**, 343 (1971).

[10] J. Simon et E. Debreczeny, *J. Thermal Analys.*, **3**, 303 (1971).

Les méthodes intégrales utilisées pour l'évaluation des paramètres cinétiques sont basées sur les équations (6) et (9)

Pour analyser les possibilités d'établir des procédés non isothermiques de détermination des paramètres cinétiques, dans le cas des phénomènes décrits par des équations cinétiques dont les fonctions de conversion $f(\alpha)$ diffèrent de $(1 - \alpha)^n$, on prendra en considération les méthodes thermogravimétriques et thermodifférentielles. Pour chacune d'elles, on examinera séparément les méthodes différentielles et les méthodes intégrales. En ce qui concerne la forme des fonctions de conversion, on adoptera une classification d'après Sestak et Berggren,[11] qui, selon notre opinion, a l'avantage d'être plus générale car elle comprend aussi d'autres réactions que celles décrites par l'équation chimique (1). On excluera cependant de cette classification les processus contrôlés par le déplacement de l'interphase, dont la cinétique est décrite par l'équation (1) pour différentes valeurs de n et qui se trouvent ainsi encadrées dans le « modèle de l'ordre de réaction ».

2. MÉTHODES THERMOGRAVIMÉTRIQUES DIFFÉRENTIELLES POUR LA DÉTERMINATION DES PARAMÈTRES CINÉTIQUES DES RÉACTIONS HÉTÉROGÈNES

2.1. L'équation (5), arrangée sous une autre forme et logarithmée, pevient :

$$\log \frac{\mathrm{d}\alpha/\mathrm{d}T}{F(\alpha)} = \log \frac{A}{a} - \frac{E}{2{,}303}\,\frac{1}{T} \tag{10}$$

et nous permet d'élaborer un groupe de procédés pour l'évaluation des paramètres cinétiques obtenus des données thermogravimétriques.

Dans ce qui suit, on présente les équations cinétiques différentielles, les fonctions de conversion $f(\alpha)$, ainsi que les formules de calcul de type (10) qui leur correspondent. On discute aussi la manière d'utiliser ces formules pour la détermination des paramètres cinétiques.

2.1.1. RÉACTIONS CONTRÔLÉES PAR LA FORMATION DES GERMES (NUCLÉATION)

A. *Nucléation suivant la loi cinétique*[4,12]

$$\frac{\mathrm{d}\alpha}{\mathrm{d}t} = k\,\alpha^m \tag{11}$$

$$m < 1$$

$$f(\alpha) = \alpha^m \tag{12}$$

---

[11] J. Sestak et G. Berggren, *Termochimica Acta*, 3, 1 (1971).

[12] D. A. Young, « Decomposition of Solids », Ier vol., Pergamon Press, Oxford, 1966.

$$\log \frac{\mathrm{d}\alpha}{\mathrm{d}T} - m \log \alpha = \log \frac{A}{a} - \frac{E}{2{,}303\,R}\,\frac{1}{T} \qquad (13)$$

La valeur de l'exposant m peut être déterminée en tenant compte que, suivant la relation (13), pour différentes vitesses d'échauffement dans des conditions isothermiques, on obtient en dérivant par rapport à $\log \alpha$:

$$\left[\frac{\mathrm{d}\log \dfrac{\mathrm{d}\alpha}{\mathrm{d}T}}{\mathrm{d}\log \alpha}\right]_{T=\mathrm{const.}} = m + \frac{\mathrm{d}\log\left(\dfrac{1}{a}\right)}{\mathrm{d}\log \alpha} \qquad (14)$$

Autrement dit, si le processus étudié est décrit par l'équation cinétique différentielle (11), la représentation graphique des valeurs $\dfrac{\mathrm{d}\log\left(\dfrac{\mathrm{d}\alpha}{\mathrm{d}t}\right)}{\mathrm{d}\log \alpha}$ en fonction de $\dfrac{\mathrm{d}\log\left(\dfrac{1}{a}\right)}{\mathrm{d}\log \alpha}$ conduit à une droite dont l'ordonnée en origine permet de déterminer la valeur de l'exposant m. En connaissant cette valeur, les deux autres paramètres cinétiques, c'est-à-dire l'énergie d'activation et le facteur préexponentiel, peuvent être déduits de la pente et de l'ordonnée en origine de la droite $\left[\left(\log \dfrac{\mathrm{d}\alpha}{\mathrm{d}t} - m \log \alpha\right), 1/T\right]$, pour une certaine valeur de la vitesse d'échauffement.

On observe que l'équation (13) est valable pour des valeurs quelconques de m, positives et négatives, et non nécessairement moindres que l'unité. Cette équation peut donc être appliquée aussi pour la description cinétique de processus différents de ceux présentés dans ce paragraphe.

B. *Nucléation suivant la loi cinétique*[4,13]

$$\frac{\mathrm{d}\alpha}{\mathrm{d}t} = k \quad \alpha^{n}(1-\alpha)^{m} \qquad (15)$$

$$1/2 < n < 1 \text{ et } 0{,}556 < m < 0{,}774$$

$$f(\alpha) = \alpha^{n}(1-\alpha)^{m} \qquad (16)$$

$$\log \frac{\mathrm{d}\alpha}{\mathrm{d}t} - n \log \alpha - m \log(1-\alpha) = \log \frac{A}{a} - \frac{E}{2{,}303\,R}\,\frac{1}{T} \qquad (17)$$

---

[13] B. V. Erofeev, « Reactivity of Solids » Elsevier, Amsterdam, 1961, p. 273.

Les valeurs des paramètres n et m peuvent être évaluées en tenant compte que, pour différentes valeurs de la vitesse d'échauffement, dans des conditions isothermiques,

$$\left[\frac{\mathrm{d}\log\dfrac{\mathrm{d}\alpha}{\mathrm{d}T}}{\mathrm{d}\log\alpha}\right]_T - \left[\frac{\mathrm{d}\log\left(\dfrac{1}{a}\right)}{\mathrm{d}\log\alpha}\right]_T = n - m\,\frac{\alpha}{1-\alpha} \tag{18}$$

En représentant graphiquement les valeurs de la différence $\left[\frac{\mathrm{d}\log\frac{\mathrm{d}\alpha}{\mathrm{d}T}}{\mathrm{d}\log\alpha}\right]_T - \frac{\mathrm{d}\log\left(\frac{1}{a}\right)}{\mathrm{d}\log\alpha}$ en fonction des valeurs $\frac{\alpha}{1-\alpha}$, on obtient une droite dont la pente et l'ordonnée en origine permettent d'évaluer m et, respectivement, n.

En connaissant ces valeurs, l'énergie d'activation et le facteur préexponentiel se déduisent de la pente et de l'ordonnée en origine de la droite $\left\{\left[\log\frac{\mathrm{d}\alpha}{\mathrm{d}T}.n\log\alpha - m\log(1-\alpha)\right], 1/T\right\}$. Dans ce cas aussi, le procédé est plus général, les formules (17) et (18) étant valables pour des valeurs de l'exposant m situées en dehors de l'intervalle qui caractérise les processus de la catégorie 2.1.1.B.

2.1.2. RÉACTIONS CONTRÔLÉES PAR LA NUCLÉATION SUIVIE D'UNE CROISSANCE DE VOLUME DES GERMES

A. *Période d'induction*[4,14]

$$\frac{\mathrm{d}\alpha}{\mathrm{d}t} = k\,\alpha^n$$

$$n = 3/4$$

Cette équation cinétique différentielle représente de fait un cas particulier de l'équation (11), ainsi que pour la détermination des paramètres cinétiques on applique le procédé indiqué au point 2.1.1A.

B. *Croissance bidimensionnelle des germes*[4,15] (*équation d'Avrami*)

$$\frac{\mathrm{d}\alpha}{\mathrm{d}T} = k(1-\alpha)\ [-\ln(1-\alpha)]^{1/2} \tag{19}$$

$$f(\alpha) = (1-\alpha)\ [-\ln(1-\alpha)]^{1/2} \tag{20}$$

---

[14] K. L. Mampel, *Z. phys. Chem.*, **A 187**, 235 (1940).

[15] M. Avrami, J. Chem. Phys., **7** 1103 (1939) ; **8**, 212 (1940) ; **9**, 177 (1941).

$$\log \frac{\mathrm{d}\alpha}{\mathrm{d}T} - \log(1-\alpha) - \frac{1}{2}\log\left[-\ln(1-\alpha)\right] = \log\frac{A}{a} - \frac{E}{2{,}303\,R}\,\frac{1}{T} \tag{21}$$

On peut utiliser l'équation (21) sans pour cela enregistrer les courbes (α, T) pour plusieurs valeurs de la vitesse d'échauffement.

En effet, la représentation graphique des valeurs $\left\{\log \frac{\mathrm{d}\alpha}{\mathrm{d}T} - \log(1-\alpha) - \frac{1}{2}\log\left[-\ln(1-\alpha)\right]\right\}$ en fonction des valeurs réciproques de la température absolue, pour une certaine valeur de la vitesse d'échauffement, conduit à une droite dont la pente et l'ordonnée en origine permettent de déduire l'énergie d'activation et, respectivement, le facteur préexponentiel.

C. *Croissance tridimensionnelle des germes* [4,12,15] (*équation d'Avrami*)

$$\frac{\mathrm{d}\alpha}{\mathrm{d}T} = k(1-\alpha)\ \left[-\ln(1-\alpha)\right]^{2/3} \tag{22}$$

$$f(\alpha) = (1-\alpha)\ \left[-\ln\,(1-\alpha)\right]^{2/3} \tag{23}$$

$$\log \frac{\mathrm{d}\alpha}{\mathrm{d}T} - \log(1-\alpha) - \frac{2}{3}\log\left[-\ln\,(1-\alpha)\right] = \log\frac{A}{a} - \frac{E}{2{,}303\,R}\,\frac{1}{T} \tag{24}$$

L'énergie d'activation et le facteur préexponentiel se déterminent ainsi qu'on l'a indiqué au point B.

D. *Cas général*

$$\frac{\mathrm{d}\alpha}{\mathrm{d}t} = k(1-\alpha)\ \left[-\ln(1-\alpha)\right]^{n} \tag{25}$$

$$f(\alpha\,(=)\,1-\alpha)\left[-\ln\,(1-\alpha)\right]^{n} \tag{26}$$

$$\log \frac{\mathrm{d}\alpha}{\mathrm{d}T} - \log\,(1-\alpha) - n\log\left[-\ln(1-\alpha)\right] = \log\frac{A}{a} - \frac{E}{2{,}303\,R}\,\frac{1}{T} \tag{27}$$

La valeur de l'exposant n se détermine en tenant compte de

$$\left[\frac{\mathrm{d}\log\frac{\mathrm{d}\alpha}{\mathrm{d}T}\frac{1}{1-\alpha}}{\mathrm{d}\log\left[-\ln(1-\alpha)\right]}\right]_{T\,=\,\mathrm{const.}} = n + \frac{\mathrm{d}\log\left(\frac{1}{a}\right)}{\mathrm{d}\log\left[-\ln(1-\alpha)\right]} \tag{28}$$

La représentation graphique des valeurs $\dfrac{\mathrm{d}\log \dfrac{\mathrm{d}\alpha}{\mathrm{d}T}\dfrac{1}{1-\alpha}}{\mathrm{d}\log\,[-\ln(1-\alpha)]}$ en fonction de $\dfrac{\mathrm{d}\log\left(\dfrac{1}{a}\right)}{\mathrm{d}\log\,[-\ln(1-\alpha)]}$, pour différentes valeurs de la vitesse d'échauffement, conduit à une droite dont l'ordonnée en origine permet de déterminer l'exposant n *et* d'établir si le processus étudié est de type B ou bien C. En connaissant la valeur de n, on détermine l'énergie d'activation et le facteur préexponentiel, en utilisant la représentation graphique de l'équation (27), ainsi qu'on l'a montré plus haut.

2.1.3. RÉACTIONS CONTRÔLÉES PAR LA NUCLÉATION SUIVIE D'UNE CROISSANCE LINÉAIRE DES GERMES

A. *Croissance enchaînée des germes avec possibilité de ramification* [4,16]

$$-\frac{\mathrm{d}\alpha}{\mathrm{d}t} = k\alpha \tag{29}$$

Cette équation peut être traitée comme un cas particulier de l'équation (11). Etant donné que $m = 1$, il ne faut plus déterminer que l'énergie d'activation et le facteur préexponentiel pour l'évaluation desquels il suffit d'avoir une seule courbe (α, T), enregistrée pour une seule valeur de la vitesse d'échauffement.

Dans cette catégorie s'encadrent aussi les réactions explosives, caractérisées par la loi cinétique

$$\frac{\mathrm{d}\alpha}{\mathrm{d}t} = k\,\alpha^{n},\ \text{où}\ n > 1$$

Pour déterminer les paramètres cinétiques, on applique le procédé indiqué au point 2.1.1.A.

B. *Germes capables de se ramifier et d'interactionner pendant leur croissance*

$$\frac{\mathrm{d}\alpha}{\mathrm{d}t} = k\alpha(1-\alpha) \tag{30}$$

$$f(\alpha) = \alpha\,(1-\alpha) \tag{31}$$

$$\log\frac{\mathrm{d}\alpha}{\mathrm{d}T} - \log\alpha(1-\alpha) = \log\frac{A}{a} - \frac{E}{2{,}303\,R}\,\frac{1}{T} \tag{32}$$

---

[16] W. E. Garner et H. R. Hailes, *Proc. Roy. Soc.*, **A 139**, 576 (1933).

On peut déterminer les paramètres cinétiques en tenant compte du fait que l'équation (30) est un cas particulier de l'équation (15), où $m = n = 1$. Si on sait avec certitude que le phénomène étudié est réellement décrit par cette équation, les paramètres cinétiques pourront être déterminés à l'aide d'une seule courbe (α, T), correspondant à une certaine vitesse d'échauffement. L'énergie d'activation et le facteur préexponentiel se déterminent à l'aide de la représentation graphique de l'équation (32).

C. *Etapes ultérieures à celles décrites aux points A et B*

$$\frac{\mathrm{d}\alpha}{\mathrm{d}t} = k\,\alpha^{n}(1-\alpha)^{m}$$

$$n < 1 \text{ et } m > 1$$

Le procédé de détermination des paramètres cinétiques a déjà été indiqué au point 2.1.1.B.

2.1.4. RÉACTIONS CONTRÔLÉES PAR LA DIFFUSION

A. *Transport unidimensionnel avec coefficient de diffusion constant* (*loi parabolique*)[17]

$$\frac{\mathrm{d}\alpha}{\mathrm{d}t} = k\alpha^{-1} \tag{33}$$

Cette équation résulte par la particularisation de l'équation (11), pour $m = -1$. Dans ce cas aussi, connaissant avec certitude la valeur de l'exposant m, on peut déterminer l'énergie d'activation et le facteur préexponentiel grâce aux données (α, T), correspondant à une seule valeur de la vitesse d'échauffement.

B. *Transport bidimensionnel* [18]

$$\frac{\mathrm{d}\alpha}{\mathrm{d}t} = k\,[-\ln(1-\alpha)]^{-1} \tag{34}$$

$$f(\alpha) = [-\ln(1-\alpha)]^{-1} \tag{35}$$

$$\log\frac{\mathrm{d}\alpha}{\mathrm{d}t} + \log[-\ln(1-\alpha)] = \log\frac{A}{a} - \frac{E}{2{,}303\,R}\,\frac{1}{T} \tag{36}$$

---

[17] K. Hauffe, « Reaktsii v tverdyk htelaklhi na ikh poverkhnosti II, I.I.L. Moscou., 1963, p. 13.

[18] G. Valensi, *Compt. rend.*, **201**, 602 (1935) ; **202**, 309 (1936).

L'évaluation des paramètres cinétiques peut aisément être effectuée à l'aide de la représentation graphique de l'équation (36).

C. *Transport tridimensionnel dans une sphère* (*Equation de Jander*[17,19])

$$\frac{\mathrm{d}\alpha}{\mathrm{d}t} = k(1-\alpha)^{1/3}[(1-\alpha)^{-1/3}-1]^{-1} \tag{37}$$

$$f(\alpha) = (1-\alpha)^{1/3}\,[(1-\alpha)^{-1/3}-1]^{-1} \tag{38}$$

$$\log\frac{\mathrm{d}\alpha}{\mathrm{d}T} - \frac{1}{3}\log(1-\alpha) + \log[(1-\alpha)^{-1/3}-1] = \log\frac{A}{a} - \frac{E}{2{,}303\;R}\,\frac{1}{T} \tag{39}$$

Les valeurs de l'énergie d'activation et du facteur préexponentiel peuvent être déduites de la pente et de l'ordonnée en origine des droites obtenues en représentant graphiquement les valeurs du membre *I* de l'équation (39), pour différentes valeurs de α, en fonction de $1/T$.

Equation Ginstling-Brounshtein.[14,20]

$$\frac{\mathrm{d}\alpha}{\mathrm{d}t} = k\,[(1-\alpha)^{-1/3}-1]^{-1} \tag{40}$$

$$f(\alpha) = [(1-\alpha)^{-1/3}-1]^{-1} \tag{41}$$

$$\log\frac{\mathrm{d}\alpha}{\mathrm{d}t} + \log\,[(1-\alpha)^{-1/3}-1] = \log\frac{A}{a} - \frac{E}{2{,}303\;R}\,\frac{1}{T} \tag{42}$$

La représentation graphiqne de l'équation (41) permet de déterminer l'énergie d'activation et le facteur préexponentiel.

On doit remarquer que les processus analysés au paragraphe 2.1.4. ne traitent pas les processus de type I, mais l'oxydation des métaux et certaines réactions en phase solide.

2.2. Les paramètres cinétiques peuvent être déterminés en établissant des procédés basés sur la généralisation de la méthode Freeman—Carroll,[21] de façon à pouvoir appliquer celle-ci pour les processus décrits par l'équation cinétique (2), où $f(\alpha) \neq (1-\alpha)^n$. Dans ce but, on considère de nouveau l'équation cinétique (2), en tenant compte de la variation de la constante cinétique avec la température, conformément à la relation (4). On obtient ainsi

$$\frac{\mathrm{d}\alpha}{\mathrm{d}t} = A\;\mathrm{e}^{-E/RT} f(\alpha) \tag{43}$$

---

[19] W. Jander, *Z. anorg. Chem.* **163**, 1 (1927).

[20] A. M. Ginstling et B. I. Brounstein, *Zhur. priklad. Khim.*, **23**, 1249 (1950).

[21] E. S. Freeman et B. Carroll, *J. Phys. Chem.*, **62**, 394 (1958).

En logarithmant, on obtient :

$$\log \frac{\mathrm{d}\alpha}{\mathrm{d}t} = \log A + \log f(\alpha) - \frac{E}{2{,}303\ R} \frac{1}{T} \tag{44}$$

En appliquant l'opérateur Δ (différence de valeurs successives) et en arrangeant de façon convenable les termes de l'équation (44), on obtient :

$$\frac{\Delta \log \frac{\mathrm{d}\alpha}{\mathrm{d}t}}{\Delta \log f(\alpha)} = 1 - \frac{\frac{E}{2{,}303\ R}\,\Delta\left(\frac{1}{T}\right)}{\Delta \log f(\alpha)} \tag{45}$$

La particularisation de la relation (45), pour différentes formes concrètes de la fonction de conversion, permet d'évaluer l'énergie d'activation. En effet, la représentation graphique $\frac{\Delta \log \frac{\mathrm{d}\alpha}{\mathrm{d}t}}{\Delta \log f(\alpha)} = f\left[\frac{\Delta\left(\frac{1}{T}\right)}{\Delta \log f(\alpha)}\right]$ conduit à une droite dont la pente permet de déterminer l'énergie d'activation. Le facteur préexponentiel peut être déterminé grâce à la relation (44).

2.2.1.A. *Pour les processus de nucléation décrits par l'équation différentielle (11), l'équation (45) devient :*

$$\frac{\Delta \log \frac{\mathrm{d}\alpha}{\mathrm{d}t}}{\Delta \log \alpha} = m - \frac{\frac{E}{2{,}303\ R}\,\Delta\left(\frac{1}{T}\right)}{\Delta \log \alpha} \tag{46}$$

La représentation graphique sous forme de droite de l'équation (46), selon le procédé démontré, permet de déterminer la valeur de l'énergie d'activation grâce à la pente de la droite, ainsi que l'exposant *m*, à l'aide de son ordonnée à l'origine.

B. *Pour les processus de nucléation décrits par l'équation différentielle (15) l'équation (45) conduit à*

$$\frac{\Delta \log \frac{\mathrm{d}\alpha}{\mathrm{d}t}}{n\ \Delta \log \alpha + m\ \Delta \log (1-\alpha)} = 1 - \frac{\frac{E}{2{,}303\ R}\,\Delta\left(\frac{1}{T}\right)}{n\ \Delta \log \alpha + m\ \Delta \log (1-\alpha)} \tag{47}$$

Si l'on suppose connue l'énergie d'activation, les valeurs des exposants *m* et *n* pourront être déterminées en utilisant quatre groupes de valeurs $\left(\alpha\cdot \frac{\mathrm{d}\alpha}{\mathrm{d}t}, T\right)$. Grâce à l'équation (47), on obtient un système d'équations qui peut être résolu en rapport des inconnues *n* et *m*. L'énergie d'activation peut être déterminée en traçant graphiquement la droite

$\frac{d\alpha}{dt}$ en fonction de $1/T$, dans des conditions d'isoconversion. En effet, l'équation (44) nous permet d'obtenir :

$$\left[\frac{d \log \frac{d\alpha}{dt}}{d\left(\frac{1}{T}\right)}\right]_{\alpha=\text{const}} = -\frac{E}{2{,}303\ R} \tag{48}$$

En connaissant les valeurs de l'énergie d'activation et des constantes n et m, le facteur préexponentiel peut être aisément déduit de l'équation (44), particularisée pour $f(\alpha) = \alpha^n(1 - \alpha)^n$.

Parmi les quelques exemples d'application des procédés non isothermiques de détermination des paramètres cinétiques pour $f(\alpha) \neq (1-\alpha)^n$, on mentionne les recherches concernant la déshydratation de l'oxalate de nickel d'hydrate.[22] Pour la période initiale de déshydratation, on a appliqué la méthode Freeman-Carroll pour $f(\alpha) = e^{(1-\alpha)}$.

On peut considérer que le procédé général d'application de la méthode Freeman—Carroll pour des fonctions de conversion quelconques, ainsi que les exemples traités ci-dessus, sont suffisants pour permettre au lecteur d'adapter cette méthode à la forme particulière de la fonction de conversion qui l'intéresse. C'est pourquoi les autres cas ne sont plus traités séparément, ainsi qu'au paragraphe précédent. L'idée à retenir, c'est que la particularisation de la formule (45) et sa représentation graphique permettent de déterminer l'énergie d'activation et, éventuellement, encore un des paramètres de la fonction de conversion. Lorsque cette fonction contient plusieurs paramètres, l'énergie d'activation se détermine dans des conditions d'isoconversion, en utilisant plusieurs valeurs de la vitesse d'échauffement. Le facteur préexponentiel se détermine à l'aide de l'équation (44).

3. MÉTHODES THERMOGRAVIMÉTRIQUES INTÉGRALES DE DÉTERMINATION DES PARAMÈTRES CINÉTIQUES DES RÉACTIONS HÉTÉROGÈNES

3.1. Dans la littérature de spécialité, on trouve un groupe de méthodes intégrales qui peuvent être généralisées, étant donné qu'elles permettent d'évaluer l'énergie d'activation sans connaître la forme de l'intégrale de conversion.[1,8,23] Ces méthodes peuvent, évidemment, être aussi appliquées à la détermination des paramètres cinétiques des réactions pour lesquelles

$$F(\alpha) \neq \begin{cases} \dfrac{1-(1-\alpha)^{1-n}}{1-n} & n \neq 1 \\ -\ln(1-\alpha) & n = 1 \end{cases},$$

n étant l'ordre de réaction.

---

[22] W. A. Hughes »Proceedings of the First International Conference on Thermal Analysis », Mac Millan & Co. London, 1965, p. 176.

[23] J. Zsako, *J. Thermal. Analysis.*, **2**, 145 (1970).

En essayant de généraliser les procédés basés sur l'utilisation d'une forme connue de l'intégrale de conversion, on pourrait éventuellement déterminer, outre l'énergie d'activation et le facteur préexponentiel, certains paramètres particuliers de cette intégrale. Dans ce but, on considère pour la fonction $p(x)$ de la relation (7), une expression approximative, obtenue en retenant seulement les deux premiers termes de son développement en série asymptotique [6]

$$p(x) = \frac{e^{x}}{x^{2}}\left(1 + \frac{2!}{x}\right) \tag{49}$$

Etant donné la signification de la variable x qu'on introduit dans (7), on obtient :

$$F(\alpha) = \frac{A}{a}\,\frac{RT^{2}}{E}\left(1 - \frac{2RT}{E}\right)e^{-E/RT} \tag{50}$$

C'est sur une approximation de cette sorte qu'est basée la méthode élaborée par Coats et Redfern [24] pour la détermination des paramètres cinétiques. On déduit les formules de calcul en logarithmant la relation générale (50)

$$\log\frac{F(\alpha)}{T^{2}} = \log\frac{AR}{aE}\left(1 - \frac{2RT}{E}\right) - \frac{E}{2{,}303\,R}\,\frac{1}{T} \tag{51}$$

En effet, la représentation graphique $\left[\log\frac{F(\alpha)}{T^{2}},\ 1/T\right]$ conduit à une droite dont la pente et l'ordonnée en origine permettent de déterminer les valeurs de l'énergie d'activation et du facteur préexponentiel.

En se limitant pour le moment à cette approximation, on analyse dans ce qui suit les possibilités de détermination des paramètres cinétiques pour tous les cas du paragraphe 2.1. Dans ce but, on doit établir la forme analytique de l'intégrale de conversion pour chaque cas à part.

On présente plus loin les intégrales de conversion, les formules de calcul et, en cas de nécessité, certaines indications pour leur utilisation, afin de déterminer les paramètres cinétiques.

3.1.1. RÉACTIONS CONTRÔLÉES PAR LA FORMATION DES GERMES (NUCLÉATION)

A. *Nucléation suivant la loi cinétique (11)*

Il est aisé d'obtenir l'intégrale de conversion, en tenant compte de l'équation (11) et en intégrant :

$$F(\alpha) = \int_{0}^{\infty}\frac{d\alpha}{\alpha^{m}} = \frac{\alpha^{1-m}}{1-m} \tag{52}$$

---

[24] A. W. Coats et J. P. Redfern, *Nature*, **201**, 68 (1966).

Grâce à ce résultat, la formule (51) devient :

$$\log \frac{1}{T^2} \frac{\alpha^{1-m}}{1-m} = \log \frac{AR}{aE}\left(1 - \frac{2RT}{E}\right) - \frac{E}{2{,}303\ R} \frac{1}{T} \tag{53}$$

relation valable pour $m < 1$ et pouvant être appliquée graphiquement de la manière connue. La représentation graphique $\left[\log \frac{1}{T^2} \frac{\alpha^{1-m}}{1-m}, \frac{1}{T}\right]$ est linéaire seulement pour la valeur correcte de l'exposant m. Autrement dit, faute d'informations supplémentaires, la valeur de m se détermine par essais successifs.

B. *Nucléation suivant la loi cinétique (15)*

$$F(\alpha) = \int_0^{\alpha} \alpha^{-n}(1 - \alpha)^{-m}\, d\alpha \tag{54}$$

Pour intégrer, on doit effectuer un développement binomial :

$$(1 - \alpha)^{-m} = 1 + \sum_{p=1}^{\infty} \frac{m(m+1)\ldots(m+p-1)}{p!}\, \alpha^p \tag{55}$$

En multipliant par α^{-n} et en intégrant, on obtient

$$F(\alpha) = \frac{\alpha^{1-n}}{1-n} + \sum_{p=1}^{\infty} \frac{m(m+1)\ldots(m+p-1)}{p!} \cdot \frac{\alpha^{p-n+1}}{p-n+1} \tag{56}$$

L'intégrale de conversion peut être approximée, en gardant un nombre de termes d'autant plus réduit que les valeurs du degré de transformation sont plus petites. Ainsi, par exemple, pour $n = m = 1/2$ et $\alpha = 0{,}90$, le quatrième terme de l'intégrale de conversion (le troisième terme de la somme) représente une valeur approximativement égale à 3,4% de la somme des quatre termes. On déduit de (56) que la valeur de l'exposant n doit être inférieure à l'unité.

Tenant lieu des relations (53) et (56), on détermine les paramètres cinétiques en utilisant la formule de calcul suivante :

$$\log \frac{1}{T^2}\left[\frac{\alpha^{1-n}}{1-n} + \sum_{p=1}^{\infty} \frac{m(m+1)\ldots(m+p-1)}{p!} \cdot \frac{\alpha^{p-n+1}}{p-n+1}\right] =$$

$$= \frac{AR}{aE}\left(1 - \frac{2RT}{E}\right) - \frac{E}{2{,}303\ R} \frac{1}{T} \tag{57}$$

L'application de cette formule implique des informations supplémentaires sur les valeurs des exposants n et m, ou bien des essais successifs pour déterminer des valeurs de n et m compatibles avec une représentation graphique parfaitement linéaire.

3.1.2. RÉACTIONS CONTRÔLÉES PAR LA NUCLÉATION SUIVIE D'UNE CROISSANCE DE VOLUME DES GERMES

A. *Période d'induction*

Etant donné la similitude des équations cinétiques, le problème peut être formellement encadré dans le cas 3.1.1.A.

B. *Croissance bidimensionnelle des germes (équation d'Avrami)*

L'intégrale de conversion a la forme :

$$F(\alpha) = 2\,[-\ln(1-\alpha)]^{1/2} \tag{58}$$

En introduisant cette expression dans (51), on obtient la formule de calcul suivante :

$$\log\frac{2}{T^2}[-\ln(1-\alpha)]^{1/2} = \log\frac{A}{a}\frac{R}{E}\left(1-\frac{2RT}{E}\right) - \frac{E}{2{,}303\;R}\frac{1}{T} \tag{59}$$

C. *Croissance tridimensionnelle des germes (équation d'Avrami)*

$$F(\alpha) = 3\,[-\ln(1-\alpha)]^{1/3} \tag{60}$$

$$\log\frac{3}{T^2}[-\ln(1-\alpha)]^{1/3} = \log\frac{A}{a}\frac{R}{E}\left(1-\frac{2RT}{E}\right) - \frac{E}{2{,}303\;R}\frac{1}{T} \tag{61}$$

D. *Cas général*

$$F(\alpha) = n[-\ln(1-\alpha)]^{1/n} \tag{62}$$

$$\log\frac{n}{T^2}[-\ln(1-\alpha)]^{1/n} = \log\frac{AR}{aE}\left(1-\frac{2RT}{E}\right) - \frac{E}{2{,}303\;R}\frac{1}{T} \tag{63}$$

La valeur de la constante n peut être déterminée par des essais successifs. En effet, c'est seulement pour la valeur correcte de n que la représentation graphique $\log\left\{\frac{n}{T^2}[-\ln(1-\alpha)^{1/n}],\ 1/T\right\}$ conduit à une droite.

3.1.3. RÉACTIONS CONTRÔLÉES PAR LA NUCLÉATION, SUIVIE D'UNE CROISSANCE LINÉAIRE DES GERMES

A. *Croissance enchaînée des germes, avec possibilité de ramification*

Quoique, du point de vue formel, ce cas pourrait être traité comme le cas 3.1.1.A, une analyse plus détaillée du problème nous démontre que, pour $\alpha = 0$, l'intégrale de conversion deviendrait égale à l'infini. C'est pourquoi les paramètres cinétiques sont déterminés par le procédé qui suit.

En intégrant l'équation différentielle (2), pour $f(\alpha) = -\alpha$, et tenant compte des relations (3) et (4), on obtient :

$$\ln\frac{1}{\alpha} = \frac{A}{a}\int \mathrm{e}^{-E/RT}\,\mathrm{d}T + C \tag{64}$$

ou bien [25] :

$$\ln\frac{1}{\alpha} = \frac{A}{a}\,\frac{RT^2}{E}\left(1 - \frac{2RT}{E}\right)\mathrm{e}^{-\frac{E}{RT}} + C \tag{65}$$

Pour deux valeurs de la vitesse d'échauffement, utilisées dans des conditions d'isoconversion, on obtient :

$$\left.\begin{aligned} \ln\frac{1}{\alpha} &= \frac{A}{a_1}\,\frac{R}{E}\,T_1^2\left(1 - \frac{2RT_1}{E}\right)\mathrm{e}^{-\frac{E}{RT_1}} + C \\ \ln\frac{1}{\alpha} &= \frac{A}{a_2}\,\frac{R}{E}\,T_2^2\left(1 - \frac{2RT_2}{E}\right)\mathrm{e}^{-\frac{E}{RT_1}} + C \end{aligned}\right\} \tag{66}$$

d'où :

$$\frac{a_2}{a_1}\left(\frac{T_1}{T_2}\right)^2 \frac{1 - \dfrac{2RT_1}{E}}{1 - \dfrac{2RT_2}{E}} = \mathrm{e}^{\frac{E}{R}\left(\frac{1}{T_1} - \frac{1}{T_2}\right)} \tag{67}$$

Grâce à la relation (67), on peut déterminer l'énergie d'activation.

Pour deux valeurs de la vitesse d'échauffement, dans des conditions isothermiques, la relation (65) devient :

$$\left.\begin{aligned} \ln\frac{1}{\alpha_1} &= \frac{A}{a_1}\,\frac{RT^2}{E}\left(1 - \frac{2RT}{E}\right)\mathrm{e}^{-\frac{E}{RT}} + C \\ \ln\frac{1}{\alpha_2} &= \frac{A}{a_2}\,\frac{RT^2}{E}\left(1 - \frac{2RT}{E}\right)\mathrm{e}^{-\frac{E}{RT}} + C \end{aligned}\right\} \tag{68}$$

---

[25] I. M. Ryjic et I. S. Gradstein, « Tabele de integrale, sume, serii și produse », Ed. tehnică, 1955, p. 104.

Par soustraction, on obtient :

$$\ln\frac{\alpha_2}{\alpha_1} = A\,\frac{RT^2}{E}\left(1-\frac{2RT}{E}\right)\left(\frac{1}{a_1}-\frac{1}{a_2}\right)\mathrm{e}^{-\frac{E}{RT}}, \tag{69}$$

formule qui permet d'évaluer le facteur préexponentiel.

Pour les réactions explosives décrites par une équation cinétique avec $f(\alpha) = \alpha^n (n > 1)$, on utilise un procédé similaire. L'énergie d'activation se détermine en appliquant la relation (67). Si on connaît la valeur de n, le facteur préexponentiel pourra être déterminé à l'aide de la relation

$$\frac{\alpha_1^{1-n}}{1-n}-\frac{\alpha_2^{1-n}}{1-n} = A\,\frac{RT^2}{E}\left(1-\frac{2RT}{E}\right)\left(\frac{1}{a_1}-\frac{1}{a_2}\right)\mathrm{e}^{-\frac{E}{RT}} \tag{70}$$

déduite de la même façon que la relation (69).

B. *Germes capables de se ramifier et d'interactionner pendant leur croissance*

Etant donné la difficulté d'évaluer l'intégrale de conversion pour $\alpha = 0$, on applique le même procédé qu'au point A, c'est-à-dire qu'on effectue l'intégration en éliminant ensuite la constante d'intégration. En intégrant l'équation (30), on obtient :

$$\ln\frac{\alpha}{1-\alpha} = \frac{A}{a}\,\frac{RT^2}{E}\left(1-\frac{2RT}{E}\right)\mathrm{e}^{-\frac{E}{RT}} + C \tag{71}$$

Dans des conditions d'isoconversion, pour deux valeurs de la vitesse d'échauffement, a_1 et a_2, on retrouve la formule (69) pour le calcul de l'énergie d'activation. Quant au facteur préexponentiel, celui-ci peut être évalué à l'aide de la formule

$$\ln\frac{\alpha_1}{\alpha_2}\,\frac{1-\alpha_2}{1-\alpha_1} = A\,\frac{RT^2}{E}\left(1-\frac{2RT}{E}\right)\left(\frac{1}{a_1}-\frac{1}{a_2}\right)\mathrm{e}^{-\frac{E}{RT}}, \tag{72}$$

déduite des conditions isothermiques.

C. *Etapes ultérieures à celles décrites aux points A et B*

Au point de vue formel, l'intégration de l'équation cinétique différentielle (15), pour $n < 1$ et $m > 1$, nous conduit de nouveau à l'équation (57), avec la mention que cette fois la valeur de l'exposant m est supérieure à l'unité.

3.1.4. RÉACTIONS CONTRÔLÉES PAR LA DIFFUSION

A. *Transport unidimensionnel avec coefficient de diffusion constant (loi parabolique)*

On déduit l'intégrale de conversion et la formule de calcul en introduisant $m = -1$ dans les relations (52) et (53).

B. *Transport bidimensionnel*

En tenant compte de l'équation (34), l'intégrale de conversion devient

$$F(\alpha) = \int_0^\infty [-\ln(1-\alpha)]\, \mathrm{d}\alpha \tag{73}$$

Afin d'intégrer, on utilise le développement en série suivant[11] :

$$\ln(1-\alpha) \cong -\left[\alpha + \frac{1}{2}\alpha^2 + \frac{1}{3}\alpha^3 + \frac{1}{4}\alpha^4 + \dots\right] \tag{74}$$

En introduisant dans (73) et en intégrant, on obtient :

$$F(\alpha) = \sum_{n=2}^{\infty} \frac{\alpha^n}{n(n-1)} \tag{75}$$

Il est aisé de calculer la somme de l'expression (75) (Annexe I), qui nous conduit à la forme suivante de la fonction intégrale de conversion :

$$F(\alpha) = \alpha + (1-\alpha)\ln(1-\alpha) \tag{76}$$

En introduisant dans (51), on obtient la formule de calcul pour la détermination des paramètres cinétiques :

$$\log \frac{1}{T^2}[\alpha + (1-\alpha)\ln(1-\alpha)] = \log \frac{\Delta R}{aE}\left(1 - \frac{2RT}{E}\right) - \frac{E}{2{,}303}\frac{1}{RT} \tag{77}$$

C. *Transport tridimensionnel dans une sphère*

Equation de Jander

$$F(\alpha) = 3\left\{\frac{1}{2}[1 + (1-\alpha)^{2/3}] - (1-\alpha)^{1/3}\right\} \tag{78}$$

$$\log \frac{3}{T^2}\left\{\frac{1}{2}[1 + (1-\alpha)^{2/3}] - (1-\alpha)^{1/3}\right\} = \log \frac{AR}{aE}\left(1 - \frac{2RT}{E}\right) - \frac{E}{2{,}303}\frac{1}{RT} \tag{79}$$

Equation Guinstling—Brounshtein

$$F(\alpha) = \frac{3}{2}[1 - (1-\alpha)^{2/3}] - \alpha \tag{80}$$

$$\log \frac{1}{T^2}\left\{\frac{3}{2}\left[1-(1-\alpha)^{2/3}-\alpha\right]\right\}=\frac{A}{a}\frac{R}{E}\left(1-\frac{2RT}{E}\right)-\frac{E}{2{,}303}\frac{1}{RT} \tag{81}$$

3.2. On peut aussi élaborer des méthodes de détermination des paramètres cinétiques des réactions hétérogènes qui ne soient pas encadrées dans le modèle de l'ordre de réaction, en utilisant d'autres approximations de l'intégrale de température. Ainsi, par exemple, on peut appliquer l'approximation de van Krevelen et collaborateurs[26] qui déterminent les paramètres cinétiques en utilisant la formule générale de calcul suivante :

$$\log F(\alpha)=\log\left[\frac{A}{a}\left(\frac{S}{T_m}\right)^{\frac{E}{RT_m}}\frac{1}{e^{\frac{E}{RT_m}}+1}\right]+\left[\frac{E}{RT_m}+1\right]\log T, \tag{82}$$

où T_m représente la température correspondant à la vitesse de réaction maximale, S est une constante égale à 0,368 et la signification des autres grandeurs est connue. La représentation graphique [$\log F(\alpha)$, $\log T$] conduit à une droite dont la pente et l'ordonnée en origine permettent de déterminer l'énergie d'activation et, respectivement, le facteur préexponentiel.

On peut aussi élaborer des méthodes intégrales de détermination des paramètres cinétiques en utilisant des programmes d'échauffement hyperbolique. En logarithmant l'expression (9), on obtient la formule générale de calcul

$$\log F(\alpha)=\log\frac{AR}{bE}-\frac{E}{2{,}303\ R}\frac{1}{T}, \tag{83}$$

dont la représentation graphique permet de déterminer l'énergie d'activation et le facteur préexponentiel.

4. MÉTHODES THERMODIFFÉRENTIELLES DIFFÉRENTIELLES POUR LA DÉTERMINATION DES PARAMÈTRES CINÉTIQUES DES RÉACTIONS HÉTÉROGÈNES

4.1. Dans l'équation (10), le degré de transformation et la vitesse de réaction $\frac{d\alpha}{dT}$ peuvent être approximés grâce aux relations[27]

$$\alpha=\frac{a}{\mathcal{A}} \tag{84}$$

$$\frac{d\alpha}{dt}=\frac{\Delta T}{\mathcal{A}} \tag{85}$$

---

[26] D. W. van Krevelen, C. van Heerden et F. J. Huntjes, *Fuel*, 30, 253 (1951).

[27] D. Fătu, *J. Thermal Analys.*, 1, 285 (1969).

où a représente la surface limitée par la courbe *ATD*, la ligne de base et la parallèle à l'axe des ordonnées correspondant au moment t ou à la température T, $\mathcal{A}$ — la surface encadrée par la courbe ATD et la ligne de base, et ΔT — la différence de température par rapport à la ligne de base, mesurée sur la courbe ATD correspondant au moment t ou à la température T. C'est ainsi qu'on obtient :

$$\log\frac{\Delta T}{\alpha} - \log f\left(\frac{a}{\mathcal{A}}\right) = \log\frac{A}{a} - \frac{E}{2{,}303\,R}\,\frac{1}{T} \tag{86}$$

En introduisant dans la formule générale de calcul (86) différentes fonctions $f\left(\frac{a}{\mathcal{A}}\right)$ correspondant à différentes fonctions de conversion $f(\alpha)$, on peut établir des procédés thermodifférentiels pour la détermination des paramètres cinétiques, similaires aux procédés thermogravimétriques décrits dans le paragraphe 2.1. On remarque que, dans les formules (84) et (85), les surfaces a et $\mathcal{A}$ sont exprimées par des unités de température au carré.

4.2. En revenant à l'équation (44) et en tenant compte de,[27]

$$\alpha = \frac{a}{\mathcal{A}} \tag{84'}$$

et

$$\frac{\mathrm{d}\alpha}{\mathrm{d}t} = \frac{\Delta T}{\mathcal{A}}, \tag{85'}$$

où a et $\mathcal{A}$ ont les significations déjà connues, mais exprimées cette fois en unités de température × unités de temps, on obtient :

$$\log\frac{\Delta T}{\mathcal{A}} = \log A + \log f\left(\frac{\mathrm{a}}{\mathcal{A}}\right) - \frac{E}{2{,}303\,R}\,\frac{1}{T} \tag{87}$$

En appliquant à (87) l'opérateur Δ, cette relation devient

$$\frac{\Delta\log\Delta T}{\Delta\log f\left(\frac{\mathrm{a}}{\mathcal{A}}\right)} = 1 - \frac{\frac{E}{2{,}303\,R}\,\Delta\left(\frac{1}{T}\right)}{\Delta\log f\left(\frac{\mathrm{a}}{\mathcal{A}}\right)} \tag{88}$$

Cette nouvelle relation peut être représentée graphiquement ainsi qu'on l'a montré au paragraphe 2.2., ce qui permet de déterminer l'énergie d'activation. Le facteur préexponentiel résulte de l'équation (87).

Freeman et Carroll ont utilisé pour le degré de transformation et la vitesse de réaction des formules plus exactes, selon Borchardt et Daniels[28]

$$\alpha = \frac{Cp\,\Delta T + Ka}{K\mathcal{A}} \tag{89}$$

$$\frac{\mathrm{d}\alpha}{\mathrm{d}t} = \frac{Cp\dfrac{\mathrm{d}\,\Delta T}{\mathrm{d}t} + K\,\Delta T}{K\mathcal{A}} \tag{90}$$

où K et Cp représentent le coefficient de transfert thermique et, respectivement, la capacité calorique de l'échantillon.

En tenant compte des relations (89) et (90), l'équation (44) devient :

$$\log \frac{Cp\dfrac{\mathrm{d}\,\Delta T}{\mathrm{d}t} + K\,\Delta T}{K\mathcal{A}} = \log \mathcal{A} + \log f\left(\frac{Cp\,\Delta T + Ka}{K\mathcal{A}}\right) - \frac{E}{2{,}303}\,\frac{1}{RT} \tag{91}$$

L'application de l'opérateur de différence Δ à (91) conduit à :

$$\frac{\Delta \log\left(Cp\dfrac{\mathrm{d}\,\Delta T}{\mathrm{d}t} + K\,\Delta T\right)}{\Delta \log f\left(\dfrac{Cp\,\Delta T + Ka}{K\mathcal{A}}\right)} = 1 - \frac{\dfrac{E}{R}\,\Delta\left(\dfrac{1}{T}\right)}{\Delta \log f\left(\dfrac{Cp\,\Delta T + Ka}{K\mathcal{A}}\right)}, \tag{92}$$

relation dont la représentation graphique permet de déterminer l'énergie d'activation, à condition de connaître les grandeurs K et Cp. Le facteur préexponentiel résulte de l'équation (91).

5. MÉTHODES THERMODIFFÉRENTIELLES INTÉGRALES DE DÉTERMINATION DES PARAMÈTRES CINÉTIQUES DES RÉACTIONS HÉTÉROGÈNES

Comme point de départ pour ces méthodes, on peut utiliser, par exemple, l'équation (50), en appliquant la formule (84) pour exprimer le degré de transformation.

Dans ces conditions, toutes les méthodes thermogravimétriques présentées au paragraphe 3.1. peuvent être exprimées de façon correspondante en méthodes thermodifférentielles. De même, on peut élaborer des procédés thermodifférentiels basés sur l'utilisation de l'équation (82).

Evidemment, l'évaluation des paramètres cinétiques par un procédé thermodifférentiel au lieu d'un procédé thermogravimétrique doit être acceptée avec une certaine réserve, étant donné les erreurs spécifiques des méthodes ATD[29].

---

[28] J. Borchardt et F. Daniels, *J. Amer. Chem. Soc.*, **79**, 41 (1957).

L'auteur considère que la détermination des paramètres cinétiques par un procédé thermodifférentiel est utile surtout pour les processus non accompagnés de variations de masse, ainsi que les réactions dans les systèmes solide-solide ou bien les transformations de phase.

CONCLUSIONS

Les méthodes non isothermiques permettent, en principe, de déterminer les paramètres cinétiques des plus différents processus hétérogènes décrits par des lois cinétiques qui ne soient pas obligatoirement encadrées dans le modèle de l'ordre de réaction.

Ce mémoire ne se propose pas d'épuiser toutes les possibilités de ce domaine de recherches, mais de stimuler l'intérêt pour une description fidèle des phénomènes, en tenant lieu de leurs lois particulières de déroulement, par la présentation de quelques principes généraux d'utilisation des données expérimentales.

---

[29] D. Fătu, *Studii și Cerc. Chim.*, București, **20**, 141 (1972).

Revue Roumaine de Chimie, 18, 9, 1577–1580 (1973)

TRANSIENT SPECIES FROM THE REACTION OF THE HYDRATED ELECTRON WITH HEXACYANOCOBALTATE. III

ION MIHALCEA* and ROBERT R. HENTZ**

* Department of Chemistry, University of Bucharest, Bd. Republicii 13, Romania
** University of Notre Dame, Department of Chemistry and the Radiation Laboratory,[1] Notre Dame, Indiana 46556, USA

Received April 3, 1973

The nanosecond pulse radiolysis of aqueous solutions of hexacyanocobaltate (III) has been investigated. The results of this work indicate that e^-_{aq} and $Co(CN)_6^{3-}$ react with $k = (3.3 \pm 0.1)10^9\ M^{-1}\ sec^{-1}$ to give one transient species (with $\varepsilon_{max} = 4 \times 10^3 M^{-1}\ cm^{-1}$ at 280 nm) which decays with $t_{1/2} = 10.4 \pm 0.4\ \mu sec$.

Venerable and co-workers [2] have reported that pulse radiolysis of aqueous solutions of hexacyanocobaltate (III) gives two distinct transient species as the initially observed products following decay of the hydrated electron, e^-_{aq}. Formation of the two transient species was attributed to approximately equally probable alternative reactions of e^-_{aq} with $Co(CN)_6^{3-}$. One of the transient species was reported to have a half-life of $\sim 10^{-3}$ sec and optical absorption maxima at 280 nm and 965 nm with $\varepsilon = 7 \times 10^3 M^{-1}$ cm^{-1} and $\varepsilon \approx 5 \times 10^2 M^{-1}\ cm^{-1}$, respectively; the other transient species was reported to have a half-life of 10^{-5} sec and an optical absorption maximum at 270–275 nm with $\varepsilon \approx 10^3 M^{-1} cm^{-1}$. In the course of a pulse-radiolysis study of the reduction of a number of cobalt complexes by Co^+, Mn^+ and Pb^+, we have examined the pulse radiolysis of aqueous solutions of hexacyanocobaltate (III) under conditions somewhat different from those of Venerable *et al.* Our results follow.

Solutions containing $K_3Co(CN)_6$, from Alfa—Inorganics, and 0.2 M *t*-butanol (Baker Analyzed) were prepared with triply distilled water; the solutions were deaerated by argon bubbling and introduced into 1 cm square suprasil cells under argon. Solutions were irradiated at about 29° with 5 nsec pulses of $\sim$8 MeV electrons at currents up to 5 A from the Notre Dame Arco Model LP—7 Linear Accelerator. Initial concentrations of e_{aq}^-, determined spectrophotometrically, were usually about 10 μM. The light source for measurement of optical absorption was a 450-W xenon lamp (Ushio UXL 451-0) that was pulsed to 50 times the steady-state output for a 5-msec period within which the absorption was recorded. Transmitted light was focussed onto the slits of a Heath monochromator with slit widths at 1—2 mm. Light intensity was measured with an RCA-1 P 28 photomultiplier, and the transient absorption signal was displayed on a Tektronix 7704 oscilloscope and permanently recorded on Polaroid 410 high-speed film. Initial light intensity was recorded on a Tektronix 564 storage oscilloscope.

---

[1] The Radiation Laboratory of the University of Notre Dame is operated under contract with the U. S. Atomic Energy Commission. This is AEC Document N° COO—38—862.

[2] G. D. Venerable II, E. J. Hart, and J. Halpern, *J. Amer. Chem. Soc.*, 91, 7538 (1969).

Response time of the system was less than 25 nsec.

Typical results are presented in figure 1 for a deaerated neutral solution with 2×10^{-3} M $Co(CN)_6^{3-}$ and 0.2 M *t*-butanol. Corresponding results were obtained with 5×10^{-4} M $Co(CN)_6^{3-}$ at $pH = 13$ and with other concentrations of the complex. The presence of 0.2 M *t*-butanol in each solution serves to remove OH (k[3] $= 2.5 \times 10^8 M^{-1} sec^{-1}$) with a half-life of 14 nsec.

Curves obtained for decay of the absorption at 578 nm after a 5-nsec pulse, such as the curve in figure 1 (b), conform to first-order kinetics and give $k = (3.3 \pm 0.1) \times 10^9 M^{-1} sec^{-1}$ for the reaction of e_{aq}^- with $Co(CN)_6^{3-}$. Such a value is somewhat lower than the $k = (5.0 \pm 0.5) \times 10^9 M^{-1} sec^{-1}$ of Venerable. *et al.*[2], but agrees well with other published values of [4] $k = 3.6 \times 10^9 M^{-1} sec^{-1}$ and[5] $k = 2.7 \times 10^9 M^{-1} sec^{-1}$. Coincident with the decay in absorption at 578 nm, a growth in absorption was observed at 280 nm. With the assumption that absorption at 280 nm is attributable to a product of the reaction of e_{aq}^- with $Co(CN)_6^{3-}$, first-order kinetic analysis of the growth curves gives for that reaction $k = (3.4 \pm 0.1) \times 10^9 M^{-1} sec^{-1}$ which is increased to $3.6 \times 10^9 M^{-1} sec^{-1}$ by inclusion of a small correction in the kinetic analysis for a possible contribution of H atoms to formation of the transient species observed at 280 nm. From the good agreement between such values of k and that obtained from decay of the absorption at 578 nm, it follows that the absorption at 280 nm is attributable indeed to a product of the reaction of e_{aq}^- with $Co(CN)_6^{3-}$.

For the experimental conditions given in figure 1, the results and conclusions reported by Venerable and co-workers (summarized in the introductory paragraph) lead to the following expectations : (1) the absorption spectrum cosequent on e_{aq}^- decay will show some evidence of two maxima in the 270—290 nm region with decay at 280 nm being slower than decay at 270—275 nm ; (2) the optical density at $\sim$280 nm will increase to a maximum and then, owing to the decay of the transient species with $t_{1/2} \approx 10^{-5}$ sec. will decrease in 40—50 μsec to about 7/8 of the maximum value and finally will decrease to zero with $t_{1/2} \approx 10^{-3}$ sec. Clearly, such expectations are not fulfilled by the results shown in figure 1. As shown in figure 1 (a), there is no evidence of two maxima and , indeed, no significant change in the spectrum in the 270 – 290 nm region over a period of 1 – 20 μsec.

---

[3] G. E. Adams, J. W. Boag, J. Currant, and B. D. Michael in "Pulse Radiolysis", M. Ebert, J. P. Keene, A. J. Swallow, and J. H. Baxendale, eds, Academic Press, London, 1965, p. 131.

[4] M. Anbar and E. J. Hart, *J. Phys. Chem.*, **69**, 973 (1965).

[5] J. H. Baxendale, E. M. Fielden, and J. P. Keene, *Proc. Royal Soc.*, **286 A**, 320 (1965).

Certainly, decay at 280 nm is not slower than decay at 270 – 275 nm. Further, the decay at 280 nm, as shown in figure 1(c), is essentially complete in 40 μsec and conforms very well to the first-order decay of a single species with $t_{1/2} = 10.4 \pm 0.4$ μsec. For the transient product species, $\varepsilon = 3 \times 10^3 M^{-1} cm^{-1}$ at 280 nm is calculated as the product of $\varepsilon = 10.6 \times 10^3 M^{-1} cm^{-1}$ for e_{aq}^- at 578 nm[6] and the ratio of the maximum optical density at 280 nm to the initial optical density at 578 nm.

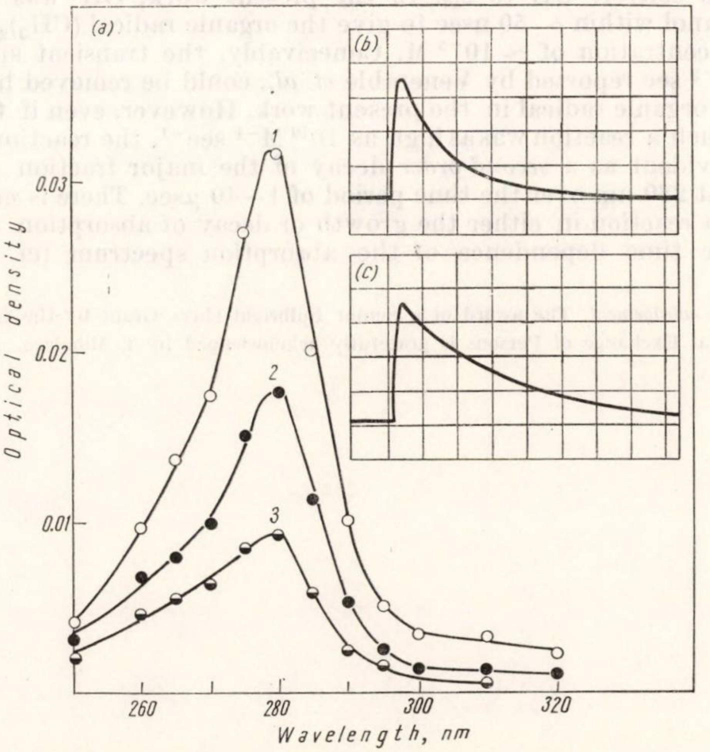

Fig. 1. – The 5-nsec pulse radiolysis of deaerated neutral aqueous solutions containing 2×10^{-3} M $Co(CN)_6^{3-}$ and 0.2 M *t*-butanol: (a) optical absorption spectra at 1 (*1*), 10 (*2*), and 20 (*3*) μsec after the pulse; (b) decay of the absorption at 578 nm in units of 5% absorption and 100 nsec *per* division on the ordinate and abscissa, respectively; (c) decay of the absorption at 280 nm in units of 2.6% absorption and 5 μsec *per* division on the ordinate and abscissa, respectively.

In summary, results of this work indicate that e_{aq}^- and $Co(CN)_6^{3-}$ react with $k = (3.3 \pm 0.1) \times 10^9 M^{-1} sec^{-1}$ to give one transient species (with $\varepsilon_{max} = 3 \times 10^3 M^{-1} cm^{-1}$ at 280 nm) which decays with $t_{1/2} =$

---

[6] J. Rabani, W. A. Mulac, and M. S. Matheson, *J. Phys. Chem.*, **69**, 53 (1965).

$= 10.4 \pm 0.4$ μsec. The transient product species appears to correspond to the species with $t_{1/2} \approx 10^{-5}$ sec reported by Venerable *et. al.*,[2] and, as suggested by them is most plausibly identified as the electron adduct $Co(CN)_6^{4-}$.

In the work of Venerable *et. al.*, the presence of H_2 and a pH=13 served to convert OH to e_{aq}^-. In the present work, OH was scavenged by *t*-butanol within ~ 50 nsec to give the organic radical $(CH_3)_2C(OH)CH_2$ at a concentration of $\sim 10^{-5}$ M. Conceivably, the transient species with $t_{1/2} \approx 10^{-3}$ sec reported by Venerable *et. al.*, could be removed by reaction with the organic radical in the present work. However, even if the specific rate of such a reaction was as high as $10^{10}\ M^{-1}\ sec^{-1}$, the reaction would be clearly evident as a *second-order* decay of the major fraction of optical density at 280 nm over the time period of 1—40 μsec. There is *no* evidence of such a reaction in either the growth or decay of absorption at 280 nm or in the time dependence of the absorption spectrum (cf. figure 1).

Acknowledgement. The award of a Senior Fulbright-Hays Grant by the Committee on International Exchange of Persons is gratefully acknowledged by I. Mihalcea.

Revue Roumaine de Chimie, 18, 9, 1581–1585 (1973)

CONTRIBUTION À L'ÉTUDE DE L'ALCOOLYSE ALCALINE DU CHLORURE DE *n*-BUTYLE

RENÉE STERNBERG

Centre de Chimie Physique
31, str. Galaţi, Bucarest 13, Roumanie

Reçu le 27 janvier 1973

L'auteur montre que l'alcoolyse alcaline du chlorure de *n*-butyle a lieu d'après un mécanisme bimoléculaire du 2ème ordre. On détermine l'énergie d'activation, le facteur de fréquence et l'entropie d'activation. Pour des concentrations différentes de *n*-butylate de sodium, l'énergie d'activation est la même, mais la constante de vitesse croît avec la dilution.

Dans un article précédent[1] nous avons montré que la solvolyse du chlorure de *n*-butyle avec l'isoamylate de Na découle d'après un mécanisme bimoléculaire. On y observe l'apparition d'un effet de dilution, la constante de vitesse de la réaction respective augmentant avec la diminution de la concentration de l'isoamylate de Na. Cet effet a été expliqué par la réaction d'une molécule avec un ion négatif produit par la dissociation incomplète de l'électrolyte et est spécifique des électrolytes faibles.

En continuant les recherches entreprises, on présente ici les résultats obtenus dans l'étude de l'alcoolyse alcaline du chlorure de *n*-butyle avec le *n*-butylate de Na. Pour éviter la réaction secondaire, conduisant à la formation des oléfines respectives, signalée par de la Mare[2] pour l'alcoolyse du bromure de tert. butyle, nous avons choisi comme solvant l'alcool *n*-butylique facile à anhydriser, le réactant étant le butylate de Na. Le chlorure de *n*-butyle et l'alcool *n*-butylique ne réagissant pas dans les conditions choisies, l'alcoolyse alcaline étudiée ne peut pas être troublée par une réaction secondaire appréciable entre le solvant et le chlorure d'alkyl. Dans ces conditions, la réaction doit respecter l'équation globale :

$$\mathrm{BuCl + BuONa \longrightarrow BuOBu + NaCl}$$

---

[1] F. Bărbulescu et R. Sternberg, *Analele Univ. Buc. seria Chimie XVI*, **1**, 19 (1967).

[2] P.B.D. de la Mare, *J. Chem. Soc.*, **1955**, 3180.

Cette réaction s'avérant être bimoléculaire, si l'on prend des concentrations équimoléculaires, l'équation de la vitesse de réaction devient par intégration :

$$k = \frac{1}{t}\left(\frac{1}{a-x} - \frac{1}{a}\right)$$

qu'on peut aussi écrire :

$$k = \frac{1}{at}\left(\frac{a}{a-x} - 1\right)$$

Le terme $\frac{a}{a-x}$ de la parenthèse a été évalué par le rapport des volumes d'acide employé pour le titrage.

A l'aide de l'équation d'Arrhénius :

$$k = A\mathrm{e}^{-E/RT}$$

on a obtenu la variation de la constante de vitesse avec la température et on a déterminé l'énergie d'activation. De l'énergie d'activation calculée, on a déduit le facteur de fréquence A et l'entropie d'activation $\Delta\ S^*$, employant la formule d'Eyring

$$A = \nu\ \frac{kT}{h}\ \mathrm{e}^{\Delta S^*/R}$$

où le facteur de transmision ν a été considéré égale à 1. On a trouvé une bonne concordance entre les valeurs du facteur de fréquence A, calculées à l'aide de l'équation d'Arrhenius et celles obtenues à l'aide de la formule de Herzfeld [3] :

$$A = \frac{kT}{h}$$

MODE DE TRAVAIL

Le chlorure de *n*-butyle employé a été préparé d'après la méthode décrite par Copenhaver et Whaley[4] et, après bidistillation avait : point d'ébullition 78,6/760 mm et indice de réfraction $n_D^{25} = 1{,}3986$. L'alcool *n*-butylique a été anhydrisé par reflux pendant 24 heures sur du Mg métallique activé avec de l'iode. Pour préserver l'alcool de l'humidité, on a travaillé dans une atmosphère d'azote.

On établit les concentrations du butylate de Na par titrage avec une solution décimoléculaire d'acide salicylique dans de l'alcool anhydre.

---

[3] K. Herzfeld, *Ann. Physik.*, **57**, 635 (1919).

[4] J. E. Copenhaver et A. M. Whaley, « Organic Syntheses » Coll. vol., IIe éd., John Willey & Sons, New York, 1 951.

La réaction découle dans des ballons de verre thermostatés avec une approximation de quelques centièmes de degré. A des intervalles de temps déterminés on a extrait à l'aide d'une seringue, par le bouchon de caoutchouc étanche, des volumes déterminés de solution qu'on a refroidie subitement. En titrant l'alcoolate on a déduit la perte de concentration correspondant à l'étape donnée.

RÉSULTATS ET DISCUSSIONS

Dans le tableau 1 se trouvent les valeurs obtenues pour une de nos expériences. Les données expérimentales ont permis de mettre en évidence le caractère bimoléculaire de la réaction. Le tableau 2 présente les données obtenues dans l'étude de la vitesse de réaction pour 3 concentrations et quatre températures différentes, représentées schématiquement dans la fig. 1.

Partant de la variation du logarithme de la constante de vitesse en fonction de l'inverse de la température absolue, on a calculé pour chaque concentration l'énergie d'activation, qui, comme on le voit dans le tableau 2, est indépendante de la concentration des réactants.

Tableau 1

Variation de la concentration fonction du temps, pour l'alcoolyse du chlorure de *n*-butyle par le *n*-butylate de Na

$a=0{,}75\times10^{-3}$ mole cm^{-3}		$T = 373$°K
t sec	cm^3 cons.	k cm^3/mole.sec.
0	3,73	
900	3,33	0,177
1800	3,00	0,180
3600	2,51	0,180
5400	2,14	0,183
7200	1,87	0,182
9000	1,67	0,183
11700	1,42	0,184
15420	1,21	0,180
18000	1,08	0,182
	Moyenne	0,181

La quatrième colonne présente les valeurs de la constante de vitesse calculées à partir des valeurs moyennes du facteur préexponentiel obtenues de la relation d'Arrhenius.

On constate une bonne concordance entre les données théoriques et celles expérimentales.

Comme on le remarque dans le tableau 2, les constantes de vitesse augmentent à mesure que les concentrations de *n*-butylate diminuent. Un

Tableau 2

Constante de vitesse et paramètres d'activation pour la réaction n-BuCl + n-BuONa

BuONa : BuCl $a = b$ mole/cm^3	t°C	k cm^3/mole.sec. obs.	k cm^3/mole.sec. calc.	E cal/mole	log A	ΔS^* cal/mole g
1,00 × 10^{-3}	80	0,0313	0,0313	19 292	10,439	
	90	0,0672	0,0673		10,442	
	100	0,1387	0,138		10,445	
	110	0,2699	0,269		10,439	
					10,449	−9,81
0,75 × 10^{-3}	80	0,0419	0,0419	19 169	10,489	
	90	0,0893	0,0893		10,491	
	100	0,181	0,181		10,48	
	110	0,353	0,353		10,485	
					10,486	−9,6
0,5 × 10^{-3}	80	0,0500	0,0500	19 169	10,566	
	90	0,1135	0,113		10,595	
	100	0,221	0,2257		10,584	
	110	0,426	0,4195		10,566	
					10,578	−9,19

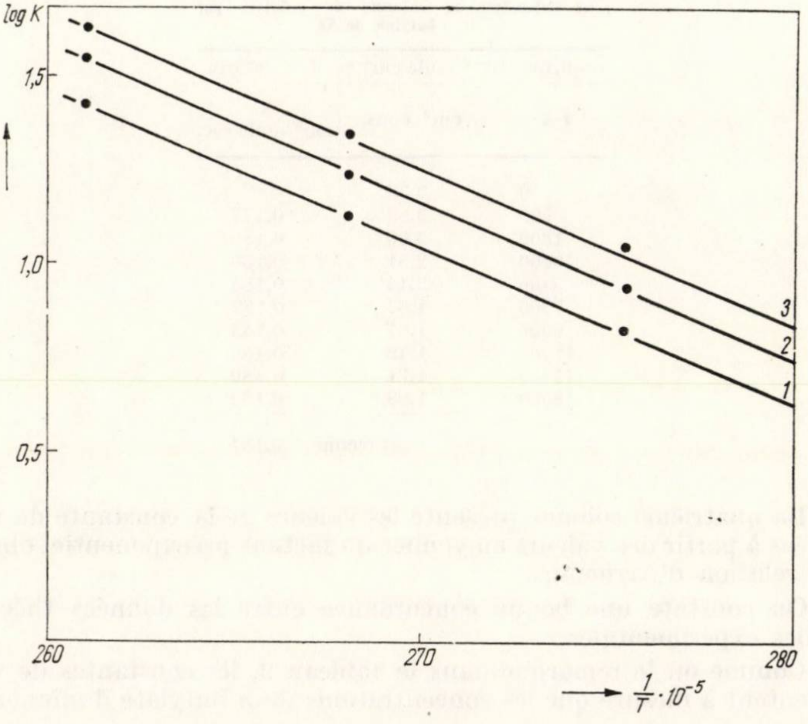

Fig. 1. — Vérification de la loi d'Arrhenius pour la réaction d'alcoolyse du n-BuCl.

comportement analogue a été décrit pour de nombreuses réactions d'alcoolyse.[5-8,9]

Pour mettre en évidence l'influence du réactant et du solvant sur la vitesse de réaction, on présente un tableau comparatif des données obtenues dans l'alcoolyse du chlorure de *n*-butyle avec du *n*-butylate et de l'isoamylate de Na.

Tableau 3

Influence du réactant sur la vitesse de réaction pour l'alcoolyse du *n*-BuCl

$RCl + R'ONa$ $a = b$ mole/cm³	t°C	k obs cm³/mole.sec.	
		$R' = C_4H_9$	$R' = \text{iso } C_5H_{11}$
$1{,}00 \cdot 10^{-3}$	90	0,0672	0,0356
	100	0,1387	0,0729
	110	0,2699	0,1522
$0{,}5 \times 10^{-3}$	100	0,2210	0,133
	110	0,4260	0,268

On voit que les valeurs de la constante de vitesse correspondant à l'alcoolyse du chlorure de *n*-butyle avec le *n*-butylate de Na sont plus grandes que celles obtenues dans la réaction avec l'isoamylate de Na.

---

[5] J. F. ACREE, *J. Amer. Chem. Soc.*, **48**, 352 (1912).

[6] H. VON HALBAN, *Z. Phys. Chem.*, **91**, 597 (1961).

[7] E. A. MELVIN HUGES, « The Kinetics of Reaction in Solution », 2nd ed. Oxford, Univ. Press, New York, 1947.

[8] S. W. BENSON, « The Foundations of Chemical Kinetics », Mc Graw-Hill, New York, 1960, p. 552.

[9] Ya. I. GHERASIMOV, V. P. DREVING, E. H. EREMIN, A. V. KISELEV, V. P. LEBEDEV, G. M. PANCHENKOV et A. I. CHLIGIN, « Kurs fizicheskoi khimii », 2ème vol « Chimia », Moscou, 1966, p. 186.

Revue Roumaine de Chimie, **18**, *9*, 1587–1594 (1973)

SUCCESSIVE CHEMISORPTION OF GASES ON SEMICONDUCTOR THIN FILMS IN THE DARK AND UNDER IRRADIATION. I

THE OXYGEN, CARBON MONOXIDE AND HYDROGEN ON ZINC OXIDE SYSTEM

MIHAELA CONSTANTINESCU and E. SEGAL

Centre of Physical Chemistry, str. Dumbrava Roșie 23, Bucharest, Romania

Received July 4, 1972

Successive chemisorption of oxygen, carbon monoxide and hydrogen on thin zinc oxide films in the dark and under irradiation has been studied by the method of electrical resistance variation. The influence of the pretreatment on the chemisorptive properties of zinc oxide films is evidenced.

Zinc oxide is a catalyst used in a large number of chemical reactions. It has good oxygen, carbon monoxide and hydrogen adsorbing capabilities and is extremely sensitive to their presence on its surface. Irradiation in the fundamental absorption band has an obvious effect upon its adsorptive properties.

In this paper we report an experimental study on successive adsorption of oxygen, carbon monoxide and hydrogen on thin zinc oxide films.

EXPERIMENTAL

A high vacuum device previously described[1] has been used. The working cell and the procedure for obtaining and introducing the gases have also been presented in earlier works.[2,3]

The zinc oxide film was obtained by air oxidizing at 450°, for four hours, a metallic zinc film, prepared by evaporation in vacuum. Before introducing gases the film was outgassed for five hours at 400° and then brought to the working temperature.

For the dark chemisorption, measurements were carried out at three different temperatures : −196°, 20°, and 250° ; under irradiation, measurements were made only at two temperatures $-196°$ and $20°$, because the irradiation effects were observed to decrease with the rise in the temperature.

---

[1] E. Segal and M. Constantinescu, *Rev. Roumaine Chim.*, **12**, 75 (1967).

[2] E. Segal and M. Constantinescu, *Rev. Roumaine Chim.*, **13**, 1449 (1968).

[3] M. Constantinescu and E. Segal, *Rev. Roumaine Chim.*, **16**, 801 (1971).

The gases were introduced each time in the same order. Oxygen was introduced first and the variation of the electrical resistance was observed for nearly 20 minutes, until a constant value was reached. The variation of the electrical resistance was further determined for carbon monoxide adsorption and finally, for hydrogen adsorption.

Under irradiation, the gases were introduced after a previous irradiation of the outgassed zinc oxide film. The previous irradiation was maintained until no more variation of the electrical resistance was observed. The same order as above was kept for the introducing of the gases.

The photosorptive properties of zinc oxide films vary depending on the surface pretreatment. This fact was experimentally evidenced by the comparative study of hydrogen photosorption on a gas pretreated surface in the dark and on a surface having preadsorbed gases under irradiation.

RESULTS

The interaction of gases with the surface of zinc oxide is accompanied by an increase or a decrease of the electrical resistance, determined by the nature of the gases, the film temperature and the conditions of darkness or irradiation during the chemisorption.

1. SUCCESSIVE ADSORPTION OF GASES IN THE DARK

At a temperature of $-196°$, the oxygen adsorption determines a positive variation of the electrical resistance. The introduction of carbon monoxide is also followed by an increase of the electrical resistance.

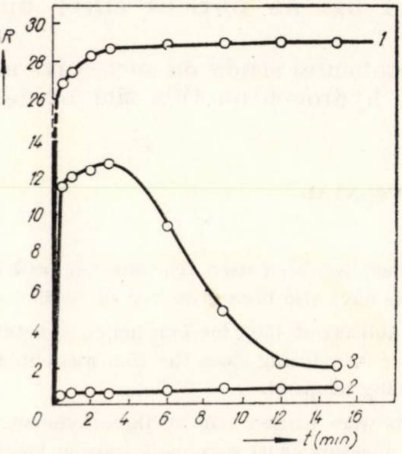

Fig. 1. — Electrical resistance variation of zinc oxide film in relation to time at the temperature of $-196°$ during adsorption of oxygen (*1*), carbon monoxide (*2*) and hydrogen (*3*) in the dark.

Hydrogen initially causes a strongly positive variation, which tends to revert; an increase of the electrical resistance is finally obtained in this case too. The experimental results are shown in figure 1.

Slightly different results are obtained when working at the temperatures of 20° and 250°. Oxygen and carbon monoxide determine also in these cases positive variation while hydrogen adsorption is followed by a decrease of the electrical resistance. The resistance variations recorded at the temperature of 250° are far more pronounced than those obtained at 20°. The experimental results obtained at the temperature of 250° are shown in figure 2.

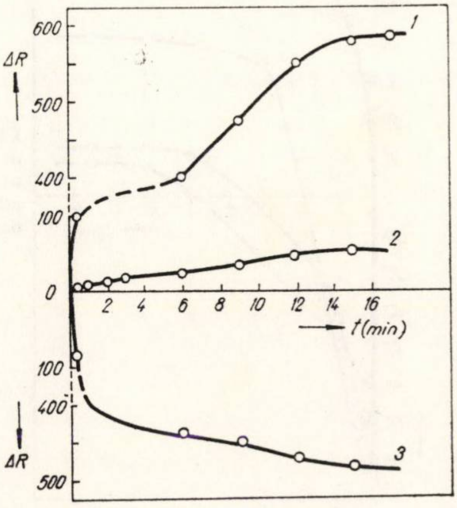

Fig. 2. — Electrical resistance variation of zinc oxide film in relation to time at the temperature of 250° during adsorption in the dark of: oxygen (*1*), carbon monoxide (*2*) and hydrogen (*3*).

2. SUCCESSIVE ADSORPTION OF GASES UNDER IRRADIATION

Previous irradiation in vacuum is followed by a decrease of the electrical resistance of zinc oxide film. A stronger variation is obtained at the temperature of −196° than at 20°.

When the electrical resistance of the film under irradiation varies no more, oxygen is introduced followed by carbon monoxide and hydrogen. The results obtained show different variations for the two temperatures under study, except for oxygen which determines in both cases increases of the electrical resistance (figures 3 and 4, curve *1*).

As it results from figure 3, carbon monoxide introduced in two successive doses (curves *2* and *2''*) with an interval of 20 minutes, produces at the beginning a sudden decrease of the electrical resistance of the zinc oxide film on which oxygen was previously adsorbed. This is followed by a return towards the original value, which is overpassed after 9 minutes, finally resulting in a positive variation of the electrical resistance. Hydrogen determines a qualitative similar behaviour except that both negative and positive variations are stronger (figure 3, curve *3*).

At the temperature of 20° (figure 4), contrary to the case of −196°, carbon monoxide determines a slightly negative variation, which becomes equal to zero in time. Hydrogen introduction is followed by no effect.

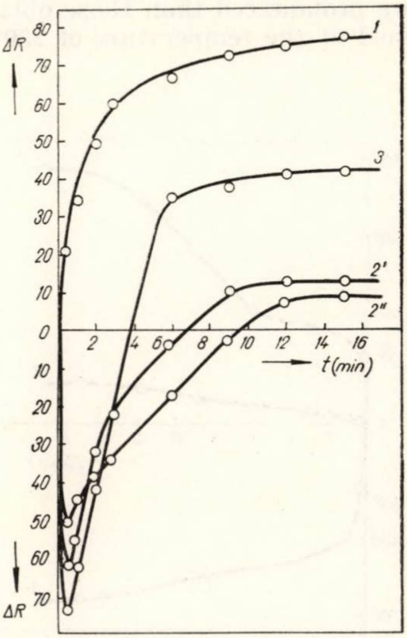

Fig. 3. — Electrical resistance variation of zinc oxide film in relation to time at the temperature of −196° during adsorption of oxygen (*1*), carbon monoxide (*2'* and *2"*) and hydrogen (*3*) under irradiation.

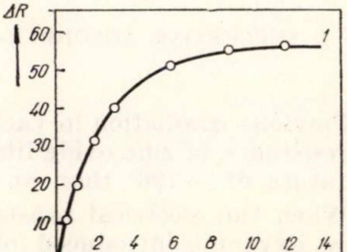

Fig. 4. — Electrical resistance variation of zinc oxide film in relation to time at the temperature of 20° during adsorption of : oxygen (*1*) and carbon monoxide (*2*) under irradiation.

3. HYDROGEN PHOTOSORPTION ON PRETREATED FILMS

The hydrogen photosorption on pretreated films has been studied in the two following cases :

— in films with gases adsorbed in the dark and followed by irradiation and evacuation under irradiation ;

— in films with gases adsorbed under irradiation and then kept in the dark for a period, followed by an evacuation period in the dark and by another irradiation.

In the first case, the hydrogen photosorption at the temperature of −196° determines at the beginning a sudden increase of the electrical resistance which drops afterwards to the original value and continues to decrease below this value. The results are shown in figure 5.

In contrast to the results obtained at a temperature of −196° at 20° and 250° the evacuation under irradiation causes an increase of the electrical resistance and hydrogen introduction is accompanied by a continuous decrease of the electrical resistance.

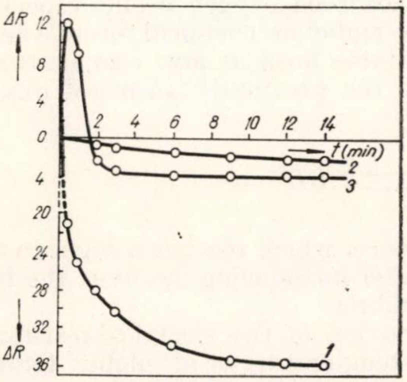

Fig. 5. — Electrical resistance variation of zinc oxide film in relation to time at the temperature of −196° after gas adsorption in the dark during irradiation (*1*), evacuation under irradiation (*2*) and hydrogen photosorption (*3*).

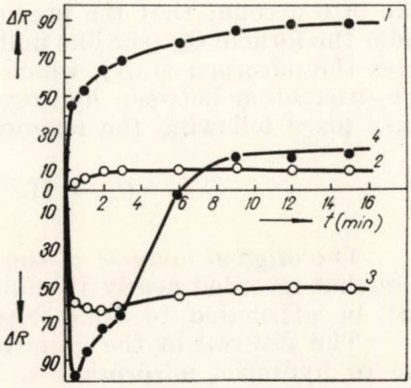

Fig. 6. — Electrical resistance variation of zinc oxide film in relation to time at the temperature of −196° after gas photoadsorption, in the dark (*1*) during evacuation in the dark (*2*), irradiation (*3*) and hydrogen photosorption (*4*).

The case of hydrogen photosorption on a film with preadsorbed gases under irradiation is essentially different from the previous case. This time, the variations of the electrical resistance produced by hydrogen photosorption are similar to those which accompany the hydrogen photosorption after the introduction of carbon monoxide (compare figure 3, curve *3* with figure 6, curve *4*).

At the temperature of 20°, the introduction of hydrogen under irradiation is accompanied by no effect.

DISCUSSION

1. SUCCESSIVE ADSORPTION OF GASES IN THE DARK

At the temperature of −196°, the oxygen acceptor adsorption approximating saturation (figure 1, curve *1*) leads to a reduced adsorption of carbon monoxide. The phenomenon is probably due to the surface blockage by oxygen. If we admit that both gases are adsorbed on the same type of centers, then the previous oxygen adsorption will consume almost the entire stock of active surface centers. The stronger adsorption of carbon monoxide on a clean surface,[4] confirms the hypothesis that both gases are adsorbed on the same type of centers. More detailed considerations on the chemisorptive mechanism of these gases on clean zinc oxide films have been presented in previous works.[1,2]

In order to interpret the positive variation of the electrical resistance recorded with hydrogen adsorption (figure 1, curve *3*), one must take into account that the previously adsorbed oxygen occurs especially under the form of O_2^- (the line under the symbol or chemical formula designates the adsorbed state), which is a stable form at low temperatures.[5] The interaction between hydrogen and the previously adsorbed oxygen takes place following the reaction

$$O_2^- + \mathrm{H}_2 + \mathrm{e} \rightleftarrows 2\ OH^- \tag{I}$$

The original increase of the resistance, which reaches a higher value than that recorded nearly 12 minutes after introducing gas over the film, may be attributed to some false equilibria.

The reversal in the variation direction of the electrical resistance, due to hydrogen adsorption at room temperature or at higher temperatures, may be attributed to the generation of the same charge carriers following the processes:

$$2\mathrm{H}_2 + O_2^- \rightleftarrows 2\mathrm{H}_2\mathrm{O} + \mathrm{e} \tag{II}$$

$$\mathrm{H}_2 + \mathrm{O}^- \rightleftarrows \mathrm{H}_2\mathrm{O} + \mathrm{e} \tag{III}$$

2. SUCCESSIVE ADSORPTION OF GASES UNDER IRRADIATION

The increase of the electrical resistance of the film at the temperature of −196° after oxygen adsorption is obviously due to the acceptor nature of this gas adsorption.

The electrical resistance variation of irradiated films with carbon monoxide adsorption may be explained by a mechanism based on the following processes

$$\mathrm{CO} + O_2^- \rightleftarrows CO_2 + O + \mathrm{e} \tag{IV}$$

$$O + O \rightleftarrows O_2 \tag{V}$$

$$O_2 + \mathrm{e} \rightleftarrows O_2^- \tag{VI}$$

$$O + 2\mathrm{e} \rightleftarrows O^{--} \tag{VII}$$

---

[4] M. Constantinescu and E. Segal, *Rev. Roumaine Chim.*, (under press).

[5] T. Kwan and Y. Fujita, *J. Res. Inst. Catalysis Hokkaido Univ.*, **7**, 24 (1959).

Process (IV) explains the initial decrease of the electrical resistance, and processes (V), (VI) and (VII) account for the subsequent increase of this property. As to the hydrogen adsorption under irradiation, it determines at the beginning a donor adsorption

$$H_2 \rightleftarrows H_2^+ + e \qquad \text{(VIII)}$$

which is afterwards reversed, and the initial effect reduced. Further on, the hydrogen action determines an acceptor adsorption of this gas, illustrated by an increase of the electrical resistance. The phenomenon is probably due to some negatively charged hydrogen surface molecular forms.

At room temperature, the variation of the electrical resistance of the zinc oxide film, after introducing the oxygen under irradiation, also indicates an acceptor adsorption of this gas. As regards the much more reduced variation of the electrical resistance when introducing carbon monoxide, it may be related to processes of types (IV), (V) and (VI). The fact that the variation of the electrical resistance remains negative throughout, can be explained by the same processes.

Under these conditions, hydrogen is probably adsorbed in a neutral molecular form

$$H_2(g) \rightleftarrows H_2 \qquad \text{(IX)}$$

which does not consume or generate any charge carriers.

3. HYDROGEN PHOTOSORPTION ON PRETREATED FILMS

a. *Pretreatment with gases adsorbed in the dark*

The significant decrease of the electrical resistance of zinc oxide films after irradiation at −196° (figure 5, curve *1*) may be attributed to the desorption of acceptor gases. Subsequent evacuation completes the action of irradiation (figure 5, curve 2).

The initial positive variation of the electrical resistance of the zinc oxide film, after hydrogen adsorption under irradiation, may be attributed to some acceptor adsorption forms of this gas, which are unstable, changing into a normal donor form (figure 3, curve *3*).

The electrical resistance decrease observed at room temperature after irradiation is probably due to the desorption of some forms of negatively charged oxygen. The increase of the electrical resistance, observed during evacuation, may be attributed to hydrogen desorption, that is, to the reversal of some equilibria of the types I, II and III.

The negative variation of the electrical resistance of films interacting with hydrogen under irradiation is due to the donor adsorption of this gas on the centers formed by irradiation.

b. *Pretreatment with gases adsorbed under irradiation*

Discontinuing the irradiation of the film at the temperature of −196°, after successive adsorption of oxygen, carbon monoxide and hydrogen under irradiation (figure 6, curve *1*), mainly leads to the disappearance of charge carriers, which was observed experimentally by the increase of the electrical resistance.

The increase of the electrical resistance observed, when evacuating the zinc oxide films in the dark, may be attributed to the desorption of some hydrogen donor forms, and the decrease of the electrical resistance corresponding to irradiation is due to the generation af some charge carriers. Reintroducing hydrogen under irradiation leads to an effect similar to that observed when introducing hydrogen under irradiation after oxygen and carbon monoxide (figure 3, curve 3).

CONCLUSIONS

1. The successive chemisorption of hydrogen, carbon monoxide and hydrogen on zinc oxide films was studied both in the dark and under irradiation, applying the method of the electrical resistance variation.

2. The experimental data support the conclusions on the common nature of the adsorption centres for oxygen and carbon monoxide.

3. The variation direction of the electrical resistance of zinc oxide films, after their interaction with carbon monoxide and hydrogen, depends on the working temperature, the previous surface treatment and the adsorption conditions (in the dark or under irradiation).

4. The irradiation of the outgassed films, in the fundamental adsorption band ($\lambda = 365$ mλ), leads to the decrease of the electrical resistance, due to the occurrence of charge carriers, which may behave as active adsorption centres.

Revue Roumaine de Chimie, **18**, 9, 1595–1600 (1973)

REACTIONS OF COORDINATED LIGANDS. II[1]

REACTION OF TRIPHENYLALUMINIUM WITH NICKEL, PALLADIUM AND COPPER BISDIMETHYLGLYOXIMATES

N. VOICULESCU, I. POPESCU and LUCIA ROMAN

Institute of Macromolecular Chemistry "P. Poni", Aleea Grigore Ghica Vodă, 41–A, Jassy, Romania

Received June 7, 1972

The preparation methods and the characteristics of the derivatives resulting from the reaction of $Al(C_6H_5)_3$ with Ni(II), Pd(II) and Cu(II) are described. The reaction products, in powder form, were isolated and characterized. The chemical analyses, the magnetic measurements and the interpretation of the IR spectra suggest that these new compounds appear through the substitution of the hydrogen of the $O-H \cdots O$ bond of the bisdimethylglyoximates with $Al(C_6H_5)_2$ groups, according to a given mechanism. The X ray diffraction image show that all the compounds are amorphous.

The reactions of coordination compounds were classified into four categories,[2] namely :

- the substitution of a ligand by another
- the intramolecular isomerization
- the reaction of the central metallic atom (oxidation or reduction)
- the reactions of the coordinated ligands.

A special interest was shown in literature to the first three types of reactions. Only few papers have dealt with the reaction of coordinated ligands, and only lately some interest for them has arisen.

The reactivity of coordinated dimethylglyoxime with bivalent transitional metals was the object of several papers[3–11] which have pointed out the disappearance of etherification and esterification properties characteristic of non-coordinated dimethylglyoximates. The experiments on the reactivity of Ni(II), Pd(II) and Cu(II) dimethylglyoximates with boron[12,13] and aluminium[1] compounds have resulted in a new class of compounds corresponding to formula I,

---

[1] N. Voiculescu and I. Popescu, *Rev. Roumaine Chim.*, **17**, 719 (1972).

[2] R. A. Krause, D. C. Jicha and D. H. Busch, *J. Amer. Chem. Soc.*, **83**, 528 (1961).

[3] M. F. Barker, *Chem. News*, **130**, 99 (1925).

[4] E. Thilo and K. Friedrich, *Ber. dtsch. chem. Ges.*, **62 B**, 2990.

[5] L. A. Ciugaev, *J. Chem. Soc.*, **105**, 2187 (1914).

[6] R. C. Voter, C. V. Banks, V. A. Fassel and P. W. Kehres, *Analyt. Chem.*, **23**, 1730 (1951).

[7] O. L. Brady and M. M. Muers, *J. Chem. Soc.*, **1930**, 1599.

[8] M. M. Jones, "Ligand Reactivity and Catalysis", Academic Press, New York and London, 1968, p. 125.

[9] A. G. Sharpe and D. B. Wakefield, *J. Chem. Soc.*, **1957**, 496.

[10] A. G. Sharpe and D. B. Wakefield, *J. Chem. Soc.*, **1957**, 3323.

[11] F. Feigl and H. A. Suter, *J. Chem. Soc.*, **1957**, 3323.

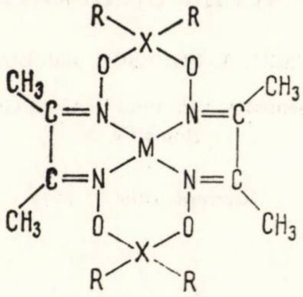

where M(II) = Ni(II), Pd(II), Cu(II), Fe(II); X = Al and R, in the case of compounds with boron, can be a halide or an aliphatic radical, and in the case of compounds with aluminium, can be an aliphatic or aromatic radical.

In this paper we give the preparation methods and some physicochemical characteristics of the compounds resulting from the reaction of $Al(C_6H_5)_3$ with Ni(II) $(DMGH)_2$, Pd(II) $(DMGH)_2$ and Cu(II) $(DMGH)_2$ — (DMGH being the radical of coordinated dimethylglyoxime

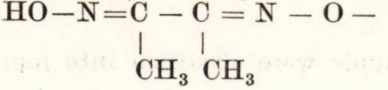

$$HO-N=\underset{\underset{CH_3}{|}}{C}-\underset{\underset{CH_3}{|}}{C}=N-O-$$

EXPERIMENTAL

The Ni(II), Pd(II) and Cu(II) bisdimethylglyoximates were obtained according to the method given by Basu.[14]

The $Al(C_6H_5)_3$ was obtained starting from $Hg(C_6H_5)_2$ and aluminium powder[15] heated at 130–140° and purified by crystallization in benzene-*n*-heptane.

REACTION OF $Al(C_6H_5)_3$ WITH NICKEL, PALLADIUM AND COPPER BISDIMETHYLGLYOXIMATES

The reaction of $Al(C_6H_5)_3$ with $Ni(II)(DMGH)_2$, $Pd(II)(DMGH)_2$ and $Cu(II)(DMGH)_2$ was carried out in a glass apparatus with provisions against moisture and atmospheric oxygen.

---

[12] G. N. Schrauzer, *Chem. Ber.*, **95**, 1438 (1962).

[13] F. Umland and D. Thierig, *Angew. Chem.*, **74**, 388 (1962).

[14] C. Basu, G. M. Cook and R. L. Belford, *Inorg. Chem.*, **3**, 1361 (1964).

[15] E. Krause and P. Dittmar, *Ber. dtsch. chem. Ges.*, **63**, 2401 (1930).

The bisdimethlyglyoximates of the metals were triturated, dried and put into a Schlenk vessel, in an actionless atmosphere. To the powders thus processed was added the benzene solution of $Al(C_6H_5)_3$. The reaction vessel was heated for a few hours up to the benzene reflow. The powders resulting from the reaction are insoluble in benzene and were thus separated by decanting. They were washed with benzene till the $Al(C_6H_5)_3$ in excess were completely removed. The total removal of the benzene and the drying of the products were carried out in vacuum. The compounds were handled in an actionless atmosphere (nitrogen or argon). The rough formulae, the colour, the analyses and the magnetic measurements are given in table 1.

Table 1

Analysis and characteristics of analysed products

The compound	Colour	Magnetic features	Analyses				
			C *Calcd.* % *Found* %	H *Calcd.* % *Found* %	Al *Calcd.* % *Found* %	N *Calcd.* % *Found* %	*M* (II) *Calcd.* % *Found* %
$Ni(II)(DMG)_2Al_2(C_6H_5)_4$	brown	diamagnetic	59.16	4.93	8.32	8.62	9.09
			58.80	5.11	8.32	8.61	9.10
$Pd(II)(DMG)_2Al_2(C_6H_5)_4$	greenish-grey	diamagnetic	55.09	4.59	7.74	8.03	15.35
			55.05	4.58	7.70	8.02	16.11
$Cu(II)(DMG)_2Al_2(C_6H_5)_4$	reddish-brown	diamagnetic	58.71	4.89	8.25	8.56	9.78
			58.55	4.89	8.25	8.60	9.75

The X ray diffraction patterns of the compounds were registered by the powder method with a URK-5 apparatus using CuK rays and a nickel filter. To avoid the humidity and the dispersion of the radiation due to the contact with air, the samples were inserted into special capillaries and exposed for two hours in a vacuum chamber at 40 kV, 25 mA. The film — sample distance was 40 mm.

The IR spectra of the compounds, pelleted in KBr, were recorded by means of an Unicam SP—200 apparatus.

RESULTS AND DISCUSSION

We have informed in an earlier paper about the way of obtaining some aluminium-organic [1] complex compounds resulting from the reaction of $Al(i-C_4H_9)_3$ on Ni(II), Pd(II) and Cu(II) bisdimethylglyoximates and free dimethylglyoxime. To establish the physicochemical features of this new class of compounds, we have synthetized a new series of combinations letting $Al(C_6H_5)_3$ react on the same chelates. The empiric formula of the series is : $M(II)\ (DMG)_2\ Al_2(C_6H_5)_3$, where M(II) can be Ni(II), Pd (II) or Cu (II). The general reaction can be represented by equation (1):

$$2Al(C_6H_5)_3 + M(II)(DMGH)_2 \quad M(II)(DMG)_2\, Al_2(C_6H_5)_4 + 2C_6H_6 \qquad (1)$$

Taking into account the electron deficit of the aluminium atoms and the structure characteristics of the bisdimethylglyoximates taking part in the reaction, we suggest a reaction-mechanism as represented by equation (2):

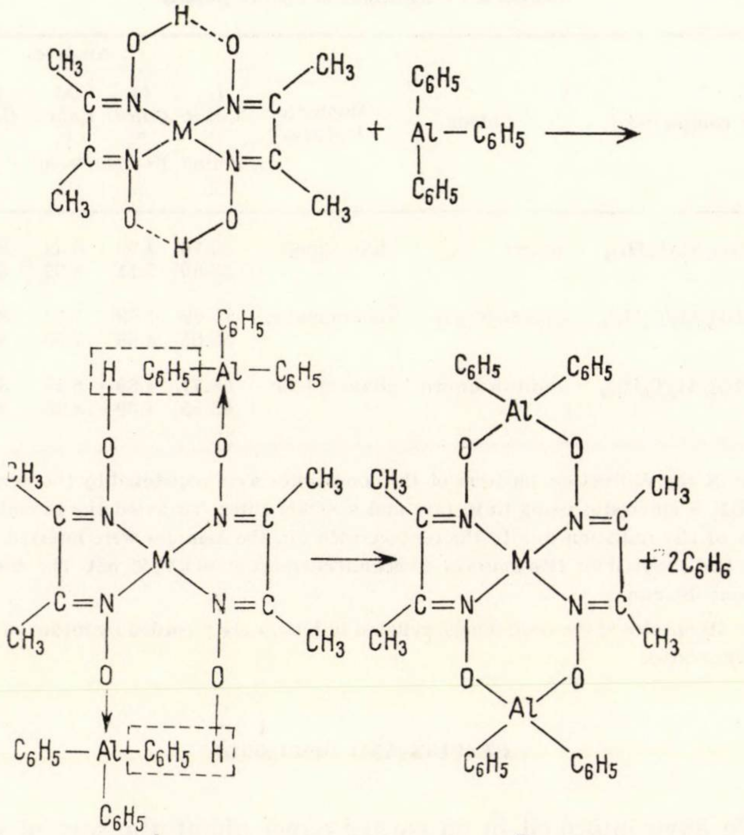

At the beginning (phase A), an adduct is formed between one bisdimethylglyoximate molecule and $Al(C_6H_5)_3$ molecules, and two dative O–Al bonds are formed. Later on in phase B, the formation of the final products of the reaction takes place through the elimination of two benzene molecules. We believe that the dative O–Al bond of phase (A) is formed between the aluminium and the oximic oxygen free of hydrogen.

This seems less likely for Ni(II) $(DMGH)_2$ as the X ray[16,17] and IR[18,19] studies suggest that the hydrogen atom of the OH... O bond in the chelate occupies a symmetrical position between the two oxygen atoms. It would hence result that the two oxygen atoms take equaly part in achieving the dative bonds O—Al. For Pd(II)$(DMGH)_2$ [16,17,19] and Cu(II) $(DMGH)_2$[19-21] compounds, the study of the structure have pointed out the asymmetrical position of the hydrogen atom, given the situation of the oxygen atoms, the hydrogen atom being nearer to the oxygen atom to which it is bound in a covalent way. The dative O—Al bond for these chelates is achieved with oximic oxygen free of hydrogen.

In the final products, resulting through the reduction of two benzene molecules, the aluminium atom achieves two bonds with the oximic oxygen atoms, which seem to be different, especially in the case of Cu(II)$(DMG)_2$ $Al_2(C_6H_5)_4$ and Pd(II)$(DMG)_2$ $Al_2(C_6H_5)_4$ compounds. Though, up to the present, we have no proof that might confirm or refute our opinion, we believe that the aluminium atom holds a nearly symmetrical position between the two oxygen atoms, owing to an intermolecular rearrangement.

The chemical analyses of the powders (table 1) point out the fact that the Al/M(II) ratio is 2 for all products, this value thus showing the maximal number of $Al(C_6H_5)_3$ molecules entering into reaction with each molecule of bisdimethylglyoximate in the above described reaction conditions.

The aluminium-organic derivatives of the bisdimethylglyoximates are insoluble in organic solvents which do not contain chlorine atoms or other functional groups which might react with the compounds. They are decomposed by water, acids and bases. It is worth mentioning that these compounds are more stable in a humid medium than those formerly described.[1]

The characteristic IR absorptions of this series are given in table 2, *versus* those of the original compounds. The 3.500—650 cm^{-1} spectral range is characterized by the disappearance of the absorption maxima of the OH groups of the bisdimethylglyoximates. Similarly, the band appearing as a shoulder in the 1600—1800 cm^{-1} range, with a variable intensity and position[18,22-24] in the initial products, is absent in their compounds with aluminium organic compounds.

The valency oscillations of the C=N bond of the aryl-aluminium derivatives are less displaced than the same oscillations of the alkyl-

---

[16] L. E. Godycki and R. E. Rundle, *Acta Cryst.*, **6**, 487 (1953).

[17] D. E. Williams, G. Wohlauer and R. E. Rundle, *J. Amer. Chem. Soc.*, **81**, 755 (1959).

[18] R. E. Rundle and M. Parasol, *J. Chem. Phys.*, **20**, 1487 (1952).

[19] K. Burger, I. Ruff and F. Ruff, *J. Inorg. Nuclear Chem.*, **27**, 179 (1965).

[20] J. E. Caton Jr. and C. V. Banks, *Inorg. Chem.*, **6**, 1670 (1967).

[21] E. Frasson, R. Zannetti, R. Bardi, S. Bezzi and G. Giacometti, *J. Inorg. Nuclear Chem.*, **8**, 452 (1958).

[22] R. Blinc and D. Hadzi, *J. Chem. Soc.*, **1968**, 4536.

[23] R. Blinc and D. Hadzi, *Spectrochim. Acta*, **16**, 852 (1960).

[24] K. Nakamoto, M. Margoshes and R. E. Rundle, *J. Amer. Chem. Soc.*, **77**, 6480 (1967).

Table 2

IR absorption characteristics

The compound	OH	OH	C=N	NO	OH
$Ni(DMGH)_2$	2350	1780	1560	1235	900
$Ni(II)(DMG)_2Al_2(C_6H_5)_4$	—	—	1590	1240	—
$Pd(DMGH)_2$	2340	1710	1550	1230	910
$Pd(II)(DMG)_2Al_2(C_6H_5)_4$	—	—	1590	1230	—
$Cu(DMGH)_2$	2600	1820	1550	1212	860
$Cu(II)(DMG)_2Al_2(C_6H_5)_4$	—	—	1595	1205	—

aluminium derivatives, which shows that the charges of the nitrogen and transitional metal atoms undergo a lesser change through the formation of the new compounds. This spectral range is also characterized by the appearance of the oscillations due to the benzene cycle of the $Al(C_6H_5)_2$ groups.

Though the substances with which we start have a crystalline structure, the new compounds, such as can be seen on the diffraction images shown in figure 1, are typically amorphous, differing fundamentally from the starting compounds. The hydrolysis reaction restores the chelates and meanwhile their crystalline structure.

The diamagnetism of the compounds synthetized by us points out the fact that the plane structure of the chelates is not changed by the substitution of the hydrogen by the $Al(C_6H_5)_2$ group.

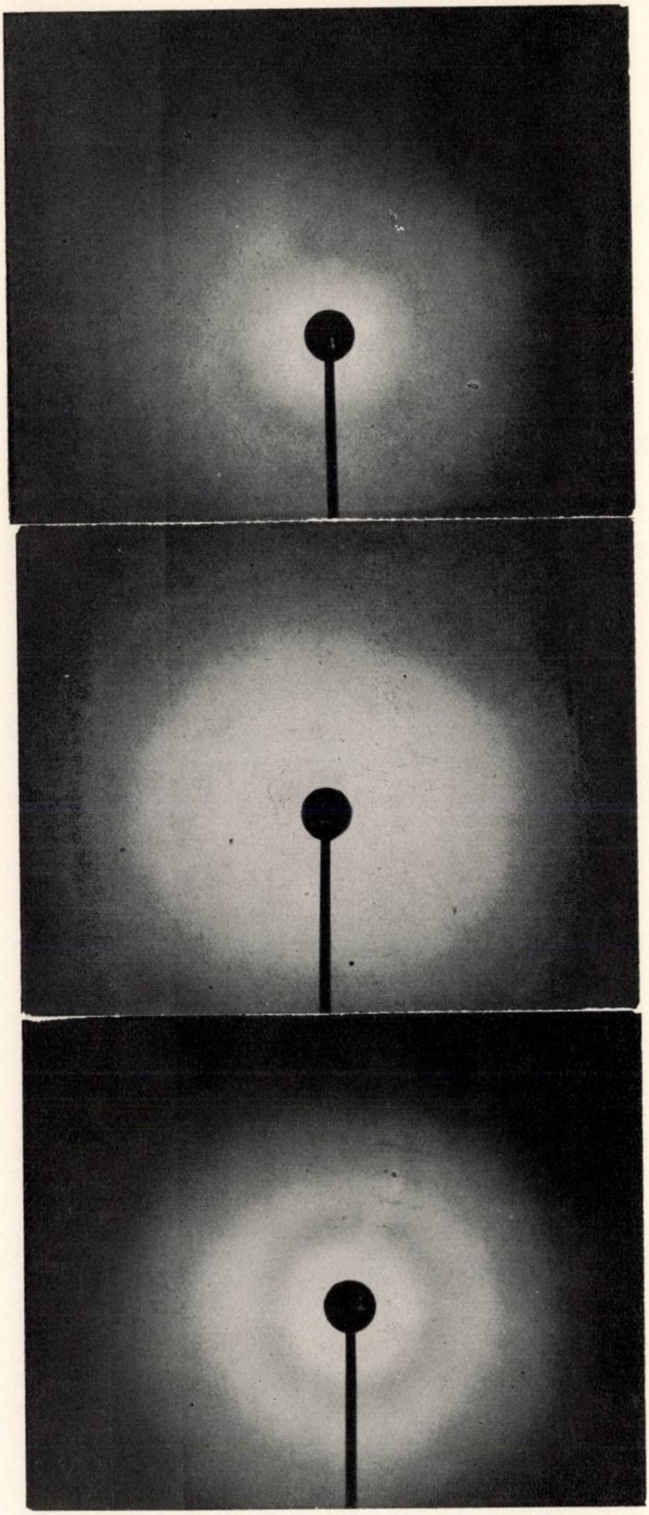

Fig. 1 *a*, *b*, *c* — Diffraction images by X rays.

a) $Ni(DMG)_2Al_2(C_6H_5)_4$;

b) $Pd(DMG)_2Al_2(C_6H_5)_4$;

c) $Cu(DMG)_2Al_2(C_6H_5)_4$.

cd. 3144 Rev. Chimie d. p. 1600

Revue Roumaine de Chimie, **18**, 9, 1601–1608 (1973)

REACTIONS OF COORDINATED LIGANDS. III[1]

ALUMINIUM-ORGANIC COMPOUNDS OF COORDINATED SALICYLALDOXIME

N. VOICULESCU, I. POPESCU and N. LUCHIAN

Institute of Macromolecular Chemistry, Aleea Grigore Ghica Vodă, 41-A, Jassy, Romania

Received July 25, 1972

A series of tetraphenyl-aluminium-bis-salicylaldoximates was obtained by reacting triphenylaluminium on Ni(II), Pd(II) and Cu(II) bis-salicylaldoximates. The reaction products were isolated as coloured powders, insoluble in the usual organic solvents. The chemical analyses, the magnetic measurements and the IR spectra show that in every case the new compounds are formed by substitution of the hydrogen bridges existing in the coordinated oximes, by $Al(C_6H_5)_2$ groups, according to a suggested mechanism. The resulting products give, by X rays diffraction, images corresponding to an amorphous structure, fundamentally different from the initial compounds, which have a crystalline structure. The new aluminium organic compounds form with the amines adducts with the formula: $M(II)(C_7H_5O_2N)_2Al_2(C_6H_5)_4L_2$, where L can be pyridine, aniline, picoline or lutidine. Among the amine adducts only the adducts with pyridine were isolated to confirm their formulae and the binding manner.

The theoretical and practical outlook on the use of salicylaldoxime in chemical analyses was discussed in several papers[2–12] dealing, at the same time, with the structure and changes taking place at the chelatinisation by different metallic ions. It is known that salicylaldoxime[4] binds the metallic ions in two ways, as shown by the formulae I and II.

---

[1] N. Voiculescu, I. Popescu and L. Roman, *Rev. Roumaine Chim.*, **18**, 1595 (1973).

[2] N. Voiculescu and I. Popescu, *Rev. Roumaine Chim.*, **17**, 719 (1972).

[3] R. Ripan, Z. Szekeli and G. Kiss, *Studii și Cercetări Chim. Acad. R.P.R. Fil. Cluj*, **12**, 201 (1961).

[4] K. Burger, F. Ruff, I. Ruff and I. Egyed, *Acta Chim. Acad. Sci. Hung.*, **46**, 1 (1965).

[5] I. Császar and I. Szeghalmi, *Acta Univ. Szeged.*, *Acta Phys. Chem.*, **12**, 117 (1966).

[6] B. S. Krishna Rao and O. E. Hileman, *Talanta*, **14**, 299 (1967).

[7] N. K. Pshenitsyn and G. A. Necrasova, *Izvest. Sektora Platiny i Drug. Blagorod Metal. Inst. Obschei i Neorg. Khim. Akad. Nauk. S.S.S.R.*, **30**, 59 (1955).

[8] M. Robtelsky and E. Jungreis, *J. Inorg. Nuclear Chem.*, **3**, 38 (1956).

[9] Reinosure Hara, *J. Pharm. Soc. Japan*, **71**, 1140 (1951).

[10] J. Császar, *Acta Chim. Acad. Sci. Hung.*, **32**, 345 (1962).

[11] K. Burger and I. Egyed, *Magyar Kém. Folyóirat*, **71**, 143 (1965).

[12] K. K. Ramaswamy and D. N. Sen, *Indian J. Chem.*, **3**, 517 (1965).

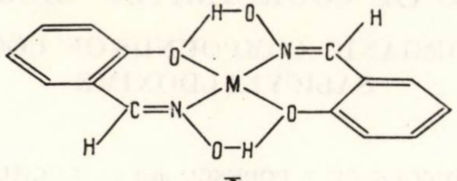

I

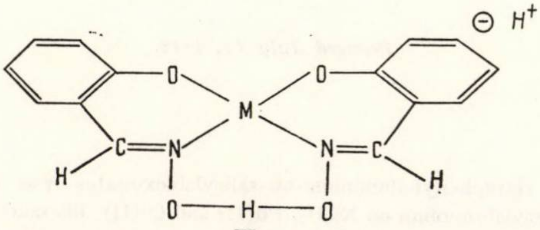

II

The bis-salicylaldoximates studied by us correspond to formula I. Some of the characteristic reactions of the functional groups of the free ligands are masqued or diminished through coordination, which may also be supposed in the case of salicylaldoxime. These changes were not much studied.

The attempt to acetylate [13] $Cu(II)(C_7H_6O_2N)_2$ with acetic anhydride and acetyl chloride has led to the obtention of a diacetylated derivative pointing out a certain resistance towards the esterification of coordinated salicylaldoxime. Trying to determine if the hydrogen bridges of these chelates behave in the same way as those of the bis-dimethylglyoximates of the same metals[1,2] *versus* the aluminium organic derivatives, we have succeeded to synthetize the series of phenylaluminium – organic derivatives of the Ni(II), Pd(II) and Cu(II) bis-salicylaldoximates (formula III) as well as their adducts with amines.

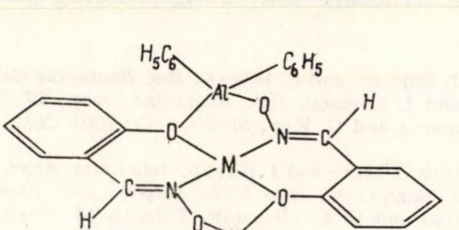

III

---

[13] K. K. Ramaswamy and D. N. Sen, *Indian J. Chem.*, **3**, 516 (1965).

The compounds were characterized by chemical and magnetic analyses, by IR spectra and X ray diffraction.

EXPERIMENTAL

The Ni(II), Pd(II) and Cu(II) bis-salicylaldoximates were obtained according to the methods given in literature.[14–16]

The $Al(C_6H_5)_3$ [17] was obtained starting from $Hg(C_6H_5)_2$ and aluminium powder, by heating up to 130–140°, and was purified by recrystallization from benzene and *n*-hexane.

The synthesis of the aluminium-organic derivatives of the Ni(II), Pd(II) and Cu(II) bis-salicylaldoximates was carried out in Schlenk vessels by adding the benzene solution of $Al(C_6H_5)_3$, in 2 : 1 ratio, to the finely ground and dried chelate powders. The reactions were carried out at room temperature, as well as by heating for several hours, at the solvent reflow temperature. In both cases, coloured powders, insoluble in benzene, were obtained. These were washed several times with hot benzene to remove any traces of $Al(C_6H_5)_3$. The products were dried in vacuum. Independently of the processing temperature, the resulting compounds have the same chemical characteristics and structures, confirmed by chemical analyses and magnetic measurements (table 1), by IR spectra (table 2) and by X-ray diffraction. The reaction and the handling of the compounds were carried out in an actionless and moistless atmosphere.

Table 1

Analyses and characteristics of the synthetized products

The compound	Colour	Magnetic characteristics	Analyses: C Calcd. % / Found %	H Calcd. % / Found %	Al Calcd. % / Found %	N Calcd. % / Found %	M Calcd. % / Found %
$Ni(C_7H_5O_2N)_2Al_2(C_6H_5)_4$	yellowish-brown	diamagnetic	66.02 66.04	4.34 4.32	7.81 7.84	4.05 4.05	8.50 8.51
$Pd(C_7H_5O_2N)_2Al_2(C_6H_5)_4$	grey	diamagnetic	61.75 61.80	4.06 4.08	7.31 7.31	3.78 3.75	14.40 14.43
$Cu(C_7H_5O_2N)_2Al_2(C_6H_5)_4$	green	diamagnetic	65.56 65.60	4.31 4.32	7.76 7.75	4.02 4.04	9.13 9.13
$Ni(C_7H_5O_2N)_2Al_2(C_6H_5)_4$	yellow	diamagnetic	67.88 67.85	4.71 4.73	6.36 6.36	6.59 6.60	6.92 6.96
$Pd(C_7H_5O_2N)_2Al_2(C_6H_5)_4Py$	grey	diamagnetic	64.25 64.30	4.46 4.45	6.02 6.00	6.24 6.25	11.87 11.90
$Cu(C_7H_5O_2N)_2Al_2(C_6H_5)_4Py_2$	yellow-green	diamagnetic	67.48 67.50	4.68 4.65	6.32 6.35	6.56 6.58	7.44 7.44

---

[14] F. Ephraim, *Ber. dtsch. chem. Ges.*, **63 B**, 1928 (1930).

[15] F. Ephraim, *Ber. dtsch. chem. Ges.*, **64**, 1210, 1215 (1931).

[16] E. G. Cox, F. W. Wardlaw and K. C. Webster., *J. Chem. Soc.*, **1 935**, 459.

[17] E. Krause and P. Dittmar, *Ber. dtsch. chem. Ges.*, **63**, 2401 (1930).

The adducts with amines were obtained by adding the previously anhydrized amines to the new compounds in powder form. The powders are solved in the amines and change their colour. The separation of the adducts was carried out by removing the amine in excess, or by precipitating with *n*-hexane, *n*-heptane or methylcyclohexane in which the adducts do not solve. The solvent and the amine in excess were removed by evaporating at low pressure. Though adducts are humidity-resistant, the reactions were carried out in an actionless and moistless atmosphere. Among adducts with amines, those with pyridine were analysed. The results of the chemical analyses, the colour and the magnetic properties are given in table 1.

The X-ray diffraction images of the compounds were obtained by the Debye Scherer method with an URK-5 and TUR M-60 apparatus by using the CuK$_\alpha$ radiation and a nickel filter. To avoid any trace of humidity, the test-samples were inserted into sealed glass-tubes. Working with the URK-5, the exposures were carried out in a vacuum chamber at 40 kV and 25 mA, for two hours, while with the TUR M−60, the exposures at 40 kV and 14 mA required eight hours.

The magnetic properties were checked with a Gouy balance in a nonhomogeneous magnetic field.

RESULTS AND DISCUSSION

The two oxygen atoms of the Ni(II), Pb(II) and Cu(II) salicylaldoximates corresponding to formula I are bound differently and are not symmetrical as are those of the nickel bis-dimethylglyoximate, in which Rundle and Parasol[18] consider that a symmetrical hydrogen bond exists. The determinations of the structure have pointed out the fact that in $Ni(II)(C_7H_6O_2N)_2$ [19] $Cu(II)(C_7H_6O_2N)_2$[20] and $Pd(II)\ (C_7H_6O_2N)_2$, [21] the hydrogen bonds are very short and probably asymmetrical. This asymmetry may be explained through the interpolation of the hydrogen between the oxygen atom of the oximic group and the oxygen atom of the phenolic group (formula I). The phenolic oxygen atom, being coordinated to the central atom, has a much lower capacity of binding the proton of the hydrogen bridge than the oxygen atom of the oximic group. This particularity of the Ni(II), Pd(II) and Cu(II) bis-salicylaldoximates hydrogen bond can also be pointed out by their reaction with the $Al(C_6H_5)_3$. Differing from the bis-dimethylglyoximates [1] of the same metals, the salicylaldoximates react more easily with the $Al(C_6H_5)_3$. The 2 : 1 ratio between $Al(C_6H_5)_3$ and the salicylaldoximates was determined by the existence of two hydrogen bridges as is shown by the stoichiometry of the reaction :

$$M(II)(C_7H_6O_2N)_2 + 2Al(C_6H_5)_3 = M(II)\,(C_7H_5O_2N)_2\,Al_2(C_6H_5)_4 + 2C_6H_6$$

We believe that this reaction takes place according to the mechanism suggested in the case of the bis-dimethylglyoximates,[1] a mechanism by which, in the first phase (formula IV) the formation of an instable adduct takes place between two $Al(C_6H_5)_3$ molecules and a chelate molecule, followed by the elimination of two benzene molecules, and the formation of the stable compounds, represented by formula III.

---

[18] R. E. Rundle and M. Parasol, *J. Chem. Phys.*, **20**, 1487 (1952).

[19] L. L. Merritt Jr., C. Guare and A. E. Lessor, *Acta Cryst.*, **9**, 253 (1956).

[20] M. A. Jarski and E. C. Lingafelter, *Acta Cryst.*, **17**, 1109 (1964).

[21] C. E. Pfluger, *Diss. Abs.*, **18**, 1644 (1958).

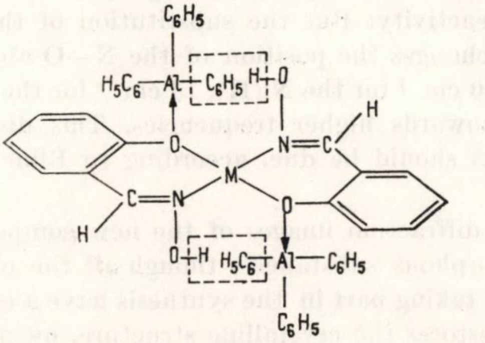

IV

This formula is corroborated by the chemical analyses and the magnetic characteristics (table 1), as well as by the interpretation of the IR spectra of the compounds (table 2).

Table 2

IR absorption spectra of $M(C_7H_5O_2N)_2\,Al_2(C_6H_5)_4$ (Values given in cm⁻¹)

Ni	Pd	Cu	Assigned to
1610	1600	1618	C=N
1558	1555	1560	Distortion of C=N
1496	1492	1500	*Ortho*
1460	1480	1464	
1322	1300	1303	C–H in the plane
1280	1200	1215	N–O
1158	1150	1160	Vibration due to the benzene ring
1125	1122	1135	
1040	1035	1045	C–O
924	922	938	N–O
760	760	775	C–H outside the plane

This table gives the approximate values of the characteristic absorption maxima in the 1650–650 cm⁻¹ range assigned to the corresponding vibrations. The high frequencies[22] found between 1650 and 1640 cm⁻¹ in the Ni(II) (1642 cm⁻¹), Pd(II) (1650 cm⁻¹) and Cu(II)

---

[22] K. K. Ramaswamy, C. I. Jose and D. N. Sen, *Indian J. Chem.*, **5**, 156 (1967).

(1647 cm^{-1}) salicylaldoximates due to the OH groups, are not to be found in the aluminium-organic compounds of the chelates, this confirming the substitution of the hydrogen by $Al(C_6H_5)_2$ groups. The fact that the characteristic absorptions of the C = N groups are only very slightly affected by the substitution of the hydrogen, shows that this group does not change its reactivity. But the substitution of the hydrogen by the $Al(C_6H_5)_2$ group changes the position of the N–O absorption maximum, displacing it by 60 cm^{-1} for the Ni(II), 13 cm^{-1} for the Pd(II) and 22 cm^{-1} for the Cu(II), towards higher frequencies. This displacement towards higher frequencies should be due, according to Blinc and Hadzi,[23] to a polar structure.

The X-ray diffraction images of the new compounds are characteristic to the amorphous substances, though all the chelates [19-21] as well as the $Al(C_5H_6)_3$[24] taking part in the synthesis have a crystalline structure. The hydrolysis restores the crystalline structure, owing to the rebuilding up of the chelates.

The diamagnetism of the new compounds (table 1) shows the conservation of the square-plane structure of the chelates, even after the creation of the chelate – Al_2R_4 bond.

The synthetized aluminium-organic salicylaldoximates compounds, contrary to those formerly presented by us,[1,2] react with amines forming stable compounds, in solid state. The $Ni(II)(C_7H_6O_2N)_2$[5,8,25] gives compounds with the pyridine only in solution, and with the same amines solid products are obtained. The reaction with amines of the Ni(II) $(C_7H_6O_2N)_2$ leads to the formation of compounds where Ni is hexacoordinated (formula V) with a D_{2h}[5] symmetry. The diamagnetic square-plane symmetry [10] is transformed into a paramagnetic octahedral symmetry.

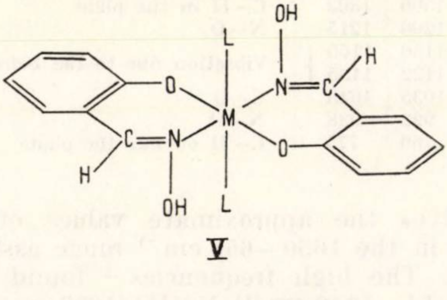

V

---

[23] R. Blinc and D. Hadzi, *J. Chem. Soc.*, **1958**, 4536.

[24] J. F. Malone and W. S. McDonald, *Chem. Comm.*, **1967**, 444.

[25] F. Maggio, V. Romano, T. Pizzino and L. Pellerito, *Ann. Chim.* (*Ital.*), **58**, 725 (1968).

Our attempts to obtain compounds corresponding to formula VI through the reaction of the aluminium-organic derivatives of the Ni(II), Pd(II) and Cu(II) salicylaldoximates with amines (pyridine, aniline, picoline, lutidine) have not enabled us to obtain paramagnetic compounds corresponding to the octahedral configuration (formula VI).

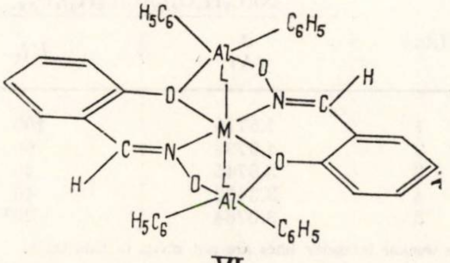

VI

The diamagnetism of these compounds forces us to suppose that the corresponding adducts are obtained through an acido-basic Lewis reaction in which the acid part is played by the aluminium atom of the aluminium-organic-salicylaldoximate derivatives (formula VII).

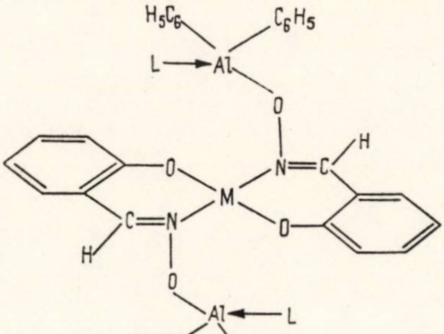

VII

The square-plane structure is thus not changed, and consequently neither is the diamagnetism.

The ease with which the adducts with amines are obtained is a confirmation of the fact that the aluminium atom is only feebly bound to the phenolic oxygen atom. The number of amine molecules bound in the solid compound is confirmed by the chemical analyses (table 1).

The X-ray analyses of the adducts with pyridine confirm a crystalline structure for the Ni(II) (table 3) and Pd(II) derivatives, and the preservation of the amorphous structure in the case of copper.

Table 3

Roentgenographic data

Line	$Ni(C_7H_5O_2)_2Al_2(C_6H_5)_4Py_2$	
	d (Å)	I/I_0
1	4.5715	100
2	4.0733	60
3	3.6745	40
4	3.3482	40
5	3.0764	20[a]

[a] The weaker intensity lines are not given in this table.

Revue Roumaine de Chimie, **18**, *9*, 1609–1612 (1973)

REACTION OF PYRYLIUM SALTS WITH NUCLEOPHILES

X[1] N (12)-SUBSTITUTED 11,13-DIMETHYL-[9](2,6)-PYRIDINOPHANIUM PERCHLORATES

ALEXANDRU T. BALABAN

Institute of Atomic Physics, P.O.B. 35, Bucharest, Romania

Received April 7, 1973

11,13-Dimethyl-[9](2,6)-pyrylophanium perchlorate (I) reacts normally with methylamine and aniline affording pyridinium salts IV and V, but with hydrazine and phenylhydrazine the reaction products II and III differ from those currently obtained from alkyl-substituted pyrylium salts.

REACTION OF 11,13-DIMETHYL-[9](2,6)-PYRYLOPHANIUM PERCHLORATE (I) WITH HYDRAZINE AND PHENYLHYDRAZINE

The reaction of pyrylium salts with hydrazine yields according to the reaction conditions and structure of the pyrylium salt, 5-, 6-, or 7-membered heterocyclic compounds : 2,4,6-triarylpyrylium salts afford 1,2-diazepines ; [1,2] 2,4,6-trialkylpyrylium salts with equimolar amounts of hydrazine yield N-aminopyridinium salts,[3] while with excess hydrazine they form pyrazolines.[3] Aryl-substituted pyrazolines result from 2,4,6-triarylpyrylium pseudobases and hydrazine.[1,4] It had been found earlier that phenylhydrazine reacts with both 2,4,6-triarylpyrylium salts and their pseudobases leading to pyrazolines.[5] With excess phenylhydrazine, bis-phenylhydrazones of pseudobases were reported to result.[6] Methylhydrazine and aryl-substituted pyrylium salts afford mainly pyrazolines (or pyrazoles by a subsequent aromatization) with small amounts of 1,2-diazepine derivatives.[7] There findings can be rationalized in a common mechanism.[1]

In the present paper we describe the reaction of hydrazine with an alkyl-substituted pyrylium salt, 11,13-dimethyl-[9](2,6)-pyrylophanium perchlorate (I)* which is readily available from the diacetylation of cyclododecene with acetic anhydride and perchloric acid.[9] Its NMR spectrum in $CDCl_3-(D_3C)_2SO$ evidences the methyl proton peak (s, 6H, τ 7.08), the pyrylium ring proton (s, 1H, τ1.28) and the three kinds of methylene protons (a-type, t, 4H, τ7.03 ; b-type, m, τ8.08 ; c-type, m, 10H, τ8.80)**.

---

[1] Preceding part, A. T. Balaban, *Tetrahedron*, **26**, 739 (1970).

[2] O. Buchardt, C. L. Pedersen, U. Svanholm, A. M. Duffield and A. T. Balaban, *Acta Chem. Scand.*, **23**, 3125 (1969).

[3] G. N. Dorofeenko, A. N. Narkevich and Yu. A. Zhdanov, *Khim. Geterotsikl. Soedin.*, **1867**, 1130.

[4] G. I. Zhungietu, I. V. Shantsevoi and D. D. Buburuz, *Khim. Geterotsikl. Soed.*, **1971**, 281 ; G. I. Zhungietu, I. V. Shantsevoi and S. V. Krivun, *ibid.*, **1973**, 45.

[5] A. T. Balaban, *Tetrahedron*, **24**, 5059 (1968).

[6] W. Schneider and W. Müller, *Liebigs Ann. Chem.*, **438**, 147 (1924).

[7] V. Snieckus and G. Kan, *Chem. Commun.*, **1970** , 1208.

In ethanolic solution, even with excess hydrazine, only one product is formed from I. It is a perchlorate which evidences two NH stretching bands in the infrared absorption spectrum at 3361 and 3282 cm^{-1}, which on deuteration are shifted to 2500 and 2395 cm^{-1}; incompletely deuterated samples present a third band at 2441 cm^{-1} due to NHD. On deuteration, also the NH bending band at 1625 cm^{-1} disappears. The NMR spectrum, in acetonitrile, presents the γ-proton at 1.97 τ, and an NH_2 peak at 3.96 τ; in deuterochloroform—hexadeutero-dimethylsulphoxide, these peaks appear at τ 2.03 and τ 3.15, respectively (on deuteration, the latter peak disappears). In trifluoroacetic acid, the γ-proton appears at 1.94 τ but the NH_2 group no longer appears ; the six methyl protons appear at 7.15τ. In $CDCl_3-(D_3C)_2SO$, the methyl protons appear at 7.07τ (a-type, triplet $J = 5.5$Hz) ; 8.10 τ (b-type), and 8.90 τ (c-type). These data indicate that the product is N(12)-amino-11,13-dimethyl—[9](2,6)-pyridinophanium perchlorate (II) :* since it is readily formed without any special precautions, the steric factors which characterize compound I must be responsible for this behaviour, different from that of other alkyl-substituted pyrylium salts.

Phenylhydrazine in excess reacts in ethanol with I affording a colourless product III presenting an N-H stretching band at 3340 cm^{-1} and strong aromatic bands at 1509 and 1600 cm^{-1}.The NMR spectrum presents in $CDCl_3$ two methyl peaks at 8.31 and 8.44 τ, and three one-proton peaks at 5.65 τ (doublet, $J=2$ cps), 6.68 τ (doublet, $J = 11$ cps) and 7.04 τ ($J=2$ and 11 cps) in addition to aromatic (10 H) and methylene protons (18 H). The mass spectrum and elemental analysis evidence that the product originates from one mole I and two moles of phenylhydrazine : parent peak at m/e 430, prominent peak at m e 338 (M—PhNH), 323 ($M-PhN_2H_2$), 283, 171 and 93.

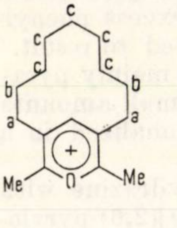

I

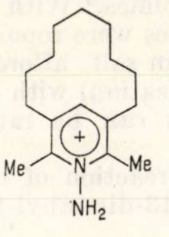

II

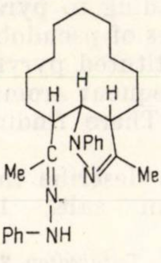

III

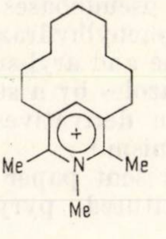

IV

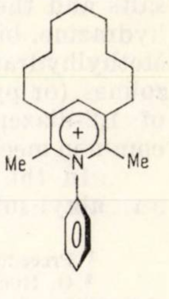

V

---

* Named after ref.[8]

** Abbreviations : singlet (s), triplet (t), multiplet (m). În ref.[8] the NMR spectrum of I in F_3CCOOH was reported, where the ring proton resonated closely to the F_3CCOOH proton.

[8] E. Vögtle and P. Neumann, *Tetrahedron*, **26**, 5847 (1970).

[9] A. T. Balaban, *Tetrahedron Letters*, **1968**, 4643.

REACTION OF (I) WITH PRIMARY AMINES : METHYLAMINE AND ANILINE

Pyrylium salts are converted by primary amines into three products, depending on the structure of both reagents : a pyridinium salt, a keto-dienamine, and (if α-methyl groups are present) an N-alkyl-aniline.[10] Methylamine and aniline usually lead to high yields of pyridinium salt. In the present case, (I) reacts normally with these two primary amines yielding the N-methyl- (IV) and N-phenylpyridinium salts (V) respectively. Their IR and NMR spectra agree with the structure. In the NMR spectra, recorded in trifluoracetic acid, the γ-proton appears at 1.80 τ (IV) and 1.86 τ (V), the N-methyl at 5.73 τ (IV), a triplet (J = 7 cps) centered at 6.88 τ (IV) and 7.12 τ (V) is due to the four a-type CH_2 protons adjacent to the pyridinium ring, broad peaks are due to the four b-type CH_2 protons adjacent to the latter at 8.07 τ (IV) and 8.23 (V), and broad peaks are due to the remaining five CH_2 groups (c-type) from the cyclododecene moiety : 8.75 τ (IV) and 8.81 τ (V). The most pronounced difference between the NMR spectra of IV and V appears for the six C-methyl protons : 7.12 τ for IV and 7.78 τ for V. The upfield shift of 0.66 ppm is analogous to other N-methyl- *versus* N-phenyl-2,6-dimethyl-pyridinium salts.[10] Owing to steric hindrance the N-phenyl group in the latter salts cannot be coplanar with the pyridinium ring and therefore shields the α-methyl groups attached to the pyridinium ring. In 2,4,6-trimethyl-pyridinium salts, an X-ray structure determination found a dihedral angle between the pyridinium and phenyl planes of 85°,[11] and even the unsubstituted N-phenylpyridinium chloride evidences a dihedral angle of 47° in the crystal.[12]

In conclusion, (I) behaves normally in its reaction with primary amines like aniline and methylamine, but the reaction with hydrazine and phenylhydrazine affords products which differ from those currently obtained with alkyl-substituted pyrylium salts.

EXPERIMENTAL PART

Diacetylation of cyclododecene. Cyclododecene (168 g, 1 mole) and acetic anhydride (1l) were stirred energetically, and 70 % perchloric acid (1 mole) was added dropwise in a flask provided with immersed thermometer and reflux condenser. The rate of addition for $HClO_4$ was controlled so that the temperature rises gradually and the mixture refluxes gently. After refluxing for two hrs the mixture was left overnight, then 1 l of ether was added under stirring and the black liquid was decanted after 24 hrs, leaving large wedge-shaped crystals. These were recrystallized from several portions of hot 1 % aqueous perchloric acid with charcoal until no more perchlorate separated on cooling the filtrate. The white perchlorate (I) was filtered off and dried in the air : 80 g (24% yield), m.p. 170°. The perchlorate I, $C_{16}H_{25}O^{\oplus}$ $ClO_4^{\ominus}$* is readily soluble in hot ethanol but less in hot 1% $HClO_4$.

---

[10] C. Toma and A. T. Balaban, *Tetrahedron*, **22**, Suppl. 7, 9 (1966).
[11] A. Camerman, L. H. Jensen and A. T. Balaban, *Acta Cryst.*, **25** B, 2623 (1969).
[12] L. H. Jensen and A. T. Balaban, to be published.

Reaction of I with hydrazine. A solution of I (1 g) in 20 ml ethanol was treated with excess hydrazine hydrate and refluxed for five minutes after the initial exothermal reaction. Then, a slight excess of 20% perchloric acid was added to neutralize the hydrazine, water was added to the warm solution until it became cloudy, and the solution was cooled. The crystallized product II was filtered off and recrystallized from ethanol or water. Colourless crystals, m.p. 249°. *Found* : N, 7.6%, $C_{16}H_{27}N_2^{\oplus}$ $ClO_4^{\ominus}$ requires : N, 8.07%.

The product was also recrystallized from deuterium oxide or from CH_3COOD for exchange of labile hydrogens.

Reaction of I with phenylhydrazine. Addition of phenylhydrazine to an alcoholic solution of I affords a red solution, which becomes yellow with excess phenylhydrazine. Brief refluxing and dilution with water yields on oily product which crystallizes on refluxing in ethanol. Colourless needles (III), m.p. 172° (from ethanol), slightly soluble in ethanol. *Found* : N, 13.38 · $C_{28}H_{38}N_4$ requires N, 13.01%.

Reaction of I with methylamine. A solution of I (1 g) in methanol (15 ml) was treated with an excess of methylamine (30% aqueous solution). After the exothermal reaction subsided, the product IV crystallized on cooling. It was filtered off, washed with methanol and recrystallized from aqueous methanol with charcoal. Colourless prisms, m.p. 226°. *Found*: N, 4.37. $C_{17}H_{28}N^{\oplus}$ $ClO_4^{\ominus}$ requires N, 4.05%.

Reaction of I with aniline. Perchlorate I was dissolved in ethanol and treated with an excess of aniline, refluxed for five minutes, cooled, and treated with 10% aqueous perchloric acid. The product V was filtered off, washed with ethanol, and recrystallized from ethanol with charcoal. Colourless leaflets m.p. 174°. *Found* : N, 3.55. $C_{22}H_{30}N^{\oplus}$ $ClO_4^{\ominus}$ requires : N, 3.43%.

Spectra. Infrared absorption spectra were recorded with a Jena UR–10 instrument, NMR spectra with a Tesla (80 MHz) and a Varian HR–100 instruments.

Acknowledgements. Thanks are expressed to Mrs. Alice Vasilescu and Mr. C.C. Renţia for Tesla NMR spectra, to prof. A. R. Katritzky and dr. A. J. Boulton for the Varian NMR spectra and for the mass spectra, to Mrs. Cornelia Popescu for elemental analyses, to Mrs. Elena Romaş for IR spectra, and to Hüls A.G. for a generous gift of cyclododecene.

---

* A misprint in the formula occurred in ref.[9] : $C_{16}H_{25}O^{+}ClO_4^{-}$ requires C, 57.7 ; H,7.6%.

Revue Roumaine de Chimie, 18, 9, 1613–1616 (1973)

DARSTELLUNG UND UNTERSUCHUNG DER HYDROACRIDINE. XI[1]

DER STERISCHE ABLAUF DER QUATERNIERUNG VON N-METHYL-α-PERHYDROACRIDIN UND N-METHYL-β-PERHYDROACRIDIN MIT TRIDEUTEROMETHYLJODID

N. BĂRBULESCU und F. POTMISCHIL

Organisch-Chemisches Laboratorium der Universität Bukarest, Spl. Independenţei 89

Eingegangen am 7. März 1973

Der sterische Ablauf der Quaternierung von N-Methyl-α-perhydroacridin (I, R= =CH_3) und N-Methyl-β-perhydroacridin (II, R=CH_3) mit CD_3I wird bei 23° und 95° untersucht. Bei I, R=CH_3, erfolgt der Angriff des CD_3I zu 65 % äquatorial und zu 35 % axial, und das Verhältnis ist von der Temperatur nicht abhängig. Bei II, R = CH_3, erfolgt der Angriff bei 23° zu 75 % äquatorial und zu 25 % axial; bei 95° wird eine Erhöhung des Anteils axialen Angriffes auf 35 % festgestellt. Es wird auch ein Überblick über das Gesamtbild der Stereochemie der Quaternierungen von N-Alkyl-Derivaten des α- (I) und β-Perhydroacridins (II) gemacht.

In der vorangehenden Mitteilung[1] wurden die Quaternierungen der N-Methyl-, N-Äthyl- und N-Benzyl-Derivate (R = CH_3, C_2H_5 und bzw. $CH_2C_6H_5$) des α- (I) und β-Perhydroacridins (II) mit je Methyl-, Äthyl- und Benzyljodid (R′ = CH_3, C_2H_5 und bzw. $C_6H_5CH_2$) beschrieben; in den Fällen mit unterschiedlichen „R" und „R′" konnte, anhand der NMR-Spektren der Quaternierungs-Produkte, der sterische Ablauf der Reaktionen besprochen werden:

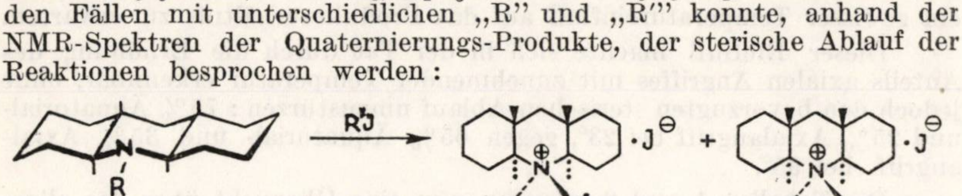

I III V

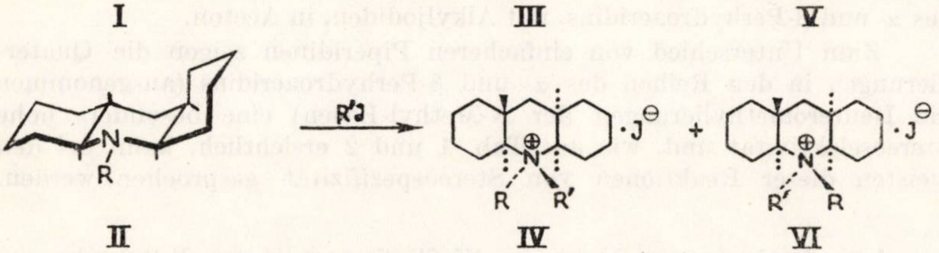

II IV VI

X[1]. Mitteilung : N. Bărbulescu und F. Potmischil, *Liebigs Ann. Chem.*, **752**, 22 (1971).

Die vorliegende Arbeit ergänzt dieses Kapitel der Perhydroacridin-Chemie mit dem sterischen Ablauf der Quaternierung von N-Methyl-α-perhydroacridin (**I**, $R = CH_3$) und N-Methyl-β-perhydroacridin (**II**, $R = CH_3$) mit Methyljodid-d_3, in Aceton, bei Raumtemperatur und bei 95° (Wärmeschrank).

DISKUSSION

N-Methyl-α-perhydroacridin + CD_3I. Das prozentuale Intensitäts-Verhältnis der $N^{\oplus}$-CH_3-Banden im NMR-Spektrum des Quaternierungs-Produktes von **I**, $R = CH_3$, mit CD_3I, bei 23°, beträgt ca. 65 : 35 zu Gunsten der axialen $N^{\oplus}$-CH_3-Gruppe[*], woraus 65% Äquatorial- und 35% Axialangriff des CD_3I erfolgt (die aus Meßfehlern herrührenden Abweichungen von den tatsächlichen Werten werden auf ±3% geschätzt).

Bei 95° wurde derselbe sterische Ablauf wie bei 23° festgestellt. Hier muß allerdings erwähnt werden, daß schon am Weg zum Wärmeschrank Bildung einer nicht unbedeutenden Menge quartären Salzes beobachtet wurde; man kann aber trotzdem—rücksichtlich der konformationellen Starrheit des α-Perhydroacridin-Gerüstes —ruhig annehmen, daß auch ohne diesem Vorfall das gleiche Ergebnis gebucht geworden wäre, da der sterische Ablauf der Quaternierung (bei selbem Quaternierungsagens) hauptsächlich von der Stellung und Konfiguration der C-Substituenten des Piperidin-Rings abhängig ist[2] (siehe auch Text unterhalb).

N-Methyl-β-perhydroacridin + CD_3I. Die bewegliche *cis*-Verknüpfung zwischen dem Piperidin-Ring und dem einen der Cyclohexan-Ringe des β-Perhydroacridin-Gerüstes macht, durch deren Inversion unter gewisser Energiezufuhr von außen, die Änderung der Raumverhältnisse um das Stickstoffatom möglich. Daher war (im Gegensatz zum α-Isomeren) ein gewisser Temperatureinfluß auf das Produktverhältnis zu erwarten.

Dieser Einfluß machte sich in der Tat durch die Erhöhung des Anteils axialen Angriffes mit zunehmender Temperatur erkennbar, ohne jedoch den bevorzugten sterischen Ablauf umzustürzen : 75% Äquatorial- und 25% Axialangriff bei 23°, gegen 65% Äquatorial- und 35% Axialangriff, bei 95°.

Die Tabellen 1 und 2 erlauben nun eine Übersicht über das allgemeine Bild der Stereochemie der Quaternierungen von N-Alkyl-Derivaten des α- und β-Perhydroacridins, mit Alkyljodiden, in Aceton.

Zum Unterschied von einfacheren Piperidinen zeigen die Quaternierungen in den Reihen des α- und β-Perhydroacridins (ausgenommen die Deuteromethylierungen der N-Methyl-Basen) eine besonders hohe Stereoselektivität und, wie aus Tab. 1 und 2 ersichtlich, kann bei den meisten dieser Reaktionen von Stereospezifizität gesprochen werden.

---

[*] Die Zuordnungen der Banden der $N^{\oplus}$-CH_3-Gruppen in den Methojodiden von N-Methyl-α- und N-Methyl-β-perhydroacridin wurden bereits in der X. Mitteilung geklärt.

Tabelle 1

Sterischer Ablauf der Quaternierungen von N-Alkyl-Derivaten des α-Perhydroacridins (I) mit Alkyljodiden (R'I), in Aceton

R	R′	Reakt.-Temp. °C	% III (ax.-Angriff)	% V (äq.-Angriff)
CH_3	CD_3	23	35	65
CH_3	CD_3	95	35	65
CH_3	C_2H_5	23	0–10	90–100
CH_3	$C_6H_5CH_2$	23	0	100
C_2H_5	CH_3	23	90–100	0–10
C_2H_5	C_2H_5	90a)	b)	b)
C_2H_5	$C_6H_5CH_2$	23	0	100
$CH_2C_6H_5$	CH_3	23	100	0
$CH_2C_6H_5$	C_2H_5	90a, c)	—	—
$CH_2C_6H_5$	$C_6H_5CH_2$	90a, d)	—	—

a) Bei Raumtemperatur konnte keine Bildung quartären Salzes beobachtet werden.

b) Obgleich das quartäre Salz keinen greifbaren Beweis liefern kann, ist, unter Berücksichtigung der Ergebnisse der anderen Quaternierungen in welchen eine Äthyl-Gruppe als „R" oder „R′" teilnimmt, mit weit überwiegendem Äquatorialangriff zu rechnen.

c) Bei 90° wurde nur N-Äthyl-α-perhydroacridin-hydrojodid in sehr schwacher Ausbeute erhalten.

d) Bei 90° wurde nur α-Perhydroacridin-hydrojodid in sehr schwacher Ausbeute erhalten.

Tabelle 2

Sterischer Ablauf der Quaternierungen von N-Alkyl-Derivaten des β-Perhydroacridins (II) mit Alkyljodiden (R'I), in Aceton

R	R′	Reakt-Temp. °C	%IV (ax.-Angriff)	%VI (äq.-Angriff)
CH_3	CD_3	23	25	75
CH_3	CD_3	95	35	65
CH_3	C_2H_5	90a)	0	100
CH_3	$C_6H_5CH_2$	23	0	100
C_2H_5	CH_3	90a	100	0
C_2H_5	C_2H_5	90a, b)	—	—
C_2H_5	$C_6H_5CH_2$	90a, c)	—	—
$CH_2C_6H_5$	CH_3	90a, d)	—	—
$CH_2C_6H_5$	C_2H_5	90a, e)	—	—
$CH_2C_6H_5$	$C_6H_5CH_2$	90a, f)	—	—

a) Bei Raumtemperatur konnte keine Bildung quartären Salzes beobachtet werden.

b) Bei 90° wurde nur N-Äthyl-β-perhydroacridin-hydrojodid in schwacher Ausbeute erhalten.

c) Ebenso, in 72%-Ausbeute.

d) Bei 90° wurde N-Methyl-β-perhydroacridin-methojodid zusammen mit unidentifizierten Produkten erhalten.

e) Bei 90° wurde β-Perhydroacridin-hydrojodid in 41%-Ausbeute erhalten.

f) Bei 90° wurde ein unidentifiziertes Produkt erhalten.

Stereospezifische Quaternierungen wurden bisher bloß bei einigen Chinolizidin-Derivaten begegnet.*)

Die Autoren danken Herrn Prof. Dr. A. R. Katritzky, University of East Anglia, Norwich, für die Überlassung des zu dieser Arbeit benötigten Trideuteromethyljodids.

BESCHREIBUNG DER VERSUCHE

NMR-Spektren wurden mit einem „Varian A60—A"-Gerät aufgenommen; als Lösungsmittel diente Chloroform, mit TMS als innerer Standard.

Die Quaternierungen wurden in geschlossenen Glasröhren ausgeführt.

---

*) Der sterische Ablauf der Quaternierungen von N-Alkyl-Derivaten einfacherer Piperidine sowie auch bicyclischer Abkömmlinge (Decahydrochinoline, Camphidine, Tropane u. Chinolizidine) wurde besonders im vergangenen Jahrzehnt ziemlich eingehend untersucht. Das Thema, in seiner ganzen Vielfältigkeit von Aspekten, ist in zwei ausgezeichneten „Reviews"[2,3] (Literatur bis 1969 berücksichtigt) besprochen; in dem seit dann verstrichenen Zeitraum sind noch einige Arbeiten[4—9] auf dem Gebiet erschienen.

[2] J. McKenna, *Top. Stereochem.*, **5**, 275 (1970); siehe auch: J. McKenna, *Conform. Anal., Pap. Int. Symp., Brussels, Sept.* **1969**, S. 165. Herausgegeben von G. Chiurdoglu, Academic Press, New York, N. Y., 1971.

[3] A. T. Bottini, *Selec. Org. Transform.*, **1**, 89 (1970).

[4] R. A. Y. Jones, A. R. Katritzky und P. G. Mente, *J. Chem. Soc.* (*B*), **1970**, 1210.

[5] I. Weisz, P. Agócs, A. Szabó und K. Kovács, *Acta Chim. Acad. Sci. Hung.*, **64**, 257 (1970).

[6] G. Fodor, R. V. Chastain, Jr., D. Frehel, M. J. Cooper, N. Mandava und E. L. Gooden, *J. Amer. Chem. Soc.*, **93**, 403 (1971).

[7] J. H. Supple und E. Eklum, *J. Amer. Chem. Soc.*, **93**, 6684 (1971).

[8] U. O. de la Camp, A. T. Bottini, C. C. Thut, J. Gal und A. G. Bellettini, *J. Org. Chem.*, **37**, 324 (1972).

[9] R. P. Duke, R. A. Y. Jones, A. R. Katritzky, J. R. Carruthers, W. Fedeli, F. Mazza und A. Vaciago, *Chem. Comm.*, **1972**, 455.

Revue Roumaine de Chimie, **18**, *9*, 1617–1626 (1973)

POTENTIAL ANTICANCER AGENTS. VIII [1-4]

NEW AROMATIC AND HETEROAROMATIC NITROGEN MUSTARDS

I. NICULESCU-DUVĂZ*, MARIA ROTARU*, V. FEYNS* and O. MAIOR**

* Oncological Institute, Bd. 1 Mai 11, Bucharest, Romania

** University of Bucharest, Faculty of Chemistry, Splaiul Independenţei, 89, Romania

Received November 25, 1972

New aromatic and heteroaromatic nitrogen mustards have been prepared and studied. UV and IR spectra and antitumour activity are also reported. Relationships between the hydrolysis rate of nitrogen mustards and the basicity of precursor amines are pointed out.

As a part of our research programme concerning the synthesis of new anticancer compounds and structure-chemical reactivity correlations in the class of aromatic nitrogen mustards[1-4] derivatives Ic and IIc containing the phenoxathiin ring were synthesized and studied.

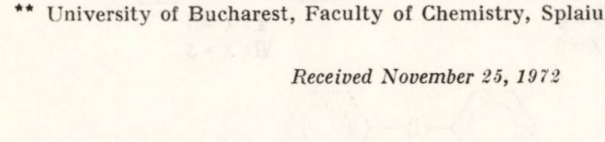

I II

a. $R = NH_2$
b. $R = N(CH_2CH_2OH)_2$
c. $R = N(CH_2CH_2Cl)_2$

Fig. 1. — Phenoxathiin derivatives.

The synthesis of the corresponding amines was previously reported.[5,6] Their conversion into nitrogen mustards was achieved by the classical procedure involving hydroxyethylation in acetic acid solution and chlorination of the N,N-bis (2-hydroxyethyl) derivatives with thionyl chloride or phosphorus oxychloride.

---

[1] I. Niculescu-Duvăz, M. Ionescu, A. Cambanis, M. Vitan and V. Feyns, *J. Med. Chem.*, **11**, 500 (1968).

[2] A. Cambanis, V. Dobre and I. Niculescu-Duvăz, *J. Med. Chem.*, **12**, 161 (1969).

[3] I. Niculescu-Duvăz, V. Feyns, V. Savaniu, M. Ionescu and A. Cambanis, *Rev. Roumaine. Chim.*, **14**, 535 (1969).

[4] I. Niculescu-Duvăz, G. Botez and A. Şerban, *Neoplasma*, **17**, 143 (1970).

[5] J. F. Nobis, A. J. Blardinelli and D. Blaney, *J. Amer. Chem. Soc.*, **76**, 3384 (1953).

[6] O. Maior and M. Stanciu, *Rev. Chim. (Bucureşti)*, **20**, 529 (1969).

In order to investigate the influence of the phenoxathiin ring closure on the basicity of the amines and on the activity of the respective nitrogen mustards, the diphenylamines IIIa. . . VIIa were prepared and converted into nitrogen mustards in the same way (indicatives a, b, c, have the same meanings as above).

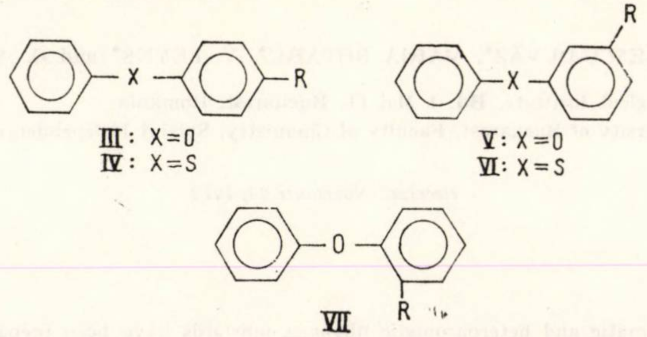

Fig. 2. – Diphenylether and diphenylsulphide derivatives.

PHYSICO-CHEMICAL DATA

The basicity constants of amines Ia. . . VIa were spectrophotometrically determined (see table 1) and correlated with the hydrolysis rates of compounds Ic. . . VIc determined according to Ross's standard method.[7] An approximative linear relationship ($r = 0.92$) was established (see also fig. 5):

$$-\log k_{66} = 8.40 - 0.98\ pK_a$$

Table 1

Amines basicity and hydrolysis rate of the corresponding nitrogen mustards

Compound	$\sigma_{(m,p)}$	pKa (R-NH$_2$)		%Hydrolysis	$-\log k_{66}$ (s^{-1})
		Exp. determ.	Calcd.*	$R = N(CH_2CH_2Cl)_2$	
I	$-0.028+0.153$	—	4.22	14.06	4.09
II	$-0.028+0.70$	2.51 ± 0.03	2.69	0.26	5.95
III	-0.028[9]	4.66 ± 0.04	4.64	27.70	3.75
	-0.320[10]		5.47		
IV	0.42*	3.38 ± 0.04	—	0.80	5.36
V	0.153*	4.14 ± 0.03	—	4.32	4.62
VI	0.70[11]	2.52 ± 0.04	2.60	2.88	4.79
VII	—	3.72 ± 0.03	—	46.82	3.46

* according to Biggs – Robinson[8].

---

[7] W. C. J. Ross, *J. Chem. Soc.*, **1949**, 183.

[8] A. J. Biggs and R. A. Robinson, *J. Chem. Soc.*, **1961**, 388.

[9] H. H. Jaffé, *Chem. Rev.*, **53**, 191 (1953).

[10] D. H., Mc. Daniel and H. C. Brown, *J. Org. Chem.*, **23**, 1420 (1958).

[11] I. A. Jdanov, "Korelatzionni analiz v organitcheskoy khimii", Izdatelstvo Rostovskovo Universiteta, Rostov, 1966.

As expected, an exaltation of the hydrolysis rate was noted in the case of the *ortho*-substituted diphenylether derivative VII, which can be accounted for by a steric inhibition of resonance.[4]

According to Biggs and Robinson equation[8] ($pK_a = 4.57 - 2.81\ \Sigma\sigma_i$), one can calculate for the substituent C_6H_5S-the following pair of values

$$\sigma_m = 0.153\ ; \qquad \sigma_p = 0.42$$

It is also noteworthy that for the substituent C_6H_5-O-, only the value $\sigma_m = -0.028$[9] is in good agreement with our experimental data.

SPECTRAL DATA

1. *Ultraviolet* UV spectra of the new nitrogen mustards in ethanolic solution are presented in figs. 3 and 4.

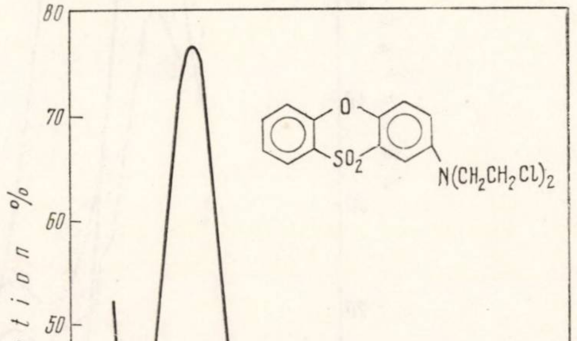

Fig. 3. — U. V. spectra of phenoxathiin — S, S — dioxide nitrogen mustard.

It is well known that in Ph-X-Ph type compounds (X = O, S), the molecule has a nonplanar steric arrangement, without interaction between the benzene rings, resulting in a similarity of spectra between Ph-X-Ph and Ph-X-Alk types of compounds.[12] The difference between O- and S-derivatives consists in the effects of the substituents on the UV-spectra.

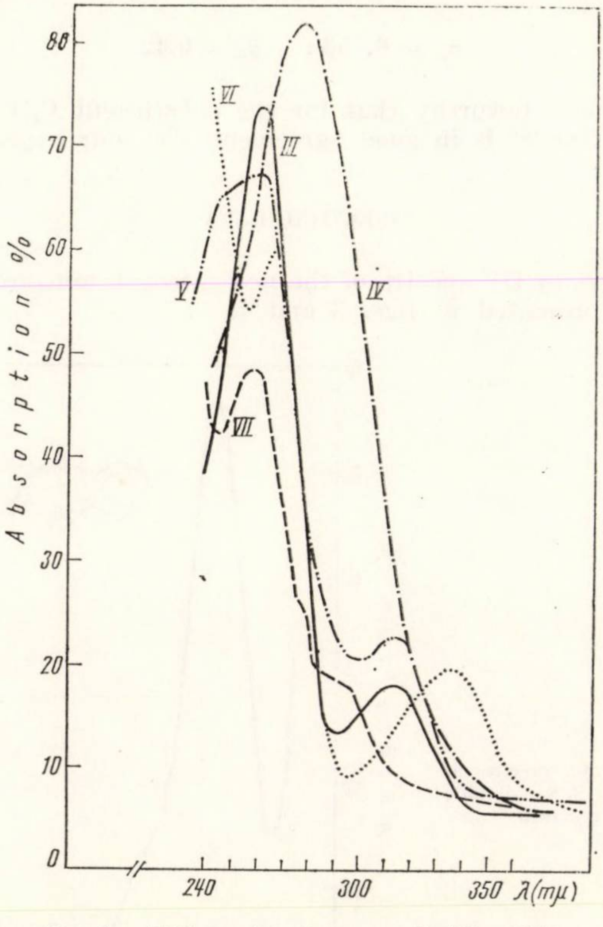

Fig. 4. — U.V. spectra of compounds IIIc—VIIc.

In the spectra of *o*- and *p*-amino-substituted aromatic ethers both B and K bands show definite bathochromic shifts, which increase in the case of N,N-bis-2(chloroethyl) derivatives (see table 2).

Due to the strong + M effect of the sulphur atom, the effect of an amino substituent on the UV spectra of diphenylsulphide is negligible,

---

[12] A. I. Kiss and B. R. Muth, *Acta Chim. Acad. Sci. Hung.*, **24**, 231 (1[illegible]

Table 2

Ultraviolet spectra [a]

Compound	λ_{max}, mμ (log)	
	B band	K band
I, $R = H^{13,14}$	295	238
Ia	298	240
II, $R = \cdot H^{14}$	295	—
IIa	288 320 290	250
IIc	352 (3.74)	270(4.45)
III, $R=H^{12}$	271	224
IIIa	295	241
IIIc	314 (3.51)	262 (4.34)
IV, $R=H^{15}$	275	250
IVa[15,16]	?	254
IVc	?	278 (4.42)
V, $R=H^{15}$	275	250
Va	274	250
Vc	316 (3.65)	260 (4.28)
VI, $R=H^{15}$	266	235
VIa[16]	312	—
VIc	337 (3.55)	270 (4.16)
VII, $R=H^{12}$	271	224
VIIa	277	—
VIIc	290(3.47)	259 (3.97)

a) EtOH solution.

but in the spectra of the corresponding nitrogen mustards the shifts of the bands are important.

In the spectra of the diphenylsulphone derivatives, which are also nonplanar, but where an interaction between the benzene rings through a 3d orbital of the sulphur atom takes place, the influence of the substituents is much more pronounced.[13]

The 2-amino group has practically no effect on the UV spectra of phenoxanthiin, just as in diphenylsulfide.

In S,S-dioxide-derivatives II, the shift of the bands produced by the donor substituents are important, as in the diphenylsulfone series.

2. *Infrared spectra* (table 3) were used for structure assignments and to follow the course of some reactions (for instance, the disappearance of ν_{OH} band during the final chlorination).

The hydroxyethylation of amines Va and VIa by the standard procedure gave final products exhibiting medium absorptions at about 1740 cm^{-1} (esters). Without structural assignment the reaction products were subjected to a HCe hydrolysis which led to the disappearance of the above mentioned band and to the isolation of the desired hydroxyethyl-derivatives.

---

[13] H. J. Skine and R. J. Small, *J. Org. Chem.*, **30**, 2140 (1965).

[14] N. Marziano, *Ricerca sci.*, **31**, 87 (1961).

[15] H. H. Jaffé and M. Orchin, "Theory and Applications of Ultraviolet Spectroscopy", John Wiley & Sons, New York, 1962.

[16] A. Manzihi, *Gazz. chim. Ital.*, **84**, 73 (1954).

The O—H stretching vibration bands in the di-hydroxyethyl-derivatives were found both in the intermolecular ($\sim$ 3250 cm^{-1}) and in the intramolecular (3400—3470 cm^{-1}) selfassociation ranges, in solid state as well as in solution.

As already reported for other nitrogen mustards studied in our laboratory,[17] both P_H and P_X bands were observed for the *trans* and *gauche* C-Cl conformers[18] (see table 6).

Assignment of the controversial C—S band in aromatic sulfides was based on recent studies[19] which consider this band a so-called X-sensitive mode of the ring.

The aromatic ether linkages were identified by means of the asymmetrical stretching vibration.[20]

The alkylation of the aminic N atom led to the well-known shift of the C—N stretching frequency.[21]

BIOLOGICAL DATA

Tests were carried out on rats bearing Walker carcinosarcoma, by daily inoculation of doses within 0.2—0.3 LD_{50}, for a period of 14 days. Treatment began 7 days after tumour transplantation. Testing data are listed in table 4.

EXPERIMENTAL

Infrared spectra were run on a UR 10 Carl Zeiss-Jena spectrophotometer in KBr disks, CCl_4 and $CHCl_3$ solutions.

Ultraviolet determinations were carried out with a CF4 Optica Milano spectrophotometer.

The pK_a values were determined by ultraviolet spectroscopy. The amines were of chromatographical purity and were characterized by their melting points : Ia — 94—5$^{\circ5}$; IIa —

---

[17] F. Chiraleu, *Rev. Roumaine Chim.*, **11**, 999 (1966).

[18] S. Mizushima, T. Shimanouchi, N. Nakamura, M. Hayadshi and S. Tsuchiya, *J. Chem. Phys.*, **26**, 970 (1957).

[19] M. Goldstein, M. A. Russell and H. A. Willis, *Spectrochim. Acta*, **25** A, 1275 (1969).

[20] L. J. Bellamy, "The Infrared Spectra of Complex Molecules", Methuen and Co., ondon, 1960.

[21] C. N. R. Rao, "Chemical Applications of Infrared Spectroscopy", Academic Press, New York, 1963.

Table 3

Infrared spectra[a]

Compound	$\nu_{as}C-S$	$\nu_{s}SO_2$	$\nu_{as}SO_2$	$\nu_{as}C-O$ ether	$\nu C-NR_2$	$\delta N-H$
Ia	1076[b]	—	—	1214	—	1616
Ib	1075	—	—	1222	1359	—
Ic	1077	—	—	1235	1359	—
IIa	1080[c]	1171	1301	1238	—	
IIb	1080	1155	1306	1230	1360	—
IIc[d]	1082	1170				
		1153	1301[e]	1237[f]	1360[g]	—
		1170				
IIIa	—	—	—	1231	—	1632
IIIb	—	—	—	1242	1374	—
IIIc[h]	—	—	—	1243	1358	—
IVa	1082[i]	—	—	—	—	1621
IVb	1074	—	—	—	1359	—
	1099?					
IVc	1080	—	—	—	1355	—
	1103?					
Va[d]	1079	—	—	—	—	1620
Vb[h]	1082	—	—	—	1355	—
	1102					
Vc	1084	—	—	—	1357	
	1105?					
VIa	1099	1155	1303	—	—	1626
VIb	1082	1150	1305	—	1361	—
	1106	1174	1315			
VIc	1105	1154	1305	—	1362	—
	1077					
VIIa	—	—	—	1218	—	1619
VIIc[h]	—	—	—	1230	1367	—

[a] KBr disks, except where otherwise noted. All frequencies in cm^{-1}; [b] lit. 1076 cm^{-1},[22]; [c] lit. 1079 cm^{-1},[22]; [d] $CHCl_3$ soln; [e] in KBr disk: 1335, 1284, 1274 cm^{-1}; [f] 1235 cm^{-1} (KBr); [g] 1372 cm^{-1} (KBr); [h] CCl_4 soln; [i] lit. 1083 cm^{-1},[23].

Table 4

Biological activity

Compound	LD_{50} mg/kg	Daily dose mg/kg	% Inhibition Walker carcinosarcoma
Ic	300	100	29*
IIc	—	—	—
IIIc	500	100	22
IVc	—	—	—
Vc	210	40	0
VIc	500	—	38
VIIc	500	100	16
		300	21

* Jensen sarcoma.

---

[22] H. Mantsch and O. Maior, *Rev. Roumaine Chim.*, **10**, 1245 (1965).

[23] N. Marciano, G. Montaudo and R. Passerini. *Ann. Chim. (Ital.)*, **52**, 121 (1962).

– 167–8°[6]; IIIa – 85°[24]; IV – 96°[25,26]; Va.H_2SO_4 – 187–9° (*Calcd.* N = 4.68 %; *Found* N = 4.76 %) [25,26]; VI[a] – 114°; VIIa – 46°.

Hydrolysis rates were determined by potentiometric titration with $AgNO_3$ of the Cl^- ions, after refluxing for 30 minutes in water : acetone 1 : 1.[7] Rate constants k_{66} were calculated assuming a monomolecular kinetics.

The relationship between hydrolysis rates of the nitrogen mustards and basicity of the precursor amines is presented in fig. 5.

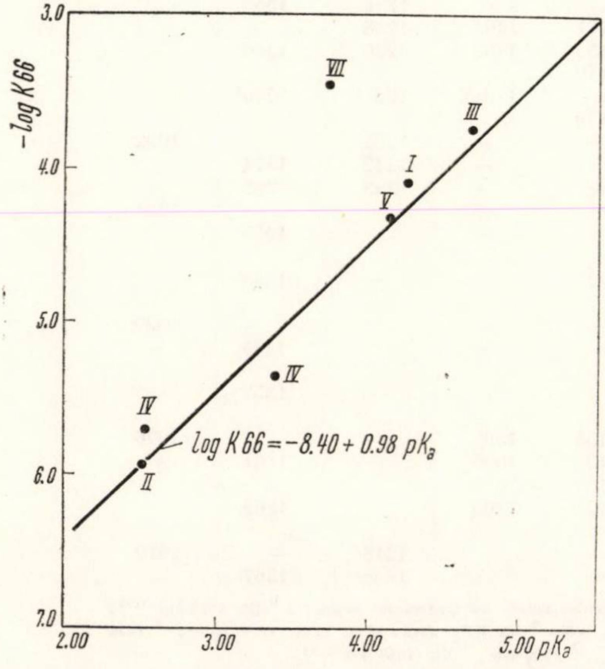

Fig. 5. – Relationship between amines basicity and hydrolysis rate of the nitrogen mustards.

2-/*N*,*N*-*bis* (2-*hydroxyethyl*)*amino*/-*phenoxathiin* (Ib). To a cooled (5°) and stirred solution of 2.2g (0.01 mole) of Ia in 30 ml of glacial acetic acid, was added 1.5 ml (0.2 mole) of ethylene oxide. The reaction mixture was allowed to stand for 2 days at room tempera-

Table 5

N,N-Bis (2-hydroxyethyl) derivatives

Compound	Formula	m.p. °C	%N Calcd.	%N Found	Yield %	Recrystallyzed solvent
Ib	$C_{16}H_{17}NSO_3$	126–128	4.62	4.53	91	MeOH :H_2O 1 :1
IIb	$C_{16}H_{17}NSO_5$	oil	4.18	4.12	83	—
IIIb	$C_{16}H_{19}NO_3$	127–129	5.13	5.09	—	MeOH : H_2O 3 :1
IVb	$C_{16}H_{19}NO_2S$	100–102	4.84	4.81	—	toluene
Vb	$C_{16}H_{19}NO_2S$	oil	4.84	4.73	—	—
VIb	$C_{16}H_{19}NO_4S$	85	4.36	4.43	—	C_6H_6 :$CHCl_3$
VIIb	$C_{16}H_{19}NO_3$	oil	5.13	5.13	—	—

---

[24] C. M. Suter, *J. Amer. Chem. Soc.*, **51**, 2583 (1929).

[25] C. M. Suter, *Ber. dtsch. chem. Ges.* **39**, 3597 (1906).

[26] R. Adams, W. Reifschneider and M. D. Noir, *Croat, Chim. Acta*, **29**, 277 (1957).

Table 6

New aromatic nitrogen mustards

Compound	m.p. °C	Recrystallized solvent	Element analysis								Yield %	IR* spectra	
			Calculated				*Found*					νc-ce, cm^{-1}	
			C	H	N	Cl	C	H	N	Cl		*trans*	*gauche*
Ic	92–94	C_6H_6 : petroleum ether	56.47	4.71	4.11	20.90	56.60	4.49	3.93	21.33	—	732	653
IIc	142–4	C_6H_6 : petroleum ether	51.61	4.03	3.76	19.09	51.86	4.25	3.77	19.45	22	744	654
IIIc	40	petroleum ether	61.93	5.48	4.51	22.90	62.00	5.61	4.52	22.61	50	739	669
IVc	50–2	petroleum ether	58.85	5.21	4.28	21.74	58.50	5.70	4.13	21.40	48	750**	663**
Vc	oil	—	58.89	5.21	4.29	21.74	54.26	5.64	4.25	21.37	43	738**	666**
Vc.HCl	80	EtOH(HCl)	—	—	3.89	—	—	—	3.74	—			
VIc	85	C_6H_6 $CHCl_3$	53.63	4.74	3.91	19.83	53.05	5.00	4.00	19.42	50	733	659
VIIc	oil	—	61.93	5.48	4.57	22.90	61.93	5.60	4.32	22.41	50	—	—

* KBr disks.
** CS_2 solution.

ture. The solvent was distilled under reduced pressure and the traces of solvent were removed by codistillation with 50 ml of benzene. Recrystallization from ethanol : water 1 : 1 afforded 2.8 g (91 %) of analytically pure Ib (see table 5).

The other hydroxyethyl derivatives listed in table 5 were similarly prepared.

2-/N,N-bis (2-chlorethyl)amino/phenoxathiin (Ic). 5.1 g (0.02 mole) of Ib were solved under stirring in 80 ml of $POCl_3$ freshly distilled and cooled at 0°. After heating for 0.5 hr on steam bath, excess $POCl_3$ was removed *in vacuo* and the oily residue was poured on crushed ice. The gum thus formed was extracted with benzene-ethyl acetate 1 :1, the extract was dried over anhydrous $MgSO_4$, treated with charcoal and evaporated under reduced pressure. Recrystallization of the crude product from benzene : petroleum ether (b. p. 60—90°) gave Ic of analytical purity.

Similarly were prepared compounds IIc—VIIc (see table 6).

Acknowledgement. The authors wish to thank Dr. V. Dobre for kindly marking the screening data available to us, Mrs. E. Tărnăuceanu and G. Botez for performing analytical and spectroscopic measurements.

Revue Roumaine de Chimie, **18**, *9*, 1627–1635 (1973)

PEPTIDES. XIV[1]

THE SYNTHESIS OF SEVERAL PEPTIDE SEQUENCES RELATED TO THE Glu^5 – AND Asn^5-ELEDOISINS

E. VARGHA,* A. BALOG,** F. GÖNCZY,** D. BREAZU** and LUCIA BEU**

* Department of Organic Chemistry, Babeş-Bolyai University, str. Arany János 11, Cluj, Romania

** Institute for Chemical and Pharmaceutical Research, str. Fabricii 126, Cluj, Romania

Received January 31, 1973

Using the AE, CP and BA* residues as amino protecting groups, and applying mixed anhydride techniques for the process of coupling, some dipeptides related to the 5–11 sequences and tripeptides related to the 5–9 sequences of eledoisins were obtained. The pentapeptide related to the 5–9 sequences of the Asn^5-eledoisins was synthetized according to the stepwise elongation method and starting from methyl glycinate as the C-terminal amino acid.

The eledoisin, an endecapeptide amide, isolated by Erspamer and Anastasi[2] from the salivary glands of *Eledone moschata* and *Aldrovandi*, possesses powerful vasodilator and hypotensive properties.[3] For this hormone the following amino acid sequence was determined by the same authors[2] and confirmed at the same time by its first synthesis by Sandrin and Boissonnas[4]:

$$\begin{array}{l}\ulcorner\!\!\rule{0pt}{0pt}\text{—Glu-Pro-Ser-Lys-Asp-Ala-Phe-Ile-Gly-Leu-Met-NH}_2\\ \quad\;\;1\quad\;\; 2\quad\;\; 3\quad\;\; 4\quad\;\; 5\quad\;\; 6\quad\;\; 7\quad\;\; 8\quad\;\; 9\quad\; 10\quad 11\end{array}$$

A considerable number of eledoisin analogs have been prepared in order to study the relationship between structure and activity of this hormone.[5-11] Thus, it was shown that the Asp^5 residue could be replaced by the asparaginyl, or glutamyl residue without considerable modification of the biological activity.

---

[1] Previous paper: E. Vargha, F. Gönczy and A. Balog, *Stud. Univ. Babeş-Bolyai, Chem.*, **17**, 125 (1972).

* The abbreviations for amino acids and their substituents are those recommended by the IUPAC-IUB Commission on Biochemical Nomenclature, published in *J. Biol. Chem.*, **247**, 977 (1972).

The other abbreviations used in this paper are: AE=1-ethoxycarbonyl-propen-2-yl; CP=2-ethoxycarbonyl-cyclopenten-1-yl; BA=1-benzoylpropen-2-yl. PAc=phenacyl (CH$_2$–CO–Ph). AcOH=acetic acid, AcOEt=ethyl acetate, DCHA=dicyclohexylamine, DMF=dimethylformamide, EtOH=ethanol, Et$_2$O=ethyl ether, MeOH=methanol, TEA=triethylamine, THF=tetrahydrofuran.

[2] V. Erspamer and A. Anastasi, *Experientia*, **18**, 58 (1962).

[3] V. Erspamer and G. F. Erspamer, *Brit. J. Pharmacol. Chemotherapy*, **19**, 337 (1962); *Chem. Abstr.*, **57**, 17323 (1962).

[4] E. Sandrin and R. A. Boissonnas, *Experientia*, **18**, 59 (1962).

The different methods reported for the synthesis of eledoisin and its analogues are based on the fragment condensation.[6a] These syntheses were performed according to the azide,[4] dicyclohexylcarbodiimide[8] or activated ester [10] methods.

According to the excellent results obtained by us for the protection of the α-amino group with β-dicarbonyl compounds, we have investigated the synthesis of several dipeptides and tripeptides related to the partial 5−11** and 5−9 sequences of the Asp^5- and Glu(OBzl)^5-eledoisin.

The protection of the α-amino group was performed with ethyl acetoacetate, 2-ethoxycarbonyl cyclopentanone or benzoylacetone according to the usual method.[12] The N-protected amino acids were preferentially isolated as dicyclohexylammonium salts, which were fairly soluble in organic solvents used for peptide syntheses.

For the activation of the carboxyl group the mixed anhydride method was used. The mixed anhydrides were prepared from the N-protected amino acid salts with ethyl chloroformate, trimethylacetyl (pivaloyl) chloride or benzoyl chloride. The precipitated dicyclohexylammonium hydrochloride had to be removed by filtration before adding the amino acid (or peptide) ester hydrochloride or hydrobromide.

The removal of the N-protecting β-dicarbonyl (AE and CP*) residues* occurred in very mild conditions, at room temperature, by acidification to pH 2−1.5, carried out in adequate medium (acetone, ethanol, methanol or ethyl acetate) with hydrochloric acid in ethanol, or hydrobromic acid in water or anhydrous acetic acid. Most of the peptide ester hydrochlorides or hydrobromides crystallized in good yields. Some of these compounds, already reported in the literature, are in good agreement with the similar ones obtained by us.

---

[5] E. Sandrin and R. A. Boissonnas, *Helv. Chim. Acta*, **47**, 1294 (1964).

[6] *a*. E. Schröder and K. Lübke , *Experientia*, **20**, 19 (1964); *b*. E. Schröder and K. Lübke, ,,The Peptides", Academic Press, NewYork and London, 1966.

[7] L. Bernardi, G. Bosisio, F. Chillemi, G. De Caro, R. De Castiglione, V. Erspamer, A. Glaesser and O. Goffredo, *Experientia*, **20**, 306 (1964).

[8] K. Lübke, E. Schröder, R. Schmiechen and H. Gibian, *Liebigs Ann. Chem.*, **679**, 195 (1964).

[9] F. Chillemi, *Gazz. chim. Ital.*, **93**, 1079 (1963); F. Chillemi, *Società Farm. Italia*, Fr. Pat. 1337576 (1963).

[10] S. Bajusz., *Acta Chim. Acad. Sci. Hung.*, **42**, 383 (1964).

** In the course of the preparation of our work W. Voelter, K. Zech and G. Jung published in *Tetrahedron*, **28**, 2649 (1972) a solid phase synthesis of natural sequence 5−11 of eledoisin.

[11] F. Cuiban, V. Badea and S. Cilianu in "Peptides 1968" North-Holland Publ. Comp., Amsterdam, 1968, p. 256.

[12] a. A. Balog, D. Breazu, E. Vargha, F. Gönczy and L. Beu, *Rev. Roumaine Chim.* **15**, 1375 (1970); *b*. A. Balog, E. Vargha, D. Breazu, L. Beu and F. Gönczy, *Rev. Roumaine Chim.*, **15**, 1391 (1970).

The symbols for the dipeptide and tripeptide derivatives we have obtained, are listed as follows:

DIPEPTIDE DERIVATIVES

10 11
1.1 AE-Leu-Met-NH$_2$
1.2 $^{+}$H$_2$-Leu-Met-NH$_2$.Cl^{-}
1.3 H-Leu-Met-NH$_2$
1.4 AE-D-Leu-D-Met-NH$_2$
1.5 $^{+}$H$_2$-D-Leu-D-Met-NH$_2$.Cl^{-}

9 10
2.1 AE-Gly-Leu-OPAc

8 9
3.1 AE-Ile-Gly-OMe
3.2 $^{+}$H$_2$-Ile-Gly-OMe.Cl^{-}
3.3 BA-Ile-Gly-OMe
3.4 AE-Ile-Gly-OEt
3.5 $^{+}$H$_2$-Ile-Gly-OEt.Cl^{-}
3.6 AE-Ile-Gly-OPAc

7 8
4.1 AE-Phe-Ile-OPAc
4.2. $^{+}$H$_2$-Phe-Ile-OPA.Br^{-}

6 7
5.1 AE-Ala-Phe-OMe
5.2a $^{+}$H$_2$-Ala-Phe-OMe.Cl^{-}
5.2b $^{+}$H$_2$-Ala-Phe-OMe.Br^{-}
5.3 AE-Ala-Phe-OPAc
5.4 $^{+}$H$_2$-Ala-Phe-OPAc.Cl^{-}

5 6
6.1 AE-Asn-Ala-OPAc
6.2 AE-Glu(OBzl)-Ala-OMe
6.3 AE-Glu(OBzl)-Ala-OPAc
6.4 $^{+}$H$_2$-Glu(OBzl)-Ala-OPAc.Cl^{-}

TRIPEPTIDE DERIVATIVES

7 8 9
7.1 AE-Phe-Ile-Gly-OMe
7.2 $^{+}$H$_2$-Phe-Ile-Gly-OMe.Cl^{-}
8.1 AE-Ala-Phe-Ile-OPAc
8.2 $^{+}$H$_2$-Ala-Phe-Ile-OPAc.Cl^{-}

5 6 7
9.1 AE-Glu(OBzl)-Ala-Phe-OPAc
9.2 $^{+}$H$_2$-Glu(OBzl)-Ala-Phe-OPAc.Br^{-}
9.3 AE-Gln-Ala-Phe-OPAc
9.4 CP-Gln-Ala-Phe-OPAc

Employing the stepwise approach and performing all the whole coupling cycle by the mixed anhydride method, the pentapeptide related to the 5–9 sequences of Asn^5-eledoisin, was prepared according to the scheme:

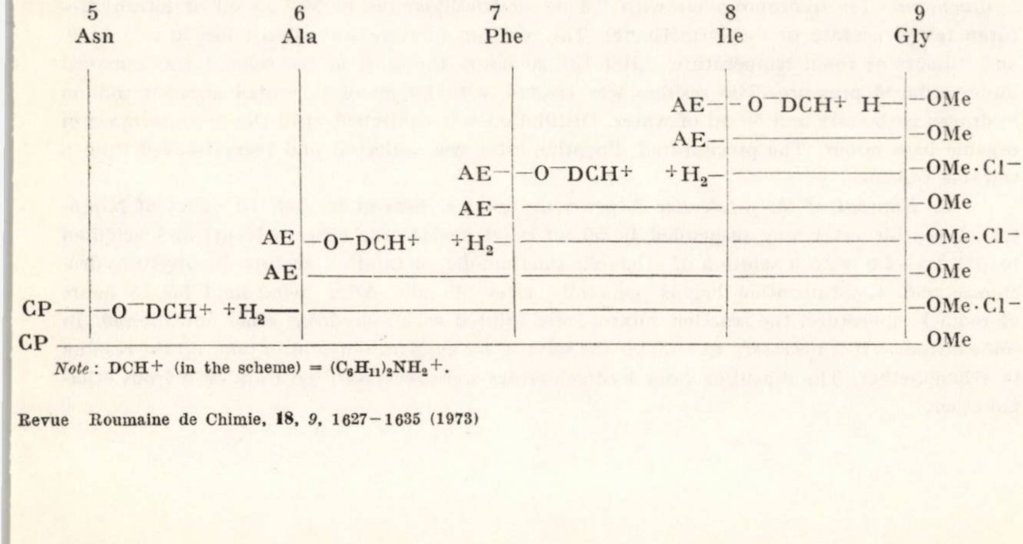

Note: DCH^{+} (in the scheme) = (C$_6$H$_{11}$)$_2$NH$_2$$^{+}$.

We remark the high yields of the 6—9 tetrapeptide (83%) and those of the 5—9 pentapeptide (80%). We hope that the use of β-dicarbonyl compounds for N-protection of amino acids opens by all means a new and promising perspective in the peptide synthesis. Thus, the Asn^5-, Gln^5- and Glu(OBzl)^5-pentapeptides related to the 5—9 sequences of eledoisin analogs, were synthesized by isolating only the ester hydrochlorides of the intermediate peptides. The results of these investigations will be published later.

EXPERIMENTAL

Melting points were taken in capillary tubes and are not corrected. Samples for analysis were dried for 3—4 hours at 64° and 16—20 Torr over phosphorous pentoxide. Optical rotations were measured on a polarimeter type Metra 400/a Praha in a 2 dm tube at 20—26° except otherwise stated.

A. *Protection of the amino acids with β-dicarbonyl compounds. General method.* A mixture of 20 mmol of amino acid, 20—25 mmol of β-ketoester or β-diketone and 20 mmol (4 ml) of dicyclohexylamine in 50 ml of methanol was heated under reflux till an almost clear solution resulted. The unreacted amino acid was eliminated by filtration and the solution was evaporated to dryness under reduced pressure. Dry benzene (2 × 25 ml) was added to the residue and the distillation repeated twice.

Dicyclohexylammonium salts of benzoylacetone N-protected amino acids (BA-derivatives) were purified by recrystallization from ethyl acetate — petroleum ether; those obtained with ethyl acetoacetate (AE-amino acid salts) or with 2-ethoxycarbonyl-cyclopentanone (CP-amino acid salts) by dissolving in anhydrous ether, filtering off and allowing the solvent to evaporate.

B. *Peptide bond formation through the mixed anhydride procedure. General method.* A solution of 20 mmol of dicyclohexylammonium salt of the N-protected amino acid in 100 ml of tetrahydrofuran or anhydrous ethyl acetate was treated below —10° with 20 mmol of ethyl chloroformate (pivaloyl chloride or benzoyl chloride) and 1—2 drops of N-methylmorpholine was added. After 15 min stirring the separated dicyclohexylamine hydrochloride was collected and washed with tetrahydrofuran (or with ethyl acetate) and anhydrous ether. The collected filtrates were treated with the amino acid ester, set free from 20 mmol of ester hydrochloride (or hydrobromide) with 2.8 ml of triethylamine in 50—60 ml of tetrahydrofuran (ethyl acetate or dichlormethane). The reaction mixture was stirred for 30 min at 0° and 3 hours at room temperature. After 12—20 hours the most of the solvent was removed under reduced pressure. The residue was treated with 50 ml of saturated aqueous sodium hydrogen carbonate and 50 ml of water. Distillation was continued until the disappearance of organic base odour. The precipitated dipeptide ester was collected and recrystallized from a suitable solvent.

C. *Removal of the β-ketoester N-protecting groups. General method.* 10 mmol of N-protected peptide ester was suspended in 50 ml ethyl acetate (or other solvent) and acidified to pH 1.5—2.0 with a solution of ethanolic (methanolic, or in ethyl acetate dissolved) hydrochloric acid. Crystallization begins generally after 30 min. After being kept for 12 hours at room temperature, the reaction mixture was diluted with anhydrous ether and filtered. In some instances it is necessary to remove the solvent by evaporation and to take up the residue in ethanol-ether. The dipeptide ester hydrochlorides were recrystallized from anhydrous ethanol-ether.

The removal of the protective groups (AE, CP) can be performed in the same conditions with a solution of hydrobromic acid in water (63 %) or in acetic acid (25–30 %), peptide ester hydrobromides being isolated in this manner.

DIPEPTIDES

1.1. *N-(1-Ethoxycarbonyl-propen-2-yl)-L-leucyl-L-methionine amide* (*AE-Leu-Met-NH$_2$*). A mixed anhydride was prepared from AE-Leu-O$^-$ DCHA $\cdot$H$^+$[12a] (25.4 g, 60 mmol) and ethyl chloroformate (6 ml, 60 mmol) in 200 ml of ethyl acetate at −5 −0° by adding 1–2 drops of N-methyl morpholine. The separated dicyclohexyl amine hydrochloride was eliminated by filtration and to the filtrate a solution of L-methionine methyl ester (10 g, 62 mmol) in 10 ml ethyl acetate was added. The reaction mixture was allowed to stand overnight at room temperature, treated with saturated aqueous sodium hydrogen carbonate (30 ml) and evaporated *in vacuo*. The residue was extracted with 3 × 50 ml of ethyl acetate and washed with water. After drying over anhydrous sodium sulphate, the solution was concentrated *in vacuo* to yield 22.5 g (96.5 %) of AE-Leu-Met-OMe as a yellow oil. The protected dipeptide ester was dissolved in 100 ml of anhydrous methanol and saturated at −10° with ammonia, sealed and kept for four days at room temperature. The reaction-mixture was refluxed for a short time to remove the excess of ammonia and evaporated to dryness. The residue recrystallized from ethanol afforded 11 g (49 %) of white solid ; m.p. 164–165° ; $[\alpha]_D$ +144 ·9° (c = 1, DMF).
$C_{17}H_{31}N_3O_4S$ (373.5) *Calcd.*, C, 54.66 ; H, 8.36 ; N, 11.26
Found, C, 55.00 ; H, 8.67 ; N, 11.00

1.2. *L-Leucyl-L-methionine amide, hydrochloride.* A suspension of 6.2 g (16.5 mmol) of AE-Leu-Met-NH$_2$ in 100 ml of ethyl acetate was acidified to pH 1.5–2.0 with a solution of hydrochloric acid in ethyl acetate (16 %). After 15 minutes, the crystals were filtered, washed with ethyl acetate, ether and dried *in vacuo* to yield 4.5 g (92%) hydrochloride ; m.p. 181–184° (marked sintering at 88°). After recrystallization from methanol-ether yielded 2.75 g pure dipeptide amide hydrochloride, m.p. 182–186°, $[\alpha]_D$+ 7.3° (c = 2, water)[10] ; according to Lübke[8] the product crystallized from methanol-ether with 1 mol methanol, m.p. 126–127°, $[\alpha]_D$ + 10.2° (c = 1, water).

1.3. *L-Leucyl-L-methionine amide.* This compound was obtained as described by Bentley and co-workers[13] from the previous ester hydrochloride **1.2** in 68 % yield, m.p. 130–131°, $[\alpha]_D$ −6.1° (c = 2, DMF). Lit.[13] m.p. 130–131°, $[\alpha]_D$ −6.3° (c = 2, DMF).

1.4. *N-(1-Ethoxycarbonyl-propen-2-yl)-D-leucyl-D-methionine amide* (*AE-D-Leu-D-Met-NH$_2$*). This compound was obtained in the same way as described above for the corresponding L–L isomeric derivative **1.1** from 12.7 g (30 mmol) of AE-D-Leu-O$^-$ DCHA.H$^+$, 3.6 g (30 mmol) pivaloyl chloride and 5 g (31 mmol) D-methionine methyl ester. Yield 5 g (45 %) ; m.p. 162–163° (from EtOH) ; $[\alpha]_D$ −121° (c = 1, DMF).
$C_{17}H_{31}N_3O_4$ S (373.5) *Calcd.*, C, 54.66 ; H, 8.37 ; N, 11.25
Found, C, 54.35 ; H, 8.76 ; N, 11.19

1.5. *D-Leucyl-D-methionine amide hydrochloride.* 1 g of AE-D-Leu-D-Met-NH$_2$ was dissolved in 100 ml of ethyl acetate and acidified with a solution of hydrochloric acid in ethyl acetate (16 %). After stirring for two hours at 0°, the oily product crystallized and it was filtered to yield 0.51 g (64 %) of hygroscopic crystalls, m.p. 180–185° (sintering at 90°).

---

[13] P. H. Bentley, H. Gregory, A. H. Laird and J. S. Morley, *J. Chem. Soc.*, **1964**, 130.

1.6. *D-Leucyl-D-methionine amide.* Prepared as the L-L isomer **1.3** with 63% yield, m.p. 130—131° (AcOEt); $[\alpha]_D^{28}$ + 6.3 (c = 0.6, DMF).

2.1. *N-(1-Ethoxycarbonyl-propen-2-yl)-glycyl-L-leucine phenacyl ester (AE-Gly-Leu-OPAc).* A mixed anhydride was prepared from 2.6 g (12 mmol) of AE-Gly-O^-K^+[12a] and 1.2 ml (12 mmol) of ethyl chloroformate in 50 ml of tetrahydrofuran by adding one drop of N-methyl morpholine. After stirring for 30 min, it was treated with H-Leu-OPAc, set free from 3.45 g (12 mmol) of hydrobromide with 1.6 ml of triethylamine in 35 ml of tetrahydrofuran. The reaction mixture was worked up in the usual manner to yield 4.5 g (95%) dipeptide ester. Recrystallization from benzene-petroleum ether gave 3 g (62%) of pure product, m.p. 118—119°; $[\alpha]_D$ —82.8° (c = 1, MeOH).

$C_{22}H_{30}N_2O_6$ (418.5) *Calcd.*, C, 63.14; H, 7.22; N 6.70
Found, C, 62.92; H, 7.60; N 6.80

3.1. *N-(1-Ethoxycarbonyl-propen-2-yl)-L-isoleucylglycine methyl ester (AE-Ile-Gly-OMe).* Prepared from 30 mmol of AE-Ile-O^-DCHA $\cdot H^+$ and freshly distilled glycine methyl ester according to the ethoxycarbonyl mixed anhydride method in a 71% yield, m.p. 115—116° (from AcOEt-petroleum ether); $[\alpha]_D$ +165° (c = 1, MeOH). Lit.[1] m.p. 117—118°.

3.2. *L-Isoleucylglycine methylester hydrochloride* obtained from 6 g (19 mmol) of AE-Ile-Gly-OMe by removal of the N-protecting group according to the Method C in ethyl acetate solution. Yiel 2.7 g (75%); m.p. 181—182°; $[\alpha]_D$ +17.5° (c = 1, AcOH). Lit.[8] m.p. 181—182°; $[\alpha]_D$ +16.3° (c = 1, AcOH).

3.3. *N-(1-Benzoyl-propen-2-yl)-L-isoleucylglycine methyl ester (BA-Ile-Gly-OMe).* Prepared according to the general method B from 13.7 g (30 mmol) of Ba-Ile-O^-DCHA $\cdot H^+$[12a] and 30 mmol of ethyl chloroformate in tetrahydrofuran. Yield 9.2 g (88%). Recrystallization from 2-propanol gave 4.3 g, m.p. 160—160.5°; $[\alpha]_D$ +242.4° (c = 1, MeOH).

$C_{19}H_{26}N_2O_4$ (346.4) *Calcd.*, C, 65.88; H, 7.56; N, 8.09
Found, C, 65.60; H, 7.69; N, 7.98

This product cannot be deprotected at pH 1.5—2.0.

3.4. *N-(1-Ethoxycarbonyl-propen-2-yl)-L-isoleucylglycine ethyl ester (AE-Ile-Gly-OEt).* Obtained according to the Method B through the ethoxycarbonyl mixed anhydride in a 84% yeield, m.p. 109—111° (AcOEt-petroleum ether); $[\alpha]_D$ +159.9° (c = 1, MeOH).

$C_{16}H_{28}N_2O_5$ (328.4) *Calcd.*, C, 58.52; H, 8.60; N, 8.59
Found, C, 59.22; H, 9.07; N, 8.50

3.5. *L-Isoleucylglycine ethyl ester hydrochloride.* The N-protecting group of the dipeptide ester **3.4** was removed according to the Method C.M.p. 136—137° ($EtOH—Et_2O$, 1 : 5); $[\alpha]_D$ +12.9° (c = 1, EtOH). Lit.[14] m.p. 136—137°; $[\alpha]_D$ +13.9° (in EtOH).

3.6. *N-(1-Ethoxycarbonyl-propen-2-yl)-L-isoleucylglycine phenacyl ester (AE-Ile-Gly-OPAc).* Prepared according to the Method B from 10 mmol of AE-Ile-O^-DCHA $\cdot H^+$[12a] through the ethoxycarbonyl mixed anhydride, with $^+H_2$-Gly-OPAc.Cl^-[12]. Almost theoretical yield; m.p. 108—110° (AcOEt-petroleum ether); $[\alpha]_D$ +145° (c = 1, MeOH).

$C_{22}H_{30}N_2O_6$ (418.5) *Calcd.*, N, 6.69; *Found*, N, 6.49

4.1. *N-(1-Ethoxycarbonyl-propen-2-yl)-L-phenylalanyl-L-isoleucine phenacyl ester (AE-Phe-Ile-OPAc).* Obtained according to the Method B from 5.5 g (12 mmol) of AE-Phe-O^-DCHA $\cdot H^+$ and 4 g (about 12 mmol) of $^+H_2$-Ile-OPAc $\cdot Br^-$[1]. After recrystallization from ethanol yielded 3.2 g (52%) pure product; m.p. 140—141°; $[\alpha]_D$—4.4° (c = 1, MeOH).

$C_{29}H_{36}N_2O_6$ (508.6) *Calcd.*, C, 68.48; H., 7.13; N, 5.54
Found, C, 68.97; H, 7.51; N, 5.57

4.2. *L-Phenylalanyl-L-isoleucine phenacyl ester hydrobromide.* 2.9 g (5.7 mmol) of AE-Phe-Ile-OPAc was suspended in 50 ml of anhydrous acetone and treated with 3 ml solution of hydrobromic acid (30%) in acetic acid. The solvent was allowed to evaporate at room temperature, the separated ester hydrobromide was collected and recrystallized from ethanol-ether to yield 2.2 g (81%); m.p. 135–137°; $[\alpha]_D -4°$ (c = 1, MeOH).

---

[14] I. R. GEIGY, Belg P., 630.332, oct. 21.1963; *Chem. Abstr.*, **60**, 14606b (1964).

$C_{25}H_{29}BrN_2O_4$ (477.4) *Calcd.*, C, 57.86; H, 6.12; N, 5.87; Br, 16.74
Found, C, 57.69; H, 6.65; N, 5.73; Br, 15.81

5.1. *N-(1-Ethoxycarbonyl-propen-2-yl)-L-alanyl-L-phenylalanine methyl ester (AE-Ala-Phe-OMe).* Obtained according to the general procedure B, from 7.7 g (20 mmol) of AE-Ala-O^- DCHA·H^+[11]; yield nearly 100%. M.p. 144–145.5° (EtOH); $[\alpha]_D +220.9°$ (c = 1, dioxan), +218° (c = 1, MeOH) respectively.

$C_{19}H_{26}N_2O_5$ (362.4) *Calcd.*, C, 62.97; H, 7.22; N, 7.73
Found, C, 63.30; H, 7.70; N, 7.83

5.2. *L-Alanyl-L-phenylalanine methyl ester.*

a. The *hydrochloride* was prepared according to the Method C from 1.6 g (4.5 mmol) of **5.1** and a solution of ethanolic hydrochloric acid (16%). Yield 1.1 g (65%); m.p. 170–172°; $[\alpha]_D +7.3°$ (c = 2, water), +14.3° (c = 1, MeOH) respectively. Lit. [15] m.p. 155–156°; $[\alpha]_D +4.2 \pm 0.5°$ (c = 2, water).

b. The *hydrobromide* was obtained according to the same Method C in 90% yield from **5.1** by adding a solution of hydrobromic acid in acetic acid, m.p. 148–149°; $[\alpha]_D +10.9°$ (c = 1, MeOH).

$C_{13}H_{19}BrN_2O_3$ (331.2) *Calcd.*, C, 47.14; H, 5.77; N, 8.46; Br, 24.13
Found, C, 47.30; H, 5.85; N, 8.39; Br, 23.00

5.3. *N-(1-Ethoxycarbonyl-propen-2-yl)-L-alanyl-L-phenylalanine phenacyl ester (AE-Ala-Phe-OPAc).* This dipeptide ester was obtained in almost quantitative yield from 3.3 mmol AE-Ala-O^-K^+[12a] and 3.3 mmol $^+H_2$-Phe-OPAc.Cl^-[12b] in tetrahydrofuran by the pivaloyl mixed anhydride Method B. M.p. 162–163.5° (EtOH); $[\alpha]_D -201°$ (c = 0.5, MeOH), –174° (c = 1.5, dioxan).

$C_{26}H_{30}N_2O_6$ (466.5) *Calcd.*, C, 66.98; H, 6.48; N 6.00
Found, C, 67.19; H, 6.98; N 5.96

5.4. *L-Alanyl-L-phenylalanine phenacyl ester hydrochloride.* The removal of the dipeptide ester N-protecting group was performed in 70% yield, according to the general way (Method C) M.p. 170–172° (MeOH–Et_2O); $[\alpha]_D -17.8°$ (c = 0.77, MeOH).

$C_{20}H_{23}ClN_2O_4$ (390.3) *Calcd.*, C, 61.45; H, 5.93; N, 7.17; Cl, 9.07
Found, C, 61.07; H, 6.43; N, 6.93; Cl, 9.70

6.1 *N-(1-Ethoxycarbonyl-propen-2-yl)-L-asparaginyl-L-alanine phenacyl ester (AE-Asn-Ala-OPAc).* A mixed anhydride was prepared from 4.2 g (15 mmol) of AE-Asn-O^-K^+[16] and 1.8 ml (15 mmol) of benzoyl chloride and two drops of N-methyl morpholine in 100 ml of tetrahydrofuran. After 3 hours stirring, the mixture was treated with L-alanine phenacyl ester obtained from its hydrochloride[12b] (3.7 g, 15 mmol) with 15 mmol of triethylamine in 50 ml of methylene chloride. Working up to the general Method B, yielded 5.2 g (80%) protected dipeptide ester. M.p. 170–171°, identical with an authentic sample prepared by us earlier.[16]

6.2. *N-(1-Ethoxycarbonyl-propen-2-yl(-O^5-benzyl-L-glutamyl-L-alanine methyl ester (AE-Glu(OBzl)-Ala-OMe)* was obtained from 16 g (30 mmol) of AE-Glu(OBzl)-O^-DCHA·H^+[12a] in a solution of tetrahydrofuran, through the ethoxycarbonyl mixed anhydride, according to the Method B. Yield 10.4 g (80%), m.p. 84–86° (benzene-petroleum ether), $[\alpha]_D +19°$ (c = 1, MeOH).

---

[15] H. NIEDRICH and P. LÖWE, *J. prakt. Chem.*, **35**, 213 (1967).
[16] A. BALOG and co-workers, *in preparation.*

$C_{22}H_{30}N_2O_7$ (434.5) *Calcd.*, C, 60.72 ; H, 6.96 ; N, 6.44
Found, C, 60.90 ; H, 7.44 ; N, 6.23

6.3. *N-(1-Ethoxycarbonyl-propen-2-yl)-O^5-benzyl-L-glutamyl-L-alanine phenacyl ester (AE-Glu(OBzl)-Ala-OPAc)*. Was prepared according to the Method B from 5.3 g (10 mmol) of AE-Glu-(OBzl)-O$^-$DCHA·H$^+$[12a]. After recrystallization from ethanol yielded 4.5 g (84%), m.p. 114—115°, $[\alpha]_D$ +54.4° (c = 1, dioxan).

$C_{29}H_{34}N_2O_8$ (538.6) *Calcd.*, C, 64.67 ; H, 6.36 ; N, 5.20
Found, C, 64.75 ; H, 6.70 ; N, 5.44

6.4. *O^5-Benzyl-L-glutamyl-L-alanine phenacyl ester hydrochloride* was obtained from the above N-protected dipeptide ester **6.3** in 80% yield. M.p. 142—143° (EtOH—Et_2O), $[\alpha]_D$ —23.1° (c = 1, MeOH).

$C_{23}H_{27}ClN_2O_6$ (462.9) *Calcd.*, C, 59.68 ; H, 5.88 ; N, 6.06 ; Cl, 7.66
Found, C, 59.11 ; H, 6.43 ; N, 6.44 ; Cl, 7.20

TRIPEPTIDES

7.1. *N-(1-Ethoxycarbonyl-propen-2-yl)-L-phenylalanyl-L-isoleucylglycine methyl ester(AE-Phe-Ile-Gly-OMe)*. This tripeptide derivative was obtained according to the Method B from 4.6 g (10 mmol) of AE-Phe-O$^-$DCHA·H$^+$ and 2.4 g (10 mmol) of $^+H_2$-Ile-Gly-OMe·Cl$^-$. Yield 3.4 g (75%) ; m.p. 179—180° (MeOH) ; $[\alpha]_D$ —36.8° (c = 1, dioxan), —38.6° (c = 1, DMF).

$C_{24}H_{35}N_3O_6$ (461.6) *Calcd.*, C, 62.45 ; H, 7.64 ; N, 9.10
Found, C, 62.20 ; H, 7.81 ; N, 9.28

7.2. *L-Phenylalanyl-L-isoleucylglycine methyl ester hydrochloride* was obtained from the protected tripeptide ester **7.1** by removal of the N-protecting group in 93% yield ; m.p. 202—204°. After recrystallization from ethanol, m.p. 213—215° (dec.) ; $[\alpha]_D$ —27.8° (c = 1, MeOH). Lit.[13] m.p. 213—215° (hemihydrat, separated from methanol-ether).

$C_{18}H_{28}ClN_3O_4$ (385.9) *Calcd.*, C, 56. 02 ; H, 7.31 ; N, 10.88
Found, C, 56.12 ; H, 7.65 ; N, 10.92

8.1. *N-(1-Ethoxycarbonyl-propen-2-yl)-L-alanyl-L-phenylalanyl-L-isoleucine phenacyl ester (AE-Ala-Phe-Ile-OPAc)*. This protected tripeptide ester was prepared from 4.6 mmol of AE-Ala-O$^-$DCHA·H$^+$ and 4.6 mmol of $^+H_2$-Phe-Ile-OPAc.Br$^-$ (**4.2**) according to the Method B in 88% yield (2.4 g). M .p. 178—179° (EtOH) ; $[\alpha]_D$ +121.8° (c = 1, dioxan).

$C_{32}H_{41}N_3O_7$ (579.7) *Calcd.*, C, 66.30 ; H, 7.13 ; N, 7.25
Found, C, 66.75 ; H, 7.07 ; N, 7.25

8.2. *L-Alanyl-L-phenylalanyl-L-isoleucine phenacyl ester hydrochloride.* The removal of the N-protecting group of **8.1** was performed by the Method C in 62 % yield ; m.p. 180—181.5° (EtOH) ; $[\alpha]_D$ —14.5° (c = 1, dioxan).

$C_{26}H_{34}ClN_3O_5$ (504.0) *Calcd.*, C, 61.56 ; H, 6.80 ; N, 8.33 ; Cl, 7.03
Found, C, 62.20 ; H, 7.27 ; N, 8.73 ; Cl, 6.75

9.1. *N-(1-Ethoxycarbonyl-propen-2-yl)-O^5-benzyl-L-glutamyl-L-alanyl-L-phenylalanine phenacyl ester (AE-Glu(OBzl)-Ala-Phe-OPAc*, was obtained according to the Method B from 10 mmol of AE-Glu(OBzl)-O$^-$DCHA·H$^+$[12a] and 10 mmol of $^+H_2$-Ala-Phe-OPAc.Cl$^-$ (**5.4**) in 75% yield (after recrystallization from ethanol). M.p. 140—141° ; $[\alpha]_D$ +29.1° (c = 1, dioxan).

$C_{38}H_{43}N_3O_9$ (685.8) *Calcd.*, C, 66.55 ; H, 6.32 ; N, 6.12
Found, C, 66.10 ; H, 6.55 ; N, 6.01

9.2. *O^5-Benzyl-L-glutamyl-L-alanyl-L-phenylalanine phenacyl ester hydrobromide.* A suspension of 4 g (5.8 mmol) of the above protected tripeptide ester **9.1** in 25 ml of anhydrous ethanol was treated with 2 ml of 30% hydrobromic acid in acetic acid. After evaporation of the obtained clear solution, the tripeptide ester hydrobromide crystallized as needles. After recrystallization from anhydrous ethanol-ether yielded 1.5 g (30%), m.p. 176–178°; $[\alpha]_D$ (−14.5° (c = 1, MeOH).

$C_{32}H_{36}BrN_3O_7$ (654.6) *Calcd.*, C, 58.72; H, 5.54; N, 6.42; Br, 12.2
Found, C, 58.60; H, 6.28; N, 6.63; Br, 11.9

9.3. *N-(1-Ethoxycarbonyl-propen-2-yl)-L-glutaminyl-L-alanyl-L-phenylalanine phenacyl ester AE-Gln-Ala-Phe-OPAc*) was obtained according to the general Method B. M.p. 189–192°; $[\alpha]_D^{35}$ +19.4° (c = 1, MeOH).

$C_{31}H_{38}N_4O_8$ (594.7) *Calcd.*, C, 62.61; H, 6.44; N, 9.42
Found C, 61.88; H, 7.10; N, 8.72

9.4. *N-(2-Ethoxycarbonyl-cyclopenten-1-yl)-L-glutaminyl-L-alanyl -L- phenylalanine methyl ester* (*CP-Gln-Ala-Phe-OMe*). This protected tripeptide ester was prepared according to the general Method B from 6.1 g (13 mmol) of $\text{CP-Gln-O}^-\text{DCHA}\cdot\text{H}^+$[16] and 3.7 g (13 mmol) of $^+\text{H}_2\text{-Ala-Phe-OMe-Cl}^-$ (5.2). Yield 5.5 g (82%); the crude product melted at 214–216°. Recrystallization from ethanol-ethyl acetate, or dioxan gave an analytical sample, m.p. 219–220°; $[\alpha]_D$ +39.8° (c = 0.12, DMF).

$C_{26}H_{36}N_4O_7$ (516.6) *Calcd.*, C, 60.45; H, 7.02; N, 10.84
Found, C, 60.67; H, 6.90; N, 11.06

TETRAPEPTIDE AND PENTAPEPTIDE

10.1. *N-(1-Ethoxycarbonyl-propen-2-yl)-L-alanyl-L-phenylalanyl-L-isoleucylglycine methyl ester* (*AE-Ala-Phe-Ile-Gly-OMe*). A mixed anhydride was prepared from 3.5 g (9 mmol) of $\text{AE-Ala-O}^-\text{DCHA}\cdot\text{H}^+$[12a] and 0.95 ml of ethyl chloroformate in tetrahydrofuran, according to the Method B. To the filtered solution of the mixed anhydride a mixture of $^+\text{H}_2\text{-Phe-Ile-Gly-OMe.Cl}^-$ (**7.2**) (3.5 g, 9mmol) and triethylamine (1.3 ml) in methylene chloride was added. The mixture was stirred one hour at −5°, then two hours at room temperature. After standing overnight an excess of saturated aqueous sodium hydrogen carbonate was added and the organic solvents were removed under reduced pressure at 30–40°. The solid residue was dried to yield 4 g (83%) crude product, m.p. 222–228°. The tetrapeptide ester may be purified by recrystallization from dioxan, yielding 75%, m.p. 244–246°; or DMF, m.p. 240–242°. $[\alpha]_D$ +103.8° (c = 1, DMF).

$C_{27}H_{40}N_4O_7$ (532.6) *Calcd.*, C, 60.89; H, 7.57; N, 10.52
Found, C, 61.00; H, 7.91; N, 10.80

10.2. *L-Alanyl-L-phenylalanyl-L-isoleucylglycine methyl ester hydrochloride.* Obtained according to the Method C from 3.7 g (7 mmol) of N-protected tetrapeptide ester **10.1**, in ethyl acetate by adding to pH 2–2.5 a solution of ethanolic hydrochloric acid 18%. Yield 3.2 g (95%); m.p. 208–209°. After recrystallization from ethyl acetate, m.p. 213–215°; $[\alpha]_D$ −4.4° (c = 1, DMF). Lit.[13] m.p. 210°; $[\alpha]_D$−5.7° (c = 2,DMF).

$C_{21}H_{33}ClN_4O_5.H_2O$ (475.0) *Calcd.*, C, 53.10; H, 7.40; N, 11.80
Found, C, 53.30; H, 7.89; N, 11.42

10.3. *N-(2-Ethoxycarbonyl-cyclopenten-1-yl)- L -asparaginyl-L-alanyl-L-phenylalanyl- L - isoleucylglycine methyl ester* (*CP-Asn-Ala-Phe-Ile-Gly-OMe*). Obtained according to the Method B from 7.4 mmol of $\text{CP-Asn-O}^-\text{DCHA}\cdot\text{H}^+$ by means of the ethoxycarbonyl mixed anhydride in ethyl acetate solution by adding 7.4 mmol of the above tetrapeptide ester **10.2**. The crude product yielded 3.7 g (80%) of protected pentapeptide ester, m.p. 212–216° (dec.); after recrystallization from DMF, m.p. 214–216°; $[\alpha]_D$ +50° (c = 1, DMF).

$C_{33}H_{48}N_6O_9$ (672.8) *Calcd.*, C, 58.91; H, 7.12; N, 12.49
Found, C, 58.79; H, 7.60; N, 12.32

Revue Roumaine de Chimie, **18**, *9*, 1637–1641 (1973)

LIQUID MEMBRANE-ELECTRODES. II*

THE *n*-BUTANOL-FRIT ELECTRODE IN ACID-BASE POTENTIOMETRIC TITRATION

MARIA MIOŞCU, ELENA HOPÎRTEAN and C. LITEANU

University of Cluj, Chair of Analytical Chemistry, str. Arany J., 11, Cluj, Romania

Received December 13, 1972

The results obtained in a series of potentiometric acid-base titrations using the *n*-butanol-frit membrane as indicating electrode, are presented. The following acids : HCl, HNO_3, $HClO_4$, HIO_3, H_2SeO_4, H_3PO_4, and bases : KOH, $Ba(OH)_2$, NH_3, have been titrated. Accuracy of the performed titrations was expressed in comparison with the results obtained with glass electrode.

The liquid membrane-electrodes are one of the recently discovered types of electrodes. The first liquid membrane-electrode was discovered by Ross in 1967.[1] According to their working mechanism there are up to now two known types of liquid membrane-electrodes : ion exchange liquid membrane-electrodes[2-8] and membrane-electrodes working by extraction.[9,10] The tricresylphosphate liquid electrode in frit used in the potentiometric precipitation titration[11] is of this second category.

As a series of liquid organic substances show extracting properties, we have considered it useful to try to obtain new types of liquid membrane-electrodes with a working mechanism based on this quality.

Having studied, in a previous paper,[12] the behaviour of the *n*-butanol/water interface membrane-electrode in acid-base potentiometric titrations, we have continued the study in this paper, aiming at obtaining an impregnated *n*-butanol membrane-electrode in a suitable support.

---

* Part I : E. Hopîrtean, A. Tîrşar and C. Liteanu, *Studia Univ. Babeş-Bolyai, Chem.* **17**(2), 99 (1972).

[1] J. W. Ross, *Science*, **156**, 1378 (1967).

[2] T. M. Hseu and Z. F. Lin, *Anal. Lett.*, **1**, 23 (1967).

[3] S. S. Potterton and W. D. Shults, *Anal. Lett.*, **1**, 11 (1967).

[4] R. M. Carlson and J. L. Paul, *Analyt. Chem.*, **40**, 1292 (1968).

[5] T. G. Lee, *Analyt. Chem.*, **41**, 391 (1969).

[6] G. A. Rechnitz and Z. F. Lin, *Anal. Lett.*, **1**, 23 (1967).

[7] A. R. Pioda Lavinia, V. Stankova and W. Simon, *Anal. Lett.*, **2**, 665 (1969).

[8] F. Conti and G. Eisenman, *Biophys. J.*, **6**, 227 (1966).

[9] C. J. Coetzee and H. Freiser, *Analyt. Chem.*, **40**, 2071 (1968).

[10] C. J. Coetzee and H. Freiser, *Analyt. Chem.*, **41**, 1128 (1969).

[11] E. Hopîrtean, A. Tîrşar and C. Liteanu, *Studia Univ. Babeş-Bolyai, Chem.*, **17** (2), 99 (1972).

[12] C. Liteanu and M. Mioşcu, *Talanta*, **19**, 889 (1970).

The paper contains the results obtained in the analytical evaluation of the *n*-butanol-frit electrode, on the potentiometric determination of some acids and bases.

EXPERIMENTAL

1. *Obtention of the membrane-electrode.* The membrane-electrode was obtained by impregnating the **dry** support with *n*-butanol. Different porous materials : frit, ultrafilter, parchment paper were tried to choose a suitable support. As the best results were obtained with the G_4 frit support, the later was the only one to be used henceforth. The inner used solution was 10^{-4}N KCl, the potential of the membrane being taken over by means of two saturated calomel electrodes (Fig. 1).

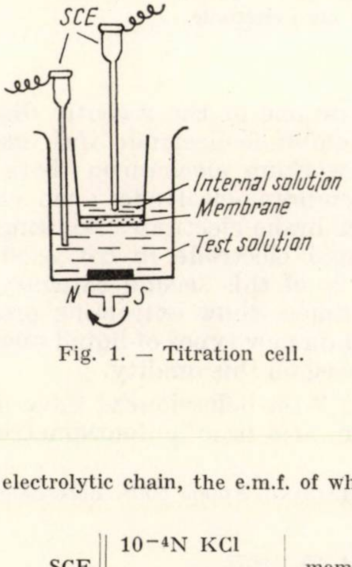

Fig. 1. – Titration cell.

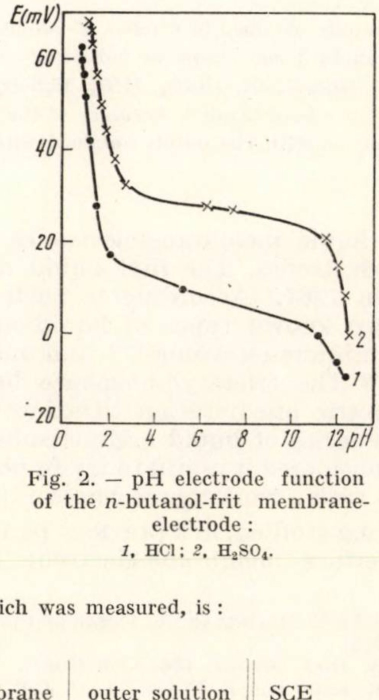

Fig. 2. – pH electrode function of the *n*-butanol-frit membrane-electrode : *1*, HCl ; *2*, H_2SO_4.

The electrolytic chain, the e.m.f. of which was measured, is :

$$\mathrm{SCE} \left\| \begin{matrix} 10^{-4}\mathrm{N\ KCl} \\ \text{inner solution} \end{matrix} \right| \text{membrane} \;\Big|\; \text{outer solution} \;\Big\|\; \mathrm{SCE}$$

The potential measurements were carried out by means of a MV 11 pH-meter, at room temperature, at restirring conditions.

2. *The pH electrode function* was determined in HCl and H_2SO_4 solutions. The corresponding pH values were determined with a glass electrode. The obtained electrode functions are given in figure 2. The response of the electrode is not nernstian.

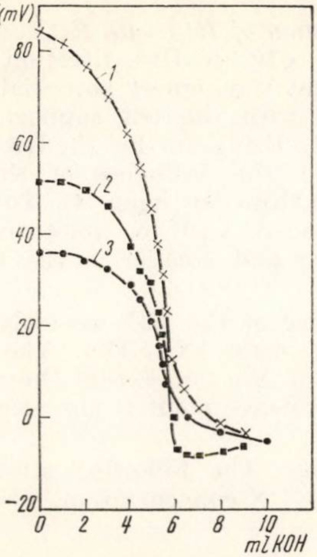

Fig. 3. — Influence of support on the HCl with KOH titration : *1*, G_4 frit ; *2*, ultrafilter ; *3*, parchment paper.

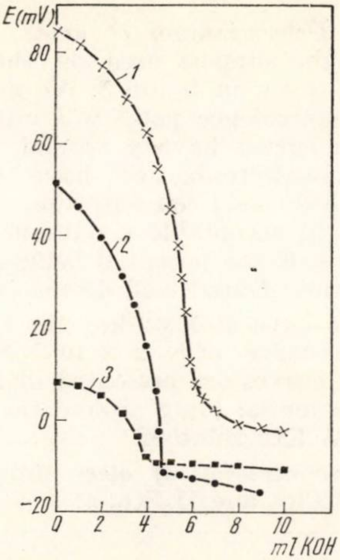

Fig. 4. — Influence of concentration on the HCl with KOH titration : *1*, $c = 2 \times 10^{-1}$ N ; *2*, $c = 2 \times 10^{-2}$ N ; *3*, $c = 2 \times 10^{-3}$ N.

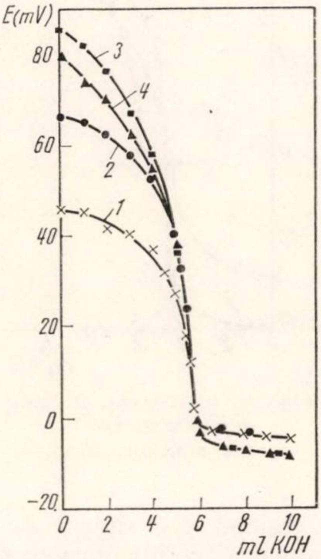

Fig. 5. — Influence of the KCl concentration on the HCl with KOH titration : *1*, 10^{-1} M KCl ; *2*, 5×10^{-1} M KCl ; *3*, 1M KCl ; *4*, 5M KCl.

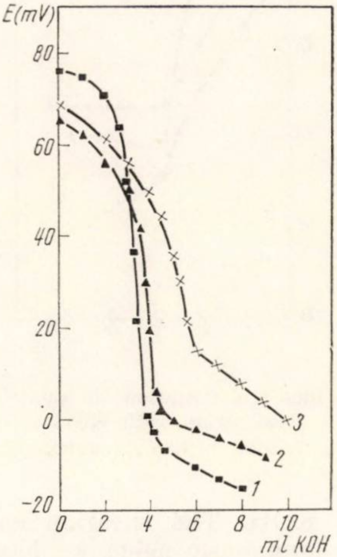

Fig. 6. — Titration of some strong acids with KOH : *1*, HNO_3 ; *2*, $HClO_4$; *3*, H_2SO_4.

3. *Determination of acids. Titration of HCl with KOH.* The influence of the support used on the $\sim 2 \times 10^{-1}$N HCl titration with 1N KOH is given in figure 3. We note that the highest potential variation at the equivalence point was obtained with the frit support G_4. The titration curves have a normal aspect. Using further the frit-*n*-butanol membrane-electrode, we have studied the influence of the titrated hydrochloric acid concentration on the titration (figure 4). The titration develops in acceptable conditions up to a 2×10^{-3}N concentration, the variations of the potential being smaller and smaller as the concentration of the titrated acid decreases.

We have also studied the influence of the KCl electrolyte on the titration curve of $\sim 2 \times 10^{-1}$ N HCl with 1N KOH. The obtained titration curves are presented in figure 5. We notice that the magnitude of the potential jump around the equivalence point is not affected even for a 5M KCl solution.

Determination of other strong acids. The following strong acids: HNO_3, $HClO_4$ and H_2SO_4, at a $\sim 2 \times 10^{-1}$ N concentration, were titrated with 1N KOH. The titration curves obtained are shown in figure 6. For the monobasic acids we have obtained titration curves similar to the curve of HCl, while the titration curve of H_2SO_4 has a different form, which may be explained by a higher marked extraction possibility of H_2SO_4 in *n*-butanol, as compared to that of the other titrated acids.[13]

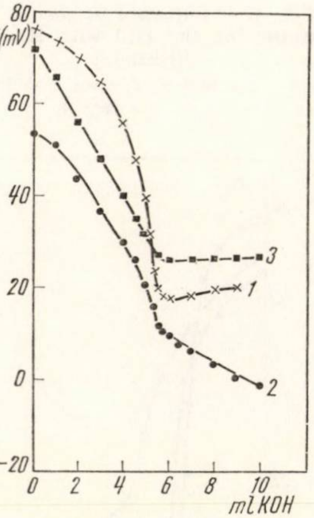

Fig. 7. — Titration of some weak acids with KOH:
1, HIO_3; *2*, H_2SeO_4; *3*, H_3PO_4.

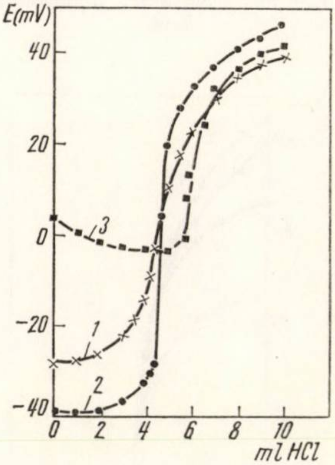

Fig. 8. — Titration of some bases with HCl:
1, KOH; *2*, $Ba(OH)_2$; *3*, NH_3.

---

[13] Z. Sh. Golynko, D. J. Skorovarov, V. F. Smirnov and N. V. Skvortsov, *Zhur. prikl. Khim.*, **38**, 271 (1965).

Determination of some weak acids. Among the weak acids we have titrated HIO_3, H_2SeO_4, H_3PO_4, at a $\sim 2 \times 10^{-1}$N concentration, with 1N KOH. The titration curves are given in figure 7. We note the analogy between the form of the titration curve of H_2SeO_4 and H_2SO_4 (figure 5), probably based on a close extraction possibility of the two acids. The titration curve of H_3PO_4 is a curve with an intersection point.

We have also attempted the titration of the acids HCOOH, $CHCl_2COOH$ and CH_3COOH, without obtaining valuable results. The organic character of the acid probably influences the electrode quality of the *n*-butanol membrane.

Determination of some bases. The following bases: KOH, $Ba(OH)_2$ and NH_3 were titrated, at a $\sim 2 \times 10^{-1}$N concentration, with 1N HCl. The titration curves obtained are given in figure 8. One notes that the shape of the titration curves comes near to that of the classical one recording a clear potential jump at the equivalence point.

The data of the above titrations are included in table 1. The values of the equivalence volumes for the titrations with the membrane-electrode were calculated by means of the Hahn-Weiler[14] interpolation method, excepting the H_2SeO_4 and H_3PO_4 titrations in which they were graphically localized. These values were compared to those obtained on titrating in the presence of the glass electrode.

Table 1

Results of acid-base titrations obtained by using the *n*-butanol-frit membrane-electrode

Titration	V_e (ml)		e(%)
	glass electrode	membrane electrode	
$HCl \sim 2 \times 10^{-1}N + KOH\ 1\ N$	5.77	5.75	− 0.3
$HNO_3 \sim 2 \times 10^{-1}N + KOH\ 1\ N$	3.71	3.65	− 1.6
$HClO_4 \sim 2 \times 10^{-1}N + KOH\ 1\ N$	4.10	4.06	− 0.9
$H_2SO_4 \sim 2 \times 10^{-1}N + KOH\ 1\ N$	5.45	5.49	+ 0.7
$HIO_3 \sim 2 \times 10^{-1}N + KOH\ 1\ N$	5.40	5.41	+ 0.1
$H_2SeO_4 \sim 2 \times 10^{-1}N + KOH\ 1\ N$	5.73	5.78*)	+ 0.8
$H_3PO_4 \sim 2 \times 10^{-1}N + KOH\ 1\ N$	5.55	5.60*)	+ 0.9
$KOH \sim 2 \times 10^{-1}N + HCl\ 1\ N$	4.30	4.33	+ 0.7
$Ba(OH)_2 \sim 2 \times 10^{-1}N + HCl\ 1\ N$	4.50	4.51	+ 0.2
$NH_3 \sim 2 \times 10^{-1}N + HCl\ 1\ N$	5.41	6.01	+11.0

* Graphically determined values.

Excepting the NH_3 titration, the errors are generally lesser than 1%, hence the *n*-butanol-frit membrane-electrode may be successfully used in the acid-base potentiometric titration.

---

[14] F. L. Hahn and G. Weiler, *Z. analyt. Chem.*, **69**, 417 (1926).

Revue Roumaine de Chimie, **18**, 9, 1643–1647 (1973)

LIQUID MEMBRANE-ELECTRODES. III*

ELECTRODES WITH WATER-IMMISCIBLE ORGANIC LIQUIDS IN FRIT. APPLICATIONS IN POTENTIOMETRIC ACID-BASE TITRATIONS

C. LITEANU, ELENA HOPÎRTEAN and MARIA MIOŞCU
University "Babeş-Bolyai", Chair of Analytical Chemistry, Str. Arany J. 11, Cluj, Romania

Received February 12, 1973

A series of liquid membrane-electrodes have been obtained by impregnating of frit with some water immiscible organic liquids as : alcohols, ketones, aromatic compounds, hydrocarbons as well as their derivatives. Electrode behaviour of the membranes obtained was tested in potentiometric titration of HCl with NaOH. Accuracy of titrations performed was expressed in comparison with results obtained with glass electrode.

Membrane electrodes with active component parts which function by extraction,[1-3] are one of the recently discovered types of liquid membrane-electrodes.

The present paper deals with the investigation of some water immiscible organic compounds as liquid membrane-electrodes in the potentiometric acid-base titrations. The membrane-electrodes used have been obtained by impregnation of dry G_4 frit with the organic substances used : alcohols, ketones, aromatic compounds, hydrocarbons as well as their derivatives. The titration cell used is presented in figure 1. In most cases the internal solution consisted of the same organic liquid as that in frit. The e.m.f. of the following electrolytic cell was measured using a MV–11 pH-meter

$$\text{S.C.E.} \;\Big\|\; \begin{matrix}\text{internal}\\ \text{solution}\end{matrix} \;\Big|\; \text{membrane} \;\Big|\; \begin{matrix}\text{external}\\ \text{solution}\end{matrix} \;\Big\|\; \text{S.E.C.}$$

Potentiometric titration of $\sim 2 \times 10^{-1}$N HCl with 1 N KOH has been performed. The reading of potential values was made at room temperature in quiet solutions.

---

* Part. II : M. Mioşcu, E. Hopîrtean and C. Liteanu, *Rev. Roumaine Chim.*, **18**, (1973).

[1] C. J. Coetzee and H. Freiser, *Analyt. Chem.*, **40**, 2071 (1968).

[2] C. J. Coetzee and H. Freiser, *Analyt. Chem.*, **41**, 1128 (1969).

[3] E. Hopîrtean, A. Tîrşar and C. Liteanu, *Studia Univ. Babeş-Bolyai, Chem.*, **17** (2), 99(1972).

1. *Membrane-electrodes with alcohols-frit.* The following membrane-electrodes have been used : butyl-alcohol-frit, amyl-alcohol-frit and cyclohexanol-frit. The titration curves obtained are presented in figure 2. One can observe the somewhat different shape of the titration curves as well as the greater potential breaks registered with cyclohexanol-frit electrodes.

The equivalence points can be easily localized by the intersection of the two linear portions of the titration curves in the immediate vicinity of the equivalence.

2. *Membrane-electrodes with ketone-frit.* Methyl-ethyl-ketone, acetyl-acetone and cyclohexanone were impregnated in frit. The titration curves obtained are presented in figure 3. Though in the case of ketones very small potential variations were registered, the equivalence point was always clearly perceptible.

The small potential variations are probably due to the low electric conductibility of these substances.

Diminishing the thickness of the organic liquid and introducing 10^{-4}N KCl as internal solution, the curves in figure 4 were obtained. In this case a greater potential variation was obtained without modifications in the localization of the equivalence point.

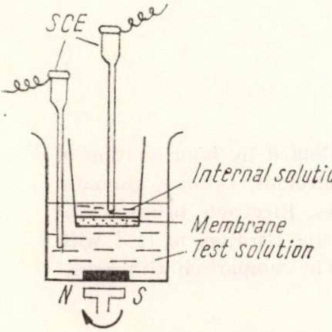

Fig. 1. — Titration cell.

3. *Membrane-electrodes with aromatic-derivative frit.* Electrodes obtained by the impregnation of the frit with benzene, nitrobenzene, toluene and xylene have been experienced, too. In the case of benzene and nitrobenzene the titrations were performed in usual conditions. The membrane-electrodes of toluene and xylene did not present stable electrode potentials because of their too high electric resistance. This electric resistance was diminished by saturation with 10^{-1}N KCl. The titration curves obtained in these conditions are presented in figure 5. It can be remarked that the behaviour of the xylene electrode was less suitable. In the case of nitrobenzene and toluene a perceptible improvement of the electrode behaviour was obtained using 10^{-4}N KCl as internal solution (Fig. 6).

4. *Membrane-electrodes with hydrocarbon-frit.* Suitable membrane-electrodes of pentane and petroleum ether have been obtained only by increasing the electric conductibility by saturation with 10^{-1}N KCl. Titration curves obtained in these conditions are represented in figure 7.

5. *Membrane-electrodes with halogen derivatives of hydrocarbons.* For this purpose $CHCl_3$ and CCl_4 saturated with 10^{-1}N KCl have been used. Using chloroform-frit membrane-electrode the curve from figure 8 has been obtained. The results obtained with a carbon tetrachloride membrane-electrode were negative.

Using 10^{-4}N KCl as internal solution better results have been obtained. The titration curves are presented in figure 9.

The accuracy of the titrations was expressed considering the difference between the graphically localized equivalence volumes as compared to the equivalence volumes, calculated according to the Hahn-Weiler method,[4] the titrations being performed in the presence of the glass elec-

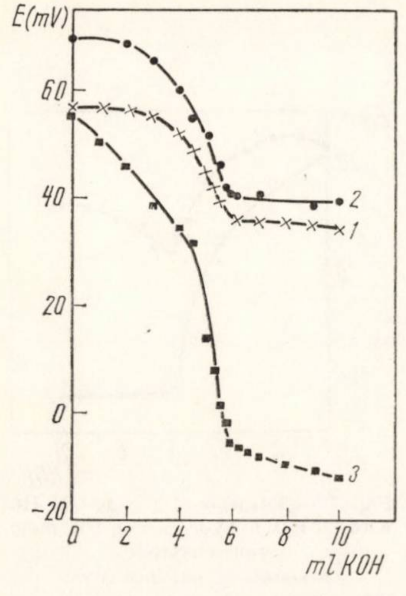

Fig. 2.—Titration of 2×10^{-1}N HCl with 1 N KOH ; alcohol-frit membrane-electrode :

1, butyl-alcohol ; *2*, amyl-alcohol ; *3*, cyclohexanol.

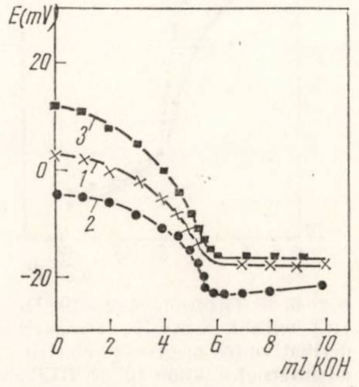

Fig. 3. — Titration of 2×10^{-1} N HCl with 1N KOH ; ketone-frit membrane-electrode :

1, methyl-ethyl-ketone ; *2*, acetyl-acetone ; *3*, cyclohexanone.

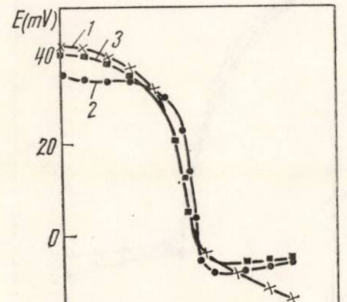

Fig. 4. — Titration of 2×10^{-1}N HCl with 1 N KOH ; ketone-frit mebrane-electrode (internal solution 10^{-4}N KCl) :

1, methyl-ethyl-ketone ; *2*, acetyl-acetone ; *3*, cyclohexanone.

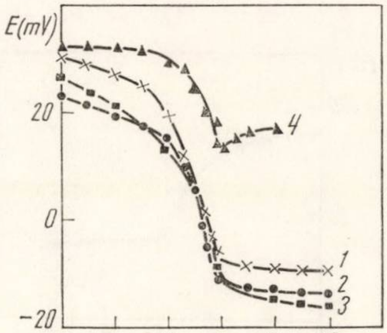

Fig. 5. — Titration of 2×10^{-1} N HCl with 1 N KOH ; aromatic derivative-frit membrane-electrode :

1, benzene ; *2*, nitrobenzene ; *3*, toluene ; *4*, xylene.

---

[4] F. L. Hahn and G. Weiler, *Z. analyt. Chem.*, **69**, 417 (1926).

trode. The results obtained are presented in table 1. There are not too great errors. Except for the xylene, the errors de not exceed 1.3%. The values in table 1 referred to the membrane-electrodes which had as internal solution the respective organic liquid (saturated or unsaturated with KCl).

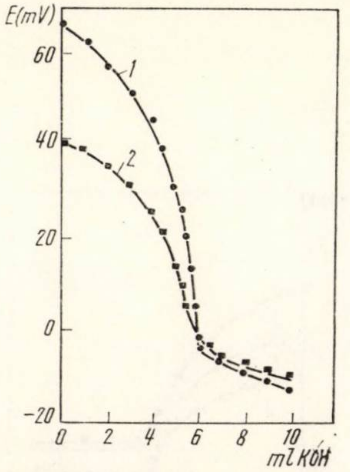

Fig. 6. — Titration of 2×10^{-1}N HCl with 1 N KOH; aromatic derivative-frit membrane-electrode (internal solution 10^{-4}N KCl):

1, nitrobenzene; *2*, toluene.

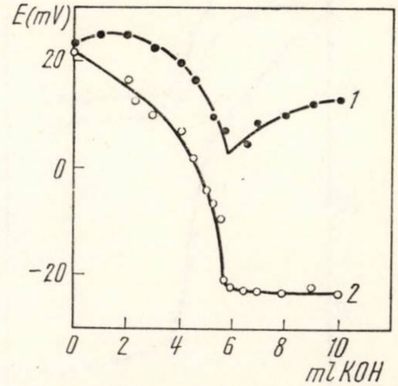

Fig. 7. — Titration of 2×10^{-1}N HCl with 1N KOH; hydrocarbon-frit membrane-electrode:

1, pentane; *2*, petroleum ether.

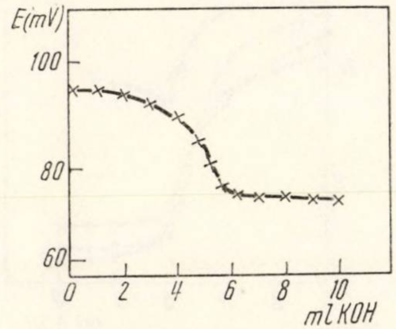

Fig. 8. — Titration of 2×10^{-1}N HCl with 1N KOH; chloroform-frit membrane-electrode.

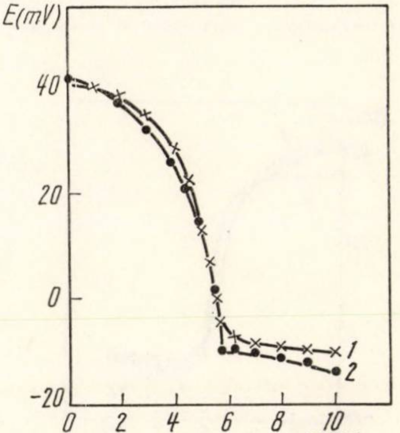

Fig. 9. — Titration of 2×10^{-1}N HCl with 1N KOH; halogene derivative-frit membrane-electrode (internal solution 10^{-4}N KCl):

1, chloroform; *2*, carbon tetrachloride.

As a conclusion, the water immiscible organic liquids tested with good results, are able to constitute electrode-active compounds in acid-base potentiometric titrations.

Table 1

Results of titration of ~ 2×10^{-1} N HCl with 1 N KOH obtained with electrodes with water immiscible organic-liquids in frit

Membrane generating liquid	V_e (ml)		e(%)
	glass electrode	membrane-electrode	
n-butyl alcohol	5.82	5.90	+1.3
amyl alcohol		5.82	0
cyclohexanol		5.80	−0.3
methyl-ethyl-ketone	5.82	5.90	+1.3
acetyl-acetone		5.80	−0.3
cyclohexanone		5.90	+1.3
benzene	5.82	5.84	+0.3
nitrobenzene		5.90	+1.3
toluene		5.90	+1.3
xylene		5.94	+2
pentane	5.82	5.90	+1.3
petroleum ether		5.78	−0.6
chloroform	5.82	5.80	−0.3

Revue Roumaine de Chimie, 18, 9, 1643–1647 (1973)

Revue Roumaine de Chimie, **18**, *9*, 1649–1657 (1973)

POLAROGRAPHIC BEHAVIOUR OF ISOCINCHOMERONIC ACID

LUIGI CAMPANELLA, PIER LUIGI CIGNINI and GIORGIO DE ANGELIS

Institute of Analytical Chemistry, University, Rome, Italy

Received January 19, 1973

Polarographic and oscillopolarographic behaviour of isocinchomeronic acid is characterized by the presence of three waves and peaks. While the first (at less negative potentials) process is of a mixed nature, involving both a catalytic reduction of hydrogen ions and the reduction in the ring of the acid, the other two ones are only catalytic discharges of hydrogen.

The polarographic behaviour of heterocyclic compounds containing an N atom in their molecule is quite complicated because in addition to normal waves these compounds can yield also catalytic ones, generally ascribed to the hydrogen discharge. The shape and the height of these waves are largely varying according to the experimental conditions, particularly those referring to pH, ionic strength, concentration, scanning rate of potential, presence and nature of the buffer system. A research is being performed in our laboratory[1–3] on the chemical and electrochemical behaviour of pyridinemonocarboxylic acids, aiming at getting useful information about the equilibria in solution among the species of the acids and about the electrochemical activity of some of these species in comparison with others.

We refer here particularly to the polarographic and oscillopolarographic behaviour of 2,5-pyridinedicarboxylic acid (isocinchomeronic: melting point 236–237°, dissociation constants 4.95×10^{-3} and 8.77×10^{-6}). The data reported in literature are scarce and only limited to the analytical aspects of the problem. Particularly Volke and his coworkers[4,5] determined isocinchomeronic acid by the polarographic method in a mixture containing several pyridinemono- and di-carboxylic acids.

Paper presented at the 23rd Meeting of the International Society of Electrochemistry (formely CITCE), Stockholm 27/8–2/9 (1972).

[1] L. Campanella and G. De Angelis, *Rev. Roumaine Chim.*, **16**, 545 (1971).

[2] L. Campanella, *Rev. Roumaine Chim.*, **17**, 1087 (1972).

[3] L. Campanella, E. Chiacchierini and M. Palchetti, *Rev. Roumaine Chim.*, **17**, 647 (1972).

[4] J. Volke and V. Volkova, *Coll. Czech. Chem. Comm.*, **20**, 1332 (1955).

[5] J. Volke and V. Volkova, *Coll. Czech. Chem. Comm.*, **20**, 908 (1955).

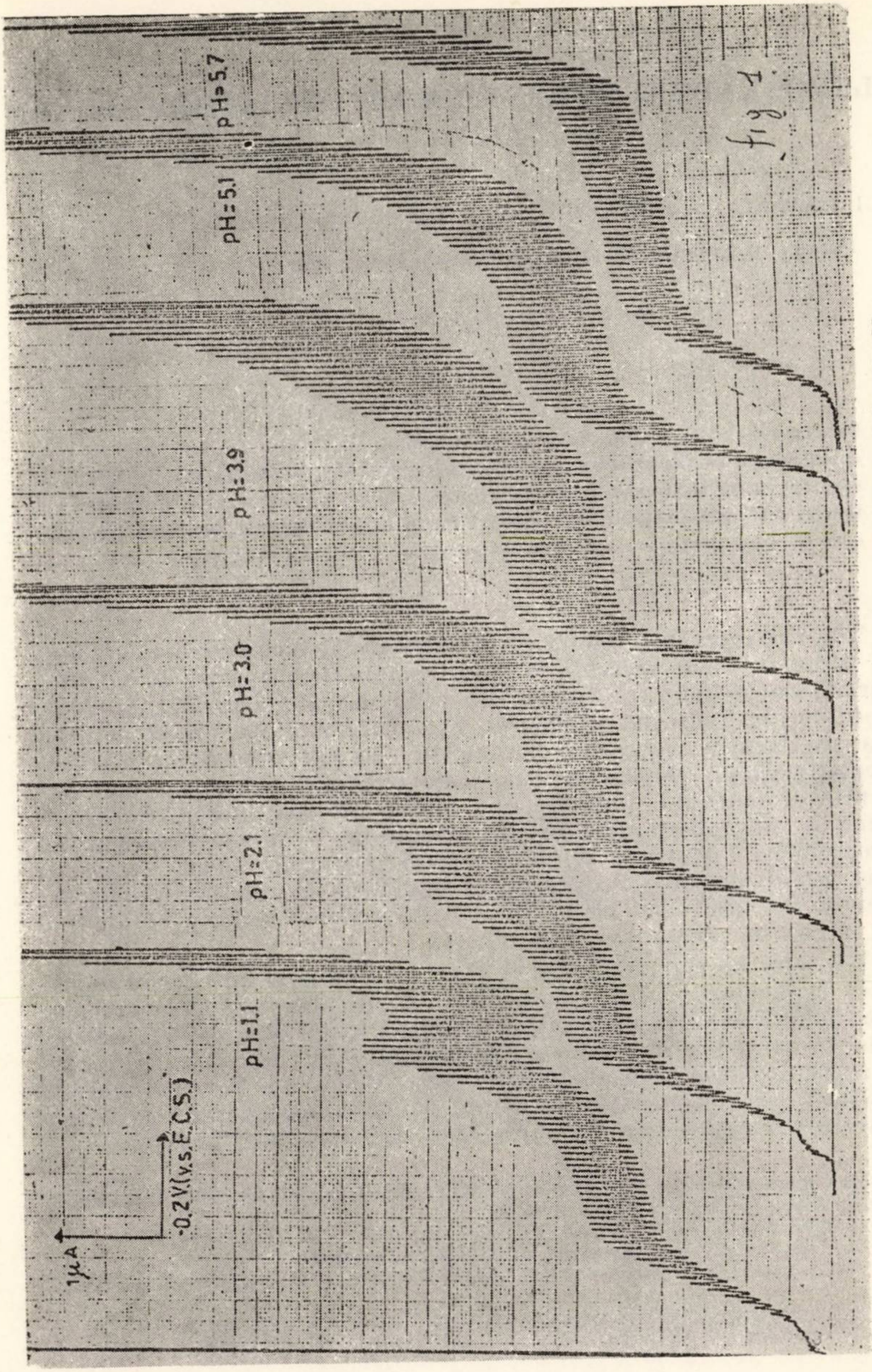

Fig. 1. – Polarographic behaviour of isocinchomeronic acid at different pH.

The study was performed by us at $\mu = 1$ M ($NaClO_4$), $T = 25.0 \pm \pm 0.5$ °C, $C = 10^{-3}$ M in the presence of 0.02 M citric buffer. The field of the very high acidities was also investigated, in this case fixing the ionic strength at 2M ($HClO_4 + NaClO_4$).

RESULTS

The polarographic behaviour of isocinchomeronic acid is characterized by the presence of three waves differently evidenced depending on pH. Only for pH < 3 all the three waves can be observed in the same polarographic curve (fig. 1).

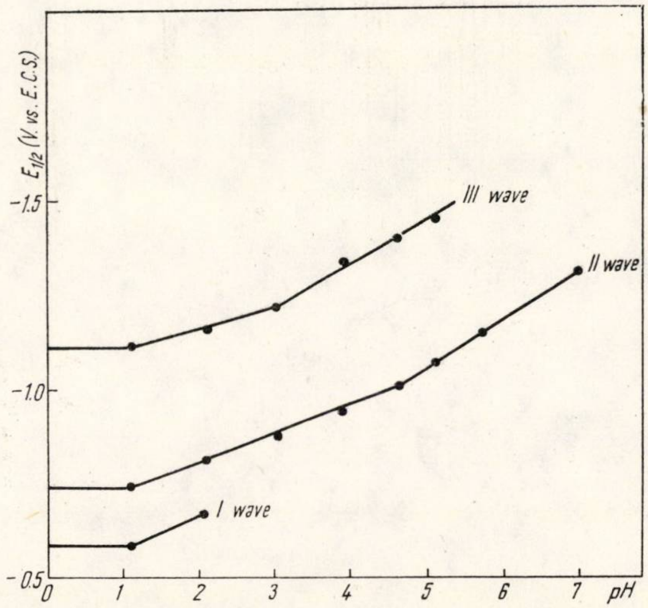

Fig. 2. — $E_{1/2}$ of the three waves as function of pH.

The first wave involves three electrons, the second and the third ones only one electron. The $E_{1/2}$ is for all the three waves a linear function of pH with some breaking points at pH $= 1.1$ (1st, 2nd, 3rd wave), 3.0 (3rd wave), 4.6 (2nd wave) (fig. 2).

The existence fields of the three waves are from very acid medium — we studied up to 2.5 M $HClO_4$ solutions — to pH $= 3$ for the first wave, pH $= 7$ for the second one and pH $= 6$ for the third wave. In alkaline solutions none of the three waves appears.

The influence of the concentration on the limiting currents obeys generally to Ilkovich equation, the only irregularities being observed for pH > 4 and concentration $< 1.4 \times 10^{-3}$ (fig. 3).

The influence of the mercury column height on the value of the limiting current was studied by the Kheifets curves (i.e. log i_d *vs* lg h_{Hg}):

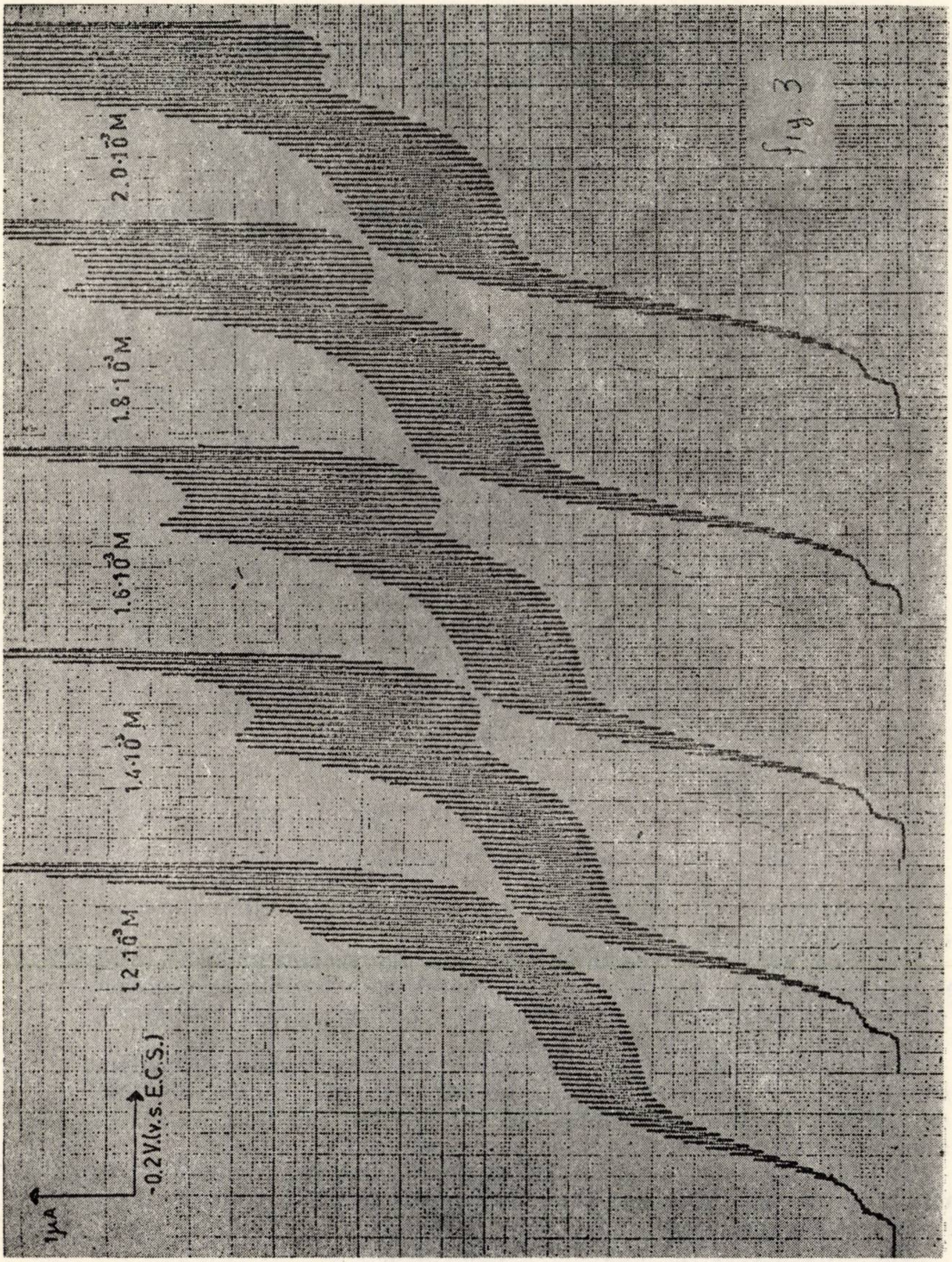

Fig. 3. — Polarographic curves at different concentrations of isocinchomeronic acid.

we obtained straight lines of slope = 0.75 ; 0.70 ; 0.80 respectively for the first, second and third wave (figs. 3,4).

Oscillopolarographic analysis yielded results well agreeing with the polarographic ones. So the oscillopolarographic peaks corresponding to the three polarographic waves can be recorded; their peak currents are depending on pH with a behaviour similar to that of the polarographic limiting currents with the only exception of the third peak for solution at $pH > 6$. The peak potential values are linear function of pH, with breaking points corresponding to variations of the slope, as the corresponding $E_{1/2}$ values. In solution at $pH < 4$ the influence of the concentration on the peak currents obeys the Randles-Sevcik equation (ensuring the proportionality between the concentration of the electrochemically active species and the peak current) (figs. 5, 6) and the peak potentials become more negative with increasing concentration. At $pH > 4$ the above proportionality is still observed only for the second and the third peak, the potentials of which do not depend on the concentration. In very acid solution the peak currents of the first and third peaks are proportional to the hydrogen ion concentration.

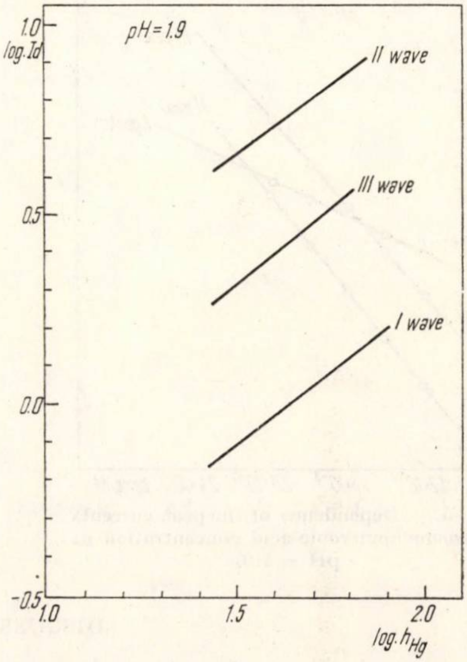

Fig. 4. — Dependence of the height of the three waves on the height of the mercury column.

At very negative potentials (about — 2V *vs* SCE) another peak is observed. This peak is characterized by anomalously high values of the current —10^2 times greater than those of the other three peaks,—so that its recording in measurable terms needs the employment of the poorest sensitivity ranges of the polarographic recorder, while at the usual sensitivities the peak looks just as a point of slope change and remains covered by the supporting electrolyte discharge. The height of this peak increases with decreasing pH.

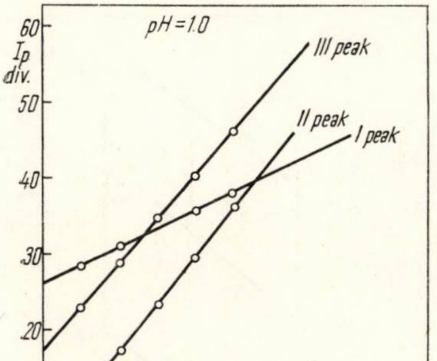

Fig. 5. — Dependence of the peak currents on isocinchomeronic acid concentration at pH = 1.0.

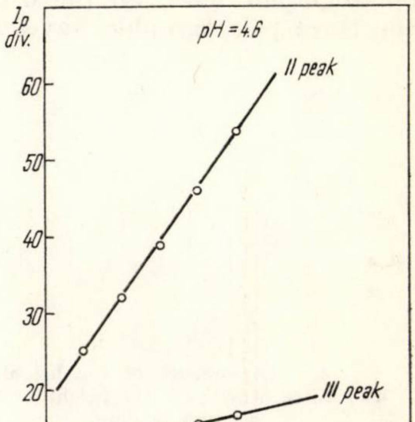

Fig. 6. — Dependence of the peak currents on isocinchomeronic acid concentration at pH = 4.6.

DISCUSSION

The interpretation of the experimental results must start from the consideration of the equilibria concerning the species of isocinchomeronic acid in aqueous solution (fig. 7).

By the analysis of the described results it can be deduced that among the species under which isocinchomeronic acid can exist in aqueous solution the bivalent anionic completely deprotonated species is the only one for which any polarographic activity can be excluded. Moreover the presence in very acid medium of all the three observed waves induces to postulate that, as for pyridine-monocarboxylic acids previously studied in our laboratory,[1,2] also for isocinchomeronic acid the protonated cationic species is the most electroactive one, both directly and through a kinetic process of equilibrium with the other species that are transformed into the cationic one at the electrode/solution interface :

$$H_2PC + H^+ \rightleftarrows H_3^+PC$$
$$HPC^- + 2H^+ \rightleftarrows H_3^+PC$$

where H_2PC and HPC^- represent the species of the acid at the protonation levels 0 and −1.

The increasing acidity degree plays two roles in the above equilibria : on the one side the concentration of H_2PC and HPC^- is lowered, on the other one the two reactions are kinetically and thermodinamically favoured.

The rate of the above transformations plays an extremely important role : indeed, if it is sufficiently high the protonated cationic species can be emphasized in a wider range of pH than expected based on values of the equilibria constants among the species of acids.

On the basis of the existence fields of the waves and peaks, of the number of electrons involved in the electrode processes, of the $\Delta E_{1/2}|\Delta pH$ slopes, of the dependence of the height of waves and peaks on the experimental conditions, particularly those referring to pH and temperature the following processes can be postulated :

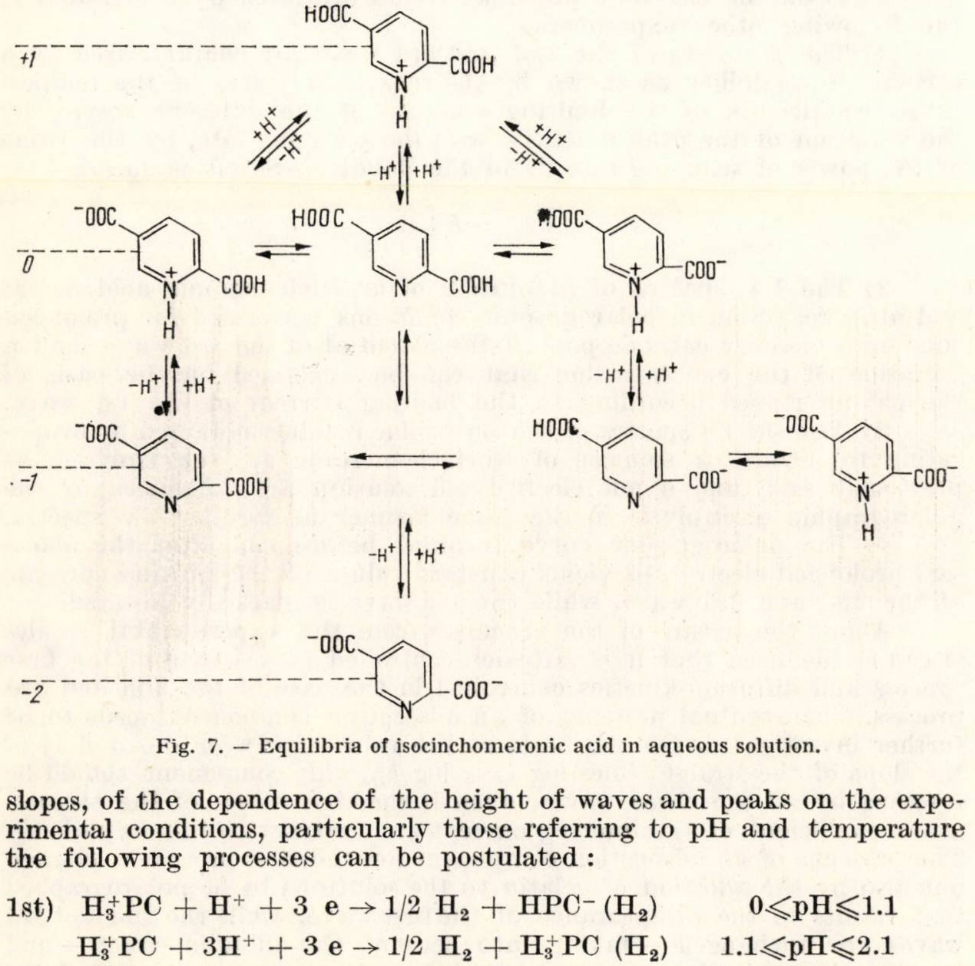

Fig. 7. – Equilibria of isocinchomeronic acid in aqueous solution.

1st) $H_3^+PC + H^+ + 3\ e \rightarrow 1/2\ H_2 + HPC^-\ (H_2)$ $\quad 0 \leqslant pH \leqslant 1.1$

$H_3^+PC + 3H^+ + 3\ e \rightarrow 1/2\ H_2 + H_3^+PC\ (H_2)$ $\quad 1.1 \leqslant pH \leqslant 2.1$

2nd) $H_3^+PC + 1\ e \rightarrow 1\ 2\ H_2 + H_2PC$ $\quad 0 \leqslant pH \leqslant 1.1$

$H_2PC + H^+ \rightleftarrows H_3^+PC \xrightarrow{e} 1/2\ H_2 + H_2PC$ $\quad 1.1 \leqslant pH \leqslant 4.6$

$HPC^- + 2H^+ \rightleftarrows H_3^+PC \xrightarrow{e} 1/2\ H_2 + H_2PC$ $\quad 4.6 \leqslant pH \leqslant 7.0$

3rd) $H_3^+PC + 1\ e \rightarrow 1/2\ H_2 + H_2PC$ $\quad 0 \leqslant pH \leqslant 1.1$

$H_2PC(zwitt) + H^+ \rightleftarrows H_3^+PC \xrightarrow{e} 1/2\ H_2 + H_2PC$ $\quad 1.1 \leqslant pH \leqslant 3.0$

$HPC^-\ (zwitt) + 2H^+ \rightleftarrows H_3^+PC \xrightarrow{e} 1/2\ H_2 + H_2PC$ $\quad 3.0 \leqslant pH \leqslant 5.1$

where H_3^+PC, H_2PC, HPC^- are the conjugated acids of the base PC^{--} (bivalent anion pyridinedicarboxylato), zwitt means zwitterion form and (H_2) indicates a species reduced in the ring (dihydroderivative).

While the first process is of a mixed nature, involving both a catalytic reduction of hydrogen ions and the reduction in the ring of the acid, the other two ones are only catalytic discharges of hydrogen. The hypothesis on the electrode processes is substantiated by the results of the following other experiments.

1) The processes of the 2nd and 3rd wave are characterized by a certain irreversibility as shown by the very high values of the temperature coefficients of the limiting currents of the different waves, by the variation of the peak potential with the scanning rate, by the value of the power of scanning rate Vs in the Randles—Sevcik equation

$$i_p = KVs^x$$

2) The UV spectra of a solution of isocinchomeronic acid before and after reduction in polarographic conditions performed for prolonged time on a mercury cathode pool at the potential of the 3rd wave show a variation of the concentration that can be explained on the basis of the charge passed according to the limiting current of the 1st wave.

3) Also the IR spectra of the crystalline residues obtained by evaporating to dryness a solution of isocinchomeronic acid electrolysed, as previously said, and a not electrolysed solution are influenced by the polarographic electrolysis in the same manner as for the UV spectra.

4) The polarographic curve recorded before and after the above said prolonged electrolysis yields constant values of the limiting currents of the 2nd and 3rd wave, while the 1st wave is markedly lowered.

About the nature of the processes from the experimental results it can be deduced that it is diffusion-controlled in the case of the first process and diffusion-kinetics controlled in the case of the 2nd and 3rd process. The eventual presence of an adsorption component needs to be further investigated. On the basis of the values (between 0.5 and 1) of the slope of the straight lines log i_d *vs* log h_{Hg} this component should be foreseen by all the three waves, even if the high values of the temperature coefficient of the limiting current are contrary to this hypothesis. The presence of an adsorption component for the first process is pointed out also by the addition of gelatin to the solutions to be polarographed that results in the disapearance of the first wave, while the 2nd and 3rd waves are unchanged — taking into account the dilution effect — and by the electrocapillary curves, recorded in the presence and not of the organic acid, from which the adsorption at the mercury electrode of a cationic species is evidenced (fig. 8).

Two objections can be advanced to the proposed mechanism. The first concerns the different $E_{1/2}$ values which result for the same process in the pH range 0—1.1 (hydrogen discharge catalysed by H_3^+PC); however, the nature of the process can account for this; at the potential of the first process gaseous hydrogen is formed on the dropping mercury electrode that becomes polarized so that an excess of tension must be applied in order to maintain the process.

A second objection regards the Kheifets slope. For diffusion-kinetics mixed processes this slope should fall in the interval 0–0.5, the limits of which take respectively for only kinetics and only diffusion-controlled processes, while our experimental values are higher than 0.5. This can be due to the increase of the mean electrode surface following the increase of the mercury height. Consequently the diffusion current and the electrode concentration of the reduced species increase, too. As according to our hypothesis the reducible species can be regenerated by the reduced ones, the recombination rate becomes higher. The kinetics component of the wave currents is thus enhanced; this increase must be added to that of the diffusion current: hence a slope higher than that expected of the Kheifets line.

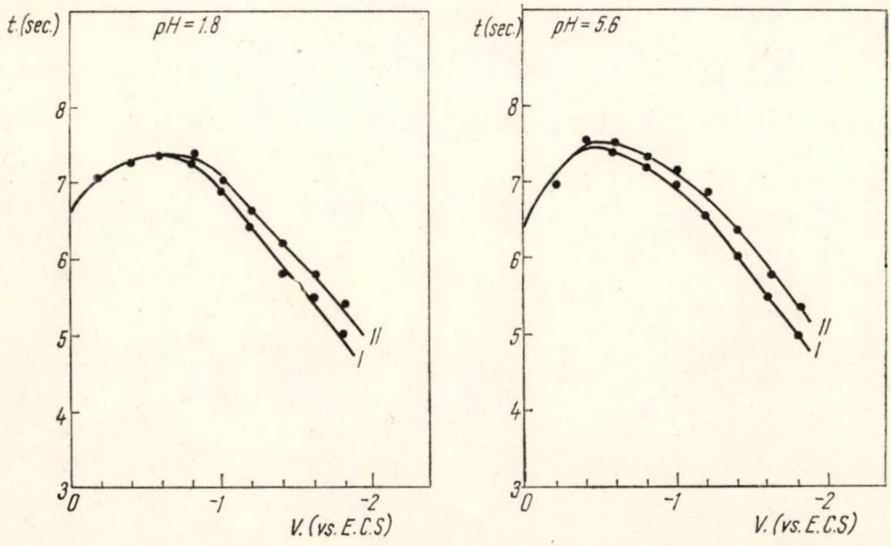

Fig. 8. — Electrocapillary curves in $NaClO_4$ 1 M (curve II) and in $NaClO_4$ containing isocinchomeronic acid (curve I).

Revue Roumaine de Chimie, **18**, *9*, 1659–1662 (1973)

SPECTROPHOTOMETRIC DETERMINATION OF THE PARTITION CONSTANT USING VARIABLE AMOUNTS OF SOLVENT

L. M. BĂLOIU

Technology Department, Academy of Economic Studies, Piaţa Romană, 6, Bucharest, Romania

Received January 4, 1973

A spectrophotometric method for the determination of the partition constant of compounds consisting of a basic dyestuff and a complex anion is proposed. Two extractions are performed, starting from identical aqueous solutions but using different amounts of solvent. From the absorbances of organic layers the partition constant can be calculated.

1. INTRODUCTION

In order to continue our researches concerning the determination of thermodynamic constants of systems consisting of complex anions and basic dyestuff cations,[1,2] we established a new method for the determination of the partition constant. The method of double extraction proposed before,[1] presents two disadvantages that, sometimes, could become important. First, the method can hardly be applied to systems with high partition constants. A rather complicated and more laborious technique, including the "slopes method"[1] must be used in this case. The second disadvantage is due to the fact that the separation of the two phases, during the first extraction, is not perfect, the second extraction being thus influenced.

The method proposed in this paper tries to avoid these disadvantages. Two identical samples are prepared and extracted, but with different amounts of solvent. The absorbances of the organic phases are afterwards compared and the partition constant is computed from these values.

---

[1] V. Armeanu, S. Oancea, S. Rusenescu and L. M. Băloiu, *Rev. Roumaine Chim.*, **17**, 925 (1972).

[2] L. M. Băloiu, *Rev. Roumaine Chim.*, **17**, 1065 (1972).

2. THEORETICAL PART

As the volume of the organic solvent is equal to the volume of the aqueous phase, the partition constant[3] is:

$$P = \frac{C_0}{C_w} = \frac{C_0}{C_i - C_0} \tag{1}$$

where C_i is the initial concentration of the studied compound in the aqueous phase (i.e. before extraction), C_w is the concentration of the compound in the aqueous phase after extraction and C_0 is the concentration of the compound in the organic phase.

According to Lambert-Beer's law

$$C_0 = \frac{A}{kl} \tag{2}$$

where A is the absorbance of the organic solution, k is the molar absorbance coefficient of the compound and l is the length of the cell.

Combining (1) and (2)

$$P = \frac{A}{klC_i - A} \tag{3}$$

In equation (3) P and k are not known.

If the extraction is carried out using a volume of organic solvent larger or smaller than the volume of aqueous phase, so that $V_0 = nV_w$ (n may be higher or smaller than unity)

$$P = \frac{C_0'}{C_w'} = \frac{C_0}{C_i - nC_0} \tag{4}$$

and, again

$$P = \frac{A}{klC_i - nA'} \tag{5}$$

The partition constant being "constant", the relations (3) and (5) allow to obtain P and k

$$P = \frac{A - A'}{nA' - A} \tag{6}$$

$$k = \frac{AA'(n-1)}{lC_i(A - A')} \tag{7}$$

---

[3] Iupac, *Information Bulletin*, **26**, 31 (1966).

Equations (6) and (7) can be demonstrated also considering the amounts of the substance in the two phases instead of the concentrations.

Let us have g grams of the compound solved in V_w cm³ of aqueous solution.

$$C = \frac{g}{V_w} \tag{8}$$

Through extraction, x grams pass in the organic solvent

$$P = \frac{\dfrac{x}{V_0}}{\dfrac{g-x}{V_w}} \tag{9}$$

When $V_0 = V_w$, equation (9) becomes

$$P = \frac{x}{g-x} \tag{10}$$

When $V_0 = nV_w$, we have

$$P = \frac{x'}{n\,(g-x')} \tag{11}$$

If x and x' are expressed in terms of the Lambert—Beer's law, we found immediately the relations (6) and (7).

3. APPLICATIVE PART

The method exposed has been verified by comparing it with the double extraction method, on the system $[Au(CN)_2]^-$—Paranitral Green.[4] The results obtained with the two methods are given in tables 1 and 2.

Table 1

The determination of the partition constant using the double extraction method

Solvent: benzene; $t° = 24°C$; $V_W = 10$ cm³; $V_0 = 10$ cm³; $l = 2$ cm

A	0.56	0.88	1.14	
A'	0.105	0.16	0.215	
P	4.28	4.50	4.30	*4.36*

---

[4] C. G. Călin, E. Diamandescu and L. M. Băloiu, *Rev. Roumaine Chim.*, **17**, 1765 (1972).

Table 2

The determination of the partition constant using the new method

Solvent = benzene ; $t^\circ = 24^\circ C$; $V_w = 10\ cm^3$; $l = 2$ cm ;
$A = 0.88$

n	1.2	1.5	2.0	0.5	
A'	0.76	0.63	0.485	1.49	
P	4.50	4.16	4.39	4.52	*4.39*

From the data presented, a good fitting can be observed, this proving the validity of the new method.

ORSZÁGOS MŰSZAKI KÖNYVTÁR ÉS DOKUMENTÁCIÓS KÖZPONT 1883

Revue Ruomaine de Chimie, 18, 9, 1663–1664 (1973)

COMPTES RENDUS

G. **MAIER**, *Valenzisomerisierungen*, Verlag Chemie, Weinheim/Bergstr., 1972 (Chemische Taschenbücher, N° 17)

The first review on valence isomerizations to be published in book form and the most complete so far, appears at a time when this field is in a period of fast development. Such a book is therefore both timely and stimulating, even though the rapidly accumulating new facts resolve some of the controversial issues and add new open questions.

The book is conceived in a highly pedagogical manner. The first pour chapters are introductory and describe respectively the basic definitions, the classification, the methods for investigation, and the Woodward-Hoffmann rules providing the theoretical basis of valence isomerizations. The next three chapters describe valence isomerizations in systems possessing only carbon atom chains : sigmatropic reactions involving conservation of the number of single and double bonds (including degenerate valence isomerizations), electrocyclic reactions involving the conversion of a double into a single bond, and intramolecular cycloadditions involving the conversion of a pair of double bonds into a pair of single bonds (in these conversions, the double bond becomes a single bond). The remaining five chapters describe valence isomerizations of systems with heteroatoms : oxygen, nitrogen, various other heteroatoms, ionic systems, and metallic complexes.

The literature coverage is excellent and reflects the wide interest of the author who is personally responsible for a significant number of developments in this fascinating field.

The graphical conditions are excellent and the clarity and abundance of formulas make the reading both pleasant and highly instructive. Perhaps broken lines for overlapping bonds would have helped in assisting a tridimensional grasp of molecular geometries. Further suggestions for future editions concern the more consistent use of symbol M for metal (instead, Me is once used on page 250), and the inclusion of a brief reference to olefin disproportionation (metathesis) in the last chapter. Finally, a more clear definition of "valence isomers" would have been convenient. Indeed, the definition on page 2 (bonding isomers) is not precise enough because it could incorrectly accomodate benzene (I) and fulvene (II) as valence isomers. A more strict (though technical) definition is that valence isomeric molecules are those which can be represented by connected graphs with the same partition of vertex degrees when only atoms with valence $\geqslant 2$ are considered. Of course, any definition has certain problems, and the author does not shun the difficulties raised by degenerate rearrangements which become non-degenerate on isotopic or substituent labelling (page 3) or the difference between valence tautomerism

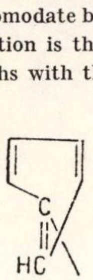

I

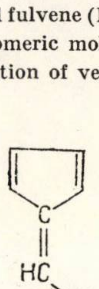

II

and mesomerism (pages 6—9) illustrated by semibullvalene with activating substituents or heteroatoms as proposed by R. Hoffmann.

In conclusion, the book is a well documented, clear and commendable review for all those interested in an up-to-date presentation of a rapidly expanding field in modern organic chemistry.

A. T. Balaban

F. A. COTTON and G. WILKINSON, "Advanced Inorganic Chemistry. A comprehensive text". Interscience Publishers, New York, 1972, 1145 p.

This volume is the third revised edition of the leading comprehensive text in the field. It contains a comprehensive bibliography of the rapidly growing literature of inorganic chemistry in its varied aspects (inorganic ring systems, complexes of — acceptor ligands, organometallic compounds, etc.). The bibliography covers the literature through mid—1971.

The book is organized into three major parts: (I) General Theory, (II) Chemistry of Nontransition Elements and (III) Chemistry of the Transition Elements. In the first part there is a brief theoretical introduction that contains a more extensive discussion of molecular symmetry, polyhedral structures and stereochemical nonrigidity and fluxionality. In comparison with the second edition, part two contains a more detailed descriptive and structural chemistry of inorganic ring systems. The major part of the book deals with the chemistry of the transition metals and incorporates the following topics: homogeneous catalysis and nitrogen activation by low-valent metal complexes; bio-inorganic chemistry of the transition metals; metal-metal bonding; complexes with CO, CNR, O_2, N_2 and NO ligands.

Any inorganic chemist who, like the present reviewer, became acquainted with "Advanced Inorganic Chemistry" as a graduate student and found it exceptionally stimulating can still profit from its critical and comprehensive survey of the inorganic chemistry.

The authors and the publisher are to be complimented on their effort, and this book is warmly commended to translation into Romanian.

Cezar Ungurenaşu

NOTE POUR LES AUTEURS

La *Revue Roumanie de Chimie* publie des articles en anglais, français, russe, allemand ou espagnol. Les auteurs sont priés d'envoyer des articles, notes, communications et comptes rendus inédits.

Les manuscrits seront dactylographiés à deux intervalles. Les tableaux seront dactylographiés sur feuilles séparées, de même que la légende des figures. Les diagrammes seront tracés à l'encre de Chine sur papier calque. Les tableaux et les figures seront numérotés par des chiffres arabes, en nombre strictement nécessaire. Prière de ne pas inscrire les mêmes données dans les tableaux et les figures. Les formules chimiques seront incluses dans le texte ; en outre, elles seront transcrites sur des feuilles séparées. Les auteurs sont priés d'indiquer les caractères italiques (en soulignant les lettres au crayon), ainsi que tout autre caractère spécial. L'ordre des références bibliographiques sera celui de leur mention dans le texte ; le nom de l'auteur sera précédé de l'initiale du prénom ; les publications périodiques seront présentées suivant les prescriptions internationales. Les références seront ajoutées à la fin de l'article ; elles paraîtront comme des notes, au bas de la page. Le texte sera précédé d'un résumé comprenant 15 lignes au maximum.

L'entière responsabilité du contenu des articles appartient aux auteurs. On publie des articles dus aux collaborateurs roumains ou étrangers. Les auteurs recevront 50 tirés à part.

PRINTED IN ROMANIA

TRAVAUX PARUS AUX ÉDITIONS DE L'ACADÉMIE DE LA RÉPUBLIQUE SOCIALISTE DE ROUMANIE

MARIA FIFI, **Dozimetria chimică a radiațiilor ionizante** (La dosimétrie chimique des radiations ionisantes), 1973, 240 p., 13,60 lei.

MIHAI FLORESCU, **Eficiența economică a cercetării științifice** (L'efficience économique de la recherche scientifique), 1972, 115 p., 15 lei.

GEORGETA LĂZĂRESCU, **Sistematizarea informațiilor în Chimia organică** (La systématisation des informations dans la chimie organique), 1972, 252 p., 10,15 lei.

P. BALTĂ et E. BALTĂ, **Introducere în chimia fizică a stării vitroase** (Introduction à la chimie physique de l'état vitreux), 1971, 240, 15,50 lei.

LYDIA-MARIA VAICUM, **Biodegrabilitatea detergenților** (La biodégrabilité des détergents), 1971, 254 p., 16 lei.

TIBERIU NĂSCUȚIU, **Metode radiometrice de analiză** (Méthodes radiométriques d'analyse), 1971, 346 p., 19,50 lei.

I. ZUGRĂVESCU et L. STOICESCU-GRIVETZ, **Polimeri heterociclici** (Polymères hétérocycliques), 1971, 190 p., 9,50 lei.

CRISTOFOR SIMIONESCU et C. V. UGLEA, **Fracționarea compușilor macromoleculari** (Fractionnement des composés macromoléculaires), 1962, 292 p., 18,50 lei.

I. MAXIM, **Materiale nucleare** (Matériaux nucléaires), 1969, 444 p., 30 lei.

CRISTOFOR SIMIONESCU et CLEOPATRA VASILIU-OPREA, **Mecanochimia compușilor macromoleculari** (La mécanochimie des composés macromoléculaires), 1967, 344 p., 23,50 lei.

CORNEL BODEA et collab., **Tratat de biochimie vegetală**, partea I, **Fitochimie** (Traité de biochimie végétale, Ire partie, Phytochimie), Ier vol., 1964, 747 p. + 4 annexes + 2 pl., 41 lei ; IIe vol., 1965, 1262 p., 1 pl., 56 lei ; IIIe vol., 1967, 773 p., 35 lei.

V. GHEȚIE et V. MICUȘAN, **Analiza imunochimică. Teorie și practică** (Analyse immunochimique. Théorie et pratique), 1966, 369 p., 28 lei.

R. PORTOCALĂ et L. POPA, **Acizii ribonucleici celulari și virali** (Les acides ribonucléiques cellulaires et viraux), 1966, 375 p., 8 pl., 26 lei.

D. PURDELEA et R. VÎLCEANU, **Chimia compușilor organici ai fosforului și ai acizilor lui** (La chimie des composés organiques du phosphore et de ses acides), 1965, 540 p., 37 lei.

1974 IAN 24

I.P.I. — c. 3144

43 426

Lei 25.—

F 1103

R

REVUE ROUMAINE DE CHIMIE

REFERÁLVA

TOME 18
N° 10
Octobre 1973
RRCHAX, **18**, *10*, 1665–1838 (1973)

ÉDITIONS DE L'ACADÉMIE DE LA RÉPUBLIQUE SOCIALISTE DE ROUMANIE

Rev. Roumaine Chim. **18**, *10*, p. 1665–1838 (1973), Bucarest

COMITÉ DE REDACTION

Rédacteur en chef:

I. G. MURGULESCU, membre de l'Académie de la République Socialiste de Roumanie

Rédacteurs en chef adjoints:

A. T. BALABAN et V. EM. SAHINI, membres correspondants de l'Académie de la République Socialiste de Roumanie

Collège de rédaction:

C. DRĂGULESCU, RALUCA RIPAN, CR. SIMIONESCU, membres de l'Académie de la République Socialiste de Roumanie; EM. BRATU, ECATERINA CIORĂNESCU-NENITZESCU, P. SPACU, membres correspondants de l'Académie de la République Socialiste de Roumanie; MARGARETA AVRAM, D. I. MARCHIDAN, G. NIAC et D. SĂNDULESCU

La Revue Roumaine de Chimie paraît 12 fois par an. Toute commande de l'étranger (fascicules ou abonnements) sera adressée à Intreprinderea Rompresfilatelia, Boîte Postale 2001, telex 011631, Bucarest, Roumanie

Les manuscrits, les livres et les revues proposés en échange, ainsi que toute correspondance seront envoyés à la rédaction:

REVUE ROUMAINE DE CHIMIE
23, Str. Dumbrava Roşie, Bucarest, Roumanie

ÉDITIONS DE L'ACADÉMIE DE LA RÉPUBLIQUE SOCIALISTE DE ROUMANIE
3 bis, str. Gutenberg, Bucarest

REVUE ROUMAINE
DE
CHIMIE

Tome 18, N° 10 Octobre 1973

I.G. MURGULESCU and EUGENIA IVANA, Absorption spectra of $PbCl_2$ and $PbBr_2$ in vapour phase . . . . 1667–1680 Ref
D.I. MARCHIDAN and SPERANŢA MATEI-TĂNĂSESCU, Thermodynamic data by solid state EMF technique and phase boundaries for some non-stoichiometric uranium oxides . . . . 1681–1684 Bcf
I.A. SCHNEIDER et G. RIESS, Influence du degré de dispersion sur la stabilité thermique des mélanges polystyrène-polyisoprène comportant du copolymère séquencé 1685–1688
CONSTANŢA HERDLICKA and S. STERNBERG, The interdiffusion coefficient of Pb^{2+} ion in fused alkali chlorides by the chronopotentiometric method . . . . 1689–1698 Ref
D. CISMARU and C. RADOVICI, The reaction kinetics in sub-micronic powders. The $ZrO_2 + CaO$ system . . . . 1699–1708 Ref
D. FĂTU, SANDA FĂTU et E. SEGAL, Cinétique des transformations du nitrate d'ammonium en régime non isothermique 1709–1714
S. PETRESCU, S. STERNBERG and VALERIA PETRESCU, The galvanostatic study of the electrochemical adsorption process on the chlorine – active carbon electrode in molten salts. II. Remanent potential 1715–1729
L.G. IONESCU, Some aspects of the chemistry of xenon and other noble gases 1731–1747
D. NEGOIU, VASILICA MUREŞAN and CORNELIA FULEA, Contributions to the chemistry of thiocomplexes. III. Complex compounds of Pd(II) with thioamides 1749–1757
J. ZSAKÓ, J. SATA und CS. VÁRHELYI, Electronic spectra of transition metal complexes. I. Ligand field parameters of some dimethylglyoximato-diamino-cobalt(III) complexes 1759–1767
I. DRIMUŞ and I.T. IONESCU, The influence of carbonyl or hydroxyl position on the breaking point of the linear twelve-membered carbon chain, by molecular oxygen 1769–1776
D. SUCIU and Z. GYÖRFI, Electronic spectra and acidity constants of some 2-amino-5-substituted 1,3,4-thiadiazoles 1777–1779
SCHELY AVRAMOVICI, A. AIRINEI et IOANA CIOCOIU, Les spectres électroniques de quelques bases de Schiff à noyaux benz- et naphtothiazoliques 1781–1792

Rev. Roumanie Chim. **18,** *10,* p. 1665–1838 (1973), Bucarest

JAMES W. PAVLIK, N. FILIPESCU, P.T. FRANGOPOL and MARIA FRANGOPOL, Photochemical addition of anthronylidene to alkenes 1793–1803

ATH. TRUŢIA and M. VODĂ, Spectrophotometric determination of Co^{2+} in $CdCl_2$ lattice 1805–1810

C. LITEANU, I.C. POPESCU and M. PREDA, Studies on the electroanalytical behaviour of membrane-electrodes under current. II. The *E*-pH electrode function and the use of a membrane-electrode of parchment paper impregnated with $BaSO_4$ in acid-base potentiometric titrations under constant direct current 1811–1817

I.C. POPESCU, C. LITEANU and M. PREDA, Studies on the electroanalytical behaviour of membrane-electrodes under current. III. The use of a membrane-electrode of parchment paper impregnated with $BaSO_4$ in potentiometric titrations by precipitating at constant direct current 1819–1824

Bq LUIGI CAMPANELLA, P.L. CIGNINI and G. DE ANGELIS, Influence of drying temperature on water content and cristalline characteristics of isocinchomeronic acid 1825–1827

CORNELIA BALABAN, GH. DOBRĂNIŞ and R. MIHAIL, Mass transfer in the absorption from a freely rising gas bubble under the action of mechanical vibrations 1829–1838

Revue Roumaine de Chimie, **18**, *10*, 1667–1680 (1973)

ABSORPTION SPECTRA OF $PbCl_2$ AND $PbBr_2$ IN VAPOUR PHASE

I.G. MURGULESCU and EUGENIA IVANA

Centre of Physical Chemistry,
Str. Galaţi 31, Bucharest, Romania

Received May 25, 1973

The absorption spectra of lead chloride and bromide were obtained in vapour phase in the 230–380 mμ range and the 530–660° temperature range. The absorption spectra were assigned to the gaseous $PbCl_2$ and $PbBr_2$ species. The vaporization heat was calculated for each species.

1. INTRODUCTION

The study of the vapour phase of lead halides [1–7] has suggested the conclusion that the only species present in the vapour phase are PbX_2 ($X = F$, Cl, Br).

Akishin [1] has nevertheless shown that the possibility of existing PbX species cannot be excluded. Klemperer *et al.*, [8] studying the geometry of gaseous lead halides have identified the PbI species in PbI_2 vapours.

Margrave *et al.*, [9] too, using the mass spectrometry method, have shown that at temperatures over 1000°, the PbF_2 in vapour phase is partly disproportioned in Pb and PbF_4; the gaseous lead reacts with PbF_2, and there results the PbF species in a 2% proportion.

The presence of PbCl and PbBr species in the $PbCl_2$ and $PbBr_2$ vapours was not proved by vapour pressure measurements, [2–4,6] though there exist certain indications on their formation at high temperatures and low pressures, and when the vapours are not in equilibrium with the condensed phase.[1,8,10-12]

---

[1] P. A. Akishin, V. P. Spiridonov and A. N. Khodcenko, *Zhur. fiz. Khim*, **32**, 1679 (1958).

[2] J. L. Barton and H. Bloom, *J. Phys. Chem.*, **60**, 1413 (1956).

[3] a. H. Bloom and J. W. Hastie, *Austr. J. Chem.*, **19**, 1003 (1966); b. H. Bloom, S. R. Richards and D. J. Williams, *Austr. idem*, **25**, 2077, (1972).

[4] H. Bloom and J. O'M Bookris, *J. Amer. Chem. Soc.*, **80**, 2044 (1958).

[5] L. C. George, R. M. Doerr and A. Visnapuu, *J. Chem. and Eng. Data*, **14**, 23 (1969).

[6] H. von Wartenberg and O. Borse, *Z. Elektrochem.*, **28**, 384 (1922).

[7] R. H. Hauge, H. W. Hastie and J. L. Margrave, *J. Phys. Chem.*, **72**, 3510 (1968).

[8] A. Buchler, J. L. Stauffer and W. Klemperer, *J. Amer. Chem. Soc.*, **86**, 4544 (1964).

[9] K. Zmbov, J. W. Hastie and J. L. Margrave, *Trans. Faraday Soc.*, **64**, 861 (1968).

Margrave,[13] studying the IR spectrum of gaseous $PbCl_2$ embedded in solid argon matrices, has observed new bands that he has assigned to the $(PbCl_2)_2$ species. This assignment is questionable, taking into account the matrix effects.

In this paper we have studied the absorption spectra in UV and visible of $PbCl_2$ and $PbBr_2$ vapours in equilibrium with the liquid in the 530—630° temperature range.

2. EXPERIMENTAL

The $PbCl_2$ and $PbBr_2$ were obtained by precipitating from Pb $(NO_3)_2$ *p.a.* with KCl and HBr, respectively. The KCl and $Pb(NO_3)_2$ were previously recrystallized. After a preliminary drying in a dry box, the halides were dried in vacuum and then melted. Gaseous HCl or gaseous HBr argon was passed for a few minutes through the melt to remove the acids. The $PbBr_2$ was then purified by vaporization in vacuum.

Since $PbCl_2$ and $PbBr_2$ have low vapour pressures at the melting point, we have built a furnace able to reach 1000° in order to have the possibility of using a wide range of temperatures (figure 1).

The furnace is made of the following parts:

1) a block of thermoinsulating brick;

2) a cooling mantle;

3) the heating resistance;

4) optical quartz windows;

5) pipe for cooling water.

The furnace has two independent heating systems, which are necessary to achieve an uniform temperature in the whole system. To make up for the heat losses through the two windows and meanwhile to avoid the vapour condensation surfaces of the cells, the furnace has an additional resistance fed separately at the ends.

The quartz cells with optical surface, built at the glass workshop of the Institute, are shown in figure 2.

The cell is made of: 1) optical windows; 2) a small reservoir for the substance; 3) a capillary to be closed by flame; 4) a ground glass tap for the direct insertion of the substance into the reservoir; 5) a vacuum tap to connect the device to the vacuum pump.

The cell used has a 2—5.5 cm length and a 2—3 cm diameter.

Before inserting the substance, the cell was washed for 20 minutes with dried and deoxygenated argon. It was then degased for approximately two hours and then closed by flame.

---

[10] Y. K. Delimarski, N. K. Tumanov and M. U. Prihodko, *Ukrain Khim. Zhur.*, **36** 1167 (1970).

[11] F. Morgan, *Phys. Rev.*, **49**, 47 (1936).

[12] G. A. Oldershaw and K. Robinson, *J. Chem. Soc. A*, **1971**, 2963.

[13] R. H. Hauge and J. L. Margrave, *High. Temp. Science*, **3**, 56 (1971).

The spectra were recorded by means of a "Standard GIBI" Carl Zeiss Jena recorder coupled to the monochromator of the VSU-1 spectrophotometer. A deuterium lamp was used as ultraviolet source.

We have found that after carring out the measurements and the gradual cooling of the cells, the solidified salt contains, included in it, a grey material. If the same sample is again brought to a vapour state, at the same temperature at which the former measurements were carried out, the absorption values are not perfectly reproducible. These changes observed could be the results of the thermal dissociation reaction :

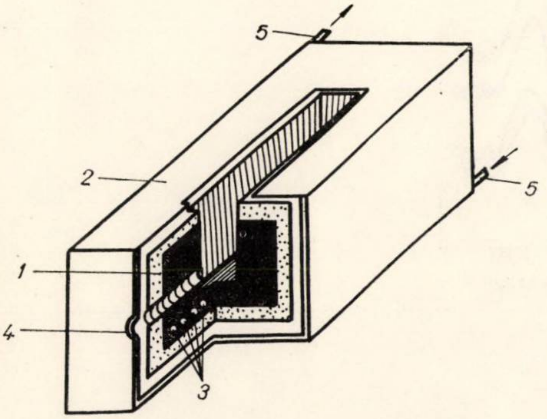

Fig. 1. — Furnace for high temperatures.

1, a block of thermoinsulating brick; 2, a cooling mantle; 3, the heating resistance; 4, optical quartz windows; 5, pipe for cooling water.

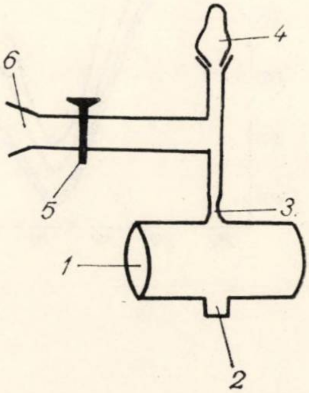

Fig. 2. — Quartz cell with optical windows.

1, optical windows; 2, a small reservoir for the substance; 3, a capillary to be closed by flame; 4, a ground glass tap; 5, a vacuum tap.

$$PbX_2(g) \rightarrow Pb(g) + X_2(g) \tag{I}$$

$$PbX_2(g) \rightarrow PbX(g) + 1/2\, X_2(g) \tag{II}$$

RESULTS AND DISCUSSIONS

The absorption spectra of the $PbCl_2$ and $PbBr_2$ vapours in equilibrium with the liquid are given in figures 3 and 4. Tables 1 and 2 give absorbance and the molecular absorption constants calculated according to the Lambert-Beer's law, for different wavelengths :

$$A = \chi cl \tag{1}$$

where : c — is the concentration, in moles/liters, and
l — is the thickness of the absorbant layer, in cm.

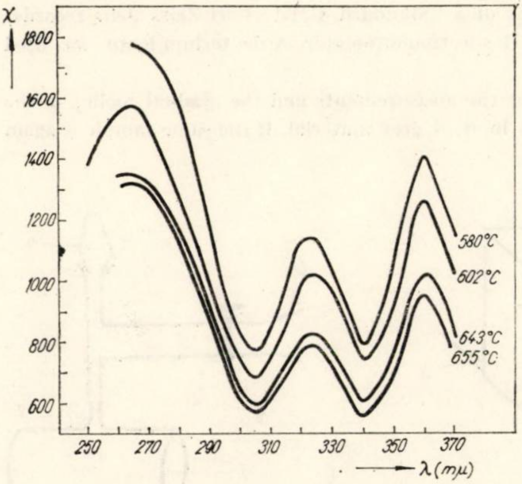

Fig. 3. — Absorption spectrum of gaseous $PbCl_2$.

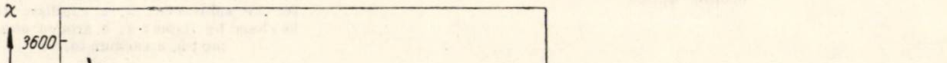

a

b

Fig. 4*a*. — UV absorption spectrum of gaseous $PbBr_2$; *b* — Visible absorption spectrum of gaseous $PbBr_2$.

Table 1

Absorption of gaseous $PbCl_2$

	$T = 853$ K $c=0.4\times10^{-4}$ mol/l $l = 5.5$ cm		$T = 875$ K $c=0.15\times10^{-4}$ mol/l $l = 2.3$ cm		$T = 928$ K $c=1.9\times10^{-4}$ mol/l $l = 3.2$ cm		$T = 916$ K $c=1.5\times10^{-4}$ mol/l $l = 2.3$ cm	
	A	*K*	*A*	*K*	*A*	*K*	*A*	*K*
250	—	—	0.206	1377	—	—	—	—
255	—	—	0.220	1471	—	—	—	—
260	—	—	0.223	1537	0.789	1297	0.462	1339
265	0.390	1778	0.229	1579	0.810	1332	0.465	1348
270	0.382	1741	0.215	1482	0.781	1284	0.448	1298
275	0.371	1694	0.212	1418	0.745	1225	0.425	1231
280	0.342	1559	0.192	1284	0.700	1151	0.404	1171
285	0.300	1367	0.173	1157	0.609	1001	0.355	1028
290	0.251	1144	0.146	976	0.516	848	0.300	869
295	0.214	975	0,124	829	0.440	723	0.255	739
300	0.181	825	0.110	735	0.373	613	0.216	626
305	0.167	761	0.102	681	0.346	569	0.205	594
310	0.183	834	0.112	749	0.370	608	0.212	614
314	0.2075	946	0.123	822	0.408	671	0.243	704
320	0.247	1126	0.145	999	0.468	769	0.277	802
324	0.249	1135	0.152	1016	0.479	787	0.289	837
330	0.2278	1038	0.139	956	0.444	730	0.268	776
340	0.171	779	0.109	729	0.327	539	0.203	588
350	0.235	1071	0.134	896	0.431	708	0.255	739
354	0.276	1258	0.164	1096	0.515	847	0.313	907
360	0.3092	1409	0.188	1257	0.577	949	0.352	1020
364	—	—	0.178	1190	—	—	0.342	991
370	0.250	1139	0.153	1023	0.476	782	0.288	834

The concentration was calculated from the vapour pressure by means of the ideal gas equation. The variation of vapour pressure with the temperature of the $PbCl_2$ and $PbBr_2$ was obtained from the equation established by Bloom *et al.* [2,4] by the boiling point method.

The linear dependence of the absorption on the vapour concentration, as required by the Beer's law is given in figures 5 and 6. Heats of vaporization of $PbCl_2$ and $PbBr_2$ were calculated from the graphical plot of the expression $\lg (A/l)T$ *versus* $1/T$ (figures 7 and 8), the resulting slopes having the value $-\Delta H/2.303$ R.

For lead chloride we found a vaporization enthalpy of 34 kcal/mol, and for lead bromide of 30 kcal/mol, in good agreement with the values obtained by other methods. [2,4,5]

Table 2

Absorption of gaseous $PbBr_2$

	$T = 815$ K $c = 0.4 \times 10^{-4}$ mol/l $l = 1.92$ cm		$T = 848$ K $c = 0.38 \times 10^{-4}$ mol/l $l = 3.2$ cm		$T = 886$ K $c = 1.82 \times 10^{-4}$ mol/l $l = 1.92$ cm		$T = 903$ K $c = 2.48 \times 10^{-4}$ mol/l $l = 3.2$ cm	
	A	*K*	*A*	*K*	*A*	*K*	*A*	*K*
250	0.271	3478	—	—	1.197	3429	—	—
255	0.228	2926	—	—	0.974	2790	—	—
260	0.206	2644	0.668	2491	0.834	2398	—	—
265	0.170	2182	0.547	2039	0.692	1982	—	—
270	0.138	1771	0.455	1700	0.581	1664	—	—
275	0.121	1553	0.400	1491	0.516	1478	—	—
280	0.114	1463	0.375	1398	0.468	1340	1.061	1336
285	0.109	1399	0.367	1368	0.455	1303	1.000	1260
290	0.111	1424	0.374	1395	0.474	1361	1.073	1352
295	0.131	1681	0.401	1495	0.505	1447	1.118	1408
300	0.137	1772	0.433	1615	0.528	1510	1.196	1504
305	0.146	1876	0.449	1674	0.544	1558	1.225	1536
308	0.146	1876	0.454	1693	0.544	1558	1.227	1546
310	0.144	1848	0.446	1663	0.540	1545	1.221	1538
314	—	—	0.436	1625	0.520	1492	1.131	1425
320	0.128	1643	0.402	1499	0.496	1421	1.035	1304
330	0.098	1258	0.325	1211	0.401	1149	0.868	1093
340	0.080	1026	0.252	939	0.306	876	0.652	821
350	0.066	847	0.196	731	0.239	684	0.531	669
360	0.062	795	0.178	664	0.216	618	0.431	543
370	0.062	795	0.176	656	0.212	610	0.428	539
380	0.059	757	0.157	585	0.191	547	—	—
400	0.103	1763	0.166	1289	0.356	1178	—	—
402	0.117	2003	0.185	1434	0.382	1264	—	—
404	0.120	2054	0.189	1465	0.395	1307	—	—
406	0.127	2176	0.196	1519	0.409	1354	—	—
408	0.138	2370	0.202	1565	0.428	1417	—	—
410	0.129	2208	0.195	1511	0.424	1403	—	—
412	0.122	2089	0.196	1519	0.412	1364	—	—
414	0.121	2071	0.187	1449	0.395	1308	—	—
418	0.109	1893	0.179	1356	0.363	1201	—	—
420	0.109	1893	0.153	1186	0.339	1122	—	—
424	0.111	1900	0.141	1093	0.309	1023	—	—
428	0.092	1575	0.119	922	0.263	870	—	—
430	0.079	1352	0.113	875	0.238	788	—	—
434	0.066	1130	0.094	728	0.200	662	—	—
440	0.056	958	0.075	581	0.149	490	—	—

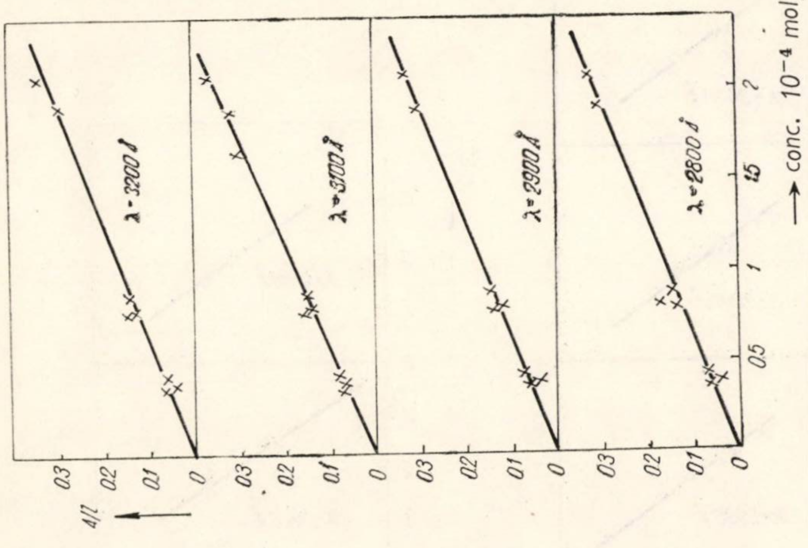

Fig. 6. — Dependence of the gaseous $PbBr_2$ absorption on concentration.

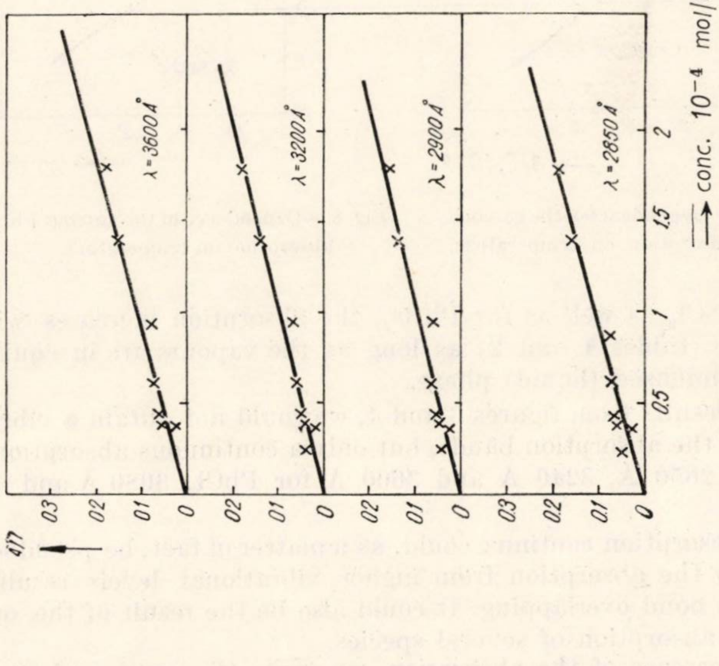

Fig. 5. — Dependence of the gaseous $PbCl_2$ absorption on concentration.

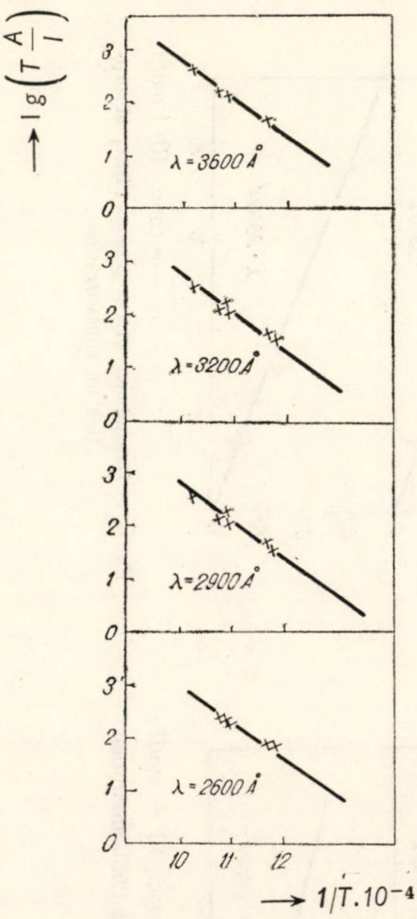

Fig. 7. — Dependence of the gaseous $PbCl_2$ absorption on temperature.

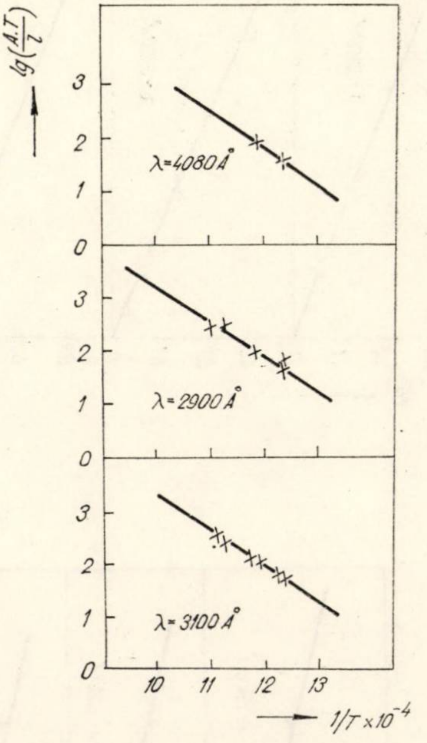

Fig. 8. — Dependence of the gaseous $PbBr_2$ absorption on temperature.

For $PbCl_2$ as well as for $PbBr_2$, the absorption increases with the temperature (tables 1 and 2) as long as the vapours are in equilibrium with the condensed (liquid) phase.

As it results from figures 3 and 4, we could not obtain a vibrational structure of the absorption bands, but only a continuous absorption, with maxima at 2650 Å, 3240 Å and 3600 Å for $PbCl_2$, 3080 Å and 4080 Å for $PbBr_2$.

The absorption continua could, as a matter of fact, be pseudocontinuous due to the absorption from higher vibrational levels resulting in considerable bond overlapping. It could also be the result of the overlapping of the absorption of several species.

The decrease of the absorption constants (figures 3 and 4) calculated from equation (1) with the temperature increase is particularly striking. The phenomenon is brought about by the thermal dissociation [14–19] of the lead halides, according to equation (1). The absorption of the lead vapours (very low concentration [20]), in the temperature range in which the absorption measurements were carried out, is negligible, scarcely exceeding the experimental errors (table 3).

Table 3

Absorption of Pb vapours

	$T = 851$ K $c = 3.7 \times 10^{-9}$ mol/l	$T = 920$ K $c = 5 \times 10^{-8}$ mol/l
	A/l	A/l
240	0.018	0.01
250	0.014	0.009
260	0.01	0.01
270	0.011	0.01
290	0.007	0.008
310	0.005	0.005
320	0.006	0.007
330	0.006	0.007
350	0.006	0.006

As the chlorine [21] absorbs very little in the wavelength range used, the phenomenon is exceedingly simple in the case of lead chloride, where the decrease of the absorption constants is partly due to the decrease of the concentration of its vapours which advances with the temperature increase. Therefore, we shall first consider the absorption of the lead chloride vapours.

Writing α the dissociation degree and χ_0 the real absorption constant, we may write (for a certain wavelength):

$$A = \chi_0(1 - \alpha)cl \tag{2}$$

From (1) and (2) there results:

$$\alpha = 1 - (\chi/\chi_0) \tag{3}$$

---

[14] A. Kaldor and D. A. Somorjai, *J. Phys. Chem.*, **70**, 3538 (1966).

[15] D. J. Morentz, R.A.M. Scott and J. J. Shortland, *J. Phys. Chem. Solids*, **33** 1235 (1972).

[16] C. Renz, *Z. anorg. Chem.*, **116**, 62 (1921).

[17] W. C. Tennant, *J. Phys. Chem.*, **70**, 3523 (1966).

[18] K. J. De Vries and J. H. von Santen, *Physica*, **30**, 2051 (1964).

[19] J. F. Verwey, *J. Phys. Chem. Solids*, **31**, 163 (1970).

[20] A. N. Nesmeianov, "Vapour Pressure of Chemical Elements", Academic Press, New York, 1963, p. 352.

[21] a. G. E. Gibson and N. S. Bayliss, *Phys. Rev.*, **44**, 193 (1933); b. G. Zimmerman and F. C. Strong, *J. Amer. Chem. Soc.*, **79**, 2063 (1957).

The real constant χ_0 may be estimated by extrapolating the values of the experimental constants at a temperature at which it turns practically to nil. We have chosen the melting temperature of the lead salt as the extrapolation temperature, at which we suppose that, in the given conditions, its thermal dissociations is negligible.

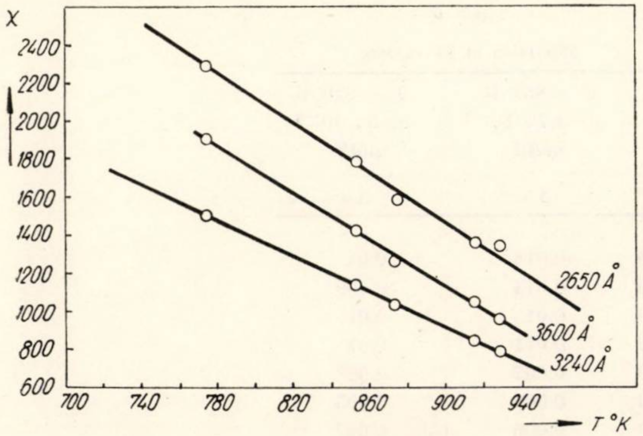

Fig. 9. — Dependence of χ on temperature for gaseous $PbCl_2$.

Figure 9 gives the extrapolation of the maximal absorption constants of lead chloride for the three above mentioned wavelengths.

We thus obtain the values : 2290 $l \cdot cm^{-1} \cdot mol^{-1}$; 1500 $l \cdot cm^{-1} \cdot mol^{-1}$ and 1900 $cm^{-1} \cdot mol^{-1}$ for 2650 Å, 3240 Å and 3600 Å. Table 4 gives the values of α calculated according to equation (3).

Table 4

Dissociation degree of $PbCl_2$ calculated according to equation (3)

(Å)	853 K	875 K	916 K	928 K
2650	0.224	0.330	0.411	0.418
3240	0.244	0.321	0.441	0.477
3600	0.259	0.338	0.460	0.500
α_m	0.242	0.329	0.437	0.465

Proceeding in the same way as for lead chloride to estimate the degree (equation 3) of lead bromide, χ_0 was obtained by extrapolating the absorption constants only for the 3080 Å maximum, in visible, the contribution of the bromide absorption being high (figure 10).

Table 5 contains the values of the dissociation degree of the lead bromide.

From table 4 and 5 it results that the dissociation degree of lead bromide is higher than that of lead chloride at approximately the same temperature. This fact is in agreement with the variation of lead halides properties when passing from chlorides towards iodides.

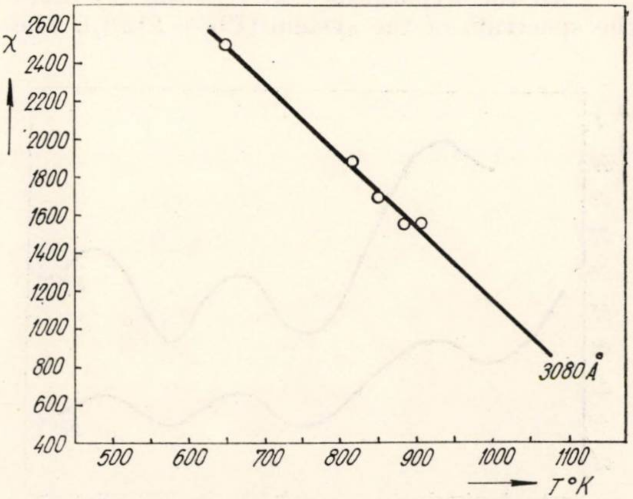

Fig. 10. — Dependence of χ on temperature for gaseous $PbBr_2$.

Since the extrapolation temperature, used for evaluating the true constant χ_0, is arbitrary, the dissociation degree includes large uncertainties; the equilibrium constant cannot be therefore estimated from these values.

Table 5

Dissociation degree of $PbCl_2$ calculated according to equation (3)

815 K	848 K	886 K	903 K
0.23	0.32	0.36	0.39

The presence of the dimer $(PbX_2)_2$ does not result from the study of the influence of the temperature on the spectra of the $PbCl_2$ and $PbBr_2$ vapours. Even if the former should exist, its high instability would bring about the decrease of its concentration with the temperature. Neither the vapour pressure measurements, nor mass spectrometry [3b] have pointed out the presence of dimers.

The lead resulting from reaction (i) can react with PbX_2 vapours in two ways :

$$Pb_{(e)} + PbX_{2(e)} \rightarrow 2PbX_{(e)} \qquad (a)$$

$$Pb_{(g)} + PbX_{2(g)} \rightarrow 2PbX_{(g)} \qquad (b)$$

The ESR [22] measurements on PbX_2, irradiated in UV at the liquid nitrogen temperature, have shown the presence of Pb^+ formed as an intermediary state in the photochemical decomposition. The formation of the Pb^+ ion resulting from reaction (a) was also proved by polarographic studies. [10,23]

In the hypothesis that reaction (b) takes place, we have obtained the spectrum of the system ($Pb + PbCl_2$). The spectra are very similar (figure 11) to those obtained in the absence of lead. The maximum intensity absorption appears at the same wavelength; the absorption has nearly the same values for lower temperatures. At higher temperatures, the differences remain very small.

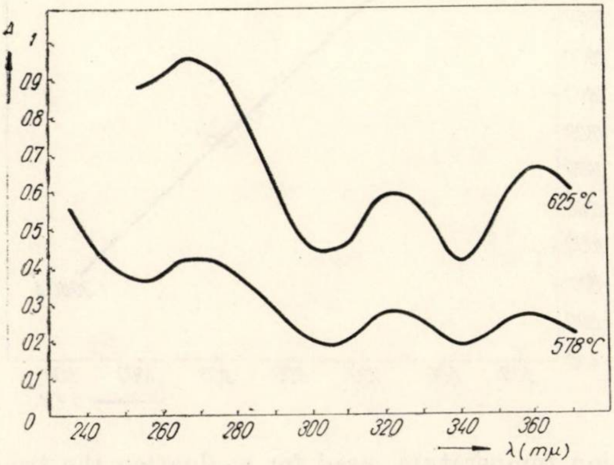

Fig. 11. — Absorption spectra of the $Pb + PbCl_2$ system.

The $PbX_{(g)}$ concentration [24] resulting from reaction (b), if this reaction takes place indeed, is extremely small, taking also into account the very low concentration of $Pb_{(g)}$.

Wieland *et al.* [25] have shown that at 1000°, at low pressure and when the vapours are not in equilibrium with the liquid phase, the following (thermal dissociation) reaction takes place :

$$PbCl_2 \rightarrow PbCl + 1/2\ Cl_2 \qquad \text{(III)}$$

$$PbCl_2 \rightarrow Pb + Cl_2 \qquad \text{(IV)}$$

at a percentage of 0.05%.

In our actual working conditions (temperatures under 700°, pressures higher than $5 \cdot 10^{-2}$ atm and equilibrium of the vapours with the liquid), the concentration of the PbX resulting from reaction (3) can only be very low.

---

[22] J. Arendsy and J. F. Verwey, *Phys. Status. Solidi*, **23**, 137 (1967).

[23] J. J. Egan, *J. Phys. Chem.*, **65**, 2222 (1961).

[24] A. W. Searcy, "Progress in Inorganic Chemistry", vol. III, Ed. F. A. Cotton, 1962, p. 102.

[25] K. Wieland and R. Newburgh, *Helv. Phys. Acta*, **25**, 87 (1952).

On the basis of the results given in literature — as mentioned above — we must underline that the PbX (X = Cl, Br) does not result normally in the vaporization process, but appears owing to the working conditions : thermal dissociation (in the mentioned conditions) and/or photochemical decomposition.

Butkow[26] and Samuel[27] have supposed that the first high wavelength absorption range would be due to the photodissociation reaction :

$$PbX_2 \rightleftarrows PbX + 1/2\ X_2 \qquad (V)$$

Margrave,[7,28,29] on the contrary, using the extended Hückel calculation method has shown that for $PbCl_2$ the absorption with a maximum at 3600 Å (the first band towards the high wavelengths) corresponds to the transition $^1A_1$ —— $^1B_1$. Contrary to Butkow, Margrave has considered the photochemical decomposition of type (V) reaction as responsible for the continuous absorption to be found at 31000 cm^{-1} (3.83 eV) in the $PbCl_2$ spectrum and at 31044 cm^{-1} (3.84 eV) for the $SnCl_2$.

Taking into account the way in which the strength of the F-MF and F-A varies, when substituting Sn by Pb and F by Cl, for the same metal (Sn or Pb), we reach the conclusion that the value of the breaking energy[12] of the Pb-Cl bond cannot exceed 4.37 eV (35293 cm^{-1}), the breaking energy of the Sn-Cl bond.

In our experiments, the sample was continuously irradiated with radiations in the 540000—280000 cm^{-1} range, which means that the radiation energy was far higher than what was needed for the PbX dissociation.

We admit that the absorption is due to the PbX_2 species (X = Cl, Br) with very small contributions of the Pb, Br and Cl vapours. Thus, the chlorine[21] which absorbs in this range also contributes to the continuous absorption in the $PbCl_2$ spectrum with a maximum intensity at 3200 Å.

The absorption of the bromine vapours in UV[30] has little effect, this taking place under 2500 Å and over 4000Å. In visible, the contribution to the absorption due to the bromine is higher, being well-known the fact that it has a maximum around 4240 Å.

The assignment of the observed spectra to the $PbCl_2$ and $PbBr_2$ species is based on the following facts :

— the temperatures are much lower than those given by Morgan,[11] Rochester[31] and Wieland[24] to form the PbX species ;

— the vapours were in equilibrium with the liquid phase ;

---

[26] K. Butkow, *Phys. Z. Sow.*, 4, 906 (1933).

[27] R. Samuel, *Rev. Mod. Phys.*, **18**, 103 (1946).

[28] J. W. Hastie, R. H. Hange and J. L. Margrave, *J. Mol. Spectroscopy*, **29**, 152 (1969).

[29] J. W. Hastie and J. L. Margrave , *J. Phys. Chem.*, **73**, 1105 (1969).

[30] A. A. Passchier, J. D. Christian and N. W. Gregory, *J. Phys. Chem.*, **71**, 937 (1967).

[31] G. D. Rochester, *Proc. Roy Soc.*, **153**, 407 (1936).

— the vaporization heat calculated (figures 7, 8) for the wavelength, where the intensity is maximum (on both sides), has the same value: 34 kcal/mol for $PbCl_2$ and 30 kg/mol for $PbBr_2$, values nearly equal to those obtained by other methods.[2,4,5]

— the proportionality coefficient of the absorption variation with the concentration has the same value for the wavelengths where the intensity is maximal;

— within the sensitivity ranges of the apparatus — if we resume the measurements for a sample cooled at room temperature — we notice that the differences are very small and that the temperature variation of the absorption is the same as in the first measurements;

— the presence of PbX species should have given in the spectrum an absorption with a maximum intensity at 4.36 eV (2843 Å) for PbCl, and for PbBr a strong absorption between 2700 and 3000 Å, corresponding to the transition $^2\Sigma - {}^2\Pi$.

Revue Roumaine de Chimie, **18**, *10*, 1681–1684 (1973)

THERMODYNAMIC DATA BY SOLID STATE EMF TECHNIQUE AND PHASE BOUNDARIES FOR SOME NONSTOICHIOMETRIC URANIUM OXIDES

D.I. MARCHIDAN and SPERANŢA MATEI-TĂNĂSESCU

Centre of Physical Chemistry,
Str. Galaţi 31, Bucharest, Romania

Received May 8, 1973

Electromotive force measurements on high-temperature galvanic cells containing solid electrolyte have been carried out in order to obtain thermodynamic data for some uranium oxides which are part of the two-phase region $U_4O_9 + U_3O_{8-y}$. Partial molar free energies, enthalpies and entropies of solution of oxygen in uranium oxides and the corresponding relative integral quantities as a function of temperature, as well as the equilibrium pressures of oxygen over the oxides have been calculated.

The phase relationships in the uranium-oxygen system have been studied by many authors by means of different experimental techniques and methods. [1–5] But, although many of the high temperature thermodynamic data for uranium compounds in the $UO_2-U_4O_9-U_3O_{8-y}$ regions are now well established, a number of inconsistencies still remain because there are still some doubts concerning the precise position of the phase boundaries.

In previous papers [6,7] we have related the values of the thermodynamic properties of some uranium oxides with nonstoichiometric compositions which within certain temperature ranges are found disproportioned in two phases. The method used was that of electromotive force measurements on galvanic cells with solid electrolyte.

In the present paper, the oxides $UO_{2.28}$ and $UO_{2.30}$ are discussed. Determinations were made with a high-temperature galvanic cell of the type:

Fe, wüstite | (0.85 ZrO_2 + 0.15 CaO) | Uranium oxide

---

[1] S. Aronson and J. Belle, *J. Chem. Phys.*, **29**, 151 (1958).

[2] K. Kiukkola, *Acta Chem Scand.*, **16**, 327 (1962).

[3] T. L. Markin, L. E. J. Roberts and A. Walter, "Thermodynamics of Nuclear Materials", Ed. I.A.E.A., Vienna, 1962, p. 693.

[4] P. E. Blackburn, *J. Phys. Chem.*, **62**, 897 (1958).

[5] F. J. Grønvold, *J. Inorg. Nuclear Chem.*, **1**, 357 (1955).

[6] D. I. Marchidan and S. Matei, *Rev. Roumaine Chim.*, **17**, 195 (1972).

[7] D. I. Marchidan and S. Matei, *Rev. Roumaine Chim.*, **17**, 9 (1972).

EXPERIMENTAL

The cell assembly consisting of the electrolyte tablet between the two electrode tablets was inserted into a quartz cell, the form and construction of which have been previously shown[8,9].

The EMF measurements were carried out in a vacuum installation at the residual gas pressure of about 133.322 × 10^{-6} N.m^{-2}. The apparatus, the experimental procedure and the techniques of preparing the tablets were also minutely described in the above mentioned papers.[8,9]

RESULTS AND DISCUSSION

The nonstoichiometric oxides $UO_{2.28}$ and $UO_{2.30}$ were studied in the temperature range of 1123–1373 K.

The EMF values for these compositions are practically identical (fig. 1) indicating the presence of a two-phase region. Actually, as the phase diagram[10-12] shows it, it is the two-phase region $U_4O_9 + U_3O_{8-y}$.

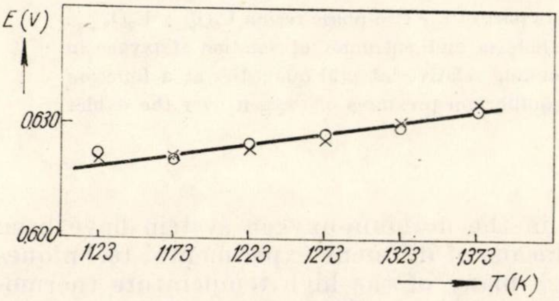

Fig. 1. – Variation of EMF with the temperature for $UO_{2.28}$ and $UO_{2.30}$.

At higher temperatures, they are in excellent agreement with the results obtained by other methods for compositions within the range $UO_{2.25}$ to $UO_{2.60}$.

The $\Delta\bar{G}_{O_2}$ values obtained by the EMF method on two samples of compositions $UO_{2.28}$ and $UO_{2.30}$ are plotted as a line in fig. 2. We observed that the values of partial molar free energy do not practically change with composition and, even more, the values are practically identical with those obtained for the oxides $UO_{2.37}$ and $UO_{2.54}$ (fig. 2), indicating that the four oxides are part from the same two-phase region.

The determination of the lower and upper limits of the U_4O_9 and U_3O_8 phases has been the object of a great number of investigations. However, the equilibrium composition of each phase is somewhat uncertain.[11] The determinations of the U_4O_9 phase boundaries by Blackburn

---

[8] D. I. Marchidan and S. Matei, *Rev. Roumaine Chim.*, **15**, 1491 (1970).

[9] D. I. Marchidan and S. Matei, *Studii şi Cercetări Chim. Acad. R.S.R.*, **18**, 617 (1970).

[10] L. E. J. Roberts and A. Walter, *J. Inorg. Nuclear Chem.*, **22**, 213 (1961).

[11] M. H. Rand and O. Kubaschewski, "The Thermochemical Properties of Uranium Compounds", Oliver and Boyd, Edinburgh, 1963, p. 26.

[12] "Thermodynamic and Transport Properties of Uranium Dioxide and Related Phases", Technical Report Series N° 39, Ed. I.A.E.A., Vienna, 1965, p. 3.

are scattered (varying irregularly from $UO_{2.254}$ to $UO_{2.279}$), while Roberts and Walter found that the upper limit of this phase is practically constant at $UO_{2.25}$.

We have measured for $UO_{2.28}$ and $UO_{2.30}$ at 1273, 1323, 1373 K identical pressures. This fact together with scattering of Blackburn's points determined us to agree with Roberts and Walter's measurements and take $UO_{2.25}$ as the upper limit of the U_4O_9 phase. This may be considered the upper limit at all temperatures up to 1395 K since, as Roberts and Walter showed, the U_4O_9 phase dissociates at about 1396 K; at higher temperatures a limiting UO_{2+x} phase is in equilibrium with U_3O_{8-y}.

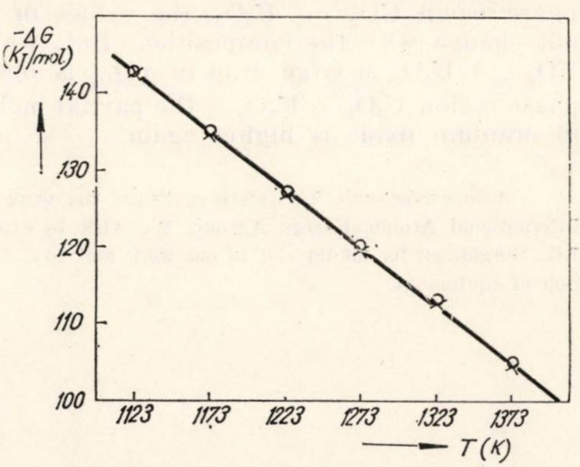

Fig. 2. – Variation of $\Delta\overline{G}_{O_2}$ with the temperature for $UO_{2.28}$ and $UO_{2.30}$.

The lower limit of the U_3O_{8-y} phase was given by Biltz and Müller[13] as $UO_{2.607}$ at 1273 K and by Blackburn[4] as $UO_{2.607}$ to $UO_{2.616}$ at 1125 K to 1399 K, as suggested by the equilibrium measurements. The results

Table 1

Thermodynamic data for the two-phase region $U_4O_9 + U_3O_{8-y}$ obtained from measurements on $UO_{2.28}$ and $UO_{2.30}$

Temp. K	$-\Delta\overline{G}_{O_2}$ ($KJ\cdot mol^{-1}$)	$-\Delta G$ ($KJ\cdot mol^{-1}$)	$-\Delta G/n_{UO_2}$ (KJ/g atom uranium)	$\log p_{O_2}$ ($N\cdot m^{-2}$)
1123	142.745	17.526	19.982	1.574
1173	135.264	16.610	18.936	0.954
1223	127.398	15.643	17.836	0.374
1273	120.264	14.765	16.836	−0.136
1323	113.097	13.886	15.832	−0.606
1373	104.959	12.886	14.694	−1.076

$-\Delta\overline{H}_{O_2}$ ($KJ\cdot mol^{-1}$) = 311.197 $-\Delta\overline{S}_{O_2}$ ($KJ\cdot mol^{-1}$) = 0.035

$-\Delta H$ ($KJ\cdot mol^{-1}$) = 38.215 $-\Delta S$ ($KJ\cdot mol^{-1}$) = 0.0184

$-\Delta H/n_{UO_2}$ ($KJ\cdot mol^{-1}$) = 43.569 $-\Delta S/n_{UO_2}$ ($KJ\cdot mol^{-1}$) = 0.021

---

[13] W. Biltz and H. Müller, *Z. anorg. Chem.*, **163**, 257 (1927).

of Markin and Roberts indicate that the limiting composition is constant from 1396 to 873 K and probably nearly so from 1723 to 873 K. We have accepted the limit [3] as $UO_{2.61}$ from 873 to 1473 K.

Anyway, more data are required on partial molar quantities in the U_3O_{8-y} region at all temperatures and in the U_4O_{9-y} region below 1273 K.

From data given in table 1, one may see that similar to the two-phase region $UO_{2+x} + U_4O_9$, the values of partial molar free energy do not change with the composition. But, while for the two-phase region $UO_{2+x} + U_4O_9$, a large drop in $\Delta\overline{H}_{O_2}$ is observed, for the second two-phase region $U_4O_9 + U_3O_{8-y}$ the partial molar heat of solution of oxygen in uranium oxide is higher again.

Acknowledgements. This work continues the work performed under a contract with the International Atomic Energy Agency. We wish to express our deep gratitude to Professor I.G. Murgulescu for his interest in our work and to C. Volcovici, for his help in the construction of equipment.

Revue Roumaine de Chimie, **18**, *10*, 1685–1688 (1973)

INFLUENCE DU DEGRÉ DE DISPERSION SUR LA STABILITÉ THERMIQUE DES MÉLANGES POLYSTYRÈNE-POLYISOPRÈNE COMPORTANT DU COPOLYMÈRE SÉQUENCÉ

I. A. SCHNEIDER * et G. RIESS **

* Laboratoire de Chimie-Physique, Université de Jassy, Roumanie
** École Supérieure de Chimie, Mulhouse, France

Reçu le 16 mars 1973

Par méthode thermogravimétrique on étudie les alliages de polymères formés de polystyrène (PS) et de polyisoprène (PI). L'addition de copolymère séquencé PS-PI permet de régler le degré de dispersion de ces mélanges. En opérant dans des conditions thermiques standards et pour une composition globale en PS donnée, on montre qu'il existe une corrélation directe entre la stabilité thermique, exprimée par l'énergie d'activation apparente, et le degré de dispersion d'une phase polymère dans l'autre.

L'interaction dans des mélanges de polymères a été étudiée par Schneider et ses collaborateurs [1] à l'aide d'une méthode thermogravimétrique en connexion avec un examen de microscopie optique. En opérant dans des conditions standards, ces auteurs ont montré qu'il existe une correspondance entre la stabilité thermique, exprimée par l'énergie d'activation apparente pour ces conditions opératoires, et la « compatibilité apparente », c'est-à-dire le degré de dispersion d'une phase polymère dans l'autre. Ils ont ainsi observé que pour des mélanges de deux homopolymères il existe des proportions caractéristiques pour lesquelles cette « compatibilité apparente » est obtenue et qui peuvent présenter de ce fait une stabilité thermique accrue.

Par ailleurs, Riess et ses collaborateurs [2] ont montré que le degré de dispersions d'un mélange de deux polymères A et B peut être réglé par addition de copolymères séquencés ou greffés A–B correspondant aux homopolymères.

---

[1] C. Vasile, F. Sandru, I. A. Schneider et N. Asandei, *Makromol. Chem.*, **110**, 20 (1967) ; C. Vasile, S. Ioan, N. Asandei et I. A. Schneider, *Angew. Makromol. Chem.*, **6**, 24 (1969) ; I. A. Schneider et C. Vasile, *European Polymer J.*, **6**, 687, 895 (1970) ; **7**, 1205 (1971).

[2] J. Kohler, A. Banderet, G. Riess et C. Job, *R.G.C.P. « Plastiques »*, **46**, 1317 (1969) ; G. Riess, Iupac Meeting, Budapest, 1969 ; J. Periad, A. Banderet et G. Riess, *Angew. Makromol. Chem.*, **15**, 37, 55 (1971).

Le degré de dispersion d'une phase dans l'autre pouvant ainsi être ajusté de façon précise, il était intéressant de confirmer la corrélation entre la stabilité thermique, donnée par l'énergie d'activation apparente, et les dimensions des phases polymères.

Une telle étude a donc été effectuée pour le système polystyrène-polyisoprène comportant des proportions variables de copolymère biséquencé polystyrène-polyisoprène (Cop SI) ou triséquencé (Cop SIS).

PARTIE EXPÉRIMENTALE

Les homopolymères et les copolymères séquencés ont été préparés par polymérisation anionique selon Szwarc [3] dans le but d'obtenir des polymères relativement monodispersés et comparables entre eux du point de vue structure. Les caractéristiques des polymères utilisés dans ce travail sont présentées dans le tableau 1.

Tableau 1

Caractéristiques des polymères et copolymères

Polymère	Notation	Composition	Poids moléculaire
Polystyrène radicalaire	PS-r		M_w = 300 000
Polystyrène anionique	PS-a		M_w = 396 000
Polyisoprène anionique	PI		M_w = 41 500
Copolymère biséquencé	SI-17	61S/39I	M_n = 94 000
Copolymère biséquencé	SI-18	68S/32I	M_n = 40 500
Copolymère biséquencé	SI	25S/75I	M_n = 109 000
Copolymère triséquencé	SIS	13S/87I	M_n = 85 000

En employant le polystyrène radicalaire PS-r, un polyisoprène anionique de M_w = 53300 et le copolymère biséquencé SI-17, trois alliages de polymères ont été préparés, qui comportent des proportions croissantes du copolymère pour augmenter le degré de dispersion et par la «compatibilité apparente» du système PS-PI incompatible. Les alliages de polymères ont été obtenus par dissolution dans un solvant commun, suivie d'une précipitation dans le méthanol. Par cette voie nous avons préparé des alliages de même composition globale (70,9—71,1 % styrène et 29,1—28,9 % isoprène) et en modifiant seulement le degré de dispersion par addition de quantités croissantes de copolymère séquencé (tableau 2).

Dans cette série, le mélange des homopolymères PS-PI a le degré de dispersion le plus grossier, tandis que le copolymère SI-18, ayant pratiquement la même composition, présente le degré de dispersion le plus fin. La dégradation thermique des polymères et des alliages de polymères a été effectuée en présence d'air, à l'aide d'un Dérivatographe MOM-Budapest dans des conditions thermiques dynamiques. Les valeurs de l'énergie d'activation apparente sont calculées par la méthode de Freeman-Carroll.[4]

---

[3] M. Szwarc, *Makromol. Chem.*, **35**, 132 (1960).

Tenant compte du fait que les paramètres cinétiques de la dégradation des polymères dans des conditions thermiques dynamiques dépendent non seulement du degré de transformation, mais aussi de la vitesse de chauffage,[5] nous avons appliqué des conditions standards pour l'évaluation de « l'énergie d'activation apparente » qui caractérise la stabilité thermique des polymères étudiés. Nous avons ainsi employé des échantillons de 20 mg et une vitesse de chauffage de 4,4—4,8°/mn. Les valeurs de l'énergie l'activation ont été calculées pour le même domaine des degrés de transformation (0,05 à 0,25).

Tableau 2

Composition des alliages de polymères

Alliage	Composition			Taux S/I
	PS-r	PI (53300)	SI-17	
A	71	29	—	71/29
B	58,7	21,3	20	71,1/28,9
C	54,4	18	27,6	70,9/29,1
Copolymère SI-18	pour comparaison			68/32

RÉSULTATS ET DISCUSSION

Ces valeurs de l'énergie d'activation apparente sont présentées dans la figure 1 en fonction de la composition des systèmes de polymère étudiés. Le fait que les alliages des polymères montrent des déviations négligeables de l'additivité suggère l'absence de forces d'interaction importantes dans le mélange de homopolymères et confirme par là leur incompatibilité.[6]

La variation de « l'énergie d'activation apparente » dans les systèmes avec la même composition globale ($S/I = 71/29$) en fonction de la quantité du copolymère biséquencé ajouté indique une augmentation de la stabilité thermique (fig. 2) qui est en concordance avec l'augmentation observée du degré de la dispersion.[7]

Par là se trouve confirmée l'hypothèse de Schneider et ses collaborateurs concernant l'existence d'une corrélation entre la stabilité thermique des mélanges de polymères et leur degré de dispersion, qui peut être ajusté grâce aux copolymères séquencés.[2]

Les auteurs remercient sincèrement M^{ne} Natalia Hurduc, D^{r} à l'Université de Jassy et M. Jacques Periard, D^{r} ingénieur à l'Ecole Supérieure de Chimie de Mulhouse, pour l'aide précieuse apportée au cours de ce travail.

[4] E. S. FREEMAN et B. CARROLL, *J. Phys. Chem.*, **62**, 398 (1958).

[5] I. A. SCHNEIDER, *Rev. Roumaine Chim.*, **17**, 291 (1972).

[6] C. VASILE, N. ASANDEI et I. A. SCHNEIDER, *Rev. Roumaine Chim.*, **11**, 1247 (1966).

[7] G. RIESS, « Extrait de Mécanique-Matériaux-Électricité », Editions Sci. et Industrie, 1970, p. 1.

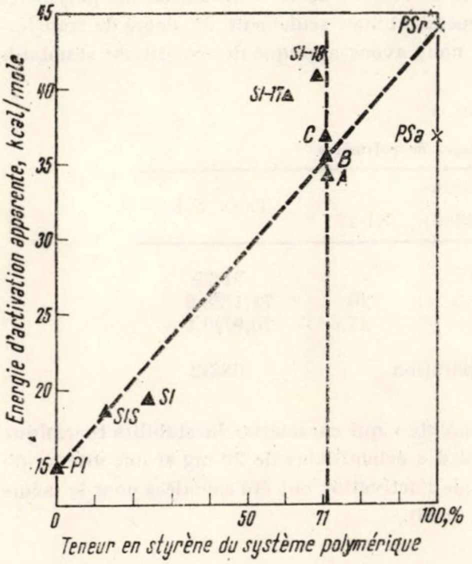

Fig. 1. — Energie d'activation apparente en fonction de la quantité croissante de styrène dans les systèmes étudiés.

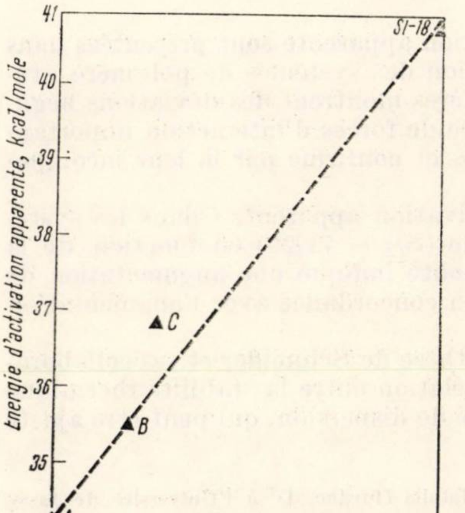

Fig. 2. — Energie d'activation apparente en fonction de la quantité croissante de copolymères séquencés.

Revue Roumaine de Chimie, **18**, *10*, 1689–1698 (1973)

THE INTERDIFFUSION COEFFICIENT OF Pb^{2+} ION IN FUSED ALKALI CHLORIDES BY THE CHRONOPOTENTIOMETRIC METHOD

CONSTANŢA HERDLICKA and S. STERNBERG

Institute of Physical Chemistry,
str. Galaţi 31, Bucharest, Romania

Received January 18, 1973

The interdiffusion coefficients and activation energies, for the diffusion of lead ion in LiCl, NaCl, KCl, RbCl and CsCl, have been determined by the chronopotentiometric technique. The interdiffusion coefficients of Pb^{2+} at 850° in the series of alkali chlorides are 9.67×10^{-5}; 6.85×10^{-5}; 6.38×10^{-5}; 5.71×10^{-5}; 6.24×10^{-5} cm²/sec while the activation energies obtained from the Arrhenius equations are in the same order, 7479; 8492; 8165; 9097; 8568 cal/mol, respectively.

The diffusion data of Pb^{2+} in alkali chlorides are compared to other interdiffusion data and correlated with the self-diffusion coefficient, volume increase at melting, the dimension and charge of the ion.

INTRODUCTION

Several chronopotentiometric works on molten salts have been published recently, their majority dealing with the study of diffusion coefficients of some metallic ions in the same solvent.

The influence of the nature of the solvent upon the diffusion of a metallic ion has scarcely been studied by chronopotentiometric as well as other experimental techniques.

There are Sjöblom's data [1] on Ag^+ diffusion in the series of alkali nitrates obtained by the gravimetric technique; Gustafsson and coworkers [2] have used an interferometric technique for the study of interdiffusion in fused alkali nitrates.

In previously published papers, [3–5] the interdiffusion coefficients and activation energies for the diffusion of silver ion in all the series of alkali nitrates and chlorides as well as the mixture KCl — NaCl of equimolecular composition obtained by the chronopotentiometric method have been reported.

---

[1] C. A. Sjöblom and A. Behn, *Z. Naturforsch.*, **23a**, 1774 (1968).

[2] S. E. Gustafsson, L. E. Wallin and T.E.G. Arvidsson, *Z. Naturforsch.*, **23a**, 1261 (1968).

[3] S. Sternberg and C. Herdlicka, *Rev. Roumaine Chim.*, **14**, 991 (1969).

[4] S. Sternberg and C. Herdlicka, *Rev. Roumaine Chim.*, **15**, 343 (1970).

[5] S. Sternberg and C. Herdlicka, *Rev. Roumaine Chim.*, **17**, 343 (1972).

In the present paper the chronopotentiometric technique is used in the diffusion study of lead ion in fused LiCl, NaCl, KCl, RbCl and CsCl at different temperatures.

Some researches have studied the diffusion of lead ion in mixtures of fused alkali halides as KCl – NaCl (equimolecular composition)[6–9] and the eutectic mixture LiCl – KCl.[10–14] The single alkali halides have been scarcely used as diffusion media for the lead ion.[6]

EXPERIMENTAL

The working cell, the block diagram and experimental procedure have been described elsewhere.[3,4,5,15]

The working electrode was a platinum plate attached to a platinum wire; the effective surface area of the plate was of 0.4–0.7 cm^2.

The potential of the working electrode has been measured across the reference electrode Ag/AgCl (0.1 M) + solvent/silica. The electrical contact between the reference and the studied electrolyte has been effected through the thin quartz wall of the silica tube which contained the reference electrode.

The electrolysis current has been obtained from a stabilized power supply of 250 V connected in series with 3 adjustable resistors (10, 1, 0.1 MΩ) in order to control the current.

The chronopotentiogrammes have been recorded at values of current densities between 25×10^{-3} and 65×10^{-3} A/cm^2 and concentrations of $PbCl_2$ from 3×10^{-5} to 8×10^{-5} mole/cm^3.

The concentration of $PbCl_2$ has been calculated from the masses of components which form the molten mixture and the equations of temperature dependence of solvent densities[16].

Chemicals. $PbCl_2$ was prepared from lead nitrate and concentrated hydrochloric acid, both pro analysis.

The *p.a.* alkali chlorides were recrystallized from aqueous solutions, dried and pre-melted in gaseous HCl atmosphere.

The more hygroscopic salts, i.e. LiCl and NaCl, were handled in a dry box with dry nitrogen atmosphere.

In the working cell the melting of the salt took place in argon atmosphere; dry argon was long bubbled through the melt in order to remove HCl traces. All solvents were checked up for purity by recording the potential-time curves in the absence of $PbCl_2$; the sudden increase of potential up to the value of the decomposition potential of the salt is a proof for the purity of the melt.

---

[6] Yu. M. Riabukin and E. A. Ukshe, *Doklady Akad. Nauk S.S.S.R.*, **145**, 366 (1962).

[7] E. A. Ukshe and N. G. Bukun, *Zhur. fiz. Khim.*, **34**, 2689 (1961).

[8] R. B. Stein, *J. Electrochem. Soc.*, **106**, 528 (1959).

[9] Yu. K. Delimarskii, A. V. Gorodyskii and V. V. Kuzmovitch, *Coll. Czech. Chem. Comm.*, **25**, 3056 (1960).

[10] H. A. Laitinen and H. C. Gaur, *Analyt. Chim. Acta*, **18**, 1 (1958).

[11] R. J. E Hens and J. J. Egan, *J. Electrochem. Soc.*, **107**, 824 (1960).

[12] C .E .Thalmayer, S. Bruckenstein and D. M. Gruen, *J . Inorg. Nuclear Chem.*, **26**, 347 (1964).

[13] I. I. Naryshkin, V. P. Yurkinskii and P. T. Stangrit, *Electrokhimya*, **5**, 1043, 1476 (1969).

[14] W. K. Behl, *J. Electrochem. Soc.*, **118**, 889 (1971).

[15] C. Herdlicka, Thesis, Bucharest, 1972.

[16] G. J. Janz, "Molten Salt Handbook", Academic Press, New York, 1967.

RESULTS

The interdiffusion coefficient has been calculated from the slope of $i_0\tau^{1/2}$ *vs.* C straight line according to Sand's eq.:

$$\tau^{1/2} = nF\pi^{1/2}D^{1/2}C/2i_0$$

where τ (sec) is the transition time, i_0 (A/cm²) the current density, D (cm²/sec) the diffusion coefficient, C (mole/cm³) the volume concentration of the reacting species, n the number of electrons participating to the electrode reaction, F (coulombs) the Faraday constant.

In tables 1–5 the experimental diffusion coefficients of Pb^{2+} in LiCl, NaCl, KCl, RbCl, CsCl obtained at different temperatures are given.

The values of the diffusion coefficient for each temperature and the per cent errors which are listed in tables 1–5, columns 3 and 4, respectively, were calculated from the least squares plots of log D *vs.* $1/T$.

Table 1

The diffusion coefficient of Pb^{2+} in LiCl

Temperature °C	$D_{Pb^{2+}} \cdot 10^5$(cm^2.sec^{-1})		Per cent deviation
	Exp.	Calcd.	
630	4.21	4.25	1.01
644	4.43	4.53	2.28
646	4.70	4.57	−2.88
683	5.57	5.35	−3.99
737	6.54	6.61	1.07
745	6.66	6.81	2.06
776	7.24	7.59	4.69
801	8.50	8.25	−3.04
821	8.82	8.79	−0.23
877	10.53	10.40	−1.26

Table 2

The diffusion coefficient of Pb^{2+} in NaCl

Temperature °C	$D_{Pb^{2+}} \cdot 10^5$ (cm^2.sec^{-1})		Per cent deviation
	Exp.	Calcd.	
814	5.94	6.00	1.14
827	6.27	6.29	0.31
831	6.41	6.38	−0.56
841	6.66	6.60	−0.88
859	6.92	7.02	1.39
863	7.27	7.11	−2.22
874	7.43	7.37	−0.76
877	7.44	7.44	0
882	7.49	7.57	1.02
890	7.73	7.76	0.38
914	8.24	8.36	1.47
918	8.57	8.46	−1.27

Table 3

The diffusion coefficient of Pb^{2+} in KCl

Temperature °C	$D_{Pb^{2+}} \cdot 10^5$ ($cm^2 . sec^{-1}$)		Per cent deviation
	Exp.	Calcd.	
791	5.22	5.18	−0.76
806	5.53	5.46	−1.17
815	5.67	5.64	−0.55
821	5.66	5.75	1.69
836	5.90	6.05	2.62
842	6.19	6.18	−0.27
859	6.50	6.53	0.44
870	6.91	6.76	−2.19
877	6.89	6.91	0.31
882	6.97	7.01	0.67
890	7.47	7.41	−0.80

Table 4

The diffusion coefficient of Pb^{2+} in RbCl

Temperature °C	$D_{Pb^{2+}} \cdot 10^5$ ($cm^2 . sec^{-1}$)		Per cent deviation
	Exp.	Calcd.	
733	3.54	3.53	−0.34
748	3.88	3.78	−2.70
786	4.36	4.43	1.73
798	4.51	4.65	3.11
826	5.28	5.19	−1.75
844	5.44	5.55	2.00
847	5.60	5.61	0.21
887	6.62	6.46	−2.52

Table 5

The diffusion coefficient of Pb^{2+} in CsCl

Temperature °C	$D_{Pb^{2+}} \cdot 10^5$ ($cm^2 . sec^{-1}$)		Per cent deviation
	Exp.	Calcd.	
665	2.79	2.91	4.17
694	3.36	3.34	−0.57
696	3.43	3.37	−1.85
700	3.39	3.43	1.22
720	3.76	3.75	−0.37
723	3.77	3.79	0.72
756	4.55	4.36	−4.40
760	4.52	4.44	−1.88
780	4.76	4.80	0.88
800	5.34	5.18	−3.01
811	5.55	5.40	−2.77
830	5.50	5.78	4.79
857	6.17	6.35	2.85
863	6.49	6.47	−0.21

Examination of fig. 1 shows that the temperature dependence of Pb^{2+} diffusion coefficient in all alkali halide media follows an Arrhenius eq.:

$$D = D_0 \exp\left(-E/RT\right)$$

where D_0 (cm^2/sec) and E (cal/mol) are the pre-exponential factor and the diffusion activation energy, respectively, both being temperature independent constants.

The numerical values of D_0 and E were also obtained from the experimental data by the least squares method.

The following equations hold for the diffusion coefficient of Pb^{2+} in alkali halides, $D_{Pb^{2+}}$, within the temperature ranges in which the measurements have been carried out:

$PbCl_2 + LiCl$

$$D_{Pb^{2+}} = (2.74 \pm 0.30) \times 10^{-3} \exp\left(-\frac{7479 \pm 222}{RT}\right) \qquad (630-877°)$$

$PbCl_2 + NaCl$

$$D_{Pb^{2+}} = (3.06 \pm 0.37) \times 10^{-3} \exp\left(-\frac{8492 \pm 271}{RT}\right) \qquad (814-918°)$$

$PbCl_2 + KCl$

$$D_{Pb^{2+}} = (2.46 \pm 0.34) \times 10^{-3} \exp\left(-\frac{8165 \pm 303}{RT}\right) \qquad (791-900°)$$

$PbCl_2 + RbCl$

$$D_{Pb^{2+}} = (3.34 \pm 0.57) \times 10^{-3} \exp\left(-\frac{9097 \pm 365}{RT}\right) \qquad (733-887°)$$

$PbCl_2 + CsCl$

$$D_{Pb^{2+}} = (2.88 \pm 0.35) \times 10^{-3} \exp\left(-\frac{8568 \pm 250}{RT}\right) \qquad (665-865°)$$

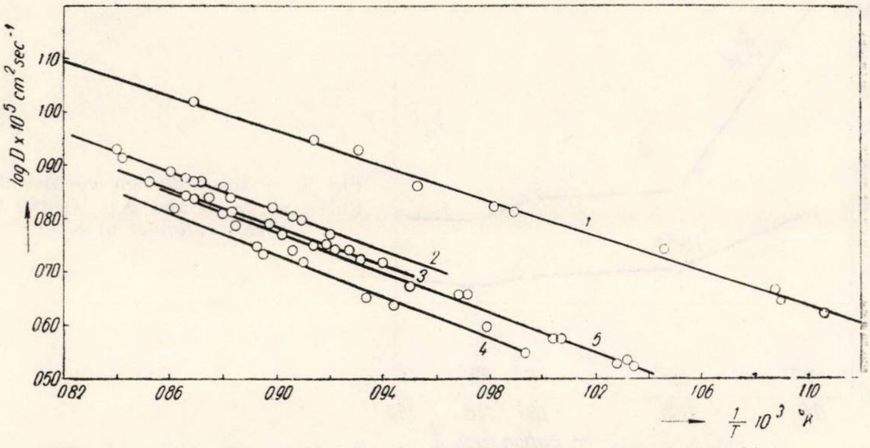

Fig. 1. — Arrhenius eq. plot for the interdiffusion coefficient of Pb^{2+} in: *1*, LiCl; *2*, NaCl; *3*, KCl; *4*, RbCl; *5*, CsCl.

The errors given for D_0 and E are standard deviations. The average per cent standard deviations of $D_{Pb^{2+}}$ for different diffusion media are: 2.76% in LiCl, 1.16% in NaCl, 1.35% in KCl, 2.19% in RbCl and 2.7% in CsCl.

DISCUSSION

Examination of data in this work as well as data previously published on diffusion of Ag^+ in fused alkali chlorides suggests the following regularities: as comes out from figs 2 and 3 there is a similitude between the D_{Ag^+} and $D_{Pb^{2+}}$ dependence on solvent cation radius. Thus, at the solvent melting temperature, the interdiffusion coefficients decrease with increasing alkali cation radius except for $D_{Pb^{2+}}$ in LiCl (fig. 2).

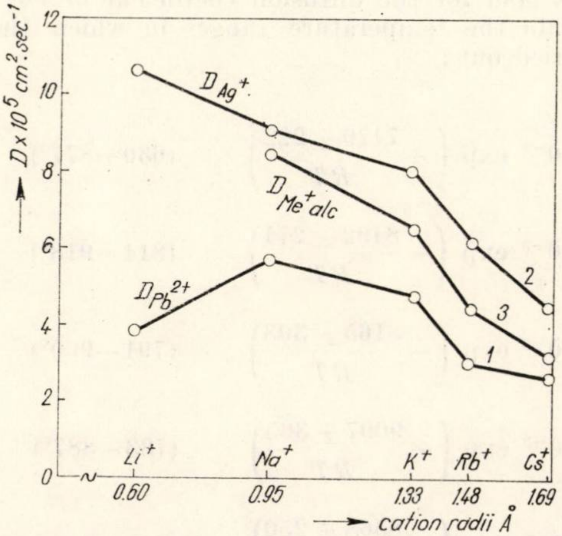

Fig. 2. — Diffusion coefficient *vs.* alkali cation radius at the solvent melting temperatures.

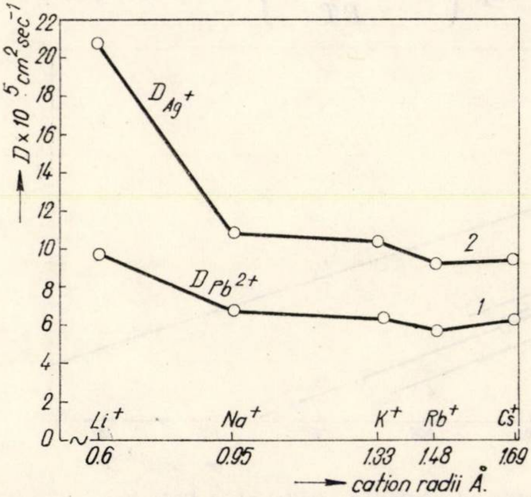

Fig. 3. — Interdiffusion coefficients of Pb^{2+} (curve *1*) and Ag^+ (curve *2*) in alkali chlorides at 850°.

At a common temperature, higher than the melting temperature, e.g. 850°, the values of the diffusion coefficient for foreign ions tend to become equal with each other in alkali chlorides except for Ag^+ and Pb^{2+} in LiCl (fig. 3).

In the same solvent, the value $D_{Pb^{2+}}$ is approximately twice lower than D_{Ag^+}, excepting LiCl in which $D_{Rb^{2+}}$ is three times lower than D_{Ag^+}.

The crystallographic radii of Ag^+ and Pb^{2+} being very close to each other ($r_{Ag^+} = 1.13$ Å and $r_{Pb^{2+}} = 1.17$ Å according to Ketelaar[17]) the difference between their diffusion coefficients in the same solvent may be ascribed to the different charge of the two ions. The charge density on Pb^{2+} surface being higher than on Ag^+, its complexing power is higher so that the radius of the kinetic unit involved in the diffusion process is probably different from Pb^{2+} crystallographic radius.

Since the chronopotentiometric experiments are carried out in solutions which are very diluted in the diffusion component, it is expected that the diffusion of the foreign ions to be strongly influenced by the structure of the diffusing medium.

The volume increase at melting decreases from LiCl to CsCl (table 6, 2nd column). If we admit that this volume change represents a free volume due to holes formed in the liquid, it is to be expected that the diffusion to be faster in LiCl and to get slower from LiCl to CsCl. Our experimental data confirm this expectation. The same behaviour was found out for the cationic self-diffusion coefficient in alkali chlorides (from the series the diffusion of Li^+ in LiCl is missing) determined by Bockris and co-workers[18,19] which are represented in fig. 2. If the values of the diffusion coefficients (calculated at the melting point of the solvent with the Arrhenius equations) are divided by the relative volume change, an approximate constant value is obtained for each group of data (table 6).

Table 6

The relationship between the diffusion coefficients and the relative volume change at the solvent melting temperature

Solvent	$\frac{\Delta V}{V}$ %	$D_{Ag^+}/\frac{\Delta V}{V}$	$D_{Pb^{2+}}/\frac{\Delta V}{V}$	$D_{Me^+}/\frac{\Delta V}{V}$
LiCl	26	$4.1 \cdot 10^{-4}$	$1.5 \cdot 10^{-4}$	—
NaCl	25	$3.6 \cdot 10^{-4}$	$2.4 \cdot 10^{-4}$	$3.4 \cdot 10^{-4}$
KCl	17.3	$4.6 \cdot 10^{-4}$	$2.7 \cdot 10^{-4}$	$3.7 \cdot 10^{-4}$
RbCl	14.3	$4.3 \cdot 10^{-4}$	$2.1 \cdot 10^{-4}$	$3.0 \cdot 10^{-4}$
CsCl	10.0	$4.5 \cdot 10^{-4}$	$2.6 \cdot 10^{-4}$	$3.1 \cdot 10^{-4}$

D_{Me^+} refers to the self-diffusion coefficients of the alkali metal in alkali chlorides.[18,19]

---

[17] J. A. A. Ketelaar, "Chemical Constitution", Elsevier Publishing Company Inc., New York, 1958.

[18] J. O'M Bockris and G. W. Hooper, *Discuss. Faraday Soc.*, **32**, 218 (1961).

[19] J. O'M Bockris, S. R. Richards and L. Nanis, *J. Phys. Chem.*, **69**, 1627 (1965).

A comparison of our results for interdiffusion coefficients of Ag^+ in chlorides [5] and alkali nitrates [3,4] and Pb^{2+} in alkali chlorides, with the cationic self-diffusion coefficients in the corresponding media, shows that D_+(inter)/D_+(self) is approximately equal to the ratio between the radius of the solvent cation and the radius of the foreign ion multiplied with their charge (table 7). The cathodic self-diffusion coefficients are taken according to Dworkin and co-workers [20] for alkali nitrates and according to Bockris and co-workers [18,19] for alkali chlorides.

Table 7

The relationship between the interdiffusion and self-diffusion coefficients, the radii and charges of ions in different diffusion media at the solvent melting temperature

Solvent	Nitrates	Chlorides		$\frac{r_{Me^+}}{r_{Ag^+}}$	$\frac{r_{Me^+}}{2r_{Pb^{2+}}}$
	D_{Ag^+}/D_{Me^+}	D_{Ag^+}/D_{Me^+}	$D_{Pb^{2+}}/D_{Me^+}$		
Li^+	0.66	—	—	0.61	—
Na^+	1.08	1.08	0.67	0.97	0.40
K^+	1.27	1.27	0.73	1.35	0.56
Rb^+	1.30	1.38	0.70	1.51	0.63
Cs^+	1.40	1.44	0.84	1.72	0.72

The Ag^+ radius was considered equal to 1Å.

Table 8

D_{Ag^+} (inter) /D_{Me^+} (self) *versus* temperature

Alkali chlorides

$\frac{D_{Ag^+}}{D_{Na^+}}$	Temp. °C	$\frac{D_{Ag^+}}{D_{K^+}}$	Temp. °C	$\frac{D_{Ag^+}}{D_{Rb^+}}$	Temp. °C	$\frac{D_{Ag^+}}{D_{Cs^+}}$	Temp. °C
1.07	801	1.27	772	1.44	717	1.44	645
1.08	830	1.25	801	1.41	750	1.45	693
1.08	860	1.26	848	1.38	780	1.45	735
1.09	890	1.27	880	1.36	801	1.44	794
1.10	920	1.28	906			1.44	830
						1.44	865

Alkali nitrates

$\frac{D_{Ag^+}}{D_{Li^+}}$	Temp. °C	$\frac{D_{Ag^+}}{D_{Na^+}}$	Temp. °C	$\frac{D_{Ag^+}}{D_{K^+}}$	Temp. °C	$\frac{D_{Ag^+}}{D_{Rb^+}}$	Temp. °C	$\frac{D_{Ag^+}}{D_{Cs^+}}$	Temp. °C
0.66	254	1.09	310	1.27	337	1.29	316	1.40	417
0.68	272	1.08	317	1.27	357	1.30	357	1.40	440
0.72	296	1.06	365	1.26	385	1.30	378	1.40	460
0.84	315	1.10	398	1.21	409	1.31	417	1.40	480

---

[20] A. S. Dworkin, R. B. Escue and E. R. Arstdalen, *J. Phys. Chem.*, **64**, 872 (1960)

Examination of table 7 shows that the D_{Ag^+}(inter)/D_{Me^+}(self) ratio takes similar values in nitrates and alkali chlorides for the same alkali cation. It should be mentioned that this ratio remains constant over a wide temperature interval (table 8).

In connection with the temperature dependence of interdiffusion coefficients it was found out that the activation energy is a function of structural parameters of both the diffusing substance and diffusion medium.

In $AgNO_3$ — Alk. NO_3 [3,4] and AgCl — Alk.Cl, [5] the activation energies for the diffusion of Ag^+ are close to the activation energies for the self-diffusion of alkali metal [18,19,20] and are higher as the melting temperature of the solvent is higher. In the same solvent the activation energy for Pb^{2+} diffusion is higher than for Ag^+.

Nagarajan and Bockris [21] consider that the activation energy for diffusion is formed of the sum of two terms : one of them representing the energy for holes formation and another one the energy the ion needs to jump from one hole to another.

On the basis of the hole model, Bockris and Hooper [18] have found that the energy for hole formation is $E_D = 3.75\ RT_\infty$ (with T_m the melting point of the salt). As it comes out from figure 4, this equation holds for the experimental values of the activation energy, for the interdiffusion Ag^+ and self-diffusion of the alkali metal in alkali nitrates and chlorides (except for E_{Ag^+} in $LiNO_3$) *. In $PbCl_2$ + Alk.Cl systems, Bockris and Hooper's equation does not hold (fig. 4).

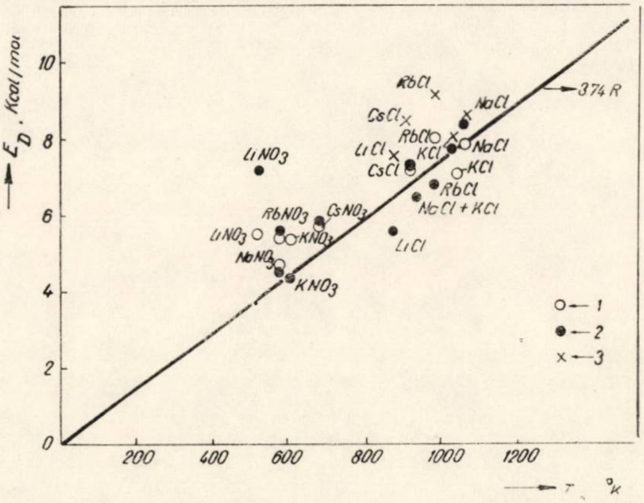

Fig. 4. — Activation energy for cationic self-diffusion and Ag^+ interdiffusion in fused alkali nitrates and chlorides according to the hole model.

1, alkali cation self-diffusion; *2*, silver ion interdiffusion; *3*, lead ion interdiffusion.

---

[21] M. K. Nagarajan and J. O'M Bockris, *J. Phys. Chem.*, **70**, 1854 (1965).

* In a previous work, [3] the activation energy for Ag^+ diffusion in $LiNO_3$ proved to be 7900 cal/mole; the measurement has lately [15] been resumed and the following equation has been found :

$$D_{Ag^+} = (8.36 \pm 4) \times 10^{-3} \exp\left(-\frac{7166 \pm 493}{RT}\right)$$

One may say that in a mono-monovalent mixture with common anion, if the foreign cation has a radius which is close to or smaller than the solvent cation radius, the activation energy consists of the energy required to form holes (into the solvent structure) of such size as to be able to accomodate the foreign ion. For the diffusion of an ion with higher charge density and complexing power (as Pb^{2+}) the jump energy is probably considerable.

Revue Roumaine de Chimie, **18**, *10*, 1699–1708 (1973)

THE REACTION KINETICS IN SUB-MICRONIC POWDERS
THE $ZrO_2 + CaO$ SYSTEM

D. CISMARU * and C. RADOVICI **

* Centre of Physical Chemistry Str. Galați, 31, Bucharest, Romania

** ICECHIM, Splaiul Independenței, 202, Bucharest, Romania

Received February 5, 1973

The kinetic study of the reaction $ZrO_2 + CaO$ in mixtures of sub-micronic crystals, in the temperature range 900–1150°, has shown that the reaction takes place according to an equation of the Avrami-Erofeyev type : $1-z = \exp(-Kt^n)$ with $n < 1$, and the factor controlling the reaction rate is the formation of new germs. Between 900 and 1000° the activation energy was also determined at 53.9 kcal/mol. Over 1000° the phase transitions influence considerably the reaction mechanism.

1. INTRODUCTION

The reaction rate in solids in powder form depends on the size of the particles taking part in the reaction and the literature gives enough references on the matter. [1,2]

For large particles and crystals (over 10μ), the increase of the reaction rate with the decrease of their dimensions is explained by the increase of the reaction surface and the decrease of the maximum thickness of the reaction product layer separating the reactants.

For small crystals (under 1μ), besides the large contact surface and the small thickness of the layer of the reaction product formed, there also intervenes the high superficial energy, which can substantially modify the kinetics of the reaction.

In table 1 we give an illustrative calculation of the superficial energy of sub-micronic particles of ZrO_2. The table shows the increase of the specific surface ($S = 6/\rho D$) and of the superficial energy ($E_S = \sigma S$) with the decrease of the size of the crystals (D). It is assumed that the ZrO_2 particles have the shape of cubes or spheres, a $\sigma = 1.13 \times 10^{-4}$

---

[1] D. Cismaru, *Studii și Cercetări Fiz. Acad. R.P.R.*, **4**, 435 (1955).

[2] D. Cismaru and C. Radovici, *Rev. Roumaine Chim.*, **17**, 69 (1972).

Joules/cm^{2}[3,4] specific superficial energy, a $\rho = 5.82$ g/cm^3 density, and that σ and ρ are the same for all sizes of the crystals. The table shows that E can take values of tenths of kilocalories per mol, of the same order of activation energies as for reactions in solids. Column 4 of the table gives the "temperatures", $t = E_S/C_p$, ($C_p = 13.308$ cal/mol.°C)[5] of different size crystalls. The 10 Å crystals are by 2500° "hotter" than the 10μ ones. This explains the well-known fact that in small ZrO_2 crystals, and at room temperature, there take place phase transformations, which in the case of large crystals appear at 1150 and 2300°.[2,3]

Table 1

Calculated values of the surface *S* and of the surface energy *versus* the diameter *D* of the undermicronic particles

D μm	*S* m^2/gr	E_s cal/mol	*t* (°C)
10.000	0.103	3.42	0.26
1.000	1.05	34.2	2.57
0.500	2.06	68.5	5.15
0.100	10.30	343	25.7
0.050	20.60	685	51.5
0.030	34.35	1143	85.9
0.010	103.0	3430	257.5
0.005	206.0	6850	514.8
0.003	343.5	11430	859
0.0015	686.6	22860	1717
0.0010	1030	34300	2575

We must also underline another aspect of the reactions in submicronic powders: the rapid increase of the specific surface, respectively of the superficial energy, with the increase of the reaction degree z. To illustrate this, we give in table 2, the values $r_1/r_0 = \sqrt[3]{1 - z}$ *versus* the reaction degree z, calculated for a sphere with an initial radius r_0, assuming that the reaction takes place uniformly on their whole surface. For the initial crystals of 10μ and $z = 0.95$, the size of the crystals left will be 3.7 μ and the variation of the superficial energy of 80 cal/mol; for the initial crystals of 0.01 μ, at $z = 0.95$, the dimension will be of 0.0037 μ and the variation of the superficial energy of 8,000 cal/mol as the reaction is going on, the reactivity of the left material increases rapidly.

Another aspect of the reactions in sub-micronic powders is determined by the small dimension of the reaction product crystals formed and by the existence of flaws in their crystal lattice. Both factors considerably increase the diffusion rate of the reactants through the layer of the reaction product, reducing its role as parameter determining the reaction rate.

---

[3] R. C. Garvie, *J. Phys. Chem.*, **69**, 1238 (1965).

[4] I. M. Polejaev, *Zhur. fiz. Khim.*, **41**, 2958 (1967).

[5] J. P. Coughlin and E. G. King, *J. Amer. Chem. Soc.*, **72**, 3262 (1950).

Taking into account the above mentioned aspects, it should be expected that the reaction kinetics in sub-micronic powders should differ from the reaction kinetics in super-micronic powder. The thermodynamic study of these reactions is rendered more difficult by the dependence of the thermodynamic parameters on the size of the crystals[6] as well as by their variation with the reaction degree.

The high reactivity of the crystals and the homogeneity of the materials resulting from the reactions are largely used in industry, and this explains the increasing interest for the kinetics and the mechanism of the reactions in sub-micronic powder reactions.

The $ZrO_2 - CaO$ system was the subject of many studies in connection to the obtention of stabilized zirconium dioxide,[7,8] but the kinetic study of this reaction is not mentioned in literature.

Table 2

Calculated values of the ratio r_1/r_0 *versus* the reaction degree, z

z	r_1/r_0 %
0.00	100
0.05	98.3
0.10	96.5
0.20	92.8
0.30	88.8
0.40	84.3
0.50	79.4
0.60	73.7
0.70	66.9
0.80	58.5
0.90	46.4
0.95	36.8

2. PROCEEDINGS

The ZrO_2 used was heated twice at 1200° to remove volatile impurities and to obtain crystals with a stable size at subsequent heatings below 1200°, making use of the reversible monoclinic $\rightleftarrows$ tetragonal phase transformation at 1150°.

The material thus processed had : ZrO_2 content — 99.71 % (gravimetrically determined by precipitation with mendelic acid ; main impurities : Si, Fe, Hf $\sim$ 0.1 % ; Mg, Pt $\sim$ 0.01 % ; Cu, Pb $\sim$ 0.001 %) ; monoclinic crystalline structure ($a = 5.147$ Å ; $b = 5.203$ Å ; $c = 5.316$ Å ; $\beta = 99°23'$) ; density measured by the picnometer method $\rho = 5.819$ g/cm^3 at 25° ; density measured by the roentgenographic method 5.825 g/cm^3 at 28° ; specific surface BET = 4.2 m^2/g ; average size of crystals determined by the roentgenographic method $D = 773$ Å.

The calcium oxide was obtained by heating pure $CaCO_3$ at 1100°. Main impurities : insoluble in HCl = 0.012 % ; SO_4^{-2} = 0.010 % ; Pb$\sim$ 0.003 % ; Fe $\sim$ 0.005 % ; Na, K $\sim$ 0.05 % ; $CO_2 \sim$ 0.02 %.

The calcium oxide was mixed to zirconium bioxide in a 5 :1 ratio ; in this ratio the effect of imperfect homogenization and the influence of CaO concentration on the kinetics and thermodynamics of the reaction is excluded, as the concentration of the CaO remains practically constant during the reaction. The mixture was homogenized with distilled water without CO_2 and heated at 600° up to the constant weight. All the processing was carried out in an Ar atmosphere to avoid the poisoning by CO_2. By washing this mixture with a diluted HCl (pH = 3) solution, the CaO is totally removed and the remaining ZrO_2 has the same characteristics as the initial ZrO_2. Of this mixture $\sim$ 5 g portions were heated in an argon atmosphere, in a platinum combustion boat, in a quartz tube, by means of a horizontal electric oven with a silicium carbide tube. The adjustment of the temperature was carried out at the level of the silicium carbide tube by means of a Pt-PtRh thermocouple and a thermal adjusting device, and the temperature was measured at the sample level, by means of another Pt-PtRh thermocouple, coupled to a galvanometre. The variations of the temperature in time, at the sample level, were of ± 5°. The reaction time was corrected for the time necessary to allow the sample to reach the reaction temperature. After heating, the mixture was suddenly cooled in air and washed with a diluted HCl (pH = 3) solution, to remove the CaO in excess, and then with distilled water, dried at 120° and analysed. The dosing of the ZrO_2 was carried out gravimetrically by precipitating with mandelic acid and calcinating at 1200°. The precision of the measurements was of ± 0.05%. The dosing of the CaO was achieved volumetrically by titrating with potassium permanganate. The precision of the measurements was of ± 0.1%. The results are given in table 3.

---

[6] K. Torkar, "Reactivity of Solid", Proc. 4th Int. Simp., Elsevier, 1961, p. 400.

[7] W. Baucal and R. Scheidegger, *Ber. dtsch. keram. Ges.*, **H 12**, 45 (1968).

[8] P. Duwez, F. Odell and F. H. Brown, *J. Amer. Ceram. Soc.*, **35**, 107 (1952).

The phase qualitative analysis was carried out by the roentgenographic method with a TUR-M-61 diffractometer with horizontal goniometer, G.M. counter, and automatic recording. Velocity of the goniometer arm: 15'/min, velocity of the paper: 200 mm/h. A Bragg-Brentano scheme with 0.5 × 1.0 × 0.5 × 9 mm slits, with Co_{K_α} radiation filtered with Fe was used. In all mixtures we have identified only orthorombic $CaZrO_3$ ($a = 11.15$ Å; $b = 8.003$ Å; $c = 11.491$ Å) [9] and monoclinic ZrO_2 with the same parameters as the initial ZrO_2.

For a quantitative dosing of ZrO_2 and $CaZrO_3$ we have plotted point by point the 111 and 200 maxima, using a Tesla impulsion counter. The measuring time was thus chosen as not to let the statistic deviation exceed ± 5%. The maxima thus plotted were cut out, and their surfaces were determined by weighting. The dosing was carried out by means of the gauging, curves in figure 1, plotted for synthetic ZrO_2 and $CaZrO_3$ mixtures. As it was to be expected, taking into account the near linear absorption coefficients ($ZrO_2 = 957.4$; $CaZrO_3 = 785.8$) the dependence of concentration on intensity differs only slightly from a straight line. The results of the quantitative phase analysis are given in table 3. The precision of the measurements was ± 2% for ZrO_2 and ± 3% $CaZrO_3$.

The interplanar distances d_{111} ZrO_2 and d_{200} $CaZrO_3$ were determined taking into account the position of the lines, considering the diffraction angle θ given by the middle of half-breadth wave, according to the Bragg formula. No corrections were made for: the zero position of the goniometer, the absorption in the sample, refraction and temperature. The reproducibility of the interplanar distances determined in this way is of ± 0.02%.

To determine the D, average sizes of the crystals, we have measured the half-breadth β_0 of the diffraction maxima plotted in every particular case (point by point), the precision of the measurements being ±2%. It was corrected for the instrumental half-breadth β_i according to the formula $\beta^2 = \beta_2^0 - \beta_i^2$ (β_i was determined making use of tetragonal $ZrSiO_4$ powder with the size of crystals 5–20 μ, maximum 200) and introduced into the Scherrer formula $D = K\lambda/\beta \cos \theta$, where $K = 0.85$. The reproductibility of these determinations is of ±3%. The absolute values of the average sizes D thus obtained are systematically affected by a series of other factors. (This will be dealt with in a future paper). We only mention that the D values refer to the sizes of the crystalline fields scattering coherently the X rays. In the present paper they are only used to compare from this point of view the analysed materials.

---

[9] N. N. Padurov, C. Schlusterius, *Ber. dtsch. keram. Ges.*, **32**, 292 (1955).

The results are given in table 4. For ZrO_2, only the half-breadth β_0 is given, as the difference between it and the instrumental half-breadth is of the order of measuring errors for the majority of cases. It shall be compared to the half-breadth for initial ZrO_2 $\beta_0 = 0.256°$.

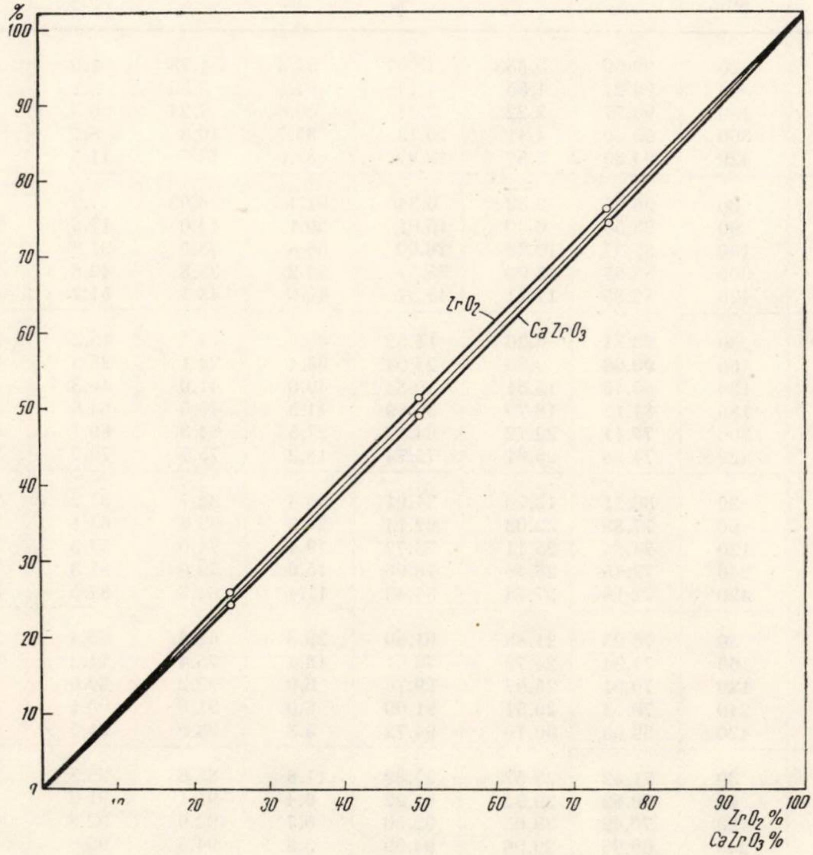

Fig. 1. — Standard curves for roentgenographic dosing of ZrO_2 and $CaZrO_3$.

3. RESULTS AND DISCUSSIONS

On the basis of the results of chemical analyses, we have calculated the reaction degree z_g, considering, according to the results of the qualitative phase analysis, that the entire CaO quantity is bound to ZrO_2 in the form of $CaZrO_3$. The results obtained are in agreement with the reaction degree z_{d_1}, calculated on the basis of monoclinic ZrO_2 concentration, determined by the roentgenographic method, in the limit of the determination errors. Table 3 gives the data of the reaction kinetics $ZrO_2 + CaO$ for the 900–1150° range.

Table 3

The values obtained for the transformation of ZrO_2 and CaO into $CaZrO_3$ and the values of the transformation degree

t °C	Time min.	ZrO_2 %	CaO %	z_g %	ZrO_2M %	z_{d_1} %	$CaZrO_3$ %	z_{d_2} %
900	30	99.09	0.883	1.957	97.5	1.73	1.8	1.25
	90	98.21	1.85	4.14	94.5	3.85	3.1	2.20
	180	96.77	3.22	7.31	89.8	7.24	6.3	4.47
	300	95.60	4.41	10.13	85.7	10.3	8.7	6.25
	420	94.36	5.57	12.97	82.6	12.7	11.5	8.37
950	30	98.05	2.83	6.34	91.4	6.03	7.9	5.5
	90	93.58	6.39	15.01	80.1	14.6	17.5	12.8
	180	89.37	10.58	26.00	66.8	25.5	31.6	24.3
	300	85.97	13.92	35.57	55.2	35.8	42.8	34.2
	420	82.85	17.11	45.37	45.6	45.1	51.2	42.5
1000	30	93.81	6.20	14.52	80.5	14.3	15.2	11.1
	60	90.08	9.86	24.04	68.4	24.1	25.8	19.7
	120	84.45	15.51	40.34	49.6	41.0	46.3	37.7
	180	81.12	18.79	50.89	41.5	49.5	54.6	46.2
	300	77.41	22.72	64.47	27.5	64.3	69.7	61.8
	420	74.28	25.61	75.74	18.2	75.7	79.5	73.5
1050	30	86.21	13.70	34.91	56.4	34.7	37.2	29.6
	60	77.89	22.03	62.14	29.2	62.4	64.1	56.5
	120	74.84	25.11	73.72	19.4	74.0	77.3	70.9
	240	73.45	26.40	78.96	15.6	79.0	81.3	76.0
	420	72.18	27.74	84.43	11.4	84.3	87.5	83.3
1100	30	78.03	21.88	61.60	29.8	61.8	65.4	57.6
	60	74.34	25.72	76.01	18.4	75.4	74.2	68.5
	120	70.91	28.97	89.76	6.9	90.2	89.0	86.2
	240	70.54	29.51	91.00	6.0	91.6	90.1	87.8
	420	69.95	30.16	94.72	5.3	93.0	91.5	89.9
1150	30	71.42	28.57	87.89	11.8	85.8	86.5	82.2
	60	70.62	29.32	91.22	6.4	91.1	91.2	88.7
	120	70.42	29.65	92.50	5.7	92.0	92.8	90.4
	240	69.95	29.96	94.09	3.8	94.5	95.0	93.3
	420	69.50	30.40	96.03	2.5	96.3	96.7	95.6

The obtained data do not check up with Jander's equation, neither with the other equations of this type, except for the 900° temperature. We have tried an Avrami-Erofeyev [10,11] $1 - z = \exp(-Kt^n)$ type equation. The graphs of the $\lg[\lg 1/(1-z)]$ dependences of $\lg t$ are given in figure 2.

For the 900, 950 and 1000° temperatures, the points find a satisfactory place on the curves which enable us to find the values for n and K. The dependence $\lg K$ of $1/T$ for these temperatures is also linear (figure 3) and we must hence assume that the reaction mechanism is the same. The activation energy and the pre-exponential factor inferred by this dependence are 53.9 kcal/mol, and respectively 1.53×10^{7}.

---

[10] M. Avrami, *J. Chem. Phys.*, **9**, 177 (1941).

[11] V. Erofeyev, *Compt. rend. Acad. Sci. U.R.S.S.* **52**, 511 (1946).

For the temperatures 1050 and 1100° the lg [lg $1/(1-z)$] dependence of lg t is no more linear, but becomes again linear for 1150°, having nevertheless a much smaller n. As shown by Whitney,[12] the Avrami-Erofeyev type of equation, with n values < 1, verifies the kinetic experimental data for the transformation of low temperature tetragonal ZrO_2 (that is formed exactly owing to the small size of the crystals) into monoclinic ZrO_2. The values obtained (between $n = 0.14$ and $n = 0.40$, according to the reaction temperature) are in agreement with the values obtained by us ($n = 0.145$). We must assume that the deviation of the dependence lg [lg $1/(1-z)$] of lg t from linearity for the temperatures 1050 and 1100° is due to the superposition, on the initial reaction mechanism, of the phase transformation mechanism $ZrO_2(M) \rightleftarrows ZrO_2(T)$ at 1150°. At 1150° the initial mechanism is practically entirely replaced by the mechanism of phase transformation.

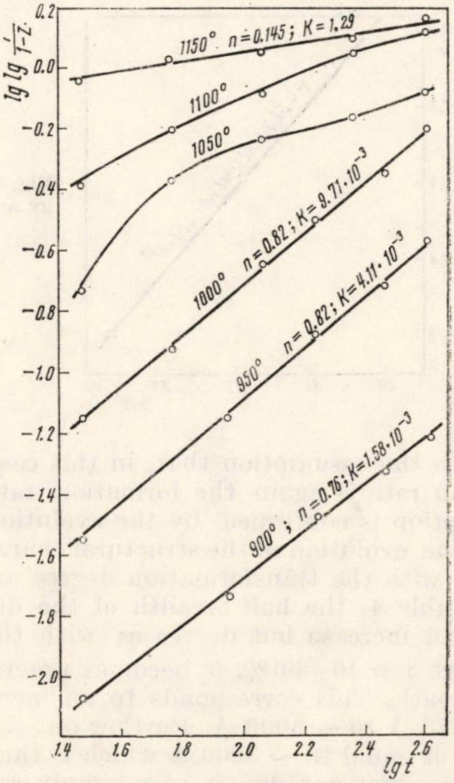

Fig. 2. — Kinetics of the reaction $ZrO_2 + CaO = CaZrO_3$.

In the phase transitions, the formation rate of the new phase germs is the factor controlling the reaction rate in most cases, as shown by

---

[12] E. Dow Whitney, *Trans. Faraday Soc.*, **61**, 1991 (1965).

Czanderma *et al.* [13] and Kroger. [14] The fact that the reaction $ZrO_2 + CaO = = CaZrO_3$ takes place at the temperatures 900, 950 and 1000° according to the Avrami-Erofeyev equation, specific for the phase transformations in general and especially for the $ZrO_2(T) - ZrO_2(R)$ transformation, leads to the assumption that, in this case too, the factor controlling the reaction rate is again the formation rate of the new phase germs. This assumption is confirmed by the evolution of the crystals sizes. Table 4 gives the evolution of the structural characteristics of the ZrO_2 and $CaZrO_3$ phases with the transformation degree and temperature. As may be seen from table 4, the half-breadth of the diffraction maxima 111 of ZrO_2 does not increase but decreases with the reaction degree.

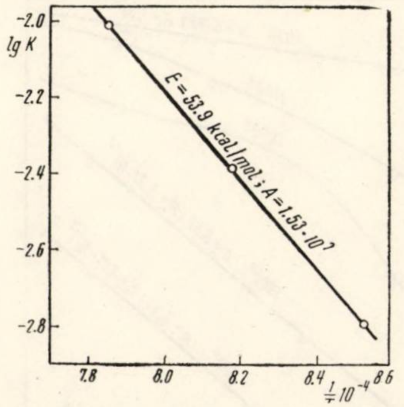

Fig. 3. — Finding of the activation energy and of the pre-exponential factor of equation $K = Ae^{-E/RT}$.

At $z = 40-50\%$, β_0 becomes practically equal to the instrumental half-breath. This corresponds to an increase of the average crystal size from 773 Å to ~ 3000 Å. Further on, the average size of the crystals is higher or equal to ~ 3000 Å which is the sensitivity limit of the method. This apparent paradox is very simply explained if we take into account that the ZrO_2 crystals are actually not homogeneous in size and perfection, but are distributed on a fairly large interval (between ~0.03 and ~ 1μ). In smaller and, thus, more reactive crystals, the germs of the new phase form quicker and they also disappear quicker from the distribution, so that the average distribution shifts towards the maximum size of the initial ZrO_2 crystals. In the large crystals, the formation of the new phase germs do not affect too much the size, and this process once closed, the reaction advances rapidly putting them out of the distribution. This hypothesis is confirmed by the evolution of the average size of the $CaZrO_3$ crystals. At lower reaction degrees, there are formed crystals of small sizes, but of the same order of magnitude as the small ZrO_2 crystals. As z increases, the average size of the $CaZrO_3$ crystals also increases, eventually exceeding the average size of the initial ZrO_2 crystals. We hence

---

[13] A. W. Czanderna, C. N. Ramachandra Rao, and J. M. Honig, *Trans. Faraday Soc.*, **54**, 1069 (1958).

[14] F. A. Kroger, "Khimia nesovershenykh cristalov", MIR, Moskva, 1969, p. 627.

Table 4

Evolution of the structural characteristics of the ZrO_2 and $CaZrO_3$ phases wiht the transformation degreeand temperature

t °C	time min	z %	ZrO_2 monoclinic			$CaZrO_3$			
			θ°	d Å	β°	θ°	d Å	β°	D Å
900	30	1.96	16.431	3.1645	0.256	12.87	4.016	—	—
	90	4.14	16.432	3.1643	0.255	12.870	4.0168	—	—
	180	7.31	16.431	3.1645	0.248	12.872	4.0165	0.39	286
	300	10.13	16.428	3.1651	0.240	12.876	4.0159	0.26	325
	420	12.97	16.429	3.1649	0.241	12.873	4.0164	0.35	345
950	30	6.34	16.431	3.1645	0.250	12.871	4.0167	0.38	297
	90	15.01	16.431	3.1645	0.238	12.868	4.0170	0.356	331
	180	26.00	16.433	3.1641	0.232	12.871	4.0167	0.318	407
	300	35.57	16.429	3.1649	0.228	12.870	4.0168	0.302	457
	420	45.37	16.434	3.1639	0.230	12.872	4.0165	0.295	483
1000	30	14.52	16.432	3.1643	0.242	12.880	4.0155	0.336	366
	60	24.04	16.433	3.1641	0.234	12.876	4.0159	0.308	437
	120	40.34	16.429	3.1649	0.228	12.869	4.0169	0.292	497
	180	50.89	16.431	3.1645	0.232	12.872	4.0165	0.272	611
	300	64.47	16.432	3.1643	0.228	12.871	4.0167	0.276	580
	420	75.74	16.432	3.1643	0.226	12.873	4.0164	0.270	623
1050	30	34.91	16.434	3.1639	0.236	12.871	4.0167	0.302	457
	60	62.14	16.437	3.1634	0.236	12.880	4.0155	0.266	660
	120	73.72	16.433	3.1641	0.234	12.073	4.0164	0.268	641
	240	78.96	16.439	3.1630	0.228	12.879	4.0156	0.264	680
	420	84.85	16.436	3.1636	0.230	12.878	4.0157	0.256	779
1100	30	61.60	16.432	3.1643	0.230	12.870	4.0168	0.260	723
	60	76.01	16.433	3.1641	0.236	12.877	4.0158	0.256	779
	120	89.76	16.434	3.1639	0.231	12.872	4.0165	0.256	779
	240	91.90	16.440	3.1628	0.234	12.881	4.0154	0.242	1116
	420	94.72	16.438	3.1632	0.240	12.880	4.0155	0.236	1482
1150	30	87.89	16.432	3.1643	0.236	12.873	4.0164	0.261	712
	60	91.22	16.428	3.1651	0.232	12.871	4.0167	0.242	1116
	120	92.50	16.436	3.1636	0.233	12.876	4.0159	0.238	1323
	240	94.09	16.435	3.1637	0.234	12.874	4.0163	0.240	1205
	420	96.03	—	—	—	12.876	4.0159	0.236	1482

have to deal with an increasing of the crystal size process, as it usually happens in phase transitions; the crystals of the new phase, once formed, are used as germs by the neighbouring crystals, in which the germs of the new phase have not yet appeared.

In table 3 we notice the fact that the reaction degree z_{d_2}, calculated according to the quantity of $CaZrO_3$ determined by the roentgenographic method, is systematically smaller than the one calculated from the chemical analysis and the roentgenographic dosage of monoclinic ZrO_2. This can certainly be explained partly by the presence of flaws in the crystal lattice of the $CaZrO_3$ (the difference decreases with the increase of the $CaZrO_3$ crystals sizes), but the differences are too large and persistent even for the crystals with a bigger average size than that of the initial ZrO_2. The interplanar distances d_{111} ZrO_2 and d_{200} $CaZrO_3$ remain the same in the precision limit of the measurements ($\pm$ 0.02%), which shows that no solid solutions are formed to affect the intensity of the diffraction maxima and, hence, the quantitative phase analysis. It seems likely to assume the presence of an amorphous or quasi-crystalline phase with a chemical structure somehow similar to that of $CaZrO_3$, transforming itself into $CaZrO_3$ with a much higher rate than the rate at which it is formed, and which was not identified by the roentgenographic method, being present only in small quantities (a few percentages). Such a phase could be the cubic solution $xZrO_2yCaO$ with a fluorite structure that is formed in ZrO_2CaO mixtures with ZrO_2 excess, at temperatures similar to those at which $CaZrO_3$ was obtained. It would be interesting to see if the kinetics of the formation of this solid solution is the same as the kinetics of the formation of $CaZrO_3$ in the presence of a CaO excess.

4. CONCLUSIONS

The kinetic study of the reaction $ZrO_2 + CaO = CaZrO_3$ in mixtures of undermicronic crystals with a 1 :5 molar ratio has shown that :

1) The kinetics of this reaction is described by an Avrami-Erofeyev type equation: $1 - z = \exp(-Kt^n)$, with $n < 1$. The reaction rate is controlled by the formation of the germs of the new phase.

2) For the 900, 950 and 1000° temperatures, the mechanism of the reaction is the same and the activation energy is 53.9 kcal/mol. At temperatures of 1050°, 1100 and 1150°, the initial reaction mechanism is influenced by the phase transition monoclinic $ZrO_2 \rightleftarrows$ tetragonal ZrO_2.

3) At 1150° the mechanism of the reaction is similar to the phase transition mechanism. The equation describing this process is the same, but n takes other values.

Revue Roumaine de Chimie, **18**, *10*, 1709–1714 (1973)

CINÉTIQUE DES TRANSFORMATIONS DU NITRATE D'AMMONIUM EN RÉGIME NON ISOTHERMIQUE

D. FĂTU, SANDA FĂTU et E. SEGAL

Chaire de théorie cinétique de la matière et cinétique chimique de
l'Université de Bucarest, 13, Bd. Republicii

Reçu le 20 décembre 1972

On a déterminé les paramètres cinétiques des transformations du nitrate d'ammonium en utilisant plusieurs vitesses de chauffage. Dans ce but on a eu recours aux données de l'analyse thermique différentielle.

Le comportement du nitrate d'ammonium pendant le chauffage et le refroidissement a constitué l'objet de nombreuses recherches. Ainsi Early et Lawry [1] ont établi qu'à la température de 169,6° le nitrate d'ammonium cristallise dans le système cubique et par refroidissement à 125,2° se transforme dans la forme quadratique. En continuant le refroidissement, on obtient la forme monoclinique à 84,2° (Valerant [2]). Après Behn,[3] celle-ci se transforme dans la phase rhomboédrique. Erofeev et Mitzkevitch [4] considèrent que la vitesse des transformations de phase est contrôlée par le processus de nucléation. Le nitrate d'ammonium se décompose conformément à une réaction exothermique qui, selon les résultats de Wood et Wise [5], est du type autocatalytique.

En ce qui suit, nous nous proposons d'aborder du point de vue cinétique ces processus.

PARTIE EXPÉRIMENTALE

Les processus de transformation du nitrate d'ammonium pendant le chauffage sont accompagnés d'effets thermiques considérables qui peuvent être mis en évidence par la méthode d'analyse thermique différentielle.

---

[1] R. G. Early et T. M. Lowry, J. *Chem. Soc.*, **115**, 1387 (1919).

[2] F. Valerant, *Compte rend.*, **137**, 805 (1903) ; **140**, 264 (1905) ; **142**, 100, 217 (1906).

[3] F. Behn, *Proc. Roy. Soc.*, **80**, 444 (1908).

[4] B. V. Erofeev et N. J. Mitzkevitch, *Sbornic naucinykh rabot Instituta khimii AN B.S.S.R.*, (**1**), *5*, 3 (1956).

[5] B. J. Wood et H. Wise, *J. Chem. Phys.*, **23**, 693 (1955).

Etant donné que la décomposition conduit à la diminution de la masse du réactif on a utilisé pour l'étude de celle-ci l'analyse thermogravimétrique et thermogravimétrique dérivée.

Les courbes thermogravimétrique T.G., thermogravimétrique dérivée T.G.D. et d'analyse thermique différentielle A.T.D. ont été enregistrées simultanément à l'aide d'une thermobalance « Derivatograph » M.O.M. Budapest, type Paulik-Paulik-Erdey. On a utilisé du nitrate d'ammonium «Reactivul» et comme substance de référence α-Al_2O_3 calcinée, au préalable, à 1 000°.

Les granules du réactif ont été triés et on a retenu la fraction ayant les dimensions de 0,09 à 0,1 mm.

RÉSULTATS ET DISCUSSIONS

La figure 1 présente les courbes A.T.D. données par la décomposition du nitrate d'ammonium en utilisant deux vitesses de chauffage, $\beta_1 = 2°/mn$ (courbe inférieure) et $\beta_2 = 10°/mn$ (courbe supérieure).

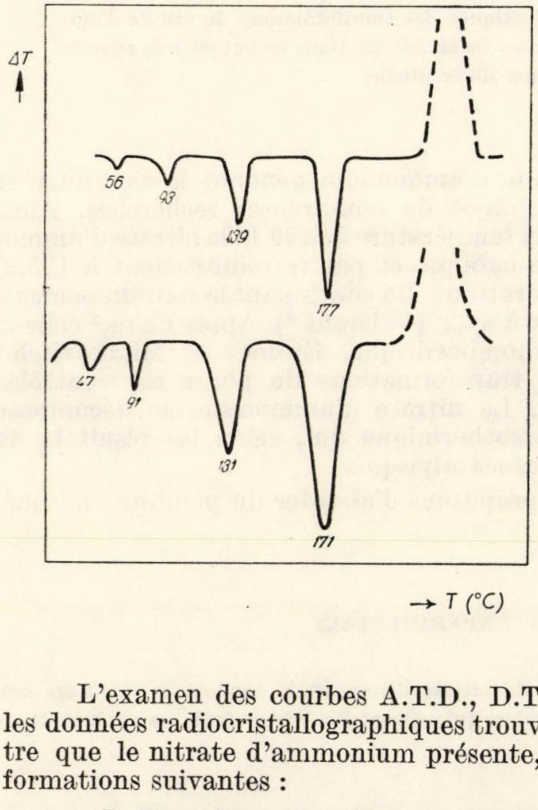

Fig. 1. — Courbes d'A.T.D. pour les transformations du nitrate d'ammonium.

L'examen des courbes A.T.D., D.T.G. et T.G., en corrélation avec les données radiocristallographiques trouvées dans la littérature [1-3], montre que le nitrate d'ammonium présente, pendant le chauffage, les transformations suivantes :

I. Transformation de forme rhomboédrique en monoclinique (quasi quadratique) ;

II. Transformation de forme monoclinique en quadratique.

III. Transformation de forme quadratique en cubique.

IV. Fusion de forme cubique.

V. Décomposition du sel fondu (273°).

Les transformations de phase I—IV sont endothermiques.

Le processus de décomposition présente un caractère explosif et conduit à un dégagement considérable de chaleur.

Les températures où l'on enregistre les pics A.T.D. « $T_{\max}$ » sont sensiblement affectées par la vitesse de chauffage.

Généralement, la vitesse du processus de transformation exprimée par la dérivée du degré de transformation par rapport au temps ($\mathrm{d}\alpha/\mathrm{d}t$) est fonction de la température et du degré de transformation.

$$\frac{\mathrm{d}\alpha}{\mathrm{d}t} = Z\mathrm{e}^{-E/RT} f(\alpha) \tag{1}$$

où : Z — facteur préexponentiel ;
R — constante des gaz ;
E — énergie d'activation ;
T — température absolue.

Dans l'hypothèse que l'ordonnée de la courbe A.T.D. est proportionnelle à la vitesse de transformation et que $\alpha_{\max} = \mathrm{const}$,. on peut analyser du point de vue cinétique les données expérimentales par la méthode Kissinger. [6]

On peut calculer l'énergie d'activation à l'aide de la relation suivante :

$$E = -4{,}575 \frac{\log \dfrac{\beta_1}{T^2_{\max_1}} - \log \dfrac{\beta_2}{T^2_{\max_2}}}{\left(\dfrac{1}{T_{\max}}\right)_1 - \left(\dfrac{1}{T_{\max}}\right)_2} \tag{2}$$

où : $T_{\max_1}$ et $T_{\max_2}$ — représentent les températures où l'on enregistre les pics A.T.D. pour les vitesses de chauffage β_1 et β_2 respectivement.

Un procédé semblable est celui proposé par Ozawa. [7] Par ce procedé on aboutit à l'équation :

$$\log \beta = -0{,}457\, E/RT_{\max} - 2{,}315 - \log ZE/R - \log F(\alpha_{\max}) \tag{3}$$

où :

$$F(\alpha_{\max}) = \int \frac{\mathrm{d}\alpha}{f(\alpha)} \tag{4}$$

$$\beta = \Delta T / \Delta t \tag{5}$$

---

[6] H. Kissinger, *Analyt. Chem.*, **29**, 1702 (1957).

[7] T. Ozawa, *J. Thermal. Anal.*, **2**, 301 (1970).

La vérification des équations (2) et (3) pour les transformations du nitrate d'ammonium a été faite par le procédé graphique.

À titre d'exemple on présente dans la figure 2 *a* et *b* les diagrammes du premier processus.

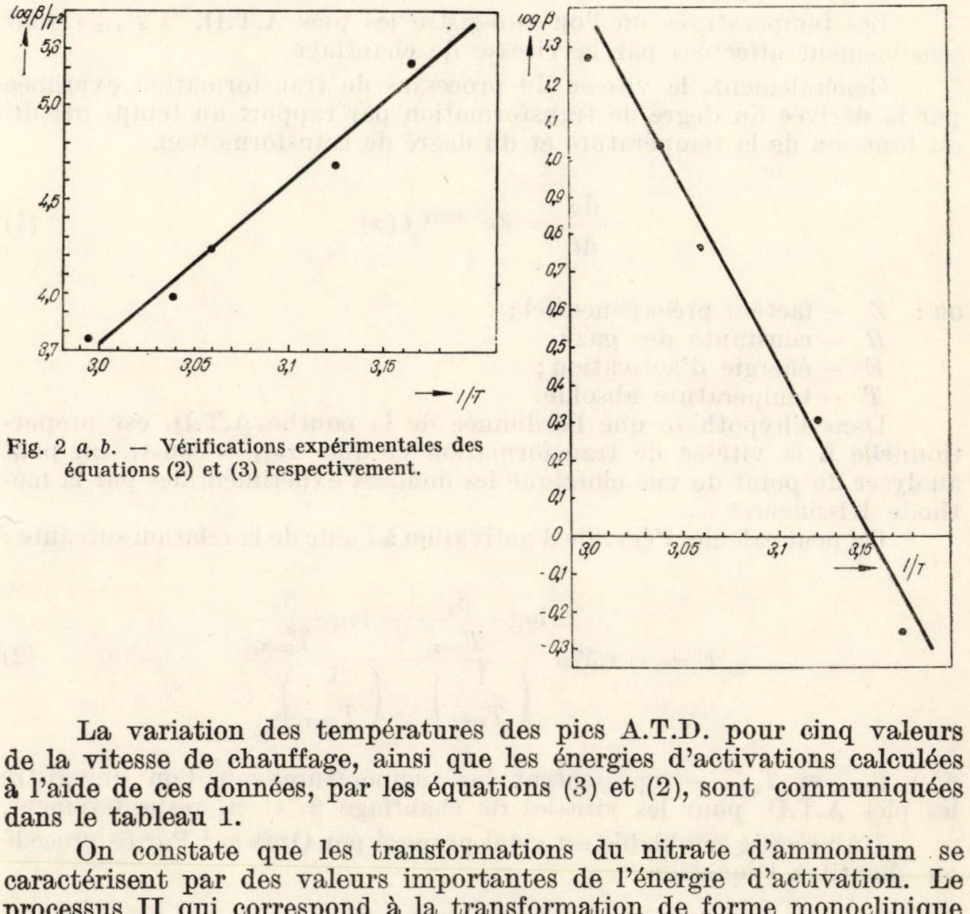

Fig. 2 *a*, *b*. — Vérifications expérimentales des équations (2) et (3) respectivement.

La variation des températures des pics A.T.D. pour cinq valeurs de la vitesse de chauffage, ainsi que les énergies d'activations calculées à l'aide de ces données, par les équations (3) et (2), sont communiquées dans le tableau 1.

On constate que les transformations du nitrate d'ammonium se caractérisent par des valeurs importantes de l'énergie d'activation. Le processus II qui correspond à la transformation de forme monoclinique en quadratique se caractérise par la plus grande valeur de l'énergie d'activation, en accord avec l'observation que la température du pic ATD généré par ce processus est peu sensible à la vitesse de chauffage.

La valeur du paramètre E, pour le processus IV, qui consiste dans la fusion de la forme cubique, est d'ordre de grandeur de l'énergie du réseau ionique. Ce paramètre n'a donc pas la signification d'une énergie d'activation.

Pour le processus de décomposition, qui conduit à une diminution de la masse du réactif, on a calculé l'énergie d'activation en utilisant aussi la courbe T.G. et T.G.D. par le procédé proposé par Freeman et Carroll.[8]

---

[8] E. S. Freeman et B. Carroll, *J. Phys. Chem.*, **62**, 394 (1958).

Tableau 1

Valeurs des paramètres β, T_{max} et E pour les transformations (I−V) du nitrate d'ammonium

Processus / Paramètre	I	II	III	IV	V
β = 0,56°C/mn		log β = 1,7482			
T_{max}	316	362	402	442	526
$T^{-1}_{max}.10^3$	3,1646	2,7624	2,4876	2,2624	1,9011
$\log(\beta T^{-2}_{max})$	−5,2514	−5,3691	−5,4602	−5,5427	−5,6938
β = 2.07°C/mn		log β = 0.3160			
T_{max}	320	364	404	444	546
$T^{-1}_{max}.10^3$	3,1250	2,7473	2,4753	2,2523	1,8315
$\log(\beta . T^{-2}_{max})$	−4,6945	−4,8062	−4,8967	−4,9887	−5,1582
β = 5,72°C/mn		log β = 0.7574			
T_{max}	327	365	408	447	556
$T^{-1}_{max}.10^3$	3,0581	2,7397	2,4510	2,2371	1,7986
$\log(\beta . T^{-2}_{max})$	−4,2716	−4,3671	−4,4640	−4,5432	−4,7326
β = 11,2°C/mn		log β = 1,0492			
T_{max}	329	366	412	450	560
T^{-1}_{max}	3,0395	2,7322	2,4272	2,2222	1,7857
$\log(\beta . T^{-2}_{max})$	−3,9850	−4,0778	−4,1805	−4,2568	−4,4473
β = 19,2°C/mn		log β = 1,2833			
T_{max}	334	369	418	454	573
$T^{-1}_{max}.10^3$	2,9940	2,7100	2,3923	2,2026	1,7452
$\log(\beta . T^{-2}_{max})$	−3,7628	−3,8509	−3,9590	−4,0306	−4,2328
$-4{,}575\ (\Delta \log\beta / \Delta T^{-1}_{max})$	$E = 42$	$E = 135$	$E = 76{,}3$	$E = 116$	$E = 44$ kcal/mole
$(R/-4{,}575)\ (\Delta \log \beta T^{-2} / \Delta T^{-1}_{max})$	$E = 40$	$E = 120$	$E = 64$	$E = 105$	$E = 45$ kcal/mole

Revue Roumaine de Chimie, 18, *10*, 1709−1714 (1973)

On obtient ainsi une valeur de 39 kcal/mole en accord satisfaisant avec la méthode A.T.D. qui est moins précise.

Pour l'ordre de la réaction il en résulte une valeur de 1/3, ce qui montre que le processus est contrôlé partiellement par la diffusion [9] des produits gazeux de la réaction (N_2, O_2, H_2O) à travers la masse visqueuse du sel fondu.

CONCLUSIONS

Les transformations présentées par le nitrate d'ammonium pendant le chauffage se caractérisent par des valeurs importantes de l'énergie d'activation. Les valeurs appréciables de l'énergie d'activation sont caractéristiques en général du processus de nucléation qui constitue l'étape limitante de vitesse des transformations de phase.

La décomposition présente une valeur fractionnaire de l'ordre de la réaction ce qui constitue une indication que celle-ci est contrôlée partiellement par la diffusion des produits gazeux à travers la masse fondue du sel.

---

[9] I. G. Murgulescu, D. Fătu et E. Segal, *J. Thermal Anal.*, **1**, 97 (1969).

Revue Roumaine de Chimie, **18**, *10*, 1715–1729 (1973)

THE GALVANOSTATIC STUDY OF THE ELECTROCHEMICAL ADSORPTION PROCESS ON THE CHLORINE–ACTIVE CARBON ELECTRODE IN MOLTEN SALTS. II[1]

REMANENT POTENTIAL

S. PETRESCU, S. STERNBERG and VALERIA PETRESCU

Polytechnical Institute, Str. Polizu 1, Bucharest, Romania

Received December 12, 1972

The results obtained in the experimental study of the electrochemical adsorption of chlorine on active carbon electrode in the molten salt system $AgCl + KCl$ ($x_{AgCl} = 0.7$) are used in order to find out which of the following models is better : the thin film model, the model of diffusion in adsorbed layer and the model of partially filled pore. The partially filled pore model is in good agreement with the experimental data.

In the experimental study of the electrochemical adsorption of chlorine on active carbon electrode in the molten salts system it appears a remanent potential. [1,2] The active carbon electrode was subjected to an anodic galvanostatic polarization up to a certain value of the electrode potential. Then, the active carbon electrode was subjected to a cathodic galvanostatic polarization up to the zero value of the electrode potential. At that moment the discharge current was interrupted. It was observed an increasing of the electrode potential without any external cause. The maximum value of the electrode potential obtained by relaxation is called relaxation potential. The time interval, in which this relaxation potential is reached, is called time of relaxation. In fig. 1 it is represented such a charge — discharge — relaxation cycle using experimental results presented in a previous paper. [1]

The existence of the remanent potential has suggested the presence of a concentration polarization during the discharge process. In order to make evident this possible process, a step by step discharge has been effectuated after each step waiting for the relaxation time. Thus, were obtained the relaxation curves seen in figure 2. These types of curves constitute a qualitative confirmation of the hypothesis of chlorine diffusion in the pores.

---

[1] S. Sternberg and V. Petrescu, *Rev. Roumaine Chim.*, in press.

[2] S. Sternberg and I. Galasiu, *Rev. Roumaine Chim.*, **15**, 1169 (1970).

In figure 2, is shown the charge curve $o-a$ having a duration $t_c = 50$ minutes and a current intensity $I_c = 0.1$ A, at the 400° temperature. In the point *a* the discharge current was cut off and the self-discharge curve *a-b* was obtained. From the point *c*, a process of discharge started with a current intensity $I_d = 0.1$ A, which lasts $t_d = 5$ minutes, obtaining the curve *c-d*. In the point *d*, the discharge current was cut off and an increasing of the electrode potential was noticed without any external cause, having as a result a typical relaxation curve *d-e*. After the relaxation time (point *e*) a new discharge process *f-g* has started, with a

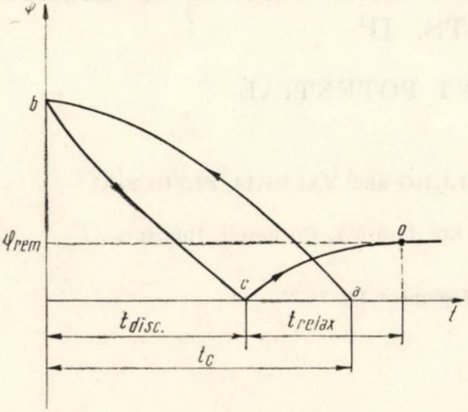

Fig. 1. — A charge — discharge cycle.

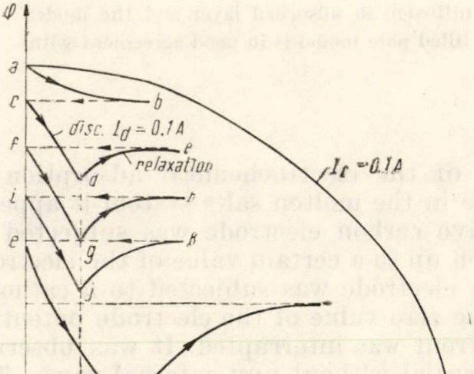

Fig. 2. — Discharge—relaxation processes.

$t_d = 5$ minutes duration. It was proceeded in a similar way obtaining the relaxation curves *g-h*, *j-k*, *m-n* ($t_d = 10$ minutes for the discharge curve *l-m*).

Although the relaxation curves presented in fig. 2 suggest evidently the presence of a chlorine diffusion phenomenon in the active carbon pores, yet we have not any information regarding the mechanism of this process ; we do not know whether the diffusion takes place in the liquid phase (molten salt) or in the gas phase (in the gas "bag" of the pore). In order to elucidate these questions there were processed the experimental data in the following three hypotheses :

— the thin film model ;
— the model of diffusion in adsorbed layer ;
— the partially filled pore model.

1. PRELIMINARY CONSIDERATIONS

Before discussing these models, we present some preliminary considerations about the diffusion process without going into details regarding the particularities of the phase in which the diffusion takes place.

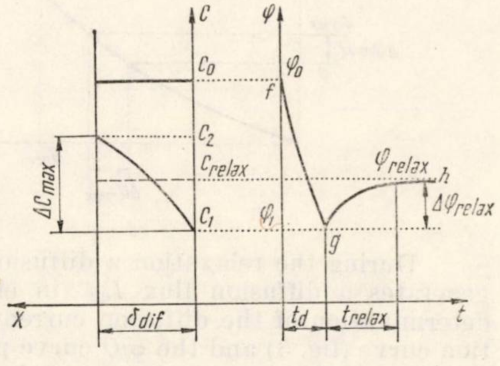

Fig. 3. — Distribution of concentration corresponding to a relaxation process.

In fig. 3 it has been represented in c/x coordinates the distribution of concentration in that phase in which the diffusion takes place when the discharge process, which have provoked the disequilibrium of concentration, ends. In the same figure is shown one of the discharge — relaxation processes (*f-g-h*, fig. 2) in φ/t coordinates. The curve *g-h* represents the increase of the electrode potential in time as a consequence of the concentration equalization by the diffusion in process the respective phase. The curves of this type are called potential relaxation curves ; they correspond to a phenomenon of concentration relaxation of chlorine into the carbon pores.

The following notations are used:

t_d — cathodic polarization time;
φ_0 — potential value at the beginning of the discharge;
φ_1 — potential value at the end of the discharge and at the beginning of the relaxation;
φ_{relax} — potential value at the end of relaxation;
$\Delta\varphi_{\text{relax}}$ — increasing of the potential during the relaxation time;
δ_{dif} — thickness of the diffusion layer;
c_0 — chlorine concentration at the equilibrium state in the phase in which the diffusion takes place, at the beginning of the discharge;
c_1 — chlorine concentration in the exterior part of the phase in which the diffusion takes place; it corresponds to the potential φ_1;
c_2 — chlorine concentration in the interior part of the phase in which the diffusion takes place;
c_{relax} — the average chlorine concentration which is attained in the respective phase, after the relaxation time t_{relax};
$\Delta c_{\max}$ — the maximum difference of concentration $= c_2 - c_1$.

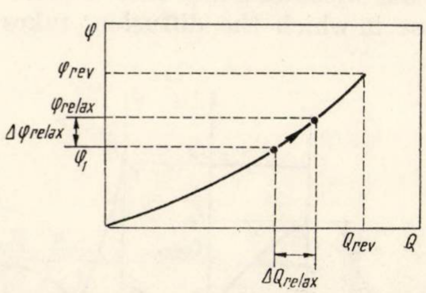

Fig. 4. — φ/Q curve for 400°.

During the relaxation a diffusion transfer of chlorine occurs which generates a diffusion flux I_{dif} (in electrical units). The experimental determination of the diffusion current can be made by using the relaxation curve (fig. 3) and the φ/Q curve presented in fig. 4 (this type of curves has been studied in a previous paper [1]). During the t_{relax} (relaxation time), a transportation of a quantity of chlorine Q_{dif} takes place. The average diffusion flux which transports this quantity of chlorine is equal to:

$$I_{\text{dif. med}} = Q_{\text{dif}}/t_{\text{relax}} \tag{1}$$

The diffusion process which takes place in the relaxation time is a nonstationary process, the chlorine diffusion flux decreasing from a maximum to zero value. This process was assimilated with a stationary one taking into account an average diffusion flux:

$$Q_{\text{dif}} = \Delta Q_{\text{relax}}/2 \tag{2}$$

There results :

$$I_{\mathrm{dif.med}} = \Delta Q_{\mathrm{relax}}/2t_{\mathrm{relax}} \tag{3}$$

where $\Delta Q_{\mathrm{relax}}$ represents the change of the adsorbed chlorine quantity corresponding to the change of the potential during the relaxation process (*g-h*, fig. 3) $\Delta\varphi_{\mathrm{relax}}$. $\Delta Q_{\mathrm{relax}}$ can be obtained using the φ/Q curve (fig. 4). From experimental data we have calculated the average diffusion flux $I_{\mathrm{dif.med}}$, using the relation (3) (table 1).

2. THE THIN FILM MODEL

In this model it is assumed that the molten salt penetrates into the pores of the carbon electrode wetting the walls of the pores and producing a thin film of thickness δ, which is the thickness of the diffusion layer (fig. 5).

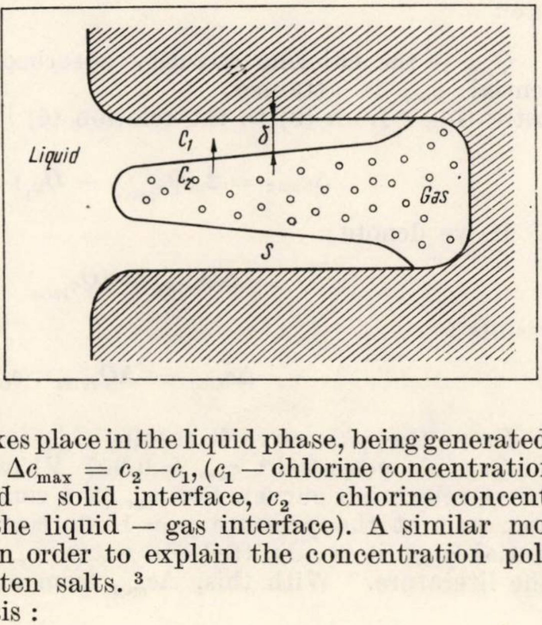

Fig. 5. — Thin film model.

The diffusion process takes place in the liquid phase, being generated by the concentration difference $\Delta c_{\max} = c_2 - c_1$, ($c_1$ — chlorine concentration in the molten salt at the liquid — solid interface, c_2 — chlorine concentration in the molten salt at the liquid — gas interface). A similar model was used by Wassan *et al.* in order to explain the concentration polarization in a fuel cell in molten salts. [3]

Assuming the hypothesis :

$$c_{\mathrm{relax}} = (c_1 + c_2)/2 \tag{4}$$

c_2 can be expressed as a function of c_{relax}.

$$c_2 \simeq 2c_{\mathrm{relax}} - c_1 \tag{5}$$

---

[3] D. T. Wasan, T. Schmidt and B. S. Baker, *Chem. Eng. Progr. Symp.*, **77**, 16 (1967).

Using the relation (5) it results for $\Delta c_{\max}$:

$$\Delta c_{\max} = 2\,(c_{\text{relax}} - c_1) \tag{6}$$

The concentration of the chlorine dissolved in the liquid phase is proportionally to the quantity of chlorine adsorbed on the active carbon electrode Q_φ (corresponding to the electrode potential φ)

$$c = KQ_\varphi \tag{7}$$

K is calculated for the reversible potential :

$$K = c_{\text{rev}}/Q_{\text{rev}} \tag{8}$$

Then :

$$c = Q_\varphi \, . \, c_{\text{rev}}/Q_{\text{rev}} \tag{9}$$

where :

Q_{rev} — the chlorine quantity adsorbed in the case the reversible potential φ_{rev} is attained.
Substituting c from (9) to the relation (6) it is obtained :

$$\Delta c_{\max} = 2\,(Q_{\varphi_{\text{relax}}} - Q_{\varphi_1}) \cdot c_{\text{rev}}/Q_{\text{rev}} \tag{10}$$

If we denote :

$$\Delta Q_{\text{relax}} = (Q_{\varphi_{\text{relax}}} - Q_{\varphi_1}) \tag{11}$$

it results :

$$\Delta c_{\text{med}} = \Delta Q_{\text{relax}} \cdot c_{\text{rev}}/Q_{\text{rev}} \tag{12}$$

From the φ/Q curve it results $Q_{\text{rev}} = 192$ coul (corresponding to the reversible potential[4] $\varphi_{\text{rev}} = 0.947$ V) and $\Delta Q_{\text{relax}} = 8.4$ coul (for the first relaxation curve). For c_{rev} (the concentration of chlorine in the molten salt at the pressure $p = 1$ at, corresponding to the reversible potential φ_{rev}) it is admitted the value $c_{\text{rev}} = 10^{-16}$ moles/cc indicated in the literature.[3] With this, Δc_{med} from relation (12) becomes :

$$\Delta c_{\text{med}} = \frac{10^{-6}}{192}\, 8.4 = 4.37 \times 10^{-8} \text{ moles/cc} \tag{13}$$

The first Fick's law yields the following expression for average diffusion current :

$$I_{\text{dif.med}}/nF = D \cdot \Delta c_{\text{med}} \cdot S/\delta \tag{14}$$

---

[4] I. Murgulescu and S. Sternberg, *Rev. Chim.* (*Bucureşti*), **2**, 251 (1957).

in which :

D — diffusion coefficient of chlorine in the molten salts estimated[5] to be 10^{-5} sq·cm/sec ;

δ — thickness of the diffusion film (fig. 5) was estimated [3] to be 10^{-4} cm ;

S — active surface wetted by the thin film is admitted [1] to be 0.2×10^5 sq·cm.

Therefore,

$$I_{\text{dif.med}} = 10^{-5} \times 4.37 \times 10^{-8} \times 0.2 \times 10^5 \times 2 \times 96500/10^{-4} = \\ = 16.9 \text{ coul/sec} \tag{15}$$

It can be seen that the thin film model is not satisfactory because the resulting values are greater than those presented in table 1.

Table 1

Computation of the average diffusion flux $I_{\text{dif med}}$

N° of the discharge—relaxation curve	φ (mv)	Q_φ (coul)	ΔQ_{relax} (coul)	t_{relax} (sec)	$I_{\text{dif med}}$ (A)
0 (*ab*)	790	156	—	—	—
1 (*cde*)	$\varphi_{\text{relax}} = 670$ $\varphi_1 = 630$	128.4 120.0	8.4	150	0.028
2 (*fge*)	$\varphi_{\text{relax}} = 560$ $\varphi_1 = 490$	103.2 88.8	14.4	270	0.0267
3 (*ijk*)	$\varphi_{\text{relax}} = 445$ $\varphi_1 = 360$	80.4 62.4	18.0	420	0.0214
4 (*lmn*)	$\varphi_{\text{relax}} = 220$ $\varphi_1 = 10$	60 1.2	58.8	900	0.0327

3. THE MODEL OF DIFFUSION IN ADSORBED LAYER

In this model it is assumed that a chlorine transport appears along the wall of the pores due to the superficial concentration gradient.

In fig. 6 is represented a pore of the carbon electrode partially filled with liquid. The following notations are used :

S_g — surface of the carbon in the "gas bag", on which chlorine is adsorbed in gas phase ;

S_l — surface wetted by the liquid, on which chlorine is adsorbed from the molten salt ;

---

[5] A.J. SWINKELS and R.N. SEEFURTH, *J. Electrochem. Soc.*, **115**, 994 (1968).

$I_{dif.p}$ — diffusion current in the adsorbed layer (on the wall);
c_{sg} — chlorine superficial concentration on the surface in contact with the gas;
c_{sl} — chlorine superficial concentration on the surface in contact with the molten salt;

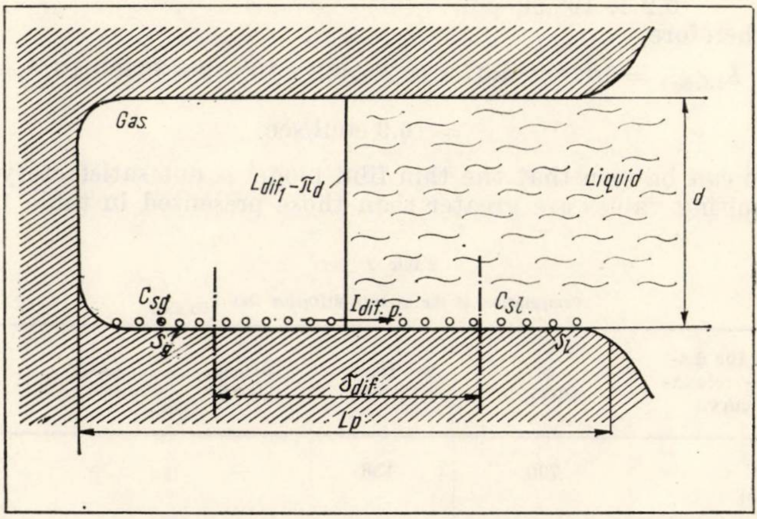

Fig. 6. — Model of diffusion in adsorbed layer.

δ_{dif} — length of the diffusion layer on the wall;
d — pore diameter;
L_p — pore length.

We can write the following relation for the total quantity of adsorbed chlorine:

$$Q_{ads} = S_l \cdot c_{sl} + S_g \cdot c_{gs} = Q_{ads.l} + Q_{ads.g} \tag{16}$$

in which the following notations are used:

$Q_{ads.}$ — total chlorine quantity adsorbed on the active carbon (in electrical units);
$Q_{ads.l}$ — chlorine quantity adsorbed on the active carbon in the liquid zone;
$Q_{ads.g}$ — chlorine quantity adsorbed in the gas zone.

As a result, superficial concentration definitions are the following:

$$c_{sl} = Q_{ads.l}/S_l \tag{17}$$

$$c_{sg} = Q_{ads.g}/S_g \tag{18}$$

Evidently, the following relation exists between surfaces :

$$S_l + S_g = S \tag{19}$$

where S represents the total active surface of the carbon electrode.

Starting the process of cathodic depolarization with a current intensity I_d, the superficial concentration existing in the liquid zone c_{sl} decreases and a concentration gradient appears between the surface of the liquid zone and that of the gas zone. This gradient :

$$\Delta c_s = c_{sg} - c_{sl} \tag{20}$$

generates a diffusion flux which increases at the same time with the increase of Δc_s. The value of Δc_s and consequently the value of $I_{\mathrm{dif.}p}$ attain their maximum just at the moment of interrupting the cathodic polarization (point g from fig. 3) :

$$\Delta c_{s_{\max}} = c_{sg_1} - c_{sl_1} = c_2 - c_1 \tag{21}$$

in which :

c_{sl_1} — superficial concentration in the liquid zone at the moment of interrupting the discharge I_d, which corresponds to the potential φ_1 ;

c_{sg_1} — superficial concentration in the gas zone at the same moment ;

c_{sl_1} corresponds to c_1 (shown in fig. 3) and c_{sg_1} corresponds to c_2 (shown in the same figure). Consequently, $\Delta c_{\max}$ can be written in accordance to relation (6) :

$$\Delta c_{s_{\max}} = 2\,(c_{\mathrm{relax}} - c_1) \tag{22}$$

Taking into account relation (17) $\Delta c_{s_{\max}}$ becomes :

$$\Delta c_{s_{\max}} = 2(Q_{\mathrm{ads}.l\ \varphi\mathrm{relax}}/S_l - Q_{\mathrm{ads}.l\ \varphi_1}/S_l) \tag{23}$$

In can be admitted that:

$$Q_{\mathrm{ads}.l} \simeq Q_{\mathrm{ads}.g} \simeq Q_{\mathrm{ads}.}/2 \tag{24}$$

$$S_l \simeq S_g \simeq S/2 \tag{25}$$

With (24) and (25) the relation (23) becomes :

$$\Delta c_{s_{\max}} = (Q_{\varphi_{\mathrm{relax}}} - Q_{\varphi_1})2/S \tag{26}$$

The difference:

$$\Delta Q = Q_{\varphi_{\text{relax}}} - Q_{\varphi_1} \tag{27}$$

can be deduced from the φ/Q curve (fig. 4) which was shown previously.

In accordance with the Fick's law applied to the diffusion process in adsorbed layer we can calculate the average diffusion intensity current:

$$I_{\text{dif. med}} = D_s \cdot \Delta c_{s\max} \cdot L_{\text{dif}}/2\,\delta_{\text{dif}} \tag{28}$$

where:

D_s — diffusion coefficient in adsorbed layer [6] $= 10^{-3}$ sq.cm/s;

L_{dif} — total length of the solid-liquid-gas interface, through which the diffusion process takes place.

For one pore the length of this interface is equal to the perimeter of the circle with diameter d:

$$L_{\text{dif. }1p} = \pi d \tag{29}$$

Denoting by N the total number of pores:

$$L_{\text{dif. tot}} = N\pi d \tag{30}$$

The total number of pores N can be estimated from the total adsorption surface S related to the surface of one pore:

$$N = S/\pi d L_p \tag{31}$$

It results:

$$L_{\text{dif.tot}} = (S_{\text{tot}}/\pi d L_p) \times \pi d = S/L_p \tag{32}$$

Therefore:

$$I_{\text{dif.}p.\text{med}} = (D_s\ \ \Delta c s_{\max}/2\,\delta_{\text{dif}}) \times S/L_p \tag{33}$$

With $\Delta c s_{\max}$ from (26) in (33) one obtains:

$$I_{\text{dif.}p.\text{med}} = D_s\ \ \Delta Q/\delta_{\text{dif}}\ \ L_p \tag{34}$$

It can be assumed:

$$\delta_{\text{dif}} = L_p\ /2 \tag{35}$$

---

[6] D. P. TIMOFEEV, "Kinetica adsorpţii", USSR Acad. Sci. Ed., Moskva, 1962.

With $\Delta Q = 8.4$ coul and $I_{\text{dif. }p\text{. med}} = 0.028$ A deduced experimentally for the first relaxation curve (*d-e*, fig. 2) for the pore length L_p the following is obtained

$$L_p = \sqrt{2D_s \Delta Q / I_{\text{dif.}p\text{. med}}} = \sqrt{2 \times 10^{-3} \times 8.4/0.028} = 0.776 \text{ cm} \tag{36}$$

This value is too large comparatively to the value indicated in literature [7] : $L_p = 10^{-2}$ cm. For the next relaxation curves one obtains for L_p greater values than 7.76 mm (for example for *g-e* curve, fig. 2, $L_p = 10.5$ mm being greater than the thickness of the active carbon electrode used).

4. THE PARTIALLY FILLED PORE MODEL

Fig. 7 represents a section through one pore of the active carbon partially filled with molten salt. The chlorine concentration on the wetted surface of the pore decreases during the discharge process, due to the electrochemical reaction of chlorine which leaves the active surface passing into the molten salt as ion. As a consequence of this concentration decrease, a concentration gradient appears in the liquid, which generates a chlorine diffusion through the diffusion liquid layer of the δ_{dif} thickness (which represents the average diffusion thickness).

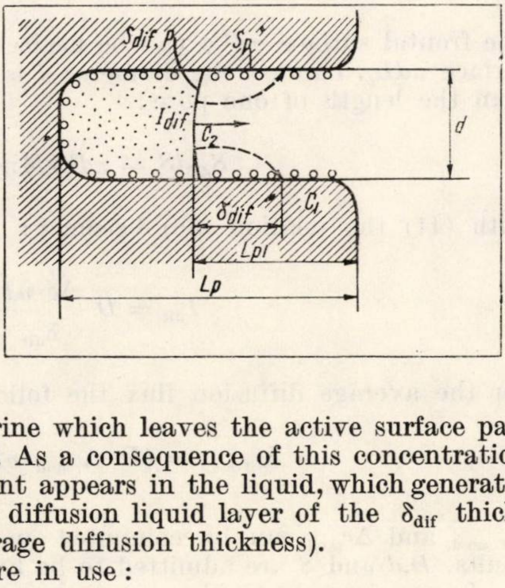

Fig. 7. – Partially filled pore model.

The following notations are in use :

L_p — wetted pore length ;
$S_{\text{dif. }p}$ — diffusion layer surface of one pore ;
S_p — total adsorption surface of one pore ;
S — total adsorption surface of the active carbon electrode (for all pores) $S = S_p \cdot N$;
S_{dif} — total diffusion surface $S_{\text{dif}} = N \cdot S_{\text{dif }p}$.

In accordance with the Fick's law one obtains a chlorine quantity transported in a unit of time for the total diffusion surface S_{dif} :

$$M = D \cdot \Delta c \cdot S_{\text{dif}}/\delta \tag{37}$$

Writing this relation in electrical units one obtains for the total diffusion flux :

$$I_{\text{dif}} = D \cdot \Delta c \cdot S_{\text{dif}} \cdot nF/\delta \tag{38}$$

S_{dif} can be expressed as a function of the total adsorption surface S :

$$S_{\text{dif}} = \frac{\pi d^2}{4} N \tag{39}$$

$$S = NS_p = N\,(S_{\text{lat.}\,p} + S_{\text{front.}\,p}) = N\left(\pi d L_p + \frac{\pi d^2}{4}\right) \tag{40}$$

The frontal surface $\pi d^2/4$ can be neglected comparatively to the lateral surface $\pi d L_p$, because the diameter d is usually $10 - 100$ times smaller than the length of one pore :

$$S_{\text{dif}}/S = \pi d^2 N/4\pi d\, L_p\, N = d/4L_p \tag{41}$$

With (41) the relation (38) becomes :

$$I_{\text{dif}} = D\frac{\Delta c \cdot nF}{\delta_{\text{dif}}} \cdot \frac{d \cdot S}{4L_p} \tag{42}$$

For the average diffusion flux the following relation can be written :

$$I_{\text{dif.med}} = (D \cdot \Delta c_{\text{med}} \cdot nF/\delta_{\text{dif}}) \cdot Sd/4L_p \tag{43}$$

$I_{\text{dif. med.}}$ and Δc_{med} can be computed on the basis of the experimental results. D, d and S are admitted to be known. In this case, the product $\delta_{\text{dif}} \cdot L_p$ can be calculated :

$$\delta_{\text{dif.}}\, L_p = \frac{nFD}{S} \cdot \frac{Sd \cdot \Delta c_{\text{max}}}{I_{\text{dif. med}}} \tag{44}$$

where one admits :

$$\Delta c_{\text{med}} = \Delta c_{\text{max}}/2 = (c_2 - c_1)/2 \tag{45}$$

In accordance with the hypothesis also admitted in the thin film model (7) :

$$c = KQ = c_{\text{rev}}.Q/Q_{\text{rev}} \tag{46}$$

one obtains for $\Delta c_{\max}$:

$$\Delta c_{\max} = (Q_2 - Q_1)c_{\text{rev}}/Q_{\text{rev}} \tag{47}$$

Q_1 can be deduced from the φ/Q curve corresponding to φ_1 (table 1) and Q_2 results from the relation :

$$Q_2 = Q_0 - I_{\text{dif.med}}\ t_d \tag{48}$$

where Q_0 is the total quantity of chlorine adsorbed, supposing that the system is in equilibrium, at the beginning of the discharge (fig. 3) *f-g* (the time discharge is t_d).
With (48) in relation (47) one obtains :

$$\Delta c_{\max} = K\,(Q_0 - I_{\text{dif. med}}\, t_d - Q_1) \tag{49}$$

As an example of computation for the relaxation curve *f-g-h* one can write :

$$\Delta c_{\max} = (128.4 - 0.0267 \times 5 \times 60 - 88.8)\text{K} = 31.58\ \text{K} \tag{50}$$

Admitting the hypothesis :

$$\delta_{\text{dif}} = \frac{L_p}{4} \tag{51}$$

and using computed values for $I_{\text{dif.med}}$ (table 1), $\Delta c_{\max}$ (table 2) and estimating for $S = 10^5$ sq·cm, $D = 10^{-5}$ sq·cm/s, $d = 10^{-4}$ cm the length of pore L_p can be calculated (table 2).

If we consider a constant value for L_p (for example the L_p value for the first relaxation curve; $L_p = 1.41 \times 10^{-2}$ cm) an increase of δ_{dif} results when the potential φ decreases. This result could be explained by the following hypothesis.

During the discharge process, the liquid wets the pore more and more, replacing chlorine which leaves the "gas bag" by diffusion in the molten salt. Computing the coefficient of displacement of the liquid in the pore (table 2)

$$\alpha = \frac{\delta_{\text{dif.}}}{\delta_{\text{dif.1}}} \tag{52}$$

Table 2

Computation of the diffusion thickness δ_{dif}

Nº of the discharge—relaxation curve	$\Delta c_{max}/K$ (coul)	$\delta_{dif}\ L_p$ (sq.cm)	L_p (cm)	δ_{dif} (cm)	$\alpha = \frac{\delta_{dif}}{\delta_{dif_1}}$
1 *(cde)*	27.6	49.7×10^{-6}	1.41×10^{-2}	0.353×10^{-2}	1
2 *(fgh)*	31.58	59.5×10^{-6}	1.54×10^{-2}	0.422×10^{-2}	1.196
3 *(ijk)*	34.4	80.2×10^{-6}	1.79×10^{-2}	0.57×10^{-2}	1.615
4 *(lmn)*	61.2	94.0×10^{-6}	1.94×10^{-2}	0.666×10^{-2}	1.885

(where $\delta_{dif.1} = 0.353 \times 10^{-2}$),

one can see that the maximum displacement is equal to the maximum variation of δ_{dif} :

$$\Delta\delta_{dif.max} = \delta_{dif.4} - \delta_{dif.1} = \alpha_4\ \delta_{dif.1} - \delta_{dif.1} = \delta_{dif.1}(\alpha_4 - 1) = \\ = (1.885 - 1)\,\delta_{dif.1} = 0.885\ \delta_{dif.1} \tag{53}$$

Admitting the hypothesis (51), it results :

$$\Delta\delta_{dif.max} = \frac{0.885}{4} L_p = 0.221\, L_p \tag{54}$$

This would correspond to a wetting of another active surface which represents 22.1 % from the total surface S (during the liquid displacement inside of the pores).

On the other hand, by computing the quantity of diffused chlorine :

$$Q_{dif} = t_d \cdot I_{dif.med} = 25 \times 0.0255 = 0.637 \text{ A min} = 38.2 \text{ coul} \tag{55}$$

we can see that it represents 21.2 % from the total quantity of adsorbed chlorine (for the process of anodic polarization with $t_c = 60$ minutes and $I_c = 0.1$ A). The nearest values of the two percentages are a confirmation of the hypothesis of the liquid displacement as a consequence of chlorine diffusion outside of the pores. This result together with the value obtained for the length of the pore $\simeq 10^{-2}$ cm, (in agreement with those indicated in literature[7]) are the confirmations of the partially filled pore model.

---

[7] E. S. Argano, T. Schmidt and D. T. Wasan, *Chem. Eng. Progr. Symp.*, **77**, 26 (1967).

Besides the advantage of this model for the phenomenon explanation, we can perceive the possibility of using it as a method of determination of the pore dimensions in the active carbon electrode.

5. CONCLUSIONS

On the basis of the models discussed we can admit the following hypothesis regarding the remanent potential. In the cases when there exists "remanent potential", the pores of the activated carbon electrode are not completely "filled" with molten salt. It remains a "bag" in which the halide agglomerates itself, probably also in the adsorbed or condensed state.

In the stationary conditions, before the starting of the discharge process, an equilibrium exists between the chlorine which is present in the "bag", the chlorine dissolved in the molten salt and the adsorbed chlorine on the active carbon at the electrode — molten salt interface (the last generates the value of electrode potential). During the discharge process, the chlorine concentration at the electrolyte — electrode interface decreases proportionally to the quantity of anodic current. When the discharge process ceases, a concentration gradient exists between the "bag" and the interface which generates a chlorine flux, respectively a gradual increase of the electrode potential — the process of relaxation. The previous discussion indicates that the global diffusion velocity is controlled by the most slowly phase of the process, namely the chlorine diffusion in molten salt.

Revue Roumaine de Chimie, **18**, *10*, 1715–1729 (1973)

Revue Roumaine de Chimie, **18**, *10*, 1731–1747 (1973)

SOME ASPECTS OF THE CHEMISTRY OF XENON AND OTHER NOBLE GASES

LAVINEL G. IONESCU[1]

Department of Chemistry,
University of California, Santa Barbara, California 93106

Received May 19, 1972

The present article reviews some interesting aspects of the discovery and historical development of the chemistry of xenon and other rare gases. The different types of noble gas "compounds" are discussed with special emphasis on the clathrates or gas hydrates. The physiological properties and the interaction of xenon with respiratory pigments are treated in some detail.

1. DISCOVERY OF THE RARE OR NOBLE GASES

The suggestion of the possible existence of rare gases in the earth's atmosphere was first presented by Henry Cavendish in 1785.[2] He observed that a small amount of air, not more than 1/120 of the original, remained unabsorbed after prolonged electrical sparking when oxygen and nitrogen from air combined to form nitrous acid. These results were substantiated by Gay-Lussac and Humboldt in 1804 by means of Volta's eudiometric explosion procedure.[3]

In 1894, while studying the density of nitrogen at the Royal Institution in London, Lord Rayleigh found that atmospheric nitrogen was always heavier than nitrogen prepared from ammonia by about 0.1 percent.[4] Passing carefully purified atmospheric nitrogen over red-hot magnesium turnings, Lord Rayleigh and William Ramsay succeeded in isolating a gas approximately twenty times heavier than hydrogen.[5] Ramsay sent samples of the new gas to A. Schuster and W. Crookes, England's most renowned spectroscopists. Both concluded that although the gas contained some nitrogen impurity, it had a characteristic spectrum different from all the other elements.[6]

---

[1] Present address: Department of Chemistry, New Mexico Highlands University, Las Vegas, N. Mexico USA 87701.

[2] H. Cavendish, *Phil. Trans. Roy. Soc. Lond.*, **75**, 372 (1785).

[3] L. J. Gay-Lussac and F. H. A. von Humboldt, *J. de Phys.*, **60**, 129 (1805).

[4] Lord Rayleigh, *Proc. Roy. Soc. Lond.*, **55**, 340 (1894).

[5] Lord Rayleigh and W. Ramsay, *Phil. Trans. Roy. Soc. Lond.*, **A 186(1)**, 187 (1895).

[6] "Noble-Gas Compounds", H. H. Hyman, Ed., University of Chicago Press, Chicago and London, 1963.

The new gas seemed to undergo no chemical reaction with any of the known elements, and because of its apparent inertness was named argon, a word that comes from the Greek *aergon* which means lazy or not doing any work.[7]

During the next few years Ramsay and Travers succeeded in isolating krypton, neon and xenon by fractionation of liquid air.[8]

Krypton (the hidden one) was isolated in May 1898, and neon (the new one) in June of the same year. Neon gave a "blaze of crimson" light when an electric discharge was passed through a sample and the phenomenon was so spectacular that Travers remarked: "For the moment the actual spectrum of light did not matter in the least, for nothing in the world gave a glow such as we had seen".[8] Shortly afterwards xenon was also discovered by the same investigators.

The name of helium comes from the Greek *helios*, which means sun. The D_3 spectral line of helium was first observed in the sun's chromosphere by Pierre J.C. Janssen.[9] He made his discovery while studying the solar eclipse of 1868 in India. Soon afterwards J.N. Lockyer and G. Rayet suggested that it was due to a new element not yet discovered on earth. Helium was first reported on earth by L. Palmieri, who observed the D_3 line upon spectroscopic examination of gas obtained from solid volcanic matter deposited on the slopes of Vesuvius.[7] The American chemist W.F. Hillerbrand collected samples of helium in 1888 by treatment of uraninite with acid.[7]

Radon was discovered in 1900 as a byproduct in the radioactive decay of radium and thorium by Ernest Rutherford[10] and Friedrich E. Dorn.[11]

Many of the physical properties of the noble gases were thoroughly studied during the first half of the century. For example, Karl S. Olzewski[12] of the University of Cracow and H. Kamerlingh Onnes of Leiden[13] studied their behavior at low temperature. The heat capacities, compressibility[5,14] and thermal conductivity[15,16] were also determined. Vasilesco[17] and Van Itterbeek and his co-workers[18,19] made extensive measurements of the viscosity of the rare gases over wide ranges of temperature. The spectra of the noble gases were thoroughly explained and clarified mainly by the work of Herzberg[20] and Paschen.[21]

---

[7] G. A. Cook, Ed., "Argon, Helium and the Rare Gases", Vol. I, Interscience Publishers, New York and London, 1961.

[8] W. M. Travers, "Discovery of the Rare Gases", Edward Arnold, London, 1928.

[9] I. Asimov, "The Noble Gases", Basic Books Inc., New York, 1966.

[10] E. Rutherford, *Phil. Mag.*, **49**, 1 (1900).

[11] F. E. Dorn, *Abhl. Naturf. Ges. Halle*, **23**, 1 (1901).

[12] K. S. Olzewski, *Phil. Trans. Roy. Soc. Lond.*, **A 186**, 253 (1895).

[13] H. K. Onnes and C. A. Crommelin, *Commun. Phys. Lab. Univ. Leiden*, **147d**, (1916).

[14] J. P. Martinez and H. K. Onnes, *ibid.*, **164** (1923).

[15] W. G. Kannuluik and E. H. Corman, *Proc. Roy. Soc. Lond.*, **65 B**, 701 (1952).

[16] H. L. Johnson and E. R. Grilly, *J. Chem. Phys.*, **14**, 233 (1946).

[17] V. Vasilesco, *Ann. de Phys.*, **20**, 137–176, 292–334 (1945).

[18] A. Van Itterbeek and O. Van Paemel, *Physica*, **7**, 265–272, 273–283 (1940).

[19] J. M. J. Coremans, A. Van Itterbeek, J. J. M. Beenakker, H. F. P. Knaap and P. Zanderbergen, *Physica*, **24**, 557 (1958).

[20] C. Herzberg, "Atomic Structure and Atomic Spectra", translated by J.W.T. Spinks, 2nd ed., Dover, New York, 1944.

[21] F. Paschen and R. Götze, "Seriengesetze der Linienspektren", Springer, Berlin, 1922.

The discovery of conventional xenon compounds in the 1960's has added considerable impetus to the study or reevaluation of many properties of the rare gases by experimental as well as theoretical methods. The condensation coefficients of Ar, Kr and Xe have been measured with a quartz microbalance [22] and comparisons have been made between experimental results and predictions of a molecular theory of condensation. [23] Lattice dynamical calculations of thermodynamic properties of the noble gases using anharmonic effects on a two body potential have led to results that agree well with experiments [24,25] Jelinek has obtained zero pressure thermal and elastic data, equations of state and melting lines for crystalline argon, krypton and xenon using the Born-Huang method of homogeneous deformations. [26] The densities of liquid Ar, Kr and Xe have been studied along the orthobaric curve and the shape of the dense fluid isochores has been determined. [27,28] Various equations of state describing the behavior of rare gases at higher pressures have been proposed. [29,30] The adsorption of noble gases on graphite, [31–33] tungsten,[34] pyrex, [35] nickel and palladium, [36] and the adsorption of helium on xenon and krypton crystals [37,38] have been studied in great detail. The solubility of the rare gases in water has been determined over a wide range of temperatures. [39,44]

Contrary to what one of the names implies, the noble gases are not rare. Table 1 gives the composition of atmospheric air near the earth's surface [9,45].

Table 1

Composition of atmospheric air near the earth's surface [9,45]

Gas	Percent by volume	Gas	Percent by volume
Nitrogen	78.084	Methane	2.0×10^{-4}
Oxygen	20.946	Krypton*	1.14×10^{-4}
Argon*	0.934	Hydrogen	5.0×10^{-5}
Carbon dioxide	0.033	Nitrous oxide	5.0×10^{-5}
Neon*	1.82×10^{-3}	Xenon*	8.7×10^{-6}
Helium*	5.24×10^{-4}	Radon*	6.0×10^{-18}

* Noble gas.

---

[22] L. L. Levenson, *J. Vac. Sci. Technol.*, **8**, 629 (1971).

[23] G. Armand, *Surface Sci.*, **9**, 145 (1968).

[24] J. W. Leech and J. A. Reissland, *J. Phys. C: Solid St. Phys.*, **3**, 975, 987 (1970).

[25] A. A. Maradudin and P. A. Flinn, *Ann. Phys.* (*N.Y.*), **22**, 223 (1963).

[26] J. E. Jelinek, *Phys. Rev.*, **B3**, 2716, 2724 (1971).

[27] M. J. Terry, J. T. Lynch, M. Bunclark, K. R. Mansell and L. A. K. Staveley, *J. Chem. Thermodyn.*, **1(4)**, 413 (1969).

[28] F. Theeuwes and R. J. Bearman, *J. Chem. Thermodyn.*, **2(4)**, 507, 513 (1970).

[29] E. Whalley, Y. Lupien and W. G. Schneider, *Can. J. Chem.*, **33**, 633 (1955).

[30] E. M. Holleran, *J. Phys. Chem.*, **72**, 1230 (1968).

[31] D. P. Poshkus, *Discuss, Faraday Soc.*, **40**, 195 (1965).

[32] S. Ross and J. P. Olivier, *Adv. in Chem.*, **33**, 301 (1961).

[33] A. Thomy and X. Duval, *J. Chim. Phys.*, **67**, 286 (1970).

[34] T. Engel and P. Gomer, *J. Chem. Phys.*, **52**, 5572 (1970).

[35] A. Schrau, *Proc. Int. Vac. Congr.*, 4th, 1968, Pt. 1, p. 106.

[36] B. G. Baker, *J. Catal.*, **16 (1)**, 102, 108 (1970).

Near the earth's surface, argon is more abundant than many of the commonly used elements. Table 2 illustrates the estimated abundance of the noble gases in the earth's surface (including the oceans and the atmosphere) compared with silicon.[46]

Large amounts of the noble gases are found in the Universe. After hydrogen, helium is the most common component of stellar atmospheres. Table 3 gives the atomic abundances estimated by Suess and Urey.[47] In fact, all the rare gases except radon have been found in stony meteorites and in many cases seem to be of primordial origin.[48]

Table 2

Estimated abundance of noble gases in the earth's surface compared to silicon[46]

Element	Weight percent	Element	Weight percent
Helium	8×10^{-7}	Xenon	2.9×10^{-9}
Neon	5×10^{-7}	Radon	4×10^{-17}
Argon	3.5×10^{-4}	Silicon	25.7
Krypton	1.9×10^{-8}		

Table 3

Estimated abundance of noble gases in the universe related to one atom of silicon[47]

Element	Atoms	Element	Atoms
Helium	3.08×10^{3}	Krypton	5.13×10^{-5}
Neon	8.6	Xenon	4.0×10^{-6}
Argon*	1.5×10^{-1}	Radon**	—

* Excluding ^{40}Ar.

** No estimate available.

Mineralogic and isotopic investigation of lunar rock brought to earth by the Apollo 11 and 12 missions indicates that all the rare gases except

[37] F. Ricca, C. Pisani and E. Garrone, *J. Chem. Phys.*, **51 (9)**, 4079 (1969).

[38] F. Ricca and E. Garrone, *Trans. Faraday Soc.*, **66 (4)**, 959 (1970).

[39] T. J. Morrison and N. B. Johnstone, *J. Chem. Soc.*, **1954**, 3441.

[40] D. Wood and R. Caputi, U. S. Naval Radiobiological Defense Laboratory, Report TR-988, San Francisco, California, 1966.

[41] G. J. Ewing and S. Maestas, *J. Phys. Chem.*, **74**, 2341 (1970).

[42] S. Maestas "Thermodynamics of the Interaction of Xenon and Myoglobin", Doctoral Dissertation, New Mexico State University, Las Cruces, N. M., September 1968.

[43] G. J. Ewing and L. G. Ionescu, *J. Phys. Chem.*, **76**, 591 (1972).

[44] L. G. Ionescu, "Attempts to Study the Interaction of Leguminous Hemoglobin with Nitrogen and Xenon", Doctoral Dissertation, New Mexico State University, Las Cruces, N. M., April 1970.

[45] E. Glueckhauf, "Composition of Atmospheric Air" in "Compendium of Meteorology", American Meteorological Society, Boston, 1951.

[46] J. S. Anderson, *J. Proc. Roy. Soc. N. S. Wales*, **76**, 329 (1943).

[47] H. E. Suess and H. C. Urey, *Rev. Mod. Phys.*, **28**, 56 (1956).

[48] J. Zähringer, *Geochim. et Cosmochim. Acta*, **32**, 209 (1968).

radon are also present in lunar material.[49-52] Most of the noble gases on the moon seem to result from two sources. There is a spallation component arising from nuclear reactions due to solar wind and cosmic rays, and a radiogenic component resulting from natural fission. Xenon may also have a third trapped component that appears to be present in samples of lunar rock taken from the interior which have not been exposed to solar wind. The low mass xenon isotopes (^{128}Xe and ^{130}Xe) are believed to be the result of spallation, while the heavier isotopes (^{134}Xe and ^{136}Xe) are thought to be formed mainly as a result of natural fission.

The relative paucity of xenon in the earth's atmosphere compared to meteorites and chondrites has been explained in terms of physical adsorption of the rare gas on terrigenous sediments,[53] and the xenon isotope anomalies observed in meteorites have been interpreted in terms of mass fractionation.[54,55] The observed relative ratio of lighter to heavier xenon isotopes in lunar soil, meteorites, chondrites and terrestrial matter has led to questions about the similarity and common origin of lunar and terrestrial material[56] and to estimates of the early temperature of the solar system.[57]

2. HISTORICAL DEVELOPMENT OF CHEMISTRY OF XENON AND OTHER RARE GASES

Travers and Ramsay discovered xenon accidentally in July 1898, while they were attempting to purify krypton by fractional distillation.[8] They named it xenon (the stranger or strange one) because of its high density and relative scarcity in air. Xe has a density of 5.897 g/l at 0° and 1 atm and a boiling point of −108.12°.[58] The erroneous suggestion that the rare gases were chemically inert is due to their discoverers Ramsay and Rayleigh.[5,59] Their suggestion was based on the observations that the rare gases failed to react with oxygen and magnesium and did not undergo any chemical change after sparking with hydrogen, carbon tetrachloride, chlorine, or even after passage through red hot tubes containing gaseous sodium, tellurium, sulfur or phosphorus.

---

[49] D. D. Bogard, J. G. Funkhouser, O. A. Schaeffer and J. Zähringer, *Trans. Amer Geophys. Union*, **51**, 345 (1970).

[50] The Lunar Sample Preliminary Examination Team, *Science*, **167**, 1325 (1970).

[51] A. L. Albee, D. S. Burnett, A. A. Chodos, E. L. Haines, J. C. Hueneke, D. A. Papanastassiou, F. A. Podosek, G. Price Russ III and G. J. Wasserburg, *Earth. Planet. Sci. Letters*, **9**, 137 (1970).

[52] E. C. Alexander, *Earth Planet. Sci. Letters*, **9**, 201 (1970).

[53] F. P. Fanale and W. A. Cannon, *Earth Planet. Sci. Letters*, **11**, 362 (1971).

[54] P. K. Kuroda and O. K. Manuel, *Nature*, **227**, 1113 (1970).

[55] E. C. Alexander, R. S. Lewis and J. H. Reynolds, *Science*, **172**, 837 (1971).

[56] E. Kondaiah, *Nucl. Phys. and Solid State Phys. Symposium*, Madurai, 1970, Vol. 2, p. 167.

[57] P. K. Kuroda, *Nature Phys. Sci.*, **230(2)**, 40 (1971).

[58] H. H. Claassen, "The Noble Gases", D. C. Heath and Co., Boston, Mass., 1966.

[59] G. J. Moody and J. D. R. Thomas, "Noble Gases and Their Compounds", MacMillan Co., New York, 1964.

These results were substantiated by Moissan,[60] who failed to notice any chemical reaction after sparking or arcing fluorine and argon between two carbon poles. Moissan performed the experiments with a sample of argon given him by Ramsay in March 1895 on the occasion of Ramsay's visit to Paris to lecture before the Société Chimique de Paris.

Other investigators obtained completely different results during the same period. Their studies were not taken seriously mainly because the experiments described could not be reproduced in other laboratories and the rare gas compounds reported to be formed were usually stable only for very short periods of time. For example, Marcellin Berthelot announced before the Académie des Sciences in 1895 that the sample of argon received from Rayleigh combined with benzene and carbon disulfide vapors under silent discharge,[61] while Oddo[62] and Schloesing[63] contradicted Ramsay and presented reasons for which the rare gases should react with halogens and magnesium.

The period from 1910 to 1962 was marked by little enthusiasm as far as the study of the noble gases is concerned. Only a limited number of articles were published, more or less evenly divided on the issue of the reactivity of the rare gases. However, it was during this period that the chemistry of the noble gas clathrates and noble gas-metal compounds was elucidated and some especially noteworthy contributions were made.

Villard[64] prepared the first clathrate of argon and water in 1896 and de Forcrand[65-67] extended the work to include krypton and xenon. Von Stackelberg and his associates confirmed the existence of these clathrates, obtained their unequivocal stoichiometry and determined their structure by x-rays.[68-71]

Damianovich and his coworkers in Argentina made significant contributions during the 1920's and 1930's to the understanding of the halides and other noble gas-metal compounds.[72,73] The formation of Pt_3He, WHe_2, PdHe, FeHe and HgHe by electric discharge in the presence of helium has been reported.[72-75]

It was only in 1962, when Neil Bartlett of the University of British Columbia synthesized $XePtF_6$ from platinum hexafluoride and xenon, that the existence of rare gas compounds was accepted without any more reservations. In an elegantly designed experiment, xenon at a higher pressure was allowed to flow into the red vapor of platinum (VI) fluoride. [76] The yellow, dense vapor of $XePtF_6$, which later condensed on the walls of the glass reaction vessel, was formed at room temperature. The product was stable under normal conditions and the reaction was soon reproduced in other laboratories. At last, one of the old myths of chemistry was dead. The "inert gas myth", as H.A. Bent had called it, stopped serving chemistry "as an approximation to the truth" and "showed that out of test tubes may still come surprising things".[77]

---

[60] H. Moissan, *Compt. Rend.*, **120**, 966 (1895).

[61] M. P. E. Berthelot, *Compt. Rend.*, **120**, 235, 581, 1316 (1895).

[62] G. Oddo, *Gazz. Chim. Ital.*, **63**, 380 (1933).

[63] T. Schloesing, *Compt. Rend.*, **121**, 525, 664 (1895).

[64] P. Villard, *Compt. Rend.*, **123**, 337 (1896).

[65] R. de Forcrand, *Compt. Rend.*, **135**, 959 (1902).

[66] R. de Forcrand, *Compt. Rend.*, **176**, 335 (1923).

[67] R. de Forcrand, *ibid.*, **181**, 15 (1925).

[68] M. von Stackelberg, *Naturwiss.*, **36**, 327, 359 (1949).

[69] M. von Stackelberg and W. Jahns, *Z. Elektrochem.*, **58**, 162 (1954).

[70] M. von Stackelberg and H. R. Müller, *ibid.*, **58**, 25 (1954).

[71] M. von Stackelberg, *Z. Elektrochem.*, **58**, 104 (1954).

[72] C. L. Chernick, *Rec. Chem. Progress*, **24**, 139 (1963).

[73] H. Damianovich, *Anales Soc. Espan. Fis. Quim.*, **26**, 365 (1928); Chem. Abstr., *23*, 1537 (1929).

[74] H. Damianovich and J. J. Trillat, *Compt. Rend.*, **188**, 991 (1929).

[75] J. G. Waller, *Nature*, **186**, 429 (1960).

The impact of the "yellow mist" was immeasurable. In the few years that have elapsed, numerous scientists in all corners of the globe turned their attention to the rare gases. Many were motivated by the search for the unknown, the mysterious or the truth, that is so characteristic of science. Notable are the contributions of Bartlett, the group at Argonne National Laboratory headed by Claassen, Malm, Selig and Chedrick, of Volavšek and Slivnik from Ljubljana, and of Allen and Hyman. Yost, who unsuccessfully tried to react xenon with fluorine and chlorine in 1933 [78], noted sarcastically that quantum chemistry, "the reigning queen of science was coy about predicting the existence of noble gas compounds" and used an old Latin proverb in his remark —"varia et mutabile semper femina".

3. COMPOUNDS OF XENON

The known compounds of xenon can be divided into three classes : the xenon-metal compounds, the clathrates, and the substances formed by the reaction of xenon with halides.

3.1 XENON METAL COMPOUNDS

There is substantial evidence, mainly from adsorption and x-ray studies, for the existence of "compounds" of helium and such elements as Pt, [73,74] W, Hg, Pb, I, S, P, and Bi. [72] Other experiments, mostly spectroscopic in nature, seem to indicate the formation of "compounds" between neon and K, Na, Rb, Zn, In, Tl, and between Tl and argon. [79] HgXe [80] and CsXe [81] have also been detected by spectroscopic means. Some are formed when vapors of Cs or Hg are pressurized with rare gases and the mixture is sparked between electrodes. Such a system of course involves many excited-state interactions. [82] Because of the small energies of dissociation, such compounds have only very narrow bands in the emission spectrum (of the order of a few Angstroms) and these are situated close to the emission lines of the metal. The existence of "molecules" of these "compounds" is hard to place in doubt in view of all the evidence available. However, these are not compounds in the ordinary sense, since under normal conditions their lifetime is extremely small and their concentration is minute. Molecules such as HgHe and HgXe probably owe their formation to van der Waals forces and for this reason are sometimes called van der Waals molecules or quasi-molecules. The energies of dissociation range from about 0.07 kcal/mole for HgHe to 0.97 kcal/mole for HgXe. [80] For purposes of comparison, suffice is to mention that the energy of dissociation of the xenon-water clathrate is about 16 kcal/mole [44,68] while that of a more conventional chemical compound such as XeF_4 is 60 kcal/mole. [6] Although additional experiments indicate the formation of xenon-metal compounds, according to some authors the available evidence is by no means conclusive and Waller [75] has suggested as late as 1960 that such compounds do not appear to exist.

---

[76] N. Bartlett, *Proc. Chem. Soc.*, 218 (1962).
[77] H. A. Bent, *Science*, **143**, 1425 (1964).
[78] D. M. Yost and H. L. Kaye, *J. Am. Chem. Soc.*, **55**, 3890 (1933).
[79] H. Krefft and R. Rompe, *Z. Physik*, **73**, 681 (1931).
[80] R. Heller, *J. Chem. Phys.*, **9**, 154 (1941).
[81] G. Thomas and L. Herman, *Compt. Rend.*, **229**, 1313 (1949).
[82] H. C. Jacobson, *Phys. Rev.*, **A 4**, 1363 (1971).

3.2 CLATHRATES

A clathrate is a compound consisting of two distinct components, the host and the guest. The guest, usually a gas or a solvent, is held in a cage provided by the crystalline structure of the host. In fact, the word clathrate was coined by Powell [83] from the Latin *clathratus*, which means enclosed by gratings or caged in. The forces holding a clathrate together are usually of the van der Waals type. De Forcrand [67] was the first to prepare and study the Xe-H_2O clathrate in 1925, [67] although the hydrate of argon had been reported by Villard as early as 1896. [64] The main reason for the delay was the unavailability of xenon. The clathrate of krypton was described by de Forcrand [66] in 1923. Von Stackelberg and his associates confirmed the existence of the noble gas clathrates, obtained their unequivocal stoichiometry and studied their structure in detail. [68-71]

Clathrates of xenon with water, phenol, hydroquinone, cyclodextrin and other compounds have been reported. [84-87] They have some interesting uses. Hydroquinone clathrates have been used for the storage and transportation of noble gases, monoamminenickel (II) cyanide has been employed in the purification of benzene, and clathrates have also been proposed as regenerable sorbers and portable life support for certain gases in space cabins. [88] The clathrates may also be used to study the properties of an enclosed molecular gas free of interactions between molecules of the same gas. Of course, the interactions now present are between the caged gas molecule and the atoms or molecules of the host.

Crystallographic studies of the water clathrates or gas hydrates indicate that the unit cell is cubic in nature with a lattice constant of 12 Å and consists ideally of 48 water molecules and 8 gas molecules, with the resulting stoichiometry Gas.$6H_2O$. [68,70,89] In actuality there are two crystalline forms of the gas hydrates, both cubic, one with a lattice constant of 12 Å and the other of 17 Å. [68,70] The simple gas hydrates, such as the xenon-water clathrate, have the 12 Å structure, while the larger structure with a cell constant of 17 Å is more common in double or mixed clathrates.

---

[83] H. M. Powell, *J. Chem. Soc.*, 298, 300, 468 (1950).

[84] L. Mandelcorn, *Chem. Rev.*, **59**, 827 (1959).

[85] M. von Stackelberg and W. Meinhold, *Z. Elektrochem.*, **58**, 40 (1954).

[86] M. von Stackelberg and H. Fruchbuss, *ibid.*, **58**, 99 (1954).

[87] M. von Stackelberg and B. Meuthen, *ibid.*, **62**, 130 (1958).

[88] R. B. Martin, NASA Spec. Publ., 1969, SP–234, pp. 379–389.

The smaller crystalline form with a lattice constant of 12 Å belongs to the octahedral symmetry group O_h^3. The eight cavities present in this unit cell are not geometrically equivalent. They are all surrounded by 24 water molecules, but two of the "cages" or "holes" are somewhat smaller than the rest. The smaller cavities, with the water molecules arranged regularly about the center of the hole, have a diameter of 5.8 Å. The remaining six have a diameter of about 6.6 Å. [68,70] Gases such as helium and neon, with van der Waals molecular diameters of 2.65 and 2.60 Å, do not form clathrates even under high pressures, probably because they are too small to be trapped in the cage of the crystalline lattice. Xenon (diameter of 4.02 Å) forms more stable hydrates than krypton (3.69 Å) and argon (2.94 Å). The clathrate of radon (diameter of 4.28 Å) has not yet been prepared, but it is believed to be more stable than the xenon hydrate. Some thermodynamic properties of the noble gas clathrates are given in table 4.

Table 4

Some thermodynamic properties of the noble gas clathrates

Clathrate	Dissociation pressure at 0 °C (atm)	Decomposition temperature at 1 atm (°C)	ΔH formation from liquid H_2O and rare gas (kcal/mole)
$Ar.6H_2O$	98.5 [66]	−39.2 [66]	14.9 [66]
	105 [64]	−42.8 [68]	
$Kr.6H_2O$	14.5 [66]	−24.8 [66]	−14.7 [66]
	14.5 [68]	−27.8 [68]	−14.5±0.5 [68]
$Xe.6H_2O$	1.15 [67]	− 1.13 [67]	−18.27 [67]
	1.50 [68,71]	− 3.4 [68]	−16.8±0.5 [68]
	1.52 [44]	− 3.6±0.4 [44]	−15.5±0.2 [44]
$Rn.6H_2O$	0.5* [71]		

* Estimated value.

The standard free energy of formation of $Xe.6H_2O$ and the standard entropy have been determined experimentally and estimated by different techniques. [44,68] The standard free energy of formation at 5°, $\Delta G_{5°}$, is $+0.504$ kcal/mole and $\Delta S_{5°}$, the standard entropy, is -54.0 eu, indicative of a high degree of ordering in the system. [44] The experimental standard heats of formation for $Xe.6H_2O$, with values of -15.5 and -8.9 kcal/mole with xenon at 1 atm and 1 molal and liquid water as the standard states, seem to indicate that the clathrate is first probably formed in the liquid state and that it subsequently undergoes a phase transition and it solidifies. [44]

The kinetics and thermodynamics of formation of clathrates from ice crystals and argon, krypton and xenon at temperatures as low as $-183°$ have been thoroughly studied by Barrer and his associates.[90,91]

For the larger crystalline form of mixed hydrates, the unit cell consists of 136 water molecules and contains eight large holes and sixteen smaller ones. Double clathrates containing a noble gas and acetone, methylene chloride, chloroform, or carbon tetrachloride have been described in detail.[83,85–87] This type of mixed hydrate has the stoichiometry $A.2B.17H_2O$, where A is the organic component and B is the rare gas.

3.3 CONVENTIONAL COMPOUNDS OF XENON

The reaction of xenon with halogens and the subsequent transformations of the xenon halides in the presence of other reagents constitute one of the most active fields of chemical research today and no attempt will be made to present a comprehensive treatment of this subject. It has been reviewed by several authors.[72,92] Only a few illustrative compounds will be discussed in order to bring into evidence some of the more interesting aspects.

Bartlett and Lohman[93] observed in 1960 that oxygen combined with platinum (VI) fluoride according to the reaction

$$O_2 + PtF_6 \rightarrow O_2^+PtF_6^-$$

Platinum (VI) fluoride is a stronger oxidizing agent than fluorine and has an electron affinity of approximately 170 kcal/mole compared to 83.5 kcal/mole for fluorine. As illustrated below, the first ionization potential for molecular oxygen is 12.2 ev, while that

$$O_2 \longrightarrow O_2^+ + e \qquad \text{I.P.} = 1.2.\ \text{ev}$$

$$Xe \longrightarrow Xe^+ + e \qquad \text{I.P.} = 12.13\ \text{ev}$$

for xenon is 12.13 ev. Because of the similarity between the two ionization potentials, Bartlett suggested that xenon should react with PtF_6 just as readily as oxygen and when the reaction was tried the expected product was obtained.[76] As previously mentioned, this was the first unequivocal synthesis of a "true compound" of a noble gas. Soon afterwards, Claassen, Malm and Selig reported the preparation of XeF_4.[94]

In the years that followed, numerous investigators have entered the field and compounds ranging from simple halides such as XeF_2, XeF_4, XeF_6, XeF_8[95–97] to XeO_3, XeO_4, $XeOF_4$[96] and complexes such as CsF

[89] W. F. CLAUSSEN, *J. Chem. Phys.*, **19**, 259, 1425 (1951).

[90] R. M. BARRER and D. J. RUZICKA, *Trans. Faraday Soc.*, **58**, 2253, 2262 (1962).

[91] R. M. BARRER and A. V. J. EDGE, *Proc. Roy. Soc.*, **A 300**, 1 (1967).

[92] J. G. MALM and E. H. APPELMAN, *Atomic Energy Rev.*, **7**, 3 (1969).

[93] N. BARTLETT and D. H. LOHMAN, *J. Chem. Soc.*, 5253 (1962).

[94] H. H. CLAASSEN, H. SELIG and J. G. MALM, *J. Am. Chem. Soc.*, **84**, 3593 (1962).

[95] J. SLIVNIK, B. BRČIĆ, B. VOLAVŠEK, A. SMALC, B. FRELC, R. ZEMLJIČ, A ANZUR and Z. VEKSLI, *Croat. Chem. Acta*, **34**, 187, 253 (1962).

[96] C. L. CHERNICK in "Noble Gas Compounds", H. H. HYMAN, Ed., University of Chicago Press, 1963, pp. 35–38.

[97] S. M. WILLIAMSON and C. W. KOCH, *Science*, **139**, 1046 (1963).

$XeOF_4$, $3RbF.XeOF_4$ and $3KF.XeOF_4$[98] have been synthesized and studied. Table 5 illustrates the standard heats of formation for some typical xenon compounds.[6,58]

Xenon fluorides and some xenon oxyfluorides are stable under normal conditions. XeF_6 and XeF_8 are very stable at room temperature. On the other hand, XeO_3 and XeO_4 explode at 25°. $Xe(OH)_4$ or $XeO_2.2H_2O$ detonates at 30–40°, while XeO_6 is said to have an explosive potential equivalent to T.N.T.[99]

Table 5

Heats of formation of some representative xenon compounds at 25°C [6,58]

Compound	ΔH formation in kcal/mole	Compound	ΔH formation in kcal/mole
XeO	+ 38	$XeOF_2$	+15.0
XeO_3	+ 95.8	$XeOF_4$	− 9
XeO_4	+153.5	$XeOF_6$	−32
XeF_2	− 19.4	XeO_2F_2	+153
XeF_4	− 60	XeO_2F_4	+ 29
XeF_6	− 79		
XeF_8	− 94		

The influence of Ti, V, Vr, Mn, Fe, Co, Ni and Cu fluorides on the reaction rate between xenon and fluorine and the reaction of XeF_2 with the fluorides of the first row transition elements has been studied recently and compounds such as $XeMnF_6$, XeF_2, VF_5, and $XeCr_2F_{10}$ have been synthesized.[100–104] The reaction of XeF_2 with organosilicon compounds has also been recently reported.[105]

The formation of the stable methyl xenonium ion (CH_3Xe^+) has been observed during the reaction of xenon and methyl fluoride in the gas phase and xenon-carbon and krypton-carbon bond strengths in the rare gas molecular ions of 43±8 and 21±5 kcal/mole, respectively, have been estimated.[106]

No conventional compounds of helium, neon or argon have yet been prepared. KrF_2 has been synthesized[107,108] and some of its properties have been studied.[107–109]. The existence of KrF_4 and KrO_3 has not been confirmed unequivocally. The study of the chemistry of radon has been somewhat hindered by the fact that it has short-lived isotopes. Radon has been reported to react and form compounds with O_2F_2, ClF_3, KrF_2

[98] H. Selig, *Inorg. Chem.*, **5**, 183 (1966).

[99] C. L. Chernick, *New Scientist*, **19** , 444 (1963).

[100] S. Rüdinger and H. Meinert, *Z. Chem.*, **9**, 434 (1969).

[101] B. Žemva and J. Slivnik, Inst. Jozef Stefan Report, R-589, 1970.

[102] J. Slivnik and B. Žemva, *Z. Anorg. Allg. Chem*, **385**, 137 (1971).

[103] J. Slivnik and B. Žemva, Inst. Jozef Stefan Report, R-598, 1971.

[104] B. Žemva, J. Zupan and J. Slivnik, *J. Inorg. Nucl. Chem.*, **33**, 3953, 3955 (1971).

[105] J. A. Gibson and A. F. Janzen, *Can. J. Chem.*, **49**, 2168 (1971).

[106] D. Holtz and J. L. Beauchamp, *Science*, **173**, 1237 (1971).

[107] J. J. Turner and G. C. Piementel, *Science*, **140**, 974 (1963).

[108] D. R. Mackenzie, *Science*, **141**, 1171 (1963).

[109] F. Schreiner, J. G. Malm and J. C. Hindman, *J. Am. Chem. Soc.*, **87**, 25 (1965)

and the xenon fluorides.[92,110] Heats of formation of −7.6, −75 and −86 kcal/mole have been calculated for $RnCl_2$, RnF_2 and RnF_4 respectively, but these substances have not been prepared.[111]

4. USES OF XENON

Because of its high cost (approximately $25/liter at normal conditions), the use of xenon for large-scale practical applications has been limited. Some of the more common uses are in the following :

a. Fluorescent lamps. These contain a Xe-Hg mixture and have a characteristic greenish blue color.

b. Bubble chambers used for the detection of mesons and gamma particles. Liquid Xe is used in this case because it vaporizes faster than mercury.

c. Geiger-Müller tubes. Xenon is used to some extent along with argon for filling G-M tubes.

d. Lasers. Like all the rare gases, in which population inversion can be easily produced, xenon has been employed to make several lasers, mostly in the infrared region.

e. Scintillators. Gaseous Ar, Kr and Xe produce scintillations in the ultraviolet region of the spectrum when struck by radioactive or other energetic particles. These flashes or sparks are subsequently converted to visible light and measured by a photomultiplier most effective in that region. Liquid and solid xenon has the advantage over the gas because it has a greater stopping power for the radiations.

f. Radiography. Xenon -135 is employed as a gamma source of radiation for exploring the interior of metals and the detection of structural flaws.

g. Clinical Applications. Xenon has been used for hematocrit measurements (relative amounts of plasma and corpuscles) in blood.[112] Xe-133 has been employed for pulmonary function evaluations,[113–116] cerebral, renal and muscle blood flow,[117–119] rate of solute absorption from tissue depots,[120] and to study clearance in arthritic joints.[121]

---

[110] P. R. Fields, L. Stein and M. H. Zirin, *J. Am. Chem. Soc.*, **84**, 4164 (1962).

[111] I. J. Vasilescu, *Rev. Roum. Chim.*, **12**, 835 (1967).

[112] A. M. Andersen and J. Ladefoged, *J. Pharm. Sci.*, **54**, 1684 (1965).

[113] J. R. Medina, P. L'Heureux and M. K. Loken, *Minn. Medicine*, **52**, 1455 (1969).

[114] K. E. Corrigan, J. Mantel and H. H. Corrigan, *Radiology*, **96**, 571 (1970).

[115] Z. V. Vorob'eva and A. I. Kabakov, *Med. Radiol.*, **16(4)**, 37 (1971).

[116] R. M. Martin, J. Wilson and N. R. Anthonisen, *Bull. Phys. Pathol. Resp.*, **7**, 291 (1971).

[117] T. M. Darbinyan, K. D. Kalantarov and B. I. Khersonskii, *Eksp. Khir. Anesleziol.*, **16 (1)**, 54 (1971).

[118] W. Graban, *Pol. Przegl. Radiol. Med. Nukl.*, **34**., 127 (1970).

[119] P. Bolme and L. Edwall, *Acta Physiol. Scand.*, **82(1)**, 17 (1971).

[120] R. E. Gosselin and G. R. Stibitz, *Pflügers Arch.*, **318**, 85 (1970).

[121] W. S. Dick, S. D. Deodhar, C. J. Provan, G. Nuki and W. W. Buchanan, *Clin. Sci.*, **40**, 327 (1971).

h. Hyperbaric Organ Preservation. The hyperbaric conservation of kidneys has been studied using different gases at various pressures. Measurements of concentration of nucleotides and cytochromes, activity of different enzymes as well as respiratory capacity of intact tissue and structural electron microscope studies, seem to indicate than xenon at a pressure of 2 atm provides the best preservation medium.[122]

e. Anesthesia. Xenon alone, as well as mixtures of xenon with halothane, cyclopropane and other gases, have been used to induce anesthesia in man.[123,124]

5. PHYSIOLOGICAL PROPERTIES OF XENON

Although the high solubility of argon in equine blood (0.42 ml/l of blood) had been observed by Régnard and Schloesing[125] as early as 1897, the suggestion that the rare gases might have physiological effects was not presented until about 1935.[126]

Narcotic effects of xenon on mice, cockroaches, paramecium, drosophila, and even of the mold neurospora crassa have been noted. As a rule all the rare gases are not anesthetic below 1 atm, but all except helium and neon have been shown to produce narcotic effects at higher pressures. Xenon has a marked depressant action at pressures of 1 atm only in man among all animals tested. The use of xenon as an anesthetic agent for human beings was first reported by Cullen and Gross in 1951.[123]

Carpenter showed that xenon alters tissue metabolism both *in vivo* and *in vitro*, and reported that it also blocks the transmission of impulses in isolated peripheral nerve fibers.[127] Gottlieb and his associates reported that xenon, krypton and nitrous oxide reversibly inhibited sodium active transport through frog skin and caused reversible conduction blockade in frog sciatic nerve.[128] The effect of increased pressure of rare gases on phospholipid membranes and the possible role of electrolyte imbalance in the mechanism of rare gas anesthesia has been studied extensively by Bennett and his coworkers.[129-132]

It is interesting to add that the influence of xenon on higher plants had not been noted and studied until very recently,[133] although the toxic effects of other anesthetic gases had been observed as early as 1908.[134]

---

[122] R. Voss, A. Rickart, K. Ruile, H. R. Schoen, R. Hans and W. Kunz, *Verh. Deut. Ges. Pathol.*, **54**, 145 (1970).

[123] S. C. Cullen and E. G. Gross, *Science*, **113**, 580 (1951).

[124] S. C. Cullen and E. I. Ezer, *Anesthesiology*, **31**, 305 (1969).

[125] P. Régnard and T. Schloesing, *Compt. Rend.*, **124**, 302 (1897).

[126] A. P. Rinfert and G. F. Dobbler, in "Argon, Helium and the Rare Gases", Vol. II, G. A. Cook, Ed., Interscience, New York, 1961.

[127] F. G. Carpenter, *Fed. Proc.*, **18**, 22 (1959).

[128] S. F. Gottlieb, A. Cymerman and A. V. Metz, *Aerosp. Med.*, **39**, 449 (1968).

[129] P. B. Bennett and A. J. Hayward, *Nature*, **213**, 938 (1967).

[130] P. B. Bennett, D. Papahadjopoulos and A. D. Bangham, *Life Siences*, **6**, 2527 (1967).

[131] P. B. Bennett, *Science J.*, **4**, 53 (1968).

[132] P. B. Bennett and A. J. Hayward, *Aerosp. Med.*, **39**, 301 (1968).

[133] J. Weigl, *Z. Naturforsch.*, **B 23 (9)**, 1253 (1968).

[134] W. Crocker and L. I. Knight, *Botan. Gaz.*, **46**, 529 (1908).

Xenon is considerably more soluble in water than are nitrogen and oxygen, and it has a tendency to accumulate in fatty tissues. The high solubility of xenon in lipids and in certain proteins is very evident. An explanation of the physiologic properties of the noble gases in terms of their physicochemical and biochemical properties has been given by Roth.[135] Several theories have been presented to explain anesthesia. Pauling has proposed a mechanism that involves the formation of clathrate microcrystals, which would subsequently alter the environment of the brain.[136] A clathrate model for the thermodynamics of the interaction of metmyoglobin and krypton, xenon and cyclopropane has been recently presented by Rothstein and Featherstone.[137] Several authors have suggested simple solubility of xenon in lipids, while others have proposed that the basic process in narcosis involves van der Waals forces and is a result of the polarizability and the excluded molar volume of the anesthetic gas.[138]

6. INTERACTION OF XENON WITH RESPIRATORY PIGMENTS

Respiratory pigments are a distinct class of conjugated proteins found in living systems and concerned with the transport of gases. In general, a respiratory pigment consists of a basic colorless protein called globin and a prosthetic group which is usually responsible for the color. The two components can be readily cleaved by acids or bases. The globin, which consists of amino acids linked by peptide bonds, varies from species to species. The prosthetic group is in most cases a coordination compound of ferrous iron and protoporphyrin IX and is called heme. Some of the more common respiratory pigments are myoglobin, hemoglobin, erythrocruorin, hemerythrin, hemocyanin and leguminous hemoglobin or legoglobin. All of the above are red respiratory pigments with the exception of hemocyanin which is blue, has no heme and contains copper instead of iron as the metal atom.

It has been known for some time that xenon is carried by the blood stream,[139] and studies related to xenon transport have shown that there exists an interaction between the rare gas and the respiratory pigments.[140] The interaction has been studied by manometric methods, radiochemical counting techniques, x-ray crystallography and some attempts have been made with ultraviolet and infrared spectroscopy. The conclusions presented early in the literature were contradictory. While there seemed to be no doubt about the reversibility of the xenon-respiratory pigment interaction, some early authors suggested that the process was a mere solubility while others indicated evidence for a stoichiometric reaction.

---

[135] E. M. Roth, *Space Sci. Rev.*, **6**, 452 (1967).

[136] L. Pauling, *Science*, **134**, 15 (1961).

[137] E. Rothstein and R. M. Featherstone, *J. Mol. Biol.*, **50**, 199 (1970).

[138] R. M. Featherstone and C. A. Muehlbacher, *Pharmacol. Rev.*, **15**, 97 (1963).

[139] R. M. Featherstone, C. A. Muehlbacher, F. L. De Bon and J. A. Forsaith. *Anesthesiology*, **22**, 977 (1961).

[140] C. A. Muehlbacher, F. L. De Bon and R. M. Featherstone, *Molec. Pharmacol.*, **2**, 86 (1966).

Mortimer and Bauer[141] studied the affinities of leguminous hemoglobin, myoglobin and hemoglobin for the gases N_2, H_2 and Ar by a manometric method, and concluded that the absorption of the gases followed Henry's Law in the range of 0 to 6 atmospheres. The free energy changes for the gas uptake were found to be in the range of $+1.5$ to $+2.8$ kcal/mole, depending on the gas used and the oxidation state of the protein.

The study of the absorption of nitrogen in aqueous solutions containing the main components of leguminous hemoglobin at 5, 15 and 25° in the 0–5 atm pressure range, has shown that nitrogen interacts with both ferri- and ferroleghemoglobin in an approximate 1 :1 molar ratio. The thermodynamic quantities obtained for the interaction of nitrogen with ferrilegoglobin at 15° were $\triangle G^\circ = -4.06 \pm 0.03$ kcal/mole, $\triangle H^\circ = + 15.7 \pm 0.1$ kcal/mole and $\triangle S^\circ = +69 \pm 1$ eu. For the nitrogen ferrolegoglobin interaction at 15°, $\triangle G^\circ = -3.8 \pm 0.21$ kcal/mole, $\triangle H^\circ = +13 \pm 1$ kcal/mole and $\triangle S^\circ = +57 \pm 2$ eu.[43,44] The nitrogenleghemoglobin interaction is of a weak nature and probably involves forces of the van der Waals type. The large positive entropy changes suggest a considerable disordering of the leghemoglobin molecule during the absorption of nitrogen.[43,44] A similar study of the interaction of leguminous hemoglobin with xenon, provided evidence for a weak interaction, but the experimental errors were so large in comparison to the interaction that the stoichiometry could not be determined.[43,44]

Conn has shown by the use of radioactive ^{133}Xe and ^{135}Xe that the absorption of the rare gas by oxidized and reduced canine and human hemoglobin obeys Henry's Law in the 0–700 mm range.[142] A similar result was obtained for krypton and xenon by Yeh and Peterson.[143] Schoenborn has also suggested that the absorption of Xe by horse hemoglobin follows Henry's Law from 0.5 to 1.5 atmospheres.[144] However, in the same article, Schoenborn also reported the results of x-ray studies which indicate that xenon is bound at four sites of the equine hemoglobin, one Xe molecule to each alpha and beta subunit. Schoenborn and his coworkers have also reported similar results for sperm whale metmyoglobin[145,146] and sperm whale deoxymyoglobin.[147] The resulting energy at the interaction site is attributed to charged induced dipole moments, dipole-dipole, and London forces. The calculated energy of interaction is 10.2 kcal/mole for metmyoglobin and 12 kcal/mole for deoxymyoglobin.

Crystallographic studies have indicated the presence of two hydrophobic sites near the heme group of sperm whale myoglobin.[147,148] The site on the distal side, called *A*, is usually occupied by ligands such as O_2,

---

[141] R. G. Mortimer and N. Bauer, *J. Phys. Chem.*, **64**, 387 (1960).

[142] H. L. Conn, Jr., J. *Appl. Physiol.*, **16**, 1065 (1961).

[143] S. Y. Yeh and R. E. Peterson, *J. Appl. Physiol.*, **20**, 1041 (1965).

[144] B. P. Schoenborn, *Nature*, **208**, 760 (1965).

[145] B. P. Schoenborn, H. Watson and J. C. Kendrew, *Nature*, **207**, 28 (1965).

[146] B. P. Schoenborn, *ibid.*, **214**, 1120 (1967).

[147] B. P. Schoenborn and C. L. Nobbs, *Molec. Pharmacol.*, **2**, 491 (1966).

[148] C. L . Nobbs in "Hemes and Hemoproteins", B. Chance, R. W. Eastbrook and T. Yonetani, Eds., Academic Press, New York, 1966, pp. 143–147.

H_2S, $CH_3CH_2CH_2CN$, which bind to the iron atom. Site *B* on the proximal side is histidine linked, involves a different kind of bonding and is occupied by molecules such as Xe and HgI_3^-. [148,149] The introduction of xenon at site *B* seems to produce a minimal rearrangement of the surrounding residues. According to Nobbs, [148] the ligands at site *A* are held to the iron by direct chemical bonds, while the xenon at site *B* is held merely by weak interactions of the van der Waals type with the surrounding groups. Fourier analysis of the crystallographic data shows that the xenon atom is located deep in the protein at 5.37 Å from Fe, at approximately half the distance between the metal and the proximal ring of histidine. [147] Recent high resolution nuclear magnetic resonance experiments indicate that the major xenon binding site in ferrimyoglobin cyanide is the same in the hemoprotein solution and in the crystal. [150]

There has been some evidence presented for the existence of another one or two binding sites for xenon in hemoproteins, in addition to the primary one described above. [41,147,151–153] About 17% of the xenon appears to be bound at these subsidiary sites. [147]

Ewing and Maestas have reported the results of manometric studies which indicate a stoichiometric interaction between xenon and equine metmyoglobin. [154] This is the first direct evidence for stoichiometric interaction obtained from solubility measurements. The same results were obtained for horse myoglobin and cyanometmyoglobin. The standard free energies of reaction at 25° vary from -2.7 kcal/mole for metmyoglobin to -2.9 kcal/mole for myoglobin and cyanometmyoglobin. [41,42] Attempts were also made to study the interaction of xenon and metmyoglobin spectrophotometrically at 700 mm of Xe by scanning in the 400–440 mμ and 500–550 mμ regions, but no detectable changes in absorption were noticed. [42] On the basis of the equilibrium constants for the xenon-myoglobin interaction evidence was presented for the existence of a primary and possibly a secondary site for xenon binding. [41,42]

Catchpool reported in 1968 that at 20° and 1 atm of xenon, 1.67 moles of the noble gas were absorbed per mole of hemoglobin. [155] At about the same time, Keyes and Lumry [151] noted that at a pressure of 2 atm, xenon had no appreciable effect on the oxygen association curve of myoglobin, but enhanced the bonding of CO. They proposed the existence of three binding sites for xenon atoms, which interact to a larger extent in carbon monoxide myoglobin than in oxymyoglobin. According to their explanation, the second and third sites were not observed in the x-ray studies because their occupancy was very low.

Wishnia has studied the binding of alkanes to hemoproteins and has concluded that this interaction takes place at two different loci. He has also suggested that in both ferrihemoglobin and ferrimyoglobin, xenon and pentane compete for the same two interacting sites. [152,156]

---

[149] W. S. Caughey, *Ann. Rev. Biochem.*, **36**, 611 (1967).

[150] R. G. Shulman, J. Peisach and B. J. Wyluda, *J. Mol. Biol.*, **48**, 517 (1969).

[151] M. Keyes and R. Lumry, *Fed. Proc.*, **27**, 895 (1968).

[152] A. Wishnia, *Biochemistry*, **8**, 5064 (1969).

[153] R. P. Schoenborn, J. *Mol. Biol.*, **45**, 279 (1969).

[154] S. Maestas and G. J. Ewing, *Curr. Mod. Biol.*, **1**, 148 (1967).

[155] J. F. Catchpool, *Fed. Proc.*, **27**, 884 (1968).

[156] A. Wishnia, *Biochemistry*, **8**, 5070 (1969).

The evidence presented by the x-ray studies of Schoenborn and associates [144-147] and the solubility measurements of Ewing and Maestas [41,154] indicate that the interaction between xenon and myoglobin and hemoglobin is stoichiometric. The adherence of hemoprotein solutions to Henry's Law observed by the earlier authors [141-143] and by Schoenborn [144] is not necessarily an indication that a stoichiometric reaction or adsorption at a specific site is not taking place. According to Mortimer and Bauer, [141] for moderate pressure (0 to 6 atm), which usually represent a region below the saturation pressures, the adsorption isotherms tend toward linearity. If the concentration of the hemoprotein-gas complex, (Hp. G), is small compared to the concentration of the hemoprotein (Hp) and gas (G), the dependence of (Hp. G) on the gas concentration or pressure must be linear when these species, i.e. Hp. G ,Hp, and G are in chemical equilibrium.

It is clear that the interaction of xenon with respiratory pigments falls in the "weak-bond" category and that the binding of xenon to hemoproteins is not strong iron — ligand bonding as in the case of O_2, CN^- and CO. However, the processes that take place during the interaction at the molecular level are still not well understood. The use of newer techniques such as fluorescent probes, spin labels, optical rotatory dispersion and circular dichroism might shed additional light about the sites of attachment of gases and conformational changes in the hemoprotein molecules during the interaction.

Revue Roumaine de Chimie, **18**, *10*, 1749–1757 (1973)

CONTRIBUTIONS TO THE CHEMISTRY OF THIOCOMPLEXES. III

COMPLEX COMPOUNDS OF Pd(II) WITH THIOAMIDES

D. NEGOIU [*], VASILICA MUREŞAN [**] and CORNELIA FULEA [*]

[*] Department of Chemistry, University of Bucharest, Splaiul Independenţei, 89, Romania

[**] Department of Chemistry, University of Craiova, Calea Bucureşti, 165, Romania

Received January 26, 1973

Complex compounds of palladium (II) with thioamides of the phenylthioacetamide series and with unsaturated aromatic thioamides, of the type PdL_2Cl_2(L = phenylthioacetamide, 2,5-diphenylthioacetamide, cynamthioamide, *p*-methoxy-cynamthioamide and *o*-tolylthioacetamide) and $PdLCl_2$(L = diphenylthioacetamide) were obtained. These complex compounds are characterized by means of chemical analysis and IR spectrophotometric analysis. The study is completed with electronic reflexion spectra, by means of which we make attributions of the absorption bands.

The ability of aliphatic thioamides to form complex compounds, with thioacetamide (TAA) as the main representative, was studied by numerous authors,[1–9] while the aromatic thioamides were much less studied. Thus, Ishikova[10] obtained the complexes of a whole series of aromatic thioamides with mercuric chloride of the $HgCl_2.2R.CS.NH_2$ type, but without going deeper into the matter. Gagliardi and Haas,[11] also, have obtained some complexes of metals with aromatic thioamides, but without analysing the obtained substances. They suppose, according

---

[1] E.G. Cox, N. Wardlaw and K.C. Webster, *J. Chem. Soc.*, **1936**, 775.
[2] D. Rosenthal and I.J. Taylor, *J. Amer. Chem. Soc.*, **82**, 4169 (1960).
[3] M. Nardelli and I. Chierici, *Gazzetta*, **87**, 1478 (1957).
[4] M. Nardelli and I. Chierici, *Gazzetta*, **88**, 359 (1958).
[5] S. Petri and T. Lipiec, *Roczniki Chem.*, **39**, 1725 (1965).
[6] C.D. Flint and M. Goodgame, *J. Chem. Soc.*, A, **1968**, 750.
[7] A.V. Ablov and V.N. Shafranskii, *Zhur. neorg. Khim.*, **9**, 585 (1964).
[8] E. Spinner, *Spectrochim. Acta*, **15**, 95 (1959).
[9] M.R. Trutter, *J. Chem. Soc.*, **1960**, 997.
[10] S. Ishikova, *Chem. Zentr.*, **98**, 1765 (1928).
[11] E. Gagliardi and W. Haas, *Mikrochim. Acta*, **1954**, 593.

to Kinder's hypothesis,[12] that the thiobenzamide $C_6H_5.CS.NH_2$ reacts in an alkaline medium with the metallic ions Ag^+, Hg_2^{2+}, Pb^{2+}, Cu^{2+}, Cd^{2+}, Bi^{3+} and Tl^+ giving the respective sulphides.

Kasparek and Mollin[13] studied the behaviour of thiobenzamide in an acid medium *versus* the following metallic ions : Ag^+, Hg^{2+}, Cu^{2+}, Au^{3+} Pt^{4+}, Pd^{2+}, Ir^{4+}, Fe^{3+} and OsO_4.

The complexes obtained are described and analysed from the chemical point of view. It is shown that thiobenzamide can act in the two tautomeric forms, A and B.

$$R-CS-NH_2 \qquad\qquad R-C(SH)=NH$$

A B

We notice, hence, that the aromatic thioamides form also well-defined and stable complex compounds with the main representatives of the class (b) of metallic ions.[14]

In this paper we aim to continue the study begun in the former papers[15,16] on the complex compounds of class (b) metals with aromatic thioamides ; in fact we deal here with the complex compounds of Pd(II) with thioamides of the phenylthioacetamide series : phenylthioacetamide (PTAA)$^{(I)}$, *o*-tolylthioacetamide (OTTAA)$^{(II)}$, 2,5-dimetylphenylthioacetamide (2,5 DMPTAA)$^{(III)}$, diphenylthioacetamide (DPTAA)$^{(IV)}$ and two nonsaturated thioamides cynamthioamide (CTA)$^{(V)}$ and *p*-methoxycynamthioamide (*p*-MCTA)$^{(VI)}$.

$$PhCH_2-CS-NH_2 \qquad o-CH_3-C_6H_4-CH_2-CS-NH_2$$

I II

$$2{,}5-(CH_3)_2C_6H_3-CH_2-CS-NH_2 \qquad Ph_2CH-CS-NH_2$$

III IV

$$PhCH=CH-CS-NH_2 \qquad p-MeO-C_6H_4-CH=CH-CS-NH_2$$

V VI

The complex compounds were studied by chemical methods as well as by means of their IR and electronic reflexion spectra.

RESULTS AND DISCUSSION

All the complex compounds described in this paper were obtained by the same method : an ethanol solution of thioamide was added to an

---

[12] K. Kinder, *Liebigs Ann. Chem.*, **10**, 450 (1926).

[13] F. Kásparek and J. Mollin, *Coll. Czech. Chem. Comm.*, **25**, 2919 (1960).

[14] S. Ahrland, J. Chatt and N.R. Davies, *Quart. Rev.*, **12**, 265 (1958).

[15] D. Negoiu and V. Mureşan, *Anal. Univ. Bucureşti Chim.*, **1971**, 121.

[16] D. Negoiu, V. Mureşan and C. Fulea, *Anal. Univ. Bucureşti Chim.* (under press).

aqueous palladium dichloride solution. The complex compounds obtained are solid substances, coloured in different brown shades, stable in time, difficult to solve or only partially soluble in inorganic or organic solvents, with higher melting points than those of the corresponding thioamides.

The data obtained through elementary chemical analysis (table 1) lead us to the following formulae:

$Pd\ L_2\ Cl_2$ (L = OTTAA, 2,5-DMPTAA, PTAA, CTA and *p*MCTA)

$Pd\ L\ Cl_2$ (L = DPTAA).

Table 1

Elementary analysis of the complexes of Pd(II)

The complex studied	Analysed element							
	Pd %		S %		C %		H %	
	Theor.	Exper.	Theor.	Exper.	Theor.	Exper.	Theor.	Exper.
$Pd\ (OTTAA)_2Cl_2$	21.08	21.20	12.67	12.34	42.69	44.03	4.35	3.97
		21.25		12.22		43.92		4.02
$Pd\ (DMPTAA)_2Cl_2$	19.89	19.78	11.96	11.74	44.80	45.89	4.88	4.12
		19.81		11.45		46.02		4.23
$Pd\ (PTAA)_2Cl_2$	22.41	22.36	13.47	13.33	40.33	41.90	3.78	3.09
		22.22		13.38		41.30		3.12
$Pd\ (DPTAA)Cl_2$	26.37	26.45	7.90	7.43	41.52	42.84	3.21	3.00
		26.28		7.55		42.63		2.97
$Pd\ (CTA)_2Cl_2$	21.19	21.23	12.73	12.47	42.89	43.10	3.57	3.12
		21.40		12.33		43.23		3.19
$Pd\ (MCTA)_2Cl_2$	18.91	18.90	11.37	11.11	42.54	43.61	4.25	4.07
		18.89		11.20		43.70		3.98

To be able to refer to the character of the bond effected at the formation of the complexes, we have carried out the spectral analysis in IR.

The comparative studies undertaken on the ligands and the corresponding complexes (figures 1, 2, 3, 4, 5 and 6) are systematized and discussed separately.

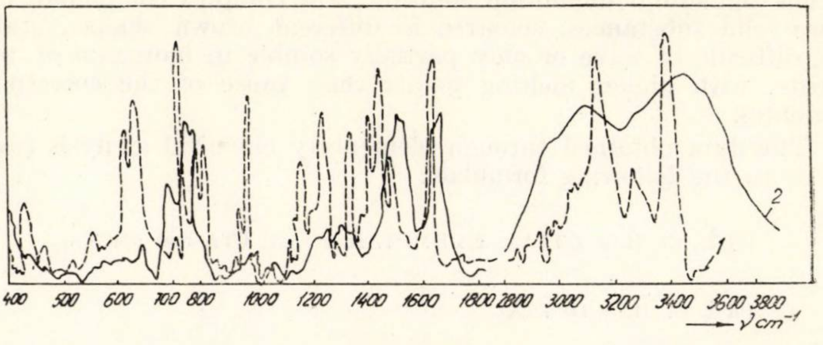

Fig. 1. – IR spectrum of *o*-tolylthioacetamide (...). IR spectrum of Pd(OTTAA)$_2$Cl$_2$ (—).

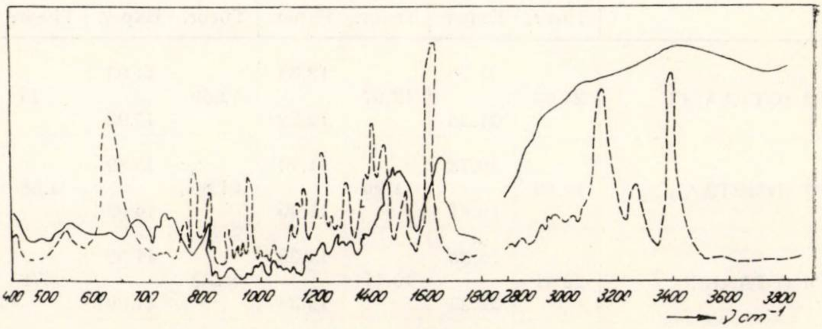

Fig. 2. – IR spectrum of 2,5-dimethylphenylthioacetamide (...). IR spectrum of Pd(DMPTAA)$_2$Cl$_2$. (—).

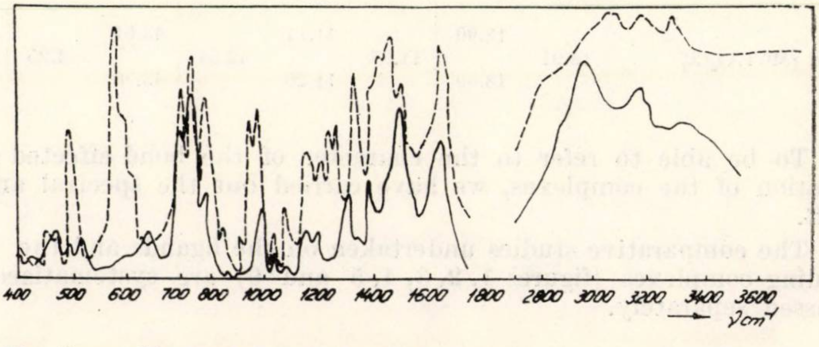

Fig. 3. – IR spectrum of phenylthioacetamide (...). IR spectrum of Pd (PTAA)$_2$Cl$_2$ (—).

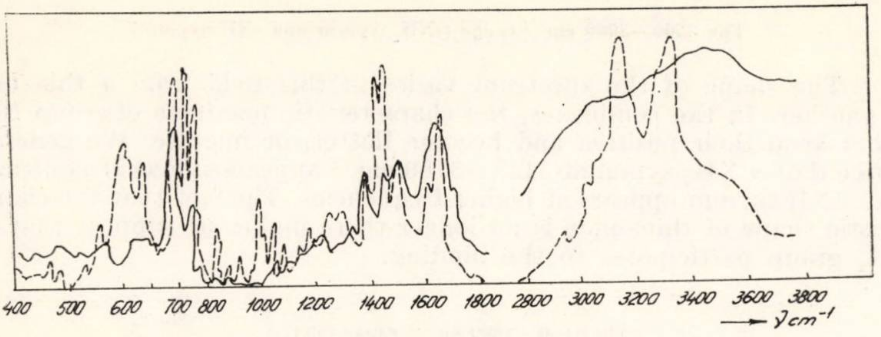

Fig. 4. – IR spectrum of diphenylthioacetamide (. . .). IR spectrum of $Pd(DPTAA)Cl_2$ (—).

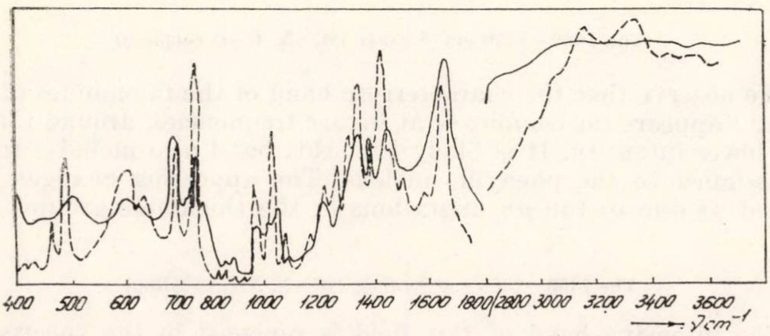

Fig. 5. – IR spectrum of cynamthioamide (. . .). IR spectrum of $Pd(CTA)_2Cl_2$ (—).

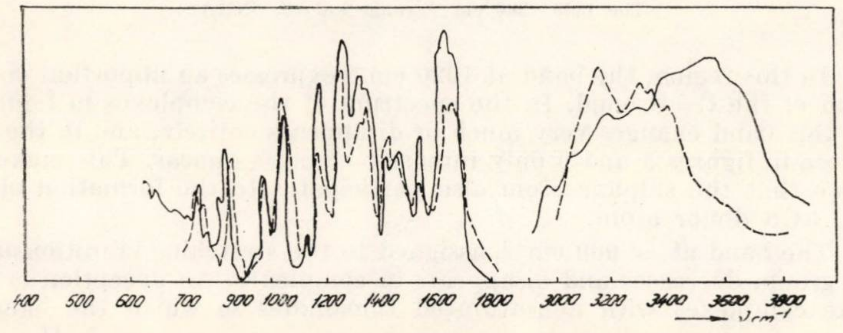

Fig. 6. – IR spectrum of *p*-methoxicynamthioamide (. . .). IR spectrum of $Pd(MCTA)_2Cl_2$ (—).

The 3500 – 3000 cm^{-1} range (νNH_2 symm and νNH asymm)

The shape of the spectrum varies in this field from a thioamide to another. In the complexes, the characteristic maximae of group NH_2, either keep their position and become flatter, or migrate. We generally notice that ν NH_2 symm at 3145 – 3180 cm^{-1} appears at lower frequencies, and ν NH asymm appears at higher frequencies. The fact that the characteristic shape of thioamide is no longer there makes us suppose that the NH_2 group participates to the binding.

The 1650 – 1600 cm^{-1} range (δNH_2)

The characteristic band of the stretching vibration of the NH_2 group appears in complexes at higher frequencies, but with a variable intensity. This fact confirms the previous assumption.

The 1600 – 1450 cm^{-1} range ($\nu C-N$, $C-C$ coupling)

We observe that the characteristic band of the thioamides at 1440 – 1420 cm^{-1} appears for complexes at higher frequencies, around 1550 cm^{-1}, with a lower intensity. It is likely that this band also includes the weak band assigned to the phenylic nucleus. The appearing changes may be explained as due to the $p\pi$ migrations in the thioamide group

The 1450 – 1350 cm^{-1} range ($\nu C-N$, NH_2 coupling)

The intensive band of this field is replaced in the spectra of the complexes by a small and weak band, in positions oscillating around the band characteristic to thioamides. At complexes with CTA and *p*MCTA the same shapes as for thioamides are approximately kept.

The 1350 – 900 cm^{-1} range ($\nu C=S$, δNH_2)

In this region, the band at 1220 cm^{-1} expresses an important contribution of the C=S bond. In the spectrum of the complexes in figures 1 to 4, this band changes very much or disappears entirely, and in the case of those in figures 5 and 6 only intensity changes appear. This makes us assume that the sulphur atom also participates to the formation of the bond, as a donor atom.

The band at ∼ 960 cm^{-1}, assigned to the stretching vibration of the NH_2 group, decreases and disappears in complexes. An exception is that of the complexes with nonsaturated thioamides in which the band at 970 cm^{-1} is maintained, as characteristic to the group

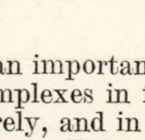

$$\begin{array}{ccccc} & & & & H \\ & \diagdown & & \diagup & \\ & & C=C & & \\ & \diagup & & \diagdown & \\ H & & & & \end{array}$$

.

The 900 – 700 cm^{-1} range (NCS)

In this field the bands disappear or decrease, only the characteristic bands of the substituted benzene nucleus remaining.

The 700 – 600 cm^{-1} range (C = S)

The very intensive band in the 550–640 cm^{-1} region of the thioamide spectrum, generally assigned to the C=S vibration, disappears or appears as a shoulder in the spectrum of complexes. In the case of complexes with thioamides the bands stay on, but their intensity changes.

These results confirm our assumption that the sulphur also participates to the achievement of the bond with NH_2 of the thioamide function.

Another aspect of the undertaken study of the palladium (II) complexes with thioamides is offered by the electronic reflexion spectra obtained in visible, shown in figure 7.

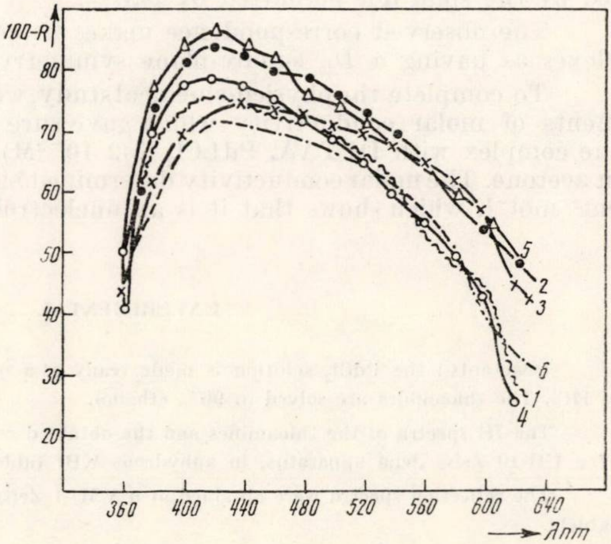

Fig. 7. — Electronic reflexion spectra of the complexes:
1, $Pd(OTTAA)_2Cl_2$;
2, $Pd(DMPTAA)_2Cl_2$;
3, $Pd(PTAA)_2Cl_2$;
4, $Pd(DPTAA)Cl_2$;
5, $Pd(CTA)_2Cl_2$;
6, $Pd(MCTA)_2Cl_2$.

Gray and Ballhausen [17] used the molecular orbitals theory to explain the spectra of the metallic square-plane complexes. The electronic spectra ($\bar{d}$-d transitions and charge-transfer spectra) are discussed for complex halides and cyanides of the d^8 configurational elements in the pattern of the molecular orbitals.

---

[17] H.B. Gray and C.J. Ballhausen, *J. Amer. Chem. Soc.*, **85**, 260 (1963).

Being on the direction of the bond, the orbital $d_{x^2-y^2}$ is less stable than all the other orbitals "d". Based on the same electrostatic effects, they reach the conclusion that the orbital d_{xy} is less stable than orbitals d_{xz} and d_{yz} (double degenerated) and d_{z^2}. Yet the position of orbital d_{z^2} is not precisely defined. Gray and Ballhausen [17] suggest the following sequence of the $5d$ orbitals : (dxz, dyz), d_{z^2}, d_{xy}, $d_{x^2-y^2}$, while Chatt *et al.*, [18] and more recently Martin [19] suggest the sequence : d_{z^2}, (d_{xz}, d_{yz}), dxy, $d_{x^2-y^2}$.

By correlating the bands observed in the electronic spectra of the Pd(II) complexes with those of $PdCl_4^{2-}$(solid state) we suggest the following assignments :

a) it is possible that the band at 23,809 cm^{-1} (420 nm), respectively 22,727 cm^{-1} (440 nm) appearing in the complexes should correspond to the band at 23,300 cm^{-1} in ($PdCl_4^{2-}$) with the assignment of transition $^1A_{1g} \rightarrow {}^1E_{1g}$ $[e_g(\pi^*) \rightarrow b_{1g}(\sigma^*)]$, a *d-d* transition, allowed by the spin, not permitted by parity.

b) we suppose that the shoulder appearing at 16,666 cm^{-1} (600 nm) corresponds to the band at 16,700 cm^{-1} in $PdCl_4^{2-}$ with assignment of the transition $^1A_{1g} \rightarrow {}^1A_{2g}$ $[b_{2g}(\pi^*) \rightarrow b_{1g}(\sigma^*)]$, a *d-d* transition, permitted by the spin, not permitted by parity.

The observed correspondence makes us consider the obtained complexes as having a D_{4h} square-plane symmetry structure.

To complete the physico-chemical study, we have carried out measurements of molar conductivity which gave sure results only in the case of the complex with DPTAA, $PdLCl_2$ (1/2 10^{-3}M), the only complex soluble in acetone. The molar conductivity determined has the value $\lambda = 2.28\ \Omega^{-1}$ cm^2 mol^{-1}, which shows that it is an unelectrolyte.

EXPERIMENTAL

Reactants : the $PdCl_2$ solution is made ready at a 0.02 M concentration, weakly acid in HCl. The thioamides are solved in 96% ethanol.

The IR spectra of the thioamines and the obtained complexes were recorded by means of a UR-10 Zeiss Jena apparatus, in anhydrous KBr tablets.

The reflection spectra were obtained at a VSU-1 Zeiss Jena spectrophotometer in MgO tablets.

The electrical conductivity was measured at a "Conductometer II" (Czechoslovakia) apparatus, with a cell having a 0.52 constant.

$Pd(OTTAA)_2Cl_2$ Complex

To 10 ml $PdCl_2$, 0.02 M was added, drop by drop, and under continuous stirring to the ligand ethanol solution till complete precipitation. The precipitate is left to settle for an hour. Taking into account the fineness of the precipitate, the filtering is carried out through a G_4

---

[18] J. Chatt, G.A. Gamlen and L.E. Orgel, *J. Chem. Soc.*, **1958**, 487.

[19] D.S. Martin, M.A. Tucker and A.J. Kassman, *Inorg. Chem.*, **1965**, 1682.

crucible. It is washed with ethanol and dried in vacuum. The complex has the appearance of a brown mass. It is stable in time, offers an average solubility in organic solvents and a low solubility in inorganic solvents.

Complexes PdL_2Cl_2 *(L = 2,5 DMPTAA, PTAA, CTA,* p-*MCTA) and* $PdLCl_2$ *(L = =DPTAA)* are obtained according to a similar working technique.

The complexes obtained are solid substances, stable, coloured in different shades of brown and orange, solving with difficulty in inorganic solvents and incompletely soluble in organic solvents (excepting Pd(DPTAA)Cl_2 easily soluble in acetone).

CONCLUSIONS

The complex compounds of Pd(II) with the aromatic thioamides described in this paper are of the type:

PdL_2Cl_2 (L = PTAA, OTTAA, 2,5-DMPTAA, CTA and *p*-MCTA)

Pd L Cl_2 (L = DPTAA)

From the correlation of the elementary chemical analysis and the study of the IR spectra, which bring proofs in the achievement of the bond by means of the sulphur as well as of the nitrogen, we infer that the following structural formulae are possible:

Pd L_2Cl_2

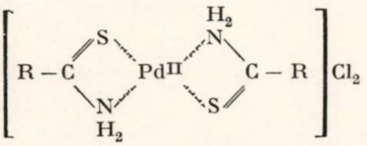

Pd LCl_2

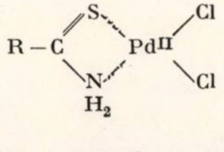

We notice that in these complexes the thioamides participate in the "thioceto" form.

The ligand of the phenylthioacetamide series, DPTAA, behaves differently to the other members of the series, generating complexes of the M^{II} L Cl_2 (M^{II} = Pd, Hg) [16] type. The fact that only one molecule of thioamide participates to the formation of the complex receives an explanation in the steric hindrances brought about by the two phenyl radicals. The formulae of the complexes M^{II} LCl_2 showing them as non-electrolytes are confirmed by the molar conductivity measurements achieved for the complex Pd(DPTAA)Cl_2.

The electronic reflexion spectra of the palladium (II) complexes bring us to the conclusion that they are square-plane, belonging to the symmetry group D_{4h}.

[illegible]. It is washed with [illegible] and dried in vacuum. The complex has the appearance of a brown mass. It is stable in the air [illegible] soluble in organic solvents and has low solubility in inorganic solvents.

Complexes [illegible] and Pd(L)$_2$Cl$_2$ [illegible] are obtained according to a similar working technique.

The complexes obtained are [illegible] stable, coloured [illegible], insoluble in water, [illegible] of inorganic solvents and [illegible] soluble in a [illegible].

CONCLUSIONS

The complex compounds of Pd(II) with the aromatic thioamides [illegible] in this paper are of the type:

Pd(L)$_2$Cl$_2$ (L = TAA, DPTAA, [illegible])

[illegible] Cl$_2$ (L = DPTAA)

From the correlation of the elementary chemical analysis and the study of the IR spectra, which bring proofs of the achievement of the bond by means of the sulphur as well as of the nitrogen, we infer that the following structural formulae are possible:

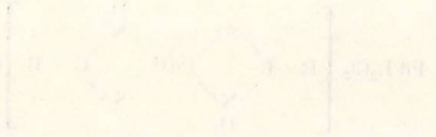

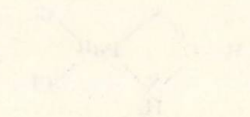

We notice that in these complexes the thioamides participate in the "thioenic" form.

The ligand of the phenylthioacetamide series, DPTAA, behaves differently to the other members of the series, generating complexes of the M^{II}LCl$_2$ (M = Pd, Hg) type. The fact that only one molecule of thioamide participates to the formation of the complex receives an explanation in the steric hindrance brought about by the two phenyl radicals. The formulae of the complexes M^{II}LCl$_2$ showing them as non-electrolytes are confirmed by the molar conductivity measurements achieved for the complex Pd(DPTAA)Cl$_2$.

The electronic reflexion spectra of the palladium (II) complexes bring us to the conclusion that they are square-planar, belonging to the symmetry group D_{4h}.

Revue Roumaine de Chimie, **18**, *10*, 1759–1767 (1973)

ELECTRONIC SPECTRA OF TRANSITION METAL COMPLEXES. I

LIGAND FIELD PARAMETERS OF SOME DIMETHYLGLYOXIMATO-DIAMINO-COBALT(III) COMPLEXES

J. ZSAKÓ, J. SATA und CS. VÁRHELYI
Faculty of Chemistry, "Babeş-Bolyai" University,
Cluj, str. Arany János 11, Romania

Received January 17, 1973

Electronic spectra of tris-dimethylglyoximato-Co(III) : $[Co(DH)_3]$ and of several bis-dimethylglyoximato-diamino-Co(III) complexes : $[Co(DH)_2(amine)_2]X$ have been recorded. The ligand field, charge transfer and ligand transition bands have been identified. The Racah parameters B, the tetragonal perturbation parameters Dt, Ds, as well as the nephelauxetic ratio β have been derived from the position of the ligand field transition bands. The character of the Co-N bond is discussed. The relative position of the energy levels has been evaluated.

The electronic spectra of the dimethylglyoximato-cobalt(III) complexes are very little studied. Spectra have been recorded by Ablov and Filippov [1] and these authors made an attempt to assign the absorptions bands observed to various transitions. Matsumoto *et al.* [2] have studied the charge transfer bands of some Co(III)-dioximine complexes. No attempt has been reported to derive some quantitative parameters from the Laporte forbidden *d-d* transition bands.

The $[Co(DH)_2 Am_2]^+$ type complexes (DH_2 stands for a molecule of dimethylglyoxime and Am for a molecule of ammonia or of an amine) can be considered to be of D_{4h} symmetry. Spectral characteristics of D_{4h} complexes can be approximated as a tetragonal perturbation of the octahedral problem.

Since all Co(III) complexes (excepting $[CoF_6]^{3-}$) are diamagnetic, the electronic configuration of Co^{3+} in octahedral environment is t_{2g}^6 in the ground state and it has just the one term $^1A_{1g}$. The $t_{2g}^5\, e_g^1$ first excited state has the terms $^1T_{1g}$, $^3T_{1g}$, $^1T_{2g}$ and $^3T_{2g}$.

---

[1] A.V. Ablov and M.P. Filippov, *Zhur. neorg. Khim.*, **3**, 1565 (1958); **4**, 2204, 2213 (1959).

[2] C. Matsumoto, T. Kato and K. Shinra, *Nippon Kagaku Zasshi*, **86**, 1266 (1965); *Chem. Abstr.*, **65**, 13027 (1966).

By using the Tanabe-Sugano approach [3] and the expression of the diagonal elements of the electrostatic matrix, [4-6] we have for the energy levels in O_h relative to the d-electron energy in crystal field of spherical symmetry the following expressions [7]:

$$E(^1A_{1g}) = -24\,Dq\,;\; E(^1T_{1g}) = -14\,Dq - C\,;$$

$$E(^1T_{2g}) = -14\,Dq + 16\,B - C\,;\; E(^3T_{1g}) = -14\,Dq - 3C\,;$$

$$E(^3T_{2g}) = -14\,Dq + 8B - 3C$$

where B and C are the Racah parameters. [8]

There are 4 possible transitions from the ground state in the first excited state:

$$^1A_{1g} \to {}^1T_{1g} \quad \text{with} \quad \widetilde{\nu}_1 = 10\,Dq - C\,;$$

$$^1A_{1g} \to {}^1T_{2g} \quad \text{with} \quad \widetilde{\nu}_2 = 10\,Dq + 16\,B - C$$

$$^1A_{1g} \to {}^3T_{1g} \quad \text{with} \quad \widetilde{\nu}_{f_1} = 10\,Dq - 3C\,;$$

$$^1A_{1g} \to {}^3T_{2g} \quad \text{with} \quad \widetilde{\nu}_{f_2} = 10\,Dq + 8\,B - 3C.$$

In the visible region, 2 absorption bands are generally observed, which can be assigned to the spin allowed transitions, characterized by $\widetilde{\nu}_1$ and $\widetilde{\nu}_2$. Besides these, a very weak band, frequently only an inflexion point, is also observed, assigned to the spin forbidden $^1A_{1g} \to {}^3T_{1g}$ transition, characterized by $\widetilde{\nu}_1$. Thus, the above given expressions allow us to derive from spectral data the parameters 10 Dq, B and C:

$$10\,Dq = \frac{3\widetilde{\nu}_1 - \widetilde{\nu}_{f_1}}{2}\,;\; B = \frac{\widetilde{\nu}_2 - \widetilde{\nu}_1}{16} \text{ and } C = \frac{\widetilde{\nu}_1 - \widetilde{\nu}_{f_1}}{2} \tag{1}$$

In a field of D_{4h} symmetry the degenerated terms are splitted as follows:

$$T_{1g} \to A_{2g} + E_g \quad \text{and} \quad T_{2g} \to B_{2g} + E_g$$

One may presume the tetragonal perturbation to be not too strong as compared to the interaction of the electrons. Thus, instead of the 2 terms E_g, we must use two linear combinations of them. [9]

$$E_g^+ = \frac{3}{2}\,E_{g1} + \frac{1}{2}\,E_{g2} \text{ and } E_g^- = \frac{1}{2}\,E_{g1} - \frac{3}{2}\,E_{g2} \tag{2}$$

---

[3] Y. Tanabe and S. Sugano, *J. Phys. Soc. Japan.*, **9**, 753, 766 (1954).

[4] J.S. Griffith and L.E. Orgel, *J. Chem. Soc.*, **1956**, 4981.

[5] D.L. Wood, J. Ferguson, K. Knox and J.P. Dillon, Jr., *J. Chem. Phys.*, **39**, 890 (1963).

[6] R.A.D. Wendthworth and T.S. Piper, *Inorg. Chem.*, **4**, 709 (1965).

[7] J.S. Griffith, "The Theory of Transition-Metal Ions", University Press, Cambridge, 1964, p. 226.

[8] J.S. Griffith, "The Theory of Transition-Metal Ions", University Press, Cambridge, 1964, p. 83.

[9] M. Bán and J. Császár, *Magyar Kém. Folyóirat*, **73**, 509 (1967).

Taking into account the diagonal elements of the electrostatic matrix, one obtains the following energies for the singlet terms in D_{4h}, relative to the d-electron energy level in spherical symmetry[9]:

$$\begin{aligned}
E(^1A_{1g}) &= -24\,Dq + 14\,Dt + 5\,B + 8\,C \\
E(^1E_g^+) &= -14\,Dq + \frac{21}{4}\,Dt + 5\,B + 7\,C \\
E(^1A_{2g}) &= -14\,Dq + 14\,Dt + 5\,B + 7\,C \\
E(^1B_{2g}) &= -14\,Dq - 4\,Ds + 9\,Dt + 21\,B + 7\,C \\
E(^1E_g^-) &= -14\,Dq + 2\,Ds + \frac{31}{4}\,Dt + 21\,B + 7\,C
\end{aligned} \tag{3}$$

where *Dt* and *Ds* are the tetragonal perturbation parameters[6,10,11] and *B* and *C* the Racah parameters.

From the $^1A_{1g}$ ground state 4 spin allowed transitions are possible

$$\begin{aligned}
&^1A_{1g} \rightarrow {}^1E_g^+ && \text{with} && \tilde{\nu}_1(\mathrm{I}) = 10\,Dq - \frac{35}{4}\,Dt - C \\
&^1A_{1g} \rightarrow {}^1A_{2g} && \text{with} && \tilde{\nu}_1(\mathrm{II}) = 10\,Dq - C \\
&^1A_{1g} \rightarrow {}^1B_{2g} && \text{with} && \tilde{\nu}_2(\mathrm{I}) = 10\,Dq - 4\,Ds - 5\,Dt + 16\,B - C \\
&^1A_{1g} \rightarrow {}^1E_g^- && \text{with} && \tilde{\nu}_2(\mathrm{II}) = 10\,Dq + 2\,Ds - \frac{25}{4}\,Dt + 26\,B - C
\end{aligned}$$

We can consider the two spin allowed transition bands of the octahedral, characterized by $\tilde{\nu}_1$ and $\tilde{\nu}_2$, to be splitted in the case of D_{4h} complexes in two components each. Experimentally, it can be observed only the splitting of the first band,[6] i.e.

$\tilde{\nu}_2(\mathrm{I}) = \tilde{\nu}_2(\mathrm{II})$, and therefore

$$D_s = \frac{5}{24}\,D_t \text{ and } \tilde{\nu}_2(\mathrm{I,\,II}) = 10\,Dq - \frac{35}{6}\,Dt + 16\,B - C \tag{4}$$

If the first band is splitted, the parameter *Dt* can be obtained according to the formula

$$D_t = \frac{4}{35}\,[\tilde{\nu}_1(\mathrm{II}) - \tilde{\nu}_1(\mathrm{I})] \tag{5}$$

---

[10] M. Bán and Császár, *Magyar Kém. Folyóirat*, **73**, 512 (1967).
[11] T.S. Piper and R.L. Carlin, *J. Chem. Phys.*, **33**, 1208 (1960).

In order to derive the Racah parameters, we must know 10 Dq, which can be obtained in first approximation from the spectrum of an analogous octahedral complex by means of formula (1). In this case we have

$$C = 10\,Dq\,(O_h) - \tilde{\nu}_1(\mathrm{II}) \tag{6}$$

and

$$B = \frac{6\,\tilde{\nu}_2(\mathrm{I,\,II}) - 60\,Dq\,(O_h) + 35\,Dt + 6\,C}{96} \tag{7}$$

If the first band is not splitted either, we can consider the energy to be the arithmetical mean of the energies of the two transitions, i.e.

$$\tilde{\nu}_1(\mathrm{I,\,II}) = \frac{\tilde{\nu}_1(\mathrm{I}) + \tilde{\nu}_1(\mathrm{II})}{2} = 10\,Dq - \frac{35}{8}D_t - C \tag{8}$$

For deriving the unknown parameters, we must presume also $10\,Dq = 10\,Dq\,(O_h)$ and as a second presumption we may take $C = C(O_h)$. Thus we have:

$$D_t = \frac{8}{35}\,[\tilde{\nu}_1(O_h) - \tilde{\nu}_1(\mathrm{I,\,II})] \text{ and}$$

$$B = \frac{6\,\tilde{\nu}_2(\mathrm{I,\,II}) - 60\,Dq\,(O_h) + 35\,D_t + 6\,C(O_h)}{96} \tag{9}$$

As is seen, it is necessary to have the spectrum of an octahedral "parent" compound. As parent compound the $[\mathrm{Co(DH)_3}]$ non-electrolytic complex has been taken. Its spectrum is given in fig. 1 and the wave number of the absorption bands in table 1.

We can see the compound to have a strong absorption in the whole UV region between 25 and 50 kK, where appear both the own transitions of the ligand and the charge transfer (CT) transitions. These strong bands are superposed in part on the weak *d-d* transition bands, masking them. The first transition ($\tilde{\nu}_1$) appears as an inflexion point at 21.2 kK (*a* in table 1). The second one ($\tilde{\nu}_2$) is completely masked by a CT transition (*b*). No asymmetry of this band can be observed and, therefore, there is no possibility to decompose it. The only possible assumption is to take for $\tilde{\nu}_2$ the wave number of this CT band, i.e. to presume

$$\nu_2 = 28 \text{ kK}$$

The position of the spin forbidden band has been found on the base of the reflexion spectrum of the compound to be

$$\tilde{\nu}_{f_1} = 12.4 \text{ kK}$$

The above data allow us to derive the parameters characterizing the octahedral field. Formulae (1) give the following results:

$$10\,Dq = 25.6 \text{ kK}, \quad B = 0.425 \text{ kK}, \quad C = 4.4 \text{ kK} \tag{10}$$

In the spectrum of [Co(DH)$_3$] there are two inflexions at 32.5 (*c*) and 38.2 kK (*d*), respectively. These can be assigned to the coordinated dimethylglyoximate ligands. The dimethylglyoxime has in free state [12] a strong band at 37.7 and a weaker one at 31.5–32.0 kK. The shift of these bands in the complex molecule towards higher wave numbers pleads for the partial covalent character of the Co–N bond.

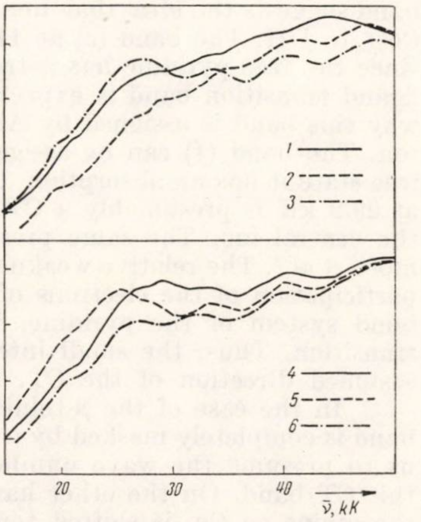

Fig. 1.—Visible and UV absorption spectrum of : *1*, [Co(DH)$_3$]; *2*, [Co(DH)$_2$(pyridine)$_2$] (NO$_3$); *3*, [Co(DH)$_2$ (*p*-toluidine)$_2$] Cl; *4*, [Co(DH)$_2$(aniline)$_2$] Br; *5*, [Co(DH)$_2$ (*m*-xylidine)$_2$] Cl; *6*, [Co(DH)$_2$(NH$_3$)$_2$] Cl.

The absorption band (*b*) at 28 kK has been assigned by Matsumoto *et al.* [2] to a CT from the Co^{3+} towards the DH ligand and the strongest band at 44 kK (*e*) to a CT from the DH ligand towards the central ion.

Electronic spectra of the tetragonal [Co(DH)$_2$ Am$_2$]$^+$ type complexes are very similar to the spectrum of the parent compound. They are also given in fig. 1.

The wave numbers, corresponding to the absorption maxima and inflexion points of the spectrum are presented in table 1.

Table 1

Wave number of the absorption bands of some [Co(DH)$_2$Am$_2$]$^+$ type complexes (in kK)

Am	(*a*)	(*b*)	(*c*)	(*d*)	(*e*)	(*f*)
1/2 DH	20.3	27.3	29.3	35.1	41.5	
pyridine	21.2	28.0	32.5	38.2	44.0	47.6
p-toluidine	20.35	27.1	32.9	40.4	48.5	
aniline	20.3	27.4	28.6	32.35	40.3	49–50
m-xylidine	20.35	25.35	27.1	33.0	40.3	50
NH$_3$	20.5	27.2	32.3	40.5	50.0	

It cannot be observed the splitting either of the first or of the second *d-d* transition bands. The strong CT and ligand transition bands are also in these cases partially superposed on the *d-d* bands and, therefore, the accurate determination of the position of the *d-d* bands is not possible. Nevertheless, the first inflexion (*a*) can be assigned in all cases to the first *d-d* transition, i.e. its wave number can be taken for $\tilde{\nu}_1$ (I, II).

---

[12] G. Kortüm, *Z. phys. Chem.*, **B. 43**, 271 (1939).

In the spectrum of the pyridine derivative, the second inflexion (*b*) at 27.3 kK can be assigned to the second *d-d* transition, i.e. its wave number can be considered as $\tilde{\nu}_2$ (I, II). The strong band (*d*) at 35.1 kK is due presumably to a pure ligand transition of DH, but the intensity of this band suggests the idea that here takes place also a CT transition from the Co^{3+} to DH. The band (*e*) at 41.5 kK seems to be also a composed one, since the free pyridine has a transition at 39.8 kK [13] and the other DH ligand transition band is expected to be also in this region. This is why this band is assigned by Ablov and Filippov [1] to the $Co(DH)_2$ skeleton. The band (*f*) can be assigned to the coordinated pyridine, since in free state it has an absorption band at 47—50 kK. [13] The weak band (*c*) at 29.2 kK is presumably a CT band, involving a CT from the amine to the central ion. The same presumption has been made also by Matsumoto *et al* [2]. The relative weakness of this band might be explained by the participation of the electrons of the donor N atom in the delocalized π-bond system of the pyridine, which lessens the probability of the CT transition. Thus, the small intensity of this band pleads for the above assumed direction of the CT.

In the case of the *p*-toluidine derivative, the second *d-d* transition band is completely masked by a CT band (*b*). Its symmetrical shape allows us to presume the wave number $\tilde{\nu}_2$(I, II) to be identical with the $\tilde{\nu}$ of this CT band. On the other hand, this band, which involves a CT from the amine to Co, is shifted towards lower energies as compared to the analogous band in the pyridine derivative, and its intensity is much higher. This is in agreement with the presumption that the CT occurs from the amine to Co^{3+}, since the CT is easier in this case due to the electron repulsive effect of the CH_3 group, linked to the aromatic ring. For the free *p*-toluidine, an absorption band at 33.8 kK has been reported, [14] but at higher wave numbers the spectrum was not studied. One may presume the *p*-toluidine to have another band at about 40 and 50 kK like the other aromatic amines. In the case of the complex ion, bands (*d*) and (*e*) are probably the corresponding ligand bands, but both bands might be composed ones, since the CT from the DH to Co^{3+} must appear also at about 40.4 kK as band (*d*) and in the case of band (*e*) it is possible also a contribution of a $Co^{3+} \rightarrow p$-toluidine CT transition. [15] The band (*c*) at 32.9 kK has an asymmetrical shape and it arises presumably from 3 different transitions. In this region the *p*-toluidine ligand band must be expected which appears at 33.8 kK in the free amine. Here must be situated a ligand band of the DH, as well as Co → DH CT band.

In the spectrum of the aniline derivative, the second *d-d* transition band can be presumed to have the same wave number as the CT band (*b*). For the free aniline 3 absorption bands have been reported, [16] at 35.0, 42.5 and 50.5 kK, respectively. The corresponding ligand bands must be the components of the bands (*d*), (*e*) and (*f*). All these bands have other contributions, too. In the case of band (*d*) one might presume a contribution of one DH ligand band, and of a Co-DH CT band. The band (*e*) must contain also a component due to a DH ligand transition and to a DH → Co CT transition. Band (*f*) is presumed to contain also a Co-aniline CT transition band. [15] Band (*c*) can be assigned to an aniline → Co CT transition, which occurs at higher energies as in the case of the analogous toluidine derivative, because of the absence of the electron repulsive effect of the CH_3 group.

---

[13] C.W.F. Spiers and J.P. Wibaut, *Rec. Trav. chim*, **56**, 573 (1937).

[14] K.L. Wolf and W. Herold, *Z. phys. Chem.*, **B.13**, 201 (1931).

[15] J. Császár, *Magyar Kém. Folyóirat*, **78**, 154 (1972).

[16] H. Ley and H. Speeker, *Ber. dtsch. chem. Ges.*, **72**, 192 (1939).

In the spectrum of the *m*-xylidine derivative, band (*b*) can be assigned to an amine → Co CT transition. Its position at lower energies, as in the previous cases, is in a perfect agreement with our above considerations concerning the effect of CH_3 groups. The intensity of this band makes difficult the localization of the second *d-d* band, which causes presumably the asymmetry of the band (*b*) and the slight inflexion at 27.1 kK (*c*).

The spectrum of the free *m*-xylidine has not been studied in the whole UV region. A single band has been reported [17] at 34.0 kK, but other bands can be expected near the values 40 and 50 kK. Bands (*d*), (*e*) and (*f*) can be presumed to contain the corresponding ligand transition bands, but their asymmetrical shape pleads for the complex character of these bands. To band (*d*) must contribute indeed both a DH ligand transition and a Co → DH CT transition. To band (*e*) as well, a DH ligand transition and a DH → Co CT transition correspond.

Band (*f*) must be due maily to a *m*-xylidine transition, but its maximum is so flat, that suggests a contribution of a CT transition, too.

In the case of the ammonia derivative band (*b*) can be assigned to an NH_3 → Co CT transfer and we might presume the second *d-d* transition band to have the same position. The band (*c*) is situated in the region where a DH ligand band can be expected, but the large intensity of the band suggests the presence of CT band, too. [2]

Band (*d*) could be assigned to a DH ligand transition and to a DH → Co CT transition. The last band (*e*) corresponds presumably to the absorption of the coordinated NH_3 and to a Co → NH_3 CT transition.

On the basis of the above discussion, we can take the wave numbers of inflexion (*a*) for $\tilde{\nu}_1$ (I, II) and we have some uncertain values for $\tilde{\nu}_2$ (I, II). An approximate calculation can be performed for the D_{4h} field parameters by using formulae (4) and (9), as well as the octahedral field parameters (10). On the basis of the Racah parameter B, calculated in this way, the nephelauxetic ratio

$$\beta = \frac{B}{B_0} \tag{11}$$

can be derived, taking 1.065 kK for the Racah parameter B_0 of the gaseous Co^{3+} ion, as indicated by Tanabe and Sugano. [3]

---

[17] A. Nakahara and R. Tsuchida, *J. Amer. Chem. Soc.*, **76**, 3103 (1954).

In table 2 are presented the results of these calculations. The magnitude $100(1-\beta)$, given in the last column, can be considered as a "percentage of the covalent character" of the metal-ligand bonds.

By using the *B* value obtained for the parent $[Co(DH)_3]$ complex, $100(1-\beta) = 60$ is obtained, i.e. the substitution of DH by two amine molecules diminishes the covalent character of the bond, but in a very small degree. Taking into account that both in the case of DH and of the amines, the Co is linked directly to a nitrogen atom, this small variation is quite understandable. On the other hand, this explains the very small *Dt* and *Ds* values, characterizing the distortion of the octahedron. This distortion is very small, since all the metal-ligand bonds are similar. Nevertheless, a nephelauxetic series can be established, indicating the increasing covalent character of the bond : aniline $<$ pyridine $<$ *p*-toluidine $<$ *m*-xylidine $<$ NH_3 $<$ DH.

Table 2

Ligand field parameters of some $[Co(DH)_2Am_2]^+$ type complexes

Am	Dt(K)	Ds(K)	B(K)	$100(1-\beta)$
NH_3	160	33.3	433	59.3
m-xylidine	194	40.4	438	58.9
p-toluidine	194	40.4	440	58.7
pyridine	206	42.9	457	57.1
aniline	206	42.9	462.5	56.6

The succession of the ligands in this series is very similar to the succession of increasing basicity of the amines.

Table 3

Spectral terms (in kK) of some $[Co(DH)_2Am_2]^+$ type complexes relative to the *d*-electron term in ligand field of spherical symmetry

Am	$^1A_{1g}$	$^1E_g^+$	$^1A_{2g}$	$^1B_{2g}$, $^1E_g^-$
NH_3	−21.83	−2.03	−0.63	+5.36
m-xylidine	−21.33	−1.83	−0.13	+5.74
p-toluidine	−21.32	−1.82	−0.12	+5.78
pyridine	−21.07	−1.67	+0.03	+6.24
aniline	−21.04	−1.65	+0.16	+6.35

Using the experimental parameters (10) and those given in table 2, we can make a rough evaluation of the energy of the ground state and of the excited singlet states on the basis of formulae (3). The results are presented in table 3.

EXPERIMENTAL

The parent compound $[Co(DH)_3]$ has been synthesized as described by Nakahara [17,18] and the amine derivatives $[Co(DH)_2Am_2]$ X according to the Ablov's method. [19]

Electronic spectra in the visible and UV ranges have been determined, using a Carl Zeiss Jena spectrophotometer VSU 1, in solution and in the case of the parent compound $[Co(DH)_3]$ also in solid state. The reflectance spectrum has been determined using a reflexion equipment attached to the VSU 1 spectrophotometer. Measurements have been carried out in methanolic solution at room temperature, 10—15 minutes after dissolution of the samples, excepting the parent compound which is very sparingly soluble in methanol. This compound can be solved in water in the presence of strong acids, due to the protonation of the coordinated dimethylglyoxime [20].

This is why the spectrum of this compound has been recorded in 0.1 M aqueous $HClO_4$, 30 minutes after dissolution.

---

[18] A. Nakahara, *Bull. Chem. Soc. Japan.*, **27**, 560 (1954.)

[19] A.V. Ablov, *Bull. Soc. chim. France*, **4**, 1783 (1937).

[20] J. Zsakó, Z. Finta and Cs. Várhelyi, *Stud. Univ. Babeş-Bolyai, Chem.*, **14** (2), 145 (1969).

Revue Roumaine de Chimie, 18, *10*, 1769–1776 (1973)

THE INFLUENCE OF CARBONYL OR HYDROXYL POSITION ON THE BREAKING POINT OF THE LINEAR TWELVE-MEMBERED CARBON CHAIN, BY MOLECULAR OXYGEN

IOSIF DRIMUŞ and IOAN T. IONESCU

Organic Technology Department, Polytechnical
Institute, Bucharest, Calea Victoriei, 149, Romania

Received February 12, 1973

The five dodecanone isomers and the six dodecanol isomers were submitted to liquid phase oxidation, with molecular oxygen. The peroxidic and carboxylic oxygen accumulation during the oxidation was established with the aid of peroxide and acidity numbers. The oxidation process was stopped at low conversions in the acids, in order to avoid their degradation. The resulted oxidation product was processed in order to separate the acids, which were then analysed by gas chromatography. On the basis of the acids composition, conclusions were drawn regarding the breaking point of the chain produced by the molecular oxygen, depending on the carbonyl or hydroxyl group.

The reaction between *n*-dodecane and oxygen is characterized by a number of consecutive, parallel and induced reactions.

At low conversions the *n*-dodecylhydroperoxides, isolated from the reaction mixture, were transformed in a mixture of *n*-dodecanols and *n*-dodecanones by thermal decomposition. [1]

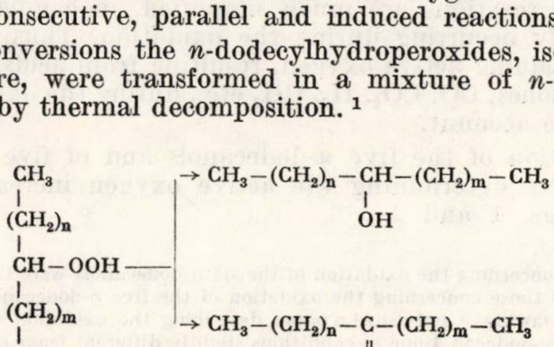

$$\begin{array}{l} \mathrm{CH_3{-}(CH_2)_n{-}(CH{-}OOH){-}(CH_2)_m{-}CH_3} \rightarrow \mathrm{CH_3{-}(CH_2)_n{-}\underset{\displaystyle OH}{\underset{|}{CH}}{-}(CH_2)_m{-}CH_3} \\ \mathrm{CH_3{-}(CH_2)_n{-}(CH{-}OOH){-}(CH_2)_m{-}CH_3} \rightarrow \mathrm{CH_3{-}(CH_2)_n{-}\underset{\displaystyle O}{\underset{\|}{C}}{-}(CH_2)_m{-}CH_3} \end{array}$$

$$n + m = 9$$

---

[1] I. Drimuş, "Studies on the Dodecane Oxidation", Thesis, Cluj University, 1966.

The *n*-dodecan-1-ol is lacking between the reaction products obtained by molecular oxygen oxidation of *n*-dodecane at 155°. This could be a proof that hydroperoxidation does not occur at a primary carbon atom.

Using the gas chromatographic technique, the *n*-dodecan-2-ol and *n*-dodecan-2-one were determined to be about 10% from the total amount of alcohols and ketones, the *n*-dodecan-3-ol and *n*-dodecan-3-one in slightly larger quantities, the rest consisting of *n*-dodecan-4-ol, *n*-dodecan-5-ol and *n*-dodecan-6-ol and *n*-dodecan-4-one, *n*-dodecan-5-one and *n*-dodecan-6-one (determined together, the separation by gas-chromatography being impossible).

In order to study the mechanism of the oxidation process and taking into account that the formed hydroperoxides give, besides other products, five secondary *n*-dodecanols and five secondary *n*-dodecanones, these ten substances were synthesized and submitted to oxidation in the same conditions as *n*-dodecane itself. *

Supposing that during the oxidation process the secondary *n*-dodecanols are oxidized to the corresponding *n*-dodecanones and then to the acids, according to Langenbeck and Pritzkow [4] the following sequence can be admitted :

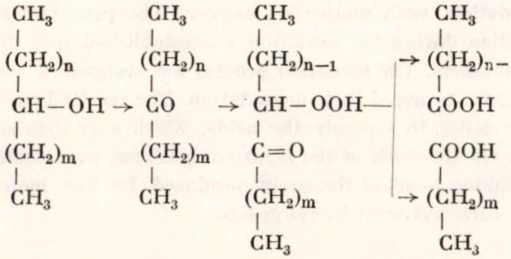

$$\begin{array}{lllll} CH_3 & CH_3 & CH_3 & & CH_3 \\ | & | & | & & | \\ (CH_2)_n & (CH_2)_n & (CH_2)_{n-1} & \rightarrow & (CH_2)_{n-1} \\ | & | & | & & | \\ CH-OH \rightarrow & CO \rightarrow & CH-OOH- & & COOH \\ | & | & | & & \\ (CH_2)_m & (CH_2)_m & C=O & & COOH \\ | & | & | & & | \\ CH_3 & CH_3 & (CH_2)_m & \rightarrow & (CH_2)_m \\ & & | & & | \\ & & CH_3 & & CH_3 \end{array}$$

$n + m = 9$

The above reactions are much simplified, in comparison with the reactions actually occurring during the oxidation. Thus, the formation of products containing active oxygen, resulting from acids, as well as the formation of lactones, CO, CO_2, H_2, CH_4 etc., during the oxidation process, is not taken into account.

The oxidation of the five *n*-dodecanols and of five *n*-dodecanones was controlled by determining the active oxygen increase in time, as illustrated in figs. 1 and 2.

---

* Our works concerning the oxidation of the six *n*-dodecanols were finished and communicated in 1965 [2] and those concerning the oxidation of the five *n*-dodecanones in May 1966. [1] In December 1966, Dawkins [3] published a paper describing the oxidation of *n*-dodecan-2-one, *n*-dodecan-3-one and *n*-dodecan-4-one in conditions slightly different from our conditions, with results in good agreement with ours.

[2] I. Drimuş and I. Ionescu, Unpublished data.

[3] A.W. Dawkins, *European Chem. News.*, **1966**, 49.

[4] D. Langenbeck and W. Pritzkow, *Chem. Techn. Fette Seifen*, **67**, 399 (1955).

Active oxygen compounds are attributed to the primordial (hydro) peroxidation of alcohols and ketones, to the (hydro) peroxidation of esters and acids, to the hydrogen peroxide accumulation, etc.

As can be observed from fig. 1, in the case of n-dodecanols oxidation, the shorter the distance of the hydroxyl group from the middle of the chain, (the more symmetrical the molecule), the easier the peroxidation occurs. Exception is made by n-dodecan-1-ol, which is the most easily oxidizable (the mechanism of this primary alcohol oxidation is probably different from that of the secondary alcohols). As for the form of the curves obtained, this is characteristic for the first product formed in the consecutive reactions, the curves presenting a maximum.

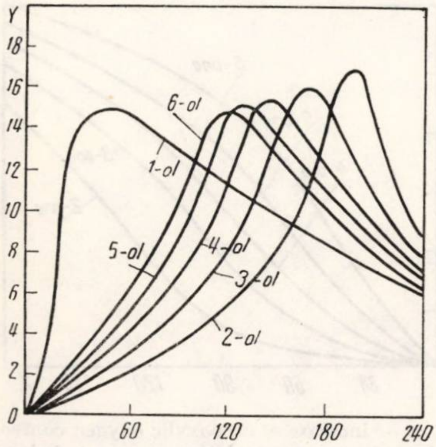

Fig. 1. — Increase of peroxidic oxygen content in time, during the oxidation of pure n-dodecanols. X = time in minutes ; Y = peroxide number expressed in mg oxygen/g oxidized product.

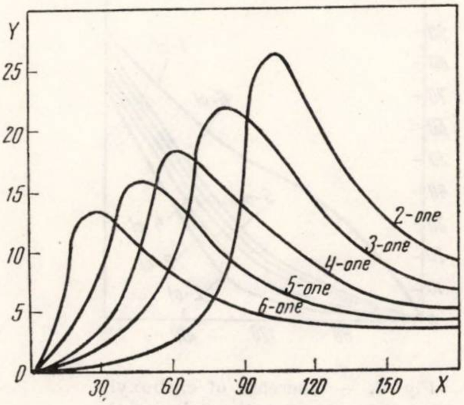

Fig. 2. — Increase of peroxidic oxygen content in time, during the oxidation of pure n-dodecanones. X = time in minutes ; Y = peroxide number expressed in mg oxygen/g oxidized product.

In the case of n-dodecanones too (fig. 2), the shorter the distance of the carbonyl group from the middle of the chain the larger the degree of oxidizability, but the maxima are larger the more asymmetrical the molecules are.

Carboxylic oxygen increase was also determined and the results obtained are illustrated in figs. 3 and 4.

As could be observed from figs. 3 and 4, the more symmetrical the molecule the easier the carboxylic group formation (n-dodecan-1-ol makes an exception). Table 1 presents the acidity and ester numbers obtained by the n-dodecanones oxidation at 155° and different times in the view to obtain comparable acid conversions.

It must be pointed out that the oxidation product of n-dodecan-2-one has an ester number 5-6 times greater than in the case of the other n-dodecanones, showing that the esters formed by the oxidation of *n*-dodecan-2-one are more resistant to oxidative degradation than those formed by the oxidation of *n*-dodecan-3-one, *n*-dodecan-4-one,*n*-dodecan-5-one and *n*-dodecan-6-one.

n-Dodecanols behave similarly with *n*-dodecanones.

In order to establish the point of chain breaking, we decided to isolate the free acids from the oxidation products of the five *n*-dodecanones and five *n*-dodecanols, and by gas-chromatographic analysis of their methyl esters to conclude about the acids chain length.

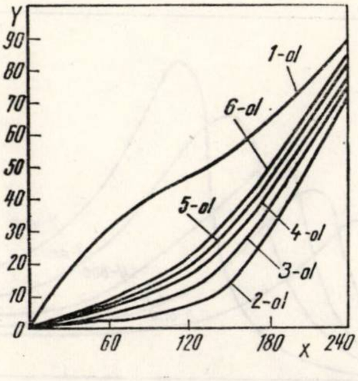

Fig. 3. — Increase of carboxylic oxygen content in time, during the oxidation of pure *n*-dodecanols. X = time in minutes ; Y = acidity number expressed in mg oxygen/g oxidized product.

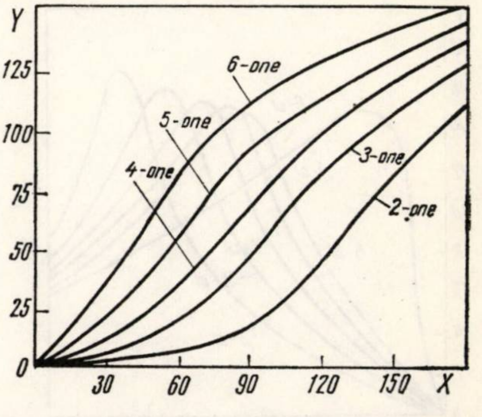

Fig. 4. — Increase of carboxylic oxygen content in time, during the oxidation of pure *n*-dodecanones. X = time in minutes ; Y = acidity number expressed in mg oxygen/g oxidized product.

Table 1

***n*-dodecanones oxidation with the view to obtain approximate equal conversions (20% free acids expressed in hexanoic acid)**

Compound	Oxidation time min	Acidity number mg O/g	Ester number mg O/g
n-dodecan-2-one	130	42.0	57.0
n-dodecan-3-one	90	47.3	8.1
n-dodecan-4-one	80	53.5	11.5
n-dodecan-5-one	60	57.0	9.0
n-dodecan-6-one	40	51.0	8.0

It has to be mentioned that *n*-dodecanones or *n*-dodecanols could be attacked by the molecular oxygen in two points :

— at the adjacent carbon placed towards the end of the chain (labelled α) ;

— at the adjacent carbon placed towards the middle of the chain (labelled α').

In each case, an intermediate product is probably formed and this is further split into two acids.

Therefore, each *n*-dodecanone or *n*-dodecanol being attacked in the α or α' position will give rise to two pairs of acids (two lower ones and two higher ones).

The following simplified reactions can be written (the radicals and other intermediate products were eliminated).

n-Dodecan-2-one oxidation in 1 (α) position

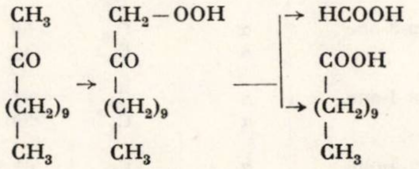

n-Dodecan-2-one oxidation in 3 (α′) position

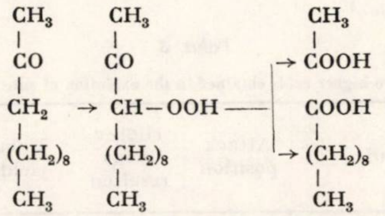

The oxidation of the other *n*-dodecanones occurs by the same reactions as well as the oxidation of *n*-dodecanols, as they are first oxidized to the corresponding *n*-dodecanones.

In our experiments only the pairs of higher acids were determined. The lower acids (with less than 5 carbon atoms) were not determined quantitatively but only identified.

A special mention is worth for the hexanoic acid obtained by *n*-dodecan-6-one oxidation, only half of the total amount being taken into account as higher acid (the rest is arbitrarily considered lower acid and was neglected as in the case of the other dodecanones oxidation). The same mention is worth for the *n*-dodecan-6-ol oxidation. The results are shown in tables 2 and 3.

For a better understanding of the oxidation process, the oxidation at low conversions of butyl ester of octanoic acid and hexyl ester of hexanoic acid were also studied.

Active oxygen and carboxylic oxygen increases at the oxidation of these two esters are illustrated in figs. 5 and 6.

Table 2

Ratios of the two higher acids obtained in the oxidation of pure *n*-dodecanones

Compound	Attack position	Higher acids resulted	Molar yields	α/α'
Lauryl aldehyde*	α	C_{12}	100	∞
	α'	C_{11}	0	
n-dodecan-2-one	α	C_{11}	42	
	α'	C_{10}	58	0.73
n-dodecan-3-one	α	C_{10}	58	
	α'	C_9	42	1.38
n-dodecan-4-one	α	C_9	61	
	α'	C_8	39	1.56
n-dodecan-5-one	α	C_8	61.5	
	α'	C_7	38.5	1.59
n-dodecan-6-one	α	C_7	51.4	
	α'	C_6	48.6	1.05

* After Dawkins. [4]

Table 3

Ratios of the two higher acids obtained in the oxidation of pure *n*-dodecanols

Compound	Attack position	Higher acids resulted	Molar yields	α/α'
n-dodecan-2-ol	α	C_{11}	39.5	
	α'	C_{10}	60.5	0.65
n-dodecan-3-ol	α	C_{10}	58.5	
	α'	C_9	41.5	1.41
n-dodecan-4-ol	α	C_9	63.0	
	α'	C_8	37.0	1.70
n-dodecan-5-ol	α	C_8	66.0	
	α'	C_7	34.0	1.94
n-dodecan-6-ol	α	C_7	53.0	
	α'	C_6	47.0	1.13

The oxidation conditions and the characteristics of the products obtained by the oxidation of the two esters are the following:

a) Butyl ester of octanoic acid oxidized at 155° for 3 hours, the obtaining product having the following characteristics:

Acidity number ...	25.3	mg	oxygen/g	oxidized product
Peroxide number ...	2.2	”	”	”
Saponification number ...	175	”	”	”
Carbonyl number ...	27	”	”	”
Hydroxyl number ...	8.3	”	”	”

The free acid obtained is mainly octanoic acid containing traces of heptanoic and hexanoic acids. Butyric acid was only detected but not determined quantitatively.

b) Hexyl ester of hexanoic acid was oxidized in the same conditions, the oxidate having the following characteristics :

Acidity number ...	21.3	mg oxygen/g oxidized product
Peroxide number ...	10.7	” ” ”
Saponification number ...	169.0	” ” ”
Carbonyl number ...	32.8	” ” ”
Hydroxyl number ...	6.8	” ” ”

The free acid separated is mainly hexanoic acid and small quantities of pentanoic acid.

These results indicate that oxidation occurs at the methylene group bound to the oxygen of the functional group.

Based on the data from tables 2 and 3, we present in fig. 7 a plot of the $\alpha:\alpha'$ ratio against carbonyl (1) or hydroxyl (2) position in the chain, in the case of 12 carbon atoms chain.

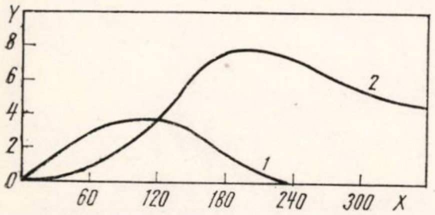

Fig. 5. — Increase of peroxidic oxygen content in time, during the oxidation of butyl ester of octanoic acid (*1*) and hexyl ester of hexanoic acid (*2*). X = time in minutes ; Y = peroxide number expressed in mg oxygen/g oxidized product.

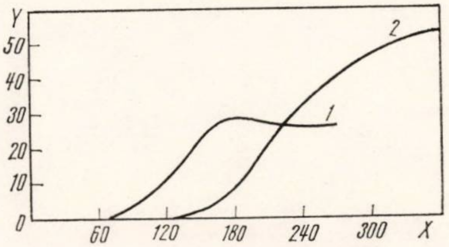

Fig. 6. — Increase of carboxylic oxygen content in time, during the oxidation of butyl ester of octanoic acid (*1*) and hexyl ester of hexanoic acid (*2*). X = time in minutes ; Y = acidity number expressed n mg oxygen/g oxidized product.

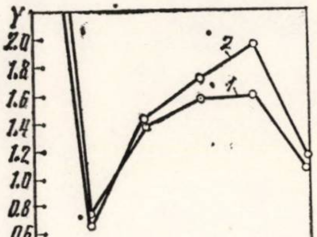

Fig. 7. — X = hydroxyl of carbonyl position in the chain ; $Y = \alpha/\alpha'$ ratio.

The $\alpha:\alpha'$ ratio (a statistical indication of the breaking point of the carbon chain in the oxidation of n-dodecanols or n-dodecanones by molecular oxygen) and the other results presented above permit the following conclusions :

1) By lauryl aldehyde oxidation as well as by dodecan-1-ol oxidation, the same oxidation product (lauric acid) is obtained, indicating that the oxygen attack is directed only toward α position.

2) In the case of the oxidation of *n*-dodecan-2-ol or *n*-dodecan-2-one the oxidation occurs preferentially in the α′ position.

3) In the case of the oxidation of *n*-dodecan-3-ol, *n*-dodecan-4-ol, *n*-dodecan-5-ol and of *n*-dodecan-3-one, *n*-dodecan-4-one, *n*-dodecan-5-one the attack is directed preferentially toward α position.

4) In the case of *n*-dodecan-6-ol or *n*-dodecan-6-one the oxidations in α and α′ positions are practically equal.

5) In the case of the esters studied, the attack by molecular oxygen takes place at the methylene group directly bound to the oxygen of the functional group.

Revue Roumaine de Chimie, **18**, *10*, 1777–1779 (1973)

ELECTRONIC SPECTRA AND ACIDITY CONSTANTS OF SOME 2-AMINO-5-SUBSTITUTED 1,3,4-THIADIAZOLES

D. SUCIU and Z. GYÖRFI

Oncological Institute, Str. Republicii 34–36, Cluj, Romania

Received January 6, 1973

The transmission of polar effects in 2-amino-5-substituted 1,3,4-thiadiazoles was studied on the basis of the ultraviolet spectra and acidity constants. It is probable that the nitrogen bridge in the thiadiazole ring is responsible for the transmission of both inductive and mesomeric effects of the 5-substituted groups.

The electronic spectra and acidity constants of some 2-amino-5-substituted thiazoles indicate that the thiazole ring allows the transmission of polar effects between the 2-amino group and an electron attracting 5-substituted group.[1] It is the purpose of this work to investigate, by means of the electronic spectra and acidity constants, the transmission of polar effects in the thiadiazole ring of some 2-amino-5-substituted 1,3,4-thiadiazole derivatives.

Protonation of 2-amino-1,3,4-thiadiazole (**1**) as well as of 2-aminothiazole takes place at the endocyclic nitrogen atom belonging to the amidine system[2]. The acid dissociation constants of compounds **1**–**14** (table 1) were determined utilizing the hipsochromic shifts in their ultraviolet spectra on ionization. The mesomeric forms *b* and *c* (Scheme 1) show the charge polarization of the amidine system of 2-amino-1,3,4-thiadiazole (**1**). Because of the presence of the second nitrogen atom located in position 4 of the ring, which produces a charge polarization as described in structures *d* and *e*, it is expected that the charge density at the site of protonation should be lower as compared with that of 2-aminothiazole. Indeed, 2-aminothiazole has $pKa = 5.39^2$ and **1** has a pKa value of 3.39 (table 1). This difference corresponds to a free energy change of 2.73 Kcal/mole.

As could be seen from table 1 the protonation of 2-amino-5-substituted 1, 3, 4-thiadiazoles is strongly influenced by the substituent located in position 5 of the ring. The effect of the 5-alkyl groups (**2**–**10**) produces the increase of the pKa values in the series: methyl

---

[1] D. Suciu, *Rev. Roumaine Chim.*, **18**, 677 (1973).

[2] H. Dorn, G. Hilgetag and A. Rieche, *Angew. Chem.*, **16**, 560 (1961).

<ethyl<propyl< butyl< pentyl< hexyl = sec. butyl < isopropyl < tert. butyl. No correlation could be established ($r < 0.80$) between the polar effect of these alkyl groups on the protonation of 2-amino-5-alkyl substituted 1,3,4-thiadiazoles (**2**–**10**) (table 1) and their corresponding Hammett constants σp or σm which have been determined in the aromatic series.[3]

Table 1

Ultraviolet maxima and acidity constants of some 2-amino-5-substituted 1,3,4-thiadiazoles

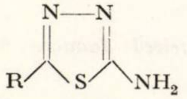

Compound	R	Ethanol		0.1 N−HCl in ethanol		*pKa*	$\lvert\Delta F\rvert$ (cal/mole)
		λ_{max} (nm)	log ε	λ_{max} (nm)	log ε		
1	H	255	3.72	243	3.78	3.39	—
2	CH_3	255 252 a)	3.74 3.70	245	3.79	3.49	140
3	CH_2CH_3	256	3.77	245	3.89	3.53	190
4	$(CH_2)_2CH_3$	256	3.80	247	3.89	3.58	260
5	$CH(CH_3)_2$	256	3.74	245	3.85	3.70	420
6	$(CH_2)_3CH_3$	256	3.85	247	3.91	3.62	310
7	$CH_2CH(CH_3)_2$	257	3.79	247	3.88	3.67	380
8	$C(CH_3)_3$	257	3.72	247	3.81	3.74	480
9	$(CH_2)_4CH_3$	257	3.68	247	3.76	3.66	370
10	$(CH_2)_5CH_3$	256	3.80	247	3.89	3.67	380
11	C_6H_5	300	4.20	284	4.26	2.90 2.90 b)	660
12	$C_6H_4-OCH_3(p)$	246 305	3.49 4.26	300	4.25	2.95	600
13	$C_6H_4-NO_2(m)$	308	3.98	274 300	3.95 3.91	2.53	1170
14	$C_6H_4-NO_2(p)$	252 352	3.88 4.17	246 347	3.88 4.06	2.30	1490

a) Determined by GOERDELER.[4] b) Determined by TESTA *et al.*[5]

[3] H.H. JAFFÉ, *Chem. Rev.*, **53**, 191 (1953).

[4] J. GOERDELER, *Chem. Ber.*, **87**, 57 (1954).

[5] E. TESTA, G.G. GALLO and F. FOVA, *Gazz. chim. Ital.*, **88**, 1272 (1958).

The derivatives **12**—**14** (table 1) containing an electron withdrawing group in position 5 of the ring have lower *pKa* values than the corresponding unsubstituted compound **1**, according to the decrease of the charge density at the site of protonation. This effect could be observed if we correlate the structures *b* and *f* (Scheme 1).

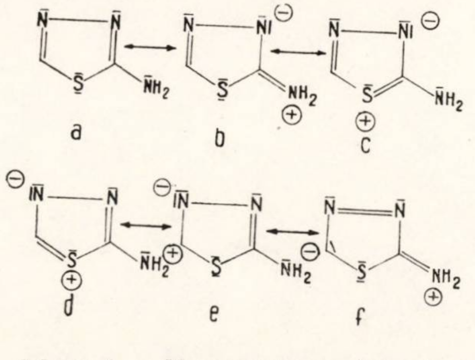

Scheme 1. — Mesomeric forms of 2-amino-1,3,4-thiadiazole.

The free energy change which corresponds to the protonation of each of the compounds **2**—**14** according to the polar effect of the 5-substituted group was calculated following the relation :

$$\Delta F = - RT \ln K$$

where *K* is the ratio of the acid dissociation constants corresponding to the 5-substituted compounds **2**—**14** and the *Ka* value of **1** (table 1).

The results indicate that both inductive and mesomeric effects of the 5-substituted groups are intensively transmitted in the nucleus of 2-amino-5-substituted 1,3,4-thiadiazoles. According to the structures *b*, *e*, *f* (Scheme 1) the major role in the transmission of these effects must be attributed to the nitrogen bridge.

EXPERIMENTAL

The compounds employed were synthetized as it was previously described: **1**—**3**[6], **3**—**10**[7], **11**[8], **12**,[9] **13**[10] and **14**.[11]

The ultraviolet spectra were recorded with a VSU-2 P(Carl Zeiss Jena) spectrophotometer.

The acidity constants were determined in glycine-HCl and Na citrate-HCl buffer solutions with the standard spectrophotometric technique. The *pKa* data (table 1) represent the mean values of 4 determinations carried out near the pH of equivalence (25°).

---

[6] Giichi Funatsukuri and Mitsuo Ueda (to Sumitomo Chemical Co., Ltd.), *Japan Pat. 20 944 ('66), 22 Feb. 1964*; *Chem. Abstr.*, **66**, 46430 f (1967).

[7] F.L. Chubb and J. Nissenbaum, *Canad. J. Chem.*, **37**, 1121 (1959).

[8] G. Young and W. Eyre, *J. Chem. Soc.*, **79**, 54 (1901).

[9] K.C. Das and M.A. Rout, *J. Sci. Ind. Res.*, **14B**, 98 (1955); *Chem. Abstr.*, **49**, 14744 d (1955).

[10] H. Weidinger and J. Kranz, *Chem. Ber.*, **96**, 1059 (1963).

[11] J. Eckenstein, E. Brogle, E. Sorkin and H. Erlenmeyer, *Helv. Chim. Acta*, **33** 1353 (1950).

The derivatives 12–14 (table 1) containing an electron withdrawing group in position 5 of the ring have lower pKa values than the corresponding unsubstituted compound 1 according to the decrease of the charge density at the site of protonation. This effect could be observed if we compare the structures b and f (Scheme 1).

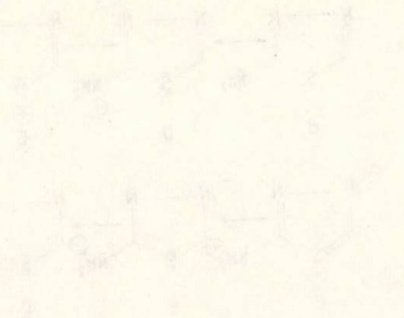

Scheme 1. — Mesomeric forms of 4-amino-1,2,4-triazole.

The free energy change which corresponds to the protonation of each of the compounds 2–14 according to the polar effect of the substituted group was calculated following the relation:

$$\Delta F^{\circ} = -RT \ln K$$

where K is the ratio of the acid dissociation constants corresponding to the substituted compounds 2–15 and the Ka value of 1 (table 1).

The results indicate that both inductive and mesomeric effects of the substituted groups are intensively transmitted in the nucleus of 4-amino-1,2,4-triazole. According to the structures b, e, f (Scheme 1) the major role in the transmission of these effects must be attributed to the nitrogen atoms.

EXPERIMENTAL

The compounds employed were synthesized as was previously described: 1–8, [illegible] 11[8], 12[9], 13[10] and 14[11].

The ultraviolet spectra were recorded with a VSU 2 P Carl Zeiss (Jena) spectrophotometer.

The acidity constants were determined in aqueous HCl and Na acetate–HCl buffer solutions with the standard spectrophotometric technique. The pKa data (table 1) represent the mean values of 5 determinations carried out near the pH of equivalence [12].

---

[8] [illegible] Fănărescu and [illegible], [illegible] (1966); [illegible] 62, 4655 [illegible] (1967).

[9] [illegible] and [illegible], J. Chem. [illegible], 188 (19[illegible]).

[10] G. Young and [illegible], J. Chem. Soc., 79, [illegible] (1901).

[11] [illegible] and [illegible], [illegible] 132, [illegible] (1950); Chem. Abstr., [illegible] (1952).

[12] [illegible] and [illegible], Chem. Ber., 88, 1059 (19[illegible]).

[13] [illegible], [illegible] and [illegible], [illegible] 30, [illegible] (1950).

Revue Roumaine de Chimie, **18**, *10*, 1781–1792 (1973)

LES SPECTRES ÉLECTRONIQUES DE QUELQUES BASES DE SCHIFF À NOYAUX BENZ- ET NAPHTO-THIAZOLIQUES

SCHELY AVRAMOVICI, A. AIRINEI*, IOANA CIOCOIU
Chaire de Chimie Organique, Université « Al.I. Cuza », Jassy
* Institut de Chimie Macromoléculaire « P. Poni », Jassy

Reçu 15 janvier 1973

On étudie, à l'aide des spectres électroniques l'influence de la nature et de la position des substituents, ainsi que l'influence de la polarité des solvants sur la force de liaison hydrogène intramoléculaire d'une série de salicylidène-aniles à noyau benz- et naphto-thiazolique. On trouve que le plus puissant effet bathochrome est dû à la présence du noyau naphto-thiazolique. On étudie aussi le changement de direction de la liaison hydrogène intramoléculaire sous l'influence d'un groupement NO_2 introduit en position *ortho* vis-à-vis d'OH, ainsi que le rôle de l'éthanol et de l'acétonitrile dans le processus de solvatation des produits.

Au cours des dernières années on a fait de nombreuses études pour établir la structure et expliquer les propriétés photochimiques des bases de Schiff, en utilisant à cette fin les données obtenues par la détermination des spectres électroniques dans divers solvants. De cette manière, on a montré que les molécules des benzylidènes-aniles ne sont pas coplanaires, la conjugaison π présentant une interruption chez l'atome d'azote[1–6].

On a établi aussi que dans le cas des *o*-hydroxy-benzylidènes-aniles se forme une liaison hydrogène intramoléculaire. Il y a donc la possibill'té de l'existence de deux formes, l'une énol-iminique (benzénoïde) (Ia), l'autre céto-aminique (*cis*-quinoïde) (Ib) qui se rétablissent en fonction de la polarité du solvant,[7–11] et qui peuvent coexister auprès d'une forme

---

[1] V. A. Ismailskii et E. A. Smirnov, *Zhur. obshchei Khim.*, **26**, 3042 (1956).

[2] P. Brocklehurst, *Tetrahedron*, **18**, 299 (1962).

[3] V. I. Minkin, Yu. A. Zhdanov, E. A. Medyantzeva et Yu. A. Ostrounov, *Tetrahedron*, **33**, 3651 (1967).

[4] M. El. Bayoumi Ashraf, M. El. Aasser et F. Abdel-Halim, *J. Amer. Chem. Soc.*, **93**, 586 (1971).

[5] M. El. Aasser, F. Abdel-Halim et M. [illegible] El. Bayoumi, *J. Amer. Chem. Soc.*, **93**, 590 (1971).

[6] N. Ebara, *Bull. Chem. Soc. Japan*, **33**, 534 (1960).

[7] P. W. Alexander et R. I. Sleet, *Austral. J. Chem.*, **23**, 1183 (1970).

[8] J. J. Charette, G. Faltlhansl et Ph. Teyssie, Spectrochim. Acta, **20**, 597 (1964).

[9] L. N. Ferguson et L. Kelly, *J. Amer. Chem. Soc.*, **73**, 3707 (1951).

[10] M. D. Cohen et S. Flavian, J. Chem. Soc. (B), **1967**, 321.

[11] R. Tsuchida et T. Tsumachi, *Bull. Chem. Soc. Japan*, **13**, 537 (1938).

trans-quinoïdique (Ic) :

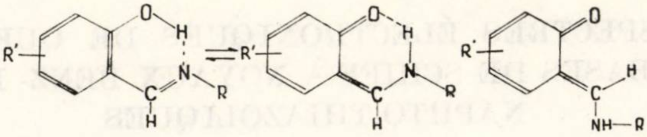

Ia Ib Ic

Ces deux aspects ont été étudiés de même liés au problème de la possibilité d'ionisation et de transfert de protons entre le solvant et les molécules étudiées.[12]

Dans un seul cas on a étudié des *o*-hydroxy-aniles ayant dans leurs molécules un noyau benz- ou naphto-thiazolique.[13]

Dans ce travail on présente l'étude des bases Schiff obtenues par la condensation de l'aldéhyde salicylique prise comme telle ou diversement substituée, avec le 2-aminobenzothiazole substitué[14] et le *p*-dimétylaminoaniline. Ils correspondent aux formules générales :

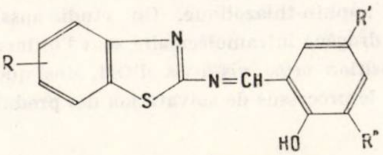

II

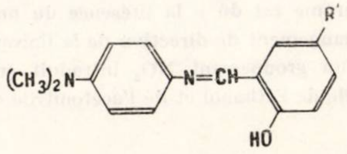

III

où R, R' et R'' prennent diverses valeurs.

Les substituents de différentes natures des composés du type II sont inscrits dans le tableau 1.

Tableau 1

Nature des substituents des molécules d'aniles du type II étudiés

Nº du comp.	R	R′	R″	Nº du comp.	R	R′	R″
II–A	(6) OCH_3	H	H	II–H	(6) CH_3	Br	H
II–B	(6) OCH_3	NO_2	H	II–I	(6) CH_3	H	NO_2
II–C	(6) OCH_3	Br	H	II–J	(6) CH_3	Br	NO_2
II–D	(6) OCH_3	H	NO_2	II–K	(5)–CH=CH–CH=CH–(6)	H	H
II–E	(6) OCH_3	Br	NO_2	II–L	(5)–CH=CH–CH=CH–(6)	NO_2	H
II–F	(6) CH_3	H	H	II–M	(5)–CH=CH–CH=CH–(6)	Br	H
II–G	(6) CH_3	NO_2	H	II–N	(5)–CH=CH–CH=CH–(6)	H	NO_2

[12] F. Kristek, J. Klicnar et P. Vetesnik, *Coll. Czech. Chem. Comm.*, **36**, 3608 (1971).

[13] M. Conte, R. Guglielmetti et J. Metzger, *Bull. Soc. chim France*, **8**, 2834 (1967).

[14] S. Avramovici, I. Ciocoiu, A. Airinei et I. Soifer, *Anal Şti., Univ. „Al. I. Cuza" Iaşi, Secţ. I*, **18**, 61 (1972).

Les substituents des molécules des aniles du type III étudiés :

III−A $R'=H$

III−B $R'=NO_2$

III−C $R'=Br$

Parallèlement on a étudié aussi trois diamines secondaires formées en même temps que les bases de Schiff correspondantes à la suite d'un processus de condensation trimoléculaire entre deux molécules d'amine et une molécule d'aldéhyde salicylique disubstituée. Elles correspondent à la formule générale :

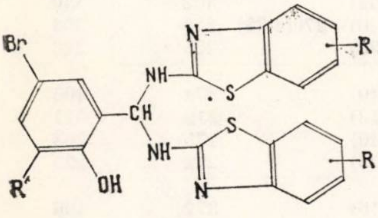

IV

IV−A $R=(6)-OCH_3$ $R'=-H$

où IV−B $R=(6)-CH_3$ $R'=-NO_2$

IV−C $R=(5)-CH=CH-CH=CH-(6)$ $R'=-NO_2$

L'oxhydryle du reste aldéhydique permet l'apparition de l'équilibre tautomère, mentionné plus haut, entre la structure énol-iminique (Ia) et celle céto-aminique (Ib). Chez les aniles étudiés par nous, l'existence de cet équilibre a été déduite des données spectrales IR et RMN[14] et aussi confirmée par les résultats obtenus par d'autres chercheurs.[13,15,16] Il restait à vérifier si les données des spectres électroniques le confirmeront et à voir quelles précisions ces données apporteront sur la disposition en plan des cycles, et sur l'influence exercée par la nature et la position des substituents, ainsi que par la nature des solvants sur le déplacement de l'équilibre tautomère.

PARTIE EXPÉRIMENTALE

Les spectres sur les produits décrits en [14] ont été enregistrés sur un spectrophotomètre UNICAM SP 800 B, en employant des cuves d'une épaisseur de 1 cm.

On a travaillé à la température ordinaire avec cinq solvants de polarités différentes : benzène (0 D), dioxanne (0,45 D) dichlorméthane (1,55 D), éthanol (1,68 D) et acétonitrile (3,37 D). Les maximums d'absorption et les coefficients d'extinction sont présentés dans le tableau 2 :

---

[15] R. Exelby et R. Grinter, *Chem. Rev.*, **65**, 247 (1965).

[16] V. I. Minkin, O. A. Osipov et V. N. Scheinker, *Zhur. fiz. Khim.*, **44**, 23 (1970).

Tableau 2

Maximums d'absorption en UV pour les produits étudiés

Nº du comp.	$\lambda_{max(nm)}$, lg ε_{max}				
	C_6H_6	$C_4H_8O_2$	CH_2Cl_2	C_2H_5OH	CH_3CN
II–A	393(4,31) 286(4,15)+281(4,15)	389(4,22) 283(4,09)+277(4,12) 226(4,31)	391(4,38) 285(4,23)+279(4,25) 237(4,23)	390(4,25) 278(4,15) 219(4,45)	385 276 226
II–B	394(4,34) 322(4,11) 286(4,30)+281(4,31)	388(4,31) 316(4,15) 275(4,41) 224(4,40)	408(4,34)+392(4,36) 320(4,14) 274(4,38) 239(4,21)	386 310 276 224	410 311 266 229
II–C	381(4,33) 320(4,22) 279(4,22)	376(4,41) 317(4,30) 374(4,40)+270(4,43) 223(4,43)	379(4,44) 319(4,32) 275(4,40)+270(4,38) 237(4,36)	376 302 273 225	400 350 303 226
II–D	394(4,30) 325(4,04) 286(4,21)+281(4,23)	390(4,35) 320(4,12) 273(4,36) 226(4,36)	394(4,40) 324(4,13) 272(4,40) 237(4,25)	374 312 275 222	406 311 263 225
II–E	413(4,09)+400(4,11) 335(3,96) 287(4,18)+280(4,21)	395(4,17) 274(4,28) 228(4,42)	400(4,16) 335(4,02) 275(4,31) 236(4,28)	372 305 266 223	406 378 310 228
II–F	384(4,10) 301(3,70) 279(4,05)	381(4,11) 305(3,78) 272(4,18) 229(4,44)	382(4,19) 301(3,83) 275(4,22)+270(4,23) 237(4,33)	381 300 268 223	377 305 270 227
II–G	374(4,10) 318(4,20) 278(4,20)	397(4,31) 284(4,14)+278(4,17) 241(4,30) 229(4,38)	410(4,25) 284(4,07)+278(4,10) 246–238(4,21)	394 274 222	396 272 227
II–H	394(4,28) 278(4,03)	390 276 228	393 276 240	389 274 226	386 274 227
II–I	388(4,23) 335(4,05) 279(4,00)	385(4,30) 275(4,20) 262(4,30) 226(4,32)	385(4,33) 275(4,22) 264(4,30) 236(4,22)	472 354 302 271 225	429 266 226
II–J	398(3,99) 301(3,87) 280(4,02)	391(3,98) 303(3,86) 263(4,24) 230(4,60)	393(4,04) 300(3,88) 261(4,28) 237(4,35)	372 301 263 225	410 302 261 225
II–K	410(4,20)+398(4,22) 292(4,26)	394(4,30) 284(4,39) 267(4,43) 244(4,62) 227(4,67)	397(4,44) 290(4,53) 266(4,49) 247(4,71)	396 312 290 265 260 247	391 287 264 244 225

Tableau 2 (suite)

Nº du comp.	$\lambda\ max_{(nm)}$, $\lg\ \varepsilon_{max}$				
	C_6H_6	$C_4H_8O_2$	CH_2Cl_2	C_2H_5OH	CH_3CN
II–L	413(4,20)+398(4,21) 287(4,37)	406(4,32)+393(4,34) 307(4,37) 284(4,58) 267(4,53)	411(4,31) 397(4,31) 310(4,31) 284(4,51) 266(4,50) 243(4,57)	450 374 312+301 265+258 231	414 313+302 264+257 232
II–M	416(4,27)+408(4,27) 290(4,28)	404(4,38) 287(4,45) 247(4,67)	409(4,37) 287(4,44) 247(4,66)	404 315 287 268+260 245 227	402 343 312+298 264+258 230
II–N	413(4,26)+398(4,29)	406(4,30)+394(4,31) 307(4,30) 284(4,48) 269(4,43) 243(4,51)	410+394 308 283 243	443 313+302 267 262 232	412 312 301 264 258 233
III–A	390(4,39) 334(3,98) 279(3,82)	387(4,37) 333(3,96) 247(4,24) 226(4,17)	392(4,38) 335(3,98) 249(4,27)	386 330 246 225	384 320 246 226
III–B	404(4,39) 318(4,13) 280(4,04)	399(4,34) 317(4,10) 262(4,17) 248(4,24)	406(4,48) 318(4,20) 262(4,31) 249(4,33)	404 317 260 249 206	401 317 260 246 218
III–C	400(4,49) 332(3,94) 280(3,89)	396(4,38) 333(3,86) 251(4,30) 234(4,31)	401(4,53) 335(3,97) 252(4,43) 237(4,46)	395 329 250 232 209	397 334 250 232
IV–A	402(4,30) 286(4,07)+281(4,08)	397(4,48) 284(4,28)+278(4,31) 243(4,43) 229(4,52)	402(4,52) 278(4,37) 245–237(4,49)	397 276 222	396 274 229
IV–B	395(4,45) 279(4,16)	390(4,53) 276(4,38) 229(4,86)	393(4,53) 277(4,37) 245(4,40)+239(4,42)	390 275 224	366 273 224
IV–C	410(4,12) 349(3,91) 335(3,88) 312(4,04) 290(4,26)	403(4,37) 313(4,30) 288(4,54) 266(4,93) 258(4,91)	404–410(4,29) 348(4,13) 333(4,10) 311(4,22) 287(4,46) 264(4,85) 255(4,89)	402 347+335 311+299 264+257 231	402 344 332 311 299 290 264 257 230

DISCUSSION DES RÉSULTATS

Ainsi que [13] dans les spectres des aniles étudiés, nous ne retrouvons que rarement les maximums caractéristiques du benzothiazole ou de l'aldéhyde salicylique dans les positions classiques : $\lambda_{max} = 294$ nm et 216 nm pour le benzothiazole[17,18] et $\lambda_{max} = 252-257$ nm et $323-331$ nm, en fonction de la polarité du solvant, pour l'aldéhyde salicylique,[7] les spectres présentant, plus ou moins, une superposition des maximums des deux parties de la molécule. Cela nous indique que les molécules étudiées possèdent, au moins en solution, une structure non coplanaire (V) favorisée d'ailleurs du point de vue énergétique. La paire d'électrons non participants de l'azote interrompt la conjugaison continue sur toute la molécule, en facilitant l'apparition de la liaison hydrogène intramoléculaire :

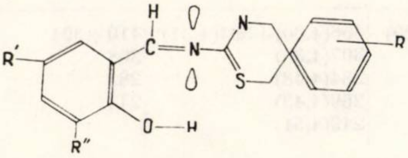

V

Grâce à la complexité structurale des produits , ainsi que de la polarité variée des solvants utilisés, on discutera les résultats obtenus, en tenant compte des critères suivants:

— l'influence de la nature des solvants

— l'influence de la nature et de la position des substituents du reste aldéhydique

— l'influence de la nature et de la position des substituents du reste aminique

Ces influences se mêlent étroitement et c'est pourquoi on les interprétera dans leur ensemble.

Dans la bibliographie consultée on admet, en général, [11,19,20] que les maximums d'environ 400 nm sont caractéristiques de la liaison hydrogène intramoléculaire et c'est pour cette raison que nous prendrons en considération seulement les variations de la position et de l'intensité de ce maximum. Dans le cas des aniles du type II la nature du substituent du noyau benzothiazolique exerce un effet bathochrome qui peut être représenté par deux ordres de succession :

a) $\lambda_{(6)CH_3} < \lambda_{(6)OCH_3} < \lambda_{(5)-CH=CH-CH=CH-(6)}$

b) $\lambda_{(6)OCH_3} < \lambda_{(6)CH_3} < \lambda_{(5)-CH=CH-CH=CH-(6)}$

---

[17] B. Ellis, P. J. F. Griffiths, *Spectrochim. Acta*, **21**, 1881 (1965).

[18] A. R. Katritzky, ,,Physical Methods in Heterocyclic Chemistry'', IIe vol., Acad. Press., New York – London, 1963, p. 59.

[19] J. Hires, *Acta Chem. et Phys. Szeged. (N.S.)*, **4**, 120 (1958).

[20] A. Kiss et E. Varga, *Acta Chem. et Phys. Szeged. (N.S.)*, **1**, 155 (1943).

L'ordre de succession a) est respecté par la majorité des produits, indifféremment de la nature des solvants. Font exception, en respectant le schéma b), les dérivés auxquels $R' = Br$ dans tous les solvants, excepté l'acétonitrile, les dérivés auxquels $R' = NO_2$ en alcool et en dioxanne, les dérivés auxquels $R'' = NO_2$ en alcool et en acétonitrile et les dérivés à $R' = Br$, $R'' = NO_2$ en acétonitrile.

Les diamines étudiées respectent, dans tous les solvants, l'ordre de succession a).

Mais dans tous les cas on retrouve l'effet bathochrome le plus puissant chez les aniles du β-naphtothiazole, grâce à la structure qui contient un système conjugué plus large.

Si on considère maintenant le problème en tenant compte de la nature des substituents du reste aldéhydique on constate que :

Les aniles du type II sans substituents dans le reste aldéhydique (II-A, II-F et II-K) présentent les maximums d'environ 400 nm à des positions qui se déplacent hypsochrome dans un ordre qui respecte approximativent l'augmentation de la polarité des solvants :

c) $\lambda_{C_6H_6} > \lambda_{CH_2Cl_2} > \lambda_{C_4H_8O_2} \approx \lambda_{C_2H_5OH} > \lambda_{CH_3CN}$

Le même ordre est respecté aussi par les trois diamines (IV-A, IV-B et IV-C), bien qu'elles possèdent des substituents dans le reste aldéhydique, avec la seule mention que, dans certains cas, les valeurs des maximums sont identiques pour des paires de solvants voisins.

Nous concluons donc que, en général, dans tous ces cas, on rencontre les absorptions pour les plus grandes longueurs d'onde dans les solvants non polaires et pour les moindres longueurs d'onde dans les solvants à polarité maximum. Cette constatation générale concorde avec les données de la littérature[7], selon lesquelles l'effet hypsochrome exercé par les solvants polaires est caractéristique des composés à liaisons hydrogène intramoléculaires.

La situation est différente pour les aniles de type II, dont la molécule contient des substituents divers dans le reste aldéhydique. Les variations de la position de la bande d'absorption autour de 400 nm ne sont pas identiques pour les mêmes substituents, étant influencées par l'interaction entre ceux-ci et les substituents du reste aminique. Dans ces cas, pour les dérivés 5-Br, 5-NO_2 et 3-NO_2, ainsi que pour ceux 3-NO_2, 5-Br on trouve les successions hypsochromes indiquées dans la schéma 1.

Dans le cas des dérivés 5-NO_2 substitués ou ne peut faire aucun rapprochement entre les divers composés. Dans les deux autres cas des produits monosubstitués on constate les mêmes successions hypsochromes pour les aniles qui ont un substituent alkylique dans le reste aminique, indifféremment si celui-ci est saturé ((6)$-CH_3$) ou non saturé ((5)$-CH{=}CH-CH{=}CH-$(6)).

La présence du groupement $-OCH_3$ dans la position 6 du reste aminique mène, indifféremment de la nature du substituent du reste aldé-

Schéma 1

Variation de la position de la bande d'absorption d'environ 400 nm en fonction du solvant

Produits substitués avec du Br dans la position 5 du reste salicylaldéhydique

II–C $\lambda_{CH_3CN} > \lambda_{C_6H_6} > \lambda_{CH_2Cl_2} > \lambda_{C_4H_8O_2} > \lambda_{C_2H_5OH}$

II–H $\lambda_{C_6H_6} > \lambda_{CH_2Cl_2} > \lambda_{C_4H_8O_2} > \lambda_{C_2H_5OH} > \lambda_{CH_3CN}$

II–M $\lambda_{C_6H_6} > \lambda_{CH_2Cl_2} > \lambda_{C_4H_8O_2} > \lambda C_2H_5OH > \lambda_{CH_3CN}$

III–C $\lambda_{CH_2Cl_2} > \lambda_{C_6H_6} > \lambda_{CH_3CN} \geqslant \lambda_{C_4H_8O_2} > \lambda_{C_2H_5OH}$

Produits substitués avec du NO_2 dans la position 5 du reste salicylaldéhydique

II–B $\lambda_{CH_3CN} > \lambda_{CH_2Cl_2} > \lambda_{C_6H_6} > \lambda_{C_4H_8O_2} > \lambda_{C_2H_5OH}$

II–G $\lambda_{CH_2Cl_2} > \lambda_{C_4H_8O_2} > \lambda_{C_2H_5OH} = \lambda_{CH_3CN} > \lambda_{C_6H_6}$

II–L $\lambda_{C_2H_5OH} > \lambda_{CH_3CN} > \lambda_{C_6H_6} > \lambda_{CH_2Cl_2} > \lambda_{C_4H_8O_2}$

III–B $\lambda_{CH_2Cl_2} > \lambda_{C_2H_5OH} = \lambda_{C_6H_6} > \lambda_{CH_3CN} > \lambda_{C_4H_8O_2}$

Produits substitués avec du NO_2 dans la position 3 du reste salicylaldéhydique

II–D $\lambda_{CH_3CN} > \lambda_{C_6H_6} > \lambda_{CH_2Cl_2} > \lambda_{C_4H_8O_2} > \lambda_{C_2H_5OH}$

II–I $\lambda_{C_2H_5OH} > \lambda_{CH_3CN} > \lambda_{C_6H_6} > \lambda_{CH_2Cl_2} = \lambda_{C_4H_8O_2}$

II–N $\lambda_{C_2H_5OH} > \lambda_{CH_3CN} > \lambda_{C_6H_6} > \lambda_{CH_2Cl_2} = \lambda_{C_4H_8O_2}$

Produits substitués avec du NO_2 dans la position 3 et du Br dans la position 5 du reste salicylaldéhydique

II–E $\lambda_{C_6H_6} > \lambda_{CH_3CN} > \lambda_{CH_2Cl_2} > \lambda_{C_4H_8O_2} > \lambda_{C_2H_5OH}$

II–J $\lambda_{CH_3CN} > \lambda_{C_6H_6} > \lambda_{CH_2Cl_2} > \lambda_{C_4H_8O_2} > \lambda_{C_2H_5OH}$

hydique, à l'apparition d'un puissant effet bathochrome dans l'acétonitrile et d'un puissant effet hypsochrome dans l'éthanol, le seul produit d'une autre série qui présente la même caractéristique étant II–J. Dans ce dernier cas il est possible que les actions cumulées des substituents du reste aldéhydique annihilent totalement l'effet du substituent du reste aminique. Dans les autres cas, il est à croire que le groupement OCH_3 intervient par un effet de conjugaison.

Il est possible que l'effet bathochrome exercé par l'acétonitrile soit dû à son action de solvatation qui pourrait mener à la stabilisation des quelques formes de résonance avec la contribution prédominante de certaines structures dipolaires cétoaminiques privées de liaison intramoléculaire.

L'effet hypsochrome exercé par l'éthanol ne peut être expliqué qu'en admettant que celui-ci, quoique solvant polaire, rende stable par solvatation les molécules dans une forme non polaire. Si pour les autres aniles, qui contiennent dans le noyau benzothiazolique un substituent (6)$-CH_3$ ou (5)$-CH=CH-CH=CH-$(6) les structures suivantes sont possibles à la solvatation en alcool :

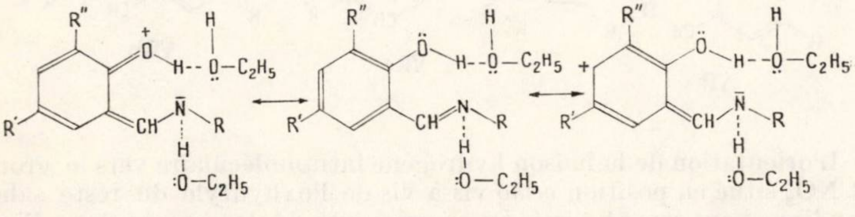

VI a VI VI b

pour les aniles au groupement méthoxy dans la position 6 du reste benzothiazolique il semble que l'alcool n'affaiblit pas la liaison hydrogène intramoléculaire dans le processus de solvatation, mais qu'il forme des liaisons intermoléculaires avec les électrons non participants de l'oxygène du groupement méthoxy, en produisant ainsi des complexes, cités par d'autres chercheurs aussi,[19] où, il y a au moins deux liaisons hydrogène. Notre affirmation est bassée sur le fait que l'alcool est le seul des solvants utilisés qui soit capable de former des liaisons hydrogène intermoléculaires avec ses protons.

La manière différente d'agir de l'alcool en comparaison d'autres solvants est évidente aussi lorsqu'on groupe ces aniles à$-OCH_3$ dans la position 6 du reste aminique en des successions hypsochromes, fonction de la nature du substituent du reste aldéhydique :

C_6H_6 : $II-E > II-D = II-B \geqslant II-A > II-C$
$C_4H_8O_2$: $II-E > II-D \geqslant II-A \geqslant II-B > II-C$
CH_2Cl_2 : $II-B > II-E > II-D > II-A > II-C$
C_2H_5OH : $II-A > II-B > II-C > II-D > II-E$
CH_3CN : $II-B > II-E = II-D > II-C > II-A$

On constate que dans l'alcool diffère complètement, tandis que dans les autres solvants, à l'exception du CH_2Cl_2 et CH_3CN où il y a une petite inversion, on trouve l'absorption à la plus grande longueur d'onde chez les dérivés qui possèdent un groupement NO_2 dans la position 3 du reste aldéhydique. Dans ces cas on admet que le groupement NO_2 voisin de l'oxydryle phénolique pourrait rendre stable la molécule en attirant vers lui l'hydrogène du groupement phénolique et en formant avec celui-ci une liaison intramoléculaire (VII c) capable de se structurer, indifféremment de la polarité du solvant, selon le schéma :

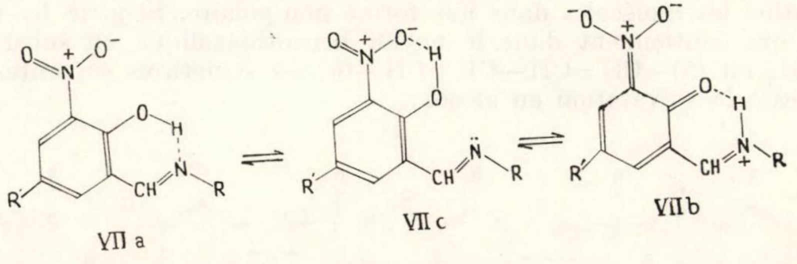
VII a

VII c

VII b

L'orientation de la liaison hydrogène intramoléculaire vers le groupement NO_2 situé en position *ortho* vis-à-vis de l'oxhydryle du reste salicylaldéhydique peut être observée aussi grâce aux déplacements dans l'infrarouge du maximum de la bande d'absorption qui correspond à la vibration symétrique du groupement NO_2. En pastille de KBr ce maximum paraît à 1360 cm^{-1} différemment de la vibration symétrique du groupement NO_2 de la position 5, qui apparaît à 1380 cm.

En solution chloroformique la vibration symétrique du groupement NO_2 de la position 3 du reste salicylaldéhydique est située environ à 1375 cm^{-1}, tandis que la même vibration pour le groupement NO_2 de la position 5 est située à environ 1350 cm^{-1}, indépendemment de la dilution. (L'étude a été effectuée avec les produits II—G et II—I.)

En alcool, la possibilité de détachement de la liaison intramoléculaire et de formation de liaisons intermoléculaires avec les protons du solvant mène à des effets différents. On trouve l'action bathochrome la plus puissante justement à l'anile non substitué dans le reste salicylaldéhydique et la plus forte action hypsochrome aux produits qui possèdent le groupement NO_2 dans la position 3 de ce reste.

On a fait aussi des recherches sur la variation de l'intensité de la bande d'absorption étudiée en fonction de la température. On a travaillé dans l'intervalle de 20° à 80° en dioxanne. On constate que dans tous les cas à chaud a lieu une décroissance de l'intensité de la bande d'absorption sans être accompagnée par un aplatissement cité par d'autres chercheurs.[13] Au refroidissement, l'intensité de la bande augmente de nouveau sans atteindre pourtant la valeur initiale. A titre d'exemple, les résultats obtenus pour le produit II—M sont représentés fig. 1.

On a représenté aussi l'énergie des transitions $\pi \rightarrow \pi^*$ dans tous les solvants, pour tous les aniles étudiés. Nous présentons les valeurs de ces transferts aux aniles au groupement méthyle dans la position 6 du reste benzothiazolique en dioxanne (fig. 2) et en acétonitrile (fig. 3).

La succession décroissante des transitions pour tous les saliclydenaniles non substitués ou monosubstitués étudiés est inscrite dans

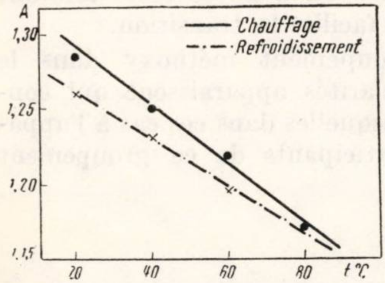

Fig. 1. — Variation de l'intensité de la bande d'absorption du produit II_M, au chauffage.

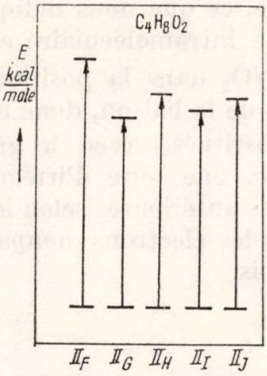

Fig. 2. — Energie de transition $\pi \to \pi^*$ pour les aniles $II_F \to II_J$ en dioxanne.

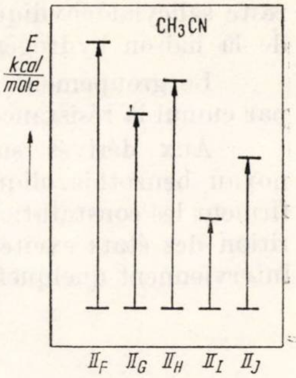

Fig. 3. — Energie de transition $\pi \to \pi^*$ pour les aniles $II_F \to II_J$ en acétonitrile.

le schéma 2 :

Schéma 2

Variation d'énergie des transitions $\pi - \pi^*$ aux salicylidenaniles non substitués et monosubstitués étudiés

Produits avec le groupement OCH_3 dans la position 6 du reste benzothiazolique

C_6H_6 : $II-B = II-D \approx II-A < II-C$
$C_4H_8O_2$: $II-A < II-B \approx II-D < II-C$
CH_2Cl_2 : $II-B < II-D < II-A < II-C$
C_2H_5OH : $II-A < II-B < II-C < II-D$
CH_3CN : $II-B < II-D < II-C < II-A$

Produits avec le groupement CH_3 dans la position 6 du reste benzothiazolique

C_6H_6 : $II-H < II-I < II-F < II-G$
$C_4H_8O_2$: $II-G < II-I < II-H < II-F$
CH_2Cl_2 : $II-G < II-H < II-I < II-F$
C_2H_5OH : $II-I < II-G < II-H < II-F$
CH_3CN : $II-I < II-G < II-H < II-F$

Produits avec le groupement $(5)-CH=CH-CH=CH-(6)$ dans le reste benzothialozique

C_6H_6 : $II-M < II-L \approx II-N < II-K$
$C_4H_8O_2$: $II-L \approx II-N < II-M < II-K$
CH_2Cl_2 : $II-L \approx II-N < II-M < II-K$
C_2H_5OH : $II-L < II-N < II-M < II-K$
CH_3CN : $II-L < II-N < II-M < II-K$

Il résulte que pour les dérivés substitués qui contiennent un reste alkylique dans le noyau benzothiazolique, la plus grande énergie de transition $\pi - \pi^*$ est présentée par les produits sans substituents dans le reste salicylaldéhydique, ce que nous indique que c'est là que la rupture de la liaison hydrogène intramoléculaire est la plus difficile.

Le groupement NO_2 dans la position 3 ou 5 de ce reste affaiblit par cumul la résistance de la liaison, donc il facilite la transition.

Aux dérivés substitués, avec le groupement méthoxy dans le noyau benzothiazolique, une série d'irrégularités apparaissent qui confirment les constatations antérieures selon lesquelles dans ces cas à l'apparition des états excités les électrons nonparticipants de ce groupement interviennent quelquefois.

Revue Roumaine de Chimie, 18, *10*, 1793–1803 (1973)

PHOTOCHEMICAL ADDITION OF ANTHRONYLIDENE TO ALKENES

JAMES W. PAVLIK
Department of Chemistry, Wisconsin State University
River Falls, Wisconsin 54022 USA

NICOLAE FILIPESCU
Department of Chemistry, The George Washington University,
Washington, D.C. 20006 USA

P.T. FRANGOPOL * and MARIA FRANGOPOL *
Institute of Atomic Physics, P.O. Box 35, Bucharest

Received January 26, 1973

Photochemically generated anthronylidene has been reported to undergo anomalous reactions with alkenes. Thus, although anthronylidene adds stereospecifically to *trans*-alkenes, hydrogen abstraction is the only reaction observed with *cis*-alkenes. We have investigated the photochemistry of 10-diazoanthrone *1* in order to understand these anomalous results.

The photolysis of *1* in acrylonitrile or styrene solutions leads to the addition of anthronylidene to the alkene with formation of the corresponding *spiro*-cyclopropane anthrone adducts. Although addition to styrene is not altered by added benzene, when photolysis is carried out in benzene solution containing diethyl fumarate, hydrogen abstraction leading to 10,10′-bianthrone competes with stereospecific addition of anthronylidene to the alkene. In benzene solution of diethyl maleate, or in neat benzene, however, hydrogen abstraction is the sole reaction. Despite its efficient hydrogen abstracting ability, anthronylidene shows unusual selectivity when generated in benzene solutions containing one equivalent of triphenylphosphine. Hydrogen abstraction does not compete with anthronylidenetriphenylphosphorane formation under these conditions suggesting that singlet anthronylidene survives multiple collisions with solvent to react with the nucleophilic triphenylphosphine. This evidence indicates that cyclopropane formation results from attack by the weakly electrophilic singlet anthronylidene on the nucleophilic alkene. In the absence of a sufficiently reactive alkene, singlet anthronylidene undergoes intersystem crossing to the triplet ground state which is an unusually efficient hydrogen abstractor.

---

* Postdoctoral Research Associates at George Washington University, 1970–1971.

INTRODUCTION

Because of its mechanistic and preparative importance, the synthesis of cyclopropane derivatives by photolytic decomposition of diazoalkanes in the presence of alkenes has received considerable attention. Although at least one exception has been reported,[1] such reactions are generally assumed to involve initial photochemical generation of a carbene intermediate which subsequently adds to the alkene by either a concerted (stereospecific) or two-step (non-stereospecific) mechanism. The stereochemistry of the cyclic products has been used to diagnose the spin-state of the reacting carbene intermediate.[2–6]

Because of the general use of stereochemistry as a mechanistic probe in carbene addition reactions, it is interesting that photochemically generated anthronylidene *2* adds stereospecifically to *trans*-stilbene but fails to add to the *cis*-isomer. Instead, when the carbene precursor, 10-diazoanthrone *1*, was photolyzed in the presence of *cis*-stilbene, the only product was 10, 10′-bianthrone *4*, presumably *via* hydrogen abstraction and coupling of the resulting radical.[7]

We have previously investigated the mechanism and stereochemistry of the thermally initiated addition of *1* to olefins with various configurations.[8] In this paper we report on the photochemical reactions of *1* with monosubstituted and stereoisomeric disubstituted alkenes. We also present mechanistic considerations suggested by the configuration of the products and observed relative reactivities

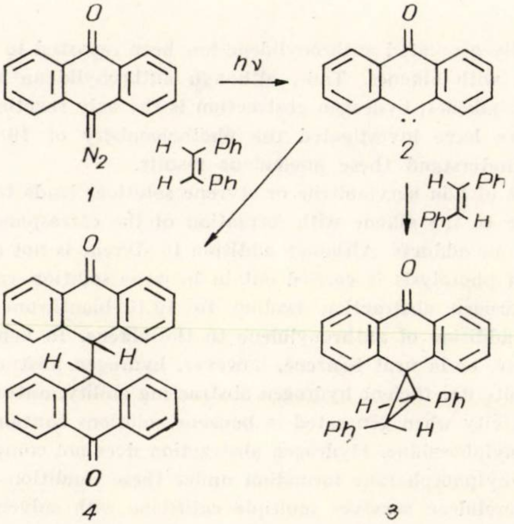

---

[1] N. Filipescu and J. R. DeMember, *Tetrahedron*, **24**, 5181 (1968).

[2] S. Murahashi, I. Moritani, and M. Nishino, *J. Amer. Chem. Soc.*, **89**, 1257 (1967).

[3] M. Jones, Jr. and K. R. Rettig, *J. Amer. Chem. Soc.*, **87**, 4013 (1965).

[4] *ibid*, **87**, 4015 (1965).

[5] W. von E. Doering and M. Jones, Jr., *Tetrahedron Letters*, **1963**, 791.

[6] A. Schonberg, A. Mustafa, and N. Latif, *J. Amer. Chem. Soc.*, **75**, 2267 (1953).

[7] G. Cauquis and G. Reverdy, *Tetrahedron Letters*, **1967**, 1493.

[8] N. Filipescu and J. W. Pavlik, *J. Chem. Soc., Sect. C*, **1970**, 1851.

RESULTS AND DISCUSSION

PHOTOLYSIS OF 10-DIAZOANTHRONE IN NEAT OLEFINS. THE EFFECT OF ADDED SOLVENT

Photolysis of *1* in neat styrene or acrylonitrile led to the formation, in high yield, of *spiro* cyclopropane anthrones *5* and *6*, respectively. Furthermore, the outcome of the reaction with styrene remained virtually unchanged when benzene replaced up to 70 mole percent of the styrene solvent.

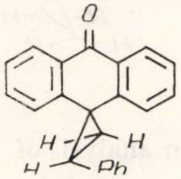

5

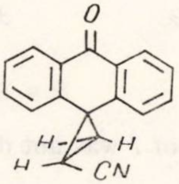

6

Although cyclopropane formation may result from addition of anthronylidene to the olefin, attack of the olefin by a short-lived excited 10-diazoanthrone singlet with initial formation of a 1-pyrazoline cannot be excluded. Because of the thermal instability of the intermediate pyrazolines,[8] this mechanism would not be distinguishable from that involving loss of nitrogen prior to olefin attack.

The reaction between an electronically excited diazo compound and an olefin would be severely curtailed, however, by the presence of an added solvent which does not react with the excited diazo singlet. The presence of an inert diluent greatly increases the number of non-reactive collisions and allows unimolecular processes such as loss of N_2 and deactivation to compete more efficiently with bimolecular addition to alkene. Thus, although a 1-pyrazoline resulted from photolysis of 9-diazofluorene in neat norbornadiene, in the presence of diethyl ether diluent, hydrogen abstraction by fluorenylidene predominated over pyrazoline formation by a ratio of 10 :1. [1] The behavior of diazofluorene, however, is in marked contrast to that of 10-diazoanthrone, since added benzene did not significantly alter the course of the photolysis of *1* in the presence of styrene. Consequently, it seems that a reaction between styrene and a short-lived excited diazo singlet is highly improbable. More likely, *spiro*cyclopropanes *5* and *6* are formed by addition of anthronylidene to the respective alkenes.

PHOTOLYSIS OF 10-DIAZOANTHRONE IN THE PRESENCE OF STEREOISOMERIC ALKENES

The stereochemistry of the photoaddition of *2* to substituted olefins was studied by irradiating *1* in benzene solutions of diethyl fumarate or diethyl maleate.

Photolysis in 30 :70 mole percent diethyl fumarate-benzene at 0° led to isolation of 31% *trans*- 2′, 3′-dicarbethoxy*spiro*[anthrone-10, 1′-cyclopropane] *7* and one percent 10,10′-bianthrone *4*. The *cis*-dicarbethoxy isomer of *7* was not detected by nmr analysis of the cyclopropane fraction.[9]

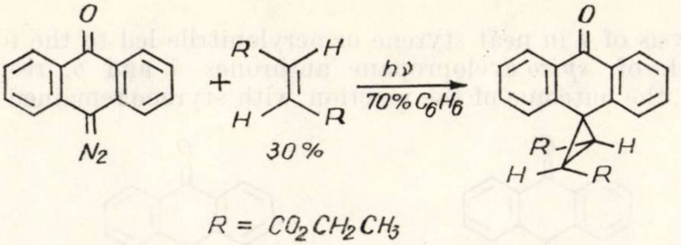

Usually, stereospecific addition is associated with a singlet carbene mechanism and concerted bond formation (Scheme 1).[10] In the case of diethyl fumarate, however, stereospecific addition need not necessarily preclude a triplet carbene mechanism. Because of the large size of the carbethoxy substitutents, the energy difference between *cis* and *trans* intermediate diradicals (*7a* and *7b*) could be large enough to result in total population of the *trans*-conformation *7a* during the "open" period and lead only to the *trans*-cyclopropane *7*. The overall results would thus be essentially indistinguishable from those obtained from concerted addition of a singlet carbene.

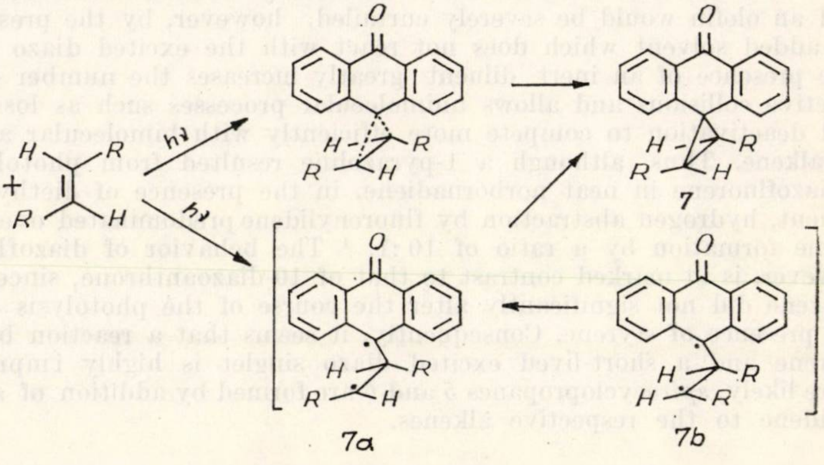

SCHEME 1 ($R=CO_2CH_2CH_3$)

The other isolated product, 10,10′-bianthrone *4*, is the result of hydrogen abstraction by anthronylidene. Its formation in the reaction with diethyl fumarate indicates that hydrogen abstraction can compete with addition to the alkene. In contrast, addition to styrene was faster and did not allow formation of this side product.

---

[9] NMR analyses of purposely prepared mixtures of the *cis* and *trans* isomers showed that as little as 2% of the *cis*-isomer could have been detected. See reference[8].

[10] P. S. Skell and R. C. Woodworth, *J. Amer. Chem. Soc.*, **78**, 4496 (1956).

The decreased reactivity of anthronylidene with diethyl fumarate may be due to the increased steric hindrance to addition that the disubstituted alkene offers the bulky anthronylidene. If so, removal of one of the carbethoxy groups from diethyl fumarate would alleviate the hindrance to addition and result in a higher *spiro*cyclopropane yield and decreased hydrogen abstraction. Such a possibility was contradicted by the results of the photolysis of *1* in 30 :70 mole percent ethyl acrylate-benzene. Irradiation at 0° gave 33 percent 2′-carbethoxy*spiro*-[anthrone-10, 1′-cyclopropane] *8* and one percent 10, 10′-bianthrone.

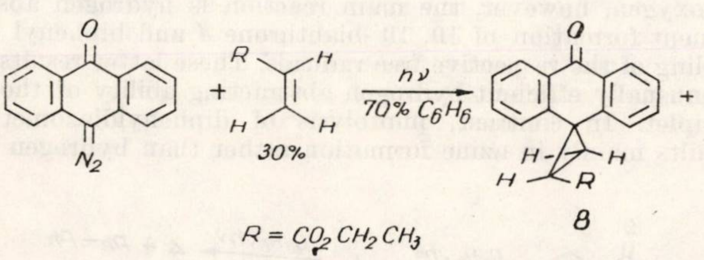

Thus, anthronylidene exhibits comparable reactivity toward diethyl fumarate and ethyl acrylate.

By comparison with the reaction between fluorenylidene and diethyl maleate,[11] the analogous reaction of anthronylidene would be expected, to yield predominately the *trans*-dicarbethoxy*spiro*cyclopropane, *7*. Photolysis of *1* in 30 : 70 mole percent diethyl maleate-benzene, however followed a completely different course and led exclusively to hydrogen abstraction resulting in the isolation of 10,10′-bianthrone in 50 percent yield. No *spiro*cyclopropane product was detected by nmr analysis.[9]

Previous attempts to explain the failure of anthronylidene to add to *cis*-disubstituted olefins were based on steric hindrance between H_4 and H_5 of anthronylidene and the *cis*-substituents of the olefin.[7] It was not explained, however, how two substituents could completely preclude addition when they are *cis* but allow addition when they are *trans*. Furthermore, it was not explained how two *cis*-substituents could sterically preclude addition of anthronylidene but allow addition of the equally bulky fluorenylidene carbene.[11] We will offer a more plausible explanation below, after discussing the spin-state of the photochemically formed anthronylidene.

[11] E. Funakubo, I. Moritani, T. Nagai-, S. Nishida, and S. Murahashi, *Tetrahedron Letters*, **1963**, 1096.

PHOTOLYSIS OF 10-DIAZOANTHRONE IN THE ABSENCE OF OLEFINS. EFFECTS OF OXYGEN AND TRIPHENYLPHOSPHINE

Esr experiments with samples of 10-diazoanthrone photolyzed in rigid matrix indicate that anthronylidene has a triplet ground state.[12] Since on the average the carbene generated photochemically in fluid solution undergoes many collisions before it reacts (see effects of added solvent, above) it may seem reasonable to assume that it is the triplet species that finally reacts. This indeed seems to be the case when *1* is photolyzed in benzene solution since in the presence of dissolved oxygen an almost quantitative yield of 9,10-anthraquinone is obtained. Oxygen, a triplet ground state molecule, is known to react rapidly with triplet carbenes[13-15] but is relatively inert towards singlet carbenes.[16,17] In the absence of oxygen, however, the main reaction is hydrogen abstraction and subsequent formation of 10, 10′-bianthrone *4* and biphenyl by symmetric coupling of the respective free radicals. These latter results demonstrate the unusually efficient hydrogen abstracting ability of the anthronylidene triplet. In contrast, photolysis of diphenyldiazomethane in benzene results mainly in azine formation rather than hydrogen abstraction.[15]

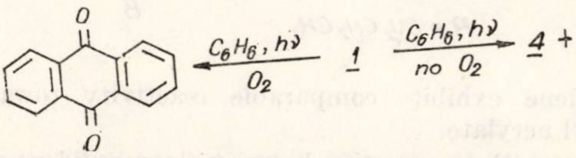

The above results are thus best interpreted in terms of a carbene reacting in its triplet ground state. In spite of such results, however, in the presence of different co-reactants there is no *a priori* reason to exclude reactions involving the originally formed singlet carbene which may be stable enough to survive multiple collisions with the solvent.[18]

Thus, in view of the highly reactive nature of the anthronylidene triplet it is significant to note that if *1* is photolyzed in benzene containing one equivalent of triphenylphosphine, the only isolated product is anthronylidenetriphenylphosphorane *9* in 85 percent yield.[19] It is conceivable that *9* could form *via* a thermally generated anthraquinone

---

[12] Esr experiments were carried out by M. B. LAMOTTE, Laboratoire de Resonance Magnetique, Centre d'Etudes Nucleaires de Grenoble, Grenoble, France and communicated to the authors privately. Unpublished esr experiments by Dr. A. D. BRITT, Department of Chemistry, The George Washington University, were also consistent with a triplet ground state. Other structurally related *p*-diazoquinones, *viz*, 4-diazocyclohexa-2,5-dienone and 4-diazo-1(H)-naphthalenone, also have esr verified triplet ground states. See E. WASSERMAN and R. W. MURRAY, *J. Amer. Chem. Soc.*, **86**, 4203 (1964).

[13] A. M. TROZZOLO, R. W. MURRAY and E. WASSERMAN, *J. Amer. Chem. Soc.*, **84**, 4990 (1962).

[14] H. STAUDINGER, E. ANTHES and F. PFENNINGER, *Ber. dtsch. chem. Ges.*, **49**, 1928 (1916).

[15] W. KIRMSE, L. HORNER and H. HOFFMAN, *Liebigs Ann. Chem.*, **614**, 19 (1958).

[16] H. M. FREY, *Proc. Chem. Soc.*, **1959**, 318.

[17] H. M. FREY, *J. Amer. Chem. Soc.*, **82**, 5947 (1960).

[18] Recent published results show that despite its triplet ground state, the reactions of singlet phenylcarbene with alkenes are not affected by dilution with inert solvent. See R. A. MOSS and ULF-HELGE DOLLING, *J. Amer. Chem. Soc.*, **93**, 954 (1971).

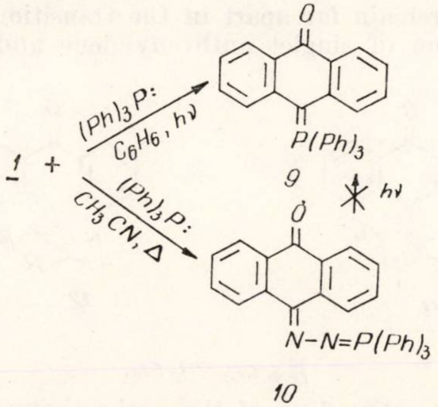

triphenylphosphazine intermediate *10*.[20] [21] However, this possibility was removed by the fact that photolysis of *10* in benzene did not lead to *9*.

Such a high degree of selectivity in the presence of triphenylphosphine is inconsistent with the high reactivity demonstrated by the hydrogen-abstraction-from-benzene reaction and suggests a difference in the nature of the reacting carbenes involved in the two reactions. Most likely, the initially formed singlet carbene is sufficiently long-lived to be captured by the triphenylphosphine. The relative reactivity of a singlet carbene with various reagents has been previously shown to parallel the nucleophilicity of the co-reactant.[22] It thus appears that in *the absence of a sufficiently nucleophilic reagent, singlet anthronylidene undergoes intersystem crossing to its triplet ground state which is an unusually efficient hydrogen abstractor.*

A singlet carbene is the conjugate base of a carbonium ion and is similarly stabilized by electron-releasing substituents. Overlap of the vacant *p*-orbital of the divalent carbon atom in singlet anthronylidene with the two adjacent *p*-orbitals in the benzene rings should thus result in considerable resonance stabilization and reduced electrophilic character.

Cyclopropane formation resulting from attack by the weakly electrophilic singlet anthronylidene on the nucleophilic alkene thus competes with intersystem crossing to the triplet anthronylidene. The relative reactivity of anthronylidene with styrene and ethyl acrylate thus parallels the expected relative reactivity of the two alkenes toward an electrophilic reagent.[23] The relative reactivity of singlet anthronylidene with diethyl fumarate and diethyl maleate (or with *cis* and *trans*-stilbene) also parallels the relative reactivity of *cis* and *trans*-alkenes toward a singlet carbene.

---

[19] J. C. Fleming and H. Shechter, *J. Org. Chem.*, **34**, 3962 (1969).

[20] M. Regitz, *Ber. dtsch. chem. Ges.*, **97**, 2742 (1964).

[21] W. Ried and M. Ritz, *Liebigs Ann. Chem.*, **691**, 50 (1966).

[22] J. Hine and A. M. Dowell, Jr., *J. Amer. Chem. Soc.*, **76**, 2688 (1954)

[23] P. B. D. de la Mare, *Quart. Rev.*, **3**, 126 (1949).

Heats of hydrogenation reveal that because of steric interference between the *cis*-carbethoxy groups, diethyl maleate is less stable than diethyl fumarate (ΔHcis − ΔHtrans = 4.22 kcal).[24] The *trans*-carbethoxy groups continue to remain far apart in the transition state *11* resulting from the combination of singlet anthronylidene and diethyl fumarate.

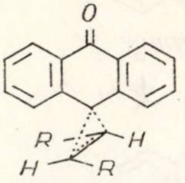

11

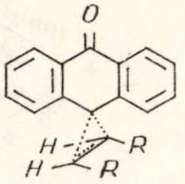

12

$R = CO_2CH_2CH_3$

In contrast, however, crowding of the carboethoxy groups in the *cis*-transition state *12* is considerably increased relative to diethyl maleate.

The increased crowding in *12* would thus sterically inhibit the rate of addition to the *cis*-alkene. A free energy of activation difference of only about 120 calories has been shown to result in a relative reactivity of 1 :1.3 for singlet dichlorocarbene with *cis* and *trans*-2-pentene.[25] Certainly, the much larger steric interference between *cis*-carbethoxy groups would lead to a much larger difference in the free energies of activation leading to *11* and *12*.

Thus, with a lower ΔF^*, addition of anthronylidene singlet to diethyl fumarate can successfully compete with intersystem crossing to the ground triplet state whereas the corresponding addition to diethyl maleate cannot. After reaching the ground triplet state, the only noticeable reaction is hydrogen abstraction.

EXPERIMENTAL

GENERAL

All photochemical reactions were carried out in a pyrex reactor previously described.[26] Two 100-W spot lamps placed at a 45° angle to each other and 10 cm from the reactor were used as a light source. Cooling to 0° was accomplished by circulating an aqueous alcohol solution through the outer jacket of the reactor by way of a spiraled copper tube submerged in a cooling bath maintained at −20°. Unless otherwise specified, all solutions were purged with Cr(II) purified nitrogen for one hour before photolysis.[27] Evolved nitrogen was collected over water. Nmr spectra were recorded at 60 MHz on a Hitachi-Perkin Elmer R-20 Spectrometer with TMS as internal standard and ir spectra were determined in double beam with a Beckman IR5A Spectrophotometer.

[24] E. L. Eliel, "Stereochemistry of Carbon Compounds", McGraw-Hill, To., New York, N.Y., 1962, p. 338.

[25] W. von E. Doering and W. A. Henderson, Jr., *J. Amer. Chem. Soc.*, **80**, 5247 (1958).

[26] J. W. Pavlik, *J. Chem. Educ.*, **46**, 568 (1969).

[27] L. Meites, "Technique of Organic Chemistry", Vol. 1, 3rd ed., John Wiley and Sons, Inc., New York, N. Y., 1941, p. 60.

10-DIAZOANTHRONE

This was prepared in 95 % yield from anthrone and *p*-toluenesulfonyl azide according to the method of Regitz. [20]

PHOTOLYSIS OF 10-DIAZOANTHRONE IN NEAT ACRYLONITRILE

Irradiation of 1.10 g (5.0 mmole) of 10-diazoanthrone in 85 ml of acrylonitrile was accompanied by the evolution of one equivalent of nitrogen. The resulting yellow solution was evaporated to dryness *in vacuo* and the residual solid was dissolved in ethanol, treated with decolorizing carbon, and allowed to crystallize. Filtration yielded 0.992 g (81 %) of 2′-cyano*spiro* [anthrone-10,1′-cyclopropane] *6* mp 184–185° (lit. [8] 184–185°).

PHOTOLYSIS OF 10-DIAZOANTHRONE IN NEAT STYRENE

Irradiation of 0.440 g (2.0 mmole) of 10-diazoanthrone in 54.7 ml (0.479 mole, styrene at 0° for 5 hours brought about the liberation of one equivalent of nitrogen. Excess styrene was removed from the resulting pale yellow solution by short-path distillation at 1 mm Hg and the residual solid dissolved in 3.0 ml warm benzene. Standing at room temperature for 24 hours and seeding with authentic 10,10′-bianthrone failed to yield any of the latter compound. The solution was diluted with 25 ml of ethanol, treated with decolorizing carbon, concentrated to 10 ml, and allowed to crystallize. Filtration gave 0.521 g (88 %) of 2′-phenyl*spiro*[anthrone-10,1′-cyclopropane] *5*, mp 153–154° (lit. [7] 154°).

PHOTOLYSIS OF 10-DIAZOANTHRONE IN 30 MOLE PERCENT STYRENE – 70 MOLE PERCENT BENZENE

Irradiation of 0.440 g (2.0 mmole) of 10-diazoanthrone in a mixture of 14.66 g (0.141 mole) styrene and 26.4 g (0.338 mole) benzene at 0° for 5 hours brought about the evolution of one equivalent of nitrogen. The resulting pale yellow solution was worked up as above. No 10,10′-bianthrone was obtained from the reaction mixture.

PHOTOLYSIS OF 10-DIAZOANTHRONE IN 30 MOLE PERCENT DIETHYL FUMARATE – 70 MOLE PERCENT BENZENE

0.440 g (2.0 mmole) of 10-diazoanthrone and 26.4 g (0.338 mole) of dry benzene were placed in the photochemical reactor and the temperature was lowered to 5°. To the resulting dark red solution was added 24.25 g (0.141 mole) of diethyl fumarate. The temperature was lowered to 0° and the solution was purged with purified nitrogen and irradiated for 5 hours to bring about the liberation of one equivalent of nitrogen. Benzene was removed from the pale yellow solution by rotary evaporation at the water pump and excess diethyl fumarate was removed by short-path distillation at 0.1 mm Hg. The resulting light yellow semi-solid was dissolved in 3.0 ml warm benzene and allowed to stand at room temperature for 24 hours. Filtration gave 4 mg (1 %) of 10,10′-bianthrone identified by a comparison of its infrared spectrum with that of authentic material.[28] The filtrate was added to 25 ml of hot cyclohexane, treated with decolorizing carbon, and concentrated to 10 ml. Cooling gave 0.226 g (31 %) of *trans*-2′,3′-dicarbethoxy*spiro*[anthrone-10,1′-cyclopropane] *7*, mp 114–115° (lit.[8] 114–115°). Nmr analysis of the filtrate gave no indication of the *cis*-isomer of *7*.[9]

PHOTOLYSIS OF 10–DIAZOANTHRONE IN 30 MOLE PERCENT ETHYL ACRYLATE —70 MOLE PERCENT BENZENE

Irradiation of a solution of 0.440 g (2.0 mmole) of 10-diazoanthrone in 26.4 g (0.338 mole) of benzene and 14.1 g (0.141 mole) of ethyl acrylate, prepared as above, for 5 hours brought about the evolution of one equivalent of nitrogen. Excess benzene and ethyl acrylate were removed from the resulting pale yellow solution by short-path distillation at 1 mm Hg and the residual yellow oil was dissolved in 3.0 ml warm benzene. Standing at room temperature for 24 hours gave 4.2 mg (1 %) of 10,10′-bianthrone. The filtrate was evaporated to dryness, dissolved in 50 ml hot *n*-hexane, treated with decolorizing carbon, and concentrated to 10 ml. Cooling gave 0.193 g (33 %) of white needles, mp 72–74°. Repeated recrystallizations from *n*-hexane gave an analytical sample of 2′-carbethoxy*spiro*[anthrone-10,1′-cyclopropane] *8*, mp 75–76°.

Anal. *Calcd.* for $C_{19}H_{16}O_3$: C, 78.08 ; H, 5.48. *Found* : C, 77.87 ; H, 5.21. Physical data were the following : infrared ($CHCl_3$), 1725 (ester C = 0), 1658 (anthrone C = 0), 1600 (aromatic C = C), 1460, 1390, 1318, 1190, 1100, 1030, and 935 cm^{-1} ; nmr ($CDCl_3$) δ0.82 triplet (3H, J = 7.2 Hz, CH_3), 2.2–2.8 ABX system (3H, cyclopropane) 3.76 quartet (2H, J = 7.2 Hz, $-CH_2$), 6.9–7.1 complex (1H, aromatic), 7.2–8.0 complex (5H, aromatic), 8.1–8.4 complex (2H, aromatics peri to C = 0).

PHOTOLYSIS OF 10-DIAZOANTHRONE IN 30 MOLE PERCENT DIETHYL MALEATE — 70 MOLE PERCENT BENZENE

A solution of 0.440 g (2.0 mmole) of 10-diazoanthrone in 26.4 g (0.338 mole) of benzene and 24.25 g (0.141 mole) of diethyl maleate was prepared and irradiated as above. After the liberation of one equivalent of nitrogen, benzene was removed from the resulting yellow solution by rotary evaporation at the water pump and excess diethyl maleate was removed by short-path distillation at 0.1 mm Hg. The residual yellow-orange paste was dissolved in 5.0 ml hot benzene. Standing at room temperature for 24 hours gave 0.191 g (49.5 %) of 10,10′-bianthrone. Nmr analysis of the filtrate indicated the presence of excess diethyl maleate and an additional trace of 10,10′-bianthrone. No *spiro*cyclopropane anthrone products were detected.

DETERMINATION OF THERMAL REACTIVITY AT 0°

To solutions of 70 mole percent benzene and 30 mole percent olefin at 0° was added the required amounts of 10-diazoanthrone. Aliquots were immediately withdrawn with a cold syringe, placed in an infrared cell, and the percent transimssion determined at 2060 cm^{-1} (diazo absorption). Aliquots withdrawn after 5 hours in the dark at 0° and similarly analysed at 2060 cm^{-1} showed no significant change in percent transmission thus eliminating "dark-reactivity" under the conditions of photolysis.

---

[28] O. Dimroth, *Ber. dtsch. chem. Ges.*, **34**, 219 (1901).

PHOTOLYSIS OF 10-DIAZOANTHRONE IN BENZENE SATURATED WITH OXYGEN

0.55 g (2.5 mmole) of 10-diazoanthrone was dissolved in 80 ml dry benzene. The resulting red solution was placed in the photochemical reactor and purged with oxygen for one hour. Irradiation of the solution brought about the evolution of one equivalent of nitrogen. The resulting pale yellow solution was evaporated to dryness *in vacuo* leaving 0.51 g (98 %) of 9,10-anthraquinone identified by its mp, lack of melting point depression when mixed with authentic 9,10-anthraquinone, and by its infrared spectrum.

PHOTOLYSIS OF 10-DIAZOANTHRONE IN BENZENE WITHOUT OXYGEN

0.55 g (2.5 mmole) of 10-diazoanthrone was dissolved in 80 ml dry benzene. The resulting red solution was placed in the photochemical reactor and purged with Cr (II) purified N_2 for one hour. Irradiation of the solution brought about the evolution of approximately one equivalent of nitrogen. Filtration of the resulting pale yellow solution gave 0.021 g (2 %) of 9,10-anthraquinone azine characterized by comparison with an authentic sample.[20] The filtrate was evaporated to dryness *in vacuo* and the remaining semi-solid residue was dissolved in 10 ml warm benzene and placed on an alumina column (25 × 350 mm, Neutral, Brockman Activity I) packed in pet ether (60–80°). The column was eluted with 200 ml pet ether, 200 ml 90 percent pet ether 10 percent diethyl ether, 200 ml 80 percent pet ether 20 percent diethyl ether, 400 ml 70 percent pet ether 30 percent diethyl ether, 200 ml 60 percent pet ether 40 percent diethyl ether, and finally 500 ml of diethyl ether ; 50 ml fractions were collected. Fractions 1–2 gave 0.054 g (29 %) of biphenyl characterized by comparison with a commercial sample, and fractions 14–16 gave 0.197 g (44 %) of 10,10′-bianthrone as the only identifiable products.

PHOTOLYSIS OF 10-DIAZOANTHRONE IN BENZENE CONTAINING TRIPHENYLPHOSPHINE

Irradiation of a solution of 0.440 g (2.0 mmole) of 10-diazoanthrone and 0.524 g (2.0 mmole) of triphenlyphosphine in 80 ml dry benzene was accompanied by the evolution of nitrogen and the formation of a heavy orange precipitate on the walls of the reactor. Irradiation was interrupted several times for the removal of this precipitate by filtration and the filtrate was returned to the photochemical reactor, repurged with nitrogen, and photolysis continued. In this manner one equivalent of nitrogen was finally evolved and 0.772 g (85 %) of anthronylidenetriphenylphosphorane *9* was obtained. The product was recrystallized from absolute ethanol to give orange needles, mp 214–215° (dec.) (lit.[19], 211–214°).

Acknowledgement. Support of this research by the Atomic Energy Commission Contract AT-(40–1)-3797 is gratefully acknowledged.

Revue Roumaine de Chimie, **18**, *10*, 1805–1810 (1973)

SPECTROPHOTOMETRIC DETERMINATION OF Co^{2+} IN $CdCl_2$ LATTICE

ATH. TRUŢIA and M. VODĂ

Institute of Physics, Bd. Păcii 222,
Bucharest, Romania

Received January 27, 1973

The physical conditions for a spectrophotometric quantitative analysis of Co^{2+} ion in a $CdCl_2$ single crystal lattice have been investigated. Two absorption bands of the $(CoCl_6)^{4-}$ complex in $CdCl_2$: Co samples have been found to be proper for such a purpose, at $\tilde{\nu}_0 = 17{,}300\ cm^{-1}$ ($^4\Gamma_4(F) \to {}^4\Gamma_4(P)$ transition) and $\tilde{\nu}_1 = 19{,}000 cm^{-1}$ ($^4\Gamma_4(F) \to {}^2\Gamma_1(G)$ transition). The corresponding extinction coefficients have been found to be $\varepsilon_0 = 9.80 \pm 0.60$ l/mol · cm and $\varepsilon_1 = 2.20 \pm 0.05$ l/mol · cm.

1. INTRODUCTION

The quantitative spectrophotometric analysis is based on the optical absorption of different chemical species. If the extinction coefficient, ε, is known for a given substance, then by measuring the thickness, x, and the transmittance of the sample one may determine the concentration, c, of the absorbing component, by using the Lambert-Beer law :

$$I = I_0 10^{-\varepsilon c x} \tag{1}$$

This method is widely used especially with liquid samples (solutions) where x is very easily measured and ε is a usually well-known constant of material.

When $CdCl_2 : Co^{2+}$ single crystals are concerned ($CdCl_2$ has a diamagnetic lattice which is transparent in the interesting spectral region, the only absorbent being the Co^{2+} ion) ε is no longer a constant. It depends on its cobalt content.

The dependence of ε on the crystal thickness is observed at large concentrations of cobalt and is due exclusively to light scattering on colloids of a second phase, pure $CoCl_2$, imbedded in the host lattice. This phenomenon is easily observed : the "zero line" of a single beam spectrophotometric curve is slowly going up towards shorter wavelengths. Evidently, the better the crystals, the smaller the scattering. For very good crystals (true solid solutions) no such effect is observed.

The concentration dependence of ε (deviation from the Beer's law) is due, this time, to some symmetry effects of the crystal field. It is well known that in the $CdCl_2$ lattice (similar to that of $CoCl_2$) the cobalt ion, Co^{2+}, is surrounded by six negative chlorine ions, Cl^-, situated at equal distances on the three cartesian axes, forming what is called an octahedron. Consequently, the cobalt ion is a centre of symmetry of the $(CoCl_6)^{4-}$complex, which is responsible for the optical spectra of such crystals.

There are two kinds of energy levels of the free Co^{2+} : quartets, with a total spin of 3/2 (^4F, ^4P) and doublets, having a total spin of 1/2 (^2G, ^2H, ^2P, etc.). These levels, degenerated in a spherical symmetry (free ion) are split up, in a lower symmetry (octahedral, O_h, in our case) into several components,[1] fig. 1, and the new states are described by symmetrical wavefunctions as long as the geometry of the complexes is perfect (undeformed). The optical transitions we are interested in are electric dipole, P, transitions which have an antisymmetric behaviour to permutation of particles. The result is that the transition moment π_{ij} of any combination of two energy levels i and j is zero :

$$\pi_{ij} = \int \psi_i P_{ij} \psi_j \, \mathrm{d}\tau = 0 \tag{2}$$

i.e. all transitions are forbidden : there should be no spectrum at all. This is what is called Laporte interdiction, or selection rule.

The intercombination transitions (between quartets and doublets) in a geometrically perfect octahedral complex are forbidden by the spin rule too, so that we should not have these transitions either.

This is what is forseen theoretically. Experimentally, we observed both kinds of the above mentioned spectra. This is because the octahedron undergoes different types of deformations some of which are static (due to defects, impurities, etc. in the immediate vicinity of the complex) the other having a dynamic character (as for example nonsymmetric vibrations). Jahn-Teller deformation could also play a role in the relaxation of the Laporte rule.

The energy levels of the nonsymmetric deformed octahedral complexes are no longer described by simple symmetric wave functions, but by a liniar combination of such expressions, some of them being antisymmetric :

$$\psi_m = c_{m1}\psi_{m1} + c_{m2}\psi_{m2} + \ldots + c_{mi}\psi_{mi} + \ldots = \sum_{n} c_{mn}\psi_{mn} \tag{3}$$

The corresponding transition moment :

$$\pi_{ij} = \int \sum_{k} c_{ik}\, \psi_{ik} P_{ij} \sum_{l} c_{jl}\, \psi_{jl} \, \mathrm{d}\tau \neq 0 \tag{4}$$

will be nonzero this time since there are always some terms in (4) which are behaving properly. Obviously in such cases the intensity of the spectrum strongly depend on the temperature of the sample (the dynamic effect) and on the topographic defects or chemical impurities. In $CdCl_2:Co^{2+}$ crystals, cobalt itself introduces the major perturbation of the host lattice so that we expect the extinction coefficient, ε, to vary with the cobalt concentration.

---

[1] A. D. Liehr, *J. Phys. Chem.*, **67**, 1314 (1963).

As the spin forbidden transitions are concerned, they are expected to appear when spin-orbit or spin-spin interactions take place in the sample. The observed bands are attesting that such is the case in a $(CoCl_6)^{4-}$ complex[2] at least for some of the spin forbidden bands.

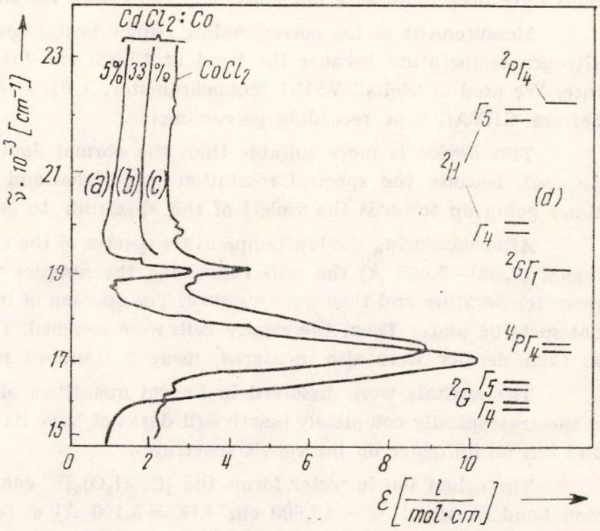

Fig. 1. — The absorption spectra of $CoCl_2$ and $CdCl_2:Co$ single crystals measured at liquid nitrogen temperature. On the right, the energy levels of the cobalt ion of O_h symmetry in crystalline field are indicated.

Returning to permanent deformations of the complex we expect to assume different values in pure $CoCl_2$ and in $CdCl_2:Co^{2+}$ depending on cobalt concentration in the last case, but we do not expect these variations to be the same for all bands because there is a specific way in which the deformations modify the wave functions of the states. We shall analyse the behaviour of two absorption bands of $(CoCl_6)^{4-}$ in order to establish a criterion for quantitative analysis of divalent cobalt in a $CdCl_2$ lattice. The only bands which could be comfortably used in this scope are those resulting from $^4\Gamma_4(F)\rightarrow{}^4\Gamma_4(P)$ and $^4\Gamma_4(F)\rightarrow{}^2\Gamma_1(G)$ transitions, situated at $\tilde{\nu}_0 = 17{,}300\ cm^{-1}$ ($\lambda_0 = 5780$ Å) and $\tilde{\nu}_1 = 19{,}000\ cm^{-1}$ ($\lambda_1 = 5260$ Å) respectively, fig. 1, at liquid nitrogen temperature.

2. EXPERIMENTAL

$CdCl_2:CoCl_2$ single crystals having molar cobalt concentrations ranged from zero to 17% and pure $CoCl_2$ single crystals have been grown as reported earlier.[3]

---

[2] ATH. TRUŢIA and M. VODĂ, to be published.

[3] M. VODĂ and ATH. TRUŢIA, *Rev. Roumaine Phys.*, **14**, 551 (1969).

Due to the structure of the $CdCl_2$ (or $CoCl_2$) lattice consisting of two chlorine sheets alternated with a metal one, the crystal cleaves easily providing very good optical surfaces. There is no need of being further polished for spectrophotometric measurements.

The crystals obtained in good growing conditions are blue, perfectly transparent (unturbid). The X ray diffraction performed on doped crystals has shown a modification of the parameters of the host lattice, indicating that Co^{2+} goes by substitution into the $CdCl_2$ lattice. [2]

Preparation of crystals for optical absorption measurements consists of cleavage, introduction of the samples in quartz cells and sealing by high vacuum grease. All these operations have been done on a hot plate ($t \simeq 140°$) since the samples are, all, hygroscopic.

Measurement of the corresponding (single beam) spectra has been performed at liquid nitrogen temperature because the band at 19,000 cm^{-1} is not well resolved at room temperature. We used a "Zeiss" VSU-1 Monochromator, a FEU-18A photomultiplier, connected to a Sefram GRVAC type recording galvanometer.

This device is more suitable than the normal double beam spectrophotometer at our disposal, because the spectral resolution was higher and we could use the "zero line" (sometimes going up towards the violet) of the spectrum to get a higher precision.

After measuring the low temperature spectra of the samples in the 13,500—20,000 cm^{-1} region (7,400—5,000 Å) the cells containing the samples were left to warm slowly up to the room temperature and then were weighed. The opening of the cells has been made again on the hot metallic plate. Then, the empty cells were weighed. The thickness of the crystals as well as their density were also measured, using a standard method.

The crystals were dissolved in known quantities of bidistilled water. Here, too, $CdCl_2$ is spectroscopically completely inactive (it does not have its own bands in the interesting region and has no influence on the cobalt spectrum).

The cobalt ion in water forms the $[Co(H_2O)_6]^{2+}$ complex having a well-defined absorption band at about $\tilde{\nu} = 19{,}600\ cm^{-1}$ ($\lambda = 5{,}100$ Å) at room temperature. This band comes from the same quartet transition as that in $CdCl_2$ crystal, namely, ${}^4\Gamma_4(F) \rightarrow {}^4\Gamma_4(P)$.

The entire quantity of cobalt makes water complexes so that by using the corresponding coefficient $\varepsilon = 4.95$ l/mol · cm (determined from measurements on standard solutions of pure $CoCl_2$ in water) we can get the total quantity of cobalt in the $CdCl_2$ single crystals with a very good precision. As the weight, density and thickness of the $CdCl_2 : Co^{2+}$ samples are known, we have calculated their cobalt concentrations expressed in mol/l and from here ε_0 (at $\tilde{\nu}_0 = 17{,}300\ cm^{-1}$) and ε_1 ($\tilde{\nu}_1 = 19{,}000\ cm^{-1}$) in these crystals.

Table 1

Extinction coefficients *

	1 %	3.3 %	4.5 %	5 %	17 %	100 %
ε_0	9.20	9.5	9.7	9—8	10.3	6.8
ε_1	2.20	2.20	2.20	2.20	2.20	2.20

* Measured against "zero line".

The concentrations of the samples used were 1 %, 3 %, 4 %, 5 %, 17 % and 100 % (pure $CoCl_2$) for comparison. The corresponding extinction coefficients measured against "zero line" are given in table 1.

3. DISCUSSION

The thickness, weight and density of the crystals as well as the optical density of aqueous solutions resulting from their dissolution and, consequently, also the cobalt concentration of the crystals have been measured with a usual precision met in optical spectrophotometry. There is no reason to think of significant errors in evaluating ε_0 and ε_1 from aqueous solutions. Nevertheless, taking into account that we have measured the entire quantity of cobalt in the crystals, regardless of its phase in the samples and that it is possible in some cases (bad crystals) that a fraction of this quantity do not contribute to the octahedral spectrum of the crystals as being in another phase than the substitutional position in the $CdCl_2$ lattice, we may expect to have important errors on ε_0 and ε_1. The first condition to avoid such errors is then to have crystals which are perfectly clear, showing no light scattering ("zero line" of the spectrum is not going up towards the violet) i.e. representing good solid solutions. The second condition that must be fulfiled concerns the quality of the surfaces of the samples : they must be perfectly plane and without layer edges in the measuring region.

These conditions have been rigorously observed in our case. The results for the two bands are, as we expected, different : the band at 19,000 cm^{-1} has always, with a good approximation, the same value for its extinction coefficient, $\varepsilon_1 = 2.2$ l/mol·cm, while the other, the most intense, at 17,300 cm^{-1}, varies from one $CdCl_2:Co^{2+}$ sample to another, having $9.20 < \varepsilon_0 < 10.30$. The samples differ by their cobalt concentration and this is connected with the deformation degree of the complex, i.e., with the corresponding transition probability. On the other hand, it is possible that the growing conditions of the crystals are also important, independent of the cobalt content of the crystals.

The lack of parallelism in the behaviour of the two bands of the complex could be at least partially explained by taking account of the fact that the quartet transition band is a consequence of pure geometric deformation, while the transition to the doublet state is due also to a spin-orbit coupling.

Regardless of the theoretical explanations, the experimental fact has shown that the band at $\tilde{\nu}_1 = 19,000$ cm^{-1} is the best to be used for quantitative analysis : its ε_1 value is the same in all conditions investigated.

4. CONCLUSIONS

a) The divalent cobalt concentration in a $CdCl_2$ single crystal lattice may precisely be determined under the mentioned quality conditions of the body and surfaces of the crystals using $\varepsilon_1 = 2.20$ l/mol·cm as measured against "zero line" ("single beam" curve) for the band at 19,000 cm^{-1} resulting from the $^4\Gamma_4(F) \rightarrow {}^2\Gamma_1(G)$ transition of the $(CoCl_6)^{4-}$ complex.

b) When the cobalt concentration is very small, the $\tilde{\nu}_0 = 17{,}300$ cm^{-1} band ($^4\Gamma_4(F) \rightarrow {}^4\Gamma_4(P)$ transition) whose $\varepsilon_0 = 9.80 \pm 0.60$ l/mol·cm may be used. In such a case the expected error on cobalt concentration is within $\pm 6\%$.

We mention that the spectra of $CdCl_2:Co^{2+}$ crystals have to be measured at liquid nitrogen temperature.

Revue Roumaine de Chimie, **18**, *10*, 1811–1817 (1973)

STUDIES ON THE ELECTROANALYTICAL BEHAVIOUR OF MEMBRANE-ELECTRODES UNDER CURRENT. II [*]

THE *E*-pH ELECTRODE FUNCTION AND THE USE OF A MEMBRANE-ELECTRODE OF PARCHMENT PAPER IMPREGNATED WITH $BaSO_4$ IN ACID-BASE POTENTIOMETRIC TITRATIONS UNDER CONSTANT DIRECT CURRENT

C. LITEANU [**], I.C. POPESCU [**] and M. PREDA [***]

[**] Chair of Analytical Chemistry, "Babeş-Bolyai" University,
Str. Arany Janos, 11, Cluj, Romania
[***] University of Craiova, Calea Bucureşti, 165, Romania

Received February 12, 1973

A direct and constant electric current, differing from zero, when passing through a membrane of parchment paper impregnated with $BaSO_4$, influences the use of the respective membrane-electrode as an indicator of the end of an acid-base potentiometric titration. This influence is studied and an explanatory hypothesis is stated.

The first attempt of putting analytically into value the behaviour of membrane-electrodes, through which a direct and constant electric current is passed, belongs to Bersier and co-workers.[1] These authors, using a polarized membrane-electrode (of a Al_2O_3 foil), carry out different potentiometric titrations by precipitation. Meanwhile they point out the fact, of exceptional analytical importance, that under the influence of the polarizing current, the potential jump at equivalence increases.

A year later, Geyer and Niklas[2] obtain remarkable results with acid-base titrations by using two polarized membrane-electrodes (of solid ionites). But the magnitude of the indication signal, of a differential type, is very seriously affected by the presence of alien electrolytes.

Starting from these favourable premises, and knowing the behaviour of the membrane-electrode of parchment-paper impregnated with $BaSO_4$,[3-5] we present in this paper a possibility of using this electrode to indicate the acid-base titrations at constant current.

---

[*] Part I. C. Liteanu and I. C. Popescu, *Rev. Roumaine Chim.*, **18**, 319 (1973).
[1] P. Bersier, J. Bersier and F. Hügli, *Helv. Chim. Acta*, **42**, 2514 (1959).
[2] R. Geyer and P. Niklas, *Z. analyt. Chem.*, **177**, 166 (1960).
[3] P. Hirsch-Ayalon, *Electrochim. Acta*, **10**, 773 (1965).
[4] E. P. Honig and J. H. Hengst, ibidem, **15**, 491 (1970).
[5] C. Liteanu and I. C. Popescu, *Rev. Roumaine Chim.*, **18**, 319 (1973).

EXPERIMENTAL

Apparatus. A power source (S) with adjustable tension in the 0–45 V field (Electromagnetica , PMG-RS) was used to deliver the direct electric polarization current. The intensity of the polarization current was measured by means of a microampermeter of class 1 precision (Metra Blansko, DU-20). The potential of the membrane-electrode was determined by means of an electronic potentiometer (P) (Clamann-Grahnert MV-11).

Assembling. The source of constant current used to polarize the electrode was achieved according to the assembling device in fig. 1.

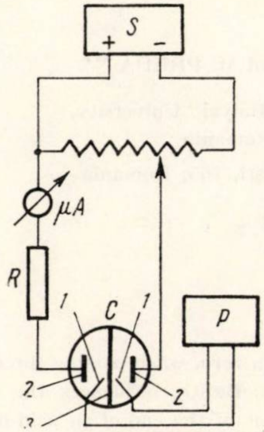

Fig. 1. — The block diagram of the assembling used for potentiometric titrations under current.

S — power source ; R — resistance (330 kΩ) ; P — electronic potentiometer ; C — working cell ; 1, SCE, 2, Pt-platined electrodes, 3, membrane.

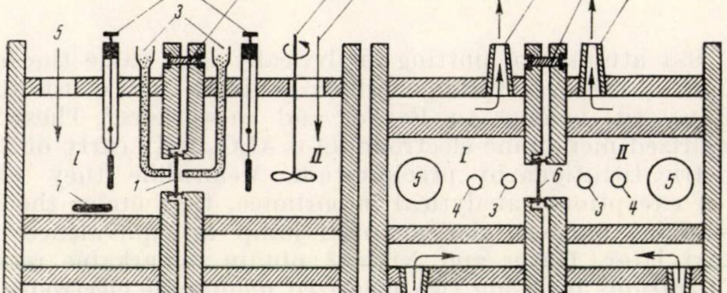

Fig. 2. — The cell used for potentiometric titrations under current.

a) I-reference compartment ; II-working compartment ; 1, membrane, 2, coupling screws ; 3, Luggin capillary with KNO_3 0.1 M agar-agar ; 4, Pt-platined electrodes (1 cm^2 area) ; 5, burette ; 6, mechanic stirrer ; 7, magnetic stirrer. *b*) 1, to thermostat ; 2, coupling screws ; 3, Luggin capillary holes ; 4, polarizing electrodes holes ; 5, burette, stirrer hole ; 6, membrane.

The membrane-electrode of parchment paper impregnated with $BaSO_4$, obtained according to the previously described method, [6] was fitted to the measuring cell used (figure 2).

---

[6] C. Liteanu and M. Mioşcu, *Rev. Roumaine Chim.*, **10**, 903 (1965).

The cell is made of two coupled independent compartments (I and II in figure 2). Each compartment has approximately 50 cm^3, is thermostatic and allows the stirring of the solution. In compartment I, which is air-tight and provided with magnetic stirring, we had a Ba(OH)$_2$ 5×10^{-2}N solution during the whole experiment.

Reactants were of *p.a.* purity and used without any previous purification.

Working routine. The possibility of analytically turning into account the effect of a direct and constant electric current, passing through the studied membrane-electrode, was tested by tracing the *E*-pH electrode function at different current intensities, during the anodic polarization. (We have named "anodic polarization" the state corresponding to the positivation of the Pt-platinized electrode of the reference compartment *versus* the electrode in the working compartment, and "cathodic polarization" the opposite situation). The electrode functions were obtained in the usual manner, using NaOH$-$H$_2$SO$_4$$-H_2$O test solutions of a known pH ($j = 7.5 \times 10^{-1}$N). The electrode potential was estimated measuring the e.m.f. of the electrochemical cell:

SCE ‖ KNO$_3$ 0.1N agar-agar ‖ Test solution | Membrane |

working compartment

| Ba(OH)$_2$ 0.05 N ‖ KNO$_3$ 0.1 N agar-agar ‖ SCE (1)

reference compartment

Based on the *E*-pH curves obtained, we have supposed that the membrane-electrode of BaSO$_4$-parchment paper may be used in acid-base potentiometric titrations under current, with better results than those at zero current. The hypothesis was checked in the case of titrating H$_2$SO$_4$ with NaOH in the $10^{-2}-10^{-3}$ M field, for different intensities of anodic polarization current.

RESULTS

The E-pH electrode function under current. By means of the contraption in figure 1, we have measured the potential of the membrane-electrode, actually the e.m.f. of cell (1), for test solutions of $\text{pH} = 1-11$ ($j = 7.5 \times 10^{-1}$ N), at different polarization intensities (figure 3). The solutions were stirred and thermostated at 25 ± 0.1°.

We notice that under the action of the external electric current in the alkaline field, the membrane-electrode reaches an unusual high sensitivity. For instance, at $i = 68$ μA between $\text{pH} = 9$ and $\text{pH} = 10$, $\Delta E \cong 800$ mV.

Acid-basic potentiometric titrations under current. By anodic polarization of the membrane-electrode at different intensities, we have titrated 20 ml H$_2$SO$_4$ 5×10^{-2} N with NaOH, 5×10^{-1} N (figure 4) and 20 ml H$_2$SO$_4$ 5×10^{-3} N with NaOH 5×10^{-2} N (figure 5).

The results of the titrations under current carried out with the studied membrane-electrode, were checked statistically from the point of view of exactness and precision (criterion "t", respectively, criterion "F"). We have used for comparison the results of the similar conductometric titrations (table 1).

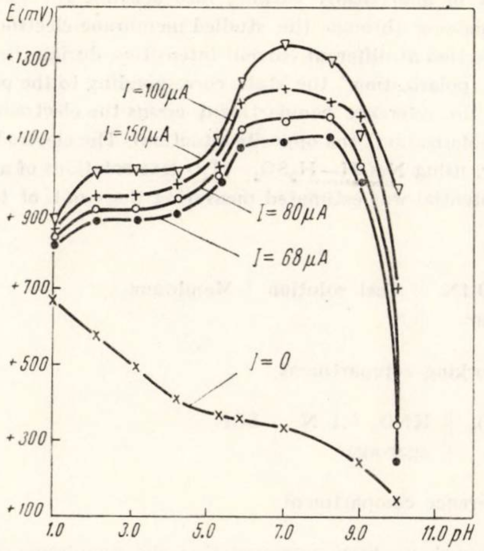

Fig. 3. — The $E-p$H electrode function under current.

Table 1

The results of the exactness check for H_2SO_4 with NaOH titration under current

H_2SO_4 concentration (N)	NaOH concentration (N)	Number of titrations (n)	I (μA)	$\overline{V}_i + s_{\overline{V}i} \cdot t_{(\alpha=0.95)}$ (ml)		"t"$_{(\alpha=0,95)}$	
				I.S.M.E.	Conductometric	calcd.	tab.
5×10^{-2}	5×10^{-1}	5	0	2.05 ± 0.00	2.04 ± 0.04 ($n=4$)	1.70	2.37
		2	68	2.05 ± 0.00		1.45	2.78
		5	80	2.05 ± 0.00		1.70	2.37
		5	100	2.09 ± 0.22		1.15	2.37
		5	150	2.07 ± 0.05		2.31	2.37
5×10^{-3}	5×10^{-2}	5	0	2.06 ± 0.02	2.32 ± 0.08 ($n=4$)	21.80	2.37
		5	68	2.20 ± 0.07		6.9	2.37
		2	80	2.30 ± 0.60		0.8	2.78
		5	100	2.33 ± 0.10		0.5	2.37
		5	150	2.35 ± 0.09		1.5	2.37

In the same way, the results of the titrations under current were compared to those obtained at zero current from the point of view of the indication clearness (table 2).

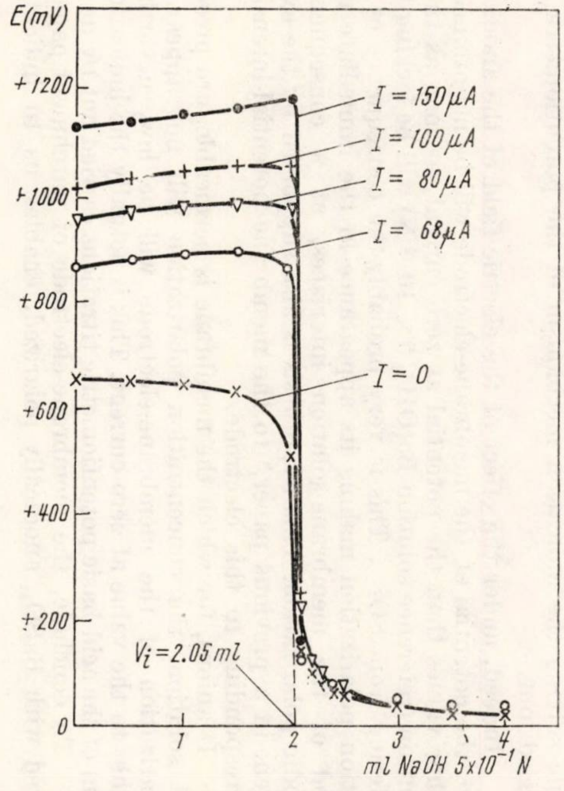

Fig. 4. — The 5×10^{-2} NH_2SO_4 titration with anodic polarized $BaSO_4$-parchment paper membrane-electrode.

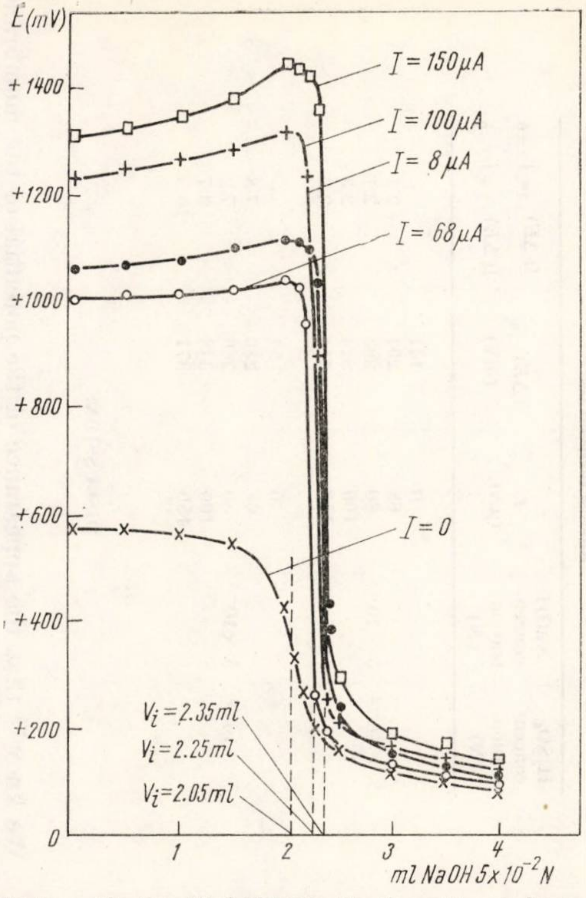

Fig. 5. — The 5×10^{-3} NH_2SO_4 titration with anodic polarized $BaSO_4$-parchment paper membrane-electrode.

Table 2

The influence of the polarization current intensity on the H_2SO_4 with NaOH titration sharpness index

H_2SO_4 concentration (N)	NaOH concentration (N)	I (μA)	$(\Delta E)_{\pm 1\%}$ (mV)	$\frac{[(\Delta E)_{\pm 1\%}]_{I \neq 0}}{[(\Delta E)_{\pm 1\%}]_{I=0}}$
5×10^{-2}	5×10^{-1}	0	141	—
		68	294	2.1
		80	298	2.1
		100	324	2.3
		150	414	2.9
5×10^{-3}	5×10^{-2}	0	32	—
		68	280	7.8
		80	260	7.2
		100	348	9.7
		150	371	10.3

DISCUSSIONS

We know[7,8] that the appearance of the potential of the membrane-electrode of parchment paper impregnated with $BaSO_4$ is based on a selective diffusion process: the H^+ and OH^- ions can pass across the membrane, while the Ba^{2+} and SO_4^{2-} ions cannot. Knowing this, one can easily explain the behaviour of the membrane-electrode under current,[9] meanwhile solving the indication mechanism of the potentiometric titrations carried out.

Indeed, under the effect of the electric field of the anodic polarization, the potential of the membrane-electrode will be maintained at much higher values than the potential at zero current, as long as the working solution (reference solution $Ba(OH)_2$ 5×10^{-2} N) will be lacking the anions differing from SO_4^{2-} . This is very probably the consequence of a concentration polarization making its appearance in the immediate neighbourhood of the membrane-solution interfaces, as a consequence of the anodic polarization. This hypothesis is also supported by the explanation given, in a previous paper,[9] to the membrane potential-intensity curves corresponding to this electrode.

If anions, for which the membrane is permeable, are present in the test solution, the concentration polarization will not appear, and the polarization of the membrane-electrode will be low, nevertheless yet higher to the value at zero current. This is actually the indication mechanism of the acid-basic potentiometric titrations carried out by us (figure 6).

To conclude, the membrane-electrode of parchment paper impregnated with $BaSO_4$, anodically polarized, enables us to indicate exactly

---

[7] P. Hirsch-Ayalon, *Rec. Trav. chim.*, **75**, 1056 (1956).

[8] C. Liteanu and I. C. Popescu, *Talanta*, **19**, 974 (1972).

[9] C. Liteanu and I. C. Popescu, *Rev. Roumaine Chim.*, **18**, 319 (1973).

the end of the acid-base titrations, with a precision which can be compared to the conductometric titration (table 1), but much clearer than the similar titration at zero current (table 2). It is also to be noted that the relative accuracy index increases with the increase of the polarization current intensity.

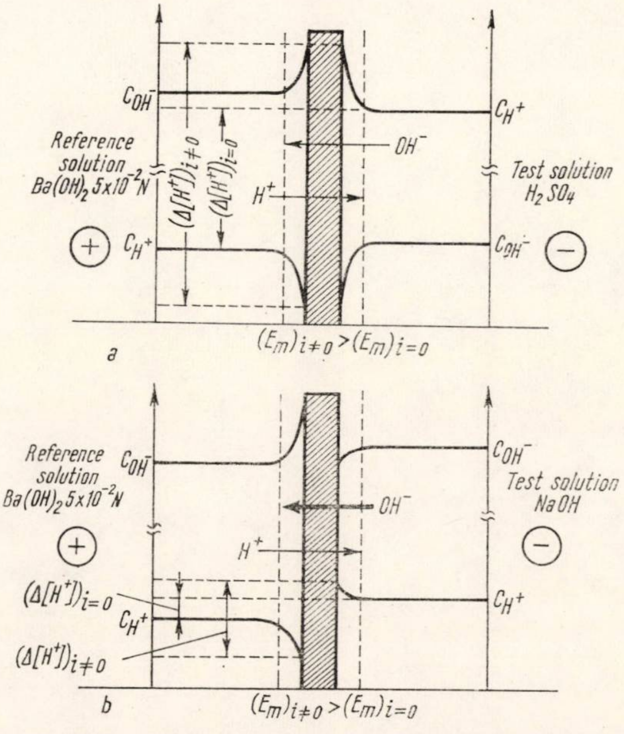
C_{OH^-}
Reference solution $Ba(OH)_2$ $5\times10^{-2}N$
$(\Delta[H^+])_{i\neq0}$
$(\Delta[H^+])_{i=0}$
H^+
OH^-
C_{H^+}
Test solution H_2SO_4
+
C_{H^+}
C_{OH^-}
−
a
$(E_m)_{i\neq0} > (E_m)_{i=0}$
Reference solution $Ba(OH)_2$ $5\times10^{-2}N$
C_{OH^-}
C_{OH^-}
Test solution NaOH
OH^-
H^+
+
−
$(\Delta[H^+])_{i=0}$
C_{H^+}
C_{H^+}
$(\Delta[H^+])_{i\neq0}$
b
$(E_m)_{i\neq0} > (E_m)_{i=0}$

Fig. 6. — The indicating mechanism of the $BaSO_4$-parchment paper membrane-electrode in acid-base titration, under current.

a) before equivalence; b) after equivalence.

Revue Roumaine de Chimie, **18**, *10*, 1819–1824 (1973)

STUDIES ON THE ELECTROANALYTICAL BEHAVIOUR OF MEMBRANE-ELECTRODES UNDER CURRENT. III*

THE USE OF A MEMBRANE-ELECTRODE OF PARCHMENT PAPER IMPREGNATED WITH $BaSO_4$ IN POTENTIOMETRIC TITRATIONS BY PRECIPITATING AT CONSTANT DIRECT CURRENT

I. C. POPESCU*, C. LITEANU* and M. PREDA**

* Chair of Analytical Chemistry, "Babeş-Bolyai" University,
Str. Arany Janos, 11, Cluj, Romania

** University of Craiova, Calea Bucureşti, 165, Romania

Received February 12, 1973

The behaviour of the membrane-electrode of parchment paper impregnated with $BaSO_4$ was studied in argentometric titration at direct and constant current of KCl, KBr and KI. These are linearized to interpret the obtained titration curves, and the results are used to clarify the working mechanism of the electrode.

In a previous paper[1] we have noticed that, under the influence of a direct and constant electric current, the marking of the end of the titration with the $BaSO_4$-parchment paper membrane-electrode is clearly improved. By this opportunity, we have advanced the hypothesis that the electrode acts in this situation as a result of the interaction of a selective diffusion process,[2,3] characteristic to the electrode, with a phenomenon of concentration polarization, brought about by the external polarization.[4]

On the other hand, the parchment paper – $BaSO_4$ membrane-electrode was used as indicator electrode in the argentometric titration of Cl^-, Br^- and I^- at zero current.[5] The basis of the indicating mechanism was supposed to be the potential depressor mechanism of the halide ions, an effect of a mixed diffusional-adsorptive nature.

This being known, we have undertaken a study on the behaviour of the $BaSO_4$-parchment paper membrane-electrode, anodically polarized during the argentometric titration of Cl^-, Br^- and I^- ions. The obtained results, given in the present paper, serve to get deeper into the characteristics of membrane-electrodes under current, meanwhile offering new experimental proofs helping to clear up the indicating mechanism suggested previously.[1]

---

* Part II., C. Liteanu, I. C. Popescu and M. Preda, *Rev. Roumaine Chim.*, **18**, 1811 (1973).

[1] C. Liteanu, I. C. Popescu and M. Preda, *Rev. Roumaine Chim.*, **18**, 1811 (1973).

[2] P. Hirsch-Ayalon, *Rec. Trav. chim.*, **75**, 1056 (1956).

[3] C. Liteanu and I. C. Popescu, *Talanta*, **19**, 974 (1972).

[4] C. Liteanu and I. C. Popescu, *Rev. Roumaine Chim.*, **18**, 319 (1973).

[5] C. Liteanu and I. C. Popescu, *Rev. Roumaine Chim.*, **15**, 973 (1970).

EXPERIMENTAL

The constant current source and the device previously described [1] were used to carry out the potentiometric titrations with the anodically polarized membrane-electrode. The anodical polarization was chosen to make the experimental results comparable to those obtained previously.

The potential of the membrane-electrode adapted to the measuring cell previously described [1] was estimated by measuring the e.m.f. of the cell :

SCE ‖ Salt bridge KNO_3 0.1 M agar-agar ‖ Test solution | Membrane | Reference solution $Ba(OH)_2$ 5×10^{-2}N ‖

‖ Salt bridge KNO_3 0.1M agar-agar ‖ SCE (1)

The solutions adjacent to the membrane were stirred and kept at a constant 25 ± 0.1° temperature. The necessary reactants, of *p.a.* purity, were used without any further purification.

EXPERIMENTAL RESULTS

The E-pX electrode function under current. The $E-p$X electrode functions ($X = Cl^-$, Br^-, I^-) were traced under anodic polarization for different current intensities, using standard KCl, KBr and KI solutions. The results are given in figures 1—3.

Potentiometric titrations by precipitation at constant current. Potentiometric titrations of KCl, KBr and KI of $2\cdot10^{-2}$M with Ag_2SO_4 10^{-2} M ($f = 1.000$) were carried out under current using silver sulphide as titrant, as the SO_4^{2-} ion does not have a potential depressing effect.[5] Figure 4 shows the KCl titration with Ag_2SO_4 at different polarization intensities.

The end of the titration is signaled by the sudden change of the titration curve slope, but, as may be noticed (figure 4), it is not possible to localize the equivalence point directly on the titration curves from $i \geqslant 30$ μA. We have therefore tried to linearize them, finding suited, for the curvilinear branch up to the equivalence point, the relationship[5] :

$$V/E = a + bV \tag{2}$$

We have calculated the equation of the $V/E - V$ line by means of the least squares method. The value of the equivalence volume was determined from the intersection of the $V/E - V$ and $E =$ const. lines, corres-

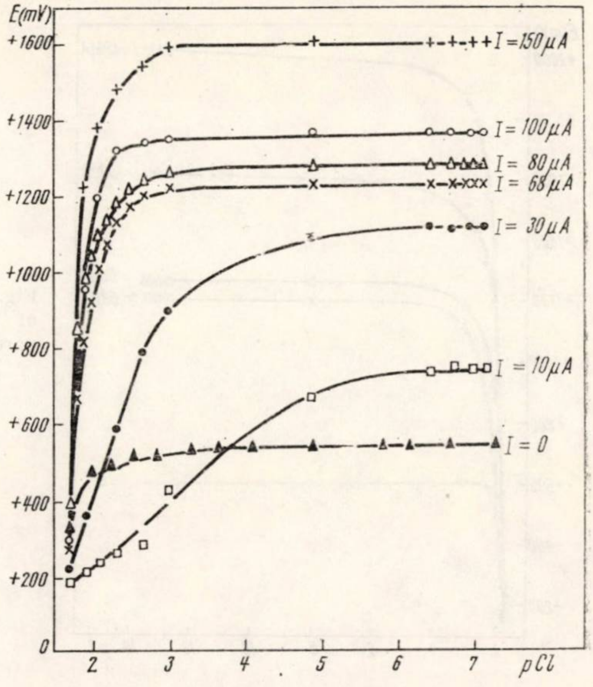

Fig. 1. — The $E-p$Cl electrode function of the anodic polarized $BaSO_4$-parchment paper membrane-electrode.

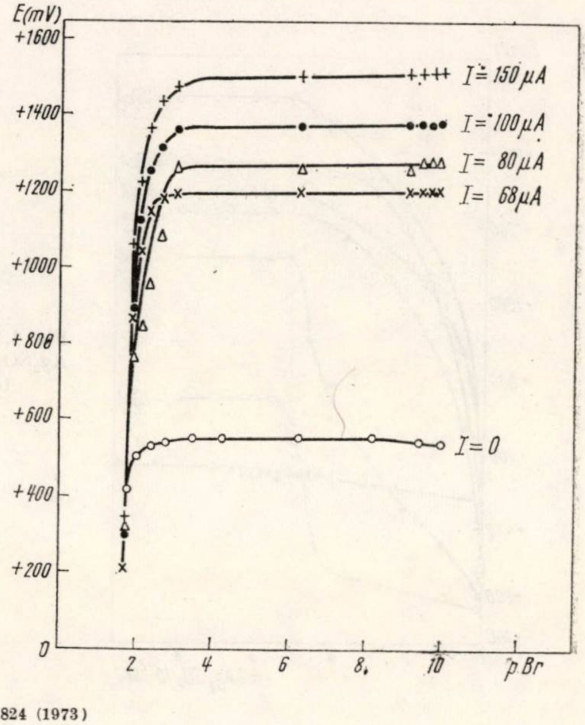

Fig. 2. — The $E-p$Br electrode function of the anodic polarized $BaSO_4$-parchment paper membrane-electrode.

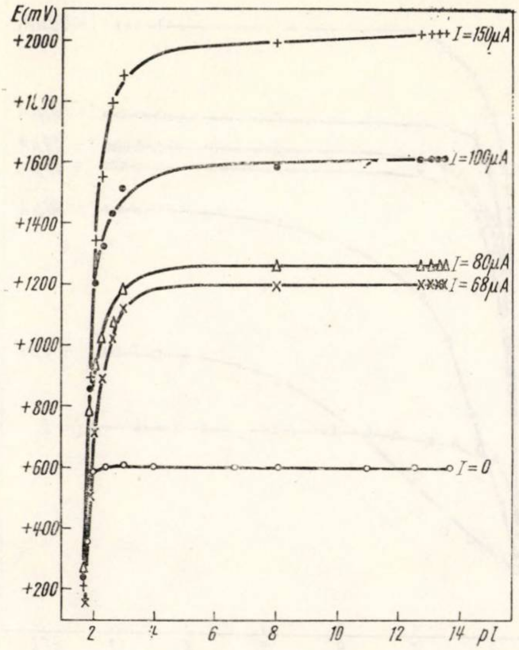

Fig. 3. — The E-pI electrode function of the anodic polarized $BaSO_4$-parchment paper membrane electrode.

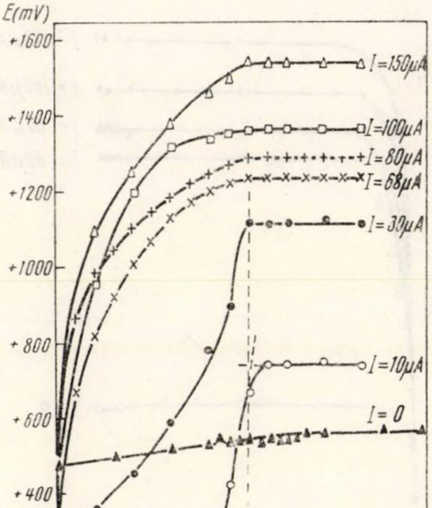

Fig. 4. — The 2×10^{-2} M KCl with 10^{-2}M Ag_2SO_4 titration at different current intensities (anodic polarization).

ponding to the two branches of the titration curves. Figure 5 shows the titration of KCl with Ag_2SO_4 and its linearization.

The same proceedings were used in the case of KBr and KI titrations with Ag_2SO_4. The titration curves at $i = 68$ μA are given in figures 6 and 7.

DISCUSSIONS

By examining the E-pX electrode functions obtained we may reach two conclusions. Firstly, we must note the fact, of great analytical importance, that according to the intensity of the anodic polarization current we can achieve unusual high sensitivities (figures 1—3) in narrow pX fields. Secondly, we can state that the shape of the electrode functions obtained entirely corresponds to the previously stated hypothesis referring to the working mechanism of this electrode at zero current[3] and at a current differing from zero.[4]

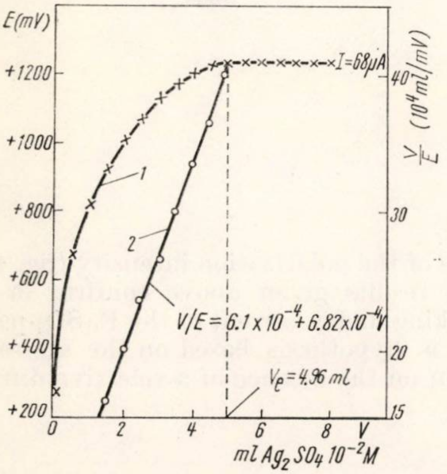

Fig. 5. —The 2×10^{-2}M KCl with 10^{-2}M Ag_2SO_4 titration with anodic polarized membrane-electrode (curve *1*) and its $V/E-E$ linearization (curve *2*).

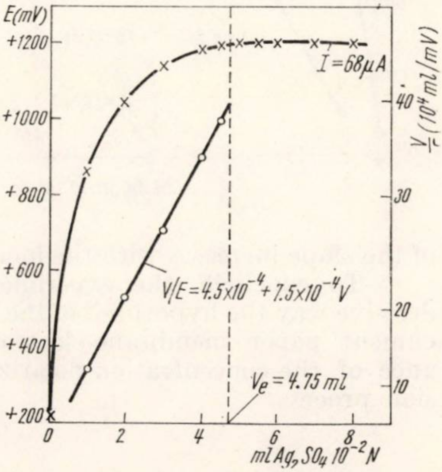

Fig. 6. — The 2×10^{-2}M KBr with 10^{-2}M Ag_2SO_4 titration with anodic polarized membrane-electrode.

Indeed, the presence of the halide ions in the test solution adjacent to the anodically polarized membrane-electrode, brings along the depolarization of the electrode, as the X^- ions will not be transported through the membrane in the direction of the polarization current. As the concentration of the halide ions decreases, the electrode will be gradually re-polarized (figures 1—3).

The obtained titration curves will evidently be interpreted in the same sense. Thus, during the titration, as a result of the X^- ions being blocked in the precipitate, the membrane-electrode is repolarized, a process that ceases with their integral consumption. This fact appears on the titration curve under the shape of a slope (figures 4, 6, 7). The height of the slope increases with the increase of the polarization intensity (fig. 4).

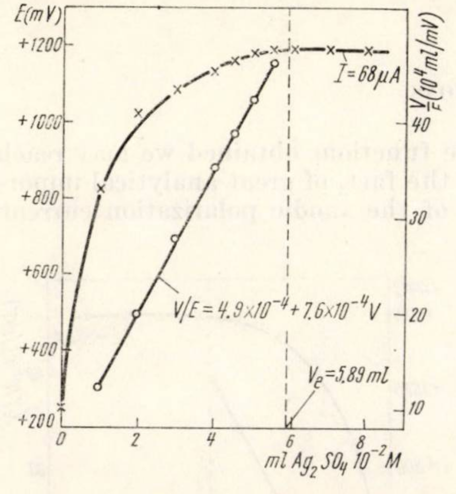

Fig. 7. — The 2×10^{-2}M KI with 10^{-2}M Ag_2SO_4 titration with anodic polarized membrane-electrode.

To conclude, the experimental results given above confirm in a decisive way the hypothesis of the working under current of the $BaSO_4$-parchment paper membrane-electrode, a hypothesis based on the appearance of the concentration polarization on the essence of a selective diffusion process.

Revue Roumaine de Chimie, **18**, *10*, 1825–1827 (1973)

INFLUENCE OF DRYING TEMPERATURE ON WATER CONTENT AND CRYSTALLINE CHARACTERISTICS OF ISOCINCHOMERONIC ACID*

LUIGI CAMPANELLA, PIER LUIGI CIGNINI and GIORGIO DE ANGELIS

Institute of Analytical Chemistry, University of Rome, Italy

Received January 27, 1973

Different powder spectra are given for isocinchomeronic acid according to various drying temperatures. The weight loss, between 40 and 60°, corresponds to 10 % of the initial weight of the acid recrystallized from water.

Going on with the study of the X-ray powder characteristic spectra of pyridinecarboxylic acids [1] we noted that isocinchomeronic acid (2,5-pyridine-dicarboxylic acid) is characterized by different powder spectra according to its degree of dryness — that means according to the ex-

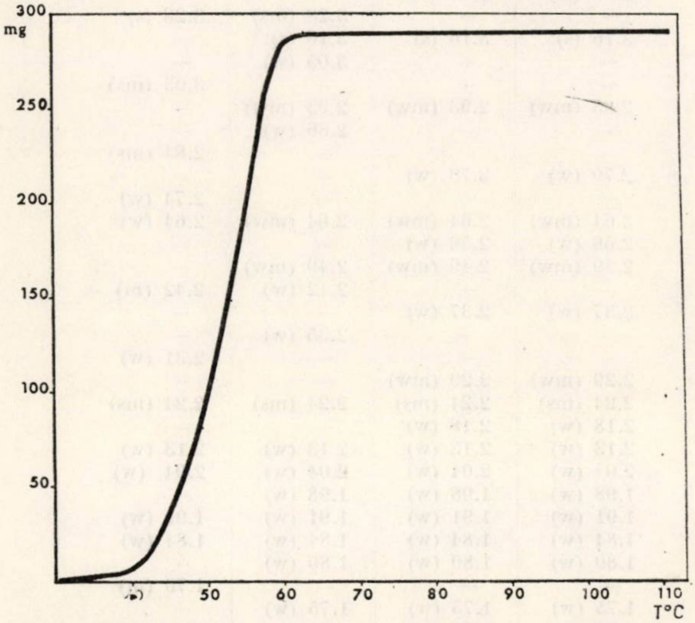

Fig. 1. — Thermogravimetric curve — weight loss *vs* temperature — of isocinchomeronic acid (initial weight = 2,684 g) ; at each temperature the sample is maintained up to constant weight.

---

* Work carried out with the aid of Italian C.N.R.

[1] L. Campanella and P. L. Cignini, Rev. Roumaine Chim., **18**, 000 (1973).

Table 1

X Ray powder spectra of isocinchomeronic acid dried at various temperatures

32°C	40°C	50°C	60°C
—	—	—	8.50 (mw)
6.70 (m)	6.70 (m)	6.72 (m)	—
—	—	—	6.55 (mw)
5.46 (mw)	5.46 (mw)	—	—
—	—	5.41 (w)	—
—	—	—	5.27 (m)
4.99 (s)	4.99 (s)	4.99 (s)	—
—	—	—	4.84 (s)
4.57 (w)	4.57 (w)	—	—
—	—	4.26 (w)	4.26 (w)
4.23 (m)	4.23 (m)	—	—
—	—	—	4.09 (m)
—	—	4.02 (w)	—
3.94 (mw)	3.94 (mw)	—	—
—	—	—	3.76 (mw)
—	—	3.73 (w)	—
3.71 (w)	3.71 (w)	—	—
—	—	—	3.63 (w)
3.50 (ms)	3.50 (ms)	3.50 (ms)	—
—	—	—	3.47 (w)
3.32 (w)	3.32 (w)	—	—
—	—	3.28 (ms)	3.28 (s)·
3.16 (s)·	3.16 (s)·	3.16 (s)·	—
—	—	3.05 (w)	—
—	—	—	3.03 (ms)
2.93 (mw)	2.93 (mw)	2.93 (mw)	—
—	—	2.86 (w)	—
—	—	—	2.84 (ms)
2.79 (w)	2.79 (w)	—	—
—	—	—	2.74 (w)
2.64 (mw)	2.64 (mw)	2.64 (mw)	2.64 (w)
2.56 (w)	2.56 (w)	—	—
2.49 (mw)	2.49 (mw)	2.49 (mw)	—
—	—	2.42 (w)	2.42 (m)
2.37 (w)	2.37 (w)	—	—
—	—	2.35 (w)	—
—	—	—	2.31 (w)
2.29 (mw)	2.29 (mw)	—	—
2.24 (ms)	2.24 (ms)	2.24 (ms)	2.24 (ms)
2.18 (w)	2.18 (w)	—	—
2.13 (w)	2.13 (w)	2.13 (w)	2.13 (w)
2.04 (w)	2.04 (w)	2.04 (w)	2.04 (w)
1.98 (w)	1.98 (w)	1.98 (w)	—
1.91 (w)	1.91 (w)	1.91 (w)	1.91 (w)
1.84 (w)	1.84 (w)	1.84 (w)	1.84 (w)
1.80 (w)	1.80 (w)	1.80 (w)	—
—	—	—	1.76 (m)
1.75 (w)	1.75 (w)	1.75 (w)	—
1.70 (w)	1.70 (w)	1.70 (w)	1.71 (w)
1.66 (w)	1.66 (w)	1.66 (w)	—
—	—	—	1.64 (w)
1.62 (w)	1.62 (w)	1.62 (w)	—

(continued)

32°C	40°C	50°C	60°C
1.58 (mw)	1.58 (mw)	1.58 (mw)	1.59 (w)
—	—	—	1.56 (w)
1.52 (w)	1.52 (w)	1.52 (w)	—
1.47 (w)	1.47 (w)	1.47 (w)	1.47 (w)
1.40 (w)	1.40 (w)	1.40 (w)	—
—	—	—	1.38 (w)
—	—	—	1.33 (w)
1.32 (w)	1.32 (w)	1.32 (w)	—
—	—	—	1.30 (w)
1.26 (w)	1.26 (w)	1.26 (w)	1.26 (w)
1.24 (w)	1.24 (w)	1.24 (w)	1.24 (w)
—	—	—	1.22 (w)
1.21 (w)	1.21 (w)	1.21 (w)	1.21 (w)
—	—	—	1.20 (w)
1.18 (w)	1.18 (w)	1.18 (w)	1.18 (w)
1.17 (w)	1.17 (w)	—	—
1.16 (w)	1.16 (w)	1.16 (w)	—
—	—	—	1.15 (w)
1.14 (w)	1.14 (w)	1.14 (w)	1.13 (w)
—	—	—	1.11 (w)

w = weak, mw = middle weak, m = middle, ms = middle strong, s = strong

perimental temperature of drying — after the recrystallization from water (table 1).

Consequently, any chance of recording reproducible spectra with analytical or diagnostic aims is conditioned by a good reproducibility of the drying conditions. It is well known[2] that isocinchomeronic acid crystallizes from water as monohydrate. The thermogravimetric curve, reported in fig. 1, shows that the weight loss occurs between 40 and 60°; as this loss corresponds to 10% of the initial weight and the molecular weights of isocinchomeronic acid and water are of 10 :1, it can be deduced that at 60° all the water is released by the acid.

In agreement the X-ray powder is unaffected by the drying temperature if the acid is dried at a temperature higher than 60°.

In conclusion, if isocinchomeronic acid must be employed as analytical reagent, its thermal behaviour must be taken into account, so that drying after recrystallization has to be performed at a temperature not lower than 60°.

---

[2] C. D. Hodgman, R. C. Weast and S. M. Selby, "Handbook of Chemistry and Physics", Chemical Rubber Publishing Co., Cleveland, Ed. 39, 1957, p. 1002.

Revue Roumaine de Chimie, **18**, *10*, 1829 – 1838 (1973)

MASS TRANSFER IN THE ABSORPTION FROM A FREELY RISING GAS BUBBLE UNDER THE ACTION OF MECHANICAL VIBRATIONS

CORNELIA BALABAN, GH. DOBRĂNIŞ and R. MIHAIL

Polytechnical Institute, Chair of Chemical Engineering,
Str. Polizu 1, Bucharest, Romania

Received May 8, 1973

The mass transfer from a freely rising gas bubble (CO_2) to a liquid column (distilled water) is intensified by mechanical vibrations in horizontal or vertical direction. Mass transfer coefficients, calculated using relationships adapted to vibrated systems, indicate an increase of approximately 30 %, when referring to non-vibrated systems.

Mass transfer from gas or vapour bubbles to a continuous liquid phase is the main process in many chemical engineering operations, such as distillation, absorption, evaporation, etc. Although industrial operations involve simultaneously many bubbles, in order to understand the fundamental phenomena in mass transfer, it is necessary to follow the process taking place on the surface of a single bubble. Several theoretical and experimental papers were written on this topic.[1–11] Recently, a review of papers published on this topic during 1968 – 1970 has appeared.[12]

From the studies mentioned above, it results that mass transfer between the surface of a bubble and the liquid phase is determined by the shape and the magnitude of the bubble, the hydrostatic pressure,

---

[1] J. H. Leonard and G. Houghton, *Chem. Eng. Sci.*, **18**, 133 (1963).
[2] J. H. Leonard and G. Houghton, *Nature*, **190**, 687 (1961).
[3] A. C. Lochiel and P. H. Calderbank, *Chem. Eng. Sci.*, **19**, 485 (1964).
[4] Pang-Sheng Li, *Scientia Sinica*, **13**, 499 (1964).
[5] C. W. Bowman and A. J. Johnson, *Canad. J. Chem. Eng.*, **40**, 139 (1962).
[6] M. H. Baird and J. F. Davidson, *Chem. Eng. Sci.*, **21**, 87 (1963).
[7] A. J. Johnson, F. Besik and A. E. Hamielec, *Canad. J. Chem. Eng.*, **47**, 559 (1969).
[8] F. Hirose and M. Moo-Young, *Chem. Eng. Sci.*, **25**, 729 (1970).
[9] K. R. Weller, *Canad. J. Chem. Eng.*, **49**, 154 (1971).
[10] K. R. Weller, *Canad. J. Chem. Eng.*, **50**, 49 (1972).
[11] T. Ishii and A. I. Johnson, *Canad. J. Chem. Eng.*, **47**, 272 (1969).
[12] L. L. Tavlarides, C. A. Coulaloglou, M. A. Zeitlin, G. E. Klinzing and B. Gal-or, *Ind. Eng. Chem.* **62**, 6 (1970).

the rising velocity, i.e. factors which determine the hydrodynamic conditions of the interface. Usually, these factors vary during the rising of the bubble in the column, influencing thereby the intensity of the mass transfer.

In order to intensify the mass transfer from a gas bubble to a liquid phase, one can act either on the parameters characterizing one of the phases (gas or liquid) or simultaneously on the parameters of both phases. Thus, for the intensification of mass transfer one can have recourse to transient regimes involving pulsations, sonic vibrations, ultrasonic or mechanical vibrations.

Experimental results have been obtained on the action of sonic vibrations in the range from 20 to 200 cps[13,14] or other ranges[15–18] on swarms of bubbles, when an appreciable increase of mass transfer was obtained. Using vertical mechanical vibrations, the vibration conditions were determined when cyclic migration of bubbles in the liquid column takes place.[19]

If in the liquid column which oscillates vertically the bubble can be maintained in a stationary position,[20–22] the observation of the transfer process is very much facilitated. The necessary conditions for this stationarity are characterized by frequency limits of 1000–2000 cps and by vibrational amplitude limits of 2–7 mm. In the theoretical treatment of this problem the simulation of the bubble by a solid sphere, although reflecting less exactly the essence of the phenomena, evidences better the hydrodynamic conditions within the pulsed liquid.[23,24] The mathematical expression of the movement and of the mass transfer from a gas bubble or a liquid drop to the liquid phase in systems submitted to sonic vibrations, ultrasonic vibrations, mechanical vibrations or pulsations, is difficult. For liquid drops in a pulsated medium, hydrodynamical studies were performed, obtaining the falling velocity of the drop as a function of its volume.[25] Other investigations effected at low Reynolds numbers allowed a relationship to be deduced for calculating the mass transfer coefficient from a gas bubble to a liquid oscillating under the action of vertical mechanical vibrations.[26]

The present paper deals with the mass transfer from a single gas bubble to a continuous liquid phase. The system gas bubble liquid column was vibrated mechanically both in horizontal and vertical directions, in

---

[13] K. L. Harbaum and G. Houghton, *Chem. Eng. Sci.*, **13**, 90 (1960).

[14] K. L. Harbaum and G. Houghton, *J. Appl. Chem.*, **12**, 234 (1962).

[15] M. H. J. Baird, *Chem. Eng. Sci.*, **18**, 685 (1963).

[16] M. H. J. Baird, *Canad. J. Chem. Eng.*, **41**, 52 (1963).

[17] S. Bretsznajder and W. Pasiuk, *Bull. Acad. polon. Sci., Ser. Sci. chim.*, **7**, 591 (1958).

[18] I. Ia. Gorodețki, V. M. Olevski, R. P. Levitanite and L. A. Legocikina, *Kim. Prom.* **41**, 834 (1965).

[19] H. R., Buchanan, G. J. Jameson and D. Oedjoe, *Ind. and Eng. Chem.* (*Fundamentals*) **1**, 81 (1962).

[20] G. J. Jameson, *Trans. Inst. Chem. Engineers*, **44**, 91 (1966).

[21] G. J. Jameson and G. F. Davidson, *Chem. Eng. Sci.*, **21**, 29 (1966).

[22] G. J. Jameson, *Chem. Eng. Sci.*, **21**, 35 (1966).

[23] J. Molinier, G., Kuychoukov and H., Angelino, *Chem. Eng. Sci.*, **26**, 1401 (1971).

[24] G. Houghton, *Proc. Roy. Soc.*, **33**, A 272 (1963).

[25] A. Chnowski and H. Angelino, *Canad. J. Chem. Eng.*, **50**, 23 (1972).

[26] E. Ruckenstein and O. Muntean, *Chem. Eng. Sci.*, **25**, 1159 (1970).

separate experiments. The amounts of absorbed gas in different vibration conditions were compared with those transferred during the free ascension of the gas bubble in the non-vibrated liquid column ; thus, a measure of the intensification of the absorption through the mechanical vibrations was obtained. By photographing the gas bubbles during the absorption under vibrations, qualitative observations were made on the behaviour of gas bubbles in various vibration conditions.

EXPERIMENTAL

The intensification of the mass transfer under the action of mechanical vibrations was followed by using the installation shown in fig. 1. It consists of the absorption column (*1*), the device for the introduction of the gas and formation of the bubble (*2*) and the system for measuring the gas volume which was introduced or absorbed (*3*). A glass column was used, with outer diameter 5 cm and 50 cm height, mounted on a mechanical vibrator with adjustable frequency and amplitude. The vibrational energy was provided by an electrical motor of 1 kW power and 1390 rpm. The gas was injected from a calibrated syringe under the metallic spoon (*4*). By rotating the spoon, the gas bubble is set free and allowed to rise in the column filled with

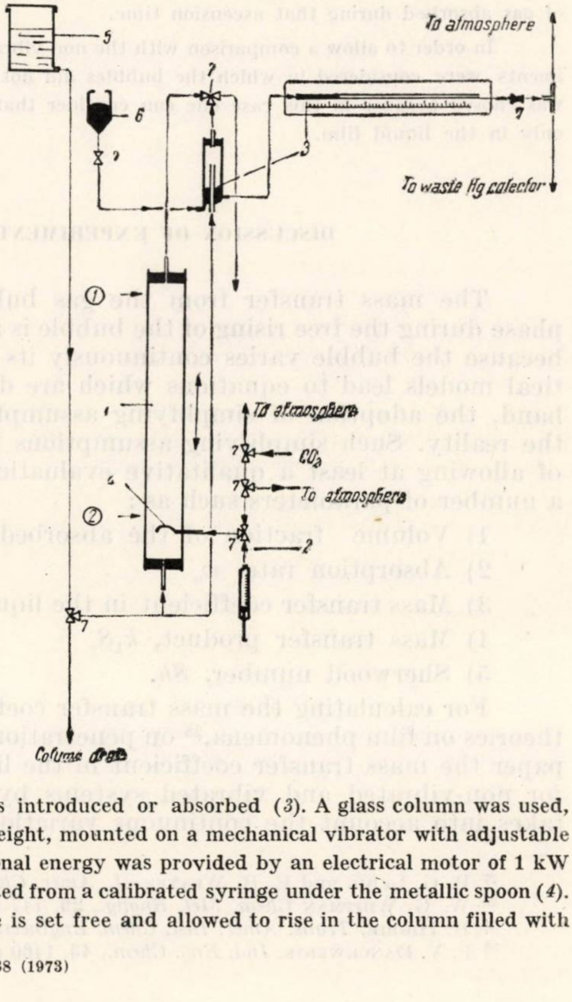

Fig. 1. — Experimental apparatus.
1, glass column. 2, gas injection system. 3, gas volume measuring system, 4, metallic spoon. 5, distilled water reservoir. 6, mercury level control system. 7, stopcocks.

liquid. In our experiments the liquid was distilled water and the gas was carbon dioxide. The measurements of the absorbed gas volume were performed by following the volume variations in a system open to atmosphere, using the method of Ledig and Weaver [23], improved by Johnson, Besik and Hamielec. [7] By suitable adjustments of stopcocks from the injection and measurements devices, one can inject the gas into the column, reset the mercury in the capillary tube, evacuate or fill the column and also evacuate the non-absorbed gas. The magnitude of the linear displacements of the mercury column in the capillary tube is directly proportional to the volume of gas injected or absorbed; the proportionality constant was determined by a previous calibration. The sensitivity of the measuring system is about $3 \cdot 10^{-3}$ ccm. The variation range of the experimental parameters was:

— initial volume of the bubble, V_1: 0.1—1.0 ccm

— frequency of vibrations, f: 15—28 cps

— amplitude of vibrations, a: 1—3 mm

— directions of vibration: horizontal and vertical, in separate experiments.

In each experimental run, the following parameters were measured: volume of gas introduced into the column, duration of the ascension of the bubble between two fixed marks, amount of gas absorbed during that ascension time.

In order to allow a comparison with the non-vibrated reference system, only those experiments were considered in which the bubbles did not break. The CO_2-distilled water system was chosen because in this case one can consider that the resistance to mass transfer occurs only in the liquid film.

DISCUSSION OF EXPERIMENTAL RESULTS

The mass transfer from the gas bubble to the continuous liquid phase during the free rising of the bubble is a complex phenomenon mainly because the bubble varies continuously its shape and volume. Mathematical models lead to equations which are difficult to solve. On the other hand, the adoption of simplifying assumptions introduces distortions of the reality. Such simplifying assumptions have, however, the advantage of allowing at least a qualitative evaluation of the influence exerted by a number of parameters such as:

1) Volume fraction of the absorbed gas, V_a
2) Absorption rate, w_a
3) Mass transfer coefficient in the liquid film, k_1
4) Mass transfer product, $k_1 S_e$
5) Sherwood number, Sh.

For calculating the mass transfer coefficient one can use the known theories on film phenomena,[28] on penetration,[29] or renewal.[30] In the present paper the mass transfer coefficient in the liquid film was calculated both for non-vibrated and vibrated systems by means of relation (1) which takes into account the continuous variation of hydrostatic pressure and

---

[27] P. G. Ledig and E. R. Weaver, *J. Amer. Chem. Soc.*, **46**, 650 (1924).
[28] W. G. Whitman *Chem. Met. Engng.*, **29**, 147 (1923).
[29] R. Higbie, *Trans. Amer. Inst. Chem. Engineers*, **31**, 365 (1935).
[30] P. V. Danckwerts, *Ind. Eng. Chem.*, **43**, 1460 (1951).

of bubble velocity during its rise. In this equation, the parameters may be calculated for the vibrated and non-vibrated situations[7] :

$$k_1 = \frac{4(P_1 - P_2)}{4.84\, RTH_c} \; \frac{(PV)_1^{1/3} - (PV)_2^{1/3}}{P_1^{4/3} - P_2^{4/3}} \tag{1}$$

The volume fraction of absorbed gas V_a is represented in figures 2*a* and 2*b* against the bubble volume, depending on the vibration conditions. At equal bubble volume, the absorbed volume fraction increases with increasing vibration frequency. The absorption rate w_a is a function of the initial bubble volume, of the vibration frequency and the vibration amplitude. The dependence of the mass transfer coefficient on vibration conditions is represented in figures 3*a* and 3*b*. The intensification of mass transfer expressed by the increase of the mass transfer coefficient is directly proportional with the frequency of the vibrations and inversely proportional with the equivalent diameter of the bubble for horizontal vibrations. For vertical vibrations, the mass transfer coefficient increases with the vibration frequency and with the equivalent diameter of the bubble. The variation of the mass transfer product and of the Sherwood number against the bubble volume is presented in figures 4, 5*a*, 5*b*, as a function of vibration conditions.

The dependence of the absorption rate, of the transfer product and of the Sherwood number *versus* the vibrational acceleration $\omega^2 a$, shown in figures 6—9, presents a cyclic variation. This can be explained by accepting the idea that the mass transfer process is modulated by vibrations. This phenomenon occurs in processes taking place in systems influenced by an external factor which varies as a sine function. Jameson[20], who studied the absorption of a set of gas bubbles in vertically vibrated liquids, obtained a cyclic variation of the amount of absorbed gas as a function of the vibration frequency. He supposed that the presence of absorption maxima could be due to frequencies at which the amount of gas present in the liquid makes this mixture more compressible than a continuous liquid phase.

When studying the absorption of single bubbles, the compressibility of the system cannot be modified. Therefore, this compressibility can be considered to be equal to that of the continuous liquid phase. Therefore, the compressibility of the system cannot constitute the only explanation of this cyclic character represented in figures 6—8.

Plot 10 represents the Reynolds number for various bubble magnitudes as a function of the vibrational acceleration. By combining the information contained in the last figure with those obtained from plots 6—8, it results that there exist vibration conditions for which the absorption is minimal, and those conditions coincide with minimal values of the Reynolds number, thus the influence of the hydrodynamic situation in the absorption is evidenced, at least indirectly. This influence is manifested in several ways. For a given height of the liquid column, the vibration increases the residence time of the bubble. From the experimental data,

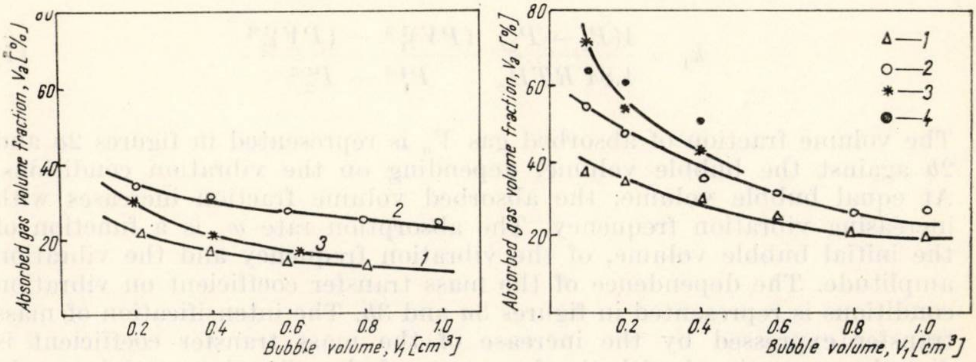

Fig. 2. — Absorbed gas volume fraction ;

a) Horizontal vibrations *1*, non-vibrated ; *2*, vibrated : f = 15 cps ; a = 12 mm ; *3*, vibrated ; f = 10 cps ; a = 2 mm ;
b) Vertical vibrations. *1*, non-vibrated ; *2*, vibrated : f = 15.5 cps ; a = 1 mm ; *3*, vibrated : f = 15.5 cps ; a = 2 mm ;
4, vibrated : f = 21 cps ; a = 1 mm.

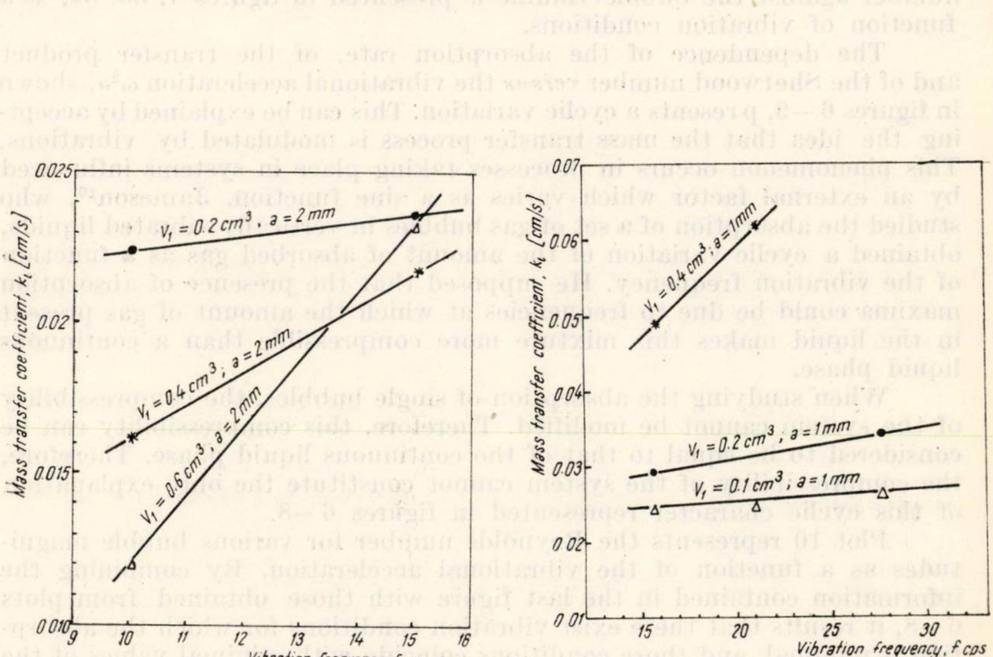

Fig. 3. — Mass transfer coefficient ; *a*) Horizontal vibrations ; b) Vertical vibrations.

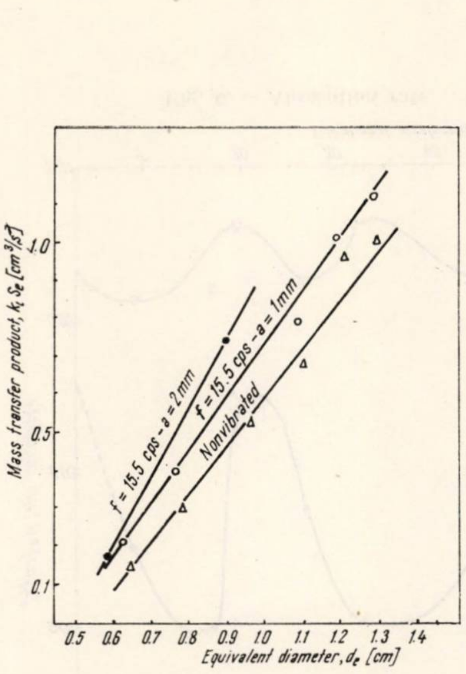

Fig. 4. — Mass transfer product.

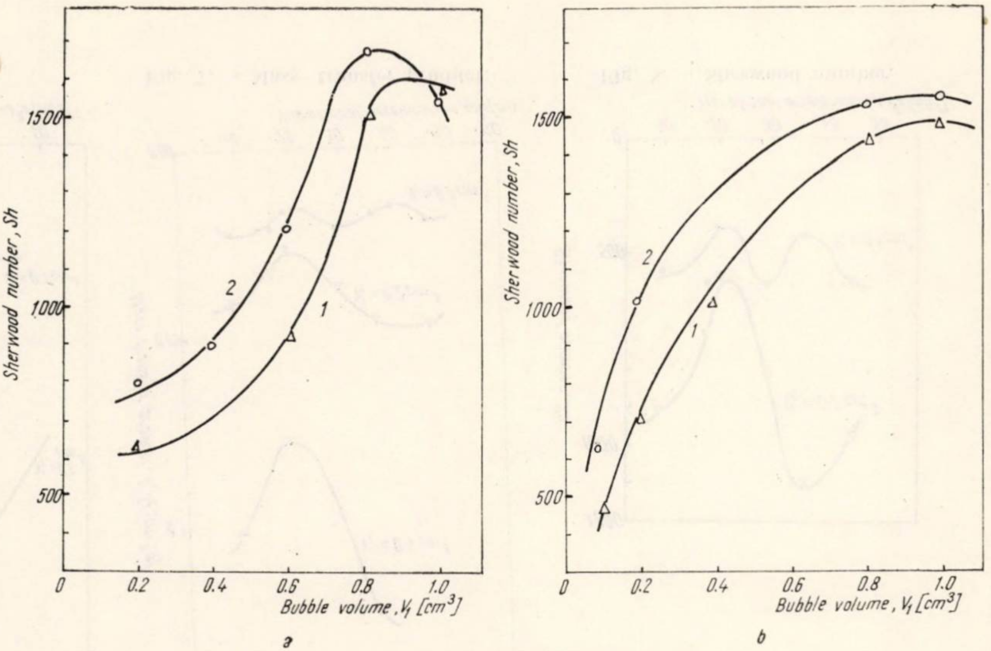

Fig. 5. — Sherwood number.

a) **Horizontal vibrations: *1*, non-vibrated; *2*, vibrated; $f = 15$ cps; $a = 2$ mm. *b)* Vertical vibrations: *1*, non-vibrated; *2*, vibrated; $f = 15.5$ cps; $a = 1$ mm.**

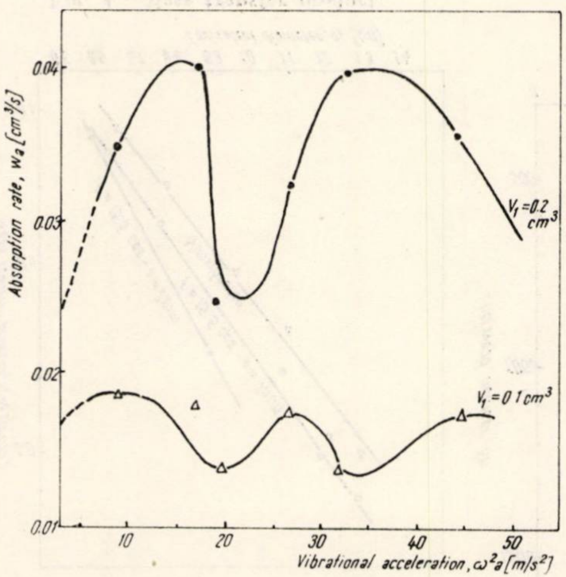

Fig. 6. – Absorption rate,

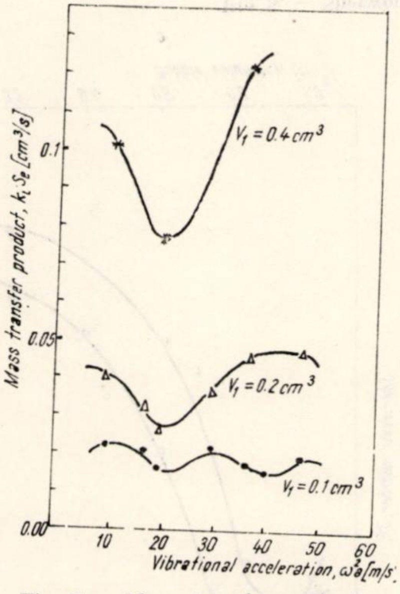

Fig. 7. – Mass transfer product.

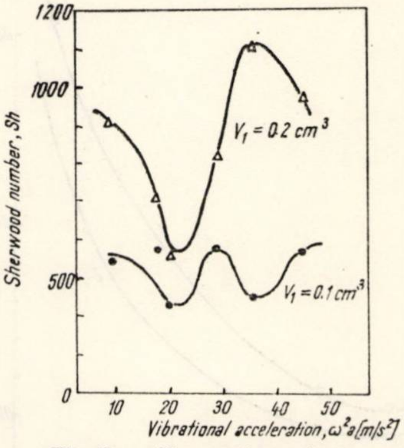

Fig. 8. – Sherwood number.

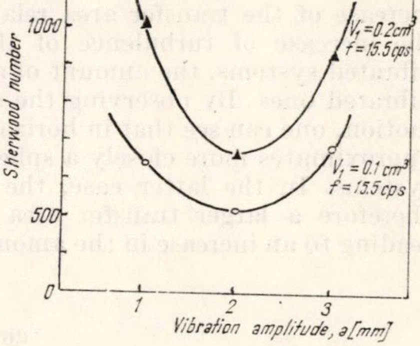

Fig. 9. — Sherwood number.

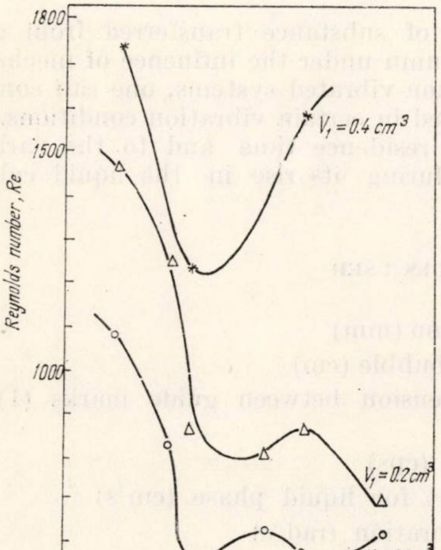

Fig. 10. — Reynolds number.

one can observe that time of rising of the bubble increases with increasing frequency and amplitude of the vibrations in the working conditions employed in the present paper. One must also take into account the effect of the periodical renewal of the liquid limiting layer adjacent to the bubble, which constitutes the major resistance to mass transfer. This renewal results in the increase of the mass transfer coefficient.

Since the measurements were carried out in conditions in which the bubble does not break, it results that the increase of the amount of transferred substance from the gas bubble to the liquid during the free rising of the gas bubble in the vibrated system can be ascribed also to the continuous change in the bubble shape. This change acts both on the increase of the transfer area relative to a non-vibrated bubble and on the increase of turbulence of the gas-liquid interface. In horizontally vibrated systems, the amount of absorbed gas is smaller than in vertically vibrated ones. By observing the shape of the bubble during its ascending motion, one can see that in horizontally vibrated systems the bubble shape approximates more closely a sphere than in the case of vertically vibrated systems. In the latter case, the bubble takes the shape of a spheroid, therefore a larger transfer area is available for the same gas volume, leading to an increase in the amount of transferred gas.

CONCLUSIONS

By comparing the amount of substance transferred from a gas bubble rising freely in a liquid column under the influence of mechanical vibrations with that obtained in non-vibrated systems, one can conclude that mass transfer can be intensified in certain vibration conditions. This is due both to the increasing of residence time and to the variation of the external bubble area during its rise in the liquid column.

SYMBOLS USED

a — Amplitude of the vibration (mm)
d_e — Equivalent diameter of bubble (cm)
t — Duration of bubble ascension between guide marks (1) and (2) (s)
f — Frequency of vibration (cps)
k_l — Mass transfer coefficient for liquid phase (cm/s)
ω — Angular velocity of vibration (rad/s)
S_e — Area of the bubble with diameter d_e (cm^2)
V_1, V_2 — Bubble volume at guide marks (1) and (2) (cm^3)
P_1, P_2 — Local hydrostatic pressure, (atm)
R — Universal gas constant, $82.06 \dfrac{\mathrm{atm \cdot cm^3}}{\mathrm{mole\ K}}$
T — Absolute temperature (K)
H_c — Slope of liquid concentration-partial pressure equilibrium curve $\left(\dfrac{\mathrm{mole}}{\mathrm{cm^3\ atm}}\right)$
V_a — Volume fraction of the absorbed gas, $\dfrac{V_1 - V_2}{V_1}$
w_a — Absorption rate, $\dfrac{V_1 - V_2}{t} \left[\dfrac{\mathrm{cm}^3}{\mathrm{s}}\right]$

CORRIGENDUM

Dans l'article: « Chaleurs de transfert en milieux ioniques. Applications aux solutions aqueuses de KCl et HCl à 25° et 35°C » (J. Chanu et M. E. Weill), paru dans le n° 9/1973 de notre revue, à la figure 2, p. 1517 on doit insérer la bibliographie suivante:

J. C. R. Turner, cf. réf. 4; P. N. Snowdon et J. C. R. Turner, *Trans Faraday Soc.*, **56**, 1812(1960); J. Chanu, *J. Chim. phys.*, **55**, 743(1958).

Revue Roumaine de Chimie, **18**, *10*, (1973)

NOTE POUR LES AUTEURS

La *Revue Roumaine de Chimie* publie des articles en anglais, français, russe, allemand ou espagnol. Les auteurs sont priés d'envoyer des articles, notes, communications et comptes rendus inédits.

Les manuscrits seront dactylographiés à deux intervalles. Les tableaux seront dactylographiés sur feuilles séparées, de même que la légende des figures. Les diagrammes seront tracés à l'encre de Chine sur papier calque. Les tableaux et les figures seront numérotés par des chiffres arabes, en nombre strictement nécessaire. Prière de ne pas inscrire les mêmes données dans les tableaux et les figures. Les formules chimiques seront incluses dans le texte ; en outre, elles seront transcrites sur des feuilles séparés. Les auteurs sont priés d'indiquer les caractères italiques (en soulignant les lettres au crayon), ainsi que tout autre caractère spécial. L'ordre des références bibliographiques sera celui de leur mention dans le texte ; le nom de l'auteur sera précédé de l'initiale du prénom ; les publications périodiques seront présentées suivant les prescriptions internationales. Les références seront ajoutées à la fin de l'article ; elles paraîtront comme des notes, au bas de la page. Le texte sera précédé d'un résumé comprenant 15 lignes au maximum.

L'entière responsabilité du contenu des articles appartient aux auteurs. On publie des articles dus aux collaborateurs roumains ou étrangers. Les auteurs recevront 50 tirés à part.

PRINTED IN ROMANIA

TRAVAUX PARUS AUX ÉDITIONS DE L'ACADÉMIE DE LA RÉPUBLIQUE SOCIALISTE DE ROUMANIE

MARIA FITI, **Dozimetria chimică a radiaţiilor ionizante** (La dosimétrie chimique des radiations ionisantes), 1973, 240 p., 13,50 lei.

MIHAI FLORESCU, **Eficienţa economică a cercetării ştiinţifice** (L'efficience économique de la recherche scientifique), 1972, 115 p., 15 lei.

GEORGETA LĂZĂRESCU, **Sistematizarea informaţiilor în chimia organică** (La systématisation des informations dans la chimie organique), 1972, 242 p., 10,50 lei.

P. BALTĂ et E. BALTĂ, **Introducere în chimia fizică a stării vitroase** (Introduction à la chimie physique de l'état vitreux), 1971, 240 p., 15,50 lei.

LYDIA-MARIA VAICUM, **Biodegrabilitatea detergenţilor** (La biodégrabilité des détergents), 1971, 254 p., 16 lei.

TIBERIU NĂŞCUŢIU, **Metode radiometrice de analiză** (Méthodes radiométriques d'analyse), 1971, 346 p., 19,50 lei.

I. ZUGRĂVESCU et L. STOICESCU-CRIVETZ, **Polimeri heterociclici** (Polymères hétérocycliques), 1971, 190 p., 9,50 lei.

I. MAXIM, **Materiale nucleare** (Matériaux nucléaires), 1969, 444 p., 30 lei.

CRISTOFOR SIMIONESCU et C. V. UGLEA, **Fracţionarea compuşilor macromoleculari** (Fractionnement des composés macromoléculaires), 1969, 292 p., 18,50 lei.

CRISTOFOR SIMIONESCU et CLEOPATRA VASILIU-OPREA, **Mecanochimia compuşilor macromoleculari** (La mécanochimie des composés macromoléculaires), 1967, 344 p., 23,50 lei.

CORNEL BODEA et collab., **Tratat de biochimie vegetală**, partea I, **Fitochimie** (Traité de biochimie végétale, Ire partie, Phytochimie), Ier vol., 1964, 747 p. + 4 annexes + 2 pl., 41 lei ; IIe vol., 1965, 1962 p., 1 pl., 56 lei ; IIIe vol., 1967, 773 p., 35 lei.

V. GHEŢIE et V. MICUŞAN, **Analiza imunochimică. Teorie şi practică** (Analyse immunochimique. Théorie et pratique), 1966, 369 p., 28 lei.

R. PORTOCALĂ et L. POPA, **Acizii ribonucleici celulari şi virali** (Les acides ribonucléiques cellulaires et viraux), 1966, 375 p., 8 pl., 26 lei.

1974 MAR 26

I.P.I. – c. 3247

43 426

Lei 25.—

F 1103

R

REFERÁLVA

REVUE
ROUMAINE
DE
CHIMIE

TOME 18
N° 11
Novembre 1973

RRCHAX, **18**, *11*, 1839–2002 (1973)

ÉDITIONS DE L'ACADÉMIE DE LA RÉPUBLIQUE SOCIALISTE DE ROUMANIE

Rev. Roumaine Chim. **18**, *11*, p. 1839–2002 (1973), Bucarest

COMITÉ DE RÉDACTION

Rédacteur en chef :

I. G. MURGULESCU, membre de l'Académie de la République Socialiste de Roumanie

Rédacteurs en chef adjoints :

A.T. BALABAN et V. EM. SAHINI, membres correspondants de l'Académie de la République Socialiste de Roumanie

Collège de rédaction :

C. DRĂGULESCU, RALUCA RIPAN, CR. SIMIONESCU, membres de l'Académie de la République Socialiste de Roumanie ; EM. BRATU, ECATERINA CIORĂNESCU-NENITZESCU, P. SPACU, membres correspondants de l'Académie de la République Socialiste de Roumanie ; MARGARETA AVRAM, D. I. MARCHIDAN, G. NIAC et D. SĂNDULESCU

La Revue Roumaine de Chimie paraît 12 fois par an. Toute commande de l'étranger (fascicules ou abonnements) sera adressée à Întreprinderea Rompresfilatelia, Boîte Postale 2001, telex 011631, Bucarest, Roumanie.

Les manuscrits, les livres et les revues proposés en échange, ainsi que toute correspondance seront envoyés à la rédaction

REVUE ROUMAINE DE CHIMIE

23, str. Dumbrava Roşie, Bucarest, Roumanie

ÉDITIONS DE L'ACADÉMIE DE LA RÉPUBLIQUE SOCIALISTE DE ROUMANIE

3 bis, str. Gutenberg, Bucarest

ORSZÁGOS MŰSZAKI KÖNYVTÁR ÉS DOKUMENTÁCIÓS KÖZPONT
183

REVUE ROUMAINE DE CHIMIE

Tome 18, Nº 11 Novembre 1973

R. H. SCHUSTER und I. A. SCHNEIDER, Mediumeinflüsse bei der Solvolyse von *t*-Butylchlorid. I. Lösungsmittel- und Salzeffekte bei der Solvolyse von *t*-Butylchlorid in wässerigen Methanol- und Dioxangemischen 1841–1852

N. PETRESCU, MARIA PETRESCU, MIRELA BRIŢCHI and LIANA PAVEL, Silicide coatings on molybdenum obtained by electrotransport and diffusion from molten fluorides . . . . 1853–1858 R

A. DRĂGĂNESCU, I. BICĂ, CRISTINA PETRESCU, ANA MARIA PAVLOVSCHI, S. ŞERBAN and N. MERJANOV, Kinetics of the homogeneous reaction between methane and sulphur . . . . 1859–1863 R

JAGDISH PRASHAD, Influence of irradiation on the threshold potential in air 1865–1866

S. SOLACOLU and A. BĂRBULESCU, Crystallochemical and dielectric survey of phases in the TiO_2-ZrO_2 system prepared by coprecipitation 1867–1873

D. NEGOIU, VASILICA MUREŞAN and S. FLOREA, Contributions to the chemistry of thiocomplexes. IV. Complex compounds of Pd(II) with thioamides of the dibenzofuran series 1875–1881

GR. POPA and Ş. MOLDOVEANU, A perturbational procedure applied to the calculation of the energetic levels in the complexes obtained by organic reagents 1883–1895

J. ZSAKÓ, CS. VÁRHELYI and F. MÁNOK, Kinetics and mechanism of substitution reactions of complexes. LII. Basic hydrolysis of *trans*-di-isothiocyanato-bis-ethylene-diamine-chromium (III) ions 1897–1902

H. C. GAUR and N. P. BANSAL, Computer evaluation of the association constants of silver-chloro and-bromo complexes in molten sodium nitrate-barium nitrate eutectic 1903–1909

N. VOICULESCU and I. POPESCU, Reactions of coordinated ligands. V. Aluminium-organic compounds of coordinated salicylaldoxime. . . . . 1911–1917 R

N. VOICULESCU, Reactions of coordinated ligands. VI. Reaction of aluminium-organic derivates with oximes. . . . . 1919–1927 R

ROYSTON M. ROBERTS and ALI ALI KHALAF Modern Friedel-Crafts Chemistry. III. the isomerization of 1,1- and 1,2-diphenylbutane under the influence of aluminium chloride catalyst in benzene solvent. . . . 1929–1936 R

Revue Roumaine Chim. **18**, *11*, 1841–2002(1973), Bucarest

ROYSTON M. ROBERTS and ALI ALI KHALAF, Modern Friedel-Crafts chemistry. IV. The fragmentation and dealkylation behaviour of 1,1-diphenyl-2-methylpropane and 1,2-diphenyl-2-methylpropane under the influence of water-activated aluminium chloride at 100° 1937–1948

I. DRIMUŞ et I. T. IONESCU, Relations entre la longueur de la chaîne des *n*-alcanes et la composition des *n*-acides monocarboxyliques obtenus par leur oxydation 1949–1958

NICOLAE FILIPESCU, JAMES W. PAVLIK, P. T. FRANGOPOL and MARIA FRANGOPOL, Spectroscopic properties of trapped anthronylidene. . . 1959–1962

DIANA GIURGIU et I. POPESCU, La réactivité des composés aluminium-organiques envers des bases Lewis. Dérivés des triphénylaluminiums avec des composés 1,3-dicarbonyliques 1963–1969

GHEORGHE FACSKO und MARIA NEMEŞ, Die polarographische Bestimmung des mit dem Natriumsalz der 4-Sulfonamidobenzolsäure komplexgebundenen Quecksilbers (II), in stark alkalischem Medium. 1971–1982

I. C. POPESCU, C. LITEANU and L. SAVICI, Studies on the electroanalytical behaviour of membrane-electrodes under current. IV. The *E*-*p*Ag electrode function and the use of the ceramic membrane-electrode of Ag_2S, Ag^+-selective in potentiometric titrations by precipitating at constant direct current 1983–1992

I. FLOREA, Spektrophotometrische Dosierung Der $Cr_2O_7^{2-}$ - und CrO_4^{2-}-Ionen mit *o*-Tolidin 1993–1999

COMPTE RENDU 2001

Revue Roumaine de Chimie, 18, 11, 1841–1852 (1973)

MEDIUMEINFLÜSSE BEI DER SOLVOLYSE VON *t*-BUTYLCHLORID. I

LÖSUNGSMITTEL-UND SALZEFFEKTE BEI DER SOLVOLYSE VON *t*-BUTYLCHLORID IN WÄSSERIGEN METHANOL-UND DIOXANGEMISCHEN

R. H. SCHUSTER

Zentrum für Physikalische Chemie, Str. Galaţi 31, Bukarest.

I. A. SCHNEIDER

Lehrstuhl für Physikalische Chemie, Universität „Al. I. Cuza", Iassy

Eingegangen : am 23. März, 1973

In der vorliegenden Arbeit wurde mit Hilfe einer modifizierten Untersuchungsmethode die Solvolyse von *t*-Butylchlorid in wässerigen Methanol- und Dioxangemischen untersucht. Die kinetischen Meßergebnisse können nicht gut zu der Dielektrizitätskonstanten des Mediums in Verbindung gebracht werden. Die sich in den Aktivierungsparametern wiederspiegelnden Lösungsmitteleffekte sind mit Zuhilfenahme einiger Literaturdaten über die Lösungsmittelstruktur erklärt worden. Es wurde weiterhin gezeigt, daß die Solvolyse auch in mit KCl gesättigter Lösung abläuft, was dem von Winstein vorgeschlagenen Solvolyseschema entspricht. Aus den gemessenen Werten der Reaktionsgeschwindigkeitskonstanten bei Gleichionsalzeffekt konnte der Molbruch des durch freie Ionen zum Produkt reagierenden Reaktanten abgeschätzt werden.

In protischen, stark polaren Medien wird der Solvolyse von tertiären Alkylhalogeniden ein SN_1 – Mechanismus zugesprochen[1-3], was auch auf *t*-Butylchlorid (*t*-BuCl) zutrifft, wodurch sich die Wahl von Grunwald und Winstein, *t*-BuCl als Bezugsubstanz für ihre bekannte empirische Freie – Energie Beziehung[4] zu verwenden, erklären läßt. Es ergab sich dabei, daß die Reaktionsgeschwindigkeitskonstante, im folgenden als RGK angegeben, der Solvolyse des *t*-BuCl in verschiedenen protischen und aprotischen Gemischen mit steigendem Wassergehalt anwächst und daß die Aktivierungsparameter zu der Lösungsmittelzu-

---

[1] E. D. Hughes und G. K. Mac Nulty, *J. Chem. Soc.*, **1937**, 1283.

[2] O. T. Benfey, E. D. Hughes und C. K. Ingold, *J. Chem. Soc.*, **1952**, 2494.

[3] L. C. Bateman, K. A. Cooper, E. D. Hughes und C. K. Ingold, *J. Chem. Soc.*, **1940**, 925.

[4] E. Grunwald und S. Winstein, *J. Amer. Chem. Soc.*, **70**, 846 (1948).

sammensetzung in einem Verhältnis stehen, welches nicht gut durch Kontinuumsvorstellungen des Mediums erklärt werden kann[5,6].

Daher war es zweckmäßig als einleitende Phase der Untersuchung der Substitutionsreaktion :

$$t\text{-BuCl} + N_3^- \longrightarrow t\text{-BuN}_3 + Cl^- \qquad \text{(I)}$$

erst die Solvolyse des *t*-BuCl und die begleitenden Lösungsmitteleffekte, sowie auch den Gleichion-Salzeffekt zu untersuchen um einen Einblick in den Solvolysemechanismus zu erhalten.

EXPERIMENTELLER TEIL

Die Reaktion ist in einer auf ±0,1° thermostatierten, mit Lösungsmittel möglichst aufgefüllten Zelle durchgeführt worden, in die durch einen Injektionsstutzen eine eingewogene Menge *t*-BuCl mittels einer 0,1 ml Hamiltonspritze eingeführt wurde. Mit Hilfe von Glasspritzen die bis zu einer vorgeeichten Marke mit kaltem Aceton (−10°) angefüllt waren, wurde die Probe durch schnelles Ansaugen bis auf's volle Volumen entnommen, wobei in der Zelle jeweils ein Stickstoffüberdruck (1,5 at) gewährleistet wurde. Dieses ermöglichte sowohl ein schnelles Stoppen der Reaktion, als auch eine genaue Volumenbestimmung der Probe. Die gebildete Salzsäuere wurde mit 0,05 n methanolischem NaOH in Gegenwart von Bromphenolblau titriert.

VERSUCHSERGEBNISSE UND DISKUSSION

Die kinetischen Meßergebnisse der Solvolyse von *t*-BuCl in Methanol – Wasser und Dioxan – Wasser Gemischen mit 30,2 – 80,7 Vol. % bei 25°, 35°, 45° sind in Tabelle 1 angegeben.
Wie ersichtlich stimmen unsere Ergebnisse ziemlich gut (einige Abweichungen ausgenommen) mit den Literaturangaben überein.

Erwartungsgemäß ergab sich eine bedeutende Erhöhung der RGK bei steigenden Wasserkonzentrationen der Lösung. Bezeichnend ist, daß die RGK in Methanol – Wasser Gemischen größer als bei Dioxan – Wasser Gemischen ist, was sowohl einem Einfluß der höheren Dielektrizitätskonstanten in Methanol – Wasser Gemischen, als auch einer Beteiligung des Methanols durch spezifische Solvatation beim geschwindigkeitsbestimmenden Schritt der Solvolyse von *t*-BuCl zugeschrieben werden kann.

---

[5] A. H. Fainberg und S. Winstein, *J. Amer. Chem. Soc.*, **78**, 2770 (1956).
[6] S. Winstein und A. H. Fainberg, *J. Amer. Chem. Soc.*, **79**, 5937 (1957).

Zur Erklärung der Meßergebnisse mußte vorerst entschieden werden, ob die Vorstellungen eines kontinuierlichen[7-9] oder die eines diskontinuierlichen Mediums[10-13] für die Solvolysereaktion heranzuziehen ist.

Während im ersten Falle die reaktionskinetischen Größen in eine quantitative Beziehung zu einer makroskopischen Größe des Lösungsmittels (z. B. Dielektrizitätskonstante, Beugungsindex oder Viskosität) gebracht werden, wird im zweiten Fall eine qualitative Beziehung zwischen thermodynamischen Größen des Lösungsmittels (und somit unmittelbar der Lösungsmittelstruktur) und einem thermodynamischen Aktivierungsparameter angestrebt.

a). EINFLUSS DER DIELEKTRIZITÄTSKONSTANTEN DES MEDIUMS

Mit Hilfe der kinetischen Werte haben wir zuerst die Gültigkeit der linearen Beziehung von Laidler und Eyring[14] für Dipol—Dipol Reaktionen, die aufgrund einer elektrostatischen Kontinuumstheorie des Mediums von Kirkwood[7] abgeleitet worden ist, untersucht :

$$\begin{aligned}\ln k_1 = & \ln (\varkappa k \mathrm{T} \mathrm{K}_0^{\neq}/\mathrm{h}) - 1/\mathrm{kT}\,(\mathrm{D}-1)/(2\mathrm{D}+1)\,[\mu_{\mathrm{A}}^2/r_{\mathrm{A}}^3 + \mu_{\mathrm{B}}^2/r_{\mathrm{B}}^3 + \mu_{\mathrm{X}^{\neq}}^2/r_{\mathrm{X}^{\neq}}^3] \\ & + (\Phi_A + \Phi_B - \Phi_{X^{\neq}})/\mathrm{kT}\end{aligned} \qquad \text{(II)}$$

Den Größen der Gleichung (II) kommt folgende Bedeutung zu : k_1 = RGK ; μ = Moleküldipolmoment ; r = Molekülradius ; Φ = Nichtelektrostatischer Faktor; D = Dielektrizitätskonstante; k = Boltzmannkonstante ; T = absolute Temperatur ; $\varkappa$ = Transmissionskoeffizient; A, B = Indices für an der Reaktion beteiligte Moleküle ; $X^{\neq}$=Index für den Übergansgzustand ; $K_0^{\neq}$ = Gleichgewichtskonstante des Übergangszustandes.

Wie aus Abb. 1 und 2 hervorgeht ist in beiden Fällen die Beziehung log k_1 — Proportionalitätsfaktor der Laidler—Eyring Gleichung (D—1)/ /(2D+1) nicht linear, wobei vor allem bei tieferen Temperaturen deutlich Inflexionspunkte zu beobachten sind.

Aufgrund dieser Ergebnisse kann aber nicht entschieden werden, wem diese Abweichungen von der Linearität zuzuschreiben sind, da z.B. ein Vorzeichenwechsel des nichtelektrostatischen Gliedes in Gleichung (II) bei ungefähr 0,8 Molbruch Wasser als Erklärung dafür dienen könnte.

Ähnlich verhalten sich nach Fainberg und Winstein[5] auch die Systeme Ethanol — Wasser und Aceton — Wasser.

---

[7] J. G. Kirkwood, *J. Chem. Phys.*, **2**, 351 (1934).
[8] E. S. Amis und G. Jaffé, *J. Chem. Phys.*, **10**, 598 (1942).
[9] J. G. Kirkwood und F. N. Westheimer, *J. Chem. Phys.*, **6**, 506 (1938).
[10] J. Lennard — Jones und J. A. Pople, *Proc. Roy. Soc.*, **A 205**, 155 (1951).
[11] G. Haggis, J. B. Hasted und T. I. Buchanan, *J. Chem. Phys.*, **20**, 1452 (1940).
[12] H. S. Frank und W—Y. Wen, *Discuss, Faraday Soc.*, **24**, 133 (1957).
[13] G. Nemethy und H. A. Scheraga, *J. Phys. Chem.*, **36**, 3382 (1962).
[14] H. Eyring und K. J. Laidler, *Ann. New York Akad. Sci.*, **39**, 303 (1940).

Eine für Ion — Dipol Reaktionen charakteristische Korrelation[14] von log k_1 mit dem reziproken Wert der Dielektrizitätskonstanten, scheint vor allem bei höheren Dielektrizitätskonstanten etwas besser als die vorhergehende.

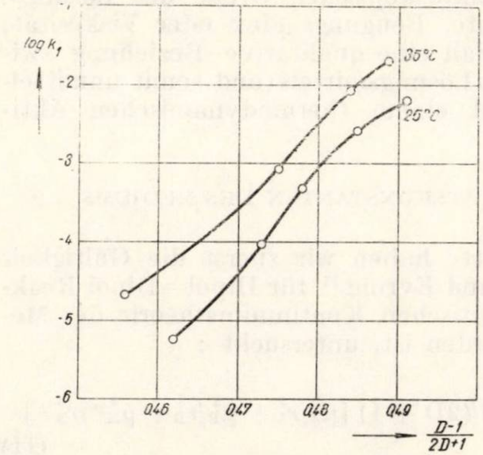

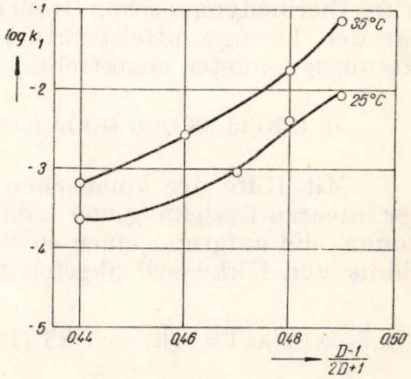

Abb. 1. — Korrelation von log k_1 mit dem Ausdruck (D—1)/(2D+1) im System Dioxan — Wasser bei 25° und 35°.

Abb. 2. — Korrelation von log k_1 mit dem Ausdruck (D—1)/(2D+1) im System Methanol—Wasser bei 25° und 35°.

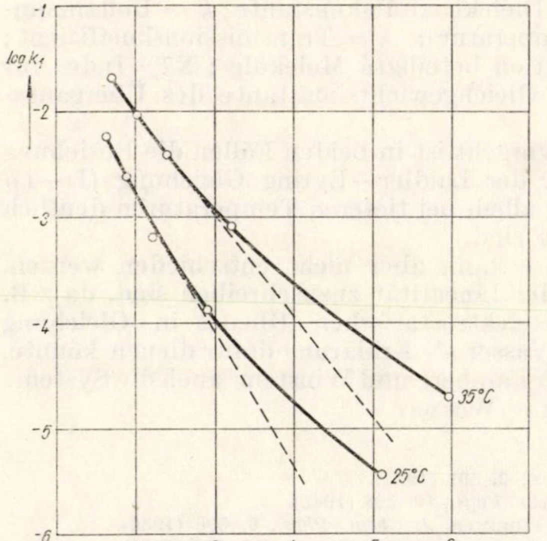

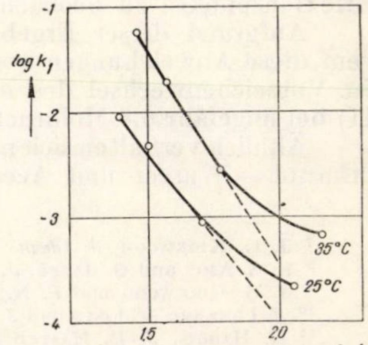

Abb. 3. — Korrelation von log k_1 mit dem reziproken Wert der Dielektrizitätskonstanten im System Dioxan — Wasser bei 25° und 35°.

Abb. 4. — Korrelation von log k_1 mit dem reziproken Wert der Dielektrizitätskonstanten im System Methanol— Wasser bei 25° und 35°.

Da bei einer Teilung von (D−1) durch (2D+1) für $D \geqslant 8$ der Ausdruck (D−1)/(2D+1) in 1/D linear wird, erscheint die Korrelation von log k_1 gegen 1/D in dem Bereich hoher Dielektrizitätskonstanten (Abb. 3 und 4) als ein Sonderfall von Gleichung (II) so daß ein eventueller Schluß, wonach der geschwindigkeitsbestimmende Schritt die produktbildende Phase der Reaktion (Ion-Dipol Reaktion) wäre, nicht statthaft ist.

Als ein weiterer Test für die Gültigkeit von elektrostatischen Theorien kann auch die Amis-Gleichung angewandt werden[15],

$$\ln k_{1,\mathrm{D}} = \ln k_{1,\infty} - 2\mu_A\mu_B/\mathrm{kTDr}^3 \qquad \text{(III)}$$

worin $r = r_A + r_B$ ist und den übrigen Größen dieselbe Bedeutung wie in Gleichung (II) zukommt.

Aus der Neigung der in Abb. 3 dargestellten Geraden kann somit der Wert für r abgeschätzt werden, wobei für Wasser das Dipolmoment, 1,84 D.E. und für *t*-BuCl 2,10 D.E. verwendet wurde. Der erhaltene Wert von näherungsweise 0,9Å ist aber viel zu klein, um für so ein großes Molekül wie *t*-BuCl auch nur in grober Annäherung zu stimmen, so daß die makroskopische Dielektrizitätskonstante in hoch wässerigen Lösungsmittelgemischen nicht zur Erklärung des Reaktionsgeschehens herangezogen werden kann.

b) AKTIVIERUNGSPARAMETER

Aus den kinetischen Daten wurden die Aktivierungsparameter für 25° berechnet. Werden diese Größen gegen den Molbruch des Wassers aufgetragen (Abb. 5 und 6) so ergibt sich in beiden untersuchten Systemen ein deutliches Minimum für die Aktivierungsenthalpie.

Dabei ist im Dioxan —Wasser System das Minimum gegen höhere Wassermolbrüche verschoben und auch etwas ausgeprägter als im Methanol — Wasser System. Da das Minimum in beiden Gemischen von Wasser, sowohl in Gegenwart eines protisch dipolaren, als auch eines aprotisch unpolaren Partners auftritt, dürften Veränderungen in der Lösungsmittelstruktur dafür verantwortlich sein. Ein Zusammenhang zwischen Lösungsmittelstruktur und partiell molaren Solvatationsenthalpien des Reaktanten und des Übergangszustandes scheint somit hier des Erklärung der beobachteten Enthalpieminima förderlich.

Es ist interessant zu erwähnen, daß Emons und Mitarbeiter bei Viskositätsmessungen im Methanol — Wasser System[16] und in gesättigten und ungesättigten NaCl und KCl Lösungen desselben Systems[17], sowie bei Kompressibilitätsmessungen in Alkalihalogenid — Methanol— Wasser Systemen[18], bei Ionen — und Lösungsmittelüberführung bei der

---

[15] E. S. Amis, *J. Chem. Educ.*, **30**, 351 (1953).

[16] H.-H. Emons, D. Dümke und M. Förtsch, *Wissenschaftl. Zeitschr. Chemie Leuna—Merseburg*, **8**, 195 (1966).

[17] F. Winkler und H.-H. Emons, *Z. Chem.*, **9**, 73 (1969).

[18] H.-H. Emons und B. Ponsold, *Z. Chem.*, **10**, 471 (1970).

Elektrolyse in Alkalimetallchlorid – Methanol – Wasser Systemen etc., im selben Bereich wie wir Extremwerte für die gemessenen Größen beobachtete.

Durch die Ausdehnung des von Frank und Wen [12] vorgeschlagenen Clustermodells für die Wasserstruktur auf binäre wässerige Gemische,

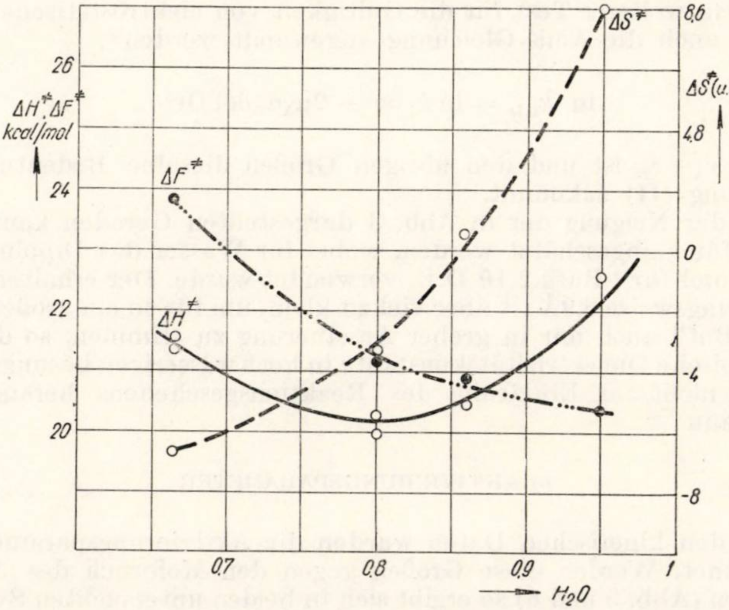

Abb. 5.—Verlauf der thermodynamischen Aktivierungsparameter $\Delta F^{\neq}$(— . . —), $\Delta H^{\neq}$ (———), $\Delta S^{\neq}$ (— — —) im System Dioxan – Wasser.

konnten Nemethy und Scheraga[13] zeigen daß durch eine Zugabe von 0,1 — 0,2 Molenbrüche eines di-oder unpolaren Nichtelektrolyten zu reinem Wasser die Wasserstruktur zunächst in einen stabileren und geordnetern Zustand gedrängt wird, der dann bei weiterem Hinzufügen des Nichtelektrolyten wieder zerstört wird. Somit durchläuft die partielle molare Solvatationsenthalpie eines dipolaren Stoffes, der in binären wässerigen Gemischen gelöst wird, ein endothermes Maximum während der Wassermolenbruch kleiner wird. Arnett und Mitarbeiter[20] konnten durch mikrokalorimetrische Messungen zeigen, daß auch die partiell molare Solvatationsenthalpie des *t*-BuCl in wässerigen Gemischen ein endothermes Maximum aufweist, wobei die Lage des Maximums mit der von uns bestimmten Lage der Aktivierungsenthalpie übereinstimmt. Es ist auch bezeichnend, daß der Wert des Minimums von cca 2 kcal/Mol, wie aus Abb. 5 und 6 hervorgeht, dem des von Arnett mitgeteilten annähernd gleichkommt.

---

[19] V. Viehweger und H.-H. Emons, *Z. anorg. Chem.*, **383**, 183 (1971).

[20] E. Mcc Arnett, P. Mcc Duggleby und J. J. Burke, *J. Amer. Chem. Soc.*, **85**, 1350 (1963).

Das Verhalten der Aktivierungsenthalpie im Gebiet des Minimums kann durch eine von der kompakteren Mischstruktur des Lösungsmittels her bewirkten schwächeren Solvatation der Reaktantenmoleküle erklärt werden, während der Übergangszustand infolge seiner elektropositiven Natur von der Solvatation wenig beeinflußt wird.

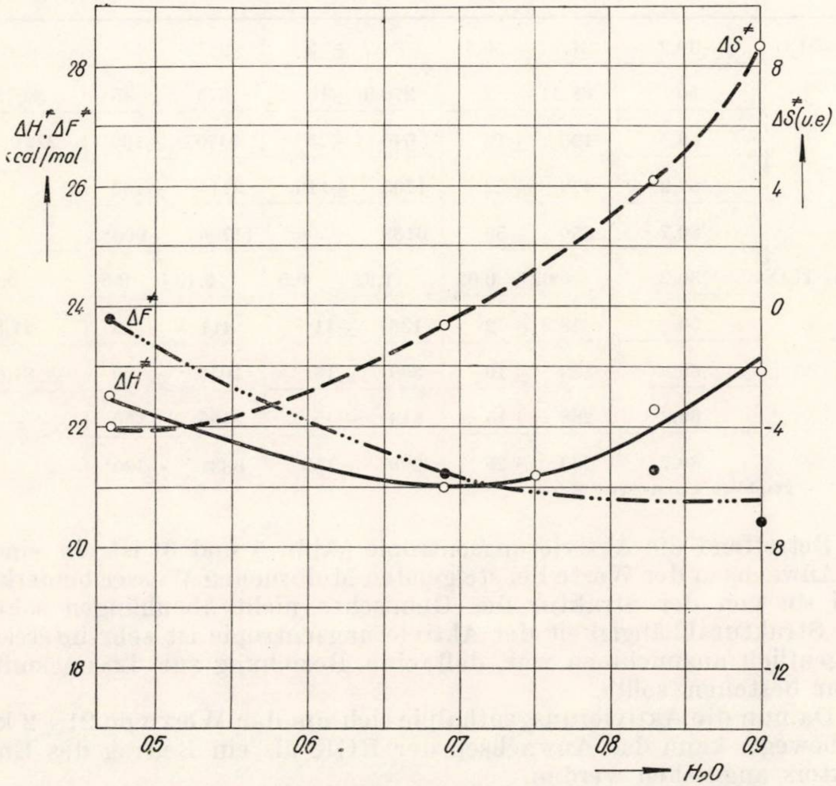

Abb. 6. — Verlauf der thermodynamischen Aktivierungsparameter $\Delta F^{\neq}$ (— . . . —), $\Delta H^{\neq}$ (———,) $\Delta S^{\neq}$(— — —) im System Methanol—Wasser.

Es ist erwähnenswert, daß der Inflexionspunkt der in Abb. 1 und 2 dargestellten Korrelationen auch in demselben kritischen Bereich liegt. Somit könnte der nichtelektrostatische Faktor wesentlich von der Art der für die Solvatation disponiblen Wechselwirkungen bestimmt sein und ein Vorzeichenwechsel im Ausdruck $\Phi_A + \Phi_B - \Phi_{X^{\neq}}$) kT beim Durchgang des Gebiets um 0,8 Molbruch Wasser erscheint nicht unwahrscheinlich.

Wie Costeanu und Mittarbeiter[21–24] feststellten, zeigt die Aktivierungsenthalpie bei der Esterhydrolyse in wässerigen Gemischen ein ähnliches Verhalten.

---

[21] G. Costeanu und O. Landauer, *Rev. Roumaine Chim.*, **17**, 1331 (1972).
[22] G. Costeanu und O. Landauer, *Rev. Roumaine Chim.*, **17**, 1339 (1972).
[23] G. Costeanu und O. Landauer, *Rev. Roumaine Chim.*, **17**, 1347 (1972).
[24] G. Costeanu und C. Mateescu, *Rev. Roumaine Chim.*, **17**, 1353 (1972).

Tabelle 1

Reaktionsgeschwindigkeitskonstanten (k_1) der Solvolyse von *t*-BuCl

Lösungsmittel	Wassergehalt Vol. %	$10^5 \times k_1 (sec^{-1})$			
		298 K	308 K	318 K	Literaturangaben 298 K
$MeOH-H_2O$	30,2	21,7 ± 0,5	67,7 ± 2	217 ±14	8,35[5]
	50	88,2 ± 2	270,0 ±16	875 ± 45	86,7[5]
	60	196 ±12	646 ±25	1470 ±100	228[5]
	69,2	479 ±22	1705 ±110	3114 ±150	–
	80,7	850 ±55	6189 ±500*	11700 ±900*	–
$Dioxan-H_2O$	30,2	0,62 ± 0,02	1,92 ± 0,5	6,46 ± 0,5	0,955[5]
	50	48,2 ± 2	138 ±11	411 ± 18	21,8[5]
	60	129 ±10	399 ±18	1050 ± 60	81,6[5]
	69,2	258 ±15	813 ±45	2406 ±150	–
	80,7	563 ±26	2298 ±150	6331 ±500*	–

* = graphisch extrapolierte Werte.

Betreffend die Aktivierungsentropie (Abb. 5 und 6) ist ein eindeutiges Anwachsen der Werte bei steigenden Molbrüchen Wasser bemerkbar, wobei sie von der Struktur des Gemisches nicht abzuhängen scheint. Diese Strukturabhängigkeit der Aktivierungsentropie ist sehr interessant da eigentlich anzunehmen war, daß eine Beziehung zur Lösungsmitteltruktur bestehen sollte.

Da nun die Aktivierunsgenthalpie sich um den Wert von 21±2 kcal/ /Mol bewegt, kann das Anwachsen der RGK als ein Beitrag des Entropiefaktors angesehen werden.

c) GLEICHION – SALZEFFEKT

Der anschließend untersuchte Gleichion-Salzeffekt steht nicht in einem direkten Verhältnis zu dem Lösungsmitteleffekt, doch wird er von uns kurz besprochen, da er uns einige zusätzliche Schlüsse über den Solvolysemechanisms ermöglichte.

Der von Ingold und Hughes [25] vorgeschlagene Reaktionsmechanismus, wobei die Ionisation geschwindigkeitsbestimmed ist,

$$RX \underset{k_{-1}}{\overset{k_1}{\rightleftharpoons}} R^+ + X^-$$

A

$$R^+ + SOH \xrightarrow{k_S} ROS + H^+$$

---

[25] E. D. Hughes, C. K. Ingold und C. S. Patel, *J. Chem. Soc.*, **1933**, 526.

ergibt für die totale RGK (k_t) den bekannten Ausdruck :

$$k_t = k_1 /(1 + k_{-1} [X^-]/k_s) \qquad \text{(IV)}$$

so daß ein Anwaschsen der Gleichionkonzentration $[X^-]$eine Verminderung der RGK bewirken muß, was nach Ingold und Hughes [26] auch als Test für den SN_1-Mechanismus gilt. Dieser Gleichion-Salzeffekt (Common ion effect) müßte bei sehr hohen Salzkonzentrationen ein Absinken der RGK auf Null bewirken falls Reaktionsschema A gültig ist,

$$\lim_{[X^-]\to\infty} k_t = 0 \qquad \text{(V)}$$

Das heißt, daß in gesättigter Lösung von $Me^+ X^-$ bei kleinen Anfangskonzentrationen von RX die Reaktion nicht ablaufen dürfte.

Winstein und Mitarbeiter [27] schlugen einem komplizierteren mehrstufigen Solvolysemechanismus vor, bei welchen die Zwischenionpaare an der Produktbildung beteiligt sind.

$$\begin{tikzcd}
RX \arrow[r, shift left, "k_1"] & R^+X^- \arrow[l, shift left, "k_{-1}"] \arrow[r, shift left, "k_2"] & R^+//X^- \arrow[l, shift left, "k_{-2}"] \arrow[r, shift left, "k_3"] \arrow[d, "SOH"', "k_s^I"] & R^+ + X^- \arrow[l, shift left, "k_{-3}"] \arrow[d, "SOH"', "k_s^{II}"] & B \\
 & & ROS & ROS &
\end{tikzcd}$$

Bei quasistationärem Reaktionszustand erhält man diesmal für die RGK den Ausdruck :

$$k_t = k_1 \{1 + (k_{-1}/k_2)\ [k_{-2} + k_s^I + k_3k_s^{II}/(k_{-3}[X^-] + k_s^{II})]/[k_s^I + \\ + k_3k_s^{II}/(k_{-3}\ [X^-] + k_s^{II})]\}^{-1} \qquad \text{(VI)}$$

so daß für sehr hohe Gleichion-Salzkonzentrationen der Ausdruck (VI) einem endlichen, von Null verschiedenen Wert zusstrebt :

$$\lim_{[X^-]\to\infty} k_t = k_1/[1 + k_{-1}\ (k_{-2} + k_s^I)/k_2\ k_s^I] = k_1^1. \qquad \text{(VII)}$$

Daher muß die Reaktion auch in mit Gleichion gesättigter Lösung stattfinden.

Es ist somit ersichtlich, daß der Gleichionsalzeffekt sowohl als Test für einen monomolekularen Solvolysemechanismus, als auch als

---

[26] L. C. Bateman, E. D. Hughes und C. K. Ingold, *J. Chem. Soc.*, **1940**, 1017.

[27] S. Winstein, E. Clippinger, A. H. Fainberg, R. Heck und G. C. Robinson, *J. Amer Chem. Soc.*, **78**, 328 (1956).

Auswahlkriterium für einen der beiden Mechanismen (A und B) verwendet werden kann.

Da wir in der Literatur nur einige vereinzelte Angaben über den Gleichion-Salzeffekt bei der Solvolyse des *t*-BuCl angetroffen haben, führten wir systematische Studien zwischen 25° und 44° und bei KCl Konzentrationen zwischen 0 und 1,85 M in Methanol — Wasser und 0 — 1,33 M in Dioxan — Wasser Systemen aus. Wie aus Tabelle 2 hervorgeht, spricht das *t*-BuCl auf den Gleichion-Salzeffekt durch eine Verminderung der RGK um 1,4 bis 4 Mal, positiv an.

Tabelle 2

Einfluß des Elektrolyten mit gleichem Anion auf die Geshwindigkeitskonstante bei der Solvolyse des *t*-BuCl

Lösungsmittel	Wassergehalt Vol. %	Temp. °C	$10^5 \times k_1$ (sec^{-1}) für KC1 (M).				
			0	0,33	0,66	1,33	1,85
$MeOH-H_2O$	50	25	88,7	77,5	64,5	45,3	—
		34	270	256	219	198	—
		44	760	578	460	266	—
	69,2	25	479	243	212	184	—
		34	1469	870	638	510	498
		44	5320	2378	1850	1258	1148
	80,7	25	850	795	—	510	276
		33	2336	1529	—	578	484
		40	5968	2942	—	1278	923
$Dioxan-H_2O$	50		0	0,3	0,5	0,8	1,0
		25	48	45,5	40,0	36,2	—
		35	138	128	98	89	—
		40	238	210	196	169	—
	80,7	25	563	520	444	322	305
		30	1384	1230	950	652	598
		35	2298	2025	1249	953	907

Dieser Effekt ist nicht sehr groß, wenn bedacht wird, daß bei der Solvolyse von z.B. *treo*-3Anysyl-2Butyl-Brombenzolsulfonat[28] eine RGK-Verminderung von 12,7 Mal in Essigsäuereanhydrid beobachtet worden ist.

---

[28] S. Winstein, R. Baker und S. Smith, *J. Amer. Chem. Soc.*, **86**, 2072 (1964).

Aus dem Verlauf der RGK bei KCl Zugabe (wofür ein typisches Beispiel in Abb. 7 für die von uns untersuchten Systeme bei 80,7 Vol. % Wasser und 33° wiedergegeben ist) ergibt sich, daß in beiden Fällen die RGK gegen einen endlichen, von Null verschiedenen Grenzwert (k_1^1) abfällt, der in gesättigter KCl Lösung gemessen wurde, so daß unserer Meinung nach, der Solvolyse ein Mechanismus nach Schema B zugeschrieben werden kann.

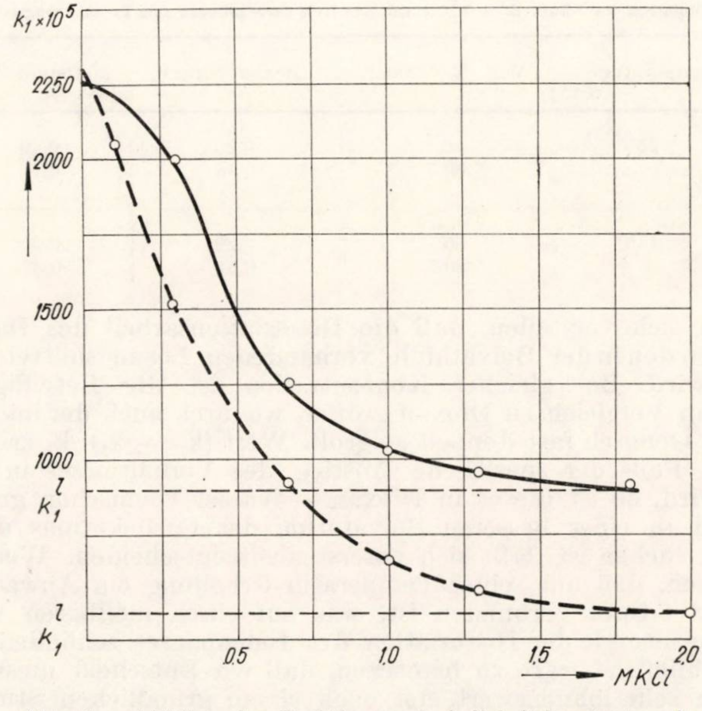

Abb. 7. — Abfallen der Reaktionsgeschwindigkeitskonstante mit dem Zusatz von Gleichionelektrolyten im Dioxan—Wasser System (———) und Methanol—Wasser System (— — —) bei 80,7 Vol. % Wasser und 33°.

Kaliumchlorid könnte außer dem Gleichion-Salzeffekt auch einen positiven Salzeffekt haben (ein solcher wurde von uns für *t*-BuCl mit KNO_3 festgestellt), so daß die von uns gemessene Größe k_1^1 noch um den Betrag des positiven Salzeffektes zu verkleinern ist, um die reelle RGK-Verminderung zu erhalten. Es wäre außerdem zu entscheiden ob der positive Salzeffekt nicht auf einer Erhöhung der Konstanten k_1, k_2 und k_3 beruhen könnte.

Da es unwahrscheinlich scheint daß ein *t*-BuCl Ionenpaar im Sinne des Schemas B in gesättigter KCl Lösung in freie Ionen dissoziert, kann k_1^1 als RGK der Solvolyse bei der durch das Ionenpaar $R^+//X^-$ das Produkt gebildet wird, angesehen werden. Das Verhältnis $(k_1 - k_1^1)/k_1$ bedeutet deshalb den Molbruch des *t*-BuCl, das über freie Ionen zum Produkt reagiert.

Einige Richtwerte sind in der untenstehenden Tabelle angegeben. Da das Vorhandensein von Methanol in der Solvathülle einiger Ionen wie z. B. Mg^{2+} in Methanol – Wasser Gemischen bewiesen worden ist [29], kann man sich vorstellen, daß die Dissoziationsarbeit des Ionenpaares $R^+//X^-$ von den in der Solvathülle vorhandenen Lösungsmittelmolekülen geleistet wird. Bei gleicher Konzentration ist die Beteilligung von Methanol in Vergleich zu Dioxan größer, wodurch auch der im Methanol – Wasser Gemisch fast doppelt so große Wert $(k_1 - k_1)/k_1$ erklärt werden kann. Falls der spezifische Anstieg des Verhältnisses in Betracht gezogen wird, so ist dieses in Dioxan – Wasser Gemischen größer. Ob der Grund in einer besseren Solvatation des Carbokations durch das Dioxan zu suchen ist, läßt sich vorerst nicht entscheiden. Weiterhin ist zu bemerken, daß mit einer Temperatur-Erhöhung ein Anwachsen des Molbruches t-BuCl verbunden ist, was auf einen meßbaren Wert der Aktivierungsenergie der Dissoziation des Ionenpaares schließen läßt.

Tabelle 3

Molbruch des *t*-BuCl $(k_1 - k_1^1)/k_1$, der über freie Carbokationen zum Produkt reagiert

Temperatur	Vol. % Wasser	Dioxan-Wasser	Methanol-Wasser
25°C	50	0,25	0,49
	80,7	0,48	0,71
44°C	50	0,29	0,65
	80,7	0,61	0,88

Abschließend wäre zu bemerken, daß ein Entscheid diesbezüglich, wenn auch sehr lohnenswert, erst nach einem gründlichen Studium der Erscheinungen möglich sein wird.

---

[29] F. WINKLER und H.-H. EMONS, *Kristall und Technik*, *4*, *511* (1969).

Revue Roumaine de Chimie, **18**, *11*, 1853–1858 (1973)

SILICIDE COATINGS ON MOLYBDENUM OBTAINED BY ELECTROTRANSPORT AND DIFFUSION FROM MOLTEN FLUORIDES

N. PETRESCU, MARIA PETRESCU, MIRELA BRIŢCHI and LIANA PAVEL

Centre of Physical Chemistry,
Str. Galaţi nr. 31, Bucharest, Romania

Received May 5, 1973

Experimental researches were performed for obtaining high temperature oxidation resisting silicide coatings on molybdenum. The treatment was carried in molten fluorides electrolytical baths wherefrom silicon was cathodically deposited on molybdenum in conditions which favoured its diffusion in the base metal. Optical microscopical informations were obtained about the diffused layer thickness as function of the current density, and about the structure of the layer. The nature of the coating layer was established by X-ray diffraction analysis and by microprobe analysis (X-ray images, quantitative analysis by direct emission X-ray spectroscopy). The obtained coating layers were compact and uniform, perfectly coherent with the base metal, with constant silicon content on their whole thickness, and were identified as consisting of $MoSi_2$, a compound which imparts to molybdenum a very good resistance to high temperatures oxidation.

The silicide coating is one of the most efficient methods for protecting molybdenum against high temperature oxidation. Above 650° molybdenum and its high strength alloys oxidize in air above the tolerable limits and protective coatings are, therefore, imperiously necessary for such service conditions.[1]

In our researches we aimed at obtaining silicon protective coatings on molybdenum by a treatment essentially different from classical coating methods (for instance spraying, pack or gaseous cementation, a.s.o.).

The method we used consists in the cathodic deposition from molten halides electrolytes, namely molten fluorides, of the coating metal, which at the high temperature of the treatment diffuses into the superficial layer of the base metal, resulting in a thin compact alloy coating, metallurgically bound to the substrate material. Reactive metals can be deposited by this method on more noble metals, protective compounds being formed as the coating metal diffuses in the substrate.[2]

---

[1] P. J. Chao, D. K. Priest and J. R. Myers, "Report of the Conference on Niobium, Tantalum, Molybdenum and Tungsten", University of Sheffield, 1960, published 1961, Amsterdam, Elsevier, p. 250.

Our experimental runs have been carried in a device comprising an electrolytic cell with molybdenum as the cathod and silicon as the anode; fragments of elemental silicon were pressed in a silver basket which ensured electrical contact. The electrolyte consisted of a mixture of alkaline fluorides of eutectic composition (LiF-KF-NaF, melting point 454°), with 10 wt% sodium fluorosilicate (Na_2SiF_6) added. The alkaline fluorides serve to maintain the silicon ions in the melt in the form of complex fluorosilicic anions; at the same time they work as a low melting solvent, allowing the treatment to be carried at convenient temperatures. The alkaline fluorides behave as an inert solvent owing to their high electrochemical stability. The large atomic diameter of the alkaline metals makes them insoluble in molybdenum, therefore the diffusion of the alkaline metals into the base metal is ruled out even if one supposes that they may be electrochemically reduced. Other advantages of using the alkaline fluorides solvent can be listed: low vapour pression which affords stability to the composition of the electrolyte, high surface tension which impedes the molten electrolyte to be carried out on the part subjected to coating, no corrosive action against molybdenum, high electrical conductivity, and an especially useful effect of fluxing, which cleans out the oxide film on the surface of the cathodic part, leaving it perfectly suited for diffusion.

The graphite electrolytic cell is sealed in a vacuum tight chamber made of stainless steel, provided with means of lifting, lowering and centering the electrodes. Argon inert atmosphere and dry salts, previously vacuum melted for eliminating hygroscopic and constitution water, have been used. During the runs, the temperature of the bath and the current intensity were kept constant.

In this research we aimed at establishing the morphological characteristics and the nature of the diffusion layer formed on the surface of molybdenum by cathodic deposition of silicon from molten fluorides.

Silicon diffusion coatings on molybdenum are of great actuality owing to some special peculiarities of molybdenum. Among the refractory metals, highly needed by modern technology, molybdenum represents a useful compromise: high melting point (2620°), relative high reserves, production and future disponibilities, and a somewhat moderate cost, comparable with that of chromium to whom molybdenum is superior by its higher melting temperature.

As the prospects for improvement in the oxidation resistance by alloying are not promising in the case of molybdenum, on account of the high volatility of the base metal oxide, the problem of the high temperature uses of molybdenum is entirely dependent on the availability of the protective coatings. Letting aside the protection of molybdenum with a thin film of platinum (as used in electronic devices, but whose life is short owing to the rapid diffusion of platinum in molybdenum) the only coating of industrial usefulness in the silicon coating with or without other minor constituents added (Cr, V, Al, W, Ta). The chief method of producing silicon coatings is cementation at high temperatures (1000 – 1200°) for relatively long periods (4 – 8 hours).

---

[2] N. C. Cook, B. A. Fosnocht and J. D. Evans, "Conference of the National Association of Corrosion Engineering", 1969, p. 520.

In our researches on coating molybdenum with silicon by cathodic deposition and diffusion from molten fluorides, the temperature was much lower than that required by the cementation process. Most of our runs were carried at 700° for 2 hours, the thickness of the coating being acted upon by modifying the current density. The relatively low temperature of the coating treatment in our runs, well below the recrystallization point of molybdenum (950°) may be interesting for long time service of molybdenum under mechanical load, since the creep resistance of molybdenum is twice if recrystallization is avoided .[3]

For establishing the character of the silicon coatings formed by this treatment, we used several investigation methods, namely optical microscopy – indirect and polarized light, scanning electron microscopy, microprobe analysis and X-ray diffraction analysis.

The silicized layer was clearly revealed by optical microscopical observation after etching; it had a granular structure different from that of the molybdenum core (fig. 1). The higher hardness of the silicized layer led to a clear delimitation of the layer by means of a shadow effect observable in inclined illumination (fig. 2).

Additional information on the layer structure were gained by observation in polarized light (fig. 3). The layer appeared with a granulation distinct from that of the core; it consisted of fine equiaxed grains.

The micrographs reveal the compact character of the layer and its perfect coherence with the base metal. The absence of a dendritic morphology in the layer shows that silicon diffused into molybdenum during the treatment.

The layer thickness was in the range 15 – 70 μm for the runs performed at 700° and 2 hours, the thickness being in general proportional to the current density when this was varied between 10 and 30 mA/cm².

The study by direct emission X-ray spectroscopy, carried out with a microprobe analyzer, allowed us to obtain an image of the distribution of the constituent elements in the specimen. On transverse section, normal to the silicized layer, a net distinction was manifest in the characteristic X-ray photons density emitted from coating and core. The X-ray image described by MoL_α photons (fig. 4) shows that molybdenum is present and uniformly distributed in the coating layer; molybdenum concentration is lower in the layer compared with the core. The X-ray image described by SiK_α photons (fig. 5) shows a high silicon concentration in the layer and its absence in the molybdenum core. The SiK_α photons recorded in the region of the core have a density quite similar to that of the parasite impulses recorded out of the specimen (fig. 5). The marginal attenuation of the layer X-ray image is a subsidiary effect accounted for by the curvature of the spectrometer crystal.

---

[3] G. L. MILLER and T. G. COX, reference 1, p. 234.

The linear analysis by direct emission X-ray spectroscopy (fig. 6) showed that the intensity of the characteristic X radiations of the constituent elements of the coating layer is constant across the thickness of the layer, manifesting a steep variation at the boundary between layer and core, namely a sharp increase of the molybdenum content in the core and a sharp decrease of the silicon content. The concentration constancy of the constituent elements in the coating layer, on its whole thickness, confirms that the diffusion of silicon in molybdenum was of the "reaction diffusion" type, resulting in a stoichiometrically defined composition of the layer.

The phase diagram Mo-Si shows that three stoichiometrical compounds can be formed in this system, namely $MoSi_2$, Mo_3Si_2 and Mo_3Si. For identifying the compound formed in our experimental runs, the coating layer was studied by X-ray diffraction analysis. By comparing the diffraction pattern of the layer with the international tables of the interplanar distances in inorganic substances a plain identity with the distances listed in the ASTM card 6−0681 belonging to the compound $MoSi_2$ was obtained. The X-ray diffraction analysis of the coating layer evinced the presence of $MoSi_2$ in the layer, but it could not rule out the possibility that other Mo-Si compounds may be present in low proportion. The problem needs attention because the oxidation resistance of the three silicides in the Mo-Si system is not the same, the best protection to molybdenum being ensured by the disilicide coating. [4,5]

In order to elucidate this aspect of the problem of the silicized layer nature, quantitative analysis by direct emission X-ray spectroscopy of the coating layer was performed. For greater certainty, the determination was carried out independently for both constituents in the same point of the layer, by measuring the intensity of the characteristic radiations $SiK_\alpha(\lambda = 7.126$ Å; $U_c = 1.837$ kV) and $MoL_\alpha(\lambda = 5.406$ Å; $U_c = 2.523$ kV). The intensity data I^{Si}_{sp} or I^{Mo}_{sp}, corrected for background and dead time, were compared with the intensity values I^{Si}_{Si}, or I^{No}_{No} emitted by pure element standards in the same excitation conditions (accelerating voltage and current of the incident electron beam). In order to derive the true concentration C_A of the analysed element in the specimen from the intensity ratio I^A_{sp} / I^A_A, the empirical calibration method based on standard alloys of known composition is seldom used, especially on account of the difficulty to prepare standard alloys of extremely high homogeneity required by the minutness of the volume subjected to analysis (some cube microns). In our case, additional difficulties of preparing standard alloys were brought about by the high melting points of the alloys in the Mo-Si system (generally above 2000°).

Therefore, we choose to derive the true concentration from the intensity ratio by means of theoretical correlation expressions, wherein the correction factors (atomic number, absorption and fluorescence corrections) take account of the complex phenomena occurring during the emission and transmission of the X-rays in the specimen, the effect of these phenomena being dependent on the specimen composition in a rather com-

---

[4] O. Kubascewski and B. E. Hopkins, reference 1, p. 181.

[5] E. Fitzer and J. Schwab, *Metall*, **9**, 1062 (1955).

Fig. 1. — Transverse section of silicized specimen ; NaOH — $K_3(CN)_6$ — H_2O etch.

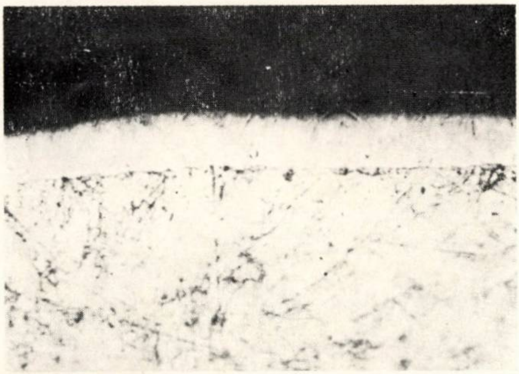

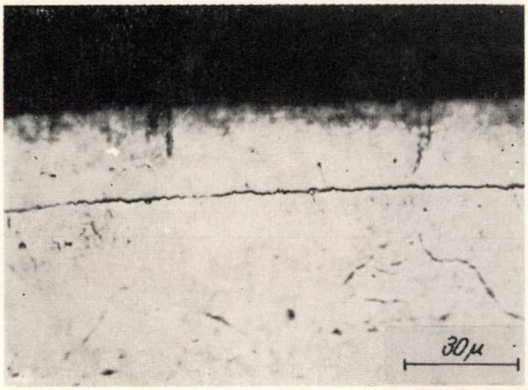

Fig. 2. — Silicized coating observed by optical microscopy (inclined illumination).

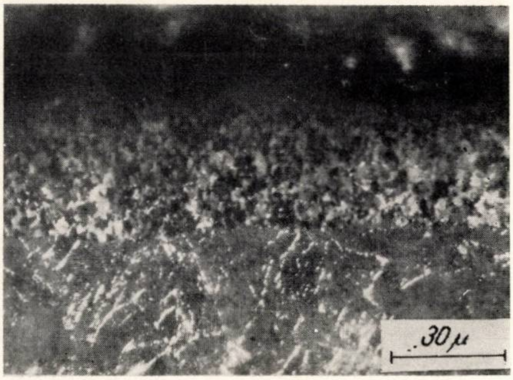

Fig. 3. — Silicized coating observed in polarized light.

Fig. 4. — X-ray image of specimen cross-section described by MoL_{α} emitted photons.

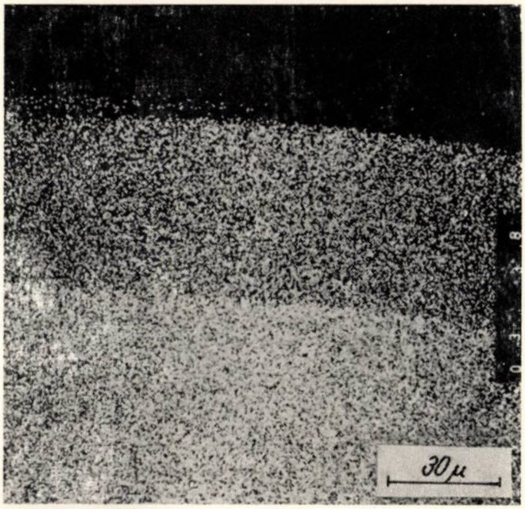

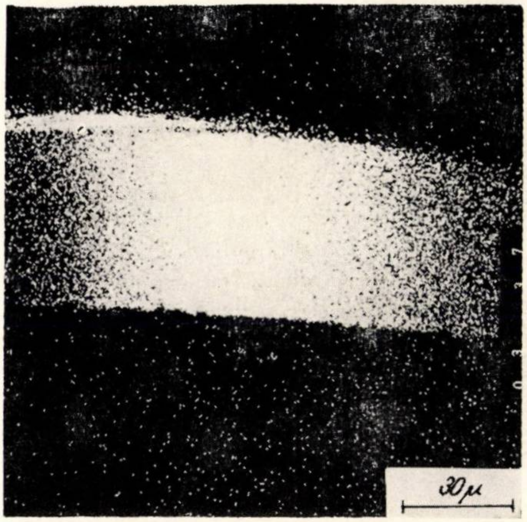

Fig. 5. — X-ray image of specimen cross-section described by SiK_{α} emitted photons.

Fig. 6. — Electron micrograph of silicized specimen and intensity profiles of characteristic radiations of molybdenum and silicon along the line A—A′.

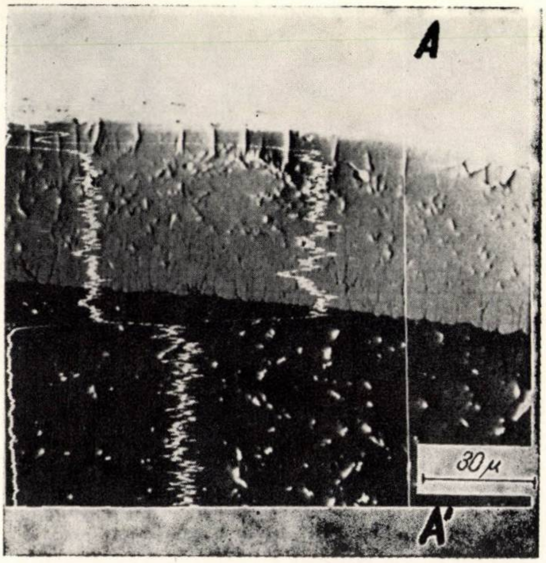

plicated manner. As a criterion of the efficacity of the correction methods a test was used that the corrected concentration value should be independent on the emission conditions of the characteristic radiation (e. g. independent on the accelerating voltage of the incident electron beam).[6] To this purpose the analyses were repeated, for silicon as well as for molybdenum, in the same point of the coating layer at different accelerating voltages. The uncorrected rough concentrations for both Si and Mo, were strongly dependent on the accelerating voltage (the solid curves in the lower part of figures 7 and 8).

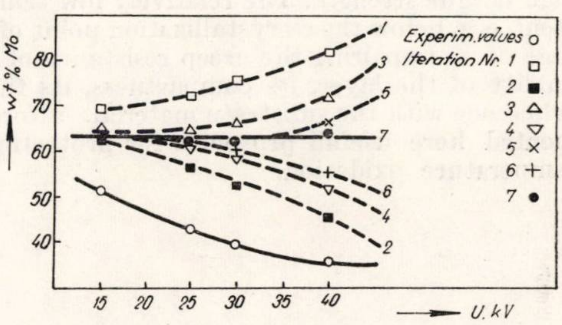

Fig. 7. — Determinations of Mo content in the coating by direct emission X-ray spectroscopy as function of the accelerating voltage of the incident electron beam, before and after atomic number—absorption correction.

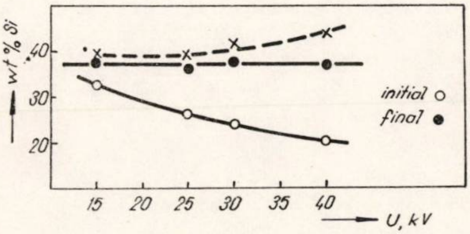

Fig. 8. — Determinations of Si content in the coating by direct emission X-ray spectroscopy as function of the accelerating voltage of the incident electron beam, before and after atomic number—absorption correction.

Since a preliminary test by applying the fluorescence correction[7] showed that for the Mo-Si alloy in the coating layer this correction was negligible, we used for deriving the true concentration an atomic number — absorption combined correction recently proposed by Büchner and Pitsch.[8] The application of the combined correction in a series of iterations attenuated more and more the dependence of the concentration on the accelerating voltage (the dotted curves in fig. 7), and finally we obtained for both Si and Mo a concentration value quite independent on the emission conditions of the characteristic radiation. This final value was taken as the true concentation and it is worthy to note that for both constituents it agrees in quite narrow error limits (±2%) with the composition of the molybdenum disilicide ($MoSi_2$), namely 63 wt% Mo and 37 wt% Si, plotted as straight horizontal lines in figures 7 and 8.

---

[6] S. Gâdea and M. Petrescu, *Rev. Roum. Sciences Techn., série Metallurgie*, under print.

[7] S. J. B. Reed, *Brit. J. Appl. Phys.* **16**, 913 (1965).

[8] A. R. Büchner and W. Pitsch, *Z. Metallkunde*, **62**, 392 (1971) ; **63**, 398 (1972).

The results of the different investigation methods used are in agreement, attesting that the coating layer obtained by the treatment applied by us consists of the $MoSi_2$ compound, present throughout the whole thickness of the coating. The well-known oxidation protective qualities of this disilicide attest that the coating method used in this work allows high temperature uses of molybdenum. Thin $MoSi_2$ layers, like those obtained here, are well suited as protective coatings for molybdenum subjected to alternating mechanical load, ensuring to the base metal a high fatigue strength. The relatively low temperature of the coating treatment, e. g. below the recrystallization point of molybdenum, has the advantage of no impairing the creep resistance of the base metal. The uniform quality of the layer, its compactness, its fine granular structure and its coherence with the substrate material, afford to the treatment experimented here usefull prospects for protecting molybdenum against high temperature oxidation.

Revue Roumaine de Chimie, **18**, *11*, 1859–1863 (1973)

KINETICS OF THE HOMOGENEOUS REACTION BETWEEN METHANE AND SULPHUR

A. DRĂGĂNESCU*, I. BICĂ*, CRISTINA PETRESCU*, ANA MARIA PAVLOVSCHI**, S. ŞERBAN** and N. MERJANOV**

*Institute of Physical Chemistry, str. Galaţi 31, Bucharest 13, Romania
**"Chimigaz" Institute, Str. Carpaţi 8, Mediaş, Romania

Received March 16, 1973

The homogeneous reaction of methane with sulphur follows a first order kinetic law with respect to both reactants for the temperature range between 600 and 700°. The following reaction rate constant (mole/cm^{3}h at^2) has been obtained:

$$k = 2.95 \cdot 10^8 \exp\ (-44.0 \cdot 10^3/RT)$$

The synthesis of carbon disulphide from methane and sulphur has been investigated mainly in heterogeneous catalysis.[1-9] Little attention has been paid to the homogeneous reaction. Thus, Fisher and Smith[10] followed this reaction in the temperature range between 550 and 625°, and Forney and Smith[4] determined the contribution of the homogeneous reaction to the silica gel catalyzed one.

The purpose of this paper is the study of the kinetics of the homogeneous gas phase reaction between methane and sulphur in the temperature range 600 — 700°.

EXPERIMENTAL

The continuous flow system used is shown in figure 1.

Sulphur was supplied in the liquid state from a reservoir (figs. 1 and 2) heated at 125. 0 ± ± 0.5°. The top of the reservoir was electrically heated to prevent the sulphur solidification

---

[1] C. M. Thacker and E. Miller, *Ind. Eng. Chem.*, **36**, 182(1944).
[2] R. F. Bacon and E. S. Boe, *Ind. Eng. Chem.*, **37**, 469(1945).
[3] H. O. Folkins, E. Miller and H. Hennig, *Ind. Eng. Chem.*, **42**, 2202(1950).
[4] R. C. Forney and J. M. Smith, *Ind. Eng. Chem.*, **43**, 1841 (1951).
[5] G. W. Nabor and J. M. Smith, *Ind. Eng. Chem.*, **45**, 1272(1953).
[6] E. Giovannini, *Ann Chim. Apl.* (*Ital.*), **39**, 671(1949).
[7] W. J. Thomas and R. F. Strickland—Constable, *Trans. Faraday Soc.*, **53**, 972 (1967).
[8] W. J. Thomas and B. John, *Trans. Inst. Chem. Engineers*, **45**, T 119(1967).
[9] A. Cybulski, *Rev. Prezemysl. Chem.*, **4**, 228(1971).
[10] R. A. Fisher and J. M. Smith, *Ind. Eng. Chem.*, **42**, 704(1950).

Liquid sulphur got into the vaporizer which was a quartz tubing provided with a capillary heated at 500°. We used this system[10] to eliminate the drawbacks of tue unusual variation of the liquid sulphur viscosity as a function of temperature.

After methane and sulphur were preheated separately they have been mixed in the reactor chamber (fig. 3) to prevent reaction in the preheating zone. Dilution of sulphur vapours proceeds with a temperature decrease due to the endothermic dissociation of sulphur[10] and, to avoid this, sulphur has been diluted with argon in the preheating zone.

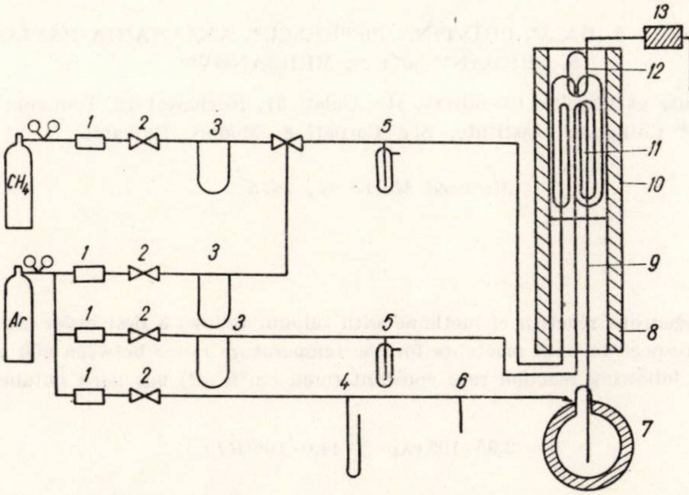
13
14
12
11
10
9
8
7
1
2
3
5
4
6
CH_4
Ar

Fig. 1. — Flow system *1*, Fine pressure reducer ; *2*, Gas regulating valve ; *3*, Flowmeters ; *4*, Manometer ; *5*, Safety traps ; *6*, Capillary ; *7*, Sulphur reservoir ; *8*, *10*, *13*, Heaters ; *9*, Sulphur vaporizer ; *11*, Preheaters ; *12*, Reactor ; *14*, Sulphur removing trap.

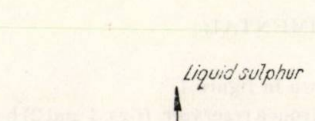
Liquid sulphur
Argon pressure
Electric mantle
Liquid sulphur
Electric heater

Fig. 2. — Sulphur reservoir.

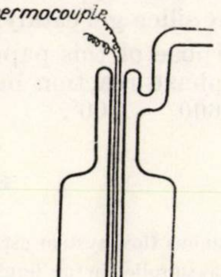
Thermocouple

Fig. 3. — Reactor.

The gases leaving the reactor furnace were kept at about 200° by an auxiliary heater in order to prevent solidification of unreacted sulphur before reaching the sulphur trap, where the most of it was removed. The finely divided sulphur was retained by glass wool filters.

Automatic electronic type EPD potentiometers have been used as furnace temperature controllers. The temperature deviation was $\pm$ 1.5°. Chromel-alumel thermocouples have been used to measure the temperature.

Heating and cooling of the apparatus has been made under argon flow.

Methane and argon of 98.6 and 99.8 % purity, respectively, have been used. The sulphur, from crude oil source, was double distilled before use. For chromatographic purposes carbon disulphide *p.a.* (Laborchemie, Apolda) and hydrogen sulphide, made from Na_2S and H_2SO_4,[11] have been used.

The reaction poducts were analysed by gas chromatography.[12]

RESULTS AND DISCUSSION

In order to determine if the methane-sulphur reaction is a homogeneous or a homogeneous-heterogeneous reaction the wall effect has been investigated. For this purpose the influence of the surface/volume ratio on the conversion was studied.

In table 1 are shown the data at 700° and at a methane-sulphur(S_2) molar ratio 0.5. One can see that a three times increase in the surface/volume ratio (from 4.37 to 13.7 cm^{-1}) has no measurable effect on the metahne and carbon disulphide percent values. Also, the reactor aging has no significant influence on the reaction of methane with sulphur.

Table 1

The influence of S/V ratio on the outlet gases composition

S/V (cm^{-1})	Space velocity (sec^{-1})	% Volumes in the outlet gases	
		CH_4	CS_2
4.37	0.315	29.0	23.4
	0.630	64.2	12.0
	1.260	89.6	3.4
13.4	0.315	29.7	21.1
	0.630	66.6	10.7
	1.260	89.6	3.4

According to our results we consider that the contribution of the methane-sulphur wall reaction to the homogeneous one, if there is any, is insignificant.

---

[11] H, MELVILLE and B. G. GOWENLOCK, "Experimental Methods in Gas Reactions", MacMillan and Co., London 1964, p. 205.

[12] A. DRĂGĂNESCU, I. BICĂ, S. ŞERBAN and A. M. PAVLOVSCHI *Rev. Roumaine Chim.*, **17**, 1779 (1972).

As known, sulphur may exhibit three allotropic species S_2, S_6, and S_8 related by the equations [13]:

$$p_{S_2} = a p_{S_6}$$

$$p_{S_2} = b p_{S_8}$$

where p_{S_2}, p_{S_6} and p_{S_8} are partial pressures of the S_2, S_6 and S_8 molecules, a and b are constants. The equilibrium is shifted to the S_2 form by increasing temperature. At temperature over 600° the S_6 form is prevalent. Thus, at 675° the S_8 form is not present and the S_6 form is only 3 % of the total sulphur. [5] Furthermore, some authors [4,10] consider that the dissociation of the S_8 and S_6 forms is comparatively fast with respect to the reaction between sulphur vapour and methane. Therefore, in our treatment we consider all sulphur only as S_2 form.

Taking into account no heterogeneous reaction, we investigated the kinetics of the homogeneous reaction. The reaction rates *vs.* partial pressures of methane and sulphur are shown in figs. 4 and 5, respectively.

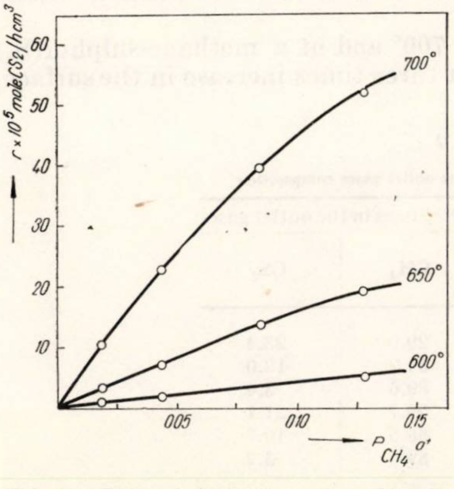

Fig. 4. — Rate of formation of carbon disulphide as a function of the inlet partial pressure of methane ($p_{S_2} = 0.153$ atm)

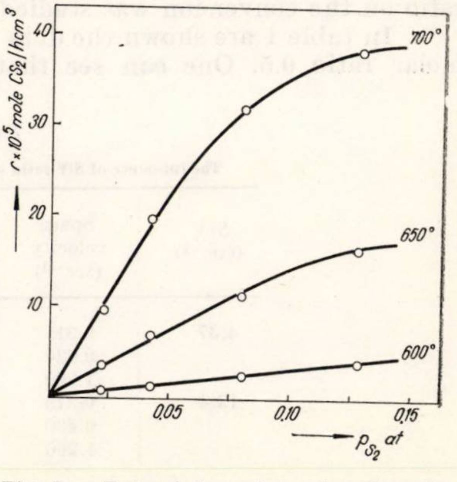

Fig. 5. — Rate of formation of carbon disulphide as a function of the inlet partial pressure of sulphur ($p_{CH_4} = 0.133$ atm)

From these figures one can see that at low partial pressures the reaction follows a first order kinetic law analogous to the silica gel catalyzed reaction. [8] The calculated reaction rate constants are shown in table 2.

The Arrhenius equation plot of these values (fig. 6) gives a satisfactory straight line whose slope corresponds to an activation energy of 44.0 Kcal/mole. The frequency factor has the value of $2.95 \cdot 10^8$ mole CS_2/cm^3 h at^2. Our k_{600} value (table 2) is nearly the Forney and Smith [4] reported value of $2.03 \cdot 10^{-3}$ mole CS_2/cm^3 h at^2 for the same temperature.

[13] G. Preuner and W. S. Schupp, *Z. phys. Chem.*, **68**, 129 (1909).

For the homogeneous reaction of methane with sulphur in a stainless steel reactor, Fisher and Smith [10] reported an activation energy of 34.4 Kcal/mole. The reported activation energy values are 38.8[3], 31.4[5] and 27.39 Kcal/mole[9] for the silica gel catalyzed reaction and 27.5 Kcal/mole[8] for the vanadium pentoxide one. The activation energy value of 44.0 Kcal/mole seems in reasonably good agreement with the above values if one takes into account that the activation value will be greater in the homogeneous reaction than the heterogeneous one.

Table 2

Reaction rate constant values for various temperatures

Temperatures °C	k (moles CS_2/cm^3 h at^2) × 10^3
600	2.61
650	10.45
700	32.60

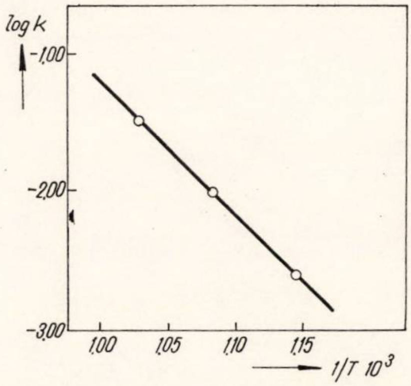

Fig. 6.—Arrhenius equation plot.

The conclusions reached regarding the homogeneous reaction of methane with sulphur within the 600 — 700° temperature range are as follows:

— At low partial pressures this reaction is first order with respect to both reactants.

— The reaction rate constant (mole CS_2/cm^3 h at^2) can be expressed as:

$$k = 2.95\ 10^8\ \exp\ (-44.0\ 10^3\ /RT).$$

Revue Roumaine de Chimie, **18**, *11*, 1865–1866 (1973)

INFLUENCE OF IRRADIATION ON THE THRESHOLD POTENTIAL IN AIR

JAGDISH PRASHAD

Chemical Laboratories, Meerut College,
Meerut–250001 – India

Received March 7, 1973

The fall of the threshold potential, V_m, under irradiation has been observed at various pressures of mercury vapour contaminated air under ozonizer excitation and was ascribed to be due to the occurrence of the positive Joshi effect, $+\Delta i$.

INTRODUCTION

The study of the threshold potential, V_m, in argon [1] revealed that V_m under irradiation, $V_{m(L)}$, is higher than that in dark, $V_{m(D)}$. It was of interest, therefore, to study the same in mercury vapour contaminated air.

EXPERIMENTAL PROCEDURE

The present study was carried out in soda glass ozonizer as reported earlier. [2,3] Air free from carbon dioxide and water vapour and at various pressures was maintained always in contact with liquid mercury at 30°. A 200 watt, 200 volt incandescent glass bulb, kept at about 25 cm from the ozonizer, served as a source of irradiation.

RESULTS AND DISCUSSION

The fall in V_m due to irradiation (cf. fig. 1) may be attributed to be due to release of photoelectrons by light ($+\Delta i$) from the adsorption-like boundary layer of low work function. The occurrence of the positive Joshi effect, $+\Delta i$, where the current under light, i_L is greater than that in dark, i_D, under constant applied potential, implies a lowering of V_m under light and hence a rise in the overvoltage $(V - V_m)$ which determines the conductivity [4]. Such a lowering of V_m by light implies its action similar to that of a higher potential in affecting the breakdown of the gas as a dielectric though the mechanism is different in the two cases. [5,6] A photo-increase of conductivity is the primary or direct consequence of Joshi's theory of the phenomenon.

---

[1] P. Jagdish, Ph. D. Thesis, Banaras Hindu University, 1961.

[2] J. Prashad, *Res. J. Hindi Sci. Academy*, **15**, 79 (1972).

[3] J. Prashad, *Roczniki Chem.*, **46**, 1629 (1972).

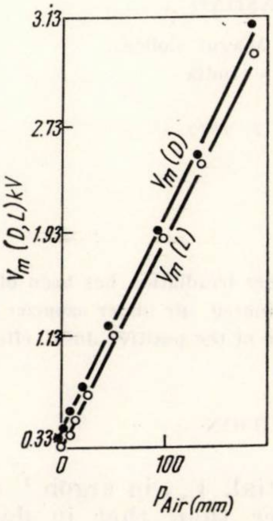

Fig. 1. — $V_{m(D,L)}$ *versus* p_{air}.

---

[4] S. S. Joshi, *Curr. Sci.*, **8**, 548 (1939).
[5] S. S. Joshi, *Proc. Indian Acad. Sci.*, **22**, 389 (1945).
[6] J. M. Meek, *Proc. Phys. Soc.*, **52**, 547 (1940).

Revue Roumaine de Chimie, **18**, *11*, 1867–1873 (1973)

CRYSTALLOCHEMICAL AND DIELECTRIC SURVEY OF PHASES IN THE TiO_2-ZrO_2 SYSTEM PREPARED BY COPRECIPITATION

S. SOLACOLU and A. BĂRBULESCU

Polytechnical Institute of Bucharest,
Str. Polizu 1, Bucharest, Romania

Received March 23, 1973

Phase formation in the TiO_2-ZrO_2 system was examined starting from non-crystalline powder mixtures prepared by coprecipitation. The thermal analysis and the phase composition prove that, under conditions of coprecipitation, the criterion of the minimum free energy governs the phase direct formation in agreement with the thermal equilibrium relations. The phases obtained are characterized by a certain non-equilibrium state which significantly influences the dielectric properties.

1. INTRODUCTION

In the field of ceramics with dielectric properties, an important place is held by compositions belonging to the TiO_2-ZrO_2 system. [1] Phase diagram of the system[2] includes the $ZrTiO_4$ compound and limited areas of TiO_2, ZrO_2 and $ZrTiO_4$ solid solutions (figure 1).

Compositions which are of interest for the production of ceramic dielectrics are situated in the $TiO_2-ZrTiO_4$ subsystem. The $ZrTiO_4$-ZrO_2 subsystem has no practical application due to the presence of the free ZrO_2 which causes the thermal instability of the ceramic mass by its polymorphous conversion accompanied by a significant volume variation.

The synthesis of $ZrTiO_4$ by solid phase reactions between TiO_2 and ZrO_2 requires high temperatures and lengthy treatments. The curve representing the compound formation becomes flattened after 5 hours at 1400 ° or 9 hours at 1300°. [3] Thermal treatment difficulties may be overcome by coprecipitating ions Ti^{4+} and Zr^{4+}. Under these conditions, $ZrTiO_4$ formation occurs at 800° within a few minutes. [4]

---

[1] N. P. Bogorodiţkii and V. V. Pasînkov, ,,Radiokeramika'', Gosenergizdat, Moskva, 1963, p. 109.

[2] L. W. Coughanour, R. S. Roth and V. A. De Prasse, *J. Res. Nat. Bur. Stand.*, **52**, 37 (1954).

[3] M. Mizuno and T. Moguchi, *Nagoya Kogyo Gijutsu Shikensho Hokoku*, 13, 124 (1964); *Chem. Abstr.*, **440**, (1965).

[4] G. H. Stöcker and R. Collouguous, *Compt. rend.*, **245**, 431 (1957).

The advantages of the chemical method for preparing mixtures, prompted us to study the conditions under which phases can be obtained in the TiO_2-ZrO_2 system, as well as their crystallochemistry and their dielectric characteristics. The results obtained are presented in this paper.

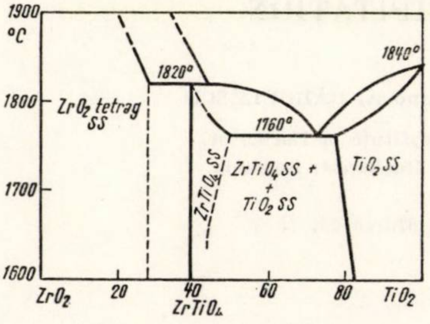

Fig. 1. — The $TiO_2 . ZrO_2$ system.[2]

2. EXPERIMENTAL

Ions Ti^{4+} and Zr^{4+} were coprecipitated from aqueous solutions by neutralization at a pH $\sim$ 7. The mixture of solutions was continuously sprinkled by injecting air in a precipitation bath heated to 80° in which the pH was kept constant by continuous NH_4OH addition. The resultant hydrogels contained over 95 % water after washing, decanting and filtering through a Buchner funnel. The freezing procedure [5] was applied to remove the water and to separate the solid phase into a practically amorphous ultrafine form.

The powdered products obtained after sedimentation and drying at 50° were characterized by differential thermal analysis. The phase composition and the crystallochemical characteristics of powders calcined under DTA conditions up to 1300° were examined by X ray analysis. Determination of the dielectric properties was made by means of disks obtained by sintering at 1360°, powders calcined at 320° and compacted at 4 t/cm^2.

A Netzsch apparatus was used for the thermal analysis. Thermograms were obtained for a 10°/min heating rate and a 0.1 mV recording sensitivity. X-ray analysis was made on a TUR M61 diffractometer with Bragg-Brentano focussing and by direct counting. The accuracy of determinations was ± 0.03 % for the lattice parameters and 5 % for intensities. A General Radio assembly was used for dielectric measurements.

3. RESULTS AND DISCUSSION

3.1. PHASE ATTAINMENT UNDER COPRECIPITATION CONDITIONS

Table 1 shows the mixtures prepared by coprecipitation of Ti^{4+} and Zr^{4+}. The processes occurring on heating the as-prepared powdered mixtures were revealed by differential thermal analysis. DTA curves (fig. 2) display a large endothermic effect in the initial period, due to dehydration. A sharp, strong exothermic effect appears over this endothermic effect or at higher temperatures relative to the composition of mixtures. Similar exothermic effects were found in zirconium dioxide gels and they are attributed to the coalescence phenomenon [6].

---

[5] A. Bărbulescu, Doctorial thesis, 1970 ; Romanian Patent, 54056, 24 June 1971.

The temperature of the exothermic effects reflected by thermograms is recorded in the composition-temperature diagram presented in figure 3. A regularity in the occurrence of coalescence effects results at roughly 300° in the field of rutile solid solutions and at about 650° in the field of Zr TiO_4 solid solutions. The position of thermal effects in the diagram proves that crystalline phases can be obtained in the system at temperatures of at most 700°. The advantages of coprecipitation are con-

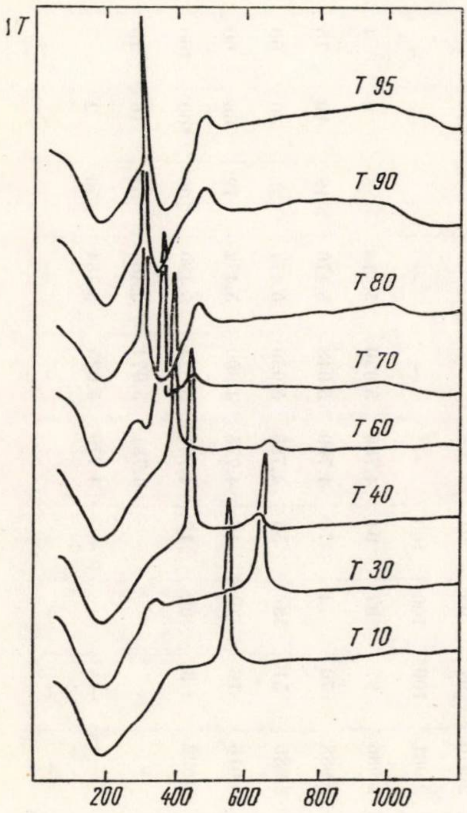

Fig. 2. — DTA curves for mixtures in the TiO_2. ZrO_2 system.

Fig. 3. — Position of exothermic effects in relation to composition.

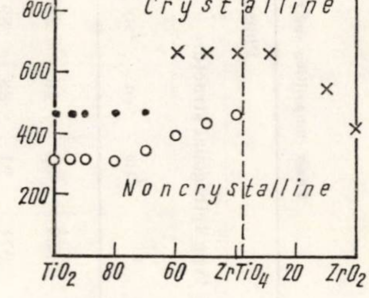

---

[6] R. C. Mackenzie, "Differential Thermal Analysis", Academic Press, London, 1970, p. 296.

Table 1

Phase composition and crystallochemical characteristics of phases in the TiO_2-ZrO_2 system

$TiO_2 : ZrO_2$ ratio	Phases. Structures. System Parameters. Relative intensities														
	TiO_2 type tetragonal structure					$ZrTiO_4$ type rhombic structure						ZrO_2 type monocline structures			
	a	c	I_{110}	I_{101}	I_{211}	a	b	c	I_{101}	I_{111}	I_{002}	d_{011}	d_{111}	I_{011}	I_{111}
100 : 0	4.588	2.959	82	80	85	—	—	—	—	—	—	—	—	—	—
95 : 5	4.600	2.971	91	88	89	—	—	—	—	—	—	—	—	—	—
90 : 10	4.603	2.976	97	95	91	—	—	—	—	—	—	—	—	—	—
80 : 20	4.608	2.981	100	100	100	—	—	—	—	—	—	—	—	—	—
70 : 30	4.612	2.986	97	97	94	4.780	5.050	5.478	5	4	4	—	—	—	—
60 : 40	4.614	2.988	70	73	74	4.799	5.048	5.476	19	19	15	—	—	—	—
50 : 50	4.617	2.985	51	58	55	4.786	5.050	5.474	38	40	50	—	—	—	—
40 : 60	4.606	3.016	16	30	16	4.778	4.990	5.472	72	66	60	—	—	—	—
30 : 70	4.607	3.022	3	32	15	4.791	5.024	5.480	100	100	100	—	—	—	—
10 : 90	—	—	—	—	—	4.781	5.074	5.464	53	16	15	3.672	3.130	50	70
5 : 95	—	—	—	—	—	4.779	5.025	5.484	56	2	5	3.674	3.137	68	78
0 :100	—	—	—	—	—	—	—	—	—	—	—	3.690	3.157	100	100

firmed, namely the possible synthesis of phases in a short time and at significantly lower temperatures than in the case of compounds formed by solid phase reactions between the crystalline components.

3.2. CRYSTALLOCHEMICAL CHARACTERISTICS OF PHASES PREPARED BY COPRECIPITATION

Studies were made on the phase composition and the crystallochemical characteristics of phases in mixtures calcined under DTA conditions up to 1300°. The phases, the lattice parameters and the relative intensities are shown in table 1.

The presence of titanium dioxide under rutile form is found to be the only phase in compositions with less than 30% ZrO_2. The increase in the dimensions of the rutile primary cell, the change of the relative intensity and the absence of lines characteristic of $ZrTiO_4$ confirm the formation of rutile solid solutions.

The presence of zirconium titanate with orthorhombic structure is found to be a main phase in 50 — 70% ZrO_2 mixtures. The lattice parameters of the pure compounds obtained under coprecipitation conditions compare well with the results, found for $ZrTiO_4$ obtained by solid phase reactions and quenching technique (table 2). The lattice parameters of type $ZrTiO_4$ phases reveal the formation of solid solutions. However, the differences found in the various mixtures reflect a certain non-equilibrium state typical of these phases.

Table 2

System parameters for the $ZrTiO_4$ compound

a	*b*	*c*	Volume (Å^3)	Observations
4.804	5.464	5.035	132.3	the present paper
4.804	5.483	5.036	132.6	rapid quenching[7]
4.802	5.483	5.034	132.5	
4.809	5.483	5.030	132.6	
4.809	5.412	5.030	130.9	gentle quenching[7]
4.806	5.447	5.032	131.7	

The presence of monocline zirconium dioxide is found in zirconium-rich mixtures. The shift of lines d_{011} and d_{111} confirms the formation of the solid solution of monocline ZrO_2.

The thermal analysis and the phase composition proves that under coprecipitation conditions, the criterion of the minimum free energy governs the phase direct formation in accordance with the phase thermal equilibrium relations.

The lattice parameters of rutile type and of $ZrTiO_4$ type phases point out the large development of solid solution fields. Considering the large volume of these fields as shown in the thermal equilibrium diagram at temperatures close to eutectic, as well as the increased volume of the $ZrTiO_4$ cell, we may assume that the phases obtained by calcination of coprecipitated mixtures represent non-equilibrium states, similar to those obtained by quenching. This finding is confirmed by the dielectric characteristics.

---

[7] R. W. Lynch and B. Morosin, *J. Amer. Ceram. Soc.*, **55**, 409 (1972).

3.3. DIELECTRIC CHARACTERISTICS OF THE PHASE PREPARED BY COPRECIPITATION

The dielectric properties of ceramic bodies obtained from mixtures prepared by coprecipitation were assessed by measuring the electric resistance, the capacitance and the dielectric losses. Values calculated for resistivity ρ, dielectric permittivity ε and the tangent of the loss angle tg δ at frequencies ranging from 1 kHz to 1 MHz, are listed in table 3.

In the field of rutile-rich compositions, there is a minimum resistivity situated at the boundary between insulators and semiconductors; the dielectric permittivity exceeds by 2 — 3 orders of magnitude the normal values for rutile ceramics and dielectric losses reach values which are incompatible with the dielectric quality. The anomaly of dielectric properties is a result of nonstoichiometric rutile phase formation. The deviation from stoichiometry produces the intensification of polarization phenomena, the increase of the electric conductivity and their dependence on frequency. The diminution of nonstoichiometric rutile amount in the two phase field determines the reduction of dielectric losses and the decrease of dielectric permittivity. In the field of $ZrTiO_4$ — based compositions, the resistivity of roughly 10^{11} ohm. cm, the permittivity around 30 and the dielectric losses below $5 \cdot 10^{-4}$ for 1MHz, reflect a normal behaviour of materials.

The results of determinations emphasize the different behaviour of the two phases under the conditions of preparation by coprecipitation: the deviation from stoichiometry is significant with TiO_2 whereas it is not found with $ZrTiO_4$. This consequence of the chemical preparation method should be considered when studying the establishment of the electric properties in the TiO_2 — based systems.

4. CONCLUSIONS

The preparation of mixtures by coprecipitation confirmed the possibility of obtaining crystalline phases in the $TiO_2 - ZrO_2$ system under profitable conditions, by calcination up to 700°.

Phase formation is governed by the criterium of the minimum free energy so that the phase composition corresponding to thermal equilibrium relations is obtained directly from the noncrystalline mixture.

The phase composition and the phase characteristics correspond to the equilibrium state at a high temperature. The increased energy content maintained at a low temperature manifests itself by the extension of rutile solid solutions up to 30% ZrO_2 and by the increased value of the $ZrTiO_4$ system parameters.

The dielectric properties of ceramic materials obtained from products prepared by coprecipitation are significantly deteriorated by rutile type phases whose deviation from stoichiometry causes a decrease of resistivity and a significant increase of dielectric losses.

Table 3

Dielectric permittivity and dielectric losses

$TiO_2 : ZrO_2$ ratio weight	1 kHz		10 kHz		100 kHz		1 MHz	
	ε	tgδ	ε	tgδ	ε	tgδ	ε	tgδ
100 :0	10750	1.97×10^{-1}	9434	6.5×10^{-2}	8096	6.8×10^{-2}	7737	8.8×10^{-2}
95 :5	7822	8.8×10^{-2}	7297	5.1×10^{-2}	6292	5.7×10^{-2}	6118	1.28×10^{-1}
90 :10	11083	1.81×10^{-1}	8068	4.63×10^{-1}	3187	4.8×10^{-1}	1449	1.53×10^{-1}
80 :20	3520	1.88×10^{-1}	2268	2.57×10^{-1}	1085	3.1×10^{-1}	969	7.7×10^{-2}
70 :30	828	2.25×10^{-1}	778	1×10^{-1}	531	5.9×10^{-2}	439	2.45×10^{-2}
60 :40	203	1.9×10^{-2}	171.5	1.52×10^{-2}	471	7.1×10^{-3}	414	4.8×10^{-3}
50 :50	45	2×10^{-4}	49.5	3×10^{-4}	28	2.5×10^{-3}	39	3×10^{-4}
40 :60	27	8×10^{-4}	39	3×10^{-4}	23	1×10^{-3}	28	2×10^{-4}
30 :70	25	5×10^{-4}	37	4×10^{-4}	21	1×10^{-3}	25	3×10^{-4}

320°

Revue Roumaine de Chimie, **18**, *11*, 1875–1881 (1973)

CONTRIBUTIONS TO THE CHEMISTRY OF THIOCOMPLEXES. IV

COMPLEX COMPOUNDS OF Pd (II) WITH THIOAMIDES OF THE DIBENZOFURAN SERIES

D. NEGOIU*, VASILICA MUREŞAN** and S. FLOREA**

* Department of Chemistry, University of Bucharest, Splaiul Independenţei 89, Romania
** Department of Chemistry, University of Craiova, Calea Bucureşti 165, Romania

Received January 26, 1973

The paper offers some theoretical views on the tendency of class (*b*) metallic ions to form stable complex compounds with thioamides. The synthesis of complex compounds of Pd(II) with thioamides of the dibenzofuran series : 3-thioacetylamino-dibenzofuran, 3-thiobenzoylamino-dibenzofuran and 3-thiofuroylamino-dibenzofuran are described. These are of the $PdLCl_2$ type and are characterized on behalf of the results of the chemical analysis and of the IR spectra. Attributions of the absorption bands are made based on the electronic reflexion spectra of the complexes and the conclusion is reached that they are square-plane, belonging to the D_{4h} symmetry group.

This paper aims to complete the theoretical discussions of our previous papers[1–3] about the tendency of the class (*b*) metallic ions to form stable complex compounds with the thioamides, to check R.G. Pearson's "principle of soft and hard acids and bases".[4,5]

Ahrland, Chatt and Davies[6] and Schwarzenbach,[7] based on the criterion of relative affinity at coordination, suggest the following series to determine the complex compounds with acceptors of the two classes :

Donor group	Stage of oxidation	Class (*a*)	Class (*b*)
7B	–I	$F \gg Cl > Br > I$	$F \ll Cl < Br < I$
6B	–II	$O \gg S > Se > Te$	$O \ll S \sim Se \sim Te$
5B	–III	$N \gg P > As > Sb$	$N \ll P > As > Sb$

---

[1] D. Negoiu and V. Mureşan, *Anal. Univ. Bucureşti. Chim.*, **1971**, 121.
[2] D. Negoiu, V. Mureşan and C. Fulea, *Anal. Univ. Bucureşti Chim.* (under press).
[3] D. Negoiu, V. Mureşan and C. Fulea, *Rev. Roumaine de Chim.* (under press).
[4] R. G. Pearson, *J. Amer. Chem. Soc.*, **85**, 3533 (1963).
[5] R. G. Pearson, *J. Chem. Educ.*, **45**, 581, 643 (1968).
[6] S. Ahrland, J. Chatt and N. R. Davies, *Quart. Rev.*, **12**, 265 (1958).
[7] G. Schwartzenbach, *Experientia Suppl.*, **1956**, 162.

Pearson[4,5] classifies the Lewis acids and bases in three categories: soft, medium and hard.

If we examine the specific character of the Lewis acids, we note that the hard acids are characterized by a small volume, a state of high oxidation, and the absence of the nonparticipating pairs of electrons in the outer valence layer, while the soft acids have a small or nil positive charge, a big volume and pairs of nonparticipating electrons (*p* or *d* electrons) in the valence layer. These characters of the soft acids bring with them a high polarizability and a low electronegativity. We notice that the class (*a*) Lewis acids correspond to hard acids, and those of class (*b*) to soft acids.

Regarding the classification of the Lewis bases, we note that the bases having N, O or F donor atoms and a high electronegativity, a low ability to polarize, and are difficult to ionize, are hard bases, while the bases having P, S, I, Br, Cl or C as donor atom and display a low electronegativity, a high ability to polarize and are easily ionized, are considered soft bases.

The correlation of these characteristics of Lewis acids and bases is materialized in "the principle of soft and hard acids and bases" stated by Pearson in 1963, according to which the hard acids have a preference for coordinating hard bases, while soft acids have a propensity for soft bases.

In this way the theoretical support of the fact that class (*b*) acceptors, which are soft Lewis acids, have an affinity for ligands with sulphur, actually thioamides, which are soft Lewis bases, is pointed out.

The present paper gives the results of chemical and physicochemical research works carried out on the complex compounds of palladium (II) with thioamides of the dibenzofuran series 3-thioacetylamino-dibenzofuran (3-TAADBF) (I) 3-thiobenzoylamino-dibenzofuran (3-TBADBF) (II) and 3-thiofuroylamino-dibenzofuran (3-TFADBF) (III) recently synthetized and described in literature.[8]

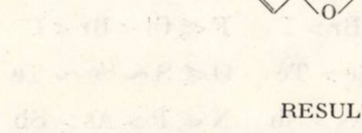

I

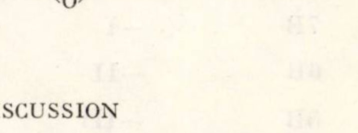

II

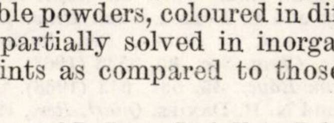

III

RESULTS AND DISCUSSION

The complex compounds of palladium (II) with these thioamides are microcrystalline, stable powders, coloured in different shades of orange brown, hardly or only partially solved in inorganic or organic solvents, having high melting points as compared to those of the respective thioamides. They were obtained by the same method : the ethanol solution of the thioamide was added to the aqueous solution of palladium dichloride.

---

[8] V. Farcaşan, S. Florea and R. Beju, *Stud. Univ. Babeş-Bolyai Chem.*, **1970**, 63.

The results of the elementary chemical analysis of the complexes obtained are given in table 1.

Table 1

Elementary analysis of the Pd(II) complexes

Studied complex	Analysed element							
	Pd %		S %		C %		H %	
	Theor.	Exper.	Theor.	Exper.	Theor.	Exper.	Theor.	Exper.
Pd (TAADBF)Cl_2	25.48	26.00 25.60	7.64	7.49 7.51	40.13	41.58 41.82	2.62	1.98 2.20
Pd (TBADBF)Cl_2	22.67	22.75 22.83	6.79	6.65 6.58	43.34	44.75 45.01	2.33	1.84 1.98
Pd (TFADBF)Cl_2	22.20	22.80 22.63	6.65	6.30 6.41	47.44	49.11 48.93	2.70	2.11 1.85

All these results are in good agreement with the formula of the type $PdLCl_2$ (L = 3-TAADBF, 3-TBADBF and 3-TFADBF) complexes. We notice that differing from the complex compounds of Pd(II) with the majority of thioamides of the phenylthioacetamide series, [3] in which two molecules of thioamide are bound in complexes of the PdL_2Cl_2 type, here only one thioamide molecule intervenes, analogous to what happens in the diphenylthioacetamide ligand. This is also explained by the large volume of the ligands leading to steric hinderings.

The IR spectra of the complexes and the corresponding thioamides are systematized and discussed in separate fields (figs. 1, 2, 3). The spectra of these thioamides have very abundant bands, well justified by their structural complexity. The literature[9] [10] shows that the thioamide group is a complex vibrational group with characteristic bands set in the 600–1650 cm^{-1} field. In the present discussions we refer especially to the bands which favour the clearing up of the problem about the character of the chemical bond in complexes.

The 3500–3000 cm^{-1} range (νNH_2 symm and νNH asymm)

The bands of the 3145–3180 cm^{-1} interval, characteristic for νNH_2 appear in complexes at lower frequencies than in the respective thioamides, and more flattened. The band assigned to νNH asymm changes in the complexes. These changes become arguments in the hypothesis that the NH_2 group also participates in the formation of the complexes.

---

[9] K. A. Jensen and P. H. Nielsen, *Acta Chem. Scand.*, **20**, 597 (1966).

[10] H. O. Desseyn and M. A. Herman, *Spectrochim. Acta*, **23**, 2457 (1967).

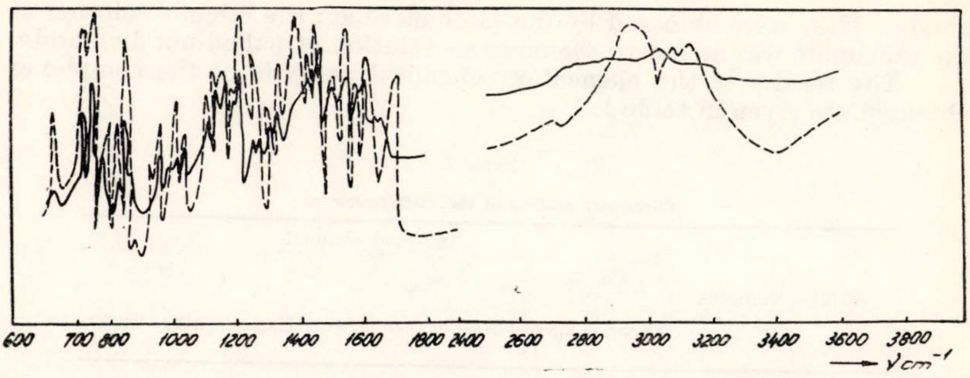

Fig. 1. – IR spectra of 3-TAADBF (. . .) and of the complex with Pd (II) (———).

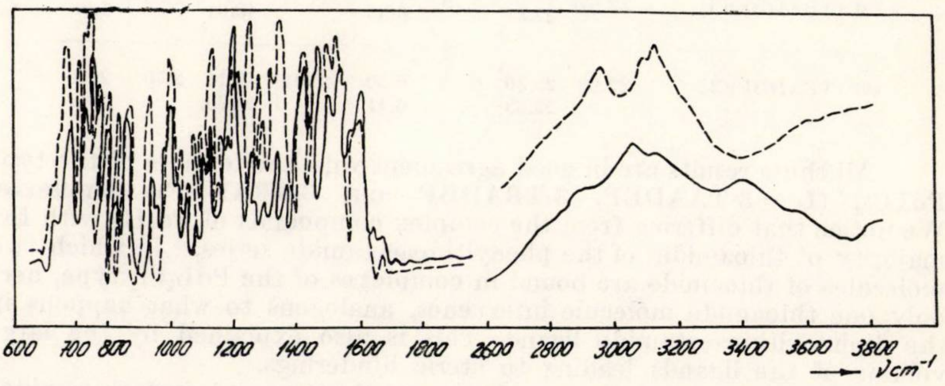

Fg. 2. – IR spectra of 3-TBADBF (. . .) and of the complex with Pd(II) (———).

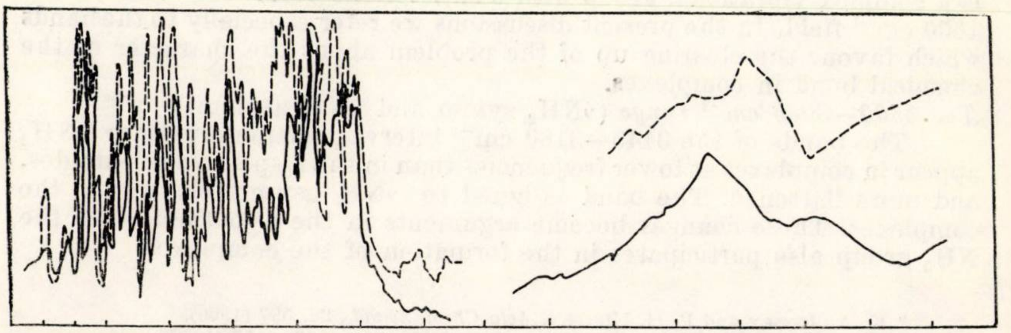

Fig. 3. – IR spectra of 3-TFADBF (. . .) and of the complex with Pd(II) (———).

The 1650–1600 cm^{-1} range (δNH_2)

The intensive band in this interval, assigned to the stretching vibration of NH_2, appears in the complexes with a smaller intensity and a slightly variable position, which confirms the former opinion.

The 1600–1450 cm^{-1} range (νC–N, C–C coupling)

The characteristic band of the thioamides at 1440–1420 cm^{-1} appears in the complexes displaced towards higher frequencies and with a lower intensity.

These changes may be explained by the electronic migrations of the thioamidic group, following the coordination.

The 1350–900 cm^{-1} range (νC=S, δNH_2)

A band very important for the discussion of the character of the bond is the one at 1220 cm^{-1}, in which the frequency of the C=S bond has an important contribution. We notice that it almost disappears. This change is an argument in favour of band narrowing down very much in complexes. This confirms the opinion that the sulphur atom participates as donor atom at achieving the chemical bond in these complexes.

The second significant band in this interval is the one at 960–980 cm^{-1} assigned to the stretching vibration of the NH_2 group, a band that is much changed, lowering its intensity, once more confirming our supposition that the NH_2 group also participates to the bond.

The 900–600 cm^{-1} range (NCS, C=S)

In this region the 630–680 cm^{-1} band is significative, generally assigned to the C=S vibration, which appears changed in the complexes, with a much lower intensity, thus confirming the opinion that the sulphur participates to the chemical bond.

The general conclusion of the IR spectral analysis is that in these complexes, the chemical bond implies the participation of the sulphur atom, as well as of the nitrogen of the thioamide group.

To complete the undertaken study of the palladium (II) complexes with these thioamides, we have carried out the electronic reflexion spectra in the visible field, as can be seen in figure 4.

The absorption bands were assigned on the basis of the data in literature, actually referring to the paper of Gray and Ballhausen,[11] which make use of the molecular orbitals theory in the case of the square-plane metallic complexes of the d^8 configuration elements : Ni(II), Au(III), Pt(II), Pd(II).

Thus, the correlation of the bands observed in the electronic spectra of the Pd(II) complexes with the thioamides of the DBF series, with those of $PdCl_4^{2-}$ (in solid state) leads to the following assignment of bands :

a) it is possible that the band at 23,809 cm^{-1} (420 nm) appearing in complexes, should correspond to the 23,300 cm^{-1} band in $PdCl_4^{2-}$, with the assignment of the transition $^1A_{1g} \rightarrow {}^1E_{1g}$ $[e_g(\pi^*) \rightarrow b_{1g}(\sigma^*)]$, $d-d$ transition, permitted by the spin, not allowed by parity.

---

[11] H. B. Gray and C. J. Ballhausen, *J. Amer. Chem. Soc.*, **85**, 260 (1963).

b) we suppose that the shoulder appearing at 16,666 cm^{-1} (600 nm) corresponds to the band at 16,700 cm^{-1} of $PdCl_4^{2-}$, with the assignment of the transition $^1A_{1g} \rightarrow {}^1A_{2g}\ [b_{2g}(\pi^*) \rightarrow b_{1g}(\sigma^*)]$, $d-d$ transition, permitted by the spin, not allowed by parity.

This observed correspondence leads us to assign to the complexes obtained a D_{4h} square-plane symmetry.

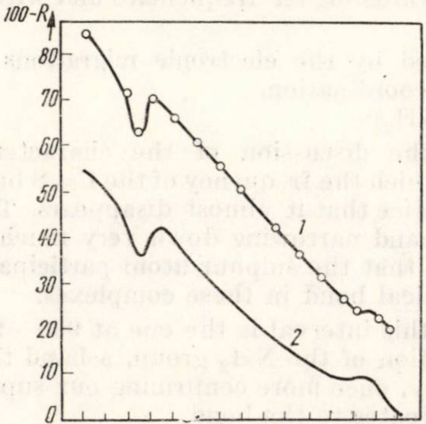

Fig. 4. — Electronic reflexion spectra of Pd (II) complexes *1*, with 3-TBADBF and *2*, with 3-TFADBF.

EXPERIMENTAL

Reactants : the $PdCl_2$ solution corresponds to a 0.02 M concentration ; it is slightly acidulated with HCl. The thioamides are solved in 96 % ethanol, by warming.

The IR spectra of the thioamides and complexes were recorded by a Perkin Elmer 157 apparatus, in anhydrous KBr tablet.

The reflexion spectra were carried out at a VSU−1 Zeiss Jena spectrophotometer, in MgO tablet.

Obtainment of the complexes

To 10 ml of $PdCl_2$ we add 0.02M in small quantities, under continuous stirring of the ethanol solution of the thioamide. A fine precipitate is formed which is left to deposit in approximately one hour.

The precipitate is filtered through a G_4 crucible, washed with ethanol and dried in vacuum. The complexes thus obtained have the appearance of microcrystalline powders, of a brown-orange colour, stable in time, with a low solubility in different organic and inorganic solvents.

CONCLUSIONS

The palladium (II) complexes with the thioamides of the dibenzofuran series are of the type :

$$PdLCl_2\ (L = \text{3-TAADBF, 3-TBADBF, 3-TFADBF})$$

The spectral analysis in IR brings proofs on the achievement of the chemical bond by means of the sulphur, as well as of the nitrogen of the NH_2 group, making it possible to draw the following formula of the complexes :

$PdLC'_2$

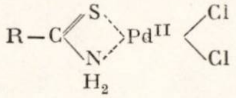

In these complexes the thioamides participate in the "thioceto" form, analogously to those described in our former paper. [3]

The electronic reflexion spectra of the complexes lead to the conclusion that they have a square-plane form, belonging to the D_{4h} symmetry group.

Revue Roumaine de Chimie, **18**, *11*, 1883–1896 (1973)

A PERTURBATIONAL PROCEDURE APPLIED TO THE CALCULATION OF THE ENERGETIC LEVELS IN THE COMPLEXES OBTAINED BY ORGANIC REAGENTS

GRIGORE POPA and ŞERBAN MOLDOVEANU

University of Bucharest, Faculty of Chemistry, Department of
Analytical Chemistry, Splaiul Independenţei 89, Romania

Received March 29, 1973

A new method of calculating the values of energetic levels in the complexes obtained by organic reagents, may be obtained by the application of the perturbational procedure indicated by P. O. Löwdin, to the atomic or molecular wave functions. For the direct application of this procedure, tables indicating the values that must be known for the calculations, are given in the paper. The procedure is then applied to the calculation of the absorption band in the visible range of zinc dithizonate.

The theoretical study of the electronic energy in the complexes obtained by organic reagents is important for the explanation of a series of properties of the above mentioned complexes, such as : the absorption spectra, the redox potentials, the stability constants, etc.

This study may be realized by means of the molecular orbital theory.

Conceiving a cluster molecule in which the central atom contains the set of atomic orbitals $\{\chi_i\}$ and considering each of atoms belonging to the ligands having the $\{\chi_x\}$ set, respectively $\{\chi_y\}$, ... sets, on the basis of usual approximations in the calculi of molecular orbitals,[1] we can obtain the values of energetic levels of molecules and molecular wave functions by solvation of the homogeneous system :

$$\sum_{n=1}^{N} c_n \left(H'_{mn} - E\,\delta_{mn}\right) = 0, \qquad m = 1, \ldots N \tag{1}$$

where $H'_{mn} = \int \chi'_m \hat{\mathcal{H}} \chi'_n \, \mathrm{d}v$

$\hat{\mathcal{H}}$ being the hamiltonian of the system and $\{\chi'_n\}$ being the set of orbitals obtained by the orthogonalization of the set $\{\{\chi_i\} \cup \{\chi_x\} \cup \ldots\}$

---

[1] C. I. Lepădatu, *Z. phys. Chem.* (*Frankfurt*), **73**, 249 (1970).

The approximate solving of the system (1) can be made following the variation procedure of P. O. Löwdin in which the orbitals are supposed to be separated into two sets A and B which bear a mutual influence. In this case, we can write:

$$c_m = \sum_{n \in A} c_n \frac{H'_{mn}(1 - \delta_{mn})}{E - H'_{mm}} + \sum_{n \in B} c_n \frac{H'_{mn}(1 - \delta_{mn})}{E - H'_{mm}}, \qquad m = 1, 2 \ldots N \tag{2}$$

or putting down for m and $n \in A$

$$U^A_{mn} = H'_{mn} + \sum_{\alpha \in B} \frac{H'_{m\alpha} \cdot H'_{\alpha n}}{E - H'_{\alpha\alpha}} + \sum_{\alpha \in B} \sum_{\beta \in B} \frac{H'_{m\alpha} \cdot H'_{\alpha\beta} \cdot H'_{\beta n}}{(E - H'_{\alpha\alpha})(E - H'_{\beta\beta})} + \ldots \tag{3}$$

we obtain:

$$c_m = \sum_{n \in A} \frac{U^A_{mn} - H'_{mn} \cdot \delta_{mn}}{E - H'_{mn}} c_n \text{ for } m \in A$$

which leads to:

$$\sum_{n \in A} c_n(U^A_{mn} - E\delta_{mn}) = 0 \tag{4}$$

It follows that, for the A set, made up of only one index corresponding to a nondegenerate state:

$$E_k = U_{kk} = H'_{kk} + \sum_{\alpha \in B} \frac{H'^2_{k\alpha}}{E_k - H'_{\alpha\alpha}} + \sum_{\alpha \in B} \sum_{\beta \in B} \frac{H'_{k\alpha} \cdot H'_{\alpha\beta} \cdot H'_{\beta k}}{(E_k - H'_{\alpha\alpha})(E_k - H'_{\beta\beta})} + \ldots \tag{5}$$

If A is made up of one set of x degenerate states of energy E^A, taking into account that we have:

$$\sum_{n \in A} c_n(U^A_{mn} - E\delta_{mn}) = 0$$

we notice that the procedure indicated in,[2] may be once and again applied parting the A set into the subsets A' and B'. Thus, we get:

$$V^{A'}_{mn} = U^A_{mn} + \sum_{\alpha \in B'} \frac{U^A_{m\alpha} \cdot U^A_{\alpha n}}{E - U^A_{\alpha\alpha}} + \ldots \tag{6}$$

When A' is made up of only one index l, we obtain for $E_l = V_{ll}$:

$$E_l = H'_{ll} + \sum_{\alpha \in B'} \frac{H'^2_{l\alpha}}{E_l - H'_{\alpha\alpha}} + \sum_{\alpha \in B} \frac{H'^2_{l\alpha}}{E_l - H'_{\alpha\alpha}} + \ldots \tag{7}$$

---

[2] P. O. Löwdin, *J. Chem. Phys.*, **18**, 365 (1950).

in which we put $H'_{l\alpha} = 0$ for the case $E_l \simeq H_{\alpha\alpha}$, in order to avoid the big errors which appear in this situation.

Thus, for the evaluation of the values for the energetic levels, we get that we can make use (not only for nondegenerate states, but also for degenerate states) of the expressions [1]:

$$E_i \simeq H'_{ii} + \sum_x \frac{H'^2_{ix}}{E_i - H'_{xx}} + \sum_y \frac{H'^2_{iy}}{E_i - H'_{yy}} + \cdots + \sum_{\substack{x \\ x \neq y \neq i}} \sum_y \frac{H'_{ix} \cdot H'_{xy} \cdot H'_{yi}}{(E_i - H'_{xx})(E_i - H'_{yy})} + \cdots \tag{8}$$

$$E_x \simeq H'_{xx} + \sum_i \frac{H'^2_{ix}}{E_x - H'_{ii}} + \sum_y \frac{H'^2_{xy}}{E_x - H'_{yy}} + \cdots + \sum_{\substack{i \\ i \neq y \neq x}} \sum_y \frac{H'_{xi} \cdot H'_{iy} \cdot H'_{yx}}{(E_x - H'_{ii})(E_x - H'_{yy})} + \cdots \tag{9}$$

As can be noticed, the relations (8) and (9) are expressions implicite in E_k. In order to get the energies, we must therefore start from an evaluation of the E_k in the members on the right of the above mentioned relations. We notice that we can have $E_k \approx H_{kk}$ and the relations:

$$H'_{ii} \simeq H_{ii} - \sum_x S_{ix} H_{ix} - \sum_y S_{iy} H_{iy} - \dots$$

$$H'_{ix} \simeq H_{ix} - S_{ix} \cdot \frac{H_{ii} + H_{xx}}{2} \tag{10}$$

. . . .

$$H'_{xx} \simeq H_{xx} - \sum_i S_{ix} H_{ix} - \sum_y S_{xy} H_{xy} - \dots$$

$$H'_{xy} \simeq H_{xy} - S_{xy} \cdot \frac{H_{xx} + H_{yy}}{2}$$

. . . .

which naturally come as a result after the orthogonalization of the set $\{\{\chi_i\} \cup \{\chi_x\} \dots\}$.[3]

The above mentioned expressions lead to the new values for E_k and the procedure, as it has been displayed above, can be repeated into its own self-consistency.

---

[3] P. O. Löwdin, *J. Chem. Phys.*, **19**, 1396 (1951).

Thus, effective calculi can be made only if H_{ii}, H_{ix}, H_{xy}, S_{ix}, $S_{xy}, \ldots$ are known; therefore, it is necessary to have their expressions. These are:

$$H_{ii} = \int \chi_i^*(\hat{\mathcal{H}}_0 + \sum_L V_L)\chi_i \mathrm{d}v = H^0_{ii} - \sum_L Z_L BI_{Li} \tag{11}$$

where V_L is the potential of electrostatic interaction between χ_i orbital and L atom of the ligand and where Z_L is the charge on L atom (or L core). Therefore

$$BI_{Li} = \int \chi_i^* \frac{1}{r_{Li}} \chi_i \mathrm{d}v$$

$$\hat{\mathcal{H}}_0 = -\nabla^{i2} + V_i, \qquad H^0_{ii} \simeq -\mathrm{VSIP}(i).^4$$

$$H_{xx} = \int \chi_x^*(\hat{\mathcal{H}}_0 + V_I + \sum_{L'} \chi_x)\mathrm{d}v = H^0_{xx} - Z_I \cdot BI_{Ix} - \sum_{L'} Z_{L'} BI_{L'x} \tag{12}$$

where χ_x does not belong to the L' atom (or L' core).

$$H_{ix} = (2 - |S_{ix}|) \cdot S_{ix} \cdot \frac{H^0_{ii} + H^0_{xx}}{2} - S_{ix} \cdot \frac{\sum_L Z_L \cdot BI_{Li} + Z_I BI_{Ix}}{2} \tag{13}$$

$$S_{zj} = \int \chi_z^* \chi_j \, \mathrm{d}v \tag{14}$$

Taking into account the orientation in space of orbitals and chemical bonds, we must rotate the coordinate systems of orbitals in order to make them parallel and with the z axis along the bond. This rotation is equivalent with a projection of the orbitals on a given direction which is determined by Eulerian angles. If the set $\{\chi_\beta\}$ belongs to the A atom and if it must be rotated on the direction determined by the bond between the atoms A and B, we have:

$$\chi_\alpha^{\text{true}} = \sum_{\beta \in A} {}^B D_{\alpha\beta} \cdot \chi_\beta \qquad \text{where } \chi_\alpha \in \{\chi_\beta\} \tag{15}$$

${}^B D_{\alpha\beta}$ being the matrix elements of the representation of the rotation operator $\hat{D}$ in$\{\chi_\beta\}$ basis. (The $D_{\alpha\beta}$ elements can be found in [5,6]). In this case, it follows that:

$$S^{\text{true}}_{\alpha\beta} = \int \sum_{\gamma \in A} {}^B D_{\alpha\gamma} \cdot \chi_\gamma \cdot \sum_{\delta \in B} {}^A D_{\beta\delta} \chi_\delta \cdot \mathrm{d}v \tag{16}$$

---

[4] C. I. Ballhausen and H. B. Gray, "Molecular Orbital Theory", W. A. Benjamin INC, New York, Amsterdam, 1964.

[5] C. E. Schäffer, *Structure and Bonding*, **5**, 68 (1968).

[6] P. Spacu and C. I. Lepădatu, *Rev. Roumaine Chim.*, **17**, 335 (1972).

and

$$S^{\text{true}}_{\alpha\beta} = \sum_{\gamma\in A}\sum_{\delta\in B} {}^{B}D_{\alpha\gamma}\,{}^{A}D_{\beta\delta}\cdot S_{\gamma\delta} \tag{16'}$$

It may be shown that the S^{true} matrix is nonnegatively definite and, therefore, physically acceptable.[7]

For $BI^{\text{true}}_{A\alpha}$ it follows that:

$$BI^{\text{true}}_{A\alpha} = \int \sum_{\beta\in B} {}^{A}D_{\alpha\beta}\chi_{\beta}\,\frac{1}{r_{A\alpha}}\sum_{\gamma\in B} {}^{A}D_{\alpha\gamma}\chi_{\gamma}\,\mathrm{d}v = \sum_{\beta\in B} {}^{A}D^{2}_{\alpha\beta}\cdot BI_{A\beta} \tag{17}$$

Therefore, we can write:

$$H^{\text{true}}_{ii} = -\,\mathrm{VSIP}(i) - \sum_{L} Z_L\, BI^{\text{true}}_{Li} \tag{11'}$$

$$H^{\text{true}}_{xx} = -\,\mathrm{VSIP}(x) - Z_I\, BI^{\text{true}}_{Ix} - \sum_{L'} Z_{L'}\, BI^{\text{true}}_{L'x} \tag{12'}$$

$$H^{\text{true}}_{ix} = -\,S^{\text{true}}_{ix}\Big[(2-|S^{\text{true}}_{ix}|)\cdot\frac{\mathrm{VSIP}(i)+\mathrm{VSIP}(x)}{2} + \frac{\sum_{L} Z_L\, BI^{\text{true}}_{Li} + Z_I\, BI_{Ix}}{2}\Big] \tag{13'}$$

. . . .

and if the index "true" is cut out, we have:

$$E_i \simeq H_{ii} + \sum_{x}\left[-S_{ix}H_{ix} + \frac{\left(H_{ix} - S_{ix}\dfrac{H_{ii}+H_{xx}}{2}\right)^2}{H_{ii} - H_{xx} + \sum_{i} S_{ix}H_{ix} + \dots} + \dots\right] + {} + \sum_{y}\left[-S_{iy}\dots\right] + \dots + \sum_{x}\sum_{y}\dots \tag{8'}$$

$$E_x \simeq H_{xx} + \sum_{i}\left[-S_{ix}H_{ix} + \frac{\left(H_{ix} - S_{ix}\cdot\dfrac{H_{ii}+H_{xx}}{2}\right)^2}{H_{xx} - H_{ii} + \sum_{x} S_{ix}H_{ix} + \dots} + \dots\right] + {} + \sum_{y}\dots + \dots + \sum_{i}\sum_{y}\dots \tag{9'}$$

---

[7] S. Moldoveanu, unpublished results.

Supposing that $S_{\alpha\beta} = \delta_{\alpha\beta}$ and $Z_{L'} \simeq 0$, these expressions become:

$$E_i \simeq -\mathrm{VSIP}(i) - \sum_L Z_L BI_{Li} \qquad (8'')$$

$$E_x \simeq -\mathrm{VSIP}(x) - Z_I \cdot BI_{Ix} \qquad (9'')$$

which shows that all the results obtained as shown above, become equivalent with those obtained by means of the cristal field theory.

In order to put into practice the (8′), (9′), (8″) and (9″) formulae, it is required to know the values of $S_{\gamma\delta}$ and $BI_{A\beta}$. Therefore, the $S_{\gamma\delta}$ values are given in table 1 for the orbitals of some usual elements. These values were obtained using Slater type orbitals.

The $S_{\gamma\delta}$ values were computed using Kruglyak's papers,[8] by means of a FORTRAN program which was executed on a IBM 360/30 computer.

The $BI_{A\beta}$ values for some elements and orbitals are given in table 2. The values were obtained using Slater type orbitals.

These values were computed using Lepădatu's papers,[9] by means of a FORTRAN program which was executed on the same computer.

In order to check the (8′) and (9′) formulae, a calculation of the values of some energetic levels in $[\mathrm{TiF}_6]^{3-}$ was made. The obtained results compared to those given in,[10] can be found in table 3.

The choosing of the basis set for the molecular wave function can also be made in another way. Taking the $\{\chi_i\}$ metal orbitals and the $\{\varphi_\alpha\}$, $\{\varphi_\beta\}\ldots$ molecular orbitals of each ligand in the basis set, we obtain:

$$\{\chi\} = \{\{\chi_i\} \cup \{\varphi_\alpha\} \cup \ldots\}$$

Following the perturbational procedure described above, we get the same results as in (8′) and (9′) or (8″) or (9″) formulae, the difference being that x must be replaced by α, y by $\beta \ldots$ and $\mathrm{VSIP}(x)$ by $E^0_\alpha \ldots$. In this case, a new problem arise: the $S_{i\alpha}$, $S_{\alpha\beta}, \ldots$ values, are not known. However, the problem can be avoided, admitting of $S_{x\gamma} = \delta_{x\gamma}$ and hence, using the (8″) and (9″) formulae for the energetic levels of the molecule.

The approximation introduced in this way is justified in the calculation of the E_α by the fact that, molecular wave functions of the ligand are usually obtained supposing $S_{\alpha\beta} = \delta_{\alpha\beta}$.[11]

Consequently, φ_α having the form $\sum\limits_x c_{x\alpha}\chi_x$ and E^0_α being the energy of the α orbital, E_α may be expressed as follows:

$$E_\alpha \simeq E^0_\alpha - Z_I \int \Big(\sum_x c_{x\alpha}\chi_x\Big) \cdot \frac{1}{r_{Ix}} \cdot \Big(\sum_x c_{x\alpha}\chi_x\Big) \mathrm{d}v = E^0_\alpha - Z_I \sum_x c^2_{x\alpha} BI_{Ix} \qquad (18)$$

The use of the (8″) formula for the calculation of the values of the E_i levels, are not satisfactory because of the neglecting of all overlap integrals between the orbitals of the central atom and those of the ligands, integrals which are not null.

---

[8] Iu. A. Kruglyak, "Metody rashcheta electronnoi structury i spectrov molecul", Naucova Dumca, Kiev, 1969.

[9] C. I. Lepădatu, private comunication.

[10] H. Basch, A. Viste and H. B. Gray, *J. Chem. Phys.*, **44**, 10 (1966).

[11] K. R. Roby, *Chem. phys. Letters*, **11**, 6 (1971).

Table 1

Values of integrals $S_{\gamma\delta}$ for σ type bonds

Orbitals	$r = 1.8$ Å	$r = 2.0$Å	$r = 2.2$Å	$r = 2.4$ Å
N 2*s* Be 2*s*	0.3069	0.2513	0.2028	
N 2*s* Na 3*s*	0.2920	0.2764	0.2578	0.2372
N 2*s* Ca 4*s*	0.2015	0.2056	0.2063	0.2039
N 2*s* Sc 3*d*	0.4726	0.4476	0.4107	0.3665
N 2*s* Sc 4*s*	0.2448	0.2435	0.2379	0.2287
N 2*s* Ti 3*d*	0.4455	0.4008	0.3483	0.2938
N 2*s* Ti 4*s*	0.2606	0.2565	0.2480	0.2356
N 2*s* V 3*d*	0.3927	0.3370	0.2788	0.2234
N 2*s* V 4*s*	0.2749	0.2679	0.2562	0.2408
N 2*s* Cr 4*s*	0.2392	0.2388	0.2342	
N 2*s* Fe 3*d*	0.1256	0.2533	0.1265	0.0888
N 2*s* Fe 4*s*	0.3099	0.2929	0.2714	0.2467
N 2*s* Co 3*d*	0.1722	0.1254	0.0873	0.0588
N 2*s* Co 4*s*	0.3189	0.2983	0.2734	0.2459
N 2*s* Ni 3*d*	0.1693	0.1229	0.0854	0.0572
N 2*s* Ni 4*s*	0.3262	0.3022	0.2742	0.2439
N 2*s* Cu 3*d*	0.0884	0.0588	0.0375	0.0231
N 2*s* Cu 4*s*	0.3068	0.2909	0.2704	
N 2*s* Zn 3*d*	0.0844	0.0588	0.0375	0.0231
N 2*s* Zn 4*s*	0.3372	0.3062	0.2722	0.2370
N 2*p* Be 2*s*	0.1929	0.1691	0.1442	
N 2*p* Na 3*s*	0.4319	0.4199	0.3998	0.3739
N 2*p* Ca 4*s*	0.3023	0.3160	0.3231	0.3239
N 2p Sc 3d	0.0785	0.1243	0.1512	0.1622
N 2p Sc 4s	0.3660	0.3731	0.3716	0.3625
N 2*p* Ti 3*d*	0.1562	0.1867	0.1945	0.1865
N 2p Ti 4s	0.3890	0.3926	0.3868	0.3731
N 2*p* V 3*d*	0.2039	0.2141	0.2031	0.1798
N 2*p* V 4*s*	0.4097	0.4093	0.3991	0.3808
N 2*p* Cr 4*s*	0.3578	0.3660	0.3658	
N 2*p* Fe 3*d*			0.1539	0.1136
N 2*p* Fe 4*s*	0.4596	0.4456	0.4210	0.3888
N 2*p* Co 3*d*	0.1872	0.1488	0.1103	0.0779
N 2*p* Co 4*s*	0.4719	0.4530	0.4236	0.3870
N 2*p* Ni 3*d*	0.1855	0.1469	0.1085	0.0762
N 2*p* Ni 4*s*	0.4819	0.4582	0.4241	0.3834
N 2*p* Cu 3*d*	0.1197	0.0839	0.0556	0.0352
N 2*p* Cu 4*s*	0.4552	0.4427	0.4197	
N 2*p* Zn 3*d*	0.1197	0.0839	0.0556	0.0352
N 2*p* Zn 4*s*	0.4961	0.4627	0.4196	0.3714
O 2*s* Be 2*s*	0.2524	0.2039	0.1624	
O 2*s* Na 3*s*	0.2404	0.2274	0.2116	0.1940
O 2*s* Ca 4*s*			0.1680	0.1662
O 2*s* Sc 3*d*	0.4432	0.4109	0.3692	0.3231
O 2*s* Sc 4*s*	0.1996	0.1944	0.1951	0.1875
O 2*s* Ti 3*d*	0.4220	0.3695	0.3127	0.2572
O 2*s* Ti 4*s*	0.2134	0.2107	0.2039	0.1935
O 2*s* V 3*d*	0.3736	0.3102	0.2484	0.1930
O 2*s* V 4*s*	0.2259	0.2207	0.2111	0.1980
O 2*s* Cr 3*d*	0.2534	0.1898	0.1363	
O 2*s* Fe 3*d*	0.1873	0.1435	0.0982	0.0653
O 2*s* Fe 4*s*	0.2571	0.2429	0.2244	0.2032
O 2*s* Co 3*d*				
O 2*s* Co 4*s*	0.2651	0.2478	0.2263	0.2024

Table 1 (continued)

Orbitals	$r = 1.8$ Å	$r = 2.0$ Å	$r = 2.2$ Å	$r = 2.4$ Å
O 2*s* Ni 3*d*				
O 2*s* Ni 4*s*	0.2719	0.2513	0.2270	0.2007
O 2*s* Cu 3*d*	0.0788	0.0484	0.0285	0.1062
O 2*s* Cu 4*s*	0.2542	0.2411	0.2236	
O 2*s* Zn 3*d*	0.0788	0.0484	0.0285	0.0162
O 2*s* Zn 4*s*	0.2820	0.2551	0.2252	0.1945
O 2*p* Be 2*s*	0.1439	0.1241	0.1041	
O 2*p* Na 3*s*	0.3707	0.3579	0.3383	0.3140
O 2*p* Ca 4*s*	0.2527	0.2643	0.2701	0.2703
O 2*p* Sc 3*d*	0.0864	0.1176	0.1329	0.1359
O 2*p* Sc 4*s*	0.3110	0.3155	0.3133	0.3044
O 2*p* Ti 3*d*	0.1534	0.1693	0.1671	0.1535
O 2*p* Ti 4*s*	0.3310	0.3332	0.3271	0.3140
O 2*p* V 3*d*	0.1938	0.1908	0.1720	0.1458
O 2*p* V 4*s*	0.3501	0.3486	0.3383	0.3210
O 2*p* Cr 3*d*	0.2067	0.1730	0.1344	
O 2*p* Fe 3*d*	0.1594	0.1475	0.1081	0.0759
O 2*p* Fe 4*s*	0.3972	0.3827	0.3589	0.3287
O 2*p* Co 3*d*				
O 2*p* Co 4*s*	0.4092	0.3899	0.3613	0.3272
O 2*p* Ni 3*d*				
O 2*p* Ni 4*s*	0.4190	0.3951	0.3623	0.3241
O 2*p* Cu 3*d*	0.1042	0.0673	0.0411	0.0240
O 2*p* Cu 4*s*	0.3929	0.3799	0.3576	
O 2*p* Zn 3*d*	0.1042	0.0673	0.0411	0.0240
O 2*p* Zn 4*s*	0.4335	0.4001	0.3588	0.3137
S 3*s* Be 2*s*	0.4482	0.3795	0.3167	0.2607
S 3*s* Na 3*s*	0.4315	0.4089	0.3833	0.3554
S 3*s* Ca 4*s*		0.3163	0.3143	0.3089
S 3*s* Sc 3*d*	0.4638	0.4699	0.4585	0.4332
S 3*s* Sc 4*s*	0.3716	0.3655	0.3553	0.3413
S 3*s* Ti 3*d*	0.4187	0.4106	0.3862	0.3505
S 3*s* Ti 4*s*	0.3915	0.3819	0.3679	0.3501
S 3*s* V 3*d*	0.3642	0.3429	0.3128	0.2735
S 3*s* V 4*s*	0.4090	0.3957	0.3780	0.3565
S 3*s* Cr 4*s*	0.4035	0.3595	0.3505	0.3377
S 3*s* Fe 3*d*	0.2509	0.1778	0.1386	0.1171
S 3*s* Fe 4*s*	0.4492	0.4245	0.3956	0.3635
S 3*s* Co 3*d*	0.1634	0.1404	0.1143	0.0887
S 3*s* Co 4*s*	0.4589	0.4305	0.3978	0.3624
S 3*s* Ni 3*d*	0.1612	0.1392	0.1130	0.0877
S 3*s* Ni 4*s*	0.4669	0.4346	0.3985	0.3600
S 3*s* Cu 3*d*	0.0909	0.0741	0.0567	0.0413
S 2*s* Cu 4*s*	0.4464	0.4227	0.3948	
S 3*s* Zn 3*d*	0.0909	0.0741	0.0567	0.0413
S 3*s* Zn 4*s*	0.4782	0.4385	0.3958	0.3517
S 3*p* Be 2*s*	0.3392	0.3077	0.2717	0.2344
S 3*p* Na 3*s*	0.5638	0.5588	0.5428	0.5179
S 3*p* Ca 4*s*	0.4258	0.4446	0.4557	0.4591
S 3*p* Sc 3*d*	0.0112	0.0980	0.1621	0.2035
S 3*p* Sc 4*s*	0.4975	0.5095	0.5113	0.5039
S 3*p* Ti 3*d*	0.1064	0.1817	0.2271	0.2463
S 3*p* Ti 4*s*	0.5219	0.5303	0.5278	0.5155
S 3*p* V 3*d*	0.1761	0.2222	0.2473	0.2452
S 3*p* V 4*s*	0.5429	0.5475	0.5405	0.5234
S 3*p* Cr 4*s*		0.5017	0.5049	0.4991

Table 1 (continued)

Orbitals	$r = 1.8$Å	$r = 2.0$Å	$r = 2.2$Å	$r = 2.4$Å
S $3p$ Fe $3d$	0.3062	0.2045	0.1658	0.1549
S $3p$ Fe $4s$	0.5884	0.5807	0.5600	0.5290
S $3p$ Co $3d$	0.1868	0.1773	0.1541	0.1253
S $3p$ Co $4s$	0.5985	0.5866	0.5612	0.5258
S $3p$ Ni $3d$	0.1846	0.1766	0.1529	0.1241
S $3p$ Ni $4s$	0.6061	0.5898	0.5603	0.5206
	0.1286	0.1103	0.0873	0.0650
S $3p$ Cu $3d$	0.5855	0.5788	0.5593	
S $3p$ Cu $4s$	0.1286	0.1103	0.0873	0.0650
S $3p$ Zn $3d$	0.6149	0.5900	0.5524	0.5053
Values of integral $S_{\gamma\delta}$ for π type bonds				
N $2p$ Ti $3d$	0.2912	0.2320	0.1806	0.1379
N $2p$ V $3d$	0.2567	0.1944	0.1437	0.1040
N $2p$ Fe $3d$	0.0997	0.1270	0.0616	0.0387
N $2p$ Co $3d$	0.1096	0.1787	0.0429	0.0258
N $2p$ Ni $3d$	0.1076	0.0681	0.0418	0.0251
N $2p$ Cu $3d$	0.0544	0.0314	0.0177	0.0098
N $2p$ Zn $3d$	0.0544	0.0314	0.0177	0.0098
O $2p$ Sc $3d$	0.2423	0.2002	0.1621	
O $2p$ Ti $3d$		0.1798	0.1368	0.1022
O $2p$ V $3d$	0.2044	0.1504	0.1080	0.0760
O $2p$ Cr $3d$	0.1371	0.0905		
O $2p$ Fe $3d$	0.1023	0.0678	0.0413	0.0247
O $2p$ Ni $3d$			0.0279	0.0091
O $2p$ Cu $3d$	0.0404	0.0217	0.0459	0.0058
O $2p$ Zn $3d$	0.0404	0.0217	0.0459	0.0058
S $3p$ Ti $3d$	0.4367	0.3676	0.3016	0.2421
S $3p$ V $3d$	0.3824	0.3075	0.2425	0.1863
S $3p$ Fe $3d$	0.2314	0.1527	0.1045	0.0743
S $3p$ Co $3d$	0.1678	0.1189	0.0818	0.0548
S $3p$ Ni $3d$	0.1658	0.1176	0.0808	0.0541
S $3p$ Cu $3d$	0.0886	0.0589	0.0380	
S $3p$ Zn $3d$	0.0886	0.0589	0.0380	

The above presented theory was applied to the calculation of the absorption band in the visible range of Zn dithizonate.

Zinc dithizonate was supposed to have a square planar structure. The molecular wave functions of dithizone were obtained by the ω technique using a QCPE, FORTRAN program which was executed on a IBM 360/30 computer. The values of the E^0_α for the n and π electrons of dithizone are given in table 4.

The values of the E_α for zinc dithizonate, obtained by applying the (9″) formula with $Z_I = +0.37$ to the E^0_{10} and E^0_{14} levels in dithizone, are given in table 5.

The value $Z_I = +0.37$ is explained by the covalent character of the bondings in zinc dithizonate.

The results which give the wavelength of the absorption band in zinc dithizonate are in good agreement with the experiment.

Table 2

$BI_{A\beta}$ (eV) values for some elements and orbitals

Element B and orbital β	r_{AB}(Å)												
	1.6	1.8	2.0	2.2	2.4	2.6	2.8	3.0	3.5	4.0	5.0	6.0	8.0
H 1*s*	8.9136	7.9602	7.1814	6.5366	5.9956	5.5362	5.1416	4.7992					
Li 2*s*	7.1724	6.7688	6.3708	5.9878	5.6257	5.2878	4.9754						
Be 2*s*			7.0325	6.4547	5.9510								
C 2*s*	8.9642	7.9871	7.1952	6.5434	5.9990			4.7995		3.5997	2.8797		1.7998
C 2*pz*	10.0075	8.7469	7.7590	6.9707	6.3294			4.9692		3.6712	2.9164	2.4210	1.8088
C 2*px* and C 2*py*	8.4425	7.6072	6.9132	6.3298	5.8338	5.4076	5.0381	4.7147	4.0605	3.5639		2.3892	
N 2*s*	8.9915	7.9972	8.7105	6.5447	5.9994	5.5380	5.1424	4.7996		3.5997	2.8797	2.3998	1.7998
N 2*pz*	9.7520	8.5382	7.5952	6.8431	6.2294			4.9174		3.6494	2.9052	2.4145	1.8060
N 2*px* and N 2*py*	8.6113	7.7266	7.0006	6.3955	5.8844					3.5748	2.8670	2.3924	1.7967
O 2*s*	8.9976	7.9989	7.1993	6.5448	5.9995	5.5380	5.1424	4.7996		3.5997	2.8797	2.3998	1.7998
O 2*pz*	9.5649	8.3990	7.4913	6.7643	6.1685	5.6709	5.2489	4.8861		3.6362	2.8984	2.4106	1.8044
O 2*px* and O 2*py*	8.7140	7.7989	7.0533	6.4351	5.9149	5.4715	5.0892	4.7563		3.5814	2.8704	2.3944	1.7976
Na 3*s*	6.1736	5.9806	5.7623	5.5272	5.2830	5.0368	4.7940	4.5590	4.0211				
Mg 3*s*	7.3752	6.9672	6.5503		5.7510	5.3867	5.0512	4.7451	4.0994				
Al 3*s*		7.5147	6.9329	6.4006	5.9224	5.4974	5.1213	4.7887		3.5993	2.8797	2.3998	1.7998
Al 3*pz*		9.2384	8.4091	7.6426	6.9571	6.3556	5.8332	5.3810		3.8581			
Al 3*px* and Al 3*py*		6.6528	6.1948	5.7795	5.4051	5.0683	4.7653	4.4926		3.4699			
P 3*s*	8.7984	7.9147	7.1646	6.5309	5.9939								
P 3*pz*	10.5096	9.2449	8.1933										
P 3*px* and P 3*py*	7.9428	7.2497	6.6502										
S 3*s*	8.9096	7.9668	7.1879						4.1139	3.5997	2.8797	2.3998	1.7998
S 3*pz*	10.3887	9.0720	8.0197						4.2736	3.7067	2.9345	2.4315	1.8132
S 3*px* and S 3*py*	8.1702	7.4142	6.7720						4.0341	3.5462			
K 3*pz*		5.0868	4.9777										
K 4*s*		3.9791	3.9557										
Ca 3*pz*		6.1975	5.9438	5.6754									

Ca 4*s*		5.0810	4.9947	4.8874							
Sc 3*s*	8.9990	7.9993	7.1993	6.5449	5.9995						
Sc 3*pz*			7.4665		6.1541		5.2398				
Sc $3dz^2$		9.2193	8.5538	7.8760	7.2244	6.6217	6.0781	5.5958	4.6323	3.9393	
Sc 4*s*			5.2031	5.0721	4.9212	4.7553					
Ti 3*s*	8.9992	7.9993	7.1994	6.5449	5.9995	5.5380					
Ti 3*pz*	9.4285	8.3009	7.4192	6.7100	6.1267	5.6280					
Ti 3*px* and											
Ti 3*py*	8.7845	7.8485	7.0894	6.4623	5.9359						
Ti $3dz^2$	10.6255	9.6229	8.6632	7.7947	7.0349	6.3825	5.8270	5.3545	4.4503		
Ti $3dx^2-y^2$ and											
Ti 3*dxy*			6.0716	5.6686	5.3070	4.9823	4.6904				
Ti 3*dxz* and											
Ti 3*dyz*	8.3133	7.6617	7.0601	6.5159		5.5978	5.2151	4.8758			
Ti 4*s*	5.6318	5.5290	5.3976	5.2410	5.0645	4.8740	4.6756	4.4746			
V $3dz^2$		9.5741	8.4723	7.5478							
V $3dx^2$-y^2 and											
V 3*dxy*			6.3420	5.8849	5.4817	5.1249	4.8079				
V 3*dxz* and											
V 3*dyz*			7.2235	6.6145	6.0863						
V 4*s*		5.7340	5.5771	5.3939	5.1914	4.9767					
Cr $3dz^2$	10.5028	9.0925	7.9921				5.4016				
Cr 3*dxz* and											
Cr 3*dyz*	9.0616	8.1085	7.3163				5.2154				
Cr 4*s*		5.2351	5.1348	5.0119	4.8695	4.7118					
Mn $3dz^2$											
Mn 4*s*		6.1191	5.9047	5.6643	5.4083	5.1462					
Fe $3dz^2$	10.2473	8.8712	7.8180	6.9945	6.3350	5.7946	5.3430	4.9594	4.2109		
Fe 3*dxz* and											
Fe 3*dyz*	9.1193	8.1297	7.3197	6.6497	6.0887	5.6134	5.2061	4.8536	4.1504		
Fe 4*s*		6.2919	6.0472	5.7780	5.4962	5.2123					
Co $3dz^2$	10.0205	8.6967	7.6896								
Co 3*dxz* and											
Co 3*dyz*	9.1435	8.1331	7.3143								
Co 4*s*		6.4576	6.1810	5.8823	5.5749	5.2699					
Ni $3dz^2$		8.5645	7.5958	6.8331	6.2155	5.7042					
Ni 3*dzx* and											
Ni 3*dyz*		8.1284	7.3058	6.6317	6.0704	5.5962					
Ni 4*s*		6.6081	6.2998	5.9726	5.6414	5.3174					
Cu $3dz^2$		8.3874	7.4728	6.7449	6.1504	5.6547					
Cu 3*dxz* and											

Table 2 (continued)

Element B and orbital β	r_{AB}(Å)											
	1.6	1.8	2.0	2.2	2.4	2.6	2.8	3.0	3.5	4.0	5.0	6.0	8.0
Cu $3dyz$		8.1108	7.2872	6.6145	6.0553	5.5831							
Cu $4s$		6.2369	6.0022	5.7424	5.4689	5.1919							
Zn $3dz^2$		8.3874	7.4728	6.7449	6.1504	5.6547	5.2346	4.8737					
Zn $3dx^2$-$y^2$and Zn $3dxy$		7.6933	6.9747	6.3752	5.8682	5.4344							
Zn $4s$		6.8798	6.5071	6.1248	5.7492	5.3915							
Zr $4dz^2$			7.3231	7.1484	6.8952	6.5856	6.2417	5.8831	5.0133	4.2715			
Zr $4dx^2$-$y^2$and Zr $4dxy$			4.7884					3.8739					
Zr $4dyz$ and Zr $4dyz$			5.6995					4.5947	4.0757				
Zr $5s$		4.2541	4.2302	4.1951	4.1474	4.0864							
Ag $4dz^2$			8.1245		6.5040		5.4415			3.6922			
Cd $4dz^2$			8.1254		6.5040		5.4415			3.6922			

Table 3

Some energetic levels in $[TiF_6]^{3-}$

Orbital x_i	E_i energy given in[10]	E_i energy found by (8)
$3dz^2$	− 9.0629 eV	−6.64 eV
$3dxy$	−11.2078 eV	−8.84 eV

Table 4

Energetic levels for dithizone obtained by ω technique the wavelengths corresponding to different transitons and experimental wavelengths

Molecular orbital in dithizone	Energy in eV	λ computed in nm	λ noticed in nm
φ_{18}	− 4.41	260	263
φ_{17}	− 4.91	290	295
φ_{16}	− 5.31	320	323
φ_{15}	− 6.43	450	445
φ_{14}	− 7.15	609	600
φ_{13}	− 7.58	771	765
φ_{12}	− 8.55		
φ_{11}	− 8.67		
φ_{10}	− 9.19		
φ_9	−10.78		
φ_8	−12.43		
φ_7	−14.18		
φ_6	−14.29		
φ_5	−14.40		
φ_4	−14.52		
φ_3	−15.53		
φ_2	−17.11		
φ_1	−17.12		

Table 5

E_α values of the energy obtained by the relation (9″)

Molecular orbital in Zn dithizonate	Energy in eV	λ computed in nm	λ noticed in nm
φ_{14}	−10.38	526	535
φ_{10}	−12.74		

Acknowledgements. The authors express their grateful thanks to Dr. C. I. Lepădatu for fruitful discussions and to the staff of the Computing Centre of the Bucharest University for assistance in obtaining tables 1 and 2.

Revue Roumaine de Chimie, **18**, *11*, 1897–1902 (1973)

KINETICS AND MECHANISM OF SUBSTITUTION REACTIONS OF COMPLEXES. LII*

BASIC HYDROLYSIS OF *TRANS*-DI-ISOTHIOCYANATO-BIS-ETHYLENE-DIAMINE-CHROMIUM (III) IONS

J. ZSAKÓ, CS. VÁRHELYI and F. MÁNOK

Faculty of Chemistry, Babeş-Bolyai University, Str. Arany János 11, Cluj, Romania

Received February 2, 1973

The hydrolysis of the complex *trans*-$[Cr(en)_2(NCS)_2]^+$ studied involves in basic solutions the pre-equilibrium $[Cr(en)(en^-)(NCS)_2]$ (I) $\rightleftarrows$ $[Cr(en^-)_2(NCS)_2]^-$ (II) $+ H^+$. Species (I) undergoes an aquation reaction and species (II) an olation reaction. Equilibrium constant of the above reaction and kinetic parameters of the aquation and olation reactions were derived from experimental data obtained at different temperatures between 50 and 65°. Results are discussed in terms of electronic structure of the complex and of electronic effects due to the deprotonation of ehtylenediamine.

In our previous paper[1] the aquation of *trans*-$[Cr(en)_2(NCS)_2]^+$ has been studied in acid solutions. In these conditions the complex studied participates in a protolytic preequilibrium, which involves the transformation of a co-ordinated ethylenediamine molecule in a deprotonated anion : en^-. Thus, the equilibrium can be expressed by means of the following equation :

$$[Cr(en)_2(NCS)_2]^+ \rightleftarrows [Cr(en)(en^-)(NCS)_2] + H^+ \quad (1)$$

and it can be characterized by the equilibrium constant K_1. Both complex species suffer an aquation. The first stage of the aquation correspond to the equations :

$$[Cr(en)_2(NCS)_2]^+ + H_2O = [Cr(en)_2(H_2O)(NCS)]^{2+} + NCS^- \quad (2)$$

$$[Cr(en)(en^-)(NCS)_2] + H_2O = [Cr(en)(en^-)(H_2O)(NCS)]^+ + NCS^- \quad (3)$$

---

[*] Part LI. Cs. Várhelyi, J. Zsakó and G. Simó, *Stud. Univ. Babeş-Bolyai, Chem.*, **18**, (2) (1973).

[1] Cs. Várhelyi, J. Zsakó and G. Simó, *Stud. Univ. Babeş-Bolyai, Chem.*, **18**, (1), (1973).

Reaction (3) is faster than (2) and it needs a lower activation enthalpy than the later. Since equilibrium (1) is shifted to left with increasing acidity, the apparent rate constant of the aquation decreases.

The firts stage of the reaction is followed by the substitution of the second NCS, *viz.* reaction (2) is followed by

$$[Cr(en)_2 (H_2O) (NCS)]^{2+} + H_2O = [Cr(en)_2(H_2O)_2]^{3+} + NCS^- \qquad (4)$$

and reaction (3) by

$$[Cr(en)(en^-)(H_2O)(NCS)]^+ + H_2O = [Cr(en)(en^-)(H_2O)_2]^{2+} + NCS^- \qquad (5)$$

Reaction (4) is very fast and it occurs practically simultaneous with reaction (2), i.e. both NCS ligands leave the complex ion at the same time. On the contrary, reaction (5) seems to have a rate comparable to that of reaction (3).

In basic solutions the analogous chloro-complex undergoes a second order olation reaction, the Cl atoms being substituted for OH groups. The rate of this olation reaction is much larger than the rate of aquation, rate constants are about 10^3 times higher at the same temperature[2]. In this respect there is a fundamental difference between the $[Cr(en)_2X_2]^+$ and the $[Co(en)_2X_2]^+$ type complexes, since in the case of the cobalt complexes the ratio of the second order olation rate constant to the first order aquation rate constant is 10^8 at 25° for the *trans*-$[Co(en)_2Cl_2]^+$ complex ion.[2]

Thus, for the complex studied, easily measurable reaction rates can be expected also in basic solutions. Our kinetic measurements have been performed between 50 and 65⁰ at OH^- concentrations comprised between $5 \cdot 10^{-4}$ and $7 \cdot 10^{-3}$. Kinetics of the reaction has been followed by measuring the concentration of NCS^- ions liberated. The graphical plot of $\log c/(c-x)$ *vs.* time, where c stands for the initial concentration of the complex and x for the concentration of NCS^- ions liberated, showed an initial linear portion, followed by positive deviations, as seen in fig. 1.

On the basis of these results the first stage of the reaction can be presumed to be of apparent first order, followed by the substitution of the second NCS. This second stage cannot be instantaneous, which allows the quite accurate construction of the zero time tangency of the kinetic curve. From the slope of these tangencies, apparent first order rate constants k_{exp} have been derived. The graphical plot of rate constants obtained *vs.* $[OH]^-$ is given in fig. 2.

The linear portion of these curves at higher $[OH^-]$ values pleads for a second order olation reaction. The first portion of the curves, especially the decreasing of rate constants with increasing $[OH^-]$ at lower $[OH^-]$values, suggests the idea that also a protolytic pre-equilibrium is involved. Presumably, also the second ethylenediamine molecule loses a proton and the equilibrium of the following reaction is established:

$$\underset{\text{I}}{[Cr(en)(en^-)(NCS)_2]} \rightleftarrows \underset{\text{II}}{[Cr(en^-)_2(NCS)_2]^-} + H^+ \qquad (6)$$

characterized by the equilibrium constant K_2.

---

[2] R. G. Pearson, R. A. Munson and F. Basolo, *J. Amer. Chem. Soc.*, **80**, 504 (1958).

Thus, the following reaction scheme has been presumed : species I undergoes the simple first order aquation reaction (3) ; species II cannot give a similar aquation reaction, it participates in the following olation reaction :

$$[\mathrm{Cr}\,(\mathrm{en}^-)_2\,(\mathrm{NCS})_2]^- + \mathrm{OH}^- = [\mathrm{Cr}\,(\mathrm{en}^-)_2\,(\mathrm{NCS})\,(\mathrm{OH})]^- + \mathrm{NCS}^- \qquad (7)$$

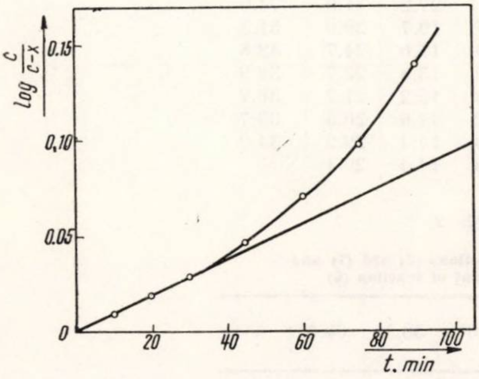

Fig. 1. — Determination of k_{exp}, 50°, $[\mathrm{OH}^-] = 5 \times 10^{-3}$.

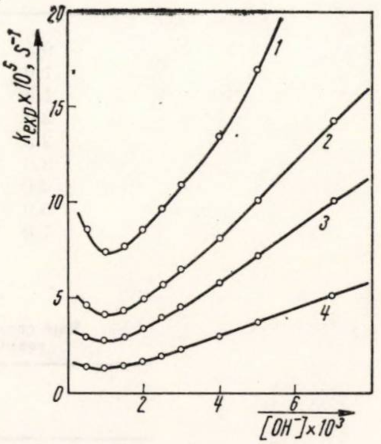

Fig. 2. — Influence of $[\mathrm{OH}^-]$ upon the rate constants k_{exp}. *1*, 65° ; *2*, 60.5° ; *3*, 56.5° ; *4*, 50°

If this scheme is true, for the apparent first order rate constant the following expression can be derived :

$$k_{\mathrm{exp}} = \frac{k_1 K_w + k_2 K_2 [\mathrm{OH}^-]^2}{K_w + K_2 [\mathrm{OH}^-]} \qquad (8)$$

taking into account equilibrium (6). In the above expression k_1 and k_2 stand for the rate constants of reactions (3) and (7), respectively, and K_w for the ionic product of water.

If the equilibrium is shifted to the right and the OH^- ion concentration exceeds sufficiently the total complex concentration, reaction (7) will be of apparent first order and the second order rate constants k_2 can be obtained as the ratio $k_{\mathrm{exp}}/[\mathrm{OH}^-]$. This ratio is given in table 1 and one can see that at higher $[\mathrm{OH}^-]$ values it has practically constant value indeed, which may be taken for k_2. Mean values of k_2 are presented in table 2.

In order to derive the corresponding k_1 and K_2 values, relation (8) has been written in the following form :

$$k_{\mathrm{exp}} = (k_{\mathrm{exp}} - k_2[\mathrm{OH}^-])\,[\mathrm{OH}^-]\frac{K_2}{K_w} + k_1 \qquad (9)$$

It is obvious that the coefficient of K_2/K_w on the right side of eq. (9) can be calculated for each temperature and each $[OH^-]$ value used.

Table 1

Ratio $10^3 \times k_{exp}/[OH^-]$, in M^{-1} sec^{-1}

$[OH^-] \times 10^3$	50°	56.5°	60.5°	65°
0.5	27.8	59.8	93.2	172
1.0	12.9	27.2	41.0	74.0
1.5	9.67	19.7	29.0	51.3
2.0	8.50	17.0	24.7	42.8
2.5	8.00	15.8	22.7	38.9
3.0	7.73	15.2	21.7	36.7
4.0	7.52	14.6	20.5	33.7
5.0	7.56	14.4	20.2	34.0
7.0	7.45	14.4	20.4	—

Table 2

Rate constants of reactions (3) and (7) and equilibrium constant of reaction (6)

	50°	56.5°	60.5°	65°
$k_1 \times 10^5$, s^{-1}	2.93	6.24	9.52	16.5
$k_2 \times 10^3$, M^{-1}, s^{-1}	7.51	14.5	20.4	33.8
$K_2 \times 10^{10}$	1.67	2.25	2.63	2.80

According to eq. (9), the graphical plot of k_{exp} for a given temperature *vs.* the coefficient of K_2/K_w must give a straight line. In fig. 3, the graphical plot of k_{exp} *vs.* $(k_{exp}-k_2[OH^-])$ $[OH^-]$ is given for the working temperatures used. As seen, a rather good linearity has been obtained, pleading for the correctness of the above given reaction scheme. The parameters of the straight lines obtained have been derived by means of the least square method. The ordinata intercept has been taken for k_1 and from the slope of the straight lines K_2 has been calculated using literature data[3] for K_w. Values obtained for k_1 and K_2 are also given in table 2.

Rate constants of reaction (3) have been derived also in our previous paper[1] from experimental data concerning the aquation in acid solutions. In these conditions $k_1 = 19.5 \times 10^{-5}$ s^{-1} has been derived for 65° which is in a rather good agreement with the value of 16.5×10^{-5} s^{-1} obtained in this paper.

As far as the activation parameters are concerned, they have been obtained by means of a graphical plot of log k/T *vs.* $1/T$, given in fig. 4.

As seen, a rather good linearity has been obtained, which enabled us to derive activation enthalpy and entropy values from the parameters of the straight lines, calculated by means of the least square method. Results are presented in table 3, together with those obtained earlier.[1]

---

[3] K. P. MISHCHENKO and A. A. RAVDEL "Kratkii spravochnik fizikokhimicheskih velichin", Izd. Khimia, Moscow, 1965, p. 106.

In the case of reaction (3), involved in the total process both in acid and basic solutions, pratically the same activation parameters have been obtained. This means, that the above given reaction scheme is consistent with our experimental data.

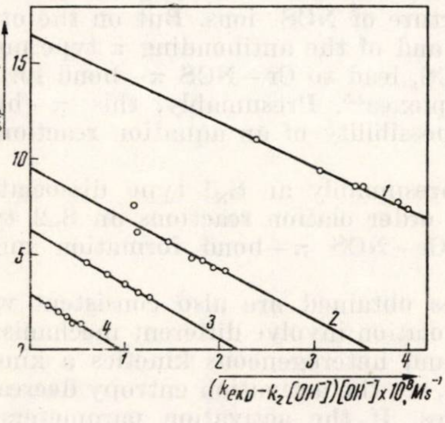

Fig. 3. — Determination of k_2 and K_2.

1, 65° ; *2*, 60.5° ; *3*, 56.5° ; *4*, 50°

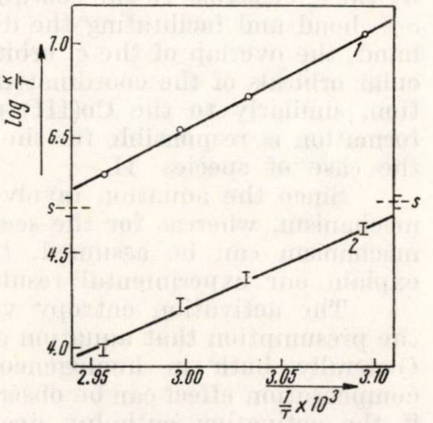

Fig. 4. — Determination of activation parameters.

1, reaction (3) ; *2*, reaction (7).

Table 3

Activation parameters of reactions (2), (3) and (7)

Reaction	$\Delta H^{\neq}$, kcal/mole	$\Delta S^{\neq}$, Cl	Reference
(2)	29.6 ± 0.7	7.3 ± 2.2	1
(3)	24.3 ± 1.2	-4.0 ± 3.1	1
(3)	24.2 ± 0.9	-4.5 ± 2.1	this paper
(7)	20.7 ± 0.7	-4.2 ± 1.5	this paper

The rather low value of K_2, as compared to K_1, which is of the order of magnitude of 10^{-3}, seems to be understandable, since both N-atoms involved are co-ordinated to the same central ion and the deprotonation of the first N-atom must exert a very important influence upon the deprotonation of the second N-atom.

The much lower activation enthalpy of reaction (3) as compared to reaction (2) has been explained[4] in terms of the electronic effects. The unshared *p*-electrons of the deprotonated N-atom exert a repulsion upon the coordinated NCS^- ions and makes easier their departure. The same effect can be expected in the case of the deprotonation of the second N-atom. In this respect, the decreasing of k_{exp} with increasing $[OH^-]$ in the first portion of the curves given in fig. 2 is quite surprising. Nevertheless, it can be explained taking into account the possibility of π-bond formation between Cr and the coordinated NCS. The Cr^{3+} ion has three

3 d electrons which occupy the t_{2g} orbitals in O_h field. In the case of our complex, the symmetry of the ligand field is D_{4h} in which the T_{eg} level is splitted in $B_{2g}+E_g$. On the one hand, the repulsion of the unshared p-electrons of the deprotonated ethylenediamine N-atom is transmitted by the e_g electrons to the coordinated NCS, thus weakening the Cr—NCS σ — bond and facilitating the departure of NCS^- ions. But on the other hand, the overlap of the e_g orbitals and of the antibonding π type molecular orbitals of the coordinated NCS, lead to Cr—NCS π—bond formation, similarly to the Co(III) complexes[4,5]. Presumably, this π—bond formation is responsible for the impossibility of an aquation reaction in the case of species II.

Since the aquation involves presumably an S_N1 type dissociation mechanism, whereas for the second order olation reactions an S_N2 type mechanism can be assumed, the Cr—NCS π—bond formation might explain our experimental results.

The activation entropy values obtained are also consistent with the presumption that aquation and olation involve different mechanisms. Generally, both in homogeneous and heterogeneous kinetics a kinetic compensation effect can be observed, *viz.* the activation entropy decreases if the activation enthalpy decreases. If the activation parameters of reactions (2) and (3) are compared, this effect can be clearly observed. On the contrary, the activation entropy of reactions (3) and (7) has practically the same value, although activation enthalpies are sensible different.

Thus, in the case of reactions (2) and (3) the same mechanism can be presumed, but for reaction (7) a different one seems to be likely.

EXPERIMENTAL

Synthesis of *trans*-$[Cr(en)_2(NCS)_2]ClO_4$ has been performed as described earlier[1].

Kinetic measurements. Samples of the complex were dissolved in preheated water. Calculated amounts of preheated NaOH and $NaNO_3$ solutions were added to ensure the needed alcalinity and the constant ionic strength of $J = 1$ M. The solutions with a total complex concentration of 2.10^{-3}M were kept in an ultrathermostat maintaining the working temperature with an accuracy of ±0.01°. The samples taken at different time intervals were poured in ice cooled 0.1 M $HClO_4$ solution in order to stop the reaction. The concentration of NCS^- ions liberated were determined by means of potentiometric titrations with $AgNO_3$ solution, using a silver wire as indicator electrode.

Acknowledgement. Authors thank to Mr. G. Hasznosi for carrying out some kinetic measurements.

---

[4] Z. Finta, Cs. Várhelyi and J. Zsakó, *J. Inorg. Nuclear Chem.*, **32**, 3013 (1970).

[5] Cs. Várhelyi, J. Zsakó and Z. Finta, *Monatsh*, **101**, 1013 (1970).

Revue Roumaine de Chimie, **18**, *11*, 1903–1909 (1973)

COMPUTER EVALUATION OF THE ASSOCIATION CONSTANTS OF SILVER-CHLORO AND -BROMO COMPLEXES IN MOLTEN SODIUM NITRATE-BARIUM NITRATE EUTECTIC

H. C. GAUR and N. P. BANSAL*

Department of Chemistry, University of Delhi, Delhi–110007, India

Received February 17, 1973

Association constants of silver-chloro and -bromo complexes in the molten eutectic $NaNO_3-Ba(NO)_3)_2$ at 350°, 375° and 400° have been evaluated using a computer method. The values of these constants have been compared with those reported earlier using the graphical extrapolation procedure. The computer method does not suggest formation of dinuclear complex species in solution.

INTRODUCTION

The computation of association constants from various types of experimental data using graphical methods has been extensively discussed by Rossotti and Rossotti[1]. The graphical procedures have been critically evaluated by Braunstein *et al.*[2] who proposed a modified graphical technique which employs a series in the stoichiometric concentrations of reactants ; this is an improvement because, *inter alia*, it eliminates the usual graphical successive approximation steps. The graphical method of Braunstein *et al.* is self-consistent, direct and simple for evaluating K_{11}, K_{12} and K_{21}. However, for higher species it becomes somewhat cumbersome and the need of other procedures which can compute these association constants becomes increasingly obvious.

In recent years, digital computers for evaluating association constants from various types of data in aqueous solutions, e.g., potentiometric[3], polarographic[4], pH-titration[5,6], etc. have been increasingly used. Several

---

[*] Present address : Ramjas College, Delhi University, Delhi–110007, India.

[1] F. J. C. Rossotti and H. Rossotti, "The Determination of Stability Constants", McGraw Hill Book Company, Inc., New York, 1961.

[2] J. Braunstein, M. Blander and R. M. Lindgren, *J. Amer. Chem. Soc.*, **84**, 1529 (1962).

[3] D. Inaman, I. Regan and B. Girling, *J. Chem. Soc.*, **59**, 348 (1964).

[4] K. Momoki, H. Sato and H. Ogawa, *Bulletin Faculty of Enginerring, Yokohama National University*, **16**, 127 (1967).

[5] R. C. Lansbury, V. E. Price and A. G. Smeeth, *J. Chem. Soc.*, **345**, 1896 (1965).

[6] I. G. Sayce, *Talanta*, **15**, 1397 (1968).

applications in molten salt solution using the potentiometric and polarographic[7-12] data have also been reported.

A comparison between the association constants from graphical and computer methods in molten salt solutions has been recently made[13]; particularly the discrepancies in the association constants of dinuclear species calculated by the two procedures have been pointed out.

In this study, the association constants for the formation of silver-chloro and -bromo complexes in the molten eutectic $NaNO_3$-$Ba(NO_3)_2$ in the temperature range 350−400° have been evaluated from the potentiometric data using a computer procedure[14] which is essentially similar to the one employed by Inman *et al* [3,12]. The values of association constants thus obtained have also been compared with those reported earlier[15-17] using the graphical extrapolation procedure.

EXPERIMENTAL

The electrolytic cell, furnace, temperature control unit, electrodes, preparation of the solvent and the general experimental technique have been described earlier.[15-18] About 250 g of the eutectic mixture was used for each experiment. All measurements were carried out under an inert nitrogen atmosphere. The melt temperature was controlled within ±1° of the set value and was measured with a calibrated chromel-alumel thermocouple. The potential measurements were made with a vernier potentiometer (Bajaj-Kaycee).

The concentration cell (A) was set up.

$$\begin{array}{c|l||l|cc} & \mathrm{AgNO_3}(T_{\mathrm{Ag}}) & \mathrm{AgNO_3}(T_{\mathrm{Ag}})^{*} & & \\ \mathrm{Ag} & & \mathrm{NaX} & \mathrm{Ag} & \mathrm{(A)} \\ & \mathrm{NaNO_3-Ba(NO_3)_2} & & & \\ & & \mathrm{NaNO_3-Ba(NO_3)_2} & & \\ (-) & & & (+) & \end{array}$$

Reference half-cell Indicator half-cell

In the absence of NaX ($X = Cl, Br$), the cell emf followed Nernst behaviour[15,16] in the concentration range $T_{Ag^+} = 7.95 \times 10^{-5}$ to $3.4 + 10^{-3}$ (moles per mole solvent). On addition of NaX to the indicator half-cell, at Ag^+ and X^- concentrations too low to precipitate the silver halide, the cell emf decreased which has been ascribed[2] to complex formation rather than to any non-ideal behaviour in the solution. For a given initial $T_{Ag}{}^*$, change in the emf of the cell (ΔE), in the presence and absence of sodium halide, was obtained as a function of T_X. This constituted one set of data. Several sets of data at T_{Ag}, varying between 1.455×10^{-4} to $1.178 \times \times 10^{-3}$ for chloro complexes and 0.833×10^{-4} to 4.372×10^{-4} for bromo complexes at 350°, 375° and 400°, were obtained.

---

* See List for symbols

[7] D. Inman, *Electrochim. Acta*, **10**, 11 (1965).

[8] S. H. White, D. Inman and B. Jones, *Trans. Faraday Soc.*, **64**, 2841 (1968).

[9] D. Inman, B. Jones and S. H. White, *J. Inorg. Nuclear Chem.*, **32**, 927 (1970).

[10] R. S. Sethi, Ph. D. Thesis, University of Delhi, 1966.

[11] D. Inman, D. G. Lovering and R. Narayan, *Trans. Faraday Soc.*, **64**, 2476 (1968).

[12] D. Inman, S. H. White, I. Wilmot (Nee Regan) and B. Jones, *J. Electroanalyt. Chem.*, **33**, 225 (1971).

[13] J. Braunstein, *J. Electroanalyt. Chem.*, **33**, 235 (1971).

[14] H. C. Gaur and G. N. Singhal (unpublished work).

[15] H. C. Gaur and N. P. Bansal, *Indian J. Chem.*, **9**, 1273 (1971).

[16] H. C. Gaur and N. P. Bansal, *J. Chem. Soc., Faraday Trans.* I, **68**, 1368 (1972).

[17] H. C. Gaur and N. P. Bansal, *Indian J. Chem.*, **10**, 202 (1972).

[18] H. C. Gaur, S. K. Jain and N. P. Bansal, *J. Electroanalyt. Chem.*, **30**, 225 (1971).

COMPUTATIONAL PROCEDURE

Considering the association equilibria involving the formation of the species * AgX, AgX_2^- and Ag_2X^+,

$$\begin{gathered} Ag^+ + X^- \rightleftharpoons AgX \\ Ag^+ + 2X^- \rightleftharpoons AgX_2^- \qquad (1) \\ 2Ag^+ + X^- \rightleftharpoons Ag_2X^+ \end{gathered}$$

in dilute solutions of $AgNO_3$ and NaX in the molten solvent $NaNO_3-Ba(NO_3)_2$ and the corresponding formation constants given by

$$\beta_{mn} = \frac{C^{-(n-m)}_{Ag_mX_n}}{C^m_{Ag}\, C^n_X} \qquad (2)$$

where m and n take up the values 1 and 2 for the above species; the total (stoichiometric) concentration of silver nitrate (T_{Ag}) and the halide (T_X) is given by the metal-balance and ligand-balance equations:

$$\begin{aligned} T_{Ag} &= C_{Ag} + C_{AgX} + C_{AgX_2} + 2C_{Ag_2X} + \dots \\ &= \beta_0 C_{Ag} + \beta_{11} C_{Ag} C_X + \beta_{12} C_{Ag} C_X^2 + 2\,\beta_{21} C_{Ag}^2 C_X + \dots \qquad (3) \\ &= C_{Ag}\,[\beta_0 + \Sigma m \beta_{mn} C^{m-1}_{Ag} C^n_X] \end{aligned}$$

$$\begin{aligned} T_X &= C_X + C_{AgX} + 2C_{AgX_2} + C_{Ag_2X} + \dots \\ &= C_X + \beta_{11}\, C_{Ag} C_X + 2\,\beta_{12}\, C_{Ag} C_X^2 + \beta_{21}\, C_{Ag}^2 C_X + \dots \qquad (4) \\ &= C_X\,[1 + \Sigma n \beta_{mn}\, C^m_{Ag} C^{n-1}_X] \end{aligned}$$

---

* Previous studies showed that these were the only significant species and hence higher species were not included in computation. Charges on the species are not written to avoid confusion with algebric operators.

It is seen from (3) that β's are a function of C_{Ag} and C_X, whereas the experimental data are in terms of ΔE and T_X. The ΔE can be correlated with the "free" (C_{Ag}) and total (T_{Ag}) silver-ion concentrations by the relation [2]:

$$\Delta E = 2.303 \frac{RT}{F} \log \frac{C_{Ag}}{T_{Ag}} \qquad (5)$$

which enables the knowledge of C_{Ag}. The C_X and β's were simultaneously evaluated using a Newton-Raphson iterative [19] procedure involving the ligand-balance equation (4), in conjunction with least squares fitting of the metal-balance equation (3) in the following manner [14]:

In the first step, C_X was approximated equal to $(T_X + C_{Ag} - T_{Ag})$, and preliminary values of β's for the first cycle were obtained from equation (3) by least squares fitting. Using these values of β's, a Newton-Raphson iteration on the ligand-balance equation (4) was carried out till constant C_X values were obtained. The complete cycle (least square fitting and Newton-Raphson iteration) was repeated using the new C_X values (obtained in a previous cycle). This cycling was continued until successive β's and C_X values were constant within a given range (0.1 %) during the final two or three cycles. The β's, C_X and the other parameters as $\sigma \Delta E, \Delta E_c, \bar{n}$ were printed out.

The data were analysed in three different ways; one of these considered the formation of only the species AgX and computed β_{11} (one degree fit). The other two programs were used for a two degree-fit of the data; one of these considered only the presence of mononuclear species AgX, AgX_2^- and evaluated β_{11}, β_{12} while the other considered AgX, AgX_2^- and Ag_2X^+ and simultaneously computed values of β_{11}, β_{12} and β_{21}.

RESULTS AND DISCUSSION

For two typical cases where $T_{Ag} = 5.608 \times 10^{-4}$ at 350° for chloro complexes and $T_{Ag} = 2.755 \times 10^{-4}$ at 400° for bromo complexes; the print out of β's, C_X and $\bar{n}$ in the final cycle and the one previous to it are presented in tables 1 and 2. Results show satisfactory constancy* in iterated ligand concentrations C_X and the formation constants β's evaluated from the experimental $\Delta E - T_X$ data. Similar constancy was observed with all the data analysed by this method.

For the silver-chloro complexes it was seen that $\sigma\Delta E$ for two-degrees fit are smaller than that for the corresponding one-degree fit, although there is wide scatter in β_{12} values obtained from different sets of data. In some of the sets β_{12} values were even negative. It appeared appropriate to use results only from one degree fit for determining the mean values of β_{11}. In the case of bromo-system, two-degrees fit gave negative values of β_{12}. This may be considered to arise from the fitting of a higher degree polynomial than is probably justified by the limited range of data for this system or the formation of the various species. Here again only the β_{11} values obtained from one-degree fit were used in taking the mean values.

---

[19] H. Margenau and G. M. Murphy, "The Mathematics of Physics and Chemistry", Affiliated East-West Press Private Ltd., New Delhi, 1963, (Indian edition).

* A small systematic error in the data is shown by the values of β_0 which are slightly different from unity. Graphically, the β_0 values cannot be distinguished from unity.

Table 1

Values β_{mn}, $\bar{n}$ C_{Cl^-} in two consecutive cycles

(Silver-chloro system)
Temp. = 350°C
$T_{Ag} = 5.608 \times 10^{-4}$ mol mol^{-1} of solvent

	Cycle 5	Cycle 6	$\sigma\Delta E$ (mV)
β_0	1.005	1.005	0.5641
B_{11}	269.01	269.01	0.5641
B_{12}	128.30	128.30	0.5641

Cycle 5		Cycle 6	
$\bar{n}$	$C_{Cl^-} \times 10^4$	$\bar{n}$	$C_{Cl^-} \times 10^4$
0.902	0.601	0.902	0.601
0.932	1.418	0.932	1.418
0.926	2.575	0.926	2.575
0.966	4.266	0.966	4.266
0.952	5.736	0.952	5.736
0.973	7.263	0.973	7.263
1.035	9.031	1.035	9.031
1.022	10.847	1.022	10.247
1.076	12.478	1.076	12.478
1.069	14.099	1.069	14.099
1.063	16.599	1.068	16.599
1.055	18.960	1.055	18.960

Table 2

Values of β_{mn}, $\bar{n}$ and C_{Br^-} in two consecutive cycles

(Silver-bromo system)
Temp. = 400°C
$T_{Ag} = 2.755 \times 10^{-4}$ mol mol^{-1} of solvent

	Cycle 92	Cycle 93	$\sigma\Delta E$ (mV)
β_1	0.996	0.996	0.2754
β_{11}	885.30	885.28	0.2754
β_{12}	23970	23960	0.2755

Cycle 92		Cycle 93	
$\bar{n}$	$C_{Br^-} \times 10^4$	$\bar{n}$	$C_{Br^-} \times 10^4$
1.088	0.4434	1.088	0.4434
1.063	0.7871	1.063	0.7871
1.046	1.1458	1.046	1.1458
1.062	1.5489	1.062	1.5489
1.002	1.9022	1.002	1.9022
1.025	3.0624	1.025	3.0624

The values of β's obtained from two-degrees fit (including dinuclear term) of the data were negative in all the cases, except one set. The results of various degree fits for this set are presented in table 3.

In table 4, K_{11} for chloro and bromo complexes of silver, as evaluated by the computer procedure, are compared with those obtained by the graphical extrapolation method. It is seen that there is a striking agreement between the K_{11} values obtained by the two methods in spite of the limitations associated particularly with the latter (computer) procedure. It may be pointed out that association constants evaluated by the computer method are not truly thermodynamic parameters as calculated by the graphical method. Also in the computer method, the error introduced in evaluating the previous association constant probably gets accumulated in the higher association constants, while it is not so with the graphical procedure.

Table 3

Silver-Chloro System

Temp. = 350°C
$T_{Ag} = 4.159 \times 10^{-4}$ mol mol^{-1} of solvent

Degree of fitting	Cycle N°	β_0	β_{11}	β_{12}	β_{21}	$\sigma\Delta E$ (mV)
one	2	0.999	345.9	—	—	0.437
Two (dinuclear) term excluded)	4	1.005	326.4	8 460	—	0.214
Two (dinuclear term included)	55	1.001	285.2	15 300	56 700	0.334

Table 4

Comparison of association constants of silver-chloro and -bromo complexes evaluated by graphical and computer methods

Temp. °C	K_{11} (Graphical)	K_{11} (Computer one-degree fit)
	Silver-chloro	complexes
350°	290^{+14}_{-14}	292^{+22}_{-22}
375°	249^{+9}_{-12}	241^{+29}_{-28}
400°	207^{+23}_{-27}	198^{+20}_{-19}
	Silver-bromo	complexes
350°	1888^{+70}_{-46}	1882^{+450}_{-441}
375°	1474^{+46}_{-92}	1290^{+165}_{-178}
400°	921^{+92}_{-46}	821^{+126}_{-96}

It would appear that while the computer method gives satisfactory and acceptable values for K_{11}, its utility for evaluating other association constants is at present limited. A possible modification would be simultaneous processing of the entire data at various initial T_{Ag}, preferably over a wide range of solutes concentration.

Acknowledgements. The authors wish to thank the Council of Scientific and Industrial Research, New Delhi, India, for finanical assistance during the progress of this work and a research fellowship to one of them (N.P.B.)

LIST OF SYMBOLS

T_{Ag} — Total (stoichiometric) silver-ion concentration
C_{Ag} — "Free" or "unbound" silver-ion concentration
T_X — Total (stoichiometric) halide-ion concentration (X = Cl, Br)
C_X — "Free" or "uncomplexed" halide ion concentration
$C_{Ag_mX_n^{-(n-m)}}$ — Concentration of the complex species $Ag_mX_n^{-(n-m)}$
K_{mn} — Stepwise association constant for the species $Ag_mX_n^{-(n-m)}$
β_{mn} — The overall formation constant of the complex $Ag_mX_n^{-(n-m)}$ and is given by $C_{Ag_mX_n^{-(n-m)}}/C_{Ag}^m C_X^n$
ΔE — The difference between the cell emf in the presence and absence of halide ions
$\sigma\Delta E$ — The standard deviation in ΔE
$\bar{n}$ — The ligand number, defined as the average number of ligands combining with each Ag

Revue Roumaine de Chimie, **18**, *11*, 1903–1909 (1973)

Revue Roumaine de Chimie, **18**, *11*, 1911–1917 (1973)

REACTIONS OF COORDINATED LIGANDS. V[1] ALUMINIUM-ORGANIC COMPOUNDS OF COORDINATED SALICYLALDOXIME

N. VOICULESCU and I. POPESCU
Institute of Macromolecular Chemistry "P. Poni",
Aleea Grigore Ghica Vodă, 41–A, Iassy, Romania

Received December 4, 1972

Tetraisobutylaluminium derivatives of nickel (II) and palladium (II) salicylaldoximates were obtained through a reaction between chelates and Al $(i-C_4H_9)_3$. Copper (II) bis-salicylaldoximate reacting with Al$(i-C_4H_9)_3$ does not form a compound similar to those obtained with nickel and palladium. Complex aluminium-organic compounds appear through the replacement of the intermolecular hydrogen bridges, existing in chelates, by aluminium bridges. The synthetized compounds form adducts with Lewis bases with nitrogen, according to the formula M(II) $(C_7H_5|O_2N)_2L_2$ (L = pyridine, lutidine, picoline). Among these only the adducts with pyridine were isolated and characterized. All synthetized compounds appear as solid coloured powders, characterized by chemical analyses, IR absorption and X-ray diffraction spectra, as well as by magnetic measurements. An explanation of the diamagnetism, encountered in the case of the compunds formerly studied and in the present paper, was attempted.

1. INTRODUCTION

We have published in previous papers [2–4] the synthesis of some complex aluminium-organic compounds, resulting from the reaction of AlR_3 ($R-C_6H_5$, $i-C_4H_9$, C_2H_5, Cl) aluminium-organic compounds with a series of coordinate oximes of analytical importance. The possibility of these reactions was determined by the structural particularities of the reaction partners, i.e. the intermolecular hydrogen bonds, differing from the normal, existing in Ni(II), Pd(II) and Cu(II) bis-dimethylglyoximates and bis-salicylaldoximates, and, on the other hand, the aluminium-organic derivatives able to give addition or substitution reactions with a series of organic compounds[5,6] in which the aluminium atom achieves a sp^3 bond. We have found no systematic study dealing with the reaction of aluminium-organic derivatives with complex compounds, though these systems are extremely used in catalysis.

---

[1] N. Voiculescu, A. Airinei and I. Popescu, *Rev. Roumaine Chim.*, **18**, 000 (1973).
[2] N. Voiculescu and I. Popescu, *Rev. Roumaine Chim.*, **17**, 719 (1972).
[3] N. Voiculescu, I. Popescu and L. Roman, *Rev. Roumaine Chim.*, **18**, 1595 (1973),
[4] N. Voiculescu, I. Popescu and N. Luchian, *Rev. Roumaine Chim.*, **18**, 1601 (1973).

Aiming at establishing a general law for the replacement of the intramolecular and intermolecular hydrogen bonds by aluminium bridges through the substitution of hydrogens by AlR_2 groups, we inform in this paper on the methods of obtaining and on some of the physicochemical characters of the compounds resulting through the reaction of $Al(i-C_4H_9)_3$ with $Ni(II)(C_7H_6O_2N)_2$, $Pd(II)(C_7H_6O_2N)_2$ and $Cu(II)(C_7H_6O_2N)_2$ as well as of the adducts with nitrogen bases of the new compounds. Only adducts with pyridine were isolated and characterized to establish their binding and characteristic.

EXPERIMENTAL

The bis-salicylaldoximates were obtained by the methods given in literature [7–9].

The synthesis of Ni (II) and Pd (II) tetraizobutyl-bissalicylaldoximattes was carried out in a Schlenk-flask by adding $Al(i-C_4H_9)_3$ in *n*-heptane solution over the chelate powder in *n*-heptane suspension. During the reaction the flask was thoroughly cooled with ice. After the reaction was finished the reaction vessel was kept at low temperature for twenty minutes. The resulting compounds are soluble in *n*-heptane. The solvent was removed by evaporation in vacuum, thus obtaining the coloured powders of the new combinations (table 1). The reactions and the handling of the compounds took place in a dry actionless atmosphere.

Table

Analytical data and characteristics

Compound	Colour	Magnetical properties	Chemical		
			Calculated		
			C	H	Al
$Ni(C_7H_5O_2N)_2Al_2(i-C_4H_9)_4$	brown	diamagnetic	58.91	7.52	8.83
$Pd(C_7H_5O_2N)_2Al_2(i-C_4H_9)_4$	grey-black	diamagnetic	54.62	6.97	8.19
$Ni(C_7H_5O_2N)_2Al_2(i-C_4H_9)_4Py_2$	greenish brown	diamagnetic	62.41	7.28	7.02
$Pd(C_7O_5N)_2Al_2(i-C_4H_9)_4Py_2$	grey-brown	diamagnetic	58.75	6.85	6.60

The reaction between $Cu(II)(C_7H_6O_2N)_2$ and $Al(i-C_4H_9)_3$ took place in the same conditions as for the Ni(II) and Pd(II) derivatives. After the reaction was finished the reaction vessel was kept in ice for a few hours, while a solid fraction, insoluble in *n*-heptane, and the liquid

---

[5] A. Ciobanu, I. Vozniuc, M. Bostan, N. Voiculescu and I. Popescu, *Rev. Roumaine Chim.*, **13**, 1497 (1968).

[6] D. Giurgiu, I. Popescu, A. Ciobanu, M. Bostan, N. Voiculescu and L. Roman, *Rev. Roumaine Chim.*, **15**, 1581 (1970).

[7] F. Ephraim, *Ber. dtsch. chem. Ges.*, **63 B**, 1928 (1930).

[8] F. Ephraim, *Ber. dtsch. chem. Ges.*, **64**, 1210, 1215 (1931).

[9] E. G. Cox, F. W. Wardlaw and K. C. Webster, *J. Chem. Soc.*, **1935**, 459.

orange-coloured fraction separated. The two phases were separated by filtering on a G_4 frit. The liquid phase was concentrated in vacuum until complete removal of the solvent. The solid compound thus obtained does not contain any copper. It has a chemical composition similar to that obtained by direct reaction between salicylaldoxime and triizobutylaluminium. The solid fraction was washed several times with *n*-heptane and was dried under vacuum. The product thus obtained is of black colour and does not contain $Al(i-C_4H_9)_2$.

The adducts with amines were obtained by two methods. One of them was to add the amines to the aluminium-organic powders of the Ni(II) and Pd(II) bis-salicylaldoximates obtained as mentioned above. The reaction was accompanied by a slight release of heat and did not imply the cooling of the reaction vessel. The excess amine was removed by evaporation in vacuum. By the second method the reaction takes place directly between $Al(i-C_4H_9)_3$ and bis-salicylaldoximates in the amine solution (the amines were dried on KOH and freshly distilled). In this case, the reaction vessel was cooled with ice. The excess amines were removed as in the first method. Whatever method applied, the resulting compounds have the same qualities and chemical structure. Table 1 gives only the adducts with pyridine. The reactions were carried out and the compunds were handled in actionless dry atmosphere.

The X-ray diffraction image of the compunds discussed in the present paper were obtained by the powder method with a TUR M–60 apparatus, using the CuK_α radiation and a nickel filter. The samples were exposed to 40 kV and 14 mA for eight hours.

The IR spectra of the compunds in solid state were recorded with a Unicam SP–1000 apparatus, in KBr tablets.

The checking of the magnetic properties was carried out with a Gouy balance in a heterogeneous magnetic field.

1

of the synthetized products

analyses

%		*Found %*				
N	M	C	H	Al	N	M
4.58	9.65	58.80	7.48	8.85	4.55	9.63
4.42	16.23	54.53	6.97	8.23	4.24	16.18
7.28	7.67	62.10	7.28	7.13	7.28	7.65
6.85	13.09	58.44	6.85	6.68	6.85	13.05

DISCUSSIONS

The isobutylaluminium compounds of Ni(II) and Pd(II) bis-salicylaldoximates appear according to reaction :

$$M(II)\,(C_7H_6O_2N)_2 + 2Al(i-C_4H_9)_3 \rightarrow M(II)\,(C_7H_5O_2N)_2Al_2R_4 + 2C_4H_{10}$$

and correspond to formula I.

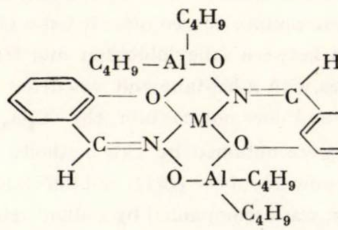

The above reaction takes probably place according to a mechanism similar to the one suggested by us for the reaction between Ni(II), Pd(II) and Cu(II) bis-salicylaldoximates with $Al(C_6H_5)_3$.

The new compounds obtained by the above reaction are easily descomposed in air, and in the presence of water, alcohols and acids deintegrate violently. Their stability în contact with air and moisture, lower than of chelates with $Al(C_6H_5)_3$ is probably due to the organic radical of the aluminium atom.

The chemical analyses of Ni(II) and Pd(II) derivatives evince the fact that the ratio Al/M is two, a value also giving the number of $Al(i-C_4H_9)_2$ groups present in the molecule of these chelates. The solubility of these compounds in organic solvents is higher than of those with $Al(C_6H_5)_2$ groups.

The formation of the adducts with a series of Lewis bases with nitrogen takes place quite easily. Being soluble in all organic solvents in which the aluminium-organic derivatives of chelates are soluble, the adducts could not be separated by precipitating them with solvents. The formation of the adducts determines an intensification of the compounds colour. The adducts with amines have a higher stability towards the action of different chemical agents, as compared to tetraisobutylaluminium Ni(II) and Pd(II) bis-salicylaldoximates.

Cu(II) bis-salicylaldoximate reacting with $Al(i-C_4H_9)_3$ has a behaviour different of that of the similar Ni(II) and Pd(II) derivatives.

On the other hand, this compound has a behaviour similar to that of Cu(II) bis-dimethylglyoximate towards $Al(i-C_4H_9)_3$. We have obtained in the working conditions mentioned the aluminium-organic derivative of uncoordinate salicylaldoxime. The synthesis and physicochemical properties of this compound shall be given later. The result of the reaction offers no surprise if we take into account the reductor character of aluminium-organic derivatives and the ease with which bivalent copper passes to a lower valence.

Table 2 gives the IR absorption bands in the 1650 − 650 cm^{-1} range, and we shall discuss them compared to those of derivatives with $Al(C_6H_5)_2$ groups. The remarkable thing in the IR spectrum of these compounds is the disappearance of the characteristic absorption bands of the OH groups in the usual absorption region. The maximum absorption of the other groups is only slightly affected through the replacement of the hydrogen bridges by aluminium bridges. The small displacements observed in the case of Ni(II) $(C_7H_5O_2N)_2Al_2(i-C_4H_9)_4$ take place in the same direction as those observed in the case of the deuterate form[10] of the Ni(II) bis-salicylaldoximate.

By comparing the IR spectra of these compunds and of the compounds with $Al(C_6H_5)_2$ groups we notice that the organic groups of the aluminium atom do not greatly affect the absorption spectrum of the chelates in the $1650-650\mathrm{cm}^{-1}$ range. Also, do not exist measurable differences between the spectra of the compounds with aluminium and of their adducts with pyridine in this field.

Table 2

Absorption spectra of $M(II)(C_7H_5O_2N)_2Al_2(i-C_4H_9)_4$ (values in cm^{-1})

$Ni(C_7H_5O_2N)_2Al_2(i-C_4H_9)_4$	$Pd(C_7H_5O_2N)_2Al_2(i-C_4H_9)_4$	Assignment
1635	1620	C = N
1553	1558	Stretching C = N
1490 1460	1495 1458	*ortho*-H_2
1363 1327 1293	1338 1302 —	C−H plane
1230 1205	1215 —	N−O
1152 1124	1157 1120	*ortho*-H_2
1068	1060	ring
1025	1040	CO
920	924	NO
850 752	820 750	Stretching CH

The X-ray diffraction images of these compounds are characteristic of these amorphous substances. The hydrolysis restores the chelates and their crystalline structure.

Magnetic measurements (table 1) on Ni(II) $(C_7H_5O_2N)_2$. $Al_2(i-C_4H_9)_4$ and Pd(II) $(C_7H_5O_2N)_2Al_2(i-C_4H_9)_4$ and on their adducts with pyridine show that these compounds are diamagnetic. The formation of adducts, in the case of Ni(II) bis-salicylaldoximate with a series of amines[11–16] takes place with the change of the dsp^2 square plane structure into a sp^3d^2 octaedrical structure. The adduct with pyridine of Ni(II) $(C_7H_6O_2N)_2$ contains thus two pyridine molecules to the nickel atom and is paramagnetic (formula II).

---

[10] K. K. Ramaswamy, C. I. Jose and D. N. Sen, *Indian J. Chem.*, **5**, 156 (1967).

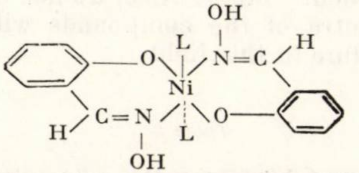

The diamagnetism observed in the case of the aluminium-organic derivatives of Ni(II), Pd(II) and Cu(II) bis-dimethylglyoximates[2,3] and bis-salicylaldoximates shows that the square plane structure and the covalent character of the chelate bonds were not changed through the replacement of the oximic hydrogens by AlR_2 groups. We believe that the abnormal diamagnetism of the derivates with copper is due to the reduction of the copper to the valence one stage, but without changing its coordination number. Thus, the diamagnetism found for these compounds is not surprising.

The binding of the amine molecules takes place in the same way as for derivatives with which it was dealt previously (formula III).

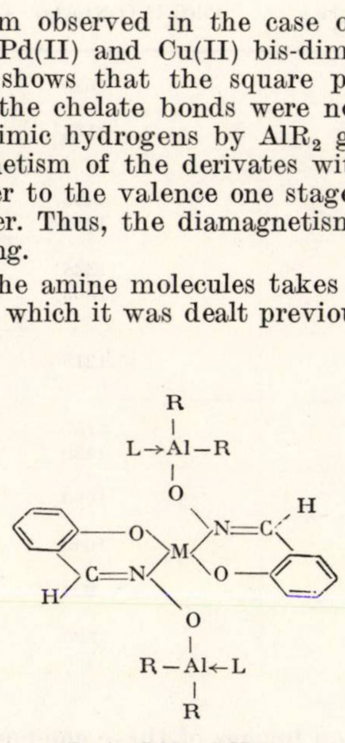

$R = i-C_4H_9,\ C_6H_5-$

---

[11] H. C. Clark and A. L. Odell, *J. Chem. Soc.*, **1955**, 3431.

[12] G. Maki, *J. Chem. Phys.*, **29**, 1129 (1958).

[13] J. Csaszar and J. Szeghalmi, *Acta Univ. Szeged., Acta Phys. Chem.*, **12**, 117 (1966).

[14] F. Maggio, V. Romano, T. Pizzino and L. Pellerito, *Ann. Chim. (Ital.)*, **58**, 725 (1968).

[15] S. Fujii and M. Sumitami, *Sci. Repts. Tohoku Univ., First Ser.*, **37**, 49 (1953).

[16] J. Csaszar, *Acta Chim. Acad. Sci. Hung.*, **32**, 345 (1962).

The formation of adducts with amines of aluminium-organic derivatives may be interpreted, as for chelates,[17,18] based on the general acid base notion. The difference lays in the fact that in the case of aluminium-organic derivatives of the chelates, the aluminium atom, and not the central metallic atom, plays the role of the acid, as in the case of chelates. In this way the diamagnetism of the adducts with amines, and the anomaly found by Schranzer[19] in the case of similar boron derivatives, is also explained.

---

[17] R. G. Pearson, *J. Amer. Chem. Sci.*, **85**, 3533 (1963).
[18] R. G. Pearson, *Chemistry in Britain*, **3**, 103 (1967).
[19] G. N. Schrauzer, *Chem. Ber.*, **95**, 1438 (1962).

Revue Roumaine de Chimie, **18**, *11*, 1919–1927 (1973)

REACTIONS OF COORDINATED LIGANDS. VI[1]

REACTION OF ALUMINIUM-ORGANIC DERIVATIVES WITH OXIMES

N. VOICULESCU

Institute of Macromolecular Chemistry "P. Poni",
Aleea Grigore Ghica Vodă, 41–A, Iassy, Romania

Received December 4, 1972

A series of aluminium-organic derivatives of dimethylglyoxime and salicylaldoxime were obtained by their reaction with Al $(i-C_4H_9)_3$, $Al(C_6H_5)_3$ and $Al(C_2H_5)_2Cl$. The resulting compounds were isolated in solid state and characterized by chemical analysis, IR absorption spectra and X-ray diffraction. In the case of aluminium organic derivatives of salicylaldoxime, their adducts with amines were also isolated, and among these, their adducts with pyridine were characterized. On behalf of the formerly published results, [1-5] we have tried to establish the similitudes and differences of behaviour between the free and the coordinated oximes with the Ni(II), Pd (II) and Cu(II) ions, *versus* the aluminium-organic derivatives.

INTRODUCTION

Dimethylglyoxime and salicylaldoxime are two important organic reagents, used in analytical chemistry. These oximes, through a rigorous control of the precipitation pH, have the quality of forming selectively, extremely stable coloured chelate compounds with the Ni(II), Pd(II) and Cu(II) ions. The coordination of the oximes with these metals determines the screening of the ligands characteristic properties. Thus, the OH groups of the coordinate oximes have no longer the typical etherification and esterification reactions.[6-8] The lack of reactivity of the OH groups in the coordinate oximes was assigned to the intermolecular hydrogen bonds O–H...O, existing in these compounds. The O–H...O hydrogen bonds of Ni(II)[9,10] Pd(II)[11,12] and Cu(II)[13,14] bis-dimethylglyoximates and bis-salicylaldoximates, are different to the usual hydrogen bonds, being shorter and stronger. They are, nevertheless, less stronger than the aluminium bridges,[15] as they may be replaced by AlR_2 ($R-C_2H_5$, C_4H_9, C_6H_5, Cl) groups.[1-5]

---

[1] N. Voiculescu and I. Popescu, *Rev. Roumaine Chim.*, **18**, 000 (1973).
[2] N. Voiculescu and I. Popescu, *Rev. Roumaine Chim.*, **17**, 719 (1972).
[3] N. Voiculescu, I. Popescu and L. Roman, *Rev. Roumaine Chim.*, **18**, 000 (1973).
[4] N. Voiculescu, I. Popescu and N. Luchian, *Rev. Roumaine Chim.*, **18**, 000 (1973).
[5] N. Voiculescu, A. Airinei and I. Popescu, *Rev. Roumaine Chim.*, **18**, 000 (1973).
[6] L. A. Ciugaev, *J. Chem. Soc.*, **1914**, 2187.
[7] M. F. Barker, *Chem. News.*, **130**, 99 (1925).
[8] E. Thilo and K. Friedrich, *Ber. dtsch. chem. Ges.*, **62 B**, 2990 (1929).

The oxygen bonds existing in the free oximes differ from those in the chelates by the way they are achieved by their strength. In dimethylglyoxime[16] the hydrogen bonds are intermolecular and are established between the oximic oxygen and the nitrogen atom of the neighbouring cell, thus determining the union of an infinite number of molecules. The atoms in the OH....N bond are not set in a straight line, but in the shape of a 140° angle.[17]

In the salicylaldoxime[18] there are inter- and intramolecular bonds. The intramolecular hydrogen bonds are established between the phenolic oxygen and the nitrogen atom O—H...N, and the intermolecular ones between the oximic oxygens O—H...O. The aluminium-organic chelates of dimethylglyoxime and salicylaldoxime examined in this paper result from the substitution of the hydrogen bonds of the oximes by aluminium-organic groups.

Based on the formerly published results,[1-5] we shall try to establish the similitudes and differences of behaviour between the free and coordinate oximes with Ni(II), Pd(II) and Cu(II) ions, *versus* aluminium-organic derivatives.

EXPERIMENTAL

The triphenylaluminium[19] was obtained from $Hg(C_6H_5)_2$ and grey aluminium, by heating at 130—140°, and was purified by recrystallization from benzene and *n*-hexane.

The method of obtaining $(DMG)_2\,Al_4\,(i-C_4H_9)_8$(DMG is the dimethylglyoxime radical) was published in a former paper. [1]

The $(DMG)_2Al_4\,(C_6H_5)_8$ was obtained by adding $Al(C_6H_5)_3$ solved in benzene on dimethylglyoxime powder. It was heated up to the reflux temperature of the solvent, till the whole quantity of dimethylglyoxime processed has been transformed into a brown powder. The total heating time was of 40 hours. The resulting product was decanted and washed several times with benzene to remove the $Al(C_6H_5)_3$ added in excess, and dried in vacuum. All operations were carried out in an actionless dry atmosphere. The chemical analyses of the product are given in table 1.

The $(DMG)_2\,Al_4(C_2H_5)_4Cl_4$ was obtained by adding $Al(C_2H_5)_2Cl$ solved in *n*-heptane over the suspension of dried dimethylglyoxime, and ground in *n*-heptane. It was heated at reflux temperature of the solvent, till the whole quantity of dimethylglyoxime processed, was transformed into a red syrup, which deposited at the bottom of the flask. The syrupy residue was separated from the liquid fraction by decantation and then dried in vacuum.

---

[9] L. E. Godycki and R. E. Rundle, *Acta Cryst.*, **6**, 487 (1953).
[10] R. C. Srivastava, E. C. Lingafelter and P. C. Jain, *Acta Cryst.*, **22**, 922 (1967).
[11] C. Panattoni, E. Fasson and R. Zanneti, *Gazz. chim. Ital.*, **89**, 2132 (1959).
[12] C. E. Pfluger, *Diss. Abs.*, **18**, 1644 (1958).
[13] E. Bua and G. Schiavinato, *Gazz. chim. Ital.*, **81**, 847 (1951).
[14] M. A. Jarski and E. C. Lingafelter, *Acta Cryst.*, **17**, 1109 (1964).
[15] E. G. Hofmann, *Liebigs Ann. Chem.*, **629**, 104 (1960).
[16] L. L. Merritt Jr. and E. Laterman, *Acta Cryst.*, **5**, 811 (1952).
[17] W. C. Hamilton, *Acta Cryst.*, **14**, 95 (1961).
[18] L. L. Merritt Jr. and E. Schroder, *Acta Cryst.*, **9**, 194 (1956).
[19] E. Krause and P. Dittmar, *Ber. dtsch. chem. Ges.*, **63**, 2401 (1930).

The $(C_7H_5O_2N)_2\ Al_2\ (i-C_4H_9)_2$ was obtained by adding an excess of salicylaldoxime over $Al(i-C_4H_9)_3$ diluted with *n*-heptane. The excess of salicylaldoxime deposited on the bottom of the flask and was separated by filtering on a G_4 frit. A solid powder was obtained after removing the solvent in vacuum. The molecular mass of the compound was determined cryoscopically in benzene (table 1).

The $(C_7H_5O_2N)_2Al_2(C_6H_5)_2$ was obtained by mixing $Al(C_6H_5)_3$ in benzene, with the suspension of the salicylaldoxime in benzene. A yellow precipitate was obtained and separated from the liquid fraction by decantation. It was washed several times with benzene and dried in vacuum.

The adducts with amines of the aluminium-organic derivatives of the salicylaldoxime were obtained by the methods described for coordinate derivatives.[1] Among these, only those with pyridine were characterized.

The reactions were carried out in Schlenk vessels, in an actionless dry atmosphere.

The chemical analyses as well as the characteristics of the synthetised compounds are given in table 1.

The X-ray diffraction images of the compounds were obtained by the powder method with a URK-5 apparat us, using the CuKα radiations and the nickel filter.

The samples were placed in special capillaries and exposed in a vacuum chamber at 40 kV and 25 mA for two hours.

The IR spectra of the compounds vere obtained with a Unicam sp. 1000 apparatus, in kBr tablets.

DISCUSSIONS

The formation reaction of the aluminium-organic derivatives of dimethylglyoxime is rendered by the following general chemical equation:

$$2\ DMGH_2 + 4AlR_3 \rightarrow (DMG)_2Al_4R_8 + 4RH$$
$$R = Cl,\ C_2H_5,\ i-C_4H_9,\ C_6H_5$$

The mechanism by which the new combinations arise is a reaction in two stages, determined by the structural particularities and the proprieties of the reactants. In the first reaction stage, the formation of an adduct between two molecules of aluminium-organic derivative and an oxime molecule occurs. The formation of the adduct takes place through the binding of the aluminium atoms to the nitrogen atoms of the oxime by a Al-N coordinative bond, determining the appearance of the free OH groups, in which the hydrogen atoms are far more mobile than in the oxime, where they are engaged in intermolecular O—H...N hydrogen bonds. The higher mobility of the hydrogens in the adducts determine the second reaction stage in which the formation of the substitution aluminium-organic derivatives of the dimethylglyoxime takes place (fig. 1).

The reaction with $Al(C_2H_5)_2Cl$ takes place with a release of ethane, and not of hydrochloric acid. The chelate compounds of the dimethylglyoxime with aluminium-organic derivatives are dimer substances. The dimerization results from the binding of the aluminium atoms to the nitrogen atoms of the neighbour cell (fig. 1) The "anti" form, appearing through a revolution of the dimethylglyoxime molecule around the central bond C—C is necessary for the formation of the dimer. The molecular weight

Table 1

Analytical data and characteristics of the synthetized combinations

Compound	Colour	Chemical analyses									
		Calculated %					*Found* %				
		C	H	Al	N	Cl	C	H	Al	N	Cl
$(DMG)_2Al_4(C_6H_5)_8$	brown	70.58	5.46	11.34	5.88	—	69.87	5.46	11.40	5.80	—
$(DMG)_2Al_4(C_2H_5)_4Cl_4$	orange-red	31.78	5.29	17.88	9.27	25.16	31.10	5.25	18.05	9.27	25.08
$(C_7H_5O_2N)_2Al_2(i-C_4H_9)_2$*	orange	60.27	6.39	12.32	6.39	—	60.15	6.39	12.40	6.39	—
$(C_7H_5O_2N)_2Al_2(C_6H_5)_2$	yellow	65.27	4.18	11.29	5.85	—	65.10	4.18	11.35	5.85	—
$(C_7H_5O_2N)_2Al_2(i-C_4H_9)_2 2Py$	orange-red	64.42	6.37	9.06	9.39	—	64.20	6.37	9.20	9.39	—
$(C_7H_5O_2N)_2Al_2(C_6H_5)_2 2Py$	yellow	67.92	4.71	8.49	8.80	—	67.40	4.65	8.65	8.60	—

* $M_{calcd.} = 438$; $M_{found} = 464$.

measurements [2] correspond to the dimer state. The formation of the dimer may also be explained by the binding of the aluminium atoms by the hydrocarbon radicals, respectively of the left chlorine atoms, or by the binding of the aluminium atoms only to the oxygen atoms. [2] The dimerization by the hydrocarbon radicals, respectively the chlorine atoms, would lead to hybride bonds of the aluminium atoms between sp^2 and sp^3, which are less stable than the hybride sp^3 bonds, formed by the nitrogen binding. The formula through O—Al—O bonds is also likely, as the aluminium-organic compounds arise through the substitution of the hydrogen bonds and the aluminium atoms are interposed between the atoms participating in this bond, atoms which in the case of dimethylgyloxime are the nitrogen and oxygen atoms O—H. . .N.

The aluminium-organic combinations of the dimethylglyoxime are coloured solid substances, instable towards water, alcohols, acids and

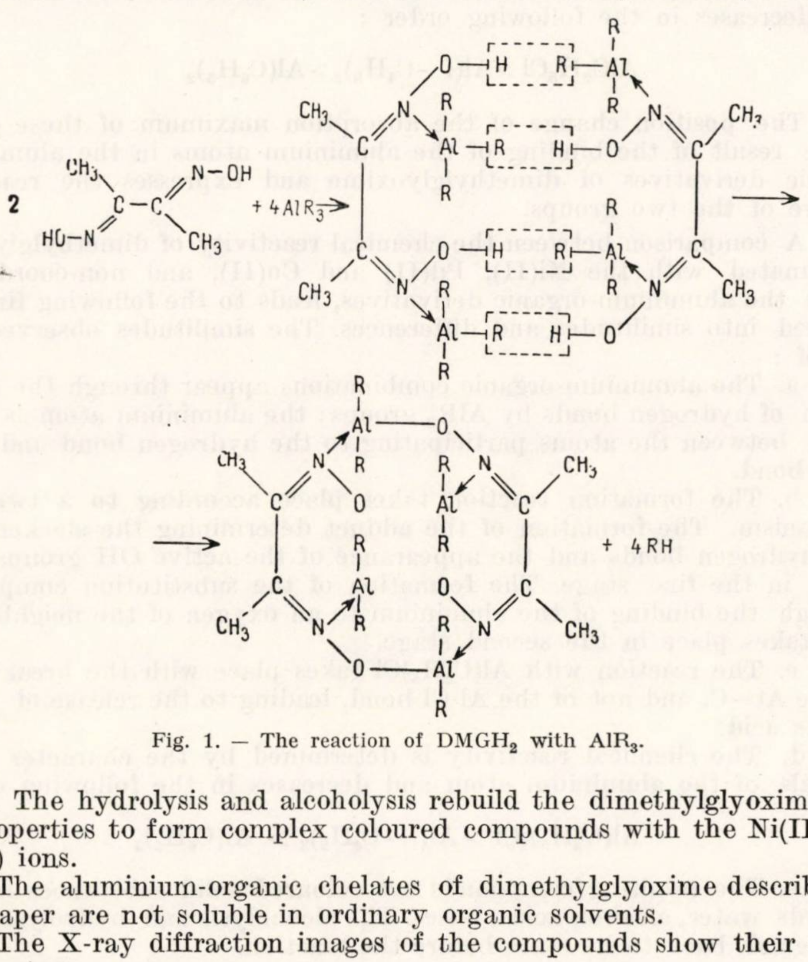

Fig. 1. — The reaction of $DMGH_2$ with AlR_3.

bases. The hydrolysis and alcoholysis rebuild the dimethylglyoxime and its properties to form complex coloured compounds with the Ni(II) and Pd(II) ions.

The aluminium-organic chelates of dimethylglyoxime described in this paper are not soluble in ordinary organic solvents.

The X-ray diffraction images of the compounds show their amorphous stage.

The replacement of oximic hydrogens by AlR_2 groups brings also about changes in the IR absorption spectrum. In the $3600-650\ cm^{-1}$ range, the absorption spectrum of the aluminium-organic combinations of the dimethylglyoxime with $Al(C_6H_5)_2$ and AlC_2H_5Cl is characterized by the absence of the absorption maxima characteristic of the OH group, placed [20] approximately at $3170\ cm^{-1}$, and by the position change of the absorption maximum of the CN and NO groups. In the $(DMG)_2Al_4(C_6H_5)_8$ spectrum, the place of absorption maximum of the CN group is at approximately $1595\ cm^{-1}$, and of the NO group at approximately $1080\ cm^{-1}$. The same maxima appear in $(DMG)_2Al_4(C_2H_5)_4Cl_4$ at $1640\ cm^{-1}$, respectively $1095\ cm^{-1}$. The two absorption maxima of the CN and NO groups of these compounds appear at much higher frequencies than for the dimethylglyoxime or even for chelates.[21] The magnitude of the displacement is determined by the character of the radicals left at the aluminium atom, and decreases in the following order :

$$AlC_2H_5Cl > Al(i-C_4H_9)_2 > Al(C_6H_5)_2$$

The position change of the absorption maximum of these groups is the result of the binding of the aluminium atoms in the aluminium-organic derivatives of dimethylglyoxime and expresses the reactivity change of the two groups.

A comparison between the chemical reactivity of dimethylglyoxime coordinated with the Ni(II), Pd(II) and Cu(II), and non-coordinated *versus* the aluminium-organic derivatives, leads to the following findings, grouped into similitudes and differences. The similitudes observed consist of :

a. The aluminium-organic combinations appear through the substitution of hydrogen bonds by AlR_2 groups ; the aluminium atom is interposed between the atoms participating to the hydrogen bond and forms a sp^3 bond.

b. The formation reaction takes place according to a two-stage mechanism. The formation of the adduct determining the slackening of the hydrogen bonds and the appearance of the active OH groups takes place in the first stage. The formation of the substitution compounds, through the binding of the aluminium to an oxygen of the neighbouring cell, takes place in the second stage.

c. The reaction with $Al(C_2H_5)Cl$ takes place with the breaking up of the Al—C, and not of the Al-Cl bond, leading to the release of hydrochloric acid.

d. The chemical reactivity is determined by the character of the radicals of the aluminium atom and decreases in the following order :

$$Al(C_2H_5)_2Cl > Al(i-C_4H_9)_3 > Al(C_6H_5)_3$$

e. The resulting compounds are coloured solid substances instable towards water, alcohol, acids, bases. The alcoholysis and hydrolysis bring the ligand back to its state before the reaction.

---

[20] G. Duyckaertes, *Bull. Soc. roy. Sci. Liège*, **21**, 196 (1952).

[21] R. Blino and D. Hadzi, *J. Chem. Soc.*, **1958**, 4536.

f. The solubility in organic solvents is determined by the character of the remaining radicals at the aluminium atom.

The observed similitudes point out the lack of influence of the central metallic atoms on the reactivity of the dimethylglyoxime and the chemical behaviour of the resulting compounds.

The differences consist of :

a) The reactivity of the free dimethylglyoxime is smaller.

b) The number of AlR_2 groups in the dimethylglyoxime molecule is double in the case of the noncoordinate form.

c) The nitrogen atoms participate to the formation of the adducts in the first reaction stage for dimethylglyoxime, and the oxygen atoms do not, as in the case of the bis-dimethylglyoximates.

d) The aluminium-organic derivatives of the free oxime result through the replacement of the intermolecular hydrogen bonds.

e) The aluminium atoms bind differently, forming a $O-Al-N$ bond in dimethylglyoxime compounds, and a $O-Al-O$ bond in the others.

These differences are the result of the influence exercised by the central metallic ions on the progress of the reaction, the binding and the behaviour of the obtained derivatives. From a chemical point of view, the influence of the central metallic ions on the reactivity of the dimethylglyoxime is the same, and no differences brought about by the character of the metal can be determined. The different behaviour of the Ni(II) and Pd(II) dimethylglyoximates and of the Cu(II) dimethylglyoximate is determined by the different behaviour of the ions, and not of the ligand, towards the aluminium organic derivatives.

The Ni (II) $(DMGH)_2$ and Pd(II)$(DMGH)_2$ are very stable combinations, compared to Cu(II)$(DMGH)_2$ and this difference probably determines their behaviour, different from that of the aluminium organic derivatives. This different behaviour of Cu(II)$(DMGH)_2$, compared to that of the ALR_3 derivatives, is not observed at the ligand, but at the central metallic ion, which, in the reaction with $Al(i-C_4H_9)_3$ and $Al(C_2H_5)_2Cl$ leaves the coordination sphere as a pure metal, and $Al(C_2H_5)_2Cl$ leaves the coordination sphere as a pure metal, and at the reaction with $Al(C_6H_5)_3$ is reduced to valence one. The reaction mechanism by which the reduction of the copper takes place implies the water molecules. The existence of water in the system is not excluded, as even Cu(II)$(DMGH)_2$ binds a water molecule, removed with difficulty. The two reactions rendering the formation of the aluminium-organic compounds and the reduction of the copper to valence one, respectively zero, are :

$$3Cu(II)(DMGH)_2 + 14AlR_3 + 3H_2O \rightarrow 3Cu + 6(DMG)(AlR_2)_2 + \\ + 18RH + Al_2O_3$$

$$6Cu(II)(DMGH)_2 + 14AlR_3 + 3H_2O \rightarrow 6Cu\,(I)(DMG)_2\,Al_2R_4 + \\ + 18RH + Al_2O_3$$

The formation of the aluminium-organic combinations of the noncoordinated salicylaldoxime takes place through the replacement of the inter- and intramolecular hydrogen bonds by AlR groups, by the following reaction which also includes the mechanism in figure 2.

The formation mechanism of the adduct is similar to the one described for the dimethylglyoxime and undergoes the same discussion. In the second stage, the condensation of two molecules of adduct takes place by closing some heterocycles with six atoms and by the removal of four hydrocarbon molecules.

The aluminium-organic combinations resulting through the replacement of the oxime and phenol hydrogens in the salicylaldoxime are coloured solid substances, stable in water, alcohol, acids and bases.

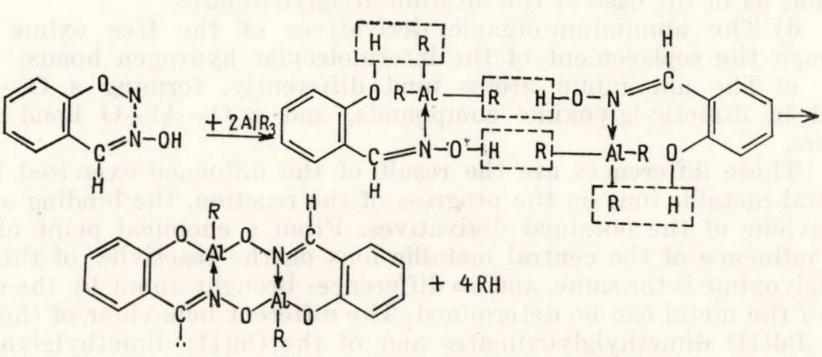

Fig. 2. — The reaction of $C_7H_7O_2N$ with AlR_3.

Compared to dimethylglyoxime, salicylaldoxime is similar by its reactivity towards the same aluminium-organic derivatives, as well as by the general chemical behaviour of the resulting combinations. The aluminium-organic derivatives of salicylaldoxime differ from those of dimethylglyoxime by the fact that they do not form dimers and in reaction with amines they produce adducts. The binding of the amine molecules takes probably place at the aluminium atom, not by the breaking of the Al-N bonds existing in the initial aluminium-organic derivatives, but changing the coordination number of the aluminium atom, which in this case becomes five. The adducts with amines of the aluminium-organic derivatives of the salicylaldoxime do not greatly change their chemical behaviour. They determine a slight intensity increase of the colour and an increase of the stability towards chemical agents.

The IR absorption spectrum of the salicylaldoxime 22 for the spectral range 3600—650 cm^{-1} undergoes some changes by the replacement of the oxime and phenol hydrogens by AlR groups. The spectra of the compound examined in this paper are given, for the spectral range 1650—650 cm^{-1} in table 2. In the spectral range 3600—650 cm^{-1}, the spectrum of these compounds lacks the characteristic absorption maxima of the oxime and phenol OH, and the change of position of the absorption maxima of the groups CN, NO and CO. The position of the absorption maxima of the groups CN and NO is moved in the same direction as for the aluminium-organic derivatives of the dimethylglyoxime, but magnitude of the displacement is much smaller and is not markedly affected by the

Table 2

IR absorption spectra of $(C_7H_5O_2N)_2Al_2(i-C_4H_9)_2$ and $(C_7H_5O_2N)_2Al_2(C_6H_5)_2$ (values in cm^{-1})

$(C_7H_5O_2N)_2Al_2(i-C_4H_9)_2$	$(C_7H_5O_2N)_2Al_2(C_6H_5)_2$	assignment
1620 1565	1620 1562	C=N
1492 1460	1498 1463	*ortho*
1310	1305	C−H
1210	1217	NO
1155 1127	1160 1127	*ortho*
1036	1040	CO
927	937	NO
830	842	CH
765	770	CH

character of the hydrocarbon radicals remaining with the aluminium atom. This points out the fact that the change in the reactivity of the CN and NO groups is determined not only by the character of the radicals remaining with the aluminium atom, but also by their number.

Important changes appear in the case of the CO bond, the absorption band of which, in the aluminium-organic compounds of salicylaldoxime appear approximately at the same wavelength as for the chelates.[22]

The absorption spectra of the aluminium-organic derivatives of the salicylaldoxime do not undergo important changes in the range discussed through the formation of adducts with the amines.

A comparison between the chemical reactivity of free and coordinated salicylaldoxime with Ni(II), Pd(II) and Cu(II) ions *versus* the aluminium-organic derivatives leads for the greater part to the conclusions drawn for the dimethylglyoxime, to which we have to add :

— The chemical reactivity of the free and coordinated salicylaldoxime *versus* aluminium-organic derivatives is the same. The resulting compounds are substitution derivatives of the oxime hydrogens with AlR_2 groups in the case of coordinate salicylaldoxime and of oxime and phenol hydrogen, with AlR groups in the case of non-coordinate salicylaldoxime.

— The number of aluminium atoms per salicylaldoxime molecule is the same, but the number of hydrocarbon radicals is double in the case of the aluminium-organic derivatives of the coordinate salicylaldoxime.

The compounds resulting in both cases have the properties of forming adducts with amines through the aluminium atoms.

---

[22] K. K. Ramaswamy, C. I. Jose and D. N. Sen, *Indian J. Chem.*, **5**, 156 (1967).

Revue Roumaine de Chimie, **18**, *11*, 1929–1936 (1973)

MODERN FRIEDEL-CRAFTS CHEMISTRY. III*

THE ISOMERIZATION OF 1,1- AND 1,2-DIPHENYLBUTANE UNDER THE INFLUENCE OF ALUMINUM CHLORIDE CATALYST IN BENZENE SOLVENT

ROYSTON M. ROBERTS** and ALI ALI KHALAF***

** Chemistry Department, University of Texas at Austin, Austin, Texas 78712, U.S.A.
*** Chemistry Department, University of Assiut, Assiut, Arab Republic of Egypt

Received February 26, 1973

The influence of aluminium chloride on 1,1- and 1,2-diphenylbutane in benzene as solvent was investigated both at room temperature and at about 70°. At room temperature, very little dephenylation and isomerization reactions were noted but more was effected when larger amounts of catalyst at higher temperature was used. Under the conditions employed, dephenylation produced *n*-butylbenzene from both isomers and isomerization was shown to follow the order : 1,1-diphenylbutane → 1,2-diphenylbutane → 1,3-diphenylbutane. Mechanisms were proposed to account for the results obtained.

In 1964 Roberts, Khalaf and Greene[1] have undertaken a detailed study of the rearrangements, dealkylations and fragmentations produced by the reaction of aluminum chloride with a number of diphenylalkanes which included 1,1-diphenyl-2-methylpropane (3), 1,2-diphenyl-2-methylpropane (6), *meso*- and *dl*- 2,3-diphenylbutane (10) and 2,2-diphenylbutane (13). These authors found that some of the aforementioned compounds underwent facile interconversions between each other upon treatment with small amounts of $AlCl_3$ at room temperature. For example, treatment of either 1,1-diphenyl-2-methylpropane (3) or 1,2-diphenyl-2-methylpropane (6) with $AlCl_3$ at room temperature for 4 hr produced a mixture containing both isomers in a ratio of about 1 : 2 in addition to smaller amounts of *dl*- and *meso*-2,3-diphenylbutane (10). Similar mild treatment of *meso*-2,3-diphenylbutane with $AlCl_3$ resulted in partial isomerization to the *dl* isomer and, to a smaller extent, to 1,2-diphenyl-2-methylpropane (6). Meanwhile, 2,2-diphenylbutane (13) was found to undergo partial isomerization in 4 hr at room temperature to *dl*- and *meso*-2,3-diphenylbutane (10). It was also noted by the same authors that the above isomerizations of diphenylbutanes were accompanied by dephenylations which led to the formation of isomeric butylbenzenes. To account for their results, Roberts, Khalaf and Greene[1] suggested the carbonium ion reactions outlined in Scheme 1.

---

* Part II: A. A. KHALAF, *Rev. Roumaine chim.*, **18**, 479 (1973).

Scheme 1

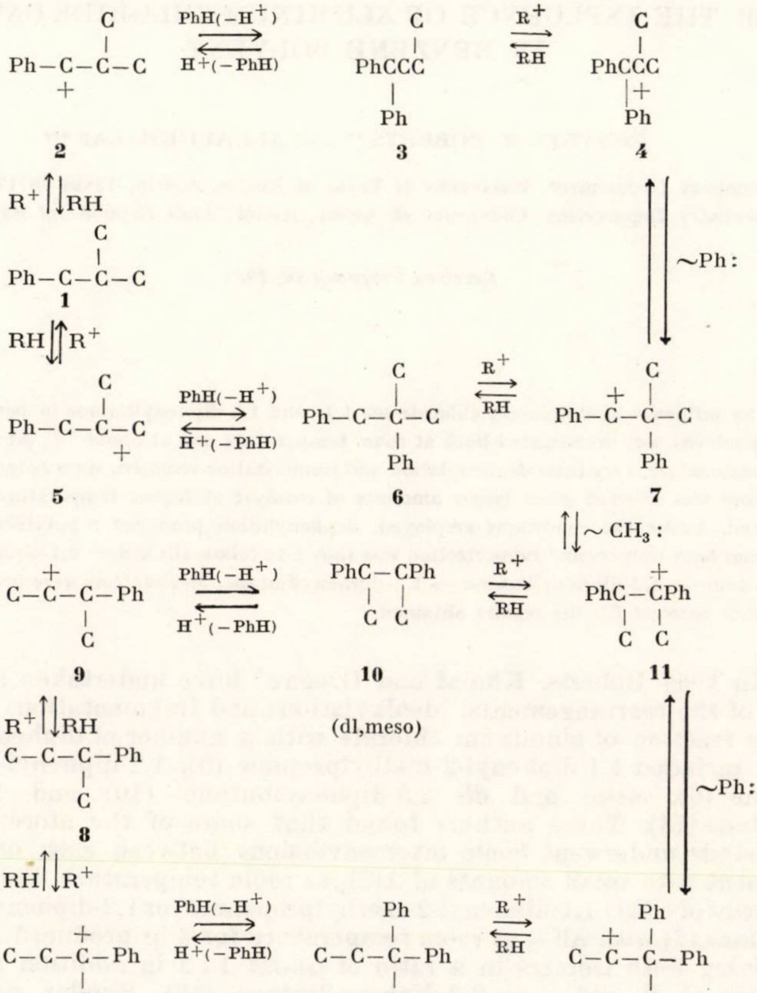

In the present paper we report on the reaction of $AlCl_3$ with the isomeric 1,1- and 1,2-diphenylbutane under a variety of conditions in which benzene was used as solvent.

---

[1] R. M. Roberts, A. A. Khalaf and R. N. Grecne, *J. Amer. Chem. Soc.*, **86**, 2846 (1964).

RESULTS AND DISCUSSION

The $AlCl_3$-catalyzed isomerization of 1,1- and 1,2-diphenylbutane in benzene was performed both at room temperature and at 68 – 70°. A summary of the conditions and results of these isomerization experiments are depicted in table 1.

Table 1

Conditions and results of the isomerizations of 1,1- and 1,2-diphenylbutane with $AlCl_3$ in benzene

Exp. N⁰	Reactants and conditions					Products, %				
	Starting diphenylbutane	$AlCl_3$ (mole)	Benzene (mole)	Temp. °C	Time hr	*n*-Butylbenzene	1,1-Diphenylbutane	1,2-Diphenylbutane	1,3-Diphenylbutane	Unidentified products
1	1,1-Diphenylbutane (0.03)	0.003	0.3	25	4.0	4.5	95.0	0.5	—	—
2	1,1-Diphenylbutane (0.1)	0.020	1.0	68 ± 2	6.5	33.0	46.0	21.0	—	—
3	1,2-Diphenylbutane (0.02)	0.002	0.2	25	4.0	2.0	—	96.0	—	2.0
4	1,2-Diphenylbutane (0.05)	0.010	0.5	70 ± 2	6.5	8.0	—	89.0	1	2.0
5	1,2-Diphenylbutane (0.05)	0.020	0.5	70 ± 2	6.5	32.0	1.0	53.0	6.0	8.0

It can be seen from the results of table 1 that the treatment of either 1,1- or 1,2-diphenylbutane with $AlCl_3$ in benzene under mild conditions (25° for 4 hr with a mole ratio of $AlCl_3 : C_4H_8Ph_2 : PhH = 1 : 10 : 100$; expts. 1 and 3) resulted mainly in little dephenylations of both isomers to *n*-butylbenzene and in inappreciable rearrangement of 1,1- to 1,2-diphenylbutane; no rearrangement of 1,2-diphenylbutane could be detected, however. Under the more vigorous conditions of expts. 2 and 4 (68 – 70° for 6.5 hr with a mole ratio of $AlCl_3 : C_4H_8Ph_2 : PhH = 2 : 10 : 100$) more dephenylation and isomerization reactions of both the 1,1- and the 1,2-diphenylbutane isomers were observed but the amount of these reactions was much more considerable with the 1,1- than with the 1,2-isomer. Considerable dephenylation and isomerization of the 1,2-diphenylbutane isomer was effected, however, when experiment 4 was repeated using a doubled proportion of catalyst ($AlCl_3/C_4H_8Ph_2$, mole ratio 0.4). See expt. 5.

Mechanistically, the isomerization and dealkylation results of table 1 can be rationalized in terms of the carbonium ion processes outlined in Scheme 2.

According to Scheme 2, the conversion of 1,1-diphenylbutane (15) into 1,2-diphenylbutane (21) and of the latter into 1,3-diphenylbutane (28) can take place by several pathways. Thus **15** can rearrange to **21** *via* any of the following three routes : (1) **15→20→18→21**, (2) **15→16→17→→18→21** and (3) **15→16→19→18→21**. Similarly, **21** can rearrange to **28** through a similar number of parallel routes : (1) **21→27→25→28**, (2) **21→23→24→25→28** and (3) **21→23→26→25→28**.

Although it is hard in the light of our present results to assume which one(s) of the above possible routes is(are) mainly involved, it can be predicted on the basis of previous reports [2–6] that the phenonium ion routes (routes number 1 in both cases) will be the most favored. Under any circumstances, however, the carbonium ion transformations involved in any of the suggested routes are expected to be difficult since they involve passing

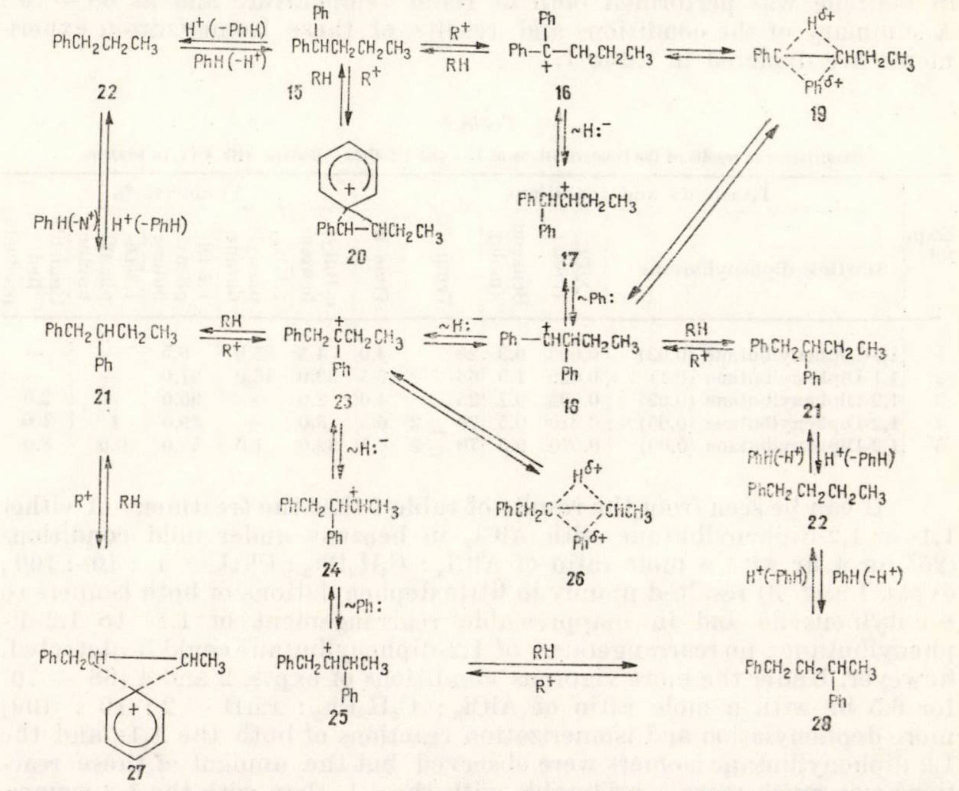
PhCH2CH2CH3
22
H+(-PhH)
PhH(-H+)
PhCHCH2CH2CH3
Ph
15
R+
RH
Ph—C—CH2CH2CH3
16
~H:−
PhCHCHCH2CH3
17
~Ph:
PhC CHCH2CH3
19
PhH(-H+)
H+(-PhH)
PhCH—CHCH2CH3
20
PhCH2CHCH2CH3
21
PhCH2CCH2CH3
23
Ph—CHCHCH2CH3
18
PhCH2CHCH2CH3
21
PhCH2CH2CH2CH3
22
PhCH2CHCHCH3
24
PhCH2C CHCH3
26
PhCH2CH CHCH3
27
PhCH2CHCHCH3
25
PhCH2CH2CHCH3
28

through some higher energy carbonium ions such as **17** and **18** in going from **15** to **21** and **24** and **25** in going from **21** to **28**. In experimental terms, the latter fact is in keeping with the observed slow reactions of both **15** and **21** in the presence of $AlCl_3$.

EXPERIMENTAL

ANALYTICAL PROCEDURES

Identification of the diphenylbutanes by v.p.c. was performed using three different columns: (1) a 6-ft, 30% Carbowax-100 on 60/80 mesh firebrick; (2) a 12-ft, 30% silicone gum rubber SE−30 on 42/60 mesh firebrick; (3) a 12-ft, 5% Bentone−34 and 5% silicone SE-52

---

[2] A. A. Khalaf and R. M. Roberts, *J. Org. Chem.*, **31**, 926 (1966).

[3] R. M. Roberts and S. E. McGuire, *J. Org. Chem.*, **35**, 102 (1970).

[4] A. A. Khalaf and R. M. Roberts, *J. Org. Chem.*, **35**, 3717 (1970).

[5] L. Schmerling, R. W. Welch and J. P. West, *J. Amer. Chem. Soc.*, **78**, 5406 (1956).

[6] L. Schmerling and J. P. West, *J. Amer. Chem. Soc.*, **76** 1917 (1954).

on 60/80 mesh Chromosorb-W. These columns were operated at 160, 190 or 220° in a Beckman GC-2 A instrument. A Beckman IR-5 A was used for infrared analysis. A Varian A-60 spectrophotometer was used for n. m. r. analysis.

MATERIALS

The required diphenylbutanes were synthesized as described below. All of the commercial starting materials and synthetic products were checked for purity by vapour-phase chromatography (v.p.c.) and infrared (i.r.) analysis. The $AlCl_3$ used was commercial anhydrous sublimed reagent grade.

SYNTHESIS OF 1,1-DIPHENYLBUTANE (15)

This was synthesized essentially by the procedure described by Serijan and Wise [7] except that 5 % palladium on charcoal was used as catalyst in the hydrogenation of the intermediate alkene. For catalytic hydrogenation, 1,1-diphenyl-1-butene was dissolved in an equal volume of 95 % ethyl alcohol and 5g of catalyst per 100 g of alkene was added. The reaction occurred at 50 psig. and the product was obtained as usual. Starting with 90 g (3.7 moles) of magnesium turnings, 612 g. (3.9 moles) of bromobenzene, 1100 ml of dry ether and 208 g (1.76 moles) of ethyl *n*-butyrate resulted in 198 g (53.6 % overall yield) of 1,1-diphenylbutane, b.p. 116–117° (2 mm), n_D^{20} 1.5566. Reported [7] b.p. 292.5° (760 mm) n_D^{22} 1.5568. The compound was found by v.p.c. to be 98–99 % pure.

SYNTHESIS OF 1,2-DIPHENYLBUTANE (21)

Preparation of 1,2-diphenyl-2-butanol. This was made by the condensation of phenylmagnesium bromide with propiophenone [7,8,9]. According to the procedure of Serijan and Wise [7] 134 g (1 mole) of freshly distilled propiophenone was condensed with 20 % excess of benzylmagnesium chloride. The latter was made from 28.8 g (1.2 moles) of dry magnesium turnings, 151 g (1.2 moles) of benzyl chloride, a small crystal of iodine and 300 ml of dry ether following the procedure given in *Organic Syntheses*.[10] Twothirds of the ether was used as solvent for the chloride and one-third was added to the magnesium in the reaction flask. The alcohol was obtained in 50 % yield and was shown by vapour chromatography and infrared spectrometry to be *ca*. 98 % pure.

Reduction of 1,2-diphenyl-2-butanol. This involved the direct catalytic hydrogenation of the carbinol. Into a 300-ml hydrogenation flask were introduced 105 g of the carbinol, 200 ml of glacial acetic acid, 8 g of 5 % palladium on charcoal and 1 ml of 70 % perchloric acid. The starting pressure was 60 psig and the mixture was hydrogenated until the calculated amount of hydrogen was absorbed. The solution was filtered to remove the catalyst. The filtrate was diluted with water and extracted with Skellysolve "B". The organic layer was washed with water, 10% sodium bicarbonate solution and again with water. It was dried over anhydrous sodium sulfate and the solvent was distilled with the aid of an aspirator. The residue, shown by vapour chromatography to be *ca.* 98% pure hydrocarbon, was distilled under vacuum. This gave 86 g (87.7%) of 1,2-diphenylbutane, b.p. 122–123° (2.2 mm), n_D^{25} 1.5485. Reported :[7] b.p.292.52° (760 mm), n_D^{20} 1.5518. The proton n.m.r. spectrum was consistent with the formulation of the compund.

---

[7] K. T. Serijan and P. H. Wise, *J. Amer. Chem. Soc.*, **74**, 365 (1952).

[8] P. Sabatier and M. Murat, *Compt. rend.*, **156**, 1430 (1913).

[9] M. Tuot and M. Guyard, *Bull. Soc. chim. France*, **14**, 1087 (1947).

[10] H. Gilman and W. E. Catlin, "Organic Synthesis", *Coll. Vol. I*, 2nd ed., A. H. Blatt, Ed. John Wiley and Sons, Inc., New York, N. Y., 1941, p. 471.

SYNTHESIS OF 1,3-DIPHENYLBUTANE (28)

The method reported by Serijan and Wise [7] was applied for the preparation of 1,3-diphenyl-3-butanol by condensation of the Grignard reagent made from 100 g (0.54 mole) of (2-bromoethyl)-benzene and 13 g (0.54 mole) of magnesium turnings with 60 g (0.5 mole) of freshly distilled acetophenone. The carbinol, obtained in *ca.* 90% yield, was reduced catalytically to the hydrocarbon following the hydrogenation procedure given before. Starting with 111 g of the crude carbinol, 200 ml of glacial acetic acid, 1 ml of 70% perchloric acid and 8 g of 5% palladium on charcoal, the yield of the crude hydrocarbon was 86 g. This was distilled under vacuum to give 65 g of 1,3-diphenylbutane, b.p. 158–159° (14 mm), n_D^{20} 1.5522. Reported [7] b.p. 302.9° dec. (760 mm), n_D^{20} 1.5523. The overall yield of hydrocarbon based on acetophenone was 62%.

ISOMERIZATION OF DIPHENYLBUTANES

General Procedure. In all experiments the hydrocarbon dissolved in benzene (dried over anhydrous sodium sulphate) was treated with anhydrous powdered $AlCl_3$ in a round-bottomed flask equipped with a magnetic stirrer and a reflux condenser protected by a calcium chloride tube. After stirring for a given time at the desired temperature, the cold reaction mixture was decomposed by adding ice-cold water and then stirring for another 15 min. The organic layer was separated using a separatory funnel and the aqueous layer was extracted two times with solvent ether. The combined extracts and organic layer were washed with 10% sodium bicarbonate solution and water, respectively, and finally dried over anhydrous calcium chloride. The ether benzene and products boiling up to butylbenzenes were distilled under atmospheric pressure using an 80-cm Nichrome spiral column. The remaining liquid was then distilled under vacuum using the same column. Vapour-phase chromatography (v.p.c.), infrared (i.r.) and nuclear magnetic resonance (n.m.r.) data were all used to identify the reaction products. Vapour phase chromatography was also used quantitatively to calculate the concentrations of the various components constituting the isomerization mixtures. Details concerning the amounts of reactants, reaction conditions and results are given separately for each experiment and are also summarized and tabulated in the discussion part.

ISOMERIZATION OF 1,1-DIPHENYLBUTANE (15)

Two experiments were carried out.

Experiment 1

1,1-Diphenylbutane, 6.3 g (0.03 mole), was treated with 0.396 g (0.003 mole) of aluminium chloride in 23.4 g (0.3 mole) of benzene at room temperature for four hours. Analysis of the crude reaction mixture by v.p.c. showed that it contained *n*-butylbenzene (4.5%),1,2-diphenylbutane (0.5%) and unchanged 1,1-diphenylbutane (95%).

Experiment 2

1,1-Diphenylbutane, 21 g (0.1 mole), was treated with 2.64 g (0.02 mole) of aluminium chloride in 78 g (1 mole) of benzene at 68 ± 2° for 6.5 hr. Vapour chromatographic analysis of the reaction mixture indicated that it consisted of *n*-butylbenzene (33 %), 1,2-diphenylbutane (21 %) and unchanged 1,1-diphenylbutane (46 %). Distillation under vacuum gave the following fractions :

Fraction N°	Pressure mm	Boiling temperature, °C	Weight, g	$n_D^{25.5}$
1	17	68	5.1	1.4867
2	2.8	121–122	4.0	1.5549
3	2.1	121–123	3.0	1.5555
4	2.1	123–124	3.0	1.5558
Residue	—	—	2.4	—

Fraction 1 was found by v.p.c. and infrared to be pure *n*-butylbenzene by comparison with authentic material (Eastman Organic Chemicals). Fractions 2, 3 and 4 were found by v.p.c. and infrared to contain 1,2-diphenylbutane (26-30%) and 1,1-diphenylbutane (74-70%). Fraction 2 was shown by v.p.c. to contain traces of diphenylmethane.

ISOMERIZATION OF 1,2-DIPHENYLBUTANE (21).

Three experiments were carried out :

Experiment 3

1,2-Diphenylbutane, 4 g (0.02 mole), was treated with 0.264 g (0.002 mole) of aluminium chloride in 15.6 g (0.2 mole) of benzene at room temperature for four hours. The solvent was removed and the residue was found by v.p.c. to contain *n*-butylbenzene (2 %), 1,2-diphenylbutane (96 %) and unidentified products (2 %). This residue was distilled to give the following fractions :

Fraction N°	Pressure, mm	Boiling temperature, °C	Weight, g	$n_D^{25.5}$
1	Atmospheric	180–185	3 drops	—
2	2	115–116	3.1	1.5481
Residue	—	—	0.5	—

Fraction 1 was found by v.p.c. to be *n*-butylbenzene. Fraction 2 was found by both v.p.c. and infrared to be pure 1,2-diphenylbutane.

Experiment 4

1,2-Diphenylbutane, 10.5 g (0.05 mole), was treated with 1.32 g. (0.01 mole) of aluminium chloride in 39 g (0.5 mole) of benzene at 70 ± 2° for 6.5 hr. Analysis of the reaction mixture by vapour chromatography indicated that it consisted of *n*-butylbenzene (8 %) and 1,2-diphenylbutane (89 %). 1,3 -Diphenylbutane was also shown in trace amounts.

Experiment 5

1,2-Diphenylbutane, 10.5 g (0.05 mole), was treated with 2.6 g (0.02 mole) of aluminum chloride in 39 g (0.5 mole) of benzene at 70 ± 2° for 6.5 hr. The reaction mixture was found by v.p.c. to consist (within ±10 %) of *n*-butylbenzene (32 %), 1,2-diphenylbutane (53 %), 1,1-diphenylbutane (1 %), 1,3-diphenylbutane (6 %) and 1,4-diphenylbutane (6 %). The remaining 2 % was composed of unidentified components.

Revue Roumaine de Chimie, **18**, *11*, 1937 – 1948 (1973)

MODERN FRIEDEL-CRAFTS CHEMISTRY. IV*

THE FRAGMENTATION AND DEALKYLATION BEHAVIOUR OF 1,1-DIPHENYL-2-METHYLPROPANE AND 1,2-DIPHENYL-2-METHYLPROPANE UNDER THE INFLUENCE OF WATER-ACTIVATED ALUMINUM CHLORIDE AT 100°

ROYSTON M. ROBERTS** and ALI ALI KHALAF***

**Chemistry Department, University of Texas at Austin, Austin, Texas 78712, U.S.A.
*** Chemistry Department, The University of Assiut, Assiut, Arab Republic of Egypt

Received February 26, 1973

The effect of water-activated aluminum chloride on both 1,1- and 1,2-diphenyl-2-methylopropane at 100° was investigated under a variety of conditions to evaluate the effect of time and catalyst ratio on the composition of the resulting fragmentation and dealkylation products. Depending upon the severity of the conditions employed, both isomers yielded varying amounts of C_2 to C_5 alkanes and C_7 to C_{10} alkylbenzenes besides isomeric diphenylbutanes and higher polymeric materials. It is suggested that the products of these reactions resulted from a combination of dealkylation, fragmentation, isomerisation, bimolecular condensation and other Friedel-Crafts type reactions.

The reactions which alkylbenzenes undergo when treated with Friedel-Crafts catalysts were formerly classified [1] as of five main types: (a) *disproportionation* (intermolecular alkyl transfers), (b) *reorientation* (intramolecular and/or intermolecular alkyl transfers), (c) *rearrangement* (internal, of side chains), (d) *dealkylation* (production of alkanes corresponding to alkyl side chains), and (e) *fragmentation* (production of alkanes smaller than alkyl side chains and smaller alkyl benzenes). With the help of modern instrumental methods of product identification, particularly vapour phase chromatography, Roberts and his collaborators have directed a part of their recent effort towards a systematic study of the mechanistic aspects of the last two reactions, namely dealkylation and fragmentation.

In a first paper published in 1963, Roberts, Baylis and Fonken [2] studied the dealkylation and fragmentation reactions of a number of monophenylalkanes including alkyl-, propyl-, butyl- and pentylbenzenes by heating them with water-activate $AlCl_3$ in a closed system at 100°. In a second paper published in 1964, Roberts, Khalaf and Greene[3] have extended the work to cover dealkylations and fragmentations of some diphenylalkanes, namely, 1,2-diphenylpropane, 2,3-diphenylbutane 2,2-diphenylbutane, 1,1-diphenyl-2-methylpropane and 1,2-diphenyl-2-methylpropane. At that time, however, the authors focused their discussions on the results obtained by treating each of the above compounds with water-activated aluminum chloride for three hours at 100°. In the present paper we wish to report the results of many experiments performed on the two closely related isomers, 1,2-diphenyl-2-methylpropane (1) and 1,1-diphenyl-2-methylpropane (2) in which the two compounds were treated with water-activated $AlCl_3$ at 100° for different reaction times and with different proportions of catalyst to study the effect of these variables upon the composition and distribution of both fragmentation and dealkylation products.

---

* Part III. R. M. Roberts and A. A. Khalaf, *Rev. Roumaine Chim.*, **18**, 1929(1973).

[1] R. M. Roberts, G. A. Ropp and O. K. Neville, *J. Amer. Chem. Soc.*, **77**, 1764 (1955).
[2] R. M. Roberts, E. K. Baylis and G. J. Fonken, *J. Amer. Chem. Soc.*, **85**, 3454 (1963).
[3] R. M. Roberts, A. A. Khalaf and R. N. Greene, *J. Amer. Chem. Soc.*, **86**, 2846 (1964).

RESULTS AND DISCUSSION

The reactions of diphenylalkanes with $AlCl_3$ were performed in the closed system described in the experimental part. The results of these reactions are summarized in tables 1 and 2 for 1,2-diphenyl-2-methylpropane (1) and in tables 3 and 4 for 1,1-diphenyl-2-methylpropane (2).

Table 1

Liquid dealkylation and fragmentation products from 1,2-diphenyl-2-methylpropane[a]

Experiment N°	Time, min	Liquid mixture, $R-C_6H_5$, Boiling Range 85−176°								
		Total, wt. % of original compound	Me %[b]	Et %[b]	o-xylene %[b]	Pr. %[b]		Butylbenzenes		
						i-	n-	t- %[b]	i- %[e]	s- %[e]
1A	5	8[c,d]	0.7	2.3	0.3	0.7	—	0.2	69	26
2A	10	10[c,d]	1.3	5.3	0.7	2.2	—	0.6	65	24
3A	15	11[c,d]	1.6	6.7	0.9	2.9	—	0.8	60	26
4A	30	11[c]	2.5	9.4	0.5	3.0	—	—	55	29
5A	60	18[c]	2.9	12.0	0.6	3.8	0.1	—	50	30
6A	120	20	5.8	16.8	0.5	5.4	0.5	—	38	33
7A	180	21	4.6	17.8	0.9	7.1	0.6	—	36	35
8A[f]	180	21	10.0	18.0	2.0	8.0	2.0	—	38	22
9A[g]	120[h] + 30[i]	18	9.6	17.6	0.7	7.6	0.6	—	35	29
10A[g]	120[h] + 60[i]	21	16.8	17.2	0.4	4.8	0.8	—	36	24
11A[g]	120[h] + 180[i]	21	26.2.	16.6	0.4	6.2	1.6	—	29	20

[a] Reactions at 100° ; reactants : hydrocarbon, 0.075 mole ; $AlCl_3$, 0.025 mole ; H_2O, 0.0125 mole. In experiments 8A−IIA, double catalyst ($AlCl_3$ and H_2O) was used.

[b] Percentage of each alkylbenzene in the liquid mixture as found by v.p.c.

[c] In experiments 1A, 2A, 3A, 4A and 5A, this contained 0.1% 0.2%, 0.2%, 0.3% and 0.4% of what is believed to be a branched C_8-paraffin and 0.6%, 0.7%, 0.9%, 0.3% and 0.2% of an unknown compound boiling in the trimethylbenzene range.

[d] In experiment 1A this contained 0.2% and in experiments 2A and 3A this contained traces of isooctane.

[e] The total percentages were found by v.p.c. and the individual percentages were found by infrared analysis.

[f] Double catalyst added in one step.

[g] Double catalyst added in two steps.

[h] With first batch of catalyst.

[i] with second batch of catalyst.

Table 2

Gaseous dealkylation and fragmentation products from 1,2-diphenyl-2-methylpropane[a]

Experiment N°	Time min	Gaseous products						
		Volume[b] ml	Total, mole %[c]	C_2H_6, %[d]	C_3H_8, %[d]	C_4H_{10}, %[d] *i*-	C_4H_{10}, %[d] *n*-	C_5H_{12}, %[d] *i*-
1A	5	42	2.5	Tr.	—	90	4	6
2A	10	42	2.5	Tr.	—	90	3	7
3A	15	42	2.5	Tr.	—	90	3	7
4A	30	60	3.5	Tr.	—	85	3	12
5A	60	73	4.3	Tr	—	85	3	12
6A	120	73	4.3	Tr.	—	71	3	26
7A	180	114	6.8	Tr.	—	74	T	26
8A[e]	180	254	15.0	Tr.	Tr.	82	1	17
9A[e]	120[f]	76	4.5	Tr.	—	75	1	24
	30[g]	60	3.5	2	Tr.	55	16	27
10A[e]	120[f]	74	4.4	Tr.	—	67	2	31
	60[g]	100	6.0	1	4	46	36	13
	120[f]	80	4.8	Tr.	—	72	1	27
11A[e]	180[g]	130	7.7	1	4	42	40	13

[a] Reactions at 100° ; reactants : hydrocarbon, 0.075 mole, $AlCl_3$, 0.025 mole, H_2O, 0.0125 mole. In experiments 8A – 11A double catalyst ($AlCl_3$ and H_2O) was used.

[b] At S.T.P.

[c] Mole % conversion to alkane based on hydrocarbon, calculated from volume of gas collected

[d] Percentage of each alkane in the gaseous mixture as found by v.p.c.

[e] Double catalyst was used.

[f] With first batch of catalyst.

[g] With second batch of catalyst.

Table 3

Liquid dealkylation and fragmentation products from 1,1-diphenyl-2-methylpropane[a]

Experiment N°	Time, min	Liquid mixture, $R-C_6H_9$, Boiling Range 85–176°								
		Total wt. % of original compound	Me %[b]	Et, %[b]	*o*-xylene %[b]	Pr %[b] *i*-	Pr %[b] *n*-	Butylbenzenes *t*- %[b]	Butylbenzenes *i*- %[c]	Butylbenzenes *s*- %[c]
1B	5	5.5[d]	0.2	3.0	0.6	3.9	0.3	Tr.[d]	61.0	31.0
2B	10	9[d]	0.5	1.4	3.4	2.4	0.3	Tr.	61.0	31.0
3B	15	10[d]	0.4	1.5	2.0	2.3	0.2	Tr.	65.5	28.1
4B	30	13[d]	0.1	1.8	0.5	2.6	0.1	Tr.	62.6	32.3
5B	60	14[c]	0.2	2.2	0.1	2.5	0.2	—	65.0	29.6
6B	120	20	0.5	6.0	Tr.	4.8	0.5	—	55.5	32.7
7B	180	20	0.8	4.6	0.4	3.5	0.7	—	56.7	33.3
8B	180	24	3.6	15.5	8.0	8.6	2.5	—	44.0	25.0

[a] Reactions at 100°; reactants : hydrocarbon, 0.05 mole ; $AlCl_3$, 0.0166 mole, H_2O, 0.008 mole. In experiment 8B the amounts of $AlCl_3$ and H_2O were doubled.

[b] Percentage of each alkylbenzene in the liquid mixture as found by v.p.c.

[c] The total percentages were found by v.p.c. and individual percentages by infrared analysis.

[d] Traces of a compound believed to be a branched octane also were found.

[e] Double catalyst ($AlCl_3$ and H_2O) was added as one batch.

Table 4

Gaseous dealkylation and fragmentation products from 1,1-diphenyl-2-methylpropane [a]

Experiment	Time min	Gaseous mixtures						
		Volume[b] ml	Total %[c]	C_2H_6 %[d]	C_3H_8 %[d]	C_4H_{10} *i*-	%[d] *n*-	C_5H_{12} %[d] *i*-
1B	5	35	3.1	—	—	80	16	4
2B	10	37	3.3	—	—	83	13	4
3B	15	33	2.9	—	—	90	4	6
4B	30	55	4.9	—	—	92	Tr.	8
5B	60	78	7.0	Tr.	—	90	Tr.	10
6B	120	129	11.5	Tr.	—	77	Tr.	23
7B	180	126	11.2	Tr.	—	74	Tr.	26
8B[e]	180	142	12.7	Tr.	Tr.	76	4	20

[a] Reactions at 100° ; reactants : hydrocarbon, 0.05 mole ; $AlCl_3$, 0.0166 mole ; H_2O, 0.008 mole. In experiment 8B double catalyst ($AlCl_3$ and H_2O) was used.

[b] At S.T.P.

[c] Mole % conversion to alkane based on hydrocarbon, calculated from the volume of gas collected.

[d] Percentage of each alkane in the mixture as found by v.p.c.

[e] Double catalyst was added as one batch.

From examining the results of tables 1 to 4 one can note some interesting changes in the fragmentation and dealkylation products with variations in reaction time and catalyst ratio. These changes can be summed up in the following points : (1) Trace amounts of *t*-butylbenzene were produced by both isomers in the early stages of the reactions (after 5, 10 and 15 minutes). Only in the case of 1,1-diphenyl-2-methylpropane traces of *t*-butylbenzene were again found after longer reaction periods (120 and 180 minutes). (2) While the ratio of isobutylbenzene : *sec*-butylbenzene produced from 1,2-diphenyl-2-methylpropane decreased from 73 : 27 (5 minutes reaction time) to 47 : 53 (after three hours) the ratio produced from 1,1-diphenyl-2-methylpropane did not change much with time (65 : 35 after five minutes and 64 : 36 after three hours). (3) Under all conditions, isobutane remained to be the major gaseous product given by both isomers and its ratio decreased with time ; in contrast, the ratio of isopentane increased with time. (4) For both isomers the ratio of *n*-butane in single catalyst experiments decreased with time. (5) After short reaction times, small amounts of branched octanes were produced from both isomers (see footnote c for table 1 and d for table 3). (6) Except for the five minute reaction, more isopropylbenzene was always produced from 1,2-diphenyl-2-methylpropane (1) than from 1,1-diphenyl-2-methylpropane (2). Moreover, the percent of this fragmentation product in the mixture from 1 increased with time. (7) Similar to increasing time effects, it can be seen from tables 1 to 6 that an increase in catalyst to hydrocarbon ratio resulted in more fragmentation, mainly, to toluene and ethylbenzene, in more dealkylation to butanes and in an enhanced production of isopentane. (8) Both 1,1- and 1,2-diphenyl-2-methylpropane showed similar but not identical dealkylation and fragmentation patterns. This is not unexpected, however, if one recalls the established facile interconversion of the two isomers in the presence of $AlCl_3$[3]. Accordingly, the observed products would result not only from the starting diphenylalkanes but also from their isomerization products.

Restricting the definition of fragmentation to mean rupture of the alkane chain[1], it can be seen from the results of tables 1 and 3 that toluene, xylene, ethylbenzene and *n*- and *i*-propyl benzene constituted the monophenylated fragmentation mixture from both 1,1 — and 1,2-diphenyl-2-methylpropane. The various carbonium ion processes believed to be involved in the formation of these fragments are visualized in Scheme 1. In addition, the formation of xylene in these reactions can be attributed to a disproportionation reaction of toluene in the presence of $AlCl_3$.[4]

Scheme 1

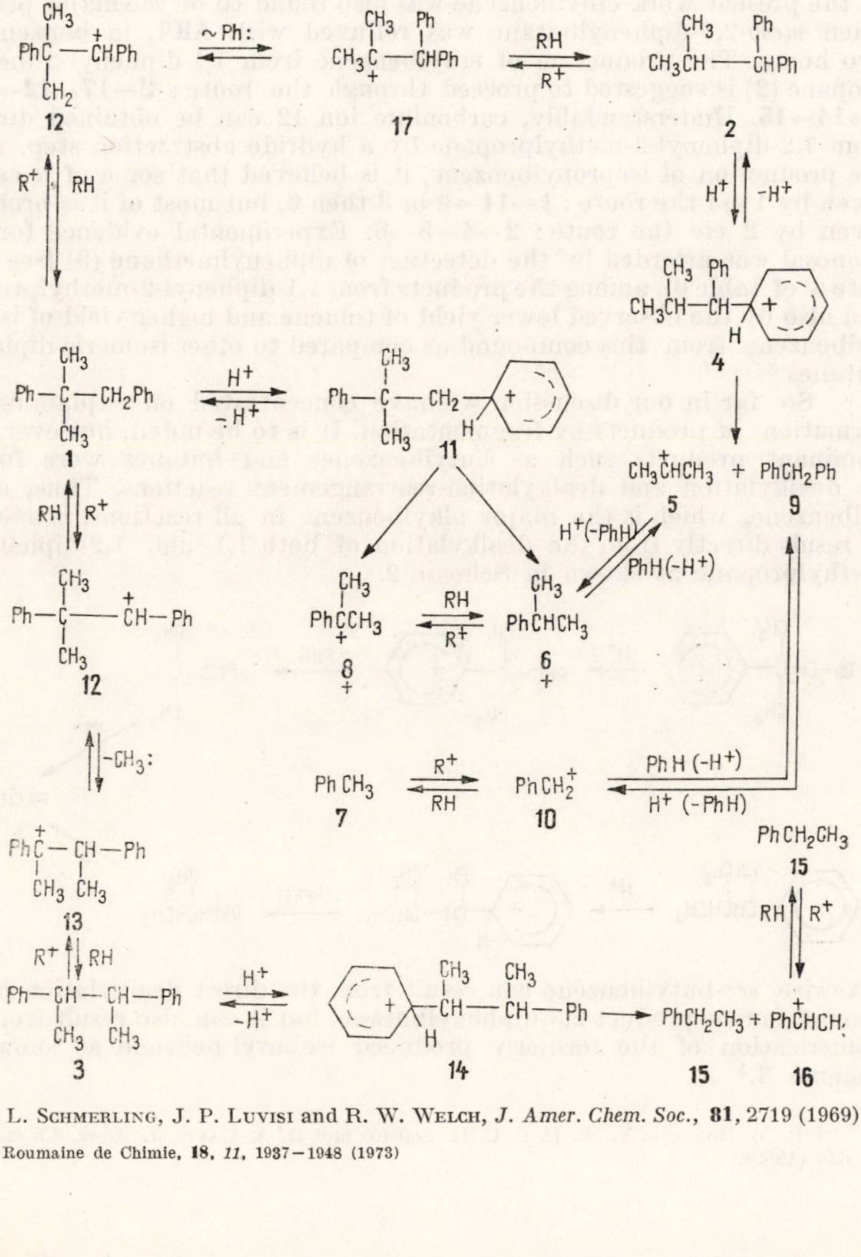

---

[4] L. Schmerling, J. P. Luvisi and R. W. Welch, *J. Amer. Chem. Soc.*, **81**, 2719 (1969).

According to Scheme 1, ethylbenzene is suggested to result from the fragmentation of 2,3-diphenylbutane (3) which is produced directly from 1,2-diphenyl-2-methylpropane (1) *via* the route **1**→**12**→**13**→**3** and from 1,1-diphenyl-2-methylpropane (2) by prior rearrangement to **1** *via* the route **2** →**17**→**12**→**1** and subsequent rearrangement of **1** to **3** as above. Experimental support for the above suggestion has been found in two facts : (a) the isolation of 2,3-diphenylbutane in these reactions (see footnotes to tables 5 and 6) and (b) the formation of ethylbenzene as the major product whenever 2,3-disphenylbutane was treated with $AlCl_3$[2,3]. In the present work ethylbenzene was also found to be the major product when *meso*-2,3-diphenylbutane was refluxed with $AlCl_3$ in benzene for two hours. The production of ethylbenzene from 1,1-diphenyl-2-methylpropane (2) is suggested to proceed through the route : **2**→**17**→**12**→**13**→**3**→**14**→**15**. Understandably, carbonium ion 12 can be obtained directly from 1,2-diphenyl-2-methylpropane by a hydride abstraction step. As to the production of isopropylbenzene, it is believed that some of it can be given by 1 *via* the route : **1**→**11**→**6** or **8** then **6**, but most of it is probably given by **2** *via* the route: **2**→**4**→**5**→**6**. Experimental evidence for this proposal was afforded by the detection of diphenylmethane (**9**) (see footnote a of table 6), among the products from 1,1-diphenyl-2-methylpropane and also by the observed lower yield of toluene and higher yield of isopropylbenzene from this compound as compared to other isomeric diphenylbutanes [3].

So far in our discussion we have concentrated on explaining the formation of products by fragmentation. It is to be noted, however, that dominant products such as butylbenzenes and butanes were formed by dealkylation and dealkylation-rearrangement reactions. Thus, isobutylbenzene, which is the major alkylbenzene in all reactions, is assumed to result directly from the dealkylation of both 1,1- and 1,2-diphenyl-2-methylpropane as shown in Scheme 2.

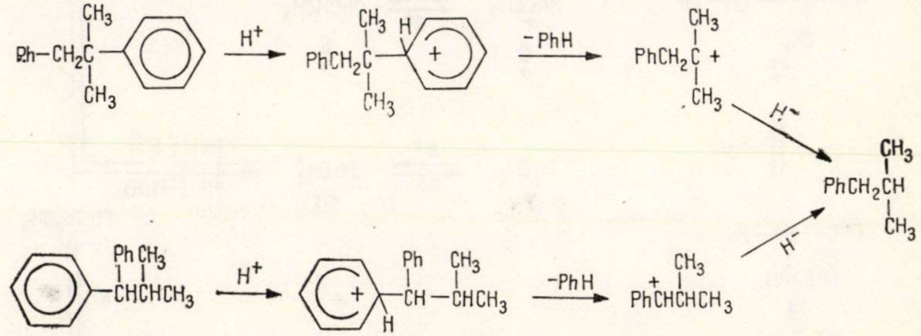

Likewise, *sec*-butylbenzene can result from the direct dealkylation of the rearrangement product 2,3-diphenylbutane, but it can also result from the isomerization of the formerly produced isobutyl-benzene as shown in Scheme 3.[5]

---

[5] R. M. Roberts, Y. W. Han, C. H. Schmid and D. A. Davis, *J. Amer. Chem. Soc.*, **81**, 640 (1959).

Concerning the gaseous products, it can be seen from tables 2 and 4 that, similar to the $AlCl_3$-catalyzed reactions of butylbenzenes at 100°, isobutane constituted most of the gaseous mixtures given by both of the two isomeric diphenylmethylpropanes. Besides isobutane, however, varying amounts of *n*-butane and isopentane were also formed. While the amount of isopentane showed an increase with increasing both time and catalyst ratio, that of *n*-butane increased mainly with increasing catalyst ratio (see experiments 9A to 11A of table 2). The modes of formation of isobutane and *n*-butane are thought to be similar to those suggested before [3] in that both the *sec*- and the isobutylbenzene produced as shown above are rapidly isomerized to *t*-butylbenzene upon mixing with the hot catalyst, and that the resulting *t*-butylbenzene immediately undergoes dealkylation to isobutane and benzene. On the other hand, *sec*-butylbenzene undergoes direct but slower dealkylation to *n*-butane and benzene.

Scheme 3

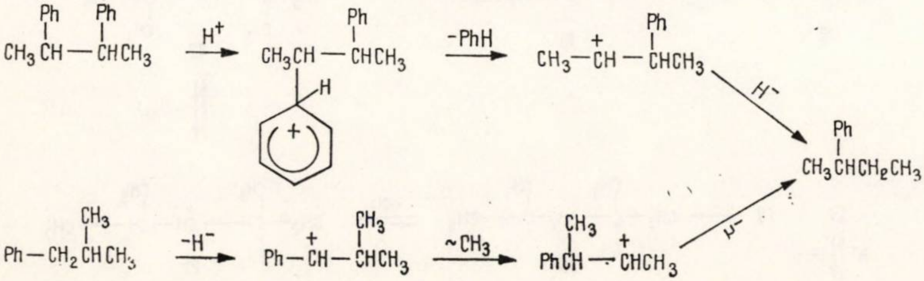

The production of isopentane from both 1,1- and 1,2-diphenylpropane in all experiments and of small but detectable amounts of isooctane and other branched C_8-paraffins in some experiments (see footnotes c and d to table 1 and footnote d to table 3) deserves some comment. The formation of isopentane can be explained reasonably in terms of a bimolecular reaction [6,7] involving the addition of *t*-butylcarbonium ion (**18**) to isobutylene (**19**) as outlined in Scheme 4. It seems from the experimental data that path (b) is more favoured since only traces of propane (**23**) were detected. In the presence of benzene, however, a third alternative path (c) is also possible. Here, **22** could alkylate benzene to yield the intermediate complex **26**. The latter, in turn, could cleave to **25** and isopropyl benzene (**6**). As a matter of fact, isopropylbenzene (**6**) was found in all of these reactions but, as has been shown before, its presence can be attributed to other reaction routes.

In Scheme 4, carbonium ions **20**, **21** and **22** might also eliminate protons to give the alkenes or abstract hydride ions to give the paraffins. In terms of the latter possibility, the detection of more than one octane isomer could be explained. Giving the steps of Scheme 4, some experimental support was the fact that when 2,2,3-trimethylpentane (which

---

[6] G. J. Karabatsos and F. M. Vane, *J. Amer. Chem. Soc.*, **85**, 729 (1963).

[7] B. S. Friedman and F. L. Morritz, *J. Amer. Chem. Soc.*, **78**, 3430 (1956).

might yield both carbonium ions 20 and 21 in the presence of strong Friedel-Crafts catalysts)[8] was treated with $AlCl_3$ at 70° for 20 min, 44% of alkane mixture consisting of 90% isobutane (18a) and 10% isopentane (24a) was evolved[3].

Scheme 4

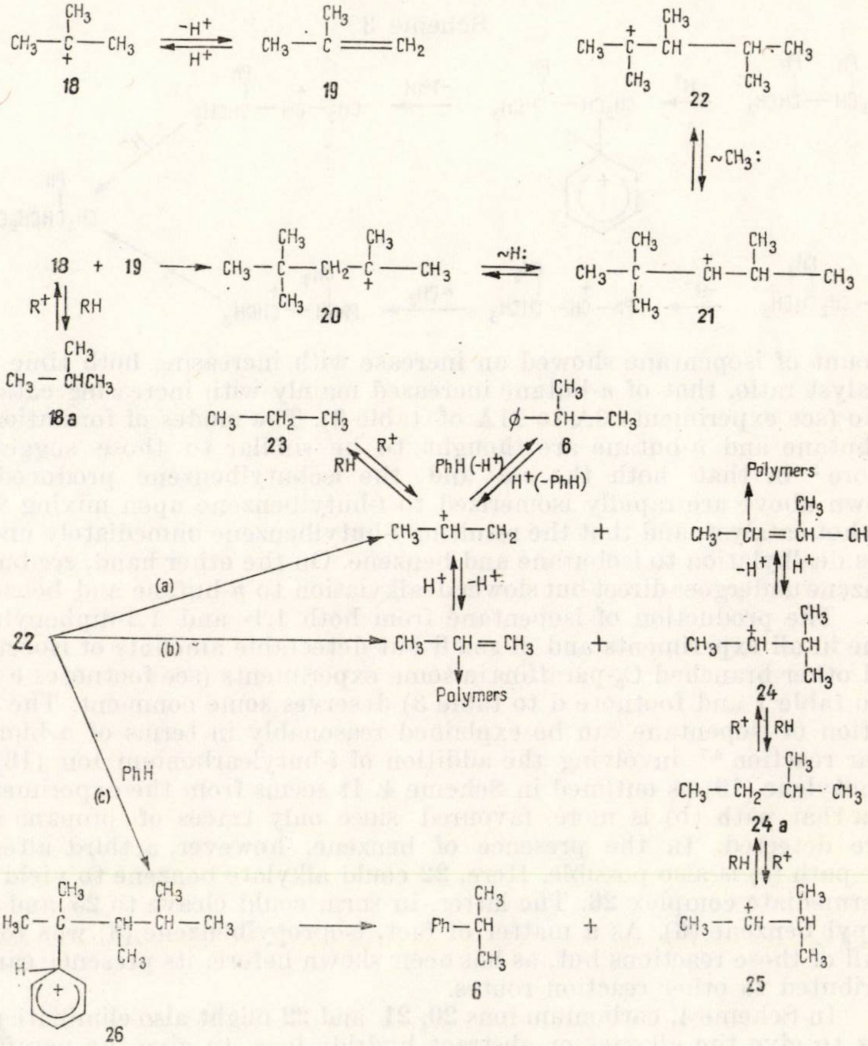
18
19
20
21
22
~CH3:
~H:
R+
RH
18a
23
6
PhH (-H+)
H+(-PhH)
Polymers
H+
-H+
(a)
(b)
(c)
PhH
24
24 a
25
26

EXPERIMENTAL

ANALYTICAL PROCEDURES

These were similar to those described before.[3]

---

[8] a) G. J. Karabatsos, F. M. Vane and S. Meyerson, *J. Amer. Chem. Soc.*, **85**, 733 (1963); b) J. D. Roberts, R. E. McMahon and J. S. Hine, *J. Amer. Chem Soc.*, **72**, 4237 (1950).

STARTING MATERIALS AND FINAL PRODUCTS

1,1-Diphenyl-2-methylpropane, 2,2-diphenyl-2-methylpropane and 2,3-diphenylbutane were prepared as described before. Isobutane, isopentane, isooctane, toluene, ethylbenzene, *n*- and isopropylbenzene, and *n*-, *sec*-, *t*- and *iso*butylbenzene were all commercially available and were obtained from the usual suppliers.

REACTIONS OF DIPHENYLALKANES WITH ALUMINUM CHLORIDE AT 100°

Apparatus

The apparatus used in all experiments is illustrated in figure 1. It was a closed system consisting of a round-bottomed flask (A) equipped with a magnetic stirrer (B), a pressure-equalizing dropping funnel (C) furnished with a helium inlet tube having a glass stopcock (D), and a spiral reflux condenser (E) cooled by tap water. The condenser was serially connected to a safety tube (F), a trap containing sodium hydroxide solution (G) and then to the upper end of an inverted separatory funnel (H) through a stopcock (I) and a three-hole rubber stopper (J). The second hole of the stopper was fitted with a tube (K) which carried the saturated salt solution displaced

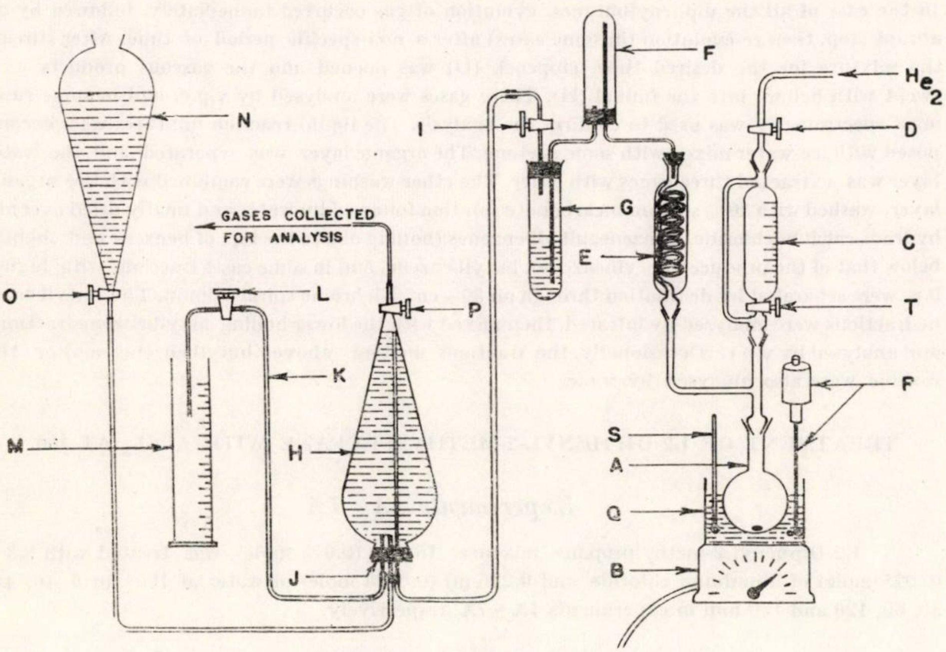

Fig. 1. – The apparatus used in the experiments.

---

[9] A. A. Khalaf and R. M. Roberts, *J. Org. Chem.*, **31**, 926 (1966).

by the gaseous products *via* stopcock (L) to a measuring cylinder (M). The third hole was connected to a reservoir (N) filled with salt solution and set at a level higher than that of the inverted funnel (H). Flow of water from (N) to (H) through stopcock (0) sweeps the gases through the upper opening of the funnel (H) from which it was collected for analysis. Reservoir (N) also was used to fill up the inverted funnel with salt solution before each experiment. An electrically-heated oil bath (Q) equipped with a mechanical stirring apparatus (R) and a thermometer (S) was used to heat the reaction flask (A).

General procedure

In all experiments, powdered analytical grade anhydrous aluminum chloride (Mallinckrodt) was weighed in the reaction flask (A). The hydrocarbon was weighed in the dropping funnel (C) and a measured volume of water was then introduced. The reaction flask was placed in the previously heated oil bath. To flush the apparatus with helium, stopcocks D, I and P were opened while L, T and 0 were closed. A stream of helium was then allowed to flow through the apparatus for two minutes. This eliminated an air peak from the vapour phase chromatographic analyses. After flushing, stopcocks D and P were closed and L and T were opened. This permitted the hydrocarbon — water mixture to pass into the reaction flask. In the case of all the diphenylbutanes, evolution of gas occurred immediately, followed by an abrupt stop, then re-evolution (in some cases) after a non-specific period of time. After stirring the mixture for the desired time, stopcock (D) was opened and the gaseous products were swept with helium into the funnel (H). These gases were analysed by v.p.c. and in some cases mass spectrometry was used to confirm the analysis. The liquid reaction mixtures were decomposed with ice-water mixed with some acetone. The organic layer was separated and the water layer was extracted three times with ether. The ether washings were combined with the organic layer, washed with 10 % sodium bicarbonate solution followed by water and finally dried over anhydrous calcium chloride. Benzene, alkylbenzenes (boiling above the b.p. of benzene and slightly below that of the produced butylbenzene), butylbenzene, and in some cases fractions with higher b.p. were separated by distillation through an 80—cm. Nichrome spiral column. The butylbenzene fractions were analysed by infrared, then mixed with the lower boiling alkylbenzene fractions and analysed by v.p.c. Occasionally, the fractions boiling above butylbenzene and/or the residue were also analysed by v.p.c.

TREATMENT OF 1,2-DIPHENYL-2-METHYLPROPANE WITH ALCL$_3$ AT 100°

Experiments 1A—7A

1,2-Diphenyl-2-methylpropane mixture, 15.75 g (0.075 mole), was treated with 3.3 g (0.025 mole) of aluminum chloride and 0.225 ml (0.0125 mole) of water at 100° for 5, 10, 15, 30, 60, 120 and 180 min in experiments 1A—7A, respectively.

Experiment 8A

1,2-Diphenyl-2-methylpropane mixture, 15.75 g (0.075 mole), was treated with 6.6 g (0.05 mole) of aluminum chloride and 0.46 ml (0.025 mole) of water at 100° for three hours.

Experiments 9A 11A

1,2-Diphenyl-2-methylpropane mixture, 15.75 g (0.075 mole), was treated with 3.3 g (0.025 mole) of aluminum chloride and 0.225 ml (0.0125 mole) of water at 100° for three hours. To the cold reaction mixture was added 3.3 g (0.025 mole) of aluminum chloride and 0.225 ml

(0.0125 mole) of water. After the addition of the second batch of catalyst, the mixture was again treated at 100° for 30, 60 and 120 min in experiments 9A, 10A and 11A, respectively.

The results of experiments 1A—11A are shown in tables 1 and 2 in the discussion section and in table 5 in this section.

Table 5

Distillation of the liquid products obtained from 1,2-diphenyl-2-methylpropane by treatment with $AlCl_3$ at 100°

Experiment N°	Distillation data, weight, g			
	Benzene	b.p. 85—165°	b.p. 165—176°	Residue[a]
1A	2.57	0.05	1.15	8.30
2A	2.60	0.10	1.53	8.45
3A	2.99	0.28	2.20	8.21
4A	3.24	0.29	2.16	7.97
5A	3.60	0.42	2.42	7.37
6A	3.61	0.39	2.65	6.90
7A	4.30	0.40	2.98	6.62
8A	2.20	1.20	2.06	5.30
9A	2.71	0.34	2.34	5.74
10A	2.90	0.98	2.27	6.60
11A	2.80	1.34	1.74	7.24

[a] Contained 1,1-diphenyl-2-methylpropane and *dl* — and meso — 2 ; 3-diphenylbutane.

TREATMENT OF 1,1-DIPHENYL-2-METHYLBUTANE WITH ALCL$_3$ AT 100°

Experiments 1B—7B

1,1-Diphenyl-2-methylpropane, 10.5 g (0.05 mole) was treated with 2.2 g (0.017 mole) of aluminum chloride and 0.15 ml (0.008 mole) of water at 100° for 5, 10, 15, 30, 60, 120 and 180 min in experiments 1B — 7B, respectively.

Experiment 8B

1,1-Diphenyl-2-methylpropane, 10.5 g (0.05 mole), was treated with 4.4 g (0.033 mole) of aluminum chloride and 0.3 ml (0.017 mole) of water for three hours at 100°.

The results of the experiments 1B to 8B are shown in table 6.

TREATMENT OF *MESO*-2,3,DIPHENYLBUTANE WITH ALCL$_3$ IN BENZENE AT REFLUX TEMPERATURE

meso-2,3-Diphenylbutane, 5.25 g (0.025 mole), was treated with 6.6 g (0.05 mole) of aluminum chloride in 39 g (0.5 mole) of benzene at 80° for two hours. No gaseous products were found. The crude mixture was analysed by v.p.c. and was shown to consist of toluene (traces), ethylbenzene (4.5 %), isopropylbenzene (2.5 %), *n*-propylbenzene (1 %), *sec-butyl-* and/or isobutylbenzene (32 %), *dl*-2,3-diphenylbutane (4 %), *meso*-2,3-diphenylbutane (1 %) and

Table 6

Distillation of the liquid products obtained from 1,1-diphenyl-2-methylpropane by treatment with $AlCl_3$ at 100°

Experiment N°	Distillation data, weight, g			
	Benzene	b.p. 85−165°	b.p 165−176°	Residue[a]
1B	1.10	0.03	0.55	6.83
2B	1.63	0.06	0.90	5.90
3B	2.20	0.08	1.00	6.30
4B	2.30	0.09	1.30	5.50
5B	2.40	0.10	1.40	5.63
6B	2.30	0.23	1.90	4.70
7B	2.70	0.24	1.80	4.60
8B	0.50	0.91	2.00	6.00

[a] Contained 1,2-diphenyl-2-methylpropane, *dl* − and *meso* −2,3-diphenylbutane and diphenylmethane,

1,3-diphenylbutane (1 %). The remaining 54 % was composed of at least 21 unidentified components; only three of these components were higher boiling than diphenylbutanes.

Revue Roumaine de Chimie, **18**, *11*, 1949–1958 (1973)

RELATIONS ENTRE LA LONGUEUR DE LA CHAÎNE DES *n*-ALCANES ET LA COMPOSITION DES *n*-ACIDES MONOCARBOXYLIQUES OBTENUS PAR LEUR OXYDATION

IOSIF DRIMUŞ et IOAN T. IONESCU

Institut Polytechnique de Bucarest, 149, Calea Victoriei

Reçu le 31 mars 1973

On a soumis à l'oxydation thermique (non catalytique) en phase liquide à l'aide de l'oxygène moléculaire les alcanes normaux ayant 12, 13, 14, 16, 17, 18, 20, 21 et 24 atomes de carbone dans leur molécule. On a étudié la composition des acides gras obtenus. On a constaté que la rupture de la chaîne de l'alcane se réalise statistiquement pour toutes les liaisons qui sont séparées du méthyle terminal avec au moins quatre atomes de carbone. On a déterminé les coefficients (sous-unitaires) pour le pourcentage molaire des acides qui se forment par la rupture des liaisons 1–2, 2–3, 3–4, 4–5 et 5–6. On a constaté que ces considérations ne sont pas valables pour le *n*-dodécane et le *n*-tridécane. On a établi une méthode de calcul concernant la composition des acides gras qu'on obtient par l'oxydation des hydrocarbures normaux C_nH_{2n+1} où *n* est compris entre 14 et 24.

Le présent ouvrage essaie d'élucider un problème très controverslé dans la littérature, concernant les points de rupture de la chaîne des *n*-alcanes pendant leur oxydation thermique à l'aide de l'oxygène moléculaire.

Le plus grand nombre des travaux concernant l'oxydation des paraffines ont été effectués sur des paraffines techniques, comprenant un mélange d'hydrocarbures. Par conséquent, les résultats obtenus ne permettent pas d'établir des conclusions générales. On présente en premier lieu les principaux travaux sur l'oxydation des *n*-alcanes purs.

Le *n*-eicosane ($C_{20}H_{42}$) a été oxydé par Wietzel [1] en 1938 ; les acides formés ont été séparés par rectification sous vide. Faute de moyens modernes de séparation, les résultats obtenus ne sont pas suffisamment concluants.

Le *n*-octadécane a été oxydé par Geisler et Asinger [2] à l'aide de l'oxygène ozonisé. Dans les produits de réactions on a pu identifier, par chromatographie sur papier, tous les acides à partir de C_1 jusqu'à C_{18}.

---

[1] G. Wietzel' *Fette u. Seifen*, **44**, 21 (1938).

[2] G. Geisler et F. Asingir, *Chem. Ber.*, **92**, 958 (1959).

Le *n*-tétradécane a été oxydé par Razumovski [3] en phase liquide à l'aide de l'oxygène moléculaire, à une température de 130° en présence de *sels de Mn et de K*. Les acides obtenus ont eu la composition suivante (en % molaires) C_1...7,4 ; C_2...4,2 ; C_3...4,3 ; C_4...3,9 ; C_5...3,9 ; C_6...5,6 ; C_7...8,8 ; C_8...13,0 ; C_9...9,2 ; C_{10}...15,7 ; C_{11}...10,1 ; C_{12}...8,8 ; C_{13}... ...3,9 et C_{14}...1,2. Ces chiffres sont assez différentes de ceux que nous avons trouvés dans le cas de l'oxydation *non catalytique* du même hydrocarbure.

Ermolaeva et ses collaborateurs[4] ont établi que les acides obtenus par oxydation non catalytique du *n*-tétradécane se trouvent dans les rapports suivants : C_{7-9}...1,0 ; C_{10} ...0,83 ; C_{11} ...0,84 et C_{12} ...0,21. Ces chiffres s'accordent assez bien avec nos résultats (tabl. 2).

Les mêmes auteurs ont étudié aussi l'oxydation du *n*-octadécane et les résultats obtenus sont similaires. Partant de considérations théoriques des plus intéressantes, ils ont élaboré une méthode de calcul de la composition des acides gras résultant de l'oxydation des *n*-alcanes ou des mélanges des *n*-alcanes.

Le *n*-hexadécane, soumis à l'oxydation par des chercheurs anglais en milieu d'acide acétique et propionique, [5] à 114...119°, sous pression, à l'aide d'un mélange d'air et d'azote, a donné les acides suivants : C_5... ...0,86% ; C_6...3,67 ; C_7...5,38 ; C_8...7,27 ; C_9...8,19 ; C_{10}...9,58% ; C_{11}...9,30 ; C_{12}...7,38 ; C_{13}...5,66 ; C_{14}...2,60 ; C_{15}...0,36 et C_{16}...1,26. Les six derniers chiffres s'accordent assez bien avec les résultats que nous avons obtenus lors de l'oxydation du même hydrocarbure, à l'aide de l'oxygène, à la pression atmosphérique, sans utilisation d'acides acétique et propionique.

On présente dans cet ouvrage la composition des acides gras obtenus par oxydation thermique (non catalytique), à 155° en phase liquide, à l'aide de l'oxygène moléculaire, de quelques *n*-alcanes purs ($C_{12}-C_{24}$).

On ne discute pas les opinions contradictoires et les nombreuses phases de la transformation des *n*-alcanes en *n*-acides; on en donne un schéma beaucoup simplifié.

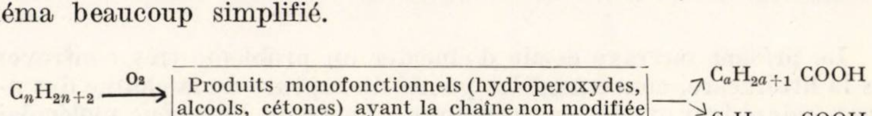

$$C_nH_{2n+2} \xrightarrow{O_2} \boxed{\begin{array}{l}\text{Produits monofonctionnels (hydroperoxydes,}\\ \text{alcools, cétones) ayant la chaîne non modifiée}\end{array}} \longrightarrow \begin{array}{l}\nearrow C_aH_{2a+1}\,COOH\\ \searrow C_bH_{2b+1}\,COOH\end{array}$$

où $a + b + 2 = n$

On considérera que, pour de faibles conversions, les réactions de dégradation sont négligeables et que, par suite de la rupture de la chaîne du *n*-alcane, il résulte une paire d'acides dont la somme des atomes de carbone est égale au nombre d'atomes de carbone du *n*-alcane soumis à l'oxydation ($a + b + 2 = n$).

On omettra les réactions secondaires menant aux acides substitués, aux produits polyfonctionnels, ainsi que les acides inférieurs (C_1-C_5)

---

[3] S. D. Razumovski, *Zhur. priklad. Khim.*, **41**, 863 (1968).

[4] L. I. Ermolaeva, I. L. Moscovici et B. C. Freidin, *Neftepererabotka i Neftekhimyia*, **1968**, 35.

[5] Boult, Wade et Tennant, Brevet Brit. 1 143 213, 19 févr. 1969 ; Chem. Abstr., **70**, 280 (1969).

pour lesquels on n'a pas encore trouvé une méthode assez précise de séparation et de dosage.

On donnera le mécanisme, beaucoup simplifié, accepté par de nombreux auteurs, de la formation des acides monocarboxyliques, par simple rupture de la chaîne de *n*-tétradécane. Dans cet exemple on considère que la première attaque s'effectue dans la position 3, quoiqu'elle puisse s'effectuer à n'importe quel des atomes de carbone. Par oxydation, à faibles conversions, du tétradécane on obtient un mélange de cétones, qui contient probablement les isomères 2, 3, 4, 5, 6 et 7. Le dosage des isomères de ce mélange n'a pu être effectué ni par spectroscopie en infra-rouge, ni par chromatographie (excepté les isomères 2 et 3). Si ce dosage était possible, les résultats devraient correspondre à la réactivité des atomes de carbone, selon leur position dans la chaîne.

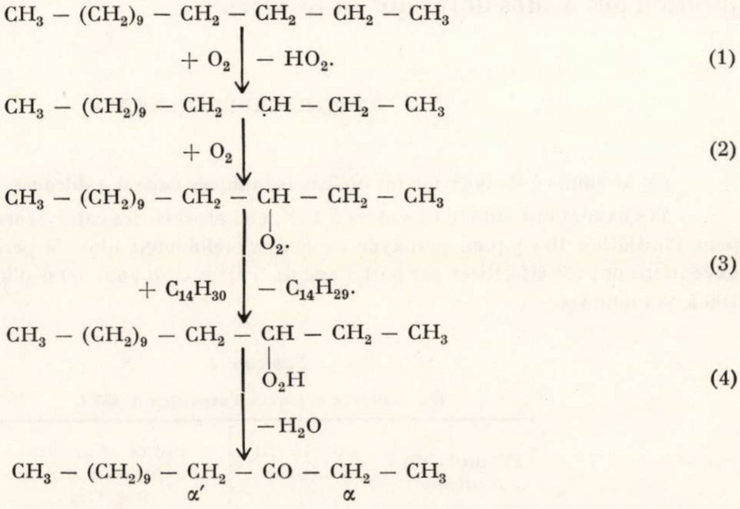

$$\begin{gathered}
\mathrm{CH_3-(CH_2)_9-CH_2-CH_2-CH_2-CH_3}\\
+\mathrm{O_2}\ \Big\downarrow\ -\mathrm{HO_2\cdot} \qquad (1)\\
\mathrm{CH_3-(CH_2)_9-CH_2-\underset{\cdot}{CH}-CH_2-CH_3}\\
+\mathrm{O_2}\ \Big\downarrow \qquad (2)\\
\mathrm{CH_3-(CH_2)_9-CH_2-\underset{O_2\cdot}{\underset{|}{CH}}-CH_2-CH_3}\\
+\mathrm{C_{14}H_{30}}\ \Big\downarrow\ -\mathrm{C_{14}H_{29}\cdot} \qquad (3)\\
\mathrm{CH_3-(CH_2)_9-CH_2-\underset{O_2H}{\underset{|}{CH}}-CH_2-CH_3} \qquad (4)\\
\Big\downarrow\ -\mathrm{H_2O}\\
\mathrm{CH_3-(CH_2)_9-\underset{\alpha'}{CH_2}-CO-\underset{\alpha}{CH_2}-CH_3}
\end{gathered}$$

Conformément au mécanisme de Langenbeck et Pritzkov [6] les cétones formées se hydroperoxydent dans la position α ou α' (réaction 5).

En admettant cette hypothèse, chacune des cétones isomères se transformera en deux paires d'acides monocarboxyliques complémentaires, soit au total quatre acides (réaction 5).

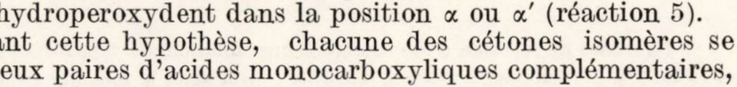

$$\mathrm{CH_3-(CH_2)_9-CH_2\overset{\alpha'}{-}CO\overset{\alpha}{-}CH_2-CH_3} \qquad (5)$$
$$\downarrow \qquad\qquad\qquad\qquad \downarrow$$
$$\begin{matrix}\mathrm{CH_3-(CH_2)_9-COOH} & \qquad & \mathrm{CH_3-(CH_2)_{10}-COOH}\\ \mathrm{CH_3-CH_2-COOH} & \qquad & \mathrm{CH_3-COOH}\end{matrix}$$

Un de nos travaux qui paraîtra prochainement confirme ce mécanisme d'oxydation pour les cétones du *n*-dodécane dans les positions α et α'.

---

[6] W. Langenbeck et W. Pritzkow, *Fette u. Seifen*, **55**, 435 et 506, (1953).

Il faut souligner qu'il existe la possibilité de formation d'autres n-acides monocarboxyliques (par exemple par la dégradation oxydante des n-acides monocarboxyliques homologues). En travaillant dans le domaine des faibles conversions, ces réactions peuvent être négligées.

On présente les résultats obtenus par l'oxydation de n-$C_{12}H_{26}$, $n-C_{13}H_{28}$, $n-C_{14}H_{30}$, $n-C_{16}H_{34}$, $n-C_{17}H_{36}$, $n-C_{18}H_{38}$, $n-C_{20}H_{42}$, $n-C_{21}H_{44}$ et $n-C_{24}H_{50}$, en déterminant pour chaque n-alcane pur la composition des acides libres qui en résultent.

PARTIE EXPÉRIMENTALE

On a soumis à l'oxydation les n-alcanes indiqués dans le tableau 1.

Les oxydations ont été exécutées à 155°, en l'absence des catalyseurs métalliques, utilisant pour l'initiation 100 p.p.m. peroxyde de lauroyl (éliminant ainsi la période d'induction). Les oxydations ont été effectuées par barbotage de 5 litres O_2/h pour 50 g d'hydrocarbure, [7] durant 105 à 140 minutes.

Tableau 1

Les n-alcanes soumis à l'oxydation à 155°C

Formule du n-alcane	Pureté du n-alcane %	Indice d'acidité du produit oxydé mg O/g
$C_{12}H_{26}$	99,4	22,32
$C_{13}H_{28}$	97,0	28,6
$C_{14}H_{30}$	98,2	23,9
$C_{16}H_{34}$	99,4	29,0
$C_{17}H_{36}$	99,2	27,2
$C_{18}H_{38}$	99,0	24,56
$C_{20}H_{42}$	96,0	24,0
$C_{21}H_{44}$	96,5	27,62
$C_{24}H_{50}$	89,7	26,59

La masse de réaction a été traitée à une solution de 5% NaOH aqueuse utilisant un excès de 5% par rapport à l'indice d'acidité ; on a agité le mélange pendant une heure à 60°. Par suite de ce traitement les acides libres ont été transformés dans leurs sels de sodium, restant en solution dans la phase aqueuse, tandis que le hydrocarbure non transformé, les alcools, les cétones, la majorité des esters, etc. sont restés en phase organique.

La phase aqueuse a été extraite trois fois par de l'éther éthylique (pour éliminer les substances non saponifiables qui s'y trouvent sous forme micellaire) et après on l'a traitée avec de l'acide sulfurique en quantité correspondant à l'hydroxyde de sodium utilisé (en excès 5%).

Par suite de ce traitement les acides gras ont été mis en liberté ; on a extrait trois fois par de l'éther éthylique ; l'extrait, séché au sulfate de sodium anhydre, a été évaporé.

Après l'évaporation de l'éther, les acides gras ont été dissous dans du méthanol anhydre saturé au trifluorure de bore, le mélange a été bouilli pendant 2 minutes ; on a ajouté de l'eau et on a extrait les esters à l'aide de l'éther de pétrole.

---

[7] I. Drimuş et C. Florescu, *Rev. Chim.* (*Bucureşti*), **24**, 345 (1973).

On a chromatographié les esters métalliques avec l'appareil GV Carlo Erba dans les conditions suivantes :

- détecteur de conductivité thermique
- colonne d'acier inoxydable au diamètre de 4 mm et à la longueur de 2 m
- Cellite 44−60 mesh imbibée de 15% succinate de diéthylenglycol
- hydrogène 70 ml/mn
- température 120→228° avec élévation de 12°/mn
- la dimension de l'échantillon injecté 10 µl.

Nous remercions l'ingénieur I. Suciu—Grupul Industrial de Petrochimie Ploiești—pour l'exécution des analyses chromatographiques.

LES RÉSULTATS OBTENUS ET LEURS INTERPRÉTATIONS

Les résultats concernant la composition des acides gras obtenus par l'oxydation des *n*-alcanes sont présentés dans les fig. 1...5 et dans le tableau 2.

L'interprétation des résultats obtenus est fondée sur les considérations suivantes :

1. On n'a pas dosé les acides C_1-C_4.
2. Pendant les expériences on a perdu la plus grande partie de l'acide pentanoïque.
3. On a enregistré des pertes de 10% de l'acide hexanoïque.
4. On a pu doser, avec une précision satisfaisante, le reste des acides et les résultats obtenus sont enregistrés dans nos figures par un point (.).
5. En admettant que la rupture des *n*-alcanes conduit à deux acides complémentaires et que la somme des atomes de carbone de ces acides paires est égale au nombre d'atomes de carbone du *n*-alcane soumis à l'oxydation, pour les acides C_1-C_6 on a calculé des pourcentages identiques par rapport aux acides complémentaires respectifs. Les chiffres complémentaires obtenus sont enregistrés dans nos figures avec un « *x* ».
6. Nous proposons une méthode de calcul qui donne la possibilité d'établir la composition des acides provenant de n'importe quel *n*-alcane $C_{14}-C_{24}$ (par extrapolation on peut l'appliquer aussi au-dessus de C_{24}). Ces chiffres, calculés, sont présentés dans nos figures par un cercle (0).

CALCUL DE LA COMPOSITION DES *n*-ACIDES MONOCARBOXYLIQUES OBTENUS PAR OXYDATION DES HYDROCARBURES NORMAUX C_nH_{2n+2} AVEC $n>13$

Les pourcentages molaires des acides s'obtiennent par la formule :

$$P_{m,n} = E_{m,n}h_n \tag{1}$$

m = nombre d'atomes de carbone de la molécule d'acide

n = nombre d'atomes de carbone de la molécule de l'hydrocarbure

Tableau 2

Coefficients des acides «terminaux» obtenus par oxydation des *n*-alcanes, en différentes conditions et par différents auteurs

Références	$C_n H_{2n+2}$ soumis à l'oxydation	Conditions de travail	Coefficients (molaires)								Observations
			n	$n-1$	$n-2$	$n-3$	$n-4$	$n-5$	$n-6$	$n-7$	
1	$C_{20}H_{42}$		0,08	0,26	0,35	0,66	0,66	1,13	0,95	0,94	Coefficients calculés à l'aide de la fig. 2 (article cité)
2	$C_{18}H_{38}$	$O_2 + O_3$	+	+	+	+	+	+	+	+	On a identifié qualitativement tous les acides
3	$C_{14}H_{30}$	130°C ;O_2 ; Mn + K	0,09	0,30	0,68	0,78	1,21	0,71	1,00	0,68	Recalculé partant de % molaires (article cité)
4	$C_{14}H_{30}$	O_2 sans catalyseur	—	—	0,21	0,64	0,83	1,0	1,0	1,0	
	$C_{18}H_{38}$	Stéarate de Mn	—	—	0,43	0,80	0,94	1,0	1,0	1,0	
5	$C_{16}H_{34}$	114—119°C Air + N_2 en milieu acide	0,09	0,03	0,26	0,57	0,70	0,95	1,06	0,99	
7	$C_{14}H_{30}$ $C_{16}H_{34}$ $C_{17}H_{36}$ $C_{18}H_{38}$ $C_{20}H_{42}$ $C_{21}H_{44}$ $C_{24}H_{50}$	O_2, 155°C sans catalyseur	0,19	0,13	0,17	0,42	0,65	0,84	1,0	1,0	Pour les autres hydrocarbures les coefficients respectifs diffèrent de ±10%
	$C_{12}H_{26}$ $C_{13}H_{28}$	Idem	0,51 0,51	0,09 0,15	0,63 0,41	1,10 0,60	1,00 1,16	0,17 1,36	0,13 1,0	0,14 0,51	Les coefficients ne sont pas valables pour C_{12} et C_{13}

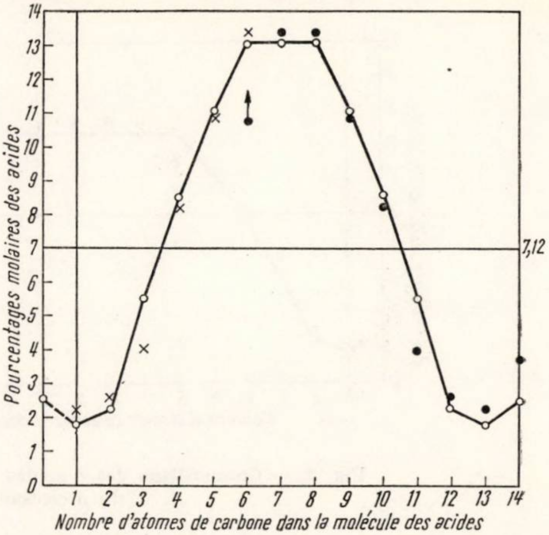

Fig. 1. — Composition des n-acides obtenus par oxydation du n-tétradécane.

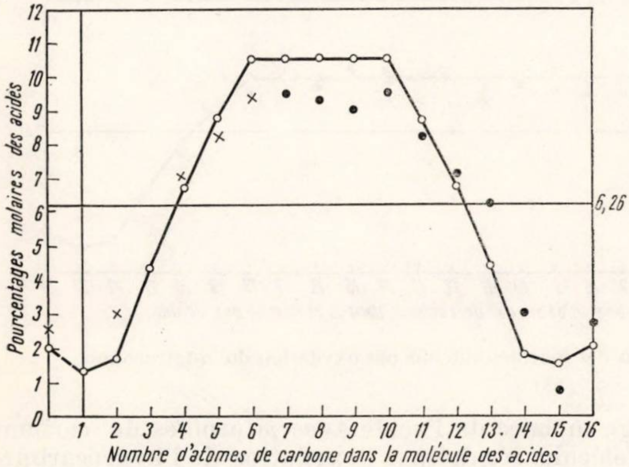

Fig. 2. — Composition des n-acides obtenus par oxydation du n-hexadécane.

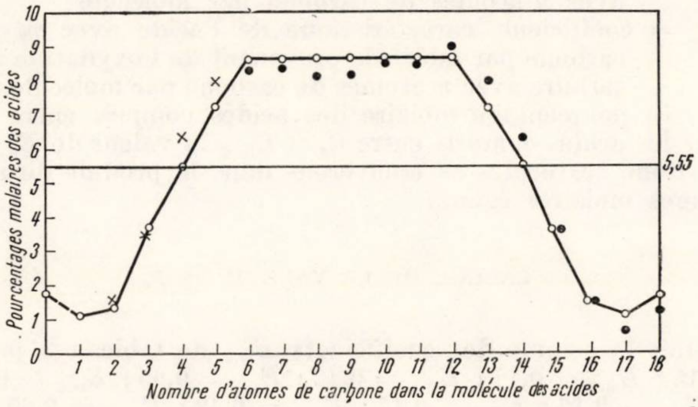

Fig. 3. — Composition des n-acides obtenus par oxydation du n-octadécane.

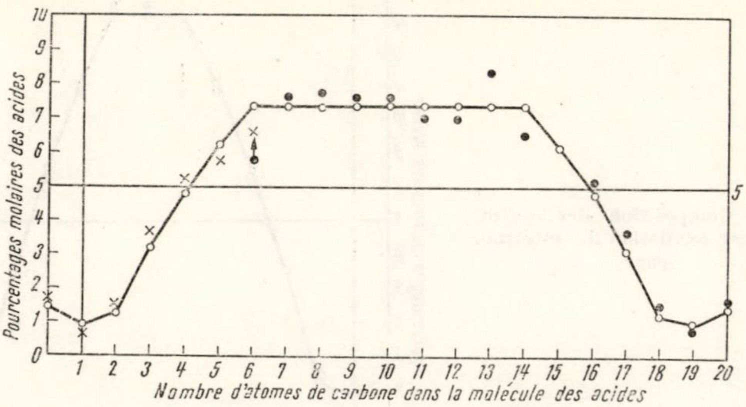

Fig. 4. — Composition des *n*-acides obtenus par oxydation du *n*-eicosane.

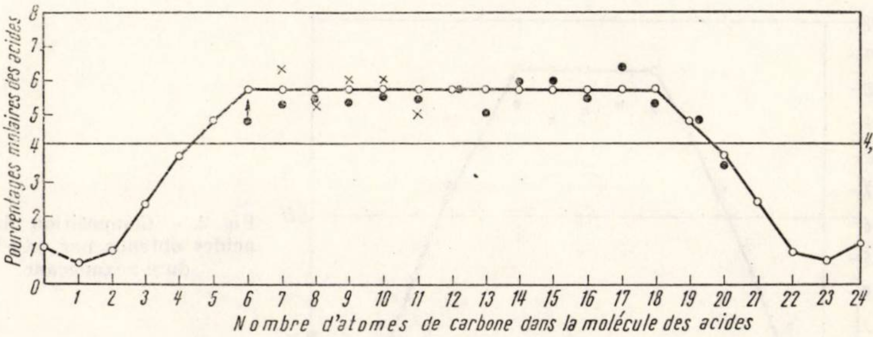

Fig. 5. — Composition des *n*-acides obtenus par oxydation du *n*-tétracosane.

$P_{m,n}$ = pourcentage molaire de l'acide avec m atomes de carbone dans la molécule, résulté par l'oxydation de l'hydrocarbure avec n-atomes de carbone par molécule

$E_{m,n}$ = coefficient caractéristique de l'acide avec m atomes de carbone par molécule provenant de l'oxydation de l'hydrocarbure avec n atomes de carbone par molécule (tableau 3)

h_n = pourcentage molaire des acides compris entre C_6 et C_{n-6}

Pour les acides compris entre C_6 et C_{n-6} la valeur de $E_{m,n}$ est égale à l'unité, donc ces acides se trouveront dans le produit de réaction en pourcentages molaires égaux.

CALCUL DE LA VALEUR DE h_n

On fait la somme des coefficients $E_{m,n}$ du tableau 3, par exemple $E_{m,1} = 0,13$; $E_{m,2} = 0,17$; $E_{m,3} = 0,42$; $E_{m,4} = 0,65$; $E_{m,5} = 0,84$; $E_m = 0,19$; $E_{m-1} = 0,13$; $E_{m-2} = 0,17$; $E_{m-3} = 0,42$; $E_{m-4} = 0,65$ et $E_{m-5} =$

Tableau 3

Valeurs du coefficient $E_{m,n}$

m	$E_{m,n}$	m	$E_{m,n}$
0	0,19	n	0,19
1	0,13	$n-1$	0,13
2	0,17	$n-2$	0,17
3	0,42	$n-3$	0,42
4	0,65	$n-4$	0,65
5	0,84	$n-5$	0,84
6	1,0	$n-6$	1,00

= 0,84 et on obtient le chiffre 4,61 valable pour les acides résultés de l'oxydation des n-alcanes C_{14-24}. On ajoute $n-5-6 = n-11$ au chiffre 4,61 obtenu.

Par exemple, dans le cas de l'oxydation de l'octadécane on obtient pour les acides compris entre C_6 et C_{18-6} le coefficient $4,61 + 7 = 11,61$.

Pour ces acides (compris entre C_6 et $C_{18-6} = C_{12}$) on obtient 100 : : 11,61 = 8,61% molaires.

Vu la relation (1) $P_{m,n} = E_{m,n}h_n$
utilisant les coefficients du tableau 3 il résulte pour les acides $C_1 \ldots C_6$ et $C_{18} \ldots C_{12}$ les pourcentages molaires suivants :

Total % mole

$(P_{0.18}) = P_{18.18} = 0{,}19 \cdot 8{,}61 = 1{,}64\%$ mole $\times 1 = 1{,}64$

$P_{1.18} = P_{17.18} = 0{,}13 \cdot 8{,}61 = 1{,}12$ $\times 2 = 2{,}24$

$P_{2.18} = P_{16.18} = 0{,}17 \cdot 8{,}61 = 1{,}46$ $\times 2 = 2{,}92$

$P_{3.18} = P_{15.18} = 0{,}42 \cdot 0{,}61 = 3{,}62$ $\times 2 = 7{,}24$

$P_{4.18} = P_{14.18} = 0{,}65 \cdot 8{,}61 = 5{,}60$ $\times 2 = 11{,}20$

$P_{5.18} = P_{13.18} = 0{,}84 \cdot 8{,}61 = 7{,}23$ $\times 2 = 14{,}46$

$P_{6.18} = P_{12.18} = 1{,}00 \cdot 8{,}61 = 8{,}61$ $\times 7 = \underline{60{,}27}$

99,97

(voir fig. 3).

CONCLUSIONS

1. On a soumis à l'oxydation les alcanes normaux ayant 14, 16, 17, 18, 20, 21 et 24 atomes de carbone dans leurs molécules.

2. On a constaté que les acides gras obtenus ayant plus de 5 atomes de carbone dans leurs molécules jusqu'aux acides qui ont $n-6$ atomes de carbone se trouvent dans le mélange de réaction en proportions molaires égales (n = le nombre d'atomes de carbone dans la molécule de l'alcane normal soumis à l'oxydation).

3. Par rapport aux acides $C_6 \ldots C_{n-6}$ qui ont le coefficient de proportionnalité égal à l'unité, les autres acides ont les coefficients suivants : $C_n \ldots 0{,}19$; $C_{1,n-1} = 0{,}13$; $C_{2,n-2} = 0{,}17$; $C_{3,n-3} = 0{,}42$; $C_{4,n-4} = 0{,}65$; $C_{5,n-5} = 0{,}84$.

Ces résultats peuvent être attribués à l'effet de répulsion des électrons des groupes méthyle terminaux de la molécule des alcanes normaux.

4. Les acides obtenus par oxydation du *n*-dodécane et du *n*-tridécane ont des coefficients de proportionnalité complètement différents de ceux des acides formés par oxydation des alcanes normaux avec plus de 13 atomes de carbone dans leur molécule.

Revue Roumaine de Chimie, **18**, *11*, 1959–1962 (1973)

SPECTROSCOPIC PROPERTIES OF TRAPPED ANTHRONYLIDENE

NICOLAE FILIPESCU and JAMES W. PAVLIK

Department of Chemistry, George Washington University, Washington, D. C. 20006 U.S.A

P. T. FRANGOPOL* and MARIA FRANGOPOL*

Institute of Atomic Physics, P. O. Box 35, Bucharest

Received January 26, 1973

Emission and excitation studies on the photolysis product of 9,10-anthraquinone diazide in organic matrix at 77 K are reported. The data substantiate the formulation of an anthronylidene structure for the resulted carbene. Evidences for efficient quintet→triplet phosphorescence obtained on excitation in the triplet manifold of anthronylidene in rigid glass are presented.

Electron spin resonance (esr) studies of carbenes formed upon photolysis of a number of 1,4-benzo- and naphthoquinone diazides [1] in an organic matrix at 77 K resulted in the assignment of a triplet ground state to these species. The esr results are consistent with a benzenoid rather than quinonoid structure for these triplets with one of unpaired electrons localized in an atomic orbital on the carbon and the other delocalized in a π-orbital, similar to the analogous phenoxy or naphthoxy radicals.

More recent reports show that reactions of 9, 10-anthraquinone diazide (I) lead to derivatives of anthrone rather than anthrol and suggest a carbene intermediate in which the two unpaired electrons are essentially localized on the methylene carbon (II)[2].

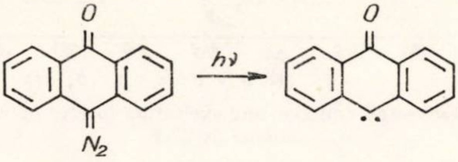

I II

---

* Postdoctoral Research Associates at George Washington University, 1970–1971.

[1] E. Wasserman and R. W. Murray, *J. Amer. Chem. Soc.*, **86**, 4203 (1964).

[2] G. Cauquis and G. Reverdy, *Tetrahedron Letters*, **1967**, 1493 ; **1968**, 1085.

Indeed, esr studies of this carbene trapped in rigid glass indicate a triplet ground state species similar to fluorenylidene [3].

We wish to report emission and excitation studies on the photolysis product of 9, 10-anthraquinone diazide in organic matrix at 77 K. These results substantiate the formulation of anthronylidene structure II for this carbene. In addition, we present evidence for efficient quintet→triplet phosphorescence obtained on excitation in the triplet manifold of anthronylidene in rigid glass.

10^{-4} M to 10^{-5} M solutions of 9, 10-anthraquinone diazide in either EPA (ethyl ether, 2-methylbutane, and ethyl alcohol in a volume ratio of 5 :5 :2, respectively) or 2-methyltetrahydrofuran were frozen in liquid nitrogen and irradiated at 410 mμ for varying lengths of time. Both excitation and emission spectra were measured as a function of irradiation time [4].

Before irradiation, as expected, no emission was observed for the diazo compound. After short irradiation time, an emission spectrum (see figure 1) could be observed which increased in intensity upon further irradiation. This spectrum was stable as long as the solution remained frozen in liquid nitrogen but disappeared if the solution was allowed to thaw and then refrozen.

The emission consists of a highly structured band in the region 400 to 500 mμ with principal maxima at 407, 436, 467, and 505 mμ. The position and structure of this band are independent of excitation wavelength in the 240 to 380 mμ range.

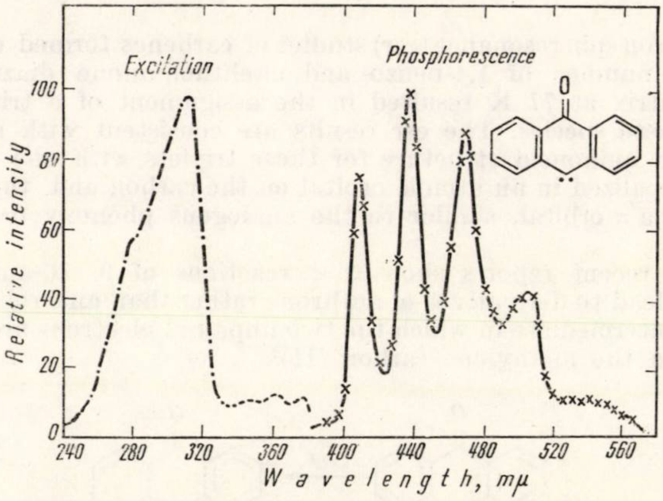

Fig. 1. Corrected emission and excitation spectra of anthronylidene at 77 K.

---

[3] Esr identification was done in cooperation with A. D. BRITT at this laboratory and was confirmed privately by B. LAMOTTE at Centre D'Etudes Nucléaires de Grenoble, Grenoble, France.

[4] Excitation and emission spectra were obtained on an Aminco-Bowman spectrophotofluorometer. Photolysis of the 9,10-anthraquinone diazide was accomplished by placing the cold-finger Dewar in the instrument sample compartment, adjusting the excitation monochromator to 410 mμ, and removing the entrance slits for the desired length of time.

The corrected excitation spectrum shows absorption in the range 240 to 380 mμ with maximum absorption at 310 mμ. The position and structure of the excitation spectrum are independent of the emission wavelength for any of the above emission maxima. When irradiated samples were allowed to thaw in the presence of air in the dark, a chemiluminescent emission was observed, the spectral distribution of which resembled that of anthraquinone phosphorescence. A similar emission was previously reported for diphenylmethylene [5].

The optical spectroscopic properties of the ground-triplet anthronylidene are of particular interest. Contrary to the reported behavior of trapped diphenylmethylenes[5-7], initial excitation in the triplet manifold of anthronylidene did not lead to $T_2 \rightarrow T_1$ fluorescence. For reasons outlined below, it seems that efficient intersystem crossing from T_2 to a lower-lying n, π^* quintet state, Q_1, leads to characteristically structured $Q_1 \rightarrow T_1$ phosphorescence. Lack of mirror image relationship with the excitation spectrum, typical aromatic carbonyl vibrational progression, and millisecond range lifetime of the emission confirm the $\pi^* \rightarrow n$ phosphorescence assignment. The emission is different from that of other possible photoproducts, *viz.*, anthraquinone or anthraquinone azine. The $Q_1 \rightarrow T_1$ characterization is consistent with emission from a trapped, reactive species, since the esr-verified ground triplet and the parallel phosphorescence signal disappeared on thawing and refreezing.

By analogy with photolysis products from 1,4-dibenzo- and naphthoquinone-diazides[1], an apparent alternative assignment for the trapped emitting species would be 9-anthranoxide diradical III — which also has a triplet ground state. However, III would be expected to emit $T-T$ fluorescence having mirror-image relationship with its excitation, with vibrational progression characteristic of anthracene derivatives, and substantially shorter decay times.

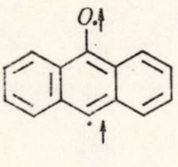

III

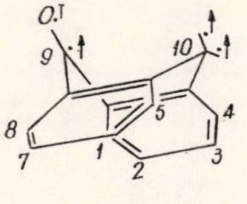

IV

The emission and excitation spectra in figure 1 closely resemble the $\pi^* \rightarrow n$ phosphorescence and excitation spectra of other aromatic ketones and especially those of anthrone. It is important to note that anthronylidene, as its precursor I, is not planar but has the steric configuration shown in IV. The structure imposed by the boat-shaped central ring should decrease the cross-conjugation of the two unpaired electrons localized on C_{10} with the two benzene rings compared to the planar diphenylmethylene. It is conceivable that electronically excited anthronylidene cannot assume a more planar configuration than the ground triplet in rigid matrix and therefore the concept of continuously delocalized π-MO's over the entire molecule is not entirely applicable. Thus, excited states involving promotion of one of the unpaired electrons to a vacant π*MO — analogous to the first excited triplet of $C_6H_5-\ddot{C}-C_6H_5$ [8] — are higher than the carbonyl *n*, π* quintet IV in which the excitation energy is essentially localized on the carbonyl group because of its rigid out-of-plane orientation with respect to the benzene rings.

---

[5] A. M. Trozzolo, R. W. Murray, and E. Wasserman, *J. Amer. Chem. Soc.*, **84**, 4998 (1962).

[6] W. A. Gibbons and A. M. Trozzolo, *J. Amer. Chem. Soc.*, **88**, 172 (1966).

[7] A. M. Trozzolo and W. A. Gibbons, *J. Amer. Chem. Soc.*, **89**, 239 (1967).

Absence of direct conjugation between the carbene electrons and the carbonyl group in IV is compatible with its trapped configuration, which, however, may allow partial crossconjugation of each C_{10} electron and $C=O$ chromophore separately with the benzene rings.

Photolysis of other *p*-quinone diazides in organic glasses at 77 K has also been studied and the results will be reported later.

Acknowledgement. This work has been supported in part by the Atomic Energy Commission on Contract AT-(40−1)−3797.

---

[8] The T_2 state of diphenylmethylene is at about 21,000 cm^{-1} above the ground T_1 state[6,7]. Distortion from planarity in II can easily elevate the analogous T_2 state by several thousand cm^{-1}.

Revue Roumaine de Chimie, **18**, *11*, 1963–1969 (1973)

LA RÉACTIVITÉ DES COMPOSÉS ALUMINIUM-ORGANIQUES ENVERS DES BASES LEWIS

DÉRIVÉS DES TRIPHÉNYLALUMINIUMS AVEC DES COMPOSÉS 1,3-DI-CARBONYLIQUES

DIANA GIURGIU et I. POPESCU

Institut de Chimie Macromoléculaire «P. Poni», 41 A, Aleea Gr. Ghica Vodă, Jassy

Reçu le 17 février 1973

On a obtenu des composés monochélatiques stables par la réaction entre le triphénylaluminium et les 1,3-dicétones, respectivement les 1,3-cétoimines. On a étudié les propriétés des nouveaux composés obtenus, la réactivité envers des bases Lewis. L'étude des spectres de diffraction des rayons-X atteste la structure cristalline des composés. Les spectres IR des composés synthétisés ont été étudiés comparativement à ceux des réactifs. Les spectres RMN-^{1}H confirment les structures proposées.

L'utilisation à grande échelle des composés aluminium-organiques dans différents systèmes catalytiques pour la polymérisation stéréospécifique a conduit à l'étude des réactions des composés alkyl- et arylaluminium avec différents ligands nucléophiliques pour élucider les mécanismes de réaction et identifier les éléments actifs responsables dans le processus de polymérisation coordinative.

Des études concernant la réaction des composés alkylaluminium avec les cétones [1] on peut détacher trois modes différents, en fonction du rapport de combinaison des réactifs, qui mènent à la formation des produits d'addition de réduction ou d'énolyse.

Surtees [2] et Mole, [3] étudiant l'action de la benzophénone sur le triphénylaluminium ont établi les conditions stœchiométriques, le mécanisme de la réaction de phénylation des cétones et identifié les produits de l'hydrolyse.

---

[1] S. Pasynkiew'cz et E. Sliwa, *J. Organometal. Chem.*, **3**, 121 (1965).

[2] J. R. Surtees, *Rev. Pure Appl. Chem.*, **13**, 91 (1936).

[3] T. Mole, *Austral, J. Chem.*, **16**, 807 (1963).

Les réactions des composés alkylaluminium avec les 1,3-di-cétones ont été moins étudiées.[4,5] Kroll[6,7] a élaboré des méthodes pour la synthèse de cette nouvelle classe de composés et pour leur utilisation dans la catalyse stéréospécifique.[8]

Dans un travail concernant la réaction entre le tris-acétylacétonate de chrome et le trialkyl-, respectivement le triphénylaluminium, Sartori et Costa[9] ont étudié les spectres IR et UV des solutions des trialkyl- et triphénylaluminium en présence de l'acétylacétone sans en isoler les produits de réaction.

En continuant nos études pour l'obtention des dérivés de type $R_2Al{-}E(R'_2)$[10] (R = phényl ; E = N, P, O ; R' = alkyl, aryle) nous avons étudié les réactions entre le triphénylaluminium et les 1,3-dicétones ou diacétamide qui étant un dérivé cétoiminique se comporte analogiquement.

On a obtenu des composés monochélatiques stables avec l'acétylacétone, la benzoylacétone, le dibenzoylméthane et le diacétamide.

On a étudié les conditions de réaction et on a proposé les structures correspondant aux analyses élémentaires, spectroscopiques, et des déterminations des poids moléculaires. Les composés sont monomères, cristallins et présentent une stabilité élevée envers l'oxygène et l'humidité, comparativement à celle du triphénylaluminium. L'eau provoque l'hydrolyse des composés conduisant à la formation de l'$Al(OH)_3$ et la reconstitution de l'énol.

Les synthèses ont été effectuées à 0°. Les réactions sont exothermiques. On chauffe après le mélange de réaction à 80°.

Les produits obtenus ne réagissent pas avec des bases Lewis, excepté l'acétylacétonate de diphénylaluminium, qui forme avec l'*o*-phénantroline et l'α, α'-dipyridyle des composés d'addition stables, au rapport molaire de 2 :1.

PARTIE EXPÉRIMENTALE

La sensibilité des composés aluminium-organiques envers l'oxygène et l'humidité a imposé les conditions des synthèses.

Les solvants utilisés ont été purifiés et anhydrisés par distillation en présence de sodium métallique et de benzophénone comme indicateur d'anhydrisation en atmosphère d'azote sec.

Le triphénylaluminium a été préparé en laboratoire en solution benzénique.

L'acétylacétone et la benzoylacétone, commerciales, ont été purifiées par distillation ou par cristallisation de benzène. Le dibenzoylméthane a été préparé à partir d'acétophénone et de benzoate d'éthyle, en présence de sodium métallique, à la température ambiante et purifié par

---

[4] M. Roha, L. C. Kreider, M. R. Frederick et W. In. Befars, *J. Polymer Sci.*, **38**, 51 (1959).

[5] B. Bogdanovici, *Angew. Chem.*, **77**, 1010 (1965).

[6] W. R. Kroll et W. Naegele, *J. Organometal. Chem.*, **19**, 439 (1969).

[7] W. R. Kroll, I. Kuntz et E. Birnbaum, *J. Organometal. Chem.*, **26**, 313 (1971).

[8] I. Kuntz et W. R. Kroll, *J. Polymer Sci. A*—1, **8**, 1601 (1970).

[9] G. Sartori et G. Costa, *Z. Elektrochem.*, **63**, 105 (1959).

[10] D Giurgiu, I. Popescu, A. Ciobanu, M. Bostan, N. Voiculescu et L. Roman, *Rev. Roumaine Chim.*, **15**, 1581 (1970).

recristallisations de benzène. Le diacétamide a été préparé aussi dans le laboratoire, à partir d'acétamide et d'anhydride acétique en présence d'acétate de sodium et recristallisé de ligroïne.

Les échantillons pour l'analyse ont été pris en système isolé, sous courant d'azote purifié et séché.

Les spectres IR ont été obtenus dans des pastilles de KBr, avec un spectrophotomètre UNICAM SP-200 pour les absorptions dans le domaine de 3500 à 700 cm^{-1}et un spectrophotomètre PERKIN-ELMER 621 pour le domaine de 700 à 300 cm^{-1}.

Les images de diffraction des rayons-X ont été obtenues avec un appareil TUR M-60 avec radiation $CuK\alpha$ et un temps d'exposition de huit heures.

Les déterminations des poids moléculaires ont été effectuées par cryoscopie en benzène.

Nous donnons, comme modèle, la synthèse du diphénylaluminium-acétylacétonate, les autres synthèses étant effectuées de façon semblable à part quelques modifications imposées par le caractère spécifique des réactants.

A une solution contenant 2 g de triphénylaluminium dans 5 ml de benzène refroidi avec de la glace on ajoute, sous forte agitation, 0,5 g d'acétylacétone fraîchement distillée. La réaction est violente exothermique. Le mélange a été progressivement chauffé à la température ambiante et après à 80° pendant une heure. Par refroidissement le produit cristallise en prismes minces blanches. Il est trois ou quatre fois lavé avec du *n*-hexane pour éloigner l'excès d'acétylacétone, séché sous vide et purifié par recristallisation de benzène.

Les propriétés et les analyses élémentaires des composés synthétisés (diphénylaluminium-acétylacétonate I, diphénylaluminium-benzoylacétonate II ,diphénylaluminium-dibenzoylméthane III, diphénylaluminium-diacétamide IV, et l'adduct diphénylaluminium-acétylacétonate-*o*-phénantroline V) sont insérées dans le tableau 1.

Le composé I réagit à chaud en solution benzénique avec l'*o*-phénantroline. Au refroidissement on a cristallisé un produit jaune pâle, qui, lavé avec un mélange de *n*-hexane et benzène 1 : 1, donne par recristallisation dans le benzène une poudre microcristalline jaune.

RÉSULTATS ET DISCUSSIONS

La préexistence d'un équilibre entre la forme cétonique et énolique déplacé vers la forme énolique[11] dans les 1,3-dicétones conduit à la formation de composés de type chélatique, tant avec les métaux transitionnels qu'avec des dérivés métal-organiques. [12–14].

Le triphénylaluminium réagit avec les 1,3-dicétones menant à la formation des composés monochélatiques par l'institution de la liaison covalente Al-O, due à la mobilité d'hydrogène énolique et d'une liaison coordinative par la paire d'électrons disponible du groupement carbonylique. Le rapport 1 :1 des réactifs est déterminé par la configuration stérique et la compensation du déficit électronique de la molécule de $(C_6H_5)_3Al$

---

[11] L. J. Bellamy et R. F. Brauch, *J. Chem. Soc.*, **1954**, 4491.

[12] B. M. Mikailov, Yu. M. Bubnow, *Izvest. Akad. Nauk. S.S.S.R., Otdel. khim. Nauk.*, **1960**, 1883.

[13] J. R. Cook et F. Martin, *J. Inorg. Nuclear Chem.*, **26**, 1249 (1964).

[14] A. Arsene, A. T. Balaban, I. Bally, A. Bordaş, M. Paraschiv et C. N. Rențea, *Spectrochim. Acta*, **23 A**, 1372 (1967).

par la formation de la liaison coordinative avec le groupement carbonylique. On a proposé le schéma de réaction :

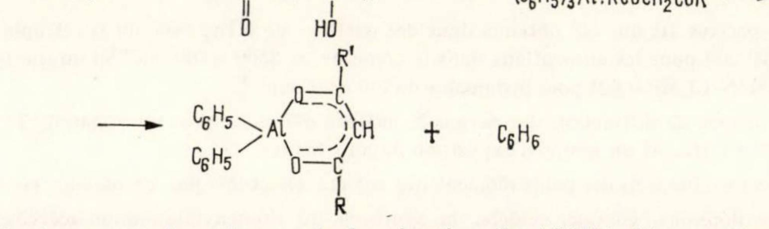

Tout comme dans le cas de la réaction du $(C_6H_5)_3Al$ avec des amines et phosphine secondaire[15] on suppose que d'abord a lieu la formation d'un adduct instable entre le triphénylaluminium et la 1,3-dicétone, suivie par une réaction protolytique avec la formation d'un composé monochélatique stable et l'élimination d'une molécule de benzène.

Le mécanisme de réaction entre le triphénylaluminium et le diacétamide est similaire, dans la réaction participe la forme énolique.

Dans le cas des dicétoimines aussi l'équilibre existant entre la forme cétonique et énolique se trouve complètement déplacé vers la forme énolique en présence d'un cation métallique capable à coordiner.[16]

La mobilité du proton énolique favorise la substitution d'un radical phénylique du $(C_6H_5)_3Al$ et l'institution d'une liaison Al—O. La formation du cycle chélatique se réalise le plus probable par le couple d'électrons disponibles du groupement carbonylique.

Les spectres IR de l'acétamide libre et du composé formé constituent des arguments pour cette hypothèse.

Tableau 1

Données analytiques et caractéristiques des composés synthétisés

Composé*	Couleur	Poids moléculaire Calculé % Trouvé %	Point de fusion	Analyses chimiques			
				C Calculé Trouvé %	H Calculé Trouvé %	Al Calculé Trouvé %	N Calculé Trouvé %
I $(C_6H_5)_2Al.C_5H_7O_2$	blanc	280	180°	72,89	6,42	9,64	—
		283		71,42	6,51	9,49	—
II $(C_6H_5)_2Al.C_{10}H_9O_2$	jaunâtre	342	décompo-	77,18	5,56	7,82	—
		360	sition	76,27	5,11	7,77	—
III $(C_6H_5)_2Al.C_{15}H_{11}O_2$	jaunâtre	404	décompo-	80,19	5,19	6,68	—
		420	sition	78,37	5,02	6,51	—
IV $(C_6H_5)_2Al.C_4H_6O_2N$	blanc	281	230°	—	—	9,46	4,98
		303		—	—	9,32	4,89
V$(C_6H_5)_2AlC_5H_7O_2.$	jaune	742	—	—	—	7,27	3,72
$\cdot N_2C_{12}H_{18}$		797		—	—	7,42	4,15

* Tous les composés sont cristallins et solubles dans du benzène et du toluène.

---

[15] D. Giurgiu, L. Roman, I. Popescu et A. Ciobanu, *Rev. Roumaine Chim.*, **16**, 1217 (1971).

[16] M. F. Hawthorne et T. Reintjes, *J. Amer. Chem. Soc.*, **86**, 5016 (1964).

Les analyses élémentaires, les poids moléculaires trouvés et les spectres IR plaident pour les structures proposées.

Les images de diffraction des rayons X montrent des structures ordonnées pour tous les composés synthétisés.

Dans le tableau 2 sont reportées les valeurs des maximums d'absorption caractéristiques dans les domaines de 3500 à 700 cm^{-1} et 700 à 300 cm^{-1} des composés étudiés, en comparaison de ceux des ligants libres.

Tableau 2

Bandes d'absorption en IR des dérivés aluminium-1, 3-dicétones (valeurs en cm^{-1})

Composé	OH	C=N	C=O	CH	C–O	CH_3	C–C	Al–C	Al–O
$(C_6H_5)_2Al.C_5H_7O_2$	—	—	*1595*	*1540*	1455	1400 *1385*	*1280* 1015 700	685 440 420	*495*
$(C_6H_5)_2Al.C_{10}H_9O_2$	—	—	*1595*	*1540* 1195 1040	1450	1410 1390	*1220* 1020 720	690 *460* 440	*475*
$(C_6H_5)_2Al.C_{15}H_{11}O_2$	—	—	*1590*	*1545* 1475 1420	1450	—	*1290* 1020 700	680 *445*	*480*
$(C_6H_5)_2Al.C_4H_6O_2N$	—	*1680*	1525	1225	1450	*1400*	*1290* 1020	695 *440*	*485*
$CH_3COCHCOHCH_3$*	2600	—	1608	—	1450	—	1249	—	—

* Les valeurs données dans la littérature.

Les bandes intenses à 2600 cm^{-1} du spectre IR de 1,3-dicétones libres confirment l'existence de la forme énolique et de la formation des ponts d'hydrogène.[17] L'absence de cette bande dans le spectre IR des composés synthétisés peut être attribuée à la substitution des ponts d'hydrogène par la réaction de l'hydrogène énolique avec l'AlR_2. Des dérivés similaires ont été obtenus dans le cas des oximes libres ou coordinées.[18]

Les fortes fréquences à 1600 cm^{-1} qui paraissent dans le cas des 1,3-dicétones libres ont été attribuées[19] aux vibrations caractéristiques de la liaison C=O. Ces fréquences sont déplacées dans les composés aluminium-organiques avec les 1,3-dicétones vers des longueurs d'onde plus grandes, respectivement 1595 à 1570 cm^{-1}. Ce déplacement peut être dû à la formation de la liaison coordinative Al–O.

L'apparition d'un maximum d'absorption dans la région 495 à 475 cm^{-1} dans les composés étudiés peut être due à l'institution de la liaison covalente Al–O, qui correspond aux données citées dans la littérature pour des composés qui contiennent la liaison Al–O.[20]

---

[17] L. J. Bellamy, G. S. Spicer et J. D. H. Strickland, *J. Chem. Soc.*, **1952**, 4653.

[18] N. Voiculescu et I. Popescu, *Rev. Roumaine Chim.*, **17**, 719 (1972).

[19] L. J. Bellamy et L. Becher, *J. Chem. Soc.*, **1954**, 4487.

[20] C. Djordjevic, *Spectrochim. Acta*, **17**, 448 (1961).

Le spectre IR du composé diphénylaluminium-diacétamide manifeste un intense maximum d'absorption dans la région 1680 cm^{-1} attribué à la liaison C=N de la cétonimine. [21] Les fréquences caractéristiques de la liaison C=O apparaissent pour ce composé dans la région 1525 cm^{-1}. Le déplacement vers des longueurs d'onde plus grandes peut être dû à un effet de chélatisation.[22] Le maximum d'absorption à 485 cm^{-1} peut être considéré aussi comme dans le cas des composés avec des 1,3-dicétones, dû à la formation de la liaison covalente Al—O.

L'acidité Lewis des composés aluminium-organiques monochélatiques, prouvée comparativement à d'autres composés de type R_2Al-ER_2,

Tableau 3

Spectres RMN—^{1}H

Composé	δ		
	C_6H_5	CH_3	CH—chélate
I 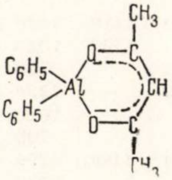	7,25	2,4	5,3
II 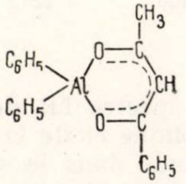	7,3	2,4	—
III 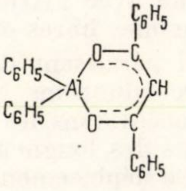	8,5	—	6,5
IV 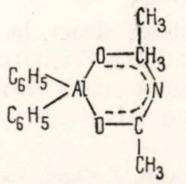	7,25	2,4	—

Les mesures RMN—^{1}H ont été effectuées en solution de Cl_3CD à la température ambiante en utilisant du TMS comme étalon.

---

[21] P. L. Pickard et T. L. Tolbert, *J. Org. Chem.*, **1961**, 4886.

[22] D. Lenormant, *Ann. Chim. (France)*, **5**, 459 (1950).

par la réaction avec des ligants qui contiennent des éléments donneurs, est diminuée ou bien insaisissable. Ces composés ne forment pas d'adducts avec les bases Lewis, excepté le composé diphénylaluminium-acétylacétonate qui réagit avec l'*o*-phénantroline et l'α, α'-dipyridyle formant des complexes stables cristallins dans le rapport molaire 2 :1.

On peut supposer qu'il y a la destruction de la liaison coordinative du groupement carbonylique et la substitution de celle-ci par une liaison de type donneur-accepteur à l'atome d'azote, étant connu que dans les réactions de déplacement des bases Lewis l'azote est un donneur plus puissant que l'oxygène. [23]

Par analogie avec les constantes de stabilité des chélates des métaux transitionnels [24] nous avons considéré que le caractère électropositif de l'atome d'aluminium dans les composés étudiés décroît dans l'ordre : diphénylaluminium-acétylacétonate > diphénylaluminium-benzoylacétonate >diphénylaluminium-dibenzoylméthane, en même temps que la stabilité du composé augmente.

La grande stabilité des composés diphénylaluminium-benzoylacétonate, respectivement diphénylaluminium-dibenzoylméthane, envers les atoms donneurs pourrait être due à l'effet inductif déterminé par la présence des cycles aromatiques des 1,3-dicétones ayant comme suite une croissance de la stabilité de la liaison coordinative Al—O.

Les spectres RMM—^{1}H indiquent des rapports quantitatifs entre les différents types de protons, ce que confirment les structures proposées.

L'élargissement du signal CH benzénique dans les composés II et III pourrait être attribué à la superposition de la résonance du proton cétonique dû à la chélatisation.

---

[23] F. G. A-Stone, *Chem. Rev.*, **18**, 101 (1958).

[24] R. L. Lintvedt et M. F. Holtzclow, *J. Amer. Chem. Soc.*, **88**, 2713 (1966).

Revue Roumaine de Chimie, **18**, *11*, 1971–1982 (1973)

DIE POLAROGRAPHISCHE BESTIMMUNG DES MIT DEM NATRIUMSALZ DER 4-SULFONAMIDOBENZOLSÄURE KOMPLEXGEBUNDENEN QUECKSILBERS (II), IN STARK ALKALISCHEM MEDIUM

GHEORGHE FACSKO und MARIA NEMEŞ

Polytechnisches Institut Timişoara, Laboratorium für Elektrochemie, Bocşa-Str. 6

Eingegangen am 26. Februar 1973

In der Arbeit wird die polarographische Bestimmung des Hg^{2+}-Ions aus einer das Natriumsalz der 4-Sulfonamidobenzoesäure und Natriumhydroxyd enthaltenden Grundlösung untersucht. Es wird gezeigt, daß das Hg^{2+} im Konzentrationsbereich 10^{-3} bis $2{,}4.10^{-3}$ Äquiv.gr./l der Konzentration genau proportionale Diffusionsgrenzströme aufweist. Die lineare Abhängigkeit des Diffusionsgrenzstromwertes von der Quadratwurzel der Quecksilbersäulenhöhe beweist, daß der Elektrodenprozeß von der Diffusion kontrolliert wird. Zwecks Bestimmung der Anzahl der am Reduktionsprozeß des Hg^{2} -Ions teilnehmenden Elektronen wurde eine mikrocoulombmetrische Technik angewandt. Die Analyse der polarographischen Kurven umfaßte graphische Darstellungen des Potentials der Quecksilbertropfelektrode in Abhängigkeit von lg $(I_d - I/I)$ bzw. lg $(I_d - I)$, sowie die Bestimmung des Einflusses des Komplexiermittels und des Hydroxyds auf das Halbstufenpotential und auf den Diffusionsgrenzstromwert.

Das Hg^{2} -Ion präzipitiert in neutralem Medium mit dem Natriumsalz der 4-Sulfonamidobenzolsäure (4-SB-Na). Der gebildete weißkäsige Niederschlag löst sich in Natriumhydroxyd unter Bildung einer komplexen Verbindung, anscheinend folgender Gleichung gemäß[1]:

$$H_2N-SO_2-C_6H_4-COO^- + Hg^{2+} + 2OH^- \rightarrow HgN-SO_2-C_6H_4-COO^- + 2H_2O \qquad (1)$$

Da im alkalischen Medium nur das Ag^+- und das Hg^{2+}-Ion mit 4-SB-Na lösliche komplexe Verbindungen bilden, wodurch sie leicht von den meisten übrigen Metallen getrennt werden können, haben wir die Möglichkeit ihrer direkten Bestimmung aus diesem Medium untersucht.

---

[1] Gh. Ciuhandu, D. Ceauşescu und Gh. Facsko, *Studii şi Cercetări Chim. Acad. Bucureşti*, **25**, 79, (1957).

In früheren Arbeiten haben wir unsere Ergebnisse betreffs der Untersuchung einiger Präzipitierungs- und Komplexierungs-,[2] sowie einiger Oxydo-Reduktionsreaktionen[3] des mit 4-SB-Na komplexgebundenen Ag^+-Ions bekanntgegeben. Ebenfalls haben wir die Möglichkeit der Anwendung dieses Komplexes als Oxydationsmittel in alkalischem Medium untersucht.[4] Ferner haben wir die potentiometrische Bestimmung des mit 4-SB-Na komplexgebundenen Hg^{2+}-Ions in stark alkalischem Medium an Hand einiger Präzipitierungs-, Komplexierungs- und Oxydoreduktionsreaktionen analysiert.[5]

In vorliegender Arbeit haben wir die Möglichkeit der polarographischen Bestimmung des Hg^{2+} aus diesem Medium untersucht, wobei auch Versuche zwecks Deutung der Form der polarographischen Treppe, sowie der Bestimmung der Anzahl der am Reduktionsprozeß des Hg^{2+}-Ions an der Tropfelektrode teilnehmenden Elektronen gemacht wurden.

ARBEITSWEISE

Die Polarogrammen wurden zum Teil mittels eines Polarographen LP 60 und zum Teil mittels eines Polarographen PO 4 aufgenommen. Als Anode wurde eine gesättigte Kalomelelektrode verwendet, die über eine Salzbrücke, bestehend aus einer durch Agar-Agar immobilisierten KNO_3-Lösung, mit der zu untersuchenden Lösung in Verbindung gebracht wurde.

Die zu polarographierenden Lösungen wurden wie folgt vorbereitet: In einem 25-cm^3-Meßkolben wurden aliqoute Volumen einer 0,5—N—NaOH- sowie einer 0,5—N—4—SB—Na-Lösung, 1 ml gesättigter Na_2SO_3-Lösung und aliquote Volumen einer $Hg(NO_3)_2$ Lösung bekannter Konzentration hinzugefügt.Nach der Zugabe von bidistilliertem Wasser bis zur Marke, wurde 10 Minuten zwecks Entfernung des gelösten Sauerstoffes gewartet, wonach bei einer Tropfzeit von 3 Sekunden, im Bereich 0—2 V polarographiert wurde. Zwecks Aufzeichnung der Eichkurven wurden die Lösungen bei +25° thermostatiert.

Zwecks Bestimmung der am Reduktionsprozeß des Hg^{2+}-Ions teilnehmenden Elektronen wurde eine mikrocoulombmetrische Technik angewendet.[6-8] Diese Methode beruht auf die Elektrolysierung einer kleinen Probe bekannten Volumens (0,2—0,3 ml) einer milimolaren Lösung unter einem bestimmten der Tropfelektrode angelegtem Potential. Das Potential wurde bei einem Wert innerhalb des Diffusionsgrenzstromes konstant gehalten. Die im Laufe der Elektrolyse verbrauchte Elektrizitätsmenge wurde durch graphische Integrierung der aufgezeichneten I—t-Kurve ermittelt. Die reduzierte Substanzmenge wurde aus der Anfangs- und Endkonzentration des Hg^{2+} Ions berechnet, nachdem diese auf Grund der Diffusionsgrenzströme an den polarographischen Eichkurven abgelesen wurden.

Die zu diesem Zweck verwendete Mikrozelle ist in Abbildung 1 wiedergegeben. Sie besteht aus zwei durch einen Schliff zusammengefügte Teile. Der Oberteil ist mit 3 Öffnungen versehen, wovon die eine der Durchführung der Kapillare der Tropfelektrode diente und die zweite der Durchführung des filierten und mit Glasfritte geschlossenen Endes eines mit gesättigter

---

[2] GH. FACSKO und R. MINGES, *Talanta*, **5**, 102 (1960).

[3] GH. FACSKO und R. MINGES, *Bul. St. şi Tehnic al I.P.T.*, **6**, 63 (1961).

[4] GH. FACSKO und R. MINGES, *Bul. şti. şi Tehnic al I.P.T.*, **7**, 265 (1962).

[5] GH. FACSKO und M. NEMEŞ, *Bul. şti. şi Tehnic al I.P.T.*, **15**, 145 (1970).

[6] S. BOGDAN, L. MEITES, E. PETERS und J. N. STURTEWANT, *J. Am. Chem. Soc.*, **73**, 1584 (1951).

[7] G. A. GILBERT und E. K. RIDEAL, *Trans. Faraday Soc.*, **47**, 396 (1951).

[8] G. F. REYNOLDS ud H. J. SHAGOLSKI, *Analyt. Chim. Acta*, **10**, 386 (1954).

KNO_3-Lösung gefüllten Hebers der die leitende Verbindung mit der Kalomelelektrode sichert. Die dritte Öffnung konnte, falls nötig, zur Einleitung eines inerten Gases verwendet werden. An Hand des Niveaugefäßes konnte ein konstantes Niveau des Quecksilbers im Elektrolysegefäß gesichert werden.

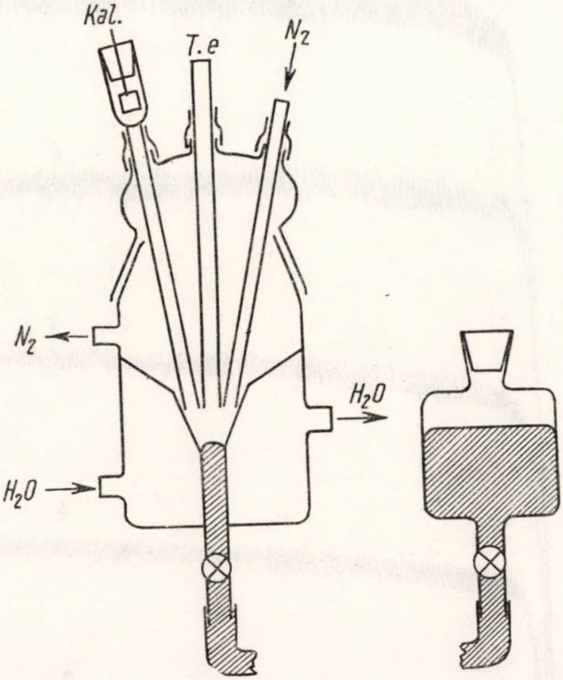

Abb. 1. — Mikrozelle zwecks Bestimmung der Anzahl, der Reduktionsprozeß des Hg^{2+}-Ions teilnehmenden Elektronen n.

Die zu elektrolysierenden Proben wurden in der gleichen Weise wie jene der Polarographie unterworfenen vorbereitet. 0,3 ml dieser Lösung wurden dann electrolysiert bei einem Potential von — 0,6 V im Vergleich zur gesättigten Kalomelelektrode (im Bereich des Diffusionsgrenzstromes) wobei die Abnahme des Diffusionsgrenzstromes mit der Zeit graphisch aufezeichnet wurde.

Die 4-Sulfonamidobenzolsäure wurde aus Chloramin T synthetisiert und zweimal aus Alkohol rekristallisiert. Die 0,5—M—4—SB—Na-Lösung wurde durch Abwägen der 4-Sulfonamidobenzolsäure, Hinzugabe von NaOH in stoicheometrischer Menge und darauffolgender Komplettierung mit bidistilliertem Wasser bis zum entsprechenden Volumen präpariert. Die anderen Reagenzien waren pro analysi.

EXPERIMENTELLE ERGEBNISSE

Das Hg^{2+}-Ion weist in einer NaOH—4. SB—Na Grundlösung eine gutausgebildete polarographische Treppe auf, deren Höhe vom Reststrom entsprechend der Grundlösung gemessen wird.

Revue Roumaine de Chimie, **18**, *11*, 1971—1982 (1973)

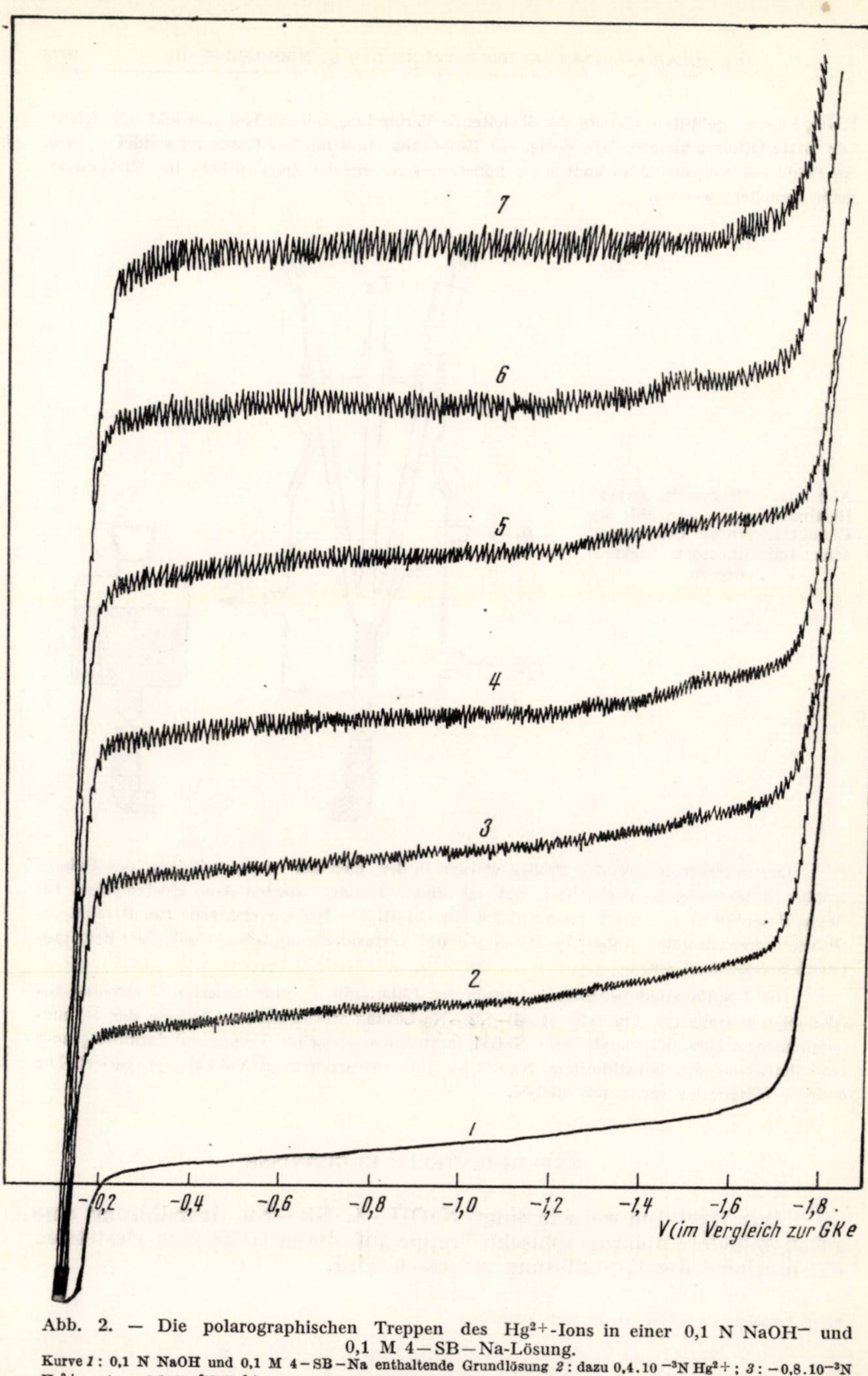

Abb. 2. — Die polarographischen Treppen des Hg^{2+}-Ions in einer 0,1 N $NaOH^-$ und 0,1 M 4—SB—Na-Lösung.

Kurve *1*: 0,1 N NaOH und 0,1 M 4—SB—Na enthaltende Grundlösung *2*: dazu $0,4.10^{-3}$N $Hg^{2}+$; *3*: $-0,8.10^{-3}$N $Hg^{2}+$; *4*: $-1,2.10^{-3}$N $Hg^{2}+$; *5*: $-1,6.10^{-3}$N $Hg^{2}+$; 6: $2 \cdot 10^{-3}$N $Hg^{2}+$; *7*: $-2,4.10^{-3}$ N Hg^{2} + Tropfzeit 3 Sekunden, Temperatur 25°C

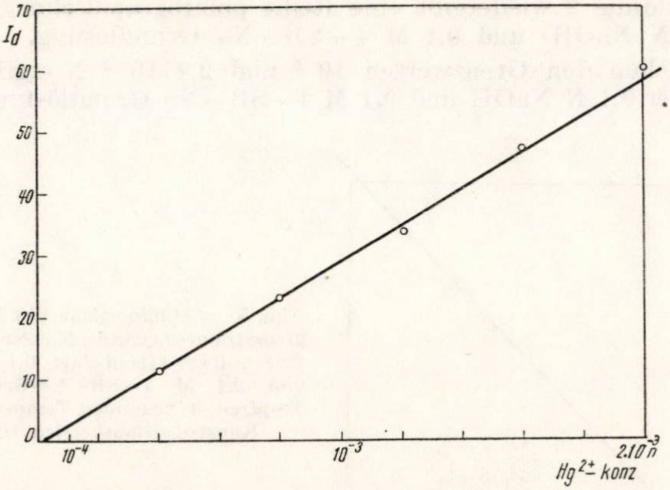

Abb. 3. – Abhängigkeit des Diffusionsgrenzstromes I_d von der Konzentration des Quecksilbers (II) in einer 0,1 N NaOH- und 0,1 M 4 – SB – Na-Grundlösung. Tropfzeit 3 Sekunden. Temperatur 25°C. Konzentrationsbereich 10^{-3}N.

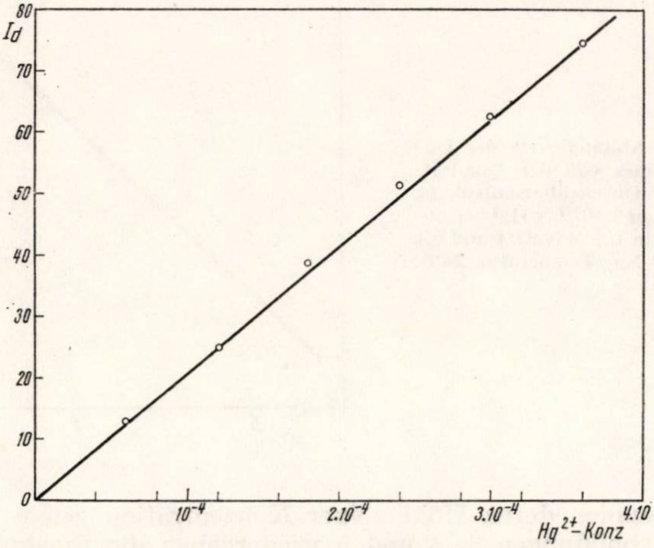

Abb. 4. – Abhängigkeit des Diffusionsgrenzstromes I_d von der Konzentration des Quecksilbers (II) in einer 0,1 N Na OH- und 0,1 M 4 – SB – Na-Grundlösung. Tropfzeit 3 Sekunden. Temperatur 25°C. Konzentrationsbereich 10^{-4} N.

Abbildung 2 wiedergibt eine Reihe polarographischer Treppen aus einer 0,1 N NaOH- und 0,1 M 4—SM—Na Grundlösung.

Zwischen den Grenzwerten 10^{-5} und $2{,}4 . 10^{-3}$ N ergibt das Hg^{2+}-Ion in einer 0,1 N NaOH und 0,1 M 4—SB—Na-Grundlösung polarographische Treppen, deren Höhe seiner Konzentration genau proportional sind. Die Abbildungen 3, 4 und 5 wiedergeben die Eichkurven für die Konzentrationsbereiche 10^{-3}, 10^{-4} und 10^{-5} Äquivalentgramm/1 Hg(II).

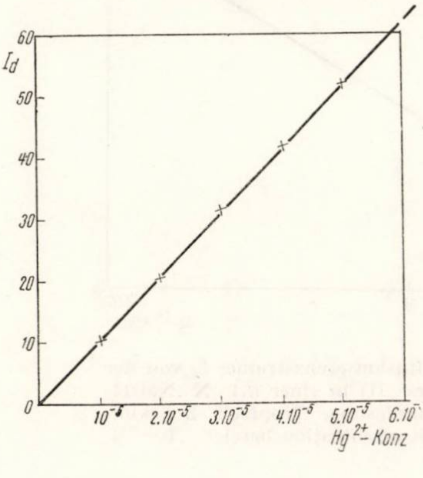

Abb. 5. — Abhängigkeit des Diffusionsgrenzstromes I_d von der Konzentration des Quecksilbers (II) in einer 0,1 N NaOH- und 0,1 M 4—SB—Na-Grundlösung. Tropfzeit 3 Sekunden. Temperatur 25°C. Konzentrationsbereich 10^{-5} N.

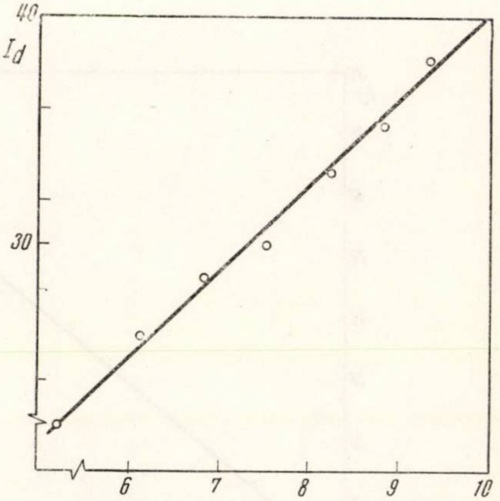

Abb. 6. — Abhängigkeit des Diffusionsstromes von der Quadratwurzel der Quecksilbersäulenhöhe im Falle einer 2.10^{-4} N Hg^{2+}-Konzentration in 0,1 N NaOH und 0,1 M 4—SB—Na. Temperatur 25°C.

Gemäß der Erwartungen, verschiebt sich das Halbstufenpotential mit steigender Hg(II)-Konzentration zu positiveren Werten, wobei die Verschiebung ungefähr 30 mV für den zehnfachen Anstieg der Quecksilberkonzentration beträgt.

Bei der Untersuchung des Einflusses der Quecksilbersäulenhöhe auf den Diffusionsgrenzstrom, wurde eine lineare Abhängigkeit des I_d von $h^{1/2}$ festgestellt. Die Ergebnisse im Falle einer 2.10^{-4} N Hg (II)- in 0,1 N NaOH und 0,1 M, 4—SB—Na-Lösung sind in Abbildung 6 wiedergegeben.

Bei der Untersuchung der polarographischen Kurven aus einer ,1 N—NaOH-Grundlösung, wobei die Konzentration des 4—SB—Na jener des Hg (II) stöchiometrisch war, wurde eine lineare Anhängigkeit zwischen dem Elektrodenpotential und dem Wert lg $\frac{I_d - I}{I}$ festgestellt. Für die Hg(II)- bzw. 4—SB—Na-Konzentration von 10^{-4}; $2,5.10^{-4}$; 5.10^{-4} und 8.10^{-4} N betrug die lineare Abhängigkeit 32, 26, 28 und 30 mV. Abbildung 7 wiedergibt diese Abhängigkeit für die beiden letzten Konzentrationen. Es wurde keine Verschiebung des Halbstufenpotentials mit der Änderung der Konzentration des Hg (II) bzw. des 4—SB—Na festgestellt.

Bei der Untersuchung der polarographischen Kurven aus einer 0,1 N NaOH- und 0,1 M 4—SB—Na-Grundlösung d.h. für den Fall, daß die Konzentration des 4—SB—Na in großem Überschuß zur Hg (II) Menge ist, wurde eine lineare Abhängigkeit zwischen dem Elektrodenpotential und dem Wert lg$(I_d - I)$ festgestellt. Für den Fall, daß die Konzentration des Hg(II) wenigstens hundertmal kleiner war als die des Komplexiermittels und des Hydroxyds, betrug diese Abhängigkeit 59—60 mV.

Abbildung 8 wiedergibt die Abhängigkeit des Potentials der Tropfelektrode vom lg $(I_d—I)$ im Falle einer 4.10^{-4} N Hg (II) în 0,1 M 4—SB—Na- und 0,1 N—NsOH Lösung.

In Anbetracht des Einflusses der Konzentration des Komplexiermittels sowie des Hydroxyds auf den Diffusionsgrenzstromwert und auf das Halbstufenpotential wurde folgendes festgestellt:

Im Bereich der Konzentration des 4—SB—Na zwischen 8.10^{-3} und 10^{-1} N (wobei die Konzentration des Hg (II) und die des NaOH bei 8.10^{-5}N bzw 0,1N konstant gehalten wurden) konnte keine Verschiebung des Halbstufenpotentials festgestellt werden, wobei der Diffusionsgrenzstrom um cca 10% herabgesetzt wurde.

Im gleichen Konzentrationsbereich, d.h. zwischen 8.10^{-3} und 10^{-1}N (wobei die Konzentration des Hg(II) und die des 4-SB-Na bei 8.10^{-5} N bzw 0,1 N konstant gehalten wurden) bewirkt das NaOH eine vernachlässigbare Verschiebung des Halbstufenpotentials zu negativeren Werten (ungefähr 15 mV bei einer zehnfachen Vergrößerung der Hydroxydkonzentration), wobei der Grenzstrom konstant blieb.

Mit Konzentrationen des 4—SB—Na und NaOH von über 0,1 N konnten wir nicht arbeiten, angesichts der Unmöglichkeit den Sauerstoff aus diesen Lösungen vollkommen zu entfernen. Die unteren Grenzen der 4—SB—Na- und NaOH-Konzentrationen wurden durch folgende Erwägung festgesetzt: um die Konzentration obiger Substanzen in unmittelbarer Elektrodennähe jener aus dem Lösungsinnern gleichsetzen zu können, muß diese wenigstens 100 mal größer sein als die Konzentration des Hg(II), um durch die Elektrodenreaktion, welche die Befreiung von 4—SB- und OH^-Ionen bewirkt, nicht fühlbar beinflußt zu werden.

Der Mikrocoulombmetrie wurden 0,3 ml einer Lösung der Hg (II)-Konzentration von 2.10^{-3} N in NaOH 0,1 N und 4 – SB – Na 0,1 M unterworfen. Die Abnahme des Diffusionsstromes mit der Zeit (bei einem kon-

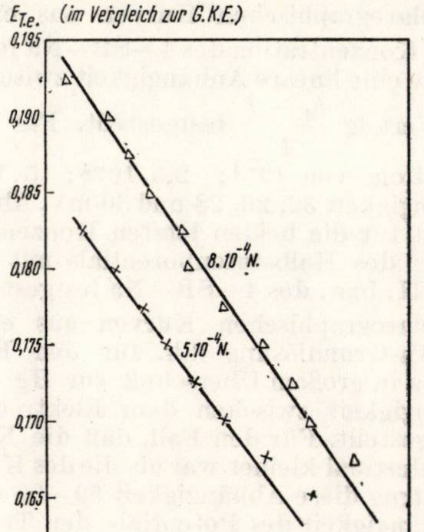

Abb. 7. – Abhängigkeit von lg $\frac{I_d-I}{I}$ vom Potential der Tropselektrode $E_{T.e.}$ für Hg^{2+}-und 4 – SB – Na-Konzentration 5.10^{-4} und 8.10^{-4} N; NaOH 0,1 N-Grundlösung. Tropfzeit 3 Sekunden.

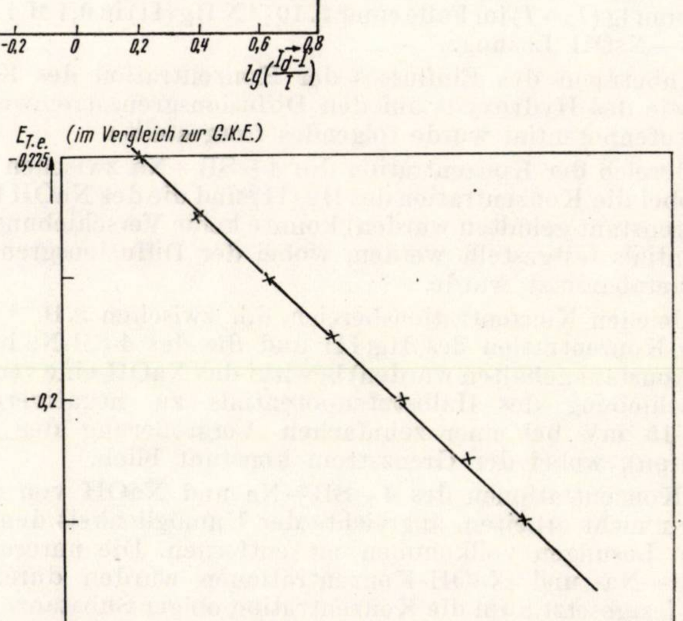

Abb. 8. – Abhängigkeit von lg $(I_d - I)$ vom Potential der Tropfelektrode $E_{T.e.}$ für die Hg (II)-Konzentration von 4.10^{-4}N in 4 – SB – Na 0,1 M und NaOH 0.1 N. Tropfzeit 3 Sekunden.

staten Potential von −0,6 V im Vergleich zur gesättigten Kalomelelektrode) wurde graphisch aufgezeichnet, bis dessen Wert ungefähr zur Hälfte des Anfangswertes sank. In Anbetracht des Umstandes daß sich obige Konzentration des Hg(II) im Bereich der genauen Proportionalität zwischen dem Diffusionsstrom und der Hg(II)-Konzentration befindet, nahmen wir an, daß sich die an der Kathode reduzierte Hg(II)-Menge aus der Abnahme des Diffusionsstromes berechnen läßt. Auf dem Diagramm, das die zeitliche Abnahme des Diffusionsstromes darstellt, verschiedene Zeitpunkte, bei denen sich dieser um 10%, 20%, 30%, 40% und schließlich um 50% des Anfangswertes verminderte, in Betracht nehmend und die entsprechende durchgeflossene Elektrizitätsmenge mittels graphischer Integrierung berechnend, erhielten wir aus der Faraday-schen Formel folgende Werte für — n — die Anzahl der am Reduktionsprozeß teilnehmenden Elektronen : 2,05 ; 1,98 : 1,91 : 1,87 ;1,87.

DISKUSSION DER ERGEBNISSE

Da die Anzahl der am Elektrodenprozeß teilnehmenden Elektronen, durch die Mikrocoulombmetrie bestimmt, 2 beträgt, kann die Reduktion des untersuchten Komplexes wie folgt geschrieben werden :

$$HgX + 2H_2O \rightarrow Hg^{2+} + H_2X + 2OH^-$$

$$Hg^{2+} + 2e^- \rightarrow Hg$$

$$HgX + 2H_2O + 2e^- \rightarrow Hg + H_2X + 2OH^- \qquad (2)$$

Mit H_2X wurde das Natrium — 4 — Sulfonamidobenzoat und mit HgX sein mit Quecksilber (II) gebildeter Komplex bezeichnet.

Die lineare Abhängigkeit des Diffusionsgrenzstromes von der Quadratwurzel der Quecksilbersäulenhöhe, beweist, daß dieser Elektrodenprozeß durch die Diffusion kontrolliert wird. Dafür spricht auch die genaue Proportionalität zwischen der Höhe der polarographischen Treppe und der Konzentration des Hg(II) in einem weiten Konzentrationsbereich.

Obiger Reaktion entsprechend, wird das Potential der Quecksilbertropfelektrode durch folgende Gleichung ausgedrückt :

$$E_{T.e.} = E^0 + \frac{RT}{2F} \ln \frac{a^0_{HgX} \cdot (a^0_{H_2O})^2}{a^0_{H_2X} \cdot (a^0_{OH^-})^2} \qquad (3)$$

worin durch a^0 die Aktivitäten der Komponenten in nächster Elektrodennähe bezeichnet sind.

Die Aktivitäten mit den Konzentrationen ersetzend und die Aktivität des Wassers gleich 1 setzend, kann Gleichung (3) in folgende Form umgeschrieben werden:

$$E_{T,\mathrm{e.}} = E^0 + \frac{RT}{2F} \ln \frac{f_{\mathrm{HgX}}}{f_{\mathrm{H_2X}} \cdot f^2_{\mathrm{OH^-}}} + \frac{RT}{2F} \ln \frac{C^0_{\mathrm{HgX}}}{C^0_{\mathrm{H_2X}} \cdot (C^0_{\mathrm{OH^-}})^2} \qquad (4)$$

Anderseits ist es bekannt, daß durch Diffusion bestimmte polarographische Stromstärke durch

$$I = K\,(C_{\mathrm{HgX}} - C^0_{\mathrm{HgX}}) \qquad (5)$$

ausgedrückt wird. Hierin ist K ein Koeffizient der alle Größen aus der Ilkovič-Gleichung mit Ausnahme der Konzentration umfaßt. $\mathrm{C_{HgX}}$ ist die Konzentration des Komplexes im Lösungsinneren. Der Diffusionsgrenzstrom wird durch

$$I_d = K \cdot C_{\mathrm{HgX}} \qquad (6)$$

wiedergegeben.

Da durch die Elektrodenreaktion H_2X-Moleküle und OH^--Ionen frei werden, wird ihre Konzentration in nächster Elektrodennähe mit dem Anstieg der Stromstärke gemäß den Gleichungen:

$$C^0_{\mathrm{H_2X}} = C_{\mathrm{H_2X}} + \frac{I}{K_1} \qquad (7)$$

und

$$C^0_{\mathrm{OH^-}} = C_{\mathrm{OH^-}} + \frac{I}{K_2} \qquad (8)$$

ansteigen. Hierin sind K_1 und K_2 Konstanten, $C_{\mathrm{H_2X}}$ und $C_{\mathrm{OH^-}}$ die Konzentrationen im Lösungsinneren.

Für den Fall, daß die zu polarographierende Lösung 4—SB—Na in stöchiometrischer Menge zum Hg(II) enthielt, war die Konzentration des Komplexes im Lösungsinneren Null, d.h.

$$\mathrm{C}^0_{\mathrm{H_2X}} = \frac{I}{K_1} \qquad (9)$$

Die Grundlösung war NaOH 0,1 N, d.h. die Konzentration der OH^--Ionen waren in großem Überschuß im Vergleich zur Konzentration des zu bestimmenden Komplexes, weswegen die Konzentration der OH^--Ionen jener aus dem Lösungsinneren gleichgesetzt werden kann.

$$C^0_{\mathrm{OH}^-} = C_{\mathrm{OH}^-} \qquad (10)$$

Durch die Zusammensetzung der Gleichungen (4), (5), (6), (9) und (10) erfolgt :

$$E_{T.e.} = E^0 + \frac{RT}{2F} \ln \frac{K_1 \cdot f_{\mathrm{HgX}}}{K . f_{\mathrm{H_2X}} \cdot f^2_{\mathrm{OH}^-}} - \frac{RT}{2F} \ln \mathrm{C}^2_{\mathrm{OH}^-} + \frac{RT}{2F} \ln \frac{I_d - I}{I} \qquad (11)$$

Demzufolge muß die graphische Darstellung des $E_{T.e.}$ als Funktion des lg $(I_d - I)/I$, für den Fall daß sich das Hg(II) und 4—SB—Na in stöchiometrischen Mengen in Anwesenheit von großem NaOH-Überschuß befinden eine Gerade mit einer Neigung von 0,029 V ergeben. Unsere Ergebnisse bestätigen zufriedenstellend diesen Wert innerhalb eines weiten Konzentrationsbereich des Hg(II).

Für den Fall daß sich sowohl das NaOH als auch das 4—SB—Na in großem Überschuß im Vergleich zum Hg(II) befinden, kann auch die Konzentration des 4—SB—Na in nächster Elektrodennähe, jener aus dem Lösungsinneren gleichgesetzt werden :

$$C^0_{\mathrm{H_2X}} = C_{\mathrm{H_2X}} \qquad (12)$$

Dann ergibt sich aus der Zuzammensetzung der Gleichungen (4), (5), (6), (10) und (12) :

$$E_{T.e.} = E^0 + \frac{RT}{2F} \ln \frac{f_{\mathrm{HgX}}}{K \cdot f_{\mathrm{H_2X}} \cdot f^2_{\mathrm{OH}^-}} - \frac{RT}{2F} \ln C_{\mathrm{H_2X}} \cdot C^2_{\mathrm{OH}^-} +$$

$$+ \frac{RT}{2F} \ln (I_d - I) \qquad (13)$$

Dementsprechend muß die graphische Darstellung von $\mathrm{E}_{T.e.}$ als Funktion von lg $(I_d - I)$ in Gegenwart eines großen Überschusses an 4—SB—Na und NaOH eine Gerade mit einer Neigung von 0,0295 V ergeben. Unsere Ergebnisse bestätigen die Linearität der Abhängigkeit zwischen $E_{T.e.}$ und lg $(I_d - I)$ für den Fall daß sich sowohl das NaOH als auch das 4—SB—Na in großem Überschuß im Vergleich zum Hg(II) befinden, die Neigung beträgt aber 0,060 V.

Aus Gleichung (11) erfolgt für das Halbstufenpotential $\mathrm{E}_{1/2}$, für den Fall, daß sich das 4—SB—Na in stöchiometrischer Menge im Vergleich zum Hg (II) befindet, in Gegenwart eines großen Überschusses an NaOH

$$E_{1/2} = E^0 + \frac{RT}{2F} \ln \frac{K_1 f_{\mathrm{Hgx}}}{K \cdot f_{\mathrm{H_2X}} \cdot f^2_{\mathrm{OH}^-}} - \frac{RT}{2F} \ln C^2_{\mathrm{OH}^-} \qquad (14)$$

Für den Fall, daß sich sowohl das 4—SB—Na als auch das NaOH in großem Überschuß im Vergleich zum Hg (II) befinden, erfolgt das Halbstufenpotential gemäß der Gleichung (13):

$$E_{1/2} = E^0 + \frac{RT}{2F} \ln \frac{f_{\mathrm{HgX}}}{K \cdot f_{\mathrm{H_2X}} \cdot f^2_{\mathrm{OH^-}}} + \frac{RT}{2F} \ln C_{\mathrm{H_2X}} \cdot C^2_{\mathrm{OH^-}} +$$

$$+ \frac{RT}{2F} \ln \frac{I_d}{2}$$

bzw., Gleichung (6) in Betracht ziehend

$$E_{1/2} = E^0 + \frac{RT}{2F} \ln \frac{f_{\mathrm{HgX}}}{2 f_{\mathrm{H_2X}} \cdot f^2_{\mathrm{OH^-}}} = \frac{RT}{2F} \ln C_{\mathrm{H_2X}} \cdot C^2_{\mathrm{OH^-}} + \frac{RT}{2F} \ln C_{\mathrm{HgX}} \quad (15)$$

Unsere Ergebnisse bestätigen beide Gleichungen (14) und (15) für das Halbstufenpotential; und zwar wurde für den Fall, daß sich das 4—SB—Na in stöchiometrischer Menge zum Hg(II) und das NaOH in großem Überschuß befand keine Verschiebung des Halbstufenpotentials mit der Änderung der Hg(II)-Konzentration festgestellt, wobei für den Fall, daß sich sowohl das 4—SB—Na als auch das NaOH in großem Überschuß im Vergleich zum Hg(II) befanden eine Verschiebung des Halbstufenpotentials zu positiveren Werten von ungefähr 30 mV bei einem zehnfachen Anstieg der Hg(II)-Konzentration zu verzeichnen war.

Aus Gleichung (15) geht hervor, daß sich das Halbstufenpotential bei der Änderung der 4—SB—Na- und NaOH-Konzentration verschieben müßte. Unsere experimentellen Ergebnisse bestätigen aber diese Abhängigkeit nicht.

SCHLUSSFOLGERUNGEN

In einer alkalischen das Natriumsalz der 4-Sulfonamidobenzolsäure enthaltenden Lösung weist das Hg(II) eine gutausgebildete polarographische Treppe auf.

Zwischen der Höhe der polarographischen Treppe und der Konzentration des Hg(II) besteht eine genaue lineare Abhängigkeit in einem weiten Konzentrationsbereich. Dementsprechend können diese Treppen einer neuen polarographischen Bestimmungsmethode des Hg(II) zu Grunde liegen.

Da in alkalischem Medium nur Hg(II) und Ag mit 4—SB—Na lösliche Komplexe bilden, wobei die Mehrheit der übrigen Ionen in diesem Medium präzipitieren, ist die dargestellte Methode zur Bestimmung des Hg(II) besonders geeignet.

Revue Roumaine de Chimie, **18**, *11*, 1983–1992 (1973)

STUDIES ON THE ELECTROANALYTICAL BEHAVIOUR OF MEMBRANE-ELECTRODES UNDER CURRENT. IV[*]

THE *E*-*p*Ag ELECTRODE FUNCTION AND THE USE OF THE CERAMIC MEMBRANE-ELECTRODE OF Ag_2S, Ag^+-SELECTIVE IN POTENTIOMETRIC TITRATIONS BY PRECIPITATING AT CONSTANT DIRECT CURRENT

I. C. POPESCU*, C. LITEANU* and L. SAVICI**

* Chair of Analytical Chemistry, "Babeş-Bolyai" University, Str. Arany Janos 11, Cluj, Romania

** Institute of Chemistry, Str. Donath 59, Cluj, Romania

Received February 12, 1973

The effect of a constant and direct electric current passing through the Ag_2S membrane-electrode on the *E*-*p*Ag electrode function, and implicitely on indicating the end of the potentiometric titration by precipitating the Ag^+ ion with this electrode is studied. This effect consists in a non-linear increase of the electrode function slope, a fact bringing with it a marked increase of the electrode sensitivity. An explanatory hypothesis, based on the appearance of a concentration polarization, is offered.

Continuing our studies on the characteristics of membrane-electrodes under current, we have examined the behaviour of the Ag_2S ceramic membrane-electrode through which a direct and constant electric current passes, in the titration of the Ag^+ ion with NaCl.

As shown,[1,2] the Ag_2S ceramic membrane-electrode is an Ag^+/S^{2-} — selective electrode. This is the consequence of the electric conductivity of the Ag_2S membrane, a conductivity exclusively achieved through the agency of the interstitial Ag^+ ions.[3–5] To be more precise, the strictly selective access of the Ag^+ ions of the solutions adjacent to the membrane in the interstices of the crystal lattice of the silver sulphide, determined by the special interfacial affinity of $Ag^+ - Ag_2S$,[6] form the decisive process in achieving the selectivity of the electrode.

---

[*] Part III: I. C. Popescu, C. Liteanu and M. Preda, *Rev. Roumaine Chim.*, **18**, 1819 (1973).

[1] C. Liteanu, I. C. Popescu and V. Ciovîrnache, *Talanta*, **19**, 985 (1972).

[2] I. C. Popescu, C. Liteanu, V. Ciovîrnache and L. Savici, *Rev. Roumaine Chim.*, **18**, 1459 (1973).

[3] M. H. Hebb, *J. Chem. Phys.*, **20**, 185 (1952).

[4] J. H. Kenedy, F. Chen and A. Clifton, *J. Electrochem. Soc.*, **115**, 918 (1968).

[5] C. Wagner, Proc. 7th Meeting Intern. Comm. Electrochem. Thermodynam. Kinetics, London, 1957, p. 361–77.

On the other hand, the working of the previously studied [7-9] $BaSO_4$-parchment paper membrane-electrode is almost entirely based on a selective diffusion process : the penetration of the ions through the membrane is, or is not forbidden, according to their possibility to precipitate in contact with the Ba^{2+}, OH^-, H^+ and SO_4^{2-} ions.

This being known, the question arises if, and how much of the unusual growth effect of the sensitivity of the $BaSO_4$-parchment paper membrane-electrode, in well chosen external electrical polarization conditions, can be found again in the case of an Ag_2S ceramic membrane-electrode, considering the clearly different share of the secondary processes (interfacial equilibria and diffusion through the membrane) participating in establishing the membrane potential in the case of the two membrane-electrodes. This is actually the aim of the present paper.

EXPERIMENTAL

The electrode function, the potentiometric titrations, and the membrane potential-current (static) curves, were obtained by means of the previously used device. [9] The potential of the Ag_2S^1 ceramic membrane-electrode ($1 cm^2$ and 1.61 mm thick Ag_2S tablet) adapted to the previously described measuring cell, [8] was identified with the e.m.f. of the cell :

SCE	Salt bridge KNO_3 $10^{-1}M$ agar-agar	Test solu- tion	Ag_2S membra- ne	$AgNO_3$ $10^{-1}M$ reference solution	Salt bridge KNO_3 $10^{-1}M$ agar-agar	SCE	(1)

The solutions adjacent to the membrane were stirred and kept at a constant 25 ± 0.1° temperature. The salt bridges were made up in the form of Luggin capillaries placed in direct contact with the surface of the membrane.

The necessary reactants, were of *p.a.* purity and were used without any further previous purifications.

RESULTS

The E-pAg electrode function under current. We have plotted the *E-p*Ag electrode function under cathodic (fig. 1) and anodic (fig. 2) polarization, at different current intensities, using the method of standard solutions (J = variable). The standard solutions were obtained by diluting from a stock solution of $AgNO_3$ 10^{-1} M obtained by weighing.

---

[6] W. L. Freiberg and P. L. de Bruyn, *J. Phys. Chem.*, **61**, 586 (1957).

[7] C. Liteanu and I. C. Popescu, *Rev. Roumaine Chim.*, **18**, 319 (1973).

[8] C. Liteanu, I. C. Popescu and M. Preda, *Rev. Roumaine Chim.*, **18**, 1811 (1973).

[9] I. C. Popescu, C. Liteanu and M. Preda, *Rev. Roumaine Chim.*, **18**, 1819 (1973).

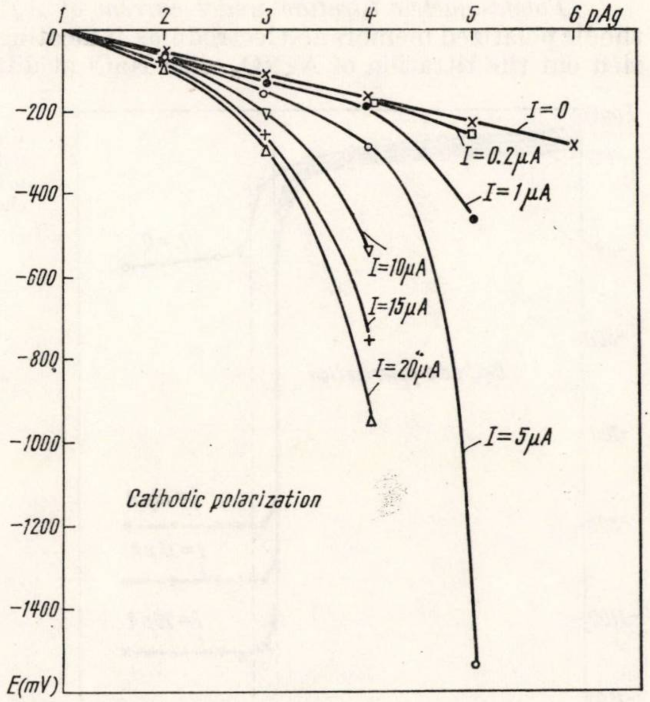

Fig. 1. — The *E*-*p*Ag electrode function under current of the Ag_2S ceramic membrane-electrode (cathodic polarization).

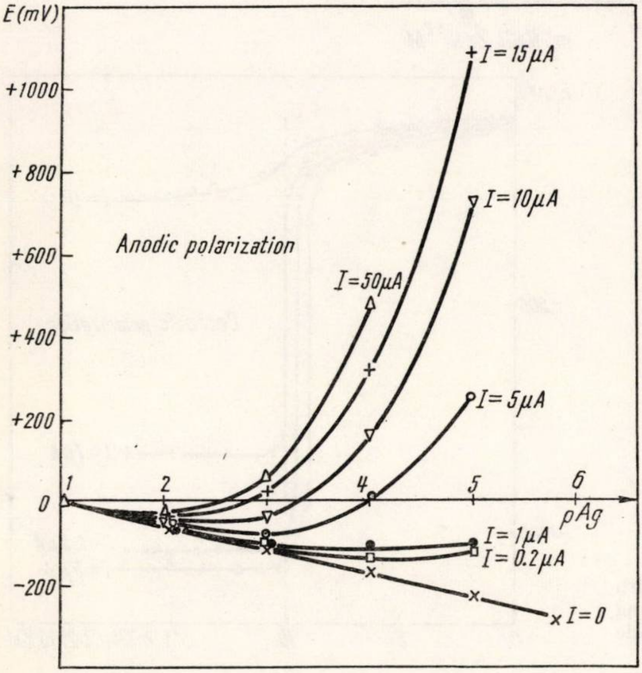

Fig. 2. — The *E*-*p*Ag electrode function under current of the Ag_2S ceramic membrane-electrode (anodic polarization).

Potentiometric titration under current of Ag^+ with Cl^-. Using a cathodic polarized membrane-electrode as indicating electrode, we have carried out the titration of $AgNO_3$ with NaCl at different current intensities

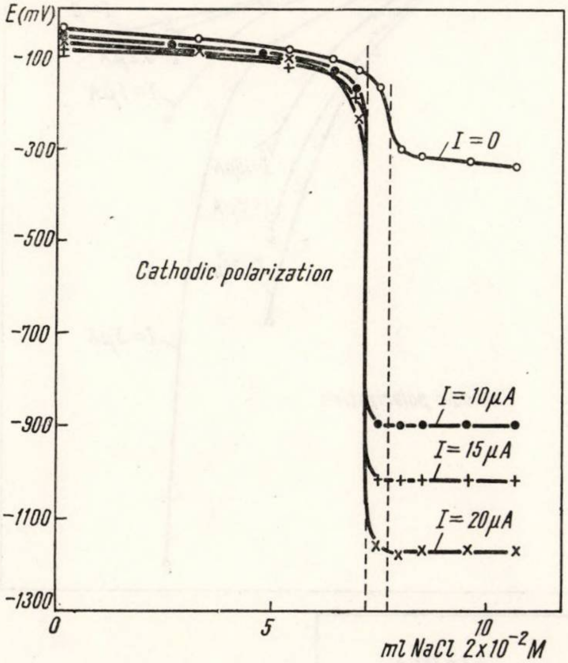

Fig. 3. – The 10^{-2} M $AgNO_3$ with 2×10^{-2} M NaCl titration using Ag_2S ceramic membrane-electrode (cathodic polarization).

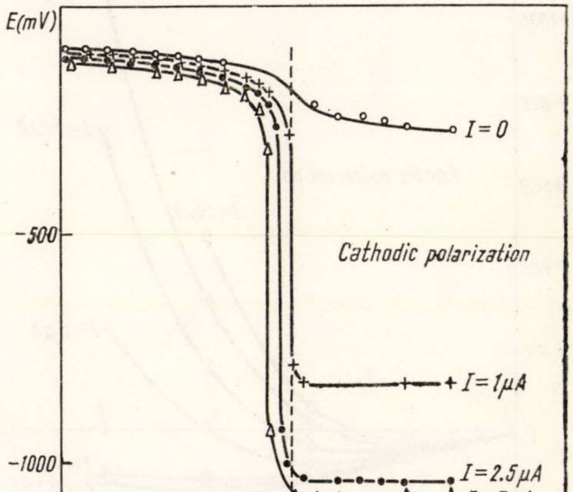

Fig. 4. – The 10^{-3}M $AgNO_3$ with 2×10^{-3} M NaCl titration using Ag_2S ceramic membrane-electrode (cathodic polarization).

and at two degrees of concentration (figures 3,4). The titrated solutions and the titrant were obtained by weighing ($f = 1.000$).

Fig. 5. – The 10^{-2}M NaCl with 2×10^{-2}M $AgNO_3$ titration using Ag_2S ceramic membrane-electrode (cathodic polarization).

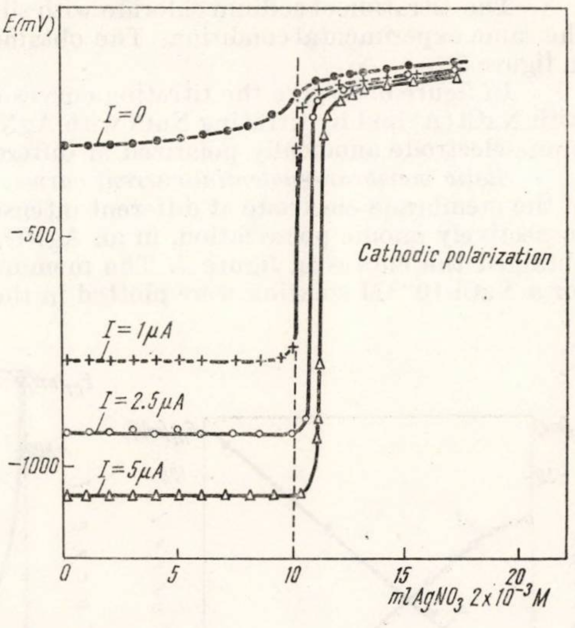

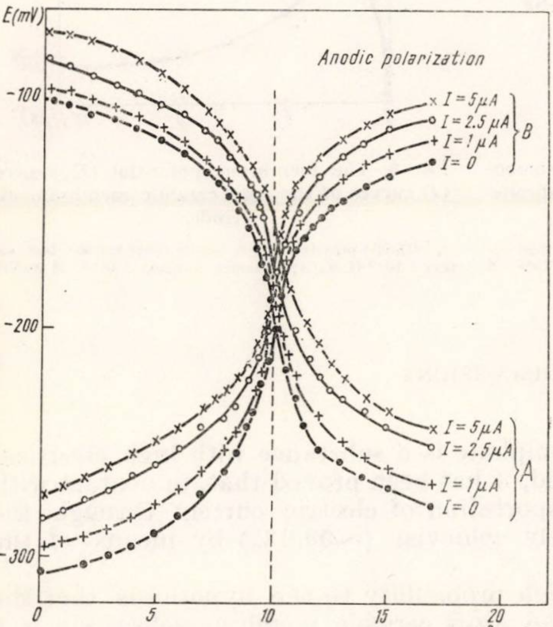

Fig. 6. – The 10^{-3} M $AgNO_3$ with 2×10^{-3}M NaCl titration (A) and 10^{-3} M NaCl with 2×10^{-3} M $AgNO_3$(B) using the Ag_2S ceramic membrane-electrode.

The titration of sodium chloride with silver nitrate was carried out in the same experimental conditions. The obtained titration curves are given in figure 5.

In figure 6 we give the titration curves obtained by titrating $AgNO_3$ with NaCl (A) and by titrating NaCl with $AgNO_3$ (B) by means of the membrane-electrode anodically polarized at different current intensities.

Static membrane-potential-current curves. By measuring the potential of the membrane-electrode at different intensities of cathodic polarization, respectively anodic polarization, in an $AgNO_3$ 10^{-3}M test solution we have obtained the curves in figure 7. The membrane potential-current curves for a NaCl 10^{-3}M solution were plotted in the same way (figure 8).

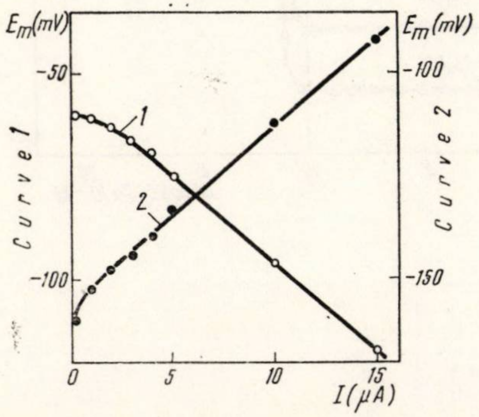

Fig. 7. — The membrane potential (E_m)-current (I) curves of the Ag_2S ceramic membrane-electrode.

1, anodic polarization ; 2, cathodic polarization (test solution : 10^{-3} M $AgNO_3$, reference solution : 10^{-1} M $AgNO_3$).

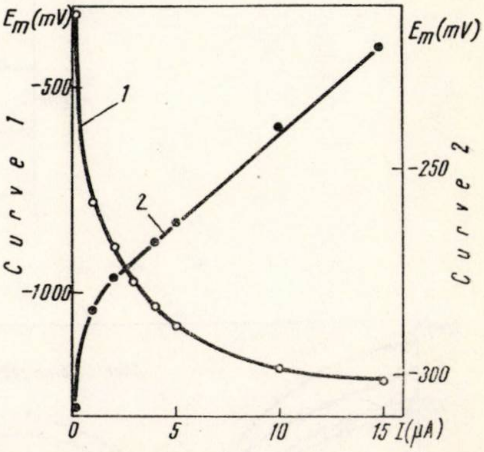

Fig. 8. The membrane potential (E_m)-current (I) curves of the Ag_2S ceramic membrane-electrode.

1, cathodic polarization ; *2*, anodic polarization (test solution : 10^{-3} M NaCl ; reference solution : 10^{-1} M $AgNO_3$).

DISCUSSIONS

It is known that silver sulphide is a substance with high electrical conductivity. On the other hand, it has been proved that, in contact with electrolyte solutions, the transportation of electric current through the membrane is almost exclusively achieved ($\sim$99.2%) by means of the silver ions.[10]

These premises offer a high probability to the hypothesis that the behaviour under current of the Ag_2S ceramic membrane-electrode is a consequence of the appearance of a concentration polarization at the membrane-test solution interface. Subsequently to this, there takes place a change of the interface potential corresponding to the actual value of the Ag^+ ion activity at this interface. For instance, in the case of cathodic polarization of the membrane-electrode, as the activity of the Ag^+ ions in the test solution decreases at the same polarization current intensity, the activity of the Ag^+ ions at the interface will also decrease, leading to the progressive negative bias of the membrane-electrode (figure 1).

---

[10] K. S. Fletcher III and R. F. Mannion, *Analyt. Chem.*, **42**, 287 (1970).

This behaviour may be expressed quantitatively if we consider as valid the model of the Nernst diffusion layer to describe the concentration polarization at the membrane-test solution interface. Thus, as a consequence of the passing of the external polarization electric current on the cathodic face of the membrane, the activity of the Ag^+ ions decreases according to the relationship:

$$a_0 = a - I\delta\ /FD \tag{2}$$

where: a_0 and a are activities of the Ag ions on the interface, respectively, in the solution; I is the intensity of the electric current; δ is the thickness of the Nernst diffusion layer; D is the diffusion coefficient of the Ag^+ ion; F is Faraday's number.

By replacing the relation (1) in Nernst's equation for the membrane-electrode potential, we obtain:

$$E_{I=0} = E_0 + \frac{RT}{F}\ln a_0 + IR_1 = E_0 + \frac{RT}{F}\ln\left(a - \frac{IS}{FD}\right) + IR_1 \tag{3}$$

where: E_0 is the standard potential of the membrane-electrode; R_1 is the electrical resistance of the aderent liquid layer and of the membrane.

If we define the overvoltage by the relationship:

$$\eta = E_{I\neq 0} - E_{I=0} \tag{4}$$

there immediately results:

$$\eta = \frac{RT}{F}\ln\left(1 - \frac{I\delta}{FD}\cdot\frac{1}{a}\right) + IR_1 \tag{5}$$

For I = constant, developing in power series the logarithmic term, and by logarithmizing both members of the obtained expression, we have:

$$\lg|\eta| = K + p\,\mathrm{Ag} \tag{6}$$

This expression offers us the possibility of checking up the hypothesis of the concentration polarization, provided we neglect the ohmic overvoltage term. A plotting of $\lg|\eta| - p\mathrm{Ag}$ must be a line (for I = constant), which is shown in figure 9, for the cathodically and anodically polarized membrane-electrode.

The hypothesis of a concentration polarization may also be supported by the possibility of interpreting the membrane potential-current curves by means of the equation describing the dependence of the current density vs the overvoltage of the kinetic theory of electrode processes. Indeed, the well-known equation:

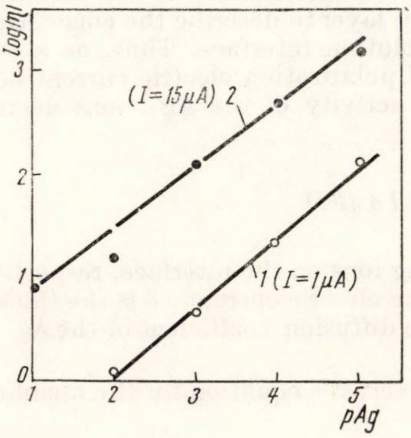

Fig. 9. — The lg $|\eta|$-pAg dependence of the Ag_2S ceramic membrane-electrode. *1*, cathodic polarization ; *2*, anodic polarization (reference solution : 10^{-1} M $AgNO_3$).

$$I = I_{\lim} \ (e^{\eta/(RT/nF)} - 1) \tag{7}$$

provided $\eta < 0.1$ V, becomes:

$$I = \frac{I_{\lim}}{RT/nF}\,\eta \tag{8}$$

an equation that is a line in coordinates $\eta - I$ (figures 10, 11, curve *1*) and provided that $\eta > 0.1$ V it is transformed into:

$$\eta = \frac{RT}{nF} \ln I - \frac{RT}{nF} \ln I_{\lim} \tag{9}$$

an equation also representing a line in coordinates $\eta - \log I$ (figure 11, curve *2*).

We also can observe that if $\eta < 0.1$ V, i.e. if the polarization concentration is at the beginning, the slopes of the $E_m - I$ curves (actually the resistance in direct current of the membrane) corresponding to the cathodic and anodic polarization of the membrane-electrode, in the same test solution (figure 7), must be identical. Indeed, $R_1 = 4.31 \times 10^3\,\Omega$ (the slope of curve *1* in figure 7) and $R_2 = 4.33 \times 10^3\ \Omega$ (the slope of curve 2 in figure 7), while the slope of the curve $E_m - I$ in figure 8 is $R_3 = 5.09 \times 10^3\Omega$ a fact that could be forseen considering the difference between the test solutions used.

In this context, the indication mechanism of the titrations carried out is evident. In the case of anodic polarization, the precision and exactness of the titrations is very good, and in the case of cathodic polarization the precision remains excellent (table 1), but a positive systematic error for the NaCl titration (figure 5), respectively a negative one for $AgNO_3$ titration (fig. 4) occurs.

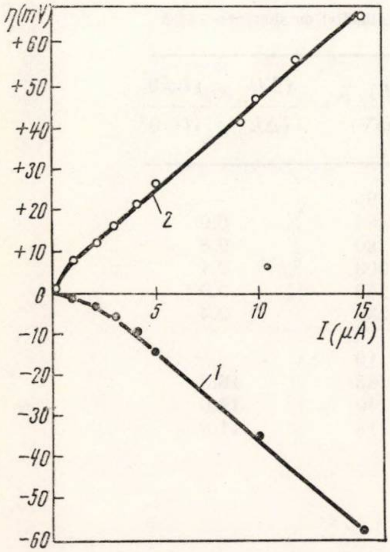

Fig. 10. — The overvoltage (η)-polarizing current intensity (*I*) curves of the Ag_2S ceramic membrane-electrode.

1, cathodic polarization ; *2*, anodic polarization (test solution : 10^{-3}M $AgNO_3$, reference solution : 10^{-1}M $AgNO_3$).

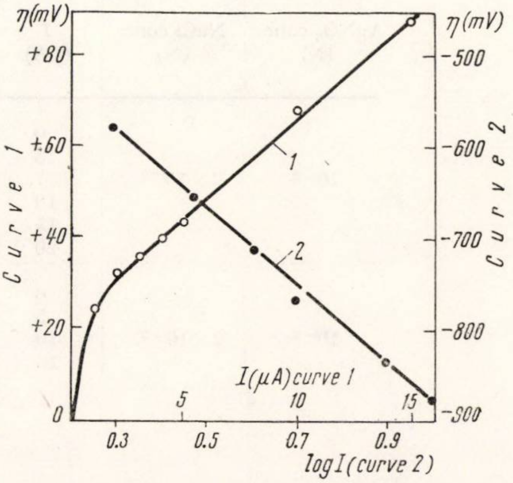

Fig. 11. — The overvoltage (η)-polarizing current intensity (*I*) curve (*1*) of Ag_2 ceramic membrane-electrode (anodic polarization) and overvoltage (η)—lg *I* curve (*2*) (cathodic polarization) (test solution : 10^{-3}M NaCl ; reference solution : 10^{-1} M $AgNO_3$).

To conclude, as a result of the polarization current action, and according to its sense and magnitude, as well as to the nature and concentration of the species present in the test solution, as a consequence of the fact that only the Ag^+ ion can pass through the Ag_2S membrane, a concentration polarization will settle at the membrane-test solution interface. This actually well-known effect is turned to good account in an analytical purpose, to increase the electrode sensitivity in an outstanding way. This statement seems obvious by derivating the relation (3) and explaining the slope of the electrode function under current :

$$\frac{(\mathrm{d}E)_{I\neq 0}}{\mathrm{d}\ln a} = \frac{RT}{F}\,\frac{a}{a-\dfrac{\delta I}{FD}} \qquad (10)$$

Relationship (10) shows that:

— at constant current, the sensitivity of the electrode increases with the *p*Ag.

— at constant concentration, the sensitivity of the electrode increases with the intensity of the polarization current.

Table 1

The influence of the polarizing current intensities (cathodic) on sharpness index of $AgNO_3$ with NaCl

$AgNO_3$ conc. (N)	NaCl conc. (N)	I (μA)	$(\Delta E)_{\pm 1\%}$ (mV)	$\frac{(\Delta E_{\pm 1\%})\, I \neq 0}{(\Delta E_{\pm 1\%}) I = 0}$
10^{-2}	2×10^{-2}	0	96	—
		5	84	0.9
		7	80	0.8
		10	203	2.1
		15	250	2.7
		20	232	2.4
10^{-3}	2×10^{-3}	0	10	—
		5	163	16.3
		10	140	14.0
		15	118	11.8

Revue Roumaine de Chimie, **18**, *11*, 1993–1999 (1973)

SPEKTROPHOTOMETRISCHE DOSIERUNG DER $Cr_2O_7^{2-}$ -UND CrO_4^{2-}-IONEN MIT *o*-TOLIDIN

I. FLOREA

Technische Hochschule ,,Traian Vuia'', Timişoara.
Laboratorium für Allgemeine Chemie, Str. Remus 14

Eingegangen am 31. Januar 1973

Man schlägt eine neue spektrophotometrische Methode zwecks Dosierung der $Cr_2O_7^{2-}$ und CrO_4^{2-} -Ionen mit *o*-Tolidin vor. Die sich bildende Verbindung ist gelb und weist ein Absorbtionsmaximum bei $\lambda = 441$ nm auf. Die durchgeführten Bestimmungen zeigen, daß die Methode die Dosierung des $Cr_2O_7^{2-}$- und CrO_4^{2-} -Ionen mit *o*-Tolidin innerhalb der Grenzen 2,16 — 49,68 μg und 5,83 — 49,60 μg ermöglicht. Die mit *o*-Tolidin erfolgte Dosierung der $Cr_2O_7^{2-}$- und CrO_4-Ionen kann man auch in Gegenwart der Ionen Na^+, K^+, NH_4^+, Cl^-, NO_3^- und SO_4^{2-} durchführen. Die Ergebnisse sind zufriedenstellend, die Empfindlichkeit der Methode ist bemerkenswert.

Für die Dosierung der $Cr_2O_7^{2-}$- und CrO_4^{2-}-Ionen sind folgende Methoden beschrieben : volumetrische[1–23], konduktometrische[24–25] poten-

---

[1] L. Erdey G. Svehla und V. Weber, *Z. analyt. Chem.*, **240**, 91 (1968) ; *Chem. Abstr.*, **69**, 92717q (1968).

[2] E. Ruzicka, *Acta Univ. Palacki. Olomuc*, **24**, 143 (1967) ; *Chem. Abstr.*, **69**, 40930j (1968).

[3] S. Arribas Jimeno, R. Rincon, R. Moro Garicia und M. L. Alvarez Bartolome, *Analyt. Chim. Acta*, **33**, 205 (1965) ; *Chem. Abstr.*, **63**, 10645c (1965).

[4] G. Svehla, L. Koltai und L. Erdey, *Analyt. Chim. Acta*, **29**, 442 (1963) ; *Chem. Abstr.*, **60**, 3466a (1964).

[5] T. S. Zhigalkina, R. S. Lev und A. I. Cherkesov, *Tr. Astrakhansk. Techn. Inst. Rybn. Prom i Khoz.*, **8**, 123 (1962) ; *Chem. Abstr.*, **60**, 3476b (1964).

[6] Yu. V. Khodakov, T. M. Zhuravleva und V. V. Mil'chenko, *Zavodskaya Lab.*, **29**, 929 (1963) ; *Chem. Abstr.*, **59**, 9322 h (1963).

[7] M. S. Jovanovic D. M. Petrovic und D. M. Pavlovic, *Glasnik Hem. Drustva, Beograd*, **27**, 89 (1962) ; *Chem. Abstr.*, **59**, 3304 h (1963).

[8] J. Vulterin, *Talanta*, **10**, 891 (1963) ; *Chem. Abstr.*, **59**, 12143 a (1963).

[9] L. Erdey, I. Buzás und K. Vigh, *Periodica Polytech.*, **3**, 1 (1959) ; *Chem. Abstr.*, **53**, 16804 e (1959).

[10] E. Ruzićka, *Chem. listy*, **51**, 1814 (1957) ; *Chem. Abstr.*, **52**, 2656 i (1958).

[11] R. V.V. Satyanarayanamurthy und M. N. Sastry, *J. Sci. Ind. Res. India*, **16 B**, 83 (1957) : *Chem. Abstr.*, **51**, 11932 c (1957).

[12] I. M. Issa und I. M. El Sherif, *Analyt. Chim. Acta*, **14**, 466 (1956) ; *Chem. Abstr.*, **51**, 5622 h (1957).

ziometrische [26–40], kulometrische [41–46], polarographische [47–49], refraktometrische [50], chromatographische [51–57], mit Ionenaustauschern [58–60], kolorimetrische [20,30,61,62] photometrische [63–65] und spektrophotometrische[66–69].

[13] Balwant Singh und Sarwam Singh, *Analyt. Chim. Acta*, **15**, 277 (1956) ; *Chem. Abstr.* **51**, 7255 a (1957).

[14] V. Simon und J. Zýka, *Chem. listy*, **50**, 360 (1956) ; *Chem. Abstr.*, **50**, 7651 c (1956).

[15] N. A. Gibson und R. A. White, *Analyt. Chim. Acta*, **12**, 413 (1955) ; *Chem. Abstr.*, **50**, 2353 i (1956).

[16] Z. G. Szabó und E. Sugár, *Analyt. Chim. Acta*, **6**, 293 (1952) ; *Chem. Zentr.*, 3611 (1953).

[17] D. V. Ramana Rao, *Current Sci*, **21**, 244 (1952) ; *Chem. Zentr.*, 8302 (1953).

[18] G. Tsatsa, *Praktika*, **10**, 235 (1935) ; *Chem. Zentr.*, **1**, 4187 (1936).

[19] D. Millin, *South African J. Sci.*, **31**, 177 (1935) ; *Chem. Zentr.*, **1**, 4187 (1936).

[20] D. Barard, *Ann. Chim. analyt. Chim appl.*, **17**, 201 (1935) ; *Chem. Zentr.*, **2**, 3269 (1935).

[21] S Kühnel Hagen, *Z. analyt. Chem.*, **95**, 414 (1933) ; *Chem. Zentr.*, **1**, 1357 (1934).

[22] Al. Ionesco-Matiu und S. Herscovici, *Bull. Soc. chim. France*, **53**, 1032 (1933) ; *Chem. Zentr.*, **1**, 2318 (1934).

[23] K. K. Chowdhry, *Lal. Bhajan, Paintindia*, (*Annual*), **67** (1968) ; *Chem. Abstr.*, **70**, 84060 a (1969).

[24] St. Ivascanu, N. Cimeanu und I. N. Ciochină, *Bul. Inst. Politeh. Iași*, **6**, 99 (1960).

[25] I. Florea, *Rev. Roumaine Chim.*, **14**, 365 (1969).

[26] A. K. Zhdanov und S. Jatrudakis, *Tr. Tashkent, Gos. Univ.* (*USSR*), **323**, 161 (1968) ; *Chem. Abstr.*, **72**, 18230 w (1970).

[27] A. K. Zhdanov, F. V. Kondeatova und N. A. Akent'eva, *Uzb. Khim. Zh.*, **13**, 13 (1969) ; *Chem. Abstr.*, **71**, 27242 h (1969).

[28] Yoshiwagi Hidemasa, Oya Hiroaki, Kashiwagi Hidemasa und Ito Hiroyuki, *Denki Kagaku, Japan*, **36**, 467 (1968) ; *Chem. Abstr.*, **69**, 102827 s (1968).

[29] L. Erdey, O. Weber und G. Svehla, *Proc. Conf. Appl. Phys.-Chem. Methods Chem. Anal., Budapest*, **1**, 240 (1966) ; *Chem. Abstr.*, **68**, 119088 d (1968).

[30] A. N. Kirghintsev und L. N. Efanov, *Izvest. Akad. Nauk SSSR, Otdel. khim. Nauk*, **4**, 625 (1965) ; *Chem. Abstr.*, **63**, 5003 a (1965).

[31] N. Jordanov und Ch. Daiev, *Talanta*, **10**, 163 (1963) ; *Chem. Abstr.*, **59**, 1063 a (1963).

[32] Tokuro Ozaki, *Bunseki Kagaku*, **11**, 241 (1962) ; *Chem. Abstr.*, **57**, 2583 c (1962).

[33] Z. A. Gallai, *Nauk Doklady* (*Ysshei Shkoly, Khim i Khim. Tekhnol.*), **3**, 498 (1958) ; *Chem. Abstr.*, **53**, 981 a (1959).

[34] M. Y. Farah und S. Z. Mikhail, *Z. analyt. Chem.*, **166**, 24 (1959) ; *Chem. Abstr.*, **53**, 16806 a (1959).

[35] N. P. Anashkina, *Gigiena Truda i Professional Zabolevaniya*, **3**, 45 (1959) ; *Chem. Abstr.*, **53**, 22645 a (1959).

[36] Kenji Maruyama und Hiroshi Hagisawa, *Bull. Inst. physic chem. Res.*, **16**, 43 (1937) ; *Chem. Zentr.*, **2**, 560 (1938).

[37] I. S. Ryss und A. A. Babalowa, *Betriebs - Lab.*, **4**, 1199 (1935) ; *Chem. Zentr.*, **1**, 4599 (1936).

[38] Enri ue Herrero Ducloux, *Rev. Fac. Ciencias quim., La Plata*, **7**, 97 (1930) ; *Chem. Zentr.*, **1**, 1692 (1932).

[39] J. L. Krassnev, R. B. Hunze und J. N. Chatfield, *J. Amer. Chem. Soc.*, **54**, 2278 (1932) ; *Chem. Zentr.*, **2**, 2489 (1932).

[40] G. S. Forbes und E. P. Bartlett, *J. Amer. Chem. Soc.*, **35**, 1527 (14/8) ; *Chem. Zentr.*, **2**, 2096 (1913).

[41] G. Kainlis und J. P. Amstutz, *Chem. Analit.*, **51**, 549 (1969) ; *Chem. Abstr.*, **72**, 62500 h (1970).

[42] J. Knoeck und D. Harwey, *Talanta*, **16**, 181 (1969) ; *Chem. Abstr.*, **70**, 74032 (1969).

[43] Takeo Takahashi und Hiroshi Sakurai, *Rep. Inst. Ind. Sci. Univ. Tokyo*, **13**, 1 (1963) ; *Chem. Abstr.*, **67**, 7748 s (1967).

[44] S. P. Tutundzic un S. N. Mladenovic, *Zhur. analit. Khim.*, **21**, 590 (1966) ; *Chem. Abstr.*, **65**, 9733 e (1966).

[45] Takeo Takahashi und Hiroshi Sakurai, *Talanta*, **10**, 971 (1963) ; *Chem. Abstr.*, **59**, 13337 h (1963).

In der Arbeit verfolgt man eine neue spektrophotometrische Methode für die Dosierung der $Cr_2O_7^{2-}$- und CrO_4^{2-}-Ionen, wobei *o*-Tolidin als Reagenz verwendet wird. Die Methode beruht auf der Entstehung eines gelbfarbenen Chinondiimins [70], das man zufolge der oxydierenden Wirkung des Bichromats und des Chromats auf *o-Tolidin erhält.* Die sich so gebildete Verbindung erlaubt die spektrophotometrische Dosierung der $Cr_2O_7^{2-}$- und CrO_4^{2-}-Ionen bei $\lambda = 441$ nm. Die Methode empfiehlt sich für $Cr_2O_7^{2-}$- und CrO_4^{2-} Quantitäten innerhalb der Mengenbereiche 2,16—49,68 μg und 5,83 — 49,60 μg. Die $Cr_2O_7^{2-}$-Ionen können auch beide zusammen dosiert werden, mit der Voraussetzung, daß ihre Gesamtmenge nicht 49,60 μg g überschreitet. Die Ionen Na^+, K^+, NH_4^+, Cl^-, NO_3^- und SO_4^{2-}

---

[46] R. S. Monk und G. C. Goode, *Talanta*, **10**, 51 (1963) ; *Chem. Abstr.*, **58**, 7371 g (1963).

[47] R. M. Issa, B. A. Abd-el-Nabey und H. Sadek, *Electrochim. Acta.*, **13**, 1827 (1968); *Chem. Abstr.*, **69**, 102492 d (1968).

[48] N. M. Milyaeva, S. T. Orlovskii und O. A. Songina, *Zhur. analit. Khim.*, **21**, 153 (1966) ; *Chem. Abstr.*, **65**, 303 h (1966).

[49] Sieji Obara und Taro Sekine, *Senki Sagaku, Japan*, **32**, 768 (1964) ; *Chem. Abstr.*, **62**, 10081 b (1965).

[50] G. G. Sade und L. L. Slepak, *Farm. Zhur (Kiev)*, **24**, 89 (1969) ; *Chem. Abstr.*, **72**, 27986 z (1970) ; *Chem. Abstr.*, **72**, 27986 z (1970).

[51] D. T. Haworth und R. M. Ziegert, *J. Chromatog.*, **34**, 544 (1968) ; *Chem. Abstr.*, **70**, 43667 k (1969).

[52] I. I. M. Elbein, A. Elbakry und M. M. Aly, *Chemist-Analyst (Univ. Cairo)*, **56**, 48 (1967) ; *Chem. Abstr.*, **68**, 18429 k (1968).

[53] W. Kielczewski und M. Schneider, *Chem. Analit.*, **9**, 693 (1964) ; *Chem. Abstr.*, **62**, 4616 c (1965).

[54] K. Suchý und E. Buchar, *Sbornik Vysoke skoly pedagog. (Prague), Priv. vedy*, **1**, 111 (1957) ; *Chem. Abstr.*, **52**, 14422 b (1958).

[55] Akira Murata, *Nippon Kagaku Zasshi*, **76**, 1040 (1955) ; *Chem. Abstr.*, **51**, 11156 i (1957).

[56] Binayendra Nath Sen, *Sci. und Cult.*, **20**, 147 (1954) ; *Chem. Zentr.*, 8714 (1956).

[57] V. I. Zolotavin und V. K. Kuznetsova, *Metody Cheruykh i Tsvetnykh Metalov*, **23**, 5 (1953) ; *Chem. Abstr.*, **51**, 1744 i (1957).

[58] W. Y. Campbell, E. F. Spano und Th. E. Green, *Analyt. Chem.*, **38**, 987 (1966) ; *Chem. Abstr.*, **65**, 11328 g (1966).

[59] Yu. Yu. Lur'e und P. S. Antipova, *Tsventnye Metally*, **34**, 11 (1961) ; *Chem. Abstr.*, **56**, 10987 c (1962).

[60] H. O. Day jr., J. S. Gill, E. V. Jones und W. L. Marshall, *Analyt. Chem.*, **26**, 611 (1954) ; *Chem. Zentr.*, 11058 (1955).

[61] E. Herzfeld, *Z. analyt. Chem.*, **115**, 127 (1938) ; *Chem. Zentr.*, **1**, 2832 (1939).

[62] F. Buscaróns und J. Artigas, *Analyt. Chim. Acta*, **16**, 452 (1957).

[63] M. Ziegler und K. Dieter, *Z. analyt. Chem.*, **204**, 413 (1964) ; *Chem. Abstr.*, **61**, 1386 h (1964).

[64] A. A. R. Wood, *Analyst*, **78**, 54 (1953) ; *Chem. Zentr.*, 6207 (1956).

[65] Konosu Hisao, Sato Masato und Mashito Yoichiro, *Nippon Kagaku Kaishi*, **1**, 53 (1972) ; *Chem. Abstr.*, **76**, 80618 q (1972).

[66] E. Ramanauskas, L. Bunikiene, M. Sapraloniene, A. Sulinniene und M. Zielenaita, *Zhur. analit. Khim.*, **24**, 244 (1969) ; *Chem. Abstr.*, **70**, 102679 r (1969).

[67] A. G. Mîrza, *Pakistan J. Sci. Ind. Res.*, **11**, 15 (1968) ; *Chem. Abstr.*, **69**, 64424 y (1968).

[68] M. Steiner und H. Kawinski, *Naturwiss.*, **42**, 344 (1955) ; *Chem. Zentr.*, 12930 (1956).

[69] M. Ariel und J. Manka, *Analyt. Chim. Acta*, **25**, 248 (1961).

[70] J. Piccard, *Ber. dtsch. chem. Ges.*, **44**, 959 (1911) ; **46**, 1843 (1913) ; **46**, 1860 (1913).

beeinflussen die Dosierung nicht, selbst wenn sie in 500-fachem Überschuß — bezogen auf die $Cr_2O_7^{2-}$ -und CrO_4^{2-}-Quanitäten — vorhanden sind.

EXPERIMENTELLES

GERÄTSCHAFT

Besteht aus der in der vorhergehenden Arbeit verwendeten [1,2].

REAGENZIEN

a) Die 1.10^{-4} molare Kaliumbichromatlösung. — Man löst 0,02942 g Kaliumbichromat *p.a.* in einem 1000 ml-Meßkolben auf. 1 ml der Lösung enthält 21,6 μg $Cr_2O_7^{2-}$.

b) Die 1.10^{-4} molare Kaliumchromatlösung. — Man löst 0,01942 g chemisch reines Kaliumchromat in einem 1000 ml-Meßkolben auf. 1 ml der Lösung enthält 19,42 μg CrO_4^{2-}.

c) Die *o*-Tolidinlösung. — Man löst in einem 100 ml-Meßkolben 0,5 g reines, durch mehrfaches Umkristallisieren aus Wasser gewonnenes *o*-Tolidin in 20 ml Eisessig auf, und ergänzt mit Wasser bis zur Marke.

d) Schwefelsäure D = 1,84, aus welcher man 6 molare Schwefelsäure zubereitet.

Die *o*-Tolidinlösung bewahrt man in einer dunklen Flasche auf.

ARBEITSWEISE

Mit Hilfe einer Mikrobürette mißt man 0,1—2,3 ml Lösung a ab, die 2,16—49.68 μg $Cr_2O_7^{2-}$ und 0,3 — 2,6 ml Lösung b, die 5,83 — 49,60 μg CrO_4^{2-} enthält, und führt diese in einen 25 ml-Meßkolben ein. Dann setzt man 1,5 ml Lösung c zu und schüttelt eine Minute lang durch. Es bildet sich eine blaue Färbung; hienach gibt man 6 molare Schwefelsäure bis zum 25 ml Volumen dazu ; man schüttelt durch. Es erscheint eine Gelbfärbung ; nach 10 Minuten — Zeit die die Stabilisierung der Farbe erfordert—wird die Extinktion bei λ = 441 nm gemessen. Als Blindprobe wird eine Lösung benützt, welche aus 1,5 ml c-Lösung auf 25 ml mit 6 molarer Schwefelsäure besteht.

ERGEBNISSE UND DISKUSSIONEN

DAS ABSORBITIONSSPEKTRUM

Die Absorbtionskurve der gebildeten Verbindung, entstanden infolge des Vermengens der Kaliumbichromat- und Kaliumchromatlösungen mit *o*-Tolidin in saurem Medium, ist in Abb. 1 dargestellt und weist ein Absorbtionsmaximum bei λ = 441 nm auf. Die entstandene Verbindung eignet sich zur spektrophotometrischen Dosierung der $Cr_2O_7^{2-}$- und CrO_4^{2-}-Ionen.

EINFLUSS DER ZEIT

Die Farbenbeständigkeit der nach der Oxydation des *o*-Tolidins mit Kaliumbichromat und Kaliumchromat in saurem Medium entstandenen Verbindung wurde während 70 Minuten verfolgt, indem man die Extinktion bei $\lambda = 441$ nm maß. Aus den Ergebnissen ist feststellbar, daß die Farbe in 10 Minuten beständig wird und weitere 10–15 Minuten lang so verbleibt.

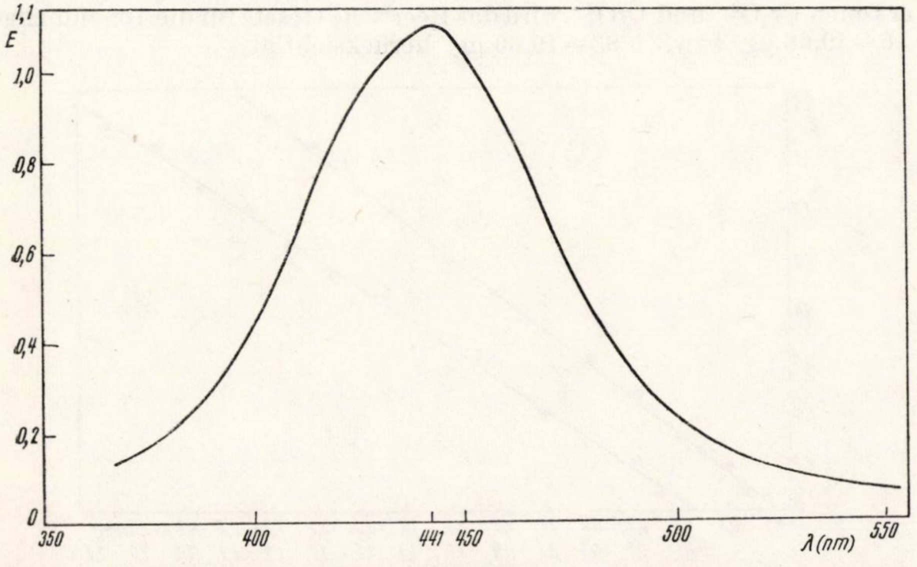

Abb. 1. — Das Absorbtionsspektrum der sich gebildeten Verbindungen, bei Verwendung der 2 cm-Küvette. 1,5 ml Lösung c + 22 ml 6 molarer Schwefelsäure.

EINFLUSS DER REAGENZIENKONZENTRATION

Die günstigsten zur Dosierung der $Cr_2O_7^{2-}$- und CrO_4^{2-}-Ionen erforderlichen Reagenzmengen für obangegebene Ionenquantitäten sind 1,5—2,0 ml 0,5%-ges *o*-Tolidin. In diesem Bereich verhält sich der Extinktionswert der Verbindung konstant, angenommen man geht von denselben $Cr_2O_7^{2-}$- und CrO_4^{2-}-Mengen aus.

EINFLUSS DER SCHWEFELSÄUREKONZENTRATION

Die Schwefelsäurekonzentration übt in der Lösung eine große Rolle auf die Farbenbeständigkeit der durch die Reaktion des Kaliumbichromats und Kaliumchromats mit *o*-Tolidin sich bildende Verbindung aus. Die bei verschiedenen Säuremolaritäten vollzogenen Extinktionsmessungen der Verbindung ergeben, daß die Beständigkeit der Farbe der Verbindung in einer 6 molaren Schwefelsäurelösung am höchsten ist.

DIE EICHKURVEN

Die Eichkurven für die Dosierung der $Cr_2O_7^{2-}$- und CrO_4^{2-}-Ionen mit *o*-Tolidin sind in Abb. 2 dargestellt. Bei der Behandlung mit *o*-Tolidin der Ionen $Cr_2O_7^{2-}$ und CrO_4^{2-} wird das Beer'sche Gesetz für die Ionenmengen 2,16—49,68 μg bzw. 5,83—49,60 μg berücksichtigt.

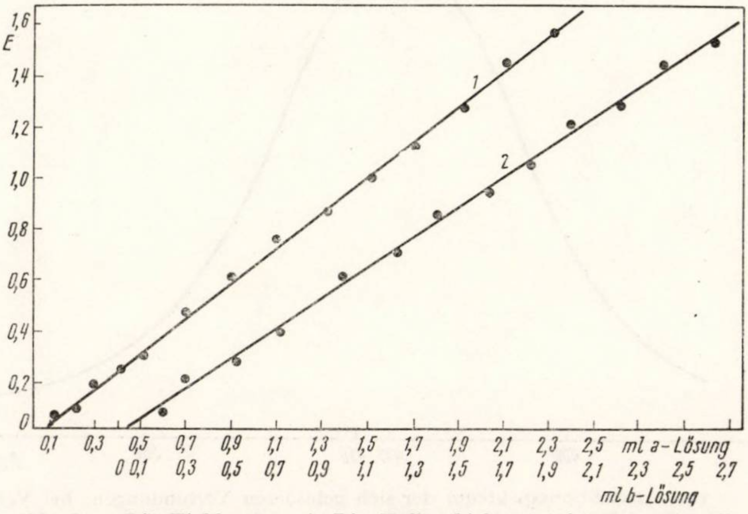

Abb. 2. — Die Eichkurven. 1. Die Kaliumbichromat lösungen, jeweils mit 1,5 ml c-Lösung versetzt und-anschließend-mit 6 molarer Schwefelsäure bis zu 25 ml ergänzt. 2. Die Kaliumchromatlösungen, jeweils mit 1,5 ml c-Lösung versetzt und—anschließend—mit 6 molarer Schwefelsäure bis zu 25 ml ergänzt.

Die experimentellen Ergebnisse sind in den Tabellen 1 und 2 zusammengefaßt.

Tabelle 1

Die spektrophotometrische Dosierung des $Cr_2O_7^{2-}$-Ions mit *o*-Tolidin

Lfd. Nr.	Verbrauchtes $Cr_2O_7^{2-}$ in μg	E $d = 2$ cm	Gefundenes $Cr_2O_7^{2-}$ in μg	E %
1	2,59	0,08	2,47	−4,63
2	7,78	0,20	7,59	+2,44
3	13,18	0,38	12,77	−3,11
4	20,74	0,62	20,27	−2,25
5	28,73	0,88	27,73	+3,48
6	38,45	1,28	37,62	−2,16
7	44,93	1,40	43,53	−3,12
8	48,38	1,52	47,63	+1,55

Die neue spektrophotometrische Methode der Dosierung der $Cr_2O_7^{2-}$ — und CrO_4^{2-} -Ionen mit *o*-Tolidin ermöglicht die bequeme Dosierung dieser Ionen, beide gleichzeitig oder einzeln, dank der großen Empfindlichkeit der Reaktion und der Farbenbeständigkeit der entstandenen Verbindungen. Die Ionen Na^+, K^+, NH_4^+, Cl^-, NO_3^- und SO_4^{2-} verhindern die Dosierung selbst im Falle großen Überschusses nicht.

Tabelle 2

Die spektrophotometrische Dosierung des CrO_4^{2-}-Ions mit *o*-Tolidin

Lfd. Nr.	Verbrauchtes CrO_4^{2-} in μg	E $d = 1$ cm	Gefundenes CrO_4^{2-} in μg	E%
1	6,21	0,10	5,93	−4,35
2	10,88	0,26	10,81	−2,90
3	15,15	0,39	14,85	+2,00
4	18,84	0,51	18,28	−2,98
5	24,86	0,70	23,91	−3,83
6	33,40	0,98	32,97	+1,30
7	40,00	1,20	39,08	−2,31
8	49,52	1,50	47,85	−3,37

ORSZÁGOS MŰSZAKI KÖNYVTÁR ÉS DOKUMENTÁCIÓS KÖZPONT 1883

Revue Roumaine de Chimie, **18**, *11*, 1993–1999 (1973)

Revue Roumaine de Chimie, **18**, *11*, 2001 (1973)

G. LIPTAY, "Atlas of thermoanalytical curves", Akadémiai Kiadó, Budapest, 1973, 160 p.

Methods of thermal analysis have developed rapidly during the last two decades, and have found widespread practical application. Today, thermoanalytical methods are important tools in research and routine analysis.

Owing to the very rapid development of thermal analysis, it seemed desirable to start the continuous publication of a collection of diagrams to assist the work of researchers and chemists in industrial laboratories engaged in thermal analysis.

This collection of diagrams is to be broadened in scope after the first volumes, so as to develop it by international collaboration (using instruments other than the Derivatograph developed by Paulik — Z. anal. Chem. 160 (1958) 241 and Talanta 13 (1966) 1405) into a handbook which can be used all over the world, and will be of good service to the steadily increasing number of thermal analysts. The present collection of diagrams (125) is part of a larger, comprehensive work in preparation. This volume is dealing with the measuring techniques and practical problems of thermalanalysis. In order to ilustrate the differences caused by the conditions of recording, this Atlas contains several curves for each substance taken under different experimental conditions. These diagrams have been especially prepared for this purpose and for this Atlas.

The experimental conditions selected may seem rather arbitrary. However, the selection was made in consideration of having due regard the practical uses and possibilities, to the ICTA recommendations. The authors use this opportunity to call the attention of scientists and researchers active in the field of thermal analysis to the possibility of joint work.

The Atlas containing the collection of diagrams is very useful and will furnish guidance and assistance to those engaged in thermal analysis.

Dr. doc. D. I. Marchidan

NOTE POUR LES AUTEURS

La *Revue Roumaine de Chimie* publie des articles en anglais, français, russe, allemand ou espagnol. Les auteurs sont priés d'envoyer des articles, notes, communications et comptes rendus inédits.

Les manuscrits seront dactylographiés à deux intervalles. Les tableaux seront dactylographiés sur feuilles séparées, de même que la légende des figures. Les diagrammes seront tracés à l'encre de Chine sur papier calque. Les tableaux et les figures seront numérotés par des chiffres arabes, en nombre strictement nécessaire. Prière de ne pas inscrire les mêmes données dans les tableaux et les figures. Les formules chimiques seront incluses dans le texte ; en outre, elles seront transcrites sur des feuilles séparées. Les auteurs sont priés d'indiquer les caractères italiques (en soulignant les lettres au crayon), ainsi que tout autre caractère spécial. L'ordre des références bibliographiques sera celui de leur mention dans le texte ; le nom de l'auteur sera précédé de l'initiale du prénom ; les publications périodiques seront présentées suivant les prescriptions internationales. Les références seront ajoutées à la fin de l'article ; elles paraîtront comme des notes, au bas de la page. Le texte sera précédé d'un résumé, comprenant 15 lignes au maximum.

L'entière responsabilité du contenu des articles appartient aux auteurs. On publie des articles dus aux collaborateurs roumains ou étrangers. Les auteurs recevront 50 tirés à part.

PRINTED IN ROMANIA

1974 MAR 20

TRAVAUX PARUS AUX ÉDITIONS DE L'ACADÉMIE DE LA RÉPUBLIQUE SOCIALISTE DE ROUMANIE

MARIA FITI, **Dozimetria chimică a radiaţiilor ionizante** (La dosimétrie chimique des radiations ionisantes), 1973, 210 p., 13,50 lei.

MIHAI FLORESCU, **Eficienţa economică a cercetării ştiinţifice** (L'efficience économique de la recherche scientifique), 1972, 115 p., 15 lei.

GEORGETA LĂZĂRESCU, **Sistematizarea informaţiilor în Chimia organică** (La systématisation des informations dans la chimie organique), 1972, 252 p., 10,50 lei.

P. BALTĂ et E. BALTĂ, **Introducere în chimia fizică a stării vitroase** (Introduction à la chimie physique de l'état vitreux), 1971, 240, 15,50 lei.

LYDIA-MARIA VAICUM, **Biodegrabilitatea detergenţilor** (La biodégrabilité des détergents), 1971, 254 p., 16 lei.

TIBERIU NĂŞCUŢIU, **Metode radiometrice de analiză** (Méthodes radiométriques d'analyse), 1971, 346 p., 19,50 lei.

I. ZUGRĂVESCU et L. STOICESCU-GRIVETZ, **Polimeri heterociclici** (Polymères hétérocycliques), 1971, 190 p., 9,50 lei.

CRISTOFOR SIMIONESCU et C. V. UGLEA, **Fracţionarea compuşilor macromoleculari** (Fractionnement des composés macromoléculaires), 1962, 292 p., 18,50 lei.

I. MAXIM, **Materiale nucleare** (Matériaux nucléaires), 1969, 444 p., 30 lei.

CRISTOFOR SIMIONESCU et CLEOPATRA VASILIU-OPREA, **Mecanochimia compuşilor macromoleculari** (La mécanochimie des composés macromoléculaires), 1967, 344 p., 23,50 lei.

CORNEL BODEA et collab., **Tratat de biochimie vegetală**, partea I, **Fitochimie** (Traité de biochimie végétale, Ire partie, Phytochimie), Ier vol., 1964, 747 p. + 4 annexes + 2 pl., 41 lei ; IIe vol., 1965, 1262 p., 1 pl., 56 lei ; IIIe vol., 1967, 773 p., 35 lei.

V. GHEŢIE et V. MICUŞAN, **Analiza imunochimică. Teorie şi practică** (Analyse immunochimique. Théorie et pratique), 1966, 369 p., 28 lei.

R. PORTOCALĂ et L. POPA, **Acizii ribonucleici celulari şi virali** (Les acides ribonucléiques cellulaires et viraux), 1966, 375 p., 8 pl., 26 lei.

I.P.I.—o. 3355

43 426

Lei 25.—

F 1103

R

REFERÁLVA

REVUE ROUMAINE DE CHIMIE

TOME 18
Nº 12
Décembre, 1973
RRCHAX, 18, *12*, 2003–2188 (1973)

ÉDITIONS DE L'ACADÉMIE DE LA RÉPUBLIQUE SOCIALISTE DE ROUMANIE

Rev. Roumaine Chim. 18, *12*, p. 2003–2188 (1973), Bucarest

COMITÉ DE REDACTION

Rédacteur en chef:

I. G. MURGULESCU, membre de l'Académie de la République Socialiste de Roumanie

Rédacteur en chef adjoints:

A. T. BALABAN et V. EM. SAHINI, membres correspondants de l'Académie de la République Socialiste de Roumanie

Collège de rédaction:

C. DRĂGULESCU, RALUCA RIPAN, CR. SIMIONESCU, membres de l'Académie de la République Socialiste de Roumanie; EM. BRATU, ECATERINA CIORĂNESCU-NENITZESCU, P. SPACU, membres correspondants de l'Académie de la République Socialiste de Roumanie; MARGARETA AVRAM, D. I. MARCHIDAN, G. NIAC et D. SANDULESCU

La Revue Roumaine de Chimie paraît 12 fois par an. Toute commande de l'étranger (fascicules ou abonnements) sera adressée à Intreprinderea Rompresfilatelia, Boîte Postale 2001, telex 011631, Bucarest, Roumanie

Les manuscrits, les livres et les revue proposés en echange, ainsi que toute correspondance seront envoyés à la rédaction:

REVUE ROUMAINE DE CHIMIE

23, str. Dumbrava Roşie, Bucarest, Roumanie

ÉDITIONS DE L'ACADÉMIE DE LA RÉPUBLIQUE SOCIALISTE DE ROUMANIE
3 bis, str. Gutenberg, Bucarest

REVUE ROUMAINE
DE
CHIMIE

Tome 18, N° 12 **Décembre 1973**

Page

M. CONTINEANU, O. CONSTANTINESCU and TATIANA ONCESCU, EPR study in the radiolysis of polycrystalline azibenzyl 2005–2010

D. R. ARMSTRONG, R. C. W. KING and P. G. PERKINS, The electronic structures of some six-membered sulphur-nitrogen and sulphur-oxygen ring systems 2011–2016

K. GRJOTHEIM, J. L. HOLM and H. A. ØYE, Physico-chemical properties of molten salts of significance to magnesium electrolysis . . . . 2017–2020 C

O. RADOVICI, CECILIA VASS and I. SOLACOLU, Electroplating of copper from pyrophosphate baths. II. The effect of electrolyte temperature 2021–2029 R

N. I. IONESCU and B. AURIAN-BLĂJENI, On the logarithmic law used in the kinetics of the solid-gas chemisorption processes 2031–2035

MELANIA BOZEŞANU, Gas chromatographic separation of formic aldehyde, methyl alcohol, water and hydrogen peroxide . . . . 2037–2038 C

MARIA BREZEANU and IOANA JITARU, Cu (II) coordination compounds with 3-amino-1-propanol 2039–2050

SILVIA PLOŞTINARU and P. SPACU, Mixed lanthanide compounds with neutral ligands containing donor oxygen atom. I. Lanthanide chlorosalicylates with triphenylphosphinoxide 2051–2058

D. NEGOIU and LIDIA PARUTA, Complex combinations of transition metals with tertiary stibines. I. Complex combinations of palladium (II) with tritolyl-stibines 2059–2066

IULIA I. GEORGESCU, M. MORARIU and DOINA ŢARINA, Mössbauer effect in complexes of isonicotinic acid hydrazide with Fe (II) — isothiocyanate $(INAH)_2 Fe(NCS)_2 H_2O$ 2067–2075

N. S. BIRADAR and V. B. MAHALE, Addition compounds of tin (IV) chloride with tetradentate Schiff bases 2077–2082

V. PIACENTE and G. BALDUCCI, Vapour pressure of antimony trichloride 2083–2085

ALICE MARIE GLATZ, FLORIN BADEA, ZSOLT ARVAY, VALERIAN

Revue Roumaine de Chimie 18, *12*, 2003–2188 (1973)

DRĂGUŢAN, FILIP CHIRALEU et ALEXANDRU C. RĂZUŞ, Condensations d'acides insaturés sur le benzène catalysées par le chlorure d'aluminium. V. Acide sorbique 2087–2096
SORIN MAGER and ERNEST L. ELIEL, Conformational equilibrium of 5-fluoro-1,3-dioxane by NMR spectroscopy 2097–2102
MARCELA FĂRCĂŞAN, R. CHIRA, GH. CIURDARU and VIORICA I. DENES, Heterocyclic methylene bases. X. 2(ω-acyl-ω-arylazo)methylene derivatives of N-containing heterocycles 2103–2112
C. TĂRĂBĂŞANU-MIHĂILĂ, L. FLORU and MARIA OLTEANU, Heterocyclic derivatives with thiazolic rings. II. Electrophilic substitutions of 6-aminothiazolo [4,5-f] indazole 2113–2125
I. MOŢOC und F. KEREK, Matrizielle Charakterisierung der Struktur und Topologie der organischen Verbindungen. IV. Prochiralität, Pseudochiralität 2127–2133
LILIANA D. PETROVA, La concentration critique micellaire de quelques sels quaternaires d'alkylpyridine 2135–2141
T. HODIŞAN, C. LITEANU and SILVIA GOCAN, Thin layer thermochromatography. VII. Comparison between temperature gradient chromatography resolution and nonsaturated chamber resolution 2143–2148
GHEORGHIŢA I. JINESCU und HANS H. REHNER, Strömungstechnische Fragen ungleichkörniger Wirbelschichten 2149–2164

INDEX DES AUTEURS 2165–2177

INDEX DES SUJETS 2177–2187

Revue Roumaine de Chimie, **18**, *12*, 2005–2010 (1973)

EPR STUDY IN THE RADIOLYSIS OF POLYCRYSTALLINE AZIBENZYL

M. CONTINEANU, O. CONSTANTINESCU and TATIANA ONCESCU

Department of Physical Chemistry, University of Bucharest, Bd. Republicii 13, Romania

Received May 16, 1973

The kinetics of radical formation and their disappearance with temperature in irradiated polycrystalline azibenzyl was studied. An appropriate mechanism of radiolysis was proposed.

1. INTRODUCTION

The study of the thermal and photochemical decomposition of diazo compounds (diphenyldiazomethane, diazofluorene, azibenzyl, diazophenantrone, etc.) by EPR has formed the object of several investigations.[1–4].

In a previous paper, we studied the kinetics of intermediate radicals occurring from azibenzyl thermal decomposition.[5] It was thought profitable to extend the study by EPR to the γ irradiation of the polycrystalline azibenzyl, in order to investigate the nature of the formed radicals and the kinetics of their formation and decay.

2. EXPERIMENTAL

Materials. Azibenzyl was prepared by oxidizing the corresponding hydrazone with HgO.[6] Hydrazone was obtained from benzyl and hydrazine hydrate.[7]

Irradiations. Samples were irradiated at 216 Ci and 10,000 Ci ^{60}Co sources with doses ranging between 10^7-10^8 Rad.

---

[1] R. W. Murray, A. M. Trozzolo, F. Wasserman and W. A. Yager, *J. Amer. Chem. Soc.*, **84**, 3212 (1962).

[2] A. M. Trozzolo, *Accounts Chem. Res.*, 329 (1968).

[3] O. Constantinescu, M. Contineanu, T. Oncescu and I. Pascaru, *Rev. Roumaine. Chim.*, **16**, 1279 (1971).

[4] L. S. Singer and I. C. Lewis, *J. Amer. Chem. Soc.*, **90**, 4212 (1968).

[5] T. Oncescu, M. Contineanu and O. Constantinescu, to be published.

[6] C. D. Nenitzescu and E. Solominica, "Organic Syntheses", Coll. Vol. II, John Wiley and Sons Inc., New York, 1943, p. 496.

[7] O. Grummit and A. Jenkins, *J. Amer. Chem. Soc.*, **68**, 914 (1946).

[8] W. Benson, "Thermochemical Kinetics, Methods for the Estimation of Thermochemical Data and Rate Parameters" John Wiley Sons. Inc. New York, London, Sydnye, 968, p. 66.

EPR measurements: EPR spectra were recorded at room temperature with the spectrograph ART-5 operating in the X band having high-frequency modulated magnetic field (100 Kc/s). The spectroscopic splitting factor was determined by using peroxylamine disulfonated as a standard.

Spectrophotometric measurements: UV and IR spectra were carried out with an SP 1800 Pye-Unicam and with an U.R. 10 Zeiss Jena device, respectively.

3. RESULTS

The polycrystalline azibenzyl γ irradiated at room temperature presents a rather simple EPR spectrum (fig. 1) with a symmetrical line without a hyperfine structure, with $g = 2.0033 \pm 0.0002$ and $\Delta H = 8.5$ G.

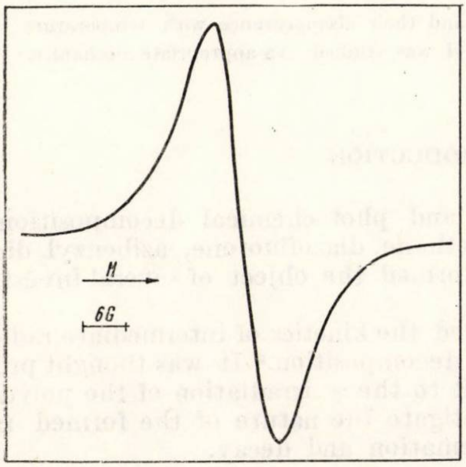

Fig. 1. — EPR spectrum of the polycrystalline azibenzyl γ irradiated at room temperature with a 4.1×10^7 Rad dose ($B_\gamma = 0.86$ MR/h).

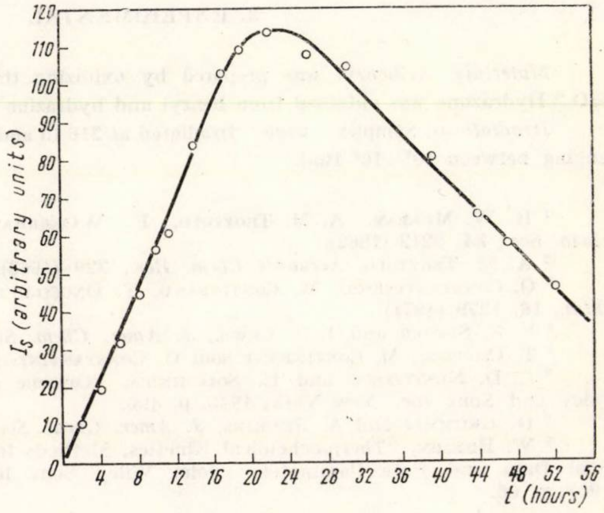

Fig. 2. — Dependence of the signal intensity on the irradiation time for a polycrystalline azibenzyl sample, at room temperature (Rate dose 9.5×10^6 Rad/h).

The radical formation by γ irradiation as a function of the dose was monitored. Figure 2 exhibits the variation of the signal intensity relative to the irradiation time (the total dose).

We have also investigated the effect of temperature on the thermal stability of radicals formed by γ irradiation of azibenzyl. For this purpose, γ irradiated samples were heated for 6 minutes from five to five degrees at a temperature range between 30–70°, measuring the relative signal intensity. Results are given in fig. 3.

We also recorded the variation of signal intensity *versus* the time for the temperatures 40, 50, 55, 60 and 65°. As an illustration, figure 4 shows the isotherm of 60°.

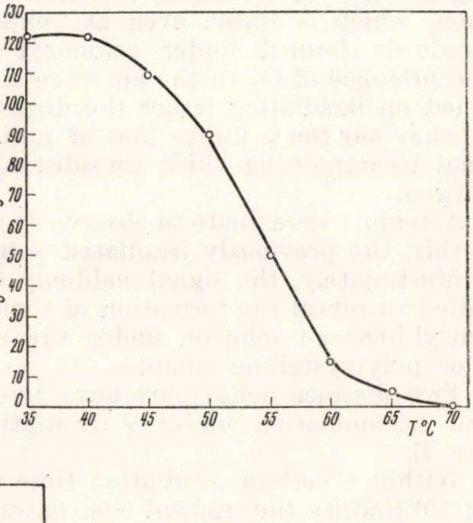

Fig. 3. – Isochronous variation of the EPR signal intensity of an irradiated polycrystalline azibenzyl sample as a function of the temperature.

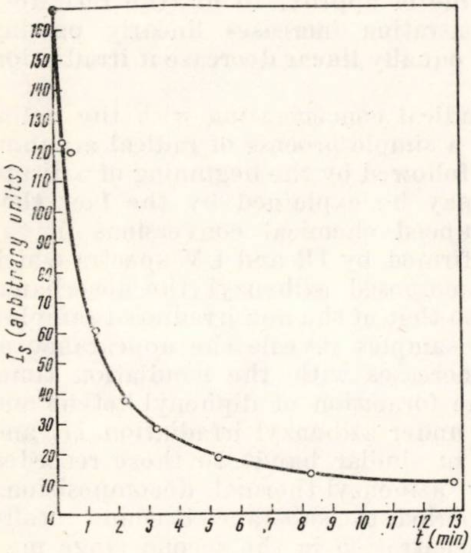

Fig. 4. – Variation of the signal intensity of the irradiated azibenzyl sample as a function of time, at a temperature of 60°.

UV and IR spectra of irradiated samples up to a dose of 15 × 10^7Rad display the same bands as in the case of non-irradiated samples.

It is noteworthy that UV and IR spectra indicate the disappearance of azibenzyl in the case of a long irradiation of about 50 hours, and are identical to those obtained for the air-thermal decomposition of azibenzyl.

4. DISCUSSION

The signal recorded under azibenzyl γ irradiation is relatively stable up to approx. 40° and totally disappears at 70° (fig. 3), being thus distinguished from the signal recorded in the azibenzyl thermal decomposition, which is stable even at temperatures beyond 200°. Likewise, the radicals formed under azibenzyl γ irradiation are not influenced by the presence of O_2 in the air since similar radical concentrations are obtained on irradiating either the degassed or the undegassed samples. This behaviour too is unlike that of radicals obtained from the azibenzyl thermal decomposition which are substantially influenced by the presence of oxygen.

Attempts were made to observe the hyperfine structure. To accomplish this, the previously irradiated samples were dissolved in benzene but unfortunately, the signal suddenly disappeared on solving. In fact, we failed to reveal the formation of some radicals even when irradiating azibenzyl benzene solution under the same dose conditions as in the case of polycrystalline samples.

Two distinct behaviours have been observed with regard to the radical accumulation under γ irradiation of polycrystalline azibenzyl (figure 2).

Within a certain irradiation time of approx. 15 hr (the rate dose 9.5 × 10^6 Rad/h) the radical concentration increases linearly passing through a maximum and showing an equally linear decrease if irradiation is continued.

The recorded variation of the radical concentration with the radiation dose suggests the occurrence of a simple process of radical accumulation up to a certain total dose, also followed by the beginning of a disappearance process. This behaviour may be explained by the fact that the substance undergoes no pronounced chemical conversions in the first stage. In fact, this has been confirmed by IR and UV spectra which are similar to those of the non-decomposed azibenzyl (the absorbance of the irradiated sample is identical to that of the non-irradiated sample). The second stage of the irradiated samples reveals the appearance of some viscous droplets whose size increases with the irradiation time. These viscous domains are due to the formation of diphenyl-ketene and also of its polymerization products, under azibenzyl irradiation. IR and UV spectra evidence the existence of similar bands to those recorded from similar products obtained by azibenzyl thermal decomposition.[5]

During a long irradiation time period, the substance becomes totally viscous. The decrease of radical concentration in the second stage may be caused by their facilitated recombination in these viscous domains, a phenomenon which was shown to occur very rapidly when dissolving the sample in benzene where the mobility of the species is greater.

It must also be mentioned that the melting temperature of the azibenzyl sample, irradiated with a dose of $15 \cdot 10^7$ Rad, decreases to 76° compared to 80° for the non-irradiated azibenzyl.

As seen in figure 2, both the accumulation and the disappearance verify a zeromolecular kinetics. The calculation of the rate constants led to $k_a = 5.83 \times 10^{10}$ radic. $g^{-1}s^{-1}$ for the accumulation and to $k_d = 2.45 \times 10^{10}$ radic. g^{-1} s^{-1} for the disappearance.

By studying the stability of radicals formed under irradiation with the temperature we observed for all the considered temperature ranges a linear dependence when we plotted $\frac{1}{I_s}$ (where I_s is the signal intensity) as a function of the heating time. As an example, the plot for the temperature of 60° is given in fig. 5.

Table 1 presents the rate constants calculated from the slopes of the straight lines.

By plotting lg k as a function of $1/T$ we calculated the activation energy of the bimolecular process of radical disappearance under the action of temperature (fig. 6) obtaining for E_a a value of 73.12 Kcal/mole. The activation entropy was also calculated,[8] obtaining a value of $\Delta E^* = +105$ e.u.

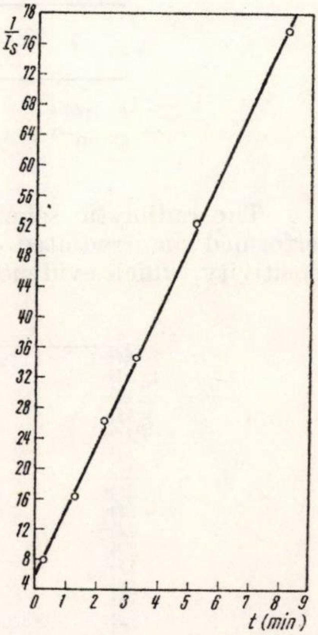

Fig. 5. — Time-dependent variation of $\frac{1}{I_s}$ at 60° for radicals formed in the irradiated azibenzyl.

Considering the characteristics of the recorded EPR spectra and using the kinetic data obtained by radical accumulation under polycrystalline azibenzyl irradiation and their disappearance by heating to various temperatures, we may suppose the following radiolysis mechanism which involves the paramagnetic species studied

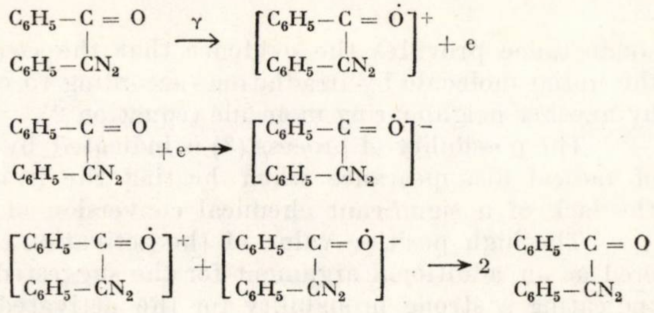

1 $$\begin{matrix}C_6H_5-C=O\\ |\\ C_6H_5-CN_2\end{matrix} \xrightarrow{\gamma} \left[\begin{matrix}C_6H_5-C=\dot{O}\\ |\\ C_6H_5-CN_2\end{matrix}\right]^{+} + e$$

2 $$\begin{matrix}C_6H_5-C=O\\ |\\ C_6H_5-CN_2\end{matrix} + e \longrightarrow \left[\begin{matrix}C_6H_5-C=\dot{O}\\ |\\ C_6H_5-CN_2\end{matrix}\right]^{-}$$

3 $$\left[\begin{matrix}C_6H_5-C=\dot{O}\\ |\\ C_6H_5-CN_2\end{matrix}\right]^{+} + \left[\begin{matrix}C_6H_5-C=\dot{O}\\ |\\ C_6H_5-CN_2\end{matrix}\right]^{-} \longrightarrow 2 \begin{matrix}C_6H_5-C=O\\ |\\ C_6H_5-CN_2\end{matrix}$$

In this manner, the possible processes (1) and (2) will account for the singlet EPR spectra without a hyperfine structure recorded from azibenzyl irradiation.

Table 1

The kinetics parameters for the radical disappearance with temperature

T °C	40	50 I	55	60	65
$k \times 10^{20}$ g.rad^{-1} s^{-1}	0.18	14.9	87.2	395.4	2353.9

The radiolytic scheme agrees with the conductivity measurements performed on irradiated crystals, by means of a device with a 10^{-9} A sensitivity, which evidenced no electric conductance. The lack of electric conductance provides the evidence that the electrons withdrawn from the initial molecule by irradiation (according to equation 1) are trapped by another neighbouring molecule (equation 2).

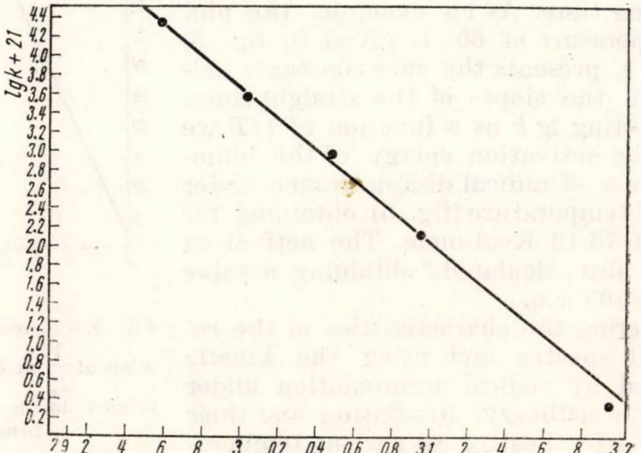

Fig. 6. — Dependence of lg k as a function of $1/T$.

The possibility of process (3) is indicated by a second order kinetics of radical disappearance when heating the irradiated sample and by the lack of a significant chemical conversion of the substance.

The high positive value of the activation entropy may be considered as an additional argument for the suggested radiolysis mechanism, indicating a strong probability for the activated complex formation in a transitional state, which leads to the reformation of azibenzyl molecules.

Revue Roumaine de Chimie, **18**, *12*, 2011–2016 (1973)

THE ELECTRONIC STRUCTURES OF SOME SIX-MEMBERED SULPHUR-NITROGEN AND SULPHUR-OXYGEN RING SYSTEMS

D. R. ARMSTRONG, R. C. W. KING and P. G. PERKINS

Department of Pure and Applied Chemistry, University of Strathclyde, Glasgow
Gl 1XL, Scotland

Received March 21, 1973

Calculations within the CNDO MO framework have been performed on a sulphur-oxygen and three sulphur-nitrogen ring systems. The results indicate that small but significant sulphur-sulphur bonds are present in all four molecules. There is also partial double bonding in the sulphur-nitrogen cyclic molecules but only single bonds are found in the sulphur oxygen network. The electron distribution over the framework atoms reveals that the sulphur and the particular first row atom are respectively, positively and negatively charged.

In a recent communication [1] the electronic structures of a planar trimeric and a planar tetrameric phosphazene were examined. It was discovered that a special feature of their bonding arises from significant interactions between pairs of phosphorus atoms. Since this bonding augments the normal mechanism of electron delocalisation within the ring it undoubtedly helps to stabilise these cyclic compounds. In order to determine whether this intra-ring bonding is unique to ring systems containing phosphorus or is a property of cyclic compounds containing second row atoms in general, it was decided to investigate the electronic structure of some six membered sulphur-nitrogen and sulphur-oxygen ring systems.

The choice of system for study was governed by the availability of geometrical data from molecular or crystal structures since sulphur-nitrogen compounds do not always possess simple structures. The three sulphur-nitrogen compounds selected were; a cyclotrithiazene $(ClSN)_3$, a trioxocyclotrithiazene $(ClOSN)_3$ and a hexaoxocyclotrithiazene $(O_2SN)_3^{3-}$. The structures of these compounds are presented in figure 1 (*a*–*c*). There are two possible isomeric formulae for the hexaoxocyclotrithiazene anion, *c* (1) and *c* (2), in which the unit charge is considered to be located at the oxygen and nitrogen atoms, respectively. This site would presumably be the position of attachment of the protons in the hypothetical parent acid $(O_2SNH)_3$. It was thought that calculations should aid in distinguishing between the two isomers. All the structures except *c* (2) invoke double bonding within the ring whilst all the molecules except *a* have sulphur in a formally hexavalent state. Clearly resolution of the true situation is highly desirable.

---

[1] D. R. Armstrong, G. H. Longmuir, and P. G. Perkins, *J. Chem. Soc.* (*Chem. Comm.*), **1972**, 464.

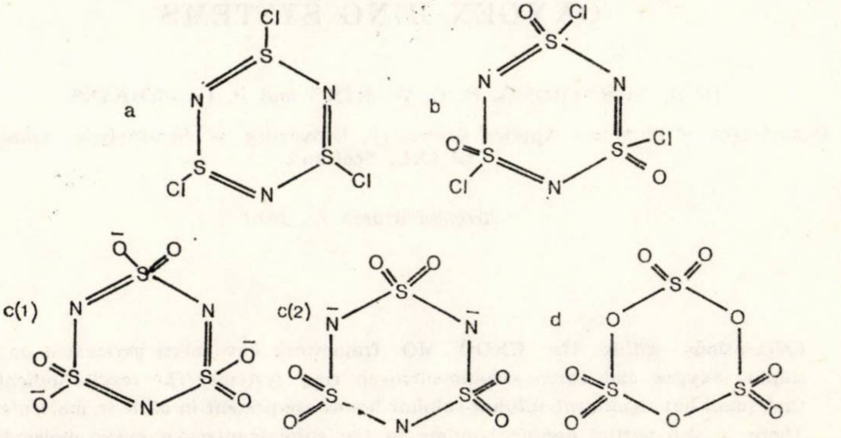

Fig. 1. — Structures of $(SNCl)_3$, $(SNOCl)_3$, $(SNO_2)_3{}^{3-}$ and $(SO_3)_3$.

The fourth system studied was the six-membered sulphur-oxygen cyclic compound hexaoxocyclotrithioxane $(O_2SO)_3$. This is isoelectronic with the $(O_2SN)_3^{3-}$ anion and hence should provide the basis for a meaningful comparison between sulphur-oxygen and sulphur-nitrogen cyclic systems. This compound is also of course the trimeric form of sulphur trioxide.

The calculational procedure used an improved version [2] of the standard CNDO/2 method [3] within the LCAO—MO—SCF framework. The input parameters for the valence orbitals, including *d* orbitals for sulphur and chlorine were abstracted from the work of Levison and Perkins.[4] The crystal and molecular structures are given in references. [5-9]

RESULTS

The electron densities, bond indices, and the atomic valencies for the five compounds are presented in table 1. The latter two quantities have recently been defined quantitatively by Armstrong, Perkins, and

---

[2] D. R. Armstrong, P. G. Perkins, and J. J. P. Stewart, *J. Chem. Soc.*, (*A*) **1971**, 3674.

[3] J. A. Pople, D. P. Santry and G. A. Segal, *J. Chem. Phys.*, **43**, S 129 (1965).

[4] K. A. Levison and P. G. Perkins, *Theor. Chim. Acta*, **17**, 1 (1970).

[5] G. A. Wiegers and A. Vos, *Acta Cryst.*, **20**, 192 (1966).

[6] A. C. Hazell, G. A. Wiegers and A. Vos, *Acta Cryst.*, **20**, 186 (1966).

[7] A. C. Hazell, Personal Communication.

[8] R. Pascard and C. Pascard-Billy, *Acta Cryst.*, **18**, 830 (1965).

[9] K. J. Palmer, *J. Amer. Chem. Soc.*, **60**, 2360 (1938).

Stewart[10] and are believed to afford a better picture of electron distribution and reactivity than the customary bond order and electron densities.

Table 1

The electron densities, valencies, and bond indices of $(SNCl)_3$, $(SNOCl)_3$, $(SNO_2)_3^{3-}$, $(SO_3)_3$ and SO_3

ELECTRON DENSITY		$(SNCl)_3$	$(SNOCl)_3$	$(SNO_2)_3^{3-}$	$(SO_3)_3$	SO_3
Sulphur	*s*	1.43	1.20	1.19	1.13	1.22
	p	3.46	3.03	3.18	2.75	2.93
	d	0.73	1.09	1.06	1.25	1.16
	total	5.62	5.32	5.43	5.13	5.31
Nitrogen	*s*	1.30	1.31	1.37		
	p	3.90	3.94	4.09		
	total	5.20	5.25	5.46		
Chlorine	*s*	1.78	1.72			
	p	5.27	5.27			
	d	0.13	0.17			
	total	7.18	7.16			
Oxygen (ring)	*s*				1.50	
	p				4.80	
	total				6.30	
Oxygen (equatorial)	*s*		1.63	1.61	1.61	1.63
	p		4.64	4.98	4.67	4.60
	total		6.27	6.59	6.28	6.23
Oxygen (axial)	*s*			1.62	1.56	
	p			4.89	4.73	
	total			6.51	6.29	
VALENCIES						
Sulphur		4.40	5.83	5.83	6.07	5.96
Nitrogen		2.83	2.86	2.67	—	—
Chlorine		1.64	1.80	—	—	—
Oxygen ring		—	—	—	2.40	—
equatorial		—	1.84	1.73	2.15	2.23
axial		—	—	1.71	2.09	—
BOND INDICES						
Sulphur-nitrogen		1.28	1.24	1.20	—	—
Sulphur-chlorine		1.29	1.30	—	—	—
Sulphur-oxygen (ring)		—	—	—	1.02	—
Sulphur-oxygen (equatorial)		—	1.57	1.50	1.82	2.00
Sulphur-oxygen (axial)		—	—	1.48	1.88	—
Sulphur-sulphur		0.23	0.16	0.16	0.10	—
nitrogen-nitrogen		0.04	0.04	0.03	—	—
Oxygen (ring) — oxygen (ring)		—	—	—	0.05	—

---

[10] D. R. Armstrong, P. G. Perkins and J. J. P. Stewart, *J. Chem. Soc. (Dalton)*, to be published.

The valency, V_A, of atom A is defined in terms of the density matrix elements P (equation 1). Comparison of this calculated value with a maximum attainable valency, gives an indication of the reactivity of the atom in its particular situation.

$$V_A = \sum_{\lambda \text{ on } A} 2P_{\lambda\lambda} - \sum_{\lambda \text{ on } A} \sum_{\sigma \text{ on } A} P_{\lambda\sigma}{}^2 \qquad (1)$$

The "bond index", B_{AB}, (equation 2) gives a quantitative measure of the multiplicity of the bond between two atoms A and B.

$$B_{AB} = \sum_{\lambda \text{ on } A} \sum_{\sigma \text{ on } B} P^2_{\lambda\sigma} \qquad (2)$$

a. Sulphur-nitrogen ring systems. In the three compounds studied, the sulphur carries a large positive charge whilst nitrogen and the substituents on sulphur take on excess electrons (table 1). The magnitude of the formal charge and the *d* orbital occupancy of sulphur depends on the number of substituents bonded to it. In hexafluorophosphazene[1] the phosphorus possesses a charge of +0.97 and the *d* orbitals house 0.79 electrons. The charge distribution is therefore more polarised in the sulphur systems probably due to the greater electron affinity of the sulphur *d* orbitals.

The calculations were repeated with the *d* orbitals excluded from the basis set. It was found, as expected, that the total electron density on the sulphur atom decreases. The nett loss, however, in only 0.1–0.3 electrons as the *p* orbital population of sulphur simultaneously increases. The omission of the *d* orbitals also causes considerable destabilisation of the systems, the energy rises being of the order of 60.0 eV, 78.6 eV, and 99.1 eV for $(SNCl)_3$ $(SNO_2)_3^{3-}$ and $(SNOCl)_3$, respectively. This loss in energy correlates with the *d* orbital population of the corresponding molecule.

The importance of *d* orbital participation is perhaps most manifest in the bond indices. These quantities depend strongly on the presence of *d* orbitals in the basis set and are therefore altered drastically by their exclusion, *e.g.* for $(SNCl)_3$ without *d* orbitals, we obtain the following bond indices; $B_{SN} = 0.97$, $B_{SCl} = 0.86$, $B_{SS} = 0.03$ and $B_{NN} = 0.02$. Hence, the presence of *d* orbitals ensures that more electron density can be involved in the bonding and although the *s*, *p*, and *d* orbital populations are altered by the involvement, the total electron density on the atom does not change dramatically.

The bond indices show that there is partial double bonding about the $(SN)_3$ rings and comparison with the corresponding value for benzene (1.44) indicates substantial delocalisation. The *d* orbitals of chlorine and sulphur enable fractional double bonding to occur in the sulphur-chlorine bond. Probably the strongest bond in these molecules is the sulphur-oxygen bond which is intermediate between a single and double bond. The intra-ring sulphur-sulphur bond indices have values between 0.16 and 0.23. These are slightly smaller than those in the six-membered phosphazane molecules (0.26) but they are still substantial and so, without doubt, electron density in the ring plane is an important factor which helps stabilise these cyclic compounds. The *d* orbital participation in the intra-ring bonding is indeed crucial and, as seen above, exclusion of the sulphur *d* orbitals produces a near zero value for the sulphur-sulphur bond index.

The valencies calculated for sulphur in the three molecules reveal a remarkable similarity to the formal value assumed from the "bond" structures of figure 1. This means that we expect the sulphur atoms in $(SNCl)_3$ to increase their valency in a reaction. Moreover, the nitrogen atoms in all the ring systems have valencies much less than the maximum of four [11] and so these atoms will also be reactive centres in the three molecules. From the electron population analyses, the sulphur atoms will be attacked readily be nucleophiles whilst electrophilic reagents will be attracted to the nitrogen atoms. This suggestion is supported by the reaction [12] of $(SNCl)_3$ with SO_3, a weak Lewis acid, to yield an adduct $(SNCl)_3.6SO_2$ which decomposes to $(SNCl)_3.3SO_3$ at 100° and at high temperature and pressure to $(SNOCl)_3$. In the first complex, the sulphur trioxide is bonded to the nitrogen and chlorine atoms and, in the second, to the nitrogen atoms only.

From electron density and bond index considerations we conclude that neither of the structural formulae C(1) and C(2) represents the molecular bonding fully.

The three "extra" electrons of the anion are almost evenly distributed over all the atoms, which thus gives no indication as to the structure of the parent acid $(SNOClH)_3$. The valencies show, however, that proton attack is more likely to occur at the nitrogen atom than at the oxygen atom. Therefore, we tentatively suggest that in hexaoxocyclotrithiazene the hydrogens will be associated with the nitrogen atoms.

b. Sulphur-oxygen ring system. From table 1 it can be seen that in both trimeric and monomeric sulphur trioxide, there is an electron drift from the sulphur to the oxygen atoms. As would be expected, this polarisation is more pronounced in the trimer where the sulphur is bonded to four oxygen atoms. The bonding situation in the $(SO_3)_3$ molecule is interesting, in that the S—O ring bonds are single, whilst the S—O exocyclic bonds are almost double in nature. There are only minor sulphur-sulphur intra-ring bonds, very limited electron delocalisation about the ring, and, consequently, any stabilisation due to electron conjugation will be small.

The electronic energies of the two species show that the trimer is unstable with respect to three monomer molecules. This is borne out by vapour pressure measurements [13] which indicate that at 72° the trimer is completely dissociated. Since here one molecule yields three by dissociation the entropy term also militates against polymerisation.

---

[11] D. R. ARMSTRONG, P. G. PERKINS and J. J. P. STEWART, *J. Chem. Soc.* (*Dalton*) submitted for publication.

[12] M. GOEHRING, and H. MALZ, *Z. Naturforsch*, **9 b**, 567 (1954).

[13] G. E. WALRAFEN, *J. Chem. Phys.*, **40**, 2326 (1964).

Finally, it is interesting to compare the isoelectronic species $(SO_3)_3$ and $(SNO_2)_3^{3-}$. In the former, as aforestated, there is single bonding about the ring and double bonding in the exocyclic bonds. In direct contrast the bonding in the anion consists of partial double bonding both around the ring and in the exocyclic bonds. The atomic valencies in $(SO_3)_3$ are internally satisfied whereas in $(SNO_2)_3{}^{3-}$ both the nitrogen and oxygen atoms are able to increase their valencies through electrophilic attack. We would therefore expect $(SO_3)_3$ to react *via* the breaking of the ring sulphur-oxygen bonds whilst $(SNO_2)_3^{3-}$ would suffer initial attack on the sulphur and nitrogen atoms without necessarily disrupting the S—N ring.

We thank the Scottish Education Department for a Maintenance Grant to R.C.W.K.

Revue Roumaine de Chimie, **18**, *12*, 2017 – 2020 (1973)

PHYSICO-CHEMICAL PROPERTIES OF MOLTEN SALTS OF SIGNIFICANCE TO MAGNESIUM ELECTROLYSIS

K. GRJOTHEIM, J. L. HOLM and H. A. ØYE

Institute of Inorganic Chemistry, The Norwegian Institute of Technology,
University of Trondheim, N-7034 Trondheim-NTH, Norway

Received June 1, 1973

The data on electrical conductivity, density, surface tension, viscosity, Gibbs free energy and wetting properties were surveyed and discussed in terms of ionic interactions in the alkali chloride-alkaline earth chloride mixtures.

The physico-chemical properties of the mixtures of alkali chlorides with alkaline earth chlorides [1–8] have been studied at our Institute. These mixtures are well-suited for studying the structural problems of molten salts. The wide range of properties of the salts, from the partially covalent $MgCl_2$ to the purely ionic CsCl, make these mixtures useful for evaluating structural models in ionic salts. A molten salt mixture of $MgCl_2-CaCl_2-NaCl-KCl$ often forms the basis for the electrolytic production of metallic magnesium, so these chloride mixtures are also of considerable technical interest.

The electrolyte used in the industrial production of magnesium is a compromise between material costs and several physico-chemical properties such as high electric conductivity, high density, low viscosity and low vapour pressure of magnesium and its chloride. Suitable surface properties that facilitate a good separation of liquid magnesium and chlorine gas are also important. With the present improved control of the electrolysis it is, however, possible to deviate from the more classical composition and add other exotic components, for instance $BaCl_2$ and LiCl.

---

[1] K. Grjotheim, J. L. Holm and J. Malmo, *Acta Chem. Scand.*, **24** , 77 (1970).

[2] K. Grjotheim, R. Nikolic and H. A. Øye, *Acta Chem. Scand.*, **24**, 489 (1970).

[3] D. Dumas, K. Grjotheim, B. Høgdahl and H. A. Øye, *Acta. Chem. Scand.*, **24** 510 (1970).

[4] B. Lillebuen, *Acta Chem. Scand.*, **24**, 3072, 3287 (1970).

[5] H. Ikeuchi and C. Krohn, *Acta Chem. Scand.*, **23**, 2230 (1970).

[6] K. Grjotheim, J. L. Holm B. Lillebuen and H. A. Øye, *Trans. Faraday Soc.*, **67**, 640 (1971).

[7] K. Grjotheim, J. L. Holm, B. Lillebuen and H. A. Øye, *Acta Chem. Scand.*, **26**, 2050 (1972).

[8] K. Grjotheim, A. H. Schultz and H. A. Øye, *Metall*, **26**, 236 (1972).

The following properties have been investigated:

a) *Electrical conductivity* by using an aluminium oxide capillary with a cell constant of about 50 cm^{-1}, coupled to a Wheat stone — Wagner bridge.[2]

b) *Density* by measuring the buoyancy of a platinum bob immersed in the melt.[6]

c) *Surface tension* by determining the force needed to free a platinum rod attached to the platinum bob. The surface tension was calculated from the weight of liquid lifted by the pin.[4,7]

d) *Viscosity* from the measurements of the damping of an oscillating platinum sphere.[3]

e) *Gibbs free energy* of magnesium chloride from the EMF of formation cells with magnesium and chlorine electrodes.[5]

f) *Phase diagrams* from differential thermal analysis.[1]

g) *Wetting properties* by measuring the contact angles between: Solid-salt melt-gas, solid-molten magnesium-gas, and solid-salt melt-liquid magnesium, the solids being iron, graphite and LAVA (basically a magnesium silicate produced by The American Lava Co.) and using argon and chlorine as the gas.[8]

The first four properties of the binary mixtures can be discussed in terms of excess functions:

$$F^E = F^{\text{exp}} - (X_1F_1^0 + X_2F_2^0) \qquad (1)$$

where X is the mole fraction, F^{exp} our experimental values and F^0 the property of the pure salts respectively. The excess values for some of the most interesting systems are given in fig. 1.

The discussion of the results may be based on the relative influence of the following four different effects:

a) The change in Coulomb forces by a mixing of cations with different sizes, this causing a decrease in the cation-cation repulsion.

b) The asymmetric polarization of the anion by the smallest cation, which strengthens this bond, while the bond between the other cation and the anion is weakened. Such species as $MgCl_4^{2-}$ are also formed.

c) The reduction of the covalent character of pure $MgCl_2$ by additions of $CaCl_2$ or an alkali chloride. By additions of one of these chlorides, the partly covalent structure of $MgCl_2$ in the molten state is ionized and thereby destroyed.

d) First order deviation from simple additivity of the surface tension is negative. This is expected in ideal mixtures, because the component with the lowest surface tension will be enriched on the surface.

The data for the ternary systems were compared with the calculated values from the corresponding three binary systems. The binary systems used in the calculation are chosen by drawing perpendiculars on the sides of a ternary triangular composition diagram, alternately through the corners. Good agreement was obtained without addition of further excess terms.

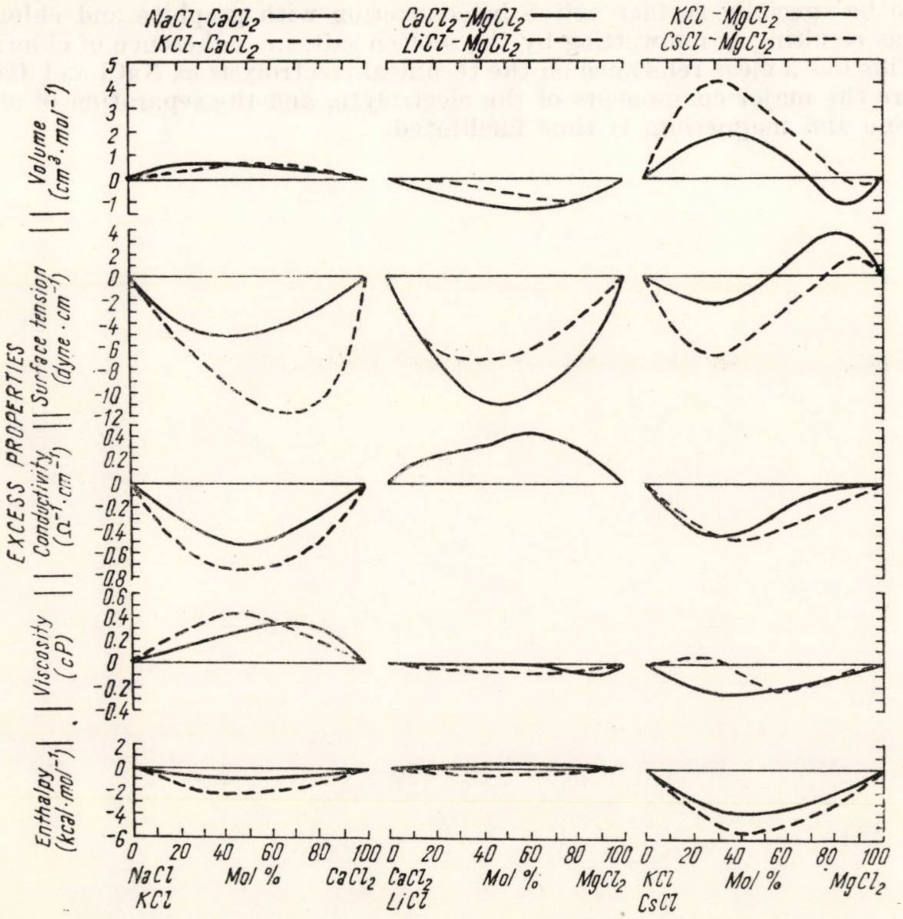

Fig. 1. — The following excess properties: volume, surface tension, conductivity and viscosity are calculated according to the equation for excess function:

$$F^{E} = F^{\exp} - (X_1F_1^0 + X_2F_2^0)$$

The enthalpy data are taken from Kleppa *et al.*: *J. Phys. Chem.*, **70**, 1249 (1966) and *J. Chem. Phys.* **47**, 2014 (1967), and T. Østvold: "A Thermodynamic Study of Some Fused Salt Mixtures Containing Alkali and Alkaline Earth Chlorides, Bromides and Iodides", Thesis, NTH 1971.

The study of the wetting properties did support the simple model for calculation of wetting angles from the surface and interfacial tensions:

$$\text{Cos } \theta_{s,i} = \frac{\gamma_{s,i} - \gamma_{s,j}}{\gamma_{ij}} \tag{2}$$

where θ is the wetting angle, s stands for the solid phase and i and j represent any two of the three combinations of the viscous phases: melt, liquid magnesium and gas. From our results NaCl and $CaCl_2$ seem to be specially surface active in connection with graphite and chlorine gas resulting in nonwetting by the molten salt, i.e. adherence of chlorine. This has a clear relevance on the technical electrolysis as NaCl and $CaCl_2$ are the major components of the electrolyte, and the separation of chlorine and magnesium is thus facilitated.

Revue Roumaine de Chimie, **18**, *12*, 2021–2029 (1973)

ELECTROPLATING OF COPPER FROM PYROPHOSPHATE BATHS. II [1]

THE EFFECT OF ELECTROLYTE TEMPERATURE

O. RADOVICI, CECILIA VASS and I. SOLACOLU

Centre of Physical Chemistry, str. Galați 31, Bucharest 13, Romania

Received April 23, 1973

The electroplating process of copper from a pyrophosphate bath has been studied in the temperature interval 25–80°, for the pH ranging between 6.5–8.5, using the potentiostatic technique. The activation enthalpy values for the anodic and cathodic process have been calculated. The temperature effect on the cathodic efficiency was studied. The structure of copper deposits has been microscopically studied and the limit of bright deposits range was established.

As shown in a previous paper [1] the electrolyte temperature is an important parameter in the pyrophosphate electrolyte baths. There are only a few papers on the temperature influence upon the copper electroplating process from different baths.[2–5] The temperature has a considerable influence in the pyrophosphate electrolyte baths both on the electrode polarization,[6,7] the cathodic efficiency and throwing power of the bath.[8]

In the present paper we deal with the temperature effect of the copper deposition pyrophosphate electrolyte on the anodic and cathodic polarization, cathodic efficiency and deposit structure.

1. EXPERIMENTAL

The working cell, electrodes and working solutions preparation, potentiostatic polarization measurements, cathodic efficiency determination and the deposit structure study have been previously described.[1]

---

[1] O. RADOVICI, C. VASS and I. SOLACOLU, *Rev. Roumaine Chim.*, **18**, 1325 (1973).

[2] D. N. GRITSAN and A. M. BULGAKOVA, *Zhur. fiz. Khim.*, **29**, 649 (1955).

[3] G. E. EMELIANENKO, *Doklady Akad. Nauk S.S.S.R.*, **105**, 1003 (1955).

[4] N. T. PAMPHYLOV, *Ukrain. khim. Zhur.*, **26**, 174 (1960).

[5] J. W. FAUST, *J. Cryst. Growth*, **1968**, 433.

[6] A. T. VAGRAMYAN and E. K. YASTREBOVA, *Zhur. fiz. Khim.*, **39**, 865 (1965).

[7] B. M. DIKOVA and N. T. KUDRYAVTSEV, *Khim. Ind. (Sofia)*, **1970**, 255.

[8] J. W. DINI, H. R. JOHNSON and J. R. HELMS, *Plating*, **54**, 1337 (1967).

The temperature working range was between 25 and 80°, the precision of thermosetting device being of ±0.1°.

The temperature effect on copper electroplating process for different values of electrolyte pH in the range 6.5–8.5 has been studied.

2. RESULTS AND DISCUSSION

2.1. THE EFFECT OF ELECTROLYTE TEMPERATURE ON THE ELECTRODE POLARIZATION

In figures 1, 2 and 3, the anodic and cathodic polarization curves for different temperatures in the range 25–80° and for electrolyte of pH 6.5, 7.5 and 8.5 respectively, in potentiostatic conditions, are shown.

Examination of these figures shows that increasing temperature always produces a decrease of the cathodic and anodic polarization of the process. The influence of temperature is more important in the range 40–60°.

The temperature effect on the polarization is better seen from the plots of the cathodic (fig. 4) and anodic (fig. 5) overpotential variation *versus* electrolyte temperature, for different current densities.

From the examination of curves in fig. 4, it comes out that the increase of temperature has a strong effect on the decreasing in polarization values, especially within the 40–60° range. The increase of the current density entails an attenuation of inflexions but the temperature effect remains the same all throughout the studied range, which can be accounted for by the increasing of the percent ohmic polarization in the total polarization of the cathodic process.

In the anodic range (fig. 5) the curves present considerable decreases up to 40°, the temperature effect within the 40–80° range being smaller.

At temperatures higher than 60° it is well known that appreciable losses of ammonia from the bath take place, which restrict the working temperature to values under this limit.

2.2. ACTIVATION ENTHALPIES

In order to calculate the values of activation enthalpies of the electrochemical processes, η was plotted *vs.* log i for each pH value and working temperature. From the extrapolation of the linear portions of the plots, the exchange current densities (i_0) were calculated; in figures 6 and 7, these plots for electrolyte solution with pH 7.5 for the cathodic and respectively, anodic process are given.

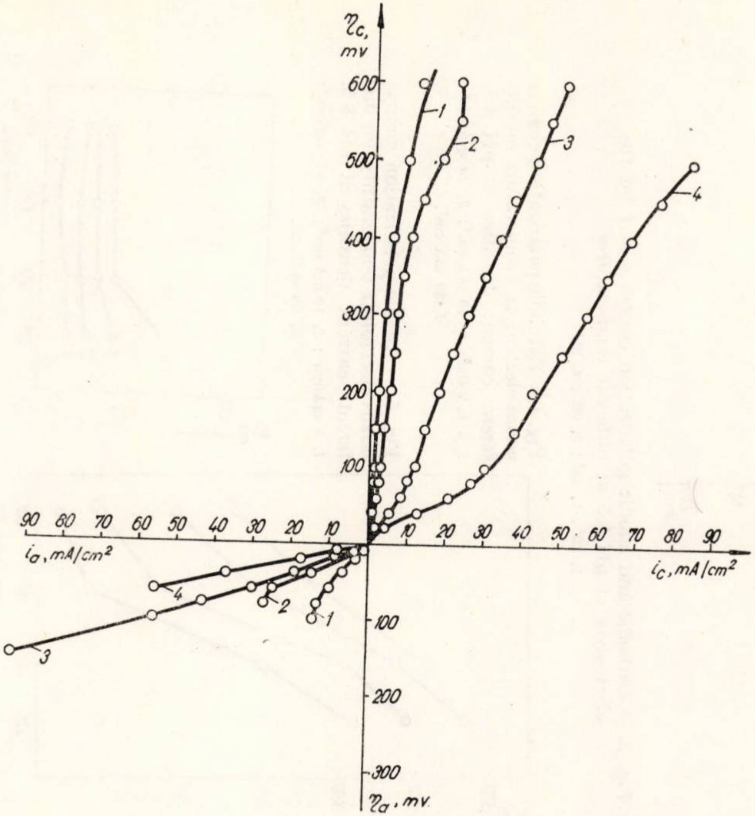

Fig. 1. – Cathodic and anodic polarization curves η *vs.i* for the electrolyte of pH 6.5 at different temperatures,
1, 25°; *2*, 40°; *3*, 60°; *4*, 80°,

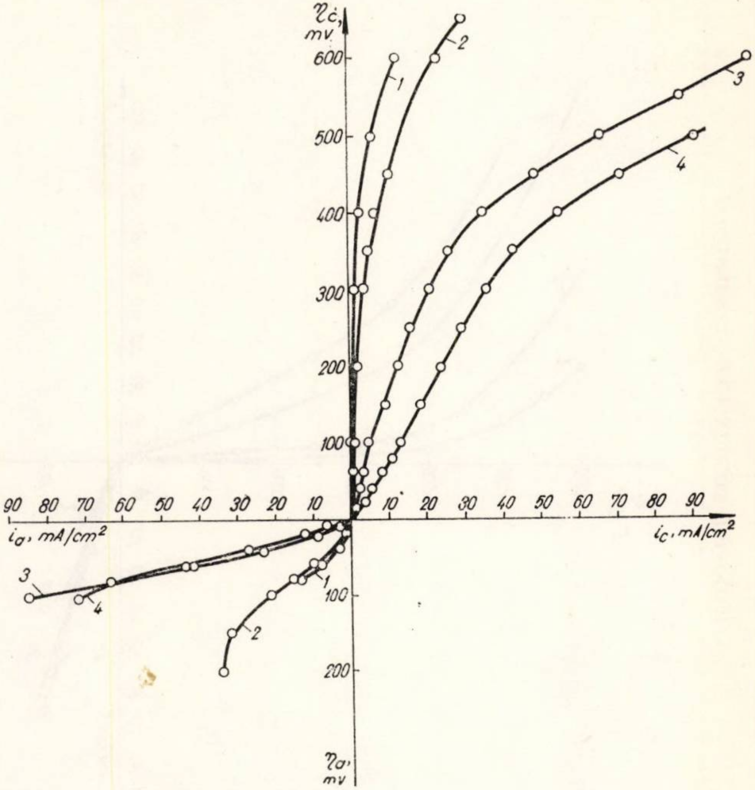

Fig. 2. – Cathodic and anodic polarization curves η *vs.i* for the electrolyte of pH 7.5 at different temperatures,
1, 25°; *2*, 40°; *3*, 60°; *4*, 80°,

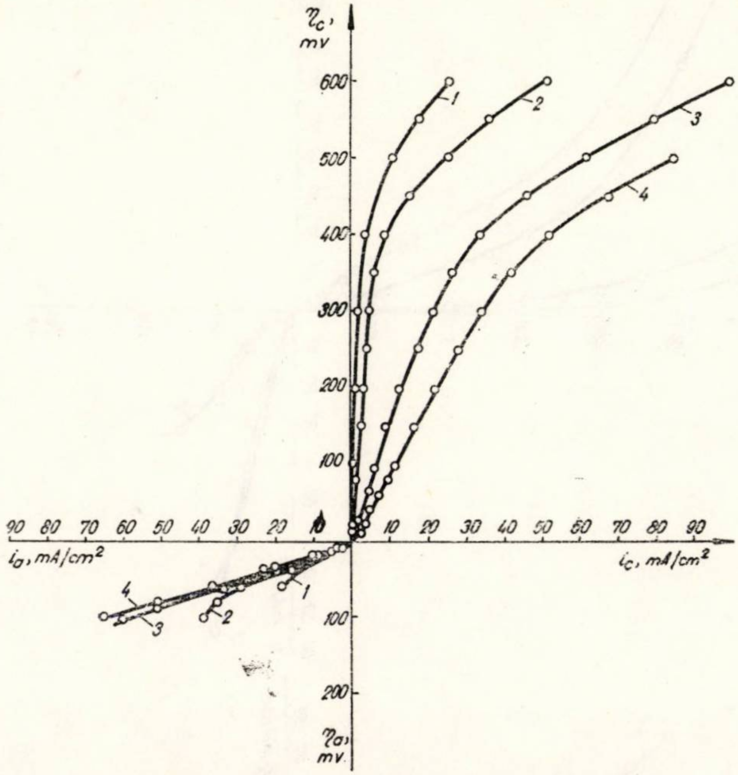

Fig. 3. — Cathodic and anodic polarization curves η *vs.i* for the electrolyte of pH 8.5 at different temperatures.
1, 25°; *2*, 40°; *3*, 60°; *4*, 80°.

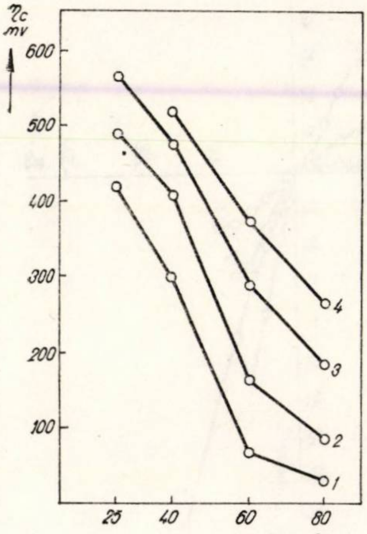

Fig. 4. — Cathodic polarization change *versus* electrolyte temperature for different current densities at pH 8.5.
1, 5 mA/cm²; *2*, 10 mA/cm²; *3*, 20 mA/cm²; *4*, 30 mA/cm².

Fig. 5. — Anodic polarization change *versus* electrolyte temperature for different current densities at pH 8.5.
1, 5 mA/cm²; *2*, 10 mA/cm²; *3*, 15 mA/cm²; *4*, 20 mA/cm².

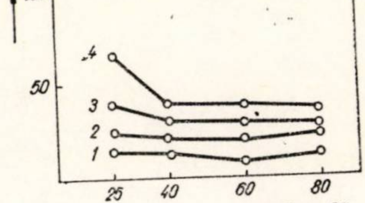

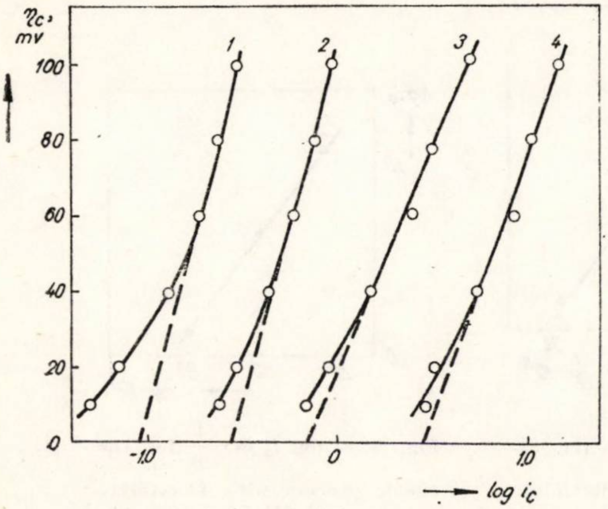

Fig. 6. $-\eta$ *vs*.log *i* curves for the cathodic process with electrolyte of pH 7.5.
1, 25°; *2*, 40°; *3*, 60°; *4*, 80°.

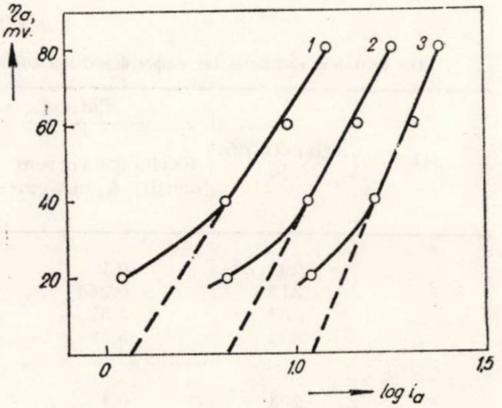

Fig. 7. $-\eta$ *vs*.log *i* curves for the anodic process with electrolyte of pH 7.5.
1, 40°; *2*, 60°; *3*, 80°.

The activation enthalpies (table 1) for the cathodic and, respectively, anodic process, at pH 7.5, were calculated from the plots log i *versus* $\frac{1}{T}$, presented in figs. 8 and 9; use has been made of the equation:

$$\frac{\partial \ln i_0}{\partial \frac{1}{T}} = -\frac{\Delta H}{R}$$

Examination of the exchange current values and of the activation enthalpies for the copper plating from complexing solution shows a considerable variation of these magnitudes with electrolyte pH. As the deposition reaction depends on pH it is clear that the mechanism of the process

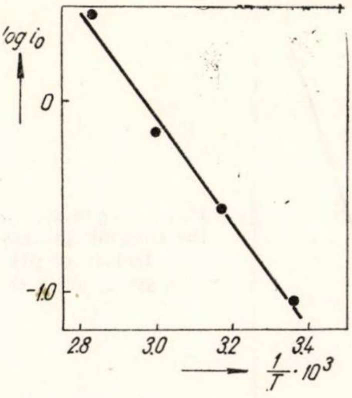

Fig. 8. — log i_0 *vs*. $\frac{1}{T}$ for the cathodic process with electrolyte of pH 7.5.

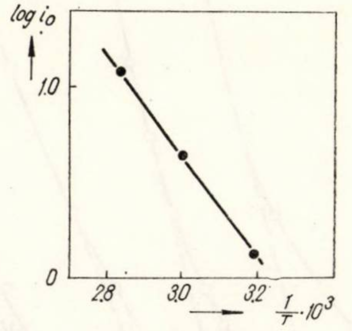

Fig. 9. — log i_0 *vs*. $\frac{1}{T}$ for the anodic process with electrolyte of pH 7.5.

Table 1

The activation enthalpies for copper deposition and dissolution process from pyrophosphate electrolytes

pH	Temperature °K	Cathodic range		Anodic range	
		Exchange current density i_0, mA/cm^2	ΔH kcal/mole	Exchange current density i_0, mA/cm^2	ΔH kcal/mole
6.5	298 313 333 353	0.1 0.263 1.32 5.49	16.45	3.31 7.58 13.06 13.31	8.06
7.5	298 313 333 353	0.1 0.275 0.69 2.88	12.43	— 1.31 4.36 12.82	12.11
8.5	298 313 333 353	0.26 0.36 1.19 2.37	10.41	— 12.76 13.0 13.1	3.45

involves complex ions, in other words that the electronic charge transfer reaction originates in the complex. Under these circumstances a deposition mechanism may be suggested with the consideration of copper complexes which may exist at different pH's of the electrolyte. Thus, at pH 8.1, with alkaline pyrophosphate excess two complexes of the pyrophosphate with Cu^{2+} are known[9]: $[Cu(P_2O_7)]^{2-}$ and $[Cu(P_2O_7)_2]^{6-}$ (the existence of a Cu^+ pyrophosphate complex has not been evidenced). In the presence of ammonia a series of complexes are formed of which we mention: $[Cu(NH_3)_4]^{2+}$, with maximum coordination number of Cu^{2+} and $[Cu(NH_3)_2]^+$ the corresponding complex of Cu^+. These complexes are formed in solutions with pH values higher than 8.1.

---

[9] N. P. Sneed, "Comprehensive Inorganic Chemistry", vol. II, van Nostrand, New York, 1959, p. 94.

Obviously there are also mixed complexes in solution, of the pyrophosphate-ammino type $[Cu(P_2O_7)(NH_3)_2]^{2-}$ but to establish the deposition mechanism one assumes the existence only of the two main types of complex ions, i.e. pyrophosphoric anions and ammino cations.

Thus, it is obvious that for the reduction of an anion at the cathode a higher activation enthalpy is necessary (since in the neighbourhood of the electric double layer there is a tendency of electrostatic repulsion between the anion and the negatively charged metallic surface) than for the reduction of a cation which can come closer to the electrode. That is clearly shown by the activation enthalpies at pH 6.5 and 7.5, where the double layer is made of pyrophosphoric anions and at pH 8.5 where it consists from ammino anions; their enthalpies are 16.45, 12.43 and 10.41 kcal/mole, respectively.

Since the stability constant of pyrophosphoric anions is 4–10 and that of the ammino-cations of the order of $4 \cdot 10^{12}$ [10] we suppose that the deposition mechanism does not involve dissociation reactions of the complex with formation of simple ions which have to be reduced to metal, but directly, metal deposition from the complex.

We further suggest the characteristic consecutive reactions, for both anion and complex cation reduction:

$$\text{a)}\ [Cu(P_2O_7)_2]^{6-} \underset{\text{rapid}}{\overset{-P_2O_7^{4-}}{\rightleftarrows}} [Cu(P_2O_7)]^{2-} + e^- \xrightarrow[\text{slow}]{}$$

$$\longrightarrow \underset{\text{unstable}}{[Cu(P_2O_7)]^{3-}} + e^- \underset{\text{rapid}}{\rightleftarrows} Cu + P_2O_7^{4-}$$

Since no pyrophosphoric complex of Cu^+ has undoubtedly been evidenced in the above consecutive reactions we considered it an unstable product. Thus, it comes out clearly that the slowest step of the process is the transfer reaction of the first electron, which leads to this unstable complex.

As to the deposition of the metallic ion from the ammino-complex, the step reduction of the complex seems possible since the ammino-monovalent copper complex is very stable. Accordingly, the sequence of the charge transfer reactions is:

$$\text{b)}\ [Cu(NH_3)_4]^{2+} + e^- \underset{\text{rapid}}{\rightleftarrows} [Cu(NH_3)_2]^+ + 2\ NH_3\uparrow \xrightarrow[\text{slow}]{+e^-} Cu + 2\ NH_3\uparrow$$

At pH 7.5 the activation enthalpy for the anodic process takes a value practically equal to that for the cathodic process, which indicates the identity of the two processes. The low activation enthalpy at pH 8.5 (3.45 kcal/mole) as compared to 12.1 kcal/mole for pH 7.5 can be explained by the existence of the ammonia within the anodic compartment and, hence, the forming of the ammino-complex more stable than the pyrophosphoric complex. This cationic complex $[Cu(NH_3)_4]^{2+}$ makes also the transfer reaction more rapid, the slow step being determined by diffusion. The relatively lower value of the activation enthalpy for the anodic process found for the electrolyte with pH 6.5 (approximately 8 kcal/mole) is due to the appearance of secondary processes which facilitate the copper anodic solving, but whose result is the appearance of a copper pyrophosphate precipitate in the anodic compartment.

---

[10] A. J. BARD, "Chemical Equilibrium", Harper and Row, London, 1966, p. 192.

2.3. THE ELECTROLYTE TEMPERATURE INFLUENCE ON THE CATHODIC EFFICIENCY

In order to check up the influence of electrolyte temperature upon the cathodic efficiency of the process, the current efficiencies at several temperatures for an electrolyte of pH 8.2 and current densities between 20 and 40 mA/cm² have been calculated (fig. 10).

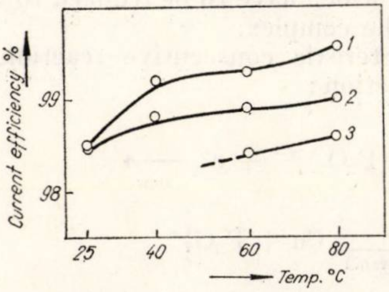

Fig. 10. — Cathodic efficiency change with temperature for an electrolyte of pH 8.2.

1, i_c = 20 mA/cm²; *2*, i_c = 30 mA/cm²; *3*, i_c = 40 mA/cm².

Examination of fig. 10 indicates that the increasing of electrolyte temperature has a favourable effect upon cathodic efficiency. Thus, for 20 mA/cm² current density, the current efficiency lies between 98.5 and 99.6 at 25 and 80°, respectively.

Although the maximum values of current efficiencies correspond to 80°, 60° is recommended as working temperature since this way important ammonia losses are avoided without an important efficiency decrease.

2.4. THE EFFECT OF ELECTROLYTE TEMPERATURE UPON THE STRUCTURE OF DEPOSITS

In order to establish the influence of electrolyte temperature on the structure of copper deposits from pyrophosphate baths, depositions on zamak supports have been made with an electrolyte of pH 8.5 at temperatures between 40 and 80° and current densities of 20 and 50 mA/cm².

Fig. 11 — The copper deposits structure from pyrophosphate electrolyte of pH 8.5 ; temperature 40°, $i_c =$ 30 mA/cm². Microphotograph, 500 X.

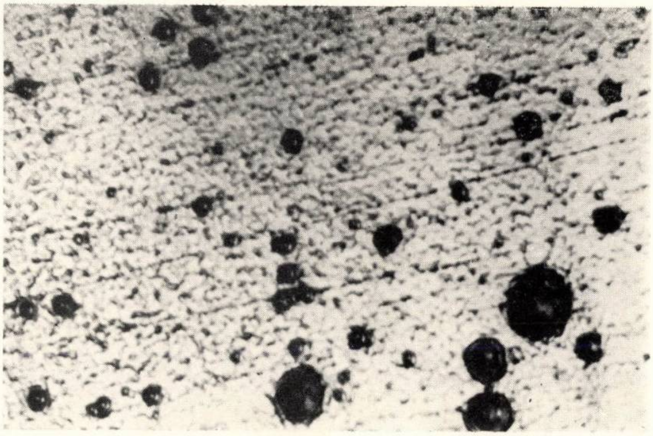

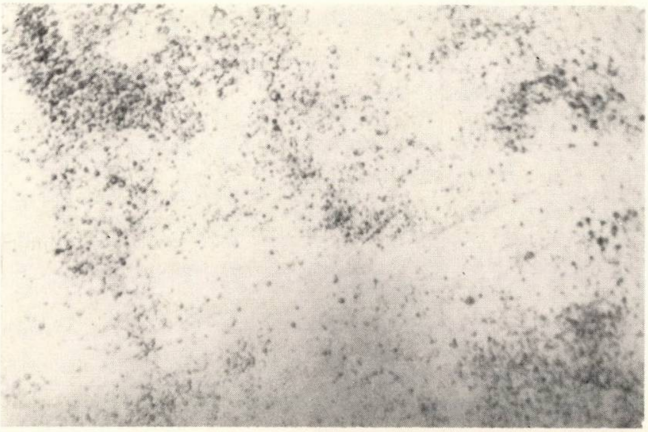

Fig. 12. — The copper deposits structure from pyrophosphate electrolyte of pH 8.5 ; temperature 60° ; $i_c =$ 30 mA/cm². Microphotograph, 500 X.

Fig. 13. — The copper deposits structure from pyrophosphate electrolyte of pH 8.5 ; temperature 40° ; $i_c =$ 40 mA/cm². Microphotograph, 500 X.

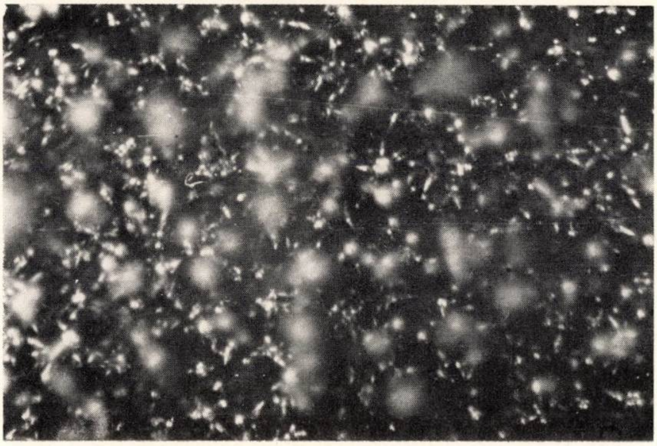

Fig. 14. — The copper deposits structure from pyrophosphate electrolyte of pH 8.5 ; temperature 60° ; i_c= 40 mA/cm². Microphotograph, 500 X.

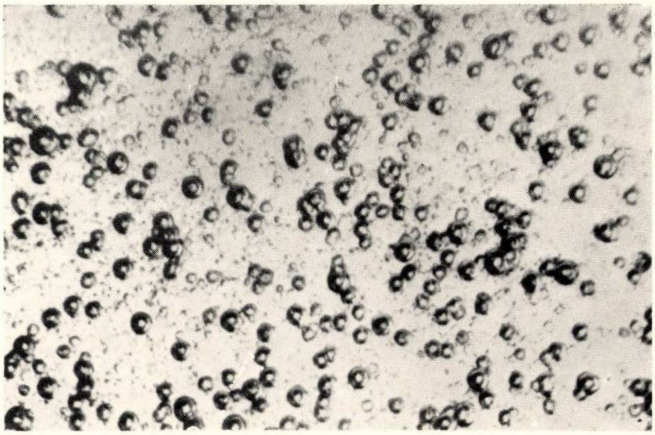

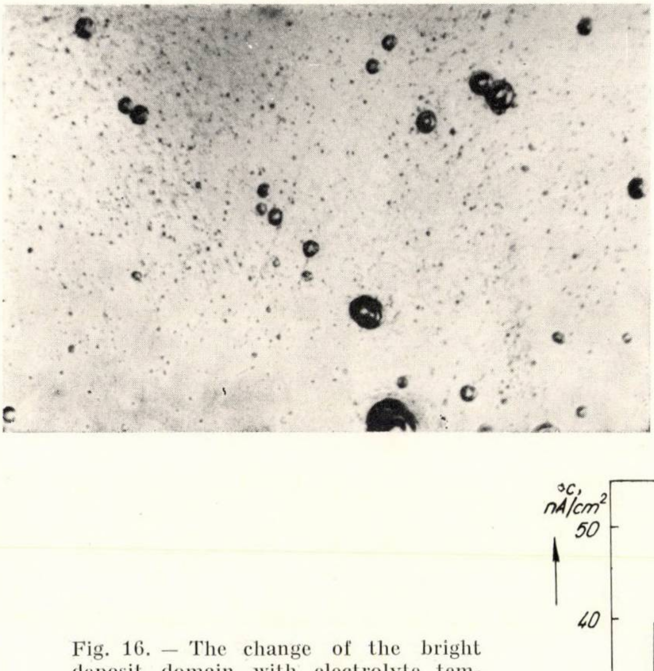

Fig. 15. — The copper deposits structure from pyrophosphate electrolyte of pH 8.5 ; temperature 80° ; i_c= 45 mA/cm². Microphotograph, 500 X.

Fig. 16. — The change of the bright deposit domain with electrolyte temperature at pH 8.5.

a, bright deposits ; *b*, semi-bright deposits ; *c*, mat deposits.

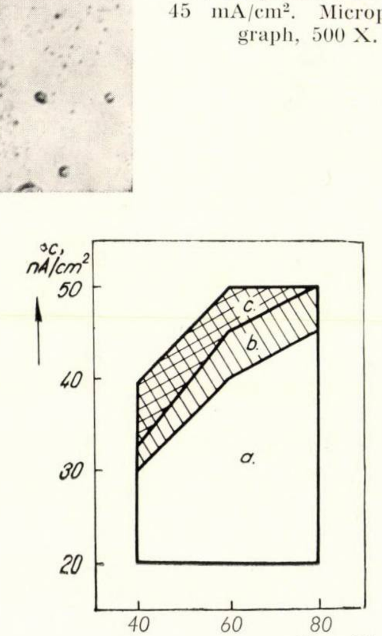

The structure of deposits has been examined by a reflexion metallographic microscope. Figures 11–15 present the microphotographs of deposits obtained in these conditions at 500 X magnification.

Examination of these microphotographs shows :

— the increasing of electrolyte temperature has a favourable effect on the structure of deposits : thus, at current densities of 30 mA/cm^2 the depositions are semi-bright at 40° and very bright at 60° (fig. 12), while at 40 mA/cm^2 the depositions are rough at 40° and semi-bright at 60° (fig. 14) ;

— at 80° bright depositions are obtained even at 45 mA/cm^2 (fig. 15).

To illustrate the effect of electrolyte temperature on the deposit structure, the extent of bright domain *vs.* temperature has been plotted in fig. 16, for an electrolyte pH of 8.5.

3. CONCLUSIONS

1. The electrolyte for copper deposition based on pyrophosphate may function in good conditions within a 40–80° temperature range.

2. The increase of electrolyte temperature brings about a reduction of cathodic and anodic polarization, the process taking place at high speed at temperatures above 40°.

3. The activation enthalpies for the overall electrochemical processes take values ranging between 10.4 and 16.5 kcal/mole and 3.45 and 12.1 kcal/mole for the cathodic and anodic processes respectively, depending on pH's.

4. The cathodic efficiency of the process increases with the working temperature. For a current density of 20 mA/cm^2 the current efficiency ranges between 98.5 and 99.6 for 25 and 80°, respectively.

5. Rising temperature over 60° is not recommended because of important ammonia losses.

6. The deposits are bright and with fine structure for current densities between 30 and 45 mA/cm^2 and temperatures between 40 and 80°, respectively.

Revue Roumaine de Chimie, **18**, *12*, 2031–2035 (1973)

ON THE LOGARITHMIC LAW USED IN THE KINETICS OF THE SOLID-GAS CHEMISORPTION PROCESSES

N. I. IONESCU and B. AURIAN-BLĂJENI

Institute of Physical Chemistry, Bucharest, str. Galaţi 31, Romania

Received January 13, 1973

The nonequivalence of the physical models leading to the integral and differential form of the logarithmic law used for the kinetic description of the solid-gas chemisorption processes is suggested. A generalization of the model leading to the integral form is obtained. This generalization might explain the use of the integral form of the logarithmic law in various fields.

The formal kinetics of chemisorption phenomena onto solid surfaces is dominated by the logarithmic law used either in its integral form:

$$q = \frac{1}{b} \ln (t + t_0) - \ln t_0 \tag{1}$$

or in its differential one:

$$\frac{\mathrm{d}q}{\mathrm{d}t} = a \exp(-bq) \tag{2}$$

where q the chemisorbed gas quantity at the t moment, a, b are constants and $t_0 = \frac{1}{ab}$, if for $t = 0, q = 0$.[1,2]

In order to justify the logarithmic equation, many models have been proposed. These models can be classified, by an attentive analysis, into three classes, the third one being nothing else than a combination between the first and the second class.[3] In the two independent classes of models the validity of the conventional kinetic formulation for a gas in contact with a set of unoccupied adsorption sites was proposed.[4]

In the present paper we aim at studying some problems concerning the existence of these first two classes of models.

---

[1] J. Zeldovich, *Acta Physicochim. U.R.S.S.*, **1**, 449 (1934).

[2] S. Z. Roginsky and J. Zeldovich, *Acta Physicochim. U.R.S.S.*, **1**, 554 (1934).

[3] C. Aharoni and F. C. Tompkins, *Adv. Catalysis*, **21**, 1 (1970).

[4] A. M. Peers, *J. Catalysis*, **4**, 672 (1965).

RESULTS AND DISCUSSION

If the chemisorption process is assimilated with a probabilistic discontinuous process Q, which progresses in discrete steps in a background of fluctuations, the most general formulation of the first class of models is[5] :

$$\frac{\mathrm{d}Q}{\mathrm{d}t} = Np \qquad -\frac{\mathrm{d}p}{\mathrm{d}t} = kNp^2 \tag{3}$$

where N is the number of events per unit time which are, in principle, capable of carrying the process forward, but have only a probability $p = p(t)$ of doing so and k a constant. The physical signification of N and p from the equations (3) in the chemisorption process is that of the number of impacts by gas molecules with the surface expressed per unit area per unit time and the number of unoccupied centers, respectively.

By integrating equations (3) one obtains a relationship analogous to (1). It is worth mentioning that the differential form of the logarithmic law is not directly justified by the first class of models; this is possible only by the use of an intermediate: the integral form.

The models from the second class assume that the activation energy of chemisorption E_a increases linearly with the coverage degree of the surface θ, according to:

$$E_a = E_0 + \alpha\theta(t) \tag{4}$$

where E_0 is the activation energy of chemisorption on the clean surface, t the time and α a constant.

The expression (4) of the activation energy is then introduced in the relation[6]:

$$\frac{\mathrm{d}q}{\mathrm{d}t} = \frac{\sigma p}{(2\pi\, mkt)^{1/2}} f(\theta) \exp(-E_a/RT) \tag{5}$$

where σ is the sticking probability of a molecule with the energy E_a, on a free surface site, p the gas pression, m the mass of a single gas molecule and $f(\theta)$ a function of the coverage. With the aid of some hypotheses concerning $f(\theta)$[6] one obtains a relationship analogous to (2). In this case too, it is worth mentioning that by this model one cannot obtain directly the integral form of the logarithmic law (1); this is possible only by using an intermediate: the differential form (2).

---

[5] P. T. Landsberg, *J. Appl. Phys.*, **33**, 2251 (1962).

[6] D. O. Hayward and B. M. W. Trapnell, "Chemisorption", 2nd Ed., Butterworths, London, 1964, chap. III.

The models of the third class lead to type (2) equations.[3] This fact may suggest the idea that the models based on the activation energy are more closed to the reality of the chemisorption phenomena.

These observations can be schematically represented in figure 1.

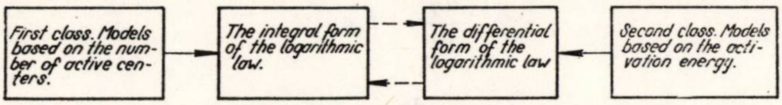
First class. Models based on the number of active centers.
The integral form of the logarithmic law.
The differential form of the logarithmic law
Second class. Models based on the activation energy.

Fig 1. — The relative positions of the forms of the logarithmic law and their generating classes of models.

The fact that each of the two presented classes of models justifies directly only a form of the logarithmic law suggests the physical nonequivalance of the models. Moreover, the possibility to pass reversibly from the form (1) to the form (2) suggests that the fitting of the experimental data with the theoretical ones obtained from a curve described by these equations does not offer conclusive indications about the mechanism of the chemisorption process.[7]

Indeed, from the verification of one of the forms of the logarithmic law it does not result unequivocally its generating class of models, owing to the mathematical equivalence of the relations (1) and (2). That is why, when a mechanism of chemisorption is looked for a justification of the logarithmic law, it should be considered which of its forms, (1) or (2), is taken into account.

Let us return to the first class of models and let be a process in which the chemisorption of a particle leads to the invalidation not of one active site but more, as it occurs, for instance, in the chemisorption of simple gases on inorganic semiconductors.

If ZnO is considered, as an example, then from the 10^{15} free sites/cm^2 only $10^{13}-10^{14}$ sites/cm^2 are occupied by oxygen chemisorption, that is 1—10% of the total number of sites.[8] The disappearance of more than one free site for a single adsorbed particle is equivalent with the association of several sites which can act as a single one in the chemisorption process.

It can be admitted that the association of sites is given by :

$$s = s\,(n) \tag{6}$$

where s is the number of associated free sites and n the number of single free sites, whose variation is supposed to have the form :

$$\frac{\mathrm{d}n}{\mathrm{d}t} = g\,(n) \tag{7}$$

where $g(n)$ is an arbitrary function, depending singly on n.

---

[7] I. S. McLintock, *J. Catalysis*, **16**, 126 (1970).

[8] K. Hauffe and R. Stechemesser, in "Symposium on Electronic Phenomena in Chemisorption and Catalysis on Semiconductors". Moscow, 1968, Walter de Gruyter, Berlin, 1969, p. 1.

If the chemisorption mechanism on single sites is admitted to be valid for the associated sites also, then the kinetic equations of the chemisorption process, according to the first class of models, are:

$$\frac{\mathrm{d}q}{\mathrm{d}t} = k_1 s \tag{8a}$$

$$-\frac{\mathrm{d}s}{\mathrm{d}t} = k_2\, s^2 \tag{8b}$$

$$s = s\,(n) \tag{8c}$$

$$\frac{\mathrm{d}n}{\mathrm{d}t} = g\,(n) \tag{8d}$$

The relation (8 c) leads to:

$$-\frac{\mathrm{d}s}{\mathrm{d}t} = -\frac{\mathrm{d}s}{\mathrm{d}n}\cdot\frac{\mathrm{d}n}{\mathrm{d}t} = -\frac{\mathrm{d}s}{\mathrm{d}n}\cdot g\,(n) \tag{9}$$

which, by comparison with equation (8b), gives:

$$-\frac{\mathrm{d}s}{\mathrm{d}n}\, g\,(n) = k_2\, s^2 \tag{10}$$

By integrating equation (10) we obtain:

$$\int_{s(n_0)}^{s(n)} \frac{\mathrm{d}s}{s^2} = k_2 \int_{n_0}^{n} \frac{\mathrm{d}n}{g\,(n)} \tag{11}$$

or:

$$\frac{1}{s} - \frac{1}{s_0} = k_2 \int_{n_0}^{n} \frac{\mathrm{d}n}{g\,(n)} \tag{12}$$

where $s_0 = s\,(n_0)$.

By introducing the expression of $s(n)$ in the relation (8a) we obtain:

$$\frac{\mathrm{d}q}{\mathrm{d}t} = s_0\, k_1 \left[\; k_2\, s_0 \int_{n_0}^{n} g^{-1}\;(n)\,\mathrm{d}n + 1 \right]^{-1} \tag{13}$$

From the relation (13) it results that the only condition which must be fulfilled by the proposed model is the integrability of the function $g^{-1}(n)$ in the interval (n_0, n). The great number of arbitrary functions satisfying this condition, some of which are presented in table 1, might constitute an explanation of the variety of different physical and chemical processes, obeying a (1)-type equation. Some of these fields have been recently reviewed.[7]

From the examination of table 1, where a, b, c, and r are constants, it results that, independently of the form of the free sites time variation law, the gas chemisorption on associated sites occurs, from the formal kinetics view-point, alike the gas chemisorption on single free sites, which also follows a logarithmic law. The only condition, in this case, is to respect the equation (8 b), the essential element of the model.

Table 1

Some functions leading to the logarithmic law

$g(n)$	n	$q \cdot \frac{k_2}{k_1}$
a	$\mathrm{at} + n_0$	$\ln[k_2 s_0 t + 1]$
bn	$n_0 \exp\ (\mathrm{bt})$	$\ln[k_2 s_0 t + 1]$
cn^r	$[ct(1 - r) + n_0^{1-r}]^{\frac{1}{1-r}}$	$\ln[k_2 s_0 t + 1]$
$\exp(n)$	$-\ln[\exp(-n_0) - t]$	$\ln[k_2 s_0 t + 1]$

In conclusion we consider that the impossibility to propose a chemisorption mechanism only on the basis of fitting the experimental data with the logarithmic law could be due both to the physical nonequivalence of the models which lead to the two forms, the differential and the integral one, and to the generalized proposed model, because more physically different mechanisms could be described in their kinetic evolution by the same formalism.

Revue Roumaine de Chimie, **18**, *12*, 2031–2035 (1973)

Revue Roumaine de Chimie, **18**, *12*, 2037 – 2038 (1973)

GAS CHROMATOGRAPHIC SEPARATION OF FORMIC ALDEHYDE, METHYL ALCOHOL, WATER AND HYDROGEN PEROXIDE

MELANIA BOZEŞANU

Centre of Physical Chemistry, Str. Galaţi nr. 31, Bucharest, Romania

Received January 30, 1973

CH_2O, CH_3OH, H_2O and H_2O_2 mixture was separated on a column filled with polyethylene glycol 20 M (Carbowax 20 M).

The study of the oxidation reaction of methane has raised the problem of a rapid method of chromatographical analysis of aqueous solutions of formic aldehyde, methyl alcohol and hydrogen peroxide.

The speciality literature [1] shows that formic aldehyde, methyl alcohol and water mixture were separated satisfactorily on a column filled with di-2-ethylhexylsebacate. However, no data on the chromatographic analysis of hydrogen peroxide are found as yet. (In the oxidation products of methane, hydrogen peroxide has been spectrophotometrically identified due to the complex formed with the titanium sulphate in acid medium).

Polyethylene glycol 400 has been also used in the chromatographical analysis of methyl alcohol and formic aldehyde,[1,2] while Carbowax 20 M in the chromatographic analysis of formic aldehyde.[3]

The present note brings forward the method of gas-chromatographical separation of aqueous solutions of formic aldehyde, methyl alcohol and hydrogen peroxide, on columns with polyethylene glycol type packings.

EXPERIMENTAL

The analyses have been performed on a CARLO ERBA type chromatograph AtC/t 400 (with thermistors). As carrier, argon was used with a 75 cm^3/min flow.

The substances used as packings have been provided by the firm CARLO ERBA, while the formic aldehyde, methyl alcohol and hydrogen peroxide used for calibrations, by the firm MERCK. The concentration of hydrogen peroxide was 25 % in weight.

---

[1] I. Iosif and I. A. Schneider, *Rev. Roumaine Chim.*, **9**, 445 (1964).

[2] G. Kyriacos, H. R. Menepace and C. E. Board, *Analyt. Chem.*, **31**, 222 (1959).

[3] I. Schepartz and P. E. Mc.Dowell, *Analyt. Chem.*, **32**, 723 (1960).

RESULTS AND DISCUSSION

The first experimental column, 1 m in length (inner diameter 4 mm) has been prepared by the impregnation of a chromosorb W of 30–60 mesh with 20% polyethylene glycol 400. The flow of the carrier gas was of 75 cm³/min, while the column temperature of 77°.

The result of the analysis of a solution of methyl alcohol and hydrogen peroxide in water is shown in figure 1.

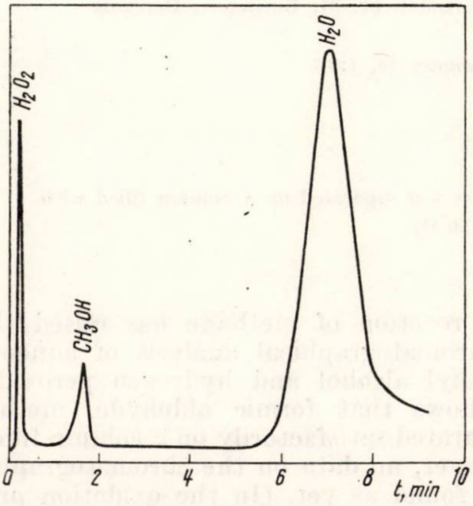

Fig. 1. – Separation of $H_2O_2CH_3OH$, H_2O on a polyethylene glycol 400 column.

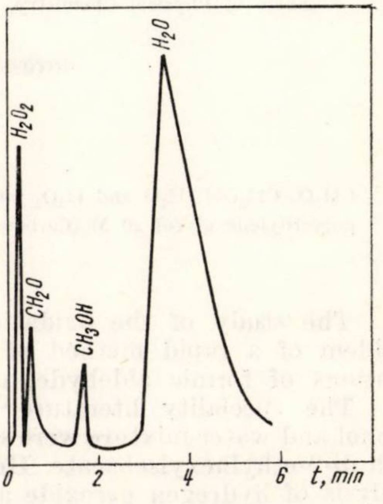

Fig. 2.– Separation of H_2O_2, CH_2O, CH_3OH and H_2O on a polyethylene glycol 20 M (carbowax 20 M) column.

Under the above working conditions, the resolution of the column for formic aldehyde and methyl alcohol is slight and, therefore, the column could not be used in the analysis of the mixture of condensable products, resulted from the oxidation reaction of methane.

Still better results have been obtained with a column of polyethylene glycol 20 M (carbowax 20 M), 20% impregnated on chromosorb P of 30–60 mesh.

The flow of the carrier gas was of 75 cm³/min and the column temperature of 85°. The chromatogram obtained on analysing an aqueous solution of formic aldehyde, methyl alcohol and hydrogen peroxide is shown in figure 2.

Under the above mentioned experimental conditions the analysis lasts 5.5. minutes.

From the aforesaid it results that the column with polyethylene glycol 20 M is the most suitable one for the analysis of the mixture of condensable products of methane oxidation, the reproducibility of the analyses being fairly good.

Revue Roumaine de Chimie, **18**, *12*, 2039–2050 (1973)

Cu(II) COORDINATION COMPOUNDS WITH 3-AMINO-1-PROPANOL

MARIA BREZEANU and IOANA JITARU

University of Bucharest, Laboratory of Inorganic Chemistry, Splaiul Independenţei 87, Bucharest, Romania

Received March 2, 1973

A series of Cu(II) coordination compounds with 1,3-aminopropanol which correspond to the following general types : $[Cu(AO)X]_2$ (X = Cl, Br, SCN, OH, CH_3COO) ; $[Cu(AOH)(AO)]X$ ($X=NO_3$, CH_3COO) ; $[Cu(AOH)(AO)X]$ (X = Cl, Br) ; $[Cu(AOH)X_2]$ (X = Cl, Br) and $[Cu(AOH)_2]SO_4.H_2O$, ($AOH = H_2N-C_3H_6-OH$ and $AO=(H_2N-C_3H_6-O)^-$ have been obtained. They were characterized by elementary chemical analysis, molecular weight determinations, molecular electrical conductivity measurements, electronic and vibrational spectra. Taking into consideration these data we try to establish the most probable stereochemistry of the obtained compounds.

The paper belongs to a larger research work on the coordination ability of some amino alcohols.

In literature there is a large number of papers dealing with the synthesis and characterization of some coordination compounds of transitional metals with ethanolamines (mono-, di- and triethanolamine).

The coordination ability of higher amino alcohols, e.g. propanolamines, is less studied.

In this direction there is a potentiometric and spectrophotometric study in aqueous solution on Cu-monopropanolamine system.[1]

Owing to this we considered a study on coordination ability of propanolamines to be interesting.

This would give us the possibility to draw a comparison between the ethanolamine and propanolamine complexes. We can also particularly study and appreciate the effect of the length of the aliphatic chain on the coordination ability of these ligands, as well as on the stabilities of coordination compounds obtained.

In this paper, we present the results we have got in the synthesis and characterization of some Cu(II) coordination compounds with monopropanolamine.

---

[1] B. Kirson, *Bull. Soc. chim. France*, **1953**, 223.

The ability of monopropanolamine to act both as neutral molecule and as anionic ligand, explains the variety of the types of coordination compounds we have got, represented through the general formulae:

$[Cu(AO)X]_2$ where $X = Cl$, Br, SCN, OH, CH_3COO;

$[Cu(AOH)(AO)]X$ where $X = NO_3$, CH_3COO;

$[Cu(AOH)(AO)X]$ where $X = Cl$, Br;

$[Cu(AOH)X_2]$ where $X = Cl$, Br and

$[Cu(AOH)_2]So_4 . H_2O$,

where AOH is monopropanolamine, $H_2N-C_3H_6-OH$, and AO, $H_2N-C_3H_6-O^-$.

The complexes obtained were characterized through elementary chemical analysis, electronic and vibrational spectra, molecular weight and electrical conductivity determinations.

RESULTS AND DISCUSSION

In order to establish the types of coordination compounds which Cu(II) can form with monopropanolamine (AOH), a ligand with many possibilities of coordination, we have studied the synthesis of these complexes under various experimental conditions. In this direction, we studied the influence of such factors as: the molar ratio Cu(II) : AOH, the medium pH, the solvent and the copper salt anion.

We must mention that among these factors there is a close interdependence, and that is why it is sometimes almost impossible to appreciate the contribution of each of them.

Referring to the first factor, it has been found that, in alcohol solution, we obtain only one type of complexes, namely $[Cu(AO)X]_2$ ($X=Cl$, Br, OH, CH_3COO) even at very high values (1 : 10 or even 1 : 20) of the molar ratio Cu (II) : AOH.

In aqueous or acetone solution, for molar ratio Cu (II) : AOH = 1 : 3, we have got the complexes $[Cu(AOH)(AO)]X$ ($X = NO_3$, CH_3COO, SO_4), respectively $[Cu(AOH)(AO)X]$ ($X = Cl$, Br).

The fact that, various compounds, in different solvents have been obtained may be assigned not only to their different solubility and stability in the respective solvents, but also to pH of the solvents used (for the same molar ratio Cu(II) : AOH).

The pH seems to have an important contribution to monopropanolamine behaviour. So that, in alcohol solution or even better in acetone solution, at acid pH ($pH \sim 3.5-4$), we obtained the complexes $[Cu(AOH)X_2]$ where monopropanolamine acts as a neutral bidentate ligand.

In neutral medium and especially in alkaline one, monopropanolamine acts as an anionic ligand. Thus, for a neutral or scarcely alkaline medium (pH ~ 7.5–8), (in acetone or aqueous solution) we got complexes of the type [Cu(AOH) (AO) X], respectively, [Cu(AOH) (AO)] X, where a molecule of monopropanolamine acts as a neutral and another one as an anionic ligand.

In alkaline medium (pH ~ 8–10) the dimer complexes of the type $[Cu(AO)\,X]_2$ were obtained, where monopropanolamine acts as an anionic ligand.

In order to establish the contribution of the copper salt anion, we used a series of salts namely, chloride, bromide, sulphocyanate, azotate, acetate and sulphate, in the synthesis of these compounds.

Under approximately the same experimental conditions (pH, molar ratio Cu(II) : AOH) the complexes obtained belong to various types in accordance with the nature of the anion.

Thus, the complexes obtained from the salts whose anion is characterized by a reduced coordination ability correspond to the general formula, [Cu(AOH) (AO)] X ($X = NO_3$, CH_3COO, SO_4), where the anion is uncoordinated. If the salt anion has a greater coordination ability, the compounds $[Cu(AO)\,X]_2$ (X = Cl, Br, SCN, OH) are obtained.

Molecular weight measurements. In order to obtain some further data referring to the nature of the studied complexes, their molecular weights have been determined (table 1). The data obtained point out the dimer character of some of them.

Table 1

Molecular weights of some obtained compounds

Compound	Melting point	Molecular weight	
		Calcd.	*Found*
$[Cu(AO)\,Cl]_2$	157 (d)	348.18	339.40
$[Cu(AO)\,Br]_2$	160	437.05	425.20
$[Cu(AO)\,OH]_2$	140 (d)	311.25	305.00
$[Cu(AO)\,CH_3COO]_2$	185	395.20	390.15
$[Cu(AO)\,SCN]_2 \cdot H_2O$	142	411.20	406.70
$[Cu(AOH)\,Cl_2]$	165	209.49	205.10
$[Cu(AOH)\,Br_2]$	150 (d)	298.41	300.50
$[Cu(AOH)\,(AO)]\,CH_3COO$	173	272.64	270.00
$[Cu(AOH)\,(AO)\,Cl]$	145 (d)	249.15	236.30
$[Cu(AOH)_2]\,SO_4 \cdot H_2O$	152	329.70	315.40

$AOH = H_2N-C_3H_6-OH$ and $AO = (H_2N-C_3H_6-O)^-$

Molecular electrical conductivity measurements. The formulation assigned to the studied complexes in the sense of the ionic dissociation nature has been confirmed by the determination of their molecular electrical conductivity.

The data obtained (table 2) show that the majority of the studied complexes are nonelectrolytes. The compounds [Cu(AOH) (AO)] X (X = $= NO_3$, CH_3COO, SO_4) present a conductivity corresponding to 1 : 1 type electrolytes.

Table 2

Molecular electrical conductivity of the obtained compounds in DMF solution *

Compound	Molar conductivity	Type of electrolyte
$[Cu(AO)\ Cl]_2$	25.20	nonelectrolyte
$[Cu(AO)\ Br]_2$	20.40	nonelectrolyte
$[Cu(AO)\ (OH)]_2$	15.10	nonelectrolyte
$[Cu(AO)\ CH_3COO]_2$	10.15	nonelectrolyte
$[Cu(AO)\ SCN]_2 . H_2O$	25.10	nonelectrolyte
$[Cu(AOH)\ Cl_2]$	20.10	nonelectrolyte
$[Cu(AOH)\ Br_2]$	25.20	nonelectrolyte
$[Cu(AOH)\ (AO)]\ NO_3$	75.20	1 : 1
$[Cu(AOH)\ (AO)]\ CH_3COO$	80.10	1 : 1
$[Cu(AOH)\ (AO)\ Cl]$	16.60	nonelectrolyte
$[Cu(AOH)\ (AO)\ Br]$	20.00	nonelectrolyte
$[Cu(AOH)_2]\ SO_4 . H_2O$	82.30	1 : 1
$[Cu(AOH)\ (AO)\ Br] . 2\ (CH_3)_2CO$	20.10	nonelectrolyte
$[Cu(AOH)\ (AO)\ Br] . 2H_2O$	22.25	nonelectrolyte

* Sol. 10^{-3} M, in $cm^2\ \Omega^{-1}\ mol^{-1}$; $t = 26°$.

Electronic spectra. To assign the most probable structure of the studied compounds, their electronic spectra have been recorded.

As it is well known,[2,3] for a square planar or pseudotetrahedral compound, the spectra of the visible range are very different, that makes possible to assign the configuration.

On the analogy of the electronic spectra (in the visible range) of the studied compounds (figs. 1—4), we conclude that all these compounds have the same structure. The large and asymmetrical band of about 600 nm, which might be splitted into several components, permits

---

[2] L. Sacconi and M. Ciampolini, *J. Chem. Soc.*, **1964**, 276.

[3] R. D. Willett, O. L. Liles and Chr. Michelson, *Inorg. Chem.*, **6**, 1885 (1967).

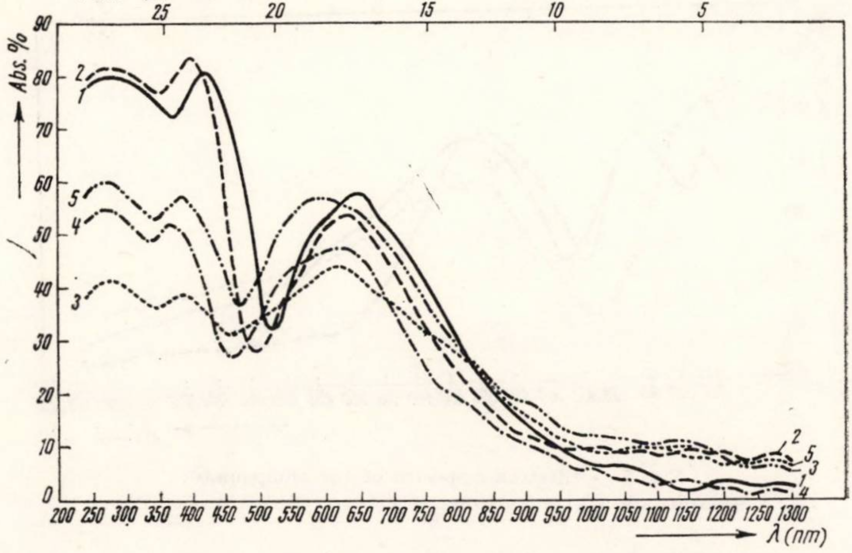

Fig. 1. — Electronic spectra of the compounds:
1, $[Cu(AO)Br]_2$; *2*, $[Cu(AO)Cl]_2$; *3*, $[Cu(AO)(OH)]_2$; *4*, $[Cu(AO)CH_3COO]_2$; *5*, $[Cu(AO)NCS]_2.H_2O$.

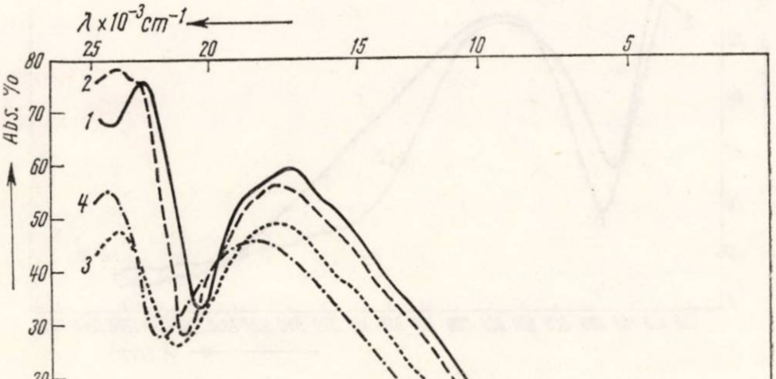

Fig. 2. — Electronic spectra of the compounds:
1, [Cu(AOH)(AO)Br]; *2*, [Cu(AOH)(AO)Cl]; *3*, $[Cu(AOH)Br_2]$; *4*, $[Cu(AOH)Cl_2]$.

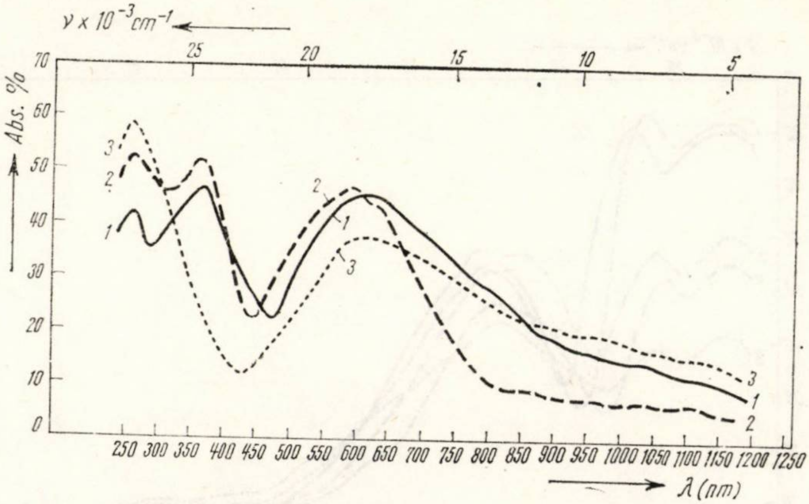

Fig. 3. — Electronic spectra of the compounds:
1, $[Cu(AOH)(AO)]NO_3$; *2*, $[Cu(AOH)(AO)]CH_3COO$; *3*, $[Cu(AOH)_2]SO_4.H_2O$.

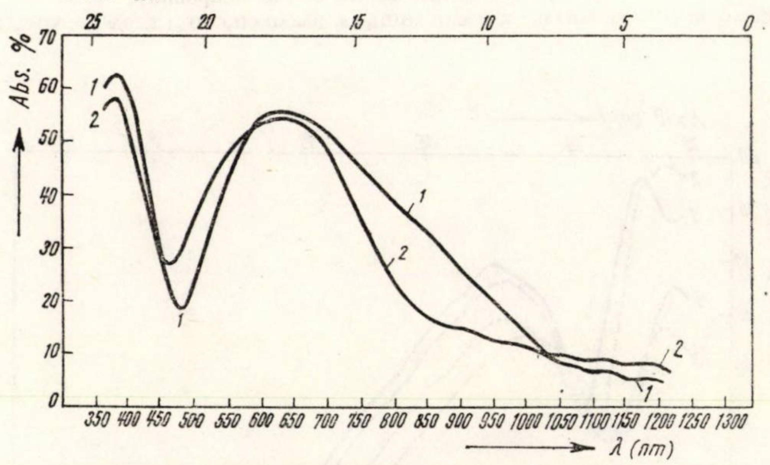

Fig. 4. — Electronic spectra of the compounds:
1, $[Cu(AOH)(AO)Br].2(CH_3)_2CO$; *2*, $[Cu(AOH)(AO)Br].2H_2O$.

the assignment of a square-planar or octahedral configuration, strongly tetragonal distorted [4,5] to the studied complexes.

In spite of the large and asymmetrical appearance, it can be noticed that the *d*—*d* band presents a hipsochromic shifting according to the anion nature for the same type of compounds (e.g. for $[Cu(AO)X]_2$ or

---

[4] D. Forster and D. M. L. Goodgame, *J. Chem. Soc.*, **1964**, 2791.

[5] A. B. P. Lever, "Inorganic Electronic Spectroscopy", American Elsevier Publishing, New York, 1968, p. 457.

$[Cu(AOH)X_2]$). This shifting permits to establish a spectrochemical series of the type: $Br < Cl < OH < CH_3COO$.

It is interesting to notice that [Cu(AOH) (AO) X] complexes spectrum is very similar with that one of $[Cu(AO)X]_2$ compounds type. This resemblance may be interpreted as pointing to the same structure of both types of compounds, very probably a square planar structure.

The assignment is in accordance with those from the literature of Cu(II) complexes with ethanolamine[6-9] or Cu(II) glycocholats.[10]

In the near ultraviolet range, the studied compounds present a rather strong band, which could be interpreted as a charge transfer band (L → M). This band presents a bathochromic shift according to the reducing character of the X ligands.

The 260 nm band belongs to monopropanolamine ligand.

Vibrational spectra. In order to bring further information referring to the stereochemistry of the obtained compounds, IR spectra were recorded.

From this point of view the most adequate spectral ranges are those where absorption is assigned to OH stretching vibrations (ν_{OH}).

In table 3, the characteristic frequencies of the obtained compounds and their probable assignments are presented.

To achieve a most fine assignment of IR spectra of the studied compounds, we have registered the free ligand spectrum, monopropanolamine, and compared it with those of monoethanolamine, known in literature.[11]

The OH stretching vibration, ν_{OH}, at 3450 cm^{-1} in monopropanolamine spectrum, points out the presence of some inter- and intramolecular hydrogen bonds.[12]

This frequency (ν_{OH}) appears at 3290 cm^{-1}, 3260 cm^{-1} and respectively 3450 cm^{-1} in $[Cu(AOH)(AO)]NO_3$, $[Cu(AOH)(AO)]CH_3COO$ and [Cu(AOH) (AO) Cl] compounds. This observation leads to the conclusion that in the first two compounds, one of monopropanolamine molecule, at least, behaves as a neutral bidentate ligand, while in the [Cu(AOH) (AO) Cl] compound, a monopropanolamine molecule, at least, behaves as a monodentate neutral ligand, (being coordinated only by nitrogen atom and having the OH group uncoordinated).

In the complexes formulated as dimers, e.g. $[Cu(AO)X]_2$, the stretching vibration, ν_{OH} disappears, pointing out the behaviour of monopropanolamine as an anionic, bidentate ligand.

In $[Cu(AO)OH]_2$ and $[Cu(AO)NCS]_2 \cdot H_2O$ complex compounds, it is more difficult to appreciate the way of monopropanolamine coordi-

---

[6] B. G. Gasanov and S. V. Grum-Grznimailo, *Kristallografiya*, **4**, 732 (1959).

[7] S. Kida, *J. Chem. Soc. Japan*, **85**, 428 (1964).

[8] E. Uhlig and K. Staiger, *Z. anorg. Chem.*, **346**, 21 (1966); **360**, 39 (1968).

[9] P. Hans Jensen, *Acta Chem. Scand.*, **25**, 1753 (1971).

[10] M. V. Artemenko and K. F. Slyusarenko, *Zhur. neorg. Khim.*, **13**, 2701 (1968).

[11] D. G. Brannon, R. H. Morrison and J. L. Hall, *J. Inorg. Nuclear Chem.*, **33**, 981 (1971).

[12] L. J. Bellamy, "The Infrared Spectra of Complex Molecules", London, New York, 1958, p. 108.

Table

Characteristic IR frequencies

Compound	$\nu_{(OH)}$	$\nu_{as(NH)}$	$\nu_{s(NH)}$	$\nu_{(NH_2)}$	$\nu_{(OH)}$
AOH	3450 (s, b)	3290 (s, b)	3170 (sh)	1615 (m, b)	1170 (w)
$[Cu(AOH)(AO)]NO_3$	3290 (s, b)	3240 (m)	3135 (m)	1585 (m)	1160 (m)
$[Cu(AOH)(AO)]CH_3COO$	3260 (s, b)	3220 (s)	3155 (s)	CH_3COO bands	1162 (s)
$[Cu(AO)(OH)]_2$	3290 (m) (ligand OH)	3250 (s)	3150 (m)	1598 (s)	1165 (s)
$[Cu(AO)SCN]_2 . H_2O$	3310 (m) (H_2O band)	3200 (w)	3150 (w)	1595 (m)	1170 (w)
$[Cu(AO)Cl]_2$	—	3190 (w)	3080 (sh)	1595 (m)	—
$[Cu(AO)CH_3COO]_2$	—	3200 (w)	3100 (w)	CH_3COO bands	—
$[Cu(AOH)(AO)Cl]$	3450 (m, b)	3175 (m, b)	3090 (w, b)	1590 (m)	—
$[Cu(AOH)_2]SO_4 . H_2O$	3300 (m, b) (H_2O band)	3280 (w, b)	3080 (w, b)	H_2O bands	SO_4 bands

s – strong, w – weak, b – broad, sh – shoulder.

nation. In $[Cu(AO)(OH)]_2$ spectrum the sharp band of 3290 cm^{-1} range could be assigned to ν_{OH} hydroxyl coordinated,[13] and in $[Cu(AO)NCS]_2 . H_2O$ spectrum, the band of 3310 cm^{-1} range may be assigned as ν_{OH} frequency of water.[14]

The second spectral range studied is the one where absorption is assigned to the stretching vibration, ν_{CO}.

In monopropanolamine spectrum, this frequency appears as a strong band. The band is found again in all the studied compounds round this value.

It is remarkable that in $[Cu(AOH)(AO)]X$ ($X = CH_3COO, NO_3$) compounds in which two AOH ligands act differently (neutral molecule and anionic ligand), ν_{CO} frequency is splitted in two distinct components, at least (the same splitting is noticed for ν_{CN} and ν_{CC} frequencies).

The stretching vibration (ν_{NH}) of the monopropanolamine amino group (which appears at 3290 cm^{-1} ($\nu_{as\,NH}$) respectively 3170 cm^{-1} (ν_{sNH})) is found again in all the studied compounds at lower values indicating coordination through azote.

The IR spectra have also been used to establish the anion function in the studied compounds (mono, bidentate, bridging or ionic ligands).

---

[13] K. Nakamoto "Infrared Spectra of Inorganic Coordination Compounds", London, New York, 1963, p. 159.

[14] K. Nakamoto, *J. Amer. Chem. Soc.*, **78**, 1347 (1956).

3

of the obtained compounds

$\nu_{(CN)}$	$\nu_{(CC)}$	$\nu_{(CO)}$	$\nu_{(NO)\,(NO_3)}$	$\nu_{(SO)\,(SO_4)}$	$\nu_{(OCO)}$ (CH_3COO)	$\nu_{(CN)}$ $\nu_{(CS)}$ $\nu_{(SCN)}$
1170 (w, b)	1075 (w, b)	1055 (s)	—	—	—	—
1160 (m)	1060 (m) 1080 (sh)	1022 (sh) 1040 (sh)	1380 (s) 830 (m)	—	—	—
1160 (m) 1183 (sh)	1085 (s)	1025 (m) 1055 (s)	1019 (m) —	—	1405 (s) 1570 (s)	—
1170 (sh)	1075 (sh)	1050 (s)	—	—	—	—
1140 (s)	1070 (s)	1045 (s)	—	—	—	2110 (s) 890 (w)
1160 (s)	1070 (m)	1040 (m)	—	—	—	—
1160 (s)	1070 (m)	1040 (m)	—	—	1415 (s) 1605 (s)	—
1140 (m) 1160 (s)	1060 (sh)	1040 (m) 1025 (sh)	—	—	—	—
SO_4 bands	SO_4 bands	1010 (sh)	—	1140 (a) 625 (a)		

From this point of view, the IR spectra analysis of $[Cu(AO)\,NCS]_2 . H_2O$ and $[Cu(AO)\,CH_3COO]_2$ dimers presents a great interest. The presence in the IR spectrum of $[Cu(AO)\,NCS]_2 . H_2O$ of a strong sharp band, unsplitted at 2110 cm^{-1} (ν_{CN}) and of a weak band at 890 cm^{-1} (ν_{CS}) leads to the assignment of a bridging SCN structure.[15]

We cannot appreciate exactly the coordination way of the OH in the $[Cu(AO)\,(OH)]_2$ compound because the range of the OH frequency is very rich in amino-alcohol bands.[13]

In $[Cu(AOH)\,(AO)\,CH_3COO]_2$ spectrum it appears a well defined sharp band at 1600 cm^{-1}, characteristic for $\nu_{as(OCO)}$ frequency.[16,17] This band is generally considered to be a sign of acetate bridging group.

In $[Cu(AOH)\,(AO)]\,CH_3COO$ spectrum, the carboxyl group stretching vibration bands appear at lower frequencies than in the former complex ($\nu_{as(OCO)}$ at 1570 cm^{-1} and $\nu_{s(OCO)}$ at 1405 cm^{-1}, characteristic for ionic acetate).[16]

In the same way, the presence of two strong unsplitted bands around 1140 cm^{-1} in the compound $[Cu(AOH)_2]\,SO_4 . H_2O$ spectrum are characteristic for SO_4 anion of Td symmetry. They advocate for the given formulation of the respective compound.[18]

---

[15] S. Chatt, and L. Duncanson, *J. Chem. Soc.* (*A*), **1971**, 1590.

[16] N. F. Curtis, *Bull. Chem. Soc. Japan*, **31**, 303 (1958).

[17] N. F. Curtis, *J. Chem. Soc.*, **1968**, 1579.

A strong unsplit band round 1380 cm^{-1} and another unsplitted medium band at 830 cm^{-1}, in spectrum of $[Cu(AOH)(AO)]NO_3$ compound indicates an NO_3 ion of C_{2v} symmetry. This agrees to the given formulation.[19]

EXPERIMENTAL

I. SYNTHESIS OF THE COMPLEX COMPOUNDS

1. *$[Cu(AO)Cl]_2$*. 0.33 ml monopropanolamine dissolved in 1.7 ml ethanol is added to the solution obtained from 0.25 g $CuCl_2 . 2H_2O$ (molar ratio Cu (II) : AOH=1 : 3) dissolved in minimum quantity of ethanol. A green crystalline substance separates, which is filtered off and washed with ethyl alcohol and acetone.

Calcd. :	Cu %,	36.55 ;	Cl %,	20.36 ;	N %,	8.04 ;
Found :		36.42 ;		20.48 ;		8.20.

2. *$[Cu(AO)Br]_2$*.0.25 ml monopropanolamine dissolved in 1.25 ml ethanol is added to the solution obtained from 0.25 g $CuBr_2$ dissolved in minimum quantity of ethanol (molar ratio Cu(II) : AOH = 1 : 3). A crystalline green compound is separated, which is filtered off and washed with ethyl alcohol and acetone (or ether).

Calcd. :	Cu %,	29.05 ;	Br %,	36.50 ;	N %,	6.41 ;
Found :		28.95 ;		36.65 ;		6.50.

3. *$[Cu(AO)(OH)]_2$*. 0.5 ml monopropanolamine dissolved in 0.5 ml water is added to the freshly prepared suspension of 0.20 g $Cu(OH)_2$ in 10 ml water (molar ratio Cu (II) : AOH = 1 : 2). This mixture is kept on a 70 degrees steam bath, for two hours, then $Cu(OH)_2$, that did not react, is filtered off. The clear solution is concentrated and is taken again with a mixture of alcohol and acetone. A crystalline light green substance separates, which is filtered off and washed with acetone.

Calcd. :	Cu %	40.83 ;	N %,	8.99 ;
Found :		40.65 ;		9.10.

4. *$[Cu(AO)CH_3COO]_2$*. 0.07 ml monopropanolamine dissolved in 0.33 ml water is added to the ordinary solution obtained from 0.25 g $Cu(CH_3COO)_2 . H_2O$ dissolved in minimum quantity of water (molar ratio Cu (II) : AOH = 1 : 2). The obtained solution is concentrated on the steam bath until the first dark blue crystals appear. When the solution dries up, a beautifully crystallized substance separates, which is filtered off and washed with small quantities of water and ethyl alcohol.

Calcd. :	Cu %,	32.64 ;	N %,	7.26 ;
Found :		32.20 ;		7.50.

5. *$[Cu(AO)SCN]_2$*. 0.75 ml monopropanolamine dissolved in 0.75 ml water and 0.4 g solid KSCN is added to the solution obtained from 0.5 g $CuSO_4 . 5H_2O$ dissolved in a minimum

---

[18] K. Nakamoto, "Infrared Spectra of Inorganic and Coordination Compounds", London, New York, 1963, p. 161.

[19] B. M. Gatehouse, S. E. Livingstone and R. S. Nyholm, *J. Chem. Soc.*, **1957**, 4222.

quantity of water (molar ratio Cu (II) : AOH : SCN = 1 : 4 : 2). A finely crystallized dark green substance is separated which is filtered off and washed with water and ethyl alcohol.

Calcd. : Cu %, 30.90 ; SCN %, 28.21 ; N %, 13.61 ;
Found : 31.15 ; 28.32 ; 13.93.

6. *[Cu(AOH) (AO)]* CH_3COO. 0.15 ml monopropanolamine dissolved in 0.65 ml water is added to a solution obtained from 0.25 g $Cu(CH_3COO)_2 . H_2O$ dissolved in a minimum quantity of water (molar ratio Cu(II) : AOH = 1 : 4). When the solution dries up, violet blue spangle like crystals separate, which are filtered off and washed with a small quantity of water and ethyl alcohol.

Calcd. : Cu %, 23.30 ; N %, 10.27 ;
Found : 23.10 ; 10.42.

7. *[Cu(AOH)(AO)]* NO_3. 0.3 ml monopropanolamine dissolved in 1.5 ml ethanol is added to a solution obtained from 0.25 g $Cu(NO_3)_2 . 3\,H_2O$ dissolved in a minimum quantity of ethanol (molar ratio Cu(II) : AOH = 1 : 3). The solution concentrates on the steam bath until the first crystals separate. When the solution dries up, a crystalline dark blue substance separates which is filtered off and washed with a small quantity of ethyl alcohol.

Calcd. : Cu %, 23.03 ; N %, 15.29 ; C %, 13.05 ;
Found : 23.15 ; 15.40 ; 13.50.

8. *[Cu(AOH)(AO)Cl]*. 0.5 ml monopropanolamine dissolved in 2.5 ml acetone is added to the solution obtained from 0.25 g $CuCl_2 . 2\,H_2O$ dissolved in a minimum quantity of acetone (molar ratio Cu(II) : AOH = 1 : 4). A green glue like substance separates which is maintained in an acetone solution. Several hours later a crystalline dark green solution separates which is filtered off and washed with acetone.

Calcd. : Cu %, 25.48 ; Cl %, 14.23 ; N %, 11.24 ;
Found : 25.32 ; 14.50 ; 11.55.

9. *[Cu(AOH)(AO) Br].2*$(CH_3)_2CO$. 0.3 ml monopropanolamine dissolved in 1.2 ml acetone is added to a diluted solution of $CuBr_2$ in acetone (0.25 g $CuBr_2$ in 20 ml acetone) (molar ratio Cu(II) : AOH = 1 : 3). Several hours later, a finely green blue crystallized substance separates which is filtered off and washed with acetone.

Calcd. : Cu %,15.51 ; Br %, 19.62 ; N %, 6.83 ;
Found : 15.70 ; 20.10 ; 7.05.

Lightly warmed at a temperature of 50–60 degrees, the substance grows dark green and loses about 3.02 % of its weight. This has been assigned to the two acetone molecules. This change is taking place in time and in dry atmosphere or in vacuum.

10. *[Cu(AOH) (AO) Br]*

Calcd. : Cu %, 21.60 ; Br %, 27.20 ; N %, 9.50 ;
Found : 21.75 ; 27.35 ; 9.73.

This compound is stable only in dry atmosphere. Being left in wet atmosphere for a time it changes its colour becoming again dark blue, because of the forming [Cu(AOH)(AO) Br].2 H_2O compound.

11. *[Cu(AOH) (AO) Br].2* H_2O

Calcd. : Cu %, 19.28 ; N %, 8.48 ; Br %, 24.55 ;
Found : 19.32 ; 8.70 ; 24.60.

12. *[Cu(AOH) Cl_2]*. A very diluted solution of monopropanolamine in acetone is added to solid 0.25 g $CuCl_2.2\,H_2O$ (molar ratio Cu(II) : AOH = 1 : 0.5). A green glue separates. This glue, in time, kept in acetone solution, becomes a crystalline green substance. It is filtered off and washed with acetone.

Calcd. :	Cu %,	30.29 ;	Cl %,	33.87 ;	N %,	6.67
Found :		30.10 ;		33.92 ;		7.05.

The same substance, but in a small efficiency, is obtained too in ethanol solution.

13. *[Cu(AOH) Br_2]*. A very diluted solution of monopropanolamine in acetone is added to solid 0.25 g $CuBr_2$ (2.5 ml monopropanolamine in 10 ml acetone) (molar ratio Cu(II) : : AOH = 1 : 0.5). Several hours later a green crystalline substance separates which is filtered off and washed in ethyl alcohol and acetone (or ether).

Calcd. :	Cu %,	21.29 ;	Br %,	53.55 ;	N %,	4.68 ;
Found :		21.10 ;		53.70 ;		4.80.

14. *[Cu(AOH)$_2$]SO_4.H_2O*. 0.25 ml monopropanolamine in 1.2 ml water is added to a solution obtained from 0.25 g $CuSO_4.5\,H_2O$ dissolved in a minimum quantity of water (molar ratio Cu(II) : AOH = 1 : 3). The solution concentrates on a 70 degrees steam bath, until the first crystals separate. When the solution dries up, a blue crystalline substance separates which is filtered and washed with a small quantity of water and ethyl alcohol.

Calcd. :	Cu %,	19.37 ;	SO_4 %,	29.29 ;	N %,	8.54 ;
Found :		19.50 ;		29.40 ;		8.80.

II. MOLECULAR WEIGHTS

The molecular weights of some compounds obtained (table 1) have been determined through the Rast minimethod, using camphor as solvent.

III. MOLECULAR CONDUCTIVITIES

Measurements of molecular electrical conductivity have been made with a Conductometer (II) (Czechoslovakia) with a constant ($K = 0.52$). The measurements have been made in 10^{-3} M DMF solutions at a temperature of 25 degrees.

The assignment of the electrolyte type has been made according to the present indication in literature referring to the methods of establishing the electrolyte type in DMF solutions.[20-22]

IV. ELECTRONIC SPECTRA

Reflection spectra have been recorded at room temperature using a spectrophotometer VSU_1, and as a referring material, magnesium oxide.

V. VIBRATIONAL SPECTRA

IR spectra have been obtained by means of a Perkin spectrophotometer using potassium bromide disk or Nujol mulls technique.

---

[20] D. J. Phillips and S. Y. Zyref, *J. Amer. Chem. Soc.*, **83**, 1806 (1961).

[21] J. V. Quagliano, J. Fujita, G. Franz, D. J. Phillips, J. A. Walmsle and S. Y. Tyree, *J. Amer. Chem. Soc.*, **83**, 3370 (1961).

[22] I. F. Jonug, R. D. Gillord and G. Willkinson, *J. Chem. Soc. (A)*, **1964**, 2176.

Revue Roumaine de Chimie, **18**, *12*, 2051–2058 (1973)

MIXED LANTHANIDE COMPOUNDS WITH NEUTRAL LIGANDS CONTAINING DONOR OXYGEN ATOM. I

LANTHANIDE CHLOROSALICYLATES WITH TRIPHENYLPHOSPHINOXIDE

SILVIA PLOŞTINARU and P. SPACU

Research Center of Physical Chemistry, Str. Dumbrava Roşie 23, Bucharest, Romania

Received May 8, 1973

The synthesis methods and properties of some lanthanide compounds of the $Ln(ClSal)_3(Ph_3PO)_2$ form, where ClSal = 5-chlorosalicylic acid. The compounds obtained were characterized according to their chemical composition, their electrical conductivity and thermogravimetrically. The electronic spectra were recorded in UV and visible range. The coordination of the neutral ligand was proved by the shift of P → O frequencies found in the IR spectra.

We have studied in previous papers the mixed compounds of lanthanide oxycarboxylates with bidentate neutral ligands with donor nitrogen atom.[1,2] A characteristic of the chemistry of lanthanides is their higher possibility to form complex compounds with polydentate ligands, rather than with monodentate ligands.[3] This feature is characteristic of the metals forming labile complexes, while a series of other metals such as Pt(IV) or Co(III), forming less active complexes have a higher coordination possibility with monodentate ligands. In the case of lanthanides, this behaviour is a result of the thermodynamic instability of the complexes towards certain hydrated ions coupled to their kinetic instability, which makes these compounds impossible to be isolated from aqueous solution. This does not mean that the lanthanide complexes are weak in the sense of a weak metal-ligand bond. Even if the numerical data concerning the stability constants for this type of compounds are scarce, the often very high thermal stability observed on the solid complexes, is a proof of the existence of a strong enough metal-ligand bond, in which the available *s* and *d* orbitals of the lanthanide ion are especially involved.

---

[1] P. Spacu and S. Ploştinaru, *Rev. Roumaine Chim.*, **17**, 697 (1972).

[2] P. Spacu and S. Ploştinaru, *Rev. Roumaine Chim.*, (in press).

[3] Th. Moeller, *Chem. Rev.*, **65**, 1 (1965).

Among the monodentate ligands, those containing the donor oxygen atom have an easier possibility to form complex compounds with lanthanides owing to the special affinity of these elements towards oxygen. In the present paper we have studied the properties and the behaviour of the mixed complexes of lanthanides with 5-chlorosalicylic acid and triphenylphosphinoxide (Ph_3PO) owing to the fact that the literature mentions very few lanthanide compounds with this ligand and this especially in connection with the study of fluorescence properties.[4–6]

EXPERIMENTAL

Reagents. The following reagents were used : oxides (Ln_2O_3) of spectral purity (Matthey and Johnson); 5-chlorosalicylic acid (Fluka AG-Switzerland); triphenylphosphinoxide (Fluka AG-Switzerland).

Preparation method of compounds. The compounds were obtained by the liquid-liquid extraction method. The lanthanide chlorosalicylate obtained by processing an aqueous $Ln(NO_3)_3$ solution, with an aqueous ammonium chlorosalicylate solution, was extracted in 60 ml of benzene containing the neutral ligand (Ph_3PO). The organic phase was then separated, washed several times with small quantities of water and slowly evaporated at the room temperature or in vacuum. A vitreous mass was thus obtained from which, by using the usual methods of organic synthesis, we have isolated the ternary compounds which are crystalline and coloured, their colour being practically identical to that of the original ion. The compounds thus obtained were again washed with small quantities of alcohol and dried in a desiccator on P_2O_5. The colourless Ce(III) compounds have gradually changed their colour during the extraction, finally reaching a dark brown colour, probably due to the oxidation of the trivalent cerium to the tetravalent cerium.

The reaction by which the compounds are obtained may by written as follows

$$[Ln(NO_3)_3]_{aq} + [NH_4ClSal]_{aq} \longrightarrow [Ln(ClSal)_3]_{ag}$$

$$[Ln(ClSal)_3]_{aq} + [Lig]_{org} \longrightarrow [Ln(ClSal)_3(Lig)_2]_{org}$$

Table 1

Analytical data

Formula of the compound	Ln		C		H	
	Calcd.	*Found*	*Calcd.*	*Found*	*Calcd.*	*Found*
$Ce(ClSal)_3(Ph_3PO)_2$	11.57	11.61	56.52	56.38	3.46	3.73
$Pr(ClSal)_3(Ph_3PO)_2$	11.62	11.94	56.48	56.59	3.46	3.78
$Nd(ClSal)_3(Ph_3PO)_2$	11.87	12.11	56.33	56.10	3.45	3.80
$Sm(ClSal)_3(Ph_3PO)_2$	12.31	12.45	56.05	55.98	3.43	3.75
$Eu(ClSal)_3(Ph_3PO)_2$	12.43	12.68	55.97	55.76	3.43	3.90
$Dy(ClSal)_3(Ph_3PO)_2$	13.17	13.50	55.50	55.31	3.40	3.81
$Tb(ClSal)_3(Ph_3PO)_2$	12.92	13.31	55.66	55.78	3.41	3.68
$Er(ClSal)_3(Ph_3PO)_2$	13.54	13.82	55.26	55.08	3.39	3.74

---

[4] D. R. Cousins and F. A. Hart, *J. Inorg. Nuclear Chem.*, **29**, 1745 (1967).

[5] D. R. Cousins and F. A. Hart, *J. Inorg. Nuclear Chem.*, **30**, 3009 (1968).

[6] S. P. Sinha, *Z. Naturforsch.*, **25 a**, 665 (1970).

The formula was determined on the basis of the elemental chemical analysis (C, H, N, M) (table 1).

The compounds are obtained as anhydrous and non-hygroscopic microcrystalline powders. They are stable in air and very soluble in benzene, chloroform, acetone and dimethylformamide, but hardly enough soluble in ethanol or methanol. The values of the molar conductivity, measured in acetone (7.8–8.3 $ohm^{-1}cm^2mol^{-1}$) and in DMF (20 $ohm^{-1} cm^2mol^{-1}$) seem to confirm the formula given by us on the basis of the elemental chemical analysis. The data obtained, compared to those given by literature,[7] show that the compounds are non-electrolytes. We have also noticed that all the compounds are stable in time in an acetone or benzene solution and that no substitution reactions with the participation of the solvent take place.

Analyses and measurements. Chemical analyses were carried out by micromethods; C, H, N were determined by microcombustion. The metal was determined gravimetrically as oxide by ignition. The results are given in table 1.

Conductivity measurements were carried out by means of a Radelkis OK-102 conductometer, in 10^{-3} M DMF and acetone solutions. Platinum electrodes were used and the cell-constant was determined with aqueous 1 M, 0.1 M and 0.01 M KCl.

IR spectra between 400–4000 cm^{-1} were recorded by means of a UR-10 Zeiss-Yena spectrophotometer, using pelleted powders of KCl.

UV and visible spectra were measured with a VSU-2 Zeiss-Jena spectrophotometer, in 10^{-4}–10^{-5} M anhydrous ethanol solutions for the 210–340 nm region, and in 10^{-2} M benzene solutions for the 360–900 nm region. Solid reflectance spectra were measured with a VSU-1 Zeiss-Jena apparatus using MgO as a standard.

RESULTS AND DISCUSSION

UV spectra. The UV spectra were carried out in an ethanol solution with 10^{-5} M concentration for complexes and 10^{-4} M for ligands. Table 2 gives the wavelengths corresponding to the absorption maxima of the free ligands and of the complexes. The fact that no shifts of the absorption maxima appear, as a consequence of the coordination, means that the energy levels between which the transitions take place are equally perturbed, but the change in the intensity of the bands is a proof of the chemical bond formation.

Visible spectra. The very sharp bands appearing in the visible part of the spectrum, due to the *f–f* transitions inside of the 4 *f* shell are well enough affected by the ligands, as a consequence of the complexation. This is marked by the shifting of the absorption bands towards higher wavelengths (the nephelauxetic effect) and the intensification of the hypersensitive bands.

Such changes were also observed in the case of the mixed complexes studied by us. The spectra of Pr (III), Nd (III), Sm (III) and Er (III) in benzene solution and the reflectance spectra were recorded in the 400–900 nm range. These data are summarized and shown in table 3 and fig. 1.

---

[7] W. J. Geary, *Coord. Chem. Rev.*, **7**, 81 (1971).

Table 2

UV spectral data

Compound	λ_{max}	$\frac{\varepsilon_{max}}{10^{-4}}$
Chlorosalicylic acid (ClSal)	233	0.742
	316	0.368
Triphenylphosphin oxide (Ph_3PO)	260	0.168
	266	0.217
	273	0.182
$Pr(ClSal)_3(Ph_3PO)_2$	265	0.556
	273	0.455
	314	1.054
$Nd(ClSal)_3(Ph_3PO)_2$	265	0.568
	273	0.461
	316	0.966
$Er(ClSal)_3(Ph_3PO)_2$	265	0.618
	273	0.483
	318	0.898

These results show that small differences appear in the frequency of the absorption bands of the complexes as compared to the corresponding aquo ions, excepting the hypersensitive band $^4I_{9/2} \rightarrow {}^4G_{5/2}$ in the Nd (III) complex ($\Delta\bar{\nu} = 209$ cm^{-1}). The ^3P_j bands in the Pr (III) complex are slightly moved as compared with the aquo ion, while in the case of Er (III) and Sm (III) complexes there appear practically no displacements. The small shifts taking place in the case of the Pr (III) and Nd (III)

Table 3

Visible spectral data

Ln^{3+}	Transition	$\Delta\bar{\nu} = \bar{\nu}_c - \bar{\nu}_{aq}$ cm^{-1}	$\Delta\varepsilon = \varepsilon_c - \varepsilon_{aq}$
Pr^{3+}	$^3H_4 \rightarrow {}^3P_2$	101	+1.04
	$\rightarrow {}^3P_1$	137	+0.14
	$\rightarrow {}^3P_0$	129	+0.95
	$\rightarrow {}^1D_2$	200	+0.22
Nd^{3+}	$^4I_{9/2} \rightarrow {}^2G_{9/2}$	—	+1.11
	$\rightarrow {}^4G_{7/2}$	147	+1.33
	$\rightarrow {}^4G_{5/2}$	209	+8.72
	$\rightarrow {}^4F_{7/2}$	—	+0.04
	$\rightarrow {}^2H_{9/2}$	56	+0.62
Er^{3+}	$^4I_{15/2} \rightarrow {}^4F_{3/2}$	—	+1.68
	$\rightarrow {}^4F_{7/2}$	—	+1.96
	$\rightarrow {}^2H_{11/2}$	—	+12.05
	$\rightarrow {}^4S_{3/2}$	—	+0.69

complexes enable us to calculate the nephelauxetic ratio $\beta = \frac{1}{n}\sum^{n=i} \nu^{i}_{\mathrm{comp}}/\nu_{\mathrm{aq}}$, considered as a measure of the covalent character of the bonds,[8] caused by the decrease of the interelectronic repulsion parameters in the complexes.[9] It is nevertheless worth mentioning an increase in the intensity of the absorption bands of the hypersensitive transitions for all the studied complexes. This hypersensitivity as shown by Jørgensen and Judd[10] is brought about by the formation of the chemical bonds resulting in the perturbation of the f orbitals. This perturbation is due to an electrical quadrupole effect and not to an electrical dipole effect. The authors suggest that around the lanthanide ion, the electromagnetic field induces an asymmetrical distribution of the dipoles.

The same changes are observed in the solid state, in some cases even appeared new bands, which could not be observed with the solution at the respective concentration.

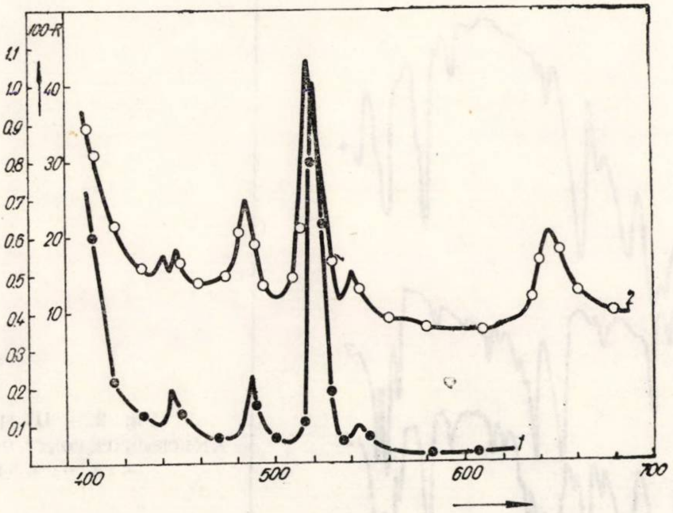

Fig. 1. — Visible absorption spectra of $Er(ClSal)_3(Ph_3PO)_2$
1, in solution; *2*, in solid state.

IR spectra. In the complexes with Ph_3PO the coordination is achieved through the oxygen atom, and this results through the shiftings of the stretching frequencies of the phosphoryl group ($P \rightarrow O$). Further details regarding the IR spectra of the free ligand and of some of its complexes with transition metals were recently presented.[11]

---

[8] C. K. Jørgensen, *Progr. Inorg. Chem.*, **4**, 73 (1962).

[9] S. P. Sinha and H. H. Schmidtke, *Mol. Phys.*, **10**, 7 (1965).

[10] C. K. Jørgensen and B. R. Judd, *Mol. Phys.*, **8**, 281 (1964).

[11] J. P. Clark, V. M. Langford and C. J. Wilkins, *J. Chem. Soc. A*, **1967**, 792.

In figure 2 are presented the IR spectra of Nd (III) and Dy (III) mixed complexes, of the neutral ligand (Ph_3PO) and of $Nd(ClSal)_3$ as representative for the simple chlorosalicylates. The spectra are complicated enough owing to the overlapping of the frequencies of both coordinated ligands. The way in which the vibration frequencies of the uncoordinated chlorosalicylic acid are changed as a consequence of the chemical bonding with the lanthanide ion, and the more important changes observed were discussed in a former paper.[2]

Regarding the neutral ligand, the presented data show that only certain vibration modes are affected through coordination. Thus, the band at 1121 cm^{-1} of the free Ph_3PO is displaced towards higher frequencies and increases in intensity through complexation. The bands observed at more than 1400 cm^{-1} due to certain C—C frequencies are overlapped on the symmetrical and asymmetrical OCO stretching of chlorosalicylate ion.

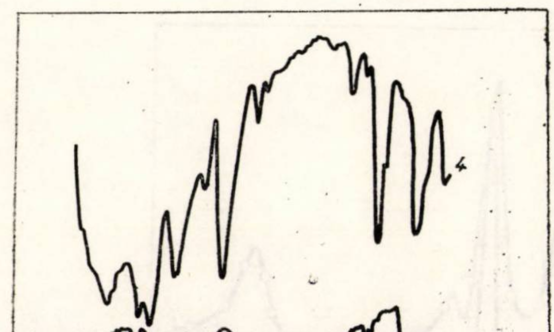

Fig. 2. — IR spectra of
1, $Nd(ClSal)_3(Ph_3PO)_2$; 2, $Dy(ClSal)_3(Ph_3PO)_2$;
3, Ph_3PO ; 4, $Nd(ClSal)_3$

The P → O stretching frequency at 1190 cm^{-1} in the free ligand appears in the complexes displaced towards smaller wavenumbers. In the case of the 3*d* transition metal complexes the displacement of νP → O towards higher wavelengths is of 40–70 cm^{-1}.[12] For the studied complexes, the decrease $\nu_{P\to O}$ varies between 29–40 cm^{-1} according to the ionic radius of the lanthanide element (table 4).

Table 4

The shift of P→O stretching vibration in $Ln(ClSal)_3(Ph_3PO)_2$ complexes

Compounds	P→O stretching cm^{-1}	$\nu_{max}^{comp} - \nu_{max}^{Ph_3PO}$
Ph_3PO	1190 (s)	—
$Ce(ClSal)_3(Ph_3PO)_2$	1150 (s)	−40
$Pr(ClSal)_3(Ph_3PO)_2$	1152 (s)	−38
$Nd(ClSal)_3(Ph_3PO)_2$	1155 (s)	−35
$Eu(ClSal)_3(Ph_3PO)_2$	1158 (s)	−32
$Dy(ClSal)_3(Ph_3PO)_2$	1160 (s)	−30

Figure 3 illustrates the manner in which the P → O bond is affected by the coordination with the lanthanide ion. As a consequence of the coordination, through an inductive effect, the positive charge on the oxygen atom increases, which brings about a strengthening of the $\sigma_{P\to O}$ bond and a weakening of the $p\pi - d\pi$ O → P bond. But the weakening of the $p\pi - d\pi$ back bonding O → P overcomes the effects connected to the strengthening of σ bond and the metal-oxygen π interaction, which leads practically to the decrease of the P → O stretching frequency.

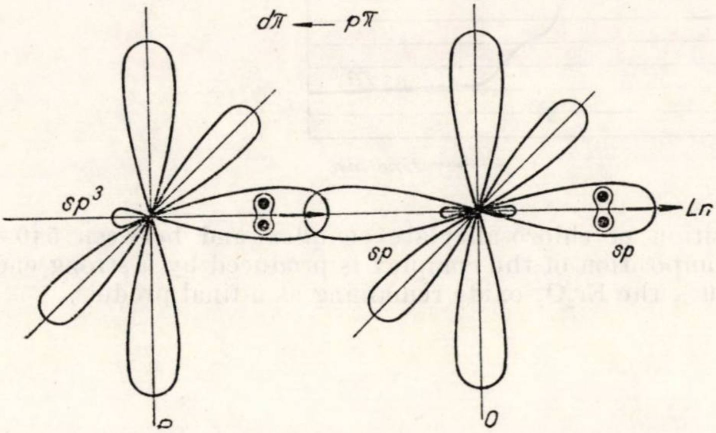

Fig. 3. – The chemical bonding between phosphorus and oxygen atoms.

Thermal behaviour. The thermal study, performed on the complexes of the type $Ln(ClSal)_3(Ph_3PO)_2$, shows that these compounds are stable till 200–220°. The TG and DTG curves (fig. 4) indicate for the $Er(ClSal)_3(Ph_3PO)_2$ a first weight loosing between 220–320° corresponding to the removal of one molecule of Ph_3PO. The total removal of Ph_3PO takes place between 320–480° when $Er(ClSal)_3$ is obtained. Between 480–540° two exothermal effects appear, corresponding to the decomposition of chlorosalicylate complex and between 540–615° the total decomposition of the complex is produced by a strong endothermal effect (580°), the Er_2O_3 oxide remaining as a final product.

---

[12] F. A. Cotton, R. D. Barnes and E. Bannister, *J. Chem. Soc. A*, **1960**, 2199.

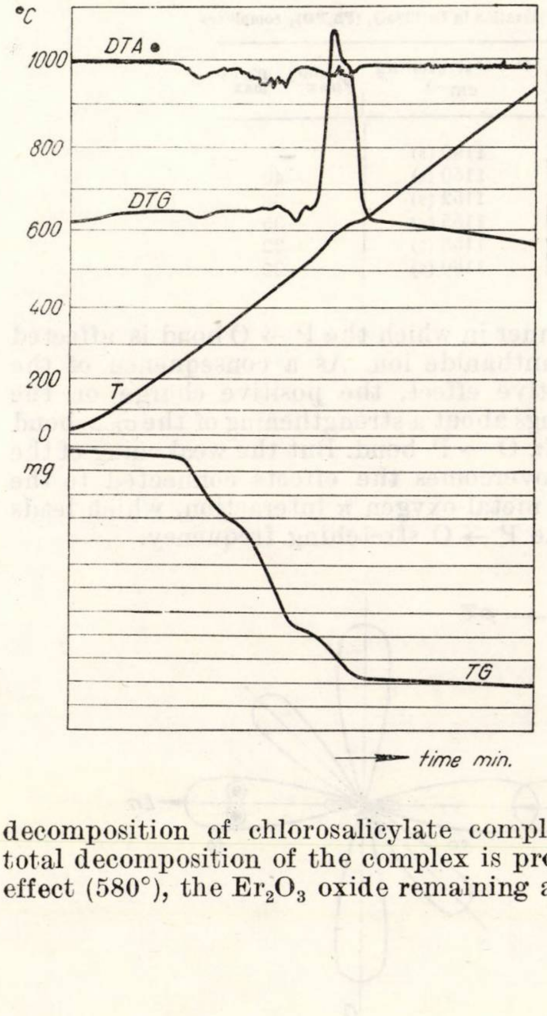

Fig. 4. – Thermal curves for $Er(ClSal)_3(Ph_3PO)_2$.

Revue Roumaine de Chimie, **18**, *12*, 2059–2066 (1973)

COMPLEX COMBINATIONS OF TRANSITION METALS WITH TERTIARY STIBINES. I

COMPLEX COMBINATIONS OF PALLADIUM (II) WITH TRITOLYL-STIBINES

D. NEGOIU * and LIDIA PARUTA**

* Faculty of Chemistry, University of Bucharest, Splaiul Independenţei, 89, Romania
** Center of Physical Chemistry, Str. Dumbrava Roşie, 23, Bucharest — 9, Romania

Received February 17, 1973

Complex combinations of Pd(II) containing aryl-stibine of the MX_2L_2, $M_2X_4L_2$ type, where M = Pd (II); L = (*ortho*-tolyl)$_3$Sb, (*meta*-tolyl)$_3$Sb and (*para*-tolyl)$_3$Sb; X = Cl^-, Br^-, I_2, NO_2^-, CN^-, SCN^-, have been prepared. The mononuclear compounds are obtained through the direct action of the ligand upon the salts of the transition metal in an adequate solvent according to the strong reduction effect of stibine at high temperatures. They are crystalline powders, brightly coloured, with a non-ionic structure and with diamagnetic properties. These combinations have a square-planar structure. The binuclear compounds are obtained either from the mononuclear compounds using an excess of the respective salt of the metal, or using the direct procedure, with the stoichiometric quantities required by the reaction. These compounds are crystalline powders brightly coloured, non-ionic, diamagnetic, with a bridged structure. Some physical and chemical properties as well as several splitting reactions of the halide bridges are presented in the case of binuclear compounds.

Similarly to the tertiary phosphines [1] and arsines [2] it was to be expected that the tertiary stibines form complex combinations with the transition metals. The most numerous and stable complex combinations are those with palladium (II); they are of the type: MX_2L_2 and $M_2X_4L_2$.

These complex combinations were studied for a long time because of their catalytic properties and researches have been intensified of late.[3] The catalytic activity is due to the presence of some empty orbitals at the central metal atom; these orbitals of low energy can form weak bonds with the hydrogen ion, as they accept electrons from the latter. The acid character of these bonds and, therefore, the catalytic activity of the compounds is highly affected by the nature of the other ligands present in the coordination sphere.

---

[1] F. G. Mann and F. H. C. Stewart, *J. Chem. Soc.*, **1955**, 1269; **1963**, 873.
[2] G. Both, *Adv. Inorg. Chem. Radiochem.*, **6**, 1 (1964).
[3] J. C. Bailar and H. Itatani, *J. Amer. Chem. Soc*, **89**, 1592 (1967).

The ligand containing phosphine or stibine was used as catalyst.

The tertiary stibines with alkyl or aryl radicals form numerous relatively stable coordinative compounds; but the capacity of coordination is stronger for the alkyl radicals than for the aryl ones. The fact is due to the strong decrease of the electronic doublet of stibium for coordination and it appears as a consequence of the configuration interaction between the aromatic ring and the free doublet of the stibium atom.

The present paper mainly describes the mononuclear combinations of the MX_2L_2 type and the binuclear combinations $M_2X_4L_2$ which were obtained for palladium (II) with tris-*o*-tolyl-stibine, tris-*m*-tolylstibine and tris-*p*-tolylstibine, where $X = Cl^-, Br^-, I^-, NO_2^-$.

We have also tried to prepare compounds analogous to the phosphines with $X = CN^-$ and SCN^- but only compounds of the type $[PdX(CN)\,L_2]$ and $[PdX(SCN)\,L_2]$ were obtained. The structure of the latter is not entirely elucidated. The same method as the one followed for the synthesis of these compounds was used with only some slight differences regarding the working conditions.

The acetone solutions of the respective tris-tolyl-stibines were treated, in water bath and under refluxing with the aqueous solutions of halides or palladium (II) nitrites in a medium of hydrochloric acid.

The corresponding complex with acetate was obtained in a reaction of double change between $[PdI_2(Sb-p-tolyl_3)_2]$ and $CH_3COO.Tl^{(I)}$.

In order to obtain binuclear compounds one can use either the above mentioned method respecting the stoichiometric ratios, or starting from the respective mononuclear compound and treating it with an excess of palladium (II) salt. Because of the reduction character of stibine which is stronger than those of phosphines or analogous arsines, the reactions are carried out between certain limits of temperature and concentration. The solvent used has an important part in the preparation of the syntheses. The complex combinations thus obtained as well as some of their properties are given in tables 1 and 2.

The stability of the combinations with phosphines, arsines, stibines, assumes lower values in this order.

These complexes crystallize with much greater difficulty are obtained with a lesser yield, and the melting points are not well defined because of their decomposition.

The mononuclear compounds, light-yellow to red-dark brown coloured, are crystalline powders, easily soluble in chloroform, little soluble in benzene and nitrobenzene and insoluble in alcohol, ether and water.

They are non-electrolytes in nitrobenzene (see table 2) and, alike all the square-planar compounds of Pd (II), have diamagnetic properties.

The first and the most general method to prepare the binuclear compounds, developed by Mann,[1] consists in treating the simple compounds PdX_2L_2 in stoichiometric ratios and under refluxing with tetrachloropalladate of ammonium. Binuclear compounds of the $Pd_2X_4L_2$ type are obtained. The reaction takes place in ethanol or acetone at an optimal temperature and is complete sometimes after a few hours, at other times, after several days.

Table 1

The analysis of Pd (II) complex combinations with *tri- ortho-*, *meta*-and *para*- tolylstibine

Compound	Analysis C % *Calcd.* *Found*	 H % *Calcd.* *Found*	 Pd % *Calcd.* *Found*	 N % *Calcd.* *Found*
$PdCl_2(Sb\text{-}p\text{-}tolyl_3)_2$	52.10 51.9	4.34 4.29	11.03 11.0	— —
$PdBr_2(Sb\text{-}p\text{-}tolyl_3)_2$	47.7 47.5	3.9 3.6	10.0 9.6	— —
$PdI_2(Sb\text{-}p\text{-}tolyl_3)_2$	43.8 43.6	3.6 3.4	9.2 8.9	— —
$Pd(NO_2)_2(Sb\text{-}p\text{-}tolyl_3)_2$	51.0 49.6	4.2 4.0	10.7 10.3	2.8 2.6
$Pd(CH_3COO)_2(Sb\text{-}p\text{-}tolyl_3)_2$	54.4 54.2	4.7 4.5	10.5 10.4	— —
$Pd(CN)\ (Sb\text{-}p\text{-}tolyl_3)_2Cl$	53.8 53.0	4.3 4.1	11.1 10.8	1.4 1.3
$Pd(SCN)\ (Sb\text{-}p\text{-}tolyl_3)_2Cl$	52.4 52.2	4.2 4.0	10.0 9.9	1.4 1.3
$Pd_2Cl_4(Sb\text{-}p\text{-}tolyl_3)_2$	44.0 43.8	3.6 3.9	9.4 9.0	— —
$Pd_2Br_4(Sb\text{-}p\text{-}tolyl_3)_2$	38.1 38.0	3.1 2.8	8.0 7.8	— —
$Pd_2I_4(Sb\text{-}p\text{-}tolyl_3)_2$	33.3 33.2	2.7 2.5	7.0 6.5	— —
$Pd_2(NO_2)_4(Sb\text{-}p\text{-}tolyl_3)_2$	42.4 42.0	3.5 3.2	8.1 8.0	4.7 4.6
$PdCl_2(Sb\text{-}m\text{-}tolyl_3)_2$	52.10 52.0	4.34 4.0	11.03 10.9	— —
$PdI_2(Sb\text{-}m\text{-}tolyl_3)_2$	43.8 43.0	3.6 3.3	9.2 9.0	— —
$Pd_2Cl_4(Sb\text{-}m\text{-}tolyl_3)_2$	44.0 43.2	3.6 3.4	9.4 9.1	— —
$Pd_2I_4(Sb\text{-}m\text{-}tolyl_3)_2$	33.3 32.8	2.7 2.5	7.0 6.9	— —
$PdCl_2(Sb\text{-}o\text{-}tolyl_3)_2$	52.10 52.0	4.3 4.0	11.03 10.8	— —
$PdBr_2(Sb\text{-}o\text{-}tolyl_3)_2$	47.7 47.1	3.9 3.5	10.0 9.5	— —
$PdI_2(Sb\text{-}o\text{-}tolyl_3)_2$	43.8 42.9	3.6 3.3	9.2 9.0	— —
$Pd(NO_3)_2(Sb\text{-}o\text{-}tolyl_3)_2$	51.0 49.4	4.2 4.0	10.7 10.2	2.8 2.7
$Pd_2Cl_4(Sb\text{-}o\text{-}tolyl_3)_2$	44.0 43.6	3.6 3.2	9.4 9.3	— —
$Pd_2Br_2(Sb\text{-}o\text{-}tolyl_3)_2$	38.1 37.6	3.1 3.0	8.0 7.6	— —
$Pd_2I_2(Sb\text{-}o\text{-}tolyl_3)_2$	33.3 33.0	2.7 2.3	7.0 6.9	— —
$Pd_2(NO_2)_4(Sb\text{-}o\text{-}tolyl_3)_2$	42.4 42.0	3.5 3.1	8.1 8.0	4.7 4.7

The complex stibines of this class are far more intensely coloured and less stable than the phosphines or the arsines of the same type. They have far more different melting points than the mononuclear compounds and are less stable in organic solvents.

These compounds are much more easily obtained than those with Pt (II).[4]

One has also tried to prepare some different classes of complex combinations with triarylstibine and to establish some transformation relations between them.[5] Thus, were obtained :

Table 2

Some properties of the complex combinations

Compound	Colour	Melting point °C	Molar conductivity $\Lambda(\Omega^{-1}mol^{-1}cm^2)$ $PhNO_3$, 22°C
$PdCl_2(Sb\text{-}p\text{-}tolyl_3)_2$	yellow-green	250	0.53
$PdBr_2(Sb\text{-}p\text{-}tolyl_3)_2$	yellow-orange	185	0.71
$PdI_2(Sb\text{-}p\text{-}tolyl_3)_2$	red-brown	192	0.70
$Pd(NO_2)_2(Sb\text{-}p\text{-}tolyl_3)_2$	yellow-green	155–160	0.80
$Pd(CH_3COO)_2(Sb\text{-}p\text{-}tolyl_3)_2$	yellow	198	0.49
$Pd(CN)\ (Sb\text{-}p\text{-}tolyl_3)_2Cl$	white-cream	110	0.60
$Pd(SCN)\ (Sb\text{-}p\text{-}tolyl_3)_2Cl$	rose-peach	170	0.65
$Pd_2Cl_4(Sb\text{-}p\text{-}tolyl_3)_2$	yellow-red	300	0.70
$Pd_2Br_4(Sb\text{-}p\text{-}tolyl_3)_2$	dark red	166	0.65
$Pd_2I_4(Sb\text{-}p\text{-}tolyl_3)_2$	brown-red	188	0.76
$Pd_2(NO_2)_4(Sb\text{-}p\text{-}tolyl_3)_2$	yellow	140–145	0.80
$PdCl_2(Sb\text{-}m\text{-}tolyl_3)_2$	light yellow	167	0.58
$PdI_2(Sb\text{-}m\text{-}tolyl_3)_2$	dark red	147	0.72
$Pd_2Cl_4(Sb\text{-}m\text{-}tolyl_3)_2$	black-brown	140	0.76
$Pd_2I_4(Sb\text{-}m\text{-}tolyl_3)_2$	brown-red	142	0.80
$PdCl_2(Sb\text{-}o\text{-}tolyl_3)_2$	yellow	205	0.90
$PdBr_2(Sb\text{-}o\text{-}tolyl_3)_2$	orange	195	0.60
$PdI_2(Sb\text{-}o\text{-}tolyl_3)_2$	brown-red	203	0.71
$Pd(NO_2)_2(Sb\text{-}o\text{-}tolyl_3)_2$	light yellow	140	0.78
$Pd_2Cl_4(Sb\text{-}o\text{-}tolyl_3)_2$	brick colour	140	0.74
$Pd_2Br_4(Sb\text{-}o\text{-}tolyl_3)_2$	brown-red	183	0.68
$Pd_2I_4(Sb\text{-}o\text{-}tolyl_3)_2$	dark-brown	190	0.85
$Pd_2(NO_2)_4(Sb\text{-}o\text{-}tolyl_3)_2$	light yellow	110–115	0.66
$PdBr_2(Sb\text{-}m\text{-}tolyl_3)_2$	brown	120	0.75

— mononuclear compounds with identical neutral ligands

$$PdX_2\ (SbR_3)_2$$

— binuclear compounds with identical neutral ligands

$$Pd_2X_4\ (SbR_3)_2$$

— mononuclear compounds with different neutral ligands

$$PdX_2\ (SbR_3)\ L$$

where : L = pyridine (py), piperidine (pip), triphenylphosphine (PPh_3) and X = Cl^-, Br^- cr I^-.

---

[4] J. Chatt and L. M. Venanzi, *J. Chem. Soc.*, **1955**, 2787; **1968**, 184.

[5] D. Negoiu and V. Şerban, *Anale. Univ. Chim.* (*Bucureşti*), ,**19** (2), 45 (1970).

Table 3

The analysis of Pd (II) mononuclear compounds with different neutral ligands

Binuclear complex with initial identic neutral ligands	L′	Mononuclear complex with different resulted neutral ligands	Colour	Melting point °C	Analysis		
					C % *Calcd.* *Found*	H % *Calcd.* *Found*	N % *Calcd.* *Found*
Pd$_2$Cl$_4$(Sb-*p*-tolyl$_3$)$_2$	py	PdCl$_2$(Sb-*p*-tolyl$_3$) py	light yellow	247	49.7 47.0	3.9 3.6	2.1 2.0
Pd$_2$Br$_4$(Sb-*p*-tolyl$_3$)$_2$	py	PdBr$_2$(Sb-*p*-tolyl$_3$) py	orange	300	42.0 41.8	3.5 3.1	1.89 1.75
Pd$_2$I$_4$(Sb-*p*-tolyl$_3$)$_2$	py	PdI$_2$(Sb-*p*-tolyl$_3$) py	red-orange	300	37.4 37.0	3.1 2.9	1.6 1.4
Pd$_2$Br$_4$(Sb-*p*-tolyl$_3$)$_2$	pip	PdBr$_2$(Sb-*p*-tolyl$_3$) pip	red-brown	d	41.8 41.2	4.4 4.2	1.8 1.7
Pd$_2$I$_4$(Sb-*p*-tolyl$_3$)$_2$	pip	PdI$_2$(Sb-*p*-tolyl$_3$) pip	brown	d	37.1 37.0	3.9 3.6	1.6 1.5
Pd$_2$Br$_4$(Sb-*p*-toyl$_3$)$_2$	PPh$_3$	PdBr$_2$(Sb-*p*-tolyl$_3$) PPh$_3$	red-orange	196d	50.7 49.8	3.9 3.6	17.3 17.2
Pd$_2$I$_4$(Sb-*p*-tolyl$_3$)$_2$	PPh$_3$	PdI$_2$(Sb-*p*-tolyl$_3$) PPh$_3$	red-brown	235	30.6 30.4	2.5 2.3	1.3 1.2

The mononuclear complex combinations with different neutral ligands were obtained starting from the binuclear compound $Pd_2X_4L_2$ and treating it with a primary amine or even a tertiary phosphine or arsine.

There occurs a splitting of the halogen bridges and two identic molecules of mononuclear compound, in which the ligands are different, appear:

$$[Pd_2X_4L_2] + 2L' \rightleftarrows 2[PdX_2LL']$$

The reaction is reversed. A decisive role is played by the temperature, the solvent used, the splitting reagent and, of course, the stoichiometric ratio.

At high temperatures, if the solution is concentrated or if there is an excess of splitting reagent, the reaction goes as follows:

$$[Pd_2X_4LL'] \longrightarrow [PdX_2L_2] + [PdX_2L'_2]$$

Generally speaking, one can assert that the following transformations may be noticed between the complex combinations of Pd (II).

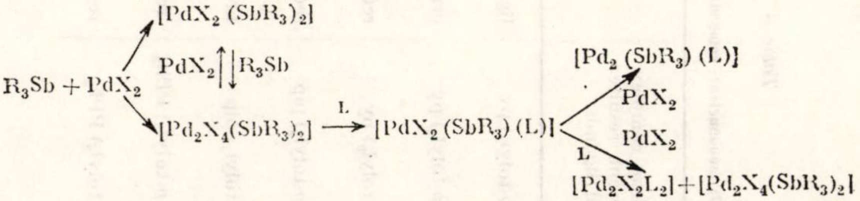

These complex compounds are crystalline powders, coloured from light yellow to dark brown, not electrolyte in nitrobenzene, with indefinite melting points, owing to the fact that they decompose when heated. They are easily soluble in organic solvents, compared to the binuclear compounds from which they derive.

EXPERIMENTAL

The *ortho-*, *meta-*, *para-*tolylstibine ligands were prepared in two steps. In the first step, $SbCl_3$ was obtained after reducing Sb_2Cl_5 with metallic stibium. In the second one, the Würtz synthesis was used to obtain the respective stibine in perfectly anhydrous solvents.

1. DICHLOROBIS-(TRI-*p*-TOLYLSTIBINE) PALLADIUM (II)

Solutions of the respective compounds in stoichiometric ratio are obtained. $PdCl_2 . 2H_2O$ (0.106 g) is solved in 10 ml water to which some drops of concentrated hydrochloric acid are added, after which it is heated up to the boiling point, until complete solvation. Small quantities of the aqueous solution of palladium chloride are added, while stirring, to the hot acetone solution of stibine. The temperature of the solution is no longer raised because the metallic palladium would rapidly be reduced (the colour of the solution becomes suddenly darker towards brown-black). After some hours, beautifully coloured crystals (light-yellow) are separated from the compound. They are filtered, washed with alcohol and dried under vacuum.

2. DIBROMOBIS-(TRI-*p*-TOLYLSTIBINE) PALLADIUM (II)

To a tri-*p*-tolylstibine solution (0.395 g) in 25 ml hot acetone is added a solution of lithium bromide (3 g LiBr in 5 ml water) and then an aqueous solution of $PdCl_2.2H_2O$ (0.106 g) in a medium of hydrochloric acid. The solution is immediately intensely coloured in red.

The solution is concentrated and about an hour later a fine yellow-red precipitate is separated at cooling. It is filtered, washed with alcohol and dried under vacuum.

3. DIIODOBIS-(TRI-*p*-TOLYLSTIBINE) PALLADIUM (II)

To the tri-*p*-tolylstibine solution (0.395 g) in 50 ml acetone, a solution of potassium iodide (3 g in 10 ml water) and a solution of $PdCl_2.2H_2O$ (0.106 g in 10 ml water) is added. A dark-red solution is formed and it is heated for a time under refluxing.

A red-brown precipitate is separated at cooling. It is filtered, washed in alcohol and dried under vacuum.

The analogous mononuclear compounds of this series are obtained in the same way, using a ten times increased quantity of natrium nitrite cyanide or alkaline thiocyanide

The binuclear complexes of the type $[Pd_2X_4(Sbtolyl_3)_2]$ can be obtained in two ways :

a) Heating under refluxing a suspension of a mononuclear complex in acetone to which a stroichiometric quantity of palladium chloride in aqueous hydrochloric solution is added.

b) By treating directly the palladium (II) halide with tritolylstibine in ethanol or acetone.

As for mononuclear complexes, bromo-, iodo-, nitroderivatives are obtained starting from a larger excess of bromide, iodide, and, respectively, alkaline nitrite.

Both for the mononuclear and binuclear complexes for the same radical, the stability increases in the $Cl < Br < I$, order so that taking also into account their lesser solubility, the tetraderivatives are often separated with quantitative efficiencies. Other compounds of the PdX_2LL' type are prepared in the following way :

DIBROMO-(TRIPHENYLPHOSPHINE-TRI-*p*-TOLYLSTIBINE) PALLADIUM (II)

To a dibromo-μ-dibromobis-(tri-*p*-tolylstibine)-dipalladium (II) suspension in chloroform is added under continuous stirring a stroichiometric quantity of triphenylphosphine. After a certain time a clear yellow-red solution is obtained.

It is left to concentrate under vacuum and then absolute ethanol is added. Brick-red coloured crystals are filtered, washed with alcohol and dried under vacuum.

DICHLORO-(PYRIDIN)-(TRI-*p*-TOLYLSTIBINE) PALLADIUM (II)

To a dichloro-μ-dichlorobis-(tri-*p*-tolylstibine) dipalladium (II) suspension in acetone, small quantities of pyridine (in acetone solution too) are added, under continuous stirring.

Eventually, a clear, yellow solution is obtained and it is concentrated by stirring with a current of dry nitrite. In the end, light-yellow crystals are separated.

They are filtered, washed with acetone and alcohol and dried under vacuum.

DIIODOPIPERIDINE-(TRI-*p*-TOLYLSTIBINE) PALLADIUM (II)

To the red diiodo-μ-diiodobis-(tri-*p*-tolylstibine) dipalladium (II) solution in methylene chloride (the solvation being quick) the piperidine solution is added in the same solvent.

The red colour of the solution immediately becomes brown. It is left for about 48 hours under vacuum.

When it concentrates, alcohol is added. Immediately, brown-red crystals may be separated. They are filtered, washed with acetone and dried under vacuum.

Revue Roumaine de Chimie, **18**, *12*, 2067–2075 (1973)

MÖSSBAUER EFFECT IN COMPLEXES OF ISONICOTINIC ACID HYDRAZIDE WITH Fe(II) – ISOTHIOCYANATE $(INAH)_2Fe(NCS)_2H_2O$

IULIA I. GEORGESCU *, M. MORARIU ** and DOINA ŢARINA **

* Polytechnical Institute of Bucharest, Str. Polizu 1, Bucharest, Romania
** Institute of Atomic Physics, Bucharest, Romania

Received February 8, 1973

The Mössbauer effect has been used to study *cis* – *trans* isomerism in some complexes of the isonicotinic acid hydrazide with Fe (II) and isothiocyanate $(INAH)_2Fe(NCS)_2 . H_2O$.

INTRODUCTION

The present work deals with the study by Mössbauer effect of some complexes of the isonicotinic acid hydrazide with Fe(II) and the isothiocyanate $(INAH)_2Fe(NCS)_2 . H_2O$, whose detailed chemical formula is given in figure 1. In this type of chelate compound, the divalent iron is in an octhaedral symmetry, analogous to that found in the $Py_4Fe(NCS)_2$ complex.[1]

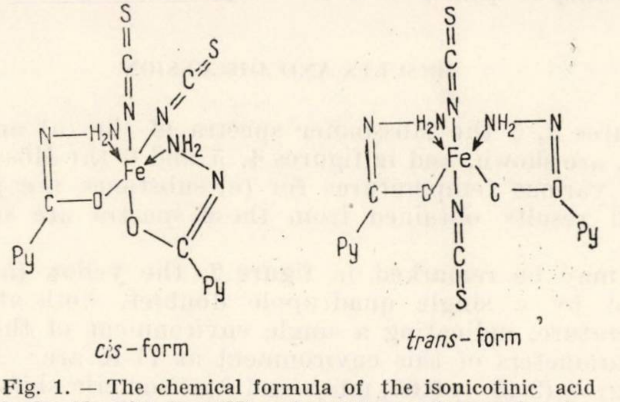

Fig. 1. – The chemical formula of the isonicotinic acid hydrazide with iron (II) and isothiocyanate complex chelate $(INAH)_2Fe(NCS)_2$.

---

[1] P. Spacu, D. Ciomârtan and M. Teodorescu, *Z. chem.*, **8**, 233 (1968).

Recently,[2] Mössbauer effect measurements have made evident the possibility of existence of the *cis* — *trans* isomerism in the above mentioned chelate compound.

In the following we intend to clarify the existence of the two isomers in the case of these substances, correlating the results of the Mössbauer study with the data obtained on the same samples [3] from the thermogravimetrical and thermodifferential analyses, from the UV reflection spectra and the X-ray diffraction analysis. The studied $(INAH)_2Fe(NCS)_2.H_2O$ complexes have been synthetised in two ways: first, by using Fe^{2+} in the synthesis, two substances were obtained, a light yellow substance marked by us with (a) and another reddish one marked with (b). The reddish substance (b) was obtained by heating the yellow precipitate in the synthesis solution up to 100°. In the second case, Fe^{3+} was used for the synthesis and a brown-black compound was obtained and marked with (c). The chemical analyses of the (a) and (b) complexes have confirmed the empirical formula for both compounds

EXPERIMENTAL METHOD

The Mössbauer spectra were obtained by means of the ELRON type equipment in a transmission arrangement described in.[4] A ^{57}Co in copper matrix source with an activity of 10 mCi was used and as a detector a NaI(Tl) crystal. The data accumulation was performed in a multichannel analyzer DIDAC-4000, Intertechnique, on 400 channels, using a source velocity of ± 10 mm/s. The fine powder samples were introduced between two mica plates. The measurements for (a) and (b) samples were performed at two temperatures, room temperature and liquid nitrogen temperature, and for (c) sample between 77 K and 463 K. The temperature stability was ± 1 K. The Mössbauer spectra were analysed by a computing program for quadrupole splitting in an ICL — type 1900 computer in the DESM code.

RESULTS AND DISCUSSION

In figures 2, 3 the Mössbauer spectra of the (a) and (b) chelate, respectively, are shown, and in figures 4, 5 and 6 the Mössbauer spectra obtained at various temperatures for (c) substance are presented. All experimental results obtained from these spectra are summarized in table 1.

As it may be remarked in figure 2, the yellow (a) substance is characterized by a single quadrupole doublet, both at 77 K and at room temperature, indicating a single environment of the Fe (II). The hyperfine parameters of this environment at 77 K are: $\Delta Q_{(a)}$ (quadrupole splitting) $= (2.43 \pm 0.03)$ mm/s and $\delta_{(a)}$ (isomeric shift) $= (+0.98 \pm \pm 0.03)$ mm/s. The spectrum of the reddish (b) substance (fig. 3) consists in the overlapping of two quadrupole doublets corresponding to two

---

[2] I. I. Georgescu, M. Hlevca, D. Barb, M. Morariu and D. Țarina, "Proceedings of the Conference on Mössbauer Spectrometry", vol. 2, Dresden, 1971, p. 470.

[3] I. I. Georgescu, D. Ciomârtan, G. Teodorescu, M. Hlevca and M. Zaharescu, *Rev. Roumaine Chim.*, **18**, 1159 (1973).

[4] D. Barb, "Efectul Mössbauer și aplicațiile sale", Ed. Academiei, București, 1972, p. 58.

Table 1

The experimental data for the (a) yellow, (b) reddish and (c) black-brown compounds. Isomer shift relative to ^{57}Co : Cu source

Sample	Colour	Temperature °K	Isomer shift δ (mm/s)			Quadrupole splitting ΔQ (mm/s)			Effect ε (%)			Observation
			trans	*cis*	Fe^{3+}	*trans*	*cis*	Fe^{3+}	*trans*	*cis*	Fe^{3+}	
(a)	yellow	77		+0.98			2.43			13.90		Prepared with $FeSO_4.7H_2O$
		296		+0.85			1.97			6.68		
(b)	reddish	77	+1.09	+1.09		3.18	2.39		17.73	5.49		
		296	+0.97	+0.99		2.43	1.85		10.65	1.76		
(c)	brown-black	77	+1.03	+0.99	+0.13	3.13	2.35	0.39	1.96	5.63	1.08	Prepared with $Fe_2(SO_4)_3$
		156	+0.99	+0.92	−0.03	3.02	1.97	0.40	0.87	2.73	0.64	
		222	+0.95	+0.68	+0.21	2.91	2.15	0.30	0.44	1.48	0.85	
		296	+0.95	+0.89	−0.25	2.99	1.83	0.35	0.66	1.78	0.35	
		322	+0.84	+0.62	−0.07	3.16	2.13	0.27	0.15	0.94	0.44	
		373	+0.67	+0.61	−0.07	2.85	2.14	0.37	0.24	0.83	0.53	
		418	+0.55	+0.55	+0.08	2.48	2.08	0.39	0.43	0.69	0.83	
		463	+0.64	+0.48	+0.15	2.35	1.71	0.31	0.59	0.44	0.95	

vicinities of the Fe(II) one with parameters identical to those of (a) substance, $\Delta Q_{1(b)} = (2.39 \pm 0.03)$ mm/s, $\delta_{1(b)} = (+1.09 \pm 0.03)$ mm/s and the other more accentuated doublet having the same isomeric shift $\delta_{2(b)} = (+1.09 \pm 0.03)$ mm/s but a larger quadrupole splitting, namely $\Delta Q_{2(b)} = (3.18 \pm 0.03)$ mm/s. The brown-black sample (c) indicates three Mössbauer vicinities : two of Fe (II) identical with those found in sample (b) as regards the values of ΔQ and δ, and one of Fe (III) whose hyperfine parameters are not characteristic for the Fe^{3+} salt used for the synthesis (ferric sulphate) and on whose nature no hypothesis was made.

As it results from the above mentioned, the Mössbauer spectra indicate two distinct vicinities of Fe(II) which are found with the same hyperfine parameters, no matter the preparation method, the synthesis with Fe^{2+} or with Fe^{3+} of the respective complexes. The authors assign these two vicinities to the presence of the two isomers, *cis* and *trans*, possible from the theoretical point of view for the $(INAH)_2Fe(NCS)_2$ complex with the octahedral symmetry. The vicinity characteristic for the yellow substance, which is more stable, is assigned to the *cis* form, the other vicinity to the *trans* form. The isomeric shifts of the two chelate isomers were found to be equal, a fact which has been already reported in publications for the *cis-trans* isomerism.[5,6] The assignment of the form *cis* or *trans* has been done taking into account the fact that the quadrupole splitting of a *trans* form is larger than that of a *cis* form,[5,6] as well as the fact that the chemical stability is higher for the configuration with the best overlap of orbitals.

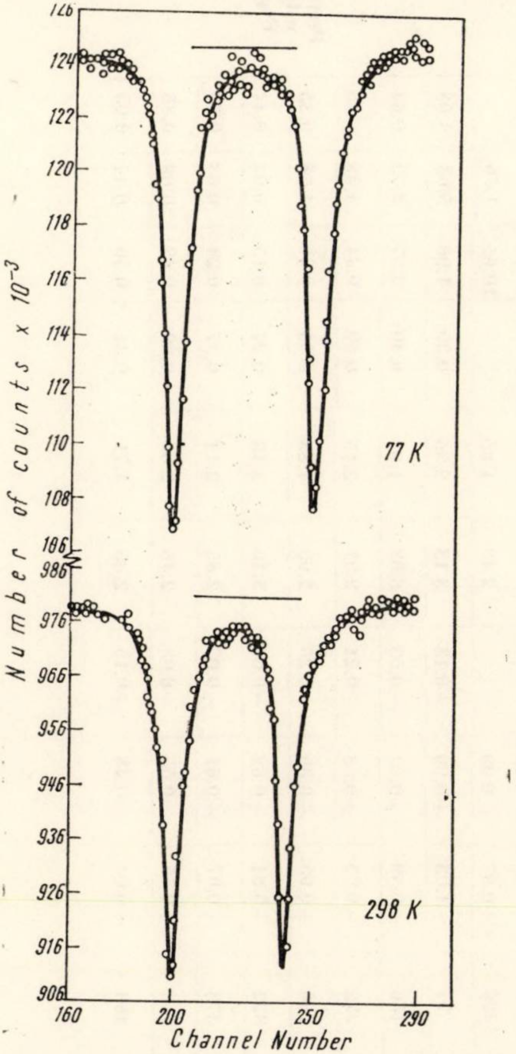

Fig. 2. — Mössbauer spectra of the (a) yellow chelate $(INAH)_2Fe(NCS)_2$ at 77 K and 298 K.

---

[5] R. B. Herber and R. G. Hayter, *J. Amer. Chem. Soc.*, **86**, 301 (1964).
[6] R. R. Berrett and B. W. Fitzsimmons, *J. Chem. Soc.* (*A*), **1967**, 525.

The X-ray diffraction analysis [3] supports the hypothesis of the existence of the two isomers. For (a) yellow and (b) reddish samples characterized by the major presence of the isomer *cis* respectively *trans*, the X-ray spectra have indicated all lattice plans of maximum intensity as being common for both substances, those corresponding to chelate (b) being more intense than those corresponding to chelate (a). These statements invalidate the supposition that the vicinity assigned to the *trans* form, predominant in the substance (b) would represent a strange compound, resulted during preparation. Moreover, the temperature dependence of the Mössbauer spectra of the (c) sample (figs. 4, 5, 6) clearly indicate the transition of the isomer *cis* into *trans* as the temperature increases. The ratio of the Mössbauer spectra areas corresponding to the two isomerical forms (table 2), proportional with the ratio of their concentration, shows that starting from about 350 K – 360 K the vicinity assigned to the *trans* form increases its concentration to the detriment of the vicinity assigned to the *cis* form. At the same time, UV reflection measurements[3] have shown that after heating at 353 K – 358 K for 10, 15 minutes, etc. and then cooling at room temperature, the UV reflection spectrum of the yellow (a) substance begins to indicate the UV reflection spectrum characteristic of (b) reddish substance. However, on the other hand, the temperature dependence of the quadrupole splitting values of the two vicinities of iron (II) in sample (c) (figure 7) proves the chemical

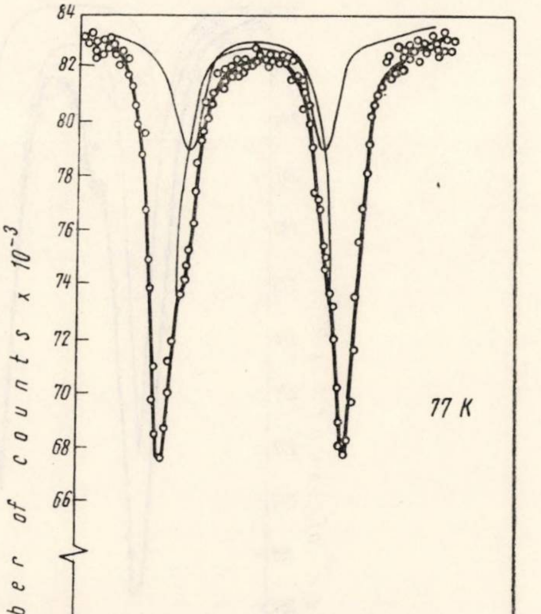

Fig. 3. — Mössbauer spectra of the (b) reddish chelate $(INAH)_2Fe(NCS)_2$ at 77 K and 298 K.

stability of these two vicinities up to 463 K. The thermogravimetrical and thermodifferential analyses [3] have also shown that substances (a), respectively (b), do not undergo any thermal decomposition up to 423 K.

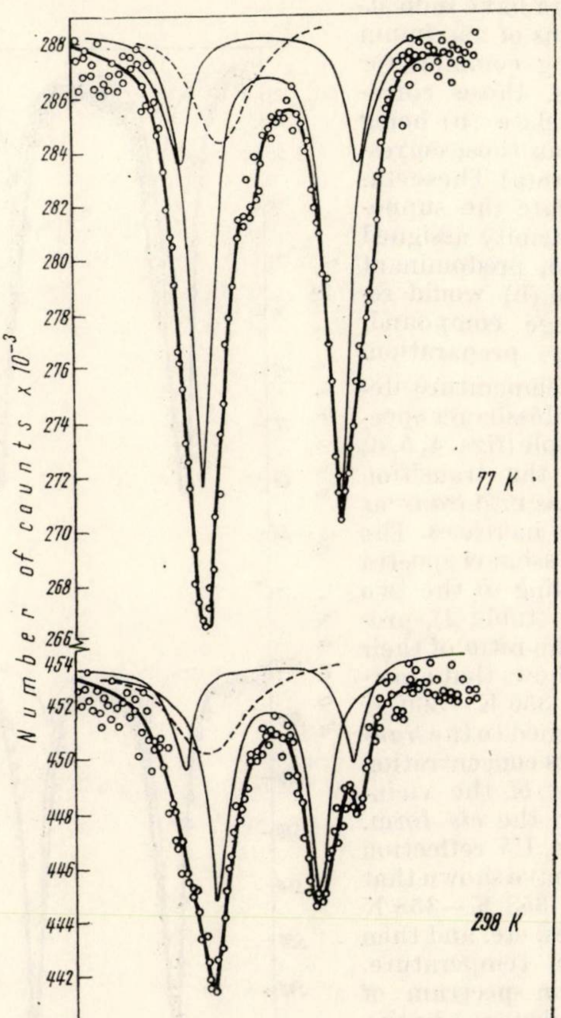

Fig. 4. — Mössbauer spectra of the (c) black-brown chelate at 77 K and 298 K.

Taking this fact into account, the increases of the rate of the *trans* vicinity to the detriment of the *cis* vicinity, remarked in Mössbauer spectra

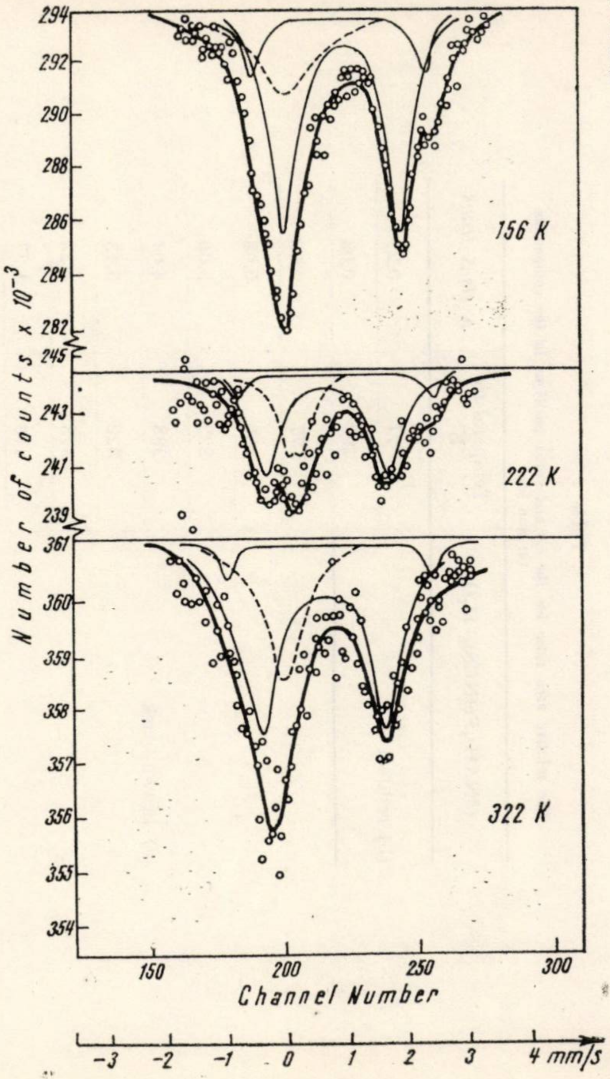

Fig.5. — Mössbauer spectra of the (c) black-brown chelate between 156 K and 322 K.

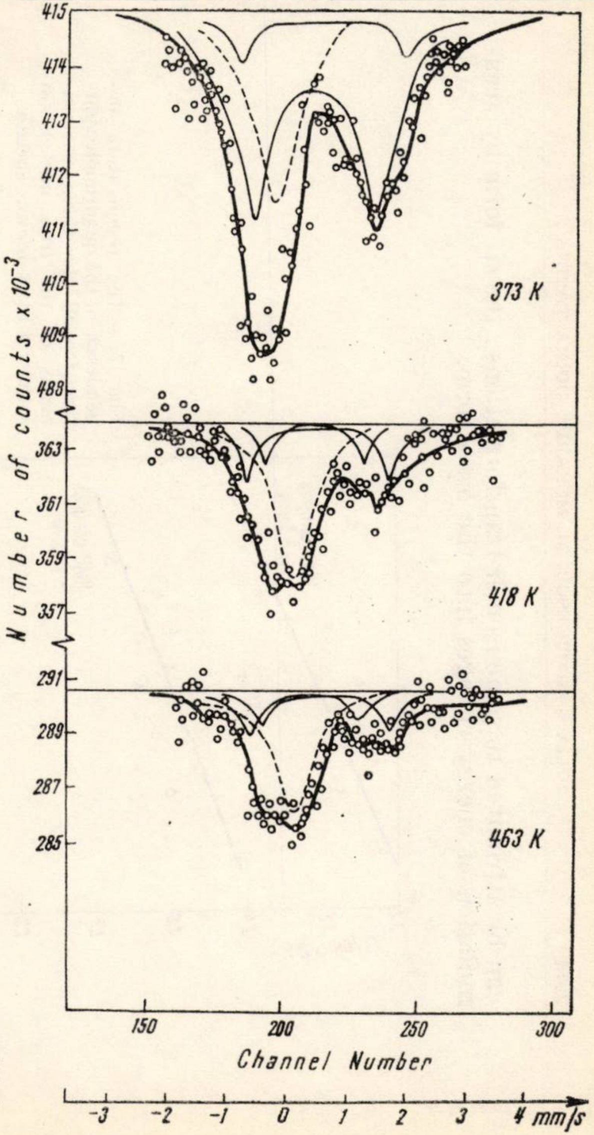

Fig. 6. — Mössbauer spectra of the (c) black-brown chelate between 373 K and 463 K.

can be attributed to some isomer transformations : the *cis* form by accumulation of energy changes into the *trans* form.

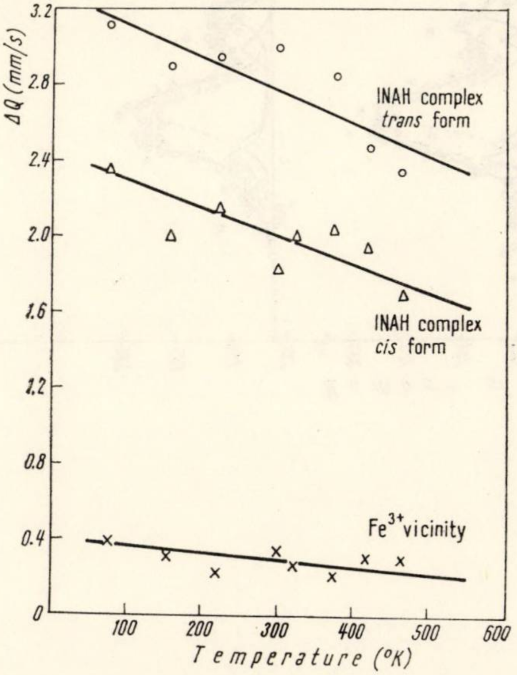

Fig. 7. — The temperature dependence of the quadrupole splitting for all the three environments of the iron nucleus in the (c) black-brown chelate.

Table 2

The relative area ratio for the *cis* and *trans* positions in the compounds (b) and (c)

$(INAH)_2Fe(NCS)_2 \cdot H_2O$	Temperature °K	A *cis*/A *trans*
(b) reddish	77	0.27
	298	0.08
(c) brown-black	77	4.06
	156	5.08
	222	3.66
	298	4.04
	322	5.13
	373	4.23
	418	1.97
	463	0.47

In fact, the obtaining of the reddish (b) substance, in which the *trans* form predominates, was due an to intentioned heating to 100° during preparation, supplying the energy necessary for the *cis* form molecules to change into the *trans* form.

In conclusion, the arguments submitted allow us to state the existence of the *cis* – *trans* isomerism in the complexes of the isonicotinic acid hydrazide with Fe (II) and isothiocyanate, mentioned in the present paper.

Revue Roumaine de Chimie, **18**, *12*, 2077–2082 (1973)

ADDITION COMPOUNDS OF TIN (IV) CHLORIDE WITH TETRADENTATE SCHIFF BASES

N. S. BIRADAR * and V. B. MAHALE

Department of Chemistry, Karnatak University, Dharwar, India

Received July 17, 1972

Addition compounds of tin(IV) chloride with tetradentate Schiff bases have been prepared in benzene medium and characterized by elemental analysis. The conductance measurements suggest that these are non-electrolytes in DMF. The infrared spectral studies show that these are all *cis* addition compounds with coordination number six. The ligands in the complexes exist in the phenolimine form and also contain intramolecular hydrogen bonding in them.

INTRODUCTION

The Schiff bases containing two coordinating centres ($-C=N$) and two active centres ($-OH$) are generally classed under tetradentate ligands.[1] These Schiff bases can behave as bidentates, if the active centres do not participate in the reaction. Recently, considerable interest has been focussed on the study of such complexes. Balmfield [2] has shown that cobalt (II) chloride forms adducts with bidentate aromatic Schiff bases and they exhibit quinonoid structures in the complexes. The recent reports have indicated that in uranium Schiff base adducts the *ortho* hydroxy oxygen involves in the coordinate bond formation.[3] It is, therefore, thought worthwhile to study the adducts of tin (IV) chloride with the tetradentate Schiff bases derived by condensing the substituted salicylaldehydes with either ethylenediamine or propylenediamine. The

---

* To whom correspondance should be addressed.

[1] H. A. Goodwin "Metal Chelates and Chelating Agents" Ed. by D. P. Mellor and F. P. Dwyer, Academic Press, New York, 1964; R. H. Holm, G. W. Everette Jr., and A. Chakravorty, "Progress in Inorganic Chemistry", Vol. 7, 1966, p. 83.

[2] P. Balmfield, *J. Chem. Soc., A.*, **1967**, 804.

[3] S. Yamada and A. Takeuchi, *Bull. Chem. Soc. Japan*, **42** 2549 (1969); *Chem. Abstr.* **72**, 27929 h (1970).

PMR studies have shown that such Schiff bases predominantly exist in phenolimine form[4] I. They can also exist in ketoamine form II.

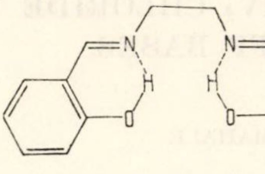

I

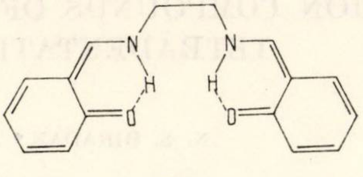

II

Hence, it is of some interest to know in which form these bases exist when complexed with tin (IV) chloride.

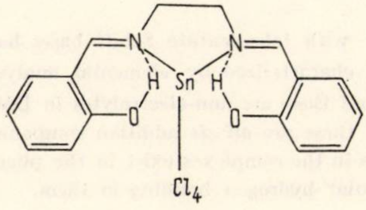

III

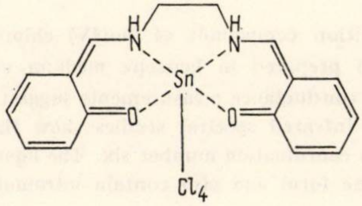

IV

The stereochemical promises allow only the formation of *cis* adducts.

In this paper we endeavour to show that the complexes of tin (IV) with these Schiff bases exist in the *cis* form having structure III.

EXPERIMENTAL

Ethylenediamine and propylenediamine were of reagent grade. Salicylaldehyde was of Bush make. The substituted salicylaldehydes were prepared by the Duff method.[5] Commercial grade benzene was purified by repeated distillation and stored over sodium wire. Tin (IV) chloride was of Riedel grade and used without further purification.

PREPARATION OF SCHIFF BASES

The diamine and aldehyde in 1 : 2 molar proportions were refluxed in alcohol medium for about an hour. The resulted Schiff base was filtered and dried in vacuum over fused calcium chloride.

---

[4] G. O. Dudeck and R. H. Holm ; *J. Amer. Chem. Soc.*, **83,** 2099 (1961) ; J. J. Charette, *Spectrochim. Acta,* **19,** 1270 (1963).

[5] J. C. Duff, *J. Chem. Soc.*, **1941,** 547.

PREPARATION OF COMPLEXES

Tin (IV) chloride in benzene medium was treated with a slight excess of Schiff base in the same medium, with vigorous shaking and left at room temperature for several hours with occasional shaking. The complex precipitated was filtered off, washed free from the reagent with benzene and dried in vacuum over fused calcium chloride.

ELEMENTAL ANALYSIS

Tin in the complexes was estimated gravimetrically as SnO_2. Chloride was determined gravimetrically as AgCl, and nitrogen by the Kjeldahl method.

PHYSICAL MEASUREMENTS

The molar conductance in DMF was determined on an ELICO conductivity bridge C.M. 82, with a cell having cell constant 0.829 cm^{-1} manufactured by the Electronic Industrial Instruments Co., Hyderabad.

The infrared spectra of the complexes in nujol mull were recorded on a Beckman IR-20.

RESULTS AND DISCUSSION

The Schiff bases under present investigation react with tin (IV) chloride in benzene medium to give yellow coloured amorphous complexes in high yield. Non-evolution of hydrogen chloride gas in the course of reaction suggests that they are adducts. The elemental analysis (table 1) is in agreement with the constitution comprising one molecule of ligand, four atoms of chlorine and one of tin. These complexes are non-electrolytes in DMF. These observations lead us to predict either hexacoordination stereochemistry (III) or octacoordination stereochemistry (IV) for these complexes. In view of the stability of the hexacoordinate complexes, it may be assumed that (III) is more favourable than (IV). This view further finds support in the study of the I.R. spectra of the complexes.

I.R. SPECTRA

The important infrared frequencies are listed in table 2, along with the assignments.

The broad weak band observed in the region 2700 – 2600 cm^{-1} in the ligands due to the intramolecular hydrogen bonded —OH is retain-

Table 1

Elemental analysis of Sn (IV) Schiff base complexes[a].

Ligands[b]	Comp. N°	Complexes	% Sn	% N	% Cl
Sal. en	V	$(C_{16}C_{16}N_2O_2)\ SnCl_4$	23.10 (22.44)	5.32 (5.27)	26.98 (26.84)
3-Me-Sal. en	VI	$(C_{18}H_{20}N_2O_2)\ SnCl_4$	21.61 (21.31)	5.05 (5.02)	26.05 (25.49)
4-Me-Sal.en	VII	$(C_{18}H_{20}N_2O_2)\ SnCl_4$	20.86 (21.31)	5.10 (5.02)	25.95 (25.49)
5-Me-Sal. en	VIII	$(C_{18}H_{20}N_2O_2)\ SnCl_4$	21.74 (21.31)	5.00 (5.02)	25.40 (25.49)
5-Cl-Sal. en	IX	$(C_{16}H_{14}Cl_2N_2O_2)\ SnCl_4$	19.50 (19.86)	4.54 (4.68)	23.76 (23.74)
2-OH-Naphthal. en	X	$(C_{24}H_{20}N_2O_2)\ SnCl_4$	18.01 (18.87)	4.50 (4.45)	22.40 (22.57)
5-Cl-Sal. pn	XI	$(C_{17}H_{16}Cl_2N_2O_2)\ SnCl_4$	20.00 (19.39)	4.16 (4.57)	23.28 (23.20)
2-OH-Naphthal. pn	XII	$(C_{25}H_{22}N_2O_2)\ SnCl_4$	17.32 (18.46)	4.54 (4.35)	22.00 (22.09)
5-Me-Sal. pn	XIII	$(C_{19}H_{22}N_2O_2)\ SnCl_4$	20.70 (20.79)	4.81 (4.90)	24.80 (24.87)

a Values in parentheses are calculated values.
b Sal = Salicylaldehyde ; Naphthal = 1-naphthaldehyde ;
en = ethylenediamine ; pn = propylenediamine.

ed in the complexes. The band due to the phenolic C—O at 1280 cm^{-1} in these bases does not show considerable shift towards higher frequency. The involvement of —OH in the bond formation usually shifts the phenolic C—O to the region between 1390 and 1300 cm^{-1}. These observations clearly suggest that the —OH groups have not taken part in the reaction, and the Schiff bases exist in the phenolimine structure.

The strong band around 1630 cm^{-1} due to the C = N stretch of the ligand shifts a little towards higher frequency and is found around 1640 cm^{-1}, indicating that the coordinate bond is formed between tin (IV) and azomethine nitrogen.

ν (Sn—N) VIBRATIONS

The metal-ligand vibrations are expected to occur in the region below 600 cm^{-1} for a number of complexes.[6] It is known that the *trans* form gives rise to only one band whereas *cis* form gives two I.R. active

---

[6] C. P. Prabhakaran and C. C. Patel, *J. Inorg. Nuclear Chem.*, **31**, 3316 (1969); B. C. Sharma, and C. C. Patel, *Indian J. Chem.*, **8**, 747 (1970); N. S. Biradar and V. H. Kulkarni, *J. Inorg. Nuclear Chem.*, **33**, 3847 (1971) and *Z. anorg. Chem.*, **387**, 275 (1972).

Table 2

Infrared frequencies (in cm^{-1}) of Sn (IV) complexes of Schiff bases and their assignments

Comp. N°	Intramolecular H-bonded-OH	ν(C=N)	ν(C−O)	ν(Sn−N)	ν(Sn−Cl)
V	2670 w	1640 s	1280 s	530 m. br 520 m. br	295 s 282 sh
VI	2670 w	1630 s	1270 s	542 s 502 s	310 sh 290 s.br
VII	2675 w	1650 s	1280 s	540 m.br 510 m.br	—
VIII	2660 w	1650 s	1280 s	534 s.br 500 s.br	294 s.br 282 sh
IX	2705 w	1640 s	1265 s	540 w 520 s	290 s 277 sh
X	2670 w	1640 s	1270 s	540 s 510 v.s	310 s 280 sh
XI	2680 w	1640 s	1280 s	545 m 505 m	305 s 280 sh
XII	2715 w	1630 s	1270 s	530 m 510 m	308 s 290 sh
XIII	2660 w	1650 s	1280 s	536 m.br 500 m.br	298 s 280 sh.

Note: In the Schiff bases the band due to the intramolecular H-bonded −OH occurrs in the region 2700−2600 cm^{-1}, phenolic C−O around 1280 cm^{-1} and C = N stretch around 1620 cm^{-1}.

bands. The strong bands found around 536 and 502 cm^{-1} in the complexes under present investigation may be assigned to ν(Sn—N) vibration. The band at 475 cm^{-1} is found in the Schiff bases and the complexes. It is, therefore, assigned to the ligand band.

ν (Sn−O) VIBRATIONS

It is reported that the M—O vibrations are found in the region 500—400 cm.$^{-1}$ [7] But no band can be assigned to ν(Sn—O) vibration in this region for these complexes since these are adducts and the bands appearing in this region are all weak.

---

[7] D. M. Adams "Metal-Ligand and Related Vibrations", Edward Arnold Ltd., London, 1967.

ν (Sn–Cl) VIBRATIONS

The Sn–Cl stretching vibration is assigned at 403 cm^{-1} by the previous workers.[8] On coordination this band shifts to lower frequency.[9] In dipyridyl and 1,10-phenanthroline complexes the Sn–Cl stretch is reported in the region 328–275 cm^{-1}. It is established that the complexes of the type *trans* MX_4L_2 with D_{4h} symmetry require only one M–X stretching to be I.R. active, whereas *cis* complexes of the type MX_4L_2 and MX_4L' (where L′ is a bidentate ligand) with C_{2v} symmetry give rise to four I.R. active bands.[10] Beattie and co-workers,[8] however, suggest that there should be at least two M–Cl bands, present for the *cis* complexes.

In all these complexes, we observe two bands in the region 312–280 cm^{-1} and these have been assigned to ν (Sn–Cl) vibrations. The presence of four bands is the indicative of the fact that the complexes of tin (IV) chloride with these tetradentate Schiff bases exist in the *cis* form. The band around 312 cm^{-1} is assigned to the characteristic band of hexacoordinated tin (IV), in view of the previous assignments.[10]

All these observations establish that these tin (IV), adducts have the structure XIV which is synonymous to III.

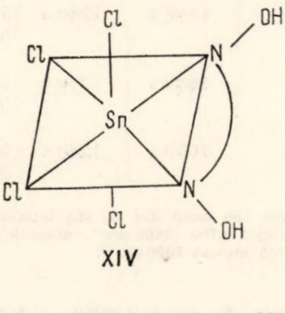

XIV

Acknowledgement. The authors wish to thank the Karnatak University for the financial assistance.

---

[8] I. R. Beattie, G. P. McQuillan, L. Rule and M. Webster, *J. Chem. Soc.*, **1963**, 1514.

[9] R. J. H. Clark, *J. Chem. Soc.*, **1963**, 1377.

[10] R. J. H. Clark, *Spectrochim. Acta*, **21**, 955 (1965).

Revue Roumaine de Chimie, **18**, *12*, 2083–2085 (1973)

VAPOUR PRESSURE OF ANTIMONY TRICHLORIDE

V. PIACENTE and G. BALDUCCI

Laboratory of Physical Chemistry and Electrochemistry
Institute of Chemistry, University of Rome, 00185 Rome, Italy

Received March 6, 1973

The vaporization behaviour of liquid $SbCl_3$ was studied by the transpiration method. Within the temperature range 360–428 K the vapour pressure equation was found to be log $P_{atm} = (4.07 \pm 0.64) - (2183 \pm 80)/T$ assuming monomeric $SbCl_3$ to be the only gaseous species. Second- and third-law calculations were performed using known and estimated thermodynamic data for $SbCl_3(g)$ and $SbCl_3(l)$ and obtaining enthalpies of vaporization.

Although thermodynamic data for the varporization of group VA trihalides are being cumulated, vapour pressure and enthalpy of vaporization values are scarce for $SbCl_3$. In addition to the early vaporization data quoted by Kelley,[1] the only vapour pressure values reported are those measured by Opperman[2] using a static method. We have measured the vapour pressure over liquid antimony (III) trichloride using a transpiration method. It was assumed that the vaporization occurs to only monomeric species according to the mass spectrometric results for $SbCl_3$[3] and by analogy with other similar systems.[4,5]

EXPERIMENTAL AND RESULTS

The measurements were made with the same transpiration apparatus which was described in details elsewhere.[6] Helium was used as carrier gas due to its high thermal conductivity and to the relatively easy purification procedure. The purification train and procedure was similar to that proposed by Bourke *et al.*[7] The vapour pressure was determined utilizing the relation

---

[1] K. K. Kelley, U.S. Bur. Mines Bull. N⁰ 383 (1935).

[2] H. Opperman, *Z. anorg. Chem.*, **356**, 1–7 (1967).

[3] P. Kusch, A. Hustrulid, and J. T. Tate, *Phys. Rev.*, **52**, 840 (1937).

[4] G. A. Gray and R. J. Sime, *J. Chem. Eng. Data*, **10**, 176 (1965) and references cited therein.

[5] D. Cubicciotti, *High Temp. Sci.*, **1**, 268 (1969).

[6] V. Piacente, A. Desideri, L. Malaspina, and A. Hallgass, *Rev. Int. Hts. Temp. et Refract.*, in press.

$$P_i = \frac{g_i}{g_i + (P_f\,\Phi\,\Delta t\,M_i)/RT_f} \qquad (1)$$

where-g_i is the amount in grams of the sample transported and condensed on the collector during the time Δt, M_i is the molecular weight, Φ is the carrier gas flow, in ml/min, measured at P_f and T_f.

The measurements were made in the range of flow 20 to 70 ml/min where the carrier gas was saturated with antimony trichloride vapours and the thermal diffusion effects were negligible. In these conditions, the measured vapour pressures were independent of the flow rate of the carrier gas.

The $SbCl_3$ (99% pure) was heated in the isothermal zone of a quartz tube furnace and the temperature was measured with a calibrated chromel-alumel thermocouple. In order to prevent as far as possible any contamination of the sample by the moisture, the operations of loading the sample into the transport tube and handling the collector with the condensate were made under inert gas anhydrous atmosphere. The amount of condensate was determined from the gain of weight of the collector after each vaporization run. Some determinations were also made using an analytical method, i.e. by volumetric titration of antimony according to a standard procedure.[8] The results obtained with the two procedures agreed within about 5%. Since the collector was water cooled, corrections were made to take into account the loss of weight of the condensate due to the sublimation which occurs at the temperature of the cooling water. Vapour pressure data for $SbCl_3(l)$ obtained from eq. (1) are reported in table 1. The equation $\log P_{\text{atm}} = (4.068 \pm 0.640) -$

Table 1

Vapour pressure and third-law enthalpy of vaporization of liquid $SdCl_3$

T (K)	Helium flow rate (ml/min)	Time (min)	Vapour pressure (atm)	$-R \ln P$	$-\Delta[(G^\circ_T - H^\circ_{298})/T]$ (eu)	ΔH°_{298} (Kcal/mole)
360	39.7	120	9.76×10^{-3}	9.202	16.02	9.08
368	34.7	110	1.24×10^{-2}	8.726	16.20	9.17
375	42.0	160	1.90×10^{-2}	7.870	16.35	9.08
380	30.4	90	2.08×10^{-2}	7.696	16.45	9.17
395	28.3	110	3.50×10^{-2}	6.658	16.85	9.28
404	46.0	110	4.88×10^{-2}	6.003	17.05	9.31
410	22.1	60	6.03×10^{-2}	5.582	17.15	9.32
413	42.8	80	6.14×10^{-2}	5.550	17.20	9.39
415	34.2	60	7.43×10^{-2}	5.166	17.20	9.28
428	29.2	60	7.58×10^{-2}	5.120	17.35	9.61
					Av.	9.3 ± 0.2

---

[7] P. J. Bourke, V. H. Denton, and H. D. Grey, AERE, R-4719 (1964).

[8] J. W. Mellor and H. V. Thompson, "A Treatise on Quantitative Inorganic Analysis", Griffin and Co., Ltd., London, 1938.

$(2183 \pm 80)/T$ was obtained by a least-squares fit of the experimental data. From this equation, the second-law heat of vaporization was calculated to be $\Delta H^\circ_{394} = 10.0 \pm 0.4$ kcal/mole. Using $C_p(\mathrm{SbCl_3}, g) = 19.83 - 1.20 \times 10^5 \mathrm{T}^{-2}$ [9] and $C_p\,(\mathrm{SbCl_3},\ l) = C_p\,(\mathrm{AsCl_3},\ l) = 31.9$,[9] the heat of vaporization at 298 K resulted to be $\Delta H^\circ_{298} = 11.2 \pm 0.4$ kcal/mole. For comparison test, the vapour pressure data were also treated by the third-law procedure. The resulting ΔH°_{298} is 9.3 ± 0.2 kcal/mole. The necessary free energy functions values for $\mathrm{SbCl_3}(g)$ were taken from Sundaram [10] and for $\mathrm{SbCl_3}(l)$ were calculated from the absolute entropy at 298 K and the heat capacity of the liquid. As experimental data are lacking, a value of 52.5 eu for the absolute entropy of $\mathrm{SbCl_3}(l)$ at 298 K has been calculated from reported thermodynamic data [11] (*viz.* heat of fusion, temperature of fusion, absolute entropy at 298°K and heat capacity for the solid). The free energy functions, $-(G^0_T - H^0_{298})/T$, for $\mathrm{SbCl_3}(l)$ so calculated were: 52.98, 53.85, and 54.97 eu at 350, 400, and 450 K, respectively. The errors in the second-law and in the average third-law enthalpy values represent only the standard deviations.

In view of the agreement between the two results, we propose for the heat of vaporization the value $\Delta H^0_{298} = 10 \pm 1$ kcal/mole, where the error is estimated and accounts for the uncertainties in the measurements and estimates.

In table 2 are shown for comparison vapour pressures and enthalpies of vaporization along with similar values of previous investigations.

Table 2

Comparison of vapour pressure equations and vaporization enthalpies of $\mathrm{SbCl_3}\ (l)$.

Temperature range (K)	$\log P_{atm} = A - B/T - C \log T$			ΔH°_{298} (2nd law) (kcal/mole)	ΔH°_{298} (3rd law) (kcal/mole)	Method	Ref.
	A	*B*	*C*				
m.p. – b.p.	26.60	3770	7.04	13.1 ±0.4	—	—	1
363–463	5.40	2676	—	13.74±0.1	—	static	2
360–428	4.07	2183	—	11.2 ±0.4	9.3±0.2	transpiration	this work

---

[9] K. K. Kelley, U. S. Bur. Mines Bull. N° 584 (1960).

[10] S. Sundaram, *Z. phys. Chem. (Frankfurt)*, **34**, 233 (1962).

[11] C. E. Wicks and F. E. Block, U.S. Bur. Mines Bull., N° 605 (1963).

[illegible] and 1/T [illegible] least-squares [illegible] of the experimental data. From this equation, the second-law heat of vaporization was calculated [illegible] for ΔH_T [illegible] Using [illegible] and C_p [illegible] the heat of vaporization at 298 K resulted to be ΔH_{298} [illegible] kcal/mole. For the third-law test, the vapor pressure data were also treated by the third-law procedure. The resulting ΔH_{298} [illegible] kcal/mole. The necessary free energy function values for [illegible] were taken from Stephenson [illegible] and for [illegible] were calculated from the absolute entropy at 298 K and the heat capacity of the liquid. [illegible] experimental data [illegible] a value of 52.5 [illegible] for the absolute entropy of [illegible] at 298 K was calculated from reported [illegible] data (viz. heat of fusion, temperature of fusion, [illegible] entropy at 298 K and heat capacity of solid). The free energy functions [illegible] calculated were 52.96, 53.86, [illegible] and for [illegible] respectively. The error in the second-law and in the third-law [illegible] enthalpy values represent only the standard deviations.

In view of the agreement between the two results, we propose for the heat of vaporization the value [illegible] 10 [illegible] kcal/mole, where the error is estimated and accounts for the uncertainties in the temperatures and [illegible].

In table 2 are shown [illegible] vapor pressures and enthalpies of vaporization along with similar values of previous investigations.

Table 2

Comparison of [illegible] and [illegible] enthalpies of vaporization of [illegible]

[illegible]	$\log P = A - B/T$	ΔH_T (kcal/mole)	ΔH_{298} (third-law) (kcal/mole)	Method	Ref.
[illegible]	[illegible]	[illegible]	[illegible]	[illegible]	[illegible]
[illegible]	[illegible]	13.7 ± 0.1	[illegible]	[illegible]	[illegible]
300–[illegible]	4.07, 2184	11.2 ± [illegible]	9.7 ± 0.2	Transpiration	this work

---

[illegible] K. K. Kelley, U. S. Bur. Mines Bull. No 584 (1960).

[illegible] Z. phys. Chem. (Frankfurt), 36, 245 (1963).

[illegible] E. [illegible], U.S. Bur. Mines Bull. [illegible] (1963).

Received [illegible]

Revue Roumaine de Chimie, **18**, *12*, 2087–2096 (1973)

CONDENSATIONS D'ACIDES INSATURÉS SUR LE BENZÈNE CATALYSÉES PAR LE CHLORURE D'ALUMINIUM. V[1]

ACIDE SORBIQUE

ALICE MARIE GLATZ *, FLORIN BADEA,** ZSOLT ARVAY,*
VALERIAN DRĂGUŢAN,* FILIP CHIRALEU* et ALEXANDRU C. RĂZUŞ *
*Centre de Chimie Organique, Bucarest, Spl. Independenţei, 202 B
** Institut Polytechnique, Bucarest, Calea Griviţei, 132, Roumanie

Reçu le 13 juin 1973

Parmi les produits de réaction obtenus par la condensation de l'acide sorbique sur le benzène, on a mis en évidence les acides : phényl-4 et -5 caproïque, *cis*- et *trans*-méthyl-3 indanylacétiques et diphényl-3,5 caproïque, ainsi que les hydrocarbures au squelette indénique : triméthyl-1, 1, 3 et diméthyl-1,3-éthyl-1-indène. Les acides monophénylés proviennent de la condensation de l'acide sorbique sur le benzène, accompagnée d'hydrogénation par transfert intermoléculaire d'hydrure. Les acides au squelette indanique, ainsi que l'acide diphénylé se forment à partir d'un acide monophénylé insaturé, intermédiaire de la réaction.

Nenitzescu, Gavăt et Cocora [2] ont montré que par le traitement de l'acide sorbique au benzène, en présence de chlorure d'aluminium on obtient l'acide phényl-5 caproïque.

La formation d'un acide monophénylé, saturé, en partant d'un acide à deux liaisons doubles, implique une condensation accompagnée d'hydrogénation.

Des transferts intermoléculaires d'hydrogène ont été depuis longtemps signalés dans la littérature.[3-5]

De telles réductions au cours de réactions Friedel-Crafts ont été observées par Nenitzescu et ses collaborateurs depuis 1931, à la condensation du chlorure d'acétyle[6-9] sur le cyclohexane et sur le cyclohexène. Cette réaction a été, plus tard, dénommée, « réaction d'acylation Nenitzescu ».[10]

---

[1] IV, A. M. Glatz, A. C. Răzuş, M. Elian et C. D. Nenitzescu, *Rev. Roumaine Chim.*, **16**, 1585 (1971).

[2] C. D. Nenitzescu, I. Gavăt et D. Cocora, *Ber. dtsch. chem. Ges.*, **73**, 233 (1940).

[3] C. D. Nenitzescu, *Studii şi Cercetări Chim. Acad. Bucureşti*, **18**, 853 (1970).

[4] C. D. Nenitzescu, « Intermolecular Hydride Transfer Reactions », dans « Carbonium Ions », IIIe vol., éd. G. A. Olah et P. von R. Schleyer, J. Wiley, 1968, New York, p. 463.

[5] C. D. Nenitzescu et A. T. Balaban, «Aliphatic Acylation», dans « Friedel-Crafts and Related Reactions» IIIe vol., éd. G. A. Olah, Interscience, New York, 1964, p. 1069.

A l'alcoylation du benzène avec du chlorure d'allyle en présence de chlorure d'aluminium humecté, Nenitzescu et Isăcescu[11] ont obtenu, en dehors de diphényl-1,2-propane, des quantités appréciables de propyle-benzène, ainsi qu'une quantité équivalente de diéthyl-9, 10-anthracène, dont le précurseur est le donneur d'hydrure, le dihydro-anthracène respectif.

A la suite de quelques résultats obtenus au cours de recherches plus récentes sur la condensation des acides insaturés alcanoïques et cycloalcoylidène-acétiques, en présence de chlorure d'aluminium, on a trouvé intéressant de reprendre l'étude du comportement de l'acide sorbique(**1**) dans les mêmes conditions de réaction,[1,2] en utilisant à cette occasion des méthodes analytiques modernes. On a séparé, en partant du produit de la réaction, par extraction alcaline, un mélange d'acides A, ainsi qu'un mélange de produits neutres B, contenant seulement des hydrocarbures (tableau 1).

Tableau 1

Produits de condensation de l'acide sorbique sur le benzène

	A						B	
Produits	**2**	**3**	**4**	**5**	**6**	**7**	**8**	**9**
moles %	43,0	50,4	0,8	3,8	2,0		32,5	21,5
rend. %	47,5*					20,0	20,6**	

* Calculé pour $C_{12}H_{16}O_2$; ** Calculé pour $C_{11}H_{14}$.

En faisant distiller le mélange A, on a eu une fraction, $Eb_2 = 168-170°$, contenant les acides : phényl-4 caproïque (**2**), phényl-5 caproïque (**3**), *cis-* et *trans*-méthyl-3 indanyl acétiques (**4** et **5**), ainsi que phényl-5 hexène-3 oïque (**6**) identifiés par chromatographie en phase vapeur effectuée sur les esters méthyliques, comparés à des échantillons préparés par d'autres voies. Le résidu de la distillation contient seulement l'acide diphényl-3,5 caproïque (**7**) F = 109–110°, identifié par analyse élémentaire, spectres IR et RMN.

---

[6] C. D. Nenitzescu et P. Cantuniari, *Liebigs Ann. Chem.*, **510**, 269 (1931).

[7] C. D. Nenitzescu et E. Ciorănescu, *Ber. dtsch. chem. Ges.*, **69**, 1820 (1936).

[8] M. Avram, *Studii şi Cercetări Chim. Acad. Bucureşti*, **19**, 583 (1971) ; idem, *Chem. Ber.*, **104**, XVII–LVII (1971).

[9] G. Baddeley, *Quart. Rev.*, **8**, 376 (1954).

[10] J. E. Gowan, T. S. Wheeler, « Name Index in Organic Reactions », éd. Longmans, Londres, 1962, p. 179.

[11] C. D. Nenitzescu et D. Isăcescu, *Ber. dtsch. chem. Ges.*, **66**, 1100 (1933).

Afin d'identifier l'acide **6** on a préparé les acides saturés : phényl-2 et -3 caproïques qui, on a constaté, ne font pas partie du mélange d'acides de la fraction $Eb_2 = 168-170°$. Dans le même but, on a préparé les acides insaturés : phényl-3 hexène-5 oïque et phényl-5 hexène-3 oïque ; ce dernier correspond au composant représentant 2% moles du mélange.

On a montré [12–14] que les produits neutres des réactions de condensation des acides alcanoïques et cyclo-alcanoïques insaturés, à une seule double liaison, sont des mélanges de cétones cycliques. Dans le cas de l'acide sorbique, les produits neutres B sont des mélanges d'hydrocarbures. Le contenu global de carbone et d'hydrogène, déterminé par analyse élémentaire, est $C_{11}H_{14}$, à partir duquel on a calculé le rendement.

De B on a séparé, par c.p.v. préparative, deux hydrocarbures. Ils ont été identifiés comme : triméthyl-1, 1, 3-indène (**8**) et diméthyl-1,3-éthyl-1-indène (**9**). Leur identification a été effectuée par analyse élémentaire et spectres RMN.

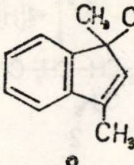

8

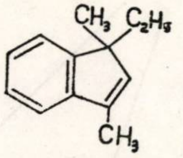

9

On donne sur le schéma 1 le mécanisme qui explique la formation des acides du mélange A.

L'addition d'un proton sur l'acide sorbique détermine la formation de deux carbocations allyliques **10** et **11**. Ceux-ci réagissent avec le benzène seulement dans la position la plus éloignée du groupe carboxyle (4 et respectivement 5) ; celà est dû à l'effet de conjugaison allylique auquel s'ajoutte l'effet inductif du groupe carboxyle. Par conséquent il en résulte les acides phénylés, insaturés **6** et **12** capables de subir diverses transformations, dans le milieu de la réaction.

L'acide **6**, reçoit un proton et, en partie, il se cyclise et donne les acides isomères *cis*- et *trans*-méthyl-3 indanyl-acétique (**4** et **5**) ; en partie, il reçoit de l'hydrogène, par un transfert intermoléculaire, et donne l'acide phényl-5 caproïque (**8**). Enfin, l'acide **6** élimine un ion d'hydrure ; il se forme un intermédiaire, le carbocation allylique-benzylique **13**. Dans ce cas le benzène se fixe dans la position 3 et, par hydrogénation, il résulte l'acide diphényl-3,5 caproïque (**7**). Ce dernier est le seul acide diphénylé décelé dans le mélange des produits de la réaction.

---

[12] A. M. Glatz, A. C. Răzuș, F. Badea et C. D. Nenitzescu, *Rev. Roumaine Chim.*, **16**, 1567 (1971).

[13] M. F. Ansell et G. F. Whitfield, *Tetrahedron Letters*, **1968**, 3075.

[14] A. M. Glatz, A. C. Răzuș et C. D. Nenitzescu, *Rev. Roumaine Chim.*, **11**, 555 (1966).

L'acide **7** aurait pu résulter par l'isomérisation d'un autre acide diphénylé **14**, formé de prime abord à partir d'un acide insaturé, phénylé dans la position 3. Afin de vérifier cette hypothèse, on a synthétisé l'acide

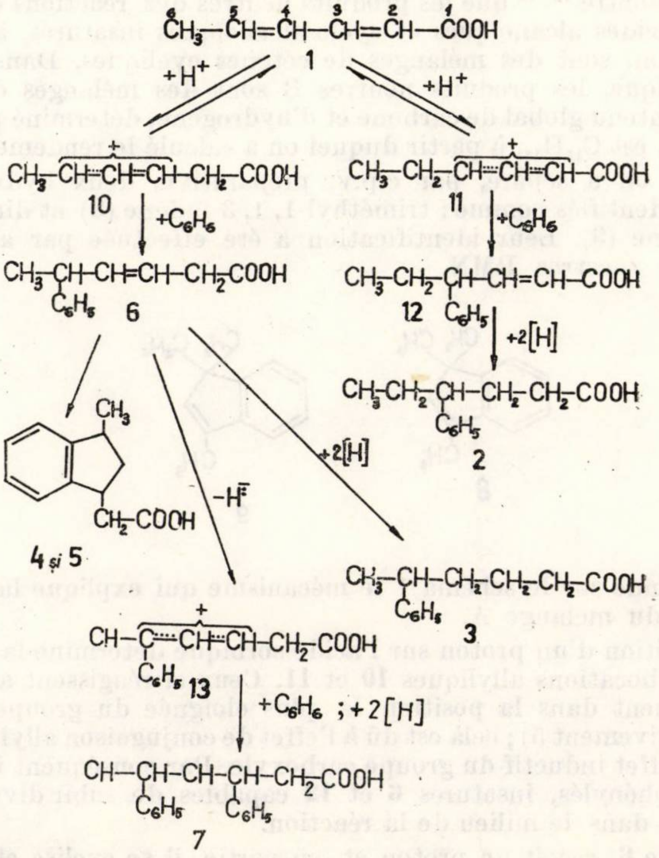

diphényl-3,4 caproïque. Celui-ci, mis dans les conditions de la réaction de condensation, ne s'est pas transformé, ce qui a infirmé l'hypothèse ci-dessus :

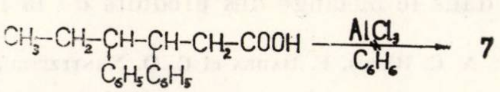
$$CH_3-CH_2-\underset{C_6H_5}{CH}-\underset{C_6H_5}{CH}-CH_2-COOH \xrightarrow[C_6H_6]{AlCl_3} 7$$

14

On peut supposer que l'intermédiaire **12** devrait subir les mêmes transformations que l'intermédiaire **6** (hydrogénation, cyclisation, élimination d'ion hydrure accompagnée de condensation sur le benzène). La présence parmi les produits de la réaction de l'acide phényl-4 caproïque (**2**) atteste un transfert intermoléculaire d'hydrogène, au cours duquel l'acide insaturé **6** a servi d'accepteur. La cyclisation de l'acide **12** devrait mener à un acide éthyl-3 indanyl-carboxylique (**15**). La comparaison par analyse c.p.v. d'un échantillon préparé par une autre voie, au mélange d'acides de la fraction $Eb_2 = 168-170°$ (esters méthyliques) indique le manque de l'acide **15**.

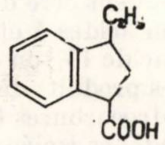

15

Une élimination d'ion hydrure mène à un carbocation allylique-benzylique **16** :

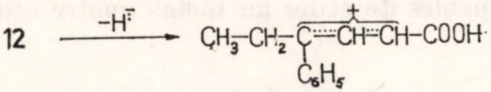

$$\mathbf{12} \xrightarrow{-H^{-}} CH_3-CH_2-\underset{\displaystyle C_6H_5}{\underset{|}{C}}\cdots CH \cdots CH-COOH$$

16

La position 2 étant, dans ce cas, inaccessible au benzène à cause de l'effet inductif du groupe carboxyle, qui, l'on sait, se manifeste le plus fortement dans cette position, l'intermédiaire **15** ne peut pas donner un acide diphénylé.

Les rendements comparables et relativement grands en acides **2**, **3** et **7** (respectivement 20,5 : 23,6 : 20,0 %) indiquent la marche principale de la réaction (condensation avec le benzène et hydrogénation).

Une fois établi le mécanisme de la condensation, il s'est posé la question de connaître le mécanisme de l'hydrogénation. Vu que pendant des réactions de transfert intermoléculaire d'ion hydrure il faut qu'il existe des donneurs et des accepteurs d'hydrure,[3,4] on a cherché à identifier ces espèces parmi les produits ou les intermédiaires de la réaction.

Dans un mémoire, plus récent, sur la condensation de l'acide cyclobutylidène-acétique on a signalé un transfert intermoléculaire d'hydrogène, en mettant en évidence les accepteurs (des acides intermédiaires phénylés insaturés), ainsi qu'un acide d'une faible teneur en hydrogène

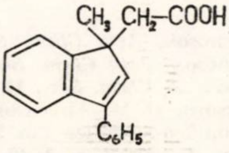

17

$C_{18}H_{16}O_2$, au squelette indénique, l'acide phényl-3-méthyl-1-indényl-acétique (**17**) dont les précurseurs ont servi de donneurs d'hydrure.

Connaissant la grande mobilité du proton chez les indènes substitués,[15-17] ainsi que leur aisance à céder de l'hydrure [18] (étant en général de bons donneurs), dans le cas de la condensation de l'acide sorbique, on peut supposer que les hydrocarbures au squelette indénique **8** et **9** sont les produits de stabilisation des précurseurs, donneurs d'hydrure, soit que ces hydrocarbures se forment à partir des intermédiaires de type allylique-benzylique **13** et **16**, soit à partir des acides **4**, **5** ou **15** (sachant que les acides indéniques peuvent être décarboxylés en milieu acide [19,20]). Observant la faible teneur en acides **4** et **5**, ainsi que l'absence, parmi les produits de la réaction, de l'acide **15**, on est porté à croire que ces acides se transforment dans d'autres produits dès leur formation. Le mécanisme par lequel se forment les hydrocarbures **8** et **9** n'a pas encore été élucidé.

La faible quantité d'indènes isolée à partir du mélange de produits de la réaction ne correspond pas à toute la quantité d'hydrogène nécessaire aux produits hydrogénés de la réaction (**2**, **3** et **7**). Par conséquent, parmi les hydrocarbures qui n'ont pas été identifiés, il doit y avoir des hydrocarbures au squelette polynucléaire, provenant d'autres donneurs d'ion hydrure, capables de céder au moins quatre atomes d'hydrogène.

PARTIE EXPÉRIMENTALE

Les points de fusion ne sont pas corrigés. Les analyses élémentaires ont été effectuées par Mmes E. Şliam et V. Daniel; les spectres IR ont été déterminés sur un spectrophotomètre UR 20 Zeiss-Iéna. Les spectres RMN ont été effectués en solution de CCl_4 sur un appareil Varian A-60 A, en utilisant le TMS comme standard interne.

Les analyses chromatographiques en phase vapeur ont été effectuées par Mlle Doina Georgescu sur un appareil Carlo Erba, modèle D ; pour les esters on a utilisé une colonne 20% éthylène-glycol-succinate/chromosorb W 60—80 mesh ; 3 m × 2 mm ; temp. col. 160° ; temp. dét. 280° ; gaz porteur : l'hydrogène ; débit 17,5 cm^3/mn. La chromatographie préparative a été effectuée sur un appareil Willy Giede. On a utilisé une colonne de 20% éthylène-glycol-adipate/chromosorb P 60—80 mesh ; 1 m × 2 mm ; temp. col. 120° ; gaz porteur : l'hydrogène ; débit 100 cm^3/mn.

CONDENSATION DE L'ACIDE SORBIQUE (1) SUR LE BENZÈNE À 40—45°

À une suspension de 40 g (0,3 moles) chlorure d'aluminium et 100 cm^3 benzène anhydre, on introduit, goutte à goutte, sous agitation, pendant 4 heures, une solution de 22,4 g (0,2 moles) acide sorbique [21] dans 300 cm^3 benzène anhydre, en maintenant la température

---

[15] A. M. Weidler et G. Bergson, *Acta Chem. Scand.*, **17**, 862, 1798, 2724 (1963).

[16] A. M. Weidler et G. Bergson, *Acta Chem. Scand.*, **18**, 1484, 1487 (1964).

[17] C. K. Ingold et R. Piggott, *J. Chem. Soc.*, **123**, 1469 (1923).

[18] C. D. Nenitzescu, I. Necşoiu, et M. Adlersberg, «Aspecte din Chimia Hidrocarburilor», «Lucrările Consfătuirii Româno-Sovietice din 3—4 dec. 1959», Bucarest, p. 213.

[19] H. Ahmed et N. Campbell, *J. Chm. Soc.*, **1960**, 4115.

[20] H. Cristol et F. Plenat, *Bull. Soc. chim. France*, **1962**, 1325.

[21] C. F. H. Allen et I. Van Allan, Org. Synth., IIIe vol., J. Wiley, New York, 1955, p. [illegible]

à 40–45°. On décompose par eau et glace. La couche benzénique est lavée par une solution de 10% d'hydroxyde de sodium, on sépare les deux couches.

Mélange d'acides A. La solution alcaline, aqueuse, contenant le mélange d'acides, acidulée à l'acide chlorhydrique est extraite à l'éther. On sèche sur sulfate de magnésium la solution éthérée, et, après avoir chassé l'éther, on distille sous pression réduite. Il en résulte une fraction, $Eb_2 = 168-170°$; rend. = 47,5%. $C_{12}H_{16}O_2$ Calculé : C 74,95 ; H 8,39 ; Trouvé : C 74,78 ; H 8,42%.

Cette fraction estérifiée au diazométhane, en solution éthérée donne une huile, $Eb_2 = 150°$.

$C_{13}H_{18}O_2$ *Calculé* : C 75,69 ; H 8,79
Trouvé : C 75,80 ; H 8,93

Le résidu de la distillation donne 10,6 g cristaux incolores, F = 109–110° (hexane) ; rend. = 20,0%.

$C_{18}H_{20}O_2$ *Calculé* : C 80,55 ; H 7,53
Trouvé : C 80,43 ; H 7,78

Ester méthylique, cristaux incolores, F = 41° (alcool).

$C_{19}H_{22}O_2$ *Calculé* : C 80,81 ; H 7,85
Trouvé : C 80,92 ; H 8,06

Identification des acides **2**, **3**, **4**, **5** et **6**

L'analyse c.p.v. du mélange des esters méthyliques de la fraction A, $Eb_2 = 168-170°$ indique cinq composants. La comparaison des temps de rétention de ces composants avec ceux des échantillons respectifs donne le rapport molaire du tableau 1.

Synthèse des échantillons *. *L'acide phényl-4 caproïque* (**2**) a été préparé d'après une méthode décrite par nous.[14]

Ester méthylique. Sur le chromatogramme (c.p.v.) son pic se superpose à celui du composant du mélange qui représente 43,0% moles.

L'*acide phényl-5 caproïque* (**3**) a été préparé par la condensation de la lactone de l'acide hydroxy-5 caproïque sur le benzène, en présence de chlorure d'aluminium.[14]

L'*ester méthylique* est superposable (c.p.v.) au composant qui représente 50,4% moles du mélange.

Acides cis- *et* trans-*méthyl-3 indanyl-acétiques* (*4 et 5*)

L'*acide phényl-2 pentène-4 oïque* a été préparé par condensation de l'ester phénylmalonique sur le bromure d'allyle, en présence de sodium, saponification et décarboxylation de l'ester résulté par cette voie ; huile, $Eb_2 = 140-143°$.

$C_{11}H_{12}O_2$ *Calculé* : C 74,98 ; H 6,86
Trouvé : C 74,76 ; H 7,27

L'*acide phényl-3-hexène-5 oïque* a été préparé à partir du précédent par rallongement de chaîne d'après Arndt-Eistert ; huile, $Eb_2 = 151-152°$.

$C_{12}H_{14}O_2$ *Calculé* : C 75,76 ; H 7,42
Trouvé : C 75,56 ; H 7,24

Ester méthylique, $Eb_2 = 120°$, huile.

$C_{13}H_{16}O_2$ (204,3) *Calculé* : C 76,43 ; H 7,87
Trouvé : C 76,43 ; H 8,09

* Tous les esters méthyliques ont été préparés par traitement d'une solution éthérée d'acide avec une solution éthérée de diazométhane.

Spectre RMN (CCl_4 ; δ ppm) : 7,17 (singulet, 5 protons aromatiques) ; 5,3−6,0 (12 lignes, J = 17,5 ; 9 ; 6,5 ; 6,5 Hz, = C−H) ; (multiplet, 2 protons = CH_2) ; 3,52 (singulet, 7 protons, CH_3 estérique) ; 2,9−3,4 (multiplet, un proton CH) ; 2,54 (doublet, 2 protons $CH_2-COOCH_3$) ; (triple triplet, 2 protons = $CH-CH_3$). Cet ester ne correspond (c.p.v.) à aucun composant du mélange.

Les *acides* cis- *et* trans-*méthyl-3 indanyl-acétiques* (**4** et **5**) ont été préparés à partir du précédent, traité par le chlorure d'aluminium, en solution benzénique, rapport molaire respectif : 1 : 1,5 : 20, dans les conditions habituelles (4 heures, à 40−45°). On obtient un mélange d'acides **4** et **5**, $Eb_2 = 164°$; F = 64°.

$C_{12}H_{14}O_2$ *Calculé* : C 75,78 ; H 7,42
Trouvé : C 76,22 ; H 7,59

Dans le *spectre RMN* de ce mélange on observe, à δ = 1,26−1,32 ppm, deux doublets correspondant à des groupes méthyle, dus à la présence des deux isomères *cis* et *trans*.

L'analyse c.p.v. des esters méthyliques ($Eb_2 = 150°$) indique deux composants qui se superposent aux composants du mélange d'acides qui représente 0,8 et respectivement 3,8 % moles.

L'acide phényl-2 caproïque a été obtenu par la condensation du bromure de *n*-butyle sur l'ester phényl-malonique, saponification et décarboxylation ; huile, $Eb_2 = 170°$.

$C_{12}H_{16}O_2$ *Calculé* : C 74,95 ; H 8,39
Trouvé : C 74,98 ; H 8,53

Spectre RMN (CCl_4 ; δ ppm) : 7,1−7,4 (multiplet, 5 protons aromatiques) ; 3,46 (triplet, J = 7,5 Hz, 1 proton CH) ; 1,05−2,3 (multiplet, 6 protons CH_2) ; 0,86 (triplet, J = 7,5 ; 3 protons CH_3) ; 10 (singulet, 1 proton COOH).

Ester méthylique, $Eb_2 = 150°$, huile.

$C_{13}H_{18}O_2$ *Calculé* : C 76,43 ; H 7,89
Trouvé : C 76,12 ; H 8,07

Il ne se superpose à aucun des composants du mélange de la réaction (analyse c.p.v.).

Acide phényl-5-hexène-3 oïque (**6**). Cet acide a été préparé à partir de l'acide phényl-5 hexadiénoïque,[22] qui a été réduit par amalgame de sodium 2 %, dans l'eau.

L'ester méthylique de cet acide, huile, $Eb_2 = 130°$, est superposable (analyse c.p.v.) au composant du mélange qui représente 2 % moles.

$C_{13}H_{16}O_2$ *Calculé* : C 76,43 ; H 7,89
Trouvé : C 75,70 ; H 7,88

Spectre RMN (CCl_4 ; δ ppm) : 7,13 (5 protons aromatiques ; singulet élargi) ; 5,68 et 5,53 (2 protons insaturés ; J = 5 Hz) ; 3,58 (singulet, 3 protons, CH_3 estériques) 3,2−3,75 (1 proton CH, multiplet) ; 2,96 (2 protons CH_2, doublet, J = 5 Hz) ; 1,35 (3 protons, un CH_3, doublet ; J = 7 Hz).

Acide éthyl-3 indanyl-carboxylique (**15**), mélange d'isomères *cis* et *trans*.

L'*hydoxy-1-éthyl-3-indane* a été obtenu par réduction de l'éthyl-indanone avec $LiAlH_4$. Cristaux incolores, F = 74° (alcool/eau).

$C_{11}H_{14}O$ *Calculé* : C 81,45 H 8,70
Trouvé : C 81,32 ; H 8,89

Spectre RMN (CCl_4 ; δ ppm) : 7,25 (4 protons aromatiques, singulet élargi) ; 5,07 (1 proton vicinal OH ; J = 6,5 Hz) ; 3,05−2,39 (3 protons ; multiplet) ; 2,22−1,2 (3 protons, multiplet) ; 0,97 (3 protons CH_3, triplet ; J = 7 Hz).

---

[22] S. Julia et Y. Bonnet, *Bull. Soc. chim. France*, **1957**, 1352.

Le remplacement du groupe hydroxyle par le brome (PBr_3), traitement par cyanure de potassium et saponification ont mené à un mélange de deux acides isomères *cis* et *trans*.

$C_{12}H_{14}O_2$ *Calculé* : C 75,76 ; H 7,42
Trouvé : C 75,62 ; H 7,65

Les esters méthyliques des acides ci-dessus ne se retrouvent pas dans le mélange des produits acides de la réaction (analyse c.p.v.).

Spectre RMN (CCl_4 ; δ ppm) : 7,5–7,0 (4 protons aromatiques, multiplet) ; 4,15–3,6 (3 protons estériques, 1 proton vicinal carbométhoxy) ; 3,5–0,85 (8 protons, multiplet).

Acide diphényl-3,4 caproïque (**14**). Par la condensation du bromure de phényl-propyle avec l'ester phényl-malonique, saponification et décarboxylation on a obtenu l'acide *diphényl-2,3 valérianique* ; cristaux incolores, F = 170° (alcool/eau).

$C_{17}H_{18}O_2$ *Calculé* : C 80,29 ; H 7,14
Trouvé : C 80,10 ; H 7,34

Spectre RMN (CCl_4 ; δ ppm) : 7,0–7,5 (multiplet, 10 protons aromatiques) ; 3,75 (doublet, J = 14,5 Hz, 1 proton CH) ; 2,9–3,4 (multiplet, 1 proton CH) ; 1,35 (quintet, J = 7 Hz, 2 protons CH_2) ; 0,55 (triplet, J = 7 Hz, 3 protons CH_3) ; 10,25 (singulet, 1 proton COOH).

Le rallongement de chaîne, d'après Arndt-Eistert de l'acide précédent, a donné l'acide **14** ; cristaux incolores, F = 154° (alcool).

$C_{18}H_{20}O_2$ *Calculé* : C 80,55 ; H 7,53
Trouvé : C 80,76 ; H 7,70

Spectre RMN (CCl_4 ; δ ppm) : 6,9–7,5 (singulet, 10 protons aromatiques) ; 2,85–3,5 (multiplet, 1 proton aromatique CH) ; 2,25–2,85 (multiplet, 1 proton CH) : 2,35 (doublet, J = 7 Hz, 2 protons CH_2) ; 1,38 (quintet, J = 7 Hz, 2 protons CH_2) ; 0,51 (triplet, J = 7 Hz, 3 protons CH_3) ; 10,0 (singulet, 1 proton COOH).

Cet acide ne s'isomérise pas, mis dans les conditions de la réaction de condensation (1 mole acide : 0,1 mole chlorure d'aluminium, 20 moles benzène anhydre, 4 heures à 40–45°).

L'ester méthylique, cristaux incolores, F = 110° (alcool), ne se superpose à aucun composant du mélange des produits.

MÉLANGE D'HYDROCARBURES B

La solution benzénique, séparée de la couche alcaline (qui représente le mélange d'acides), est lavée à l'eau jusqu'à une réaction neutre. On sèche sur sulfate de magnésium. On chasse le benzène, il en reste 3 g d'huile, Eb_2 = 70–100°. L'analyse élémentaire de ce mélange donne un rapport carbone/hydrogène : $C_{11}H_{14}$ vis-à-vis duquel on a calculé le rendement (tableau 1) ; rend. = 20,6 %.

IDENTIFICATION DES HYDROCARBURES **8** ET **9**

L'analyse c.p.v. présente 10 composants. On a pu séparer de ce mélange, par c.p.v. préparative deux composants :

Triméthyl-1, 1, 3 indène (**8**), huile, Eb_2 = 70°.

$C_{12}H_{14}$ *Calculé* : C 91,11 ; H 8,92
Trouvé : C 90,96 ; H 9,14

Le *spectre RMN* de l'hydrocarbure **8** est identique à celui décrit dans la littérature.[23]

Diméthyl-1,3 éthyl-1 indène (**9**), huile, $Eb_2 = 70°$.

$C_{13}H_{16}$ *Calculé* : C 90,10 ; H 9,84
Trouvé : C 89,62 ; H 9,40

Le *spectre RMN* (CCl_4 ; δ ppm) : 7,3—7,0 (4 protons aromatiques) ; 5,9 (quartet, J = 1,5 Hz ; 1 proton insaturé) ; 2,09 (doublet, J = 1,5 Hz ; 3 protons $CH_3-C=$) ; 1,25 (singulet, 3 protons $CH-CH_3$) ; 1,72 (quartet, J = 7 Hz, 2 protons CH_2) ; 0,62 (triplet, J = 7 Hz ; 3 protons CH_3).

Ce spectre met en évidence la présence de deux groupes méthyle, l'un lié à un atome de carbone saturé, l'autre à la double liaison, ainsi qu'un groupe éthyle lié à un atome de carbone saturé.

Les signaux du proton insaturé ainsi que ceux du groupe méthyle de $\delta = 2,09$ ppm sont pratiquement identiques à ceux des indènes substitués avec des groupes méthyle en position 3.[23,24] La position singulière du signal de $\delta = 0,62$ ppm est due à l'écranage que subit le groupe méthyle de la part du groupe phényle voisin. Cet effet a été observé aussi dans le cas d'un autre dérivé indénique substitué par un groupe éthyle en position 1.[25]

---

[23] J. Buddrus, *Chem. Ber.*, **101**, 4152 (1968).

[24] A. Bosche et R. W. Braun, *Canad. J. Chem.*, **42**, 1718 (1964).

[25] E. T. McBee, G, W. Calundann et T. Hodgins, *J. Org. Chem.*, **31**, 4260 (1966).

Revue Roumaine de Chimie, **18**, *12*, 2097–2102 (1973)

CONFORMATIONAL EQUILIBRIUM OF 5-FLUORO-1,3-DIOXANE BY NMR SPECTROSCOPY

SORIN MAGER * and ERNEST L. ELIEL **

Department of Chemistry, University of Notre Dame,
Notre Dame, Indiana, U.S.A.

Received May 5, 1973

5-Fluoro-1,3-dioxane was synthesized and its conformational equilibrium established by ^{19}F NMR spectroscopy using the equation $\Delta G^\circ = - RT\ln \frac{\nu_a - \nu}{\nu - \nu_e}$. ν_a and ν_e were taken as the fluorine signals of *cis-* and *trans*-2-isopropyl-5-fluoro-1,3-dioxanes. The free energy difference ΔG° was found to be +0.78 kcal/mol corresponding to a concentration of 79% of the *cis* (axial) isomer at equilibrium.

In order to acquire more information concerning the stereochemistry of 1,3-dioxane derivatives and especially to confirm the unexpected strong preference for the axial position of fluorine in the 2-isopropyl-5-halo-1,3-dioxanes [1,2] (in contrast to chlorine and bromine which both prefer the equatorial position), 5-fluoro-1,3-dioxane was synthesized and its conformational equilibrium (fig. 1) established by ^{19}F NMR spectroscopy.

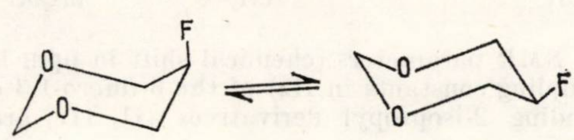

Fig. 1. — Conformational equilibrium of 5-fluoro-1,3-dioxane.

---

* Permanent address: Chair of Organic Chemistry, Babeş Bolyai University, Cluj, Romania.

** Present address: Department of Chemistry, University of North Carolina at Chapel Hill 27514, U.S.A.

[1] E. L. Eliel and M. K. Kaloustian, *Chem. Comm.*, **1970**, 290.

[2] R. J. Abraham, H. D. Banks, E. L. Eliel, O. Hofer and M. K. Kaloustian, *J. Amer. Chem. Soc.*, **94**, 1913 (1972).

The synthesis of 5-fluoro-1,3-dioxane was carried out by the sequence of reactions (1) and (2)

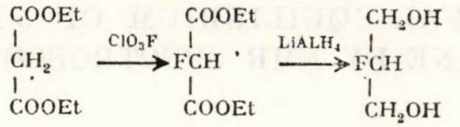
COOEt
CH₂
COOEt
ClO₃F
COOEt
FCH
COOEt
LiALH₄
CH₂OH
FCH
CH₂OH

(1)

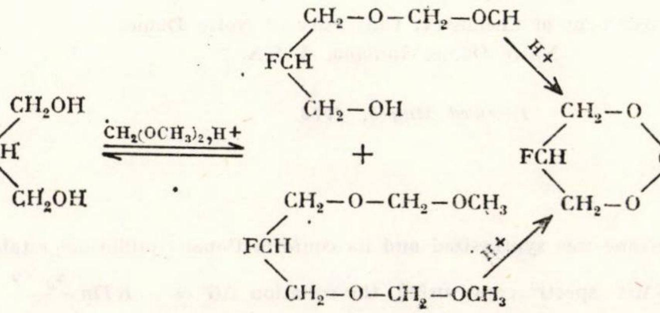
CH₂OH
FCH
CH₂OH
CH₂(OCH₃)₂,H+
CH₂—O—CH₂—OCH
FCH
CH₂—OH
+
CH₂—O—CH₂—OCH₃
FCH
CH₂—O—CH₂—OCH₃
H+
CH₂—O
FCH
CH₂
CH₂—O
H+

(2)

As was shown in detail by means of gas chromatography in the case of the synthesis of 5,5-difluoro-1,3-dioxane,[3] the probable path of dioxane formation, starting from both mono and diether is probably that shown by reactions (3) and (4)

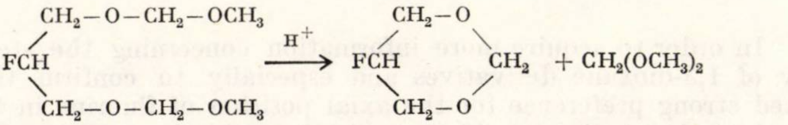
CH₂—O—CH₂—OCH₃
FCH
CH₂—O—CH₂—OCH₃
H+
CH₂—O
FCH
CH₂
CH₂—O
+ CH₂(OCH₃)₂

(3)

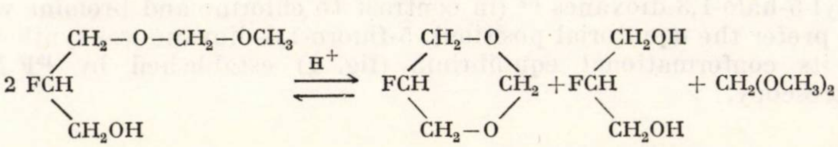
CH₂—O—CH₂—OCH₃
2 FCH
CH₂OH
H+
CH₂—O
FCH
CH₂
CH₂—O
+FCH
CH₂OH
CH₂OH
+ CH₂(OCH₃)₂

(4)

The ^{19}F NMR parameters (chemical shift in ppm in the Φ scale[4] and $^{19}F/^{1}H$ coupling constants in Hz) of the 5-fluoro-1,3 dioxane (I) and the corresponding 2-isopropyl derivatives (II, III) are presented in table 1.

The conformational free energy for the equilibrium shown in fig. 1 was established by means of NMR spectroscopy[5–8] using equation (5)

$$\Delta G^\circ = -RT \ln K \tag{5}$$

---

[3] E. L. Eliel and S. Mager, in press (*J. Org. Chem.*)

[4] G. Filipovich and G. V. D. Tiers, *J. Phys. Chem.*, **63**, 761 (1959).

[5] R. V. Lemieux, R. K. Kullnig, H. J. Bernstein and W. G. Schneider, *J. Amer. Chem. Soc.*, **80**, 6098 (1958).

[6] E. L. Eliel *Chem Ind.* (*London*), **1959**, 568.

[7] H. S. Gutowski and A. Saika, *J. Chem. Phys.* **21**, 1688 (1953).

[8] E. L. Eliel, *Angew. Chem. Internat. Edn.*, **4**, 761 (1965).

*Table 1**

The ^{19}F NMR parameters of 5-fluoro-1,3-dioxane (I) and the corresponding 2-isopropyl derivatives (II, III)

Compound	Φ	$J_{F_5H_5}$	$J_{F_aH_{4(6)a}}$	$J_{F_aH_{4(6)e}}$	$J_{F_aH_{2a}}$	$J_{H_{2a}H_{2e}}$
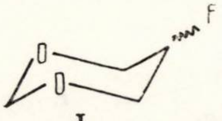 I	191.9	47.2	24	~6.5	—	6.2
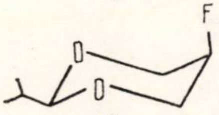 II	191	47	37	17.5	3.7	—
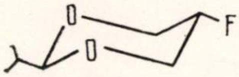 III	200	47.2	—	—	—	—

* The notations *a* and *e* refer to the orientation in the major conformation for compound I.

in which the conformational equilibrium constant K may be computed as

$$K = \frac{\nu_a - \nu}{\nu - \nu_e} \tag{6}$$

where ν represents the fluorine chemical shift in the rapidly equilibrating 1,3-dioxane system and ν_a and ν_e are the axial and equatorial fluorine chemical shifts in the fixed (biased) *cis*- and *trans*-2-isopropyl-5-fluoro-1,3-dioxanes (fig. 2) which were synthesized for this purpose.

It is known that the $\Delta G°$-value for the equilibrium shown in fig. 3 is very large, 4.2 kcal/mol (99.9% in the favour of the *e* isomer)[9] so that the alternate conformation of II and III in fig. 2 (with axial isopropyl) as well as twist boat forms[10,11] may be disregarded because of their high energy.

Introducing, in equations (6) and (5), the experimental values found for ν, ν_a and ν_e, (see experimental part) the conformational equilibrium constant was found to be $K = 0.27$ corresponding to a free energy difference $\Delta G° = +0.78$ kcal/mol in CCl_3F which shows a predominance of the axial (*cis*) isomer to the extent of 79%. This conclusion, though only semiquantitative in view of the inherent uncertainties of the NMR method of conformational analysis,[12] especially using ^{19}F NMR,[13] is in agreement with that obtained by means of the equilibration method,[2] which shows a similar strong preference for the axial (*cis*) isomer in the case of the 2-isopropyl-5-fluoro-1,3-dioxane (e.g. $\Delta G^\circ = 0.62$ kcal/mol in solvent ether).

---

[9] F. W. Nader and E. L. Eliel, *J. Amer. Chem. Soc.*, **92**, 3050 (1970).

[10] K. Pihlaja, *Acta Chem. Scand.*, **22**, 716, 2401 (1968).

[11] E. L. Eliel, *Accounts Chem. Research*, **3**, 1 (1970).

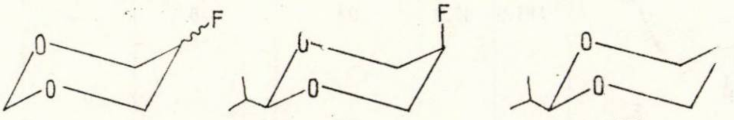

I II III

Fig. 2. — Conformational structures of 5-fluoro-1,3-dioxane (I), *cis*- and *trans*-2-isopropyl-5-fluoro-1,3-dioxane (II, III).

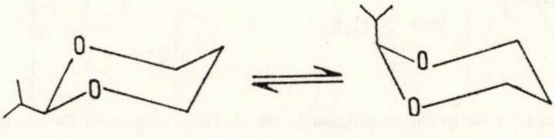

Fig. 3. — Conformational equilibrium of 2-isopropyl-1,3-dioxane.

Thus, the surprising preference of fluorine for the axial position at C-5 in a 1,3-dioxane is confirmed beyond any doubt. Comparison of the obtained ΔG° value with the corresponding ΔG° value in the case of cyclohexyl fluoride[13] ($\Delta G^\circ = -0.13$ kcal/mol in carbon disulfide) clearly shows the pronounced shifting of the equilibrium towards the axial position of the fluorine, as the two CH_2-groups in cyclohexane are replaced with the two oxygen atoms in the 1,3-dioxane. By way of an explanation, an electron-nuclear attraction dominating the F/O non-bonded potential at the distance involved in the axial (*cis*) isomer was suggested.[2]

After this paper was accepted for publication we learned of the study by L. D. Hall and R. N. Johnson,[14] in which these authors also examine I, II and III by ^1H and ^{19}F NMR spectroscopy. From averaging of H/H and H/F coupling constants, the authors compute the percentage of the axial conformer of 5-fluoro-1,3-dioxane to be 58% in cyclohexane, 81–83% in 1 : 1 cyclohexane-acetic acid, and 86–95% in polar solvents (acetone, methylene chloride, chloroform, etc.). Our data concerning the position of the equilibrium are in agreeement with those of Hall and Johnson.

---

[12] F. R. Jensen, C. H. Bushweller and B. H. Beck, *J. Amer. Chem. Soc.*, **91**, 344 (1969).

[13] E. L. Eliel and R. J. L. Martin, *J. Amer. Chem. Soc.*, **90**, 682, 689 (1968).

[14] L. D. Hall and R. N. Johnson, *Org. Magn. Resonance*, **4**, 369 (1972).

EXPERIMENTAL

^{19}FMR spectra were recorded on a Varian XL-100 Model spectrometer operating at 94.1 MHz. Chemical shifts are reported in Φ scale proposed by Filipovich and Tiers [4] using trichlorofluoromethane as both reference and solvent. The values found for ν, ν_e and ν_a were 94172417.3 Hz, 94172038 Hz and 94172519.5 Hz, respectively.

DIETHYLFLUOROMALONATE[15]

a) To a suspension of 12 g NaH in 1600 ml dry toluene, 80 g diethyl malonate was added dropwise, maintaining the temperature between 20–25°. The mixture was stirred for one more hour at 25°. A strong stream of perchloryl fluoride was bubbled through the solution for about 40 minutes allowing the temperature to rise to 35°. The reaction product was checked by g.l.p.c. using a 20% Carbowax 20 M on Firebrick column at about 150°. The order of the peaks in the chromatogram was : difluorinated malonic ester, malonic ester, monofluorinated ester whose proportions were 30%, 30%, 40%. The solution was concentrated and the components separated using a Nester Faust preparative gas chromatograph (Model 850 Prepkromatic) with a Biwall column filled with 20% Carbowax 20 M on Chromosorb W, at 145°, He flow 200 cc/min.

Retention times were 5′, 11′ and 20′, respectively.

b) Starting from ethyl fluoromalonate and ethyl chloroformate the procedure of Bergman [16] was followed.

2-FLUORO-1,3-PROPANEDIOL

To a suspension of 6.9 g (0.18 mol) $LiAlH_4$* in 200 ml anhydrous ether, 21.6 g (0.12 mol) diethylfluoromalonate in 250 ml anhydrous ether was added slowly, maintaining a gentle reflux. Refluxing was continued for another two hours. After cooling, 6.9 ml water was added dropwise cautiously, followed by 6.9 ml 15% Na OH solution and again 19.7 ml water. After stirring for 1 hour, the precipitate was filtered and extracted four times with 200 ml hot tetrahydrofuran. The solution was concentrated and, from the reaction product, 2-fluoro-1,3-propanediol was obtained by preparative g.l.p.c. A 4-foot 20% Carbowax 20 M on Firebrick (80–100 mesh) column was used and the separation performed at 185° with a 240 ml/min He flow. Retention time : 19′. M.p. = 41–42° (lit.[17] 38–39°) ^{19}F NMR parameters : $J_{FH(gem)} = 50$ cps. ; $J_{FH(vic)} = 25$ cps. Anal. *Calcd.* for $C_3H_7O_2F$: C, 38.29; H, 7.50. *Found:* C, 38.78; H, 7.52.

---

* Using larger amounts of $LiAlH_4$ led to the formation of 1,3-propanediol as a by-product in a proportion up to about 35% of the fluorinated compound. It is probably better to add the $LiAlH_4$ in small portions to the ethereal solution of diethylfluoromalonate.

[15] H. Gershon, J. A. A. Renwick, W. K. Wynn and R. D'Arcoli, *J. Org. Chem.* **31**, 916 (1966).

[16] E. D. Bergman, S. Cohen and I. Shahak, *J. Chem. Soc.*, **1959**, 3286.

[17] V. Tolman and K. Veres, *Coll. Czech. Chem. Comm.*, **37**, 2962 (1972).

CIS- AND *TRANS-*2-ISOPROPYL-5-FLUORO-1,3-DIOXANE, SEE [2]
5-FLUORO-1,3-DIOXANE

2-Fluoro-1,3-propanediol (0.5 g) was boiled for 4 hours with 15 ml dimethoxymethane in the presence of a catalytic amount of Amberlyst-15 (polystyrenesulphonic acid). The excess of dimethoxymethane was distilled and the residue transferred to a small distillation flask. Fresh Amberlyst-15 was added and the content of the distillation flask was gradually heated to 130–135° at a vacuum of 10–20 mm Hg. From the distillation product, the pure 5-fluoro-1,3-dioxane was obtained by preparative gas-liquid chromatography using a 4-foot 20% Carbowax 20 M on Firebrick (mesh 80–100) column at 100° with a 230 ml/min He flow.

Retention time 12′. Anal. *Calcd.* for $C_4H_7O_2F$: C, 45.28, H, 6.65. *Found* : C, 45.65 ; H, 6.60.

This work was supported by a grant (GP-24,910) of the National Science Foundation, U.S.A. We thank Mr. Don Schifferl for assistance in recording the NMR spectra.

Revue Roumaine de Chimie, **18**, *12*, 2103–2112 (1973)

HETEROCYCLIC METHYLENE BASES. X[1]

2-(ω-ACYL-ω-ARYLAZO) METHYLENE DERIVATIVES OF N-CONTAINING HETEROCYCLES

MARCELA FĂRCĂŞAN, R. CHIRA, GH. CIURDARU and VIORICA I. DENES

Institute of Chemistry, str. Donath 65–103, Cluj, Romania

Received December 18, 1972

Three different series of 2-(ω-acyl-ω-arylazo)methylene derivatives of N-containing heterocycles were prepared by two methods. The structure of these compounds is discussed on the basis of their IR spectral data.

The so-called "methylene bases" (A, a = b = H) of the N-containing heterocycles react readily with electrophiles affording mono- and disubstituted derivatives in the side chain. Two types of symmetrical disubstituted compounds are described in the literature namely the bis-azo (A, a = b = N = N—Ar)[2] and the bis-mercapto (A, a = b = S—Ar)[3] derivatives. They have been prepared either in a single step using two moles of electrophile to one mole of methylene base, or by acting one mole of electrophile with one mole of monosubstituted derivative. Unsymmetrical substituted compounds have been also reported such as 2-(ω-formyl-ω-azo),[4] 2-(ω-sulphonyl-ω-azo)[5] and 2-(ω-mercapto-ω-acyl)[3] derivatives of certain 2-methylene-azolines.

The acyl-arylazo-methylene derivatives of the N-containing heterocycles (A, a = COR, b = N = N—Ar) which the paper is dealing with, were hitherto unknown. We undertook their preparation in the hope of obtaining compounds with interesting physical, chemical and possibly dyeing properties.

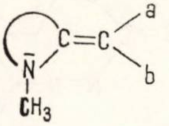

A

---

[1] Part IX. Gh. Ciurdaru, M. Fărcăşan, and V. I. Dénes, *Rev. Roumaine Chim.*, **15**, 1975 (1970).

[2] H. Wahl, and M. T. Le Bris, *Bull. Soc. chim. France.*, **1954**, 248, 251, 587, 1281.

[3] V. I. Dénes, M. Fărcăşan and Gh. Ciurdaru, *Chem. Ber.*, **96**, 174 (1963).

[4] P. Lochon and H. Wahl, *Chimia.*, **19**, 218 (1965).

[5] R. G. Dubenko, Iu. Ushenko and P. Pelkis, *J. Heterocycl. Soedin.* (*Riga*)., **1**, 76 (1968).

Two routes were followed in order to synthetize these compounds :

— Diazonium salts coupling 2-acyl-methylene derivatives (B)[6,7,8,9] (Route 1) ;

— Acyl chlorides addition to monoazo-methylene derivatives (C)[10] (Route 2).

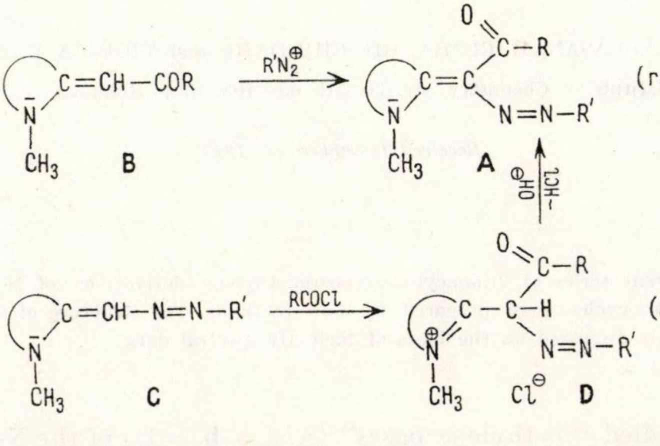

The route 2 is less convenient due to the rather complicated synthesis of the monoazo compound C. On the contrary, the route 1 makes possible the easy preparation of a large number of various acyl-azo compounds A. Following this route we prepared two different series of acyl-azo-methylene-benzothiazolines, namely :

— Compounds type I, in which R was maintained unchanged, by coupling various diazonium salts with 3-methyl-2-(benzoyl-methylene)-benzothiazoline ;

— Compounds type II, in which R′ is maintained unchanged, by coupling of 4-nitrophenyldiazonium chloride with various acyl-methylene derivatives.

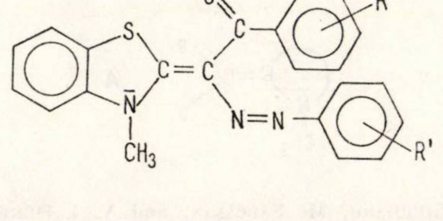

---

[6] V. I. Dénes, Gh. Ciurdaru and M. Fărcăşan, *Chem. Ber.*, **96**, 2691 (1963).
[7] V. I. Dénes, Gh. Ciurdaru and M. Fărcăşan, *Rev. Roumaine Chim.*, **9**, 375 (1964).
[8] V. I. Dénes, Gh. Ciurdaru and M. Fărcăşan, *Rev. Roumaine Chim.*, **10**, 1045 (1965).
[9] Gh. Ciurdaru and V. I. Dénes, *Rev. Roumaine Chim.*, **14**, 1063 (1969).
[10] H. Wahl and M. T. Le Bris, *Bull. Soc. chim. France*, **1954**, 1277.

I. $R = H$	II. $R' = 4'-NO_2$
a. $R' = 4'-OCH_3$	a. $R = 4-OCH_3$
b. $R' = 4'-CH_3$	b. $R = 4-CH_3$
c. $R' = H$	c. $R = H$
d. $R' = 4'-Cl$	d. $R = 4-Cl$
e. $R' = 4'-Br$	e. $R = 4-Br$
f. $R' = 3'-Cl$	f. $R = 3-Cl$
g. $R' = 3'-Br$	g. $R = 3-NO_2$
h. $R' = 3'-NO_2$	h. $R = 4-NO_2$

A third series III, in which R and R′ are constant and varies only the heterocyclic ring, was prepared by coupling 4-nitrophenyldiazonium chloride with 2-benzoylmethylene derivatives of different N-containing heterocycles.

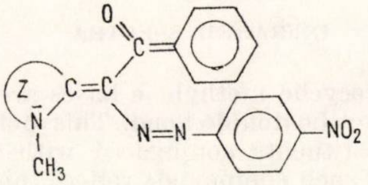

III

a. Z = N-methyl-benzoselenazoline

b. Z = 3, 4, 5-trimethyl-thiazoline-4

c. Z = 1,3-dimethyl-benzimidazoline

d. Z = 1-methyl-1,2-dihydroquinoline

In order to check the route 2 we treated some monoazomethylene compounds [10] with benzoyl chlorides. The strongly polarized double bond reacted smoothly under very mild conditions with the reagent used affording the expected quaternary salts IV. The occurrence of a strong C = O stretching band in the IR spectra of these compounds supports their formulation as addition products.

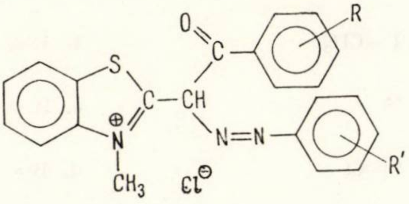

IV

a. $R = H$; $R' = H$ $\nu_{C=O}$: 1705 cm^{-1}

b. $R = H$; $R' = 4'-NO_2$ $\nu_{C=O}$: 1685 cm^{-1}

c. $R = 4 - NO_2$; $R' = 4'-NO_2$ $\nu_{C=O}$: 1685 cm^{-1}

Treatment of compounds IVa and IVb with bases resulted in the formation of acyl-azo-methylene compounds Ia and Ib; they were proved to be identical with those prepared following route 1. By acting with bases (pyridine, triethylamine) on compound IVc a cleavage of the acyl group leading to the initial monoazomethylene derivative was observed.

INFRARED SPECTRA

Actually the heterocyclic methylene bases are enamines possessing a strongly polarized exocyclic double bond. This polarization is transmitted to unsaturated substituents conjugated with the enaminic double bond. The IR spectra of such compounds reflect this phenomenon. Thus, in the spectra of 2-acylmethylene-azolines[1] the $\nu_{C=C}$ and $\nu_{C=O}$ bands appear both shifted downwards to 1615–1570 cm^{-1}. Consequently, the dipolar structures E and F must be considered to contribute substantially to the resonance hybride of these compounds.

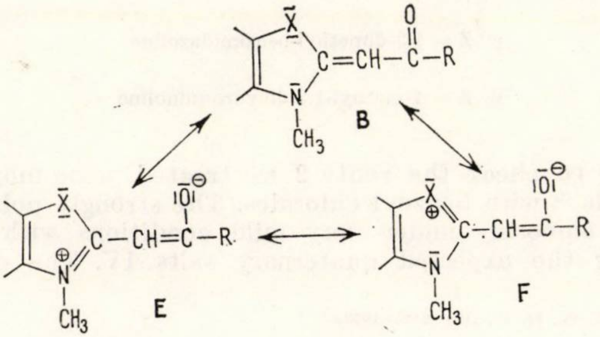

In the acyl-azo-methylenes the participation of the $-N=N-$ group to the double bond delocalization is to be expected. Consequently, the resonance hybride will contain besides the fully covalent structure four dipolar structures as shown below:

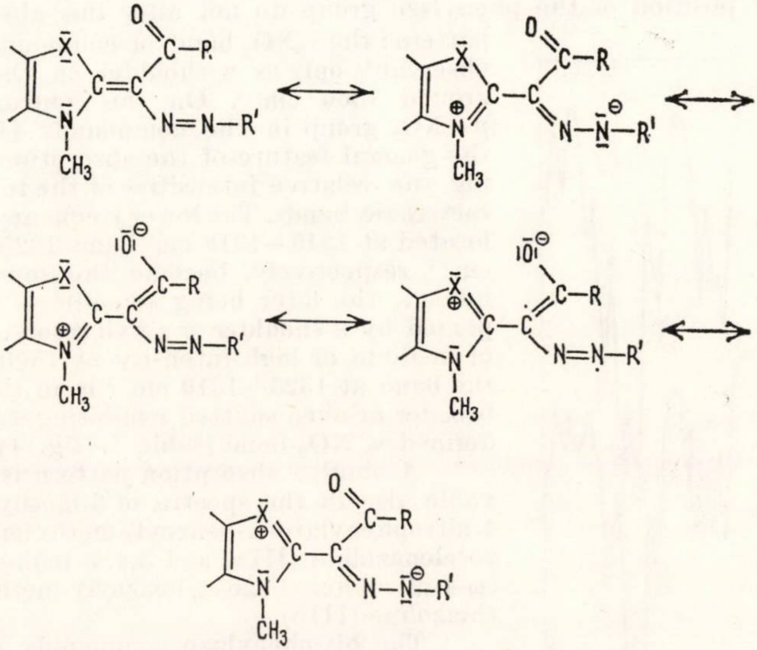

The data concerning the IR absorption of the $-N=N-$group found in the literature are very different. None of them is sufficiently reliable to permit a sure identification of this group. Le Fèvre *et al.*[11] investigating 36 aromatic azo compounds found two bands at 1577 ± 8 cm^{-1} and 1406 ± 14 cm^{-1}, respectively, and mentioned that these could be produced also by the aromatic ring. Authors working later in this field accepted either the one or the other of these two ranges for the characterization of the azo group. Fernandez-Alonso and Oliete[12] reported in the spectra of azonaphthalenes a band around 1505 cm^{-1} and correlated it with the azo group. Bassignana and Cogrossi[13] working on 110 azo dyes assigned to the $-N=N-$ group a band at 1410 ± 30 cm^{-1} and to the $-C=N-$ group another one at 1145 ± 15 cm^{-1}.

We did not expect that these data would be confirmed or invalidated by the IR measurements carried out on our strongly polarized acyl-azo-methylenes. Indeed, we found in the spectra of compounds I a characteristic absorption pattern which consists of four bands: two very strong at 1375–1368 cm^{-1} and 1362–1355 cm^{-1}, respectively, and two of lower intensities at 1405–1395 cm^{-1} and 1330 cm^{-1}, respectively. An illustrative example is the spectrum of compound I f pictured in fig. 1. Substituents such as CH_3-, CH_3O-, or a halogen atom, in the *para* position of the phenylazo group do not alter this absorption pattern; the $\nu_S NO_2$ band of compound I h is observable only as a shoulder on the band around 1360 cm^{-1}. On the contrary, the $p-NO_2$ group in the compounds II alters the general feature of the absorption changing the relative intensities of the four characteristic bands. The lower frequency bands located at 1340–1318 cm^{-1} and 1325–1295 cm^{-1}, respectively, become the most prominent, the later being sometimes accompanied by a shoulder or a well resolved band of medium or high intensity at 1300 cm^{-1}; the band at 1325–1310 cm^{-1} is in this case broader or even splitted exhibiting a clearly defined $\nu_S NO_2$ band (table 1, fig. 1).

---

[11] R. J-W. Le Fèvre, M. F. O'Dwyer and R. L. Werner, *Chem. and Ind.*, **1953**, 378.

[12] J. I. Fernandez-Alonso, and J. L. Oliete, *Chem. Abstr.*, **62**, 4783 h (1965).

[13] P. Bassignana and C. Cogrossi, *Tetrahedron*, **20**, 2361 (1964).

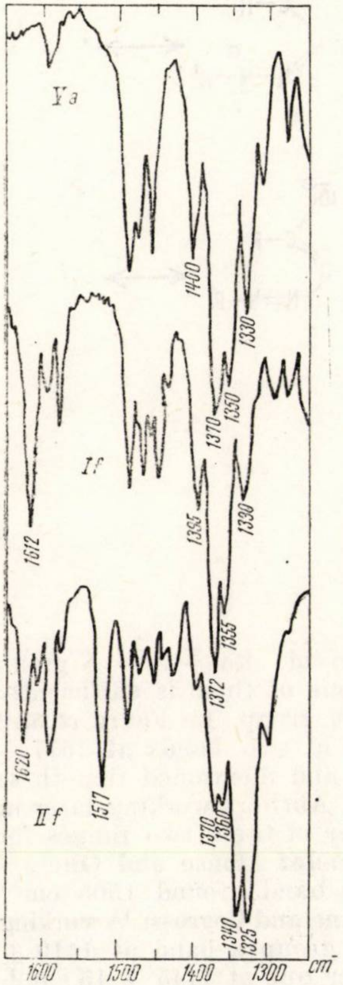

Fig. 1. — IR spectra in the 1650–1250 cm^{-1} region of compounds If, IIf, and Va.

A similar absorption pattern is observable also in the spectra of 3-methyl-2-(ω-4-nitrophenylazo-ω-benzoyl)-methylene-benzoselenazoline (IIIa) and 3,4, 5-trimethyl-2-(ω-4-nitrophenyl-azo-ω-benzoyl) methylene-thiazoline (IIIb).

The bis-phenylazo compounds Va and Vb, prepared according to Wahl,[2] were found to exhibit an analogous quadruplet in the same region.

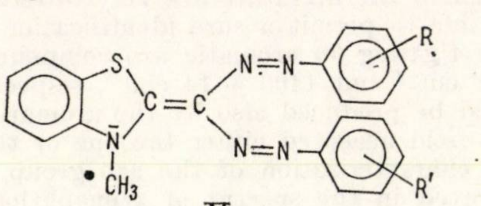

V

a. R = R′ = H

b. R = R′ = 4 – Cl

The band at 1625–1610 cm^{-1} present in the spectra of acyl-azo-methylenes and lacking from those of bis-phenylazo compounds (V) was consequently assigned to the strongly polarized C = O group.

Since the four strong bands discussed above are observable either in the spectra of our acylazo compounds or in those of bis-azomethylenes, they may be correlated with the polarized —N = N-group. The high intensity of these bands is due to the ionic character of the double bond as in the case of fulvenes in which the strongly polarized double bond entails a very strong absorption band.

Consequently, the actual structure of the acyl-azo-methylene derivatives of the N-containing heterocycles seems to be closer to a dipolar structure G than to a nonpolar one.

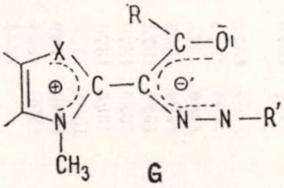

G

EXPERIMENTAL

3-METHYL-2-(ω-ACYL-ω-ARYLAZO) METHYLENE DERIVATIVES

Route 1. General Method. An ice cold acetone solution of 2-acylmethylene-azoline (B) was treated with an equimolecular amount of diazonium salt solution. The pH was then brought to 5–6 with a saturated sodium acetate solution. After 1 hour standing the precipitate is filtered and purified as shown in table 2.

Coupling in acidic medium. The 2-acylmethylene-azoline (B) is dissolved in acetone and the solution is brought to pH 1.5–2 with HCl 2N, cooled at 0° and treated with the aqueous solution of the diazonium salt. After 2 hours standing the precipitate (IIa resp. IIIa) is filtered.

Route 2. General Method. To a stirred solution of 2-(arylazo) methylene-benzothiazoline[10] (C) in CH_2Cl_2 or $CHCl_3$ an equimolecular amount of acyl chloride dissolved in the same solvent was added. The quantitatively precipitated addition product IV was filtered and purified by dissolution in methanol and precipitation with ether.

3-METHYL-2-(ω-BENZOYL-ω-PHENYLAZO) METHYL-BENZOTHIAZOLIUM CHLORIDE (IV a) : M.p. 227°

$C_{22}H_{18}ClN_3OS$ %Cl : *Calcd.* : 8.69 ; *Found* : 8.10

3-METHYL-2-[ω-BENZOYL-(4′-NITROPHENYLAZO)] METHYL-BENZOTHIAZOLIUM CHLORIDE (IV v): M.p. 257°

$C_{22}H_{17}ClN_4OS$ %Cl : *Calcd.* : 7.82 ; *Found* : 7.45

3-METHYL-2-[ω-(4-NITROBENZOYL)-ω-(4′-NITROPHENYLAZO)] METHYL-BENZOTHIAZOLIUM CHLORIDE (IV c)

The compound is unstable. A fast m.p. gives 231° (dec.).

Free bases. The salts IV were dissolved in aqueous methanol and the free bases (Ic, IIc), identical with those prepared following route 1, were precipitated by addition of triethylamine or pyridine.

IR spectra. The spectral measurements were carried out in KBr pellets (0.3 g substance to 300 mg KBr) using a UNICAM SP 200 G spectrophotometer.

Table 1

Absorptions of 3-methyl-2-(ω-acyl-ω-arylazo)methylenes in the 1650 – 1300 cm⁻¹ region

Substance	C = O	C = C arom.		NO_2	C = C skeleton and C – H bending vibrations									Characteristic range of the polarized N = N group				
Va		1590				1485	1473	1455						*1400*	**1370**	**1350**	*1330*	
Vb		1588				1482	1472	1455						*1388*	**1365**	**1350**	*1330*	
Ia	1613	1600	1575		1510	1480	1465	1455		1445	1428			*1402*	**1375**	**1360**	*1330*	
					1500													
Ib	1610	1595	1575		1500	1480	1465	1455		1448	1425			*1400*	**1372**	**1362**	*1330*	
Ic	1613	1597	1578			1485	1470	1455	1450	1445	1436			*1405*	**1370**	**1362**	*1330*	
Id	1618	1595	1575			1485	1470	1460	1450	1445	1435		1418	*1400*	**1370**	**1360**	*1330*	
Ie	1615	1595	1570			1482	1468	1460	1448	1440	1432		1415	*1395*	**1368**	**1360**	*1330*	
If	1612	1590	1575			1482	1465	1455		1445	1432			*1395*	**1372**	**1355**	*1330*	
Ig	1618	1595	1578			1485	1470	1460		1450	1430			*1395*	**1370**	**1360**	*1330*	
Ih	1612	. . .	1575	1530		1482	1470	1448		1445				*1395*	**1370**	**1360**	*1330*	
IIa	1625	1600	1595	1510		1485	1470	1450		1440	1432			1385	*1368*	*1353*	**1320**	**1310**
IIb	1625	1605	1585	1515	1505	1482	1468	1448			1435			1390	*1362*	*1352*	**1335**	**1315**
IIc	1620	1602	1585	1515		1482	1465	1450			1435	1422		1390	*1365*	*1355*	**1335**	**1320**
IId	1622	1605	1586	1515		1482	1470	1448			1435		1405		*1365*	*1355*	**1338**	**1322**
IIe	1622	1605	1587	1517		1482	1470	1450			1438	1425		1400	*1365*	*1355*	**1338**	**1322**
IIf	1620	1605	1587	1517		1485	1470	1450			1438	1425		1395	*1370*	*1360*	**1340**	**1325**
IIg	1600	1585	1565	1525		1485	1468	1448			1440	1425		1395	*1365*	**1358**	**1325**	**1300**
				1510														
IIh	1620	1590		1520		1480	1468	1448			1433	1421						
				1510										1393	*1370*	*1350*	**1340**	**1325**
IIIa	1628	1600	1585	1515		1483	1470	1458	1448			1422		1388			**1318**	**1295**
IIIb	1620	1595	1582	1515		1480	1470	1445				1420		1360				

italicized – strong bands, bold-faced – very strong bands.

Table 2

3 Methyl-2-(ω-acyl-ω-arylazo)methylene derivatives

Substance	M.p. Colour Solvent	Empirical formula	Analysis			
			%N		%S	
			Calcd.	*Found*	*Calcd.*	*Found*
Ia	202° Brick-red DMFA	$C_{23}H_{19}N_3O_2S$	10.47	10.70	7.99	8.08
Ib	210° Brick-red DMFA	$C_{23}H_{19}N_3OS$	10.91	10.97	8.32	8.29
Ic	193° Orange DMFA	$C_{22}H_{17}N_3OS$	11.32	11.63	8.63	8.16
Id	232° Orange DMFA	$C_{22}H_{16}ClN_3OS$	10.36	10.60	7.90	7.95
Ie	242.5° Orange DMFA	$C_{22}H_{16}BrN_3OS$	9.33	9.54	7.12	6.90
If	212° Cinnabar red Chlf. + EtOH	$C_{22}H_{16}ClN_3OS$	10.36	10.62	7.90	7.36
Ig	214–16° Orange Chlf.	$C_{22}H_{16}BrN_3OS$	9.33	9.85	7.12	6.81
Ih	232° Orange DMFA	$C_{22}H_{16}N_4O_3S$	13.46	13.76	7.70	7.39
IIa	262° Red DMFA	$C_{23}H_{18}N_4O_4S$	12.55	12.60	7.18	7.16
IIb	260–1° Red DMFA	$C_{23}H_{18}N_4O_3S$	13.02	13.47	7.45	7.55
IIc	244° Cyclamen red Benzene	$C_{22}H_{16}N_4O_3S$	13.46	13.70	7.70	7.80

Table 2 (continued)

Substance	M.P. Colour Solvent	Empirical formula	Analysis %N *Calcd.*	 *Found*	 %S *Calcd.*	 *Found*		
IId	263–4° Cinnabar red DMFA	$C_{22}H_{15}ClN_4O_3S$	12.44	12.61	7.12	7.50		
IIe	268° Cinnabar red DMFA	$C_{22}H_{15}BrN_4O_3S$	11.32	11.57	6.48	6.57		
IIf	243° Cinnabar red DMFA	$C_{22}H_{15}ClN_4O_3S$	12.44	12.16	7.12	7.01		
IIg	274° Orange DMFA	$C_{22}H_{15}N_2O_5S$	15.18	15.35	6.95	6.83		
IIh	281° Cinnabar red DMFA	$C_{22}H_{15}N_2O_5S$	15.18	15.17	6.95	6.93		
IIIb	245–6° Brick-red DMFA	$C_{20}H_{18}N_4O_3S$	14.21	14.45	8.13	7.55		
					%C		%H	
IIIa	279–80° Red DMFA	$C_{22}H_{16}N_4O_3Se$	12.09	12.31	57.00	57.32	3.47	3.35
IIIc	271° Red DMFA	$C_{23}H_{15}N_5O_3$	16.95	16.97	66.81	66.75	4.63	4.71
IIId	224–5° Brown violet Chlf. + Pet. et.	$C_{24}H_{18}N_4O_3$	13.65	13.70	70.23	70.43	4.42	4.59

Revue Roumaine de Chimie, **18**, *12*, 2113–2125 (1973)

HETEROCYCLIC DERIVATIVES WITH THIAZOLIC RINGS. II[1]

ELECTROPHILIC SUBSTITUTIONS OF 6-AMINOTHIAZOLO [4,5-f] INDAZOLE

C.TĂRĂBĂŞANU-MIHĂILĂ, L. FLORU and MARIA OLTEANU

Laboratory of Chemistry and Technology of Organic Dyes, Polytechnic Institute of Bucharest,
Calea Victoriei 149, Romania

Received April 17, 1973

Studies have been carried out on the possibility of obtaining certain halogenated, nitrated and sulfonated derivatives of 6-aminothiazolo [4,5-f] indazole.

1. INTRODUCTION

The direct substitution of benzothiazolic and indazolic heterocyclic system has formed the object of many studies in recent years. Dahn and co-workers,[2] Tărăbăşanu and co-workers [3] analysed the nitration possibilities of benzothiazoles and of their substituted derivatives and Sureau and co-workers [4–6] investigated the possibilities for the nitration and sulfonation of indazole.

Halogenation of aminoindazoles [7] has been known for a long time, leading to 3-substituted compounds in all cases.

The utilization of benzothiazoles and indazoles substituted in the synthesis of dyes leads to interesting results.

The presence of halogen atoms increases the resistance of dyes [7] to light and wet treatments and the electron-accepting groups cause strong bathochrome effects,[2] sometimes even providing the green colour which is missing in common monoazo-dyes.

---

[1] C. Tărăbăşanu-Mihăilă, L. Floru, E. Baltă and A. Predescu, *Rev. Roumaine Chim.*, **18**, 889 (1973).

[2] J. W. Dehn, N. Y. Bayside, R. Eltonhead, N. J. Englewood and R. A. Pizzarello, (Interchemical Corporation, New York, N.Y., a corporation of Ohio), U.S. Pat. 3057848, Oct. 1962.

[3] C. Tărăbăşanu-Mihăilă, L. Floru and E. Frank, *Rev. Roumaine Chim.*, **18**, (1973).

[4] P. Petelcolos and R. Sureau, *Bull. Soc. chim. France*, **1950**, 466.

[5] R. Sureau and R. Pernot, *Bull. Soc. chim. France*, **1958**, 152.

[6] R. Sureau and R. Pernot, *Bull. Soc. chim. France*, **1960**, 32.

[7] H. Sanielevici, *Coloristica*, **13**, 9 (1969).

Based on these findings and considering the outstanding results obtained by introducing 6-aminothiazolo [4,5-f] indazole into the structure of dispersion dyes,[1] we tried to obtain some of its substituted derivatives, not mentioned in the literature, which would provide further means for preparing a large scale of dyes.

The present paper reports the results of investigations regarding the synthesis of certain halogenated, nitrated and sulfonated compounds of 6-aminothiazolo [4,5-f] indazole, with the intention of presenting the tinctorial properties of derivated monoazo-dyes in further papers.

The succession of reactions used is shown in the scheme at page 2115·

2. EXPERIMENTAL AND DISCUSSION

2.1. HALOGENATION OF 6-AMINOTHIAZOLO [4,5-f] INDAZOLE

The action of chlorine or bromine on the aqueous solution of compound III hydrochloride at temperatures ranging between 40–50° leads to the formation of 3-chlorine-6-amino-thiazolo [4,5-f]indazole (VII, $X = Cl$) or 3-bromine-6-aminothiazolo [4,5-f]indazole (VII, $X = Br$) respectively, which precipitate in the reaction mass. The insolubility of these compounds in 5% HCl permits a good separation from the unreacted intermediate III. Yields are good, reaching 85–90% and the purity of products is remarkable.

In view of precisely defining the position of the halogen atom, type VII products were also obtained starting from 3-halogen-6-amino indazoles (V) obtained according to indications found in the literature [7] by sulfocyanuration followed by cyclization in an acid medium.

We also mention the possibility of preparing 3-halogen-5-sulfocyan-6-amino indazole (VI) from 6-amino indazole (I), using an excess of halogen in the sulfocyanuration reaction.

Halogeno-6-aminothiazolo [4,5-f]indazoles obtained by applying the three procedures proved to be identical, a fact which assesses the presence of the halogen atom in position 3. Data referring to the synthesis of those compounds are listed in tables 1 and 2.

2.2. NITRATION OF 6-AMINOTHIAZOLO [4,5-f] INDAZOLE

The action of nitric acid in a 98% sulfuric acid medium on compound III at temperatures ranging between –5 and 90° determines the formation of a nitro-derivative (IV ; $Y = NO_2$). Since the synthesis of a similar product from nitro-6-aminoindazoles was not possible (these compounds can no more be sulfocyanurated due to the strong electron-

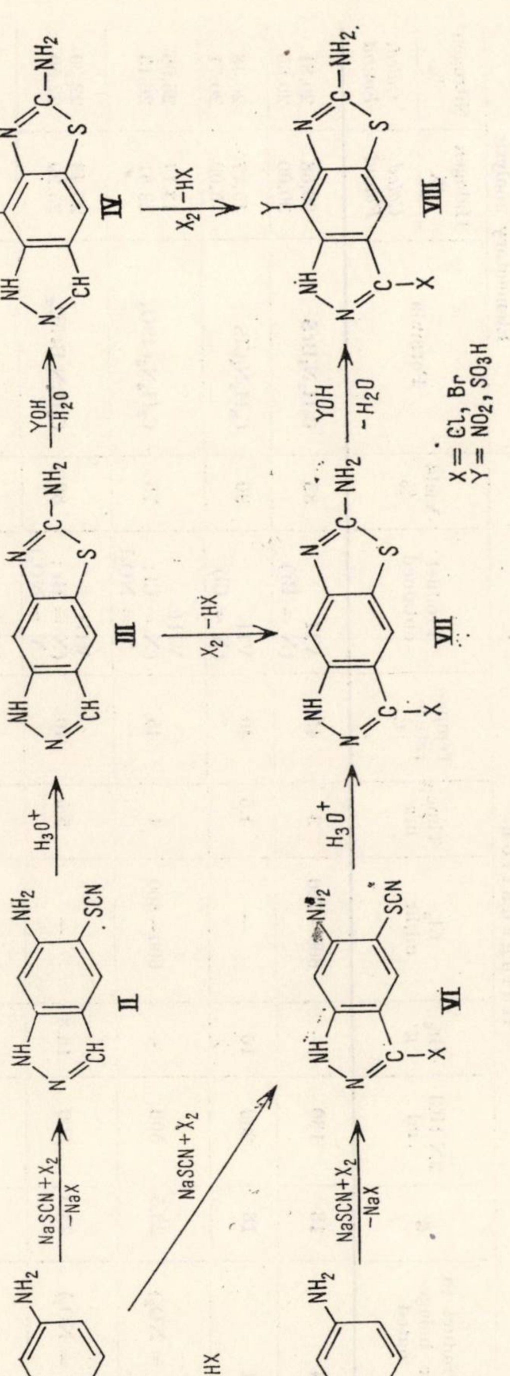
I
II
III
IV
V
VI
VII
VIII
NaSCN + X₂, −NaX
NaSCN + X₂
X₂, −HX
H₃O⁺
YOH, −H₂O
X = Cl, Br
Y = NO₂, SO₃H

Table 1

Data regarding synthesis of the compound of VII and VIII type

Halogenation									Elementary analysis		
Product to be halogenated	g	2N HCl ml	Br_2 g	Cl_2 ml/hr	Time hrs	Temperature °C	Product obtained	Yield %	Formula	Halogen % *Calcd.* *Found*	Nitrogen % *Calcd.* *Found*
III	18	180	—	600—700	3	45	VII (X = Br)	85	$C_8H_5N_4BrS$	29.68 30.00	20.81 20.65
III	18	200	16	—	4.5	40	VII (X = Cl)	90	$C_8H_5N_4ClS$	15.77 15.09	20.48 20.71
IV ($Y = NO_2$)	23.5	500	—	600—800	4	45	VIII (X = Cl; $Y = NO_2$)	75	$C_8H_4N_5ClSO_2$	13.14 13.31	25.96 26.13
IV ($Y = NO_2$)	23.5	500	16.8	—	5.5	40	VIII (X = Br; $Y = NO_2$)	80	$C_8H_4N_5BrSO_2$	25.43 25.20	22.29 22.50
IV ($Y = SO_3H$)	27	300	—	600	4.5	45	VIII (X = Cl; $Y = SO_3H$)	65	$C_8H_5N_4ClS_2O_3$	11.63 11.85	18.41 18.72
IV ($Y = SO_3H$)	27	300	16.8	—	4	40	VIII (X = Br; $Y = SO_3H$)	40	$C_8H_5N_4BrS_2O_3$	22.88 23.00	16.04 15.87

Table 2

Data regarding synthesis of the compounds of VII type

Sulfocyanuration								Cyclization				Elementary analysis		
Product to be sulfocyanurated	g	CH_3COOH ml	NaSCN g	Br_2 g	Cl_2 ml/hr	Time hrs	Temperature °C	2N HCl ml	Refluxing time hrs	Product obtained	Yield %	Formula	Halogen %	Nitrogen %
													Calcd. *Found*	*Calcd.* *Found*
V (X = Cl)	17	250	29	—	800	4 10	15 28	600	6	VII (X = Cl)	78	$C_8H_5N_4ClS$	15.77 15.97	20.48 20.15
V (X = Cl)	17	250	29	16	—	4 12	5 25	600	6	VII (X = Cl)	75	$C_8H_5N_4ClS$	15.77 15.88	20.48 20.21
I	13.3	200	29	—	800–1000	2 10	15 25	600	8	VII (X = Cl)	60	$C_8H_5N_4ClS$	15.77 15.50	20.48 20.71
V (X = Br)	20	300	27.5	—	800	4 10	5 28	1000	8	VII (X = Br)	70	$C_8H_5N_4BrS$	29.68 30.00	20.81 20.68
V (X = Br)	20	300	27.5	16	—	4 12	5 25	1000	8	VII (X = Br)	85	$C_8H_5N_4BrS$	29.68 29.91	20.81 21.01
I	13.3	200	29	16	—	2 10	15 25	800	6	VII (X = Br)	55	$C_8H_5N_4BrS$	29.68 29.35	20.81 20.73

accepting effect of the nitro group), the placement of the nitro group in position 8 was assigned by IR spectral analysis of this compound.

Data concerning the synthesis and the main properties of 6-amino-8-nitrothiazolo [4,5-f]indazole (IV; Y = NO_2) are presented in table 3.

Table 3

Data regarding synthesis of the compounds of IV and VIII type

Nitration (sulfonation)								Elementary analysis		
Product to be substituted	g	98% H_2SO_4 ml	80% HNO_3 g	Temperature °C	Time hrs	Product obtained	Yield %	Formula	Halogen	Nitrogen
									Calcd. *Found*	*Calcd.* *Found*
III	19	150	8	−5 10 90	1 6 4	IV (Y = NO_2)	76	$C_8H_5N_5SO_2$	—	29.77 30.00
III	19	200	—	60 110	1 5	IV (Y = SO_3H)	40	$C_8H_6N_4S_2O_3$	—	23.81 23.65
VII (X = Cl)	22.4	160	8	−5 10 90	1 6 6	VIII (X = Cl; Y = NO_2)	75	$C_8H_4N_5ClSO_2$	13.14 13.21	25.96 26.08
VII (X = Br)	26.9	250	8	−5 10 90	1 6 6	VIII (X = Br; Y = NO_2)	75	$C_8H_4N_5BrSO_2$	25.43 25.60	22.29 22.07
VII (X = Cl)	22.4	250	—	60 110	1 5	VIII (X = Cl; Y = SO_3H)	25	$C_8H_5N_4S_2ClO_3$	11.63 11.48	18.41 18.57
VII (X = Br)	26.9	250	—	60 110	1 5	VIII (X = Br; Y = SO_3H)	25	$C_8H_5N_4S_2BrO_3$	22.88 23.14	16.04 16.41

The yield of nitration reaction is 85–80%. The product may be recrystallized from dimethylformamide, dimethylsulfoxide or triethylene glycol.

2.3. SULFONATION OF 6-AMINOTHIAZOLO [4,5-f] INDAZOLE

The action of 98% sulfuric acid upon compound III at temperatures between 60–110° results in its sulfonation. Neither in this case was the synthesis of the standard samples possible since the behaviour of the sulfonic acids of 6-amino-indazole in the sulfocyanuration reaction is similar to that of the nitro-derivative.

The placement of sulfonic group in position 8 was assigned by IR spectral analysis of this compound.

Table 3 presents data concerning the synthesis and the main properties of 6-aminothiazolo [4,5-f] indazole 8-sulfonic acid.

2.4. SYNTHESIS OF DISUBSTITUTED 6-AMINOTHIAZOLO [4,5-f] INDAZOLES (VIII)

Two methods were applied for the synthesis of 3-chlorine-6-amino-8-nitrothiazolo [4,5-f] indazole (VIII ; $X = Cl$, $Y = NO_2$) and of 3-bromine-6-amino-8-nitrothiazole [4,5-f] indazole (VIII ; $X = Br$, $Y = NO_2$) : halogenation of compounds IV ($Y = NO_2$) and nitration of derivatives VII ($X = Cl, Br$). The reaction conditions are identical to those used in the substitution of compound III. The 3-chlorine-6-aminothiazolo [4,5-f] indazole sulfonic acid (VIII ; $X = Cl$, $Y = SO_3H$) and the 3-bromine-6-aminothiazolo [4,5-f] indazole sulfonic acid (VIII ; $X = Br$, $Y = SO_3H$) were also synthesized by two methods : halogenation of compounds IV ($Y = SO_3H$) and sulfonation of derivatives VII ($X = Cl, Br$). The reaction conditions are identical to those used in the case of analogous substitutions based on compound III.

Data concerning the synthesis and the main properties of these products are listed in tables 2 and 3.

3. IR SPECTRA OF 6-AMINOTHIAZOLO [4,5-f] INDAZOLE SUBSTITUTED DERIVATIVES

3.1. 3-HALOGENO-6-AMINOTHIAZOLO [4,5-f] INDAZOLE (VII)

Sullivan showed [8] that in the case of type IX compounds the general aspect of the spectrum is affected by the nature of R_1 and R_2 substituents only by the introduction of their own bands.

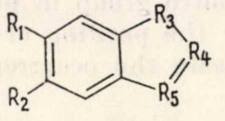

$R_3 = CH_2, O, NH, CO, SO_2$
$R_4, R_5 = N, CH$

IX

We extended this finding to type III compounds, where two compactly condensed heterocyclic systems maintain their spectral individuality.[1] Hence, all halogenated derivatives in position 3 of 6 aminothiazolo [4,5-f] indazole are expected to reproduce in the IR spectrum the characteristic bands of 3 halogeno indazoles (V) and those specific to the benzothiazole system (IX ; $R_1 = R_2 = H$; $R_3 = S$; $R_4 = C{-}NH_2$; $R_5 = N$).

The spectral data presented in table 4 confirm this fact. The main fundamental bands of compound III are maintained in the case of products VIII except for ν_{CH} values situated at 3065 and 2935 cm^{-1}. This is a normal fact since this grouping dissappears after halogenation.

---

[8] D. G. O'SULLIVAN and J. SADLER, *J. Org. Chem.*, **22**, 283 (1957).

The following bands have been assigned :

1. Bands situated within the 658–660, 635–630 and 620 cm^{-1} regions, corresponding to the C–S bond, a fact that has been reported by Surede and co-workers ;[9]

2. Bands situated at 980, 920 and 895 cm^{-1}, specific of the thiazole system ; [1]

3. Bands situated at 1632, 1580, 1540 and 1510 cm^{-1}, specific of the benzothiazole system.[10,11]

4. All characteristic bands of the indazole system : $\nu_{NH} = 3160\ cm^{-1}$, as well as all bands situated within the 1380–1975 and 850–720 cm^{-1} regions.[12]

5. Bands $\nu_{NH_2 asym}$ at 3375 and $\nu_{NH_2 sym}$ at 3315 cm^{-1} which confirm the presence of amino group.

We mention that these bands are found in the spectra of all the substituted compounds of 6-aminothiazole [4,5-f] indazole (table 4).

3.2. 6-AMINO-8-NITROTHIAZOLO [4,5-f] INDAZOLE IV ($Y = NO_2$) AND ITS HALOGENATED DERIVATIVES VIII ($X = Cl, Br$; $Y = NO_2$)

Since two isomers may be obtained by nitration of 6 amino-thiazolo [4,5-f] indazole III (having the nitro group in positions 4 and 8, respectively) we undertake to identify the position of the nitro group, because the experimental results indicate the occurrence of a unitary product by nitration.

Since the synthesis of standard samples was not possible we intend to identify the position of the nitro group based on the position of ν_{NH} and $\nu_{NO_2 asym}$ bands.

The extremely low frequency of ν_{NH} band (3145 cm^{-1}) in type IV and VIII compounds (table 4) and the stretched aspect of the band suggest that this group takes part in the formation of hydrogen bonds, knowing that the higher the hydrogen bonding capacity, the lower are the values of ν_{NH} in indazole compounds.

---

[9] K. S. Suresh, J. Ramachandran and G. N. R. Rao, *J. Sci. Ind. Res. India*, **208**, 2031 (1961).

[10] J. M. Bonnier, M. Gelus and B. Papoz, *Bull. Soc. chim. France*, **9**, 2485 (1965).

[11] A. Taurins, J. G. E. Fenyes and R. N. Janes, *Canad. J. Chem.*, **35**, 423 (1957)

[12] D. G. O'Sullivan, *J. Chem. Soc.*, **8**, 3278 (1960).

In the case of nitroindazoles,[1] the hydrogen bonds are achieved without participation of nitro groups, being exclusively intermolecular. This finding pleads for the structures X and XI:

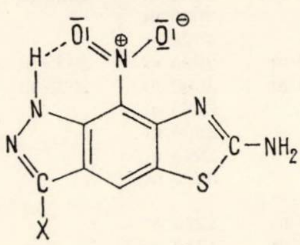

X

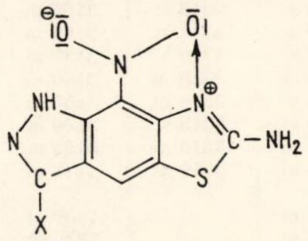

XI

$X = H, Cl, Br$

For these reasons, the presence of nitro groups in position 8 seems highly probable in the case of certain compounds of type IV and VIII.

The following conclusions may result from the analysis of the position of bands $\nu_{NO_{2}asym}$ at 1525 cm^{-1} and $\nu_{NO_{2}sym}$ at 1340 cm^{-1} (bands which are identical for all type IV and VII compounds).

The examination of the symmetric vibration is largely affected by the fact that the amine C—N valency vibration is also found in its absorption region of 1300—1360 cm^{-1},[13-16] an accurate assignment of bands being hardly to achieve.[17-18] On the other hand, Brown[19] shows that substituents found in the aromatic nucleus of nitroderivatives have a significantly more pronounced influence on $\nu_{NO_{2}asym}$ than on $\nu_{NO_{2}sym}$.

For this reason, our discussion will refer to $\nu_{NO_{2}asym}$ alone.

In the case of substituted *ortho* aromatic nitroderivatives, the reciprocal actions may be of two types: on the one hand, formation of some orthoquinoide structures, on the other hand, a field effect oriented in an opposite direction.

As has been reported by Franck and co-workers,[20] the field effect has a predominant action in most cases, due to the low distance between substituents. Its occurrence in the case of the compounds mentioned above may be justified by the mesomeric structures X and XI.

The fact that $\nu_{NO_{2}asym}$ ranges within the 1510—1525 cm^{-1} region, established by Franck[20] for *ortho* substituted nitroderivatives pleads for the presence of the mentioned mesomeric structures.

---

[13] R. R. Randle and D. H. Whiffen, *J. Chem. Soc.*, **1952**, 4153.

[14] R. I. Francel, *J. Amer. Chem. Soc.*, **74**, 1265 (1952).

[15] J. F. Brown, *J. Amer. Chem. Soc.*, **77**, 6341 (1955).

[16] R. D. Kross and V. A. Fassel, *J. Amer. Chem. Soc.*, **78**, 4225 (1956).

[17] N. B. Colthup, *J. Opt. Soc. Amer.*, **40**, 397 (1950).

[18] R. B. Barnes, R. G. Gore, R. W. Stafford and V. Z. Williams, *Analyt. Chem.*, **20**, 402 (1948).

[19] J. F. Brown, *J. Amer. Chem. Soc.*, **77**, 6341 (1955).

[20] B. Franck, H. Hormann and S. Scheibe, *Chem. Ber.*, **1957**, 90.

Table

Infrared bands of the compounds

1	3380 s	3315 s	3160 m	3065 m	3030 m	2935 m	2885 m
2	3375 s	3313 s	3160 m		3025 m		
3	3380 s	3315 s	3165 m		3025 m		2880 m
4	3385 s	3320 s	3145 m	3070 m	2995 m	2935 m	2850 m
5	3365 m	3310 m	3150 m	3075 m	3000 m	2935 m	2870 m
6	3380 s	3310 m	3155 m		2985 m		2900 m
7	3385 s	3315 s	3160 m		2990 m		2895 w
8	3370 m	3315 m	3155 m		3025 m		2890 w
9	3365 m	3310 m	3148 m		3015 m		2890 m
1	1380 m		1330 m	1245 m	1210 w		1132 m
2	1385 m		1330 m	1245 m	1215 w		1130 m
3	1375 m		1320 m	1240 w			1135 m
4	1392 m	1340 m	1310 m	1250 w			1126 m
5	1385 m		1300 m	1240 m	1208 w	1140 m	1160 m
6	1375 m	1330 m	1290 m	1228 m	1190 w		1145 m
7	1380 m	1340 m	1295 m	1235 w	1200 w		1140 m
8	1395 m		1330 w	1250 w		1145 m	1130 w
9	1400 m		1290 w	1245 m		1145 m	1135 w
1	826 w	795 m	775 m	745 w	720 w	690 w	658 w
2		795 m	775 m	740 w	718 w		660 w
3	825 w		780 m	740 w			660 w
4	816 w		794 s		730 w	706 s	
5	826w	800 m	785 m	740 w	720 w	685 s	658 w
6			780 m		710 w	695 w	
7			795 s			685 w	
8	830 w	795 m	775 m	730 w		680 w	
9	820 w	795 m		735 w		690 w	

1 – Compound III
2 – Compound VII (X = Cl)
3 – Compound VII (X = Br)
4 – Compound IV (Y = NO_2)
* IR spectra were taken in a KBr disk using a UR-10 spectrophotometer.

IR spectra of compounds IV and VIII reveal the presence of a shoulder near 1545 cm^{-1} in all cases. This frequency resembles to that of an aliphatic nitro group and is likely to result from molecules in which the NO_2 group is deviated from the molecule plane, these structures being no more capable of resonance.

All these considerations plead for position 8 of the nitro group in type IV and VIII compounds.

3.3. 6-AMINOTHIAZOLO [4,5-f] INDAZOLE 8-SULFONIC ACID (V,Y = SO_3H) AND ITS HALOGENATED DERIVATIVES VIII (X = Cl, Br; Y = SO_3H)

There are few papers dealing with IR spectra of sulfonic acids. The bands within the 1150—1260, 1010—1080 and 600—700 cm^{-1} regions were suggested for identification purposes.[21]

---

[21] L. J. Bellamy, "Infrared Spectra of Complex Molecules", Londra, Methuen Co., 1959, p. 351.

4

III IV, VII and VIII *

2805 w	2765 w	1632 s	1580 w			1510 m	1420 m
		1632 s	1580 w	1540 w		1515 m	
		1630 s	1575 w			1510 m	1420 m
2785 w		1615 s			1525 m	1490 m	1425 w
		1625 s	1562 w			1503 m	1415 m
	2700 w	1620 s	1570 w		1520 m	1490 m	1420 m
		1630 s	1565 w	1530 w	1520 m	1520 m	1425 m
	2780 w	1615 s		1550 w		1490 m	1410 w
	2780 w	1615 s				1510 w	1400 w
1105 m	1075 w		1032 m	980 m	920 s	855 m	838 w
1100 m	1075 w			985 m	915 s	855 m	840 w
1100 m			1030 m	980 w	917 s	850 m	
1092 m			1025 m	980 w	930 m		850 m
1107 m		1065 m		990 m	890 m		830 w
1105 m	1060 w			960 m	890 s	860 m	845 w
1100 m	1070 w			970 w	900 s	870 m	
1090 w	1080 w	1060 m		965 m	915 s		845 w
1100 w	1085 w	1070 m		960 w	930 m		850 w
630 w	620 w						
635 w	620 w						
635 w							
630 w							
640 w	624 w						
625 w							
625 w							

5 – Compound IV ($Y = SO_3H$)
6 – Compound VIII ($X = Cl$; $Y = NO_2$)
7 – Compound VIII ($X = Br$; $Y = NO_2$)
8 – Compound VIII ($X = Cl$; $Y = SO_3H$)
9 – Compound VIII ($X = Br$; $Y = SO_3H$)

Since the thiazolo [4,5-f] indazole system reveals numerous bands in these regions,[1] the identification of bands is extremely difficult and arbitrary even in the case of symmetric and asymmetric ν_{SO_2}.

For this reason we discuss only the frequency ν_{NH} situated at 3150 cm^{-1} in all type V and VIII compounds. The marked closeness in the position of this band for nitroderivatives and sulfonic acids suggests that the NH group takes part in the hydrogen bond formation. This supports for the presence of sulfonic group in position 8 when the mesomeric structures XII and XIII are possible. In this case, the field effect seems to have a significant weight. The fact that electrophil substitutions occur in position 8 on the thiazolo [4,5-f] indazole nucleus, suggests that NH and N groups are not protonated in a 98% sulfuric acid medium since in this case the orientation of the substitution would occur in position 4. An experimental verification of this assumption was not possible because of the amino group oxidation reactions occurring when more diluted sulfuric acid is used in the reaction (when dissociation becomes possible for the sulfuric acid).

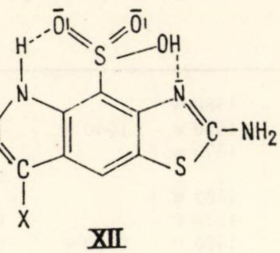

XII

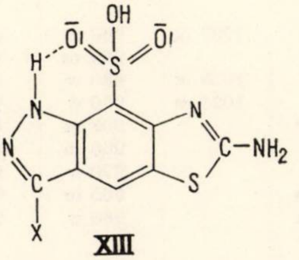

XIII

In our further works we shall present the substitution reactions of 8 acetyl aminothiazolo [4,5-f] indazole in which nitration and sulfonation in position 4 becomes possible by using 75% sulfuric acid.

4. EXPERIMENTAL

4.1. HALOGENATION OF 8-AMINOTHIAZOLO [4,5-f] INDAZOLE AND OF ITS SUBSTITUTED DERIVATIVES (TABLE 1)

The amine hydrochloride to be halogenated is passed into a 4-neck flask fitted with a stirrer, a bubble flask (dropping funnel) and an ascending refrigerent with a thermometer. Chlorine is bubbled (bromine is dropped) after the experiment temperature has been reached.

The reaction mass is filtered on completion of the reaction. The precipitate is washed with much water until a neutral pH has been obtained for the filtrate.

The resulted halogenoderivative is then dried at 65—70° in vacuum.

4.2. SULFOCYANURATION OF 6-AMINO INDAZOLE AND OF ITS HALOGENATED DERIVATIVES (TABLE 2)

Glacial acetic acid is passed into a four-neck flask fitted with an ascending refrigerent, a stirrer, a thermometer and a dropping funnel. The amine to be sulfocyanurated is then dissolved with vigorous stirring. Sodium sulfocyanide is added to the acetic acid after dissolution of the amine and after reaching the experiment temperature, followed by the dropwise addition of bromine solution (the oxidizing agent). After 24 hours of standing, the formed sulfocyanurated derivative is filtered and dried at 100°.

4.3. CYCLIZATION OF SULFOCYANURATED DERIVATIVES OF THIAZOLE COMPOUNDS (TABLE 2)

Cyclization of sulfocyanurates occurs by boiling them in 2 n hydrochloric acid (1 mole sulfocyanurated compounds to 5 l solution). The solution is filtered to remove the possible impurities. The thiazole compound is separated by alkalination of the filtrate with sodium bicarbonate. It is then washed and dried at 85–90° in vacuum.

4.4. NITRATION OF 8-AMINOTHIAZOLO [4,5-f] INDAZOLE AND OF ITS SUBSTITUTED DERIVATIVES (TABLE 3)

98% sulfuric acid is introduced into a 4-neck flask fitted with a stirrer, a thermometer, a dropping funnel and an ascending refrigerent. When the working temperature has been reached, the compound to be nitrated is added. After its total dissolution, the sulfonitric mixture is added, dropwise. The thermal conditions are presented in table 3.

On completion of the reaction, the reaction mass is poured over ice water, precipitating nitroderivatives. They are washed with water and dried at 70° in vacuum.

4.5. SULFONATION OF 8-AMINOTHIAZOLO [4,5-f] INDAZOLE AND OF ITS SUBSTITUTED DERIVATIVES (TABLE 3)

98% sulfuric acid is introduced into a 3-neck flask. The mixture is cooled to 0° and the compound to be sulfonated is then added. After its total dissolution, the temperature is increased in accordance with the thermal conditions mentioned in table 3. The reaction mass is then poured over ice water. A portion of the sulfonic acid precipitates as such, the remaining being separated as potassium salt by salination with potassium chloride. It is dried at 50°.

5. CONCLUSIONS

1. Studies on halogenation, nitration and sulfonation possibilities of the thiazolo [4,5-f] indazole system in view of obtaining certain mono- and disubstituted derivatives were made.
2. The position of the substituent was established by synthesis of some standard samples (in the case of halogenated derivatives) and was assigned by IR spectral analysis for the rest of compounds.
3. Halogenation of thiazolo [4,5-f] indazole takes place in position 3 in all cases. In mediums in which protonation of azogroups in the heterocycle is not possible, nitration and sulfonation of thiazolo [4,5-f] indazole occurs in position 8.
4. IR spectra have an additive character in the case of 6-aminothiazolo [4,5-f] indazole substituted in positions 3 and 8, exhibiting the proper bands of the indazole and thiazole rings.

Revue Roumaine de Chimie, **18**, *12*, 2113–2125 (1973)

[illegible] dissolution of the azide and after reaching the experimental temperature, followed by the dropwise addition of bromine solution [illegible] agent. After 24 hours of standing, the [illegible] derivative is filtered and dried at 100°.

4.3. CYCLIZATION OF SULFOCYANATED DERIVATIVES OF THIAZOLE COMPOUNDS (TABLE 4)

Cyclization of sulfocyanated derivatives occurs by boiling [illegible] compounds [illegible] The [illegible] compound is separated by [illegible] It is then washed and dried at 60° in vacuum.

4.4. NITRATION OF 2-AMINOTHIAZOLO [4,5-f] INDAZOLE AND OF ITS 3-SUBSTITUTED DERIVATIVES (TABLE 5)

[illegible] sulfuric acid is introduced into a neck flask fitted with a stirrer, a thermometer, a dropping funnel and [illegible] When the working temperature has been reached, the compound to be nitrated is added. After its total dissolution, the sulfonitric mixture is added dropwise. The reaction conditions are presented in table 5.

At the end of the reaction, the reaction mass is poured onto ice water, [illegible] derivatives, thus [illegible] washed with water and dried at 60° in vacuum.

4.5. SULFONATION OF 2-AMINOTHIAZOLO [4,5-f] INDAZOLE AND OF ITS 3-SUBSTITUTED DERIVATIVES (TABLE 6)

98% sulfuric acid is introduced into a 3-neck flask. The solution is cooled to 0° and the compound to be sulfonated is then added. After its total dissolution, the temperature is [illegible] in accordance with the reaction conditions, mentioned in table 6. The reaction mass is then poured over ice water, [illegible] of the sulfonic acid precipitates [illegible] the [illegible] being separated as potassium salt by [illegible] with potassium chloride. It is dried at 60°.

5. CONCLUSIONS

1. Studies on halogenation, nitration and sulfonation possibilities of the thiazolo [4,5-f] indazole system in view of obtaining certain mono- and disubstituted derivatives were made.

2. The position of the substituent was established by synthesis of some standard samples (in the case of halogenated derivatives) and was assigned by IR spectral analysis for the rest of compounds.

3. Halogenation of thiazolo [4,5-f] indazole takes place in position 3 in all cases. In mediums in which protonation of azogroups in the heterocycle is not possible, nitration and sulfonation of thiazolo [4,5-f] indazole occur in position 8.

4. IR spectra have an additive character in the case of 6-aminothiazolo [4,5-f] indazole substituted in positions 3 and 8, exhibiting the proper bands of the indazole and thiazole rings.

Received [illegible]

Revue Roumaine de Chimie, **18**, *12*, 2127–2133 (1973)

MATRIZIELLE CHARAKTERISIERUNG DER STRUKTUR UND TOPOLOGIE DER ORGANISCHEN VERBINDUNGEN. IV.[1–3]

PROCHIRALITÄT, PSEUDOCHIRALITÄT

I. MOŢOC und F. KEREK
Organisch Chemisches Laboratorium des Polytechnischen Instituts, Timişoara,
Postfach 103, Rumänien

Eingegangen am 8. Mai 1973

Als Fortsetzung der Versuche zur Anwendung des matriziellen Formalismus zur mathematischen Beschreibung der Konstitution, beziehungsweise der chiralen Konfigurationen und Konformationen wurden die Probleme der Prochiralität, beziehungsweise der Pseudochiralität studiert. Es wurden Beziehungen mit Operatoren folgender Form: $\tau^1 \; M_1 = \tau^2 M_1$ für die Beziehung der Prochiralität, beziehungsweise $\mathscr{C}^{\varphi_0} \overline{M} \sim \overline{M}^{\top}.\ F$ für die Beziehung der Pseudochiralität abgeleitet.

1. EINLEITUNG

Der matrizielle Formalismus erwies sich als geeignet in der Beschreibung der Konstitution der Moleküle.[1] Dieser Formalismus ermöglichte ebenfalls die mathematische Beschreibung der Beziehungen der molekularen Chiralität konfigurativer,[2] beziehungsweise konformativer Natur.[3]

Ugi und Mitarbeiter [4,5,6] gelang es, unter Anwendung der sogenannten *be* Matrizen zur Darstellung isomerer Struktur von Molekülen, eine neue Beschreibungsart der strukturellen Daten zu erziehen. Sie leiten ebenfalls die mathematischen Gleichungen, die den Vorgang der Umwandlung eines Isomers in das andere sowie einen chemischen Vorgang im allgemeinen ausdrücken, ab.

In Fortsetzung der Versuche [1–3] den matriziellen Formalismus für die Beschreibung der stereoisomeren Beziehungen anzuwenden wurden nun Aspekte im Zusammenhang mit der Prochiralität bzw. der Pseudochiralität analysiert.

---

[1] F. Kerek und I. Moţoc, *Rev. Roumaine Chim.*, **18**, 283 (1973).

[2] I. Moţoc und F. Kerek, *ibid.*, **18**, 000 (1973).

[3] F. Kerek und I. Moţoc, *ibid*, **18**, 000 (1973).

[4] I. Ugi, D. Marquarding, H. Klusacek, G. Gokel und P. Gillespie, *Angew. Chem.*, **82**, 741 (1970).

[5] I. Ugi und P. Gillespie, *Angew. Chem.*, **83**, 980 (1971).

[6] I. Ugi, P. Gillespie und C. Gillespie, *Trans. New York Acad. Sci. II*, **34**, 417 (1972).

2. PROCHIRALITÄT

Erhält man eine chirale Struktur, indem man einen Liganden aus einer endlichen Ligandenmenge ersetzt, so ist letztere in dem von Hanson [7] festgelegten Sinn: „prochiral".

Für den einfachen Fall eines Zentrums mit vier Liganden kann man in der Abb. 1 beobachten, daß die chirale Struktur (B) durch das Ersetzen eines Liganden *g* durch den Liganden *h* in der ursprünglichen Struktur (A) — die also prochiral ist — erhalten wird.

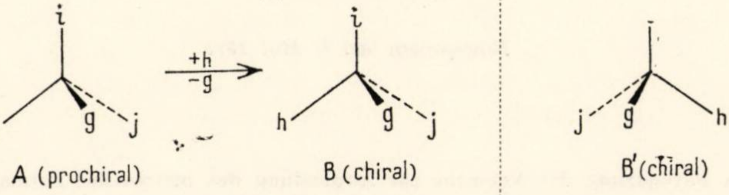

Abb. 1

Es gibt selbstverständlich auch verschiedene Fälle der axialen und planaren Prochiralität (siehe Abb. 2). Die Beziehung der Prochiralität ist für enzymatische Reaktionen, bzw. für die N.M.R.-Spektroskopie von besonderer Bedeutung. [8]

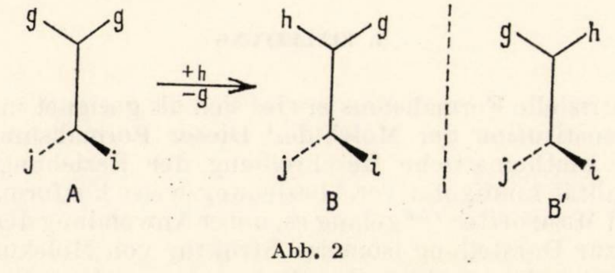

Abb. 2

Es ist notwendig die Tatsache zu unterstreichen, daß der Begriff der Prochiralität seinen wahren Sinn für die komplexeren Fälle der Chiralität verliert. Wir werden diese Fälle, die Ruch [9] in die Kategorie *b* der molekularen Chiralität einstuft, nicht in Betracht ziehen.

Analog der vorhergehenden Betrachtungen [2,3] werden auch hier nur die, der von Ruch [9] eingeführten Kategorie *a* angehörende Chiralität Fälle diskutiert.

Hanson schlug die Erweiterung des Nomenklatur-Systems R—S von Cahn, Ingold und Prelog vor [10] und führte die Symbole pro-R, pro-S zur Spezifikation der prochiralen Formationen ein.[7] Dieser Vorschlag wurde auch von der IUPAC[11] Komission angenommen.

---

[7] K. R. Hanson, *J. Amer. Chem. Soc.*, **88**, 2731 (1966).

[8] K. Mislow und M. Raban, "Topics in Stereochemistry", Vol. I, edited by E. Eliel and N. Allinger, Interscience New York, 1967, p. 1—38.

[9] E. Ruch, *Accounts of Chem. Res.*, **5**, 49 (1972).

[10] R. S. Cahn, C. K. Ingold und V. Prelog, *Angew. Chem.*, **78**, 413 (1966).

In allen Fällen der Prochiralität liegt eigentlich eine gewisse Identität der Liganden vor, und zwar solcher Natur, daß die Abänderung nur eines einzigen Liganden schon zu einer chiralen Struktur führt.

2.1. DIE MATRIZIELLE CHARAKTERISIERUNG DER PROCHIRALITÄT

Mit $\mathcal{M}$ wird die Menge der dem untersuchten Chiralitätselement zugeordneten kanonischen Matrizen bezeichnet

$$\mathcal{M} = \{M_k \mid M_i\, M \sim M_j\} \tag{1}$$

Es sei nun τ^1 jener Operator, der mit den, den Elementen der konfigurativen Matrix entsprechenden Indizen, wie folgt, operiert:

$$\tau^1 : (11) \rightarrow (21) \tag{2}$$

Wenn man also die Matrix $\begin{bmatrix} a & b \\ c & d \end{bmatrix}$ betrachtet, so ist folgende Beziehung erfüllt:

$$\tau^1 \begin{bmatrix} a & b \\ c & d \end{bmatrix} = \begin{bmatrix} c & b \\ a & d \end{bmatrix}$$

Folgende Eigenschaften des Operators τ sind offensichtlich:

$$\tau^1 . \tau^1 \ldots \tau^1 = \tau^{1+1+\ldots+1} \tag{3}$$

$$\tau^{2k+1} \equiv \tau^1 \quad , \qquad k \in N \tag{4}$$

$$\tau^{2k} : (11) \rightarrow (11), \qquad k \in N \tag{5}$$

$$\tau^{2k} : (21) \rightarrow (21)$$

τ^1 ist also der Einheitsoperator. $\{\tau^1, \tau^2\}$ stellt infolgedessen eine Gruppe in Bezug auf die durch die Beziehung (2) definierte Multiplikation.

Das durch die Menge der kanonischen Matrizen $\mathcal{M}$ beschriebene Zentrum ist also prochiral, wenn eine Matrix $M_l \in \mathcal{M}$ existiert, die folgende Gleichung mit Operatoren erfüllt:

$$\tau^1 M_l = \tau^2 M_l \tag{6}$$

---

[11] IUPAC, „Tentative Rules for the Nomenclature of Organic Chemistry", Section E. *J. Org. Chem.*, **35**, 2849 (1970).

Bemerkung. In der Gleichung (6) wurde in der rechten Seite als Einheitsoperator verwendent.

3. PSEUDOCHIRALITÄT

In dem in den Abb. 1 und 2 veranschaulichten Übergang von einer prochiralen in eine chirale Formation, existiert auch eine Zwischenmodalität. In dem Falle, in dem die Liganden, deren Identität beseitigt wird, chiral sind, kann man nur ihre Konfiguration ändern, wie dies aus Abb. 3 ersichtlich ist :

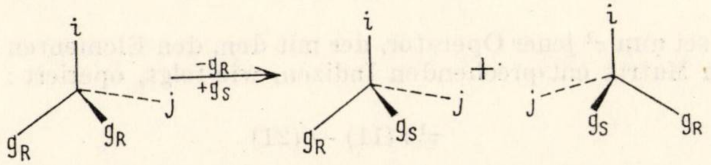

Abb. 3

Die zwei erhaltenen Strukturen sind nicht identisch ohne aber Enantiomere zu sein. Da g_R das Spiegelbild des Liganden g_S ist, weisen sie eine Symmetrieebene auf, und können also nicht mehr chiral sein. Übereinkunftsgemäß [10] werden sie pseudochiral genannt.

3.1. DIE MATRIZIELLE CHRAKTERISIERUNG DER PSEUDOCHIRALITÄT

In dem allgemeineren Fall existiert ein Chiralitätselement, an das die Liganden L gebunden sind (Abb. 4) :

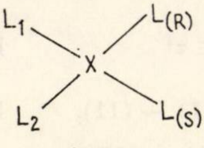

Abb. 4

Zwei der Liganden $L_{(R)}$ und $L_{(S)}$ sind von derselben konstitutiven Natur, aber mit entgegengesetzter Konfiguration. Das Element ist also pseudochiral. Jedem Liganden wird eine kanonische, konfigurative Matrix, gemäß dem in [2] angeführten Verfahren, zugeordnet.

Wir können annehmen, daß wir zu folgenden Beziehungen gelangen :

$$L_1 \leftrightarrow M_1 \tag{7}$$

$$L_2 \leftrightarrow M_2 \tag{8}$$

$$L_{(R)} \leftrightarrow M \tag{9}$$

$$L_{(S)} \leftrightarrow M^T \tag{10}$$

wobei M die entsprechenden kanonischen Matrizen darstellen. Es ist notwendig, daβ L_1 und L_2 verschieden sind also $L_1 \neq L_2$. Ohne die Allgemeingültigkeit zu beeinträchtigen, kann man annehmen daß

$$L_1 > L_2 \tag{11}$$

L_2 ist der Ligand kleinsten Ranges gemäß der Standard Sequenzregel.[10] Die Beziehungen (9) und (10) sind offensichtlich wahr, da es ja bekannt ist daβ, der Interkonversion der Konfiguration

$$R \rightleftarrows S$$

matriziell, folgende Beziehung entspricht:

$$M \rightleftarrows M^T$$

Eine der dem Zentrum X zugeordneten kanonischen Matrizen, ist folgende:

$$\overline{M} = \begin{bmatrix} M & M^T \\ M_1 & M_2 \end{bmatrix} \tag{12}$$

Zieht man die Abb. 5 in Betracht, so ist es offensichtlich, daß die Matrix (12) eine kanonische ist:

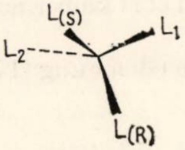

Abb. 5

Setzt man voraus, daß

$$L_{(R)} > L_{(S)} > {}_1 > L_2$$

so erfüllt die Matrix $\overline{M}$ folgende Gleichung mit Operatoren:

$$\mathscr{C}^{\varphi} \; \overline{M} = \mathscr{L}^{-} \; M \tag{13}$$

Wenn $\overline{M}$ eine Matrix einer chiralen Konfiguration ist, dann erfüllt die Matrix $\overline{M}'$ des entsprechenden Enantiomers folgende Operatorengleichung:

$$\mathscr{C}^{\varphi} \overline{M}'' = \mathscr{L}^{+} \overline{M}' \tag{14}$$

Gemäß [2] kann man schreiben:

$$\overline{\mathrm{M}}' = \overline{\mathrm{M}}^{\mathrm{T}} \,.\, \mathrm{F} \tag{15}$$

$$\text{weil } \mathrm{F} = \begin{bmatrix} \delta & 0 \\ 0 & \delta \end{bmatrix}, \text{ wobei } \delta = |^{\mathrm{T}}$$

Infolgedessen wird also

$$\overline{\mathrm{M}}' = \begin{bmatrix} \mathrm{M} & \mathrm{M}^{\mathrm{T}} \\ \mathrm{M}_1 & \mathrm{M}_2 \end{bmatrix}^{\mathrm{T}} \cdot \begin{bmatrix} \delta & 0 \\ 0 & \delta \end{bmatrix}$$

$$\overline{\mathrm{M}}' = \begin{bmatrix} \mathrm{M} & \mathrm{M}_1 \\ \mathrm{M}^{\mathrm{T}} & \mathrm{M}_2 \end{bmatrix} \cdot \begin{bmatrix} \delta & 0 \\ 0 & \delta \end{bmatrix}$$

$$\overline{\mathrm{M}}' = \begin{bmatrix} \mathrm{M}^{\mathrm{T}} & \mathrm{M}_1^{\mathrm{T}} \\ \mathrm{M} & \mathrm{M}_2^{\mathrm{T}} \end{bmatrix} \tag{16}$$

Man kann aber feststellen daß:

$$\mathscr{C}^{\varphi}\overline{\mathrm{M}}' = \mathscr{C}^{\varphi}\,(\overline{\mathrm{M}}^{\mathrm{T}} \,.\, \mathrm{F}) = \mathscr{L}^{-}\overline{\mathrm{M}}' \tag{17}$$

Die Matrix $\overline{\mathrm{M}}$, hat gemäß (17) kein Enantiomer, ist also keine Matrix einer chiralen Konfiguration.

Das erzielte Ergebnis, die Gleichung (17), war zu erwarten. Man kann folgendes bemerken:

$$\mathscr{C}^{3}\overline{\mathrm{M}}' \sim \overline{\mathrm{M}} \tag{18}$$

Die zwei Matrizen sind also konfigurativ gleichwertig, da der Operator $\mathscr{C}^{\varphi}$ die Konfiguration unangetastet läßt.

Die Gleichung (18) beweist, daß die beiden Konfigurationen $\overline{\mathrm{M}}$ und die widerspiegelte Konfiguration von $\overline{\mathrm{M}}$ kongruent sind. Dieselbe Information ist auch in der Gleichung (19) enthalten.

Als Schlußfolgerung kann man zeigen, daß falls $\overline{\mathrm{M}}$ folgende Eigenschaft besitzt:

$$\mathscr{C}^{\varphi}\overline{\mathrm{M}} = \mathscr{L}^{+}\overline{\mathrm{M}} \Rightarrow \mathscr{C}^{\varphi}\overline{\mathrm{M}}^{\mathrm{T}}.\mathrm{F} = \mathscr{L}^{+}\overline{\mathrm{M}}^{\mathrm{T}}.\mathrm{F} \tag{19}$$

$$\mathscr{C}^{\varphi}\overline{\mathrm{M}} = \mathscr{L}^{-}\overline{\mathrm{M}} \Rightarrow \mathscr{C}^{\varphi}\overline{\mathrm{M}}^{\mathrm{T}}.\mathrm{F} = \mathscr{L}^{-}\overline{\mathrm{M}}^{\mathrm{T}}.\mathrm{F} \tag{20}$$

ist sie eine, einer pseudochiralen Konfiguration zugeordnete Matrix.

Eine der den Gleichungen (19) und (20) gleichwertige Definierung der Pseudochiralität, stellt die Gleichung (21) dar. Wenn für jedwelche kanonische Matrix ein φ_0 existiert, so daß

$$\mathscr{C}^{\varphi_0}\overline{\mathrm{M}} \sim \overline{\mathrm{M}^{\mathrm{T}}}.\mathrm{F} \tag{21}$$

dann beschreibt $\overline{\mathrm{M}}$ eine pseudochirale Konfiguration.

4. SCHLUSSFOLGERUNGEN

Die für die Charakterisierung der Prochiralität und Pseudochiralität abgeleiteten Operatorgleichungen bringen die wesentliche topologische Eigenschaft dieser Beziehungen in mathematischer Darstellungsweise zum Ausdruck.

Revue Roumaine de Chimie, 18, 12, 2127–2133 (1973)

Revue Roumaine de Chimie, **18**, *12*, 2135–2141 (1973)

LA CONCENTRATION CRITIQUE MICELLAIRE DE QUELQUES SELS QUATERNAIRES D'ALKYLPYRIDINE

LILIANA D. PETROVA

Institut de recherches chimiques (CNIRO-THP),
Section de Technologie chimique organique,
Iskarsko Sosé 14, Sofia, Bulgarie

Reçu le 20 janvier 1973

On a étudié les concentrations critiques micellaires et les points Krafft de quelques sels quaternaires d'alkylpyridine, en déterminant les courbes de solubilité et de conductibilité électrique. On a obtenu des courbes caractéristiques pour les colloïdes électrolytiques d'association. Pour les composés du type B (sels quaternaires de N-alkylpyridylcarbinol) et du type C (mélange du composé B et d'iodhydrate de pyridylcarbinol), solubles dans l'eau les valeurs des concentrations critiques micellaires et des points Krafft augmentent par rapport à la longueur de la chaîne hydrocarbonée de la molécule, tandis que pour les composés du type A, solubles dans le diméthylformamide (iodhydrates de 2-oxyméthyle-4-alkylpyridine), ces valeurs en sont indépendantes. On a discuté les résultats expérimentaux compte tenu de la structure amphypatique de la molécule qui détermine la formation des micelles.

Afin d'élargir leur domaine d'application, on a étudié, par différentes méthodes, les agents tensioactifs cationiques du point de vue colloïdal et on a établi la formation des micelles lors du dépassement d'une certaine concentration, leur structure et leur forme, ainsi que les facteurs qui peuvent les modifier. On a étudié surtout les sels d'ammonium quaternaire, à longue chaîne hydrocarbonée et moins ceux d'alkylpyridine.

Ainsi, en mesurant la conductibilité électrique et le nombre de transport du bromure d'alkylpyridine [1,2] on a mis en évidence l'existence de la couche fixe de contre-ions (Br^-) qui se déplacent en même temps que la micelle. La micelle sphérique de type Hartley a une mobilité accrue à la concentration de formation des micelles (CMC), tandis que celle des contre-ions diminue fortement. Au contraire, c'est aux concentrations plus élevées que la mobilité des micelles diminue.

Par des études sur le comportement conductométrique des solutions de chlorure de cétylpyridine à de fortes tensions (l'effet Wien),[3]

---

[1] G. S. Hartley, *Trans. Faraday Soc.*, **34**, 283 (1938).

[2] G. S. Hartley, B. Collie et C. Samis, *Trans. Faraday Soc.*, **32**, 795 (1936); *J. Chem. Educ.*, **27**, 312 (1950).

[3] Z. Malsh et G. S. Hartley, *Z. Phys. Chem.*, **170 A**, 321 (1934).

on a démontré que les micelles ioniques conduisent mieux le courant électrique que les ions individuels. En étudiant l'influence de la température sur CMC des halogénures d'alkylpyridine,[4] ainsi que de la formation des micelles,[5] on a mis en évidence, d'une part, le rôle joué par la chaîne alkylique et, d'autre part, celui joué par le noyau pyridinique sur la structure des micelles ainsi que les propriétés des solutions de ce type.

La solubilité des substances tensioactives (tensides) ioniques dans le domaine des concentrations faibles augmente lentement par rapport à l'élévation de la température jusqu'à un certain degré surnommé le point Krafft [6]; au-delà de ce point, la solubilité augmente brusquement et les solutions deviennent parfaitement claires. Cette augmentation brusque de la solubilité à une certaine température et à une certaine concentration indique la formation des micelles.

Compte tenu de l'intérêt théorique et pratique présenté par les quelques nouveaux composés que nous avons récemment synthétisés, dans le but d'établir leur caractère colloïdal en solutions, nous avons déterminé les concentrations critiques micellaires à partir de leurs courbes de solubilité et de conductibilité électrique. Par la dernière méthode on peut également mettre en évidence l'existence du caractère de colloïde électrolytique des substances étudiées dans des solutions aqueuses.

Nous avons étudié des composés de différents types :

A = iodhydrates de 2-oxyméthyle-4-alkylpyridine;

B = sels quaternaires des n-alkylpyridylcarbinol et

C = mélange du composé de type B et d'iodhydrate de pyridylcarbinol, le radical R ayant 8, 10, 12 et 18 atomes de carbone.

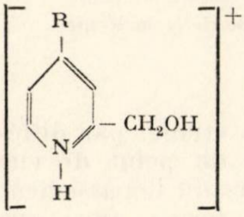

type A

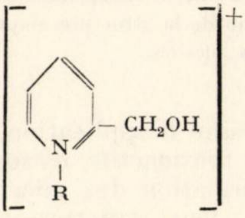

type B

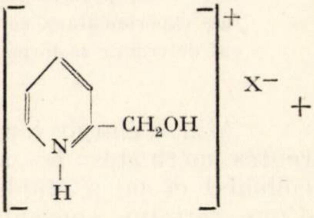

type C

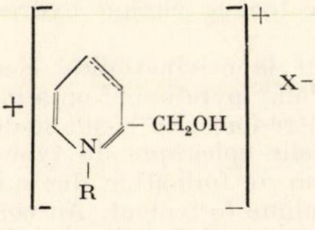

Sans déterminer exactement le rapport des composés du mélange nous avons établi [7] que la proportion du composé quaternaire B dans le

[4] J. A. Stead et H. Taylor, *J. Colloid Interface Sci.*, **30**, 483 (1969).

[5] V. A. Vilshansky et A. Yurjenko, *Kolloid. Zhur.*, **33**, 35 (1971).

[6] F. Krafft et H. Wiglow, *Ber. dtsch. chem. Ges.*, **28**, 2566 (1895).

[7] C. Simionescu, E. Comaniţă et L. Petrova, *Bul. Inst. Politehnic Iaşi*, sous presse.

mélange diminue par rapport à l'accroissement de la longueur du radical R. Lorsque le radical alkylique a 18 atomes de carbone, l'élimination du radical R du cycle pyridylcarbinol est presque total ; on obtient l'iodhydrate du 2-pyridylcarbinol à traces de sel quaternaire de type B.

RÉSULTATS EXPÉRIMENTAUX

A. SOLUBILITÉ

On a déterminé la solubilité des composés du type B et C dans l'eau et celle du composé du type A dans le diméthylformamide, en explorant le domaine de température de 10 à 70° de 5 en 5°. On a choisi ces températures en fonction de la longueur de la chaîne hydrocarbonée de la molécule.

On a introduit dans une éprouvette une quantité connue de la substance étudiée et on l'a placée dans un bain thermostaté. On a maintenu une température constante avec une précision de ±0,05°. Ensuite, on a ajouté petit à petit (avec une micropipette), des quantités connues de l'eau conductométrique, en agitant continuellement. L'équilibre thermique des phases du système ayant été établi et la solution étant devenue limpide, on note la quantité totale de l'eau ajoutée et on en calcule la concentration. On diminue la température de 5° ; la solution devient trouble à cause de la diminution de la solubilité et donc de l'apparition des cristaux. En maintenant une température constante on procède de la même manière que lors de la température antérieure. On continue de baisser la température en déterminant la solubilité de la substance (g% ml de solution) pour chaque intervalle de 5° jusqu'à ce qu'on obtienne une courbe complète de solubilité.

B. CONDUCTIBILITÉ ÉLECTRIQUE

On a préparé les solutions aqueuses des substances mentionnées en les chauffant légèrement (35°) jusqu'à leur dissolution complète. Les concentrations ont été exprimées tout d'abord en grammes par 100 ml de solution, pour être transformées par la suite en équivalents – gramme par 1000 ml de solution.

On a utilisé l'eau conductométrique tridistillée ayant la conductibilité spécifique $\lambda_{sp}=2-4\times10^{-4}$ ohm^{-1} cm^{-1}. La conductibilité électrique a été mesurée avec une précision de ±1 %, à l'aide d'un appareil type « Radelkis », ayant une cellule à électrodes de Pt platinées. La constante de la cellule a été déterminée à l'aide d'une solution de KCl de différentes concentrations. La reproductibilité des résultats a été vérifiée sur plusieures solutions de la même concentration des composés.

DISCUSSIONS

A. SOLUBILITÉ

Dans les figures 1, 2 et 3 on a représenté la variation de la solubilité, en fonction de diverses températures pour les composés du type B et C, dans l'eau, et du type A, dans le diméthylformamide.

On remarque que l'allure des courbes est typique des colloïdes électrolytiques d'association, soit anioniques[8,9], soit cationiques.[10]

L'augmentation accusée de la solubilité des composés peut être expliquée par la formation des micelles. On a supposé [8] que, au-dessous

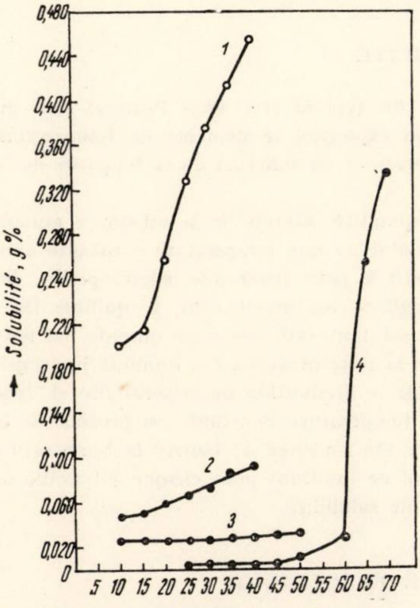

Fig. 1. — Solubilité dans l'eau des composés de type B aux R = C_8 (*1*), C_{10} (*2*), C_{12} (*3*) et C_{18} (*4*), en fonction de la température.

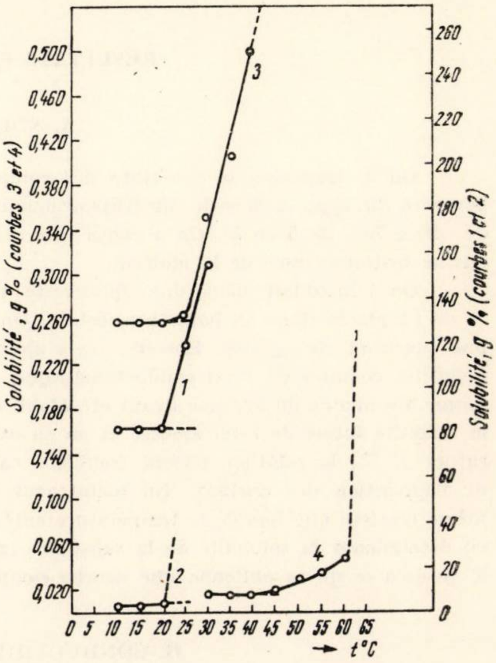

Fig. 2. — Solubilité dans l'eau des composés du type C aux R = C_8 (*1*), C_{10} (*2*), C_{12} (*3*) et d'iodhydrate de pyridilcarbinol pur (*4*), en fonction de la température.

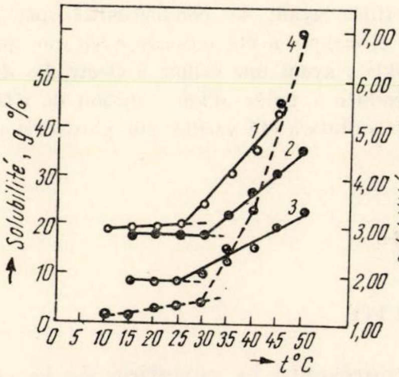

Fig. 3. — Solubilité dans le diméthylformamide des composés du type A aux R = C_8 (*1*), C_{10} (*2*), C_{12} (*3*) et C_{18} (*4*), en fonction de la température.

---

[8] H. Tartar et K. Wright, *J. Amer. Chem. Soc.*, **61**, 539 (1939).

[9] H. Lange et M. Schwuger, *Kolloid-Z.*, **223**, 145 (1968).

[10] E. Angelescu, A. Nicolescu et E. Bărbulescu, *Studii şi Cercetări Chim. Acad. R.P.R.*, **9**, 357 (1961).

de la concentration critique micellaire, la solubilité dépend seulement de l'équilibre établi entre les ions et la phase cristalline; elle est réduite à cause de la partie non polaire d'ion (la chaîne hydrocarbonée) et devient toujours moins accusée au fur et à mesure de l'accroissement de la chaîne hydrocarbonée. Au-dessus de CMC la solubilité augmente à cause de la couche d'hydratation des groupes polaires qui sont orientés vers la surface des micelles. Dans ce domaine de concentration la solubilité dépend seulement de l'équilibre existant entre les micelles, les contre-ions et les ions de la substance tensioactive. Aussi peut-on en déduire graphiquement le CMC et les points Krafft d'après la méthode connue de la variation brusque de la solubilité.

Le tableau 1 comprend les valeurs des points Krafft des substances solubles dans l'eau (type B et C) ou dans le diméthylformamide (type A).

On remarque que le point Krafft augmente par rapport à l'accroissement de la longueur de la chaîne hydrocarbonée des composés du type B et C. Lorsque la molécule contient 18 atomes de carbone il y a une augmentation bien accusée de la solubilité ; par conséquent le point Krafft est déplacé de 25° à 60°. Dans le cas des composés du type C on obtient également des courbes de solubilité caractéristiques, ce qui prouve que la présence des sels quaternaires du type B, bien qu'ils ne représentent que de faibles quantités ou seulement des traces, leur imprime le caractère de colloïde électrolytique d'association.

La classe des substances du type A, insolubles dans l'eau, a un comportement tout à fait différent : ces substances ont des points Krafft très proches (entre 25° et 30°), indépendants de la longueur de la chaîne hydrocarbonée (fig. 3, tableau 1).

Tableau 1

Points Krafft (°C) des composés du type A dans le diméthylformamide et du type B et C dans l'eau

R / Type du composé	C_8	C_{10}	C_{12}	C_{18}
Composés A	25	30	25	30
Composés B	15	15	25,5	60
Composés C	20	20	25	60

B. CONDUCTIBILITÉ ÉLECTRIQUE

On a suivi l'influence de la longueur de la chaîne hydrocarbonée sur le caractère lyophile des composés B et C.

La caractère lyophile d'un colloïde électrolytique influence non seulement le CMC mais aussi le degré de dispersion. Ce fait a été mis en évidence par la conductibilité électrique [11,12] :

a) l'accroissement du degré de dispersion produit une augmenta-

---

[11] E. Angelescu, *Kolloid-Z.*, **92**, 94 (1940) ; *Rev. Roumaine Chim.*, **7**, 21 (1962).

[12] E. Angelescu et M. Radu, *Studii si Cercetări Chim. Acad. R.P.R.*, **6**, 403 (1958) ; *Rev. Roumaine Chim.*, **11**, 113 (1966).

tion du nombre des molécules qui passent à la surface des micelles. Par leur dissociation le nombre des contre-ions libres s'accroît, la charge spécifique aussi et la conductibilité électrique s'intensifie ;
b) la réduction du nombre des micelles conduit à l'accroissement de leur mobilité et, donc, de leur conductibilité électrique.

En tenant compte des faits mentionnés ci-dessus les concentrations choisies pour mesurer la conductibilité électrique ont été déterminées à l'aide de la courbe de solubilité des composés.

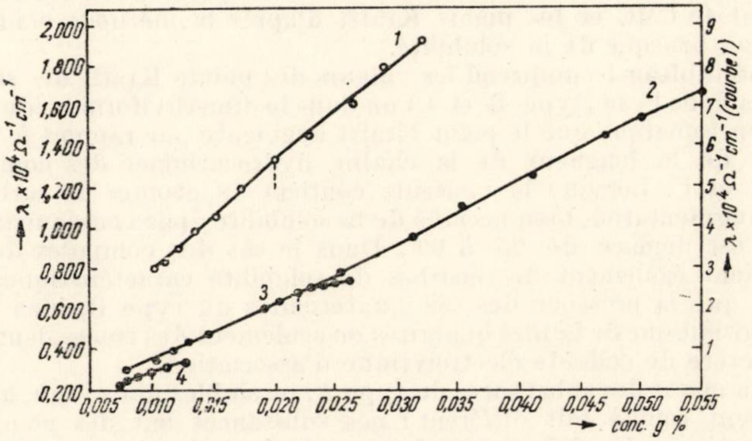

Fig. 4. – Variation de la conductibilité électrique spécifique des composés du type B aux R = C_8 (*1*), C_{10} (*2*), C_{12} (*3*) et C_{18} (*4*) en fonction de la concentration ; température = 30°.

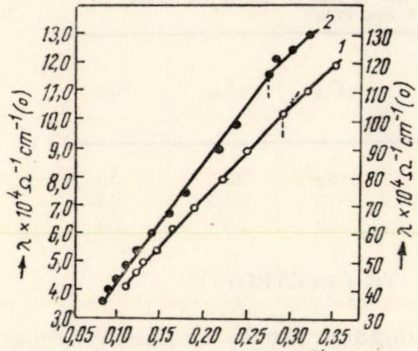

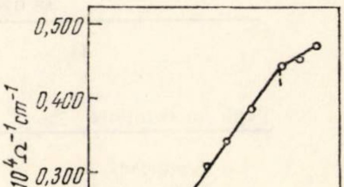

Fig. 5. – Variation de la conductibilité électrique spécifique des composés du type C aux R = C_{10} (*1*) et C_{12} (*2*), en fonction de la concentration du mélange ; température = 30°.

Fig. 6. – Variation de la conductibilité électrique spécifique du composé du type C ayant R = C_{18}, en fonction de la concentration du mélange ; température = 30°.

Dans les figures 4–6 on a représenté la variation de la conductibilité électrique spécifique en fonction de la concentration des composés étudiés, à 30° ; dans le tableau 2 on voit les valeurs des concentrations critiques micellaires déduites tant des courbes de conductibilité électrique que de celles de solubilité.

Il faut mentionner que dans le cas du composé de type C ayant R = 8 atomes de carbone, on n'a pas mesuré la conductibilité électrique à cause de sa grande solubilité dans l'eau ; ceci indique le fait que dans les domaines habituels de concentration il se présente comme un électrolyte normal. Il est possible qu'il ne forme des agrégats micellaires que dans des concentrations très élevées. Ceci est dû, d'une part, à la grande solubilité de l'iodhydrate de pyridylcarbinol et, d'autre part, à sa courte chaîne hydrocarbonée (C_8), respectivement à la partie hydrophobe de la molécule qui atténue le caractère amphipatique nécessaire à la formation des micelles.

Tableau 2

Concentrations critiques micellaires (CMC), en g% ml

Type du composé \ R	C_8		C_{10}		C_{12}		C_{18}	
	a	b	a	b	a	b	a	b
Composés A	20,38	—	18,57	—	8,85	—	1,49	—
Composés B	0,215	0,200	0,050	0,040	0,026	0,022	0,005	0,010
Composés C	—	—	3,30	2,91	0,260	0,273	0,015	0,013

a – CMC par solubilité. *b* – CMC par conductibilité électrique.

La concordance, assez bonne, des valeurs de CMC obtenues à partir des courbes de la conductibilité électrique et de la solubilité (tableau 2) fait ressortir la réduction du caractère lyophile des sels cationiques par rapport à l'accroissement de la chaîne hydrocarboné de la molécule, phénomène bien connu, d'ailleurs, pour les colloïdes électrolytiques d'association.

On remarque la différence accentuée entre les sels d'ammonium quaternaire (composés du type B) et leurs mélanges avec l'iodhydrate de 2-pyridylcarbinol (composés du type C) : indépendamment de la longueur de la chaîne hydrocarbonée, les derniers composés ont des CMC élevés par rapport à celles des sels purs cationiques d'ammonium quaternaires. Ce fait met en évidence l'accentuation de leur caractère lyophile à cause de la présence de la molécule fortement hydrophile d'iodhydrate de 2-pyridylcarbinol. Par conséquent, CMC et le degré de dispersion augmentent lorsque les valeurs de la conductibilité électrique montent.

En conclusion, les sels quaternaires d'alkylpyridine étudiés présentent des propriétés colloïdales caractéristiques des colloïdes électrolytiques d'association. Les valeurs des concentrations critiques micellaires et des points Krafft augmentent par rapport à la longueur de la chaîne hydrocarbonée de la molécule pour les composés solubles dans l'eau et sont indépendantes pour ceux solubles dans le diméthylformamide.

L'auteur exprime ses remerciements chaleureux aux Dr G. Popescu et Dr M. Radu de l'Institut de Chimie Macromoléculaire « P. Poni », Secteur des Colloïdes, Bucarest, pour l'appui accordé.

Revue Roumaine de Chimie, **18**, *12*, 2143–2148 (1973)

THIN LAYER THERMOCHROMATOGRAPHY. VII*
COMPARISON BETWEEN TEMPERATURE GRADIENT CHROMATOGRAPHY RESOLUTION AND NONSATURATED CHAMBER RESOLUTION

T. HODIŞAN, C. LITEANU and SILVIA GOCAN

Department of Chemistry, Chair of Analytical Chemistry, "Babeş-Bolyai" University,
Str. Arany Janos, 11, Cluj, Romania

Received April 27, 1973

A series of variants of the conventional chromatography, aiming at achieving some separations that could not be carried out by the classical method, have appeared in literature in the last 20 years. Among these, the chromatography in a chamber nonsaturated by the eluent vapours, was, and still is, of a frequent use. This paper aims to show the efficiency of this technique as compared to that of the temperature gradient, by means of quantitative measurements. The separation possibility of components was expressed quantitatively by the resolution. This study shows that by achieving an optimal resolution in a shorter time, we may consider the temperature gradient chromatography superior to the nonsaturated chamber technique.

The retention of a component in a given chromatographic system depends on a series of factors. The most important among these are: the saturation degree of the chromatographic chamber, the composition of the vapours in the chamber and the water content of the plate. All these agents are connected to the stationary phase that is formed. The latter is sometimes extremely important, owing to its permanent presence in the surrounding atmosphere.

For normal repartition or reversed phases chromatography it is necessary to saturate adequately the atmosphere of the chamber, to ensure an as constant as possible structure of the two phases in contact.

The temperature gradient chromatography, emphasizing the effect of the chambers non-saturation by creating a vapour tension gradient, and hence a stressing of the alternation of the mobile and stationary phase composition, proves that this alteration has also a positive role in separations based on repartition. This paper will try to explain the increased efficiency of nonsaturated chambers compared to fully saturated chambers, even for separations in which the elementary process is the repartition.

---

* Part VI, T. Hodişan, Şt. Bândeanu and C. Liteanu, *Studia Univ. Babeş-Bolyai Chem.*, **18** (2), 119 (1972).

The efficiency of nonsaturated chambers is discussed controversially in literature.[1,2] The fact that this technique ensures a higher separation efficiency than the completely saturated chambers seems actually to be unanimously accepted.

De Zeeuw [3-7] demonstrates this for some particular cases, meanwhile showing that the reproducibility is the same as in the saturated chamber, provided same working conditions are granted. We shall dwell upon this point later.

The nonsaturation leads to a better separation not only owing to the flow of a supplementary volume of eluent,[4] which is about the same as an increase of the column length, but also owing to the preferential sorption of the polar component in the solvent mixture to be found in the chamber, owing to the evaporation of the eluent during the migration. An activity gradient of the stationary phase in thus created, as the upper part of the plate is longer in close contact with the vapour mixture created in the chamber.

There is just one, though fairly serious, drawback that may be ascribed to this technique, namely the difficulty of obtaining some reproducible R_f values, though de Zeeuw does not agree to this. It is very true that maintaining constant the working conditions, the reproducibility of R_f values is absolutely compulsory. This is practically very difficult to achieve. A 100% or 0% saturation degree is easily obtained, but an intermediary nonsaturation degree is difficultly checked.

For this reason, a series of scientists have found large variations of the R_f values from one experiment to another. Geiss *et al.*[8] have found 300% variations of the R_f in experiments carried out comparatively in saturated and nonsaturated atmosphere. Stahl [9,10] too has shown that in a nonsaturated chamber, the marginal zones of the plate get further of the starting line than those of the plate center. This is the so-called "marginal effect" and is due to an intensive evaporation taking place at the plate edge. This effect may be avoided by a complete saturation of the plate.

Of course the variation of the R_f values, as well as this "marginal effect", do not prove disadvantageous, when we are only interested in the separation, if this is achieved quantitatively.

---

[1] F. Geiss, *J. Chromatog.*, **14**, 79 (1964).

[2] R. A. de Zeeuw, H. Compaan, J. H. Dhont, R. P. Labadie, F. J. Ritter and C. Vinkerborg, *J. Chromatog.*, **61**, 392 (1971).

[3] R. A. de Zeeuw, *Pharm. Weekbl.*, **102**, 113 (1967).

[4] R. A. de Zeeuw, *J. Chromatog.*, **32**, 43 (1968).

[5] R. A. de Zeeuw, *J. Chromatog.*, **33**, 222 (1968).

[6] R. A. de Zeeuw, *J. Chromatog.*, **33**, 227 (1968).

[7] R. A. de Zeeuw, *Analyt. Chem.*, **40**, 2134 (1968).

[8] F. Geiss, H. Schlitt and A. Klose, *Z. analyt. Chem.*, **213**, 331 (1965).

[9] E. Stahl, *Pharm. Rundsch.*, **1**, Heft 2, 1 (1959).

[10] E. Stahl, "Dünnschicht-Chromatographie", 2 Aufl., Springer-Verlag, Berlin, 1967, pag. 70.

EXPERIMENTAL

In the experiments carried out in this study we have tried to avoid these disadvantages by using an isothermal chamber, making it possible to work at different temperatures (figure 1).

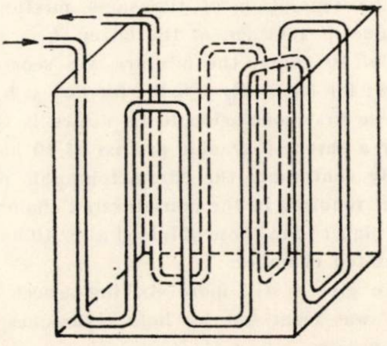

Fig. 1. — Isothermal chamber with working possibilities at various temperatures.

The chamber is a parallelepiped with double lateral sides of plexiglass ; at the bottom and the top it has two removable lids. The upper lid has two apertures : one for the control thermometer inside the chamber and one for the support of the chromatographic plate. Through the lateral sides passes a glass serpentine through which flows water provided by a thermostat at the required temperature.

The eluent is contained in a cylindrical glass vase in which there is a serpentine through which water flows. By this means the temperature of the eluent is regulated.

The vase with the eluent has an aperture in the form of a 10 cm long and 8 mm broad slit. This slit has such a small opening on purpose, to create inside the chamber an atmosphere nonsaturated by the vapours of the eluent. This chamber grants, the moment the plate is introduced, a 100 % degree of nonsaturation, and during the chromatographic process the saturation degree attained is rather small.

A mixture of Ni^{2+}, Co^{2+} and Mn^{2+} was submitted to separation, and, on the other hand, a mixture of Ni^{2+} and Mn^{2+}, to estimate the quantitative separation possibilities. Unlike Zeeuw's experiments, the working temperature was in each case 40°, to increase the efficacy of the separation.

Microcrystalline cellulose (Merck) in suspension in water, spread 0.3 mm thick on glass plates, was used as support, and *n*-butanol saturated with HCl 4N as eluent. For the chosen support and eluent, the mixture submitted to separation (Ni^{2+}, Mn^{2+}, Co^{2+}) offers great difficulties at the separation, when using the conventional working technique.

To create a 100 % nonsaturation degree we have raised the inner temperature of the chamber to 40°, then we introduced the eluent by means of a funnel inserted through the aperture of the control thermometer. After removing the funnel and re-inserting the thermometer, and after 5—8 minutes, when the eluent has reached the 40° temperature, the chromatographic plate is introduced into the eluent.

After 10 hours of chromatography the plates were removed and the zones localized by means of a solution of 0.5 % rubeanic acid in ethyl alcohol, and an ammonia atmosphere. The mixture was not separated in these conditions, though a slight beginning was noticed, but another very interesting phenomenon was noted, namely that the zones of the Co^{2+} and Mn^{2+} components have an inverse migration order than the one obtained in all the experiments carried out in isothermal chromatography with a saturated atmosphere, as well as with a temperature gradient.[11]

After 12 hours of separating process, the inversion phenomenon of the migration is still clearer, and the zones are clearly separated. The following values are obtained : for Ni^{2+}, $R_f = 0.15$; for Mn^{2+}, $R_f = 0.60$ and for Co^{2+}, $R_f = 0.82$.

The separation of the same mixture was undertaken with a temperature gradient. At a value of 1.43°/cm of the latter ($t_i = 40°$, $t_s = 60°$, $l = 14$ cm), and a chromatographic process of 10 hours, the mixture was separated quantitatively, the following values being obtained : for Ni^{2+}, $R_f = 0.48$; for Co^{2+}, $R_f = 0.55$, and for Mn^{2+}, $R_f = 0.61$.

The first conclusion to be drawn is that the temperature gradient has a higher efficacy for a chromatographic process of 10 hours.

By continuing the chromatographic process in temperature gradient up to 12 hours (the time required in the nonsaturated chamber), the differences between the R_f values were slightly higher than those obtained after 10 hours, but much smaller than those obtained in the nonsaturated chamber.

To give a still more striking aspect of the two compared techniques, a Ni^{2+}, Mn^{2+} mixture was separated by both techniques, at a constant duration of the chromatographic process.

The zones localized with rubeanic acid were photographed on the same film and in the same conditions. The film was read by means of a microphotometer, by transmission every 1 mm, and the respective densitograms were then plotted *versus* the distance covered by the zone on the plate.

RESULTS AND CONCLUSIONS

The resolution was calculated by means of the obtained densitograms. For the densitograms where the "break" between the zones is more marked, we have made use [12] of the equation :

$$R_s = \Delta z / 2\,(\sigma_1 + \sigma_2) \tag{1}$$

where Δz represents the distance measured on the densitogram, between the two peaks, and σ_1 and σ_2 are the standard deviations of the two peaks. For the densitograms where the "break" between the zones is only slightly marked (weak separations) and the measuring of the parameter σ would lead to big errors, the resolution was calculated [13] by means of the equation :

$$R_s = \sqrt[n]{1.15\,(0.3 - \log V/P)} \tag{2}$$

The ratio $V/P = h_i/h_{0_1}$ and the significance of these values are given in figure 2.

---

[11] T. Hodişan, S. Băndeanu and C. Liteanu, *Stud. Univ. Babeş-Bolyai, Chem.*, **17** (2), 119 (1972).

[12] L. R. Snyder, "Principles of Adsorption Chromatography", Marcel Dekker (ed.), New York, **1963**, p. 17.

[13] A. B. Christophe, *Chromatographia*, **4**, 455 (1971).

The variation of the resolution *versus* the duration of the chromatographic process, is given, for both techniques in figure 3.

This figure shows that for fairly small durations of the chromatographic process, the efficacy of the temperature gradient is higher. With the increase of the duration the efficacy of the nonsaturated chamber increases, exceeding the efficacy obtained in the temperature gradient, and then again decreases to a lower degree than that of the temperature gradient.

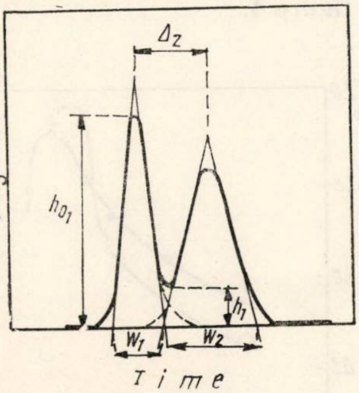

Fig. 2. — The parameters used for the count of resolution and of ratio V/P for two adjacent bands.

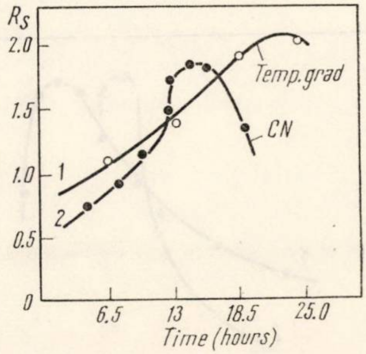

Fig. 3. — Comparison concerning the variation of resolution of $Ni^{2+} + Mn^{2+}$ mixture with development time, by temperature gradient technique *1*, and nonsaturated chamber (CN) *2*.

Yet, we must note that the optimal resolution ($R_s = 1.0$) is reached in a shorter time by means of the temperature gradient technique. It is true that better resolutions are obtained in a certain time range of the chromatographic process in a nonsaturated chamber, but the real aim of any separation process is to obtain the resolution in a minimal time interval. From this point of view, the temperature gradient technique is clearly superior to the technique of the nonsaturated chamber (in temperature gradient $R_s = 1.0$ after approximately 5.5 hours, and in a nonsaturated chamber $R_s = 1.0$ after approximately 9.5 hours).

To have a highly accurate image of the separation capacity of these two techniques, we have submitted to these separations the mixtures of the following amino acids : alanine, glutamic acid and alanine, glutamine, by both techniques.

As the temperature of the eluent bath in the nonsaturated chamber was 40°, the same temperature was applied ($t_i = 40°$) to the eluent bath for the temperature gradient chromatography. In this case the higher temperature (t_s) was 48°.

A mixture of crystalline cellulose and Kieselgur (95 : 5 in weight) in ethanol was used as support, and the upper phase of the *n*-butanol-acetic acid-water (4 : 1 : 5 v/v) was used as eluent. After visual examination with a 0.2% ethanol solution of ninhydrin, the respective densitograms were plotted, from which the resolutions were calculated, as described above.

The variation of the resolution *versus* the duration of the development, by both techniques, is given in figure 4.

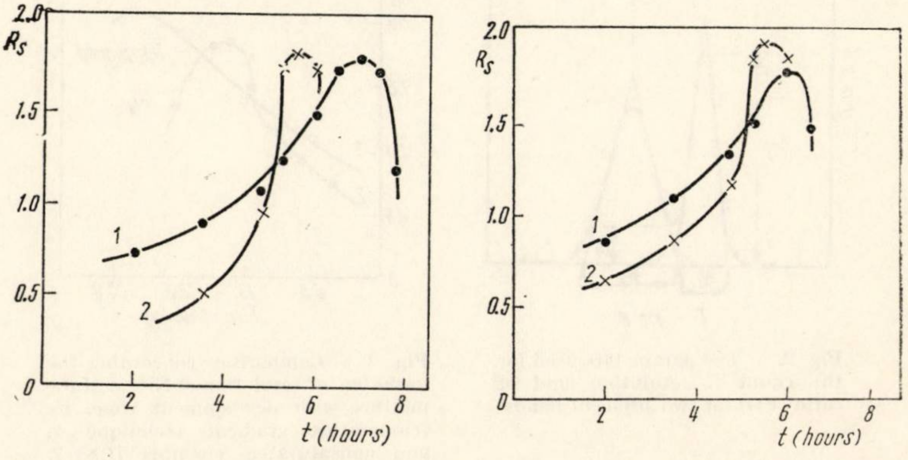

Fig. 4. – Comparison concerning the obtained resolution in temperature gradient *1*, and in nonsaturated chamber *2*, for mixtures of the following amino acids : alanine, glutamic acid and alanine, glutamine.

By analysing this figure we notice that, in these cases too, the optimal resolution is achieved in a shorter time in the conditions of a temperature gradient, than in a chamber nonsaturated by the vapours of the eluent. There is a perfect analogy between the behaviour of these amino acids mixtures and the Ni^{2+}, Mn^{2+} mixture, regarding the resolution : for small durations of the chromatographic process, the temperature gradient chromatography achieves a higher separation power. As it is in this time interval that the optimal resolution is obtained, we can consider the temperature gradient technique superior to the nonsaturated chamber technique.

Revue Roumaine de Chimie, **18**, *12*, 2149–2164 (1973)

STRÖMUNGSTECHNISCHE FRAGEN UNGLEICHKÖRNIGER WIRBELSCHICHTEN

GHEORGHIŢA I. JINESCU und HANS H. REHNER
Lehrstuhl für chemische Verfahrenstechnik und Lehrstuhl für Silikatschemie, Polytechnisches Institut, Bukarest, Str. Polizu N° 1, Rumänien

Eingegangen am 8. Mai 1973

Ungleichkörnige Wirbelschichten haben statt eines Lockerungspunktes einen Lockerungsbereich, dessen Größe von der Gleichmäßigkeitszahl n und der Dichte des Feststoffes abhängt. Es wird eine Methode für die Berechnung der Lockerungsgeschwindigkeit der gesamten Schicht angegeben, wobei die für gleichkörnige Schichten gültigen Gleichungen und die statistische Korngrößenverteilung nach Rosin-Rammler verwendet wird.

1. EINLEITUNG

Die Wirbelschichttechnik als Arbeitsverfahren behält auch weiterhin einen wichtigen Platz und erwirbt sich ständig neue Anwendungsgebiete in der chemischen Technologie und in anderen Industriezweigen.[1–6] Da die Fluidisierung ein äußerst komplexer Vorgang ist, so ergeben sich oftmals Nachteile, die die Erzielung von optimalen Arbeitsbedingungen erschweren. Einen wesentlichen Beitrag zur praktischen Anwendung der Wirbelschicht leistete hierbei in den letzten Jahren die Erforschung der Struktur der Wirbelschicht, der Berührung und Strömung der Phasen, der Möglichkeiten zur Verwirklichung und Beibehaltung optimaler strömungstechnischer Bedingungen u.a.

Die meisten strömungstechnischen Forschungen bezogen sich auf gleichkörnige Schichten oder auf Schichten mit einem engen Korngrößenbereich. Da man diese jedoch in der Praxis selten antrifft, so

---

[1] S. ELMAHEN und R. BEN AIM, ,,Purification of the Gaseous Mixture Containing SO_2 by Absorption in Fluidized Bed'', Mitteilung beim 4-ten Kongreß CHISA, Prag, 1972.

[2] V. N. ANOKIN und I. P. MUKHLIONOW, ,,Fundamental Processes in the Technology of Bound Nitrogen in a Fluidized Bed of Catalyst'', Mitteilung beim 4-ten Kongreß CHISA, Prag, 1972.

[3] K. E. MACHORIN, ,,Vapour-Gas-Activation of Anthracite in a Fluidized Bed'', Mitteilung beim 4-ten Kongreß CHISA, Prag, 1972.

[4] M. A. DOHEIM, ,,Fluidization in the Ferrous Industry'', Mitteilung beim 4-ten Kongreß CHISA, Prag, 1972.

[5] D. WORMALD und E. M. BURNELL, *Brit. Chem. Eng.*, **16**, 376 (1971).

[6] P. LE GOFF, F. VERGNES, F. COEURET und J. BORDED, *Ind. Eng. Chem.* **61** (10), 9 (1969).

ergeben sich naturgemäß Unterschiede zwischen dem Verhalten der industriellen Wirbelschichten und den auf Grund von Laboratoriumsversuchen gemachten Voraussagen.

Unterschiedliche Korngrößen können im Ausgangsgut vorhanden sein, wie es bei Trocknung, Absorption, Vermischung oder Wärmebehandlung zumeist der Fall ist, oder sie entstehen während der Durchwirbelung durch Abrieb [7] (z.B. bei katalytischen Verfahren), durch Platzen der Teilchen oder durch Zusammenballung kleiner Partikel.[8-11] Die Erklärungen für das abweichende Verhalten der kleinen Teilchen, die einen größeren Durchmesser als den gemessenen vortäuschen, sind :

— die Tendenz zur Zusammenballung als Folge der durch Reibung entstandenen elektrischen Aufladung der Teilchen [8-10];

— an der Teilchenoberfläche bildet sich eine Haut aus Molekülen des Trägergases, deren Dicke durch Absorbtions- und Reibungskräfte bestimmt wird [11];

— die Tendenz zur Zusammenballung als Folge von zwischen den Teilchen wirksamen Anziehungskräften.[10]

2. DAS VERHALTEN VON UNGLEICHKÖRNIGEN WIRBELSCHICHTEN

Über das abweichende Verhalten von Wirbelschichten mit großer, kleiner oder ungleichförmiger Körnung ist viel geschrieben worden.[8-16] Feinkörnige Schichten ($d_p < 25$ μm) neigen zur Bildung von Kanälen bei Geschwindigkeiten, die nur wenig über dem Lockerungspunkt liegen, um so mehr je kleiner die Teilchen sind. Bei größeren Geschwindigkeiten bilden sich dagegen Gasblasen als eigenständige Phase infolge der Zusammenballung der Teilchen.

In grobkörnigen Schichten ($d_p > 600$ μm) sind die zwischen den Teilchen wirksamen Anziehungskräfte klein, so daß die Unregelmäßigkeiten der Struktur hier einen anderen Charakter haben. Diese Wirbelschichten neigen zur Vergrößerung der Gasblasen infolge des Austausches mit dem in der kontinuierlichen Phase vorhandenen Gas. Bei größeren Geschwindigkeiten werden die Unregelmäßigkeiten instabil, was zu einer guten Durchmischung von Gas und Feststoff führt. Andererseits kann aber die Vergrößerung der Gasblasen unter Umständen zur Pfropfenbildung führen, was durch das Verhältnis H/D und die Teilchendichte ρ_p bedingt wird.

---

[7] M. A. Doheim, A. A. Chaneya und U. S. A. Rassoul, ,,Attribution and Elutriation Studies on Fluidized Iron Ores'', Mitteilung beim 4-ten Kongreß CHISA, Prag, 1972.

[8] P. Reboux, ,,Phénomène de Fluidization'', Association Française de Fluidization, Paris, S. 154.

[9] L. Essayan und M. Essayan, ,,Fluidizarea'', Ed. tehnică, Bucureşti, 1959, S.32.

[10] I. Teoreanu, Doktordissertation, Bucureşti, 1961, S. 28.

[11] J. M. Datson, *Amer. Inst. Chem. Engineers J.*, **5**, 169 (1959).

[12] J. M. Datson, *Amer. Inst. Chem. Engineers J.*, **6**, 115 (1960).

[13] G. L. Matheson, W. A. Herbst und P. H. Holt, *Ind. Eng. Chem.*, **41**, 1099 (1949).

[14] S. D. Raşeev, *Rev. Chim. (Bucureşti)*, **12**, 439 (1962).

[15] Gh. I. Jinescu, Doktordissertation, Bucureşti, 1970, S. 190.

[16] G. Geldart, ,,Types of Gas Fluidization'', Mitteilung beim 4-ten Kongreß CHISA, Prag, 1972.

Experimentelle Untersuchungen von Mehrkornschüttungen haben gezeigt, daß durch einen bestimmten Anteil an Feingut die Wirbelschichtzähigkeit bedeutend herabgesetzt und die Struktur der Wirbelschicht verbessert wird.[13,17-22] Travinki [21] definiert eine kritische Konzentration des Feingutes C_f für die optimale Struktur der Wirbelschicht durch die Beziehung :

$$C_f = \frac{0{,}565(3m + 3m^2 - r)}{1 + 0{,}565\,(3m + 3m^2 - r)} \tag{1}$$

wobei $r = H_f/H_0$ und $m = d_{pf}/d_p$. Ein Überschuß an Feingut führt zur Bildung von Kanälen als Folge der Kohäsionskräfte, während eine zu geringe Menge an Feingut die Pfropfenbildung fördert.

Da die Korngrößenzusammensetzung des Feststoffes einen großen Einfluß auf die Eigenschaften der Wirbelschicht hat, wird dem Studium der ungleichkörnigen Schichten ein großes Interesse gewidmet, da das Verhalten dieser Schichten komplizierter ist als dasjenige der gleichkörnigen Schichten.

Ungleichkörnige Schüttungen kennzeichnen sich durch eine allmähliche Lockerung. Mit steigender Gasgeschwindigkeit werden zuerst die kleinsten Teilchen verwirbelt, die größeren folgen nach, bis die ganze Schicht durchwirbelt wird. Es gibt also einen Übergangszustand zwischen Schüttschicht und ausgebildeter Wirbelschicht, wobei der Impulsaustausch zwischen den kleinen und großen Teilchen eine wichtige Rolle für die Verwirbelung letzterer spielt.[23-25]

Die Lockerungsgeschwindigkeit wird von den meisten Forschern aus der Diskontinuität des Druckverlust-Geschwindigkeits-Diagramms $\Delta p = f(u)$ bestimmt. Für ungleichkörnige Wirbelschichten sind nur einzelne Zusammenhänge $\Delta p = f(u)$ für Güter mit engem Kornband bekannt [23] (Abb. 1). Vergleicht man die Druckverlust-Geschwindigkeits-Diagramme für gleichkörnige [26] (Abb. 2) und ungleichkörnige Wirbel schichten [23] (Abb. 1), so bemerkt man, daß bei letzteren ein Druckverlustmaximum $\Delta\pi$ am Lockerungspunkt fehlt. Das Druckverlustmaximum wird durch einen zusätzlichen Energieverbrauch für die Über-

---

[17] M. Leva, ,,Fluidization'', McGraw-Hill Book Co., London, 1959, S. 132.

[18] I. M. Rasumow, ,,PseWdooshishenie i pneWmatitscheskii transport syputschich materialow'', Isd. Chimia, Moskau, 1964, S. 8.

[19] Iu. P. Gupalo, R. B. Rosenbaum N. N. Petrenko und C. M. Todes, *Isvest. Akad. Nauk S.S.S.R. Metalugia i topliwa*, 4, 123 (1961).

[20] F. A. Zenz, *Petrol Rafiner*, **36**, 261 (1957).

[21] N. Travinski, *Chem. Ing. Tech.*, **25**, 201 (1953).

[22] A. S. Fournol, M. A. Bergougnou und C. G. J. Baker, ,,Solids Entrainment in a Larger Gas Fluidized Bed'', Mitteilung beim 4-ten Kongreß CHISA, Prag. 1972.

[23] N. B. Kondukow, *Inj. fiz. Zhur.*, **4**, 31 (1961).

[24] N. B. Kondukow, *Inj. fiz. Zhur.*, **5**, 27 (1962).

[25] N. B. Kondukow und M. H. Sosna, *Khim. Prom.*, **1965**, 402.

[26] N. I. Ghelperin, V. G. Ainstein und V. B. Kwascha, ,,Osnowy techniki psewdooshishenja'', Chimia, Moskau, 1967, S. 50.

windung der Kohäsionskräfte der Feststoffteilchen hervorgerufen und hängt von ihrer Form, Oberflächenbeschaffenheit und räumlichen Anordnung ab. Das Fehlen eines Maximums $\Delta\pi$ in ungleichkörnigen Schüttungen wird durch die allmähliche Verwirbelung der unterschiedlich großen Teilchen und den Impulsaustausch zwischen denselben erklärt.

Vorliegende Arbeit hat sich das Ziel gesetzt, die strömungstechnischen Größen der ungleichkörnigen Wirbelschicht in der Nähe des Lockerungspunktes als Funktionen der Körnungsparameter darzustellen.

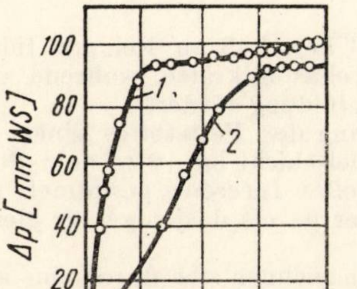

Abb. 1. — Druckverlust — Geschwindigkeitsdiagramm für Eisenerz [23]:

1, Kornfraktion 0,112 – 0,175 mm, Trägergas Wasserstoff;
2, Kornfraktion 0,25 – 0,5 mm, Trägergas Stickstoff.

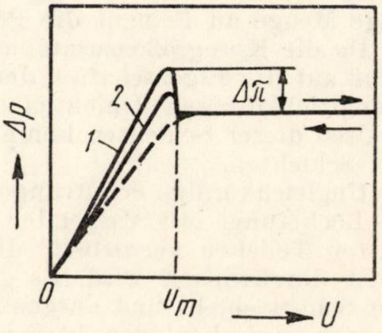

Abb. 2. — Abhängigkeit des Druckverlustes in einer Gleichkornwirbelschicht von der Trägergasgeschwindigkeit [26]:

1, bei kompakter Anordnung der Teilchen; *2*, bei loser Anordnung der Teilchen.

3. KÖRNUNGSCHARAKTERISTIKEN DES WIRBELGUTES

Für Wirbelgut mit einem engen Kornband wird als Teilchengröße ein mittlerer Durchmesser d_p eingesetzt. Da jedoch die Teilchen meist eine unregelmäßige Form haben, so muß neben dem Wert der mittleren Korngröße auch angegeben werden, wie sie bestimmt wurde. [10–18]

Es gibt verschiedene Methoden zur rechnerischen Bestimmung der mittleren Korngröße. Meistens wird hierzu die Trennung in verschiedene Kornfraktionen mit Hilfe von Normsieben verwendet. Die mittlere Korngröße d_i einer zwischen zwei Sieben erhaltenen Kornfaktion bestimmt man als arithmetisches oder geometrisches Mittel der beiden Sieböffnungen d_i' und d_i'':

$$d_i = \frac{d_i' + d_i''}{2} \tag{2}$$

oder

$$d_i = \sqrt{d_i' \cdot d_i''} \tag{3}$$

Kondučov [23,24] empfiehlt statt dessen die Beziehung:

$$d_i = \sqrt[3]{\frac{2d_i'^2 \cdot d_i''^2}{d_i' + d_i''}} \tag{4}$$

Zur Bestimmung der mittleren Korngröße des Wirbelgutes werden am häufigsten folgende Beziehungen verwendet:

$$\frac{1}{d_p} = \sum \frac{x_i}{d_i} \tag{5}$$

und

$$d_p = \Sigma x_i \cdot d_i \tag{6}$$

Die mittlere Korngröße kann aber auch auf die geometrischen Eigenschaften der Teilchen bezogen werden,[27] was zu folgenden Arten der Mittelbildung führt:

– Volumenmittel

$$d_p = \sqrt[3]{\frac{\Sigma x_i}{\Sigma(x_i/d_i^3)}}\,; \tag{7}$$

– Oberflächenmittel bezogen auf die mittlere Oberfläche

$$d_p = \sqrt{\frac{\Sigma(x_i/d_i)}{\Sigma(x_i/d_i^3)}}\,; \tag{8}$$

– Oberflächenmittel bezogen auf die spezifische Oberfläche

$$d_p = \frac{\sum x_i}{\sum(x_i/d_i)} \tag{9}$$

Die Berechnung der mittleren Korngröße für ein und dasselbe Gut mit Hilfe der obigen Beziehungen (2–9) ergibt Werte, die sich mitunter größenordnungsmäßig voneinander unterscheiden, um so mehr, je größer die Kornbandbreite ist.

---

[27] Em. A. Bratu, „Operaţii şi utilaje in industria chimică", Ed. tehnică, Bucureşti, 1961, S. 391.

Die Güte einer Wirbelschicht wird durch ihre strömungstechnischen Größen ausgedrückt, die ihrerseits von der Korngröße des Wirbelgutes bestimmt werden. So wachsen Dichte ρ_s und Zähigkeit η_s der Wirbelschicht mit der Korngröße d_p. Feine Teilchen vermindern des Zähigkeit einer grobkörnigen Schicht.[13,28] Der Hohlraumanteil ε wird durch das Verhältnis d_p/D bestimmt:

$$\varepsilon = a \cdot (d_p/D)^b \tag{10}$$

Die Vergrößerung des Verhältnisses d_p/D führt zur Verschlechterung der Anordnung der Teilchen in Wandnähe und somit zur Vergrößerung des Lückenvolumens.[29,30]

Die Lockerungsgeschwindigkeit u_m wächst ungefähr mit dem Quadrat der Korngröße, wie es folgende Beziehungen zeigen :

— nach Lewis und Mitarbeiter [31] :

$$u_m = \frac{1}{200} \cdot \frac{\varepsilon^3}{1-\varepsilon} \cdot \frac{d_p^2 \cdot \rho_p \cdot g}{\eta} \cdot \varphi_p^2 ; \tag{11}$$

— nach Leva u. Mitarbeiter [32] :

$$u_m = 9{,}35 . 10^{-3} \frac{d_p^{1,82}}{\nu^{0,88}} \cdot \left(\frac{\rho_p - \rho}{\rho} \right)^{0,94} ; \tag{12}$$

gültig für laminare Strömung, oder :

— nach Gupalo [33] :

$$\mathrm{Re} = \frac{\mathrm{Ar} . \varepsilon^{4,75}}{18 + 0{,}6 \sqrt{\mathrm{Ar} . \varepsilon^{4,75}}} ; \tag{13}$$

— nach Rowe [34] :

$$u_m = 0{,}00081 \, (\rho_p - \rho) \cdot g \cdot d_p^2 / \eta ; \tag{14}$$

gültig unabhängig von der Art der Strömung.

---

[28] W. HARVAT und O. HAVEL, *Paliva*, **23**, 253 (1953).

[29] A. M. SYTSCHEWA und N. N. EGOROW, *Chim. i techn. topliv i masel*, **1963**, 10.

[30] IA TSCHIBOROWSKI, ,,Prozessy chimitscheskoi technologii'', Goschimisdat, Moskau, 1958, S. 8.

[31] W. K. LEWIS, E. R. GILLILAND und W. C. BAUER, *Ind. Eng. Chem.*, **41**, 1104 (1949).

[32] M. LEVA, S. TAKASHI und C. WEN, *Génie chim.*, **75**, 33 (1956).

[33] IU. P. GUPALO, *Inj. fiz. Zhur.*, **5**, 96 (1962).

[34] P. N. ROWE, *Trans. Inst. Chem. Engineers*, **39**, 175 (1961).

Für die Berechnung des Druckabfalls in der Schicht wurde folgende Beziehung vorgeschlagen[28]:

$$\Delta p = \xi \cdot \frac{H_0}{d_p} \cdot \frac{u^2}{2} \cdot \rho, \tag{15}$$

wobei der Widerstandsbeiwert

$$\xi = 85\,\mathrm{Re}^{-0,75} . (d_p/d_M)^{0,6} . (\rho_p/\rho)^{0,25} \tag{16}$$

Die im Schrifttum abgeleiteten Beziehungen für u_m haben als gemeinsamen Ansatzpunkt die Abhängigkeit des Reibungsbeiwertes von der Reynoldszahl und die gleichzeitige Lösung der Gleichungen für den Druckverlust in der Schüttung bzw. in der Wirbelschicht.[31,32,34]

Der Unterschied zwischen den mit obigen Beziehungen berechneten und den experimentell gefundenen Werten ist mitunter groß, vor allem bei Schichten mit sehr feinen Körnungen, bei Schichten mit einer großen Kornbandbreite oder bei großen Reynoldszahlen. Der Grund dieser Unterschiede ist in der Verwendung einer oft ungenauen mittleren Korngröße und dem häufig schwierigen Abschätzen von Formfaktor und Mindestlückenvolumen zu suchen. Aus dem unterschiedlichen Verhalten von ungleichkörnigen Wirbelschichten mit gleicher mittlerer Korngröße folgt die Notwendigkeit beim Studium des strömungstechnischen Verhaltens ungleichkörniger Wirbelschichten neben der mittleren Korngröße einen zweiten Parameter einzuführen, der die Breite des Kornbandes angibt. Ein derartiger Parameter ergibt sich aus der Kornverteilungskurve.

Die in Europa am häufigsten verwendete Darstellung von Durchgangs- bzw. Rückstandssummenkurven ist das Rosin-Rammler-Sperling-Netz.[35] Grundlage hierfür ist das sogenannte Rosin-Rammler'sche Gesetz, das einen rein empirischen Zusammenhang zwischen Rückstand und Korngröße beschreibt:

$$R = 100\,\mathrm{e}^{-(d/d')^n} \tag{17}$$

Durch zweimaliges Logarithmieren erhält man aus dieser Formel:

$$\lg\left(\lg\frac{100}{R}\right) = n \cdot \lg d + \lg(\lg e) - n \cdot \lg d' \tag{18}$$

Die beiden letzten Glieder sind konstant, d.h. daß zwischen dem Logarithmus der Korngröße und dem Ausdruck $\lg\left(\lg\frac{100}{R}\right)$ ein linearer

---

[35] O. LAUER, „Feinheitsmessungen an technischen Stäuben", Mayer, Augsburg, 1970, S. 85.

Zusammenhang besteht. Wird auf der Abszissenachse der Logarithmus der Korngröße und auf der Ordonatenachse der $\lg\left(\lg\frac{100}{R}\right)$ aufgetragen, so erhält man eine Gerade (Abb. 3). Dies ist erfahrungsgemäß für sehr viele Körnungen der Fall. Abweichungen können am unteren und oberen Ende des Kornbandes auftreten. Die Gleichmäßigkeitszahl n, eine Materialkonstante, erscheint im Rosin-Rammler-Sperling-Netz als der Anstieg der Körnungslinie. Die Bezugskorngröße d' ist diejenige Korngröße, die 36,8% Rückstand aufweist. Eine Körnung kann also durch zwei Größen charakterisiert werden: n und d'. Statt d' wird häufig die mittlere Korngröße d_{50} verwendet, der ein Rückstand von 50% entspricht. Sie

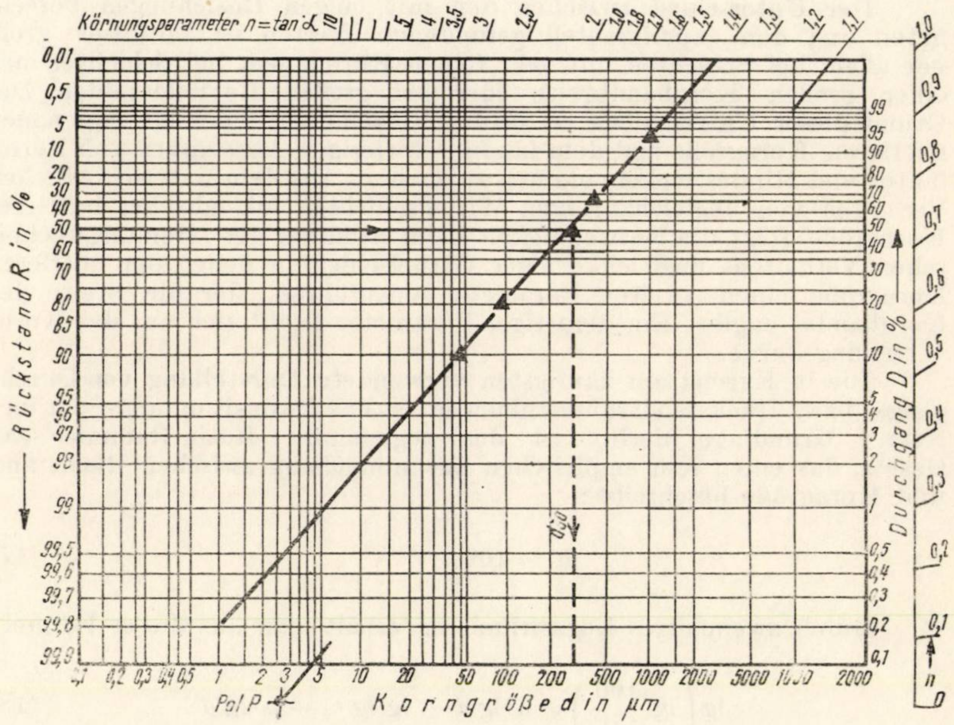

Abb. 3. — Rosin—Rammler—Sperling-Diagramm für Schlackensand: $d' = 440\,\mu\mathrm{m}$, $n = 1{,}59$.

kann ebenfalls aus dem Rosin-Rammler-Sperling-Netz abgelesen werden. Zwischen d_{50} und d' besteht der Zusammenhang

$$d_{50} = \sqrt[n]{0{,}694\,.\,d'} \tag{19}$$

4. DIE BESTIMMUNG DER LOCKERUNGSGESCHWINDIGKEIT VON MEHRKORNSCHICHTEN

Für die Berechnung der Lockerungsgeschwindigkeit von Mehrkornschichten sind wenige Gleichungen bekannt. Petrow [36,37] untersuchte den Zusammenhang zwischen Strömungsmenge des Trägergases, Hohlraumanteil und Kornzusammensetzung für Schichten mit 2 oder 3 verschiedenen Kornfraktionen im Bereich von der Schüttung bis zur pneumatischen Förderung und fand folgende Beziehung:

$$\mathrm{Re}_i = \frac{\mathrm{Ar}_i}{150\frac{1-\varepsilon_0}{\varepsilon^3}\left[1+\sum_{i=1}^{i=N-1} x_i\,(D_i-1)\right]^2 + \sqrt{\frac{1{,}75}{\varepsilon_0^3}}\left[1+\sum_{i=1}^{i=N-1} x_i\,(D_i-1)\right]\sqrt{\mathrm{Ar}_i}} \qquad (20)$$

wobei $D_i = d_N/d_i$ ($D_1 = d_N/d_1$; $D_2 = d_N/d_2 \ldots$);
$d_1, d_2 \ldots d_N$ – mittlere Durchmesser der Kornfraktionen nach Gl. (2);
ε_0 – Hohlraumanteil der Schüttung;
Ar_i und Re_i – wurden mit dem mittleren Durchmesser der größten Kornfraktion berechnet. Die Beziehung gilt für laminare und turbulente Strömung.

Nach Karpow [38] kann die Lockerung geschwindigkeit von Mehrkornschüttungen mit folgender Gleichung berechnet werden:

$$\mathrm{Re} = 0{,}049\ \mathrm{Ar}(1-\varepsilon)^{0{,}8}\,(d_M/d_p)^{0{,}48}\,(\rho/\rho_p)^{0{,}2} \qquad (21)$$

Hier wird die Korngrößenverteilung duch das Verhältnis d_M/d_p berücksichtigt, wobei d_p nach Gl. (4) und (5) berechnet wird.

Ungleichkörnige Schichten mit großen Partikeln haben den Lockerungspunkt im turbulenten Strömungsbereich. Für die Berechnung der Lockerungsgeschwindigkeit von Schichten mit Teilchen von 5–30 mm gilt nach Masurow [39] für $2200 < \mathrm{Ar} < 435000$ folgende Beziehung:

$$\mathrm{Re} = 14{,}5\ \mathrm{Ar}^{0{,}45} \qquad (22)$$

wobei: $\mathrm{Re} = \frac{u\cdot d_M}{\nu}$ und $\mathrm{Ar} = \frac{g\cdot d_M^3}{2}\left(\frac{\rho_p}{\rho} - 1\right)$ mit dem Durchmesser der größten Teilchen berechnet werden.

Die Rechnung nach den Gleichungen (11) bis (14) ergibt für die Lockerungsgeschwindigkeit ungleichkörniger Schichten viel zu kleine Werte, was auf die Verwendung eines mittleren Durchmessers und auf

---

[36] W. N. Petrow, *Isvest. W.U.S.M.W.O. S.S.S.R. Nefti i gas*, **1961**, 79.

[37] N. W. Petrow, *Isvest. W.U.S.M.W.O. S.S.S.R. Nefti i gas*, **1962**, 71.

[38] A. I. Karpow, *Isvest. W.U.S.M.W.O. S.S.S.R. Nefti i gas*, **1962**, 71.

[39] D. Ia. Masurow, *Inj. fiz. Zhur.*, **5**, 13 (1962).

die Vernachlässigung der Korngrößenverteilung zurückzuführen ist. Wird die Rechnung nach den Gleichungen (21) und (22) mit dem größten Teilchendurchmesser durchgeführt, so erhält man zu große Werte. Die unhandliche Form der Gleichung (20) erschwert ihre praktische Anwendung. Der wahre Wert der Lockerungsgeschwindigkeit befindet sich zwischen den mit obigen Gleichungen berechneten Grenzwerten; für seine Berechnung muß ein geeigneter „mittlerer" Durchmesser verwendet, aber auch die Korngrößenverteilung berücksichtigt werden.

5. VERSUCHSERGEBNISSE

Die Versuche auf Grund deren die Gleichungen (20) bis (22) aufgestellt wurden, sowie Untersuchungen neueren Datums,[40] kennzeichnen sich dadurch, daß Mischungen von 2 bis 3 verschiedener Kornfraktionen verwendet wurden.

Bei unseren Versuchen wurden dagegen als Wirbelgut technische Zerkleinerungsprodukte (Schlackensand, Koks und Silikagel) verwendet, ohne eine Trennung in Kornklassen vorzunehmen. Eine Siebanalyse ergab die jeweilige Korngrößenverteilung, die in allen Fällen im Rosin-Rammler-Sperling-Netz als Gerade dargestellt werden konnte. Es wurden auch „synthetische" (aus Kornfraktionen zusammengesetzte) Körnungen verwendet, die jedoch in ihrem Aufbau dem Gesetz von Rosin-Rammler entsprachen. Die Darstellung im Rosin-Rammler-Sperling-Körnungsnetz ergab folgende, die Körnung kennzeichnende Werte (Tabelle 1): Gleichmäßigkeitzahl n, kleinster Teilchendurchmesser d_m (99% Rückstand), größter Teilchendurchmesser d_M(1% Rückstand), Bezugskorngröße d' (36,8% Rückstand) und „mittlerer„ Durchmesser d_{50} (50% Rückstand).

Die Versuchseinrichtung bestand aus einer Glasröhre von 50 mm Durchmesser und 350 mm Höhe, mit einer porösen Platte als Rost, einem Rota-Meter, einem Differentialmanometer und einem an die Druckluftleitung angeschlossenen Luftfilter.

Die Versuche wurden mit den in Tabelle 1 angegebenen Wirbelgütern durchgeführt; sie zeigten den Einfluß der Korngrößenverteilung auf die beginnende Fluidisierung.

Für die Bestimmung der Lockerungsgeschwindigkeit wurde der Druckverlust in der Schicht Δp_s als Funktion der Trägergasmenge Q_v, sowohl bei steigender als auch bei fallender Luftmenge dargestellt. Es wurden gleichzeitig Trägergasmenge Q_v, Gesamtdruckverlust Δp_t und Höhe der Wirbelschicht H_f gemessen. Die für Δp_t und H_f angegebenen Werte wurden aus je 3 Versuchsreihen gemittelt, deren Abweichungen unter 5% betrugen. Gleichzeitig wurden visuelle Betrachtungen der Schicht vorgenommen.

Der Druckverlust in der Schicht Δp_s wurde mit folgender Beziehung berechnet:

$$\Delta p_s = \Delta p_t - \Delta p_0, \qquad (23)$$

wobei Δp_0 der im Leerlauf bei gleicher Luftmenge gemessene Druckverlust ist.

---

[40] H. BRAUNER und V. ASBECK, *Verfahrenstechnik*, **6**, 230 (1972).

Tabelle 1

Körnungsparameter der Wirbelgüter, sowie experimentell und rechnerisch bestimmte Werte der Lockerungsgeschwindigkeit

Größe	Zeichen	Maßeinheit	Wirbelgut													
			Schlackensand				Koks					Silikagel				
Teilchendichte	ρ_p	g/cm³	2,2	2,2	2,2	2,2	1,3	1,3	1,3	1,3	1,3	0,983	0,983	0,983	0,983	0,983
Kleinster Korndurchmesser	d_m	μm	8	26	60	135	56	71	130	160	200	29	33	76	150	225
Größter Korndurchmesser	d_M	μm	1350	1100	1200	910	850	850	1000	900	920	700	700	660	860	890
Bezugskorngröße	d'	μm	380	440	580	590	480	460	605	600	640	330	340	430	580	630
Mittlerer Durchmesser	d_{50}	μm	280	350	475	510	400	400	520	530	580	265	275	375	500	575
Gleichförmigkeitszahl	n	—	1,19	1,59	2,27	2,51	2,15	2,5	2,96	3,45	4,04	1,9	2,29	2,62	3,38	4,36
Anfangslockerungsgeschwindigkeit (experimentell)	u_i	cm/s	4,97	7,2	13,8	18,4	4,59	5,36	6,88	9,18	10,5	2,3	3,06	4,6	6,88	7,65
Endlockerungsgeschwindigkeit (experimentell)	u_f	cm/s	16,8	17,6	24,5	27	13	13	13,8	15,3	15,3	9,18	8,82	10,7	13,8	12
Lockerungsgeschwindigkeit nach Gl. (14) mit d_m	u_m	cm/s	0,0061	0,65	0,345	1,75	0,178	0,286	0,96	1,45	2,26	0,036	0,0468	0,248	0,97	2,18
Lockerungsgeschwindigkeit nach Gl. (14) mit d_M	$u_m \cdot 10^{-2}$	cm/s	1,75	1,16	1,38	0,795	0,544	0,41	0,567	0,46	0,48	0,211	0,211	0,188	0,317	0,34
Lockerungsgeschwindigkeit nach Gl. (14) mit d'	u_m	cm/s	13,8	18,6	32,3	33,4	13	12	20,7	20,4	23,2	4,69	4,97	7,95	14,4	17,05
Lockerungsgeschwindigkeit nach Gl. (14) mit d_{50}	u_m	cm/s	7,5	11,7	21,6	24,9	9,05	9,05	15,3	15,9	19	3,02	3,25	6,05	10,8	14,2
Lockerungsgeschwindigkeit nach Gl. (12) mit d_{50}	u_m	cm/s	6,55	9,87	17,1	19,5	7,62	7,62	12,2	12,75	15	2,75	2,98	5,25	8,85	11,4
Reynoldszahl mit u_f und d_{50}	Re	—	3,05	3,98	7,55	8,8	3,35	3,35	4,66	5,28	5,75	1,57	3,36	2,6	4,47	4,48

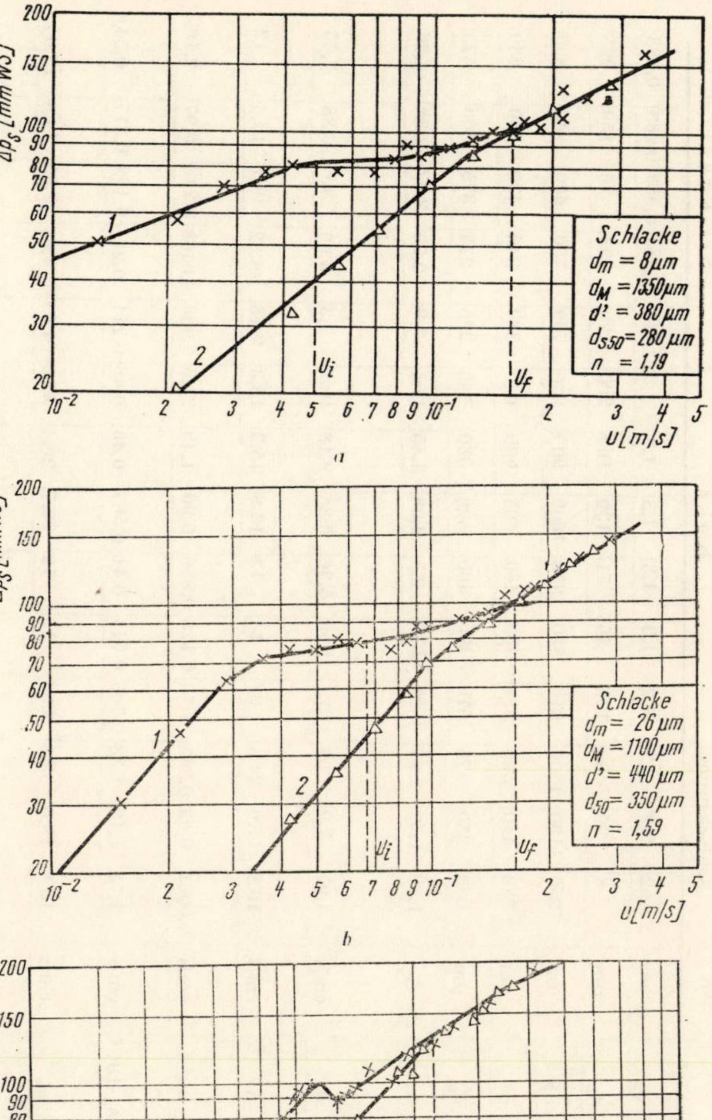

Abb. 4. – Abhängigkeit des Druckverlustes in der Wirbelschicht von der Luftgeschwindigkeit für verschiedene Körnungen:

1, bei steigender Luftgeschwindigkeit; *2*, bei fallender Luftgeschwindigkeit.

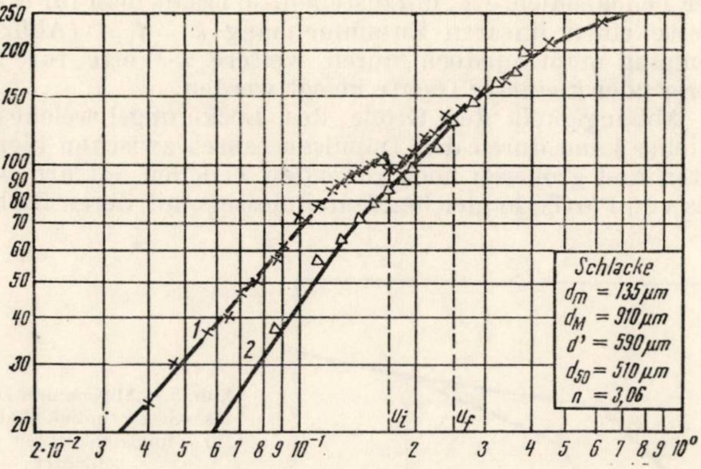

d

Auf Grund der Versuchsergebnisse wurden die Kurven $\Delta p_s = f(u)$ im logarithmischen Maßtab gezeichnet. Als Beispiel hierfür dienen die in Abbildung 4, a, b , c, d für Schlackensand dargestellten Kurven. Der Verlauf dieser Kurven kann verallgemeinert werden; man erhält auf diese Weise die generelle Darstellung der Funktion $\Delta p_s = f\,(u)$ für Schichten mit einem breiten Kornband (Abb. 5).

Im Falle von Vielkornschichten werden zuerst die kleinen Teilchen verwirbelt; bei steigender Trägergasgeschwindigkeit folgen nach und nach immer größere Teilchen. Dieses führt zur Ausbildung eines von der Anfangslockerungsgeschwindigkeit u_i und der Endlockerungsgeschwindigkeit u_f begrenzten Lockerungsbereiches, innerhalb dessen sich der Übergang von der Schüttung zur Wirbelschicht allmählich vollzieht (Abb. 4, a bis d, Tab. 1). Mit steigender Gleichmäßigkeitszahl n, also bei einem engeren Kornband, kann man das Entstehen eines Druckverlustmaximums beobachten, was den Schluß zuläßt, daß in diesem Fall der Impulsaustausch zwischen kleinen und großen Teilchen weniger wirksam ist; das Verhalten nähert sich also dem einer Gleichkornwirbelschicht.

Der Lockerungsbereich ist umso größer, je kleiner die Gleichmäßigkeitszahl n ist. Einen Überblick über diesen Zusammenhang erhält man, wenn man das Verhältnis u_f/u_i in Abhängigkeit von n im logarithmischen Maßstab aufzeichnet (Abb. 6). Für alle untersuchten Materialien erhält man in diesem Fall parallel verschobene Geraden mit der Steigung $-1{,}13$ was zu folgender Beziehung führt:

$$u_f/u_i = k\,.\,n^{-1{,}13}\,; \qquad (24)$$

k ist eine materialabhängige Konstante u. zw. $k = 4{,}1$ für Schlackensand, $k = 6{,}5$ für Koks bzw. $k = 7{,}3$ für Silikagel. Versucht man k in Abhängigkeit der Teilchendichte ρ_p darzustellen, so erhält man für die 3 verfügbaren Werte einen linearen Zusammenhang $k = f(\rho_p)$ (Abb. 7). Dieser Zusammenhang müßte jedoch durch weitere k-Werte für Materialien mit größerer oder kleinerer Dichte belegt werden.

Die Abhängigkeit der Größe des Lockerungsbereiches von der Teilchendichte kann durch den Impulsaustausch zwischen kleinen, schon verwirbelten und größeren noch ruhenden Teilchen erklärt werden, da der Impuls von Partikeln gleichen Durchmessers mit deren Dichte wächst.

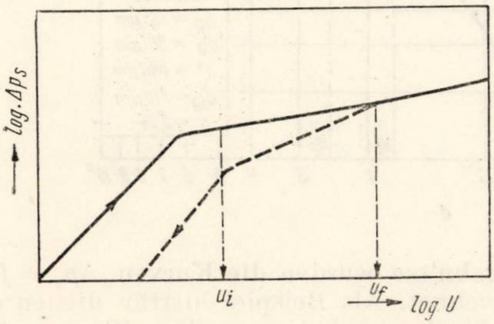

Abb. 5. — Allgemeines Druckverlust-Geschwindigkeitsdiagramm für ungleichkörnige Wirbelschichten.

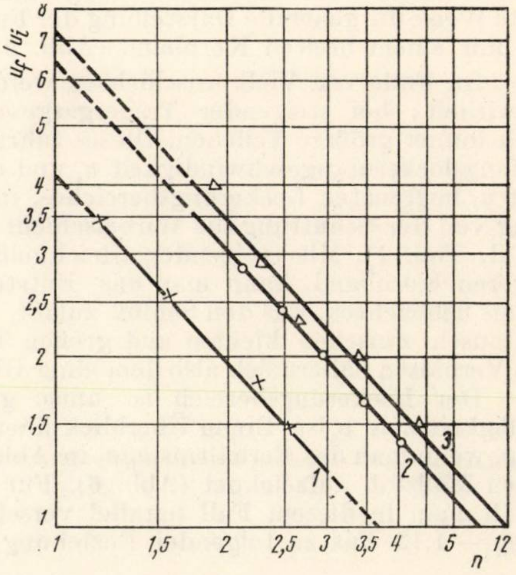

Abb. 6. — Abhängigkeit des Bruches u_f/u_i von der Gleichmäßigkeitszahl :
1, Schlackensand ; 2, Koks ; 3, Silikagel.

Aus Abb. 6 sieht man gleichfalls, daß es für jedes Material einen endlichen Grenzwert für die Gleichmäßigkeitszahl n gibt, oberhalb dessen sich die Schicht wie eine Gleichkornschicht ($n = \infty$) verhält. Die gleiche Schlußfolgerung ergab sich auch aus den Bildern für den Zusammenhang $\Delta p_s = f(u)$, wo im Falle von Schichten mit großem n ein Druckverlustmaximum $\Delta\pi$ am Lockerungspunkt zu beobachten ist.

Schließlich wurde überprüft, ob man die für Gleichkornschichten abgeleiteten Gleichungen für die Lockerungsgeschwindigkeit auch für ungleichkörnige Schichten verwenden kann, wenn ein entsprechender „mittlerer" Durchmesser eingesetzt wird. Dieser Durchmesser müßte leicht aus der Korngrößenverteilung zu ermitteln sein.

Die Ergebnisse der Rechnung nach den Formeln von Rowe (Gl. 14), bzw. Leva (Gl. 12) mit den Korngrößen d_m, d_M, d' bzw. d_{50} sind in der Tabelle 1 angegeben. Die mit d_m bzw. d_M berechneten Werte liegen ausserhalb des Bereiches $u_i - u_f$; d' ergab für die meisten der untersuchten Körnungen zu große Werte ($> u_f$). Wird jedoch d_{50} in die Beziehungen von Rowe bzw. Leva eingesetzt, so erhält man Werte zwischen u_i und u_f, bei denen, visuellen Beobachtungen zufolge, etwa 80% der Schicht verwirbelt ist. Folglich können wir für die Berechnung der Lockerungsgeschwindigkeit von Vielkornschichten die für Gleichkornschichten gültigen Beziehungen (z.B. nach Rowe oder Leva) empfehlen, wobei jedoch als Korngröße der aus dem Rosin-Rammler-Sperling-Körnungsnetz leicht ablesbare mittlere Durchmesser d_{50} einzusetzen ist.

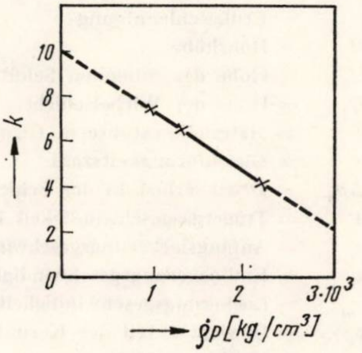

Abb. 7. — Abhängigkeit des Koeffizienten k von der Teilchendichte.

SCHLUSSFOLGERUNGEN

Die Fluidisierung technischer (ungleichkörniger) Güter ist ein komplizierter Vorgang, bei dem der Impulsaustausch zwischen kleinen schon verwirbelten und größeren noch ruhenden Teilchen eine wichtige Rolle spielt.

Der Übergang von der Schüttung zur ausgebildeten Wirbelschicht vollzieht sich in einem Geschwindigkeitsbereich, dessen Breite von der Gleichmäßigkeitszahl und der Teilchendichte abhängt. Für die Berechnung der Lockerungsgeschwindigkeit muß die Korngrößenverteilung im Rosin-Rammler-Sperling-Körnungsnetz dargestellt werden, wobei mindestens zwei Siebrückstände bekannt sein müssen. Aus dem Rosin-Rammler-Sperling-Diagramm sind Gleichmäßigkeitszahl n und mittlere

Korngröße d_{50} abzulesen. Die Lockerungsgeschwindigkeit kann mit Hilfe der für Gleichkornschichten abgeleiteten Beziehungen berechnet werden, wenn als Korngröße der mittlere Durchmesser d_{50} eingesetzt wird.

ZEICHEN

a, b = Konstanten in Gl. (10)
C_f = Feingutkonzentration in der Wirbelschicht (Gl. 1)
d = Korngröße
d' = Bezugskorngröße (36,8 % Rückstand)
d_i = mittlerer Durchmesser einer Kornklasse
d_i', d_i'' = unterer bzw. oberer Grenzkorndurchmesser einer Kornklasse
d_m = kleinster Korndurchmesser
d_M = größter Korndurchmesser
d_p = mittlere Korngröße berechnet nach Gl. (5) bis (9)
d_{pf} = mittlerer Durchmesser des Feingutes
d_{50} = mittlere Korngröße (50 % Rückstand)
D = Rohrdurchmesser
g = Erdbeschleunigung
H = Rohrhöhe
H_0 = Höhe der ruhenden Schüttung
H_f = Höhe der Wirbelschicht
k = Materialkonstante in Gl. (24)
n = Gleichförmigkeitszahl
Δp_s = Druckverlust in der Schicht
u = Trägergasgeschwindigkeit bezogen auf den Rohrquerschnitt
u_i = Anfangslockerungsgeschwindigkeit
u_f = Endlockerungsgeschwindigkeit
u_m = Lockerungsgeschwindigkeit
x_i = Gewichtsanteil der Kornklasse mit dem mittleren Durchmesser d_i
ε = Hohlraumanteil
η = dynamische Zähigkeit des Trägergases
η_s = dynamische Zähigkeit der Wirbelschicht
ξ = kinematische Zähigkeit des Trägergases
ρ = Trägergasdichte
ρ_p = Teilchendichte
ρ_s = Dichte der Wirbelschicht
Φ_p = Formfaktor der Teilchen

$$\mathrm{Ar} = \frac{g \cdot d_p^3}{\nu^2}\left[\frac{\rho_p}{\rho} - 1\right] \quad \text{Archimedeszahl}$$

$$\mathrm{Re} = \frac{u \cdot d_p}{\nu} \quad \text{Reynoldszahl.}$$

F 1103

INDEX DU TOME 18, 1973

INDEX DES AUTEURS

A

Page

Adorian, I., Temperature and concentration dependence of molar polarization in binary mixtures of polar liquids with nonpolar solvent . . . 211
—, voir Sternberg S.. 945

Airinei, A., voir Avramovici, S. . . 1781

Albescu, I., Contributions to the study of lanthanides with biguanide derivatives. V. Lanthanide compounds with hydrochloric paludrine. 599
—, Contributions to the study of lanthanides with biguanide derivatives. VI. Halogeno- and pseudohalogeno-compounds of lanthanides . . 829

Aleksić, B. D. and A. Terlecki-Baričević, Investigation of some properties of the ammonia synthesis catalysts obtained by melting natural magnetite 575

Amălinei, I., voir Cobianu N. . . . 305

Andrei, Z., voir Tomoaia, M. 1547

Angelescu, A., voir Iovu, M. 263

Angelis, G. de, voir Campanella, L. 1269
—, voir Campanella, L. . . . 1649, 1825

Armeanu, V. and E. Drăgușin, Spectrophotometric study of cadmium complex with benzthiazolylazo-2,4-dichlorophenol reagent . . . 1475

Armstrong, D. R. and R. C. W. King, P. G. Perkins, The electronic structures of some six-membered sulphur-nitrogen and sulphur oxygen ring systems 2011

Arshad, A. B. M. and M. A. Hashmi, Correlation of the physical properties of organosulphur compounds. II. Effective electronegativity of the molecules and their physical properties. 1033
— and I. A. Khan, Correlation of the physical properties of organosilicon compounds. III. Electronegativity of molecules and their boiling point, refractivity and density 1395

Arvay Z., voir Glatz, A. M. 2087

Page

Asandei, N., voir Simionescu, Cr. I. 327

Aurian-Blăjeni, B., voir Ionescu, N. I. 2031

Avram, M. and I. G. Dinulescu, F. Chiraleu, C. D. Nenitzescu, Investigations in the cyclobutane series. XXXII. The addition of bromine to derivatives of *exo. exo*-tetracyclo$[4.4.2.0^{2.5}.0^{7.10}]$ dodeca-3.11-diene 863
— and I. G. Dinulescu, C. D. Nenitzescu, R. A. Y. Jones, A. R. Katritzky, R. J. Wyatt, Configurations of substituted dibenzobicyclo [3.2.1]octadienes 441

Avramovici, S. et A. Airinei, I. Ciocoiu, Les spectres électroniques de quelques bases de Schiff à noyaux benz- et naptho-thiazoliques . . 1781
— and I. Druță, I. Zugrăvescu, On some derivatives of the hydrazinocarboxylic acid. II. Syntheses and spectral data 431

B

Bacaloglu, R. und B. D. Bader, Neue organische Pigmente - Isatinderivate. III. Studium der IR-Spektren einiger 2-Arylaminoindoxyle und 3-Aryliminooxindole 275

Badea, F., voir Glatz, A. M. 2087
—, voir Voicu, M 131

Bader, B. D., voir Bacaloglu, R . 275
—, voir Vîlceanu, R. 1225

Badiger, V. V. and S. C. Bennur, Pyrimidine. IV. Synthesis of N-aryl-N′-4-(2-methylthio-5-bromopyrimidoyl) ureas and thiourea . . . 1389
— and M. Y. M. Jamkhandi, Analogues of chloramphenicol. II. Synthesis of 2-chloroacetamido-1-(4′-chloro-3′-nitro-phenyl) propane-1,3-diol 489

Baican, R., voir Negoiță, N. . . . 995

Page

Balaban, A. T., Chemical graphs. XVI. Intramolecular isomerizations of octahedral complexes with six different ligands 841
—, Chemical graphs. XVIII. Graphs of degrees four or less, isomers of annulenes, and nomenclature of bridged polycyclic structures 635
—, Chemical graphs. XIX. Intramolecular isomerizations of trigonal-bipyramidal structures with five different ligands 855
—, Reaction of pyrylium salts with nucleophiles. X. N(12)-substituted 11,13-dimethyl-[9] (2,6)-pyridinophanium perchlorates 1605
—, voir Gârd, E. 257
—, voir Negoiţă, N. 995
—, voir Pomponiu, C. 1173

Balaban, C. and Gh. Dobrănis, R. Mihail, Mass transfer in the absorption from a freely rising gas bubble under the action of mechanical vibrations 1829

Bălănescu, Al., voir Vasilescu, D. S. 907
Balducci, G., voir Piacente, V. 2083
Balmez, M., voir Csomontaniy, G. 1367
Balog, A. and D. Breazu, V. Voinescu, M. Herman, E. Vargha, E. Ramonţian, Peptides. XII. Behaviour of the mixed anhydrides of some amino acids N-protected with β-ketoesters 123
—, voir Vargha, E. 1627

Băloiu, L. M., Spectrophotometric determination of the partition constant using variable amounts of solvent 1659
Baltă, E., voir Tărăbăşanu-Mihăilă, C. 889
Baltă, P. and L. Dollinger, Influence of alkaline cations on the sensitivity of the phototropic glasses with AgCl 399
Banciu, A. C., voir Spacu, P. 1143
Bansal, N.P., voir Gaur, H. C. 1903
Barabás, A., voir Işfan, E. 667, 1233

Bărbulescu, A., voir Solacolu, Ş. 1867
Bărbulescu, N. and M. Moraru, D. Şotcă, Bicyclo [3.3.1] nonane. The acid-catalyzed reactions of a bicyclic epoxide 873
— und F. Potmischil, Darstellung und Untersuchung der Hydroacridine. XI. Der sterische Ablauf der Quaternierung von N-methyl-α-perhydroacridin und N-methyl-β-perhydroacridin mit Trideuteromethyljodid 1613
Bardi, G., voir Maria, G. de 367
Bejan, L., voir Sternberg, S. 11
Benedek, I., voir Simionescu, Cr. I. 327
Bennur, S. C., voir Badiger, S. C. 1389

Page

Beu, L. and J. Rissu, The synthesis and spectrophotometric studies on benzoyl cyanide phenylhydrazones 723
—, voir Vargha, E. 1627
Bică, I., voir Drăgănescu, A. 1859
Biradar, N. S. and V. H. Kulkarni, Schiff base complexes with IV and V group metals 63
— and V. B. Mahale, Addition compounds of Tin (IV) chloride with tetradentate Schiff bases 2077
— and V. B. Mahale, V. H. Kulkarni, Titanium (IV) chloride complexes with cobalt (II) chelates of tetradentate Schiff bases 809
Bodea, C., voir Panea, T., 1259
—, voir Tămaş, V. 1409
Boghină, C., voir Cobianu, N. 305
Botar, A. V. und T. J. R. Weakley, Heteropolywolframate des Th(IV) 1155
Bozeşanu, M., Gas chromatographic separation of formic aldehyde methyl alcohol, water and hydrogen peroxide 2037
Braşoveanu, I., voir Fruma, Al. 803
Breazu, D., voir Balog, A. 123
—, voir Vargha, E. 1627
Brezeanu, M. and I. Jitaru, Cu(II) coordination compounds with 3-amino-1-propanol 2039
Briţchi, M., voir Petrescu, N. 1853
Bulan, St., voir Furnică, Gh. 175

C

Căldăraru, H., voir Caragheorgheopol, A. 1497
Campanella, L. and P. L. Cignini, X-ray powder spectra of pyridinemonocarboxylic acids and their use for the qualitative analysis of a mixture of these acids 1087
—, and P. L. Cignini, G. de Angelis, Influence of drying temperature on water content and cristalline characteristics of isocinchomeronic acid 1825
— and P. L. Cignini, G. de Angelis, Polarographic behaviour of isocinchomeronic acid 1649
— and P. Cignini, G. de Angelis, Polarographic, oscillopolarographic and chronopotentiometric behaviour and determination of nicotinic acid 1269
Caragheorgheopol, A. and H. Căldăraru, V. E. Sahini, Assignment of proton hyperfine splitting constants in cyclic α-ketoiminoxy radicals 1497

Page

Cecal, Al. et I. A. Schneider, Réactions d'échange isotopique entre Tl (III) complexé et ^{204}Tl (I) . . . 35
Cenuşe, Z., voir Vîlcu, R. . . . 377
Cerchez, M., voir Dinescu, R. . . . 23
—, voir Solacolu, S. . . . 203
Chanu, J. et M. E. Weill, Chaleurs de transfert en milieux ioniques : application aux solutions aqueuses de KCl et HCl à 25° et 35°C . . . 1513
Chiacchierini, E. and R. Cochieri, Behaviour of Cr (III)-poly (aminocarboxylate) ligands solutions at the dropping-mercury electrode (DME) . . . 1441
Chifu, E., voir Tomoaia, M. . . . 1547
Chira, R., Fărcăşan, M. . . . 2103
Chiraleu, F., voir Avram, M. . . . 863
—, voir Gârd, E. . . . 257
—, voir Glatz, A. M. . . . 2087
Chiriac, A., voir Vîlceanu, R. . . . 1345
Chirulescu, T. and C. Ciobanu, Gh. Şerban, Kinetic study on the reduction of nickel catalysts . . . 1333
Cignini, P. L., voir Campanella, L. . . . 1087, 1269, 1649, 1825
Cîmpeanu, G., voir Iovu, M. . . . 883
Ciobanu, C., voir Chirulescu, T. . . . 1333
Ciocoiu, I., voir Avramovici, S. . . . 1781
Ciomîrtan, D., voir Fruma, Al. . . . 803
—, voir Georgescu, I. I. . . . 1159
Ciovîrnache, V., voir Popescu, U.C. . . . 145, 1459
Cîrje, M., Über 1,2,3,4-Tetrahydroakridin-9-Carboxyl-Säure-Derivate. I. Amide . . . 1013
Cismaru, D. and C. Radovici, The reaction kinetics in submicronic powders. The ZrO_2 + CaO system . . . 1699
Cismaru, G. D. and P. Spacu, Electrical conductivity of intermetallic compounds of the cerium-thallium system . . . 1345
Ciurdaru, Gh., voir Fărcăşanu, M. . . . 2103
Ciurdaru, V., voir Tămaş, V. . . . 1409
Cobianu, N. and C. Boghină, B. Mărculescu, I. Amălinei, On the reactivity of N-vinylcaprolactam in radicalic polymerization . . . 305
Cochieri, R., voir Chiacchierini, E. . . . 1441
Coman, B., voir Vîlcu, R. . . . 1301
Coman, M., voir Simiti, I. . . . 685
Comaniţă, E., voir Petrova, L. . . . 1361
Comptes Rendus, 519, 733, 1101, 1489, 1663, 1664, 2001
Constantin, M., voir Răileanu, M. . . . 1243
Constantin, V., voir Contineanu, M. . . . 761
Constantinescu, A., voir Liteanu, C. . . . 155
— and C. Liteanu, Ionophoresis with flow gradient . . . 1273
Constantinescu, M. and E. Segal, Successive chemisorption of gases on semiconductor thin films in the dark and under irradiation. I. The oxygen, carbon monoxide and hydrogen on zinc oxyde system . . . 1587
Constantinescu, O., voir Contineanu, M. . . . 2005
Contineanu, M. and O.Constantinescu, T. Oncescu, EPR study in the radiolysis if polycrystalline azibenzyl . . . 2005
— and T. Oncescu, R. N. Schindler, Kinetics and mechanism of the thermal decomposition of azibenzyl. I. Decomposition in benzene solution . . . 549
— and T. Oncescu, R. N. Schindler, Kinetics and mechanism of the thermal decomposition of azibenzil. II. Studies in the absence of a solvent . . . 753
— and C. Podină, V. Constantin, Mass spectrum of diphenyldiazomethane . . . 761
Cornea F. et C. Fulea, A. O. Fulea, Relations concernant la structure électronique et la réactivité de quelques thioamides . . . 111
Costache, D. and S. Sasu, Kinetic determination of vanadium by the reaction between pyrogallol bromine red and potassium bromate . . . 913
Cristea, I., voir Fărcăşan, V. . . . 469
Csomontanyi, G. et M. Netta, M. Balmez, Hydrogénation catalytique de l'acétophénone . . . 1367
Cuiban, F., An improved synthesis of optically pure N^{α}-methyl-lysine . . . 463
—, Peptide syntheses with N-(acyl-o-nitrophenyl)-substituted amino acids . . . 449

D

Dănilă, D., voir Haiduc, I. . . . 1093
Demetrescu, I., voir Murgulescu, I. G. . . . 355, 523
Denes, V., voir Fărcăşan, M. . . . 2103
Dima, M., voir Petrariu, I. . . . 493
Dinescu, R. et M. Cerchez, Les équilibres de phase du système Na_2O-CaO-Al_2O_3-SiO_2. Équilibres de phase dans le sous-système Na_2O. Al_2O_3. $6SiO_2$-CaO. Al_2O_3. $2SiO_2$ $-3Al_2O_3$. $2SiO_2$$-Al_2O_3$ intéressant la céramique super-alumineuse . . . 23

Page

Dinulescu, I. G., voir Avram. 441
Dobrăniş, Gh., voir Balaban, C. . . . 1829
Dobrescu-Ciureanu, M. and V. E. Sahini, A perturbation treatment of molecular complexes. III. Iodine complexes with five-membered heteroaromatics 921
Dollingher, L., voir Baltă, P. 399
Domşa, F., voir Negoiţă, N. 995
Drăgănescu, A. and I. Bică, C. Petrescu, Kinetics of the homogeneous reaction between methane and sulphur 1859
Drăghici, C., voir Urseanu, F. 1019
Drăgulescu, C. and A. Nimară, I. Julean, D. Marandiuc, Polarographic behaviour of bismuth (III) in acid perchlorate solutions 583
— and T. Simionescu, M. Totan Curtui, Study of the thorium-purpurin complex by butanol extraction 43
— and N. Vîlceanu, Uranyl-pyrophosphate complexes. III. The monopyrophosphato-pentauranyl cation complex 49
— and N. Vîlceanu, I. Julean, Uranyl-pyrophosphate complexes. IV. Precipitation reactions of the pyrophosphato-uranylate complex anions with the Ag^+ ion 53
— and N. Vîlceanu, Uranyl-pyrophosphate complexes. V. The precipitation reaction of the sodium bis-pyrophosphato-uranylate complex with the Cd^{2+} ion 59
Drăguşin, E., voir Armeanu, V. . . . 1475
Drăguţan, V., voir Glatz, A.M., . . 2087
Drimuş I. and I. T. Ionescu, Der Einfluss der Kettenlänge einiger *n*-Alkane auf ihre Peroxydierungsgeschwindigkeit mit molekularem Sauerstoff, in flüssiger Phase . . . 269
— and I. T. Ionescu, The influence of carbonyl or hydroxyl position on the breaking point of the linear twelve membered carbon chain, by molecular oxigen 1769
— and I. T. Ionescu, Relations entre la longueur de la chaîne des *n*-alcanes et la composition des *n*-acides monocarboxyliques obtenus par leur oxydation 1949
Druţă, I., voir Avramovici, S. . . . 431
Duşoiu, N., Magnetic dispersion and magnetic absorption of some ferrimagnetic compounds in the domain of centimetre waves. I. Li-Fe-Be and Ni-Fe-Be 1339

Page

E

El-Abbady, A. M. and M. A. Omara, N. G. Kandil, γ-keto acids in the Pfitzinger reaction 899
Eliel, E. L., voir Mager, S. 1379
2097

F

Fabian, J., voir Vlassa, M.. 99
Facsko, Gh. und M. Nemes, Die polarographische Bestimmung des mit dem Natriumsalz der 4-Sulfonamidobenzoläure komplexgebundenen Quecksilbers (II), in stark alkalischem Medium 1971
Fărcăşan, M. and R. Chira, Gh. Ciurdaru, V. Deneş, Heterocyclic methylene bases. X. 2-(ω-acyl-ω-arylazo) methylene derivatives of N-containing heterocycles 2103
Fărcăşan, V. and I. Cristea, Dibenzofurans. I. The formylation of 3-dimethylamino-dibenzofuran by the Vilsmeier-Haack method 469
—, voir Panea, T. 1259
Fătu, D. et S. Fătu, E. Segal, Cinétique des transformations du nitrate d'ammonium en régime non isothermique 1709
Fătu, S., voir Fătu, D. 1709
Feyns, V., voir Niculescu-Duvăz, I. 1617
Filipescu, N., voir Pavlik, J. W. 1793
— and J. W. Pavlik, P. T. Frangopol, M. Frangopol, Spectroscopic properties of trapped anthronylidene 1959
Finta, Z. and C. S. Várhelyi, J. Zsakó, Kinetics and mechanism of substitution reactions of complexes. XLIII. Basic hydrolysis of $[Co(DH)_2(H_2O)(NCS)]$ 417
Fiti, M., Mechanism of radiolytic reduction of Cr^{VI} in aqueous solutions 511
Fitzner, K., voir Moser, Z. 557
Florea, I., Spektrophotometrische Dosierung der $Cr_2O_7^{2-}$ und CrO_4^{2-}-Ionen mit *o*-Tolidin 1993
Florea, S., voir Negoiu, D. 1875
Floru, L., voir Tărăbăşanu-Mihăilă, C. 889
2113
Frangopol, M., voir Filipescu, N. . . 1959
—M, voir Pavlik, J. W. 1793
Frangopol P.T., voir Filipescu, N. . 1959
—, voir Pavlik, J. W. 1793
Fruma, Al. und D. Ciomârtan, I. Braşoveanu, I. V., Nicolescu, Die

Page

Struktur des mit Lithium and Titan dotiertem Aluminiumoxyd . . 803
—, voir Nicolescu, I.V. 953
— und I. V. Nicolescu, Die Chemisorption von Wasserstoff, Benzol und Zyklohexan auf mit Lithium und Titan dotiertem Aluminiumoxyd. II. Adsorptionswärmen . 1131
Fulea, A.O., voir Cornea, F. 111
Fulea, C., voir Cornea, F. 111
—, voir Negoiu, D. 1749
Furnică, Gh. et M. Toader, S. Turcitu, St. Bulan, L'étude du mécanisme physico-chimique de la sorption des isotopes radio-actifs par certaines macromolécules inorganiques polyélectrolytiques. I. La sorption physique et chimique par la diatomite, la montmorillonite, la kieselguhr, le silicagel, le kaolin et la calcite, des radionucléides des éléments I, P. Na, Cs, Sr, Ba, Zn, Cu, Co, Mn et Fe 175

G

Galin, M., voir Simionescu, Cr. I. . 327
Gănescu, I., voir Várhelyi, C. . . . 823
Gârd, E. and F. Chiraleu, I. I. Stănoiu, A. T. Balaban, Isotopic exchange of active methyl hydrogens. VII. Kinetic study of 2,4,6-trimethylpyrylium salts in deuterium oxide. 257
Gaur, H. C. and N. P. Bansal, Computer evaluation of the association constants of silver-chloro and bromo complexes in molten sodium nitrate — barium nitrate eutectic . . 1903
Gaymard, F. et R. Guedj, A. Vermeglio, Sur la chloration et l'oxychloration spécifiques des cycloheptène et cyclopentène 979
Georgescu, I. I. and D. Ciomârtan, G. Teodorescu, M. Hlevca, M. Zaharescu, Complexes of isonicotinic acid hydrazide with Fe (II) and thiocyan, $(INAH)_2$ Fe $(NCS)_2$. H_2O 1159
— and M. Moraru, D. Ţarina, Mössbauer effect in complexes of isonicotinic acid hydrazide with Fe (II) —isothiocyanate $(INAH)_2$ Fe $(NCS)_2$. H_2O 2067
Georgescu, M., voir Teoreanu, I. . 623
Gigli, R., voir Maria, G. de 367
Gioabă, A. and V. E. M. Sahini, E. Volanschi, NMR spectra of some phenoxatellurine derivatives . . . 531
Giurgiu, D. et I. Popescu, La réactivité des composés aluminium-organiques envers de bases Lewis. Dérivés des triphénylaluminium avec des composés 1,3-dicarbonyliques 1963
Glatz, A. M. et F. Badea, Z. Arvay, V. Drăguţan, F. Chiraleu, A. C. Răzuş, Condensations d'acides insaturés sur le benzène catalysées par le chlorure d'aluminium. V. Acide sorbique 2087
Gocan, S., voir Hodişan, T. 2143
Gönczy, F., voir Vargha, E. 1627
Grjotheim, K. and J. L. Holm, H. A. Øye, Physico-chemical properties of molten salts of significante go magnesium electrolysis. 2017
Guedj, R., voir Gaymard, F. . . . 979
Gulută, F., voir Isăcescu, D.A. . 695
Györfi, Z., voir Suciu, D. 1777

H

Haiduc, I. and D. Dănilă, C. Liteanu, Influence of indicating electrode pretreatment on potentiometric titration parameters. V. Gold pretreated electrode in potentiometric titration of $Cr_2O_7^{2-}$ with Fe^{2+} . 1093
Hashmi, A. H., voir Khan, I. A. . . 815
Hashmi, M. A., voir Arshad, A. B. M. 1033
Hentz, R. R., voir Mihalcea, I. . . 1577
Herak, R., voir Putanov, P. 569
Herdlicka, C. and S. Sternberg, The interdiffusion coefficient of Pb^{2+} ion in fused alkali chlorides by the chronopotentiometric method . . 1689
Herman, M., voir Balog, A. 123
Hlevca, M., voir Georgescu, I. I.. . . 1159
Hodişan, T. and C. Liteanu, S. Gocan, Thin layer thermochromatography. VII. Comparison between temperature gradient chromatography resolution and nonsaturated chamber resolution 2143
Holm, J. L., voir Grjotheim, K. . 2017
Hopîrtean, E., voir Liteanu, C. . . 1643
—, voir Mioşcu, M. 1637

I

Inţa, I. and P. Mărgineanu, The ferromagnetic resonance of nickel-chromia catalyst . . . 347
Ioan, S., voir Simionescu, Cr. I . . 327
Ionescu, I., Quelques remarques sur les propriétés des bétons aux résines synthétiques et aux liants minéraux 1041

Page

Ionescu, I. T., voir Drimuş, I. . . . 269, 1769, 1949

Ionescu, I. V., voir Isăcescu, D. A. . 695

Ionescu, L. G., Some aspects of the chemistry of xenon and other noble gases 1731

Ionescu, M., voir Vlassa, M. 99

Ionescu, N. I. and B. Aurian-Blăjeni, On the logarithmic law used in the kinetics of the solid-gas chemisorption processes 2031

Iordache, O. and M. Muntean, I. Teoreanu, Stochastic modelling of chemical processes 239

Iosif, I. and I. A. Schneider, C. Volanschi, Some aspects of the cool flame and low temperature ignition of mehtane 195

Iovanovici, J., voir Putanov, P. . . . 569

Iovu, M. and A. Angelescu, Phenyl benzyl sulphides 263

— et G. Cîmpeanu, Tris-éthers. I. La condensation du bis (chlorométhyl) éther avec les phénoxydes, méthyle- et diméthyle-phénoxydes de sodium 883

— et S. Radu, Condensation du 4, 4′-azodiphénoxyde de sodium avec les dérivés chlorométhylés du benzène 473

Isăcescu, D. A. and I. V. Ionescu, F. Guluţă, C. Roncea, D. Mihăiţă, Studies in the polyethylene field. VI. Pressure-volume-temperature-crystallinity relationship in high-pressure additive-containing polyethylene 695

Işfan, E. and A. Barabás, Heterocyclic organoboron compounds. XV. Boronium chelate salts and beryllium chelates of 1,3-ketoenols with disturbed resonance in the chelate ring 667

— and C. Uncuţa, A. Barabás, Beryllium- (3-acyl-2,4- pentanedi - onates) 1233

Ivan, E., voir Spacu, P. 405, 589

Ivana, E., voir Murgulescu, I. G. 189,1667

J

Jamkhandi, M. Y. M., voir Badiger, V.V. 489

Jinescu, G. I. und H. H. Rehner, Strömungstechnische Fragen ungleichchkörniger Wirbelschichten . 2149

Jitaru, I., voir Brezeanu, M. 2039

Page

Jones, R. A. Y., voir Avram, M. . . . 441

Julean, I., voir Drăgulescu, C. . . 53, 583

K

Kandil, N. G., voir El-Abbady, A. M. 899

Katritzky, A. R., voir Avram, M. . . 441

Kékedy, L., voir Kovács, I. 1483

Kékedy, L. and F. Makkay, Zero current bipotentiometric indication with pretreated electrodes. I. Oxidimetric titration of Fe (II) using platinum electrodes 717

Kérek, F., voir Moţoc, I. 289, 2127

— und I. Moţoc, Matrizielle Charakterisierung der Topologie der organischen Verbindungen. I. Konstitution. 283

— und I. Moţoc, Matrizielle Charakterisierung der Struktur und Topologie der organischen Verbindungen. III. Konformation, Chirale Konformeren 655

Khalaf A. A., Modern Friedel-Crafts chemistry. I. Cyclialkylations of some secondary and tertiary phenylalkyl chlorides in the presence of the mild $AlCl_3/CH_3NO_2$ and $FeCl_3$ catalysts 297

—, Modern Friedel-Crafts Chemistry. II. Rearrangements accompanying benzene alkylations with 1- and 2-hydroxy-2- methyl-1-phenylpropane, 1- and 2-chloro-2-methyl-1-phenylpropane and 2-methyl-1-phenyl-1-propene in the presence of Friedel Crafts catalysts 479

—, voir Roberts R.M. 1929, 1937

Khan, I. A., voir Arshad, A.B.M. 1395

—, and A. H. Hashmi, Studies on coordination compounds. Thiourea and phosphine complexes of Ni (II) and Co (II) 815

King, R. C. W., voir Armstrong D. R. 2011

Klasinc, L., voir POP, E. 1249

— and N. Trinajstić, E. Pop, Theoretical study of isomeric thienylfurans 89

Kovács, I. and L. Kékedy, Polarographic investigation of the cadmium and zinc ethyl xanthate complexes 1483

— i B. Tökes, Poliarografichescoe issledovanie complecsoobrazovaniya etilxantoghenata caliyaa s ionami H^{2+} 1263

Page

Kudesia, V. P., Kinetics of oxidation of butan-2-ol by peroxydisulphate catalyzed by Ag (I) ion 1373
Kulkarni, V. H., voir Biradar N. S. 63, 809

L

Lazăr, D. P. and J. Turkevich, Methyl radicals on porous Vycor glass as studied by ESR spectroscopy 537
Lepădatu, C. I., voir Spacu, P. . . . 1143
Liteanu C., voir Costantinescu A. 1273
— and A. Constantinescu, Paper thermochromatography. XVII. The separation of leucine and isoleucine in temperature gradient . . 155
—, voir Haiduc, I. 1093
—, voir Hodișan, T. 2143
—, voir Mioșcu, M. 1637
— and E. Hopîrtean, M. Mioșcu, Liquid membrane-electrodes. III. Electrodes with water-immiscible organic liquids in frit. Applications in potentiometric acid-base titrations 1643,
—, voir Popescu, I. C. 145, 1451, 1459, 1819, 1983
— and I. C. Popescu, Studies on the electroanalytical behaviour of membrane-electrodes under current. I. Current-membrane potential curves for the parchment membrane-electrode impregnated with $BaSO_4$ . . 319
— and I. C. Popescu, A. Mocanu, Characterization of ceramic ion-selective membrane-electrodes. VII. AgI-Ag_2S, CN^--selective membrane electrode 1467
— and I. C. Popescu, M. Preda, Studies on the electroanalytical behaviour of membrane-electrodes under current. II. The E-pH electrode function and the use of a membrane-electrode of parchment paper impregnated with $BaSO_4$ in acid-base potentiometric titrations under constant direct current . . . 1811
Luca, C., voir Petrariu, I. 493
Luchian, N., voir Voiculescu, N. 1601

M

Mager, S. and E. L. Eliel, Conformational equilibrium of 5-fluoro-1,3-dioxane by NMR spectroscopy . . 2097

Page

— and E. L. Eliel, Synthesis and configurational equilibrium of 2-isopropyl-5-acetyl-1,3-dioxane . . 1379
Mahale, V. B., voir Biradar, N. S. 809, 2077
Maior, O., voir Niculescu-Duvăz, I. 1617
Makkay, F., voir Kékedy, L. 717
Malaspina, L., voir Maria, G. DE . 367
Mánok, F., voir Zsakó, J. 1897
Marandiuc, D., voir Drăgulescu, C. . 583
Marchidan, D. I. and S. Matei-Tănăsescu, Thermodynamic data by solid state EMF technique and phase boundaries for some non-stoichiometric uranium oxides . . 1681
— and L. Vasu, Heat of melting for eutectics formed in binary systems of $AgNO_3$ with KNO_3, $RbNO_3$, $CsNO_3$, AgCl and AgBr 1295
Mărculescu, B., voir Cobianu, N. . 305
Mărculescu, C., voir Popea, Fl. . . 247, 425
Mărgineanu, P., voir Ința, I. . . . 347
Maria, G. and L. Malaspina, G. Bardi, R. Gigli, Simultaneous determination by Knudsen effusion-microcalorimetric technique of the vapour pressure and sublimation enthalpy of antimony trifluoride. Vapour pressure of bismuth trifluoride 367
Marinescu, M., voir Vîlceanu, R. . 1225
Matei-Tănăsescu, S., voir Marchidan, D.I. 1681
Mateiovici, Ov., Study of electrochemical forming of surface oxides on the active carbon electrode. . . . 233
Mavrodin-Tărăbîc, M., Contribution à l'étude de l'hydrolyse de l'ion UO_2^{2+} en milieu perchlorique . . . 609
—, L'étude des espèces ioniques formées par l'hydrolyse de l'ion d'uranium hexavalent 73
— et I. Onaca, I. Solacolu, L'étude de la réaction d'oxydation de l'hydrogène sur les électrodes poreuses en nickel 1121
—, voir Radovici, O. 767
Mihail, R., voir Balaban, C. 1829
Mihăiță, D., voir Isăcescu, D. A. . . 695
Mihalcea, I. and R. R. Hentz, Transient species from the reaction of the hydrated electron with hexacyanocobaltate. III. 1577
Mioșcu, M. and E. Hopîrtean, C. Liteanu, Liquid membrane-electrodes. II. The *n*-butanol-frit electrode in acid-base potentiometric titration 1637
—, voir Liteanu, C. 1643
Misdolea, C., voir Vîlcu, R. 387

Page

Mocanu, A., voir Liteanu, C. 1467

Moldoveanu, S., voir Popa, Gr. 1883

Moldoveanu, S., voir Popa, Gr. 1883

Moraru, M., voir Bărbulescu, N. 873

Moraru, M., voir Georgescu, I. 2067

Moser, Z. and K. Fitzner, L. Zabdyr, On the equilibrium constant of the side reaction in the concentration cell in dilute Cd-Pb liquid solutions 557

Moţoc, I., Die mathematische Darstellung der Homologie und der homologen Serien 1419

—, voir Kerek F. 283, 655

— und F. Kerek, Matrizielle Charakterisierung der Struktur und Topologie organischer Verbindungen. II. Konfiguration, Chiralität 289

— und F. Kerek, Matrizielle Charakterisierung der Struktur und Topologie der organischen Verbindungen. IV. Prochiralität, Pseudochiralität 2127

Muntean, M., voir Iordache, O. 239

Mureşan, V., voir Negoiu, D. 1749, 1875

Murgulescu, I. G. and I. Demetrescu, On the mechanism of the reactions between benzyl bromide and alcohols 523

— and I. Demetrescu, The kinetics of reactions between benzhydryl bromide and normal alcohols 355

— and E. Ivana, Absorption spectra of $PbCl_2$ and $PbBr_2$ in vapour phase 1667

— and E. Popa, E. Ivana, Electronic absorption of silver halides in passing from solid to molten state 189

— and L. Popescu, Diffusion potentials in molten salts 737

N

Născuţiu, T., Le comportement des ions inorganiques en chromatographie sur papier avec solvants à base d'alcools-acides 161

Negoiţă, N. and R. Baican, F. Domşa, A. T. Balaban, Use of ESR spectrum simulator for determining precisely hyperfine coupling constants of stable nitrogen free radicals 995

Negoiu, D. and V. Mureşan, S. Florea, Contributions to the chemistry of thiocomplexes. IV. Complex compounds of Pd (II) with thioamides of the dibenzofuran series 1875

Page

— and V. Mureşan, C. Fulea, Contributions to the chemistry of thiocomplexes. III. Complex compounds of Pd (II) with thiomides 1749

— and L. Paruta, Complex combinations of transition metals with tertiary stibines. I. Complex combinations of palladium (II) with tritolyl-stibines 2059

Nemes, M., voir Facsko, Gh. 1971

Nenitzescu, C.D., voir Avram, M. 441, 863

Netta, M., voir Csomontaniy, G. 1367

Nicolescu, I. V., voir Fruma, Al. 803, 1131

— und Al. Fruma, Die Chemisorption von Wasserstoff, Benzol und Zyklohexan auf mit Lithium und Titan dotiertem Aluminiumoxyd. I. Adsorptionsisothermen 953

Niculescu-Duvăz, I. and M. Rotaru, V. Feyns, O. Maior, Potential anticancer agents. VIII. New aromatic and heteroaromatic nitrogen mustards 1617

Nimară, A., voir Drăgulescu, C. 583

O

Olteanu, M., voir Tărăbăşanu-Mihăilă, C. 2113

Olteneanu, M., voir Răileanu, M. 1243

—, voir Sahini, V. E. 361

Omara, M. A., voir El Abbady, A. M. 899

Onaca, I., voir Mavrodin-Tărăbîc, M. 1121

—, voir Radovici, O. 767

Oncescu, T., voir Contineanu, M. 549, 753, 2005

Øye, H. A., voir Grjotheim, K. 2017

P

Panea, T. and V. Fărcăşan, C. Bodea, Hydroxy-phenothiazine-5,5-dioxides. I. 1,7,9-trichloro-3-hydroxy-5,5-dioxi-phenothiazine 1259

Paruta, L., voir Negoiu, D. 2059

Pavel, L., voir Petrescu, N. 1853

Pavlik, J. W., voir Filipescu, N. 1959

— and N. Filipescu, P. T. Frangopol, M. Frangopol, Photochemical addition of anthronylidine to alkenes 1793

Percec, S., voir Popescu, Fl. 1067, 1427

Perişanu, Şt., voir Vîlcu, R. 1531

Page

Perkins, P. G., The electronic structure of some ladder polymers. I. Band structure of polyacenes and nitrogen substituted polyacenes . . 931
—, The electronic structure of ladder polymers. II. Excited states of *cata*-condensed benzenes, pyrazines and pyridines 1111
—, The electronic structure of some molecules and ions containing carbon, silicon, oxygen and sulphur. II. Co, SiO, CS, SiS and COS 1289
—, The electronic structure of some molecules and ions containing carbon, silicon, oxygen and sulphur. III. Anions formed by carbon, silicon and sulphur 1501
—, voir Armstrong, D. R. 2011
Petit, G., Les analyses cryométriques dans la recherche de la structure des substances dissoutes en milieu salin électrolyte fort 1521
Petrariu, I. and C. Luca, Ig. Poinescu, M. Dima, Quaternary basic ammonium polyelectrolytes. I. Quaternization reaction of some tertiary amines containing hydroxylic groups with chloromethylated polystyrene 493
—, voir Popescu Fl. 1067
Petrescu, C., voir Drăgănescu, A. . 1859
Petrescu, M., voir Petrescu, N. . . . 1853
Petrescu, N. and M. Petrescu, M. Briţchi, L. Pavel, Silicide coatings on molybdenum obtained by electrotransport and diffusion from molten fluorides 1853
Petrescu, S., and S. Sternberg, V. Petrescu, The galvanostatic study of the electrochemical adsorption process on the chlorine — active carbon electrode in molten salts. II. Remanent potential 1715
Petrescu, V., voir Petrescu, S. . . . 1715
Petrova, L. D., La concentration critique micellaire de quelques sels quaternaires d'alkylpyridine 2133
— und E. Comaniţă, Über die Synthese einiger quartären Pyridiniumsalze 1361
Piacente, V. and G. Balducci, Vapor pressure of antimony trichloride . . 2083
Pîrlog, C., voir Popea, Fl. 247
Ploştinaru, S., voir Spacu, P. . . . 971
— and P. Spacu, Mixed lanthanide compounds with neutral ligands containing donor oxygen atom. I. Lanthanide chlorosalicylates with triphenyl-phosphin-oxide 2051
Podină, C., voir Contineanu, M. . . . 761

Page

—, voir Sahini, V. E. 1283
Poinescu, Ig., voir Petrariu, I. . . . 493
—, voir Popescu, Fl.. 1067
Pomponiu, C. and A. T. Balaban, Computing program for interpreting ESR spectra of organic free radicals 1173
Pop, E., voir Klasinc, L. 89
— and L. Klasinc, N. Trinajstić, Theoretical studies of some furocoumarin isomers 1249
Popa, E., voir Murgulescu, I. G. . . . 189
Popa, Gr. and S. Moldoveanu, A perturbational procedure applied of the energetic levels in the complexes obtained by organic reagents 1883
Popea, Fl. and C. Mărculescu, New thorium complexes with pyrimidine derivatives 425
— and C. Mărculescu, C. Pirlog, New uranyl compounds with pyrimidine derivatives 247
Popescu, Fl. et S. Percec, La chlorophosphonation du polychlorure de vinyle et de l'alcool polyvinylique 1427
— et S. Percec, Ig. Poinescu, I. Petrariu, La phosphorylation des copolymères ternaires macroporeux 1067
Popescu-Haş, D., voir Solacolu, Ş. . . 3
Popescu, I., voir Giurgiu, D. 1963
—, voir Voiculescu, N. 1595, 1601, 1911
Popescu, I. C. and V. Ciovîrnache, L. Savici, C. Liteanu, Characterization of ceramic ion-selective membrane-electrodes. VI. Selectivity of the Ag^+/S^{2-}-selective Ag_2S membrane-electrode 1459
— , voir Liteanu C. 319, 1467, 1811
— and C. Liteanu, V. Ciovîrnache, Characterization of the ceramic ion-selective membrane-electrodes. IV. Influence of the obtaining conditions of Ag_2S membrane upon the working of Ag^+-selective membrane-electrode 145
— and C. Liteanu, M. Preda, Studies on the electroanalytical behaviour of membrane-electrodes under current. III. The use of a membrane-electrode of parchment paper impregnated with $BaSO_4$ in potentiometric titrations by precipitating at constant direct current 1819

Page

— and C. Liteanu, L. Savici, Characterization of ceramic ion-selective membrane-electrodes. V. Ag_2S, S^2 -selective membrane-electrode 1451
— and C. Liteanu, L. Savici, Studies on the electroanalytical behaviour of membrane-electrodes under current. IV. The E-pAg electrode function and the use of the ceramic membrane electrode of Ag_2S, Ag^+ -selective in potentiometric titrations by precipitating at constant direct current 1983
Popescu, L., voir Murgulescu, I. G. 737
Popescu, S. D., Polarographic determination of anthraquinone 2-chloroanthraquinone and 2-aminoanthraquinone 507
Potmischil, F., voir Bărbulescu, N. . 1613
Prashad, J., Influence of irradiation on the threshold potential in air 1865
—, Studies of the Joshi effect in halogens and oxygen. Influence of intersleeve exposure to brushes from a d.c. and various a.c. high tension sources 1075
Preda, M., voir Liteanu, C. 1811
—, voir Popescu, I. C. 1819
—, voir Várhelyi, C. 823
Predescu, A., voir Tărăbăşanu-Mihăilă, C.. 889
Putanov, P. i J. Iovanovici, R. Herak, Vlijanie dobavok i vosstanovitelnoi sredj na formirovanie fazovogo costava v katalizatore dlia nizkotemperaturnoi konversii ikisi ugleroda 569

R

Radovici, C., voir Cismaru, D. . . . 1699
Radovici, O. et M. Mavrodin-Tărăbîc, I. Onaca, I. Solacolu, Contribution à l'étude de la source chimique de courant $Zn/MOH/O_2$. I. L'efficacité électrochimique d'une pile à cathode activée avec de l'argent 767
— and C. Vass, Kinetics of copper electrocrystallization from pyrophosphate electrolytes 1105
— and C. Vass, I. Solacolu, Electroplating of copper from pyrophosphate baths. I. The effect of electrolyte pH 1325
— and C. Vass, I. Solacolu, Electroplating of copper from pyrophosphate baths. II. The effect of electrolyte temperature 2021
Radu, S., voir Iovu, M. 473
Rădulescu, M., voir Vîlceanu, R. . 1225
Radulian I., voir Răileanu, M. . . 1005, ... 1243

Page

Răileanu, M., and I. Radulian, Reaction of amines with phenothiazinium cation. I. Synthesis and properties of 3H-phenothiazine-3- [potassium 4-anilsulphonate], 3H-phenothiazine-3-[potassium 3-anilsulphonate] and 3H-phenothiazine-3- [potassium 2-anilsulphonate] 1005
— and I. Radulian, M. Olteanu, M. Constantin, Donor-acceptor complexes. III. Charge transfer complexes of 1,3,6,8-tetranitrocarbazole 1243
Ramonţian, E., voir Balog, A. . . . 123
Răzuş, A. C., voir Glatz, A. M. . . 2087
Rehner, H. H., voir Jinescu, G. I. . . 2149
Ries, G., voir Schneider, I.A. . . . 1685
Roberts, R. and A. A. Khalaf, Modern Friedel-Crafts chemistry. III. The isomerisation of 1,1- and 1,2-diphenylbutane under the influence of aluminium chloride catalyst in benzene solvent 1929
— and A. A. Khalaf, Modern Friedel-Crafts chemistry. IV. The fragmentation and dealkylation behaviour of 1,1-diphenyl-2-methylpropane and 1,2-diphenyl-2-methylpropane under the influence of water-activated aluminium chloride at 100° 1937
Roman, L., voir Voiculescu, N. . . 1595
Roncea, C., voir Isăcescu, D.A. . . 695
Rotaru, M., voir Nicurescu-Duvăz, I. 1617
Russu, J., voir Beu, L. 723

S

Sahini, V. E., voir Caragheorgheopol, A. 1497
— V. E., voir Dobrescu-Ciureanu, M. 921
—, voir Gioabă, A. 531
— and M. Olteneanu, Solvent effect on the anharmonicity of the $C=O$ vibration of acetophenone and benzophenone 361
— et C. Podină, M. Strul, L'étude des isomères de la nitroaniline par spectrométrie de masse 1283
— and J. Weinberg, Xylidine isomers. II. The influence of isomerism on dipole moments 1493
Sălăgeanu, I. and D. Trestianu, E. Segal, Study of the thermal decomposition of ammonium molybdate supported on alumina . . . 1537
Sasu, S., voir Costache, D. 913
Sata, J., voir Zsakó, I. 1759

Page

Savici, L., voir Popescu, I. C. 1451
. . . . 1459
. . . . 1983
Schindler, R. N., voir Contineanu, M. 549,
. . . . 753
Schneider I.A., voir Cecal, Al. . . 35
—, voir Iosif, I. 195
— et G. Riess, Influence du degré de dispersion sur la stabilité thermique des mélanges polystyrène-polyisoprène comportant du copolymère séquencé 1685
—, voir Schuster, R. H. 1841
Schuster, R. H. und I. A. Schneider, Mediumeinflüsse bei der Solvolyse von *t*-Butylchlorid. I. Lösungsmittel-und Salzeffekte bei der Solvolyse von *t*-Butylchlorid in wässerigen Methanol- und Dioxangemischen 1841
Schwartz, I., voir Simiti, I. 685
Segal, E., Méthodes non isothermiques utilisées pour la détermination des paramètres cinétiques de réactions hétérogénes décrites par des équations cinétiques non encadrées dans le modèle de l'ordre de réaction 1555
—, voir Constantinescu, M. . . . 1587
—, voir Fătu, D. 1709
—, voir Sălăgeanu, I. 1537
—, voir Solacolu, Ș. 203
Șerban, Gh., voir Chirulescu, T. . . 1333
Simionescu, Cr. I. and I. Benedek, S. Ioan, N. Asandei, M. Galin, Copolymerization reactions using organic titanium derivatives-aluminum alkyl complexes. VII. Structural aspects of acrylonitrile-methylmethacrylate copolymers prepared by the use of the soluble Ziegler-Natta catalyst system : bis (cyclopentadienyl)-titanium-dichloride-triethylaluminium 327
Simiti, I., M. Coman and I. Schwartz, Contributions to the study of hetercycles. XXIV. A study of intermediates in the Hantzsch reaction. A new method to obtain 5-acetylthiazole derivatives 685
Simon, Z., voir Vîlceanu, R. . . . 1345
Simionescu, T., voir Drăgulescu, C.. . 43
Singurel, G., voir Singurel, L. . . . 789
Singurel, L. and G. Singurel, On the oscillation spectrum of dimethyl sulphoxide(DMSO) in solution . . 789
Sinha, S. P., Simple HMO-calculations on some N-heterocyclic ligands of analytical importance 777
Șliam, E., voir Urseanu, F. 1019

Page

Solacolu, I., voir Mavrodin-Tărăbîc, M. 1121
Solacolu, I., voir Radovici, O. . . 767,
. . . . 1325
—, voir Vass, C. 2021
Solacolu, Ș. and A. Bărbulescu, Crystallochemical and dielectric survey of phases in the TiO_2-ZrO_2 system prepared by coprecipitation 1867
— and M. Cerchez, E. Segal, Kinetics of the formation reactions of oxydic compounds in solid phase through differential thermal analysis 203
— and D. Popescu-Haș, The mineralizing action of F^- ions in vitroceramic structures of the Na_2O-MgO-Al_2O_3 -SiO_2 -system on volume effects 3
Șotcă, D., voir Bărbulescu, N. . . . 873
Spacu, P. and A. C. Banciu, C. I. Lepădatu, Co (II) and Ni (II) chelates with ligands containing donor nitrogen atoms 1143
—, voir Cismaru, G. D.. 1345
— and E. Ivan, New compounds of yttrium and lanthanides with derivatives of anthranilic acid. I. The N,N bis (carboxy methyl) anthranilic acid (ANDA) 405
— and E. Ivan, New compounds of yttrium and lanthanides with N,N'-ethylenedianthranilic acid (EDAN) 589
— and S. Ploștinaru, Spectral study of some mixed ligand compounds of lanthanides 971
—, voir Ploștinaru, S 2051
Stănoiu, I. I., voir Gârd, E 257
Ștefănescu, M., voir Vasilescu, D. S. 907
Sternberg, R., Contribution à l'étude de l'alcoolyse alcaline du chlorure de *n*-butyle 1581
Sternberg, S. and I. Adorian, Thermodynamic excess properties of molten LiCl + KCl, LiCl + RbCl, NaC + RbCl and NaCl + CsCl mixtures 945
— and L. Bejan, Thermodynamic properties of the reciprocal mixtures of fused salts : AgCl + (K, Rb, Cs). I. 11
—, voir Herdlicka, C. 1689
—, voir Petrescu, S. 1715
— and M. Terzi, Surface tension of the reciprocal molten salt pairs (K, Ag ; Cl, Br). 1319
— and T. Vișan, The determination of the diffusive and capacitive current in the chronopotentiometry of

Page

the molten salt systems (Na, Ag) NO_3 and (K, Ag)NO 221
Strul, M., voir Sahini, V. E.. 1283
Suciu, D., Electronic spectra and acidity constants of some 2-amino-5-substituted thiazoles 677
— and Z. Györfi, Electronic spectra and acidity constants of some 2-amino-5-substituted 1,3,4-thiadiazoles 1777

T

Tămaș, V. and V. Ciurdaru, C. Bodea, Azlactones of carotenoids. I. Synthesis and properties of azlactones of β-apocarotenals and of diapo-carotenedials 1409
Tărăbășanu-Mihăilă, C. and L. Floru, E. Baltă, A. Predescu, Heterocyclic derivatives with thiazolic rings. I. Synthesis of 6-amino-thiazolo [4,5-f] indazole. 889
Tărăbășanu-Mihăilă, C. and L. Floru, M. Olteanu, Heterocyclic derivatives with thiazolic rings. II. Electrophilic substitutions of 6-aminothiazolo [4,5-f] indazole 2113
Țarina, D., voir Georgescu, I. . . . 2067
Teodorescu, G., voir Georgescu, I. I. 1159
Teodorescu, Gr., Methods for the determination of tolazoline. Visible and infrared spectra of the combination with ammonium reineckate 501
Teoreanu, I. and M. Georgescu, The role of clinker and of calcium chloride in the hardening process of some silicate slags 623
—, voir Iordache, O. 239
Terlecki-Baričević, A., voir Aleksić B. D. 575
Terzi, M., voir Sternberg, S. . . . 1319
Toader, M., voir Furnică, Gh. . . . 175
Tökes, B., voir Kovacs, I. 1263
Tomoaia, M. et Z. Andrei, E. Chifu, Tension interfaciale dans le système solution benzénique de tributylphosphate/ solution aqueuse de nitrate cuivrique 1547
Topor, D., Transference numbers and mobilities in molten univalent nitrates 1311
Totan-Curtui, M., voir Drăgulescu, C. 43
Trestianu, D., voir Sălăgeanu, I. . 1537
Trinajstić, N., voir Klasing, L. . . . 89
Trinajstić, N., voir Pop, E. 1249
Truția, Ath. and M. Vodă, Spectrophotometric determination of Co^{2+} in $CdCl_2$ lattice 1805
Turcitu, E., voir Furnică, Gh. . . . 175
Turkevich, J., voir Lazăr, D. P. . . 537

U

Uncuța, C., voir Ișfan, E. 1233
Urseanu, F. and C. Drăghici, R. Vintilă, E. Șliam, New syntheses of naphth [2,3-c] acridan-5,8,14-trionic dyes 1019
— and I. Zugrăvescu, New disperse dyes with naphth [2,3-c] acridan [5,6-cd] pyrazol-4,10 (2H)-dione structure 1211

V

Vargha, E., voir Balog, A. 123
— and A. Balog, F. Gönczy, D. Breazu, L. Beu, Peptides. XIV. The synthesis of several peptide sequences related to the Glu^5- and Asp^2-eledoisins 1627
Várhelyi, Cs., voir Finta, Z. . . 417
— und I. Gănescu, M. Preda, Über α-Dioximinkomplexe der Übergangsmetalle. XXXVI. Neue Dimethylglyoximin-Chelate des Kobalts (III) mit -Dipyridyl und o-Phenanthrolin 823
—, voir Zsakó J. 1759
—, voir Zsakó J. 1897
Vasilescu, D. S. and M. Ștefănescu, Al. Bălănescu, The polymerization of N-vinylcarbazole by the systems acrylonitrile-$ZnCl_2$ and acrylonitrile -$HgCl_2$ 907
Vass, C., voir Radovici, O. 1105
1325, 2021
Vasu, L., voir Marchidan, D. I. . . 1295
Vermeglio, A., voir Gaymard, F. . 979
Vîlceanu N., voir Drăgulescu C. . . 49
53, 59
Vîlceanu, R. und B. D. Bader, M. Rădulescu, M. Marinescu, Neue organische Pigmente-Isatinderivate. IV. Thermisches Verhalten 1225
— and Z. Simon, A. Chiriac, Stability of three-membered heterocycles. I. Considerations concerning thermodynamic stability and conservation of orbital symmetry . 1353
Vîlcu, R. and Z. Cenușe, Isothermal equilibrium and calculation of excess functions in the benzene-isobutyl alcohol system 377

Page

— and B. Coman, Caloric capacities of vapours of organic liquids. I. A flow calorimeter 1301

— and C. Misdolea, Significant structures theory of ionic binary liquid mixtures: heat capacities, compressibility coefficients and thermal expansion coefficients . . 387

— and Șt. Perișanu, Application of the Allen-Skinner bond energy scheme to benzenoid polynuclear hydrocarbons 1531

Vintilă, R., voir Urseanu, F. . . . 1019

Vișan, T., voir Sternberg, S. . . . 221

Vlassa, M. and M. Ionescu, J. Fabian, Electronic structure and transitions of 1,2,3-trimethoxyacridine 99

Vodă, M., voir Truția, Ath. 1805

Vodnár, J., The study of the decomposition of organic hydroperoxides on cation exchangers. II. Decomposition of cumene hydroperoxide on fine granulated Vionit CS-1 in static conditions. 797

Voicu, A., voir Voicu, M. 131

Voicu, M. and F. Badea, A. Voicu, Kinetics of solvolytic reactions. IV. Transition state in the π-route of the acetolysis of 5H-dibenzo [*a,d*]-cyclohepten-5-yl -(β-ethyl) tosylate 131

Voiculescu, N., Reactions of coordinated ligands. VI. Reaction of aluminium-organic derivatives with oximes 1919

— and I. Popescu, Reactions of coordinated ligands. V. Aluminium-organic compounds of coordinated salicylaldoxime 1911

Page

— and I. Popescu, N. Luchian, Reactions of coordinated ligands. III. Aluminium-organic compounds of coordinated salicylaldoxime . . . 1601

— and I. Popescu, L. Roman, Reactions of coordinated ligands. II. Reaction of triphenylaluminium with nickel, palladium and copper bisdimethylglyoximates 1595

Voinescu, V., voir Balog, A. . . . 123

Volanschi, C., voir Iosif, I. 195

Volanschi, E., voir Gioabă, A. . . 531

W

Weakley, T. J. R., voir Botar, A. V. 1155

Weill, M. E., voir Chanu, J. 1513

Weinberg, J., voir Sahini, V. E. . . 1493

Wyatt, R. J., voir Avram, M. 441

Z

Zabdyr, L., voir Moser, Z. 557

Zaharescu, M., voir Georgescu, I. I. . 1159

Zsakó, J., voir Finta, Z. 417

— und J. Sata, CS. Várhelyi, Electronic spectra of transition metal complexes. I. Ligand field parameters of some dimethylglyoximato-diamino-cobalt (III) complexes . 1759

— and Cs. Várhelyi, F. Mánok, Kinetics and mechanism of substitution reactions of complexes. III. Basic hydrolysis of *trans*-di-isothiocyanato-bis-ethylene-diamine-chromium (III) ions 1897

Zugrăvescu, I., voir Avramovici, S. 431

—, voir Urseanu, F. 1211

INDEX DES SUJETS

A

Absorption spectra of $PbCl_2$ and $PbBr_2$ in vapour phase, I. G. Murgulescu and E. Ivana 1667

Acétophénone, Hydrogénation catalytique de l'-, G. Csomontanyi, M. Netta et M. Balmez . . . 1367

n-Acides monocarboxyliques obtenus par leur oxydation, Relations entre la longueur de la chaîne de *n*-alcanes et la composition des-, I. Drimuș et I. T. Ionescu 1949

Addition compounds of tin (IV) chloride with tetradentate Schiff bases, N. S. Biradar and V. B. Mihale 2077

Page

Alcoolyse alcaline du chlorure de *n*-butyle, Contribution à l'étude de l'-, R. Sternberg 1581
Alkylpyridine, La Concentration critique micellaire de quelques sels quaternaires d'-, L. D. Petrova . . . 2133
Aluminium-organiques envers de bases Lewis. Dérivés des triphénylaluminium avec des composés 1,3-dicarbonyliques, La réactivité des composes-, D. Giurgiu et I. Popescu 1963
Aluminiumoxyd, Die Struktur des mit Lithium und Titan dotiertem-, Al. Fruma, D. Ciomârtan, I. Braşoveanu und I. V. Nicolescu . . . 803
Ammonia synthesis catalysts obtained by melting natural magnetite, Investigation of some properties of the-, B. D. Aleksić and A. Terlecki-Baričevič 575
Analyses cryométriques dans la recherche de la structure des substances dissoutes en milieu salin électrolyte fort, Le -, G. Petit . . 1521
Anthraquinone, 2-chloroanthraquinone and 2-aminoanthraquinone, Polarographic determination of -, S. D. Popescu 507
Anthronylidene, Spectroscopic properties of trapped-, N. Filipescu, J. W. Pavlik, P. T. Frangopol and M. Frangopol 1959
Association constants of silver-chloro and bromo complexes in molten sodium nitrate-barium nitrate eutectic, Computer evaluation of the -, H. C. Gaur and N. P. Bansal . 1903
Azibenzyl. I. Decomposition in benzene solution, Kinetics and mechanism of the thermal decomposition of-, M. Contineanu, T. Oncescu and R. N. Schindler . . 549
Azibenzyl. II. Studies in the absence of a solvent, Kinetics and mechanism of the thermal decomposition of-, M. Contineanu, T. Oncescu and R. N. Schindler 753
Azibenzyl, EPR study in the radiolysis of polycrystalline-, M. Contineanu, O. Constantinescu and T. Oncescu 2005
Azlactones of carotenoids. I. Synthesis and properties of azlactones of β-apocarotenals and of diapocarotenedials, V. Tămaş, V. Ciurdaru and C. Bodea 1409

B

Benzenoid polynuclear hydrocarbons, Application of the Allen-Skinner bond energy scheme to-, R. Vîlcu and St. Perişanu 1531
Benzhydryl bromide and normal alcohols, The kinetics of reactions between-, I. G. Murgulescu and I. Demetrescu 355
Benzyl bromide and alcohols, On the mechanism of the reactions between-, I. G. Murgulescu and I. Demetrescu 523
Beryllium -(3-acyl-2,4-pentanedionates), E. Işfan, C. Uncuţa and A. Barabás 1233
Bétons aux résines synthétiques et aux liants minéraux, Quelques remarques sur les propriétés des-, I. Ionescu 1033
Bicyclo [3,3.1.] nonane. The acid-catalysed reactions of a bicyclic epoxide, N. Bărbulescu, M. Moraru and D. Şotcă 873
Binary mixtures of polar liquids with nonpolar solvent, Temperature and concentration dependence of molar polarization in-, I. Adorian 211
Bismuth (III) in acid perchlorate solutions, Polarographic behaviour of-, C. Drăgulescu A. Nimară, I. Julean and D. Marandiuc 583
Breaking point of the linear twelve-membered carbon chain, by molecular oxygen, The influence of carbonyl or hydroxyl position on the-, I. Drimuş and I. T. Ionescu. . . . 1769
Butan-2-ol by peroxydisulphate catalysed by Ag(I) ion, Kinetics of oxidation of-, V. P. Kudesia 1373

C

Cadmium and zinc ethyl xanthate complexes, Polarographic investigation of the-, I. Kovács and L. Kékedy 1483
Cadmium complex with benthiazolylazo-2,4-dichlorophenol reagent, Spectrophotometric study of-, V. Armeanu and E. Drăguşin 1475
Caloric capacities of vapours of organic liquids. I. A flow calorimeter, R. Vîlcu and B. Coman 1301
Carbon electrode, Study of electrochemical forming of surface oxides on the active-, Ov. Mateiovici . . . 233
Ceramic ion-selective membrane-electrodes. IV. Influence of the obtaining conditions of Ag_2S membrane upon the Ag^+ -selective membrane-electrode, Characterization of the-, I. C. Popescu, C. Liteanu and V. Ciovîrnache 145

Page

Ceramic ion-selective membrane-electrodes. V. Ag_2S, S^{2-}-selective membrane-electrode, Characterization of-, I. C. Popescu, C. Liteanu and L. Savici 1451

Ceramic ion-selective membrane-electrodes. VI. Selectivity of the Ag^+/S^{2-}-selective Ag_2S membrane-electrode, Characterization of-, I. C. Popescu, V. Ciovîrnache, L. Savici and C. Liteanu 1459

Ceramic ion-selective membrane-electrodes. VII. The AgI-Ag_2S, CN^--selective membrane electrode, Characterization of-, C. Liteanu, I.C. Popescu and A. Mocanu 1467

Chaleurs de transfert en milieux ioniques : application aux solutions aqueuses de KCl et HCl a 25° et 35°C, J. Chanu et M. E. Weill 1513

Chemical graphs. XVI. Intramolecular isomerizations of octahedral complexes with six different ligands, A. T. Balaban 841

Chemical graphs. XVIII. Graphs of degrees four or less, isomers of annulenes, and nomenclature of bridged polycyclic structures, A. T. Balaban 635

Chemical graphs. XIX. Intramolecular isomerizations of trigonal-bipyramidal structures with five different ligands, A. T. Balaban 855

Chemisorption of gases on semiconductor thin films in the dark and under irradiation. I. The oxygen, carbon monoxide and hydrogen on zinc oxide system, Successive-, M. Constantinescu and E. Segal 1587

Chemisorption processes, On the logarithmic law used in the kinetics of the solid-gas-, N. I. Ionescu and B. Aurian-Blăjeni 2031

Chemisorption von Wasserstoff, Benzol und Cyclohexan auf mit Lithium und Titan dotiertem Aluminium. I. Adsorptionsisothermen, Die-, I. V. Nicolescu und Al. Fruma 953

Chemisorption von Wasserstoff, Benzol und Cyclohexan auf mit Lithium und Titan dotiertem Aluminiumoxyd. II. Adsorptionswärmen, Die-, Al. Fruma und I. V. Nicolescu 1131

Chloramphenicol. II. Synthesis of 2-chloroacetamido-1-(4′-chloro-3′-nitro-phenyl) propane-1,3-diol, Analogues of-, V. V. Badiger and M. Y. M. Jamkhandi 489

Page

Chlorophosphonation du polychlorure de vinyle et de l'alcool polyvinylique, La-, Fl. Popescu et S. Percec 1427

Chromatographie sur papier avec solvants à base d'alcools-acides, Le comportement des ions inorganiques en-, T. Născuţiu 161

Chronopotentiometry of the molten salt systems (Na, AG) NO_3 and (K, Ag)NO_3, The determination of the diffusive and capacitive current in the-, S. Sternberg and T. Vişan 221

Co(II) and Ni(II) chelates with ligands containing donor nitrogen atoms, P. Spacu, A. C. Banciu and C. I. Lepădatu 1143

Complexes. LII. Basic hydrolysis of *trans*-di-isothiocyanato-bis-ethylene-diamine-chromium (III) ions, Kinetics and mechanism of substitution reaction of-, J. Zsakó, Cs. Várhelyi and F. Mánok 1897

Complexes of isonicotinic acid hydrazide with Fe (II) and thiocyan, (INAH) $Fe_2(NCS)_2 . H_2O$, I. I. Georgescu, D. Ciomârtan, G. Teodorescu, M. Hlevca and M. Zaharescu 1159

Comptes rendus, 519, 733, 1101, 1489, 1663, 1664 2001

Condensation du 4, 4′-azodiphénoxyde de sodium avec les dérivés chlorométhylés du benzène, M. Iovu et S. Radu 473

Condensations d'acides insaturés sur le benzène catalysées par le chlorure d'aluminium. V. Acide sorbique, A. M. Glatz, F. Badea, Z. Arvay, V. Drăguţan, F. Chiraleu et A. C. Răzuş 2087

Cool flame and low-temperature ignition of methane, Some aspects of the-, I. Iosif, I. A. Schneider and C. Volanschi 195

Coordinated ligands. II. Reaction of triphenylaluminium with nickel, palladium and copper bisdimethylglyoximates, Reactions of-, N. Voiculescu, I. Popescu and L. Roman 1595

Coordinated ligands. III. Aluminium-organic compounds of coordinated salicylaldoxime, Reactions of -, N. Voiculescu, I. Popescu and N. Luchian 1601

Coordinated ligands. V. Aluminium-organic compounds of coordinated salicylaldoxime, Reactions of -, N. Voiculescu and I. Popescu 1911

Page

Coordinated ligands. VI. Reaction of aluminium-organic derivatives with oximes, Reactions of -, N. Voiculescu 1919

Copolymères ternaires macroporeux, La phosphorylation des -, Fl. Popescu, S. Percec, Ig. Poinescu et I. Petrariu 1067

Copolymerization reactions using organic titanium derivatives-aluminium alkyl complexes. VII. Structural aspects of acrylonitrile-methylmethacrylate copolymers prepared by the use of the soluble Zigler-Natta catalyst system : bis (cyclopentadienyl)-titanium-dichloride-triethylaluminium, CR. I. Simionescu, I. Benedek, S. Ioan, A. Asandei, and M. Galin 327

Copper electrocrystallization from pyrophosphate electrolytes, Kinetics of -, O. Radovici and C. Vass . . . 1105

Cr (III)-poly (aminocarboxylate) ligands solutions at the dropping-mercury electrode (DME), Behaviour of -, E. Chiacchierini and R. Cocchieri 1441

Crystallochemical and dielectric survey of phases in the TiO_2-ZrO_2 system prepared by coprecipitation, Ș. Solacolu and A. Bărbulescu . . 1867

Cu, Co, Mn et Fe, L'étude du mécanisme physico-chimique de la sorption des isotopes radio-actifs par certaines -, Gh. Furnică, M. Toader, E. Turcitu et Șt. Bulan . . . 175

Cu (II) coordination compounds with 3-amino-1-propanol, M. Brezeanu and I. Jitaru 2039

Cumene hydroperoxide on fine granulated Vionit CS-1 in static conditions, The study of the decomposition of organic hydroperoxides on cation exchangers. II. Decomposition of -, . Vodnár 797

Cyclobutane series. XXXII. The addition of bromine to derivatives of *exo. exo*-tetracyclo $[4.4.2.0^{2.5}.0^{7.10}]$ dodeca-3.11-diene, M. Avram, I. G. Dinulescu, F. Chiraleu and C. D. Nenitzescu 863

Cycloheptène et cyclopentène, Sur la chloration et l'oxychloration spécifiques des cycloheptène et cyclopentène, F. Gaymard, R. Guejd et A. Vermeglio 979

Page

D

Dibenzobicyclo [3.2.1] octadienes, Configurations of substituted -, M. Avram, I. G. Dinulescu, C. D. Nenitzescu, R. A. Y. Jones, A. R. Katritzky and R. J. Wyatt 441

Dibenzofurans. I. The formylation of 3-dimethylamino-dibenzofuran by the Vilsmeier-Haack method, V. Fărcășan and I. Cristea 469

Dimethyl sulphoxide (DMSO) in solution, On the oscillation spectrum of -, L. Singurel and G. Singurel 789

α-Dioximinkomplexe der Übergangsmetalle. XXXVI. Neue Dimethylglyoximin-Chelate des Kobalts (III) mit α, α'-Dipyridyl und *o*-Phenanthrolin, Über -, C. Várhelyi, I. Gănescu und M. Preda 823

Diphenyldiazomethane, Mass spectrum of -, M. Contineanu, C. Podină and V. Constantin 761

Donor-acceptor complexes. III. Charge transfer complexes of 1,3,6,8-tetranitrocarbazole, M. Răileanu, I. Radulian, M. Olteneanu and M. Constantin 1243

Dyes with naphth [2,3-c acridan 5,6-cd] pyrazol-4,10 (2H)-dione structure, New disperse -, F. Urseanu, and I. Zugrăvescu 1211

E

Electroanalytical behaviour of membrane-electrodes under current. III. The use of a membrane-electrode of parchment paper impregnated with $BaSO_4$ in potentiometric titrations by precipitating at constant direct current, Studies on the- I. G. Popescu, C. Liteanu and M. Preda 1819

Electrodes. I. Oxidimetric titration of Fe (II) using platinum electrodes, Zero current bipotentiometric indication with pretreated -, L. Kékedy and F. Makkay 717

Electronic spectra and acidity constants of some 2-amino-5-substituted 1,3,4-thiadiazoles, D. Suciu and Z. Györfi 1777

Electronic spectra of transition metal complexes. I. Ligand field parameters of some dimethylglyoximatodiamino-cobalt (III) complexes, J. Zsakó, J. Sata und Cs. Várhelyi 1759

Page

Electronic structures of some molecules and ions containing carbon, silicon, oxygen and sulphur. II. CO, SiO, CS, SiS and COS, The -, P. G. Perkins 1283

Electronic structures of some molecules and ions containing carbon, silicon, oxygen and sulphur. III. Anions formed by carbon, silicon and sulphur, The -, P. G. Perkins . . . 1501

Electronic structures of some six-membered sulphur-nitrogen and sulphur oxygen ring systems, The -, D. R. Armstrong, R. C. W. King and P. G. Perkins 2011

Electroplating of copper from pyrophosphate baths. I. The effect of electrolyte pH, O. Radovici, C. Vass and I. Solacolu 1325

Electroplating of copper from pyrophosphate baths. II. The effect of electrolyte temperature, O. Radovici, C. Vass and I. Solacolu . . . 2021

Energetic levels in the complexes obtained by organic reagents, A perturbational procedure applied to the calculation of the -, Gr. Popa and S. Moldoveanu 1883

Équilibres de phase du système Na_2O-CaO-Al_2O_3-SiO_2. Équilibres de phase dans le sous-système $Na_2O \cdot Al_2O_3$ $6 \cdot SiO_2$-$CaO \cdot Al_2O_3 \cdot 2SiO_2$-$3Al_2O_3 \cdot$ $2SiO_2$-Al_2O_3 intéressant la céramique superalumineuse, R. Dinescu et M. Cerchez 23

Equilibrium constant of the side reaction in the concentration cell in dilute Cd-Pb liquid solutions, On the -, Z. Moser, K. Fitzner and L. Zabdyr. 557

Excess functions in the benzene-isobutyl alcohol system, Isothermal equilibrium and calculation of -, R. Vîlcu and Z. Cenușe 377

F

Fazovogo sostava v katalizatore dlia nizkotemperaturnoi konversii okisi ugleroda, Vlianie dobavok i vostanovitelnoi sredj na formilovanie -, P. Putanov, J. Iovanovici. R. Herak 569

5-Fluoro-1,3-dioxane by NMR spectroscopy, Conformational equilibrium of -, S. Mager and L. Eliel 2097

Friedel-Crafts chemistry. I. Cyclialkylations of some secondary and tertiary phenylalkyl chlorides in the presence of the mild $AlCl_3/CH_3NO_2$ and $FeCl_3$ catalysts, Modern -, A. A. Khalaf 297

Friedel-Crafts chemistry. II. Rearrangements accompaning benzene alkylations with 1- and 2-hydroxy-2-methyl-1-phenylpropane, 1-and 2-chloro-2-methyl-1-phenylpropane and 2-methyl-1-phenyl-1-propane in the presence of Friedel-Crafts catalysts, Modern -, A. A. Khalaf . 479

Friedel-Crafts chemistry. III. The isomerisation of 1,1- and 1,2-diphenylbutane under the influence of aluminium chloride catalyst in benzene solvent, Modern -, R. M. Roberts and A. A. Khalaf 1929

Friedel-Craft chemistry. IV. The fragmentation and dealkylation behaviour of 1,1-diphenyl-2-methylpropane and 1,2-diphenyl-2-methylpropane under the influence of water-activated aluminium chloride at 100°, Modern -, R. M. Roberts and A. A. Khalaf 1937

Furocoumarin isomers, Theoretical studies of some -, E. Pop, L. Klasinc and N. Trinajstić 1249

Fused alkali chlorides by the chronopotentiometric method, The interdiffusion coefficient of Pb^{2+} ion in -, C. Herdlicka and S. Sternberg 1689

Fused salts : AgCl + (K, Rb, Cs). I., Thermodynamic properties of the reciprocal mixtures of -, S. Sternberg and L. Bejan 11

Galvanostatic study of the electrochemical adsorption process on the chlorine-active carbon electrode in molten salts. II. Remanent potential, The -, S. Petrescu, S. Sternberg and V. Petrescu 1715

Gas chromatographic separation of formic aldehyde methyl alcohol, water and hydrogen peroxide, M. Bozeșanu. 2037

H

Heat of melting for eutetics formed in binary systems of $AgNO_3$ with KNO_3, $RbNO_3$, $CsNO_3$, AgCl and AgBr, D. I. Marchidan and L. Vasu 1295

Heterocycles. I. Considerations concerning thermodynamic stability and conservation of orbital symmetry, Stability of three-membered-, R. Vîlceanu, Z. Simon and A. Chiriac 1353

Page

Heterocycles. XXIV. A study of intermediates in the Hantzsch reaction. A new method to obtain 5-acetylthiazole derivatives, Contributions to the study of -, I. Simiti, M. Coman and I. Schwartz 685

Heterocyclic derivatives with thiazolic rings. I. Synthesis of 6-aminothiazole 4,5-f indazole, C. Tărăbăşanu-Mihăilă, L. Floru, E. Baltă and A. Predescu 889

Heterocyclic derivatives with thiazolic rings. II. Electrophilic substitutions of 6-aminothiazole [4,5-f] indazole, C. Tărăbăşanu-Mihăilă, L. Floru and M. Olteanu 2113

Heterocyclic methylene bases. X. 2-(ω-acyl-ω-arylazo) methylene derivatives of N-containing heterocyles, M. Fărcăşan, R. Chira, Gh. Ciurdaru and V. Denes. 2103

Heterocyclic organoboron compounds. XV. Boronium chelate salts and beryllium chelates of 1,3-ketoenols with disturbed resonance in the chelate ring, E. Isfan and A. Barabás . . 667

Heteropolywolframate des Th (IV), A. V. Botar und T.J.R. Weakley . . 1155

Homogeneous reaction between methane and sulphur, Kinetics of the -, A. Drăgănescu, I. Bică and C. Petrescu 1859

Homologie und der homologen Serien, Die mathematische Darstellung der -, I. Moţoc 1419

Hydrazinocarboxylic acid. II. Syntheses and spectral data, On some derivatives of the -, S. Avramovici, I. Druţă and I. Zugrăvescu 431

Hydroacridine. XI. Der sterische Ablauf der Quaternierung von N-methyl-α-perhydroacridin und N-methyl-β-perhydroacridin mit Trideuteromethyljodid, Darstellung und Untersuchung der -, N. Bărbulescu und F. Potmischil 1613

Hydrolyse der l'ion UO_2^{2+} en milieu perchlorique, Contribution à l'étude de l' -, M. Mavrodin-Tărăbîc 609

Hydroxy-phenothiazine-5,5-dioxides. I. 1,7,9-trichloro-3-hydroxy-5,5-dioxi-phenothiazine, T. Panea, V. Fărcăşan and C. Bodea 1259

I

Intermetallic compounds of the cerium-thallium system, Electrical conductivity of -, G. D. Cismaru and P. Spacu 1345

Page

Ionophoresis with flow gradient, A. Constantinescu and C. Liteanu 1273

Isocinchomeronic acid, Influence of drying temperature on water content and crystalline characteristics of -, L. Campanella, P. L. Cignini and G. de Angelis 1825

Isocinchomeronic acid, Polarographic behaviour of -, L. Campanella, P. L. Cignini and G. de Angelis 1649

2-Isopropyl-5-acetyl-1,3-dioxane, Synthesis and configurational equilibrium of -, S. Mager and E. L. Eliel 1379

Isotopic exchange of active methyl hydrogens. VII. Kinetic study of 2,4, 6-trimethylpyrylium salts in deuterium oxides, E. Gârd, F. Chiraleu, I. I. Stănoiu and A. T. Balaban 257

J

Joshi effect in halogens and oxygen. Influence of intersleeve exposure to brushes from a. d.c. and various a.c. high tension sources, J. Prashad 1075

K

γ-Keto acids in the Pfitzinger reaction, A. M. El Abbady, M. S. Omara and N. G. Kandil 899

L

Ladder polymers. I. Band structure of polyacenes and nitrogen substituted polyacenes, The electronic structure of some -, P. G. Perkins . . . 931

Ladder polymers. II. Excited states of *cata*-condensed benzenes, pyrazines and pyridines, The electronic structure of -, P. G. Perkins. . . . 1111

Lanthanide compounds with neutral ligands containing donor oxygen atom. I. Lanthanide chlorosalicylate with triphenylphosphin oxide, Mixed -, S. Ploştinaru and P. Spacu 2051

Lanthanides with biguanide derivatives. V. Lanthanide compounds with hydrochloric paludrine, Contributions to the study of -, I. Albescu 599

Lanthanides with biguanide derivatives. VI. Halogeno- and pseudohalogeno-compounds of lanthanides, Contributions to the study of -, I. Albescu 829

Page

Ligand compounds of lanthanides, Spectral study of some mixed -, P. Spacu and S. Ploştinaru 971

Liquid membrane electrodes. I. The *n*-butanol-frit electrode in acid-base potentiometric titration, M. Mioşcu, E. Hopîrtean and C. Liteanu 1637

Liquid membrane-electrodes. III. Electrodes with water-immiscible organic liquids in frit. Applications in potentiometric acid - base titrations, C. Liteanu, E. Hopîrtean and M. Mioşcu 1643

M

Magnetic dispersion and magnetic absorption of some ferrimagnetic compounds in the domain of centimetre waves. I. Li-Fe-Be and Ni-Fe-Be, N. Duşoiu 1339

Mass transfer in the absorption from a freely rising gas bubble under the action of mechanical vibrations, C. Balaban, Gh. Dobrăniş and R. Mihail 1829

Matrizielle Charakterisierung der Struktur und Topologie der organischen Verbindungen. I. Konstitution, F. Kerek und I. Moţoc . . 283

Matrizielle Charakterisierung der Struktur und Topologie organischer Verbindungen. II. Konfiguration, Chiralität, I. Moţoc und F. Kerek . . 289

atrizieille Charakterisierung der Struktur und Topologie der organischen Verbindungen. III. Konformation, Chirale Konformeren, F. Kerek und I. Moţoc 655

Matrizielle Charakterisierung der Struktur und Topologie der organischen Verbindungen. IV. Prochiralität Pseudochiralität, I. Moţoc und F. Kerek 2127

Membrane-electrodes under current. I. Current-membrane potential curves for the parchment membrane-electrode impregnated with $BaSO_4$, Studies on the electroanalytical behaviour of -, C. Liteanu and I. C. Popescu 319

Membrane-electrodes under current. II. The E-pH electrode function and the use of a membrane-electrode of parchment paper impregnated with $BaSO_4$ in acid-base potentiometric titrations under constant direct current, Studies on the electroanalytical behaviour of -, C. Liteanu, I. C. Popescu and M. Preda . . . 1811

Membrane-electrodes under current. IV. The E-pAg electrode function and the use of the ceramic membrane electrode of Ag_2S, Ag^+-selective in potentiometric titrations by precipitating at constant direct current, Studies on the electroanalytical behaviour of -, I. C. Popescu, C. Liteanu and L. Savici 1983

Methyl radicals on porous Vycor glass as studied by ESR spectroscopy, D. P. Lazăr and J. Turkevich . . 537

Molecular complexes. III. Iodine complexes with five-membered heteroaromatic, A perturbation treatment of -, M. Dobrescu-Ciureanu and V. E. Sahini 921

Molten salt pairs (K, Ag ; Cl, Br), Surface tension of the reciprocal -, S. Sternberg and M. Terzi 1319

Molten salts, Diffusion potentials in —, I. G. Murgulescu and L. Popescu 737

Molten salts of significance to magnesium electrolysis, Physico-chemical properties of -, K. Grjotheim, I. L. Holm- and H. A. Oye 2017

Mössbauer effect in complexes of isonicotinic acid hydrazide with Fe (II)-isothiocyanate (INAH)$_2$Fe(NCS)$_2$ H$_2$O, I. I. Georgescu, M. Morariu and D. Ţarina 2067

N

Napthth [2,3-c] acridan-5,8,14-trionic dyes, New syntheses of -, F. Urseanu, C. Drăghici, R. Vintilă and E. Sliam 1019

Nickel catalysts, Kinetic study on the reduction of -, T. Chirulescu, C. Ciobanu and Gh. Şerban 1333

Nickel-chromia catalyst, The ferromagnetic resonance of -, I. Inţa and P. Mărgineanu 347

Nicotinic acid, Polarographic, oscillopolarographic and chronopotentiometric behaviour and determination of -, L. Campanella, P. Cignini and G. de Angelis 1269

Nitrate d'ammonium en regime non-isothermique, Cinétique des transformations du -, D. Fătu, S. Fătu et E. Segal 1709

Nitroaniline par spectrométrie de masse, L'étude des isomères de la -, V. E. SAhini, C. Podină et M. Strul 1283

Page

Nitrogen free radicals, Use of ESR spectrum simulator for determining precisely hyperfine coupling constants of stable -, N. Negoiţă, R. Baican, F. Domşa and A. T. Balaban 995

Nitrogen mustards, Potential anticancer agents. VIII. New aromatic and heteroaromatic -, I. Niculescu-Duvăz, M. Rotaru, V. Feyns and O. Maior 1617

N-heterocyclic ligands of analytical importance, Simple HMO-calculations on some -, S. P. Sinha . . 777

N^{α}-methyl-lysine, An improved synthesis of optically pure, -, F. Cuiban 463

N-vinylcarbazole by the systems acrylonitrile-$ZnCl_2$ and acrylonitrile-$HgCl_2$, The polymerization of -, D. S. Vasilescu, M. Ştefănescu and Al. Bălănescu 907

O

Organic free radicals, Computing program for interpreting ESR spectra of-, C. Pomponiu and A. T. Balaban 1173

Organosilicon compounds. III. Electronegativity of molecules and their boiling point refractivity and density, Correlation of the physical properties of -, M. A. A. Beg and I. A. Khan 1395

Organosulphur compounds. II. Effective electronegativity of the molecules and their physical properties, Correlation of the physical properties of -, M. A. A. Beg and M. A. Hashmi. 1033

Oxydation de l'hydrogène sur les électrodes poreuses en nickel, L'étude de la réaction d'-, M. Mavrodin-Tărăbîc, I. Ionaca et I. Solacolu . 1121

Oxydic compounds in solid phase through differential thermal analysis, Kinetics of the formation reactions of -, S. Solacolu, M. Cerchez and E. Segal 203

P

Paper thermochromatography. XVII. The separation of leucine and isoleucine in temperature gradient, C. Liteanu and A. Constantinescu . 155

Peroxydierungsgeschwindigkeit mit molekularem Sauerstoff, in flüssiger Phase, Der Einfluss der Kettenlänge einiger *n*-Alkane auf ihre-, I. Drimuş und I. T. Ionescu . . 269

Peptide syntheses with N- (acyl-*o*-nitrophenyl)-substituted amino acids, F. Cuiban. 449

Peptides. XII. Behaviour of the mixed anhydrides of some amino-acids N-protected with ketoesters, A. Balog, D. Breazu, V. Voinescu, M. Herman, E. Vargha and E. Ramontian 123

Peptides. XIV. The synthesis of several peptide sequences related to the Glu^5- and Asp^5 -eledoisins, E. Vargha, A. Balog, F. Gőnczy, D. Breazu and L. Beu 1627

Phenothiazinium cation. I. Synthesis and properties of 3H-phenothiazine-3- [potassium 4-anilsulphonate], 3H-phenothiazine-3- [potassium 3-anilsulphonate] and 3H-phenothiazine-3- [potassium 2-anilsulphonate], Reaction of amines with -, M. Răileanu and I. Radulian . . . 1005

Phenoxatellurine derivatives, NMR spectra of some -, A. Gioabă, V. E. Sahini and E. Volanschi 531

Phenyl benzyl sulphides, M. Iovu and A. Angelescu 263

Phenylhydrazones, The synthesis and spectrophotometric studies on benzoyl cyanide -, L. Beu and J. Russu 723

Photochemical addition of anthronylidene to alkenes, J. W. Pavlik, N. Filipescu, P. T. Frangopol and M. Frangopol 1793

Phototropic glasses with AgCl, Influence of alkaline cations on the sensitivity of the -, P. Baltă and L. Dollingher 399

Pigmente-Isatinderivate. III. Studium der IR-Spektren einiger 2-Arylaminoindoxyle und S-Arylimino - oxindole, Neue organische-, R. Bacaloglu und B. D. Bader. 275

Pigmente-Isatinderivate. IV. Thermisches Verhalten, Neue organische -, R. Vîlceanu, B. D. Bader, M. Rădulescu und M. Marinescu. . . 1225

Poliarograficheskoe issledovanie kompleso-obrazovania etilksantogenata kalia s ionami H^{2+},I. Kovacs i B. Tökes 1263

Polyethylene field. VI. Pressure-volume-temperature-crystallinity relationship in high-pressure additive-containing polyethylene, Studies in the -, D. A. Isăcescu, I. V. Ionescu,

Page

F. Guluță, C. Roncea and D. Mihăiță 695

Polystyrène-polyisoprène comportant du copolymère séquencé, Influence du degré de dispersion sur la stabilité thermique des mélanges -, I. A. Schneider et G. Riess 1685

Potentiometric titration parameters. V. Gold pretreated electrode in potentiometric titration of $Cr_2O_7^{2-}$ with Fe^{2+}, Influence of indicating electrode pretreatment on -, I. Haiduc, D. Dănilă and C. Liteanu . . . 1093

Proton hyperfine splitting constants in cyclic α-keto-iminoxy radicals, Assignement of -, A. Caragheorgheopol, H. Căldăraru and V. E. Sahini 1497

Pyridinemonocarboxylic acids and their use for the qualitative analysis of a mixture of these acids, X-ray powder spectra of -, L. Campanella and P. L. Cignini 1087

Pyridiniumsalze, Über die Synthese einiger quartärem -, L. Petrova und E. Comaniță 1361

Pyrimidine. IV. Synthesis of N-aryl-N' -4- (2-methylthio-5-bromopyrimidoyl) ureas and -thiourea, V. V. Badiger and S. C. Bennur 1389

Pyrylium salts with nucleophiles. X. N (12)-substituted 11,13-dimethyl [9] (2,6)-pyridinophanium perchlorates, Reaction of -, A. T. Balaban 1609

Q

Quaternary basic ammonium polyelectrolytes. I. Quaternization reaction of some tertiary amines hydroxylic groups with chloromethylated polystyrene, I. Petrariu, C. Luca, Ig. Poinescu and M. Dima 493

R

Radicalic polymerization, On the reactivity of N-vinylcaprolactam in -, N. Cobianu, C. Boghină, B. Mărculescu and I. Amălinei 305

Radiolytic reduction of Cr^{VI} in aqueous solutions, Mechanism of -, M. Fiti . 511

Réactions d'échange isotopique entre Tl (III) complexé et ^{204}Tl (I), Al. Cecal et I. A. Schneider 35

Réactions hétérogènes décrites par des équations cinétiques non encadrées dans le modèle de l'ordre de réaction, Méthodes non isothermiques utilisées pour la détermination des paramètres cinétiques des -, E. Segal 1555

Page

S

Silicide coating on molybdenum obtained by electrotransport and diffusion from molten fluorides, N. Petrescu, M. Petrescu, N. Brițchi and L. Pavel. 1853

Solvolyse von *t*-butylchlorid. I. Lösungsmittel- und Saltzeffekte bei der Solvolyse von *t*-butylchlorid in wässeringen methanol- und dioxangemischen, Mediumeinflüsse bei der -, R. M. Schuster und I. A. Schneider 1841

Spectres électroniques de quelques bases de Schiff à noyaux benz- et naphto-thiazoliques, Les -, S. Avramovici, A. Airinei et I. Ciocoiu 1781

Spectrophotometric determination of Co^{2+} in $CdCl_2$ lattice, Ath. Truția and M. Vodă 1805

Spektrophotometrische Dosierung der $Cr_2O_7^{2-}$ und $Cr_2O_7^{2-}$ Ionen mit *o*-Tolidin, I. Florea 1993

Strömungstechnische Fragen ungleichkörniger Wirbelschichten, G. I. Jinescu und H. H. Rehner 2149

Submicronic powders. The $ZrO_2 + CaO$ system, The reaction kinetics in -, D. Cismaru and C. Radovici. . . 1699

4-Sulfonamidobenzolsäure komplexgebundenen Quecksilbers (II), in stark alkalischem Medium, Die polarographische Bestimmung mit dem Natriumsaltz der -Gh. Facsko und M. Nemeș 1971

Schiff base complexes with IV and V group metals, N. S. Biradar and V. H. Kulkarni 63

Significant structures theory of ionic binary liquid mixtures : heat capacities, compressibility coefficients and thermal-expansion coefficients, R. Vîlcu and C. Misdolea 387

Silicate slags, The role of clinker and of calcium chloride in the hardening process of some -, I. Teoreanu and M. Georgescu. 623

Silver halides in passing from solid to molten state, Electronic absorption spectra of -, I. G. Murgulescu, E. Popa and E. Ivana 189

Solvent effect on the anharmonicity of the C=O vibration of acetophenone and benzophenone, V. E. Sahini and M. Olteneanu 361

Page

Solvolytic reactions. IV. Transition state in the π-route of the acetolysis of 5H-dibenzo [a, d]- cyclohepten-5-yl-(β-ethyl) tosylate, Kinetics of -, M. Voicu, F. Badea and A. Voicu 131

Source chimique de courant $Zn|MOH|O_2$. I. L'efficacité électrochimique d'une pile à cathode activée avec de l'argent, Contribution à l'étude de la -, O. Radovici, M. Mavrodin-Tărăbîc, I. Onaca et I. Solacolu 767

Spectrophotometric determination of the partition constant using variable amounts of solvent, L. M. Băloiu 1659

Stochastic modelling of chemical processes, O. Iordache, M. Muntean and I. Teoreanu 239

Substitution reactions of complexes. XLIII. Basic hydrolysis of $[Co(DH)_2(H_2O)(NCS)]$, Kinetics and mechanism of -, Z. Finta, Cs. Várhelyi and J. Zsakó 417

T

Tension interfaciale dans le système solution benzénique de tributylphosphate/solution aqueuse de nitrate cuivrique, M. Tomoaia, Z. Andrei et E. Chifu 1547

1,2,3,4-Tetrahydroakridin-9-Carboxyl-Suäre-Derivate. I. Amide, Über -, M. Cîrje 1013

Thermal decomposition of ammonium molybdate supported on alumina, Study of the -, I. Sălăgeanu, D. Trestianu and E. Segal 1537

Thermodynamic data by solid state EMF technique and phase boundaries for some nonstoichiometric uranium oxides, D. I. Marchidan and S. Matei-Tănăsescu 1681

Thermodynamic excess properties of molten LiCl + KCl, LiCl + RbCl, NaCl + RbCl and NaCl + CsCl mixtures, S. Sternberg and I. Adorian 945

Thiazoles, Electronic spectra and acidity constants of some 2-amino-5-substituted -, D. Suciu 677

Thienylfurans, Theoretical study of isomeric-, L. Klasinc, N. Trinajstić and E. Pop 89

Thin-layer thermochromatography. X. Comparison between temperature gradient chromatography resolution and nonsaturated chamber resolution, T. Hodişan, C. Liteanu and S. Gocan 2143

Page

Thioamides, Relations concernant la structure électronique et la réactivité de quelques -, F. Cornea, C. Fulea et A. O. Fulea 111

Thiocomplexes. III. Complex compounds of Pd (I) with thioamides, Contributions to the chemistry of -, D. Negoiu, V. Mureşan and C. Fulea 1749

Thiocomplexes. IV. Complex compounds of Pd (II) with thioamides of the dibenzofuran series, Contributions to the chemistry of -, D. Negoiu, V. Mureşan and S. Florea . 1875

Thiourea and phosphine complexes of Ni (II) and Co (II), Studies on coordination compounds -, I. A. Khan and A. H. Hashmi 815

Thorium complexes with pyrimidine derivatives, New -, Fl. Popea and C. Mărculescu 425

Thorium-purpurin complex by butanol extraction, Study of the -, C. Drăgulescu, T. Simionescu and M. Totan-Curtui 43

Threshold potential in air, Influence of irradiation on the -, J. Prashad 1865

Titanium (I) chloride complexes with cobalt (II) chelates of tetradentate. Schiff-bases, N. S. Biradar, V. B. Mahale and V. H. Kulkarni . . 809

Tolazoline. Visible and infrared spectra of combination with ammonium reineckate, Gr. Teodorescu . . . 501

Transference numbers and mobilities in molten univalent nitrates, D. Topor 1311

Transient species from the reaction of the hydrated electron with hexacyanocobaltate (III), I. Mihalcea and R. R. Hentz 1577

Transition metals with tertiary stibines. I. Complex combinations of palladium (II) with tritolyl-stibines, Complex combinations of -, D. Negoiu and L. Paruta 2059

1,2,3-Trimethoxyacridine, Electronic structure and transitions of -, M. Vlassa, M. Ionescu and J. Fabian 99

Tris-éthers. I. La condensation du bis (chlorométhyle) éther avec les phénoxyde, méthyle et diméthyle-phénoxydes de sodium, M. Iovu et G. Cîmpeanu. 883

U

Uranium hexavalent, L'étude des espèces ioniques formées par l'hydrolyse de l'ion d'-, M. Mavrodin-Tărăbîc. 73

Page

Uranyl compounds with pyrimidine derivatives, New -, F. Popea, C. Mărculescu and C. Pîrlog 247

Uranyl-pyrosphosphate complexes. III. The monopyrophosphato-pentauranyl cation complex, C. Drăgulescu and N. Vîlceanu 49

Uranyl-pyrosphosphate complexes. IV. Precipitation reactions of the pyrophosphato uranylate complex anions with the Ag^+ ion, C. Drăgulescu, N. Vîlceanu and I. Julean . 53

Uranyl-pyrophosphate complexes. V. The precipitation reaction of the sodium bis-pyrophosphato-uranylate complex with the Cd^{2+} ion, C. Drăgulescu and N. Vîlceanu . . 59

V

Vanadium by the reaction between pyrogallol bromine red and potassium bromate, Kinetic determination of -, D. Costache and S. Sasu 913

Vapor pressure of antimony trichloride, V. Piacente and G. Balducci . . . 2083

Vapour pressure and sublimation enthalpy of antimony trifluoride. Vapour pressure of bismuth trifluoride, Simultaneous determination by Knudsen effusion-microcalorimetric technique of the -, G. de Maria, L. Malaspina, G. Bardi and R. Gigli. 367

Vitroceramic structures of the Na_2O-MgO-Al_2O_3-SiO_2-system on volume effects, The mineralizing action of F^- ions in -, Ş. Solacolu and D. Popescu-Haş 3

X

Xenon and other noble gases, Some aspects of the chemistry of -, L. G. Ionescu 1731

Xylidine isomers. II. The influence of isomerism on dipole moments, V. E. Sahini and J. Weinberg 1493

Y

Yttrium and lanthanides with derivatives of anthranilic acid. I. The N, N is (carboxy methyl) anthranilic acid (ANDA), New compounds of-, P. Spacu and E. Ivan 405

Yttrium and lanthanides with N,N′-ethylenedianthranilic acid (EDAN), New compounds of -, P. Spacu and E. Ivan 589

NOTE POUR LES AUTEURS

La *Revue Roumanie de Chimie* publie des articles en anglais, français, russe, allemand ou espagnol. Les auteurs sont priés d'envoyer des articles, notes, communications et comptes rendus inédits.

Les manuscrits seront dactylographiés à deux intervalles. Les tableaux seront dactylographiés sur feuilles séparées, de même que la légende des figures. Les diagrammes seront tracés à l'encre de Chine sur papier calque. Les tableaux et les figures seront numérotés par des chiffres arabes, en nombre strictement nécessaire. Prière de ne pas inscrire les mêmes données dans les tableaux et les figures. Les formules chimiques seront incluses dans le texte ; en outre, elles seront transcrites sur des feuilles séparées. Les auteurs sont priés d'indiquer les caractères italiques (en soulignant les lettres au crayon), ainsi que tout autre caractère spécial. L'ordre des références bibliographiques sera celui de leur mention dans le texte ; le nom de l'auteur sera précédé de l'initiale du prénom ; les publications périodiques seront présentées suivant les prescriptions internationales. Les références seront ajoutées à la fin de l'article ; elles paraîtront comme des notes, au bas de la page. Le texte sera précédé d'un résumé comprenant 15 lignes au maximum.

L'entière responsabilité du contenu des articles appartient aux auteurs. On publie des articles dus aux collaborateurs roumains ou étrangers. Les auteurs recevront 50 tirés à part.

PRINTED IN ROMANIA

TRAVAUX PARUS AUX ÉDITIONS DE L'ACADÉMIE DE LA RÉPUBLIQUE SOCIALISTE DE ROUMANIE

MARIA FITI, **Dozimetria chimică a radiaţiilor ionizante** (La dosimétrie chimique des radiations ionisantes), 1973, 240 p., 13,50 lei.

MIHAI FLORESCU, **Eficienţa economică a cercetării ştiinţifice** (L'efficience économique de la recherche scientifique), 1972, 115 p., 15 lei.

GEORGETA LĂZĂRESCU, **Sistematizarea informaţiilor în chimia organică** (La systématisation des informations dans la chimie organique), 1972, 242 p., 10,50 lei.

P. BALTĂ et E. BALTĂ, **Introducere în chimia fizică a stării vitroase** (Introduction à la chimie physique de l'état vitreux), 1971, 240 p., 15,50 lei.

LYDIA-MARIA VAICUM, **Biodegrabilitatea detergenţilor** (La biodégrabilité des détergents), 1971, 346 p., 19,50 lei.

TIBERIU NĂŞCUŢIU, **Metode radiometrice de analiză** (Méthodes radiométriques d'analyse), 1971, 346 p., 19,50 lei.

I. ZUGRĂVESCU et L. STOICESCU-CRIVETZ, **Polimeri heterociclici** (Polymères hétérocycliques), 1971, 190 p., 9,50 lei.

I. V. MAXIM, **Materiale nucleare** (Matériaux nucléaires), 1969, 444 p., 30 lei.

CRISTOFOR SIMIONESCU et C. V. UGLEA, **Fracţionarea compuşilor macromoleculari** (Fractionnement des composés macromoléculaires), 1969, 292 p., 18,50 lei.

CORNEL BODEA et collab., **Tratat de biochimie vegetală**, partea I, **Fitochimie** (Traité de biochimie végétale, 1re partie, Phytochimie), Ier vol., 1964, 747 p. + 4 annexes + 2 pl., 41 lei ; IIe vol., 1965, 1962 p., 1 pl., 56 lei ; IIIe vol., 1967, 773 p., 35 lei.

CRISTOFOR SIMIONESCU et CLEOPATRA VASILIU-OPREA, **Mecanochimia compuşilor macromoleculari** (La mécanochimie des composés macromoléculaires), 1967, 344 p., 23,50 lei.

V. GHEŢIE et V. MICUŞAN, **Analiza imunochimică. Teorie şi practică** (Analyse immunochimique. Théorie et pratique), 1966, 369 p., 28 lei.

R. PORTOCALĂ et L. POPA, **Acizii ribonucleici celulari şi virali** (Les acides ribonucléiques cellulaires et viraux), 1966, 375 p., 8 pl., 26 lei.

I.P.I. — c. 3423

43 426

Lei 25.—